VOLUME 1

Neonatal and Perinatal Medicine

Atlas of the Newborn

Rudolph

VOLUME 1

Neonatal
and
Perinatal
Medicine

Atlas of the Newborn

Arnold J. Rudolph, M.D.
(Deceased)
Professor of Pediatrics
Baylor Medical College
Houston, Texas

VOLUME 1

Neonatal
and
Perinatal
Medicine

Atlas of the Newborn

Arnold J. Rudolph, M.D.
(Deceased)

1997

B.C. Decker Inc.
Hamilton • London

B.C. Decker Inc.
4 Hughson Street South
P.O. Box 620, L.C.D. 1
Hamilton, Ontario L8N 3K7
Tel: 905 522-7017
Fax: 905 522-7839
e-mail: info@bcdecker.com

Printed in Canada

96 97 98 99 00/BP/987654321

ISBN 1-55009-031-3

Sales and distribution

United States
Blackwell Science Inc.
Commerce Place
350 Main Street
Malden, MA 02148
U.S.A.
Tel: 1-800-215-1000

Canada
Copp Clark Ltd.
200 Adelaide Street West
3rd Floor
Toronto, Ontario
Canada M5H 1W7
Tel: 416-597-1616
Fax: 416-597-1617

Japan
Igaku-Shoin Ltd.
Tokyo International P.O. Box 5063
1-28-36 Hongo, Bunkyo-ku
Tokyo 113, Japan
Tel: 3 3817 5680
Fax: 3 3815 7805

U.K., Europe, Scandinavia, Middle East
Blackwell Science Ltd.
c/o Marston Book Services Ltd.
P.O. Box 87
Oxford OX2 0DT
England
Tel: 44-1865-79115

Australia
Blackwell Science Pty, Ltd.
54 University Street
Carleton, Victoria 3053
Australia
Tel: 03 9347 0300
Fax: 03 9349 3016

Notice: the authors and publisher have made every effort to ensure that the patient care recommended herein, including choice of drugs and drug dosages, is in accord with the accepted standard and practice at the time of publication. However, since research and regulation constantly change clinical standards, the reader is urged to check the product information sheet included in the package of each drug, which includes recommended doses, warnings, and contraindications. This is particularly important with new or infrequently used drugs.

Foreword

Sir William Osler stated, "There is no more difficult task in medicine than the art of observation." The late Arnold Jack Rudolph was an internationally renowned neonatologist, a teacher's teacher, and, above all, one who constantly reminded us about how much could be learned by simply observing, in his case, the newborn infant.

This color atlas of neonatology represents a distillation of more than 50 years of observing normal and abnormal newborn infants. The *Atlas* begins with a section on the placenta, its membranes, and the umbilical cord. Jack Rudolph delighted in giving a lecture entitled "Don't Make Mirth of the Afterbirth," in which he captivated audiences by showing them how much you could learn about the newborn infant from simply observing the placenta, its membranes, and the umbilical cord.

In a few more than 60 photomicrographs, we learn to read the placenta and gain insight into such disorders as intrauterine growth retardation, omphalitis, cytomegalic inclusion disease, congenital syphilis, and congenital neuroblastoma. Congenital abnormalities of every organ system are depicted along with the appearance of newborn infants who have been subjected in utero to a variety of different drugs, toxins, or chemicals. We also learn to appreciate the manifestations of birth trauma and abnormalities caused by abnormal intrauterine positioning.

More than 250 photographs are used to illustrate the field of neonatal dermatology. The collection of photographs used in this section is superior to that which I have seen in any other textbook or atlas of neonatology or dermatology; this section alone makes this reference a required addition to the library of any clinician interested in the care of infants and children. Photographs of the Kasabach-Merritt syndrome (cavernous hemangioma with thrombocytopenia), Klippel-Trénaunay syndrome, Turner's syndrome, Waardenburg's syndrome, neurocutaneous melanosis, mastocytosis (urticaria pigmentosa), and incontinentia pigmenti (Bloch-Sulzberger syndrome) are among the best that I have seen.

Cutaneous manifestations are associated with many perinatal infections. The varied manifestations of staphylococcal infection of the newborn are depicted vividly in photomicrographs of furunculosis, pyoderma, bullous impetigo, abscesses, parotitis, dacryocystitis, inastitis, cellulitis, omphalitis, and funisitis. Streptococcal cellulitis, *Haemophilus influenzae* cellulitis, and cutaneous manifestations of listeriosis all are depicted. There are numerous photomicrographs of congenital syphilis, showing the typical peripheral desquamative rash on the palms and soles, as well as other potential skin manifestations of congenital syphilis which may produce either vesicular, bullous, or ulcerative lesions. The various radiologic manifestations of congenital syphilis, including pneumonia alba, ascites, growth arrest lines, Wegner's sign, periostitis, and syphilitic osteochondritis, are depicted. Periostitis of the clavicle (Higouménaki's sign) is shown in a photograph that also depicts periostitis of the ribs. A beautiful photomicrograph of Wimberger's sign also has been included; this sign, which may appear in an infant with congenital syphilis, reveals radiolucency due to erosion of the medial aspect of the proximal tibial metaphysis.

The *Atlas* also includes a beautiful set of photographs which delineate the ophthalmologic examination of the newborn. Lesions which may result from trauma, infection, or congenital abnormalities are included. There are numerous photographs of the ocular manifestations of a variety of systemic diseases, such as Tay-Sachs disease, tuberous sclerosis, tyrosinase deficiency, and many more. Photographs of disturbances of each of the various organ systems, or disorders affecting such organ systems, also are included along with numerous photographs of different forms of dwarfism, nonchromosomal syndromes and associations, and chromosomal disorders. In short, this *Atlas* is the complete visual textbook of neonatology and will provide any

physician, nurse, or student with a distillation of 50 years of neonatal experience as viewed through the eyes of a master clinician.

Arnold Jack Rudolph was born in 1918, grew up in South Africa, and graduated from the Witwatersrand Medical School in 1940. Following residency training in pediatrics at the Transvaal Memorial Hospital for Children, he entered private pediatric practice in Johannesburg, South Africa. After almost a decade, he left South Africa and moved to Boston, where he served as a Senior Assistant Resident in Medicine at the Children's Medical Center in Boston, Massachusetts, and subsequently pursued fellowship training in neonatology at the same institution and at the Boston Lying-In Hospital, Children's Medical Center and Harvard Medical School under Dr. Clement A. Smith.

In 1961, Dr. Rudolph came to Baylor College of Medicine in Houston, Texas, the school at which he spent the remainder of his career. He was a master teacher, who received the outstanding teacher award from pediatric medical students on so many occasions that he was elected to the Outstanding Faculty Hall of Fame in 1982. Dr. Rudolph also received numerous awards over the years from the pediatric house staffs for his superb teaching skills.

He was the Director of the Newborn Section in the Department of Pediatrics at Baylor College of Medicine for many years, until he voluntarily relinquished that position in 1986 for reasons related to his health. Nevertheless, Jack Rudolph continued to work extraordinarily long hours in the care of the newborn infant, and was at the bedside teaching both students and house staff, as well as his colleagues, on a daily basis until just a few months before his death in July 1995.

Although Dr. Rudolph was the author or co-author of more than 100 published papers that appeared in the peer-reviewed medical literature, his most lasting contribution to neonatology and to pediatrics is in the legacy of the numerous medical students, house staff, fellows, and other colleagues whom he taught incessantly about how much one could learn from simply observing the newborn infant. This *Atlas* is a tour de force; it is a spectacular teaching tool that has been developed, collated, and presented by one of the finest clinical neonatologists in the history of medicine. It is an intensely personal volume that, as Dr. Rudolph himself states, "is not intended to rival standard neonatology texts," but rather to supplement them. This statement reveals Dr. Rudolph's innate modesty, since with the exception of some discussion on pathogenesis and treatment, it surpasses most neonatology texts in the wealth of clinical information that one can derive from viewing and imbibing its contents. We owe Dr. Rudolph and those who aided him in this work a debt of gratitude for making available to the medical community an unparalleled visual reference on the normal and abnormal newborn infant.

Ralph D. Feigin, M.D.
June 13, 1996

Preface

I first became attracted to the idea of producing a color atlas of neonatology many years ago. However, the impetus to synthesize my experience and compile this current collection was inspired by the frequent requests from medical students, pediatric house staff, nurses and others to provide them with a color atlas of the clinical material provided in my "slide shows." For the past few decades I have used the medium of color slides and radiographs as a teaching tool. In these weekly "slide shows" the normal and abnormal, as words never can, are illustrated.

"I cannot define an elephant but I know one when I see one."[1]

The collection of material used has been added to constantly with the support of the pediatric house staff who inform me to "bring your camera" whenever they see an unusual clinical finding or syndrome in the nurseries.

A thorough routine neonatal examination is the inalienable right of every infant. Most newborn babies are healthy and only a relatively small number may require special care. It is important to have the ability to distinguish normal variations and minor findings from the subtle early signs of problems. The theme that recurs most often is that careful clinical assessment, in the traditional sense, is the prerequisite and the essential foundation for understanding the disorders of the newborn. It requires familiarity with the wide range of normal, as well as dermatologic, cardiac, pulmonary, gastrointestinal, genitourinary, neurologic, and musculoskeletal disorders, genetics and syndromes. A background in general pediatrics and a working knowledge of obstetrics are essential. The general layout of the atlas is based on the above. Diseases are assigned to each section on the basis of the most frequent and obvious presenting sign. It seems probable that the findings depicted will change significantly in the decades to come. In this way duplication has been kept to a minimum. Additional space has been devoted to those areas of neonatal pathology (e.g., examination of the placenta, multiple births and iatrogenesis) which pose particular problems or cause clinical concern.

Obviously, because of limitations of space, it is impossible to be comprehensive and include every rare disorder or syndrome. I have tried to select both typical findings and variations in normal infants and those found in uncommon conditions. Some relevant conditions where individual variations need to be demonstrated are shown in more than one case.

As the present volume is essentially one of my personal experience, it is not intended to rival standard neonatology texts, but is presented as a supplement to them. It seems logical that references should be to standard texts or reviews where discussion on pathogenesis, treatment, and references to original works may be found.

Helen Mintz Hittner, M.D., has been kind enough to contribute the outstanding section on neonatal ophthalmology.

I have done my best to make the necessary acknowledgements to the various sources for the clinical material. If I have inadvertently omitted any of those, I apologize. My most sincere appreciation and thanks to Donna Hamburg, M.D., Kru Ferry, M.D., Michael Gomez, M.D., Virginia Schneider, PA, and Jeff Murray, M.D., who have spent innumerable hours in organizing and culling the material from my large collection. We wish to thank Abraham M. Rudolph, M.D., for his assistance in reviewing the material. We also wish to thank the following people for their photo contributions to this work: Cirilo Sotelo-Avila, Stan Connor, Avory Fanaroff, Milton Finegold, Brian Kershan, Tom Klima, Susan Landers, Gerardo Cabera-Meza, Ken Moise, Don Singer, Edward Singleton.

It is hoped that this atlas will provide neonatologists, pediatricians, family physicians, medical students and nurses with a basis for recognizing a broad spectrum of normal variations and clinical problems as well as provide them with an overall perspective of neonatology, a field in which there continues to be a rapid acceleration of knowledge and technology. One must bear in mind the caveat that pictures cannot supplant clinical experience in mastering the skill of visual recall.

1. Senile dementia of Alzheimer's type — normal aging or disease? (Editorial) *Lancet* 1989; i:476-477.

Arnold J. Rudolph, M.D.

CONTENTS

Volume I
Neonatal and Perinatal Medicine

Introduction

Although several texts provide extensive written descriptions of disorders o the newborn infant, the senses of touch, hearing and, especially, sight create the most lasting impressions. Over a period of almost five decades, my brother Jack Rudolph diligently recorded in pictorial form his vast experiences in physical examination of the newborn. The *Atlas of the Newborn* reflects a selection from the thousands of color slides in his collection, and truly represents "the art of medicine" as applied to neonatology. A number of unusual or rare conditions are included in this atlas. I consider this fully justified because, if one has not seen or heard of a condition, one cannot diagnose it.

In this, the first in a five-volume series, three main topics are covered. Although it is common practice to discard the afterbirth, or placenta and its membranes, careful examination of this fetal organ often provides insight into conditions affecting the newborn. Thus, it may reveal evidence of intrauterine infection, which may be transmitted to the neonate; of hemorrhage, which may cause asphyxia; or of vascular or developmental anomalies, which may result in intrauterine growth retardation. Many of these placental abnormalities are illustrated in this volume.

Physical forces acting during fetal development, during delivery, or after birth may be responsible for a variety of anomalies in the newborn. The influences of uterine constraint, of fetal position, and of amniotic bands are demonstrated magnificently, with resulting anomalies being related to specific fetal postures. Conditions associated with birth trauma, including fractures, nerve disruptions and other disturbances, are clearly depicted. Many examples of complications resulting from treatment of the newborn, or iatrogenic problems such as vascular complications of umbilical arterial catheterization, are shown graphically.

A major section demonstrates many of the physical anomalies resulting from fetal exposure to various chemicals, such as occurs through maternal drug abuse or administration of pharmacologic agents to the mother during embryonic or fetal development.

This volume will be enormously valuable to obstetricians and neonatologists, as well as to midwives and nurses involved in the delivery and care of the newborn.

Abraham M. Rudolph, M.D.

Chapter 1
The Placenta, Its Membranes, and the Umbilical Cord

The human placenta is a highly sophisticated organ of interface between mother and fetus, often referred to as the "gate-keeper to the fetus." Careful examination of the placenta, its membranes, and the umbilical cord can prove to be a valuable aid in the diagnosis and treatment of the neonate. Gross examination of the placenta takes five minutes, and more sophisticated examination should be considered when there is poor pregnancy outcome, recognizable malformations or abnormalities, multiple gestation, extremes of amniotic fluid volume, severe intrauterine growth retardation, short umbilical cord (< 32 cm), and profound acidemia. The maternal surface of the placenta (decidual plate) is soft, spongy and dark red; and the fetal surface (chorionic plate) is shiny and steel blue to gray. The placenta, membranes, and umbilical cord weigh approximately 400 to 600 g at birth. The ratio of fetal to placental size increases with gestation, being less than or equal to 1:1 at prior to three months, 4:1 at four to six months, and 6:1 at term. Abnormalities in structure can result in an inefficient transport of oxygen and nutrients to the developing baby. Despite this importance, it is one of the least understood and investigated human organs.

1.1

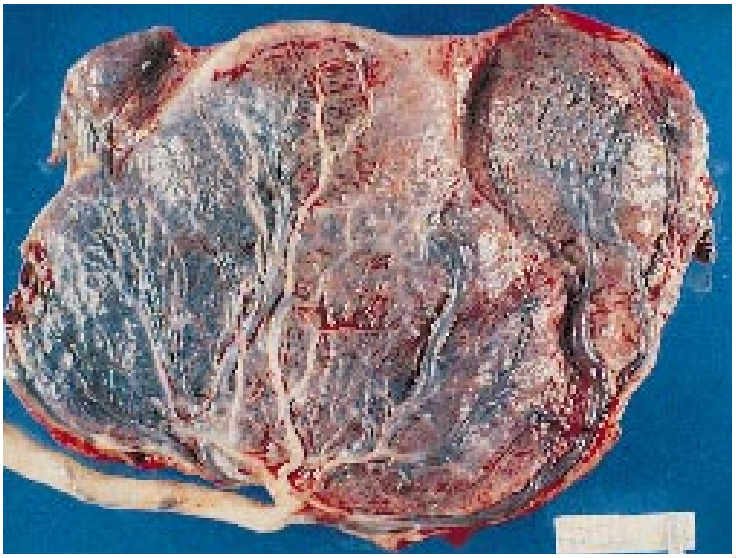

Figure 1.1. A succenturiate (accessory) lobe is common and has no effect on the fetus. This occurs in about 3 to 5% of deliveries. Its importance arises from the fact that it may be retained within the uterus and cause postpartum bleeding. (Sotelo-Avila, C.)

1.2

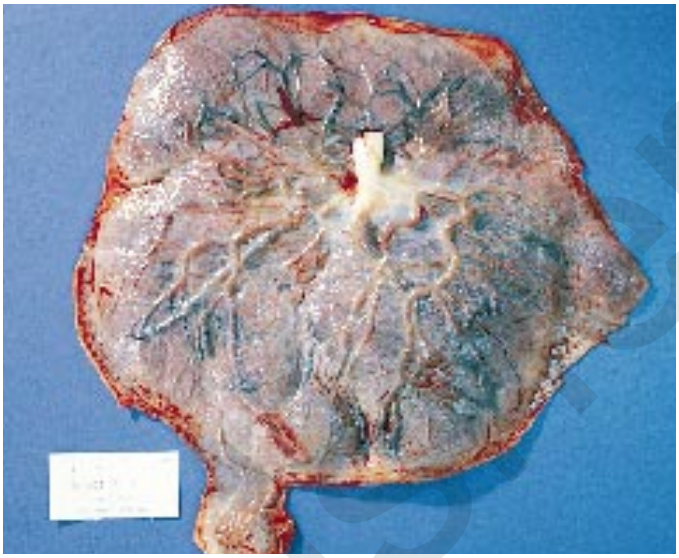

Figure 1.2. Another example of a succenturiate lobe. Note that this is very small and the diagnosis can easily be missed if the placenta is not examined carefully. (Singer, D.)

1.3

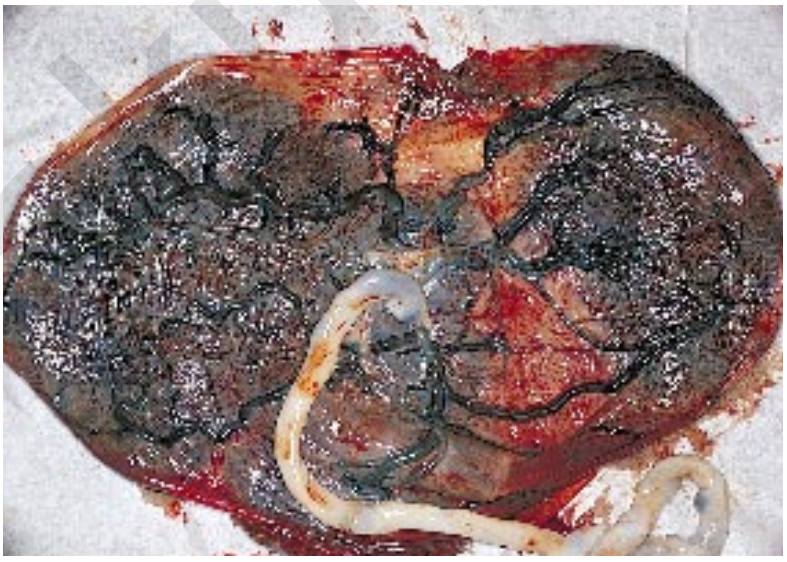

Figure 1.3. Fetal surface of a bipartite or bilobed placenta (placenta duplex). The two parts of the placenta are of nearly equal size and this occurs in about 1% of deliveries. Note that the lobes are separated by membranes. The umbilical cord may insert into one or other lobe, or may insert between the two.

1.4

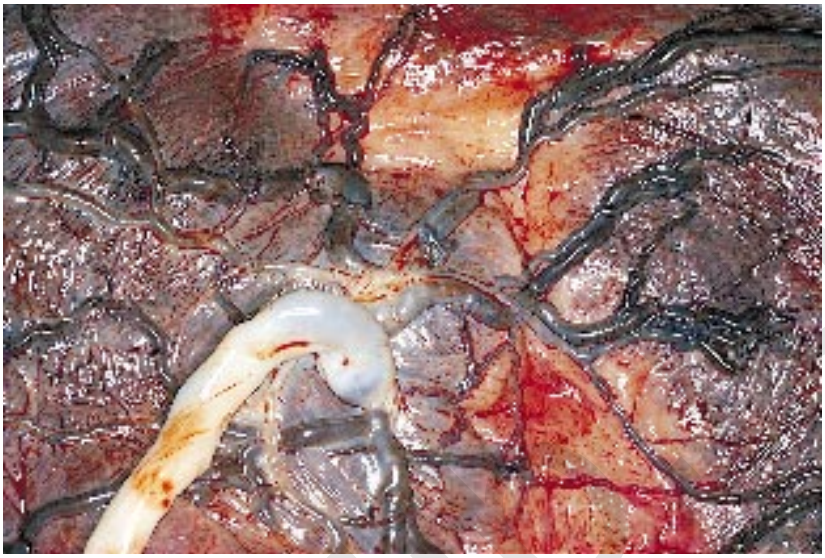

Figure 1.4. A close-up of the same placenta. The risk to the infant is that the vessels crossing the membranes may rupture, resulting in massive blood loss. It is suggested that this condition arises as a result of superficial implantation of the ovum.

1.5

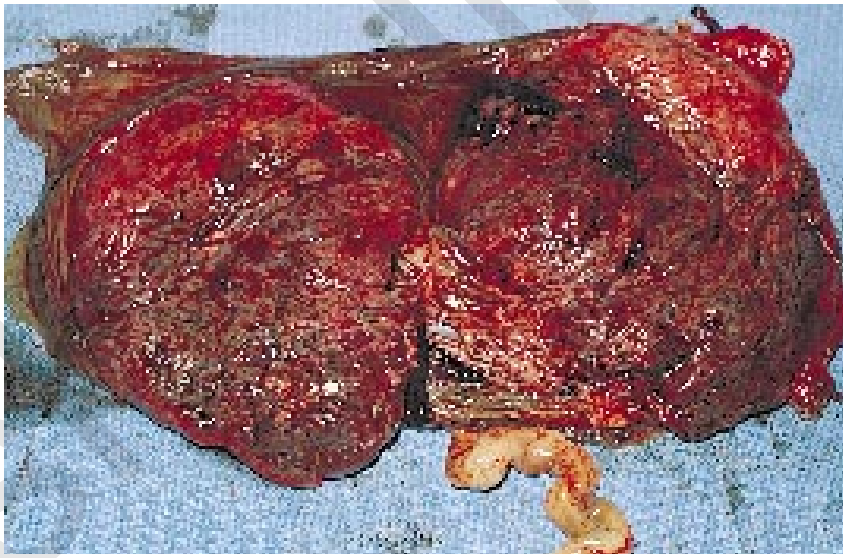

Figure 1.5. Another example of a placenta duplex showing the maternal surface.

1.6

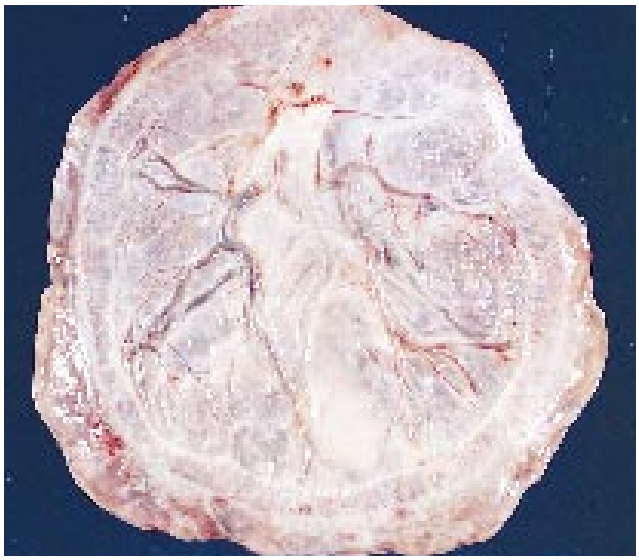

Figure 1.6. In a circumvallate (circummarginate) placenta the fetal surface may be reduced if decidual tissue has made its way between the amnion and chorion. This appears as a yellow, peripheral, hyalinized fold circumscribing the edge of the chorionic plate. This type of placenta has been reported to be a cause of antepartum bleeding and premature labor.

1.7

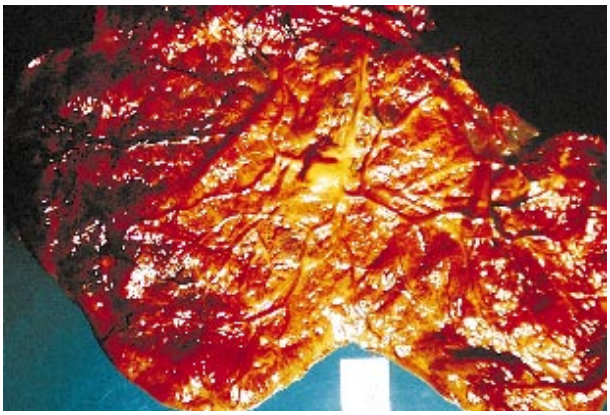

Figure 1.7. This is an example of placenta membranacea (placenta diffusa). These placentas are rare. The ovum implants too deeply, the villae of the chorion fail to regress, and the placental tissue develops over the entire surface of the chorion. The placenta is very thin and is associated with poor fetal growth and antepartum hemorrhage. There may be previa type bleeding.

1.8

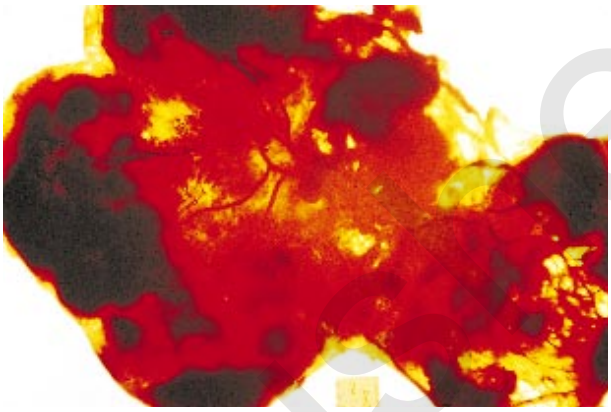

Figure 1.8. Transillumination of the same placenta shows the thinness of this type of placenta and that islets of placental tissue are present throughout the membranes. Pregnancy rarely goes to term and fetal death is common. If pregnancy continues to term, placenta accreta may occur. In this condition, there is failure of separation of the placenta during the third stage of labor and there may be severe postpartum hemorrhage.

1.9

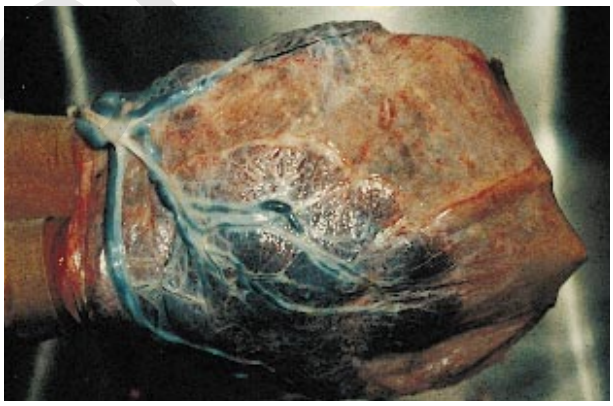

Figure 1.9. An annular ("girdle" or ring-shaped) is a rare form of placenta which resembles a segment of a hollow cylinder. Sometimes a complex ring of placental tissue is seen. More commonly a portion of the ring undergoes atrophy resulting in a placenta which is approximately horseshoe-shaped. This type of placenta is probably a variant of placenta membranacea. Its clinical significance is uncertain but it appears to be associated with a high incidence of both ante- and postpartum bleeding. The fetus is often small for gestational age. (Connor, S.)

1.10

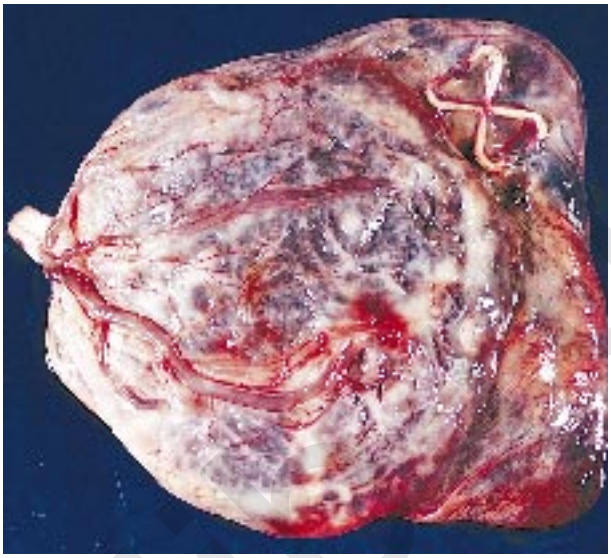

Figure 1.10. This otherwise normal placenta shows the presence of an intrauterine contraceptive device, indicating that it did not prevent pregnancy.

1.11

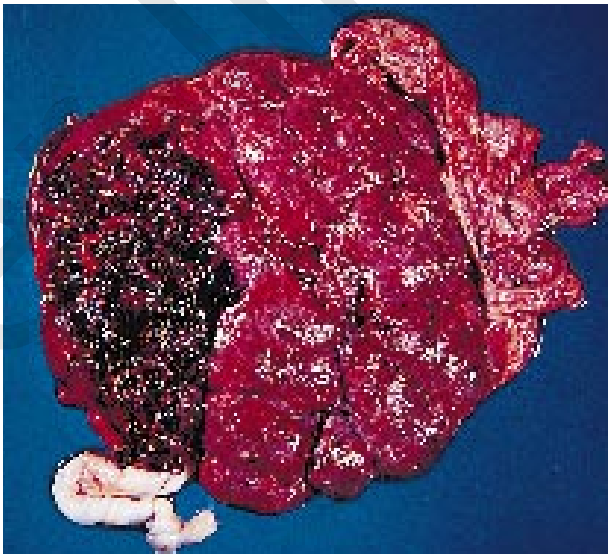

Figure 1.11. In premature separation of the placenta (abruptio placentae) there may be massive bleeding of maternal origin. Note the massive blood loss on the left of the maternal surface of the placenta. In these cases, there may be severe fetal asphyxia or death. The infant in this case had blood in stool (melena neonatorum) at birth. This was shown to be ingested maternal blood by the Apt test.

1.12

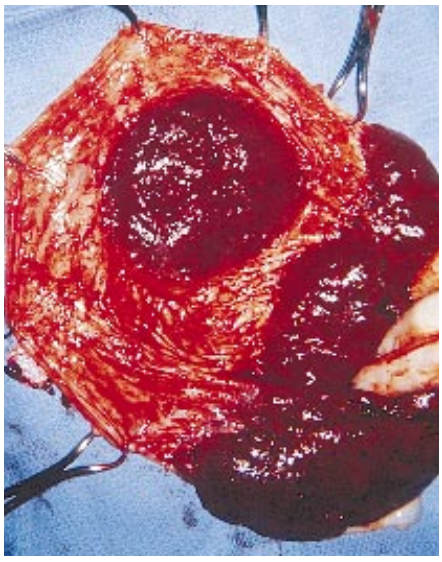

Figure 1.12. Another example of abruptio placentae. A large abruptio placentae may result in poor growth of the infant and fetal blood loss.

1.13

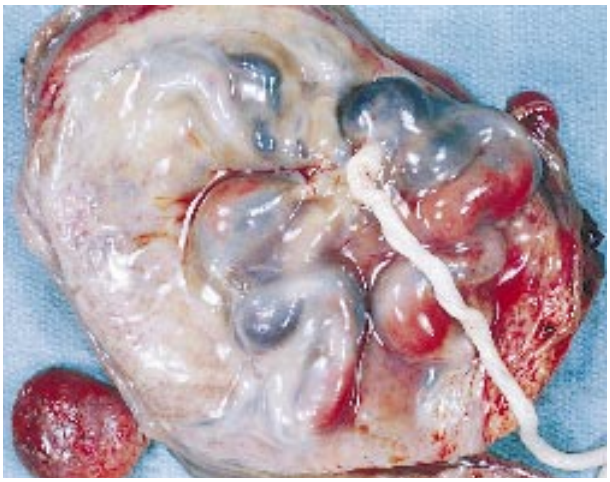

Figure 1.13. Fetal surface of a placenta with a large chorangioma (hemangioma of the placenta). These infants may present with severe nonimmune hydrops fetalis. The majority of cases of hydrops fetalis are now due to nonimmune causes.

1.14

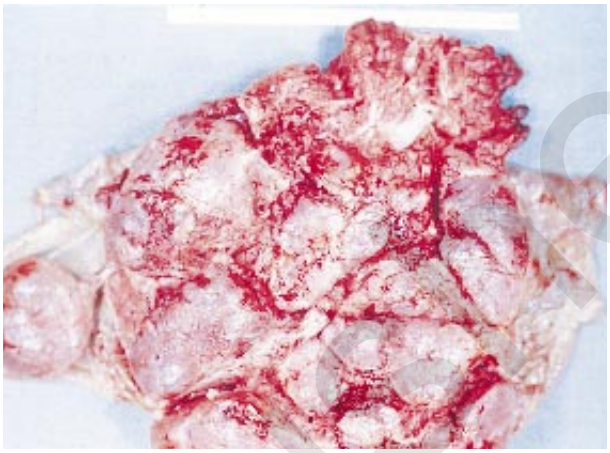

Figure 1.14. Maternal surface of the same placenta. Note the placental enlargement due to the chorangioma and edema. If the placenta is not examined, this cause of nonimmune hydrops fetalis may be missed.

1.15

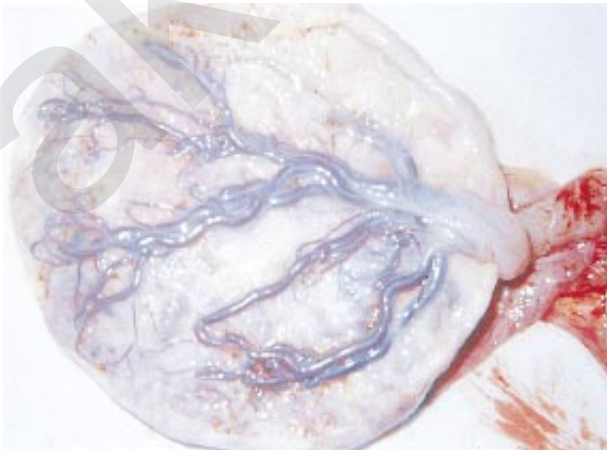

Figure 1.15. A calcified, small placenta. This infant had severe intrauterine growth retardation at term as a result of poor fetal nutrition.

1.16

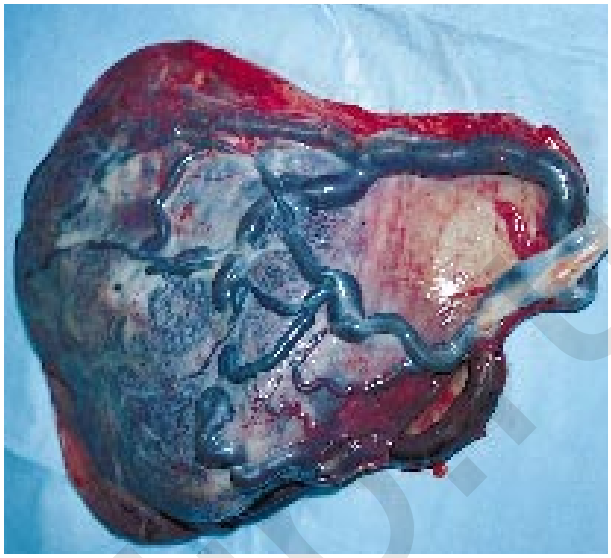

Figure 1.16. In velamentous insertion of the cord the umbilical vessels traverse the fetal membranes unsupported by either the umbilical cord or by placental tissue. If tearing of these unsupported vessels occurs before or during delivery, it can result in massive fetal blood loss.

1.17

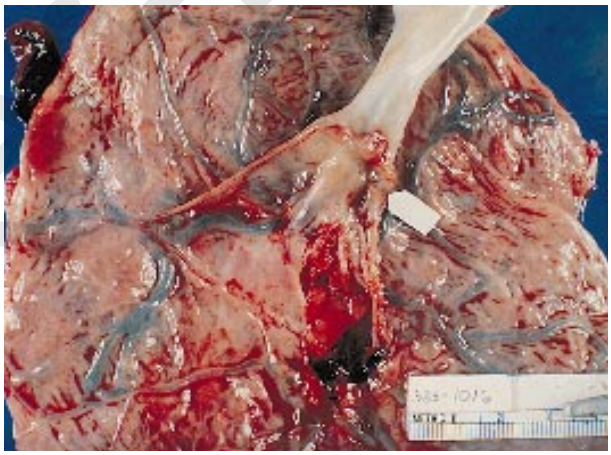

Figure 1.17. Another example of velamentous insertion of the cord. Note the vessels traversing the membranes before inserting into the fetal surface of the placenta. The vessels, lying in loose unsupported tissue, may easily stretch and tear, especially if they cross the cervical os and result in vasa previa with massive blood loss. (Sotelo-Avila, C.)

1.18

Figure 1.18. An example of velamentous insertion of the cord. Note the large vessels exposed in the membranes before they insert into the placental tissue, a section of which is shown at the top. Velamentous insertion of the cord occurs in 0.5 to 1% of singleton births, in 7% of twin births, and in 30 to 40% of triplet births. (Sotelo-Avila, C.)

1.19

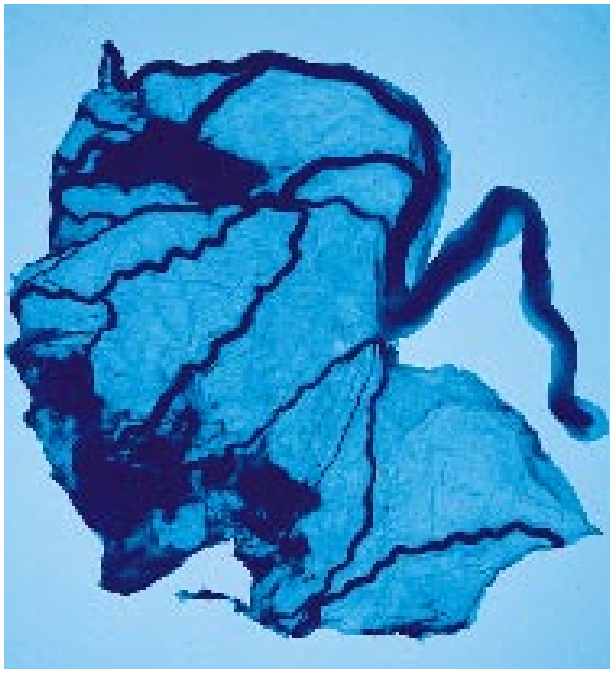

Figure 1.19. Transillumination of the placenta shown in Figure 1.18. (Sotelo-Avila, C.)

1.20

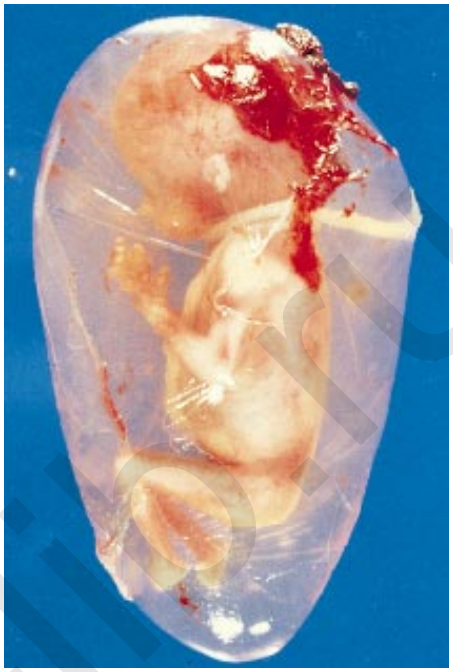

Figure 1.20. Fetus born in a caul. Note that the membranes completely surround the fetus and that the umbilical cord (nuchal cord) encircles the neck twice. A cord around the neck once occurs in about 20%, and twice in about 2% of pregnancies. Whether the cord causes any problems depends on its tightness around the neck. (Klima, T.)

1.21

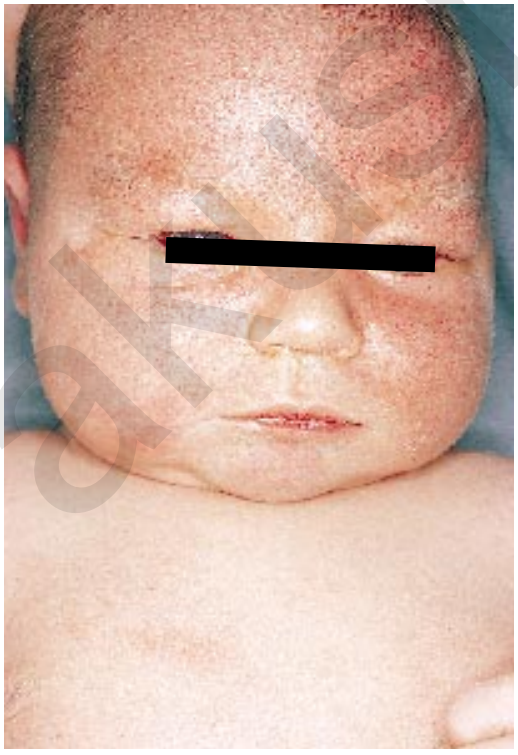

Figure 1.21. Note the petechiae of the face and head and the subconjunctival hemorrhages in this infant who had a long cord around the neck. The normal umbilical cord is 40 to 60 cm long. Long cords (>70 cm) are more apt to be looped around the neck or an extremity of the fetus or to have true knots. Extremely short cords (<30 cm) may lead to abruptio placentae, inversion of the uterus, and intrafunicular hemorrhage (bleeding within the umbilical cord).

1.22

Figure 1.22. This cord was extremely long and wrapped around the left wrist and several times around the neck resulting in intrauterine death and birth of a stillborn infant. A long umbilical cord has usually been stretched by the movement of an extremely active fetus.

1.23

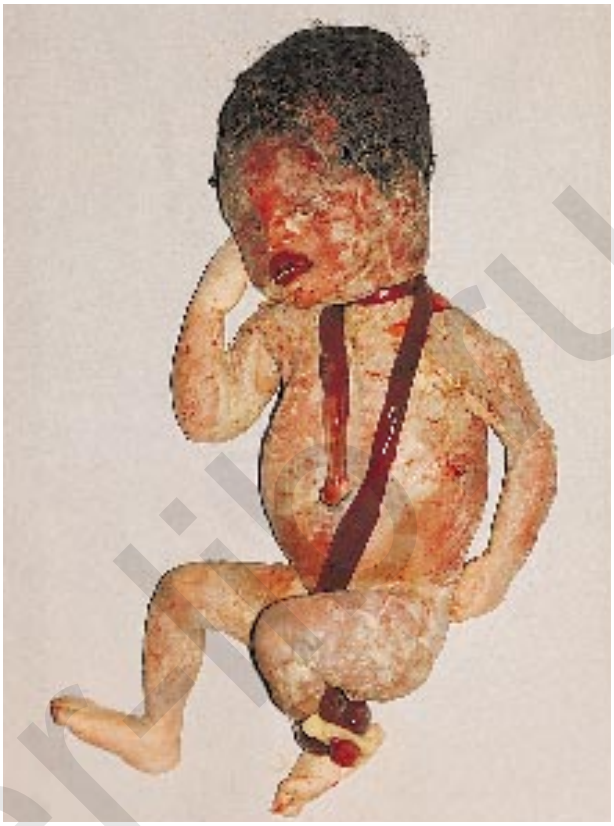

Figure 1.23. Intrauterine death as a result of a long umbilical cord which wrapped around the neck and then the left leg. As the infant moved in utero, he strangled himself.

1.24

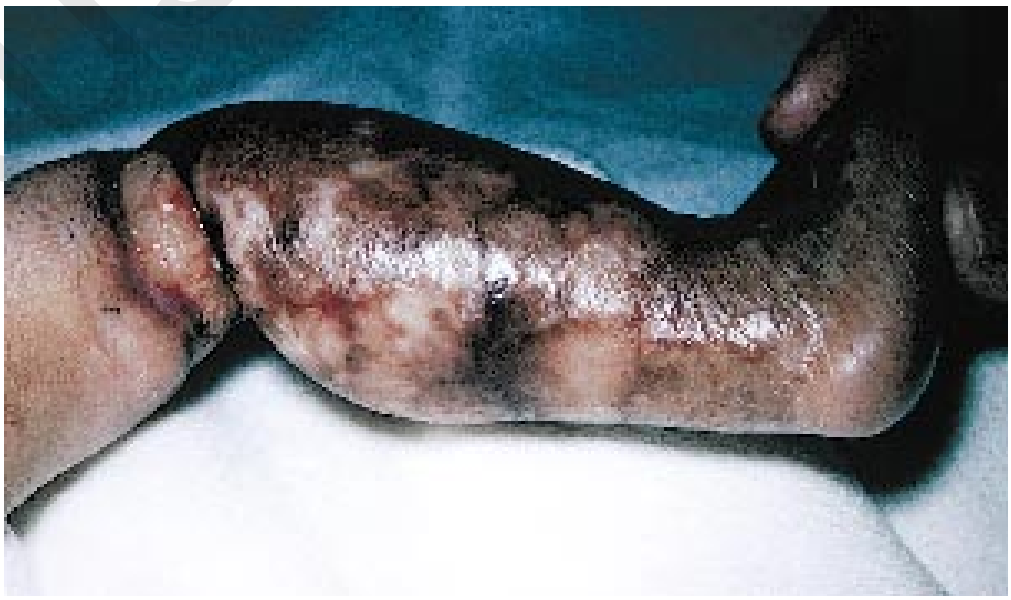

Figure 1.24. A long umbilical cord can encircle an extremity and leave recognizable grooves (furrows) with or without skin ulceration. These are not associated with a poor outcome. In this infant, the cord encircled the right knee very tightly and interfered with the circulation distally.

1.25

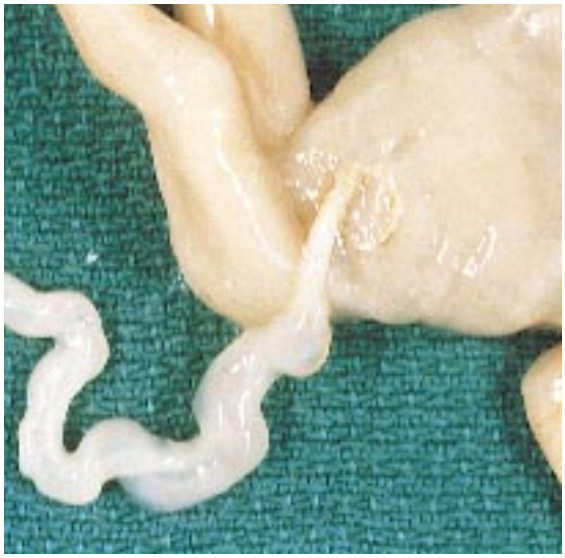

Figure 1.25. The severe umbilical cord constriction proximally resulted in intrauterine death of this fetus. (Finegold, M.)

1.26

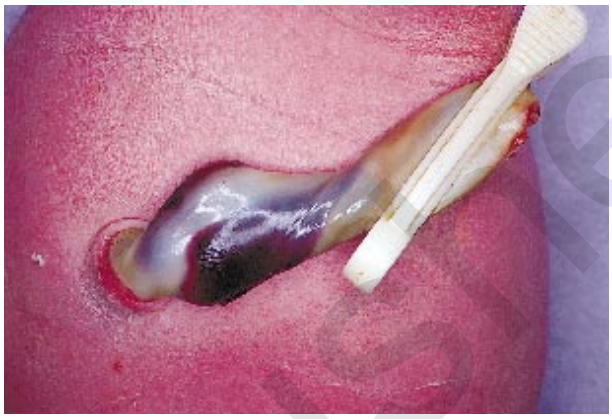

Figure 1.26. A hematoma of the umbilical cord (intrafunicular hemorrhage) resulted from a short umbilical cord. Short umbilical cords are associated with extreme intrauterine immobility, such as in the fetal akinesia syndrome.

1.27

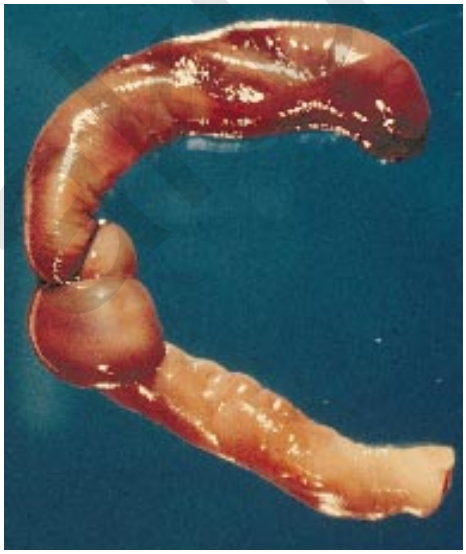

Figure 1.27. A true knot in the umbilical cord of this fetus resulted in intrauterine death. The incidence of true knots in the umbilical cord is 0.1 to 1%, and is strongly associated with long cords and other markers of vigorous fetal activity. It is associated with about 10% of stillbirths. The knots must be very tight to obstruct blood flow. At the site of a long standing knot, such as in this fetus, there is a loss of Wharton's jelly and a constriction of umbilical vessels. Wharton's jelly probably prevents umbilical cord blood vessel compression by diffusing the pressure exerted by knots. The jelly is also slippery and this makes it difficult to maintain a knot.

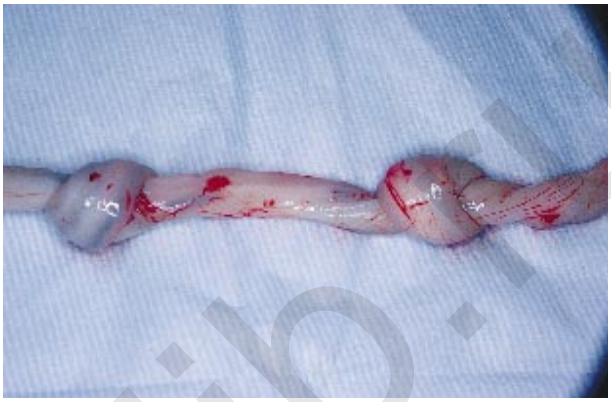

1.28

Figure 1.28. An example of two true knots in the umbilical cord in an infant who was normal at birth.

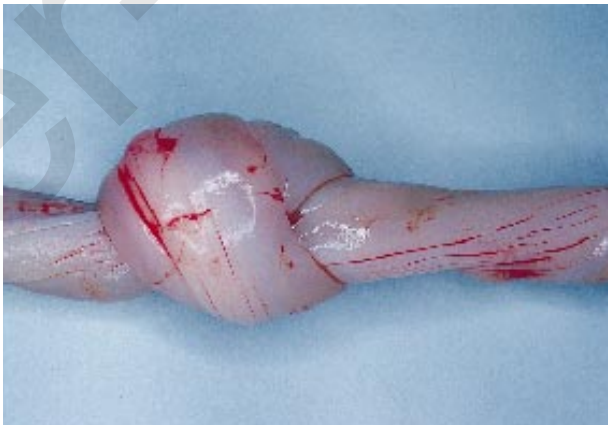

1.29

Figure 1.29. Close up of the true knot to the right in Figure 1.28. Note that the Wharton's jelly is normal and that there is no constriction of the cord. This is, therefore, a recent knot. A previously loose knot may be suddenly tightened as the infant descends during delivery.

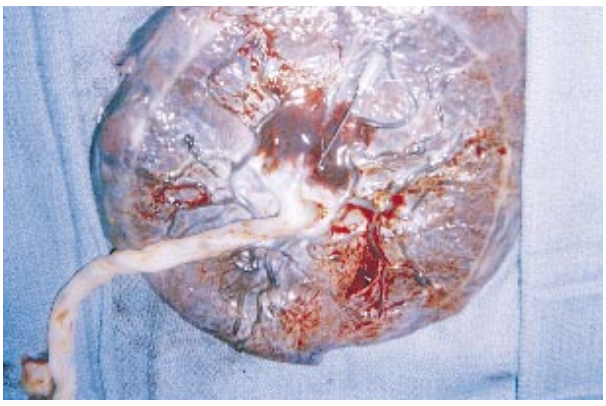

1.30

Figure 1.30. This umbilical cord transection during amniocentesis occurred several years ago, before ultrasound was used to determine the position of the amniocentesis needle. There was considerable blood loss.

1.31

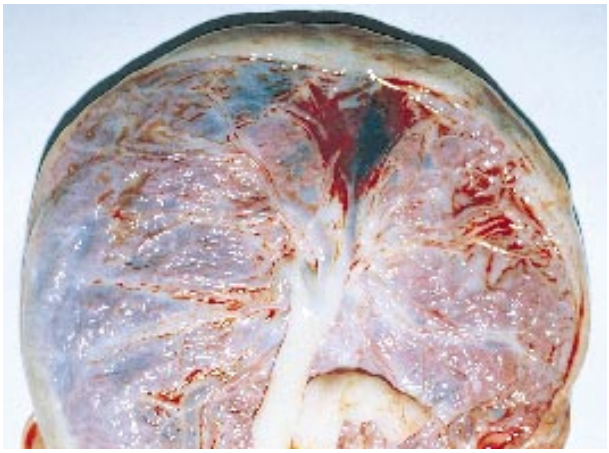

Figure 1.31. Another example of amniocentesis through a term placenta. The fetus developed tachycardia but was normal at birth. (Moise, K.)

1.32

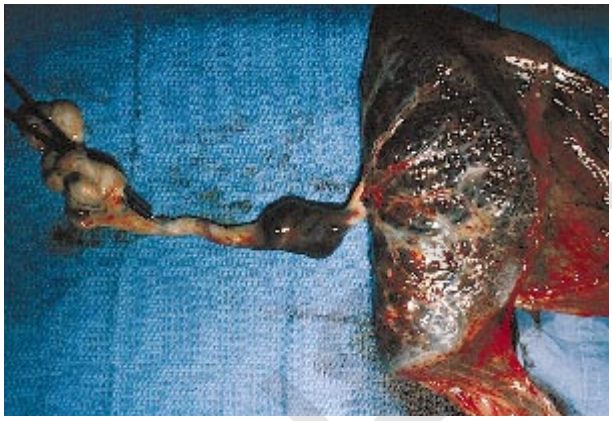

Figure 1.32. Hematoma from transection of the umbilical cord during amniocentesis. There was marked blood loss and fetal demise.

1.33

Figure 1.33. The diagnosis of single umbilical artery is made by examining a section through the surface of the umbilical cord. This anomaly is present in 0.7 to 1.0% of single placentas and in 3 to 7.0% of multiple birth placentas. The incidence is low in black infants, but is increased in infants with associated congenital malformations. Further investigation is recommended if a single umbilical artery is associated with one other major anomaly.

1.34

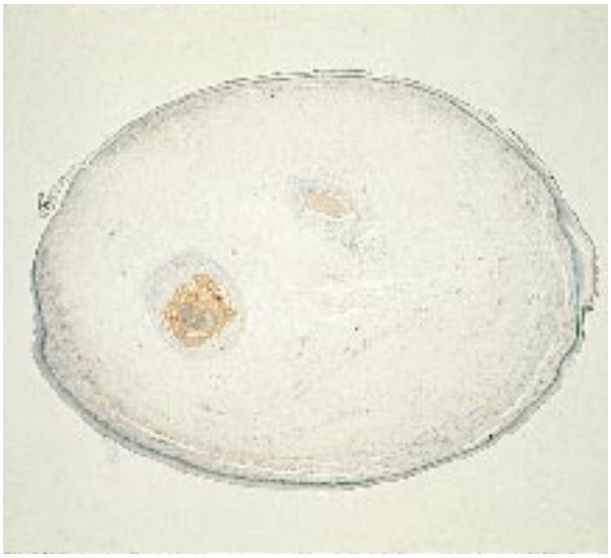

Figure 1.34. A histologic section of an umbilical cord with a single umbilical artery. Note that the thick-walled vessel is the artery and the thin-walled vessel is the vein. It may be associated with abnormal cord length, velamentous cord insertion, or circumvallate placenta. The finding of other congenital malformations is not specific for any one organ system. Cardiac, renal, gastrointestinal, and skeletal malformities have been described. There is an increased incidence of a single umbilical artery in trisomy 13 and 18.

1.35

Figure 1.35. Note the markedly enlarged, edematous umbilical cord due to excess Wharton's jelly in an infant of a diabetic mother. These cords are very friable and tear easily.

1.36

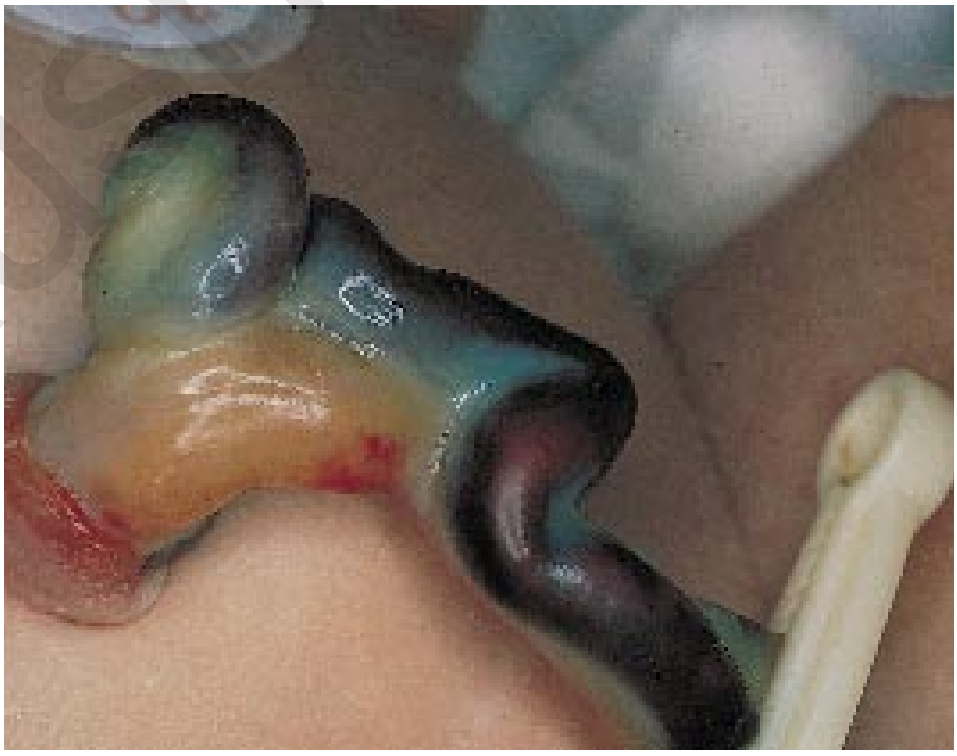

Figure 1.36. A thrombosed vessel in an umbilical cord with little Wharton's jelly. Trauma to the cord is more common when there is a lack of Wharton's jelly. The lack of Wharton's jelly is seen more commonly in postmature infants. A thrombosed vessel in the umbilical cord may compromise fetal well-being.

1.37

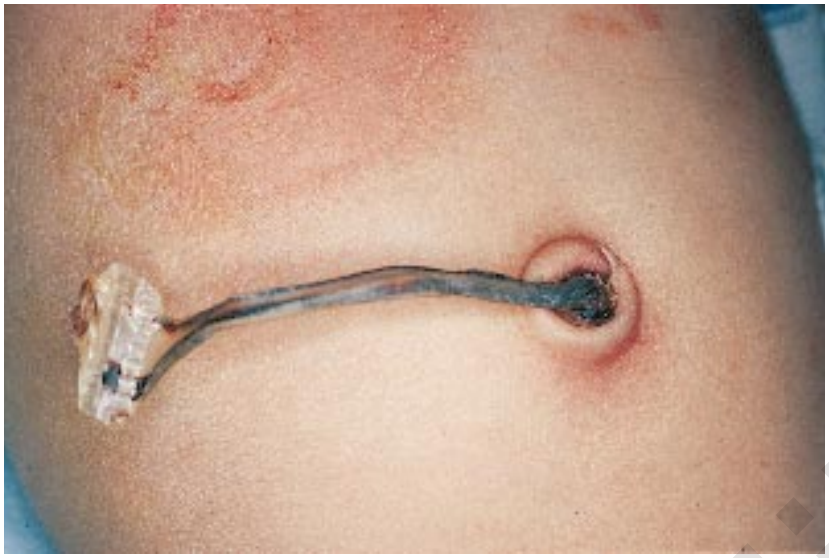

Figure 1.37. This thin, narrow umbilical cord with total lack of Wharton's jelly was present at birth in an infant with postmaturity and oligohydramnios. Cord compression is probably more frequent with a narrow cord, perhaps because the Wharton's jelly does not "cushion" the cord.

1.38

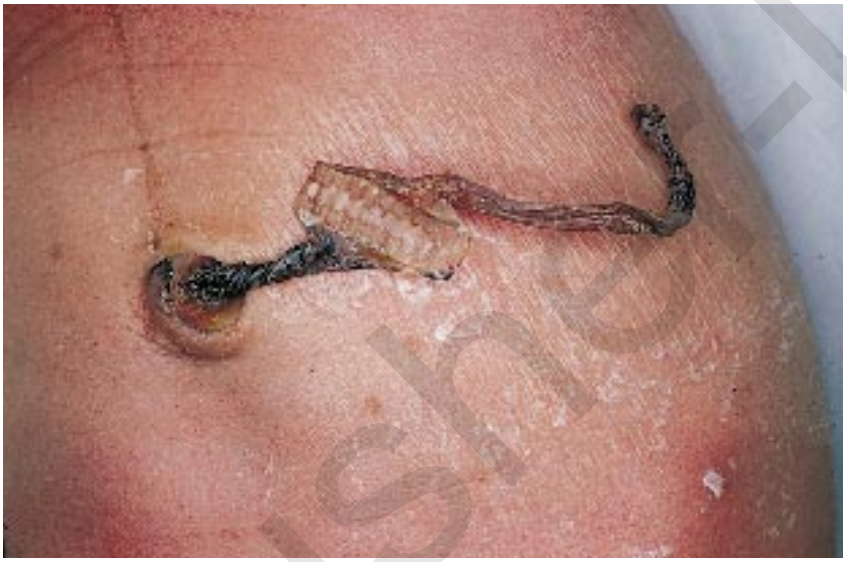

Figure 1.38. A drying umbilical cord 4 days after birth. Note that as the cord dries, the Wharton's jelly disappears rapidly.

1.39

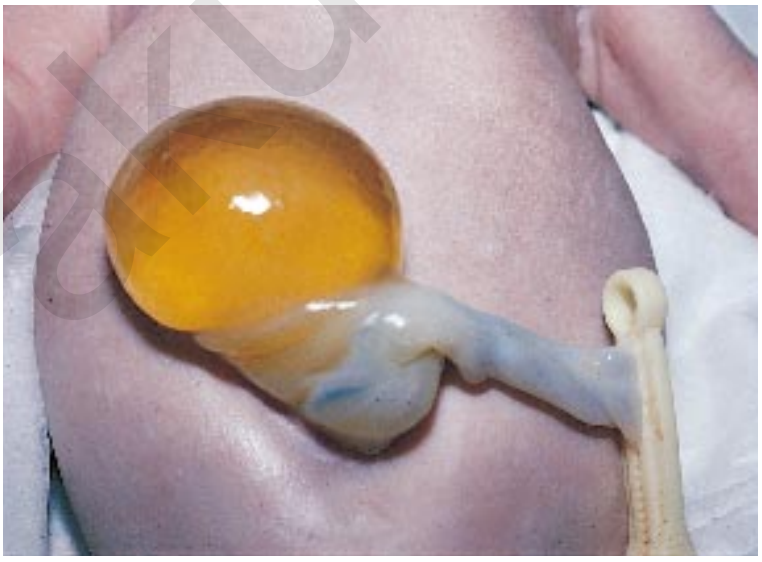

Figure 1.39. This infant has a large cyst in the umbilical cord. The chemical composition of the fluid in this cyst was that of serum rather than urine. These cysts are thought to arise from the allantois.

1.40

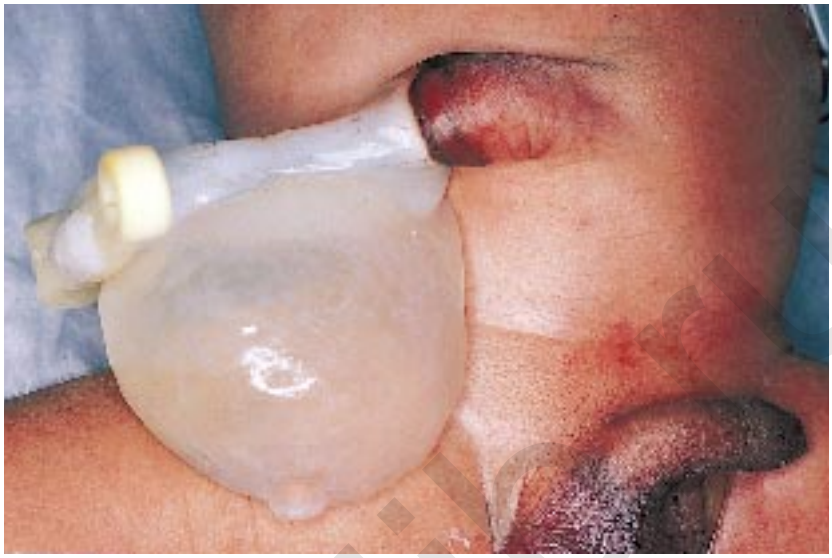

Figure 1.40. Another example of an umbilical cord cyst which is thought to arise from the allantois. These cysts are of no clinical significance.

1.41

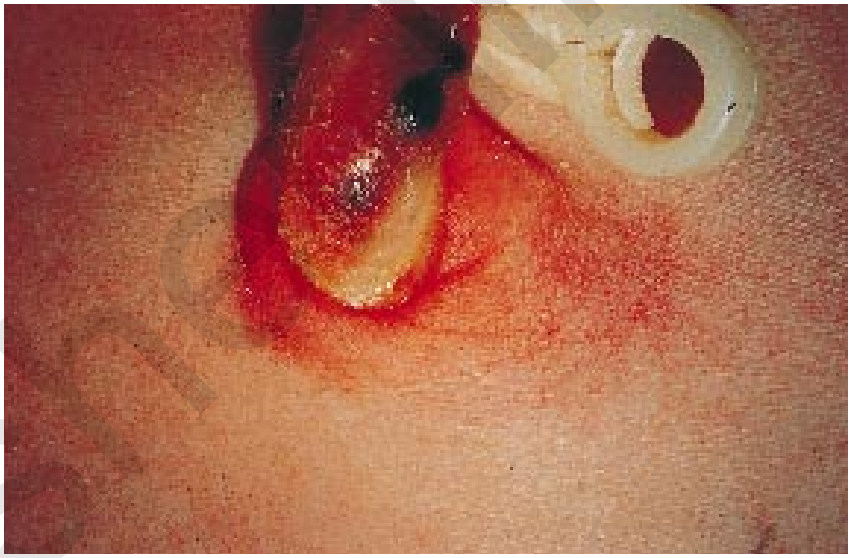

Figure 1.41. Omphalitis and funisitis in an umbilical cord. Omphalitis is an acute inflammation of the skin surrounding the umbilicus. Funisitis is an acute inflammation of the umbilical cord itself. It results from bacteria or mycoplasma in the amniotic fluid attracting fetal neutrophils to migrate out of the umbilical cord vessels. It can be associated with necrosis and calcium deposits within the cord.

1.42

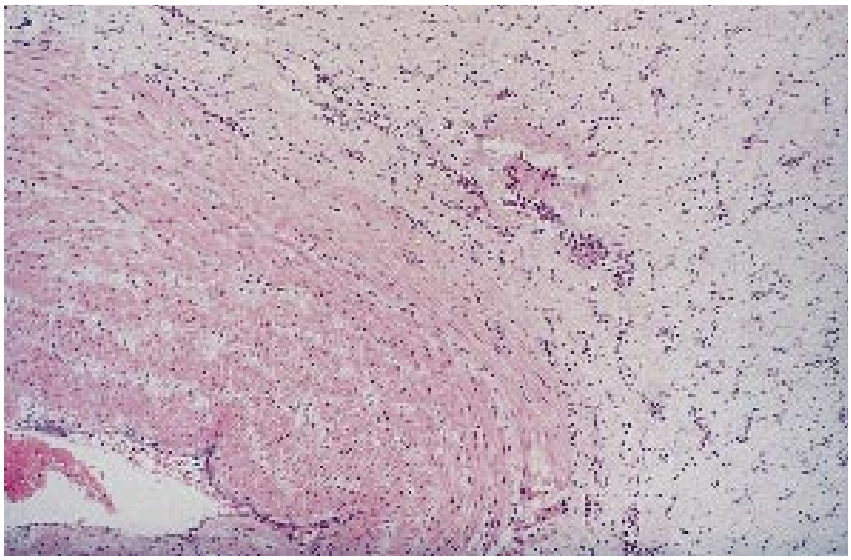

Figure 1.42. Histologic section of an umbilical cord showing funisitis. Note the marked inflammatory reaction surrounding an artery in the cord itself. (Sotelo-Avila, C.)

1.43

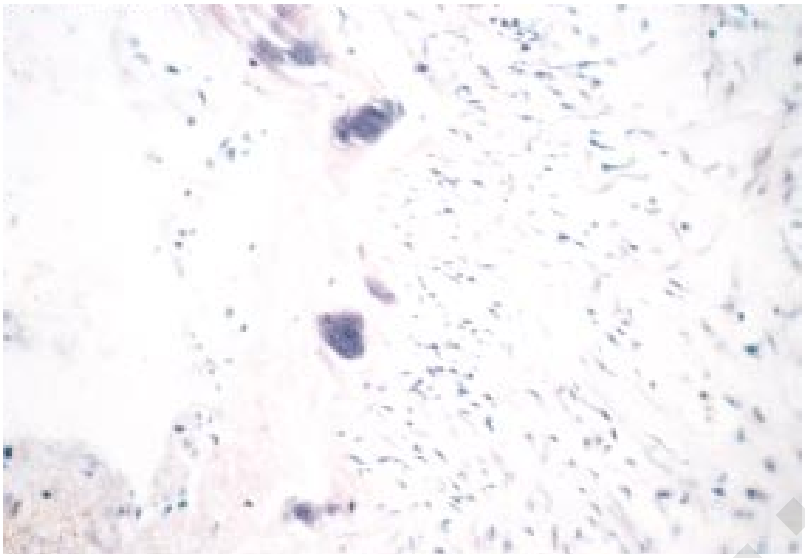

Figure 1.43. Histologic section of an umbilical cord showing marked inflammatory reaction and bacterial colonies (intensely stained blue areas) surrounding a vein in the cord itself.

1.44

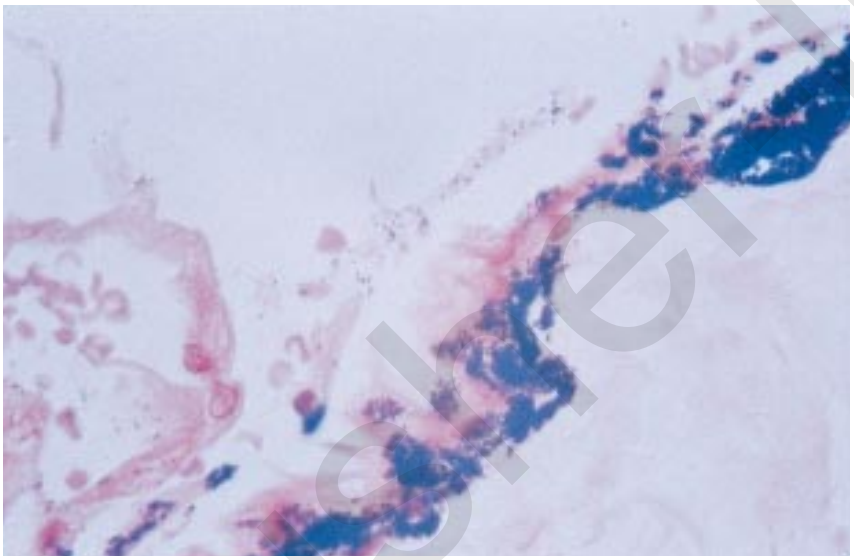

Figure 1.44. Histologic section of the umbilical cord in an infant with congenital listeriosis. Note the gram positive organisms on the surface of the umbilical cord.

1.45

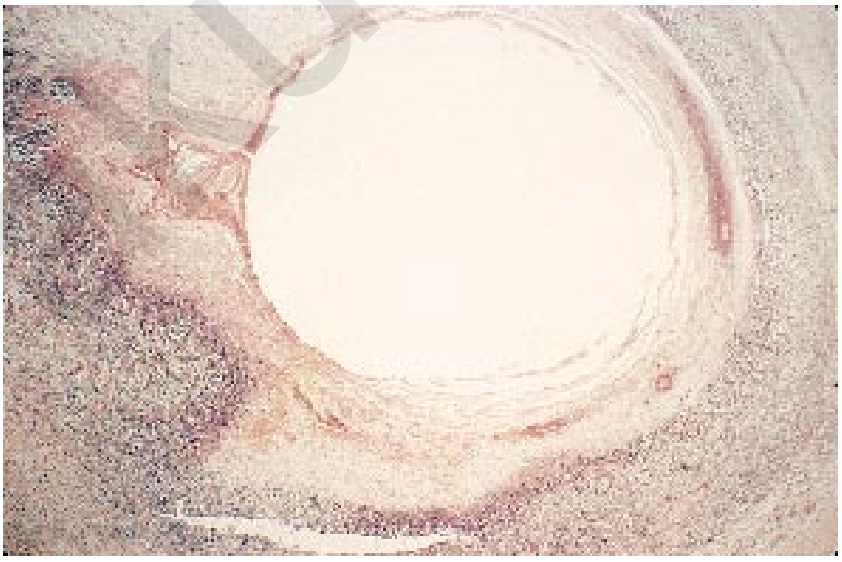

Figure 1.45. Histologic section of funisitis occurring as a result of a catheter in situ in an umbilical vessel.

1.46

Figure 1.46. The external surface of the umbilical cord shows cheesy white areas similar to thrush which suggest the diagnosis of congenital candidiasis. (Sotelo-Avila, C.)

1.47

Figure 1.47. A histologic section of the umbilical cord of the same infant showing funisitis with the hyphae of *Candida* which are stained pink. (Sotelo-Avila, C.)

1.48

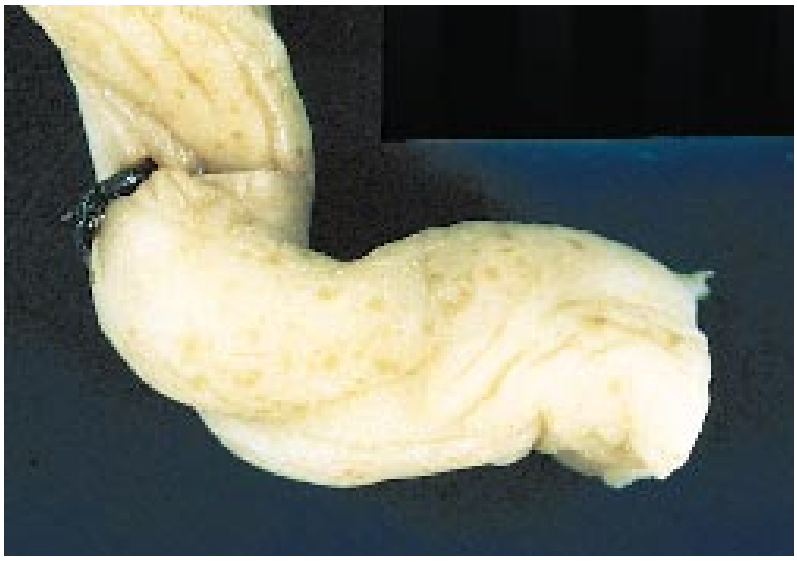

Figure 1.48. External surface of an umbilical cord with yellowish brown areas on the external surface which suggest the diagnosis of congenital candidiasis. (Fanaroff, A.)

1.49

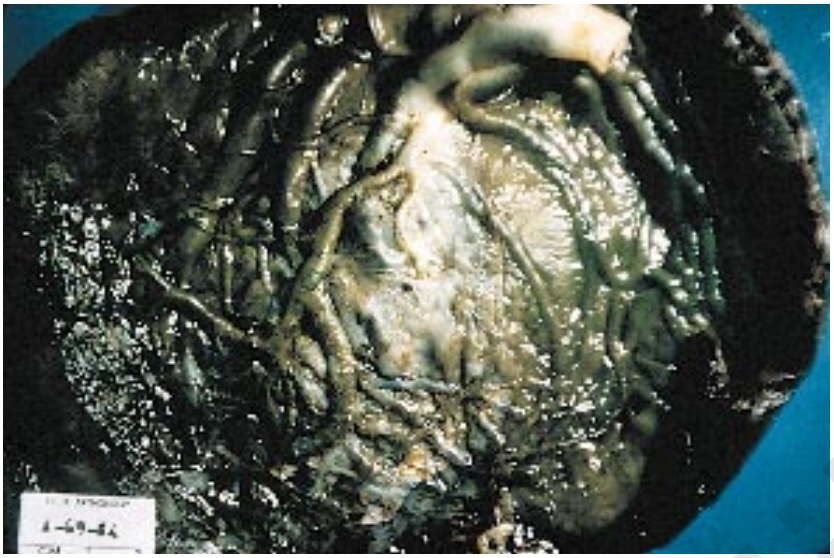

Figure 1.49. Fetal surface of a placenta showing chorioamnionitis. Normally, the fetal surface of a placenta is shiny and clear with a prominent vascular pattern. In chorioamnionitis the fetal surface appears dull and opaque with an obscure vascular pattern. The amniotic fluid is cloudy, and the placenta, membranes, and amniotic fluid may have a foul odor. Aspiration in this infected milieu by the fetus may result in neonatal pneumonia, sepsis and/or neonatal meningitis.

1.50

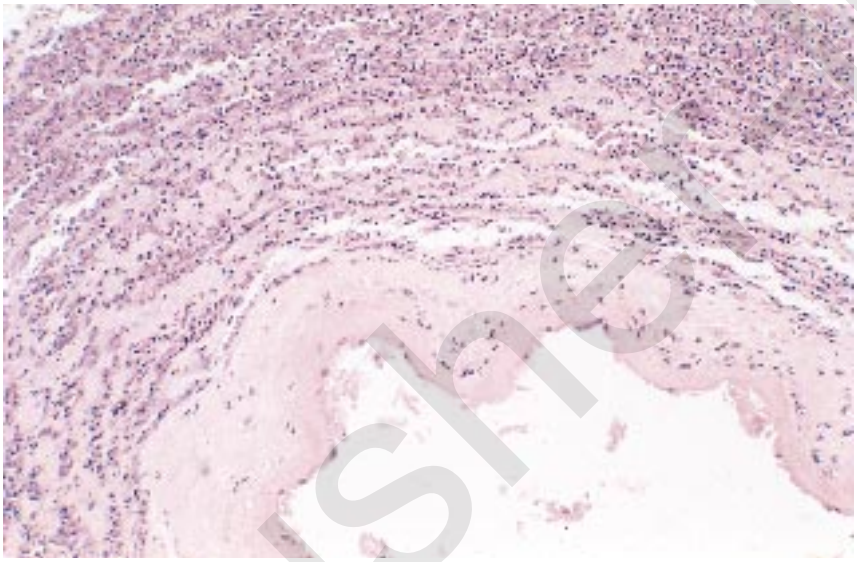

Figure 1.50. Histologic section of the placenta showing chorioamnionitis. Factors associated with increased risk of placental infection include premature and prolonged rupture of the membranes, prolonged labor, placenta previa, and multiple births. Bacterial infections are more common than viral and fungal infections.

1.51

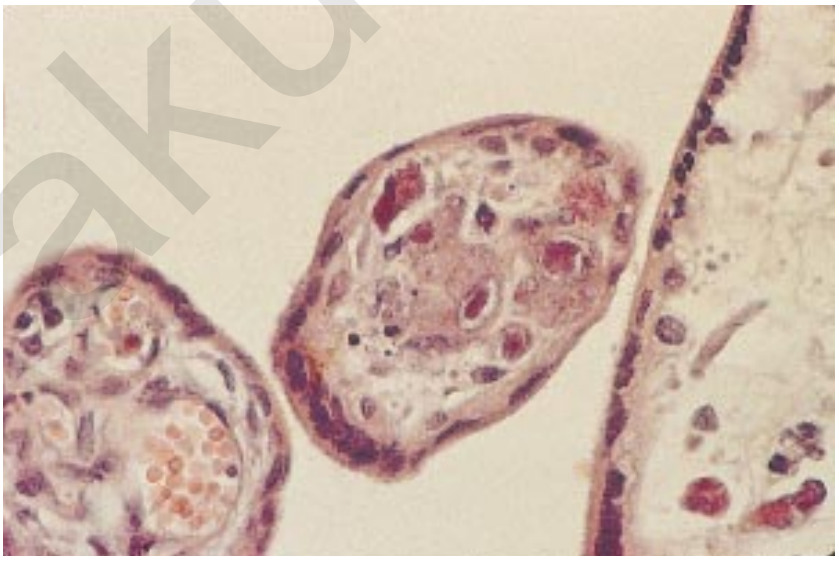

Figure 1.51. Histologic section of a placenta with cytomegalovirus infection. Note the typical "owl's eye" inclusions in the villae. Viral agents reach the fetus by hematogenous dissemination and traverse the placental villae. Since viral lesions tend to be microscopic, gross examination of the placenta is not helpful. (Finegold, M.)

1.52

Figure 1.52. Histologic section of a placenta with congenital syphilis. Note the numerous spirochetes. (Finegold, M.)

1.53

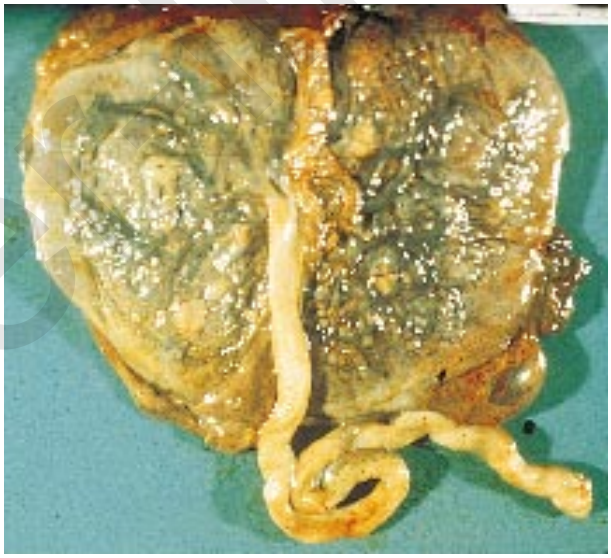

Figure 1.53. The presence of meconium staining of the amniotic fluid occurs with fetal distress and postmaturity. Meconium staining of the placenta may occur within 1 hour. In cases of chorioamnionitis, the fetal surface may be green; in listeriosis, there may be brown or chocolate staining of the amniotic fluid with similar staining of the placenta. (Finegold, M.)

1.54

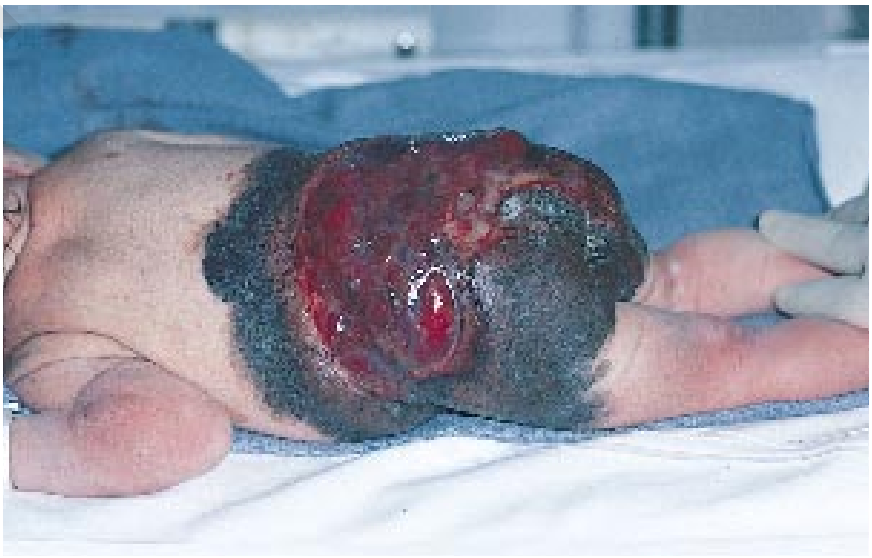

Figure 1.54. Infant with a large "garment" nevus (bathing trunk nevus). Note the marked breakdown and ulceration of the skin.

1.55

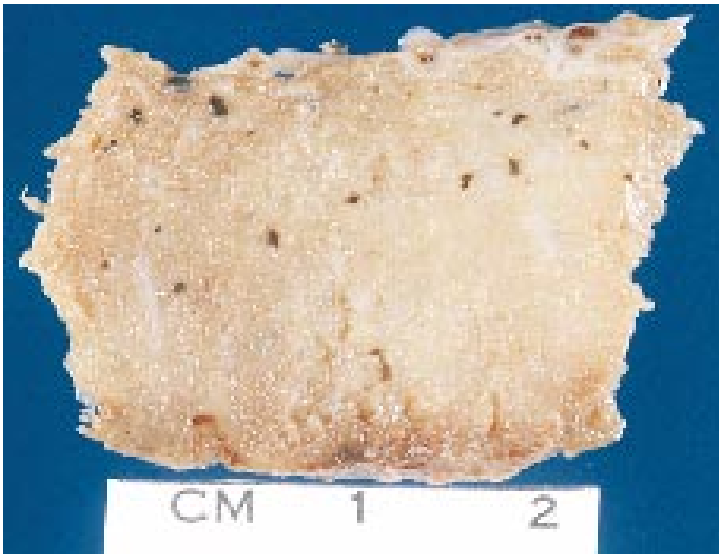

Figure 1.55. Gross section of placenta showing multiple nevi in the same infant shown in Figure 1.54. This emphasizes the importance of examining the placenta in infants born with such abnormalities. (Sotelo-Avila, C.)

1.56

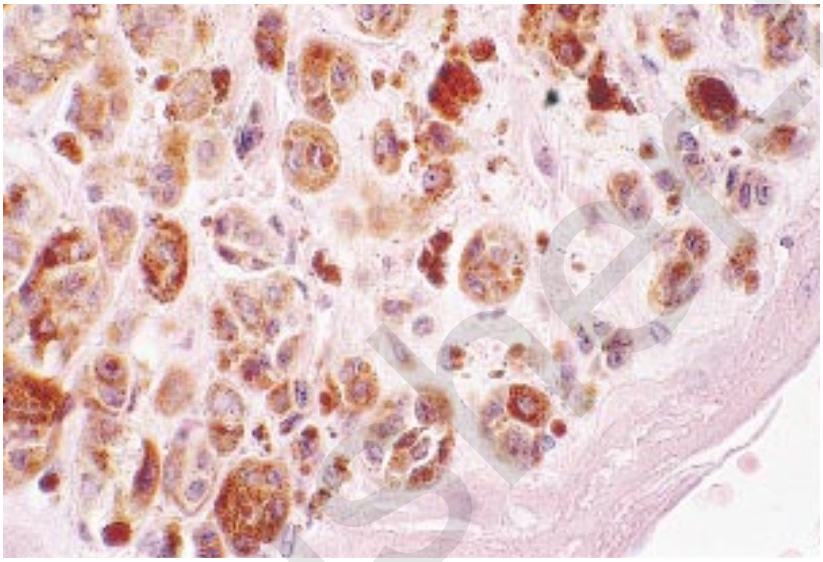

Figure 1.56. Histologic section of melanoma cells from the placenta of the same infant shown in Figure 1.54 and 1.55. Similarly lesions can be seen in the placenta of infants with congenital neuroblastoma. (Sotelo-Avila, C.)

1.57

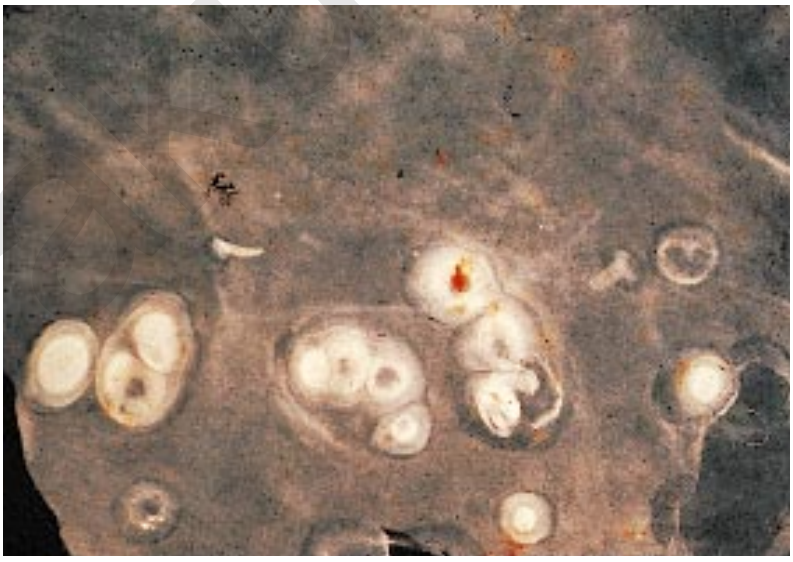

Figure 1.57. Squamous metaplasia of the amnion. In this placenta with squamous metaplasia, the amnion is stripped from the membranes. Note the concentric appearance of these nodules and their frequent umbilication. The amnion is squamous and these areas of metaplasia form with maturity. Note the tiny nodules of keratin irregularly present on the fetal surface.

1.58

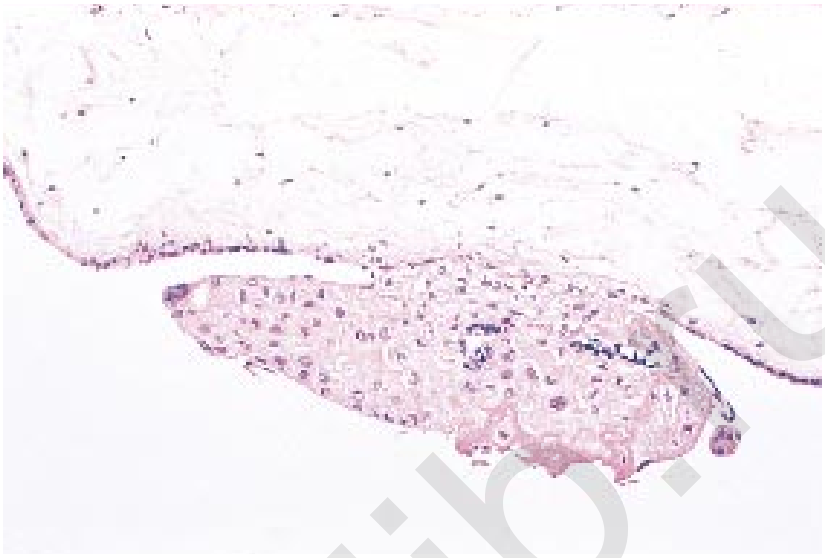

Figure 1.58. Histologic section of the amnion showing the squamous metaplasia. Squamous metaplasia differs from amnion nodosum in that the lesions *cannot* be separated readily, whereas the nodules in amnion nodosum can be picked off of the underlying amnion leaving a semi-transparent, saucer-shaped depression with somewhat ragged edges.

1.59

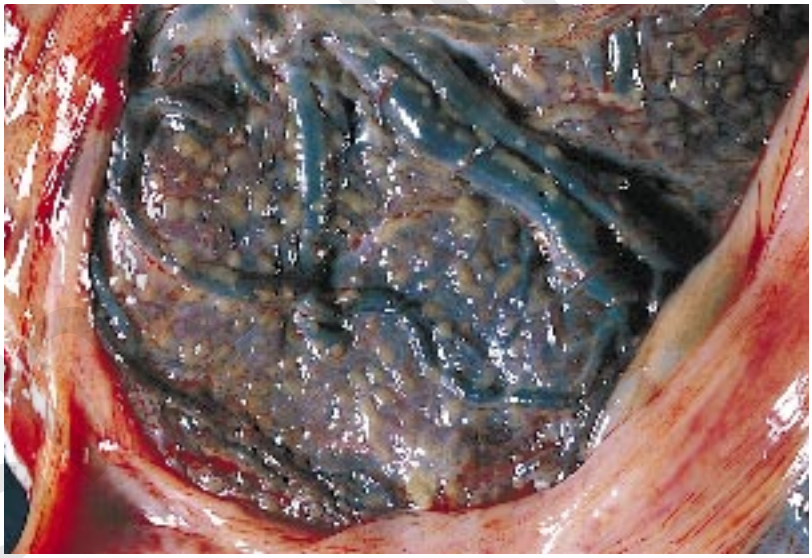

Figure 1.59. Typical amnion nodosum in one twin. This twin was an acardiac monster having no urinary tract. The amnion is rough and shows numerous fine granules which are whitish, opaque, and uniform in size. Frequently the nodules are more irregular in size and slightly yellowish brown. It is unusual to see this degree of amnion nodosum. The other twin was normal.

1.60

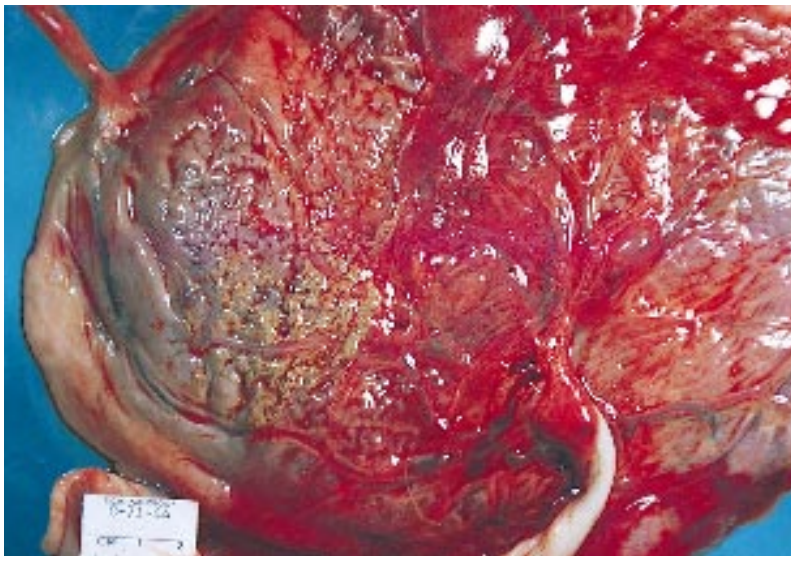

Figure 1.60. Another example of amnion nodosum in a twin placenta. Note the normal umbilical cord and placenta on the right and the small umbilical cord with a thrombosed vessel on the left. This was a twin-twin transfusion syndrome and the twin on the left became a fetus papyraceus. The amnion nodosum lesions are whitish, opaque, and uniform in size.

1.61

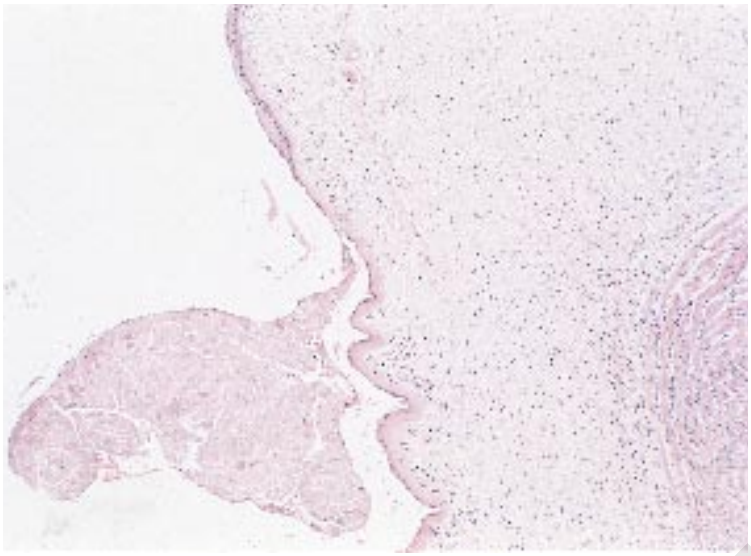

Figure 1.61. Histologic section of a placenta and membranes showing amnion nodosum on the left and chorioamnionitis on the right in an infant with renal dysgenesis and hypoplastic lungs.

1.62

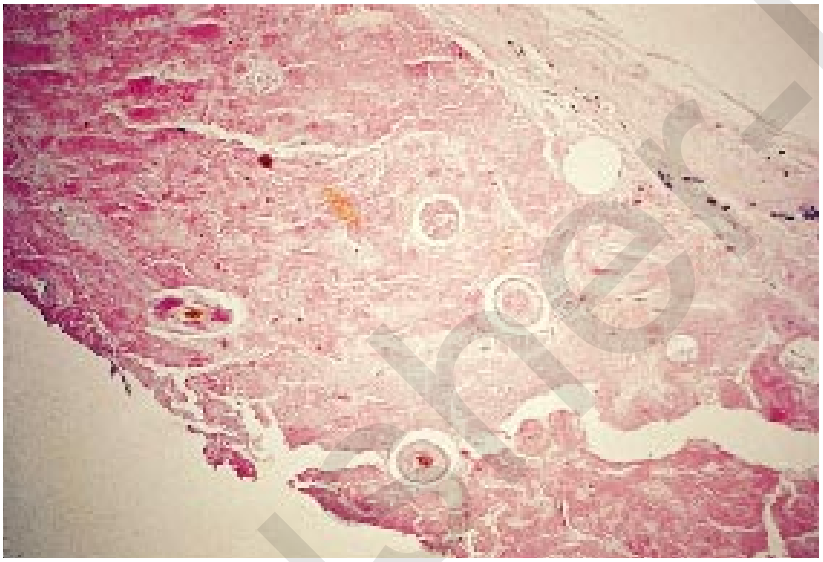

Figure 1.62. High-power histologic section of amnion nodosum which consists of lanugo, vernix caseosa, and squamous epithelial cells. With marked oligohydramnios, the fetal skin rubs against the fetal surface of the placenta and produces these lesions.

Chapter 2
Multiple Births

Multiple gestation occurs frequently in pregnancy. The most common is twinning, which occurs in about one in every 80 pregnancies. There are two types of twins: monozygous or "identical" and dizygous or "fraternal." The monozygous twin rate is 1 in every 200 pregnancies. It results from a single ovulation with subsequent splitting of the developing egg within the first 14 days. There is no familial tendency. Dizygous twinning results from double ovulation and fertilization and is probably determined by higher gonadotropin secretion rates. The rate of dizygous twinning is variable and is influenced by heredity (transmitted autosomally but expressed only in the mother), race (as high as 1 in 23 births in some West African races; as low as 1 in 300 births in Mongolian races), maternal age (increased frequency with increasing age), and drugs (incidence of twinning is 6.6% with the use of Clomid®). Examination of the placenta of multiple births is important because of the two- to three-fold higher incidence of structural defects in monozygous twins and increased potential for successful future transplant between monozygous twins. Monochorionic placentas are invariably fused and about 75% of the infants are identical twins. Dichorionic placentas may be fused or separate. Infants with a dichorionic fused placenta may be identical (monozygous) or fraternal (dizygous). The membrane which separates the two fetal cavities is the key to the evaluation of twin placenta. Typically, this runs across the middle of the fused placenta. In monochorionic twins, with one chorion covering two amnia, the dividing membrane consists of two translucent amnionic layers which can be pulled with ease from the placental surface. In 1% of monozygotic twinning, the placenta will be monochorionic-monoamnionic. In conjoined twinning, the placenta is also monochorionic-monoamnionic. In dichorionic twins, with two amnia, the dividing membrane consists of four layers, two chorionic and two amnionic; it is opaque, thicker, and does not separate from the placental surface without tearing.

2.1

Figure 2.1. These infants are normal, identical triplets born at 32 weeks gestation. They initially had mild respiratory distress, but improved rapidly. (Cabera-Meza, G.)

2.2

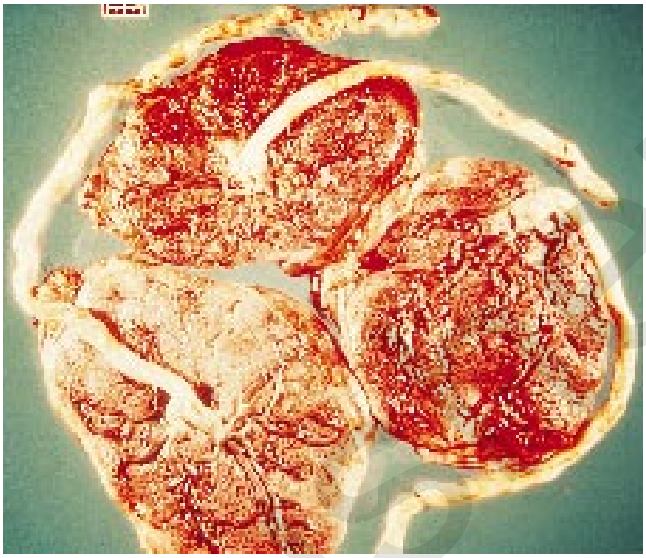

Figure 2.2. The fetal surfaces of the placentas of fraternal triplets.

2.3

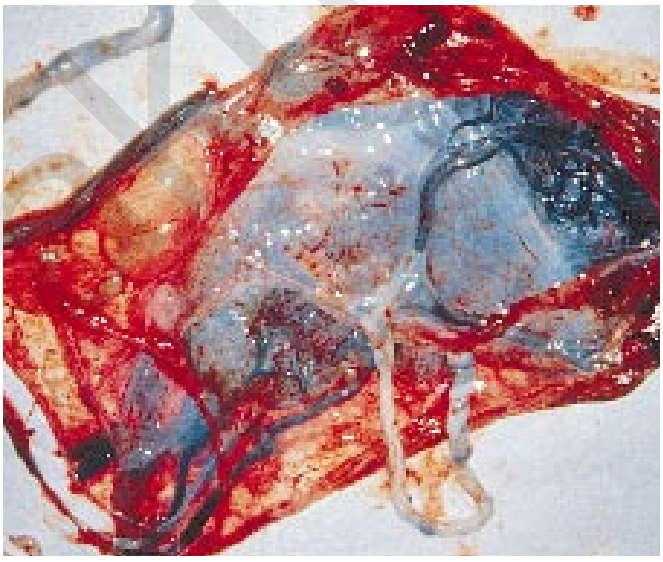

Figure 2.3. A triplet placenta showing a velamentous insertion of the cord in one of the triplets. Note that the placentas are fused and thus the pregnancy could be monozygotic.

2.4

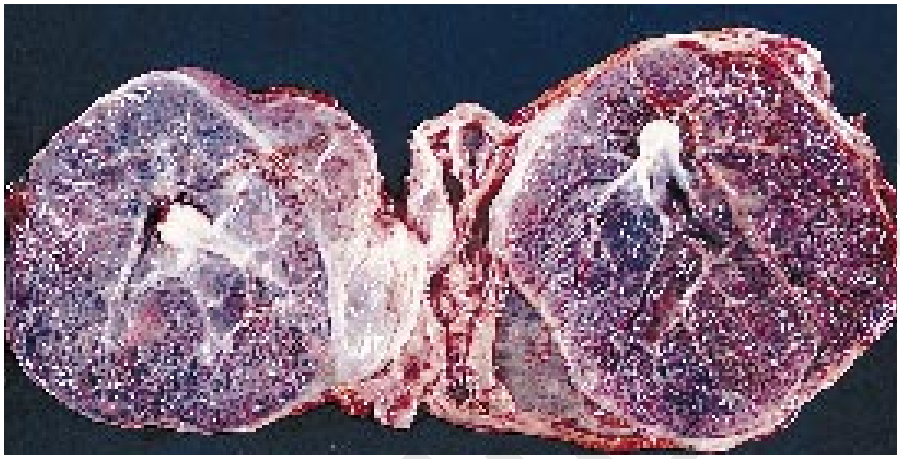

Figure 2.4. The fetal surfaces of two completely separated twin placentas. These are always dizygotic.

2.5

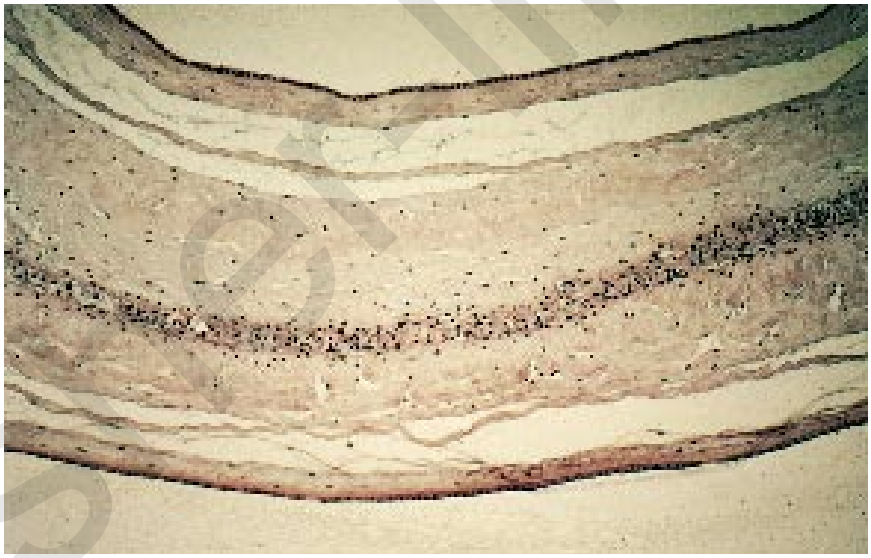

Figure 2.5. This low-power histologic section demonstrates that an amnion can be identified on each side of two chorion. Thus, this is an example of a dichorionic-diamnionic placenta. This type of dividing membranes is typically seen in all dizygotic twinning and in about 20 to 25% of monozygotic twinning.

2.6

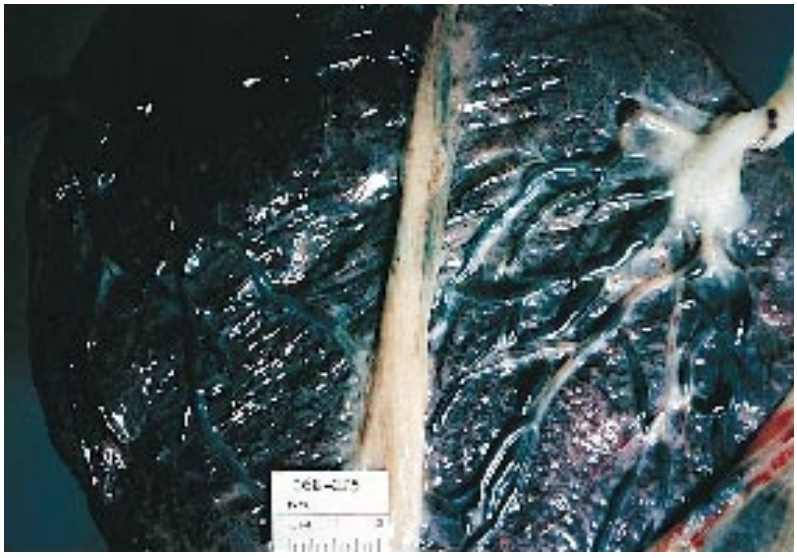

Figure 2.6. The fetal surface of this fused, twin placenta shows the dividing membranes. In this placenta, histologic examination showed that there were two amnia and a single chorion (diamnionic-monochorionic). These twins would thus be monozygotic.

2.7

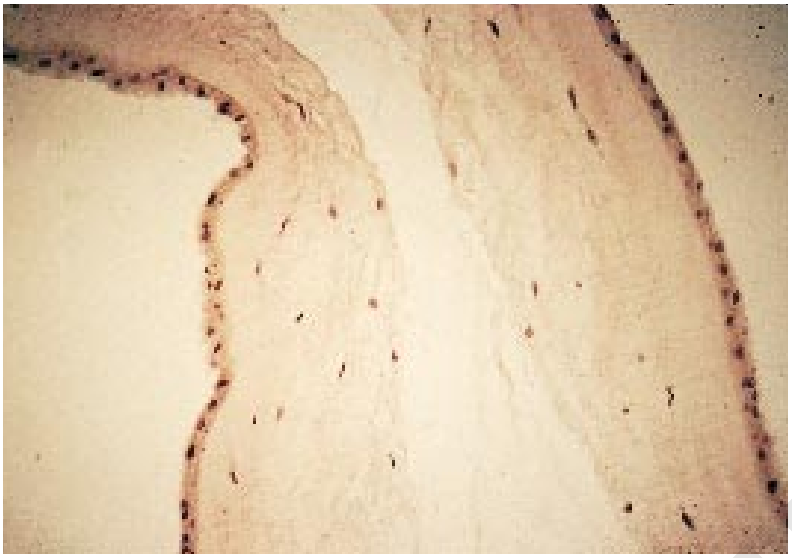

Figure 2.7. Histology of the membranes of the same placenta shows the double amnion on the outer surfaces with a single chorion (diamnionic-monochorionic).

2.8

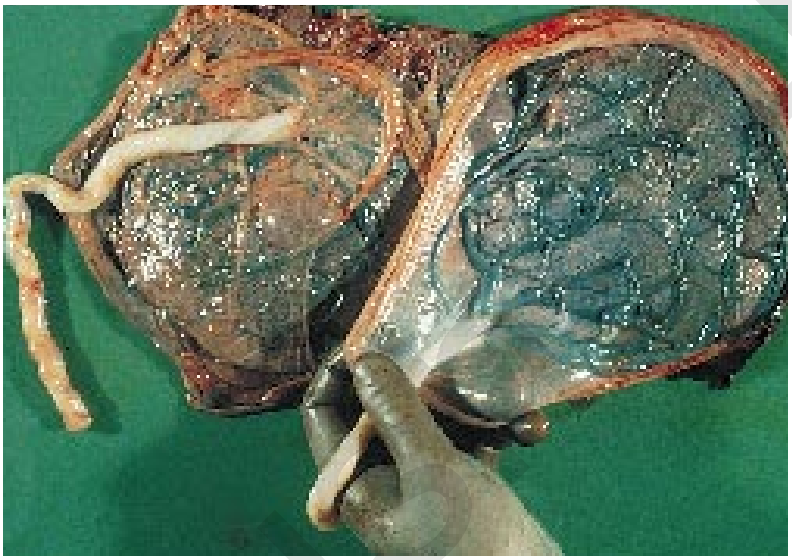

Figure 2.8. On the fetal surface of this fused, twin placenta, the dividing membrane is very thin and clear, suggesting that this is a monozygotic pregnancy. This was confirmed by histologic examination showing a single chorion. (Finegold, M.)

2.9

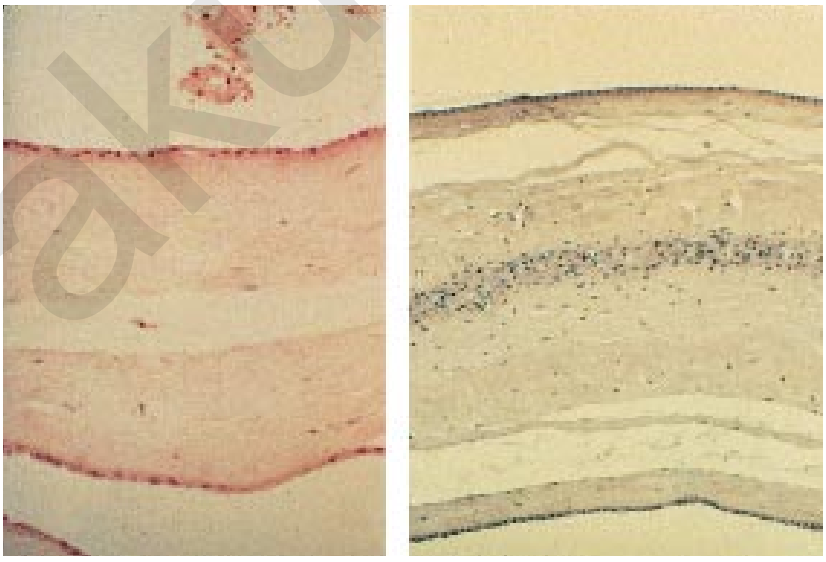

Figure 2.9. The histologic appearance of the dividing membranes in twin placentas are compared in this figure. On the left, note the diamnionic-monochorionic twin placenta, and on the right, note the diamnionic-dichorionic twin placenta.

2.10

Figure 2.10. Note the two umbilical cords inserting into the fetal surface of the placenta without the presence of dividing membranes. This is typical of a monoamnionic-monochorionic twin placenta, which occurs in 1% of twin pregnancies.

2.11

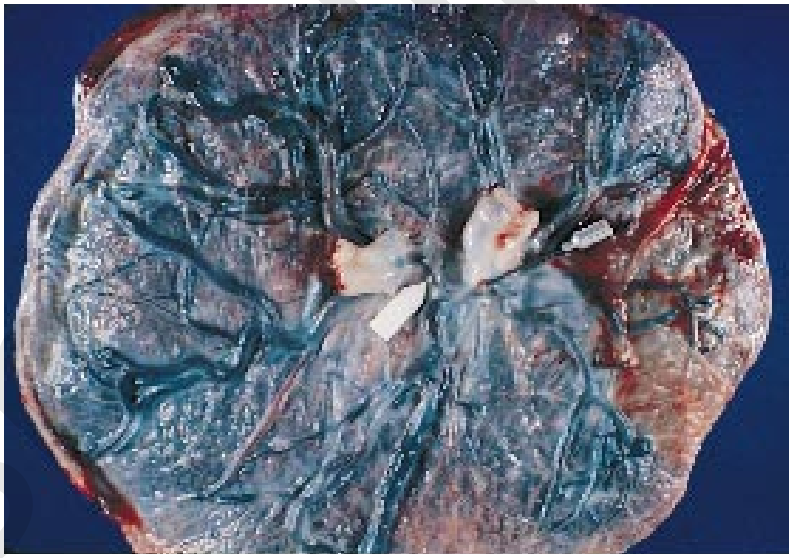

Figure 2.11. The fetal surface of a monoamnionic-monochorionic twin placenta, showing the insertion of two separate umbilical cords. (Sotelo-Avila, C.)

2.12

Figure 2.12. Close-up of the above placenta shows anastomosis of the vessels between the two umbilical cords. This results in a twin (feto-fetal) transfusion syndrome. (Sotelo-Avila, C.)

2.13

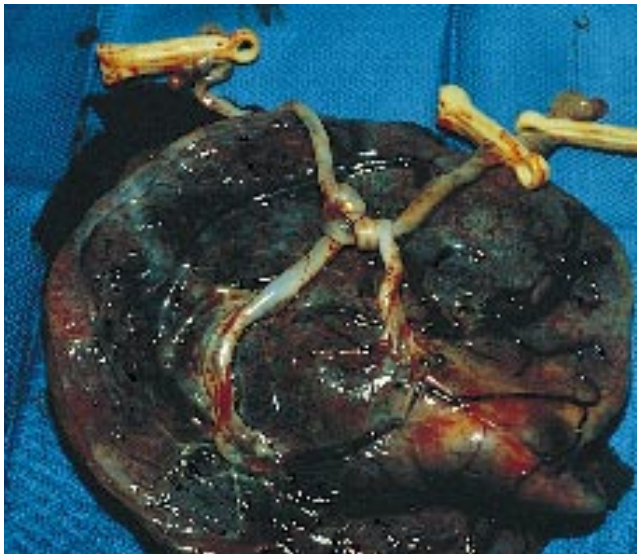

Figure 2.13. The fetal surface of a monoamnionic-monochorionic twin placenta showing the entanglement of the two umbilical cords resulting in fetal anoxia and fetal distress with meconium passage. Note the meconium-stained appearance of the fetal surface of the placenta. Entanglement of the cords is a complication which may occur because of a lack of a dividing membrane in monoamnionic-monochorionic twins. (Karishan, B.)

2.14

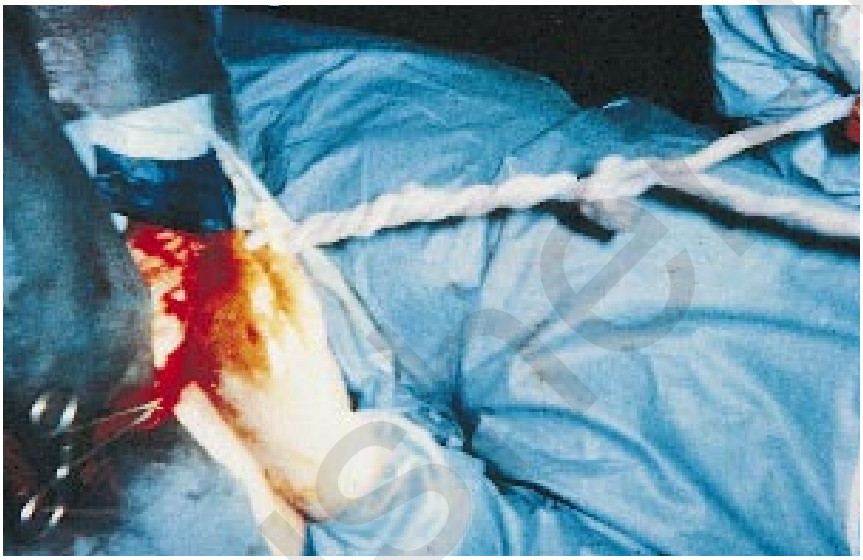

Figure 2.14. Another example of entangled cords in a monoamnionic-monochorionic twin placenta.

2.15

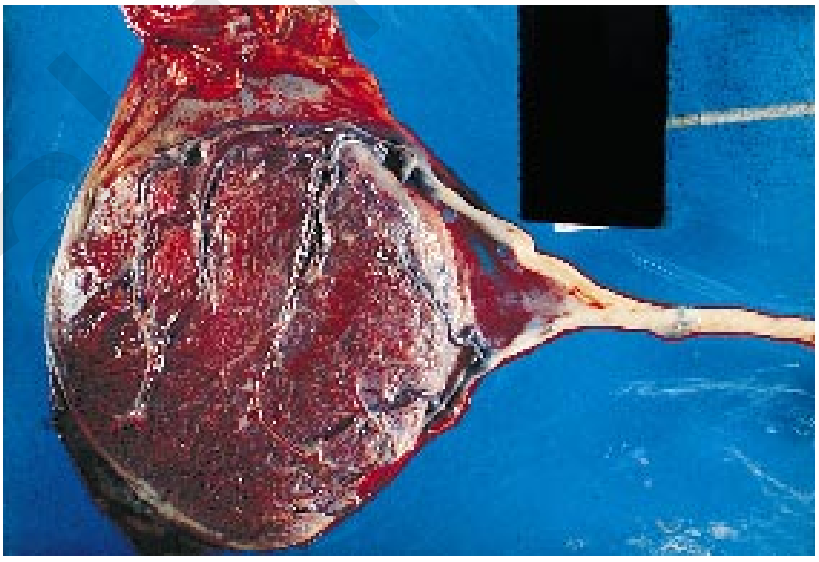

Figure 2.15. The fetal surface of this monoamnionic-monochorionic placenta in conjoined twins shows the insertion of the two umbilical cords, but note that these fuse and present as a single fused cord in thoracopagus twins. (Sotelo-Avila, C.)

2.16

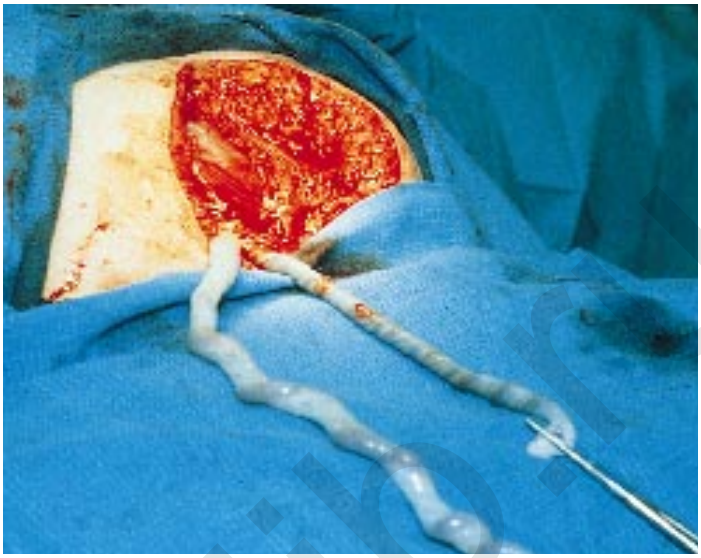

Figure 2.16. The appearance of the umbilical cords in a twin pregnancy. Note the small size of the umbilical cord in the infant who was growth-retarded as compared to the normal size of the umbilical cord in the normal twin.

2.17

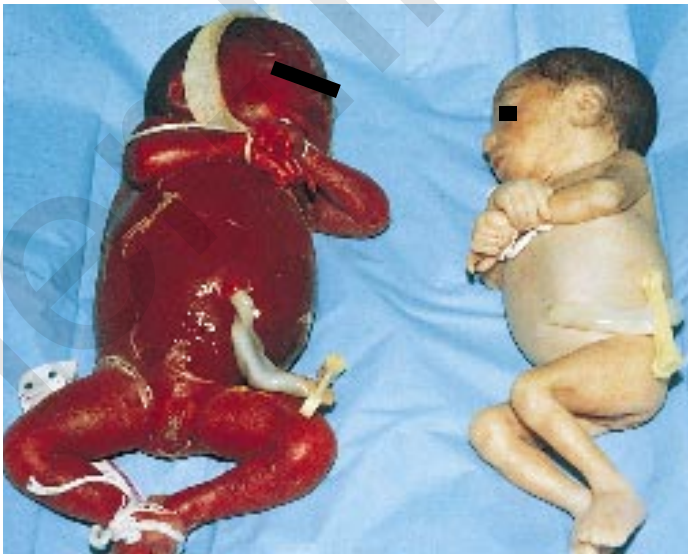

Figure 2.17. These infants born as stillbirths at 30 weeks gestation are an example of twin (feto-fetal) transfusion syndrome. In this syndrome, vascular anastomoses permit the transfer of arterial blood under high pressure from the twin on the right (donor) to the low pressure venous system of the other twin (recipient). The donor twin is thus kept hypovolemic, dehydrated, malnourished, or even in shock. His organs are small and his amniotic fluid is decreased. The recipient twin becomes hypervolemic, edematous, and plethoric (polycythemic). His organs are large, he may have congestive failure and his amniotic fluid is increased.

2.18

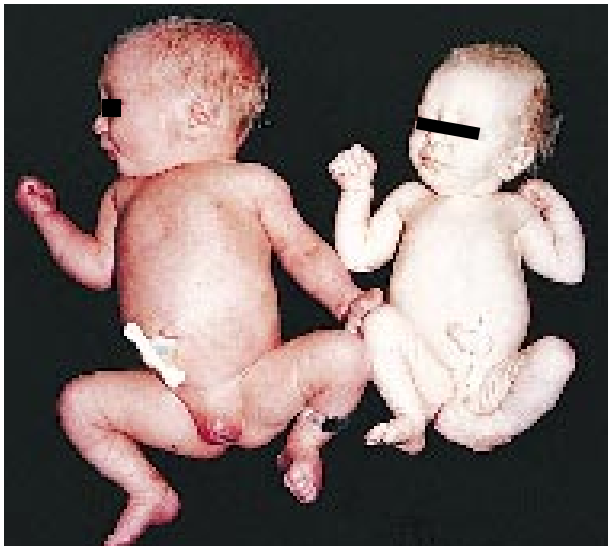

Figure 2.18. These monozygotic twins at birth represent another example of twin transfusion syndrome. The birth weight of the twin on the left was 3000 g with a central hematocrit of 86%. The birth weight of the twin on the right was 2230 g with a central hematocrit of 27%. Twin transfusion syndrome occurs only in monochorionic twins. It occurs in 15 to 30% of monochorionic pregnancies and is defined in terms of a difference of greater than 250 g birth weight and/or 20% difference in the central hematocrit between the twins. Twins in this syndrome usually do not look identical at birth although in fact they are monozygotic.

2.19

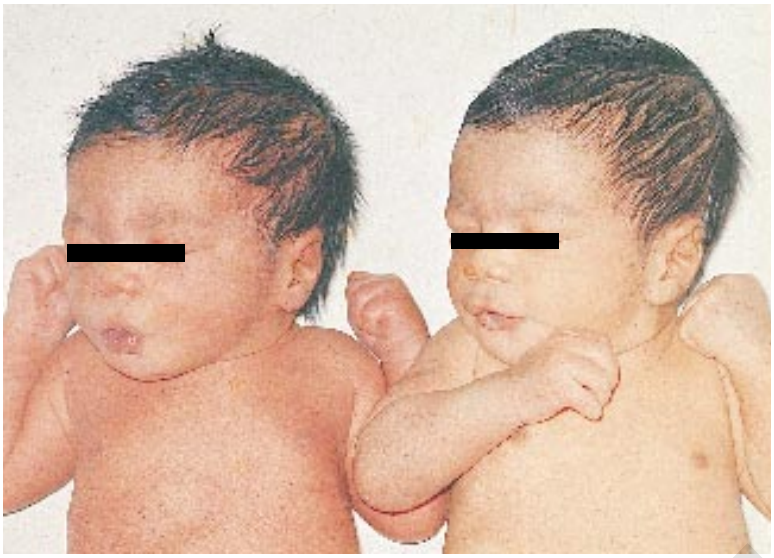

Figure 2.19. In these infants with twin transfusion syndrome, the difference in birth weight was only 180 g and the difference in central hematocrit was 32%. Thus, these infants represent a mild example of twin transfusion syndrome.

2.20

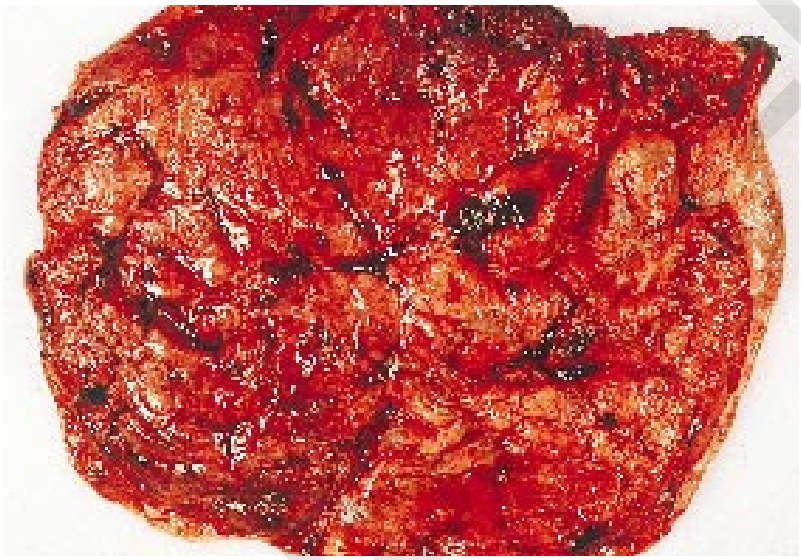

Figure 2.20. The maternal surface of a monozygotic twin placenta in infants who had the twin transfusion syndrome. Note on the left the congested appearance of the portion of the placenta supplying the recipient twin who had a central hematocrit of 69%, and note on the right the much paler appearance of the placenta supplying the donor twin who had a central hematocrit of 45%. (Singer, D.)

2.21

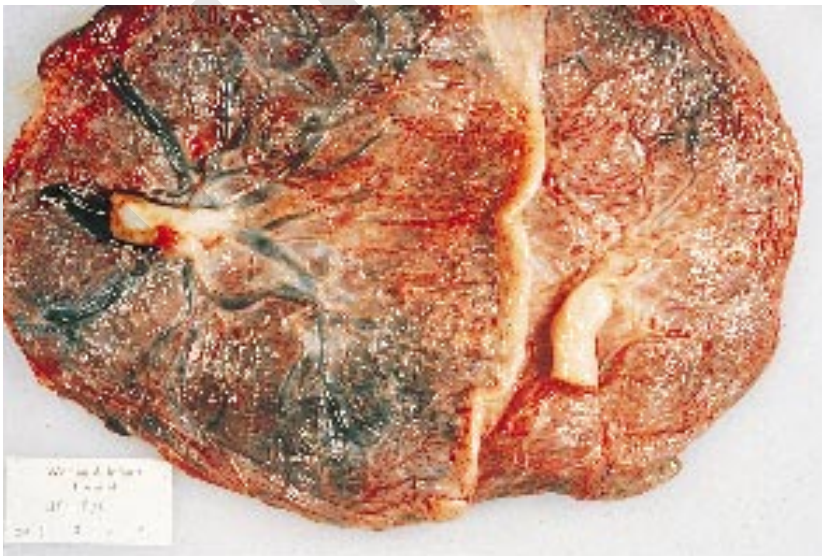

Figure 2.21. The fetal surface of the same placenta as in Figure. 2.20 showing the congested appearance on the left of the recipient portion of the twin placenta and the pallor on the right of the donor portion of the twin placenta. These vascular connections may be artery-to-artery, vein-to-vein, or artery-to-vein. Any form may significantly affect the fetuses physiologically and clinically.

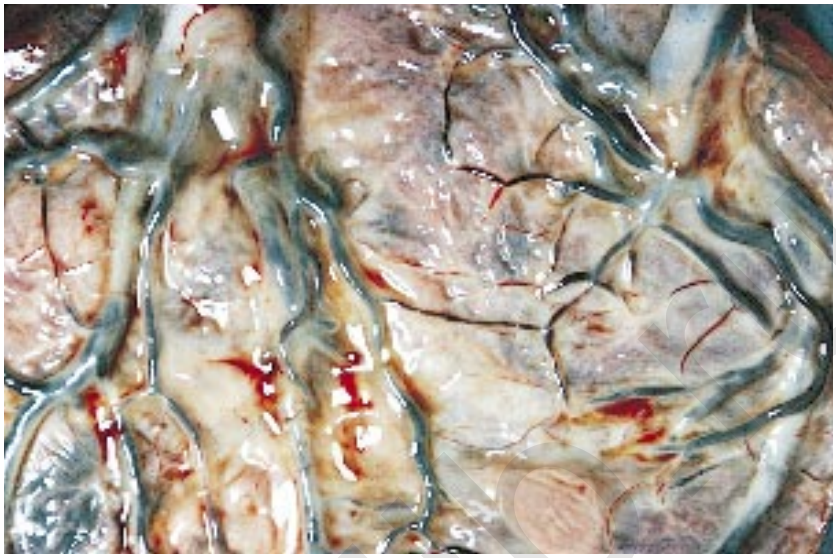

2.22

Figure 2.22. The fetal surface of placentas in twin transfusion syndrome showing the anastomoses between the two fetal circulations following the injection of infant formula, which is used as a contrast medium. Note that on the fetal surface of the placenta arteries *always* cross over veins. The anastomosis between an artery on the left and a vein on the right is shown at the junction of the left third and the right two-thirds of the figure.

2.23

Figure 2.23. This close-up view clearly shows the artery-to-vein anastomosis.

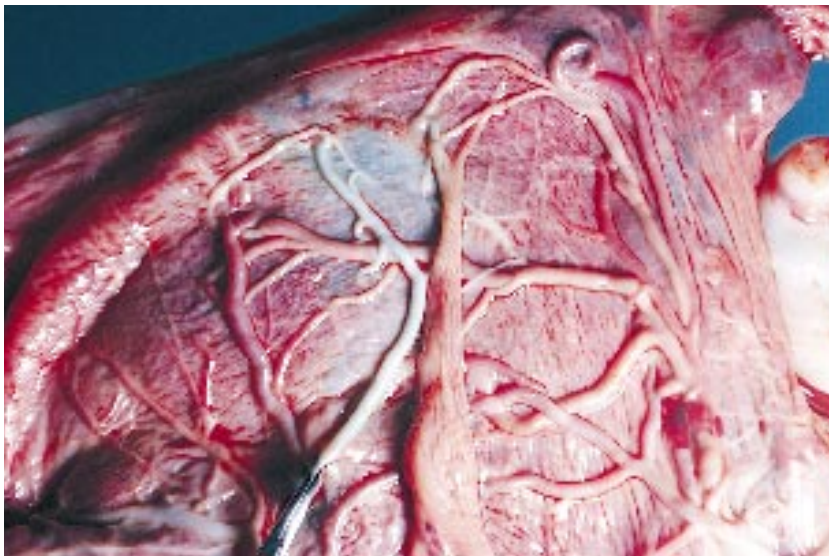

2.24

Figure 2.24. Another example of an injection of infant formula filling the arteries which cross over the veins in this vessel anastomosis.

2.25

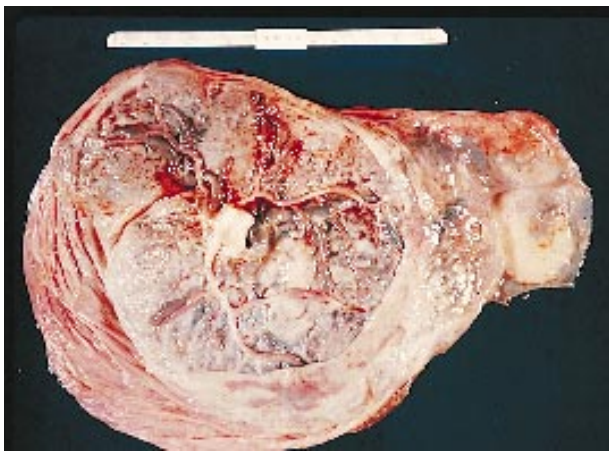

Figure 2.25. In extreme cases the transfusion syndrome may cause the death of one twin resulting in a fetus papyraceus. In this figure, there is an extrachorial placenta with a fetus papyraceus attached.

2.26

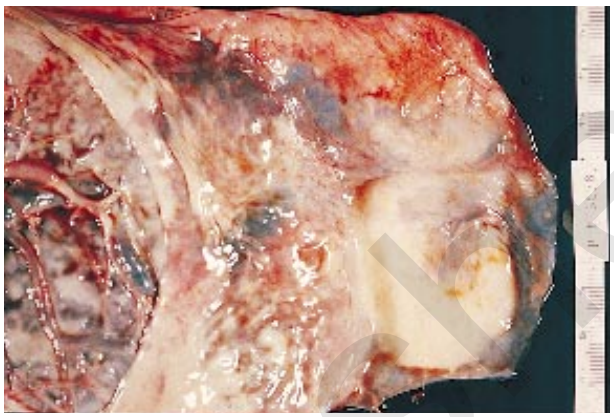

Figure 2.26. Close-up of the extrachorial placenta with the fetus papyraceus attached.

2.27

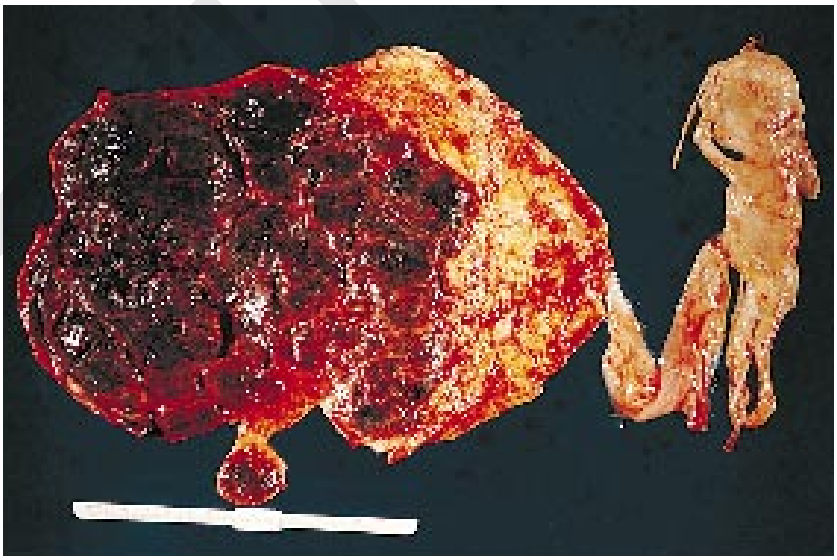

Figure 2.27. Another example of the twin transfusion syndrome. Note the maternal surface of the placenta showing the congested recipient placenta on the left and the pale donor placenta on the right with an attached fetus papyraceus.

2.28

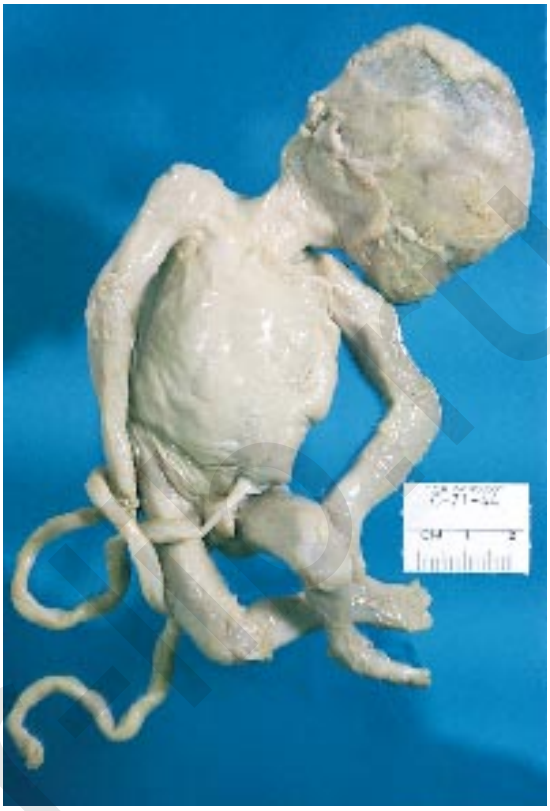

Figure 2.28. The fetus papyraceus may calcify and result in a lithopedion ("stone child") as shown in this figure.

2.29

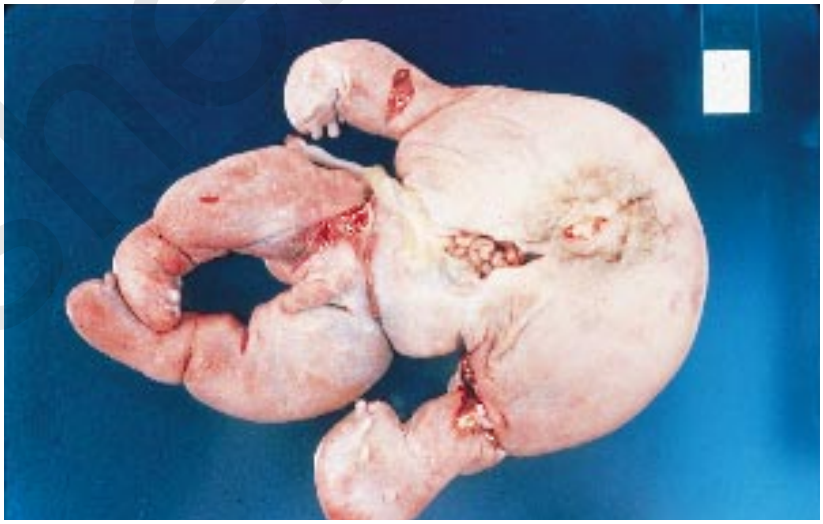

Figure 2.29. A stillborn male infant with a birthweight of 1170 g and length of 34 cm is an example of acardius acephalus. This is one of the acardiac anomalies which occurs as a consequence of abnormal umbilical artery-to-artery anastomoses between two fetuses in the presence of a fused placenta. It is sometimes referred to as the TRAP (*t*win-*r*eversed-*a*rterial-*p*erfusion) sequence. (Klima, T.)

2.30

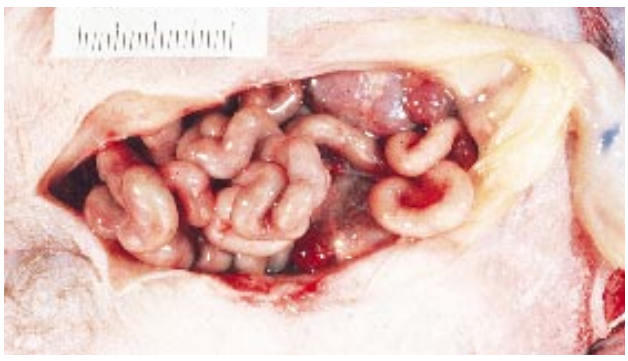

Figure 2.30. A close-up of the abdomen of the same infant shows an omphalocele; there was also hydrops, pulmonary agenesis, and polyhydramnios. Acardiac anomalies include three groups: acephalus in 60 to 75% of cases, amorphus in 20% of cases, and a well-formed head and body in 10% of cases. (Klima, T.)

2.31

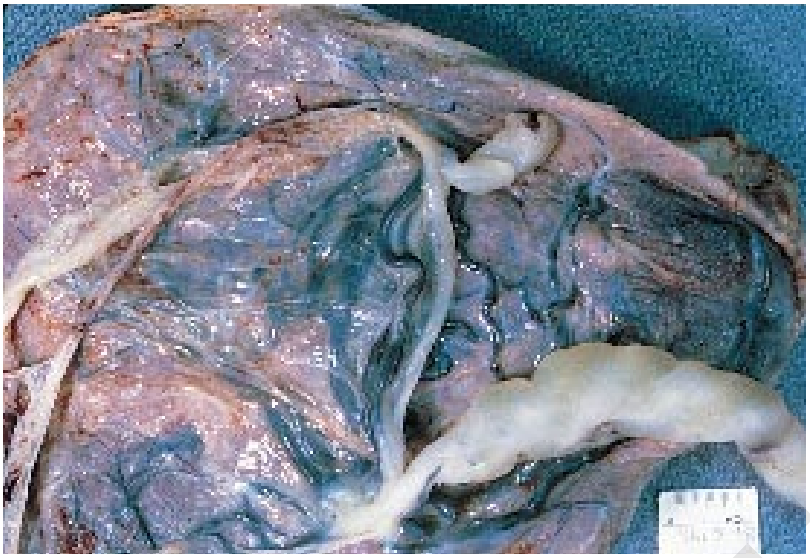

Figure 2.31. The fused placenta of the same infant with acardius acephalus shown in Figure 2.29 and 2.30. Note the large cord of the "normal" infant which had three vessels and the small cord of the infant with acardius acephalus which had two vessels. There were no separating membranes between the two cords. Note the large anastomoses between the placentas. (Klima, T.)

2.32

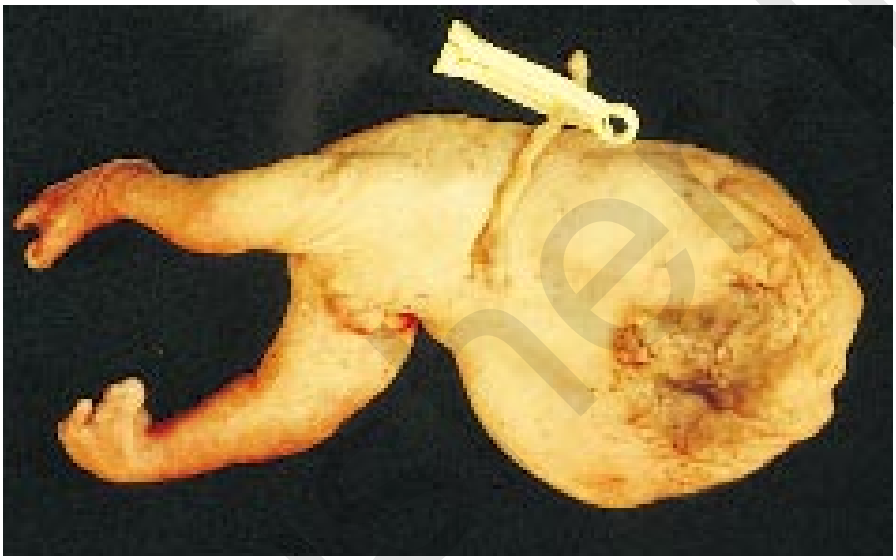

Figure 2.32. An acardius acephalus infant delivered at 30 weeks gestation. The upper body and shoulders form a fleshy mass capped by a tuft of short hairs. The lower body has two well-formed legs but has clubbed, bifid feet with two toes. (Klima, T.)

2.33

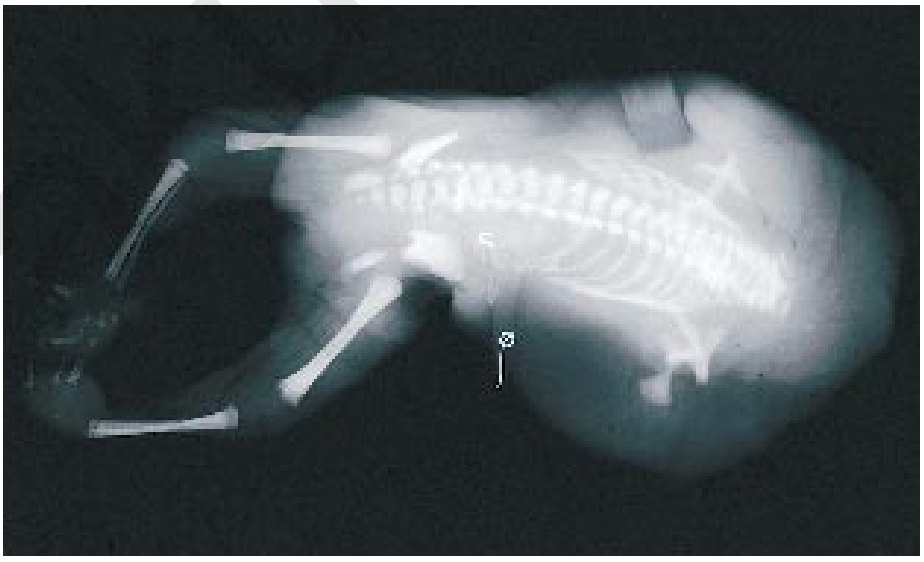

Figure 2.33. Radiograph of the infant with acardius acephalus. Note the lack of cranial development. Two clavicles and scapulae are present. The vertebral column is normal. The chest is narrow due to lack of the heart and hypoplastic lungs. The pelvis and lower extremities are well mineralized and relatively normal except for lack of some metatarsal bones.

2.34

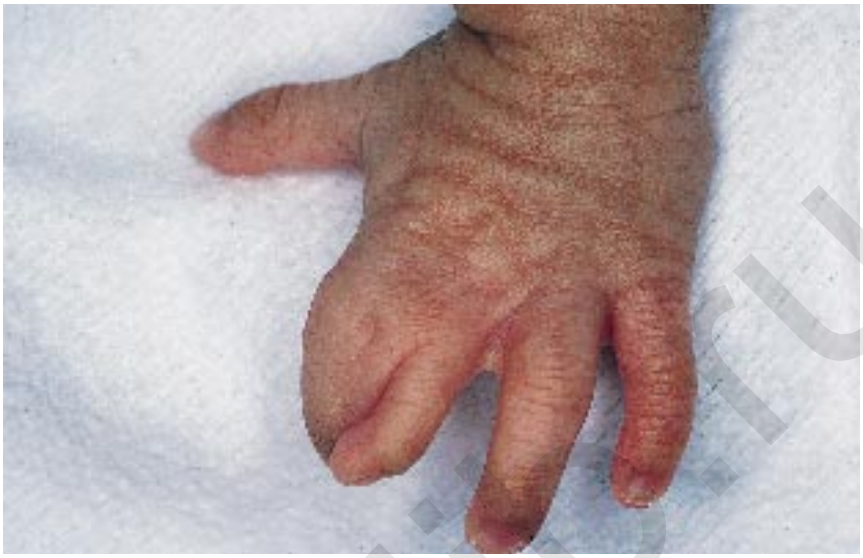

Figure 2.34. The twin with the dominant heart of the same pregnancy often shows additional anomalies such as limb reduction defects. These have been attributed to embolic disease consequent upon stasis in the acardiac fetus. This twin had some limb anomalies which included fusion of digits of the left hand as seen in this figure.

2.35

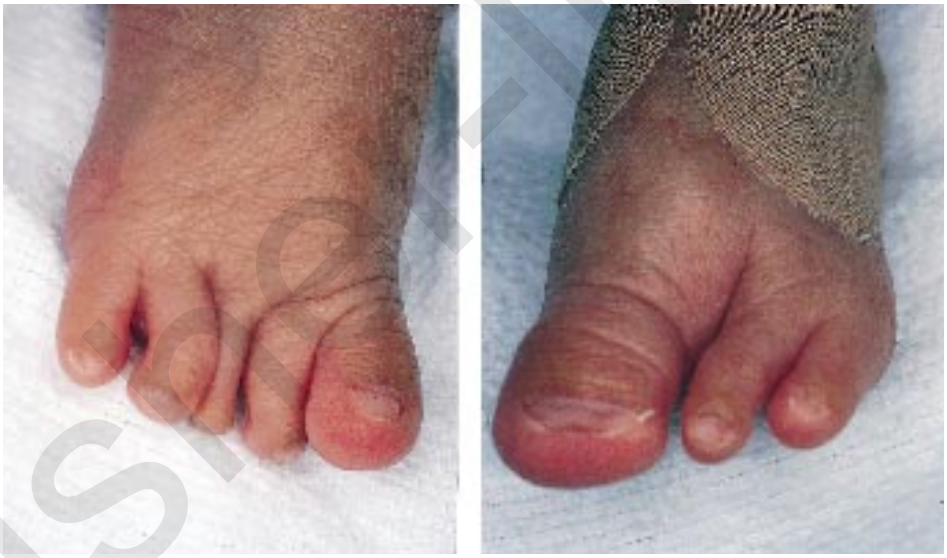

Figure 2.35. This is the same infant showing anomalies of both feet.

2.36

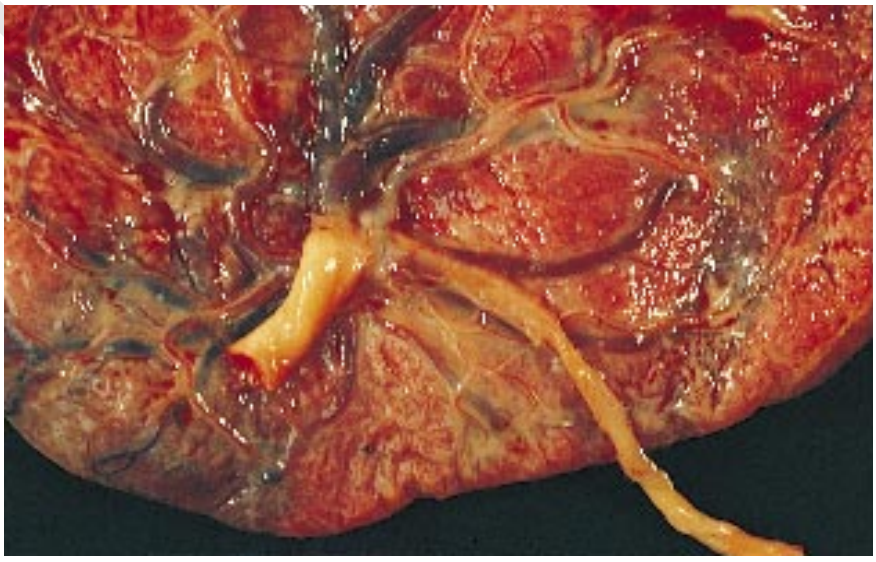

Figure 2.36. The placenta of the infants described above showing two umbilical cords with a common insertion about 5 cm from the margin of the placenta. The larger cord was approximately 10 mm in diameter and had three vessels. The smaller cord was approximately 6 mm in diameter and had two vessels. Note the congested appearance of the placental tissue and the vessels on the left and the pallor of the placental tissue and the vessels on the right. (Klima, T.)

2.37

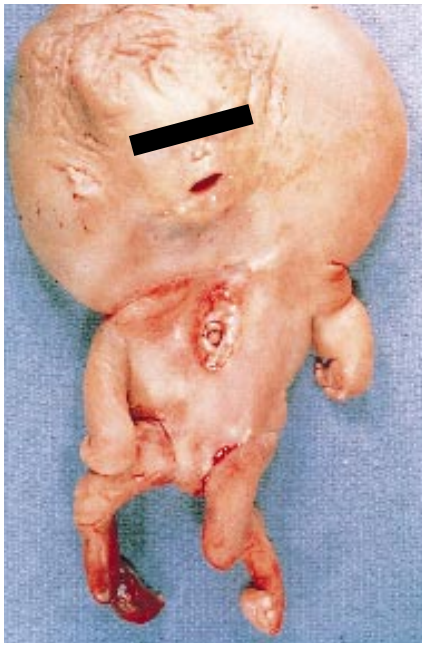

Figure 2.37. This is an example of acardius anceps (hemiacardius). The cranial portion is partially covered by hair, but no head is formed. There is a globular structure of the upper part which shows a rudimentary face with an oral opening through which a cleft palate is seen. Four extremities are present. There is a defect in the anterior abdominal wall with intestinal loops present. (Klima, T.)

2.38

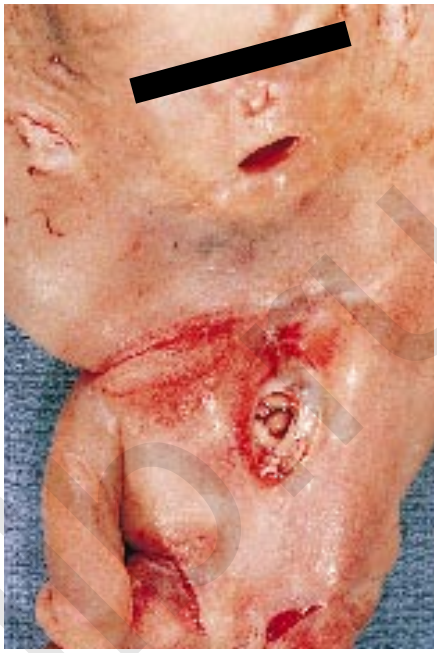

Figure 2.38. Close-up of the same infant shown in Figure 2.37. The anterior wall of the abdomen is missing and the intestinal loops are exposed. There is no umbilical cord identified. (Klima, T.)

CONJOINED TWINS

Conjoined twins are rare, one per 50,000 to 100,000 live births. They result from the failure of the zygote to completely divide. This occurs in approximately 1% of monozygotic twins. The incidence of the types of fusion is as follows: The most common types are thoracopagus twins with an incidence of one per 70,000 live births (73.4%), pygopagus twins (18.8%), ischiopagus twins (5.9%), and the most rare types are the craniopagus twins with an incidence of one per 2,000,000 to 4,000,000 live births (1.7%). Conjoined twinning occurs only in monoamnionic-monochorionic pregnancies.

2.39

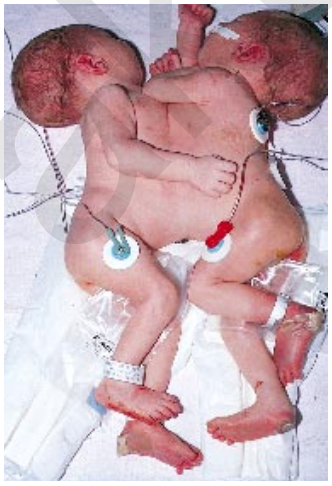

Figure 2.39. In thoracopagus conjoined twins, note the fusion at the thorax and upper part of the abdomen with a single site of umbilical cord insertion. The posture is typical for thoracopagus conjoined twins in that the heads are hyperextended and the backs are relatively straight.

2.40

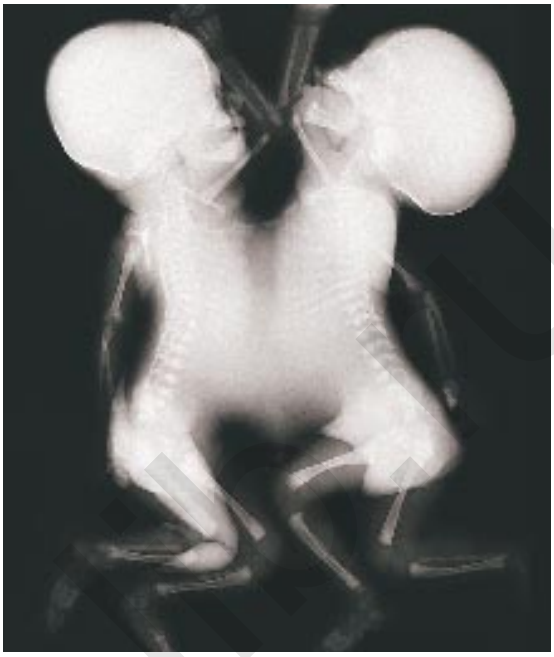

Figure 2.40. Radiograph of the conjoined twins shown in Figure 2.39 illustrates the hyperextended heads and the fusion of the thoraces and upper abdomen. On fetal radiograph, the hyperextended fetal heads at the same level were considered almost diagnostic of thoracopagus conjoined twins. With the advent of ultrasonography, the diagnosis should be made more readily.

2.41

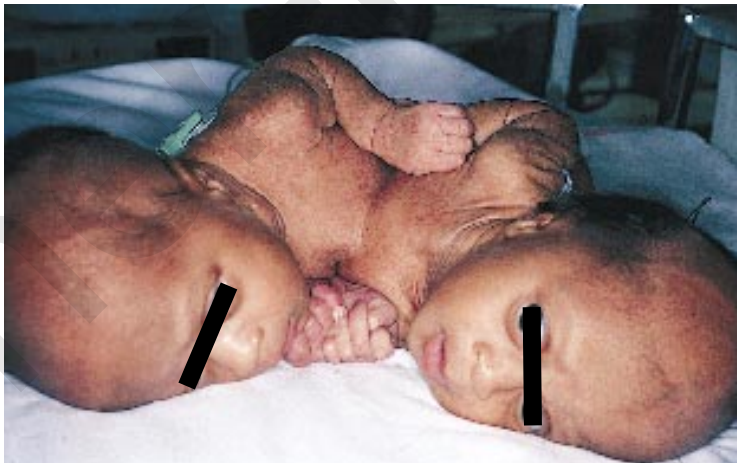

Figure 2.41. Another set of thoracopagus conjoined twins showing the typical posture of the hyperextended heads.

2.42

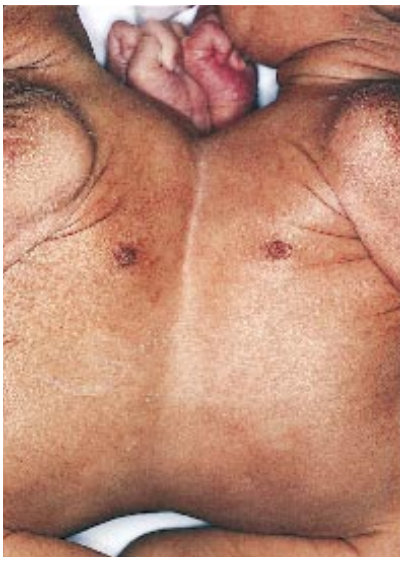

Figure 2.42. Thoracopagus conjoined twins showing the fusion from the upper thorax to the midabdomen.

2.43

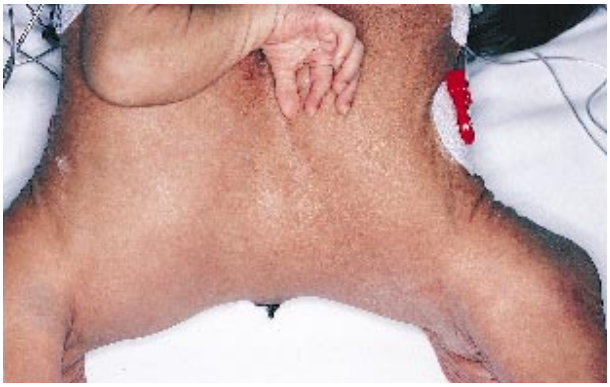

Figure 2.43. The same twins as shown in Figure 2.41 showing the fused upper abdomen and the fused umbilical cord.

2.44

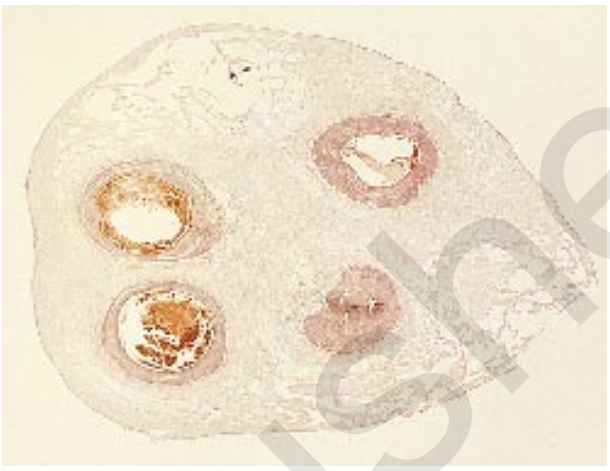

Figure 2.44. This fused umbilical cord section from the same set of thoracopagus conjoined twins shows the presence of four vessels, two arteries and two veins. In the fused umbilical cords seen in conjoined twinning, there may be from two to seven vessels. (Singer, D.)

2.45

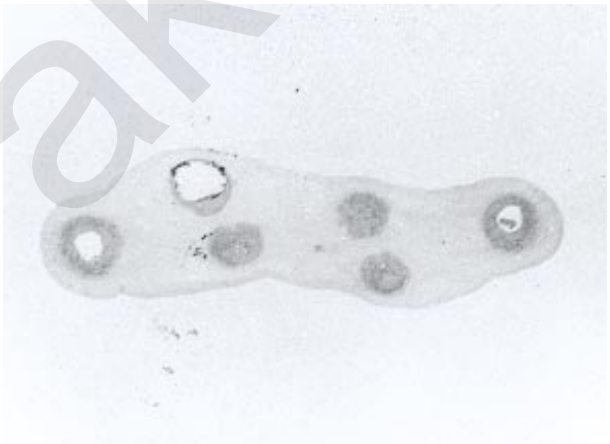

Figure 2.45. This fused umbilical cord section showing three arteries and three veins is another example from conjoined twins. (Singer, D.)

2.46

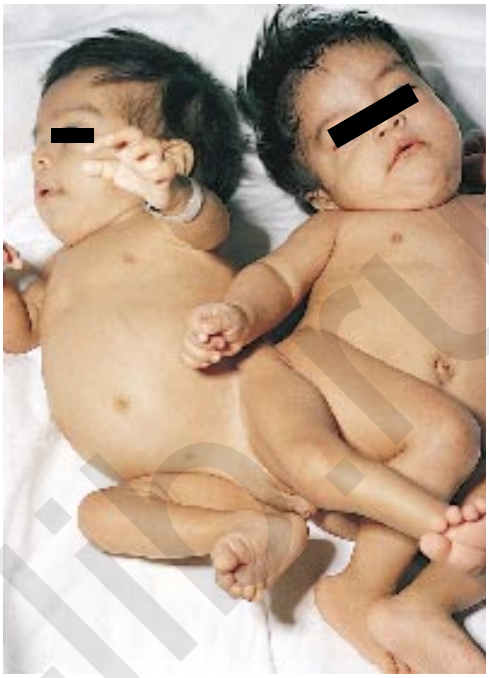

Figure 2.46. Pygopagus conjoined twins are fused at the buttocks.

2.47

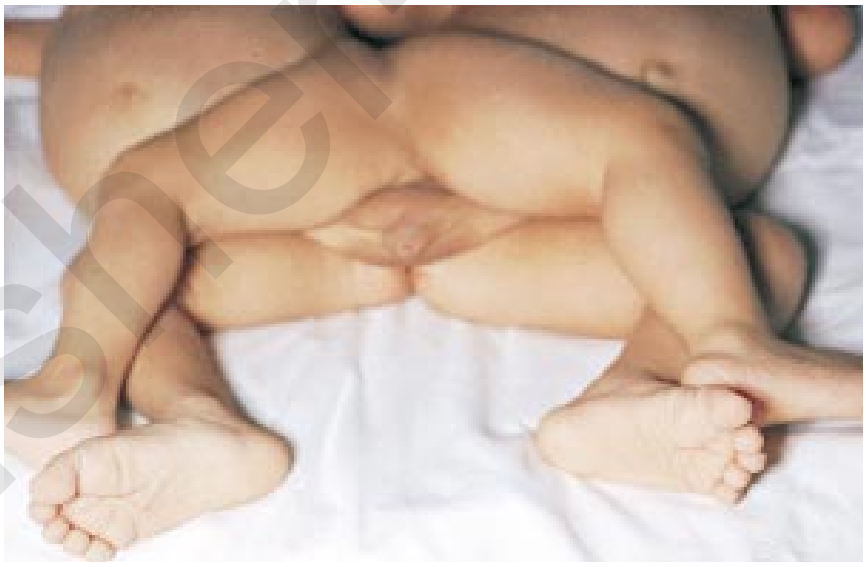

Figure 2.47. The same set of pygopagus conjoined twins showing the fused genitalia.

2.48

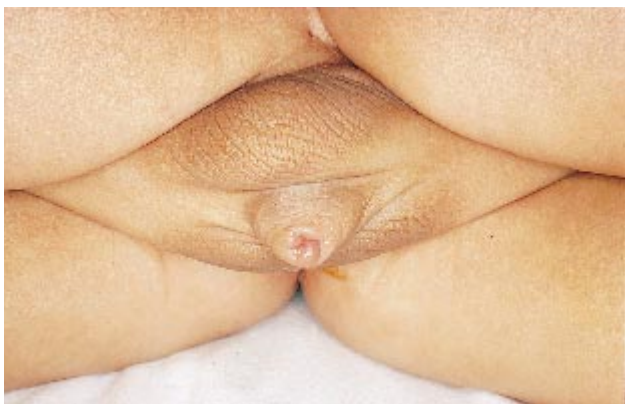

Figure 2.48. Close-up of the fused genitalia in the same set of pygopagus conjoined twins.

2.49

Figure 2.49. The twins shown in Figure 2.46 were successfully separated. This figure shows them prior to discharge from the hospital.

2.50

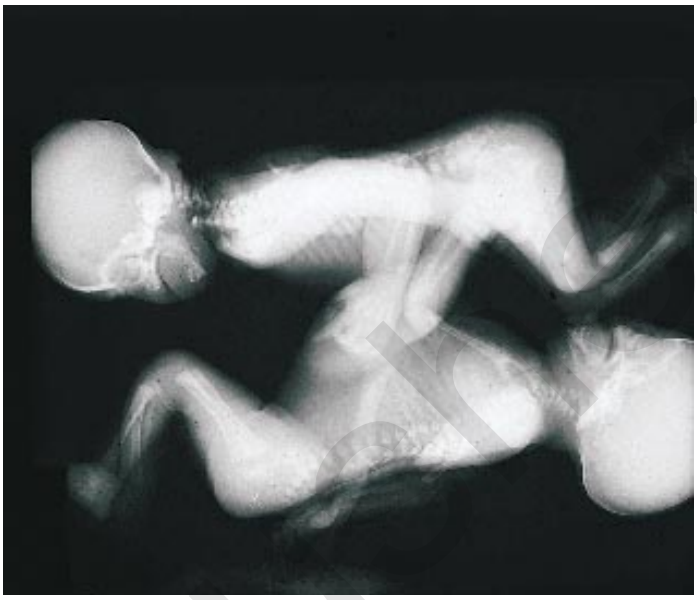

Figure 2.50. Radiograph of a set of omphalopagus twins shows the fusion at the abdominal walls and hence they could be separated.

2.51

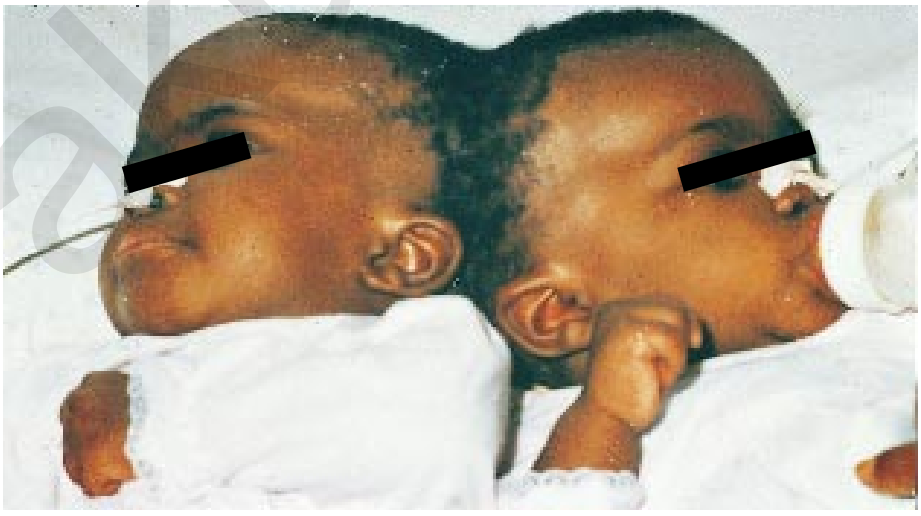

Figure 2.51. An example of craniopagus conjoined twins.

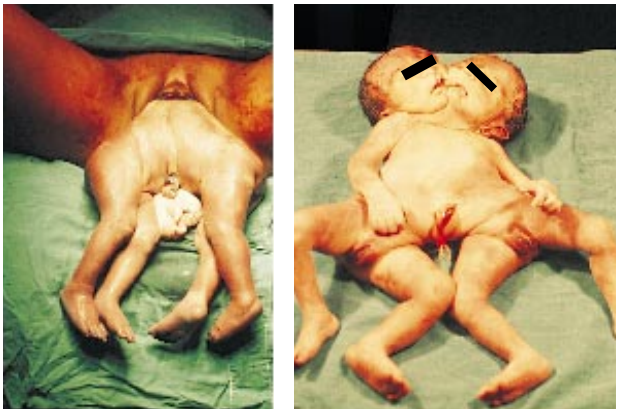

2.52

Figure 2.52. Note on the left, the vaginal delivery of prosopothoracopagus conjoined twins. On the right, note the twins following delivery. Prosopothoracopagus conjoined twins are twins united in the frontal plane with the fusion extending from the oral region through the thorax and upper abdomen. Diagnosis was not made prenatally and the twins died at delivery. Note that there are only two upper extremities (dibrachus) and four lower extremities (tetrapus). (Caberra-Meza, G.)

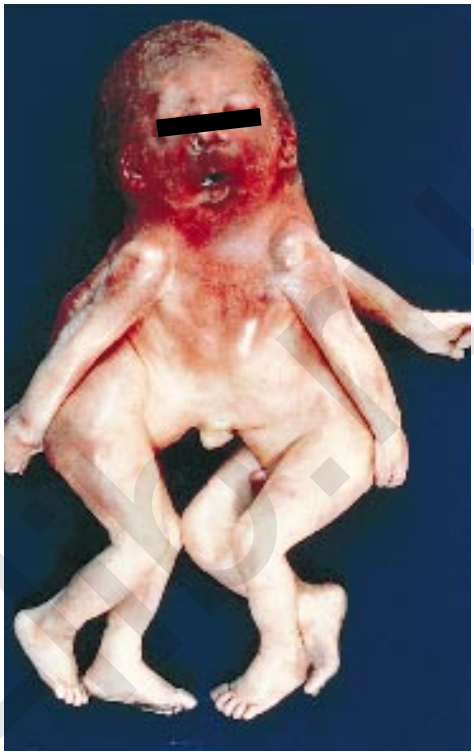

2.53

Figure 2.53. Cephalothoracopagus conjoined twins. Note the syncephalus.

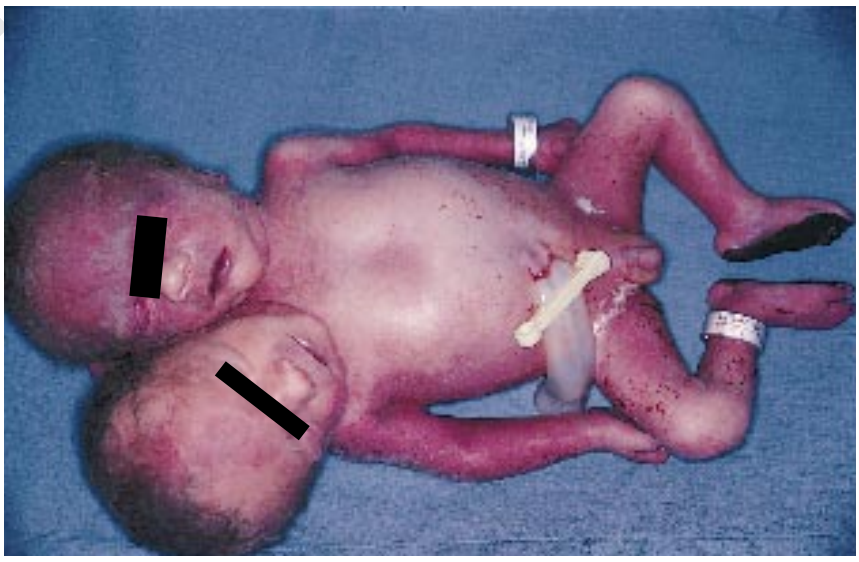

2.54

Figure 2.54. Dicephalus conjoined twins with dicephalus, three upper extremities (tribrachus), and two lower extremities (dipus). Note the two separate heads and the fused chest.

2.55

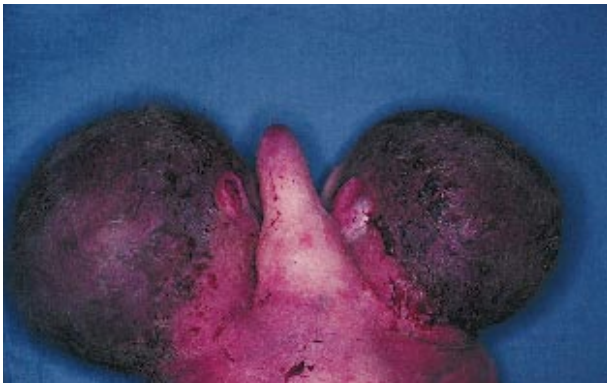

Figure 2.55. A close-up of the same twins shown in Figure 2.54 demonstrates the third upper extremity extending from the fused shoulders. There were two separate neurologic systems, two separate pulmonary systems, two gastrointestinal systems joining at the jejunum, a single genitourinary system, and conjoined hearts with complex anomalies.

2.56

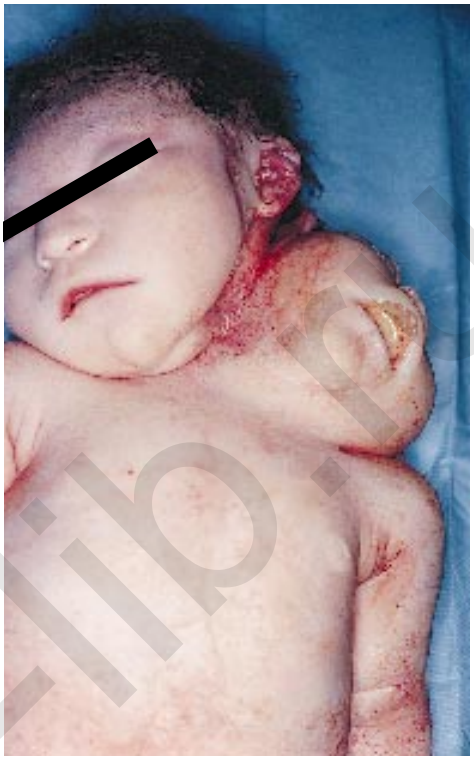

Figure 2.56. Another example of dicephalus conjoined twins. Note that the head on the left of the figure is normal but that there is anencephaly of the head on the right of the figure.

2.57

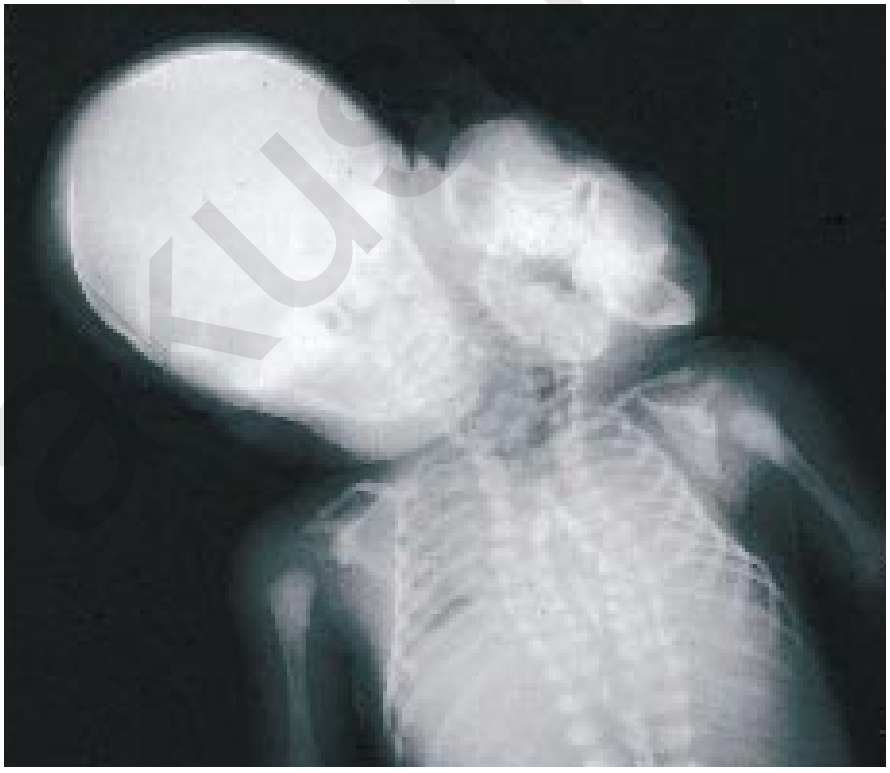

Figure 2.57. Radiograph of the same conjoined twins showing the normal head on the left of the figure and the anencephalic head on the right of the figure. Note that there are fused vertebral columns with some separation at the lower thorax and upper abdomen and that there is dibrachus.

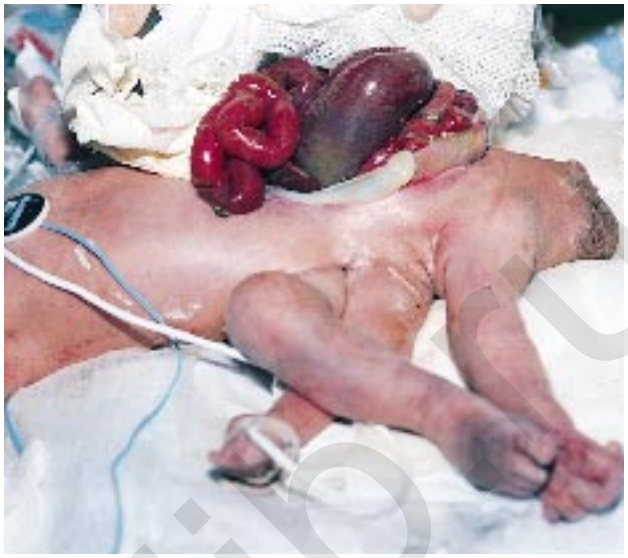

2.58

Figure 2.58. Asymmetric ischiopagus conjoined twins. Note that the twin on the right of the figure, which is attached at the ischia, is an anencephalic parasite with a partial thorax and abdomen and two upper and two lower extremities. The "normal" twin on the left of the figure had gastroschisis, imperforate anus, and rectovaginal fistula. There were two bladders, two kidneys, and two uteri present.

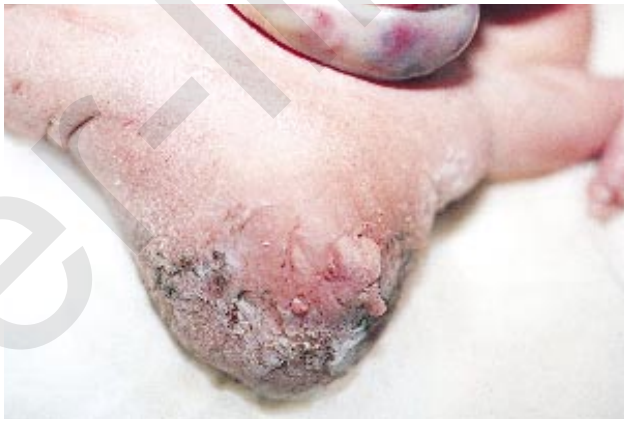

2.59

Figure 2.59. Close-up of the anencephalic parasite in the above asymmetric ischiopagus conjoined twins.

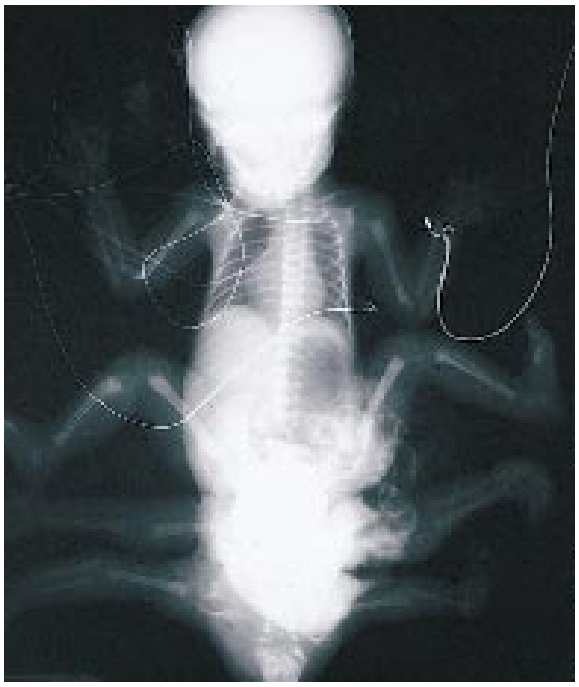

2.60

Figure 2.60. Radiograph of the asymmetric ischiopagus conjoined twins. Note at the bottom the severely anecephalic twin attached to the "normal" twin who has a large gastroschisis. Each twin has four extremities.

2.61

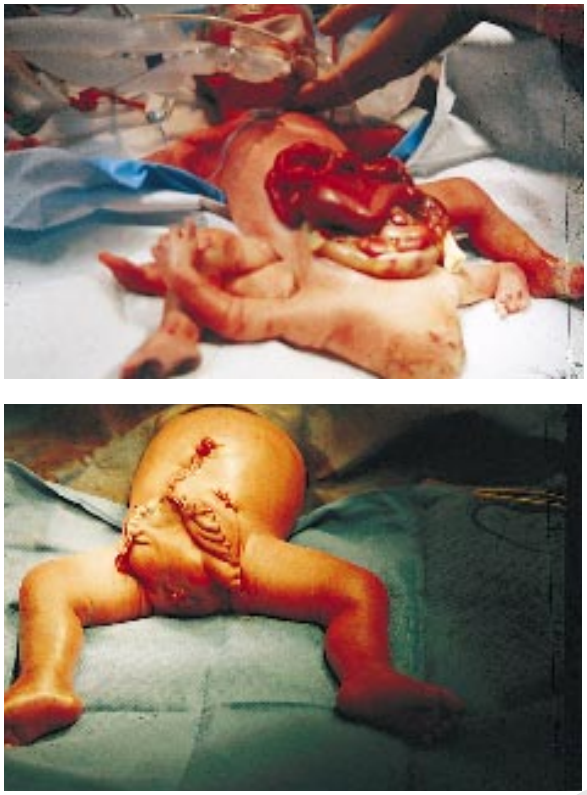

Figure 2.61. Preoperative (above) and postoperative (below) appearance of the asymmetric ischiopagus conjoined twins shown in Figures 2.58 to 2.60.

2.62

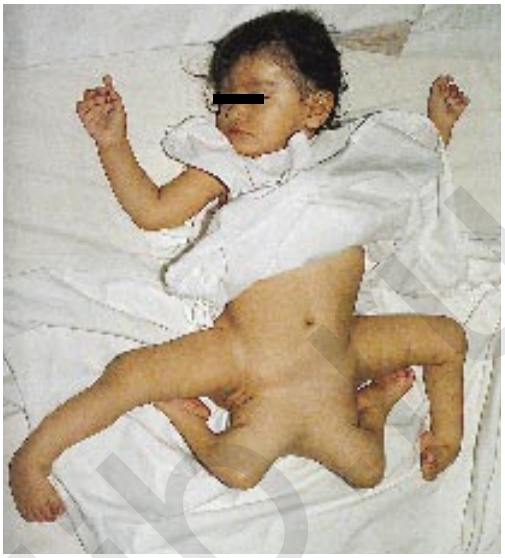

Figure 2.62. Dipygus twins. Recent work has suggested that genes are involved in establishing the body axes, metameric pattern (segmentation genes), and regional specialization (homeotic genes). This raises the possibility that many of the abnormalities of facial duplication in man are not a manifestation of incomplete twinning but may be homeotic malformations. Limb duplication may also be a result of stimulation of homeobox gene expression and thus a well-formed pair of arms and/or legs may be seen emerging.

2.63

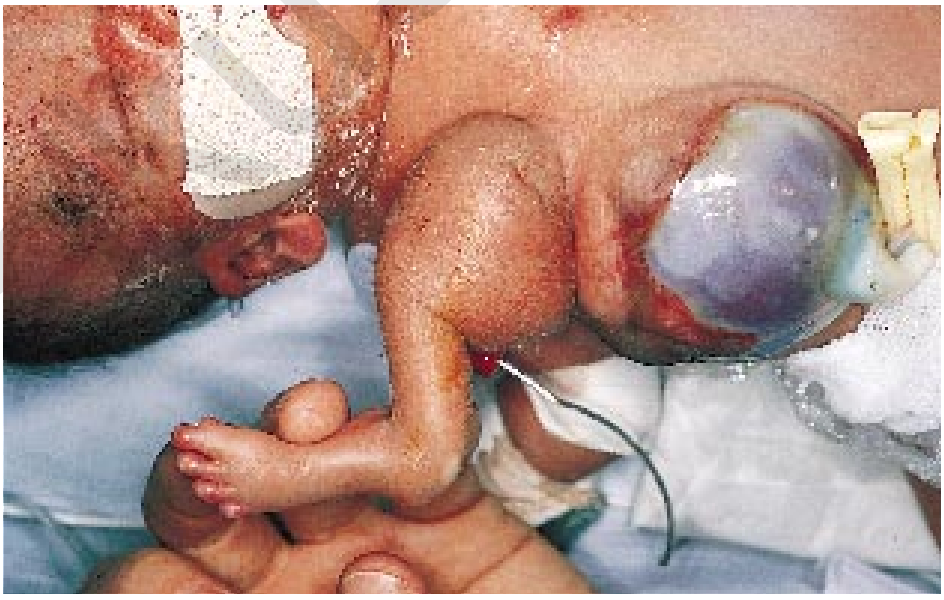

Figure 2.63. This infant has a well-developed lower extremity emerging from the chest and has been considered to be an asymmetrical double malformation – heteroadelphia (an underdeveloped *parasite* attached to a well-developed *autosite*). With the new concept, this could be an example of a homeotic malformation. Also note the large omphalocele.

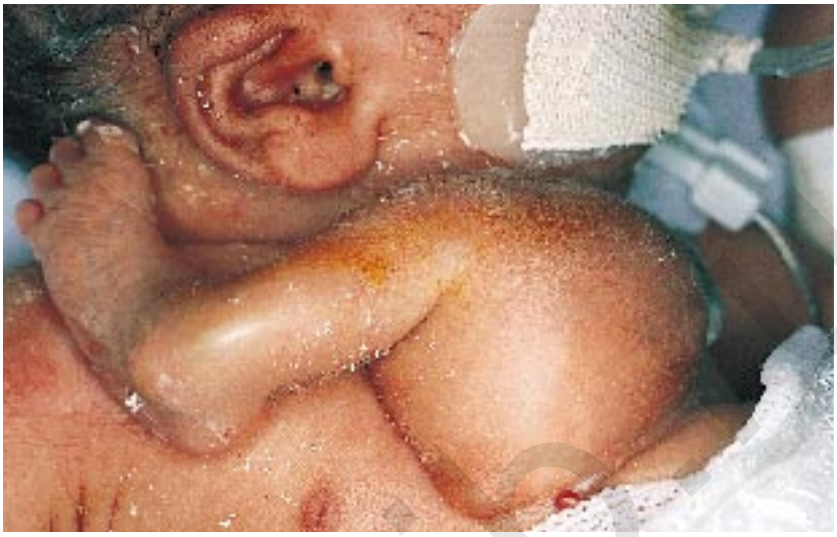

2.64

Figure 2.64. Close-up view of the same accessory lower extremity as shown in Figure 2.63.

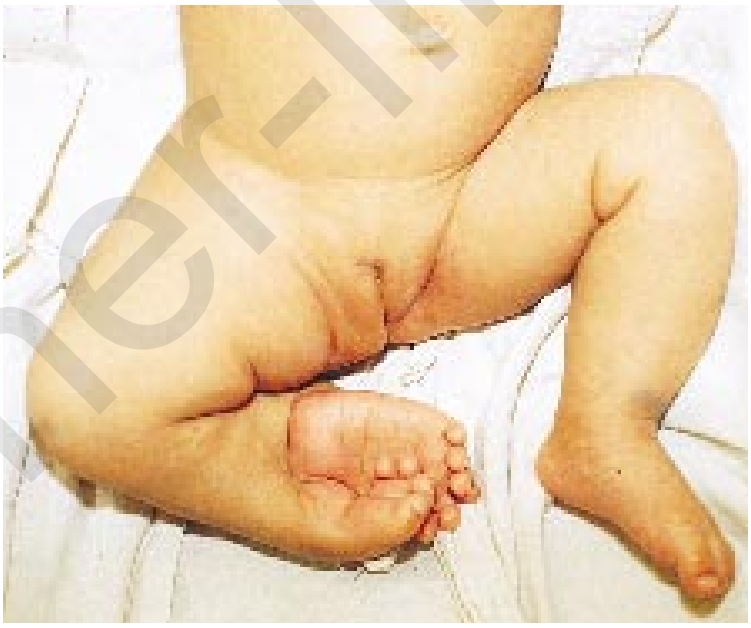

2.65

Figure 2.65. Duplication of the right leg and foot. The question again arises as to whether this is an asymmetric double monster or a homeotic malformation. (Cabera-Meza, G.)

2.66

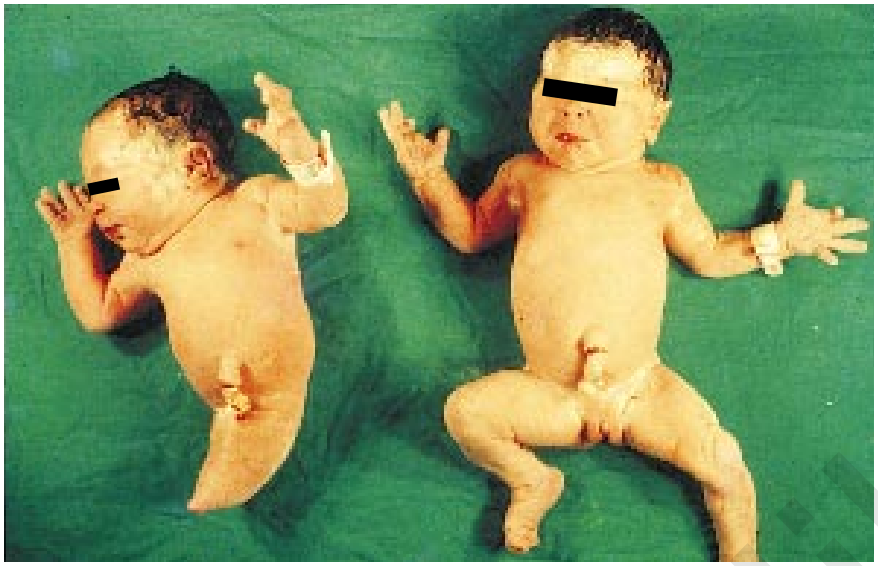

Figure 2.66. Discordant twins. The twin on the left is an example of a severe caudal regression syndrome. There was oligohydramnios, renal agenesis, imperforate anus, and lack of external genitalia. The twin on the right is normal. (Cabera-Meza, G.)

2.67

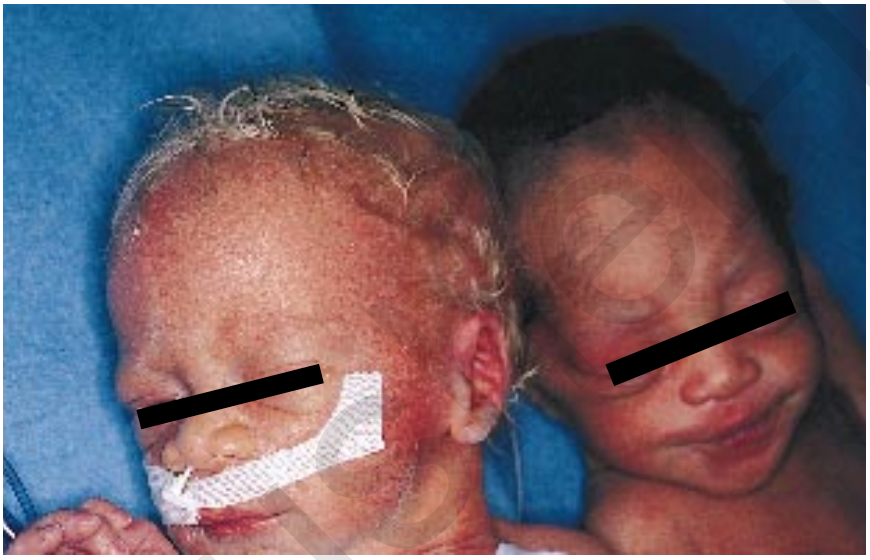

Figure 2.67. Another example of discordant twins. The twin on the left is an albino and the twin on the right is normal. This is the second set of discordant twins (one albino and one normal) born to this mother.

Chapter 3
Effects of Maternal Medication

During pregnancy, the average fetus is exposed to four physician-prescribed and five self-prescribed drugs. Every drug administered or taken by a pregnant woman presents the mother with both risks and benefits. The risks include the drug's potential as a teratogen or as a cause of toxicity in the fetus. Most human teratogens affect the embryo during a very narrow period of early development as illustrated by the time (24 to 33 days gestation) during which the fetus is susceptible to limb reduction defects caused by thalidomide. Several human teratogens, such as alcohol, androgens, cocaine, diphenylhydantoin, radiation, tetracycline, valproic acid, and warfarin have serious side effects beyond the period of organogenesis. These effects may include cell deletion, vascular disruption, necrosis, physiologic decompensation, organ pathology, and intrauterine growth retardation. Drugs taken in the third trimester may not have teratogenic effects, but may be toxic to the fetus. Some examples include indomethacin (causing oligohydramnios), propylthiouracil (causing fetal goiter), and erythromycin (causing cholestatic hepatitis). A detailed history of maternal drug use and abuse is essential in evaluating most malformations and diseases in the neonatal period.

3.1

Figure 3.1. This illustration contrasts the craniofacial features of a healthy child on the right to those of a child with fetal alcohol syndrome on the left. Note the microcephaly, short palpebral fissure, flat maxillary area, poorly developed philtrum and thin upper lip (Peter Shvartsman, Canadian Medical Association Journal, July 15, 1981 cover).

3.2

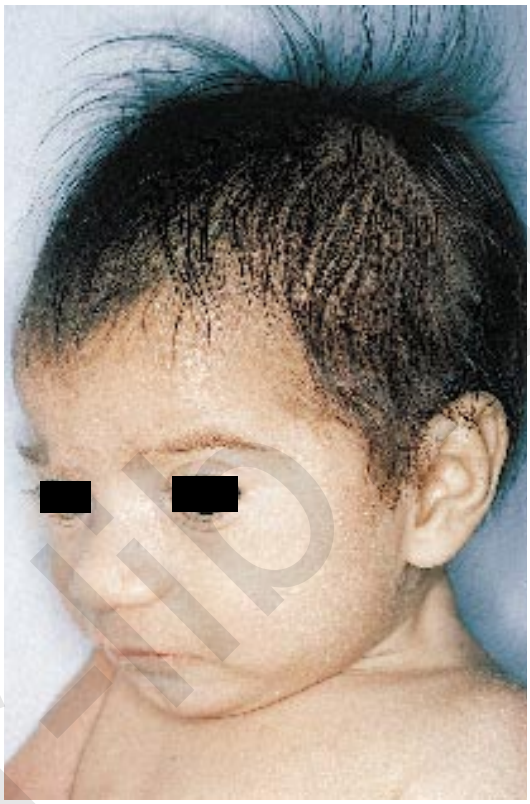

Figure 3.2. This infant, age 6 weeks, was born to a mother with severe, chronic alcoholism. There was failure to thrive and hypotonia. Note the microcephaly (head circumference less than the third percentile), short nose, absence of philtrum and thin vermilion border of the upper lip.

Findings in fetal alcohol syndrome include intrauterine growth retardation, microcephaly, dysplastic facial features, hypoplasia of the midface, and a hypoplastic philtrum with a thin vermilion border of the upper lip. Later there may be continued failure to thrive and developmental and behavioral disorders.

3.3

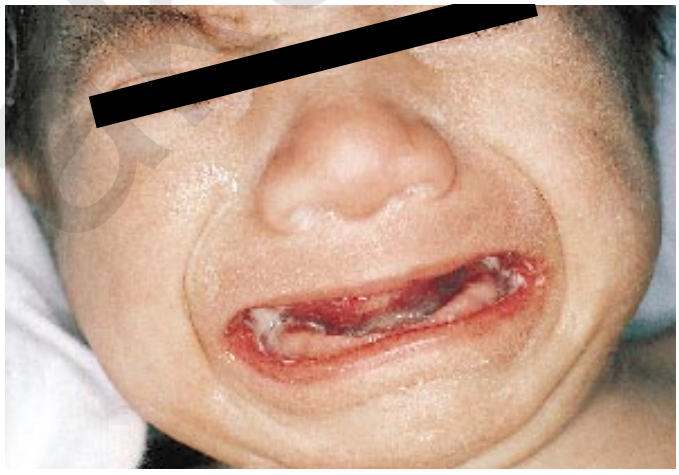

Figure 3.3. Close-up of the face of the same infant shows the short nose, absence of the philtrum, and thin vermilion border of the upper lip. Many other findings in fetal alcohol syndrome have been reported, including epicanthic folds, ptosis, hypoplastic maxilla, deep or accentuated palmar creases, and clinodactyly.

3.4

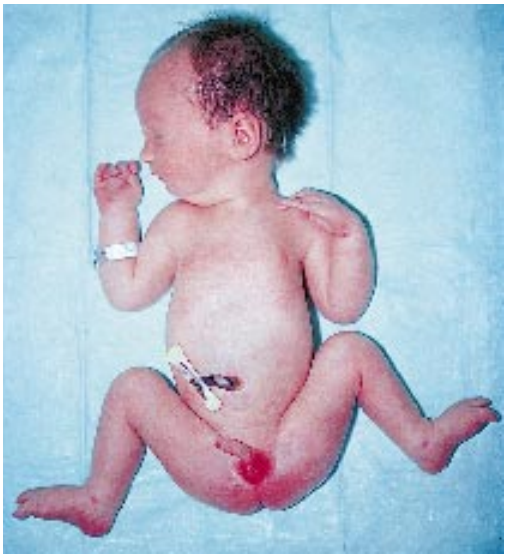

Figure 3.4. Soon after birth, this infant of a narcotic addict shows hypotonia. Note the concavity of the inner aspect of the thighs and the position of the lower extremities. This has resulted from a postural deformation in which the fetus has had its thighs flexed over its abdomen in utero. Because of the mother's narcotic habit there was minimal fetal movement in utero.

3.5

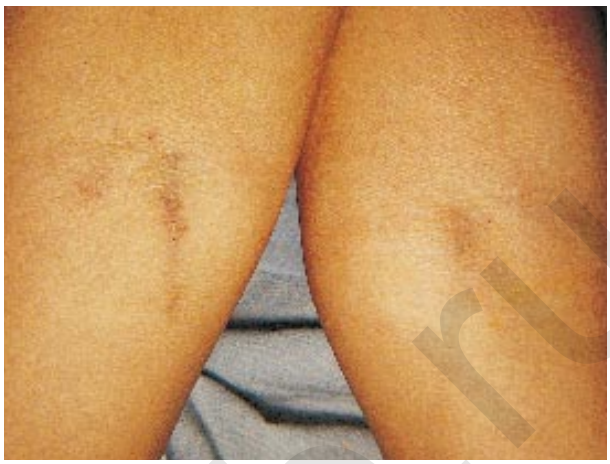

Figure 3.5. Drug withdrawal is a major problem in neonates delivered of narcotic addicted mothers. This figure stresses the fact that one should always check for signs of drug addiction in the mother. This figure shows needle tracks at both elbows of a mother.

3.6

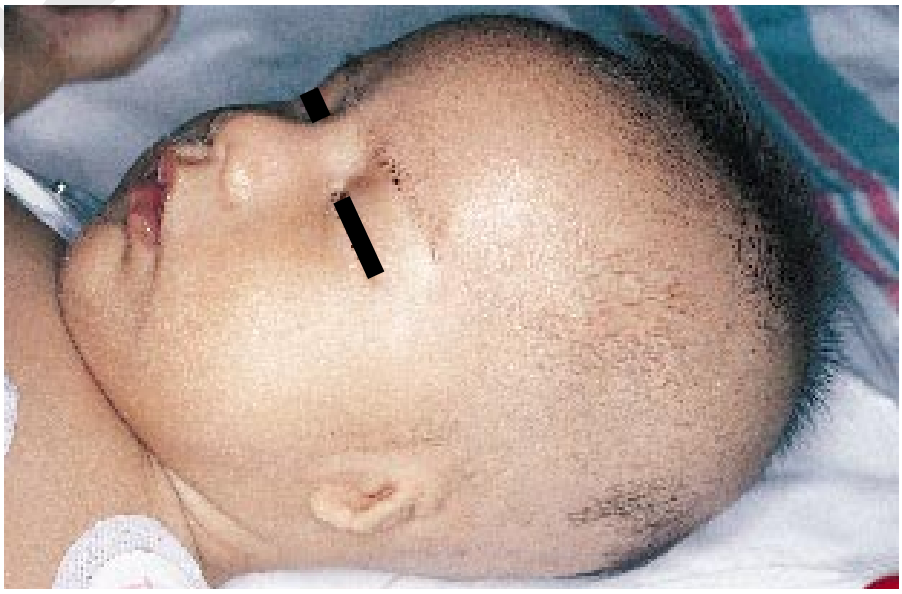

Figure 3.6. Infants with retinoic acid embryopathy (Accutane™ embryopathy) may have craniofacial, cardiovascular, and central nervous system abnormalities. In this infant note the narrow sloping forehead, flat depressed nasal bridge, mild micrognathia, and microtia with absence of the external auditory canal. In addition there was congenital heart disease. Affected infants may have hydrocephalus, microcephaly, or thymic abnormalities. This mother was treated with retinoic acid during the first month of pregnancy.

3.7

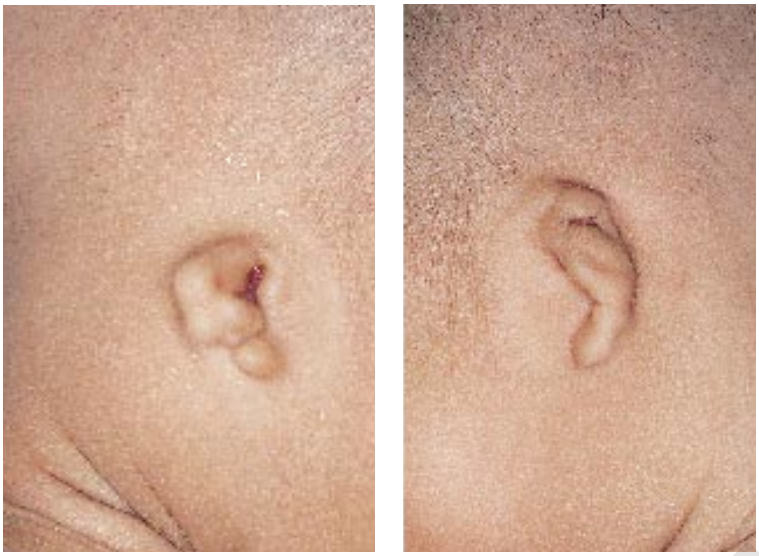

Figure 3.7. Close-up of the ears of the same infant as shown in Figure 3.6 shows the bilateral microtia with absence of the external auditory meatus.

3.8

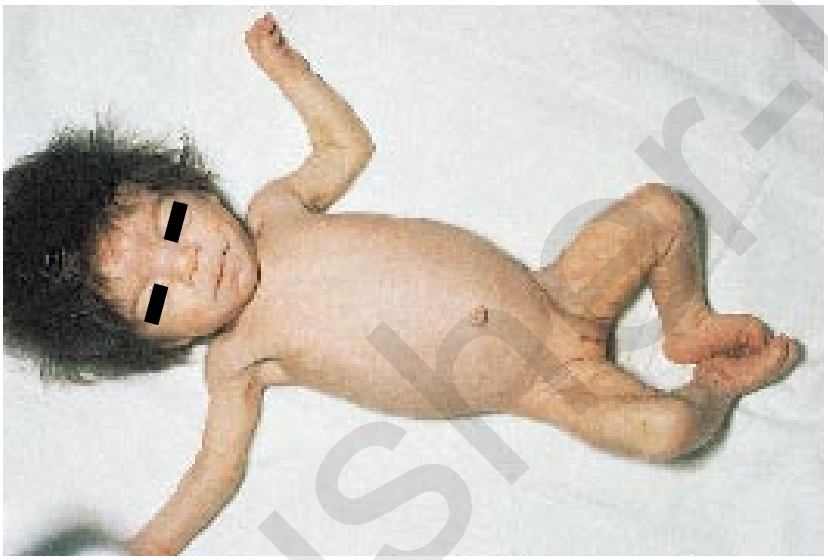

Figure 3.8. In infants with the fetal hydantoin (Dilantin™) syndrome there is moderate growth retardation, usually prenatal, a wide anterior fontanelle and metopic ridging. In this infant, note the growth retardation, profuse scalp hair, and short neck. Other findings included hypoplasia of the distal phalanges with small nails and a digital thumb.

3.9

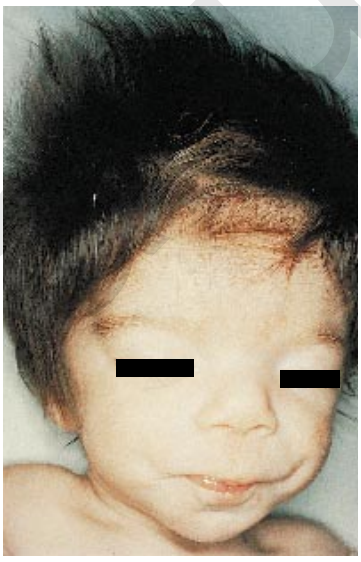

Figure 3.9. Close-up of the face of the same infant. Note the marked hirsutism, low hairline, low nasal bridge with a short upturned nose ("pug" nose), and long philtrum.

3.10

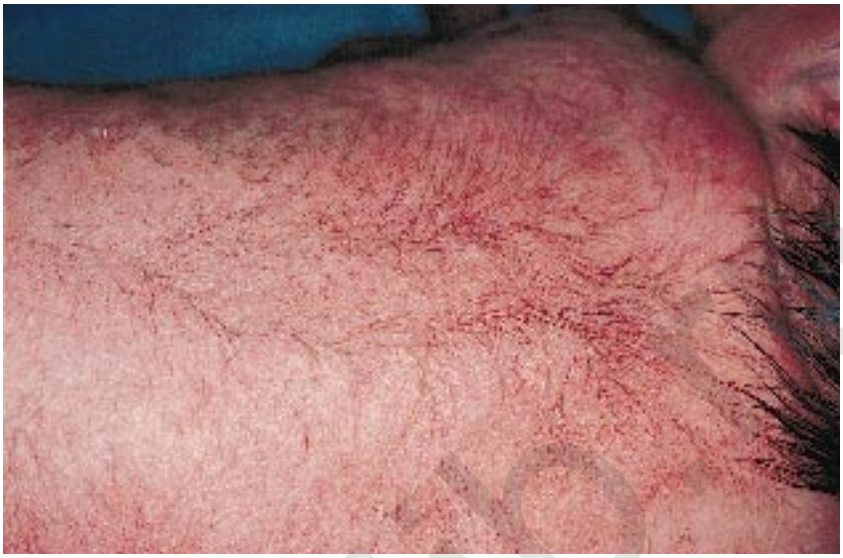

Figure 3.10. Hypertrichosis in another infant with the fetal hydantoin syndrome. Mother was treated throughout pregnancy with hydantoin. The risk of fetal hydantoin syndrome in infants of treated mothers is about 10%.

3.11

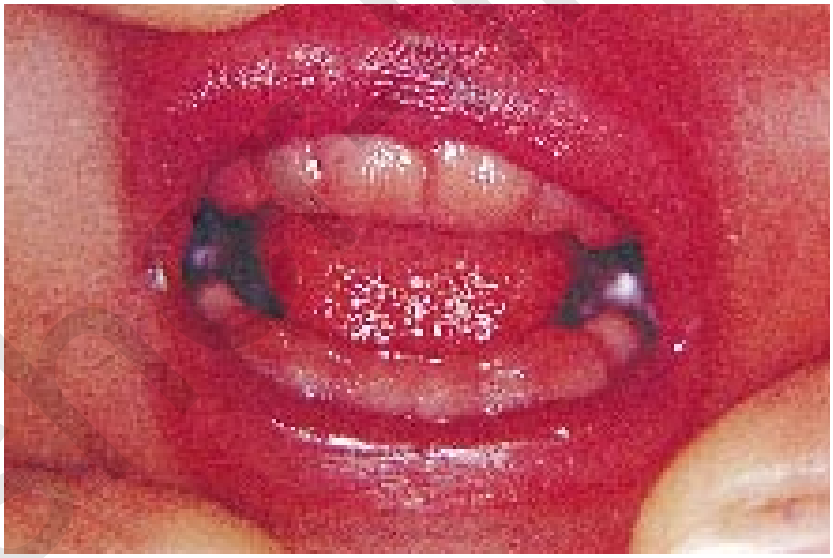

Figure 3.11. Gum hypertrophy in an infant with the fetal hydantoin syndrome. Many other findings have been reported in infants with fetal hydantoin syndrome, including widely spaced nipples, rib anomalies, abnormal palmar creases, pilonidal sinus, and congenital heart disease.

3.12

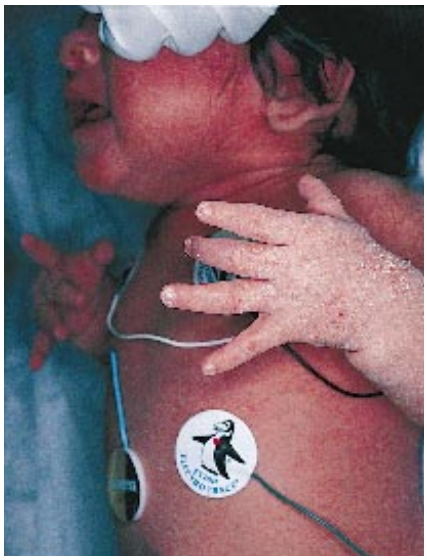

Figure 3.12. This infant of an epileptic mother on hydantoin developed seizures at the age of 36 hours. He had hypocalcemia with a calcium level of 6.4 mg/dL and a phosphorus level of 11.2 mg/dL. In fetal hydantoin syndrome the digital hypoplasia may be associated with narrow distal phalanges and hypoplastic nails.

3.13

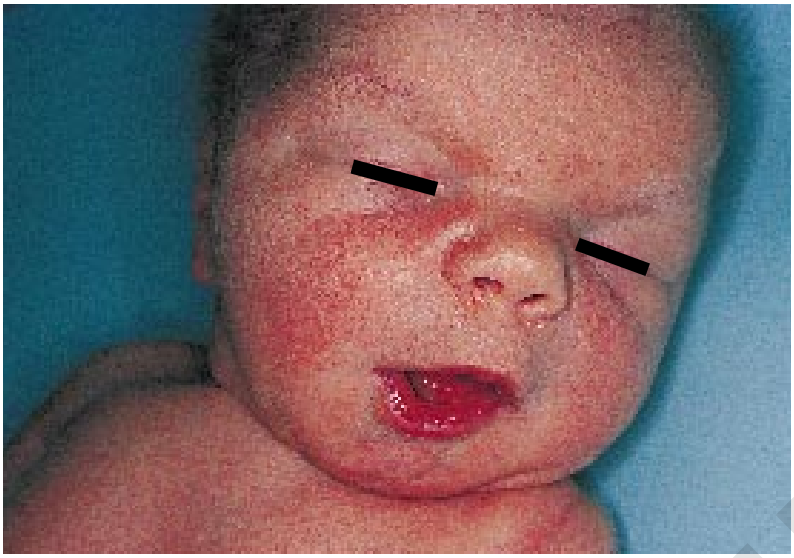

Figure 3.13. This infant with the fetal hydantoin syndrome presented with many of the findings already described. There was growth retardation, hypertelorism, small pug nose, anteverted nostrils, long philtrum, and thin vermilion border of the upper lip, and short neck.

3.14

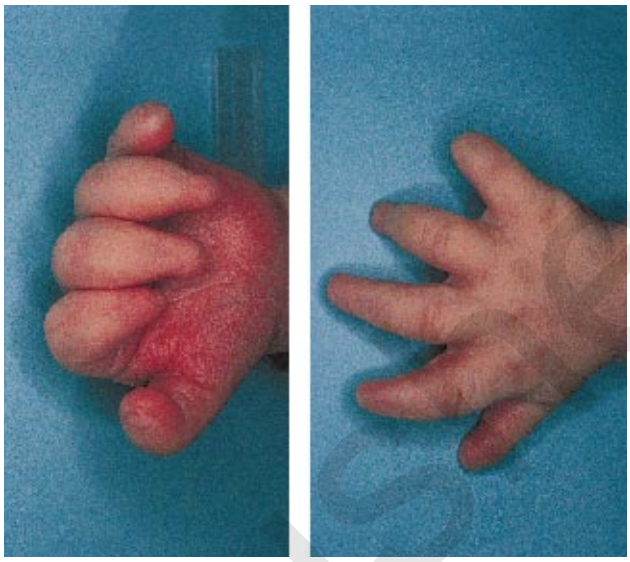

Figure 3.14. The same infant shows the characteristic changes in the fingers. Note the hypoplasia of the distal phalanges with hypoplastic or absent nails and the digital thumbs. There is mild webbing.

3.15

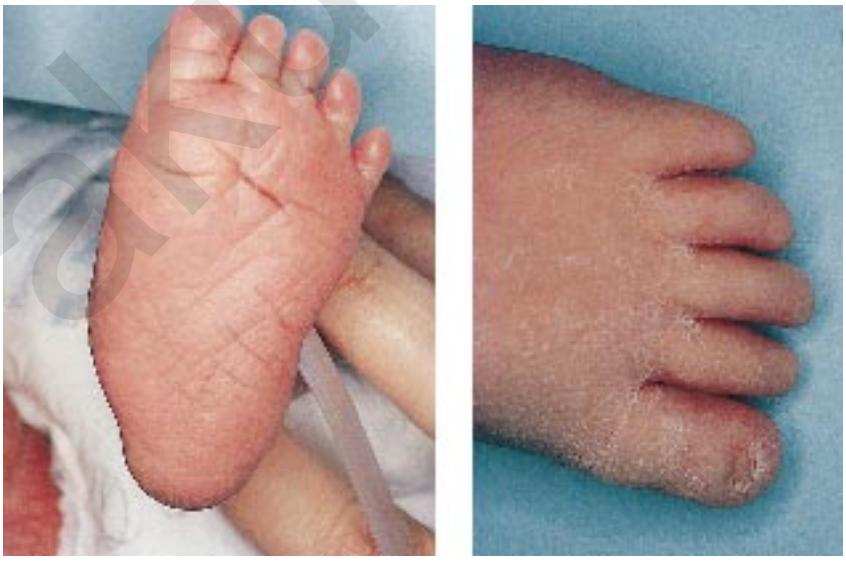

Figure 3.15. The same infant with fetal hydantoin syndrome shows the marked hypoplasia of the distal phalanges of the toes and absent or hypoplastic nails.

3.16

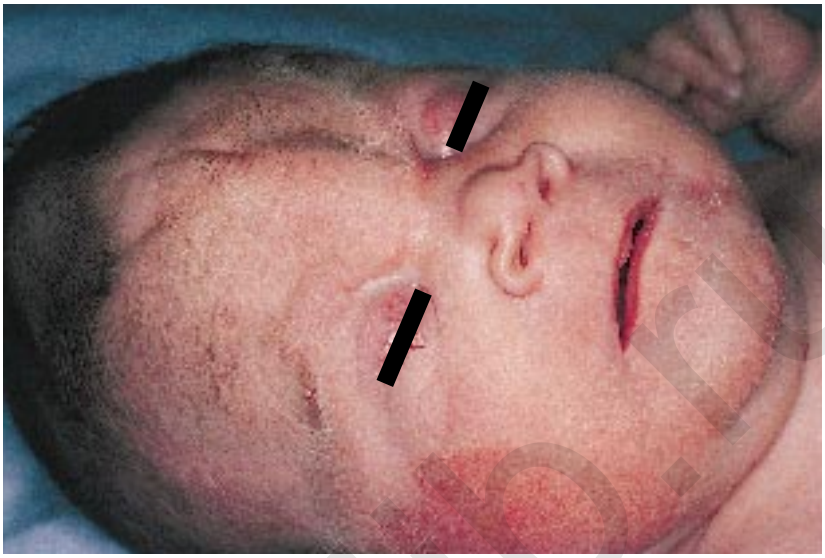

Figure 3.16. Postnatal growth deficiency and microcephaly are present in two-thirds of children exposed to valproic acid in combination with other anticonvulsants. It does not occur with monotherapy with valproic acid. This infant with the fetal vaproate syndrome shows the typical craniofacial abnormalities. Note the trigonocephaly with a prominent metopic ridge, bifrontal narrowing, outer orbital ridge deficiency, midface hypoplasia, epicanthic folds, small short upturned nose, and long flat philtrum.

3.17

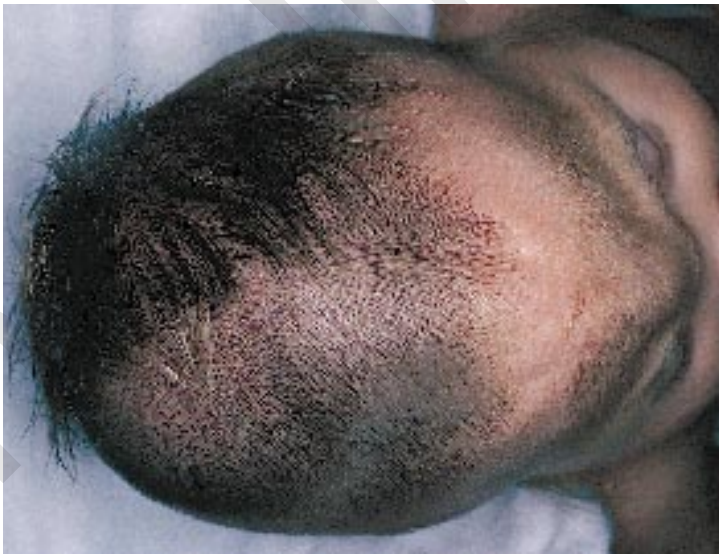

Figure 3.17. A cranial view of the same infant shows the trigonocephaly due to premature closure of the metopic suture, bifrontal narrowing, and outer orbital ridge deficiency.

3.18

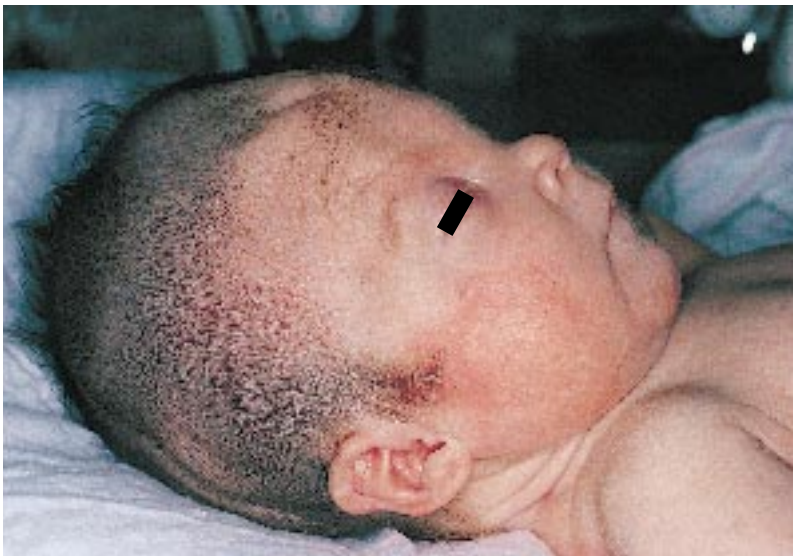

Figure 3.18. Lateral view of the head and face of the same infant shows the marked metopic ridge, small flat short nose, micrognathia and "square" ears.

3.19

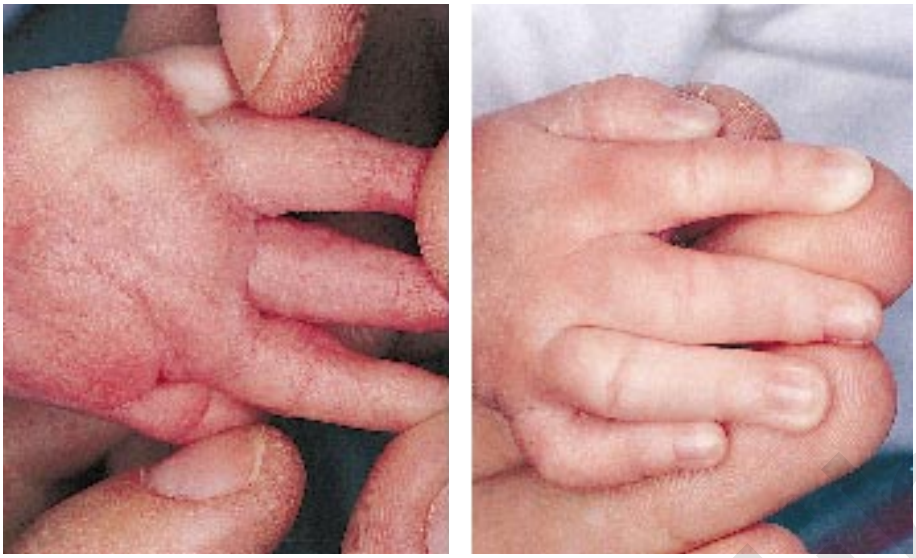

Figure 3.19. The same infant with fetal valproate syndrome as shown in Figures 3.16 to 3.18, had distal phalangeal hypoplasia and tapering of the fingers. Note the abnormal creases on the fingers and palm due to lack of fetal movement in utero. Other changes reported in infants with this syndrome include tracheomalacia, congenital heart defects, and urogenital anomalies.

3.20

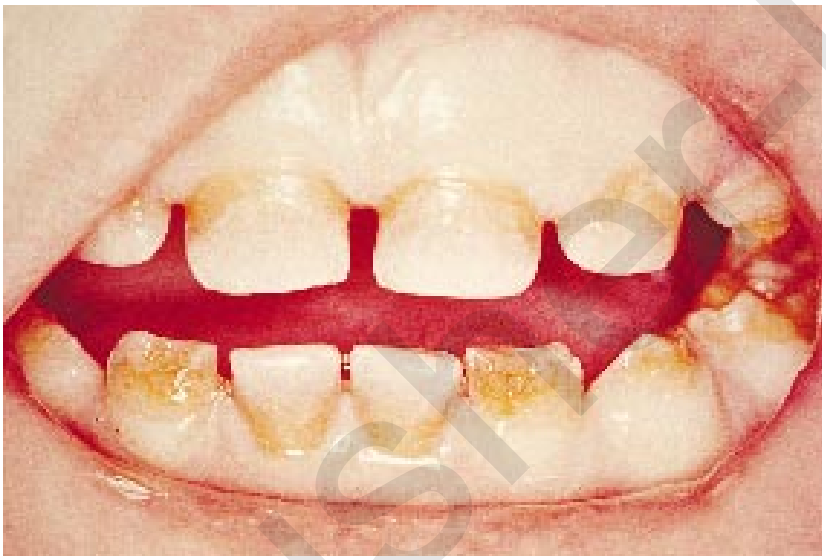

Figure 3.20. Yellow staining of the teeth in a child exposed to maternal tetracycline in utero.

3.21

Figure 3.21. A Wood's filter shows the fluorescence of the nails in an infant exposed to maternal tetracycline. If young infants are given tetracycline after birth the staining of the teeth and nails also occurs.

3.22

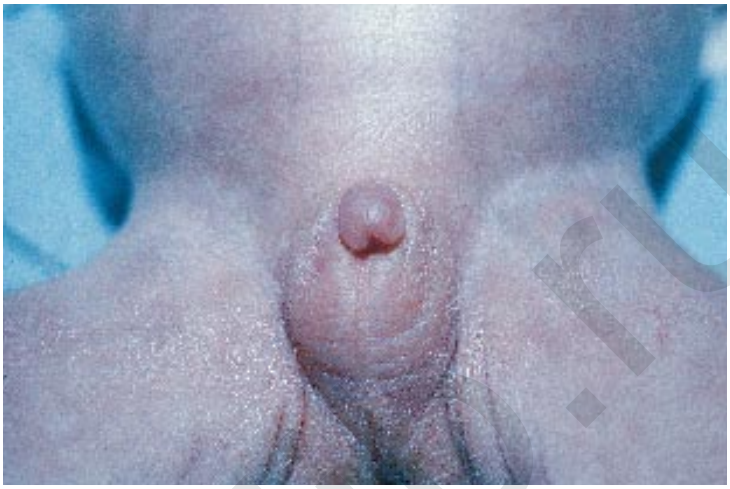

Figure 3.22. Drug-induced pseudohermaphroditism in a female infant who was virilized by progestational agents during the first trimester of pregnancy. The incidence of this condition has decreased because, with recognition of this iatrogenic cause of virilization of the fetus, there has been a decreased use of incriminating drugs such as progestational agents or androgens during the first trimester. There may be fusion of labioscrotal folds with formation of a urogenital sinus and clitoromegaly. (See Volume V, chapter 5).

3.23

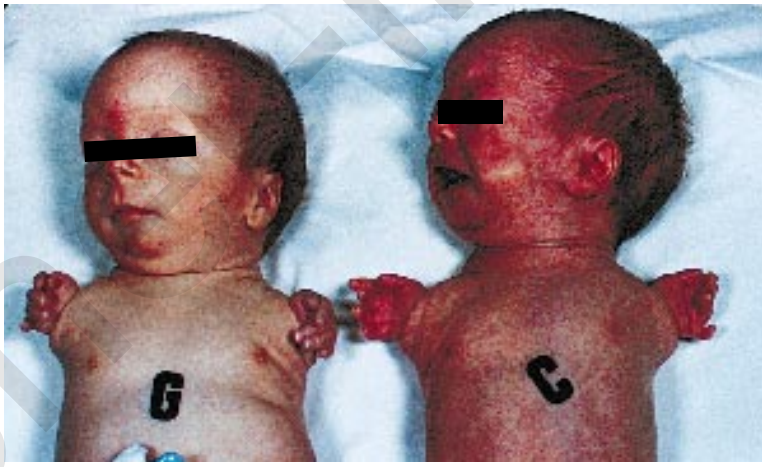

Figure 3.23. The thalidomide syndrome in twin infants born to a mother who took thalidomide early in gestation. Maternal ingestion of thalidomide between the 25th to 44th day after conception may cause malformations. In the thalidomide syndrome the limbs are usually asymmetrically involved and the malformations of the extremities are of all grades of severity (digits are usually present). There may be microphthalmia, ear deformities, and cardiac, renal and intestinal malformations.

3.24

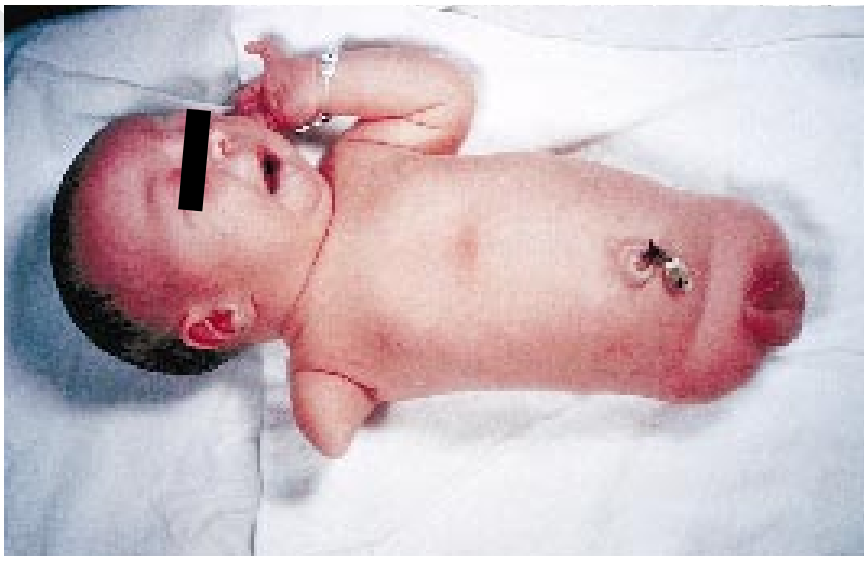

Figure 3.24. Phocomelia in another infant born to another mother who took thalidomide in early gestation. Note the asymmetric phocomelia.

3.25

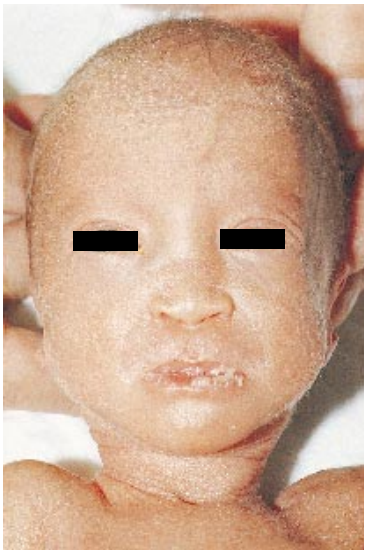

Figure 3.25. This infant with the fetal warfarin syndrome (Coumadin™ embryopathy) was born to a mother who was being treated with warfarin during the first trimester of pregnancy. These infants typically are low birthweight and have facial and skeletal abnormalities. Less commonly they may have central nervous system and eye abnormalities. In this baby note the typical facial features of a broad flat face and nasal hypoplasia with a low nasal bridge, a prominent philtrum, and micrognathia.

3.26

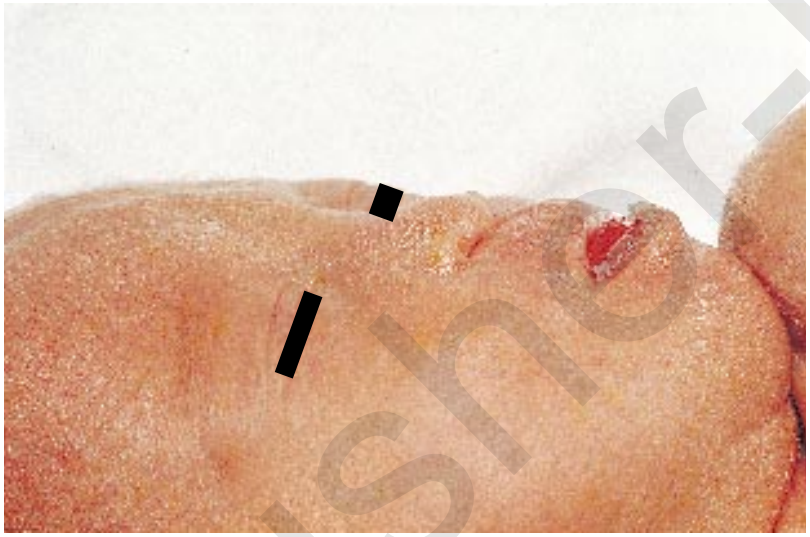

Figure 3.26. The lateral view of the face strikingly demonstrates the marked nasal hypoplasia resulting in a very flat face. Because of the marked nasal hypoplasia these infants often present with upper airway obstruction.

3.27

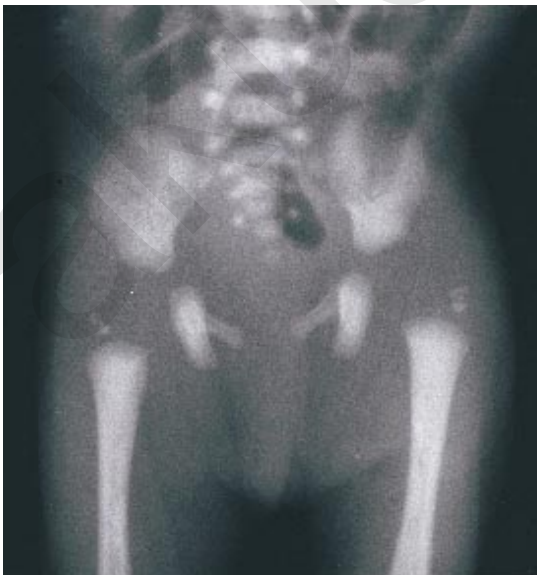

Figure 3.27. Radiograph of the lower extremities of the same infant shows the stippling of the epiphyses at the proximal femora. Stippling of the epiphyses may occur along the vertebral column and the tarsal bones. The stippling disappears in the first few years of life. Coumadin™ embryopathy is phenotypically similar to hereditary chondrodystrophia punctata and it must thus be distinguished from the different hereditary forms of Conradi-Hünermann syndrome.

Chapter 4
Birth Trauma

Birth trauma refers to those injuries sustained during labor and delivery. Despite skilled and competent obstetric care, some may be unavoidable. Factors predisposing infants to injury include macrosomia, prematurity, cephalopelvic disproportion, dystocia, prolonged labor, and abnormal presentation. In 1988, birth injuries ranked eight as major causes of neonatal mortality and caused 4.6 deaths per 100,000 live births. The clinician who cares for newborn infants must be familiar with the conditions caused by birth injury. Injuries are known to occur to the soft tissues, head, eyes, ears, vocal cords, neck and shoulder, spine and spinal cord, intra-abdominal organs, extremities, and genitalia. Although many are mild and self limited, others are serious and potentially lethal.

4.1

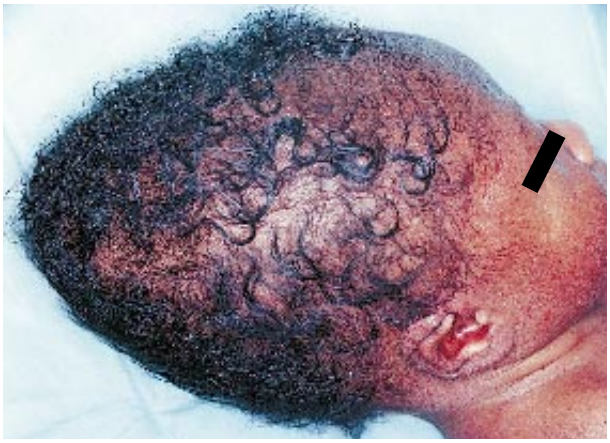

Figure 4.1. Severe molding of the head following an occipitoposterior presentation. The mobile skull bones and brain deform to comply with pressure in the birth canal. Note the flattened forehead and long occiput. It resolves spontaneously and needs no intervention.

4.2

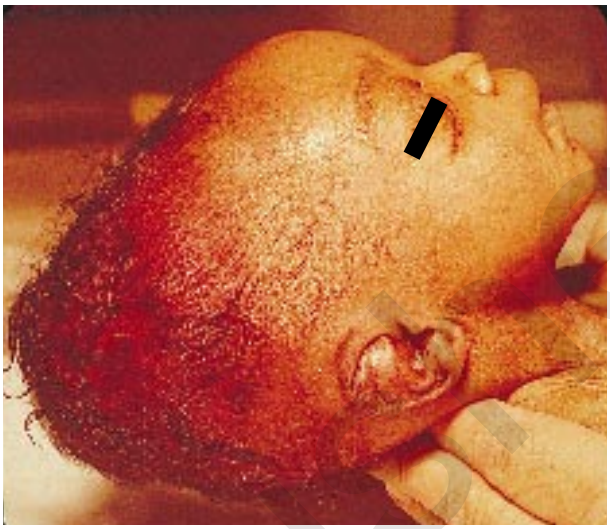

Figure 4.2. Persistent occipitoposterior presentation with marked molding and a caput succedaneum. A caput succedaneum occurs as a result of the presenting part pressing against the partly dilated cervix whose constricting rim obstructs the return flow of venous flood and lymph from the scalp leading to edema. The distribution crosses suture lines (compare with cephalhematoma) and is usually present at birth.

4.3

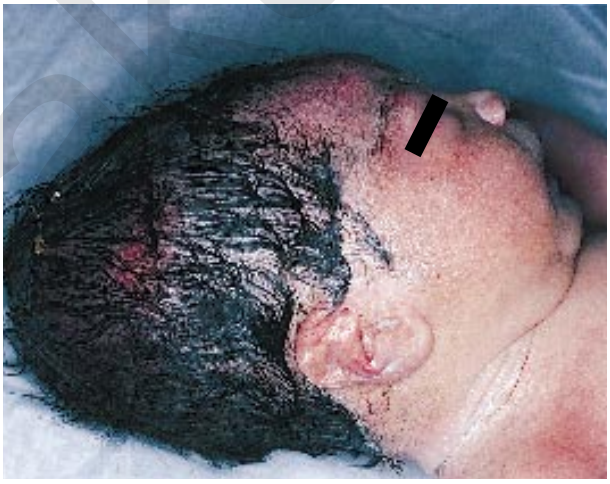

Figure 4.3. Caput succedaneum with prolonged labor. In a caput succedaneum the tissues involved are those encircled by the "girdle of contact" formed by the maternal passages. The location indicates the intrauterine lie of the fetus. In breech delivery there may be similar edema and bruising of the perineum, buttocks, or genitalia. These are really an equivalent of caput succedaneum.

4.4

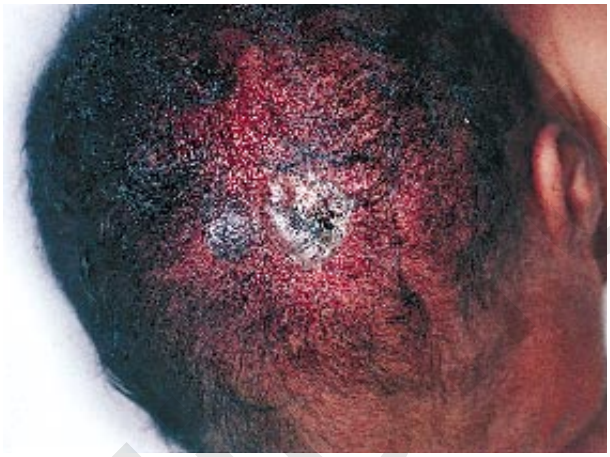

Figure 4.4. "Blisters" of the skin following prolonged labor over a caput succedaneum in an infant at the age of 1 day following prolonged labor. Aspiration of the material was sterile.

4.5

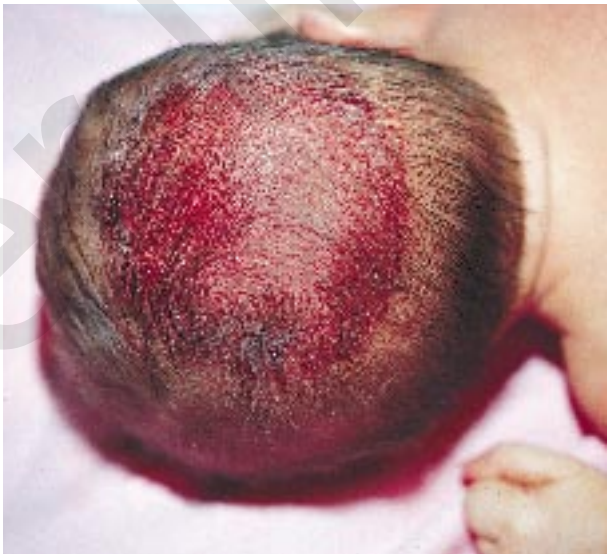

Figure 4.5. A large caput (chignon) following vacuum extractor delivery. The word "chignon" refers to the localized area of scalp edema caused by the suction of the cup of the vacuum extractor. Most cases resolve spontaneously but if associated with perinatal asphyxia there may be necrosis of the chignon leading to ulceration of the scalp.

4.6

Figure 4.6. "Caput ring." In rare cases with persistent strong contractions and a slowly dilating cervix, necrosis of the scalp may occur in the area of a caput due to pressure ischemia occurring during a prolonged labor.

4.7

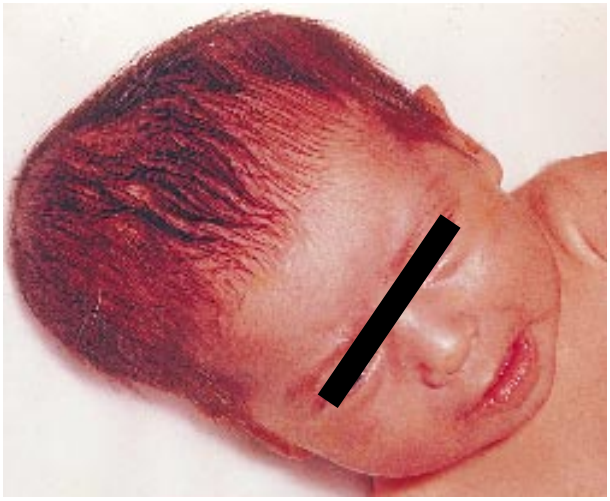

Figure 4.7. Cephalhematoma over the right parietal bone. A cephalhematoma is a subperiosteal hemorrhage occurring as a result of vessel rupture at birth. It is generally not apparent at birth but is noted in the first day or two of life. It should be distinguished from a caput succedaneum. It is most commonly seen over the parietal bones and more commonly over the right parietal than the left. A caput succedaneum and cephalhematoma may occur concurrently.

4.8

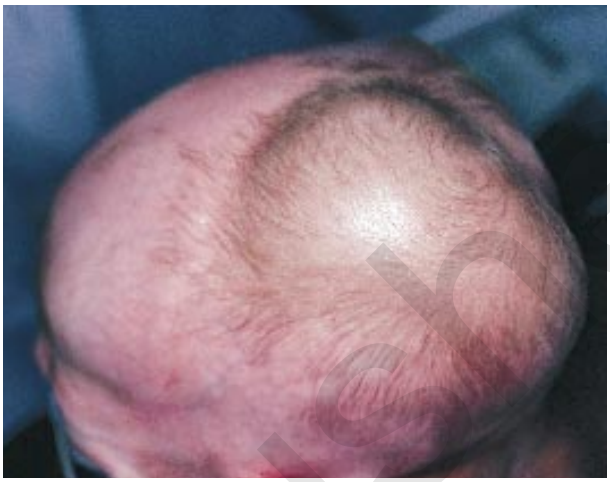

Figure 4.8. Large left parietal cephalhematoma. Note that the cephalhematoma is limited by suture lines because it is a subperiosteal hemorrhage. Cephalhematoma occurs more commonly after prolonged primigravida labor or forceps delivery especially in post term infants where suture fusion makes the skull hard and unyielding.

4.9

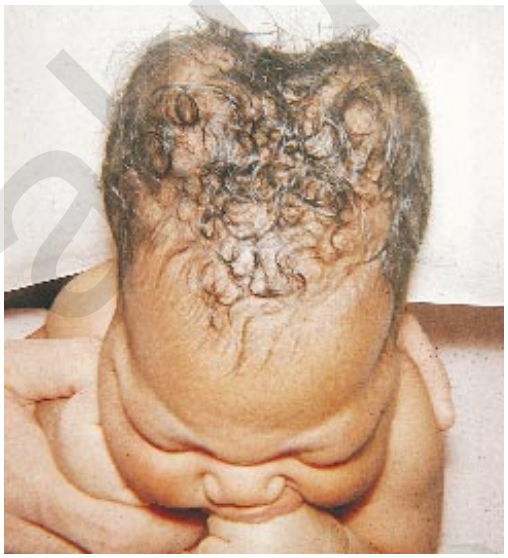

Figure 4.9. Bilateral cephalhematomas in this infant demonstrate very clearly the limitation of the cephalhematoma by suture lines. Complications of cephalhematomas include anemia, jaundice, infection, and underlying skull fracture. In general, cephalhematomas resolve spontaneously over a period of weeks to months.

4.10

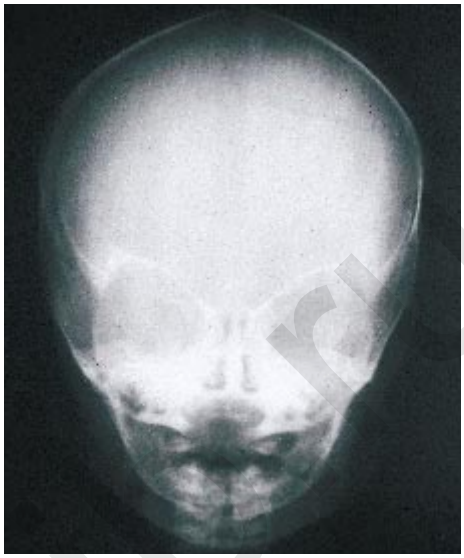

Figure 4.10. Cephalhematoma with linear fracture of the skull. This occurs in 4 to 5% of infants with a cephalhematoma.

4.11

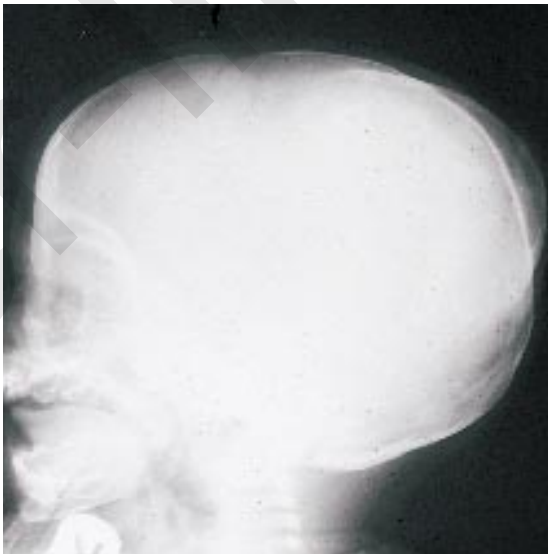

Figure 4.11. Calcification in a cephalhematoma giving the lesion an "egg shell" feel occurs as a result of deposition of calcium in the organizing blood. Periosteal new bone forms around the perimeter of the cephalhematoma and this rim of calcification may be noted for several months.

4.12

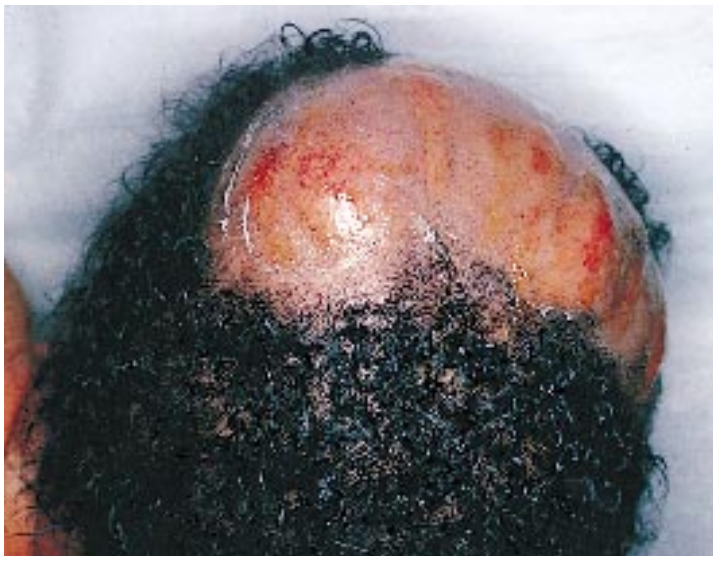

Figure 4.12. Infected cephalhematoma in an infant with *Escherichia coli* sepsis. Osteomyelitis of the underlying parietal bone was present.

4.13

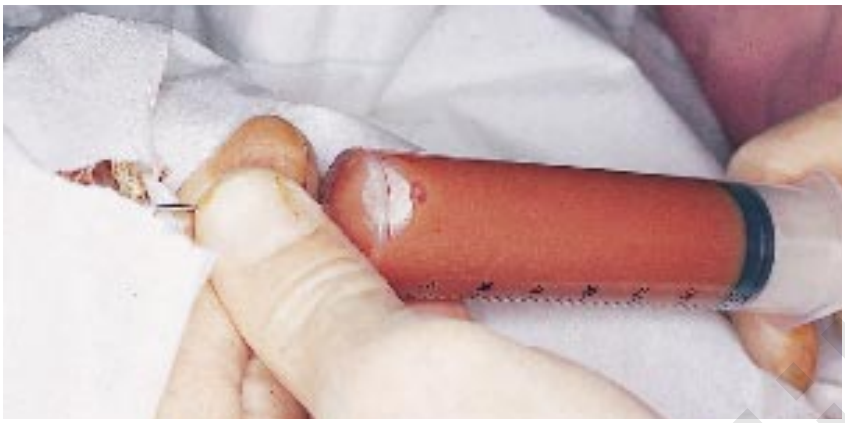

Figure 4.13. The same infant as in Figure 4.12 with pus being drained from the infected cephalhematoma (pyocephalhematoma). The pus grew pure *E. coli* in culture. In general it is recommended that cephalhematomas not be aspirated, but on rare occasions, if the infant develops sepsis due to any organism, infection may occur in the cephalhematoma requiring drainage.

4.14

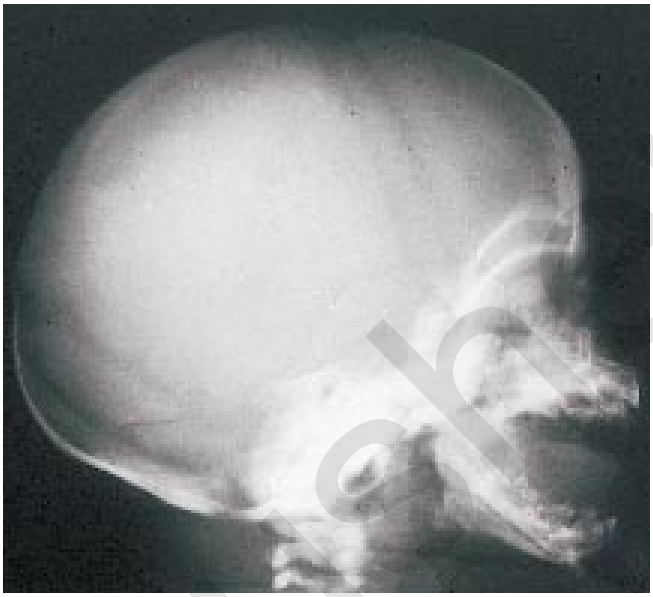

Figure 4.14. Radiograph of the skull of the same infant showing osteomyelitis of the parietal bone.

4.15

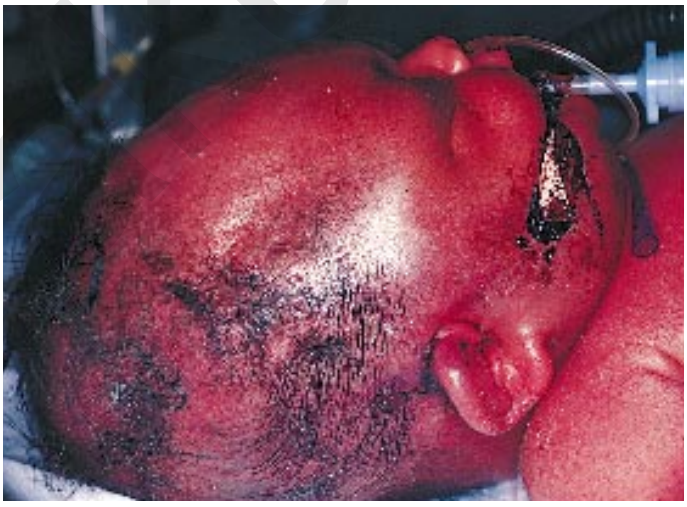

Figure 4.15. Massive scalp hemorrhage of the newborn (subgaleal hemorrhage). When there is rupture of the capillaries in the subaponeurotic area, there may be massive scalp hemorrhage with spread over the entire scalp and massive blood loss. Disseminated intravascular coagulopathy may ensue rapidly. This condition may occur as a result of a precipitous delivery or poor application of a vacuum extractor. Note the massive soft tissue swelling.

4.16

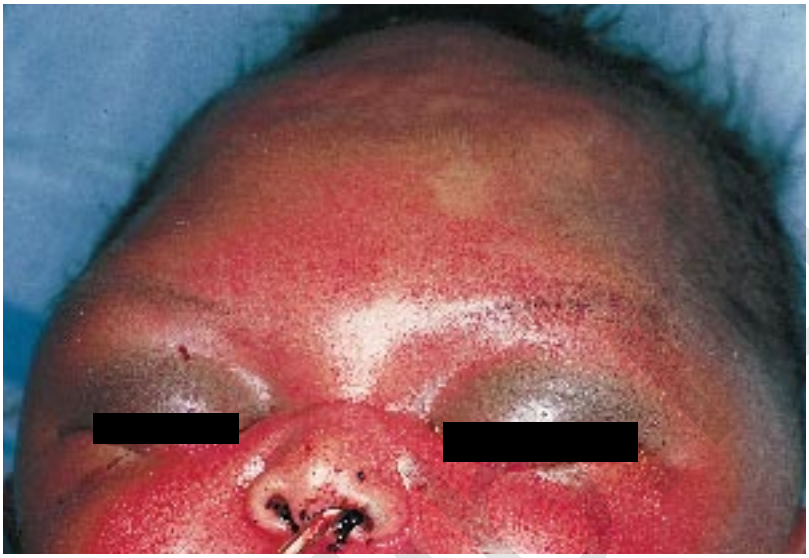

Figure 4.16. Frontal view of the same infant who had a massive scalp hemorrhage with a skull fracture. Note the ecchymoses of the upper eyelids and marked swelling from the bridge of the nose extending over the scalp. This is characteristic of a subgaleal hemorrhage as the aponeurosis of Galen attaches at the upper eyelids and has no attachment to the scalp until the nape of the neck and the sternocleidomastoid muscle on the sides, hence the massive hemorrhage in the subgaleal area of the head.

4.17

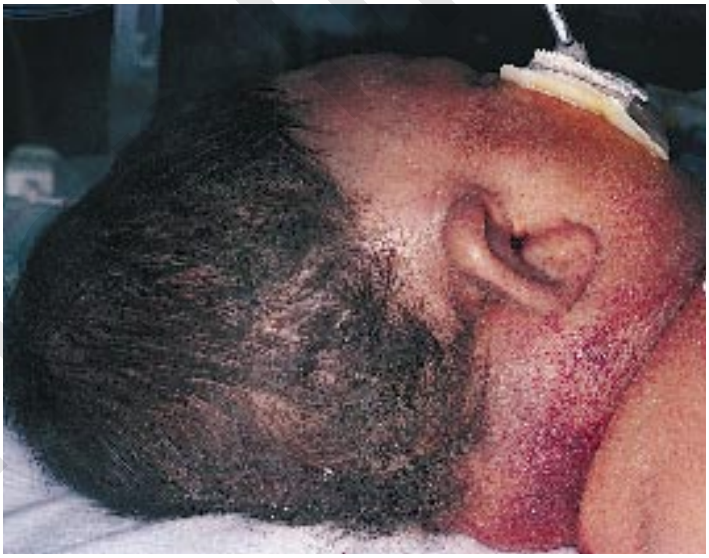

Figure 4.17. A massive scalp hemorrhage following vacuum extractor delivery. Note the limitation of bleeding at the nape of the neck and the sternocleidomastoid muscle. The bleeding into the subaponeurotic space may result in massive blood loss leading to hypovolemia and shock.

4.18

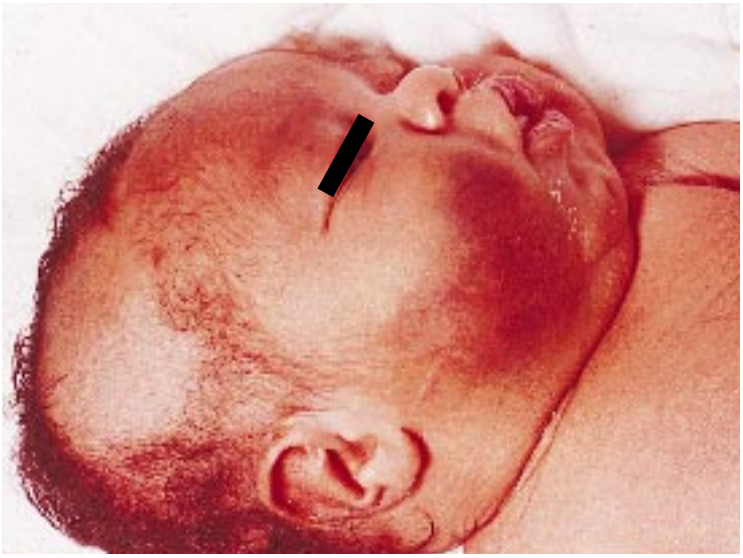

Figure 4.18. Hematoma of the right cheek and mouth which occurred during a difficult spontaneous delivery.

4.19

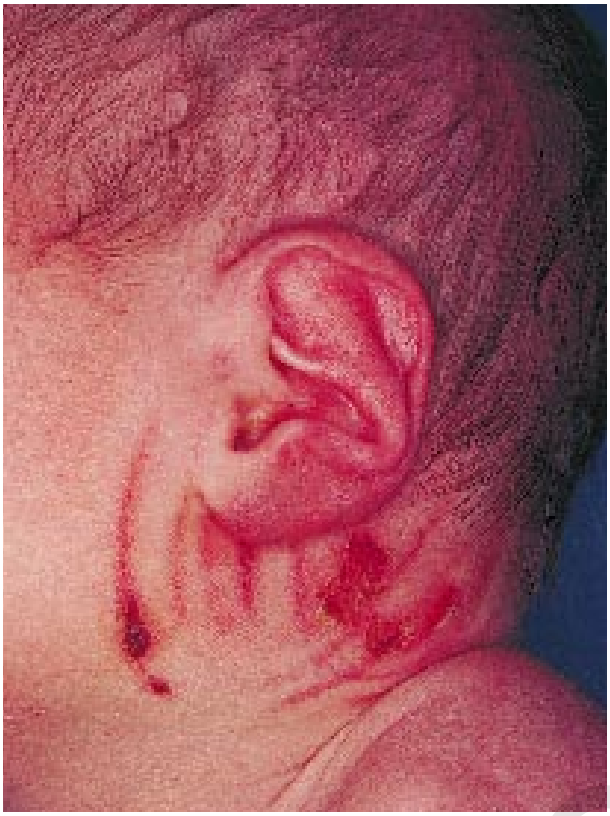

Figure 4.19. Trauma from a forceps delivery. Forceps marks on the cheek are fairly common. Rarely, a transient facial palsy may be associated with this type of trauma and occasionally the forceps may actually traumatize the skin, leading to ulceration.

4.20

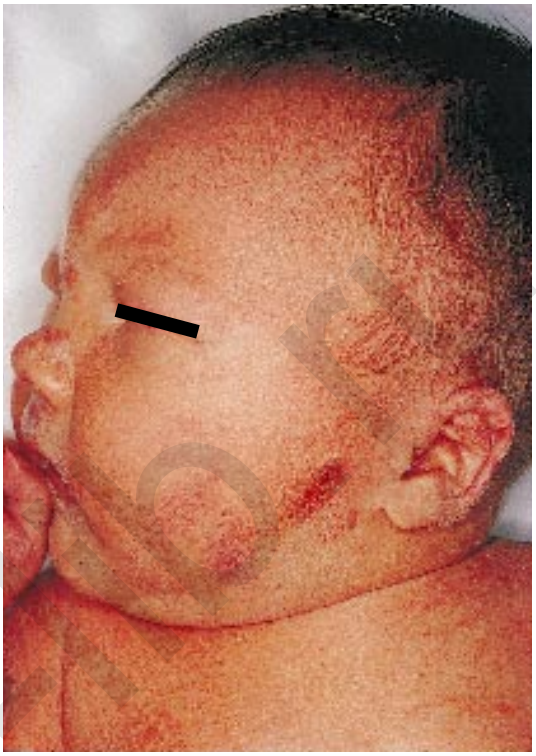

Figure 4.20. Forceps mark following delivery. The pressure of the forceps blade may result in damage to the underlying tissue and, as in this infant, subcutaneous fat necrosis may occur.

4.21

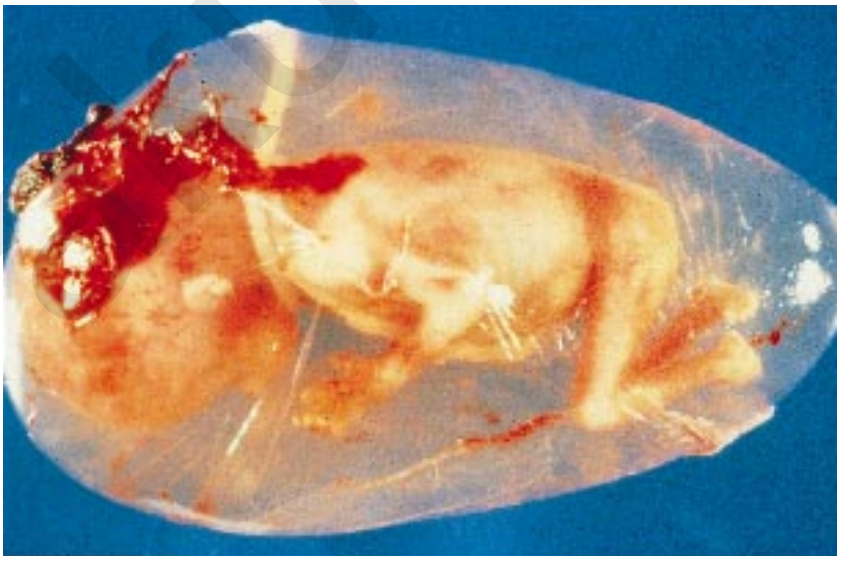

Figure 4.21. Fetus born in a caul with a nuchal cord. Cord around the neck once is present in about 20% of deliveries and, in about 2% of deliveries, there is a cord around the neck twice. This common finding generally does not cause problems unless the cord constricts the neck tightly. (Klima, T.)

4.22

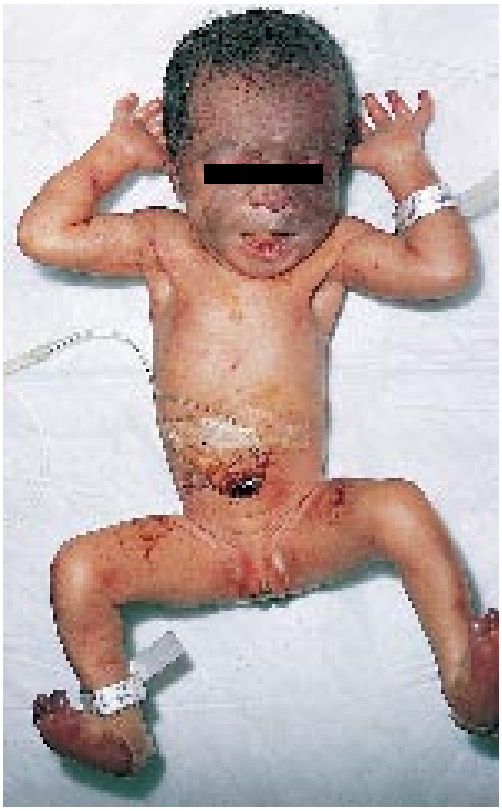

Figure 4.22. Facial suffusion due to a nuchal cord.

4.23

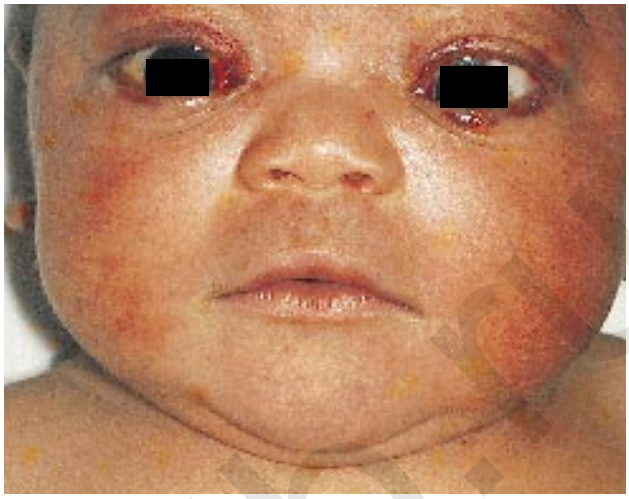

Figure 4.23. Cord around the neck interfering with circulation. Note the petechiae of the face and head and the subconjunctival hemorrhages. Petechiae are also seen in infants in whom there is abnormal delay following delivery of the head and neck before the trunk and shoulders are delivered. In subconjunctival hemorrhage a linear or lunar hemorrhage is often seen to the side of the iris. Petechiae and subconjunctival hemorrhages do not have the same ominous significance as those on the trunk or limbs and usually fade in the first few days of life.

4.24

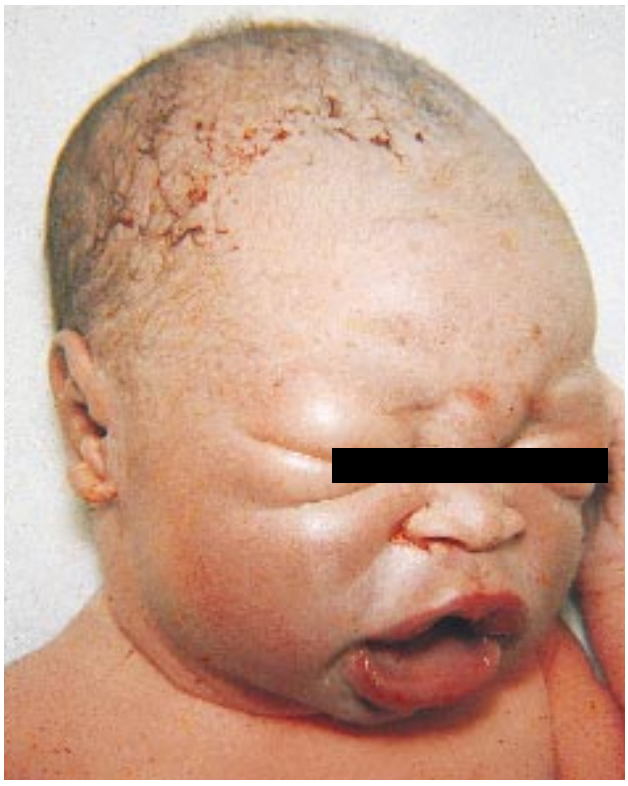

Figure 4.24. Marked suffusion and bruising of the face as a result of a face presentation. This could be considered the equivalent of a caput with the face as the presenting part. There is deep blue discoloration and swelling of the face and there may be considerable disfiguration of the face which is of short duration.

4.25

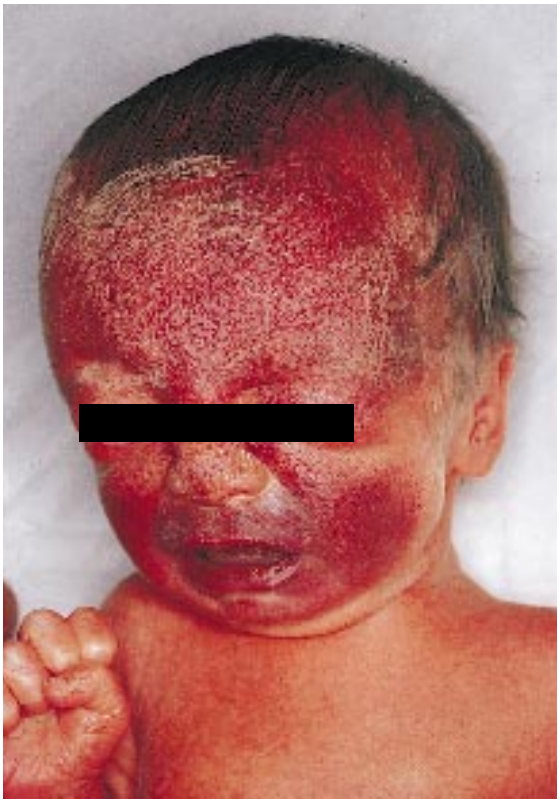

Figure 4.25. Face presentation in a premature infant of 34 weeks gestation. Note the very marked ecchymotic appearance of the face.

4.26

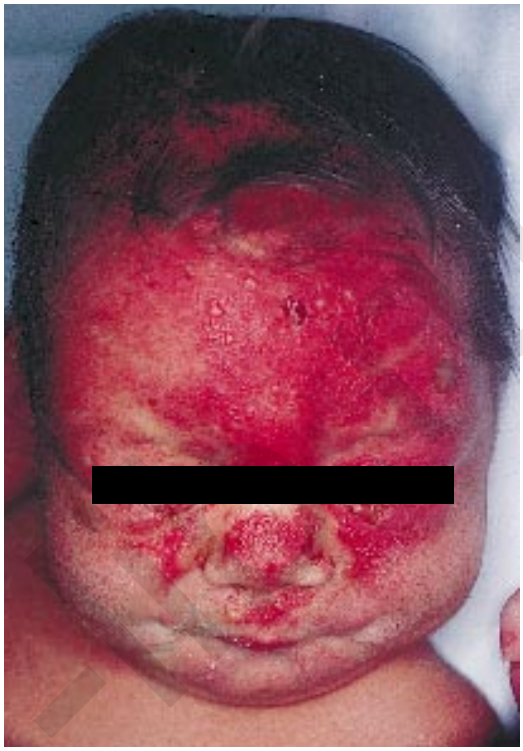

Figure 4.26. Face/brow presentation. Note the marked edema and ecchymoses over the face and brow, particularly the left eye.

4.27

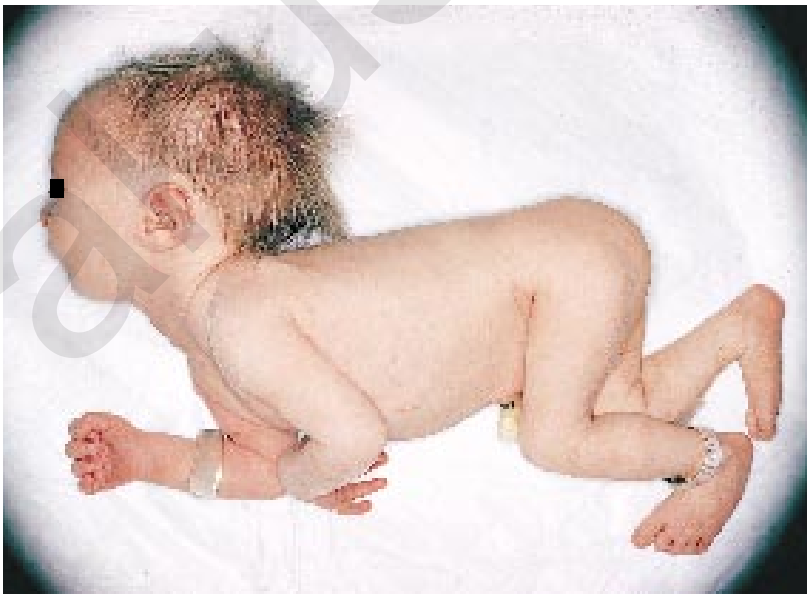

Figure 4.27. A brow presentation with hyperextension of the head. This is the classic "militaristic attitude" with head back and chin out. Opisthotonos is excluded by lack of arching of the back. As this is the baby's "position-of-comfort" in utero, during the first few days postnatally the infant will be unhappy if an attempt is made to flex the head. After several days the infant will adopt a normal posture.

4.28

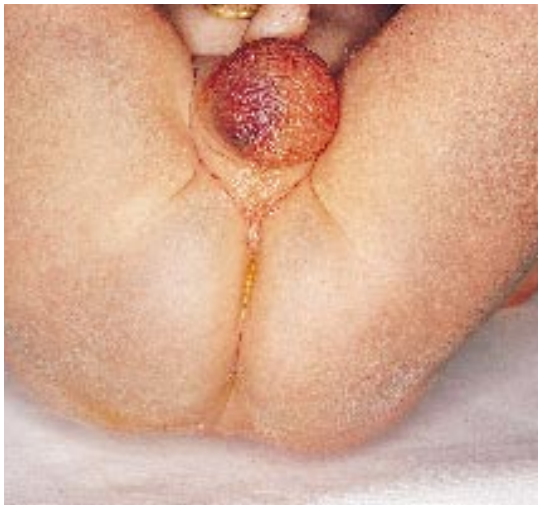

Figure 4.28. In this infant who was a breech presentation note the edema, bruising, and ecchymosis. In breech presentations the perineum, buttocks, and thighs may be severely bruised.

4.29

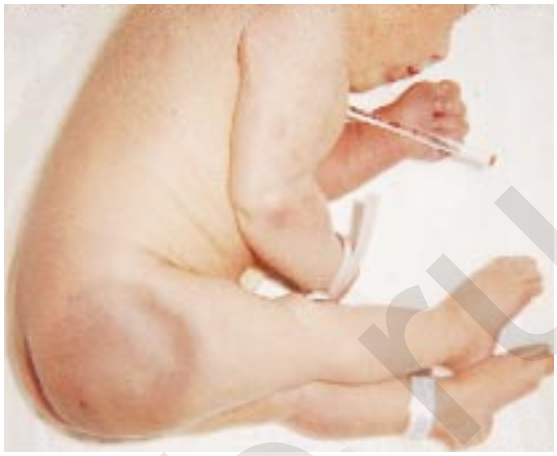

Figure 4.29. This infant is another example of a breech presentation. Note the extended legs and the equivalent of a caput over the right buttock, which was the presenting part.

4.30

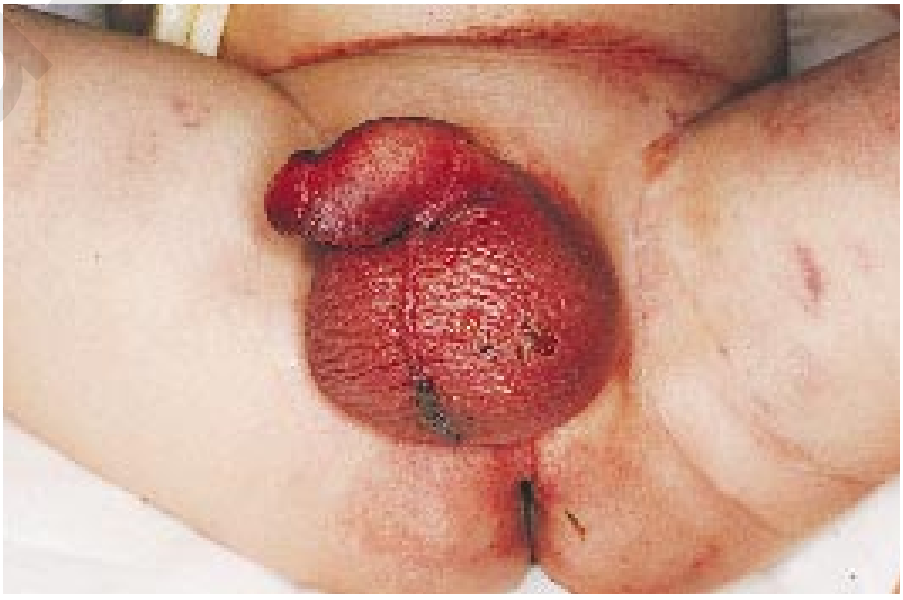

Figure 4.30. Bruising of male genitalia due to a breech presentation. Note the marked swelling of the scrotum and penis. In rare cases testicular trauma may occur.

4.31

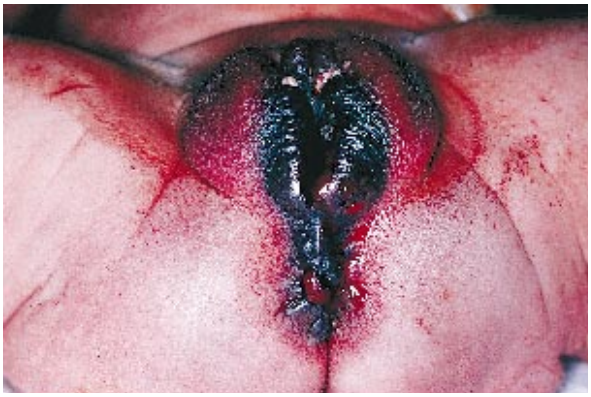

Figure 4.31. Breech presentation in a female infant with marked bruising and swelling of the genitalia. Note the swollen labia majora and bruised labia minora.

4.32

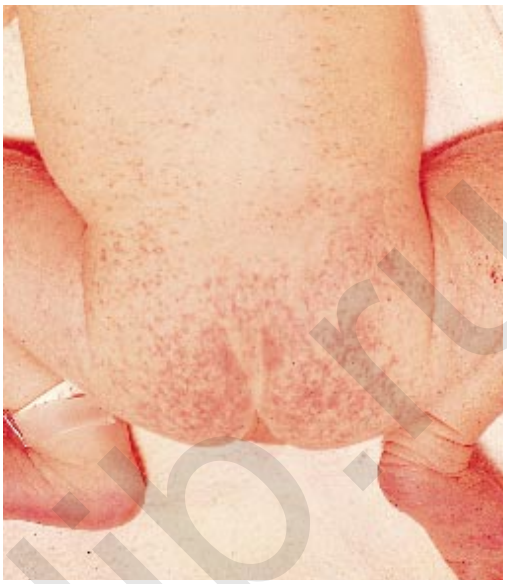

Figure 4.32. Petechiae following a breech delivery are frequently seen in otherwise normal infants. They are of no consequence and improve spontaneously in a few days.

4.33

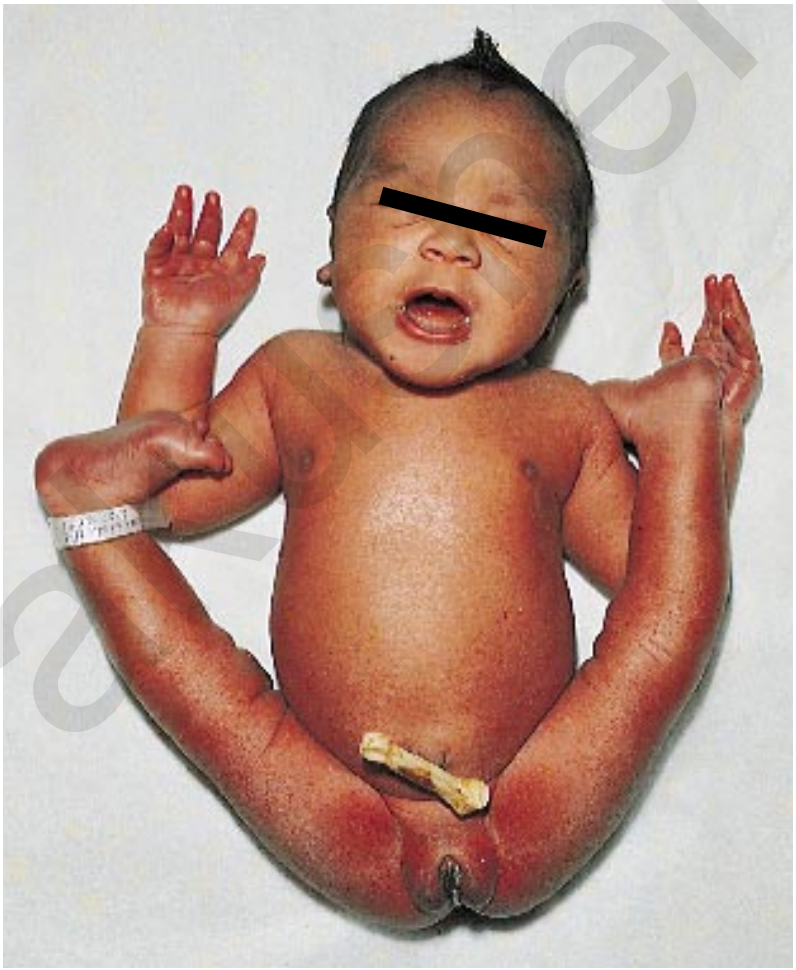

Figure 4.33. Typical position-of-comfort of an infant who was a frank breech presentation. Note the mild genu recurvatum. This infant kept her legs in extension with the knees flexed for several days. "Position-of-comfort" deformations are common in breech presentations and improve in a few days. These infants should all be checked for congenital dislocation of the hip.

4.34

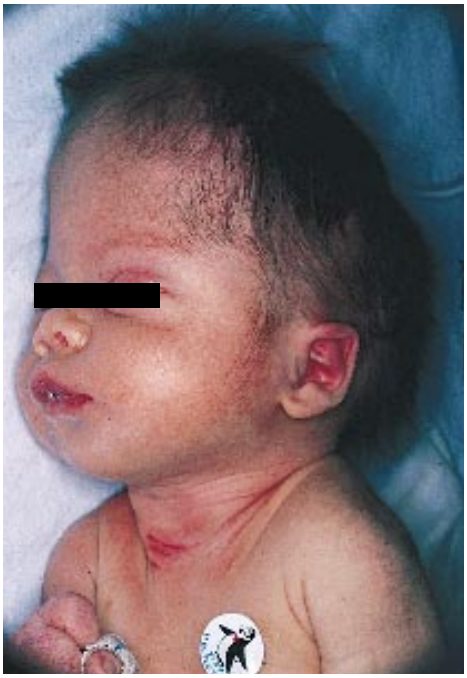

Figure 4.34. The characteristic molding of the head of an infant in a breech presentation. The frontal view shows the occipitofrontal head elongation along with a prominent occipital shelf and the neck appears long.

4.35

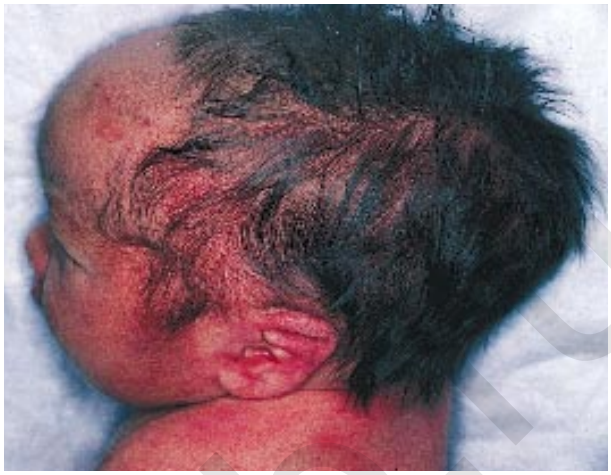

Figure 4.35. Lateral view of the head of the same infant shows the flattening of the vertex and the prominent occipital shelf. The plane of flattening is directed upward and forward from the occipital protuberance, which is quite prominent. The characteristic head results from prolonged pressure of the flexed head against the fundus of the uterus in breech presentation.

4.36

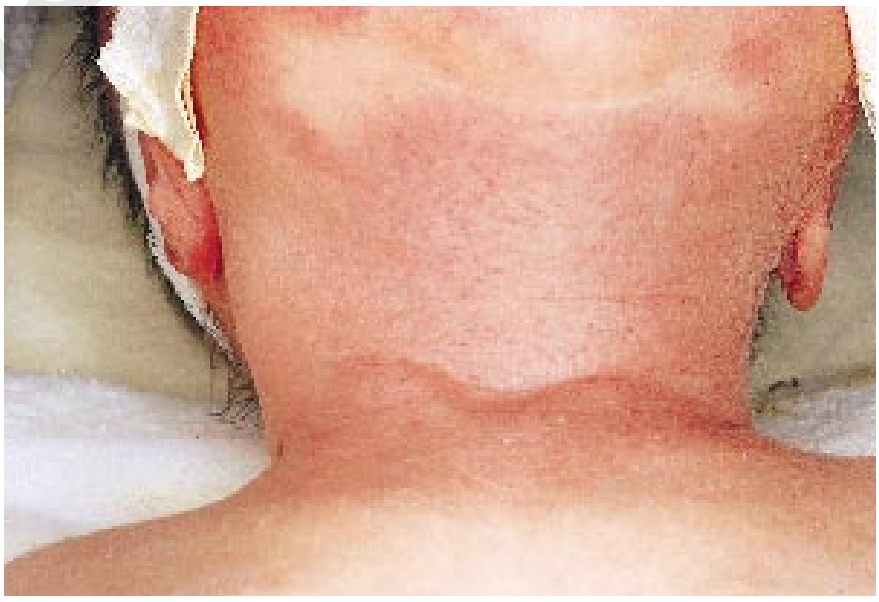

Figure 4.36. "Hanging neck" contusion in a difficult delivery of a breech presentation. The infant was extremely depressed and required ventilatory support.

4.37

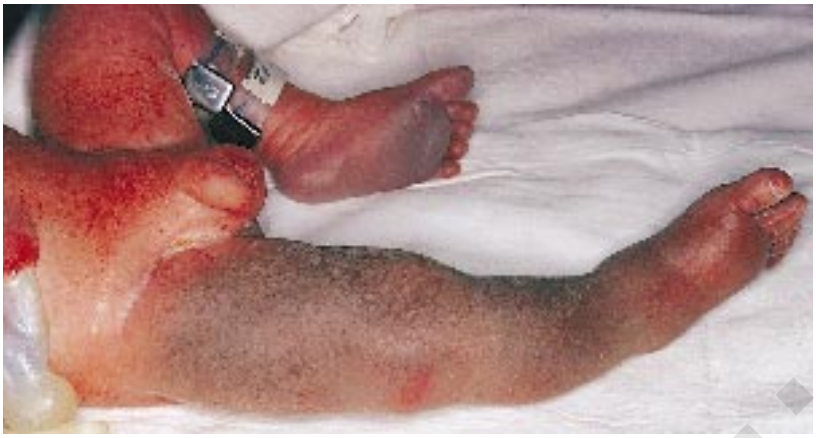

Figure 4.37. Double footling breech presentation. The right leg presented through the cervical os for 6 hours prior to delivery. Note the marked ecchymoses and edema. This resolved spontaneously but the infant developed hyperbilirubinemia.

4.38

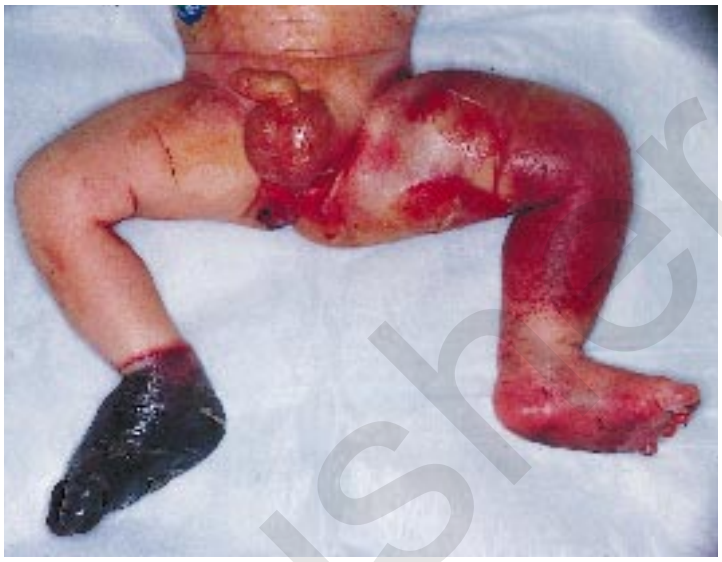

Figure 4.38. This mother had a history of a difficult previous abortion. With this pregnancy she had a spontaneous rupture of the uterus. On laparotomy a large perforation was noted in the uterus through which the infant's lower extremities presented. Note the compression edema and ecchymoses of the left leg and the gangrene of the right foot.

4.39

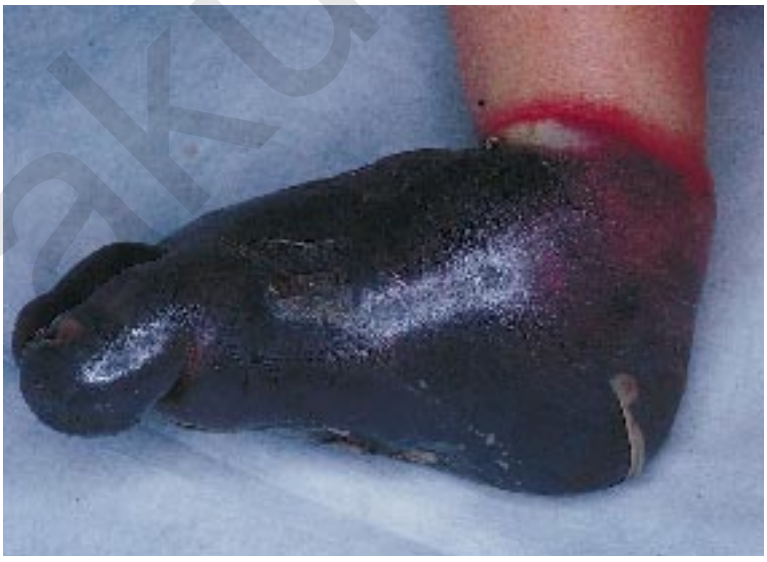

Figure 4.39. A close-up view of the gangrene of the right foot in the same infant.

4.40

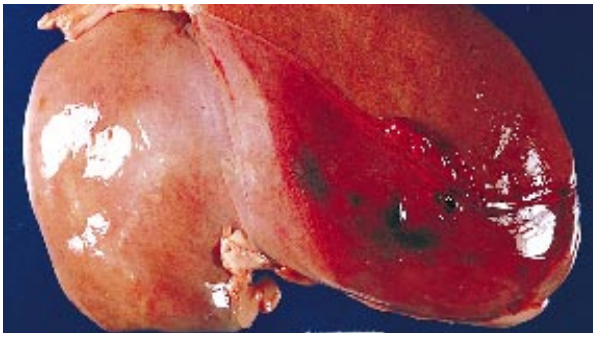

Figure 4.40. Subcapsular hematoma of the liver is generally a pathologic finding. It occurs most commonly with breech delivery especially in premature infants. Occasionally, if bleeding persists, the capsule of the liver ruptures and there is massive hemorrhage into the peritoneal cavity. This usually occurs on the third or fourth day of life. The same may occur in the course of mismanaged artificial cardiopulmonary resuscitation. Rupture of the spleen is very rare and is more common with a transverse lie.

4.41

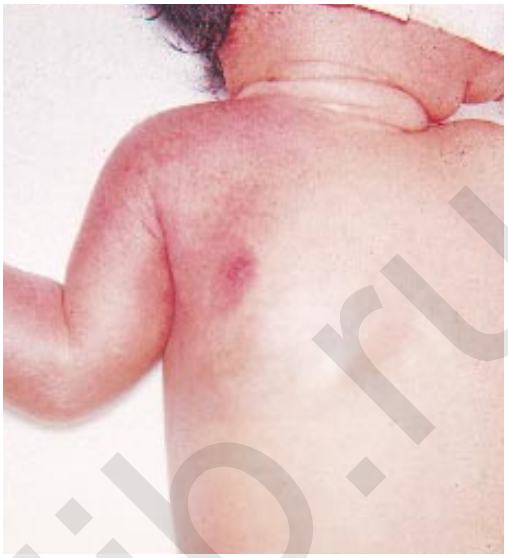

Figure 4.41. Transverse lie with a shoulder presentation. Note the marked swelling and ecchymoses of the right shoulder and upper extremity.

4.42

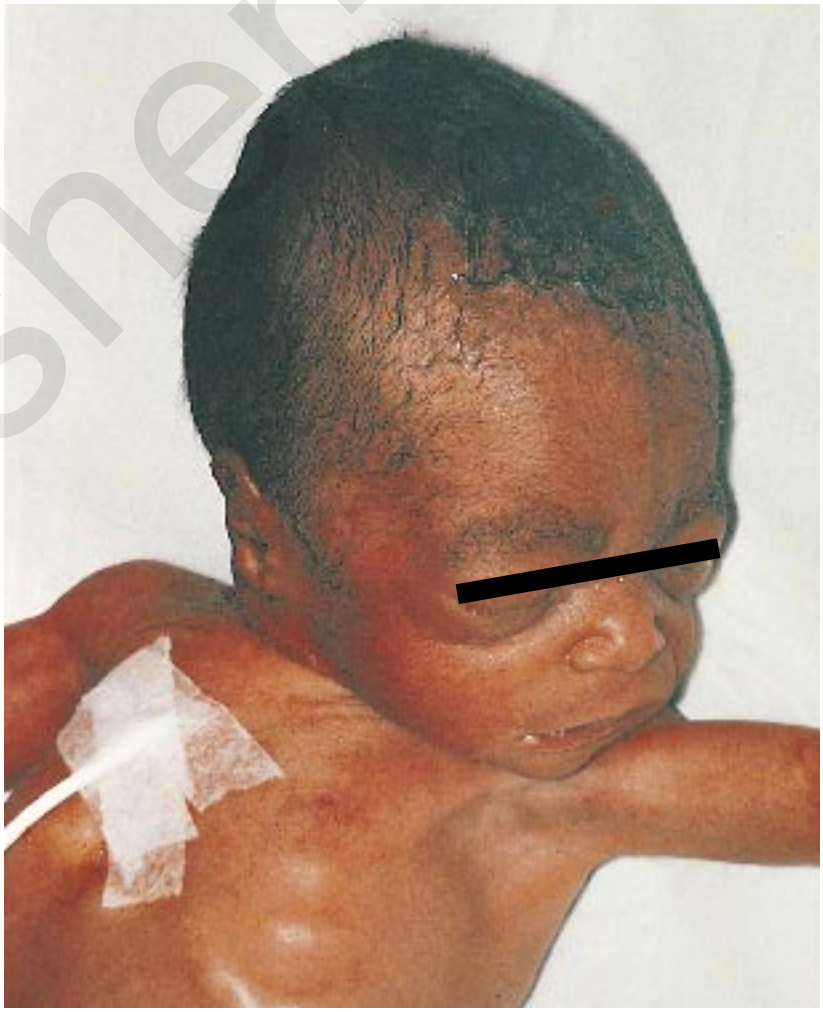

Figure 4.42. Compound presentation of the right arm, hand and vertex. Note the depression in the skull.

4.43

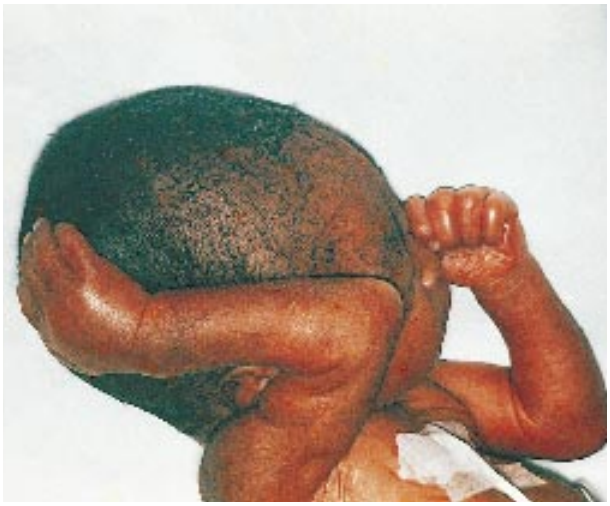

Figure 4.43. The same infant with the arm and hand placed in its in utero position. Note the marked edema of the right forearm and hand compared to that of the left arm and hand. This occurred as the result of the compound presentation.

4.44

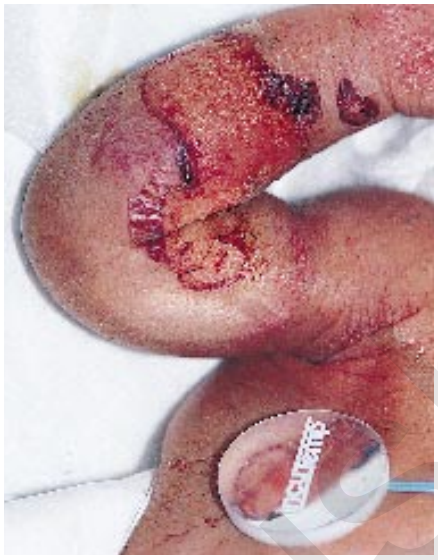

Figure 4.44. In this infant the membranes ruptured 10 days prior to delivery which was by cesarean birth for chorioamnionitis. There was difficulty in delivering the right arm which presented at the elbow. The hand is normal; therefore this was not due to an amniotic band.

4.45

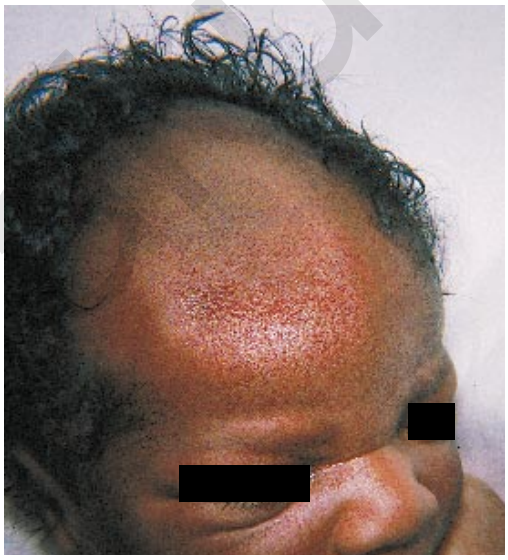

Figure 4.45. Intrauterine skull fracture (congenital molding of the skull) which occurs in cases of infants with poor mineralization of the skull where the mother has a prominent sacral promontory and has a prolonged labor or delivers precipitously. It results in a greenstick or depressed fracture of the skull.

4.46

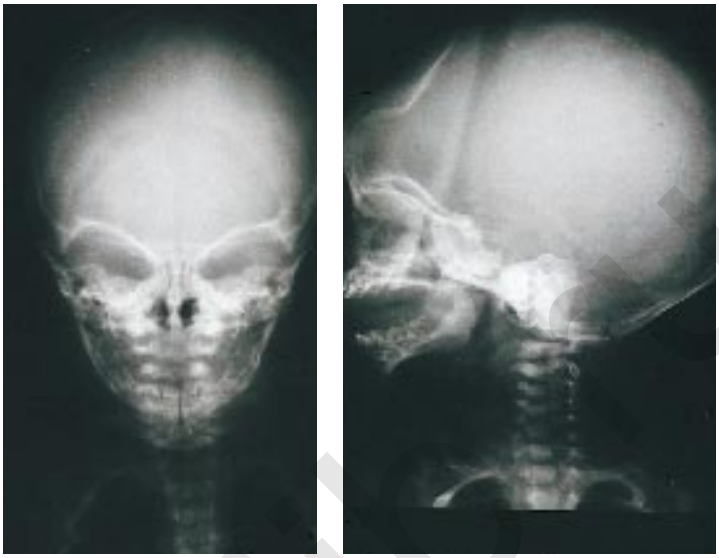

Figure 4.46. Radiograph of the skull of the infant shown in Figure 4.45 showing a depressed fracture in a poorly mineralized skull after a spontaneous vertex delivery. In these infants the fracture may improve spontaneously but there is a question as to whether treatment should be passive or surgical lifting of the fracture is indicated.

4.47

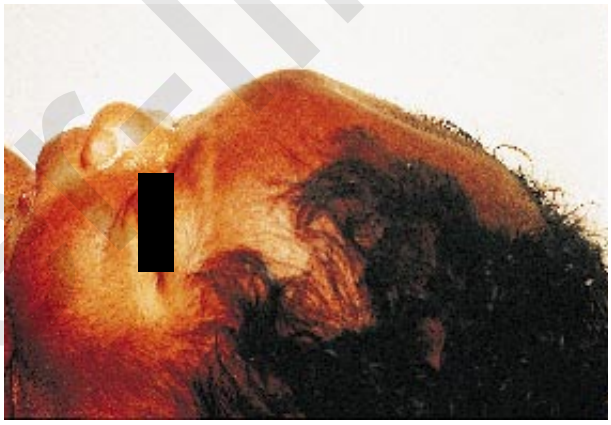

Figure 4.47. Another example of an intrauterine skull fracture (also called congenital molding of the skull).

4.48

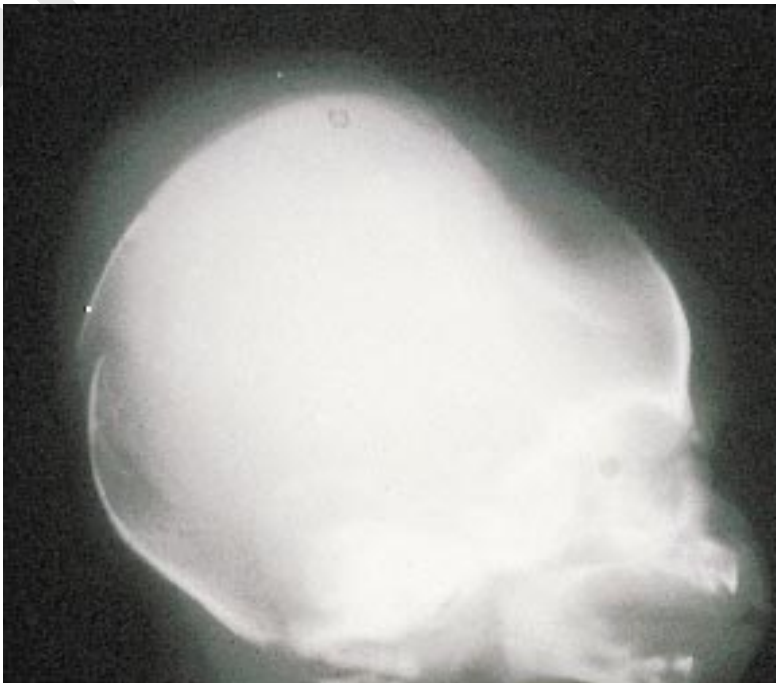

Figure 4.48. Radiograph of a depressed fracture of the skull following forceps trauma. A linear skull fracture may be seen underlying a cephalhematoma or may occur from postnatal trauma such as in an infant falling from the bed to the floor.

4.49

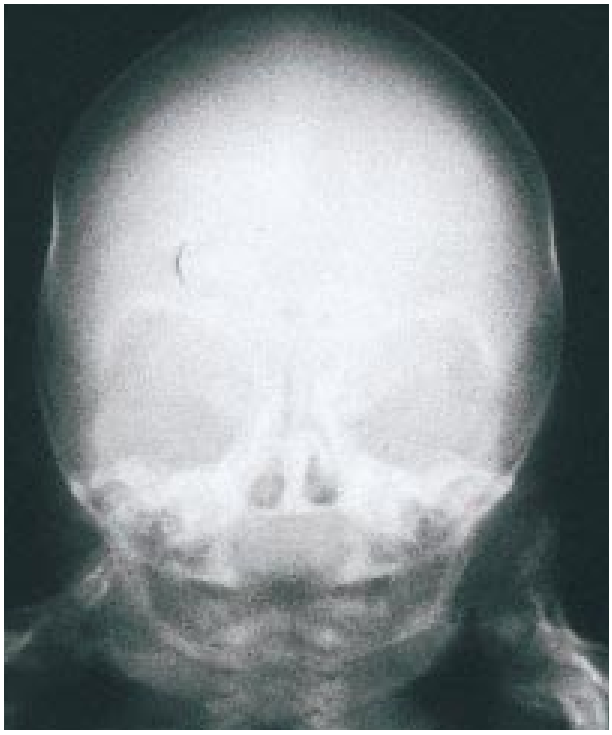

Figure 4.49. This infant had depression on both sides of its skull from its intrauterine position. Note that this is not traumatic and requires no treatment.

4.50

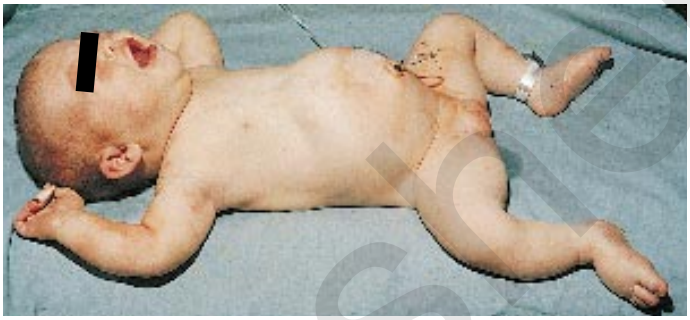

Figure 4.50. Cervical cord injury. This very rare complication is invariably associated with breech delivery. Note the crying infant lying flat on the bed in the "pithed-frog" position with abdominal distention due both to lack of muscle tone and to an enlarged bladder.

4.51

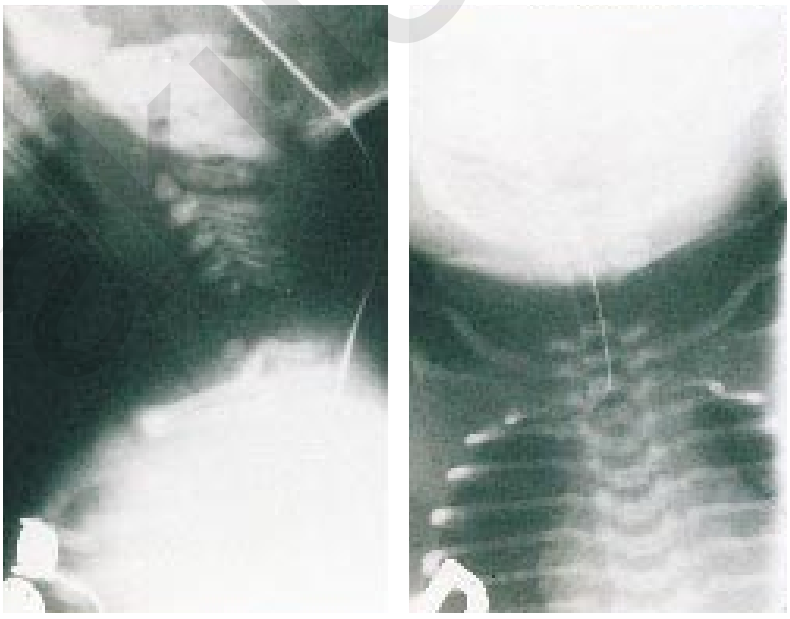

Figure 4.51. Radiograph of the neck showing the cervical cord and spinal injury following breech delivery. Note the fracture dislocation and separation involving C5 and C6.

4.52

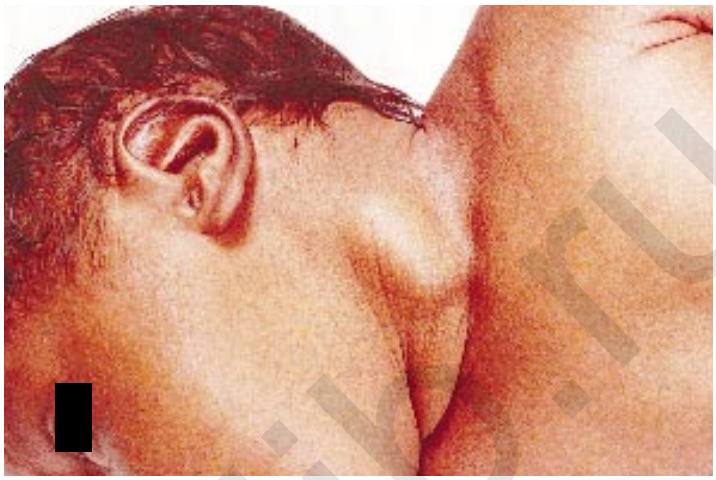

Figure 4.52. Congenital torticollis is usually not apparent at birth but within the first week a swelling is noted over the sternocleidomastoid muscle (stenomastoid tumor). This is thought to occur as a result of spasm, hemorrhage or fibrosis. It results in shortening of the sternocleidomastoid muscle and tilting of the head. It is important to recognize since it may cause astigmatism.

4.53

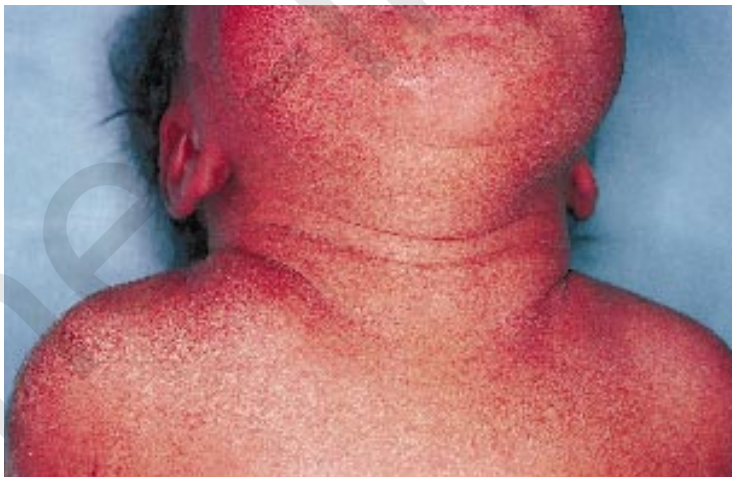

Figure 4.53. Fracture of the right clavicle in an infant at the age of 3 days. There was soft tissue swelling but not much callus formation. The baby may be asymptomatic and the first clinical sign may be a swelling over the clavicle from callus formation or there may be pseudoparesis of the upper limb on the affected side.

4.54

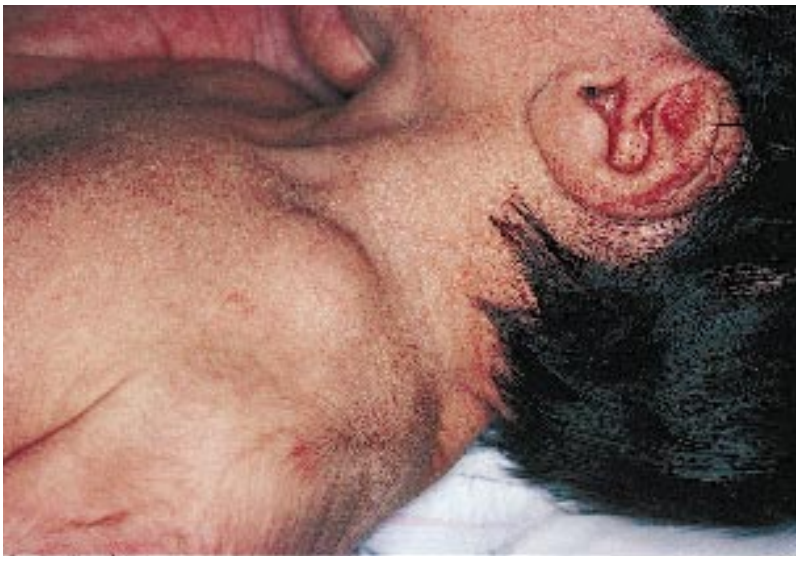

Figure 4.54. This infant did not have the fracture of the left clavicle diagnosed until the age of 10 days but the nurses had noted that the infant was irritable and restless especially when handled. Examination revealed the excessive callus due to a fracture of the left clavicle. In any infant with a fracture of the clavicle one should also check for injury to the brachial plexus, phrenic nerve, recurrent laryngeal nerve, and the sympathetic chain.

4.55

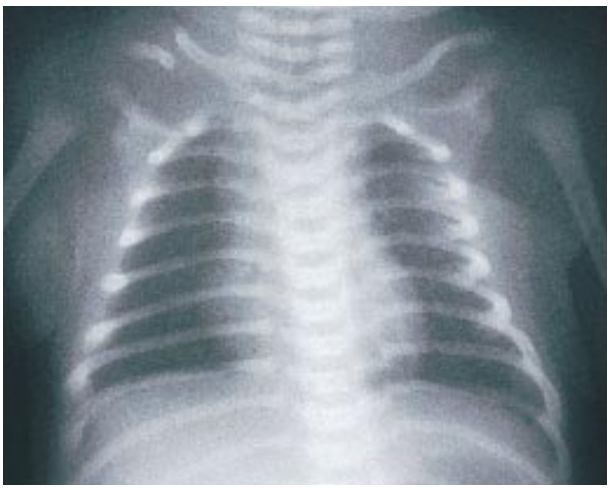

Figure 4.55. A radiograph of the chest showing a fracture of the right clavicle. The clavicle is the site of the most common fracture during delivery especially if shoulder dystocia is present. Healing is rapid because of the speed with which callus formation occurs and it is rare to have any permanent deformity.

4.56

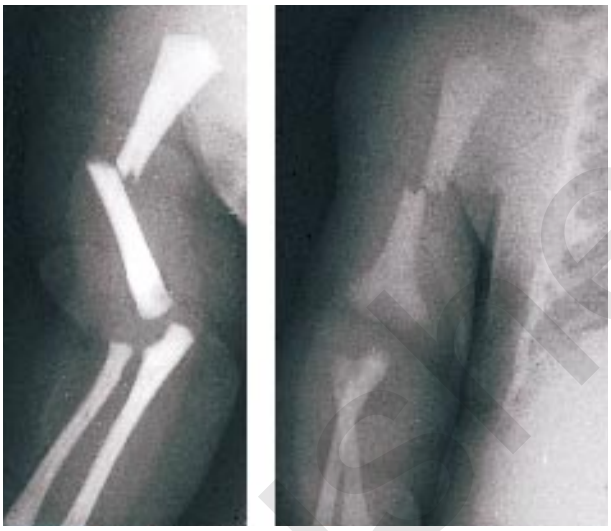

Figure 4.56. A radiograph of a fracture of the middle third of the right humerus following a difficult delivery. This commonly arises with shoulder dystocia and may be associated with lesions of the brachial plexus due to traction on the shoulder girdle. The upper arm is immobile, painful and may be swollen.

4.57

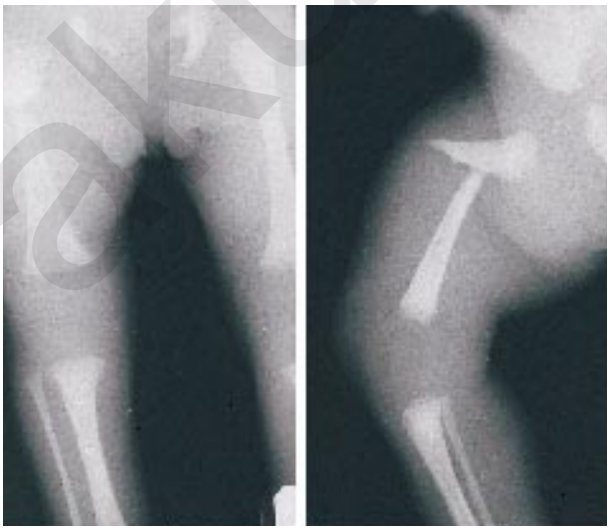

Figure 4.57. A radiograph of a fracture of the right femur occurring as a result of birth injury following breech extraction.

4.58

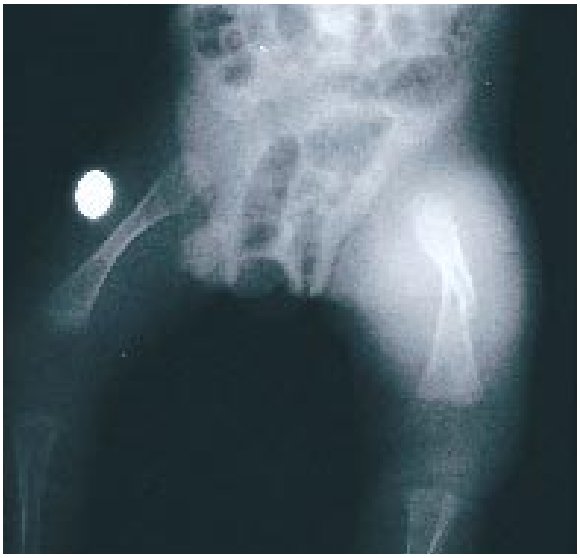

Figure 4.58. A radiograph of a fracture of the left femur with marked soft tissue swelling. Note the large right inguinal hernia.

4.59

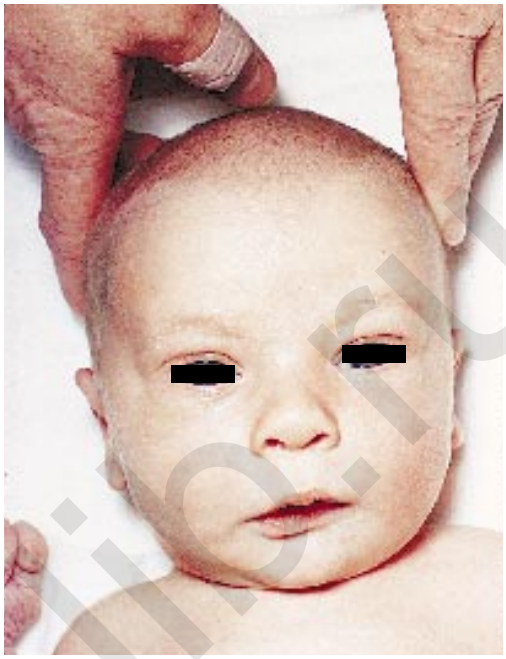

Figure 4.59. Facial nerve palsy occurred in this infant as a result of application of forceps. It may also occur following prolonged labor in a mother with a prominent sacral promontory. Note the ptosis and drooping mouth on the right side.

4.60

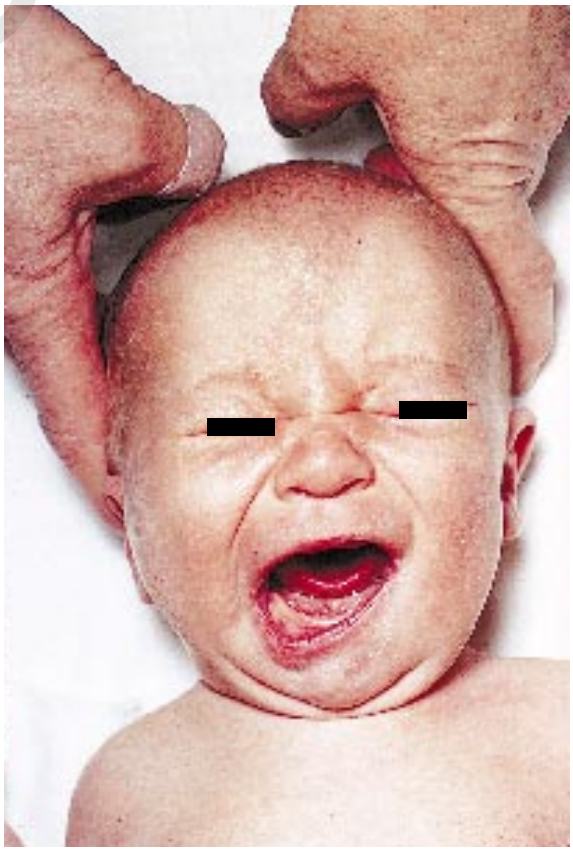

Figure 4.60. This shows the same infant crying. The facial palsy becomes readily apparent. This demonstrates how easily the diagnosis may be missed in a quiet or sleeping infant. There is diminished movement of the affected side of the face, the eye frequently but not always remains partly open, the nasolabial fold is absent and the mouth droops, being drawn over to the healthy side when the infant cries. Note that the forehead is smooth on the affected side. Restoration of normal function and disappearance of the paresis may be complete in a few days or usually within a few weeks. Permanent paralysis is exceptional and suggests a central lesion.

4.61

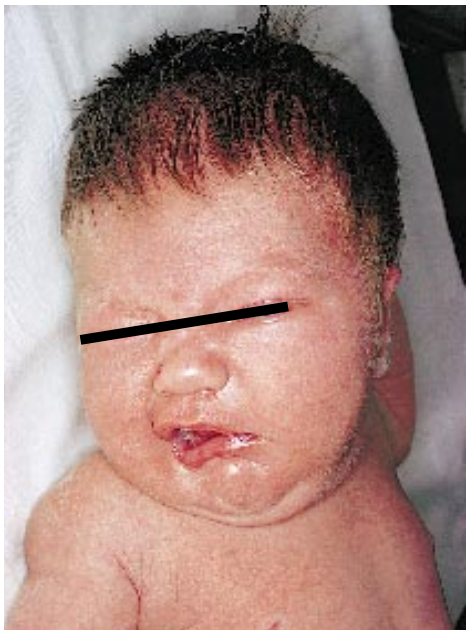

Figure 4.61. Facial palsy of the left side in an infant. This infant shows the typical findings in that he is unable to close his eye or contract the lower facial muscles and has loss of the nasolabial fold on the affected side. In traumatic facial paresis frequently only the mandibular branch of the facial nerve is affected. With central facial paresis the two lower branches are affected allowing for movement of the forehead. Facial paresis in Möbius syndrome is usually bilateral and incomplete and the face is expressionless.

4.62

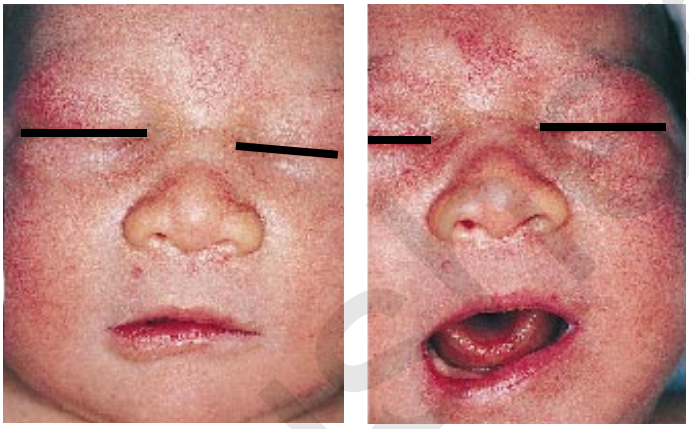

Figure 4.62. Congenital hypoplasia of the depressor anguli oris muscle (angular depressor muscle). The localized facial weakness in which the lower lip on one side fails to be depressed on crying results in an "asymmetric crying facies." The resulting facial asymmetry when the child cries may be misinterpreted. There is a weakness of the muscles controlling movement of the mouth but not those of the upper face. The nasolabial folds are normal and the affected side will not move when the infant cries. The normal side of the face is assumed to be abnormal because the lower lip on the intact side appears to be pulled down and everted. This is a benign condition and is *not* facial palsy. It lessens as the child gets older. It may be associated with other anomalies, particularly those of the cardiovascular system.

4.63

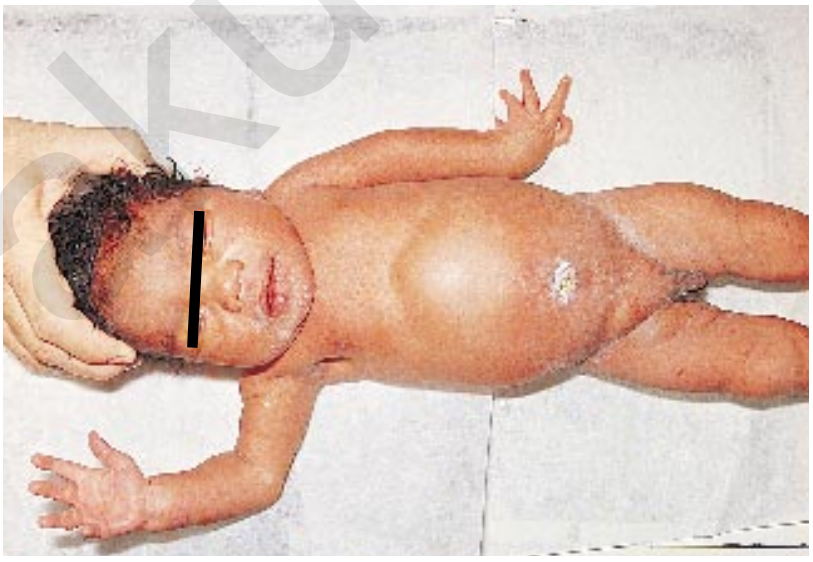

Figure 4.63. Erb's palsy (upper brachial plexus injury) occurs as a result of traction on the brachial plexus (most often the upper nerve roots, C3, C4, and C5). This type of injury occurs most commonly in cases of shoulder dystocia. It presents with the infant lying with the affected upper extremity adducted and internally rotated, the elbow extended, and the hand partially closed with the palm directed outwards and posteriorly resulting in the typical "waiter's tip" position. The majority of these injuries resolve spontaneously in 3 to 4 weeks.

4.64

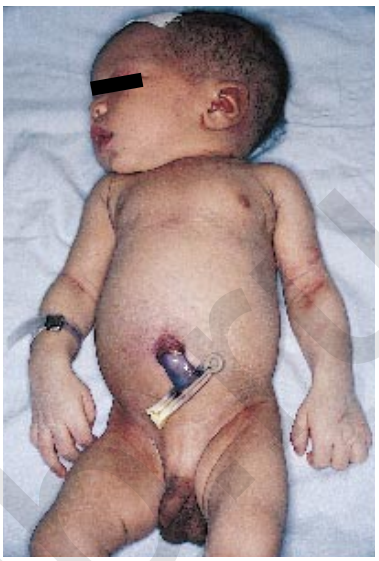

Figure 4.64. Bilateral involvement of the upper brachial plexus resulting in the typical position in both upper extremities. In the rare event of a bilateral palsy the possibility of damage to the spinal cord has to be considered. Note that infants with Erb's palsy may lack a Moro response on the affected side.

4.65

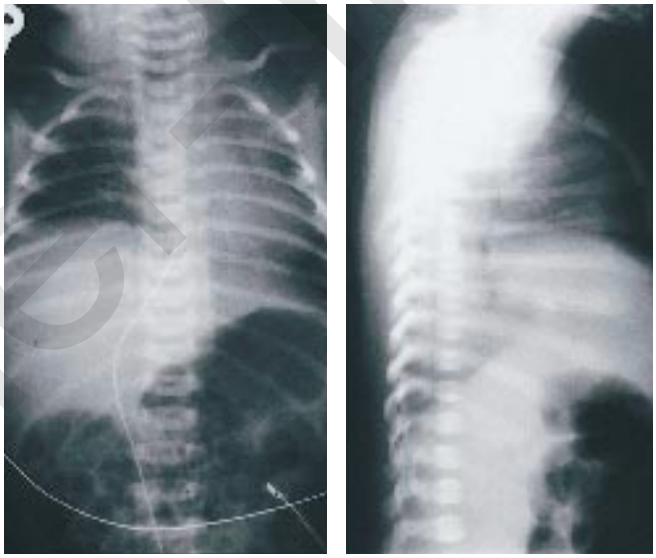

Figure 4.65. Anteroposterior and lateral radiograph of the chest in an infant with a right Erb's palsy. Note the ipsilateral paralysis of the right diaphragm due to phrenic nerve palsy which may occur in association with upper motor brachial plexus trauma. A rare complication associated with Erb's palsy is a Horner's syndrome on the same side, due to involvement of the cervical sympathetic nerves. If Horner's syndrome persists, the infant may develop heterochromia iridis caused by failure of development of secondary pigmentation in the affected eye.

4.66

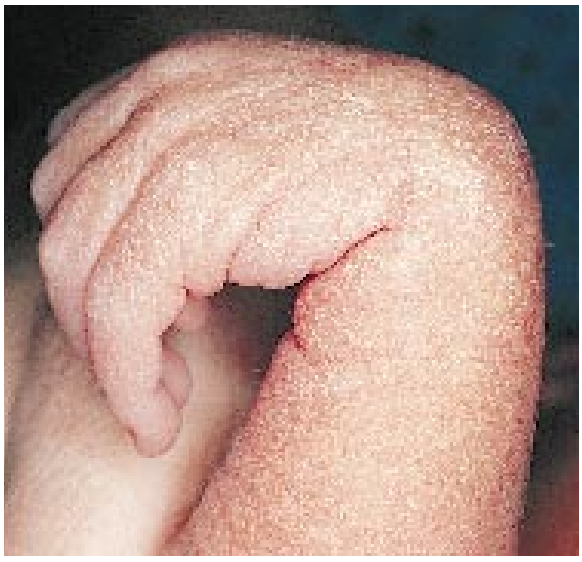

Figure 4.66. Left radial nerve palsy in a neonate presents as a typical wrist-drop. The condition probably results from interference with blood supply to the nerve if there is abnormal compression or traction during a difficult labor. With the wrist-drop there is ability to grip with the fingers and voluntary extension of the fingers. A similar appearance may occur in an infant with a postural deformity, or a pseudo "wrist-drop" may be seen in a floppy, hypotonic infant hence it is important to check for voluntary wrist extension.

Chapter 5
Deformations and Disruptions

A structural abnormality or anomaly may be a malformation, deformation, or disruption. Deformations and disruptions are the result of mechanical forces affecting normal tissue, while malformations are the result of a primary problem in morphogenesis. A deformation is a physical change in form, shape, or position caused by mechanical forces secondary to restricted intrauterine motion (e.g., clubfoot secondary to constraint of the foot). Most of these have an excellent prognosis once the fetus is released from the constraining environment. In some instances, application of an opposite force may be needed to correct the deformation. Some deformations are caused by a problem intrinsic to the fetus and are not reversible (clubfoot secondary to neuromuscular disorder). A clear distinction between deformation and malformation is important when educating parents on prognosis, management and recurrence risk. A disruption is a congenital defect resulting from an extrinsic interference with an originally normal developmental process (e.g., abnormality caused by an amniotic band). Disruptions usually result in cell death and are not correctable.

DEFORMATIONS (Congenital Postural Deformities, "Position-of-Comfort" Anomalies) and DISRUPTIONS (Amniotic band disruption complex–The Early Amnion Rupture Spectrum (TEARS))

Autoamputation of digits, furrows due to amniotic bands, and syndactyly may develop between the affected digits. Amniotic bands may cause major disruptions that lead to constriction or amputation or to craniofacial disruption. Lack of symmetry of the lesions differentiate disruption caused by amniotic bands from genetic causes of craniofacial or limb anomalies.

5.1

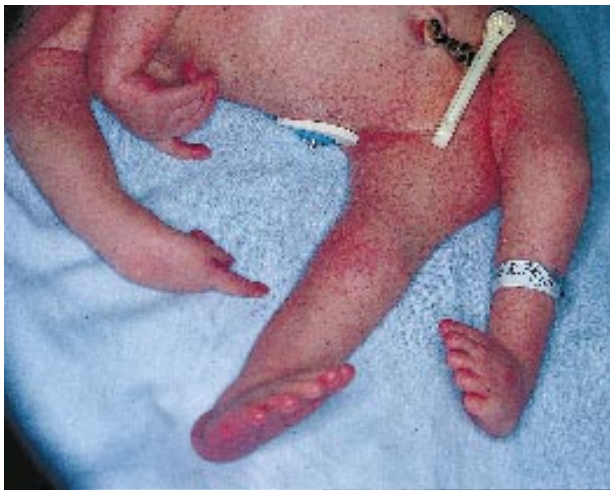

Figure 5.1. The infant in the following five figures was referred to hospital with a diagnosis of multiple congenital malformations. It should be noted that these "malformations" represent examples of congenital postural deformities. Note the position of the hands, lower extremities and the feet occurring as a result of this infant's position in utero.

5.2

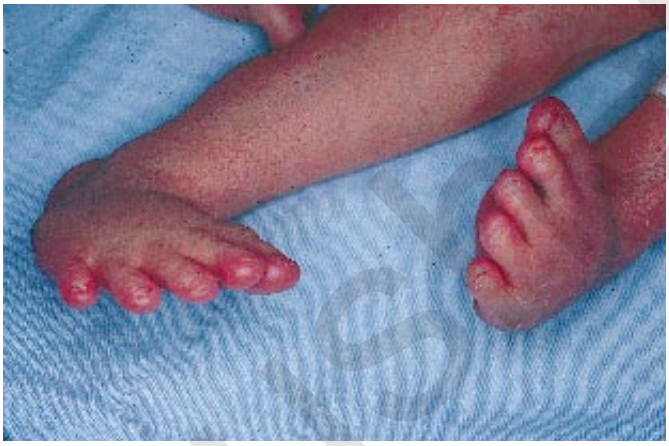

Figure 5.2. A close-up of the postural deformities involving the feet.

5.3

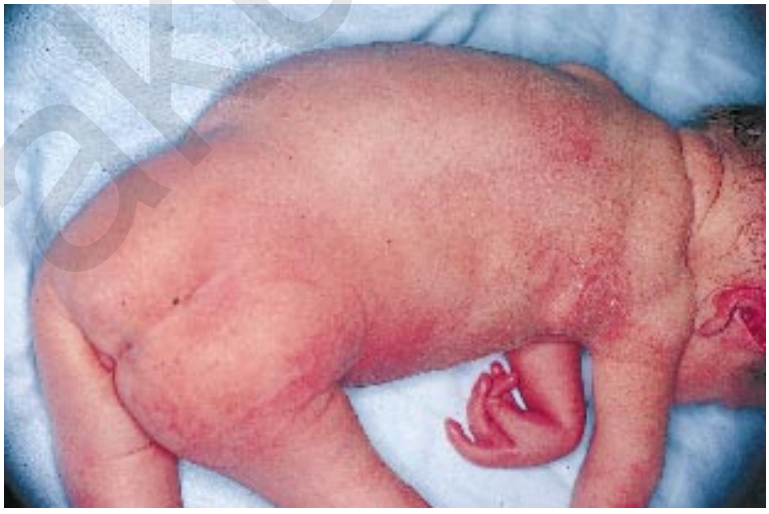

Figure 5.3. This figure demonstrates the congenital postural scoliosis and pseudo "wrist-drop."

5.4

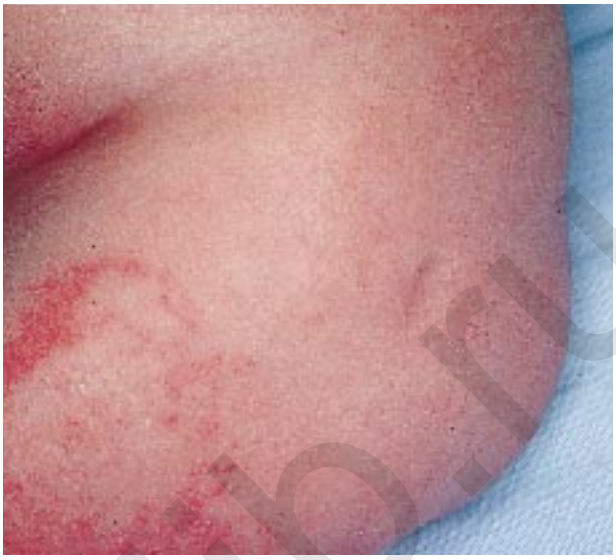

Figure 5.4. This figure of the same infant shows a skin dimple over the left hip. Skin dimples are not uncommon in association with deformations (postural deformities or "position-of-comfort" deformities).

5.5

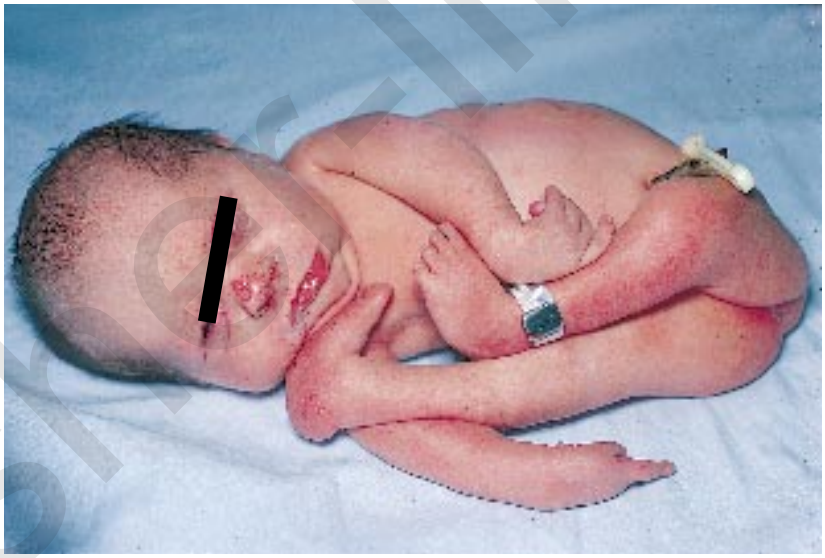

Figure 5.5. The infant has been placed into her in utero position. This demonstrates clearly how the above changes occurred as a result of the infant's "position-of-comfort" in utero. If placed in a normal position, infants with deformations will be uncomfortable and will cry, but will quiet down rapidly when allowed to return to their "position-of-comfort."

5.6

Figure 5.6. Abdominal pregnancy is associated with multiple congenital postural deformities as there is no cushion of amniotic fluid.

5.7

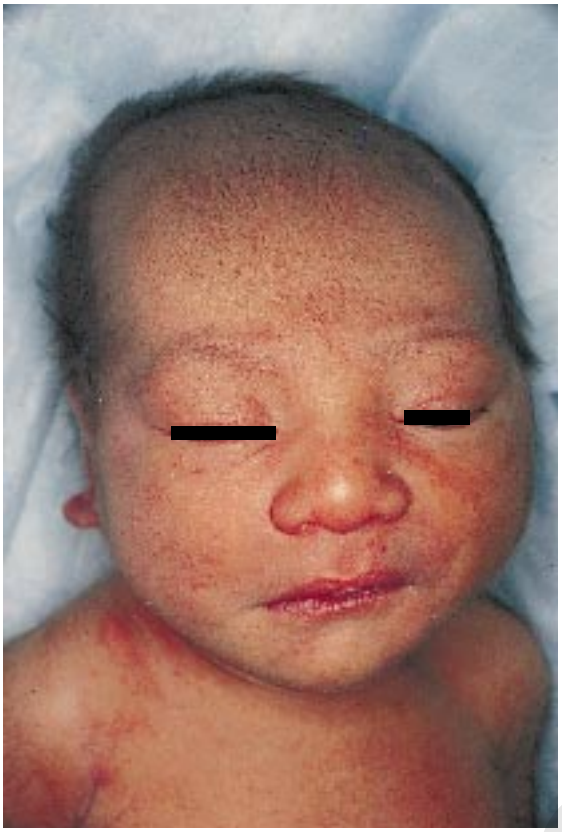

Figure 5.7. Asymmetry of the face and head in an infant at birth due to a deformation.

5.8

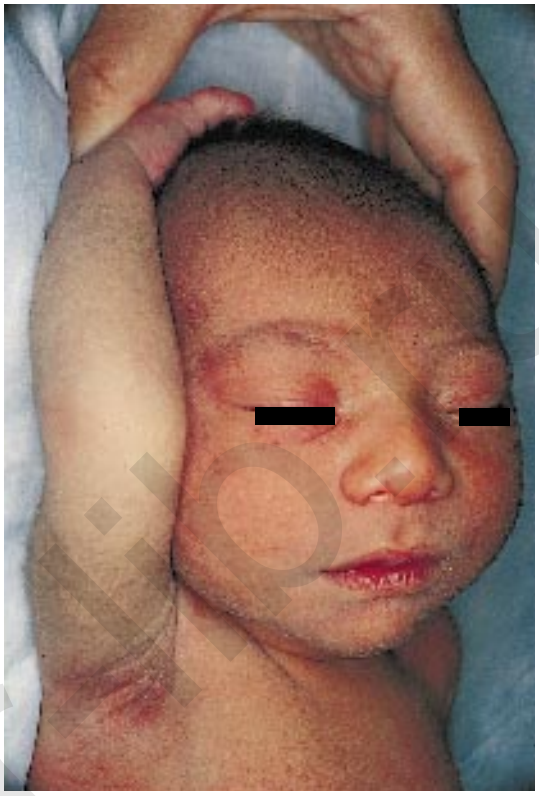

Figure 5.8. The same infant demonstrating that this occurred as a result of the right upper extremity lying in apposition to the face and head on the right side in utero.

5.9

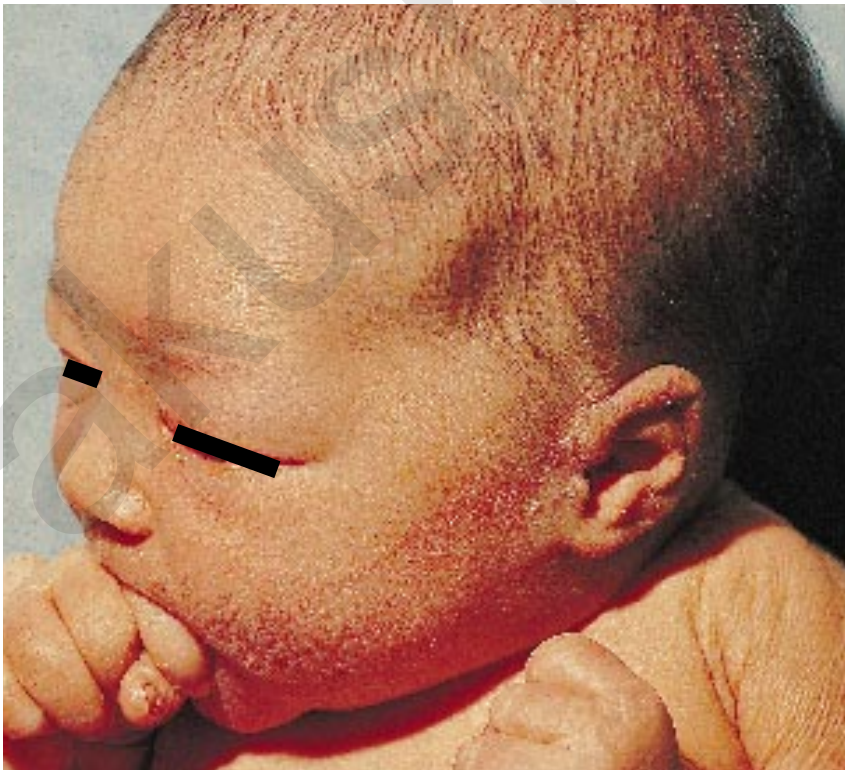

Figure 5.9. This normal infant presented at birth with a depression over its left temporal area. This occurred as a result of an in utero positional deformity.

5.10

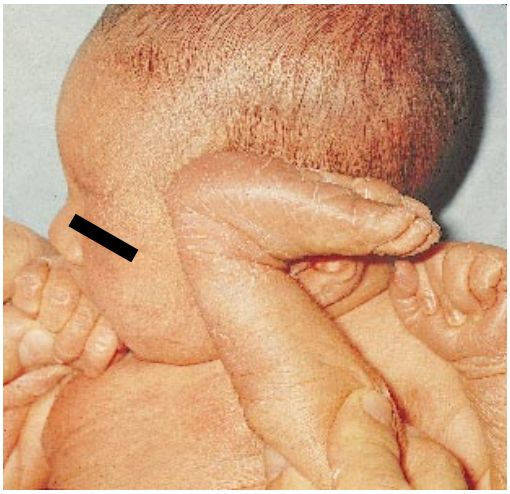

Figure 5.10. In the same infant as shown in Figure 5.9 the left temporal depression was due to pressure of the baby's left foot on the fetal skull in utero.

5.11

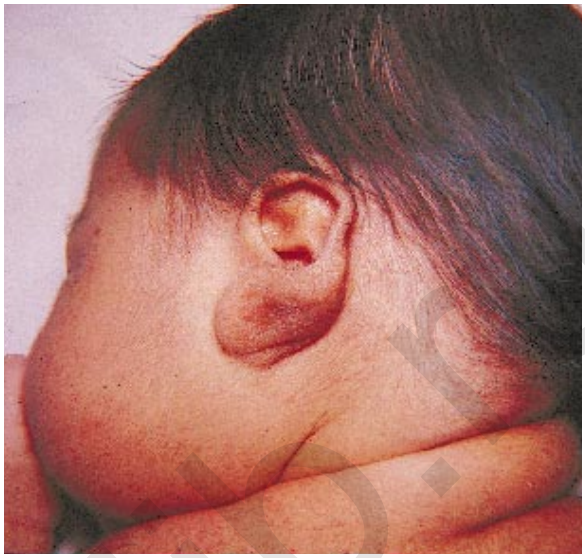

Figure 5.11. This very common finding of folding of the ear lobe occurs as a result of a postural deformity.

5.12

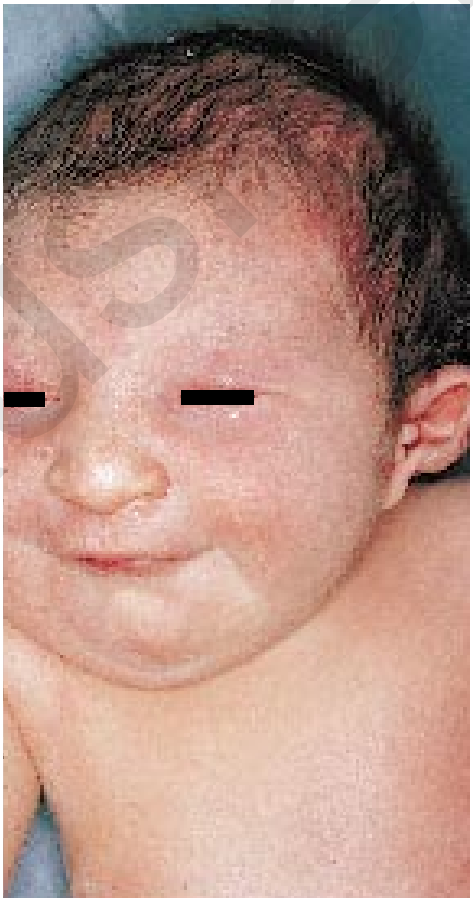

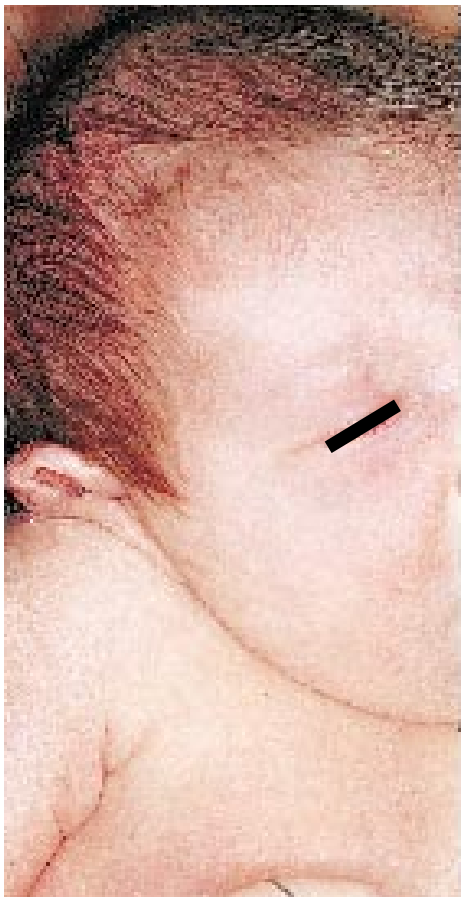

Figure 5.12. In this infant the same type of postural deformity is noted demonstrating that this occurs as a result of the shoulder pressing up against the ear lobe in utero. In general, over 90% of congenital postural deformities correct spontaneously.

5.13

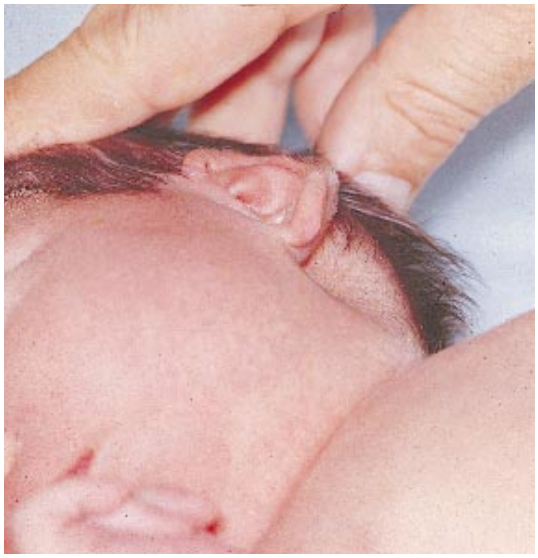

Figure 5.13. In rare cases marked pressure of the shoulder on the fetal head in utero can result in a depression over the temporal area. Note the ear is pushed forward.

5.14

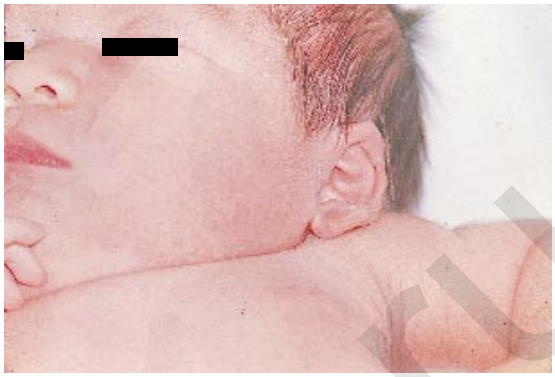

Figure 5.14. The same infant in its "position-of-comfort" shows that the shoulder caused the depression and abnormal appearance of the ear.

5.15

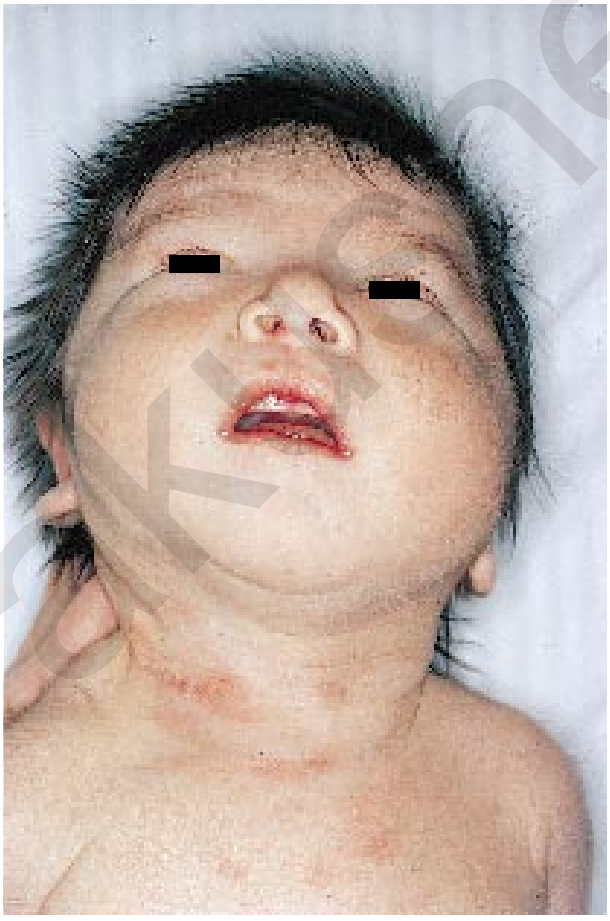

Figure 5.15. This infant with asymmetry of the jaw at birth was noted to have some abrasions on the neck. Skin abrasions can occur in relation to a postural deformity.

5.16

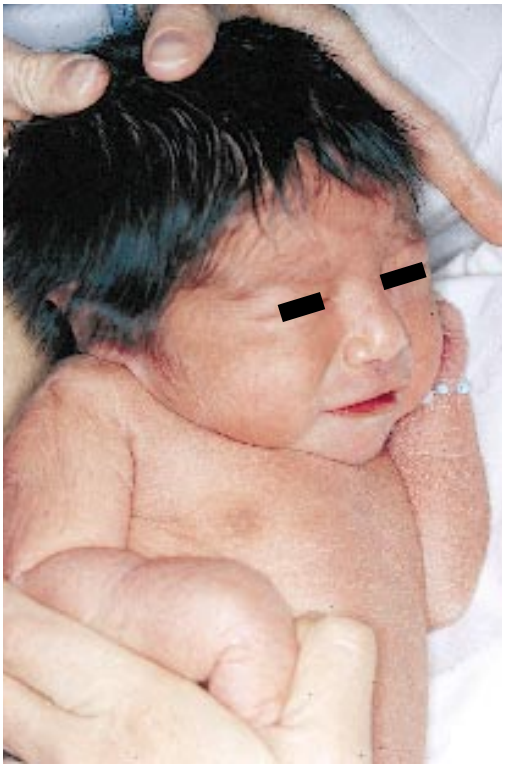

Figure 5.16. The same infant showing its "position-of-comfort" in utero.

5.17

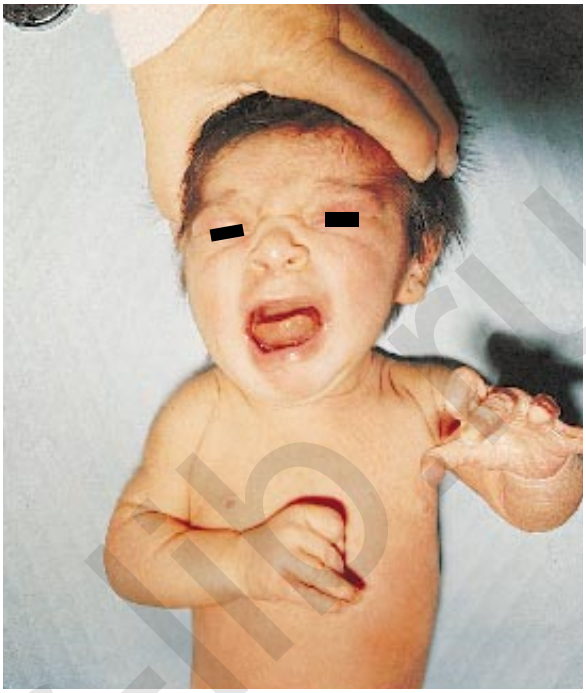

Figure 5.17. There is marked asymmetry of the face in this infant. When the face and head are straightened, the infant is very uncomfortable and cries.

5.18

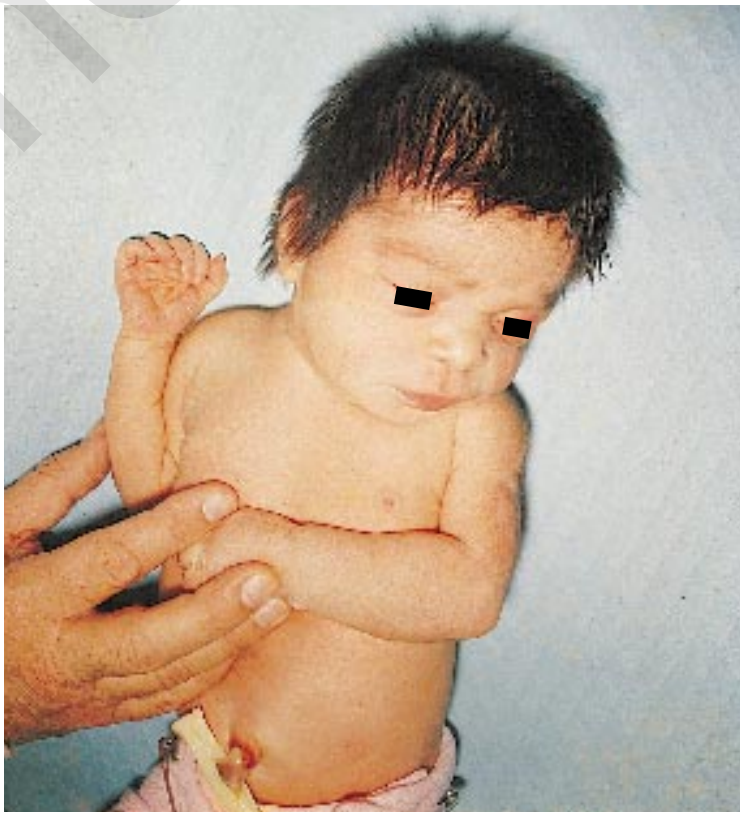

Figure 5.18. The same infant quiets down immediately when allowed to go into its "position-of-comfort" in utero. This also demonstrates the reason for the asymmetry of the face.

5.19

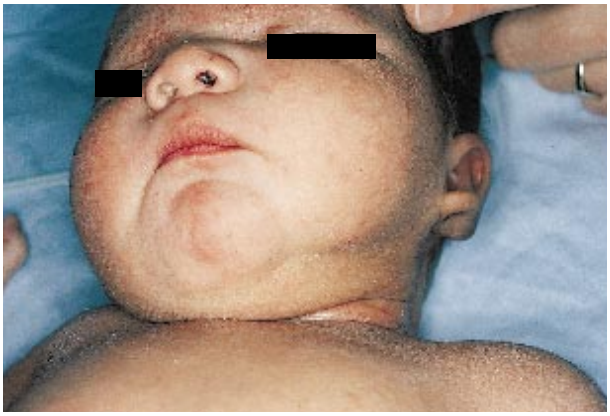

Figure 5.19. Positional deformity showing asymmetry of the face and jaw.

5.20

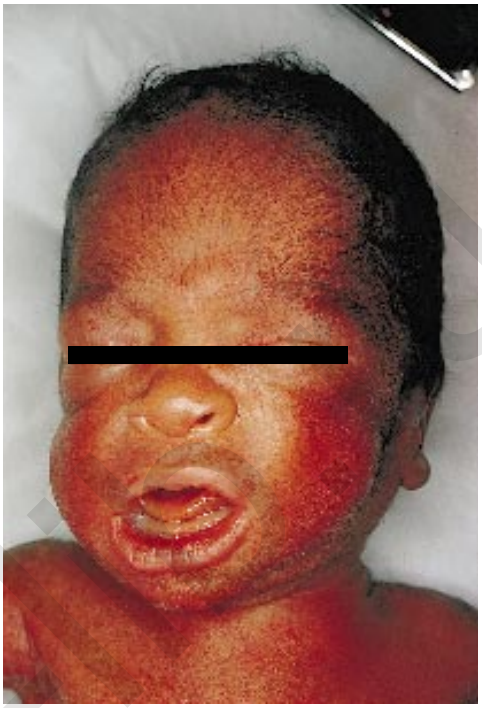

Figure 5.20. Asymmetry of the face occurring as a result of a "position-of-comfort" deformity.

5.21

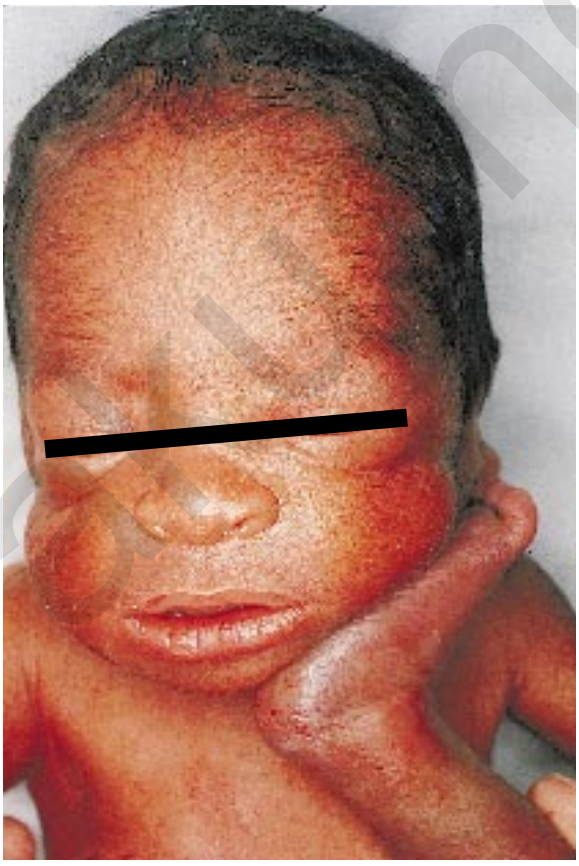

Figure 5.21. The same infant shows that the asymmetry is due to its left foot being placed up against the side of the face and jaw. Another example of "position-of-comfort" deformity.

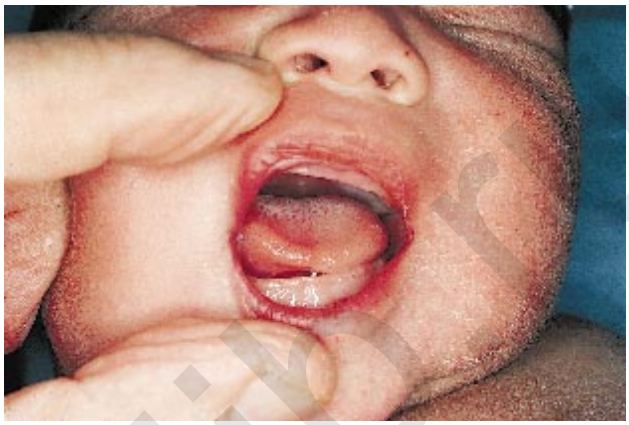

5.22

Figure 5.22. Malocclusion of the jaw may occur if there is a marked and prolonged positional deformity. Infants with malocclusion should be followed as the malocclusion may require treatment at a later date.

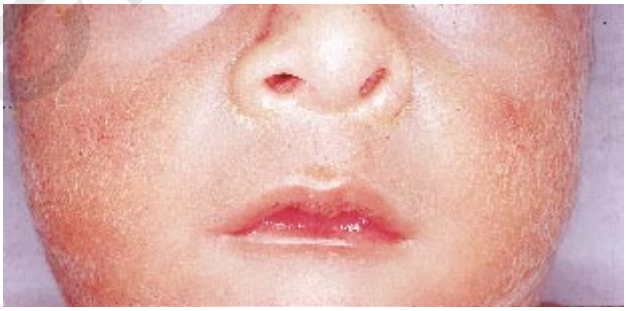

5.23

Figure 5.23. There is asymmetry of the nostrils in this infant. Note the vertical left nostril and horizontal right nostril. This can occur as a result of a postural deformity or dislocation of the nasal cartilage.

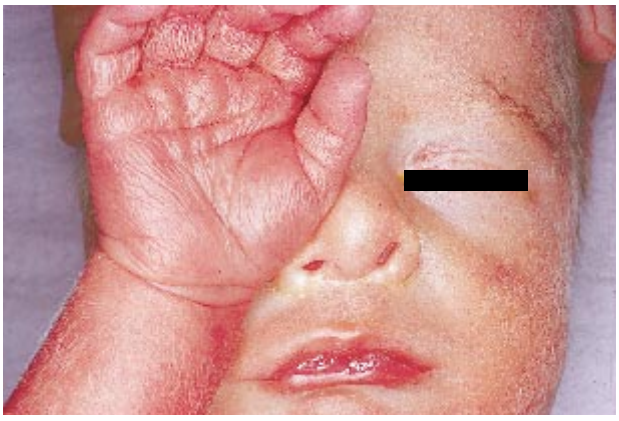

5.24

Figure 5.24. The same infant shows that the asymmetry was associated with a postural deformity due to pressure of the right hand on the nose in utero. This invariably corrects spontaneously.

5.25

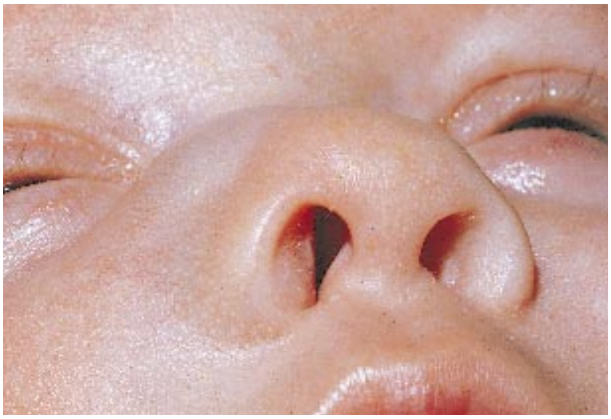

Figure 5.25. In this infant note the asymmetry of the nostrils and ecchymosis due to a dislocation of the triangular cartilage of the nasal septum, which may occur during delivery, especially if the mother has a prominent sacral promontory. When the septum is manually moved toward the midline the asymmetry persists confirming the dislocation. These infants require an otolaryngology evaluation.

5.26

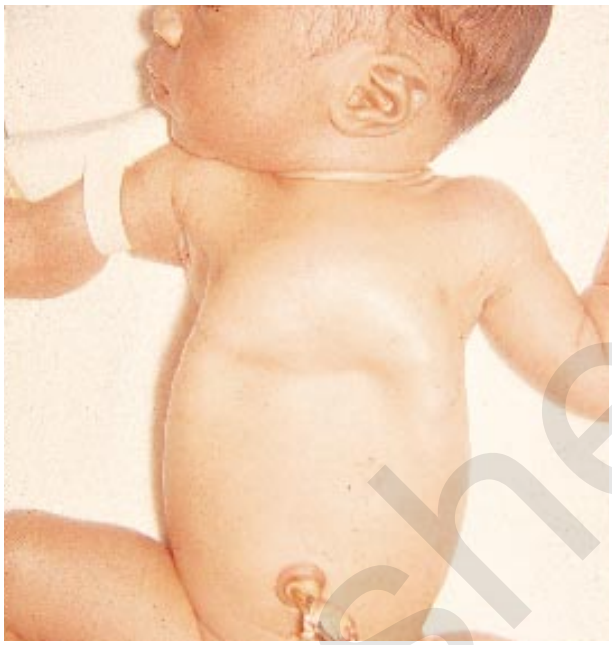

Figure 5.26. Note the subcostal depression on either side of the xiphoid in an infant who was a breech presentation.

5.27

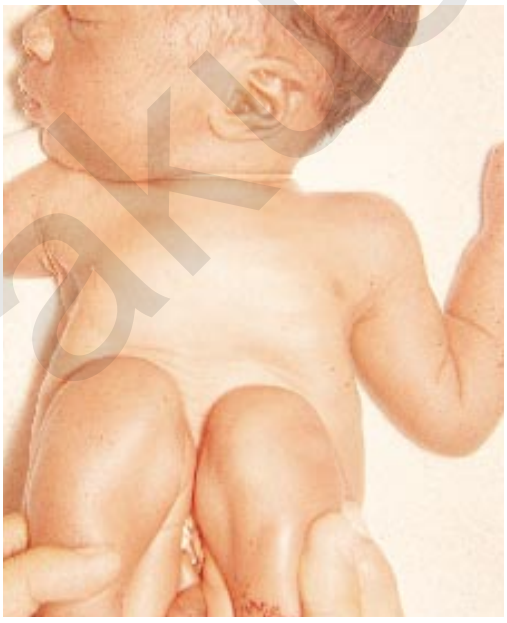

Figure 5.27. This figure shows the same infant with both knees fitting well into the depressions. This is a fairly common example of a "position-of-comfort" deformity.

5.28

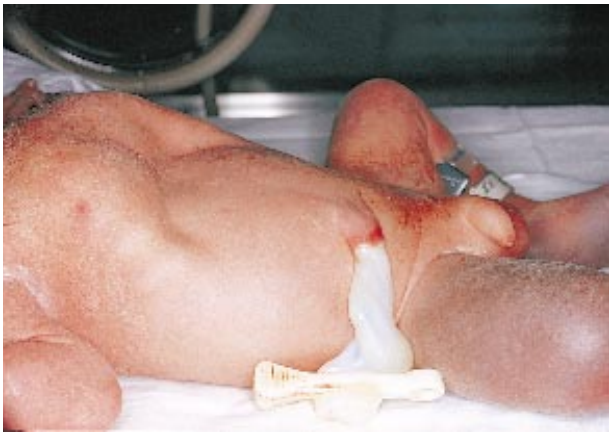

Figure 5.28. Another example of a positional deformity on both sides of the subcostal area resulting from position in utero in a breech presentation. This should not be confused with subcostal retraction in this premature infant who had respiratory distress.

5.29

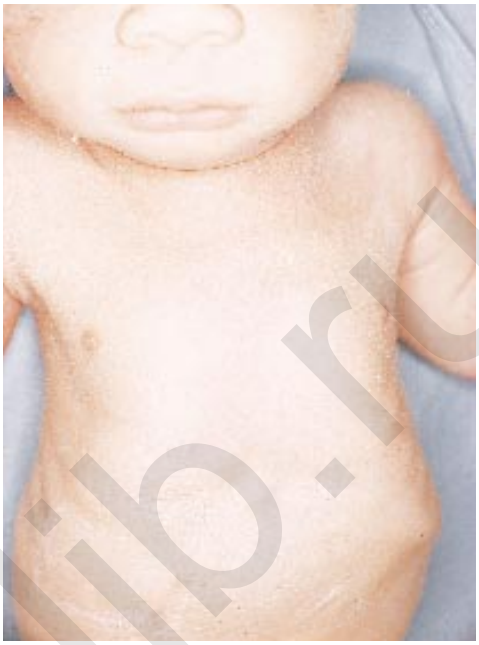

Figure 5.29. In this infant the chest appears to be narrow compared with the rest of the body.

5.30

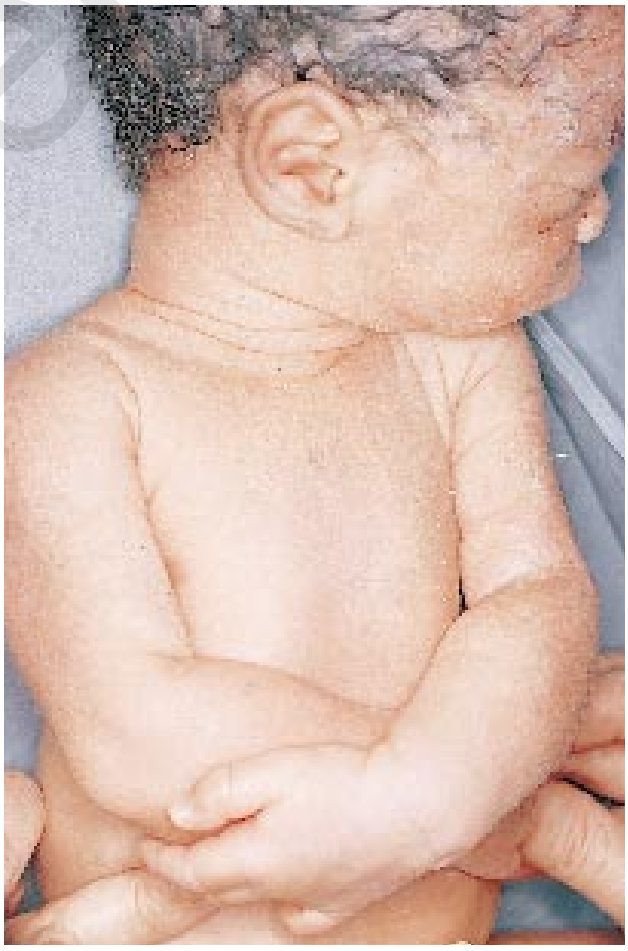

Figure 5.30. The same infant shows the arms lying along side the chest wall compressing the thorax. This is a fairly common postural deformity and should not be confused with a narrow thorax observed in cases of dwarfism.

5.31

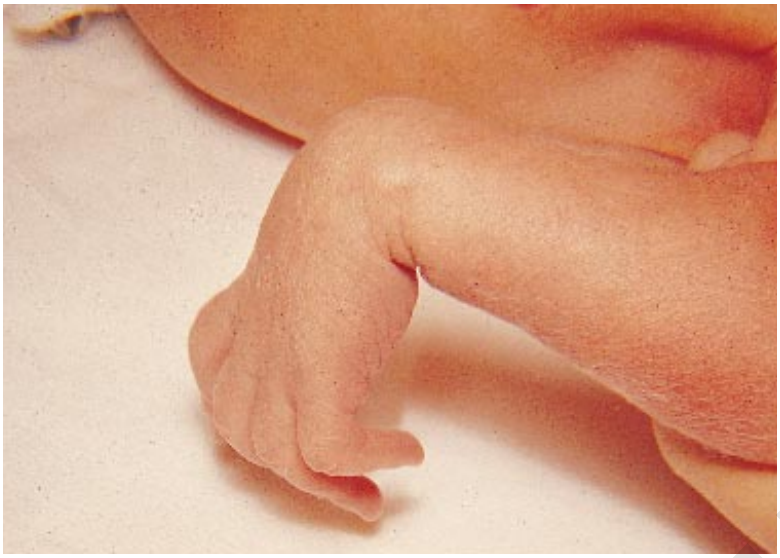

Figure 5.31. In this infant it appeared that there was a left wrist-drop and the diagnosis of radial palsy was considered. However, with stimulation the left hand moved normally and the postural deformity resolved completely in a few days.

5.32

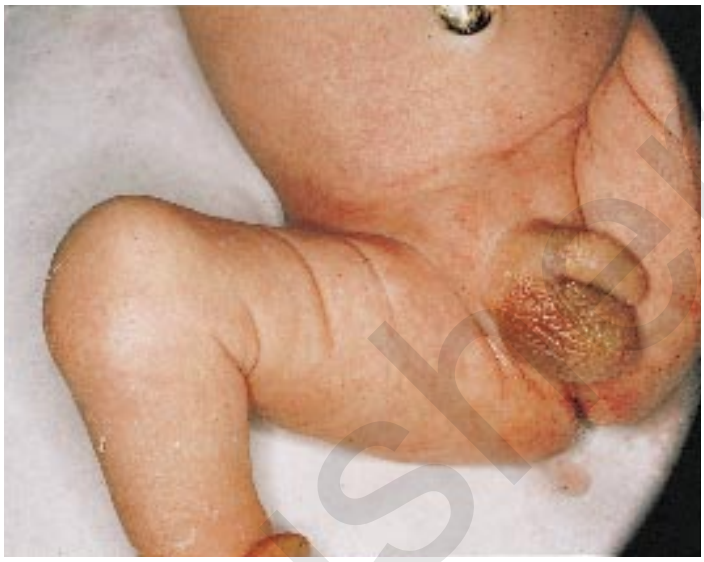

Figure 5.32. In breech presentation there may be a marked concavity of the inner aspect of the thigh. The lower extremities in a frank breech may lie up against the fetal abdomen causing a "position-of-comfort" deformity.

5.33

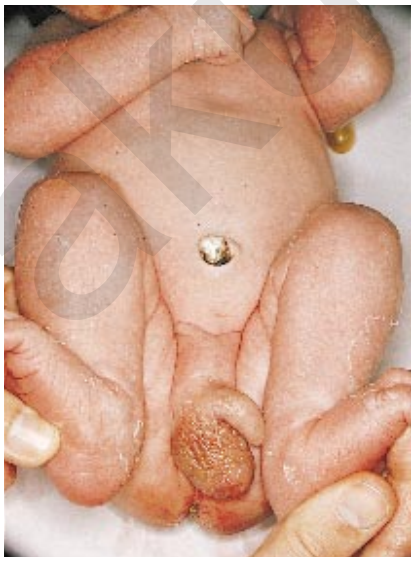

Figure 5.33. The same infant showing its "position-of-comfort." A similar concavity of the inner aspect of the thighs may occur in infants who have lack of movement in utero.

5.34

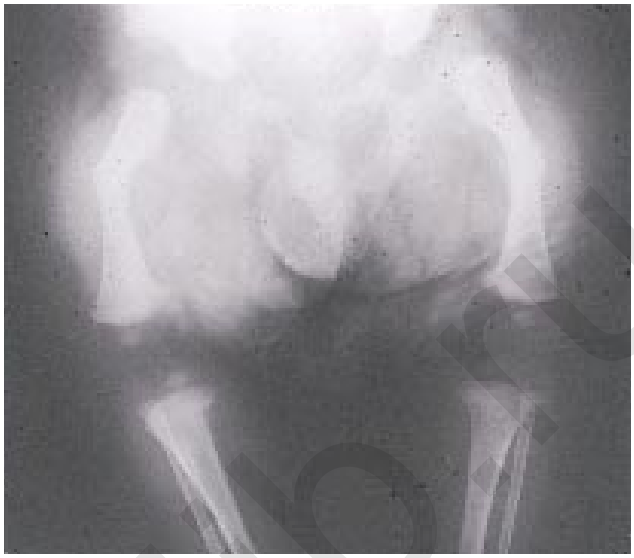

Figure 5.34. Radiograph of an otherwise normal infant with the uncommon finding of bilateral bowing of the femora occurring as a result of a "position-of-comfort" deformity. Bowing of one or both tibiae in which they curve gently toward the midline may have the soles of the feet face each other. Femoral bowing is rare but is occasionally present in babies born after prolonged breech presentation. Congenital bowing of the forearm and humerus almost never occur. These tend to improve gradually as with all deformations.

5.35

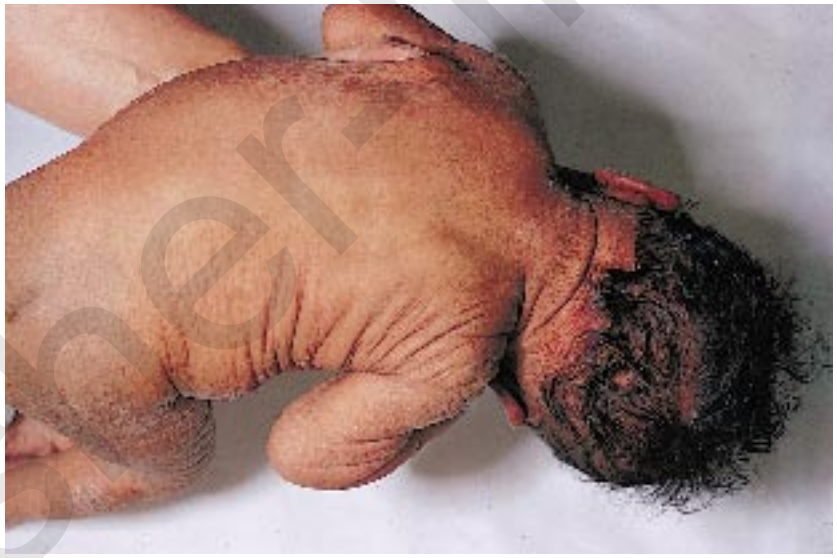

Figure 5.35. Posterior view of an infant showing congenital postural scoliosis which occurred as a result of position in utero.

5.36

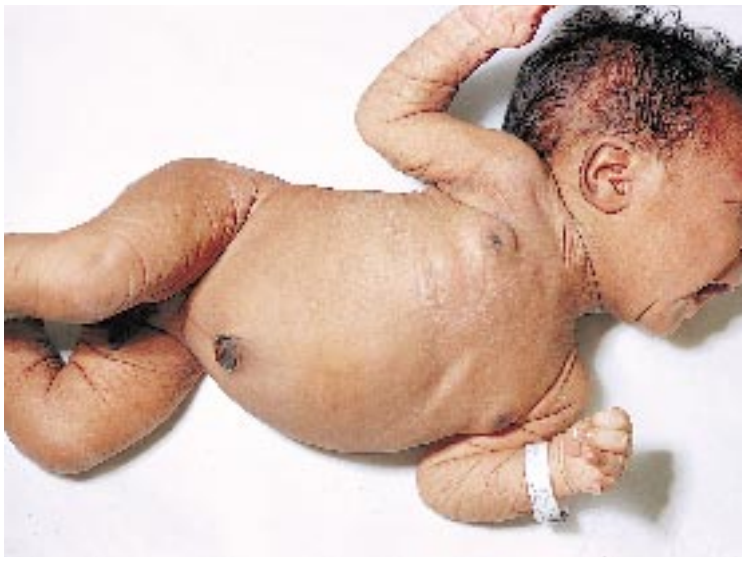

Figure 5.36. The same infant demonstrating the postural scoliosis. Postural scoliosis in the newborn is rare. If a true congenital scoliosis is present it is usually associated with a structural anomaly of the vertebral column.

5.37

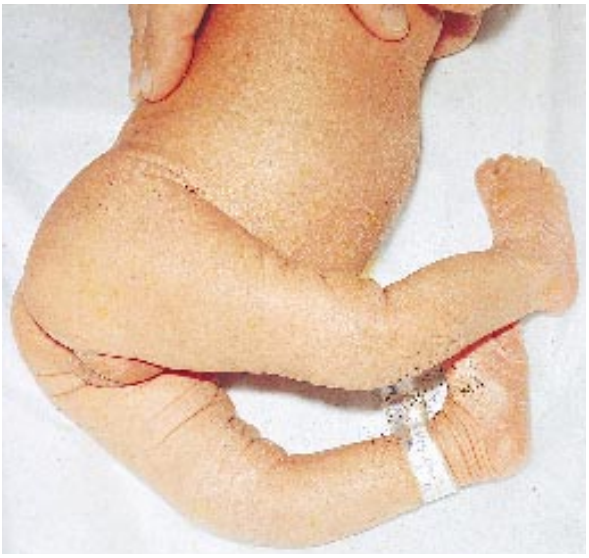

Figure 5.37. This infant has a fairly common congenital postural deformity – genu recurvatum. This "position-of-comfort" deformity gives the impression that there is a dislocation at the knees. Note the hyperextensibility at the knees and note that the creases on the thighs which are normally seen posteriorly are anteriorly placed.

5.38

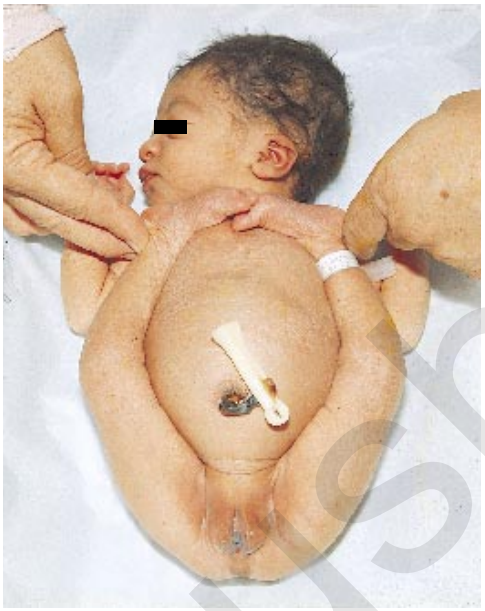

Figure 5.38. The same infant with genu recurvatum in its "position-of-comfort." When it occurs, genu recurvatum ("back knee") is almost invariably associated with breech presentations and the incidence is much more common in females. The majority correct spontaneously; in severe cases posterior splinting may be necessary.

5.39

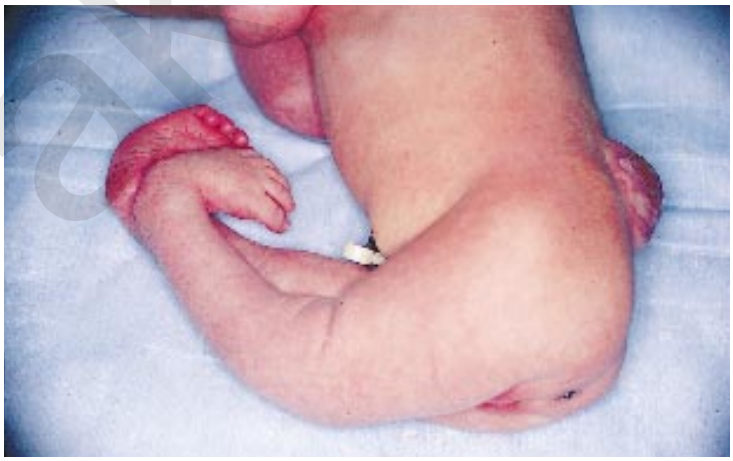

Figure 5.39. Another example of genu recurvatum in an infant with a neural tube defect. Note the bilateral clubfeet that are also considered to be postural deformities. Genu recurvatum may occur in neurologic disorders and in syndromes with generalized joint laxity and hypermobility, such as Ehlers-Danlos syndrome.

5.40

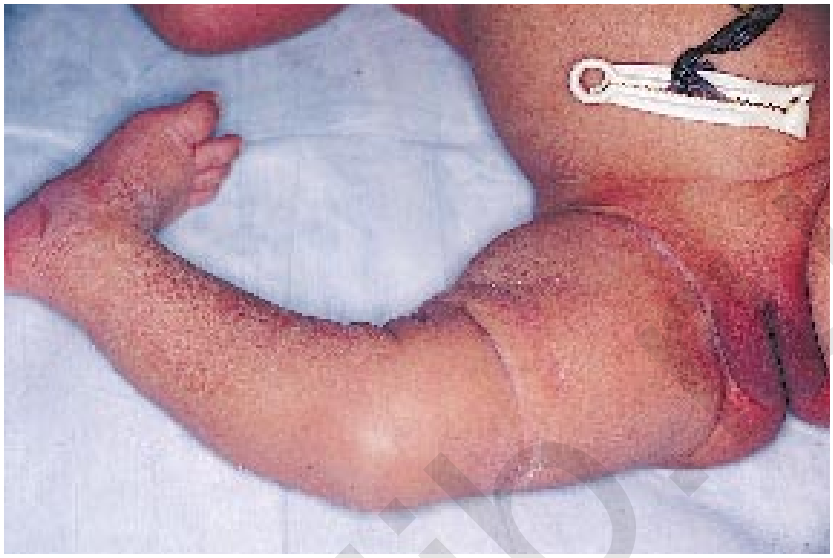

Figure 5.40. This infant has a congenital dislocation of the right knee. This uncommon finding has the same appearance as genu recurvatum. Congenital dislocations of the knee rarely occur as an isolated condition but may be seen in Larsen's syndrome, a condition in which there are multiple joint dislocations. It may be confirmed by radiography and requires treatment.

5.41

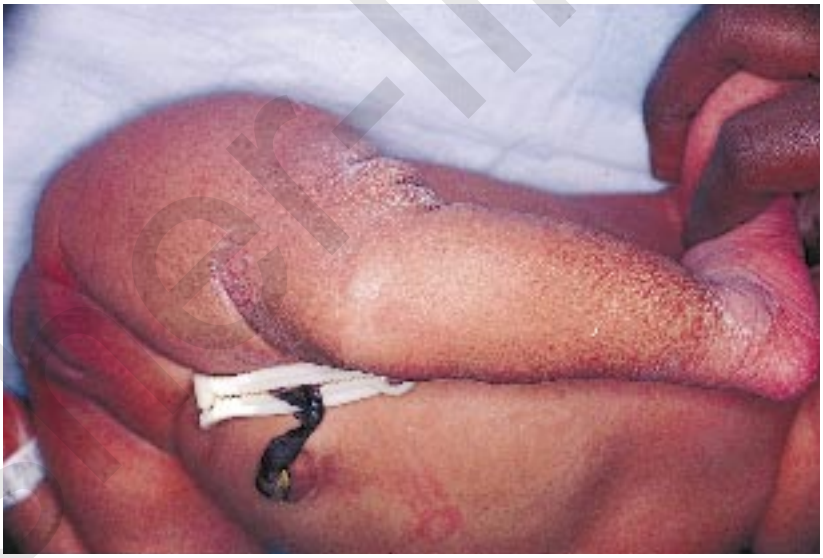

Figure 5.41. Another view of the congenital dislocation of the right knee in the same infant.

5.42

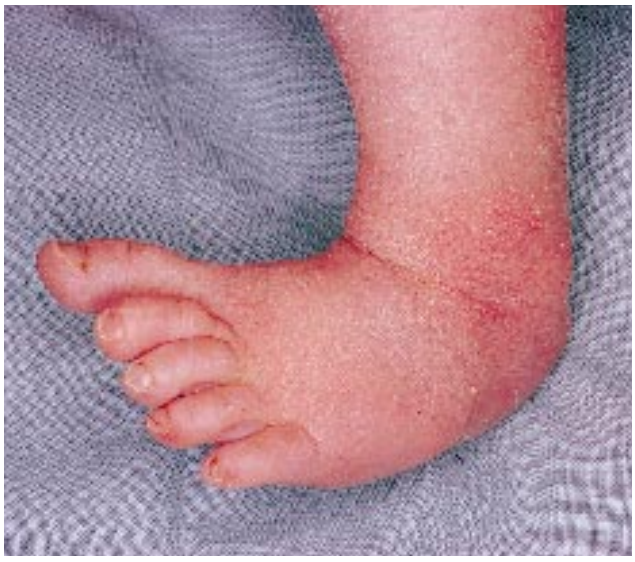

Figure 5.42. Metatarsus adductus (metatarsus varus) is a common postural deformity which requires no treatment. The forefoot is turned medially so that the lateral border of the sole is quite convex. The heel is in a neutral position and the foot can be dorsiflexed normally. If intrauterine constraint has been prolonged a deep plantar crease will be seen on the medial side.

5.43

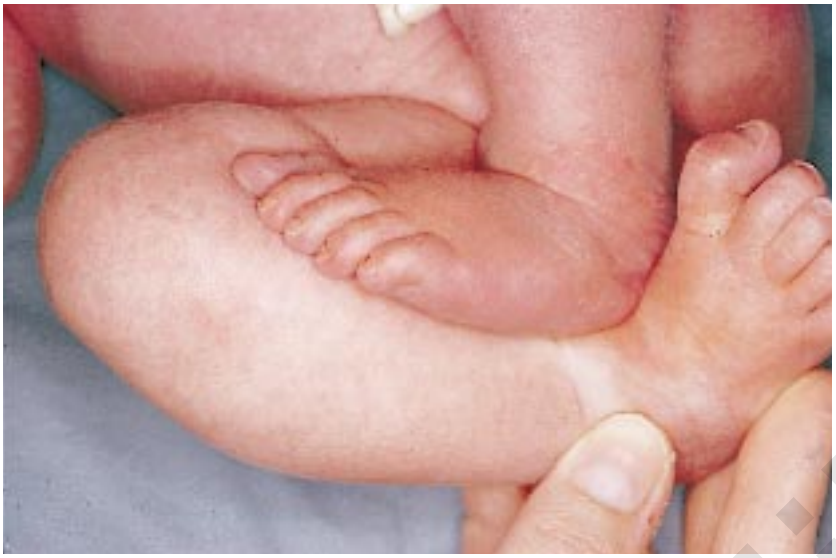

Figure 5.43. The position of the feet in utero in the same infant as shown in Figure 5.42 demonstrates how the midfoot becomes adducted.

5.44

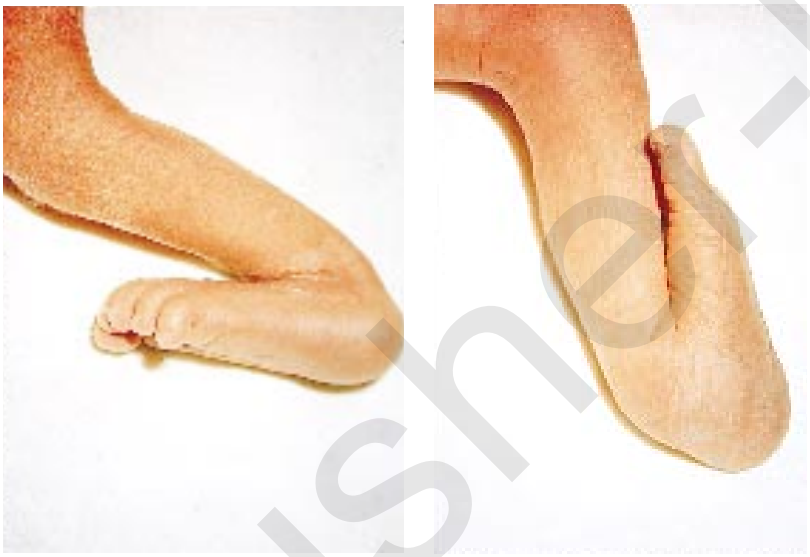

Figure 5.44. Talipes calcaneovalgus is the most common of the congenital postural deformities. The foot is dorsiflexed on the fibular side of the ankle and everted with the sole facing anterolaterally. As implied by the name, the calcaneus also is deviated laterally. A deep skin crease is often present in the plane of abnormal flexion and the subcutaneous tissue is diminished over the anterolateral region of the foot.

5.45

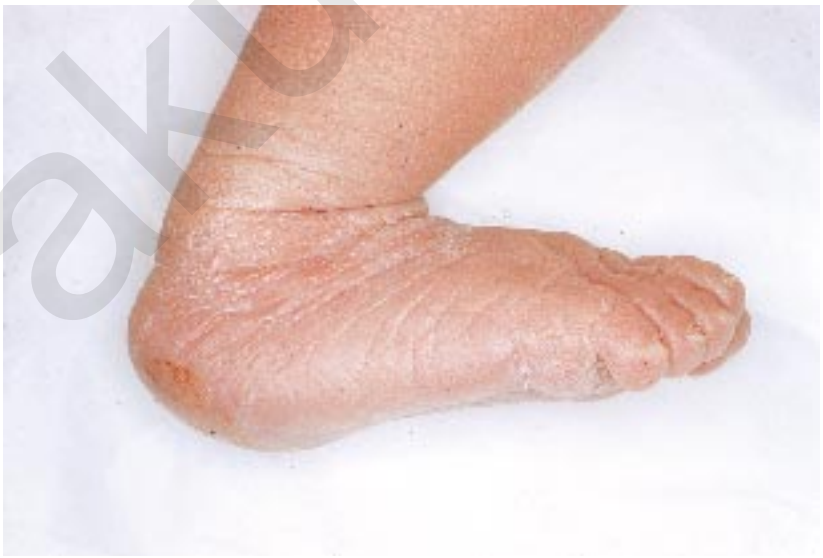

Figure 5.45. In this infant with talipes calcaneovalgus, note the marked dorsiflexion of the foot which is lying against the anterior part of the leg. Talipes calcaneovalgus may occur as a result of abnormal intrauterine posture or may be associated with lower motor neuron defects such as spina bifida. Spontaneous correction usually occurs. This anomaly is more common in babies born in the breech position, especially if the knees were flexed in utero.

5.46

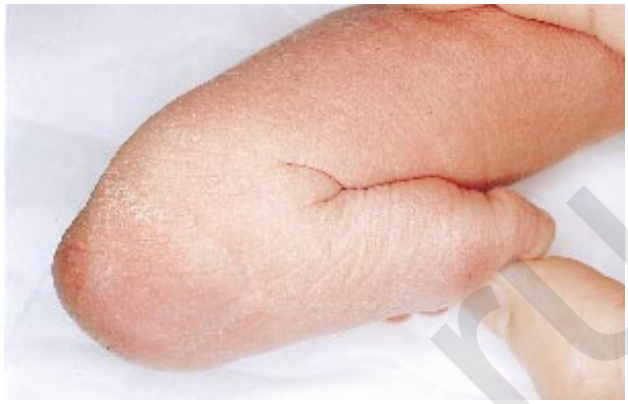

Figure 5.46. The same infant showing the flattening of the dorsum of the foot and marked concavity of the lateral side of the ankle joint.

5.47

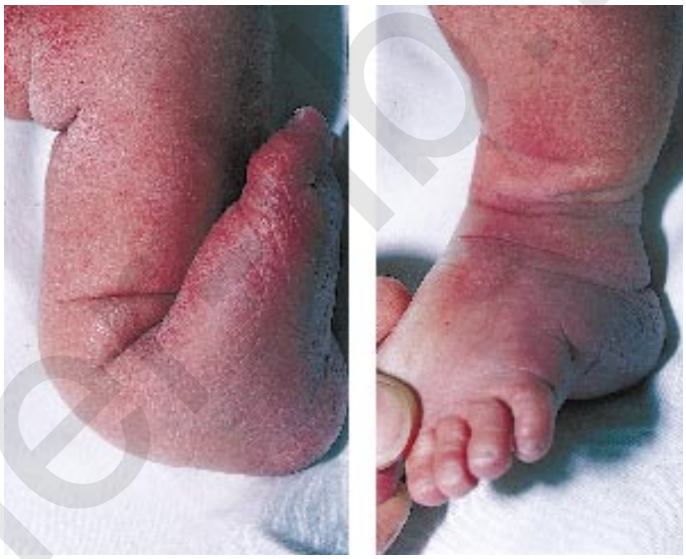

Figure 5.47. An infant with severe talipes calcaneovalgus with marked bowing of the tibia and fibula. Osseous changes such as these are uncommon. This infant required surgical correction.

5.48

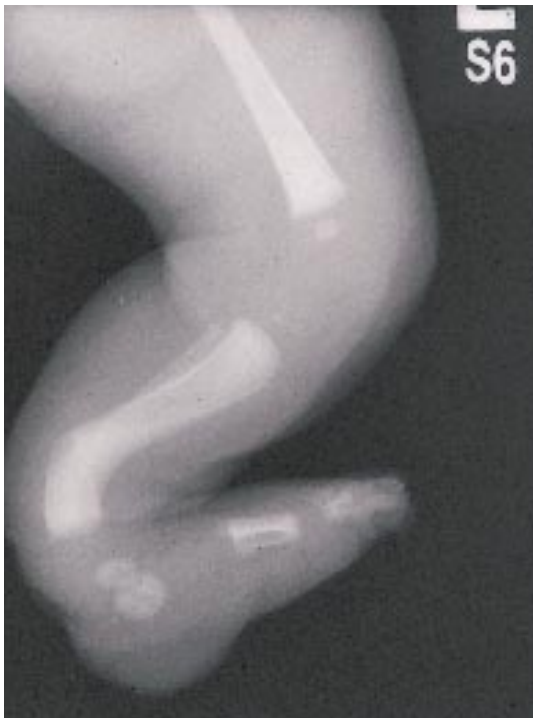

Figure 5.48. Radiograph of the same infant showing the marked bowing of the distal ends of the tibia and fibula.

5.49

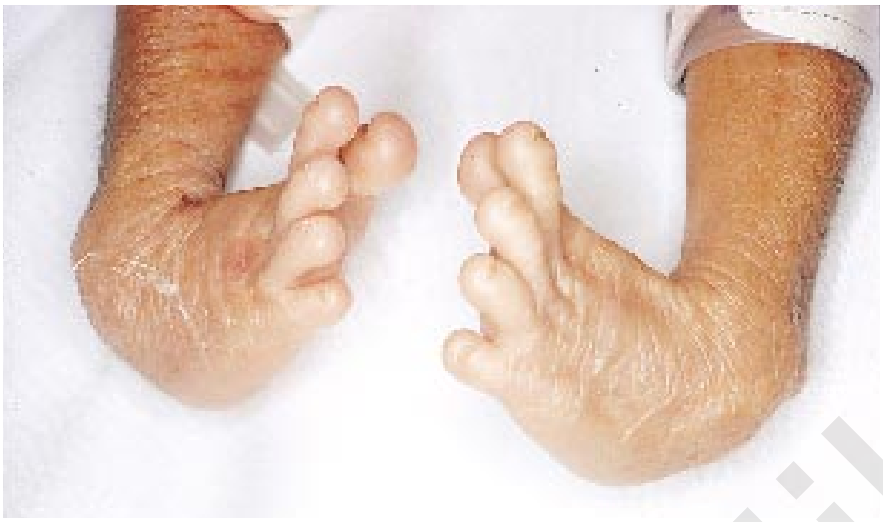

Figure 5.49. Bilateral clubfoot (talipes equinovarus). Talipes equinovarus causes the foot to be sharply plantar flexed and inverted so that the sole is toward the median plane. Note the "tip toe" position with the soles of the feet nearly facing each other. The calcaneus is in varus position and some degree of metatarsus adductus is almost always present. The skin and subcutaneous tissue over the lateral part of the joint may be thin and dorsiflexion is minimal or absent.

5.50

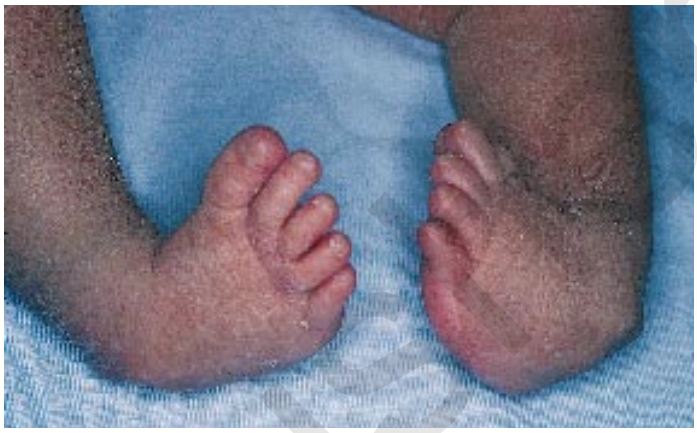

Figure 5.50. Bilateral clubfoot. The occurrence of club feet has been considered to be the result of a congenital malformation or a postural deformity. If the legs and feet are subjected to mechanical stress during the last weeks in utero, especially if the fetus is in the breech position, a clubfoot may develop. If the constraint has been relatively mild or brief, the deformity is usually flexible in that the foot can be manipulated into normal position. A fixed deformity implies either severe, prolonged immobilization with contractures of the ligaments and capsules of the joints or an intrinsic skeletal anomaly. This type is resistant to conservative treatment, and casting or surgery is the treatment of choice.

5.51

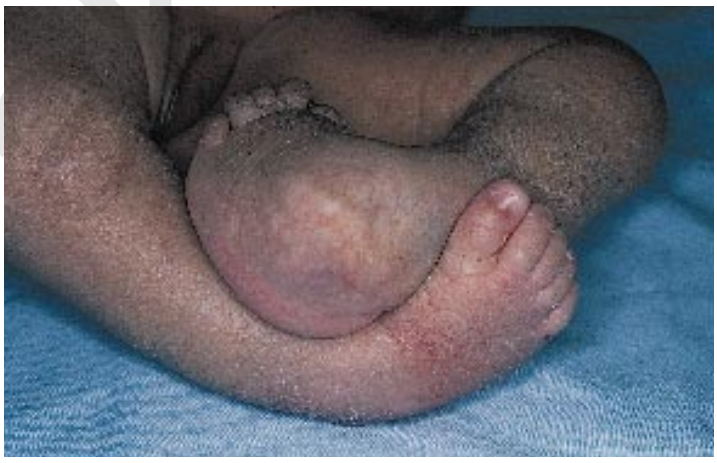

Figure 5.51. The same infant with the feet in their "position-of-comfort." Note the dimples at the ankles suggesting that this occurred as a result of a postural deformity. Some authors have suggested that the presence of dimples at the ankles in an infant with clubbing of the feet indicates that it has occurred as a result of a postural deformity.

5.52

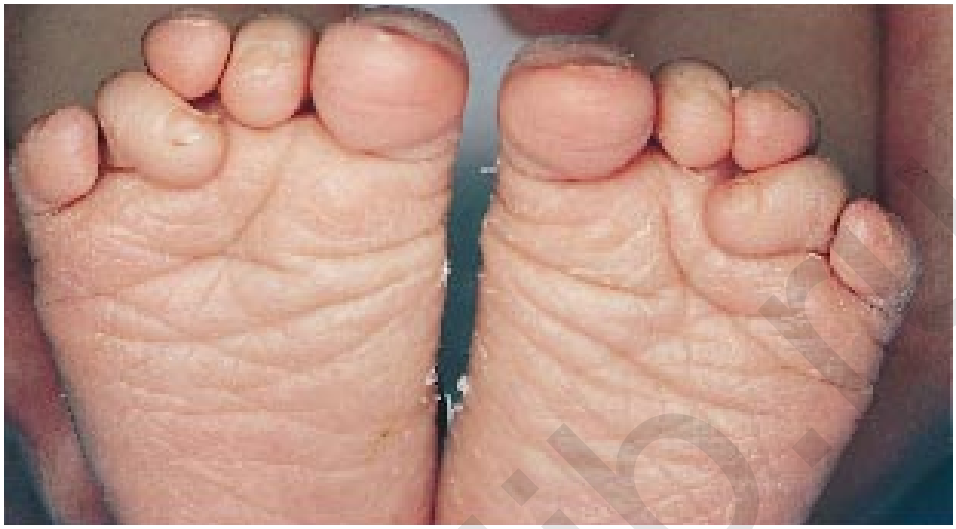

Figure 5.52. Congenital curly toes (overlapping toes) are a common finding in newborn infants. There is often a family history of the same finding in parents or siblings. Treatment is not necessary.

5.53

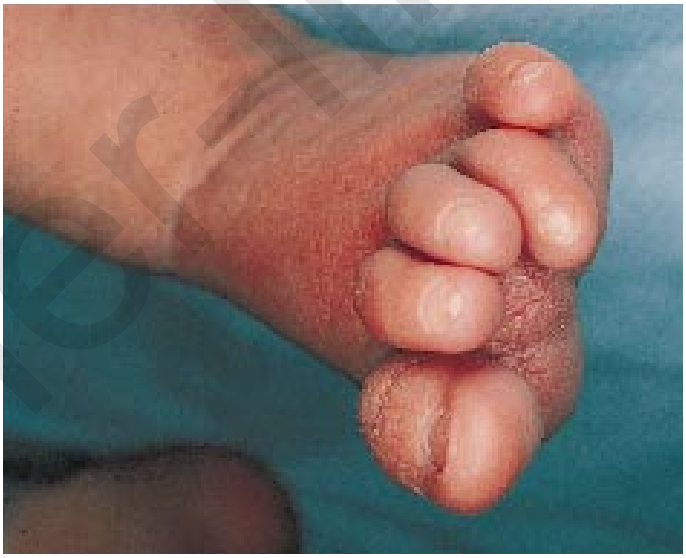

Figure 5.53. Another infant with congenital curly toes. The abnormality becomes less obvious as the infant grows.

5.54

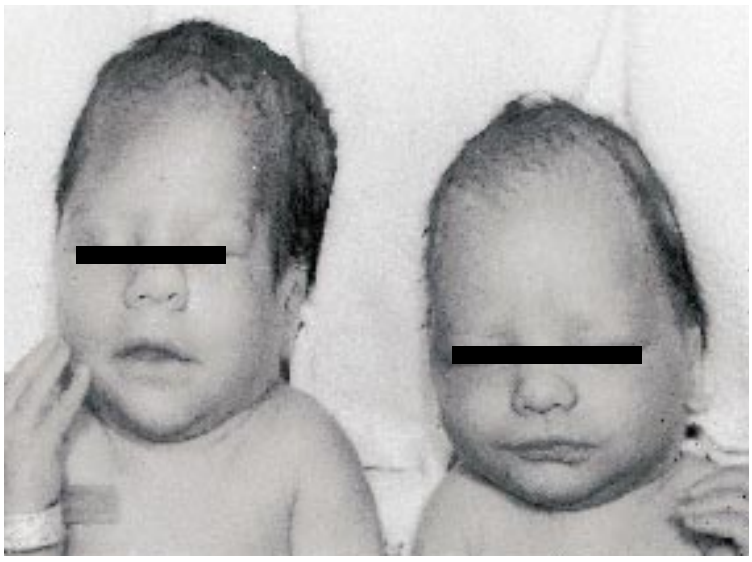

Figure 5.54. Twins with asymmetrical heads occurring as a result of an in utero positional deformity. Both infants were vertex presentations. Note how the heads "fit" together.

5.55

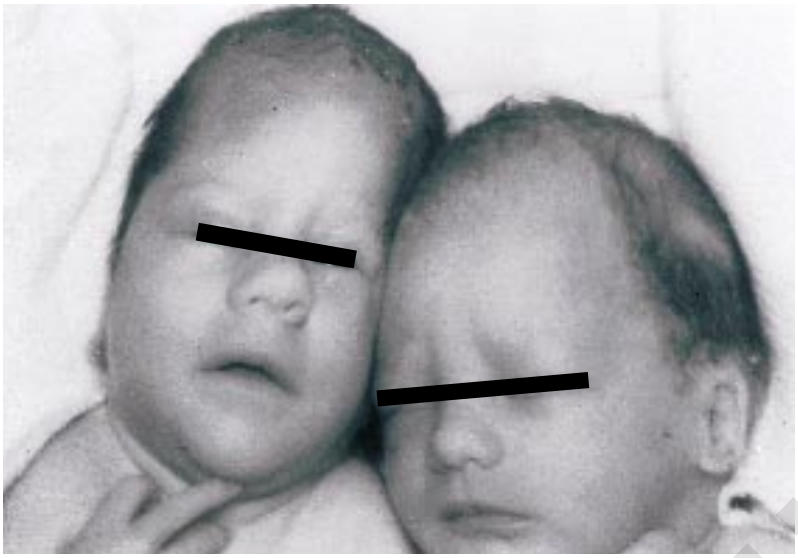

Figure 5.55. The same infants as shown in Figure 5.54 with their heads together (in utero position). As the infants grew the asymmetry improved.

5.56

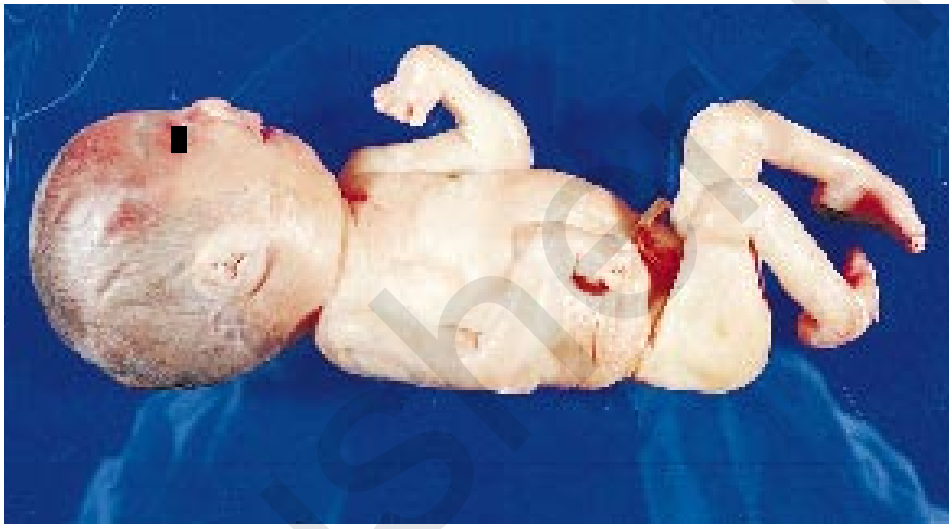

Figure 5.56. This infant with arthrogryposis demonstrates the severe congenital joint contractures. These occur as a result of lack of intrauterine movement and may be associated with muscle or neurologic pathology. Such severe contractures may be accompanied (or produced) by joint webbing (e.g., multiple pterygium syndrome or popliteal pterygium syndrome).

5.57

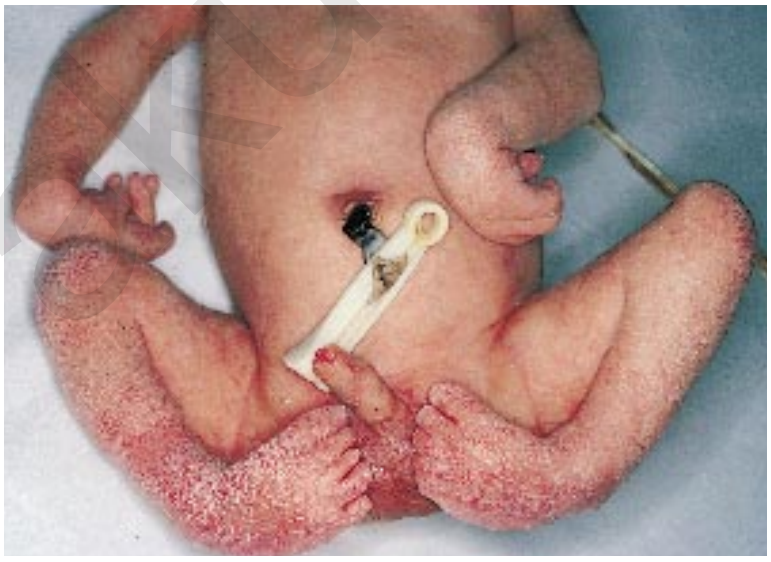

Figure 5.57. Frontal view of another infant with arthrogryposis. Extreme intrauterine compression over an extended period of time can produce such severe distortion in multiple joints that supporting ligaments become contracted and opposing tendons stretch. The muscles acting across these joints may atrophy, creating a picture indistinguishable from the intrinsic forms of arthrogryposis multiplex congenita.

5.58

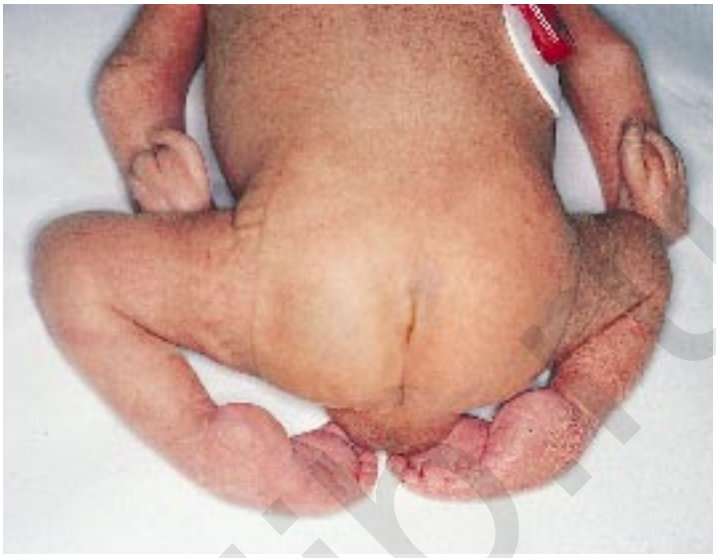

Figure 5.58. Posterior view of the arthrogryposis in the same infant as in Figure 5.57.

5.59

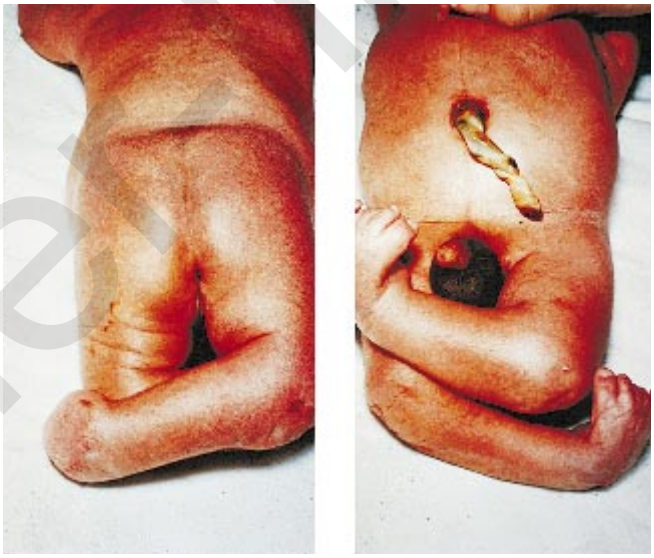

Figure 5.59. This infant is an example of arthrogryposis with joint contractures involving the lower extremities only. The upper extremities were normal. This may occur in infants with neural tube defects, caudal regression syndrome and muscle disease.

5.60

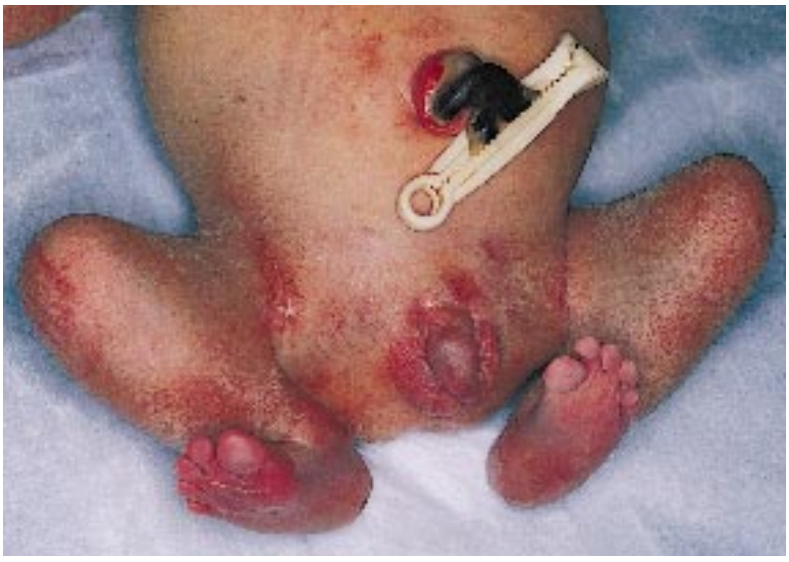

Figure 5.60. An infant with the caudal regression syndrome resulting in arthrogryposis. Note the marked underdevelopment of the hips and the webbing at the joints. There is also talipes calcaneovalgus.

5.61

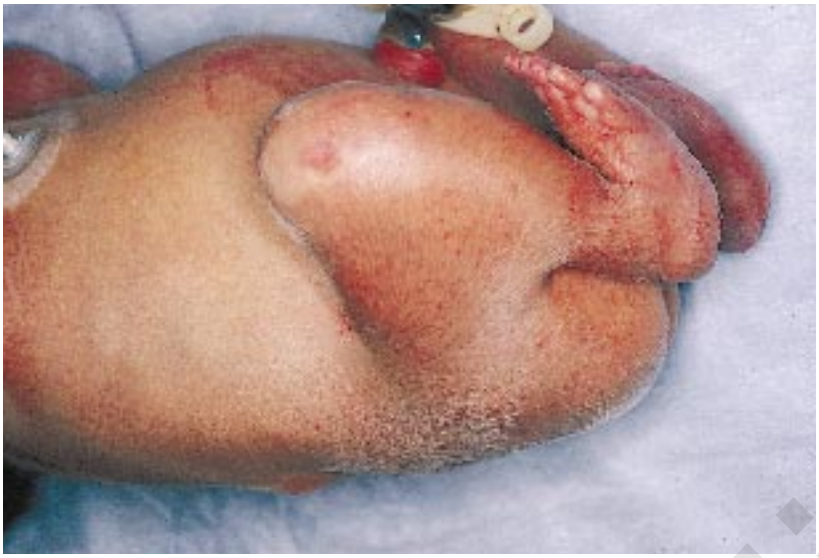

Figure 5.61. Lateral view of the same infant shows the marked underdevelopment of the hips, the arthrogryposis, webbing, and the dimples at the joints due to lack of movement. Note the talipes calcaneovalgus.

5.62

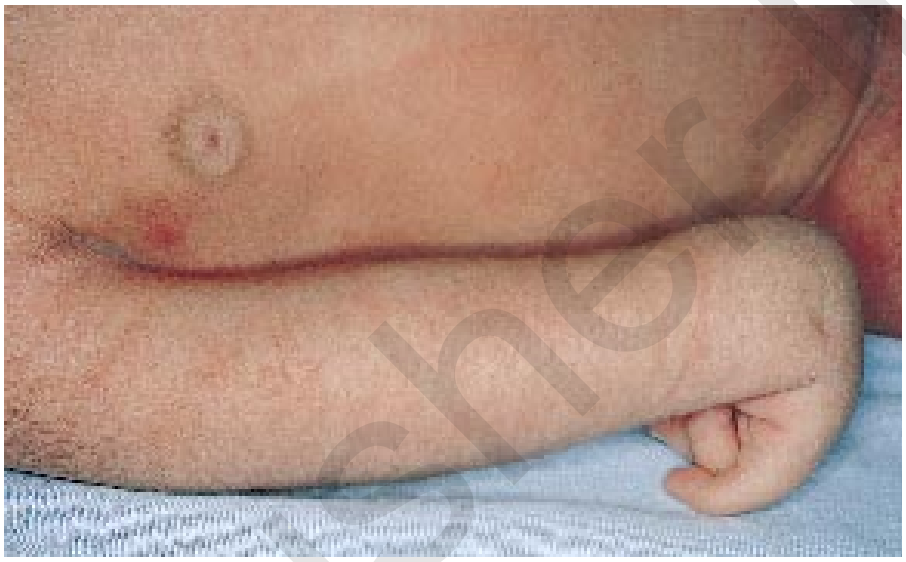

Figure 5.62. An infant with an amyoplasia congenita disruptive sequence. In this condition the elbows are usually in extension with the wrists and hands flexed.

5.63

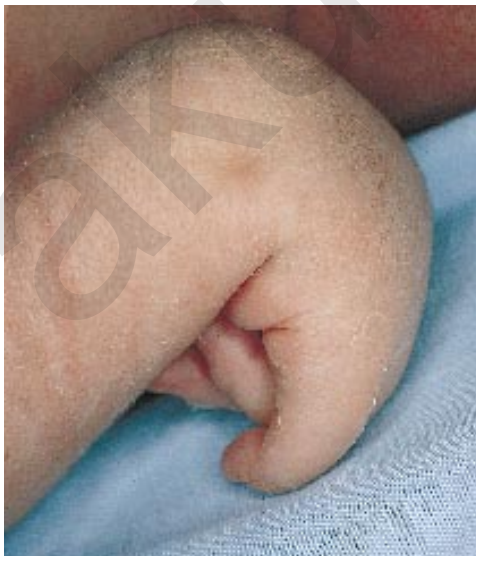

Figure 5.63. The same infant showing a close-up of the right wrist and hand. Note the dimples at the contracture site. In this condition there may be cord wrapping of the limb and amniotic bands.

5.64

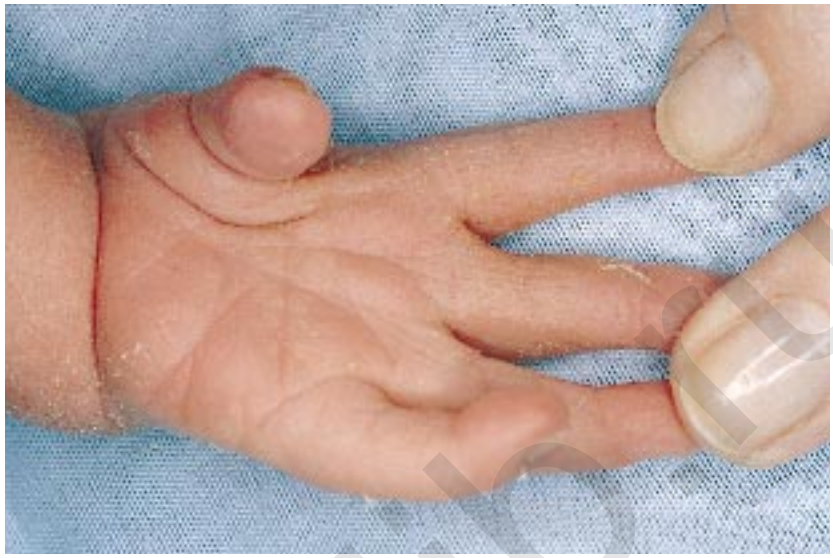

Figure 5.64. This figure shows the left hand of the same infant. Note the lack of development of the finger and hand creases. Lack of development of the creases indicates lack of fetal movement of the fingers occurring before the 10th to 12th week of gestation.

5.65

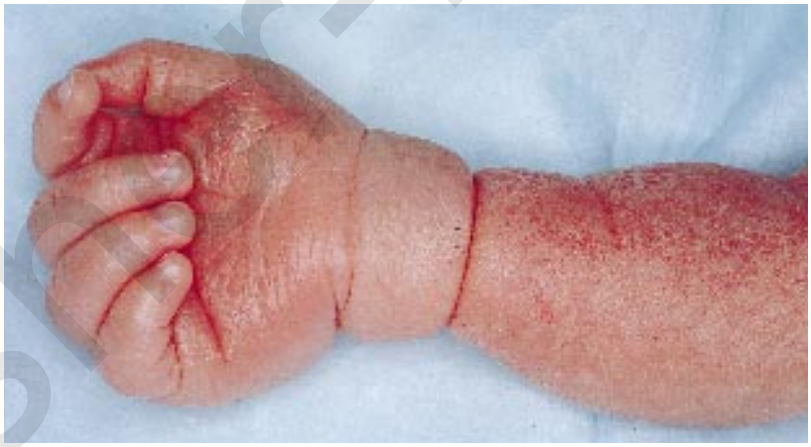

Figure 5.65. There is an intrauterine constriction band at the right wrist in this infant. Shallow constricting rings can encircle a limb at any level and destroy subcutaneous tissue sometimes producing distal edema. Amniotic bands may result in constriction or amputation (partial or complete) of extremities and are thought to occur as a result of an active fetus pushing an extremity through and tearing the amnion. This represents an example of *T*he *E*arly *A*mnion *R*upture *S*pectrum (TEARS).

5.66

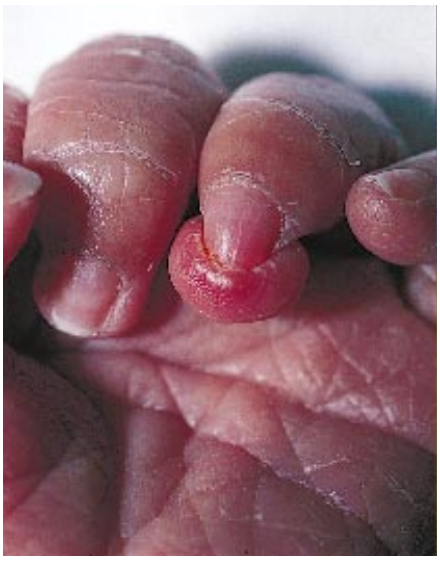

Figure 5.66. The congenital anomaly of the fourth finger of the left hand in this infant is due to an amniotic band. Also note the collodion appearance of the skin of this postmature infant. The hands and feet (and especially the digits) are the most common sites of damage from amniotic bands. If there is mild constriction, distal edema is produced; with more severe compression there can be disruption of tissue down to the periosteum with eventual loss of the distal avascular portion – a congenital amputation. The findings in such infants are bizzare and very variable.

5.67

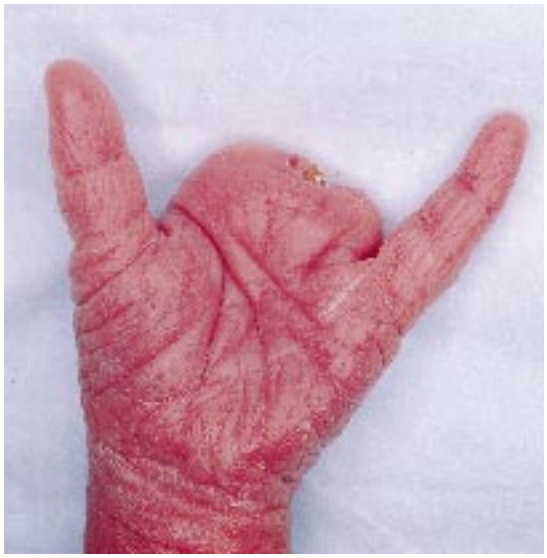

Figure 5.67. An infant with amputation of the second, third and fourth fingers occurring as a result of intrauterine constriction bands. At birth, the amputation site will be scarred and sometimes bands of fibrous tissue still will be attached to the injured area. The damage is usually asymmetric with digits affected at different levels and, occasionally, several digits will be bound together at the tips by scar tissue producing a form of pseudosyndactyly.

5.68

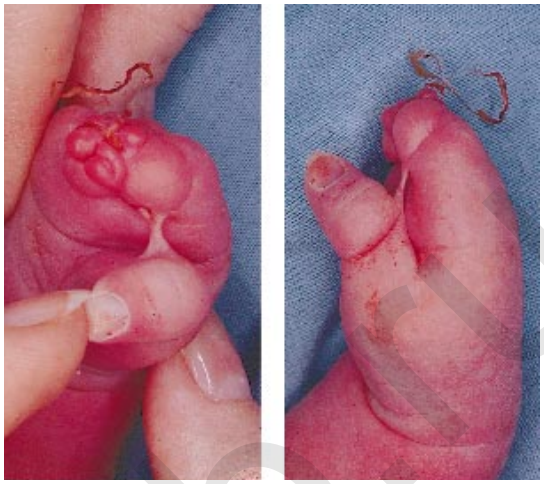

Figure 5.68. The amniotic band syndrome in this infant resulted in amputated fingers, intrauterine constriction bands and fusion of the amputated digits.

5.69

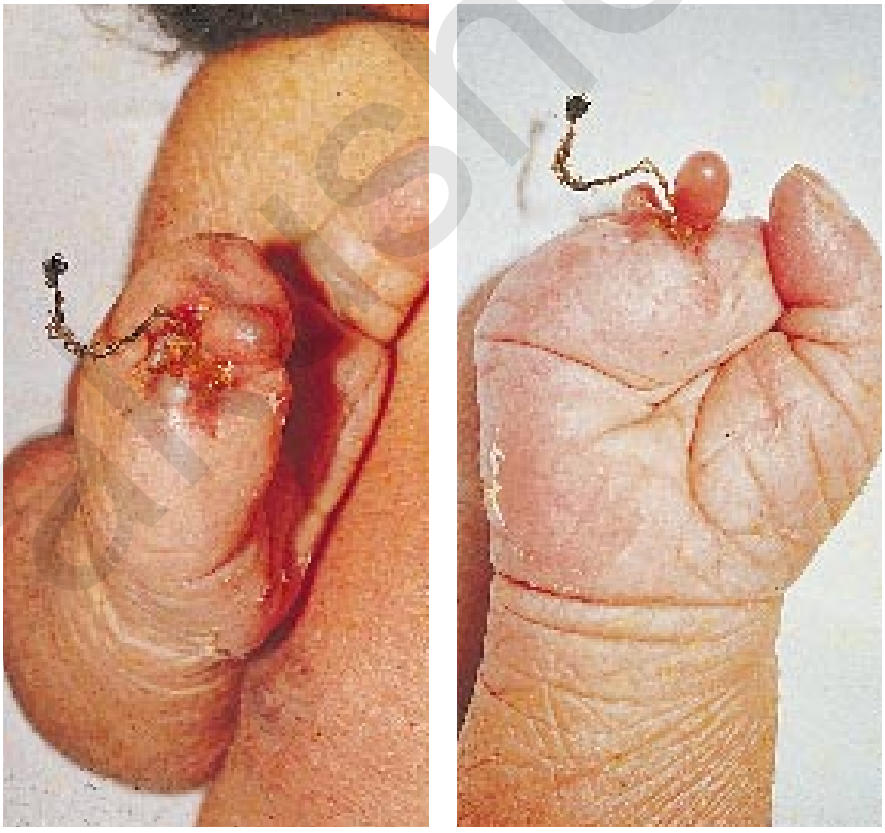

Figure 5.69. Another example of the amniotic band syndrome in which the amputated digits, raw areas and strand of amnion on the right hand can be seen.

5.70

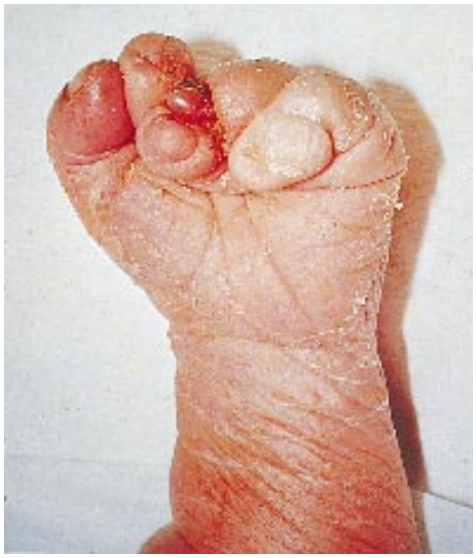

Figure 5.70. This figure of the same infant as shown in Figure 5.69 shows the involvement of the left hand as a result of the amniotic band syndrome.

5.71

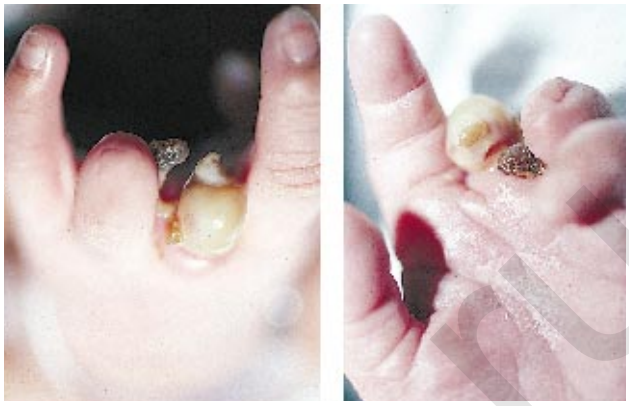

Figure 5.71. Amniotic bands involving the fingers of an infant. Note the amputated fourth finger and the constriction involving the base of the third finger resulting in gangrene.

5.72

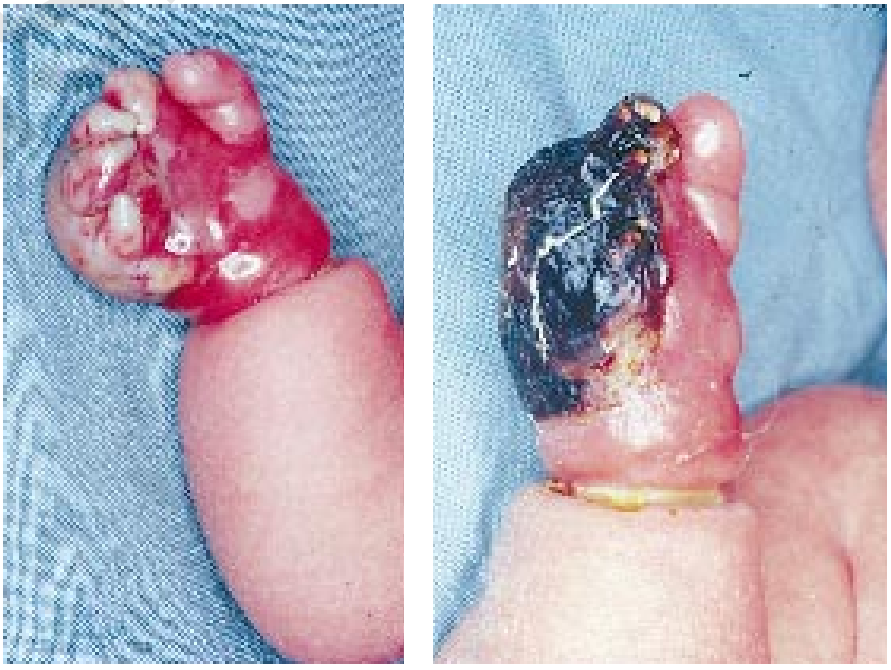

Figure 5.72. An intrauterine constriction band at the right wrist resulted in marked obstruction of circulation to the hand. Note that at the site of constriction a band has been removed, but because of the distal involvement of the circulation, the condition worsened and the infant eventually required amputation.

5.73

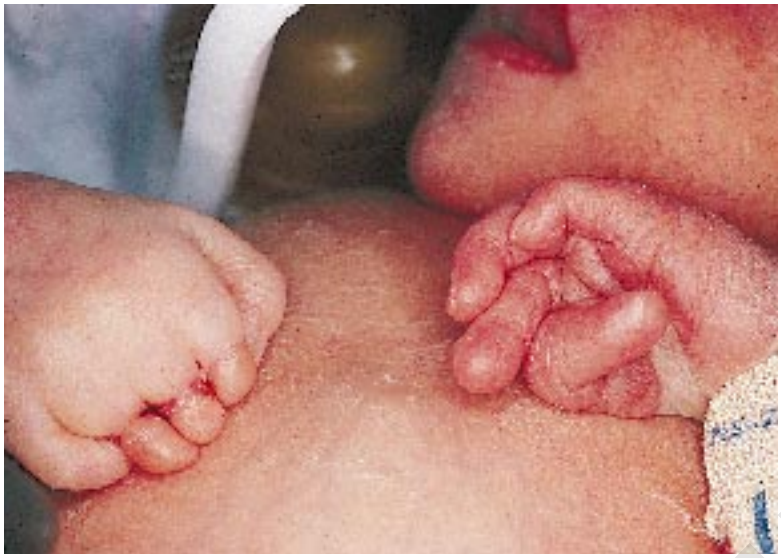

Figure 5.73. In this infant there is a disruption of the right hand due to constriction bands resulting in amputations of the second, third, and fourth fingers. Note the congenital absence of the thumb in the left hand, which was not a disruption but occurred as a result of a true congenital malformation.

5.74

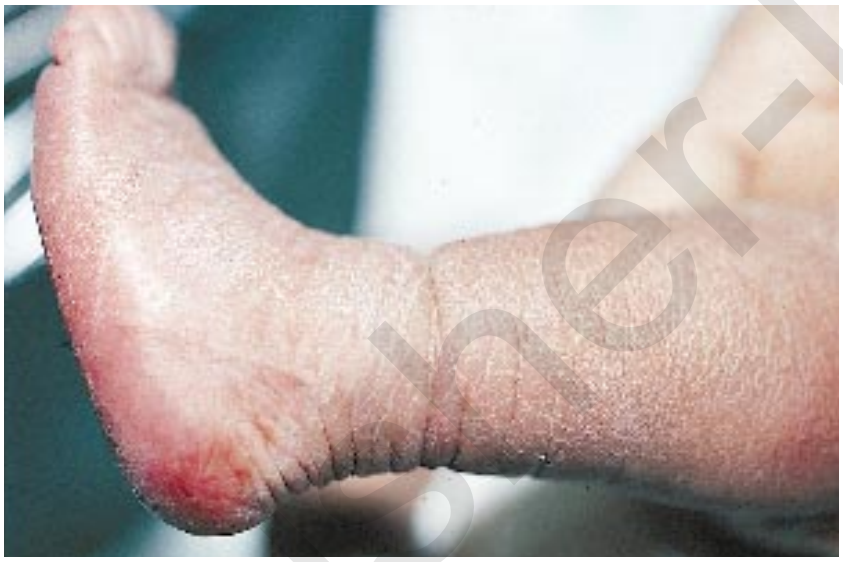

Figure 5.74. There is a minimal amniotic band at the distal part of the right foot of this infant. It should be noted that this type of finding could easily be missed on examination.

5.75

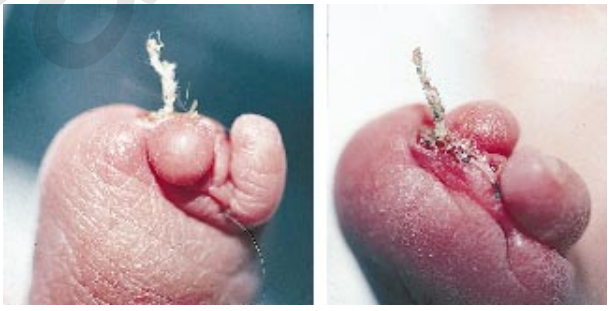

Figure 5.75. In this same infant shown in Figure 5.74 there were severe amniotic bands of the fingers and toes. Note the strands of amnion.

5.76

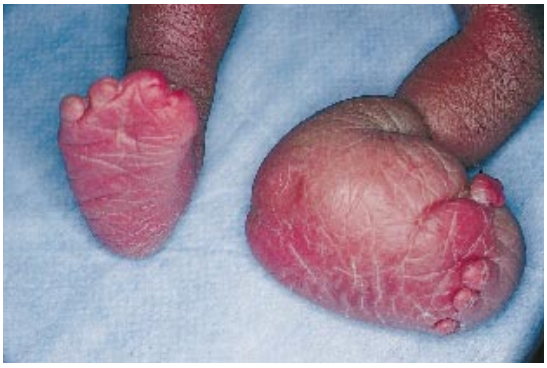

Figure 5.76. Intrauterine constriction bands (amniotic bands) may disrupt tissue growth and result in partial or complete amputation. In this infant there was amputation of the toes but a severe constriction band interfered with circulation of the left leg. Note the marked distal swelling of the left leg.

5.77

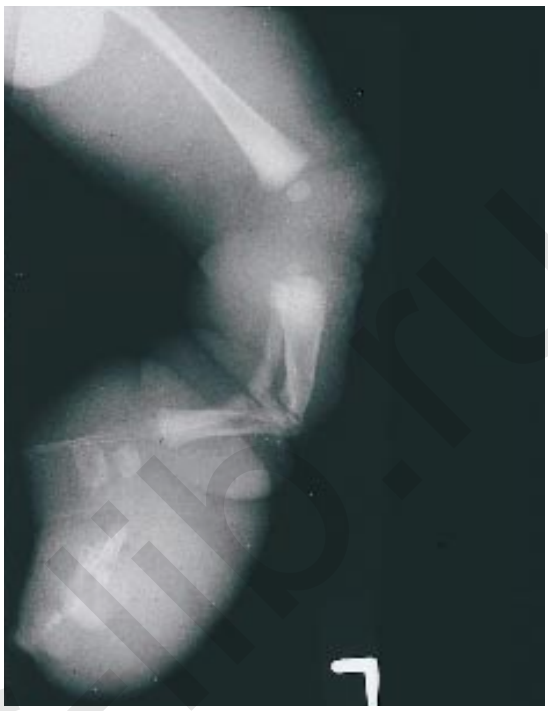

Figure 5.77. Radiograph of the same infant shown in Figure 5.76, showing marked bowing and fracture of the tibia and fibula of the left leg as a result of the constriction band. Also note the severe tissue swelling of the foot.

5.78

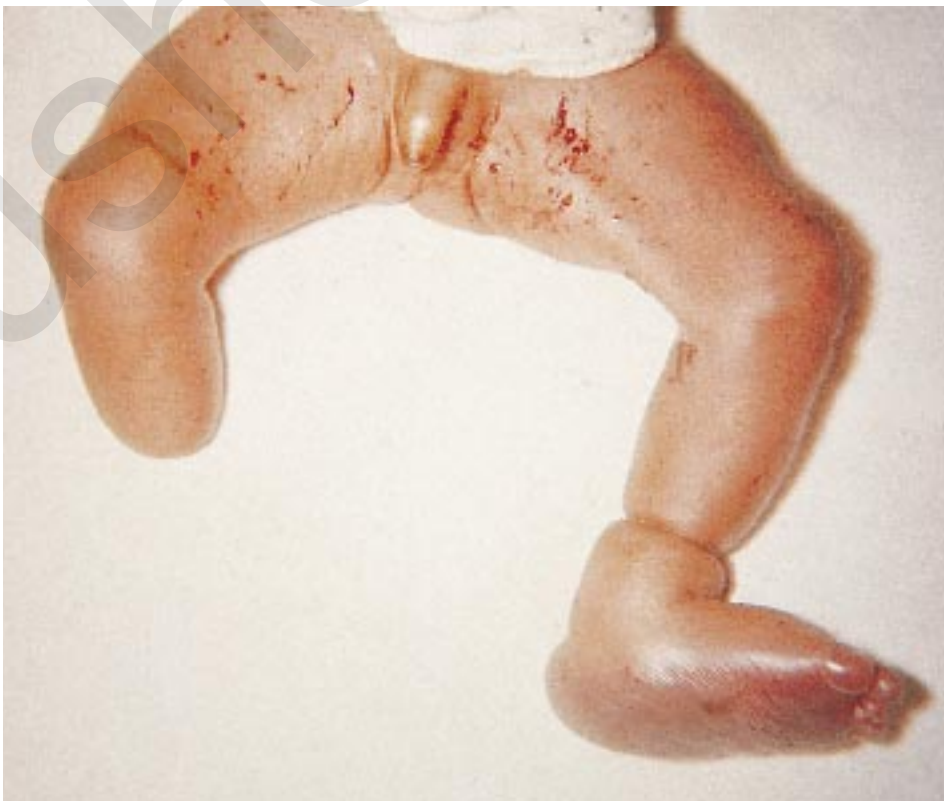

Figure 5.78. An intrauterine amputation of the right leg and a constriction band of the left leg were noted in this infant at birth. If there is a congenital amputation, consideration should be given to whether the amputation is a primary or secondary limb reduction defect. This is an example of a secondary limb reduction defect.

5.79

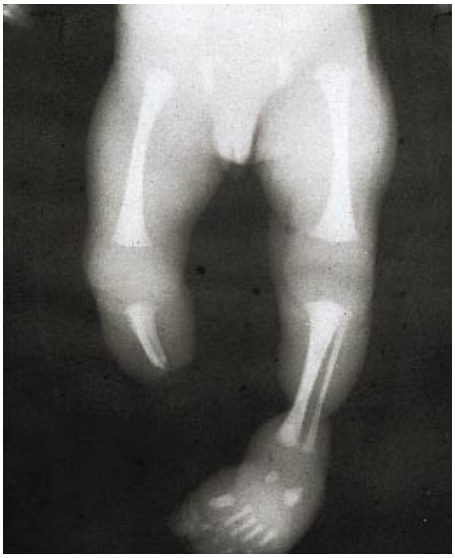

Figure 5.79. A radiograph of the same infant as shown in Figure 5.78 showing the amputation of the right leg. Note the soft tissue constriction of the distal left leg.

5.80

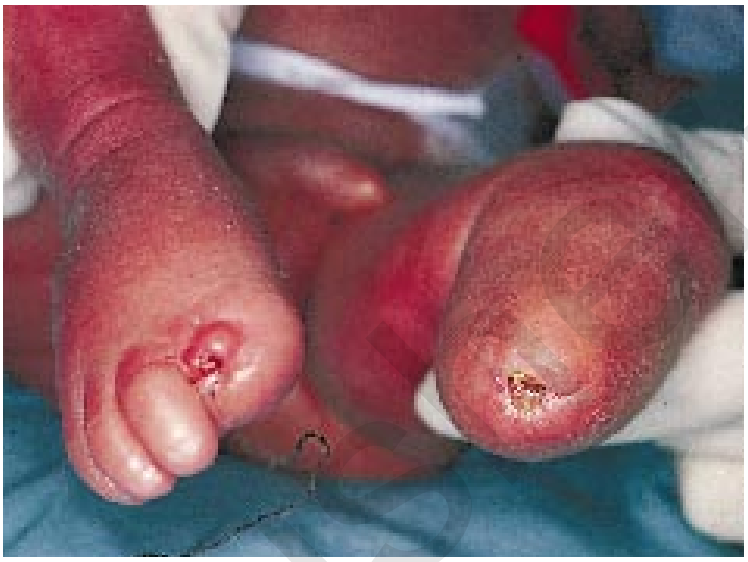

Figure 5.80. Another example of congenital amputation of the left leg and the toes of the right foot by amniotic bands. In primary limb reduction defects, the skin at the amputation is smooth and there is underlying subcutaneous tissue. In secondary limb reduction deformities, the skin shows ulceration or scarring and has no underlying subcutaneous tissue. Radiography shows the stump of the bone is smooth in primary limb reduction defects and the stump of the bone is jagged in secondary defects.

5.81

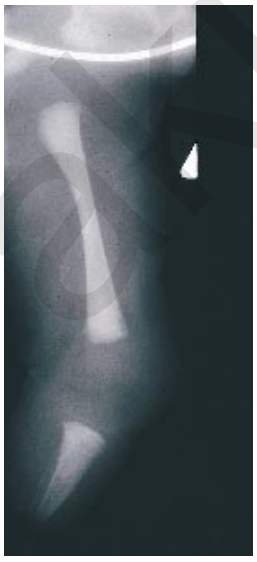

Figure 5.81. A radiograph of the same infant shown in Figure 5.80 showing the congenital amputation of the left leg at the site of the amniotic band.

5.82

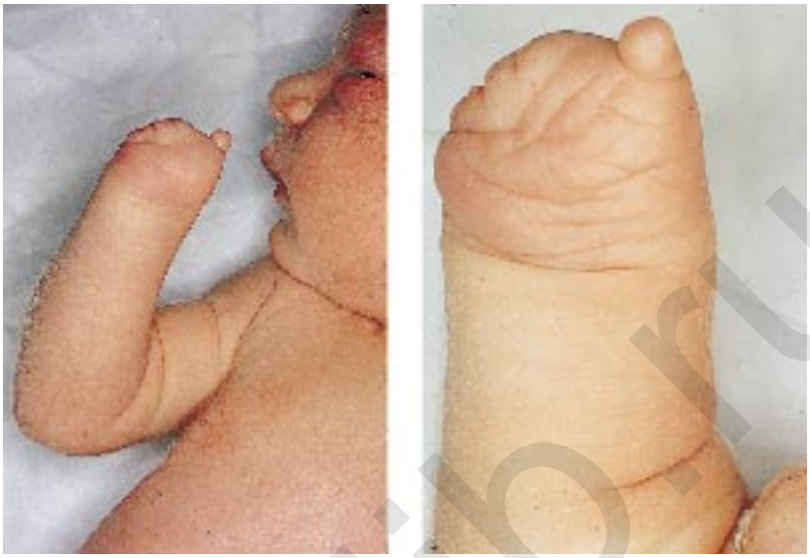

Figure 5.82. Congenital amputation of the right hand. This is a primary limb reduction defect.

5.83

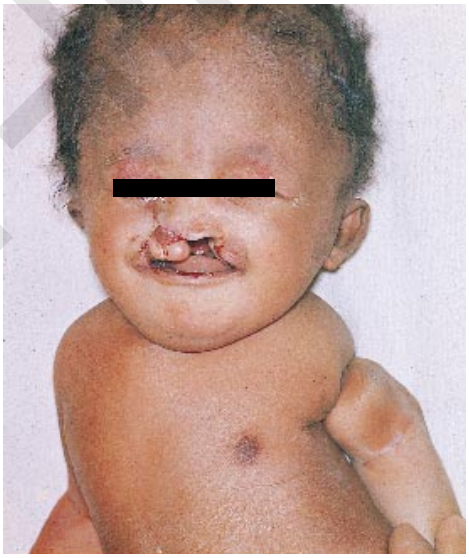

Figure 5.83. This infant presented with multiple anomalies including a bilateral cleft lip and palate, partial amputation of the right arm, and a congenital scalp defect.

5.84

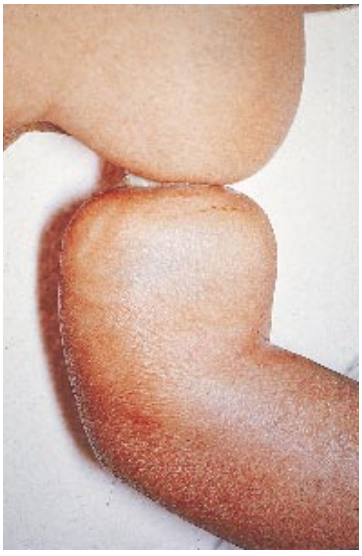

Figure 5.84. In the same infant shown in Figure 5.83, note the amniotic band constriction down to the bone almost resulting in amputation of the right arm.

5.85

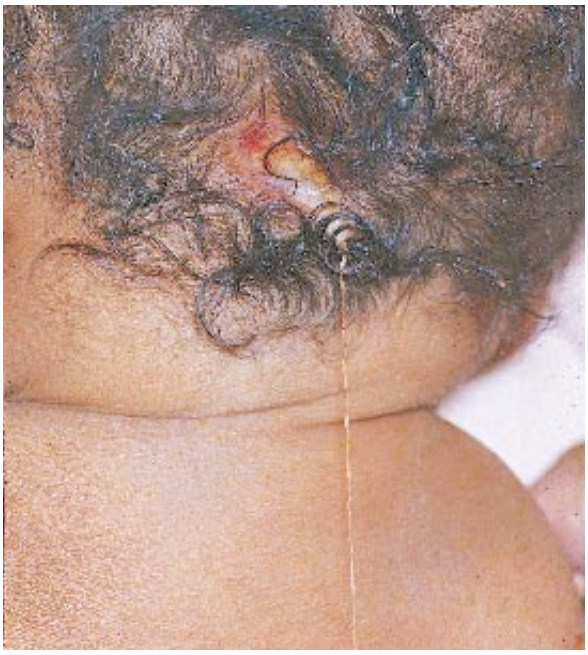

Figure 5.85. The same infant as in Figures 5.83 and 5.84 showing the congenital scalp defect in the occipital area. Note the strand of amnion attached to the defect.

5.86

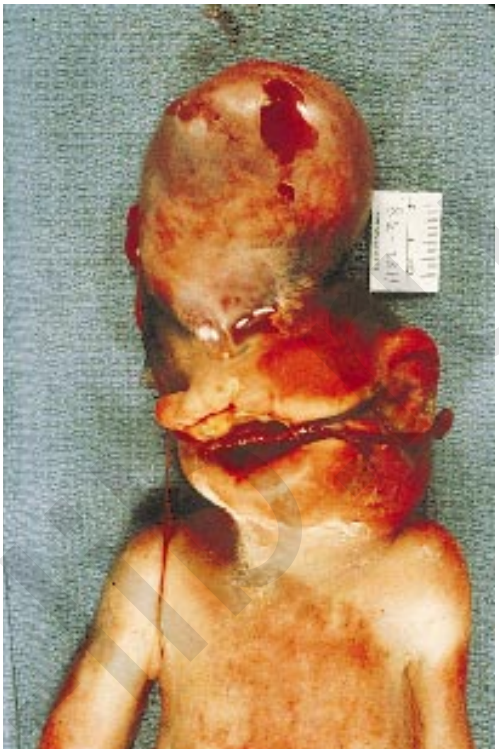

Figure 5.86. The early amnion rupture spectrum (TEARS) in this infant shows the bizarre findings involving the face and head. There is a skin defect of the scalp with an encephalocele and gross malformation of the face. The ADAM complex is an example of TEARS. The complex includes *A*mniotic *D*eformities, *A*dhesions, and *M*utilations. Findings in the ADAM complex include cleft lip, bizarre midfacial clefts, central nervous system abnormalities (hydrocephalus, microcephaly, asymmetric encephalocele), gastrointestinal abnormalities (omphalocele, gastroschisis), and ocular abnormalities (coloboma, anophthalmia, corneal opacity).

5.87

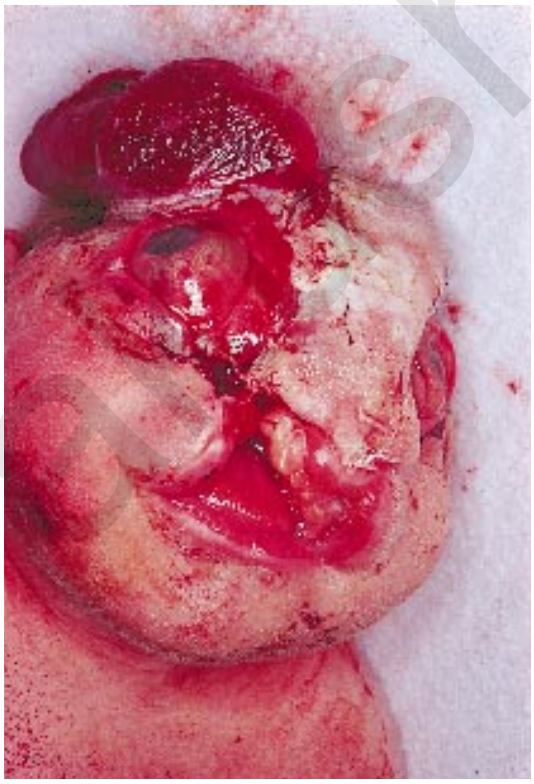

Figure 5.87. This infant is another example of the early amnion rupture spectrum. Note the asymmetric encephalocele in addition to the bizarre anomalies of the face and eye. In general, encephaloceles are midline and an asymmetric encephalocele is always suggestive of a disruption.

5.88

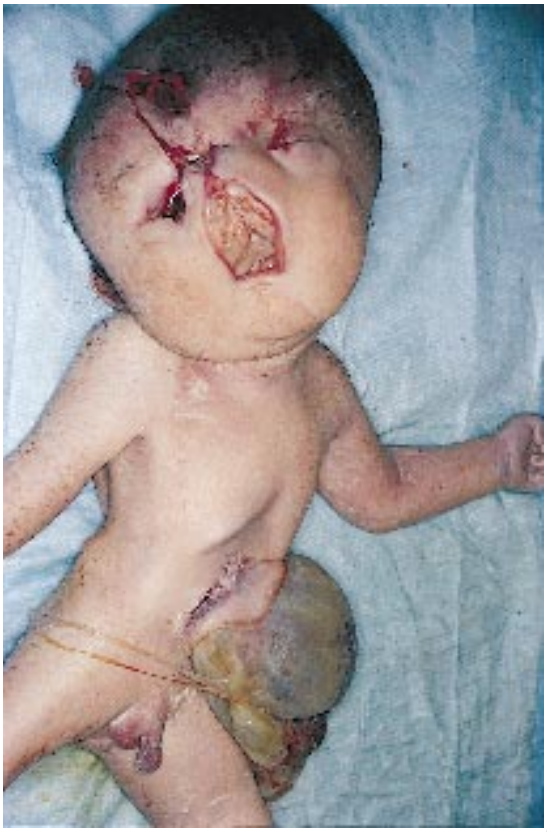

Figure 5.88. This infant with TEARS has bizarre facial clefting, a central nervous system defect, an abdominal wall defect, and limb defects.

5.89

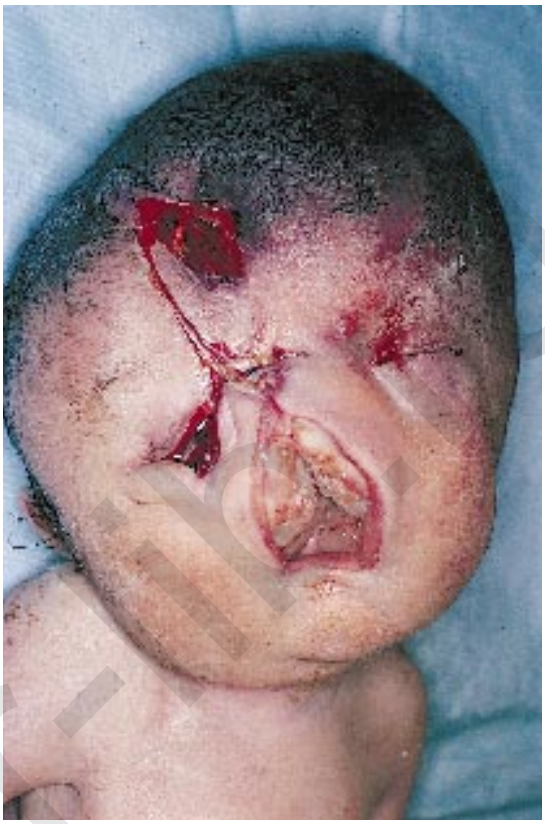

Figure 5.89. A close-up of this infant showing the bizarre facial clefting and a strand of amnion extending from the right eye to the scalp defect. Also note the severe defect of the mouth and palate. In general, bizarre facial clefting (oblique facial clefting) is noted in disruptions whereas lateral or transverse facial clefts occur in infants with syndromes (e.g., Goldenhar's syndrome).

5.90

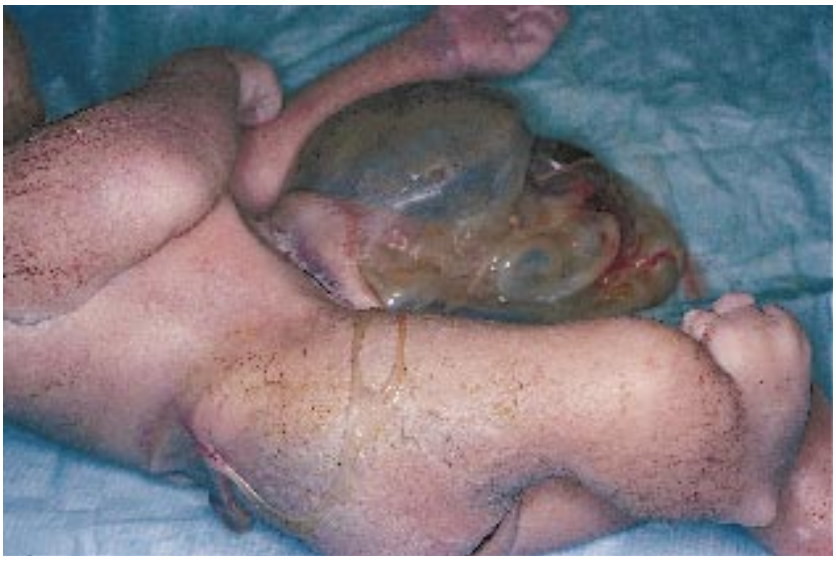

Figure 5.90. The same infant showing the abdominal wall defect (omphalocele) and strands of amnion extending from this to the central nervous system malformation.

5.91

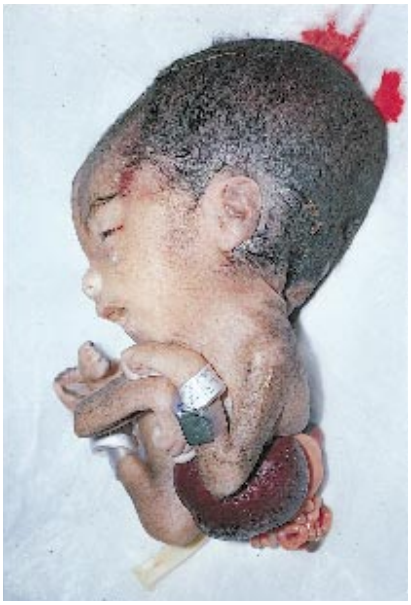

Figure 5.91. The early amnion rupture spectrum caused a limb/body wall deficiency with spine and central nervous system defects in this infant. Note the hydrocephalus.

5.92

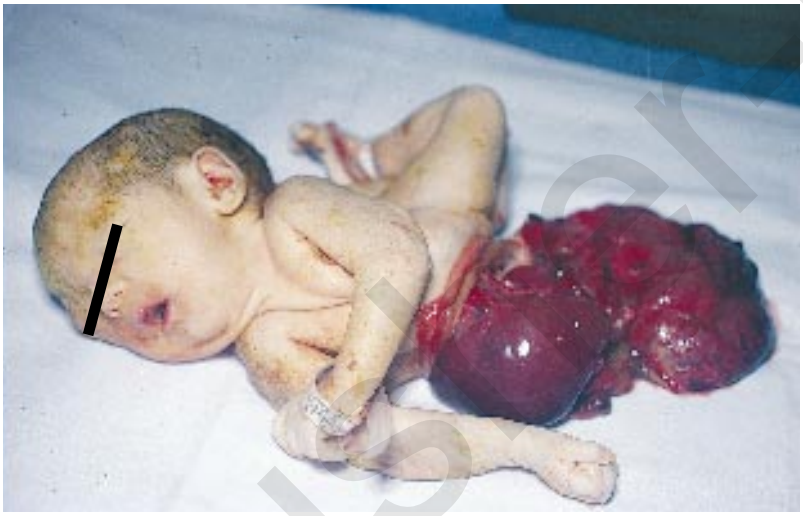

Figure 5.92. The limb/body wall deficiency in this infant caused a severe thoracoabdominal wall defect. Note the severe scoliosis and kyphosis and the short umbilical cord with the placenta attached to the abdominal viscera.

5.93

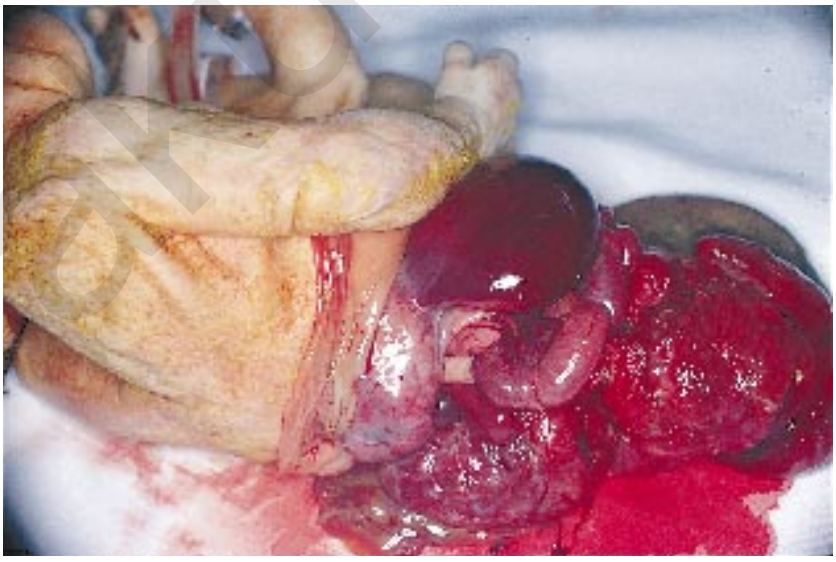

Figure 5.93. A close-up showing the right lung and the eviscerated abdominal organs with the placenta attached.

5.94

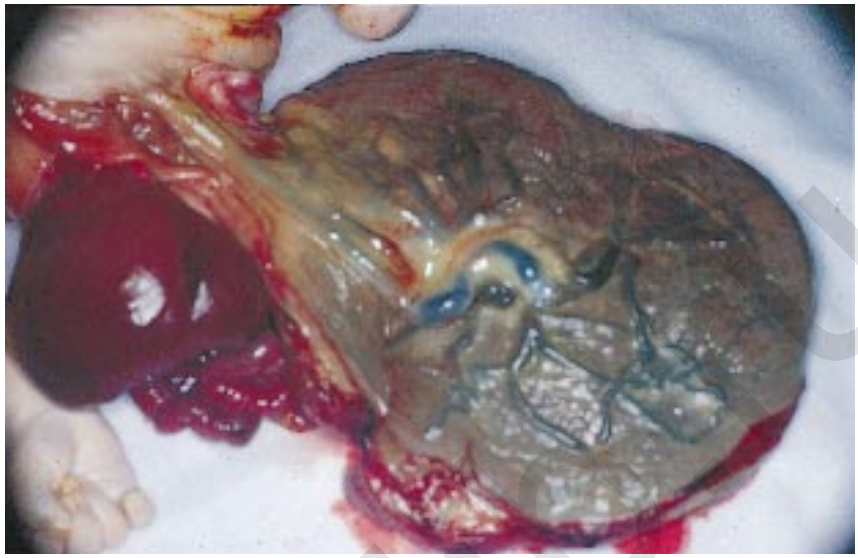

Figure 5.94. Another view showing the short umbilical cord.

5.95

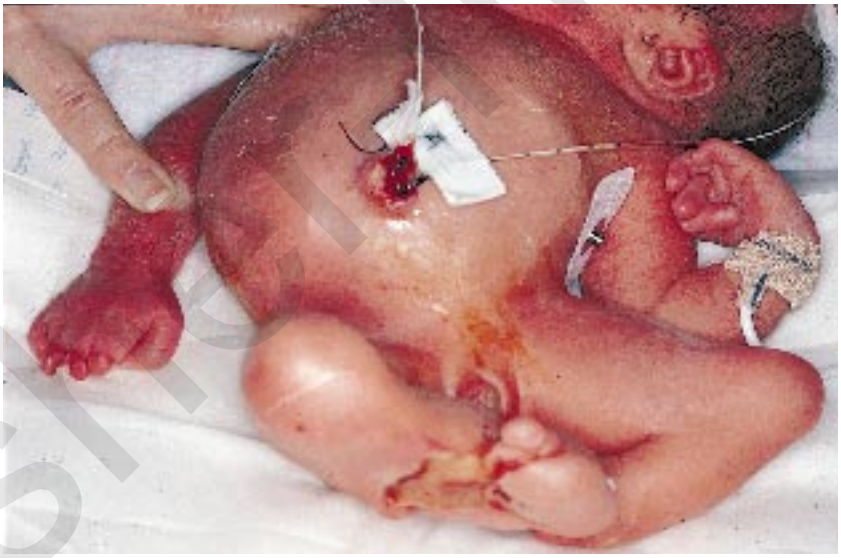

Figure 5.95. In this infant with disruption, there is severe scoliosis and the placenta was attached to the right leg. The striking difference between this infant and the other examples of disruption is that this infant also had congenital malformations.

5.96

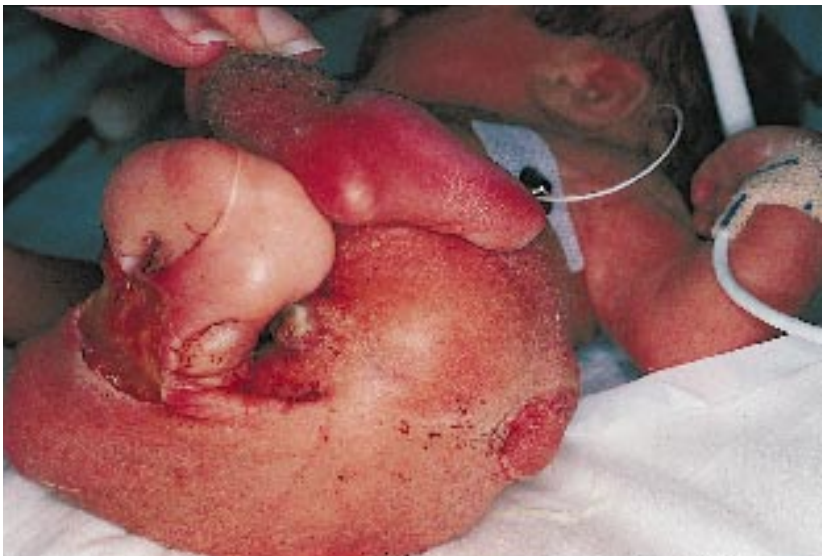

Figure 5.96. In the same infant, note that the disruption involved the lower extremities and the right hand but the infant also had an imperforate anus, lumbar spine defect and dextrocardia, plus a patent ductus arteriosus. Congenital anomalies include malformations, disruptions, and deformations. This figure should alert one to the fact that any combination of these can occur.

5.97

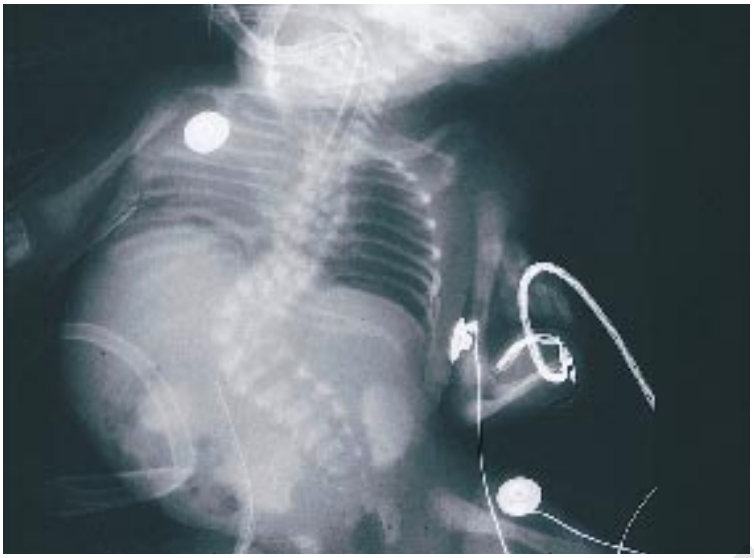

Figure 5.97. A radiograph of the same infant as in Figures 5.95 and 5.96 shows the dextrocardia, abnormalities of the ribs, and abnormal segmentation of the thoracolumbar vertebrae. In this infant the kyphosis and scoliosis was caused by both the malformation of the spine and the disruption.

5.98

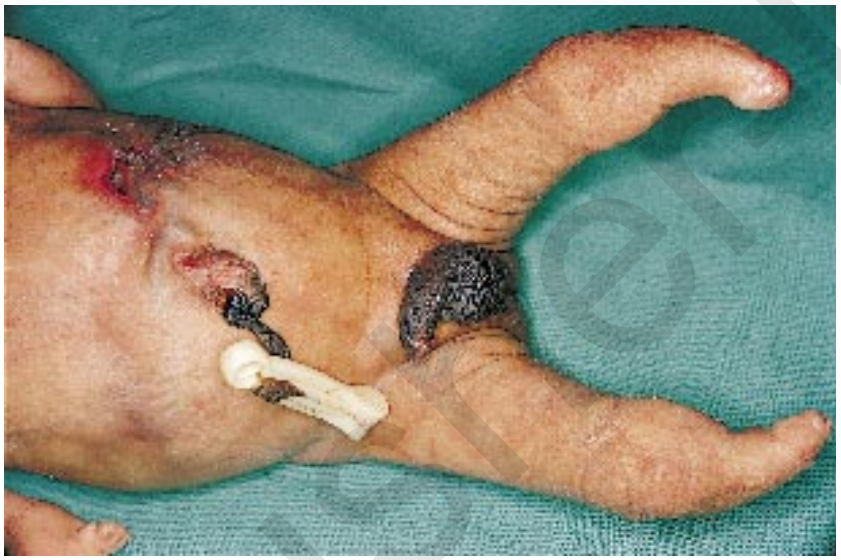

Figure 5.98. The typical reduction sequence of limb reduction anomalies and scalp and skin defects are noted in this infant with Adams-Oliver syndrome.

5.99

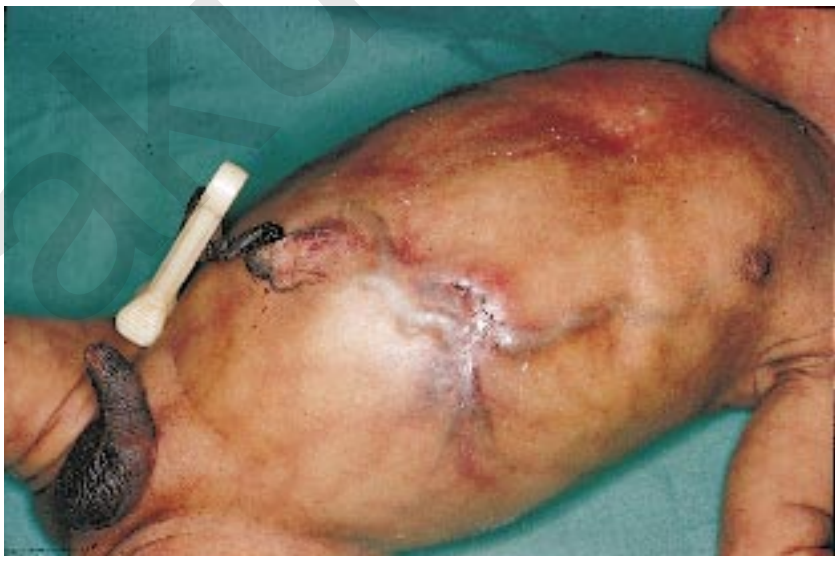

Figure 5.99. Close-up of the skin defect of the abdominal wall in the same infant.

5.100

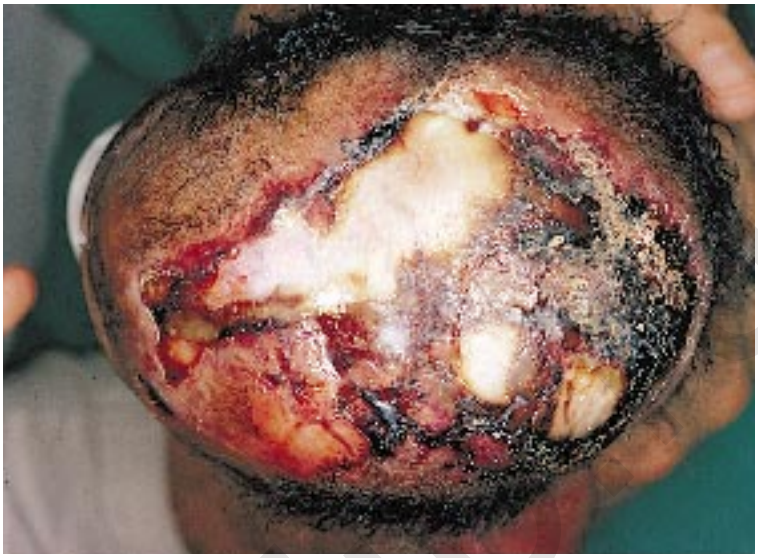

Figure 5.100. Close-up of the scalp defect in the same infant as in Figures 5.98 to 5.99.

5.101

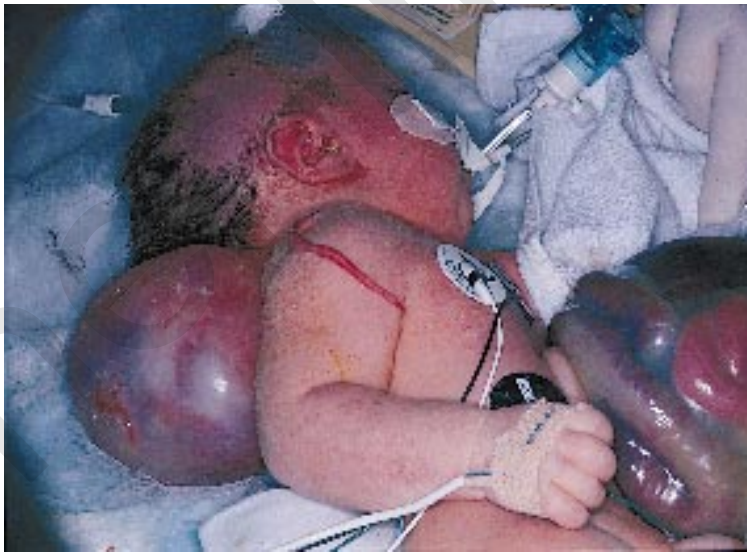

Figure 5.101. The early amniotic rupture spectrum in an infant with a cervical meningomyelocele and an omphalocele. Note the amniotic band extending across the right shoulder. There was an amniotic band 1 cm proximal to the left ankle.

5.102

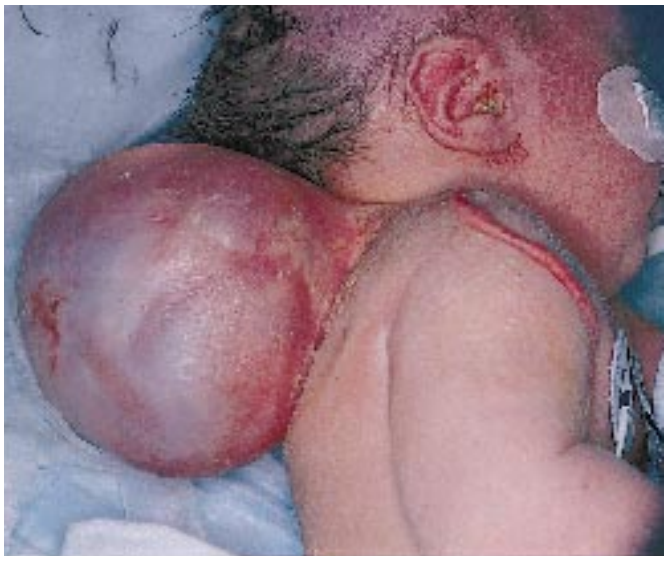

Figure 5.102. A close-up of the cervical meningomyelocele in the same infant. Note the amniotic band extending across the right shoulder.

5.103

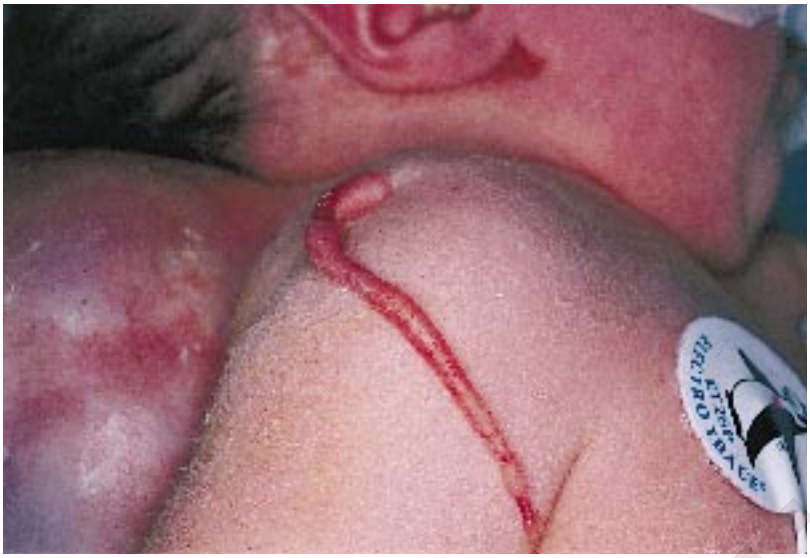

Figure 5.103. A close-up of the amniotic tissue band over the right shoulder in the same infant as shown in Figures 5.101 and 5.102.

Chapter 6
Fetal Growth and Assessment of Gestational Age

The normal term infant has completed a gestation of ≥ 37 weeks and has a birth weight ≥ 2500 g. Accurate dating of pregnancy is important in evaluating the abnormally grown infant at birth. There are two different populations of low birthweight infants, those who are 1) born premature in gestation (i.e, at < 37 weeks); or 2) small for gestational age (SGA). Infants are SGA for one of two reasons: 1) a normal intrauterine environment but abnormal development due to fetal factors (i.e., chromosomal abnormalities); or 2) an abnormal uterine environment (i.e., maternal toxemia, heart disease, etc.) leading to abnormal growth.

Many criteria have been used to estimate gestational age. Obstetrical factors employed to determine age include date of last menstrual period, auscultation of fetal heart tones (audible by Doppler at 10 weeks, and stethoscope at 20 weeks), quickening (first maternal perception of fetal movement usually occurring at 18 to 20 weeks), and fundal height (used to estimate fetal size during the first trimester). Ultrasonography with first trimester measurements of crown-rump length accurately estimates gestation ± 3 days. Up to 30 weeks gestation, measurements of the fetal biparietal diameter, femur length, and abdominal circumference are a reliable index of fetal size (body weight) and gestational age, but afterwards may be quite variable. Physical examination may also be used in assessing gestational age. Gestational age only indirectly measures maturity, and other measurements are needed to determine organ-specific maturity (e.g., amniotic fluid lactase/sucrase ratio > 2 for fetal lung maturity).

6.1A

	6 months 28 weeks	6½ months 30 weeks	7 months 32 weeks	7½ months 34 weeks	8 months 36 weeks	8½ months 38 weeks	9 months 40 weeks
1. Posture	Completely hypotonic	Beginning of flexion of thigh at hip	Stronger flexion	Frog-like attitude	Flexion of the four limbs	Hypertonic	Very hypertonic
2. Head to ear maneuver							
3. Popliteal angle	150°		110°	100°	100°	90°	80°
4. Dorsiflexion angle of foot			40–50°		40–50°		Premature reached 40wk 40° Full term
5. 'Scarf' sign	'Scarf' sign complete with no resistance		'Scarf' sign more limited		Elbow slightly passes midline		Elbow almost reaches midline
6. Return to flexion of forearm	Upper limbs very hypotonic lying in extension			Flexion of forearms begins to appear, but very weak	Strong 'return to flexion.' Flexion tone inhibited if forearm maintained 30 seconds in extension	Strong 'return to flexion.' Forearm returns very promptly to flexion after being extended for 30 seconds	

Passive tone. Increase of tone with maturity illustrated by means of six clinical tests. (From Amiel-Tison, C.: Arch. Dis. Child.,*43*:89,1968.)

6.1B

Gestational age	32wk	34wk	36wk	38wk	40wk
Lower extremity	Brief support	Excellent straightening of legs when upright			
Trunk	–	+ –	Transitory straightening	Good straightening of trunk when upright	
Neck flexors	No movement of the head.	[face view] Head rolls on the shoulder	Brisk movement head passes in the axis of trunk	Head maintained for a few seconds	Maintained in axis for more than a few seconds
Neck extensors	Head begins to lift but falls down	[profile view] Brisk movement head passes in the axis of trunk	Good straightening but not maintained	Head maintained for a few seconds	Maintained in axis for more than a few seconds

Active tone. Increase of tone with maturity illustrated by means of four tests of righting reactions. (From Amiel-Tison, C.: *In* Gluck, L. (ed.), Modern Perinatal Medicine, Chicago, Year book Medical Publishers, 1974, p. 347.)

Figure 6.1A & B. Many scoring systems have been devised to assess by exam the gestational age of infants at birth. The originals are shown here in figures A & B, published by Amiel-Tison. The Dubowitz examination is one of the most complete systems, combining the general physical examination performed in the first hours of life with the neurologic evaluation carried out when the infant is at least 24 hours old. The Ballard Method abbreviates the Dubowitz scoring system and uses only 12 physical and neurologic criteria. Statistically, however, the Ballard is as accurate in assessing gestation age (± 2 weeks) as more thorough examinations and is most useful in the busy clinical setting.

6.2

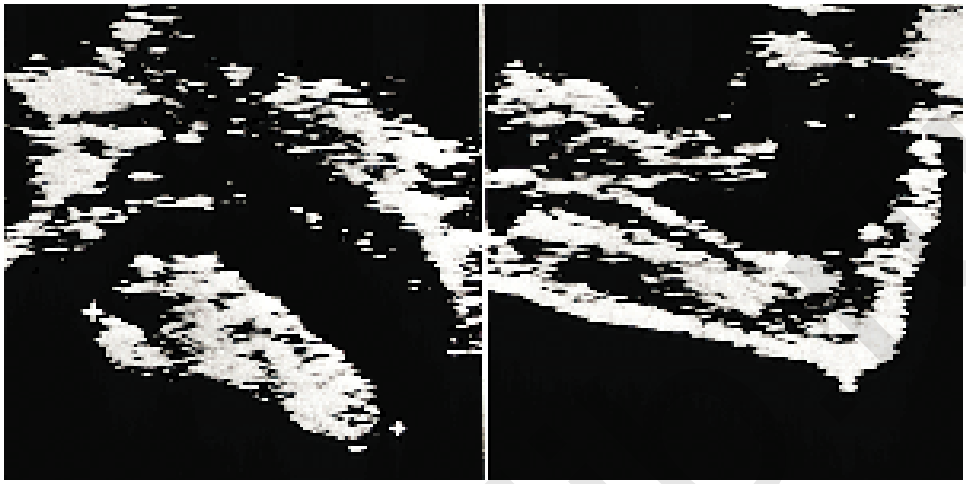

Figure 6.2. A prenatal ultrasound examination showing a view of a foot. Foot length on prenatal ultrasound has been shown to correlate well with gestational age.

6.3

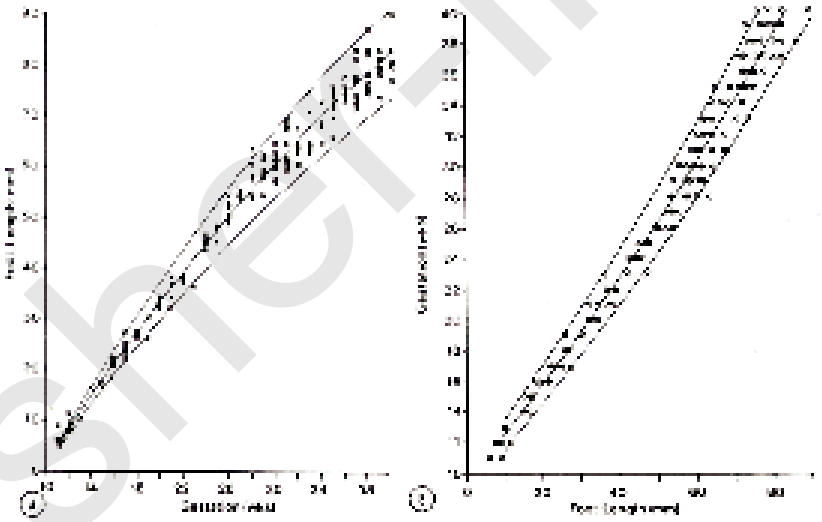

Figure 6.3. Graphic representation of the correlation between fetal foot length and gestational age. (Mercer et al. Scatter plots of ultrasonic feetus. gestational age. AM J Obstet Gynecol 1987; 156:350 Mosby Year Book, used with permission)

6.4

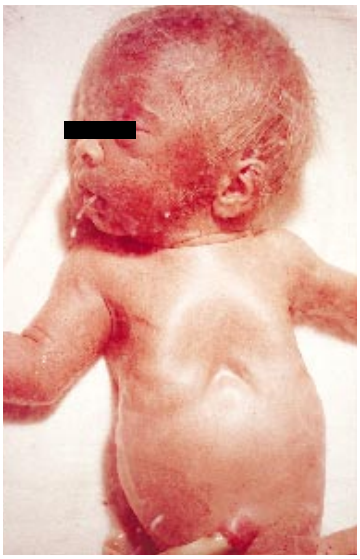

Figure 6.4. The premature infant has a large head in relation to body size and the eyes are protruding due to disproportion between the size of the eyeballs and the orbital cavity. The skin is red to pink, shiny due to edema, transparent with highly visible arterioles and venules, and is covered by lanugo. Subcutaneous tissue is poorly developed. Scalp hair is sparse and straight. Vernix is not formed and no nipples or areolae are seen. Note that the infant lies flat on the bed, in a frog-leg position with shoulders, elbows, and knees all touching the mattress. The head is to one side or other, not in line with the trunk.

6.5

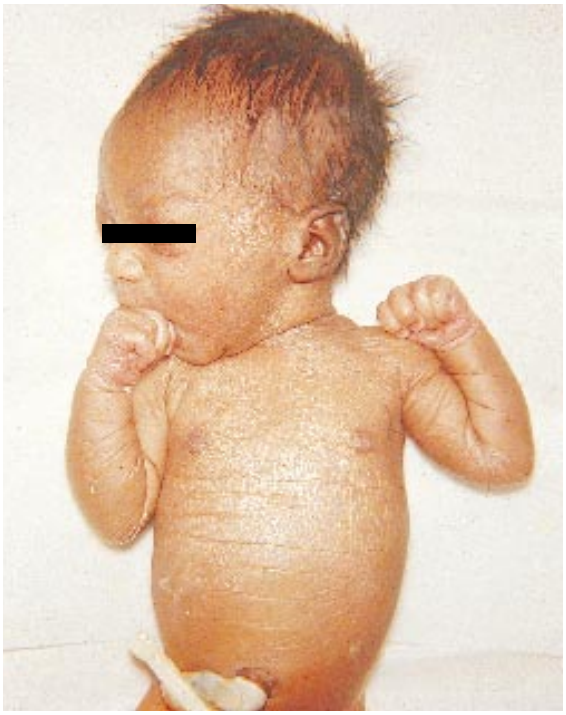

Figure 6.5. The postmature infant appears long and skinny due to decreased subcutaneous fat stores with advancing gestation near term. The skull is hard because the sutures have started to fuse. Note the wizened facies and alert expression typical of the post-term baby. These infants tend to be wakeful and have desquamation of the skin. The hands are like a washerwomen's, dry and wrinkled, with long fingernails. Meconium staining may be seen on the umbilical cord and fingernails more commonly in the post-term infants.

6.6

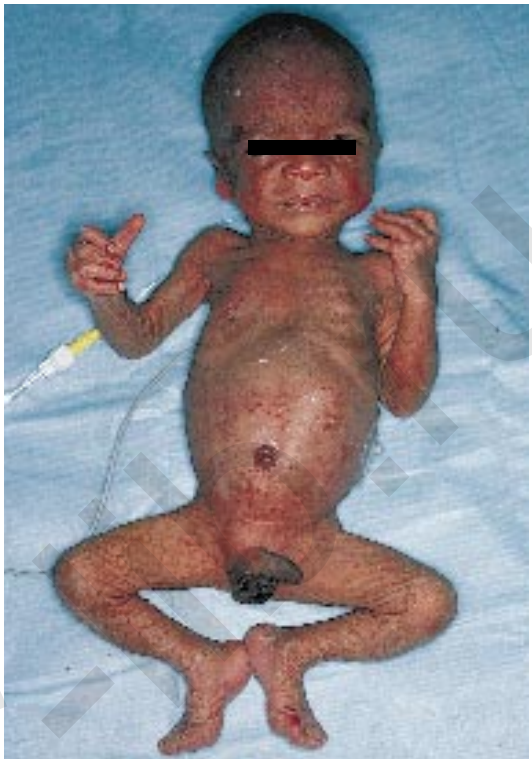

Figure 6.6. When a fetus is undergrown due to intrauterine dysfunction, the sequence begins with loss of fat and muscle mass as noted in this growth-retarded infant. This is followed by loss of mass of less essential organs (liver, thymus, spleen, adrenals), loss of mass of more essential organs (heart), and finally loss of brain mass. If head circumference is compromised, it indicates that malnutrition must have been very severe, and it carries a poor prognosis.

6.7

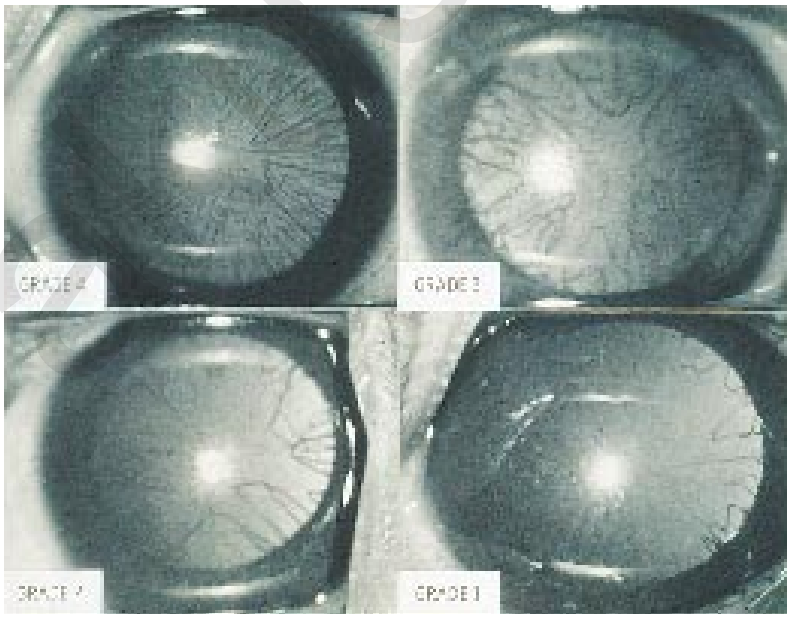

Figure 6.7. Two systems are useful clinically to determine gestational age by examination of the eye. First, examination of the anterior eye for the presence of the tunica vasculosa lentis, apparent generally from 27 to 34 weeks. Note in this composite figure the tunica vasculosa lentis Grade IV at 27 to 28 weeks completely covers the anterior surface of the lens and then gradually decreases to Grade I by 33 to 34 weeks when only peripheral remnants of the vessels are visible on the anterior surface of the lens.

6.8

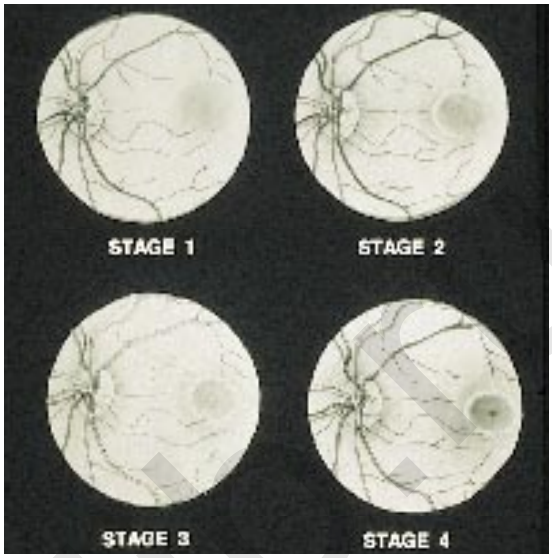

Figure 6.8. The second system used to determine gestational age involves examination of the fundus to assess macular development from 34 weeks to term. This composite figure shows Stage I – dark red pigmentation appearing, 34 to 35 weeks gestation; Stage II – the annular reflex is partially evident, 36 weeks gestation; Stage III – the complete annular reflex is present, 37 weeks gestation; Stage IV – the foveolar pit can be seen, 38 weeks gestation.

6.9

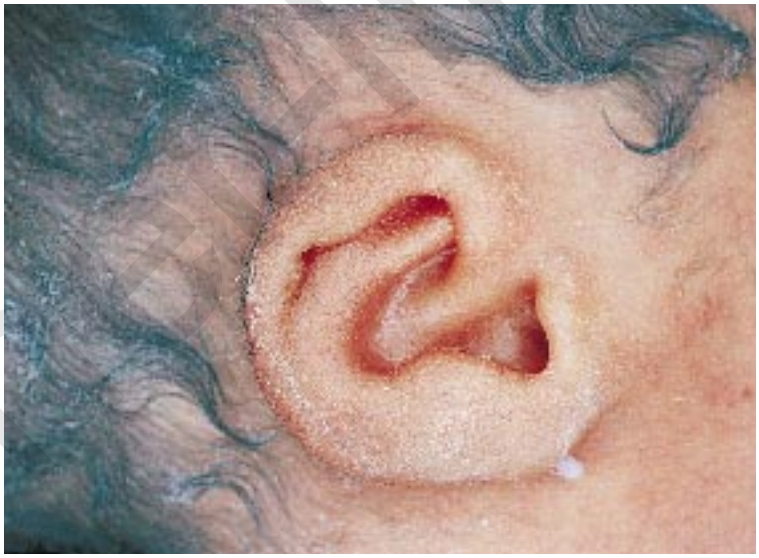

Figure 6.9. Because calcium is preferentially deposited in the last few weeks before birth, the stiffness of the baby's ear cartilage provides another test of maturity. In premature infants, the ear cartilage is deficient and the soft pinna does not spring back. On release it remains crumpled against the side of the head. At term the cartilage is more rigid similar to the adult ear.

6.10

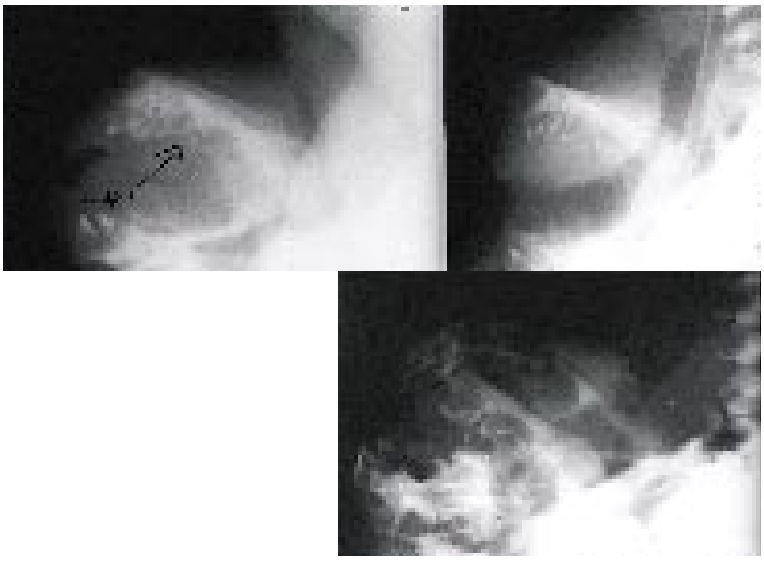

Figure 6.10. The presence of teeth seen by radiography in the jaw is a relatively accurate method of assessing gestational age. In the figure on the top left, incisors and cuspids have appeared but no molars, indicating a gestational age of less than 33 weeks. In the top right is shown the appearance of incisors and first deciduous molars consistent with 33 to 37 weeks gestation. On the bottom, the second deciduous molar and follicle of first permanent molar are present, indicating a gestation of greater than 37 weeks. This method is not useful in assessing infants with anhydrotic ectodermal dysplasia who have adentia.

6.11

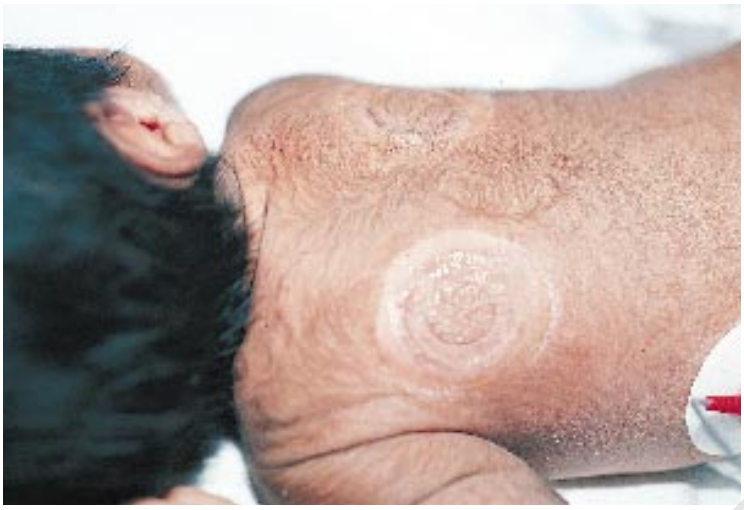

Figure 6.11. Hair, particularly on the head, is a reliable marker of maturity. Premature hair is fuzzy and the hair ends tend to clump together. In the term infant the hairs are distinct, coarse and silky. Lanugo is absent prior to 20 to 22 weeks gestation, but by 30 to 32 weeks becomes diffuse over the body. By term, lanugo has mostly disappeared. There are marked racial differences among babies with respect to lanugo characteristics. Hispanic infants, in general, have considerably more body hair persisting to term and black infants often have less than average lanugo.

6.12

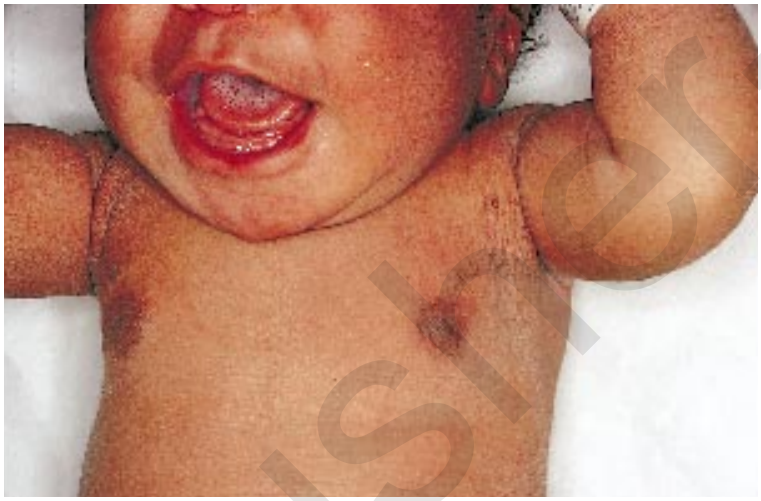

Figure 6.12. The breast analog does not respond to hormonal stimulation until near the 35th week and thus the size of the nodule can be correlated with development. Before 34 weeks the nipple and areola are identifiable, although they are immature-looking and non-pigmented. Between 34 and 36 weeks the nipple becomes erectile and a small nubbin of breast tissue can be felt under the areola. By 36 to 38 weeks, there is usually a palpable nodule and, by term, the nodule has enlarged to 5 to 10 mm in size.

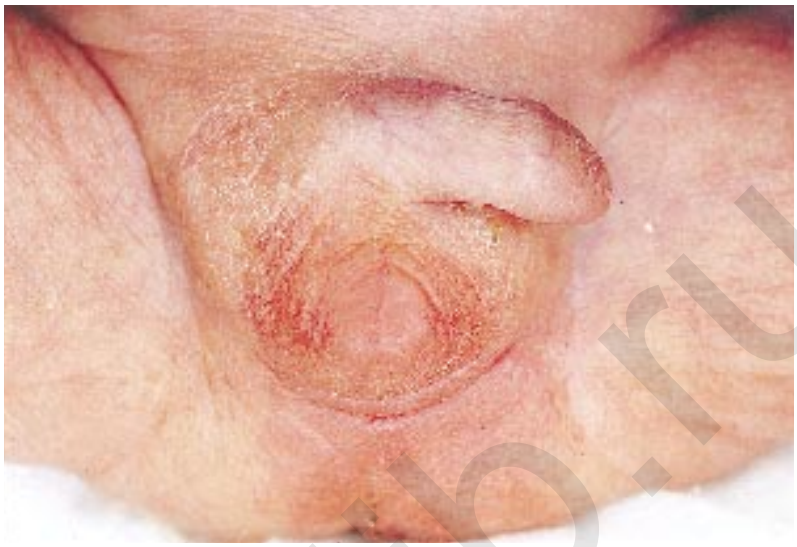

6.13

Figure 6.13. In the preterm male infant the testes are undescended and the scrotum empty, as pictured here. In the preterm female infant the clitoris is relatively large, and the vulva gapes due to separation of the labia majora and minora.

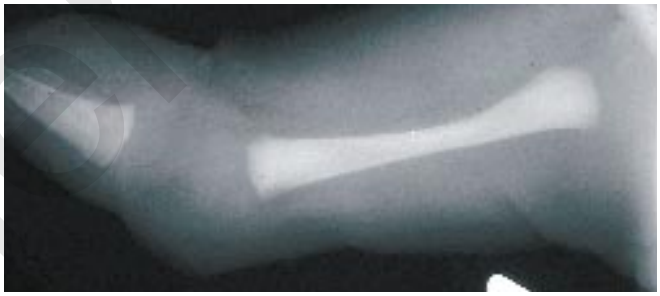

6.14

Figure 6.14. Looking for epiphyseal centers in long bone radiographs is useful in the assessment of gestational age. The lower extremity radiographs show the proximal tibial epiphyseal center, which generally appears by 36 weeks gestation, being followed by the distal femoral epiphyseal center at 38 weeks gestation. In this patient no epiphyseal centers are seen, consistent with the infant's gestational age of 35 weeks. Conditions that may alter the normal appearance of the centers include hypothyroidism, congenital viral infections, and congenital syphilis.

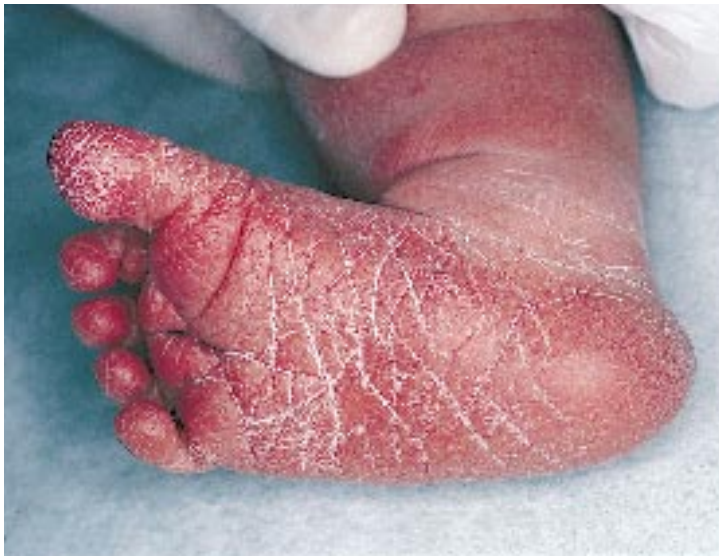

6.15

Figure 6.15. At 30 weeks or less the soles of the baby's feet are smooth. At 34 weeks, creases have started to appear on the anterior third of the plantar surface. By term, the entire plantar area is noticeably creased. In the post-term infant shown here, the soles show excessive creasing on the plantar surface together with dry peeling skin.

6.16

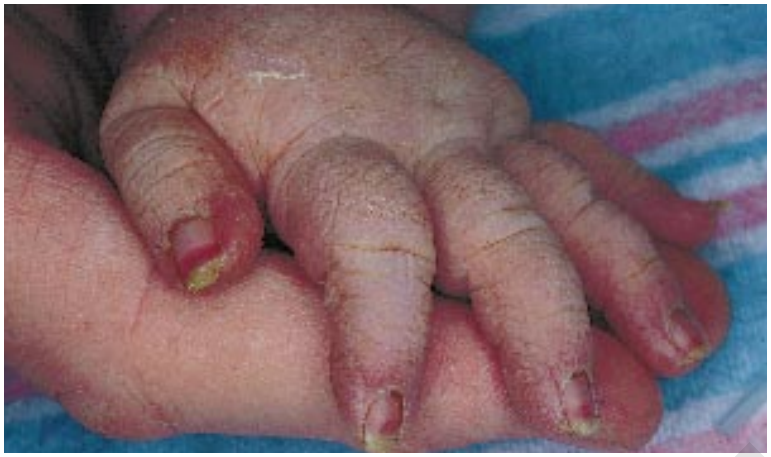

Figure 6.16. Meconium staining, as noted in this post-term infant, is a potential sign of fetal distress and is more common in the post-term infant. Meconium staining of the fingernails, as noted in this figure, suggests exposure to meconium of at least 4 to 6 hours, duration. Presence of meconium in the amniotic fluid may be helpful in assessing gestational age. In general, the fetus does not pass meconium before 34 weeks gestation; hence, the presence of meconium may either increase the estimated gestation of a premature infant or suggest that other causes of discolored amniotic fluid (such as *Listeria monocytogenes*) be considered.

6.17

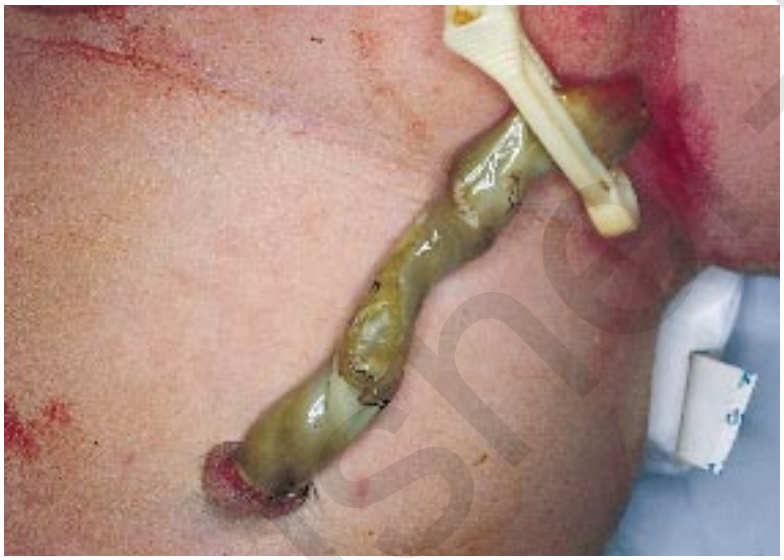

Figure 6.17. Meconium staining of the umbilical cord of the same post-term infant.

Chapter 7
Iatrogenesis

All interventions, whether intended as therapy or as monitoring, are inherently invasive and therefore have associated risks. The task of weighing risks and benefits would be simple if both were quantitatively known. Estimating the frequency of complications is difficult except for the most frequent and even those vary widely. Complications due to mechanical trauma, accidents, technique errors, or faulty equipment are potentially preventable. Complications due to interaction of the intervention with the patient (e.g., infection, thrombosis) may not be preventable until new techniques, equipment, or methods are developed. This section provides a catalogue of complications associated with intensive care in the neonate. Clinicians must continue to be vigilant and mindful of potential iatrogenic complications so that these problems may be prevented when possible and otherwise rapidly recognized and managed.

7.1

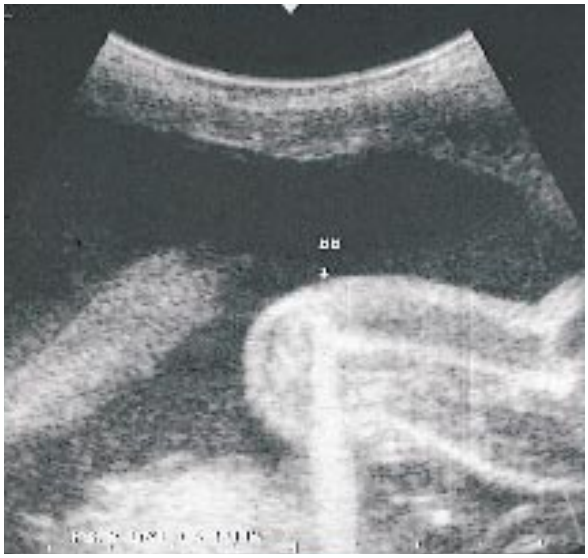

Figure 7.1. Ultrasound examination of the abdomen of a pregnant mother (gestational age 35 weeks) who was shot with a BB gun. Note the shadow from the BB pellet located in the soft tissue above the fetal femur. (Moise, K.)

7.2

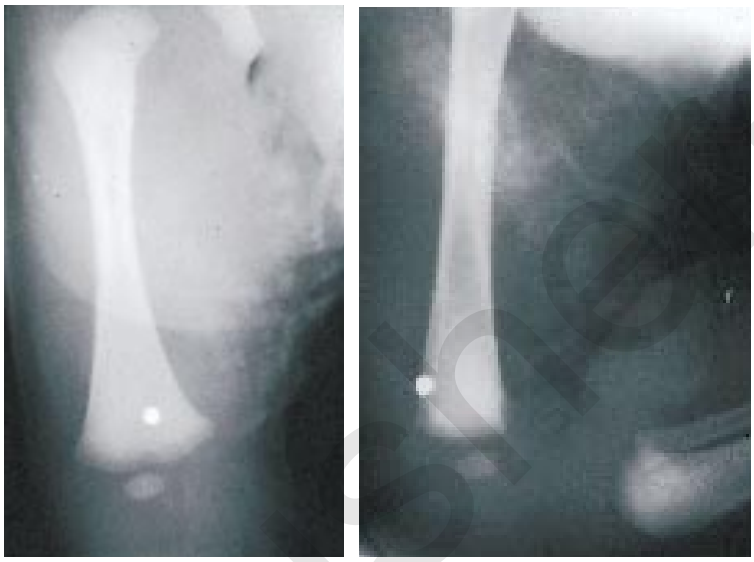

Figure 7.2. After delivery of the infant, radiography showed the presence of the BB pellet at the distal end of the femur. The infant had a normal course.

7.3

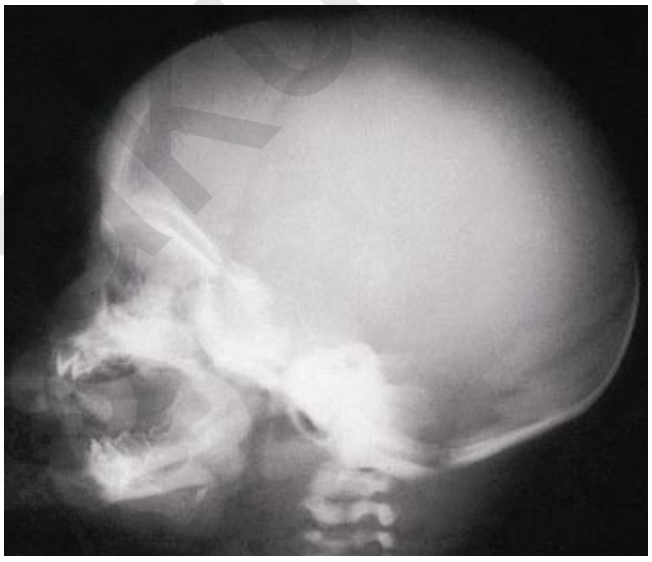

Figure 7.3. This infant developed swelling and some erythema over the frontal area. Radiography of the skull shows periosteal elevation of the frontal bone. This resulted from the application of a fetal scalp electrode.

7.4

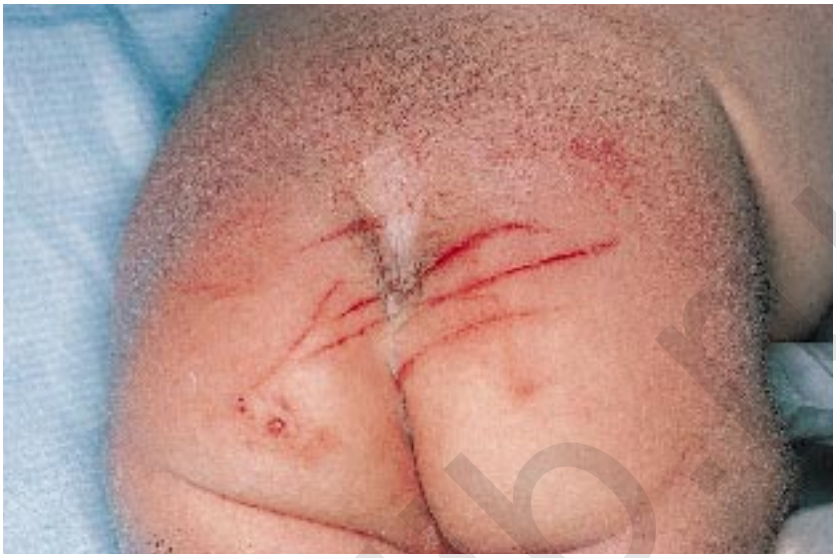

Figure 7.4. Skin incisions on the buttocks of an infant delivered by cesarean birth. It is not uncommon for infants to have iatrogenic trauma, such as facial abrasions from forceps delivery, and trauma from diagnostic-therapeutic procedures such as amniocentesis. (Landers, S.)

7.5

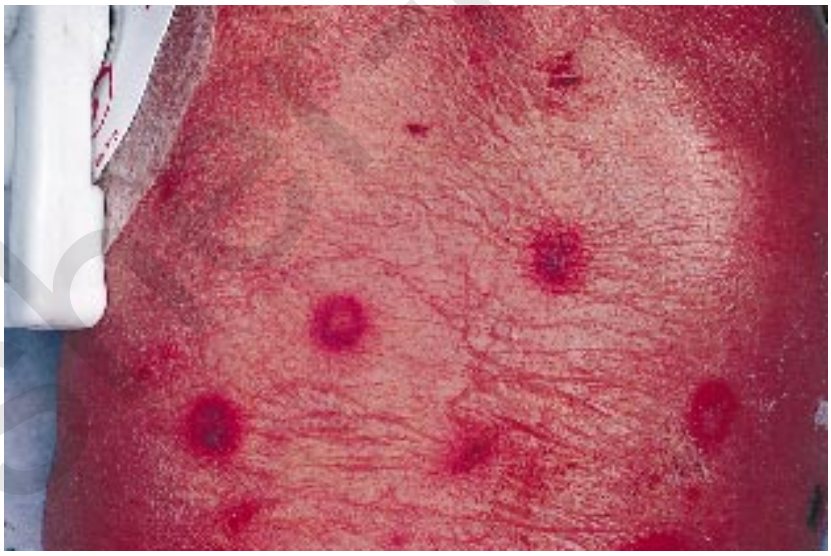

Figure 7.5. Circular lesions on the back of an infant as a result of skin burns from a faulty transcutaneous pO_2 electrode. With the advent of pulse oximetry the transcutaneous electrodes are rarely used nowadays.

7.6

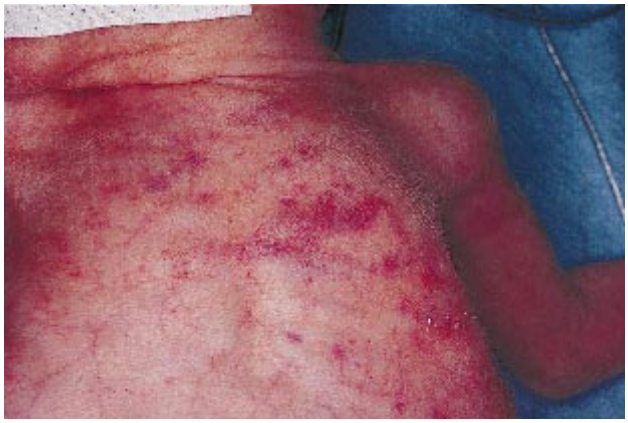

Figure 7.6. Purpuric lesions on the chest of a very small premature infant following vigorous physiotherapy.

7.7

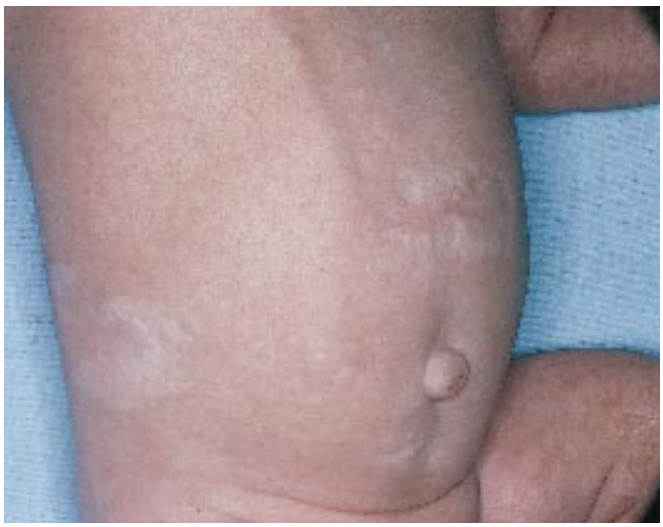

Figure 7.7. Hypopigmentation of the skin of the lower abdomen as a result of scarring from application of tape in the newborn intensive care unit. Trauma to the skin from adhesive tape is not uncommon, especially in very low birth weight infants. The hypopigmentation improves over time. (Landers, S.)

7.8

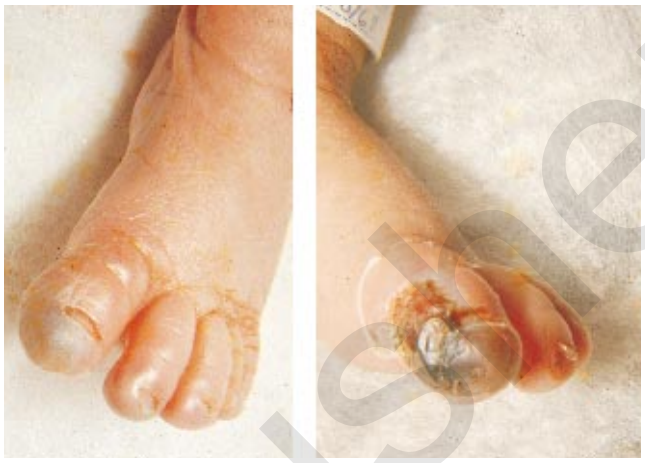

Figure 7.8. This infant developed necrosis and discoloration of the toes as the result of burns from the heater in an incubator at the time Gordon-Armstrong incubators were in use for management of premature infants. In our nursery, several infants developed burns over a short period of time. It was determined that the physician examining the infant would place the infant on top of the incubator and the burn would result from contact with a metallic instruction guide which was normally present on the incubator cover. Once the cause was determined, this problem was eliminated. The reason for including a historic figure is that in care and management of a sick neonate one should always be on the alert for possible iatrogenic problems.

7.9

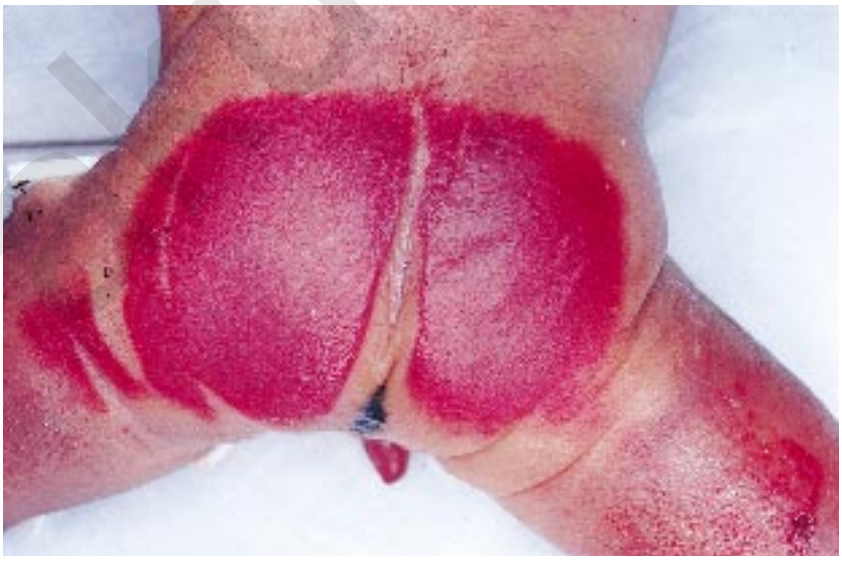

Figure 7.9. Percutaneous alcohol absorption with resultant erythema and burns to the buttocks of a premature infant. During placement of an umbilical arterial catheter, alcohol or iodine may track down the sides of the abdomen and soak the underlying sheet. Evaporation is restricted from the skin in contact with the underlying sheet and this may result in irritation, erythema, and severe burns, especially in a premature infant with very sensitive skin.

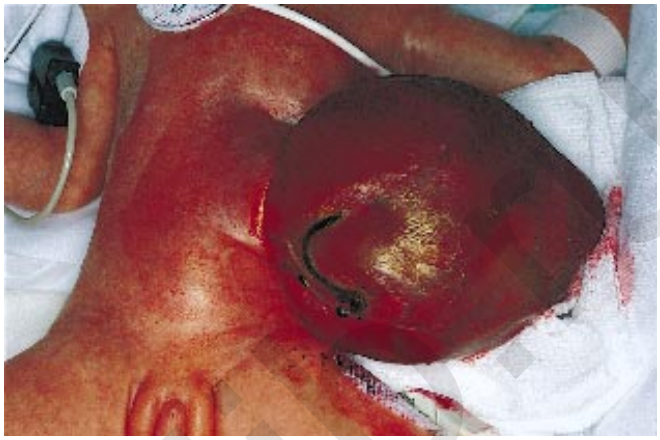

7.10

Figure 7.10. In this premature infant with a birth weight of 1000 g and severe hyaline membrane disease, it was elected to do medical management of the omphalocele. Mercurochrome was applied three times a day to the sac of the omphalocele as a topical solution. Treat-ment with organic mercurial antiseptics is controversial, since infants may develop potentially toxic levels of mercury because of the reduced skin barriers. The infant developed acute mercurial poisoning with the typical findings of acrodynia. Other preparations, such as silver nitrate, hexachlorophene, etc., have also been used with success in medical management of an omphalocele. One should always be on the alert for problems which may arise from excess absorption.

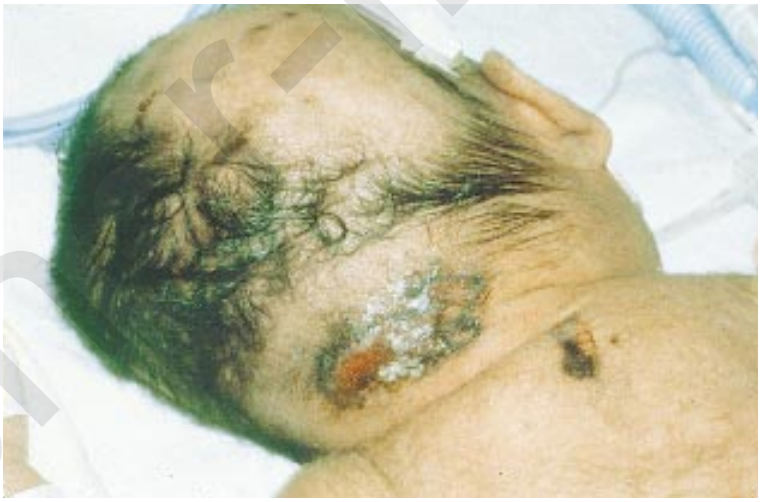

7.11

Figure 7.11. Decubitus ulceration of the back of the neck of an infant who was placed in the supine position and was on muscle relaxants for 8 days while being treated for septic shock. This stresses the importance of nursing care in these infants. (Landers, S.)

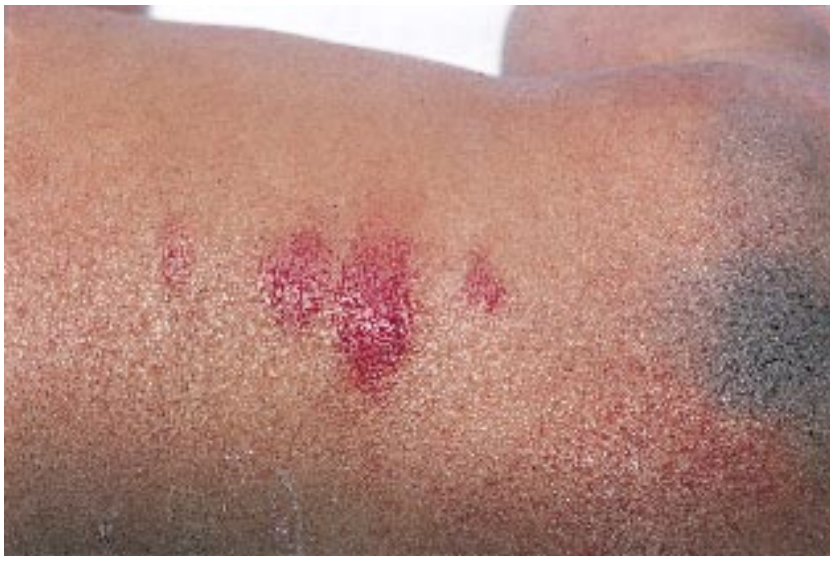

7.12

Figure 7.12. This infant had a lumbar puncture performed to exclude possible meningitis. Four days later these nodular erythematous lesions developed on the back over the sites of the lumbar puncture attempts. The lesions were those of subcutaneous fat necrosis. The possibility of infection should remain in the differential diagnosis.

7.13

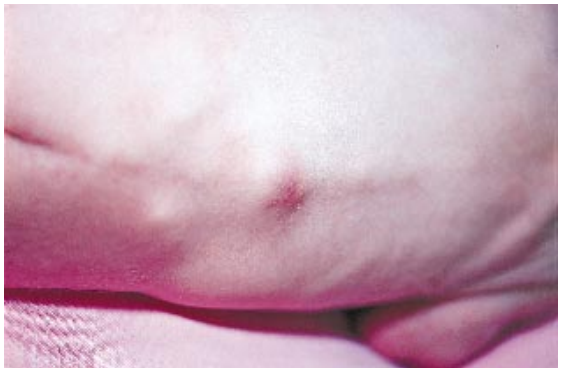

Figure 7.13. Slightly fluctuant erythematous midline back lesion in an infant with a staphylococcal abscess following lumbar puncture.

7.14

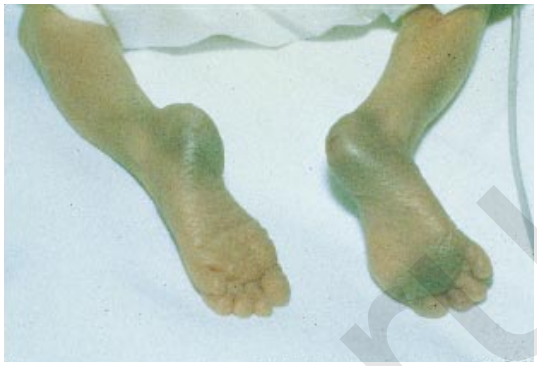

Figure 7.14. Appearance of the heels of a low birth-weight premature infant after repeated "heel-sticks." This can be avoided by warming of the heel and more gentle squeezing of the heel when collecting blood. Miscalculation of the water temperature when warming a heel may cause scalding and a skin burn. (Landers, S.)

7.15

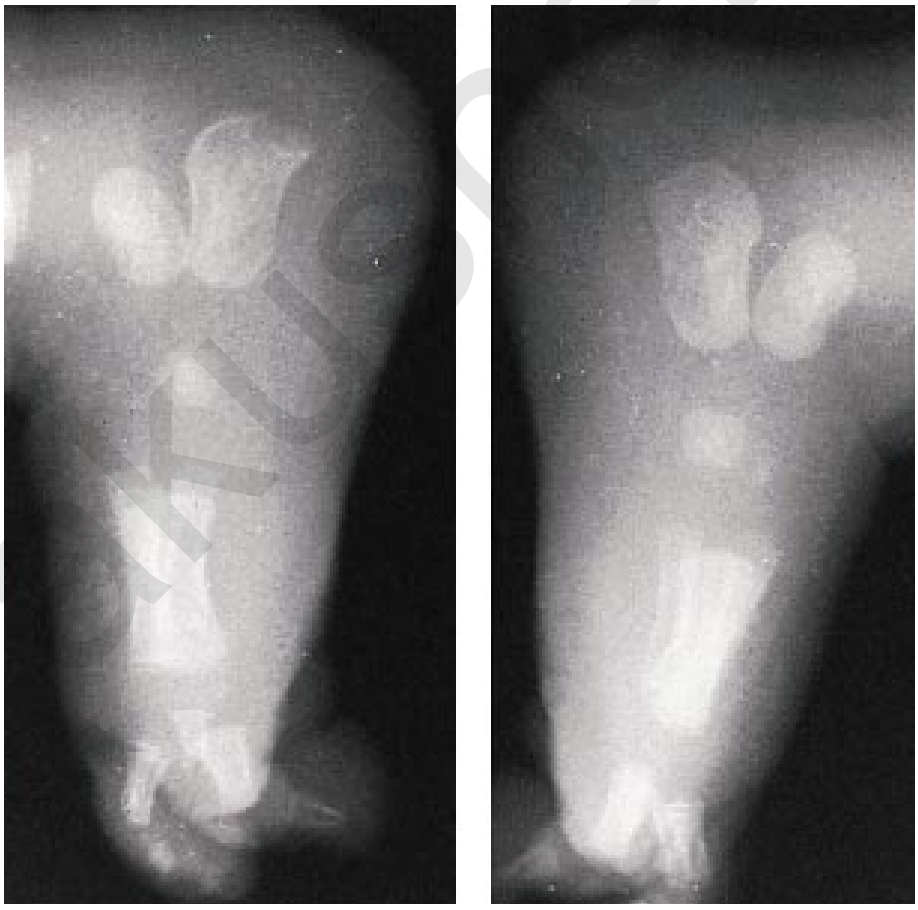

Figure 7.15. Radiograph of the feet of an infant with osteomyelitis of the calcaneus (on the left) following "heel-stick" trauma. The other heel is normal (on the right). One of the most common methods in infants of collecting laboratory blood specimens for analysis is by "heel-stick."

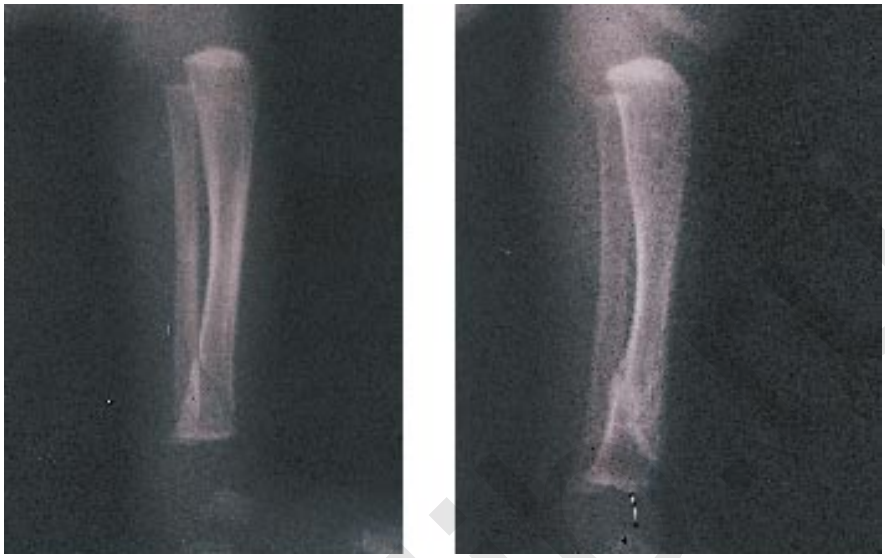

7.16

Figure 7.16. Radiograph of an infant with a spiral fracture of the distal end of the tibia. This fracture is the result of increased angulation with force applied by a technician collecting a "heel-stick" blood specimen. On the left, note the fresh fracture. On the right, note the healing fracture 3 weeks later. This infant had congenital syphilis. On initial radiographs there were growth arrest lines in the proximal tibia and distal femur, but the tibia was otherwise normal.

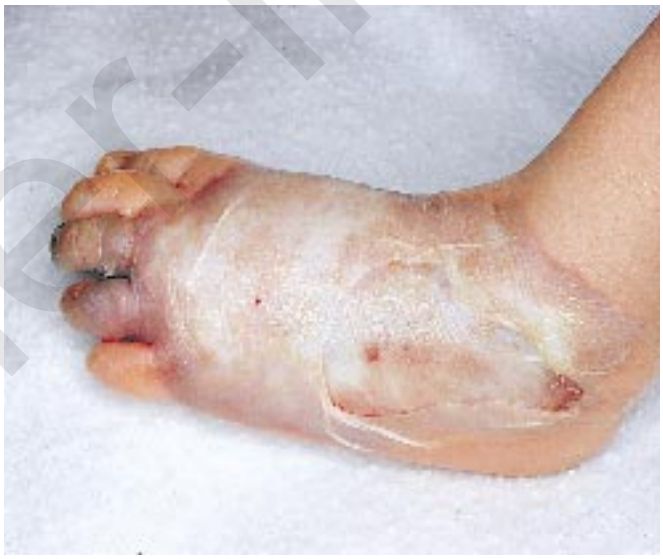

7.17

Figure 7.17. Edema, bullous excoriation and discoloration of the foot of an infant following dislodgment of the needle from an infusion pump. Ulceration due to extravasation of intravenous infusion fluid may follow subcutaneous leakage of any hypertonic solution, but those containing calcium are particularly irritating.

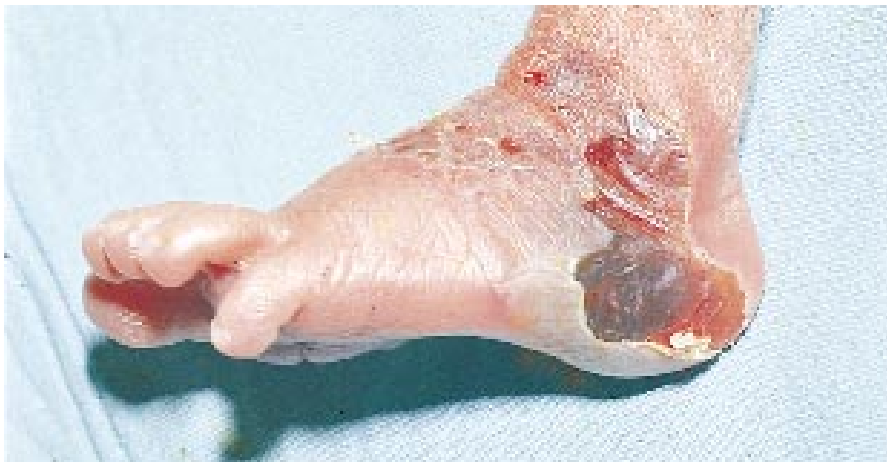

7.18

Figure 7.18. Soft tissue infiltration following continuous infusion with a needle displaced out of the vein. If these areas are large, they may subsequently require a skin graft.

7.19

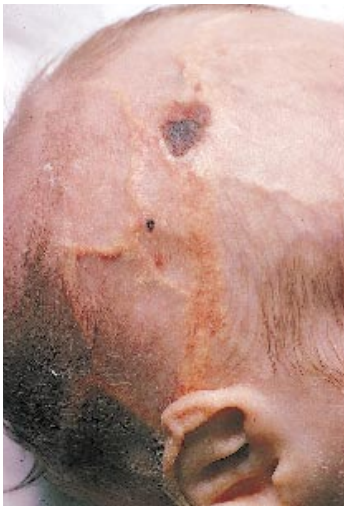

Figure 7.19. Calcification of the scalp veins following intravenous infusion of sodium bicarbonate and calcium gluconate. Deep areas of necrosis may occur following infiltration from intravenous solutions containing calcium.

7.20

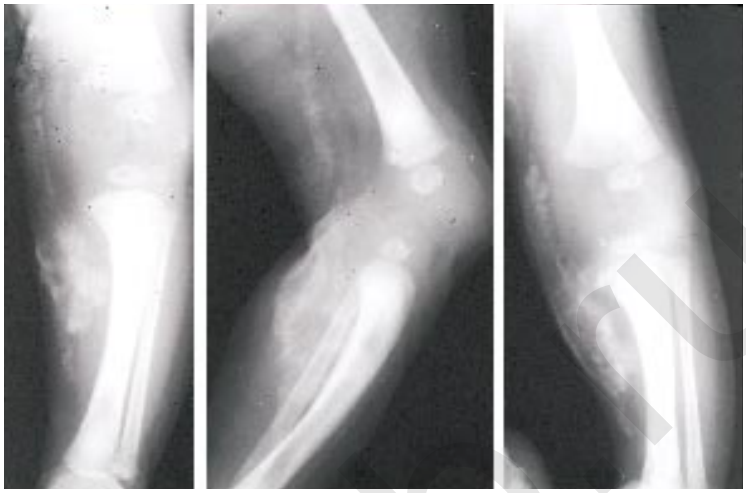

Figure 7.20. Radiographic series of an infant's leg with soft tissue and intravascular calcifications. This infant received calcium gluconate through a "cut-down" in the ankle. There are two patterns of calcification: amorphous ("bulky") and vascular (going up through the thigh).

7.21

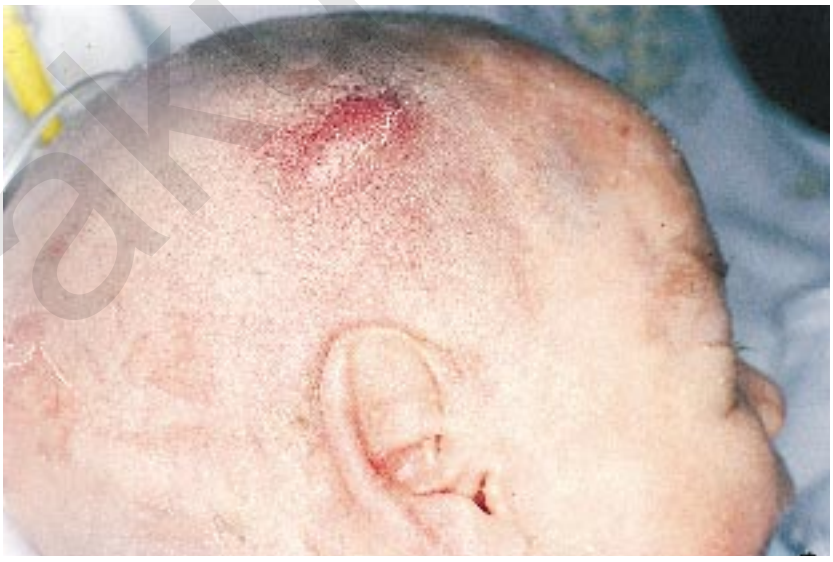

Figure 7.21. Soft tissue swelling and erythema in this infant with *Staphylococcus aureus* bacteremia and abscess. Abscess formation can occur frequently alone or in association with bacteremia at old venipuncture sites.

7.22

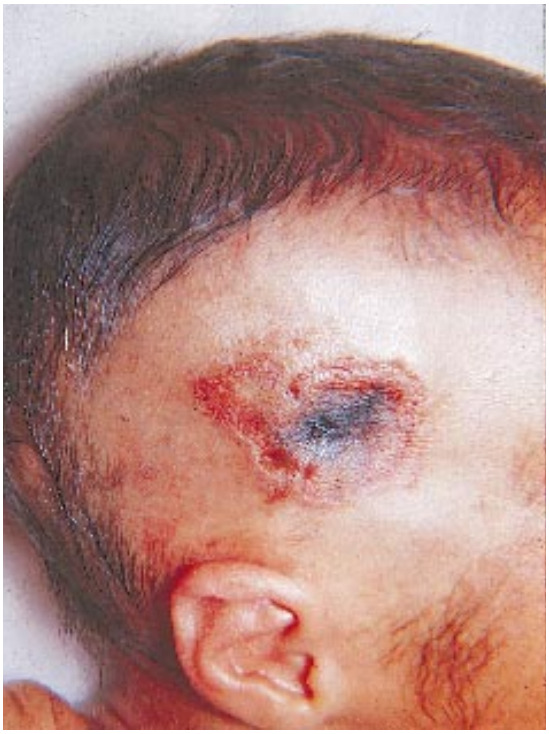

Figure 7.22. Infant with staphylococcal scalp infection following scalp vein infusion.

7.23

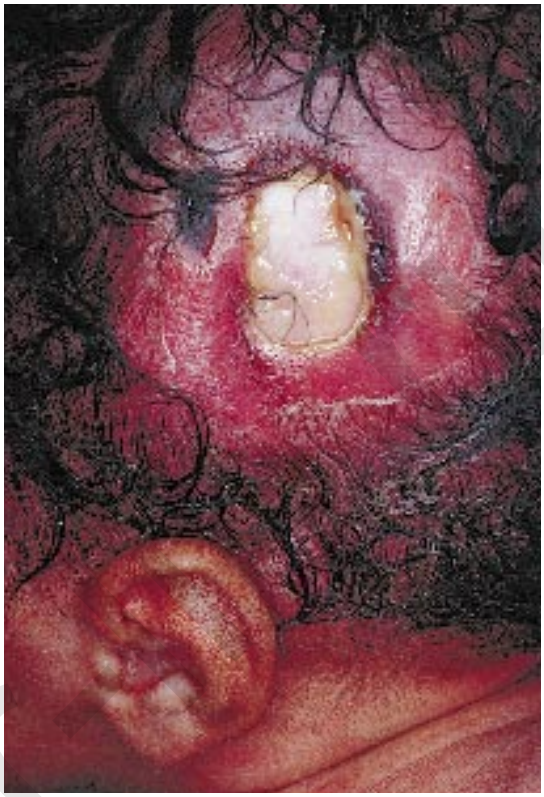

Figure 7.23. This scalp defect occurred as the result of a staphylococcal infection with an underlying osteomyelitis of the skull.

7.24

Figure 7.24. Transillumination of the scalp of an infant following infiltration of fluid from an intravenous scalp infusion. Extravasation of fluid in the scalp or scalp edema will transilluminate.

7.25

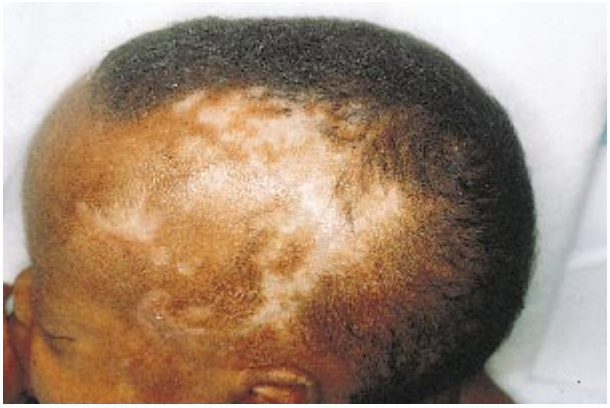

Figure 7.25. Hypopigmentation, alopecia and scarring on the scalp of a former very low birth weight premature infant (birth weight 700 g) following multiple scalp vein infiltrations.

7.26

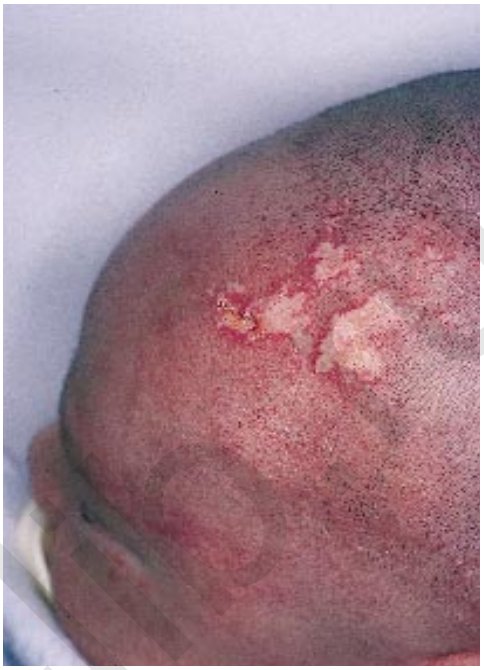

Figure 7.26. Scalp infiltration of total parenteral nutrition fluid and intralipid in an infant at the age of 7 days. This healed without residual hypopigmentation or scarring.

7.27

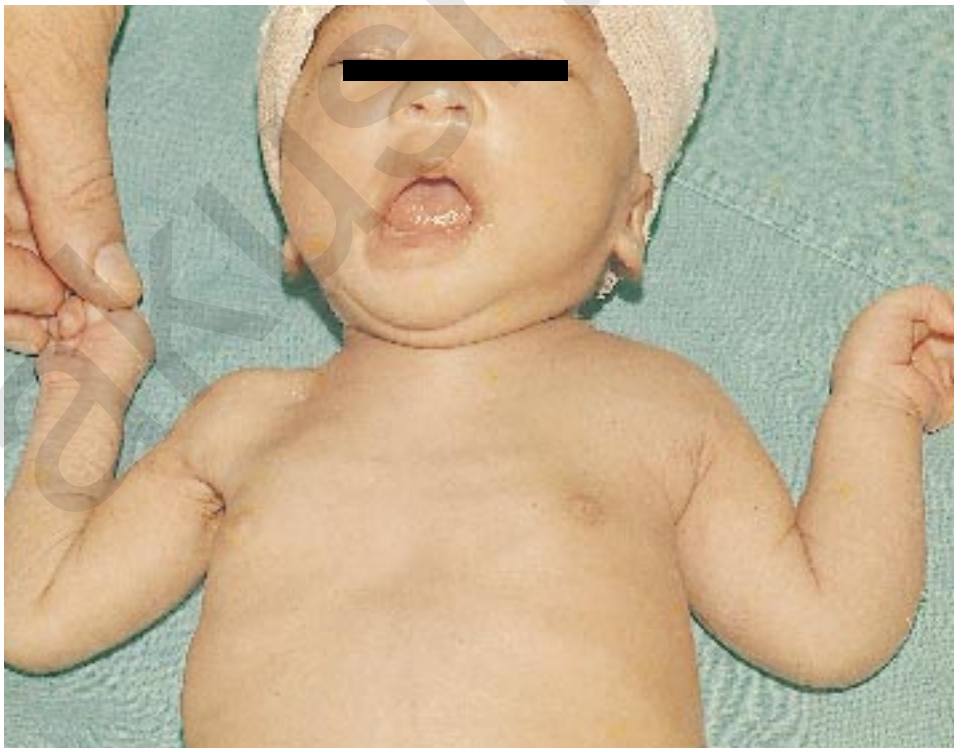

Figure 7.27. Soft tissue nonerythematous swelling of this infant's right side of neck, arm and chest occurred as the result of extravascular extravasation of central total parenteral nutrition. Note the facial palsy on the left side.

7.28

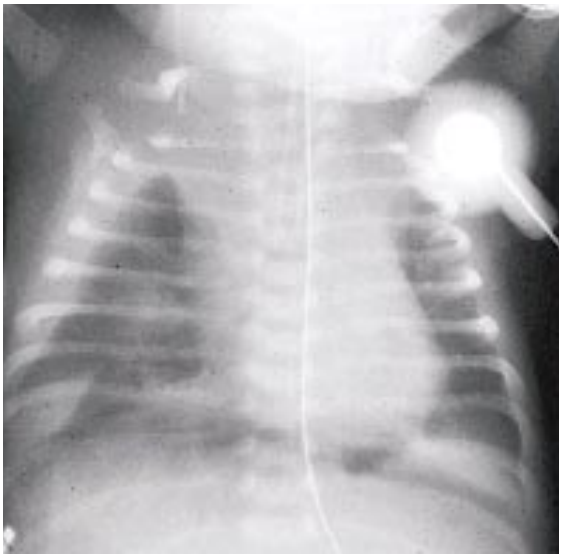

Figure 7.28. In this radiograph of the neck and chest, note the right-sided soft tissue swelling in the neck, a widened mediastinal shadow, and a large pleural effusion. These findings are the result of perforation of the vein by the central total parenteral nutrition catheter.

7.29

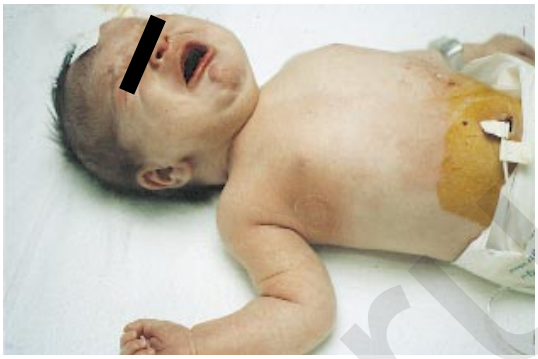

Figure 7.29. Patchy discoloration of the skin of an infant as the result of a bolus infusion of Prostaglandin E.

7.30

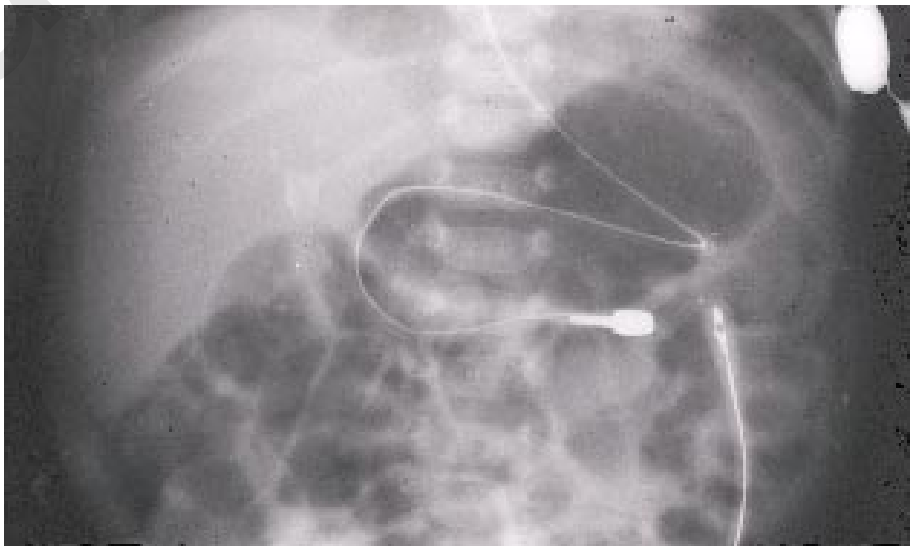

Figure 7.30. Abdominal radiograph of an infant with a gold-tip transpyloric feeding tube. Note the right upper quadrant vascular calcification of the portal vein. This is the result of sodium bicarbonate and calcium gluconate infusion given together through an umbilical venous catheter.

7.31

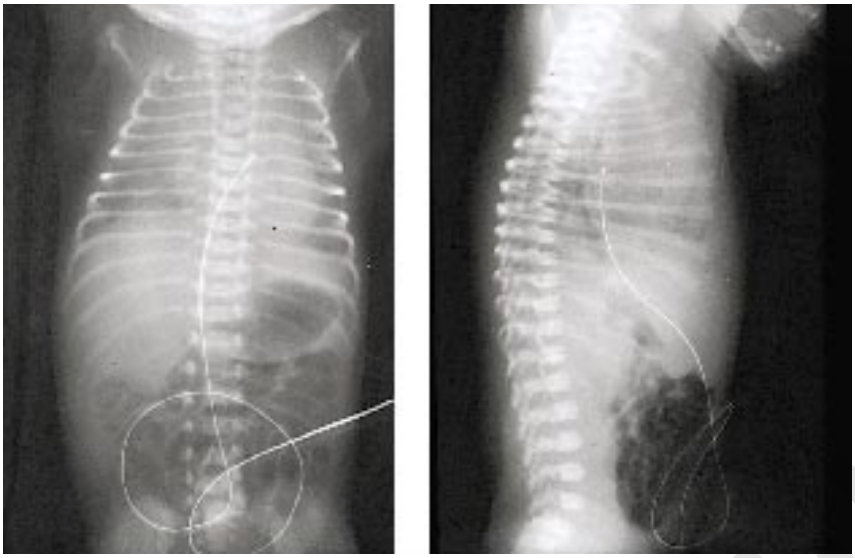

Figure 7.31. Anteroposterior and lateral radiographic views of an umbilical venous catheter placed high in the heart. It is possible to sample oxygenated left atrial blood when the catheter passes across the patent foramen ovale.

7.32

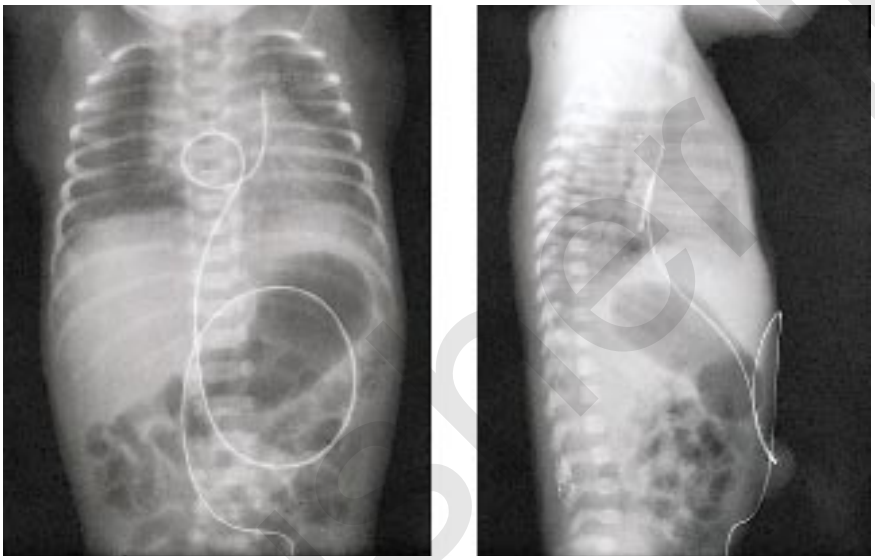

Figure 7.32. Anteroposterior and lateral radiographic views of an infant with an umbilical venous catheter placed in the left pulmonary artery. The previous figure and this figure stress the importance of checking placement of umbilical catheters following their insertion. When they are placed in such abnormal positions they should be withdrawn.

7.33

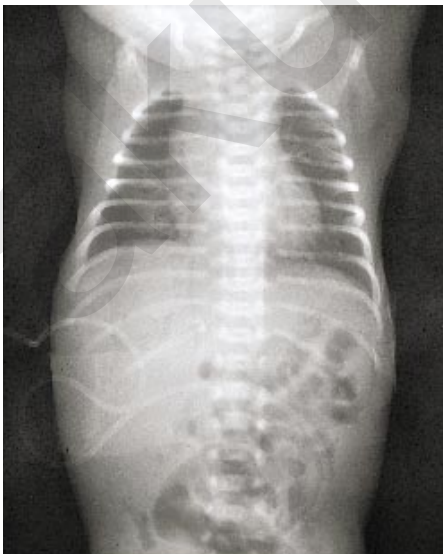

Figure 7.33. Chest and abdominal radiograph of an infant after placement of an umbilical venous catheter. Note the placement of the catheter in the liver with air outlining the portal venous system.

7.34

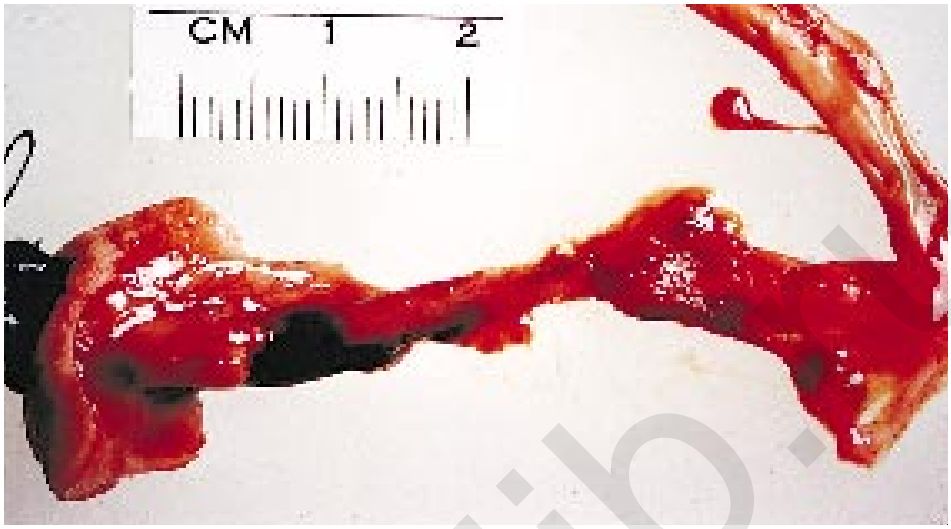

Figure 7.34. Autopsy specimen of the umbilical vessels with umbilical vein perforation from a catheter during umbilical vein placement.

7.35

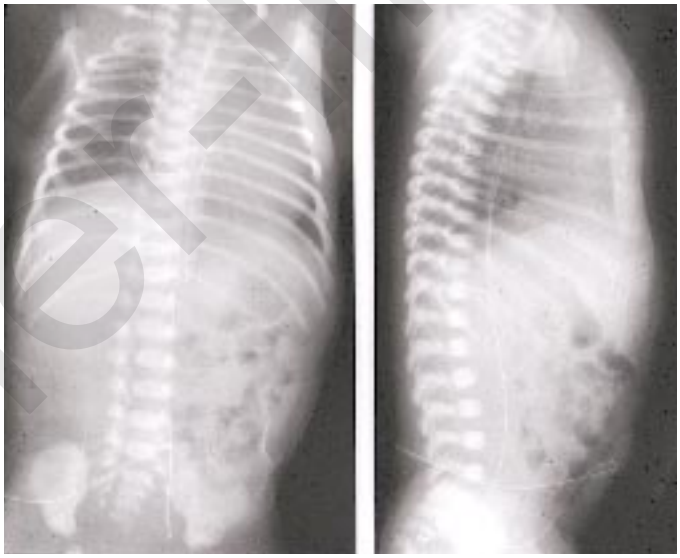

Figure 7.35. Anteroposterior and lateral radiographs in an infant showing an umbilical artery catheter which is placed high in the thoracic aorta curving on itself.

7.36

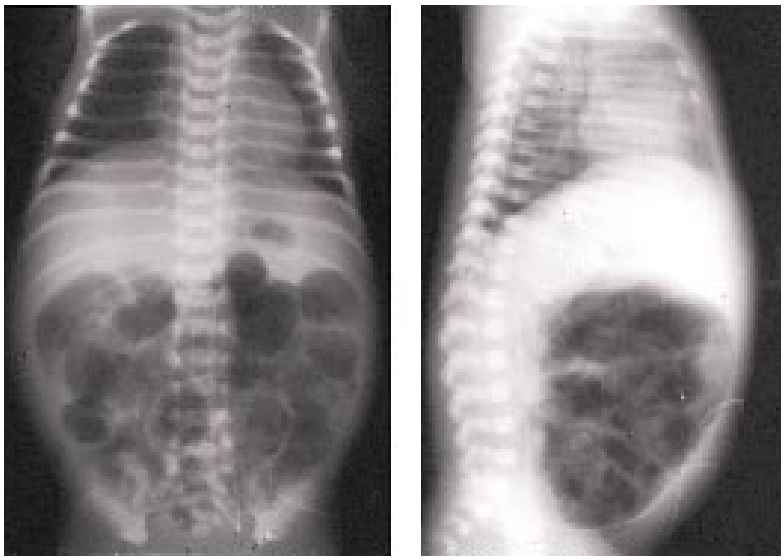

Figure 7.36. Anteroposterior and lateral radiographs of the same infant showing repositioning of the umbilical artery catheter after its initial high aortic placement. These follow-up films show the location of the catheter in the superior mesenteric artery. The infant developed abdominal distention and vomiting and had a large segment of gangrenous bowel which was removed.

7.37

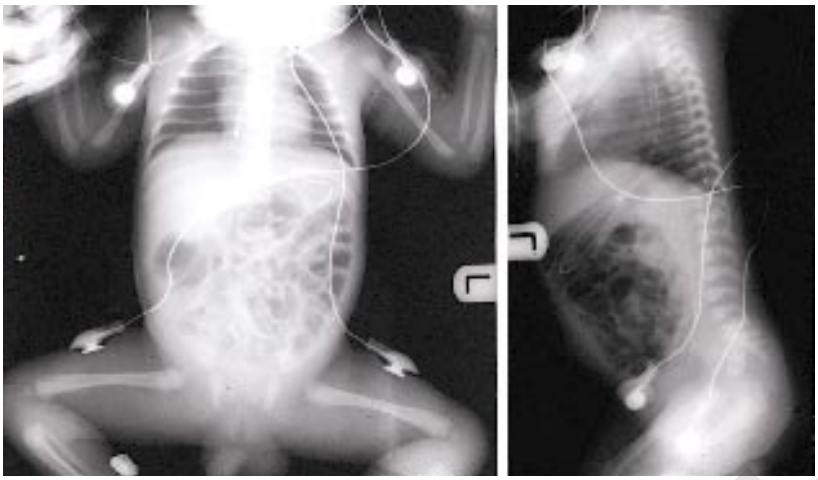

Figure 7.37. Anteroposterior and lateral radiographic views of a "free," broken umbilical artery catheter lying in the abdominal and thoracic aorta. The catheter broke at the insertion site during planned removal. The remaining catheter had to be surgically removed.

7.38

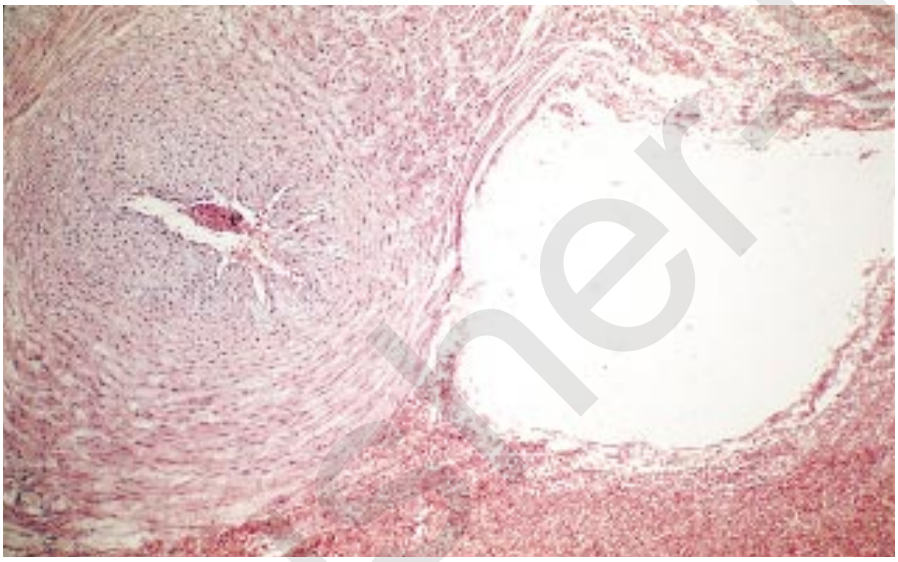

Figure 7.38. Histologic view showing on the left the umbilical artery and on the right the juxtaposed "false" catheter passage. The possibility of creating a false passage should always be considered when there is difficulty with placement of an umbilical catheter.

7.39

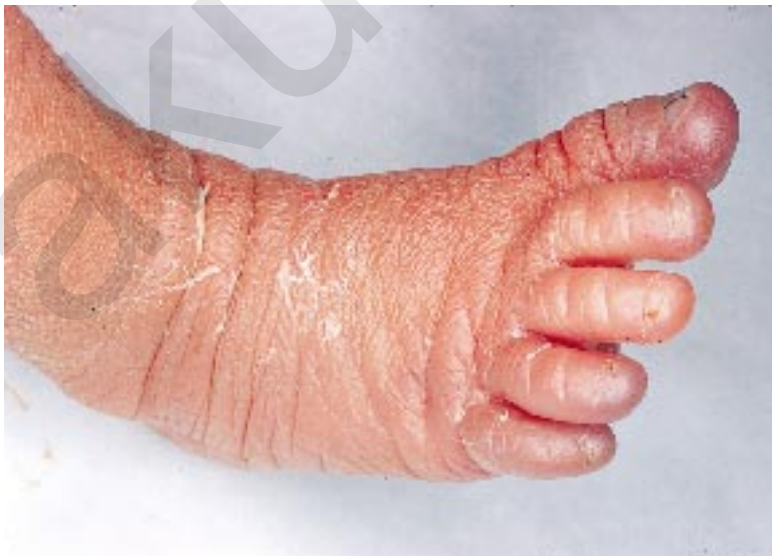

Figure 7.39. Discoloration of the great toe and little toes of the left foot in this infant followed umbilical artery catheter placement. With removal of the catheter, vasospasm subsided with subsequent normal circulation and appearance. Umbilical artery catheterization may be associated with thrombotic complications.

7.40

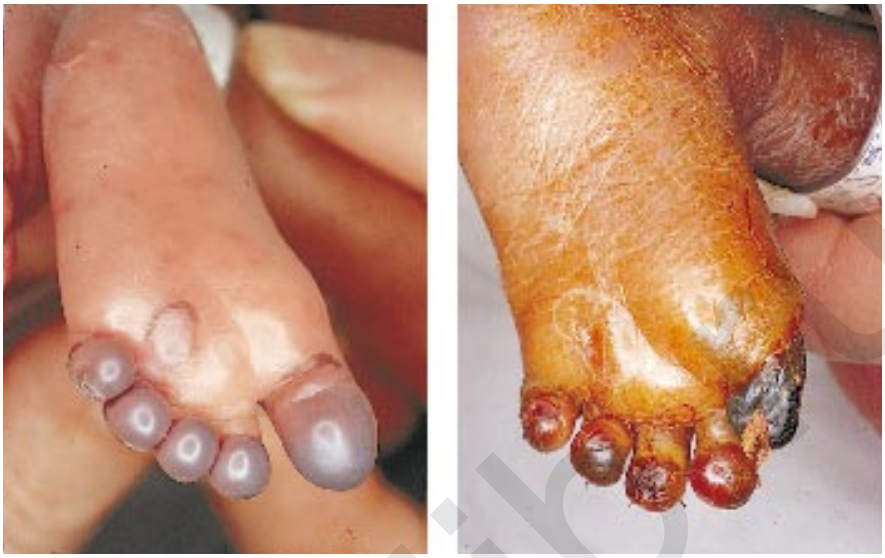

Figure 7.40. On the left, note the discoloration of the toes in an infant 4 hours after placement of an umbilical arterial catheter. There was no significant improvement after catheter removal. On the right, note the gangrenous and atrophied appearance of the same foot 15 days later.

7.41

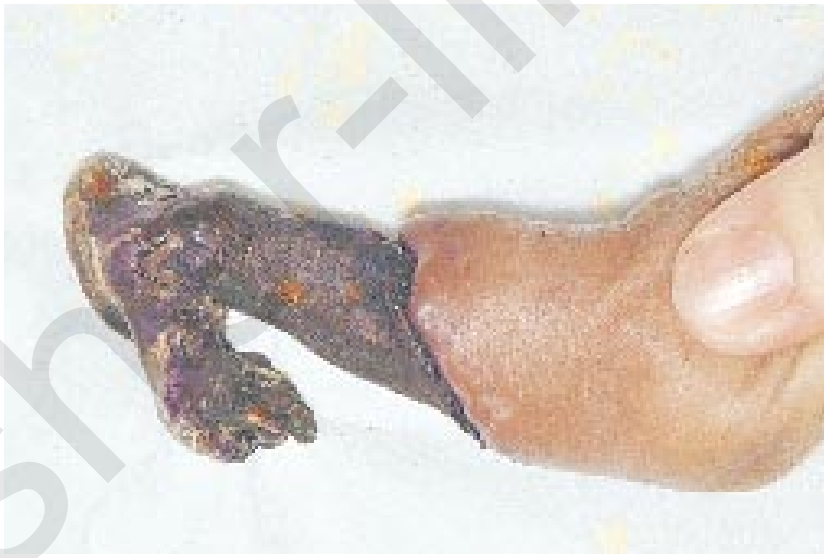

Figure 7.41. Severe atrophy and gangrene of the left lower extremity in an infant as a result of umbilical artery catheter placement. This can occur as a result of vasospasm or clot formation in a major vessel with inadequate collateral support in a very low birthweight infant.

7.42

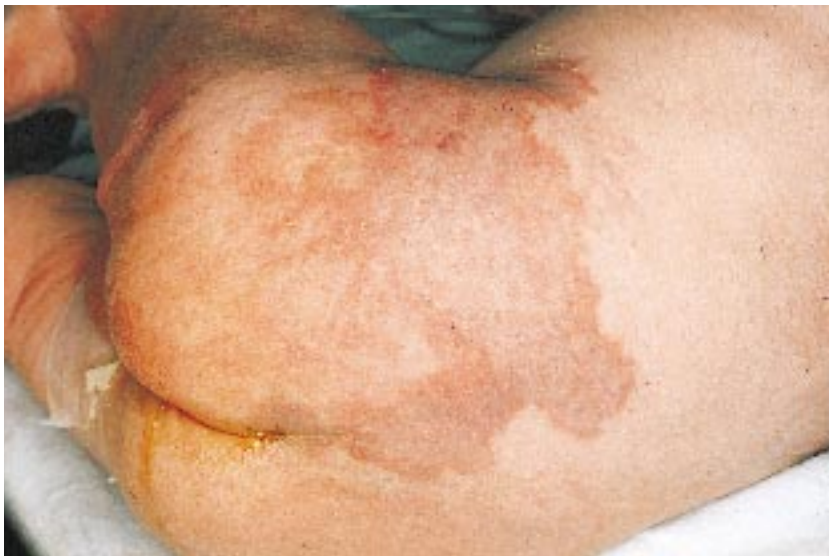

Figure 7.42. Discoloration and necrosis of the buttocks as a result of umbilical artery catheter placement in an infant at the age of 4 days. This occurs from spasm and thrombosis of the internal obturator artery which supplies the muscles of the buttock. Intra arterial injection of alkali may also be followed by gangrene of the buttock.

7.43

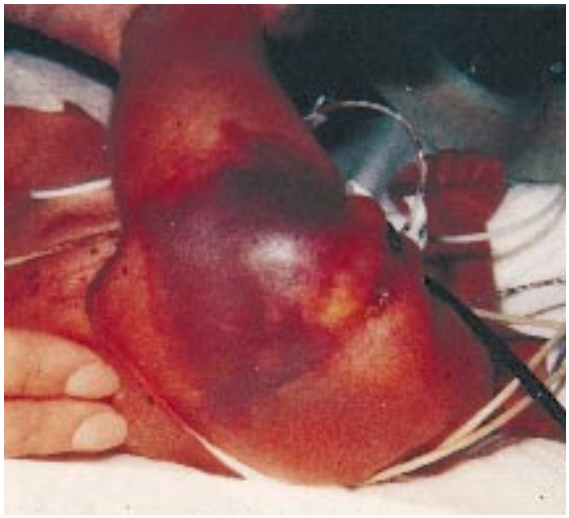

Figure 7.43. Discoloration with gangrene of the right buttock following umbilical artery catheter placement.

7.44

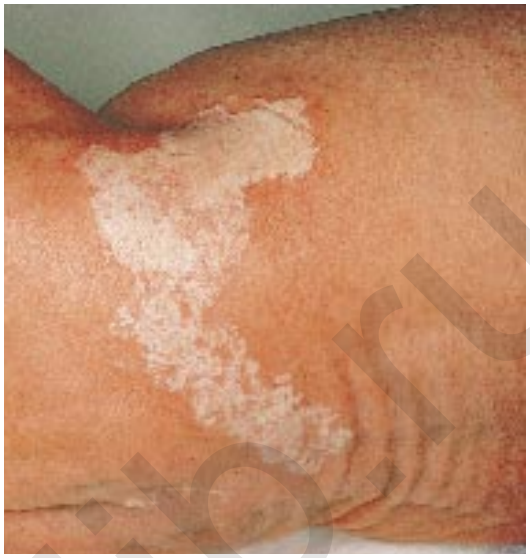

Figure 7.44. The same infant 10 days later showed marked improvement of the buttock.

7.45

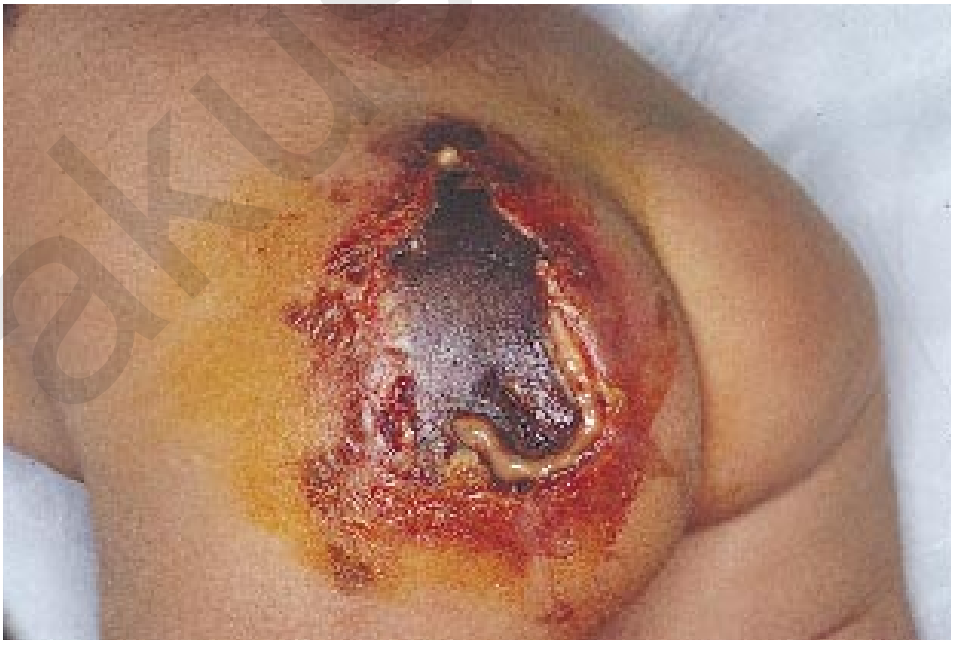

Figure 7.45. Gangrene of the left buttock following umbilical artery catherization. The umbilical artery catheter was positioned in the iliac artery radiographically. There is a well-known association between injection of medications into the umbilical artery and necrosis and gangrene of the buttock and sciatic nerve palsy.

7.46

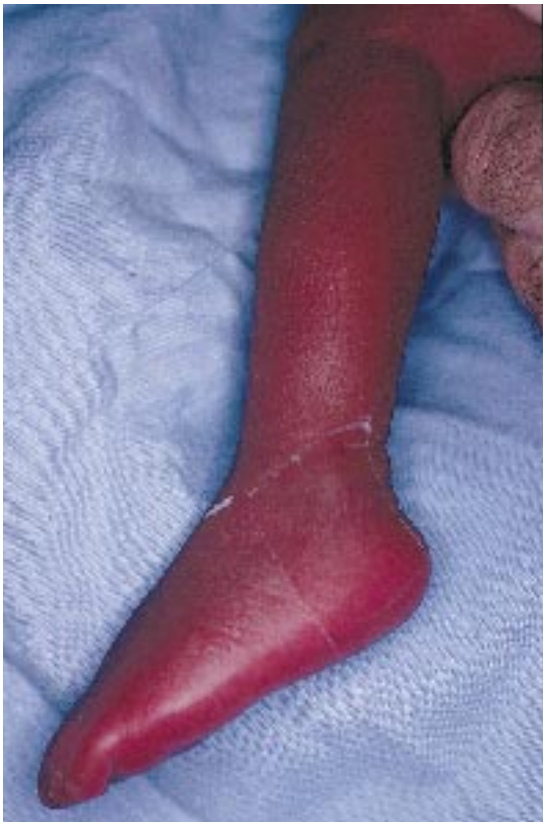

Figure 7.46. The same infant with unilateral gangrene of the buttock also had a sciatic nerve palsy as a result of the umbilical catheter being positioned in the iliac artery. Note the "foot drop."

7.47

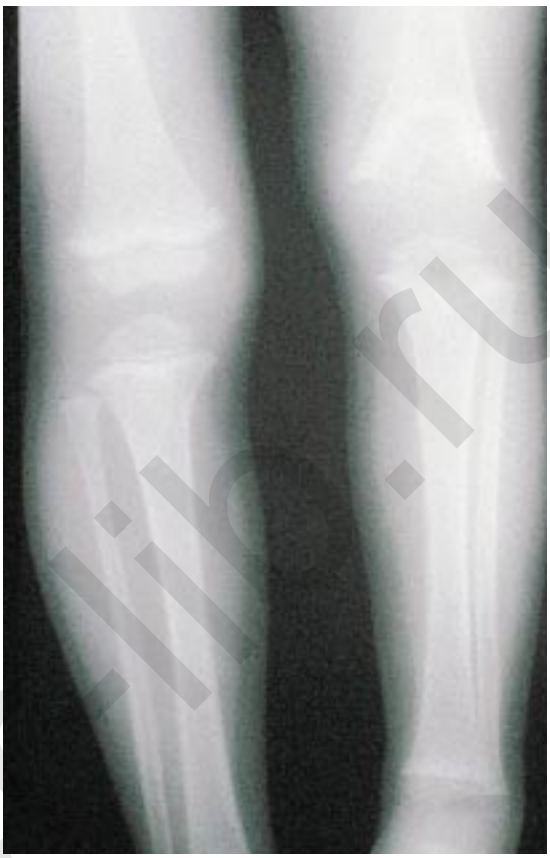

Figure 7.47. Radiograph of the lower extremities in an infant with leg length discrepancy. The soft tissue mass and bone growth of the left leg are decreased in comparison to the right. These postnatal changes were the result of femoral artery thrombosis after umbilical artery catheter placement.

7.48

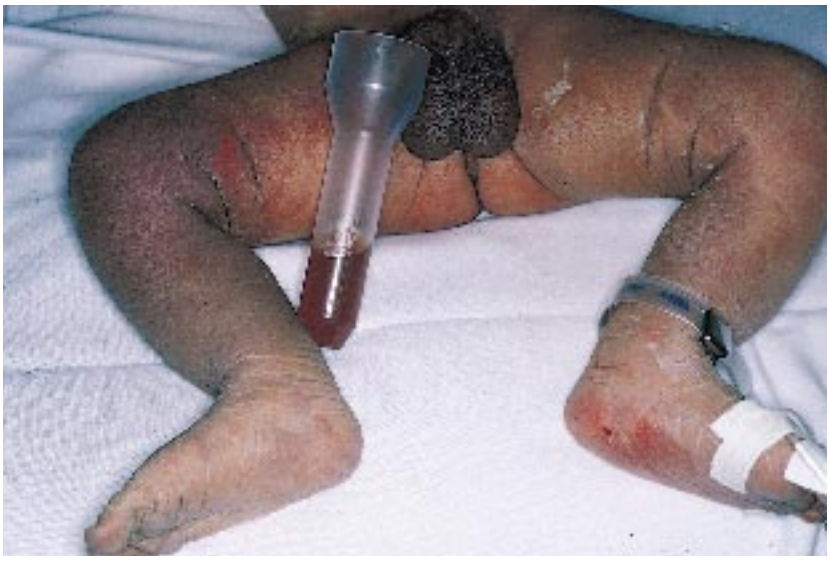

Figure 7.48. Placement of an umbilical artery catheter was difficult in this infant. On the first and second attempts the catheter went down each leg. On the third attempt the catheter was placed in the aorta. It remained in place for 4 hours when blood was noted in the urine and the legs were both noted to have some discoloration.This figure shows the status 19 hours after the catheter was removed. The infant continued to improve.

7.49

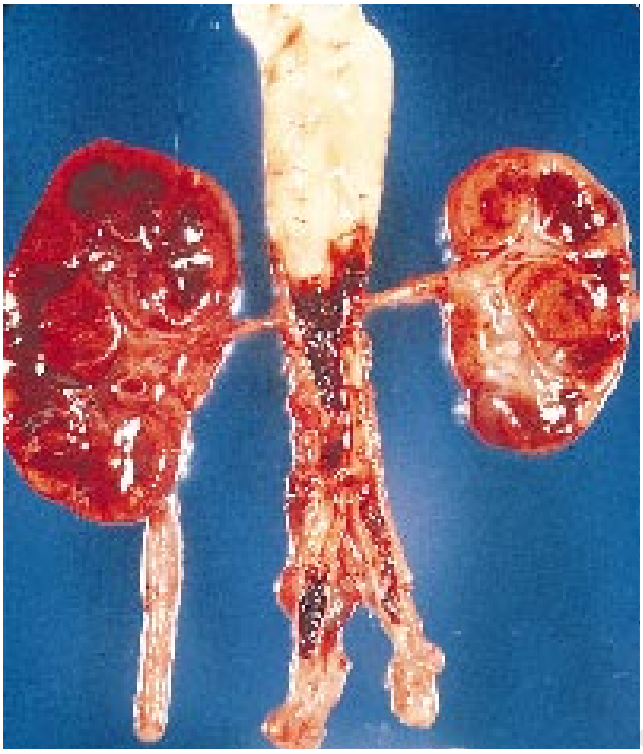

Figure 7.49. Autopsy specimen demonstrating thrombosis involving the aorta, iliac arteries and renal arteries following umbilical artery catheterization at birth. The infant died at the age of 12 days.

7.50

Figure 7.50. Autopsy specimen of the aorta with periumbilical artery catheter thrombosis.

7.51

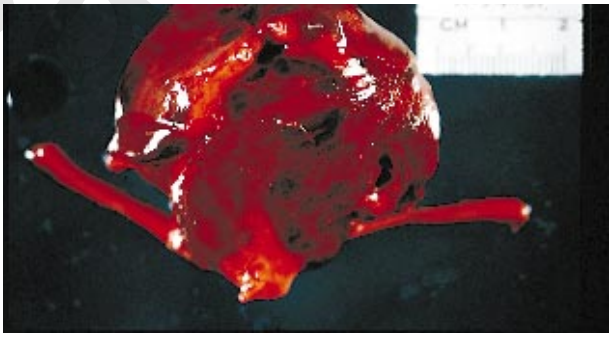

Figure 7.51. Autopsy specimen of the bladder. Note the engorged hemorrhagic bladder wall which was the result of an umbilical artery catheter perforation.

7.52

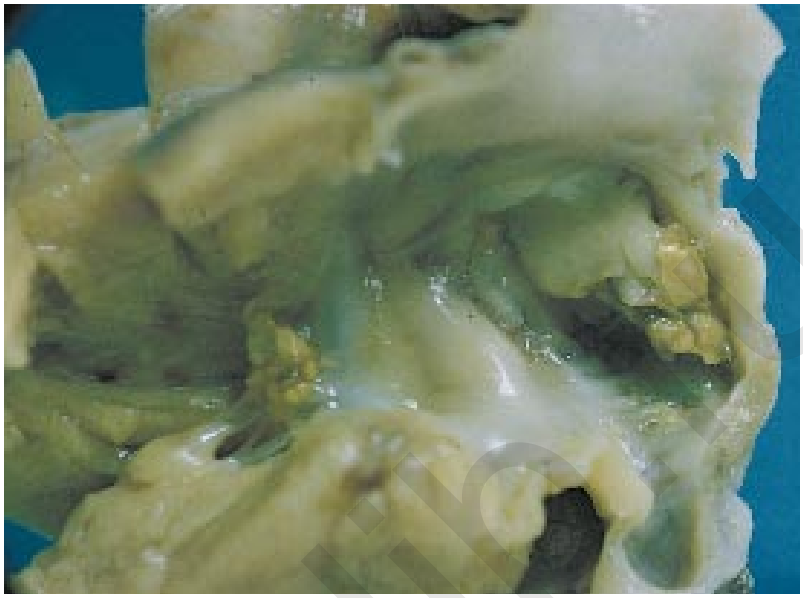

Figure 7.52. Autopsy specimen of the heart in an infant who developed vegetations as a result of prolonged umbilical venous catheter placement. Note the verrucous vegetations due to staphylococcal endocarditis.The condition was diagnosed antemortem by echocardiography. In cases of prolonged sepsis in small premature infants, the diagnosis of endocarditis should always be excluded.

7.53

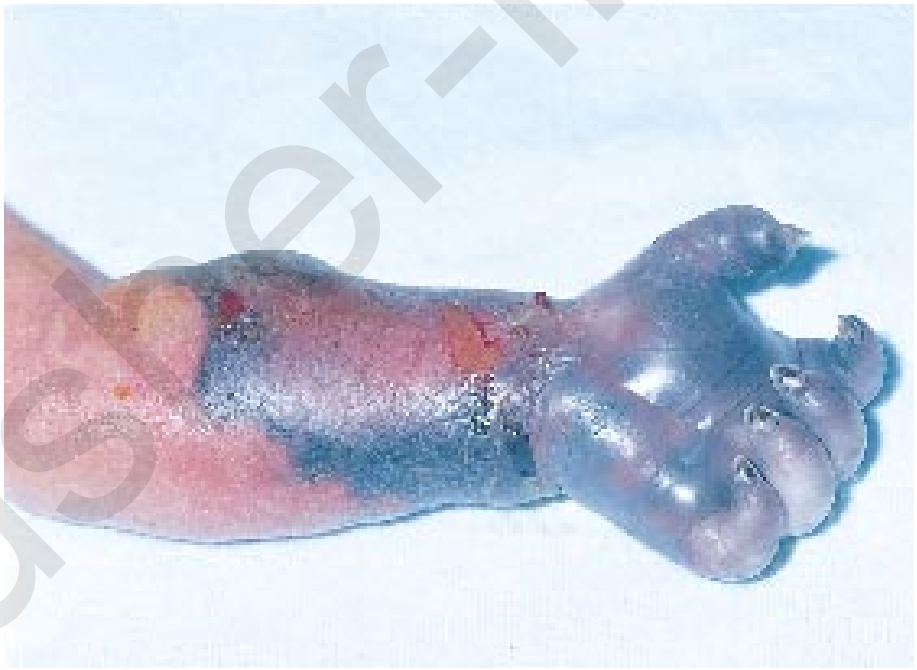

Figure 7.53. Gangrene resulting in amputation of the right arm following an infusion of 10% dextrose in the right radial artery.

7.54

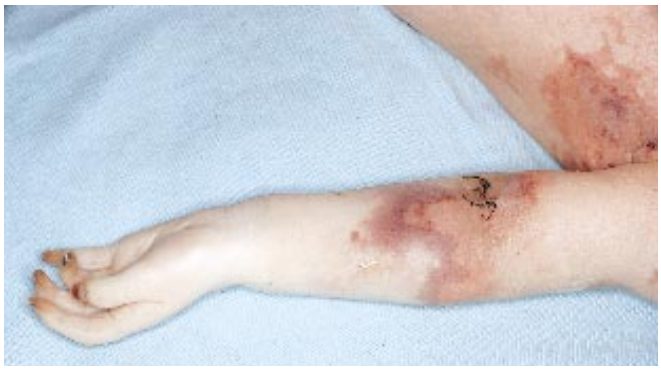

Figure 7.54. This infant developed obstruction to the circulation of the distal right forearm and hand following attempts at right radial artery catheterization. Subsequently, a cut-down was placed in the right brachial artery, resulting from thrombosis. Note the white discoloration and atrophy of the hand and distal forearm with gangrene of the distal fingertips. A sharp demarcation line separated the normal from the abnormal circulation.

7.55

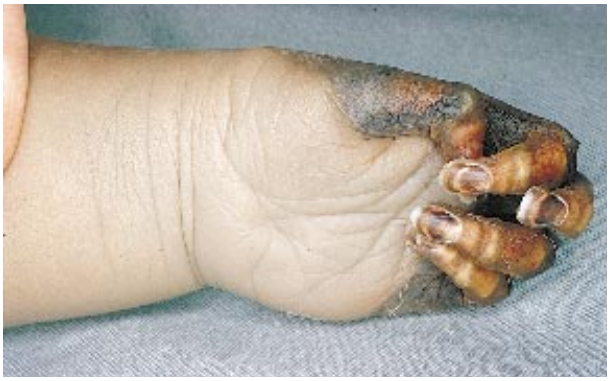

Figure 7.55. Close-up of the right hand of the same infant 2 weeks later shows the atrophy and gangrene of the right hand.

7.56

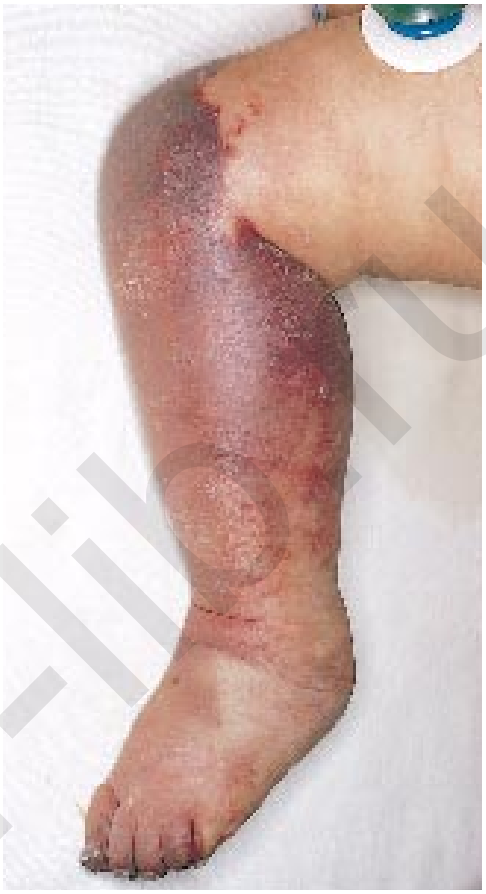

Figure 7.56. The same infant, in addition to the thromboses, had embolization from the same site which resulted in discoloration and impaired circulation of the right lower extremity. This improved.

7.57

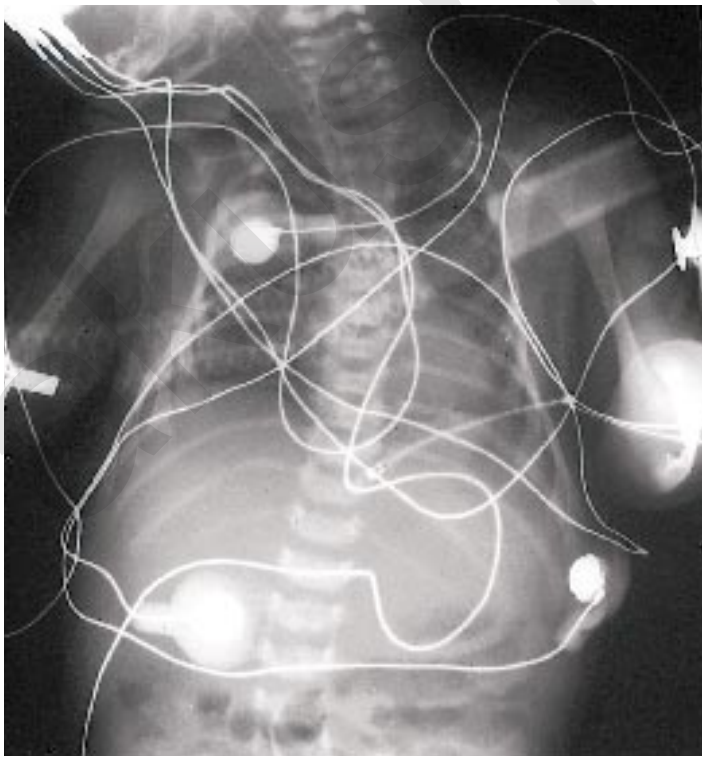

Figure 7.57. Radiograph of the chest of an infant admitted to the neonatal intensive care unit. Note the excessive neonatal equipment interfering with evaluation of the status of any cardiorespiratory pathology. When doing radiographic evaluation it is extremely important that an attempt be made to clear all the excess tubes and leads to obtain as clear a field as possible.

7.58

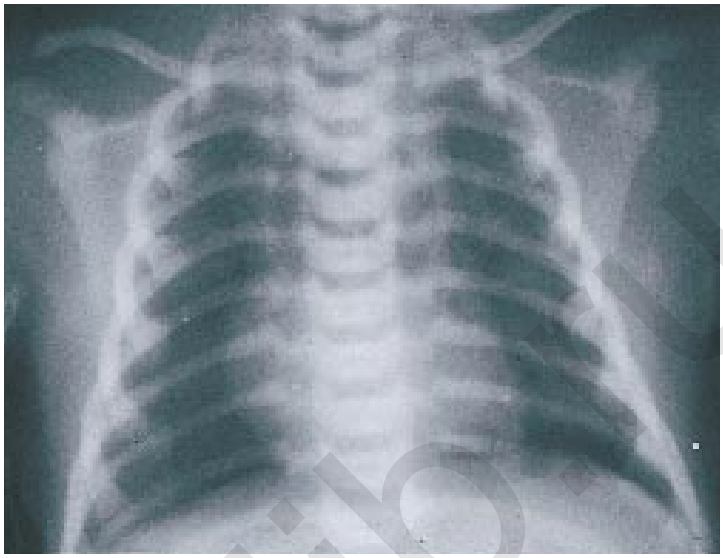

Figure 7.58. Radiograph of the chest of an infant with a translucent circular mediastinal shadow. If the radiograph is taken through the top of the incubator, it may give artifactual shadows such as this one caused by the hole in an Isolette™ .

7.59

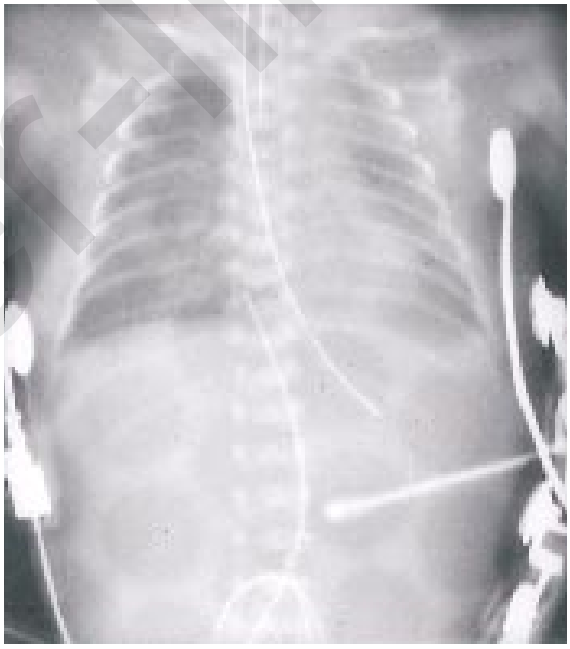

Figure 7.59. Radiograph of chest and abdomen showing artifactual shadows from placement of the infant on an air mattress. It is important to be aware of these possible artifacts when reviewing radiographic films.

7.60

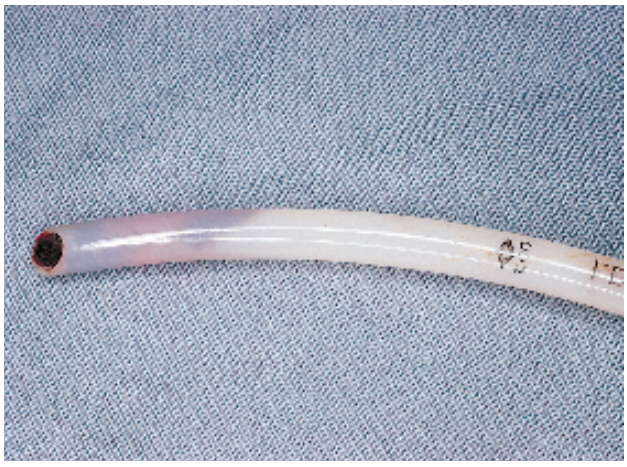

Figure 7.60. An infant with respiratory distress developed acute deterioration. It was noted that there was poor movement of air into the lungs. On removing the nasotracheal tube a blood clot was found to be obstructing the tube. With replacement of the tube there was rapid improvement.

7.61

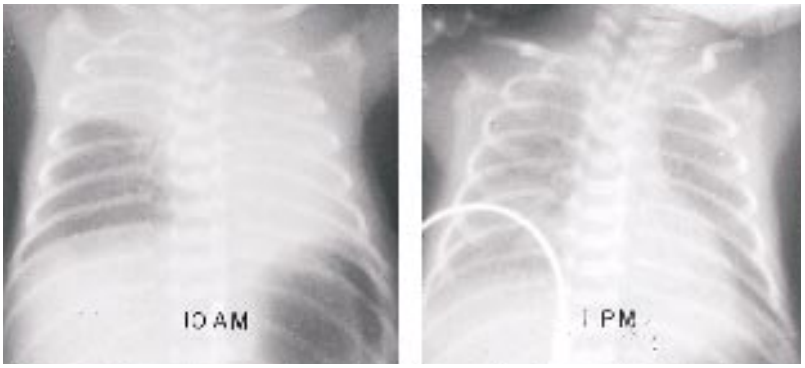

Figure 7.61. Serial chest radiographs of an infant with left lung and right upper lobe opacification as the result of right mainstem bronchus intubation (left). After repositioning the endotracheal tube there was rapid resolution of the atelectasis (right).

7.62

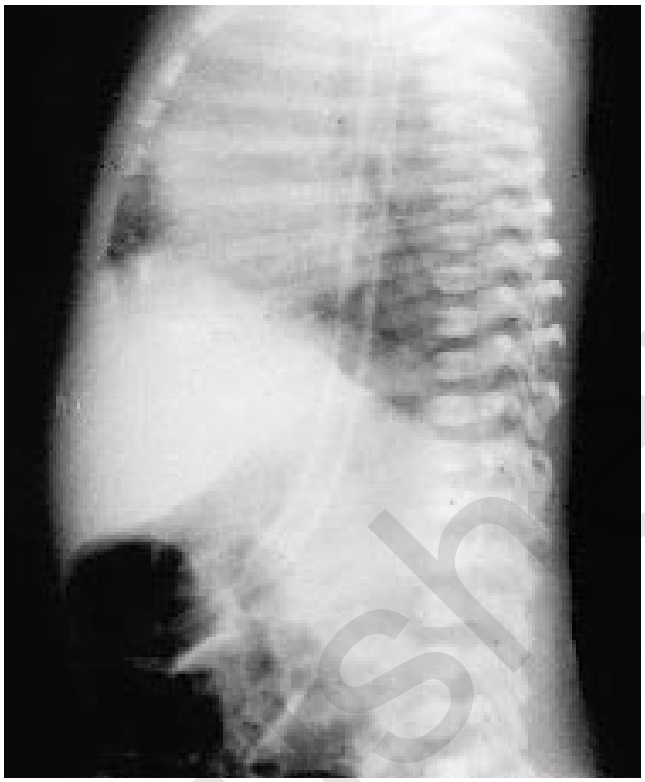

Figure 7.62. Lateral view of the chest and abdomen in an infant who has a "swallowed endotracheal tube." Note that the endotracheal tube is a cuffed tube which is rarely used at the present time. During resuscitation instead of endotracheal intubation the esophagus was inadvertently intubated and the tube was swallowed. This was successfully removed without any complication.

7.63

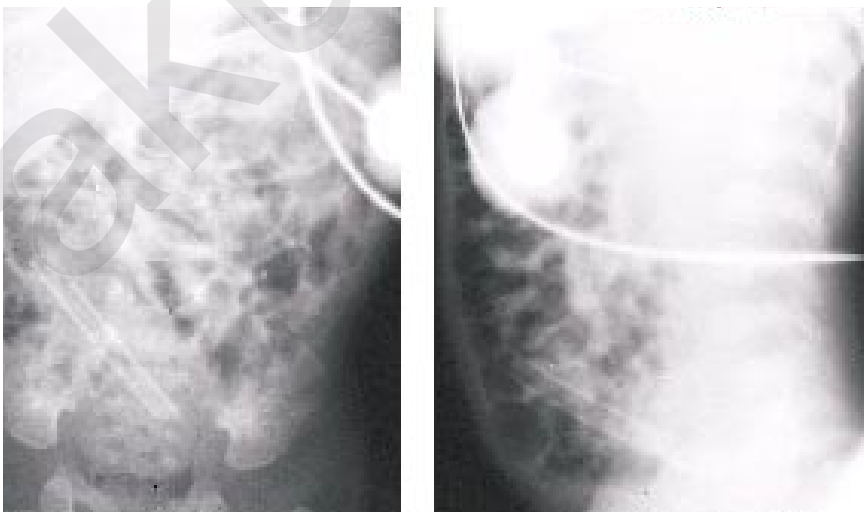

Figure 7.63. Abdominal radiographs of an infant who "swallowed a nasal CPAP tube." The tube was recovered in the stool 11 days later. (Singleton, E.)

7.64

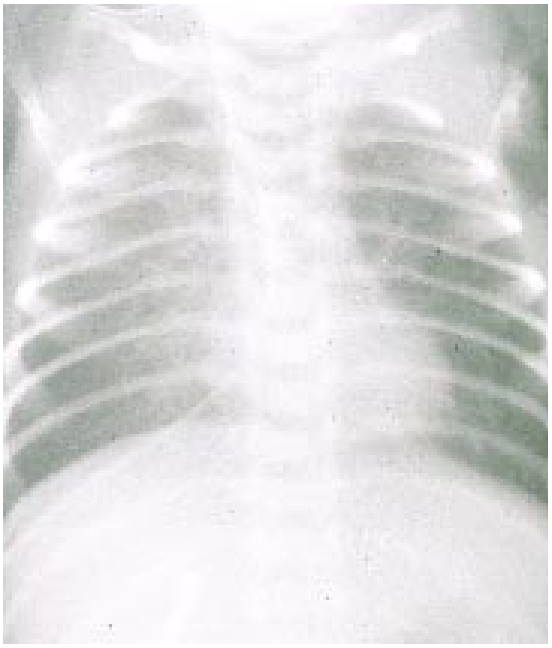

Figure 7.64. This infant developed increasing respiratory distress. Radiography of the chest showed abnormal placement of the feeding tube that tracks into the right thorax. Associated with this are increased infiltrates, most prominent in the right lung. The abnormal placement of the feeding tube occurred as a result of esophageal perforation.

7.65

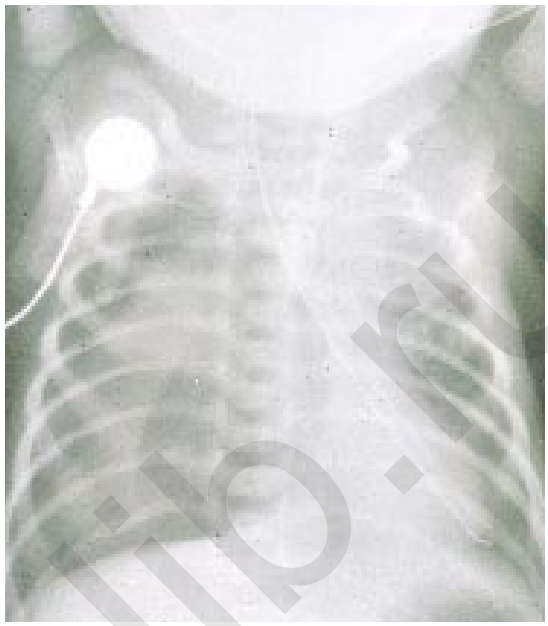

Figure 7.65. Radiograph of the chest of the same infant 24 hours later showing a right-sided pneumothorax and placement of the nasogastric feeding tube in the left thorax as the result of esophageal perforation. It should be noted that the feeding tube may pass either to the right or left side of the chest. Spontaneous perforation of the esophagus (Boerhaave's syndrome) does occur, but would be extremely rare in a neonate. Neonatal perforation is usually associated with trauma such as from a feeding tube.

7.66

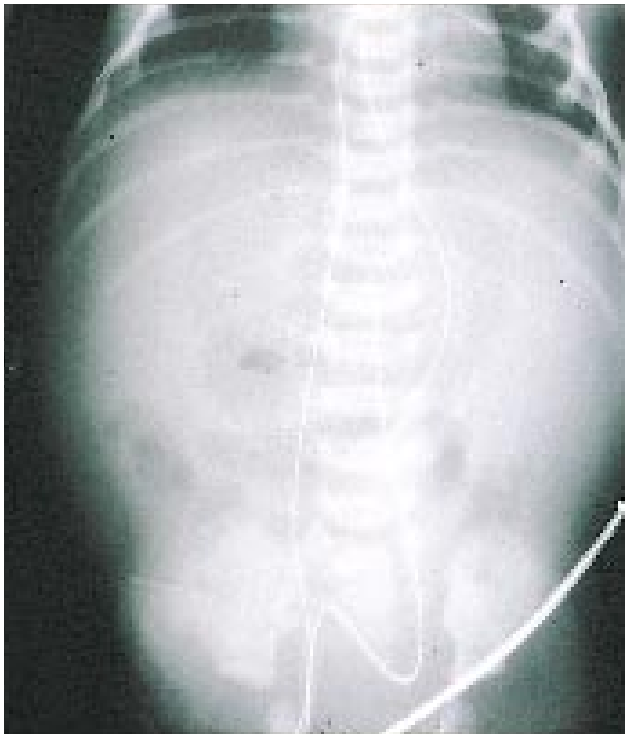

Figure 7.66. Abdominal radiograph of an infant with pneumoperitoneum as a result of nasogastric tube perforation of the stomach. Note the midline lucency, the "football sign," with visible falciform ligament. Perforation of the stomach may occur spontaneously as a result of a weakness in the wall of the stomach. It is also reported from placement of feeding catheters. Application of suction, especially if the catheter tip is up against the stomach wall, can cause damage. (Singleton, E.)

7.67

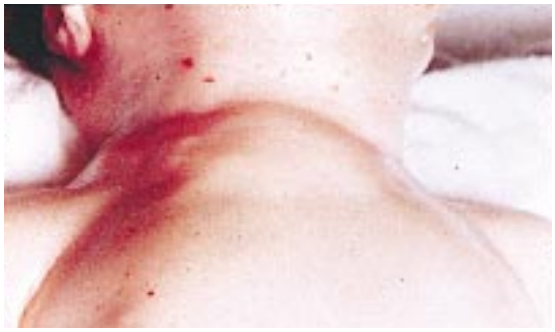

Figure 7.67. Soft tissue swelling of the neck was crepitant to palpation. This infant developed subcutaneous emphysema as a result of resuscitation. The subcutaneous emphysema absorbs spontaneously.

7.68

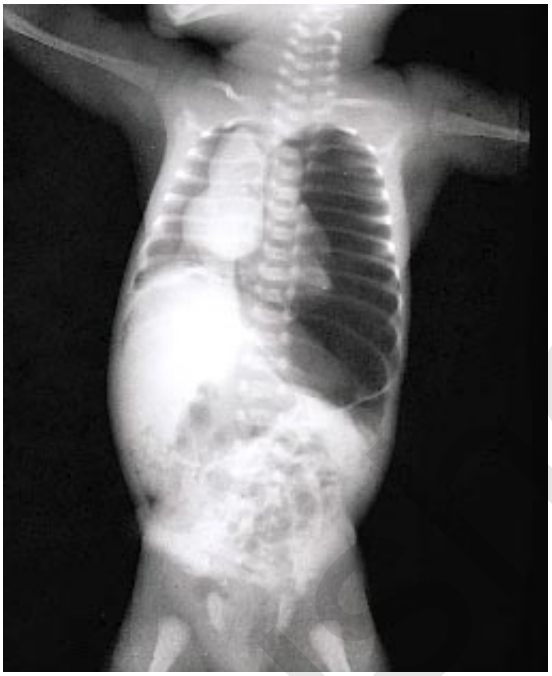

Figure 7.68. Radiograph of the chest and abdomen in an infant showing massive left pneumothorax and pneumomediastinum with displacement of the heart to the right side. On the right side some air is noted between the diaphragm and the upper border of the liver. This is a mild pneumoperitoneum from tracking down of air from the pneumomediastinum. This iatrogenic pathology occurred with vigorous bag and mask resuscitation using excessive pressures.

7.69

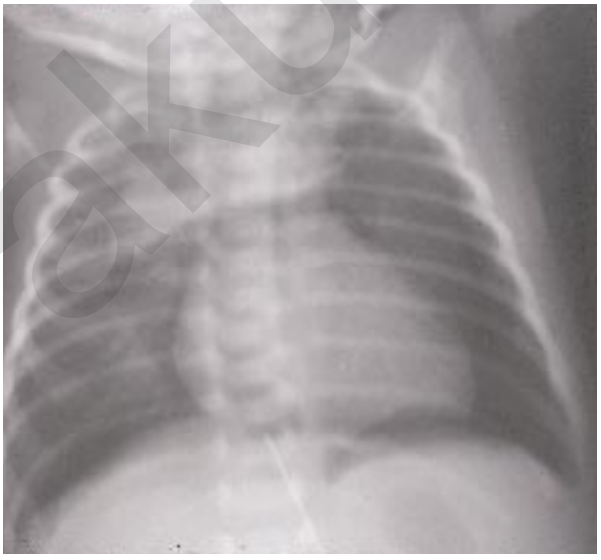

Figure 7.69. Radiograph of the chest in an infant requiring resuscitation at delivery. Note the pneumomediastinum with the lobes of the thymus gland being very prominent bilaterally ("butterfly wing" appearance) as a result of the air in the pneumomediastinum lifting up the lobes of the thymus.

7.70

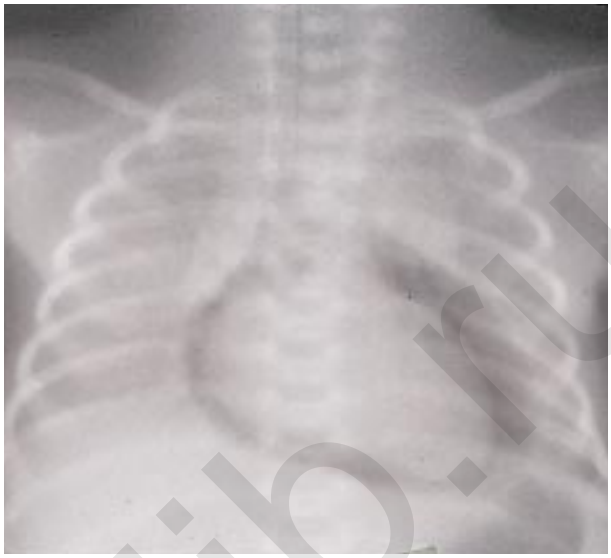

Figure 7.70. Radiograph of the chest in an infant with severe respiratory distress who developed a pneumopericardium causing cardiovascular instability.

7.71

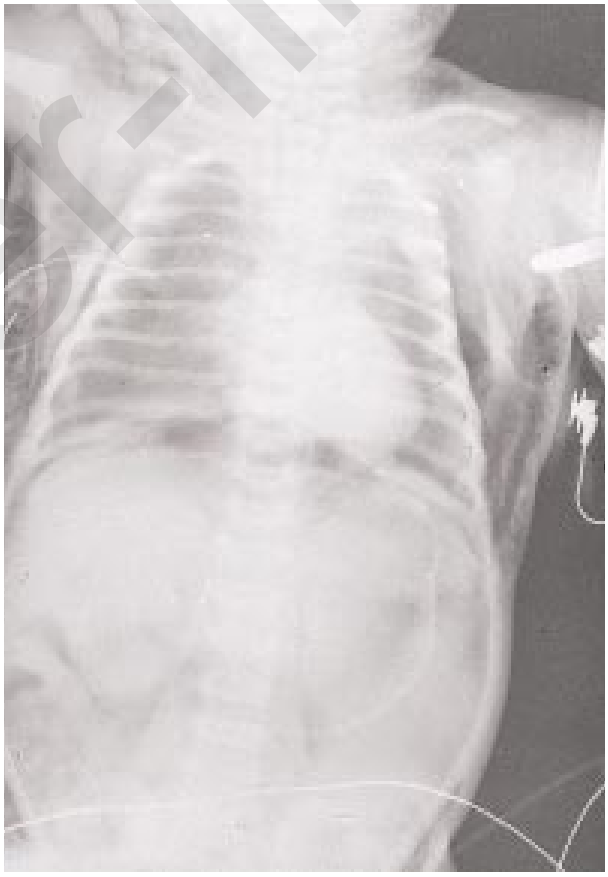

Figure 7.71. Chest and abdominal radiograph in an infant with massive air leak. Note the pneumothorax, pneumomediastinum, pneumoperitoneum and subcutaneous emphysema. This problem occurred as a result of the use of excessive pressures in ventilating the infant.

7.72

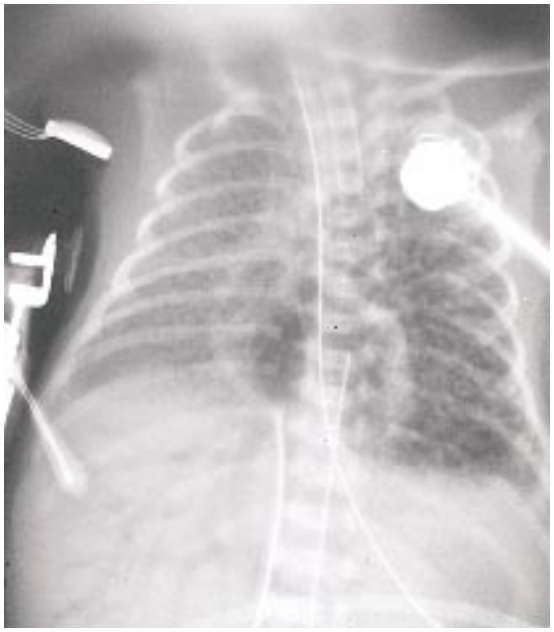

Figure 7.72. Radiograph in an infant with massive air embolism. Note the presence of air in the heart and in the vascular bed of the liver.

7.73

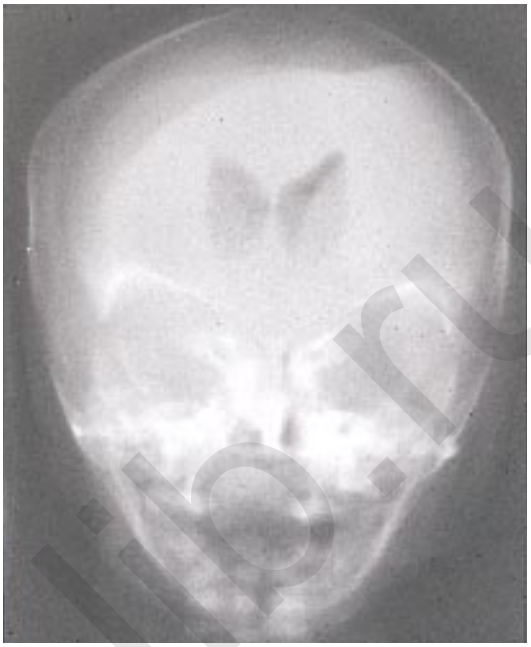

Figure 7.73. A plain radiograph of the skull in the same infant with massive air embolism shows air in the ventricular collecting system. There was also an associated large intraventricular hemorrhage. Massive air embolism is a rare complication of excessive positive pressure resuscitation or ventilation.

7.74

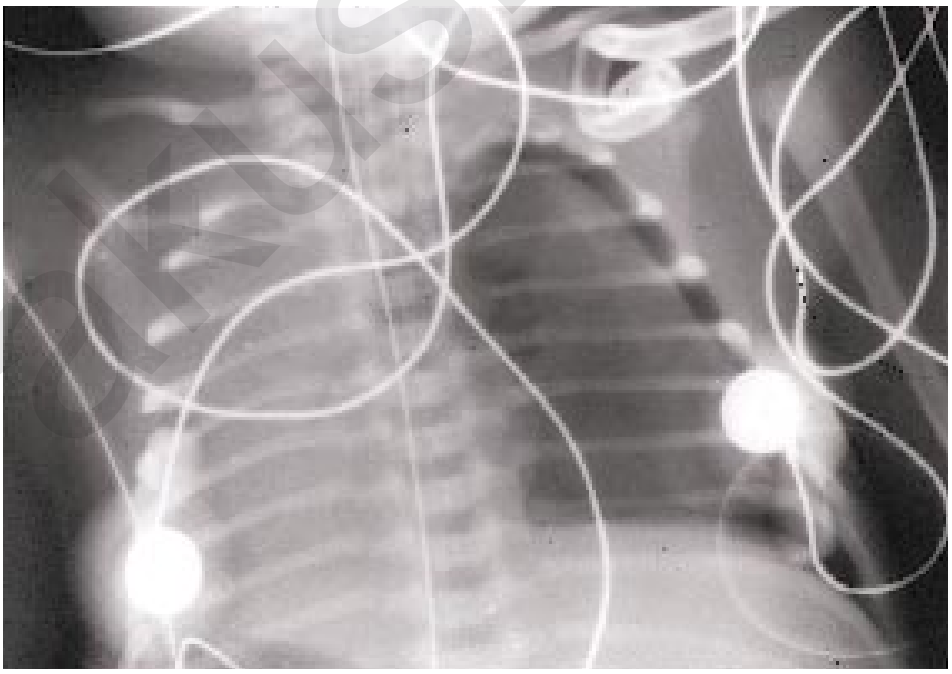

Figure 7.74. Radiograph of the chest of an infant with a left-sided pneumothorax. Note the superior location of the improperly placed chest tube which is lying outside the left thorax.

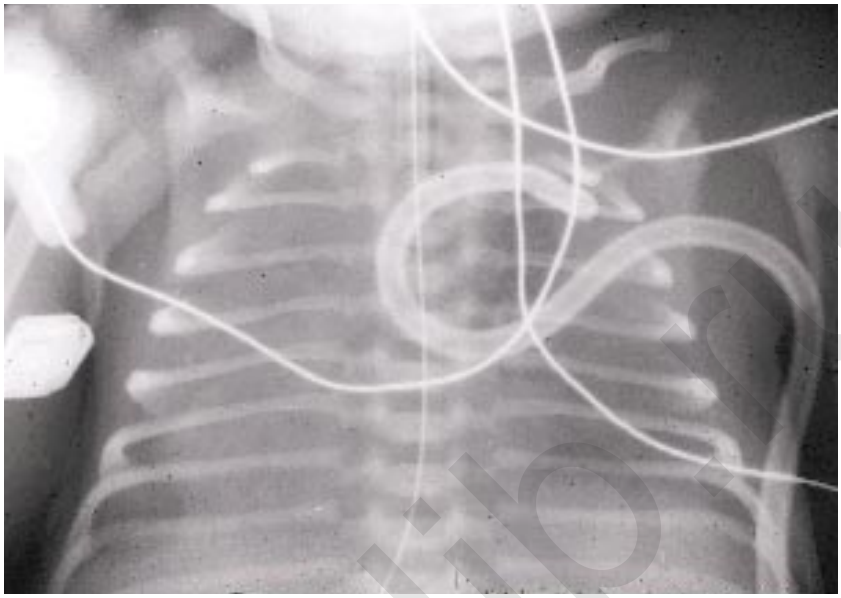

7.75

Figure 7.75. Radiograph of the chest of the same infant with rapid resolution of the pneumothorax after proper placement of the chest tube into the left thorax.

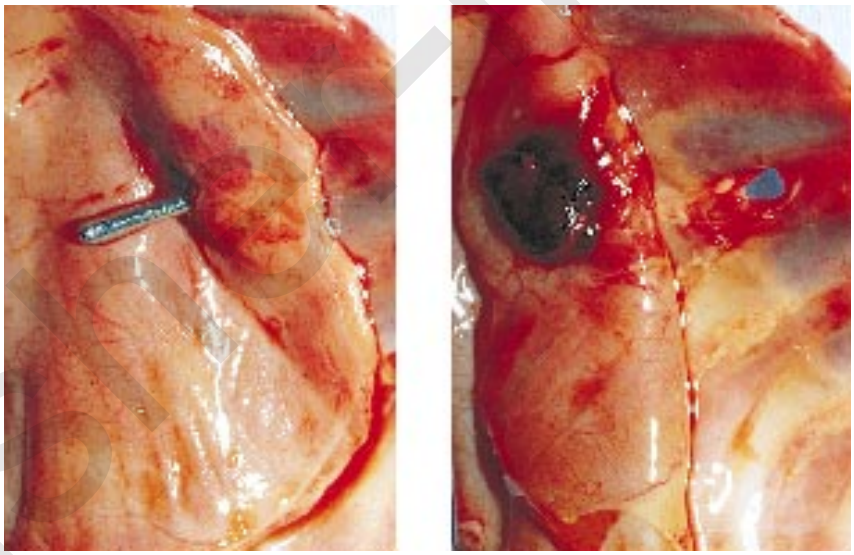

7.76

Figure 7.76. This low birth weight infant (birth weight 1440 g) developed a large pneumothorax on the right side. A chest tube was placed in the right sixth intercostal space in the anterior axillary line. The tube perforated the diaphragm and liver resulting in massive hemorrhage from the liver. At autopsy the figure on the left shows the placement of the tube through the chest wall with damage to the diaphragm. The figure on the right shows the perforation of the diaphragm which then resulted in damage to the liver and hemorrhage.

7.77

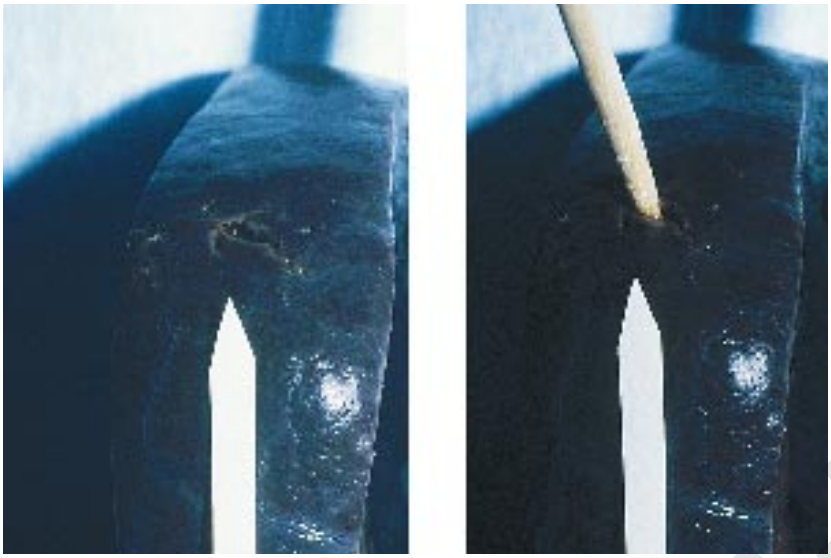

Figure 7.77. Autopsy specimen of the liver from the same infant. Note the laceration of the liver which resulted in the hemorrhage.

7.78

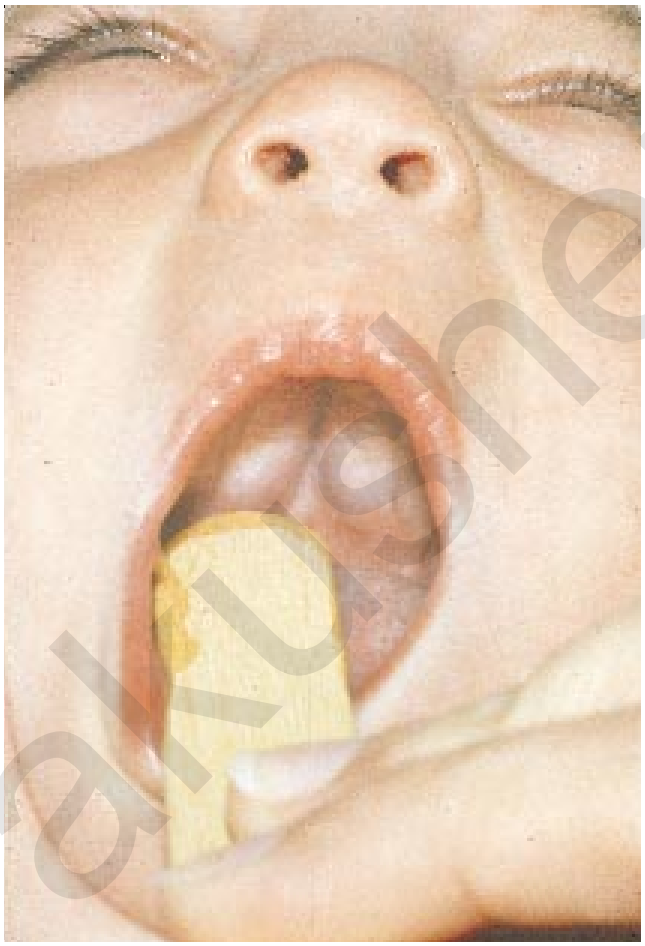

Figure 7.78. As the result of prolonged endotracheal tube intubation this infant developed ridging of the hard palate with a subsequent high arch.

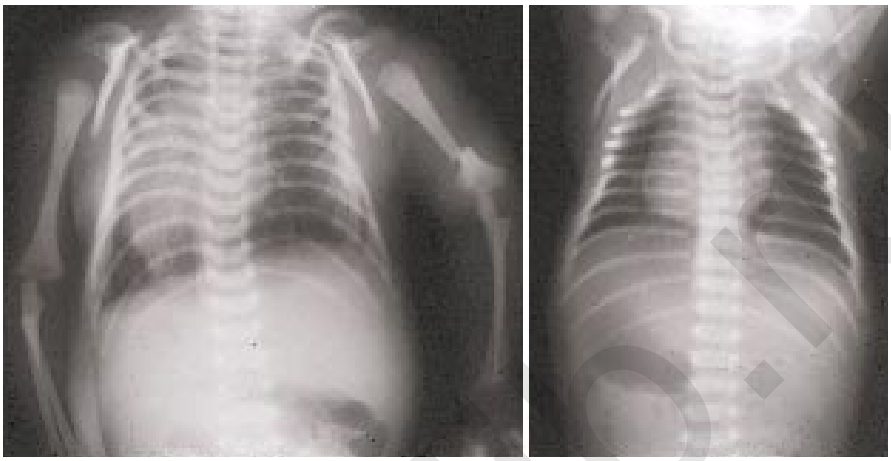

7.79

Figure 7.79. Radiographs of the chest in an infant with (on the left) an apparently normal chest soon after birth. On the right, 2 weeks later, note the fracture of the right humerus and fractures of the ribs. The etiology was obscure but was thought to be iatrogenic.

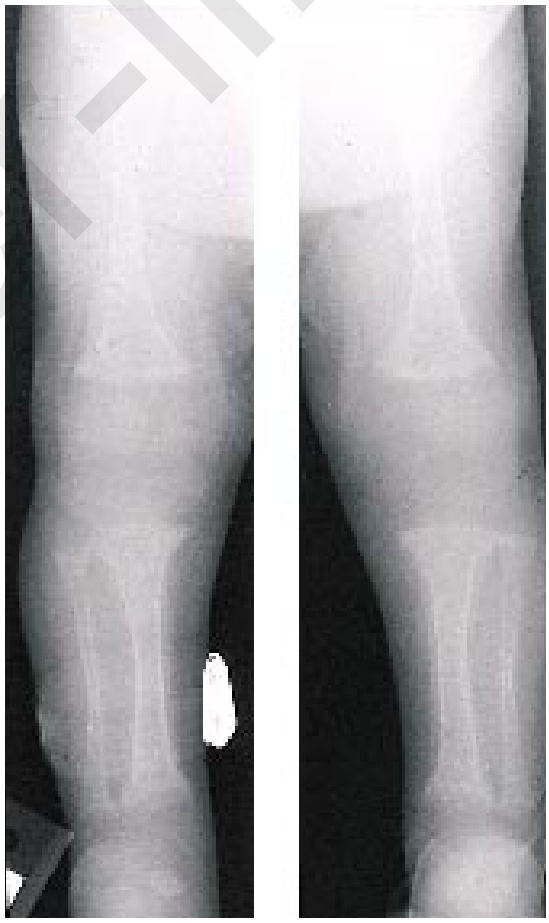

7.80

Figure 7.80. Radiograph of the lower extremities in an infant with bronchopulmonary dysplasia who developed rickets. Note the poor mineralization of the bones with metaphyseal flaring and cupping.

Index

VOLUME 2

Musculoskeletal Disorders and Congenital Deformities

Atlas of the Newborn

Rudolph

VOLUME 2

Musculoskeletal Disorders and Congenital Deformities

Atlas of the Newborn

Arnold J. Rudolph, M.D.
(Deceased)
Professor of Pediatrics
Baylor Medical College
Houston, Texas

VOLUME 2

Musculoskeletal Disorders and Congenital Deformities

Atlas of the Newborn

Arnold J. Rudolph, M.D.

1997
B.C. Decker Inc.
Hamilton • London

B.C. Decker Inc.
4 Hughson Street South
P.O. Box 620, L.C.D. 1
Hamilton, Ontario L8N 3K7
Tel: 905 522-7017
Fax: 905 522-7839
e-mail: info@bcdecker.com

Printed in Canada

9697989900/BP/987654321

ISBN 1-55009-032-1

Sales and distribution

United States
Blackwell Science Inc.
Commerce Place
350 Main Street
Malden, MA 02148
U.S.A.
Tel: 1-800-215-1000

Canada
Copp Clark Ltd.
200 Adelaide Street West
3rd Floor
Toronto, Ontario
Canada M5H 1W7
Tel: 416-597-1616
Fax: 416-597-1617

Japan
Igaku-Shoin Ltd.
Tokyo International P.O. Box 5063
1-28-36 Hongo, Bunkyo-ku
Tokyo 113, Japan
Tel: 3 3817 5680
Fax: 3 3815 7805

U.K., Europe, Scandinavia, Middle East
Blackwell Science Ltd.
c/o Marston Book Services Ltd.
P.O. Box 87
Oxford OX2 0DT
England
Tel: 44-1865-79115

Australia
Blackwell Science Pty, Ltd.
54 University Street
Carleton, Victoria 3053
Australia
Tel: 03 9347 0300
Fax: 03 9349 3016

Notice: the authors and publisher have made every effort to ensure that the patient care recommended herein, including choice of drugs and drug dosages, is in accord with the accepted standard and practice at the time of publication. However, since research and regulation constantly change clinical standards, the reader is urged to check the product information sheet included in the package of each drug, which includes recommended doses, warnings, and contraindications. This is particularly important with new or infrequently used drugs.

Foreword

Sir William Osler stated, "There is no more difficult task in medicine than the art of observation." The late Arnold Jack Rudolph was an internationally renowned neonatologist, a teacher's teacher, and, above all, one who constantly reminded us about how much could be learned by simply observing, in his case, the newborn infant.

This color atlas of neonatology represents a distillation of more than 50 years of observing normal and abnormal newborn infants. The *Atlas* begins with a section on the placenta, its membranes, and the umbilical cord. Jack Rudolph delighted in giving a lecture entitled "Don't Make Mirth of the Afterbirth," in which he captivated audiences by showing them how much you could learn about the newborn infant from simply observing the placenta, its membranes, and the umbilical cord.

In a few more than 60 photomicrographs, we learn to read the placenta and gain insight into such disorders as intrauterine growth retardation, omphalitis, cytomegalic inclusion disease, congenital syphilis, and congenital neuroblastoma. Congenital abnormalities of every organ system are depicted along with the appearance of newborn infants who have been subjected in utero to a variety of different drugs, toxins, or chemicals. We also learn to appreciate the manifestations of birth trauma and abnormalities caused by abnormal intrauterine positioning.

More than 250 photographs are used to illustrate the field of neonatal dermatology. The collection of photographs used in this section is superior to that which I have seen in any other textbook or atlas of neonatology or dermatology; this section alone makes this reference a required addition to the library of any clinician interested in the care of infants and children. Photographs of the Kasabach-Merritt syndrome (cavernous hemangioma with thrombocytopenia), Klippel-Trénaunay syndrome, Turner's syndrome, Waardenburg's syndrome, neurocutaneous melanosis, mastocytosis (urticaria pigmentosa), and incontinentia pigmenti (Bloch-Sulzberger syndrome) are among the best that I have seen.

Cutaneous manifestations are associated with many perinatal infections. The varied manifestations of staphylococcal infection of the newborn are depicted vividly in photomicrographs of furunculosis, pyoderma, bullous impetigo, abscesses, parotitis, dacryocystitis, inastitis, cellulitis, omphalitis, and funisitis. Streptococcal cellulitis, *Haemophilus influenzae* cellulitis, and cutaneous manifestations of listeriosis all are depicted. There are numerous photomicrographs of congenital syphilis, showing the typical peripheral desquamative rash on the palms and soles, as well as other potential skin manifestations of congenital syphilis which may produce either vesicular, bullous, or ulcerative lesions. The various radiologic manifestations of congenital syphilis, including pneumonia alba, ascites, growth arrest lines, Wegner's sign, periostitis, and syphilitic osteochondritis, are depicted. Periostitis of the clavicle (Higouménaki's sign) is shown in a photograph that also depicts periostitis of the ribs. A beautiful photomicrograph of Wimberger's sign also has been included; this sign, which may appear in an infant with congenital syphilis, reveals radiolucency due to erosion of the medial aspect of the proximal tibial metaphysis.

The *Atlas* also includes a beautiful set of photographs which delineate the ophthalmologic examination of the newborn. Lesions which may result from trauma, infection, or congenital abnormalities are included. There are numerous photographs of the ocular manifestations of a variety of systemic diseases, such as Tay-Sachs disease, tuberous sclerosis, tyrosinase deficiency, and many more. Photographs of disturbances of each of the various organ systems, or disorders affecting such organ systems, also are included along with numerous photographs of different forms of dwarfism, nonchromosomal syndromes and associations, and chromosomal disorders. In short, this *Atlas* is the complete visual textbook of neonatology and will provide any

physician, nurse, or student with a distillation of 50 years of neonatal experience as viewed through the eyes of a master clinician.

Arnold Jack Rudolph was born in 1918, grew up in South Africa, and graduated from the Witwatersrand Medical School in 1940. Following residency training in pediatrics at the Transvaal Memorial Hospital for Children, he entered private pediatric practice in Johannesburg, South Africa. After almost a decade, he left South Africa and moved to Boston, where he served as a Senior Assistant Resident in Medicine at the Children's Medical Center in Boston, Massachusetts, and subsequently pursued fellowship training in neonatology at the same institution and at the Boston Lying-In Hospital, Children's Medical Center and Harvard Medical School under Dr. Clement A. Smith.

In 1961, Dr. Rudolph came to Baylor College of Medicine in Houston, Texas, the school at which he spent the remainder of his career. He was a master teacher, who received the outstanding teacher award from pediatric medical students on so many occasions that he was elected to the Outstanding Faculty Hall of Fame in 1982. Dr. Rudolph also received numerous awards over the years from the pediatric house staffs for his superb teaching skills.

He was the Director of the Newborn Section in the Department of Pediatrics at Baylor College of Medicine for many years, until he voluntarily relinquished that position in 1986 for reasons related to his health. Nevertheless, Jack Rudolph continued to work extraordinarily long hours in the care of the newborn infant, and was at the bedside teaching both students and house staff, as well as his colleagues, on a daily basis until just a few months before his death in July 1995.

Although Dr. Rudolph was the author or co-author of more than 100 published papers that appeared in the peer-reviewed medical literature, his most lasting contribution to neonatology and to pediatrics is in the legacy of the numerous medical students, house staff, fellows, and other colleagues whom he taught incessantly about how much one could learn from simply observing the newborn infant. This *Atlas* is a tour de force; it is a spectacular teaching tool that has been developed, collated, and presented by one of the finest clinical neonatologists in the history of medicine. It is an intensely personal volume that, as Dr. Rudolph himself states, "is not intended to rival standard neonatology texts," but rather to supplement them. This statement reveals Dr. Rudolph's innate modesty, since with the exception of some discussion on pathogenesis and treatment, it surpasses most neonatology texts in the wealth of clinical information that one can derive from viewing and imbibing its contents. We owe Dr. Rudolph and those who aided him in this work a debt of gratitude for making available to the medical community an unparalleled visual reference on the normal and abnormal newborn infant.

Ralph D. Feigin, M.D.
June 13, 1996

Preface

I first became attracted to the idea of producing a color atlas of neonatology many years ago. However, the impetus to synthesize my experience and compile this current collection was inspired by the frequent requests from medical students, pediatric house staff, nurses and others to provide them with a color atlas of the clinical material provided in my "slide shows." For the past few decades I have used the medium of color slides and radiographs as a teaching tool. In these weekly "slide shows" the normal and abnormal, as words never can, are illustrated.

"I cannot define an elephant but I know one when I see one."[1]

The collection of material used has been added to constantly with the support of the pediatric house staff who inform me to "bring your camera" whenever they see an unusual clinical finding or syndrome in the nurseries.

A thorough routine neonatal examination is the inalienable right of every infant. Most newborn babies are healthy and only a relatively small number may require special care. It is important to have the ability to distinguish normal variations and minor findings from the subtle early signs of problems. The theme that recurs most often is that careful clinical assessment, in the traditional sense, is the prerequisite and the essential foundation for understanding the disorders of the newborn. It requires familiarity with the wide range of normal, as well as dermatologic, cardiac, pulmonary, gastrointestinal, genitourinary, neurologic, and musculoskeletal disorders, genetics and syndromes. A background in general pediatrics and a working knowledge of obstetrics are essential. The general layout of the atlas is based on the above. Diseases are assigned to each section on the basis of the most frequent and obvious presenting sign. It seems probable that the findings depicted will change significantly in the decades to come. In this way duplication has been kept to a minimum. Additional space has been devoted to those areas of neonatal pathology (e.g., examination of the placenta, multiple births and iatrogenesis) which pose particular problems or cause clinical concern.

Obviously, because of limitations of space, it is impossible to be comprehensive and include every rare disorder or syndrome. I have tried to select both typical findings and variations in normal infants and those found in uncommon conditions. Some relevant conditions where individual variations need to be demonstrated are shown in more than one case.

As the present volume is essentially one of my personal experience, it is not intended to rival standard neonatology texts, but is presented as a supplement to them. It seems logical that references should be to standard texts or reviews where discussion on pathogenesis, treatment, and references to original works may be found.

Helen Mintz Hittner, M.D., has been kind enough to contribute the outstanding section on neonatal ophthalmology.

I have done my best to make the necessary acknowledgements to the various sources for the clinical material. If I have inadvertently omitted any of those, I apologize. My most sincere appreciation and thanks to Donna Hamburg, M.D., Kru Ferry, M.D., Michael Gomez, M.D., Virginia Schneider, PA, and Jeff Murray, M.D., who have spent innumerable hours in organizing and culling the material from my large collection. We wish to thank Abraham M. Rudolph, M.D., for his assistance in reviewing the material. We also wish to thank the following people for their photo contributions to this work: Cirilo Sotelo-Avila, Stan Connor, Avory Fanaroff, Milton Finegold, Brian Kershan, Tom Klima, Susan Landers, Gerardo Cabera-Meza, Ken Moise, Don Singer, Edward Singleton.

It is hoped that this atlas will provide neonatologists, pediatricians, family physicians, medical students and nurses with a basis for recognizing a broad spectrum of normal variations and clinical problems as well as provide them with an overall perspective of neonatology, a field in which there continues to be a rapid acceleration of knowledge and technology. One must bear in mind the caveat that pictures cannot supplant clinical experience in mastering the skill of visual recall.

1. Senile dementia of Alzheimer's type — normal aging or disease? (Editorial) *Lancet* 1989; i:476-477.

Arnold J. Rudolph, M.D.

CONTENTS

Volume II
Musculoskeletal Disorders and Congenital Deformities

Introduction

Although several texts provide extensive written descriptions of disorders of the newborn infant, the senses of touch, hearing and, especially, sight, create the most lasting impressions. Over a period of almost five decades, my brother Jack Rudolph diligently recorded in pictorial form his vast experiences in physical examination of the newborn infant. The *Atlas of the Newborn* reflects his selection from the thousands of color slides in his collection, and it truly represents the "art of medicine" as applied to neonatology. A number of unusual or rare conditions are included in this atlas. I consider this fully justified because, if one has not seen or heard of a condition, one cannot diagnose it.

This, the second of the five-volume series, includes three main topics: skeletal disorders, as well as dwarfism; multiple congenital anomaly syndromes; and chromosomal disorders.

Genetic skeletal disorders include a large group of anomalies which may be associated with dwarfism of various types, and may result in forcal structural or functional disorders. The examples of these disorders shorn in this volume draws attention to their appearance in the neonate, thus permitting early recognition of these anomalies.

Patients with multiple congenital anomaly syndromes and chromosomal disorders present a real challenge to the clinician, and recognition is often particularly difficult in the neonatal period. Although many descriptions of the various syndromes have been published, few provide good graphic examples. It is of utmost importance that these multiple congenital anomaly syndromes and chromosomal disorders be recognized as early as possible, so that appropriate therapeutic options, prognosis and recurrence risks can be presented to the families. The high quality photographs of various manifestations to these disorders will be of tremendous assistance to the clinician in recognizing them in the neonatal period.

This volume will be extremely valuable, not only to obstetricians, neonatologists and nurses involved in the perinatal period, but also to orthopaedists and clinical geneticists.

Abraham M. Rudolph, M.D.

Chapter 1
Musculoskeletal Disorders

Although some congenital musculoskeletal dysplasias are among the most obvious disorders of the neonate, they are also the most unusual. Congenital absence of all or part of a limb, deformities of the feet or hands, and lesions of the neck and trunk are rarely a diagnostic problem. The most common musculoskeletal dysplasias are among the most difficult to diagnose. Congenital hip dislocation may not be diagnosed even after repeated examination by experienced observers. Musculoskeletal infections complicating sepsis produce few subtle signs and may be easily overlooked. This is further complicated by the general concept that early diagnosis and treatment results in the greatest potential for normal growth and development of the infant. The examination of the musculoskeletal system should include inspection (e.g., looking for anomalies in contour position, and in spontaneous and reflex movement) and palpation (e.g., to determine if there are abnormalities in passive motion) and should be systematic to ensure completeness.

1.1

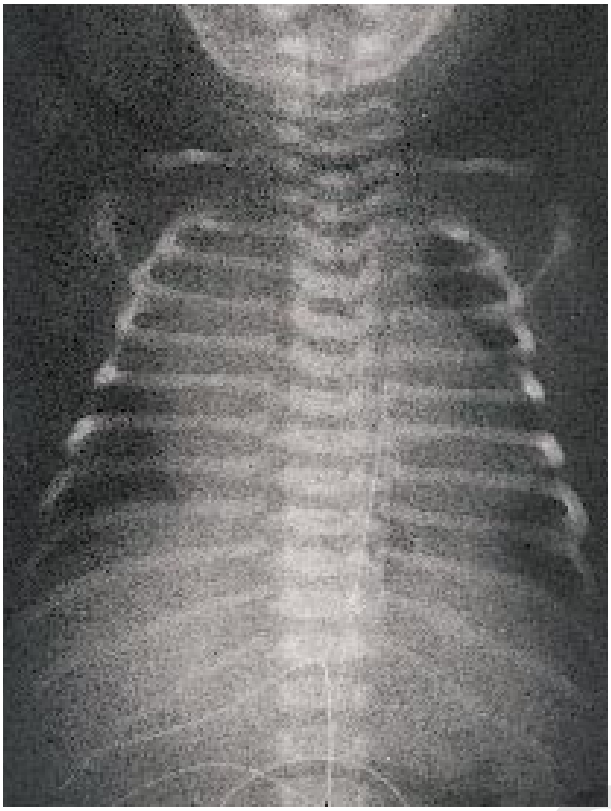

Figure 1.1. Chest radiograph showing 11 ribs. The presence of 11 ribs is not an uncommon finding in normal infants but occurs with greater frequency in infants with Down syndrome. Note the cardiac enlargement and enlarged thymus.

1.2

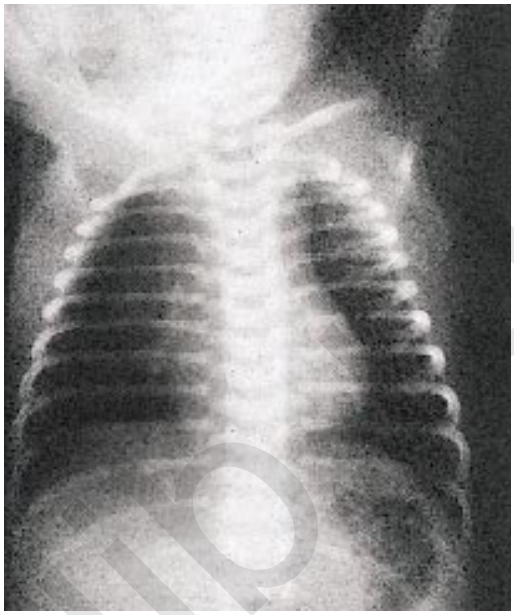

Figure 1.2. Radiograph showing 13 ribs bilaterally in an otherwise normal infant.

1.3

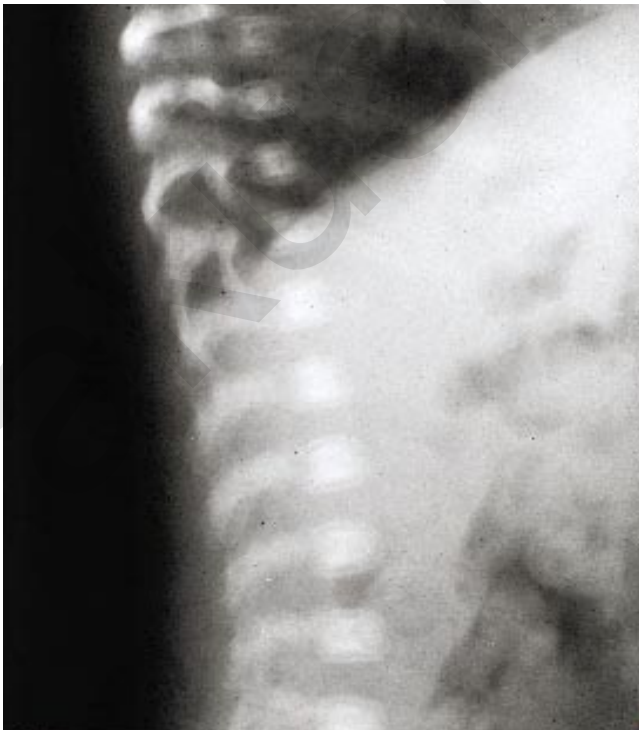

Figure 1.3. Lateral radiograph of the spine showing the "bone-in-bone" appearance of the vertebral bodies. This is a striking example of growth arrest but otherwise is a nonspecific finding.

1.4

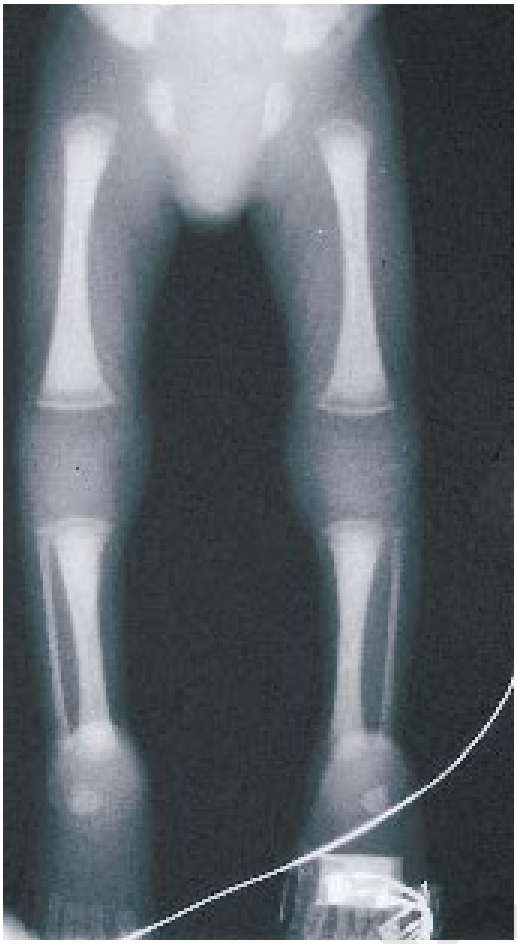

Figure 1.4. This figure shows the growth arrest lines in the long bones of a term infant with severe intrauterine growth retardation. Note the lack of the distal femoral and proximal tibial ossification centers, normally appearing at 36 and 38 weeks respectively, also caused by growth retardation. Hypothyroidism is also a consideration.

1.5

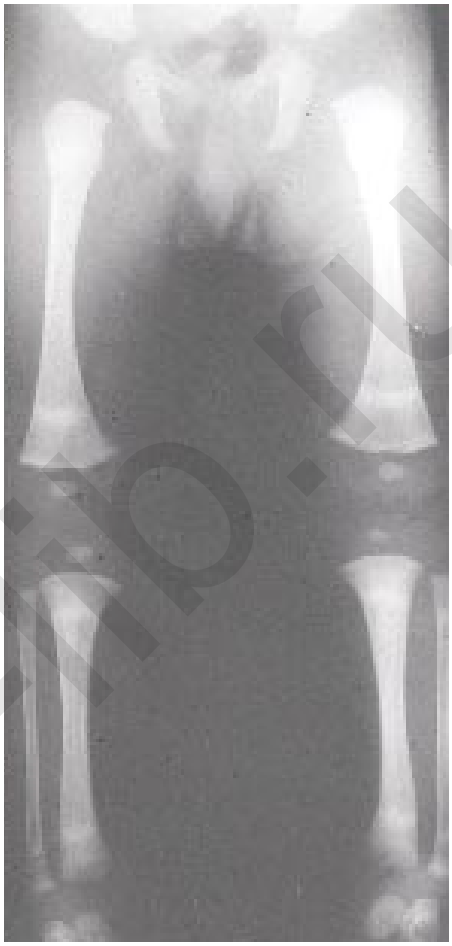

Figure 1.5. A radiograph of the lower extremities in a term infant showing the growth arrest lines. Note that in this infant the distal femoral tibial and proximal tibial ossification centers are present.

1.6

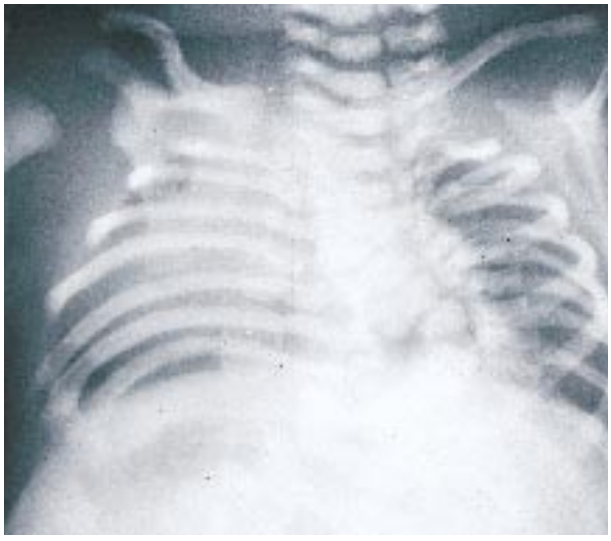

Figure 1.6. A radiograph showing faulty segmentation of vertebrae in an infant with rachischisis. This defect may be seen in infants with the VATER syndrome and other congenital anomalies.

Hemivertebrae may occur in the cervical or thoracic spine, and less commonly in the lumbar spine. An isolated hemivertebra may not be recognized clinically but can cause abnormal posture (scoliosis). More commonly, hemivertebrae are multiple and may be associated with other skeletal abnormalities, as in the ribs.

1.7

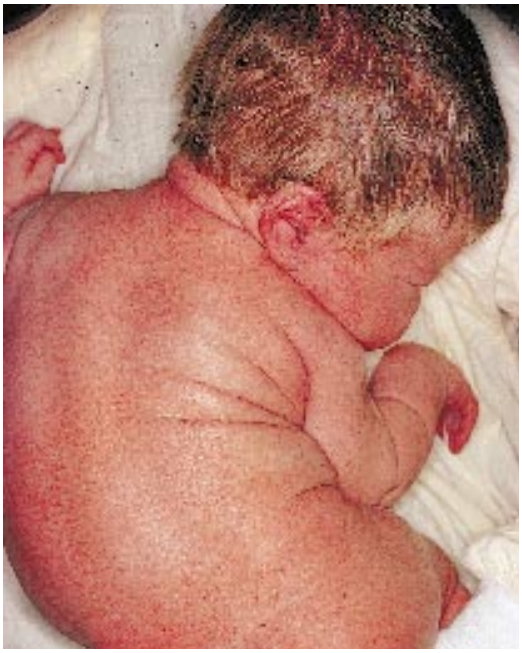

Figure 1.7. Congenital scoliosis is rare in neonates but may occur in association with structural anomalies of the vertebral spine. In this infant, the congenital scoliosis was associated with abnormal segmentation of vertebrae.

1.8

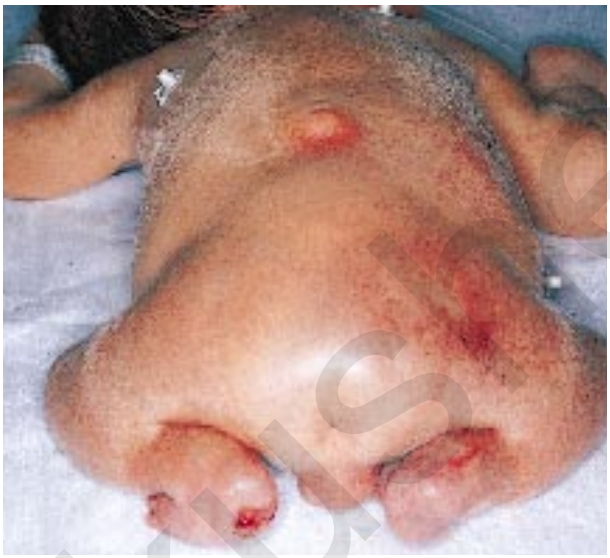

Figure 1.8. In this infant with caudal regression syndrome, the mother was a class B diabetic. Oligohydramnios was present, but renal function was normal in the infant. Note the arthrogryposis of the lower extremities.

1.9

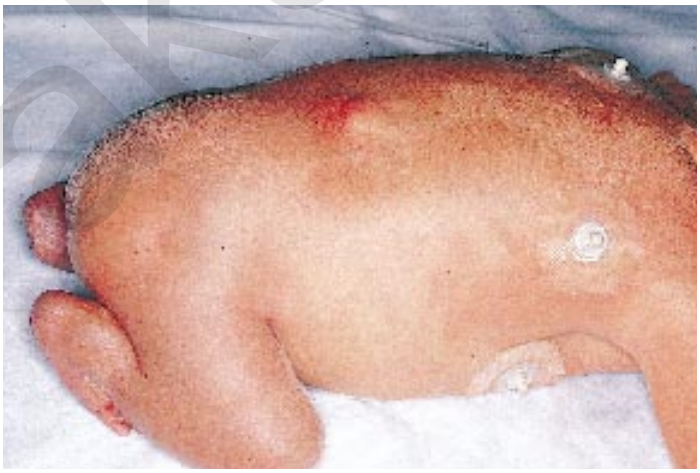

Figure 1.9. Lateral view of the same infant showing the prominent end of the spine and arthrogryposis of the lower extremities.

1.10

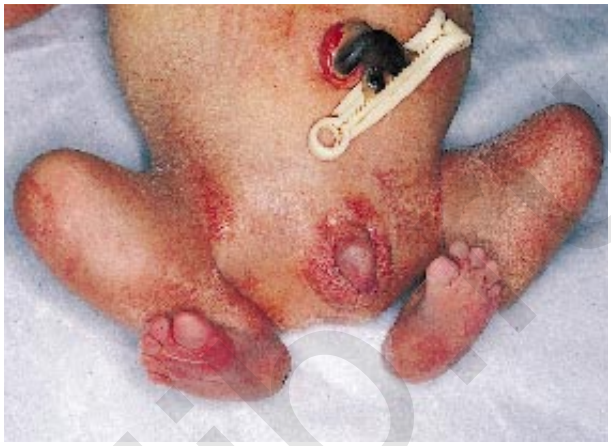

Figure 1.10. Frontal view of the same infant showing the short lower extremities due to the marked arthrogryposis affecting the hip, knee, and ankle joints. Infants with lumbosacral agenesis clinically adopt the so-called "Buddha" position.

1.11

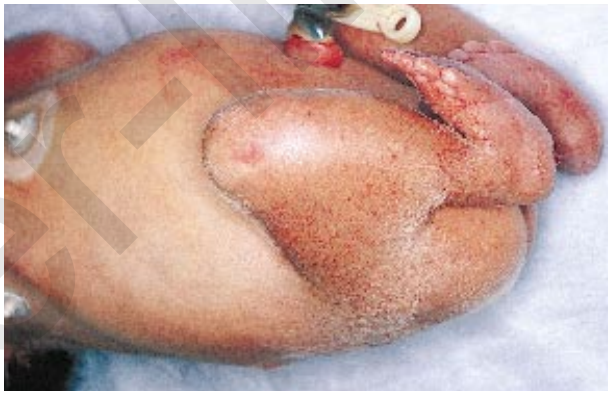

Figure 1.11. The same infant showing the arthrogryposis but note the dimple at the knee. Skin dimples such as this are associated with pressure over a joint and lack of movement.

1.12

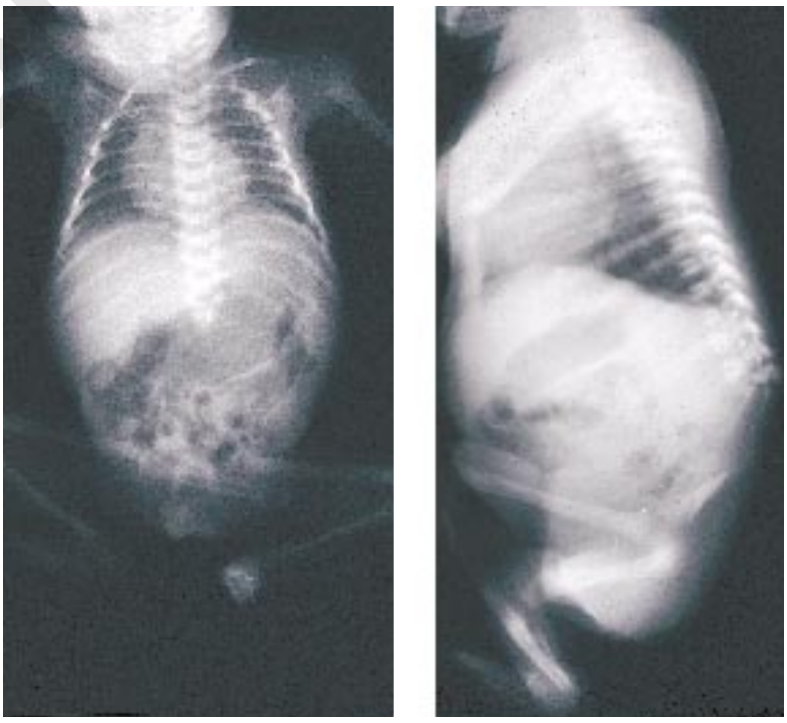

Figure 1.12. Anteroposterior and lateral radiographs demonstrating the lumbosacral agenesis.

1.13

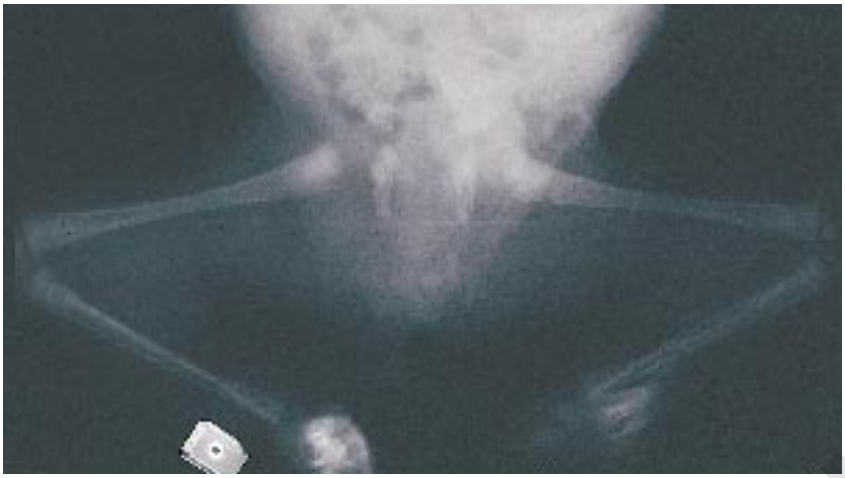

Figure 1.13. Radiograph of the lower extremities of the same infant. Note the abnormal development of the pelvis due to the lumbosacral agenesis, the thin, poorly developed bones and lack of muscle mass. This is due to lack of fetal movement and resulting arthrogryposis.

1.14

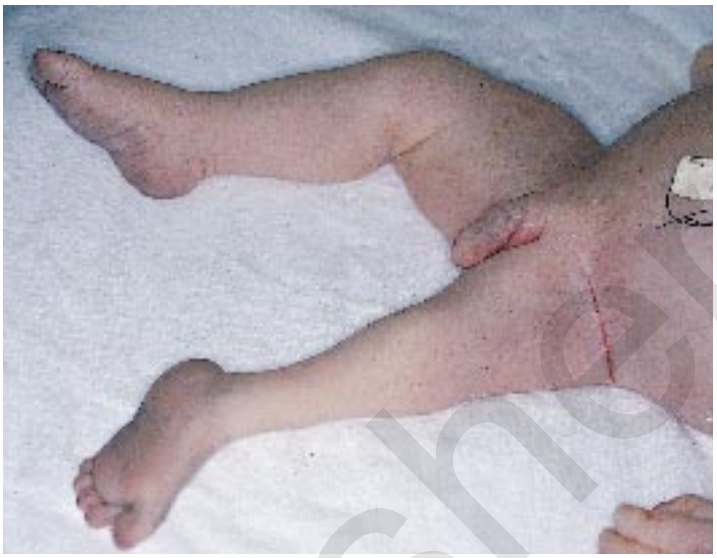

Figure 1.14. An asymmetric form of the caudal regression syndrome and hypoplastic left lower extremity associated with hypoplasia of muscles and sciatic nerve on the left side.

1.15

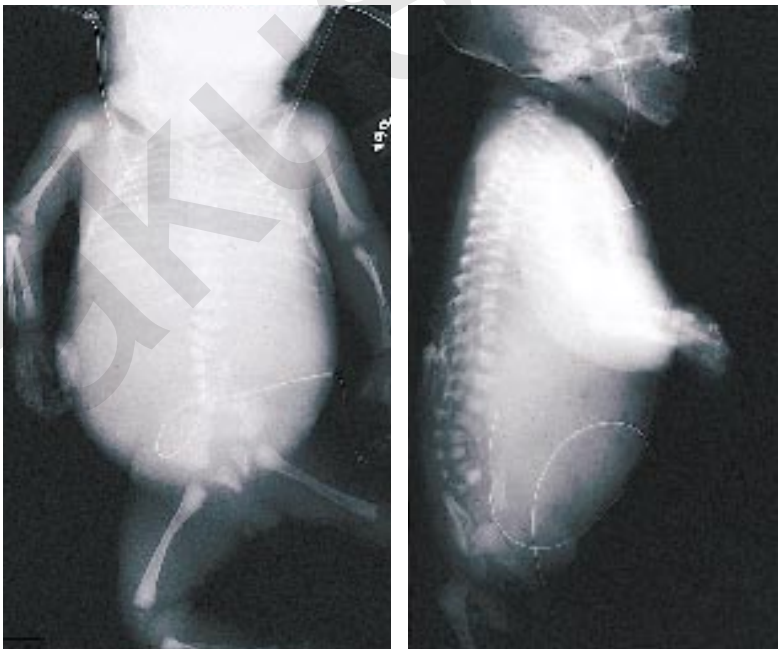

Figure 1.15. Anteroposterior and lateral radiographs of the same infant. Note the hemicaudal dysplasia. Also note the bilateral pulmonary hypoplasia.

1.16

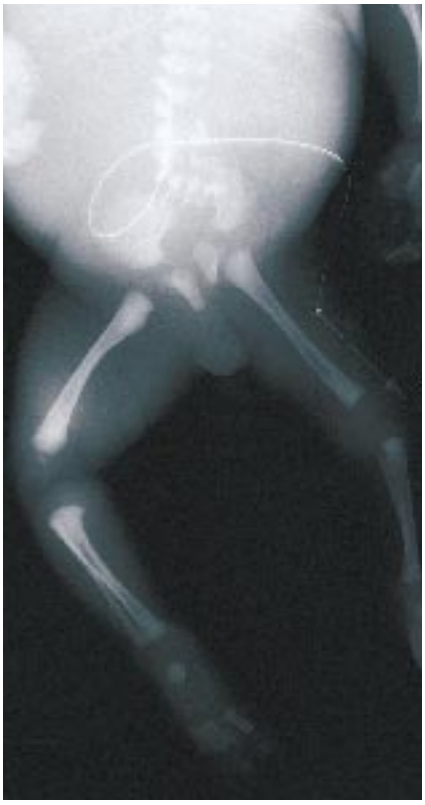

Figure 1.16. Close-up radiograph of the pelvis and lower extremities in the same infant. There are lumbar and sacral hemivertebrae with left scoliosis and vertebral fusion, hypoplasia of left pelvic bones, dislocation of the left hip, and a hypoplastic left lower extremity.

1.17

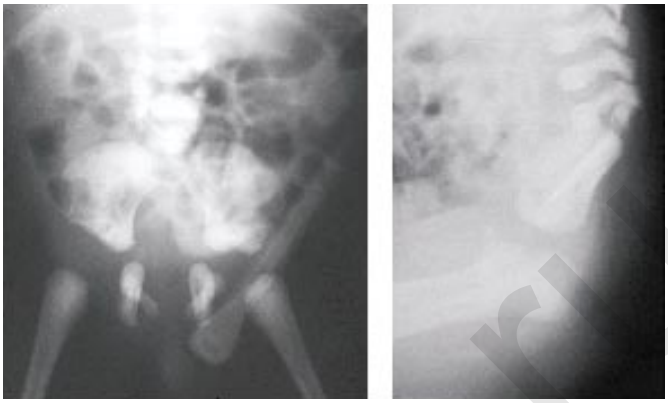

Figure 1.17. Anteroposterior and lateral radiograph of an infant with sacral agenesis, born to a diabetic mother. This is one of the classic abnormalities reported in infants of diabetic mothers.

1.18

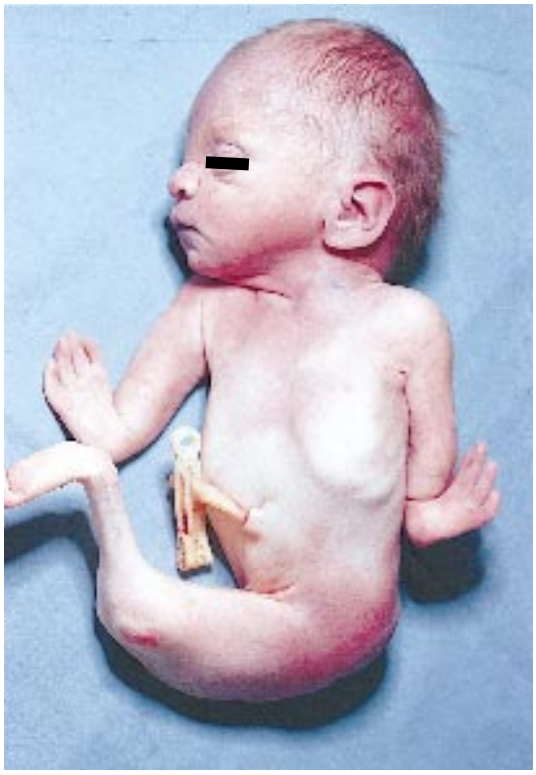

Figure 1.18. Sirenomelia ("mermaid" fetus) in an infant of a diabetic mother shows the severe postural deformities associated with the oligohydramnios which is always present in infants with sirenomelia because of renal agenesis. These infants typically lack an anus and have abnormal genitalia. Note the Potter facies, low-set ears, epicanthal folds and micrognathia associated with oligohydramnios and renal agenesis.

1.19

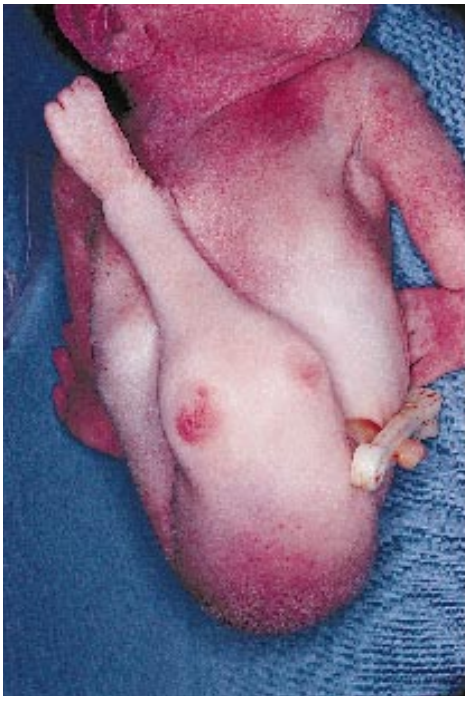

Figure 1.19. The same infant as in Fig. 1.18 placed in its position-of-comfort in utero. Note that the fused lower extremities give the typical appearance of a mermaid.

1.20

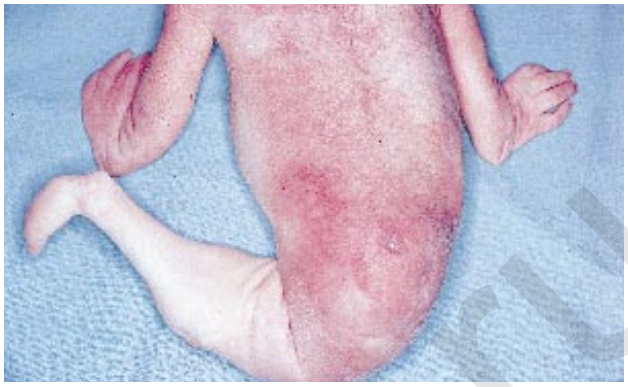

Figure 1.20. Note the anal atresia and postural deformities of the hands and lower body in the same infant.

1.21

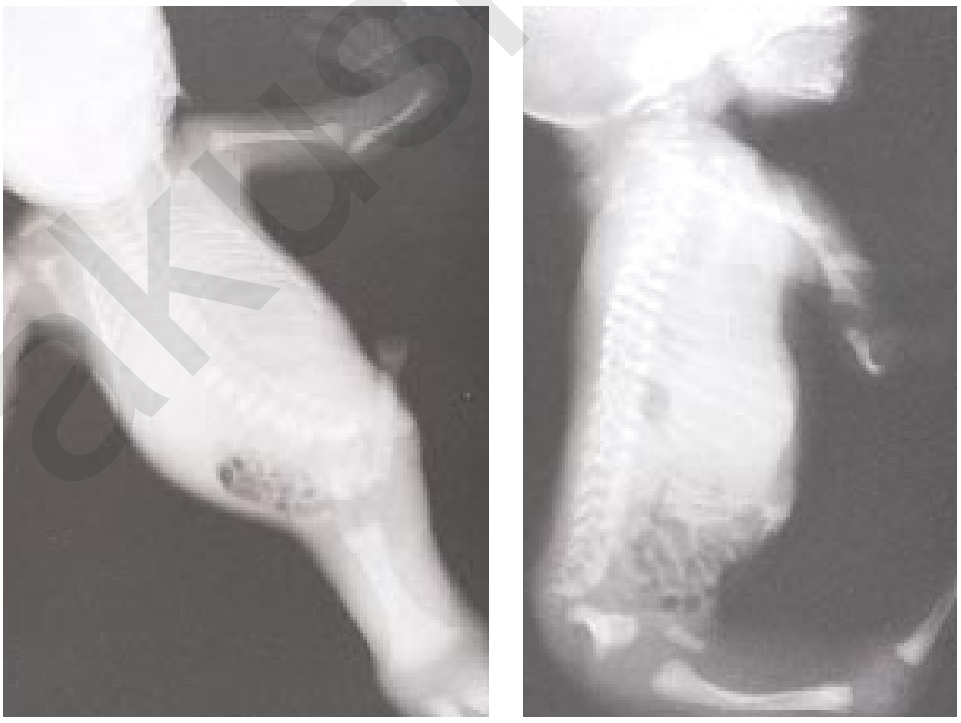

Figure 1.21. Anteroposterior and lateral radiographs of the same infant show the marked scoliosis, the abnormal pelvis and the fused femora.

1.22

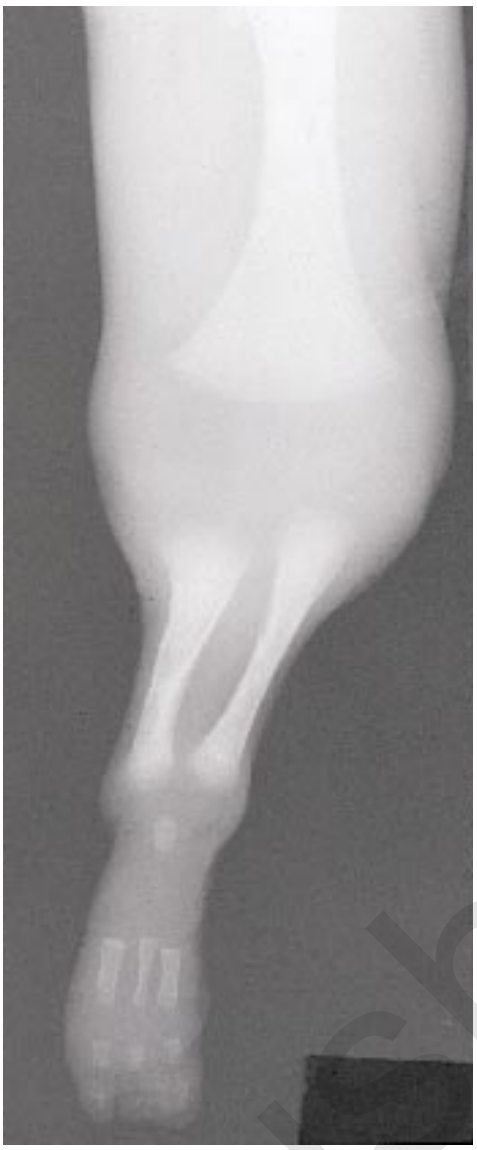

Figure 1.22. Radiograph of the same infant showing the fused femora, separate tibiae and abnormal development of the foot.

1.23

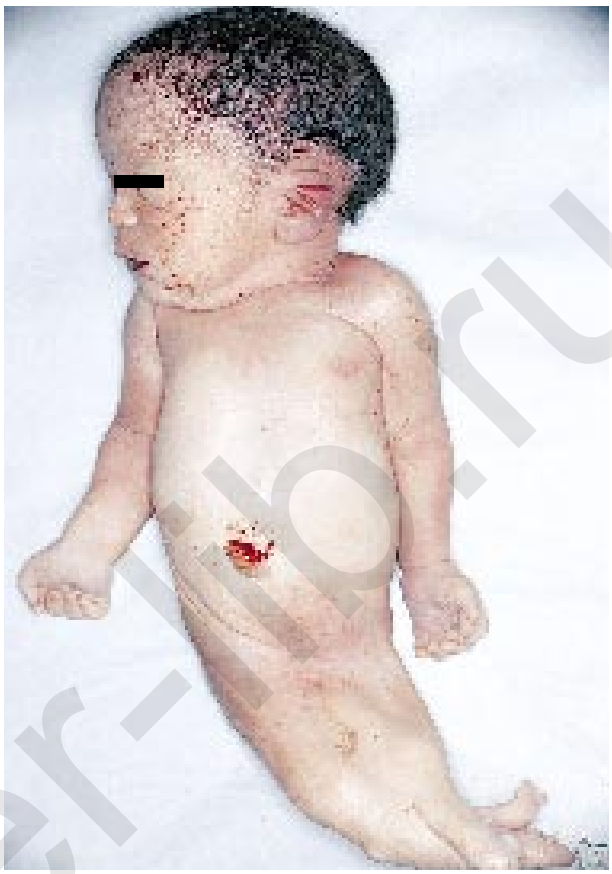

Figure 1.23. This infant of a diabetic mother exhibits sirenomelia with total lack of development of the genitalia and an imperforate anus. Associated with the renal agenesis is oligohydramnios; this infant also demonstrates the typical Potter facies. Note the low-set ear, flat nose and micrognathia.

1.24

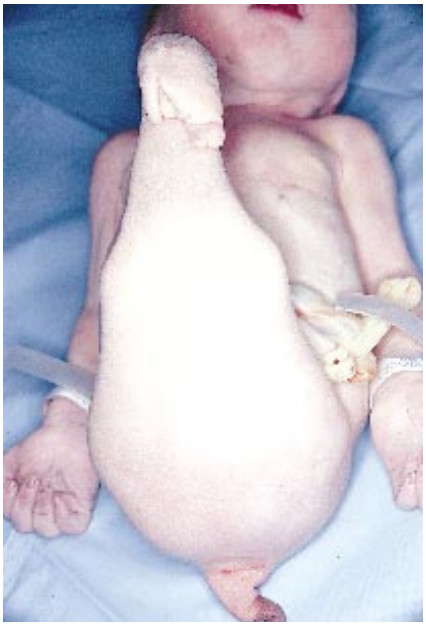

Figure 1.24. Sirenomelia in another infant of a diabetic mother; the infant had severe oligohydramnios associated with renal agenesis. There were no external genitalia and anal atresia was present, but note that this infant had a "tail" present.

1.25

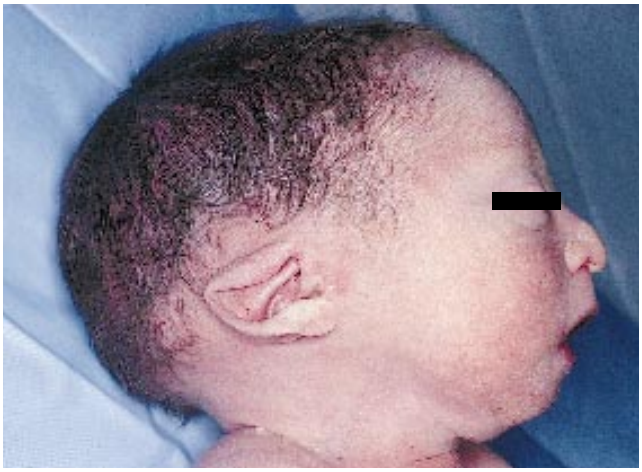

Figure 1.25. A close-up of the face of the same infant with the typical Potter facies associated with oligohydramnios and renal agenesis. Note the low-set abnormal ears, the flat nose, and micrognathia. Epicanthal folds were also present.

1.26

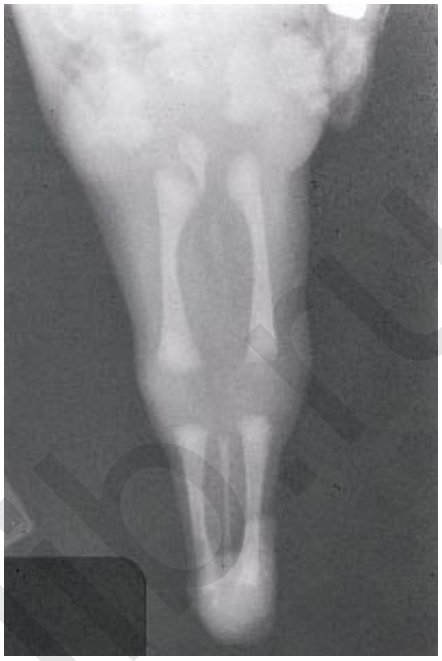

Figure 1.26. Radiograph of the lower extremities of the same infant with sirenomelia shows the presence of two separate femora with fusion of soft tissue, two separate tibiae, and a single fibula distally.

SKELETAL DEFICIENCIES

Skeletal deficiencies may be longitudinal defects which affect the limb on one side of the central axis or transverse defects in which the limb is truncated abruptly and the limb may terminate at any level but distal involvement is more common than proximal. Thus, radial aplasia with absence of the thumb and forefinger is characterized as a preaxial longitudinal hemimelia of the upper limb. Similarly, involvement of the lower limb would produce tibial aplasia. The affected limb will be curved toward the side of the deficiency and usually will be somewhat foreshortened. In transverse defects the defect closely resembles a congenital amputation but usually there is some degree of hypoplasia of the remaining proximal structures and the distal stump of the limb is not scarred but commonly small nubbins of tissue representing rudimentary digits may be present. Differentiation should be made between transverse defects, which are primary limb reduction defects, and secondary limb reduction defects which arise as a result of disruption.

1.27

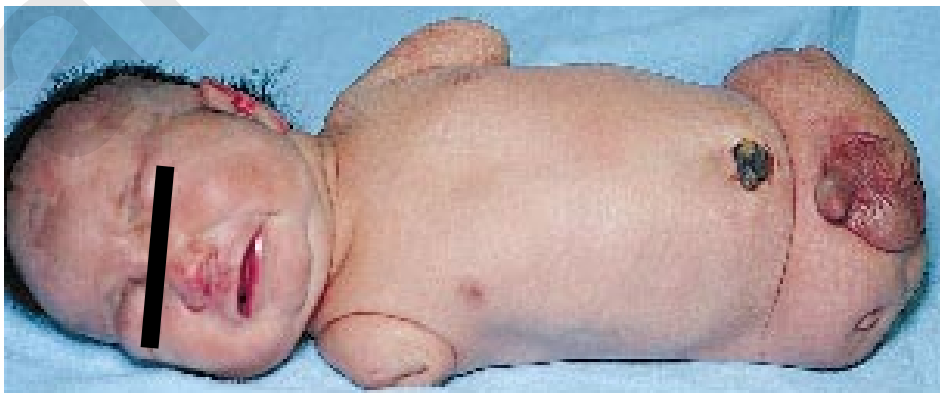

Figure 1.27. Amelia of all extremities (tetramelia). Amelia is absence of the entire limb structure. There was a history of consanguinity. Apart from the abnormalities of the extremities, this infant was normal.

1.28

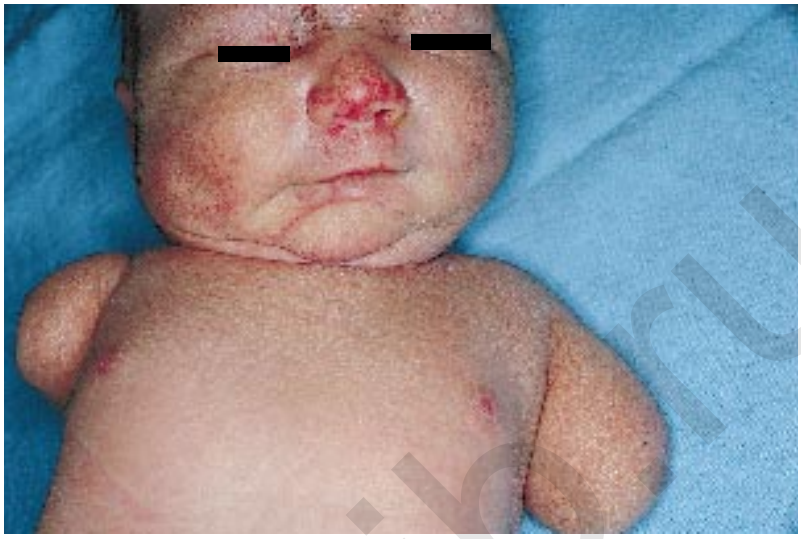

Figure 1.28. Close-up of the upper extremities of the same infant.

1.29

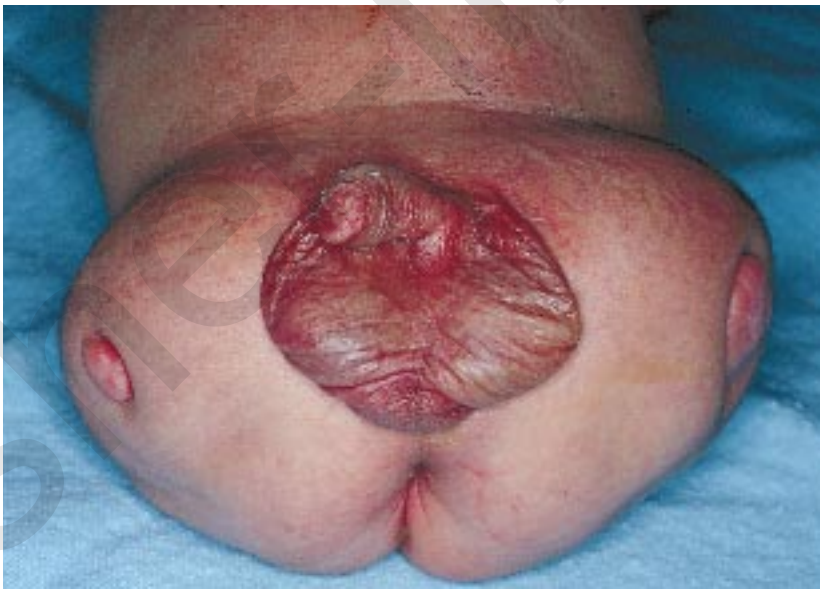

Figure 1.29. Close-up of the lower extremities of the same infant.

1.30

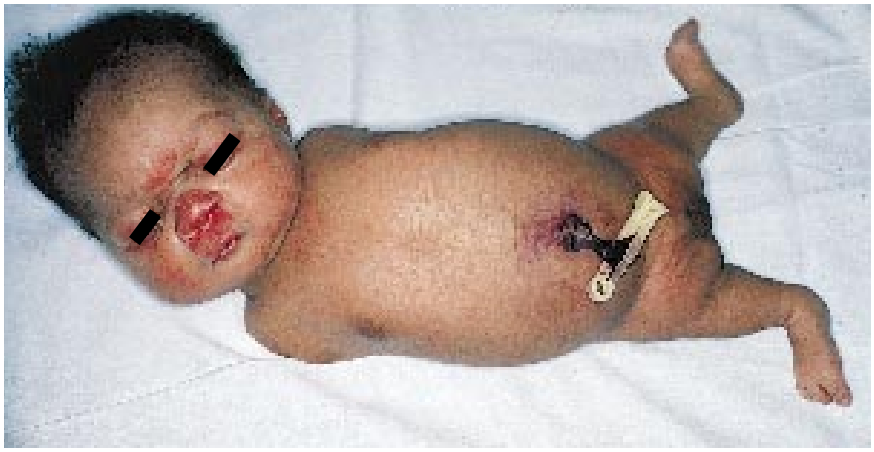

Figure 1.30. An infant with amelia of the upper extremities and ectromelia of the lower extremities. Ectromelia is the absence or incomplete development of the long bones of one or more of the limbs. This may represent the most extreme form of an intercalary defect. In total amelia, a form of ectromelia, no limb elements whatsoever are present.

1.31

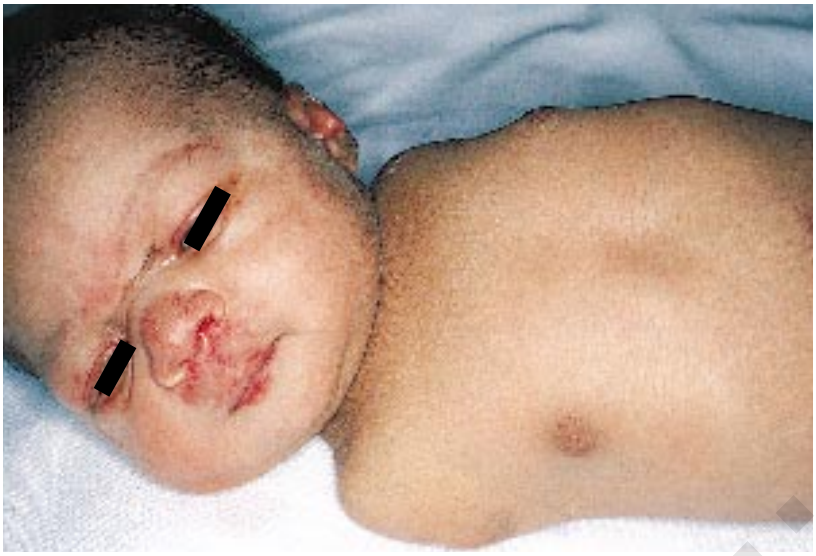

Figure 1.31. Close-up of amelia of upper extremities of the same infant. This infant had abnormal scapulae.

1.32

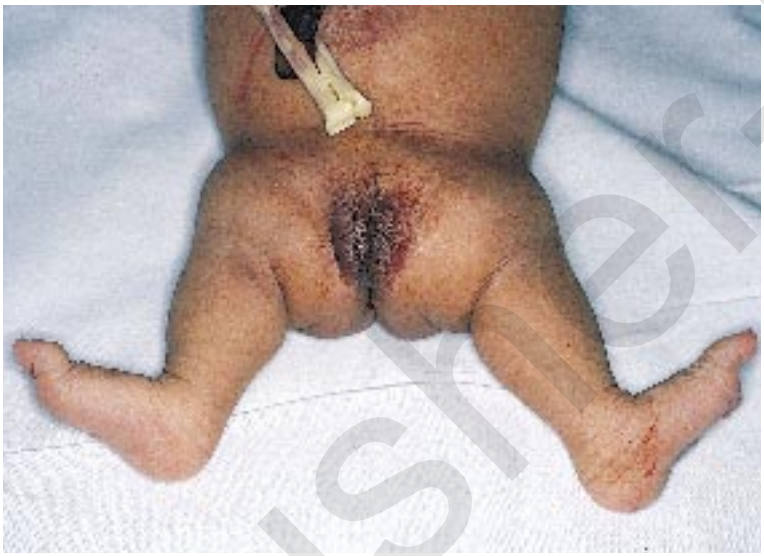

Figure 1.32. Close-up of ectromelia of the lower extremities of the same infant.

1.33

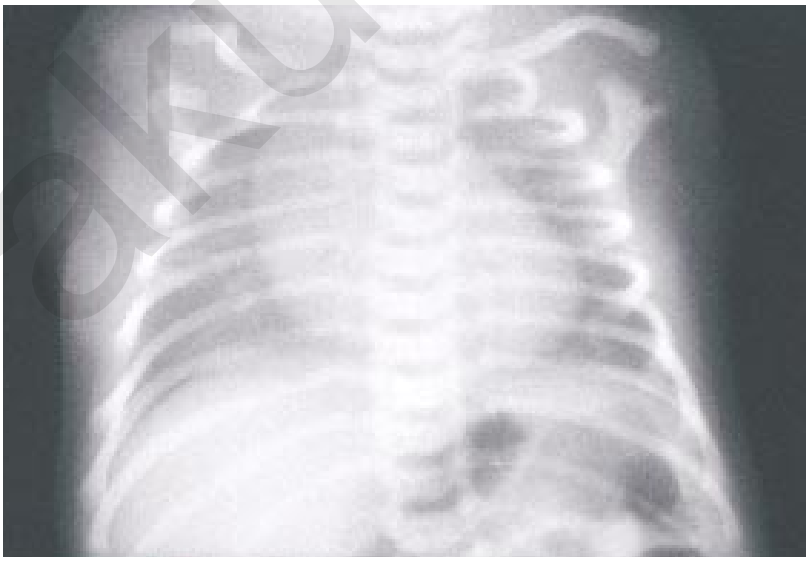

Figure 1.33. Chest radiograph of the same infant. Note the abnormal scapulae and total absence of the upper extremities. This radiograph stresses the importance of looking at the total radiograph and not the lungs alone when looking at a chest radiograph.

Figure 1.34. In a radiograph of the lower extremities of the same infant, note that there are no hip joints and that the femora and fibulae are absent bilaterally.

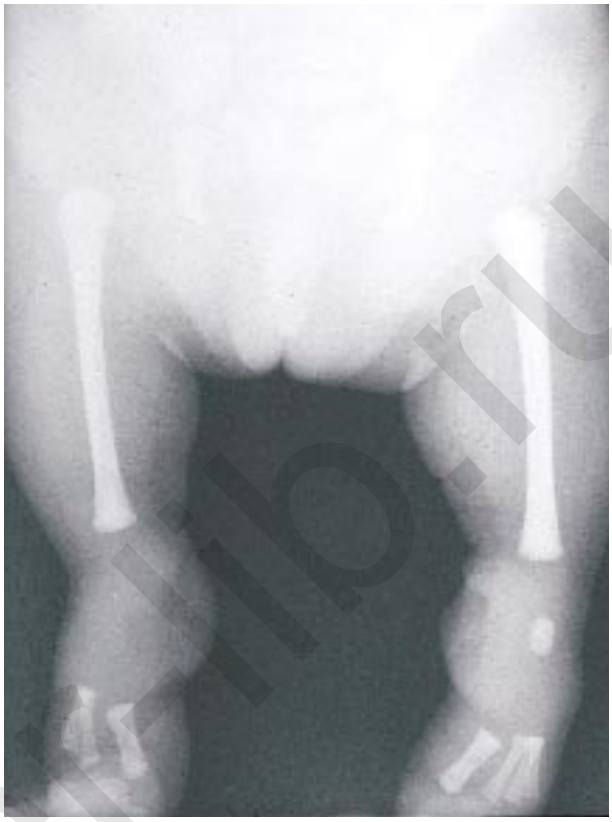

1.34

INTERCALARY DEFECTS

Intercalary defects are those in which a more proximal portion of a limb fails to develop properly but distal structures are relatively intact. An extreme example is phocomelia, which involves partial or complete underdevelopment of the rhizomelic and mesomelic limb segments. The structures of the hands and feet may be reduced to a single digit or may appear relatively normal but arise directly from the trunk like the flippers of a seal. In less severe cases, portions of the proximal limb may remain.

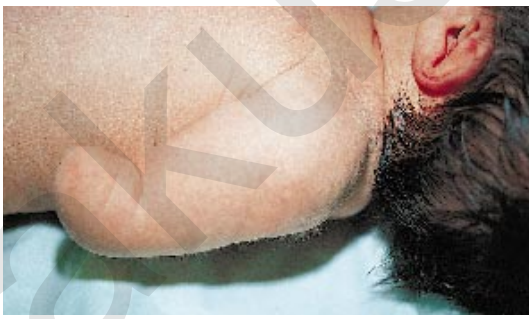

1.35

Figure 1.35. This otherwise normal infant has an isolated limb malformation of the left arm. This is a transverse defect and is a primary limb reduction defect.

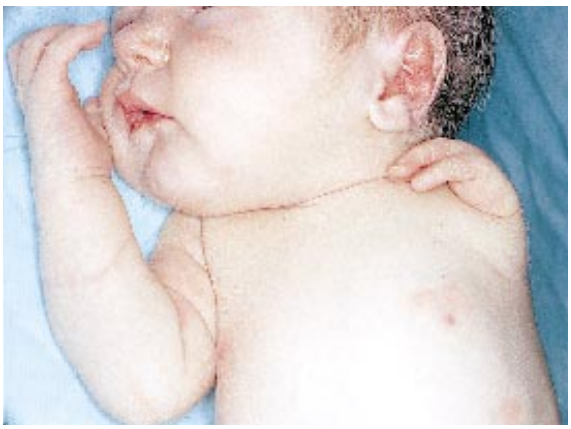

1.36

Figure 1.36. This infant represents an example of unilateral non-thalidomide-induced phocomelia. This malformation, which was common in thalidomide-exposed babies, is, otherwise, a very rare congenital malformation.

1.37

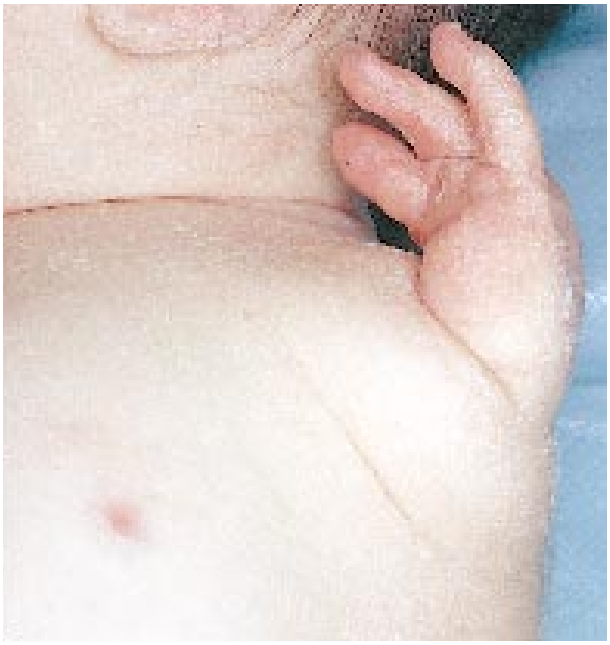

Figure 1.37. Close-up of the phocomelia in the same infant as in Figure 1.36. This is a primary limb reduction defect in that there was lack of the humerus, radius, and ulna in the left upper extremity. In phocomelia there may be absence of the femur, tibia, and fibula in the lower extremities. There may be bilateral involvement of the extremities.

1.38

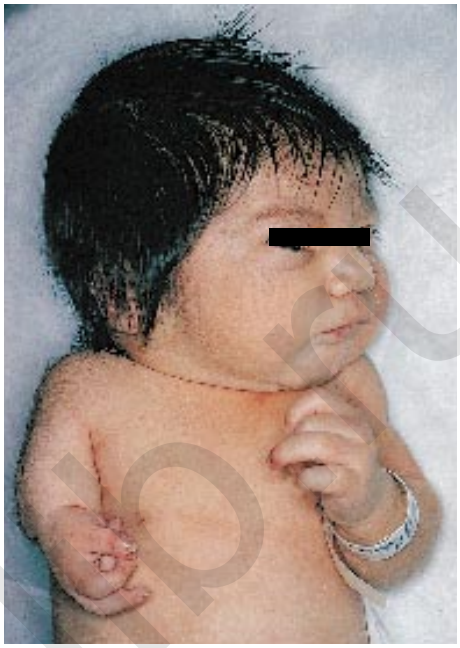

Figure 1.38. Hemimelia of the right upper extremity. This is another example of a transverse defect in which a limb is truncated abruptly. This is a primary limb reduction defect.

1.39

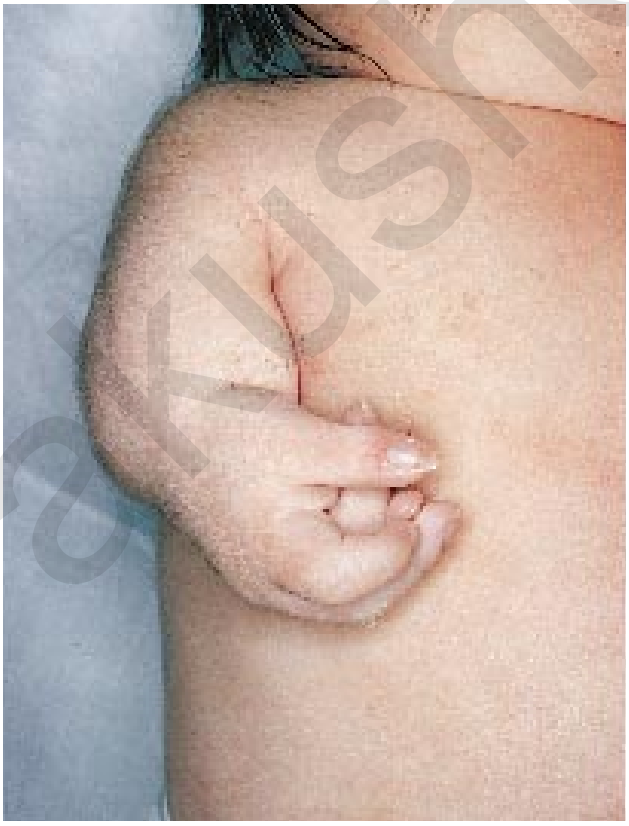

Figure 1.39. Close-up of hemimelia in same infant. Note the well-developed hand.

1.40

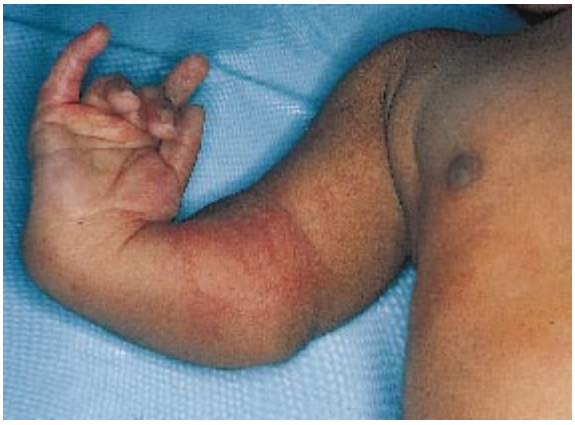

Figure 1.40. This infant has the thrombocytopenia-absent radius (TAR) syndrome. There is absence of the radius bilaterally. Note that the absence of the radius of the right forearm has resulted in a "club hand." In the TAR syndrome the thumb is always present.

Clinical signs of radial dysplasia include a shortening of the forearm with radial displacement of the hand ("club hand"). Varying degrees of dysplasia occur, ranging from complete absence of the radius with major malformations of the preaxial (radial) side of the hand to normal development of the radius and only minor anomalies of the thumb.

1.41

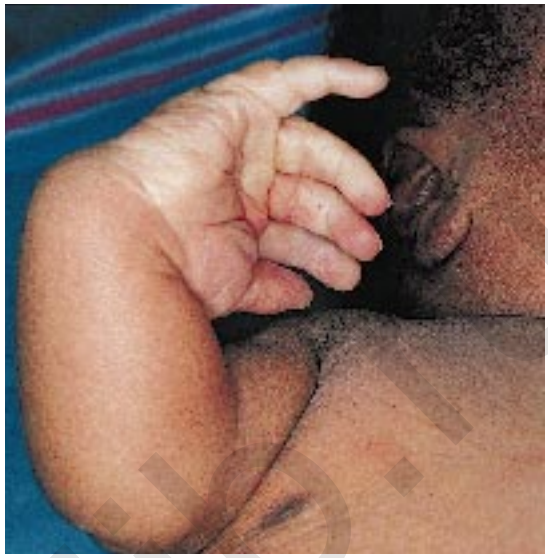

Figure 1.41. Another view of the same infant with the TAR syndrome showing the left forearm and hand. Again note the presence of the thumb. Some dysmorphic syndromes, such as the TAR syndrome, may show varying combinations of the different types of limb defect. There is a preaxial longitudinal defect (absence of the radius), but the ulna is also short and the thumb and forefinger are invariably present as expected with an intercalary defect.

Radial dysplasia may be associated with pancytopenia as in Fanconi's syndrome but may also be associated with congenital heart disease and abnormalities of other parts of the skeleton.

1.42

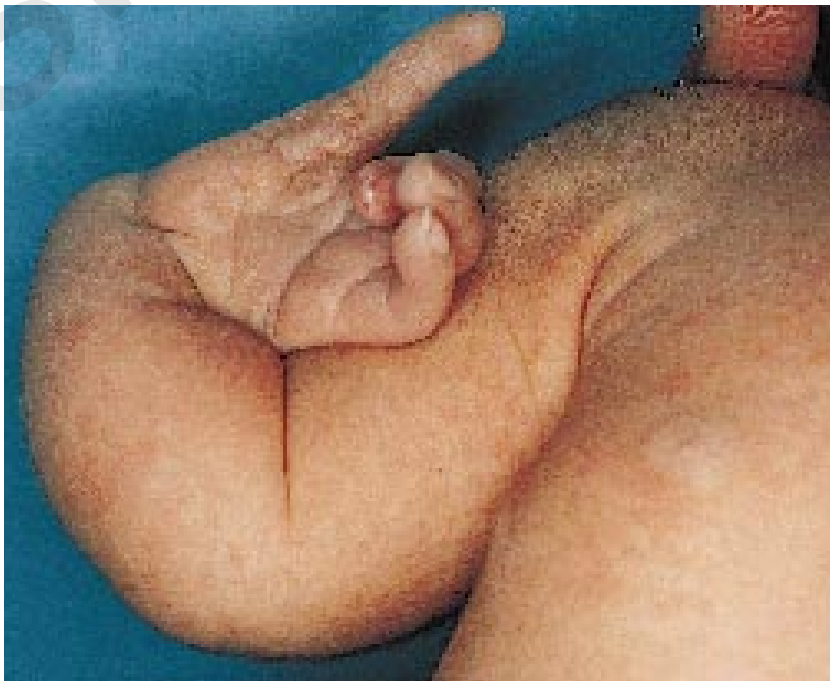

Figure 1.42. This infant has Fanconi's syndrome. Note the congenital absence of the right radius and right thumb. In Fanconi's syndrome the thumb may occasionally be present. Note the club hand with absence of the radius and the thumb. This may be unilateral or bilateral. In Fanconi's syndrome there is pancytopenia (anemia, neutropenia, and thrombocytopenia) in addition to the hypoplastic or absent thumbs and hypoplastic or absent radius.

1.43

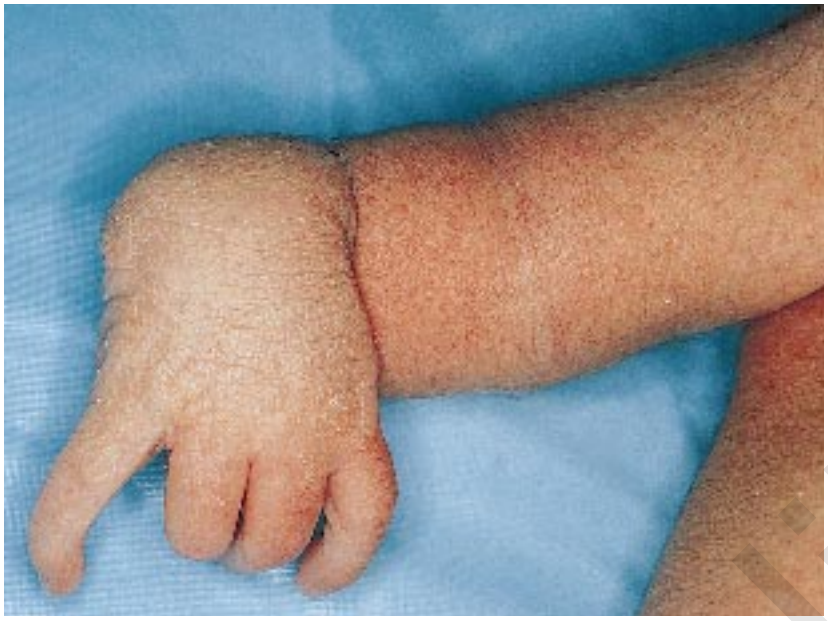

Figure 1.43. Another view of the same infant as in Figure 1.42 showing the absence of the radius and right thumb with the typical club hand.

1.44

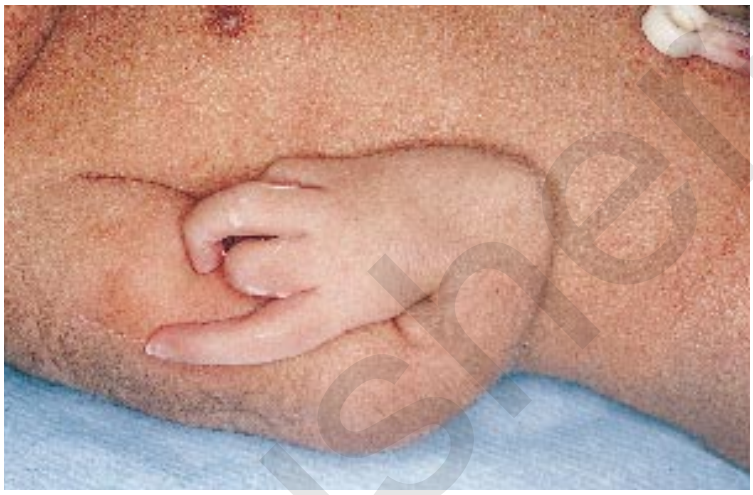

Figure 1.44. Another example of Fanconi's syndrome with congenital absence of the right radius and thumb and thrombocytopenia (platelet count of 30,000/mm^3). Note the skin dimples at the elbow which are related to the infant's position in utero.

1.45

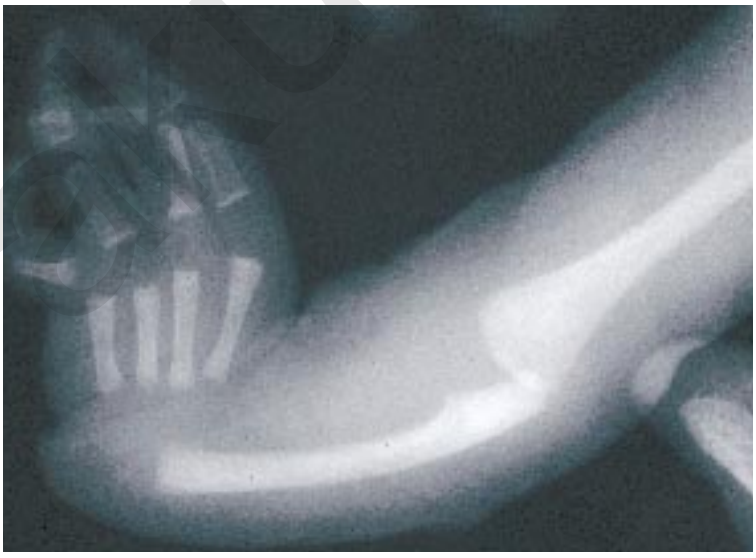

Figure 1.45. Radiograph of the right upper extremity of the same infant showing the absence of the radius and right thumb.

1.46

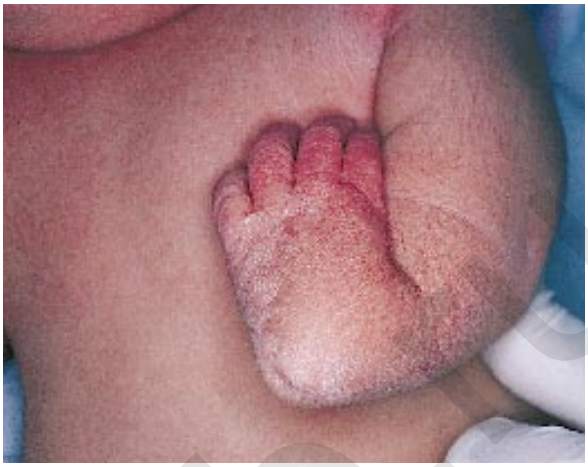

Figure 1.46. In this infant with Holt-Oram syndrome (cardiac limb syndrome), note the congenital absence of the left radius and thumb. The infant also had coarctation of the aorta. Holt-Oram syndrome may be associated with any congenital cardiac defect of which atrial septal defect is the most common. A family history of this condition is common.

1.47

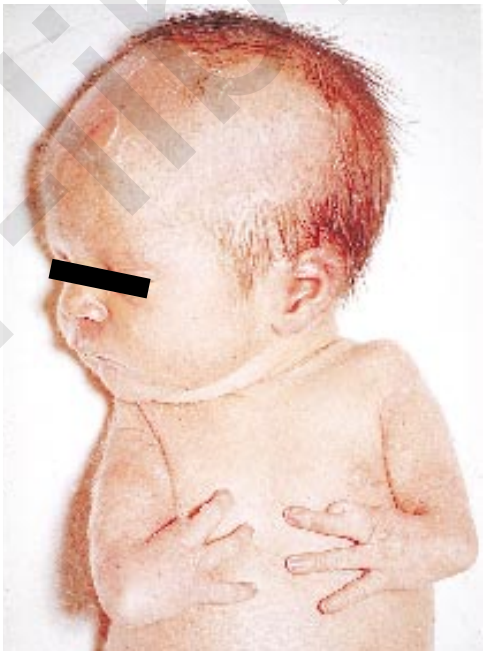

Figure 1.47. Bilateral congenital absence of thumbs and radii in an otherwise normal infant. The father of this infant had the same congenital abnormalities. It is important to obtain a good family history as this condition may be familial.

1.48

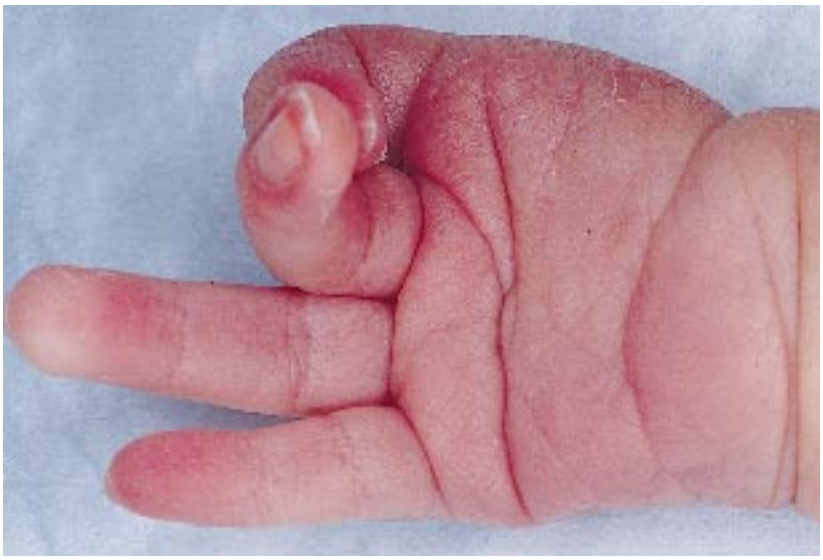

Figure 1.48. Congenital absence of the right thumb was present in this otherwise normal infant.

1.49

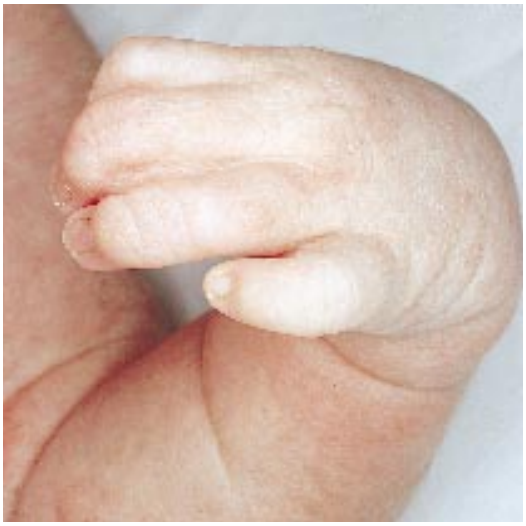

Figure 1.49. Another example of congenital absence of the thumb in an otherwise normal infant but note there is syndactyly between the third and fourth fingers.

1.50

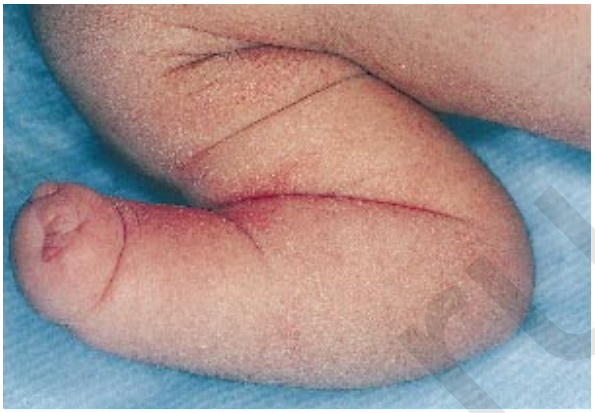

Figure 1.50. Acheiria of the right hand in an infant. This occurs because of a failure of formation of the hand as an isolated defect. The radius and ulna may be foreshortened, there are no metacarpals or phalanges seen radiologically, the thumb may be normally formed, and rudimentary nails may be present. This is an example of a transverse defect in which there is hypoplasia of all structures distal to a particular level on the limb. Usually there is preservation of the more proximal parts which may be normal or diminished in size.

1.51

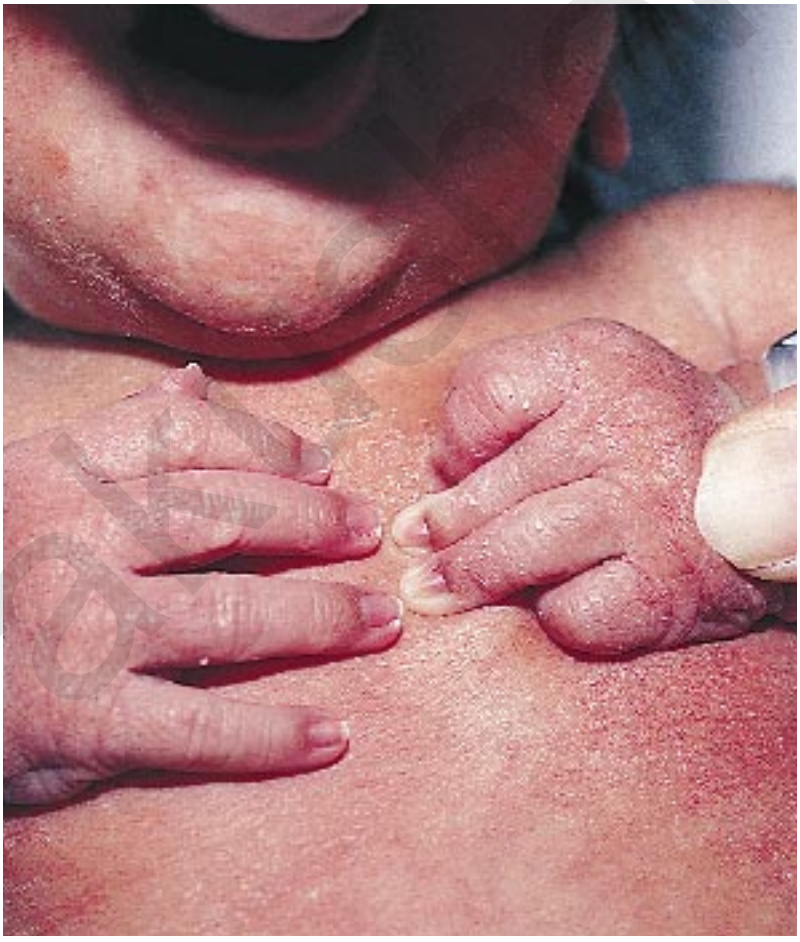

Figure 1.51. This otherwise normal infant had microcheiria of the left hand. Note the normal right hand. The normal hand is about twice as long as it is wide. If metacarpal hypoplasia is present it produces an unusually short palm.

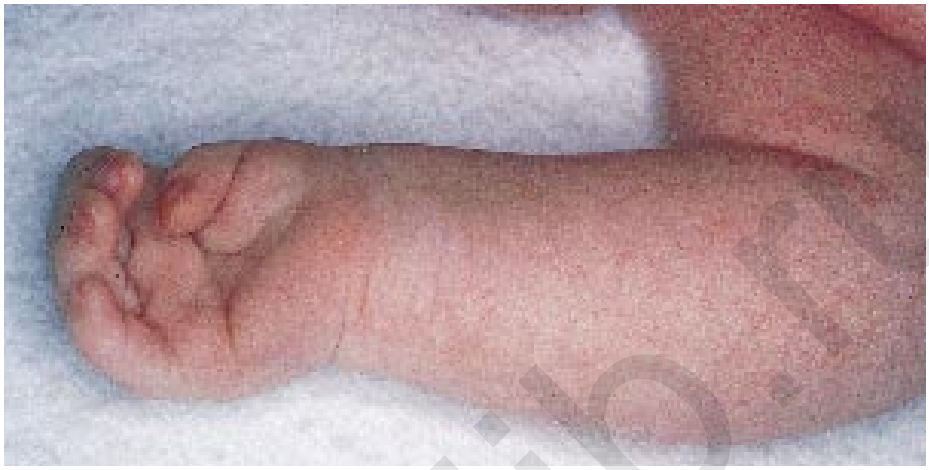

1.52

Figure 1.52. Note the microcheiria of the right hand in this infant with Cornelia de Lange's syndrome. This is not an uncommon finding in infants with this syndrome.

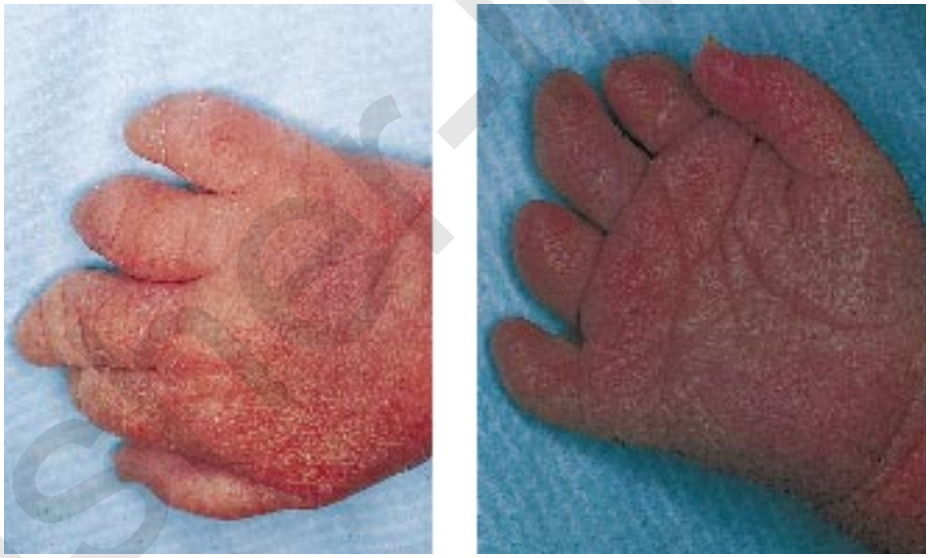

1.53

Figure 1.53. Brachydactyly of the right hand. This finding may be isolated but is seen in many syndromes.

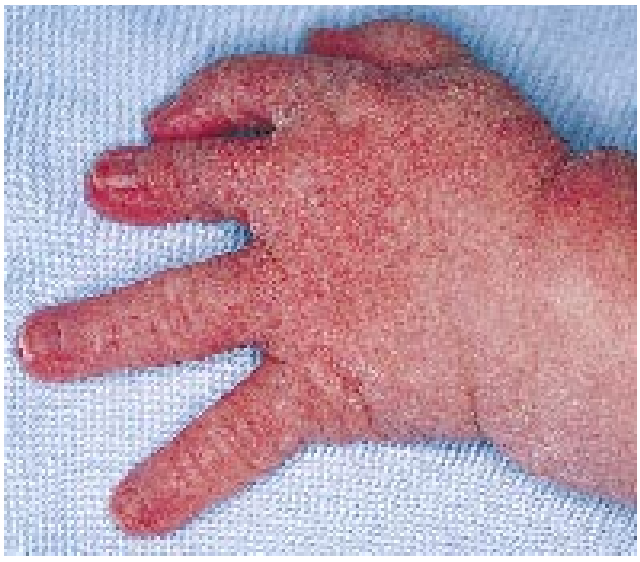

1.54

Figure 1.54. Dorsal view of congenital brachydactyly of the index and middle fingers of left hand. The father had the identical type of congenital brachydactyly.

Asymmetric length of the fingers is usually the result of hypoplasia of one or more phalanges. Tapered fingers may indicate mild hypoplasia of the middle and distal phalanges.

1.55

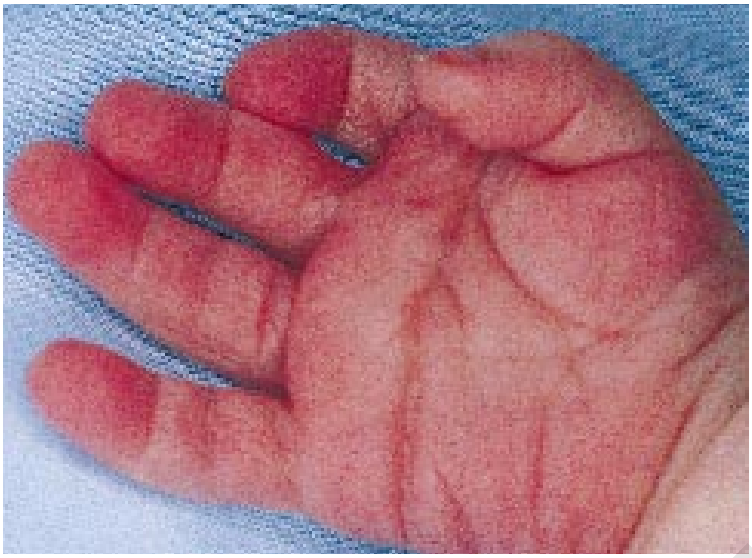

Figure 1.55. Ventral view of the right hand of the same infant as in Figure 1.54.

1.56

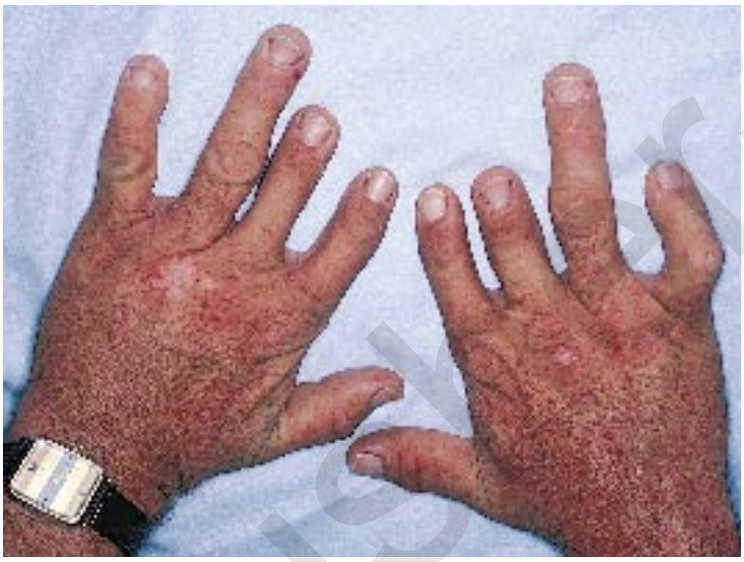

Figure 1.56. Identical bilateral congenital brachydactyly in the infant's father.

1.57

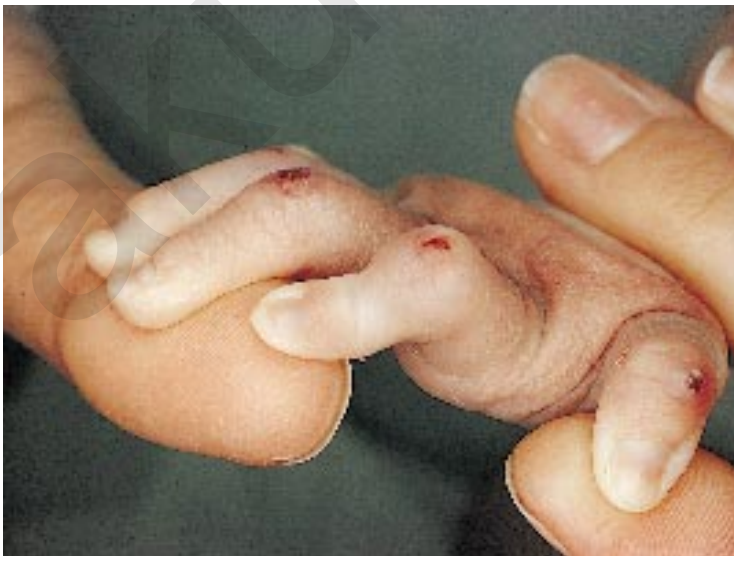

Figure 1.57. Camptodactyly (bent, contracted digits) most commonly affects the fifth, fourth and third digits in decreasing order of frequency. Presumably, it is the consequence of relative shortness in the length of the flexor tendons with respect to growth of the hand. It may occur as an isolated finding but is more commonly associated with lack of movement in utero. It is usually bilateral and symmetrical. Each finger should be extended passively to its full extent. Extension of less than 180 degrees at any joint signifies joint contracture (camptodactyly).

1.58

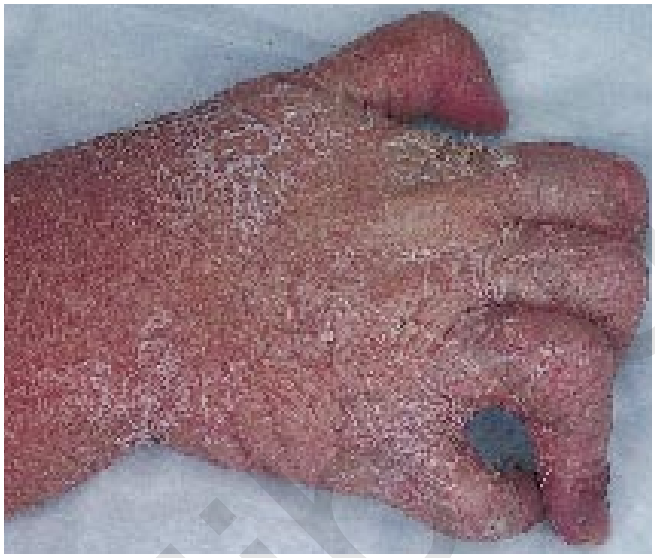

Figure 1.58. Camptodactyly of fingers in an infant with arthrogryposis.

1.59

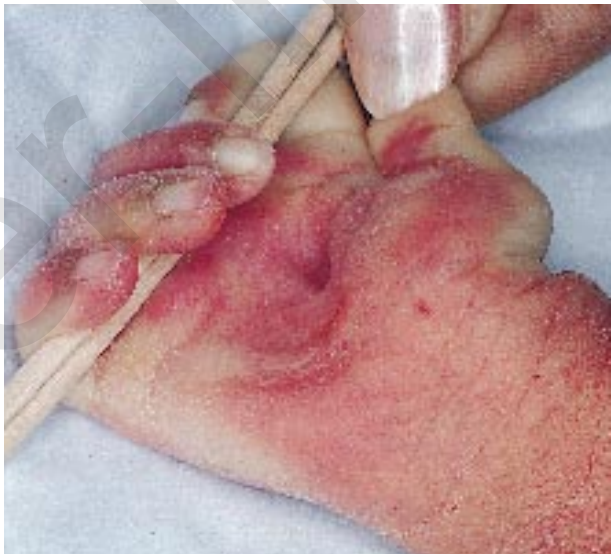

Figure 1.59. The hand of the same infant showing the severity of the contractures and lack of palmar creases due to the severe contractures. Note the depression in the palm resulting from the contracted fingers.

1.60

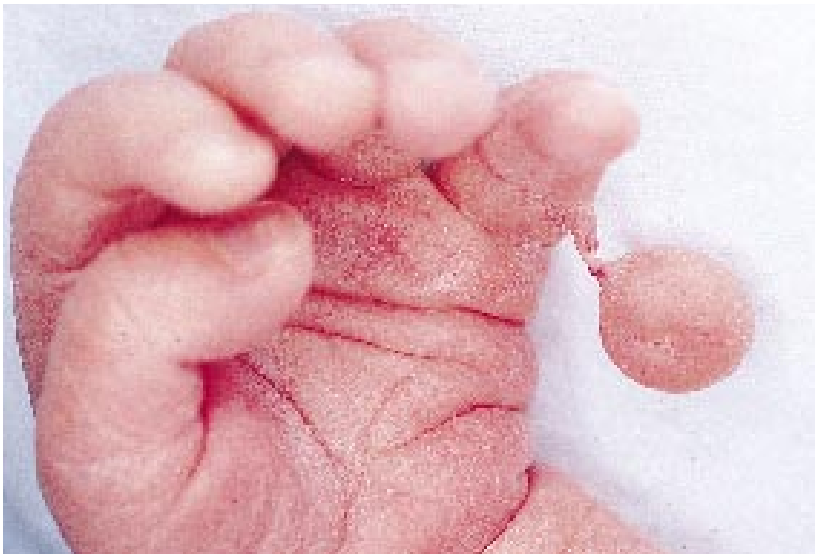

Figure 1.60. Supernumerary digit in which the thin pedicle distinguishes it from true polydactyly. In polydactyly the additional digit may consist solely of soft tissue or less commonly has skeletal elements.

1.61

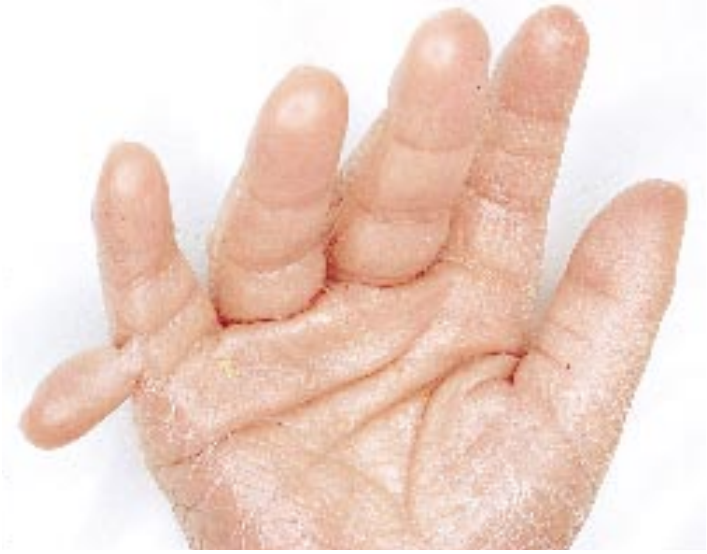

Figure 1.61. Postaxial polydactyly is most commonly seen in black infants where it occurs as an autosomal dominant trait. The polydactyly may be noted as a nubbin of scar tissue, as a pedunculated mass attached by a small pedicle, or as a fully developed digit. Polydactyly may be preaxial, occurring at the thumb or big toe, or postaxial, arising on the ulnar aspect of the fifth finger or fibular aspect of the fifth toe. Central polydactyly does occur but is extremely rare. The vast majority of infants with polydactyly have postaxial polydactyly.

1.62

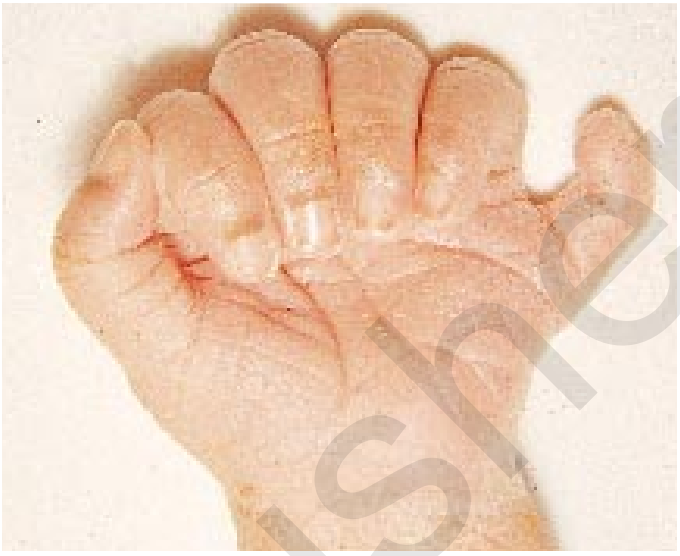

Figure 1.62. Another example of postaxial polydactyly with a well-developed digit. These digits may be fairly well formed with one or more rudimentary phalanges. Duplication of digits occurs when one or more extra digital rays are formed during the embryonic period. Polydactyly is an associated finding in many syndromes such as trisomy 13 or 18, Ellis-van Creveld syndrome, Carpenter's syndrome, etc.

1.63

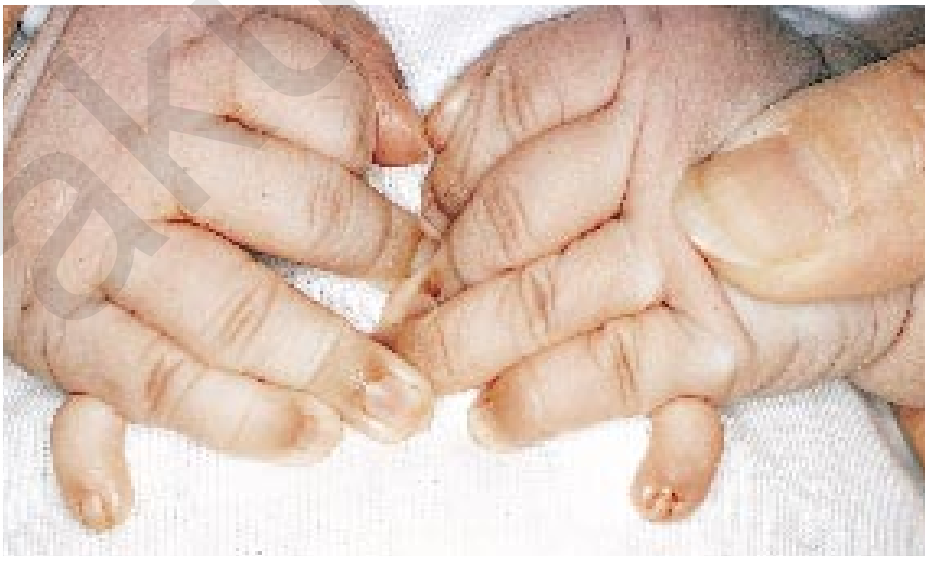

Figure 1.63. Bilateral postaxial polydactyly. Note that polydactyly may be unilateral or bilateral.

1.64

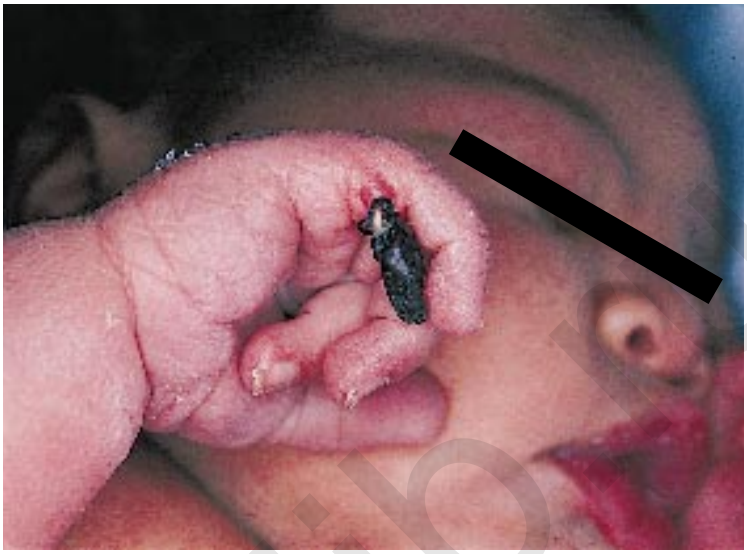

Figure 1.64. Postaxial polydactyly in an infant at birth showing a necrotic, almost amputated, extra digit due to interference with circulation. This would explain why some infants with polydactyly may only have evidence of scarring on the lateral side of the digit.

1.65

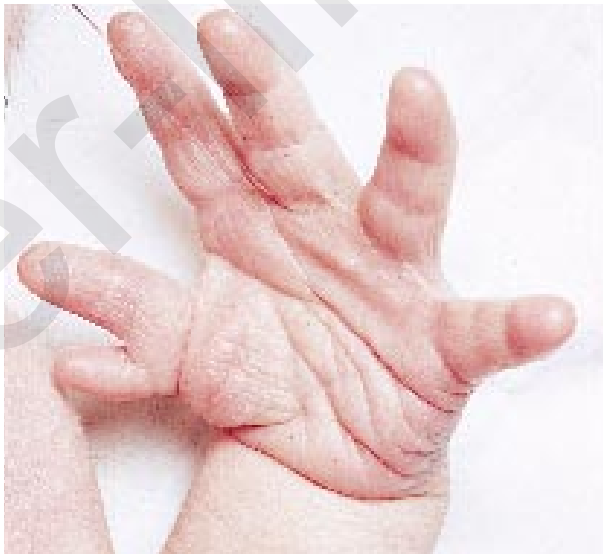

Figure 1.65. This infant has preaxial polydactyly of the right hand. Preaxial polydactyly is less common but has the same range of severity, with the accessory tissue usually arising from the midportion of the thumb or first toe.

1.66

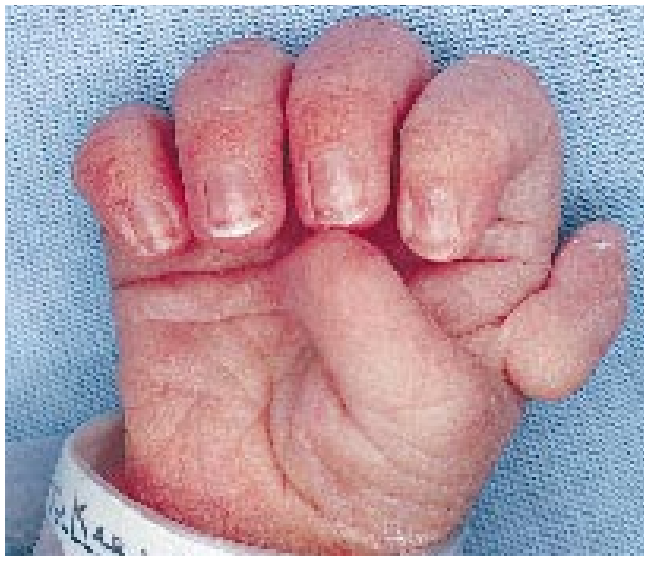

Figure 1.66. In this infant with preaxial polydactyly, note that the extra digit is poorly developed.

1.67

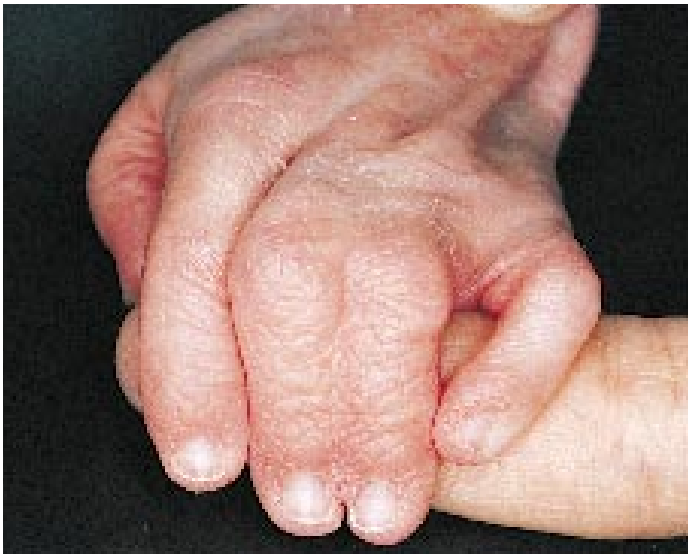

Figure 1.67. Partial cutaneous syndactyly represents an incomplete separation of the fingers and occurs most commonly between the third and fourth fingers and between the second and third toes. Syndactyly is the most frequent form of hand anomaly. It is often bilateral and may be combined with polydactyly, congenital finger amputations, and syndromes. Syndactyly refers to fusion of the soft tissues without synostosis (bony fusion). If there is synostosis, the term symphalangism is used.

1.68

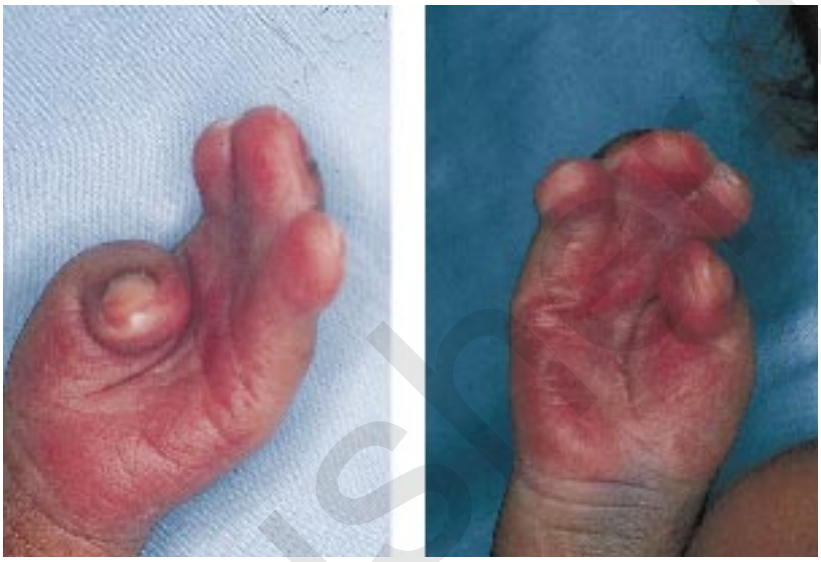

Figure 1.68. This infant with Apert's syndrome (acrocephalosyndactyly) shows symmetric syndactyly of both hands. In Apert's syndrome, total syndactyly may involve the full length of the hands or feet. They appear cupped and mitten-like and may have a single undulating band-shaped nail.

1.69

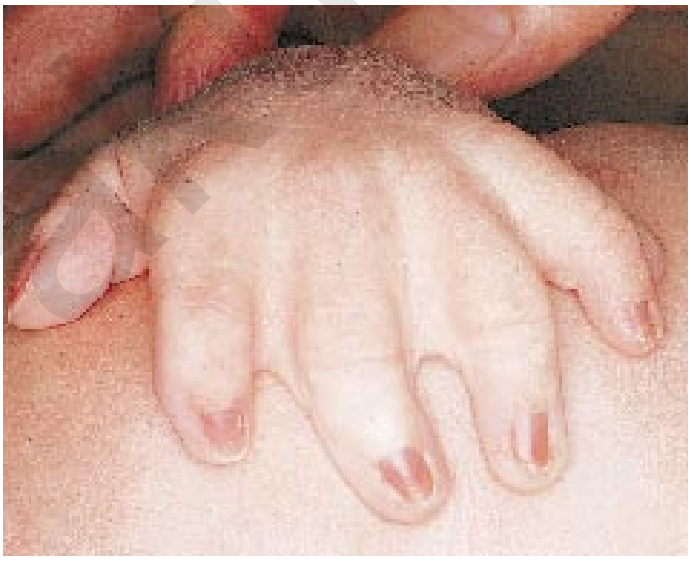

Figure 1.69. In Carpenter's syndrome (acrocephalopolysyndactyly), polysyndactyly is a prominent feature. Note the webbing between the digits; the extra digit can be noted behind the fifth digit.

1.70

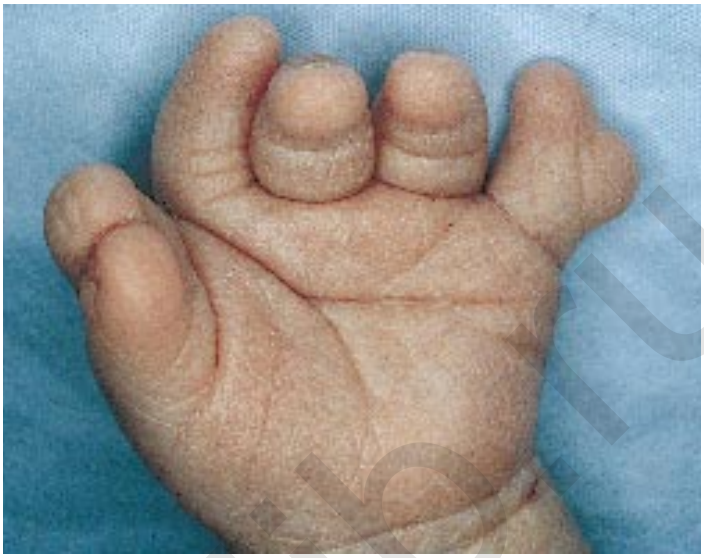

Figure 1.70. Polysyndactyly (seven digits) with brachydactyly and hypoplastic nails in an infant with Ellis-van Creveld syndrome.

1.71

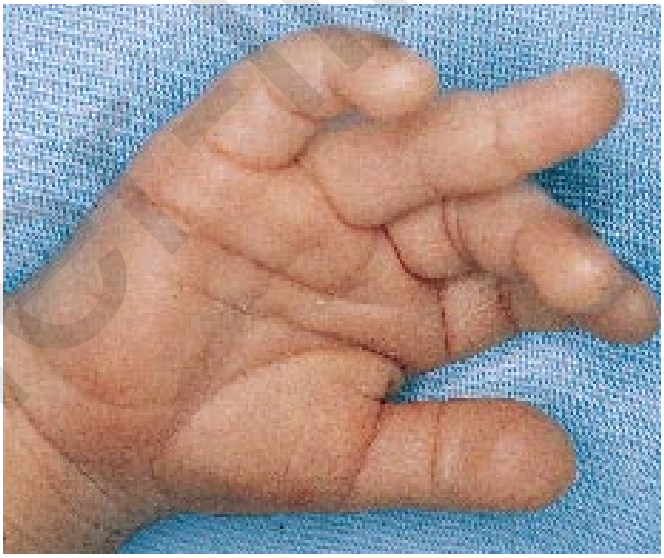

Figure 1.71. There was a family history of broad thumbs and toes in this otherwise normal infant who exhibits an overgrowth anomaly of the thumbs and big toes. Syndromes such as Rubenstein-Taybi and Larsen's syndrome should be excluded in infants with broad thumbs and toes.

1.72

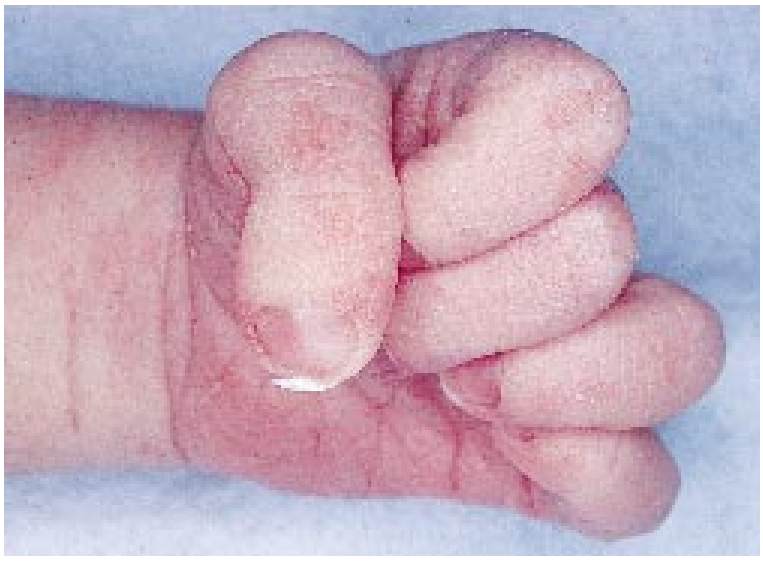

Figure 1.72. A broad spatulate thumb in an infant with Larsen's syndrome.

1.73

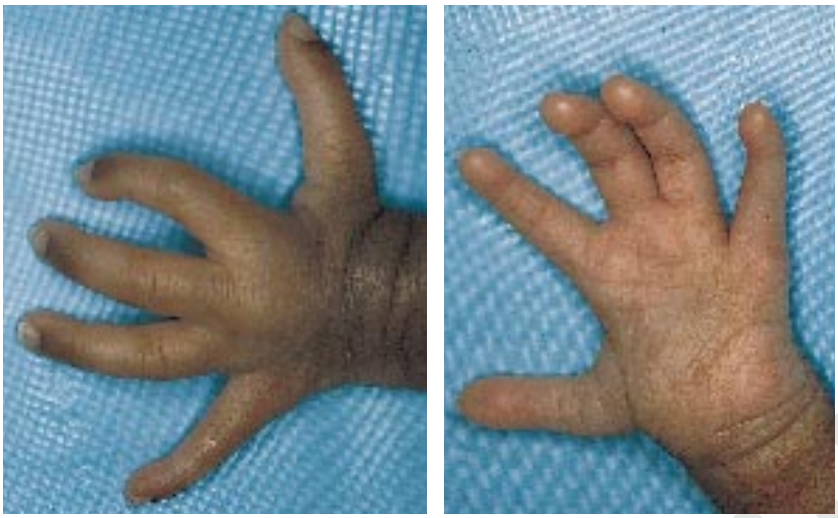

Figure 1.73. A dorsal (left) and ventral (right) view of digitalization of the right thumb in an infant with imperforate anus and microphthalmia. Karyotype was normal.

If there are three phalanges comprising the thumb (triphalangeal thumb), conditions such as Fanconi's pancytopenia syndrome and Holt-Oram syndrome should be considered in the differential diagnosis. A triphalangeal thumb lies in the same plane as the fingers.

1.74

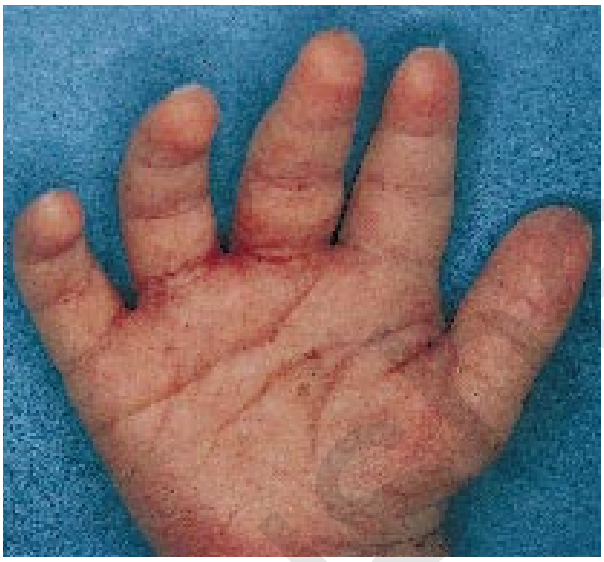

Figure 1.74. A palmar view of digitalization of the right thumb in another infant. Note the extra creases in the thumb. This infant also had bifid big toes with polydactyly.

1.75

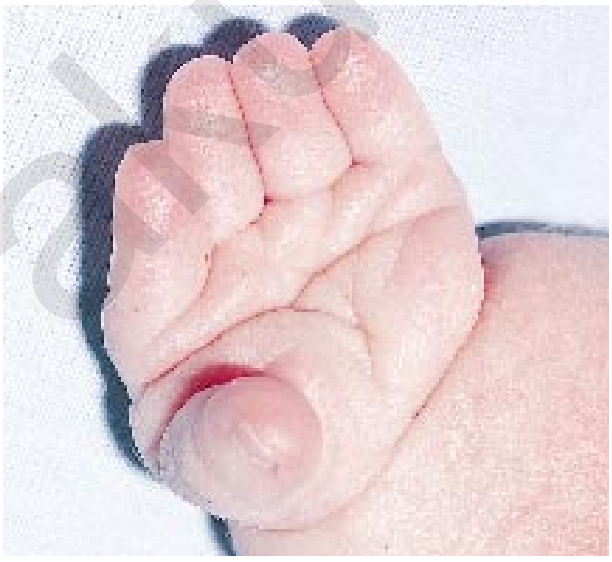

Figure 1.75. The "hitchhiker" thumb is a proximally placed thumb caused by hypoplasia of the first metacarpal. The thumb is retroflexed with hypoplasia of the thenar eminence. This type of thumb is typical in diastrophic dwarfism.

1.76

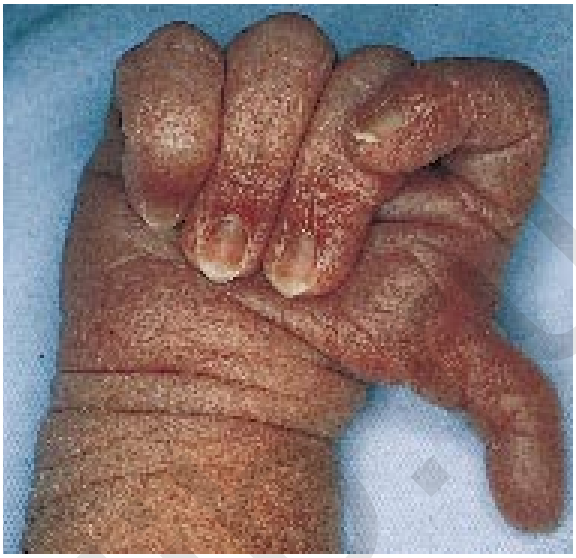

Figure 1.76. Pouce flottant ("floating" thumb) of the right hand. In this condition there is an absent or hypoplastic first metacarpal.

1.77

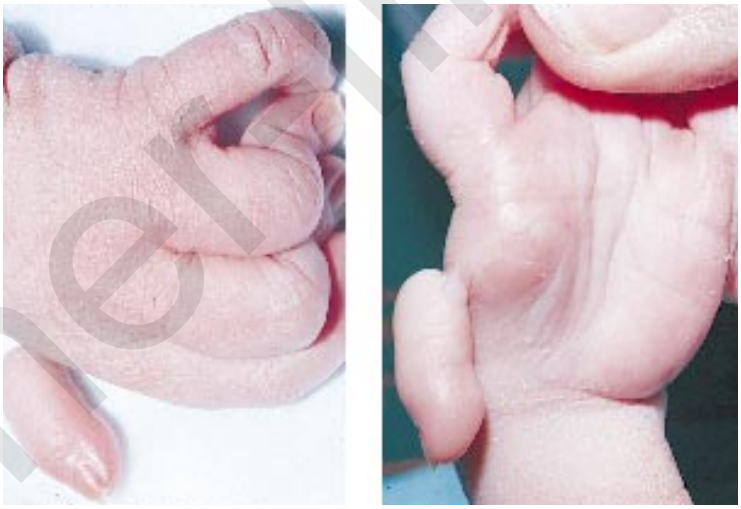

Figure 1.77. Another example of pouce flottant. There is an absence or maldevelopment of the first metacarpal with phalanges.

1.78

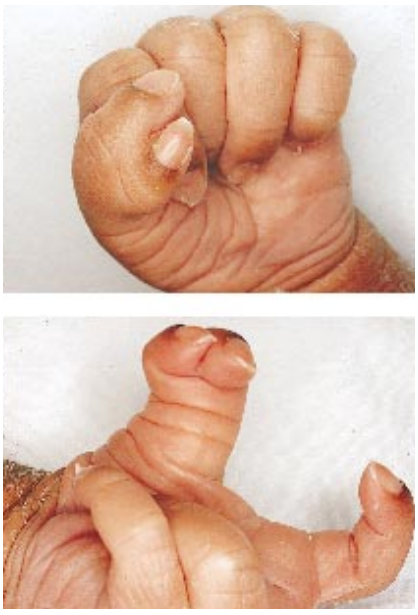

Figure 1.78. An early insult to the limb bud in the 5th to 6th embryologic week may result in a duplication of parts, especially of the hands and feet, such as this bifid thumb.

1.79

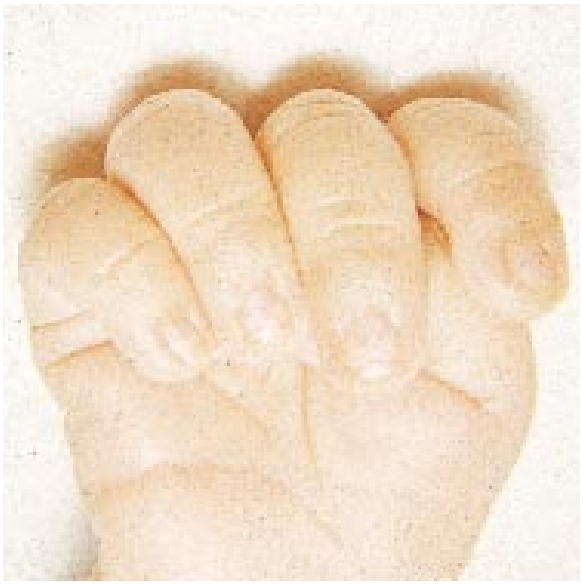

Figure 1.79. Palmar adduction ("cortical" thumb) in a normal infant. The thumbs are freely mobile but are held adducted and flexed across the palms with the fingers tightly clutched over them. "Cortical" thumbs are a manifestation of hypertonicity when they are present beyond the first 3 to 4 months. Constant palmar adduction or "clasped" thumb after this age would alert one to the possibility of central nervous system pathology. "Clasped" thumbs are held in a flexed and adducted position across the palm and cannot be abducted or extended.

1.80

Figure 1.80. In infants with neonatal Marfan syndrome, the thumb may extend beyond the fifth finger when the infant fists its hand. This infant with Marfan syndrome had an upper/lower segment ratio of 1.52. The normal upper/lower segment ratio in the neonate is 1.69 to 1.7. It is much reduced in Marfan syndrome and increased in short-limbed dwarfism and hypothyroidism. Note that the fingers are long, tubular, and relatively slender.

1.81

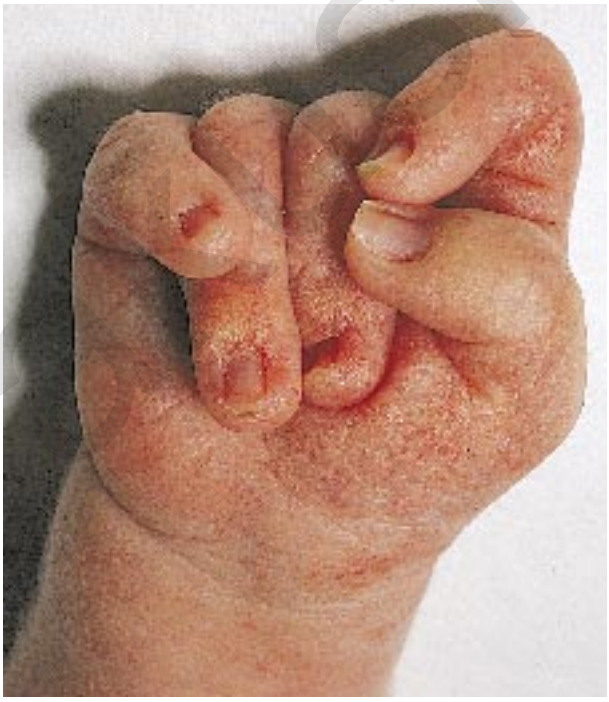

Figure 1.81. The typical appearance of the fingers in trisomy 18. Note the index finger overlapping the third finger and the fifth finger overlapping the fourth finger. Also note the hypoplastic nails.

1.82

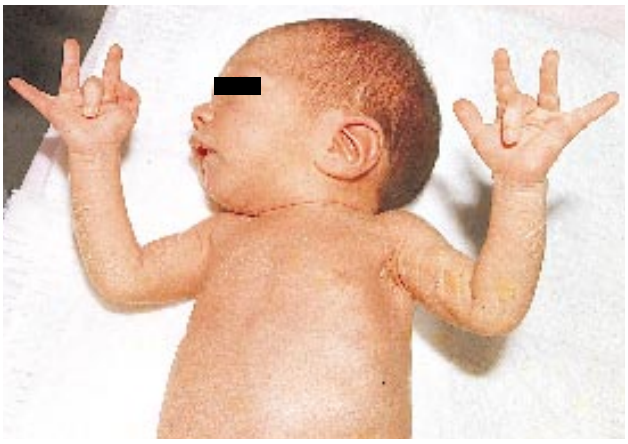

Figure 1.82. Bilateral trigger fingers in a neonate. Trigger digits may involve the thumbs or the fingers. The fingers may present with clicking, flexion contractures of the proximal interphalangeal joint, or both. They are much less commonly involved than the thumbs which present with a palpable nodule at the proximal flexor tendon pulley at the level of the metacarpophalangeal joint. Trigger thumbs must be distinguished from a congenital clasped thumb in which the deformity usually affects the metacarpophalangeal joint.

1.83

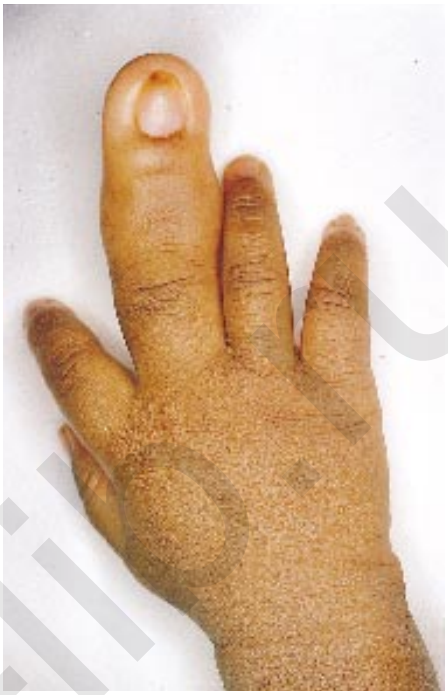

Figure 1.83. Macrodactyly of the right middle finger occurring from a localized overgrowth of a digit. This occurs most frequently as a random isolated enlargement of a finger or toe, or it may be associated with vascular or lymphatic malformations or may occur in neurofibromatosis.

1.84

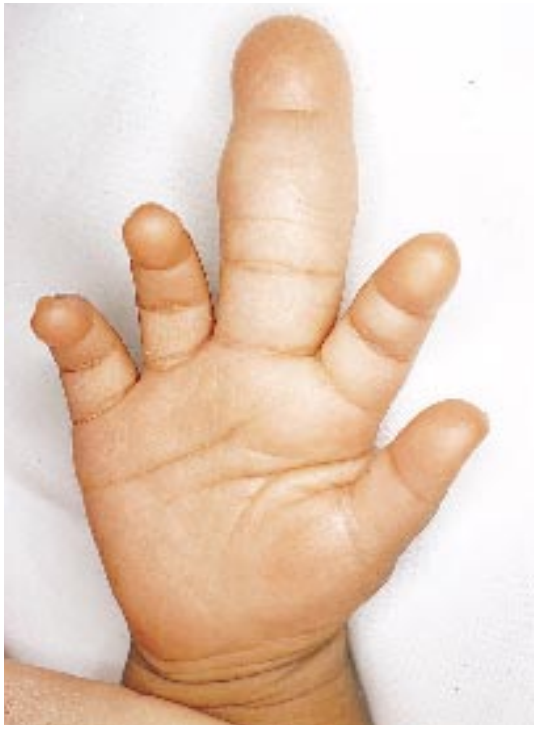

Figure 1.84. Ventral view of the macrodactyly of the right middle finger in the same infant. This was an isolated finding in this infant.

1.85

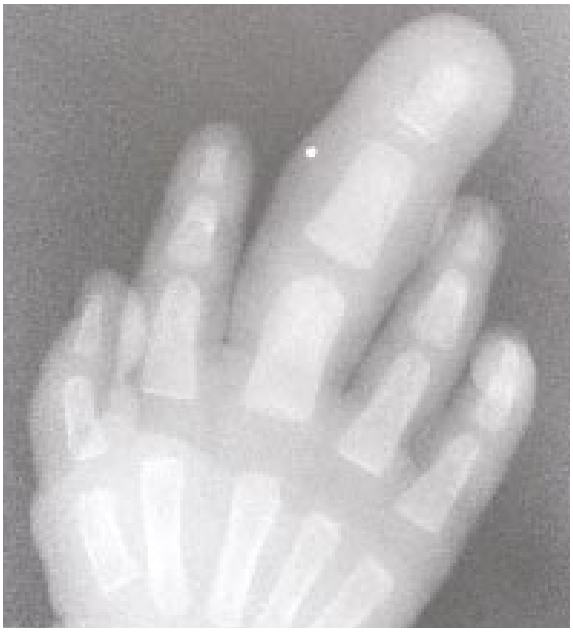

Figure 1.85. Radiograph of the hand of the infant shown in Figure 1.84 showing the macrodactyly of the right middle finger.

1.86

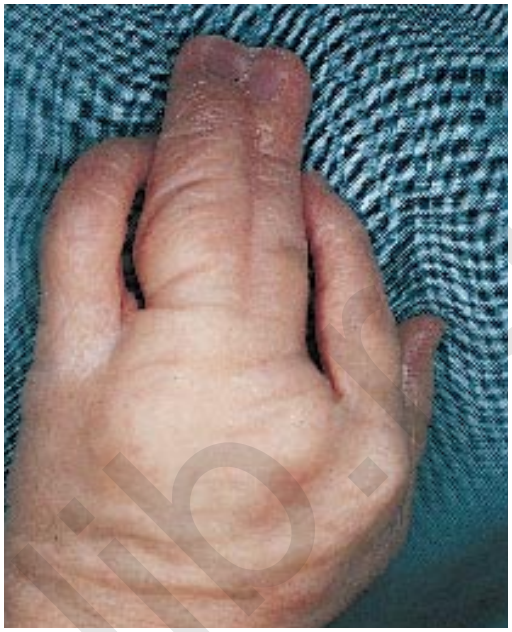

Figure 1.86. Macrosyndactyly of the third and fourth fingers of the left hand. This infant had a massive diffuse lymphangioma involving the left side of the neck, the chest, and the upper extremity.

1.87

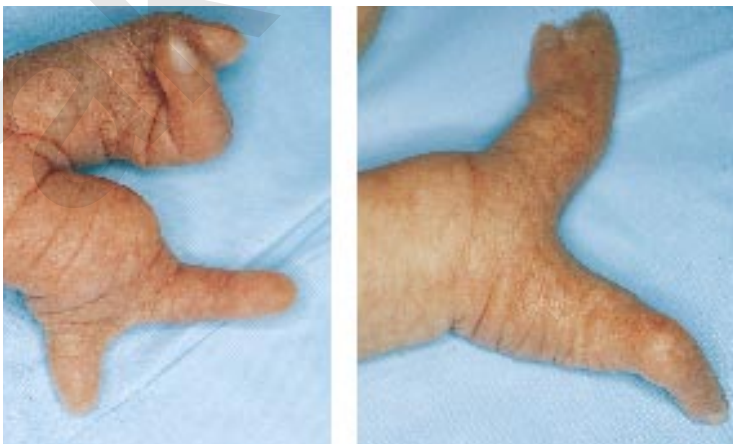

Figure 1.87. In these infants with "lobster-claw" deformity (ectrodactyly, or split hand/split foot deformation), the typical V-shaped cleft is noted on the left. In this classic form, all four limbs are involved. The feet are usually more severely affected than the hands. This type is strongly familial and is usually inherited as an autosomal dominant. The atypical type of lobster-claw deformity is seen on the right. Note that the cleft is wider (U-shaped defect) with only a thumb and small finger remaining. This atypical type has no genetic basis and usually involves a single upper extremity but always spares the feet.

1.88

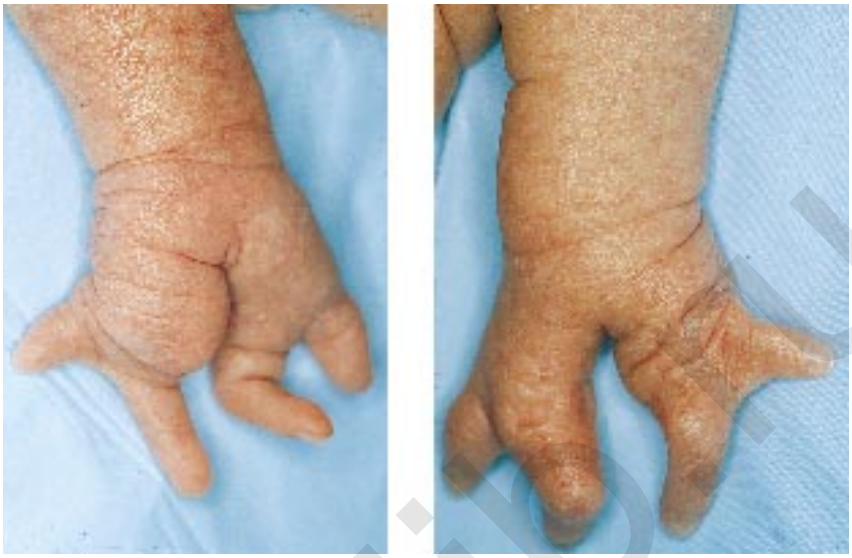

Figure 1.88. Typical V-shaped lobster-claw deformity of the hands. The lobster-claw deformity may be associated with other malformations, often as a genetically determined syndrome. In the hand, the typical deformity consists of the absence of the third digital ray, with a deep triangular cleft extending to the level of the carpal bones. Fingers bordering the cleft may show clinodactyly, camptodactyly, or syndactyly and are sometimes hypoplastic or completely missing.

1.89

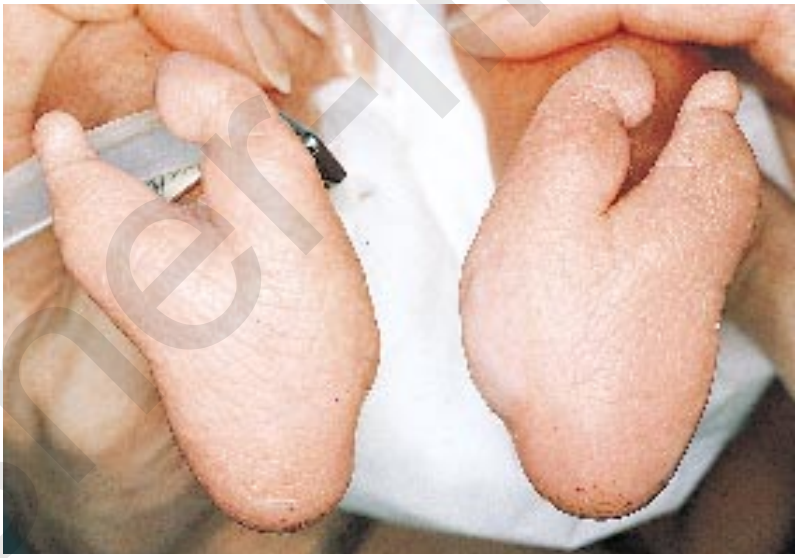

Figure 1.89. The typical V-shaped lobster-claw deformity of the feet in the same infant.

1.90

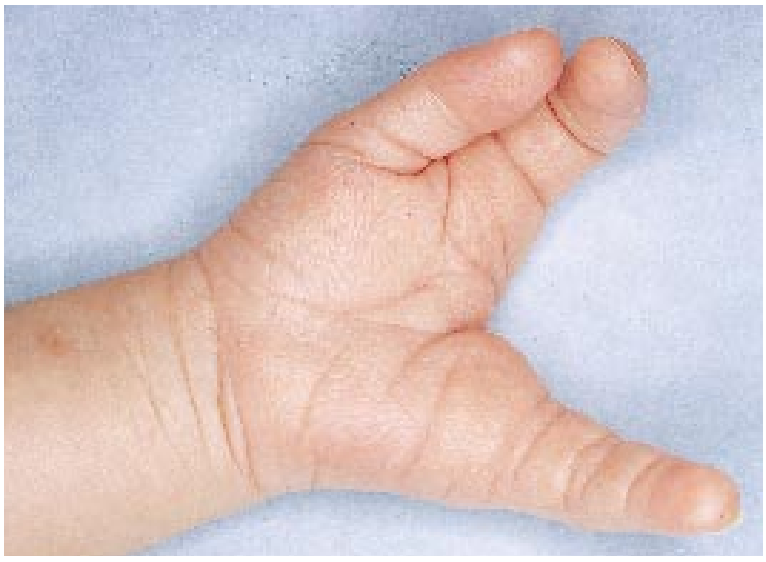

Figure 1.90. The atypical type of lobster-claw deformity (U-shaped defect) which only involved the right hand of this infant. Note the wider cleft. This is a sporadic defect.

1.91

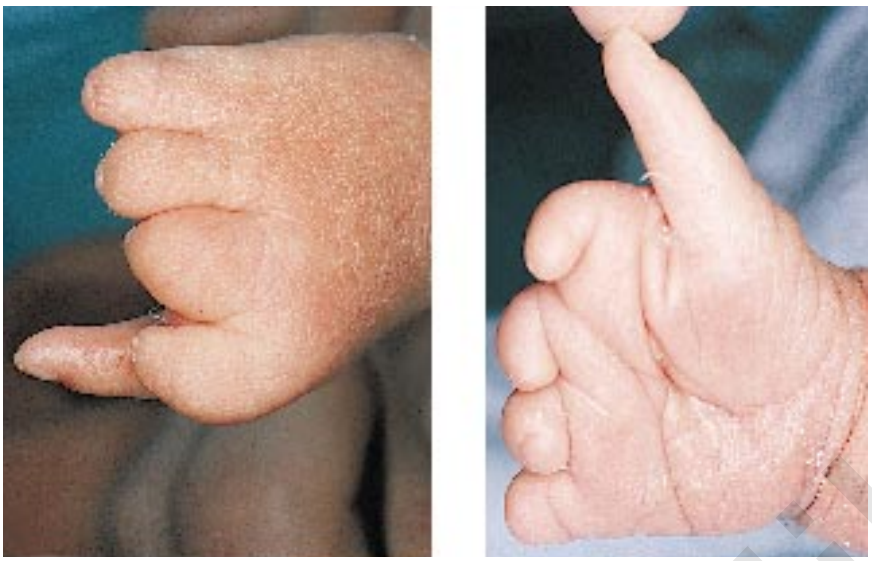

Figure 1.91. A primary reduction malformation of the fingers of the right hand.

1.92

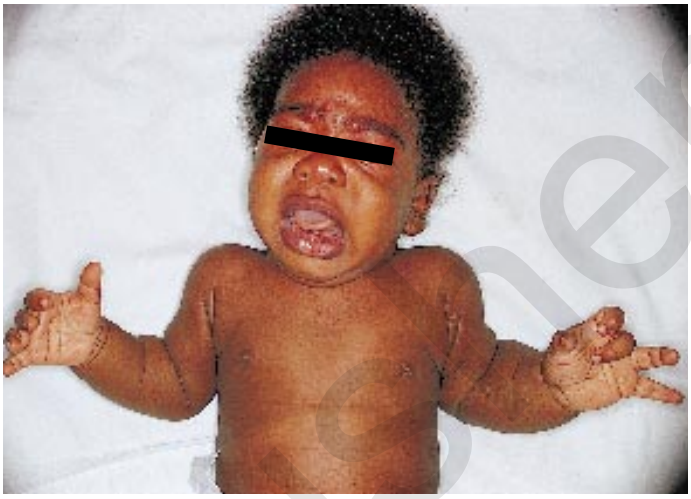

Figure 1.92. Congenital hypertrophy of the left upper extremity of an infant at the age of five months. This is also known as segmental hypertrophy or local acromegaly. This is often not obvious at birth but becomes more apparent with increasing age. Limb asymmetry can be caused by vascular anomalies that produce localized overcirculation, but more commonly is found as an isolated phenomenon. When such asymmetry affects one entire side of the body, the term hemihypertrophy is used.

Differential diagnosis of hemihypertrophy includes neurofibromatosis, Wilms' tumor, Beckwith-Wiedemann syndrome, Klippel-Trénaunay syndrome, and Russell-Silver dwarf, but most commonly this is an idiopathic finding.

1.93

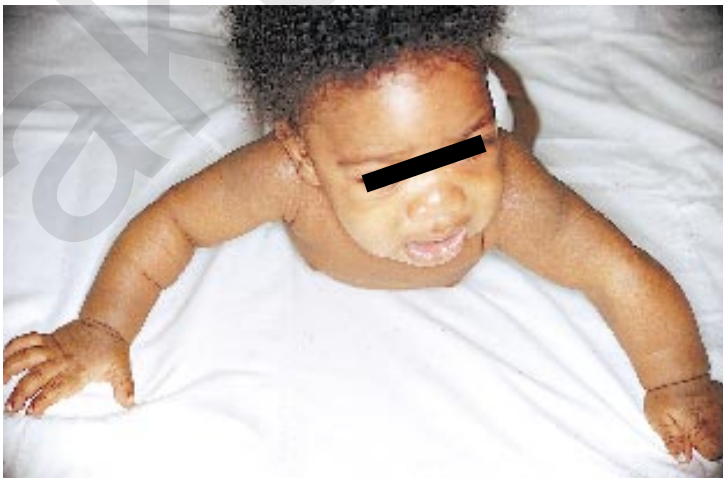

Figure 1.93. The same infant demonstrating the congenital hypertrophy of the left upper extremity.

1.94

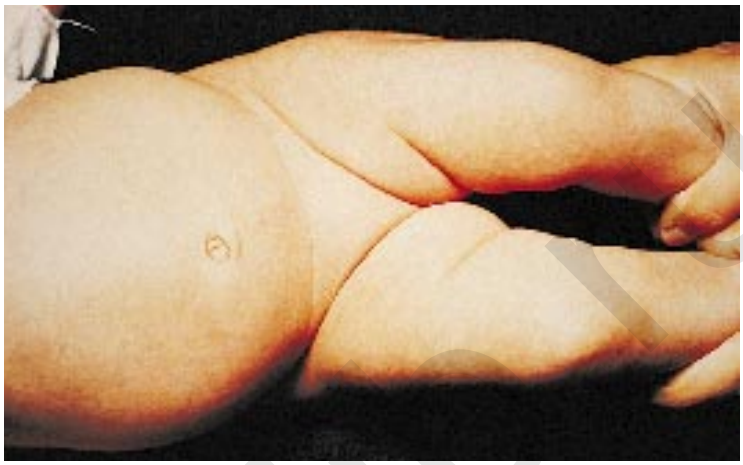

Figure 1.94. A frontal view of a neonate with congenital dislocation of the hip. Note the asymmetry of the skin folds. In congenital dislocation of the hip, asymmetry is not commonly noted in the neonatal period. Congenital dislocation is very much more common in female infants.

1.95

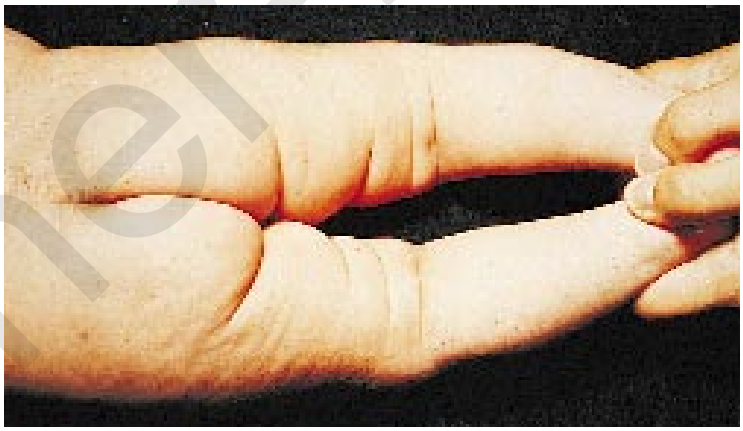

Figure 1.95. A dorsal view of the same infant shows the asymmetric gluteal folds and other skin folds. In the neonatal period the asymmetry of the gluteal folds and other skin folds is usually not as apparent as it is in this infant.

1.96

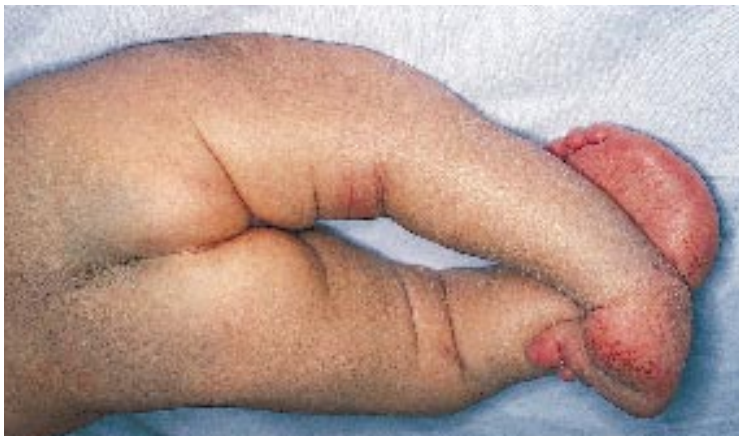

Figure 1.96. Congenital hip dislocation and bilateral club feet in an infant with Poland's anomaly. Note the asymmetry of the creases. Congenital hip dislocation is commonly associated with the presence of other congenital postural deformities. Also note the bilateral talipes equinovarus.

1.97

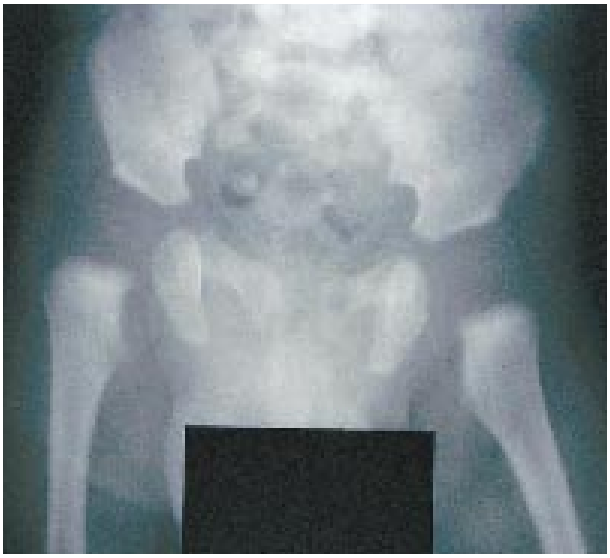

Figure 1.97. Radiograph of congenital dislocation of the hip.

1.98

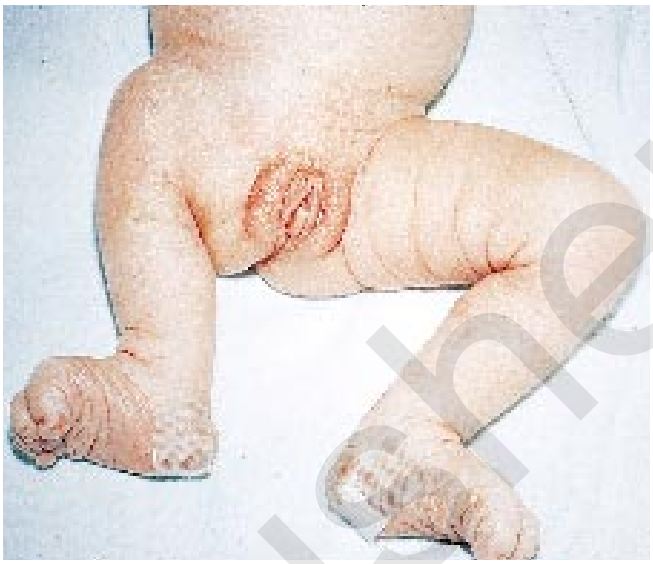

Figure 1.98. Proximal focal femoral deficiency of the right side in an otherwise normal infant. This is a congenital defect of unknown cause, usually consisting of a shortening and contracture of the proximal portion of the femur with or without involvement of the pelvic bones. The severity of the condition depends on the presence or absence of the femoral head and acetabulum. Treatment is directed towards stabilizing the hip. Correction of the leg length discrepancy may require an amputation above the knee and fitting with a prosthesis.

1.99

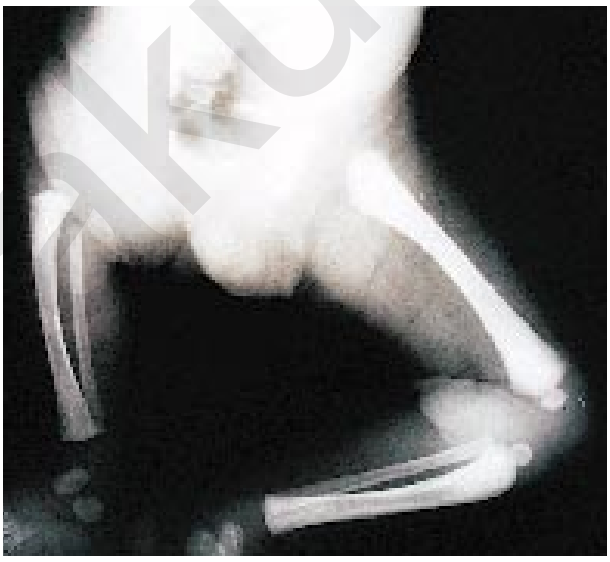

Figure 1.99. Radiograph of the same infant showing the proximal focal femoral deficiency.

1.100

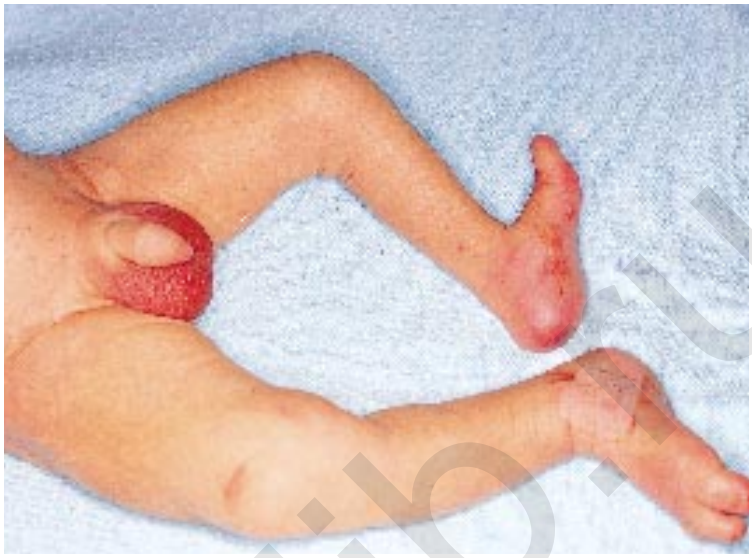

Figure 1.100. Hypotrophic left lower extremity. This may occur in the caudal regression syndrome or may be due to interference with the vascular supply to the lower extremity.

1.101

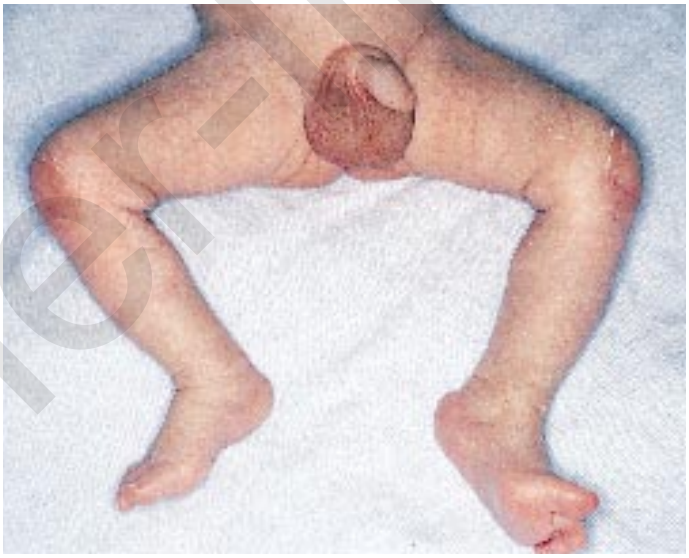

Figure 1.101. Hypoplastic right lower extremity with four toes on the right foot.

1.102

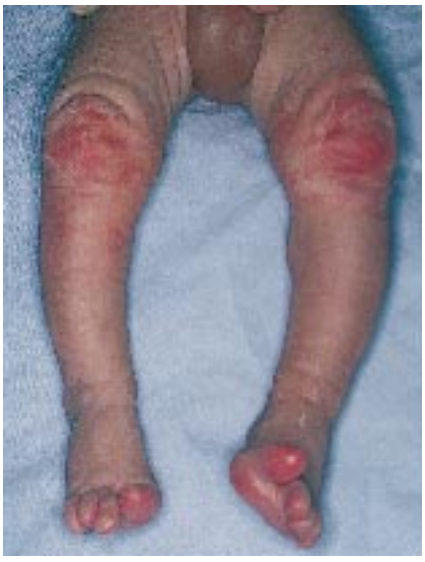

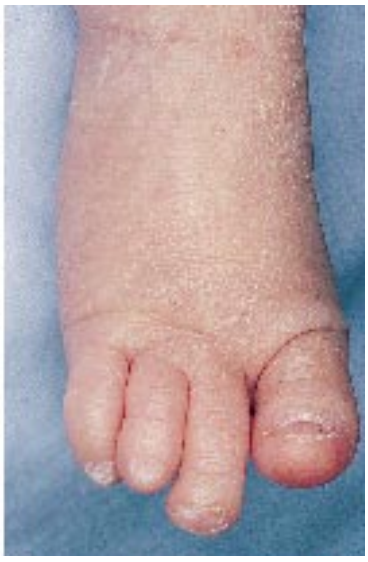

Figure 1.102. The same infant showing the hypoplasia of the right lower extremity and the presence of four toes on the right foot. Note that the hypoplasia can be subtle.

1.103

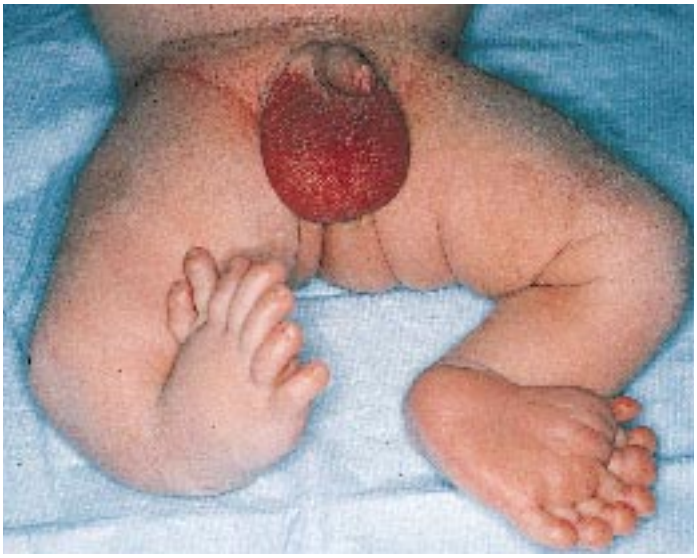

Figure 1.103. Congenital absence of patellae in a normal infant. This finding is also noted in trisomy 8 and Nievergelt syndrome.

1.104

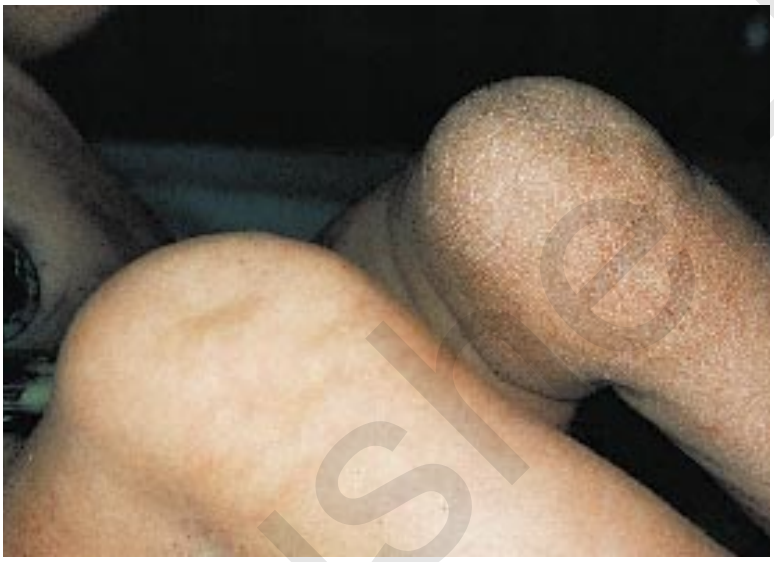

Figure 1.104. In this infant with the tibia reduction-polydactyly syndrome there is an absence of the tibiae bilaterally with septadactyly on the right foot and octadactyly on the left foot. Absence or hypoplasia of the tibia was seen in the thalidomide syndrome. It is otherwise rare, whereas absence of the fibula is more common. It is more common in males, more often unilateral and more common on the right side.

1.105

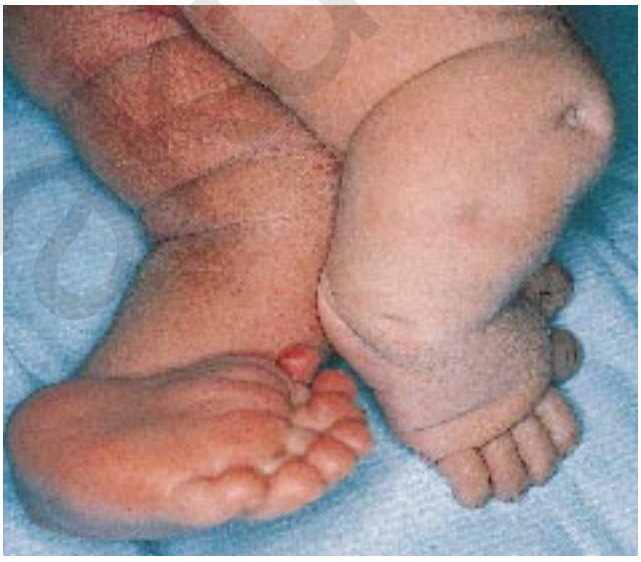

Figure 1.105. In the tibia reduction-polydactyly syndrome, the fibula may be shortened but is otherwise normal and the patella may be absent. Associated malformations are common and strikingly heterogeneous. Note the skin dimple at the knee joint and the skin dimple over the leg, and the bilateral pes equinovarus associated with the absence of the tibiae. The plantar surface of the foot is turned medially.

Skin dimples at a joint are seen normally in infants but dimples over a long bone are always associated with pathology.

1.106

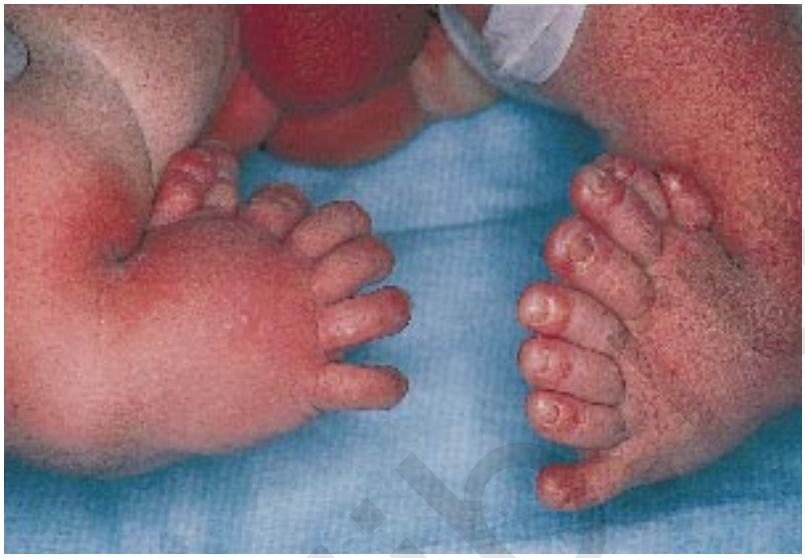

Figure 1.106. Tibia reduction-polydactyly syndrome in the same infant showing the septadactyly of the right foot, octadactyly of the left foot and bilateral pes equinovarus because of absence of the tibia.

1.107

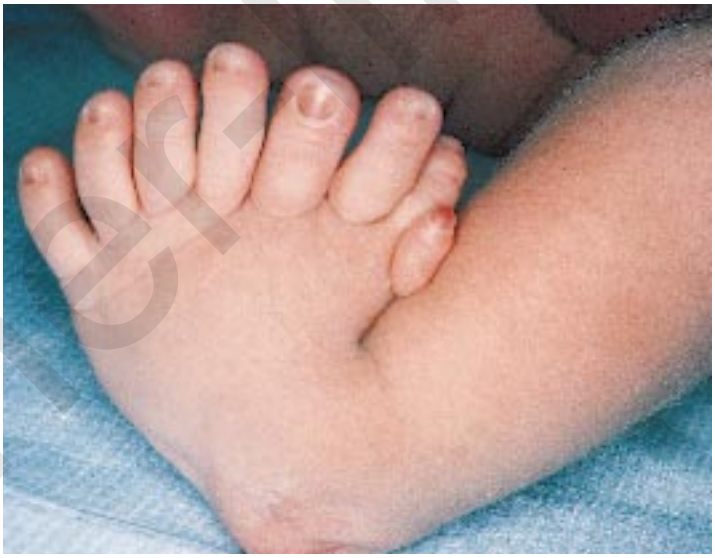

Figure 1.107. Octadactyly and pes equinovarus of the left foot in the same infant. Note the position of the big toe. The extra digits are therefore preaxial.

1.108

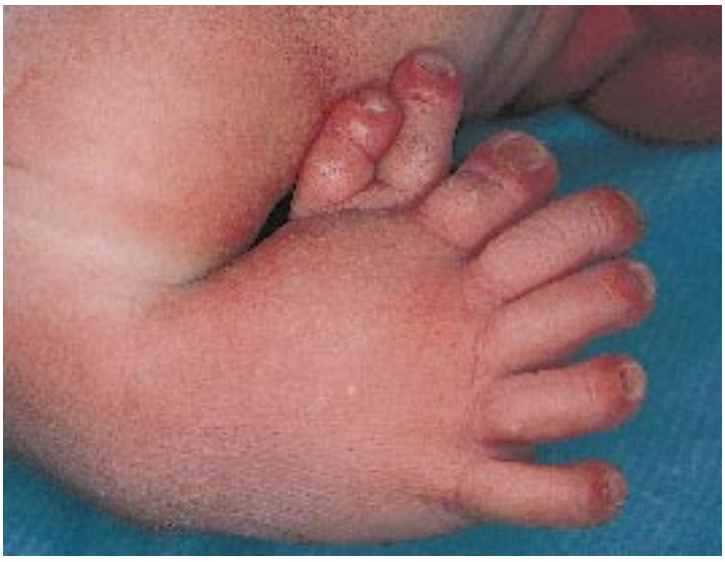

Figure 1.108. The same infant showing the septadactyly and pes equinovarus of the right foot. Note the position of the big toe. The extra digits are also preaxial.

1.109

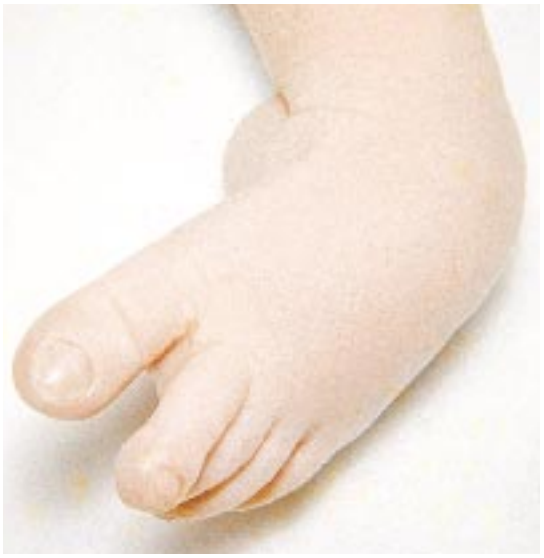

Figure 1.109. Talipes equinovarus (congenital clubfoot). There has been much discussion as to whether this is a true congenital malformation or whether it occurs as a result of a postural deformity (intrauterine molding). The foot cannot be dorsiflexed to the normal position and the heel is fixed in the varus deformity.

1.110

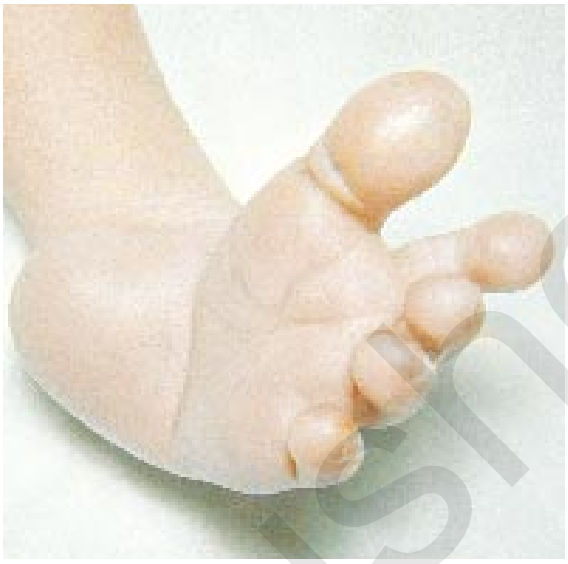

Figure 1.110. Another view of the foot of the same infant.

1.111

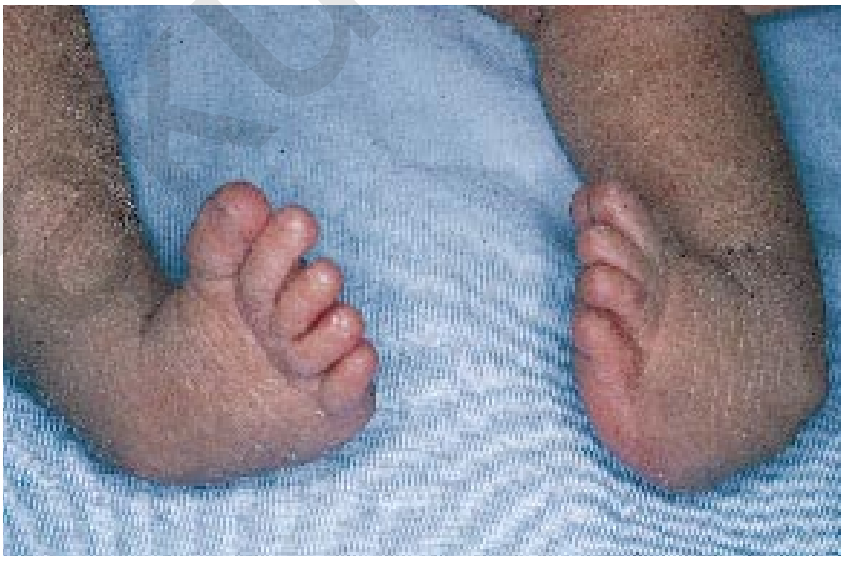

Figure 1.111. Talipes equinovarus (congenital clubfoot) in an infant with Poland's anomaly. Talipes equinovarus is frequently associated with congenital hip dysplasia, neural tube defects, and neuromuscular conditions.

1.112

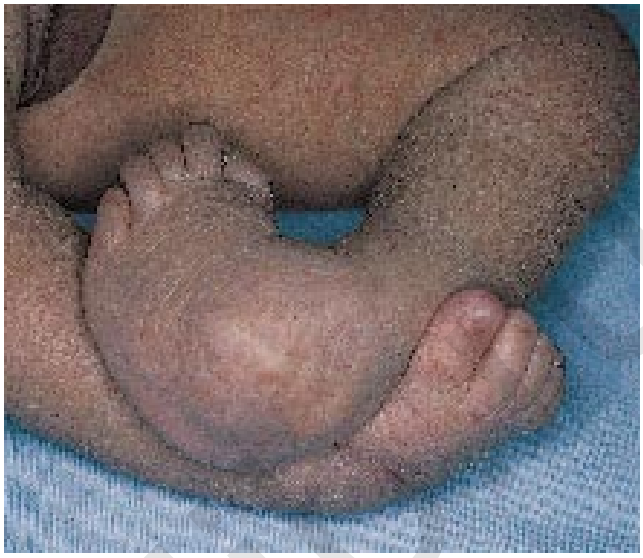

Figure 1.112. The same infant showing the position of the feet in utero, suggesting that the defect occurred as a result of a congenital postural deformity. In infants with clubfoot occurring as a congenital malformation, skin dimples are not present at the ankles, whereas in infants with clubfoot associated with postural deformations, dimples may be present over the joint as is noted in this infant.

1.113

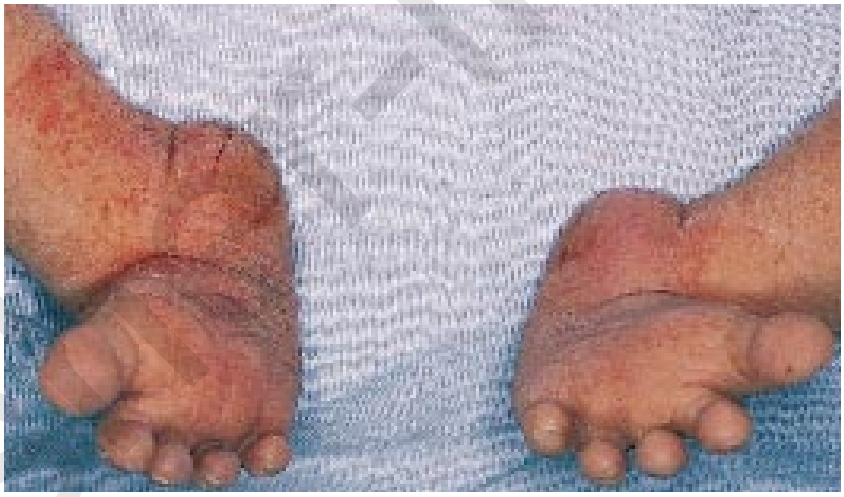

Figure 1.113. Bilateral clubfoot in an infant with myotonic dystrophy. The lack of fetal movement in utero caused this deformity. Clubfoot is commonly seen in infants with neuromuscular diseases such as neural tube defects and amyotonia congenita (Oppenheim's disease).

1.114

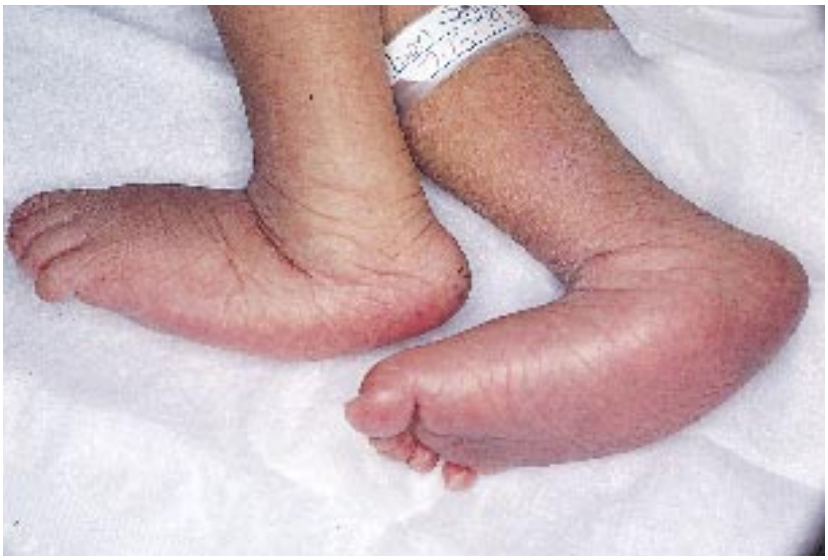

Figure 1.114. Rocker-bottom feet are noted in this infant with trisomy 18. Posterior calcaneal extension is present and the convex appearance of the sole of the foot resembles a "rocking chair."

1.115

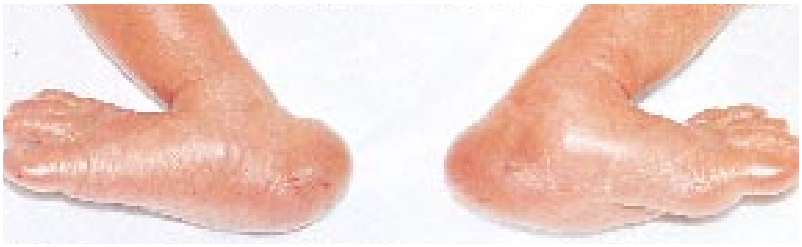

Figure 1.115. This infant with a neural tube defect presents a classic appearance of rocker-bottom feet with marked posterior calcaneal extension. Rocker-bottom feet are commonly seen in infants with neural tube defects.

1.116

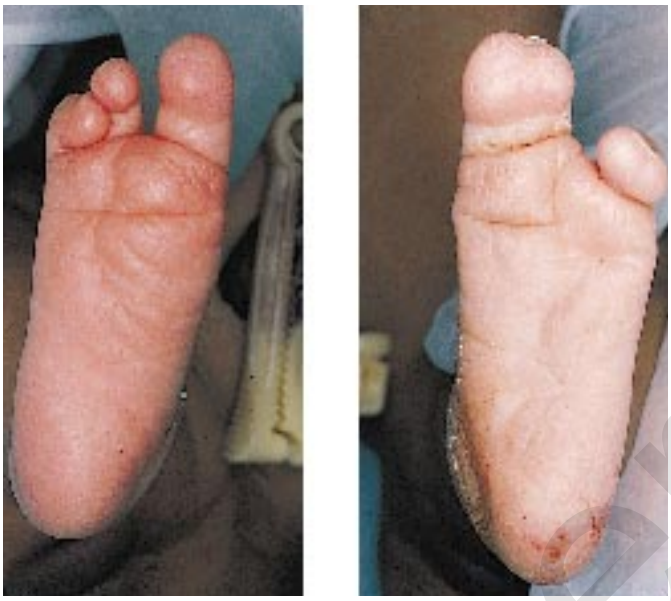

Figure 1.116. An example of ectrodactyly of both feet. Note that there are three toes on the right foot and three toes on the left foot with fusion of the first and second toes. The sole creases are poorly developed.

1.117

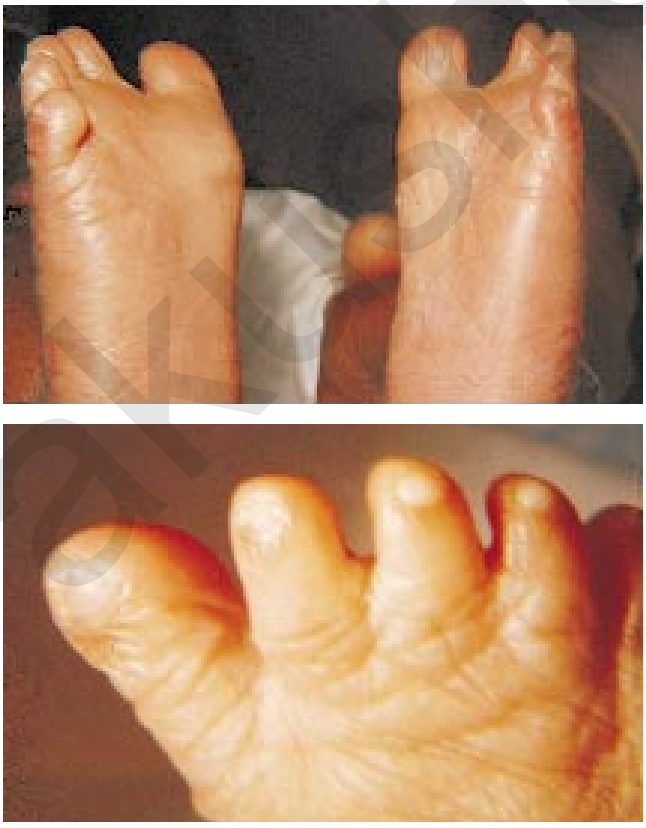

Figure 1.117. Microsyndactyly of the toes in an otherwise normal infant.

1.118

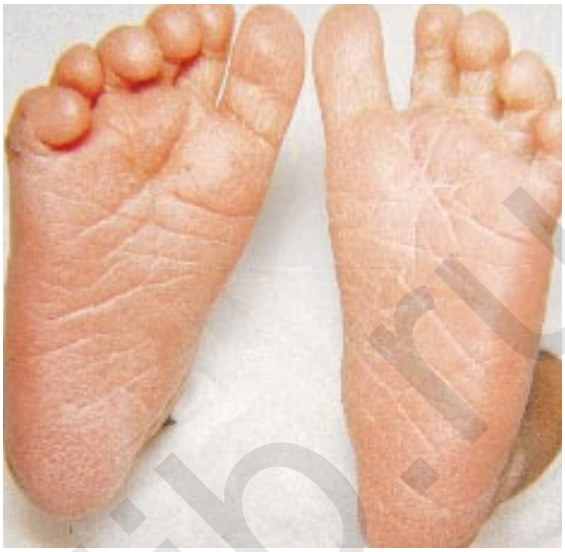

Figure 1.118. Polydactyly of toes of the right foot.

1.119

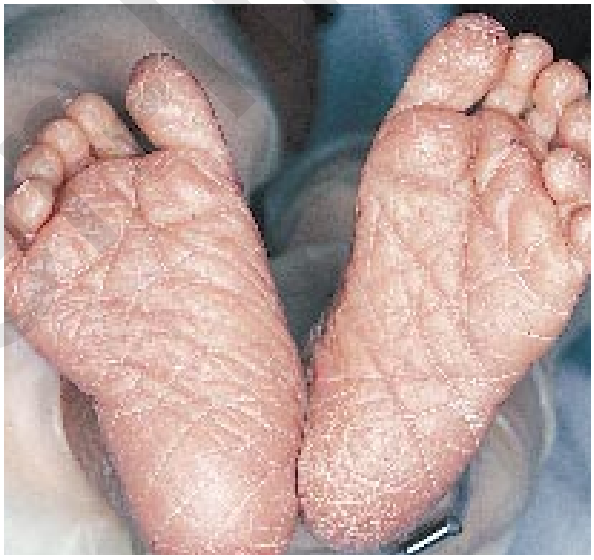

Figure 1.119. Polydactyly of the toes of both feet.

1.120

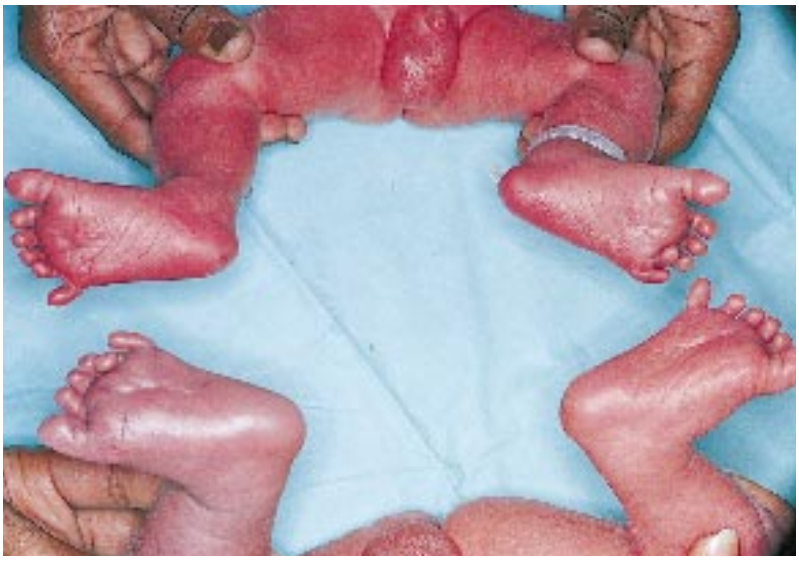

Figure 1.120. Bilateral polydactyly of toes in identical twins.

1.121

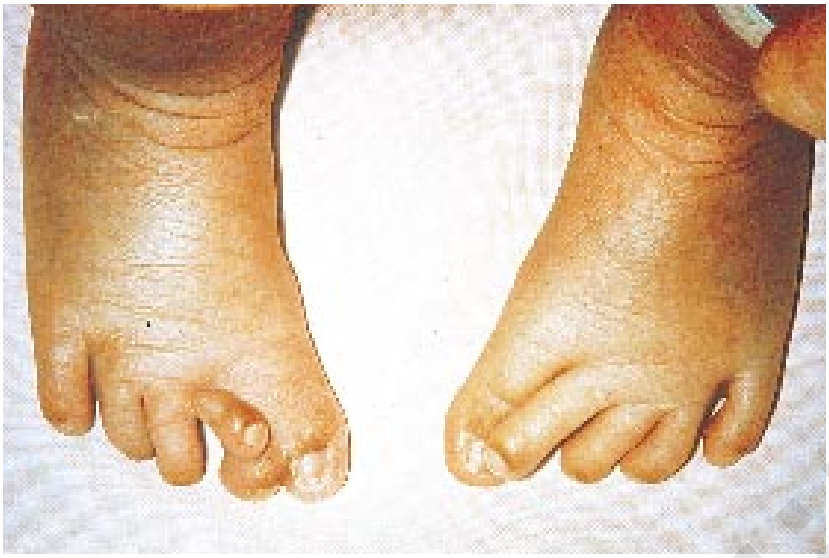

Figure 1.121. Central polydactyly and syndactyly of the first and second toes of the right foot in an infant of a diabetic mother. Otherwise, the infant was normal.

1.122

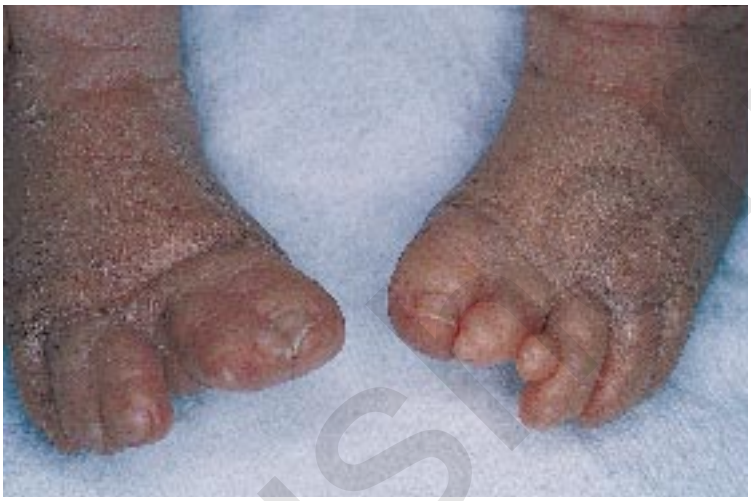

Figure 1.122. Central polydactyly of the left foot with syndactyly of the first and second toes of both feet. This infant, who clinically was not typical of a trisomy 18, had the radiographic findings of a gracile appearance of the ribs and an antimongoloid pelvis. The karyotype was a typical trisomy 18.

1.123

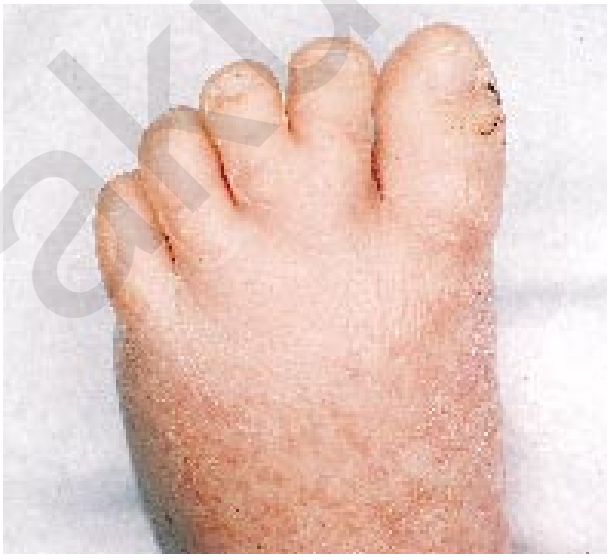

Figure 1.123. Syndactyly in an otherwise normal infant is of no medical or cosmetic significance and involves the toes more frequently than the fingers. Syndactyly refers to fusion of the soft tissues without synostosis. It is also seen in many syndromes such as Smith-Lemli-Opitz, Apert's, and trisomy 18.

1.124

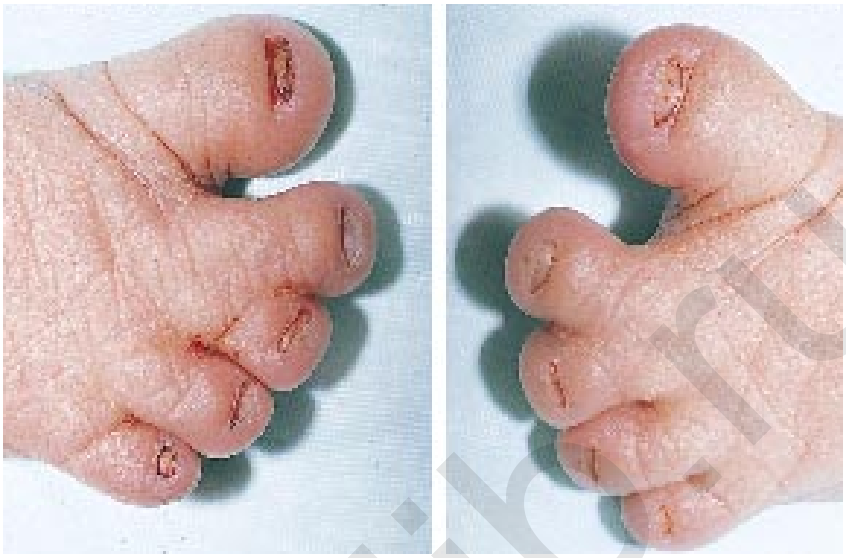

Figure 1.124. Syndactyly of the second and third toes bilaterally with markedly hypoplastic nails in an infant who also had a floating thumb of the right hand. Chromosomes were normal.

1.125

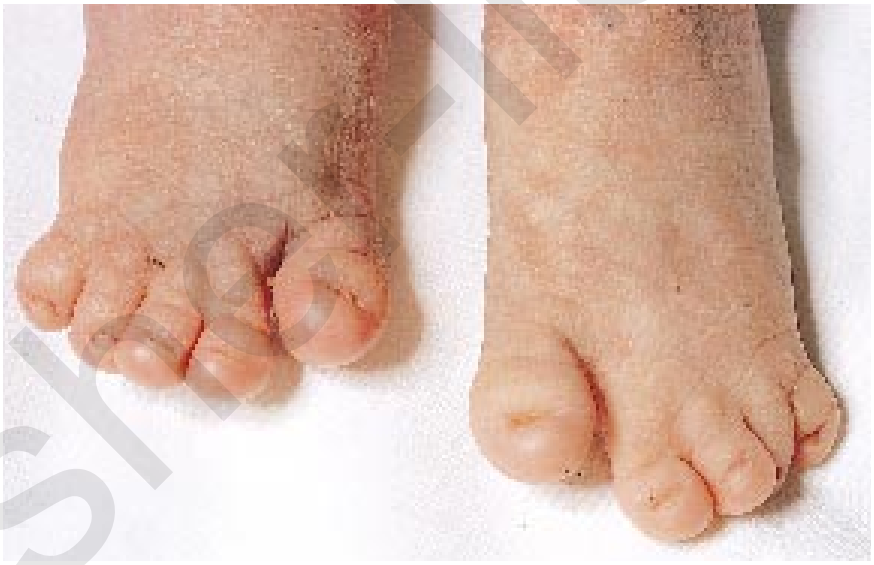

Figure 1.125. Mild syndactyly of the second and third toes in an infant with the other typical findings of trisomy 18, namely the short big toes and hypoplastic nails.

1.126

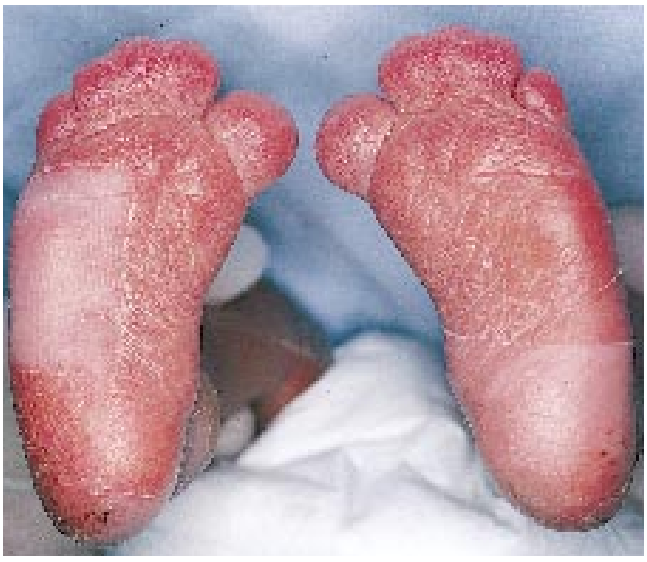

Figure 1.126. Symmetrical syndactyly of the toes in an infant with Apert's syndrome (acrocephalosyndactyly).

In symphalangism, no joint movement whatever is possible at the sites of the affected interphalangeal joints because the bony fusion has taken place. The absence of flexion creases is an excellent clue to the presence of this anomaly.

1.127

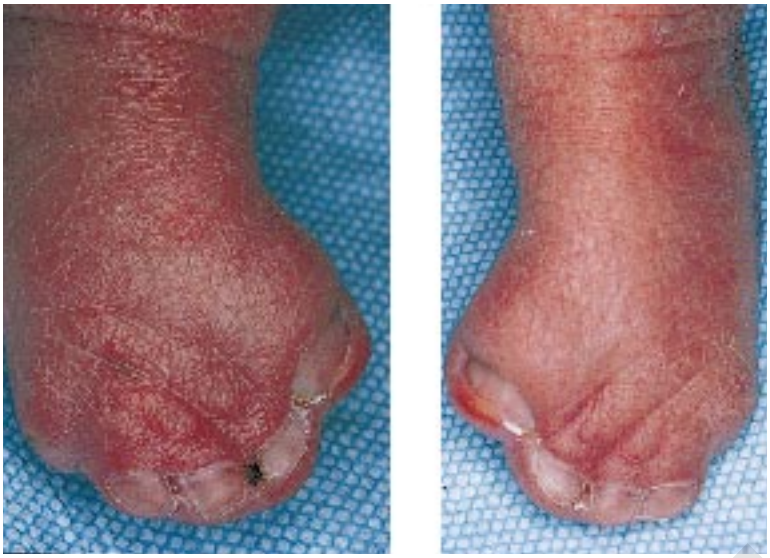

Figure 1.127. Another example of symmetrical syndactyly of the toes in Apert's syndrome.

1.128

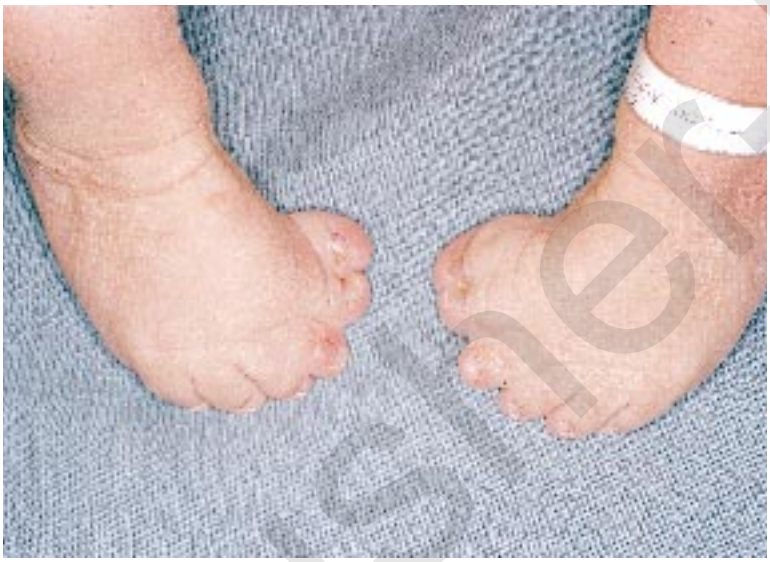

Figure 1.128. Bilateral symmetrical polysyndactyly giving the appearance of webbing between the toes in an infantwith Carpenter's syndrome (acrocephalopolysyndactyly).

1.129

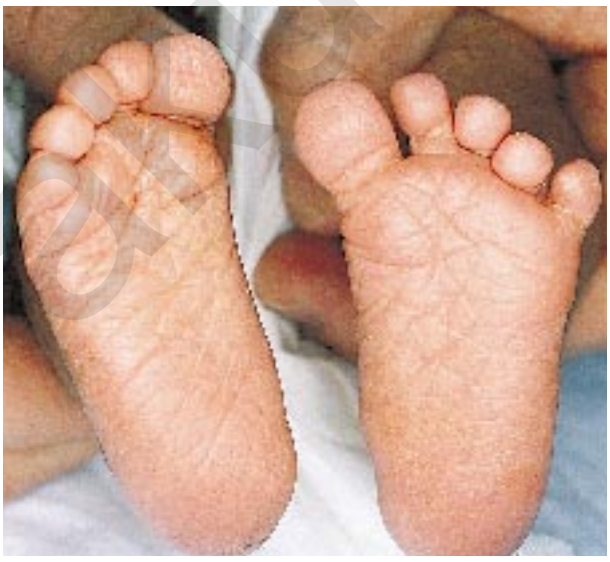

Figure 1.129. Broad toes in a normal infant. This may be familial. Broad toes are seen in certain syndromes such as Rubenstein-Taybi syndrome and Larsen's syndrome.

1.130

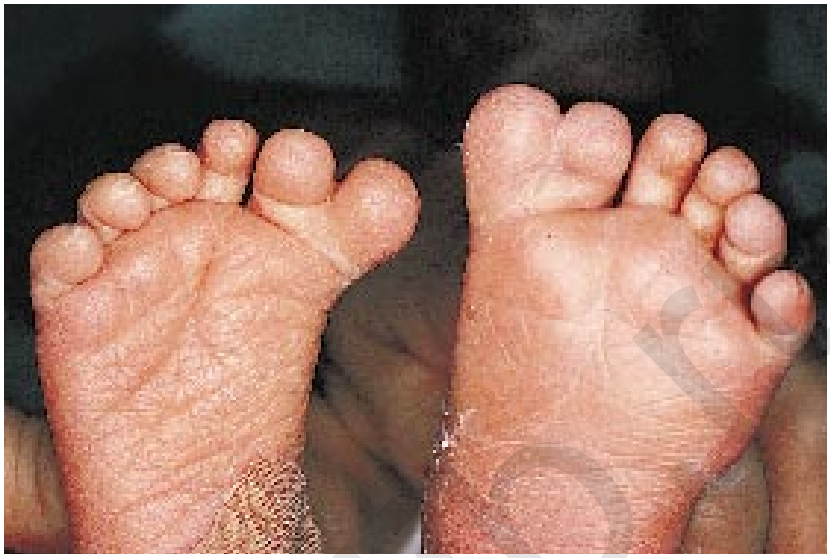

Figure 1.130. Preaxial polydactyly with bifid big toes in an otherwise normal infant.

1.131

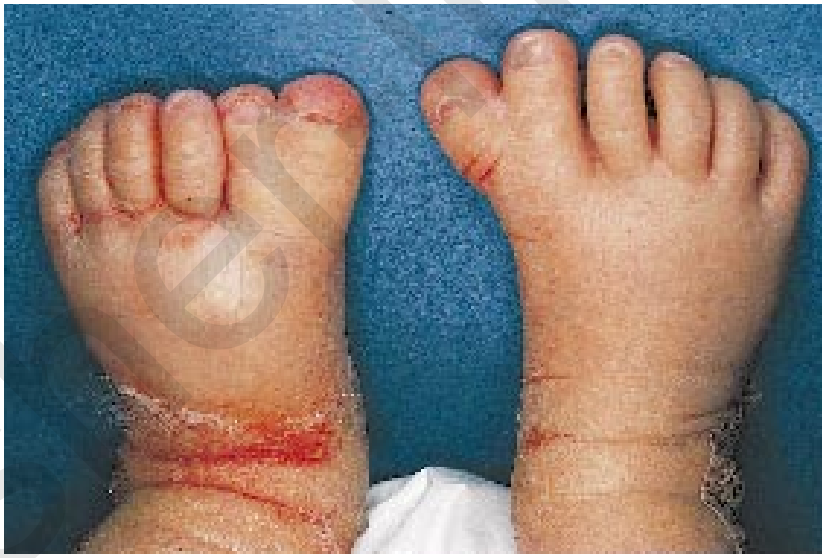

Figure 1.131. Bifid big toes with polydactyly in an infant who also has digitalization of the thumbs.

1.132

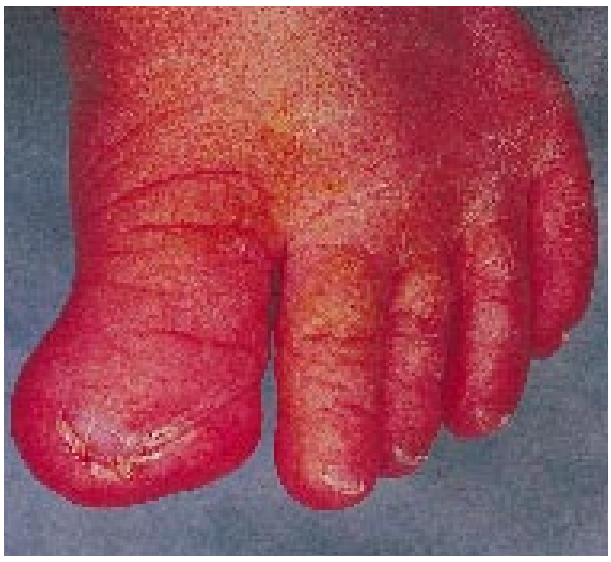

Figure 1.132. Duplication of the big toe. Radiograph showed two separate digits. This may result from an early insult to the limb bud in the 5th to 6th week of gestation.

1.133

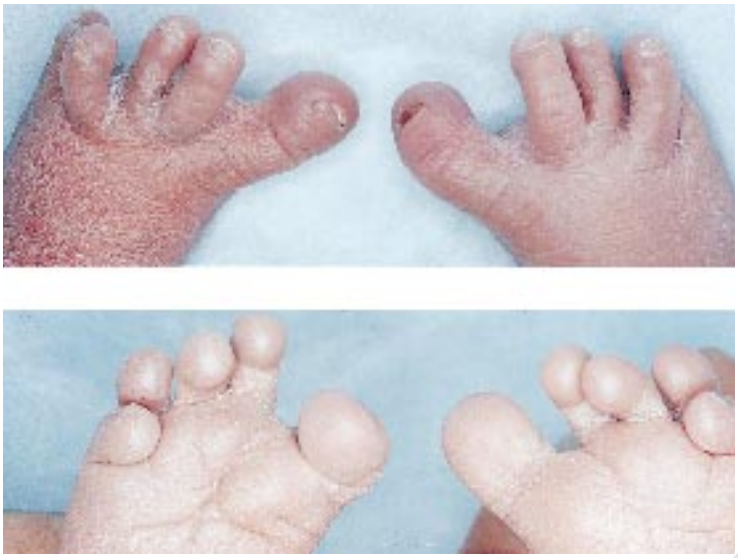

Figure 1.133. Congenital curly toes ("overlapping" toes). These are very common and are often familial. The abnormality becomes less obvious as the infant grows.

1.134

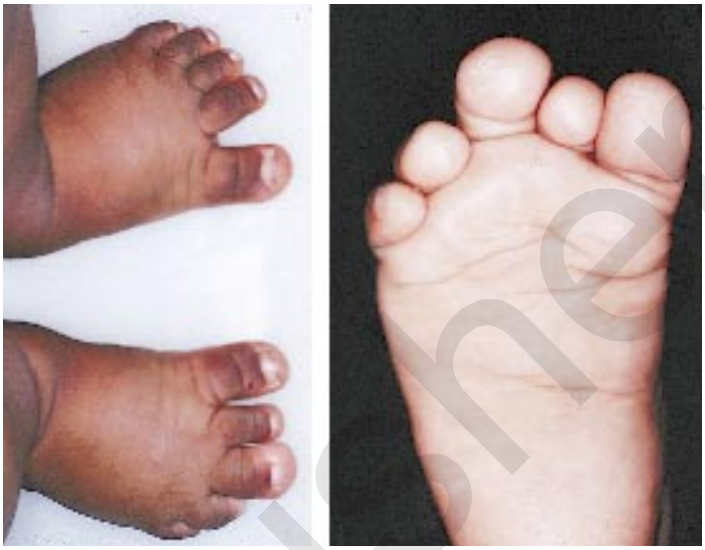

Figure 1.134. Hypertrophy of the third toe of the right foot. This may occur as an isolated finding or may be seen in neurofibromatosis or in infants with vascular malformation of a digit.

1.135

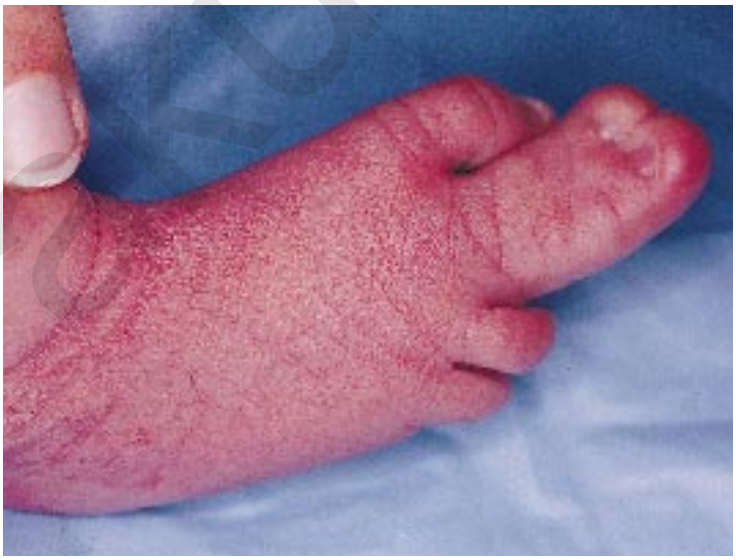

Figure 1.135. Dorsal view of macrosyndactyly of the second and third toes of the right foot.

1.136

Figure 1.136. Plantar view of the toes of the same infant.

1.137

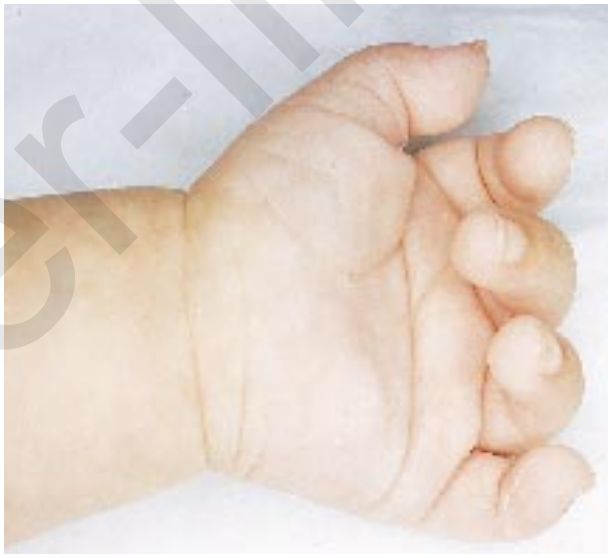

Figure 1.137. Single palmar crease and clinodactyly in the left hand of an otherwise normal infant. Single palmar creases are noted bilaterally in 1 to 2% of normal infants and unilaterally in 6% of normal infants. It is present in about 50% of patients with Down syndrome. It is twice as common in males as in females and it is associated with many syndromes. Palm creases form in response to flexion at the metacarpophalangeal joints and opposition of the thumb. Three deep creases are usually seen but there are many normal variants.

1.138

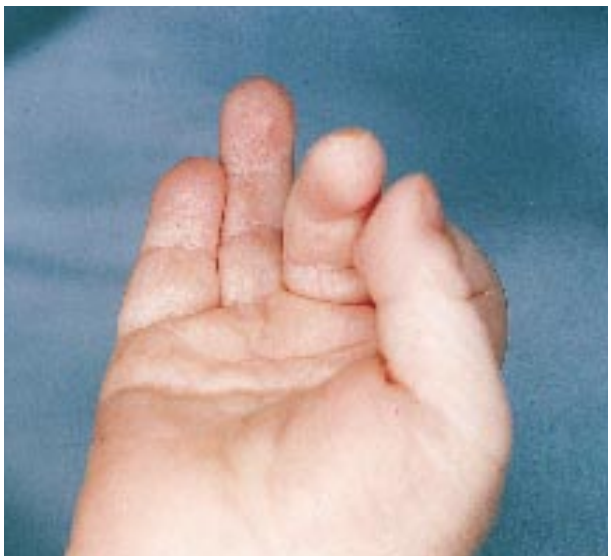

Figure 1.138. Single palmar crease and clinodactyly of the right hand. Clinodactyly is the incurving of the finger to one side, usually toward the midline, due to an absent or hypoplastic middle phalanx. Involvement of the fifth finger is most common. With an absent phalanx only two creases are present as in this infant. With a hypoplastic middle phalanx, the number of creases is normal but creases are closer together and will slope toward each other rather than being parallel. It is noted in otherwise normal infants but also occurs in many syndromes.

1.139

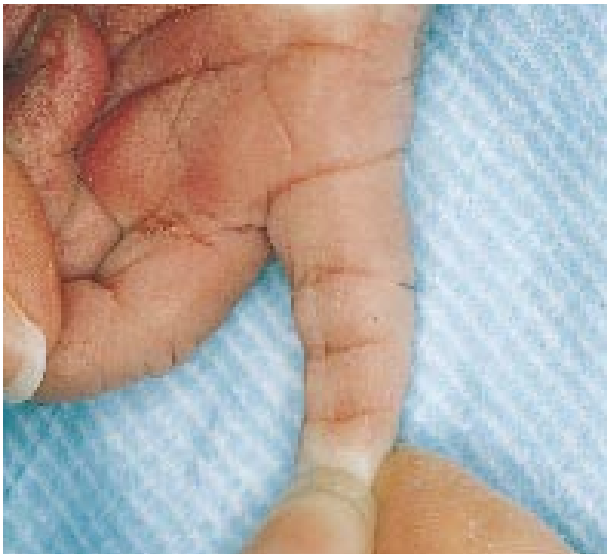

Figure 1.139. An extra crease on the fifth finger.

1.140

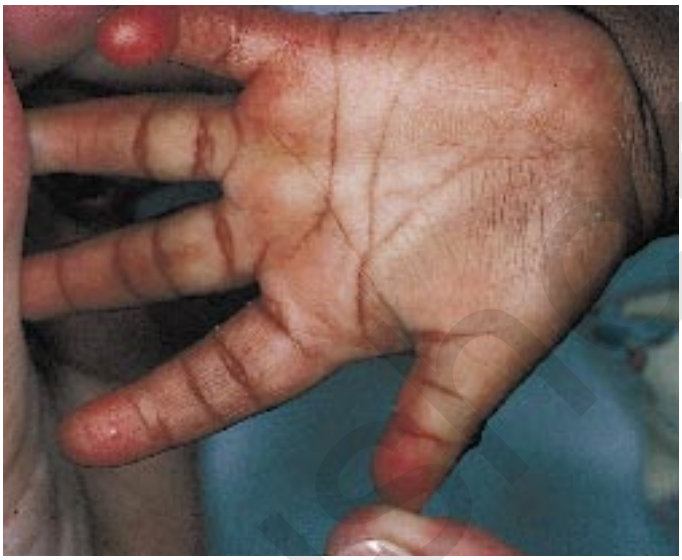

Figure 1.140. Increased number of finger creases in an otherwise normal infant. Increased finger creases may be seen in normal infants and in infants that have increased laxity of the joints such as in Larsen's syndrome and Ehlers-Danlos syndrome. They often signify increased fetal activity at 11 to 12 weeks of fetal life when the creases normally become evident. Hence, gross alteration in crease patterning is usually indicative of an abnormality in form and/or function of the hand prior to the 11th fetal week. If there is a lack of fetal movement before this period of gestation, the number of finger creases is decreased.

1.141

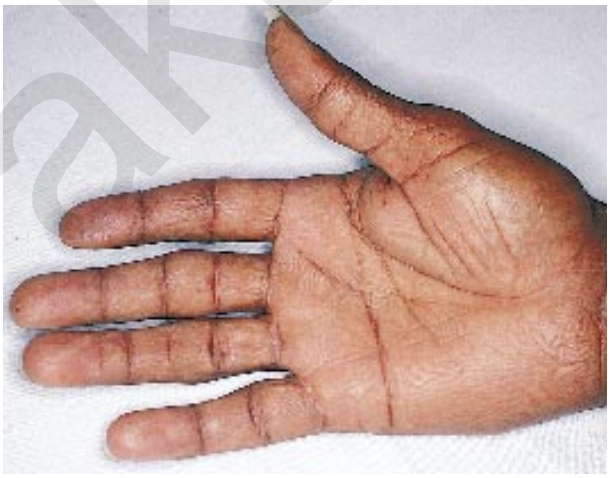

Figure 1.141. The father of the same infant also had increased finger creases. He was otherwise normal and had no problems. The thenar crease normally circles the base of the thenar eminence, extending distally to between the thumb and index fingers. The distal palmar crease traverses the palm beneath the last three fingers, beginning at the ulnar edge of the palm and curving distally to exit between the middle and index fingers. The proximal palmar crease may be less well defined. It begins over the hypothenar eminence and normally extends parallel to the distal crease to exit near or fuse with the distal portion of the thenar crease.

1.142

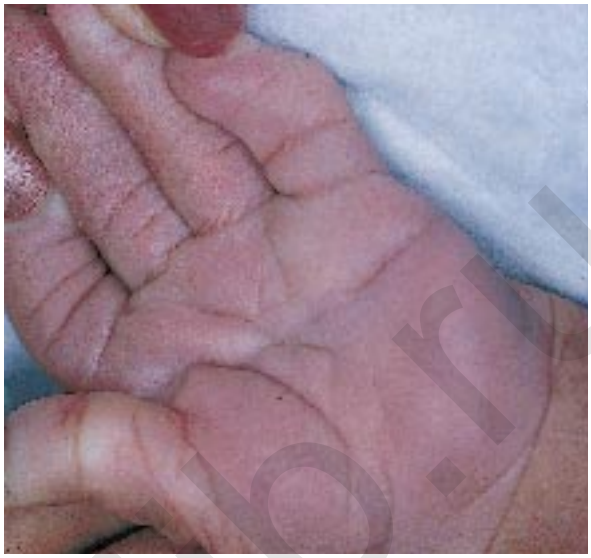

Figure 1.142. Increased and abnormal finger creases due to laxity of joints in an infant with Larsen's syndrome. Note the single palmar crease.

1.143

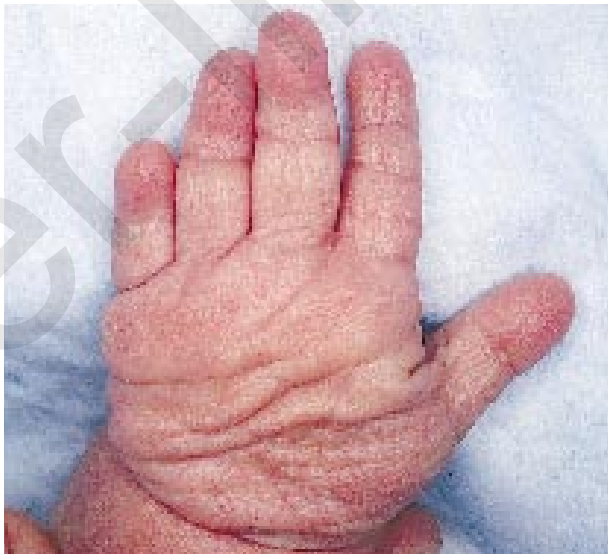

Figure 1.143. This infant has decreased creases in both the fingers and the palm due to lack of fetal movement. Absence of normal flexion creases invariably signifies inadequate movement of the underlying joints. Changes in the palmar crease include the single palmar crease (simian crease) and the bridged palmar crease (Sydney line) in which there is an extension of the proximal transverse crease which reaches the ulnar border of the hand and the medial edge of the palm between the index and middle fingers.

1.144

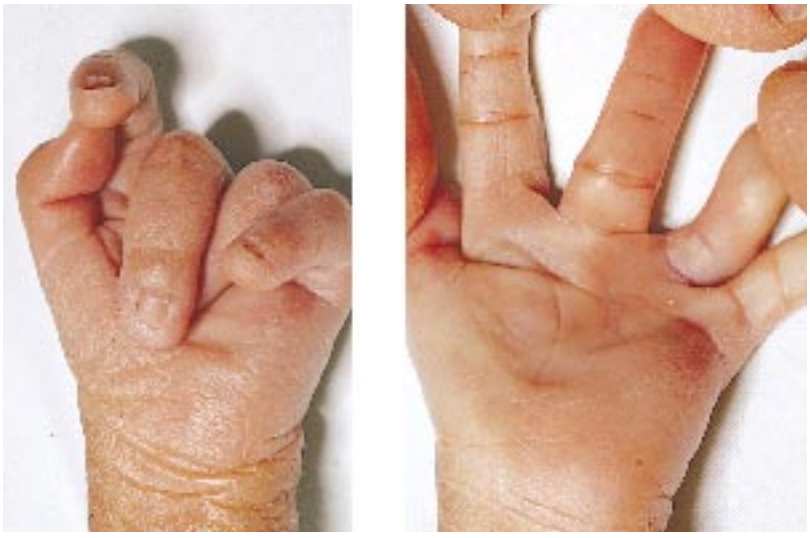

Figure 1.144. Lack of fetal movement is seen in acute infantile spinal atrophy (Werdnig-Hoffmann disease). Lack of normal development of the finger creases is due to lack of fetal movement early in gestation. On the left, note the position of comfort of the fingers with deep depression in the palm shown on the right.

1.145

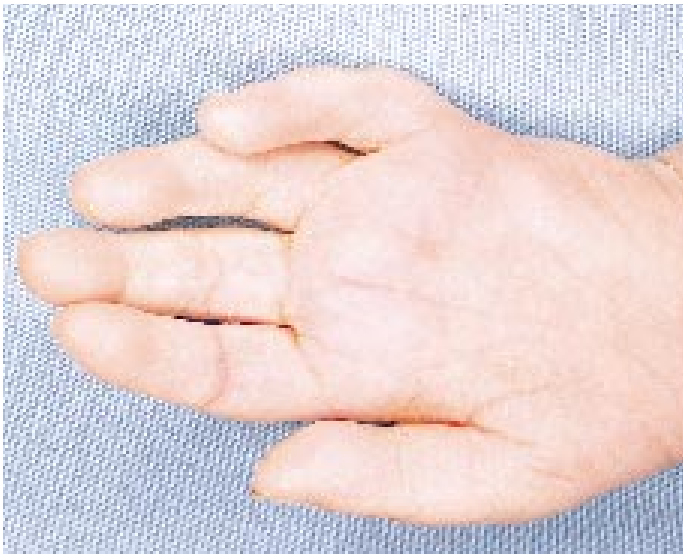

Figure 1.145. Lack of creases of the palm and fingers in an infant with amyotonia congenita.

1.146

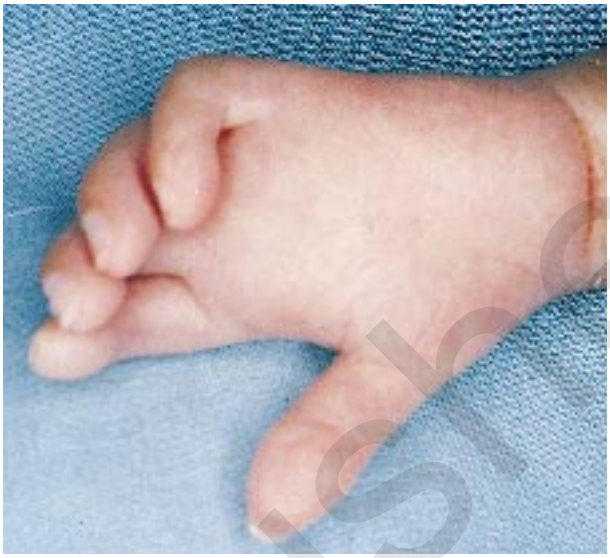

Figure 1.146. Hypoplastic (absent or sparse) dermal ridges and absence of flexion creases on the fingers and palms are seen in this infant with the fetal akinesia sequence (Pena-Shokeir phenotype).

1.147

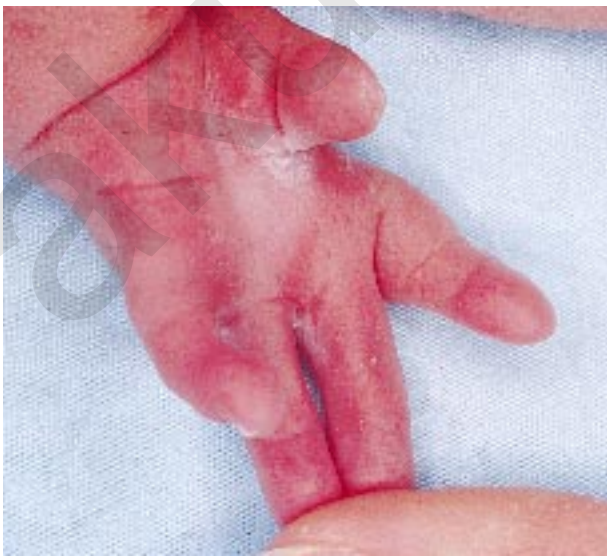

Figure 1.147. This infant with arthrogryposis multiplex congenita shows the lack of palmar and finger creases due to lack of fetal movement before the 10th to 12th weeks of gestation.

1.148

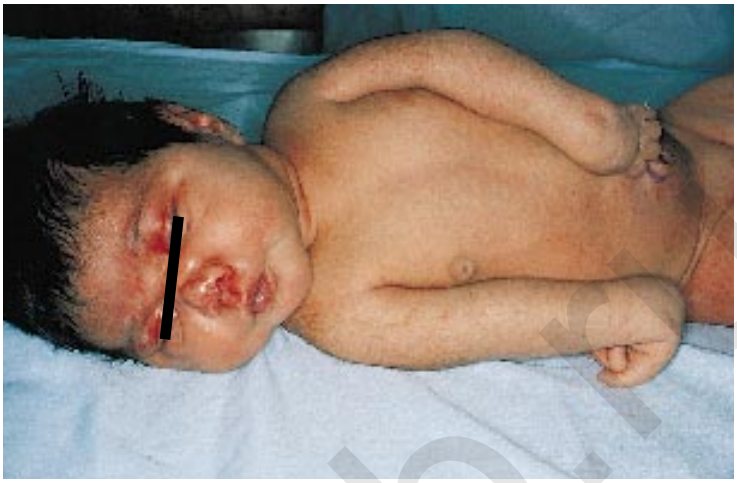

Figure 1.148. Arthrogryposis multiplex congenita in this infant shows the contractures which occur in this condition. They are usually symmetrical and involve all four extremities but may involve only the upper or lower limbs. There is muscular hypotonia, generalized thickening of the skin with dimpling, and hip subluxation; and bilateral talipes equinovarus, opisthotonos and scoliosis of the spine are common.

1.149

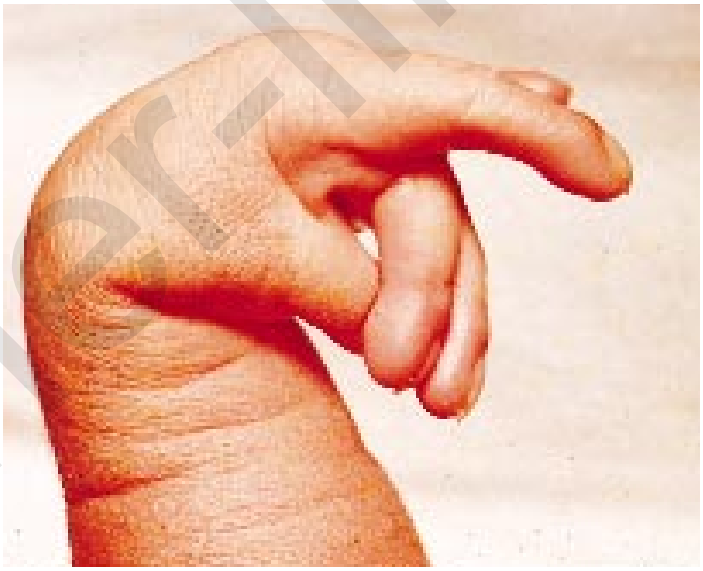

Figure 1.149. Contracture of the hand in an infant with arthrogryposis multiplex congenita.

1.150

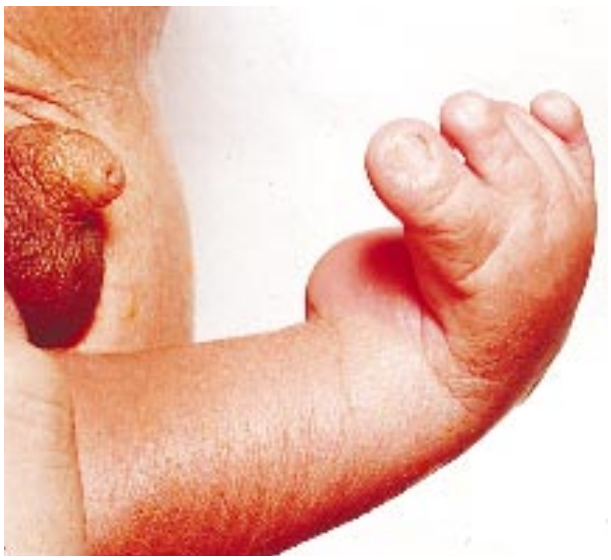

Figure 1.150. Contracture of the lower extremity in the same infant. These infants commonly have bilateral talipes equinovarus.

1.151

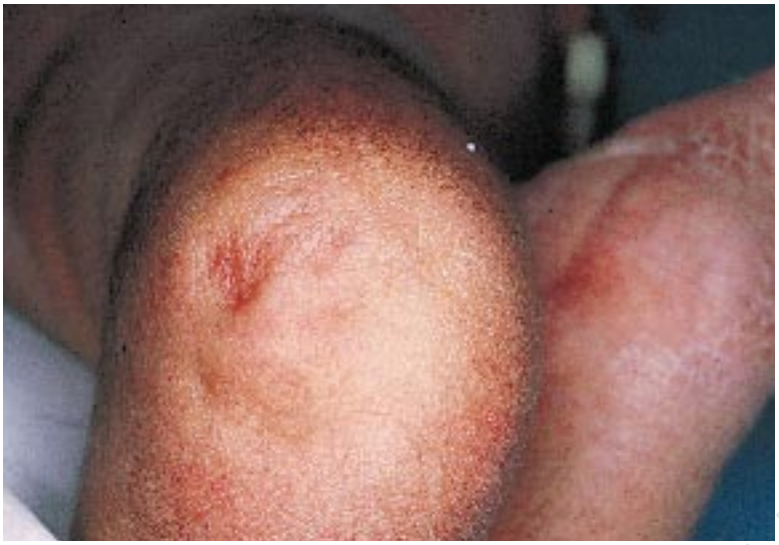

Figure 1.151. Dimples at the knee in an infant with arthrogryposis multiplex congenita. Normally dimples at a joint are of no significance, but they may occur with contractures and lack of movement as in this infant.

Chapter 2
Dwarfism

Dwarfs frequently present in the newborn period, but sometimes the diagnosis is not obvious until there is additional disproportionate growth. There are many different kinds of dwarfs and the nomenclature is descriptive of the portions of the long bones affected. Rhizomelic shortening refers to the proximal portions of the long bones (e.g., upper arms and thighs). Mesomelic shortening refers to the central segments of the long bones (e.g., forearms and legs). Acromelic shortening refers to the hands and feet. All three segments may be affected simultaneously but unequally, as in achondroplasia in which the most severe effect is in the proximal segment. All four limbs may be involved as in Conradi-Hünermann syndrome. Only the femur may be involved as in femoral hypoplasia syndrome or only the forearms may be affected as in Robinow's syndrome. A general knowledge of the various kinds of dwarfs is important in their recognition. Frequently, consultation with a radiologist, geneticist, pediatrician or neonatologist experienced in recognizing dwarfs may be necessary.

2.1

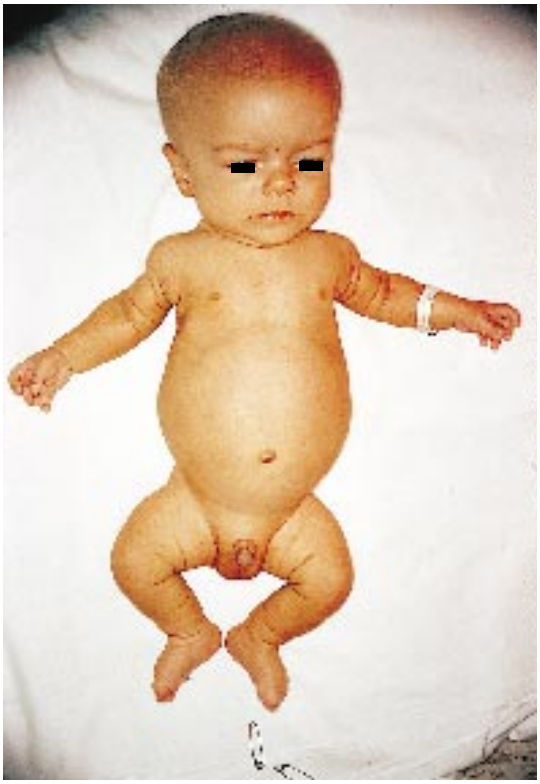

Figure 2.1. Achondroplasia (rhizomelic dwarfism). This is dominantly inherited but many cases occur by spontaneous mutation. There are short proximal parts of the arms and legs (rhizomelic micromelia), marked lordosis, caudal narrowing of the spine, and spade-like hands (short "trident" hand with short metacarpals and phalanges). Note the normally sized but laterally compressed trunk.

2.2

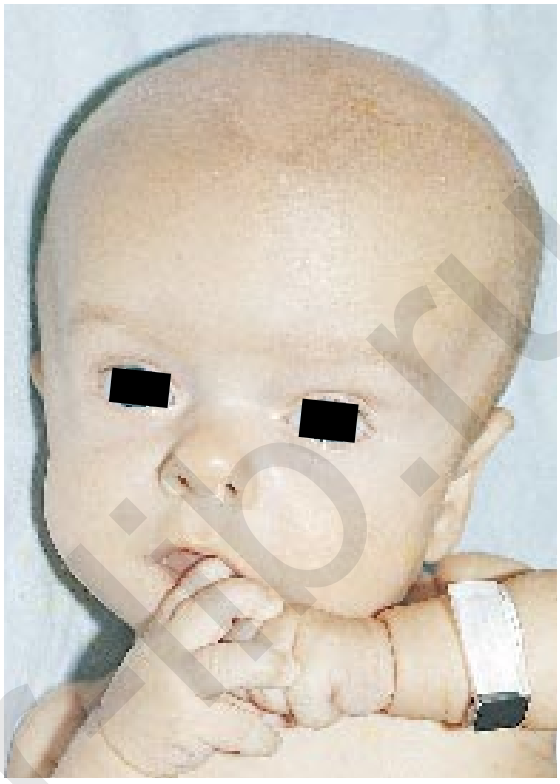

Figure 2.2. The head of the same infant showing the large square head with bossing of the forehead and a depressed nasal bridge. Infants with achondroplasia may have megalencephaly (macroencephaly).

In hypochondroplasia syndrome there is a near normal craniofacies but the limbs are short and there is caudal narrowing of the spine.

2.3

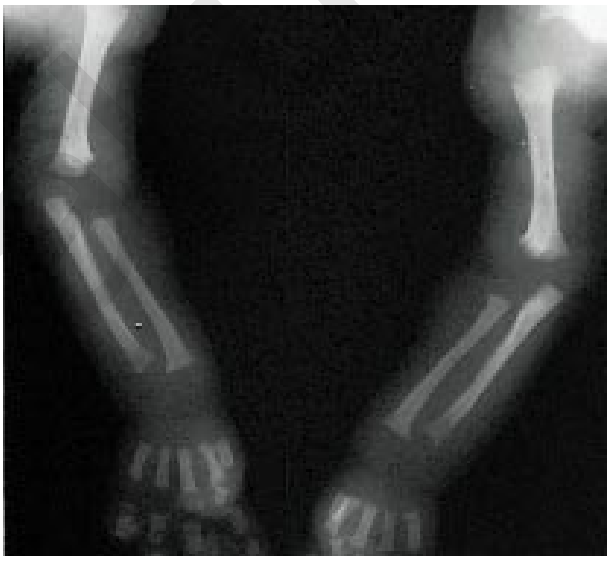

Figure 2.3. A radiograph of the upper extremities showing the short proximal parts. Note that the typical changes in the long bones are not yet present.

2.4

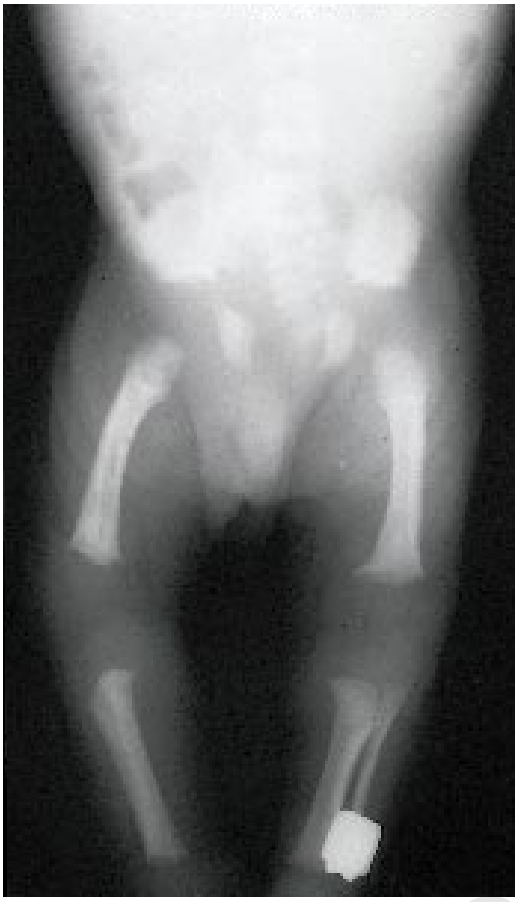

Figure 2.4. A radiograph of the lower extremities showing the short proximal parts. Note that the bones are broad and short.

2.5

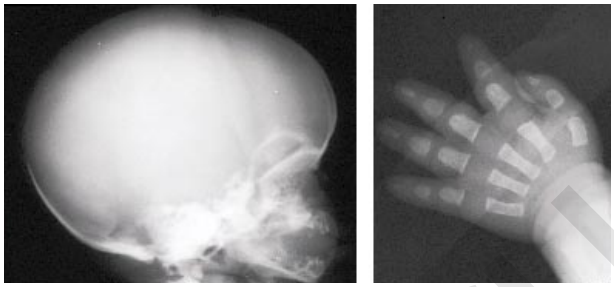

Figure 2.5. Radiograph of skull on the left showing the large size, shortened base and shallow sella turcica. This is characteristic in achondroplasia. On the right is a radiograph of the left hand showing the broad and short bones.

2.6

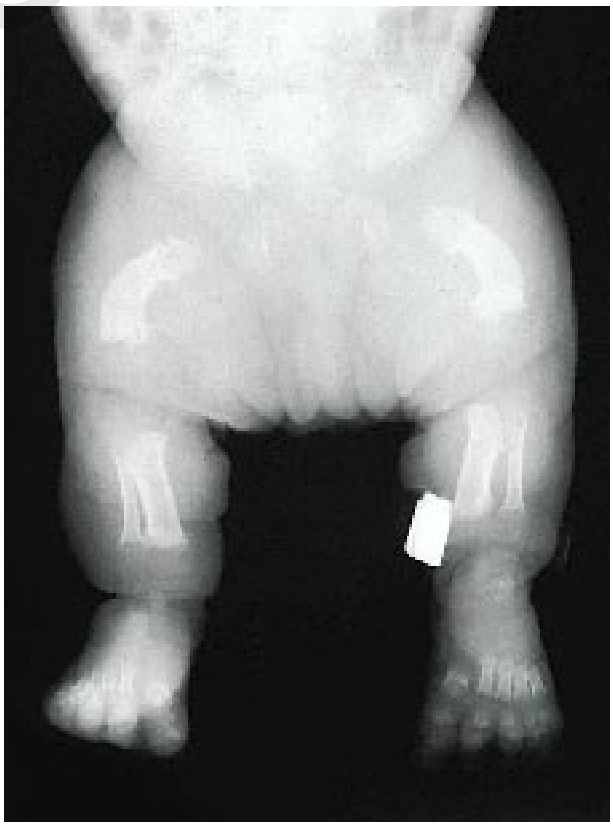

Figure 2.6. A radiograph of the lower extremities in an infant with achondroplasia. Note the broad short bones with irregular and flared epiphyseal lines. Note the typical "telephone handle" appearance of the femur.

2.7

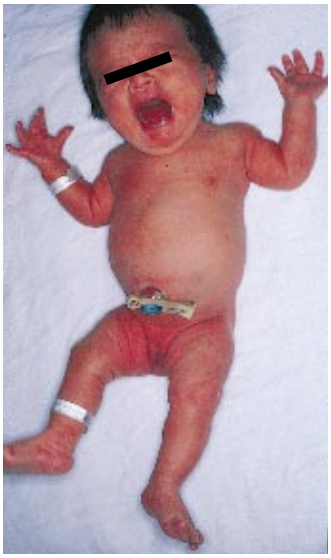

Figure 2.7. Another example of achondroplasia in a term infant. The infant's length was 45 cm with an upper/lower segment ratio of 2.3. The upper/lower segment ratio for a term infant is 1.7. The shortness of length and the increase in upper/lower segment ratio is due to the short lower extremities. The head circumference of 36 cm is above the 90th percentile.

2.8

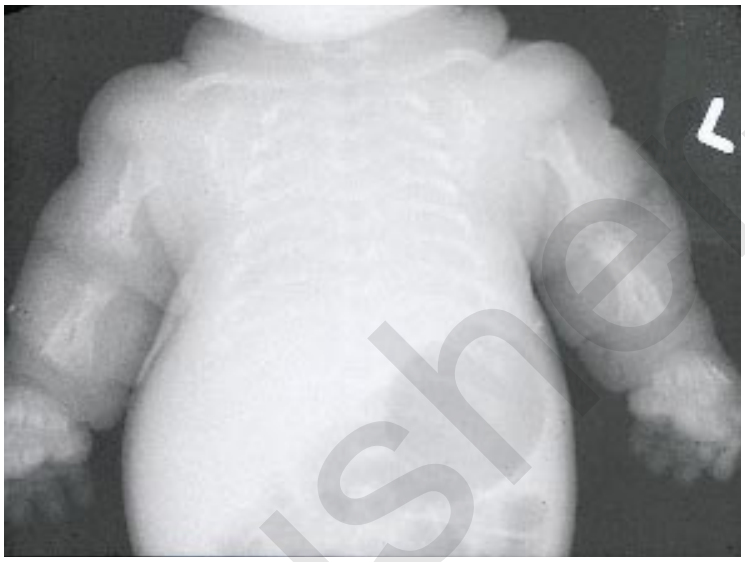

Figure 2.8. A radiograph of an infant with achondroplasia. Note the rhizomelic upper extremities and the narrow ribs which result in compression of the chest.

2.9

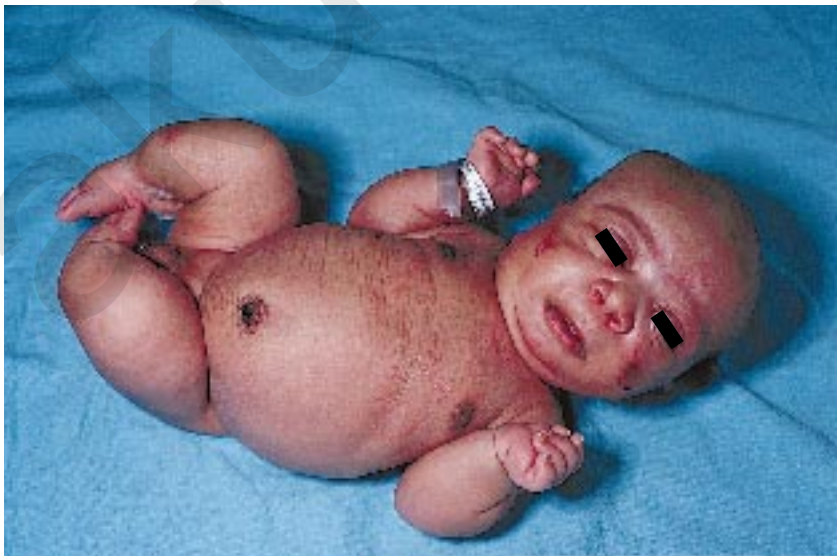

Figure 2.9. Camptomelic dysplasia. Note the short limbs and marked bowing of the tibiae in this autosomal recessive type of dwarfism. The infants have a flat facies with a low nasal bridge and micrognathia. The majority of infants die in the neonatal period from respiratory insufficiency.

2.10

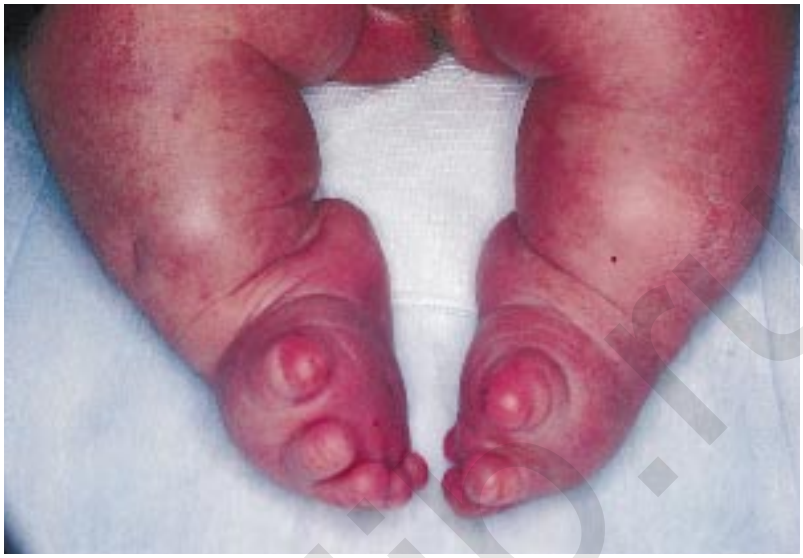

Figure 2.10. Note the bowed tibiae and the skin dimple over the mid-portion of the leg in the same infant with camptomelic dysplasia. These occur as a result of absent or hypoplastic fibulae in these infants.

2.11

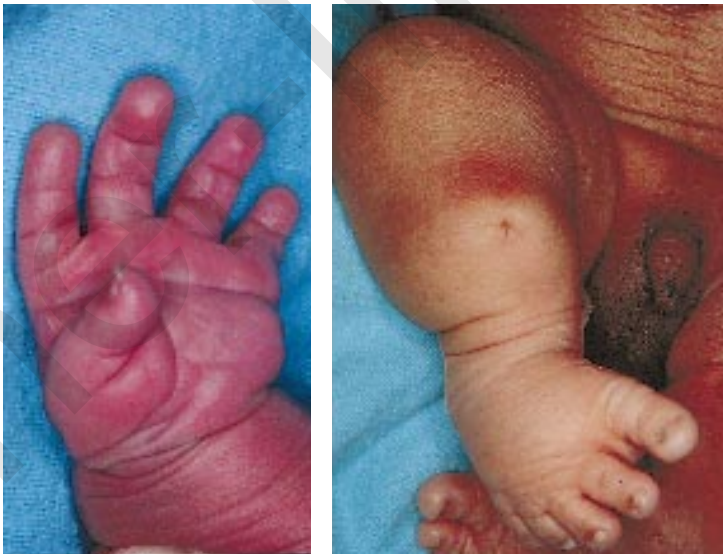

Figure 2.11. The same infant showing the left hand and the right leg. Note the short stubby fingers, single palmar crease and clinodactyly of the fifth finger and the anterior bowing of the tibia with skin dimpling over the convex area. Dimples at a joint are common and usually normal but the presence of skin dimples between joints, such as in this infant, always signifies underlying pathology.

2.12

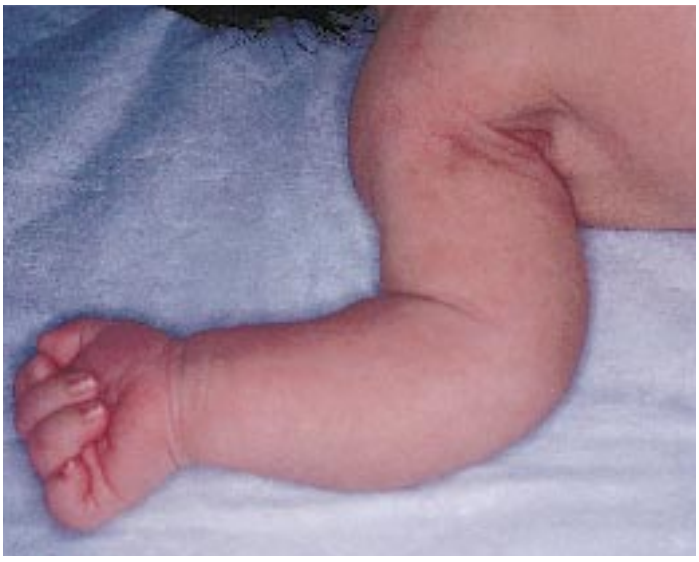

Figure 2.12. Note the marked shortening of the proximal portion of the right upper extremity compared with the distal portion in an infant with camptomelic dysplasia.

2.13

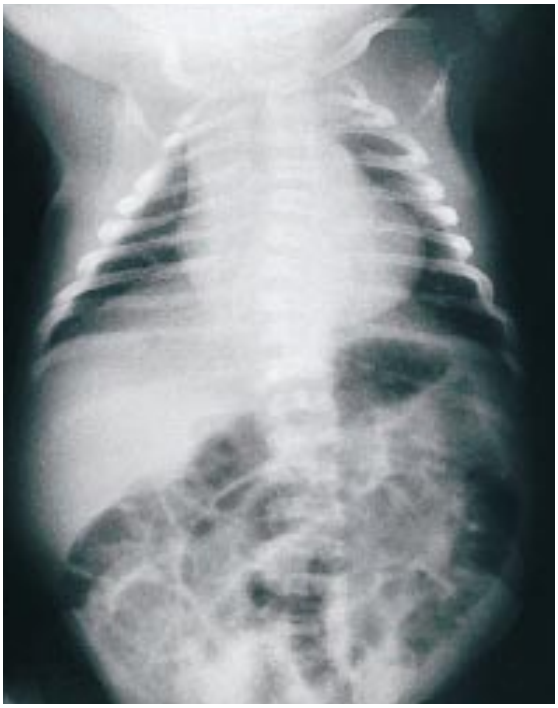

Figure 2.13. A radiograph of the chest of this infant shows the small thoracic cage with thin, short clavicles and hypoplastic scapulae. This is a typical finding in camptomelic dysplasia.

2.14

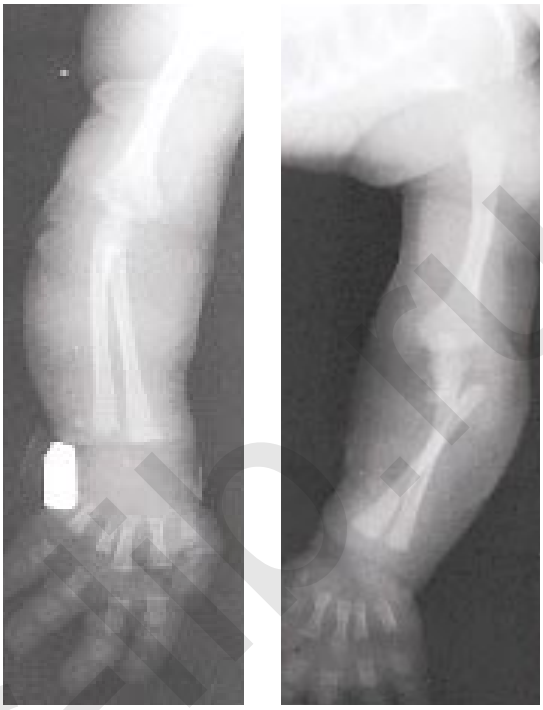

Figure 2.14. Radiograph of the upper extremities of the same infant with camptomelic dysplasia showing the hypoplastic scapulae, bowing of long bones, radioulnar dislocation and short proximal phalanges.

2.15

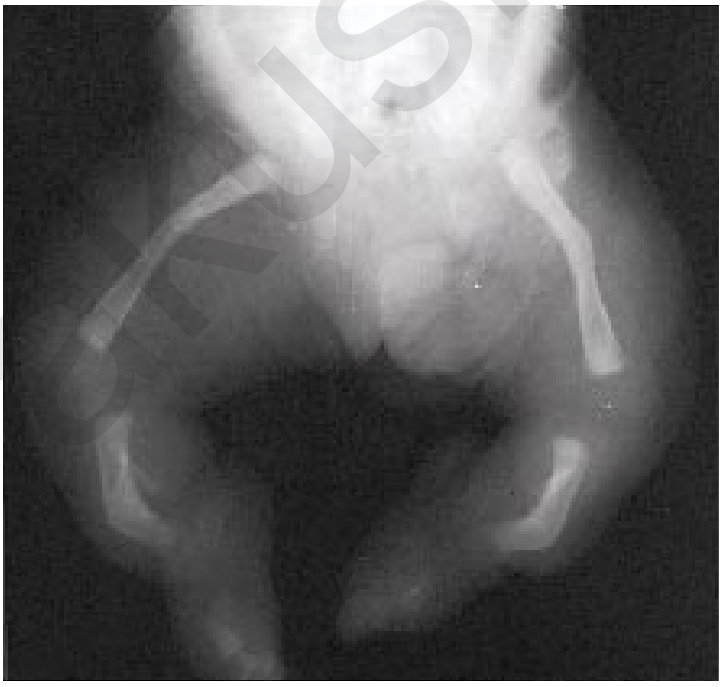

Figure 2.15. Radiograph of the lower extremities of the same infant with camptomelic dysplasia. Note the marked bowing of the long bones with cortical thickening of the concave border and thinning of the convex border. Also note the absent left fibula and hypoplastic right fibula.

2.16

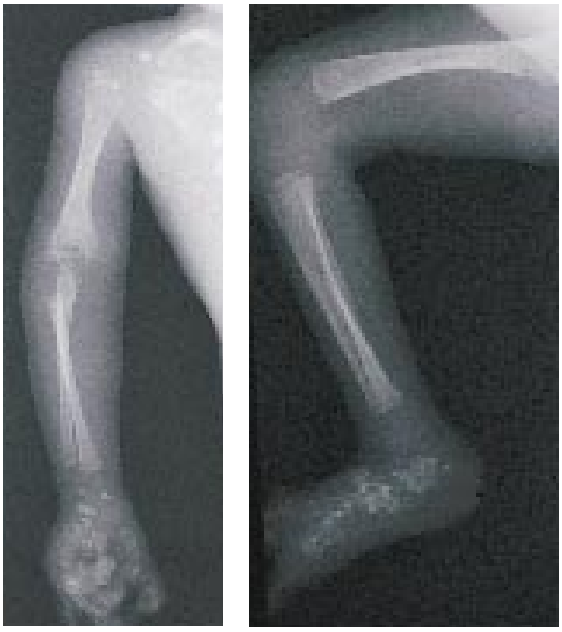

Figure 2.16. Radiograph of the upper and lower extremities showing the stippling of the epiphyses of an infant with chondrodystrophia calcificans congenita. This may occur as a rhizomelic form with a flat facies, low nasal bridge and cataracts, short humeri and femora, coronal clefts in the vertebrae, and punctate epiphyseal mineralization. It also occurs in an autosomal dominant form (Conradi-Hünermann syndrome) in which there is asymmetric limb shortness and early punctate epiphyseal mineralization. In infants with stippling of the epiphyses, consideration should also be given to the diagnoses of Zellweger syndrome and the fetal warfarin syndrome.

2.17

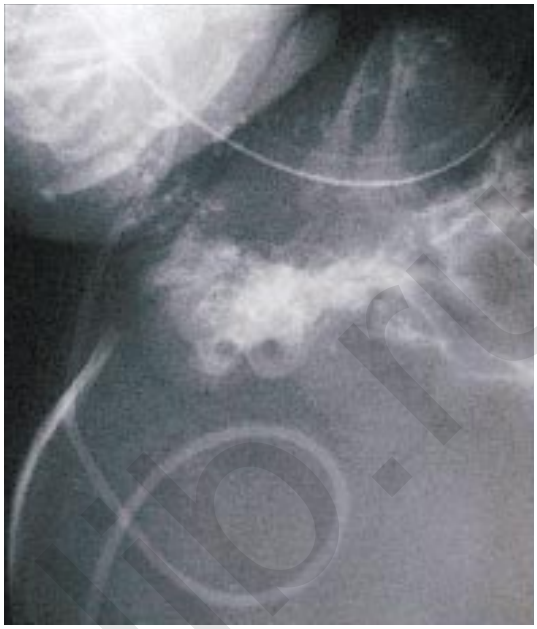

Figure 2.17. Radiograph of the neck in the same infant showing the characteristic stippling at the hyoid bone and the spine.

2.18

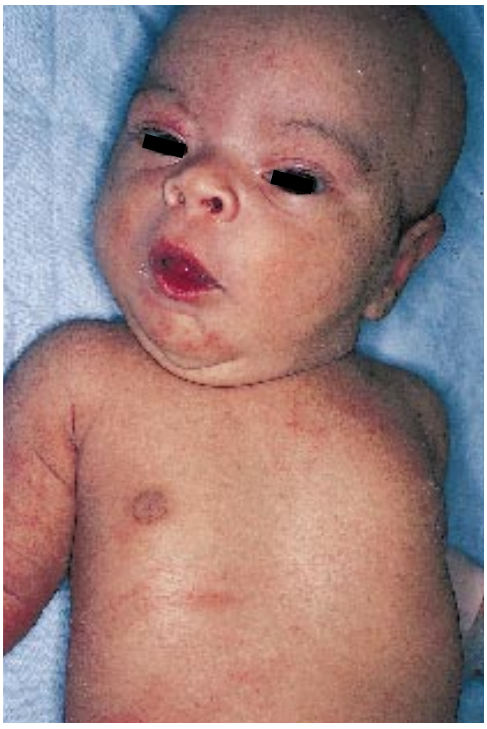

Figure 2.18. In this infant with cleidocranial dysplasia, an autosomal dominant condition, the shoulders clinically appear normal. They may present with hanging narrow shoulders, pectus excavatum, and abnormal shoulder movement due to the bilateral absence of the clavicles. In any infant with wide open sutures and fontanelles or wormian bones on clinical examination of the skull, one should always check the clavicles to exclude the diagnosis of cleidocranial dysostosis.

2.19

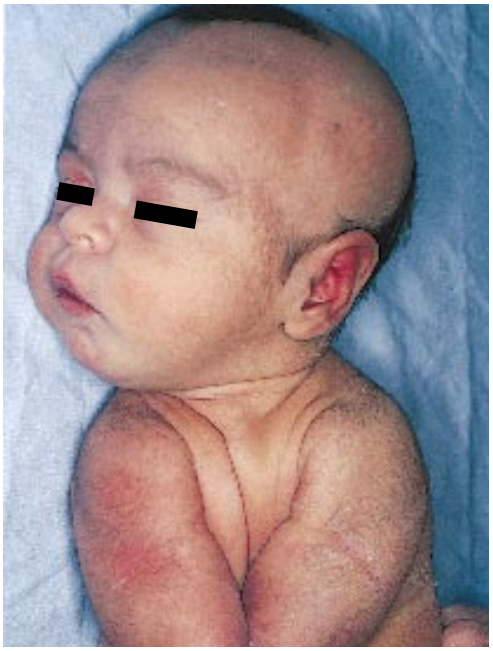

Figure 2.19. The same infant as in Figure 2.18 with cleidocranial dysplasia showing the approximation of the shoulders in front of the chest due to the absence of the clavicles. These infants present with other findings. Aplasia or defective development of the clavicles and laxity of the ligaments allow the forward folding of the shoulders. Defective mineralization of other parts of the skeleton may occur.

2.20

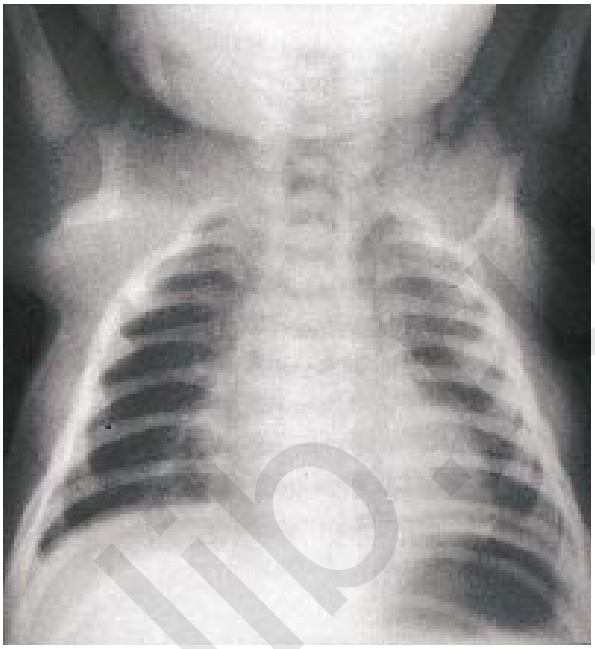

Figure 2.20. Radiograph of the chest shows the absence of the clavicles.

2.21

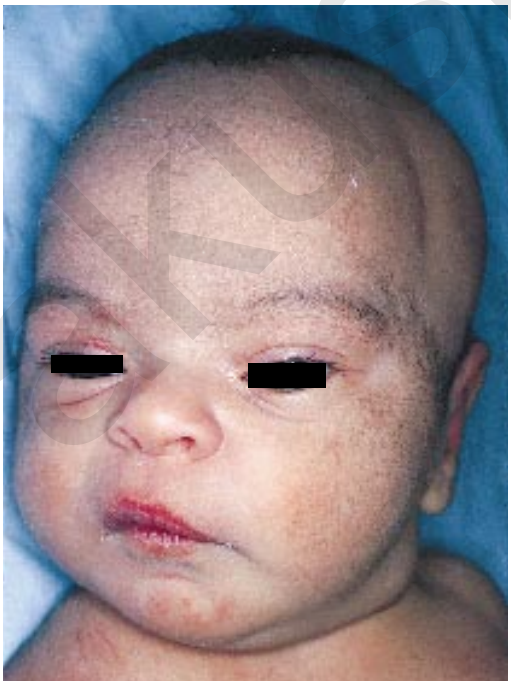

Figure 2.21. This figure shows the same infant with frontal and parietal bossing. The face appears small with a broad nose and depressed nasal bridge, and there is a groove over the metopic suture. The infant also had a large, open fontanelle.

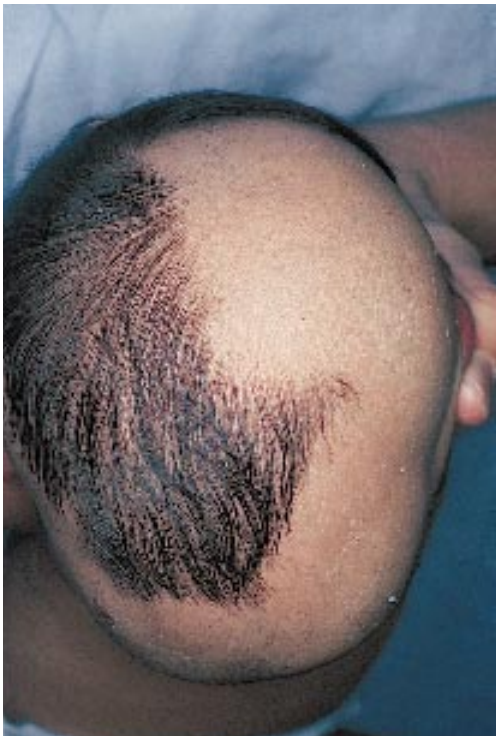

2.22

Figure 2.22. The same infant showing the brachycephalic skull and frontal and parietal bossing.

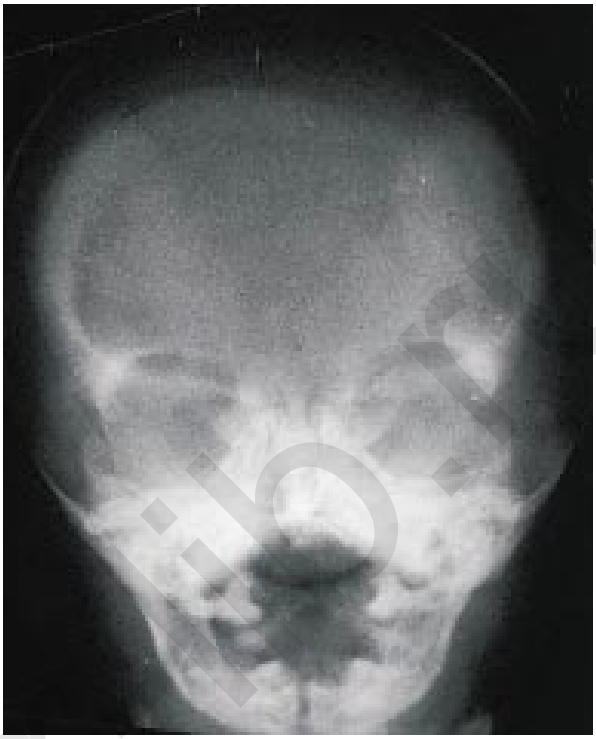

2.23

Figure 2.23. The radiograph of the skull in the same infant. Note the wide open fontanelles due to their delayed closure. There is also marked widening of the cranial sutures.

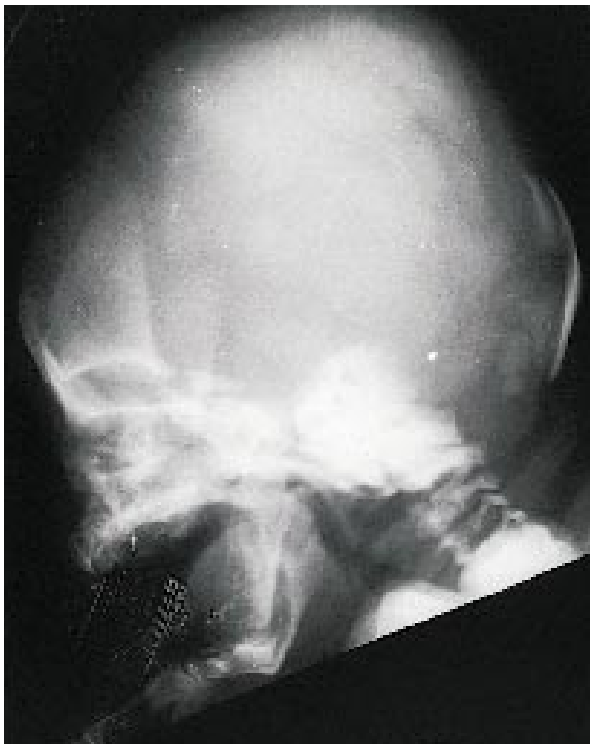

2.24

Figure 2.24. A lateral radiograph of the skull in an infant with cleidocranial dysostosis showing the marked frontal and parietal bossing and brachycephaly.

2.25

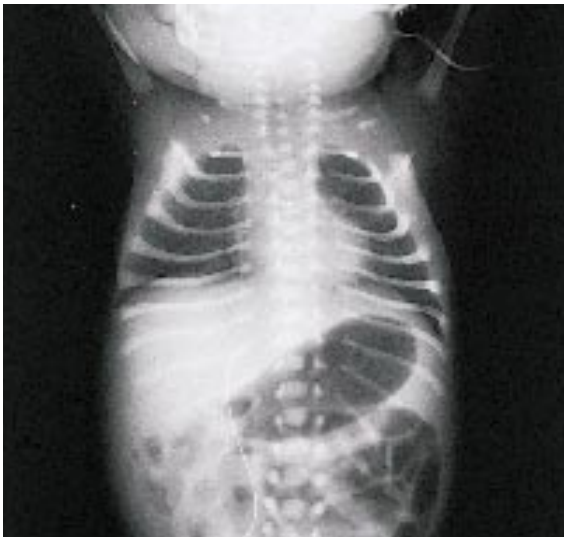

Figure 2.25. This infant with cleidocranial dysostosis has hypoplastic clavicles and had the typical findings in the skull. In cleidocranial dysostosis there may be partial to complete dysplasia of the clavicles.

2.26

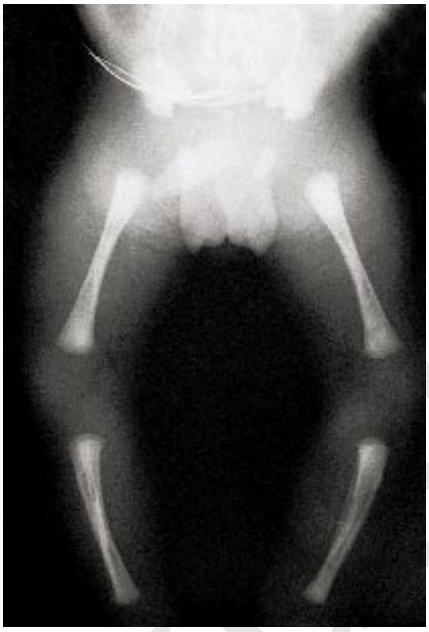

Figure 2.26. The radiograph of the pelvis and long bones of the same infant shows the poorly developed pelvis with small ilia and marked separation of the symphysis pubis.

2.27

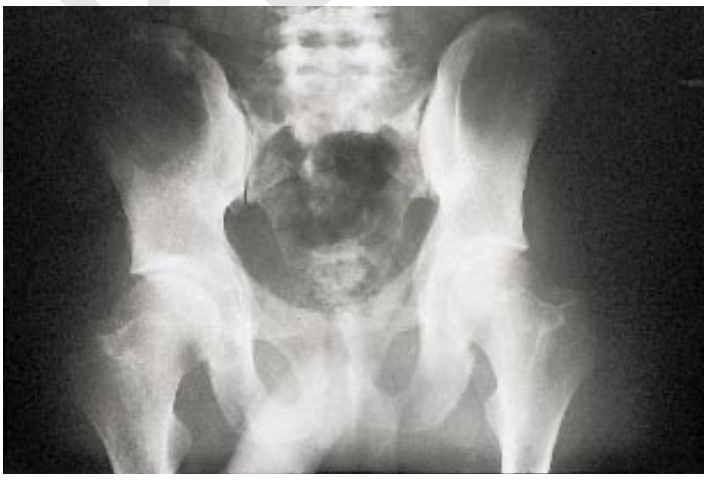

Figure 2.27. Radiograph of the pelvis of the father of the same infant at the age of 25 years. Note the retarded ossification of the corpora and inferior rami of the pubic bones and the retarded ossification of the symphysis pubis (i.e., symphysis pubis gap is not fused).

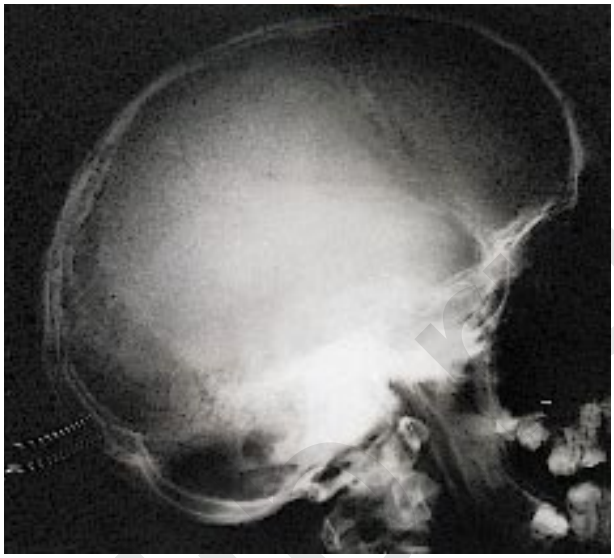

2.28

Figure 2.28. Radiograph of the father's skull showing the poor ossification and multiple wormian bones.

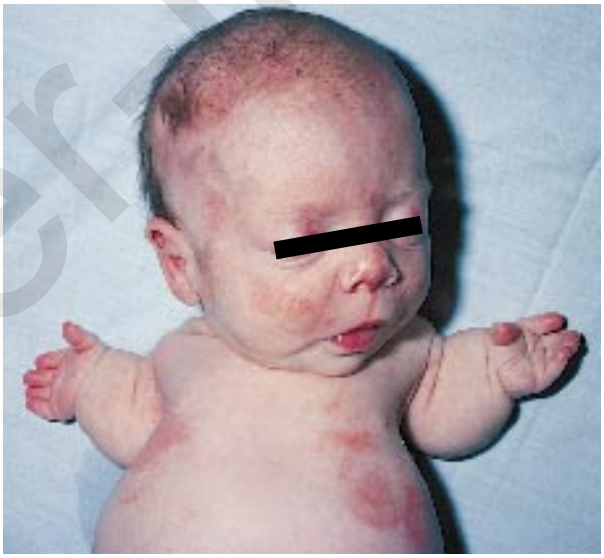

2.29

Figure 2.29. This infant with diastrophic dysplasia presents the marked narrowing of the chest, the short limbs and the typical "hitchhiker" thumbs (hyperextensible and hyperabductable). In this autosomal recessive condition there is disproportionate dwarfism (abnormal shortness of the proximal parts of the limbs), club feet, and widening between the first and second toes ("sandal" sign). The big toes are abducted.

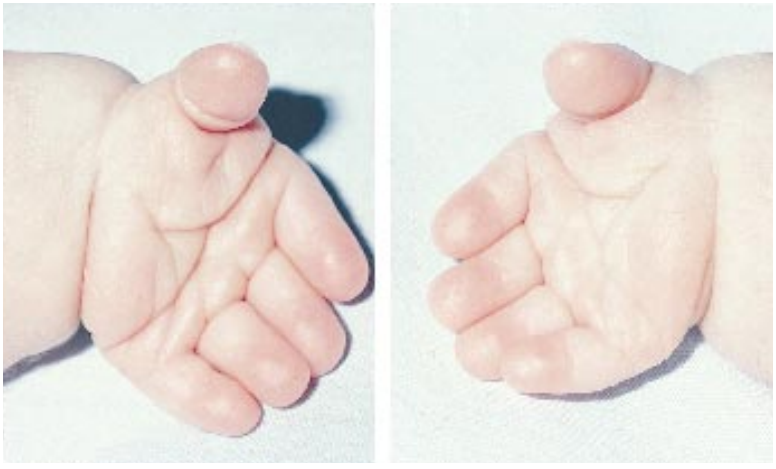

2.30

Figure 2.30. This figure is a close-up of the typical "hitchhiker" thumbs in the same infant with diastrophic dysplasia. The "hitchhiker" thumb is caused by hypoplasia of the first metacarpal, and the long axis of the digit is oriented almost horizontally in relation to the palm. The thumb is retroflexed with hypoplasia of the thenar musculature. Radiographic examination of the long bones in these infants demonstrates spreading of the metaphyses and delayed closure and deformation of the epiphyses.

2.31

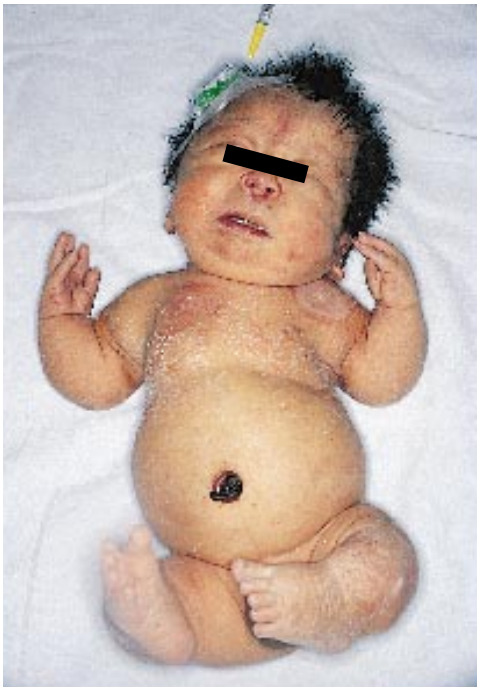

Figure 2.31. This infant has a rare form of short-limbed dwarfism. The diagnosis is anisospondylic camptomicromelic dwarfism (dyssegmental dwarfism). This condition is autosomal recessive, there is disproportionate short stature, flat facies, flat nose and micrognathia. Cleft palate is common. There is a short neck and narrow thorax with short bent extremities and decreased joint mobility. A radiograph of the spine is diagnostic in that there are short vertebral bodies with segmentation defects.

2.32

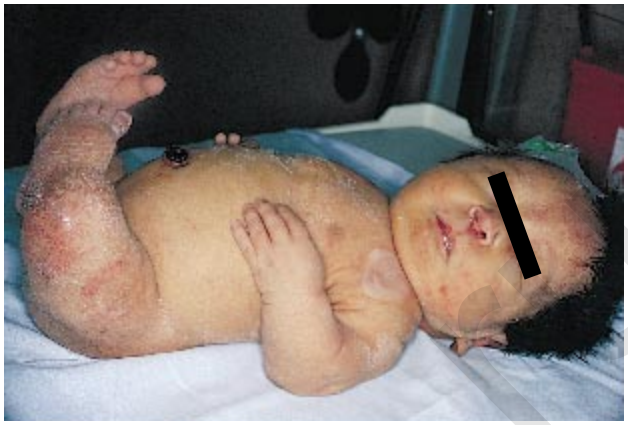

Figure 2.32. A lateral view of the same infant.

2.33

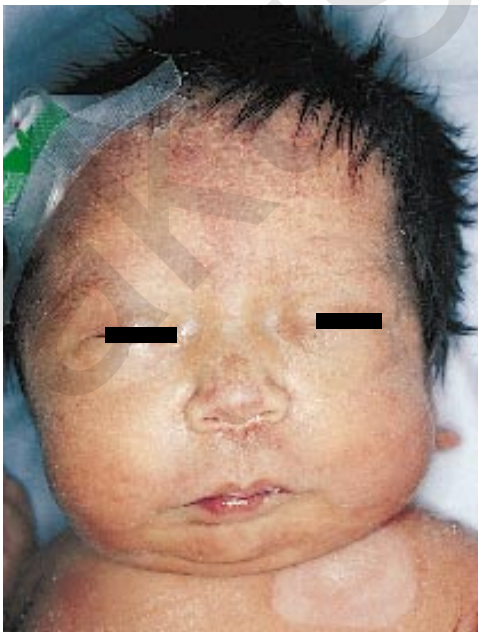

Figure 2.33. A close-up view of the same infant showing the flat facies with a flat nose, micrognathia and a short neck.

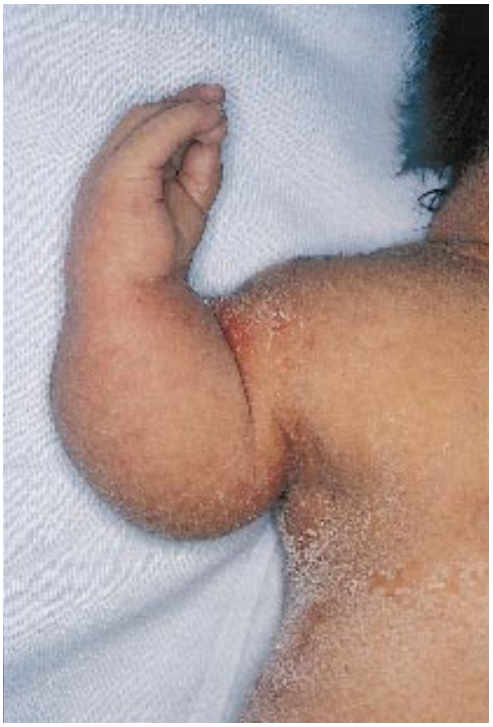

2.34

Figure 2.34. The right upper extremity of the same infant showing the camptomicromelia and the small thorax.

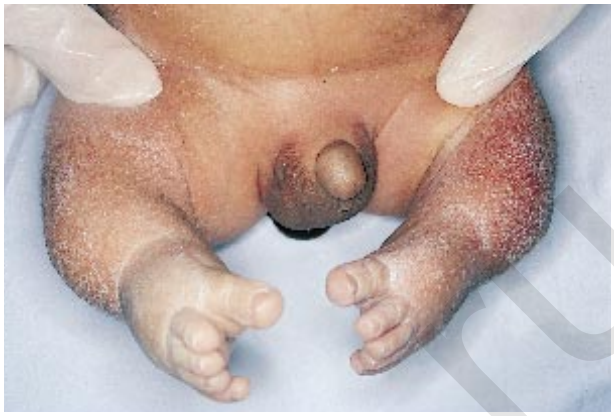

2.35

Figure 2.35. The lower extremities of the same infant showing the marked camptomicromelia.

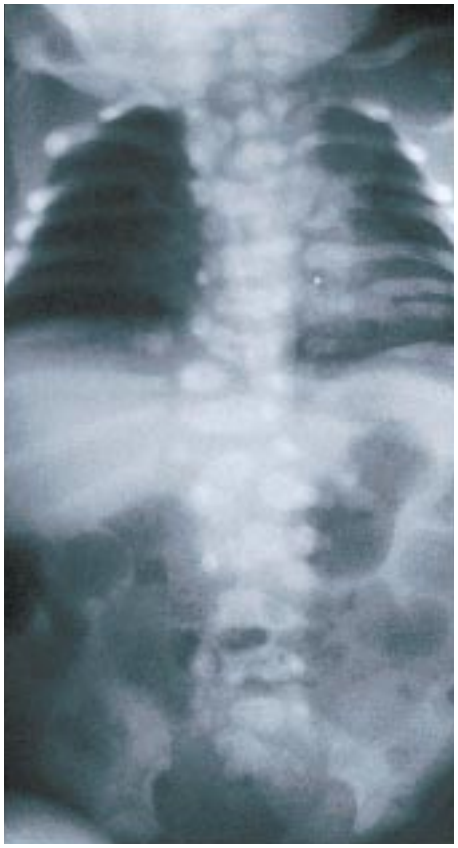

2.36

Figure 2.36. Radiograph of the chest and spine of the same infant with dyssegmental dwarfism. Note the anisospondyly (segmentation defects of the vertebral bodies), abnormalities of the ribs, hypoplastic scapulae, and ilia with irregular borders.

2.37

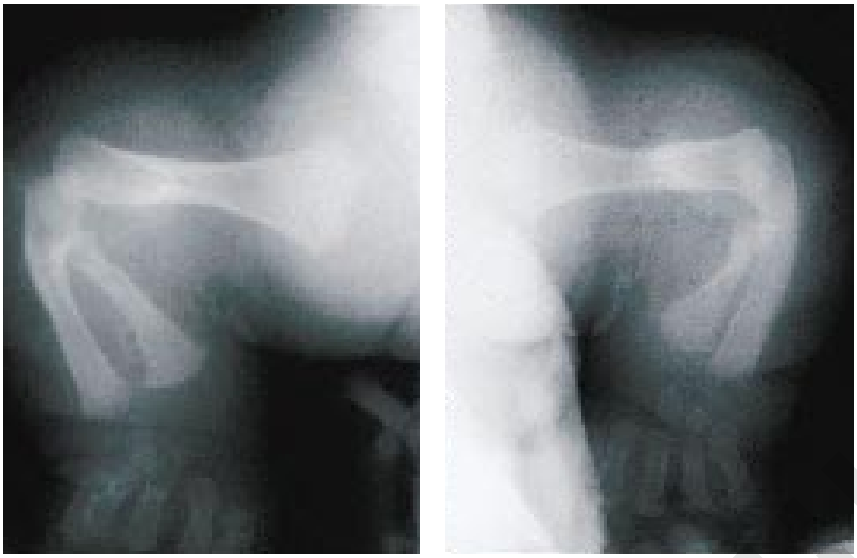

Figure 2.37. Radiograph of the upper extremities of the same infant as in Figure 2.31 showing the long bones which are markedly shortened with midshaft angulation (camptomelia) together with marked metaphyseal flaring and cupping.

2.38

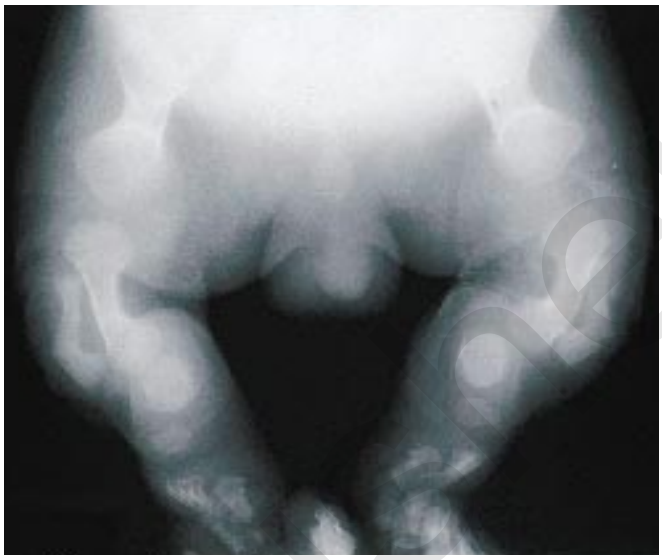

Figure 2.38. Radiograph of the lower extremities of the same infant. The long bones are markedly shortened with midshaft angulation (camptomelia) together with marked metaphyseal flaring and cupping.

2.39

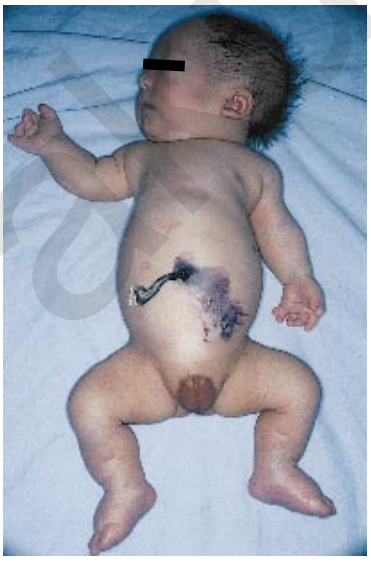

Figure 2.39. This infant with chondroectodermal dysplasia (Ellis-van Creveld syndrome) presents with the typical short distal extremities, short ribs, polydactyly, nail hypoplasia, neonatal teeth, and congenital heart disease. Although atrial septal defect is most common, this infant had a hypoplastic left heart. Note that the extremities are plump and markedly and progressively shortened distally, that is, from the trunk to the phalanges. Birthweight was 2880 g, length was 44.5 cm (<10th percentile), and fronto-occipital circumference (FOC) was 34.5 cm (50th percentile).

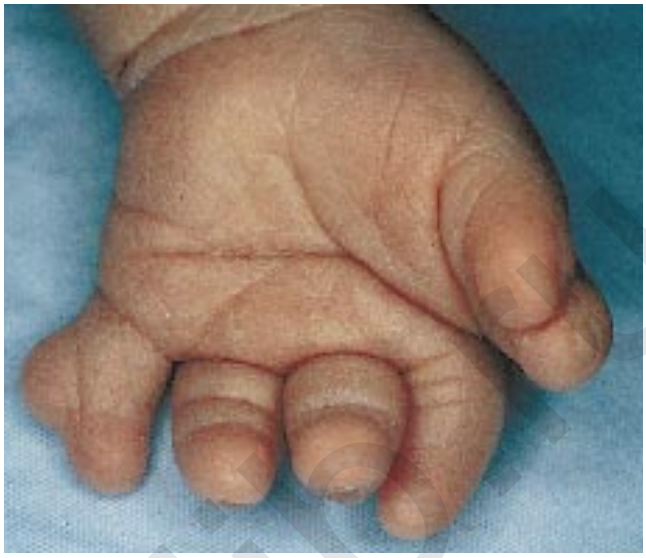

2.40

Figure 2.40. A close-up of the left hand of the infant shown in Figure 2.39 showing polydactyly (seven digits) and brachydactyly.

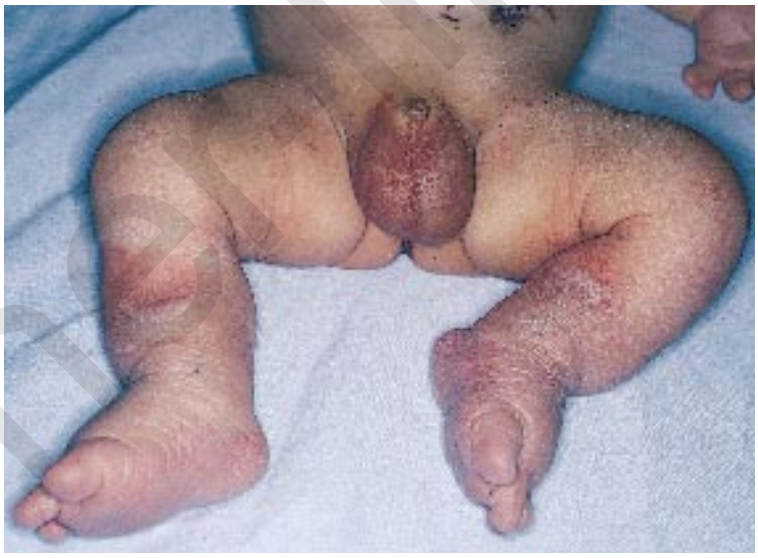

2.41

Figure 2.41. Note the typical lower extremities in the same infant. The limbs which are short and plump become markedly and progressively shortened distally, that is, from the trunk to the phalanges. Also note the very small penis (genital anomalies are not uncommon in this condition).

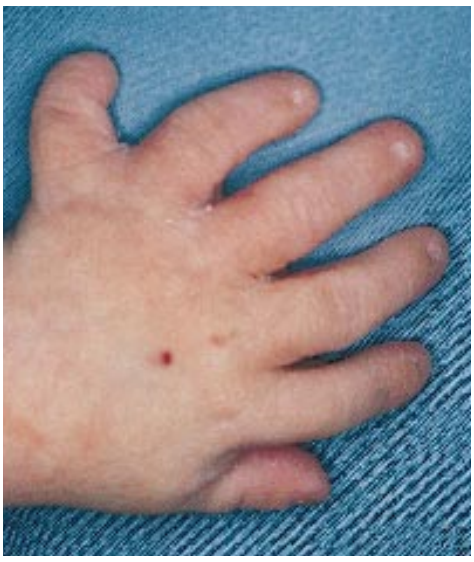

2.42

Figure 2.42. Preaxial polydactyly and brachydactyly in another infant with Ellis-van Creveld syndrome. Note the markedly hypoplastic nails.

2.43

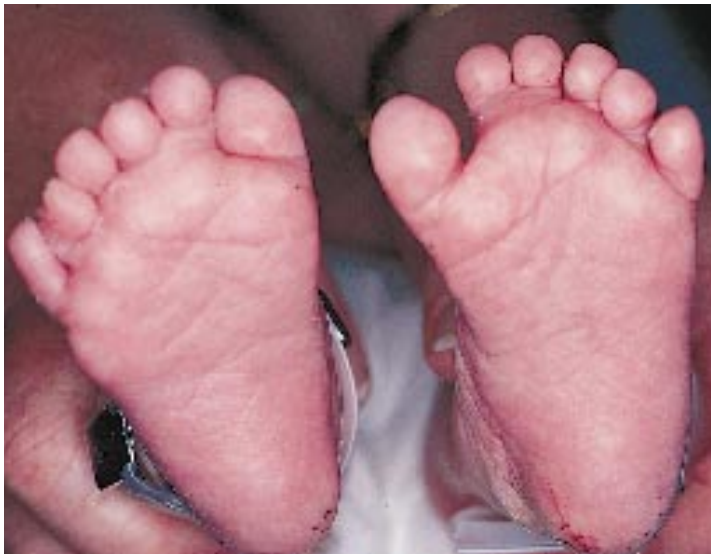

Figure 2.43. Postaxial polydactyly of the toes in an infant with Ellis-van Creveld syndrome. In this syndrome, polydactyly is noted in the fingers in 100% of cases but is present in the toes in only 10 to 20%.

2.44

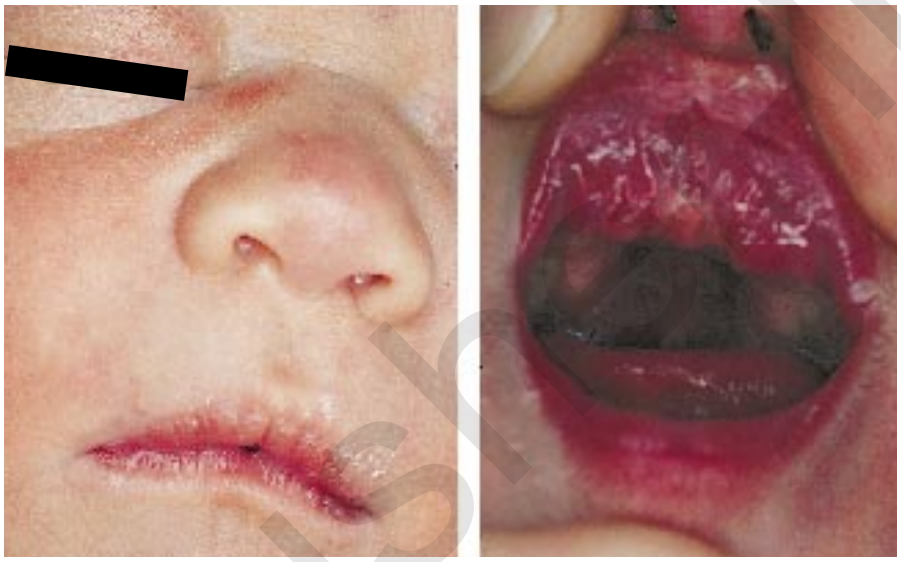

Figure 2.44. In this infant with Ellis-van Creveld syndrome, note on the left the short upper lip with midline defect due to fusion of the upper lip to the maxillary-gingival margin. On the right, note that the fusion of the upper lip to the maxillary-gingival margin results in a lack of the mucobuccal fold or sulcus which normally is present anteriorly.

2.45

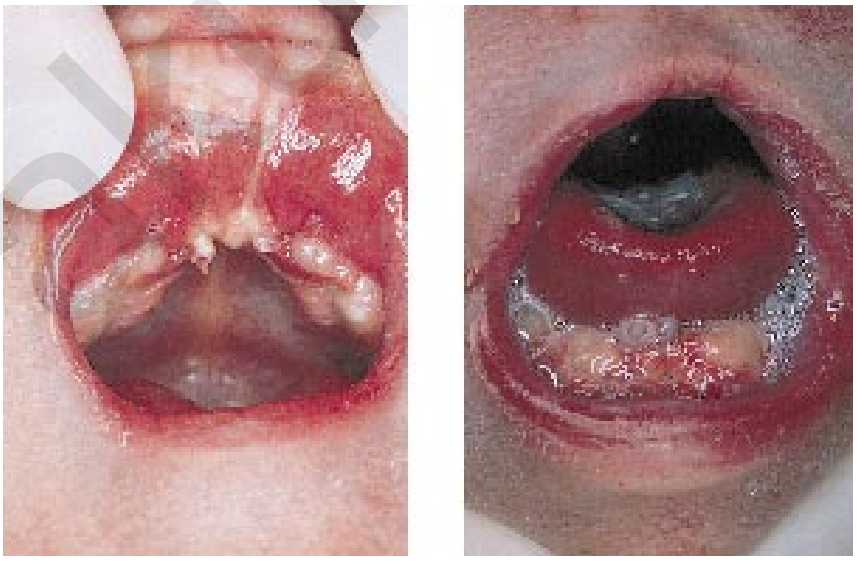

Figure 2.45. This infant with Ellis-van Creveld syndrome demonstrates on the left the fusion of the labiogingival margins so there is no sulcus to the upper lip. Also note the hypoplastic neonatal teeth in the upper jaw. On the right, note the hypoplastic neonatal teeth in the lower jaw. Neonatal teeth are present in 30% of infants with Ellis-van Creveld syndrome.

2.46

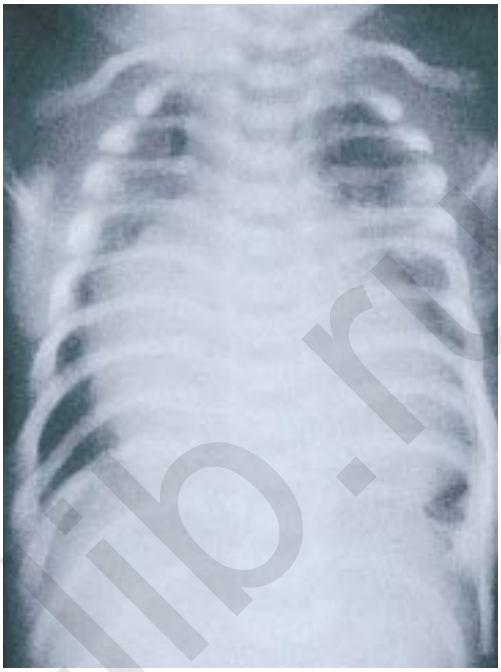

Figure 2.46. A radiograph of the chest of an infant with Ellis-van Creveld syndrome. Note the long narrow chest and short ribs with cardiac enlargement. Congenital heart disease is present in 50 to 60% of cases of Ellis-van Creveld syndrome. This infant had a large atrial septal defect, the most common lesion seen in Ellis-van Creveld syndrome.

2.47

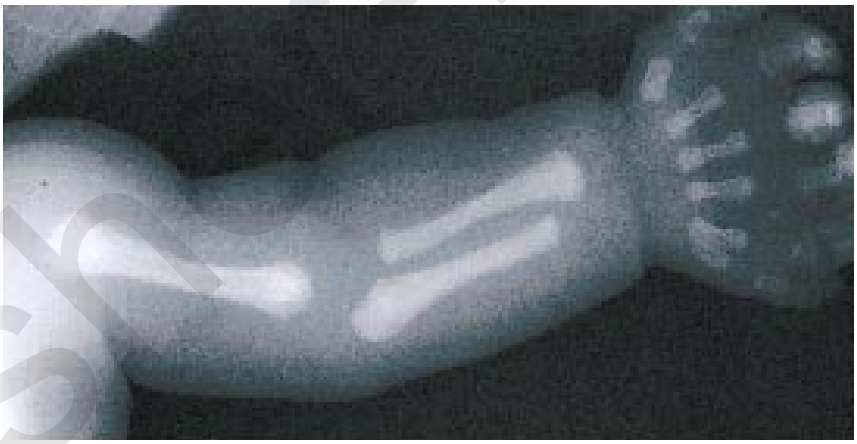

Figure 2.47. Radiograph showing the mesomelic shortening of the limbs and polydactyly. The proximal end of the ulna and distal end of the radius are swollen and bulbous giving the appearance of two parallel drumsticks that point in opposite directions.

2.48

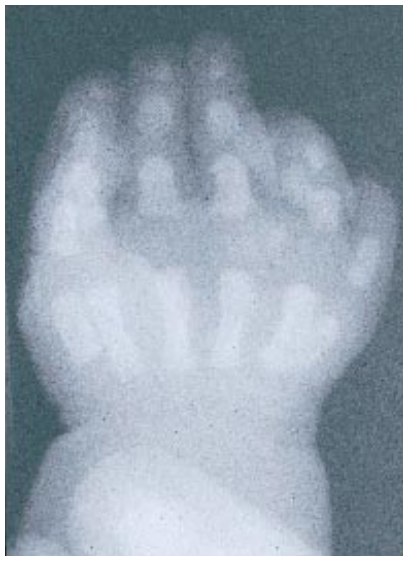

Figure 2.48. Radiograph of the hand in an infant with Ellis-van Creveld syndrome. Note that the phalanges are short but that the proximal phalanges are relatively long compared to the others. Adults, therefore, cannot make a tight fist. Also note the fusion of the fifth and sixth metacarpals.

2.49

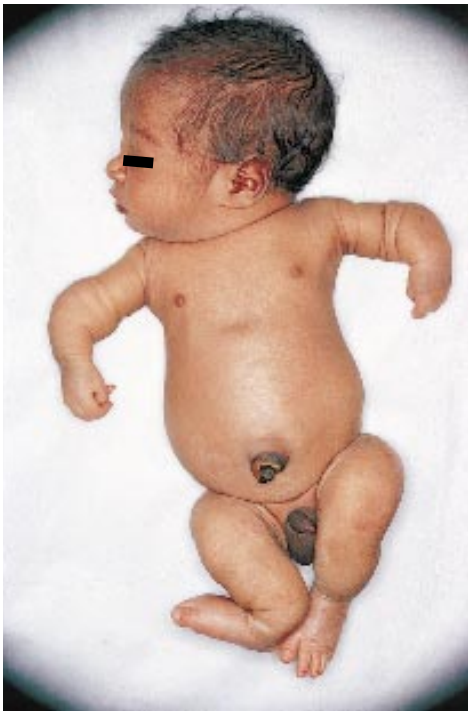

Figure 2.49. Short-limbed dwarfism in an infant with congenital hypophosphatasia. There is failure of calcification of all bones resulting in marked bowing. This autosomal recessive condition is associated with a severe deficiency of tissue and serum alkaline phosphatase. It presents with bowed lower extremities with overlying cutaneous dimpling and short ribs resulting in a small thoracic cage. Death usually occurs from respiratory insufficiency.

2.50

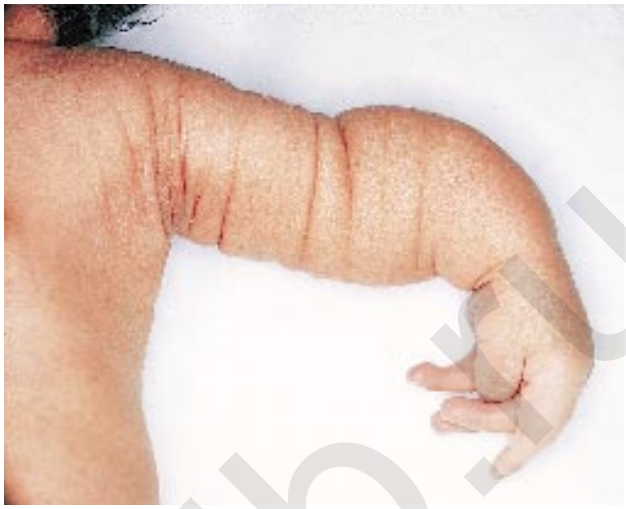

Figure 2.50. Close-up view of the arm of the same infant showing the marked bowing at the forearm.

2.51

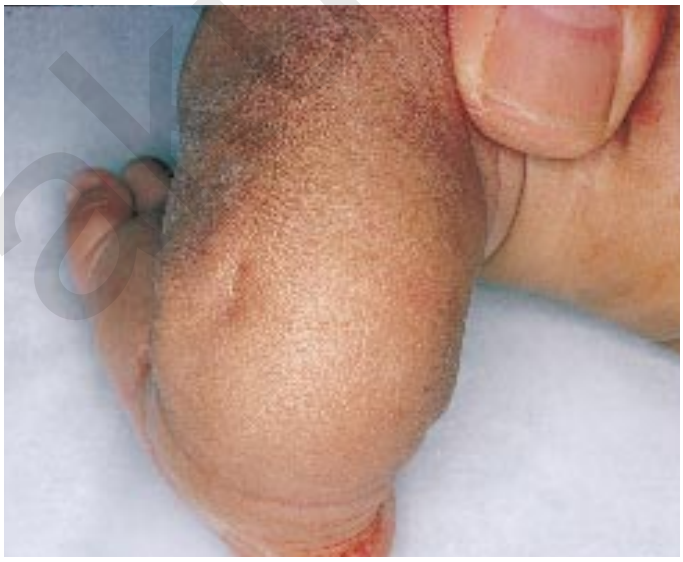

Figure 2.51. The lower right leg of the same infant showing the marked bowing with a large skin dimple over the middle of the leg. This is a classic physical sign in infants with congenital hypophosphatasia.

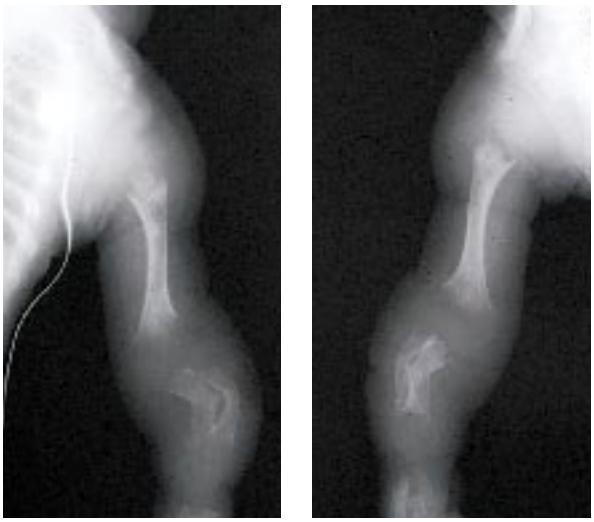

2.52

Figure 2.52. Radiograph of the upper extremity showing the osteoporosis and metaphyseal flaring with marked bowing of the radius and ulna bilaterally.

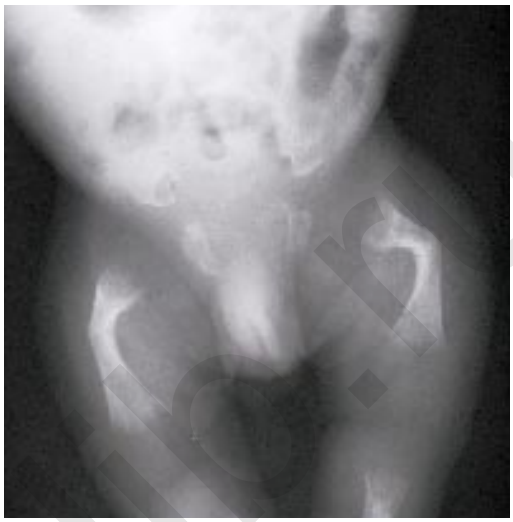

2.53

Figure 2.53. Radiograph of the lower extremities of the same infant showing the gross osteoporosis and metaphyseal flaring with marked bowing of the femora, tibiae and fibulae.

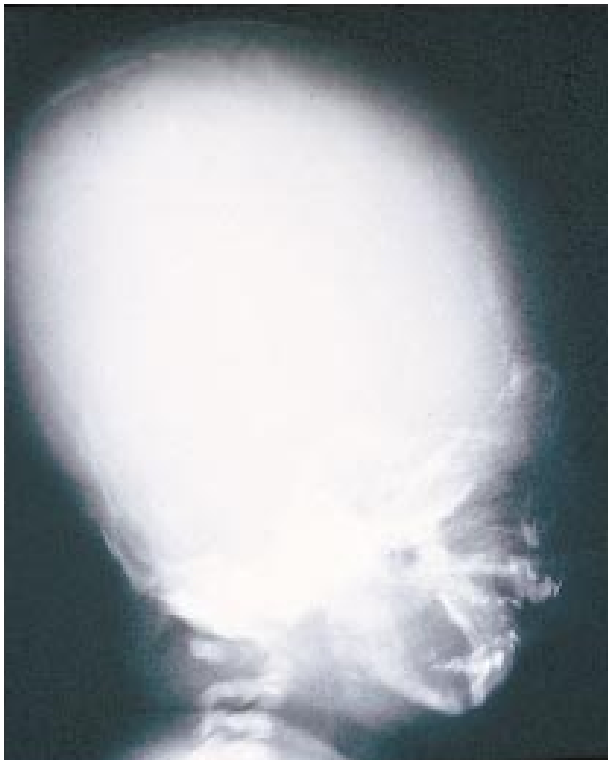

2.54

Figure 2.54. Radiograph of the skull of an infant with congenital hypophosphatasia. Note the marked lack of mineralization with deformity of the skull. Characteristic is the large size of the skull, shortened base, and a shallow sella turcica. There is late closure of the fontanelles. This appearance is comparable to the skull seen in infants with osteogenesis imperfecta.

2.55

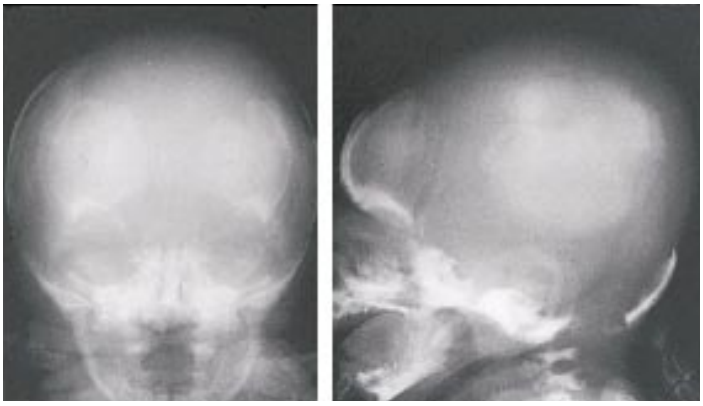

Figure 2.55. Radiograph of the skull of another infant with congenital hypophosphatasia. Note that some mineralization is present but that it is very poor.

2.56

Figure 2.56. In this infant with asphyxiating thoracic dystrophy (Jeune's syndrome) note the abnormally long and narrow thorax with high clavicles and a large abdomen. The narrow thorax due to short ribs results in limited chest wall movement. As a result of this, there is a lack of space in the subcostal area and the liver lies completely in the abdomen. These infants may have hypoplastic lungs and renal pathology in the form of cystic tubular hypoplasia and/or glomerular sclerosis.

2.57

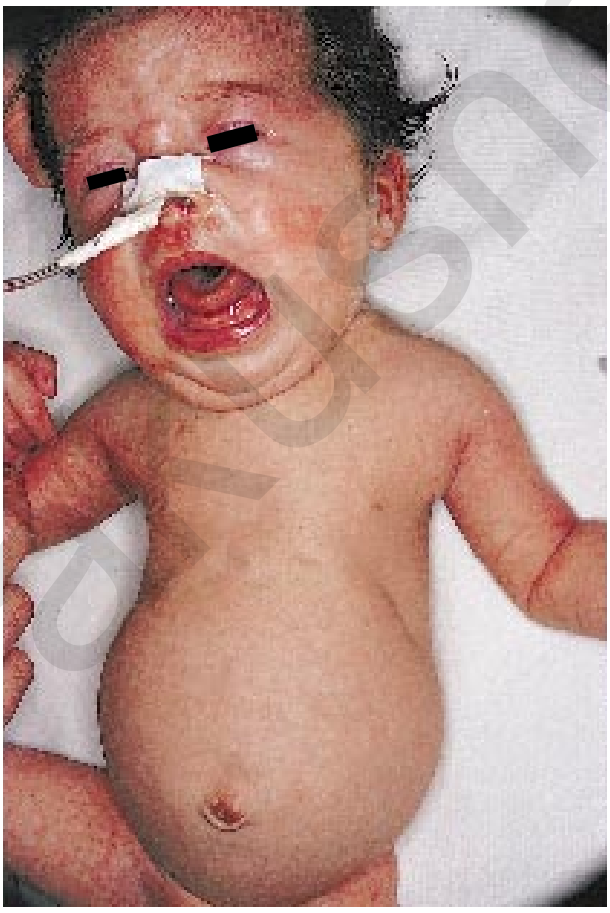

Figure 2.57. Another infant with asphyxiating thoracic dystrophy. Again note the small thorax due to short ribs, the high clavicles and what appears to be abdominal distention due to the fact that the whole liver is in the abdomen. These infants give the appearance of having widely spaced nipples. There is shortening of the arms and legs as well as an inability to extend the forearm at the elbow joint. The condition is autosomal recessive.

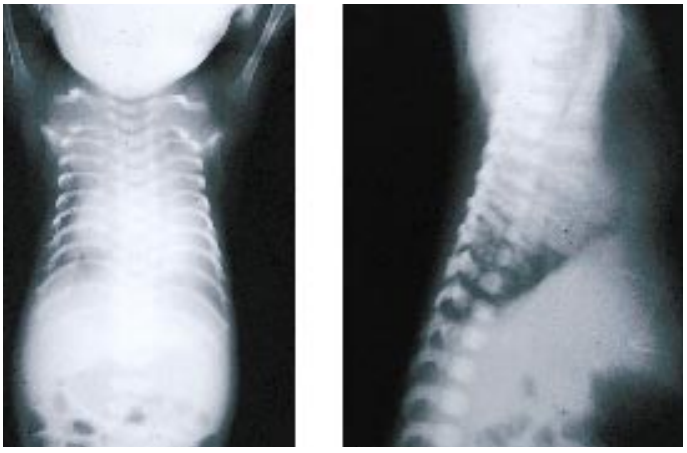

2.58

Figure 2.58. Anteroposterior and lateral radiograph of an infant with asphyxiating thoracic dystrophy. Note the short ribs which are horizontally placed, giving the appearance of a long narrow chest. The heart is normal in size but appears to be large because of the narrow thorax. Note the high clavicles, which are of normal size.

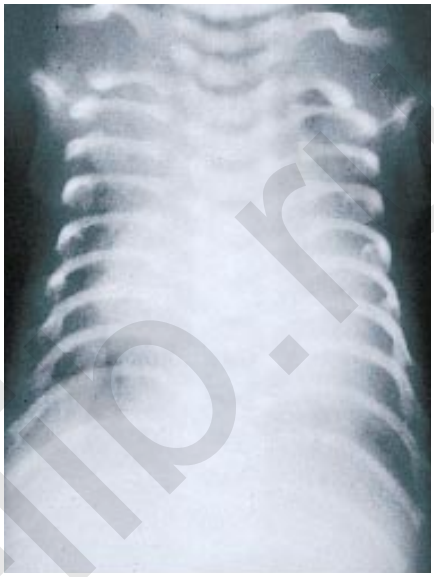

2.59

Figure 2.59. Radiograph of an infant with asphyxiating thoracic dystrophy. Note the very short ribs with a long narrow chest and the high clavicles.

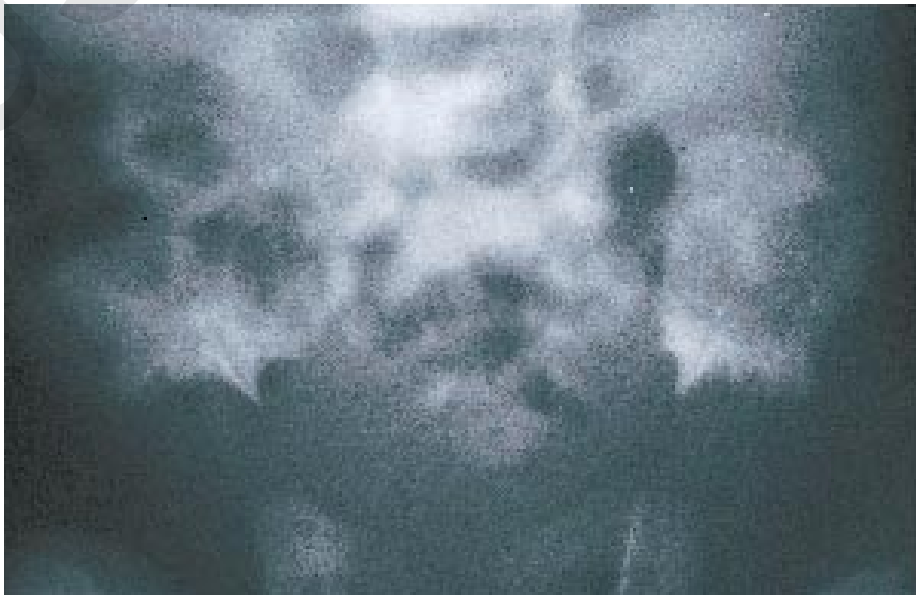

2.60

Figure 2.60. Radiograph of the pelvis of an infant with asphyxiating thoracic dystrophy. Note the hypoplastic iliac wings and flattened acetabula with spike-like projections at the lower margins of the sciatic notches.

2.61

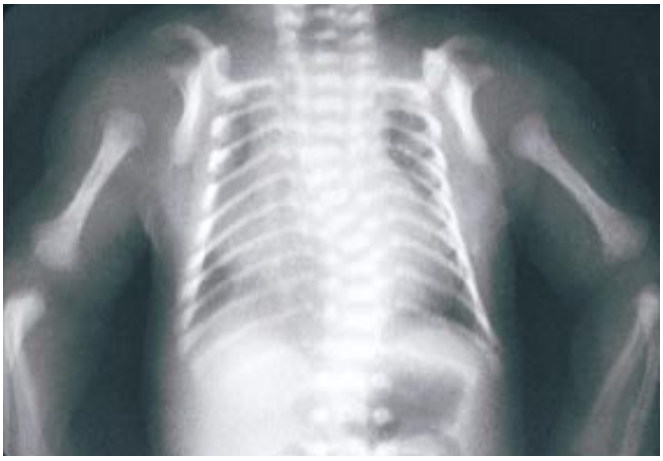

Figure 2.61. Radiograph of an infant with metatropic dysplasia. This is another form of dwarfism associated with a narrow thorax, thoracic kyphoscoliosis and metaphyseal flaring (giving the typical "dumb-bell" appearance). The proportion of the length of the trunk to the extremities reverses during childhood. At first the trunk is too long and the extremities too short. With increasing kyphoscoliosis the trunk becomes short.

2.62

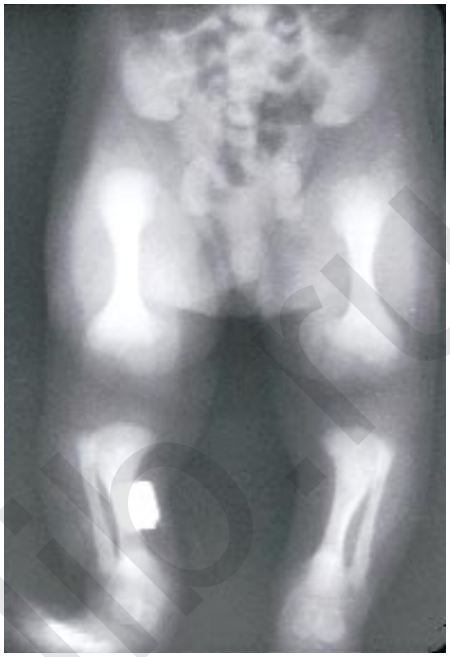

Figure 2.62. Radiograph of the lower extremities of the same infant showing the short limbs with typical "dumb-bell" appearance of the femora, which occurs as a result of huge epiphyses. There is hypoplasia of the basilar pelvis with horizontal acetabula, a short, deep sacroiliac notch, and squared iliac wings.

2.63

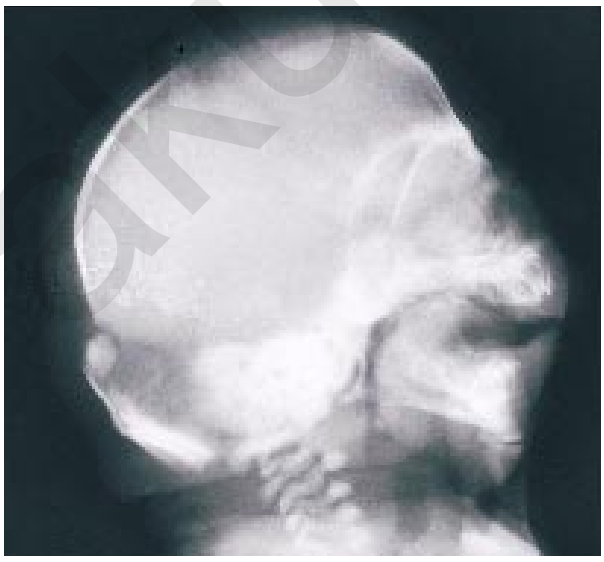

Figure 2.63. Radiograph of skull in an infant with metatropic dysplasia. Note the poor mineralization and the very prominent occiput.

2.64

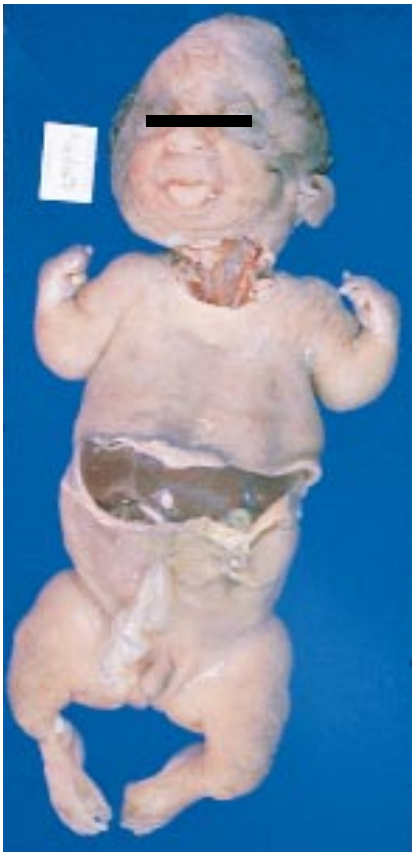

Figure 2.64. Type II osteogenesis imperfecta which is perinatally lethal. Death occurs before or shortly after birth. The lethal form is autosomally dominant but they are mostly new mutations. Rarely it is autosomally recessive. Note the markedly abnormal skull (which is soft and impressionable) and short limbs due to osteogenesis imperfecta. The damage to the neck and abdomen was present at birth.

2.65

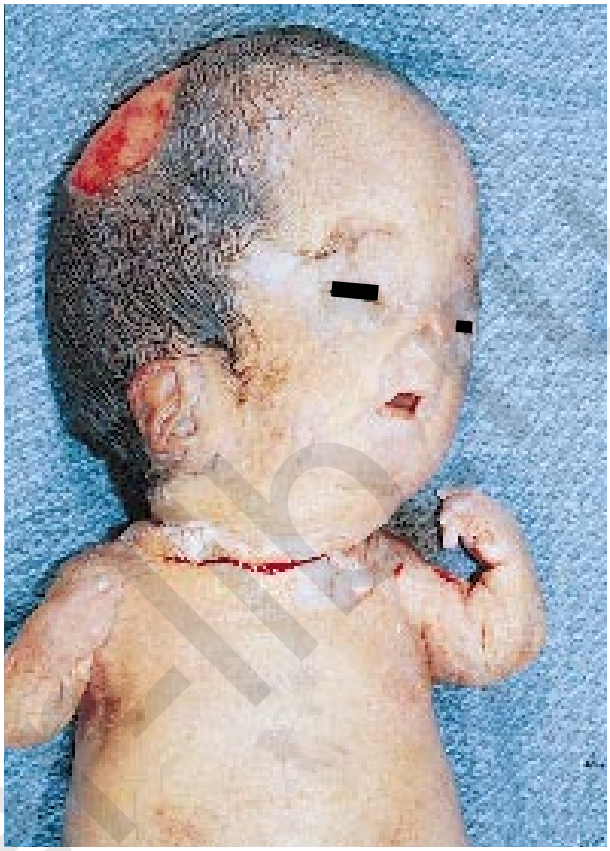

Figure 2.65. Another infant with severe osteogenesis imperfecta with marked shortening of long bones due to multiple fractures in utero as seen in the upper extremities and a grossly abnormal hand. This infant is another example of type II osteogenesis imperfecta. The head is grossly abnormal. The ear is not truly low set but gives this appearance due to the abnormal skull.

2.66

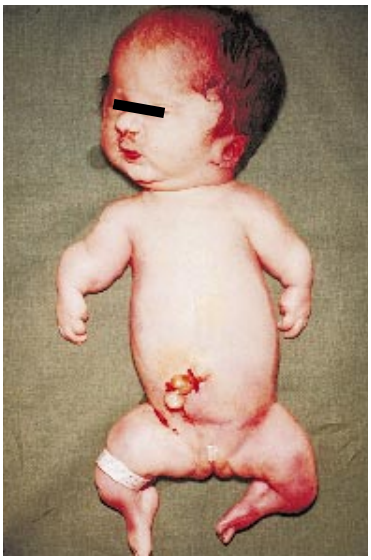

Figure 2.66. This infant with short extremities due to multiple in utero fractures is an example of type III osteogenesis imperfecta. The head is slightly enlarged, giving the ears a low-set appearance.

2.67

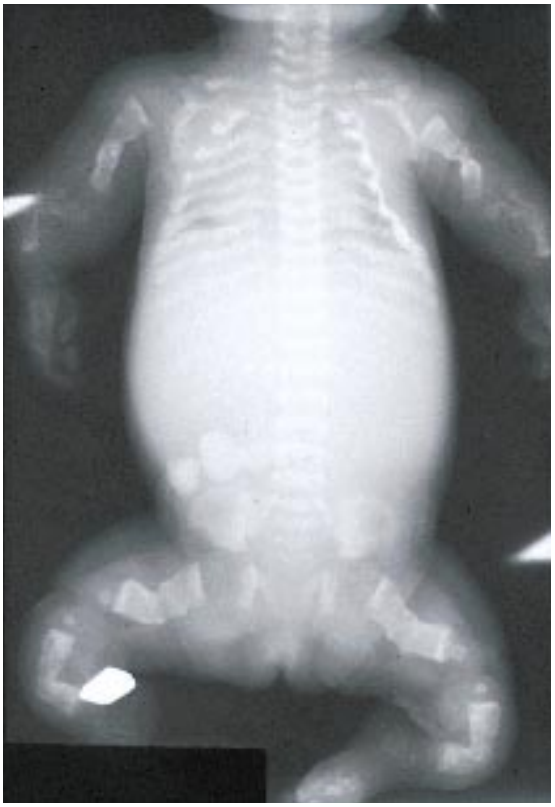

Figure 2.67. Total body radiograph of the same infant as in Figure 2.66 showing the numerous intrauterine fractures of the long bones of the extremities resulting in shortening of the extremities, and the intrauterine fractures of the ribs resulting in a narrow chest. Note the density above the right side of the pelvis. This is the umbilical cord stump which appears as an opacity in an abdominal radiograph where gas is lacking in the gastrointestinal tract.

2.68

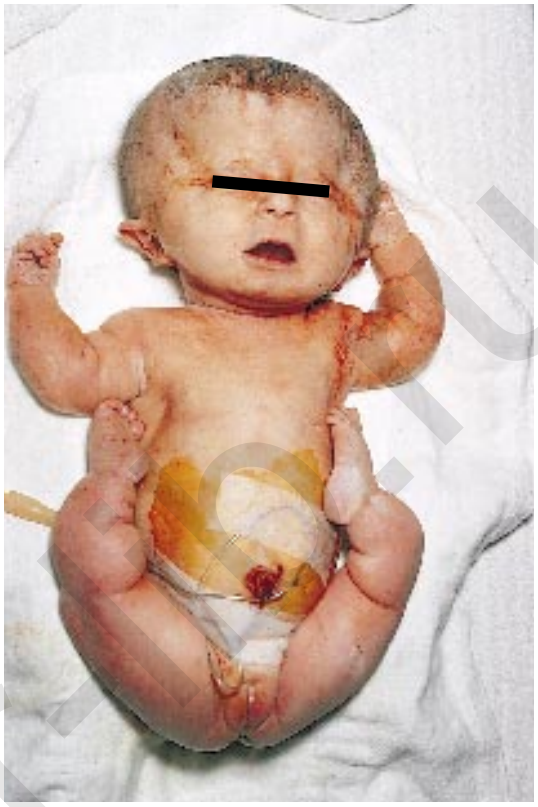

Figure 2.68. Another example of type III osteogenesis imperfecta showing the bowing and shortening of limbs due to intrauterine fractures. The skull is large and abnormal due to the lack of mineralization and multiple wormian bones. This infant also has a narrow chest due to intrauterine fractures of the ribs.

2.69

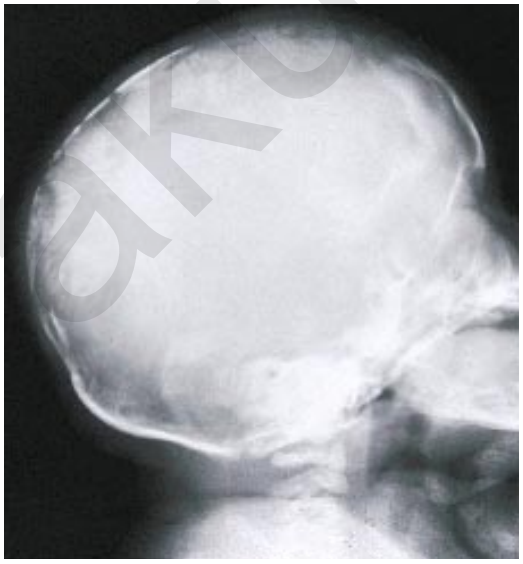

Figure 2.69. Radiograph of the skull in an infant with osteogenesis imperfecta. Note the lack of mineralization with wormian bones. Clinically one feels multiple small bones over the skull. There is a thin cortex with minimal skull ossification and generalized osteoporosis.

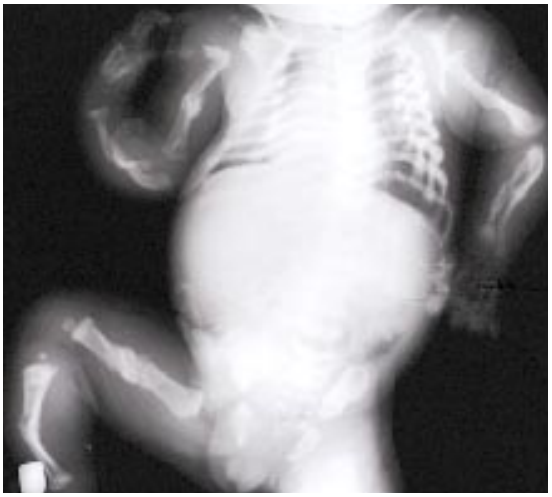

2.70

Figure 2.70. Another radiograph of an infant with type III osteogenesis imperfecta. Note the intrauterine fractures and bowing of the long bones.

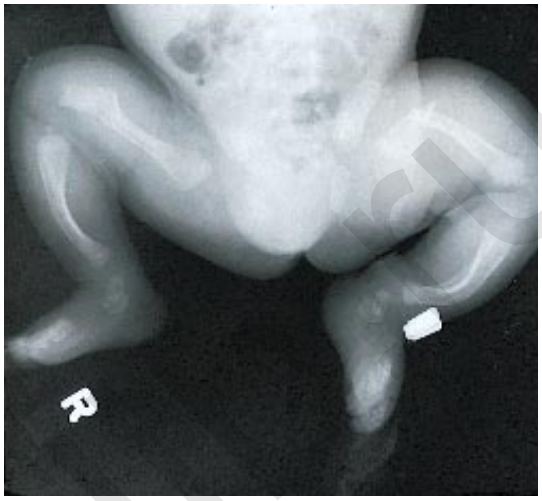

2.71

Figure 2.71. Radiograph of osteogenesis imperfecta in a neonate. Note the fracture of the proximal part of the left femur and the marked bowing of the other long bones. This alerts one to the fact that mild forms of osteogenesis imperfecta may occur.

2.72

Figure 2.72. Type III osteogenesis imperfecta in identical twins. Note the large heads and the bowing of the long bones due to mild intrauterine fractures.

2.73

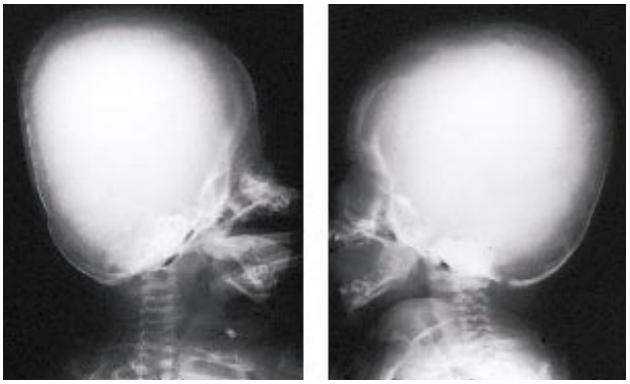

Figure 2.73. Radiograph of the skulls of the same twins as in Figure 2.72 showing the marked lack of mineralization.

2.74

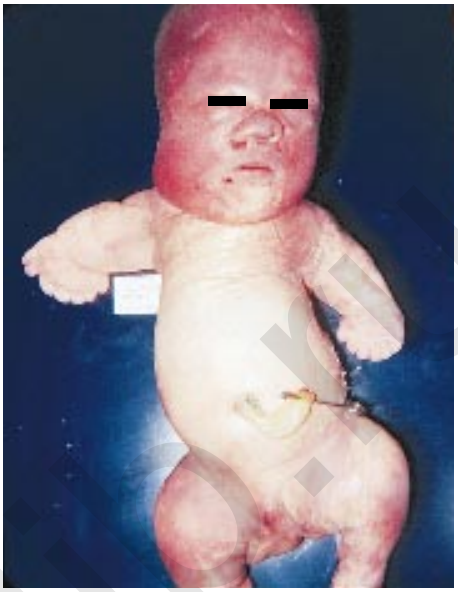

Figure 2.74. Short-limbed dwarfism in an infant with the Saldino-Noonan syndrome. This infant demonstrates the marked narrowing of the thorax with a large abdomen. The large abdomen is commonly seen in infants with a narrow thorax because the subcostal space is too small to accommodate the liver. The abdomen, per se, is normal. In this form of short-limbed dwarfism there is a narrow chest, due to short ribs, and polydactyly. (Richardson MM, Beaudet AL, Wanger ML, Malinis Rosenberg HS, Lucci JL: Prenatal diagnosis of recurrence of Saldino-Noonan dwarfism. *J. Pediatr* 91: 467-471. Reprinted with permission from Mosby Year Book, Inc., St. Louis, MO.)

2.75

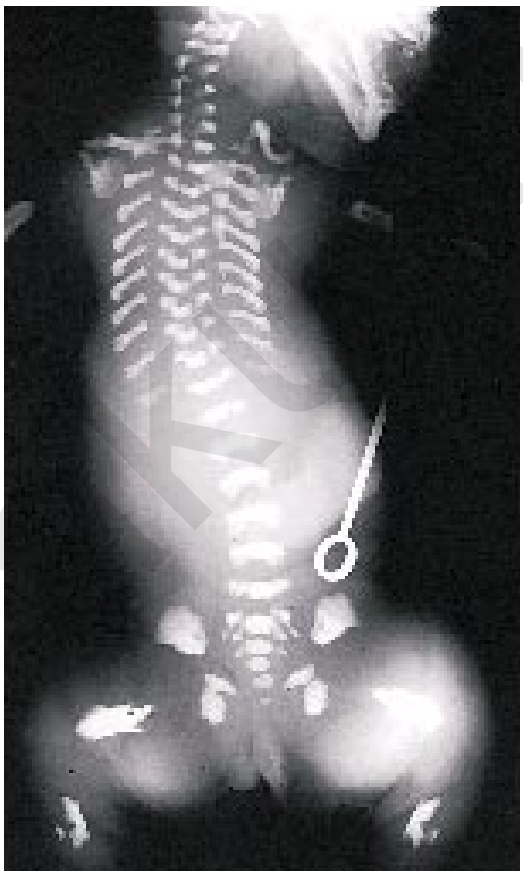

Figure 2.75. Body radiograph of an infant with Saldino-Noonan syndrome. In this form of short-limbed dwarfism, hydrops is usually present, the chest is extremely narrow due to the very short horizontal ribs, and the long bones are extremely short and jagged.

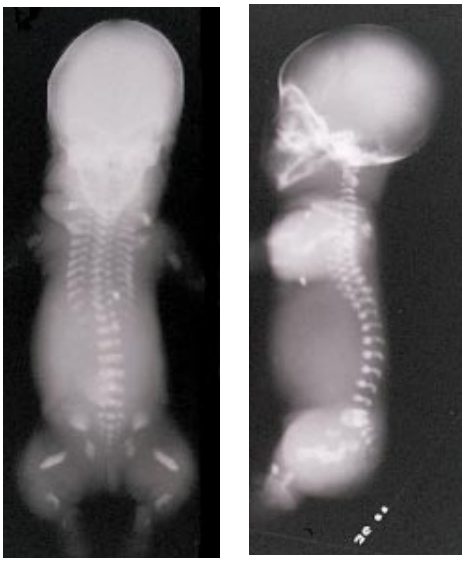

2.76

Figure 2.76. Anteroposterior and lateral radiograph of another infant with Saldino-Noonan syndrome. Note the horizontal, very short ribs, the high clavicles and the extremely short, jagged long bones.

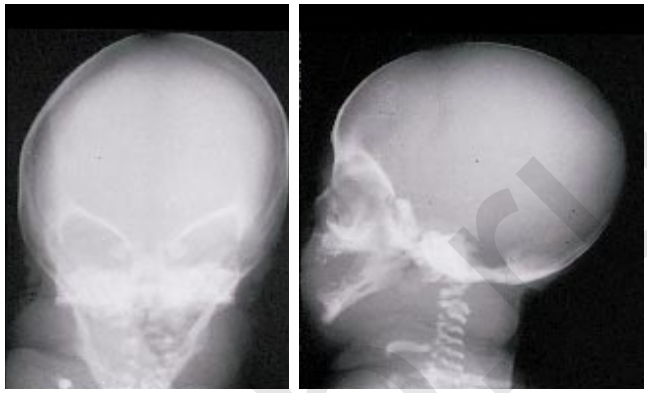

2.77

Figure 2.77. Skull radiograph, anteroposterior and lateral, showing the poor mineralization. Note the high clavicles.

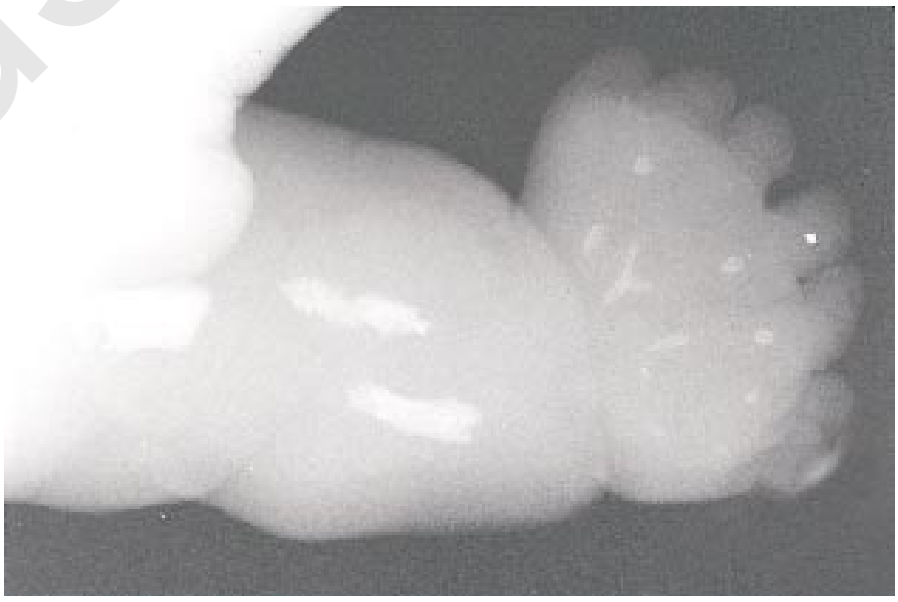

2.78

Figure 2.78. A close-up of the right upper extremity showing the extremely short, jagged long bones and poor development of the metacarpals and phalanges. Note the polydactyly.

2.79

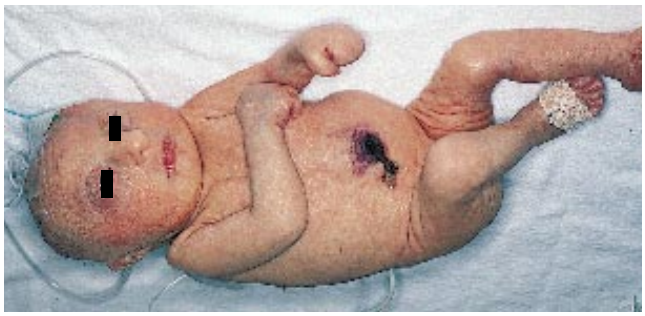

Figure 2.79. In Seckel's bird-headed dwarfism there is severe growth retardation with proportional dwarfism. This infant at 35 weeks gestation had a birth weight of 910 g, a length of 31.5 cm, and a head circumference of 23 cm, all less than the 10th percentile. There was severe microcephaly with premature fusion of all sutures, prominent eyes, a prominent beak-like nose, micrognathia, and malformed ears (low-set and lack of lobe). These infants have postnatal growth retardation and moderate to severe mental retardation.

2.80

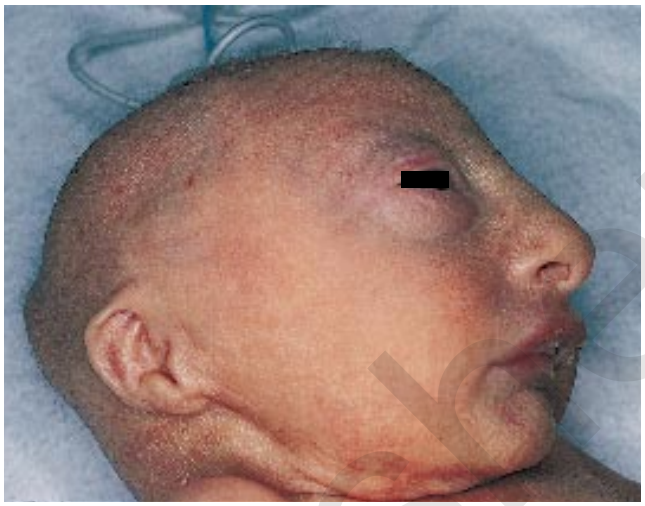

Figure 2.80. A close-up of the face of the same infant showing the severe microcephaly, the prominent eyes, the beak-like nose, and micrognathia. Note the low-set ear with lack of ear lobe. On CT scan the ventricles were barely perceptible and small in size.

2.81

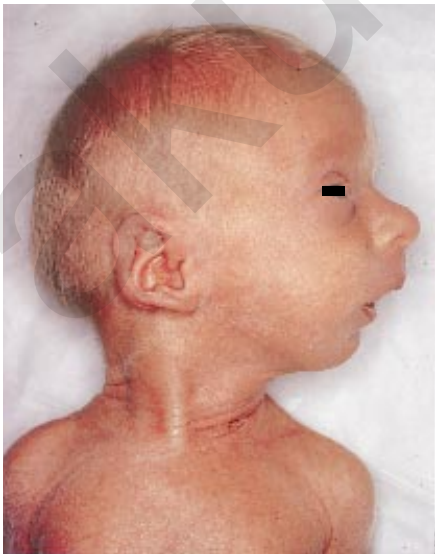

Figure 2.81. A less severe example of the Seckel's bird-headed dwarfism in which the microcephaly is striking but the other features are not as prominent.

2.82

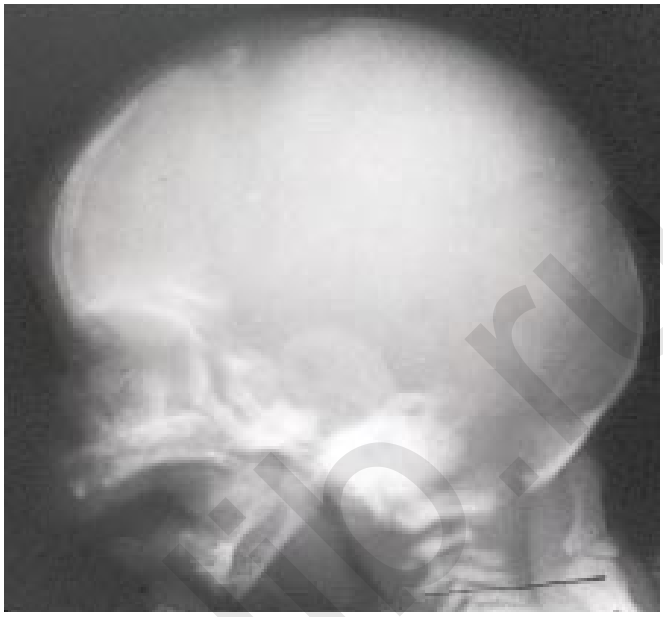

Figure 2.82. Radiograph of the skull in the same infant with Seckel's bird-headed dwarfism. Note the narrow (but not closed) sutures and tooth bud mineralization (incisors and first molars) in this infant. The tooth mineralization indicates that this infant had a gestational age of 35 weeks.

2.83

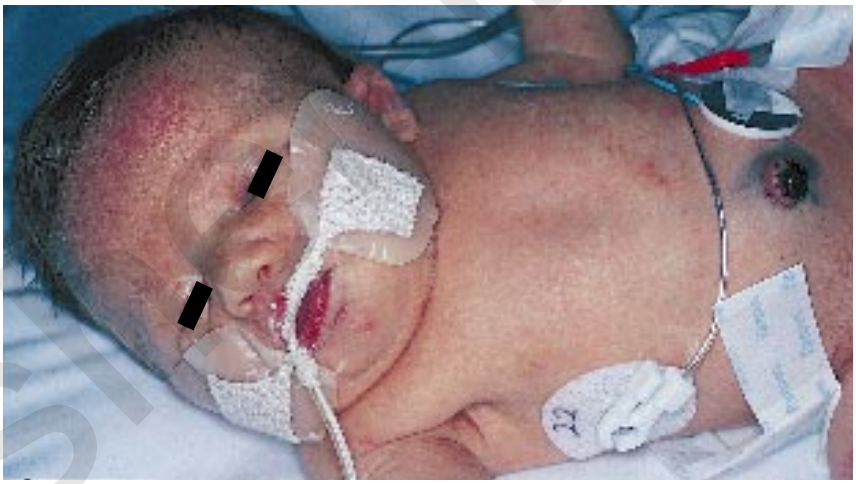

Figure 2.83. This infant is a typical example of spondylothoracic dysplasia (Jarcho-Levin syndrome). She had marked shortness of the neck and posterior aspect of the chest, with an increased diameter of the thoracic cage. The limbs were long and thin with tapering digits. Note the broad forehead and wide nasal bridge with anteverted nares. These infants typically have multiple anomalies of the vertebrae and a short thorax with a diminished number of ribs.

2.84

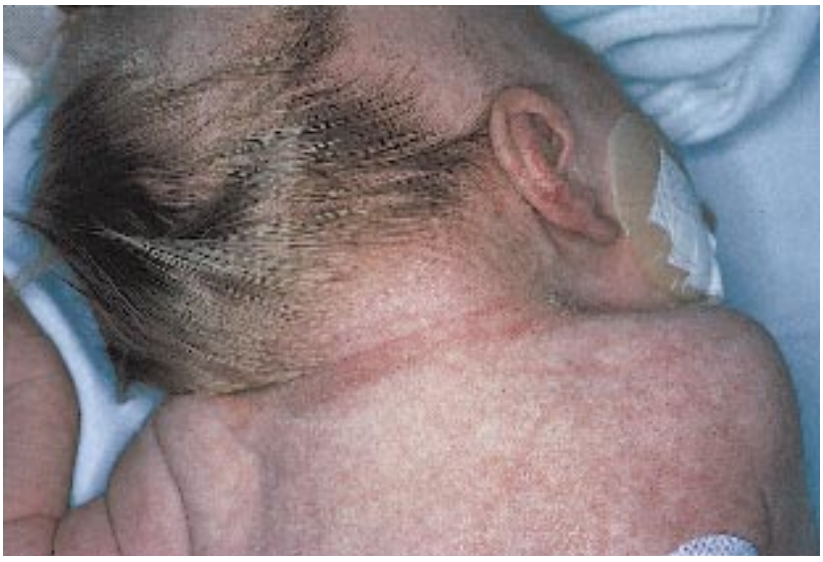

Figure 2.84. View of the back of the head and neck of the same infant showing the marked shortness of the neck and prominence of the occiput.

2.85

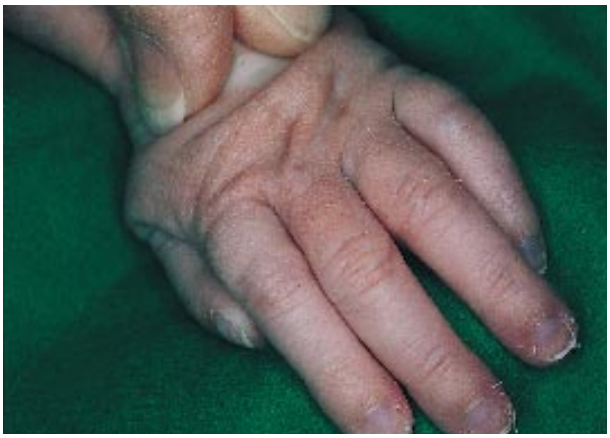

Figure 2.85. The fingers of the same infant as in Figure 2.83 and 2.84 show the typical long tapering digits (arachnodactyly) which are often noted in spondylothoracic dysplasia.

2.86

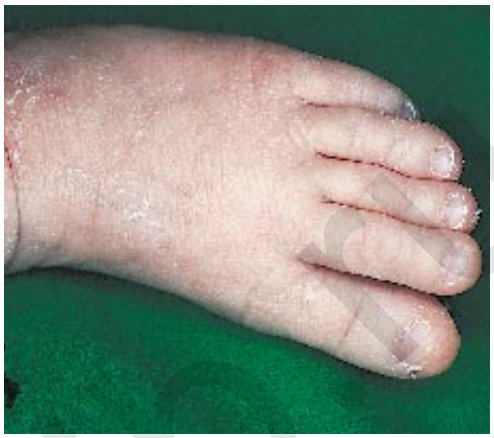

Figure 2.86. In this figure, note the extremely long tapering toes of the same infant.

2.87

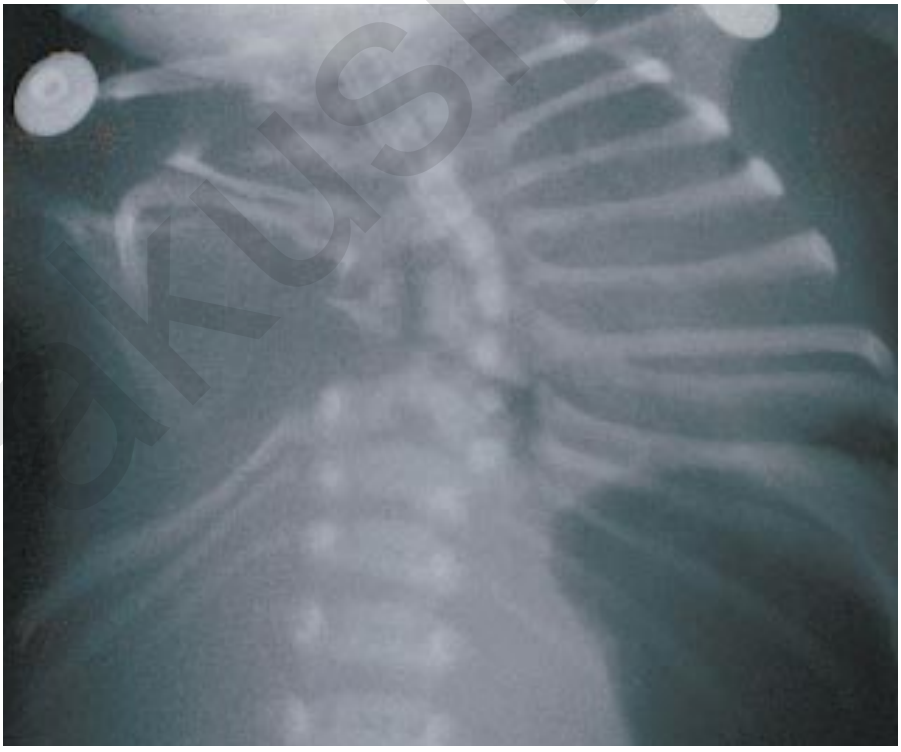

Figure 2.87. Chest radiograph of an infant with spondylothoracic dysplasia showing the grotesque and bizarre deformity of the ribs and spine. There is marked vertebral column shortening and numerous vertebral anomalies consisting of hemivertebrae, absent vertebrae, cleft vertebrae, and open neural arches. The severe deformity of the spinal column leads to posterior crowding and a fan-like appearance of the ribs on the frontal radiograms. The thorax is short on the right side due to a diminished number of ribs. The rib deformities are asymmetric.

2.88

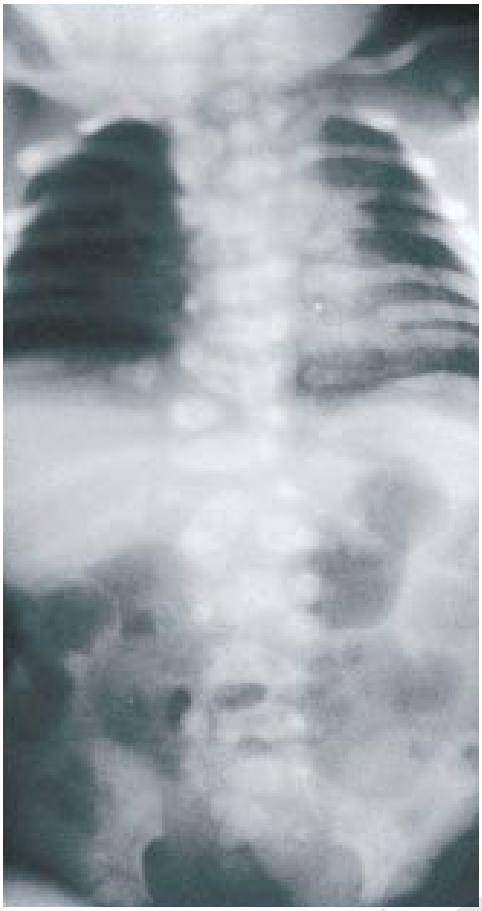

Figure 2.88. Radiograph of the thorax and abdomen in a less severe example of spondylothoracic dysplasia. Note the marked abnormalities in segmentation of the vertebrae. These abnormalities extend the total length of the spine, resulting in marked deformity of the spine (scoliosis, kyphosis).

2.89

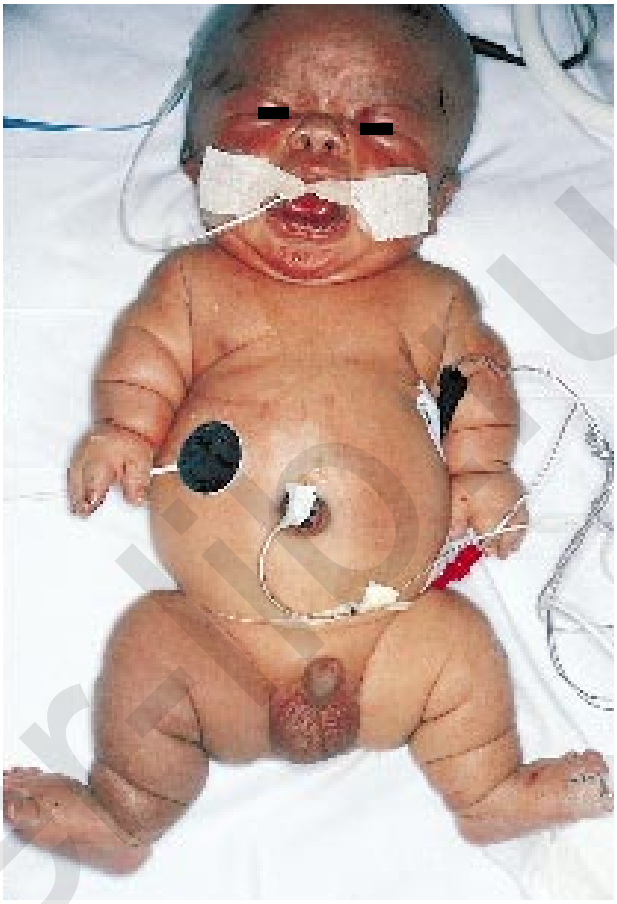

Figure 2.89. Short-limbed dwarfism in an infant with thanatophoric dysplasia. This form of dwarfism is more common in males. Note the large head and hypertelorism. The chest is markedly narrowed with a large protruding abdomen. The limbs are short and there are increased skin folds about the extremities. These infants do not survive.

2.90

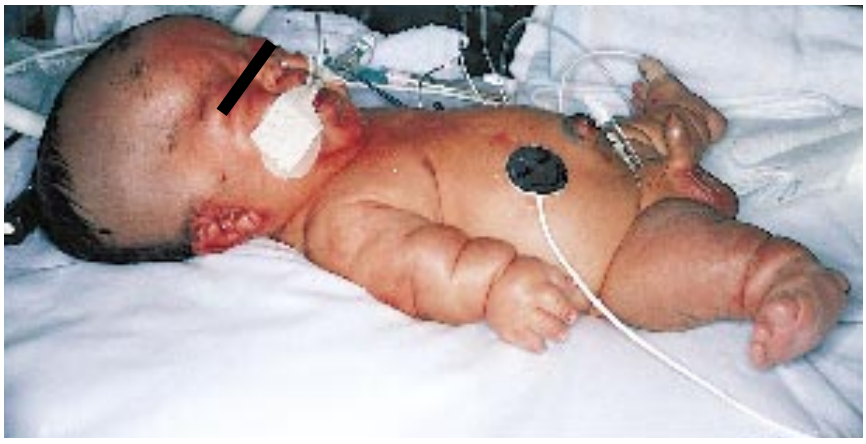

Figure 2.90. Lateral view of the same infant with thanatophoric dysplasia. The length of the infant at term was 40 cm due to the extremely shortened and bowed extremities. The head is large with a circumference of 40 cm. Note the prominent forehead.

2.91

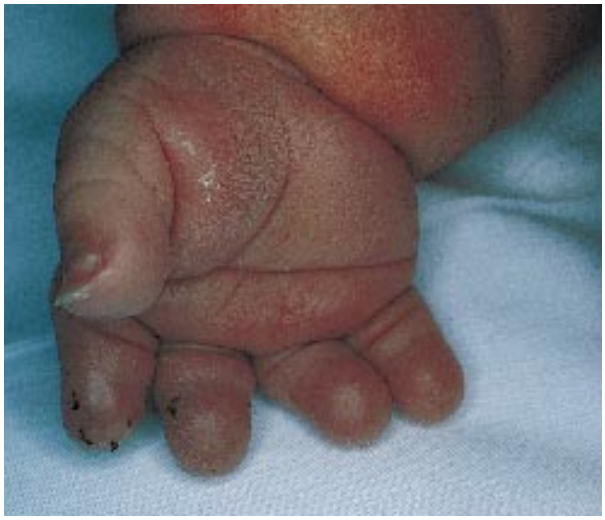

Figure 2.91. The right hand of the same infant demonstrating the marked brachydactyly and a single palmar crease.

2.92

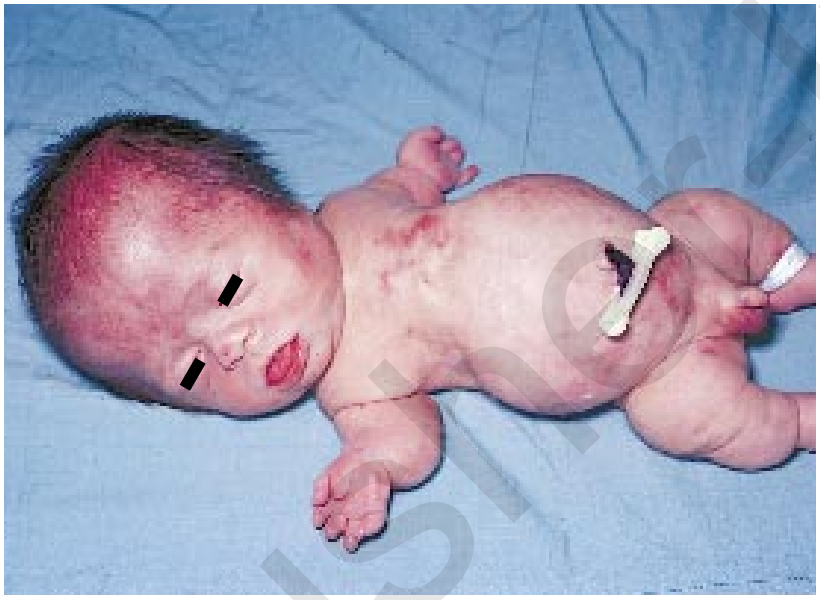

Figure 2.92. Another example of an infant with thanatophoric dysplasia. Note the hypotonia, large head, narrow thorax due to short ribs, prominent abdomen, and markedly shortened extremities. These infants with their large head and micromelia may be mistakenly diagnosed as having achondroplasia.

2.93

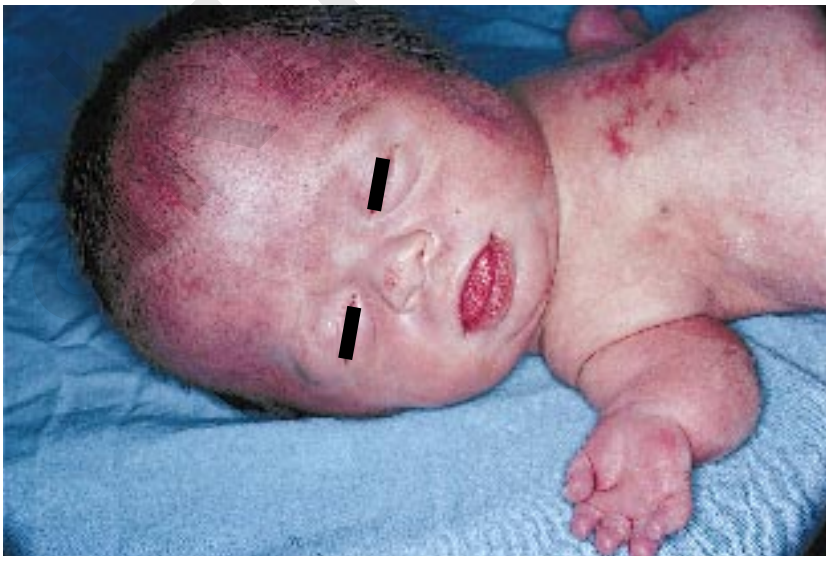

Figure 2.93. A close-up of the face of the same infant showing the large head, prominent forehead, hypertelorism, and flat nasal bridge. Note the narrow chest and short upper extremity with brachydactyly.

2.94

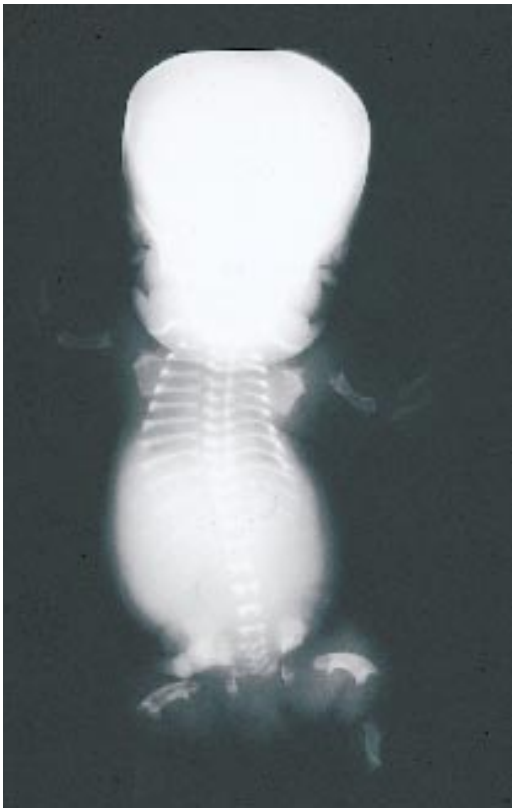

Figure 2.94. Body radiograph of an infant with thanatophoric dysplasia. Note the large head, narrow thorax due to short ribs, the typical V-shaped clavicles, and the prominent abdomen. Also note the marked flattening of the vertebral bodies. The ossification centers of the vertebrae are reduced.

2.95

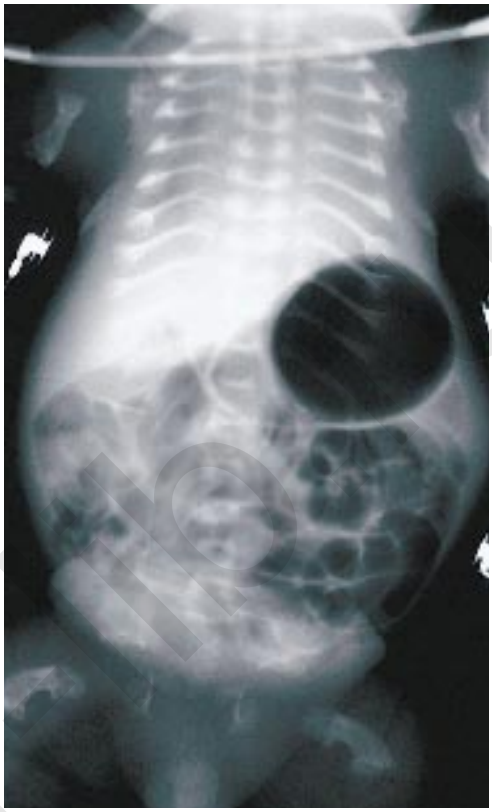

Figure 2.95. Anteroposterior radiograph of chest and abdomen in an infant with thanatophoric dysplasia. Note the short ribs which result in a narrow chest and the marked flattening of the vertebral bodies. The long bones demonstrate the marked shortening and bowing with the cupped irregular flaring of the proximal and distal metaphyses (the "telephone receiver" sign) which is especially noted in the femora.

2.96

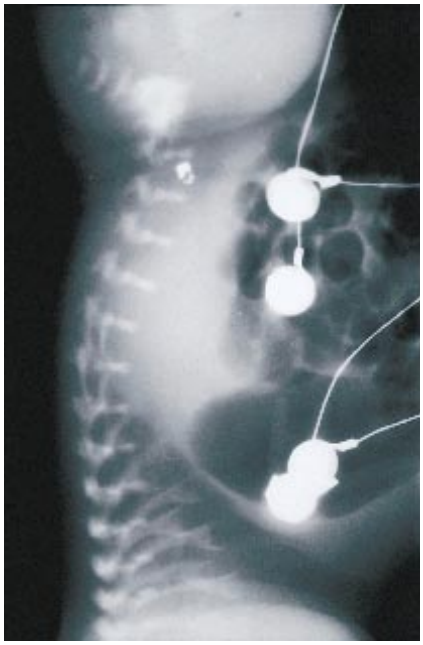

Figure 2.96. Lateral radiograph of the same infant showing the marked flattening of the vertebral bodies and flat ends to the ribs. In an infant with short-limbed dwarfism, this finding is diagnostic of thanatophoric dysplasia.

2.97

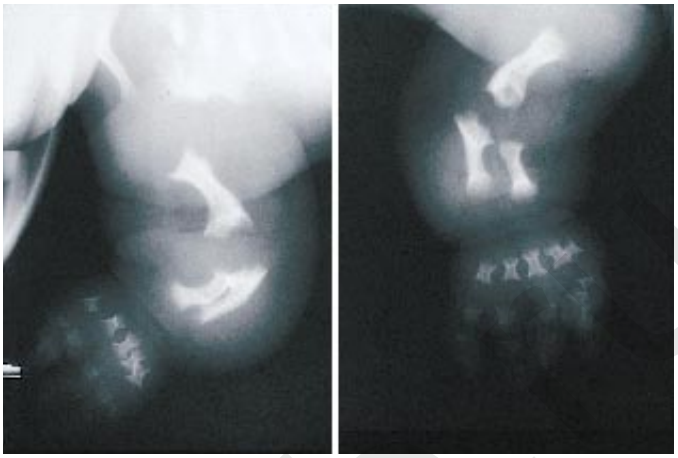

Figure 2.97. Radiograph of the upper extremities in an infant with thanatophoric dysplasia. Note the extremely shortened long bones with proximal and distal metaphyseal flaring.

2.98

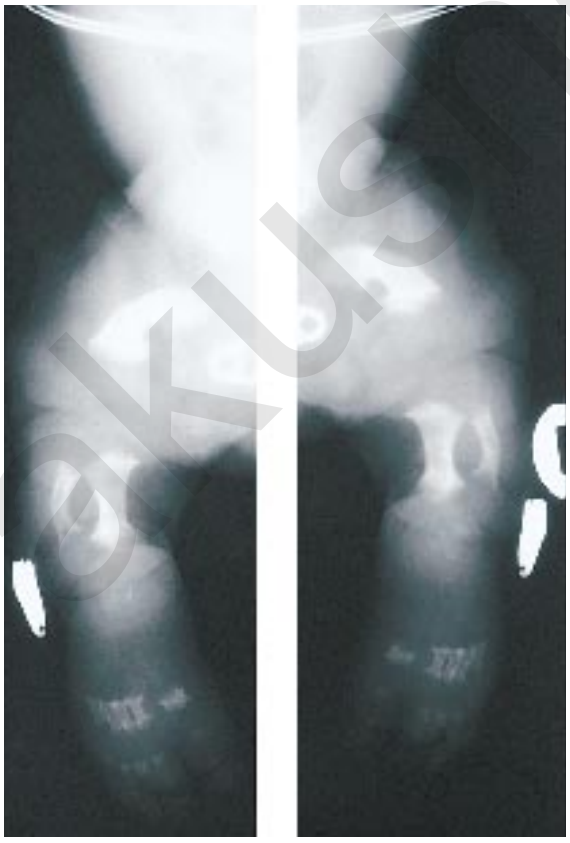

Figure 2.98. Radiograph of the lower extremities of the same infant again demonstrating the marked shortening of long bones with proximal and distal metaphyseal flaring.

Chapter 3
Non Chromosomal Syndromes, Associations, and Sequences

A syndrome, association, sequence, or complex is a constellation of abnormal physical signs, each nonspecific in isolation but resulting in a mosaic that can be diagnosed with confidence. The pathogenic mechanisms involved are variable. The clinical presentation depends on the pathogenic mechanism and the time of occurrence. Approximately 2% of all newborn infants have a significant malformation which may be relatively simple or complex. The later the defect develops in gestation, the more simple the malformation. In 10% of these infants, a chromosomal abnormality can be detected. In approximately 20%, the malformations are based on a single gene defect, with autosomal dominant disorders predominating. Multifactorial inheritance accounts for 30% of neonates with malformations. A small percentage of malformations is seen in infants born to diabetic mothers or mothers who have received a known teratogenic drug. The remaining 35% of newborn infants have no identifiable cause for their malformations. In infants with malformations, 7.5% are associated with deformations (see Volume I, Chapter 5). Malformations and deformations may recur with a similar pattern. Disruptions tend to be sporadic and no two cases are exactly alike. Due to limitations of space, this section can demonstrate only some very characteristic findings; therefore the clinician should not consider these descriptions to be complete and should refer to other references as needed.

3.1

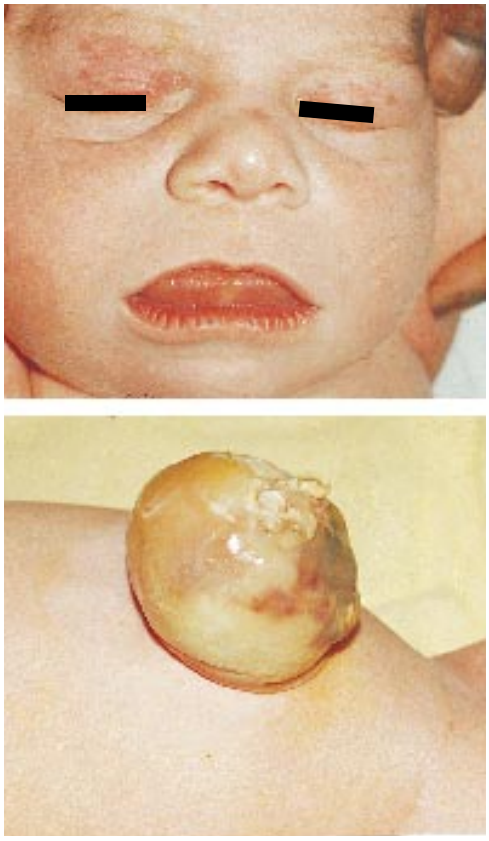

Figure 3.1. The top half of the figure shows macroglossia and a nevus flammeus; the lower portion shows an omphalocele; both in an infant with Beckwith-Wiedemann syndrome (*e*xomphalos-*m*acroglossia-*g*igantism [EMG] syndrome). It is usually sporadic and 60% of cases occur in females. Hemihypertrophy occurs in 10 to 15% of the infants.

3.2

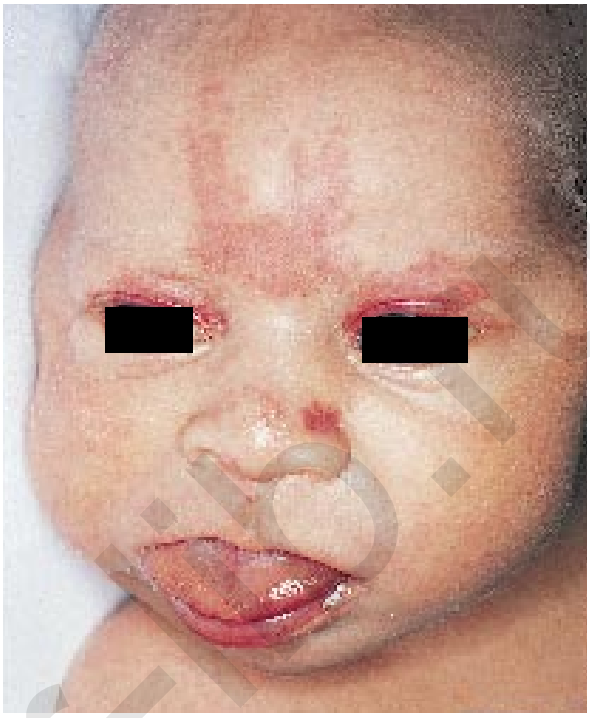

Figure 3.2. Another example of an infant with the typical macrosomia (birthweight of 3950 g), polycythemia (hematocrit 66%) and hypoglycemia. Note the macroglossia, nevus flammeus over the glabellar region and the eyelids, and the prominent eyes with relative infraorbital hypoplasia.

3.3

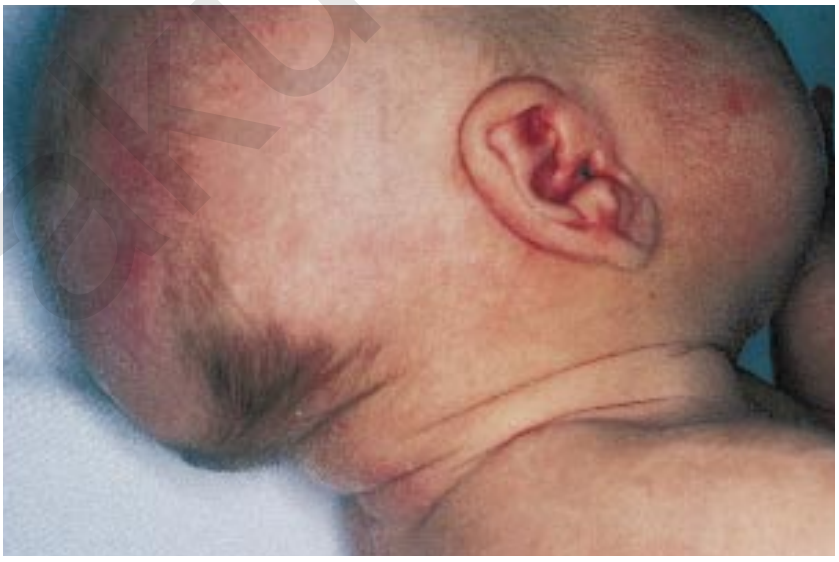

Figure 3.3. This infant with Beckwith-Wiedemann syndrome shows the prominent occiput and typical transverse crease in the lobe of the ear.

3.4

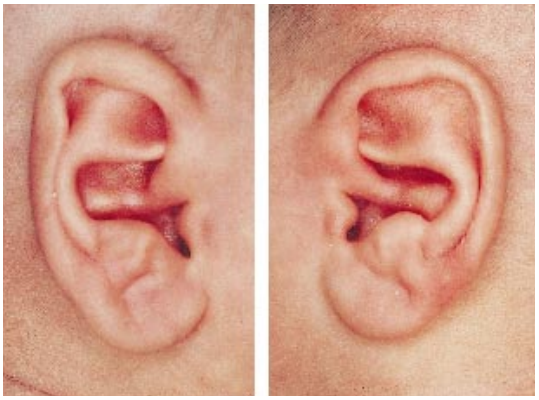

Figure 3.4. Transverse creases of the lobes of the ears in an infant with Beckwith-Wiedemann syndrome.

3.5

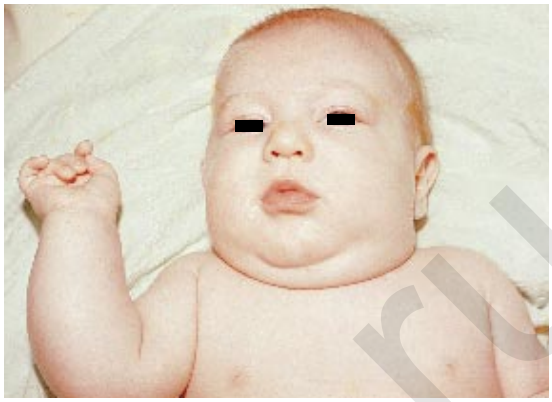

Figure 3.5. This 2-month-old infant with Caffey's syndrome (infantile cortical hyperostosis) shows the characteristic swelling of the jaw and right forearm. It usually occurs in a well-nourished infant. When the jaw is involved there is usually marked swelling of the face, mainly localized over the jaw. Most commonly this condition is diagnosed in the first few months of life, but congenital Caffey's syndrome has been reported.

3.6

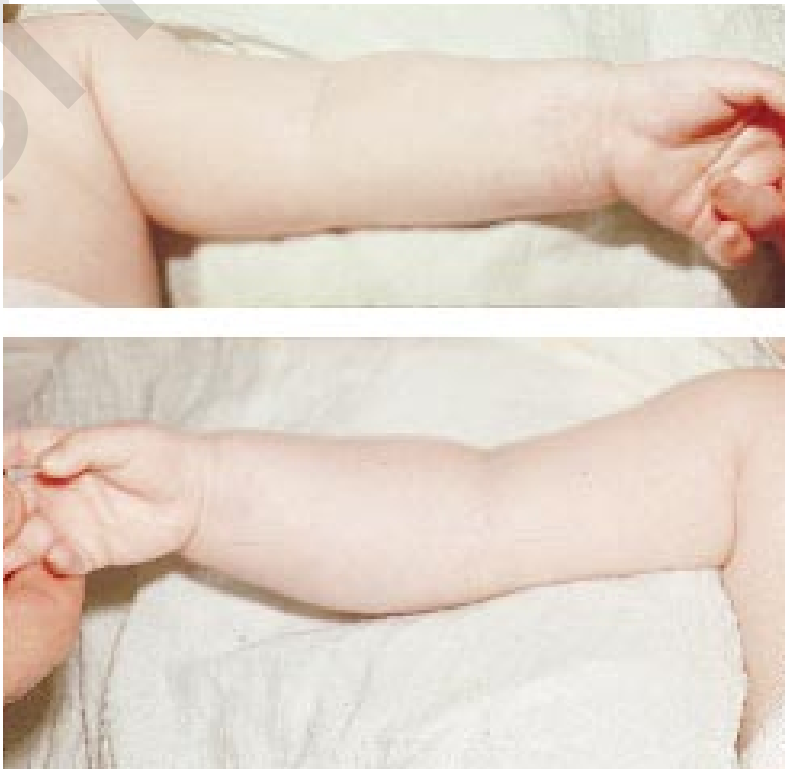

Figure 3.6. The same infant with Caffey's syndrome. Note that the left arm is normal but the right forearm is swollen and tender.

3.7

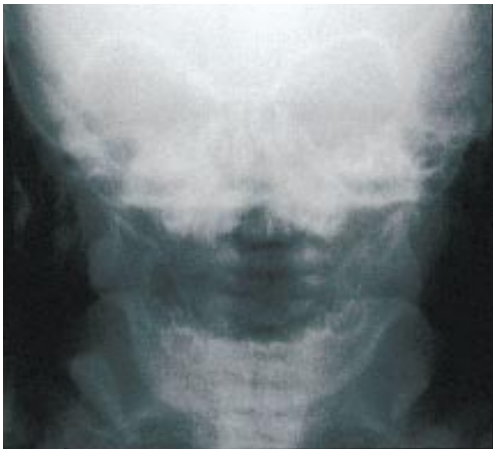

Figure 3.7. A radiograph showing the cortical hyperostosis of the jaw in an infant at the age of 4½ months.

3.8

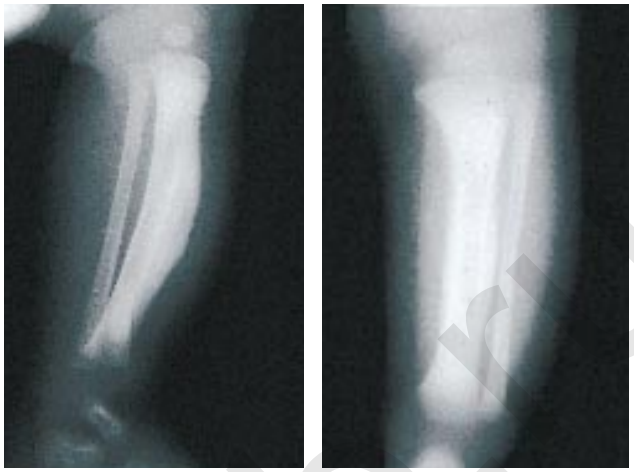

Figure 3.8. Lower extremity radiograph of the same infant at the age of 1 month. Note the early cortical hyperostosis of the femur and tibia.

3.9

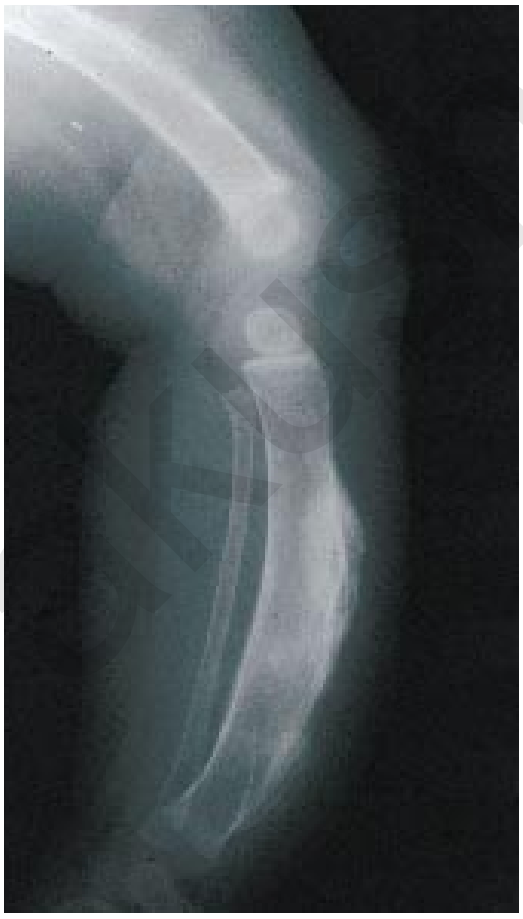

Figure 3.9. Follow-up radiograph of the lower extremity in the same infant at the age of 4½ months shows the marked cortical hyperostosis of the left tibia. Periosteal thickening of the long bones with translucent bands at the distal epiphyseal ends is diagnostic. Later, the bones expand and the cortex is thinned. The enlarged medullary cavity has little trabeculation and the soft tissue is swollen. The condition is self-limiting.

3.10

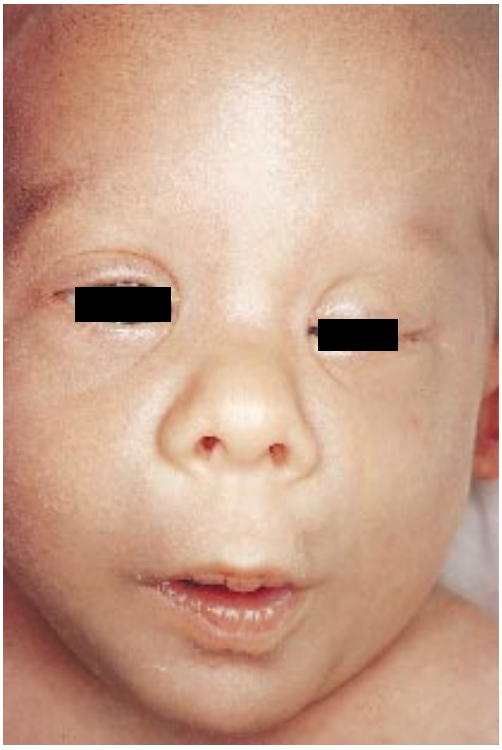

Figure 3.10. Infant with the CHARGE association. Occurrence is non-random and is characterized by *c*oloboma, *h*eart disease, *a*tresia of the choanae, *r*etarded postnatal growth and development, *g*enitourinary anomalies, and *e*ar anomalies and deafness. Most infants have some degree of mental deficiency. The coloboma commonly involves the retina but may range in severity from an isolated coloboma of the iris to anophthalmos.

3.11

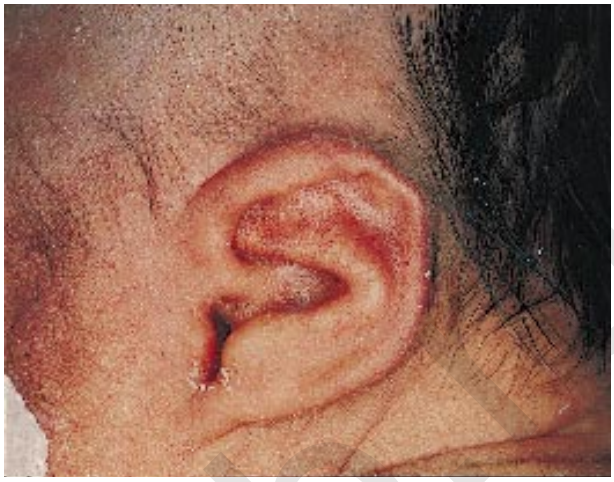

Figure 3.11. Abnormal ear in an infant with the CHARGE association.

3.12

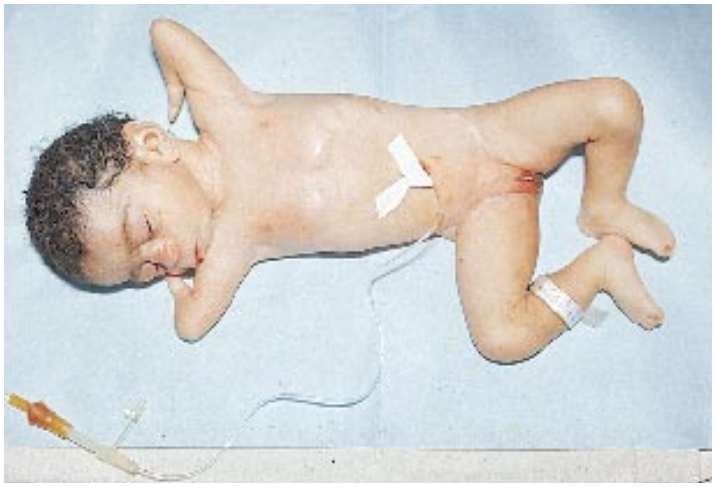

Figure 3.12. Cornelia de Lange's syndrome (Brachmann-de Lange syndrome: typus degenerativus amstelodamensis). One hundred percent of these infants have shortness of stature of prenatal onset, mental retardation and sluggish physical activity, hypoplastic nipples, initial hypertonicity and a low-pitched, weak, growling cry in infancy. Most of the infants have early feeding difficulties and early growth failure. In this infant note the bushy eyebrows and micromelia.

3.13

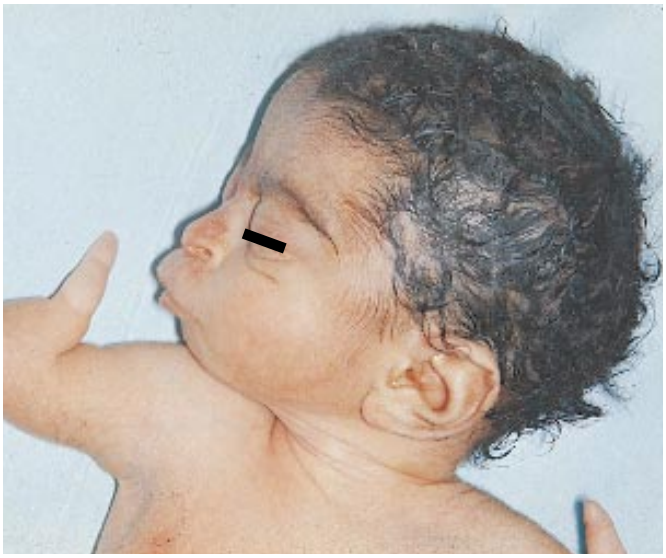

Figure 3.13. Close-up of face of the same infant as in Figure 3.12. Note the hirsutism, bushy eyebrows, downward slanting palpebral fissures, and micrognathia.

3.14

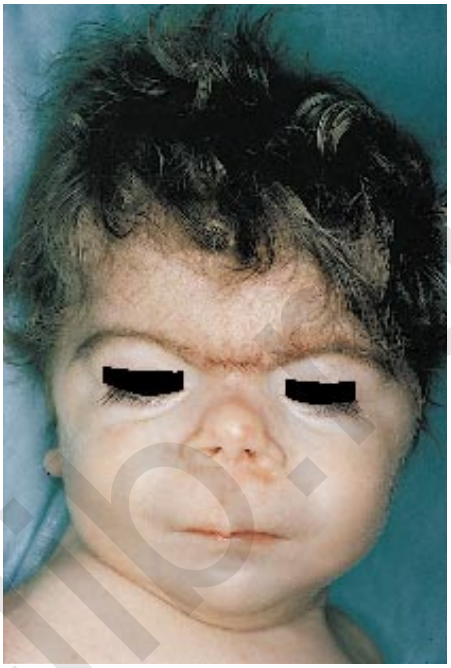

Figure 3.14. This infant with Cornelia de Lange's syndrome shows many of the characteristic findings: coarse, mop-like hair; bushy eyebrows and synophrys (confluent, thick eyebrows); long curly eyelashes; short nose with small anteverted nostrils; thin lips with a small midline beak of the upper lip; long philtrum; and downward curving of the angles of the mouth. The infants often have a mask-like expression.

3.15

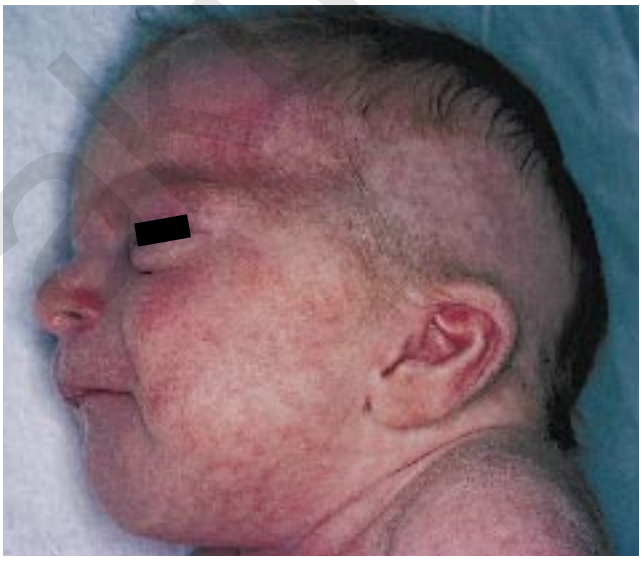

Figure 3.15. Another infant with Cornelia de Lange's syndrome showing the typical microbrachycephaly seen in over 90% of these infants, bushy eyebrows, small nose and micrognathia. Note the low-set ear and cutis marmorata which are also very common findings in Cornelia de Lange's syndrome.

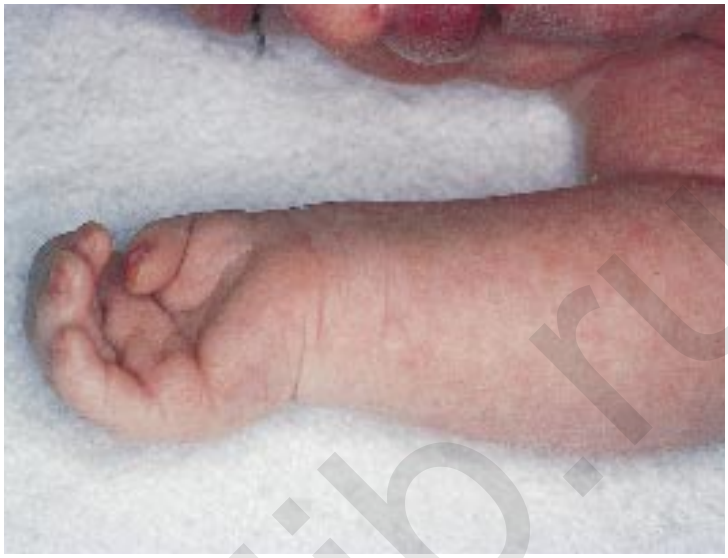

3.16

Figure 3.16. Anomalies of the extremities are common in infants with Cornelia de Lange's syndrome varying from the most severe (micromelia) to small hands and feet (microcheiria and micropodia). This infant with Cornelia de Lange's syndrome has microcheiria of the right hand. Both a single palmar crease (simian crease) and clinodactyly are very common in infants with this syndrome.

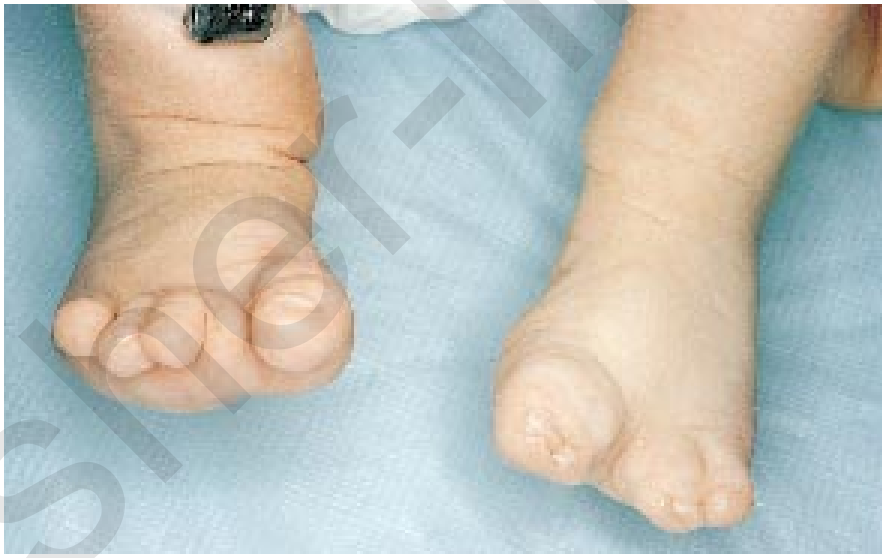

3.17

Figure 3.17. Syndactyly of the first, second, third and fourth toes in an infant with Cornelia de Lange's syndrome. The most common type of syndactyly is that of the second and third toes which is seen in many normal infants and in many syndromes.

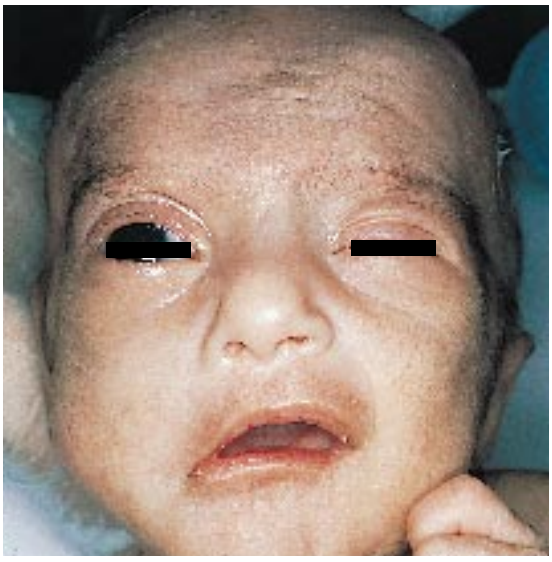

3.18

Figure 3.18. DiGeorge malformation complex. This is a primary defect of the fourth branchial arch and the third and fourth pharyngeal pouch. In this infant note the lateral displacement of the inner canthi (hypertelorism), the anteverted nares, and short philtrum with a cupid-bow mouth. This infant also had micrognathia, microcephaly, congenital heart disease (atrial septal defect and ventricular septal defect) and hypocalcemia. Note the congenital facial palsy which is not part of the complex. The EEG was grossly abnormal and the T cell count was decreased.

3.19

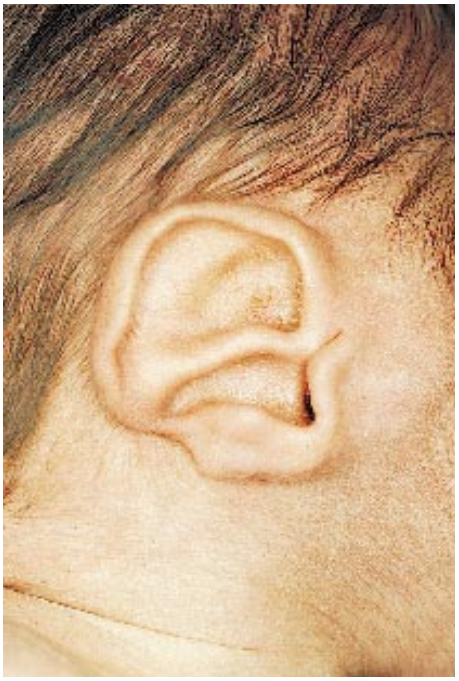

Figure 3.19. Abnormal dysplastic ear in the same infant. The acronym "CATCH 22 syndrome" has been applied to DiGeorge syndrome in that there are *c*ardiac defects, *a*bnormal facies, *t*hymic hypoplasia, *c*left palate, *h*ypocalcemia, and *22*q11 deletion.

3.20

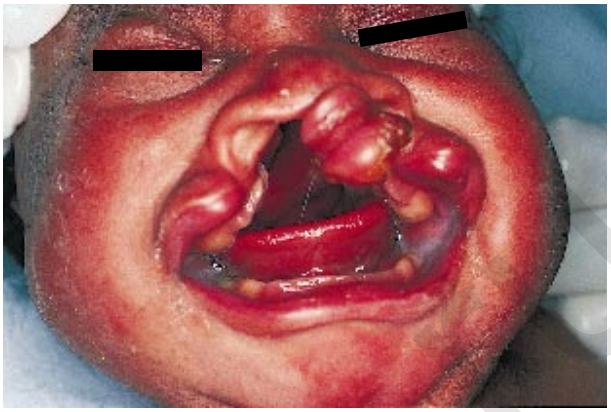

Figure 3.20. In the *e*ctrodactyly-*e*ctodermal dysplasia-*c*lefting (EEC) syndrome there are varying manifestations of lobster-claw deformity (ectrodactyly) of the hands and feet and there is cleft lip/palate. The cleft lip is usually bilateral. Other manifestations include absence of the lacrimal puncta with tearing and blepharitis; abnormal teeth; malformations of the genitourinary (GU) tract such as cryptorchidism; and alterations in the skin and hair. Scalp hair, eyelashes and eyebrows are usually sparse and hair color is light. The nails may be hypoplastic and brittle. Most of these infants have normal intelligence. In this infant note the severe bilateral cleft lip and palate.

3.21

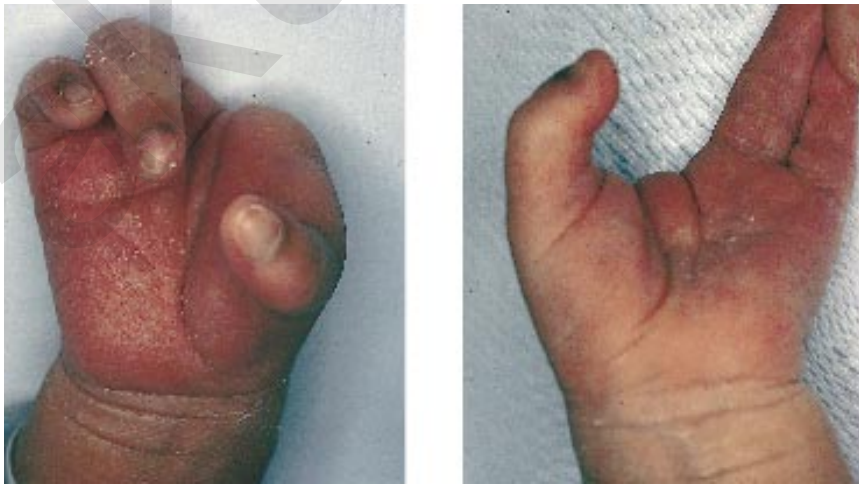

Figure 3.21. In this figure of the same infant note the ectrodactyly (lobster-clw deformity) of both hands. In this condition, usually all four extremities have a lobster-claw deformity.

3.22

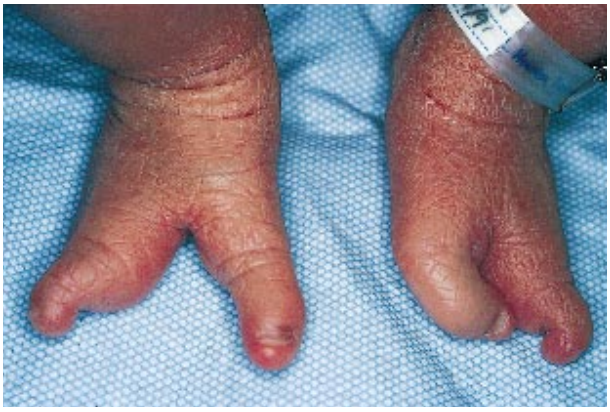

Figure 3.22. Dorsal view of the ectrodactyly of both feet of the same infant.

3.23

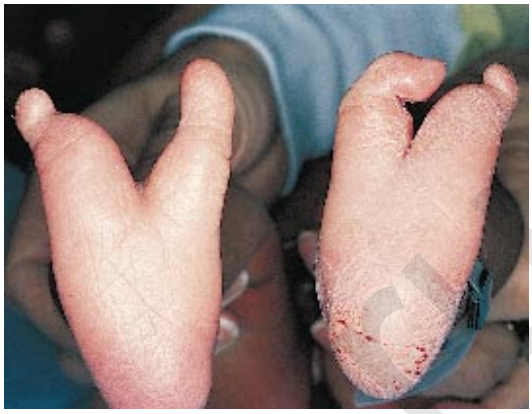

Figure 3.23. The same infant showing the soles of the feet.

3.24

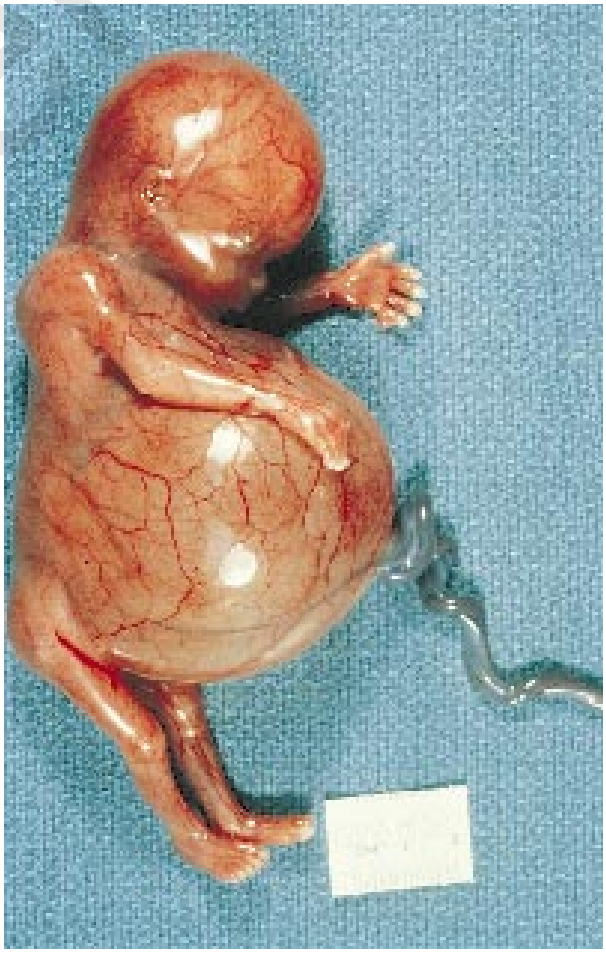

Figure 3.24. Eagle-Barrett syndrome (prune belly syndrome) is also described as the triad syndrome: absence of abdominal musculature, genitourinary tract abnormalities, and cryptorchidism. In this fetus there is a markedly distended abdomen due to a very distended bladder. It is now thought that the genitalia and urinary tract abnormalities are the precursor of the absence of abdominal musculature.

3.25

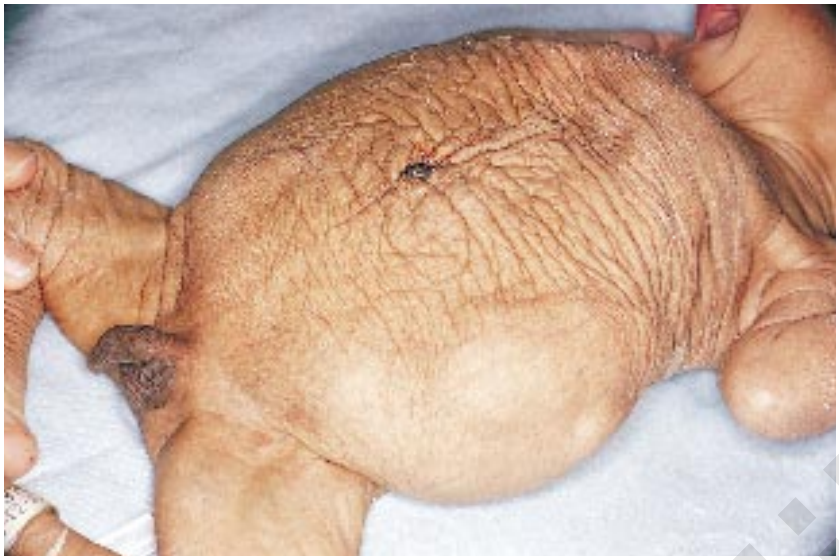

Figure 3.25. The characteristic findings of prune belly syndrome are present in this infant. Note the marked laxity of the abdominal wall giving it the appearance of a "prune," and the large mass on the left side of the abdomen due to massive dilatation of the ureter and hydronephrosis. Also note the cryptorchidism.

3.26

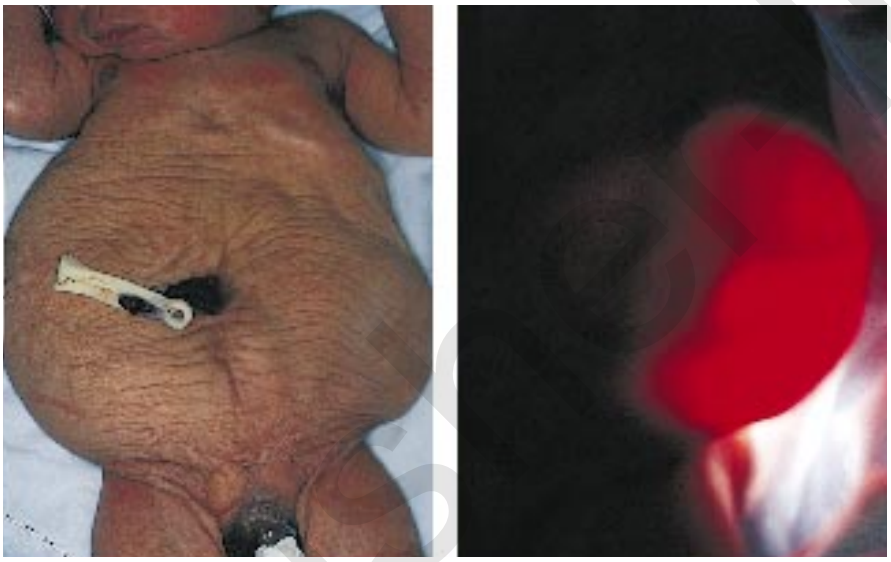

Figure 3.26. Another example of absence of abdominal musculature. Note the typical appearance of the prune belly on the left of the figure and the transillumination showing the massive hydroureter on the right.

3.27

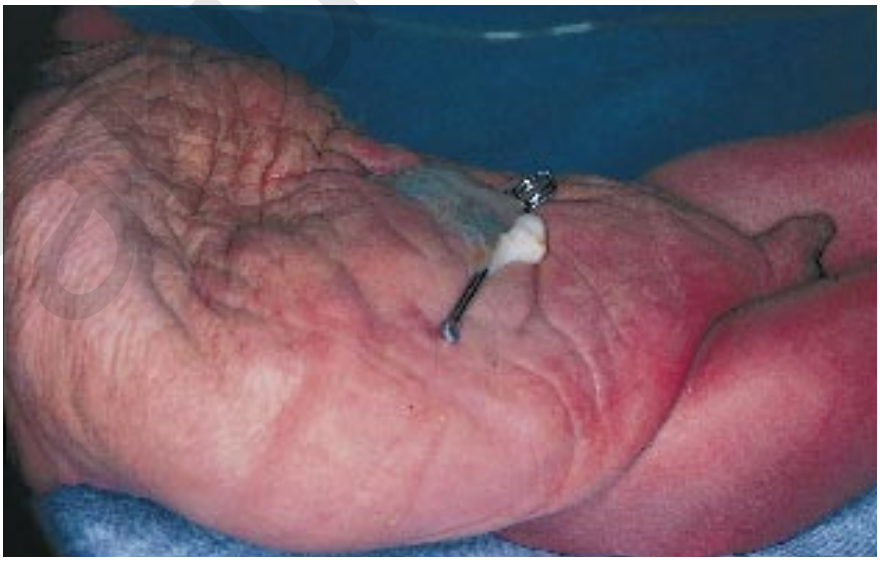

Figure 3.27. Appearance of absence of abdominal musculature in another infant.

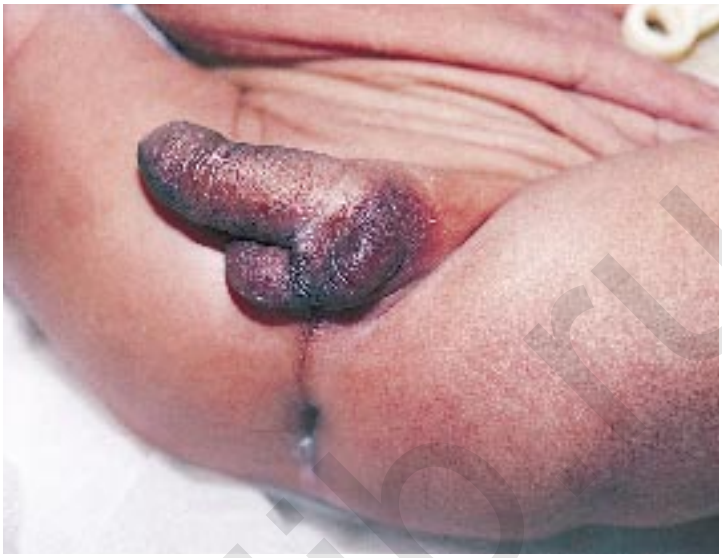

3.28

Figure 3.28. Cryptorchidism in an infant with prune belly syndrome.

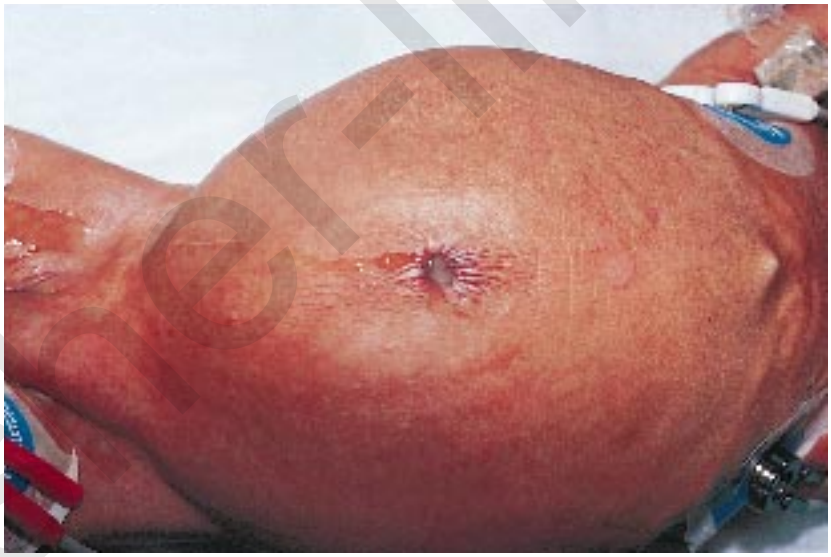

3.29

Figure 3.29. A common finding in infants with prune belly syndrome is a patent urachus.

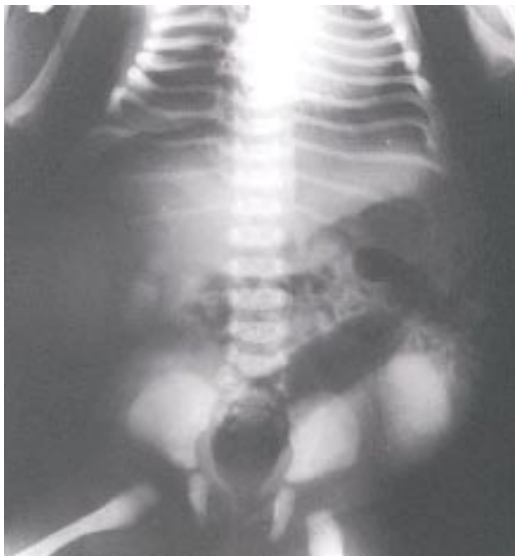

3.30

Figure 3.30. Radiograph of abdomen showing the bulging of the flanks and abnormal gas pattern due to genitourinary tract abnormalities in an infant with Eagle-Barrett syndrome.

3.31

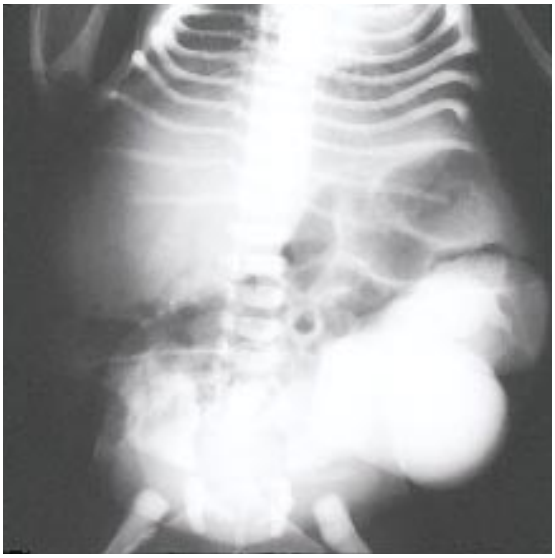

Figure 3.31. Contrast study in the same infant as in Figure 3.30 showing the massive hydroureter.

3.32

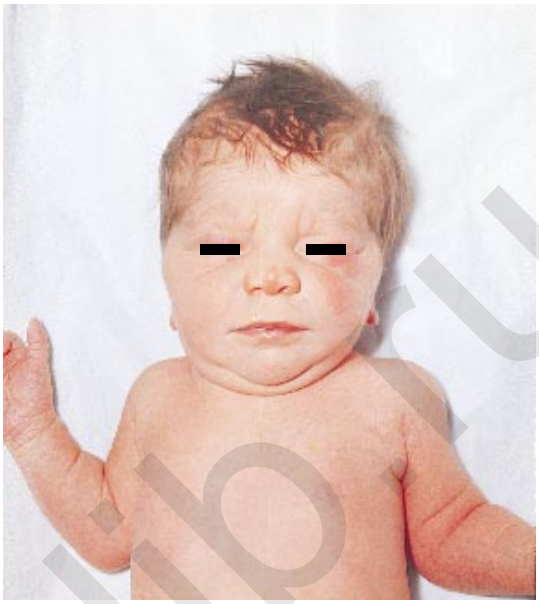

Figure 3.32. This infant with Ehlers-Danlos syndrome (cutis hyperelastica) presented at birth with marked hypotonia, joint hypermobility, and hyperextensibility of the skin. Note the epicanthal folds.

3.33

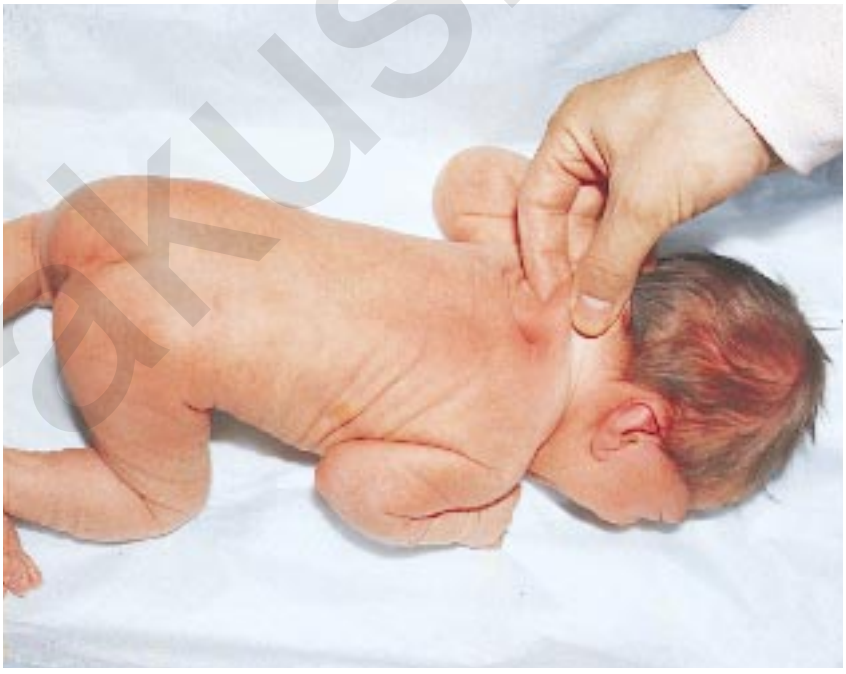

Figure 3.33. Figure of the same infant showing the webbing of the neck and hyperextensibility of the skin. The elasticity of the skin allows it to stretch and recoil, whereas in cutis laxa the skin hangs down in loose folds and does not recoil, and the joints are not hyperextensible as is seen in Ehlers-Danlos syndrome.

3.34

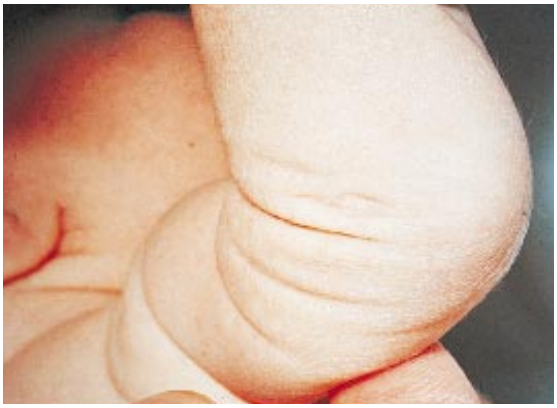

Figure 3.34. In the same infant note the hyperextensibility of the skin and the mild skin defects. There may be flat scars with paper-thin scar tissue, and hematomas occur after mild trauma in Ehlers-Danlos syndrome.

3.35

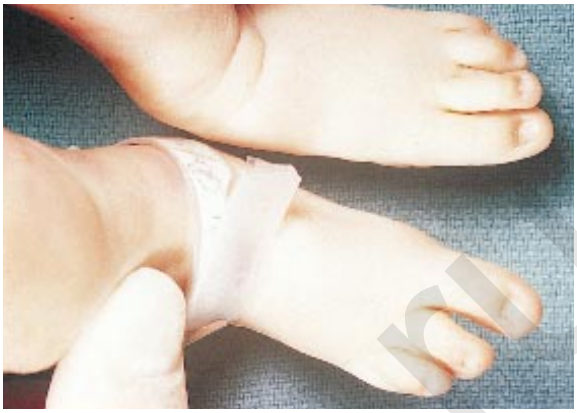

Figure 3.35. Other findings in Ehlers-Danlos syndrome include diaphragmatic hernia, congenital heart defects, and renal anomalies. There may be ectasia of portions of the gastrointestinal and respiratory tracts. The infant had an atrial septal defect, a small left diaphragmatic eventration, absence of the right mesocolon, and a double collecting system of the left kidney with an ectopic right kidney in the pelvis. The infant also demonstrates the second and fourth toes set dorsally to the first, third, and fifth toes and connected by a web.

3.36

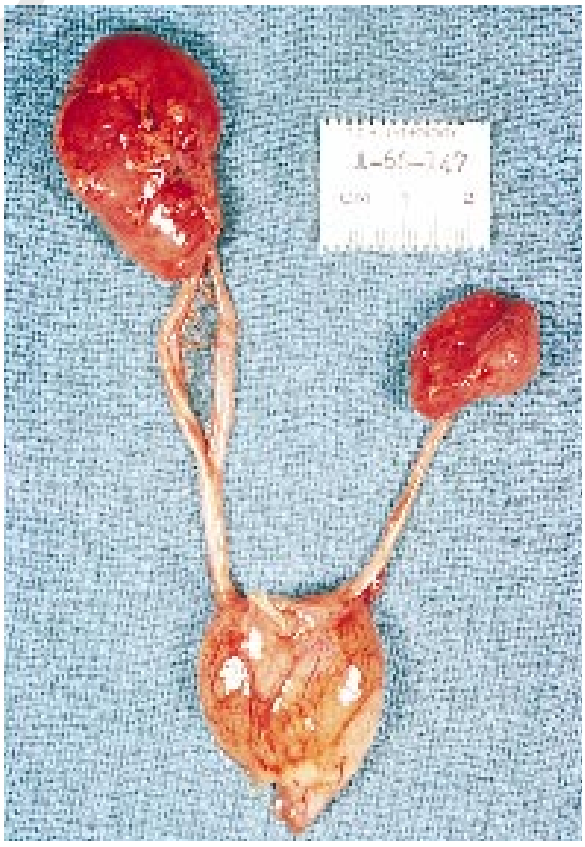

Figure 3.36. The renal system of the same infant at autopsy shows the ectopic right kidney which was in the pelvis and the left kidney with a double collecting system proximally.

3.37

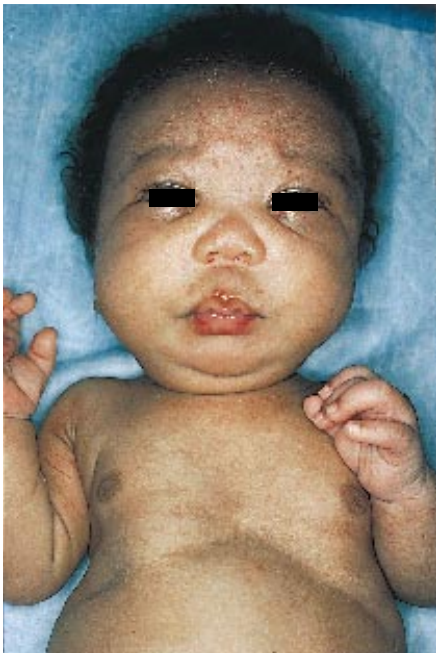

Figure 3.37. The fetal face syndrome (Robinow's syndrome or mesomelic dysplasia). These infants have slight to moderate shortness of stature, macrocephaly, a large anterior fontanelle, and frontal bossing with apparent hypertelorism, a short nose with anteverted nares, a long philtrum, and a small mouth with micrognathia. These result in a flat facial profile. The appearance of the face is similar to that of a fetus of about 8 weeks gestation. Hyperplastic alveolar ridges are present and a microphallus is a frequent finding.

3.38

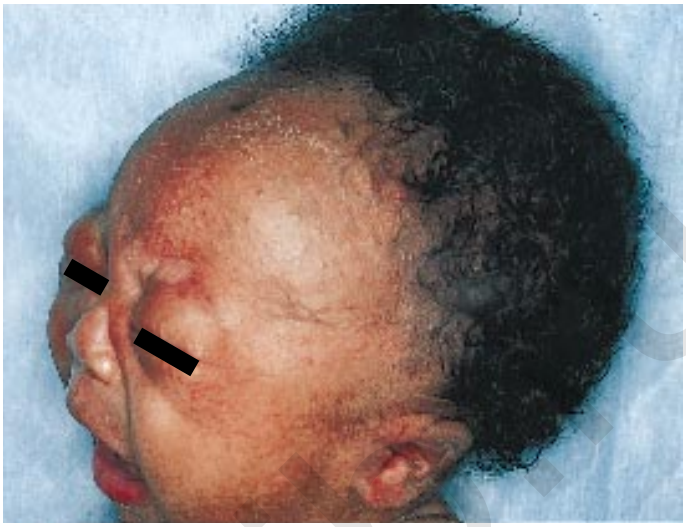

Figure 3.38. In this figure of the same infant note the marked frontal bossing, the large anterior fontanelle, the short nose, long philtrum, and micrognathia.

3.39

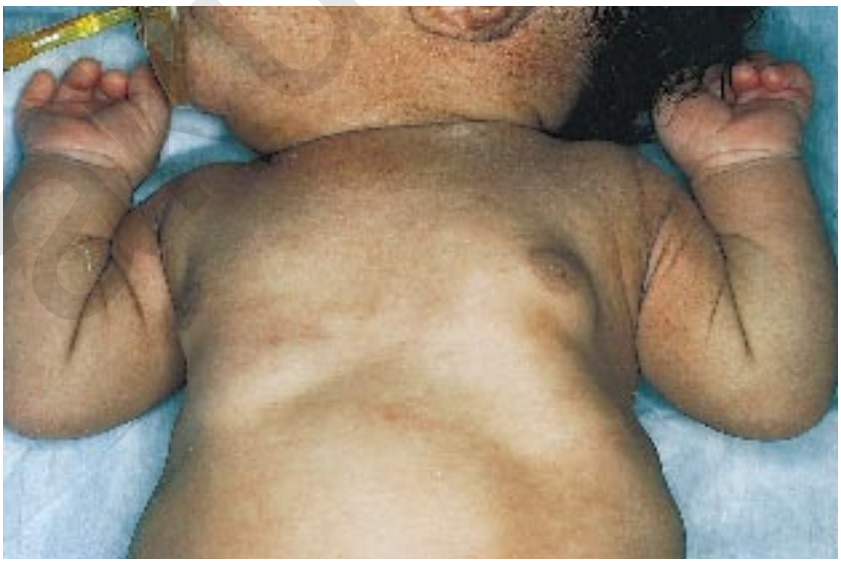

Figure 3.39. The chest and upper extremities of the same infant show the mesomelic dwarfism with the short forearms and brachydactyly. Mesomelic dwarfism affects the upper extremities more than the lower in these infants. There is mild pectus excavatum. Also note that this infant has some breast hypertrophy due to mastitis neonatorum.

3.40

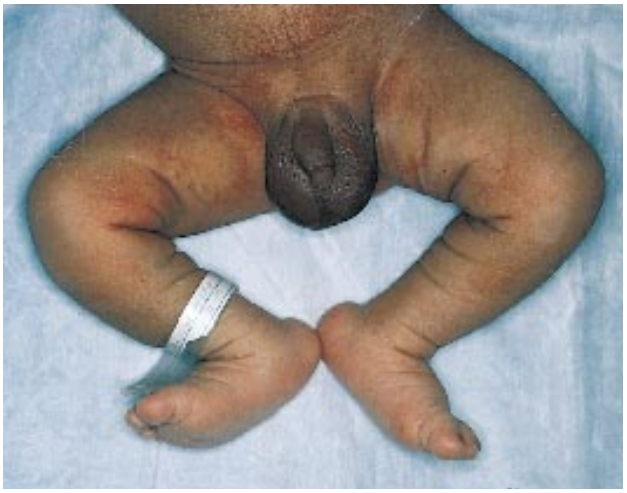

Figure 3.40. Note that the lower extremities of the same infant are normal except for the presence of bilateral rocker-bottom feet.

3.41

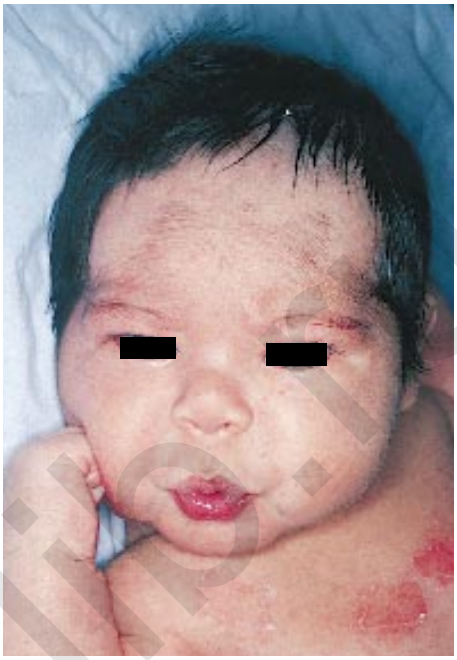

Figure 3.41. Infants with the femoral hypoplasia-unusual facies syndrome present with small stature and a typical facies. There are upslanting palpebral fissures, a short nose with hypoplastic alae nasi, a long philtrum, and a thin upper lip. A cleft palate may be present.

3.42

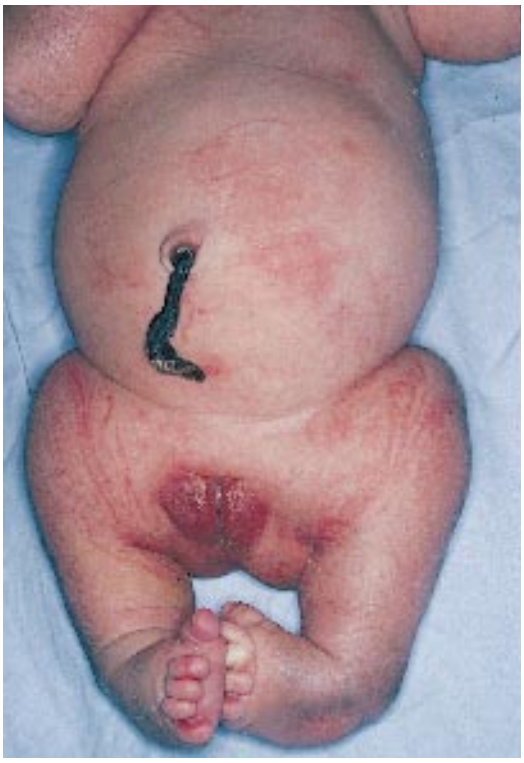

Figure 3.42. In this figure of the same infant note the abnormal lower extremities. These may be due to hypoplastic or absent femora and fibulae. In this infant the femora were absent and note also the bilateral talipes equinovarus. Hypoplasia of the humeri with restricted elbow movement may also occur in this syndrome.

3.43

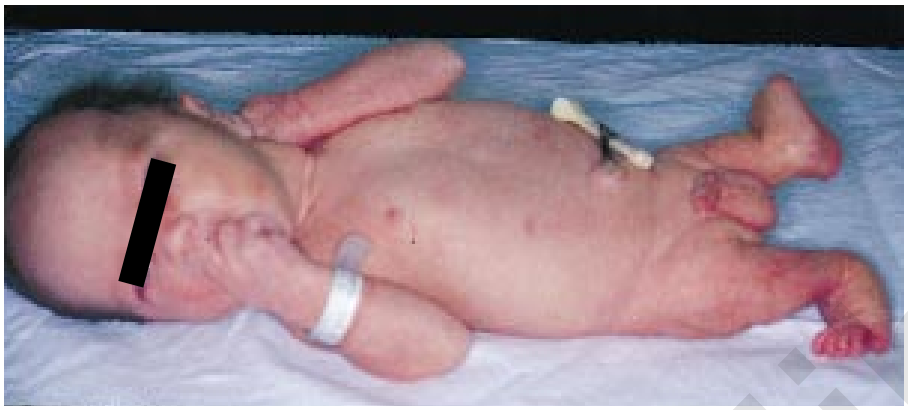

Figure 3.43. Another infant with the femoral hypoplasia-unusual facies syndrome. Note the small stature, predominantly the result of the small lower limbs.

3.44

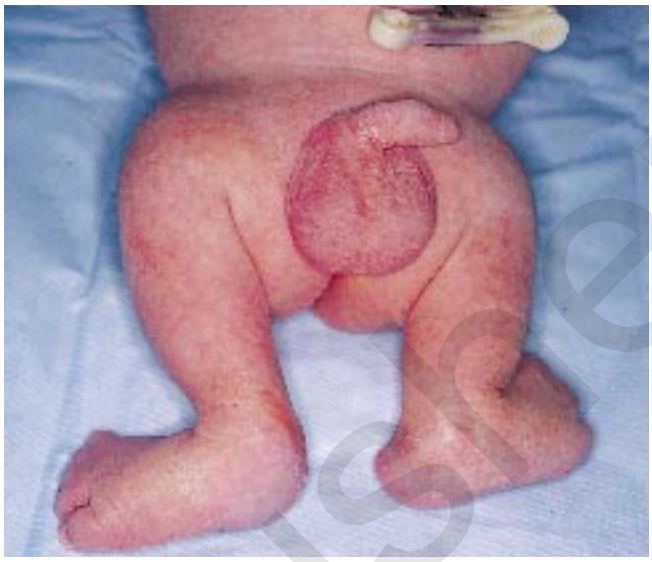

Figure 3.44. Close-up of the lower extremities of the same infant showing the absence of the femora.

3.45

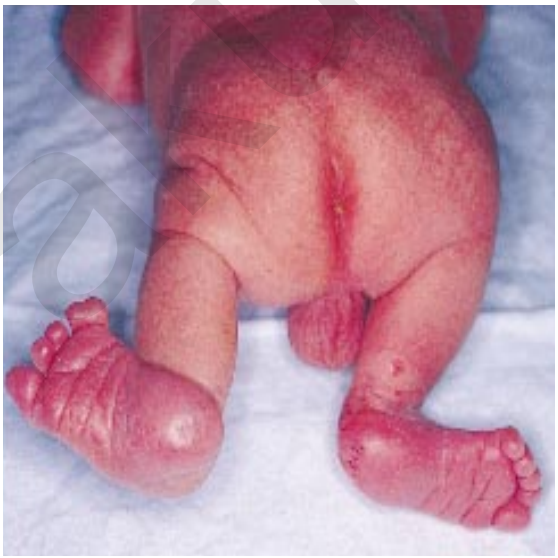

Figure 3.45. Posterior view of the lower extremities of the same infant.

3.46

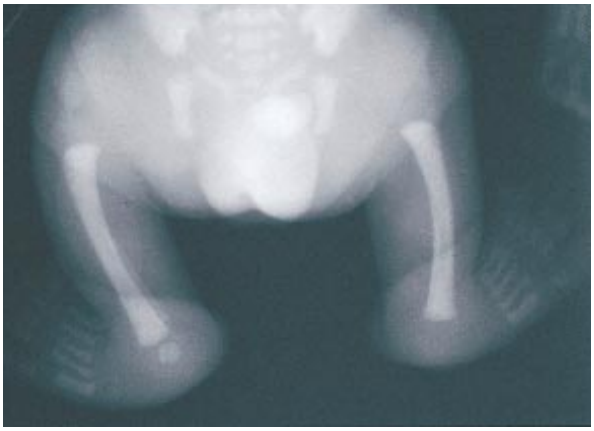

Figure 3.46. Radiograph of the lower extremities of the same infant showing the absence of femora bilaterally, a hypoplastic fibula on the right and an absent fibula on the left. In these infants, the acetabula may be hypoplastic and there may be a constricted iliac base with a vertical ischial axis.

3.47

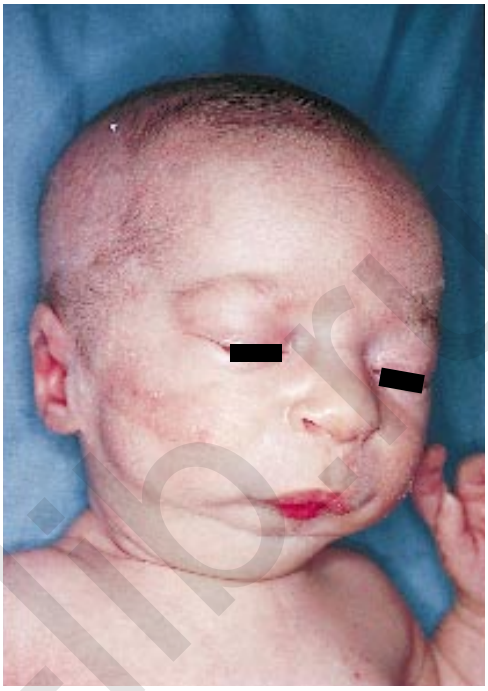

Figure 3.47. Another case of the femoral hypoplasia-unusual facies syndrome. Note the typical appearance of the face with the upslanting palpebral fissures, the short nose with hypoplastic alae nasi, long philtrum and micrognathia which was due to marked hypoplasia of the mandible. This infant also had a cleft palate which may be a part of this syndrome.

3.48

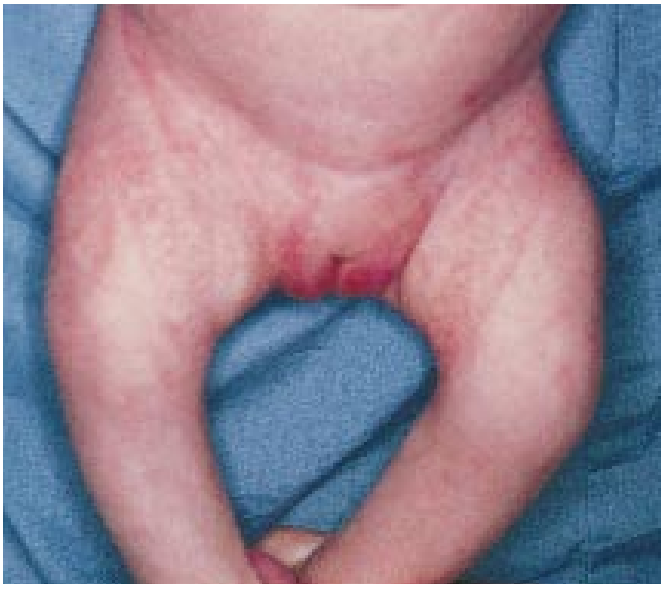

Figure 3.48. This figure of the same infant shows the short lower extremities with abnormal hypoplastic femora.

3.49

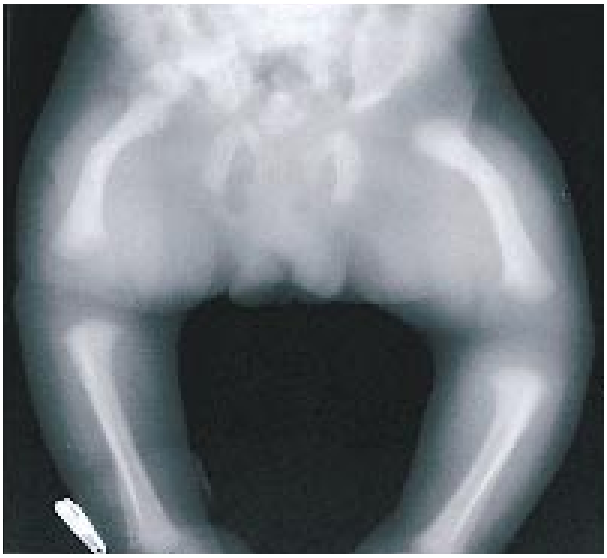

Figure 3.49. Radiograph of the same infant. The wings of the ilia are slenderized, the acetabular cavities are very shallow and ill formed, and there is bilateral dislocation of the hips. There are symmetric angular deformities in the midshafts of both femora which are shortened in length.

3.50

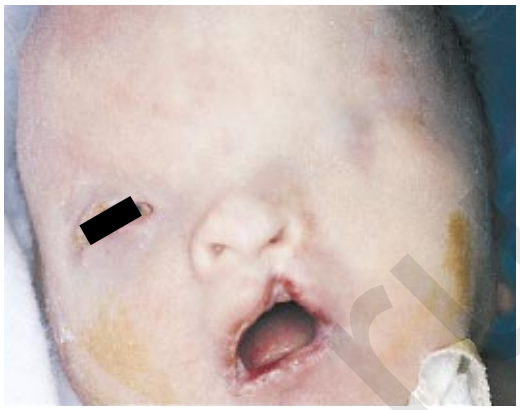

Figure 3.50. This infant, born at 35 weeks gestation, had Fraser's syndrome (cryptophthalmos syndrome). Note the cryptophthalmos on the left and the microphthalmia on the right. The infant had a cleft lip on the left and a high arched palate. There was subglottic tracheal obstruction. In Fraser's syndrome there is cryptophthalmos usually with a defect of the eye, and hair growth on the lateral forehead extends to the lateral eyebrow. Cryptophthalmos is bilateral in 50% of cases. There may be hypoplastic, notched nares and a broad nose with a depressed bridge. There are ear anomalies, most commonly cupping. Other findings in the syndrome include laryngeal stenosis or atresia, renal agenesis, and incomplete development of the male or female genitalia. There may be partial cutaneous syndactyly.

3.51

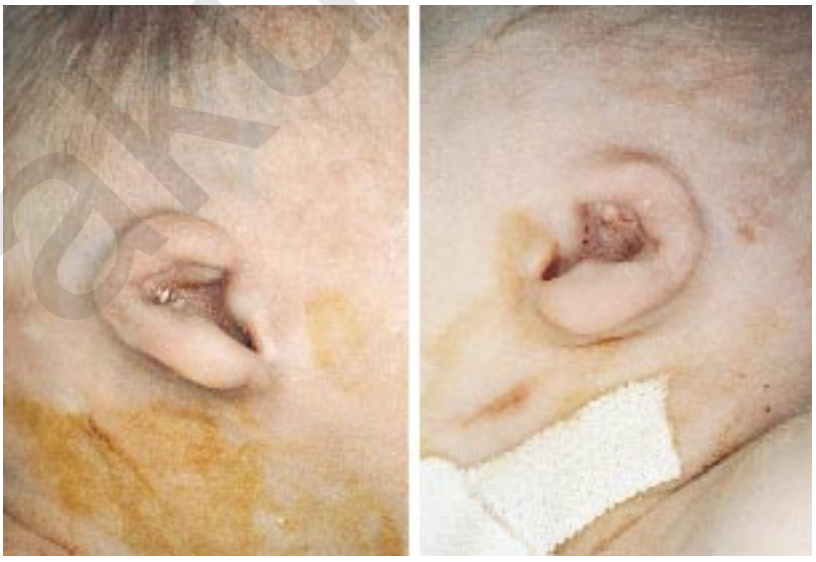

Figure 3.51. In this figure of the same infant, note the abnormal ears with marked cupping.

3.52

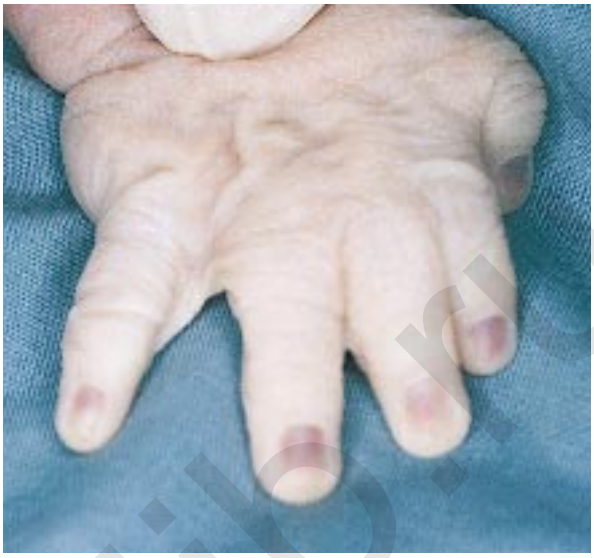

Figure 3.52. Cutaneous syndactyly (webbing) of the fingers is present in the same infant.

3.53

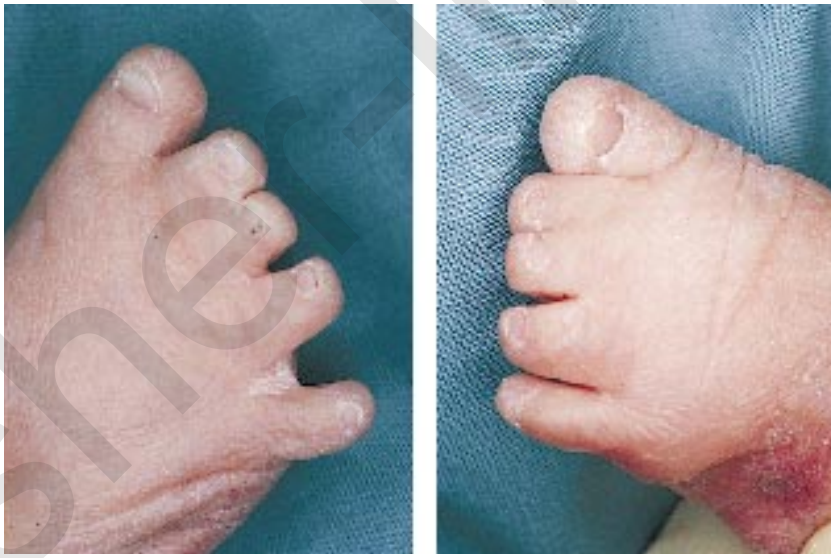

Figure 3.53. The same infant with Fraser's syndrome showing the webbing of the toes.

3.54

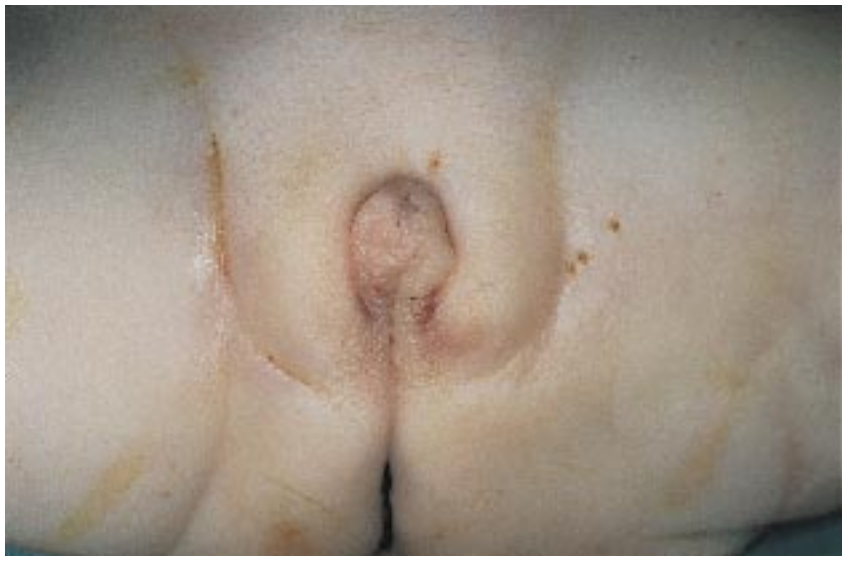

Figure 3.54. Clitoromegaly in the same infant with Fraser's syndrome. The uterus and ovaries were present on ultrasound and there was bilateral renal agenesis.

3.55

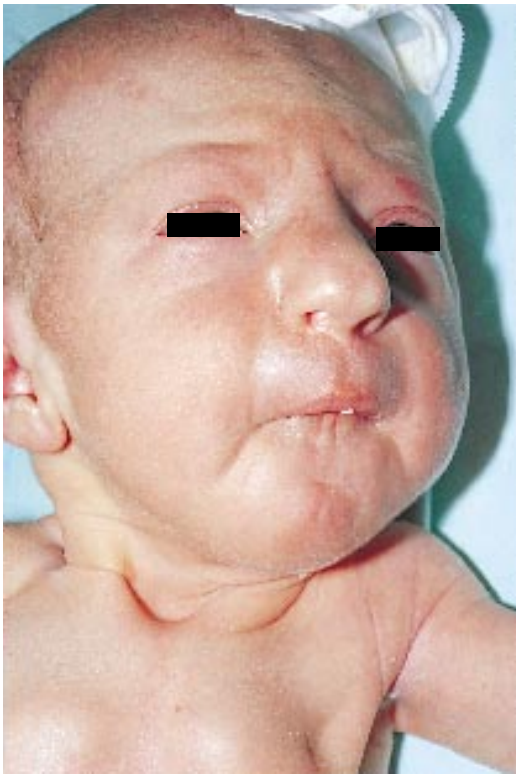

Figure 3.55. Freeman-Sheldon syndrome ("whistling face" syndrome or cranio-carpotarsal dystrophy) is an autosomal dominant condition. Note the full forehead and mask-like facies with a small mouth giving a "whistling face" appearance. There is a broad nasal bridge with deep set eyes and blepharophimosis. The nose is small with hypoplastic alae nasi and a long philtrum. Note the H-shaped cutaneous dimpling on the chin and there may be a high palate and small tongue. These infants may have failure to thrive due to swallowing difficulties, but intelligence is in the normal range.

3.56

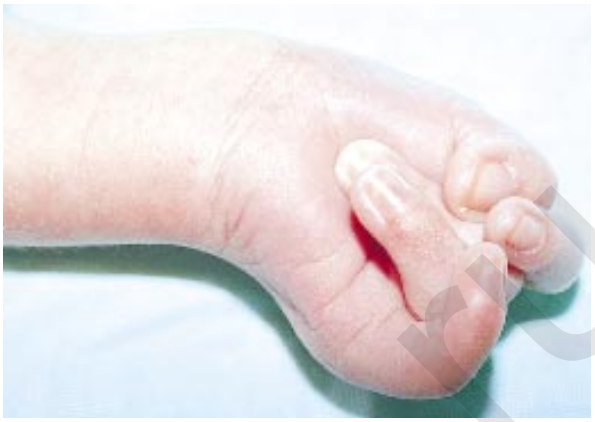

Figure 3.56. The upper extremity of the same infant with the Freeman-Sheldon syndrome. Note the ulnar deviation of the hand and contracted fingers.

3.57

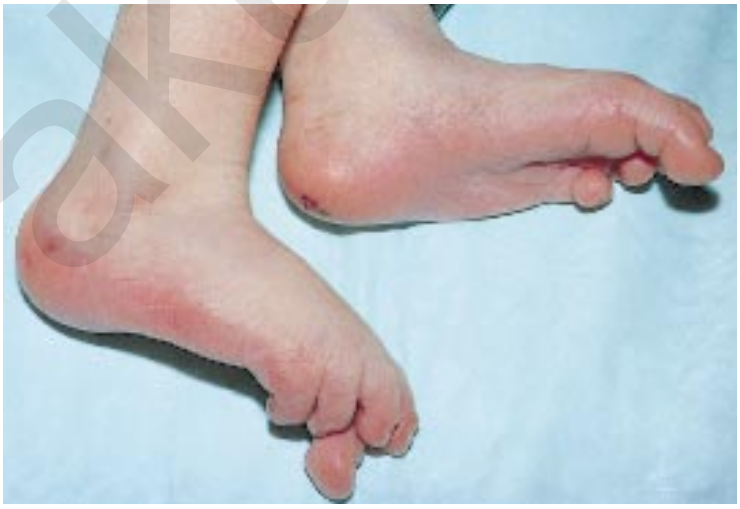

Figure 3.57. In this figure of the same infant, note the contractures of the toes. Talipes equinovarus may be present.

3.58

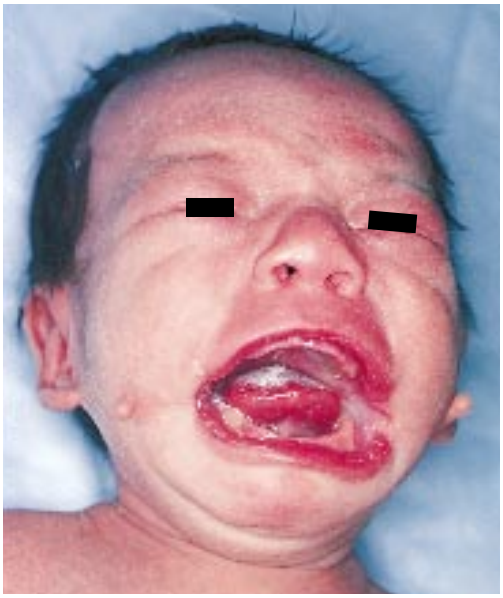

Figure 3.58. Goldenhar's syndrome (facioauriculovertebral spectrum; oculoauriculovertebral dysplasia) is associated with abnormalities of the first and second branchial arches. This infant shows the antimongoloid slant, bilateral macrostomia, and skin tags. Over 90% of these infants have ear abnormalities (small or unusually shaped ears, preauricular tags, and pits). They may have abnormalities of the cervical vertebrae, particularly hemivertebra, coloboma of the upper eyelids, and epibulbar dermoids. Congenital heart disease may be present in one-third of these infants. More than 80% of the infants have normal intelligence.

3.59

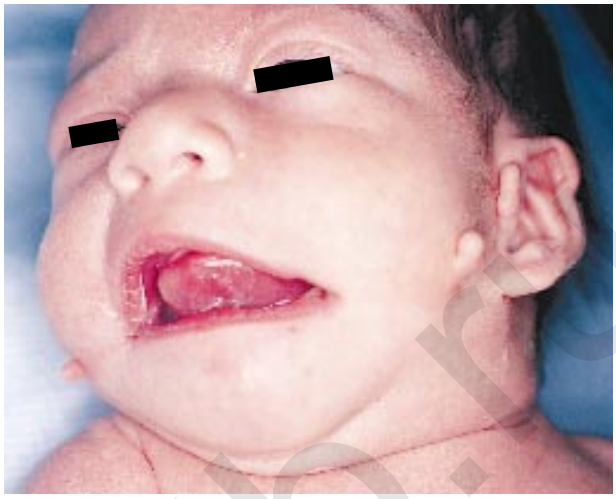

Figure 3.59. Another infant with Goldenhar's syndrome showing the abnormal ear and preauricular skin tags in a line extending from the ear to the macrostomic mouth. Characteristic of Goldenhar's syndrome is the combination of unilateral facial hypoplasia, epibulbar dermoid, ocular abnormalities, preauricular appendages, and unilateral dysplasia of the auricle.

3.60

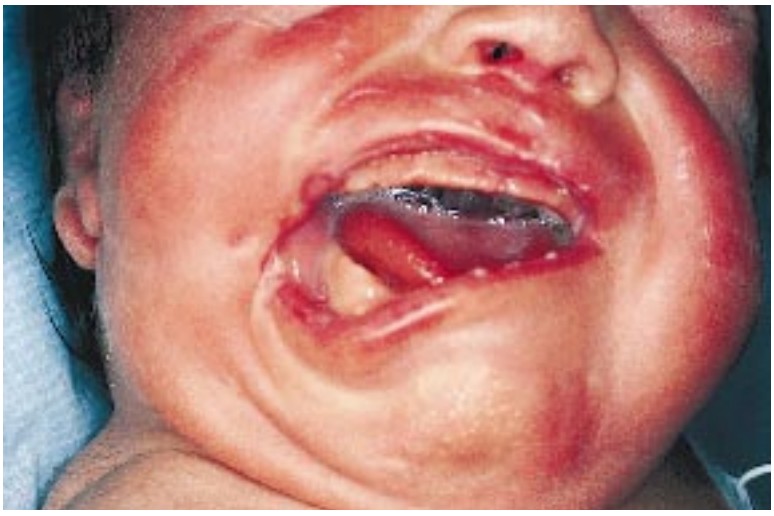

Figure 3.60. This infant is another example of Goldenhar's syndrome. She has macrostomia with a unilateral right facial cleft. In addition, there were ear epibulbar dermoids, and cardiac and vertebral abnormalities.

3.61

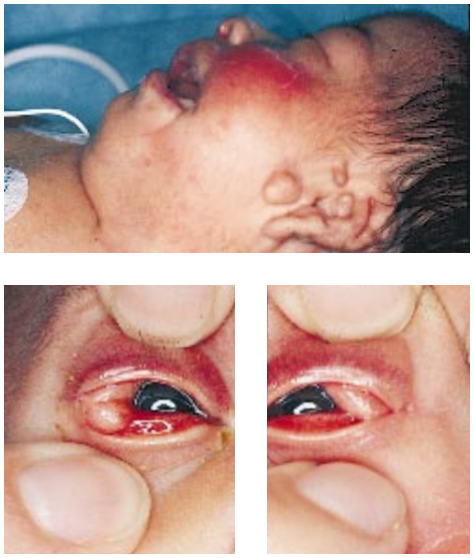

Figure 3.61. This composite figure of the same infant as in Figure 3.60 shows the abnormalities of the ears with preauricular tags and epibulbar dermoids.

3.62

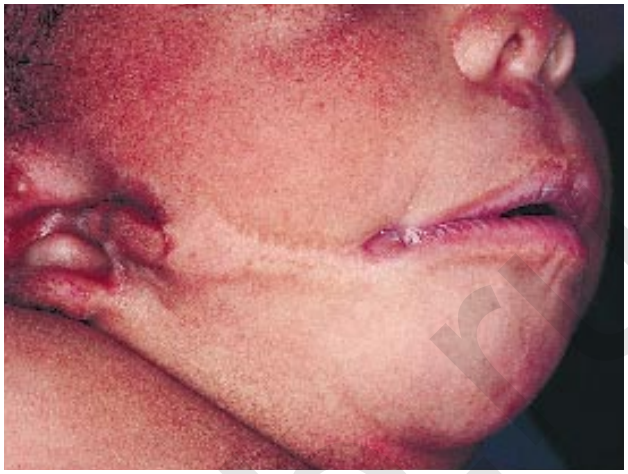

Figure 3.62. Another infant with Goldenhar's syndrome showing the lateral facial cleft, abnormal ear, preauricular skin tag, and abnormal skin from the corner of the mouth to the ear due to lack of normal fusion during development of the face.

3.63

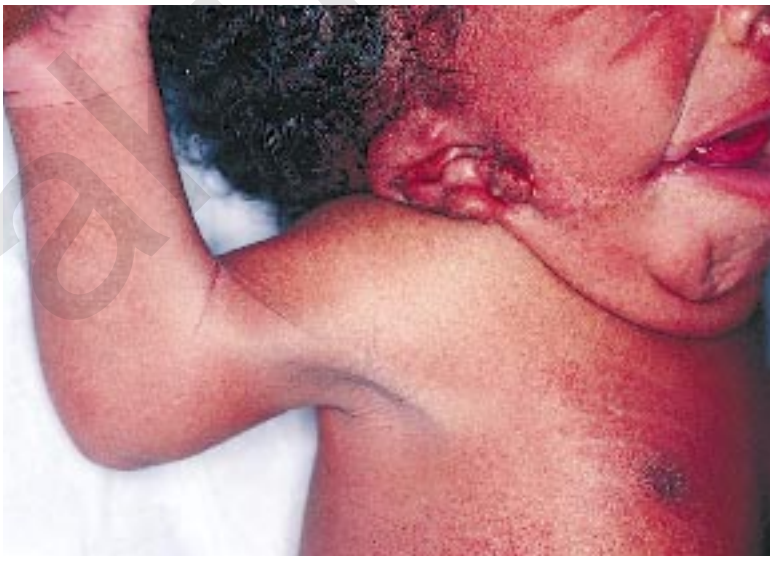

Figure 3.63. The same infant showing arthrogryposis.

3.64

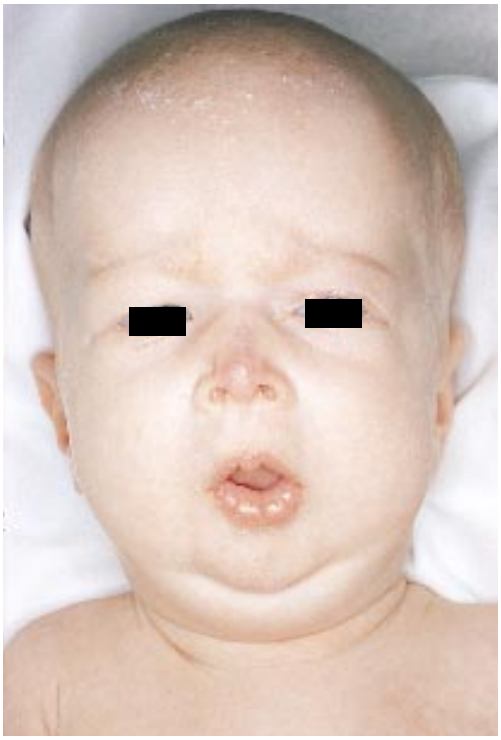

Figure 3.64. Infants with Hallermann-Streiff syndrome (oculomandibulofacial syndrome, François dyscephaly) have proportionate dwarfism. They also have brachycephaly with frontal and parietal bossing; hypotrichosis is present and the face appears small in relation to the skull. An antimongoloid slant of the eyes is common, and there is a narrow beaked nose and a hypoplastic mandible which gives the face a somewhat bird-like appearance. The mouth is small and there may be natal or supernumerary teeth. These infants often have bilateral congenital cataracts.

3.65

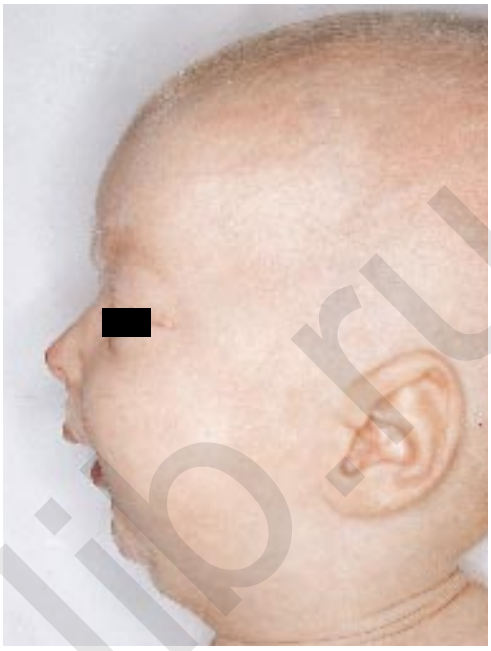

Figure 3.65. A lateral view of the same infant. Note the brachycephalic skull, small nose, micrognathia, and marked hypotrichosis. These infants have normal intelligence.

3.66

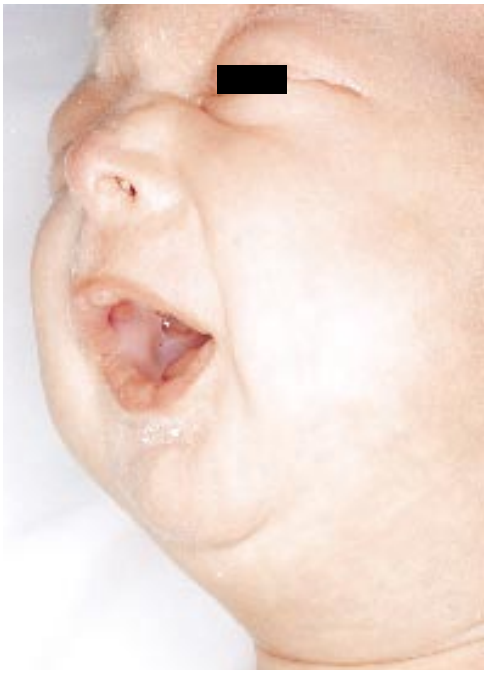

Figure 3.66. In this figure note the antimongoloid slant of the eyes, narrow beaked nose, small pinched mouth, micrognathia, hypoplastic mandible and hypotrichosis.

3.67

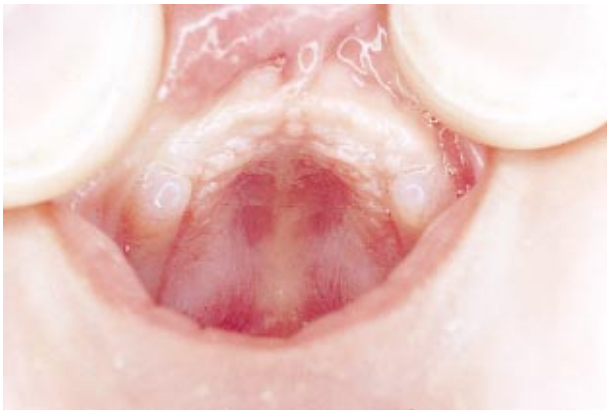

Figure 3.67. In this figure of the same infant as in Figure 3.66 note the high arched palate.

3.68

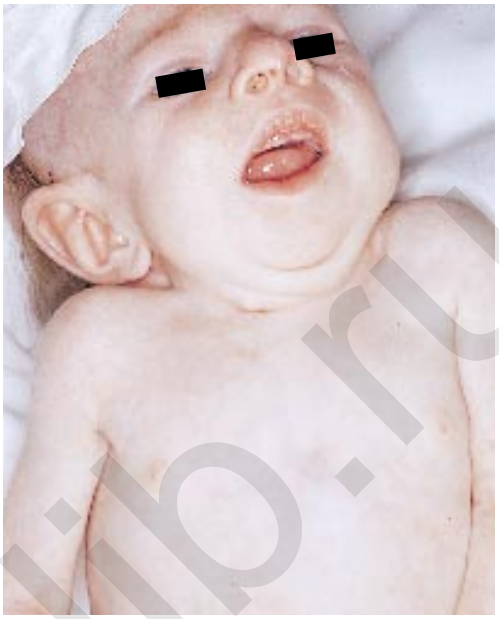

Figure 3.68. Infants with the Klippel-Feil syndrome or anomaly have a head which appears to be directly on the thorax. The facies is distorted and the ears are low set. Fusion or malformation of the cervical and upper thoracic vertebrae produces the short neck with head tilt and low posterior hairline. Strabismus is common.

3.69

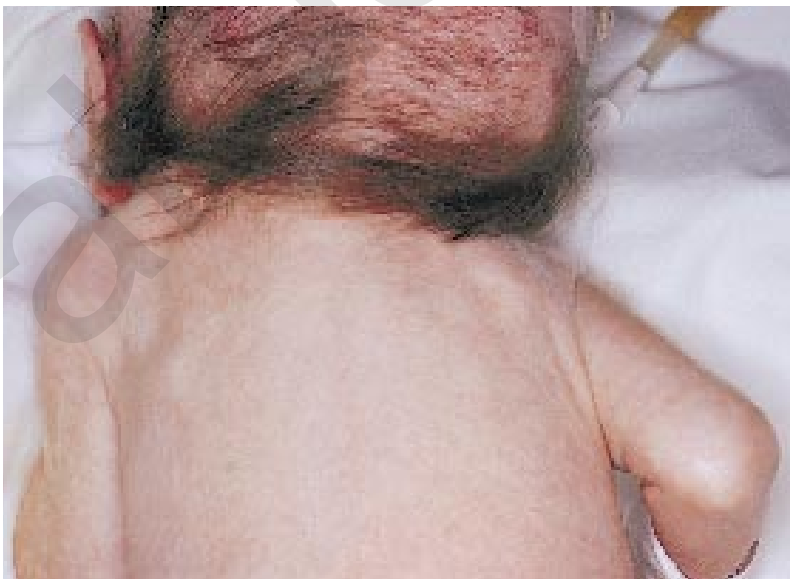

Figure 3.69. Posterior view of the same infant showing the short neck (congenital brevicollis) and the low hairline.

3.70

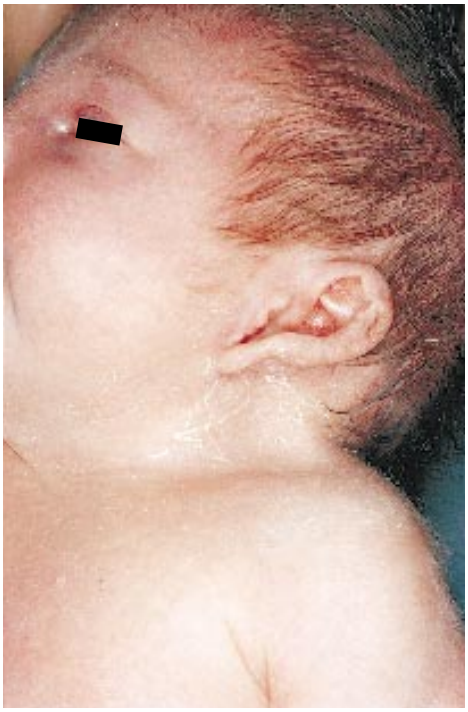

Figure 3.70. A lateral view of the face, neck and chest of another infant with Klippel-Feil syndrome. Note the extremely short neck with low hairline and very abnormal ear.

3.71

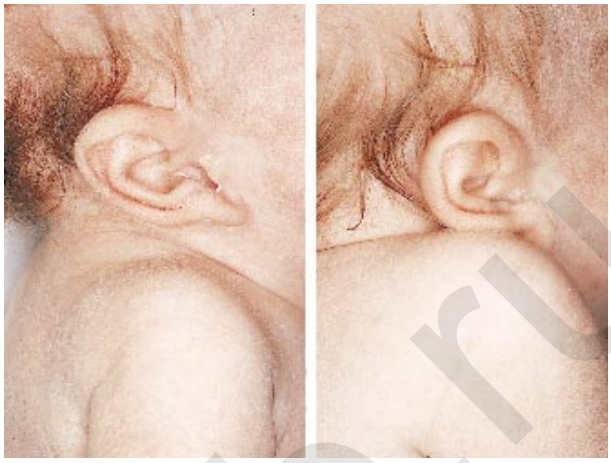

Figure 3.71. In this infant with the Klippel-Feil syndrome note the abnormal ear and short neck on the left. On the right, note that the abnormality of the ear results from pressure of the shoulder on the developing ear — a deformation.

3.72

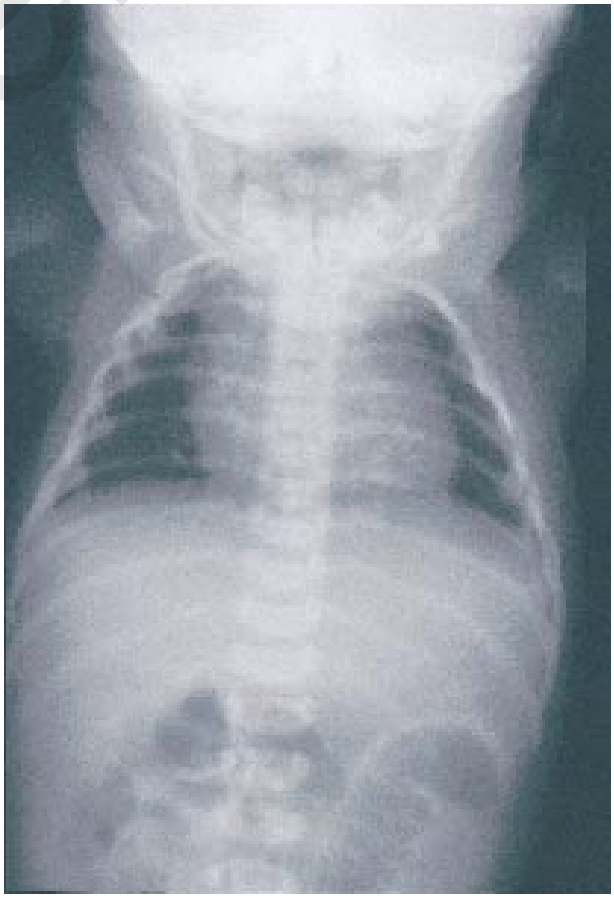

Figure 3.72. Anteroposterior radiograph of an infant with Klippel-Feil syndrome showing the numerous cervical spine vertebral body anomalies.

3.73

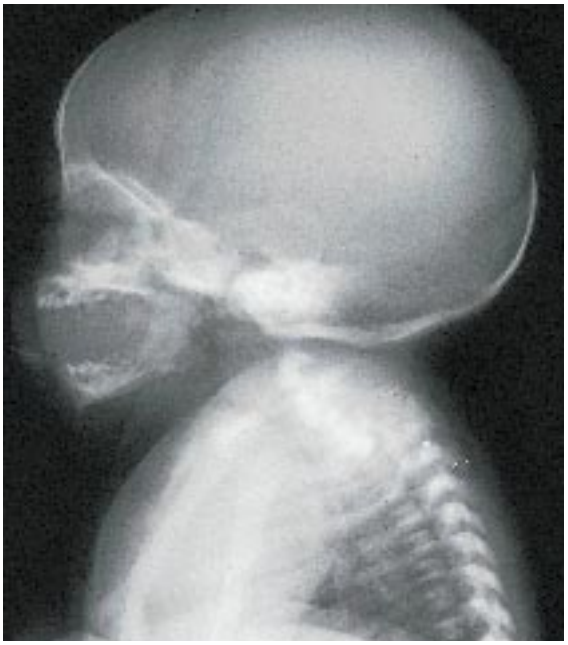

Figure 3.73. Lateral radiograph of the same infant as in Figure 3.72 with Klippel-Feil syndrome again shows cervical vertebrael anomalies resulting from abnormal fusion of the cervical vertebrae. There may be other associated skeletal defects such as the Sprengel's deformity or thoracic hemivertebrae. If the brachial plexus is involved, it may result in deformities of the hand.

3.74

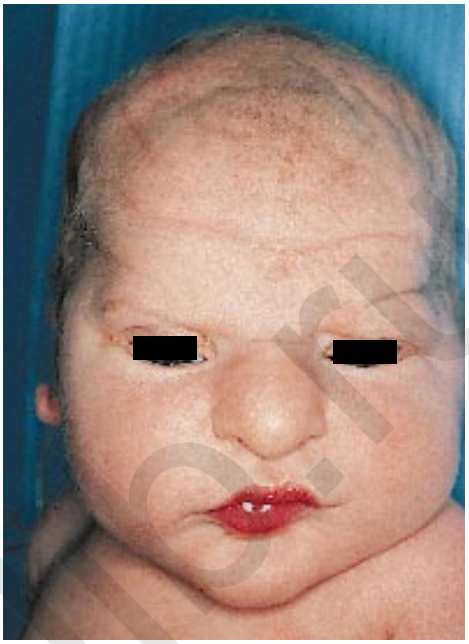

Figure 3.74. Infants with the Langer-Giedion syndrome have a bulbous nose, tented alae nasi, and a prominent elongated philtrum. There is a thin upper lip with mild micrognathia and mild microcephaly. Scalp hair is sparse. The ears are hypertrophic with excessive folding and tissue mass. The skin is redundant and loose. This infant, in addition to the above findings, had cutis verticis gyrata.

3.75

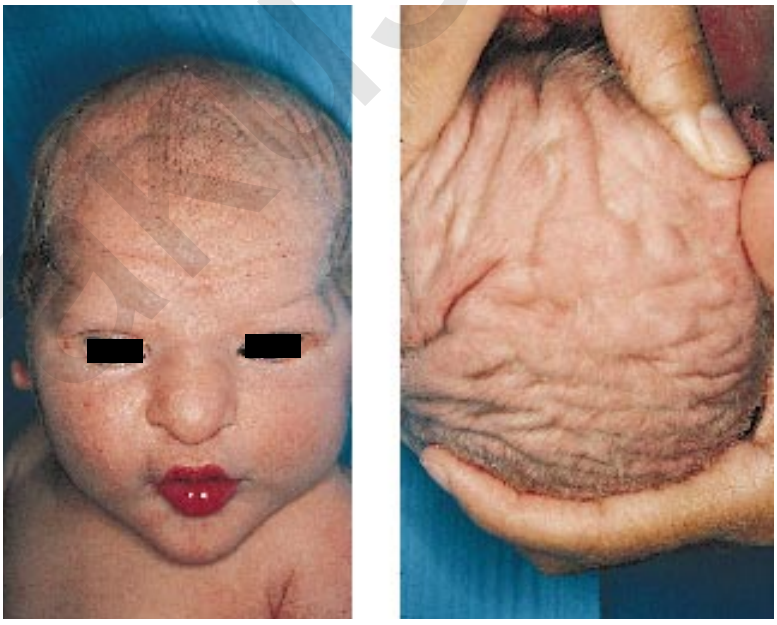

Figure 3.75. In this figure of the same infant again note the bulbous nose, thin upper lip on the left and the cutis verticis gyrata on the right. The trichorhinophalangeal syndrome has many similarities to Langer-Giedion syndrome except that the redundant skin and microcephaly are not present.

3.76

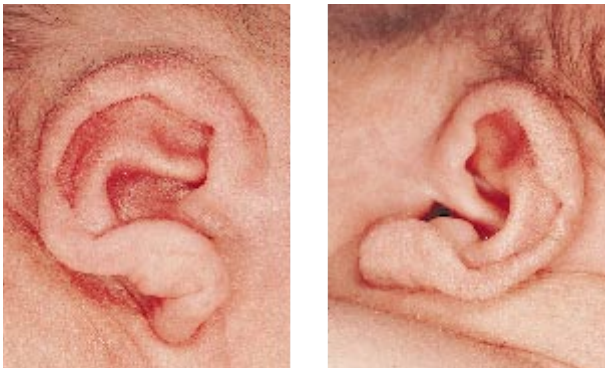

Figure 3.76. Close-up of the ears of the same infant showing the hypertrophy with excessive folding and tissue mass.

3.77

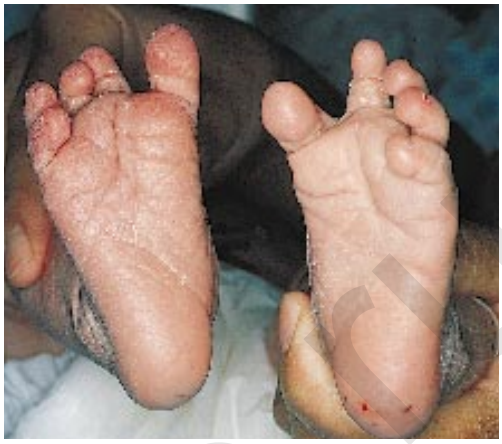

Figure 3.77. The same infant had large vertical creases on both plantar surfaces anteriorly. These are strongly associated with trisomy 8. The Langer-Giedion syndrome recently has been associated with a deletion of the long arm of chromosome 8.

3.78

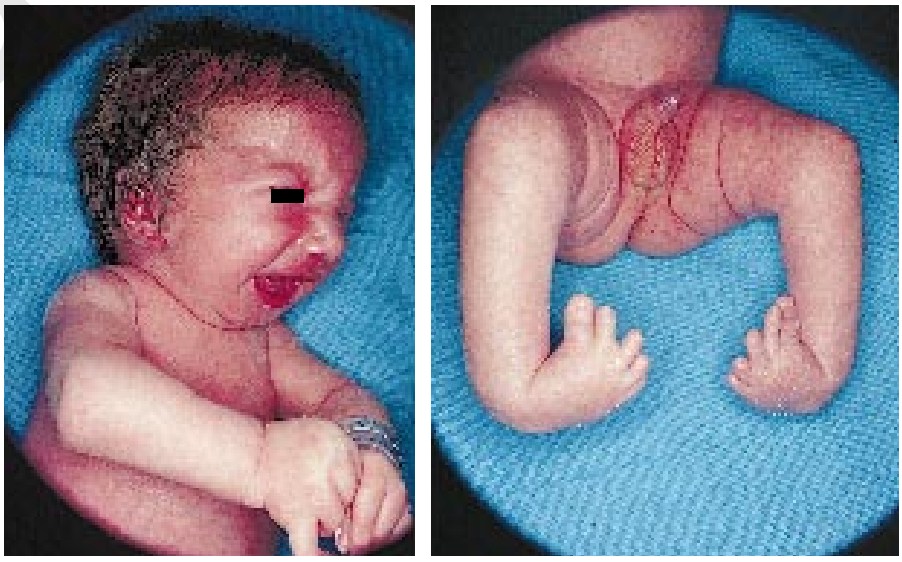

Figure 3.78. This infant with Larsen's syndrome demonstrates the prominent forehead, depressed nasal bridge, and dislocation of the elbows on the left. On the right there is dislocation of the hips, knees, and talipes equinovarus.

3.79

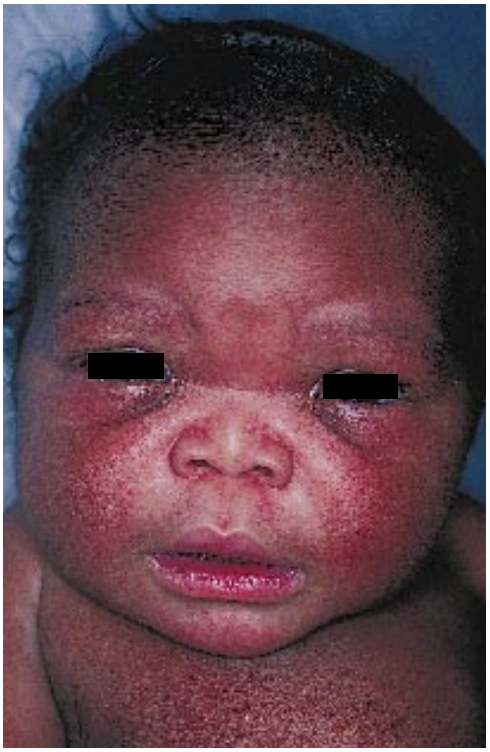

Figure 3.79. In Larsen's syndrome there is a flat facies associated with a prominent forehead, a flat and depressed nasal bridge, and the eyes are wide set.

3.80

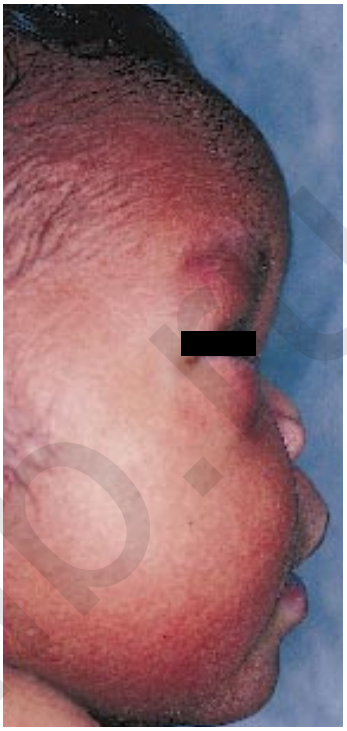

Figure 3.80. A lateral view of the face of the same infant shows the very flat facies associated with a prominent forehead and depressed nasal bridge. Note that the eyes are rather deep set.

3.81

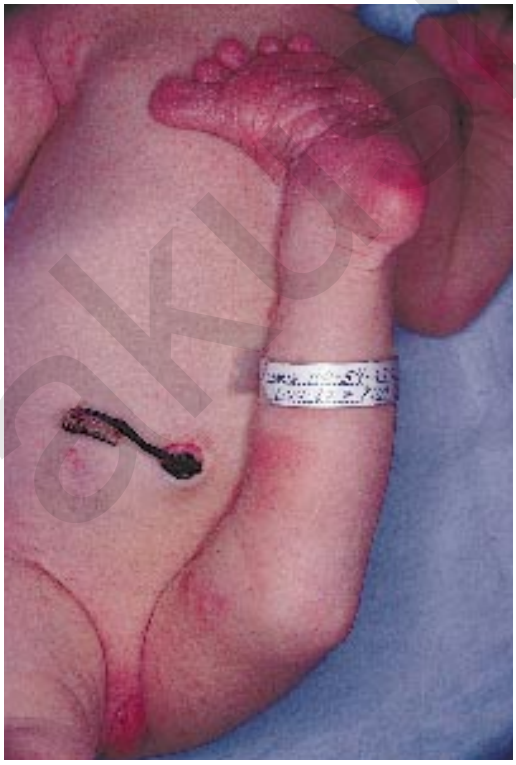

Figure 3.81. In this infant with Larsen's syndrome note the congenital dislocation of the left knee, metatarsus varus, and large big toe.

3.82

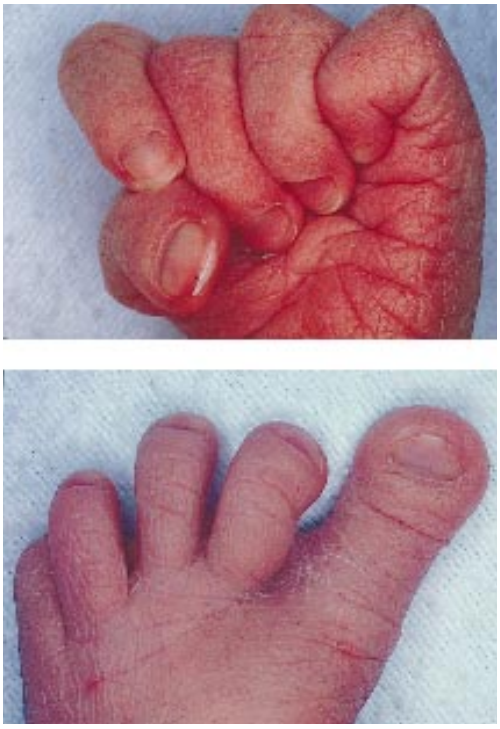

Figure 3.82. Infants with Larsen's syndrome have other characteristic findings in addition to the flat facies and multiple joint dislocations (elbows, hips, and knees). Note the broad spatulate thumb and altered hand position due to the short metacarpals (upper photo), and the big toe and hypoplastic nails (lower photo).

3.83

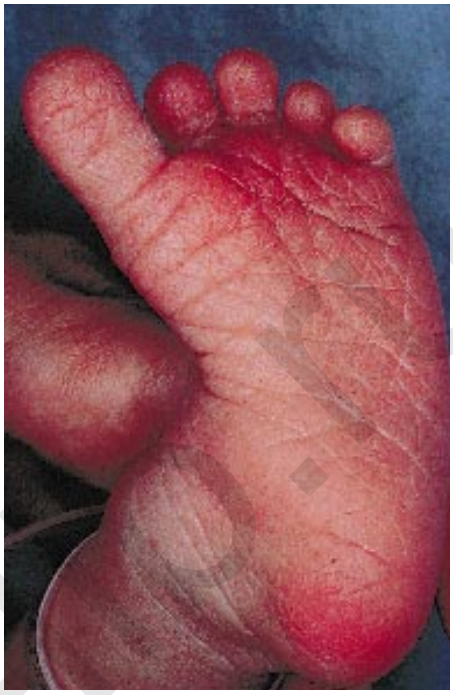

Figure 3.83. In the same infant, note the typical large big toe and metatarsus varus.

3.84

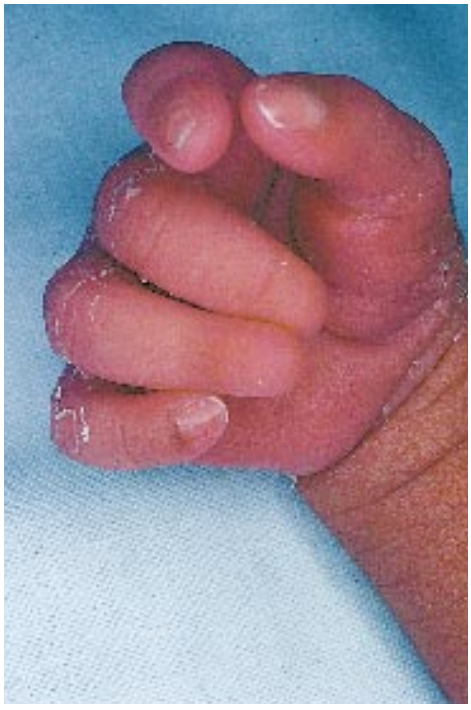

Figure 3.84. This infant with Larsen's syndrome has spatulate thumbs and shortened metacarpals. Also note the absence of nails on the third and fourth fingers of the right hand.

3.85

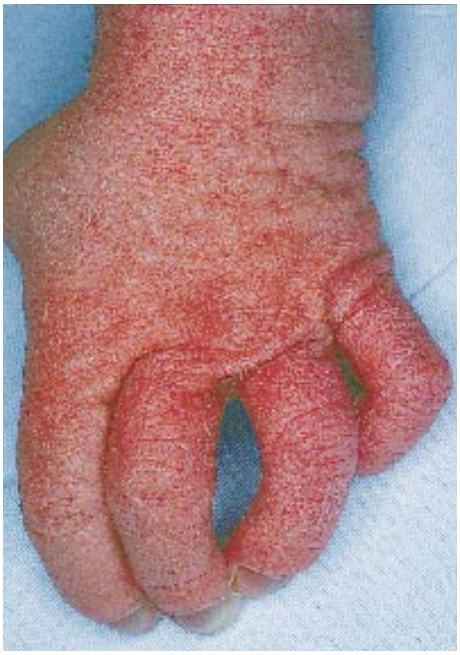

Figure 3.85. A dorsal view of the hand in the same infant shows the short metacarpals with normal fingers thus giving the appearance of a short hand.

3.86

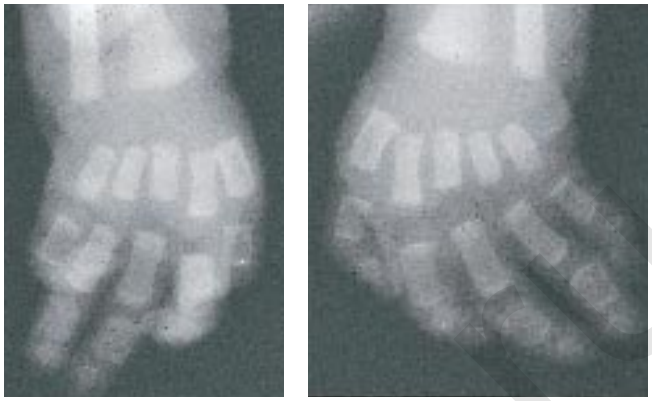

Figure 3.86. This radiograph of the hand clearly demonstrates the short metacarpals noted in Larsen's syndrome.

3.87

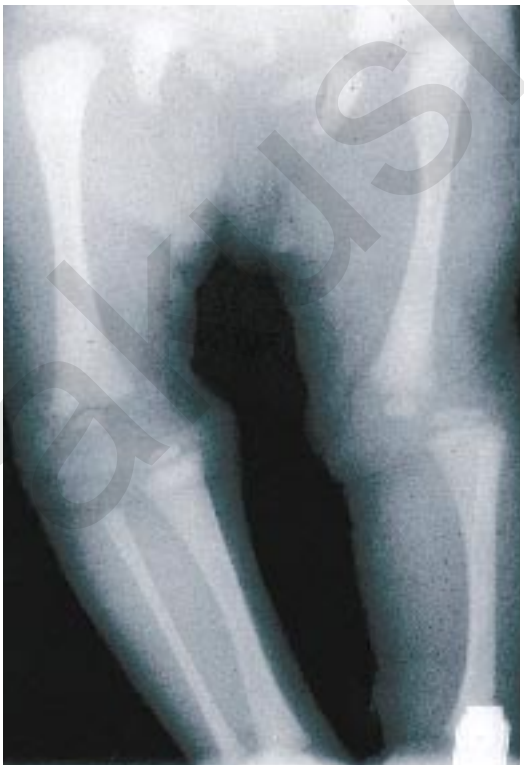

Figure 3.87. Radiograph of bilateral dislocation of the knee joints in Larsen's syndrome.

3.88

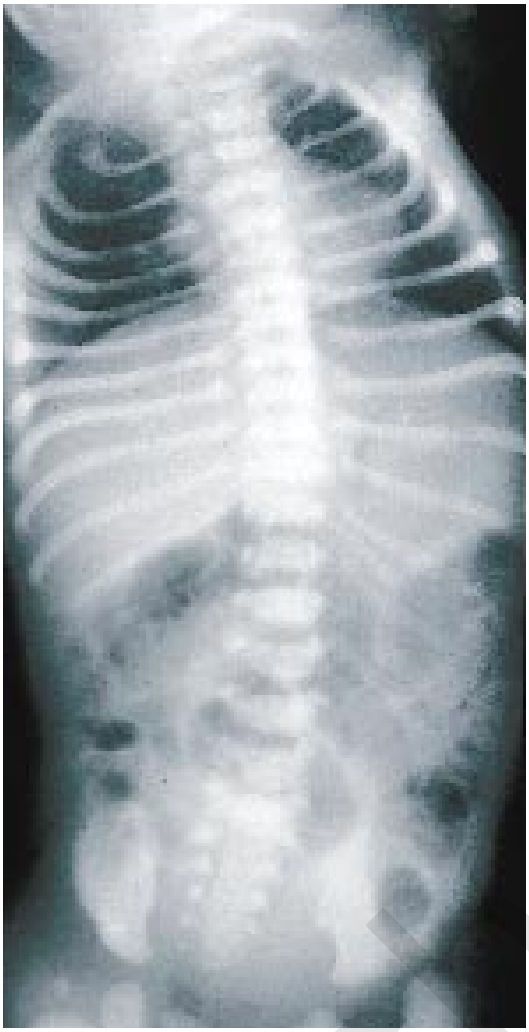

Figure 3.88. Radiograph of the spine of an infant with Larsen's syndrome showing the abnormal segmentation of the vertebrae, especially in the cervical and upper thoracic areas. Also note the dislocation of the hip joints.

3.89

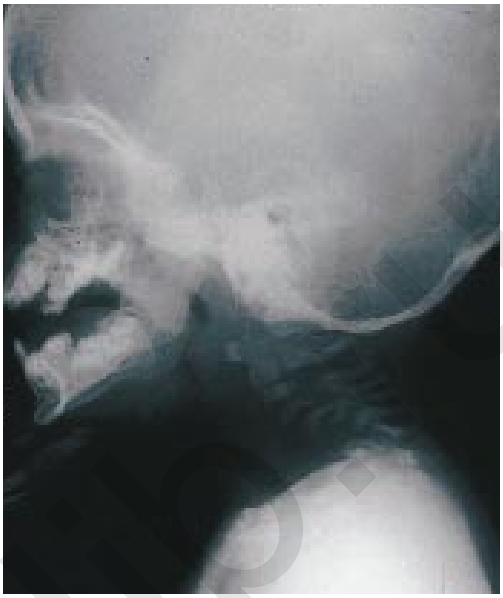

Figure 3.89. X-ray of the neck in Larsen's syndrome.

3.90

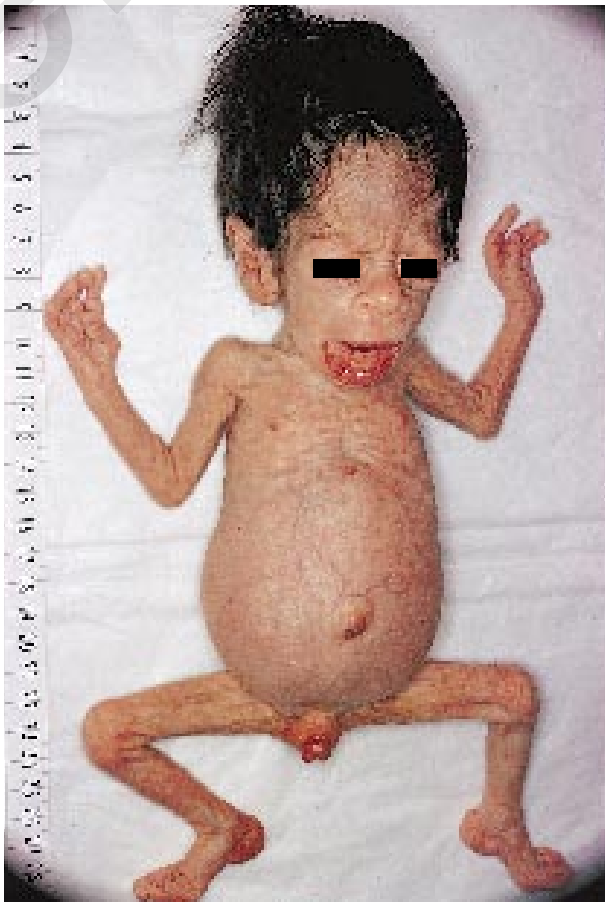

Figure 3.90. This infant with leprechaunism (Donohue's syndrome) demonstrates the very severe intrauterine growth retardation. The infant had a birth weight of 750 g at a gestational age of 37 weeks. At age 3 weeks the weight was 780 g. Note the marked hirsutism, sunken cheeks, pointed chin, large mouth, thick lips, wide nostrils, large eyes, large ears, and enlarged clitoris.

3.91

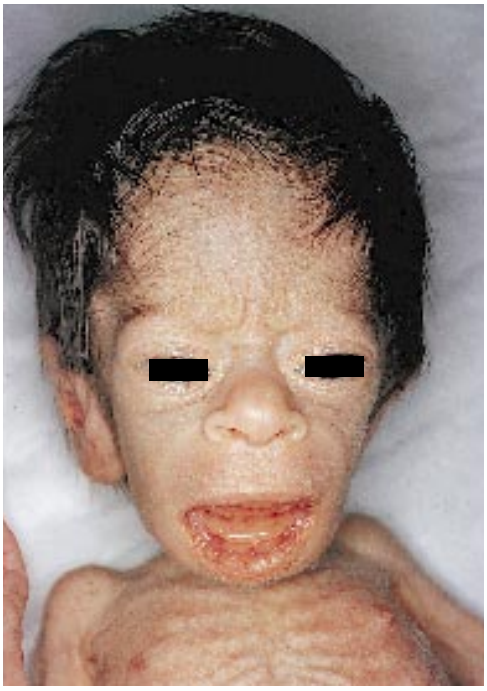

Figure 3.91. A close-up of the face of the same infant as in Figure 3.90 at the age of 3 weeks again shows the severe growth retardation, sunken cheeks, pointed chin, large mouth, large eyes that have a very alert expression, and large ears. Note the gingival hyperplasia.

3.92

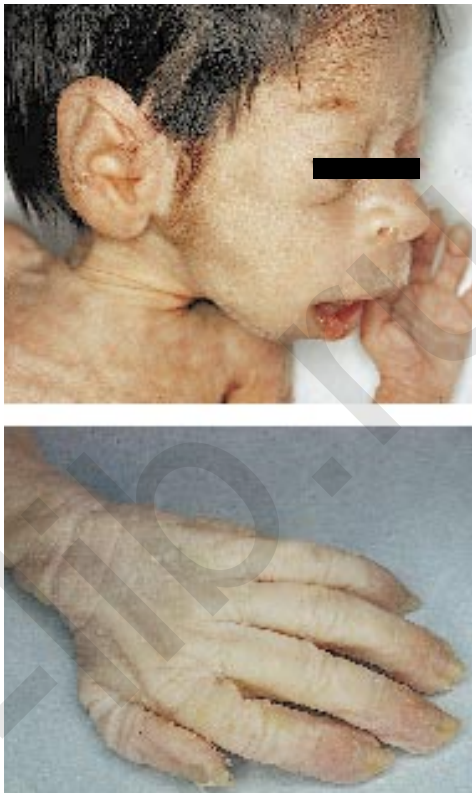

Figure 3.92. A lateral view of the face of the same infant. Note the sunken face and very large ears in the upper half of the figure. The lower portion of the figure shows the large hands that are seen in these infants. Note the marked loss of subcutaneous tissue and wrinkled, loose skin. Infants with Donohue's syndrome commonly have large hands and feet. At autopsy the infant had cystic ovaries which are typically found in this condition.

3.93

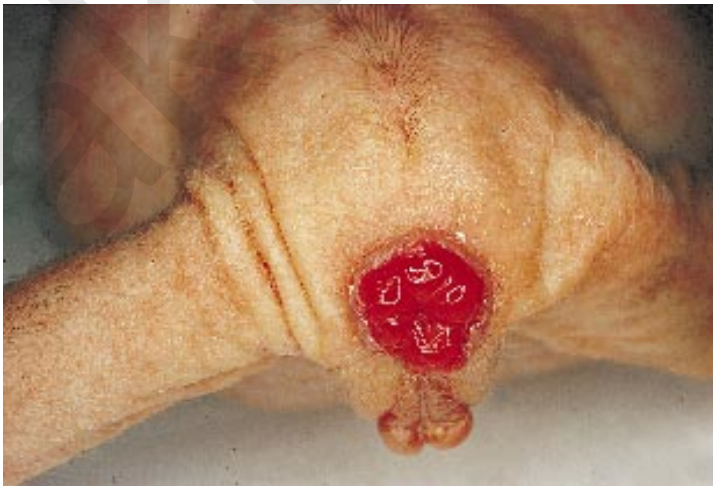

Figure 3.93. This infant, in addition, had a rectal prolapse. Note the wrinkled, loose skin associated with marked lack of adipose tissue.

3.94

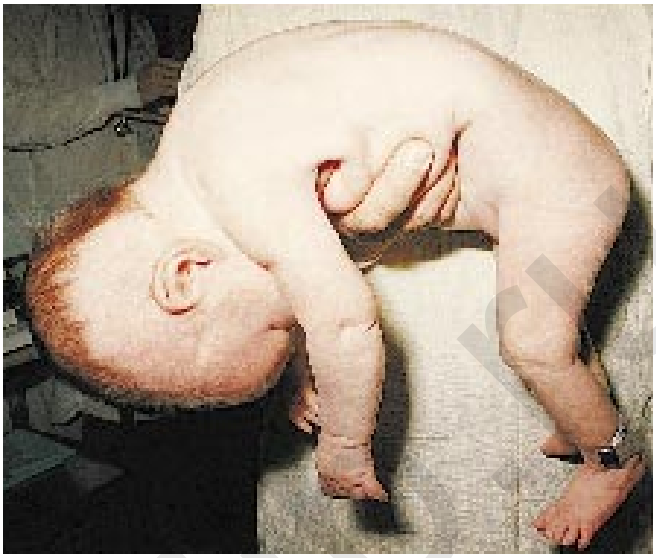

Figure 3.94. In Lowe syndrome (oculocerebrorenal syndrome) there is marked hypotonia and joint hypermobility.

3.95

Figure 3.95. The same infant with Lowe syndrome has bilateral cataracts and epicanthic folds.

3.96

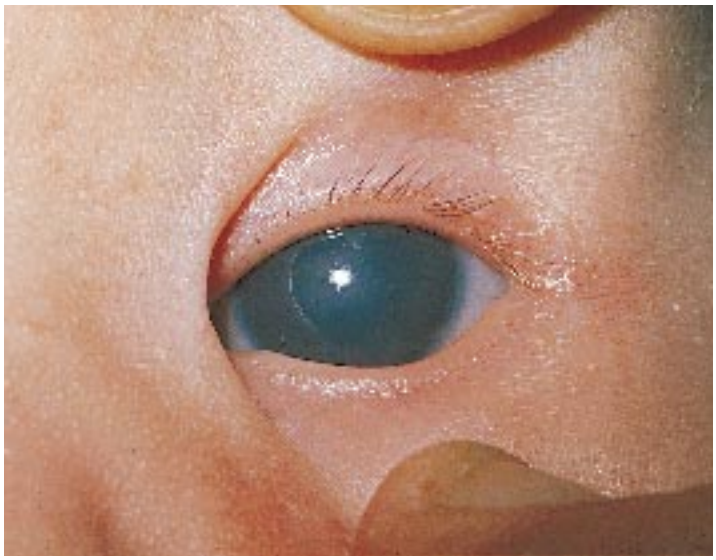

Figure 3.96. Corneal clouding and epicanthic folds are present in the same infant.

3.97

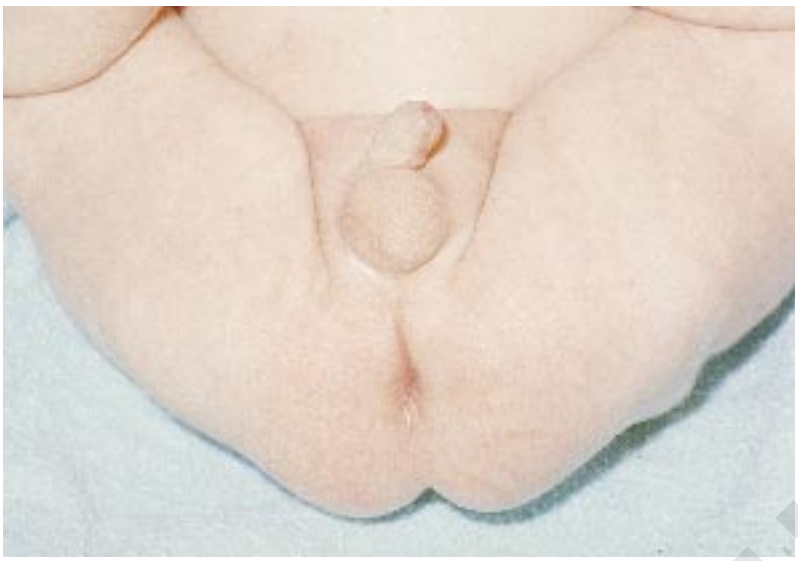

Figure 3.97. In Lowe syndrome, renal tubular dysfunction and cryptorchidism are common. Note the presence of cryptorchidism.

3.98

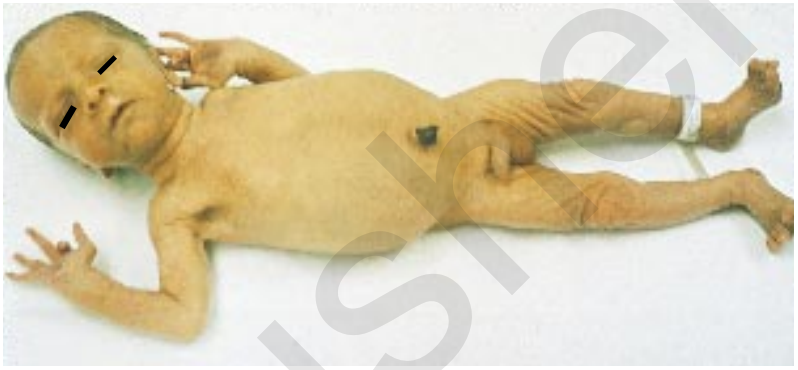

Figure 3.98. A term newborn with Marfan syndrome who had a birth weight of 3720 g and a length of 54 cm. Note the tall stature with long slim limbs and hypotonia. In Marfan syndrome, limbs are disproportionately long and trunk length is usually normal resulting in a low upper/lower segment ratio. Ophthalmologic and cardiovascular pathologies, such as dislocation of the lens and aneurysmal dilatation of the aorta, are usually noted after the neonatal period.

3.99

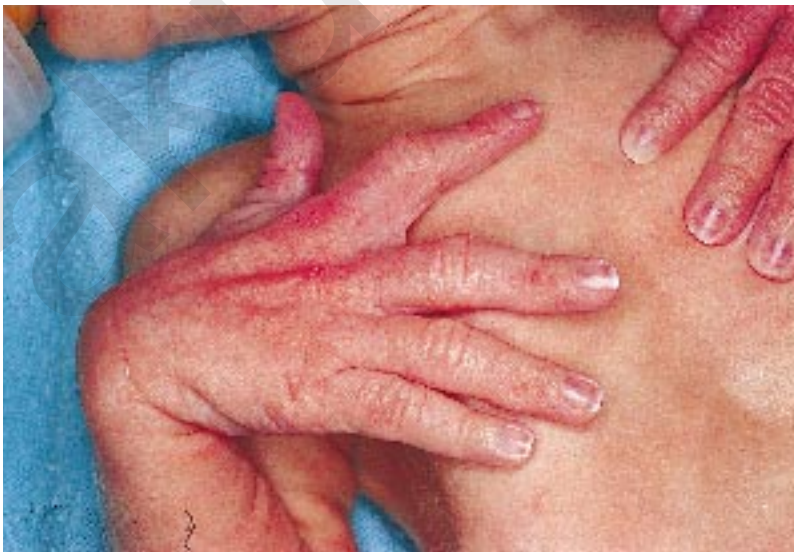

Figure 3.99. In this infant with Marfan syndrome, note the marked lengthening of the fingers (arachnodactyly). The diagnosis of Marfan syndrome may be difficult in the neonatal period because many normal infants appear to have long fingers. The combination of an increased birth length and a decreased upper / lower segment ratio should alert one to the possibility of this diagnosis. In older children the disproportion can often be detected by noting that the finger tips reach much further down the thigh than usual in the standing position.

3.100

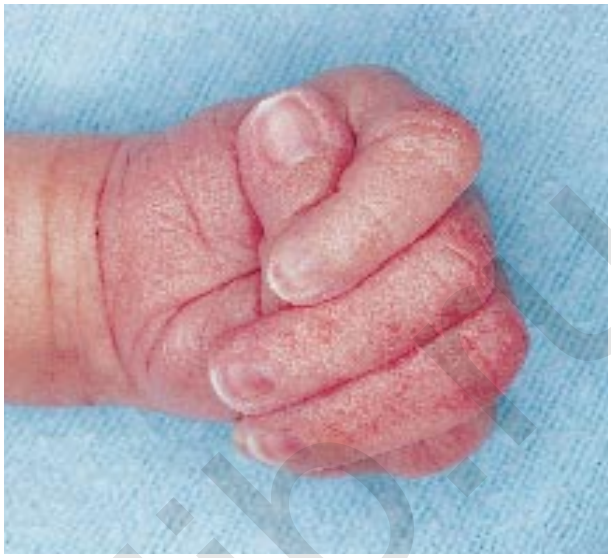

Figure 3.100. In Marfan syndrome when the patient makes a fist, the thumb often extends beyond the fifth finger as shown in the same infant.

3.101

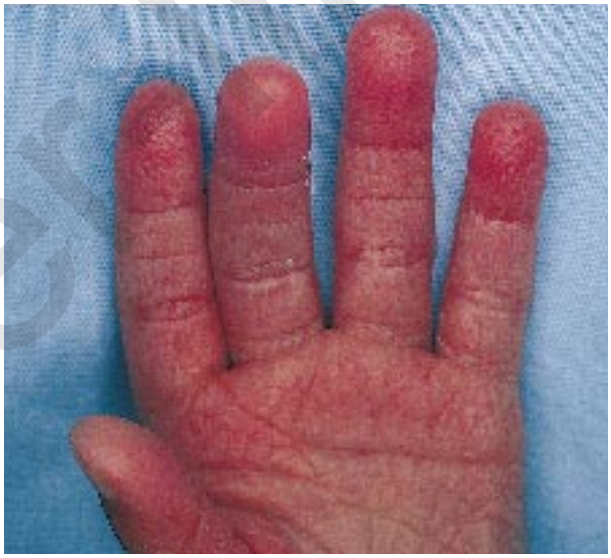

Figure 3.101. This neonate with Marfan syndrome exhibits the long fingers with increased creases on the fingers. This finding is common in infants who have increased mobility and hyperextensibility at the joints during development in utero and is seen in conditions such as Marfan syndrome and Larsen's syndrome.

3.102

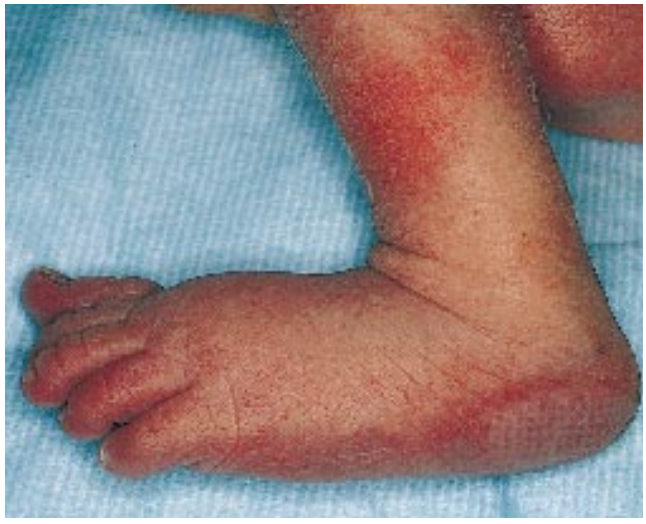

Figure 3.102. The same infant with Marfan syndrome shows the long foot and arachnodactyly.

3.103

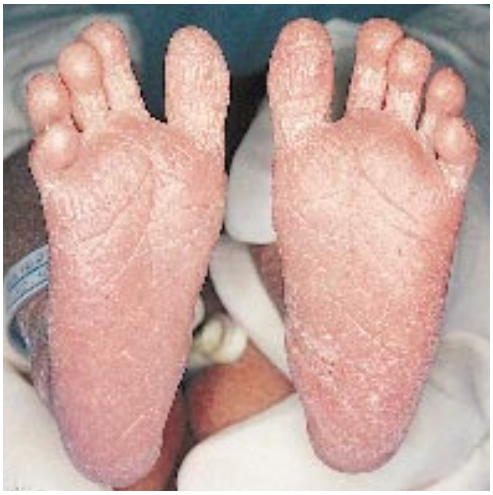

Figure 3.103. This is another example of long feet and toes in an infant with Marfan syndrome. Note the bilateral congenital curly toes. This infant had a birth length of 53 cm and an upper/lower segment ratio of 1.41. The normal upper/lower segment ratio at birth is 1.69 to 1.70. In short-limbed dwarfism and hypothyroidism it averages 1.8 or more, and in Marfan syndrome it averages 1.45.

3.104

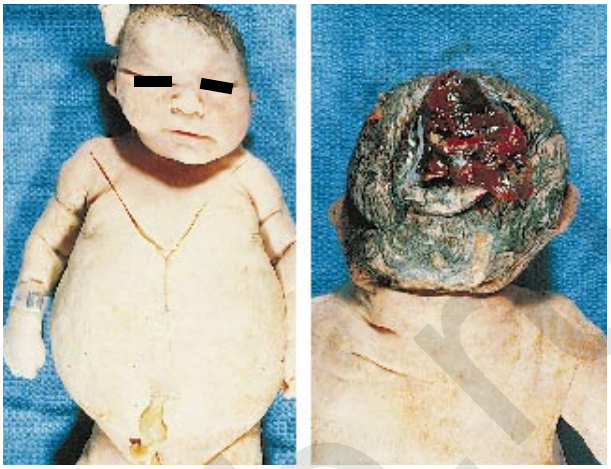

Figure 3.104. The typical findings in Meckel-Gruber syndrome (dysencephalia splanchnocystica) include encephalocele, polydactyly, and cystic dysplasia of the kidneys. In this infant there was marked oligohydramnios, deformations, encephalocele, hypoplastic lungs, infantile polycystic kidneys, and polydactyly. On the left note the marked abdominal distention due to the polycystic kidneys and on the right note the parieto-occipital encephalocele. (C. Langston)

3.105

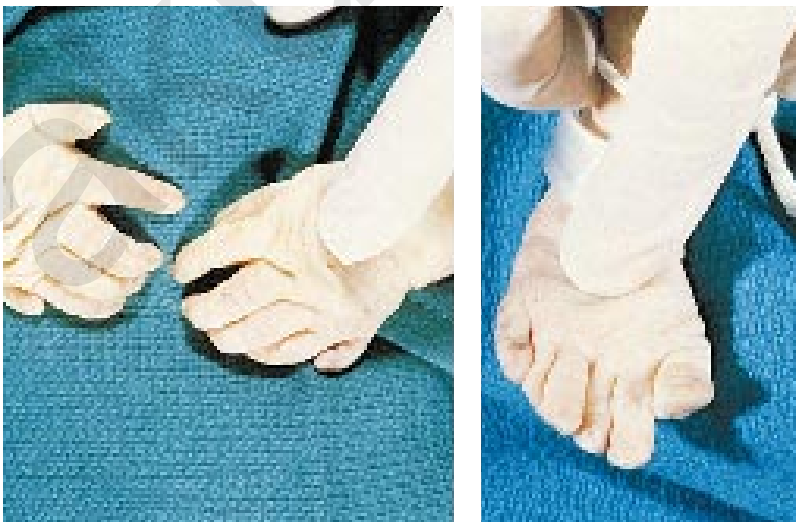

Figure 3.105. The same infant showing the polydactyly of both hands and polydactyly of the right foot. (C. Langston)

3.106

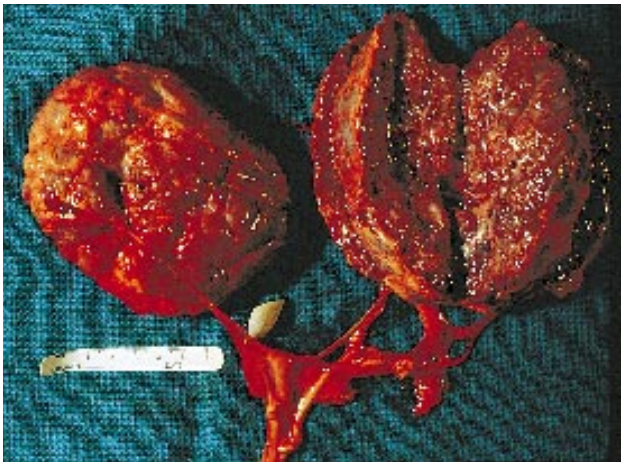

Figure 3.106. Bilateral infantile polycystic kidneys in the same infant with Meckel-Gruber syndrome. The right kidney weighed 210 g and the left kidney 200 g. (C. Langston)

3.107

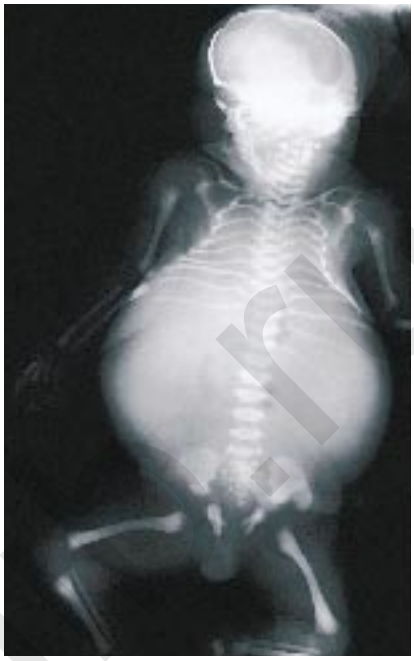

Figure 3.107. Full-body radiograph of the same infant. Note the marked skull defect associated with an encephalocele; the bell-shaped thorax and hypoplastic lungs; and the enlarged abdomen bulging in the flanks associated with the infantile polycystic kidneys.

3.108

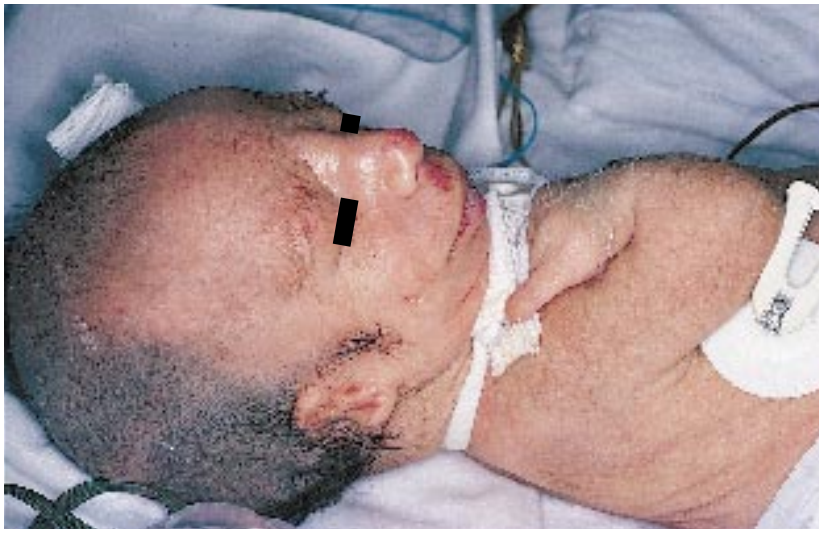

Figure 3.108. This infant with Nager's acrofacial dysostosis syndrome shows the slight antimongoloid slant, prominent nose, malar hypoplasia, micrognathia, and atresia of the external auditory canal. Associated with the hypoplastic mandible may be a bony cleft of the mandibular symphysis. In addition, the infant had radial hypoplasia and absence of thumbs. This infant required an emergency tracheostomy. Also note the projection of the scalp hair onto the lateral cheek.

3.109

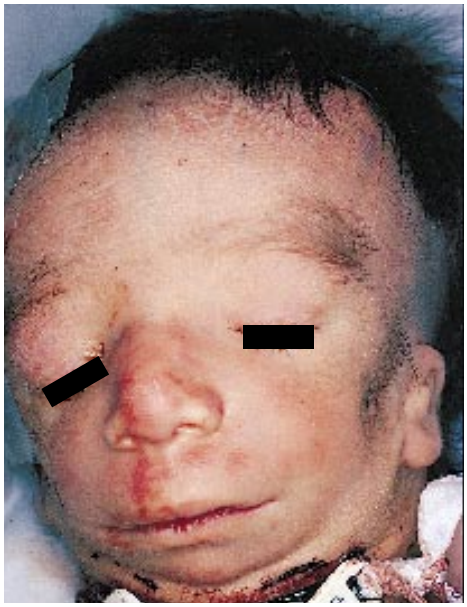

Figure 3.109. Frontal view of the face of the same infant as in Figure 3.108. The facial appearance resembles that of infants with Treacher-Collins syndrome. Note the partial absence of eyebrows which is another feature in these infants.

3.110

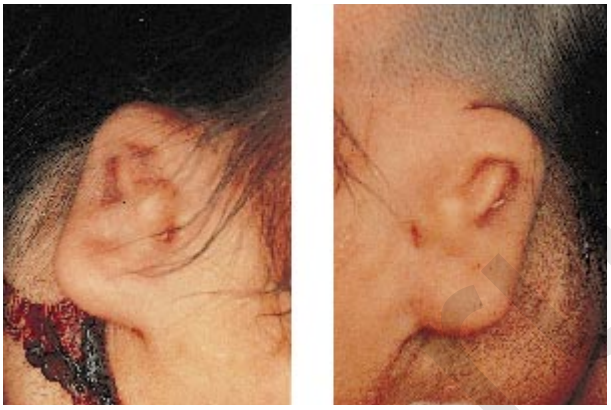

Figure 3.110. This figure shows the abnormal ears with atresia of the external auditory canals in the same infant.

3.111

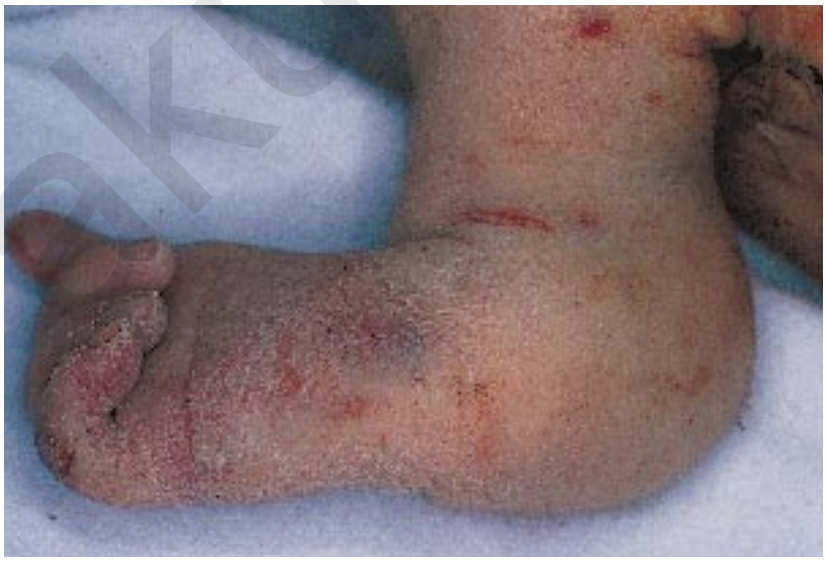

Figure 3.111. Hypoplastic radius and ulna and absent thumb in the right upper extremity of the same infant. Hypoplasia or aplasia of the radius and absence of the thumb may or may not be present in infants with Nager's syndrome. This infant also had these typical findings in both upper extremities. This results in short forearms and there may be proximal radioulnar synostosis and limitation of elbow extension. Postaxial hexadactyly of the hands and feet and synostosis of the metacarpals and metatarsals may occur.

3.112

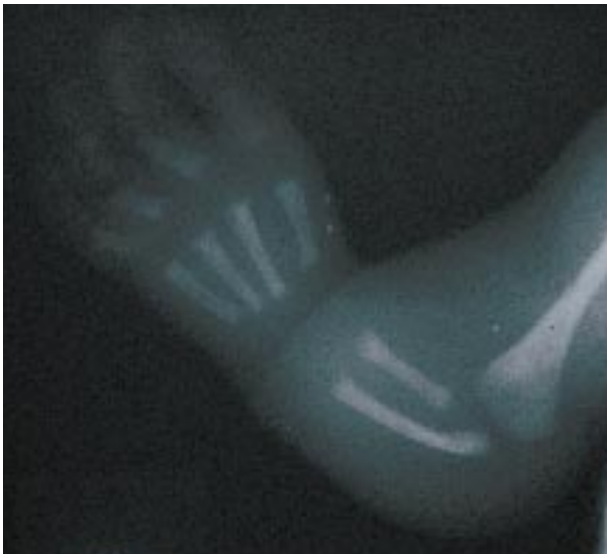

Figure 3.112. Radiograph of the right upper extremity showing the hypoplastic radius and ulna and absent right thumb.

3.113

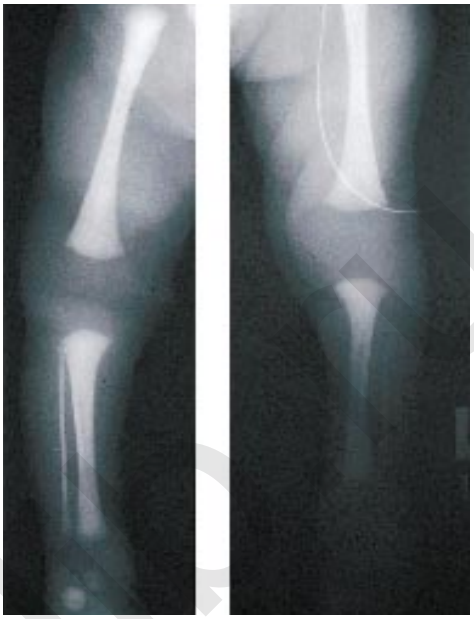

Figure 3.113. Radiograph of the lower extremities of the same infant showing hypoplasia of the right fibula and absence of the left fibula.

3.114

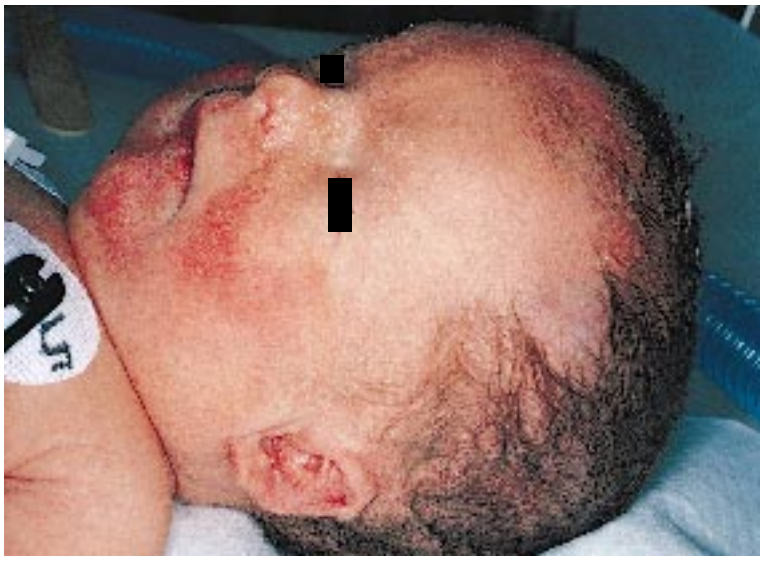

Figure 3.114. This infant with orofaciodigital syndrome type I (an X-linked dominant disorder limited to females because it is lethal in males) has an enlarged head from hydrocephalus.

3.115

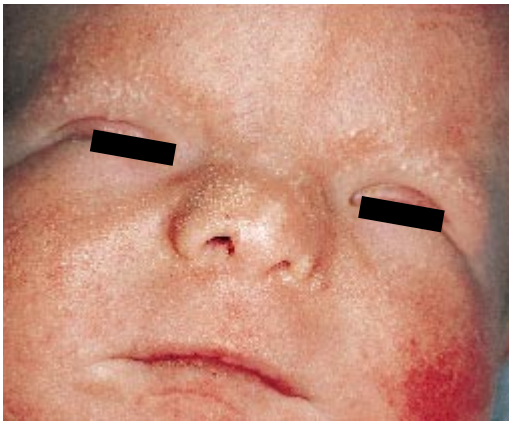

Figure 3.115. This frontal view of the same infant as in Figure 3.114 shows the typical facial appearance. Note the wide interorbital distance (euryopia), lateral displacement of the inner canthi, the flat midfacial region, and one nostril which is smaller than the other. The nasal root is broad, there is a short upper lip with a thin vermilion border, and typically milia are present in these infants.

3.116

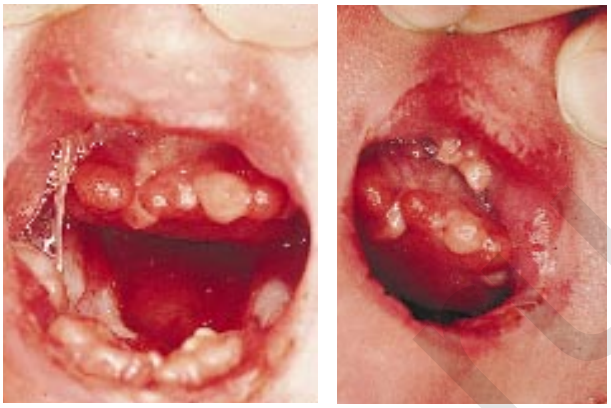

Figure 3.116. In these figures the same infant shows the clefting of the palate and the small hematomatous masses on the dorsal and ventral surfaces of the tongue. Neonatal teeth and ankyloglossia are present. There is also webbing between the buccal mucous membranes and the alveolar ridge.

3.117

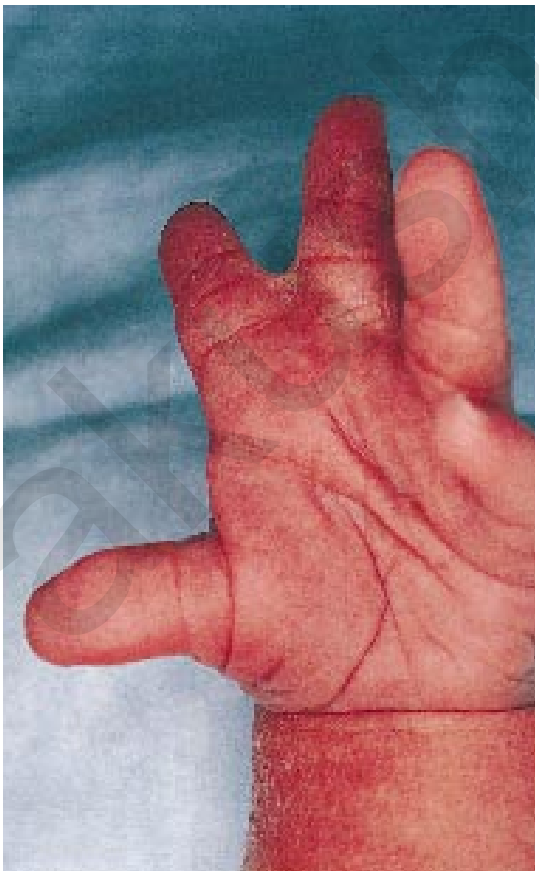

Figure 3.117. The same infant has brachydactyly, clinodactyly, and syndactyly of the fingers of the left hand.

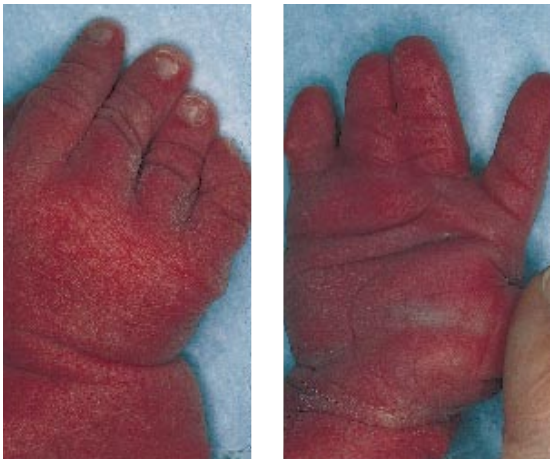

3.118

Figure 3.118. The right hand of the same infant with orofaciodigital syndrome again shows the brachydactyly and syndactyly on the right. Note the clinodactyly and prominence on the little finger due to postaxial polydactyly.

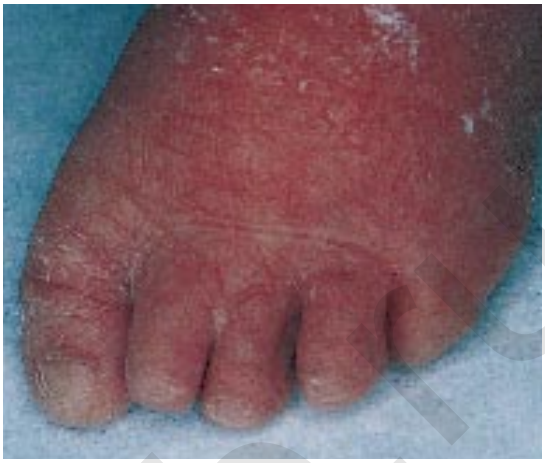

3.119

Figure 3.119. The same infant also shows marked brachydactyly of the toes. The hallux is inclined laterally and there is syndactyly of the second and third toes.

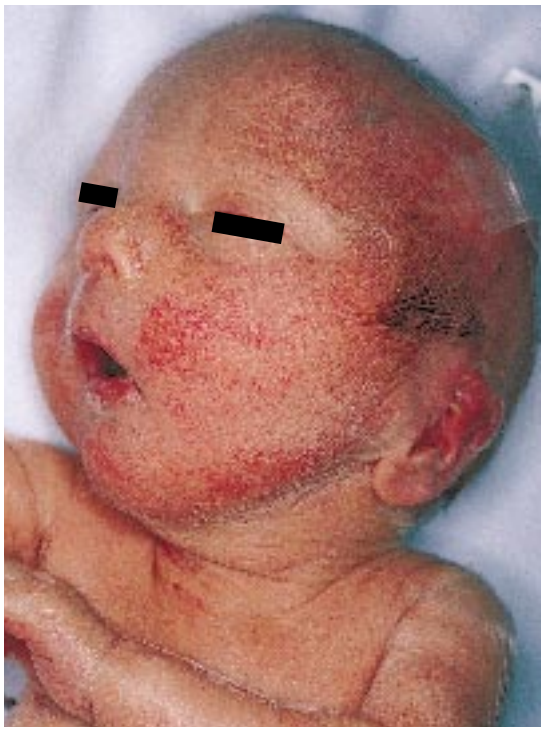

3.120

Figure 3.120. In the Pena-Shokeir phenotype type I (fetal akinesia/hypokinesia sequence), there is severe intrauterine growth retardation and diffuse atrophy of skeletal muscle resulting in arthrogryposis with the head circumference spared. There are low-set ears, a depressed tip of the nose, small mouth, and micrognathia. It is suggested that this phenotype is secondary to decreased in utero movement and as a result there is polyhydramnios (due to failure of normal swallowing) and a short umbilical cord. There may be severe neuromyopathic disease. Neuromuscular defisciency of the diaphragm and intercostal muscles results in pulmonary hypoplasia.

3.121

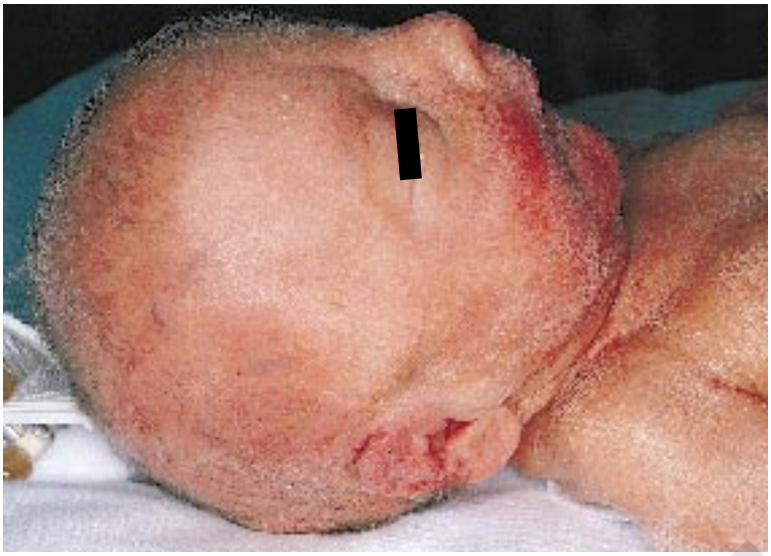

Figure 3.121. The lateral view of the same infant as in Figure 3.120 shows the poorly developed, low-set ear, depressed nasal tip, and micrognathia.

3.122

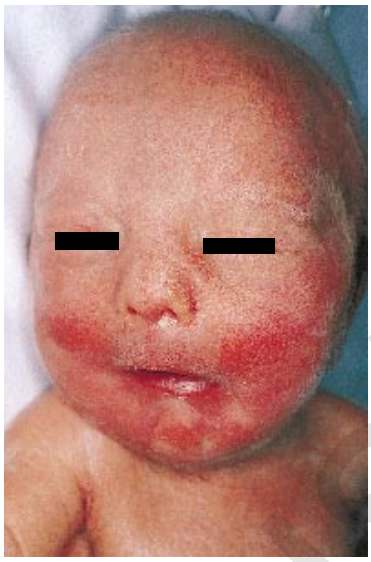

Figure 3.122. A close-up of the face of the same infant shows hypertelorism, telecanthus, and epicanthic folds, as well as the depressed nasal tip with a small mouth and micrognathia.

3.123

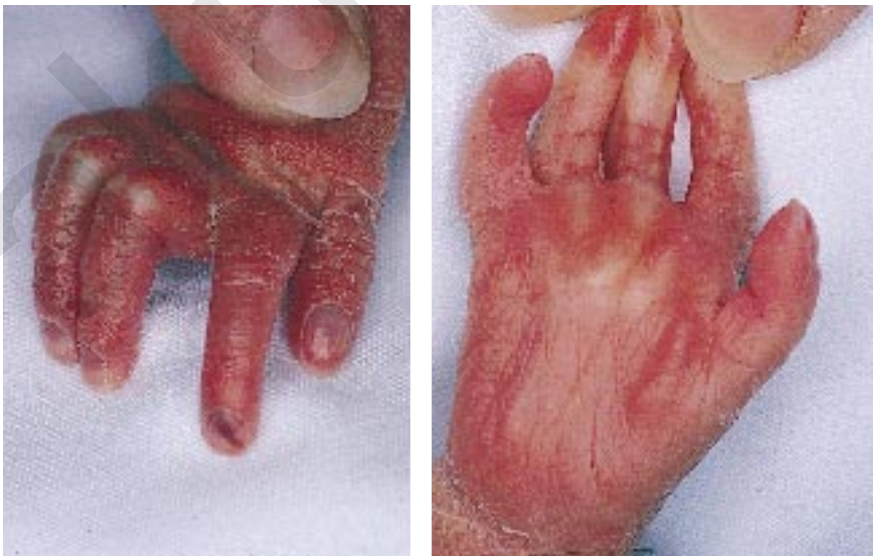

Figure 3.123. This same infant shows camptodactyly due to contractures in the fingers. Also note the poor dermal ridges and absence of flexion creases on the fingers and palms due to lack of fetal movement in the early weeks of gestation.

3.124

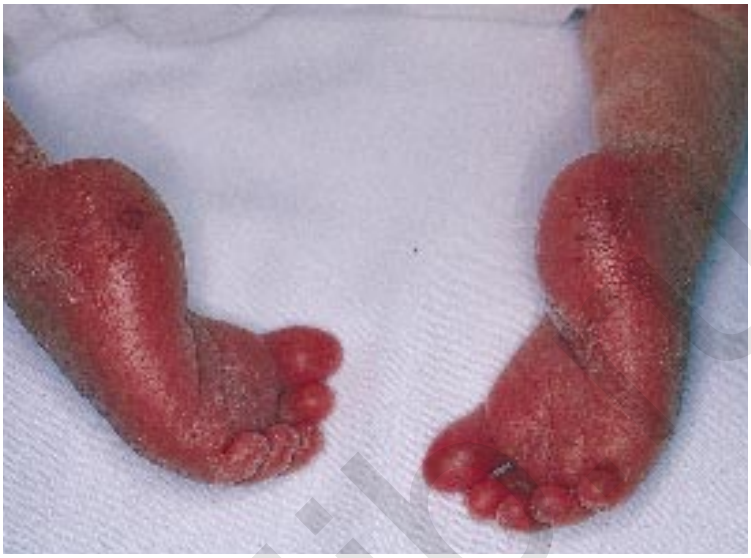

Figure 3.124. Talipes equinovarus in the same infant.

3.125

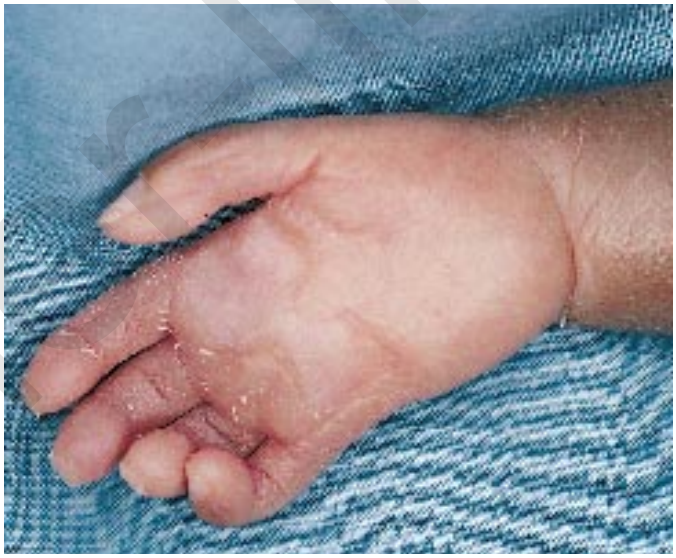

Figure 3.125. Another infant with the fetal akinesia sequence showing the marked lack of dermal ridges and creases. This infant had the typical dysmorphic features of the face, webbing of the neck, and severe intrauterine growth retardation with generalized arthrogryposis.

3.126

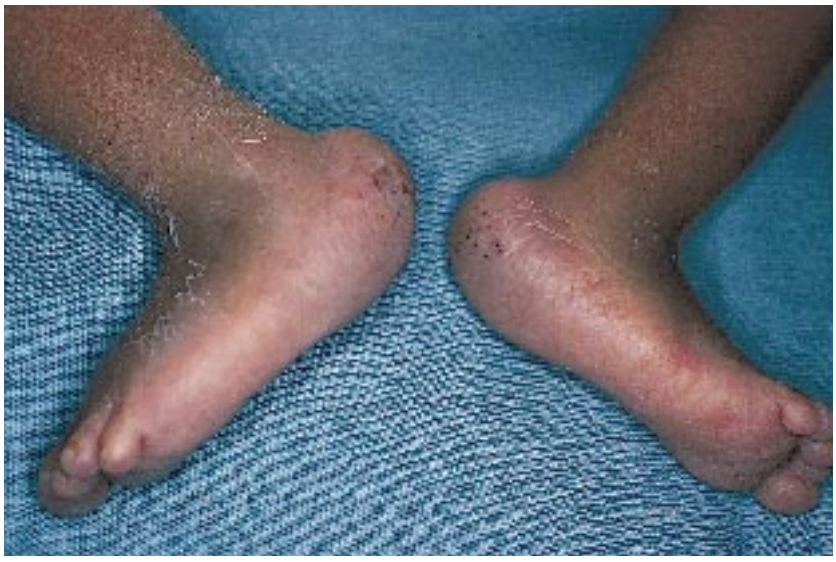

Figure 3.126. The same infant also had rocker-bottom feet.

3.127

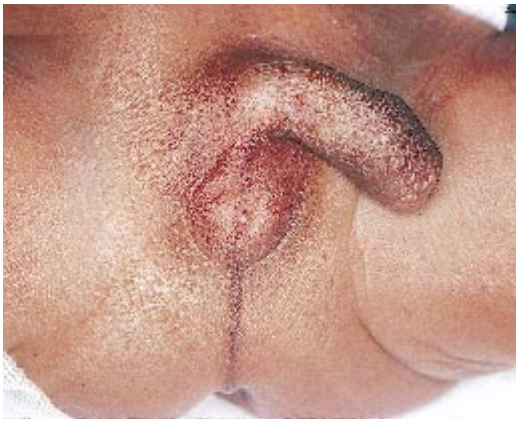

Figure 3.127. Cryptorchidism is common in infants with the fetal akinesia sequence.

3.128

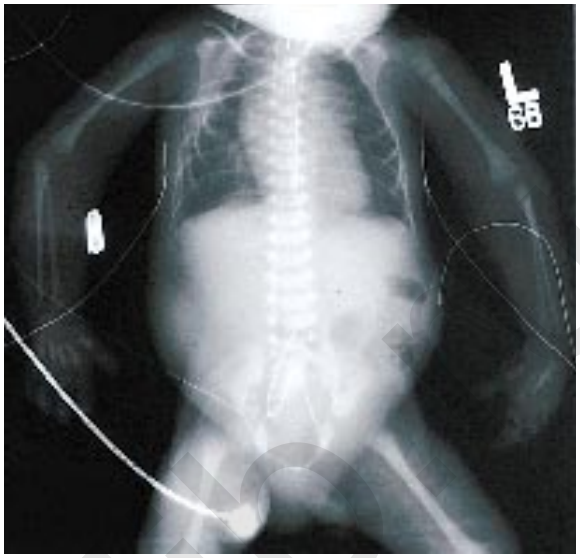

Figure 3.128. In a body radiograph of the same infant with the fetal akinesia sequence, note the thin gracile ribs, long thin clavicles, and thinning of all the long bones. The soft tissue in the extremities shows a lack of muscle mass. The appearance of the gracile ribs and long clavicles are also seen in trisomy 18 and myotonic dystrophy.

3.129

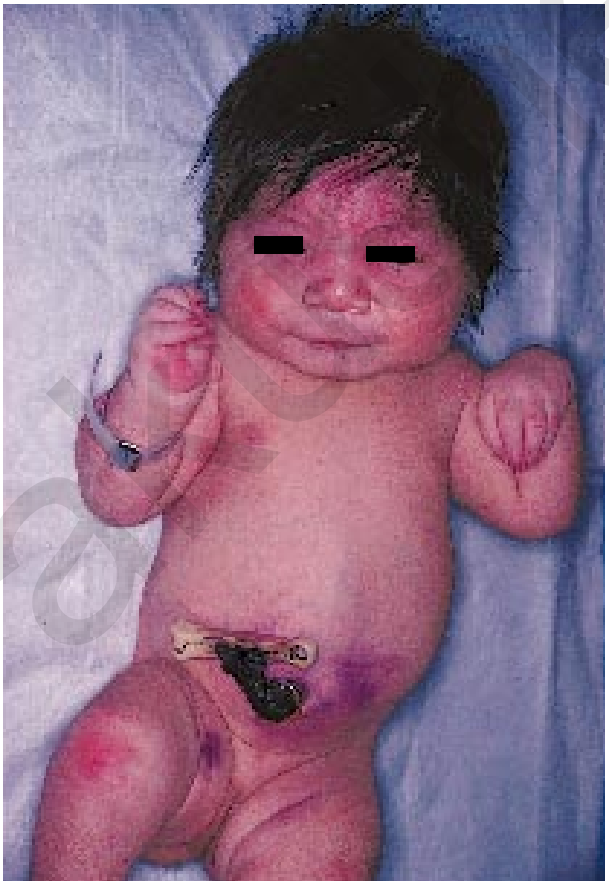

Figure 3.129. This infant with cerebrooculofacioskeletal (COFS) syndrome (Pena-Shokeir syndrome type II) presented with generalized hypotonia, hirsutism, characteristic facial features, widely spaced nipples, joint contractures, camptodactyly, and rocker-bottom feet.

3.130

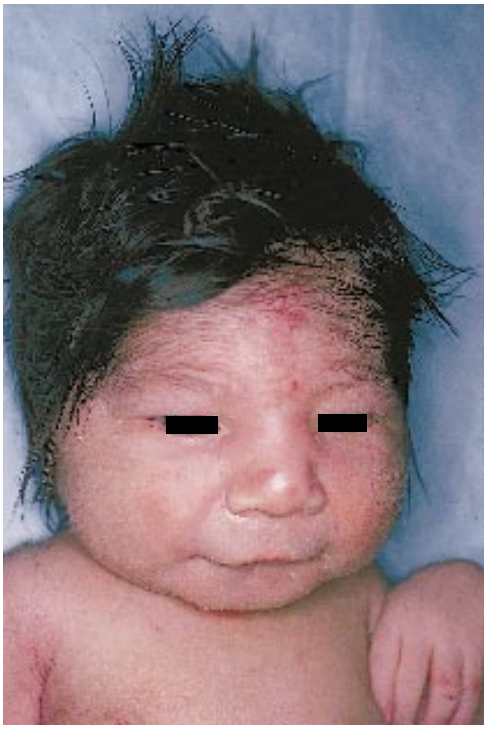

Figure 3.130. A close-up view of the face of the same infant showing the characteristic facial features. Note the hirsutism, deep-set eyes, prominent root of the nose, upper lip overlapping the lower lip, and micrognathia.

3.131

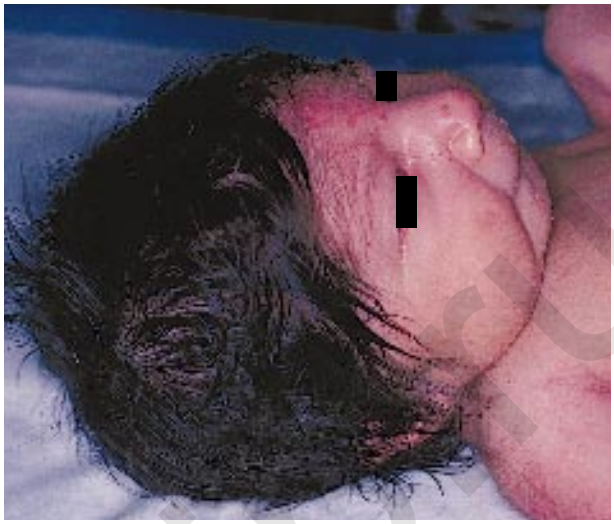

Figure 3.131. A lateral view of the head and face of the same infant shows the hirsutism, microcephaly, blepharophimosis, deep-set eyes, upper lip overlapping the lower lip, and micrognathia.

3.132

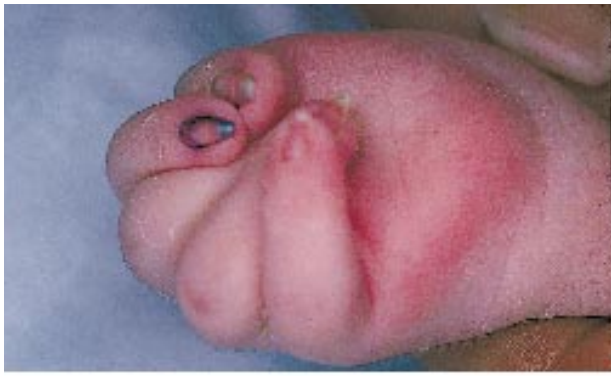

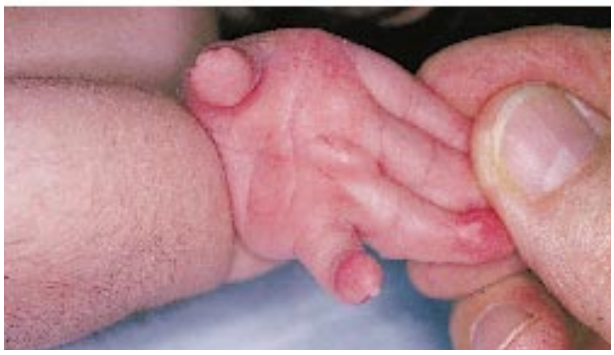

Figure 3.132. In the close-up of the hand of this infant with COFS syndrome in the upper figure note the camptodactyly, and in the lower figure with the hand open, note the absence of finger creases due to lack of fetal movement early in gestation.

3.133

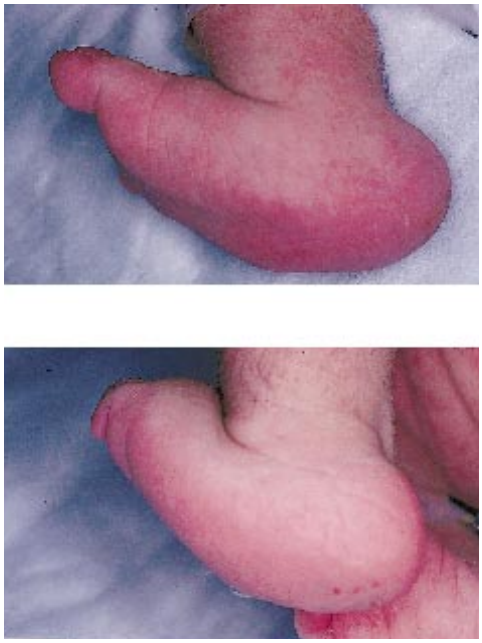

Figure 3.133. The same infant as in Figure 3.132 demonstrates rocker-bottom feet. Note the marked contracture accompanying this as seen in the right foot in the lower figure. These infants also have a longitudinal groove in the soles along the second metatarsal.

3.134

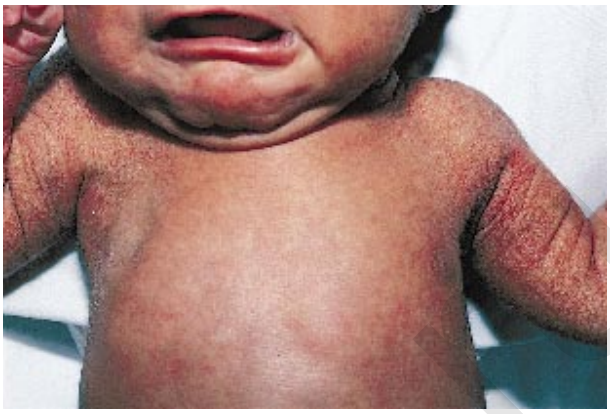

Figure 3.134. Infant with Poland's anomaly showing unilateral absence of the sternal and costal portions of the pectoralis major muscle and brachysyndactyly of the hand on the ipsilateral side. There may be absence or hypoplasia and upward displacement of the nipple and breast on the affected side.

3.135

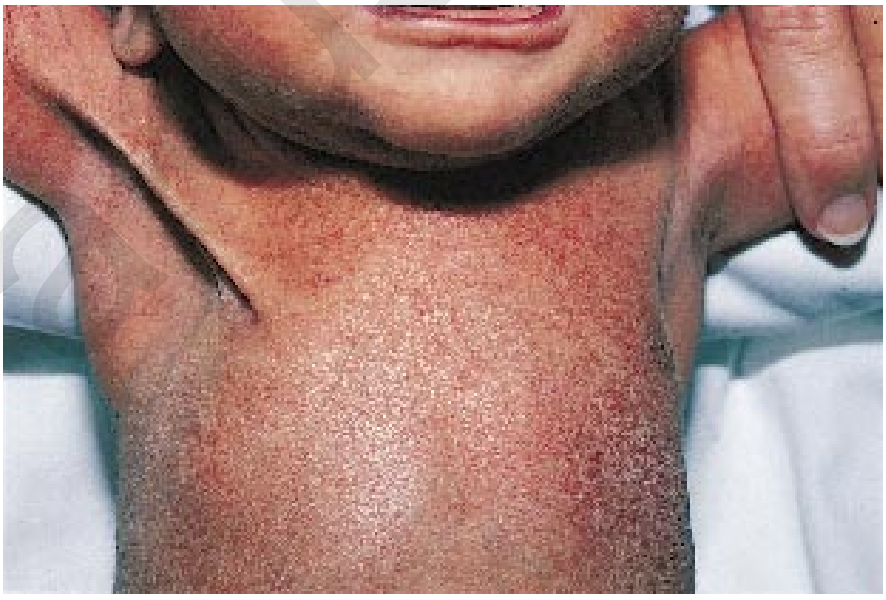

Figure 3.135. If the abnormality is not obvious, then extending the arms is a means of better demonstrating the abnormality as seen in the same infant. Note the absence of the nipple. Occasionally there may be some abnormalities underlying the defect.

3.136

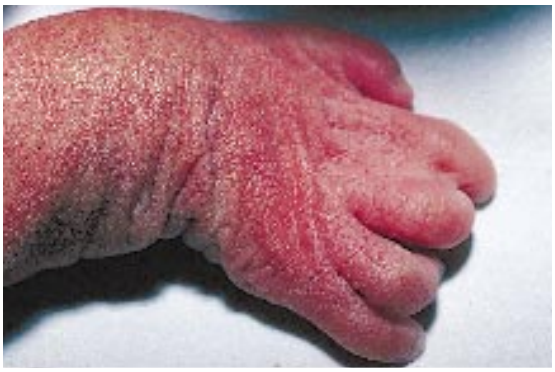

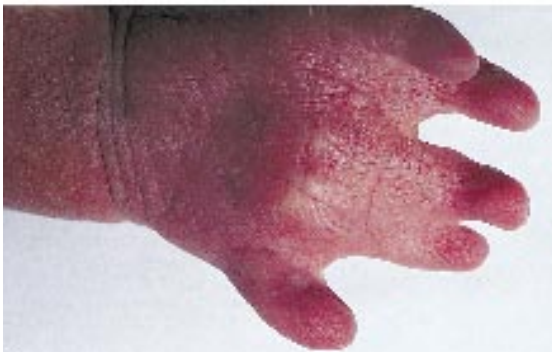

Figure 3.136. The hands of the same infant show the brachysyndactyly. The hand on the affected side is usually smaller than that on the unaffected side. There is usually no bony synostosis. Less commonly the forearm is smaller on the affected side.

3.137

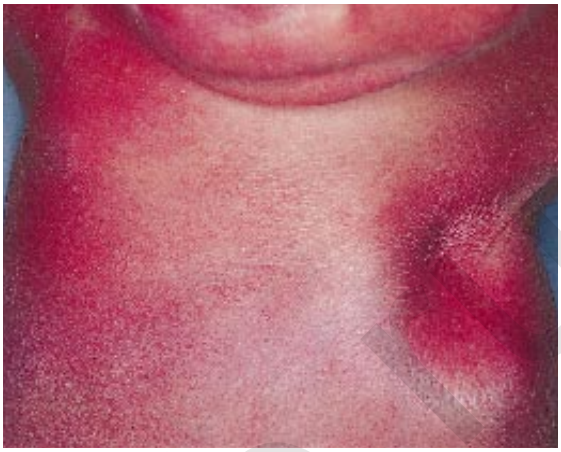

Figure 3.137. Another example of Poland's anomaly. In this infant the defect is more severe, in that in addition to the lack of the pectoralis major there are defects in other muscles such as the absence of the pectoralis minor. In Poland's anomaly, 75% of the infants are male and in 70% the right side is affected.

3.138

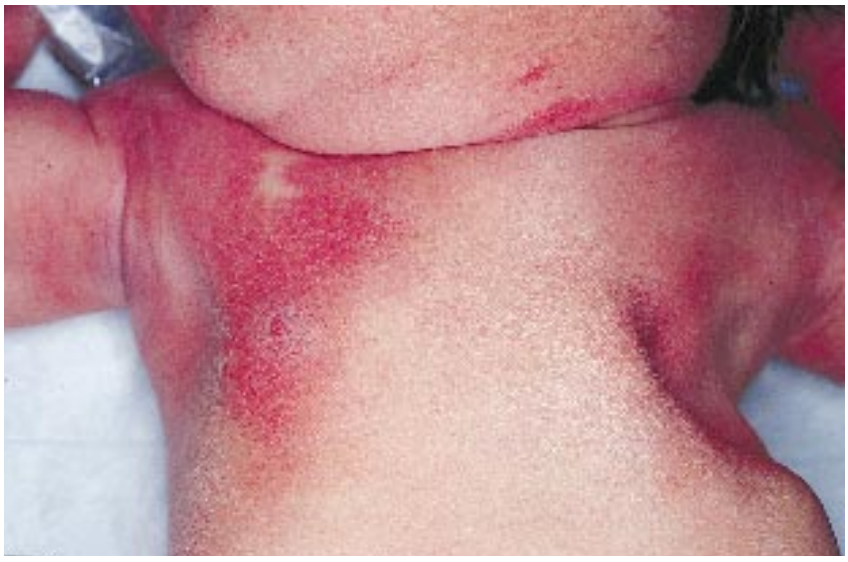

Figure 3.138. The defect the chest wall was due to a deformation resulting from the abnormal hand being held in the "position-of-comfort" where it was lodged during the last few weeks of gestation.

3.139

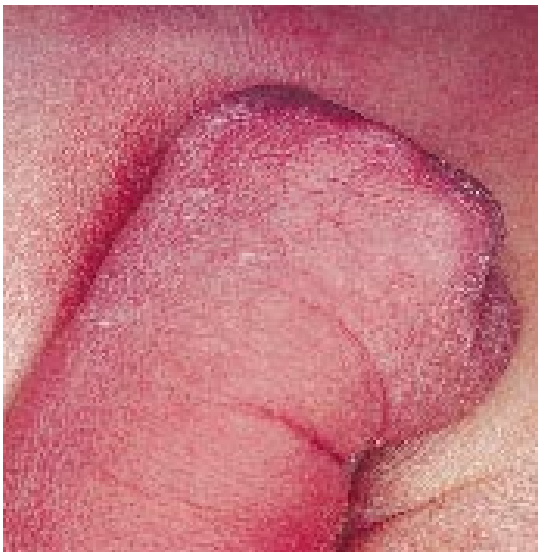

Figure 3.139. A close-up of the infant in Figure 3.138 showing the hand placed in the defect.

3.140

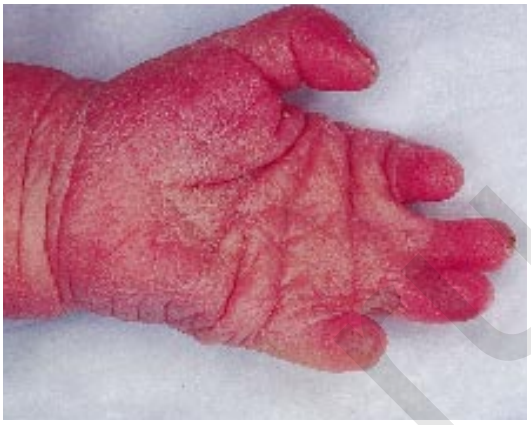

Figure 3.140. A close-up of the left hand showing the marked brachysyndactyly.

3.141

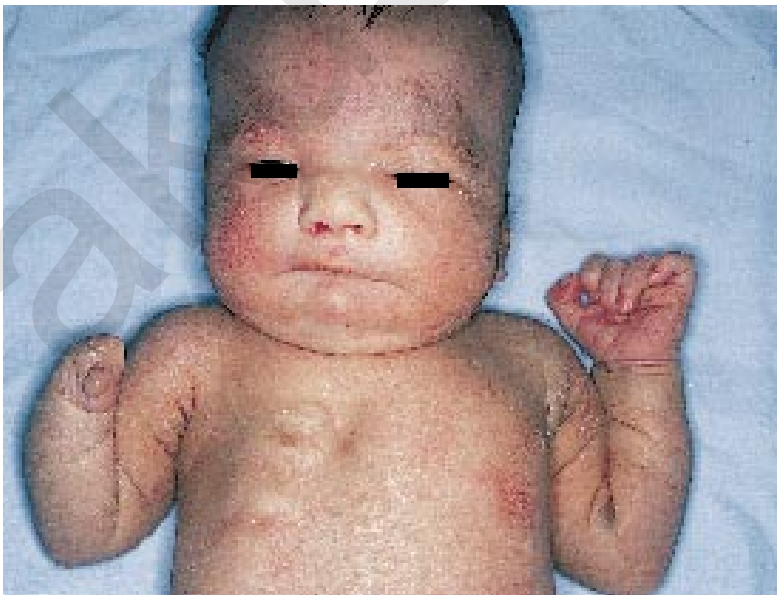

Figure 3.141. In about 15% of cases there is an association of Poland's anomaly with Möbius' syndrome. In Poland's anomaly the hand anomalies are usually unilateral, whereas in Möbius' syndrome they are usually bilateral. This infant with Poland's anomaly and Möbius' syndrome shows the mask-like facies, ptosis of eyelids, drooping of the angles of the mouth, and the absence of the right pectoralis with a hypoplastic right forearm and hand.

3.142

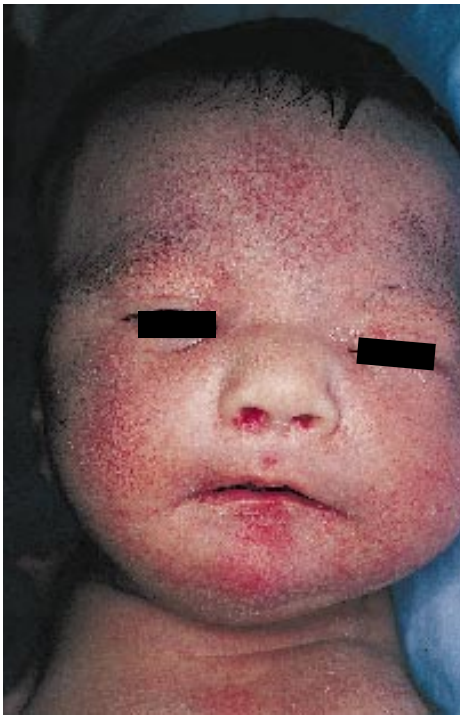

Figure 3.142. A close-up of the face of the same infant. Note the mask-like facies, eyelid ptosis, and drooping of the angles of the mouth. These infants have inefficient sucking and swallowing. In Möbius' syndrome there are usually bilateral cranial nerve palsies involving the sixth and seventh cranial nerves. Occasionally other cranial nerves (three, five, nine and twelve) may be involved.

3.143

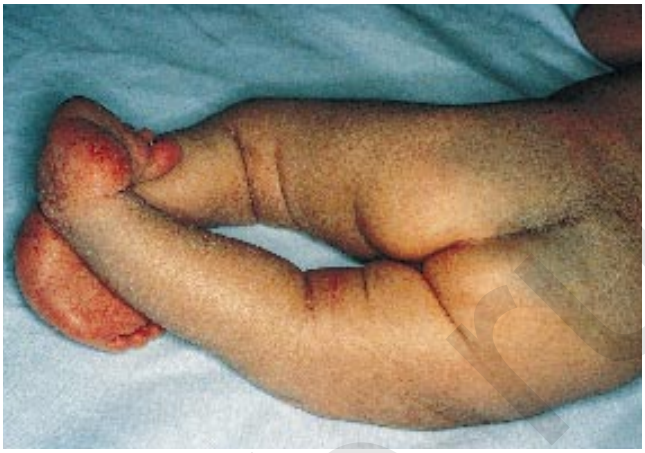

Figure 3.143. This infant has congenital dislocation of the right hip and the bilateral clubfoot. Note the asymmetric buttock creases typical of congenital dislocation of the hip. In Möbius' syndrome there may be deformities of the hands and feet and arthrogryposis is not uncommon.

3.144

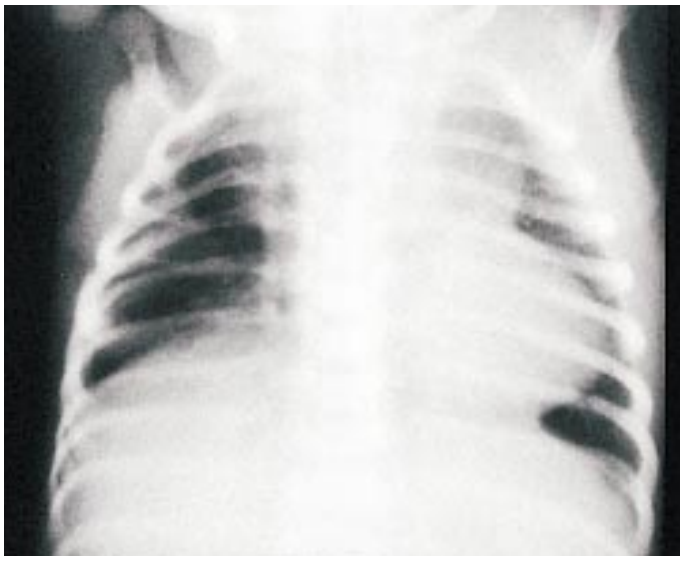

Figure 3.144. A chest radiograph in Poland's anomaly demonstrates the increased lucency of the right upper chest, especially of soft tissue, due to the absence of the pectoralis muscle. Compare the appearance of the scapulae on both sides. Note that the ribs are normal.

3.145

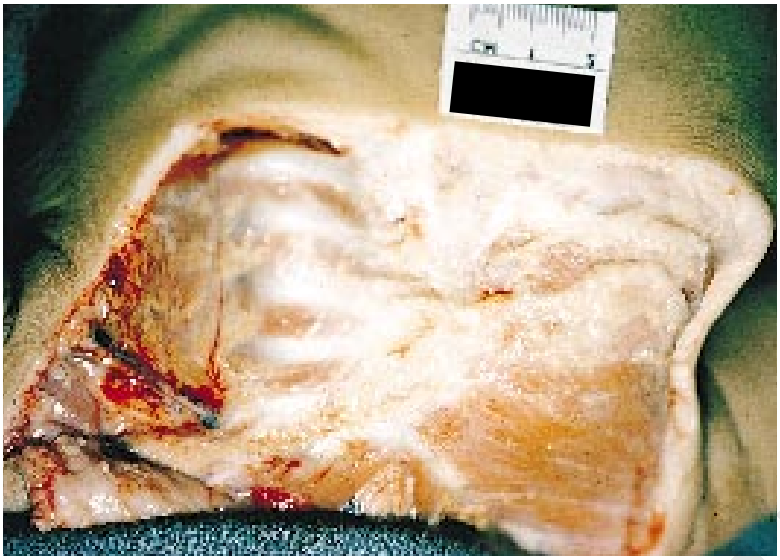

Figure 3.145. The pathologic appearance of the chest in an infant who had congenital absence of the pectoralis muscle.

3.146

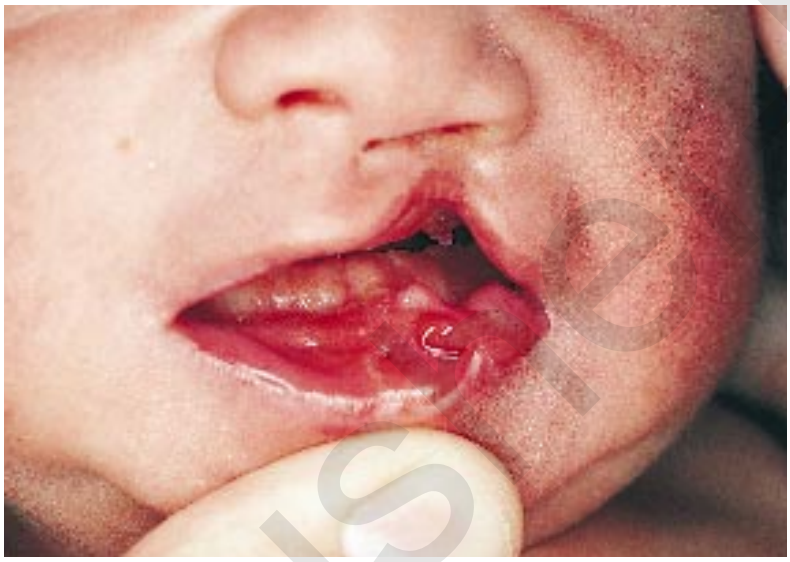

Figure 3.146. This infant with the popliteal pterygium syndrome (popliteal web syndrome) shows the unilateral cleft lip and cleft palate. There are lip pits and also note the remnants of the oral frenula which have been cut. Oral frenula are typically seen in these infants and there may be cutaneous webs between the eyelids.

3.147

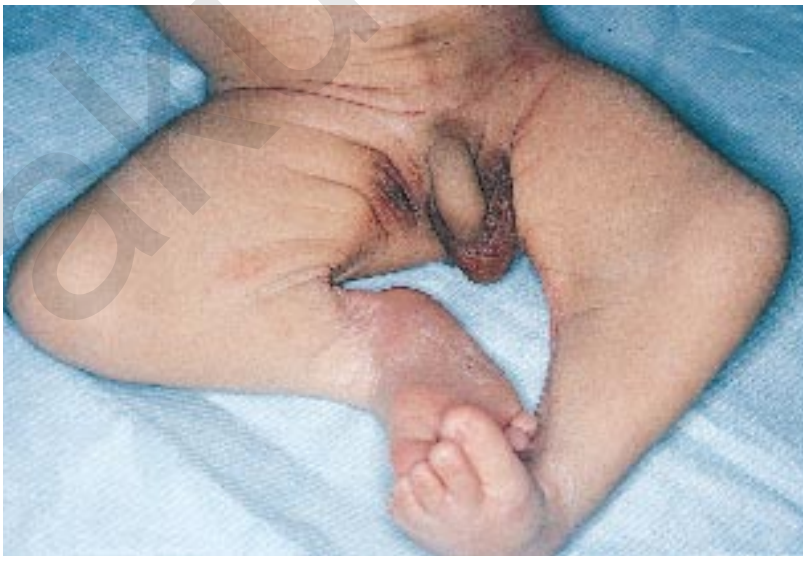

Figure 3.147. In the same infant note the very marked popliteal webbing which extends from the leg up to the thigh. Also note the divided scrotum with cryptorchidism on the right.

3.148

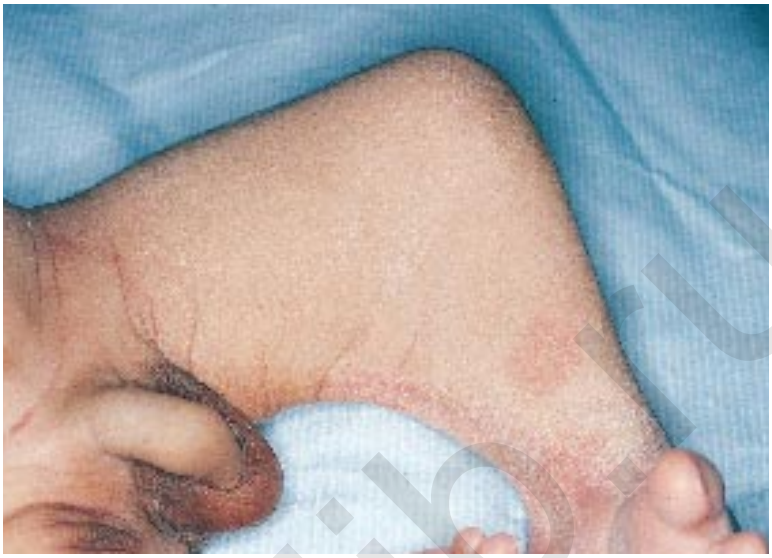

Figure 3.148. A close-up of the large popliteal web. The dense fibrous cord in the posterior portion of the popliteal pterygium may contain the tibial nerve.

3.149

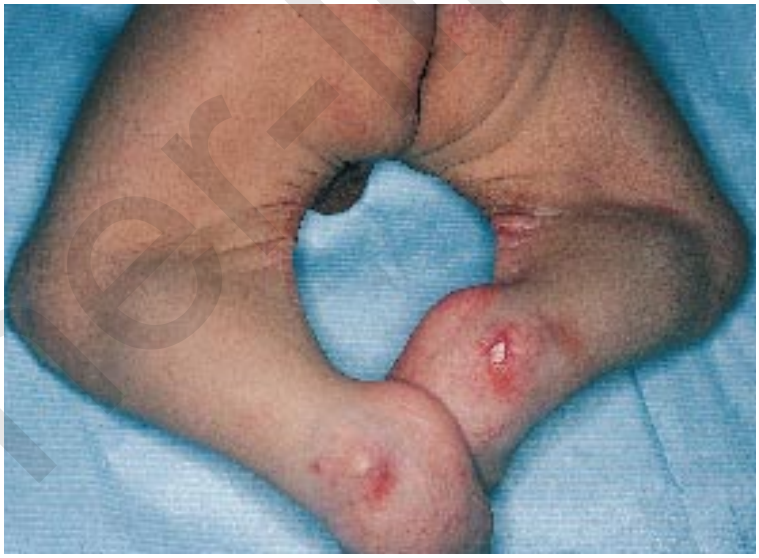

Figure 3.149. A posterior view of the lower extremities of the same infant shows the large popliteal pterygia extending from the hips to the ankles. There is also clubbing of both feet, a common finding in this condition.

3.150

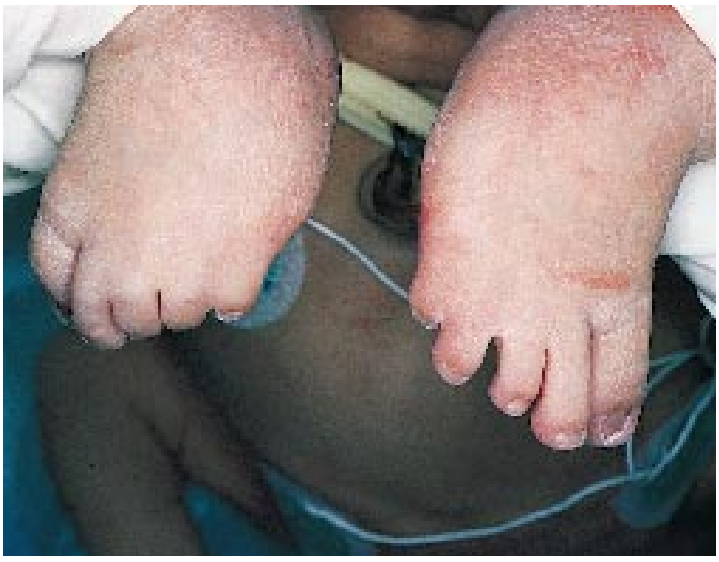

Figure 3.150. In the same infant there is syndactyly of the toes in both feet. Note the pyramidal form of the skin over the hallux which is typically seen in this condition.

3.151

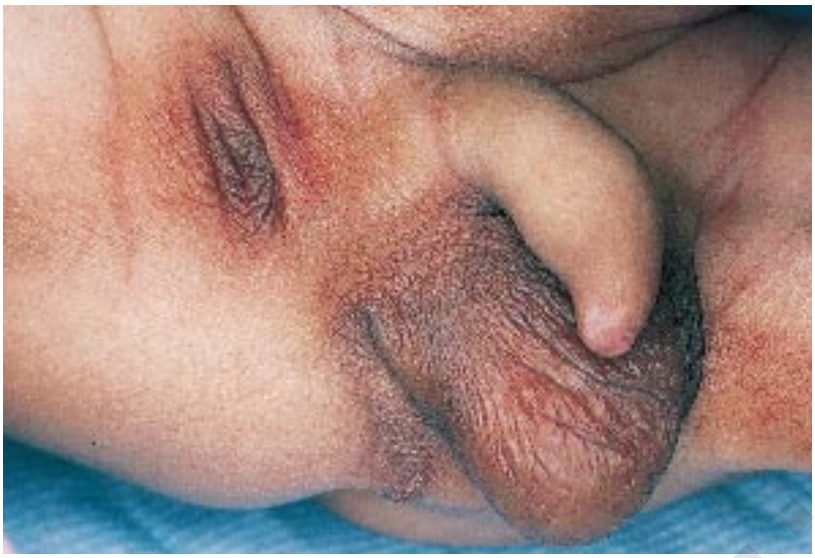

Figure 3.151. A close-up of the genitalia of the same infant as shown in Figure 3.150 shows the divided scrotum with cryptorchidism on the right. In female infants there may be hypoplastic labia minora and the genitalia may be ambiguous.

3.152

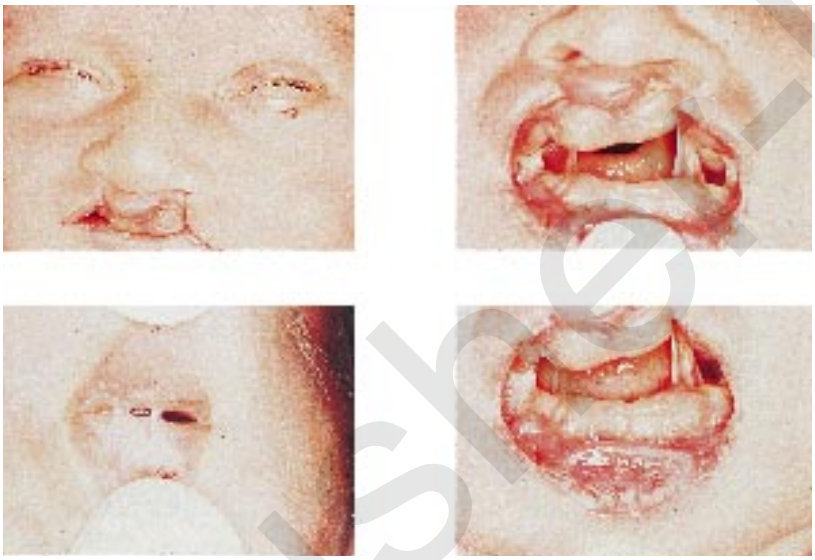

Figure 3.152. This female infant with popliteal pterygium syndrome presented with the filiform adhesions between the eyelids which are seen in 20% of patients. Cleft lip and palate are seen in 85% and pits of the lower lip are seen in 60%. The bands of tissue extending between the jaws which are well demonstrated in this patient are noted in about 35%.

3.153

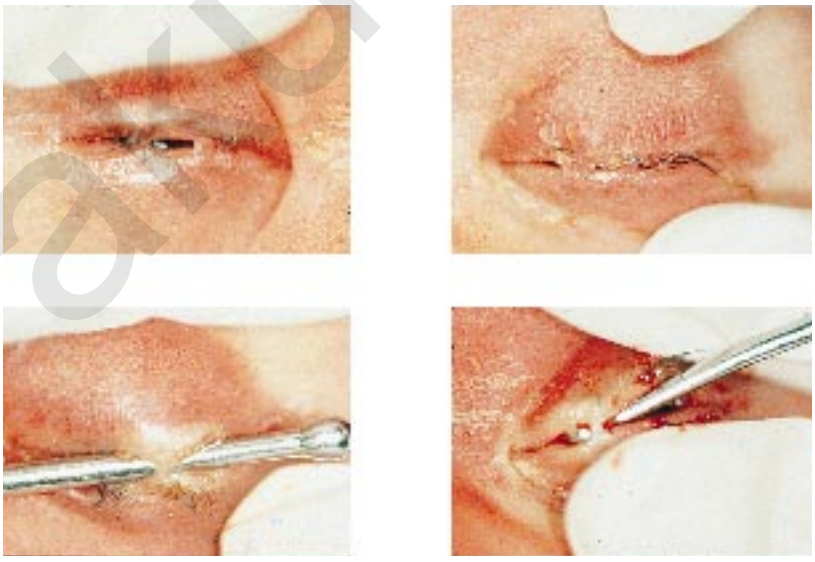

Figure 3.153. Close-up of the filiform adhesions between the eyelids of the same infant.

3.154

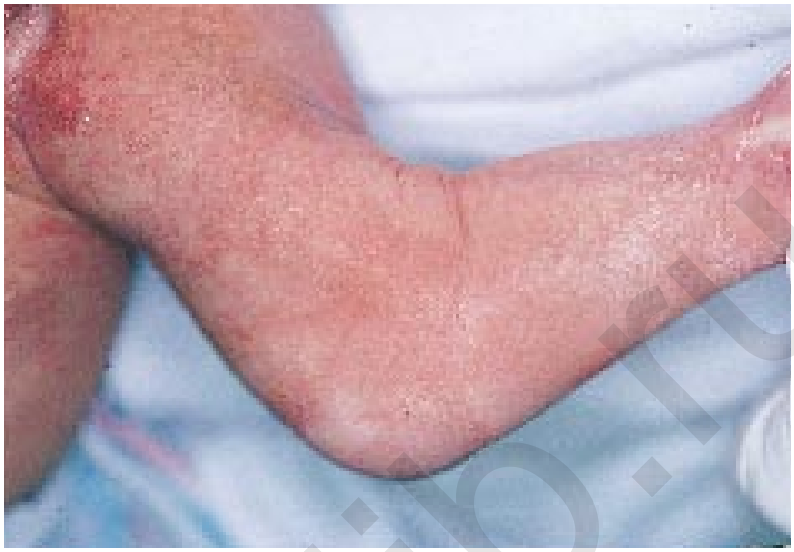

Figure 3.154. The popliteal pterygium in the same infant is not nearly as severe as in the previous example. Note the abnormal digits.

3.155

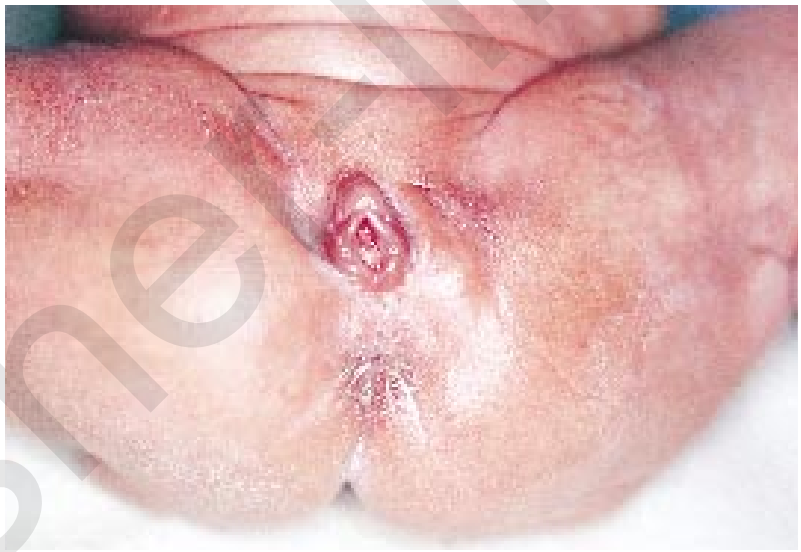

Figure 3.155. Absence of the labia majora is present in about 60% of infants with popliteal pterygium syndrome.

3.156

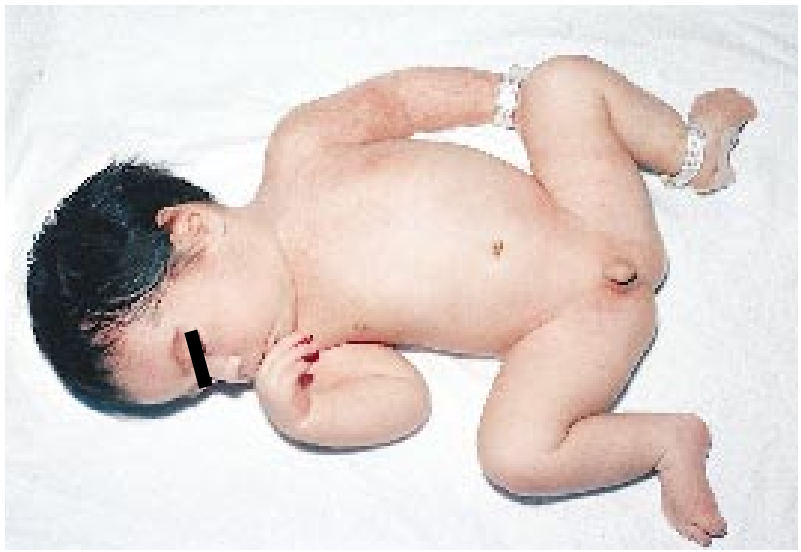

Figure 3.156. Prader-Willi syndrome presents in the neonate with marked hypotonia, a weak cry, and hypogonadism at birth. In Prader-Willi syndrome the mother may note decreased fetal activity, and there is a breech presentation in about 30% of cases. Although born at term, the infants are usually small, weighing less than 3000 g. There is a characteristic history of feeding difficulty which may result in failure to thrive. The condition is sporadic and there is a preponderance of males. In Prader-Willi syndrome, the karyotype is abnormal in about 50% of cases (deletion 15q).

3.157

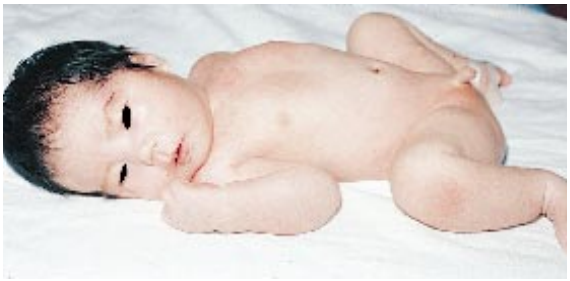

Figure 3.157. In this view of the same infant as in Figure 3.156, in addition to the hypotonia, some of the characteristic craniofacial features are apparent. Note the almond-shaped, upslanting palpebral fissures and the prominent forehead.

3.158

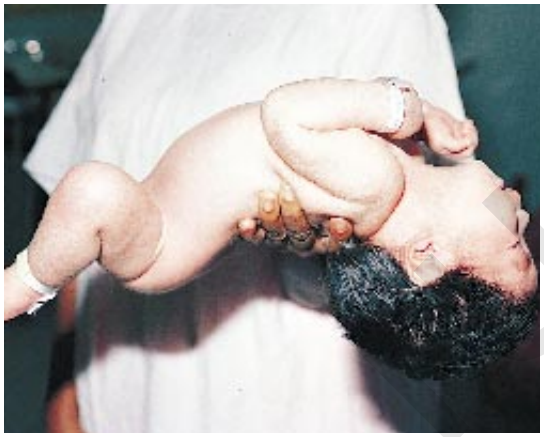

Figure 3.158. There is marked hypotonia in this infant with Prader-Willi syndrome in the prone position. It is usually severe in early infancy, and Moro's reflex and tendon reflexes are decreased or absent. Congenital dislocation of the hips is not uncommon.

3.159

Figure 3.159. Marked hypotonia in this infant with Prader-Willi syndrome when the infant is held in the supine position.

3.160

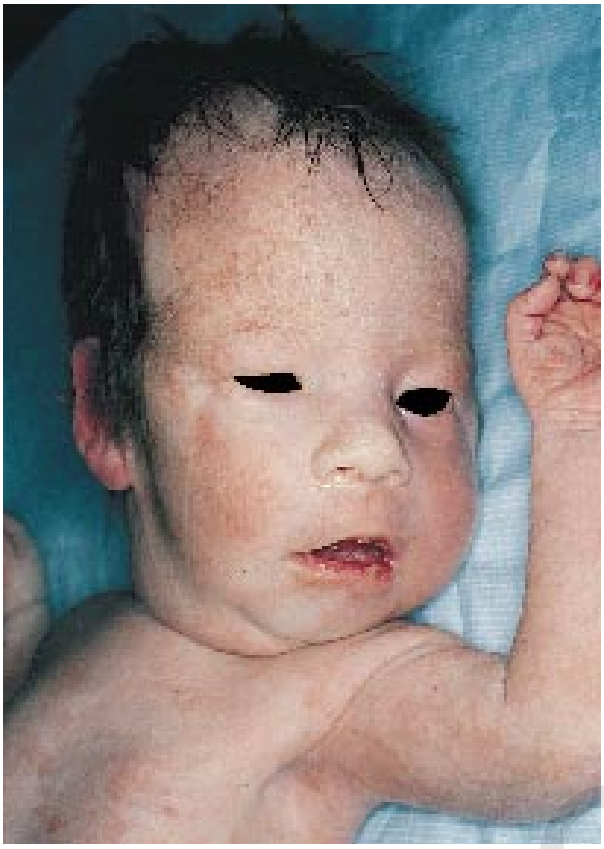

Figure 3.160. Close-up of the face of an infant showing the characteristic craniofacial features. Note the prominent forehead and a reduced biparietal diameter. The eyes are almond shaped with upslanting palpebral fissures. The ears are dysplastic and the mouth is fish-like with a triangular upper lip. Note the small hand. The hands and feet may be small and remain small. Clinodactyly and syndactyly may be present in Prader-Willi syndrome.

3.161

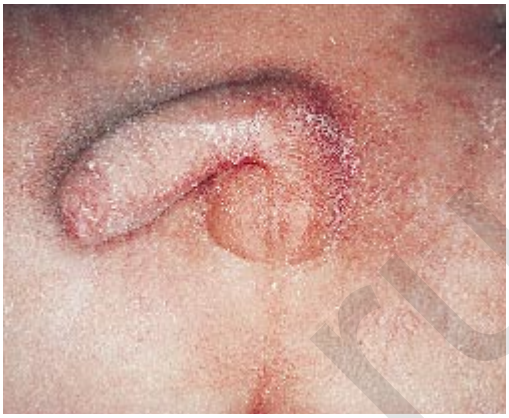

Figure 3.161. In the same infant note the cryptorchidism and a rudimentary scrotum.

3.162

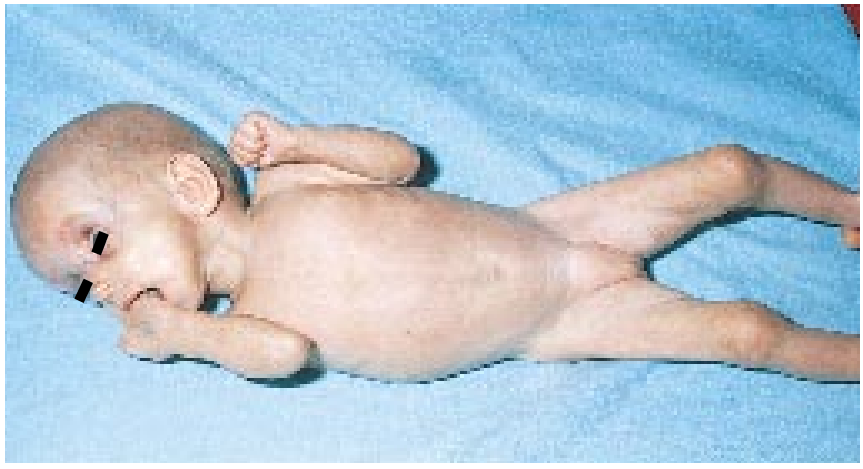

Figure 3.162. In this term infant with progeria (Hutch inson-Gilford syndrome) there was marked growth retardation (birthweight 1800 g). The face is small with a large head (pseudohydrocephalus) and there is a marked lack of subcutaneous tissue and prominence of the knees. This is a condition in which there is pseudosenility with hypertension, cardiomegaly, and atherosclerosis resulting in early death (at the average age of 14 years).

3.163

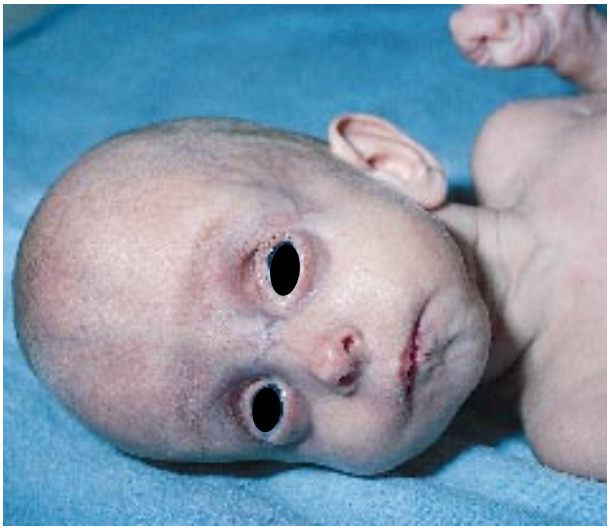

Figure 3.163. A close-up of the face of the same infant as shown in Figure 3.16 at age 6 weeks shows the small face with large head (pseudohydrocephalus), frontal and parietal bossing, hypotrichosis (scalp, eyebrows, and eyelashes), thin skin, prominent scalp veins, prominent eyes, mid-face hypoplasia, and micrognathia. The nose is thin and rather beaked.

3.164

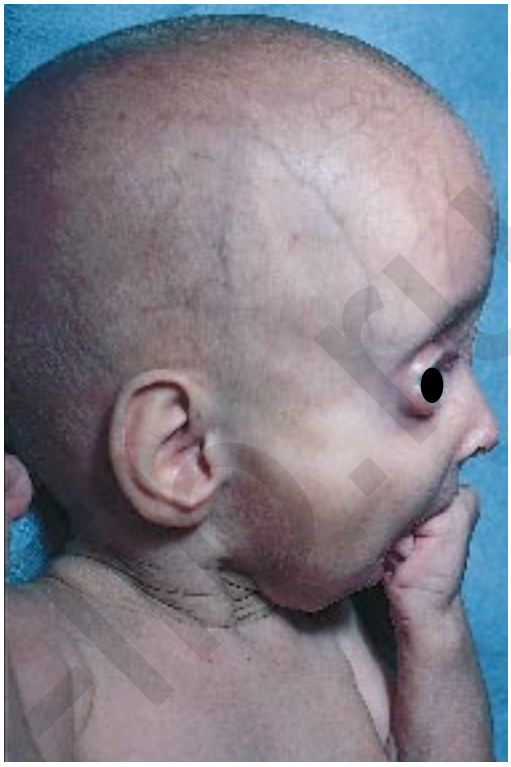

Figure 3.164. Lateral view of the head and face in the same infant. Note the pseudohydrocephalus, hypotrichosis, prominent scalp veins, prominent eyes, small beak-like nose, and micrognathia. Note the prominent buccal pads in the cheek. These infants feed well and growth is normal until about the first year of life when it plateaus.

3.165

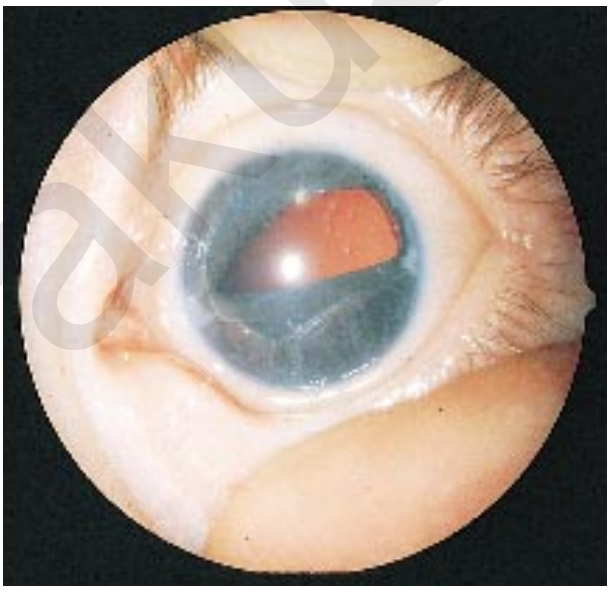

Figure 3.165. Rieger's syndrome is an autosomal dominant neural crest disorder in which there are abnormalities of the pituitary gland, teeth, and the mesenchymal structures of the eye. In this infant with Rieger's syndrome note the changes in the left eye. The pupil is distorted by peripheral anterior synechiae (adhesion of the iris to the cornea).

3.166

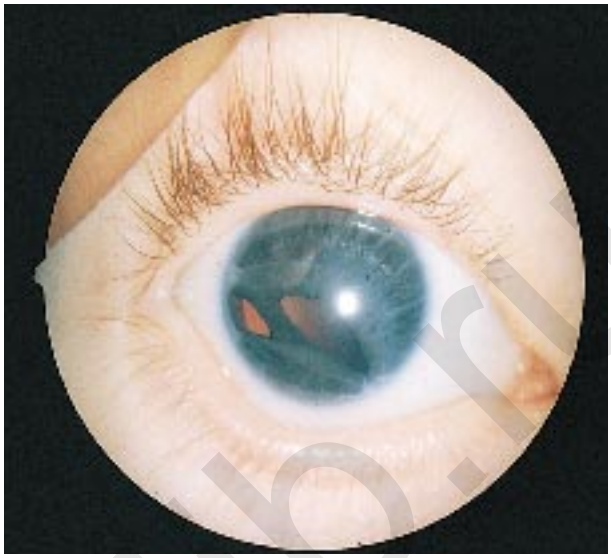

Figure 3.166. The same infant showing the changes in the right eye. Note the polycoria (multiple pupils) and peripheral anterior synechiae.

3.167

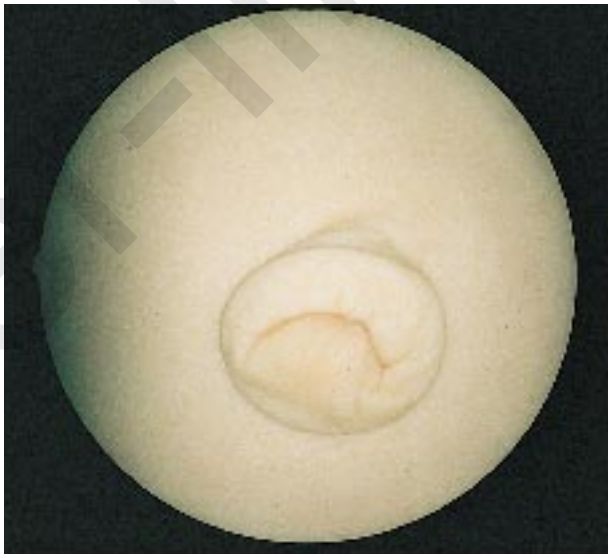

Figure 3.167. Patients with Rieger's syndrome have an unusually short umbilical cord which leaves a very characteristic umbilicus as seen in the same affected infant.

3.168

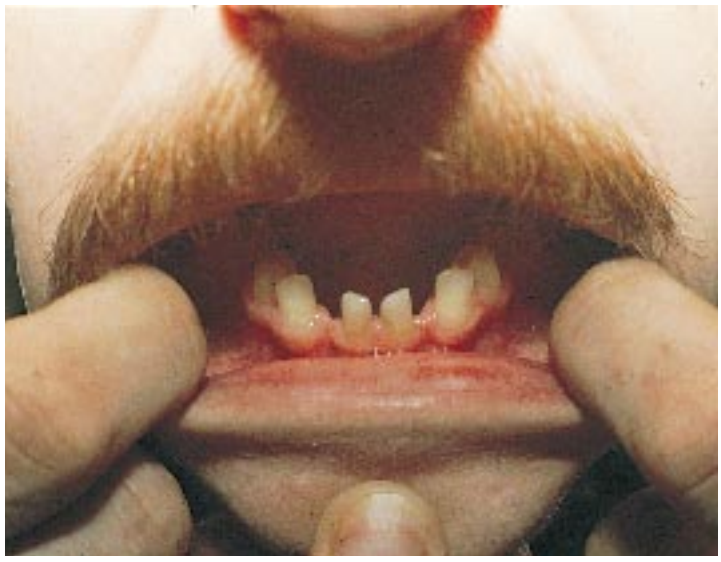

Figure 3.168. The father of the same infant shows hypodontia of the teeth. He also had ophthalmologic changes.

3.169

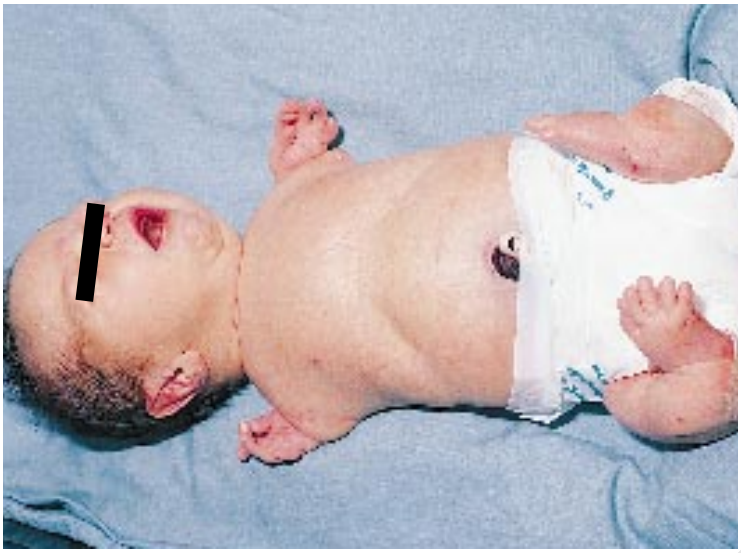

Figure 3.169. This infant with (pseudothalidomide syndrome) shows the tetraphocomelia. There is no cleft lip or palate, which would make the diagnosis the pseudothalidomide syndrome rather than Roberts' syndrome. The limb malformations are symmetric and more severe in the upper than in the lower limbs. Compare this infant to an infant exposed to maternal thalidomide in Volume I, Figure 3.23.

3.170

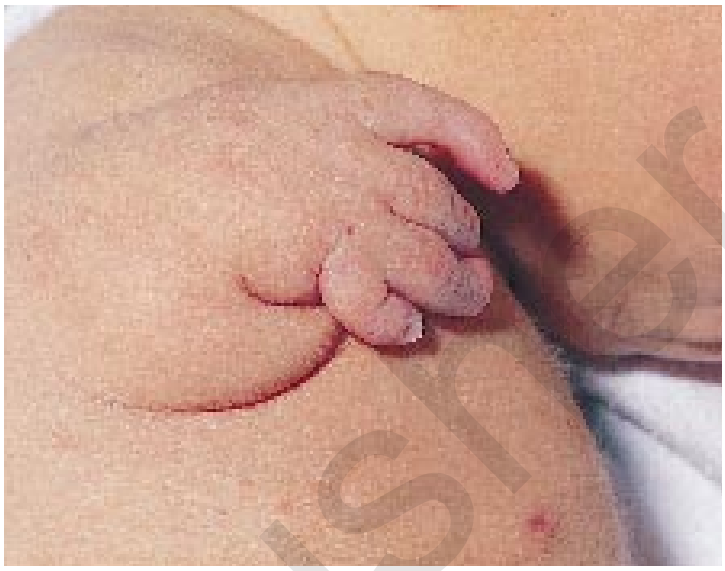

Figure 3.170. This is a close-up view of the right upper extremity of the infant. The phocomelia has resulted in absence of humeri, radii, and ulnae. In Roberts' syndrome the malformed hands may have hypoplastic or absent thumbs and there may be abnormalities of the digits.

3.171

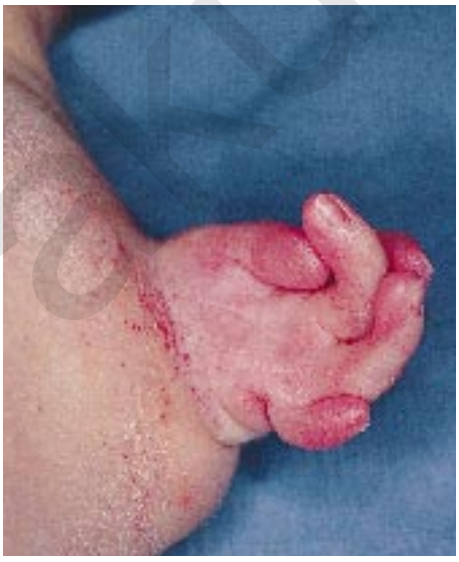

Figure 3.171. The left hand of the same infant showing the phocomelia with the abnormal hand and digits.

3.172

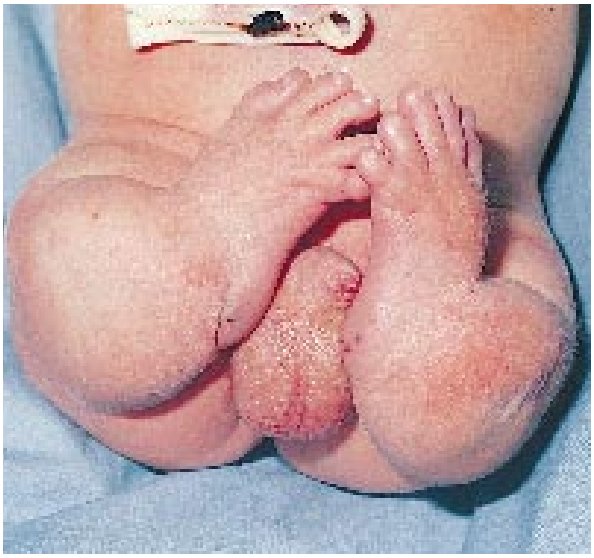

Figure 3.172. The lower extremities of the infant show the less severe changes in that the femora, tibiae, and fibulae are hypoplastic and the feet are abnormal.

3.173

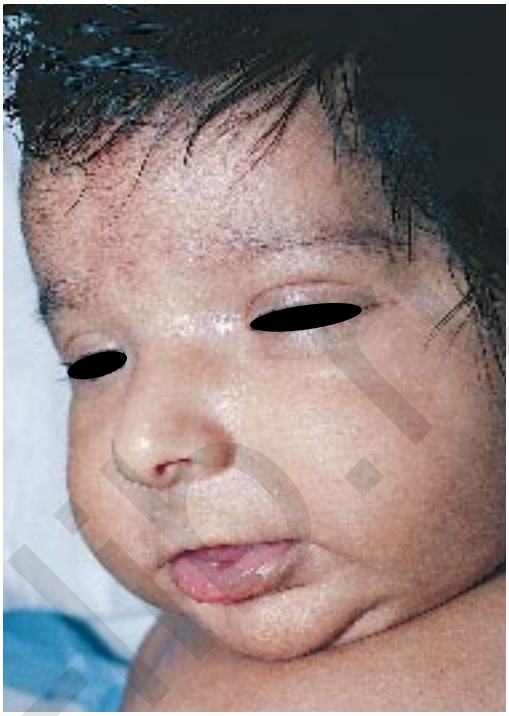

Figure 3.173. This infant with Rubenstein-Taybi syndrome presented at term with a birthweight of 2700 g and a length of 48 cm. Note the prominent forehead, hypertrichosis, downslanting palpebral fissures, epicanthic folds, long eyelashes, hypertelorism, broad nasal bridge, a beaked nose with a nasal septum extending below the alae nasi, and micrognathia. In addition to the findings above, patients with Rubenstein-Taybi syndrome commonly have microcephaly, low-set malformed ears and a high arched narrow palate.

3.174

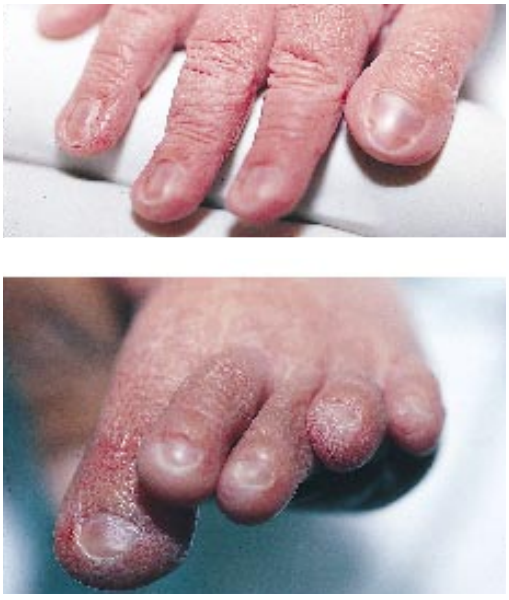

Figure 3.174. This figure shows the typical broad thumbs and broad toes which are seen in all infants with Rubenstein-Taybi syndrome. There may be shortening of thumbs and big toes. Clinodactyly of the fifth finger and overlapping of toes are seen in about 50% of these infants.

3.175

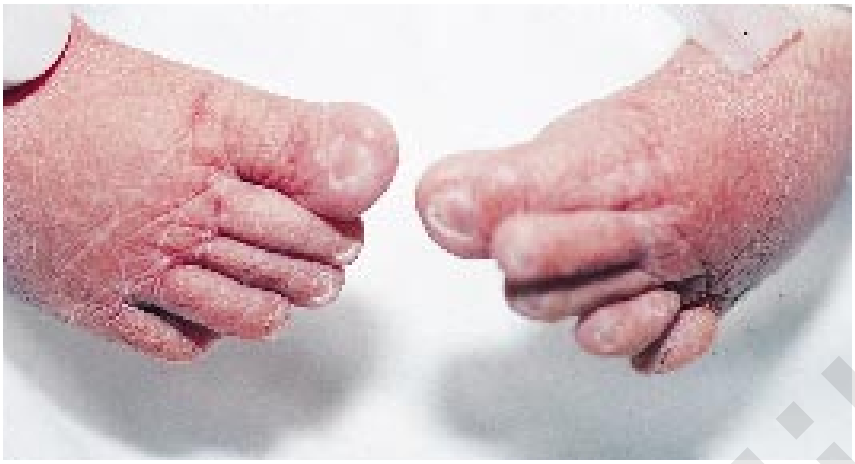

Figure 3.175. Broad thumbs and broad toes in another infant with Rubenstein-Taybi syndrome. Note the typical overlapping of toes.

3.176

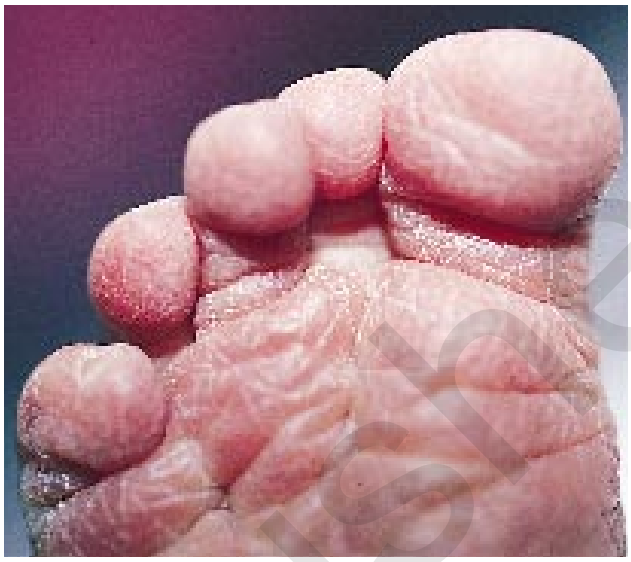

Figure 3.176. Another view of the same infant with the Rubenstein-Taybi syndrome showing the large big toe and overlapping of toes.

3.177

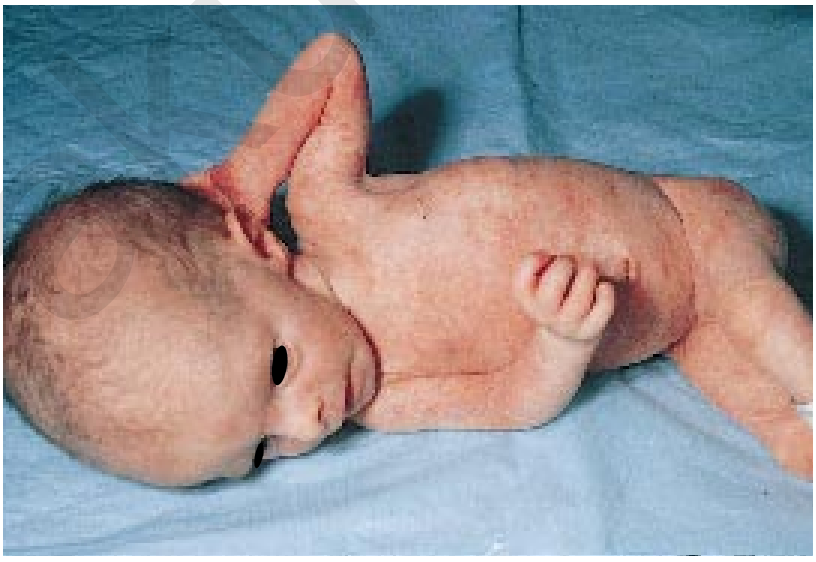

Figure 3.177. This term baby shows the typical findings of Russell-Silver syndrome in that he was unusually small for his gestational age (less than the 3rd percentile), small in stature, and had pseudohydrocephalus in that the head appeared to be disproportionately large for the small face. The proximal extremities are relatively short and the distal extremities are long (disproportionate dwarfism). Some of these infants may have skeletal asymmetry which may involve the entire body (hemihypertrophy) or which may be limited to involve only the skull or a limb.

3.178

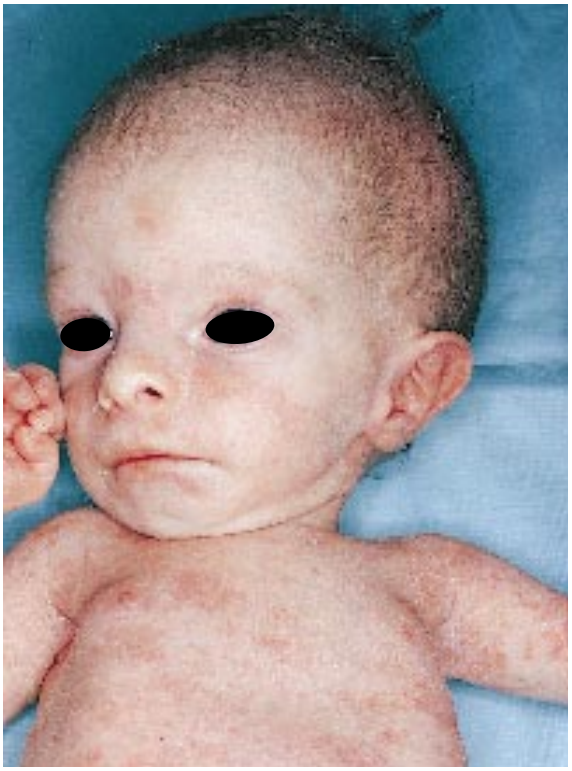

Figure 3.178. Close-up of the face of the same infant showing again the disproportion between the large head and the small face which tapers to a narrow jaw giving rise to a triangular facies. The fronto-occipital circumference is normal and the fontanelles are enlarged. Note the frontal bossing, prominent eyes, long eyelashes, and downturned angles of the mouth (giving a carp-like appearance), micrognathia, and posteriorly rotated ears.

A triangular facies is often the result of a disparity between the growth of the cranium, paced by normal brain growth, and the growth of the facial skeleton whose bones may share in an intrinsic growth deficiency.

3.179

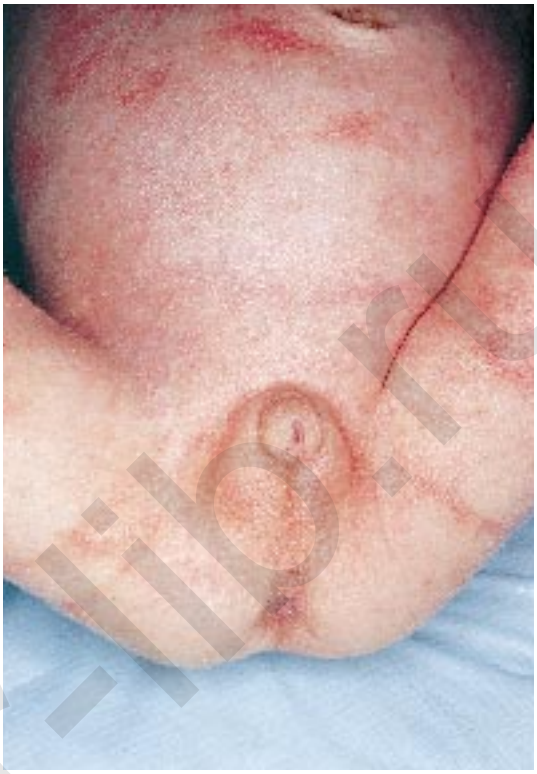

Figure 3.179. In the same infant note the cryptorchidism. Genital hypoplasia and hypogonadism are commonly present in Russell-Silver syndrome.

3.180

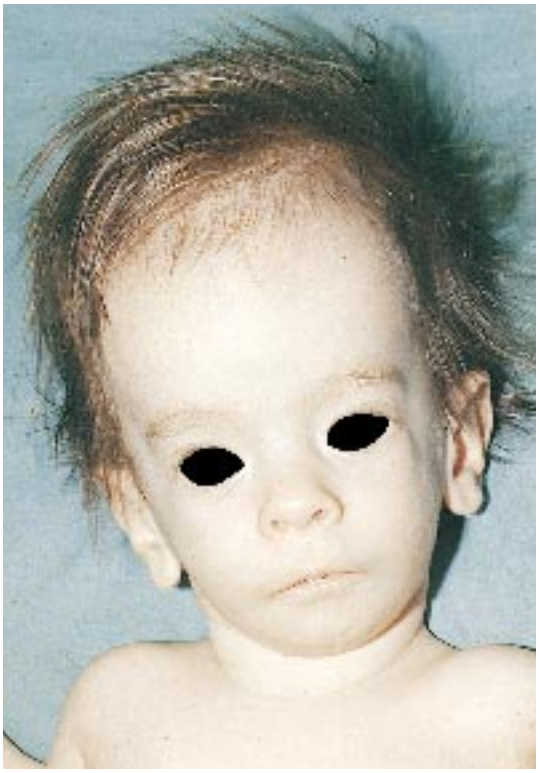

Figure 3.180. In another infant with the Russell-Silver syndrome, note the pseudohydrocephalus, prominent eyes, triangular facies, and carp-like mouth.

3.181

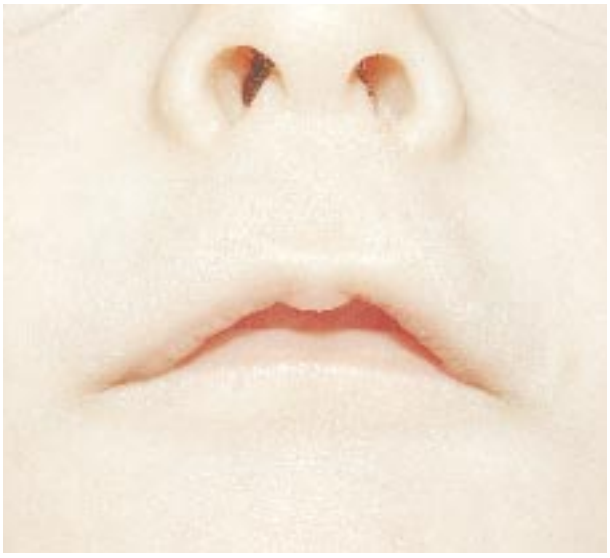

Figure 3.181. Close-up view of the mouth of the same infant as in Figure 3.180 showing the typical carp-like or inverted V-shaped appearance of the mouth.

3.182

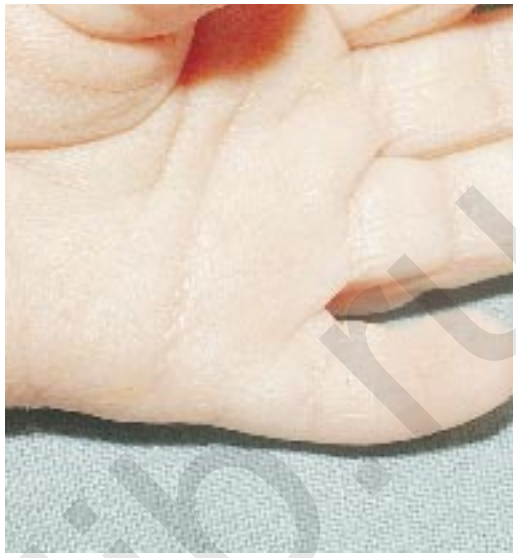

Figure 3.182. The same infant had a single palmar crease and clinodactyly of the fifth finger, which are also common findings in Russell-Silver syndrome.

3.183

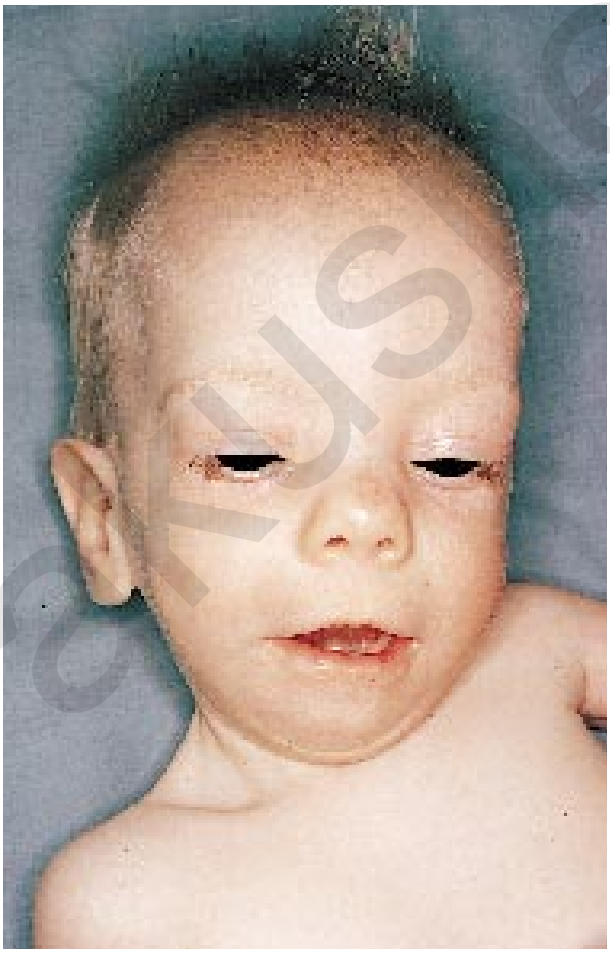

Figure 3.183. In the Smith-Lemli-Opitz syndrome the infants are small for their gestational age with a mean birthweight of 2560 g at term, commonly present as breech presentations, and have mental retardation. This is a female infant, but male infants predominate. There is microcephaly with moderate scaphocephaly, bilateral ptosis, low-set ears, a broad nasal tip with anteverted nostrils, and mild micrognathia. Other findings that may occur are an antimongoloid slant and epicanthic folds of the eyes.

3.184

Figure 3.184. Lateral view of the face of the same infant. Note the long eyelashes, the ptosis of the eyelids, anteverted nostrils and the mild micrognathia.

3.185

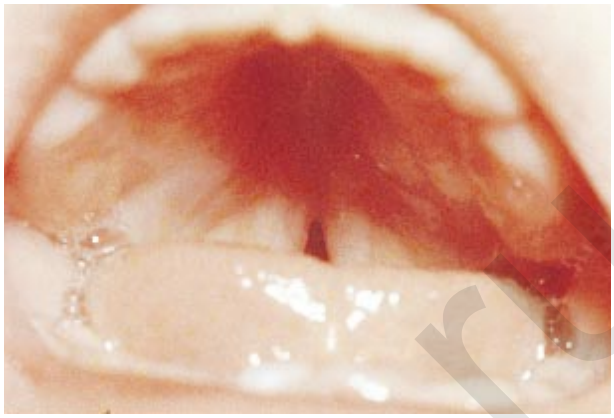

Figure 3.185. The same infant with Smith-Lemli-Opitz syndrome had a small cleft in the soft palate.

3.186

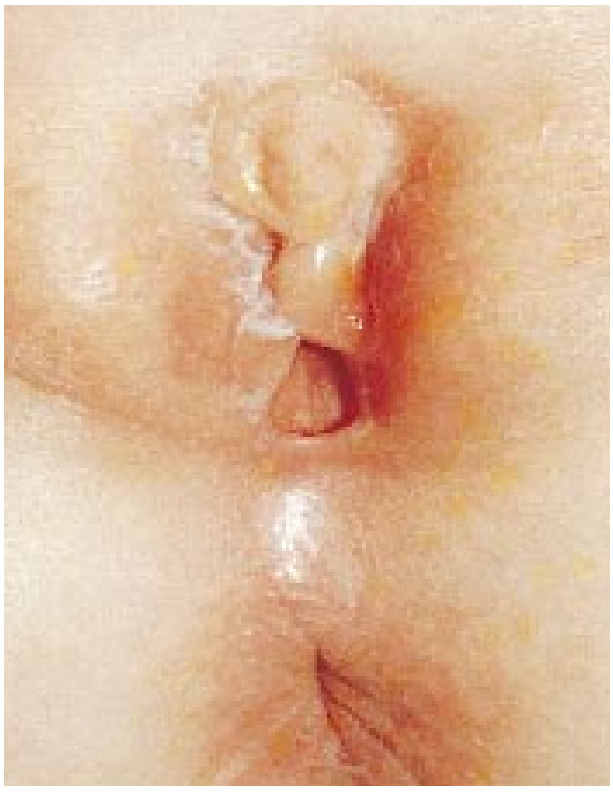

Figure 3.186. Note the hypoplastic genitalia. Males have small penises and hypogonadism.

3.187

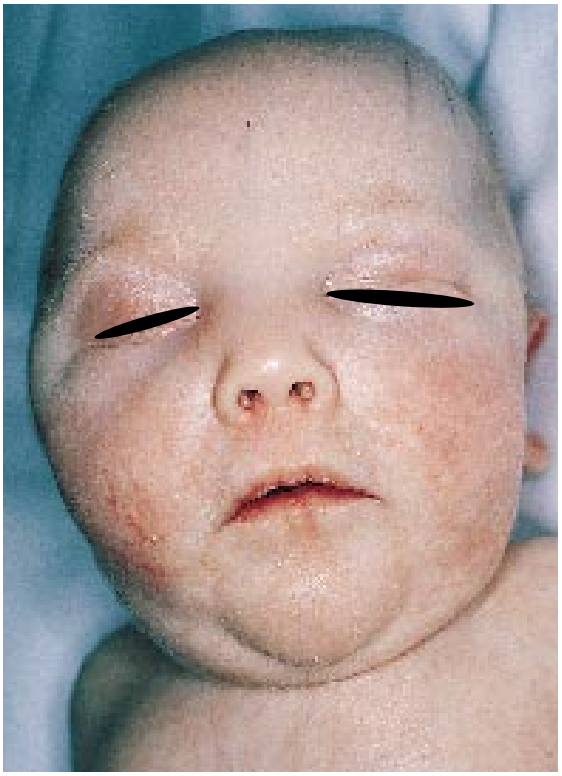

Figure 3.187. Another example of Smith-Lemli-Opitz syndrome in a male infant showing the typical appearance of the face. Note the microcephaly, closed eyes associated with ptosis, inner epicanthic folds, broad nasal tip with anteverted nostrils, and micrognathia.

3.188

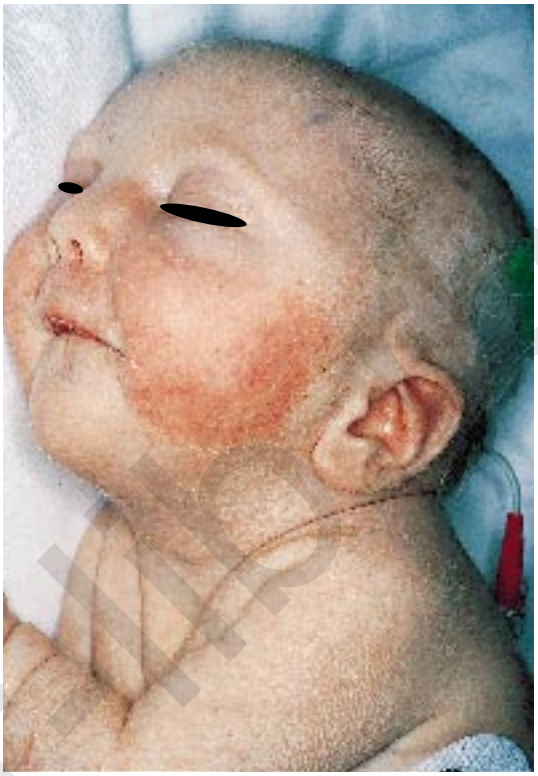

Figure 3.188. The same infant from the lateral view showing the face and head. Note the microcephaly with a tendency to scaphocephaly, low-set ears, ptosis, anteverted nostrils, and micrognathia.

3.189

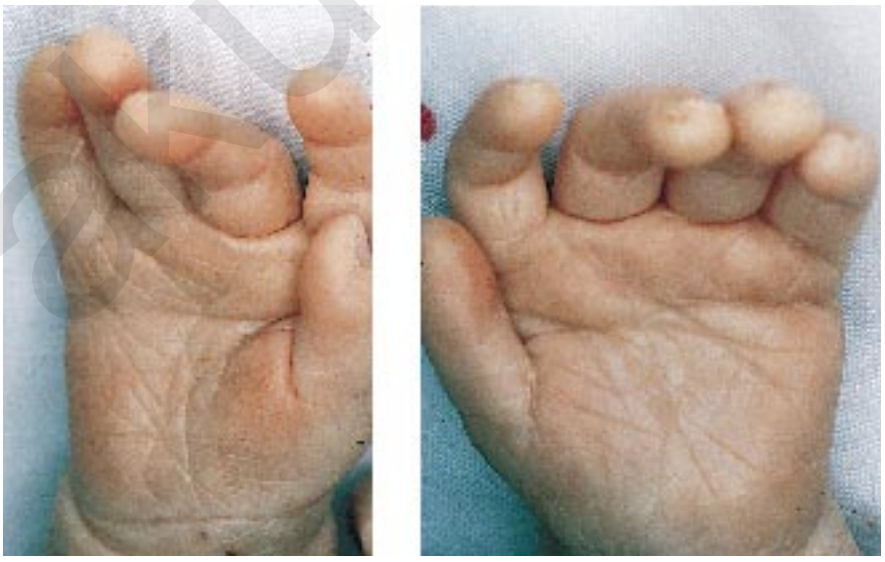

Figure 3.189. The hands of the same infant. The figure on the left shows a single palmar crease on the right hand and the figure on the right shows a Sydney line on the left hand. A Sydney line is often reported as a single palmar crease but note that there are two separate transverse palmar creases which are joined by another crease. These palmar findings are common in many normal infants and are seen in many syndromes.

3.190

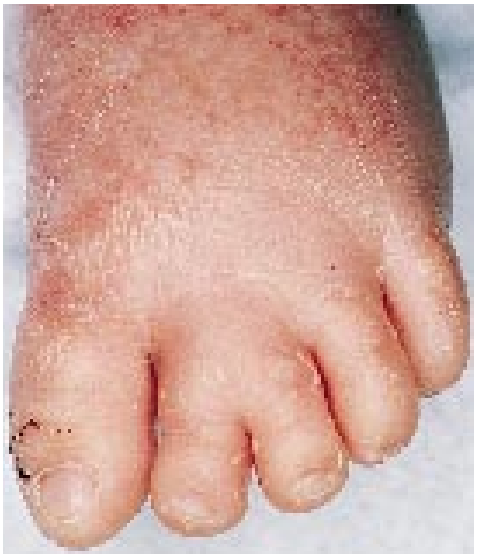

Figure 3.190. Syndactyly of the second and third toes is a common finding in Smith-Lemli-Opitz syndrome, but may occur in normal patients or in many other syndromes.

3.191

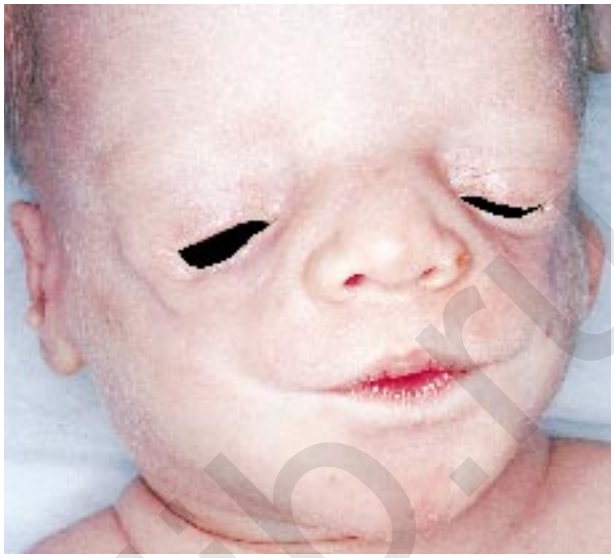

Figure 3.191. This infant with Treacher-Collins syndrome (mandibulofacial dysostosis) shows the typical findings of antimongoloid slanting palpebral fissures, colobomas of the lateral part of the lower eyelids, deficient eyelashes, hypoplasia of the zygomatic arch, micrognathia, and malformed ears. The nose is prominent.

3.192

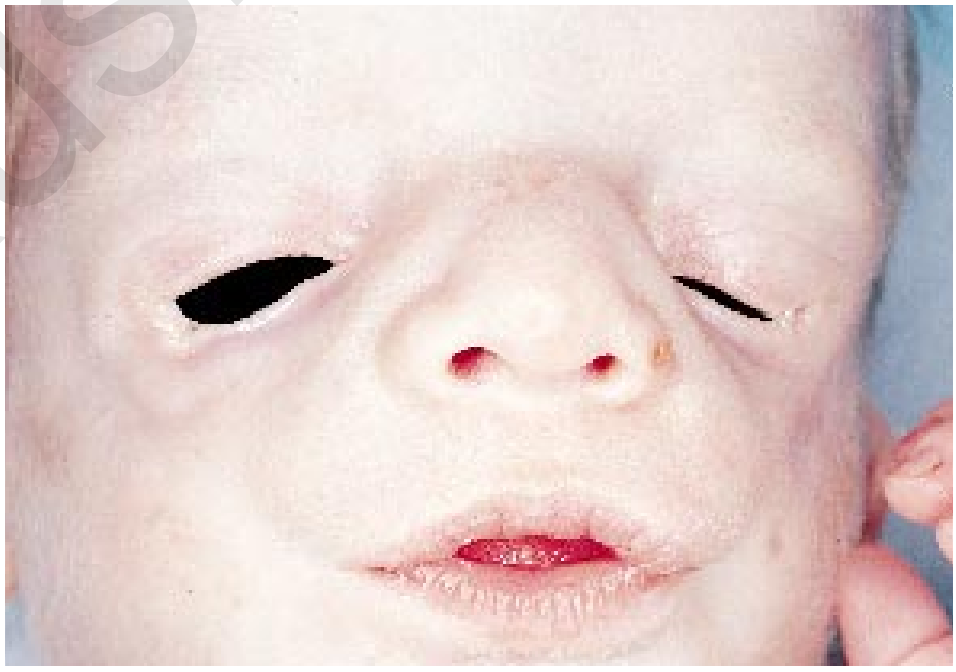

Figure 3.192. Close-up of the face of the same infant showing the antimongoloid slant and colobomas of the lower eyelids which typically occur at the junction of the inner two-thirds and outer third of the lower eyelids. Note the absence of eyebrows and eyelashes, the prominent nose and the hypoplasia of the zygomatic bone.

3.193

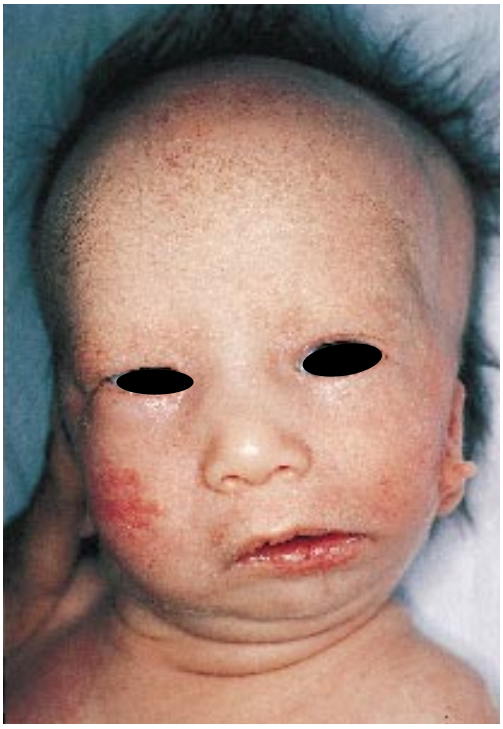

Figure 3.193. A less severe case of Treacher-Collins syndrome. Note the unilateral macrostomia and the abnormal ear. Treacher-Collins syndrome is a familial malformation involving structures originating from the first branchial arch and may have moderate expressivity.

3.194

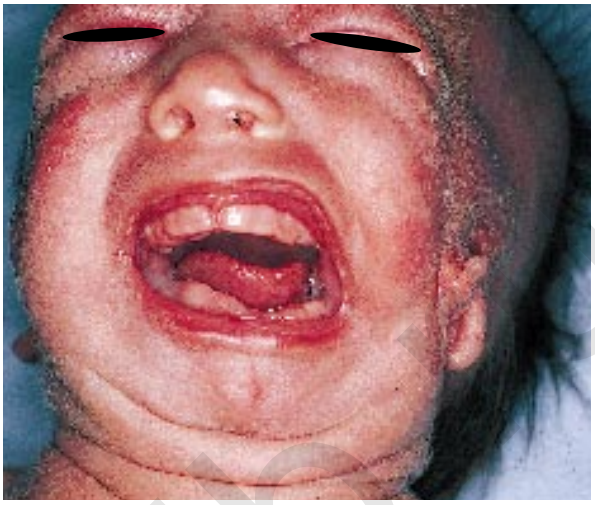

Figure 3.194. The same infant when crying better demonstrates the findings. Note the antimongoloid slant, the prominent nose, and the micrognathia. Infants with this syndrome may have a cleft of the palate, particularly of the soft palate. A finding in many of these infants is a projection of the scalp hair onto the lateral cheek.

3.195

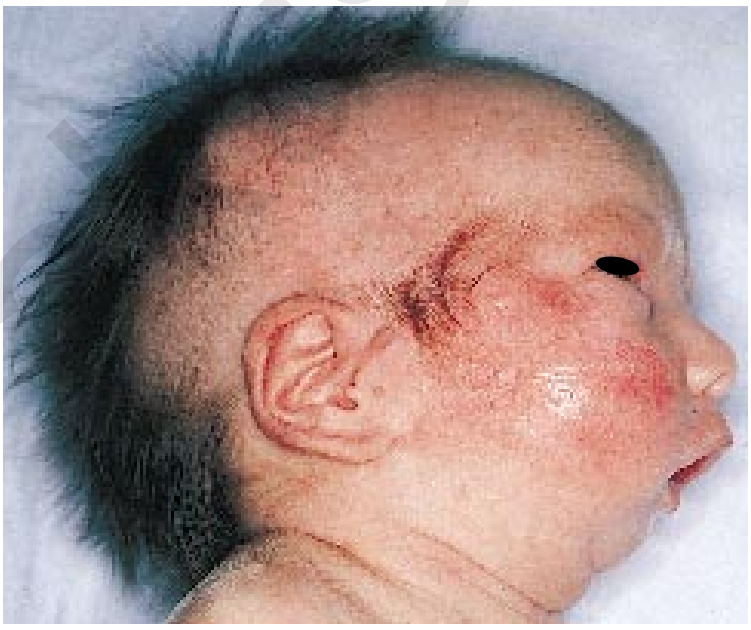

Figure 3.195. A lateral view of the same infant showing the slightly abnormal right ear with preauricular skin tags, the prominent nose and micrognathia.

3.196

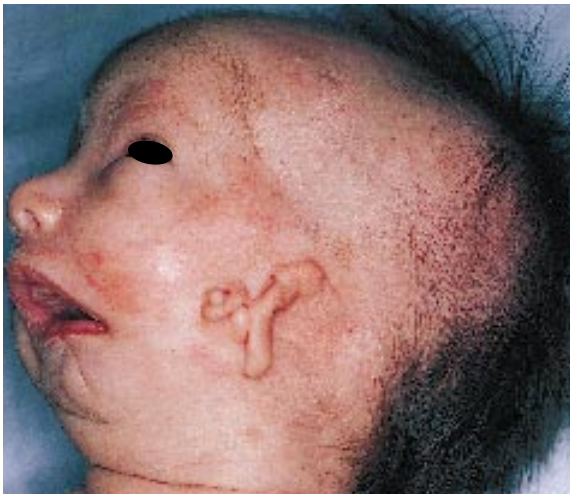

Figure 3.196. Lateral view of the same infant showing the grossly abnormal ear on the left side with atresia of the auditory canal, the antimongoloid slant, prominent nose and micrognathia.

3.197

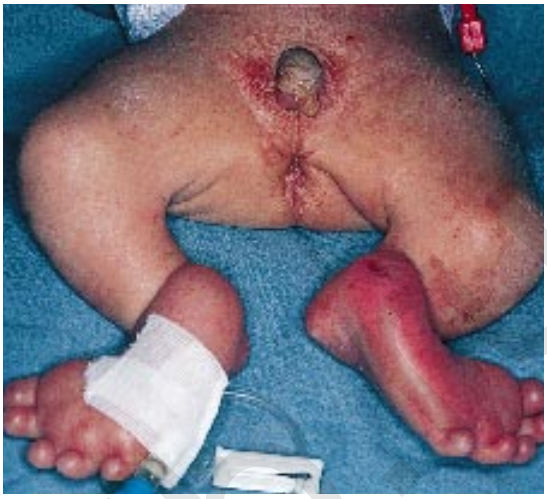

Figure 3.197. This infant with the VACTERL syndrome exhibits the following: *v*ertebral anomalies, imperforate *a*nus, *c*ardiac defects, *t*racheoesophageal fistula, *r*enal anomalies, and *l*imb defects. In cases where the acronym VATER is used, the "C" for cardiac abnormalities, and the "L" for limb defects are excluded, and the "R" stands for renal and radial anomalies. This infant had a tracheoesophageal fistula, duodenal atresia, and anal stenosis. There was a double outlet left ventricle causing congestive failure, hydronephrosis, ambiguous genitalia, and cryptorchidism. There was sacral dysgenesis and hemivertebrae, absence of the radii bilaterally, absence of tibiae bilaterally, and severe clubfoot.

3.198

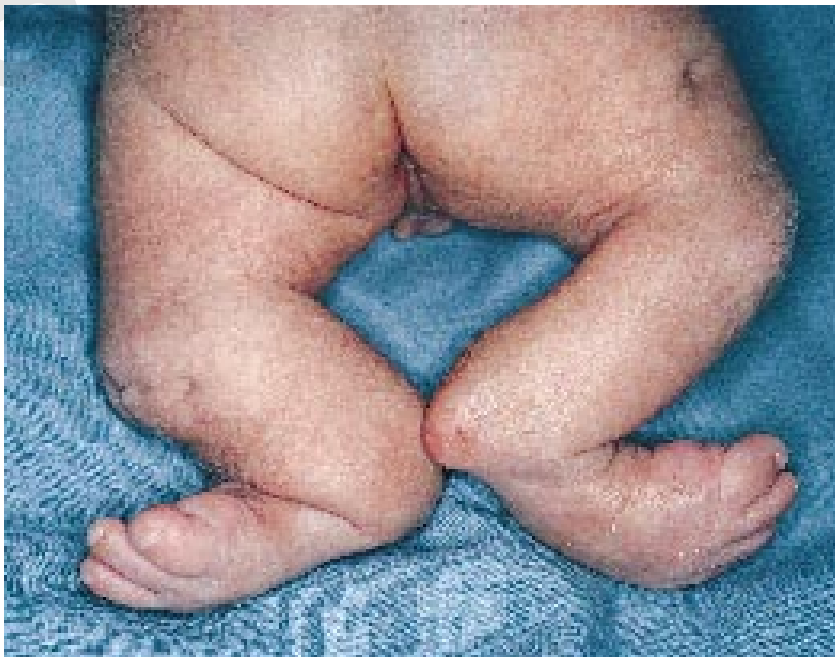

Figure 3.198. A posterior view of the pelvis and lower extremities of the same infant. Note the abnormal gluteal folds, as this infant also had bilateral dislocation of the hips. Note the skin dimples at the joints.

3.199

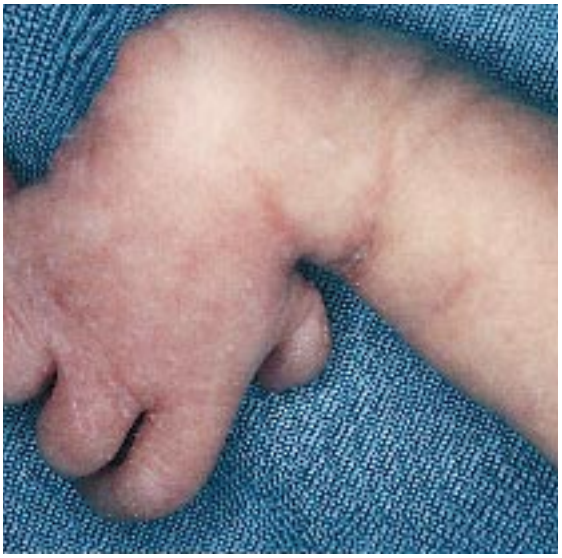

Figure 3.199. The right upper extremity of this same infant shown in Figures 3.197 and 3.198 shows the club hand due to the absence of the radius.

3.200

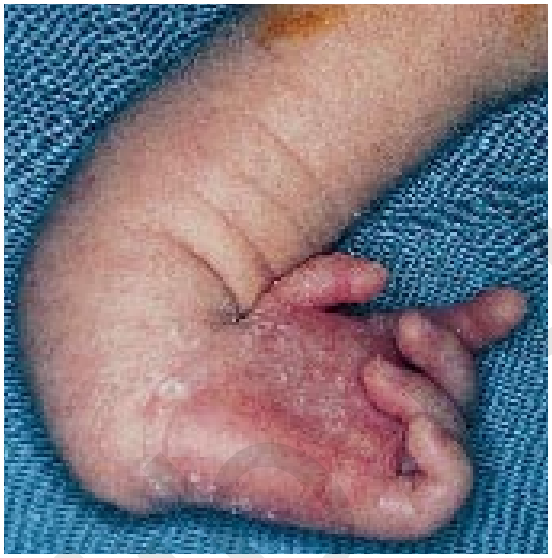

Figure 3.200. The left upper extremity of the same infant shows the absence of the radius, resulting in a club hand. Also note the abnormal thumb.

3.201

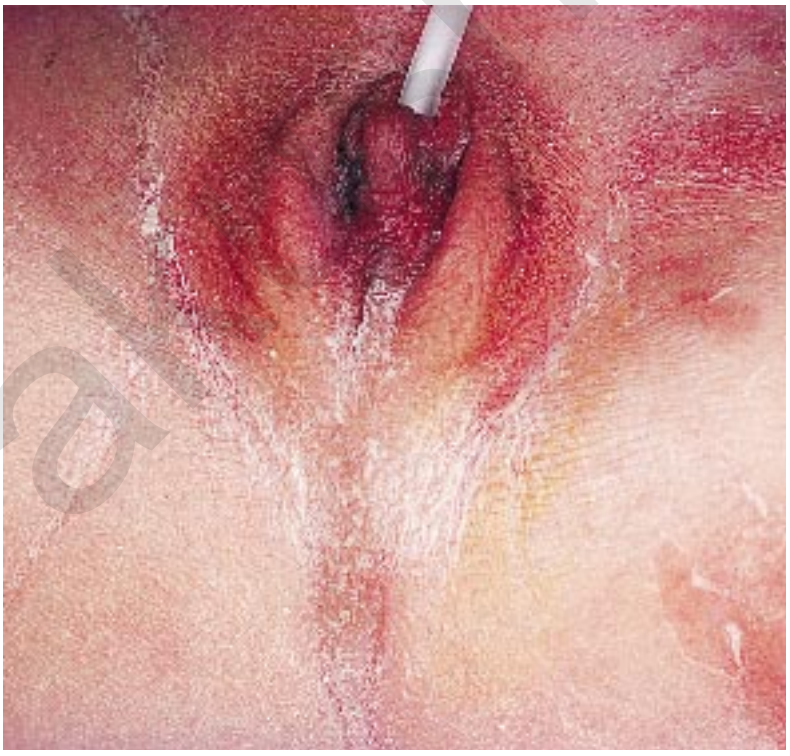

Figure 3.201. This infant with the VACTERL syndrome presented with vertebral anomalies of the lower thoracic vertebrae, an esophageal atresia, dextrocardia, imperforate anus, and ambiguous genitalia. There were no anomalies of the limbs. Note the imperforate anus and ambiguous genitalia. Karyotype was normal XX. A catheter placed in the single perineal opening appeared in the colostomy. This confirmed the presence of a cloacal sac.

3.202

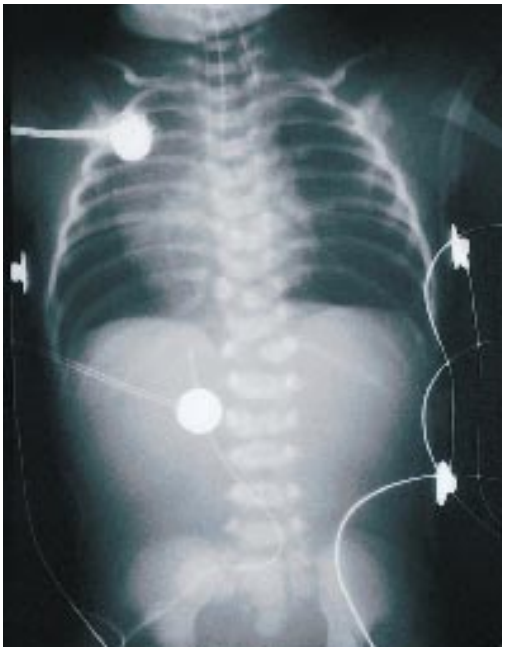

Figure 3.202. Radiograph of this infant shows the air-filled blind esophageal sac. Note that there is no communicating fistula, as the abdomen is completely opaque due to lack of air in the GI tract. There is abnormal segmentation of the distal thoracic vertebrae and anomalies of the ribs.

3.203

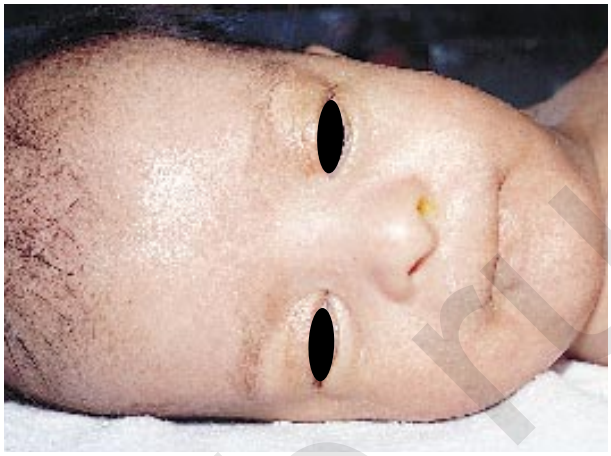

Figure 3.203. Infants with Zellweger syndrome (cerebrohepatorenal syndrome) present with hypotonia and typical craniofacial features, in addition to other finings. In the close-up of the head of this infant note the high prominent forehead and somewhat flattened facies, hypertelorism, epicanthic folds, anteverted nares, and micrognathia.

3.204

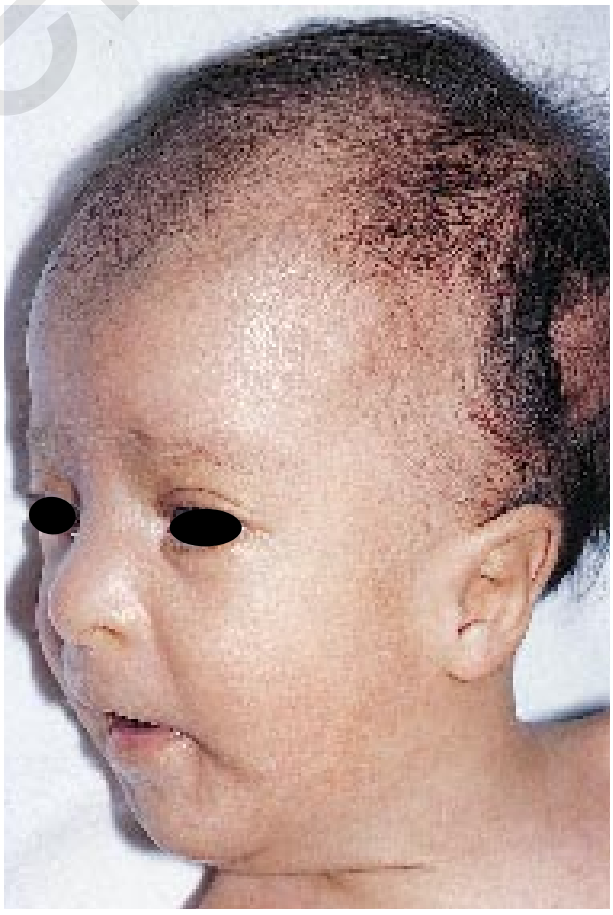

Figure 3.204. The lateral view of the face of the same infant shows the high forehead, flattened facies, micrognathia, and low-set ears. There is brachycephaly as the occiput is flat. In this infant the fontanelles were wide open, and hepatosplenomegaly, albuminuria, and ulnar deviation with a simian crease of the hand were present.

3.205

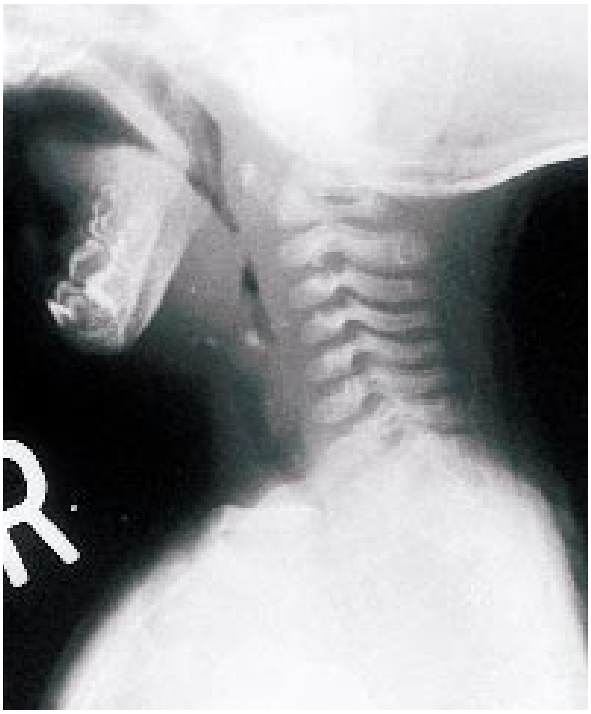

Figure 3.205. Stippling of the epiphyses and hyoid are common in Zellweger syndrome. This radiograph of the neck shows stippling at the hyoid bone.

3.206

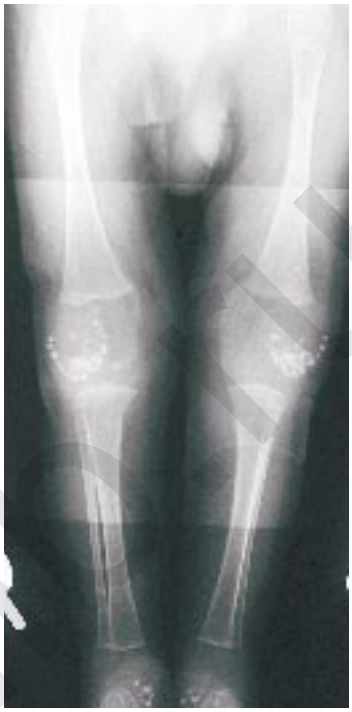

Figure 3.206. Early punctate mineralization of the patella is a common finding, and note the stippling at the knee joints and ankles.

3.207

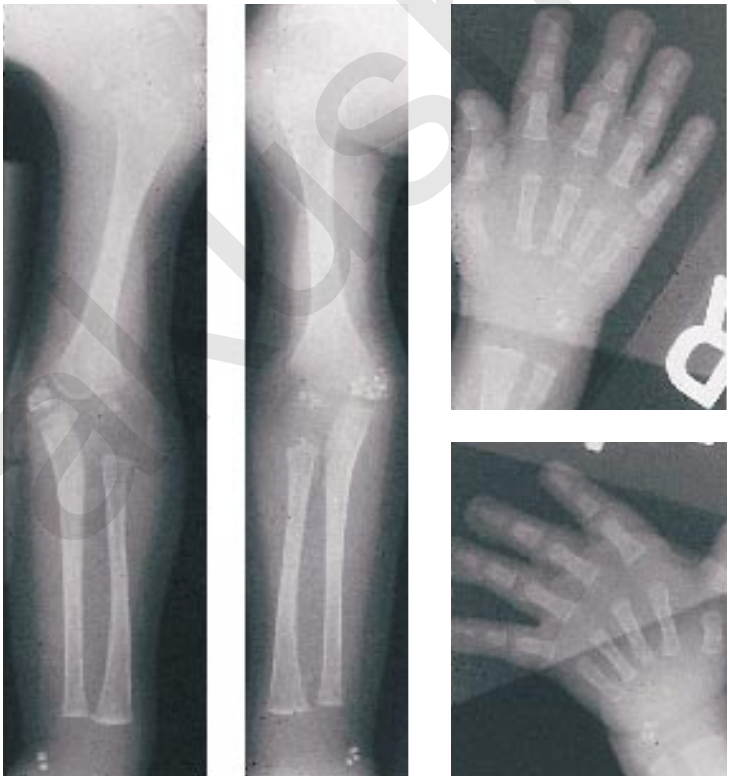

Figure 3.207. Radiographs of the upper extremities of the same infant showing the stippling at the elbows and wrists.

3.208

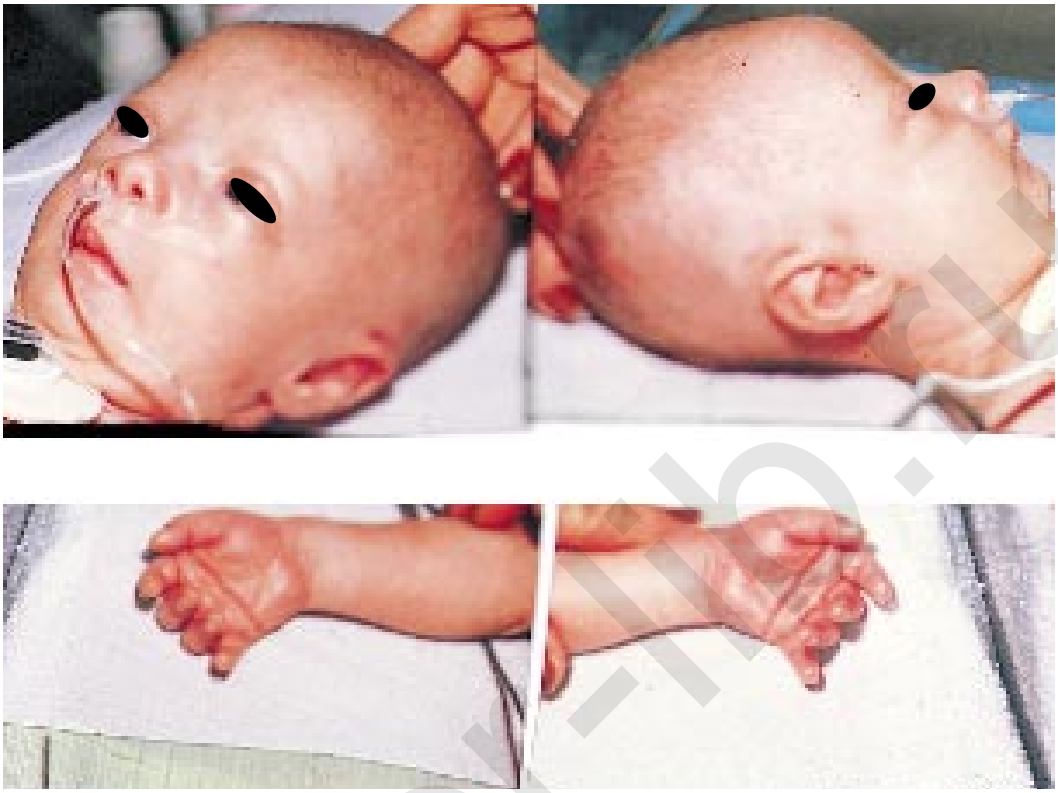

Figure 3.208. This infant with Zellweger syndrome had marked hypotonia and shows the typical appearance of the head and face, the single palmar creases, and clinodactyly. There is commonly ulnar deviation with simian creases of the hand. Brushfield's spots also occur in infants with Zellweger syndrome. Because of the hypotonia, craniofacial findings, Brushfield's spots, and simian creases, these infants often are mistaken for infants with trisomy 21.

Chapter 4
Chromosomal Disorders

Chromosomal abnormalities are fairly common. They occur in about 1 in every 200 deliveries, although many of these infants are phenotypically normal. In addition, 50% of all spontaneous abortions involve a chromosomal abnormality. Nondisjunction, where an extra chromosome (or part of a chromosome) is present (e.g., trisomy 21), is the most common cause of chromosomal disorders. Translocation syndromes, where chromosomal material breaks off from one chromosome and translocates to another, may not have classic clinical findings and may be difficult to diagnose. Usually infants with balanced translocations are only carriers and do not demonstrate clinical manifestations, while unbalanced translocations result in clinical signs. A deletion occurs when chromosomal material is missing from either the upper (p) or lower (q) arms of a chromosome (e.g., cri du chat syndrome with deletion of the upper short arm of chromosome 5 5p–). An abnormal number of X or Y chromosomes can also result in significant clinical syndromes (e.g., Turner's syndrome with absence of one of the X chromosomes 45X0). Chromosomal analysis should be considered for all stillbirths, newborns with multiple congenital anomalies, or to confirm a suspected chromosomal diagnosis.

4.1

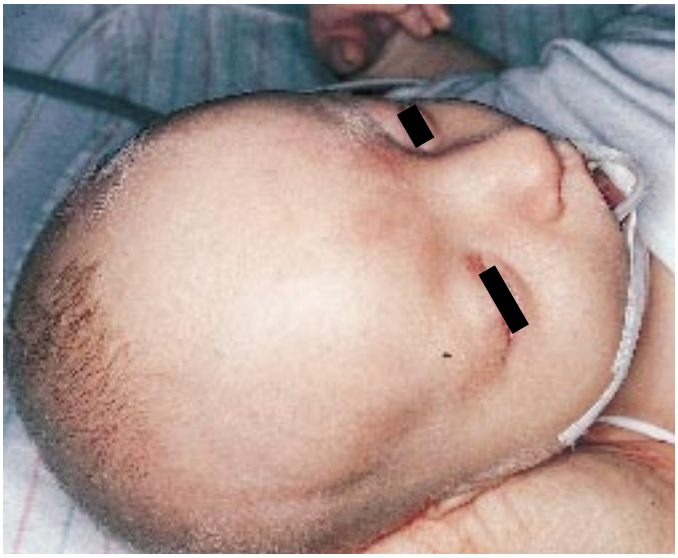

Figure 4.1. In the syndrome caused by deletion of the short arm of chromosome number 4 (4p– syndrome, Wolf-Hirschhorn syndrome), there is marked prenatal growth deficiency and decreased fetal activity. At birth the facial features are typical: microcephaly, a high forehead, prominent glabella, and a wide nasal bridge with nasal beaking (the "Grecian helmet" appearance of the head). This infant also has craniofacial asymmetry.

4.2

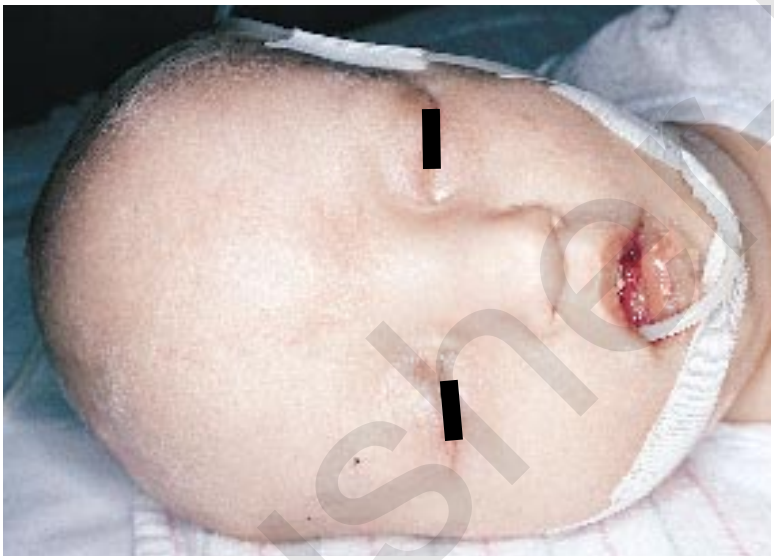

Figure 4.2. A frontal view of the same infant shows the high forehead and a prominent glabella. The eyebrows are highly arched and sparse medially. There is nasal beaking and epicanthic folds with bilateral ptosis. There is a short deep philtrum with a short upper lip and a turned-down, fish-like mouth. A cleft lip and/or palate occurs in about 10% of these infants.

4.3

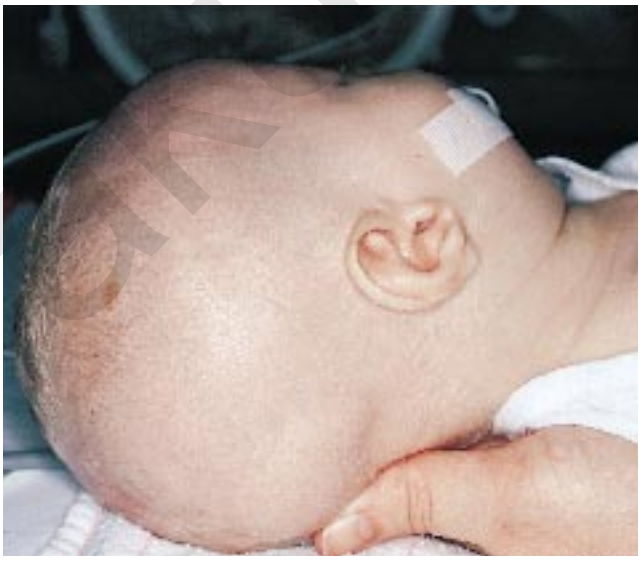

Figure 4.3. In the lateral view of the same infant note the lobeless pinnae and micrognathia. The external auditory canals are narrow.

4.4

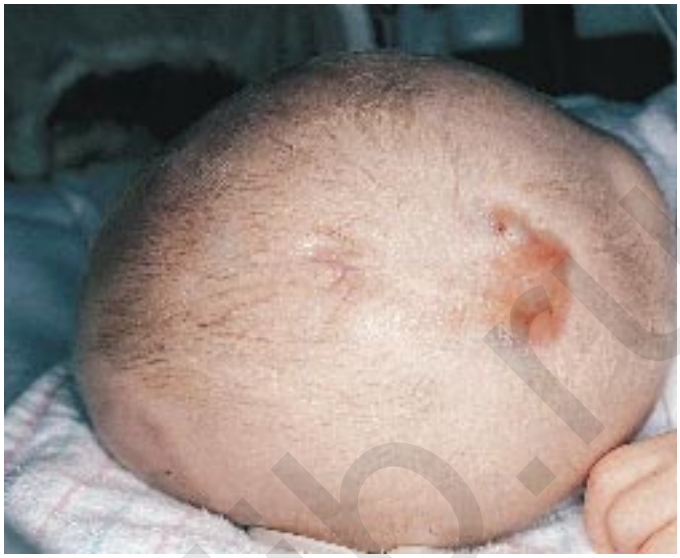

Figure 4.4. This same infant with Wolf-Hirschhorn syndrome had a posterior midline scalp defect which is seen in about 10% of these infants. He also had hypospadias and cryptorchidism, a finding frequently associated with this syndrome.

Other findings in infants with this syndrome include coloboma of the iris, simian crease, hypoplastic dermal ridges, talipes equinovarus, and cardiac anomalies. Radiologically there may be fusion of the ribs and dislocation of the hips.

4.5

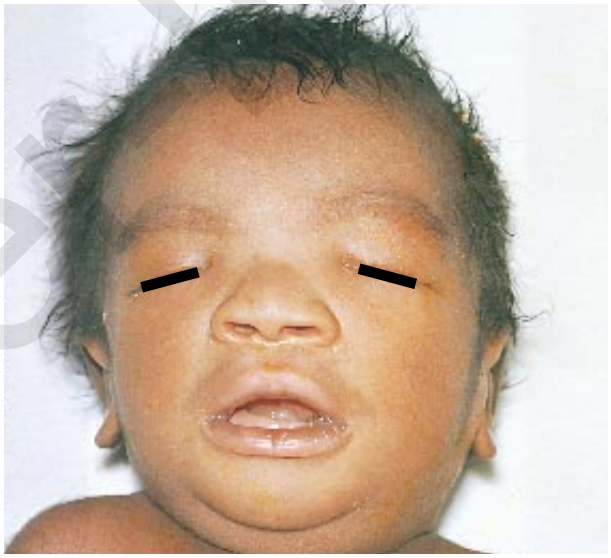

Figure 4.5. Deletion of the short arm of chromosome number 5 (5p– syndrome, cri du chat syndrome) is present in this infant; his twin was normal. Note the craniofacial disproportion, with microcephaly, round face, dysplastic low-set ears, the downward (antimongoloid) slant of the palpebral fissures, hypertelorism, and micrognathia. The typical cat cry (high-pitched mewing cry) was present. The cat cry is due to a narrow larynx, and occurs as a result of the cords being approximated anteriorly leaving a narrow opening posteriorly. It is not present in all infants and disappears as the infant grows.

4.6

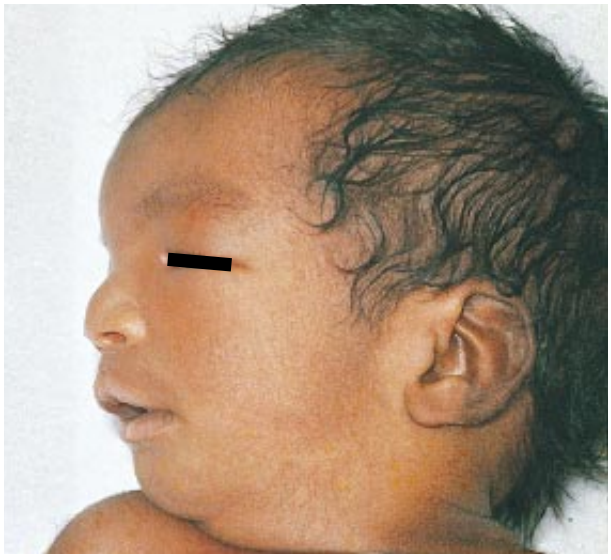

Figure 4.6. The lateral view of the same infant shows the low-set ears, flattened nose, and micrognathia.

4.7

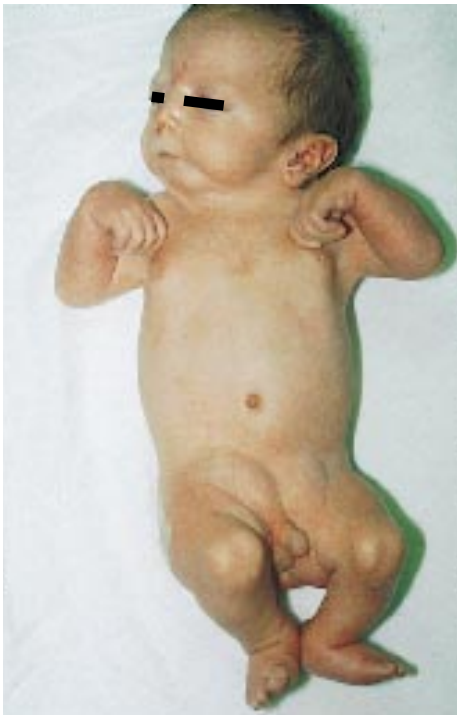

Figure 4.7. Trisomy 8 syndrome is usually a trisomy 8/normal mosaicism. Note the dysmorphic craniofacial features, micrognathia, postural deformity of the hands, cryptorchidism with bilateral inguinal herniae, and absence of the patellae.

4.8

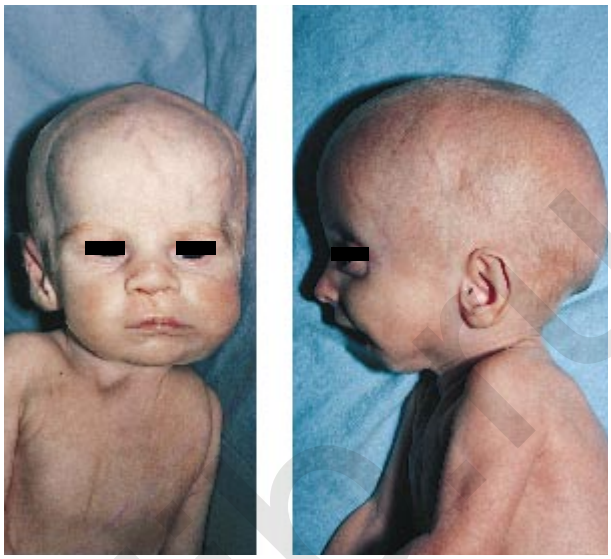

Figure 4.8. Another infant with trisomy 8 shows the dysplastic craniofacial features (short nose, broad nasal bridge, prominent nares, wide philtrum, thin upper lip, and low-set ears with thick helices).

4.9

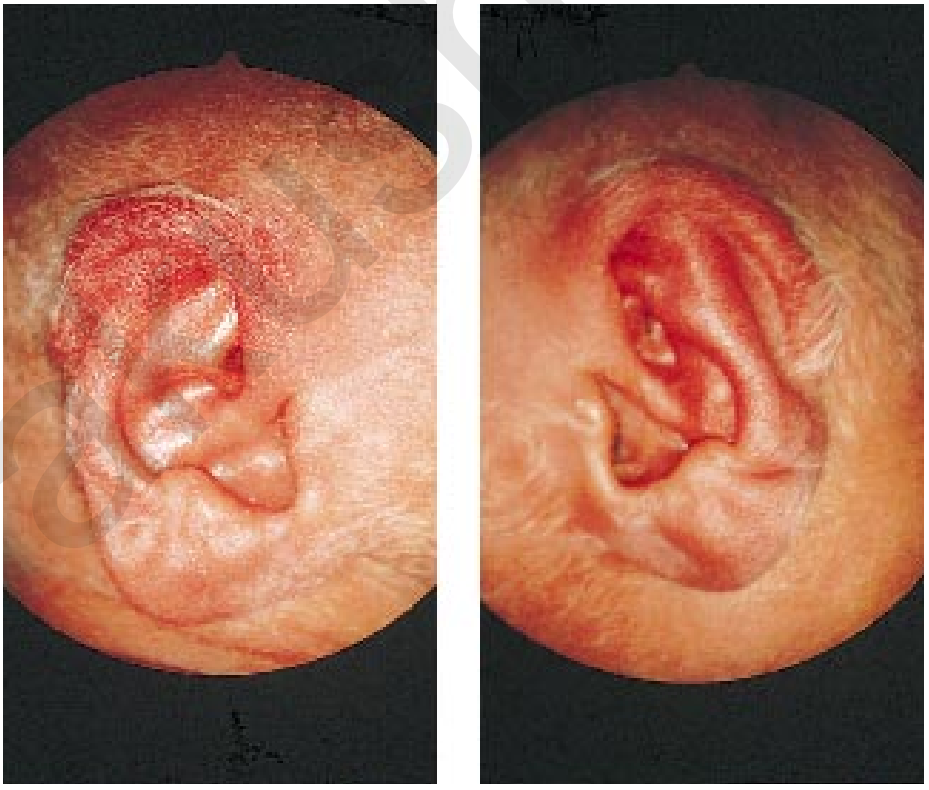

Figure 4.9. A close-up view of the ears of the same infant demonstrates the thick helices.

4.10

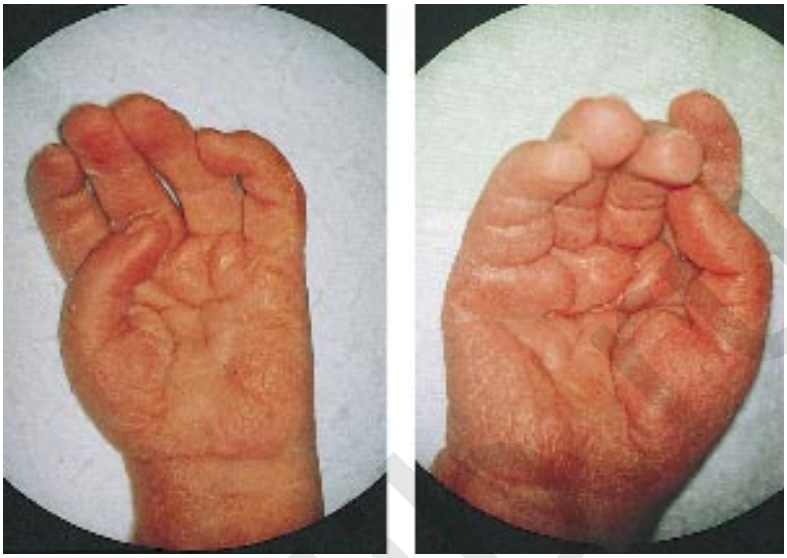

Figure 4.10. The hands of the same infant with trisomy 8 show the shortened hallux, camptodactyly, and deep flexion creases of the palms. Deep furrows are found on both the palms of the hand and soles of the feet (these regress with increasing age).

4.11

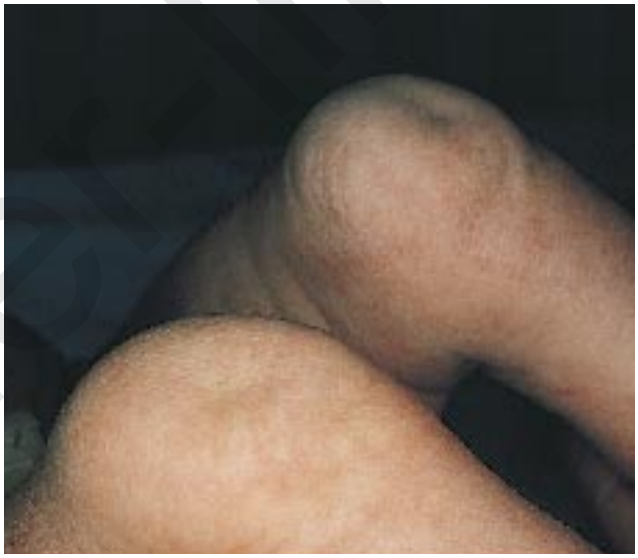

Figure 4.11. Congenital absence of the patellae is another finding in the trisomy 8 syndrome. In addition to the findings shown here in trisomy 8 other common findings include cleft palate, single palmar crease, and contractures of large joints.

4.12

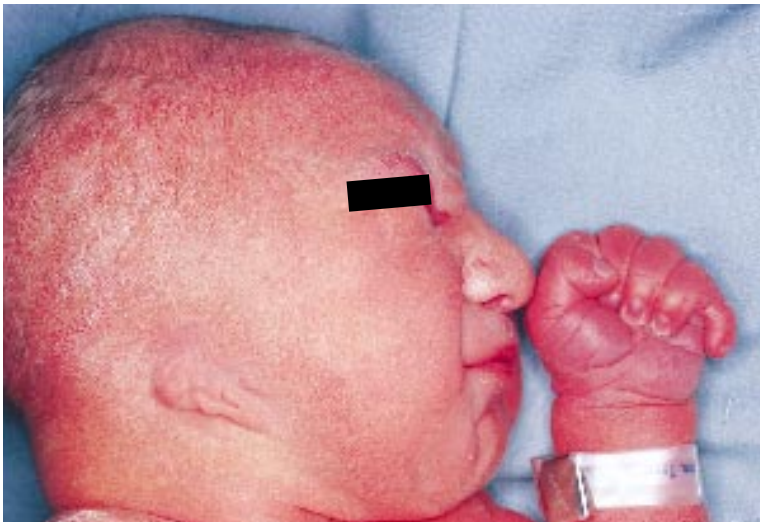

Figure 4.12. In the trisomy 13 syndrome (Patau's syndrome) there is microcephaly, a sloping forehead, grossly abnormal ears, micrognathia, and polydactyly. In this infant, in addition to these findings, there was a scalp defect and atresia of the external auditory canals. In trisomy 13 syndrome other findings include microphthalmia, anophthalmia, hypo- or hypertelorism, depressed nasal bridge, bilateral cleft lip and/or palate, congenital heart disease, omphalocele, large umbilical hernia, renal anomalies, flexion and overlapping of the fingers, single palmar crease, and a prominent heel giving rise to "rocker-bottom" feet. If the infant sur-

4.13

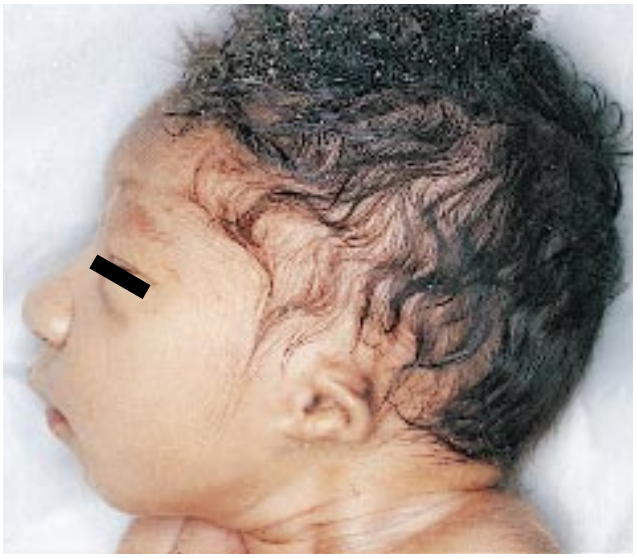

Figure 4.13. Trisomy 13 in another infant showing microcephaly, microtia with low-set ears, and micrognathia. This same infant had bilateral glaucoma.

4.14

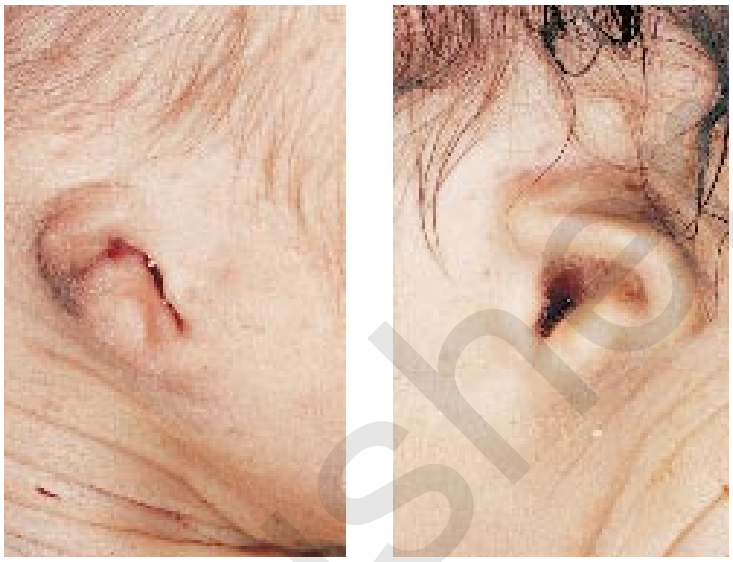

Figure 4.14. A close-up view of the ears of the same infant showing the bilateral microtia. Ear abnormalities may be minimal or there may be total absence of the external auditory canal.

4.15

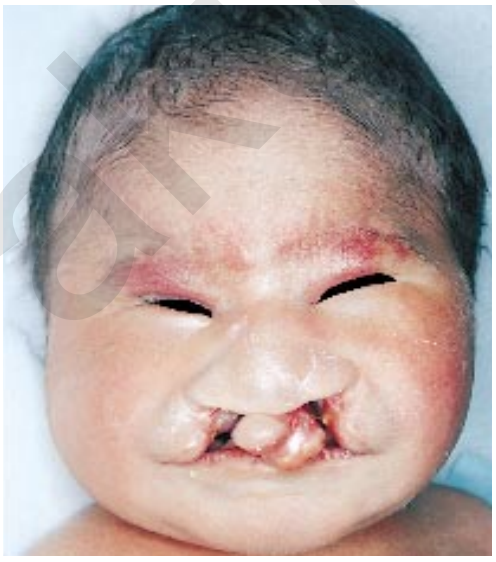

Figure 4.15. A common finding in trisomy 13 is bilateral cleft lip and palate. In this infant there is microcephaly, hypotelorism, the eyes are microphthalmic, and there is a receding forehead. On further study the infant had an alobar holoprosencephaly. In trisomy 13, central nervous system abnormalities are found in 50% or more of infants and, hence, one should check for a holoprosencephaly defect.

4.16

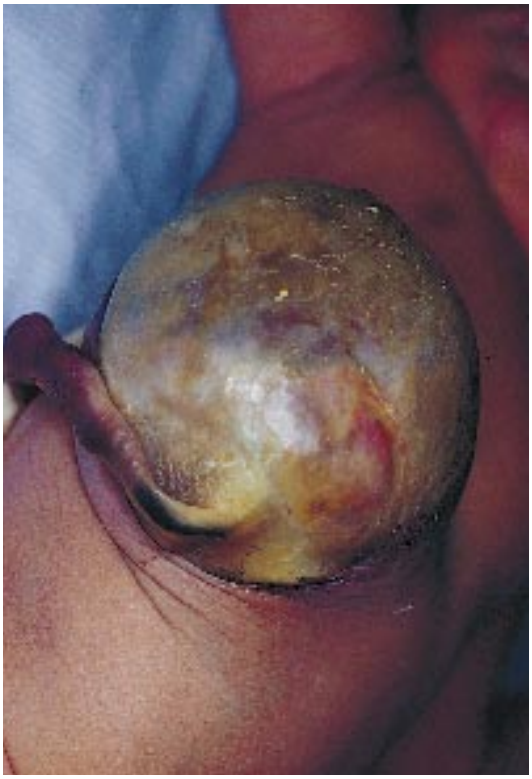

Figure 4.16. The same infant also had an omphalocele. The finding of cleft lip and palate with an omphalocele or large umbilical hernia should alert one to the possibility of the diagnosis of trisomy 13.

4.17

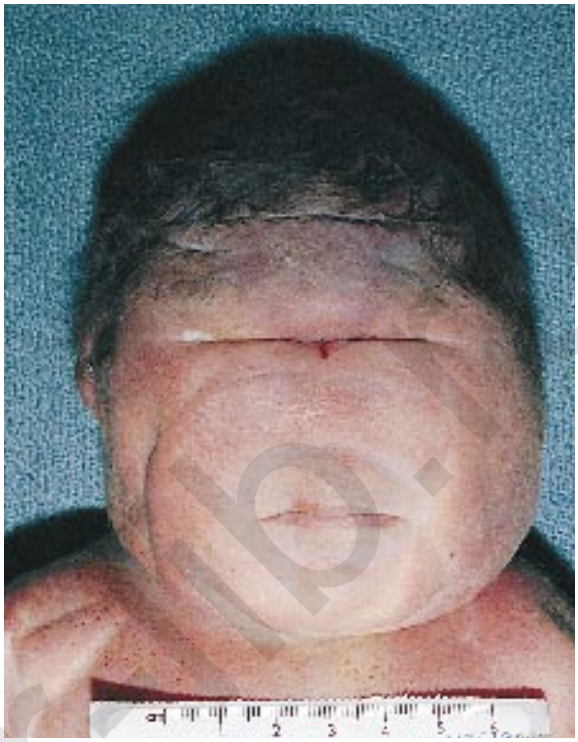

Figure 4.17. Median cleft syndrome may be associated with chromosomal defects. This infant with trisomy 13 had cyclops with anophthalmia. There is no proboscis present. There was arhinencephaly and alobar holoprosencephaly on CT scan.

4.18

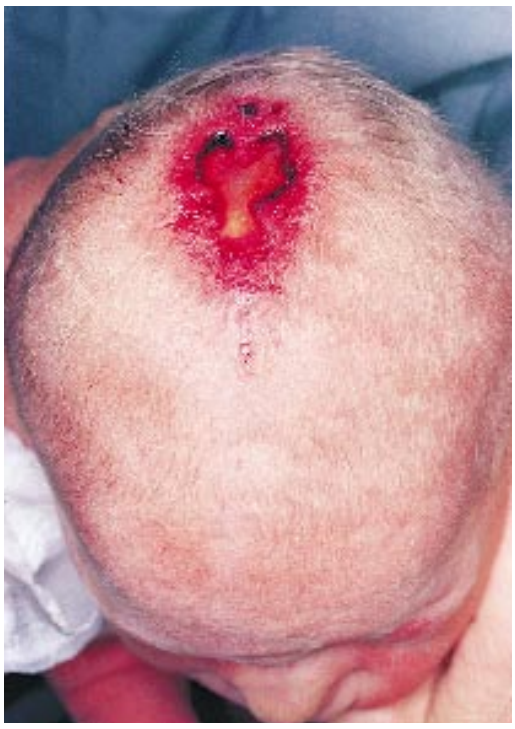

Figure 4.18. Another common finding in trisomy 13 is a midline scalp defect, which is most common in the parieto-occipital area. This infant also had abnormal ears, micrognathia, and polydactyly.

4.19

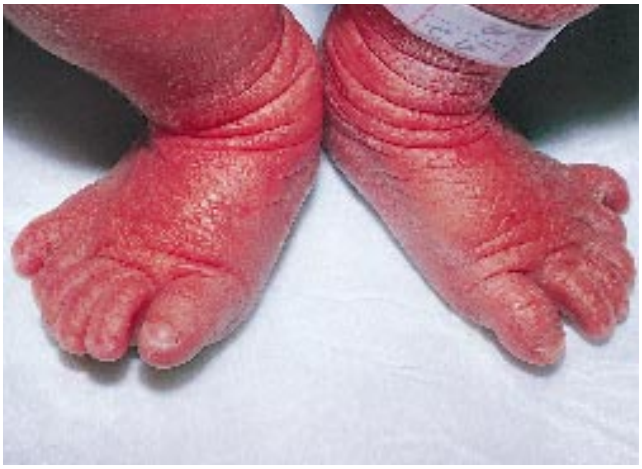

Figure 4.19. Polydactyly of the hands and feet occur frequently in infants with trisomy 13.

4.20

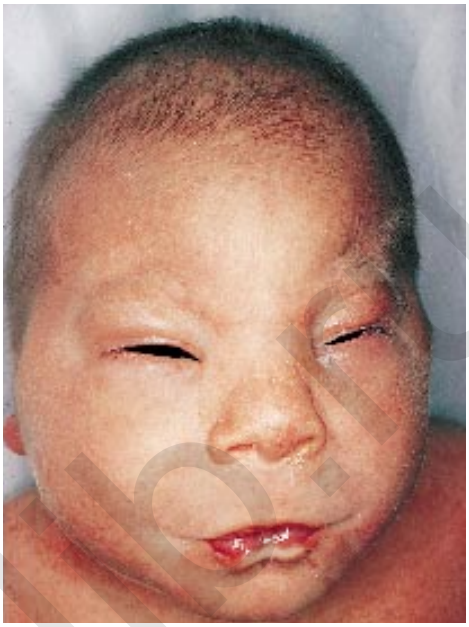

Figure 4.20. In this infant with trigonocephaly, hypotelorism, patchy alopecia, and eleven ribs, the diagnosis was that of a ring D chromosome defect (karyotype was performed in the pre-banding era). Trigonocephaly is associated with premature fusion of the metopic suture and may occur in chromosomal anomalies and in median cleft syndrome, but also occurs in normal infants.

4.21

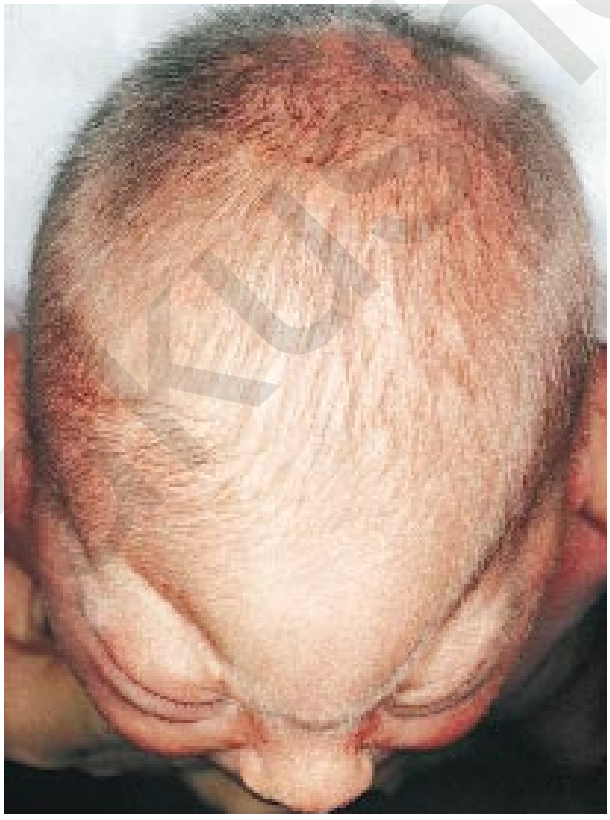

Figure 4.21. This view better demonstrates the trigonocephaly and the patchy alopecia.

4.22

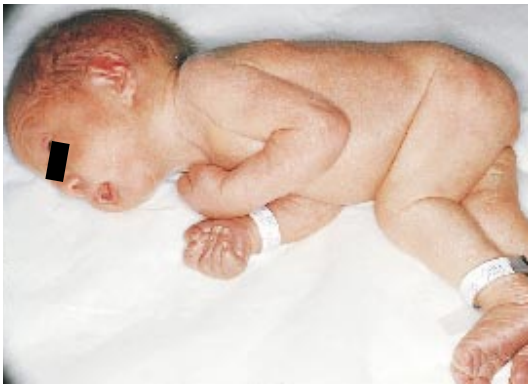

Figure 4.22. Severe intrauterine growth retardation (birthweight 1590 g at term) was noted in this infant with the typical findings of trisomy 18 (Edwards' syndrome). Note the low-set, poorly developed ears, micrognathia, and the typical overlapping position of the fingers. In trisomy 18 there is a preponderance of three females to one male infant. Other findings in trisomy 18 include prominent occiput, microcephaly, short sternum, congenital heart disease, abnormal genitalia, and renal anomalies (horseshoe kidney, polycystic kidneys, etc.). If the infant survives, there is severe mental retardation.

4.23

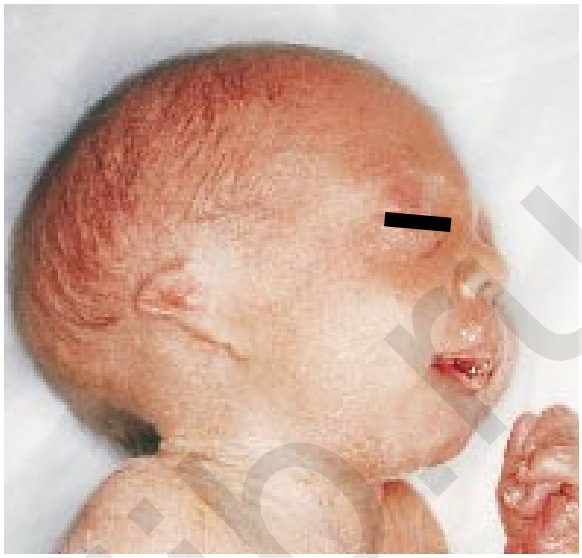

Figure 4.23. A close-up view of the face and skull in the same infant shows the characteristic prominent occiput, low-set abnormal ears with atresia of the external auditory canals (the ears often appear cupped), and micrognathia. The typical flexion deformity of the fingers can also be seen.

4.24

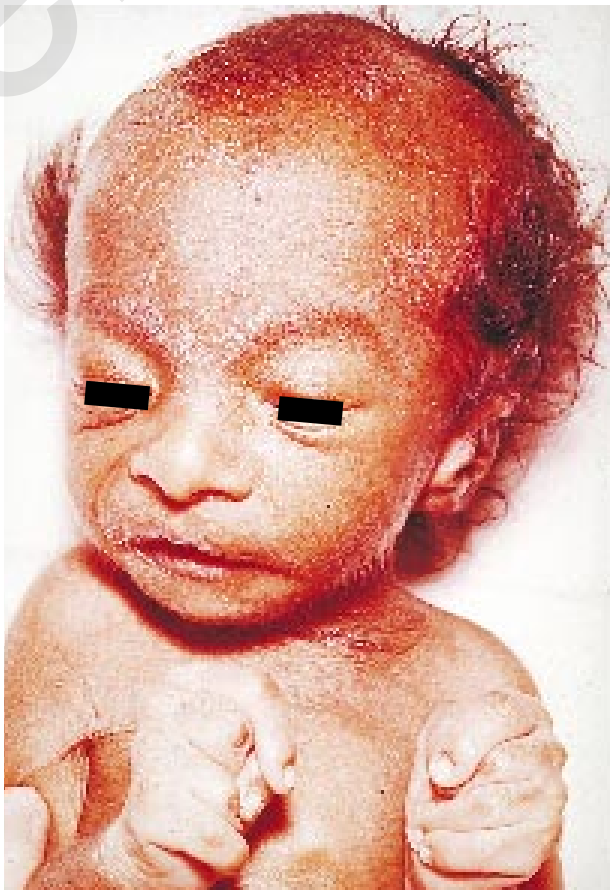

Figure 4.24. Trisomy 18 in another infant shows the intrauterine growth retardation, narrow bifrontal diameter, low-set ears, and micrognathia. Note the typical clenched hands with flexion deformities of the fingers.

4.25

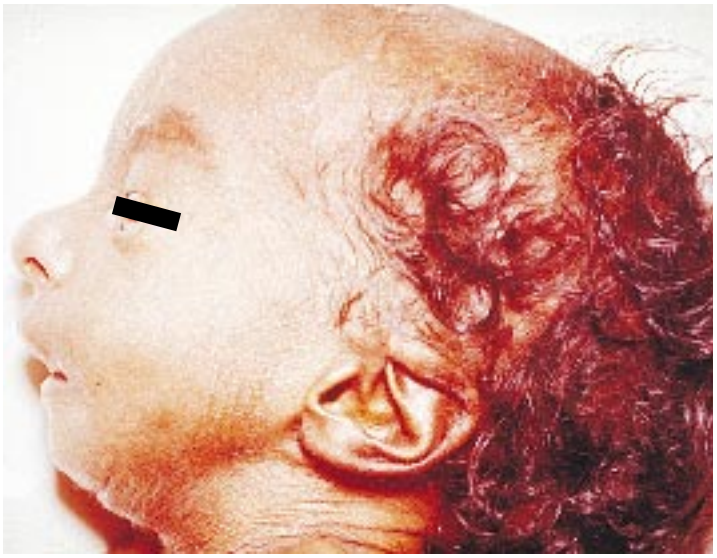

Figure 4.25. The lateral view of the same infant as in Fig. 4.24 shows the prominent occiput, low-set ears with a large pinna, and micrognathia.

4.26

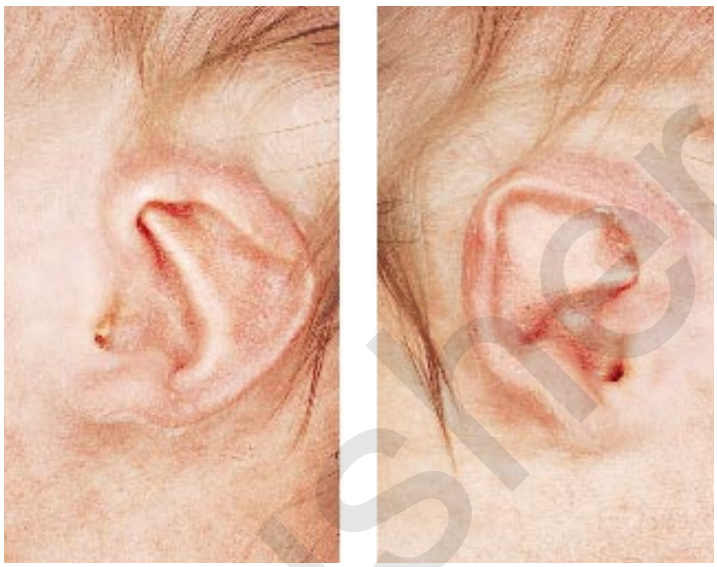

Figure 4.26. The right ear in this infant demonstrates the characteristic cupping ("tulip-shaped") deformity noted in infants with trisomy 18.

4.27

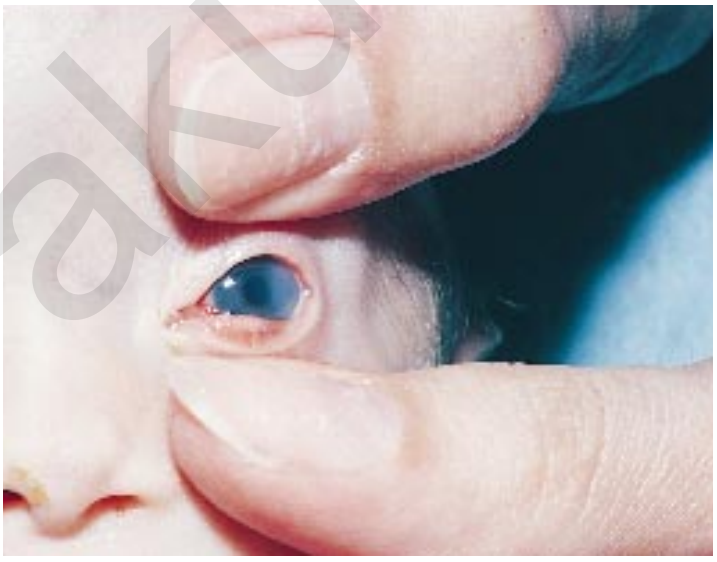

Figure 4.27. Coloboma of the left eye of this infant with trisomy 18. Other ophthalmologic findings in trisomy 18 include short palpebral fissures, hypoplasia of the orbital ridges, and corneal opacities.

4.28

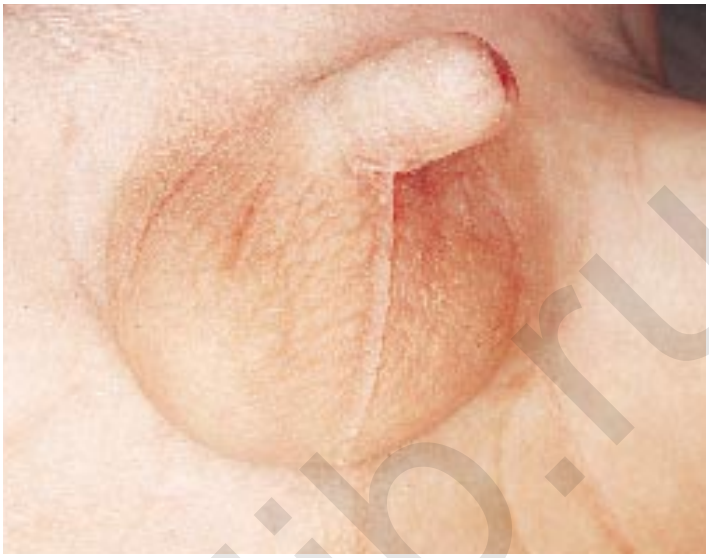

Figure 4.28. In trisomy 18, abnormalities of the genitalia are common. This male infant has cryptorchidism, and in female infants there may be hypoplasia of the labia majora with a prominent clitoris.

4.29

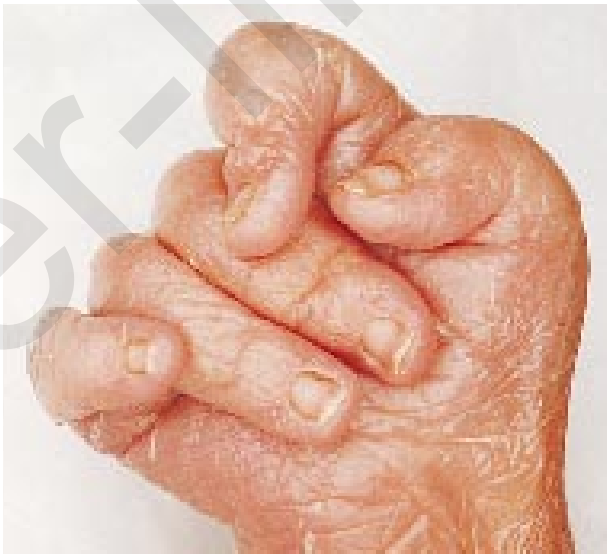

Figure 4.29. The appearance of this hand is very typical of infants with trisomy 18, occurring in about 50% of affected infants. Note the clenched hand with a tendency for the index finger to overlap the third and for the fifth finger to overlap the fourth. At times these fingers are extended, giving the appearance of the sign for "I love you" in American sign language. Infants with trisomy 18 also commonly have hypoplasia of the nails on both the fingers (especially the fifth finger) and the toes.

4.30

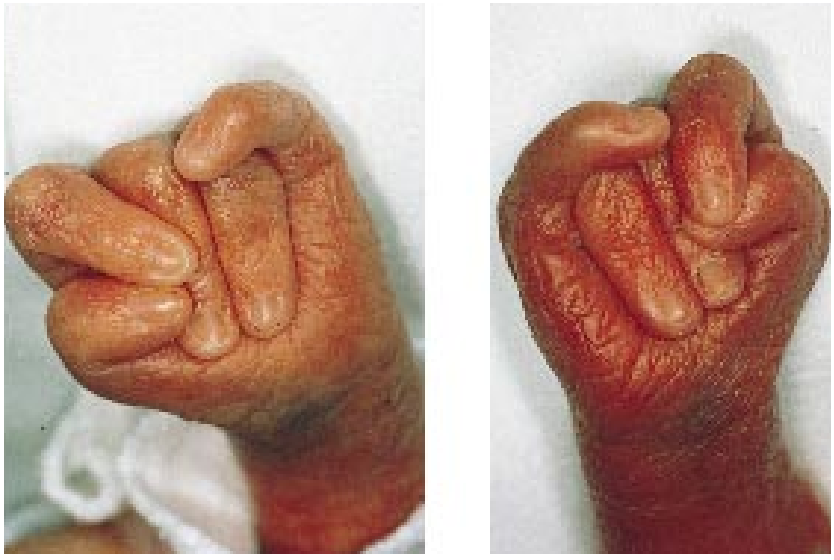

Figure 4.30. Another typical example of the hands in an infant with trisomy 18.

4.31

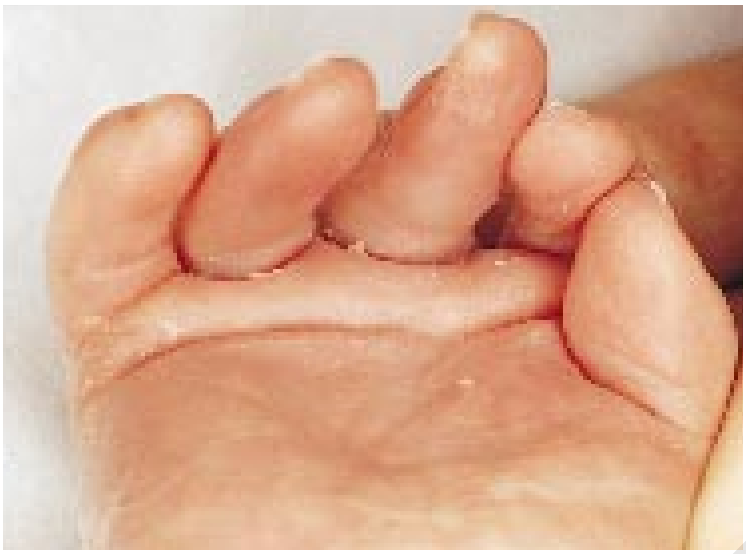

Figure 4.31. Note the single palmar crease in this infant with trisomy 18. A single palmar crease is a common finding in normal infants and is also noted in numerous syndromes. Note the lack of development of other dermal creases, indicating that there was a lack of fetal movement from early in gestation. In this infant there is an absence of finger creases on all fingers. In trisomy 18 it is not uncommon to have an absence of distal creases on the fifth finger (clinodactyly) and less commonly on the fourth and third fingers.

4.32

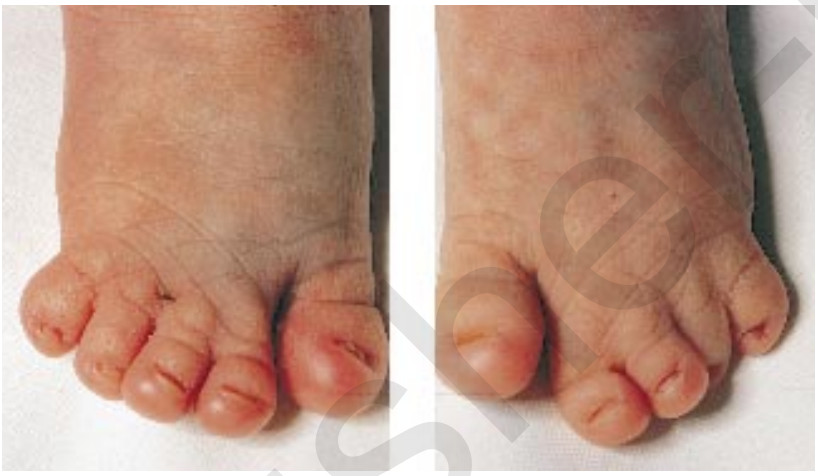

Figure 4.32. Note the short big toes and hypoplastic nails which are typically seen in trisomy 18. The short big toes are frequently dorsiflexed. There is also syndactyly of the second and third toes bilaterally in this infant, which is a common finding in normal infants and in infants with other pathologies, and is also reported in trisomy 18. Infants with trisomy 18 may have talipes equinovarus or "rocker-bottom" feet.

4.33

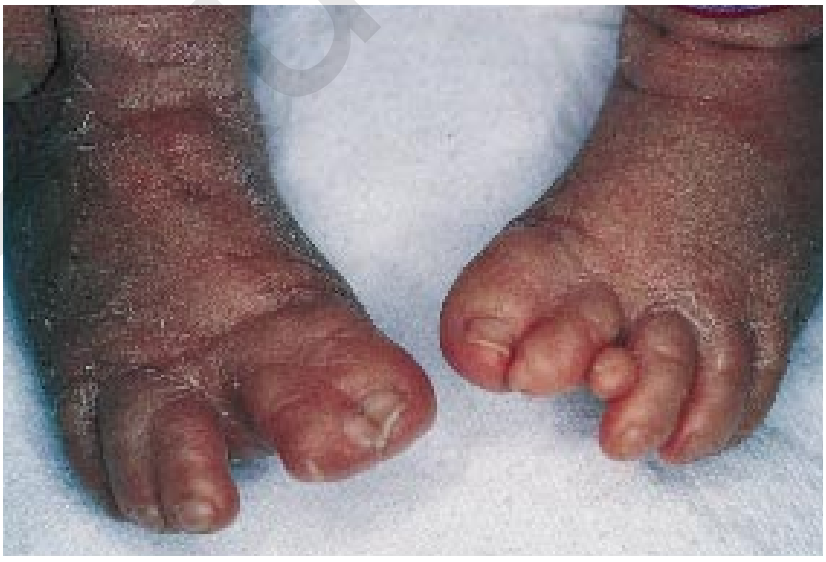

Figure 4.33. This infant did not have the typical clinical appearance of an infant with trisomy 18, but the radiographic findings of gracile ribs and antimongoloid pelvis were diagnostic. The diagnosis was confirmed by karyotype. Note the central polydactyly of the left foot and syndactyly of the right foot. Central polydactyly is an uncommon finding in normal infants and should alert one to the possible diagnosis of a chromosomal disorder.

4.34

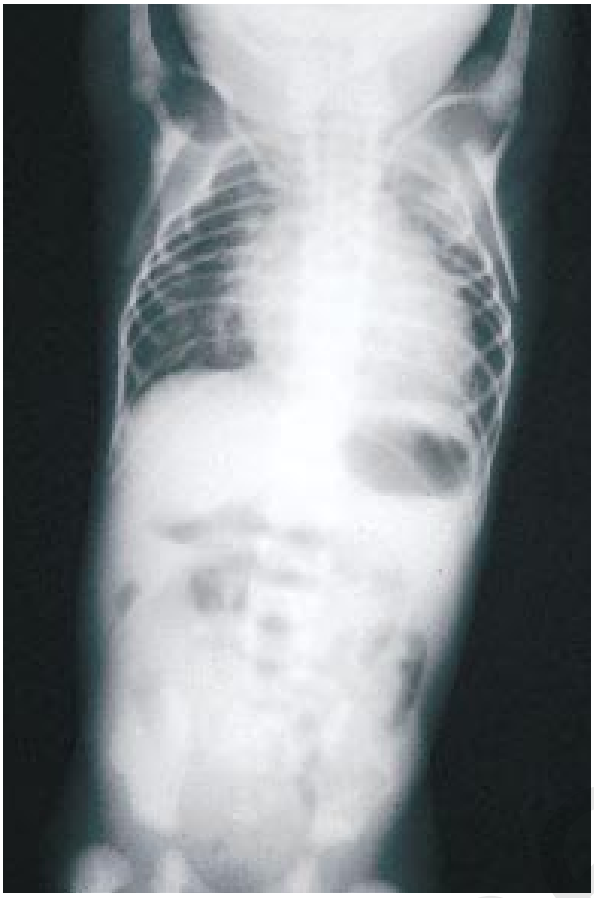

Figure 4.34. This full-body radiograph illustrates the typical findings in trisomy 18. Note the gracile (fine, delicate) ribs and the antimongoloid (very vertical) appearance of the pelvis. The infant also had cardiac enlargement which was associated with congenital heart disease (patent ductus arteriosus).

4.35

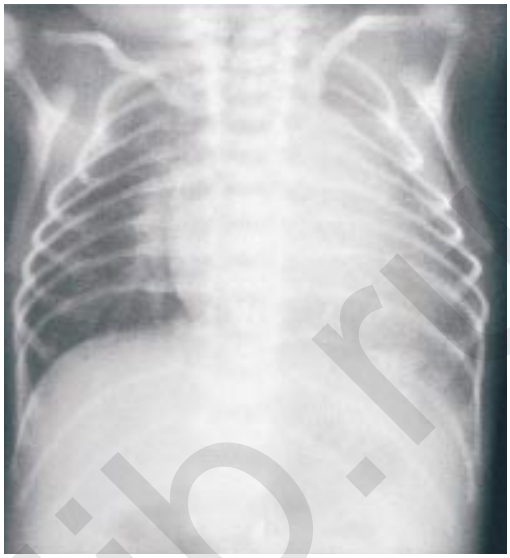

Figure 4.35. The chest radiograph of the same infant shows the gracile appearance of the ribs and the long slender clavicles, giving rise to the so-called "bicycle handle" clavicles. This radiologic appearance should always alert one to the possible diagnosis of trisomy 18.

4.36

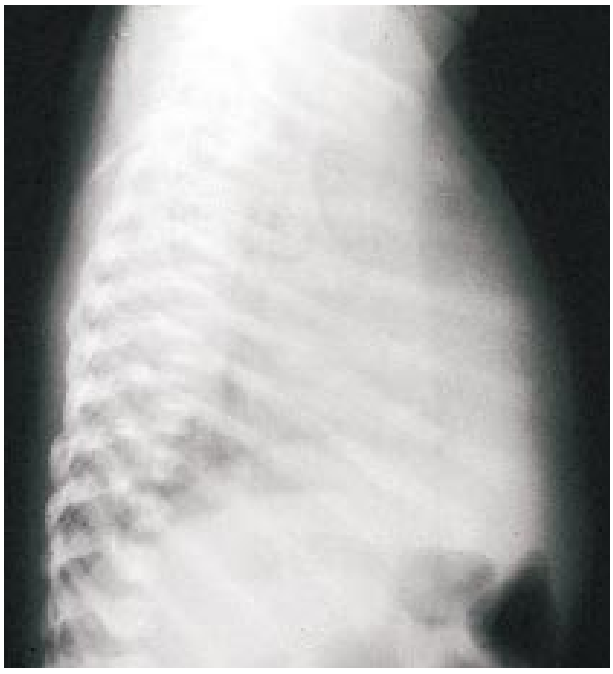

Figure 4.36. The sternum is short in trisomy 18, and sternal ossification centers are absent or decreased in number. In this lateral radiograph of the chest in another infant with trisomy 18, there are no sternal ossification centers.

4.37

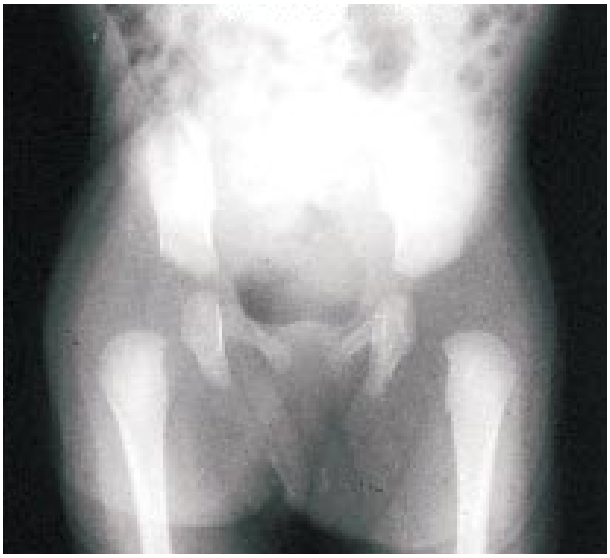

Figure 4.37. Radiograph of the pelvis in the same infant as shown in Figure 4.36 with trisomy 18 demonstrates the antimongoloid configuration. The pelvis is small, the iliac crest is narrow, and there are large acetabular angles.

4.38

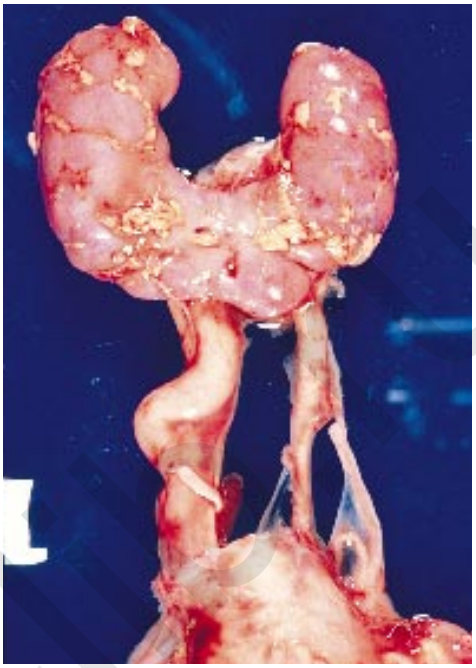

Figure 4.38. A pathologic specimen of a horseshoe kidney from an infant with trisomy 18. Note the hydroureter and hydronephrosis on the left. Horseshoe kidneys, ectopic kidneys, double ureters, and other renal anomalies are common in trisomy 18.

4.39

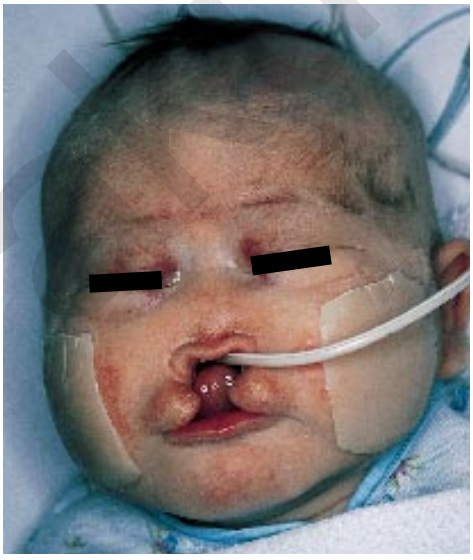

Figure 4.39. This infant with a median cleft, hypotelorism, and holoprosencephaly had an 18p– chromosomal defect. The most consistent features of the 18p– defect are ptosis, epicanthal folds, hypotelorism, rounded facies, and large protruding ears. In some cases, holoprosencephaly may be present. The hands and feet are relatively small. If the infant survives, there is severe mental retardation.

4.40

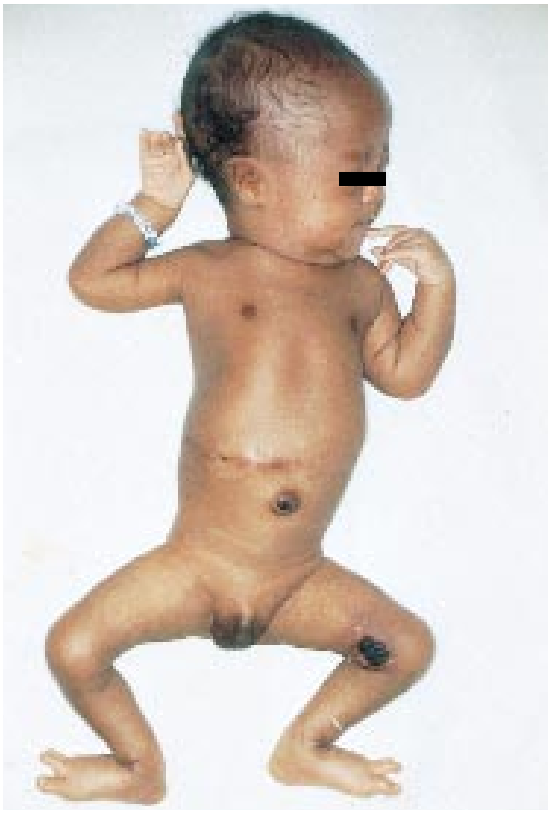

Figure 4.40. The typical appearance of an infant with trisomy 21 (Down syndrome). Note the marked hypotonia, flat facies, single palmar crease and separation of the first and second toes. The abdominal surgery was for the common finding of duodenal atresia. There is a burn at the left knee which occurred during surgery. The incidence of trisomy 21 is 1 in 700 newborns. The typical findings in trisomy 21 include hypotonia, poor Moro's reflex, hyperflexibility of joints, excess skin at the back of the neck, a flat facial profile, slanted palpebral fissures, dysplasia of the pelvis, and hand and feet abnormalities.

4.41

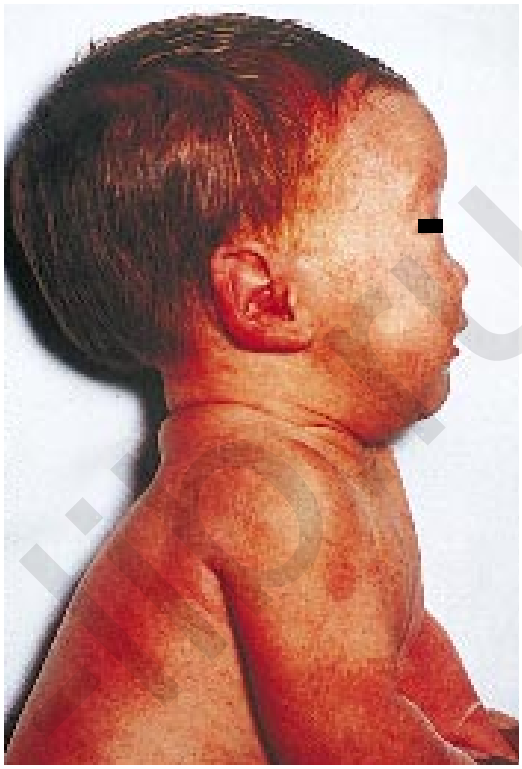

Figure 4.41. The typical flat facies ("glattegesicht") in an infant with trisomy 21 is due to a lack of the orbital ridges, a flat nose, and micrognathia, which together result in a lack of profile. Also note that there is some excess skin at the nape of the neck.

4.42

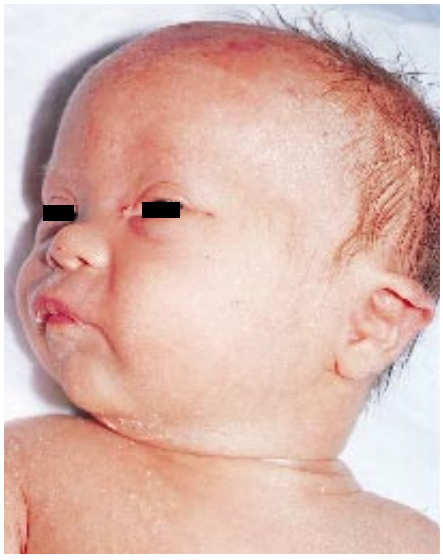

Figure 4.42. In trisomy 21 the head is small and round (brachycephaly) which occurs as a result of the flat occiput and the flat facies (compare with the prominent occiput seen in trisomy 18 [Figure 4.25]). There is a mongoloid appearance to the eyes due to the slanting palpebral fissures, the ears are low set, the nose is flat, and there is micrognathia.

4.43

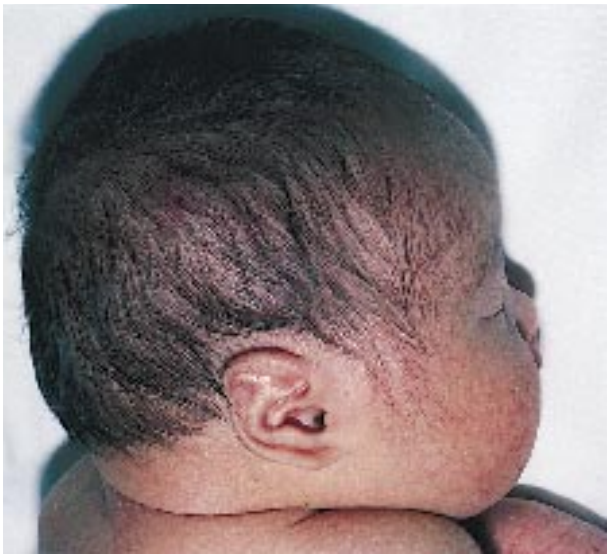

Figure 4.43. Trisomy 21 in another infant showing the typical flat facial features, flat occiput, and webbing of the neck. There was also mild microcephaly.

4.44

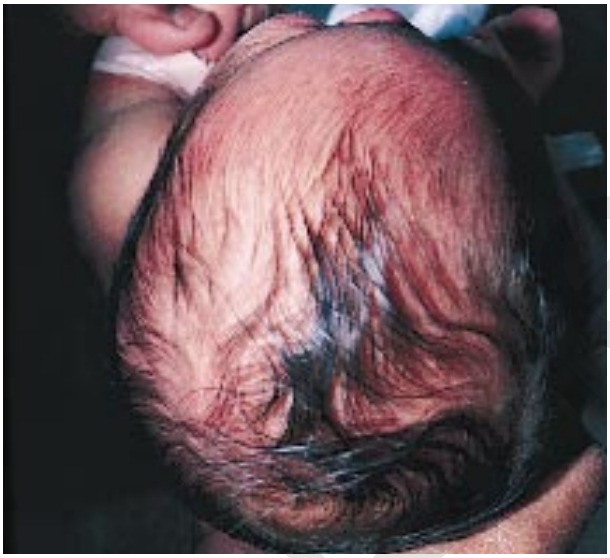

Figure 4.44. A view of the same infant's head shows the brachycephaly which results from the flat forehead and flat occiput. The sutures were normal.

4.45

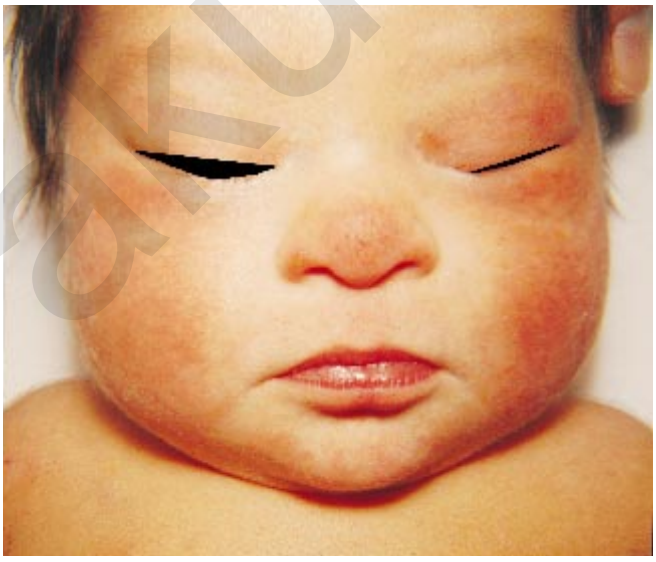

Figure 4.45. A close-up of the face of an infant with trisomy 21 shows the characteristic mongolian slant of the eyes, the hypertelorism, and the flat nose. Epicanthal folds, a common finding in Down syndrome, may be less obvious in the neonate than later in life. Epicanthal folds, which represent a vertical fold of skin on either side of the nose sometimes covering the inner canthus, are seen as a facial characteristic in normal infants as well as in syndromes such as Down syndrome. In infants with Down syndrome the tongue may protrude, giving rise to the impression that macroglossia is present. In Down syndrome there is a short palate and, hence, this is a relative macroglossia.

4.46

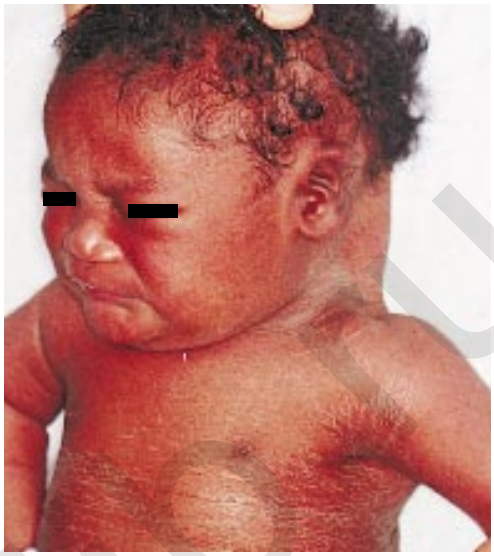

Figure 4.46. Webbing of the neck is a common finding in Down syndrome. This male infant with marked webbing of the neck and flat facies had the typical karyotype of trisomy 21. Because of the webbing, the neck may appear to be short.

4.47

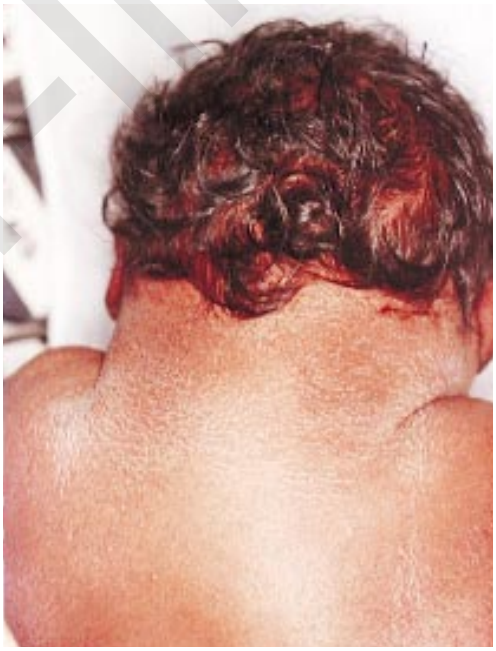

Figure 4.47. Posterior view of the same infant with trisomy 21 shows the marked webbing of the neck. Note that the hairline is high in contrast to Turner's syndrome where the hairline is low and the hair may be in whorls.

4.48

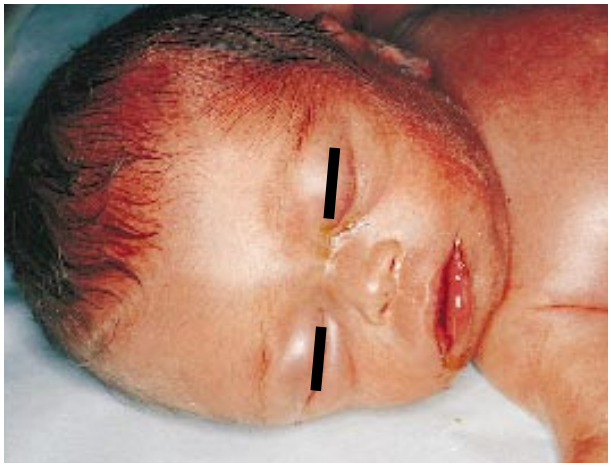

Figure 4.48. Down syndrome in a premature infant (gestational age of 33 weeks) with the typical karyotype of trisomy 21. The clinical diagnosis of Down syndrome may be difficult in small premature infants because the typical findings such as epicanthal folds, etc., are not as obvious as they are in the term infant.

4.49

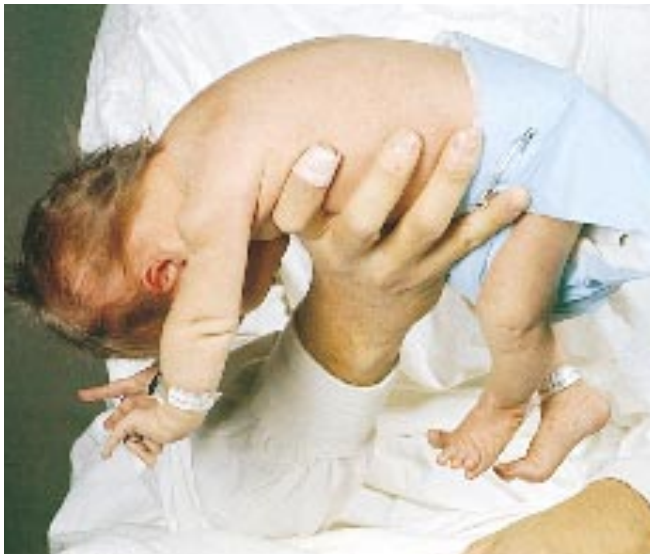

Figure 4.49. Marked hypotonia in an infant with Down syndrome. Hypotonia is present in over 80% of infants with Down syndrome. Also note the separation of the first and second toes.

4.50

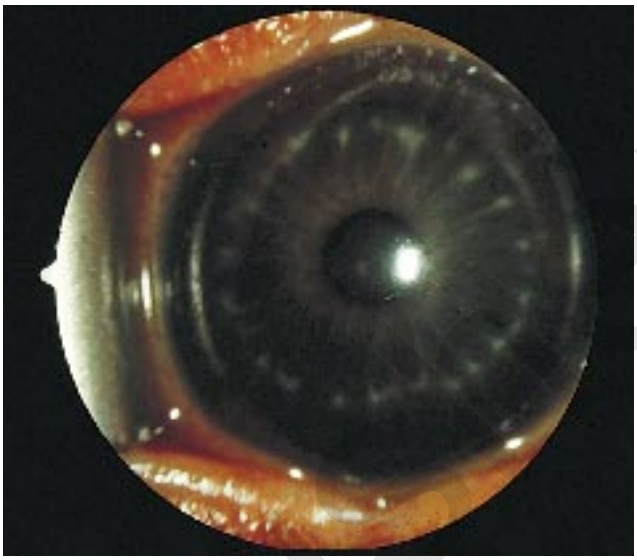

Figure 4.50. Brushfield's spots in the eyes of an infant with trisomy 21. These are aggregates of stromal fibers which form a ring around the iris near the limbus. They tend to disappear with age. Brushfield's spots may be seen in normal blue-eyed infants, but if present in infants with brown eyes they are pathologic. Brushfield's spots are also seen in infants with Zellweger syndrome.

4.51

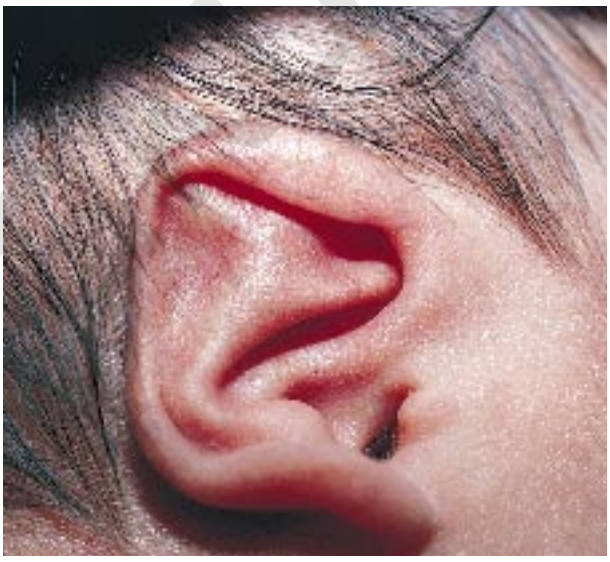

Figure 4.51. The typical square ("boxy") appearance of the ear in an infant with trisomy 21. Abnormalities of the ears are noted in at least 60% of infants with Down syndrome. Typically they are boxy, but they may be low set and small with overlapping of the helix and a prominent anthelix.

4.52

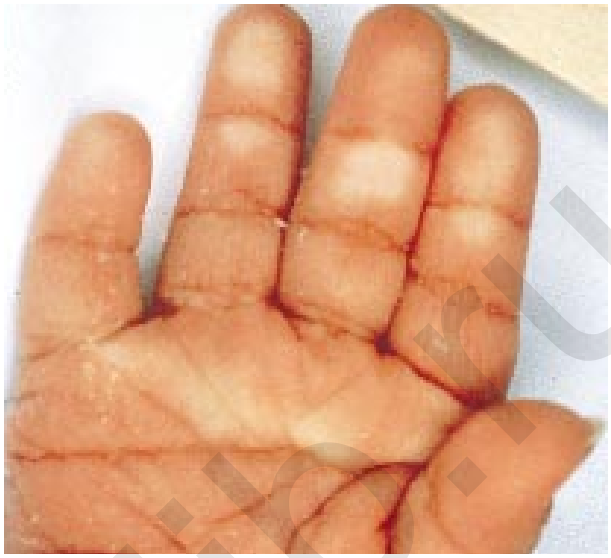

Figure 4.52. The typical short stubby fingers, single palmar (simian) crease, and clinodactyly of digit five on the right hand of an infant with trisomy 21. The short stubby fingers resulting in a short broad hand are noted in about 70% of infants with trisomy 21. A single palmar crease may be a normal variant occurring on both hands in 1 to 2% of the population and on one hand in 6%. Clinodactyly is incurving of the finger due to an absent or hypoplastic middle phalanx. Clinodactyly of the fifth digit is also seen as a normal variant and as a finding in many other syndromes.

4.53

Figure 4.53. This infant with trisomy 21 has a single palmar crease. There is no clinodactyly but there is hypoplasia of the middle phalanx of the fifth finger as noted by the decreased distance between the finger creases. The single palmar crease is seen in about 45% of infants with trisomy 21 and is a finding in many other syndromes.

4.54

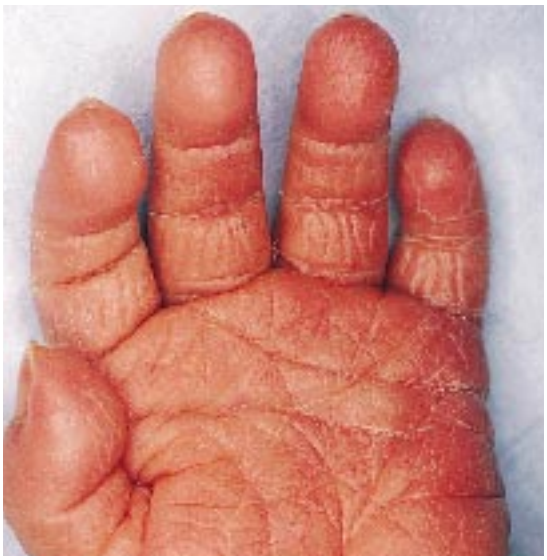

Figure 4.54. This infant with trisomy 21 has clinodactyly but normal palmar creases. Clinodactyly with an absent or hypoplastic middle phalanx of the fifth finger is present in about 50% of infants with trisomy 21.

4.55

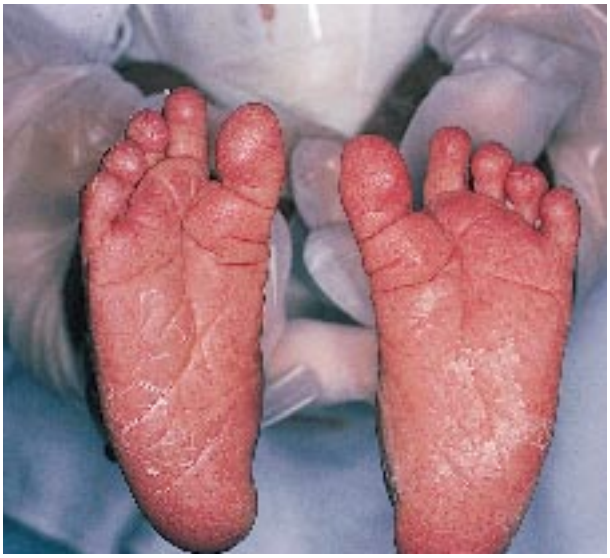

Figure 4.55. The gap between the first and second toes ("sandal" or "thong" sign) is a typical finding in trisomy 21. The feet are broad and short. The plantar surfaces are creased with a deep long furrow (ape-line) between the first and second toes.

4.56

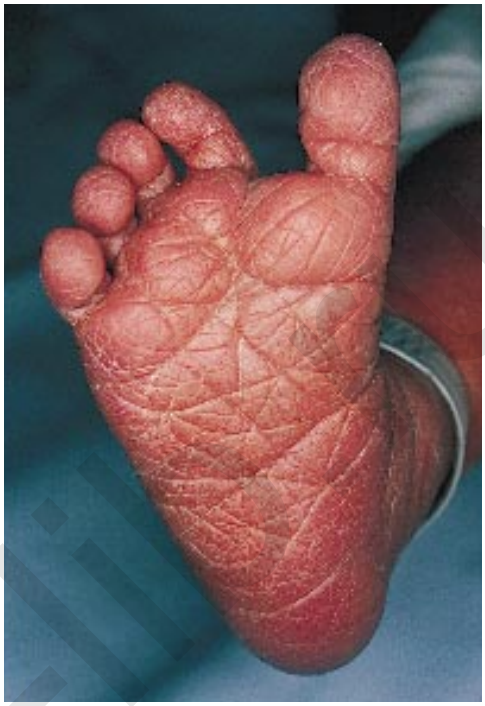

Figure 4.56. A close-up view of the broad short foot of an infant with trisomy 21 shows the marked separation of the first and second toes and the deep furrows on the sole.

4.57

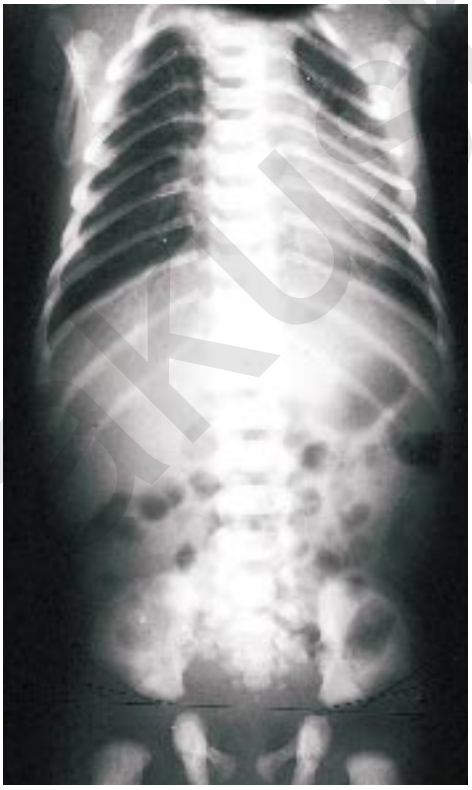

Figure 4.57. Total radiograph of an infant with trisomy 21 shows the long narrow chest cage with downslanting ribs due to hypotonia. Any infant who is hypotonic has this appearance of the chest cage. The finding of eleven pairs of ribs, as in this infant, is common in Down syndrome but also may occur as a finding in normal infants. The pelvis is a typical mongoloid pelvis. The infant also had congenital heart disease (the most common defect being an endocardial cushion defect).

4.58

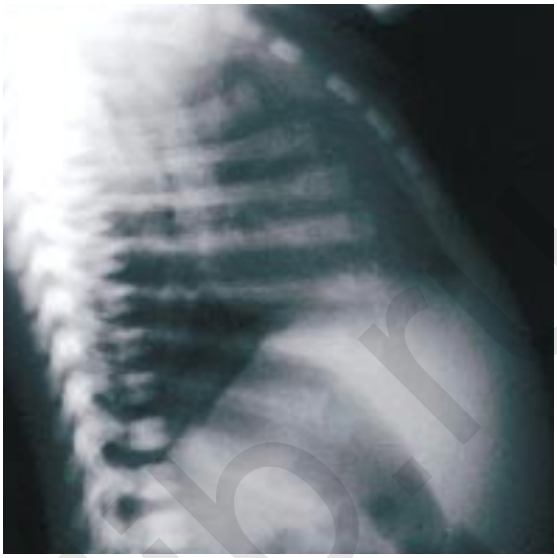

Figure 4.58. Lateral chest radiograph in another infant with trisomy 21 shows the increased number of sternal ossification centers. Compare this with trisomy 18 where ossification centers are decreased in number or absent (see Figure 4.36). Note that the ribs are normal in appearance as compared to the gracile delicate ribs seen in infants with trisomy 18.

4.59

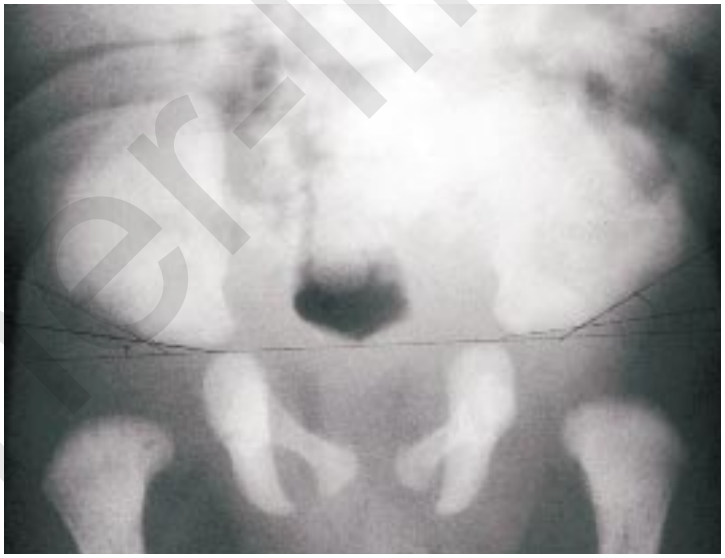

Figure 4.59. Radiograph of the typical mongoloid pelvis seen in infants with trisomy 21. Note the marked lateral flaring of the ilia giving rise to the so-called "Mickey Mouse" pelvis. There is a shallow acetabular angle. Compare this with the antimongoloid pelvis noted in infants with trisomy 18 (see Figure 4.37).

4.60

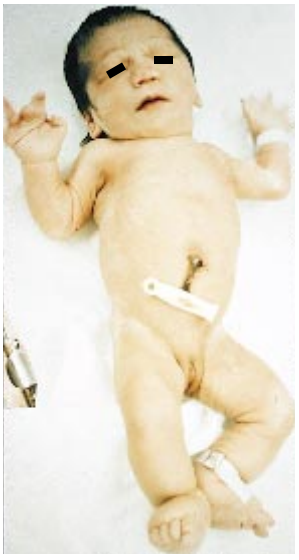

Figure 4.60. Infants with Turner's syndrome (XO syndrome) are phenotypically female although they have one of the pairs of X chromosomes missing. This term infant is short (length 43 cm) and demonstrates the short neck, shield-like chest with widely spaced nipples, and lymphedema, especially of the feet. Note also the single palmar crease on the right hand. Infants with Turner's syndrome may be small for gestational age.

4.61

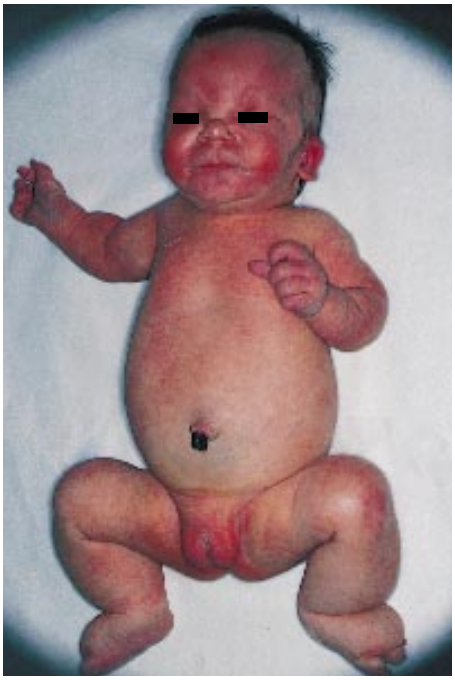

Figure 4.61. In another example of Turner's syndrome in a term infant (length 44 cm) note the marked lymphedema, especially of the lower extremities. Other findings in Turner's syndrome include a low posterior hairline with the appearance of a short neck, webbing of the neck, congenital heart disease (especially coarctation of the aorta), pigmented nevi, and skeletal abnormalities.

4.62

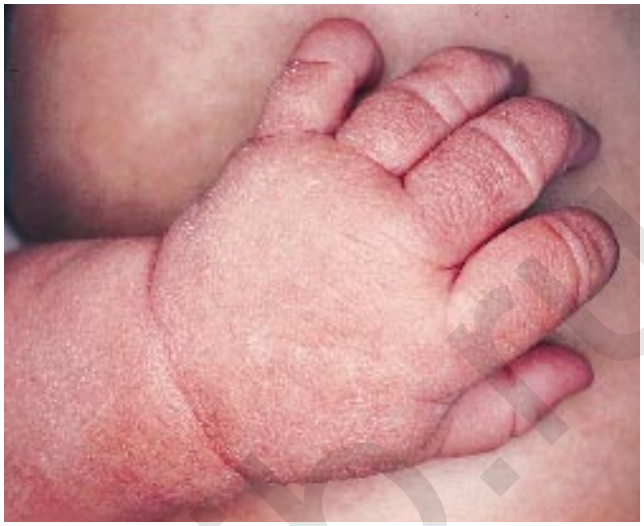

Figure 4.62. The same infant shows the marked lymphedema in the left hand. Transient congenital lymphedema with residual puffiness is noted over the dorsum of the hands and feet in more than 80% of infants with Turner's syndrome.

4.63

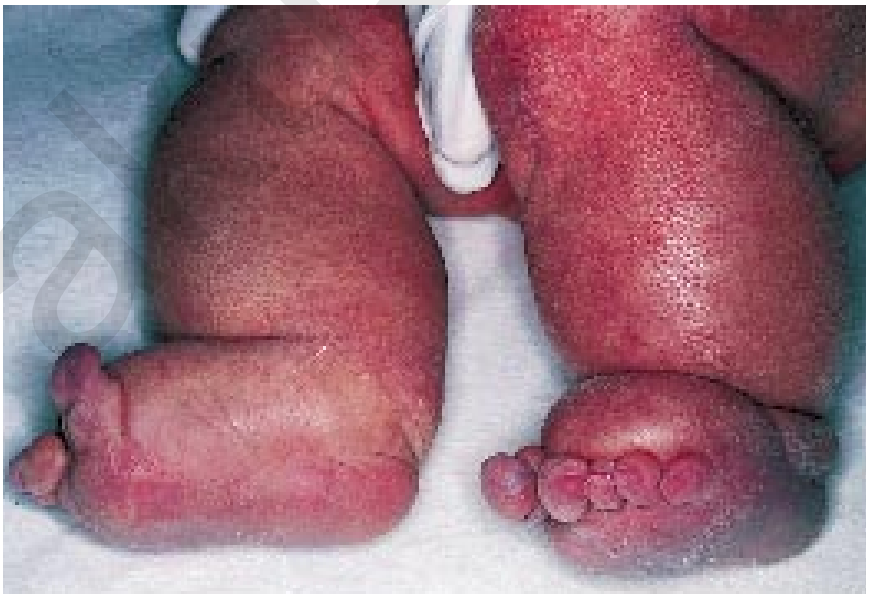

Figure 4.63. Note the hypoplastic nails in the same infant with Turner's syndrome. Hypoplastic finger and toe nails are commonly noted in infants with Turner's syndrome in that the nails are narrow, hyperconvex, and may be deep set.

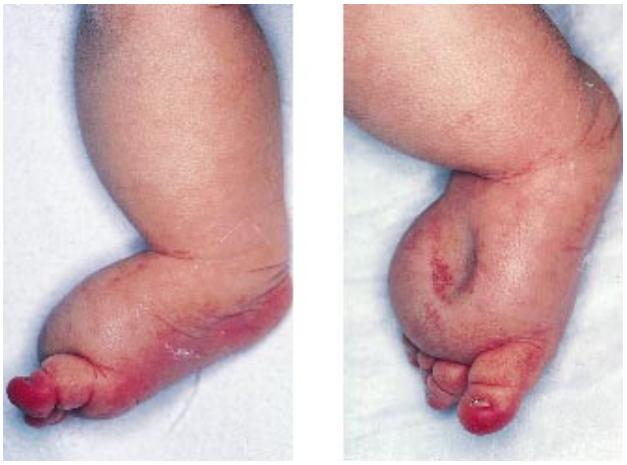

4.64

Figure 4.64. Note the marked lymphedema of both legs and feet in the same infant with Turner's syndrome. The marked lymphedema in Turner's syndrome is a pitting edema. Compare this with congenital lymphedema (Milroy's disease) where the edema is non-pitting.

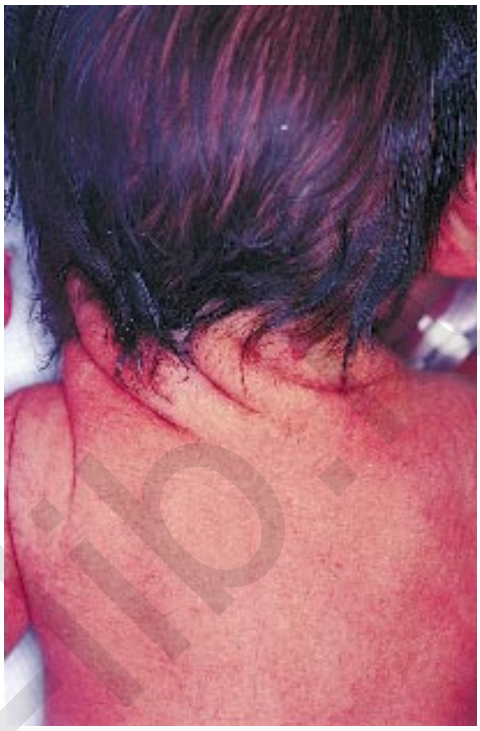

4.65

Figure 4.65. There is marked webbing of the neck in this infant with Turner's syndrome. Note the low posterior hairline. Compare this with the webbing of the neck and high hairline in trisomy 21 (see Figure 4.47). The infant also had congenital heart disease (coarctation of the aorta).

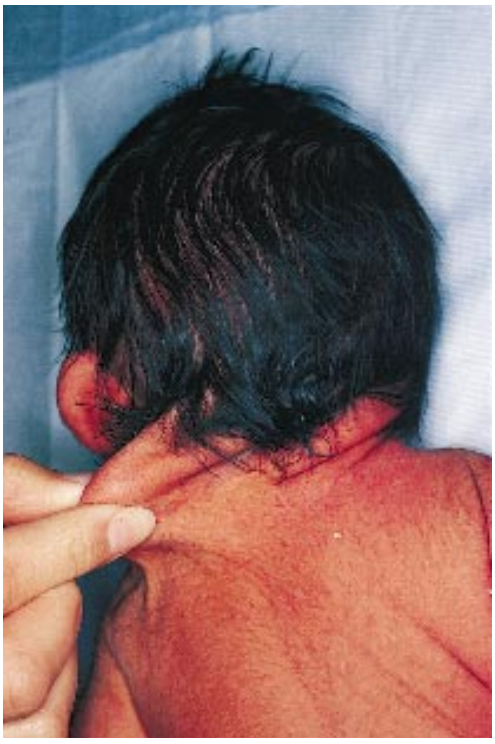

4.66

Figure 4.66. The marked webbing of the neck is again noted in this same infant with Turner syndrome. This results in the appearance of a shortened neck. The webbing of the neck occurs as a result of redundant skin.

A short neck may result from absence, malformation or coalescence of one or more cervical vertebrae, often giving the impression that the head is resting directly on the shoulders (Klippel-Feil syndrome, Jarcho-Levin syndrome). Neck webbing or high placement of the scapulae can give a similar appearance (Turner's syndrome, Down syndrome, cleidocranial dysostosis).

4.67

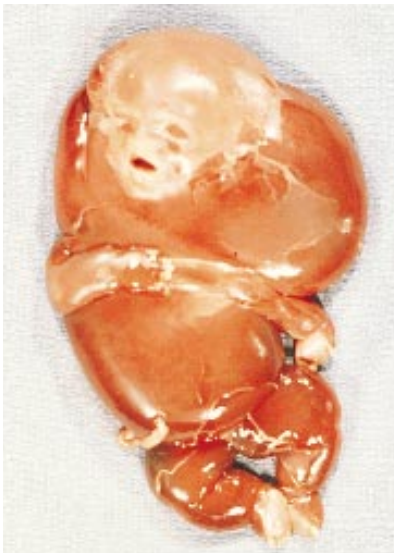

Figure 4.67. Fetal Turner's syndrome in an aborted fetus. Diagnosis was made prenatally by ultrasound and confirmed by karyotype. Note the large nuchal cystic hygromas of the neck and moderate hydrops of the limbs and body wall. This would explain the etiology of the redundant neck skin of these infants at birth. (R. Carpenter)

4.68

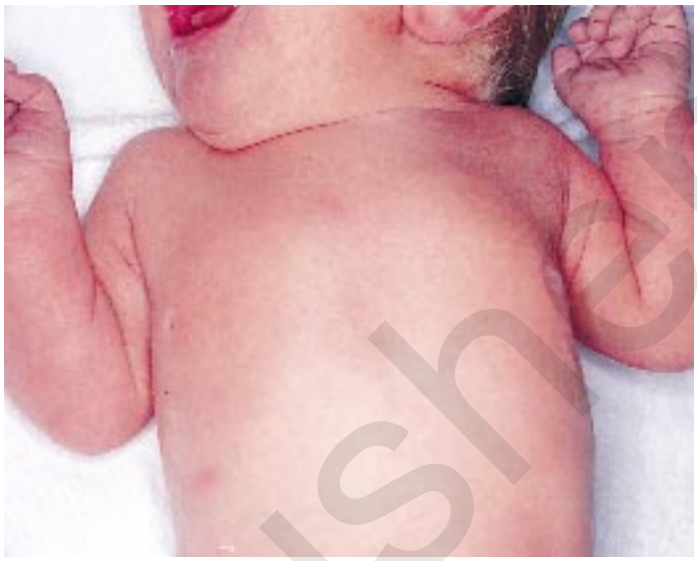

Figure 4.68. This infant with Turner's syndrome has the typical broad chest (shield-like chest) with widely spaced nipples. The nipples may be hypoplastic and/or inverted.

4.69

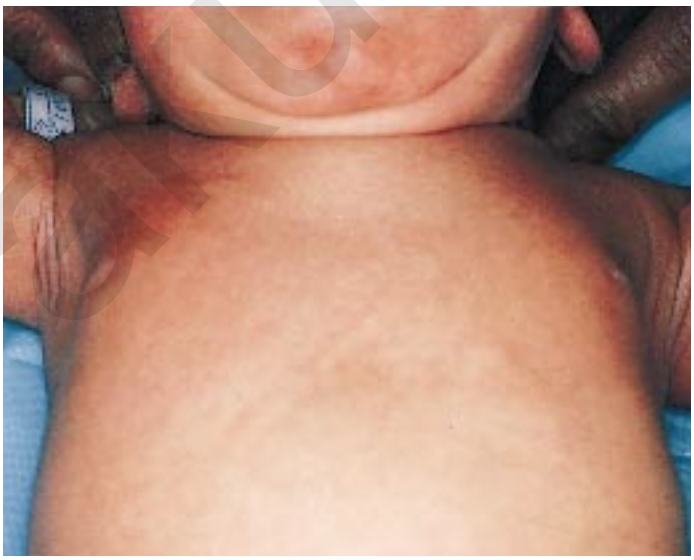

Figure 4.69. In Noonan's syndrome (Turner phenotype in the male) the typical findings are similar to those seen in Turner's syndrome. The infants are short in stature, have webbing of the neck, widely spaced nipples, lymphedema, and congenital heart disease (especially pulmonic stenosis). In this male infant with Noonan's syndrome note the shield-like chest and widely spaced nipples.

4.70

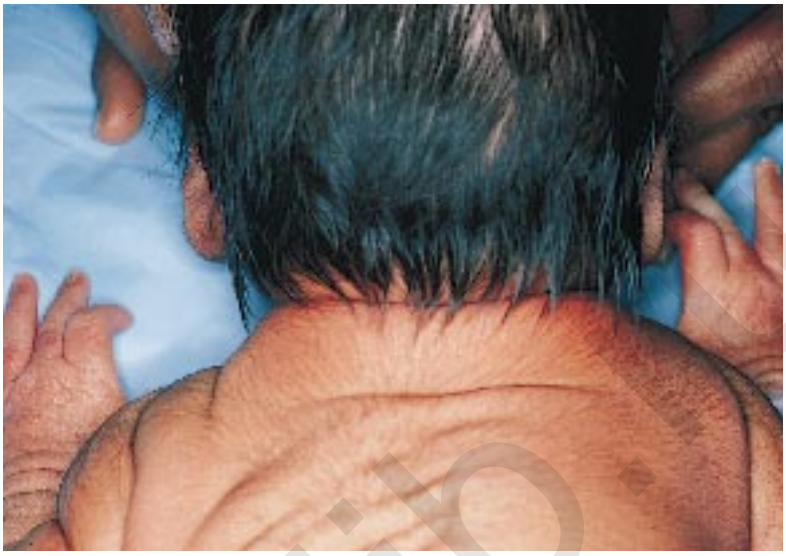

Figure 4.70. The same infant has the typical appearance of a short neck, redundant skin, and low posterior hairline.

4.71

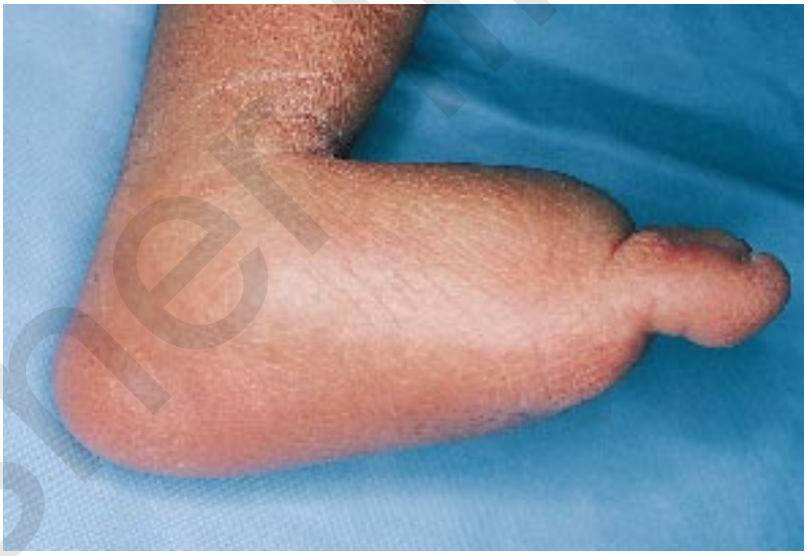

Figure 4.71. Lymphedema of the dorsum of the foot in the same infant with Noonan's syndrome.

Index

VOLUME 3

Head and Neck, Eye, Central Nervous System

Atlas of the Newborn

Rudolph

VOLUME 3

Head and Neck,
Eye,
Central Nervous
System

Atlas of the Newborn

Arnold J. Rudolph, M.D.
1918-1995

Arnold J. Rudolph, M.D.
1918–1995
Professor of Pediatrics,
Obstetrics, and Gynecology
Baylor College of Medicine
Houston, Texas

VOLUME 3

Head and Neck, Eye, Central Nervous System

Atlas of the Newborn

Arnold J. Rudolph, M.D.
1918-1995

with a chapter on neonatal ophthalamology by
Helen A. Mintz-Hittner, M.D.

1997

B.C. Decker Inc.
Hamilton • London

B.C. Decker Inc.
4 Hughson Street South
P.O. Box 620, L.C.D. 1
Hamilton, Ontario L8N 3K7
Tel: 905 522-7017
Fax: 905 522-7839
e-mail: info@bcdecker.com

Printed in Canada

97 98 99 00/BP/9 8 7 6 5 4 3 2 1

ISBN 1-55009-033-X

Sales and distribution

United States
Blackwell Science Inc.
Commerce Place
350 Main Street
Malden, MA 02148
U.S.A.
Tel: 1-800-215-1000

Canada
Copp Clark Ltd.
200 Adelaide Street West
3rd Floor
Toronto, Ontario
Canada M5H 1W7
Tel: 416-597-1616
Fax: 416-597-1617

Japan
Igaku-Shoin Ltd.
Tokyo International P.O. Box 5063
1-28-36 Hongo, Bunkyo-ku
Tokyo 113, Japan
Tel: 3 3817 5680
Fax: 3 3815 7805

U.K., Europe, Scandinavia, Middle East
Blackwell Science Ltd.
c/o Marston Book Services Ltd.
P.O. Box 87
Oxford OX2 0DT
England
Tel: 44-1865-79115

Australia
Blackwell Science Pty, Ltd.
54 University Street
Carleton, Victoria 3053
Australia
Tel: 03 9347 0300
Fax: 03 9349 3016

Notice: the authors and publisher have made every effort to ensure that the patient care recommended herein, including choice of drugs and drug dosages, is in accord with the accepted standard and practice at the time of publication. However, since research and regulation constantly change clinical standards, the reader is urged to check the product information sheet included in the package of each drug, which includes recommended doses, warnings, and contraindications. This is particularly important with new or infrequently used drugs.

Foreword

Sir William Osler stated, "There is no more difficult task in medicine than the art of observation." The late Arnold Jack Rudolph was an internationally renowned neonatologist, a teacher's teacher, and, above all, one who constantly reminded us about how much could be learned by simply observing, in his case, the newborn infant.

This color atlas of neonatology represents a distillation of more than 50 years of observing normal and abnormal newborn infants. The *Atlas* begins with a section on the placenta, its membranes, and the umbilical cord. Jack Rudolph delighted in giving a lecture entitled "Don't Make Mirth of the Afterbirth," in which he captivated audiences by showing them how much you could learn about the newborn infant from simply observing the placenta, its membranes, and the umbilical cord.

In a few more than 60 photomicrographs, we learn to read the placenta and gain insight into such disorders as intrauterine growth retardation, omphalitis, cytomegalic inclusion disease, congenital syphilis, and congenital neuroblastoma. Congenital abnormalities of every organ system are depicted along with the appearance of newborn infants who have been subjected in utero to a variety of different drugs, toxins, or chemicals. We also learn to appreciate the manifestations of birth trauma and abnormalities caused by abnormal intrauterine positioning.

More than 250 photographs are used to illustrate the field of neonatal dermatology. The collection of photographs used in this section is superior to that which I have seen in any other textbook or atlas of neonatology or dermatology; this section alone makes this reference a required addition to the library of any clinician interested in the care of infants and children. Photographs of the Kasabach-Merritt syndrome (cavernous hemangioma with thrombocytopenia), Klippel-Trénaunay syndrome, Turner's syndrome, Waardenburg's syndrome, neurocutaneous melanosis, mastocytosis (urticaria pigmentosa), and incontinentia pigmenti (Bloch-Sulzberger syndrome) are among the best that I have seen.

Cutaneous manifestations are associated with many perinatal infections. The varied manifestations of staphylococcal infection of the newborn are depicted vividly in photomicrographs of furunculosis, pyoderma, bullous impetigo, abscesses, parotitis, dacryocystitis, inastitis, cellulitis, omphalitis, and funisitis. Streptococcal cellulitis, *Haemophilus influenzae* cellulitis, and cutaneous manifestations of listeriosis all are depicted. There are numerous photomicrographs of congenital syphilis, showing the typical peripheral desquamative rash on the palms and soles, as well as other potential skin manifestations of congenital syphilis which may produce either vesicular, bullous, or ulcerative lesions. The various radiologic manifestations of congenital syphilis, including pneumonia alba, ascites, growth arrest lines, Wegner's sign, periostitis, and syphilitic osteochondritis, are depicted. Periostitis of the clavicle (Higouménaki's sign) is shown in a photograph that also depicts periostitis of the ribs. A beautiful photomicrograph of Wimberger's sign also has been included; this sign, which may appear in an infant with congenital syphilis, reveals radiolucency due to erosion of the medial aspect of the proximal tibial metaphysis.

The *Atlas* also includes a beautiful set of photographs which delineate the ophthalmologic examination of the newborn. Lesions which may result from trauma, infection, or congenital abnormalities are included. There are numerous photographs of the ocular manifestations of a variety of systemic diseases, such as Tay-Sachs disease, tuberous sclerosis, tyrosinase deficiency, and many more. Photographs of disturbances of each of the various organ systems, or disorders affecting such organ systems, also are included along with numerous photographs of different forms of dwarfism, nonchromosomal syndromes and associations, and chromosomal disorders. In short, this *Atlas* is the complete visual textbook of neonatology and will provide any

physician, nurse, or student with a distillation of 50 years of neonatal experience as viewed through the eyes of a master clinician.

Arnold Jack Rudolph was born in 1918, grew up in South Africa, and graduated from the Witwatersrand Medical School in 1940. Following residency training in pediatrics at the Transvaal Memorial Hospital for Children, he entered private pediatric practice in Johannesburg, South Africa. After almost a decade, he left South Africa and moved to Boston, where he served as a Senior Assistant Resident in Medicine at the Children's Medical Center in Boston, Massachusetts, and subsequently pursued fellowship training in neonatology at the same institution and at the Boston Lying-In Hospital, Children's Medical Center and Harvard Medical School under Dr. Clement A. Smith.

In 1961, Dr. Rudolph came to Baylor College of Medicine in Houston, Texas, the school at which he spent the remainder of his career. He was a master teacher, who received the outstanding teacher award from pediatric medical students on so many occasions that he was elected to the Outstanding Faculty Hall of Fame in 1982. Dr. Rudolph also received numerous awards over the years from the pediatric house staffs for his superb teaching skills.

He was the Director of the Newborn Section in the Department of Pediatrics at Baylor College of Medicine for many years, until he voluntarily relinquished that position in 1986 for reasons related to his health. Nevertheless, Jack Rudolph continued to work extraordinarily long hours in the care of the newborn infant, and was at the bedside teaching both students and house staff, as well as his colleagues, on a daily basis until just a few months before his death in July 1995.

Although Dr. Rudolph was the author or co-author of more than 100 published papers that appeared in the peer-reviewed medical literature, his most lasting contribution to neonatology and to pediatrics is in the legacy of the numerous medical students, house staff, fellows, and other colleagues whom he taught incessantly about how much one could learn from simply observing the newborn infant. This *Atlas* is a tour de force; it is a spectacular teaching tool that has been developed, collated, and presented by one of the finest clinical neonatologists in the history of medicine. It is an intensely personal volume that, as Dr. Rudolph himself states, "is not intended to rival standard neonatology texts," but rather to supplement them. This statement reveals Dr. Rudolph's innate modesty, since with the exception of some discussion on pathogenesis and treatment, it surpasses most neonatology texts in the wealth of clinical information that one can derive from viewing and imbibing its contents. We owe Dr. Rudolph and those who aided him in this work a debt of gratitude for making available to the medical community an unparalleled visual reference on the normal and abnormal newborn infant.

Ralph D. Feigin, M.D.
June 13, 1996

Preface

I first became attracted to the idea of producing a color atlas of neonatology many years ago. However, the impetus to synthesize my experience and compile this current collection was inspired by the frequent requests from medical students, pediatric house staff, nurses and others to provide them with a color atlas of the clinical material provided in my "slide shows." For the past few decades I have used the medium of color slides and radiographs as a teaching tool. In these weekly "slide shows" the normal and abnormal, as words never can, are illustrated.

"I cannot define an elephant but I know one when I see one."[1]

The collection of material used has been added to constantly with the support of the pediatric house staff who inform me to "bring your camera" whenever they see an unusual clinical finding or syndrome in the nurseries.

A thorough routine neonatal examination is the inalienable right of every infant. Most newborn babies are healthy and only a relatively small number may require special care. It is important to have the ability to distinguish normal variations and minor findings from the subtle early signs of problems. The theme that recurs most often is that careful clinical assessment, in the traditional sense, is the prerequisite and the essential foundation for understanding the disorders of the newborn. It requires familiarity with the wide range of normal, as well as dermatologic, cardiac, pulmonary, gastrointestinal, genitourinary, neurologic, and musculoskeletal disorders, genetics and syndromes. A background in general pediatrics and a working knowledge of obstetrics are essential. The general layout of the atlas is based on the above. Diseases are assigned to each section on the basis of the most frequent and obvious presenting sign. It seems probable that the findings depicted will change significantly in the decades to come. In this way duplication has been kept to a minimum. Additional space has been devoted to those areas of neonatal pathology (e.g., examination of the placenta, multiple births and iatrogenesis) which pose particular problems or cause clinical concern.

Obviously, because of limitations of space, it is impossible to be comprehensive and include every rare disorder or syndrome. I have tried to select both typical findings and variations in normal infants and those found in uncommon conditions. Some relevant conditions where individual variations need to be demonstrated are shown in more than one case.

As the present volume is essentially one of my personal experience, it is not intended to rival standard neonatology texts, but is presented as a supplement to them. It seems logical that references should be to standard texts or reviews where discussion on pathogenesis, treatment, and references to original works may be found.

Helen Mintz Hittner, M.D., has been kind enough to contribute the outstanding section on neonatal ophthalmology.

I have done my best to make the necessary acknowledgements to the various sources for the clinical material. If I have inadvertently omitted any of those, I apologize. My most sincere appreciation and thanks to Donna Hamburg, M.D., Kru Ferry, M.D., Michael Gomez, M.D., Virginia Schneider, PA, and Jeff Murray, M.D., who have spent innumerable hours in organizing and culling the material from my large collection. We wish to thank Abraham M. Rudolph, M.D., for his assistance in reviewing the material. We also wish to thank the following people for their photo contributions to this work: Claire Langston, Helen Mintz–Hittner, Rose Wolfson.

It is hoped that this atlas will provide neonatologists, pediatricians, family physicians, medical students and nurses with a basis for recognizing a broad spectrum of normal variations and clinical problems as well as provide them with an overall perspective of neonatology, a field in which there continues to be a rapid acceleration of knowledge and technology. One must bear in mind the caveat that pictures cannot supplant clinical experience in mastering the skill of visual recall.

1. Senile dementia of Alzheimer's type — normal aging or disease? (Editorial) *Lancet* 1989; i:476-477.

Arnold J. Rudolph, M.D.

CONTENTS

Volume III
Head and Neck, Eye, Central Nervous System

Introduction

Although several texts provide extensive written descriptions of the newborn infant, the senses of touch, hearing, and especially sight, create the most lasting impressions. Over a period of almost five decades, my brother Jack Rudolph diligently recorded, in pictorial form, his vast experiences in physical examination of the newborn infant. *Atlas of the Newborn* reflects his selection from the thousands of color slides in his collection, and truly represents the "art of medicine" as applied to neonatology. A number of unusual or rare conditions are included in this atlas. I consider this fully justified, because if one has not seen or heard of a condition, one will never be able to diagnose it.

This third volume of the five-volume series encompasses three main topics: the head and neck, the eyes, and the central nervous system.

Chapter 1 of this volume focuses on the head and neck, and includes a singular collection depicting various abnormalities of skull shape and size, demonstrating how external forces during the birth process may mold the cranial vault. Facial cleft syndromes, including midline facial defects, cleft lip, cleft palate, and other facial clefts, are graphically shown. In addition, abnormalities of the mouth, tongue, and ears are represented in outstanding photographs.

Chapter 2 concentrates on disorders of the eye, and is unique in its graphic representation of ophthalmalogic problems in the newborn. The importance of careful and systematic examination of the various components of the eye in the neonate is stressed, as often it is neglected.

Chapter 3 is dedicated to disorders of the central nervous system. In addition to pictorially representating many of the abnormalities that are noted to result from neonatal neurologic abnormalities, this chapter provides an extensive graphic description of the various forms of meningocele.

Volume III of *Atlas of the Newborn* will be extremely valuable to obstetricians, neonatologists, pediatricians and nurses involved in perinatal care, and also to clinical geneticists, surgeons, ophthalmologists and neurologists involved in the care of the newborn infant.

Abraham M. Rudolph, M.D.

Chapter 1
Head and Neck

Examination of the head should include visual inspection, palpation, auscultation (for bruits over the temporal arteries and anterior fontanelle), assessment of the shape and size relative to the rest of the body and face, distribution and character of the hair and underlying scalp, and measurement of head circumference. The hair is inspected for color, texture, distribution and directional patterns. The shape of the cranial vault reflects interaction of internal (anatomy, volume, pressure) and external (intra- and extrauterine molding, suture mobility) forces. The mode of delivery will affect the shape of the head (e.g., vaginal delivery with vertex presentation leads to a narrowed biparietal diameter and a maximal occipitomental dimension; breech presentation may accentuate the occipitofrontal dimension with parietal flattening and frontal prominence). Normal molding resolves within a few weeks, but other aberrations progress.

Normal variations in contour, size, relationships, and range of motion of the newborn neck must be distinguished from congenital anomalies and traumatic lesions. The neck should be examined passively for rotation, lateral flexion, anterior flexion, and extension. Rotation of 80° and lateral flexion of 40° should be present and symmetric to both sides. Extension and flexion are difficult to measure, but in flexion the chin should touch or nearly touch the chest wall and extension should be 45° from neutral. When rotation or lateral flexion is asymmetrical or when motion is limited, radiographs of the neck should be obtained. The neck should be extended to look for clefts and cysts. The isthmus of a normal thyroid is just palpable in the sternal notch on neck extension. Other congenital neck masses include cystic hygroma, lymphangioma, and cervical teratoma. The earlier that appropriate treatment is started, the more likely that correction can occur.

1.1

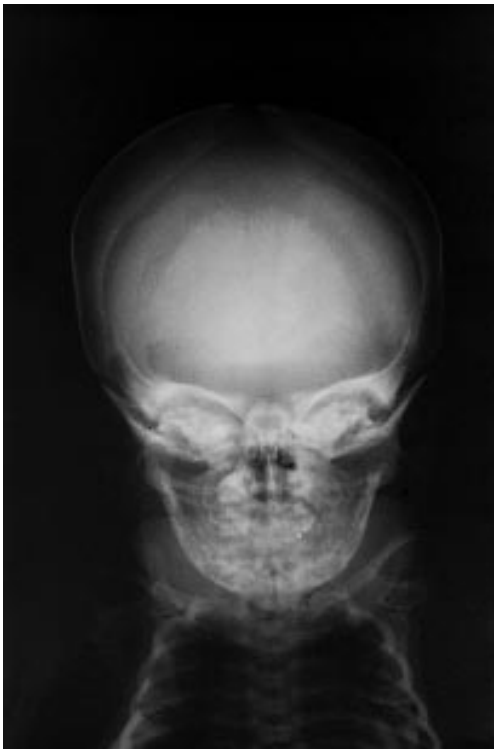

Figure 1.1. Anteroposterior radiograph of the normal newborn skull. Note the fontanelle and suture lines.

1.2

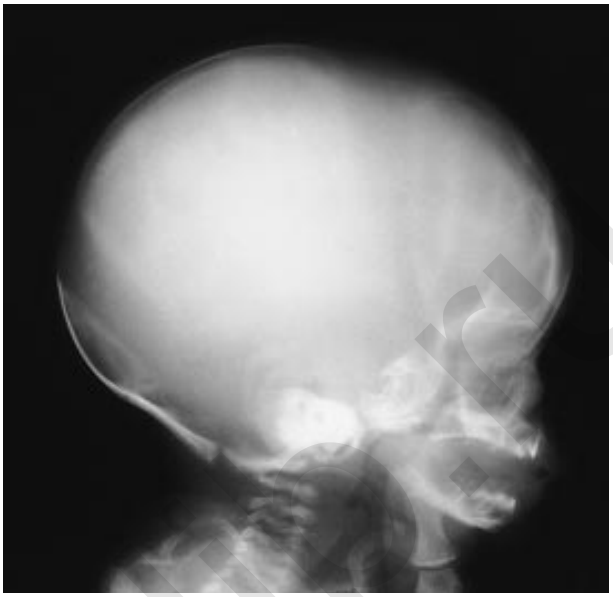

Figure 1.2. Lateral radiograph of a normal term newborn skull. Note the poor mineralization of the bones with separation of sutures. In the lateral view, mineralization of the lower teeth correlates well with gestational age. Mineralization of only the incisors indicates a gestational age of less than 33 weeks. Mineralization of the incisors and the first molars correlates with a gestational age of 33 to 37 weeks. Mineralization of the second molar in addition to the above correlates with less than 37 weeks gestation.

1.3

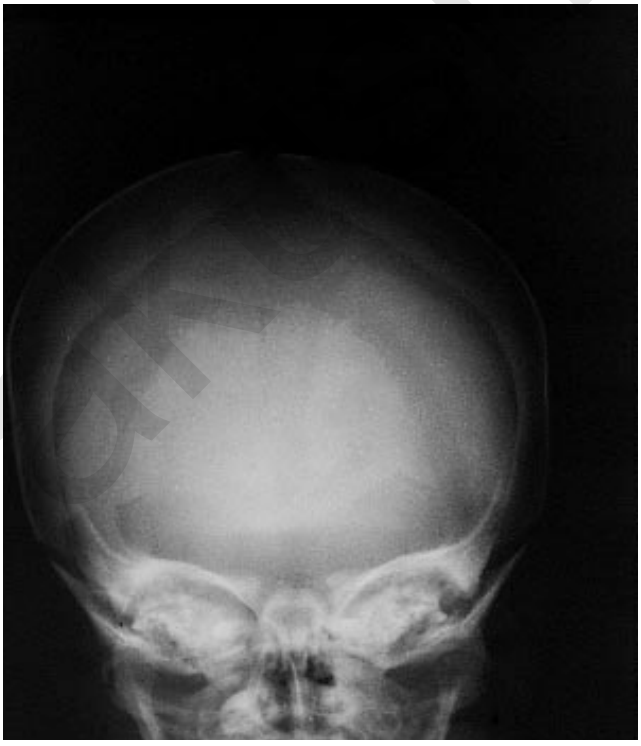

Figure 1.3. Lateral radiograph of the skull showing the presence of an anterior fontanelle bone. This infant's head is somewhat elongated. Fontanelle bones are more common over the posterior fontanelle. There are no clinical signs and as the skull mineralizes these bones become confluent with the rest of the skull. The bone may be palpable in the fontanelle.

1.4

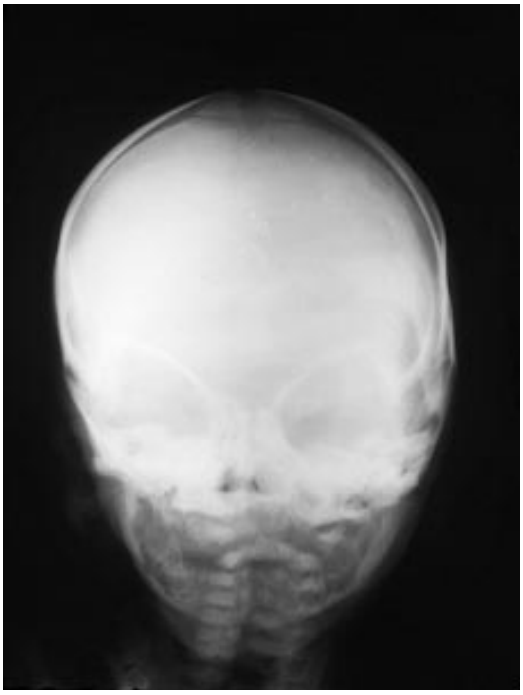

Figure 1.4. Anteroposterior radiograph of the same infant as in Figure 1.3, showing the anterior fontanelle bone. The third fontanelle is a widening of the sagittal suture near the junction of its middle and posterior thirds. It represents slowed growth of the plates of the parietal bone and may be distinguished from the posterior fontanelle by its position and round or oval appearance.

1.5

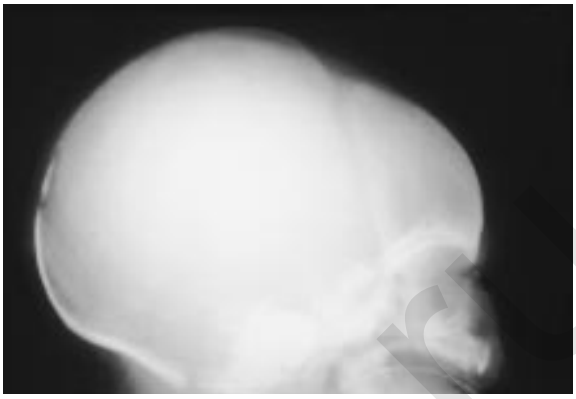

Figure 1.5. A lateral radiograph of the skull showing a posterior fontanelle bone. Note the poor mineralization of the skull in an otherwise normal infant. Mineralization of the skull may be minimal at birth in normal infants.

1.6

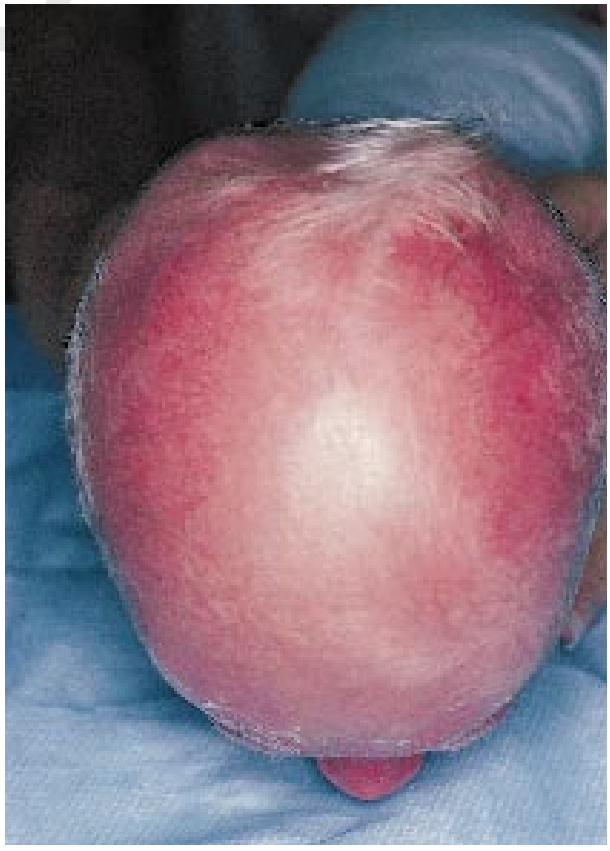

Figure 1.6. The clinical appearance of congenital parietal foramina in an otherwise normal neonate. Note that the infant is lying on his face and the depressions over the parietal area reflect the defects. These are rounded defects in the parietal bone. They are usually bilateral and vary in size from 1 mm to 3 cm. They are usually asymptomatic but may cause concern because of bulging or pulsation of the overlying scalp.

1.7

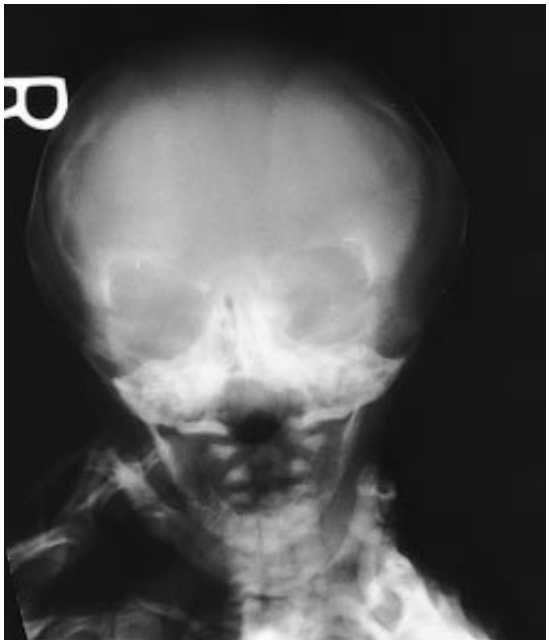

Figure 1.7. Radiograph of the skull of the same infant as in Figure 1.6. Note the posterior parietal foramina and poor mineralization of the skull with a large metopic suture.

1.8

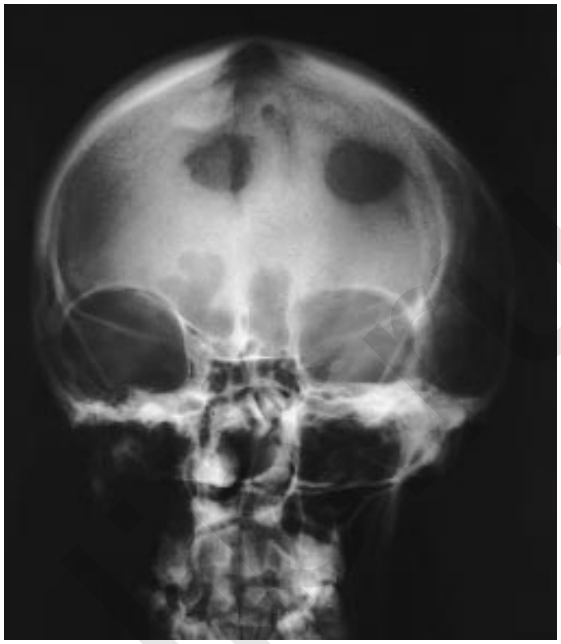

Figure 1.8. Congenital parietal foramina are often familial, as noted in this radiograph of the skull of the mother of the same infant.

1.9

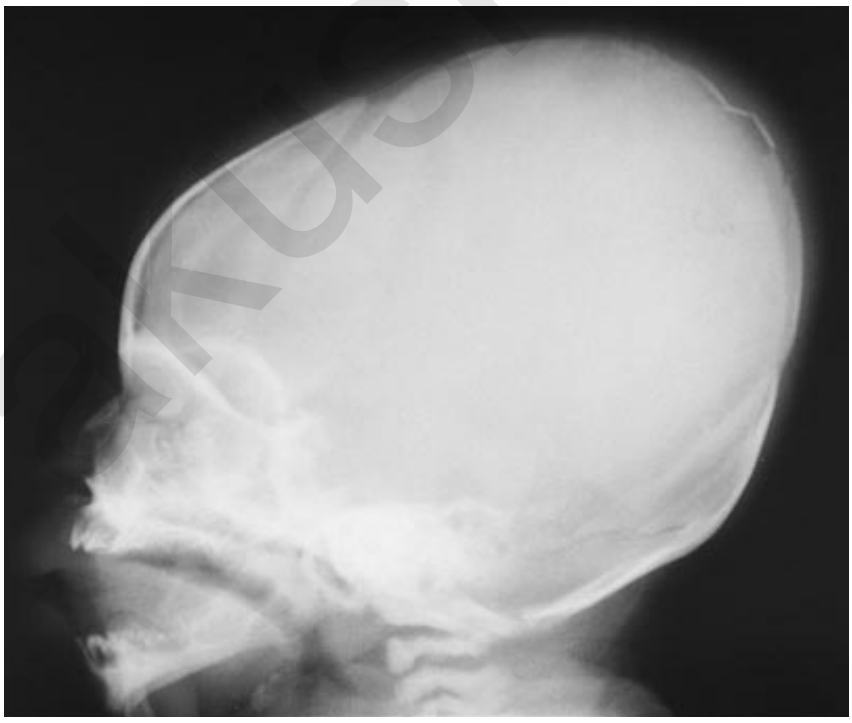

Figure 1.9. A radiograph of a linear skull fracture over the parietal bone. This is not common in the neonate but may occasionally be associated with a cephalohematoma. It can also occur as a result of trauma.

1.10

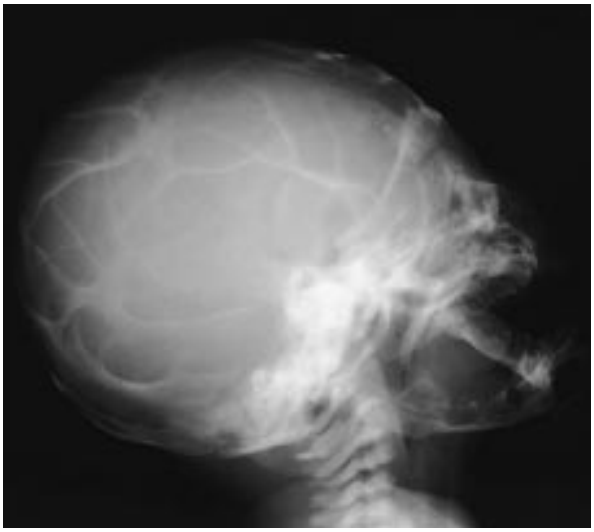

Figure 1.10. Lateral radiograph of the skull of an infant with lacunar skull (lückenschädel), which is a result of defective calcification of the skull bones. Note the characteristic honeycomb skull appearance. This malformation is commonly associated with neural tube defects (encephalocele and meningocele) and is characterized by sharply defined depressions which are usually readily palpable and situated in the frontal and parietal areas.

1.11

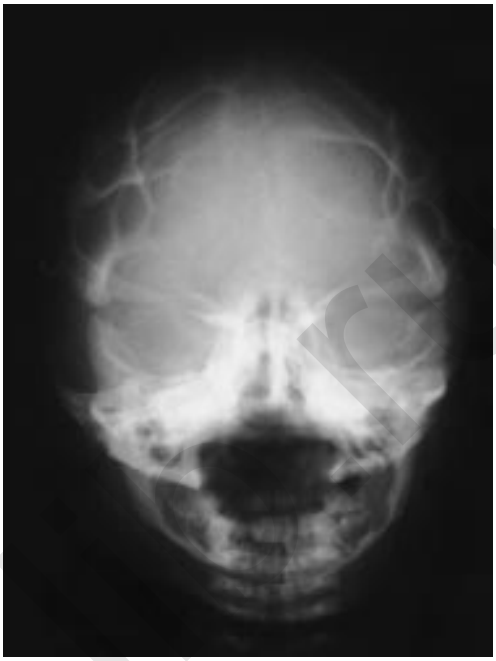

Figure 1.11. Frontal radiograph of the skull of the same infant with lückenschädel.

Compare lückenschädel with craniotabes which consists of localized areas of softening in one or several bones of the vault of the skull. The involved bones feel like parchment and are easily indented when pressed with the fingertip. When the pressure is removed, the soft bone resumes its former contour in much the same way as an indented ping pong ball recovers its shape. Craniotabes is more common in term infants than in premature infants. It is commonly found in normal infants, hydrocephalic infants, and in infants with osteogenesis imperfecta.

1.12

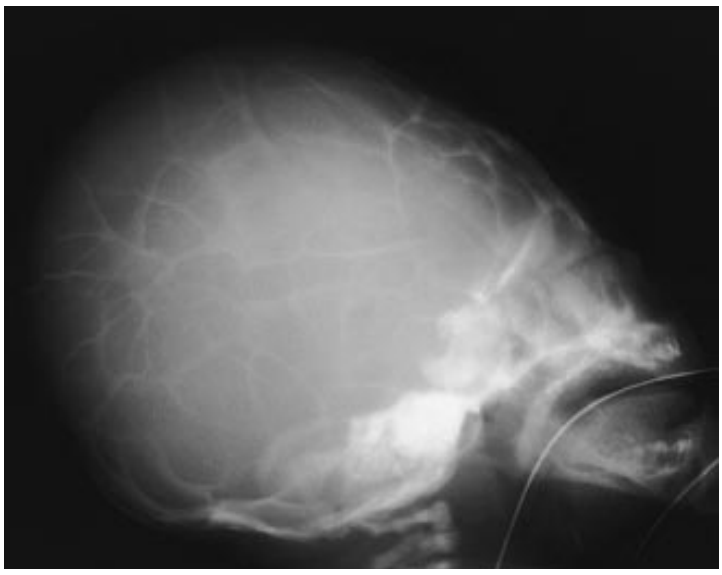

Figure 1.12. Lateral skull radiograph of lückenschädel in another infant with a lumbar meningocele, imperforate anus, and rectovaginal fistula.

1.13

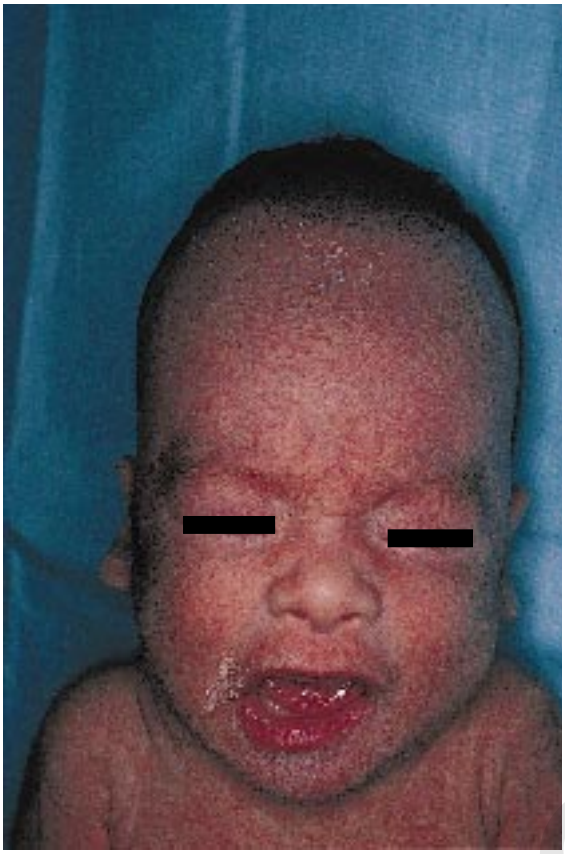

Figure 1.13. Note the typical long narrow skull of a premature infant with hypsicephaly. Hypsicephaly is a term used by anthropologists for "high heads" that are not pathologic or due to craniosynostosis. This term is used interchangeably with that of dolichocephaly when associated with prematurity.

1.14

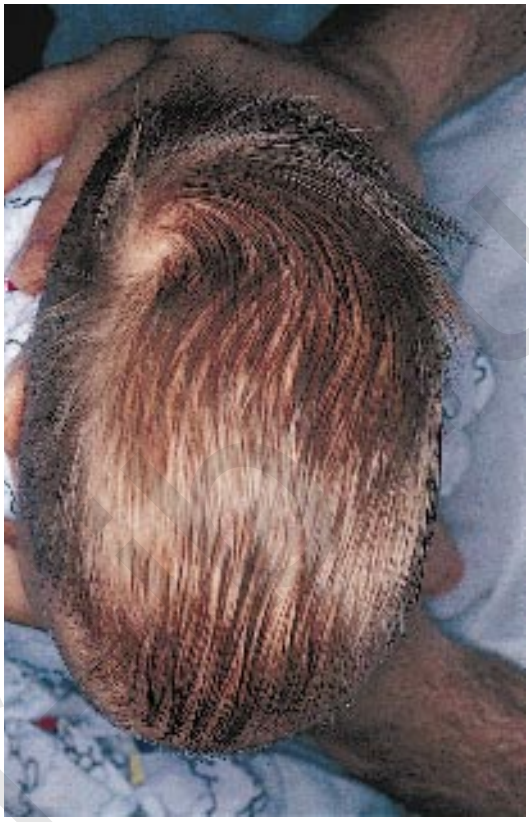

Figure 1.14. The typical appearance of dolichocephaly associated with prematurity. In these infants the sagittal suture remains open. The long, narrow head of dolichocephaly is not present at birth but results from transient molding of the skull as a result of the infant lying on its side. The large head of the small premature infant restricts frequent movement of the head, and hence this appearance is a postural deformity. Craniosynostosis with premature fusion of the sagittal suture is different from this normal postural deformity of premature infants.

1.15

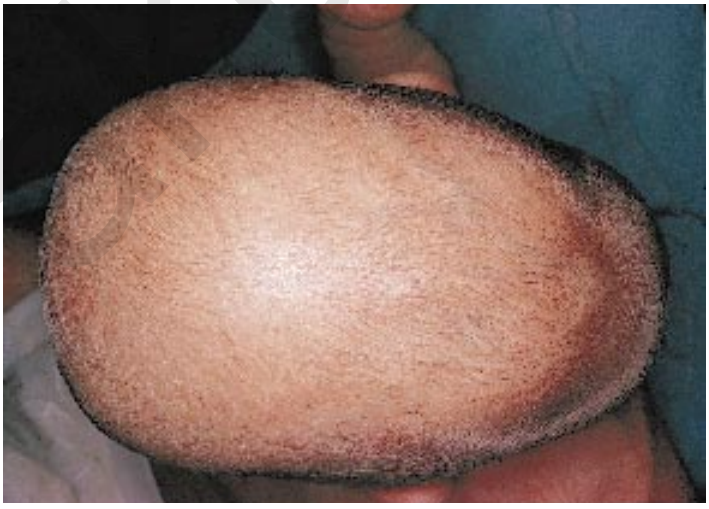

Figure 1.15. Premature fusion of the sagittal suture in this infant has resulted in scaphocephaly. Note the long, narrow head and the fused sagittal suture which presents as a ridge. This condition is more common in male infants.

1.16

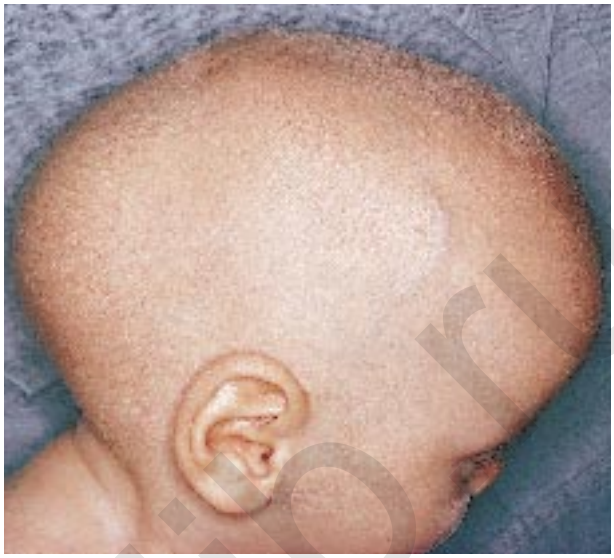

Figure 1.16. Lateral view of the head of another infant with scaphocephaly. Note the frontal and posterior bossing of the head.

1.17

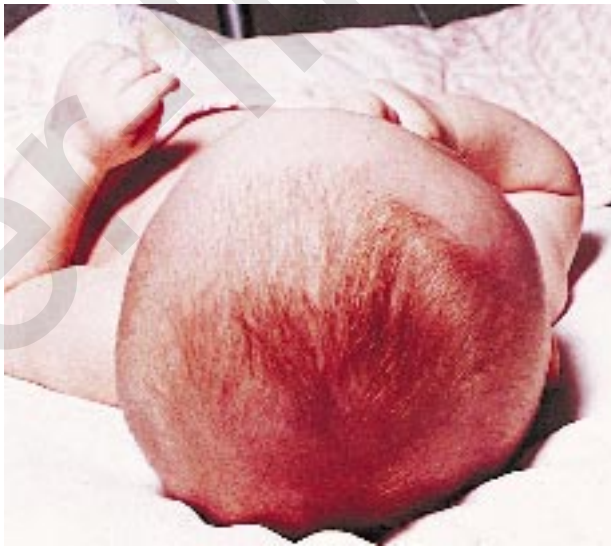

Figure 1.17. Craniosynostosis due to premature fusion of the coronal sutures has resulted in brachycephaly. Note the short, round appearance of the head with reduction of the anteroposterior diameter. This also occurs in Apert's syndrome and Carpenter's syndrome. Brachycephaly is also seen in infants with Down syndrome, Brachmann-de Lange syndrome, and cleidocranial dysostosis due to flattening of the occiput.

1.18

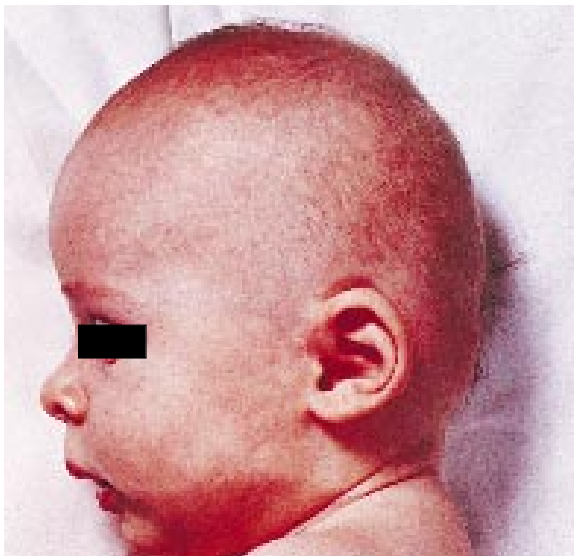

Figure 1.18. Lateral view of the head of the same infant with craniosynostosis of the coronal sutures. Note the short, round appearance of the head and the flat occiput.

1.19

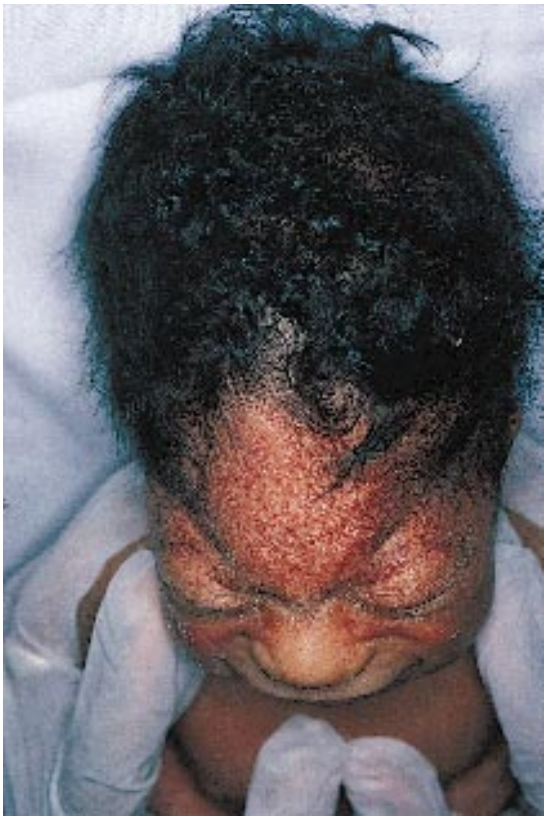

Figure 1.19. Trigonocephaly is due to premature fusion of the metopic suture and is represented clinically by a triangular-shaped head. This condition may occur in utero or in the first months of life. It may occur in otherwise normal infants, but is also seen in infants with chromosomal anomalies or the median cleft syndrome.

1.20

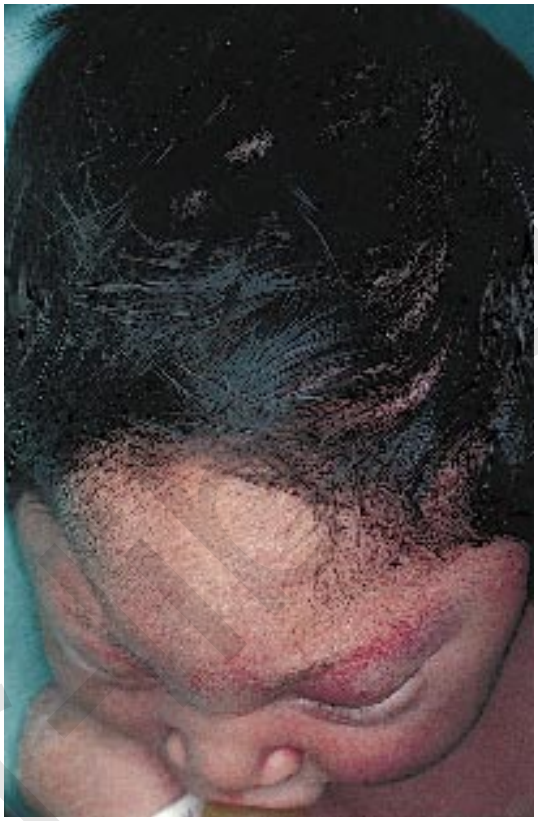

Figure 1.20. Another example of less severe trigonocephaly.

1.21

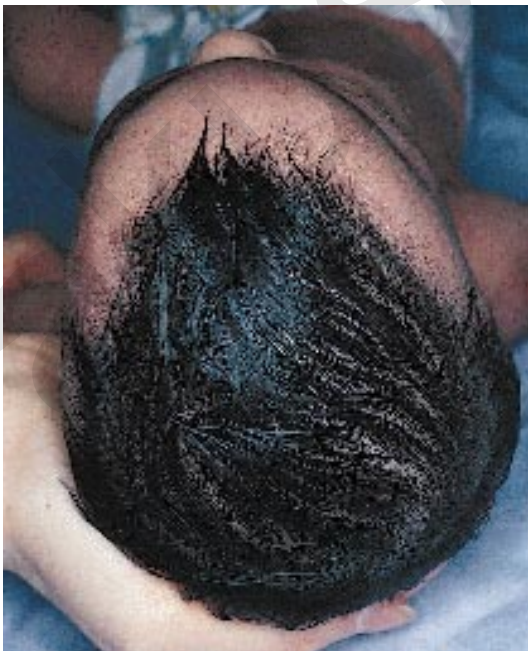

Figure 1.21. Note the asynclitism of the skull (plagiocephaly) associated with premature fusion of a single coronal suture. Plagiocephaly (oblique-shaped skull) occurs with premature fusion of a single suture (such as the coronal or lambdoidal) or with a congenital postural deformity. There is flattening of the diagonally opposite corners of the head (e.g., the right frontal and left occipital areas). In more severe cases, asymmetry of the facial features may also be seen. If plagiocephaly occurs as a result of a deformation, it is transient and corrects spontaneously. The combination of plagiocephaly and torticollis is well recognized.

1.22

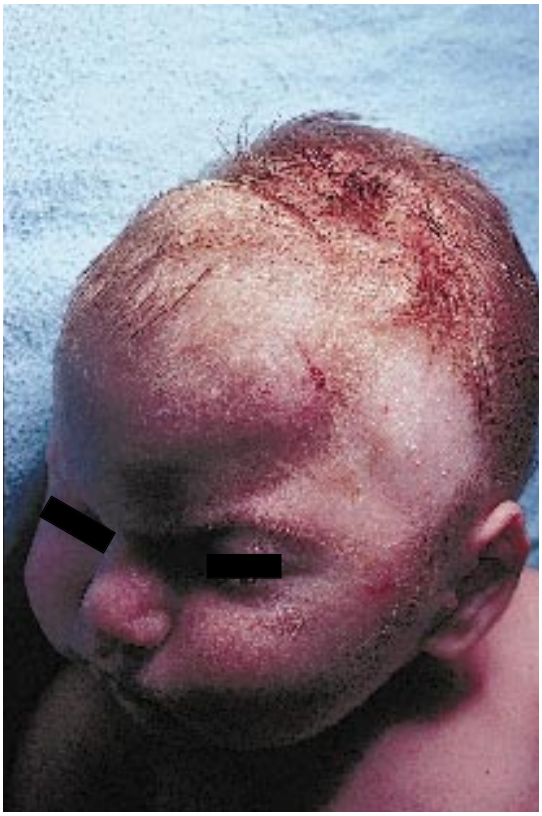

Figure 1.22. Kleeblattschädel ("cloverleaf" skull) is the result of premature fusion of the sagittal and coronal sutures. There is a trilobed appearance of the skull with indentations in the center and in the temporal regions. The ears are low set and the nasal bridge is depressed. This condition may occur in otherwise normal infants but is also noted in skeletal dysplastic conditions such as thanatophoric dwarfism.

1.23

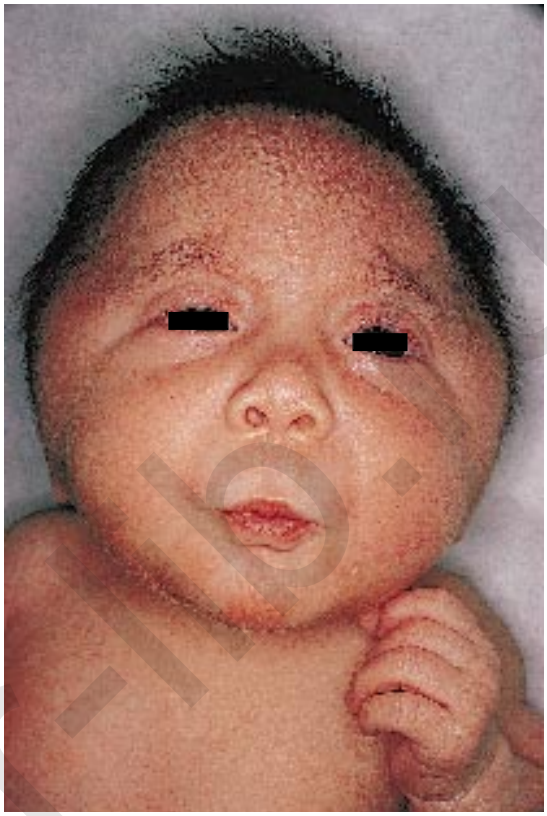

Figure 1.23. Another example of a "cloverleaf" skull. The brain is forced to grow through the anterior and temporal fontanelles resulting in upward and lateral growth.

1.24

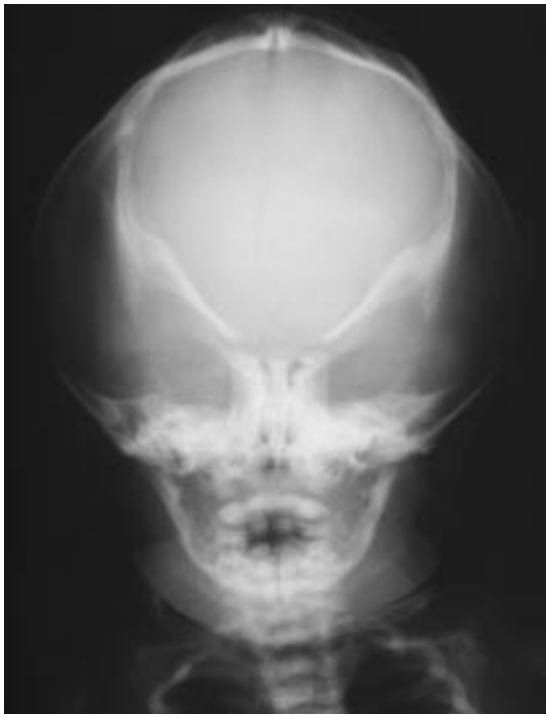

Figure 1.24. A frontal radiograph of "cloverleaf" skull in an infant exhibiting thanatophoric dwarfism.

1.25

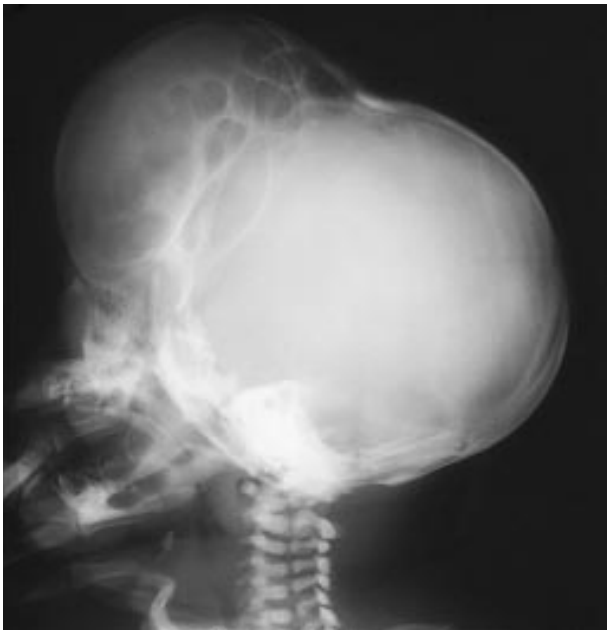

Figure 1.25. Lateral radiograph of the skull of the same infant as in Figure 1.24 with "cloverleaf" skull and thanatophoric dwarfism.

1.26

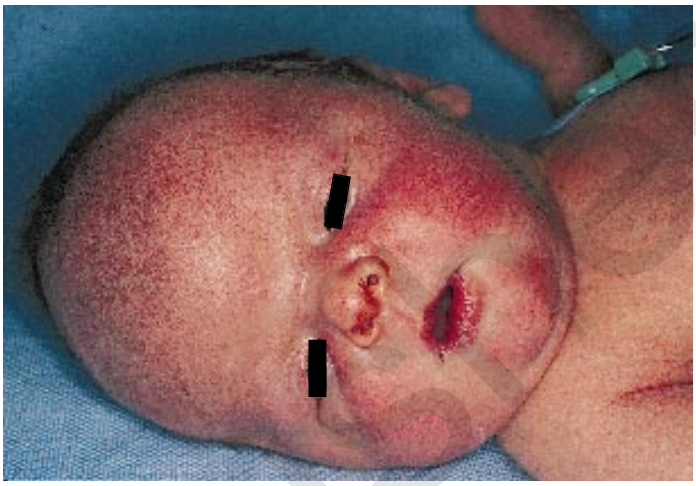

Figure 1.26. In this infant with Apert's syndrome (acrocephalosyndactyly), note the high steep frontal bone, protruding forehead, flat midface, small pinched nose, and the downward slanting of the palpebral fissures. The acrocephaly is due to premature fusion of the coronal sutures, resulting in bilateral coronal craniosynostosis. This infant also had the typical finding of a high arched palate.

1.27

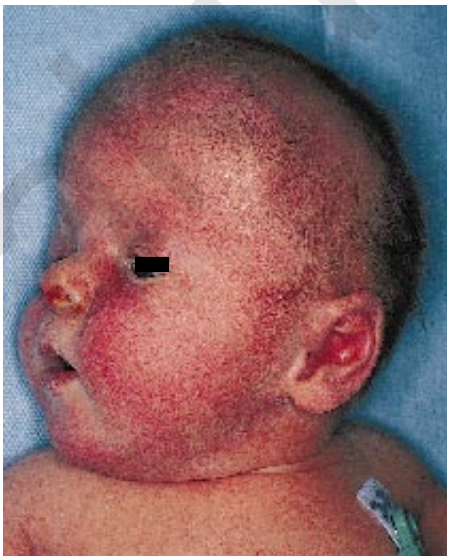

Figure 1.27. A lateral view of the head of the same infant. Again note the high steep frontal bone, protruding forehead, flat midface, small pinched nose, and the downward slanting of the palpebral fissures.

1.28

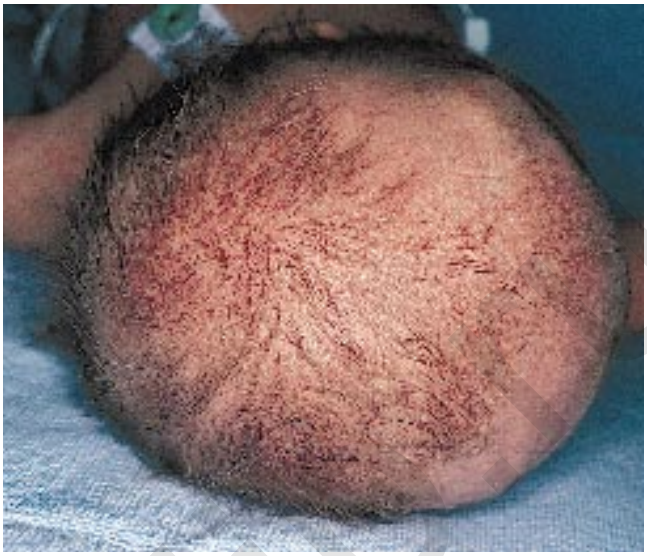

Figure 1.28. Superior view of the head of the same infant demonstrates turribrachycephaly ("tower" skull) which has occurred as a result of craniosynostosis of the coronal sutures. Note the ridges resulting from the fused sutures. The malformation of the skull occurs as a flattening of the frontal and occipital bones.

1.29

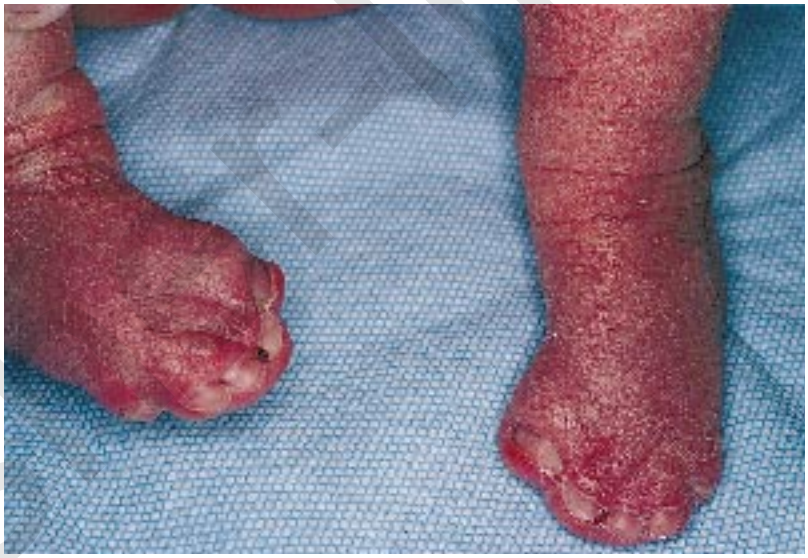

Figure 1.29. The same infant shows the characteristic symmetrical syndactyly which involves the toes. The fingers were similarly affected.

1.30

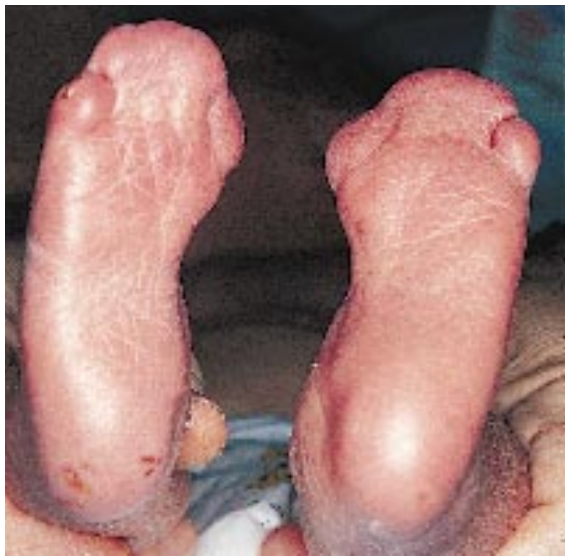

Figure 1.30. Another view of the symmetrical syndactyly of the toes in the same infant.

1.31

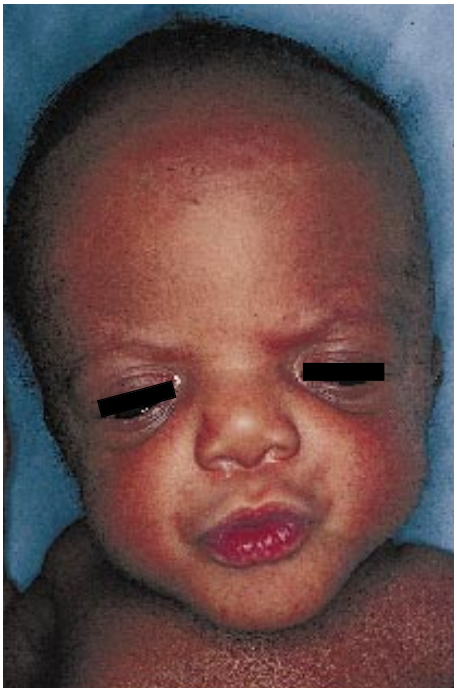

Figure 1.31. Another example of acrocephalosyndactyly in an infant whose mother had the same condition. Note the turribrachycephaly, high steep frontal bones, protruding forehead, flat midface, small pinched nose, and the downward slant of the palpebral fissures.

1.32

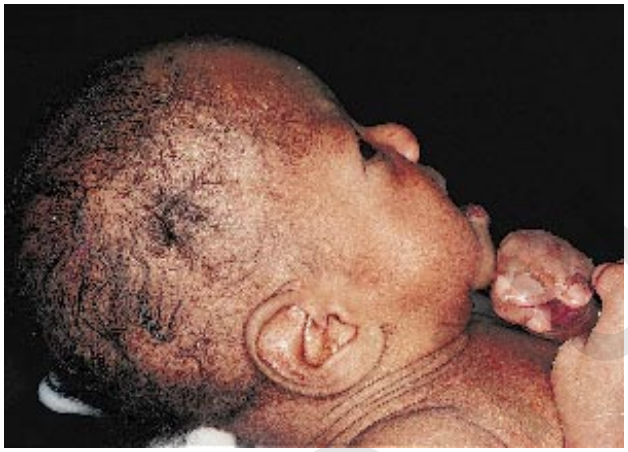

Figure 1.32. Lateral view of the same infant. Note the turribrachycephaly with the high steep forehead and note the syndactyly of the fingers of the left hand.

1.33

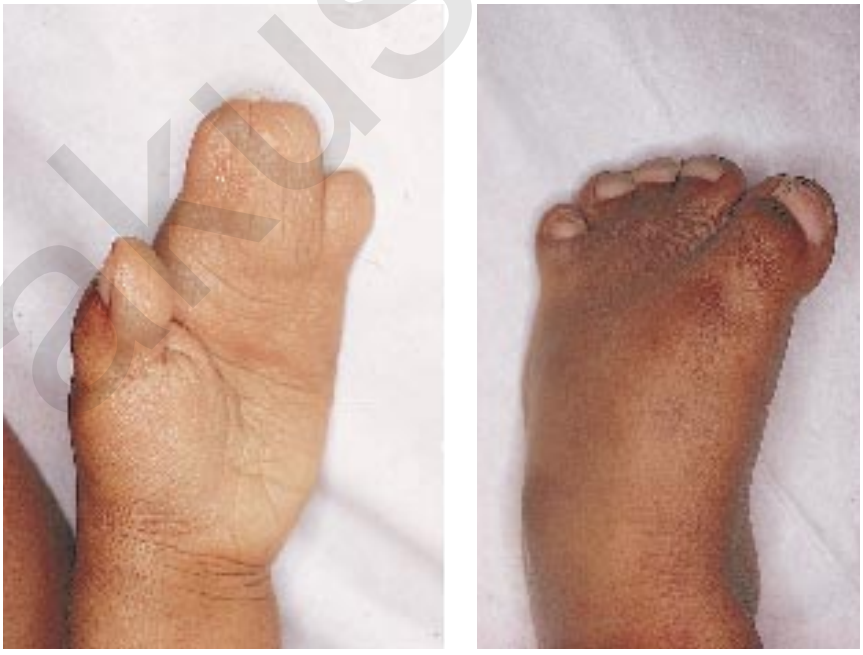

Figure 1.33. In this figure of the same infant, note on the left the syndactyly of the hand and on the right the syndactyly of the foot. These infants have symmetrical syndactyly.

1.34

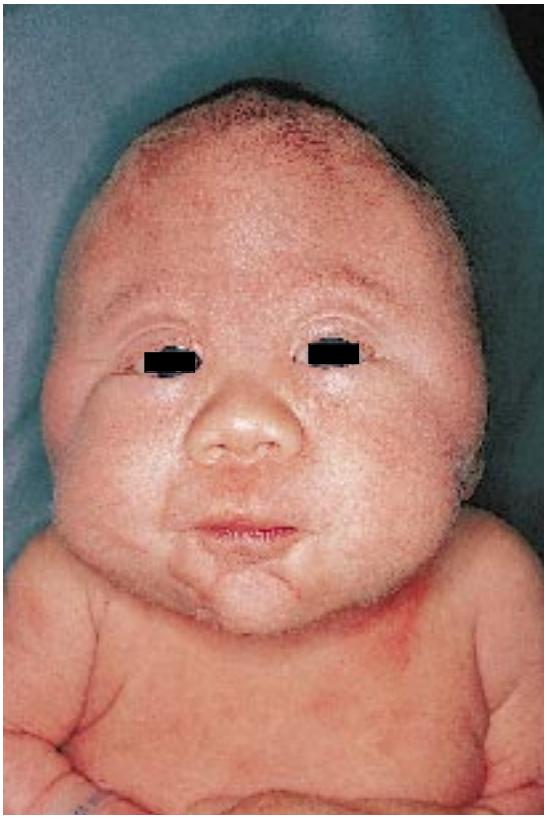

Figure 1.34. In infants with Carpenter's syndrome (acrocephalopolysyndactyly), the facial appearance is similar to that of infants with Apert's syndrome; in addition, there is polysyndactyly. This infant with Carpenter's syndrome shows the high steep protruding forehead, the flat midface, the small pinched nose, and the downward slanting of the palpebral fissures.

1.35

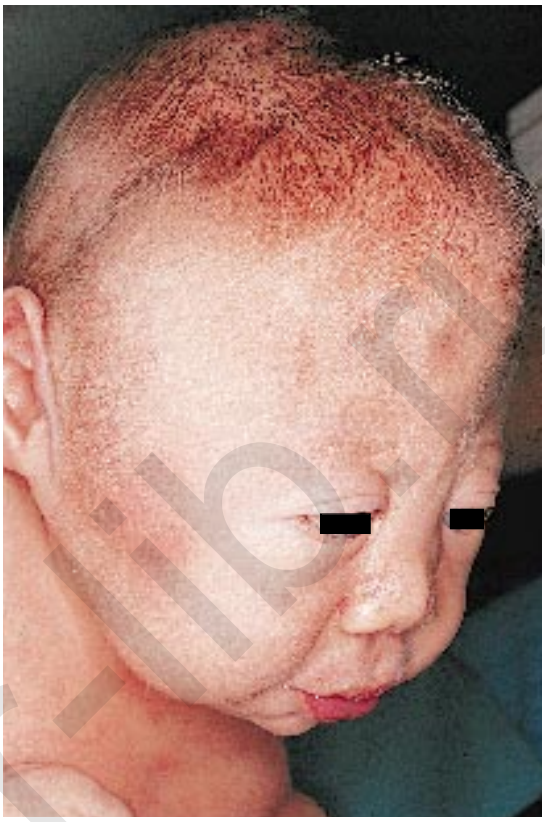

Figure 1.35. Oblique view of the same infant with Carpenter's syndrome shows the high steep forehead and turribrachycephaly. Note the ridges of the fused coronal sutures.

1.36

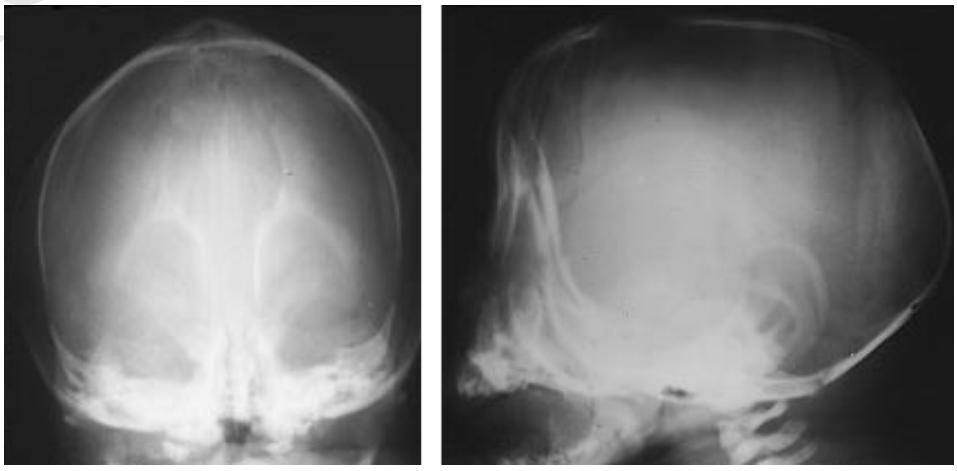

Figure 1.36. Frontal and lateral radiographs of the skull in the same infant show the premature fusion of the coronal sutures and the turribrachycephaly.

1.37

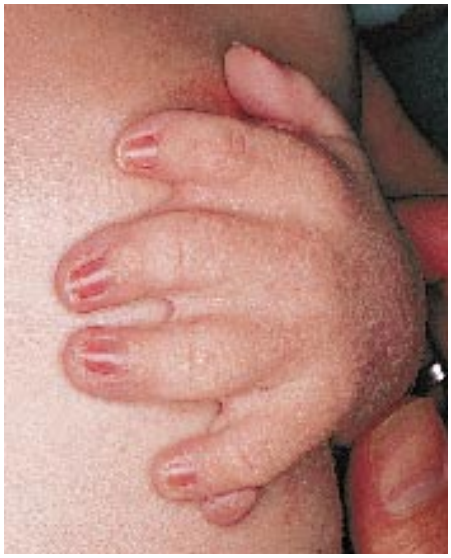

Figure 1.37. The left hand of the same infant as in Figures 1.34-1.36 with Carpenter's syndrome shows the polysyndactyly. Note the extra digit and the syndactyly which presents in the form of webbing.

1.38

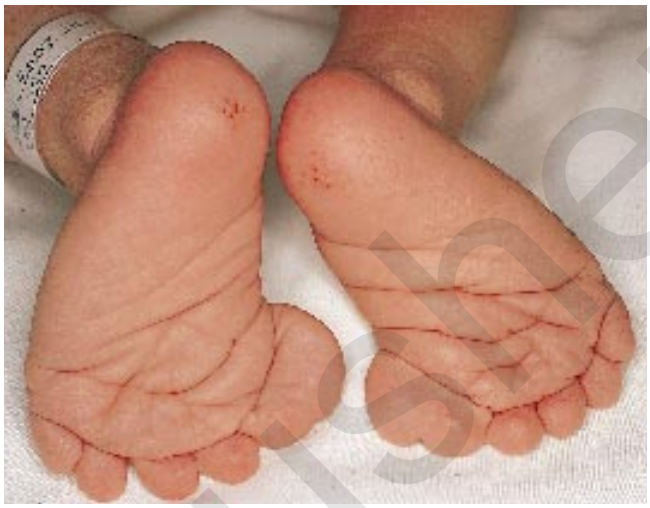

Figure 1.38. Symmetrical polysyndactyly of the feet in the same infant with Carpenter's syndrome.

1.39

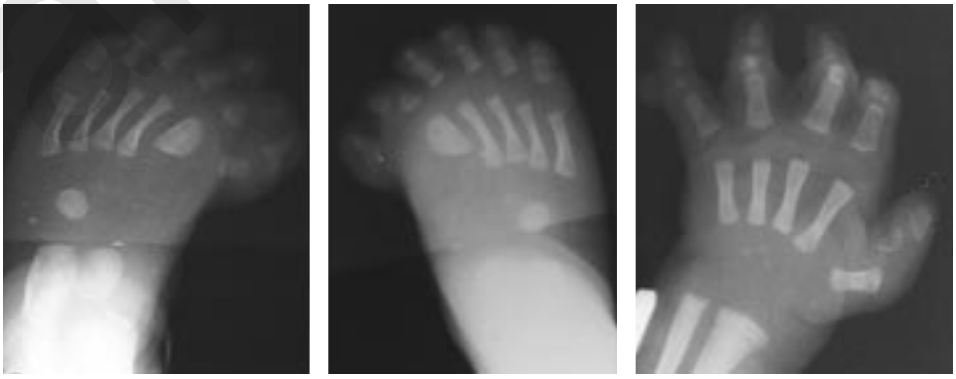

Figure 1.39. Radiographs of the feet and the right hand in the same infant with Carpenter's syndrome.

1.40

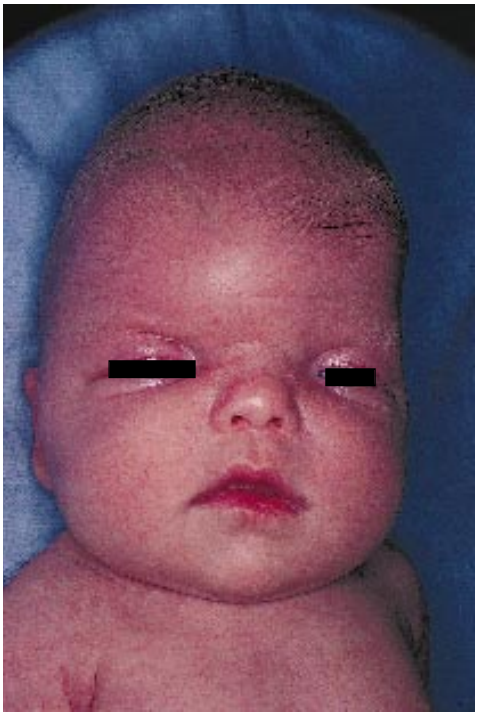

Figure 1.40. This neonate presented with the typical features of Crouzon's disease (craniofacial dysostosis). Note the deformed skull due to craniosynostosis of the coronal, sagittal, and metopic sutures. There is an antimongoloid slant to the eyes, shallow orbits with hypertelorism and hypoplasia of the facial bones. The nose is short with a low bridge. There is a short upper lip with a protruding lower lip. These infants may later develop exophthalmos.

1.41

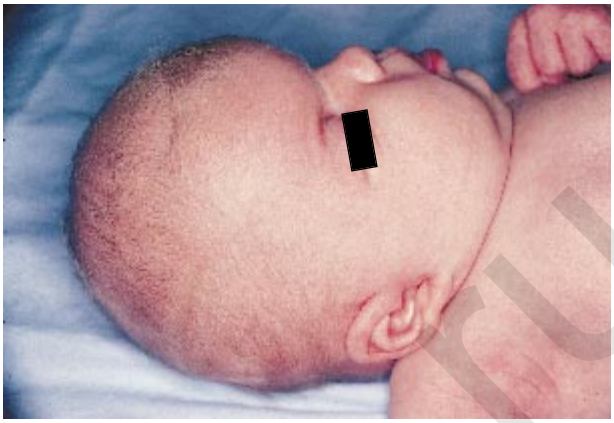

Figure 1.41. Lateral view of the same infant. Note the brachycephaly, high forehead, shallow orbits, and hypoplastic maxilla. This gives the appearance of a "dished-in" facies. The mandible may appear to be prognathic in contrast. Radiographs of the skull of these infants show premature synostosis with shortening of the base of the skull and narrowed optic foramina. Surgical treatment is essential.

1.42

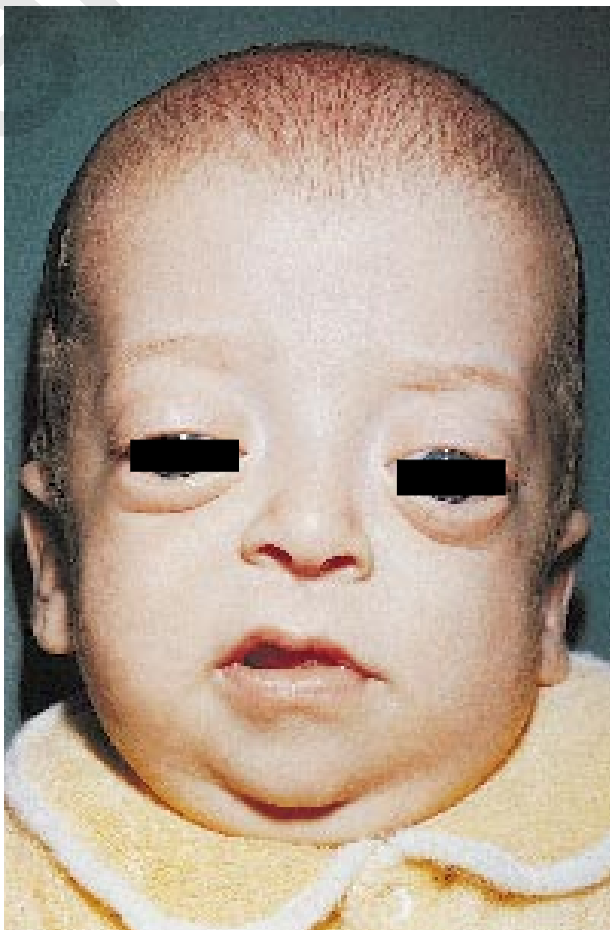

Figure 1.42. A 3-month-old infant with Crouzon's disease. Note the previous findings but in addition there is exophthalmos. Exophthalmos is not usually present at birth but develops later.

1.43

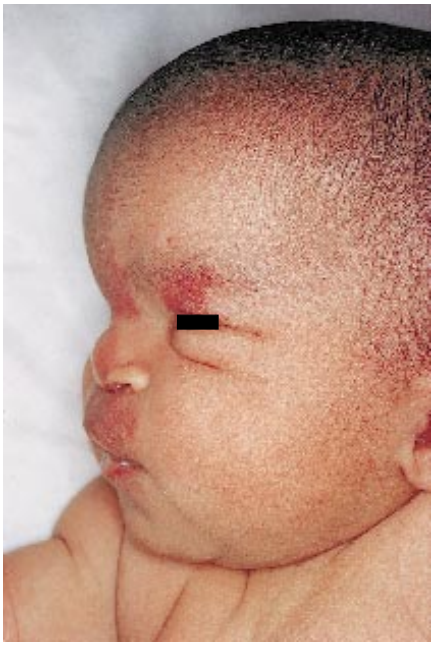

Figure 1.43. A flat facies is seen in many syndromes. It should be recognized that normal infants, such as this neonate, may present with the same appearance. Note the prominent forehead, flat nose and mild micrognathia which results in the flat facies.

1.44

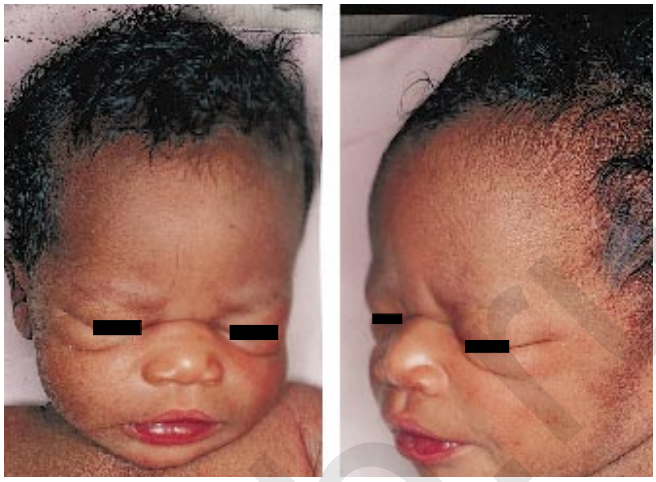

Figure 1.44. This normal infant has what appears to be a depressed nasal bridge. The mother had the same facies. Bulging over the nasal bridge, which appears when the infant cries may indicate the presence of an anterior encephalocele.

1.45

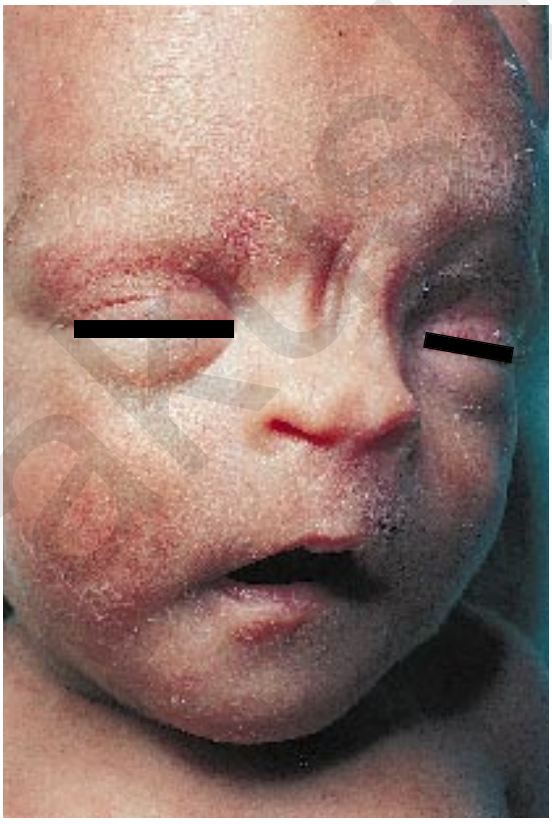

Figure 1.45. When too much tissue develops in (or migrates into) the upper midfacial zone it causes varying degrees of frontonasal dysplasia. The nasal bridge is broad, and extreme hypertelorism is always present. In severe cases there may be several centimeters of separation, with aberrant formation of the philtrum and upper lip (such as an extremely short philtrum and a tented upper lip). This infant is an example of a median cleft nose (frontonasal dysplasia). Note the prominent epicanthic folds. Although nasal clefting may be a normal variant, prominent midline clefting may be associated with holoprosencephaly, as part of the median cleft syndrome, and thus requires a diagnostic evaluation. CT scan in this infant confirmed the presence of holoprosencephaly.

1.46

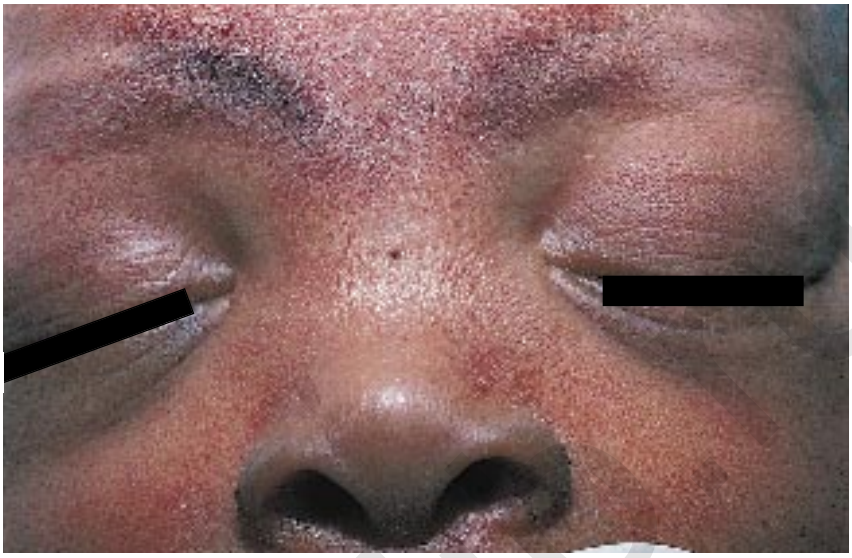

Figure 1.46. Note the median nasal pit in this infant. As with any midline lesion on the head or back, one should check to be sure this does not represent the end of a tract that communicates with the central nervous system. Danger signs include hairs implanted in the pit, fluid emerging from its depths or any underlying bony defect or cystic mass.

1.47

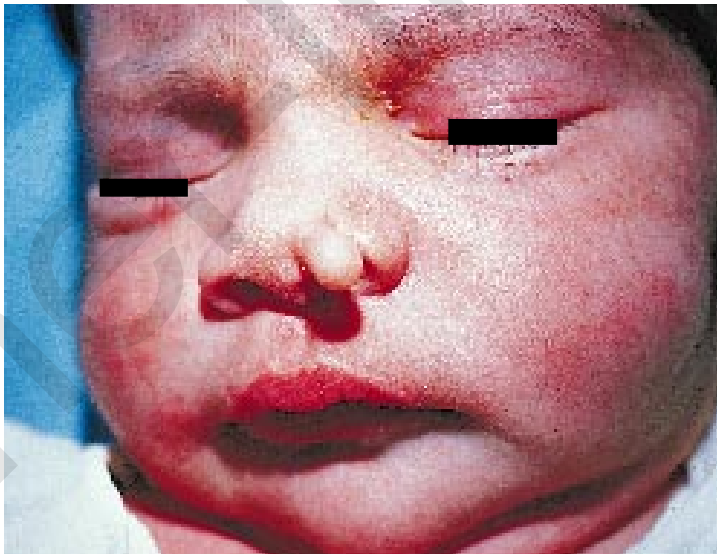

Figure 1.47. Lateral nasal clefts may occur in otherwise normal infants.

1.48

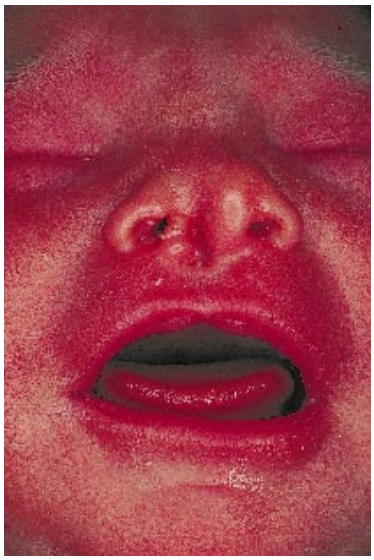

Figure 1.48. A more severe example of a lateral nasal cleft in an otherwise normal infant.

1.49

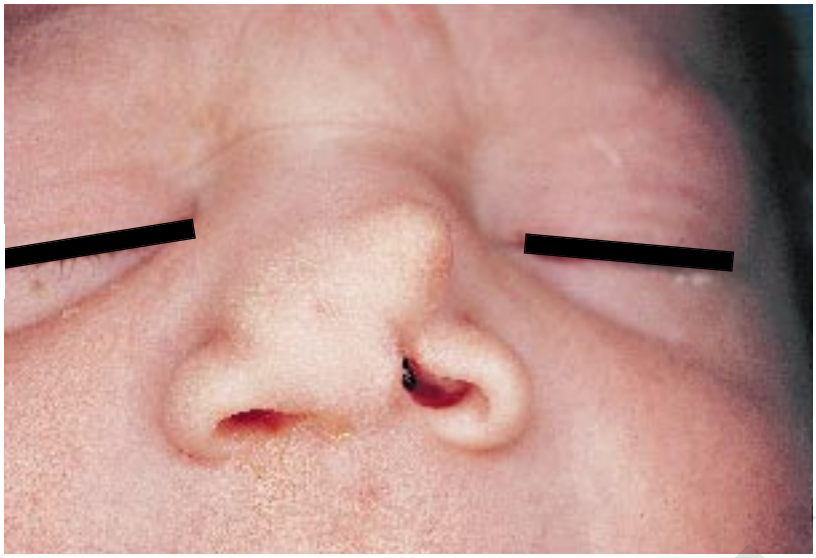

Figure 1.49. Although lateral nasal clefts, in general, are isolated findings, this infant in addition to the cleft had Holt-Oram syndrome (heart disease, in this case coarctation of the aorta, and absence of left radius and thumb).

1.50

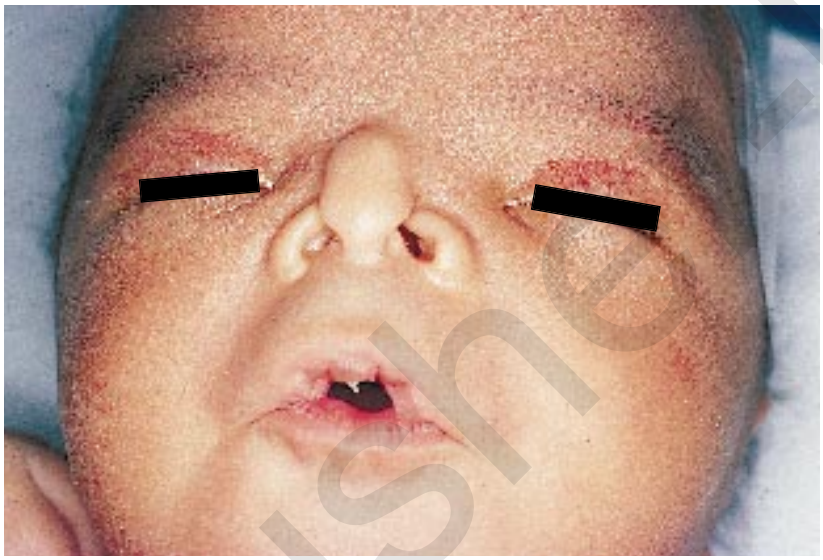

Figure 1.50. In this infant with bilateral clefting of the alae nasi, the philtrum is long and smooth because of the short nose. Note the downslanting palpebral fissures. There were bilateral cloudy corneas and congenital cataracts, a large anterior fontanelle and large metopic sutures. Karyotype was normal and MRI of the head was normal.

1.51

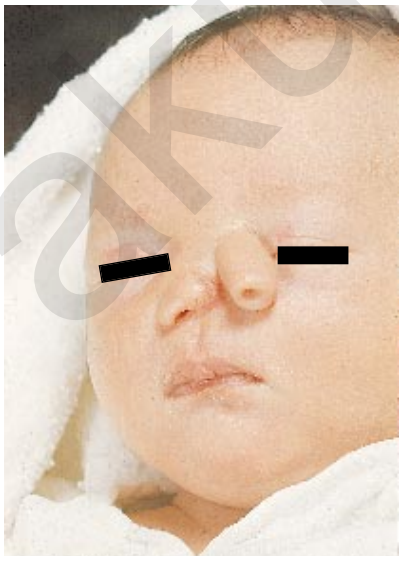

Figure 1.51. Proboscis lateralis is a congenital abnormality in which the nose fails to develop normally.

1.52

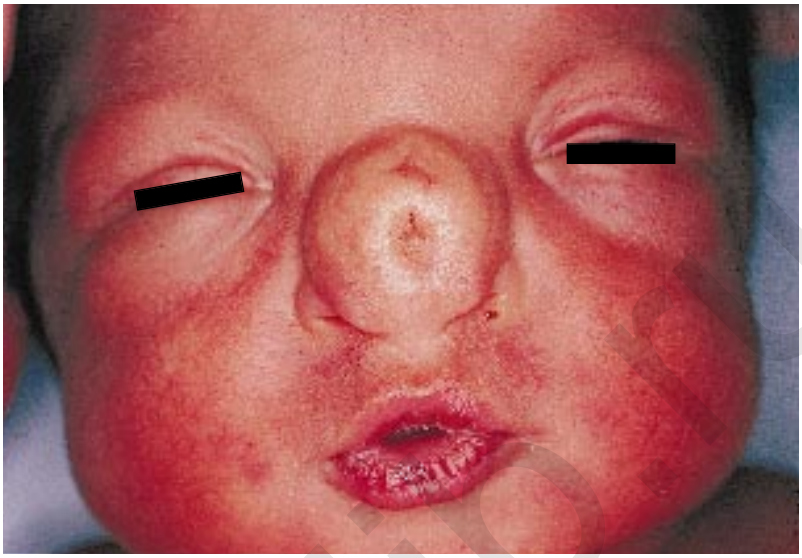

Figure 1.52. Severe midline nasal schistasis. This was confirmed to be a communicating encephalocele on CT scan.

1.53

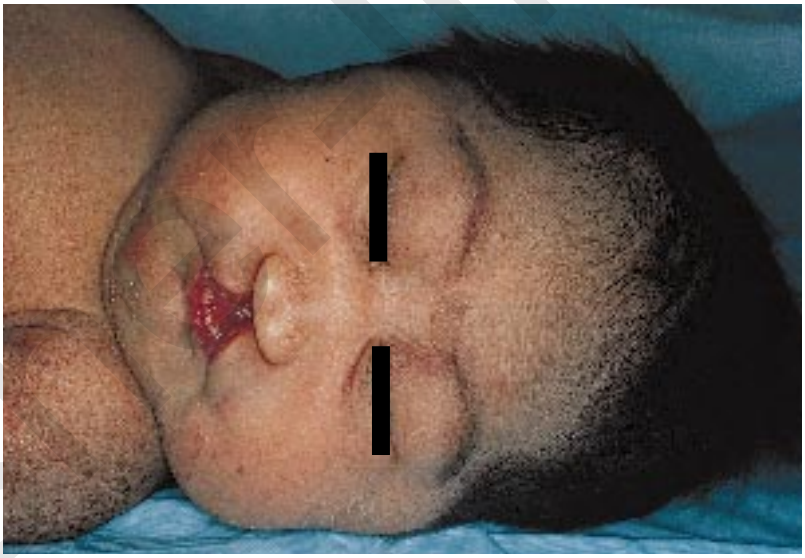

Figure 1.53. This infant has the median cleft syndrome. Note the facial features which include median cleft lip, nasal depression, hypotelorism, receding forehead, and microcephaly. A median cleft palate was also present. These findings commonly occur with alobar holoprosencephaly as a result of underdevelopment of the brain. The majority of cases of holoprosencephaly are sporadic and may occur as an isolated anomaly, in association with chromosomal abnormalities (13, 13q–, 18p–), all in syndromes associated with arhinencephaly or holoprosencephaly.

1.54

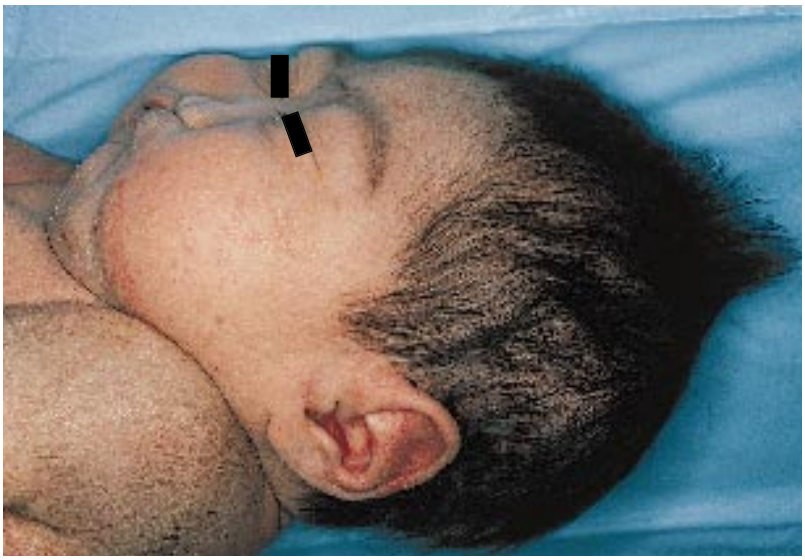

Figure 1.54. Lateral view of the same infant shows the microcephaly, receding forehead and chin, marked hypotelorism, and median cleft.

1.55

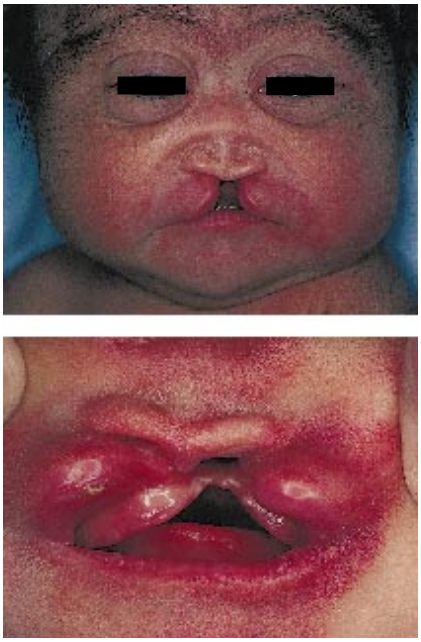

Figure 1.55. Another example of the median cleft syndrome with a normal karyotype and a head ultrasound showing holoprosencephaly. The close-up view shows clefting of the alveolar ridge which is also seen in this syndrome.
Holoprosencephaly results from maldevelopment of the forebrain (prosencephalon). It may occur as an alobar type in which there is a horseshoe-shaped single ventricle; a semilobar type in which there is partial differentiation of the ventricles, especially at the temporo-occipital horns; or a lobar type in which there is partial fusion of the frontal lobes and a narrow body of the lateral ventricles.

1.56

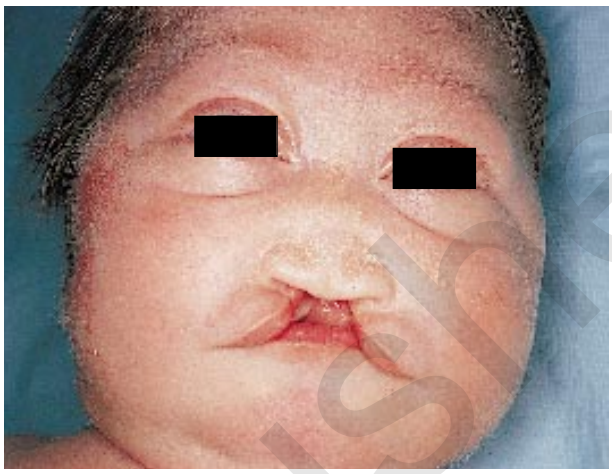

Figure 1.56. Another example of the median cleft syndrome in an infant with trisomy 13. Note the hypotelorism and midline position of the cleft lip. Embryologically this differs from the more common unilateral or bilateral cleft lip.

1.57

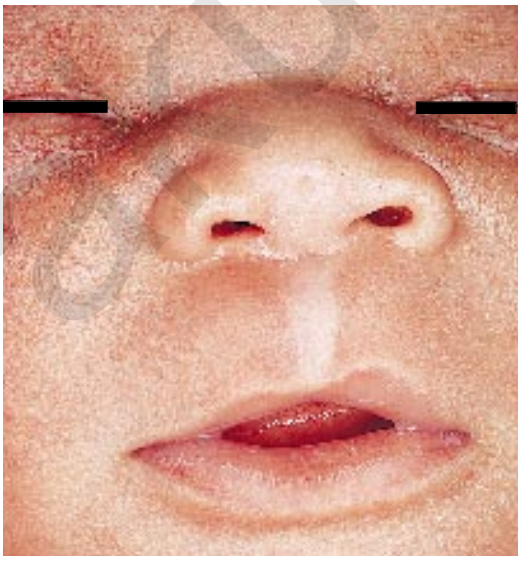

Figure 1.57. Note the midline hypopigmentation of the philtrum with lack of true clefting of the lip. This finding suggests that further evaluation should be done. Central nervous system evaluation revealed holoprosencephaly.

1.58

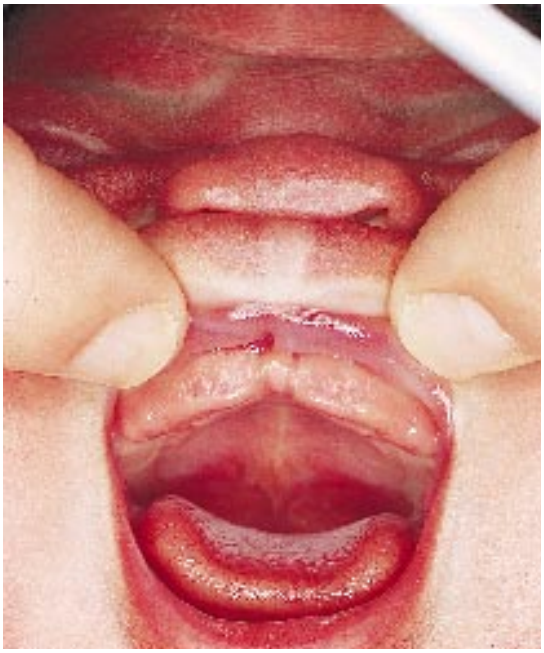

Figure 1.58. Notching of the alveolar ridge in the same infant as in Figure 1.57 with median cleft syndrome.

1.59

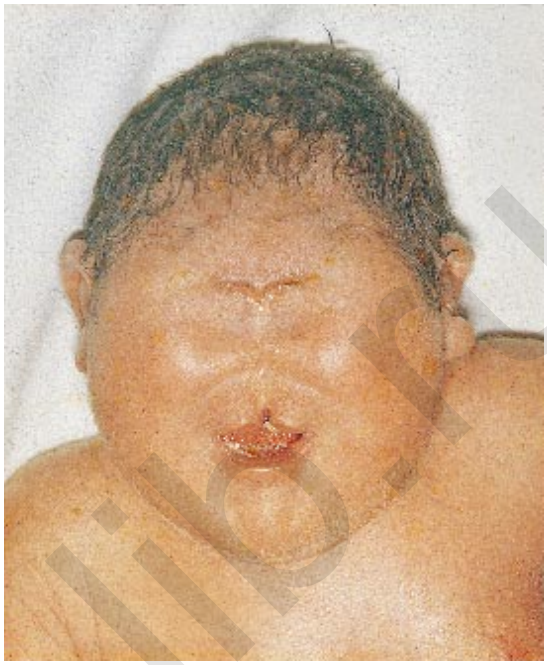

Figure 1.59. Holoprosencephaly may have other clinical manifestions. This infant is an example of cyclopia without a nose or proboscis. In cyclopia there may be a single, double or absent proboscis above or below the fused orbits. Note the marked hypotelorism resulting in fused eyes (cyclopia), lack of nose, and small median cleft of the upper lip. There is also severe microcephaly.

1.60

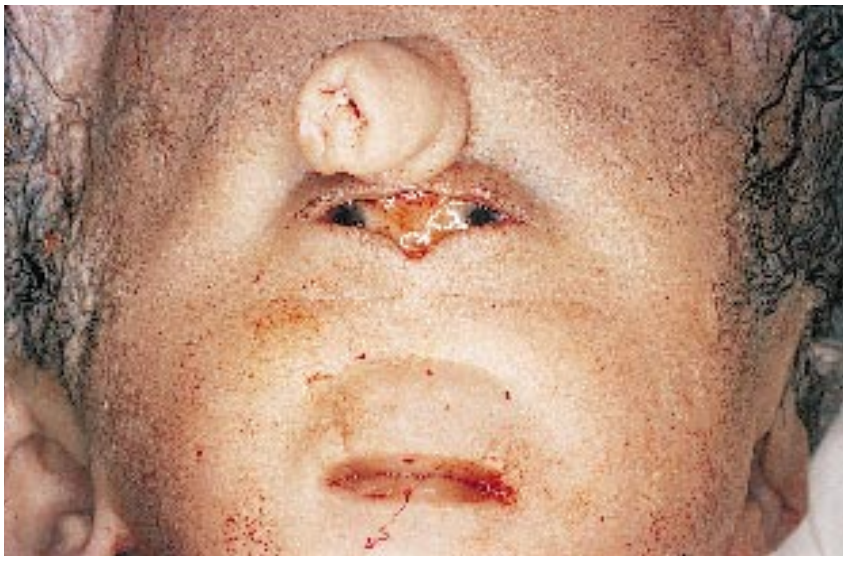

Figure 1.60. This is an example of cyclopia with a superior proboscis. Note the median cleft in the single fused lower eyelids, the fused orbits, and the hypoplasia of the facial bones. This is another example of median cleft syndrome with holoprosencephaly.

1.61

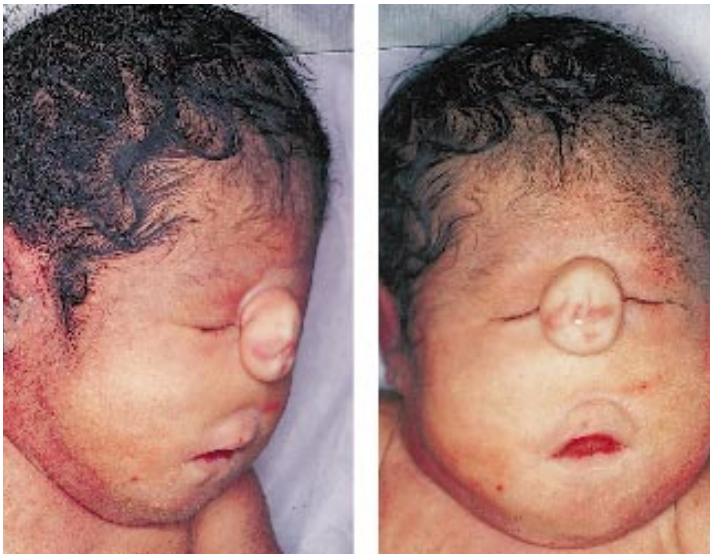

Figure 1.61. In holoprosencephaly when there are separate orbits with a proboscis above the eyes and a lack of nostril with a single or double proboscis above or below the eyes, the condition is called ethmocephaly. Note also the small mouth.

1.62

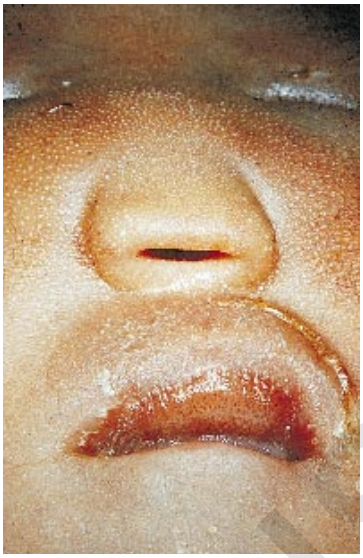

Figure 1.62. Another variant of the median cleft syndrome (holoprosencephaly) is cebocephaly in which there is a small nose with a single nostril above or below the eyes. Note the single orifice and aplasia of the nasal septum and philtrum.

1.63

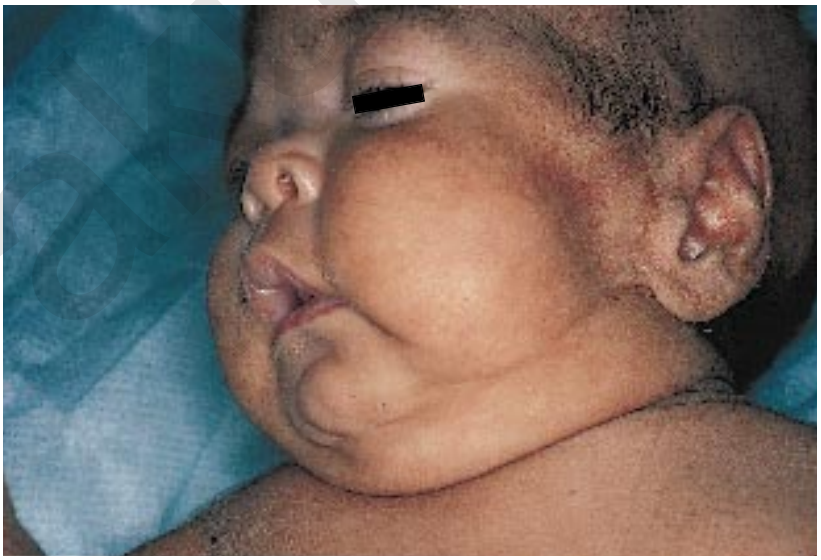

Figure 1.63. Buccal fat pads (sucking cushions) are pads of fat tissue between the fibers of the masseter muscle. When the infant is sucking they prevent collapsing of the cheeks during indrawing. These fat pads remain unaltered despite loss of adipose tissue in other body areas.

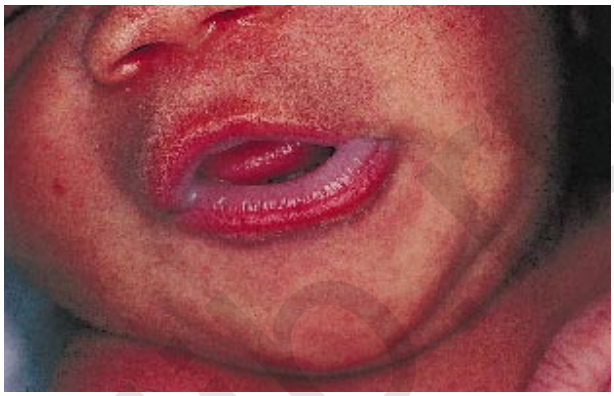

1.64

Figure 1.64. Sucking blisters (sucking calluses) on the lips are present in the newborn infant. From birth, the lips show a sharp line of demarcation where the skin meets the mucosa. The mucosa is slightly elevated, moist, glistening deep red or purple and ends abruptly with the skin which forms one-third of the visible lip. The term "sucking calluses" is a misnomer because they are not callosities due to pressure or friction. They have been seen at their most florid in infants who have never sucked (for example those with congenital heart disease). Efficient sucking requires a complete seal of the lips around the nipple, hence the development of these calluses.

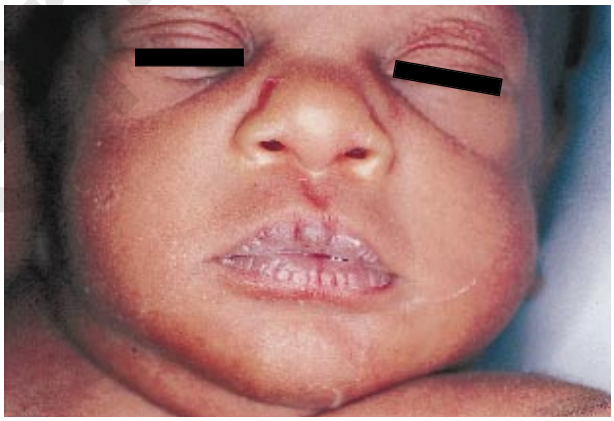

1.65

Figure 1.65. Another example of sucking blisters in an infant at 6 days of age. Note that the mucous membrane portion of the lip has a superficial furrowed appearance. With time, the outer layer dries with lifting and shedding of the cornified epithelium and new blisters may develop for a few weeks. They occur most commonly in breast-fed infants or babies who feed vigorously. Pathologically, this can also occur from overheated formula, or as an allergic reaction to the components of the nipple or the formula.

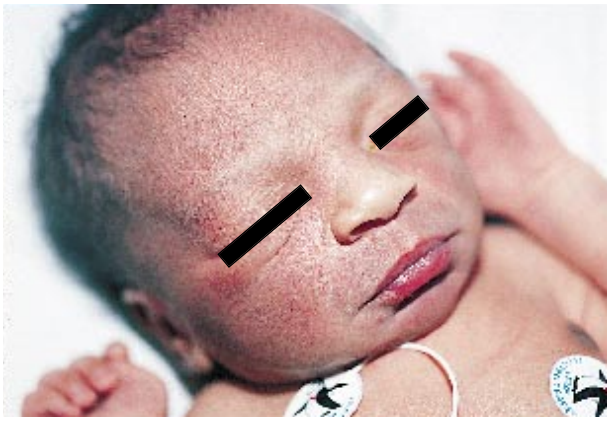

1.66

Figure 1.66. A thin vermilion border of the upper lip in a normal infant. This may also be seen in many syndromes such as the fetal alcohol syndrome.
A long philtrum may indicate a short nose and a short philtrum may indicate a long nose. Downturned corners of the mouth may reflect overgrowth in the width of the upper lip, which when combined with a short philtrum or thick lower lip results in a carp-like mouth.

1.67

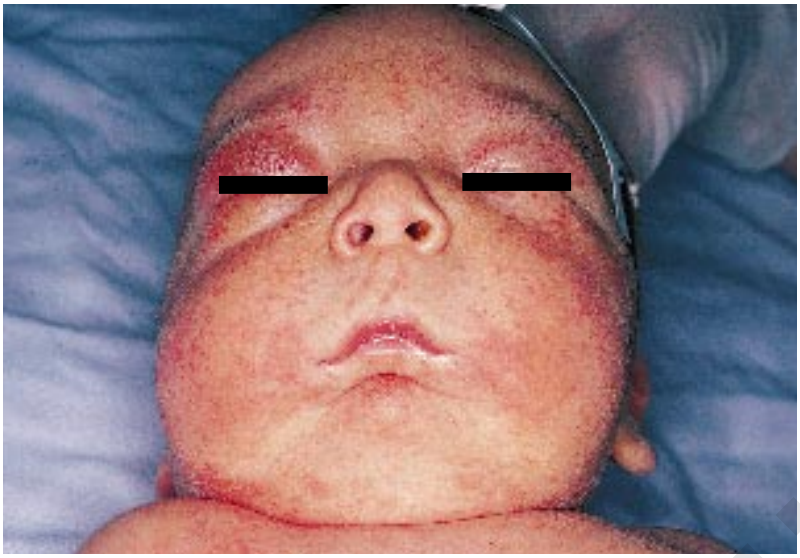

Figure 1.67. This infant is an example of microstomia occurring as a result of excessive merging of the maxillary and mandibular processes of the mandibular arch. This may occur in normal infants or is associated with many syndromes such as Hallermann-Streiff syndrome and Freeman-Sheldon syndrome. The diagnosis in this infant was mosaic trisomy 8.

1.68

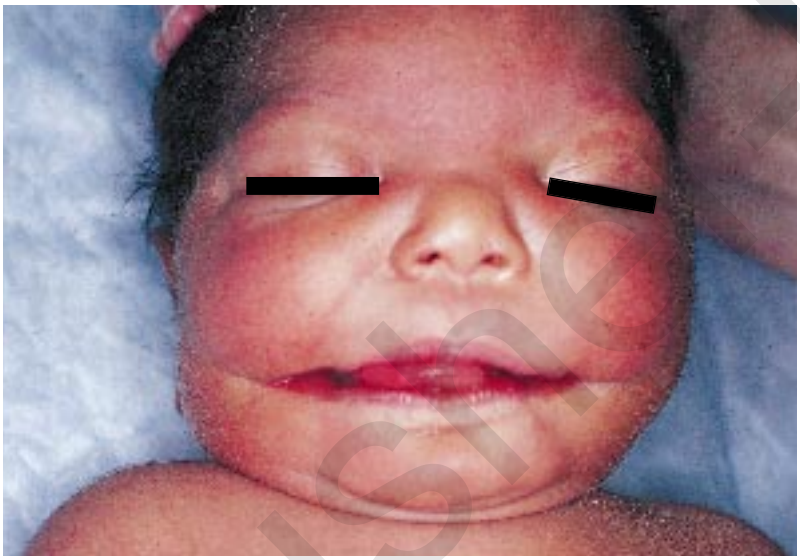

Figure 1.68. This infant with severe bilateral macrostomia is an example of a congenital lateral or transverse facial cleft which results from malformation of the mandibular arch (failure of the lateral maxillary and mandibular processes to merge). The defect may be unilateral or bilateral and is associated with deformities of the outer ear, hypoplasia of the mandible or maxilla, and cleft palate. It is also seen in Goldenhar's syndrome.

1.69

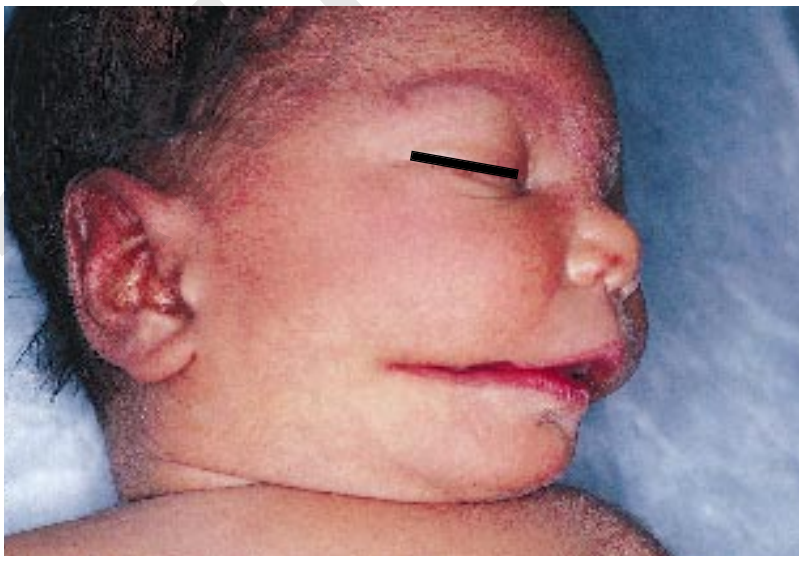

Figure 1.69. A lateral view of the severe macrostomia in the same infant. Note the micrognathia. There were no other abnormalities.
An oblique facial cleft (orbitofacial fissure) extends from the upper lip to the medial aspect of the orbit. It is often bilateral and may involve the orbit, nose, lacrimal ducts, or central nervous system. This may occur from facial clefting that results from swallowed amniotic bands and represents a disruption in that it does not follow the normal planes of fusion of the face.

1.70

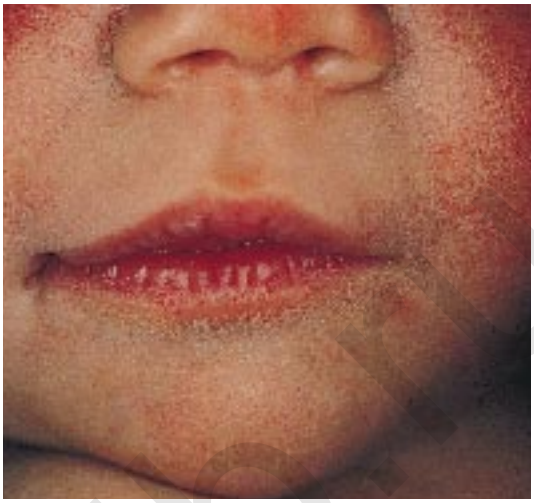

Figure 1.70. Right-sided unilateral macrostomia in an otherwise normal infant.

1.71

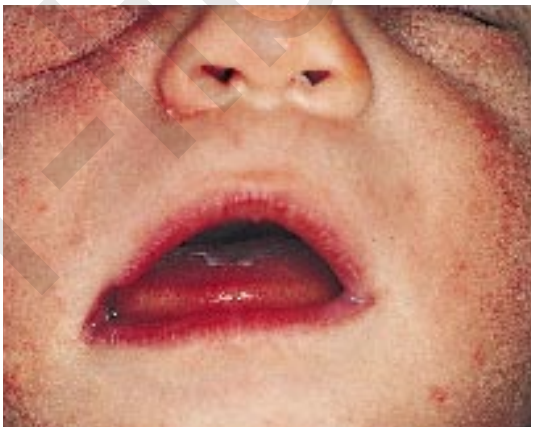

Figure 1.71. This infant with Goldenhar's syndrome has unilateral macrostomia. There was an antimongoloid slant to the eyes, preauricular skin tags, and deafness.

1.72

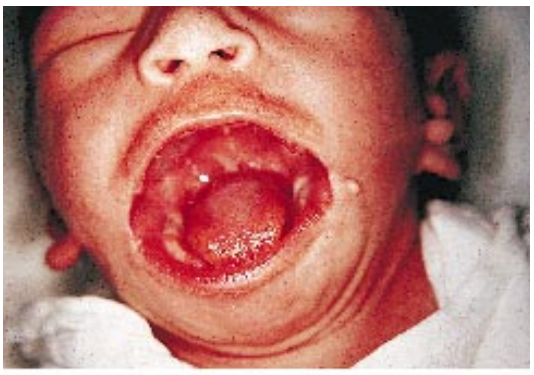

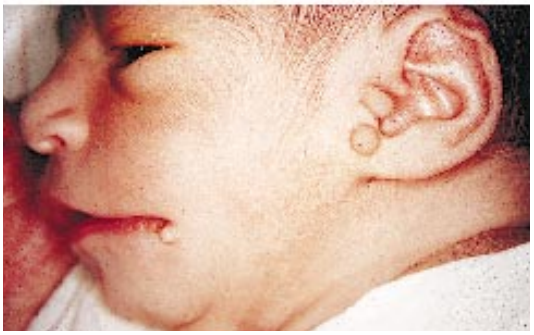

Figure 1.72. Macrostomia with cutaneous tags and preauricular skin tags. Cutaneous pits and tags may be found along a line connecting the oral commissure and the external auditory canal in Goldenhar's syndrome.

1.73

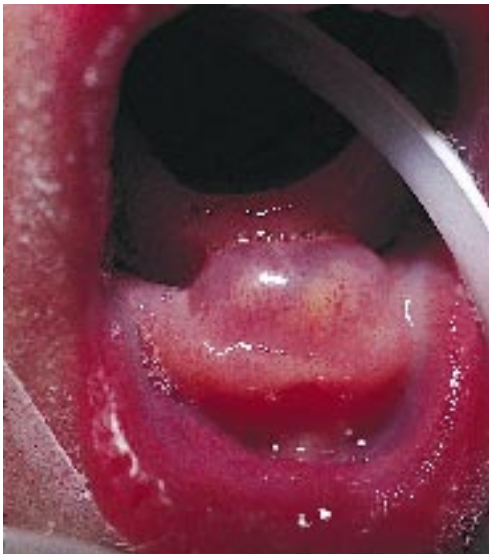

Figure 1.73. Eruption cysts in an infant at birth. Note the central lower incisors which are visible. The teeth erupted at the age of 4 days.

1.74

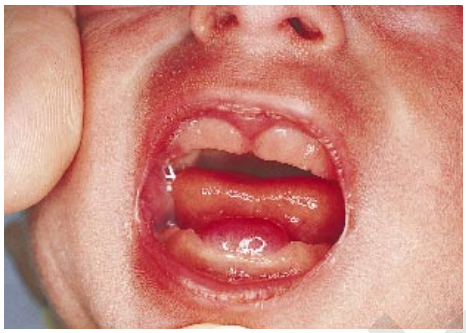

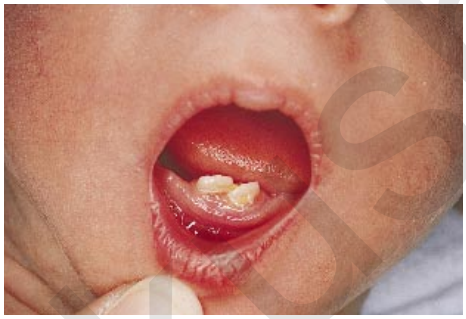

Figure 1.74. In the upper figure, note the eruption cysts which were present at birth. At the age of 7 days, both lower central incisors had erupted (lower figure). Nearly all neonatal teeth arise from the normal deciduous complement and are usually only immature caps of enamel and dentine with poor root formation. Often the eruption cyst is present on the gum at birth and the neonatal tooth appears shortly afterwards. The lower central incisors are the most common site for neonatal teeth.

1.75

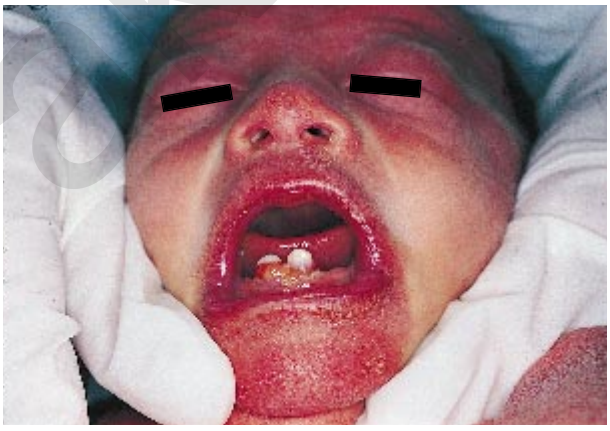

Figure 1.75. Natal teeth present at birth. Teeth that erupt after birth are neonatal teeth. These teeth have a familial pattern of occurrence and are more common in certain races such as American Indians and Eskimos. Neonatal teeth may occur in association with syndromes.

1.76

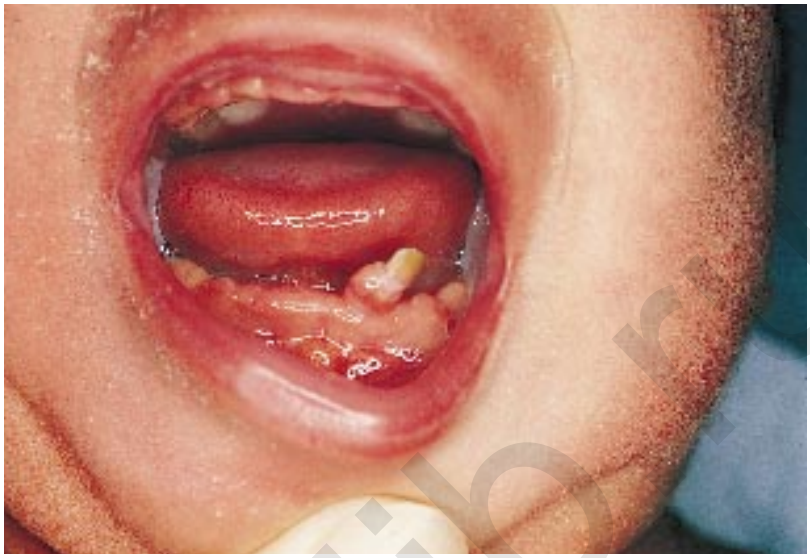

Figure 1.76. Note the poor development of this natal tooth. This should be extracted, as this may fall out spontaneously and be aspirated.

1.77

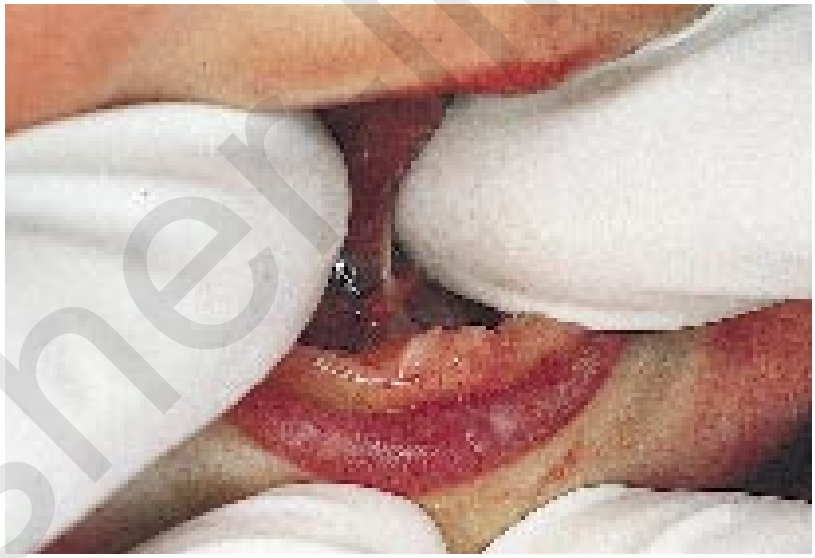

Figure 1.77. Natal teeth present at birth in a very low birthweight infant (weight 700 g).

1.78

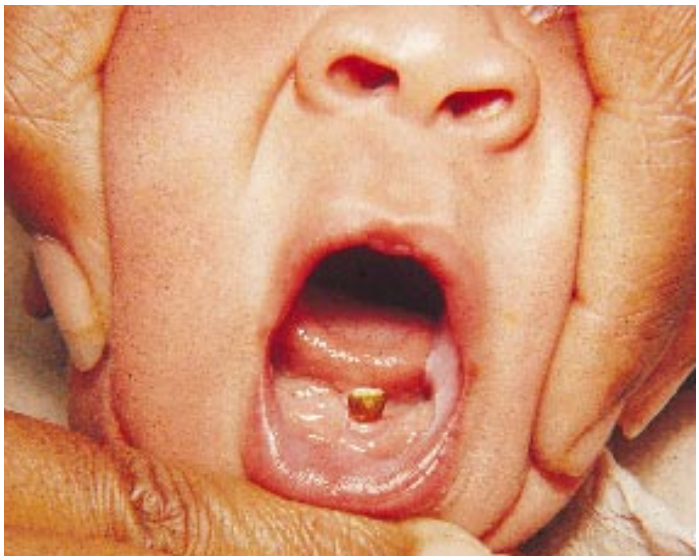

Figure 1.78. Discoloration of a natal tooth secondary to maternal treatment with tetracycline during pregnancy.

1.79

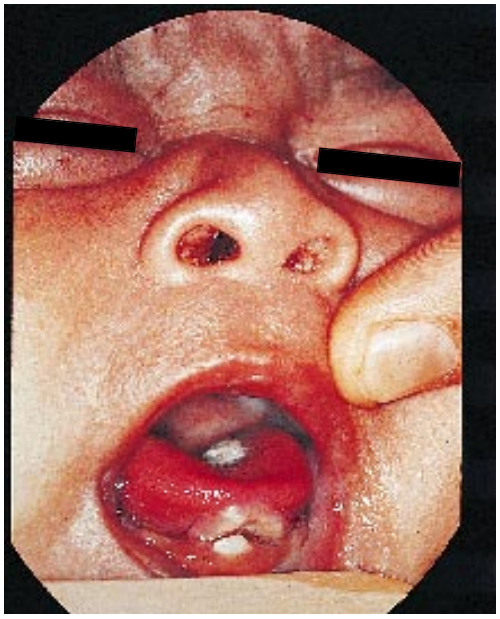

Figure 1.79. Neonatal teeth causing ulceration of the undersurface of the tongue by vigorous sucking (Riga-Fede disease). Neonatal teeth are more likely to cause this because the mucous membranes are still very delicate. These teeth require extraction to permit healing of the ulceration.

1.80

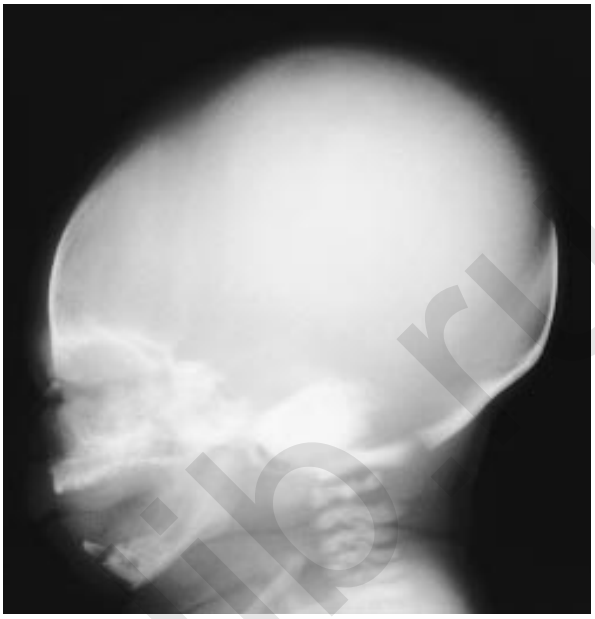

Figure 1.80. Lateral radiograph of the skull. Note the neonatal teeth.

1.81

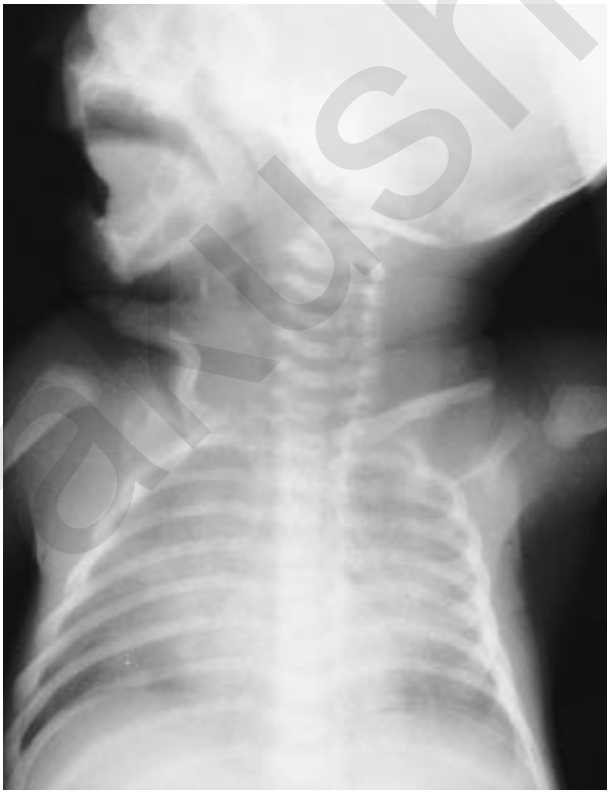

Figure 1.81. Radiograph of the face and chest showing the lack of dentition in a term infant with ectodermal dysplasia. Normally, at term there should be mineralization of the incisors and of the first and second molars.

1.82

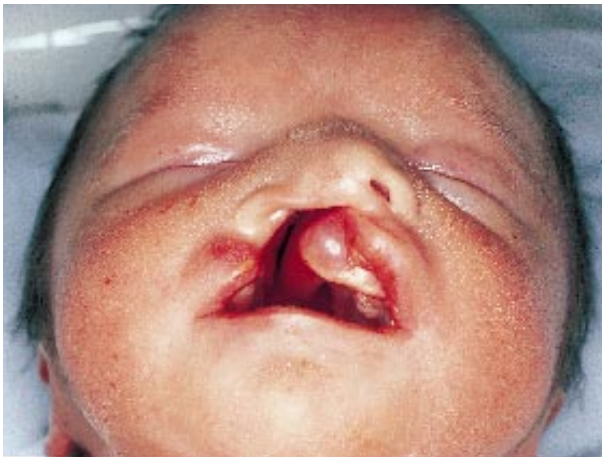

Figure 1.82. A baby with a right unilateral cleft lip and a cleft palate. Note the eruption cyst in the upper jaw. In general, neonatal teeth are more common in the lower jaw, but in the presence of a cleft lip and/or cleft palate, neonatal teeth are often present in the upper jaw.

1.83

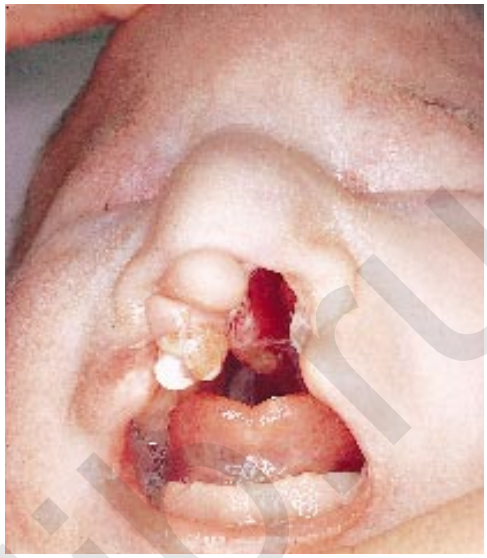

Figure 1.83. This infant with a left cleft lip and cleft palate has a neonatal tooth in the upper jaw.

1.84

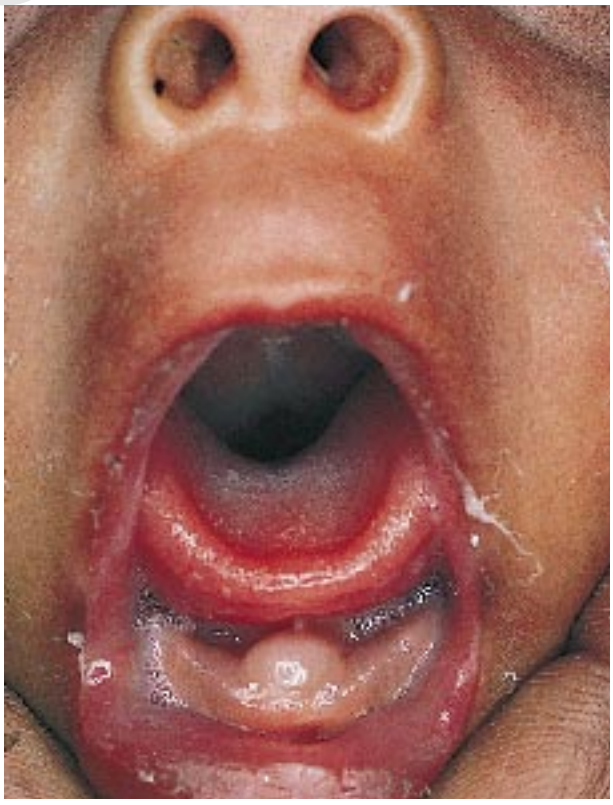

Figure 1.84. If a central eruption cyst or central mandibular incisor is present in the lower jaw, the diagnosis of median cleft syndrome must be excluded. This infant had median cleft syndrome. A single central maxillary incisor also may be seen in growth hormone deficiency.

1.85

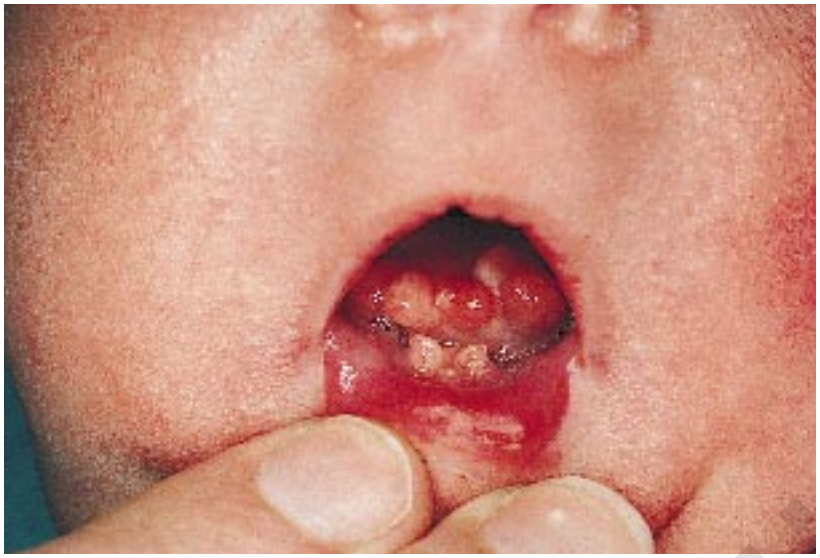

Figure 1.85. In this infant with neonatal teeth, note the small white hamartomatous masses on the ventral and dorsal surfaces of the tongue and the ankyloglossia. These findings are typical of the orofaciodigital syndrome, Type I.

1.86

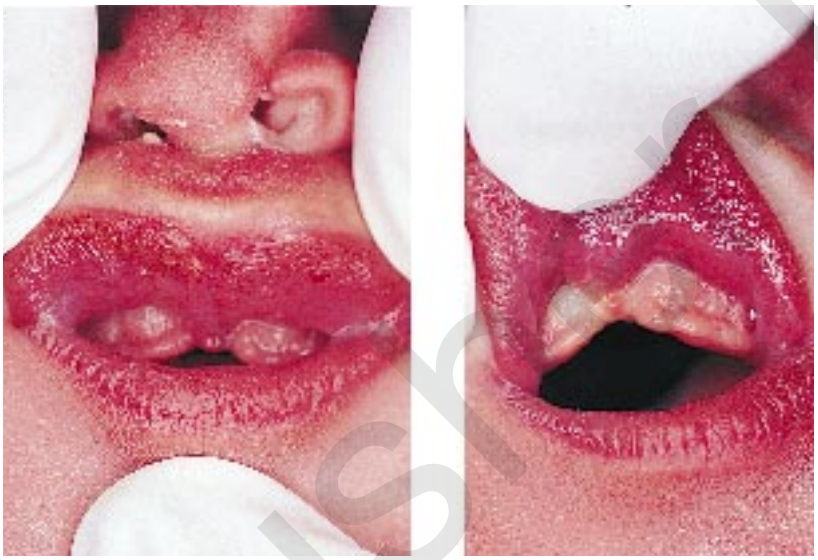

Figure 1.86. Frenulum (frenum) labialis superior. The frenulum is a continuation of the fibrous median raphe of the maxilla. It may be prominent and unusually thick and is often associated with deep notching of the alveolar ridge of the maxilla.

1.87

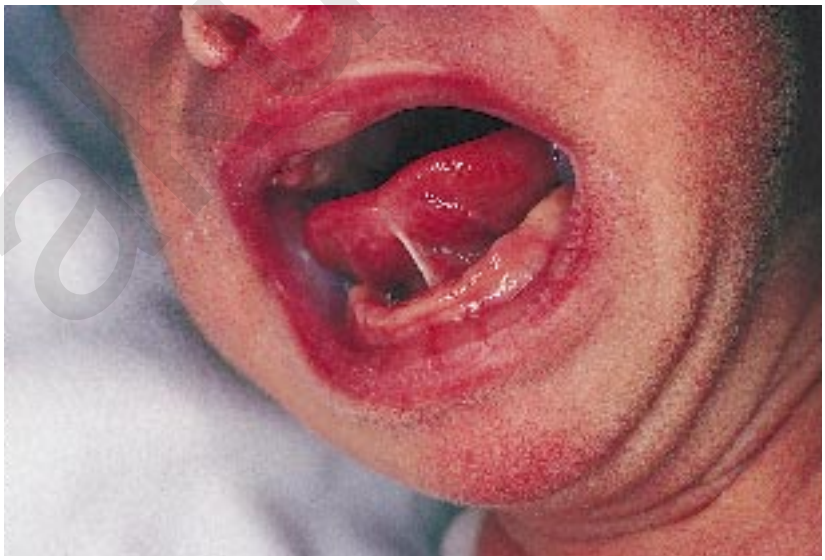

Figure 1.87. Lingual ankyloglossia ("tongue tie") in a premature infant (birthweight 1700 g). Note the indentation of the tip of the tongue. The lingual frenulum limits the movement of the tip of the tongue. True tongue tie is rare. If the tongue can be protruded beyond the lips, no intervention is necessary as the tongue grows more rapidly than the frenulum and soon becomes freely mobile.

1.88

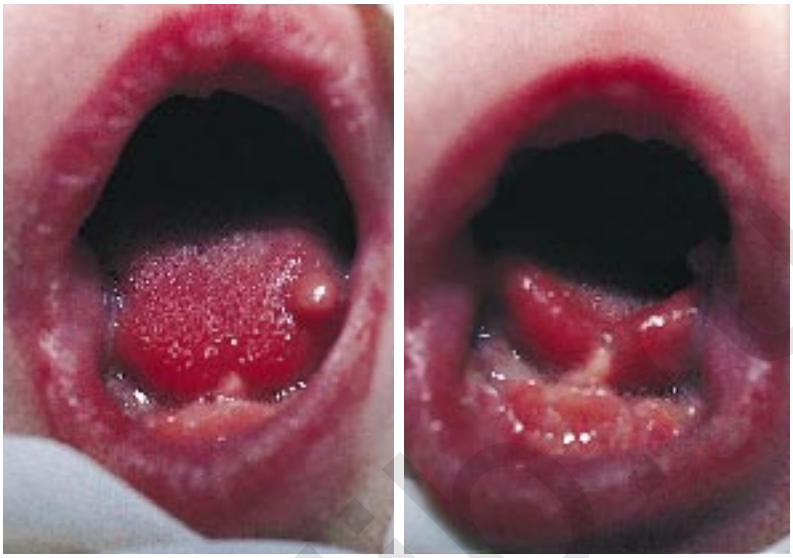

Figure 1.88. The lingual frenulum may be thick and short, and may be continuous through an alveolar notch to produce a dimpled or bifid tongue. Usually this is of no consequence. In this infant with orofaciodigital syndrome, in addition to the short frenulum, there is gum hypertrophy and a hamartoma. There was syndactyly of the second and third toes.
A thickened lingual/labial frenulum may result in a wide space (diastema) between the central incisors. As the canines begin to erupt at 9 to 11 years of age, division of the thickened frenulum allows the gap to close.

1.89

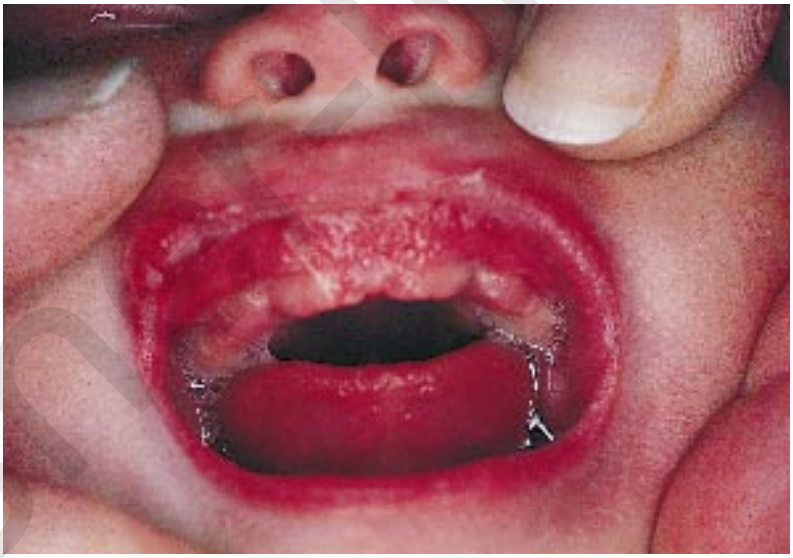

Figure 1.89. In Ellis-van Creveld syndrome (chondroectodermal dysplasia) one of the typical findings is present in the mouth. There is a defect in the upper lip due to fusion of the labiogingival margins of the upper lip so that there is no mucobuccal sulcus. Note the compartments for the individual tooth buds can be seen on the alveolar ridges.

1.90

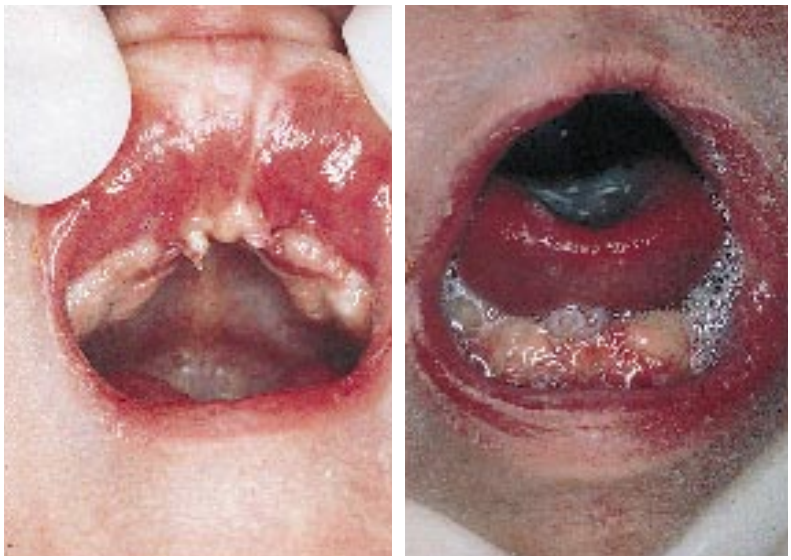

Figure 1.90. Another infant with Ellis-van Creveld syndrome showing the typical changes in the mouth. On the left, note the defect particularly in the middle of the upper lip in which there is fusion at the maxillogingival margin to the upper lip so that there is no mucobuccal sulcus. Also note the hypoplastic neonatal teeth in the upper jaw in the figure on the left and in the lower jaw in the figure on the right.

1.91

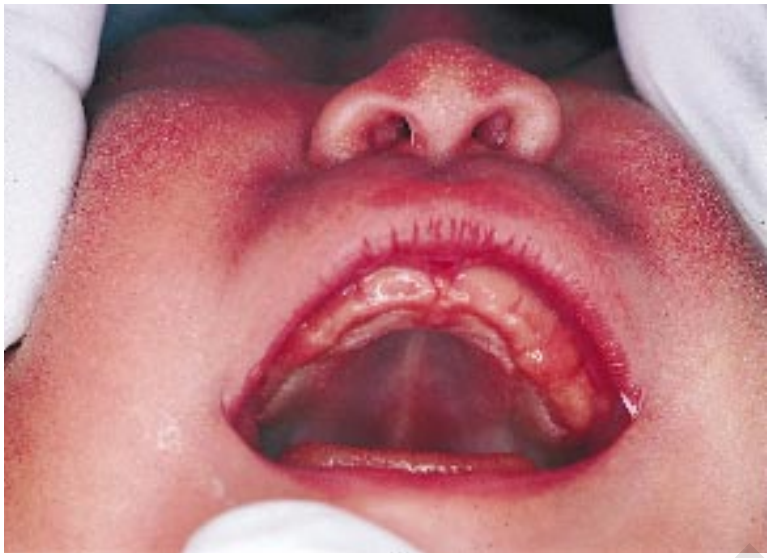

Figure 1.91. The components for each individual tooth bud can often be seen on the alveolar ridges of the maxilla and mandible in normal infants. Note the milia on the nose and the demarcation on the lip where the skin meets the mucous membrane. The sucking calluses occur on the mucous membrane part of the lip and are most prominent on the central portion.

1.92

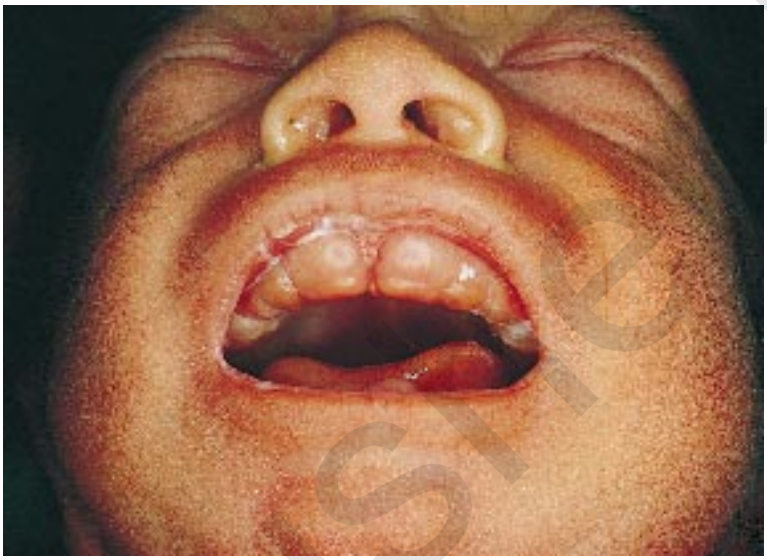

Figure 1.92. Gum hypertrophy in an infant born to a mother treated with phenytoin during pregnancy.

1.93

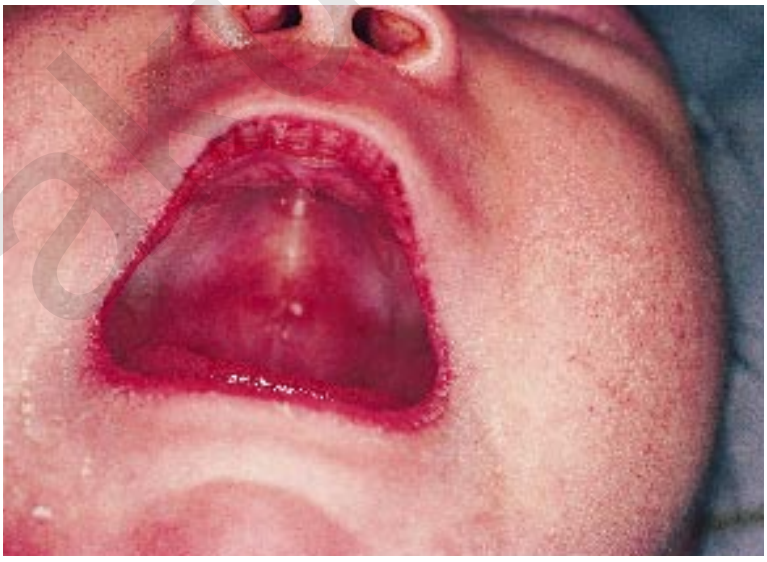

Figure 1.93. Epithelial pearls are areas where the cells are condensed in whorls or small cysts. These are most often seen in the mouth. The most common are called Epstein's pearls which consist of a small cluster of whitish-yellow swellings at the junction of the soft and hard palate in the midline.

1.94

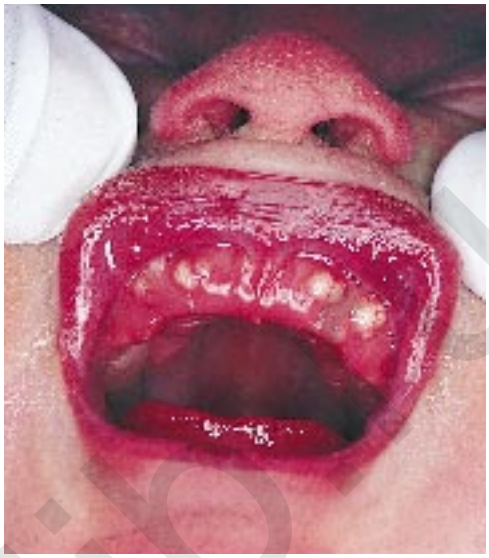

Figure 1.94. Note the Bohn's nodules (inclusion cysts) on the alveolar margin in this infant. Epithelial pearls are also seen on the areola or on the foreskin.

1.95

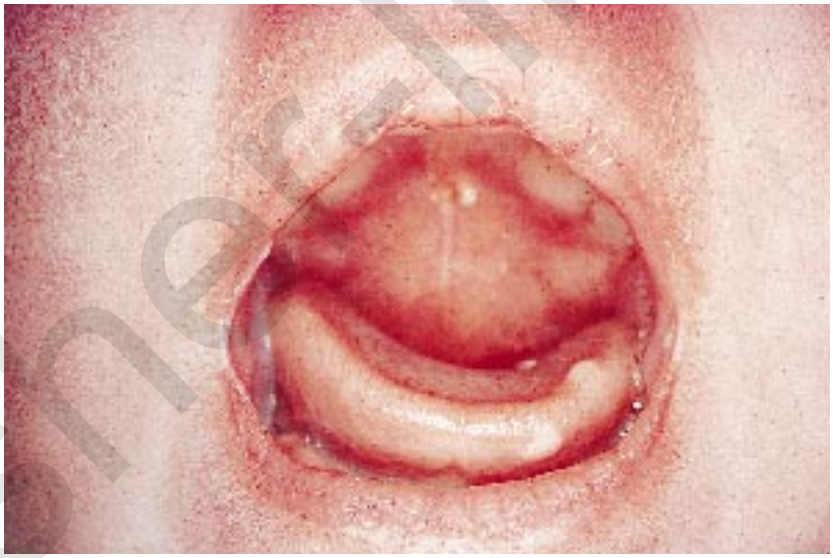

Figure 1.95. Note the inclusion cysts on the tongue and the Epstein's pearls.

1.96

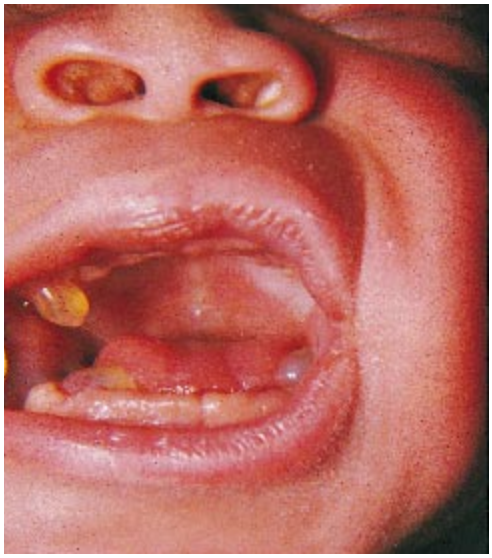

Figure 1.96. Another example of inclusion cysts which are larger. Epstein's pearls, Bohn's nodules, and inclusion cysts all improve spontanteously.

1.97

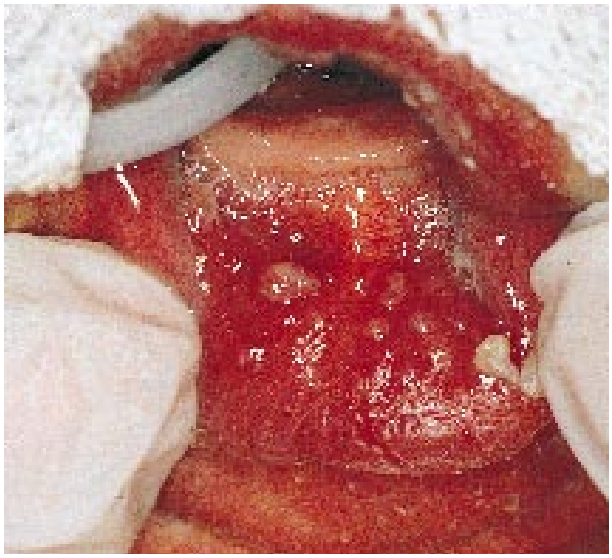

Figure 1.97. Note the mucoceles on the lower lip of this premature infant (birthweight 1200 g). Mucoceles are not true cysts but rather collections of mucus surrounded by connective tissue. They usually occur on the lower lip, are not common, and require no treatment. Differential diagnosis includes herpetic lesions.

1.98

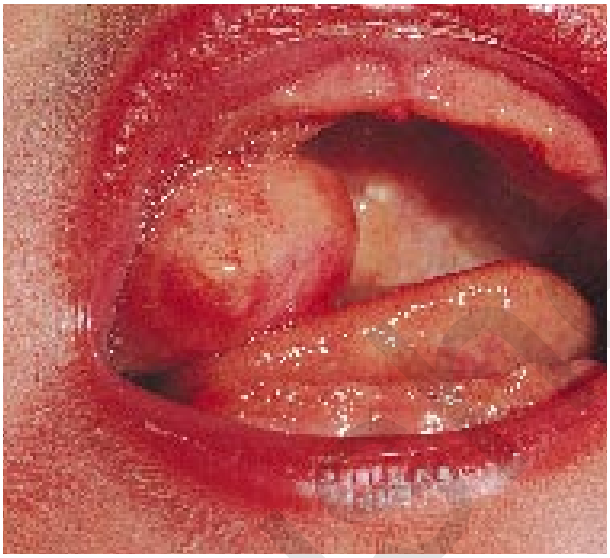

Figure 1.98. Congenital epulis may occur as a small or very large mass that protrudes from the mouth as a large tumor. They may be pedunculated and are of firm consistency. They usually occur in the region of the maxillary alveolar mucosa and are a form of embryonal hamartoma. A large epulis needs excision and rarely occurs.

1.99

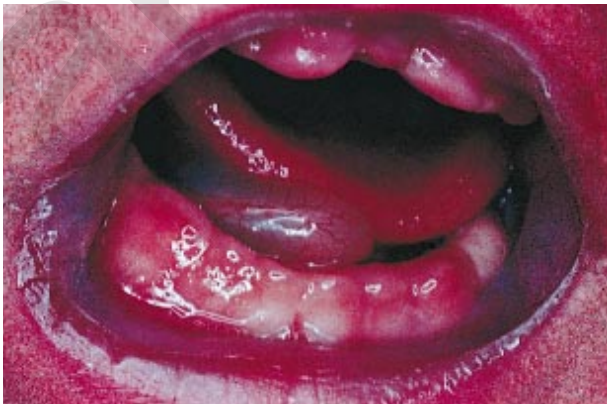

Figure 1.99. This bluish fluctuant transparent swelling in the anterior part of the floor of the mouth is a ranula which is a retention cyst arising from the sublingual gland. The term ranula originates from its similarity to the inflated bladder of a frog's throat. Ranula is a diminutive of *Rana* species of frog. Large ranulas need excision but the smaller lesions resolve spontaneously. Note the diastema in the upper jaw.

1.100

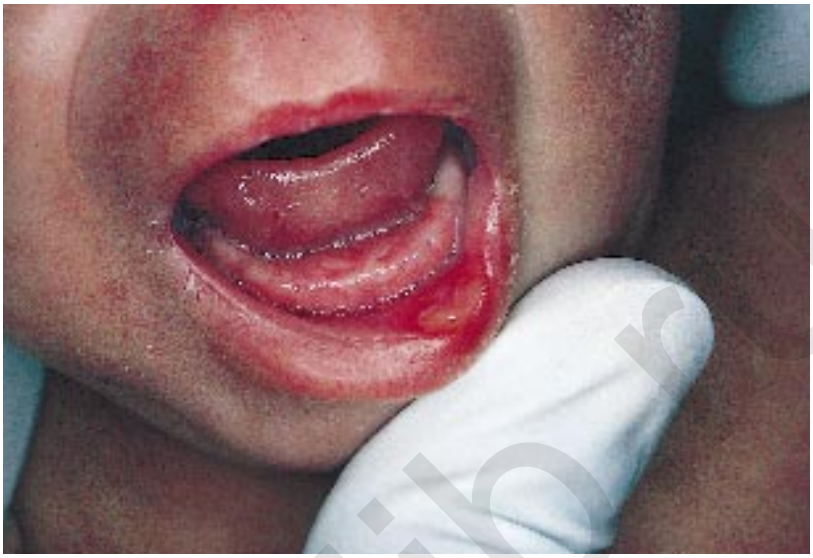

Figure 1.100. Traumatic ulcer on the lower lip of a neonate as a result of orotracheal intubation for resuscitation.

1.101

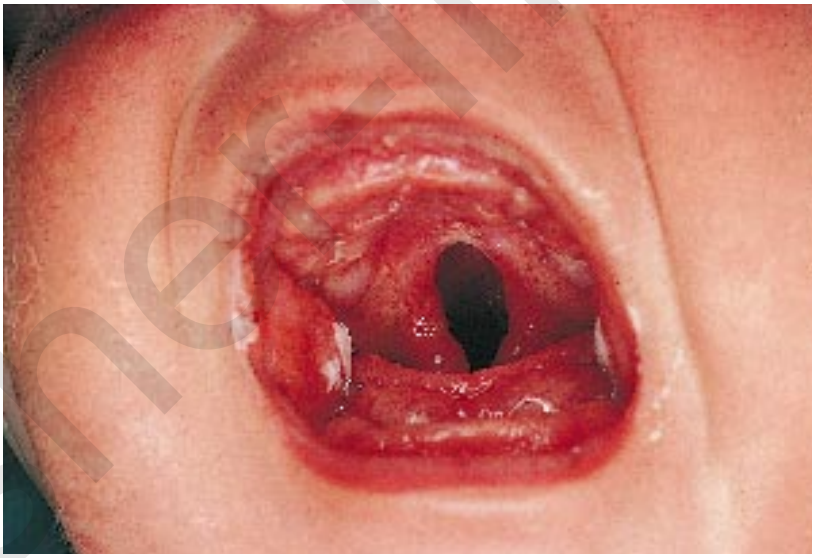

Figure 1.101. Aglossia and cleft palate in an otherwise normal infant. Aglossia occurs more frequently in the aglossia/hypoglossia adactylia syndrome. Due to the absence of a normal tongue, note how easily the cleft palate is seen. On the buccal mucosa note the oral candidiasis (thrush).

1.102

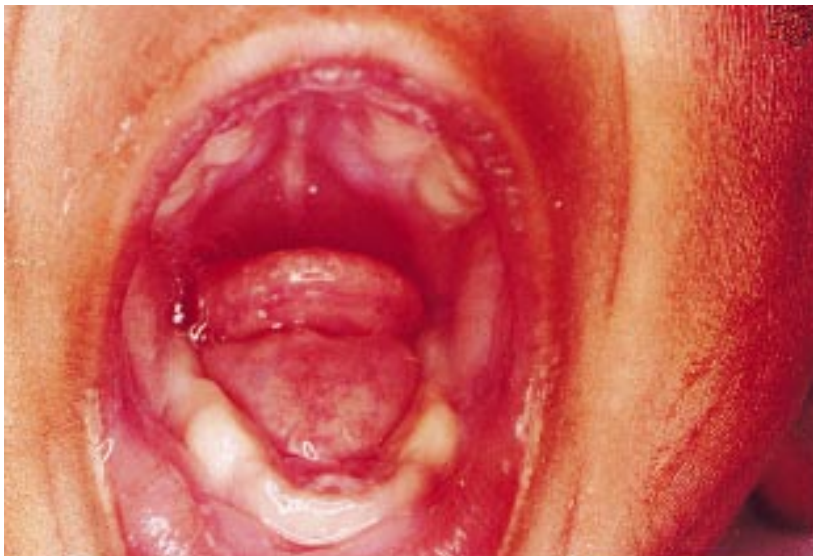

Figure 1.102. Note the small hypoplastic tongue (hypoglossia) posteriorly in this otherwise normal infant. This condition is more commonly associated with digital anomalies in the aglossia/hypoglossia adactylia syndrome.

1.103

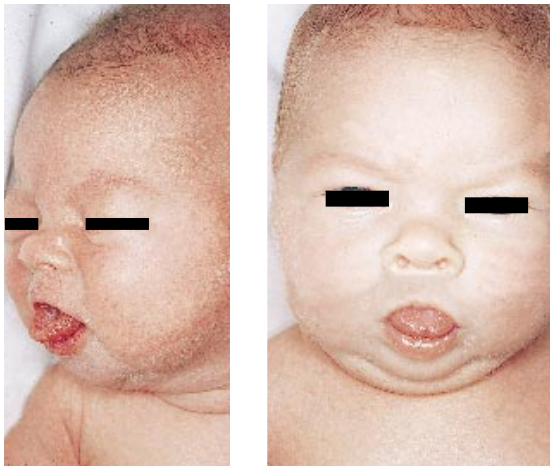

Figure 1.103. Macroglossia in an otherwise normal infant. The most common cause of macroglossia is idiopathic hypertrophy of the muscles of the tongue.

1.104

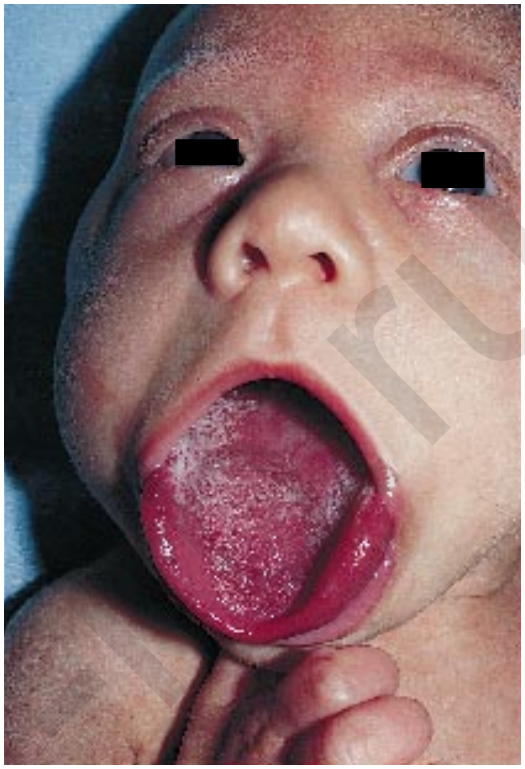

Figure 1.104. Macroglossia associated with Beckwith-Wiedemann syndrome. These infants have *e*xomphalos (omphalocele or large umbilical hernia), *m*acroglossia, and *g*igantism (EMG syndrome).

1.105

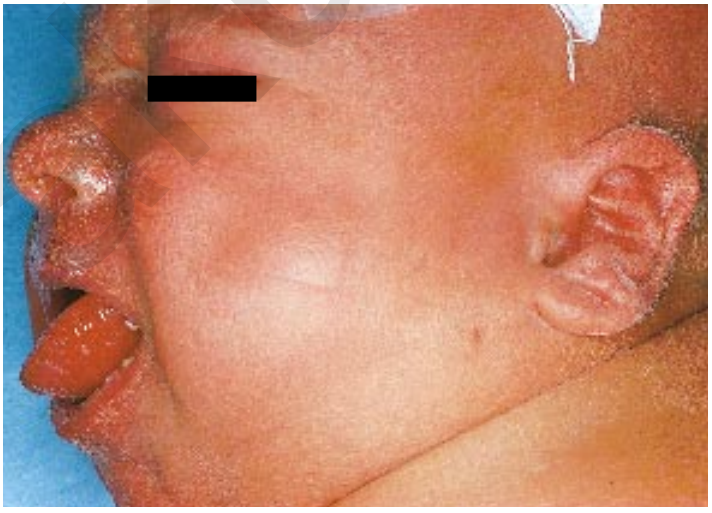

Figure 1.105. Another infant with Beckwith-Wiedemann syndrome showing the protrusion of the tongue with macroglossia. Note the other characteristic finding of a transverse crease of the earlobe.

1.106

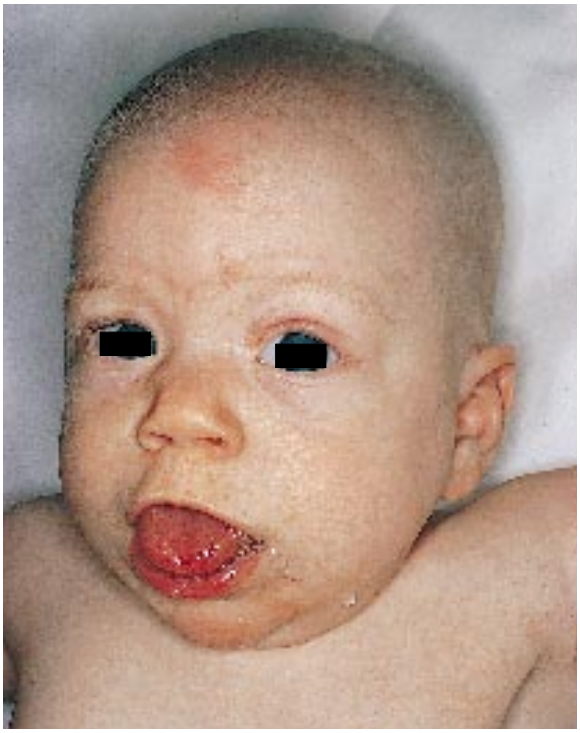

Figure 1.106. Macroglossia in a 2-month-old infant with Type II glycogen storage disease (Pompe's disease). Macroglossia is also seen in infants with congenital hypothyroidism and hemangioma or lymphangioma of the tongue.

1.107

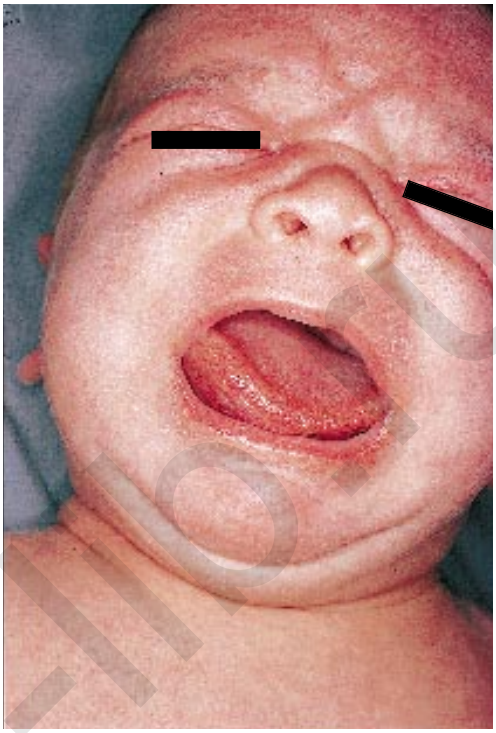

Figure 1.107. Macroglossia associated with unilateral hypertrophy of the right side of the tongue. This may be idiopathic or due to a hemangioma or lymphangioma of the tongue.

1.108

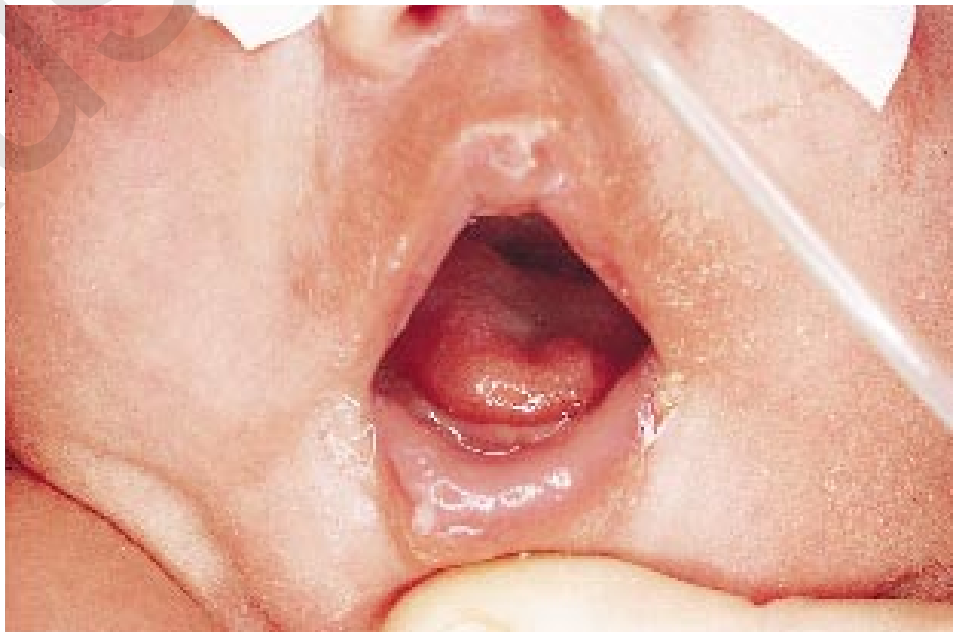

Figure 1.108. Atrophy of the left side of the tongue in an infant with Poland's anomaly and Möbius' syndrome. The association of these two conditions is not uncommon.

1.109

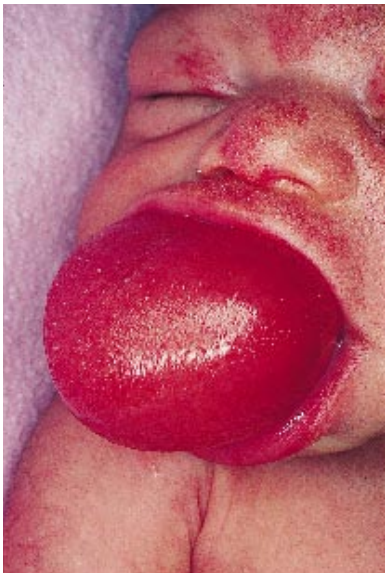

Figure 1.109. This infant with a large cystic mass of the tongue presented with severe respiratory distress. A preoperative thyroid scan was normal. The mass was resected and a diagnosis of an enterocystoma of the tongue (gastric duplication cyst) was made. The infant did well following removal of the cyst.

1.110

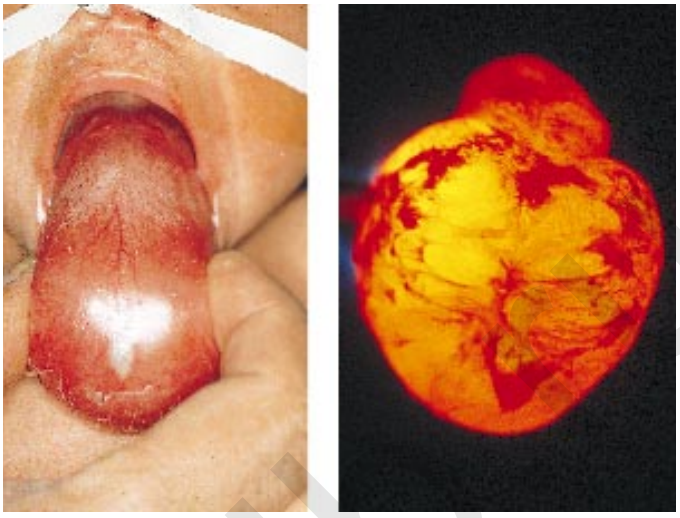

Figure 1.110. In the same infant, on the left note the large cystic swelling of the enterocystoma of the tongue. The figure on the right shows the transillumination of the cyst postoperatively.

1.111

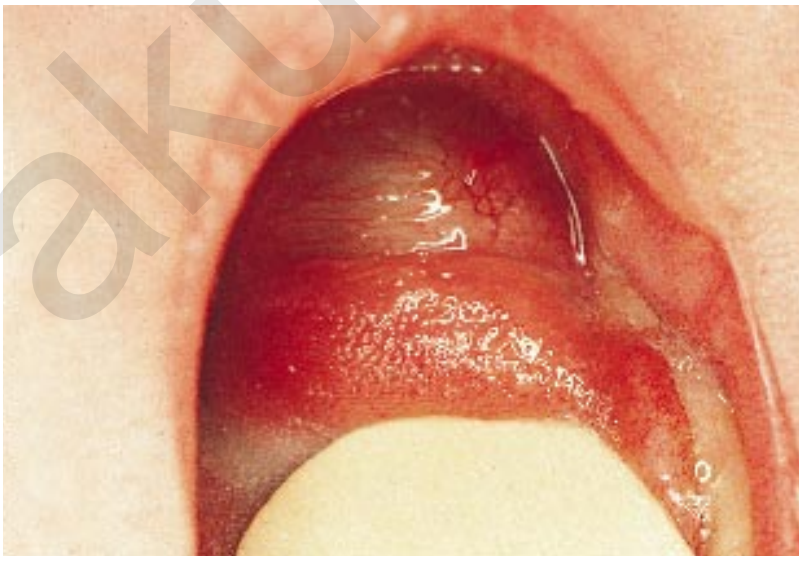

Figure 1.111. This infant presented with moderate respiratory distress and was noted to have a large cyst, especially on the left side at the base of the tongue. The cyst which was removed was diagnosed as an epithelial cyst in that it was lined by squamous epithelial cells.

1.112

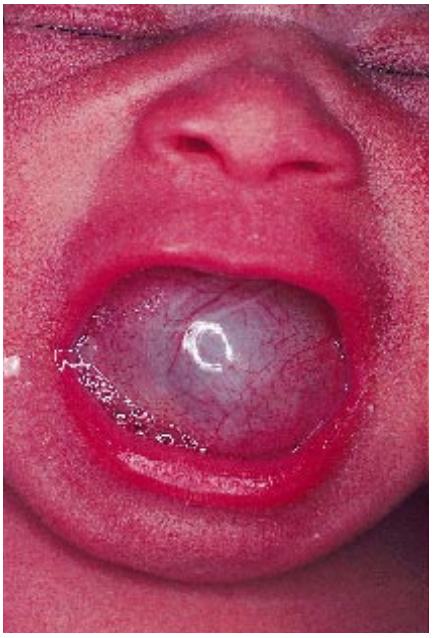

Figure 1.112. The large cystic midline swelling of the tongue in this infant was histologically diagnosed as a large thyroglossal cyst which was benign and lined by columnar epithelial cells.

1.113

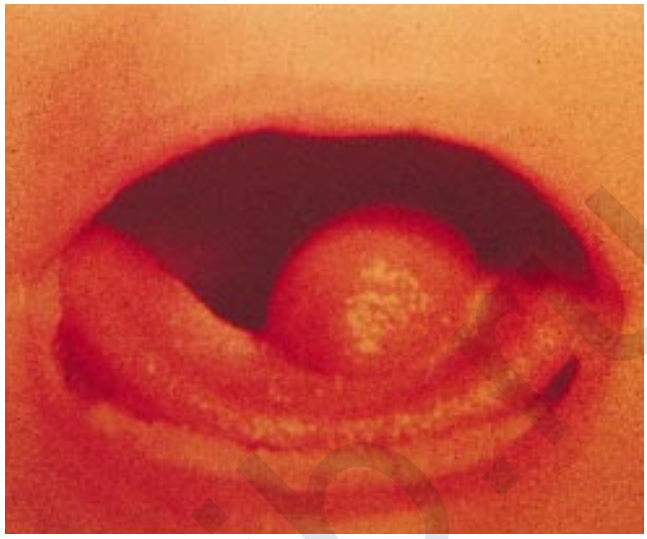

Figure 1.113. This well-circumscribed mass on the tongue was surgically removed and a diagnosis of hemangioma was made.

1.114

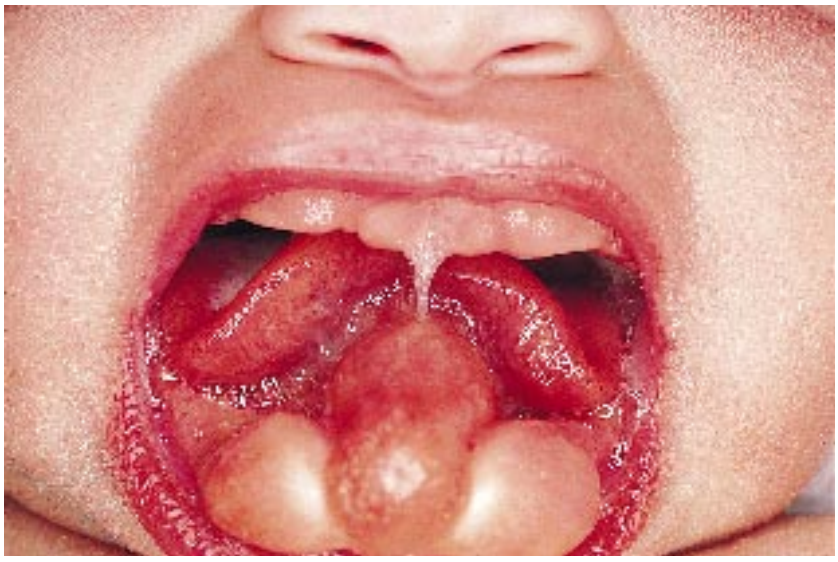

Figure 1.114. This infant at birth presented with a tumor involving the midmandible and floor of the mouth. The mass divided the tongue which was thickened and foreshortened. There was an associated midfacial cleft with a dermoid of the upper palate. With this type of defect a median cleft should be excluded. Tests for this were normal.

1.115

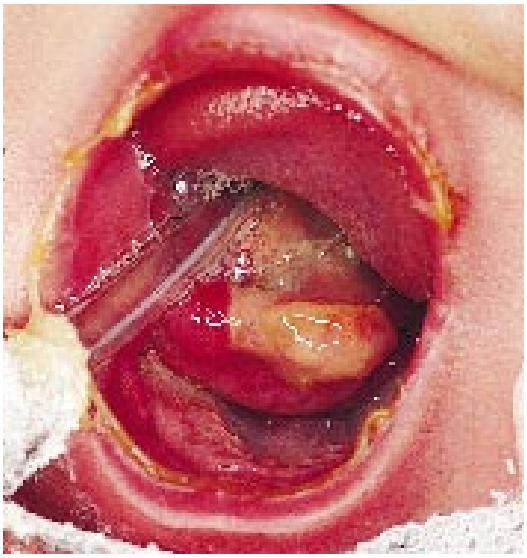

Figure 1.115. A mass involving the tongue was noted at birth in this term infant. Upon surgical removal, the diagnosis of teratoma of the tongue was confirmed. This was a benign teratoma and the infant did well.

1.116

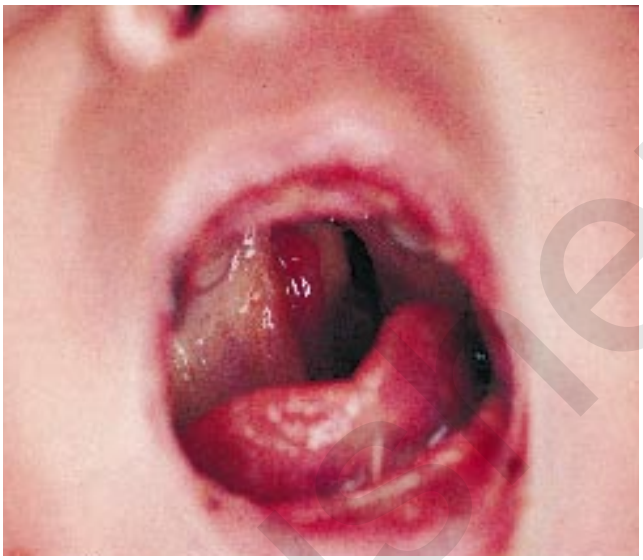

Figure 1.116. The large mass in the posterior mouth and nasopharynx in this term infant, with a cleft palate, was friable and bled easily. At surgery it was found to be a benign teratoma of the nasopharynx.

1.117

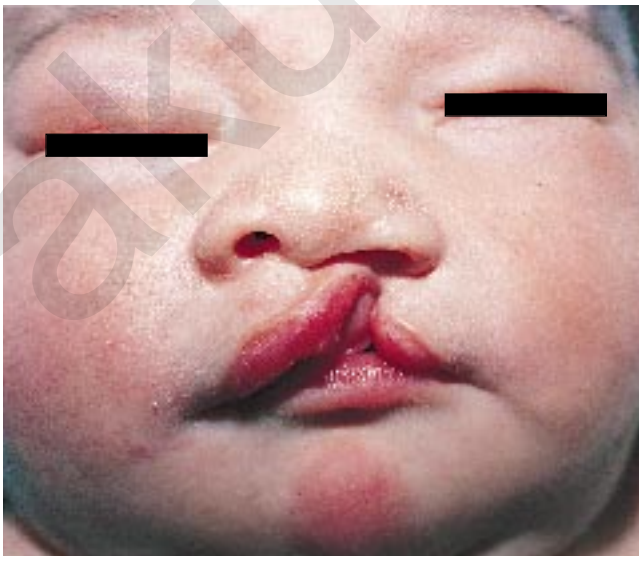

Figure 1.117. Cleft lip may be unilateral or bilateral and is often associated with a cleft palate. This normal infant has a mild unilateral cleft lip with a normal palate. The nose is flattened on the affected side. Cleft lips and palates may be seen in otherwise normal infants or in infants with syndromes or chromosomal abnormalities.

1.118

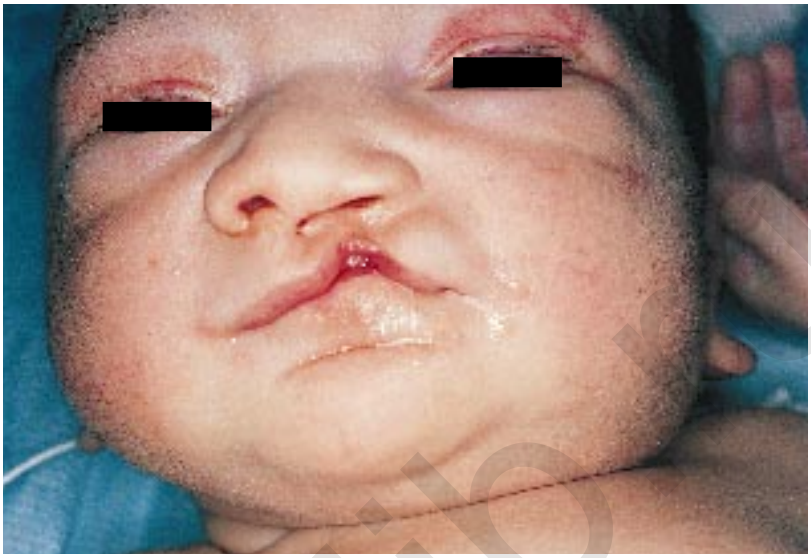

Figure 1.118. An example of a unilateral cleft lip with a normal palate in an infant with the popliteal pterygium syndrome. Note that the upper lip is indented to the left of the philtrum and the nose is flattened, but the defect does not extend into the alveolar process.

1.119

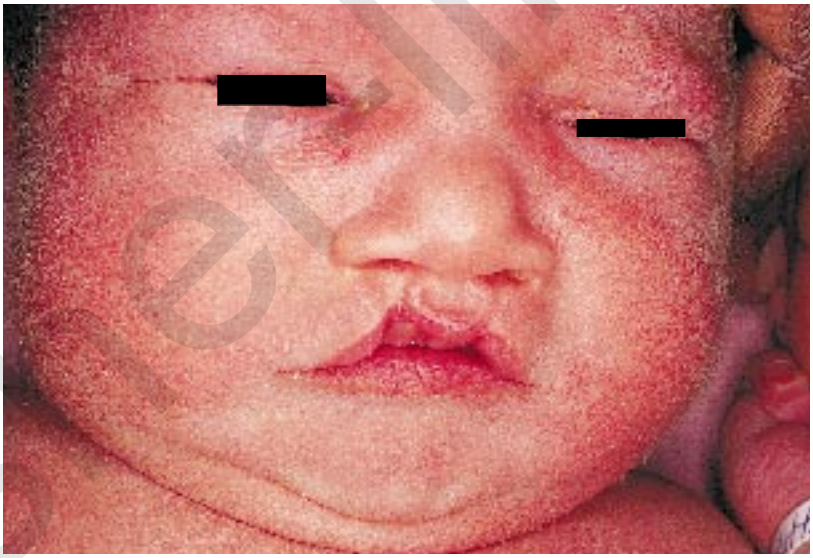

Figure 1.119. A mild bilateral cleft lip in an otherwise normal infant. In partial or complete unilateral or bilateral cleft lip, the line of clefting is paramedian and follows the ridge at either side of the philtrum.

1.120

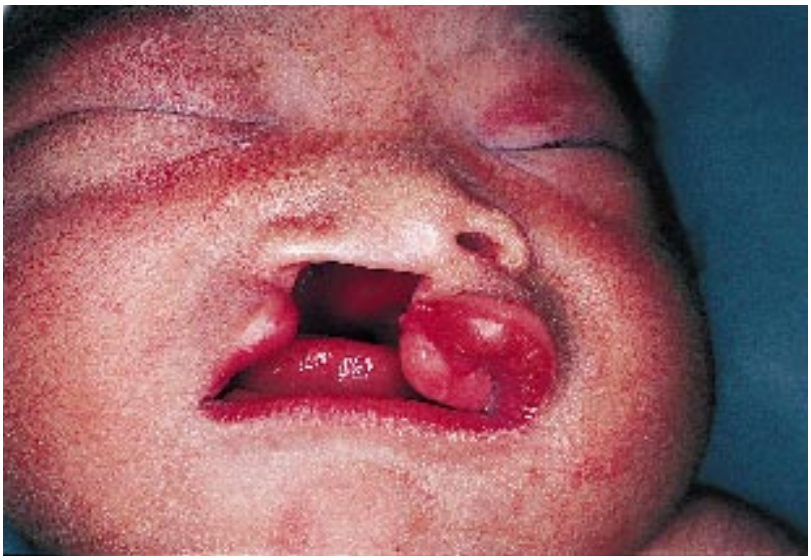

Figure 1.120. A unilateral cleft lip and cleft palate in an otherwise normal infant. The unilateral cleft lip has extended to the nostril, which is flattened and deflected. Cleft lip and palate occur in many syndromes such as trisomy 13 and the ectrodactyly-ectodermal dysplasia-clefting syndrome (EEC syndrome).

1.121

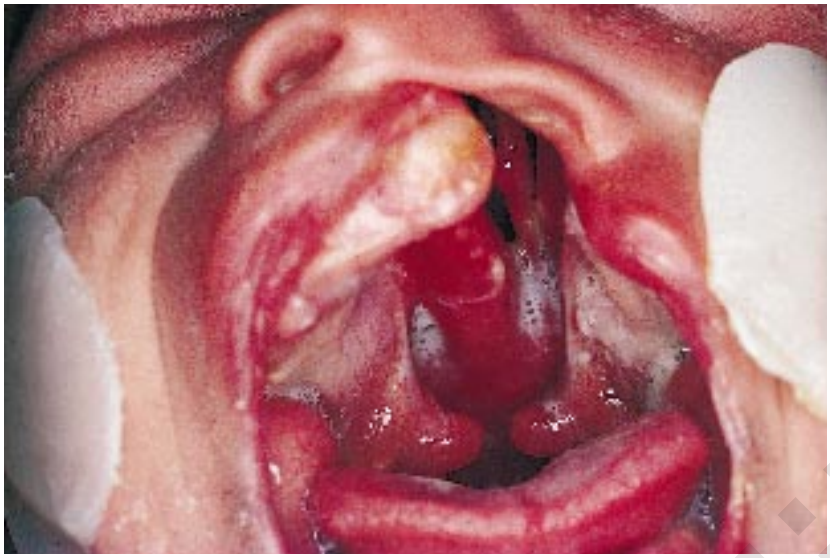

Figure 1.121. Cleft palate in an infant with a unilateral cleft lip. Note the splitting of the uvula.

1.122

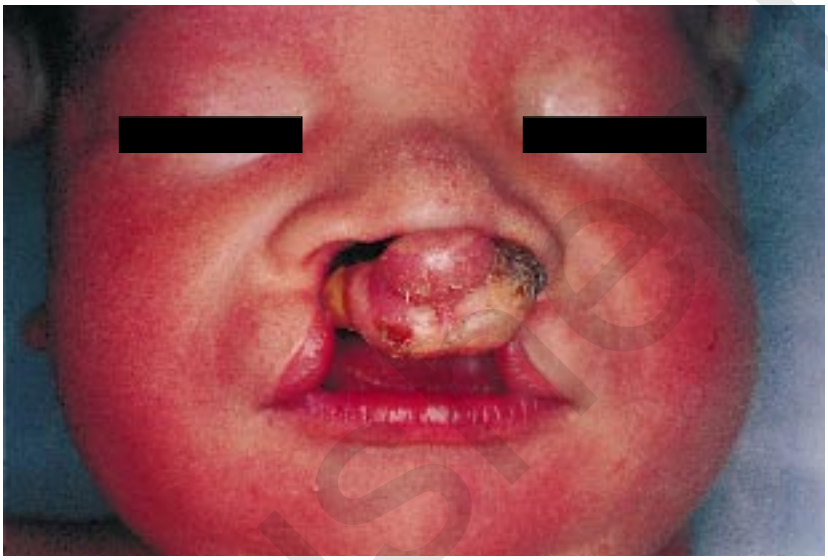

Figure 1.122. Bilateral cleft lip and cleft palate with a severe total cleft palate and incomplete bilateral cleft lip. A midline nubbin of tissue is seen attached to the columella of the nose. This represents the remnant of the intermaxillary segment, the unpaired median structure that normally would have formed the floor of the philtral groove, the center of the upper alveolar ridge, and the primary palate.

1.123

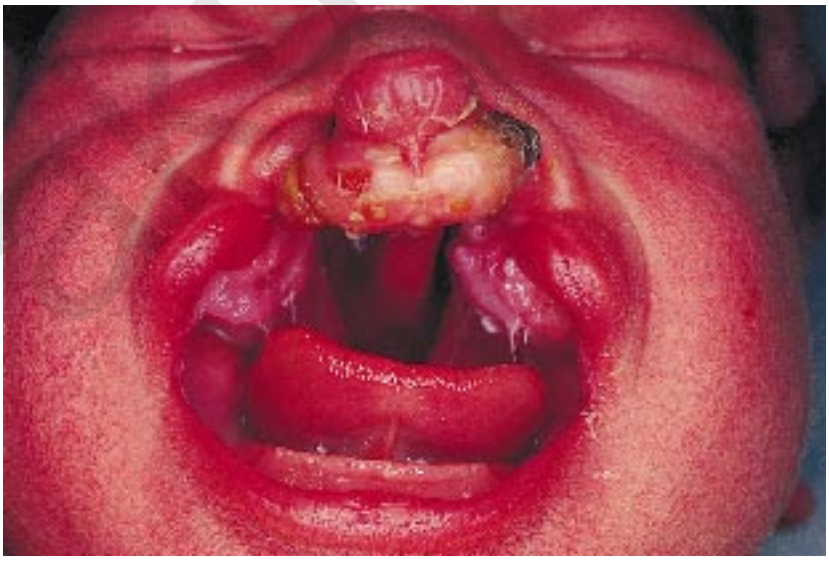

Figure 1.123. In the same infant the cleft palate is clearly demonstrated. Note the protruding vomer.

1.124

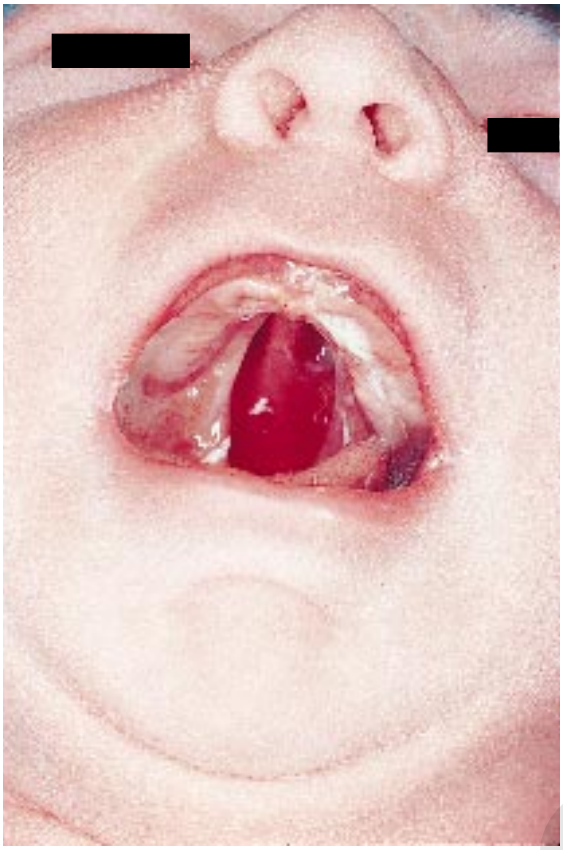

Figure 1.124. Cleft palate in an otherwise normal infant. An isolated cleft palate (either the soft palate, hard palate, or both) occurs more frequently in females and is commonly associated with other abnormalities (such as Robin's anomalad).

1.125

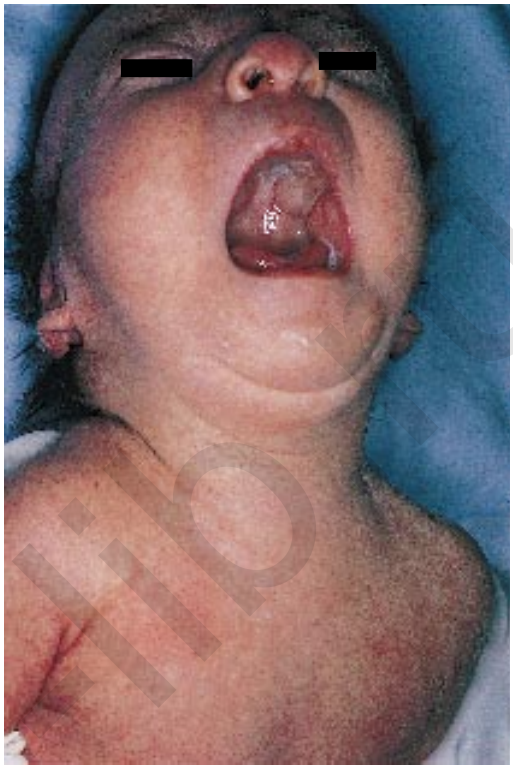

Figure 1.125. A high arched palate in a normal infant. This may occur in association with other congenital anomalies or may occur iatrogenically, secondary to prolonged orotracheal intubation.

1.126

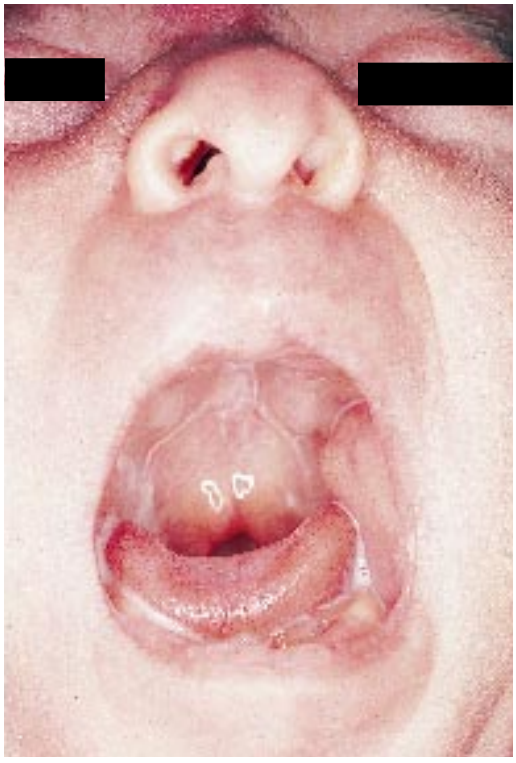

Figure 1.126. A high arched palate in an infant with a cleft of the soft palate.

1.127

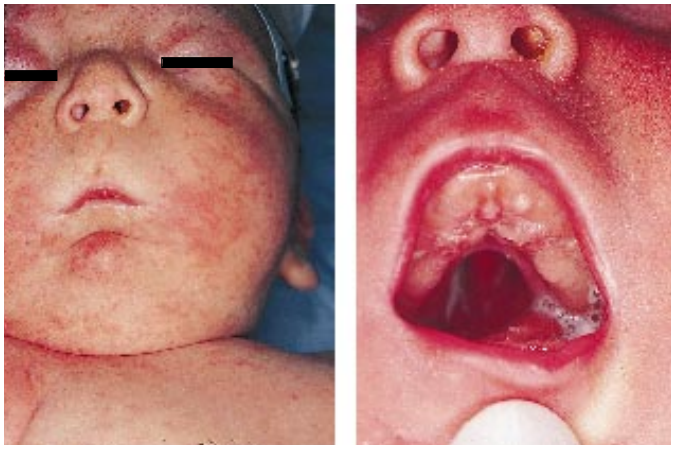

Figure 1.127. On the left, note the marked microstomia and on the right note the cleft palate, in an infant with a mosaic trisomy 8.

1.128

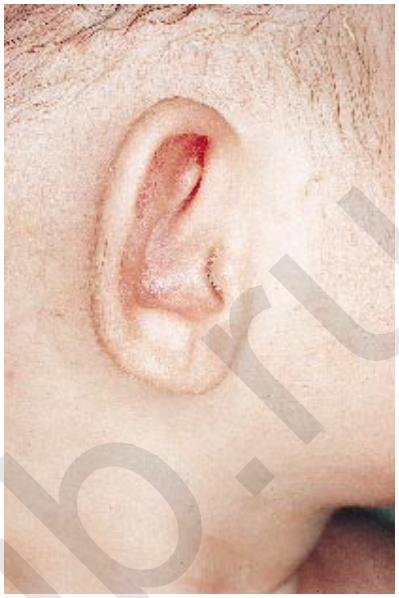

Figure 1.128. The normal ear shows many variations in the folds in relation to the cartilage. For example, in this infant poor development and deformations caused transient abnormalities in the appearance of the ears.

1.129

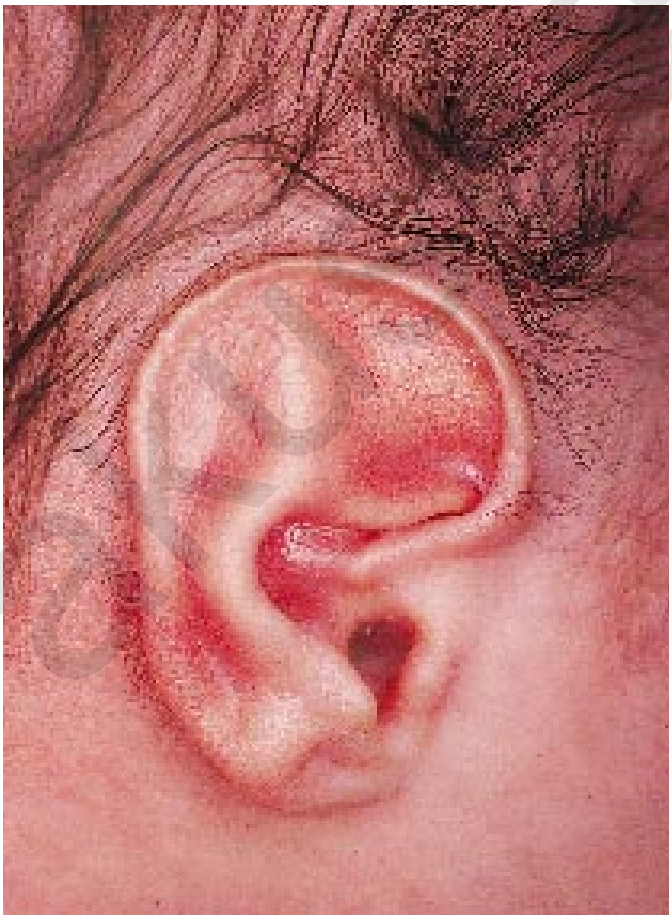

Figure 1.129. Normal ears with lack of good cartilage development may appear as large flattened ears bilaterally. These are often caused by prolonged intrauterine compression as a result of oligohydramnios.

1.130

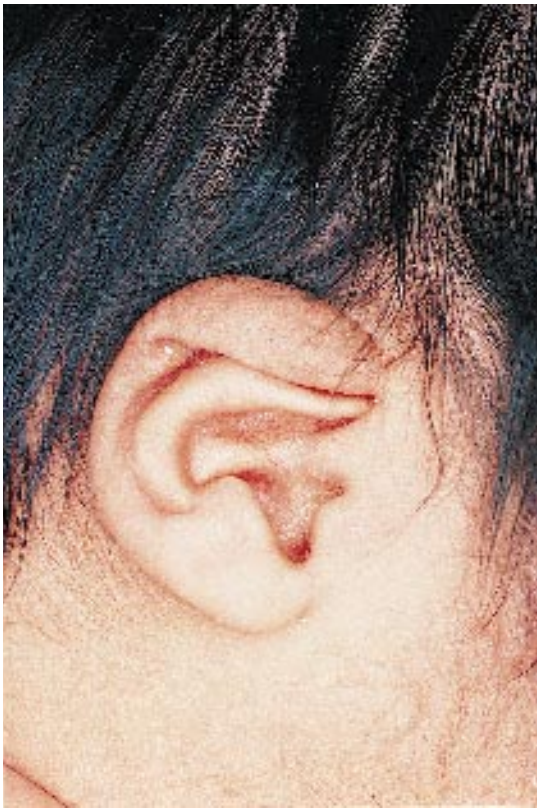

Figure 1.130. An overturned helix (a folded ear) is usually a temporary deformation secondary to in utero position.

1.131

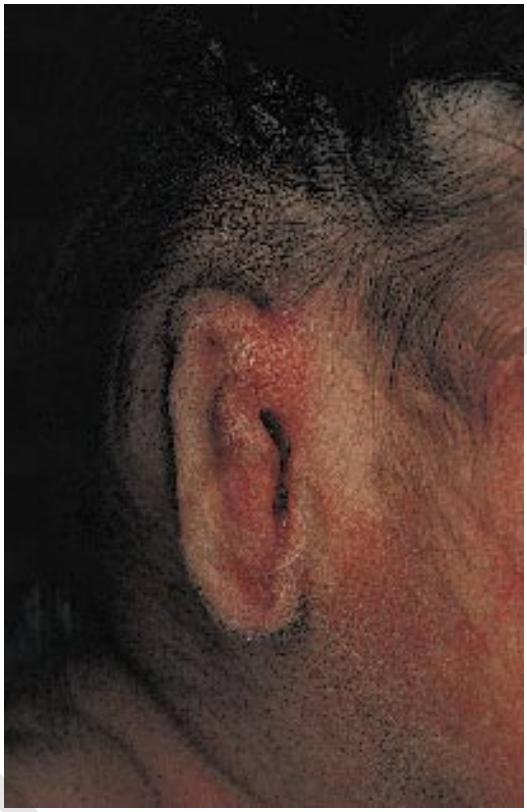

Figure 1.131. Another example of a folded helix due to in utero position.

1.132

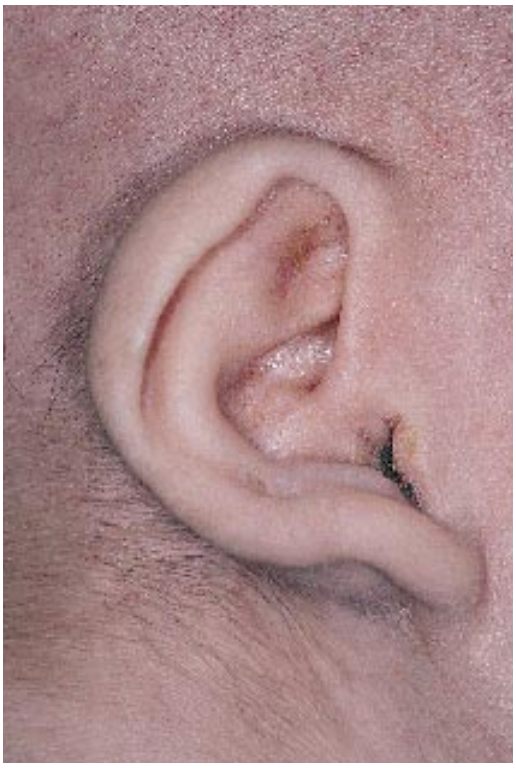

Figure 1.132. Positional deformation of a normal ear secondary to the presence of pressure of the infant's shoulder on the lobe of the ear in utero. Note that the pinna is crumpled upward and forward.

1.133

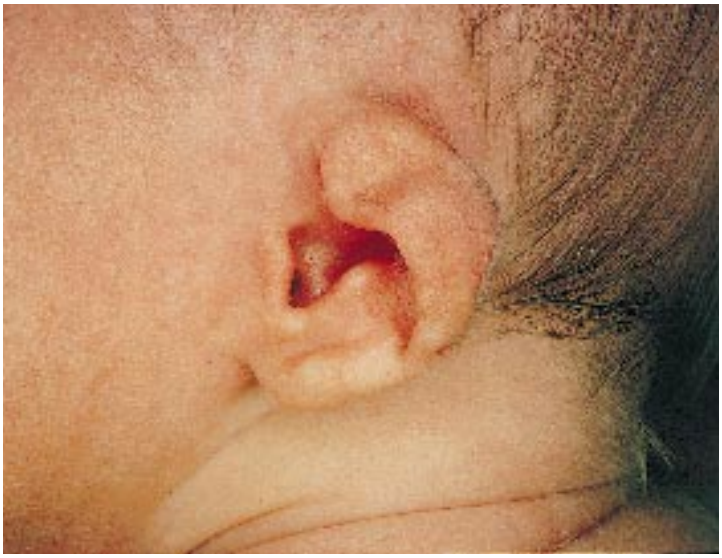

Figure 1.133. This is an example of an infant with a lop ear. Weakness or absence of the auricular muscles result in various deformities of the auricle. When the superior muscle band is absent, a lop ear occurs. If only the posterior slip is missing, a protruding ear is seen. If both muscle bands are absent, a cupped ear is formed. These characteristic abnormalities of the auricle are more commonly seen in infants with severe hypotonia.

1.134

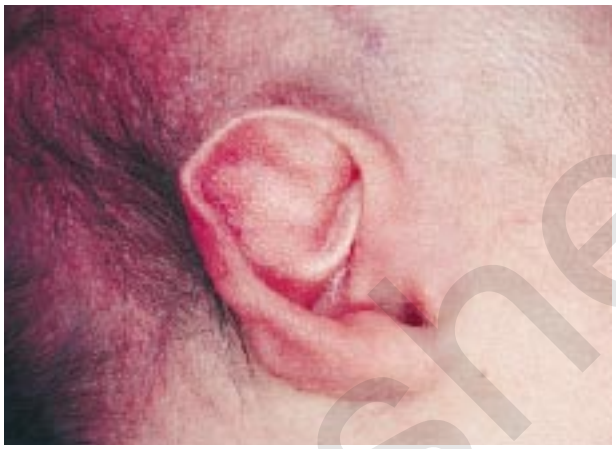

Figure 1.134. Poor development of the ear can be seen in association with a lack of or decreased fetal movement.

1.135

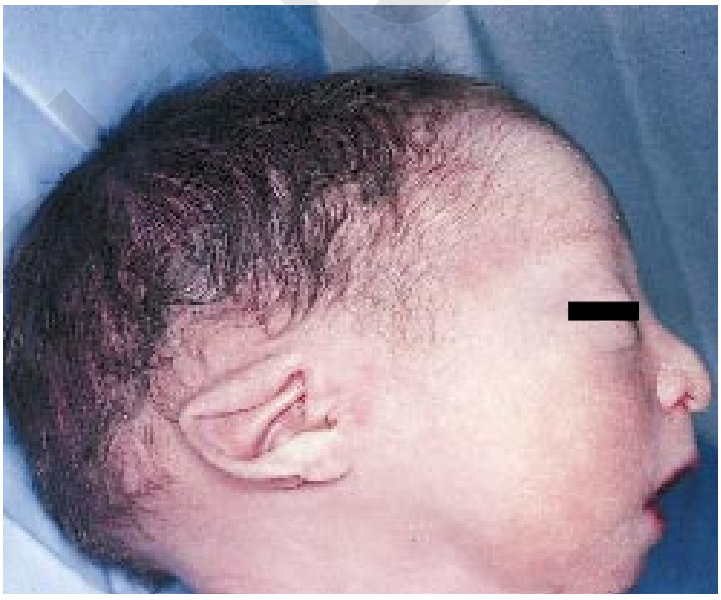

Figure 1.135. In this infant with Potter's syndrome note the slanted and low-set ear. Ears are considered slanted when the angle of slope of the auricle exceeds fifteen degrees from the perpendicular. Low placement and slanted auricles often go together and usually present a lag in morphogenesis.
Low-set ears are defined as those where the helix meets the cranium at a level below that of a horizontal plane with the corners of the orbit. The presence of low-set ears can be determined by extending a line joining both inner canthi. This accounts for any upward or downward slanting of the eyes. The illusion of low ear placement can be created by an unusually large head as is seen in hydrocephalus or by a small external ear. The pseudohydrocephalus (catch-up growth of the head) in very low birthweight infants may create the impression of low-set ears in an otherwise normal infant.

1.136

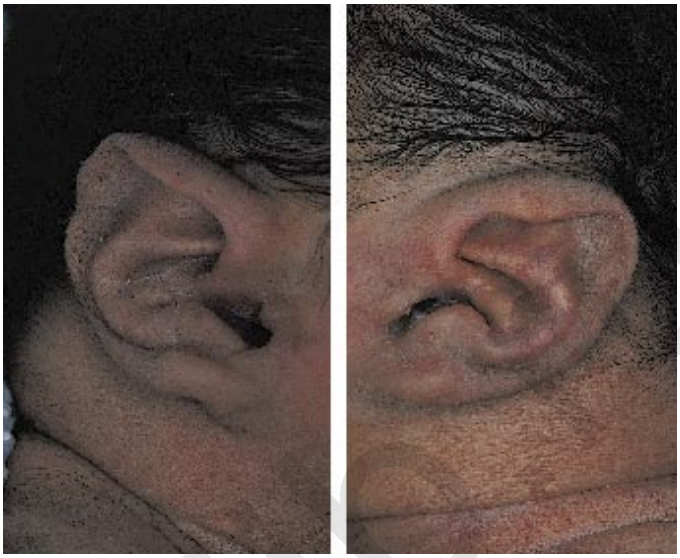

Figure 1.136. Poorly folded small and posteriorly angulated ears occurred with decreased fetal movement in this infant with the fetal akinesia syndrome.

1.137

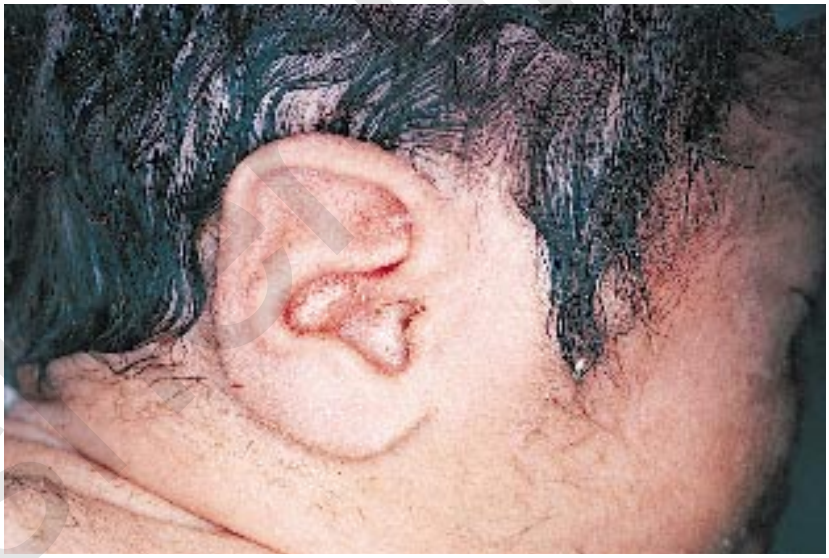

Figure 1.137. Note the attenuation and backward sweep of the upper helix in the ears of this infant. This is called the Mozart ear as it is said to have been present in Mozart and his family.

1.138

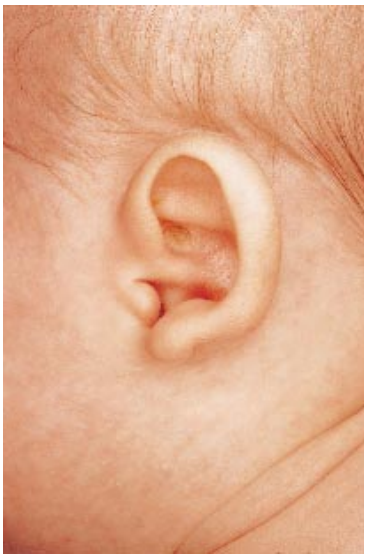

Figure 1.138. Lack of normal development of the lobule of the ear.

1.139

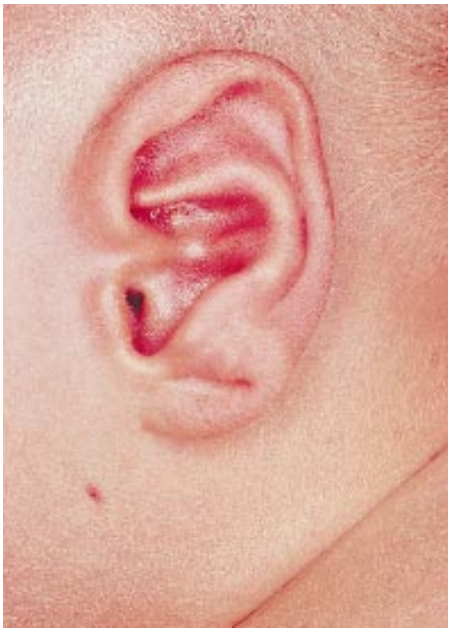

Figure 1.139. Transverse earlobe creases are a feature of some syndromes as in this infant with Beckwith-Wiedemann syndrome.

1.140

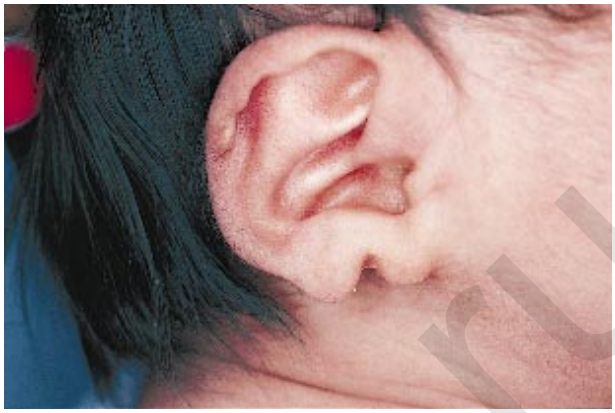

Figure 1.140. This otherwise normal infant had bilateral cleft ear lobes. This occurs as a result of incomplete fusion between the most medial embryonic hillocks.

1.141

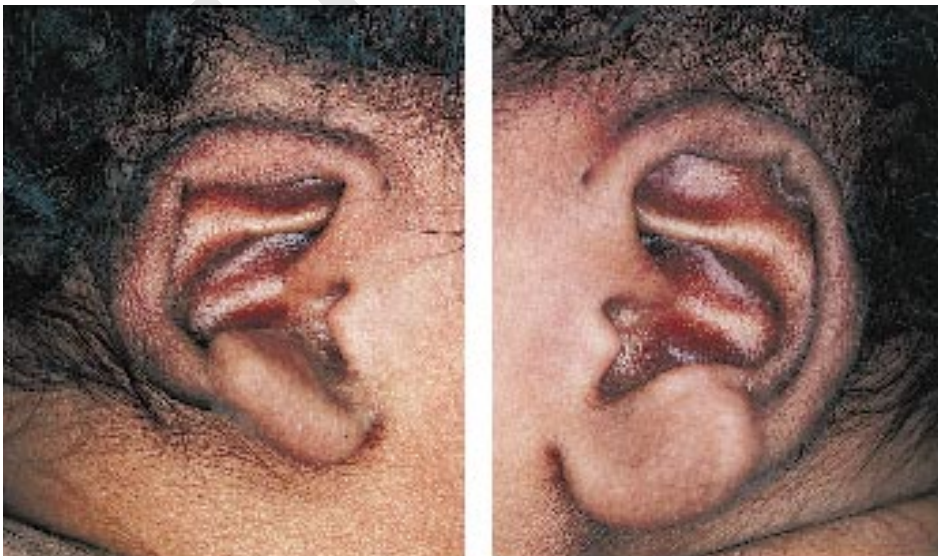

Figure 1.141. Preauricular pits in an otherwise normal infant. The mother had the same findings. Preauricular pits and preauricular tags occur in about 1% of individuals and are twice as common in females and more common in black infants. They are believed to represent remnants of early embryonic branchial cleft or arch structures.

1.142

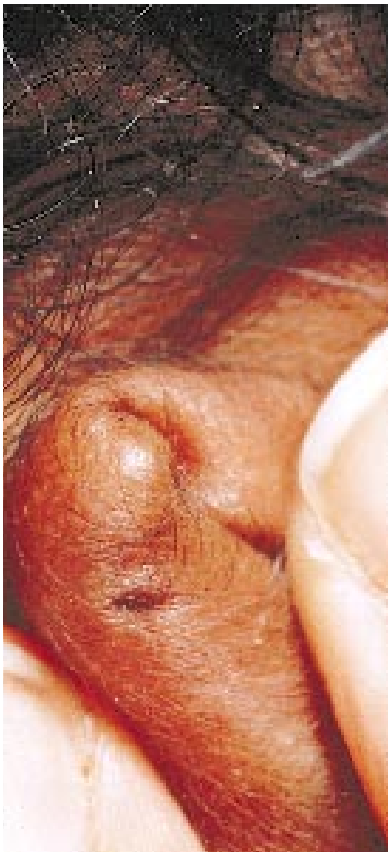

Figure 1.142. There were bilateral pits on the lobes of the ears in this otherwise normal infant.

1.143

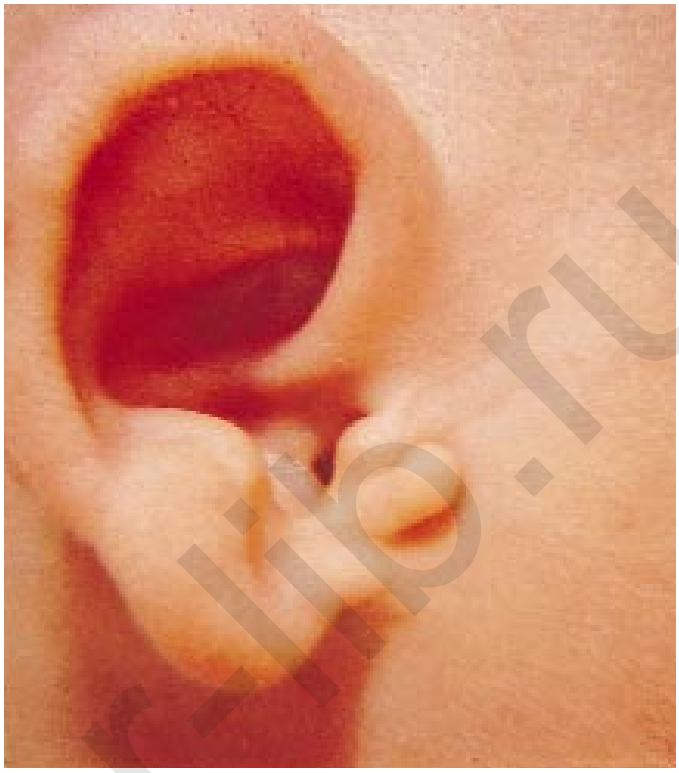

Figure 1.143. Preauricular skin tag in an otherwise normal infant. These skin tags often contain a core of cartilage and appear to represent accessory hillocks of His. Hillocks normally develop in the recess of the mandibular and hyoid arches and coalesce to form the auricle.

1.144

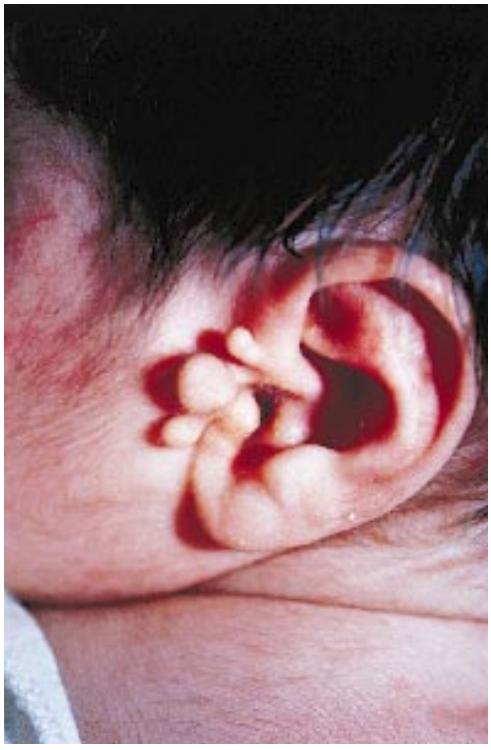

Figure 1.144. Multiple preauricular skin tags in an infant with a normal ear. Note that skin tags may be pedunculated.

1.145

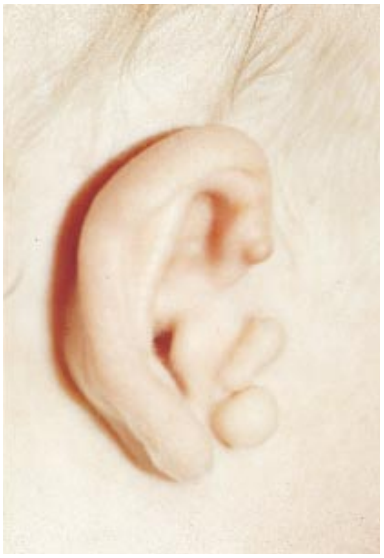

Figure 1.145. Preauricular skin tags in an infant with cupping of the ear.

1.146

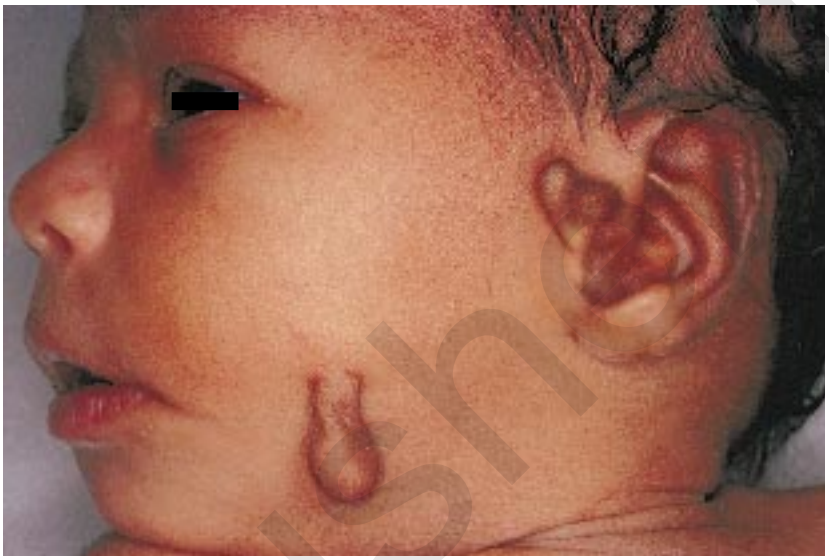

Figure 1.146. Preauricular skin tags and skin tags along a line connecting the oral commissure with the external auditory canal are seen in syndromes involving the first and second branchial arch, as in this infant with Goldenhar's syndrome.

1.147

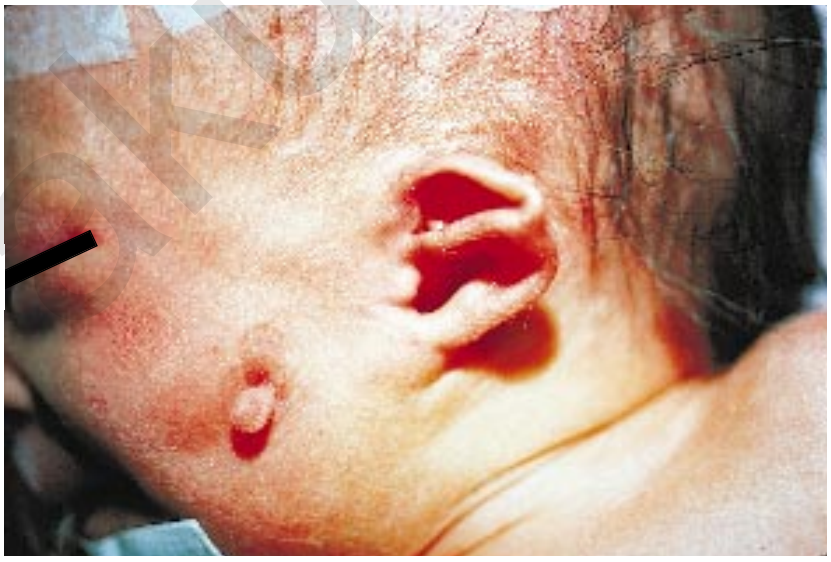

Figure 1.147. This infant exhibited abnormal ears with skin tags and a fistula. Abnormal ears, fistulae, and skin tags are seen more commonly in the first branchial arch syndrome as this infant with Treacher-Collins syndrome.

1.148

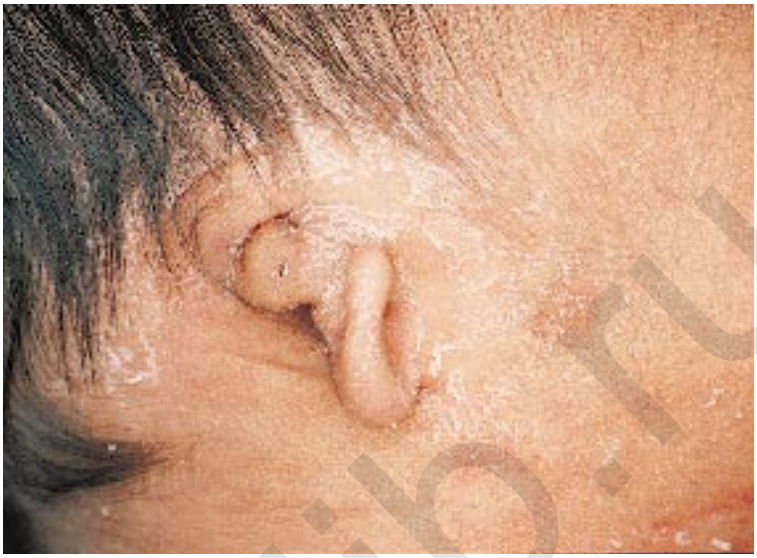

Figure 1.148. Microtia with atresia of the external auditory canal on the right side in an otherwise normal infant. Hypoplasia of the pinna or microtia ("small ear") is the most common isolated intrinsic malformation of the auricle. When microtia is unilateral, the right side is more commonly involved. The spectrum of this abnormality ranges from a small but structurally normal ear, through remnants of cartilage and skin surrounding a small external auditory canal, to total absence of auricular structures.

1.149

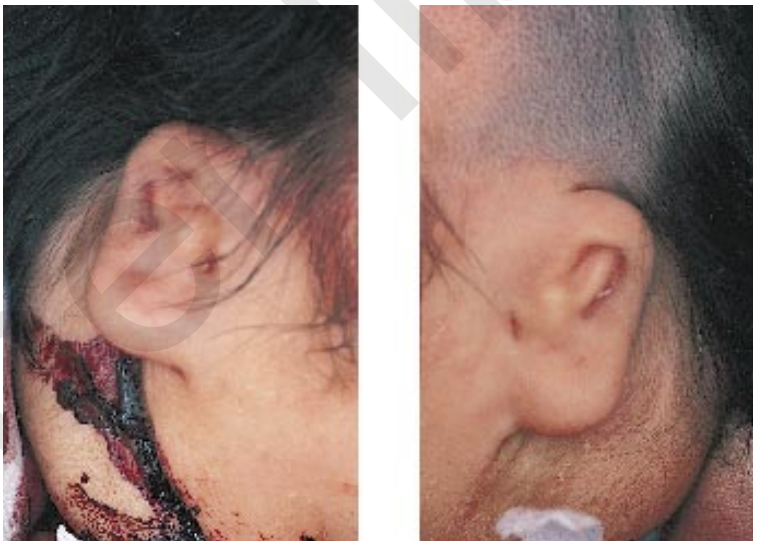

Figure 1.149. Bilateral microtia with atresia of the external auditory canals in an infant with Nager's acrofacial dysostosis syndrome. Varying degrees of microtia occur in syndromes involving the branchial arches such as Treacher-Collins, and Goldenhar's syndrome, and Nager's syndrome (acrofacial dysostosis).

1.150

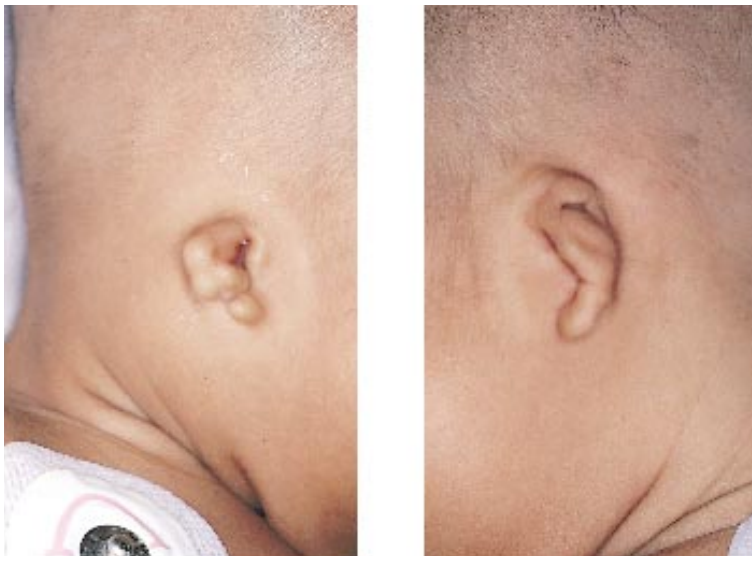

Figure 1.150. Bilateral microtia with absence of external auditory canals in the infant of a mother treated with retinoic acid during the first trimester of pregnancy.

1.151

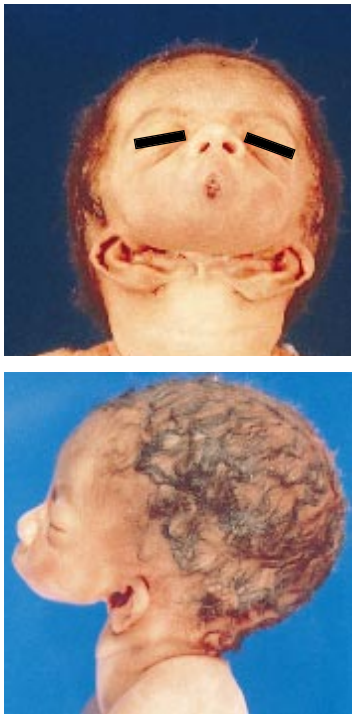

Figure 1.151. In this premature infant of 29 weeks' gestation and birthweight 1120 g there is a branchial arch embryopathy resulting in agnathia, microstomia, and small posteriorly positioned hypoplastic tongue. The ears are very low set and the lower lobes may be fused to the neck which was short and thin. Aural ascent does not occur due to the lack of development of the jaw, hence the low position of the ears. These infants typically have hypoplastic lungs. (C.Langston)

1.152

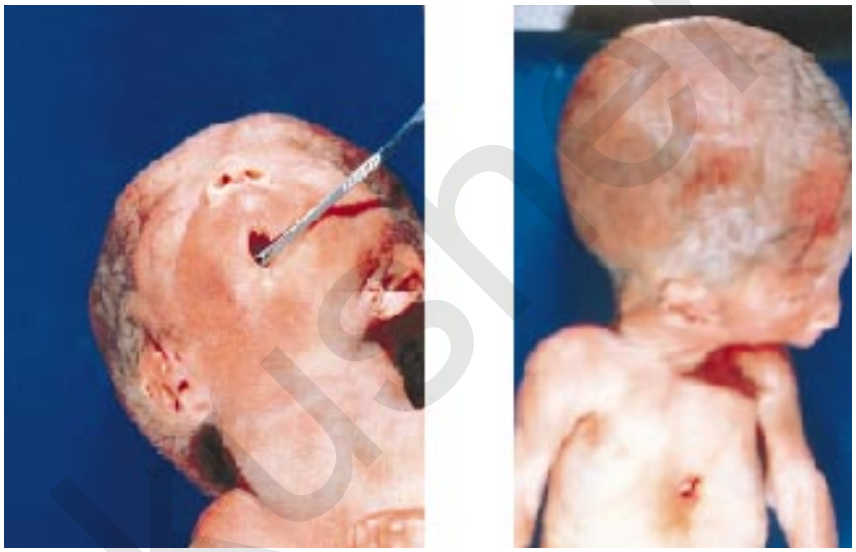

Figure 1.152. Another example of agnathia. Note the low-set ears and microstomia. Hydrocephalus and congenital heart disease are commonly present in branchial arch embryopathy. (C.Langston)

1.153

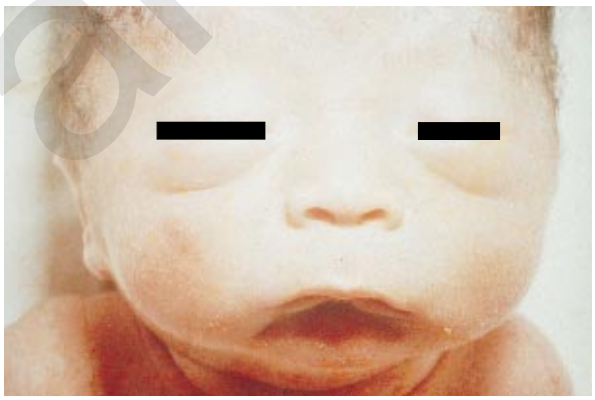

Figure 1.153. This infant with severe micrognathia had significant respiratory distress. Micrognathia is most commonly familial or idiopathic, but many syndromes are associated with this finding.

1.154

Figure 1.154. A lateral view of the same infant as in Figure 1.53 showing the marked micrognathia.

1.155

Figure 1.155. Severe micrognathia in an infant who had a small cleft palate (Robin's anomalad). This infant had respiratory distress and major problems with feeding.

1.156

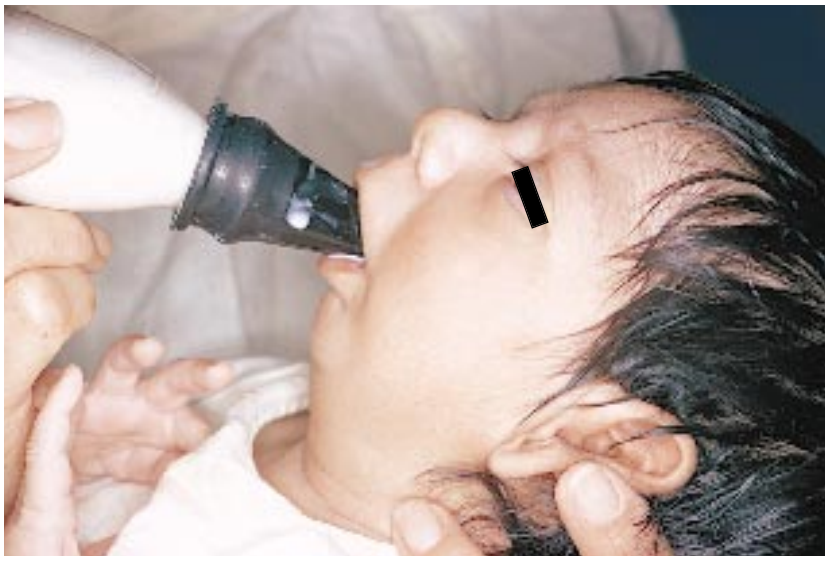

Figure 1.156. Feeding was accomplished in the same infant by the use of a lamb's nipple.

1.157

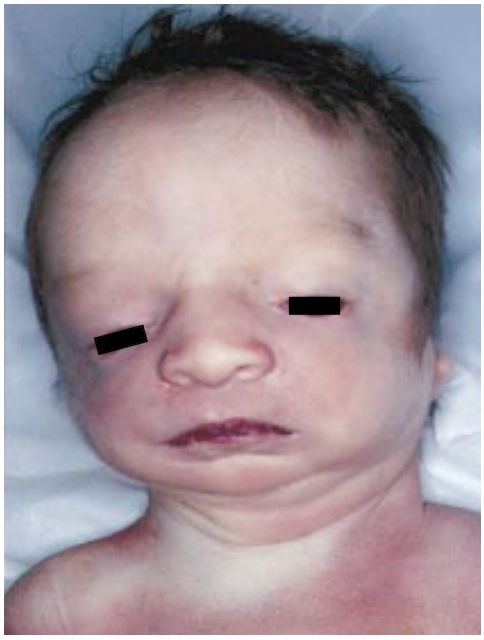

Figure 1.157. Marked micrognathia in an infant with Treacher-Collins syndrome (mandibulofacial dysostosis). In addition to the micrognathia, note the antimongoloid slant of the eyes, prominent nose, and malar hypoplasia.

1.158

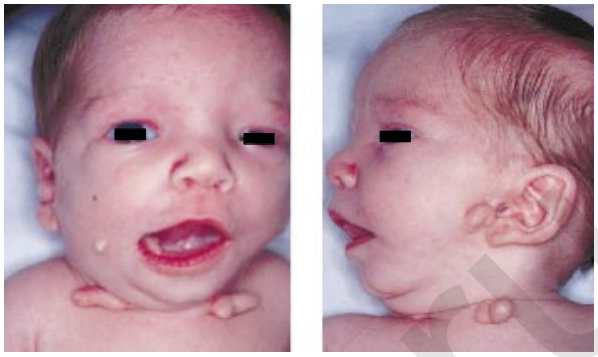

Figure 1.158. Micrognathia in an infant with Goldenhar's syndrome (hemifacial microsomia). In addition, note the preauricular skin tags, unilateral macrostomia, and skin tags due to the extra branchial arch anomalies.

1.159

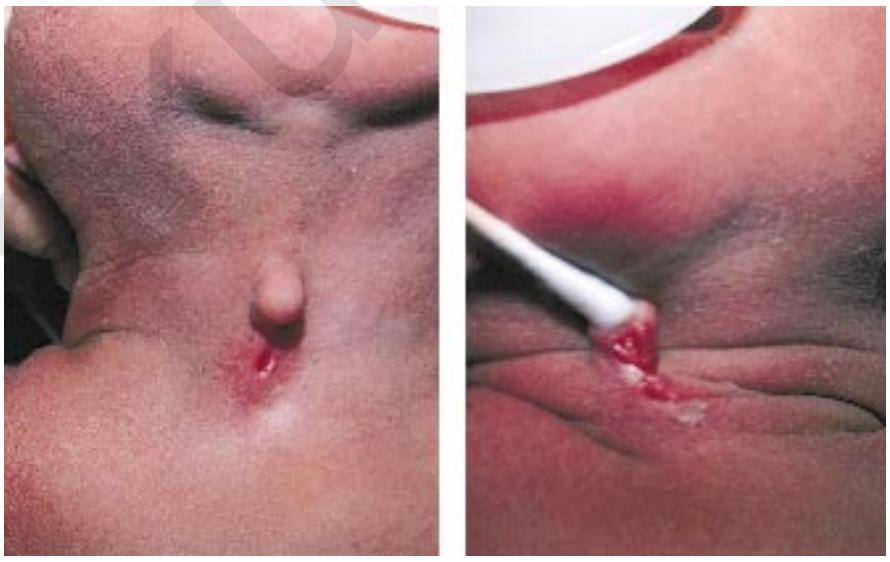

Figure 1.159. A congenital midline cervical cleft is a rare developmental anomaly. It represents failure of the branchial arches to fuse in the midline. It most commonly affects females, and presents at birth with a ventral midline defect of the skin of the neck. A reddened weeping strip of atrophic skin approximately 5 mm in width may occur at any level between the chin and sternal notch. Often there is a nipple-like projection at the upper end of the fissure and an associated sinus tract at the caudal end which may discharge mucoid material. This condition may be misinterpreted as a branchial cleft anomaly or thyroglossal duct cyst.

1.160

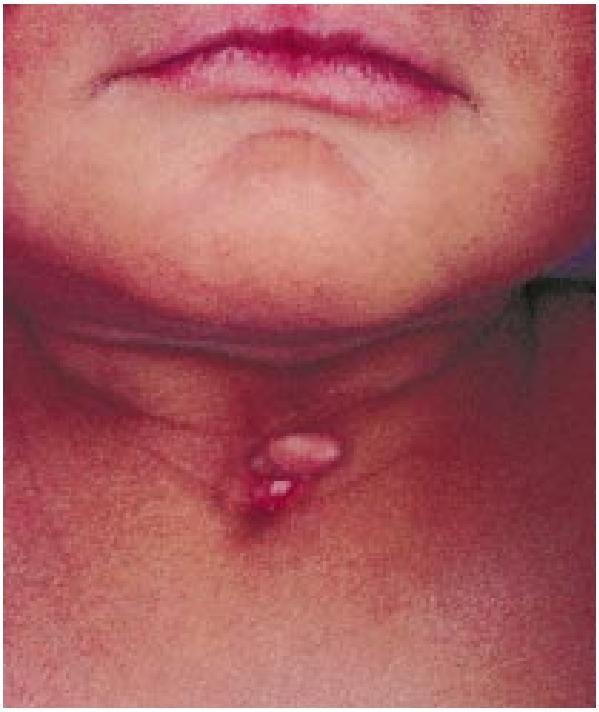

Figure 1.160. Another example of a congenital midline cervical cleft. Note the characteristic nipple-like projection, atrophic skin defect, and caudal fistulous tract. This may become a fibrous "cord" and result in a web-like contracture. This must be differentiated from a thyroglossal duct cyst/sinus which develops if the thyroglossal duct fails to close after the descent of the thyroid gland into the lower neck. It can occur anywhere on a line connecting the sternal notch and the base of the tongue.

1.161

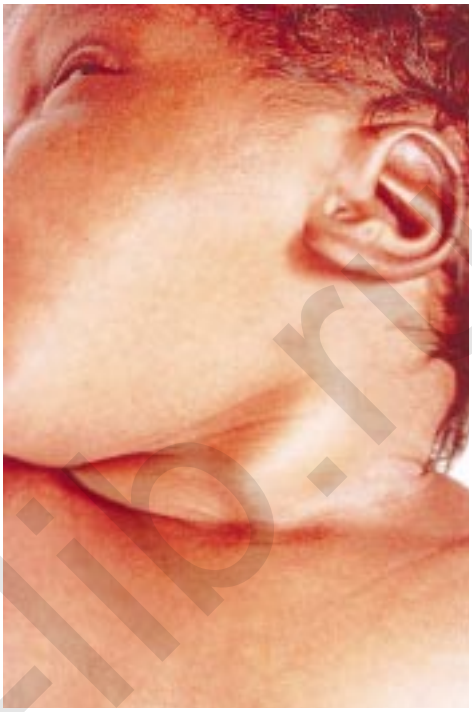

Figure 1.161. When delivery has involved excessive rotation or gross lateral rotation of the neck, a lump may appear in the sternomastoid muscle (sternomastoid tumor). This usually becomes apparent in the second week of life and commonly is situated in the lower half of the muscle. It may enlarge before resolving spontaneously, and may result in torticollis as a result of contraction of the sternomastoid muscle causing flexion of the head toward the side of the lesion. This condition must be differentiated from superior oblique palsy (IVth cranial nerve palsy) by an ophthalmologist.

1.162

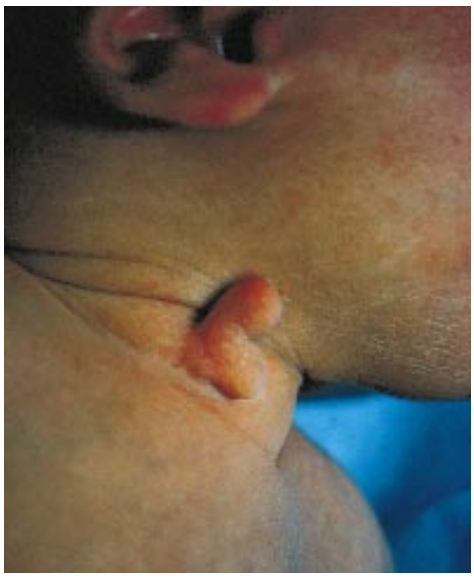

Figure 1.162. Abnormal development of the branchial clefts and arches may result in remnants, fistulae or cysts. Defects are usually unilateral and the external opening lies at the anterior edge of the sternocleidomastoid muscle, usually at the lower third. Secondary bacterial infection and cyst formation may occur. In this infant there is a branchial cleft remnant.

1.163

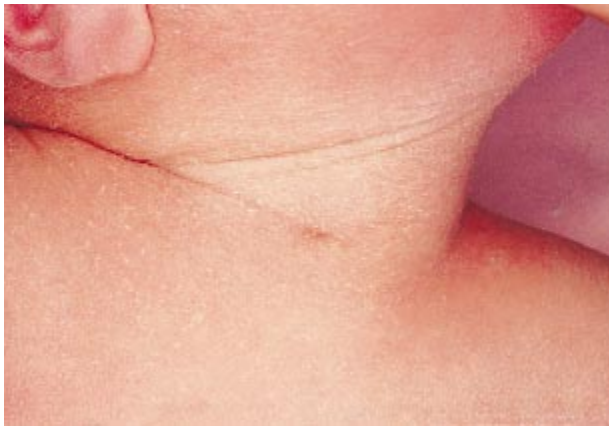

Figure 1.163. The subtle finding of a branchial sinus may be missed if examination of the infant is not thorough.

1.164

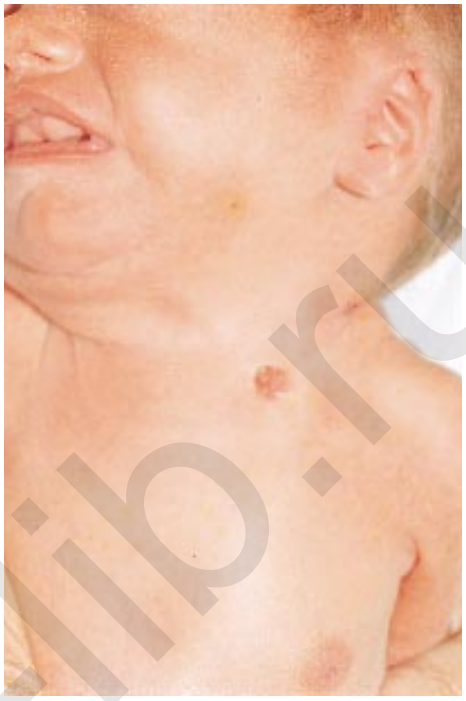

Figure 1.164. Branchial remnants tend to occur along the course of the sternomastoid muscle.

1.165

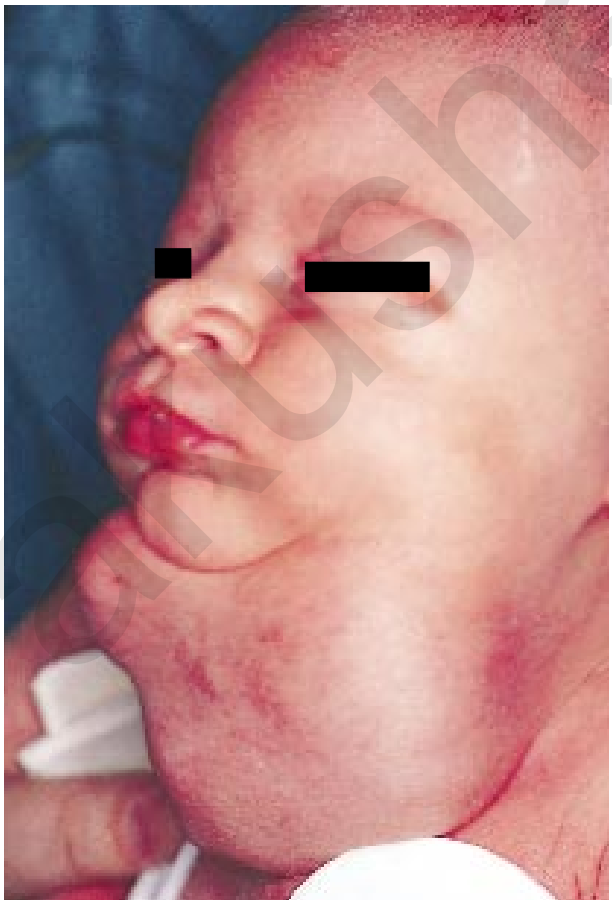

Figure 1.165. The large cystic hygroma (lymphangioma) presented in this infant as a large soft fluctuating mass. These are located most commonly in the neck and consist of proliferation of lymph vessels. Although not malignant, they may spread over the neck with extension into the mouth.

1.166

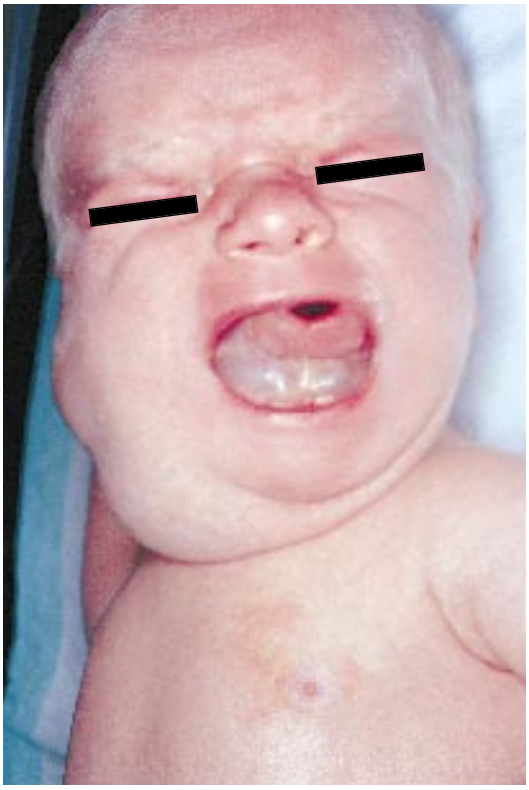

Figure 1.166. A large cystic hygroma involving the right side of the neck and face with extension into the mouth. The mass compromised respiration in this infant. Such masses in the neck should be differentiated from thyroglossal duct and cervical cysts.

1.167

Figure 1.167. Transillumination of the cystic hygroma in the same infant.

1.168

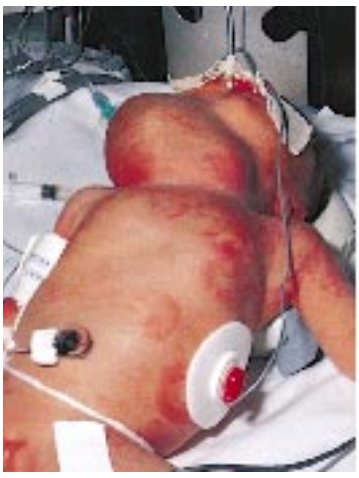

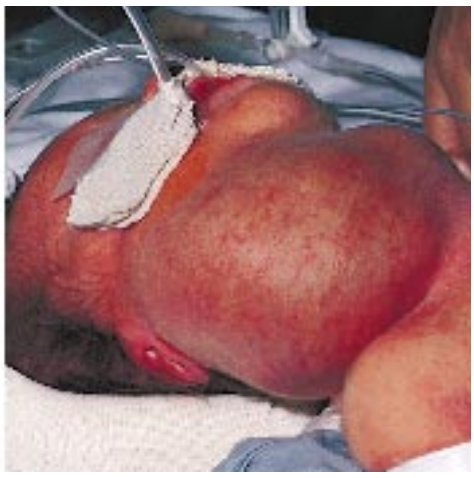

Figure 1.168. The large mass present at birth in the cervical area of this infant caused severe respiratory distress. It was a malignant teratoma of the neck.

1.169

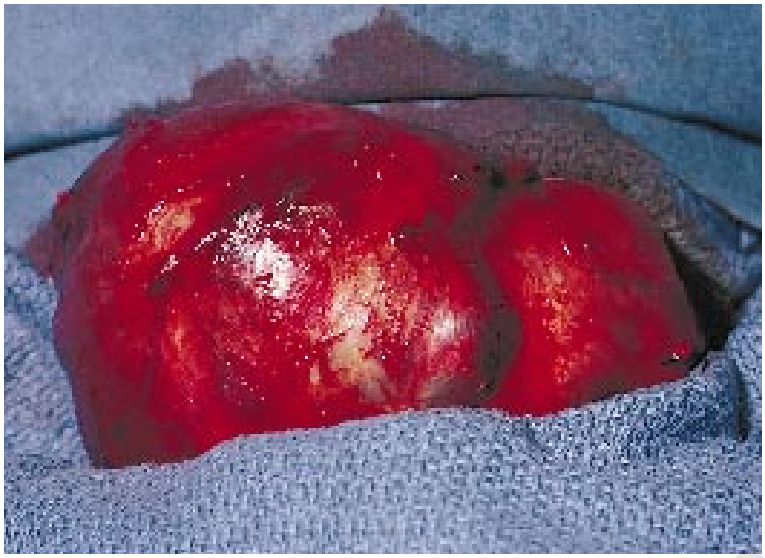

Figure 1.169. The surgical specimen of the mass of the same infant showed mixed yolk sac and embryonal remnants.

Chapter 2
Ophthalmology†

Blinding diseases can destroy useful vision unless rapidly diagnosed and treated. The initial routine examination of all infants should be carried out by the primary care physician, and should include direct ophthalmoscopy, and an orderly structural examination to include the eyebrows, lids, and lashes and lacrimal system, conjunctiva, sclera, cornea, iris (note pupils), anterior chamber, lens, vitreous, and fundus (especially optic nerve and macula). Look for symmetry of ocular structures and clarity of optical media (clear cornea, lens, vitreous). The red reflex should be bright and symmetrical. In all preterm infants ≤1250 g at birth, after an initial period of retinal development (from 4 to 6 weeks of life), an ophthalmologist trained to screen retinopathy of prematurity should initiate regular ophthalmologic examinations until inner retinal vascularization is complete, follow the progression and regression of retinopathy of prematurity (ROP), determine the need for surgical therapy for ROP, and follow the infant for the development of refractive errors, strabismus, amblyopia, etc. (all are increased in preterm infants). In any infant suspected of congenital intrauterine infections, genetic syndromes, family history of eye disease in parents or siblings, severe central nervous system abnormalities, maternal drug use or abuse, and obvious eye abnormalities or failure to obtain bilateral red reflexes, an ophthalmology consultation should be considered. The eyes are not completely developed anatomically or functionally at birth and are constantly changing during the neonatal period. It is important to recognize the normal findings during different stages of growth and understand what is abnormal.

†Photos and text for Chapter 2 provided by Helen A. Mintz-Hittner, M.D., Clinical Professor, Department of Ophthalmology and Visual Science, The University of Texas Medical School at Houston, and Clinical Professor, Department of Ophthalmology, Baylor College of Medicine, Houston, Texas.

OPHTHALMOLOGIC EXAMINATION OF THE NEWBORN

I. Examination of the Eyes should take place

A. During the initial routine examination (1st day of life) of all infants (by the pediatrician/neonatologist) to exclude obvious anomalies (must include bilateral red reflexes).

B. Following an initial period of stabilization (1st week of life) in all preterm infants ≤ 1250 grams at birth (by the pediatrician/neonatologist) to exclude obvious anomalies and to assess gestational age.

C. Following an initial period of retinal development (from 4 to 6 weeks of life) in all preterm infants ≤1250 grams at birth (by an ophthalmologist trained to screen retinopathy of prematurity [ROP]):

1. To initiate regular ophthalmologic examinations until inner retinal vascularization is complete (may not be to the ora serrata).

2. To follow the progression and regression of ROP.

3. To determine the need for surgical therapy, which is usually necessary from 32 to 42 weeks postconceptual age (gestational age + postnatal age), thus ROP occurs early in larger (higher gestational age) infants and later in smaller (lower gestational age) infants.

4. To follow for the development of refractive errors, strabismus, amblyopia, etc. (all of which are more frequent in preterm infants).

D. At any time when any of the following are suspected or proven (by an ophthalmologist):

1. congenital intrauterine infections;

2. genetic syndromes;

3. family history of eye disease in parents or siblings;

4. severe central nervous system abnormalities;

5. maternal drug use or abuse;

6. obvious eye abnormalities or failure to obtain bilateral red reflexes.

II. Examination Techniques and Normal Findings

A. The use of direct ophthalmoscopy and dilating drops (cyclopentolate 0.2% and phenylephrine 1%) is safe and effective without causing hypertension or bradycardia in all but the smallest and most unstable infants. Hold the eyelids open for a few seconds; blot away excess.

B. A functional examination — for visual acuity, visual field, motility, and refraction — is not part of the routine initial examination. Note that good fixation and following and consistently straight eyes may not be present until 6 months of age; however, if there is no visual interest, nystagmus, bilaterally dull red reflexes, asymmetrical red reflexes, or a consistently crossed eye, an examination by an ophthalmologist is recommended.

C. During an orderly structural examination, note obvious orbital abnormalities (overview) and then proceed from the anterior to the posterior parts of the eye: an external examination includes the eyebrows, lids, lashes, lacrimal system; an internal includes the conjunctiva, sclera, cornea, iris (note pupils), anterior chamber, lens, vitreous, fundus (especially optic nerve and macula). Look for symmetry of ocular structures and clarity of optical media (clear cornea, lens, vitreous). The red reflex should be bright and symmetrical.

D. Be aware of the *urgency* of ophthalmologic examinations:

1. To prevent progressive ocular damage (e.g., glaucoma, retinopathy of prematurity, etc.).

2. To prevent unilateral deprivation amblyopia due to any unilateral obstruction to the visual axis (lid tumor, ptosis, corneal clouding such as glaucoma, corneal injury such as forceps, cataract, vitreous hemorrhage, etc.). Immediately patch both eyes to prevent irreversible severe amblyopia from developing, and refer to an ophthalmologist as soon as the obstruction is recognized.

3. To prevent bilateral deprivation amblyopia due to any bilateral obstruction to the visual axes (especially cataracts). Cataract surgery and refractive correction must be completed by 6 weeks postnatal age (in a term infant) to obtain optimal visual results. Other bilateral obstructions (corneal and vitreal) are less amenable to surgical correction with optimal visual results; however, refer to an ophthalmologist as soon as the obstructions are recognized. Note: asymmetrical refractive errors can cause relative unilateral refractive amblyopia; bilateral large farsighted refractive errors can cause relative bilateral refractive amblyopia.

TRAUMA (Iatrogenic)

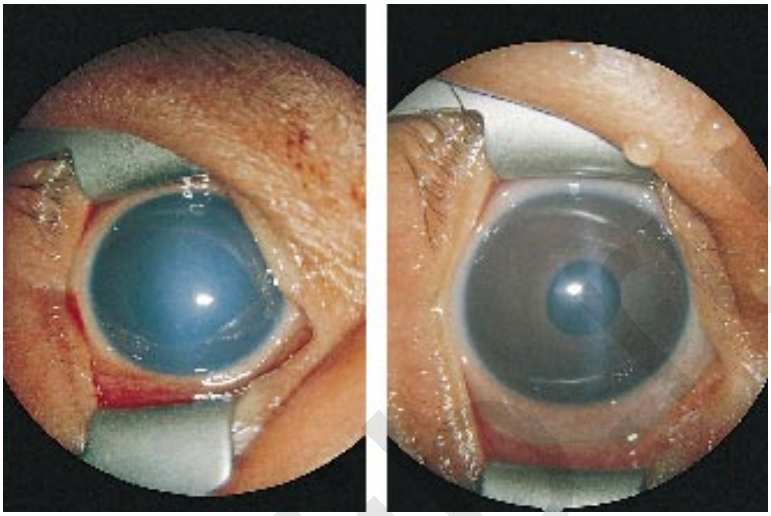

2.1

Figure 2.1. The ocular photograph on the left shows acute linear corneal edema which is transient but is usually associated with permanent corneal damage. The ocular photograph on the right shows the same eye, 2 weeks later, with breaks in Descemet's layer of the cornea which marks the axis of severe myopic astigmatism.

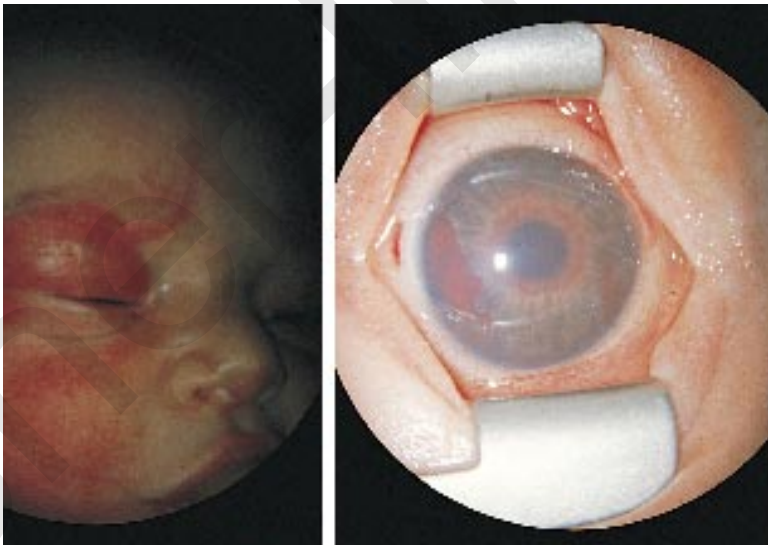

2.2

Figure 2.2. On the left is a mark on the face, directly over the eye, indicating the exact location that forceps were applied. On the right, the eyelids have been opened to reveal a partial hyphema caused by damage to the root of the iris, which resolved without any treatment or permanent ocular damage. The blood is in the anterior chamber of the eye, between the posterior corneal surface and the anterior iris surface. Blood in the anterior chamber of a neonate usually resolves rapidly without any treatment.

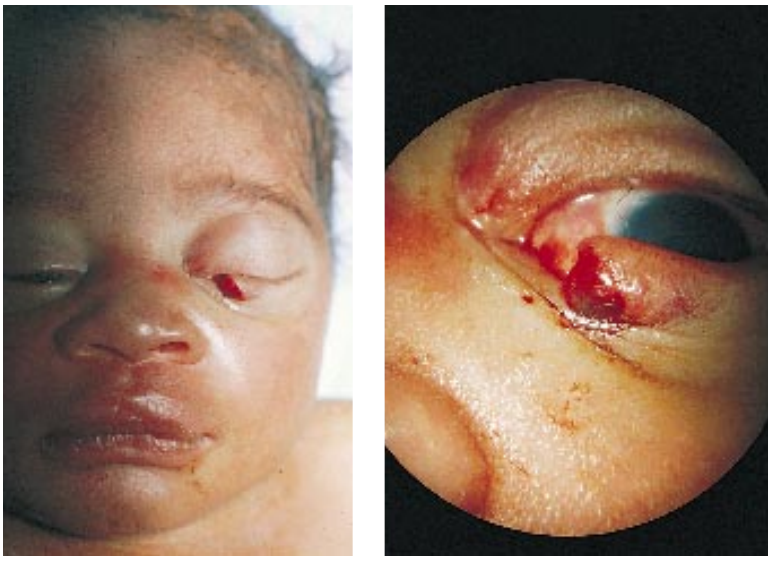

2.3

Figure 2.3. The mark on the face on the left indicates that forceps had slipped between the left eye and the nasal orbital wall. A close-up view of the same injury shows that there is a lid laceration involving the left lacrimal drainage system. Any laceration involving the lid margin should be repaired surgically as soon as possible in order to prevent permanent lid notching. When the nasal lid margin is involved, special attention must be given to repair the lacrimal system to prevent watering of the eye.

2.4

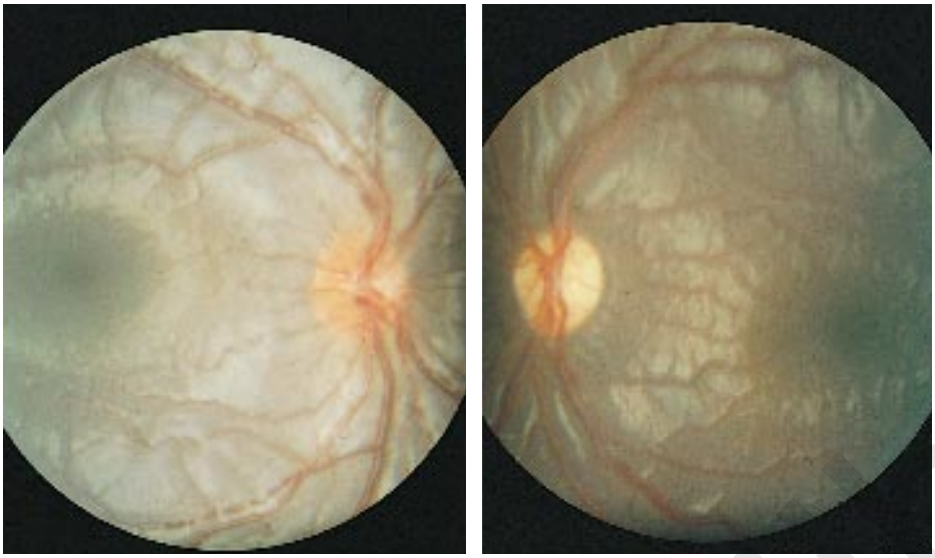

Figure 2.4. These figures are of the optic nerves of the infant shown in Figure 2.3, one year later. On the left is the normal right optic nerve; on the right is the left optic nerve which has developed complete optic nerve atrophy, related to stretching of the left optic nerve occurring when the forceps had slipped between the left eye and the nasal orbital wall. As a result, the eye is totally blind.

2.5

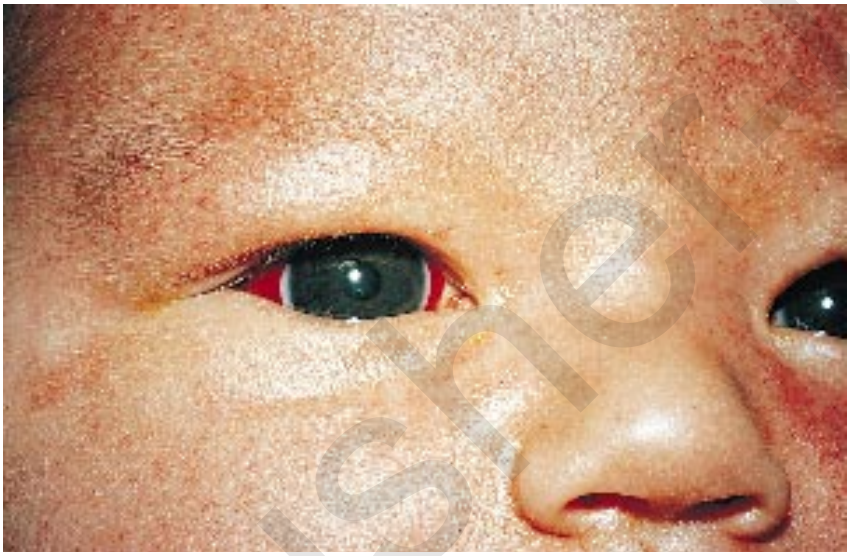

Figure 2.5. Subconjunctival hemorrhages are very common in the neonate immediately following birth. They resolve spontaneously without any consequences.

2.6

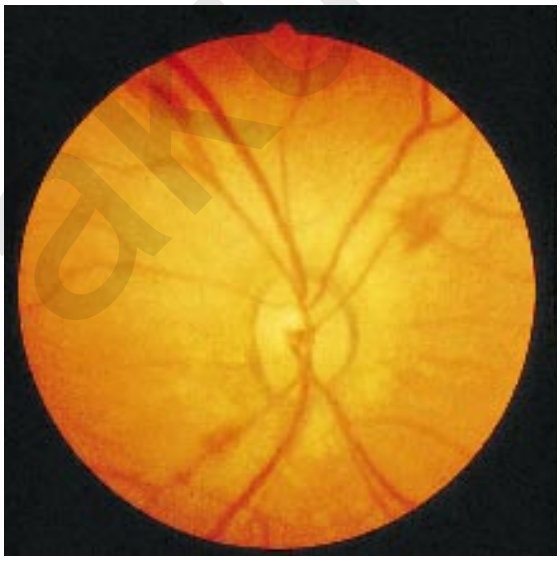

Figure 2.6. Retinal hemorrhages occur frequently in the neonate, especially following vaginal delivery. In some studies, the incidence of small retinal hemorrhages is as high as 25% irrespective of whether the delivery was spontaneous or required the application of forceps. These retinal hemorrhages resolve spontaneously without any consequences. In contrast, hemorrhages into the vitreous gel may prevent light from getting through to the retina for several days or even weeks and will cause a severe, irreversible deprivation amblyopia.

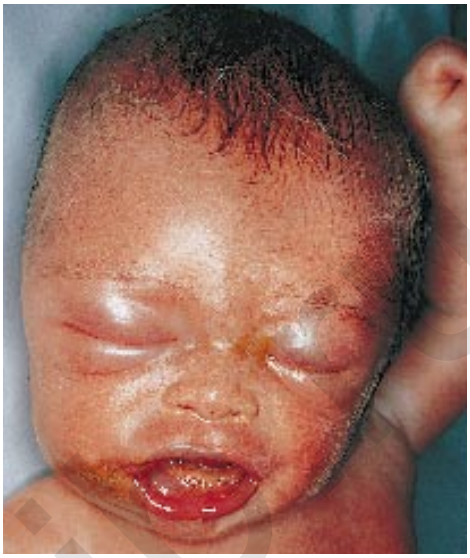

2.7

Figure 2.7. Chemical conjunctivitis in a premature infant resulting from the use of silver nitrate for Crede prophylaxis. Sometimes this is so severe that it prevents visualization of the eye on the initial examination in the nursery. This usually improves within 24 to 48 hours and an ocular examination should be performed at that time. For prophylaxis, at the present time, different antibiotic preparations have been suggested. However, because of resistant *Neisseria* gonococcus strains, many centers still use silver nitrate.

INFECTION (Acquired)

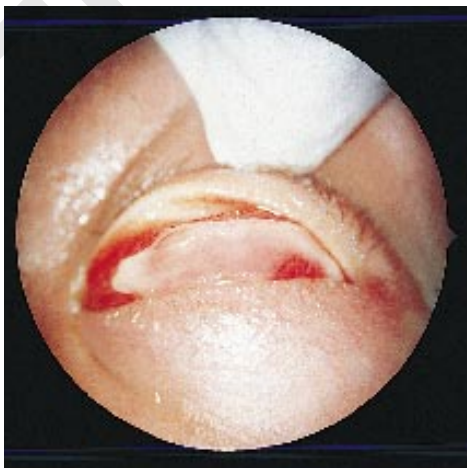

2.8

Figure 2.8. Trachoma inclusion conjunctivitis (TRIC or chlamydial conjunctivitis) usually does not become clinically apparent before the 6th day of life. This shows a dense white membrane which developed over a period of a week. TRIC is one of the few infections which cause the formation of conjunctival membranes, shown on the conjunctival surface of the upper eyelid of this eye. Tetracycline and erythromycin have been used for Crede prophylaxis in some nurseries because of the increasing incidence of chlamydial infection.

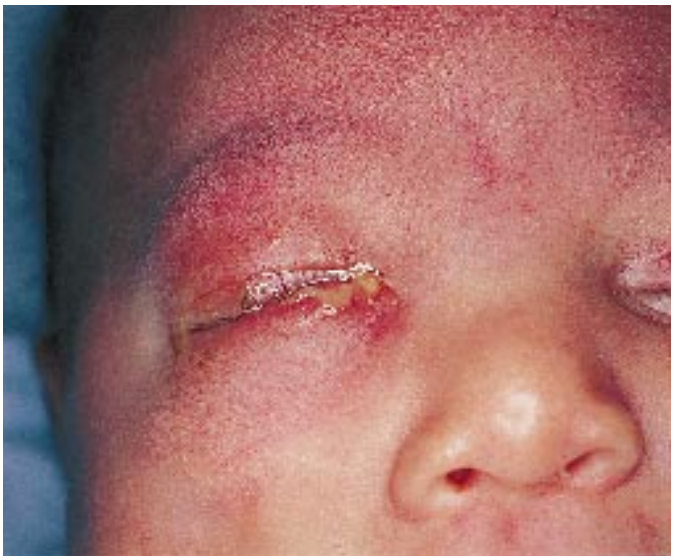

2.9

Figure 2.9. *Escherichia coli* conjunctivitis is present in this right eye. The most common conjunctivitis in the neonate in the first 24 hours of life is a chemical conjunctivitis. If the conjunctivitis is due to an infection, the most common cause is *Staphylococcus aureus*, but many other organisms may be responsible. Culture and sensitivity will suggest the appropriate antibiotic therapy.

2.10

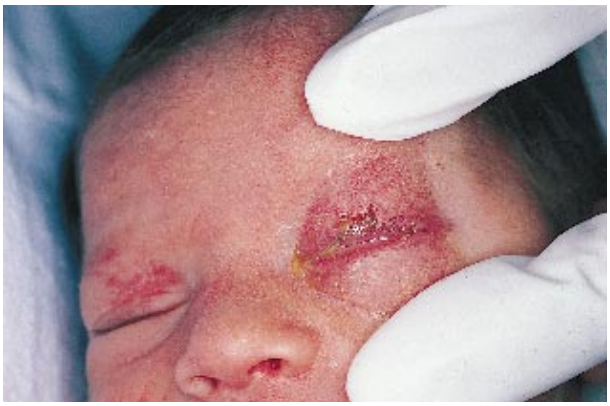

Figure 2.10. *Neisseria gonorrhoeae*: Gonococcal conjunctivitis, which became clinically apparent in this infant by the 2nd day of life, developed a purulent drainage quickly. *Neisseria* is one of the few organisms which attack the intact corneal epithelium. Because of this ability to cause corneal ulceration with perforation and subsequent endophthalmitis, *Neisseria* was once the most common cause of blindness in infants in this country.

2.11

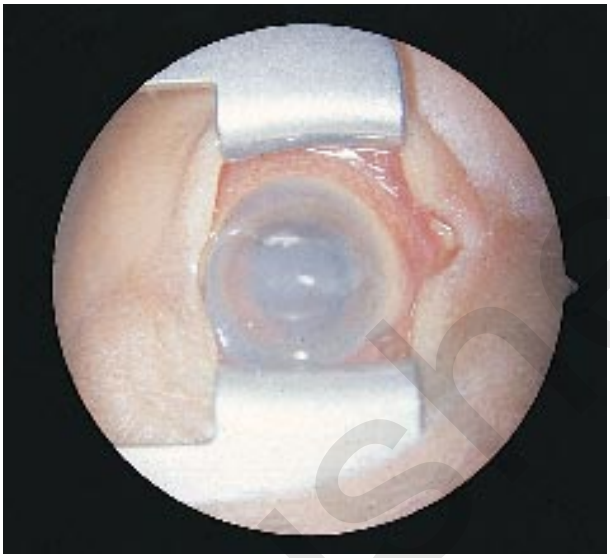

Figure 2.11. *Pseudomonas aeruginosa*: Corneal ulcer with perforation in a preterm infant. *Pseudomonas* is one of the few organisms which attack the intact corneal epithelium. Because of this ability, corneal ulceration with perforation and subsequent endophthalmitis may occur in preterm infants. Any preterm infant who is chemically paralysed while on mechanical ventilation may develop corneal exposure with subsequent corneal ulcer. Thus, it is imperative to use a lubricating ophthalmic ointment or to tape the eyes shut in this clinical setting.

2.12

Figure 2.12. *Candida albicans*: Retinitis is seen as small white infiltrates ("cotton-patches") scattered in the retina. They reflect the high blood flow through the choroidal vascular system of the eye and resolve slowly with treatment for systemic candidiasis.

INFECTION (Congenital intrauterine: TORCH diseases: Toxoplasmosis, Other, Rubella virus, Cytomegalovirus, Herpes simplex virus)

2.13

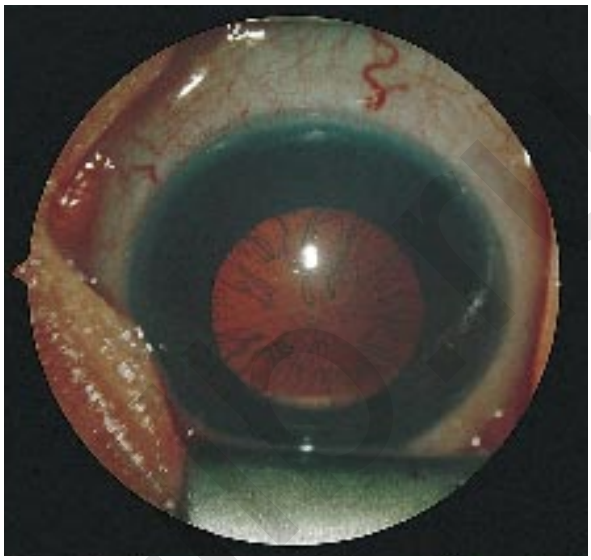

Figure 2.13. TORCH disease must be considered with persistent tunica vasculosa lentis in any small-for-gestational-age infant. This is a grade 3 tunica vasculosa lentis in an infant with congenital rubella who was 35 weeks gestational age and weighed 860 g at birth.

2.14

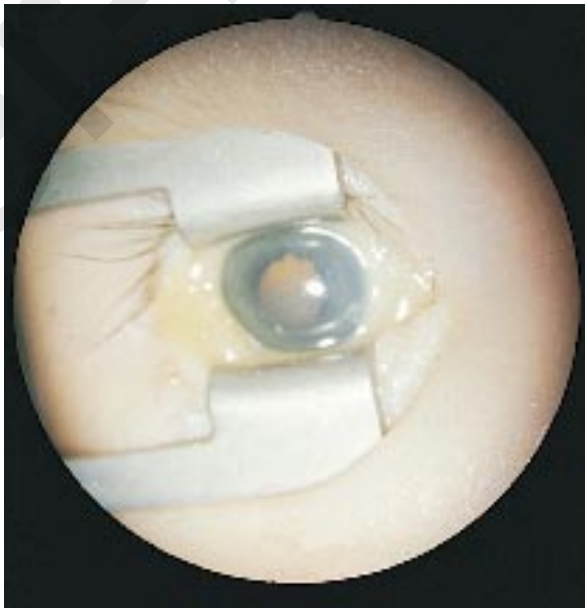

Figure 2.14. TORCH diseases must be considered with unilateral or bilateral microphthalmia in any small-for-gestational-age infant. This is a microphthalmic eye in an infant with congenital toxoplasmosis who weighed 2500 g at birth and was 39 weeks gestational age.

2.15

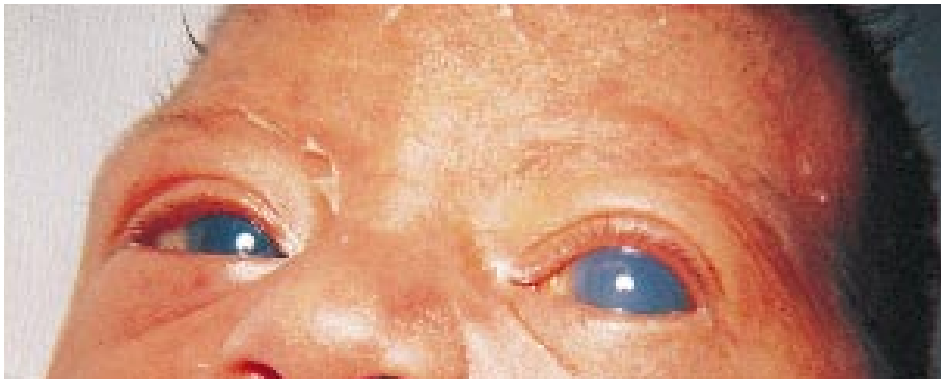

Figure 2.15. Rubella glaucoma is an uncommon ocular finding in infants with congenital rubella. Glaucoma occurs in less than 10% of infants with congenital rubella and usually is transient. It is probably related to inflammation.

2.16

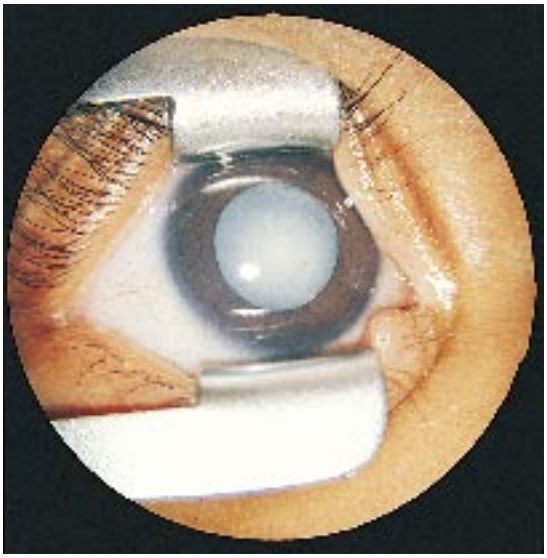

Figure 2.16. Rubella cataract is the most common ocular finding in infants with congenital rubella and occurs in up to 75% of these infants. Classically, the cataract is nuclear, and the virus can be isolated from the lens for years following birth.

2.17

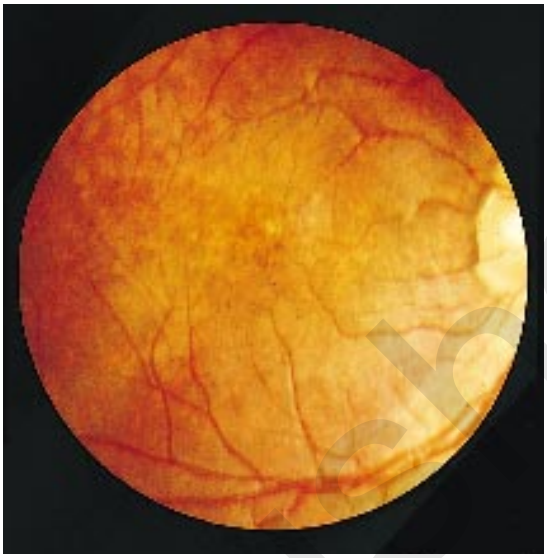

Figure 2.17. Rubella retinitis appears as a salt and pepper retinitis classically and reflects damage to the retinal pigment epithelium. It can be present without any decrease in visual acuity.

2.18

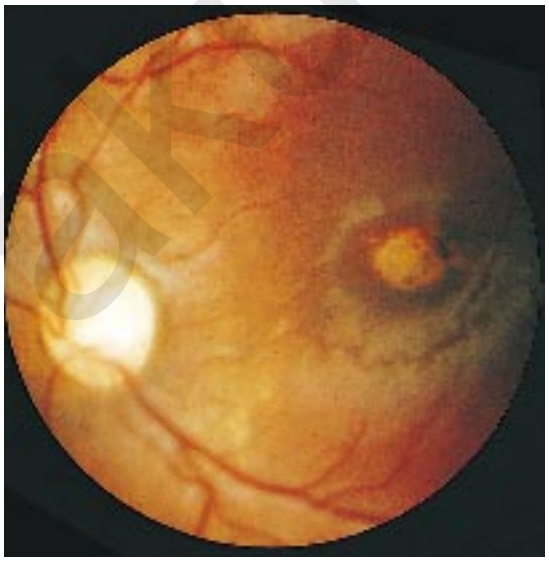

Figure 2.18. Cytomegalovirus may cause a small macular chorioretinal scar. This is the most typical lesion in cytomegalovirus infection.

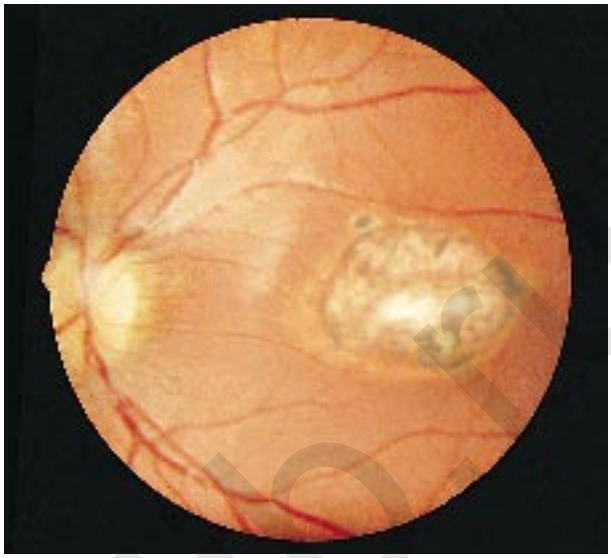

2.19

Figure 2.19. Toxoplasmosis may cause a large macular chorioretinal scar. This is the most typical lesion of toxoplasmosis infection, but it is indistinguishable clinically from a large macular chorioretinal scar of cytomegalovirus infection.

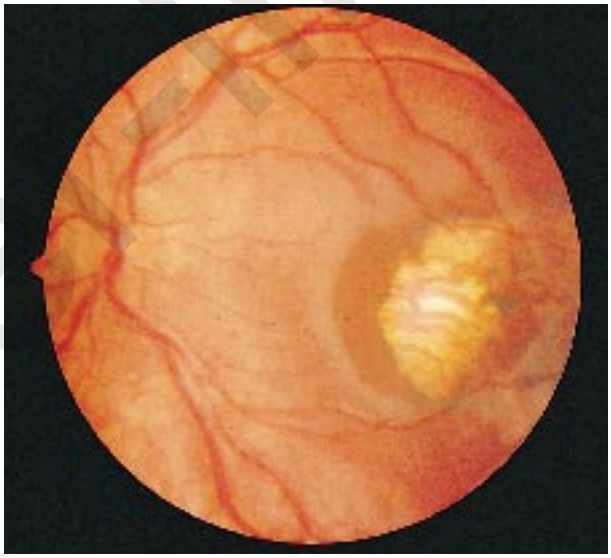

2.20

Figure 2.20. Cytomegalovirus was the cause of this large macular chorioretinal scar. It closely resembles the scar of toxoplasmosis shown in Figure 2.19.

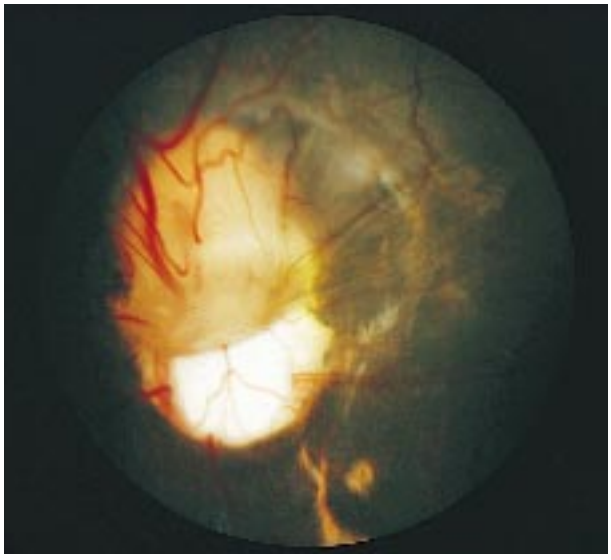

2.21

Figure 2.21. Cytomegalovirus may cause a coloboma of the optic nerve. This failure of the fetal fissure to fuse posteriorly may occur in infants with cytomegalovirus infection. When there is ocular involvement in cytomegalovirus infection, there is usually damage to the central nervous system.

2.22

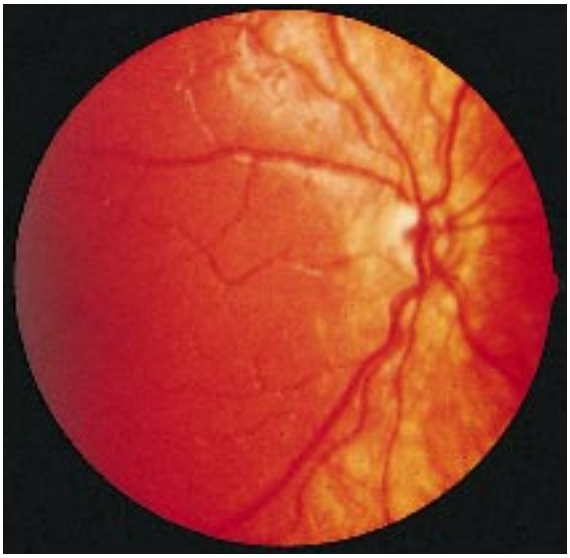

Figure 2.22. Cytomegalovirus may cause hypoplasia of the optic nerve. This lack of development of the optic nerve in infants with cytomegalovirus infection may be associated with severe damage to the central nervous system.

2.23

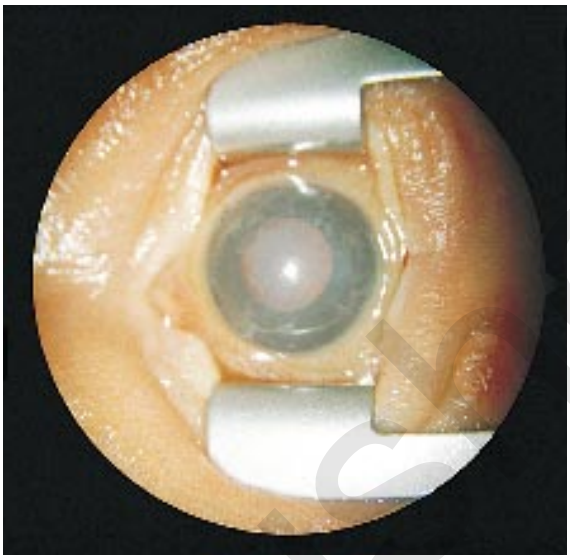

Figure 2.23. Herpes simplex infection can be devastating not only to the eye but to the central nervous system. Occasionally, a superficial herpetic corneal ulcer with edema, as shown in this figure, can allow rapid diagnosis of herpetic infection with the opportunity to institute systemic therapy immediately.

2.24

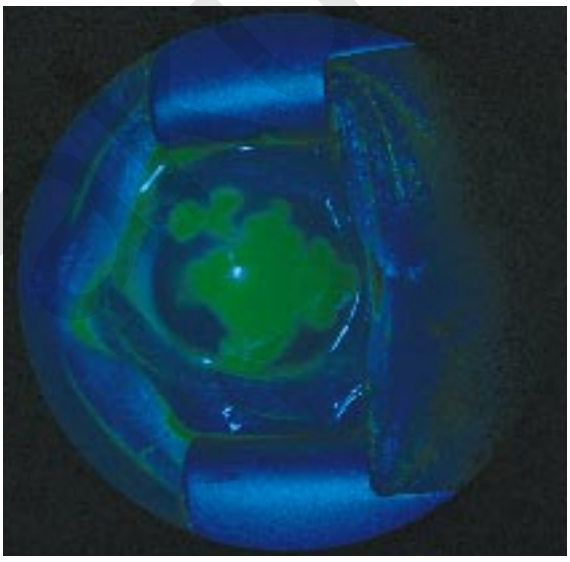

Figure 2.24. This herpes simplex corneal ulcer with dendrites, shown unstained Figure 2.23, is stained with fluorescein and viewed with a cobalt blue filter. Such a corneal lesion allows early diagnosis. If therapy is begun immediately, herpes simplex infection does not necessarily correlate with severe central nervous system damage.

2.25

Figure 2.25. Herpes simplex can cause a necrotizing chorioretinitis. It usually appears within the first few days following birth as macular or peripheral retinal edema.

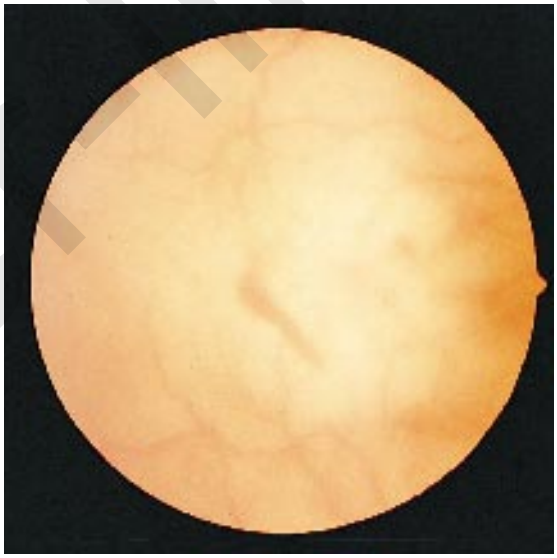

2.26

Figure 2.26. Herpes simplex necrotizing chorioretinitis usually progresses rapidly and usually correlates with severe central nervous system necrosis. This is the same eye as in Figure 2.25, 4 days later.

LACRIMAL ABNORMALITIES

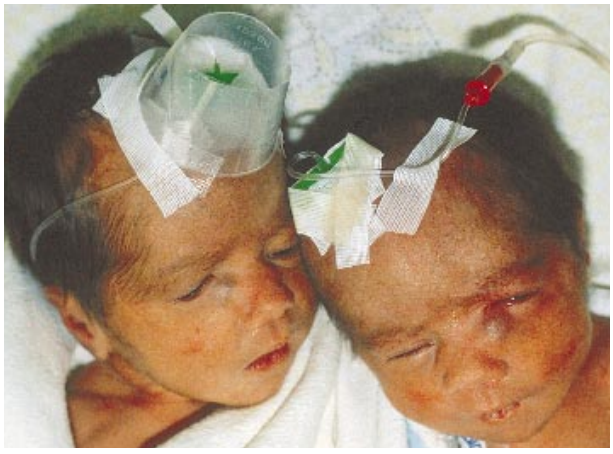

2.27

Figure 2.27. A dacryocystocele may occur as an autosomal dominant in families as exemplified by these twins. The lacrimal sac is blocked at both ends and a sterile swelling appears as a purplish swelling adjacent to the base of the nose. Simple lacrimal probing allows for a swift resolution of this problem; however, if there is anything atypical about the location or the appearance of the swelling, an ultrasound of the brain should be obtained to exclude an encephalocele.

2.28

Figure 2.28. If a lacrimal cyst becomes infected, the skin overlying the cyst becomes edematous and erythematous. Because septicemia, meningitis, and/or cavernous sinus thrombosis may occur, systemic antibiotics are indicated. Following a short period of antibiotics, probing of the lacrimal system should be performed.

LIDS

2.29

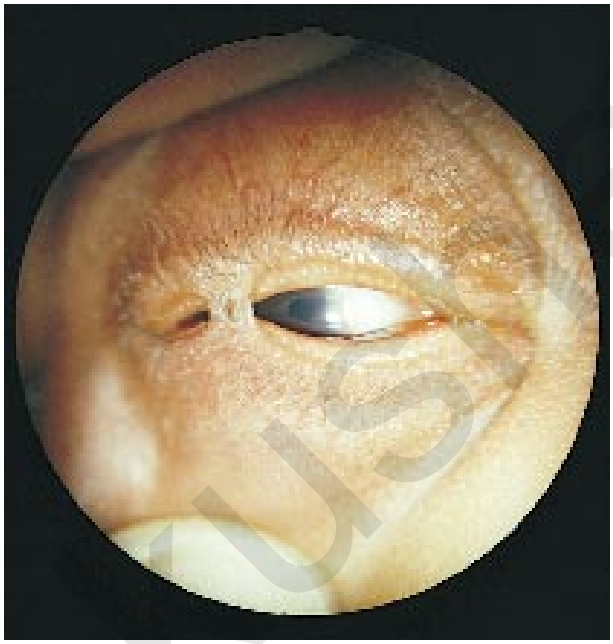

Figure 2.29. Ankyloblepharon filiforme adnatum is shown in this figure with fusion of the upper and lower eyelids by small filiform attachments which can be cut with scissors. Blepharophimosis is a narrow palpebral fissure which occurs as a congenital anomaly and should be included in the differential diagnosis of ankyloblepharon filiforme adnatum.

2.30

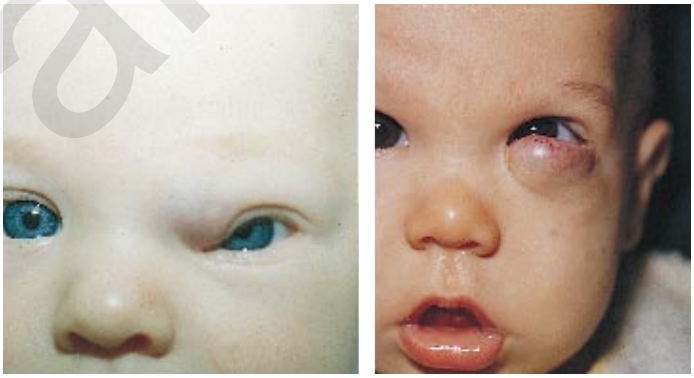

Figure 2.30. Capillary hemangiomas of the lids most frequently arise nasally from either the superior or the inferior palpebral fissure. They are poorly defined soft swellings of the eyelid with purple (red-blue) discoloration of the skin. They require treatment when rapid growth threatens the visual axis which can lead to irreversible deprivation amblyopia.

2.31

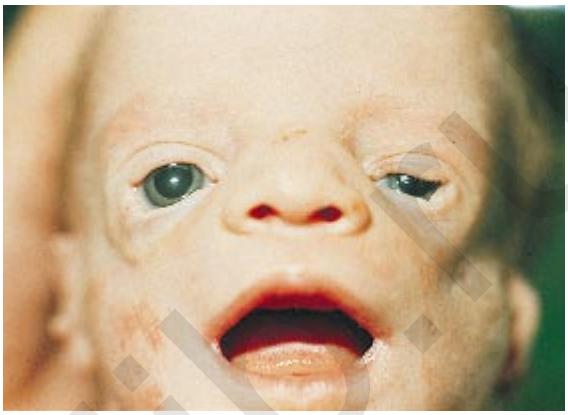

Figure 2.31. Treacher-Collins syndrome is characterized by malformations of the structures formed from the first branchial arch, groove, and pouch. Mandibulofacial dysostosis with antimongoloid slanting of the palpebral fissure and coloboma of the lower temporal lid is inherited as an autosomal dominant (5q11) disorder.

2.32

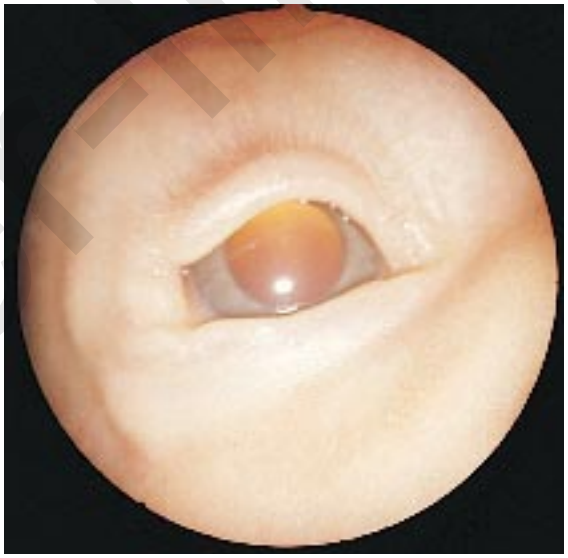

Figure 2.32. The coloboma of the lid in the Treacher-Collins syndrome involves the lateral third of the lower lid and may not affect the lid margin. Other lower lid anomalies such as absent lacrimal punctae and irregular lower lid lashes may also be present.

2.33

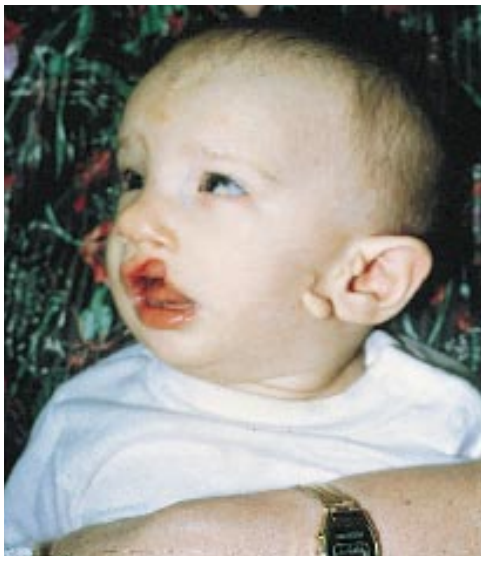

Figure 2.33. The most common findings of Goldenhar's syndrome, which is characterized by hemifacial macrosomia, are colobomas of the upper lids, solid epibulbar dermoids located at the inferotemporal border of the cornea, and solid lipodermoids located in the superotemporal sulcus near the lacrimal gland. Oculoauriculovertebral dysplasia is sporadic and the basic defect is unknown.

2.34

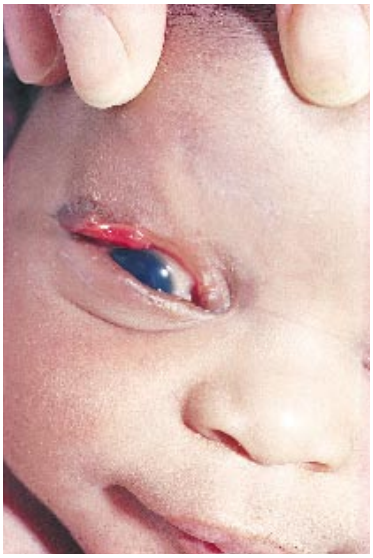

Figure 2.34. The coloboma of the lid in Goldenhar's syndrome involves the middle third of the upper lid which does affect the lid margin.

2.35

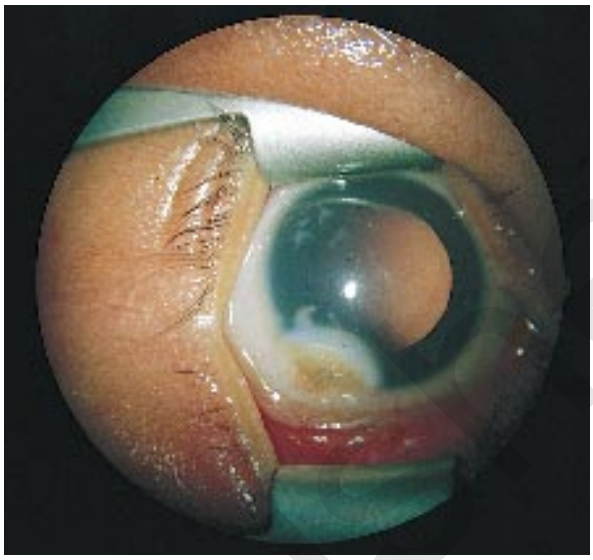

Figure 2.35. This typical dermoid of the Goldenhar's syndrome occurs as a solid mass of the conjunctiva at the inferotemporal border of the cornea. Flattening of the cornea occurs in the meridian of the dermoid, causing an associated astigmatism and occasionally a secondary amblyopia.

2.36

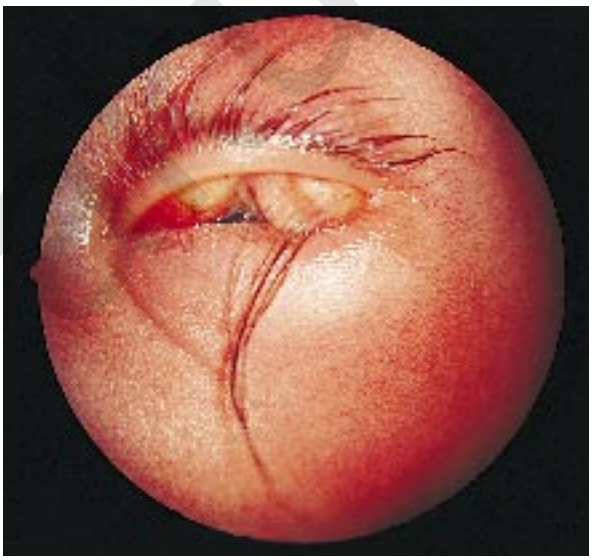

Figure 2.36. This complex choristoma located in the superotemporal sulcus of the left eye with the upper lid everted demonstrates the long lashes which may be present. This is different from the lipodermoid noted in the same position in some patients with Goldenhar's syndrome.

2.37

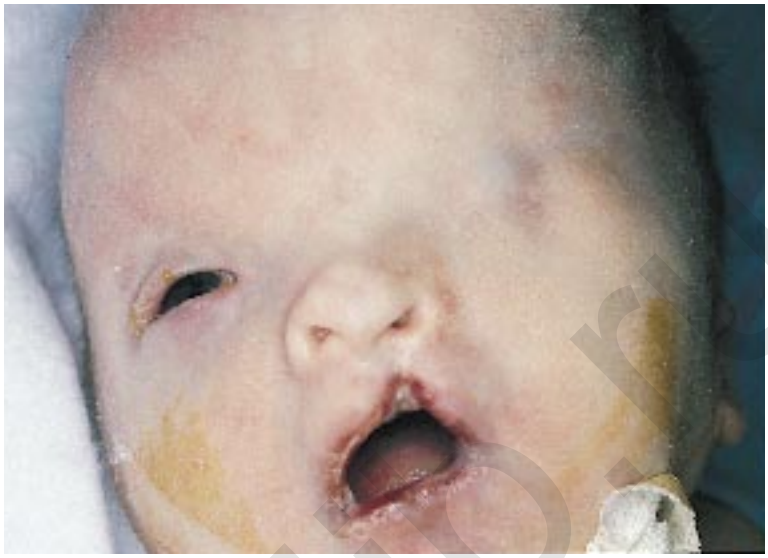

Figure 2.37. Fraser's syndrome is an autosomal recessive disorder which occurs when the maturation of the lids is interrupted and the lid folds fail to develop. This infant shows complete cryptophthalmos by the left lid (surface ectoderm) with complete coverage of the corneal epithelium.

2.38

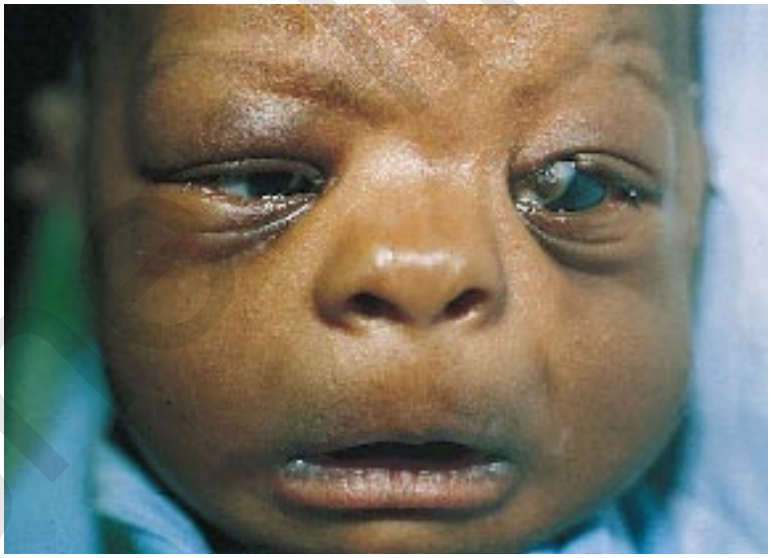

Figure 2.38. This figure demonstrates Fraser's syndrome with partial cryptophthalmos. There is a continuation of the left superonasal lid (surface ectoderm) with the corneal epithelium.

2.39

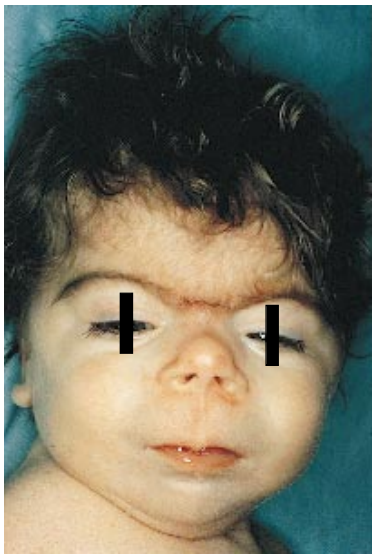

Figure 2.39. The typical confluent eyebrows, long curly eyelashes, and telecanthus associated with the Cornelia de Lange syndrome are present in this infant. Telecanthus is the lateral displacement of the inner canthi such that the medial portion of the eye is partially obscured, giving rise to the impression of strabismus and hypertelorism. In hypertelorism the eyes are widely spaced. Because a low nasal bridge may give rise to the impression of widely spaced eyes, the distance between the two eyes should always be measured.

2.40

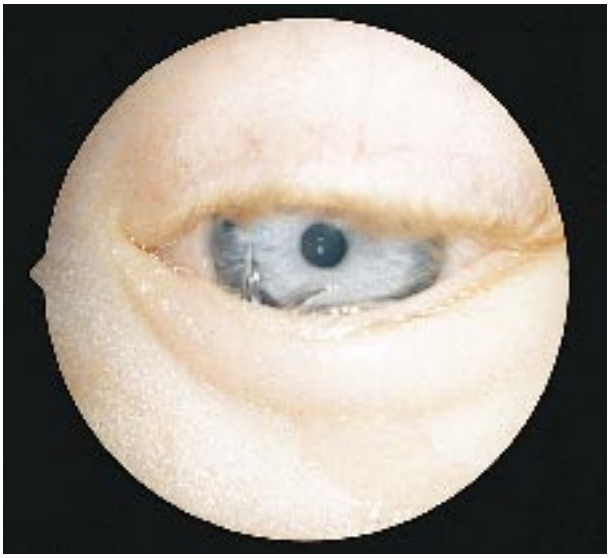

Figure 2.40. Congenital entropion is shown in this patient with epiblepharon allowing the inturning of the lower nasal lid such that the lashes irritate the cornea.

2.41

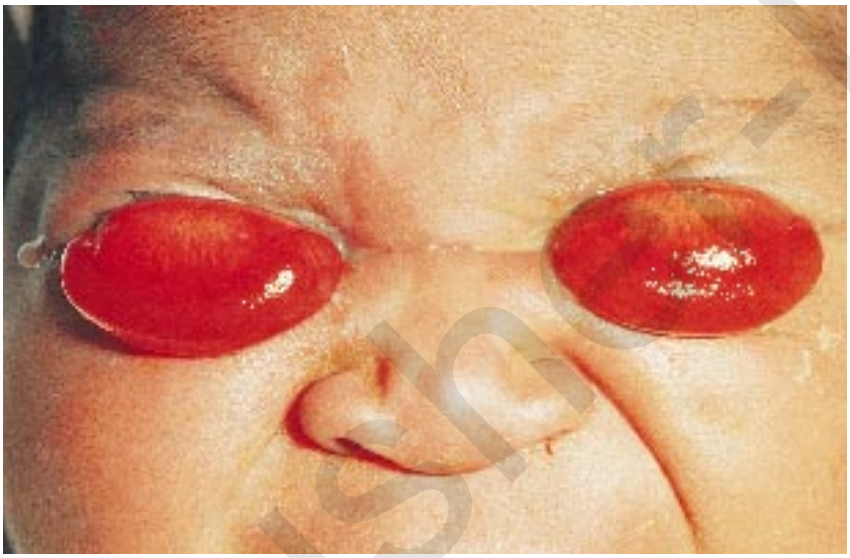

Figure 2.41. Congenital ectropion occurs as a result of intrauterine prolapse of the conjunctiva. This may require temporary taping or suturing of the lid margins. In the absence of microphthalmos, buphthalmos, or eyelid defects, primary eyelid eversion is rare and follows a benign course. The tarsal conjunctiva is chemotic, hyperemic, and protrudes outward. The lid returns to normal a few days following application of ophthalmic ointment and moist sterile gauze dressings.

2.42

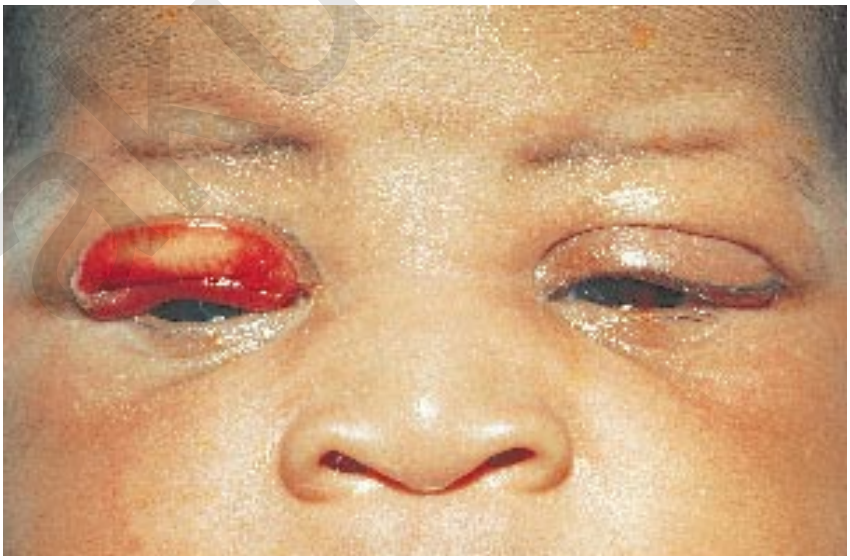

Figure 2.42. The same patient showing a residual right upper lid ectropion after five days of bilateral pressure patches. If this occurs as a unilateral condition, it is essential to tape both eyes closed to prevent deprivation amblyopia.

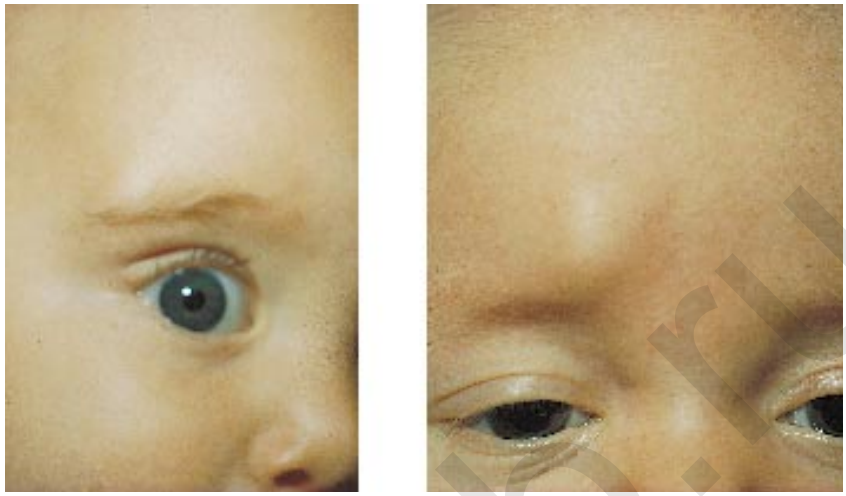

2.43

Figure 2.43. Dermoid cysts occur when surface ectodermal elements are sequestered along the closure lines of the fetal bony sutures. These cystic dermoids demonstrate the superotemporal and the superonasal locations.

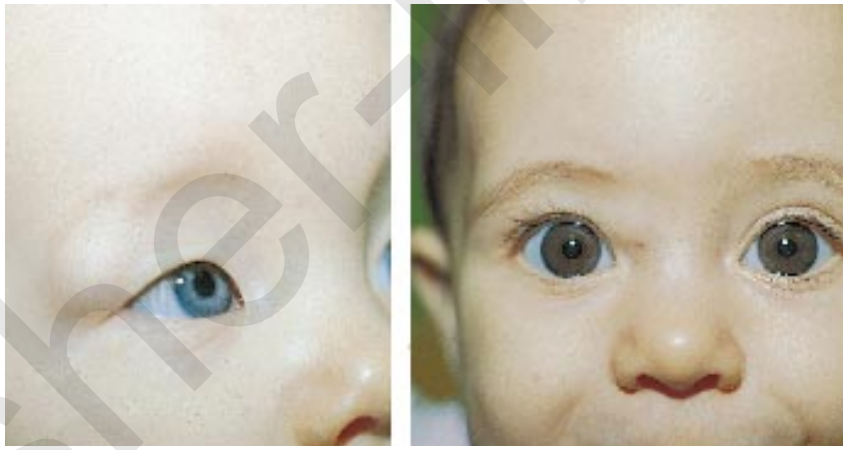

2.44

Figure 2.44. These cystic dermoids demonstrate the inferotemporal and the inferonasal locations. They are lined by keratinized squamous epithelial cells and contain hair follicles and sebaceous glands.

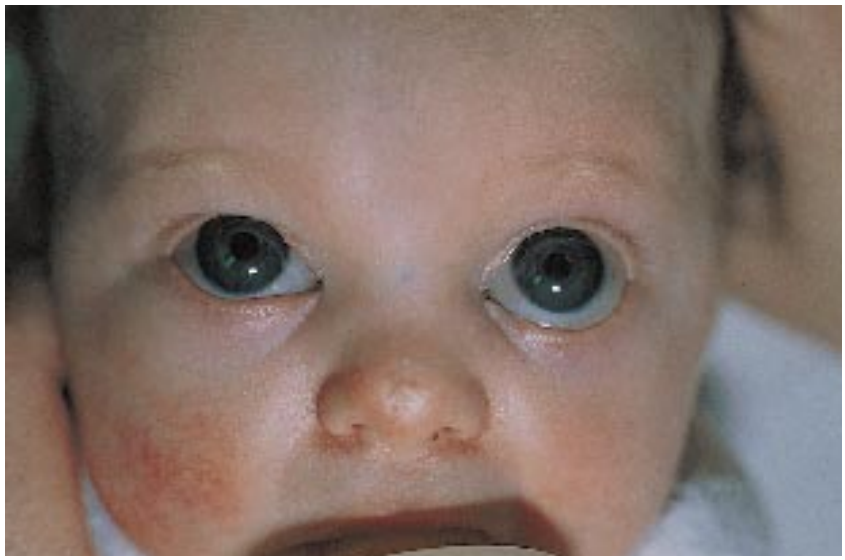

2.45

Figure 2.45. Exophthalmos and lid retraction occur infrequently. This patient demonstrates the typical lid signs of neonatal hyperthyroidism. Children with craniofacial anomalies and shallow orbits also may demonstrate severe exophthalmos and lid retraction.

2.46

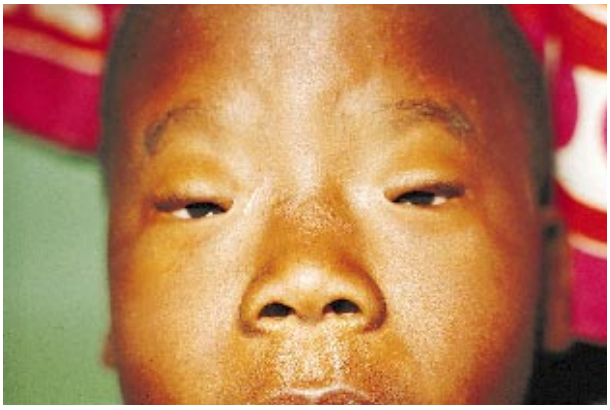

Figure 2.46. This patient demonstrates bilateral blepharoptosis, blepharophimosis, and epicanthus inversus with normal globes and normal vision which occurs as an autosomal dominant. This is distinct from bilateral anophthalmia, microphthalmia, or nanophthalmia where the globes are not present or small with absent or impaired vision. The epicanthus is a crescentic fold of skin running vertically between the lids over the inner canthus. It can be most prominent in the upper eyelid (epicanthus tarsalis); most prominent in the lower eyelid (epicanthus inversus); or equally distributed between the upper and lower eyelids (epicanthus palpebralis).

OCULAR SIZE

2.47

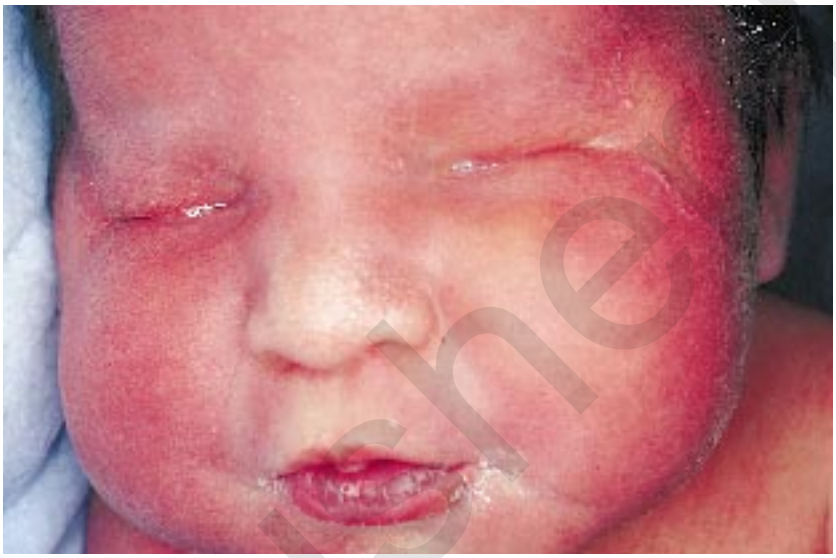

Figure 2.47. At term birth, the normal ocular sagittal length is 17.5 mm, and the normal corneal diameter is 10 mm. This is a term infant with very severe bilateral microphthalmia. The globes are virtually absent and the infant is totally blind. This may occur unilaterally or bilaterally and is often associated with other anomalies of the central nervous system.

2.48

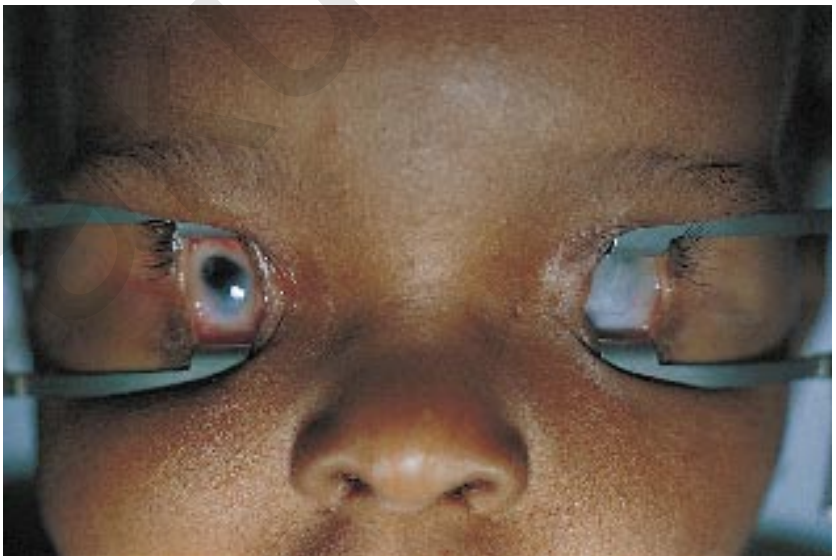

Figure 2.48. This is another term infant with severe bilateral microphthalmia. The globes are small, and vision is extremely poor. There are several forms of microphthalmia including those associated with congenital infection, chromosomal abnormalities, and the CHARGE syndrome.

2.49

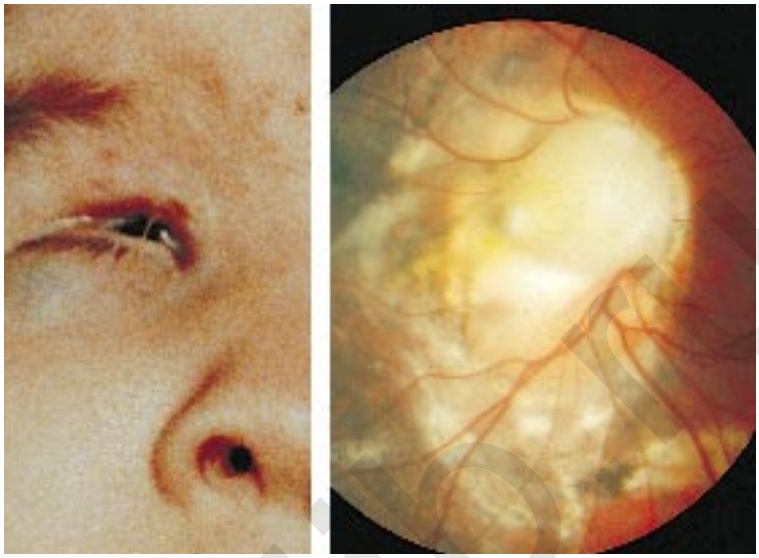

Figure 2.49. Colobomatous microphthalmia may be inherited as an autosomal dominant disorder with extremely variable expressivity. On the left is severe microphthalmia presenting as a cystic eye. On the right is a coloboma of the optic nerve with continuous coloboma of the choroid and retina which was present in another member of the same family.

2.50

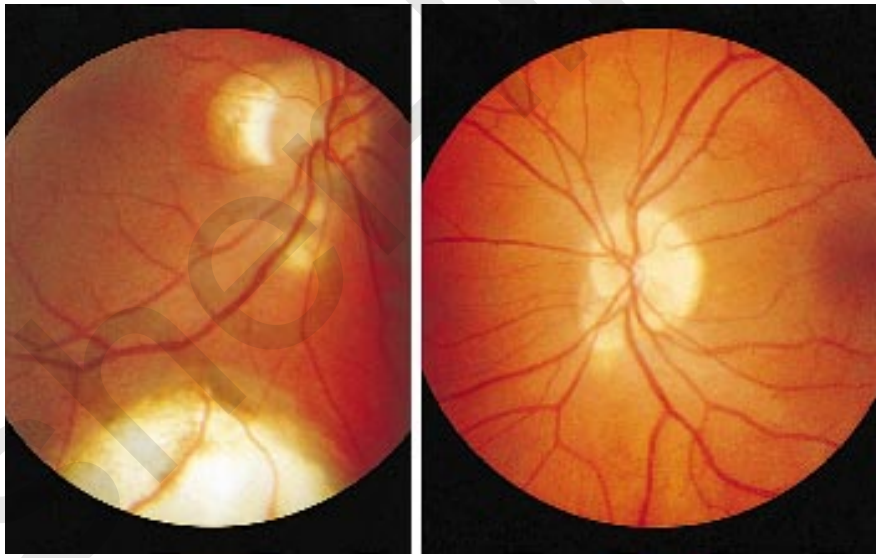

Figure 2.50. On the left is a minimal coloboma of the optic nerve with peripheral coloboma of the choroid and retina in another member of the same family. On the right is a very minimal coloboma of the choroid and retina adjacent to the normal optic nerve in a member of the same family who was totally unaware that she carried the gene for autosomal dominant colobomatous microphthalmia.

ANTERIOR SEGMENT
(Cornea, iris, and trabecular meshwork [glaucoma])

2.51

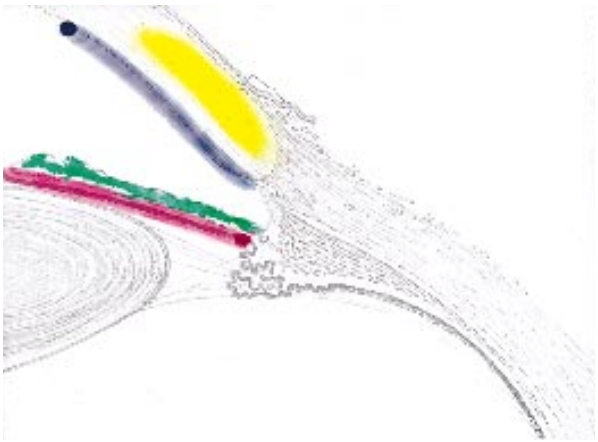

Figure 2.51. When the structures of the anterior segment are subdivided according to their embryonic layer of origin, various patterns emerge. In this figure, the neuroectoderm, consisting of the anterior rim of optic cup, iris pigment epithelium and pupillary musculature is shown in red; the 1st neural crest mesenchymal wave (corneal endothelium and trabecular meshwork) is shown in black; the 2nd neural crest mesenchymal wave (corneal stroma) is shown in yellow; and the 3rd neural crest mesenchymal wave (iris stroma) is shown in green.

2.52

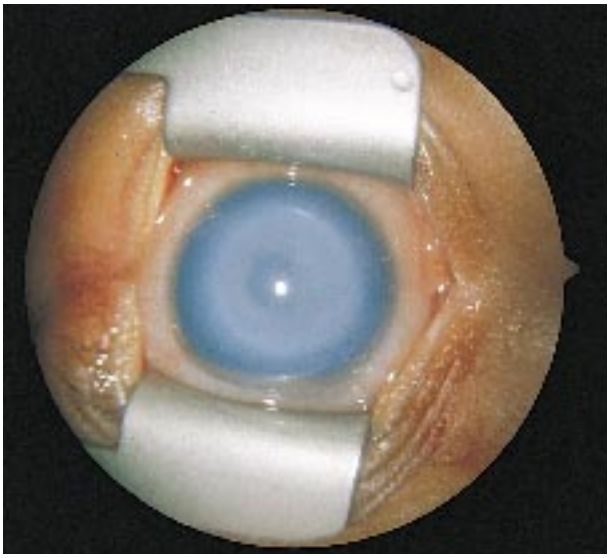

Figure 2.52. Peters anomaly is shown in this figure. Corneal clouding is marked because corneal endothelium is abnormal, and glaucoma is common because the trabecular meshwork may be altered. This photograph demonstrates severe corneal clouding which would justify a penetrating corneal transplant in at least one eye of a bilaterally affected infant even though the prognosis for a successful corneal transplant in infants is poor.

2.53

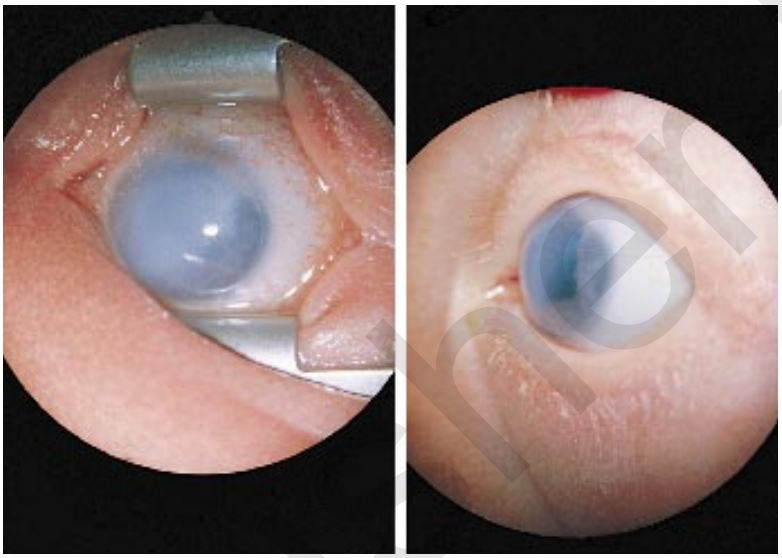

Figure 2.53. Anterior segment mesenchymal dysgenesis in one member of an autosomal dominant (4q28-31) family with variable expressivity is shown in this figure. On the left is an eye with a large area of severe corneal clouding. On the right, the same eye demonstrates the adhesions of the iris to the corneal endothelium.

2.54

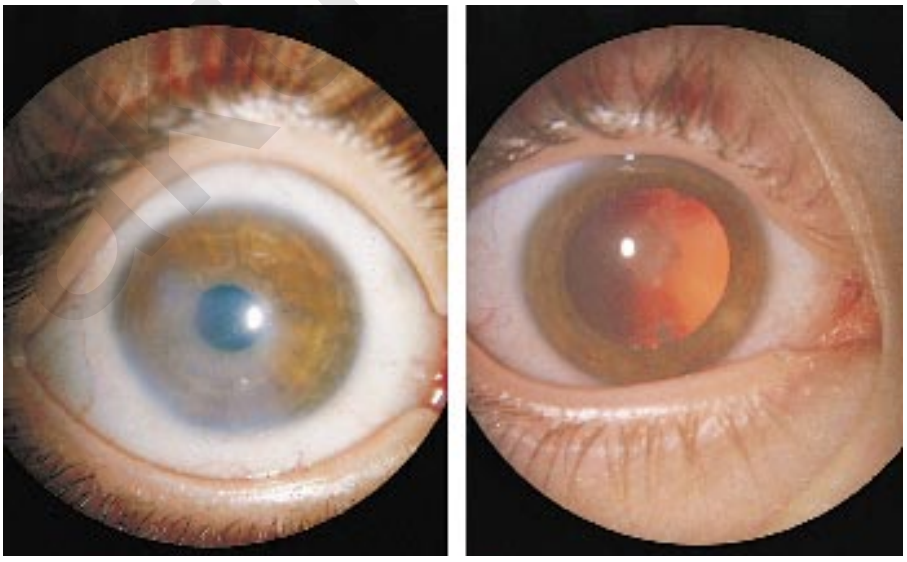

Figure 2.54. This figure shows anterior segment mesenchymal dysgenesis in members of the same family as in Figure 2.53. On the left is a smaller area of moderate corneal clouding, and on the right is a tiny area of minimal corneal opacity and a central cataract.

2.55

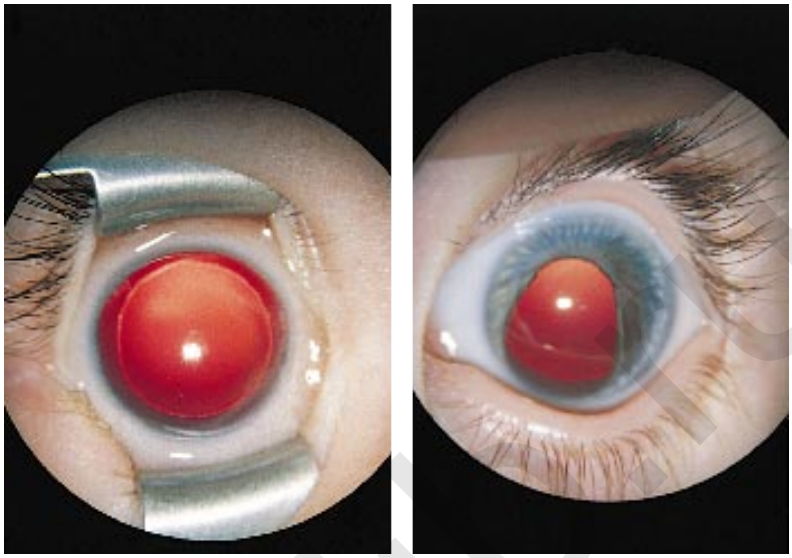

Figure 2.55. Aniridia in members of an autosomal dominant (11p13; PAX6) family with variable expressivity is shown in this figure. Neuroectodermal layers of the iris are abnormal. On the left is an eye with complete aniridia. On the right is an eye with an atypical (i.e., any location except inferonasal) iris coloboma.

2.56

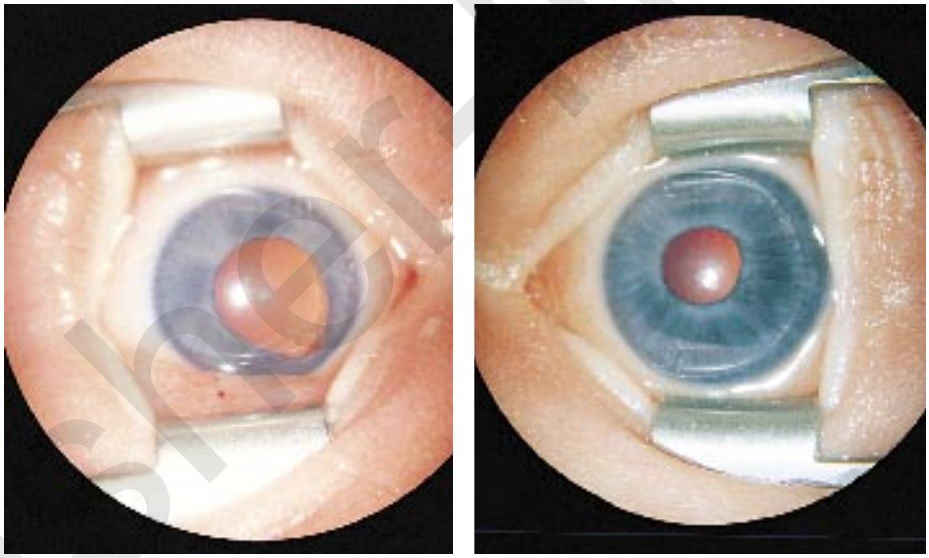

Figure 2.56. This figure shows aniridia in members of the same family, as in Figure 2.55. On the left is a typical (inferonasal location) iris coloboma. On the right is an eye with an eccentric round pupil with iris thinning and no iris collarette.

2.57

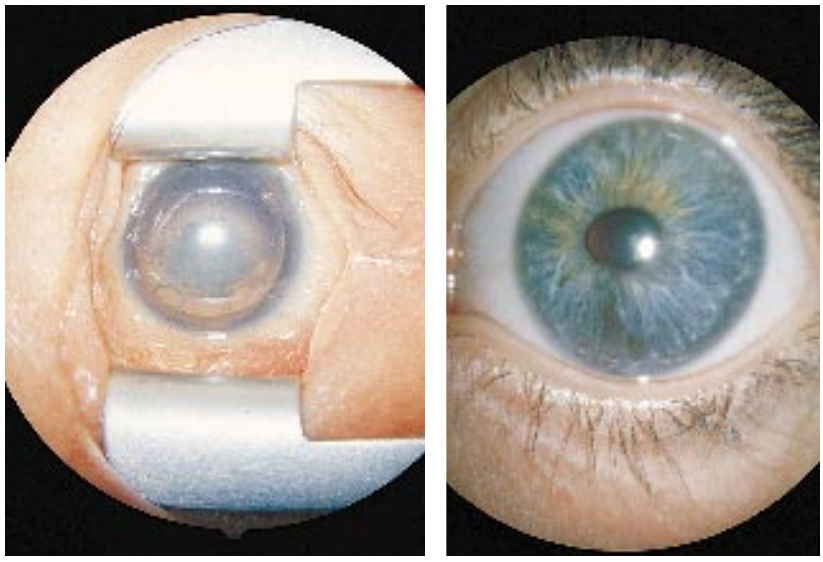

Figure 2.57. Aniridia also occurs as a deletion syndrome (del 11p13) known as the WAGR syndrome (*W*ilms' tumor, *A*niridia, *G*enitourinary anomalies, and mental *R*etardation). On the left is a nearly complete aniridia with minimal iris remnants and a dense cataract. On the right is a very minimal aniridia with an eccentric round pupil with iris thinning and no iris collarette.

2.58

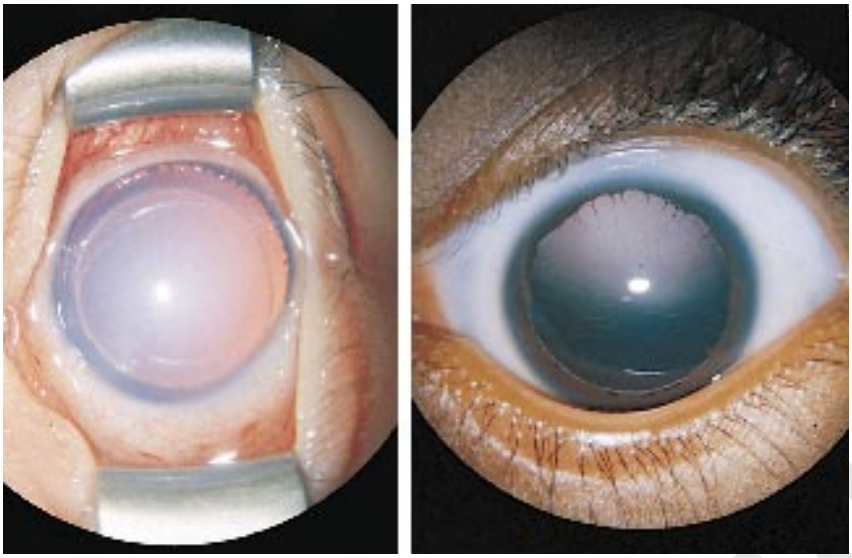

Figure 2.58. Aniridia with cerebellar malformation is an autosomal recessive disorder which seems to be associated with little variability in expression. On the left is a rather complete aniridia with corneal clouding due to glaucoma. On the right is another virtually complete aniridia with minimal iris remnants.

2.59

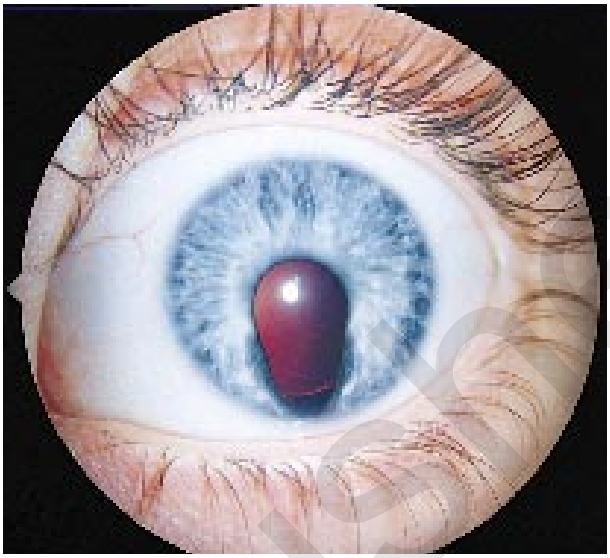

Figure 2.59. This figure shows a typical (inferonasal) isolated iris coloboma related to a failure of fusion of the optic cup at its most anterior extent. All iris structures are intact except in the inferonasal position.

2.60

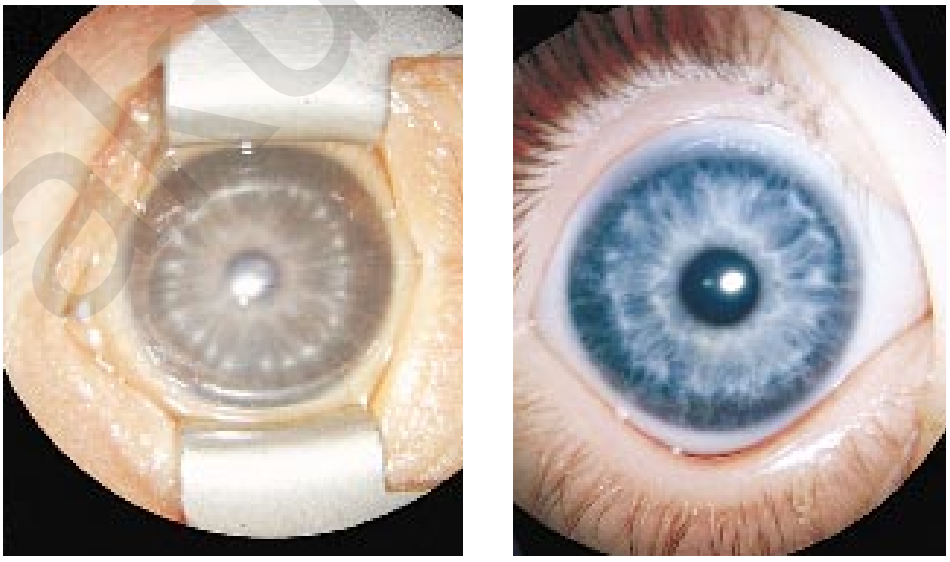

Figure 2.60. This figure demonstrates Brushfield's spots in an infant with brown irides which are pathognomonic for Down syndrome. In contrast, Brushfield's spots in an infant with blue irides is a nonspecific finding of many blue irides.

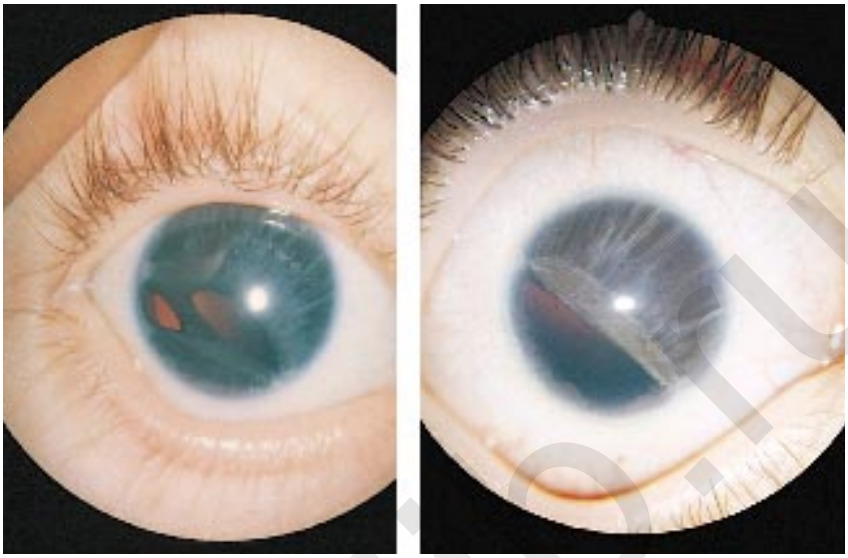

2.61

Figure 2.61. Rieger's syndrome is an autosomal dominant (4q23-q27) disorder with abnormal irides, associated with an abnormal umbilicus and malformed teeth. Abnormal iris stroma is present, and glaucoma is common. Families may exhibit variable expressivity. On the left is an eye with polycoria, dyscoria, and correctopia present at birth. On the right is the same eye several years later demonstrating early glaucoma due to progressive obliteration of the chamber angle by adhesions of the iris to an anterior Schwalbe's line.

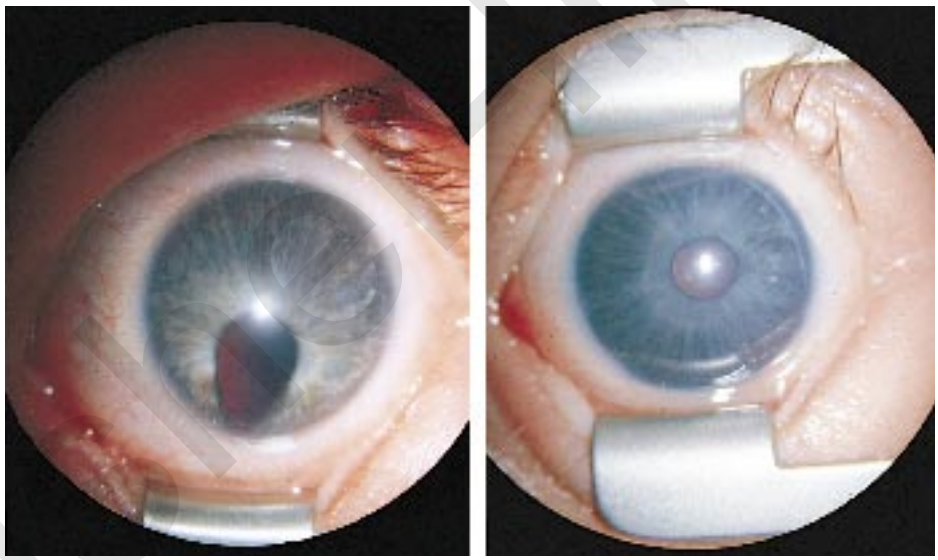

2.62

Figure 2.62. This figure demonstrates less severe anomalies of the anterior segment. On the left is an eye with dyscoria and correctopia which was present at birth resembling an iris coloboma due to a small iris adhesion to an anterior Schwalbe's line. On the right is an eye with a central pupil, which is fortuitous since glaucoma is less likely to occur in eyes with central pupils.

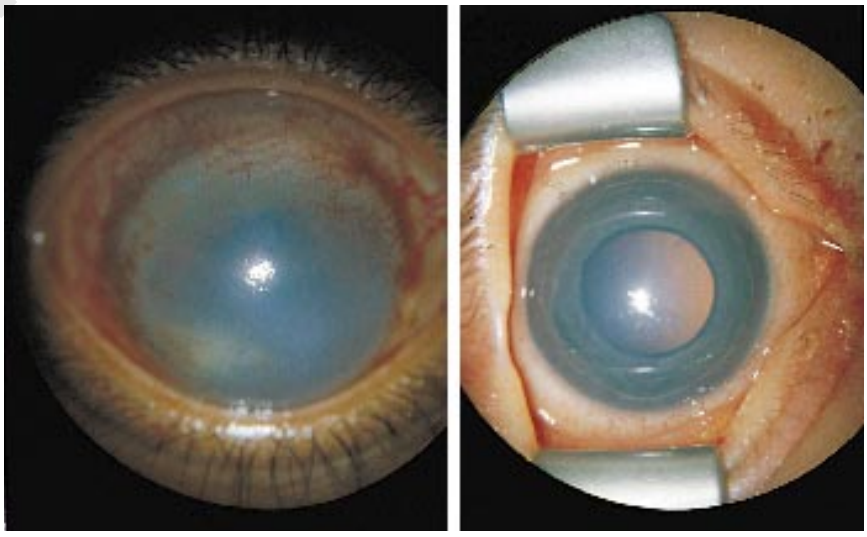

2.63

Figure 2.63. This figure shows members of a family with autosomal dominant pseudo-Rieger's syndrome which has been associated with an abnormal pituitary or an empty sella in some affected family members. An abnormal iris stroma is present and glaucoma is common. Families may exhibit variable expressivity. On the left is an eye with end stage glaucoma with secondary corneal clouding. On the right is an eye with early glaucoma with abnormal adhesions of the iris to an anterior Schwalbe's line extending 360 degrees.

2.64

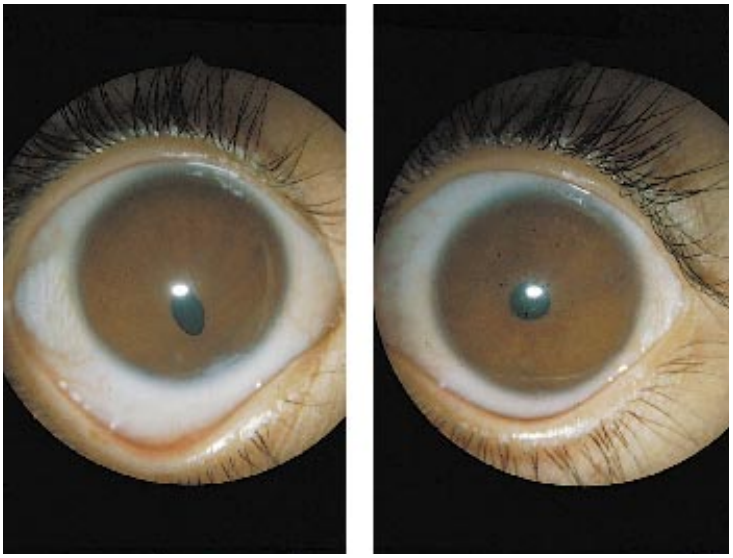

Figure 2.64. Anterior segments in members of the same family with pseudo-Rieger's syndrome are shown as in Figure 2.63. On the left is an eye with an eccentric pupil resembling an iris coloboma due to a small iris adhesion to an anterior Schwalbe's line. On the right is an eye with a central pupil which does not have an associated glaucoma.

2.65

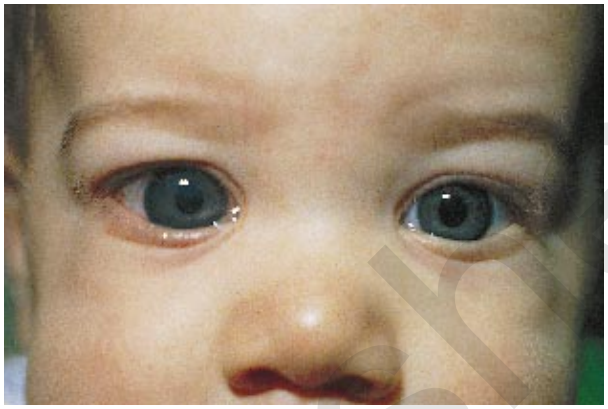

Figure 2.65. This infant demonstrates the asymmetrical eye size seen with unilateral glaucoma which is an autosomal recessive disorder. Megalocornea (a constant enlarged corneal diameter present at birth) must be considered in patients with bilateral glaucoma (a corneal enlargment which is progressive up to age 2 years). In megalocornea, the intraocular pressure is not increased. Glaucoma usually presents with excessive tearing, photophobia, and corneal clouding.

2.66

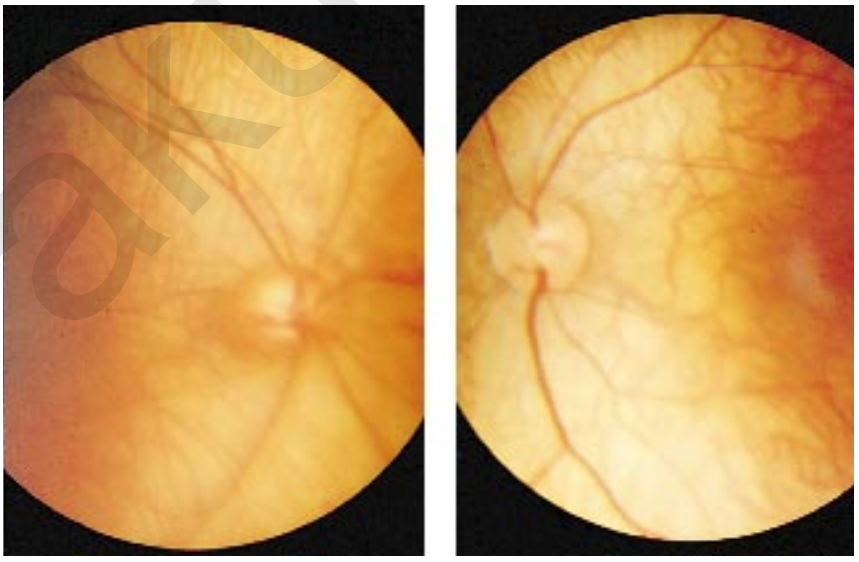

Figure 2.66. These photographs are of the optic nerves of the infant shown in Figure 2.65. The optic nerves reveal asymmetrical cupping reflecting the increased intraocular pressure in the right eye (figure left) and the normal intraocular pressure in the left eye (figure right).

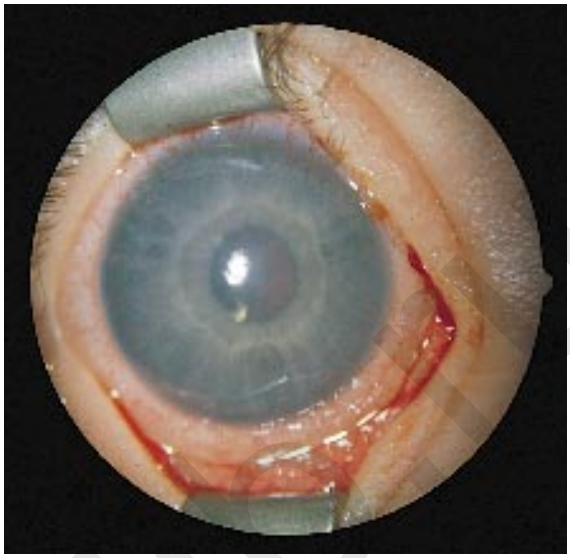

2.67

Figure 2.67. The affected eye of the same infant as in Figure 2.66 demonstrates the corneal enlargement and clouding secondary to corneal edema.

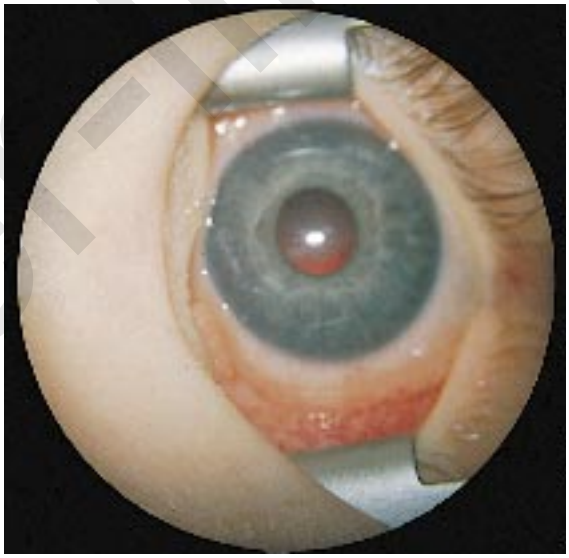

2.68

Figure 2.68. This figure is of the unaffected eye of the same infant. The asymmetry is extremely important in detecting glaucoma in early cases.

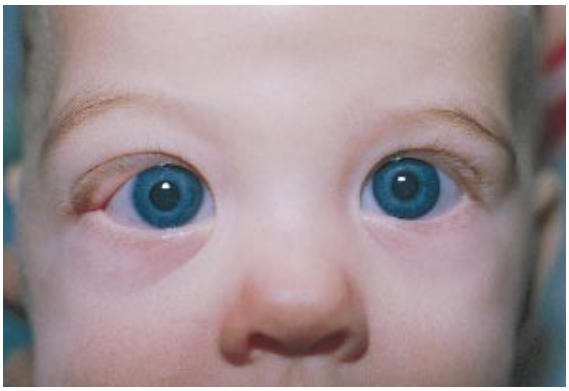

2.69

Figure 2.69. This infant has neurofibromatosis which is an autosomal dominant (Type 1, 17q11.2; Type 2, 22q11.2-q13) disorder. The asymmetrical eye size demonstrated is due to glaucoma. The thickening of the right upper temporal lid is a plexiform neuroma which is pathognomonic for neurofibromatosis.

2.70

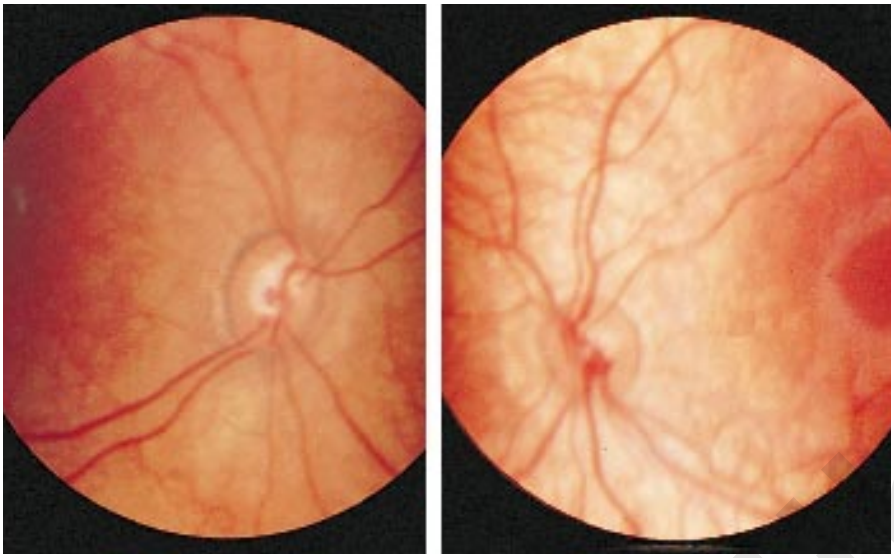

Figure 2.70. These photographs are of the optic nerves of the patient in Figure 2.69. The optic nerves reveal asymmetrical cupping, reflecting the increased intraocular pressure in the right eye (on the left) and the normal intraocular pressure in the left eye (on the right).

2.71

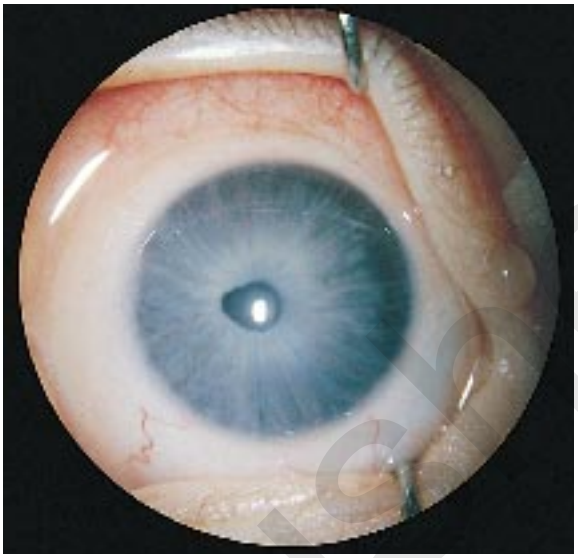

Figure 2.71. The affected eye of the same infant exhibits minimal corneal enlargement, clouding secondary to corneal edema, and ectropion uvea with displacement of the pupil temporally.

2.72

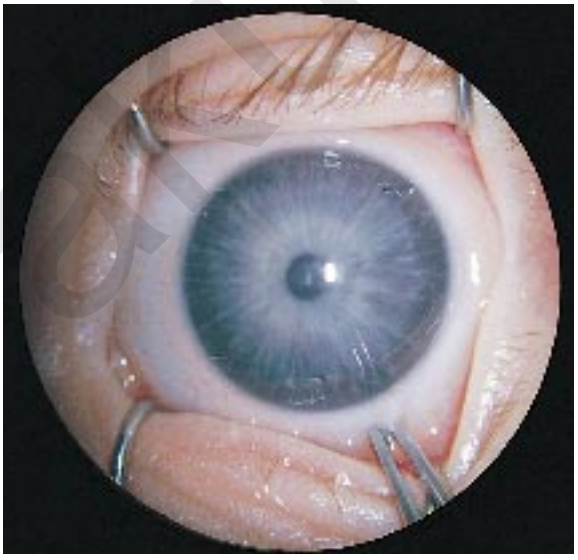

Figure 2.72. This photograph is of the unaffected eye of the same infant showing a clear cornea and central pupil. Again, the asymmetry is very important in diagnosing this glaucoma early.

2.73

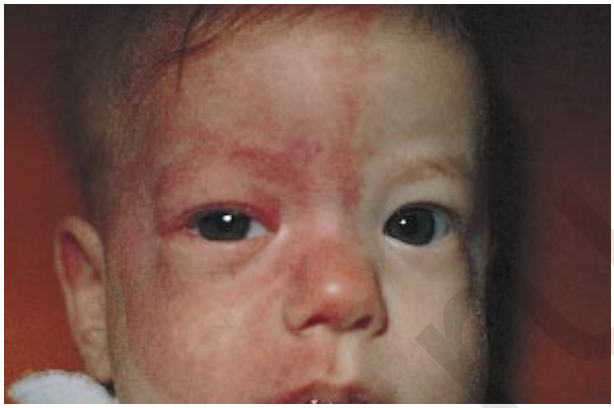

Figure 2.73. This infant has Sturge-Weber syndrome with glaucoma. The unilateral facial hemangioma is pathognomonic for Sturge-Weber syndrome, and the involvement of the upper lid and conjunctiva is associated with choroidal hemangiomas and secondary glaucoma.

2.74

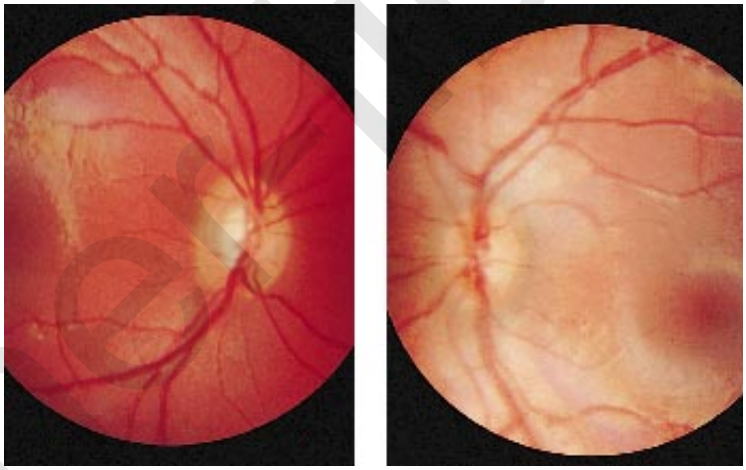

Figure 2.74. The photographs of the optic nerves in the same infant as shown in Figure 2.73 demonstrate the asymmetrical cupping reflecting the increased intraocular pressure in the right eye (on the left) and the normal intraocular pressure in the left eye (on the right).

2.75

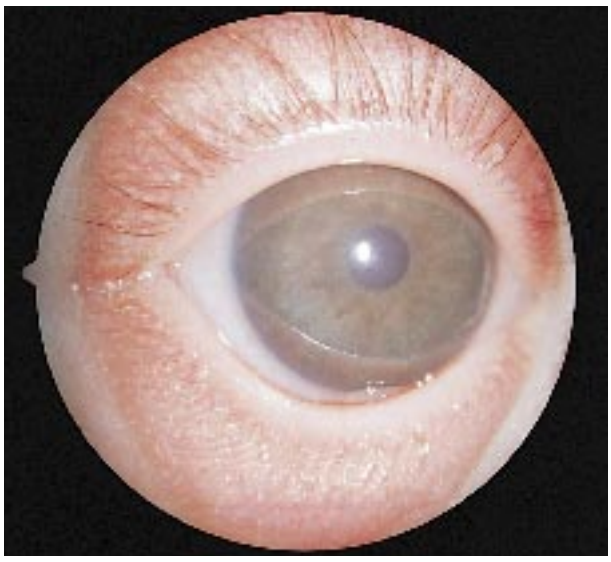

Figure 2.75. The affected eye of the same patient demonstrates minimal corneal enlargement, clouding secondary to corneal edema, and erythema of the conjunctiva reflecting the presence of a choroidal hemangioma.

2.76

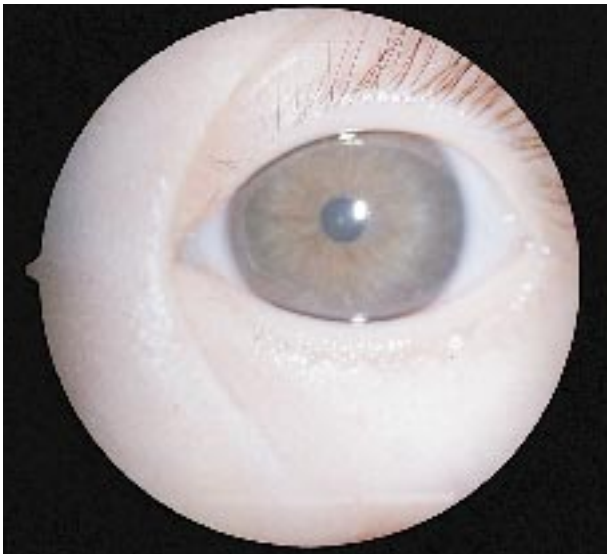

Figure 2.76. Note the clear white conjunctiva in the unaffected eye of the same infant as in Figures 2.73-2.75.

2.77

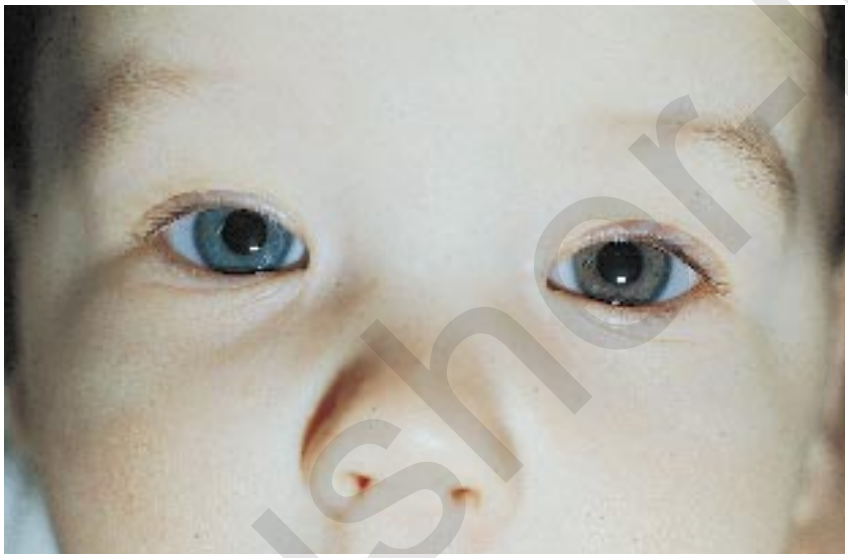

Figure 2.77. This patient demonstrates heterochromia of the irides which is occasionally seen in tuberous sclerosis, an autosomal dominant (9q33-34; 16p13) disorder. Sector iris pigmentation is also seen in tuberous sclerosis due to abnormal neural crest migration of melanocytes into the iris stroma.

2.78

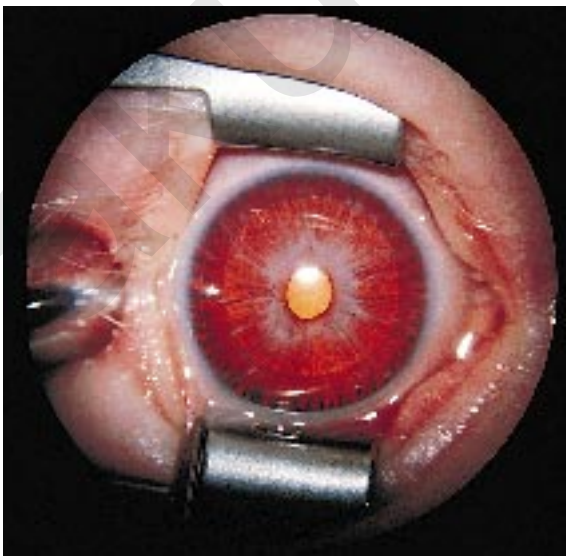

Figure 2.78. Oculocutaneous albinism is complete albinism with a lack of pigmentation in the eye and skin and is inherited as an autosomal recessive (tyrosinase deficiency; 11q14-q21) disorder. The iris pigment epithelium contains no melanin, and the iris has no color. Thus, the iris has a pink color, and the hair is totally white. This form of albinism is distinct from ocular or incomplete albinism with a partial lack of pigment in the eye and skin which is inherited as an X-linked recessive (Xp22.3) disorder. The iris pigment epithelium contains less melanin, and the iris has a light color. Thus, the iris is usually blue, and the hair is blond.

LENS

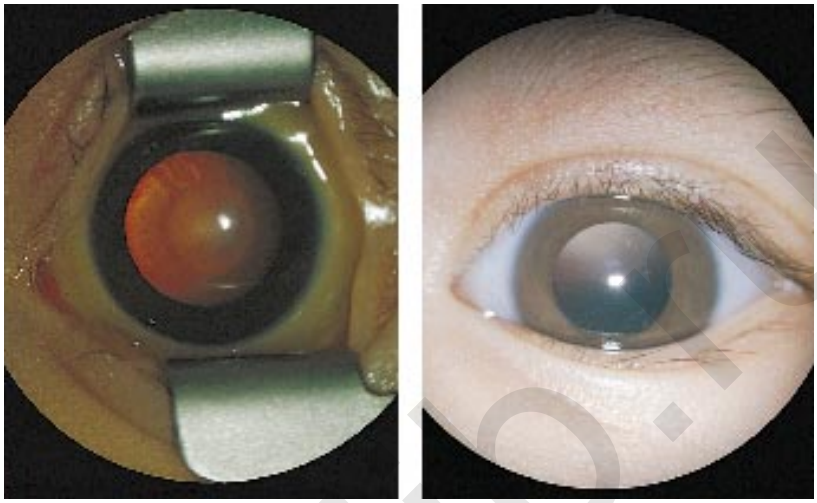

2.79

Figure 2.79. The cataract shown on the left is a classical "oil drop" cataract present at birth in an infant with galactosemia which is an autosomal recessive (galactokinase deficiency; 9p13) disorder. On the right, the same eye is shown several years later with the cataract almost completely gone after years of good dietary control.

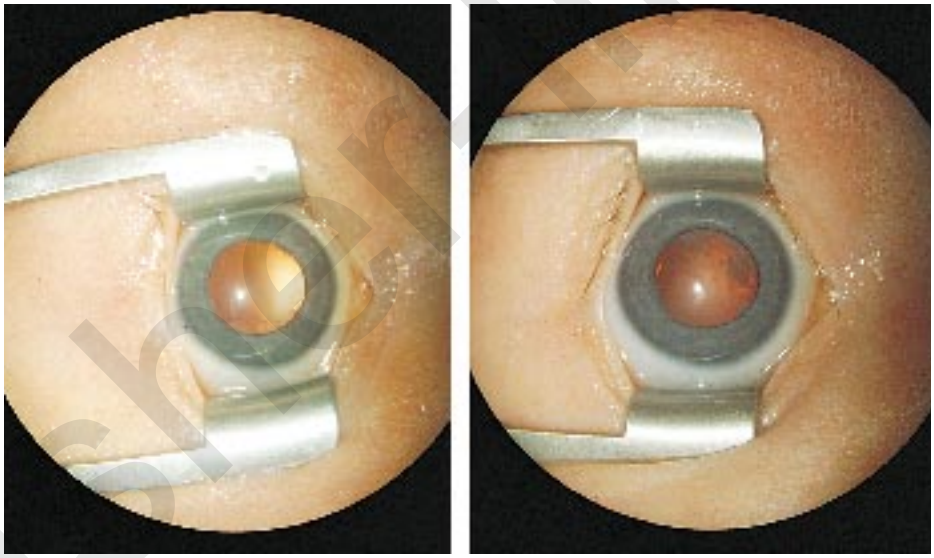

2.80

Figure 2.80. The Hallermann-Streiff syndrome is an autosomal dominant syndrome which is associated with hypotrichosis, mandibular hypoplasia, beaked nose, and endocephaly. The figure on the left demonstrates an early cataract in a child with the Hallermann-Streiff syndrome. The figure on the right is of the same eye a few weeks later showing progression to a dense cataract requiring surgery.

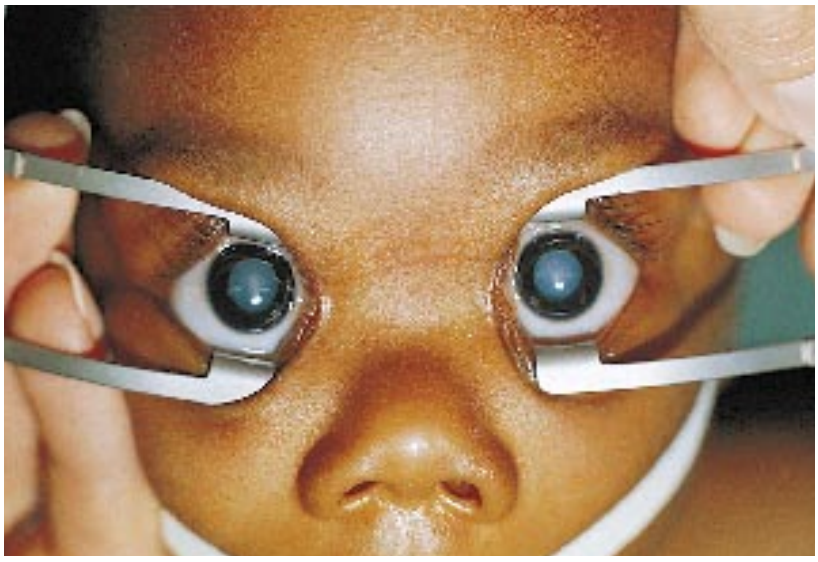

2.81

Figure 2.81. Dense bilateral cataracts represent an "ocular emergency" since immediate referral can result in normal vision (20/20) and stereoacuity. This perfect result cannot be obtained if surgery with optical correction has not been completed by the age of 6 weeks following birth.

2.82

Figure 2.82. This is the same patient shown in Figure 2.81 following bilateral removal of cataracts and immediate fitting with aphakic contact lenses. The infant developed perfect vision and binocular fusion.

2.83

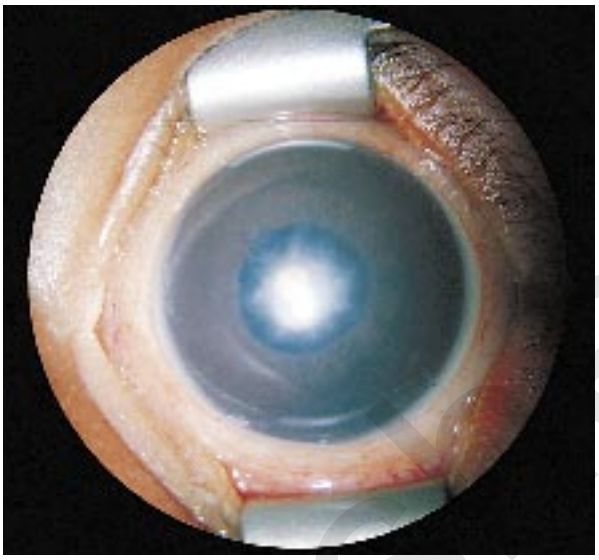

Figure 2.83. Cataracts are present in Lowe syndrome (oculocerebrorenal syndrome) which is an X-linked recessive disorder (Xq25). In this syndrome, glaucoma is also frequently present.

2.84

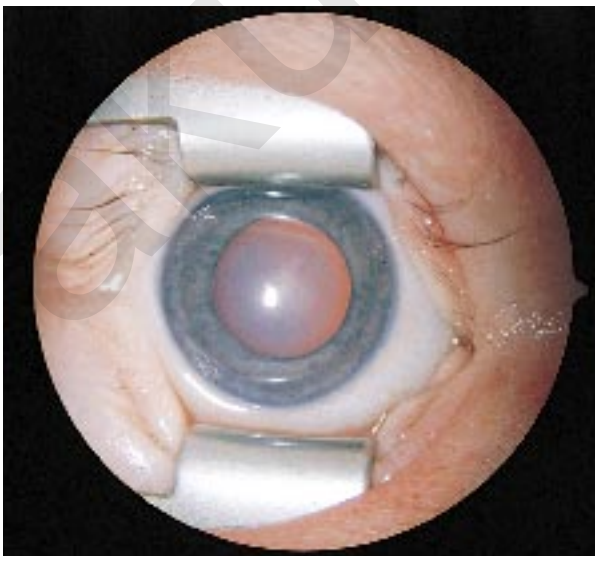

Figure 2.84. In the rhizomelic chondrodysplasia punctata syndrome, an autosomal recessive disorder, cataracts are frequently present.

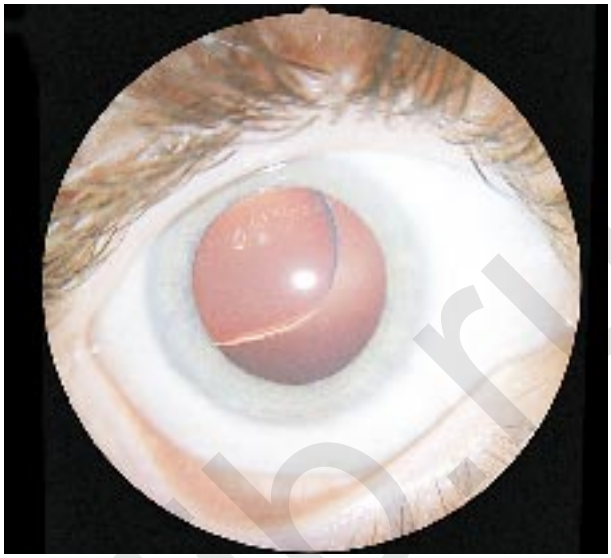

2.85

Figure 2.85. The lens is dislocated superotemporally in the infant with Marfan syndrome which is an autosomal dominant (15q15-21) disorder.

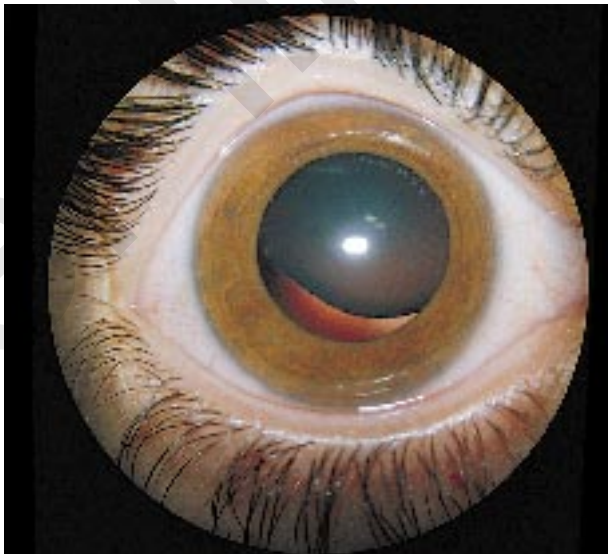

2.86

Figure 2.86. Homocystinuria is an autosomal recessive (cystathionine ß-synthetase deficiency; 21q22) disorder which is associated with lenses usually dislocated inferiorly. Patients are tall, have osteoporosis, arachnodactyly, and mental retardation.

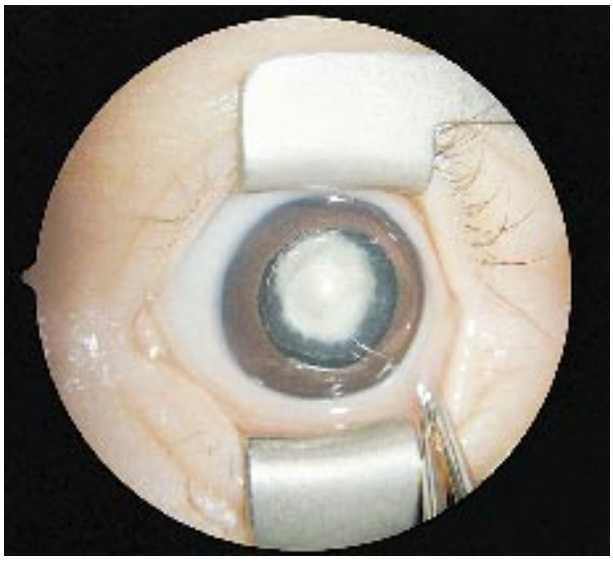

2.87

RETINA-VITREOUS

Figure 2.87. Persistent hyperplastic primary vitreous (PHPV) results from a failure of the embryonic hyaloid artery system to involute. In this eye, the persistence is primarily anterior with formation of a large cataract.

2.88

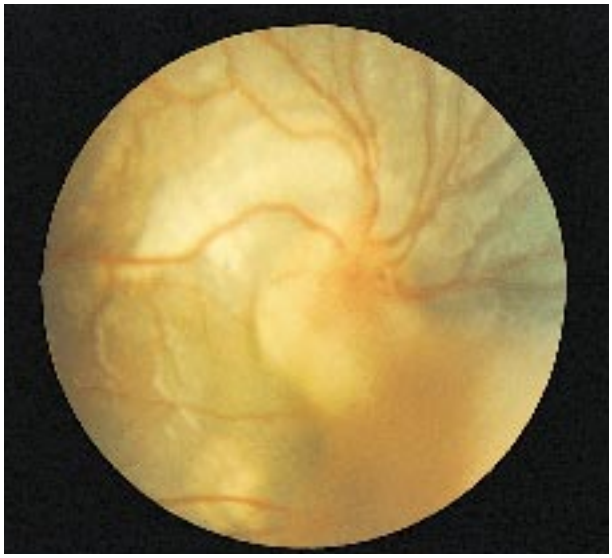

Figure 2.88. In this eye, the PHPV is primarily posterior with the presence of a large stalk to the optic nerve.

2.89

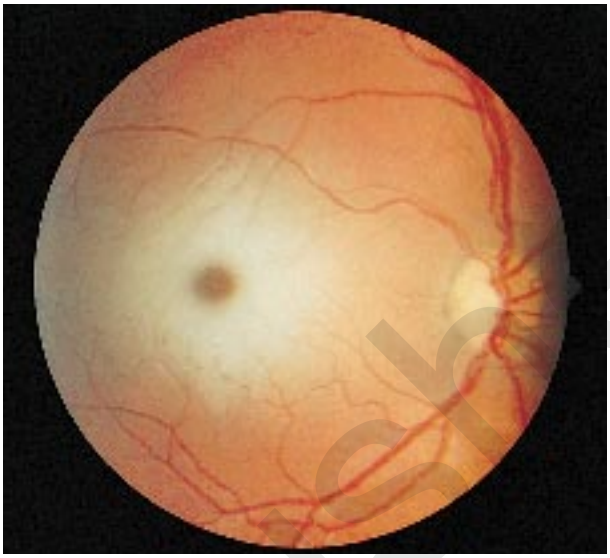

Figure 2.89. Tay-Sachs disease (GM_2 gangliosidosis Type I) is an autosomal recessive (12q22-25) disorder which develops a macular cherry-red spot due to deposition of abnormal lipid in the ganglion cell layer of the inner retina surrounding the normal macula.

2.90

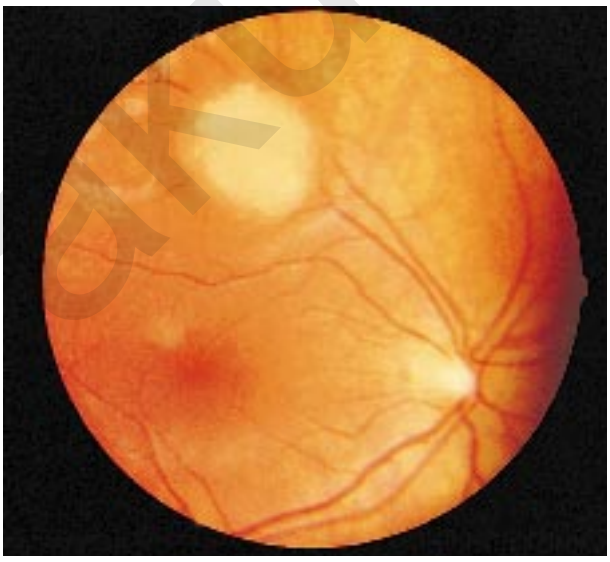

Figure 2.90. Tuberous sclerosis is an autosomal dominant (9q33-34, 16p13) disorder of neural crest origin. This figure shows a retinal astrocytic hamartoma.

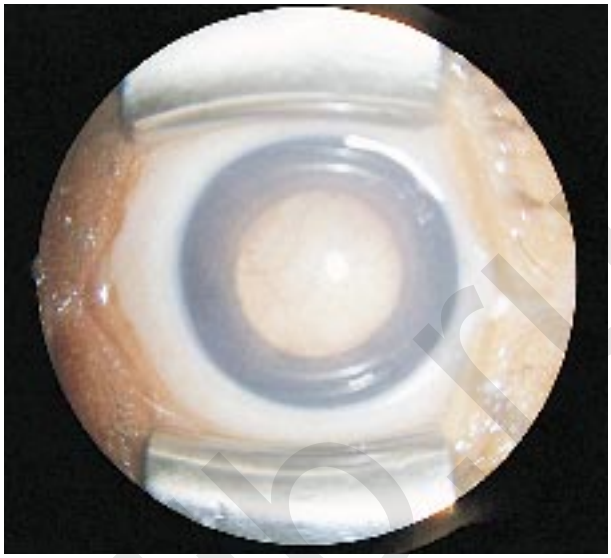

2.91

Figure 2.91. Retinoblastoma is an autosomal dominant (13q14) disorder which usually occurs without mental retardation or other systemic malformations. This is a left eye with a large tumor treated by enucleation. The differential diagnosis includes all causes of leukocoria (white pupil) including congenital cataracts, persistent hyperplastic primary vitreous, cicatricial retinopathy of prematurity, and the entities in the differential diagnosis of cicatricial retinopathy of prematurity.

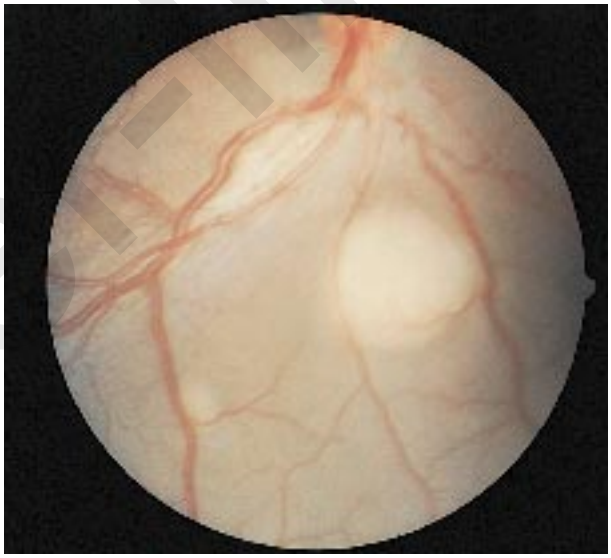

2.92

Figure 2.92. The right eye of the same patient as shown in Figure 2.91. These small tumors were treated with phototherapy.

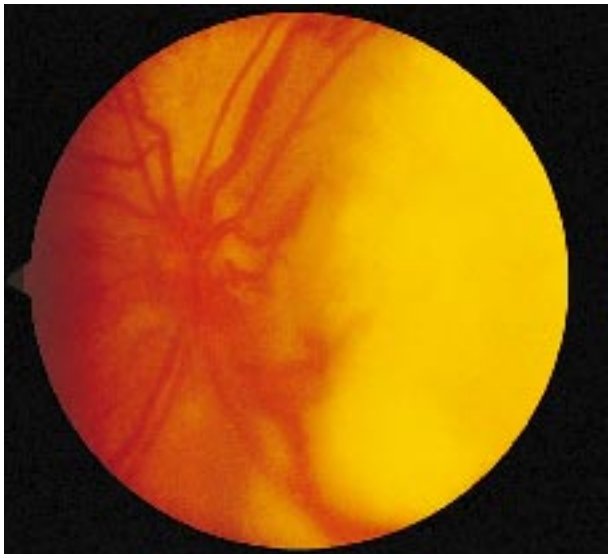

2.93

Figure 2.93. Retinoblastoma also occurs as a deletion syndrome (del 13q14) with mental retardation and other systemic malformations. This is a left eye with a large tumor treated by enucleation.

2.94

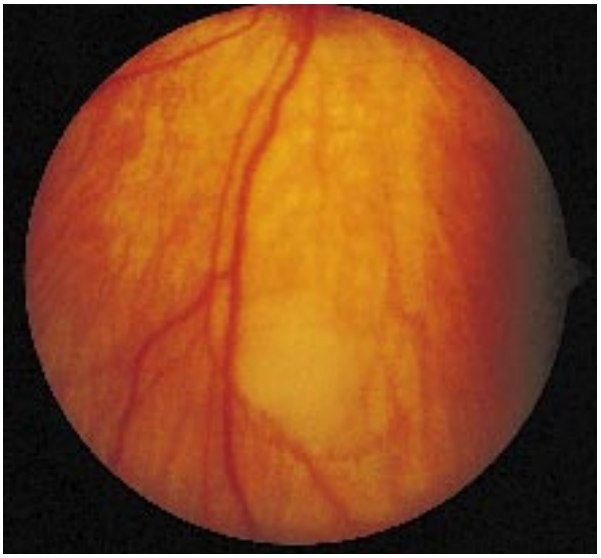

Figure 2.94. This is the right eye of the patient shown in Figure 2.93. This small tumor was treated by cryotherapy. Currently, episcleral plaque radiotherapy and carboplatin chemotherapy are used to treat small ocular tumors, especially when preservation of useful vision is possible.

RETINOPATHY OF PREMATURITY

Active Retinopathy of Prematurity

There are three parameters to the classification system known as the International Classification of Active Retinopathy of Prematurity (ICROP): location of the disease (zone), extent of the disease (clock hours), and severity of abnormal vascular response (stage). Screening for active retinopathy of prematurity should begin after 4 weeks but before 6 weeks following birth. The critical time for screening is from 32 to 42 weeks postconceptual age. Follow-up examinations vary depending on the clinical findings.

2.95

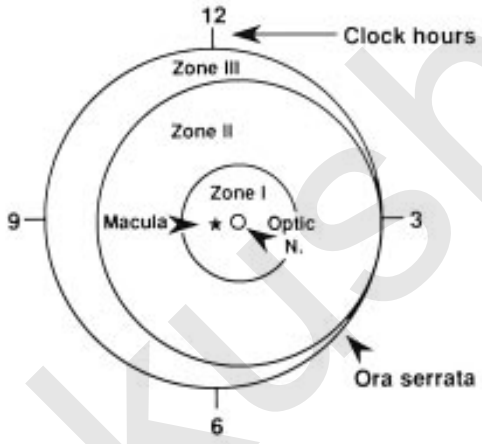

Figure 2.95. The location (zone) and extent (clock hours) of the disease must be drawn on a form similar to this.

2.96

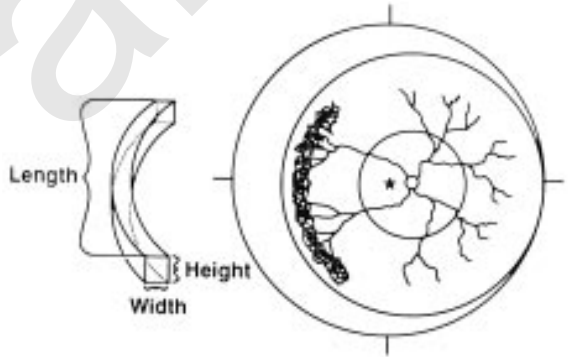

Figure 2.96. The volume (stage) of abnormal vascular response (ridge with or without extravascular fibrovascular proliferation) must be indicated for each clock hour. The location of this volume and vascular engorgement of the posterior inner retinal vessels determine when surgical intervention must be initiated.

2.97

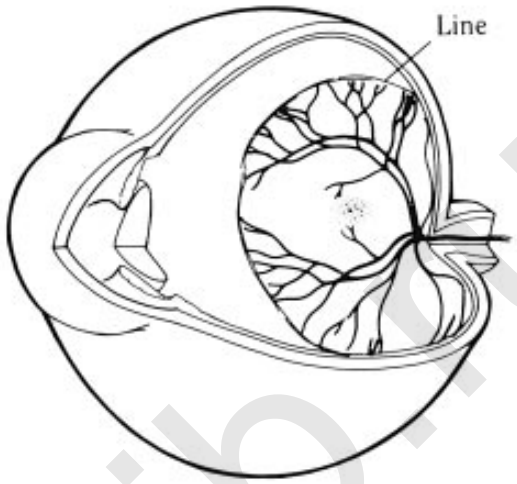

Figure 2.97. This figure depicts active retinopathy of prematurity: stage 1 (demarcation line).

2.98

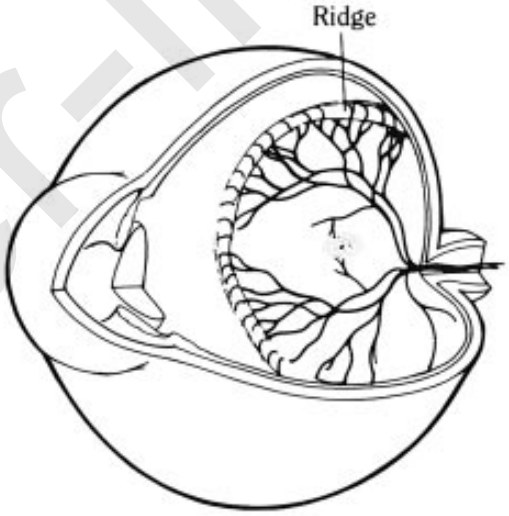

Figure 2.98. This figure depicts active retinopathy of prematurity: stage 2 (ridge).

2.99

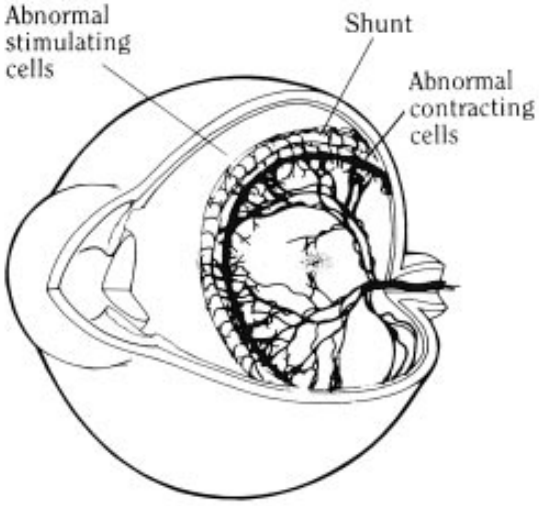

Figure 2.99. This figure depicts active retinopathy of prematurity: stage 3 (ridge with extraretinal fibrovascular proliferation).

2.100

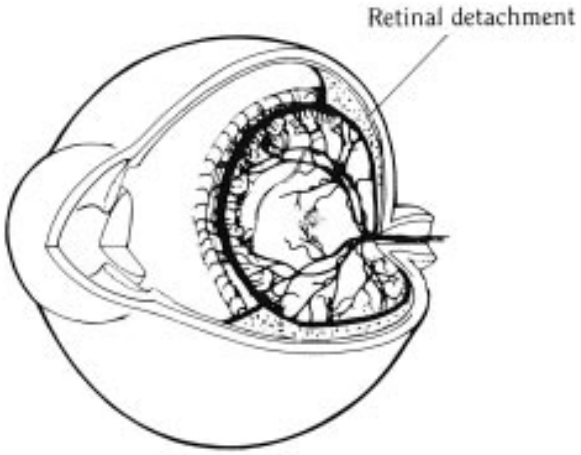

Figure 2.100. This figure depicts active retinopathy of prematurity: stage 4a (partial retinal detachment not involving the macula). More severe forms of retinal detachment (not shown) are stage 4b (partial retinal detachment involving the macula) and stage 5 (total retinal detachment).

2.101

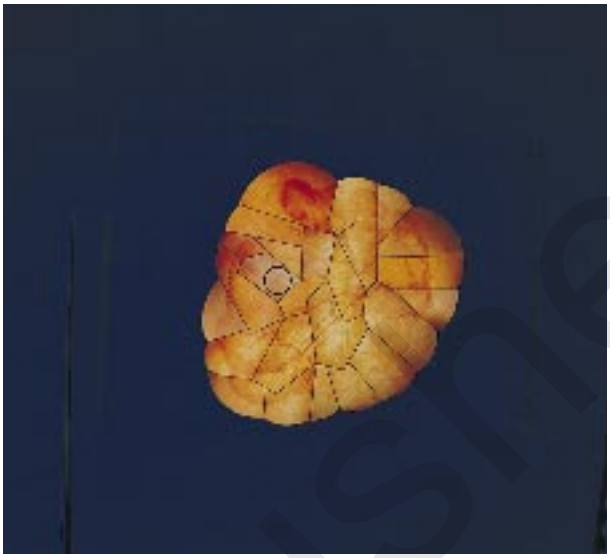

Figure 2.101. In this retinal montage there is zone I retinopathy of prematurity (stage 3 with plus disease). The same magnification is used in all four of the ROP montages.

2.102

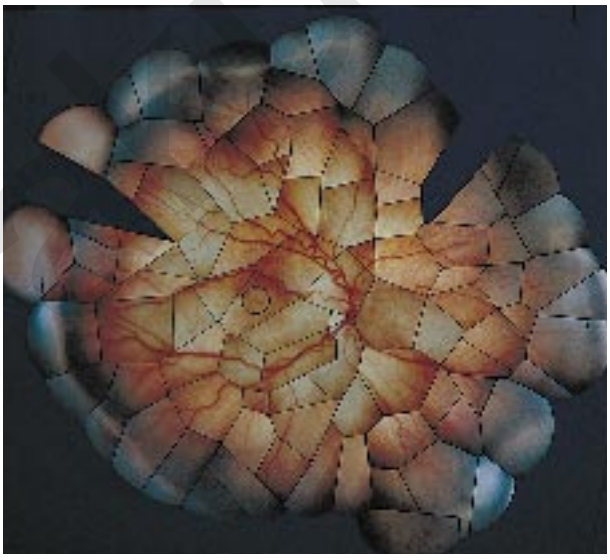

Figure 2.102. A retinal montage which shows zone II retinopathy of prematurity (stage 4a with plus disease).

2.103

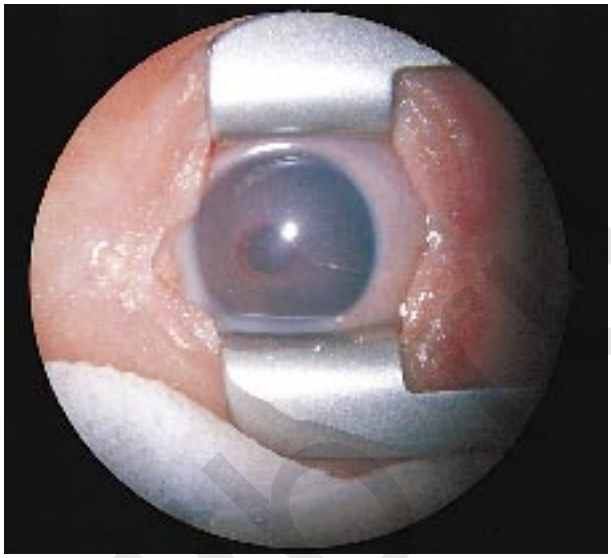

Figure 2.103. In this photograph note the vessels of the iris collarette which are engorged, making dilatation of the pupil difficult.

2.104

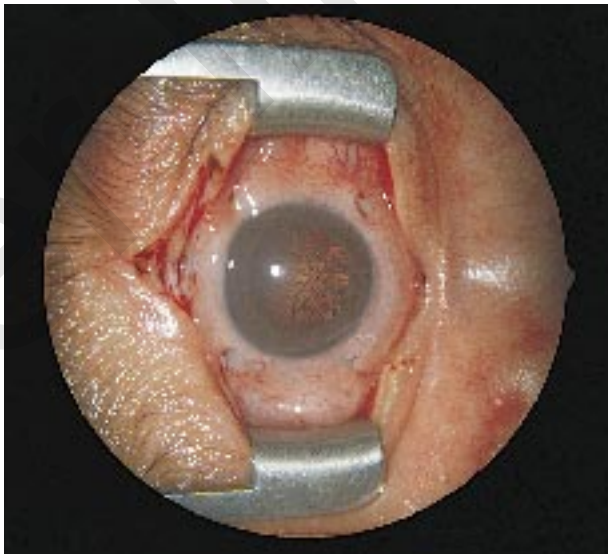

Figure 2.104. A persistent and engorged tunica vasculosa lentis occurs in those infants who are very immature and develop severe active retinopathy of prematurity.

Cicatricial (Spontaneous Regression) Retinopathy of Prematurity

The anatomical macular outcome which correlates with final visual acuity is measured by two parameters: macular ectopia and vessel traction.

2.105

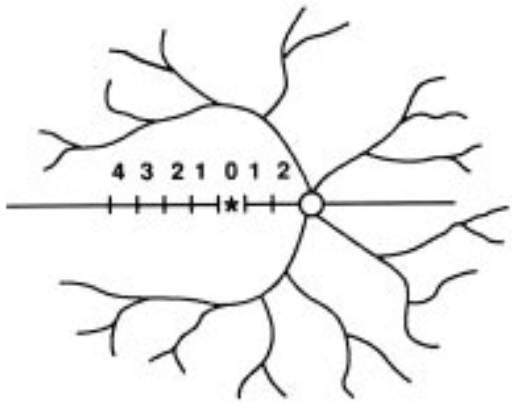

Figure 2.105. This is the grading system for macular ectopia. The normal macular position is between 2 and 3 disc diameters from the temporal margin of the optic disc. The numbering system is shown.

2.106

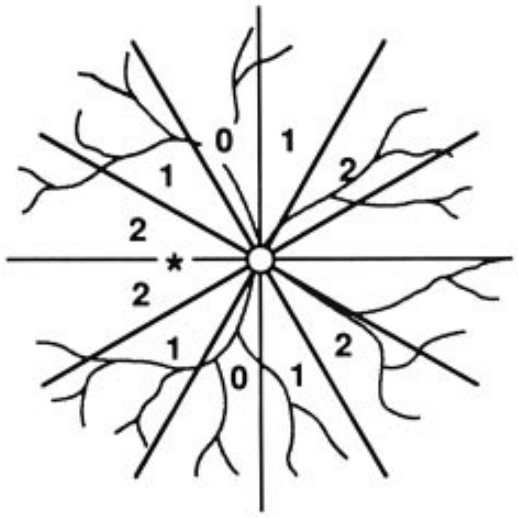

Figure 2.106. In the grading system for vessel traction, the normal position of retinal vessels for the first two disc diameters is between the vertical meridian and the 30 sectors temporal to the vertical meridian. The numbering system is shown.

2.107

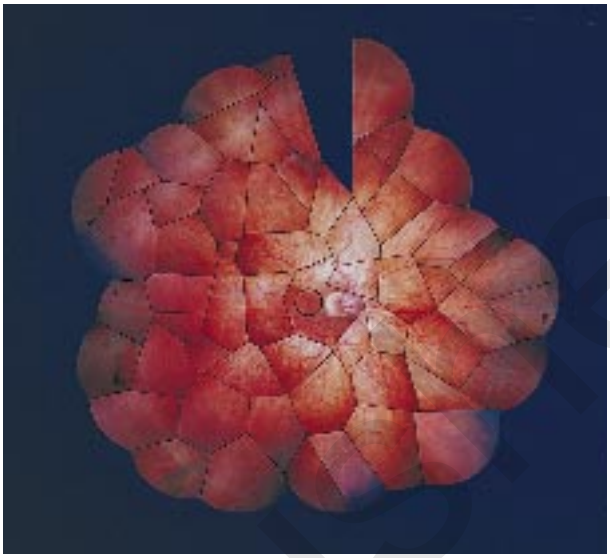

Figure 2.107. This retinal montage shows nasal dragging of the macula with macular ectopia of 2 and vessel traction of 1. Vision is 20/400.

2.108

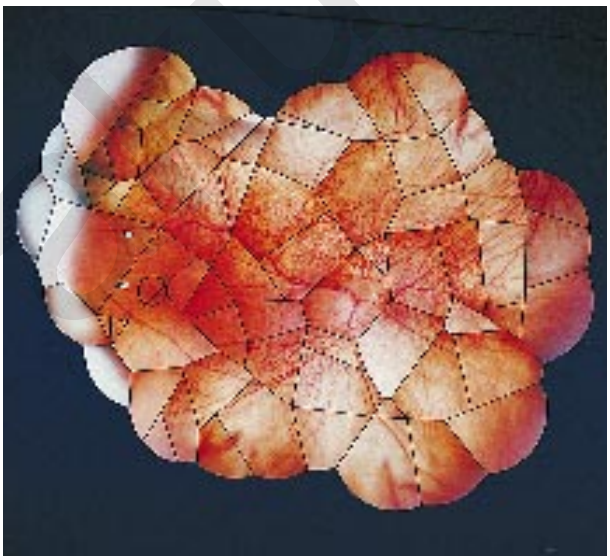

Figure 2.108. In this retinal montage note the temporal dragging of the macula with macular ectopia of 4 and vessel traction of 2. Vision is 20/400.

2.109

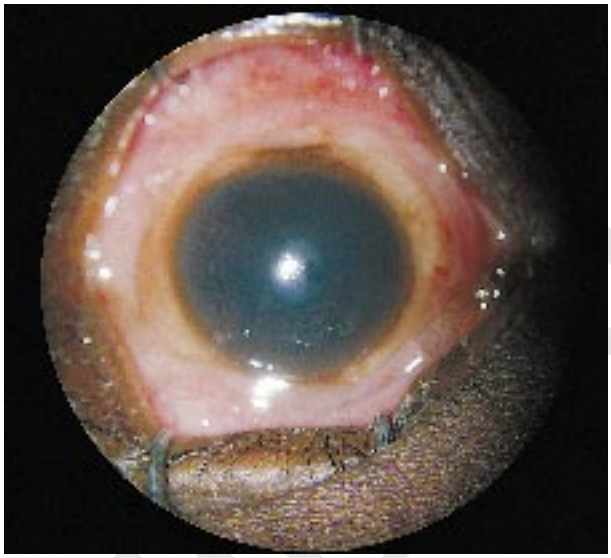

Figure 2.109. An angle closure glaucoma is a common complication of very severe ROP. Conjuctival erythema, corneal clouding, a nondilatable pupil, and a flat anterior chamber are present.

2.110

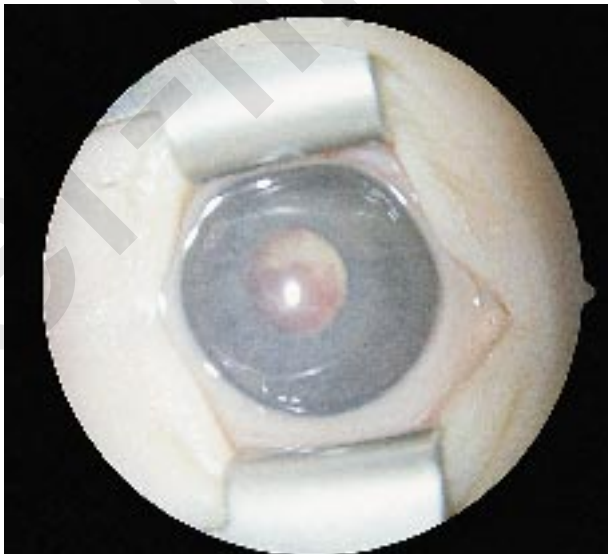

Figure 2.110. In complete retinal detachment there is a fibrovascular mass behind the lens which provided the original name for retinopathy of prematurity: "RLF" or retrolental (behind the lens) fibroplasia (fibrovascular mass).

Differential Diagnosis for Retinopathy of Prematurity

A. Abnormal neuroectodermal migration or differentiation of the retina (from inner to outer layers) can be associated with abnormal migration or differentiation of the central nervous system as in the following examples.

2.111

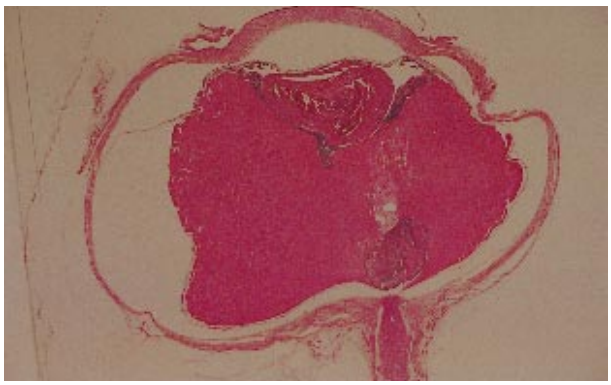

Figure 2.111. Walker-Warburg syndrome is an autosomal recessive disorder with absence of the normal cascade of retinal differentiation reflected in abnormal development of all retinal layers. Remnant retina is "retrolental" (behind the lens) and lissencephaly is present in the central nervous system.

2.112

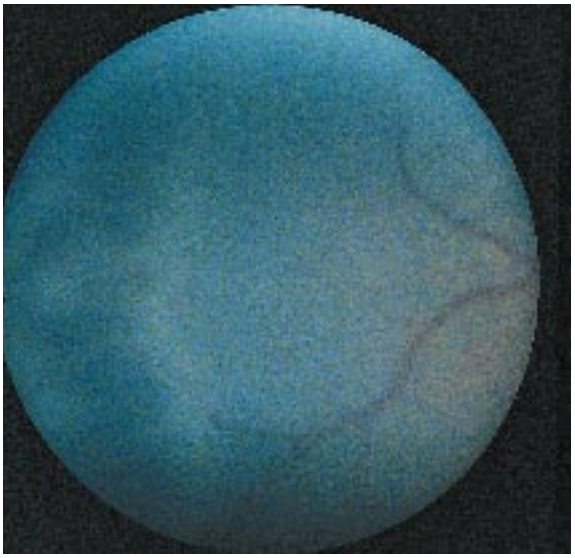

Figure 2.112. The Dandy-Walker deformity with a posterior encephalocele is another autosomal recessive disorder which demonstrates the absence of the normal cascade of retinal differentiation in the retinal periphery.

2.113

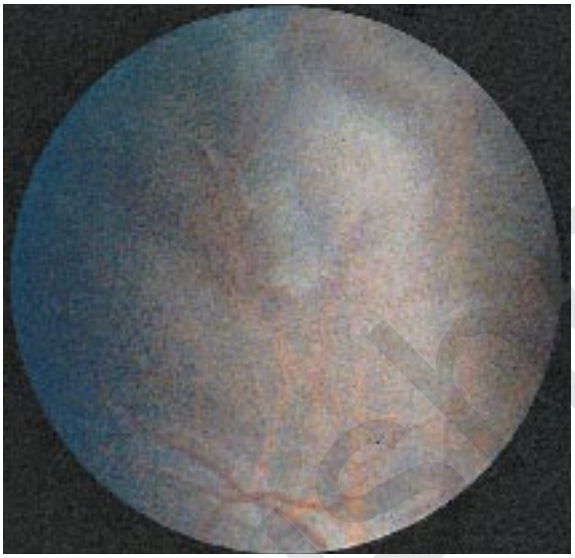

Figure 2.113. Stickler syndrome is an autosomal dominant (12q13) disorder which may be diagnosed in the newborn period by recognizing the association between the Robin's anomalad of cleft palate, small mandible, and backward displacement of the tongue. A progressive arthropathy can be identified radiographically. The Kniest syndrome may be an autosomal recessive disorder of the same gene. Abnormal thinning of the peripheral retina which precedes giant retinal tears is seen in these retinas.

2.114

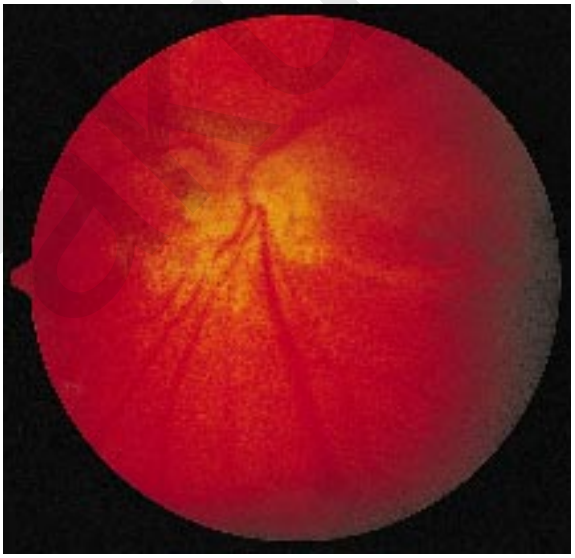

Figure 2.114. Juvenile retinoschisis is an X-linked recessive (Xp22) disorder which can present with peripheral and/or foveal involvement. Clinically this is seen as vitreous veils and strands with retinal detachment peripherally and/or a star-shaped or spoke-like configuration in the fovea. Splitting of the nerve fiber layer in the inner retina is present pathologically.

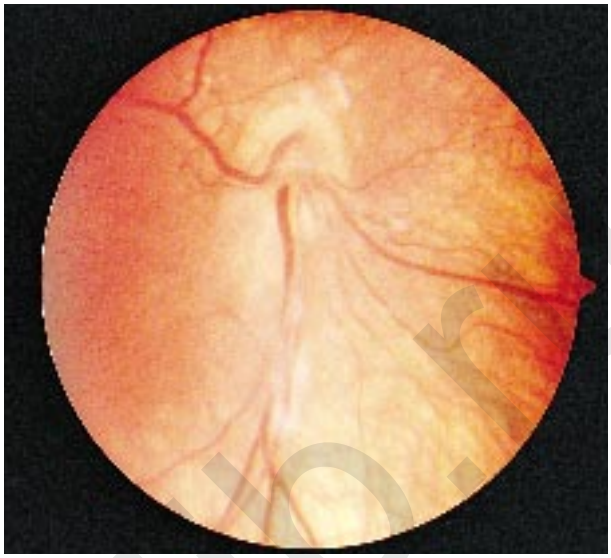

2.115

Figure 2.115. Incontinentia pigmenti is an X-linked dominant (Xq27-28) disorder (i.e., limited to females). There is abnormal melanin within the retinal pigment epithelium and abnormal vascularization of the peripheral retina. Skin, skeletal and central nervous systems are also affected in this disorder.

B. Abnormal formation of inner retinal vessels can occur due to genetic abnormality and can be associated with abnormal vascularization of other organ systems as in the following examples.

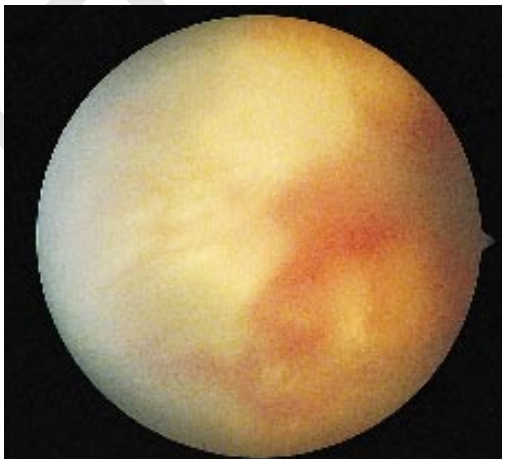

2.116

Figure 2.116. Norrie syndrome is an X-linked recessive (Xp11.3) disorder which has been classically described as congenital blindness in all patients with a dysplastic retina histologically. Hearing loss and mental retardation have been associated progressive findings. Currently, this classic definition has been revised to include other phenotypes of the Norrie disease gene.

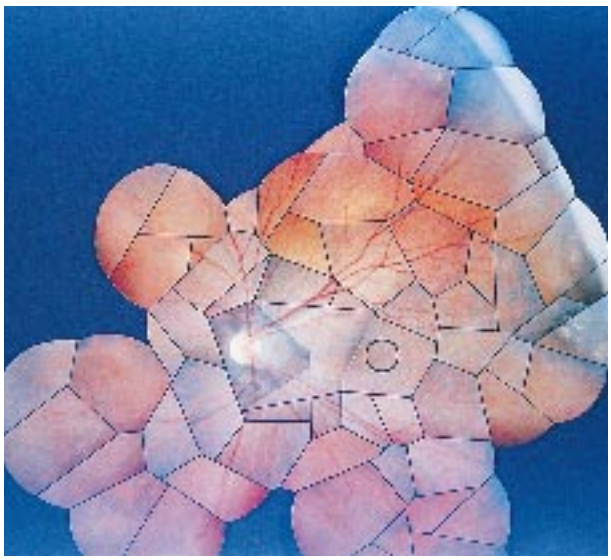

2.117

Figure 2.117. Exudative vitreoretinopathy can be a phenotype of the Norrie disease gene (Xp11.3) in term infants with ocular involvement only. Clinically, there is a progressive peripheral retinal neovascularization resembling cicatricial Grade II to IV RLF with macular ectopia as shown in this montage. An autosomal dominant (11q13) exudative vitreoretinopathy may be clinically indistinguishable.

2.118

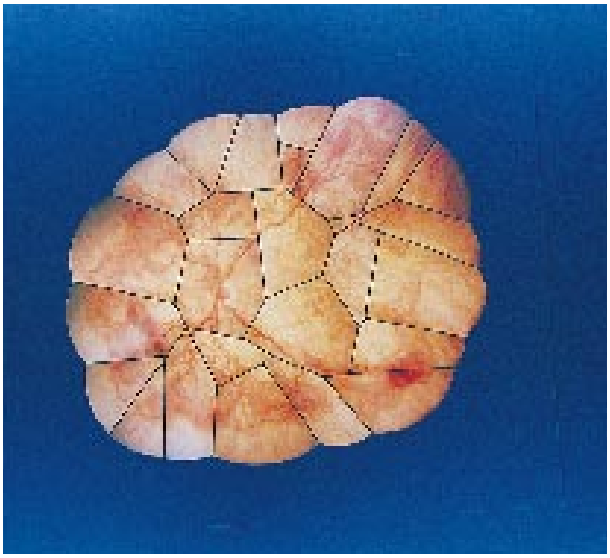

Figure 2.118. Preterm infants can present with a phenotype of the Norrie disease gene that involves all of the systems vascularized by the dorsal embryonic aortic arches (aorta, thymus, ear, brain, and eye). Clinically, there is an acute peripheral retinal neovascularization resembling active Stage III ROP as shown in this montage.

C. Abnormal formation of inner retinal vessels can occur in response to an intrauterine insult and can be associated with gross CNS changes as in the following examples.

2.119

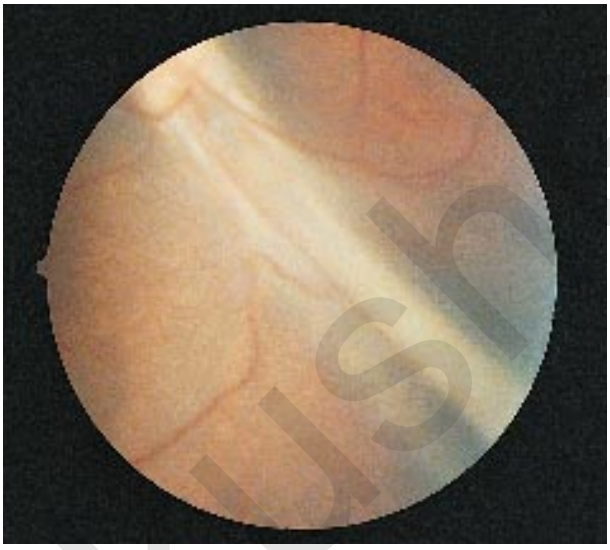

Figure 2.119. The retina of an Asian infant who presented with an anterior encephalocele. Anterior encephaloceles and this retinal picture are more common in Asians and Africans because of their thin ethmoidal structures.

2.120

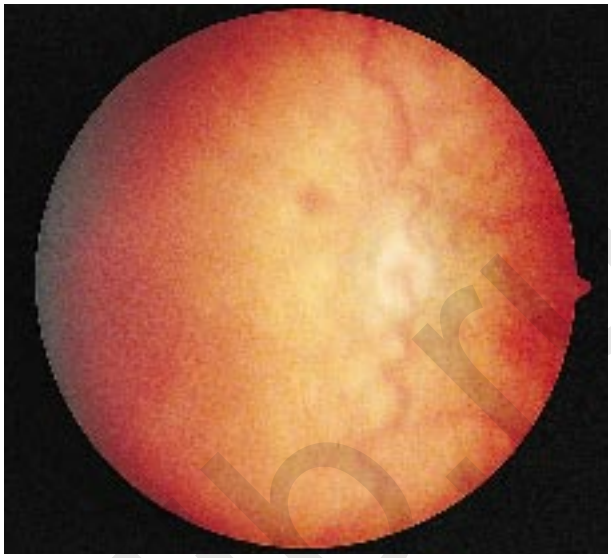

Figure 2.120. This is the retina of an infant who suffered an intrauterine infarction of both middle cerebral arteries. Similar intrauterine stresses can be associated with retinal pictures virtually indistinguishable from ROP.

OPTIC NERVE

2.121

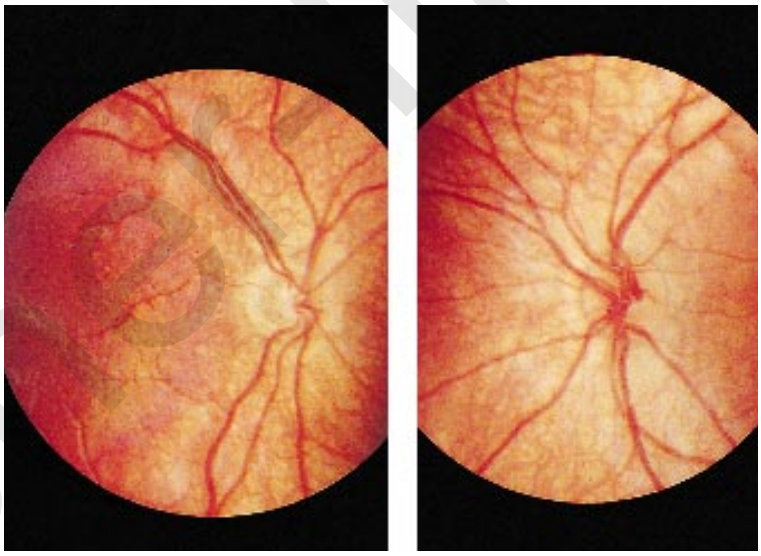

Figure 2.121. Note the hypoplastic optic nerve on the left and a normal optic nerve in the fellow eye on the right. Optic nerve hypoplasia may occur unilaterally or bilaterally, both sporadically, as part of de Mosier syndrome with absence of corpus callosum, and as part of autosomal recessive optic nerve hypoplasia. It may be necessary to evaluate the endocrine status of the infant (growth hormone and thyroid hormone are most commonly decreased).

2.122

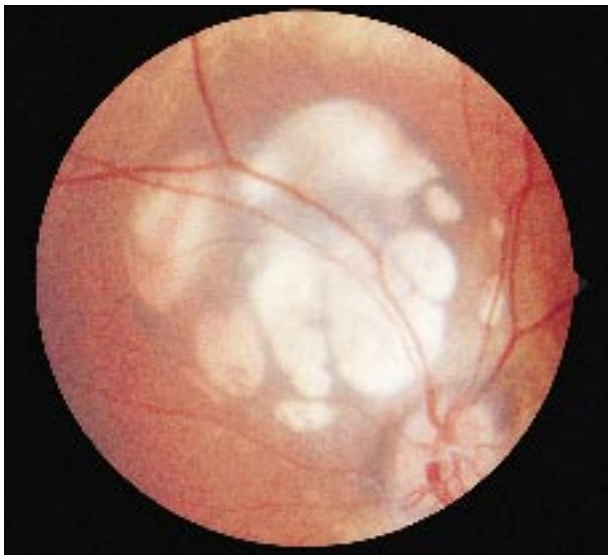

Figure 2.122. Aicardi's syndrome presents with characteristic chorioretinal "lacunar" lesions. The syndrome is an X-linked dominant (Xp22) disorder (limited to females). Optic nerve colobomas can occur. The CT scan shows agenesis of the corpus callosum and affected patients have severe mental retardation and infantile massive spasms.

2.123

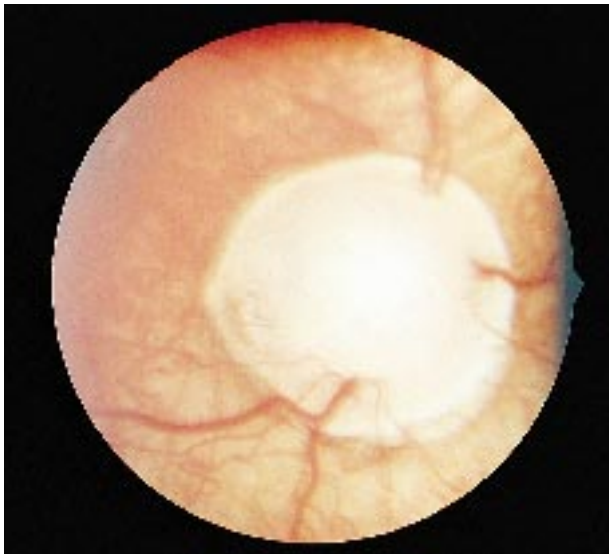

Figure 2.123. Optic nerve coloboma (without microphthalmia) may occur as an autosomal dominant or sporadically. It is appropriate to examine other family members, especially any with a history of "glaucoma," because of variable expressivity.

2.124

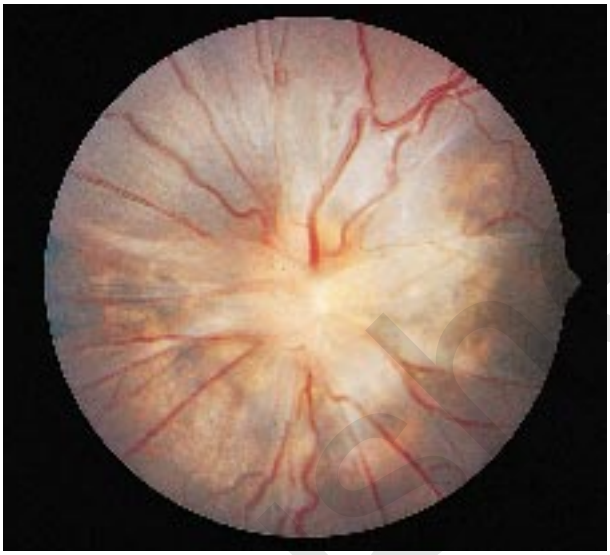

Figure 2.124. Morning glory optic nerve anomaly is characterized by an enlarged and excavated disc. Note the symmetry of the fundus excavation with respect to the disc which suggests an anomalous funnel-shaped enlargement of the distal optic stalk at its junction with the primitive optic vesicle as the primary embryological defect. Vision is always poor and there may be associated defects such as the transsphenoidal form of basal encephalocele.

Chapter 3
The Central Nervous System

Central nervous system disorders are among the three major causes of mortality in neonates. All of the conditions that affect the infant's brain do so in part because this system is developing at a rapid rate. The neurologic examination of the newborn must thus be interpreted in the context of the child's brain maturation (gestational age) and level of alertness. The examination should be brief so as to avoid hypoxemia and fluctuations in arterial blood pressure. Head circumference is a useful measure of intracranial volume, and longitudinal measurements in particular provide important information. Observation of movement and symmetry can contribute significantly to the evaluation while minimizing the effects of handling, especially in the sick neonate. These observations should include any available assessment of the fetus in the intrauterine environment. Examination of the following cranial nerves is possible: 1 (olfaction); 2 (optic fundi); 3 (pupils); 3, 4, 6 (extraarticular movements, facial sensation and masticatory power); 7 (facial motility); 5, 7, 9, 10, 12 (sucking and swallowing); 11 (sternocleidomastoid function); and 12 (tongue function). Reliable assessment of cranial nerves 2 (vision) and 8 (audition) may require testing of auditory or visual evoked responses. Motor examination should include an assessment of tone and posture, motility and strength, and tendon and plantar reflexes. Primary neonatal reflexes including Moro's reflex, palmar grasp, and tonic neck response should also be considered. Although a sensory examination is possible, it is usually very limited and can be noxious. Because of the limitations of the neurologic exam and the complex support required by the sick neonate, frequently additional, usually non-invasive, neurodiagnostics will be required. These can include brain imaging (ultrasonography, computed tomography, magnetic resonance imaging, brain scan), neurophysiologic techniques (electroencephalogram, nerve conduction, electromyography), and cerebrospinal fluid examination.

3.1

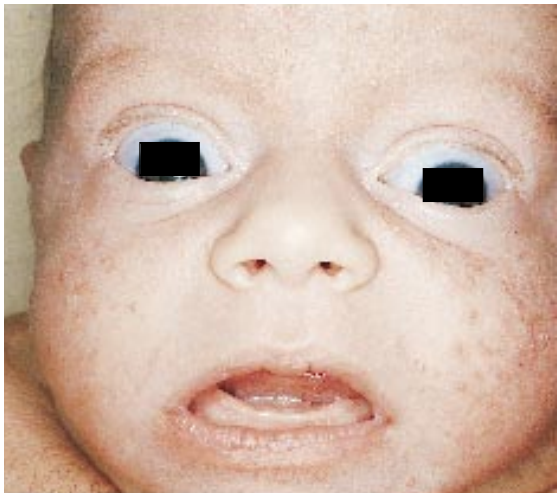

Figure 3.1. "Setting sun" sign in a normal newborn infant. The setting sun sign means that conjugate upward deviation is decreased. The upper eyelids are retracted and the irides are partly covered by the lower eyelid giving the appearance of a sunset. This is rarely observed as an isolated finding in an otherwise normal newborn infant. It may be normal if it is transient, but if it persists, it must be investigated. Note associated neonatal acne in this infant.

3.2

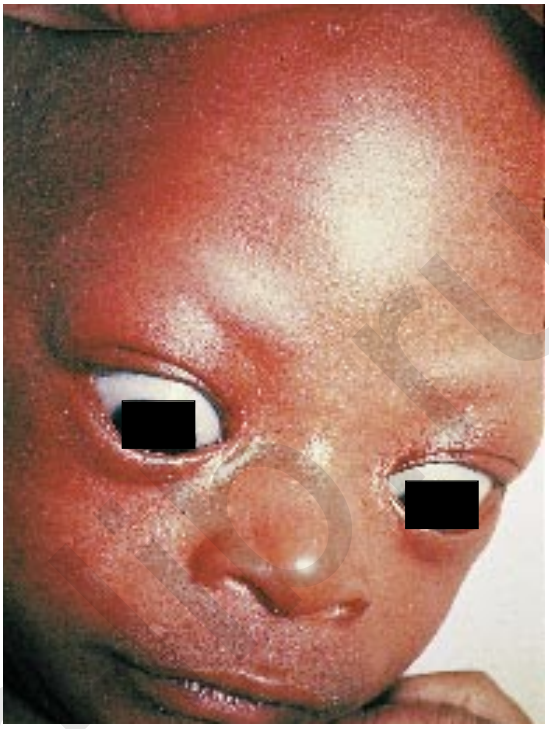

Figure 3.2. Persistent "setting sun" sign in an abnormal newborn infant. The setting sun sign is usually due to a lesion in the region of the quadrigeminal plate of the midbrain and signifies increased intracranial pressure. Increased intracranial pressure may result from hydrocephalus or subdural hematoma. It can occur in parenchymal or midbrain lesions, especially kernicterus.

3.3

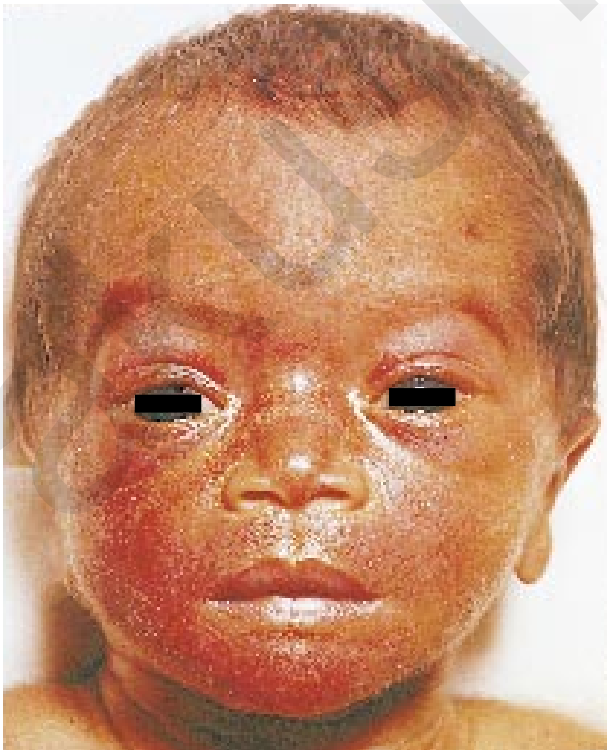

Figure 3.3. This premature infant with wide open eyes and a hyperalert expression continued to have an increased state of arousal, which is abnormal in the first hours of life. CT scan demonstrated a tentorial tear with hemorrhage. Hyperalert states may be the result of intracranial pathology or may be related to maternal drug ingestion. Infants with severe intracranial irritation may also have an anxious expression and furrowed brows.

3.4

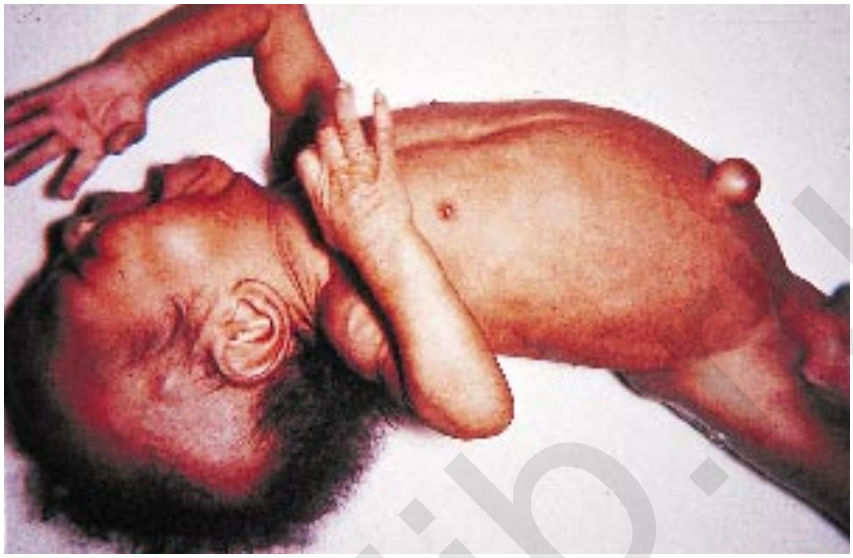

Figure 3.4. Opisthotonic posturing in an infant with congenital rubella encephalitis. Severe cortical irritation or damage may produce marked hypertonicity of the spinal muscles. The neck is hyperextended and the spine is arched. Note the flexed arms, fisted hands, and extended legs. Contractures may occur if the child remains in an opisthotonic posture.

3.5

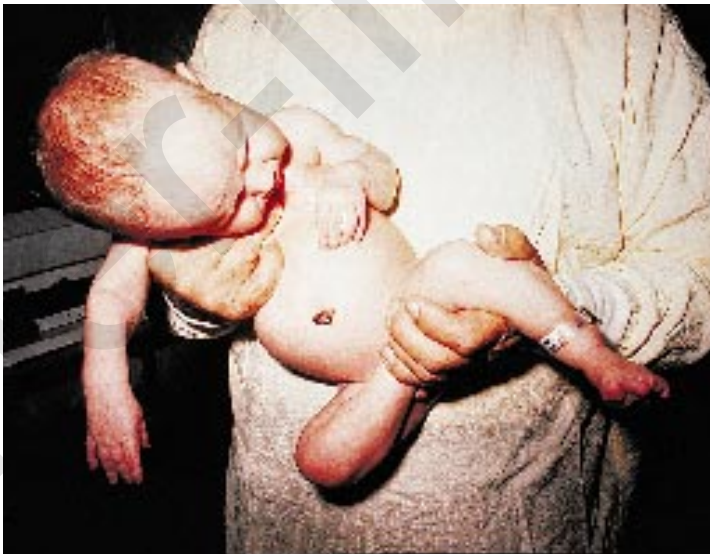

Figure 3.5. Marked hypotonia in a term infant with Lowe syndrome. Note that the infant hangs limply when supported in a prone position.

3.6

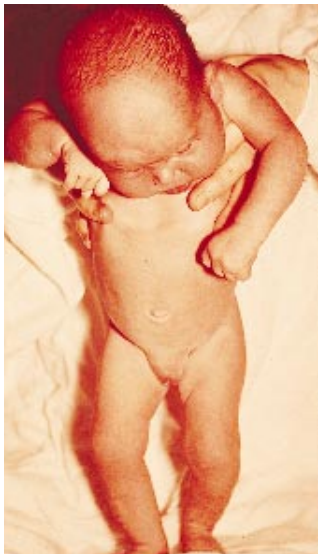

Figure 3.6. Extreme hypotonia in a term infant who appears to slip through the hands of her examiner when held upright under the arms. Most term newborns can maintain the head in the same plane as the trunk when lifted by the arms or ventrally suspended. Extreme head lag is a sign of hypotonia that can be seen in infants with Down syndrome, prematurity, or brain damage.

3.7

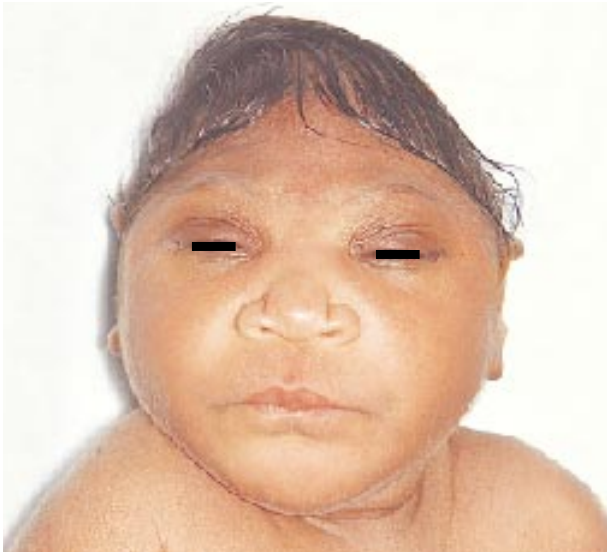

Figure 3.7. Microcephaly in a term infant with congenital rubella. Microcephaly may be idiopathic or acquired as a result of intracranial pathology. It may also result from serious perinatal brain injury in which case the FOC (fronto-occipital circumference) may be normal at birth, but then fail to increase as the brain fails to grow after birth. Severe physical and mental retardation may follow. This infant had an FOC of 30 cm and closed fontanelles.

3.8

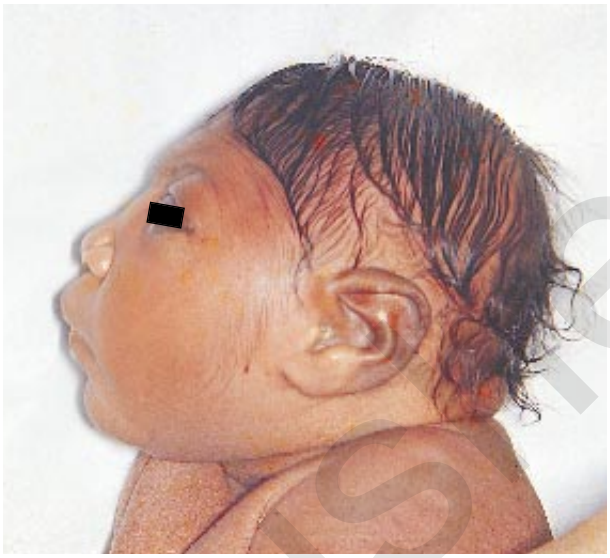

Figure 3.8. Lateral view of the same infant with microcephaly. Microcephaly occurs with intrauterine infections (rubella, cytomegalovirus, toxoplasmosis), chromosomal abnormalities (cri du chat syndrome, trisomy 13), and toxic drug effects (fetal alcohol syndrome, fetal aminopterin syndrome).

3.9

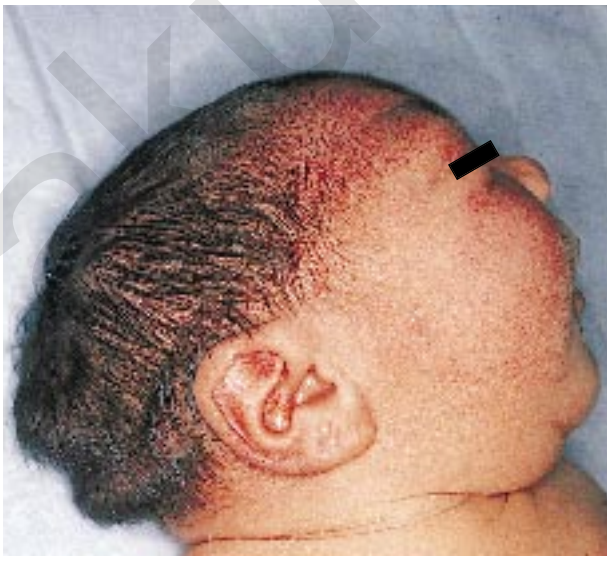

Figure 3.9. Infant with severe microcephaly of unknown etiology. One must consider heredity, infection, or irradiation.

3.10

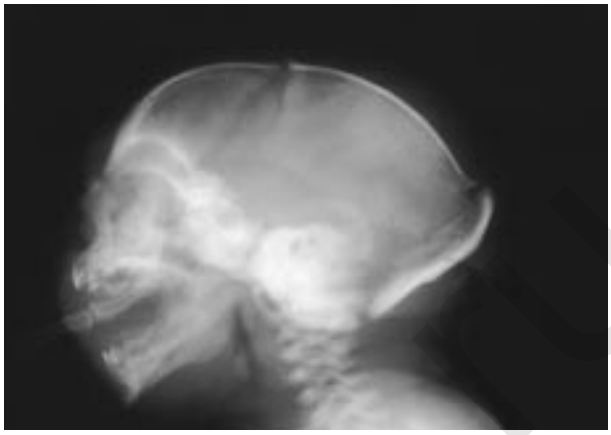

Figure 3.10. Lateral skull radiograph of the same infant. Note the severe microcephaly. The normal ratio of cranial vault to bony facial structures is 4:1.

3.11

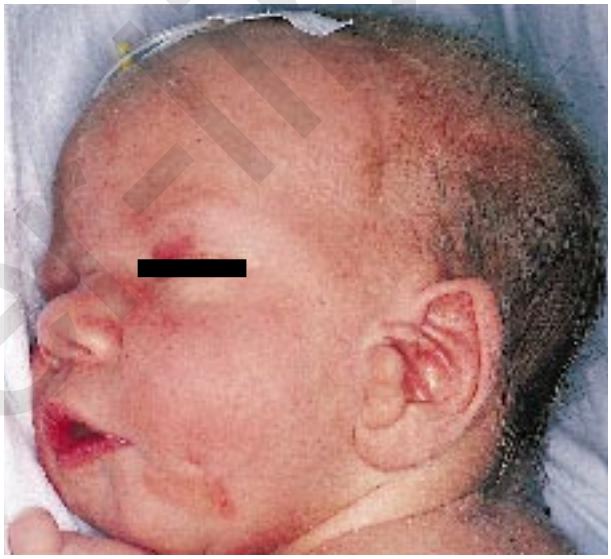

Figure 3.11. Macrocephalic head with a fronto-occipital circumference of 39 cm in a hypotonic infant with a left cheek skin pit, ear tags, and Goldenhar's syndrome. This infant had an increased head circumference at birth, a fontanelle of normal size, and cranial sutures that are not widened. The face appears relatively normal in size.

3.12

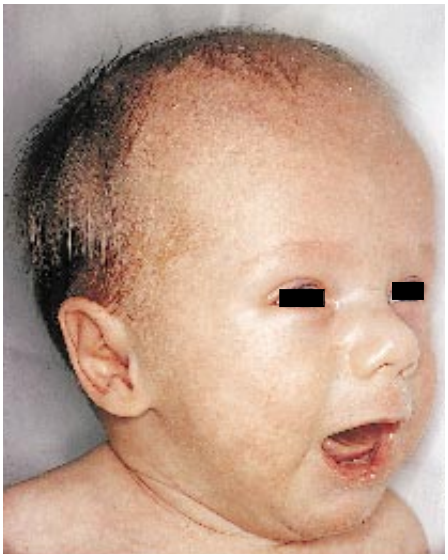

Figure 3.12. This term infant had macrocephaly, a prominent brow, and distended scalp veins. Transillumination was positive with the lack of underlying brain tissue being consistent with hydranencephaly.

3.13

Figure 3.13. Transillumination of the head of the same infant with hydranencephaly shown in Figure 3.12. This results from failure of the development of the cerebrum with resulting gross dilatation of the ventricles. Note the "jack-o-lantern" appearance of the eyes and an area of opacity in the transilluminated head. Infants with hydranencephaly may have isolated nubbins of brain tissue. This condition has an extremely poor prognosis.

3.14

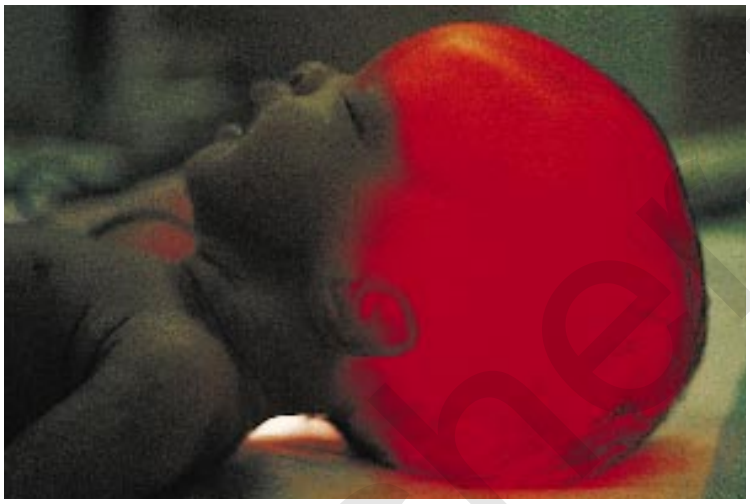

Figure 3.14. Transillumination of the lateral view of the head of another infant with hydranencephaly. Note the large head size compared with that of the face. Typically infants with hydranencephaly present with heads that are macrocephalic. Infants with hydrocephalus will also have transillumination of the skull, but this would become readily apparent only if there was massive enlargement of the head.

3.15

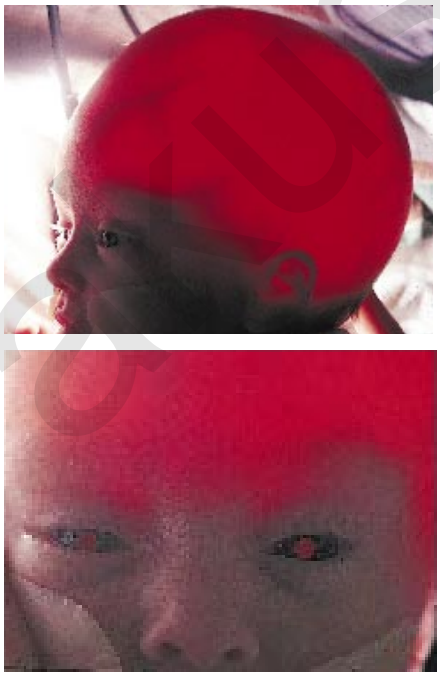

Figure 3.15. Lateral and anterior-posterior views of the head of an infant with hydranencephaly. Note the large head, some prominence of scalp veins, the "jack-o-lantern" appearance of the eyes, and the total lack of brain tissue.

3.16

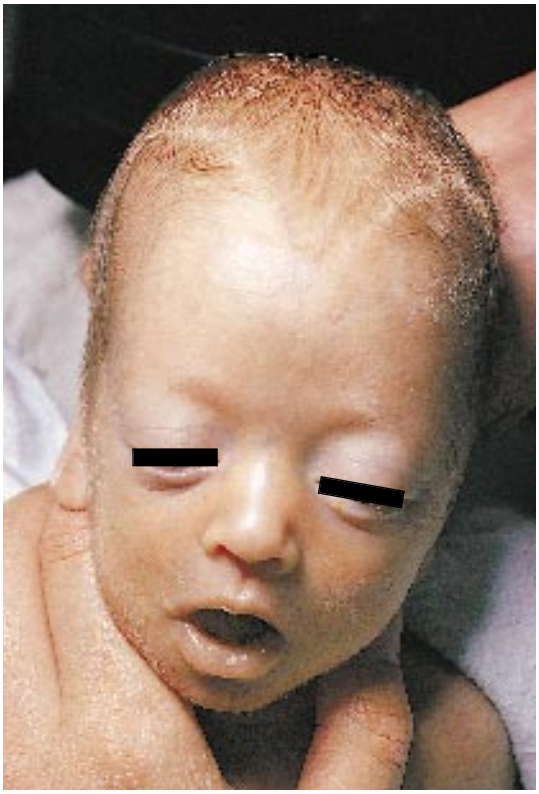

Figure 3.16. Clinical appearance of an infant with hydranencephaly. Note the prominent scalp veins and brow. There is macrocephaly and a large open anterior fontanelle associated with poor mineralization of the skull.

3.17

Figure 3.17. Transillumination of the head of the same infant with hydranencephaly. Note the "jack-o-lantern" appearance of the eyes indicating the lack of neural tissue behind the globe.

3.18

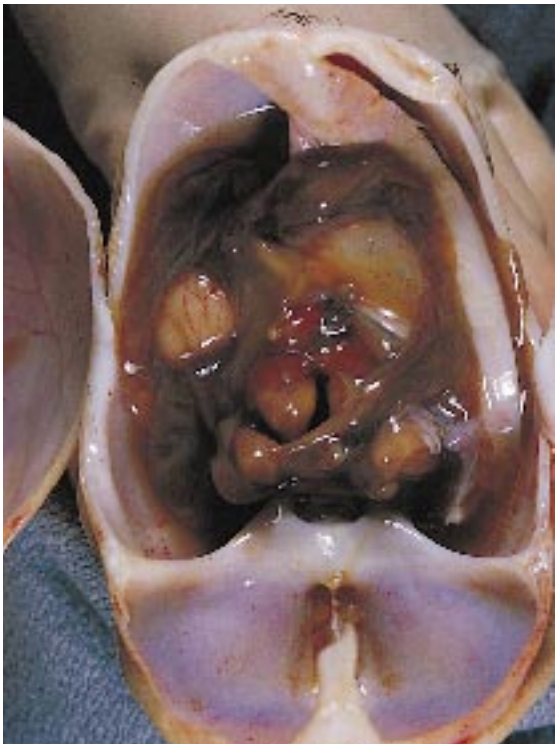

Figure 3.18. Autopsy view of the skull of the same infant with hydranencephaly. Note the empty cranial vault with lack of development of the cerebrum.

3.19

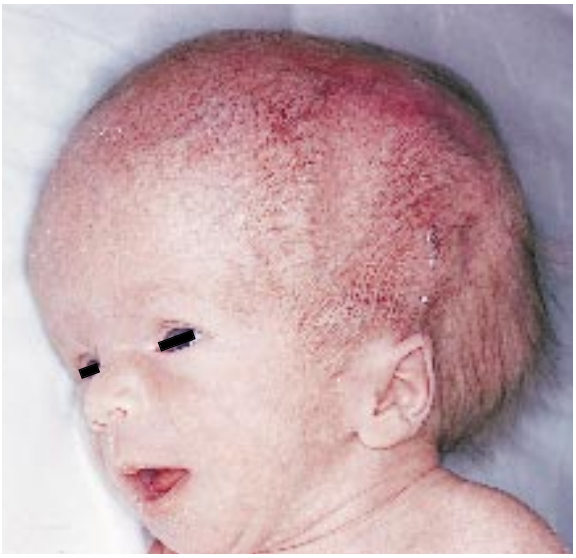

Figure 3.19. Lateral view of the head of an infant with macrocephaly due to a large porencephalic cyst.

3.20

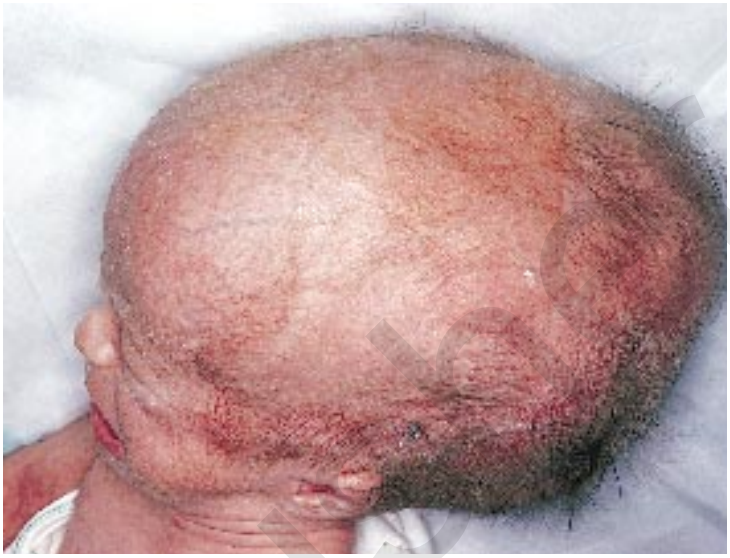

Figure 3.20. Another view of the head of the same infant showing the marked distortion of the posterior occiput and the engorged scalp veins.

3.21

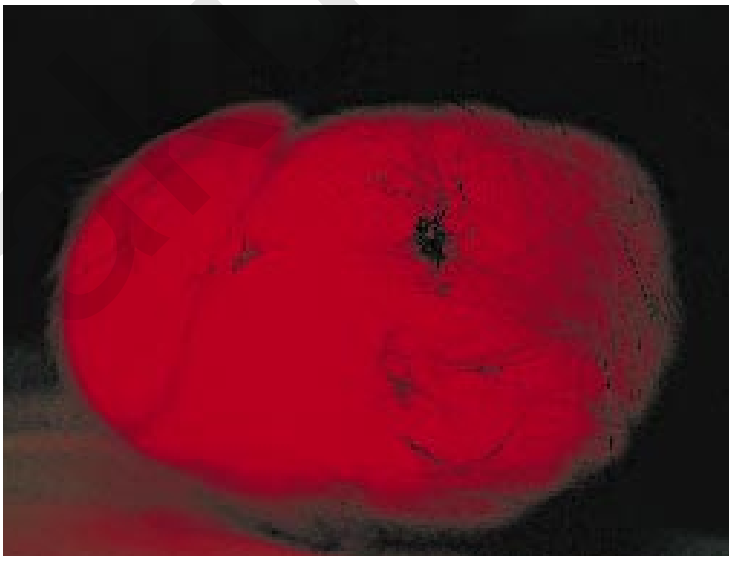

Figure 3.21. Transillumination of the skull of the same infant. The fluid-filled lobulated space-occupying cyst results in marked distortion of the cranial vault.

3.22

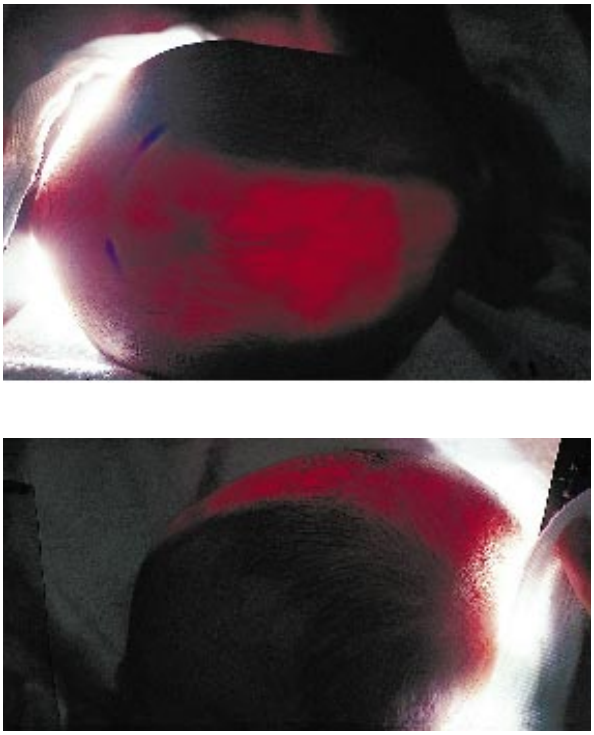

Figure 3.22. Transillumination of the skull of another infant with a smaller porencephalic cyst with the presence of some normal neural tissue.

3.23

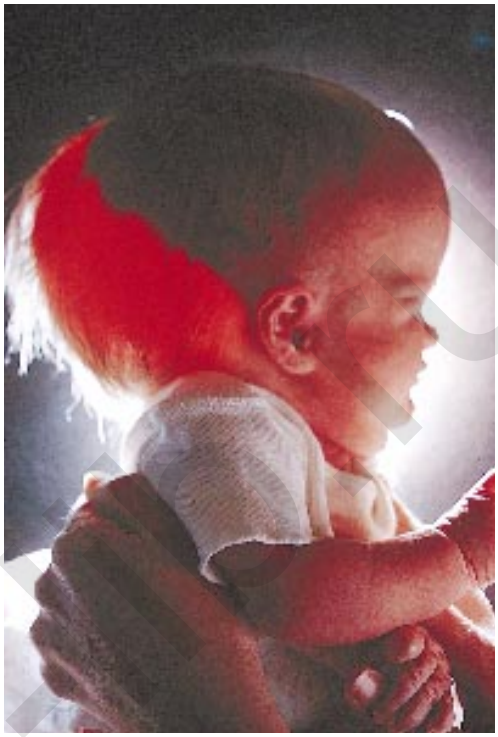

Figure 3.23. Transillumination of the skull of an infant with a Dandy-Walker malformation. Note the bulging occiput and enlargement of the head, and a large posterior fossa cyst.

3.24

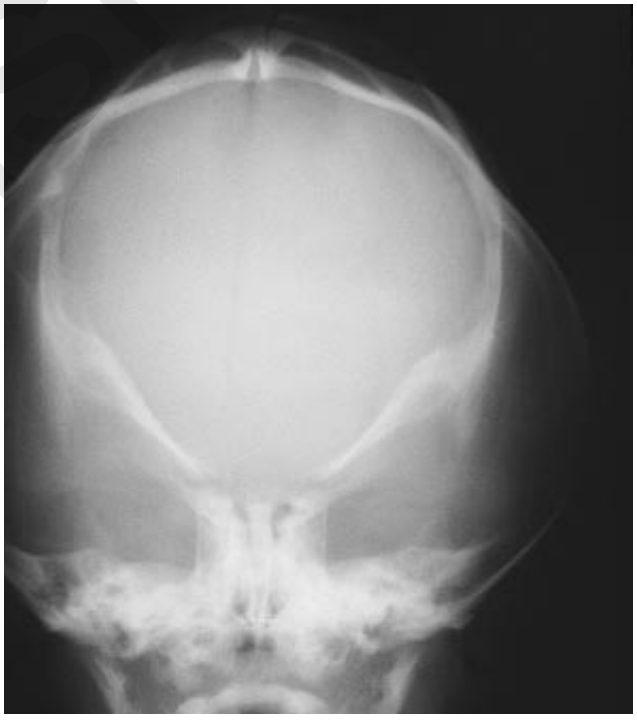

Figure 3.24. Cranial ultrasound study of an infant with an increased fronto-occipital circumference. Scanning section reveals large posterior fossa with hydrocephalus as the result of a Dandy-Walker malformation. This ultrasound marking is referred to as the "Chinese lantern" sign.

3.25

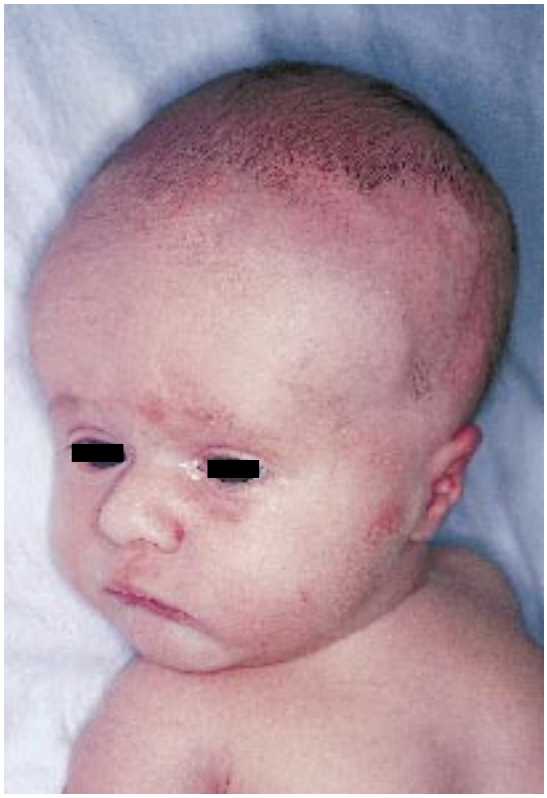

Figure 3.25. A premature infant (birth weight 1250 g) now aged two months with "pseudohydrocephalus." These infants have rapidly growing heads as a result of normal catch-up growth. Frontal bossing with prominent temporoparietal bulging suggests a diagnosis of hydrocephalus which can easily be excluded by a cranial ultrasound examination.

3.26

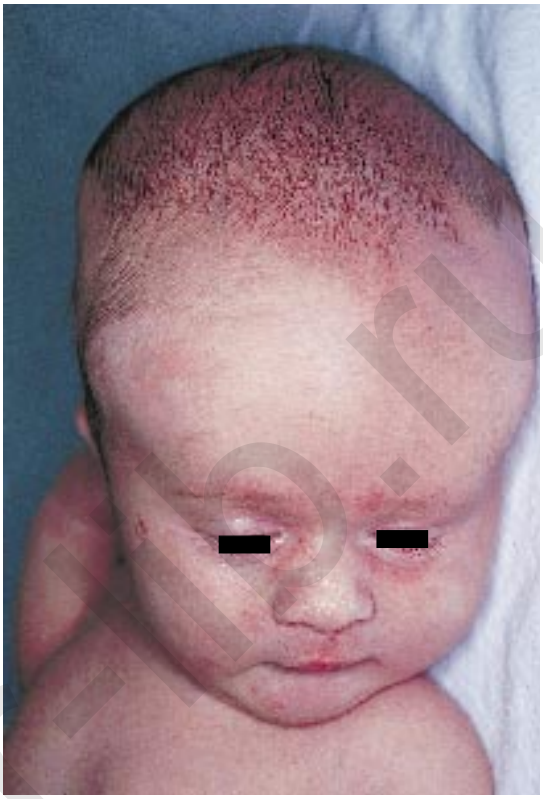

Figure 3.26. Superior view of the same infant with apparent hydrocephalus (pseudohydrocephalus of prematurity).

3.27

Figure 3.27. The same premature infant had some increased transillumination of the cranial vault. This was not pathologic but was the result of poor mineralization with transient increased skull lucency.

3.28

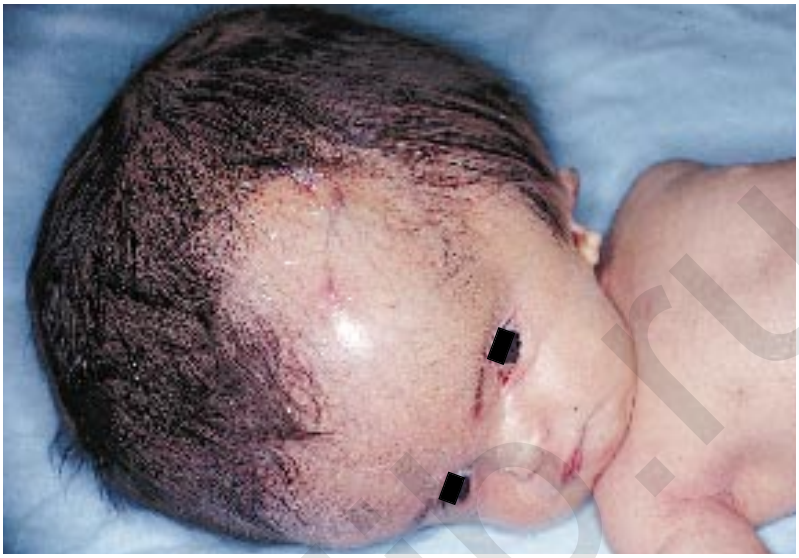

Figure 3.28. This term infant shows massive head enlargement as the result of congenital hydrocephalus. This results from overproduction or obstruction of the circulation of the cerebrospinal fluid. It can be inherited as an X-linked recessive trait in a male infant as the result of aqueductal stenosis. Other underlying brain defects may be present.

3.29

Figure 3.29. Congenital hydrocephalus in a term male infant with respiratory failure. Note the common association of the adducted thumbs, seen in the X-linked variant, and the prominent scalp veins. The birth weight of this infant was 3800 g, the length 53 cm, and the fronto-occipital circumference 52.5 cm.

3.30

Figure 3.30. Transillumination of the skull of the same infant with congenital hydrocephalus. Note the very prominent scalp veins which probably reflect the marked increase in intracranial pressure.

3.31

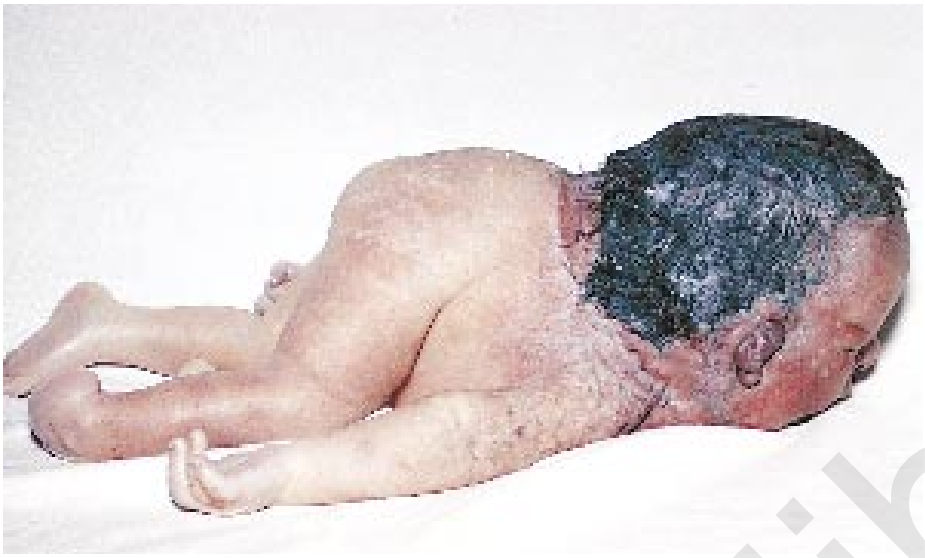

Figure 3.31. Iniencephaly is the most severe form of a closed neural tube defect. It results in enlargement of the foramen magnum and fusion of the posterior occiput with the cervicothoracic spine. It is incompatible with survival.

3.32

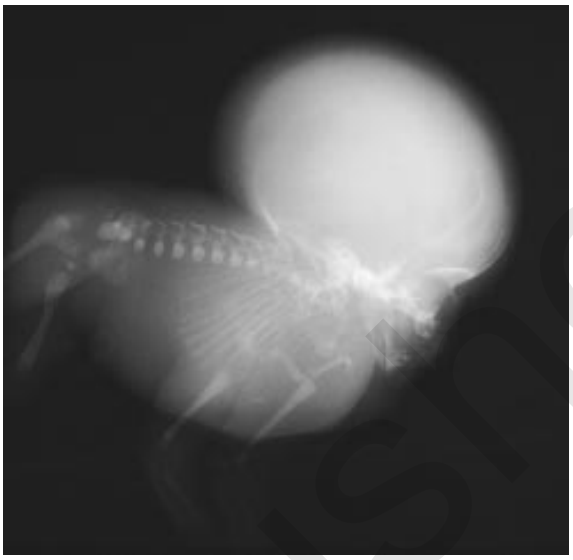

Figure 3.32. Radiograph of the same infant with iniencephaly. Note absence of the laminal and spinal processes of the cervical, dorsal, and sometimes lumbar vertebrae. The vertebrae are reduced in number and are irregularly fused.

3.33

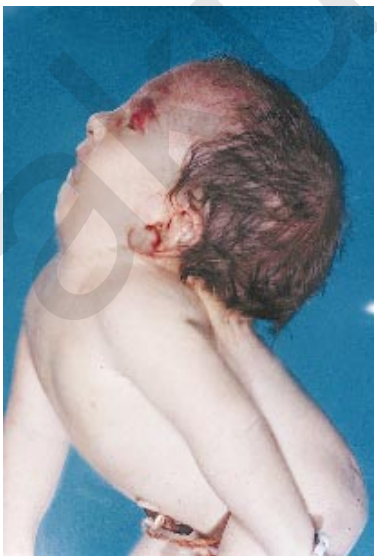

Figure 3.33. Another infant with iniencephaly showing the lack of a neck due to the fusion of the posterior occiput with the cervicothoracic spine.

3.34

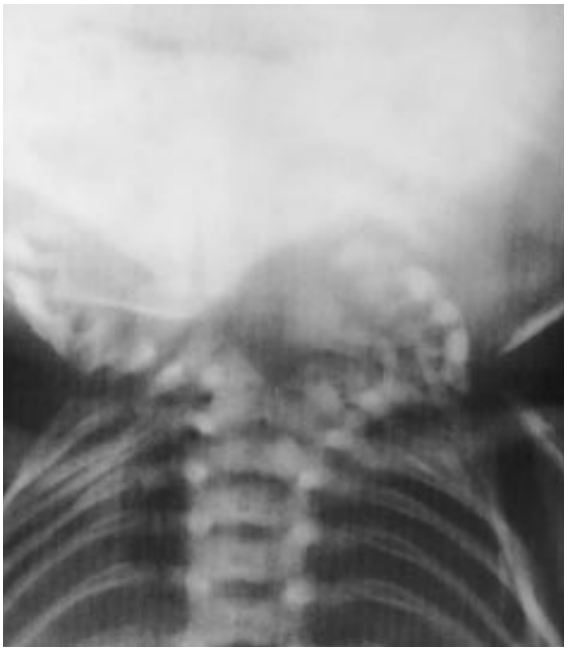

Figure 3.34. Radiograph of the same infant with iniencephaly. Note the schistasis of the cervical vertebrae.

3.35

Figure 3.35. Craniorachischisis represents the most severe form of an open neural tube defect. Note that the defect in this infant is open from the anterior to the posterior neural pore.

3.36

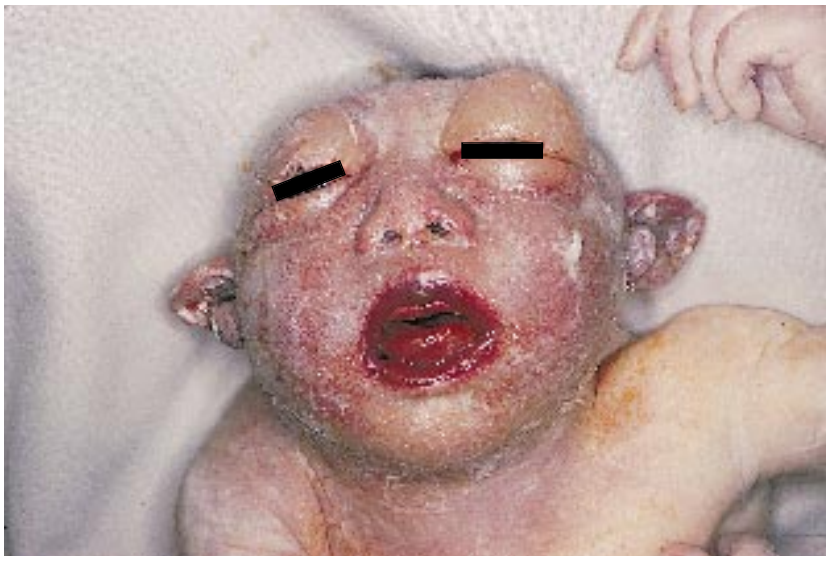

Figure 3.36. Anencephaly is a developmental defect in the brain with an open cranium resulting from failure of the anterior neural tube to close. It is a major open neural tube defect in which there is absence of skull bones, cranial vault, and incomplete development of the brain. Malformation of other organs may occur such as adrenal hypoplasia and genitourinary abnormalities. Anencephaly in this term infant left an exposed fibrotic degenerating ill-defined mass of neural tissue. Most of these infants are stillborn and the remainder die in the immediate neonatal period.

3.37

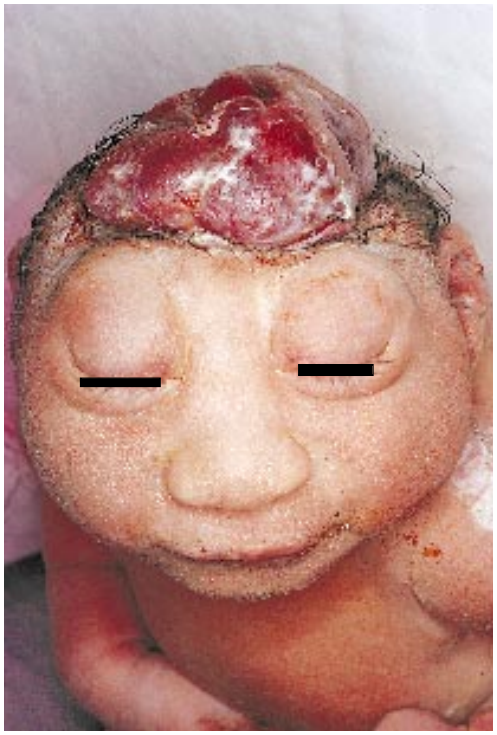

Figure 3.37. Another infant with anencephaly. Anencephaly is more common in females.

3.38

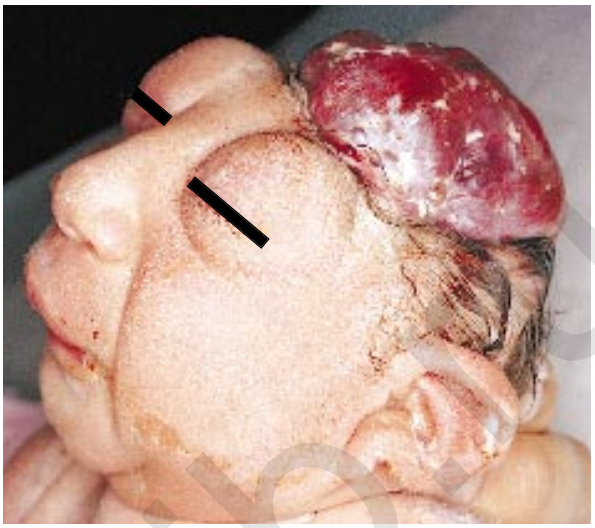

Figure 3.38. The lateral view of the same infant with anencephaly.

3.39

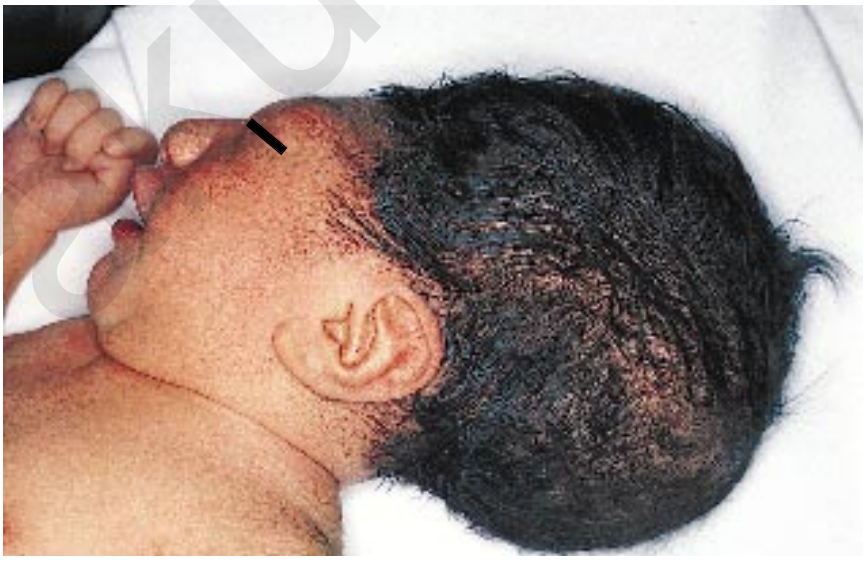

Figure 3.39. Encephaloceles may occur at any midline point in the skull and result from failure of the neuroectodermal axis to develop normally. This results in bony defects of the skull with protrusion of the meninges which may contain neural tissue. They are most common in the occipital area. The prognosis is better if the rest of the skull is normal and there is no herniation of neural tissue.

3.40

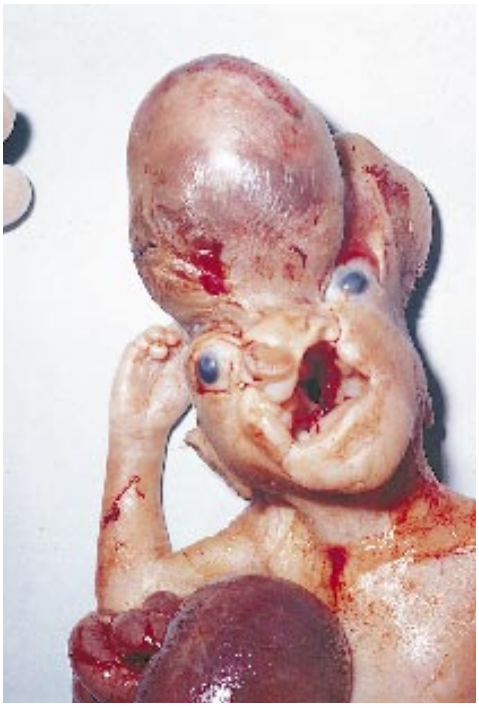

Figure 3.40. Encephaloceles occur at any midline point in the skull. The exception is the occurrence of an asymmetric encephalocele that occurs with a severe amniotic band disruption sequence. This infant with disruption shows the large asymmetric encephalocele and the involvement of the mouth, nose, eyes, and head.

3.41

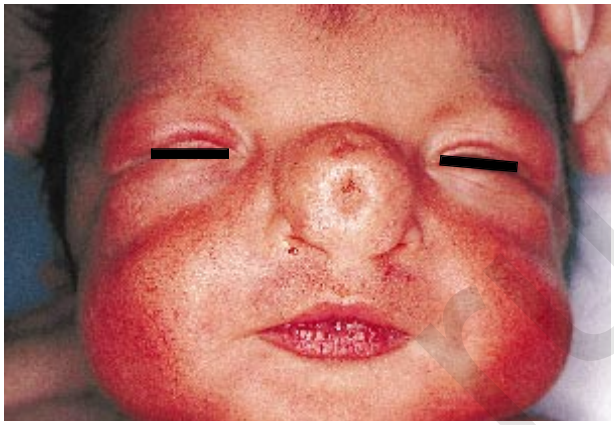

Figure 3.41. Abnormal facial and nasal appearance of an infant with an anterior encephalocele. This infant has a severe midline nasal schistasis. The external airways were obstructed. The CT scan demonstrated a communicating encephalocele. At surgery, an ethmoid encephalocele was removed.

3.42

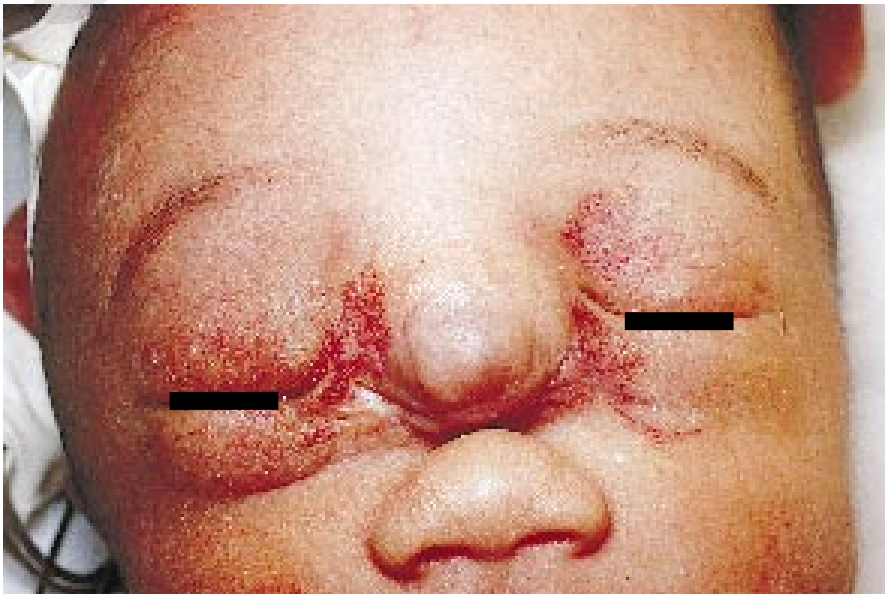

Figure 3.42. The soft tissue mass in this infant proved to be an anterior encephalocele.

3.43

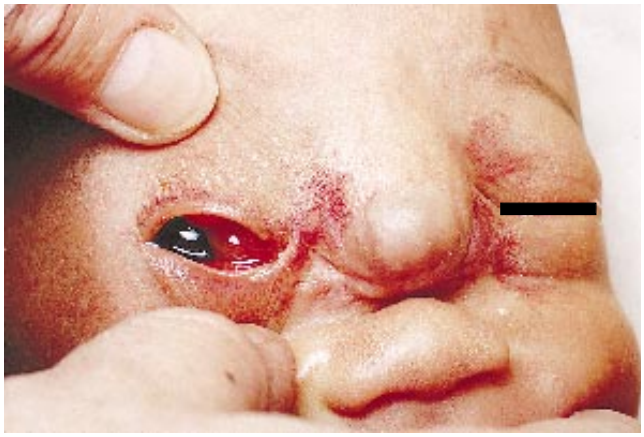

Figure 3.43. Retraction of eyelids of the same infant reveals that the soft tissue mass occupies the nasal aspect of the orbit with distortion of the globe.

3.44

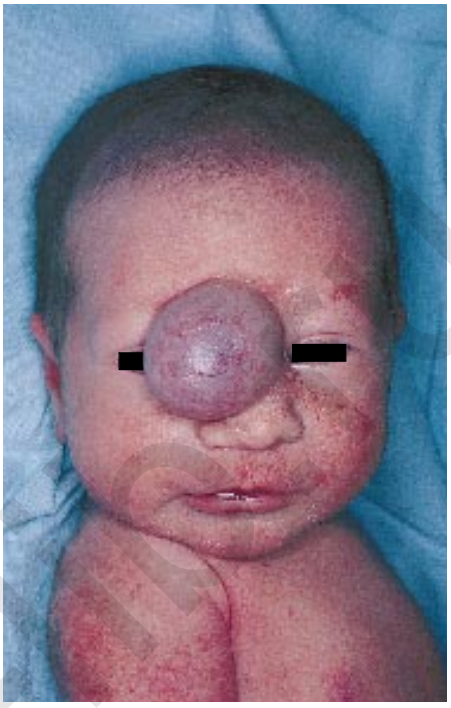

Figure 3.44. A term infant with an anterior encephalocele. In the Western hemisphere and Europe, the majority of encephaloceles are posterior, whereas in the Far East (India, Sri Lanka, Africa, etc.), the majority of encephaloceles are anterior.

3.45

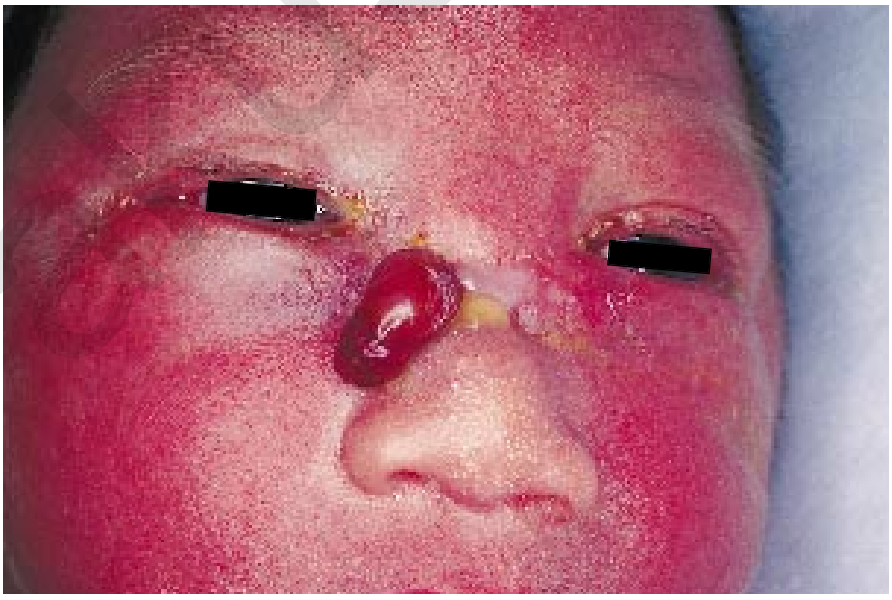

Figure 3.45. In this infant with an anterior encephalocele, the fluid draining from the mass was positive for glucose confirming the origin of the fluid as CSF (cerebrospinal fluid).

3.46

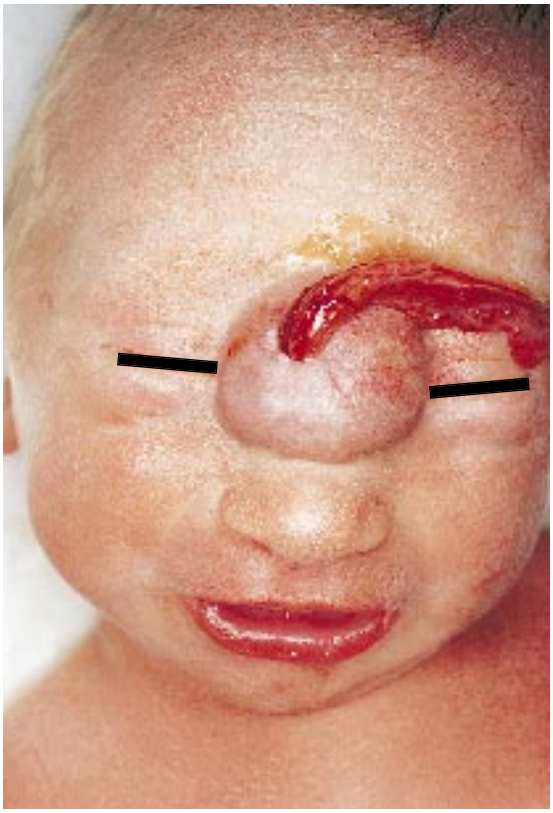

Figure 3.46. This anterior encephalocele presented as a soft tissue midline mass which caused nasal obstruction and respiratory distress.

3.47

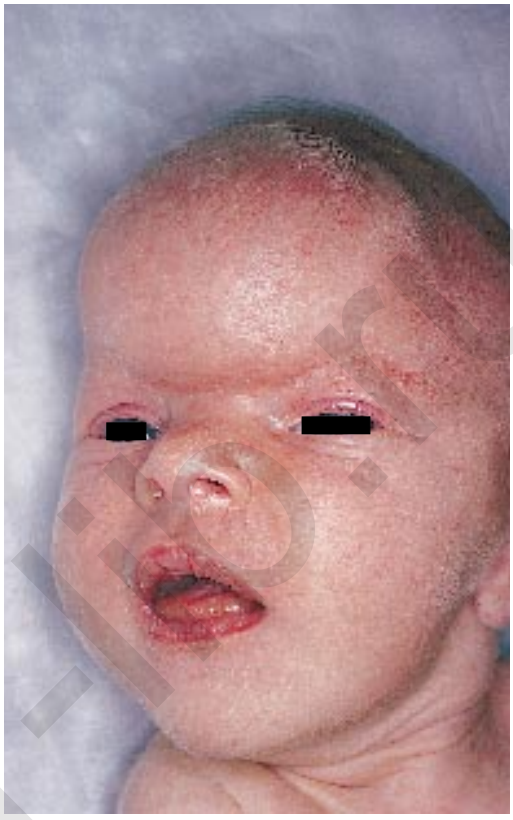

Figure 3.47. The abnormal brow appearance in this term infant is the result of a frontal encephalocele.

3.48

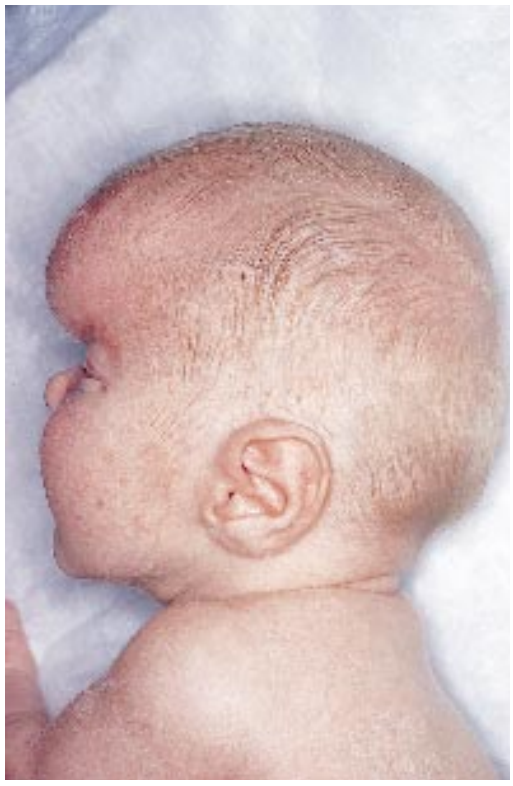

Figure 3.48. Lateral view of the same infant with a frontal encephalocele.

3.49

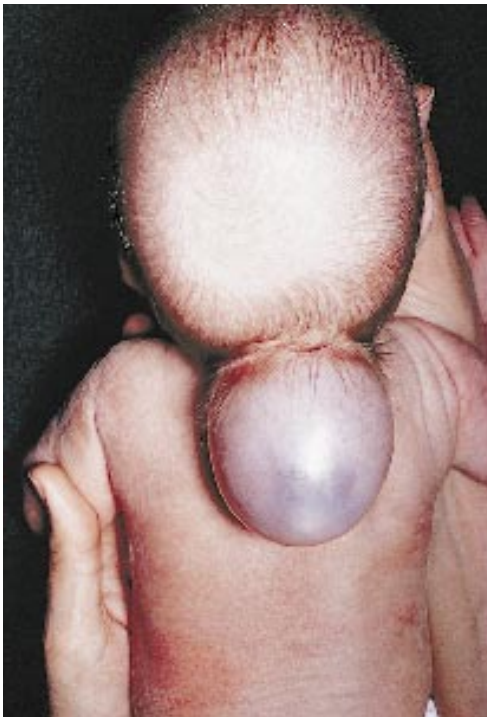

Figure 3.49. A posterior encephalocele in an infant may be difficult to distinguish from a cervical meningocele. It is both a posterior encephalocele and cervical myelomeningocele when there is involvement of both the bony skull and spine. Cervical myelomeningoceles are usually not associated with other neurologic abnormalities.

3.50

Figure 3.50. Inferior view with transillumination of the posterior structure in an occipital encephalocele. In a cranial encephalocele there is a herniation of meninges through a skull defect.

3.51

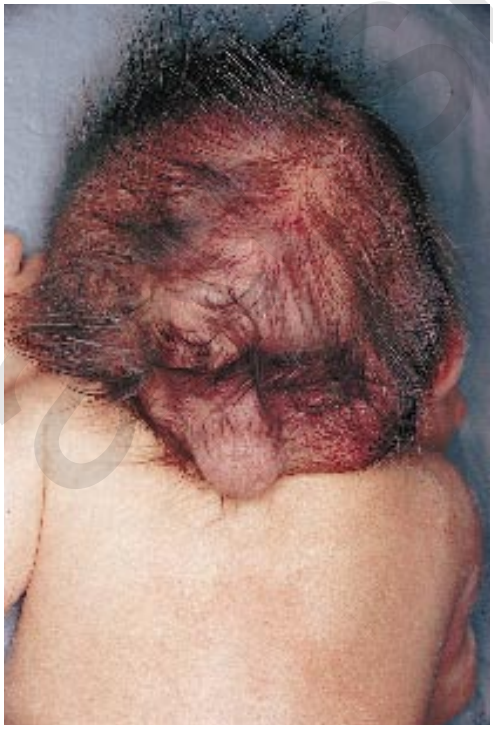

Figure 3.51. Infant with a posterior small occipital encephalocele. Occipital encephalocele present as a protruding soft tissue mass from the base of the skull.

3.52

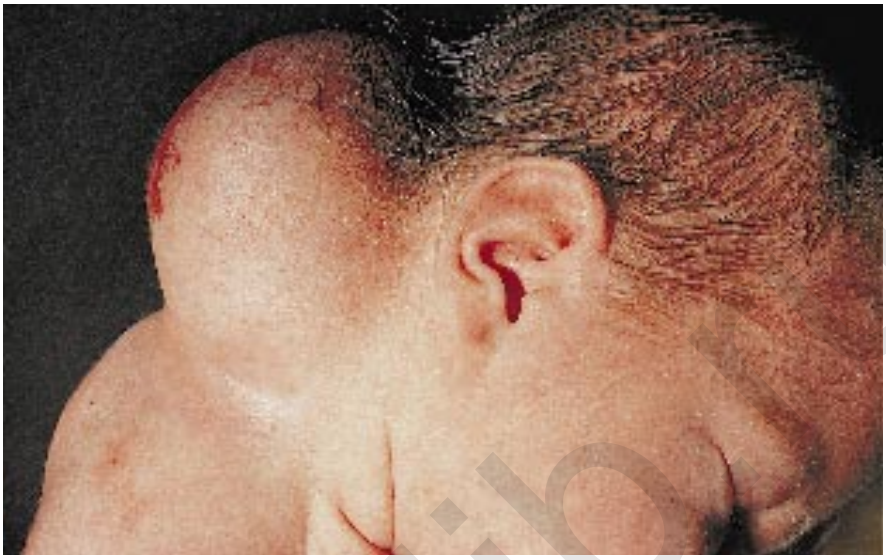

Figure 3.52. Posterior encephaloceles may be distinguished from associated cervical spine abnormalities by MRI.

3.53

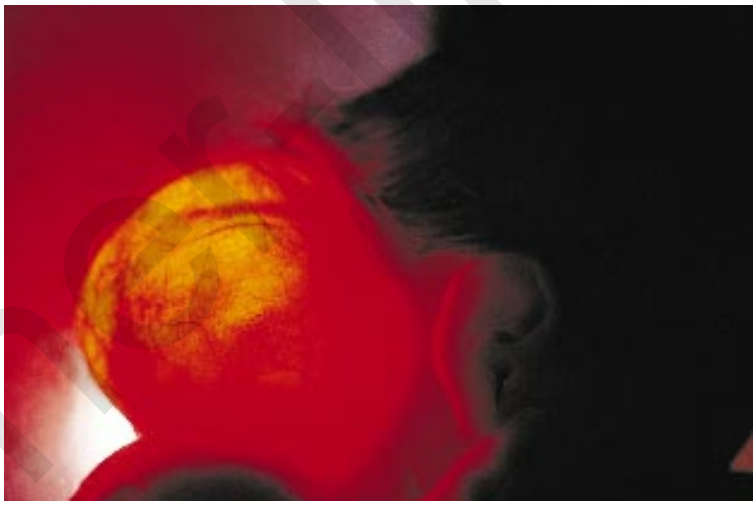

Figure 3.53. Transillumination of the posterior encephalocele in the same infant.

3.54

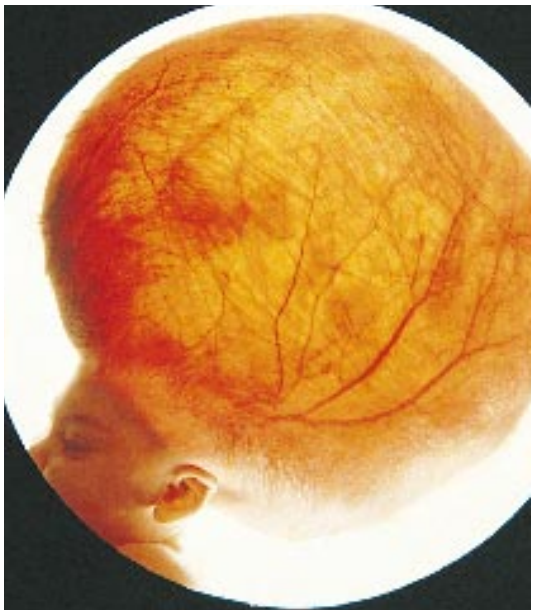

Figure 3.54. In this massive occipital encephalocele note the lack of neurologic tissue.

3.55

Figure 3.55. Rupture of a large posterior encephalocele with protrusion of neural components. This results in a poor prognosis.

3.56

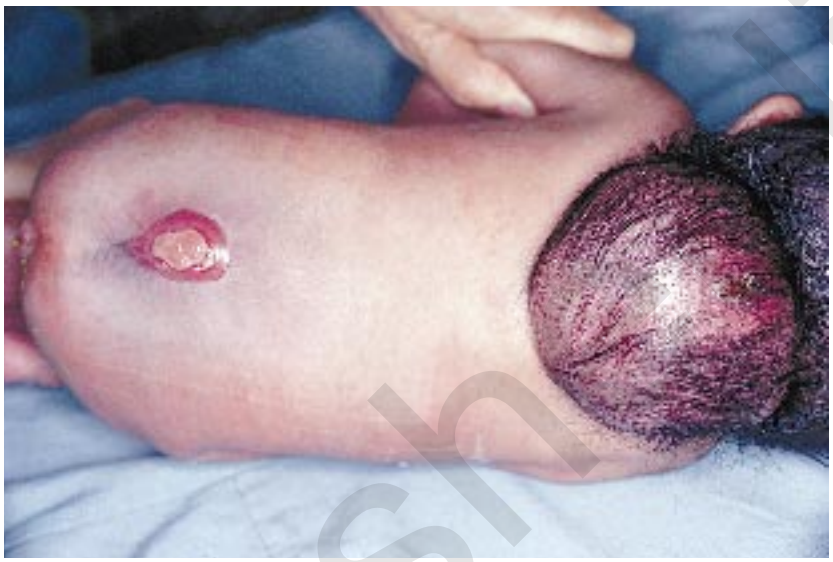

Figure 3.56. Infant with both a posterior encephalocele and a lumbar myelomeningocele. The lumbar area is the most common site for myelomeningoceles.

3.57

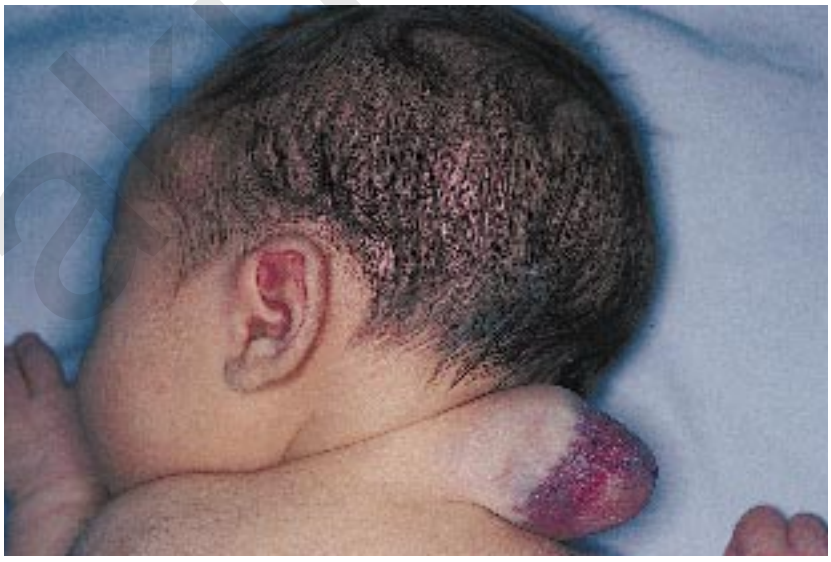

Figure 3.57. A cervical meningocele may be difficult to differentiate from an occipital encephalocele. Further study in this infant showed that this was a cervical meningocele.

3.58

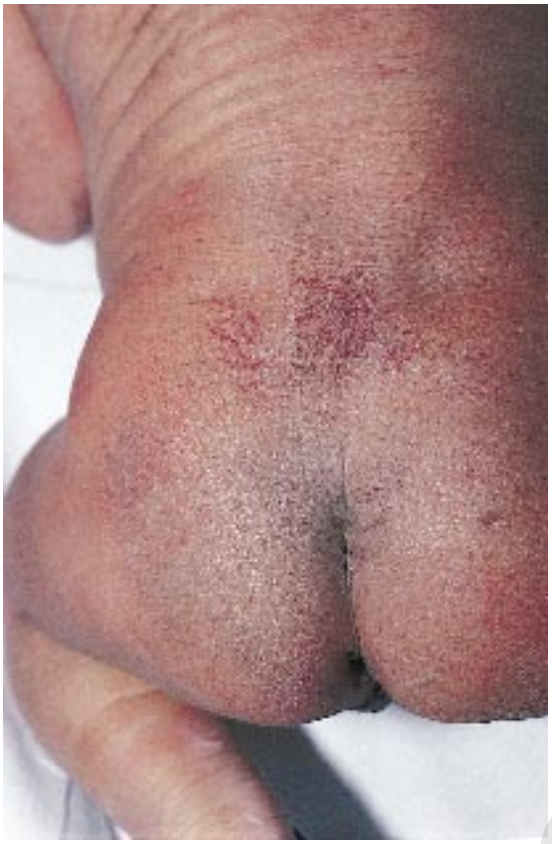

Figure 3.58. A midline hair tuft in the lumbosacral area. This infant had a tethered cord on MRI study. Hair tufts, skin tags, sinuses, and abnormal pigmentation that occur in the midline along the length of the spinal column should always alert one to the possibility of an associated underlying neurologic abnormality. With a tethered cord the neural tissue is firmly attached at its caudal end, being bound by a stout connective tissue band to the interior of the bony canal. With growth, the spinal canal normally grows more rapidly than the spinal cord resulting in traction on the cord. This may gradually pull the lower end of the brainstem down into the foramen magnum like a cork into a bottle. This is the Arnold-Chiari malformation.

3.59

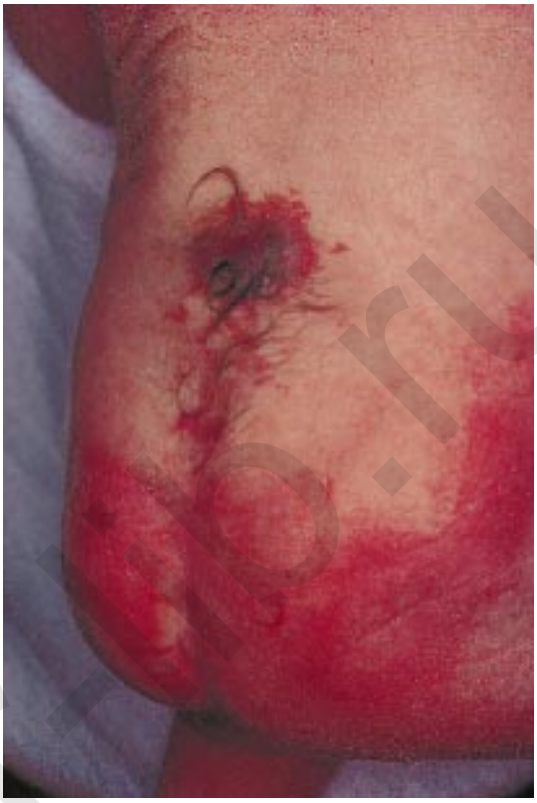

Figure 3.59. A midline tuft of hair with a pigmented nevus in the lumbosacral area. This should alert one to the possibility of an associated underlying neurologic abnormality.

3.60

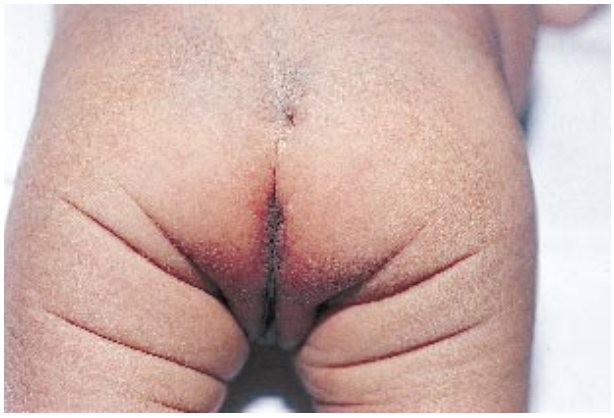

Figure 3.60. Midline pilonidal dimples or sinuses are common deformities. They represent the point of attachment of the distal end of the neural tube to the coccyx. If there is a deep dimple, an MRI should be performed to exclude a neural tube defect. The MRI was normal in this infant.

3.61

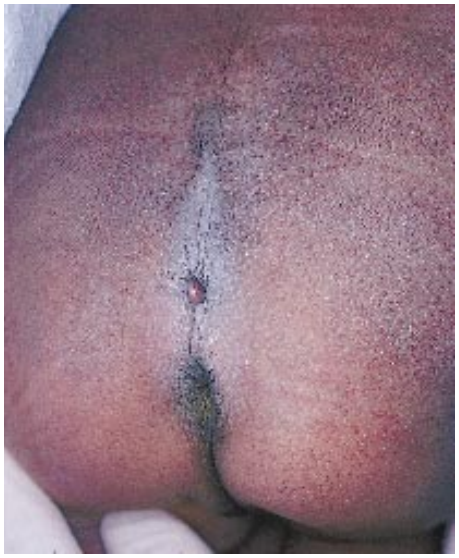

Figure 3.61. This infant had a midline small skin tag with depigmentation of the skin in the lumbosacral region. The MRI revealed a tethered cord.

3.62

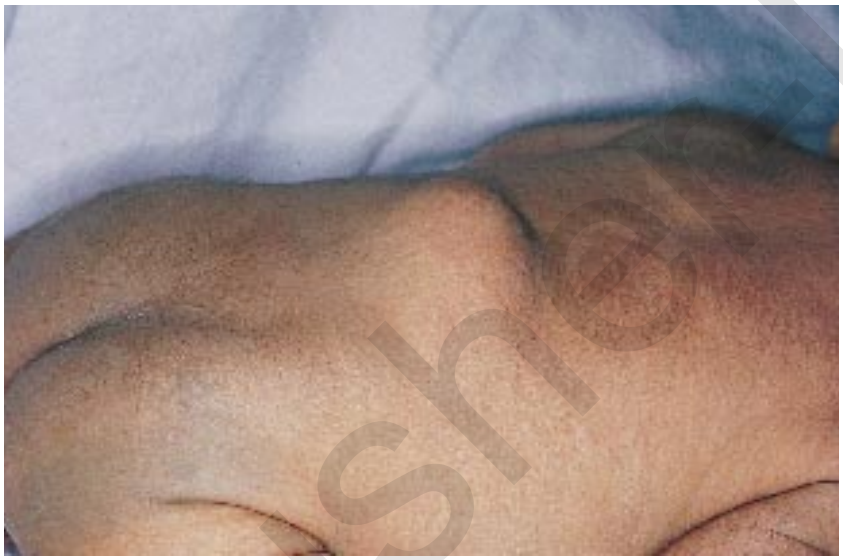

Figure 3.62. This infant has a lumbar meningocele which is an example of a closed neural tube defect. The neural tube closes by infolding from the coccyx to the nasion and defects of fusion can occur anywhere along this axis. Meningoceles occur when the membranes surrounding the spinal cord bulge outward through a dorsal defect in the bony spinal canal. The resulting mass may be tense or fluctuant and is covered by intact skin.

3.63

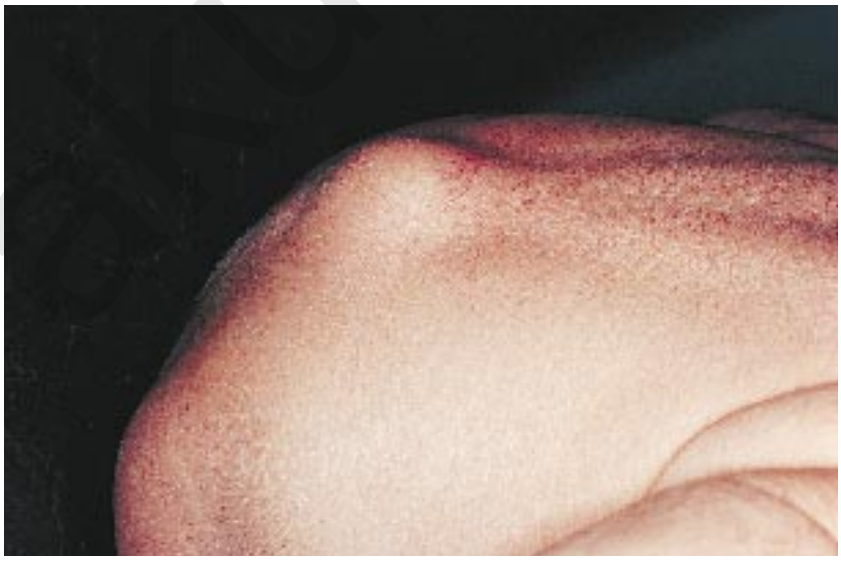

Figure 3.63. A lumbosacral meningocele is present in this infant. The lumbosacral area is the most common location for both meningoceles and myelomeningoceles. Infants with meningoceles and myelomeningoceles may have an Arnold-Chiari malformation and a high percentage develop hydrocephalus. The quality of life is influenced by the site of the neurologic lesion.

3.64

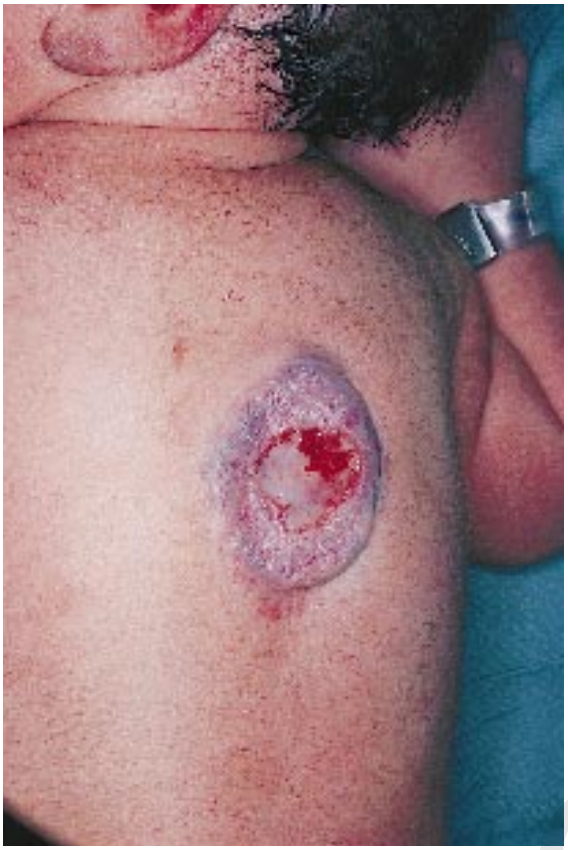

Figure 3.64. This infant has a thoracic myelomeningocele which presents as an open midline defect. Although myelomeningoceles occur most commonly at the lumbosacral level, they may affect the neural tube at any level. The posterior elements covering the spinal canal fail to form, but in this type of defect the cystic mass that bulges out posteriorly contains neural tissue and the surface of the meninges is exposed to the exterior with no skin covering. Large lesions may incorporate a large segment of the spinal cord itself.

3.65

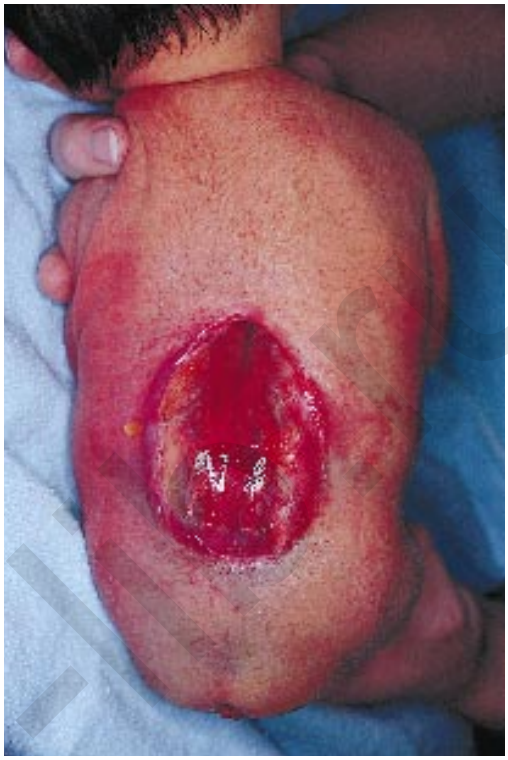

Figure 3.65. Thoracolumbosacral myelomeningocele with exposure of the central spinal canal. Note the leaking of cerebrospinal fluid. The meningeal sac often ruptures before birth or during delivery, thus exposing the neural tissue to direct injury or the risk of infection. Loss of neurologic function distal to the lesion is the rule. There may be absence of control of the urinary and anal sphincters, bladder paralysis, and variable degrees of sensory and motor deficit to the lower limbs.

3.66

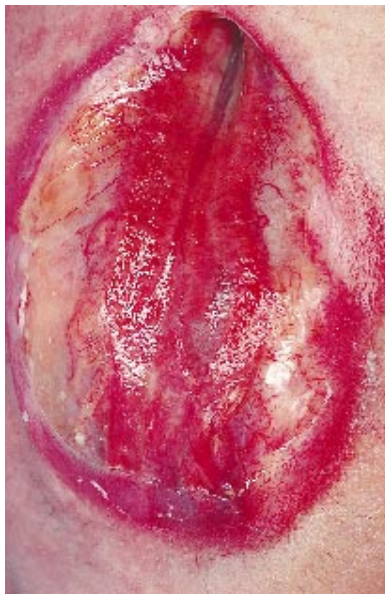

Figure 3.66. A close-up view of the thoracolumbosacral myelomeningocele with the exposed central canal visible.

3.67

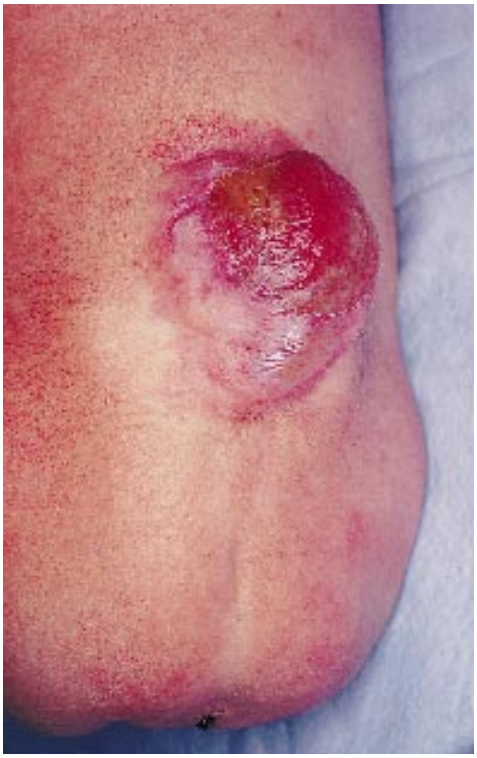

Figure 3.67. In this infant with a lumbosacral myelomeningocele note that with this low level of involvement, there was no anal wink, the hips were flexed, and there were bilateral clubfeet. Clubfeet and rocker-bottom feet are commonly associated with myelomeningoceles.

3.68

Figure 3.68. In this infant with a lumbosacral meningocele note that the sac is closed and that there is an overlying hair tuft. Trivial abnormalities such as nevi, sinuses, and hair tufts may indicate an underlying central nervous system abnormality.

3.69

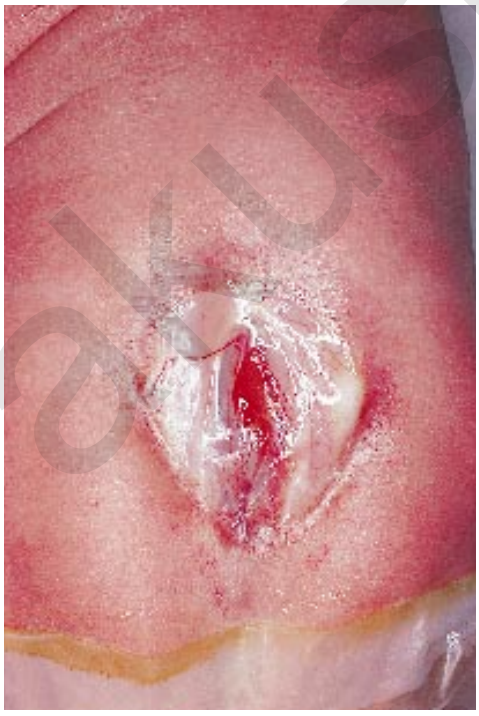

Figure 3.69. An infant with rachischisis or myelomeningocele. In contrast to encephaloceles, myelomeningoceles represent failure of closure of the posterior neuropore. There is usually lack of fusion of the vertebral arches with broadened vertebrae and dorsal protrusion of the neural tissue in an enclosed sac with a thin membrane that can easily rupture. Secondary hydrocephalus is a common association.

3.70

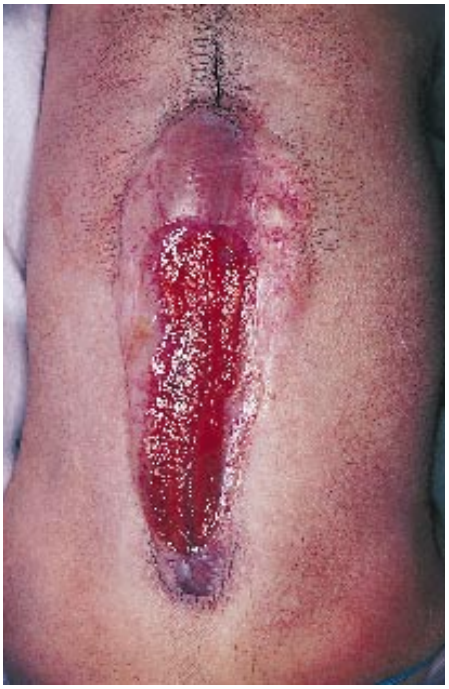

Figure 3.70. Thoracolumbar myelomeningocele in another infant. Diastematomyelia (congenital medial cleft of the spinal cord) is usually associated with spina bifida occulta. There may be tufts of hair (hypertrichosis) in the area of the mid to lower thoracic spinal column. The condition is diagnosed by MRI.

3.71

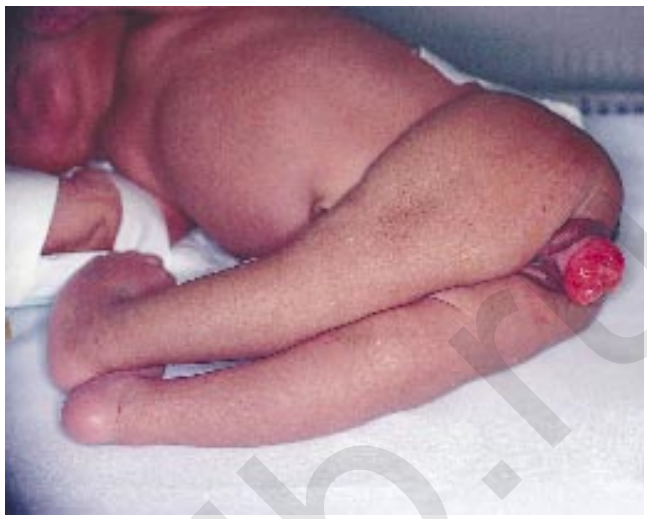

Figure 3.71. In infants with a myelomeningocele there may be associated abnormal posture. Note the severely deformed lower limbs from lack of movement in utero resulting in genu recurvatum, and the rocker-bottom feet. This infant also shows procidentia (prolapse of the uterus with protrusion of the cervix). Procidentia is a very uncommon finding in the neonate but, if present, is invariably associated with a neural tube defect.

3.72

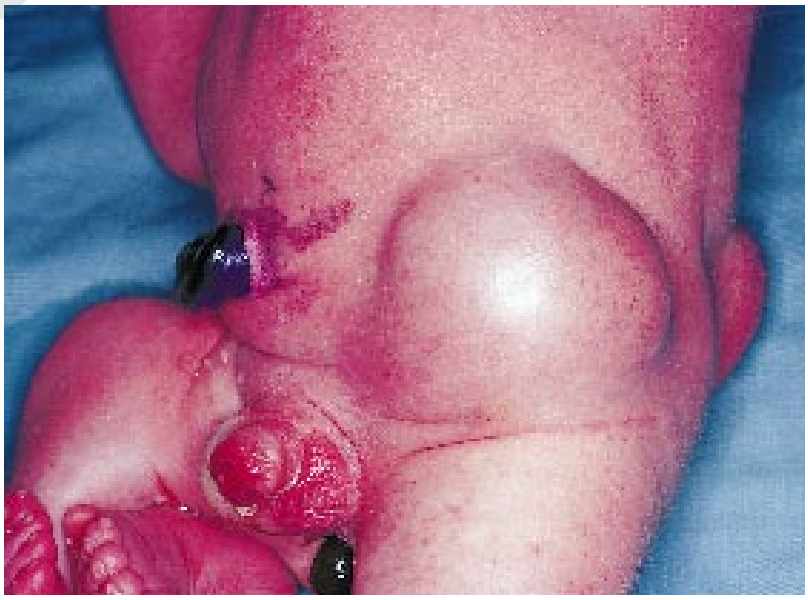

Figure 3.72. Lumbar myelomeningocele and anterior abdominal wall hernia.

3.73

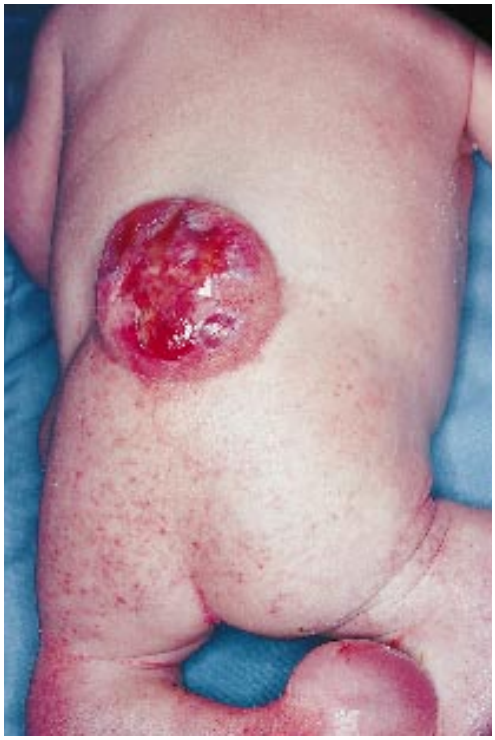

Figure 3.73. Posterior view of the same infant as in Figure 3.72 showing the lumbar myelomeningocele.

3.74

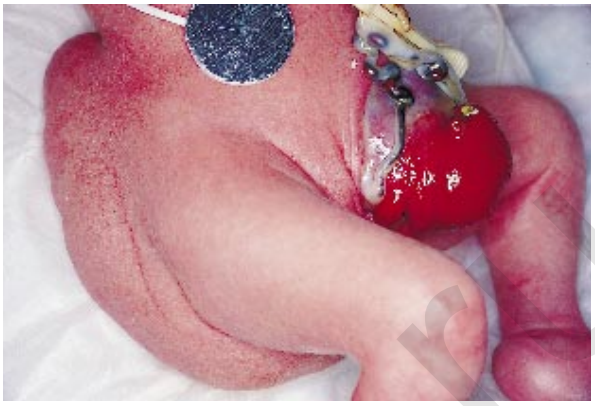

Figure 3.74. A 31-week gestation premature infant with a cloacal exstrophy sequence (exstrophy of the cloaca, imperforate anus, ambiguous genitalia, and myelocystocele). There is a myelocystocele (hydromyelia; syringomyelocele) extending from T7 to the sacrum, and the infant also had an associated Arnold-Chiari malformation.

Myelocystoceles are due to dilatation of the central canal (hydromyelia) and to protrusion over the surface of the posterior aspect of the much expanded spinal cord which may be covered by meninges and skin. In such cases, the cavity is cranially and caudally directly connected with the central canal. The spinal nerves do not traverse the cavity (as they do in the common myelomeningocele) but course around it.

3.75

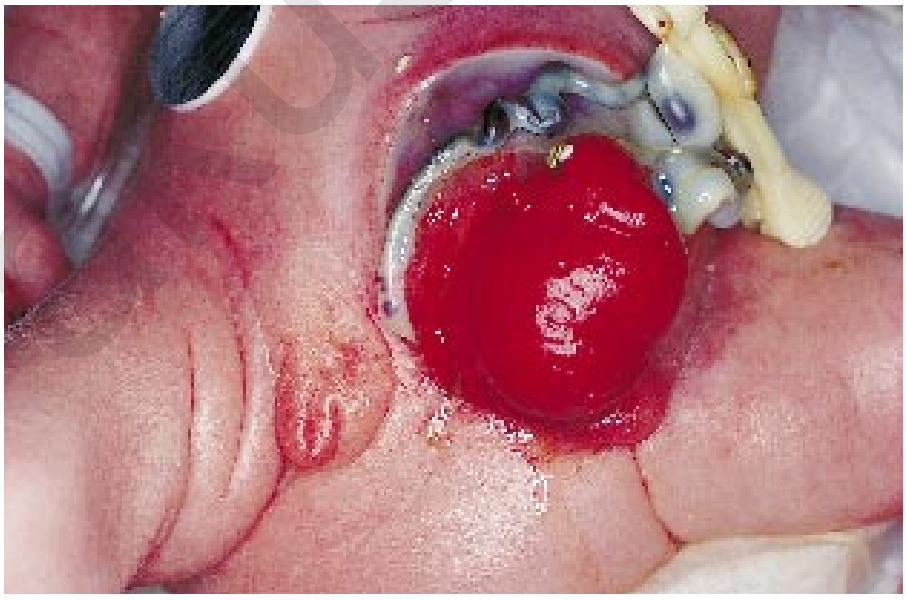

Figure 3.75. A close-up view of the exstrophy of the cloaca. Note the ureteral openings.

3.76

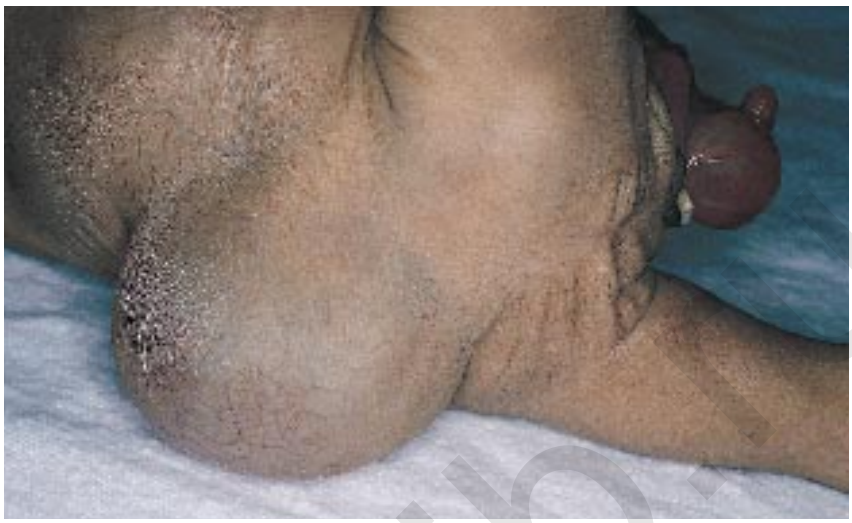

Figure 3.76. Another infant with the cloacal exstrophy sequence. Associated anomalies include imperforate anus, ambiguous genitalia, cloacal exstrophy, and lumbosacral myelocele.

3.77

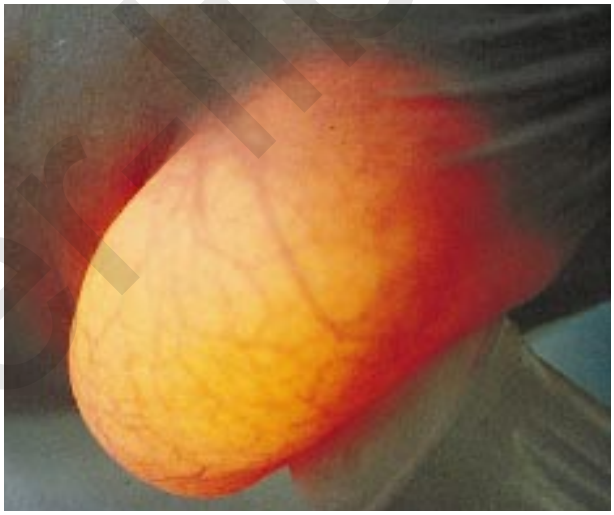

Figure 3.77. Transillumination of the lumbosacral mass of the same infant shows the myelocystocele.

3.78

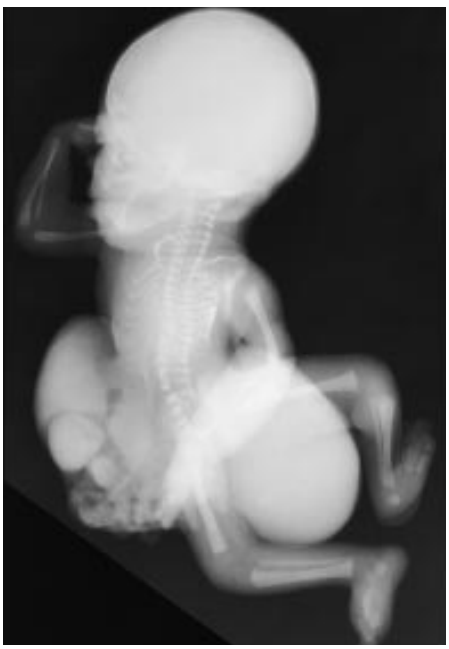

Figure 3.78. Radiograph of another infant with the cloacal exstrophy sequence. Note the large myelocystocele, omphalocele, and cloacal exstrophy.

3.79

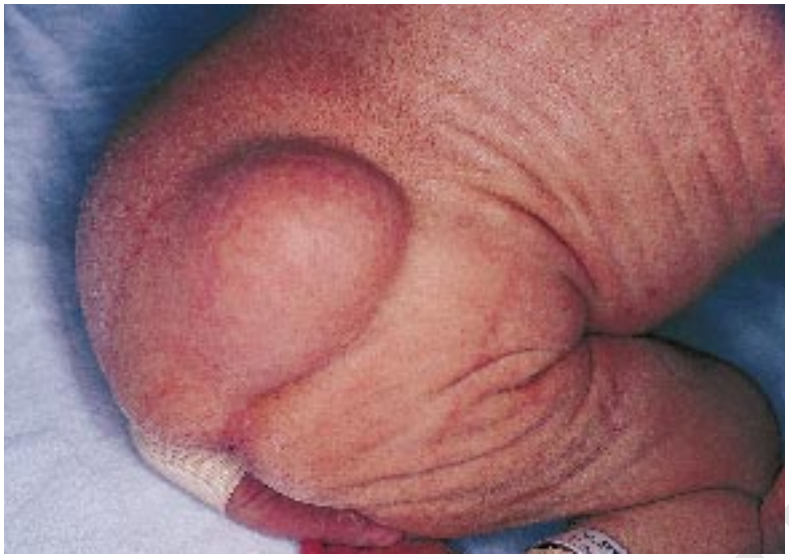

Figure 3.79. This lipomeningocele is a simple meningocele with infiltration of fibrous and fatty tissue continuous with a subcutaneous lipoma. The lipoma may even extend into the spinal canal. Because of the presence of the lipoma, as seen in this infant, the meningocele is not midline. There was an underlying tethered cord as demonstrated by MRI.

3.80

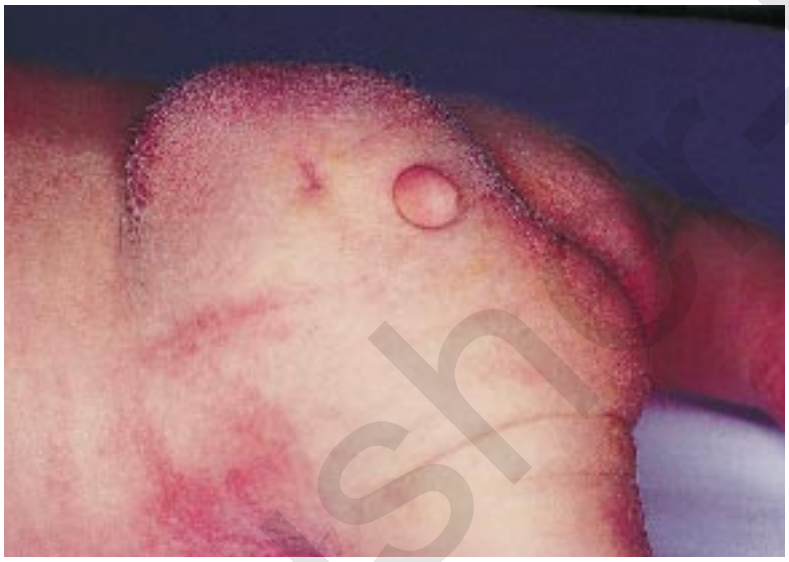

Figure 3.80. Note the associated protrusion of a skin tag in another variant of a lipomeningocele. In infants with lipomeningoceles, skin tags may be present, there may be some skin discoloration due to the presence of the lipoma, and the lesions are usually not midline because of the presence of the lipoma. Lipomeningoceles are relatively rare defects.

3.81

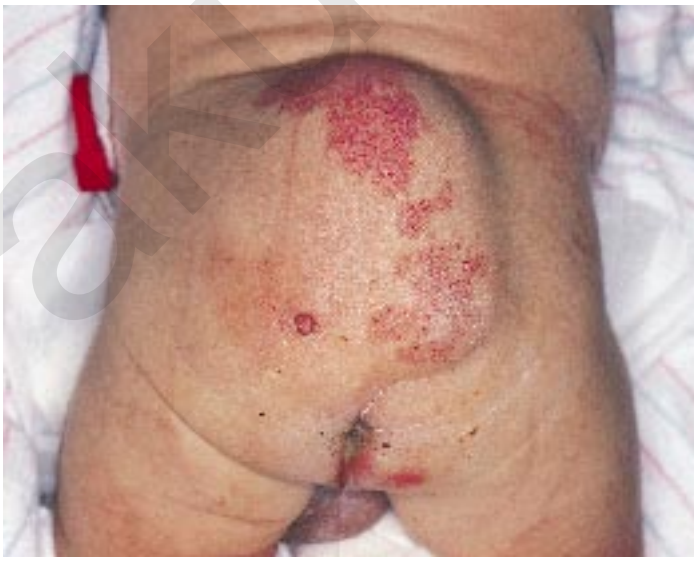

Figure 3.81. In this infant with a lipomeningocele with a tethered cord, note the associated skin discoloration with a small skin tag.

3.82

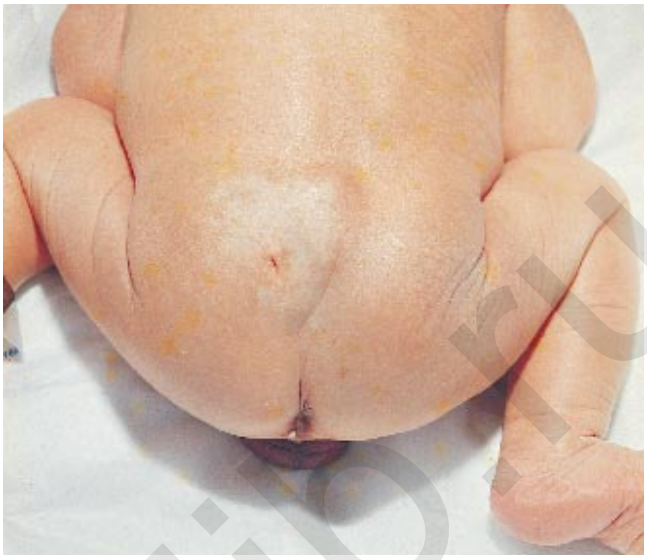

Figure 3.82. A lipomeningocele with an associated sinus tract is present in this infant.

3.83

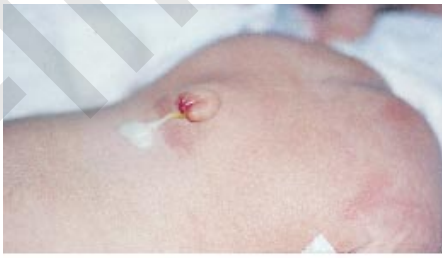

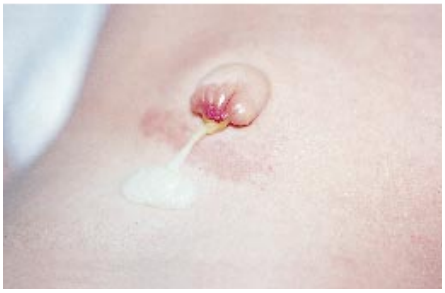

Figure 3.83. Infant with a large dermal sinus tract associated with cord tethering and spinal dysraphism. On MRI there was a tethered cord and spina bifida both above and below the lesion.

3.84

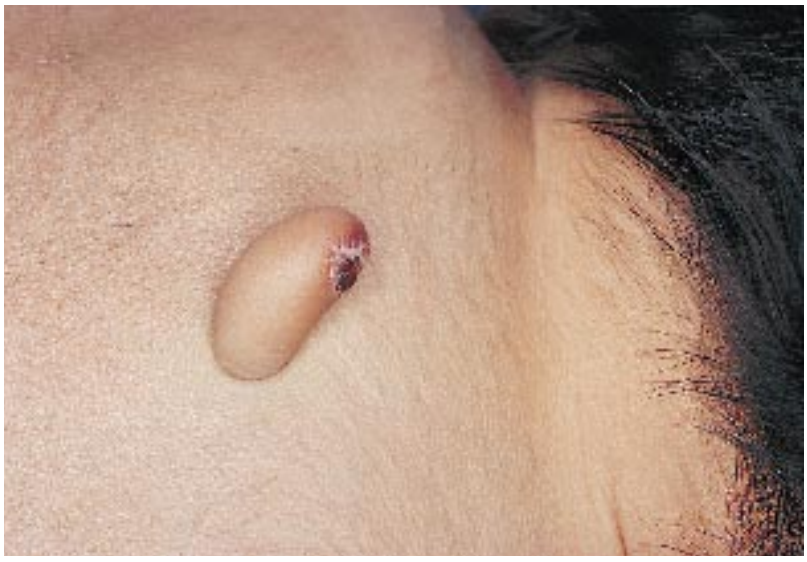

Figure 3.84. Small "finger-like" dermal tag extending from the midline of the back at the T4 level. Underlying the skin tag there was bony dysraphism with a small band of soft tissue extending toward the spinal cord. There were multiple rib anomalies with fusion of several upper thoracic ribs. MRI showed a spina bifida of the upper thoracic spine and tethering of the spinal cord distally.

3.85

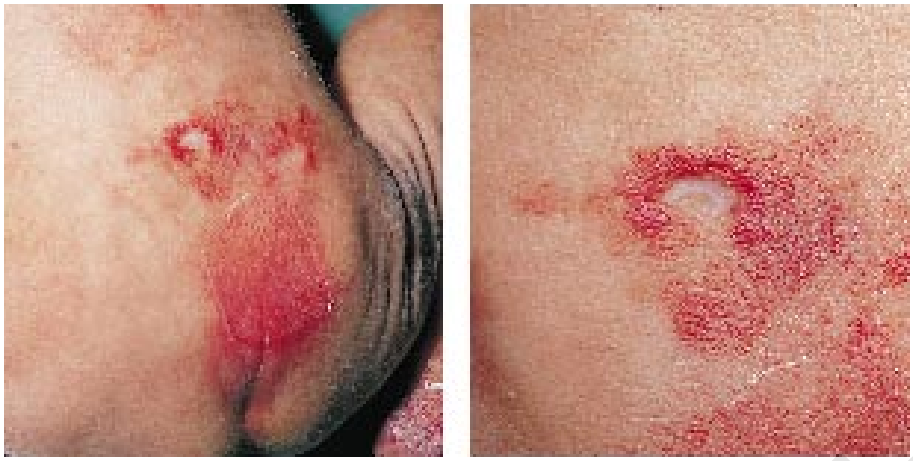

Figure 3.85. On the left is a photograph of a large midline skin defect representing a large dermal sinus. Right is a close-up of the dermal sinus.

3.86

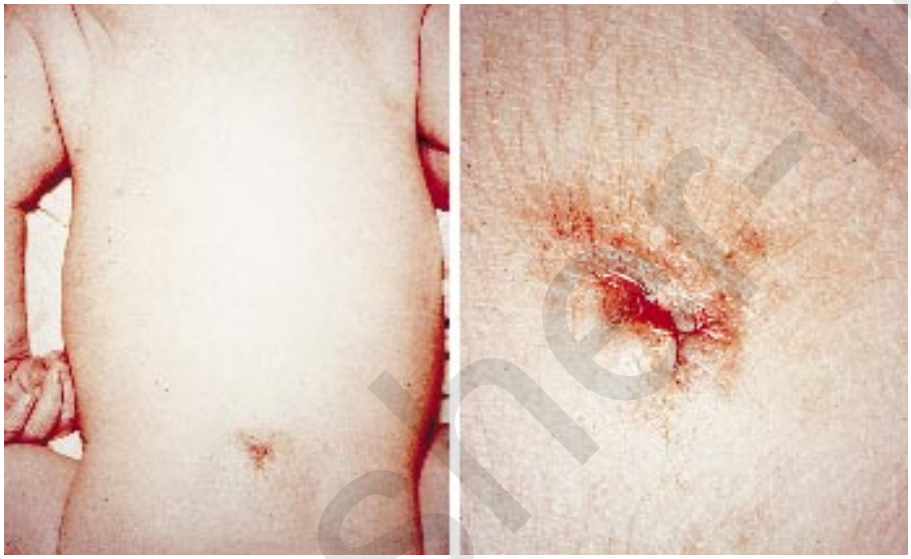

Figure 3.86. Left, photograph of another variant of a dermal sinus. Right, close-up of the same sinus. Dermal sinuses occur midline anywhere along the spinal cord and warrant examination of the central nervous system.

3.87

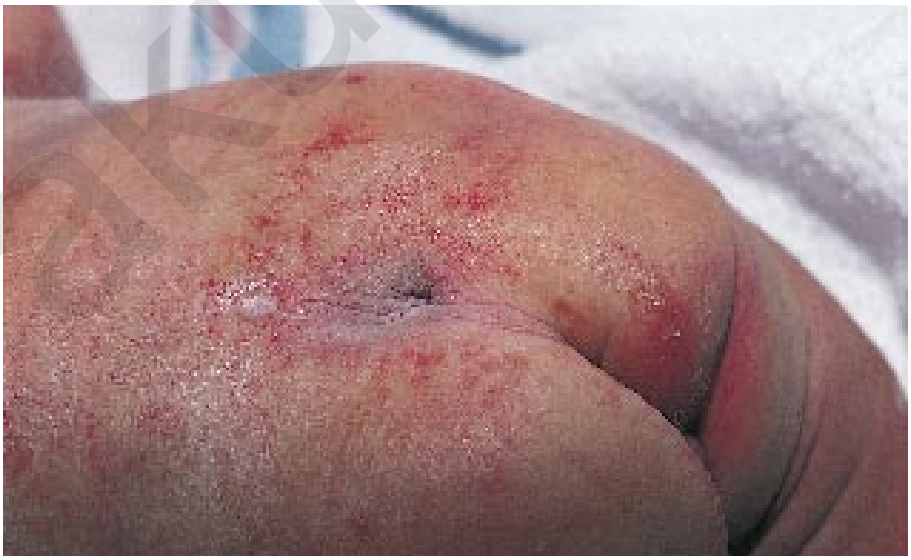

Figure 3.87. Midline skin defect with an inferior deep pilonidal dimple. MRI of the spinal column revealed a tethered spinal cord. A pilonidal sinus may connect with the underlying distal end of the spinal canal. This should be suspected when the bottom of a midline pit over the sacrum cannot be seen, if there is any fluid emerging from the depths of such a pit, or when the pit contains hairs.

3.88

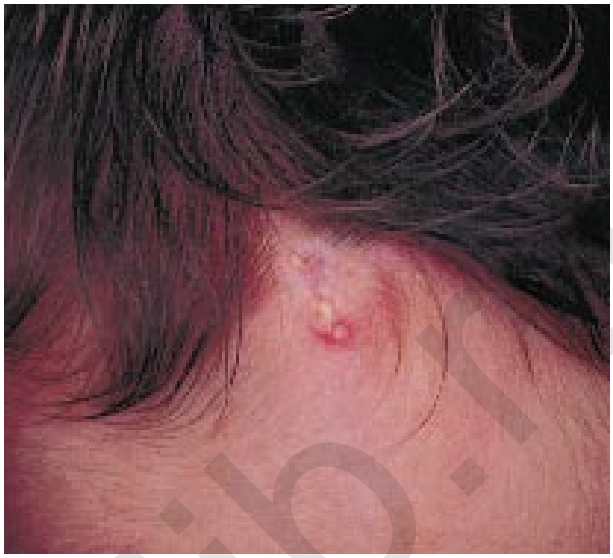

Figure 3.88. Midline skin defect at the inferior aspect of the hairline of an infant with an associated dermal sinus tract. This infant had an associated lateral nasal cleft.

3.89

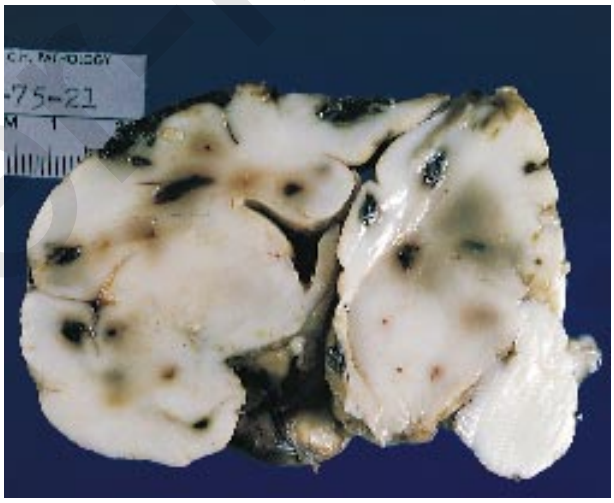

Figure 3.89. Anoxic encephalomalacia and hemorrhages in an autopsy specimen of a brain. Note the multiple areas of hemorrhage in the brain of this term infant.

3.90

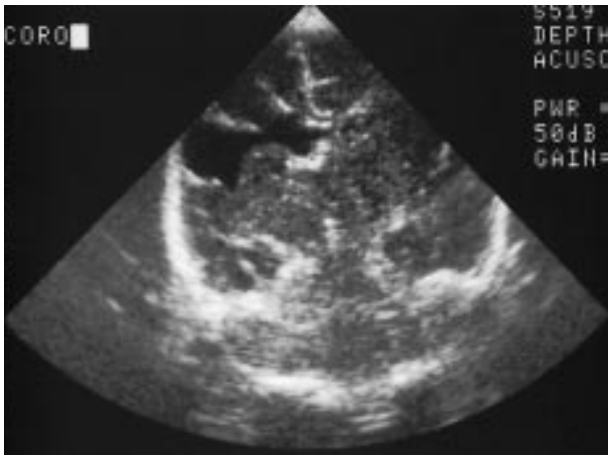

Figure 3.90. Head ultrasound examination of an infant with schizencephaly. This is the most severe of the cortical malformations as the result of abnormal migration occurring no later than the 2nd month of gestation. There is complete agenesis of a portion of the cerebral wall leaving bilateral schisms or clefts.

3.91

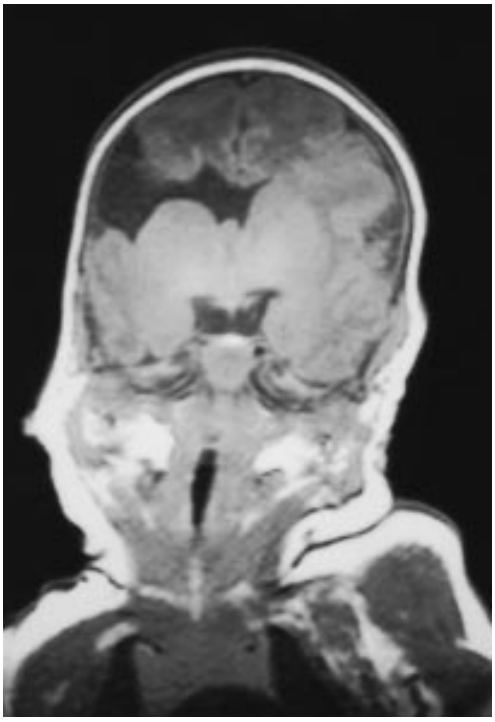

Figure 3.91. Clefts or "lips" demonstrated in the right hemisphere in the MRI of the head of an infant with schizencephaly. The lips of the clefts may become widely separated and massive dilation of the ventricles may occur. This can result in a striking degree of transillumination of the skull with an incorrect diagnosis of hydranencephaly. Infants who survive have severe seizures with marked spasticity (sometimes preceded by hypotonia), and severe retardation.

3.92

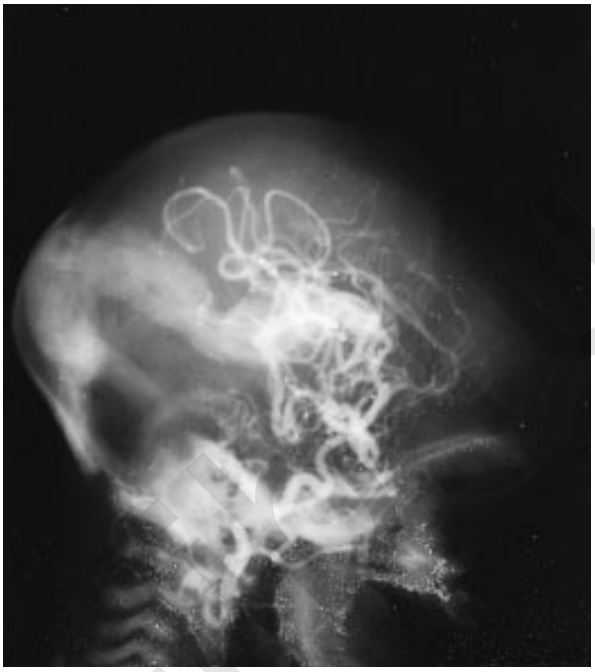

Figure 3.92. Angiogram of an infant who presented with severe congestive heart failure. Note the large arteriovenous malformation of the great vein of Galen. These malformations have been diagnosed both pre- and postnatally with the use of ultrasonography, CT scan, or MRI.

3.93

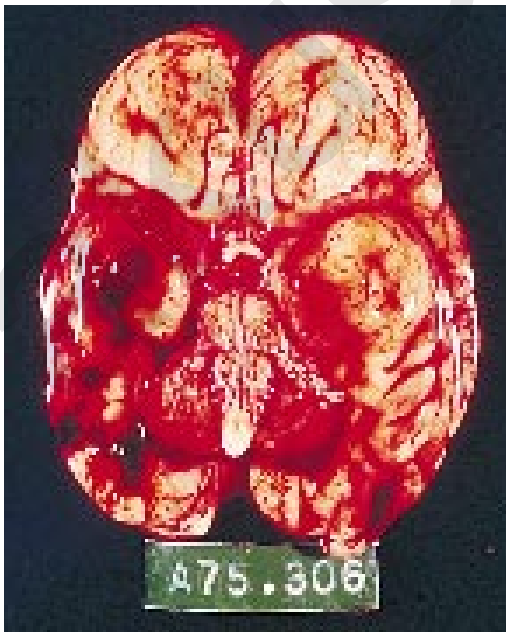

Figure 3.93. Autopsy specimen of the brain of a premature infant who suffered from a large subarachnoid hemorrhage. Note the bleeding especially around the temporal lobes.

3.94

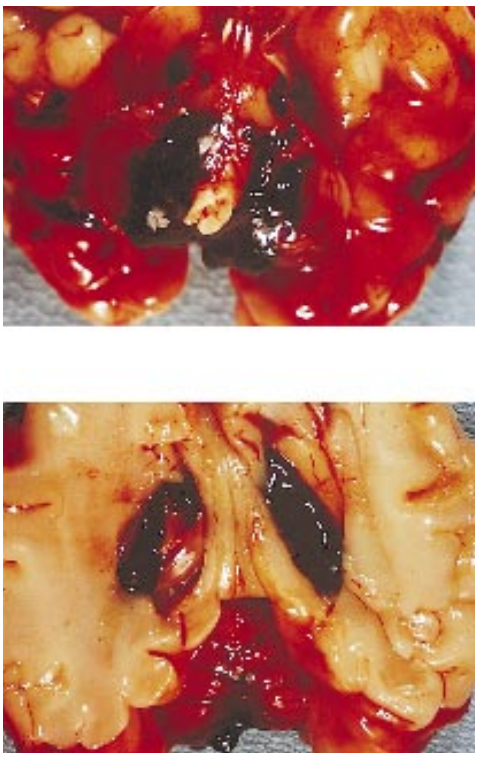

Figure 3.94. Autopsy specimens of the brains of two infants showing massive hemorrhage. Top, hemorrhages at the base of the brain. Bottom, massive bilateral intraventricular hemorrhages.

3.95

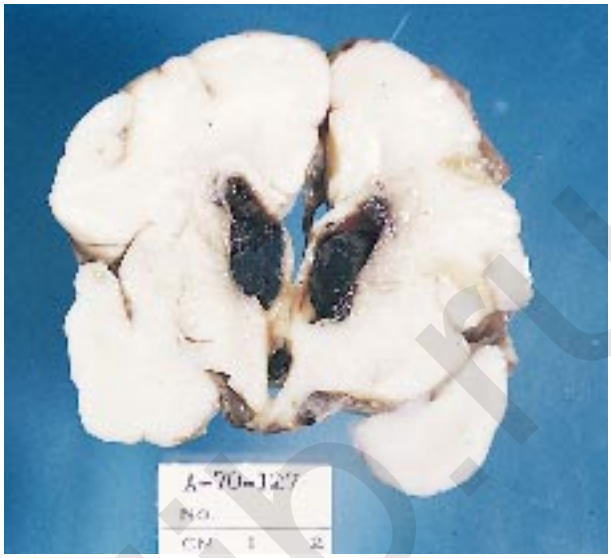

Figure 3.95. Autopsy coronal views of the brain with bilateral intraventricular hemorrhage. Note the lack of convolutions and convexities in this immature brain. The ventricles are enlarged as a result of massive bleeding.

3.96

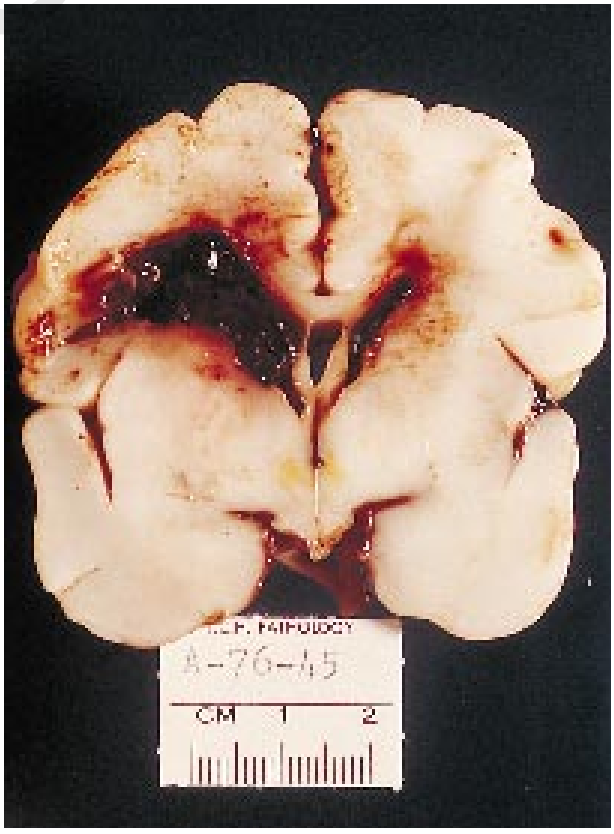

Figure 3.96. Autopsy specimen of a brain with bilateral intraventricular hemorrhage. Note the marked extension of the hemorrhage into the right cerebrum. This constitutes a grade IV intraventricular hemorrhage.

3.97

Figure 3.97. Autopsy specimens of casts of blood from a large intraventricular hemorrhage. Top, cast of the lateral ventricle; bottom, cast of the fourth ventricle.

3.98

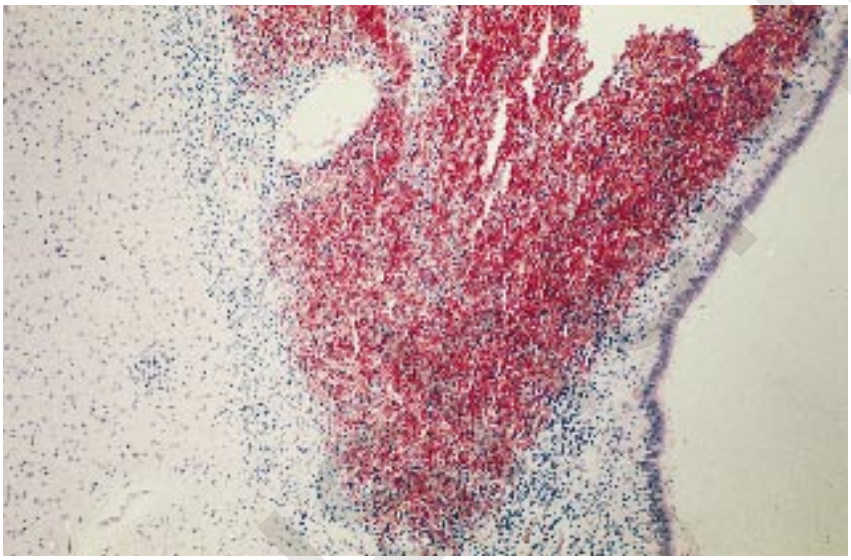

Figure 3.98. Histology of a section from the brain of a premature infant with a subependymal hemorrhage. Note, on the right, the lack of congestion/blood in the adjacent ventricle. This indicates that the subependymal hemorrhage has not broken through into the ventricle.

3.99

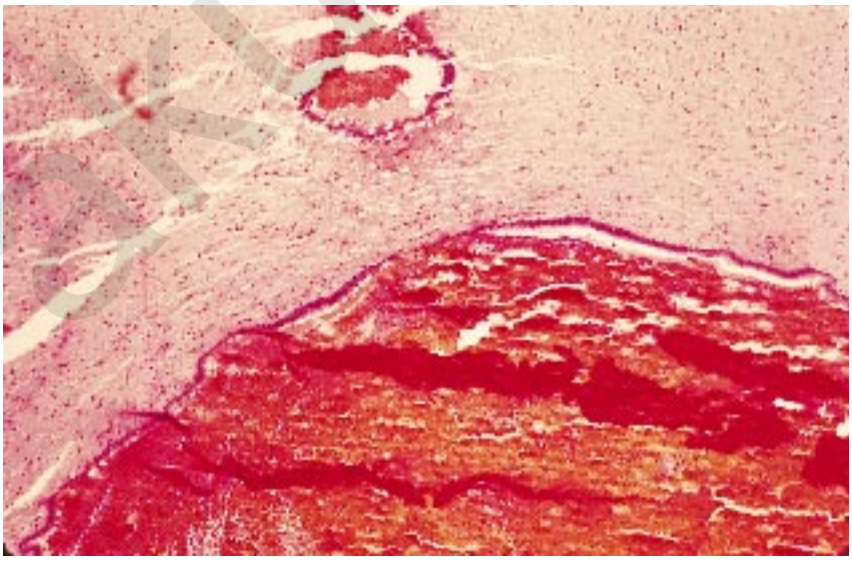

Figure 3.99. In contrast, this histology represents a section from the brain of a premature infant who has had an intraventricular hemorrhage. Note that the congestion/blood has broken through into the ventricle which is filled with blood.

Classification for periventricular-intraventricular hemorrhage (PVH-IVH):

Grade I. Subependymal hemorrhage.
Grade II. Hemorrhage into the ventricles.
Grade III. Hemorrhage into the ventricles with dilatation of the ventricles.
Grade IV. Hemorrhage into the ventricles with dilatation of the ventricles and extension into the parenchyma.

3.100

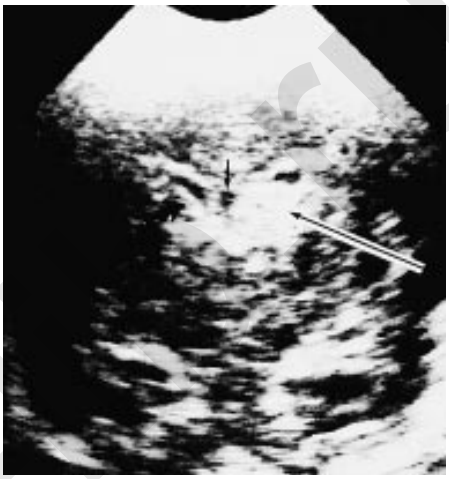

Figure 3.100. A coronal ultrasound scan through the brain of a premature infant with a grade I PVH-IVH. There is a large left-sided subependymal hemorrhage (large arrow) with a less echogenic area on the right. Note the midline septum pellucidum (small superior arrow). (Figures 3.100–3.103 are from Langston C, Wolfson R. JAMA 1983; 250:3213 and are reprinted with the permission of the American Medical Association. Copyright 1983, American Medical Association.)

3.101

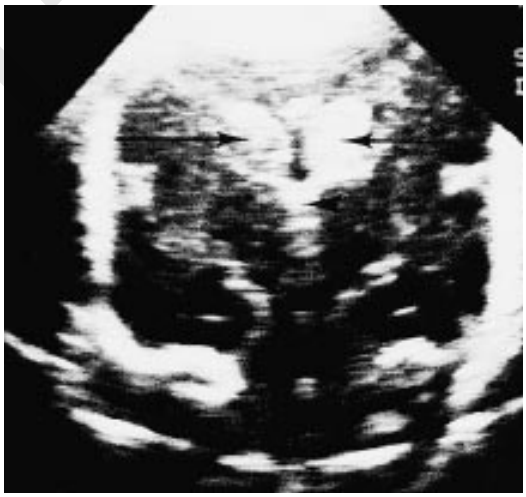

Figure 3.101. A coronal ultrasound scan shows echogenic blood in the mildly dilated lateral ventricles (arrows) and in the 3rd ventricle (arrowhead).

3.102

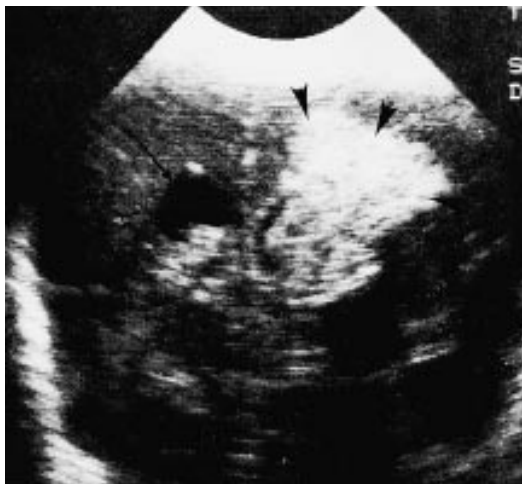

Figure 3.102. This coronal ultrasound scan shows extension of blood into the parenchyma of the brain (arrow heads). Note the large dilated right lateral ventricle (arrows).

3.103

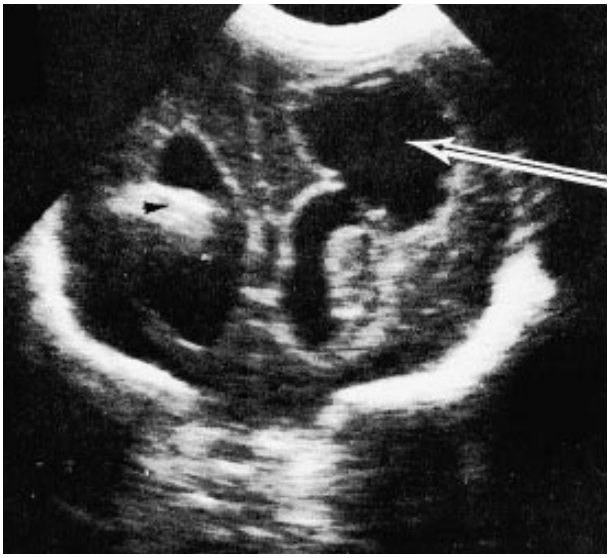

Figure 3.103. This coronal ultrasound scan shows conversion of intraparenchymal bleeding to a large area of porencephaly (arrow). The echogenic shunt tube is placed in the dilated right lateral ventricle (arrowhead).

3.104

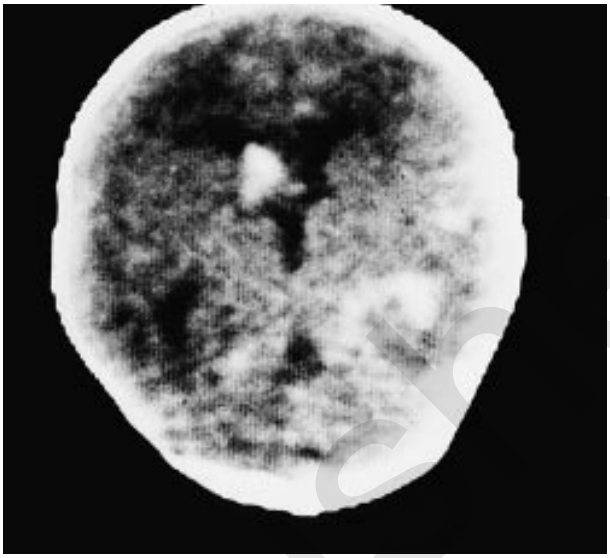

Figure 3.104. A CT scan of an infant with a grade II PVH-IVH. There is blood within the lateral ventricles without ventricular dilatation.

3.105

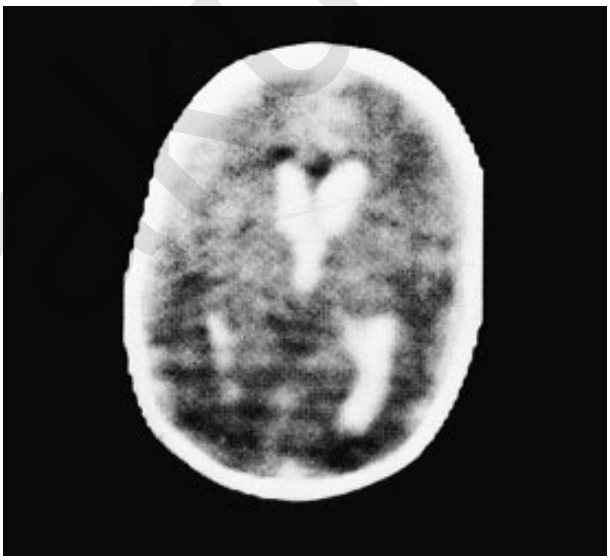

Figure 3.105. A CT scan of an infant with a grade III PVH-IVH. There is blood within the dilated lateral ventricles.

3.106

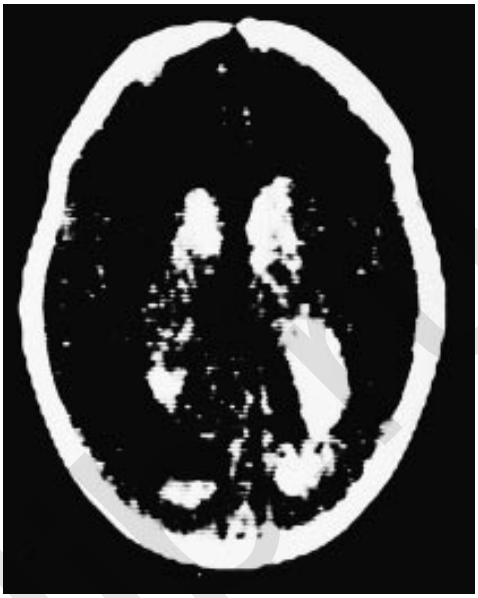

Figure 3.106. A CT scan of an infant with a grade IV PVH-IVH. Note the blood within the lateral ventricles and extension into the cerebral parenchyma.

3.107

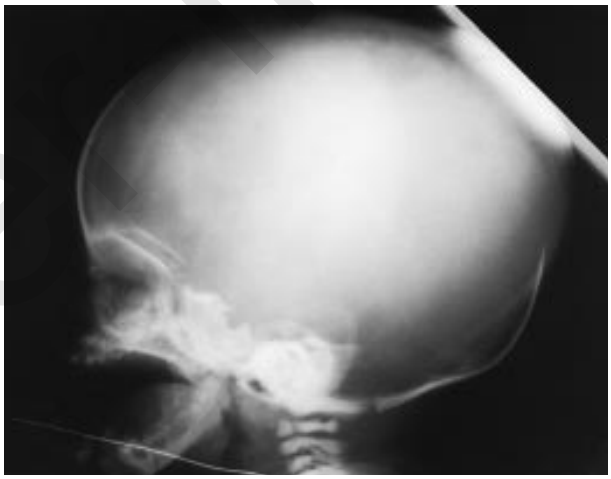

Figure 3.107. This term infant presented with marked increase in head size (fronto-occipital circumference 41 cm). A lateral skull radiograph showed the enlarged head and an increased density over the parietal area.

3.108

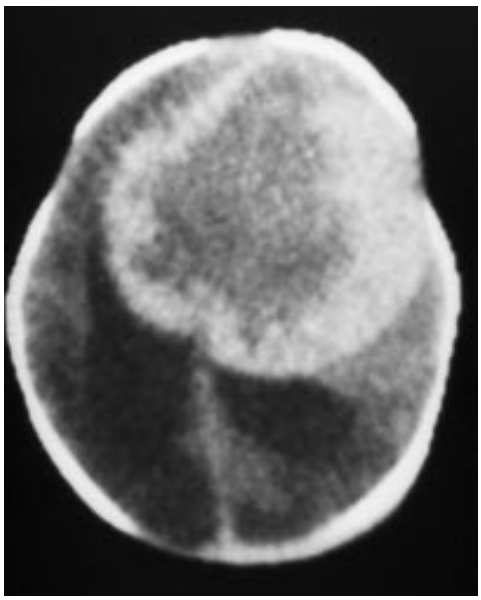

Figure 3.108. A CT scan of the same infant showed a large brain tumor. The infant died at the age of 2 days and autopsy diagnosis was glioblastoma multiforme. There was hydrocephalus and a massive brain tumor with diffuse encephalomalacia and marked distortion of the brain.

The presentation of congenital brain tumors includes:

1) Stillborn with megalencephaly, with tumor replacing nearly all of the brain.
2) Liveborn with dystocia secondary to hydrocephalus.
3) Normal at birth but with abrupt cranial enlargement within a few days.

3.109

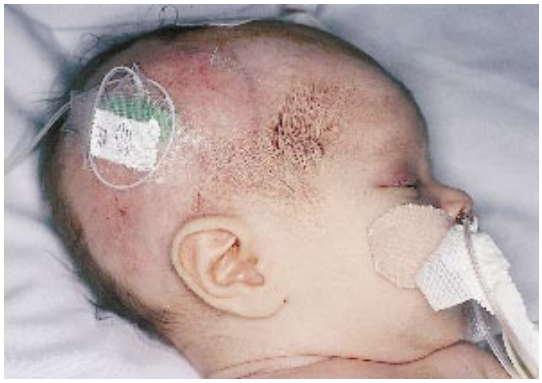

Figure 3.109. This term infant, born by spontaneous vaginal delivery, developed seizures on the first day of life and was treated with phenobarbital. The EEG showed decreased activity of the left temporal region. The fronto-occipital circumference increased rapidly in the first few days of life from 38.5 cm at birth to 41 cm at 10 days of age. Note the enlargement of the head and the illusion of low-set rotated ears.

3.110

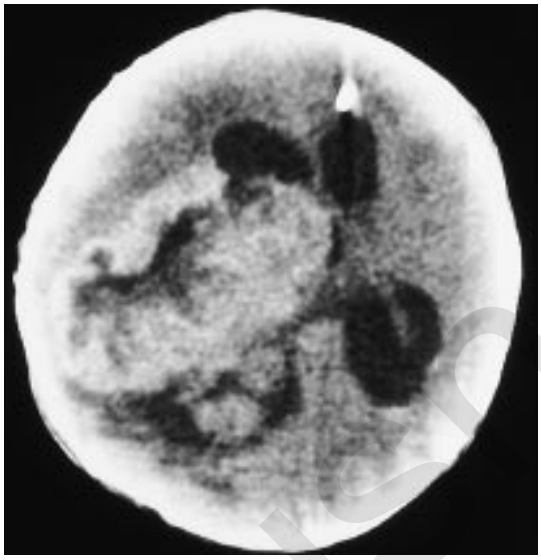

Figure 3.110. A CT scan of the same infant revealed a large choroid plexus tumor. These tumors are usually associated with hydrocephalus. Hydrocephalus may occur as a result of an increased production of CSF or may be due to obstruction of the flow of CSF. A rapid increase in the size of the tumor or hydrocephalus may be associated with hemorrhage and necrosis in the tumor as occurred in this infant.

3.111

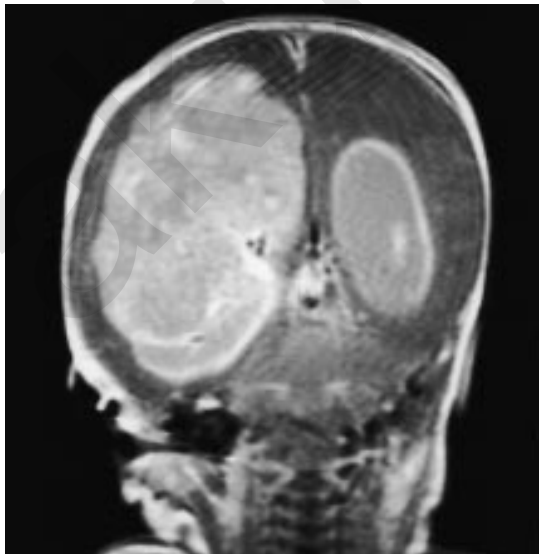

Figure 3.111. MRI of the same infant on the 9th day of life revealed a large mass on the right side extending to the midline with ventricular dilatation and hydrocephalus. The infant died at 31 days of age.

3.112

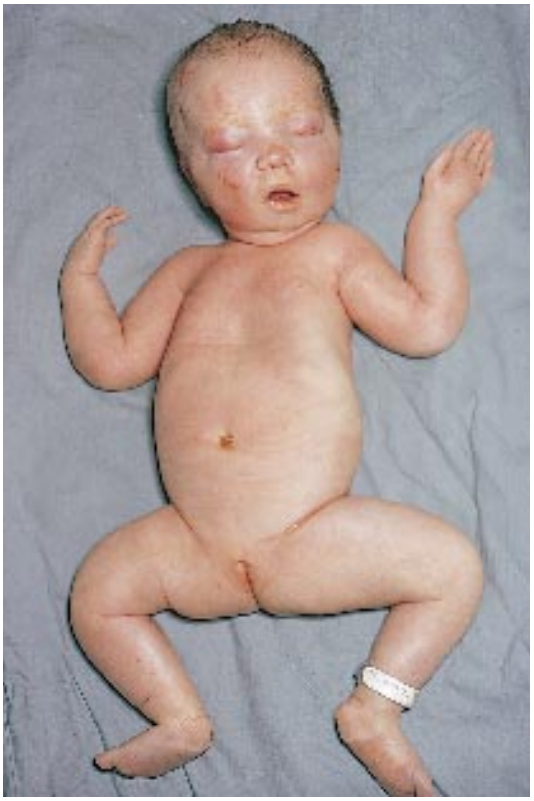

Figure 3.112. There was marked lack of fetal movement, vaginal delivery was difficult, and there was a fracture of the left humerus and of the right femur present at birth in this floppy term infant. Note the "frog leg" position with marked hypotonia, areflexia, and paradoxical respiration. The diagnosis was amyotonia congenita.

3.113

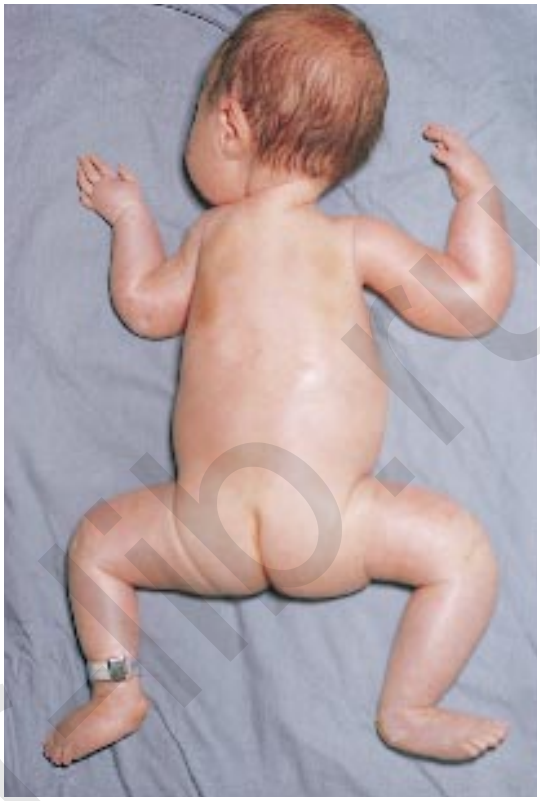

Figure 3.113. Posterior view of the same infant. Note again the hypotonia and the "frog leg" position with swelling of the left arm and the right leg. This swelling is the result of fractures at the time of birth.

3.114

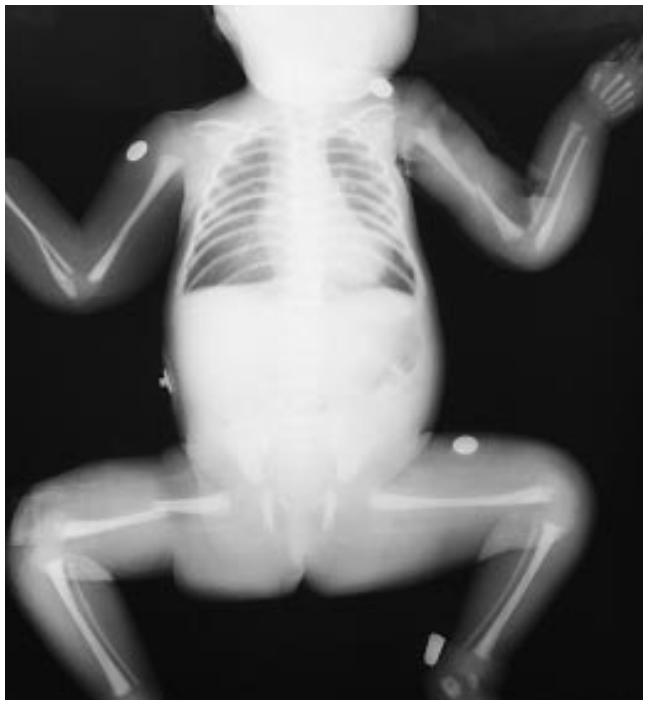

Figure 3.114. Radiograph of the same infant. Note the very thin bones, lack of muscle tissue, and fracture of the left humerus and right femur.

3.115

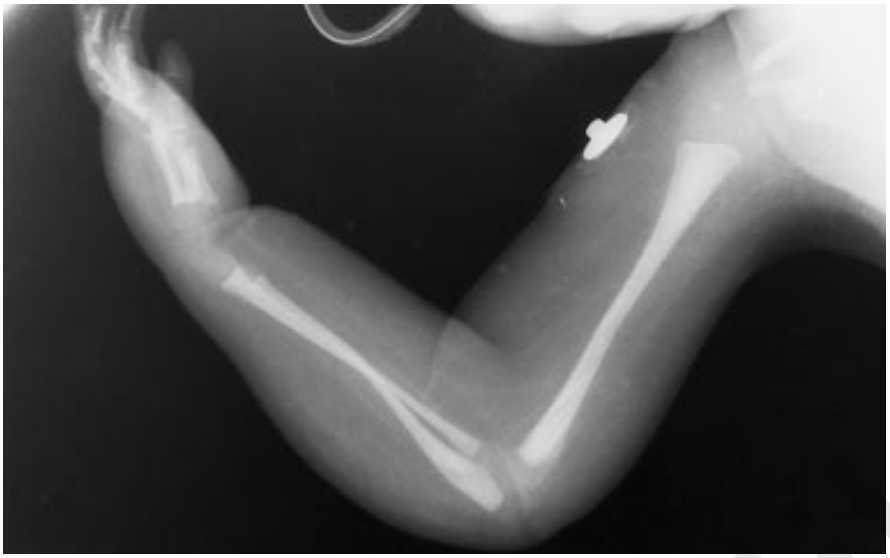

Figure 3.115. Radiograph of the right arm of the same infant shown in Figure 3.112-3.114. Note the marked thinning of the bones and lack of muscle mass. This poor development of bone and muscle results from lack of fetal movement.

3.116

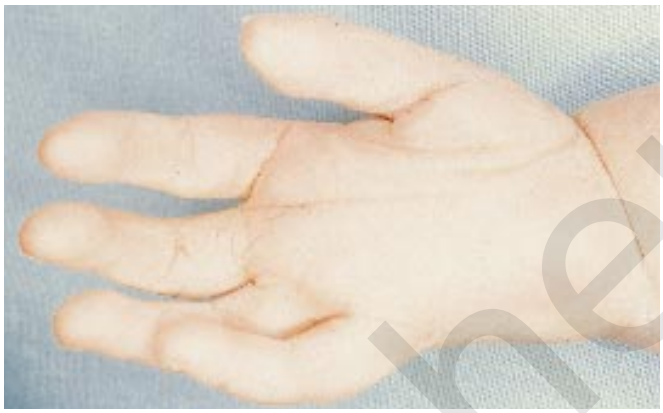

Figure 3.116. Right hand of the same infant with amyotonia congenita. Note the lack of finger creases and the abnormal appearance of the hand due to lack of intrauterine fetal movement. Finger creases normally develop at 11 to 12 weeks gestational age.

3.117

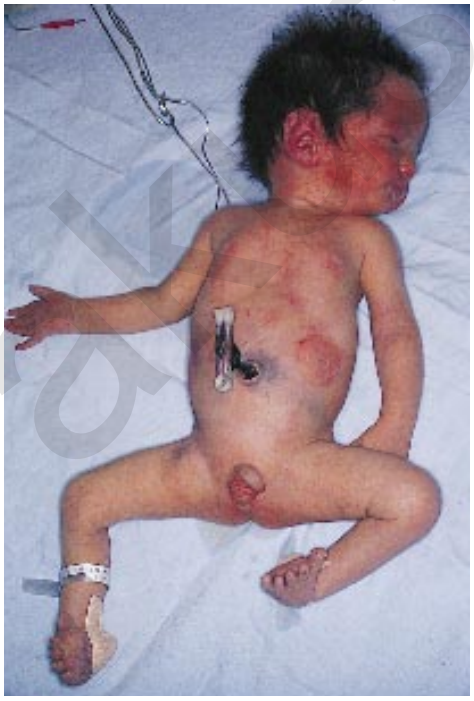

Figure 3.117. In this male infant with myotonic dystrophy, note the marked hypotonia, cryptorchidism, and clubfoot.

3.118

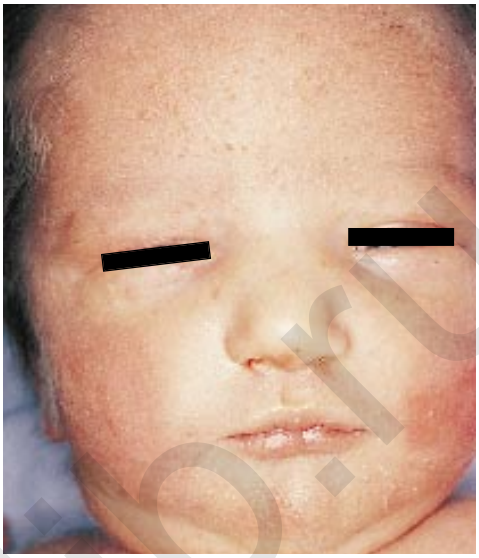

Figure 3.118. The face of the same infant as shown in Figure 3.117 shows the typical lack of expression and the bilateral ptosis seen in myotonic dystrophy. This should be differentiated from neonatal myasthenia gravis.

About 10 to 15% of infants of myasthenic mothers are affected and signs present in the baby at or shortly after birth. The clinical picture of neonatal myasthenia gravis is dominated by general hypotonia, there being symmetrical involvement of the face, trunk and limbs. In severe cases there is lack of facial expression and difficulty in sucking and swallowing. Prognosis is good, with improvement within a week; the infant may be symptomatic as long as 6 weeks.

3.119

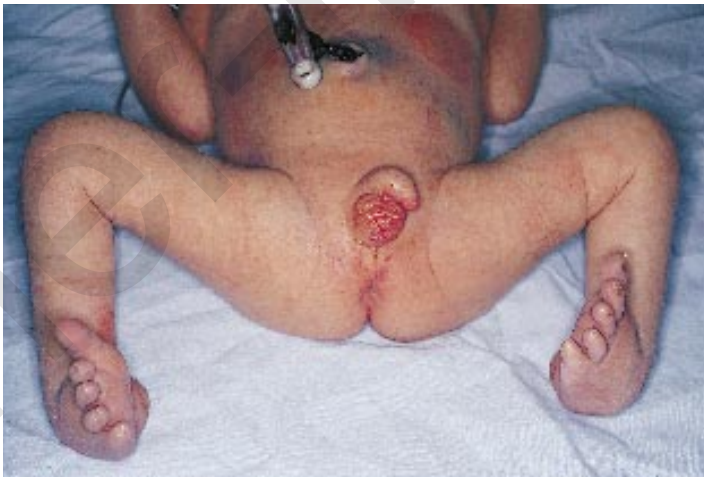

Figure 3.119. Cryptorchidism and clubfoot in the same infant with myotonic dystrophy.

3.120

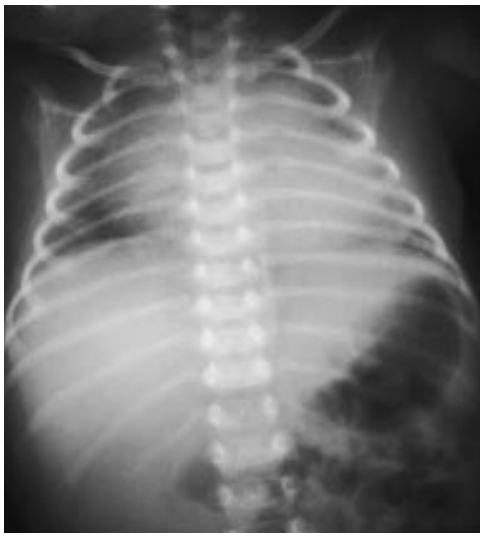

Figure 3.120. Radiograph of thorax of a hypotonic infant with the fetal akinesia syndrome. Note the thin, gracile, downslanting ribs, long thin clavicles, and splayed chest. The poor inspiration is due to poor muscle effort because of the hypotonia.

Index

VOLUME 4

Dermatology and Perinatal Infection

Atlas of the Newborn

Rudolph

VOLUME 4

Dermatology and Perinatal Infection

Atlas of the Newborn

Arnold J. Rudolph, M.D.
1918–1995
Professor of Pediatrics,
Obstetrics and Gynecology
Baylor College of Medicine
Houston, Texas

VOLUME 4

Dermatology and Perinatal Infection

Atlas of the Newborn

Arnold J. Rudolph, M.D.
1918-1995

1997
B.C. Decker Inc.
Hamilton • London

B.C. Decker Inc.
4 Hughson Street South
P.O. Box 620, L.C.D. 1
Hamilton, Ontario L8N 3K7
Tel: 905 522-7017
Fax: 905 522-7839
e-mail: info@bcdecker.com

Printed in Canada

97 98 99 00/BP/9 8 7 6 5 4 3 2 1

ISBN 1-55009-034-8

Sales and distribution

United States
Blackwell Science Inc.
Commerce Place
350 Main Street
Malden, MA 02148
U.S.A.
Tel: 1-800-215-1000

Canada
Copp Clark Ltd.
200 Adelaide Street West
3rd Floor
Toronto, Ontario
Canada M5H 1W7
Tel: 416-597-1616
Fax: 416-597-1617

Japan
Igaku-Shoin Ltd.
Tokyo International P.O. Box 5063
1-28-36 Hongo, Bunkyo-ku
Tokyo 113, Japan
Tel: 3 3817 5680
Fax: 3 3815 7805

U.K., Europe, Scandinavia, Middle East
Blackwell Science Ltd.
c/o Marston Book Services Ltd.
P.O. Box 87
Oxford OX2 0DT
England
Tel: 44-1865-79115

Australia
Blackwell Science Pty, Ltd.
54 University Street
Carleton, Victoria 3053
Australia
Tel: 03 9347 0300
Fax: 03 9349 3016

Foreword

Sir William Osler stated, "There is no more difficult task in medicine than the art of observation." The late Arnold Jack Rudolph was an internationally renowned neonatologist, a teacher's teacher, and, above all, one who constantly reminded us about how much could be learned by simply observing, in his case, the newborn infant.

This color atlas of neonatology represents a distillation of more than 50 years of observing normal and abnormal newborn infants. The *Atlas* begins with a section on the placenta, its membranes, and the umbilical cord. Jack Rudolph delighted in giving a lecture entitled "Don't Make Mirth of the Afterbirth," in which he captivated audiences by showing them how much you could learn about the newborn infant from simply observing the placenta, its membranes, and the umbilical cord.

In a few more than 60 photomicrographs, we learn to read the placenta and gain insight into such disorders as intrauterine growth retardation, omphalitis, cytomegalic inclusion disease, congenital syphilis, and congenital neuroblastoma. Congenital abnormalities of every organ system are depicted along with the appearance of newborn infants who have been subjected in utero to a variety of different drugs, toxins, or chemicals. We also learn to appreciate the manifestations of birth trauma and abnormalities caused by abnormal intrauterine positioning.

More than 250 photographs are used to illustrate the field of neonatal dermatology. The collection of photographs used in this section is superior to that which I have seen in any other textbook or atlas of neonatology or dermatology; this section alone makes this reference a required addition to the library of any clinician interested in the care of infants and children. Photographs of the Kasabach-Merritt syndrome (cavernous hemangioma with thrombocytopenia), Klippel-Trenaunay syndrome, Turner's syndrome, Waardenburg's syndrome, neurocutaneous melanosis, mastocytosis (urticaria pigmentosa), and incontinentia pigmenti (Bloch-Sulzberger syndrome) are among the best that I have seen.

Cutaneous manifestations are associated with many perinatal infections. The varied manifestations of staphylococcal infection of the newborn are depicted vividly in photomicrographs of furunculosis, pyoderma, bullous impetigo, abscesses, parotitis, dacryocystitis, inastitis, cellulitis, omphalitis, and funisitis. Streptococcal cellulitis, *Haemophilus influenzae* cellulitis, and cutaneous manifestations of listeriosis all are depicted. There are numerous photomicrographs of congenital syphilis, showing the typical peripheral desquamative rash on the palms and soles, as well as other potential skin manifestations of congenital syphilis which may produce either vesicular, bullous, or ulcerative lesions. The various radiologic manifestations of congenital syphilis, including pneumonia alba, ascites, growth arrest lines, Wegner's sign, periostitis, and syphilitic osteochondritis, are depicted. Periostitis of the clavicle (Higouménaki's sign) is shown in a photograph that also depicts periostitis of the ribs. A beautiful photomicrograph of Wimberger's sign also has been included; this sign, which may appear in an infant with congenital syphilis, reveals radiolucency due to erosion of the medial aspect of the proximal tibial metaphysis.

The *Atlas* also includes a beautiful set of photographs which delineate the ophthalmologic examination of the newborn. Lesions which may result from trauma, infection, or congenital abnormalities are included. There are numerous photographs of the ocular manifestations of a variety of systemic diseases, such as Tay-Sachs disease, tuberous sclerosis, tyrosinase deficiency, and many more. Photographs of disturbances of each of the various organ systems, or disorders affecting such organ systems, also are included along with numerous photographs of different forms of dwarfism, nonchromosomal syndromes and associations, and chromosomal disorders. In short, this *Atlas* is the complete visual textbook of neonatology and will provide any

physician, nurse, or student with a distillation of 50 years of neonatal experience as viewed through the eyes of a master clinician.

Arnold Jack Rudolph was born in 1918, grew up in South Africa, and graduated from the Witwatersrand Medical School in 1940. Following residency training in pediatrics at the Transvaal Memorial Hospital for Children, he entered private pediatric practice in Johannesburg, South Africa. After almost a decade, he left South Africa and moved to Boston, where he served as a Senior Assistant Resident in Medicine at the Children's Medical Center in Boston, Massachusetts, and subsequently pursued fellowship training in neonatology at the same institution and at the Boston Lying-In Hospital, Children's Medical Center and Harvard Medical School under Dr. Clement A. Smith.

In 1961, Dr. Rudolph came to Baylor College of Medicine in Houston, Texas, the school at which he spent the remainder of his career. He was a master teacher, who received the outstanding teacher award from pediatric medical students on so many occasions that he was elected to the Outstanding Faculty Hall of Fame in 1982. Dr. Rudolph also received numerous awards over the years from the pediatric house staffs for his superb teaching skills.

He was the Director of the Newborn Section in the Department of Pediatrics at Baylor College of Medicine for many years, until he voluntarily relinquished that position in 1986 for reasons related to his health. Nevertheless, Jack Rudolph continued to work extraordinarily long hours in the care of the newborn infant, and was at the bedside teaching both students and house staff, as well as his colleagues, on a daily basis until just a few months before his death in July 1995.

Although Dr. Rudolph was the author or co-author of more than 100 published papers that appeared in the peer-reviewed medical literature, his most lasting contribution to neonatology and to pediatrics is in the legacy of the numerous medical students, house staff, fellows, and other colleagues whom he taught incessantly about how much one could learn from simply observing the newborn infant. This *Atlas* is a tour de force; it is a spectacular teaching tool that has been developed, collated, and presented by one of the finest clinical neonatologists in the history of medicine. It is an intensely personal volume that, as Dr. Rudolph himself states, "is not intended to rival standard neonatology texts," but rather to supplement them. This statement reveals Dr. Rudolph's innate modesty, since with the exception of some discussion on pathogenesis and treatment, it surpasses most neonatology texts in the wealth of clinical information that one can derive from viewing and imbibing its contents. We owe Dr. Rudolph and those who aided him in this work a debt of gratitude for making available to the medical community an unparalleled visual reference on the normal and abnormal newborn infant.

Ralph D. Feigin, M.D.
June 13, 1996

Preface

I first became attracted to the idea of producing a color atlas of neonatology many years ago. However, the impetus to synthesize my experience and compile this current collection was inspired by the frequent requests from medical students, pediatric house staff, nurses and others to provide them with a color atlas of the clinical material provided in my "slide shows." For the past few decades I have used the medium of color slides and radiographs as a teaching tool. In these weekly "slide shows" the normal and abnormal, as words never can, are illustrated.

"I cannot define an elephant but I know one when I see one."[1]

The collection of material used has been added to constantly with the support of the pediatric house staff who inform me to "bring your camera" whenever they see an unusual clinical finding or syndrome in the nurseries.

A thorough routine neonatal examination is the inalienable right of every infant. Most newborn babies are healthy and only a relatively small number may require special care. It is important to have the ability to distinguish normal variations and minor findings from the subtle early signs of problems. The theme that recurs most often is that careful clinical assessment, in the traditional sense, is the prerequisite and the essential foundation for understanding the disorders of the newborn. It requires familiarity with the wide range of normal, as well as dermatologic, cardiac, pulmonary, gastrointestinal, genitourinary, neurologic, and musculoskeletal disorders, genetics and syndromes. A background in general pediatrics and a working knowledge of obstetrics are essential. The general layout of the atlas is based on the above. Diseases are assigned to each section on the basis of the most frequent and obvious presenting sign. It seems probable that the findings depicted will change significantly in the decades to come. In this way duplication has been kept to a minimum. Additional space has been devoted to those areas of neonatal pathology (e.g., examination of the placenta, multiple births and iatrogenesis) which pose particular problems or cause clinical concern.

Obviously, because of limitations of space, it is impossible to be comprehensive and include every rare disorder or syndrome. I have tried to select both typical findings and variations in normal infants and those found in uncommon conditions. Some relevant conditions where individual variations need to be demonstrated are shown in more than one case.

As the present volume is essentially one of my personal experience, it is not intended to rival standard neonatology texts, but is presented as a supplement to them. It seems logical that references should be to standard texts or reviews where discussion on pathogenesis, treatment, and references to original works may be found.

Helen Mintz Hittner, M.D., has been kind enough to contribute the outstanding section on neonatal ophthalmology.

I have done my best to make the necessary acknowledgements to the various sources for the clinical material. If I have inadvertently omitted any of those, I apologize. My most sincere appreciation and thanks to Donna Hamburg, M.D., Kru Ferry, M.D., Michael Gomez, M.D., Virginia Schneider, PA, and Jeff Murray, M.D., who have spent innumerable hours in organizing and culling the material from my large collection. We wish to thank Abraham M. Rudolph, M.D., for his assistance in reviewing the material. We also wish to thank the following people for their photographic contributions to this work: Gerardo Cabrera-Meza, Morven Edwards, John Kenny, Claire Langston, Moise Levy, Ken Moise and Don Singer.

It is hoped that this atlas will provide neonatologists, pediatricians, family physicians, medical students and nurses with a basis for recognizing a broad spectrum of normal variations and clinical problems as well as provide them with an overall perspective of neonatology, a field in which there continues to be a rapid acceleration of knowledge and technology. One must bear in mind the caveat that pictures cannot supplant clinical experience in mastering the skill of visual recall.

1. Senile dementia of Alzheimer's type — normal aging or disease? (Editorial) *Lancet* 1989; i:476-477.

Arnold J. Rudolph, M.D.

CONTENTS

Volume 4
Dermatology and Perinatal Infection

Introduction

Although several texts provide extensive written descriptions of the newborn infant, the senses of touch, hearing, and especially sight, create the most lasting impressions. Over a period of almost five decades, my brother Jack Rudolph diligently recorded, in pictorial form, his vast experiences in physical examination of the newborn infant. *Atlas of the Newborn* reflects his selection from the thousands of color slides in his collection, and truly represents the "art of medicine" as applied to neonatology. A number of unusual or rare conditions are included in this atlas. I consider this fully justified, because if one has not seen or heard of a condition, one will never be able to diagnose it.

This fourth volume of the five-volume series reviews two main areas; disorders of the skin, and perinatal infections.

Clinical assessment of skin disorders in the newborn infant is one of the most challenging problems confronting neonatologists and pediatricians, and many feel quite insecure in evaluating skin lesions in neonates. Chapter 1, *Dermatology,* provides a unique and elegant collection of color photographs illustrating many of the skin abnormalities that may be encountered in the newborn. The section depicting benign and transient skin lesions is of particular interest, and congenital abnormalities, vascular malformations, disorders of pigmentation, vesiculo-bullous lesions, and scaling conditions are extensively reviewed. This is perhaps the most detailed graphic presentation of dermatologic problems in the newborn infant currently available.

Chapter 2, *Perinatal Infection*, provides excellent illustrations of various organ system involvements in the neonate resulting from infection by bacteria and by syphilis, as well as prenatal viral infections such as cytomegalovirus, rubella, and varicella, and infection by protozoa such as toxoplasma. The section depicting congenital syphilis is especially comprehensive, covering the protean manifestations of this infection in the infant. The effects of neonatally-acquired infections due to bacteria, herpes virus and fungi are also elegantly illustrated.

Volume IV of *Atlas of the Newborn* will be of enormous value to general pediatricians, neonatologists, obstetricians and nurses involved in perinatal care, and also to dermatologists and infectious disease specialists.

Abraham M. Rudolph, M.D.

Chapter 1
Neonatal Dermatology

The neonatal skin must be given careful consideration for several reasons:

- It is a protective organ, especially when covered with vernix.
- Any break in integrity creates an opportunity for infection; therefore, minimize skin trauma.
- Absorption of agents through the skin, especially in premature infants, may have harmful effects (e.g., hexachlorophene, Betadine™, boric acid, etc.)
- The skin may be used therapeutically (e.g., application of safflower oil for essential fatty acid deficiency).

Neonatal skin may present a bewildering variety of lesions; some innocent, temporary and the result of a physiologic response; others the result of an episodic disease; and still others indicative of a serious, often fatal, underlying disorder.
Dermatologic manifestations of infection are presented in Chapter 2, Perinatal Infection.

BENIGN AND TRANSIENT CUTANEOUS LESIONS

These lesions are commonly observed in a normal nursery population, and none require special therapeutic consideration. Numerous benign minor variations in the skin noted in the routine care of babies who are well include skin pigmentation, desquamation, vernix caseosa, etc.

1.1

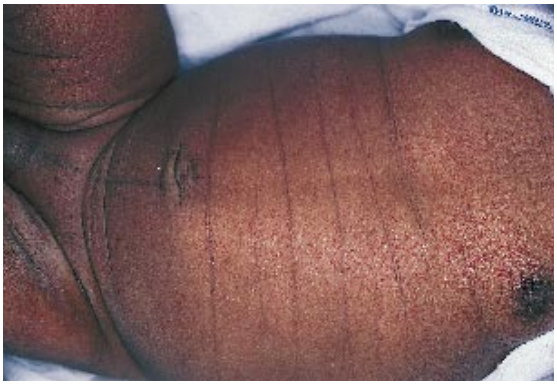

Figure 1.1. In this infant there is a regular segment-like pattern of transverse folding creases across the lower thorax and abdomen giving the trunk a "gridiron" appearance. Note the prominent linea nigra. This finding is more common in postmature infants.

1.2

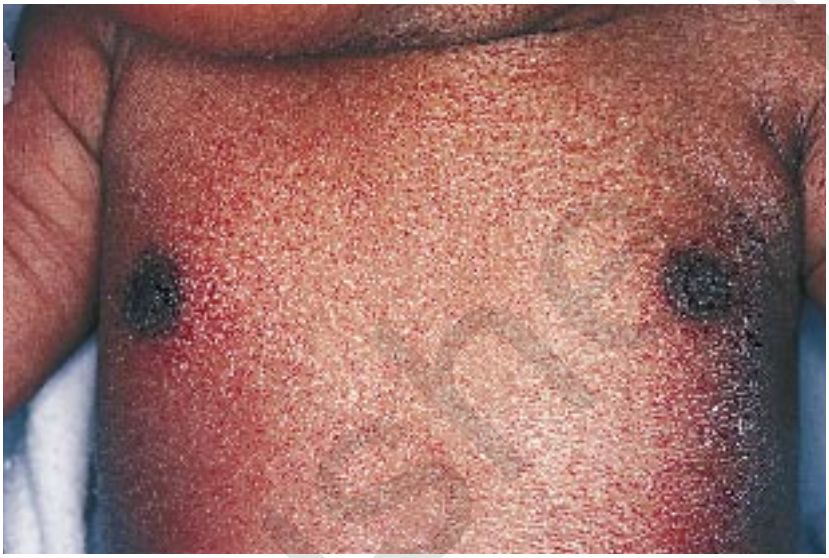

Figure 1.2. Pigmentation of the areola of the nipple in a newborn infant. Pigmentation is more marked in black infants.

1.3

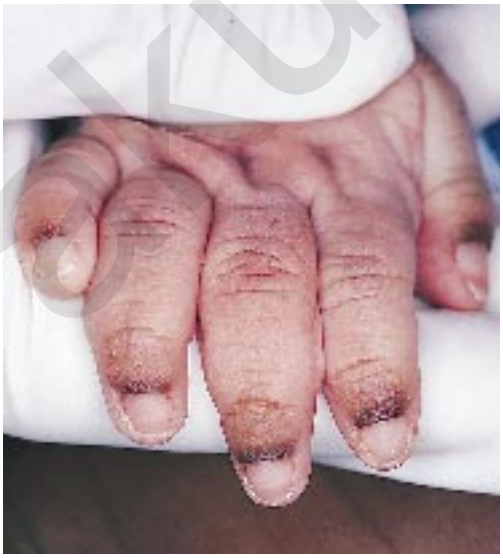

Figure 1.3. Pigmentation at the base of the nails in a black infant. There may be little pigmentation of the skin in general at birth, but the finding of pigmentation at the base of the nails, pinnae of the ears, axilla, areolae of the nipples, genitalia, and a prominent linea nigra would all suggest that the infant is a black infant.

1.4

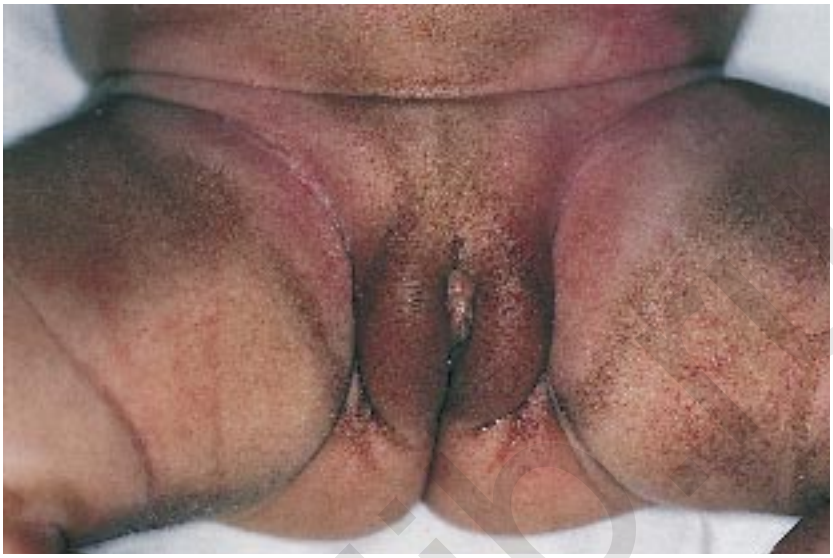

Figure 1.4. Linea nigra and pigmentation of the skin and genitalia in a black female infant. Linea nigra is the line of increased pigmentation extending from the umbilicus to the more darkly pigmented genitalia. This area of benign pigmentation becomes less prominent as the baby's skin darkens. In this postmature infant note the area of lack of pigmentation in both groins.

1.5

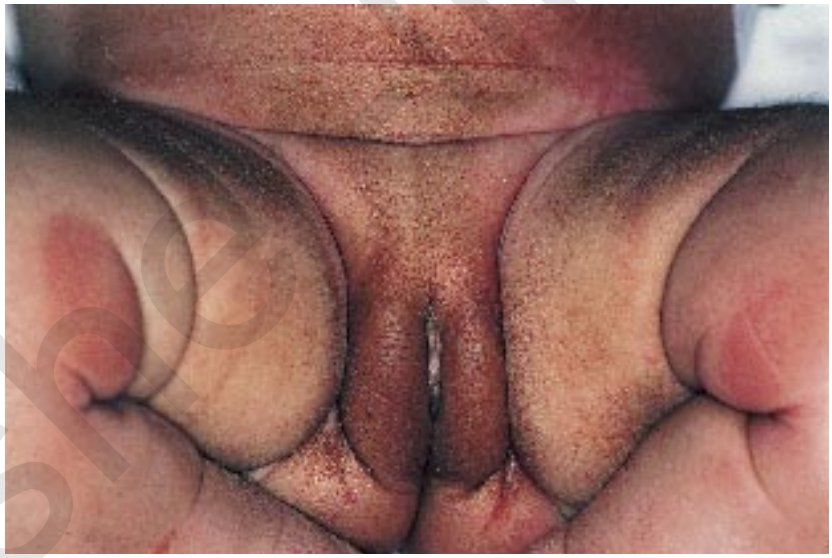

Figure 1.5. The same infant as in Figure 1.4 with her thighs adducted. Note that the areas lacking pigmentation in the groins correspond to the area protected in utero by adduction of the lower limbs.

1.6

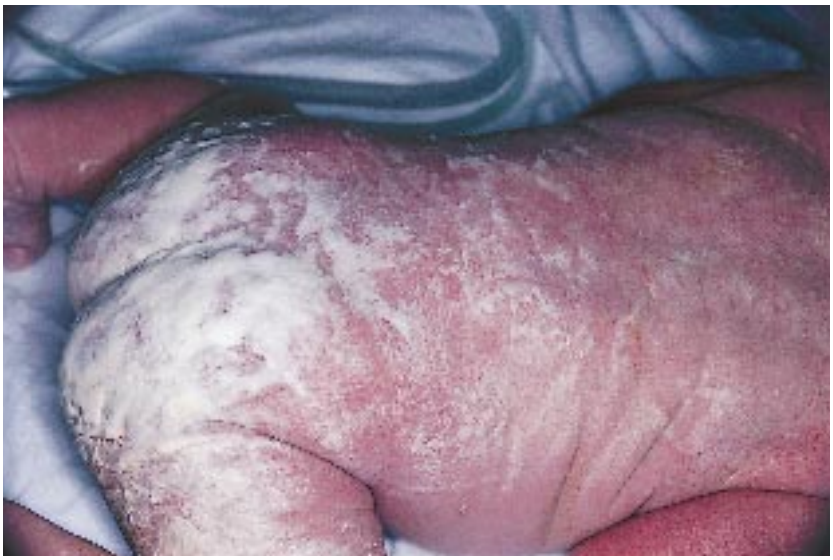

Figure 1.6. Vernix caseosa present in a term infant at birth. The vernix caseosa is a fetal product of the sebaceous glands, shed epithelial cells, and hair. It is cheesy-white in appearance and may be liberally caked all over the skin or concentrated in folds like the groins and genitalia, the axilla, or behind the ears. Its presence suggests that the infant is close to term as the vernix disappears with increasing gestational age. The vernix normally is white in color but can alter to a golden-yellow in infants that are meconium-stained from fetal distress or in infants with erythroblastosis fetalis.

1.7

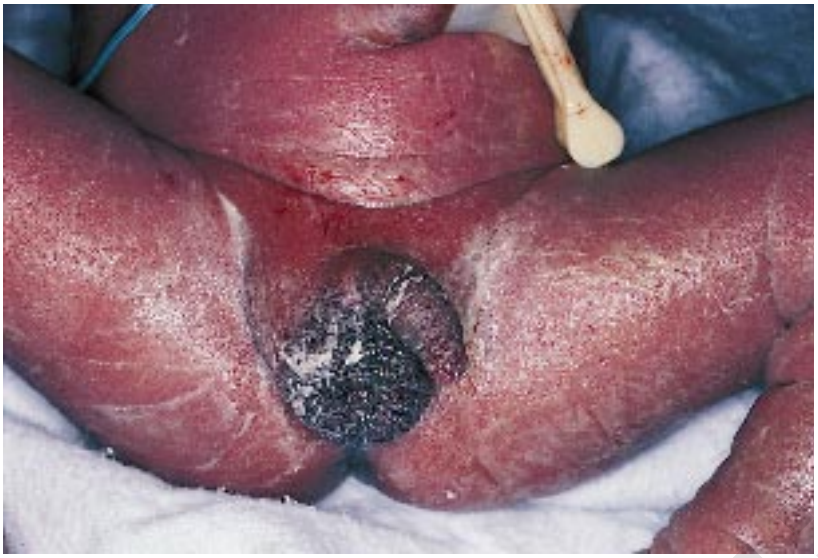

Figure 1.7. A minimal amount of vernix caseosa in the groins and genitalia of a male infant.

1.8

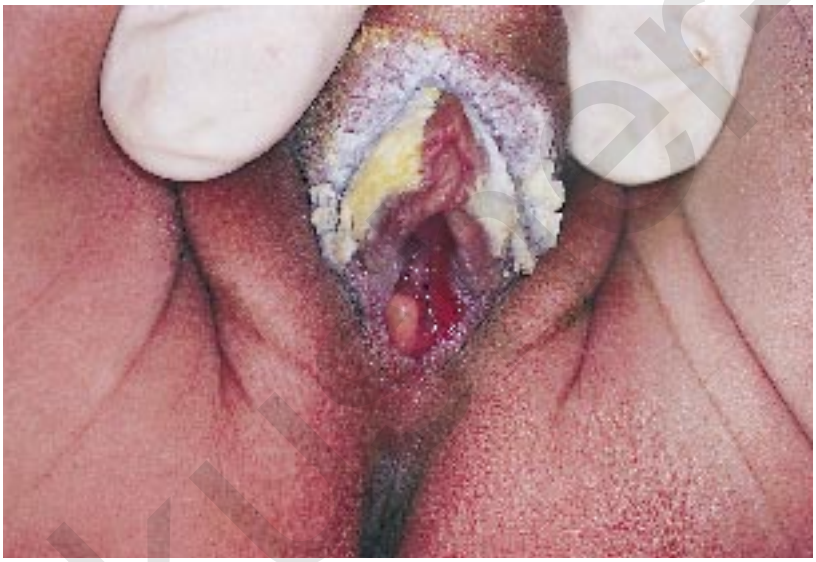

Figure 1.8. Vernix caseosa in a female infant. After birth the infant is bathed and the vernix removed by the nurse. If there is any question as to whether or not there was any meconium staining, certain areas such as the axilla, inguinal folds and genitalia, if not adequately cleaned, will reveal traces of the vernix.

1.9

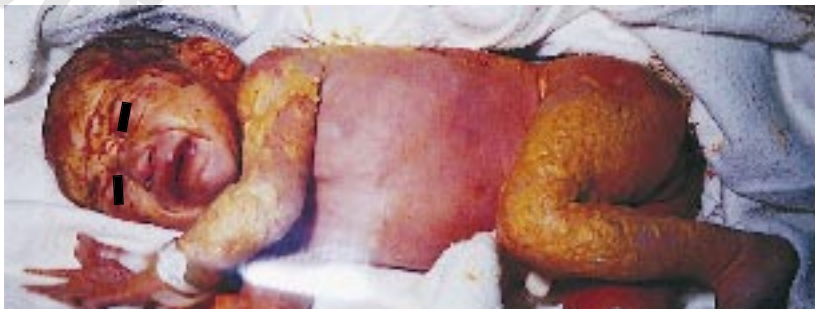

Figure 1.9. Meconium staining of the vernix and skin in an infant who had fetal distress with meconium-stained amniotic fluid.

1.10

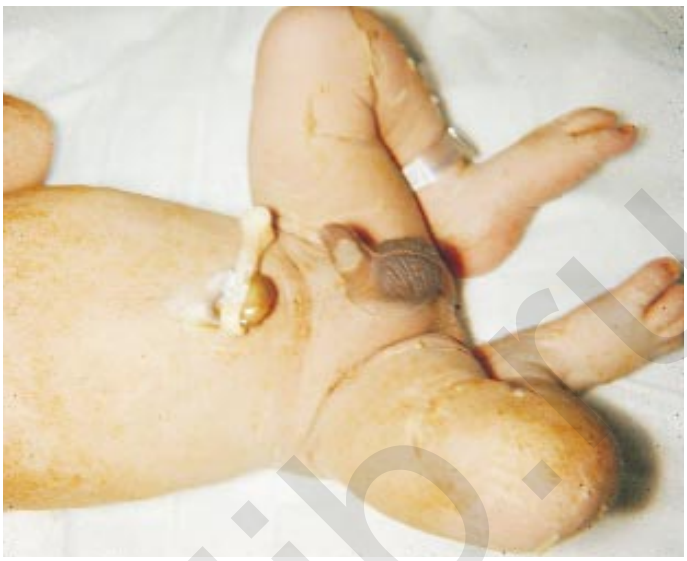

Figure 1.10. Note the meconium staining of the skin in a post-term infant. He also had marked desquamation of the skin as well as long finger nails, features common to the postmature infant.

1.11

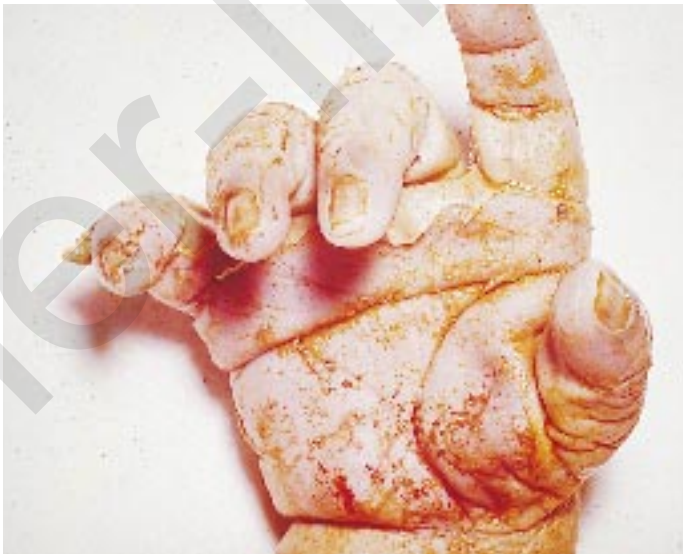

Figure 1.11. The hand of the same infant as in Figure 1.1. showing the desquamation of the skin, long finger nails, and meconium staining.

1.12

Figure 1.12. Marked desquamation of the skin in a post-term infant. This is a benign physiologic desquamation with paper-thin peeling; the underlying skin is normal. It occurs with postmaturity as the vernix disappears and the skin of the fetus is not protected from the amniotic fluid. The process is more marked in areas of irritation.

1.13

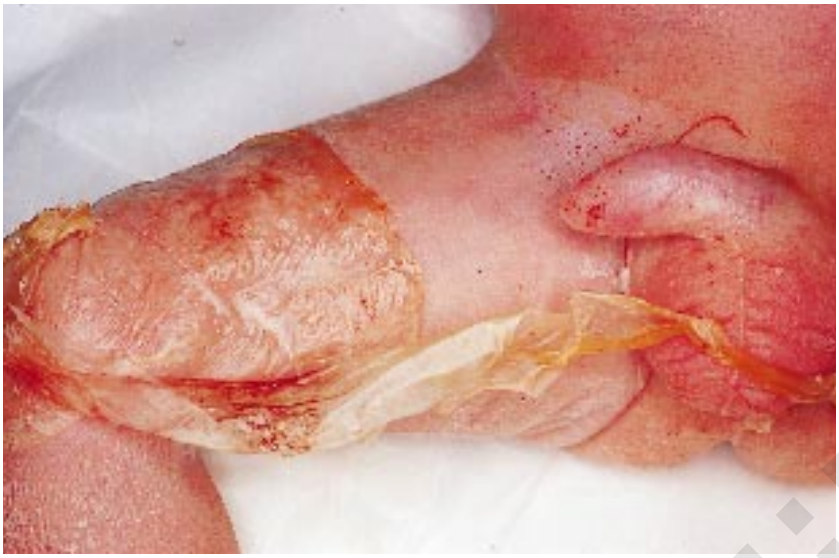

Figure 1.13. Desquamation of the skin is a very typical finding in an abdominal pregnancy in which the fetus is not protected by the amniotic fluid.

1.14

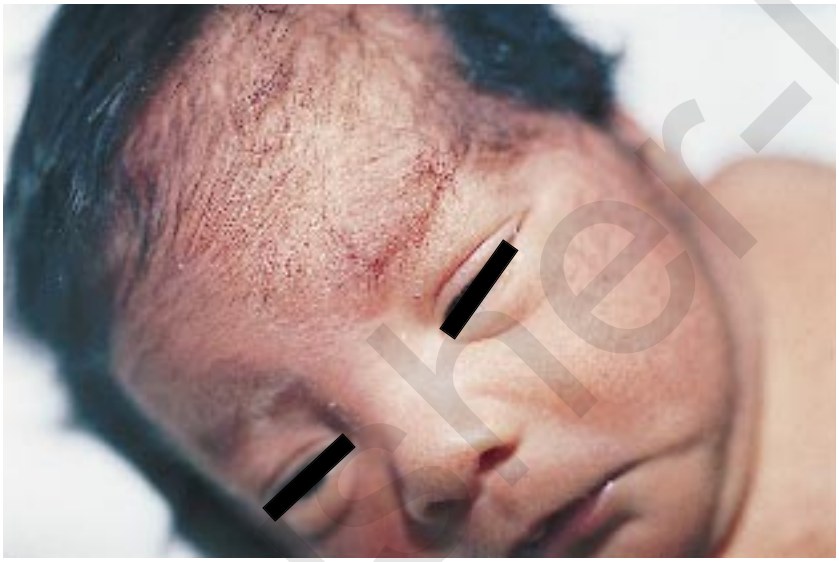

Figure 1.14. Hypertrichosis (hirsutism) is very common in normal mature Hispanic infants.

1.15

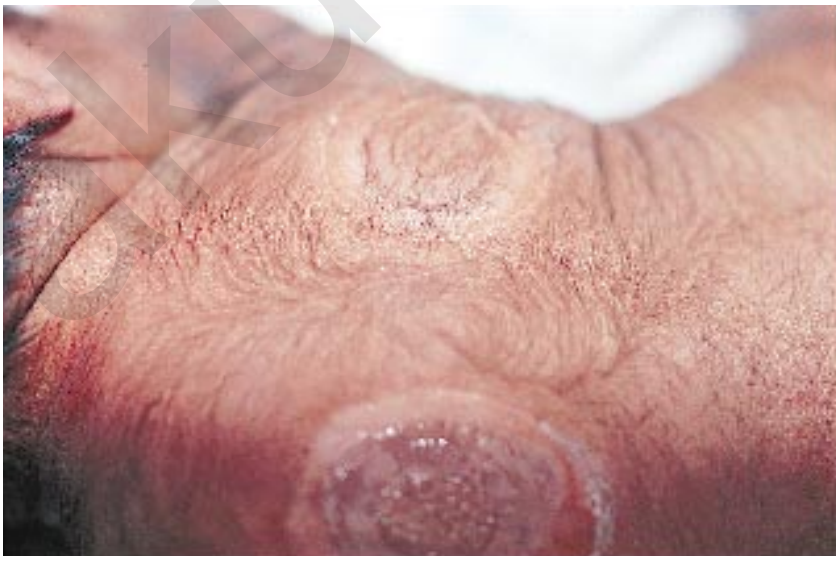

Figure 1.15. Another infant with hypertrichosis over the body at birth. Note that although this is very striking it is a normal finding in normal mature Hispanic infants.

1.16

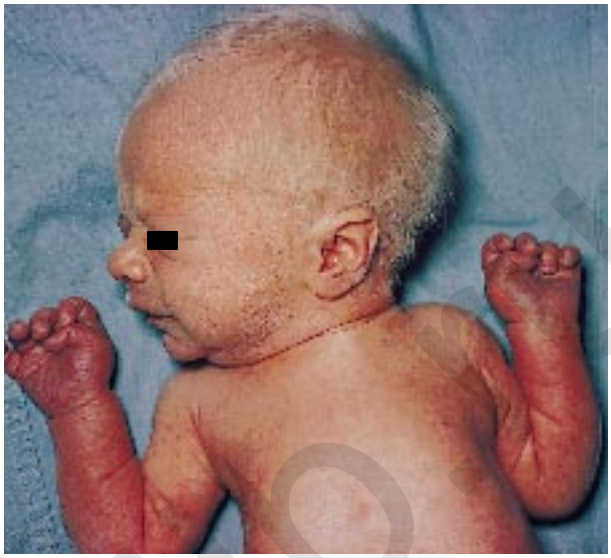

Figure 1.16. Acrocyanosis in an otherwise normal infant. Peripheral vasoconstriction occurs very commonly in normal infants and rapidly improves when the infant is warmed or cries.

1.17

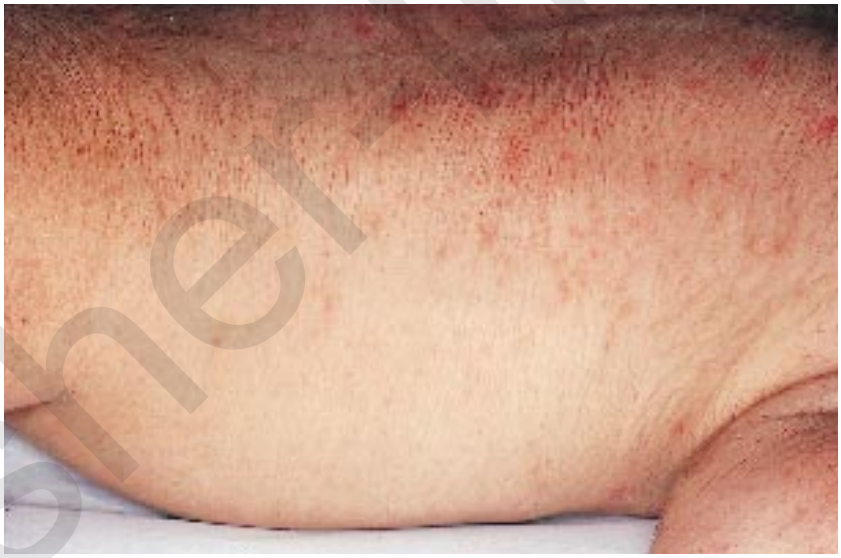

Figure 1.17. In this infant note the maculopapular rash which followed phototherapy treatment for hyperbilirubinemia. This "bilirubin rash" improves rapidly following discontinuation of phototherapy.

1.18

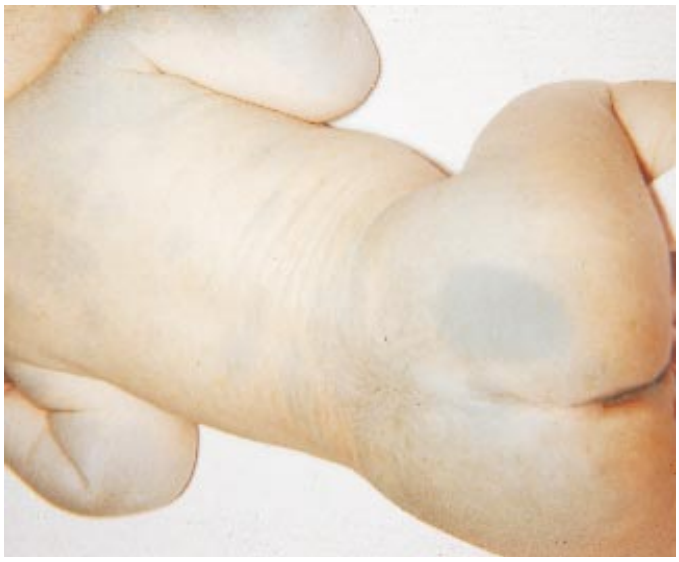

Figure 1.18. Mongolian spots in a caucasian infant. Mongolian spots are a minor anomaly commonly found in infants of darkly pigmented racial groups. They occur in 5 to 10% of caucasian infants, 70% of hispanic and oriental infants, and over 90% of black infants. The circumscribed bluish-grey to dark blue areas of discoloration are usually found over the lumbosacral area and lower back, rarely extending as far as the shoulders and neck, and can also be found on the limbs. They tend to be on the outer surfaces of the body when the infant is placed in its fetal position and are due to an accumulation of dopa-positive melanocytes.

1.19

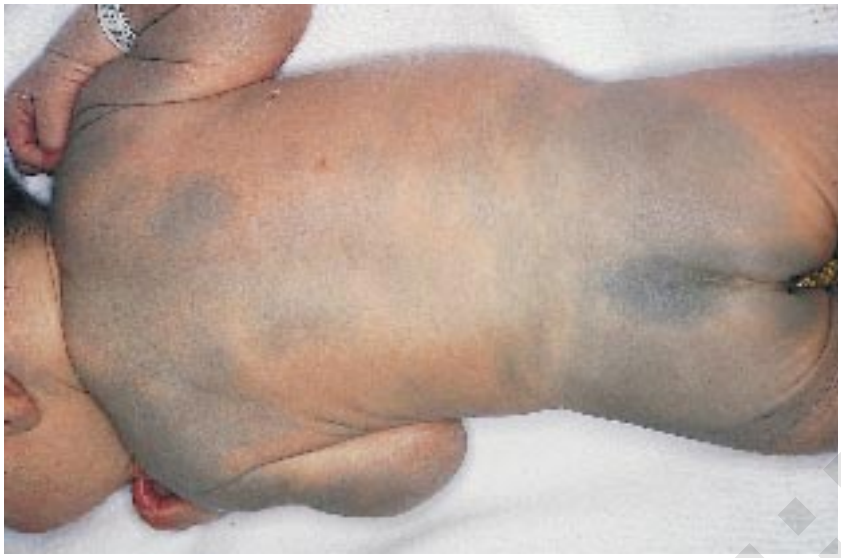

Figure 1.19. Mongolian spots in a black infant. The spots have no significance but are sometimes mistaken for bruises, causing a suspicion of child abuse. This should be kept in mind when intentional injury is questioned. They fade during childhood or appear to fade as the skin darkens. As mongolian spots are never elevated and are not palpable, they can be differentiated from a blue nevus which is raised and is located on the arms, legs, or face and persists throughout life.

1.20

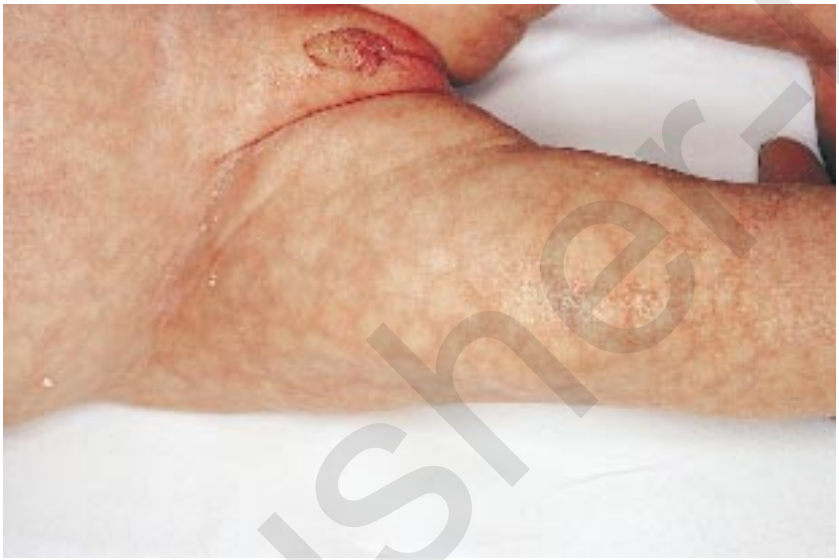

Figure 1.20. Cutis marmorata is a common finding in normal infants. This fine reticulated mottled appearance is due to vasomotor instability and thus is more commonly seen in premature infants, but should also alert one to the possibility of sepsis, hypothyroidism, and central nervous system pathology.

1.21

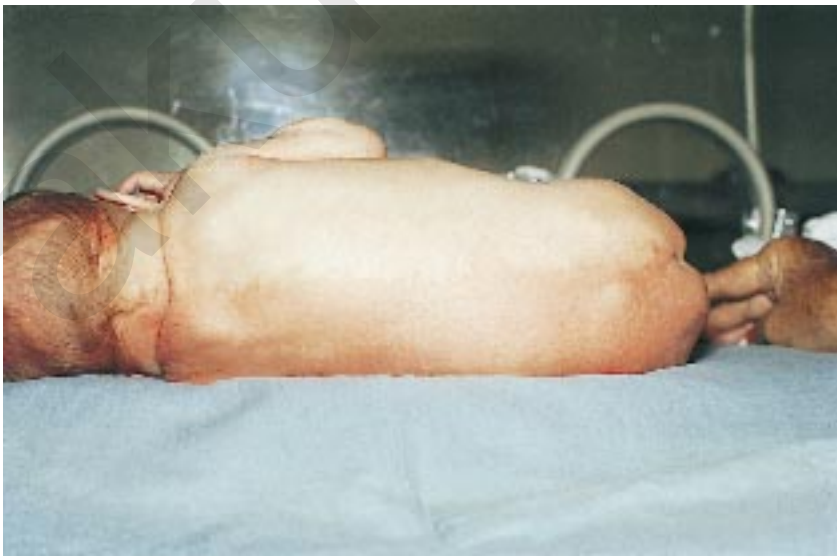

Figure 1.21. In the harlequin sign (harlequin color change) there is a vivid line of demarcation which appears down the midline. The dependent side of the skin becomes flushed (erythematous) and the uppermost side becomes pale. If the infant is turned to the other side, the appearance of the skin reverses. It is proposed that this condition results from vasomotor instability.

1.22

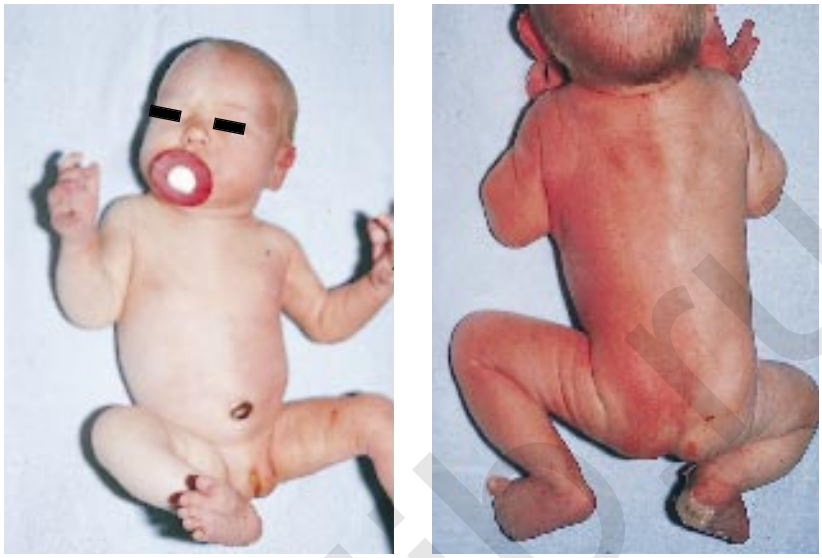

Figure 1.22. The harlequin sign in another infant showing the frontal and posterior views. This condition occurs most commonly in premature infants, is rare in term infants, and is of no pathologic significance. It may recur repeatedly in the same infant but disappears within the first few months of life. Harlequin sign is not to be be confused with the harlequin fetus (ichthyosis congenita).

1.23

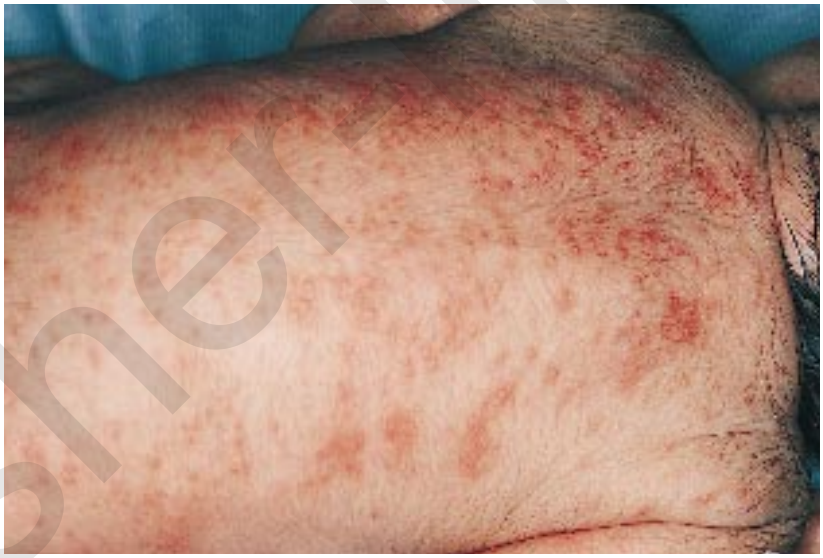

Figure 1.23. Erythema toxicum neonatorum (urticaria neonatorum) on the back of a term infant. This is the most common rash noted in the normal term infant. It is not seen in preterm and rarely seen in post-term infants. It usually appears on the 2nd or 3rd day of life (rarely in the first 24 hours) and is seldom seen after the age of 14 days. It affects about 40 to 50% of full term infants and the condition is self-limiting. Lesions may be minimal or extensive.

1.24

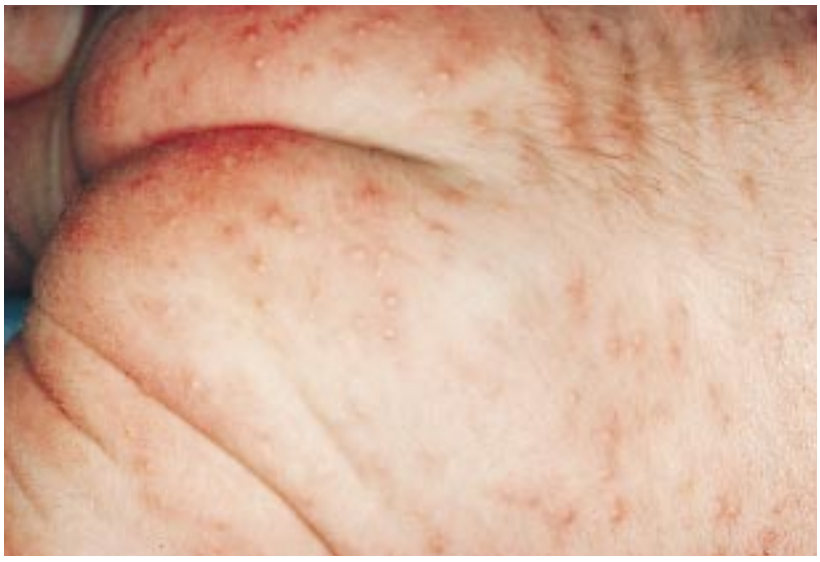

Figure 1.24. Another example of erythema toxicum neonatorum ("flea bite" dermatitis of the newborn). The lesions most frequently present are erythematous and maculopapular, but macules or papules may predominate. The lesions come and go on various sites on the trunk and limbs before they disappear permanently. The rash may become confluent and intensified in areas subject to irritation.

1.25

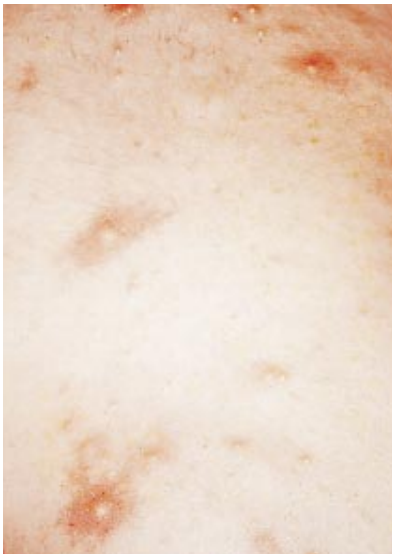

Figure 1.25. Close-up of the lesions in erythema toxicum neonatorum. The etiology is unknown but biopsy of the lesions show the presence of numerous eosinophils. It has been suggested that the presence of erythema toxicum is evidence of maturity.

1.26

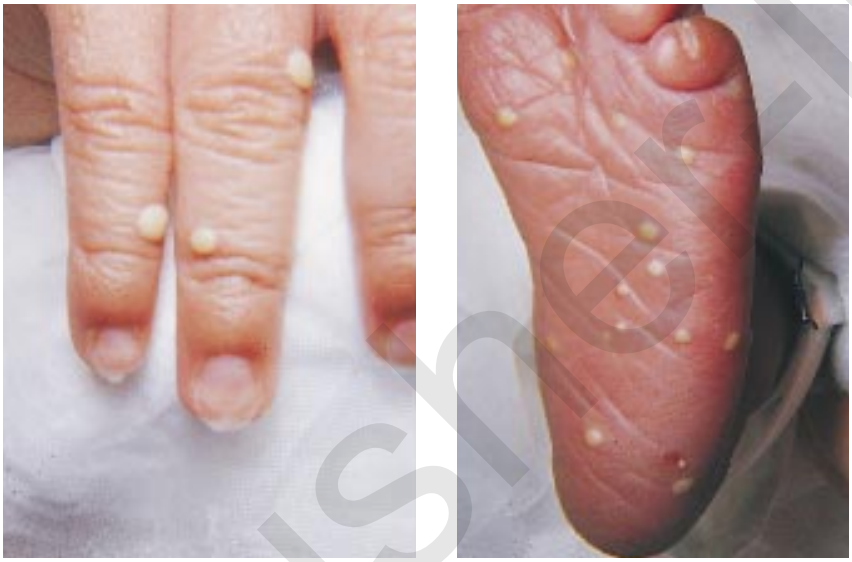

Figure 1.26. Erythema toxicum neonatorum may present as vesicular lesions, which were present at birth in this infant. Note the lack of inflammation surrounding the vesicles (which actually look like pustules). These lesions may be associated with the more usual maculopapular lesions elsewhere on the skin. The diagnosis of erythema toxicum was confirmed by examination of a stained smear from the lesions in which eosinophils alone were present and numerous. The vesicles resolved spontaneously. Differential diagnosis includes herpetic lesions and transient neonatal pustular melanosis.

1.27

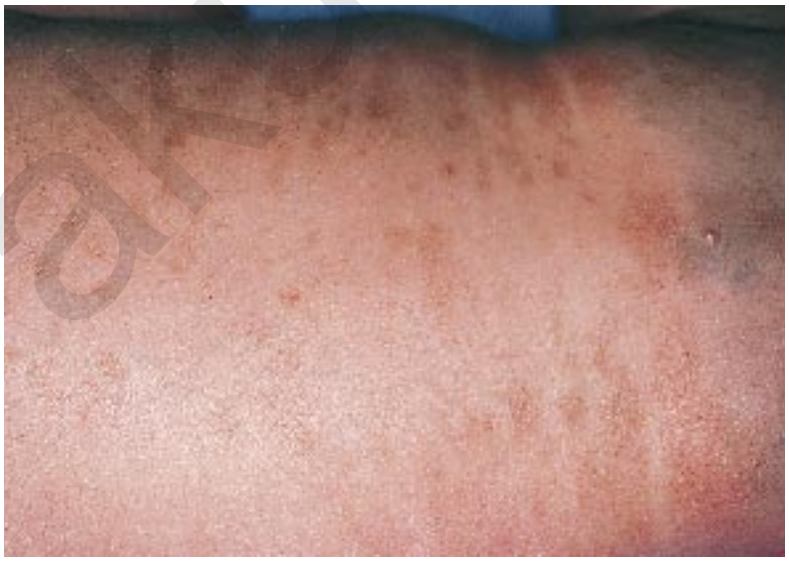

Figure 1.27. Lentigines are smooth, freckle-like, pigmented macules. They are usually present at birth, have a scattered distribution, and have been considered by some to be a manifestation of intrauterine erythema toxicum neonatorum. They usually disappear within 6 to 8 weeks.

1.28

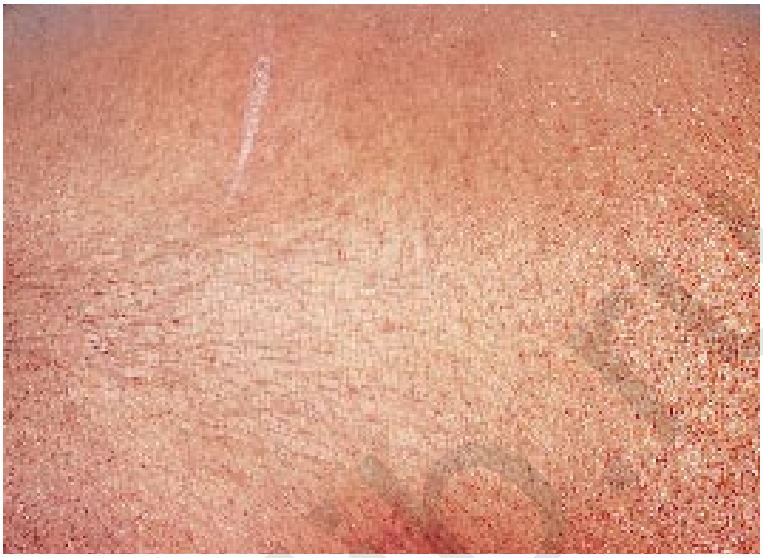

Figure 1.28. Another example of lentigines. Note the scattered distribution of the lesions which were present at birth. Lentigines should be differentiated from freckles (ephelides) which are red or light brown, well-circumscribed macules usually less than 5 mm in diameter. Freckles are not seen in infancy but appear in childhood, especially on sun-exposed areas of the skin. In general, freckles are found in clusters. Because they normally do not appear in the axilla, their presence in this area is a strong indication of neurofibromatosis.

1.29

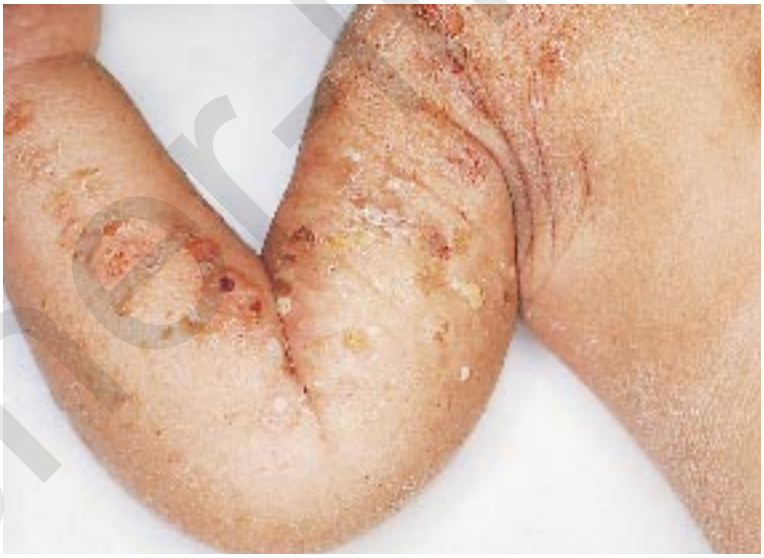

Figure 1.29. Transient neonatal pustular melanosis in an infant at the age of 3 days. This is a benign self-limiting disorder of unknown etiology characterized by superficial sterile vesiculopustular lesions that rupture early. They present as intact pustules as well as ruptured lesions which become evanescent hyperpigmented macules. These lesions are usually present at birth and are seen in 0.5 to 2% of newborns. Over 90% of the infants with this condition are black. The lesions are most often seen in clusters under the chin, and on the forehead, neck, lower back, and the extremities. They generally regress within 1 to 2 months and the hyperpigmented area eventually blends as the surrounding skin darkens.

1.30

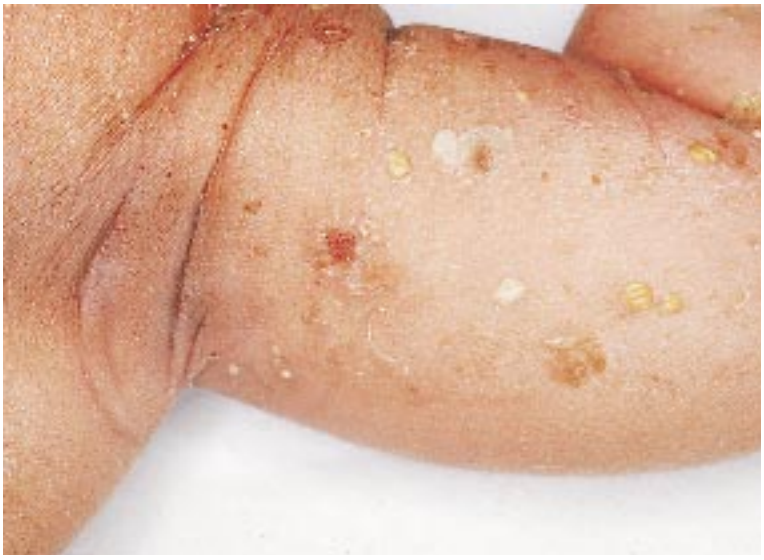

Figure 1.30. Another example of transient neonatal pustular melanosis in which the typical lesions are present. Note the vesiculopustular lesions and the brown hyperpigmented macules. The lesions of transient neonatal pustular melanosis are sterile on culture, and smears of fluid from the vesicles demonstrate neutrophils and cellular debris. There are few or no eosinophils, in contrast to the lesions of erythema toxicum neonatorum which reveal clusters of eosinophils and a relative absence of neutrophils. Differential diagnosis includes erythema toxicum and staphylococcal, herpetic, or candidal infections.

1.31

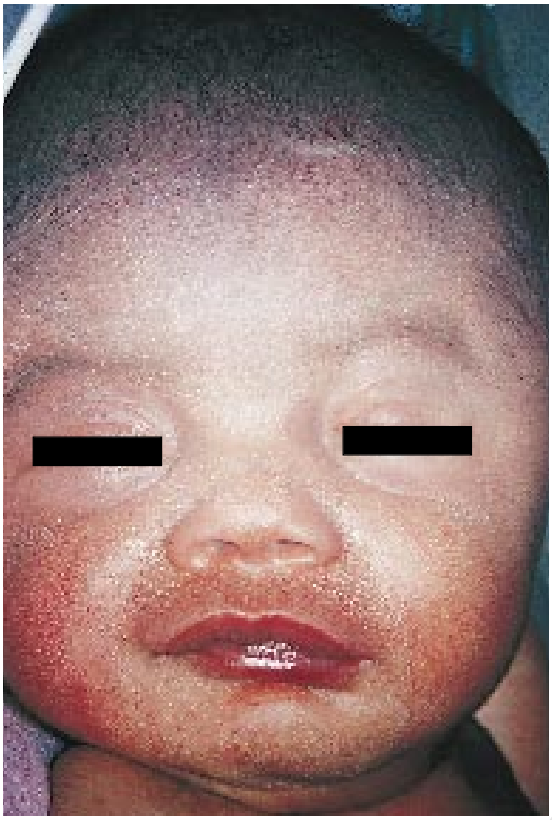

Figure 1.31. Sebaceous gland hyperplasia represents a physiologic phenomenon of the newborn manifested by multiple, yellow to flesh-colored tiny greasy-looking papules that occur on the nose, cheeks, and upper lips of full term infants. These papules, a manifestation of maternal androgen stimulation, represent a temporary disorder that resolves spontaneously within the first few weeks of life.

1.32

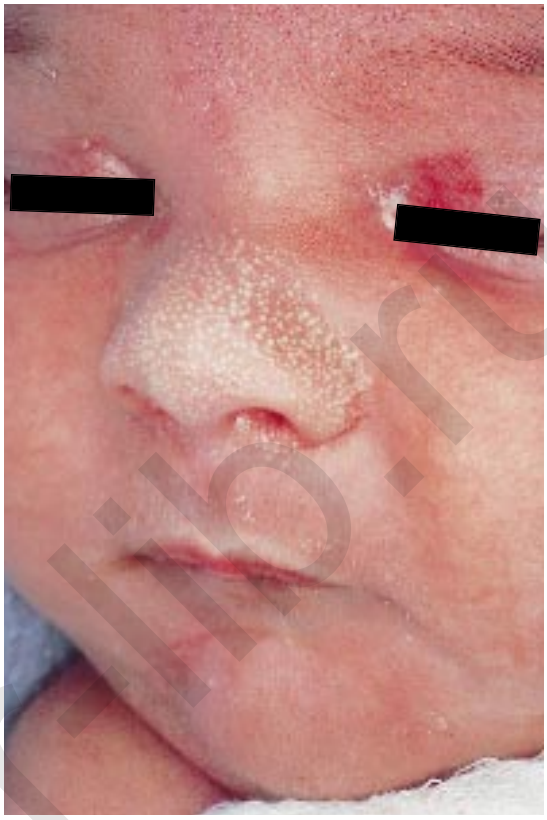

Figure 1.32. A close-up view of sebaceous gland hyperplasia.

1.33

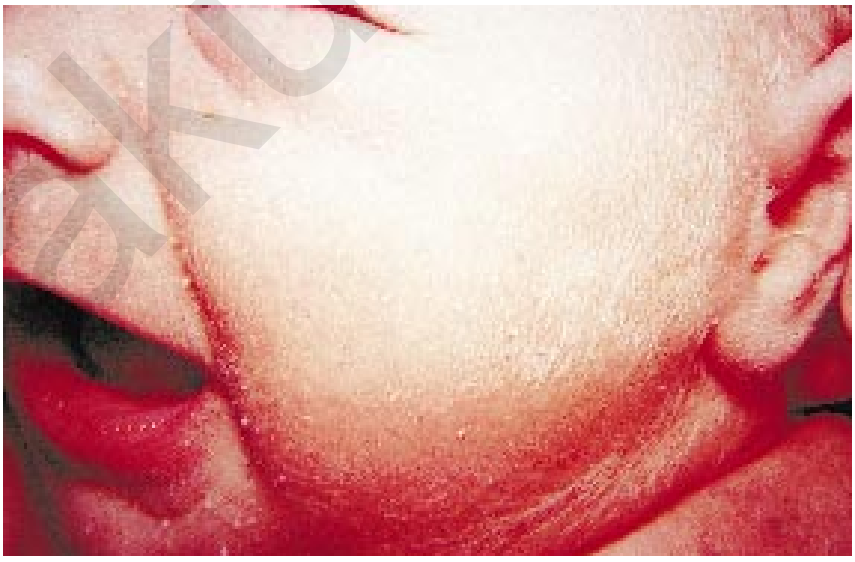

Figure 1.33. Milia occur commonly on the face of 25 to 40% of newborn infants. Histologically they are small superficial inclusion cysts that result from retention of keratin and sebaceous material within the pilosebaceous glands of the newborn, and appear as tiny 1- to 2-mm white or yellowish-white papules. The lesions are called "milia" because of their resemblance to millet seeds. Milia are particularly prominent on the cheeks, nose, chin, and nasolabial folds. The condition is self-limiting and resolves within the first month of life. Persistent and numerous milia may be seen in association with other defects (e.g., oral-facial-digital syndrome type I).

1.34

Figure 1.34. Miliaria crystallina (sudamina) consists of clear superficial pinpoint vesicles without an inflammatory areola. The lesions appear especially on the head and chest. Each vesicle is related to a sweat gland, the duct of which has been obstructed or occluded. The rash differs from milia in that the vesicles lack the white opacity of milia, generally appear a little later (in the 2nd week), and are often related to excessive warmth and humidity. The incidence is greatest in the first few weeks of life owing to the relative immaturity of the eccrine ducts which favor poral closure and sweat retention.

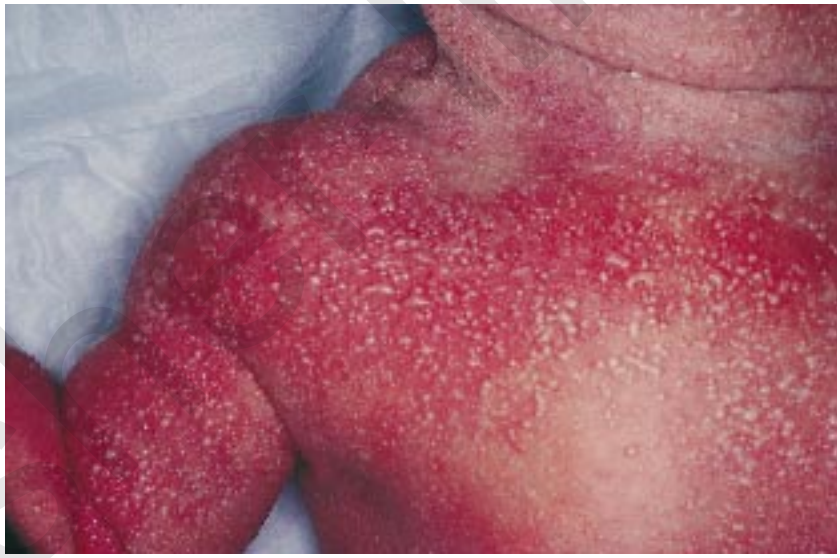

1.35

Figure 1.35. Miliaria rubra (prickly heat) is characterized by small discrete erythematous papules, vesicles, or papulovesicles which are surrounded by erythema. Lesions have a predilection for covered parts of the body where the baby gets overheated. It is important to unwrap these babies and avoid excessive heat.

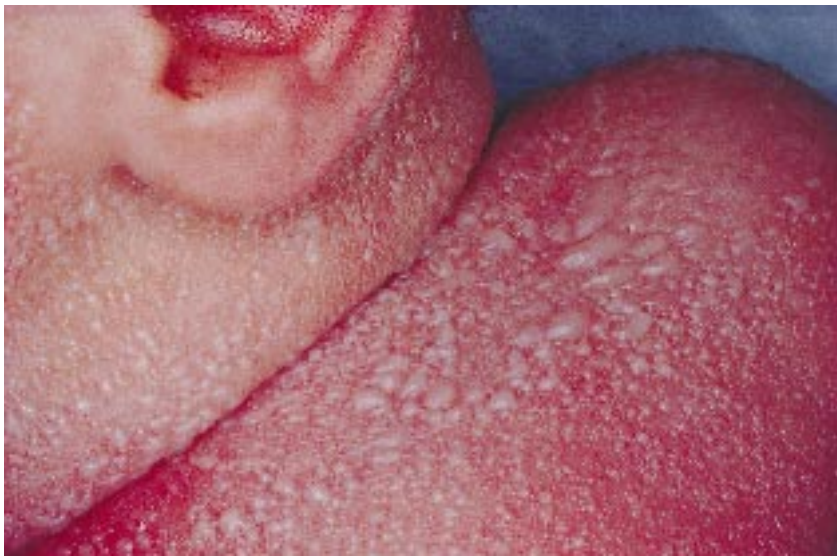

1.36

Figure 1.36. A close-up of the lesions of miliaria rubra. Note the clear vesicles and erythema of the surrounding skin.

1.37

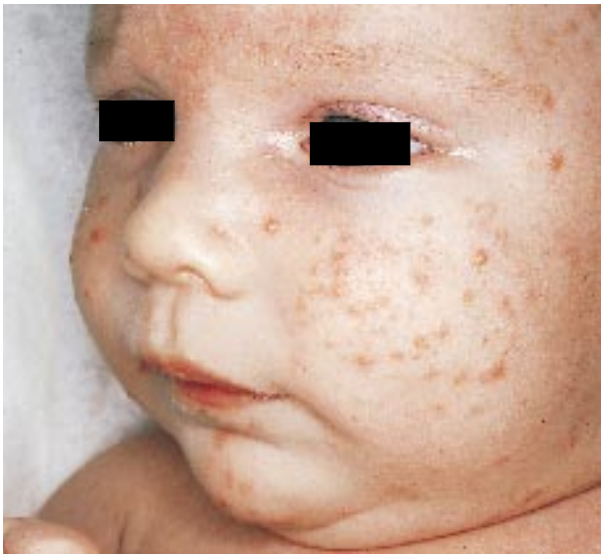

Figure 1.37. Infants with acne neonatorum have the typical facial distribution of the comedones seen in acne in adolescence. The chest and back are rarely involved. Neonatal acne appears to develop as a result of maternal androgen stimulation of sebaceous glands that have not yet involoted to their childhood state of immaturity. Acne neonatorum is a common, transitory, self-limiting disorder and should not be mistaken for an infection.

1.38

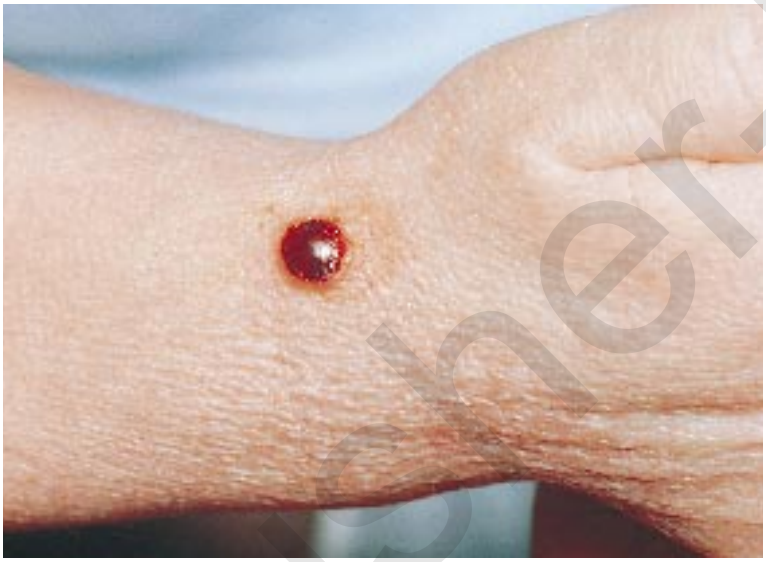

Figure 1.38. Intrauterine sucking lesions (sucking blisters) may present as small intact or ruptured bullae and are most commonly seen on the radial surface of the wrist, dorsum of the hand, or dorsum of the fingers. If unruptured, as in this infant, they may be filled with sterile serous fluid or, if sucking is vigorous, there may be a hemorrhagic component. Intrauterine sucking lesions are an example of self-induced tissue disruption in a normal newborn; the lesions are benign and require no therapy.

1.39

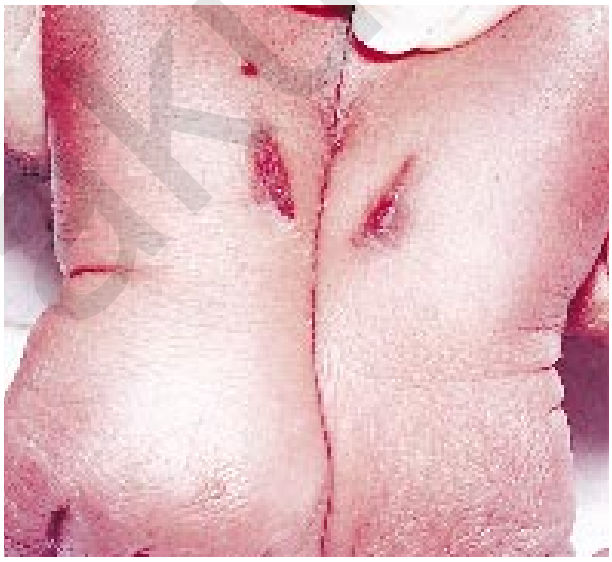

Figure 1.39. The intrauterine sucking lesions at the wrists in this infant have ruptured and left raw areas which will not heal as long as the infant continues sucking at the site.

1.40

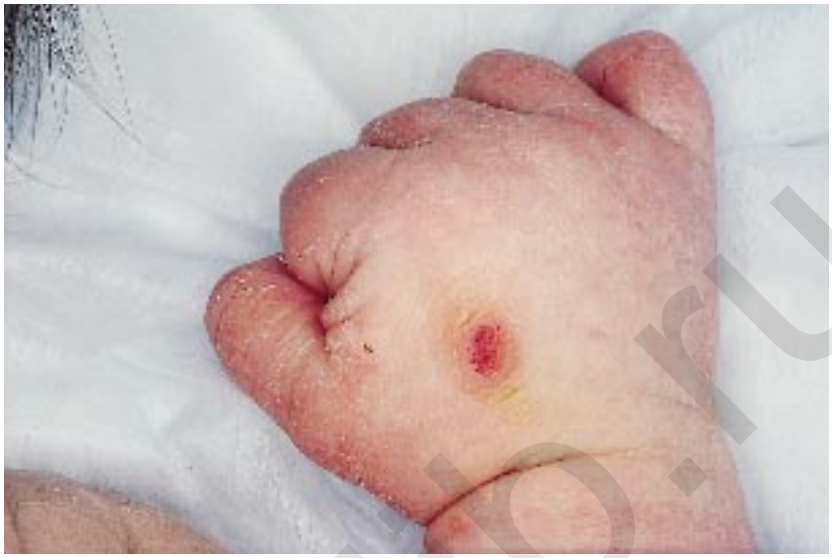

Figure 1.40. Another example of an intrauterine sucking lesion on the dorsum of the right hand.

1.41

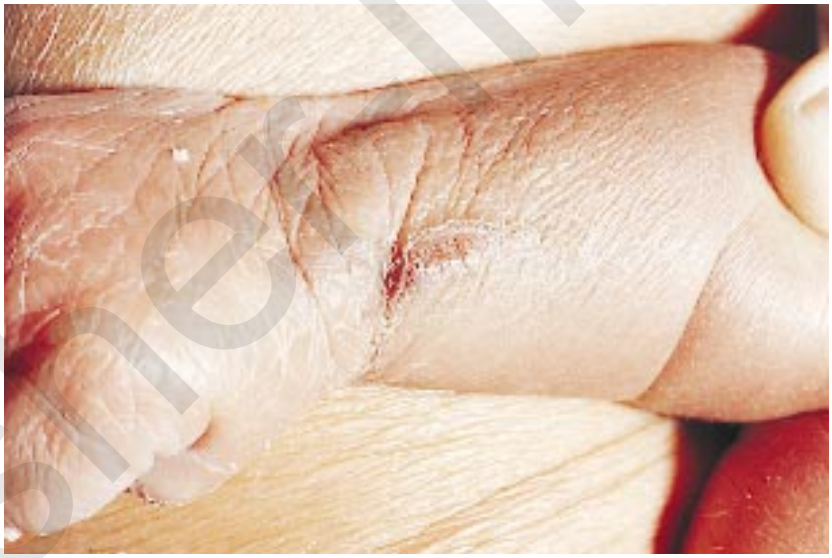

Figure 1.41. The intrauterine sucking lesions may heal and present at birth with an area of scarring, as noted in this infant.

1.42

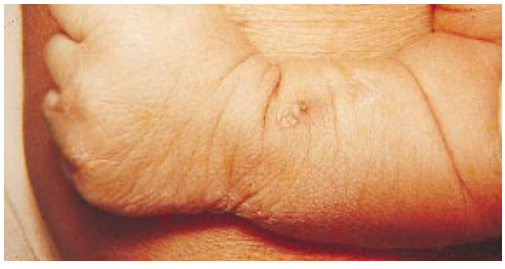

Figure 1.42. In upper panel, note another example of scarring at the left wrist in a normal newborn from an intrauterine sucking lesion. Below, this infant continued sucking its wrist after birth at the site of this lesion.

1.43

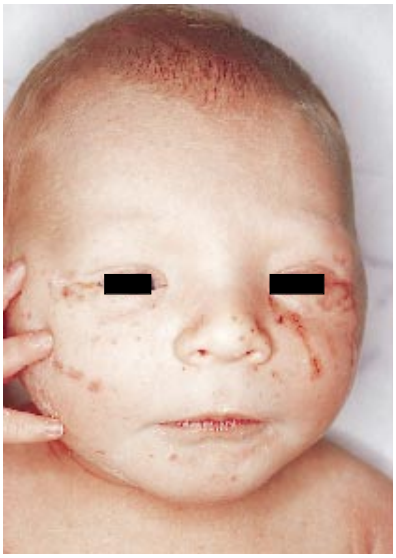

Figure 1.43. Facial abrasions in this infant were self-inflicted. This type of lesion results from hyperactivity in an infant with long finger nails and is seen more commonly in postmature infants and in infants with drug withdrawal.

1.44

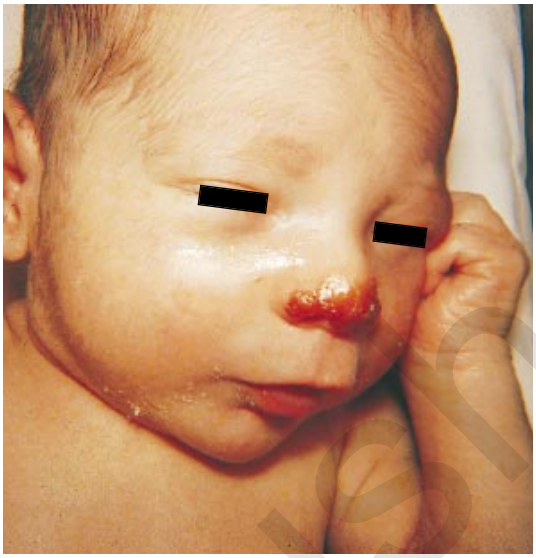

Figure 1.44. Abrasion of the nose ("sheet burns") in an infant with hyperactivity due to drug withdrawal. At the present time hyperactivity is most commonly seen with drug withdrawal, but may occur in infants experiencing pain, congenital hyperthyroidism, etc. The abrasions and erythema generally develop over prominent body parts such as the nose, ears, cheeks, elbows, and knees.

1.45

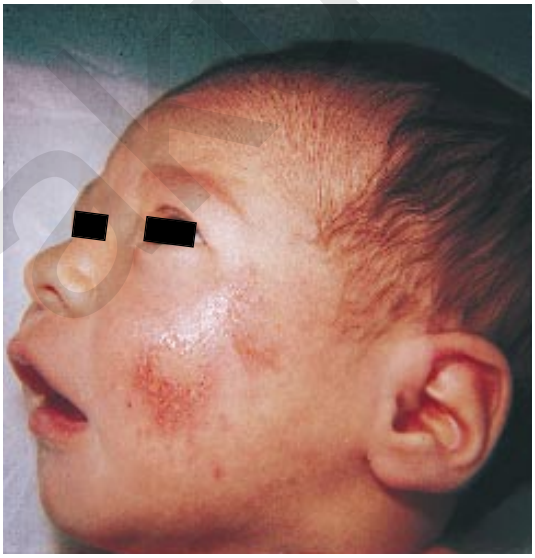

Figure 1.45. "Sheet burn" of the cheeks in a hyperactive infant who was lying in a pool of regurgitated gastric contents. A similar appearance could occur with hyperactivity in an infant with drug withdrawal alone.

1.46

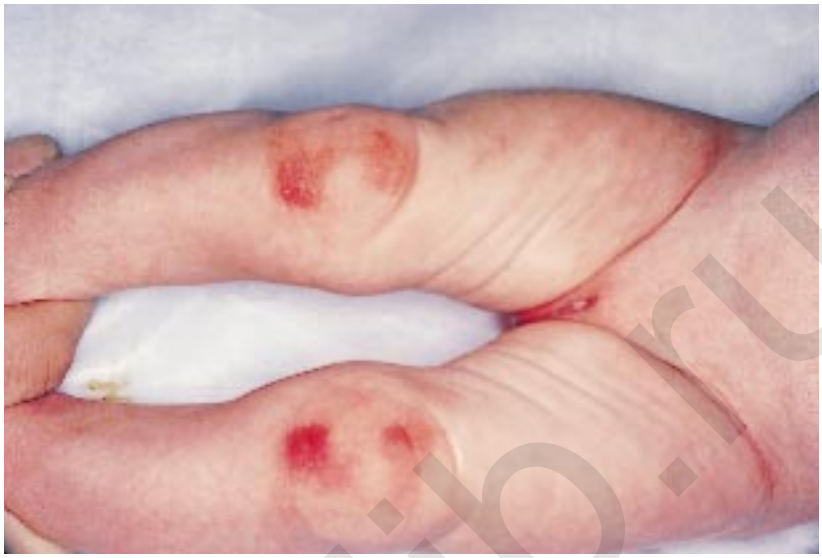

Figure 1.46. Abrasions of the knees occurring in an infant with drug withdrawal. This type of lesion, which occurs as a result of repeated hip flexion in a hyperactive infant, is very common.

1.47

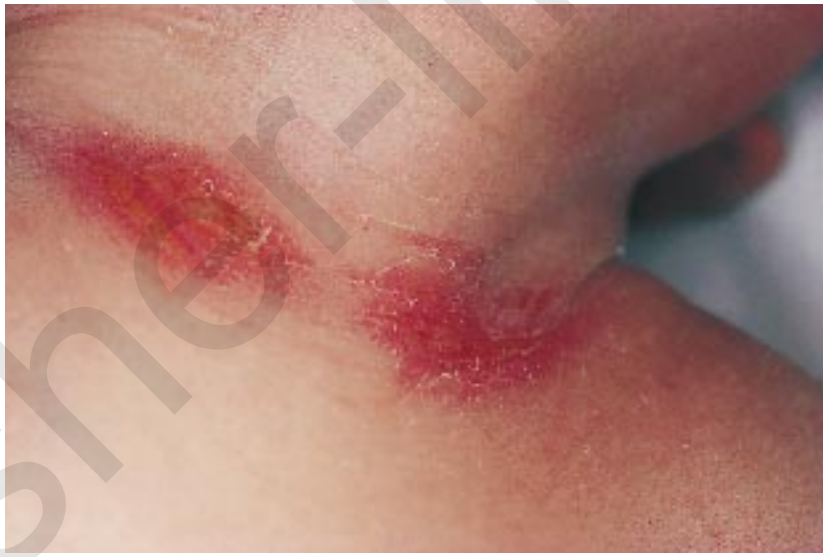

Figure 1.47. This infant presented at birth with an abraded area in the neck. The cord was around the neck three times and this was thought to be the etiology of the abrasion.

1.48

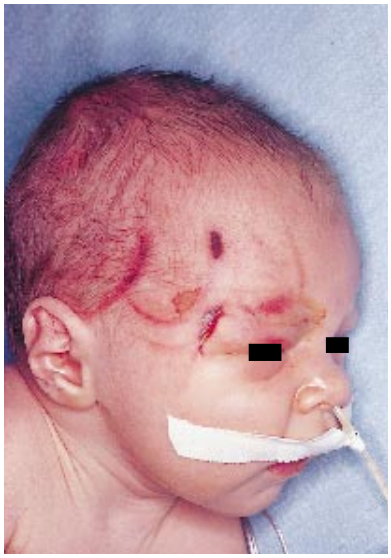

Figure 1.48. The abrasions of the head and face in this normal infant occurred with forceps delivery. There was rapid healing.

1.49

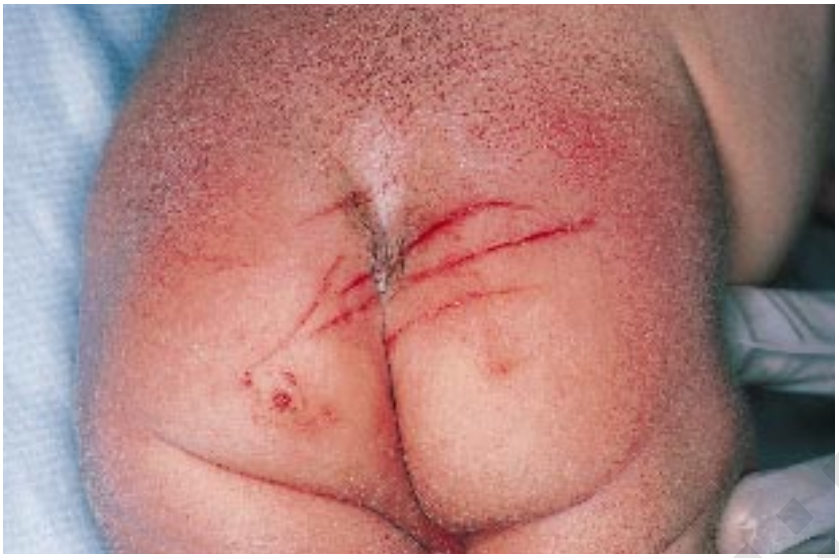

Figure 1.49. Skin incisions over the buttocks in an infant following cesarean birth.

1.50

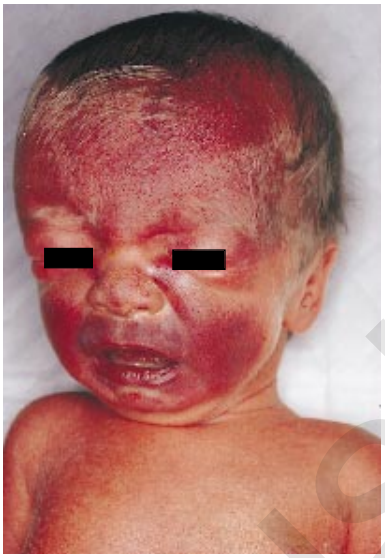

Figure 1.50. Edema and ecchymoses of the face in a premature infant who was delivered as a face presentation. These infants need to be checked for anemia and hyperbilirubinemia.

1.51

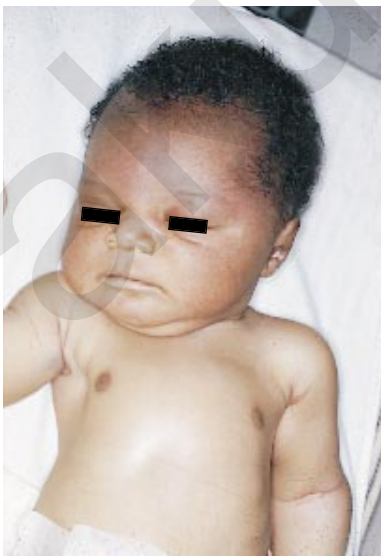

Figure 1.51. Suffusion of the face and head in an infant who had a tight nuchal cord. Note the difference in color of the face and head compared with the rest of the body.

1.52

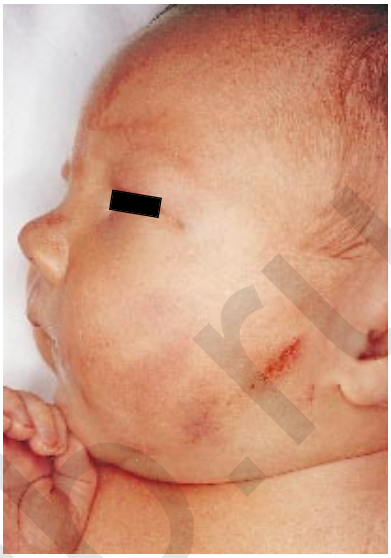

Figure 1.52. In this infant aged 6 days, note the healing abrasion from the application of forceps. In addition note the changes in the skin in that there is some reddish-purple discoloration and swelling with induration of the underlying subcutaneous tissue. This is an example of early subcutaneous fat necrosis. Subcutaneous fat necrosis occurs in areas subjected to undue pressure such as by forceps.

1.53

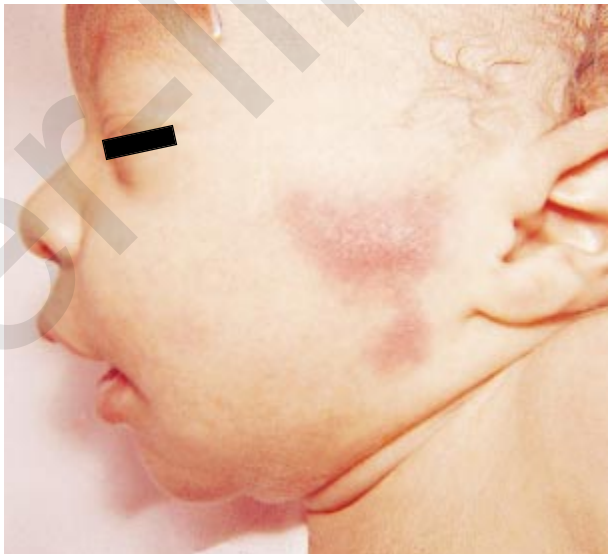

Figure 1.53. Subcutaneous fat necrosis of the cheek in an infant following forceps delivery. In subcutaneous fat necrosis, which is usually detected towards the end of the first week of life, the lesions have an inflammatory or ecchymotic appearance. The underlying tissue may be indurated and feels diffusely hardened. With breakdown of the subcutaneous tissue after several days there may be an area in the center which is fluctuant. If managed conservatively, spontaneous healing usually occurs. This condition should not be mistakenly treated as an infection.

1.54

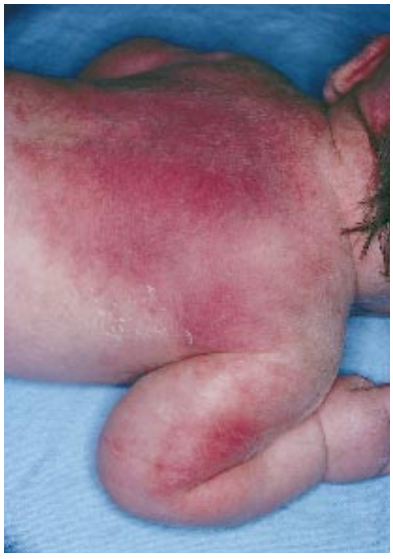

Figure 1.54. This infant, aged 5 days and delivered as a breech presentation, developed the extensive reddish-purple discoloration and swelling of the skin over the back with induration of the underlying subcutaneous tissue. This is an example of extensive subcutaneous fat necrosis. With conservative treatment, improvement occurred within 2 to 3 weeks.

Differential diagnosis includes sclerema neonatorum in which there is progressive hardening of the subcutaneous tissue associated with severe illness of the infant. In sclerema the involved areas are hard and non-pitting and the palms and soles are spared.

1.55

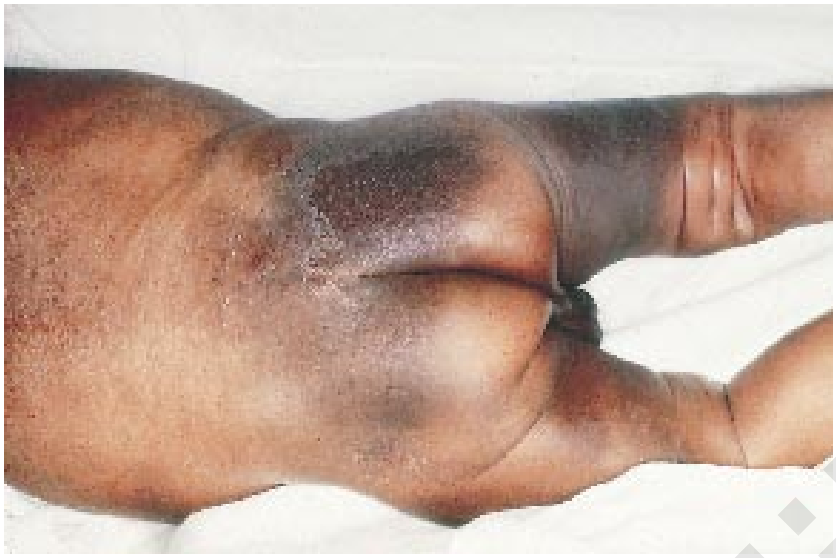

Figure 1.55. During delivery of this infant with a breech presentation there was much manipulation and handling. He developed severe generalized subcutaneous fat necrosis which presented as numerous ecchymotic lesions with marked induration of the skin. Any handling of this infant resulted in pain and discomfort. Over a period of several weeks the subcutaneous fat necrosis improved but the infant developed hypercalcemia. His serum calcium level was 15.8 mg/dL. (There is a case report of an infant with subcutaneous fat necrosis who developed a serum calcium level of greater than 20 mg/dL.)

1.56

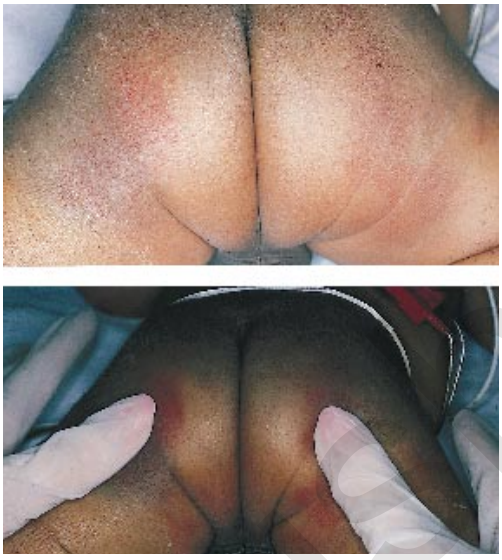

Figure 1.56. This infant delivered by emergency cesarean birth was an extremely difficult delivery and on the 4th day of life he developed an area of subcutaneous fat necrosis over each buttock as noted in the top panel. In the lower panel, note how pressure over these sites during delivery resulted in the subcutaneous fat necrosis.

1.57

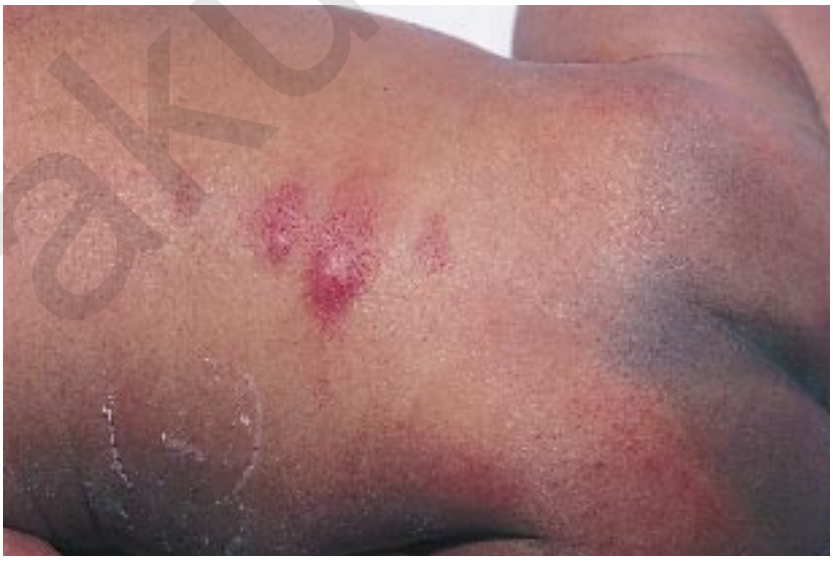

Figure 1.57. In this infant there were several attempts at performing a spinal tap for sepsis evaluation. Four days later he developed areas of subcutaneous fat necrosis over the lower lumbar area. These could easily have been mistaken for abscesses but were confirmed to be subcutaneous fat necrosis occurring from the pressure applied in performing the spinal tap. Note the mongolian spots.

1.58

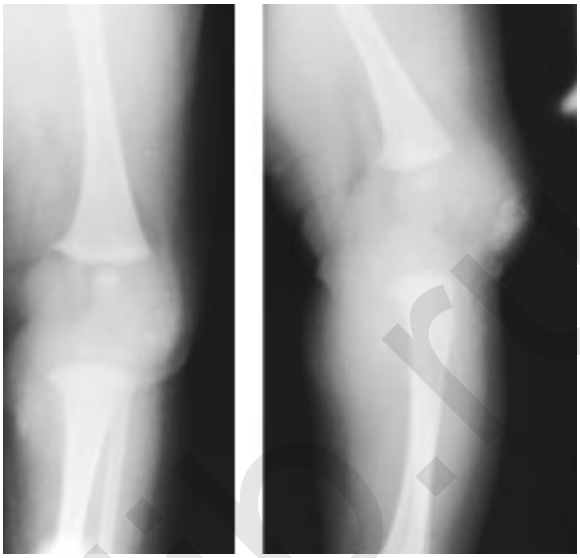

Figure 1.58. Calcification may occur in areas of subcutaneous fat necrosis. In this radiograph note the soft tissue calcifications occurring as a result of subcutaneous fat necrosis.

1.59

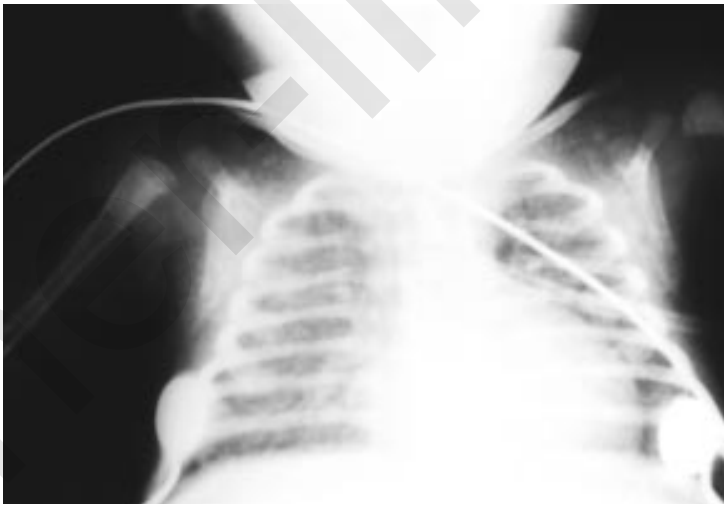

Figure 1.59. Calcifications occurred in the scapular area of this small premature infant as a result of subcutaneous fat necrosis which developed from vigorous chest physiotherapy.

DEVELOPMENTAL ABNORMALITIES OF THE SKIN

1.60

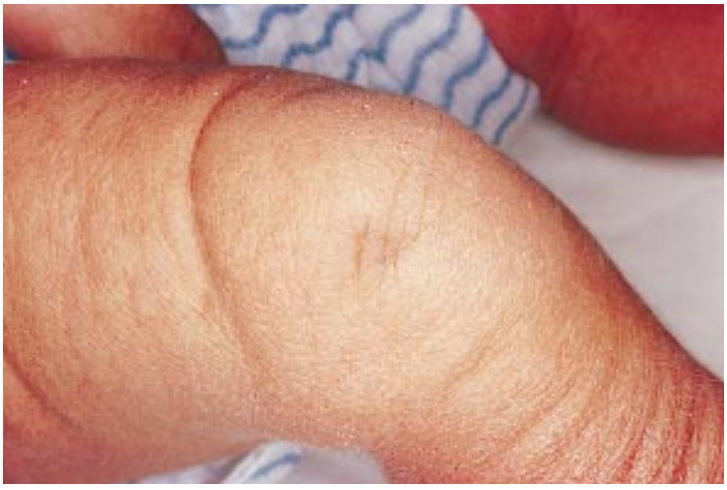

Figure 1.60. This infant has a typical pigmented skin dimple at the knee. The presence of a skin dimple over a joint, pigmented or not, is normal. Skin dimpling is frequently noted in a relatively mild form where there has been prolonged intrauterine pressure upon the bony prominences, particularly at the elbows and knees. Normal skin dimples are most commonly noted at the knee joints, over the lateral aspect of the elbows, over the acromion process, and in the lumbosacral area.

1.61

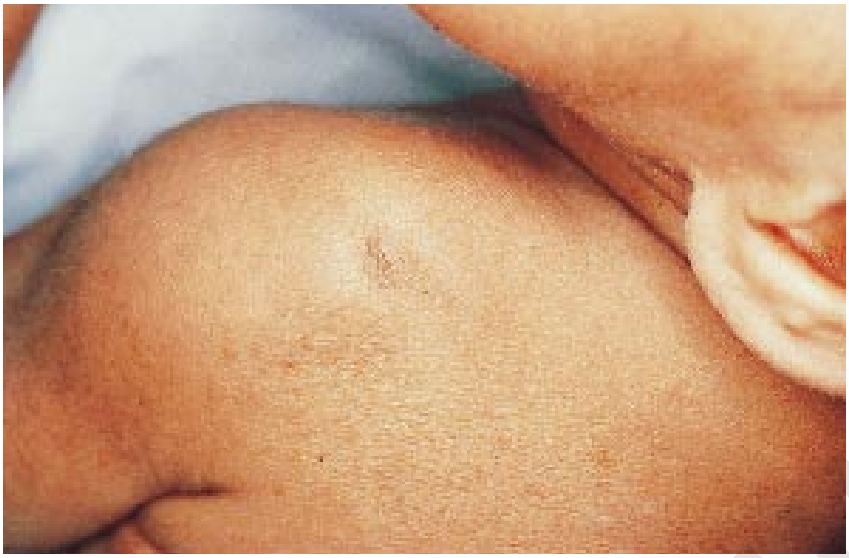

Figure 1.61. A pigmented skin dimple over the left shoulder. Normal skin dimples in general tend to occur in areas where the skin is relatively tightly bound to the underlying bony prominences.

1.62

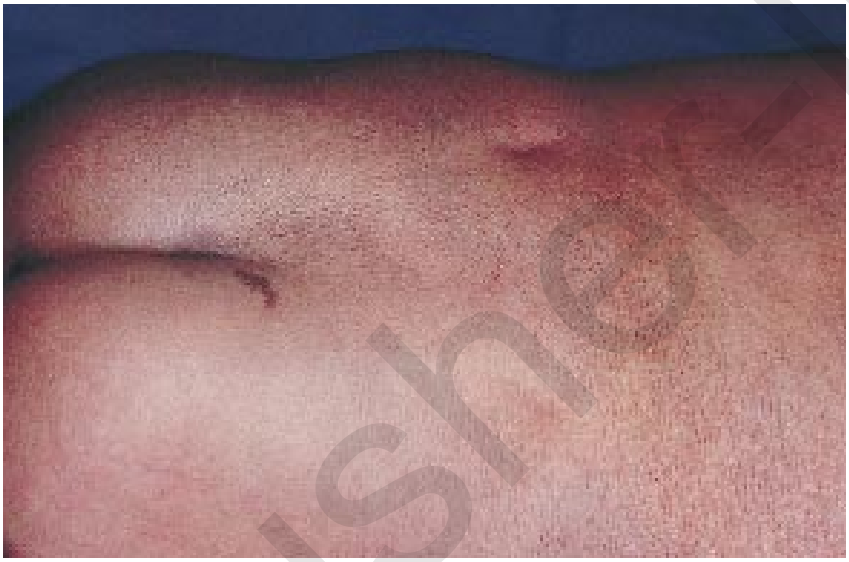

Figure 1.62. Nonpigmented skin dimples in the iliosacral area. These tend to be crease-shaped and may be multiple over the lower part of the back. If midline, they should be distinguished from a pilonidal sinus.

1.63

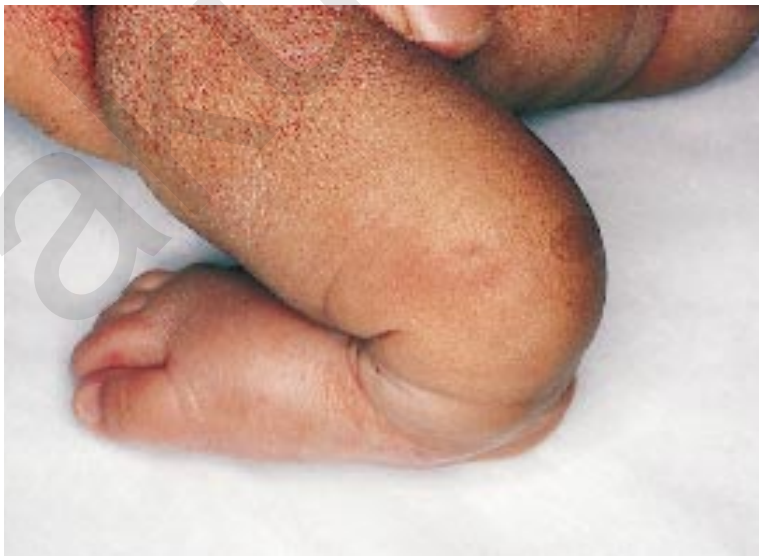

Figure 1.63. Dimples in between the joints over the long bones are considered pathologic until proven otherwise. In this infant with congenital hypophosphatasia, the skin dimple over the middle of the tibia is a very typical finding. Abnormal (aberrant) skin dimples may occur at a location where there has been a closer than usual proximity between the skin and the underlying bone structure during fetal life, resulting in deficient development of subcutaneous tissue at that locus. Such dimples may be secondary either to a loss of subcutaneous tissue or to an aberrant bony promontory. These may also cause breakdown of the dermis with ulcer formation.

1.64

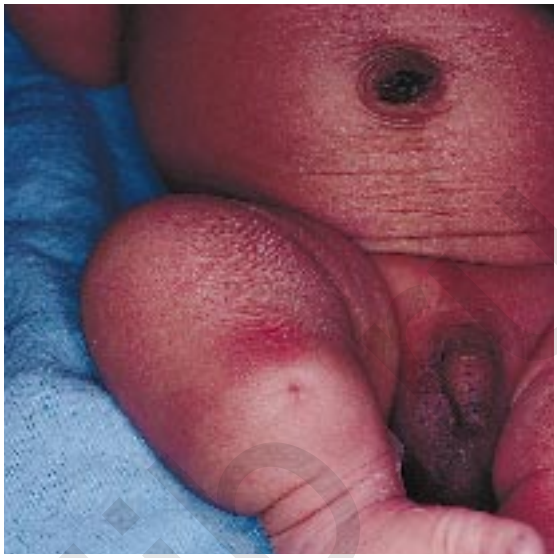

Figure 1.64. An example of an abnormal skin dimple in an infant with camptomelic dysplasia. Note the extreme prenatal distortion of the bones with the development of the aberrant skin dimples over the abnormal bony prominences. The most common site for this type of abnormal skin dimple is over the apex of a severe curvature of the tibia in cases of fibular hypoplasia, but other areas can be similarly affected.

1.65

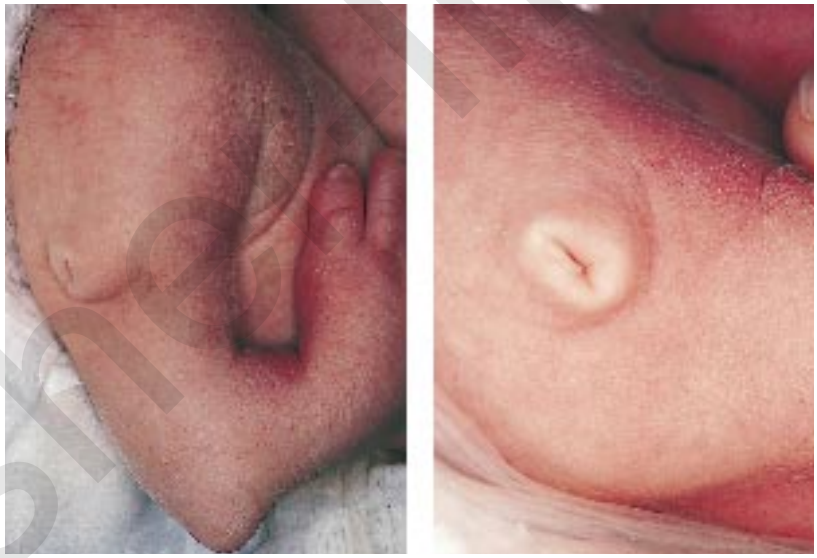

Figure 1.65. This infant with exstrophy of the cloaca sequence had a dysplastic, markedly hypoplastic right tibia with deformity of the right foot. Note the severity of the abnormal skin dimple.

1.66

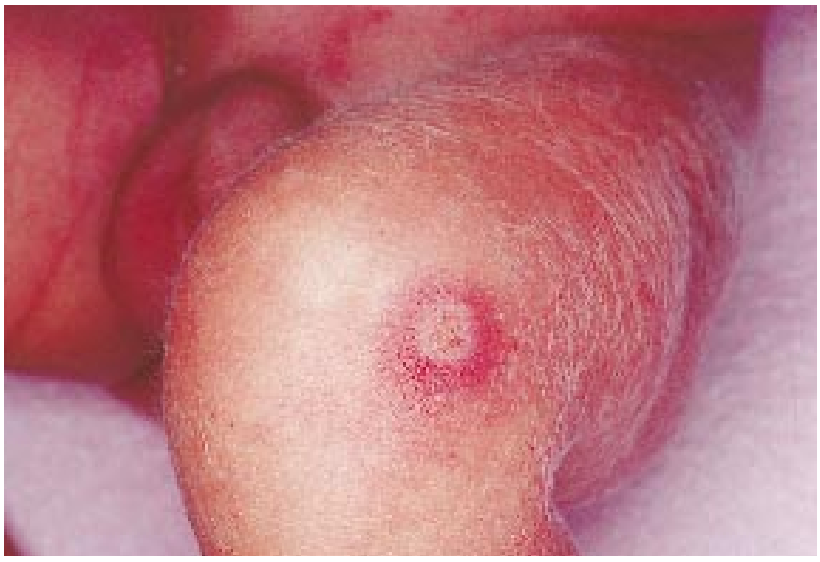

Figure 1.66. Ulceration of the skin, which was present at birth in this infant, occurred as a result of intrauterine pressure on the fetus.

1.67

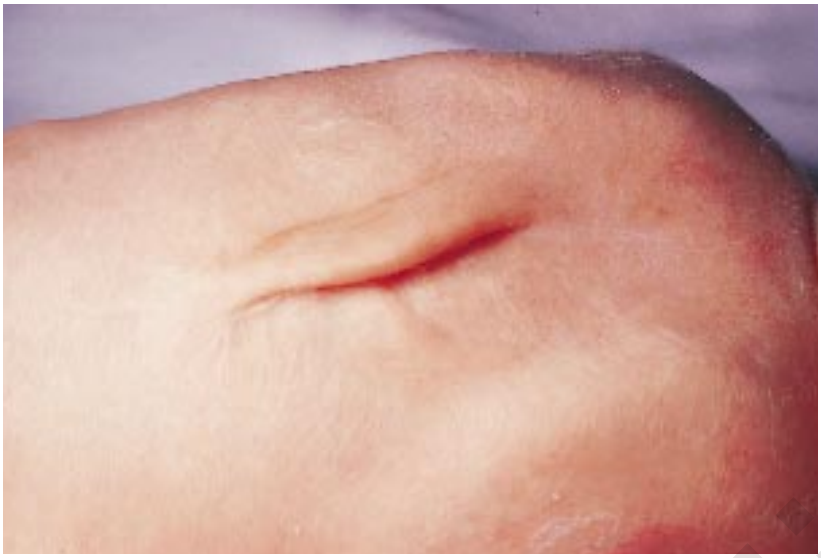

Figure 1.67. The large skin fold on the back of this infant was hard and fibrotic. It was believed to have occurred as a result of the skin being "pinched" in utero from intrauterine constraint very early in gestation.

1.68

Figure 1.68. A midline occipital defect consisting of a tag with some cystic formation is seen in this infant. In any infant with a midline lesion anywhere from the back of the neck to the lower end of the spine, it is mandatory to investigate the neural axis. The lesions may consist of small sinuses, cysts, or hemangiomas.

1.69

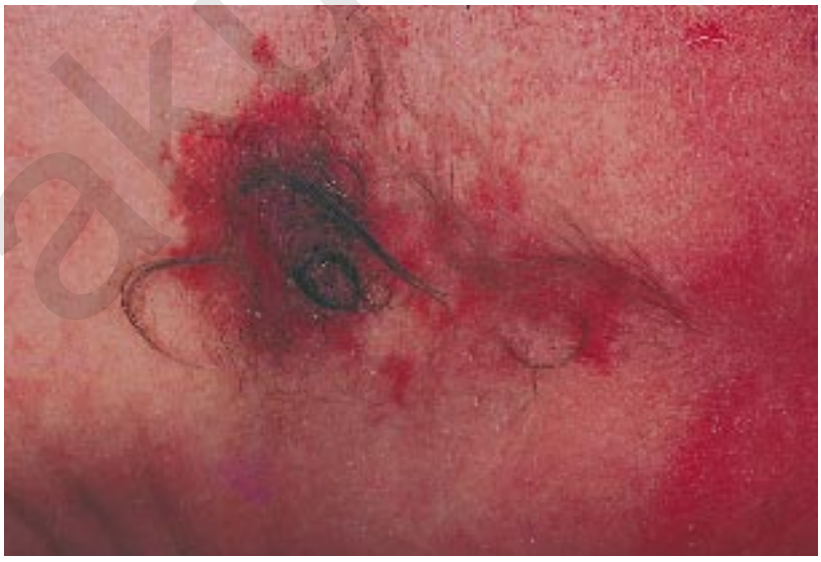

Figure 1.69. This infant presented with a midline hemangioma associated with a midline tuft of hair over the spine. Further investigation confirmed the presence of a neural axis defect. If hair tufts are associated with any of these lesions, the risk is even greater.

1.70

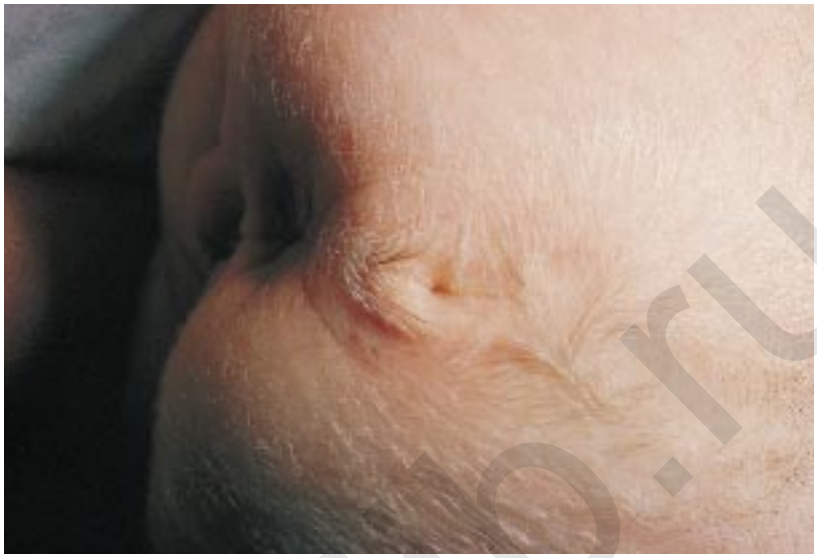

Figure 1.70. Pilonidal dimples are extremely common in neonates. If the base of the dimple can be seen easily, further investigation is not necessary. If the dimple is very deep or appears to be a sinus tract it is important to do a neurologic evaluation.

1.71

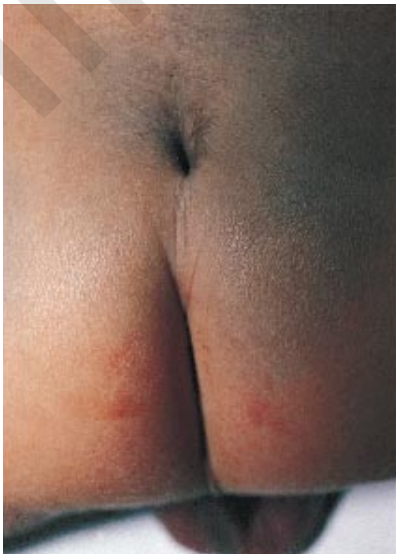

Figure 1.71. Another example of a pilonidal dimple which is deep. This infant's MRI study was normal.

1.72

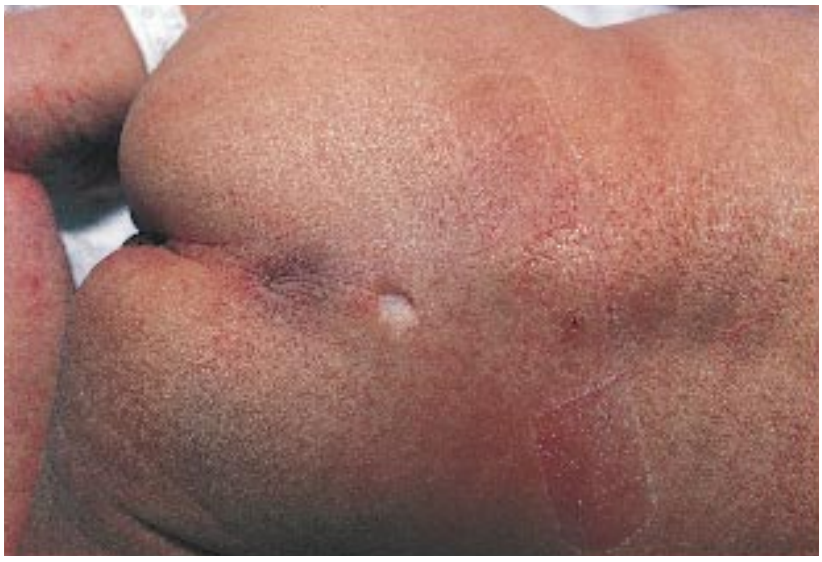

Figure 1.72. In this infant there is a midline defect over the distal end of the spine. With this type of lesion it is mandatory to do further studies. MRI confirmed the presence of a tethered cord syndrome. Note the "bandaid sign" in this infant confirming that the infant had a spinal tap performed as part of a sepsis evaluation. This was contraindicated in this infant because of the midline skin defect.

1.73

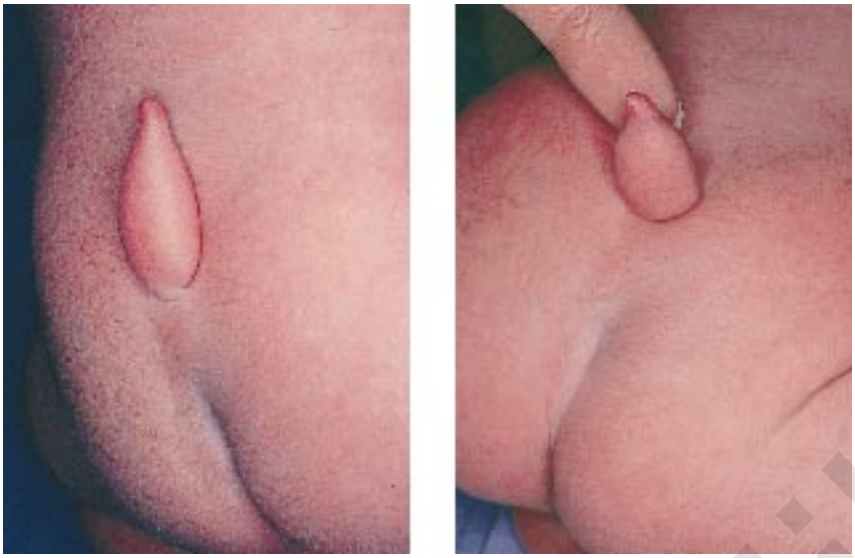

Figure 1.73. A baby with a tail. Vestigial tails are rarely seen in the neonate. They may consist of soft tissue only, as in this infant, or may contain osseous structures.

1.74

Figure 1.74. Note the preauricular and facial skin tags in this otherwise normal infant. Preauricular skin tags are extremely common, but the presence of skin tags between the ear and corner of the mouth would suggest a diagnosis of Goldenhar's syndrome.

1.75

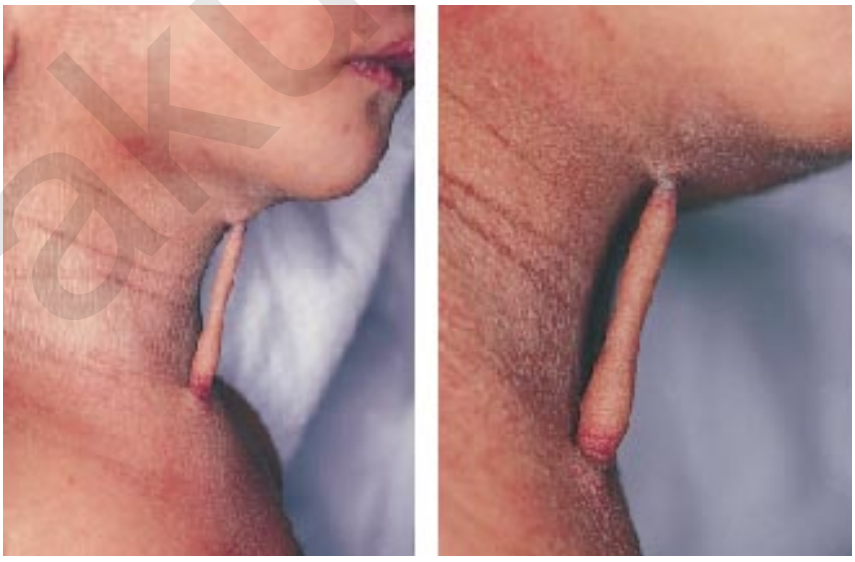

Figure 1.75. Midline skin and tissue band between the jaw and lower sternum in an otherwise normal infant.

1.76

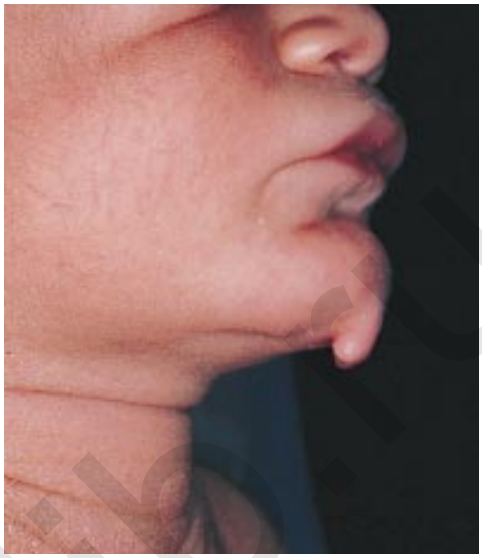

Figure 1.76. A midline skin tag of the chin. This consisted of soft tissue only. The radiograph of the mandible was normal.

1.77

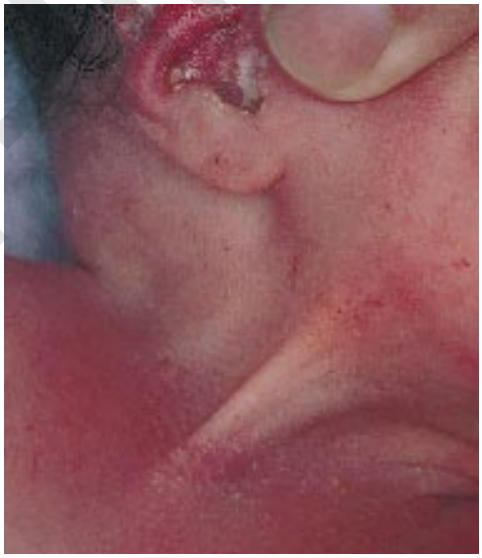

Figure 1.77. This infant has redundancy of the skin in the neck which was present at birth. It was related to the infant's position in utero in that the head was flexed on the right upper chest, resulting in the tight skin. There may be a small amount of redundant skin in the neck normally, but when there is enough to cause visible folds or webs on the lateral neck, prenatal edema in the region is almost certain to be the cause. Extensive redundancy of neck skin is seen in a number of dysmorphic conditions (e.g., Turner's and Noonan's syndromes). Once localized skin growth has taken place, it does not easily reconstitute itself if the distending forces are removed.

1.78

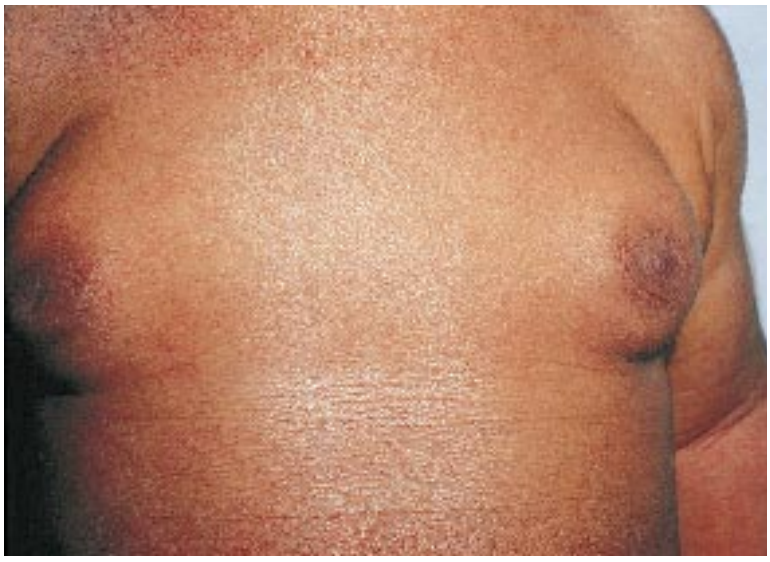

Figure 1.78. Mastitis neonatorum due to physiologic breast engorgement is the result of transplacental transfer of maternal estrogen to the fetus. Enlargement is generally symmetrical, as noted in this infant. Witch's milk (which is chemically identical to colostrum) may be expressed from the breasts, but it is not advisable to relieve the swelling by expressing the milk since infection may follow.

1.79

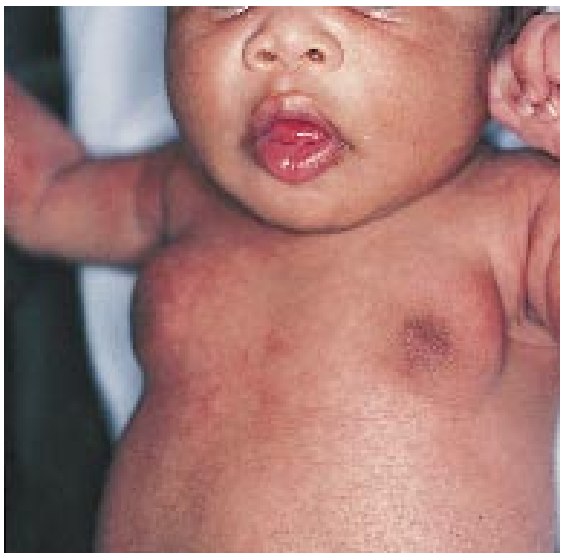

Figure 1.79. Another example of mastitis neonatorum which is asymmetrical in that it is more prominent on the right than on the left. Mastitis neonatorum is noted more frequently in postmature infants. It subsides spontaneously over the course of several weeks.

1.80

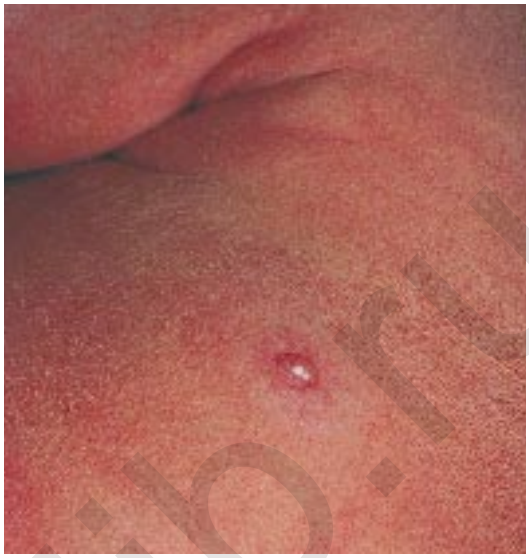

Figure 1.80. This infant has inclusion cysts of the right nipple. These require no treatment as they resolve spontaneously.

1.81

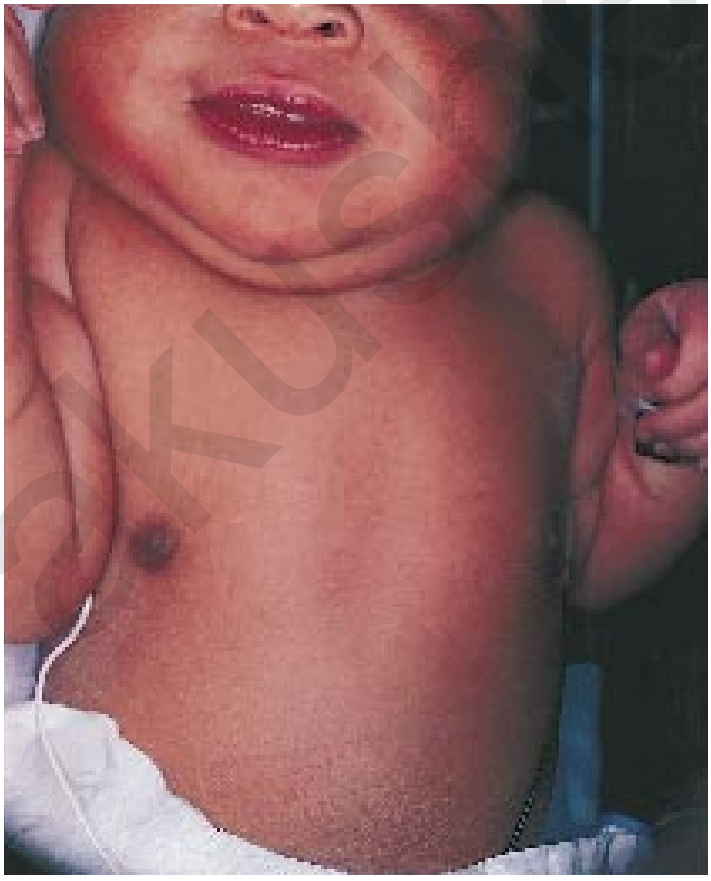

Figure 1.81. Note that the nipples are in the 5th intercostal space in this otherwise normal infant. The nipple may be found anywhere along the milk line which extends from the axilla to the pubis. Normally the nipple is located at the 4th intercostal space.

1.82

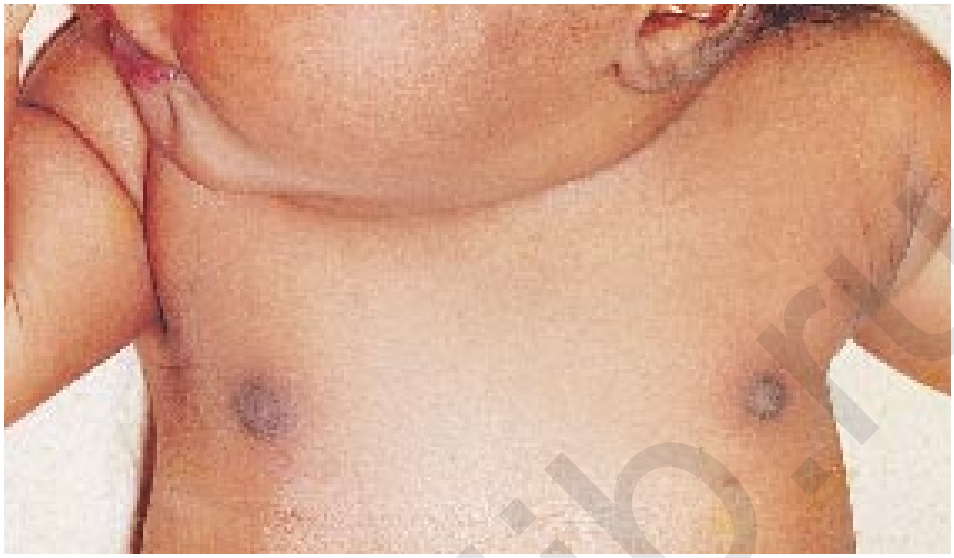

Figure 1.82. Note the bilateral supernumerary nipples in the anterior axilla and bilateral supernumerary nipples below the normal nipples in this black infant.

1.83

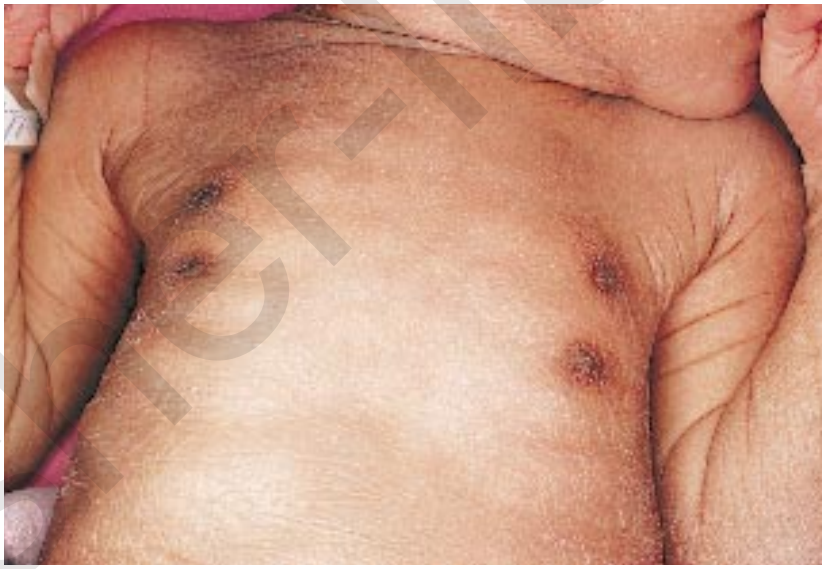

Figure 1.83. Supernumerary nipples are especially common in members of darkly pigmented racial groups. They occur anywhere along the milk line and the supernumerary breast tissue may present as an oval pigmented spot less than half the size of the normal nipple, or may present as another fully developed nipple.

1.84

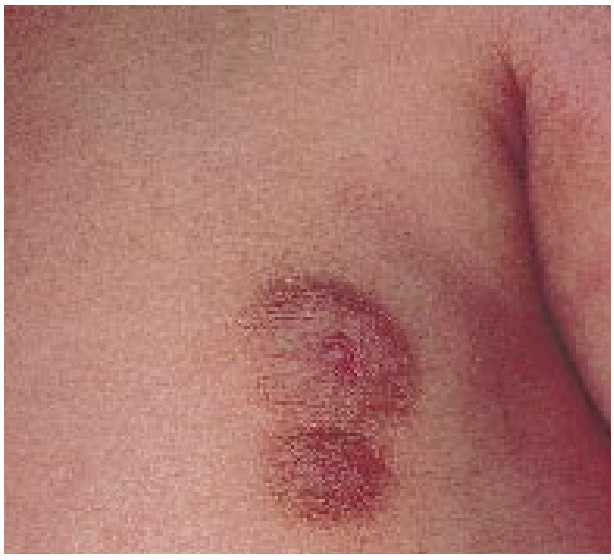

Figure 1.84. In this infant there is a unilateral supernumerary breast on the left side. Supernumerary breasts are rare. These are potentially functional and, like extra nipples, these structures occur along the embryonic milk line unilaterally or bilaterally, usually below the normal site of breast placement. The nipple and areola are quite well developed, distinguishing this anomaly from simple supernumerary nipples.

1.85

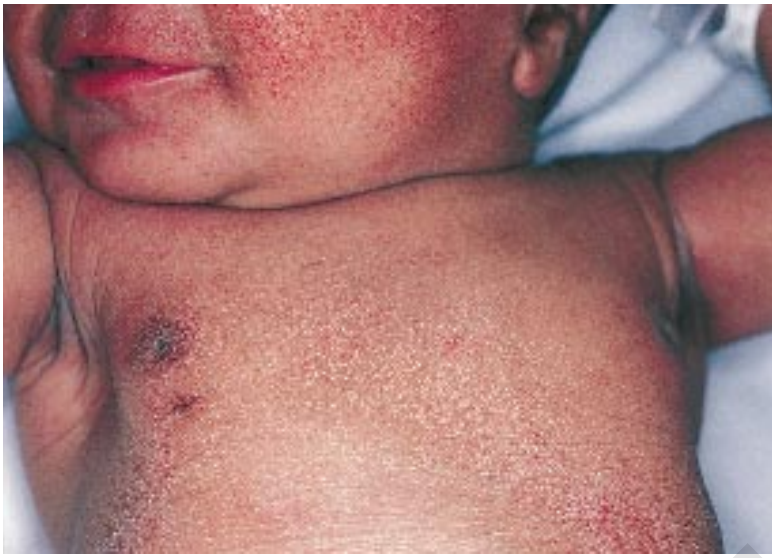

Figure 1.85. Note that the nipples are wide-spaced and there is a right-sided unilateral supernumerary nipple. In general, wide-spaced nipples occur rarely in infants with a normal chest configuration. Infants with Turner's or Noonan's syndrome have wide-spaced nipples but have a shield-like chest.

1.86

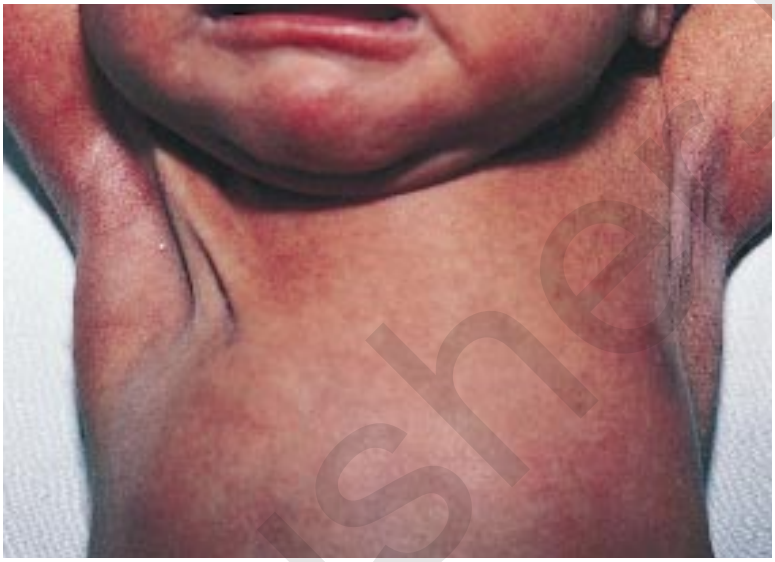

Figure 1.86. This infant with Poland's anomaly has absence of the nipple (athelia) on the right associated with the absence of the pectoralis muscle. Athelia is rare but is seen unilaterally in infants with Poland's anomaly, and bilaterally in certain forms of ectodermal dysplasia.

Hypoplastic nipples are usually poorly pigmented with a narrow or absent areolar zone and little palpable breast tissue. Both sides are equally affected. Absence of the breast (amastia) is very rare. There is no sign of nipple, areola, or mammary tissue.

1.87

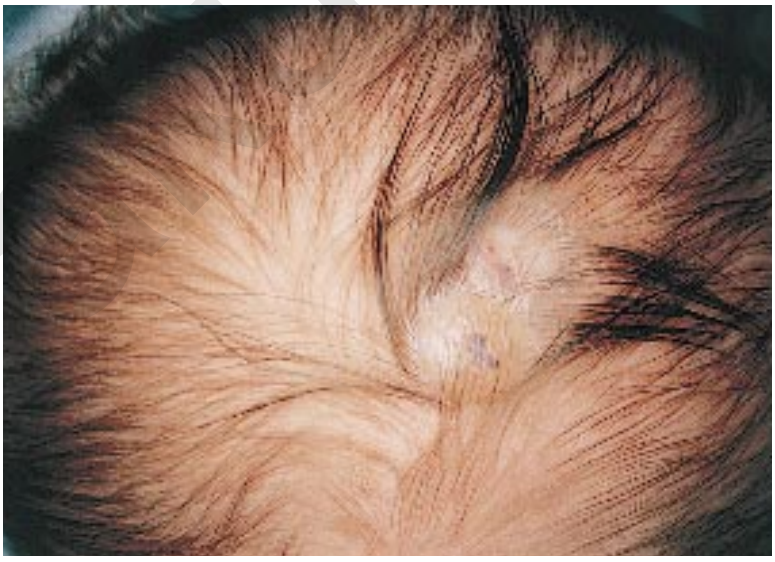

Figure 1.87. Congenital scalp defect (aplasia cutis congenita) occurs most commonly as a single small defect of the scalp, 1 to 2 cm across, and is usually located close to the normal site of a parietal hair whorl. The lesions have a well defined edge with a punched-out appearance, and may be multiple or involve a larger portion of the scalp. Etiology is unknown, and they heal with scarring leaving a zone of permanent alopecia.

1.88

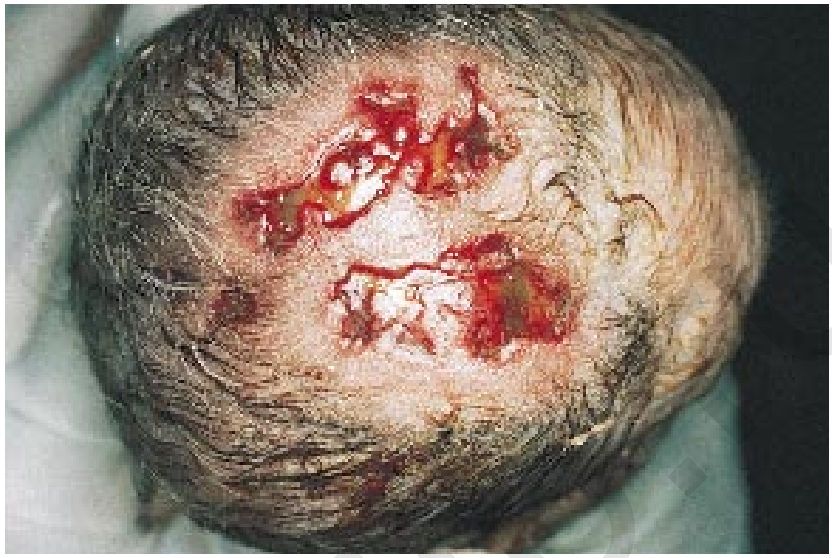

Figure 1.88. Scalp defects are a frequent finding in infants with trisomy 13, as in this infant. A more severe congenital scalp defect may have a full thickness absence of the skin with large areas of skin aplasia. This lesion may occur as a result of in utero disruption by an amniotic band.

1.89

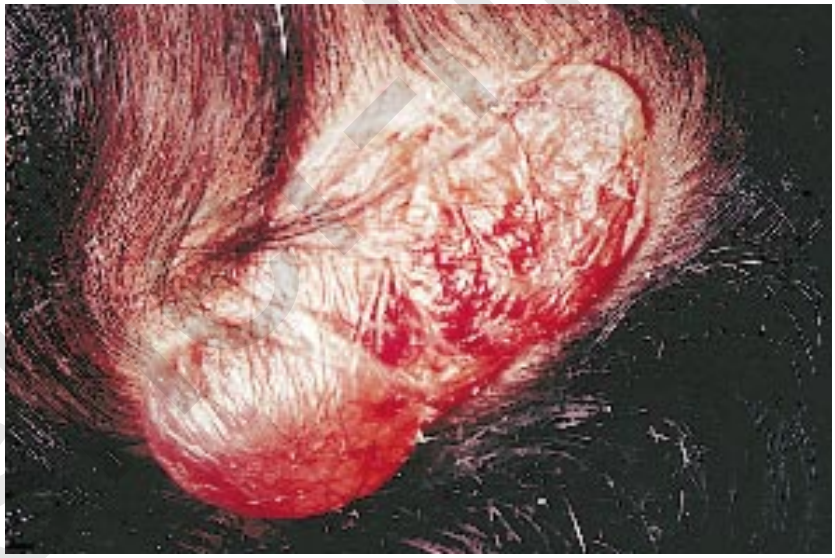

Figure 1.89. In this otherwise normal infant there is a large congenital scalp defect associated with a bullous bleb.

1.90

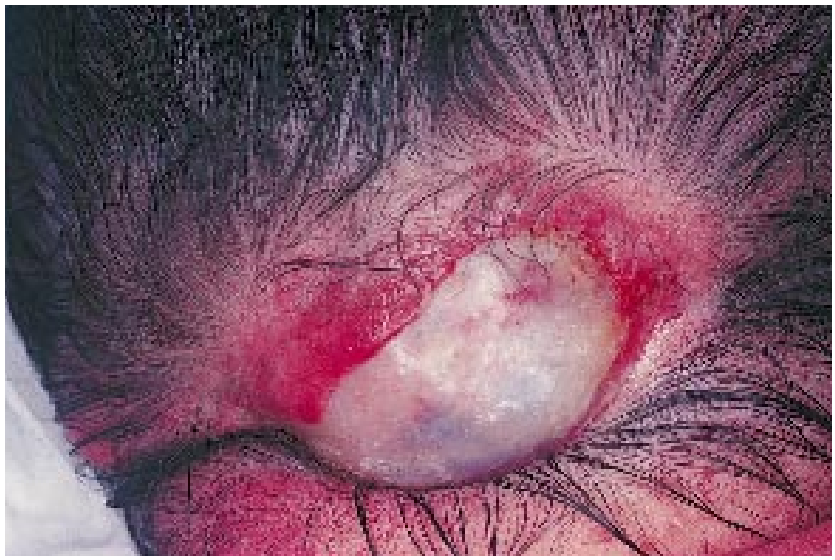

Figure 1.90. A massive congenital scalp defect which involved the skull and exposed the dura mater.

1.91

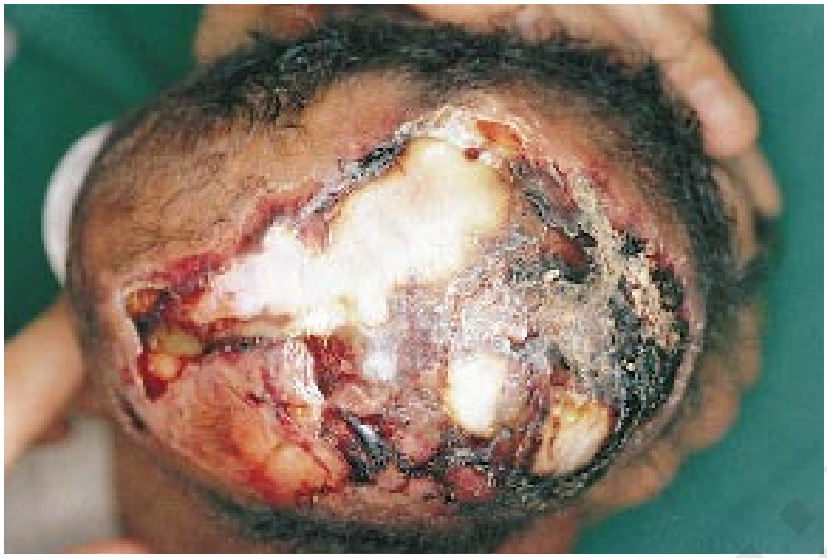

Figure 1.91. The severe congenital scalp defect in this infant occurred in the Adams-Oliver syndrome, which is a disruption sequence associated with limb reduction anomalies and scalp and skin defects as a result of amniotic bands.

1.92

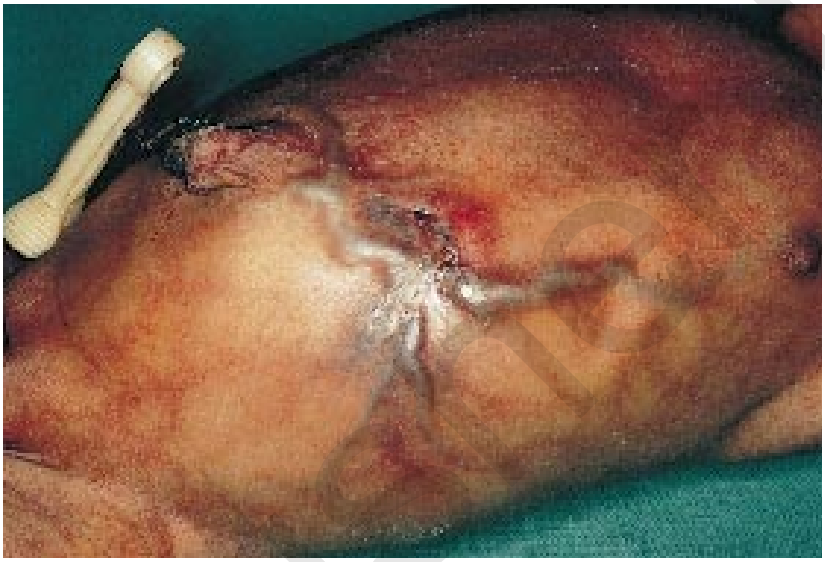

Figure 1.92. The same infant showing the marked aplasia cutis congenita in the skin of the abdomen with dilated superficial capillaries. This is an example of aplasia of the skin affecting the trunk as a result of amniotic bands. It is quite rare.

1.93

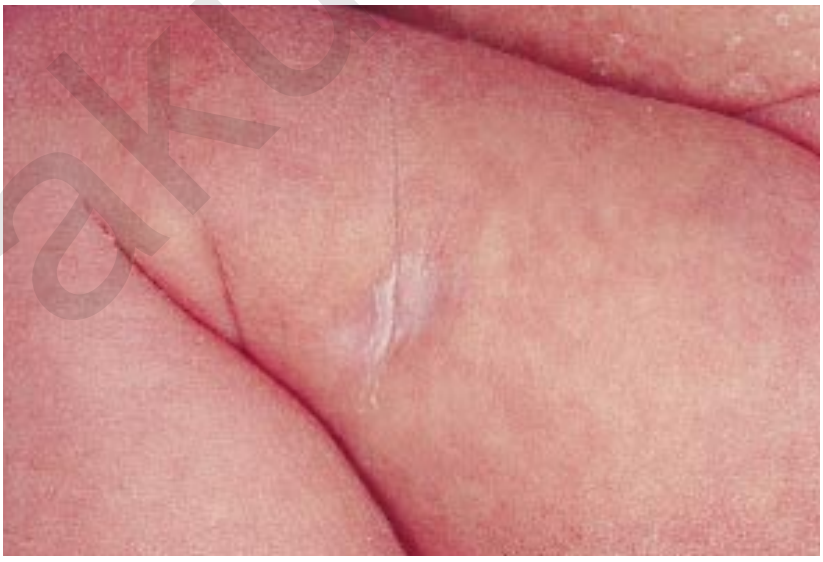

Figure 1.93. Congenital skin defect of the thigh in an infant. It is not known whether this type of disruption results from an intrinsic abnormality of the skin itself or whether aberrant bands of amniotic tissue adhere to intact fetal skin. Some cases of scarring of the skin, especially if linear, have been associated with prenatal varicella infections.

1.94

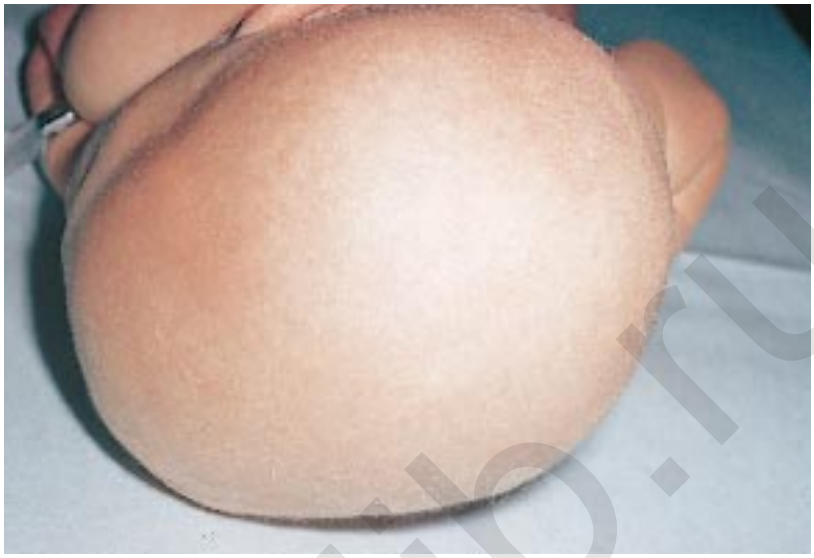

Figure 1.94. Congenital alopecia is usually an autosomal recessive disorder but may be an isolated event. Hair development begins at about week 14 of gestation, and from gestational week 20 until birth the body is covered with fine lanugo hair. This is gradually replaced during the first months of postnatal life with coarser, moderately pigmented vellus hair. Alopecia or hypotrichosis occurs in several syndromes (e.g., ectodermal dysplasia where the hair is sparse over the scalp, eyebrows, and eyelashes; progeria; Hallermann-Streiff syndrome; and cartilage-hair hypoplasia).

1.95

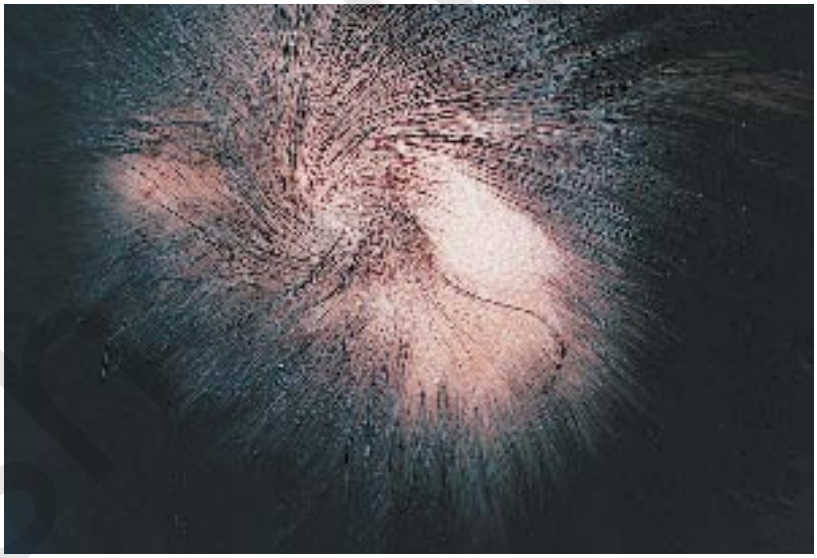

Figure 1.95. The scalp of this infant showed a patchy alopecia at birth. A hair whorl is situated over the part of the brain growing most rapidly from about 16 to 19 weeks of gestation. The normal position is slightly lateral to the midline in the posterior parietal zone. It appears that this patch of alopecia is related to this. Physiologic "frictional" alopecia usually occurs over the occipital region as a result of head rolling and friction producing hair loss on the back of the head. It is poorly circumscribed and resolves completely once the infant is able to change its position at will.

1.96

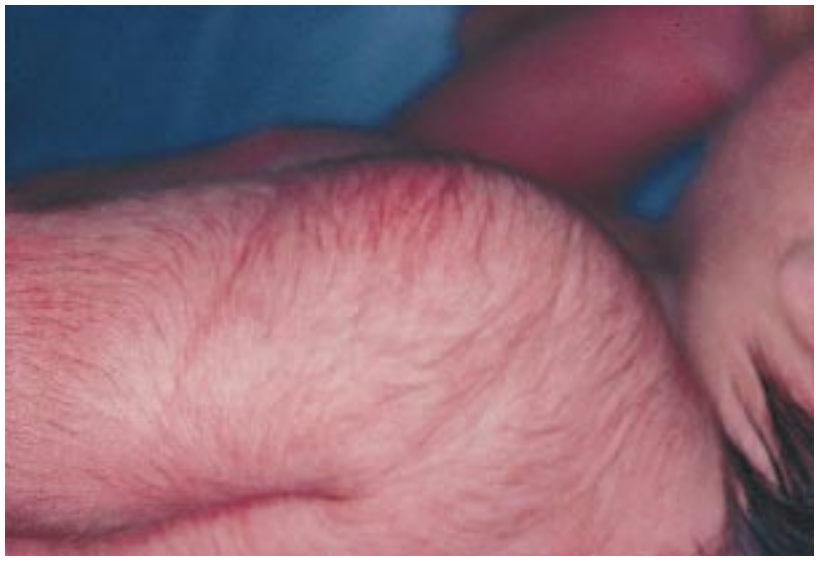

Figure 1.96. Hypertrichosis is seen in normal infants, especially in hispanic infants who tend to have more hair than caucasian or black infants. In hispanics especially there may be hairy ears with long coarse dark hair emerging from the lateral and posterior surface of the pinna.

1.97

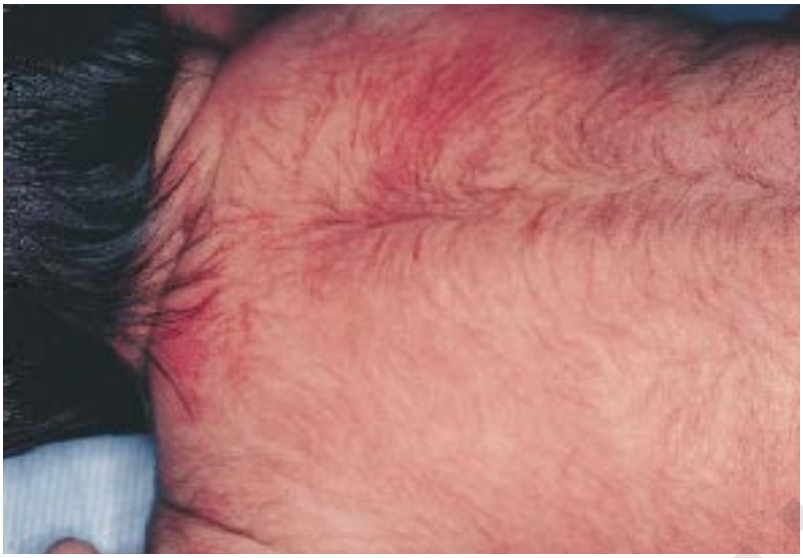

Figure 1.97. Hypertrichosis in a Hispanic infant whose mother was an epileptic treated with phenytoin throughout her pregnancy. Hypertrichosis is associated with syndromes such as Cornelia de Lange's, leprechaunism, etc. In infants with hypertrichosis associated with syndromes, there may be a low anterior hairline which is especially noted at the sides of the forehead approaching the lateral eyebrows due to a widened "sideburn."

1.98

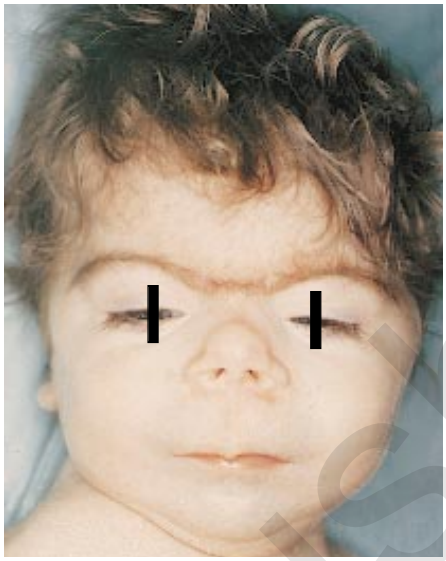

Figure 1.98. Hypertrichosis in an infant with Cornelia de Lange's syndrome. Note also the synophrys, anteverted nostrils, and lack of philtrum. Synophrys (bridging of the eyebrows in the midline) is seen in Cornelia de Lange's syndrome, Waardenburg's syndrome, and in otherwise normal infants. The skin between the eyebrows usually bears only fine vellus hairs, and when the brows encroach on this area they produce the appearance of a single band of hair above the eyes. Straight eyelashes emerge from the lid margin at a steep angle and extend straight downward rather than exhibiting the gentle upward curve. Such eyelashes are seen in children with severe neuromuscular disease and may be caused by lack of normal muscle tone in the levator palpebri superioris muscle.

1.99

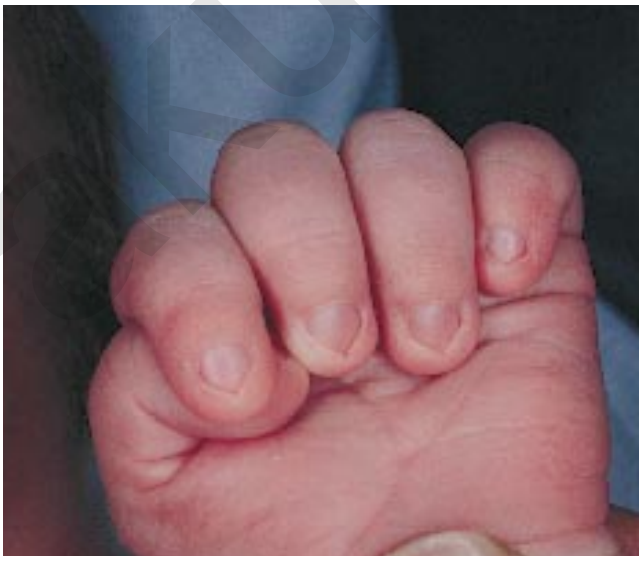

Figure 1.99. This infant's triangular nails fit into the category of tapered nails that become progressively narrower and more hyperconvex as they grow distally. The nails generally reflect the size and shape of the underlying distal phalanx (e.g., hypoplastic nail, narrow hyperconvex nail, short broad nail).

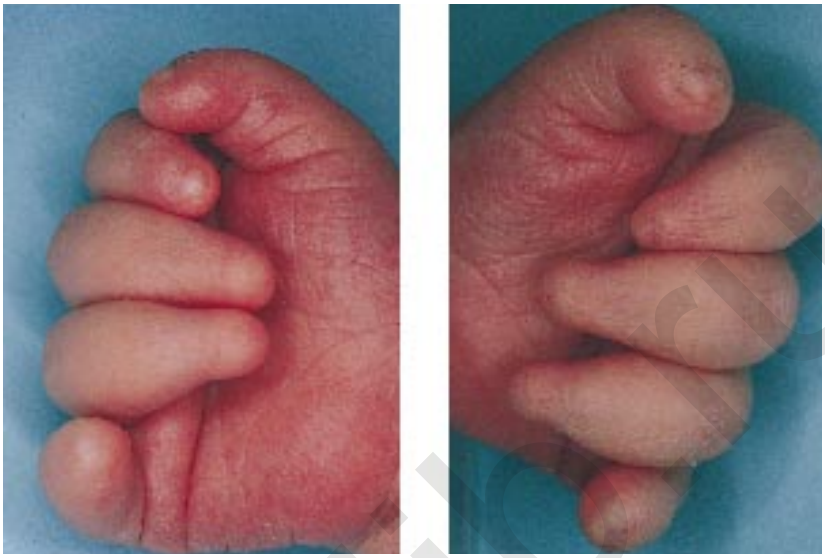

1.100

Figure 1.100. In this infant with the fetal hydantoin syndrome the nails are hypoplastic and distorted or absent over the short hypoplastic distal phalanges. Note the digitalization of the thumbs. Total nail aplasia is very rare. At birth, some or all of the fingers bear a rudimentary nail bed. In nail-patella syndrome, partial nail aplasia occurs, particularly in the thumbs and index fingers.

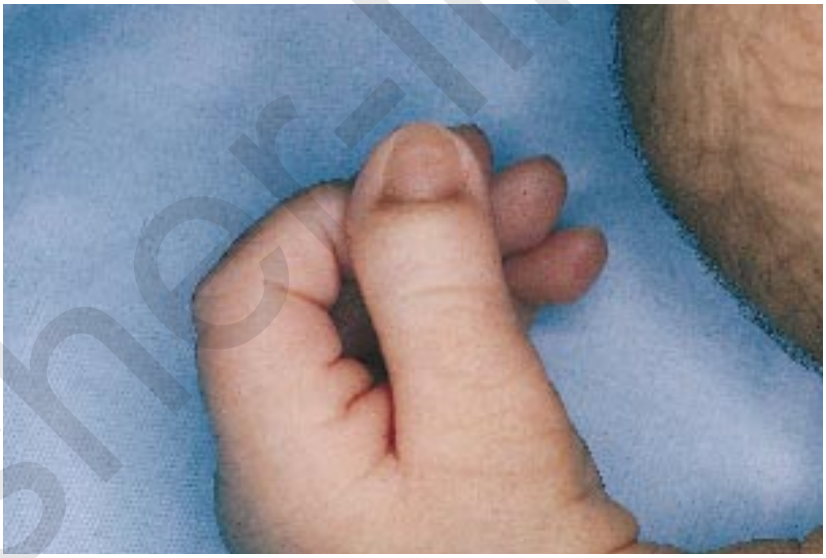

1.101

Figure 1.101. Unusually broad nails of normal length are found over digits with duplication of the distal phalanx. They are also seen in Rubenstein-Taybi syndrome and Larsen's syndrome.

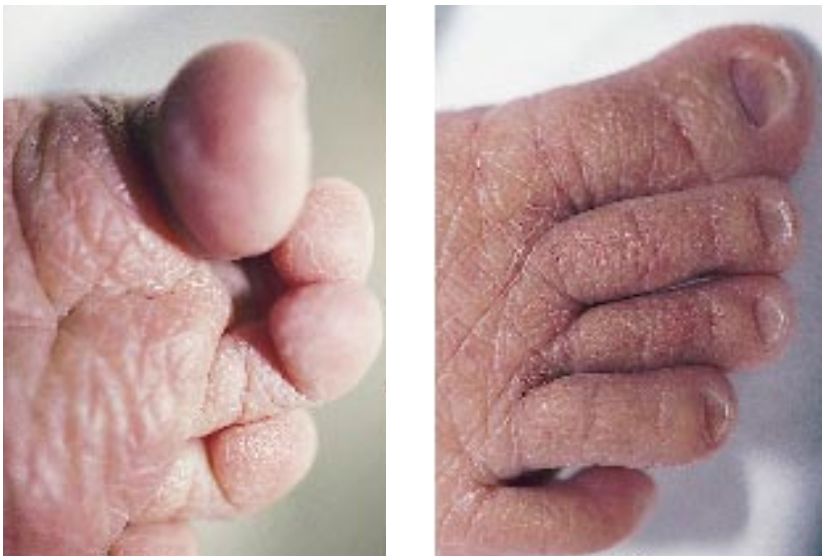

1.102

Figure 1.102. Unusually broad toes in another infant with Rubenstein-Taybi syndrome.

VASCULAR DISORDERS AND MALFORMATIONS

1.103

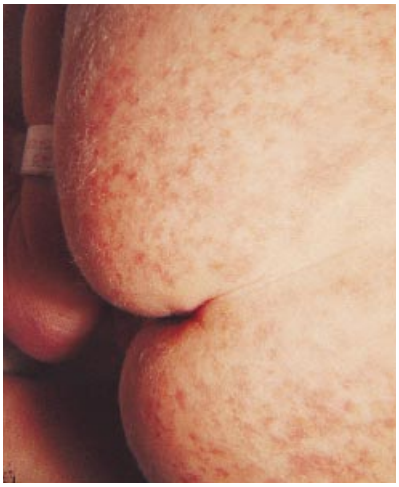

Figure 1.103. Petechiae are common in normal infants, particularly over the back and buttocks. They usually disappear within a few days. Facial petechiae are commonly seen in infants in whom there was a nuchal cord or where there was abnormal delay following delivery of the head and neck before the trunk and shoulders were delivered.

1.104

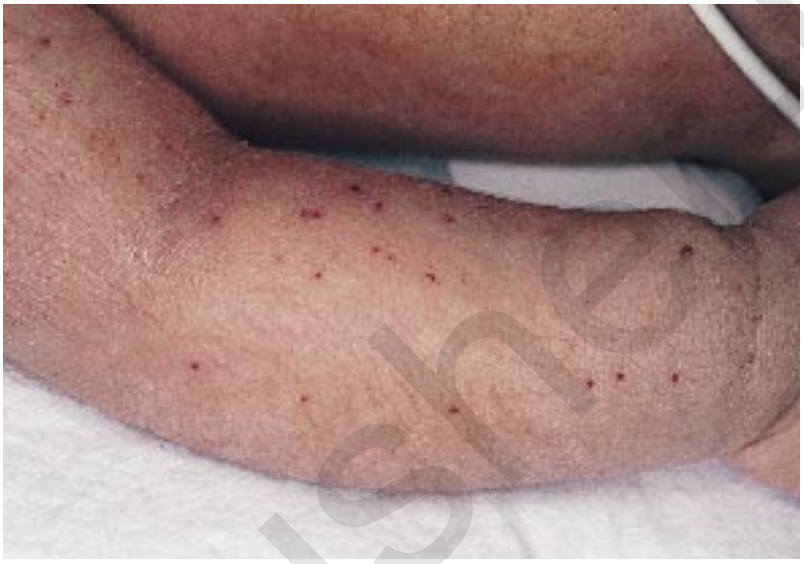

Figure 1.104. The petechiae in this infant were associated with severe birth asphyxia. The platelet count was 90,000/mm^3 and the petechiae resolved spontaneously within a few days.

1.105

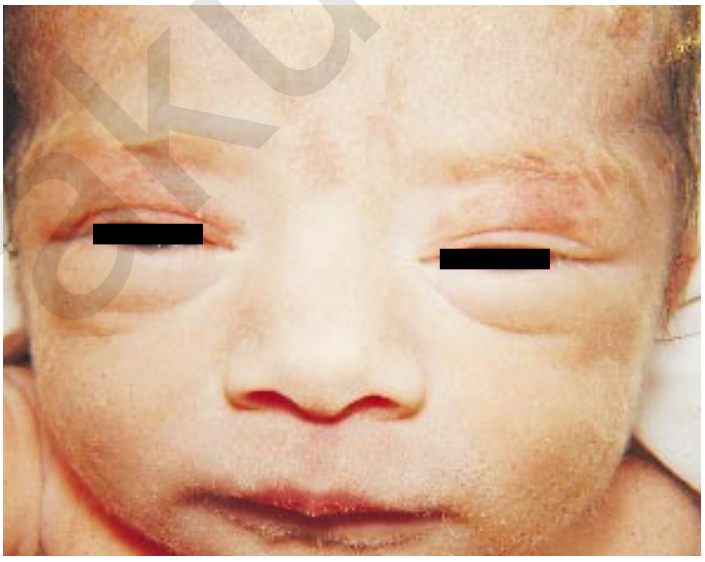

Figure 1.105. Macular hemangioma ("angel's kiss") of the eyelids in a newborn infant. Vascular nevi occur in up to 40% of newborns. They are divided into three groups (salmon patches, hemangiomas, and vascular malformations) and are classified by their histology and the degree of involvement of the skin and subcutaneous tissues. The most common are the salmon patches (macular hemangioma, nevus flammeus). They consist of dilated capillaries in the superficial layers of the dermis and are noted most commonly on the face, the midforehead, the glabella, philtrum, and the nape of the neck. Multiple sites are often affected.

1.106

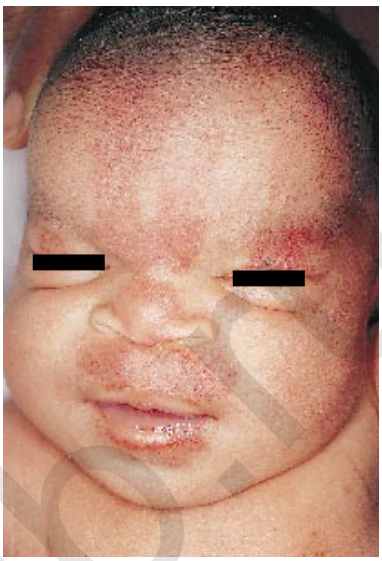

Figure 1.106. Macular hemangioma of the eyelids, glabella, and face. Macular hemangiomas (telangiectatic nevi) are poorly defined, bright red in color, and blanch easily with pressure, but the blood returns rapidly. In general these capillary hemangiomas become less visible in the first year of life as the skin becomes less translucent.

1.107

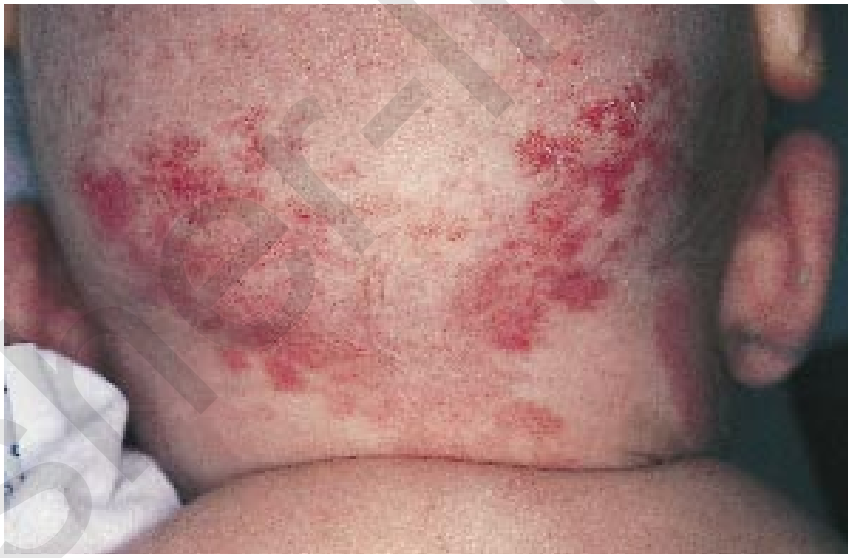

Figure 1.107. A macular hemangioma (salmon patch) in the nape of the neck is commonly called the "stork-bite" nevus. These are the most common of the macular hemangiomas and fade gradually, but are more likely to persist than other macular hemangiomas.

1.108

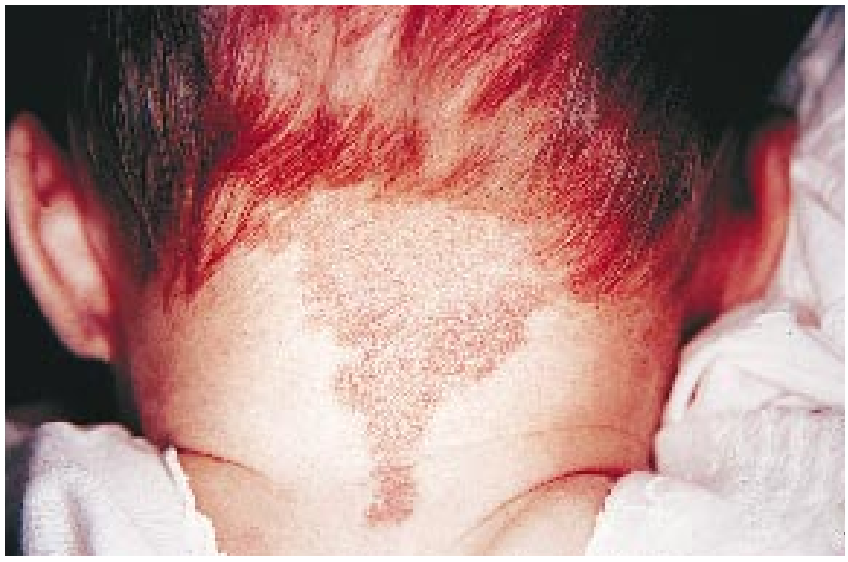

Figure 1.108. An infant at age 5 months with a "stork-bite" nevus.

1.109

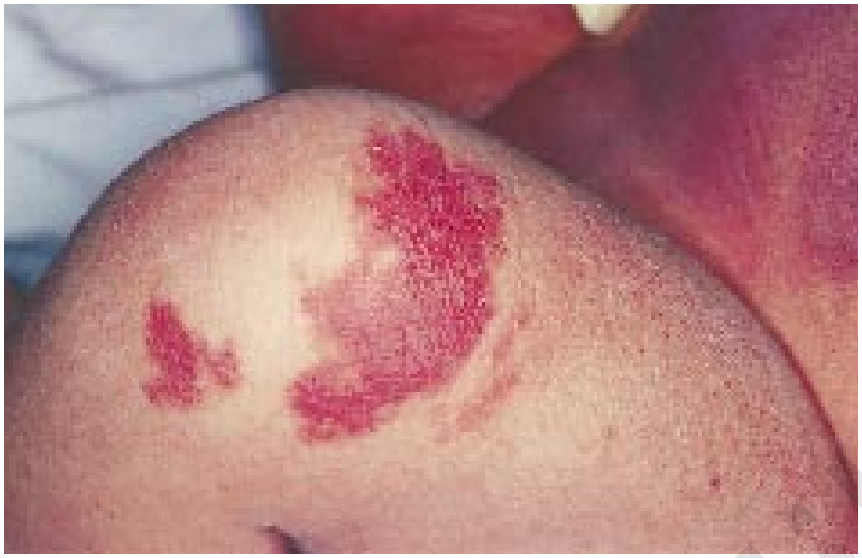

Figure 1.109. A macular hemangioma of the left knee in an infant. Lesions on the trunk and limbs may be extensive.

1.110

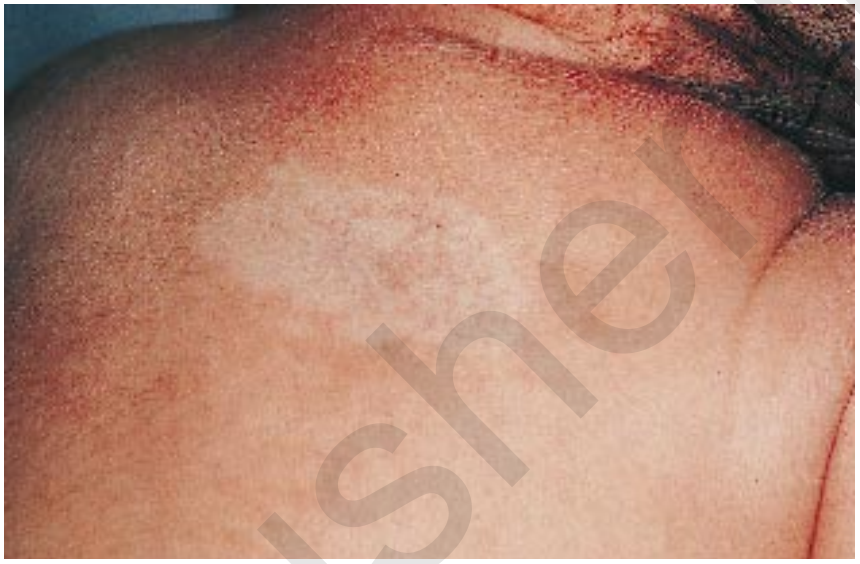

Figure 1.110. A nevus anemicus present at birth on the back of an infant. Note that the nevus is pale and has prominent capillaries. It may be the precursor of a strawberry nevus in that it starts as a fine, thread-like telangiectasis surrounded by an area of localized pallor. Both strawberry nevus and nevus anemicus involute spontaneously.

1.111

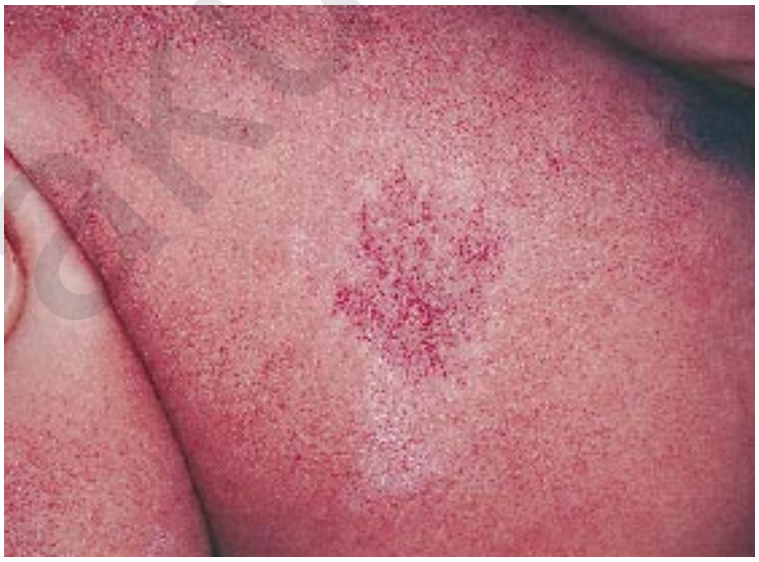

Figure 1.111. Another example of a nevus anemicus present at birth on the left thigh. Capillary hemangiomas (strawberry nevi) may be present at birth, but generally develop during the first few postnatal weeks as pale or slightly reddened, well-demarcated zones of skin a few millimeters to several centimeters in diameter. They may occur on any area of the body but are seen most commonly on the head and neck (40%) and the trunk (30%). During the first months of life, rapid growth occurs and the lesions become elevated above the surrounding skin with a spongy consistency, and attain a bright red to purple color. Although compressible, they blanch with gentle pressure but seldom empty completely.

1.112

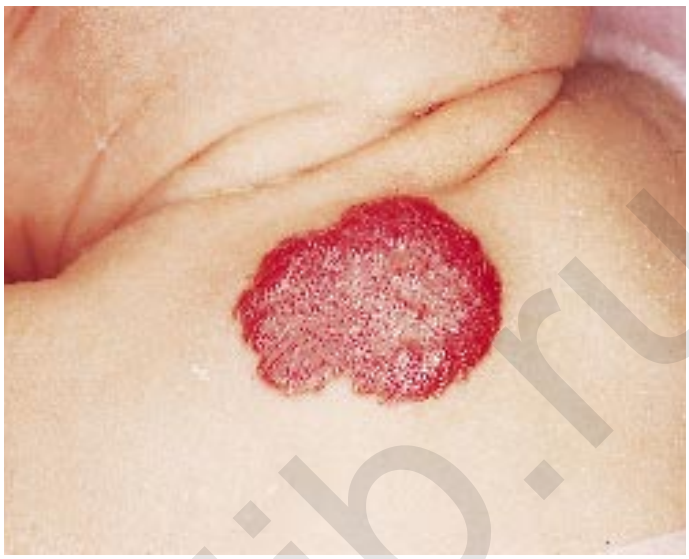

Figure 1.112. A capillary hemangioma (strawberry nevus) which developed in the upper thoracic region over the course of several weeks after birth is noted in this infant at the age of 3 weeks. The irregular surface with sharp demarcation is typical of a "strawberry" hemangioma which consists of dilated new capillaries in the dermal or subdermal area. The classic strawberry hemangioma is a raised, bright- or purplish-red lobulated tumor with well-defined borders and minute capillaries protruding from its surface, hence its "strawberry-like" appearance. Their history is usually one of continued rapid enlargement during the first few months of life followed by gradual spontaneous regression which occurs by central involution without scarring. In 50% of cases they resolve by the age of 5 years, in 70% by the age of 7 years, and in 90% by the age of 9 years.

1.113

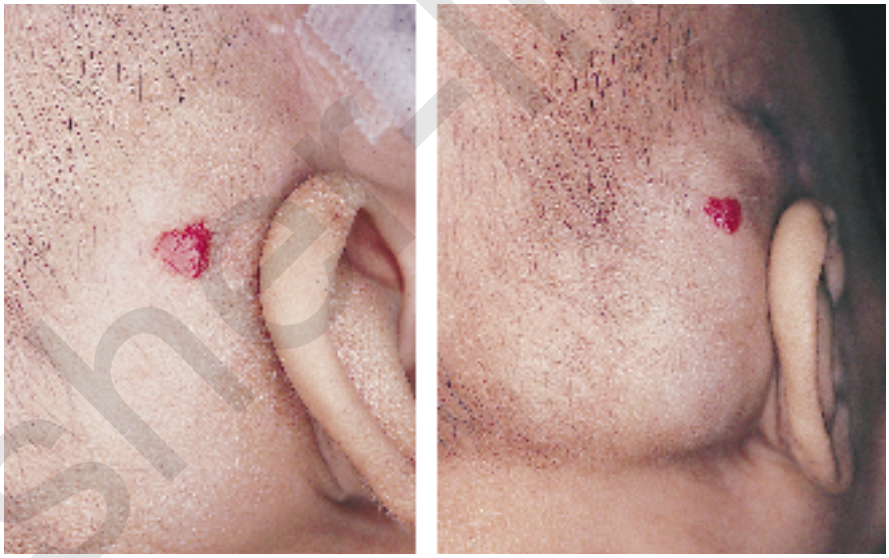

Figure 1.113. In this two and a half months old infant with a birthweight of 585 g, note the small strawberry nevus (figure left). This vascular tumor is apparently caused by a local persistence of angioblastic cells that give rise to a plexus of thin-walled capillaries with poor venous drainage. This continued to enlarge and at the age of three and one half months, note the marked enlargement of the nevus in the underlying tissue (figure right).

1.114

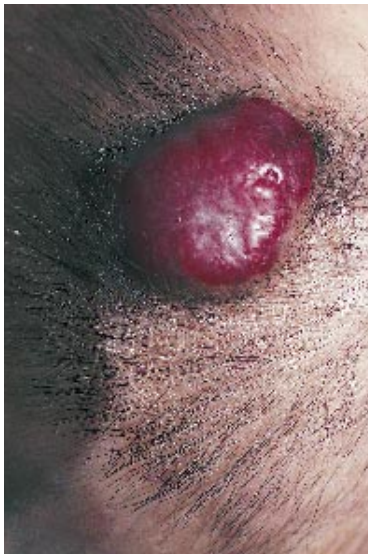

Figure 1.114. This 8-week-old premature infant with a birthweight of 900 g developed several strawberry nevi on the scalp at the age of 6 weeks. Note the rapid growth over a 2 week period. Hemangiomas are rarely seen in premature babies with a gestational age of less than 34 weeks. As the infant becomes older, hemangiomas may develop.

1.115

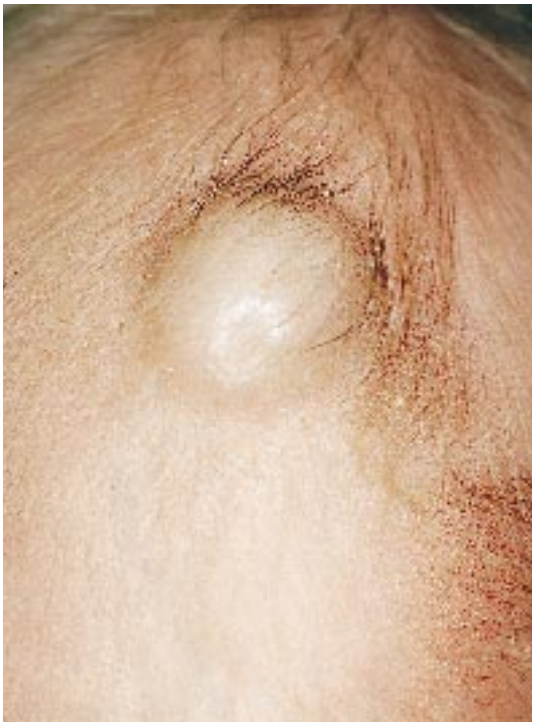

Figure 1.115. This infant shown in Figure 1.114, now at the age of 3 months, developed a cystic swelling over the scalp in the first few weeks of life. The cystic swelling increased gradually in size; note the bluish hue. On removal this was confirmed to be a strawberry hemangioma. Note that strawberry hemangiomas may have a large component visible on the surface of the skin, or may be covered by the skin, thus obscuring their characteristic appearance.

1.116

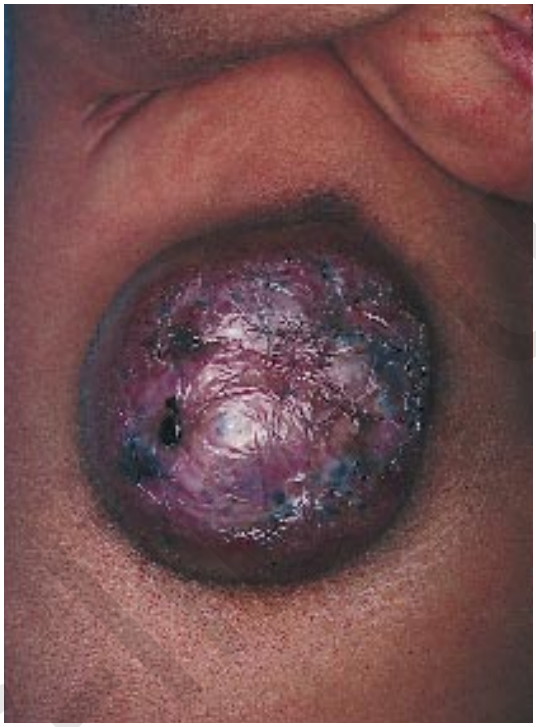

Figure 1.116. In some infants the lesion may appear to be a hemangioma but, as in this example, on biopsy the diagnosis was a hemangioendothelioma of the right chest.

1.117

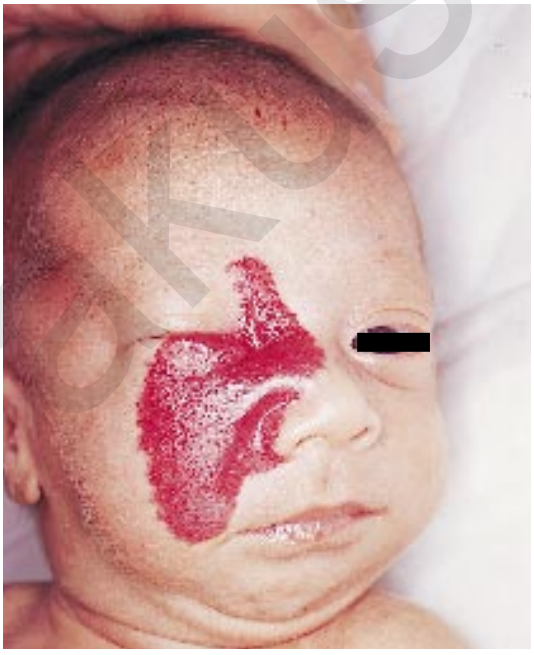

Figure 1.117. The capillary hemangioma involving the right side of the face in this infant demonstrates the fact that hemangiomas may expand sufficiently to interfere with function or may evidence bleeding or superficial infection. In this infant there would be marked interference with development of normal vision and, if untreated, this would lead to astigmatism and other problems. In such instances, treatment with steroids or laser surgery may be indicated.

1.118

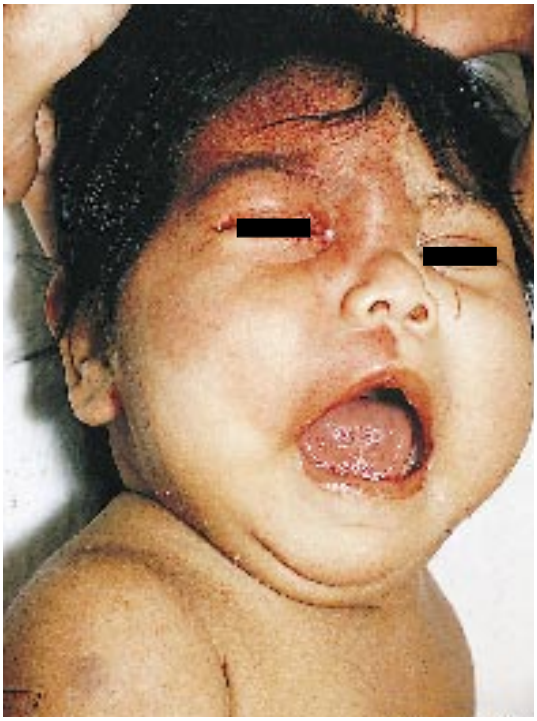

Figure 1.118. Port wine stain (nevus flammeus) is another macular hemangioma which represents a regional dilatation and enlargement of mature capillaries. It usually affects the skin of the face and neck, and the lesions are sharp-bordered and range in color from pale purple to deep burgundy. It usually does not indicate underlying abnormalities unless it extends into the area of distribution of the ophthalmic branch of the trigeminal nerve that serves the facial skin over the eyelid and up into the brow where, as in this infant, it may signal the presence of the intracranial vascular anomalies of Sturge-Weber syndrome (encephalotrigeminal angiomatosis).

1.119

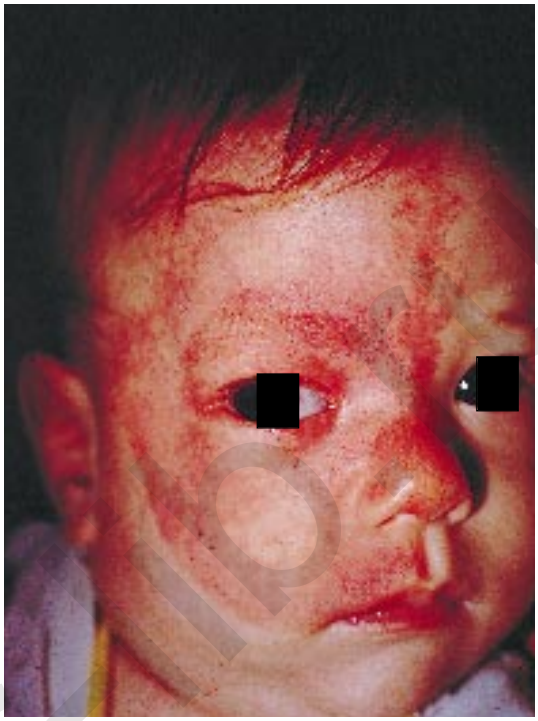

Figure 1.119. Another example of Sturge-Weber syndrome in which the distribution involves both the 1st and 2nd branch of the trigeminal nerve. Note the glaucoma of the right eye. In Sturge-Weber syndrome, lesions stop at the midline. When extensive facial involvement is present, there may be an associated glaucoma (buphthalmos). As this is one of the neurocutaneous syndromes, a CT scan of the head should be done to exclude intracranial involvement. Radiographs of the skull may reveal unilateral curvilinear, double-contoured lines of calcification in the cerebral cortex ("railroad track calcification"). The intracerebral vascular abnormalities lead to brain atrophy and ocular lesions (optic atrophy).

1.120

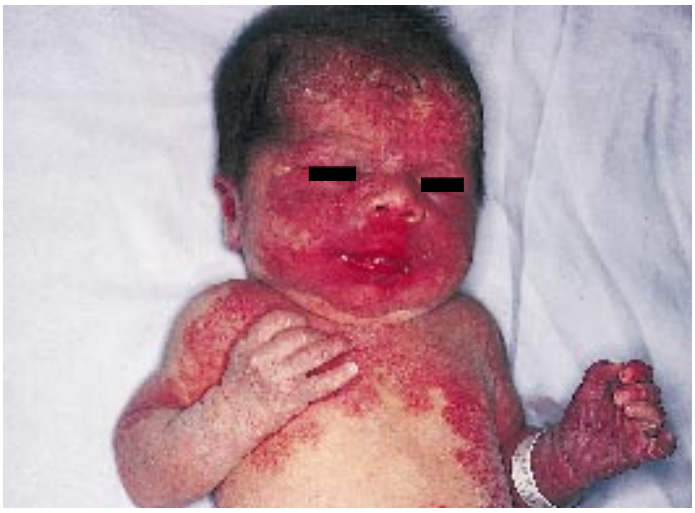

Figure 1.120. This infant with involvement of the trunk and limbs is another example of Sturge-Weber syndrome. There were bilateral congenital glaucoma, seizures at the age of 6 days, and an abnormal CT scan. In Sturge-Weber syndrome, seizures occur in 80% of infants, mental retardation in a high percentage, and an associated glaucoma in 40 to 50% of the infants, especially if both the ophthalmic and maxillary branches of the trigeminal nerve are involved.

1.121

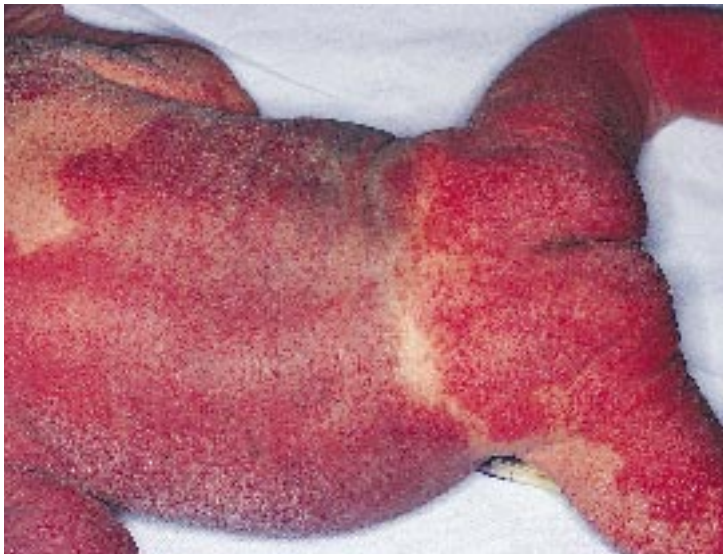

Figure 1.121. Note the widespread involvement of the trunk and limbs in the same infant. The likelihood of Sturge-Weber syndrome is greater when nevi such as these are present on the trunk and the limbs.

1.122

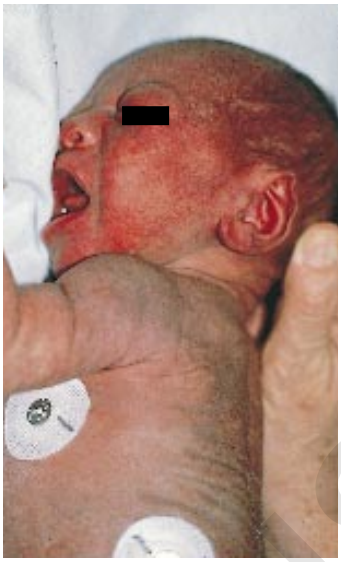

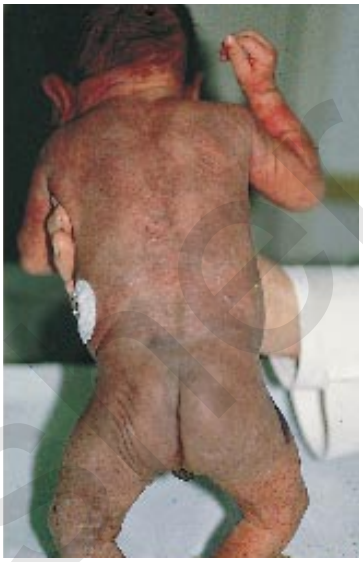

Figure 1.122. Phacomatosis pigmentovascularis is a rare condition in which there is a port wine appearance (as in Sturge-Weber syndrome) in addition to patches of slate-gray hyperpigmentation which clinically resemble mongolian spots. The infant also had a glaucoma of the left eye. This condition has been associated with glaucoma, seizures, and skeletal abnormalities.

1.123

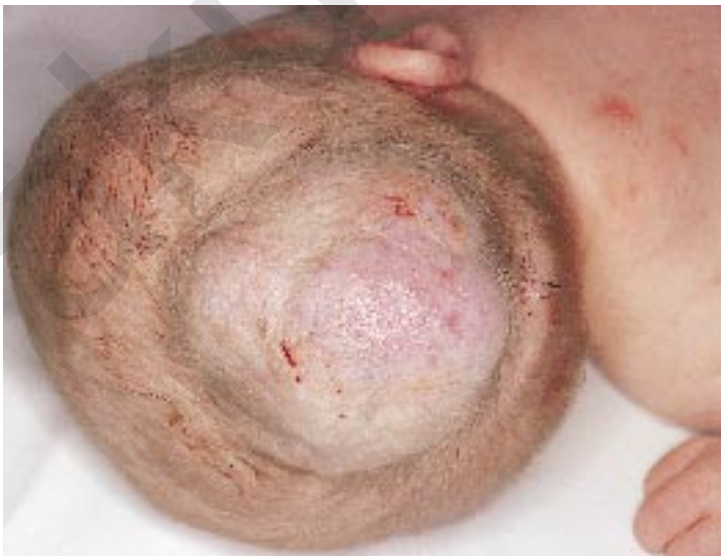

Figure 1.123. A large cavernous hemangioma was present on the scalp of this infant at birth. These are raised lesions and often do not appear until the infant is a few weeks of age. Deep cavernous hemangiomas are based on the localized failure of normal angiogenesis. They grow slowly after birth and have a blue color because of their site below the dermis. There is a soft movable nonpulsatile mass which feels like a "bag of worms." Blood flow through these tumors is very slow and, therefore, they do not compress easily or blanch with pressure.

1.124

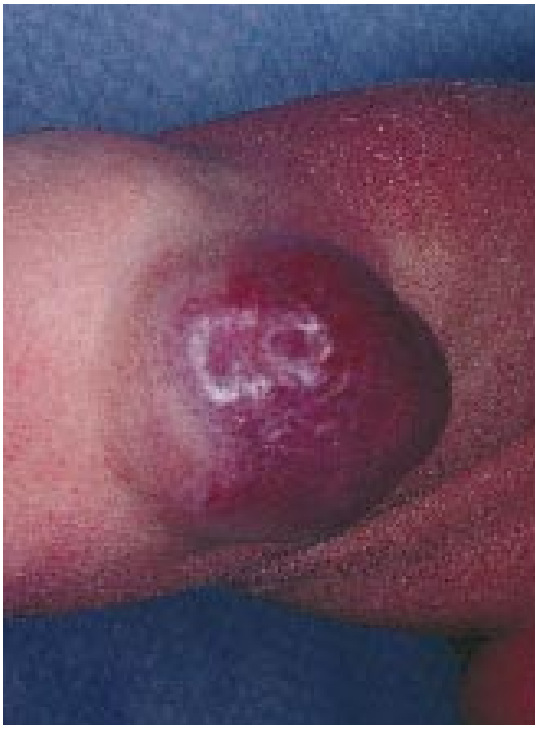

Figure 1.124. Cavernous hemangiomas occur mainly on the head and neck but may present anywhere such as this large cavernous hemangioma of the right knee. Thrombocytopenia due to platelet trapping, and marked vascular shunting leading to high output congestive heart failure may be complications associated with large cavernous hemangiomas.

1.125

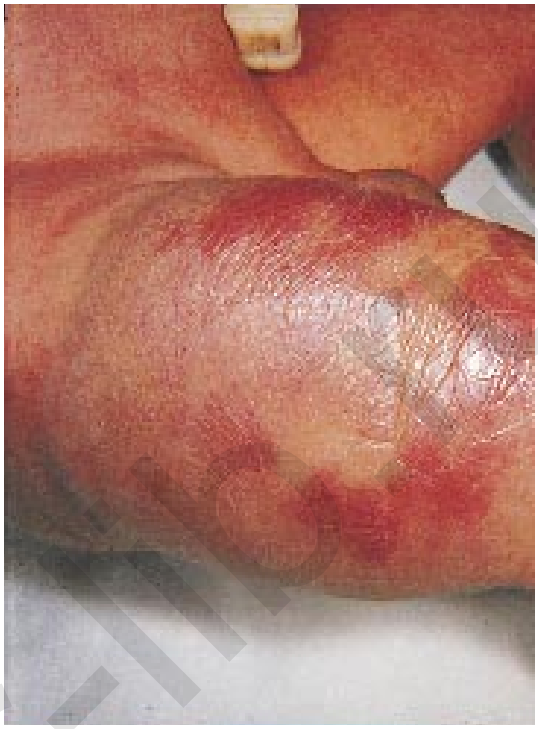

Figure 1.125. This infant with Kasabach-Merritt syndrome (cavernous hemangioma with thrombocytopenia) had a large cavernous hemangioma of the right lower thigh and knee and a platelet count of 54,000/mm^3. These infants may develop disseminated intravascular coagulopathy because of the consumption of the coagulation factors.

1.126

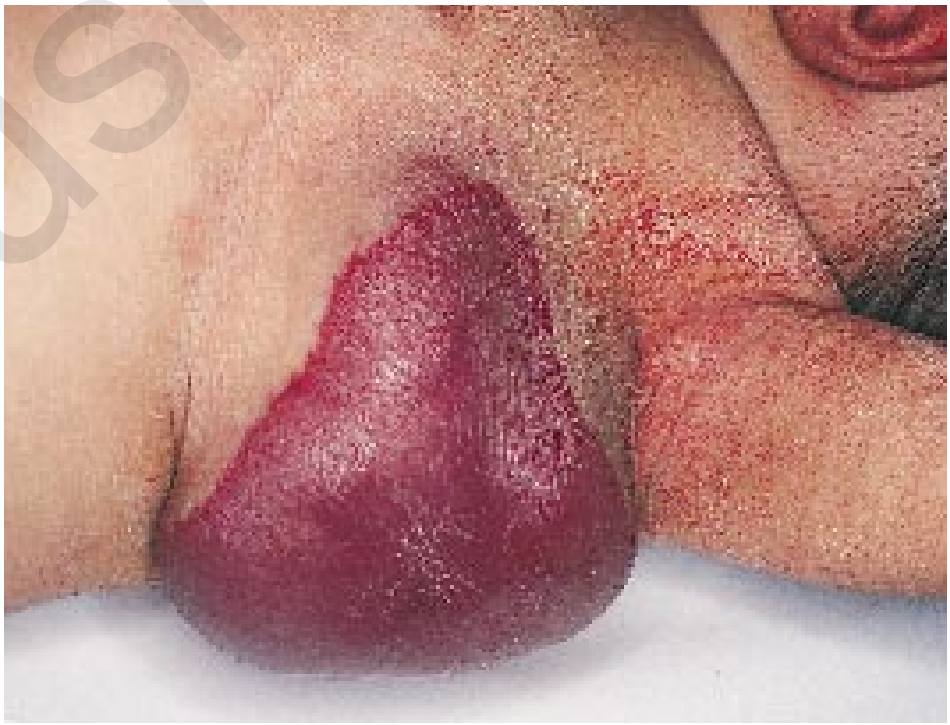

Figure 1.126. This large cavernous hemangioma of the left side of the chest was asymptomatic and the infant had a normal platelet count.

1.127

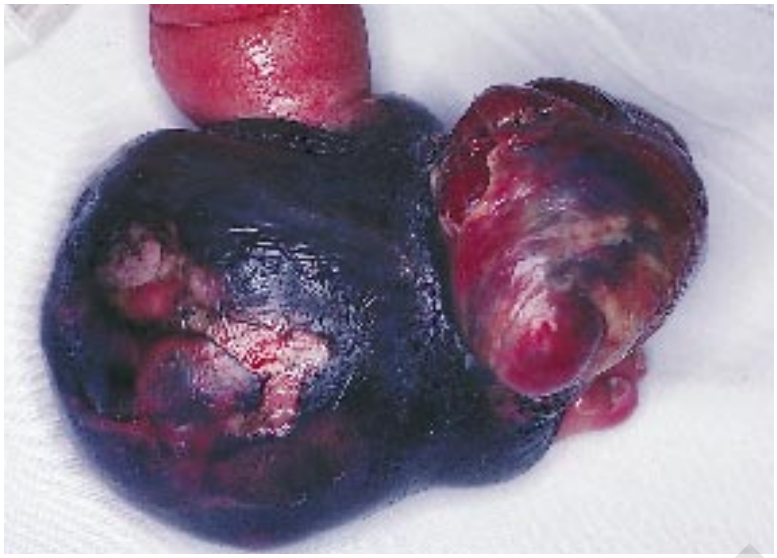

Figure 1.127. The massive cavernous hemangioma involving the left leg and foot of this infant was compromised during in utero life, resulting in gangrene. The hemangioma was removed surgically after birth. In large cavernous hemangiomas the underlying structures may be involved, such as in this infant where the underlying osseous structures were involved.

1.128

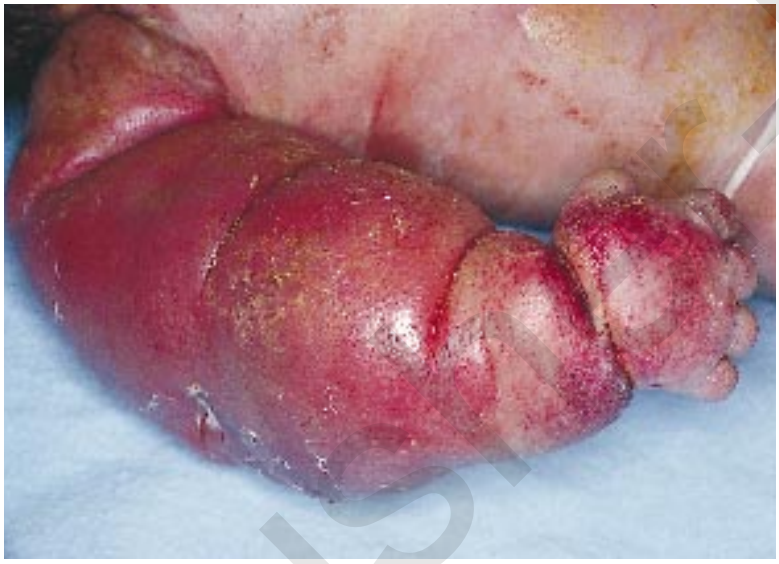

Figure 1.128. The massive cavernous hemangioma of the right upper extremity in this infant resulted in high output congestive heart failure in utero. There was marked anasarca with a total protein of 2.8 mg/dL, hematocrit of 20%, and platelet count of 26,000/mm^3.

1.129

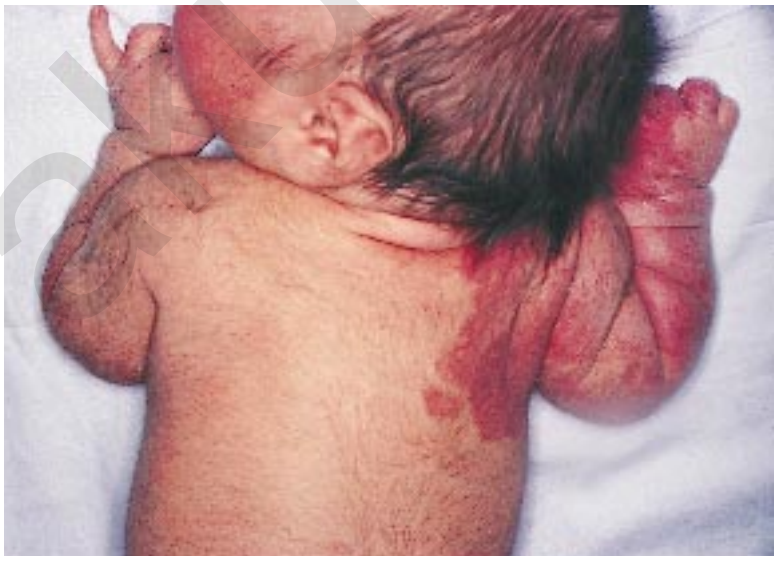

Figure 1.129. A large capillary hemangioma (nevus flammeus) involving the right shoulder and right upper extremity resulting in an asymmetric hypertrophy of the shoulder and right upper extremity. This constitutes the Klippel-Trenaunay syndrome. Unilateral distribution predominates and there may be disproportionate growth. Hypertrophy is not always present at the site of the vascular malformation. The cause of the hemihypertrophy is not definitely known, but it is suggested that it may be due to a local increased blood supply to the area.

1.130

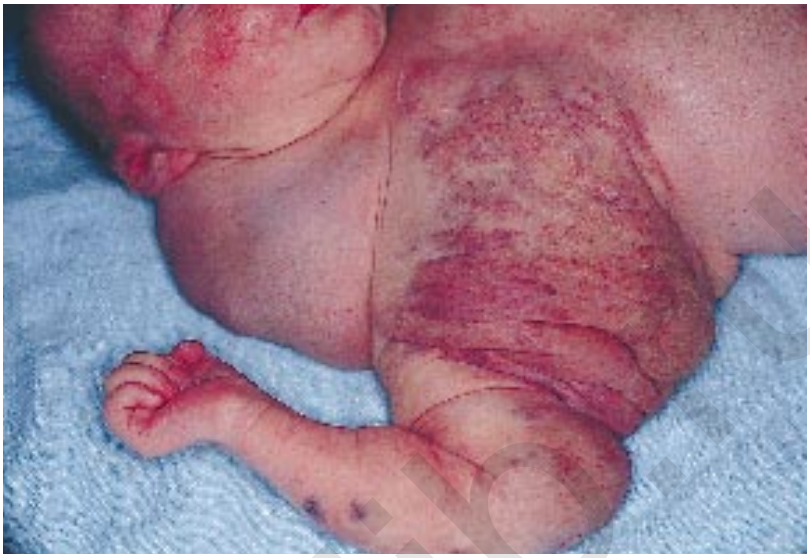

Figure 1.130. The large cavernous hemangioma involving the neck, chest, and axilla of this infant was associated with numerous other small hemangiomas over the body and resulted in hemihypertrophy of the right upper arm, the right leg, and the left foot. This is another example of Klippel-Trenaunay syndrome. In Klippel-Trenaunay syndrome one should always check for hemangiomata of the viscera, brain, and eyes in addition to the involvement of the skin.

1.131

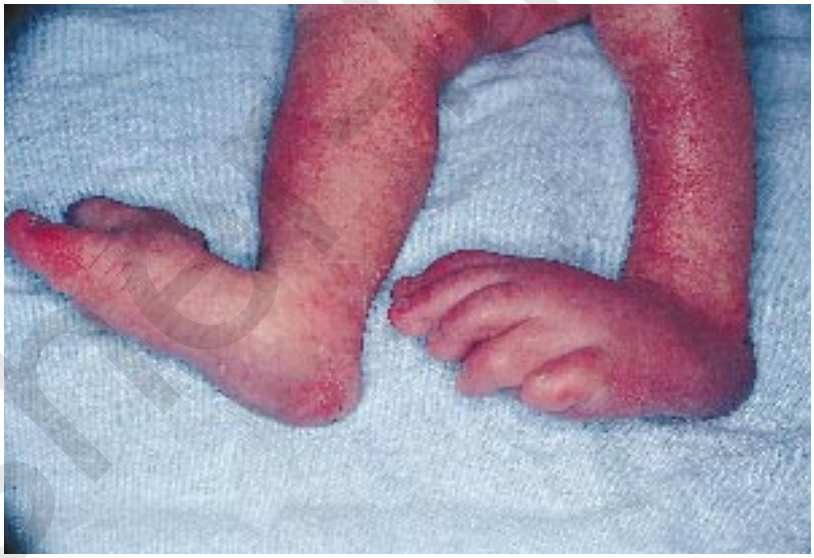

Figure 1.131. The lower extremities of the same infant as in Figure 1.130 with Klippel-Trenaunay syndrome shows the hypertrophy of the right leg and the left foot.

1.132

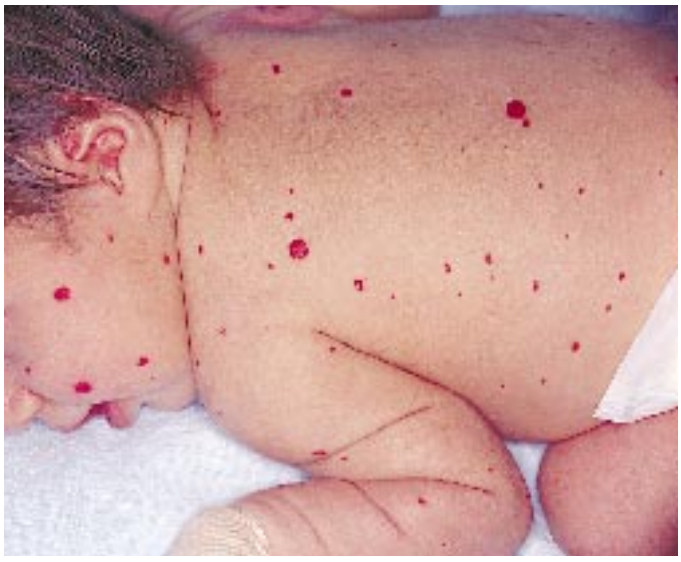

Figure 1.132. Multiple hemangiomatosis (diffuse neonatal hemangiomatosis) may present solely with cutaneous involvement, as noted in this infant, or with systemic involvement (of the liver, brain, etc.). There are numerous widely disseminated, small, red to dark blue papular cutaneous hemangiomas which are usually present at birth or develop within the first few weeks of life. In infants with cutaneous involvement only, prognosis is good. In infants with systemic involvement, prognosis is variable.

1.133

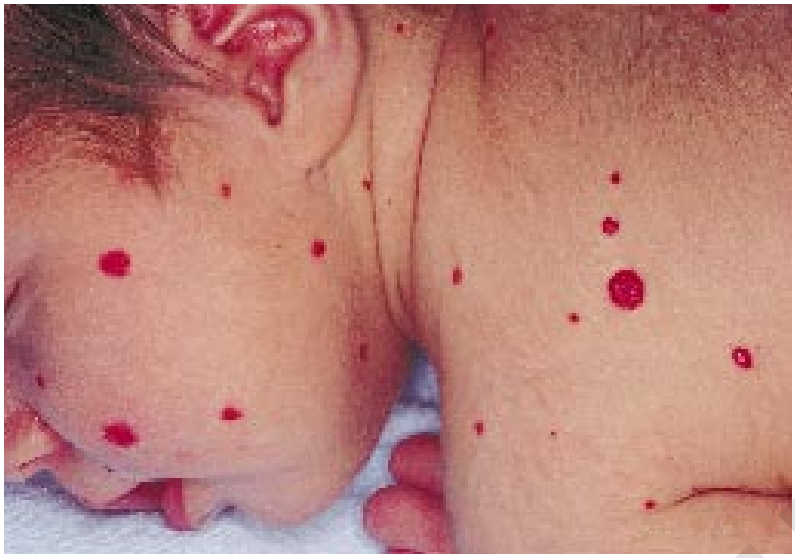

Figure 1.133. A close-up view of the multiple hemangiomata in the same infant as in Figure 1.132.

1.134

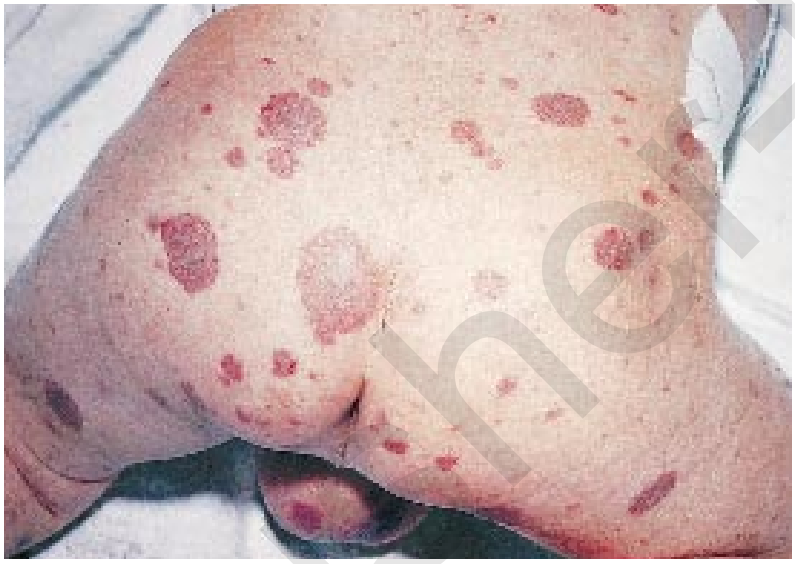

Figure 1.134. Multiple hemangiomatosis in an infant with systemic involvement. There were multiple hemangiomata in the liver and several hemangiomata in the gastrointestinal tract and brain in this infant. At the age of ten days the infant developed hematemesis and abdominal distention. At surgery it was noted the infant had massive hemorrhage from a hemangioma in the duodenum. If systemic involvement is suspected, liver and spleen scans or hepatic angiography may confirm the diagnosis. (See Figure 2.147 of Volume V for an example of systemic involvement in multiple hemangiomatosis.)

1.135

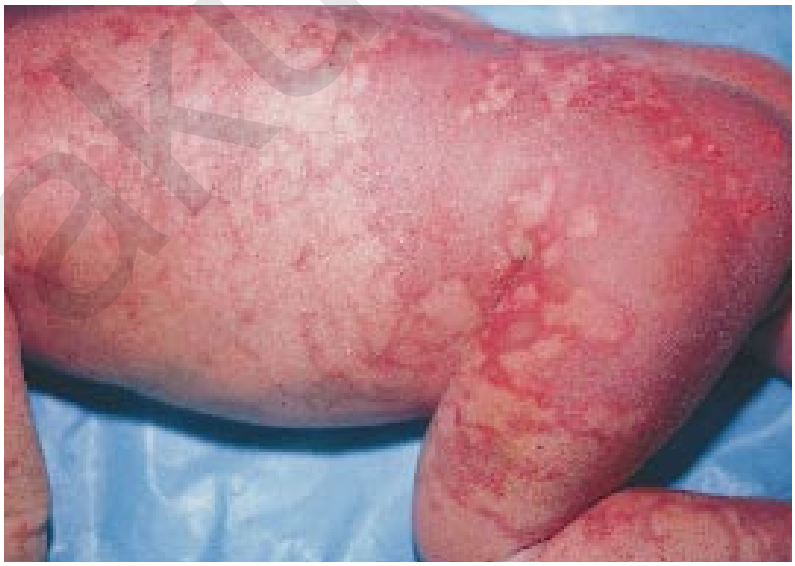

Figure 1.135. In cutis marmorata telangiectatica congenita (congenital generalized lymphangiectasia), dilated superficial venous and capillary channels are usually noted at birth. The skin appears as a reticulated network with white insulae in between. The classic appearance of reddish-blue reticulation of the skin changes with crying (becomes increasingly red) or other stimulation (becomes livid with cooling). Most cases are generalized, such as in this infant, but there may be segmental or localized involvement.

1.136

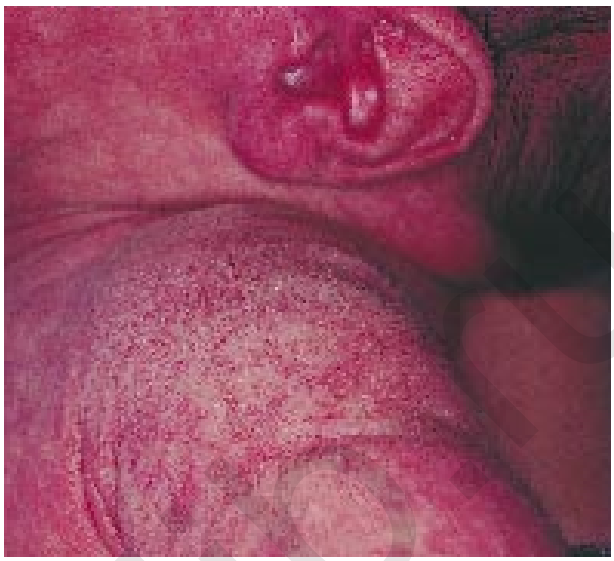

Figure 1.136. Another infant with cutis marmorata telangiectatica congenita. The condition may extend for the first few weeks and usually persists throughout life, but eventually improves during childhood. Rarely, small areas of superficial ulceration may develop.

1.137

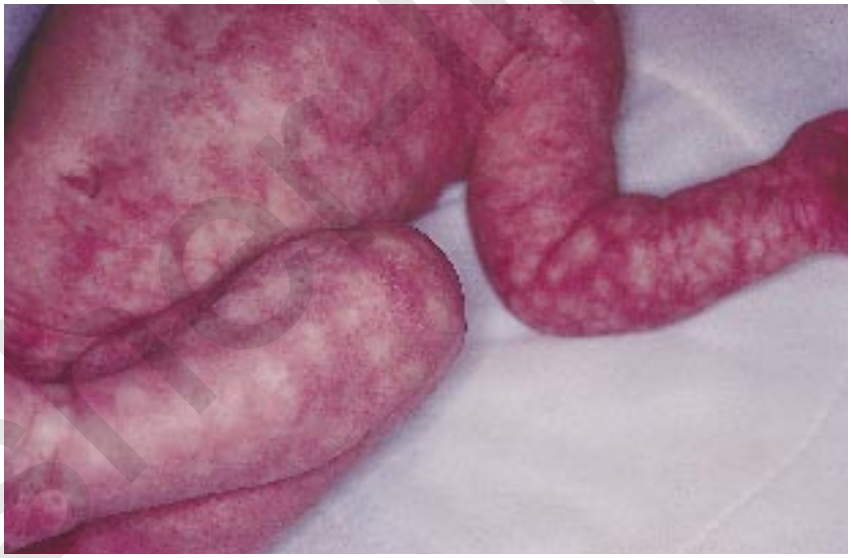

Figure 1.137. Cutis marmorata telangiectatica congenita in which the distribution is segmental. The etiology is unknown, but it seems to represent a developmental ectasia of both capillaries and veins.

1.138

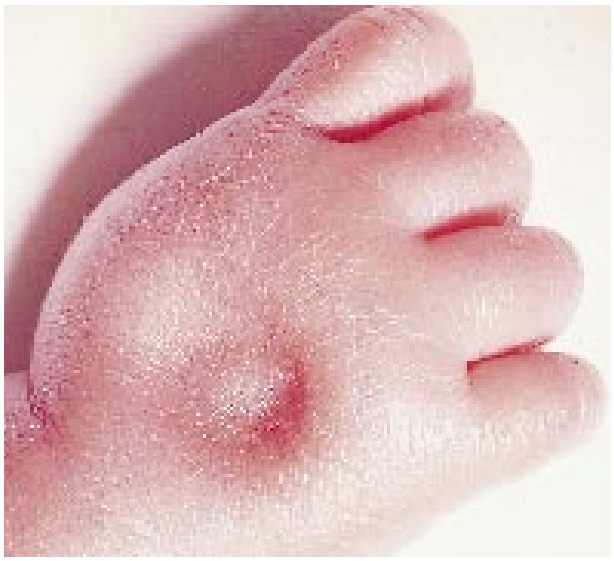

Figure 1.138. Lymphedema in an infant with Turner's syndrome shows pitting edema on the dorsum of the hand. The diffuse soft tissue swelling in lymphedema is caused by increased accumulation of lymph due to inadequate lymphatic drainage. Lymphedema may be primary (congenital) or secondary.

1.139

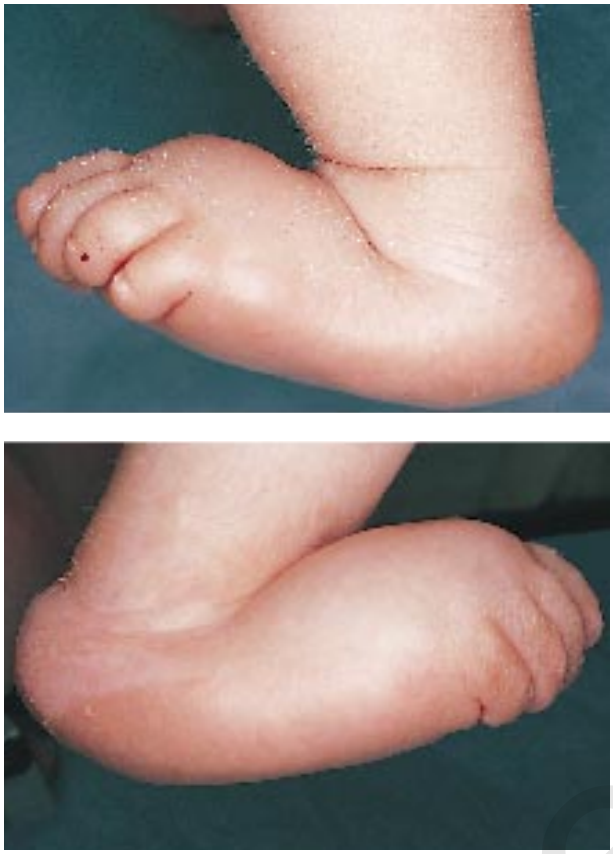

Figure 1.139. Lymphedema of both feet in an infant with Turner's syndrome. The area is swollen and firm at birth and is characterized by pitting on pressure.

1.140

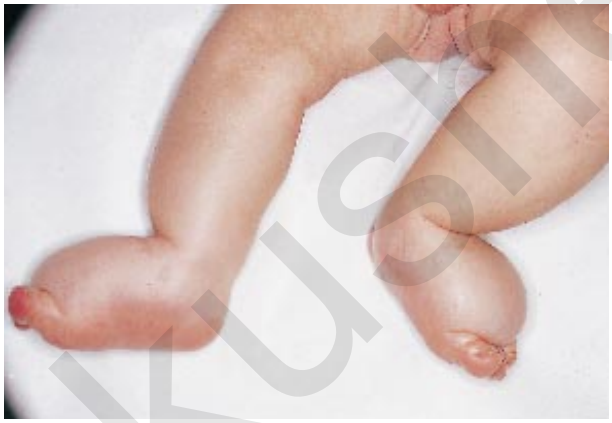

Figure 1.140. Milroy's disease is an inherited autosomal dominant condition which presents with the typical bilateral lymphedema in the lower extremities. The condition occurs as a result of absence of lymphatics and is always confined to the legs and feet.

1.141

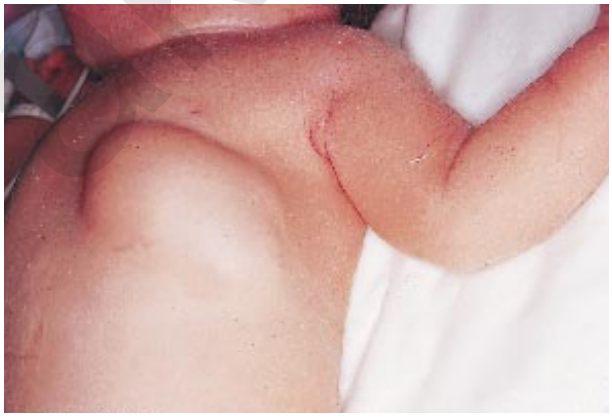

Figure 1.141. Lymphangioma simplex of the anterior chest present at birth in an infant. There are four major forms of lymphangiomas: lymphangioma simplex, lymphangioma circumscriptum, cavernous lymphangioma, and cystic hygroma. Lymphangioma simplex is a solitary, well-circumscribed, flesh-colored dermal or subcutaneous tumor. It may occur anywhere on the subcutaneous or mucosal surface and is seen most commonly on the neck, upper trunk, proximal extremities and tongue. The surface is generally smooth and it may remain stable or grow quickly.

1.142

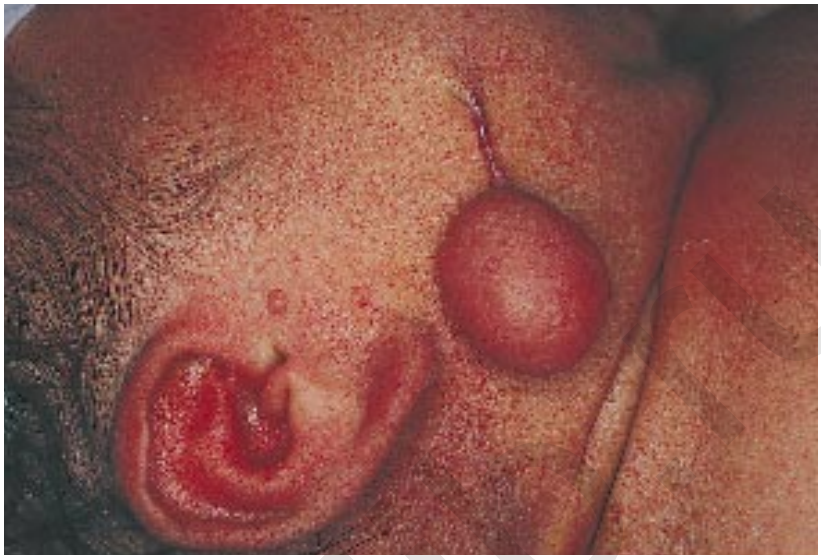

Figure 1.142. On removal, this mass attached by a stalk to the right side of this infant's face was confirmed to be a typical simple lymphangioma. The small preauricular tag was not associated with any other pathology.

1.143

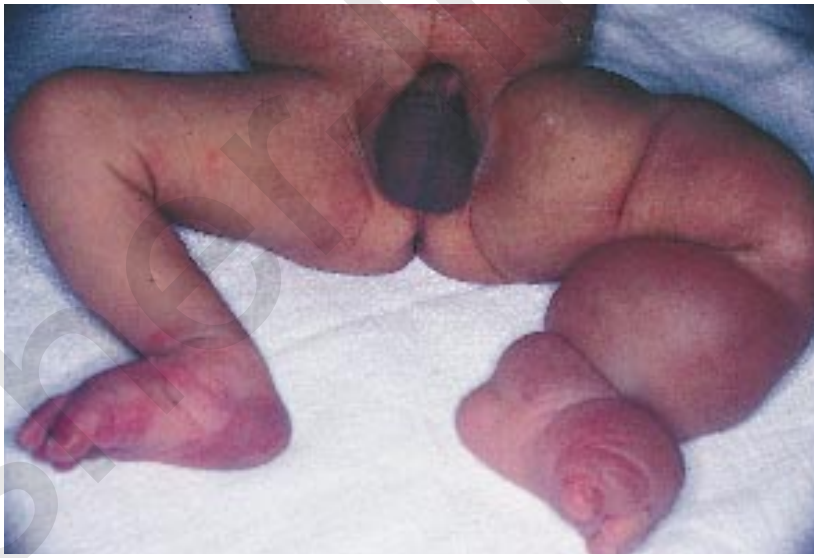

Figure 1.143. Circumscribed lymphangioma of the left lower extremity in a neonate. Lymphangioma circumscriptum is the most common form of lymphangioma. It is characterized by groups of deep-seated, thick-walled vesicles that have the appearance of "frog spawn" or "grape clusters." The common sites of involvement are the proximal limbs, shoulders, neck, axilla and adjacent chest wall, perineum, inguinal folds, tongue, and mucous membranes.

1.144

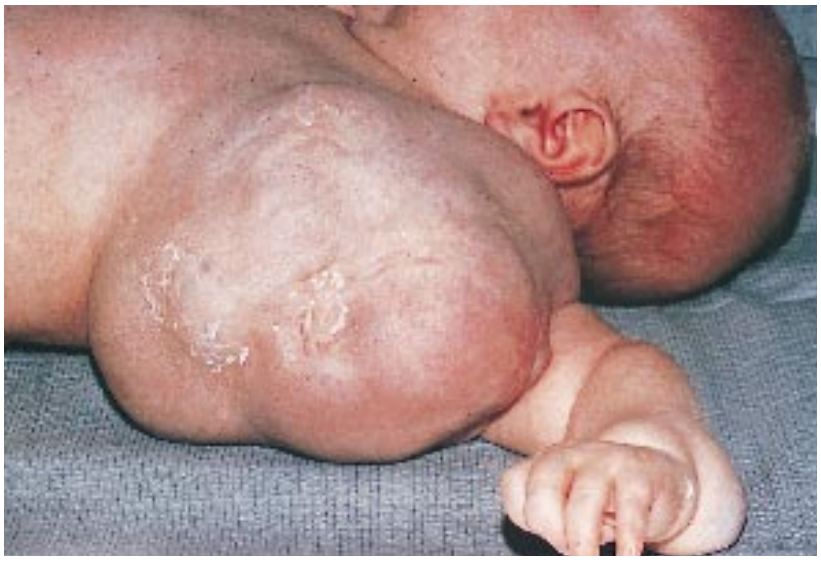

Figure 1.144. A large cavernous lymphangioma of the left axilla and anterior chest present at birth in an infant. Cavernous lymphangioma consists of diffuse soft tissue masses of large cystic dilatations of lymphatic vessels in the dermis and subcutaneous tissue, and may involve the intermuscular septa. The lesions are ill-defined and frequently involve large areas of the face, trunk, and extremities. They may occur in the tongue, resulting in macroglossia. Lymphangiomas frequently have a hemangiomatous component (hemangiolymphoma) so that some of the vesicles are filled with fresh or altered blood. Treatment is surgical but recurrences are common.

1.145

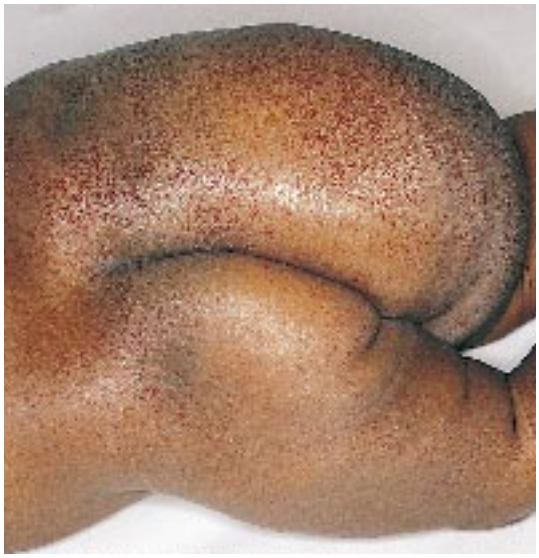

Figure 1.145. A large cavernous lymphangioma affecting the right gluteal region and proximal lower extremity of an infant. There was no osseous involvement.

1.146

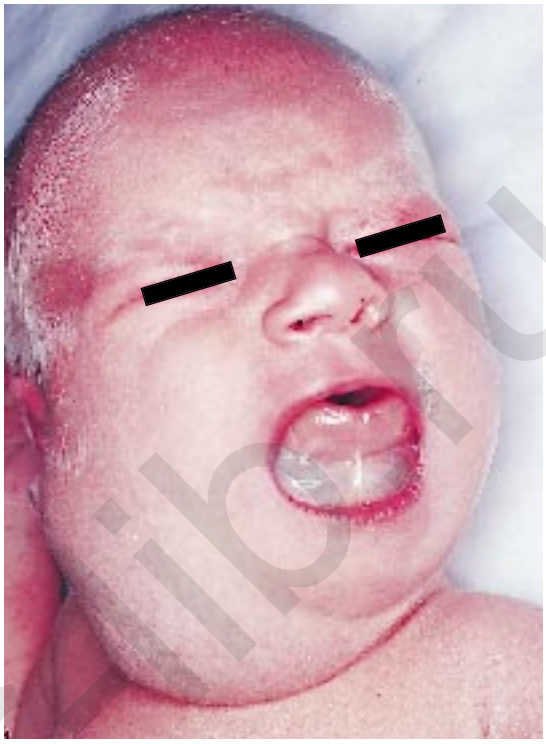

Figure 1.146. Cystic hygroma of the right side of the neck with involvement of the mucous membranes. Cystic hygroma is a benign loculated cystic mass which is soft, diffuse, impressible, and translucent due to accumulation of fluid in the lymphatics. The commonest sites are in the neck (hygroma colli), axilla, and upper arm. Rarely they are seen in the groin or popliteal fossa. They do not resolve spontaneously. Surgical treatment may be complicated and recurrences are uncommon following complete removal.

1.147

Figure 1.147. Transillumination of the cystic hygroma in the same infant as in Figure 1.146. Note the extent of involvement of the neck and mouth.

1.148

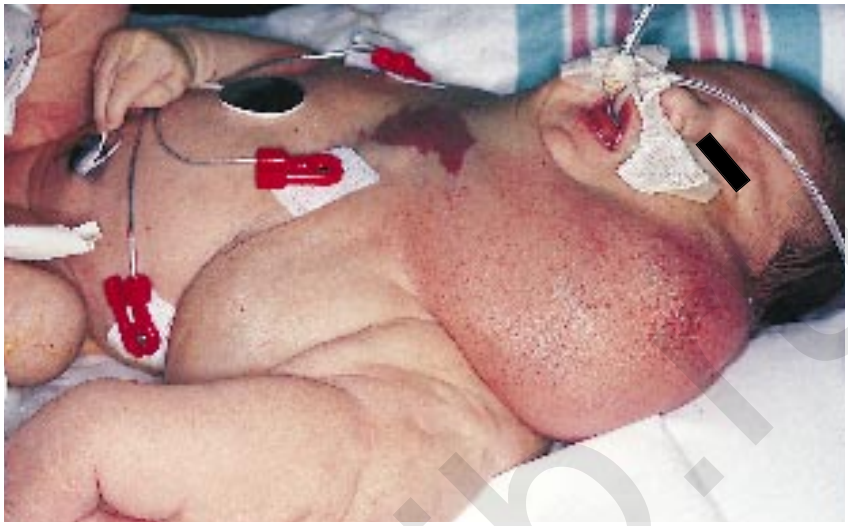

Figure 1.148. This infant with a massive diffuse lymphangioma (elephantiasis congenita angiomatosis or elephantiasis lymphangiectatica) had severely compromised respiration from the tumor and required tracheostomy. Note the large area of nevus present superficially over the anterior part of the chest. Biopsy diagnosis was a hemangiolymphoma. Note the redness of the area which was related to secondary infection, a common complication.

1.149

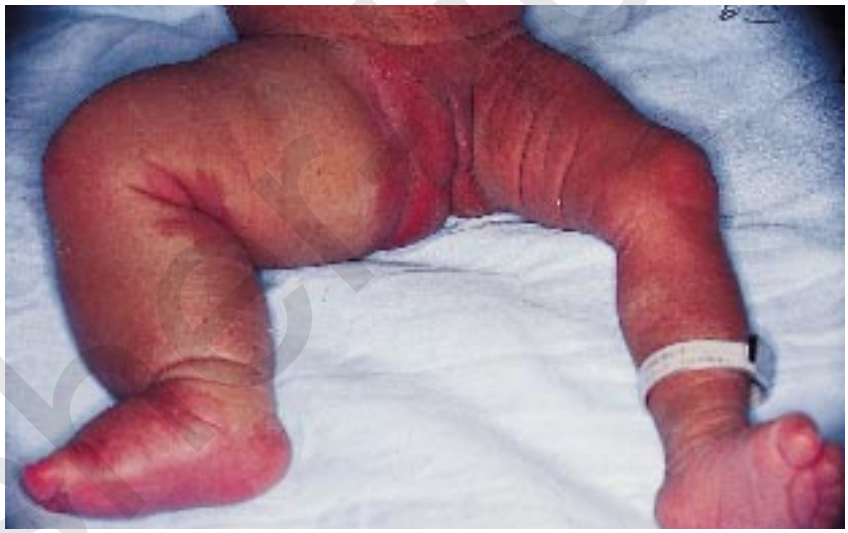

Figure 1.149. In another infant with elephantiasis congenita angiomatosis, note the massive involvement of the right lower extremity. Diffuse angiomas (elephantiasis lymphangiectatica) are large, ill-defined cystic dilatations involving the skin, subcutaneous tissue, muscles, and mucous membrane. They may involve the trunk, extremities, and large areas of the face, lips, or tongue. There is marked enlargement of the affected areas as a result of invasion by the cystic lymphatics. The areas may have a red or purplish color because of the presence in the vesicles of blood mixed with lymph.

PIGMENTATION ABNORMALITIES

Vitiligo (leukoderma) is a condition which is not commonly seen in the neonatal period. The irregularly outlined hypopigmented areas seen in vitiligo often have hyperpigmented borders, and the patches may enlarge over a period of several years but *will not darken over time*. When areas of hypopigmentation are noted they must be differentiated from the ash leaf appearance of tuberous sclerosis.

1.150

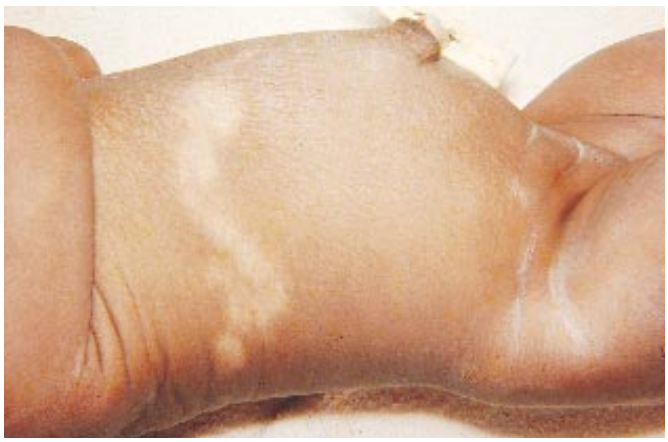

Figure 1.150. There may be iatrogenic causes of delayed pigmentation, such as a hypopigmented area over the skin where chest electrodes or tape have been placed. These hypopigmented areas occurring as a result of irritation or breakdown of the skin *darken with increasing age* and blend with the surrounding skin.

1.151

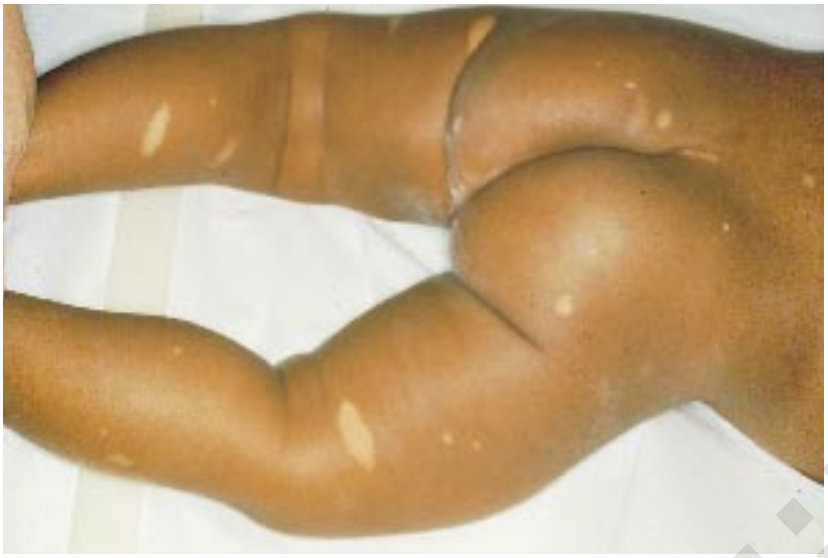

Figure 1.151. Ash leaf spots are found on the skin of the trunk, buttocks, and limbs in children with tuberous sclerosis. These dull, white areas may be linear or oval, measuring 1 cm across or less. They tend to be sharply pointed at one end and rounded at the other. Café-au-lait spots may be present. Ash leaf spots lack the characteristic milky-white appearance of lesions of vitiligo because melanocytes are present in fair numbers but the melanosomes are poorly pigmented.

1.152

Figure 1.152. Examination of the lesions under the Wood's filter shows the typical ash leaf spots in the same infant with tuberous sclerosis. Tuberous sclerosis is a neurocutaneous syndrome which, in addition to the cutaneous changes, has systemic manifestations in 80 to 90% of cases. These include central nervous system involvement (seizures, mental retardation), cardiac tumors (rhabdomyomas), renal hamartomas, retinal lesions, and osseous changes. CT scan may show tumor-like nodes in the cerebral cortex.

1.153

Figure 1.153. A close-up of a typical ash leaf macule in tuberous sclerosis showing the characteristic hypopigmented leaf shape. In tuberous sclerosis, shagreen patches are also noted; these are zones of slightly thickened and firm, yellow, irregularly outlined skin, a few centimeters across, with a finely dimpled surface resembling the skin of an orange. They are usually found on the flanks and back.

1.154

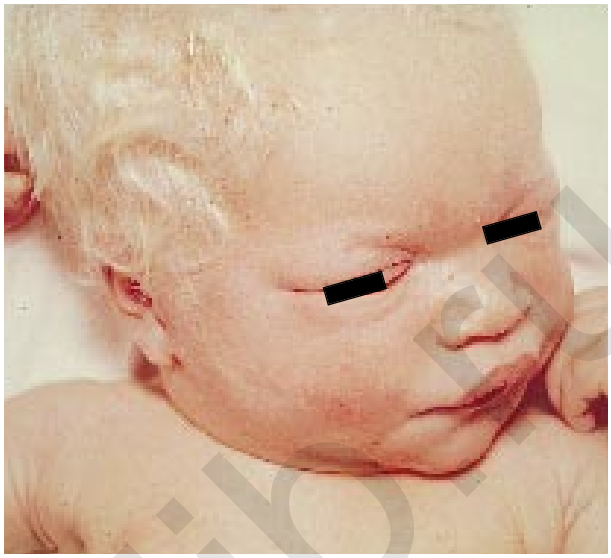

Figure 1.154. This is a black infant with total albinism, an autosomal recessive condition in which total lack of pigment is characteristic. Albinism is an uncommon disorder of melanin synthesis manifested by a total lack of pigmentation of the skin, hair, and eyes. It occurs in two forms: oculocutaneous and ocular. In oculocutaneous albinism there is generally a decrease or absence of pigment in the eyes, skin, and hair; in ocular albinism only the eye pigment is consistently abnormal. If the iris does not have the typical pink appearance seen in albinism but has a bluish-grey pigmentation, it is less likely that the child will be photophobic.

1.155

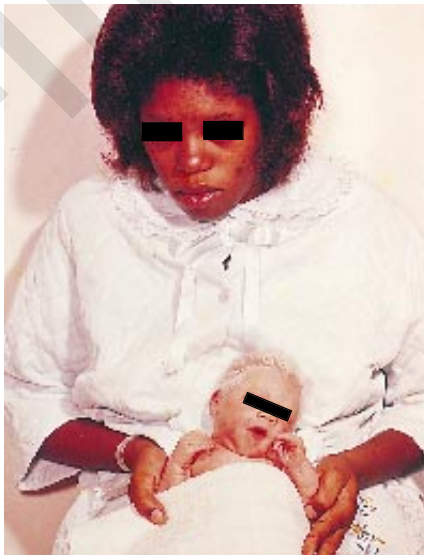

Figure 1.155. Another infant with albinism with her mother. Note the striking difference in pigmentation of mother and baby. Albinism is characterized by varying degrees of reduction of pigment in the skin and hair, translucent irides, hypopigmented ocular fundi and an associated nystagmus. Affected children have been called "moon children" because they have marked photosensitivity and photophobia, and prefer to go outdoors only at night.

1.156

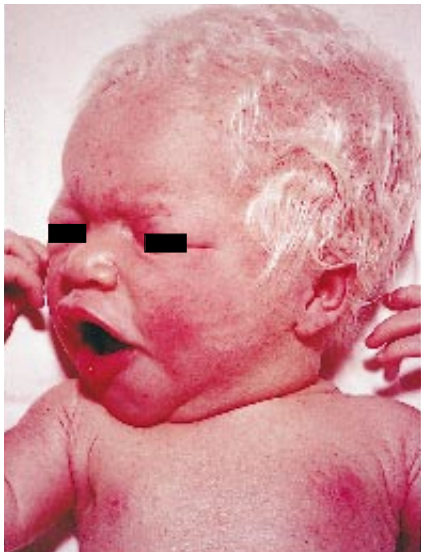

Figure 1.156. Close-up of the same infant as in Figure 1.154 showing the total lack of pigmentation.

1.157

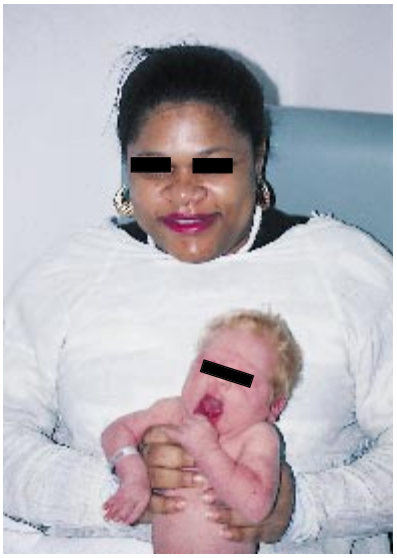

Figure 1.157. Mother and infant with tyrosinase-positive oculocutaneous albinism. Melanocytes or melanosomes are present in the affected skin and hair in normal numbers but, although they are tyrosine positive, fail to produce normal amounts of melanin in the areas of leukoderma or poliosis. There are many variants of oculocutaneous albinism but tyrosinase-positive or tyrosinase-negative are the most common. These are so designated on the basis of pigment production in plucked hair incubated in tyrosine.

1.158

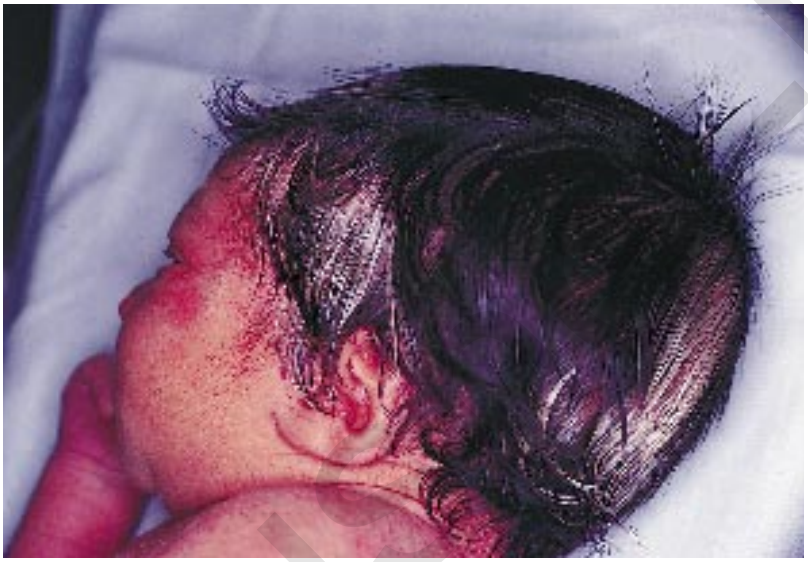

Figure 1.158. In partial albinism (poliosis circumscripta; piebaldism) there are hypopigmented areas of the scalp. Depigmented areas may also occur on the torso or the extremities with the exception of the back, hands, and feet. Decreased hair pigmentation (poliosis) is most often seen close to the anterior hairline either centrally or to one side of the midline. This condition (piebaldism) is seen in normal individuals and may follow an autosomal dominant inheritance.

1.159

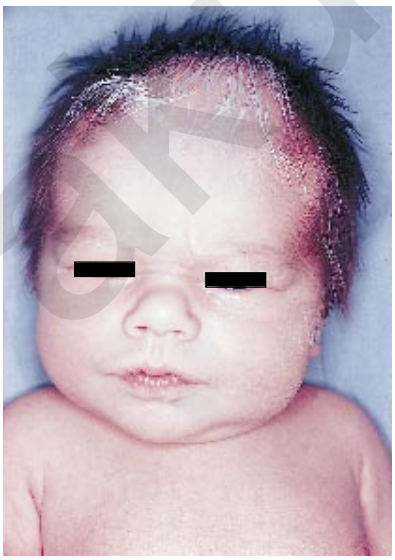

Figure 1.159. In Waardenburg's syndrome, an autosomal dominant condition, a white forelock is characteristic. It is a form of partial albinism (poliosis). In addition to the white forelock, there is dystopia canthorum (lateral displacement of the medial canthi and lacrimal puncta of the lower eyelids), synophrys, heterochromia iridis, broad nasal root, and congenital deafness. If the inner canthal distance divided by the interpupillary distance is greater than 0.6, this lateral displacement of the inner canthi may help confirm the diagnosis.

1.160

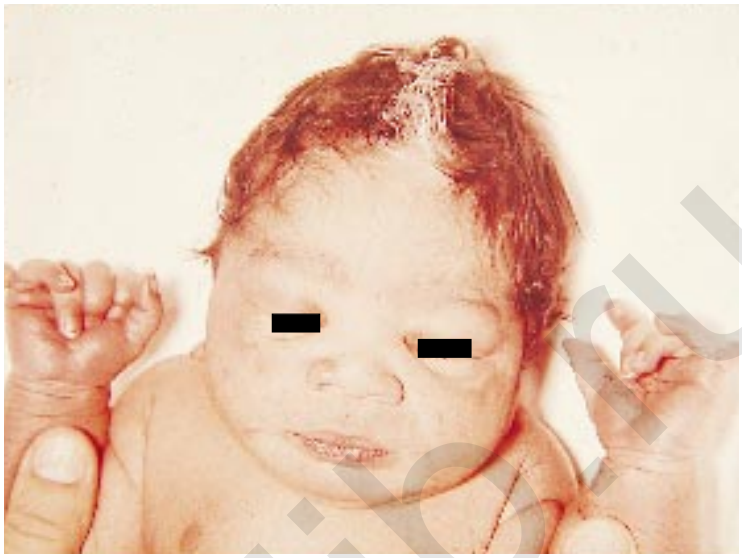

Figure 1.160. Another example of Waardenburg's syndrome. Note the white forelock and the dystopia canthorum.

1.161

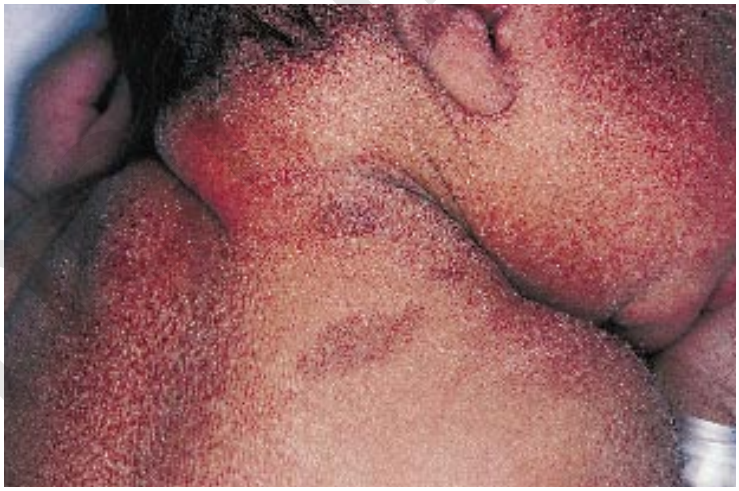

Figure 1.161. Café-au-lait spots, present in this twin infant with neurofibromatosis, are skin lesions caused by hyperpigmentation of the basal epidermal cells. They may be seen in healthy children, as well as those with neurofibromatosis, tuberous sclerosis, and the Russell-Silver syndrome. They range in size from a few millimeters to several centimeters in diameter and have a color slightly darker than that of the surrounding skin. The most common type have edges that are fairly smooth and quite clearly demarcated ("coast of California"). A second type of café-au-lait spot has a much more jagged, irregular border ("coast of Maine") and is usually larger and solitary. Such lesions are seen in McCune-Albright polyostotic dysplasia.

1.162

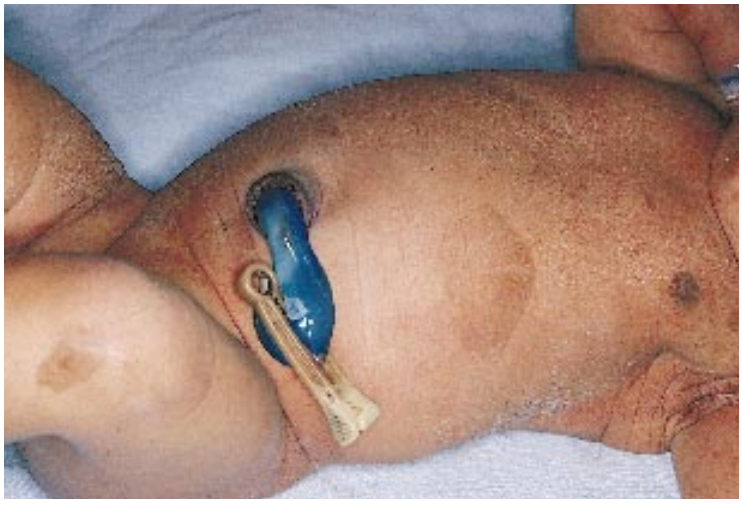

Figure 1.162. In this infant with neurofibromatosis note the multiple café-au-lait spots. About 5% of white infants and almost 15% of black infants have one such spot. Café-au-lait spots are somewhat darker in color in black infants than in caucasian infants. Neurofibromatosis is an autosomal dominant condition in which the presence of 5 or more café-au-lait spots greater than 0.5 cm in diameter in young infants is diagnostic of the disorder.

1.163

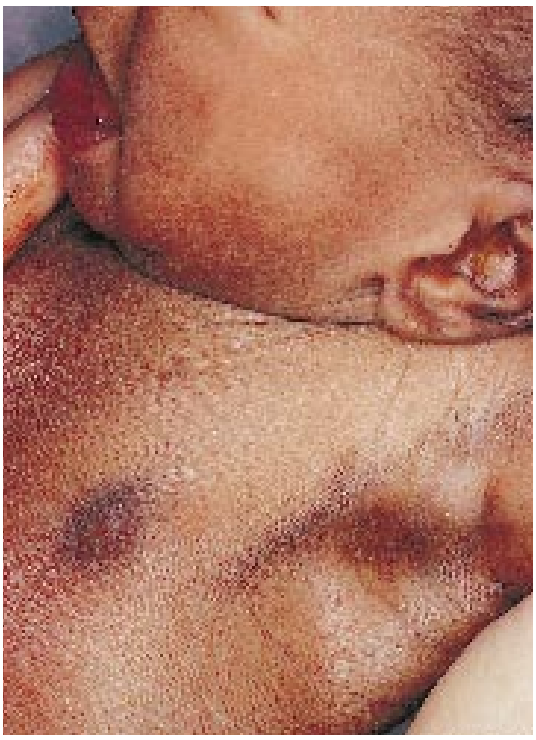

Figure 1.163. Another infant with neurofibromatosis. The presence of a single café-au-lait spot in the axilla may be diagnostic of this disorder. Crowe's sign (axillary freckling) appears as multiple 1- to 4-mm café-au-lait spots in the axillary vault and is seen in 25 to 50% of patients with neurofibromatosis.

1.164

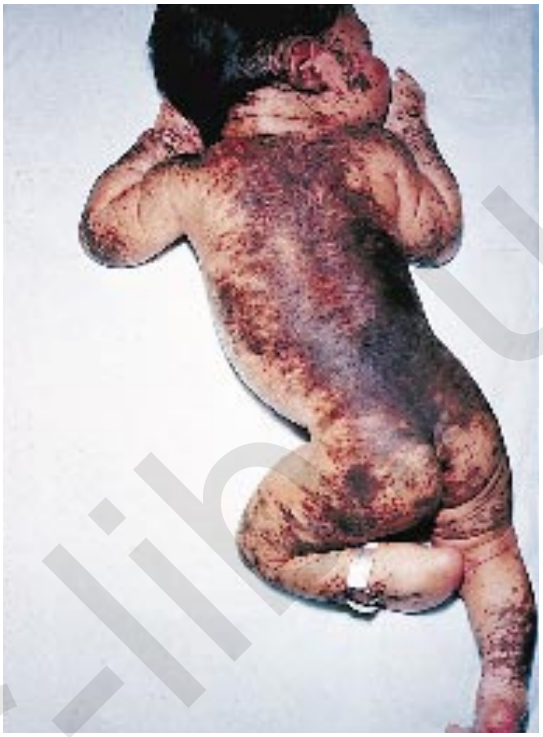

Figure 1.164. Familial progressive hyperpigmentation in a neonate is a benign form of familial hyperpigmentation that has been reported only in black families. The mother was affected and, including this infant, she had five affected children. This dominantly inherited condition presents at birth as irregular patches and streaks of hyperpigmentation which increase in size, number, and confluence with age. The pigmentation later appears in the conjunctivae and buccal mucosa, and extensive areas of the skin and mucous membranes are involved.

1.165

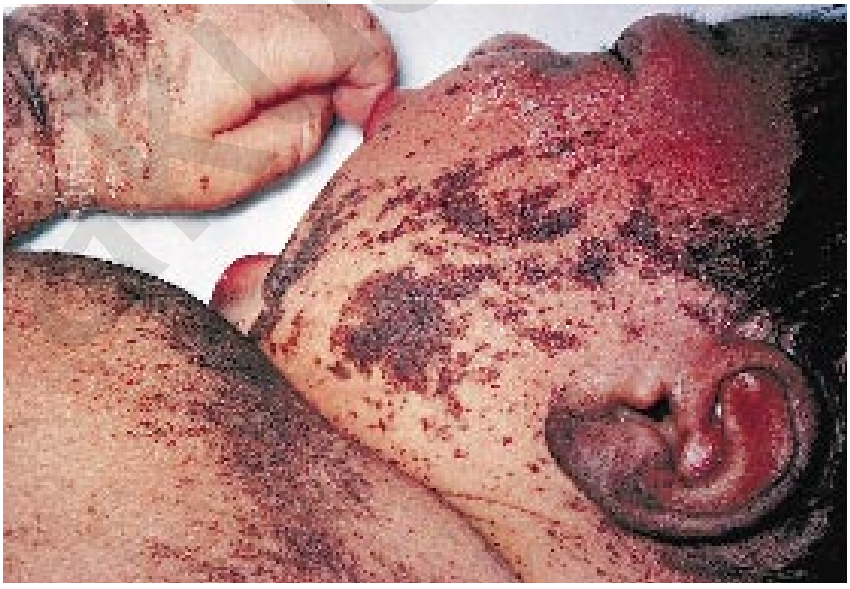

Figure 1.165. A close-up of the face of the same infant as in Figure 1.164 with familial progressive hyperpigmentation. Histopathologically the most distinctive manifestation consists of heavy melanization of the basal cell layers.

1.166

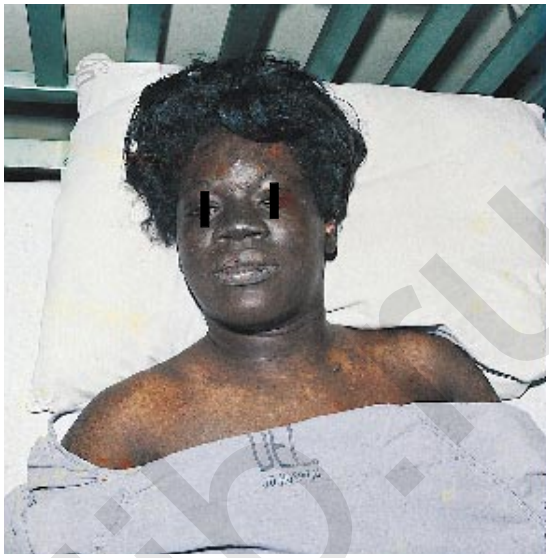

Figure 1.166. Note the marked hyperpigmentation in the skin of the mother of the infant shown in Fig. 1.165. Also note the pigmentation in the conjunctivae.

1.167

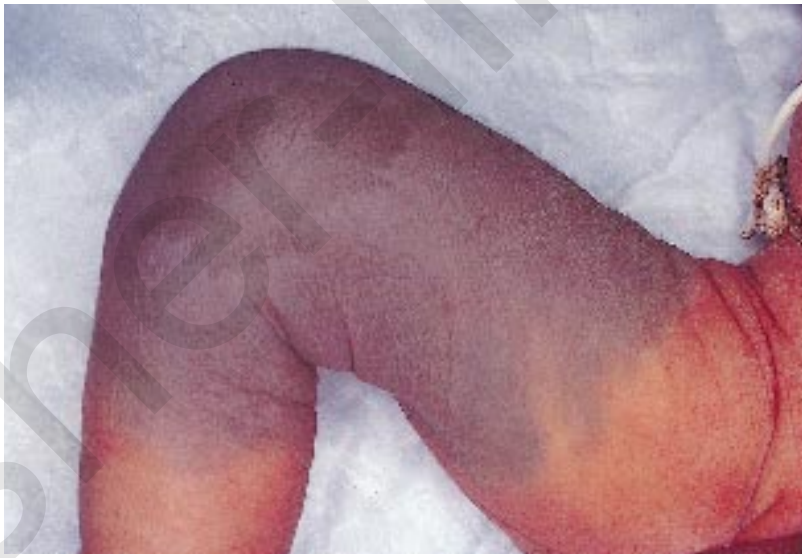

Figure 1.167. A pigmented nevus (junctional nevus) is a flat melanocytic nevus. The lesions are superficial, flat, discrete, brown, and hyperpigmented. There are usually a few lesions and they have a sharply demarcated border. Their color may vary from brown to black and they are caused by excessive numbers of melanocytes (nevocytes) at the dermal-epidermal junction. In some instances, proliferation of nevocytes down into the dermis occurs, giving rise to a raised, more or less darkly pigmented papular or verrucous lesion. These nevi are usually benign and the potential for malignant change is minimal but is greater for lesions that appear after birth.

1.168

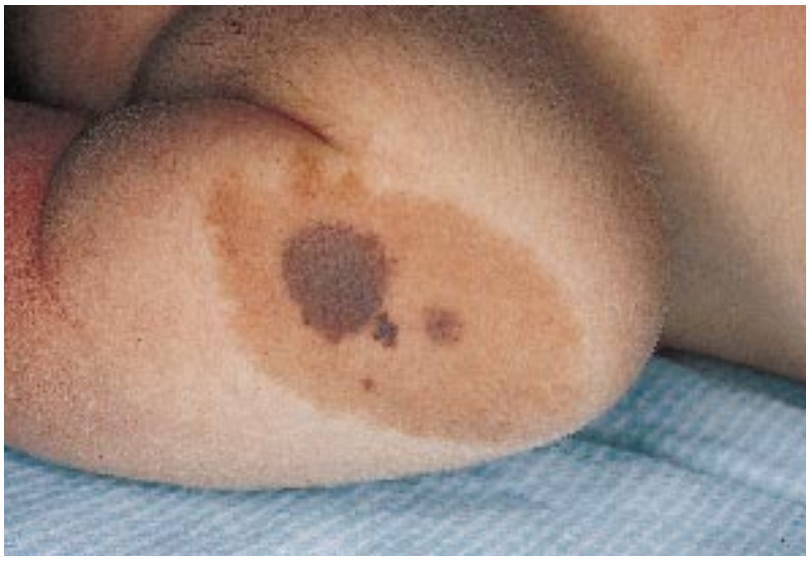

Figure 1.168. Another example of a pigmented nevus. Three types of pigmented nevi are identified: intradermal, junctional, and compound. Intradermal nevi lie within the dermis and occur most frequently in adults. Halo nevus is the term given to a darkly pigmented junctional nevus that is surrounded by a pale zone of depigmented skin. This halo represents the body's immune response to the nevocytic cells, which is affecting melanocytes in the surrounding normal skin for a short distance.

1.169

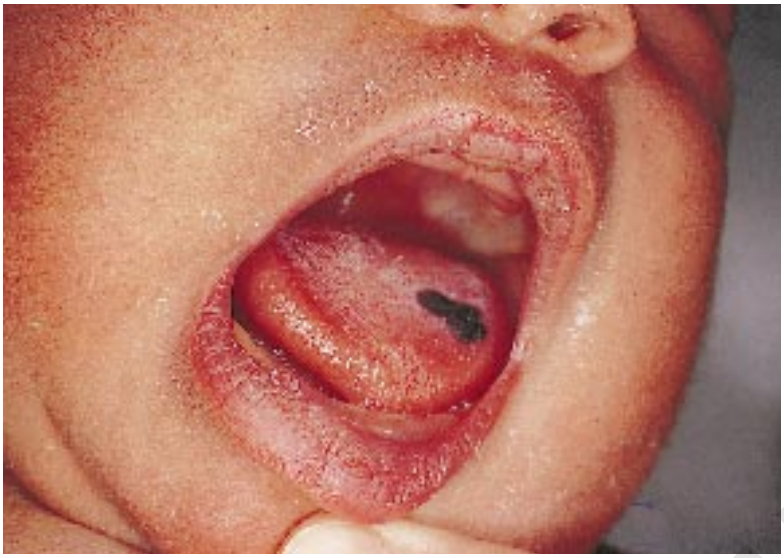

Figure 1.169. The pigmented nevus of the tongue is another example of a junctional nevus in an unusual location.

1.170

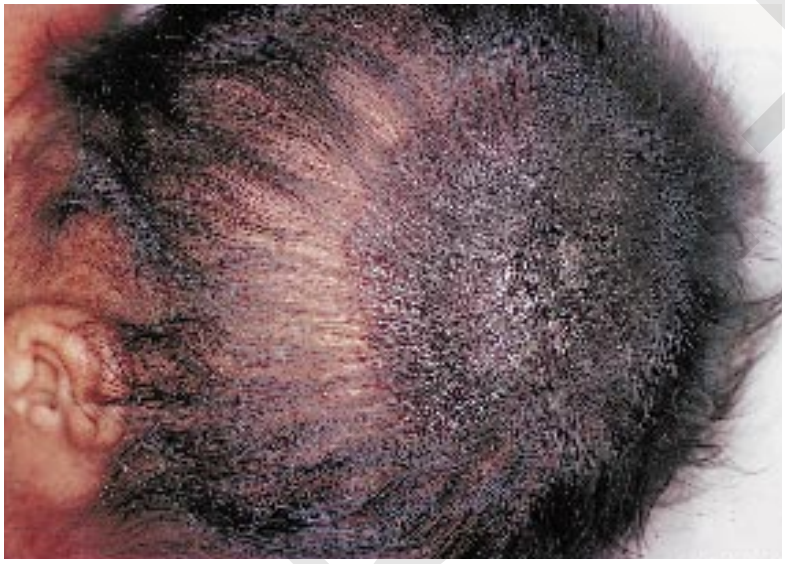

Figure 1.170. A pigmented nevus on the scalp obviously has associated hair and, because of this, tends to be much coarser in texture. These junctional nevi of the scalp may cover large areas.

1.171

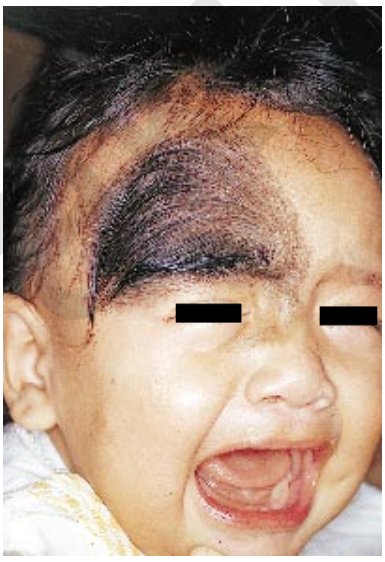

Figure 1.171. In this infant there is a large benign hairy pigmented nevus. These nevi may be pale at first with fine vellus hairs, but increasing pigmentation takes place during the first year of life, often with the growth of dark coarse hair. The hyperpigmented zones may be extremely large with numerous satellite lesions. They may occur anywhere on the body and are variable in size. Approximately 10% of giant hairy nevi develop into malignant melanomas.

Figure 1.172. A congenital giant pigmented nevus is extensive and sharply outlined. The hyperpigmented zones may be extremely large, covering the trunk, especially the lower trunk ("garment" nevus or "bathing trunk" nevus). "Garment" nevi involve a very large body surface area (e.g., the entire back or an extremity). The surface of these lesions is nodular or raised with fleshy elements and has a somewhat leathery texture. It may have dark, coarse hairs within the lesion. Histologically this would be classified as a compound nevus. A junctional nevus lies only on the epidermal surface and is flat, smooth, and relatively small. Junctional nevi over time may become compound nevi. Compound nevi possess the features of both junctional and intradermal nevi in that nevus cells are seen within the dermis as well as within the epidermis. They tend to be more elevated and vary from a slightly raised plaque to a lesion of a somewhat more papillomatous nature.

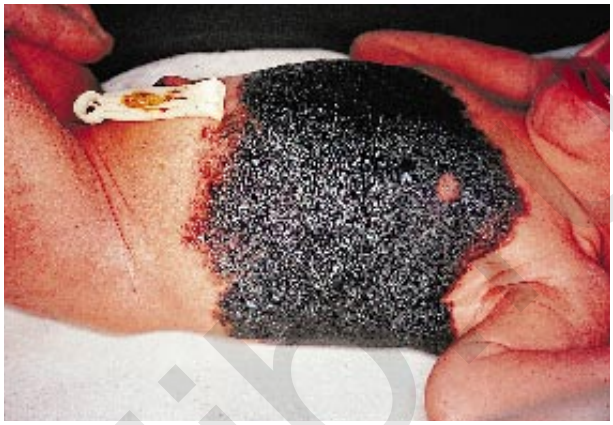

1.172

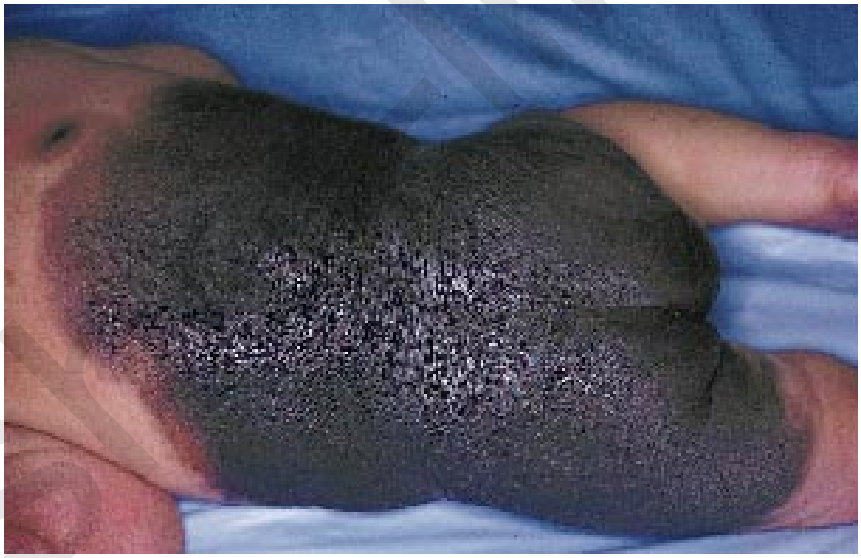

1.173

Figure 1.173. A large "garment" nevus involving most of the trunk and perineum. In infants with a giant "garment" nevus there may be widely disseminated pigmented patches which represent satellite melanocytic nevi. In these infants there is a propensity for malignant change, and therefore an aggressive surgical approach is justified.

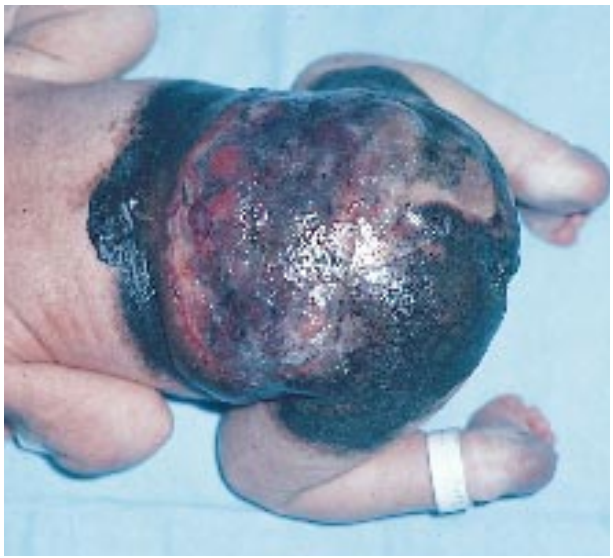

1.174

Figure 1.174. This infant with a large "garment" ("bathing trunk") nevus had skin breakdown with ulceration in utero and presented at birth with this appearance. Examination of the placenta showed numerous secondary pigmented nevi in the placental tissue. Histopathologic examination of the nevi in the placenta showed numerous melanoma cells. The mother was normal.

1.175

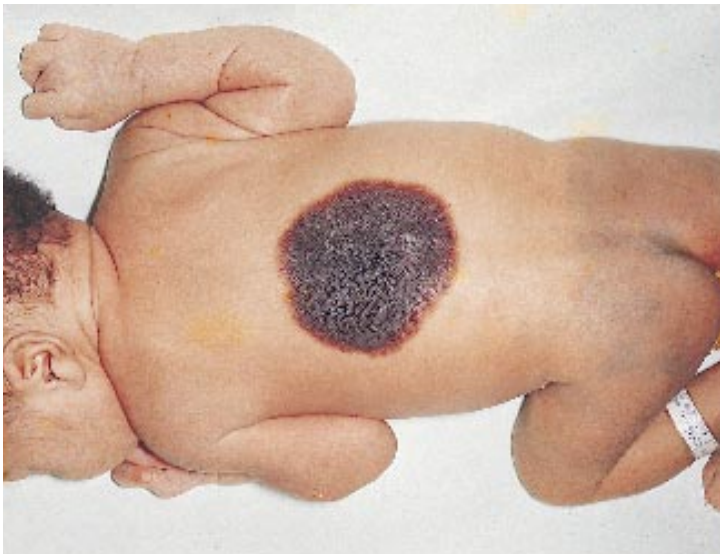

Figure 1.175. A large pigmented nevus over the midline in the thoracolumbar area of this infant may be significant in that any lesion located in the midline over the spine should alert one to the possibility of a neural tube defect. The faun-tail nevus is an elongated patch of dark skin bearing abundant long dark hair located in the midline over the lumbar spine or sacrum. It is a rare but helpful indicator of a tethered spinal cord.

1.176

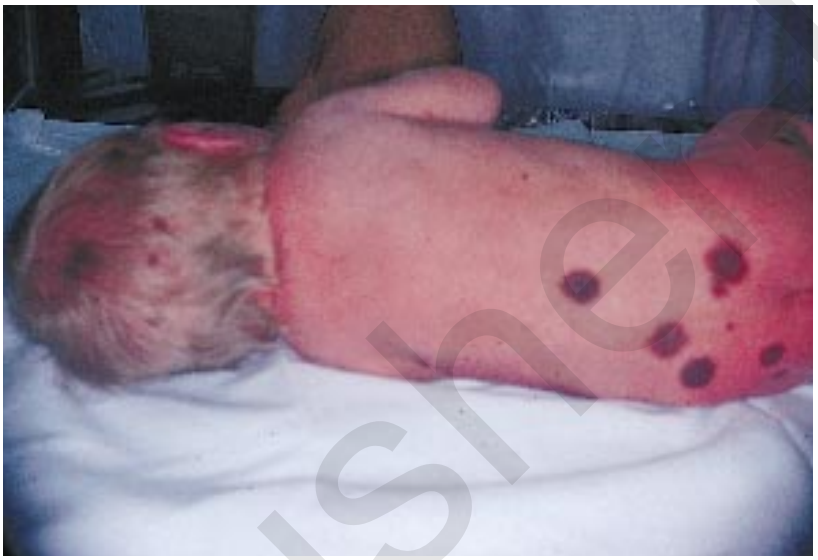

Figure 1.176. The multiple pigmented nevi involving the scalp and trunk in this infant are characteristic of the neurocutaneous melanosis sequence. There are dark pigmented multiple nevi, which are sometimes hairy and are more extensive in a bathing trunk distribution over the lower trunk, abdomen, and lower thighs. There may be leptomeningeal involvement with nests and sheets of melanoblasts, most striking at the base of the brain. This may lead to hydrocephalus, seizures, and deterioration of central nervous system function. In these cases, cells containing melanin may be detected in the cerebrospinal fluid.

1.177

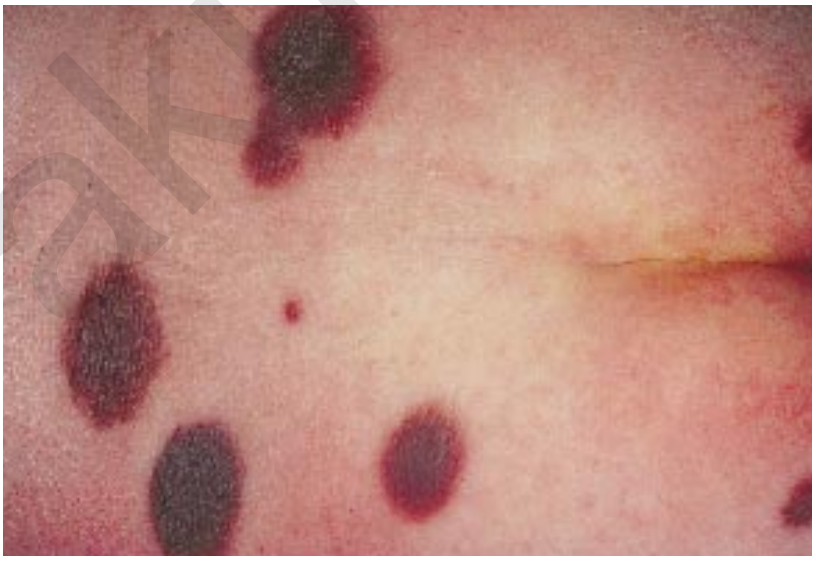

Figure 1.177. A close-up of the lesions in the lumbosacral and gluteal areas in the same infant as in Figure 1.176.

1.178

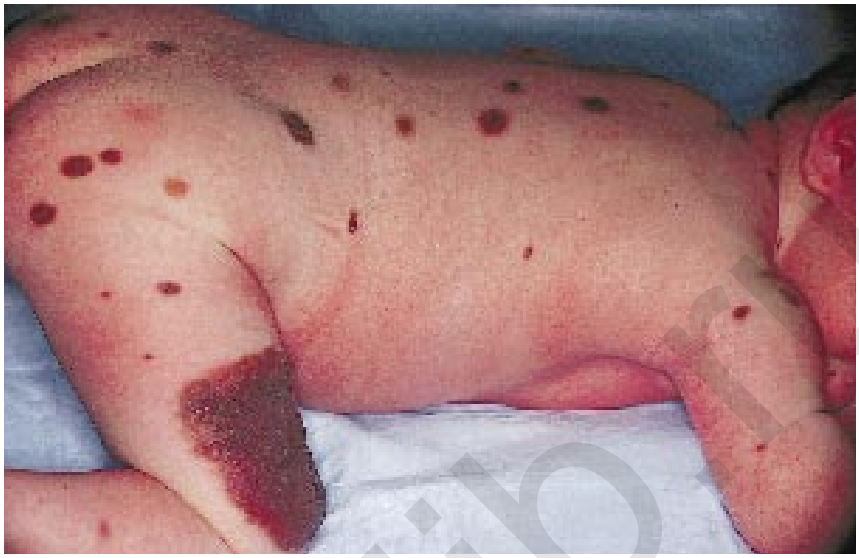

Figure 1.178. Another infant with the neurocutaneous melanosis sequence. The finding of a single giant nevus with numerous satellite lesions is not uncommon in this disorder. Cutaneous melanosis is evident at birth and central nervous system function may be normal initially, but seizures and mental deterioration occur later. The risk of malignant melanoma degeneration is 10 to 15%.

1.179

Figure 1.179. Mastocytosis (urticaria pigmentosa) is a mast cell infiltrative disorder which presents at birth or develops during the first few weeks of life. The lesions may be solitary or in groups, as in this infant. Macules, papules, nodular lesions, vesicles, and bullae may all be signs of mastocytosis. They vary in color from a slightly reddish appearance to a tan or brown appearance. Spontaneous remission of the skin lesions usually occurs. Skin biopsy shows mast cell infiltration.

1.180

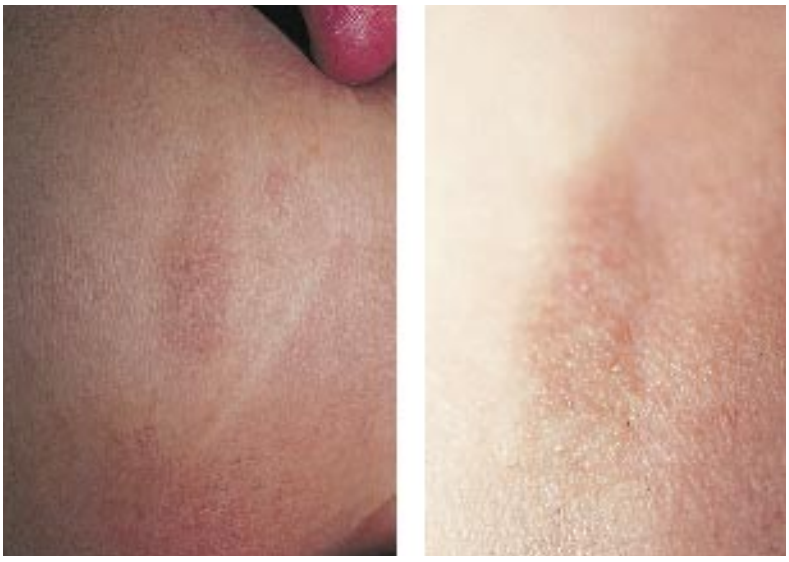

Figure 1.180. In about 5% of cases, mastocytosis is localized. In the figure on the left there is a solitary tan to brownish-colored, slightly raised lesion on the back. As seen in the figure on the right, rubbing the skin over this area results in dermatographism (Darier's sign) due to histamine release. Nodular forms of mastocytosis must be differentiated from xanthoma and juvenile xanthomagranulomas.

1.181

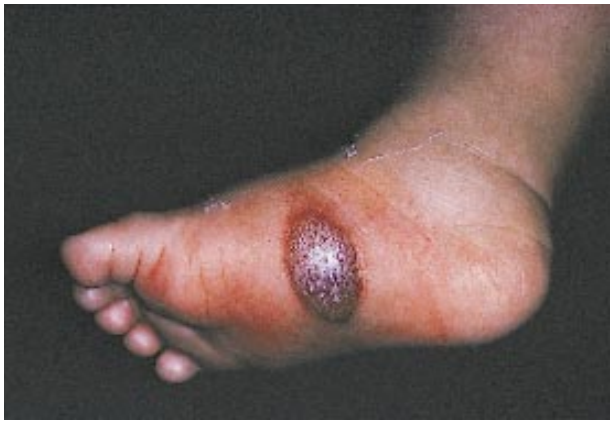

Figure 1.181. This is a lesion of bullous mastocytosis (urticaria pigmentosa) that presented at birth in this infant as a solitary bullous lesion on the sole of the right foot. Note the area of redness surrounding the lesion (dermatographism) following examination of the lesion. Spontaneous remission of the skin lesions usually occurs. It is rare for lesions to appear after the age of 3 years. Differential diagnosis includes bullous impetigo, epidermolysis bullosa, incontinentia pigmenti, and bullous congenital ichthyosiform erythroderma.

1.182

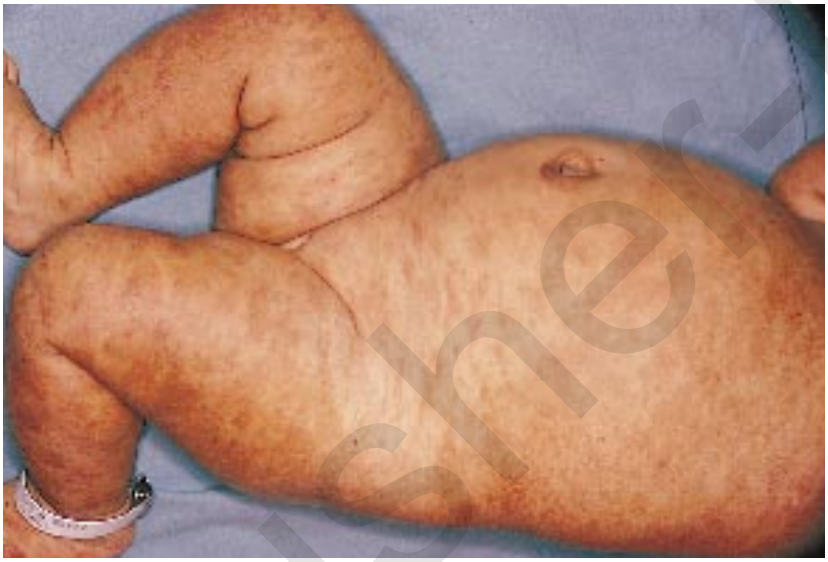

Figure 1.182. In this infant with a systemic skin rash present at birth, the diagnosis of urticaria pigmentosa was confirmed. In systemic mastocytosis there is hepatosplenomegaly and bone involvement. Biopsy shows mast cell infiltration. In localized mastocytosis, which occurs in about 5% of all cases of mastocytosis, spontaneous remission of the skin lesions usually occurs. Prognosis is usually good, provided that there are no signs of systemic mastocytosis (hepatosplenomegaly, bone involvement).

1.183

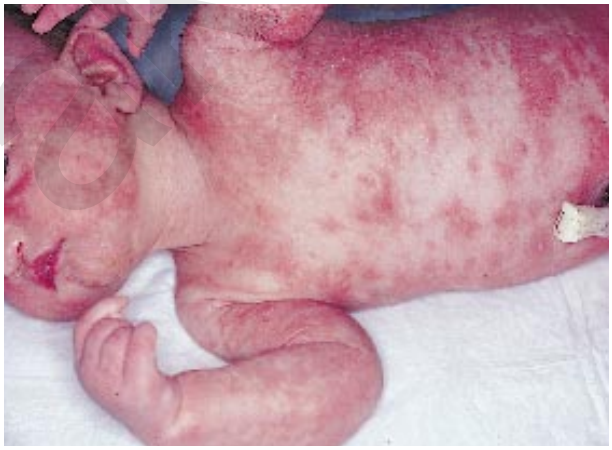

Figure 1.183. Incontinentia pigmenti (Bloch-Sulzberger syndrome) is considered to be a neurocutaneous syndrome seen only in female infants (X-linked dominant, generally lethal prenatally to the male). It has four cutaneous phases. In this infant note the early maculopapular appearance without vesicles or pigmentation. The lesions contain eosinophils, and blood eosinophilia is frequently present. In the next phase there are many vesicular lesions. These then become bullous and pustular. The bullae may be superseded by verrucous lesions in the same distribution, and after these disappear, whorls of hyperpigmentation appear. In the final phase, hypopigmented patches may occur. The patterning of the skin abnormalities follows the path of Blaschko's lines, which represent the course of early migration of primordial skin cells progressing from the dorsal to the ventral midline.

1.184

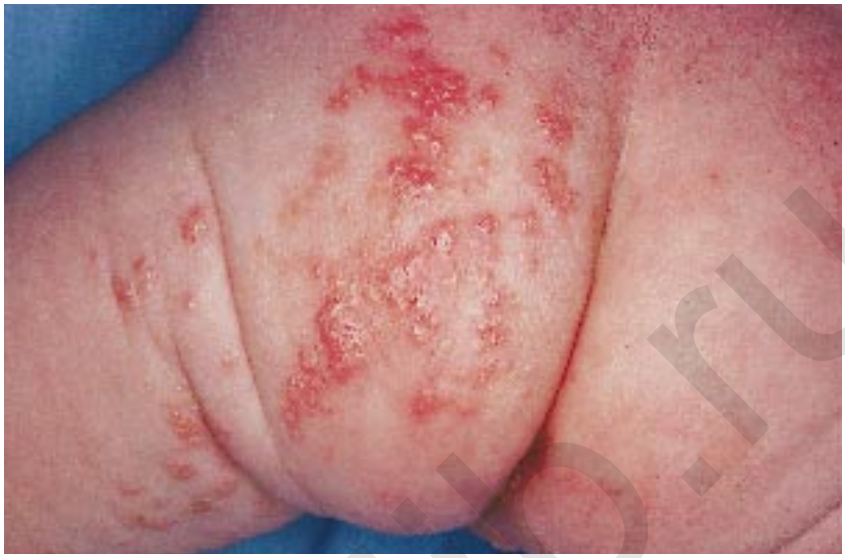

Figure 1.184. Within the first month of life in incontinentia pigmenti, the vesicular phase develops as noted in this infant. Note the linearly arranged vesicles and red nodules on the flexor surface of the upper and lower extremities. The blisters may cluster in a bizarre arrangement if they are numerous.

1.185

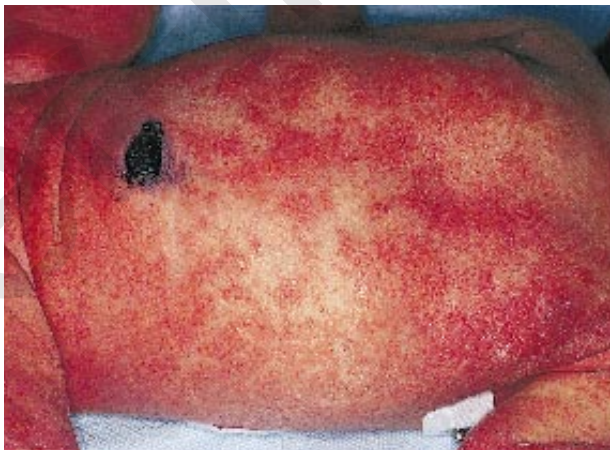

Figure 1.185. Another infant with incontinentia pigmenti. Note the maculovesicular pigmented appearance of the skin in a swirling pattern. The infant developed seizures on the 2nd day of life. Systemic manifestations occur in about 70% of infants (20% at birth). These include central nervous system (microcephaly, seizures, and retardation), ocular (cataracts, retinal dysplasia, etc.), osseous (hemivertebrae, extra ribs, hemiatrophy, etc.), dental (hypodontia, etc.), and occasionally cardiac abnormalities.

1.186

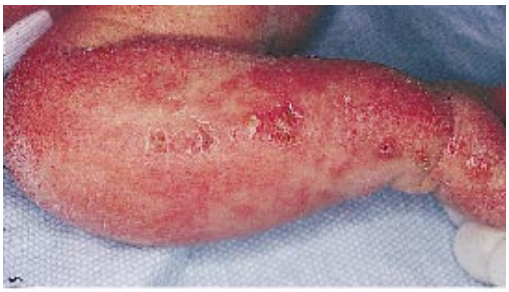

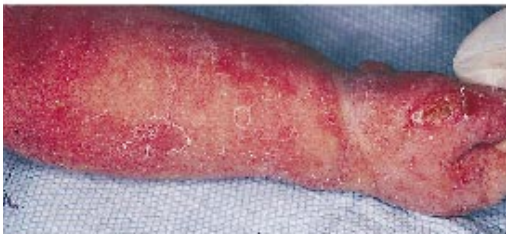

Figure 1.186. In this phase of incontinentia pigmenti, vesicles and bullae have formed and these have broken down with some increased pigmentation.

1.187

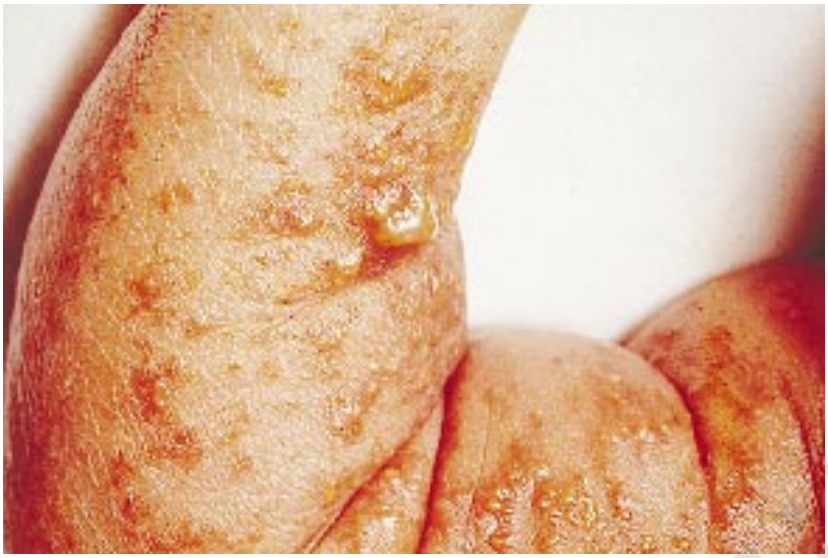

Figure 1.187. A close-up of the right upper extremity showing the vesicles with some verrucous element and increasing pigmentation with a tendency to follow Blaschko's lines.

1.188

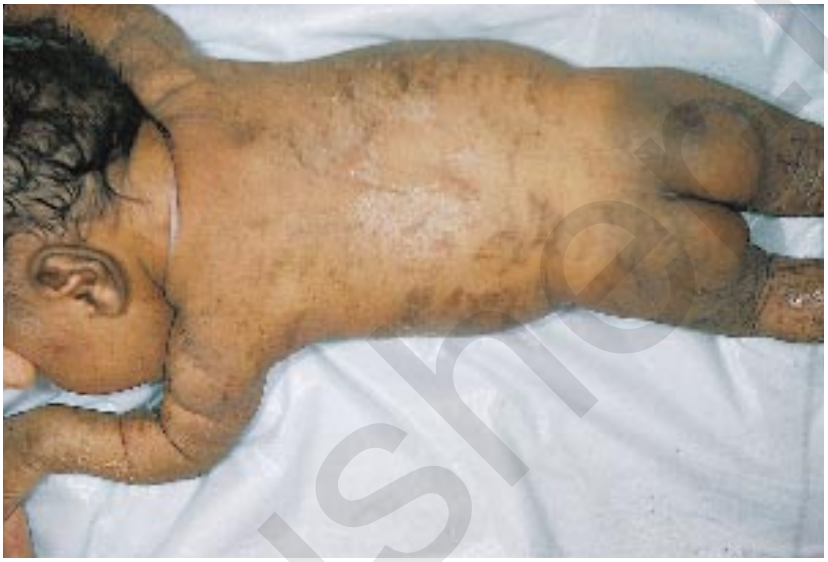

Figure 1.188. In a later phase of incontinentia pigmenti, between 6 to 12 months of age, red-brown, hyperpigmented lesions appear in a symmetric distribution on the arms and legs while other lesions have improved. Note the bizarre distribution of the lesions and the pigmentation. The pigmented zones have very irregular patterns and tend to follow the path of Blaschko's lines. They have a roughly V-shaped configuration over the back, a wavy S-shaped distribution over the anterior trunk, and a longitudinal orientation over the limbs. These lesions tend to persist.

1.189

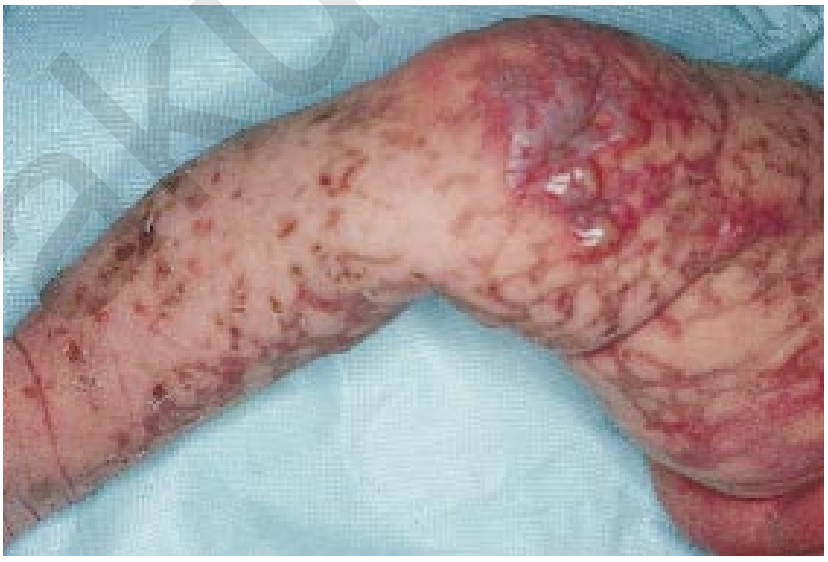

Figure 1.189. A close-up of the right lower extremity of an infant with incontinentia pigmenti. Note the presence of vesicles and the typical pattern of swirled hyperpigmentation of the skin that has been compared to that of a marble cake. This is present mainly on the extremities and trunk, and increases in intensity until the 2nd year of life. It may persist many years, then gradually fades.

1.190

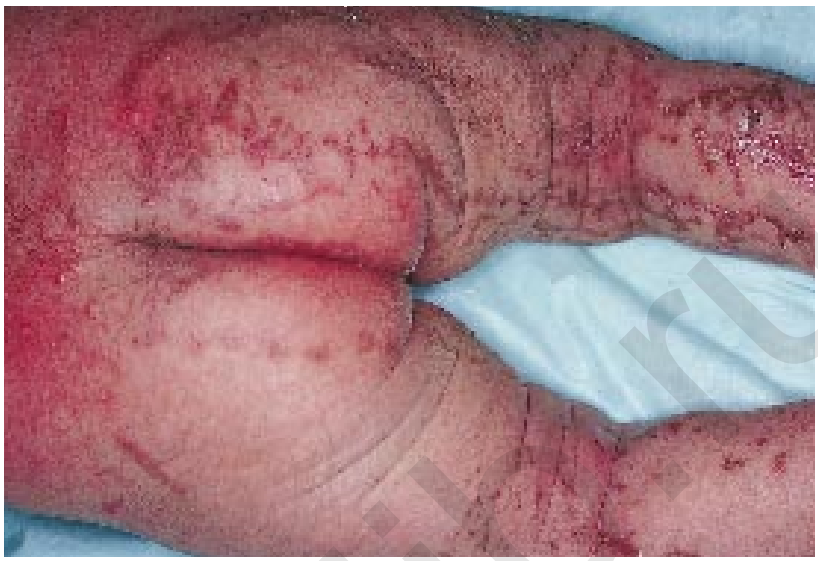

Figure 1.190. A close-up of the lower trunk, buttocks, and extremities showing the pigmentary changes which tend to follow the path of Blaschko's lines.

1.191

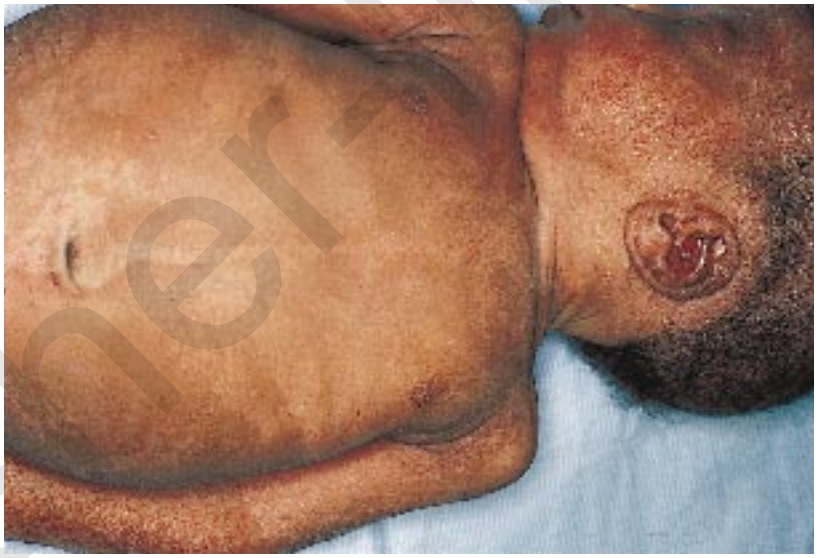

Figure 1.191. In incontinentia pigmenti achromians (hypomelanosis of Ito), a neurocutaneous syndrome, the distribution of hypopigmentation is similar to that of the hyperpigmented areas seen in incontinentia pigmenti. Note that there is a pattern of swirled hypopigmentation which looks like a photographic negative of the hyperpigmented streaks seen in incontinentia pigmenti. This disorder is associated with seizures and mental retardation. The whorls may appear without the prior development of vesicles or bullae.

1.192

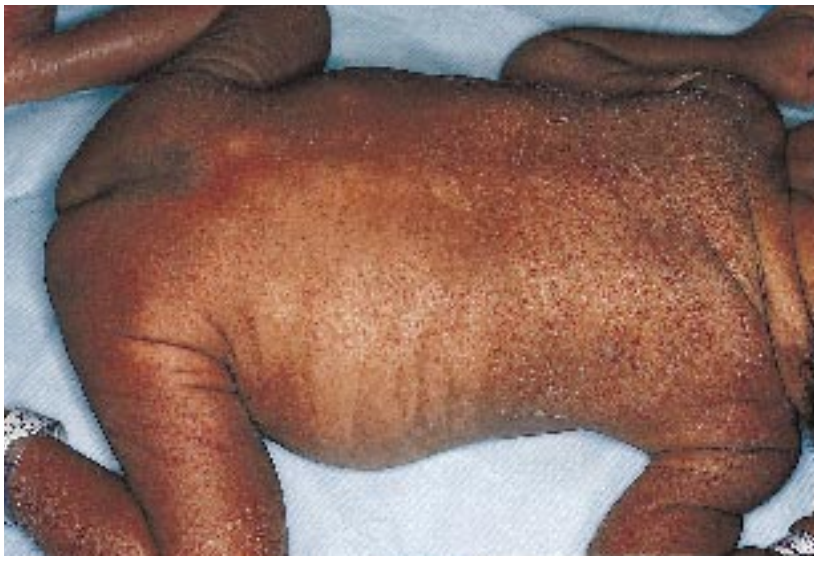

Figure 1.192. The back of the same infant as in Figure 1.191 showing the distribution of the hypopigmented lesions, again demonstrating these bizarre patterns which look like a photographic negative of the hyperpigmented streaks seen in incontinentia pigmenti and which tend to follow Blaschko's lines. In a few patients, the lesions may be patchy and confined to relatively limited areas of the body. In most cases, however, the hypopigmented areas are extensive, often bilateral, and appear to be more pronounced on the ventral surface of the trunk and the flexor surface of the limbs.

1.193

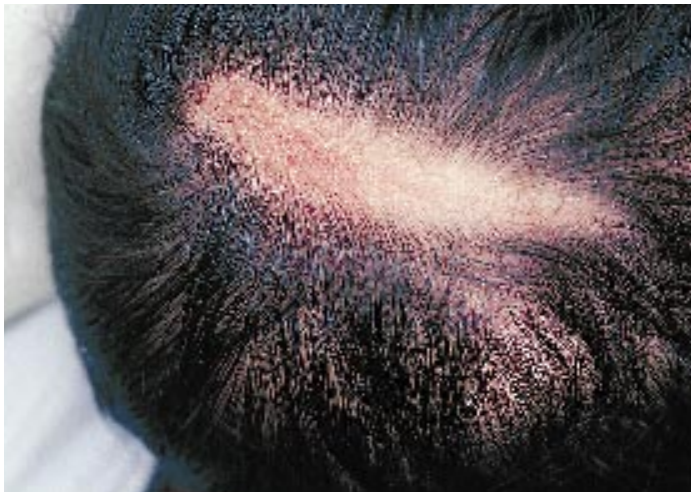

Figure 1.193. Epidermal nevus on the scalp present at birth. These are raised verrucous lesions of variable size, sometimes round but more commonly linear, and tend to follow Blaschko's lines. They may appear later in infancy and are slightly hyperpigmented or yellowish in light-skinned infants, while appearing dark brown to black in darker skinned infants. An epidermal nevus must be differentiated from a nevus sebaceus of Jadassohn.

1.194

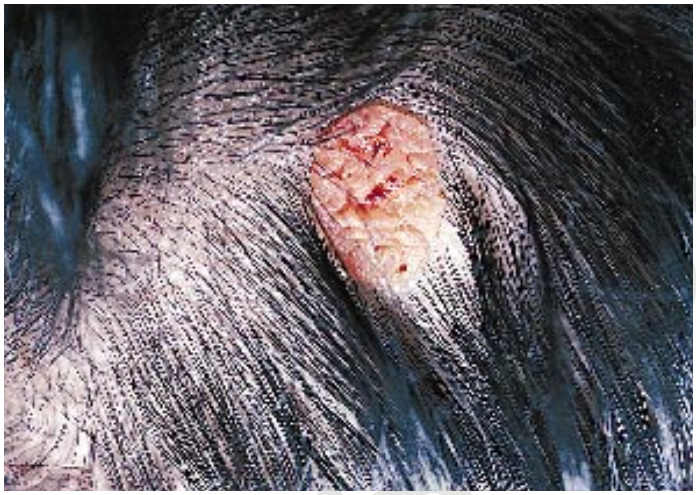

Figure 1.194. Another example of an epidermal nevus on the scalp which was present at birth but had a more verrucous and hyperpigmented appearance. An epidermal nevus is a benign congenital disorder that is characterized by circumscribed hyperkeratosis and hypertrophy of the epidermis. The diagnosis was confirmed by skin biopsy.

1.195

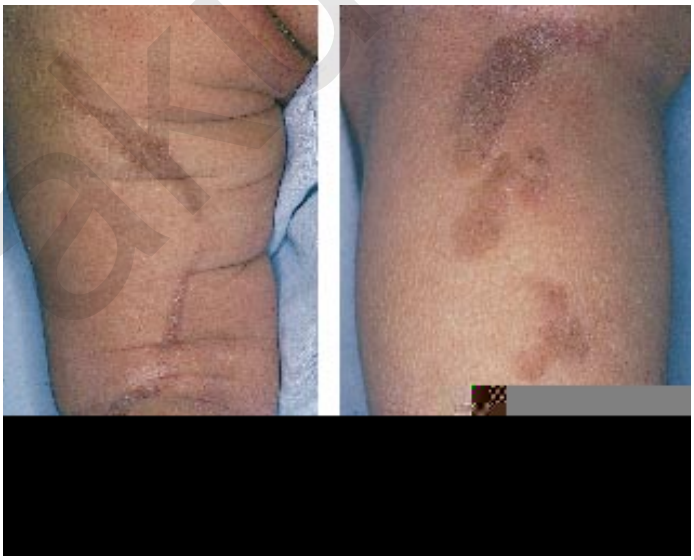

Figure 1.195. A linear epidermal nevus of the back of the left thigh and leg which was present at birth. In this infant note the linearity and the increased pigmentation of the lesions on the thigh. Epidermal nevi often favor the extremities rather than the head and neck in what appears to be a dermatomal distribution (follows Blaschko's lines). They may occur as single lesions, but generally multiple lesions are present arranged in a linear distribution.

1.196

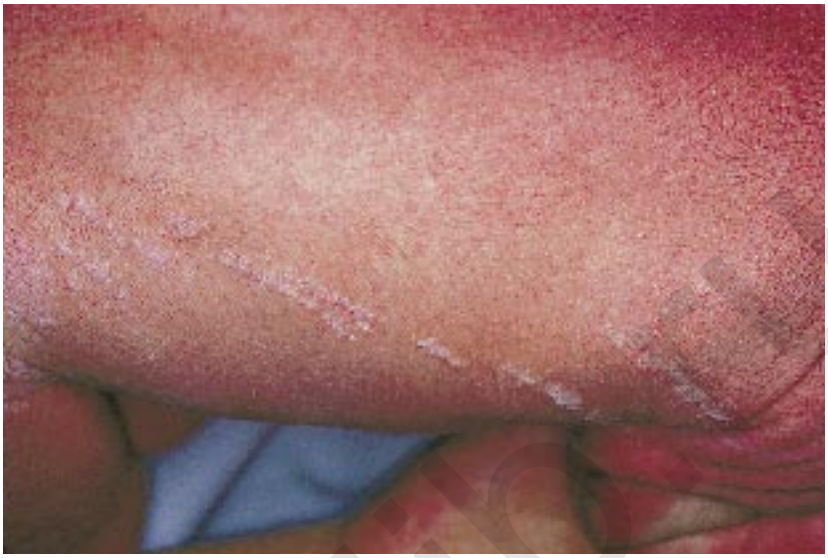

Figure 1.196. Linear verrucous epidermal nevus present at birth over the right torso of an infant. Note that this is similar to an epidermal nevus but has a more verrucous appearance and may be more hyperpigmented.

1.197

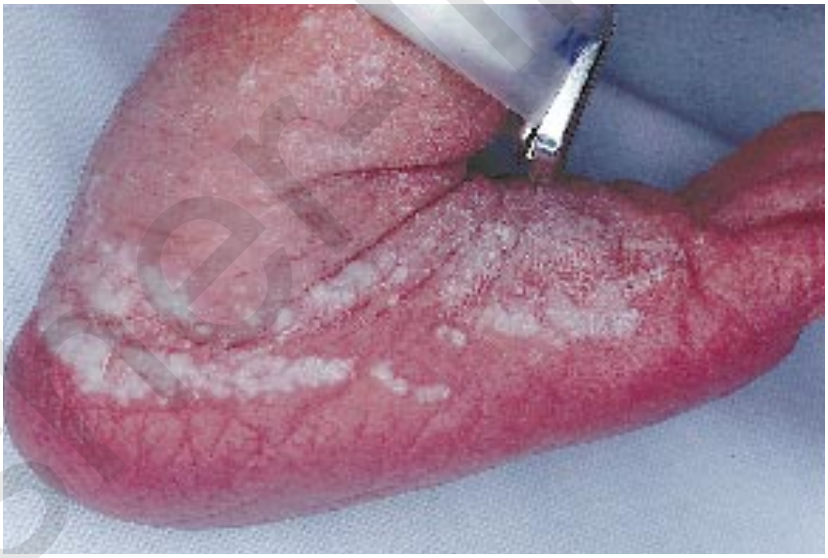

Figure 1.197. Close-up of a linear verrucous epidermal nevus which was present only on the distal part of the left leg and foot of this otherwise normal infant. A localized form (nevus verrucosus) usually consists of a solitary lesion which may be grayish to yellowish-brown in color and warty, granular, or papillomatous in appearance.

1.198

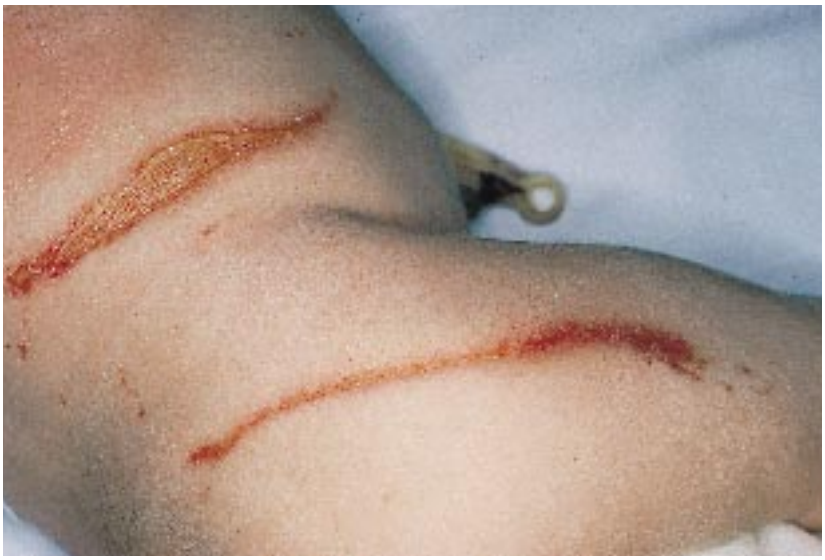

Figure 1.198. This infant presented at birth with linear erosions which were open and appeared to be traumatic. By the age of three months the erosions became hypertrophic and hyperkeratotic. New areas developed over the previous uninvolved areas of the skin, and later a verrucous appearance developed. Skin biopsy diagnosis was that of a classic linear verrucous epidermal nevus. Central nervous system, ocular, and long bone studies were normal.

1.199

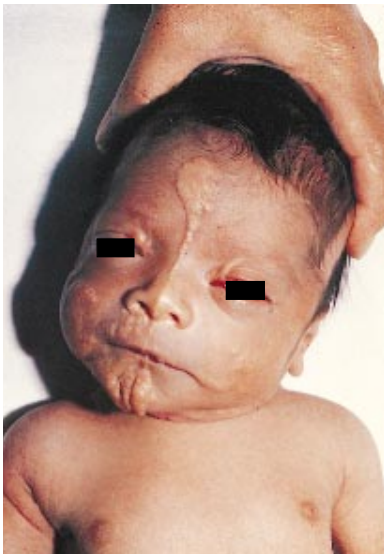

Figure 1.199. Nevus unius lateris is the term used when the lesions of epidermal nevus are extensive and systematized. It may present as a single linear or spiral warty lesion or, at times, as an elaborate, continuous, or interrupted pattern affecting multiple sites. When the scalp, face, or neck is involved, adnexal tissues such as the sebaceous glands may be affected and become enlarged. For this form, the term linear nevus sebaceus may be used. Linear nevus sebaceus should not be confused with nevus sebaceus of Jadassohn, a distinct and unrelated disorder.
In the linear nevus sebaceus syndrome, small linearly arranged verrucous yellow-orange nodules are seen on the face, neck, and limbs. Multiple sebaceous nevi may be found on the scalp and there may be pigmented nevi on the extremities. These lesions may be associated with ocular dermoids and major ophthalmic abnormalities (cloudy cornea and colobomata of the eyelid, iris, and/or choroid). In the central nervous system there may be intracranial malformations which are associated with seizure disorders. Pigmentary and skeletal abnormalities may also be present.

1.200

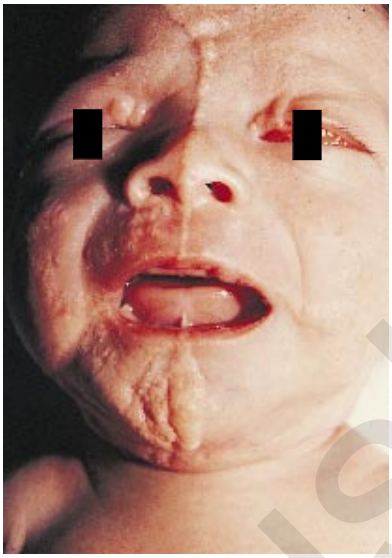

Figure 1.200. Close-up of the face of the same infant as in Figure 1.199 with the linear nevus sebaceus syndrome. Note the typical lesions in the midfacial area which extend from the forehead down into the lower jaw. Note that these are linear in distribution. Also note the dermoids of the eye. This infant developed seizures at the age of 10 days. The EEG was grossly abnormal and a diagnosis of cortical atrophy was made. The infant died at the age of 2 months.

1.201

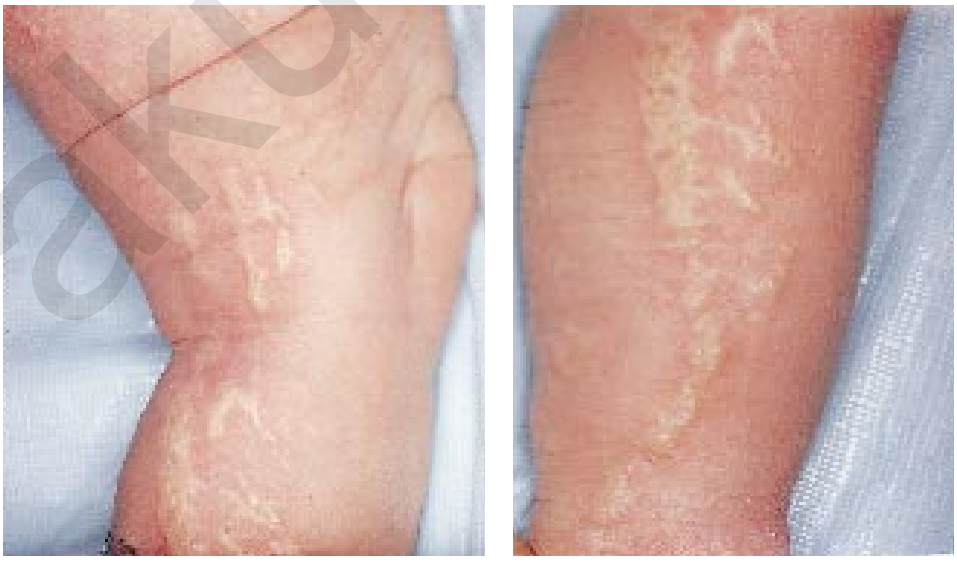

Figure 1.201. Linear epidermal nevi in another infant who had central nervous system abnormalities and seizures.

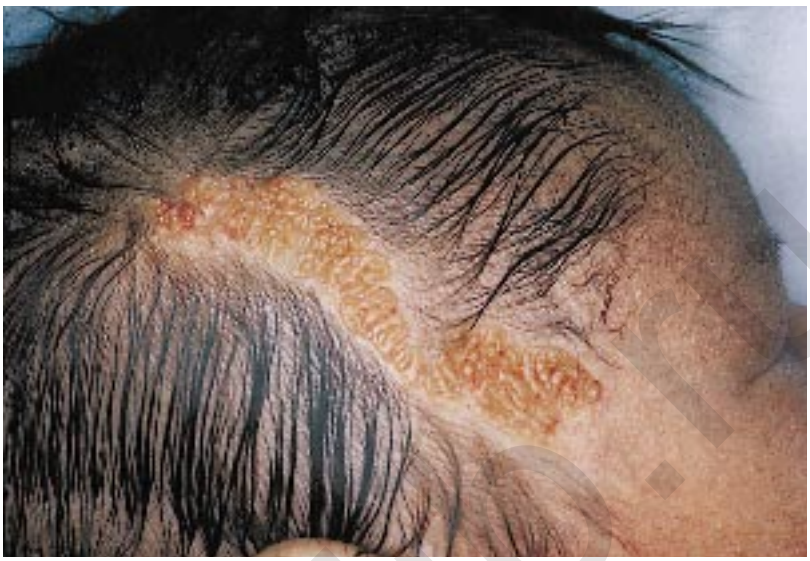

1.202

Figure 1.202. Nevus sebaceus of Jadassohn is a hamartomatous lesion with mixed tissue components that most commonly occurs on the scalp and face. These nevi are seen at birth as flat or slightly elevated, well-circumscribed, sometimes elongated, orange-yellow to yellowish-brown plaques with a greasy or waxy hairless surface. The lesions are usually solitary, round or oval on the scalp, or linear on the face and ears. They vary from a few millimeters to centimeters in diameter. The condition is not inherited but familial forms may occur, are noted with equal frequency in males and females, and occur in all races.

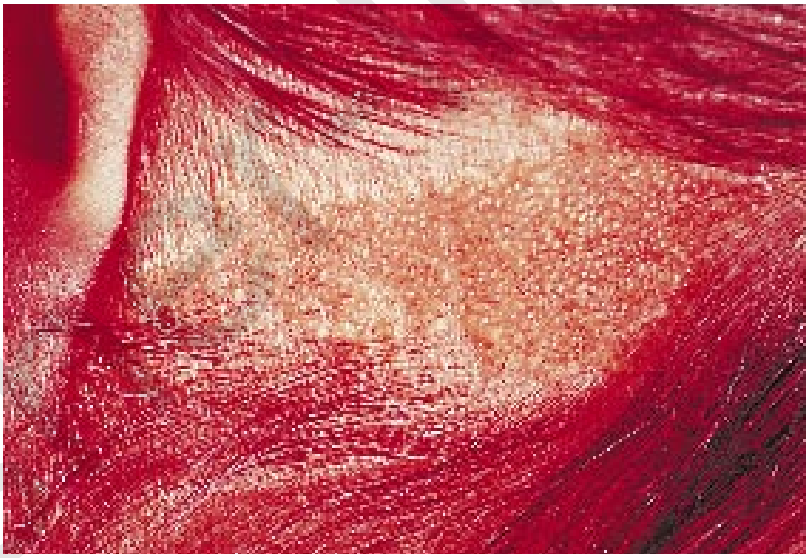

1.203

Figure 1.203. Another example of a nevus sebaceus of Jadassohn. Note that this lesion is larger and not as raised as the nevus in the previous infant. The lesions persist, enlarge gradually, and malignant degeneration may occur in 10 to 15% of lesions generally during adolescence or adult life. The most frequent change is that of a basal cell carcinoma. Rapid enlargement or ulceration of the nevus at any age may suggest malignant change.

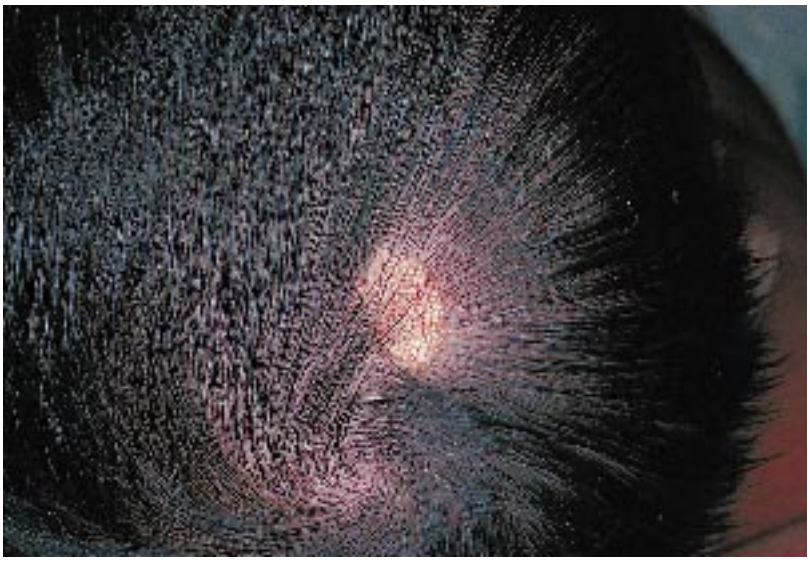

1.204

Figure 1.204. Nevus sebaceus of Jadassohn in the scalp. Note that this is a round, small lesion which could easily be missed on the initial physical examination. Linear epidermal nevi and verrucous nevi should not be confused with nevus sebaceus of Jadassohn which is a distinct and unrelated disorder.

1.205

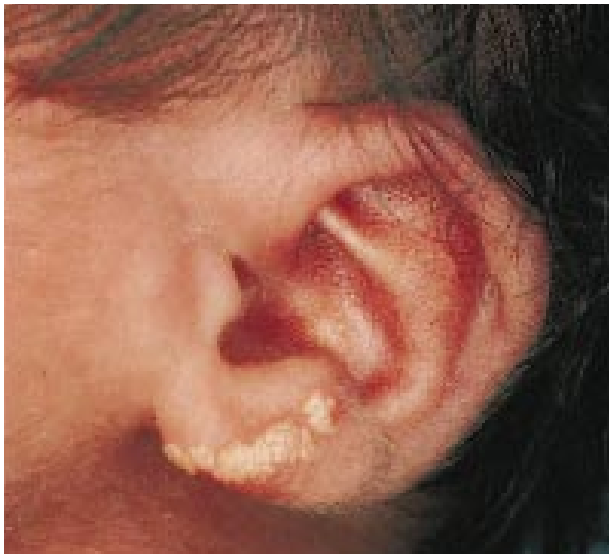

Figure 1.205. An example of a nevus sebaceus of Jadassohn involving the left ear.

1.206

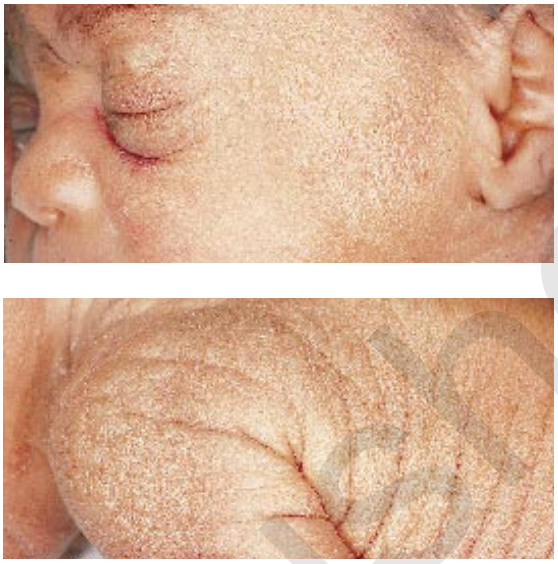

Figure 1.206. Note the raised lesions on the face (upper figure) and similar lesions on the left shoulder and back (lower figure) present at birth in this infant who was otherwise normal. Skin biopsy diagnosis was that of nevoid, unclassified. This is a benign hamartomatous nevus in which the skin lesions are of different cell types and vary considerably in size and location.

VESICULOBULLOUS ERUPTIONS

1.207

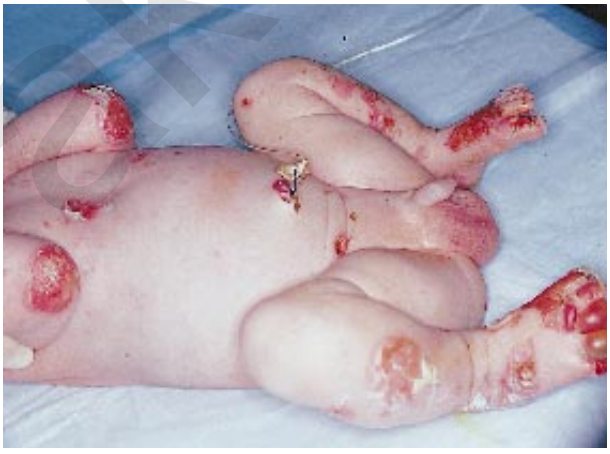

Figure 1.207. Epidermolysis bullosa is an autosomally inherited blistering and bullous disorder which is present at birth or becomes manifest soon after birth. It commonly affects the face, hands, feet, and variably the limbs and trunk and is characterized by trauma-inflicted erosions (Nikolsky's sign) and loss of the epidermis. As in this infant, the lesions are most commonly seen over the extensor surfaces and there are broken bullae with underlying erythroderma. Epidermolysis bullosa occurs in three major inherited forms: e. bullosa simplex (epidermolytic), junctional e. bullosa (letalis; gravis), and e. bullosa dystrophica (dominant and recessive forms) based on the presence or absence of scarring, the mode of inheritance, and the level of skin cleavage following minor trauma.

1.208

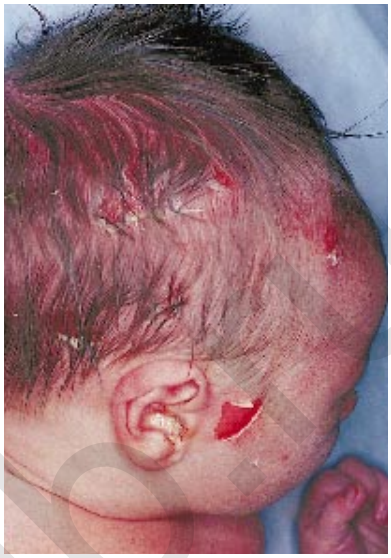

Figure 1.208. In this infant with epidermolysis bullosa, pressure of the forceps blade at delivery has resulted in a positive Nikolsky's sign. In Nikolsky's sign, firm stroking or rubbing of the skin will cause development of localized separation and tearing of the skin. In the Koebner phenomenon, minimal trauma (rubbing of the skin) may result in the formation of blebs (vesicles and bullae). Vesicles are blistering lesions less than 0.5 cm in diameter, whereas bullae are blistering lesions 0.5 to 1 cm or more in diameter.

1.209

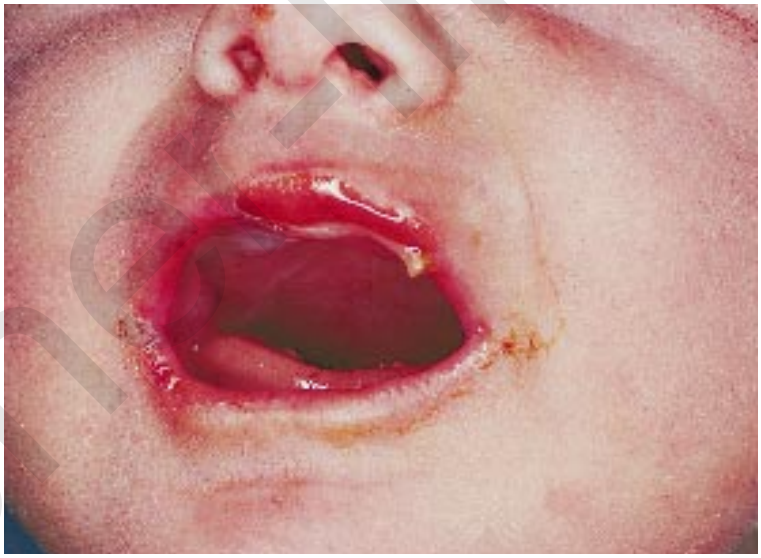

Figure 1.209. Bullous formation on the lip of the same infant as in Figure 1.208 as a result of resuscitation.

1.210

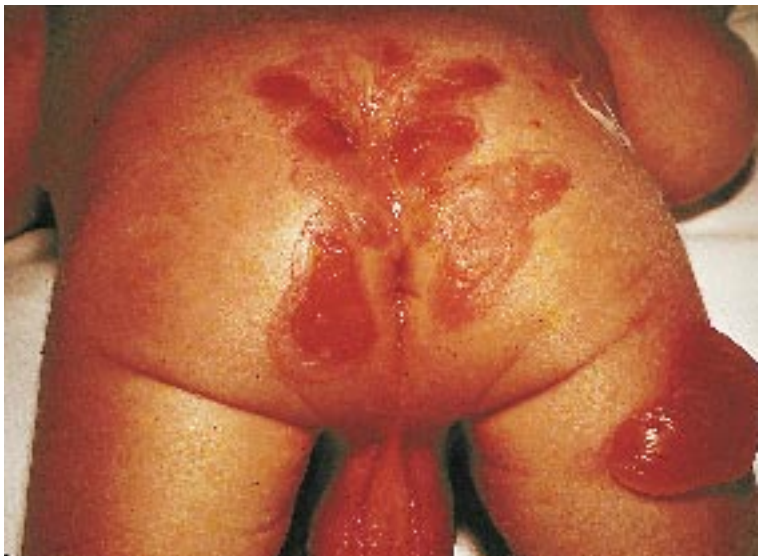

Figure 1.210. In epidermolysis bullosa simplex, an autosomal dominant condition, there is inadequate bonding between the epidermal and dermal layers with separation of the skin at the basal cell and intraepidermal junction. When the bullae break, the denuded areas resemble second degree burns but the ulcerated vesicles and bullae resolve without scarring and heal rapidly. (Sometimes in severe cases there may be mild scarring.) Mucous membranes and nails are usually not affected.

1.211

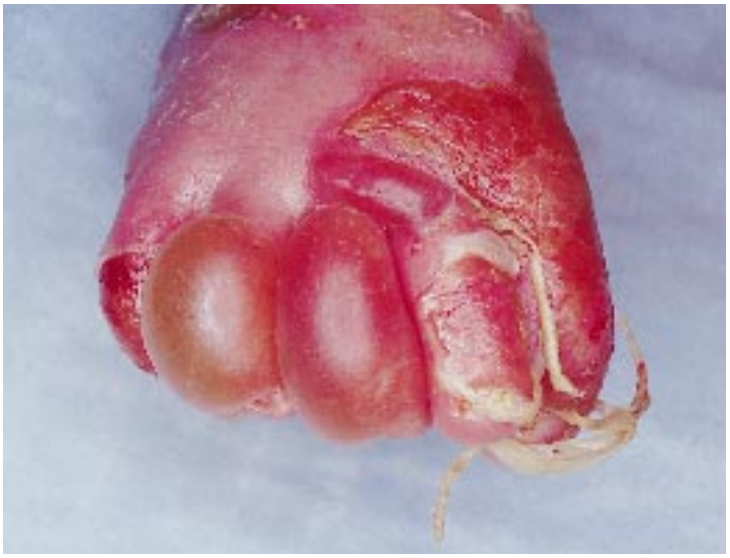

Figure 1.211. Note the bullae on the third and fourth toes and the extensive erosions (after rupture of the bullae) elsewhere on the foot of this infant with the dystrophic form of epidermolysis bullosa. In dystrophic epidermolysis bullosa, the blister forms in the papillary dermis below the basement membrane. These areas heal gradually, leaving atrophic scars, keloids, and contractures. Fingers and toes are bound together if there is loss of digits, and a mitten-like mass may form. Dystrophy of the nails may occur, leading to loss of the nails. This is an autosomal recessive condition which affects skin, mucous membranes and nails.

1.212

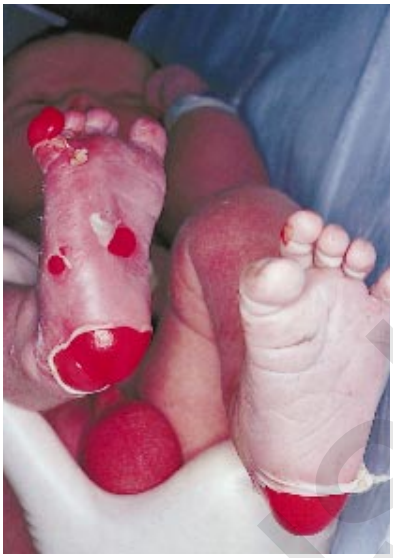

Figure 1.212. Epidermolysis bullosa in which the lesions were present at birth. The feet are one of the most commonly affected sites because babies kick their feet. If the lesions are extensive, the infant is at risk for fluid and electrolyte loss as well as infection.

1.213

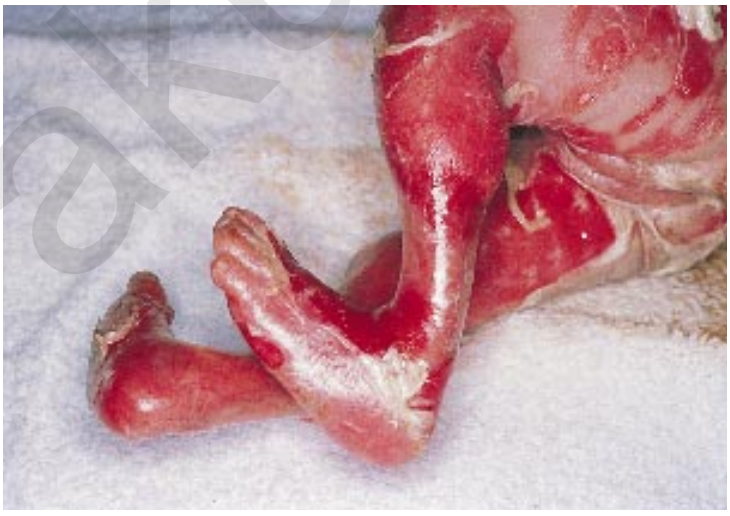

Figure 1.213. Epidermolysis bullosa letalis (junctional epidermolysis bullosa, Herlitz's disease) in an infant with generalized involvement of the skin. Note the massive involvement of the lower extremities showing the denudation, scarring, and contractures. In this form of epidermolysis bullosa, the skin separates in the lamina lucida of the dermal-epidermal junction and blistering leads to mild atrophic changes. Junctional epidermolysis bullosa is the most severe form of epidermolysis bullosa. It is characterized by blistering and large erosions, mainly on the buttocks, trunk, and scalp without scarring unless complicated by secondary infection. Approximately 50% of these infants die within the first 2 years of life; some survive into adulthood. Therefore, recently the term "letalis" has not been used.

1.214

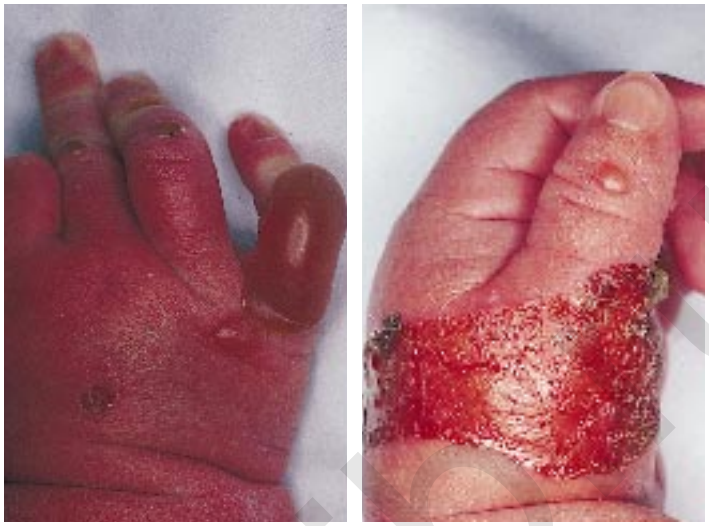

Figure 1.214. In transient bullous dermolysis of the newborn, the lesions are present at birth or shortly thereafter. With the bullous appearance of the lesions, epidermolysis bullosa should be considered in the differential diagnosis, but the family history and rapid regression of the lesions can confirm the diagnosis of transient bullous dermolysis of the newborn. The sibling of this infant had similar lesions at birth. In the figure on the left note the large bullous lesions on the 5th finger of the right hand. There were similar lesions on the left hand at birth. In the figure on the right note the healing of the lesions 5 days after birth.

SCALING DISORDERS

Different abnormalities of the stratum corneum are included under the general heading "ichthyosis." These conditions all involve faulty keratinization. The name is derived from the small plates of thickened epidermis yielding a pattern similar to the scales of a fish.

1.215

Figure 1.215. This postmature infant is an example of a so-called "collodion baby." Collodion babies are seen in postmaturity, lamellar ichthyosis, and congenital ichthyosiform erythroderma. The term "collodion" is used because of the varnished (glistening parchment-like) appearance of the skin which is similar to that resulting from collodion applied to the skin. This infant was postmature and the skin improved rapidly.

1.216

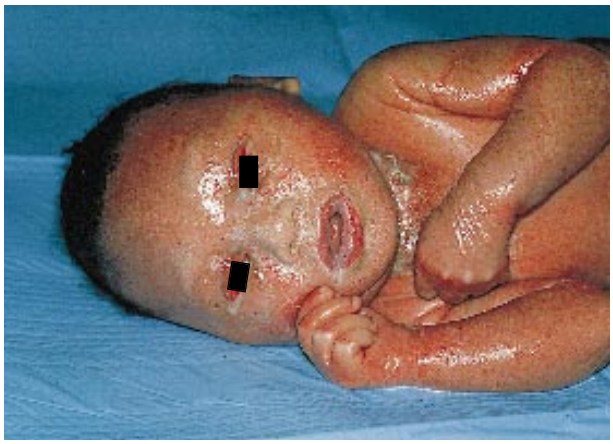

Figure 1.216. Another example of a collodion baby is this infant with lamellar ichthyosis who was born encased in a membrane. In addition to the collodion appearance of the skin, note the ectropion (eversion of the eyelids with exposure of the palpebral fissure) and eclabium (eversion of the lips which causes inability to suck) which occur as a result of the puckering of the skin, and the hyperkeratosis of the palms and soles. Mobility of the infant may be limited by the tightness of the membrane and also respiratory difficulty may occur due to restriction of chest expansion until spontaneous peeling begins in the first few days. The cutaneous covering dries out and is gradually shed in large sheet-like layers leaving a residual redness and hyperkeratosis. Lamellar ichthyosis is inherited as an autosomal recessive trait with two variants: the classic, more severe form of lamellar ichthyosis, and a milder erythrodermic variant (non-bullous ichthyosiform erythroderma). (Levy, M., Moise, K.)

1.217

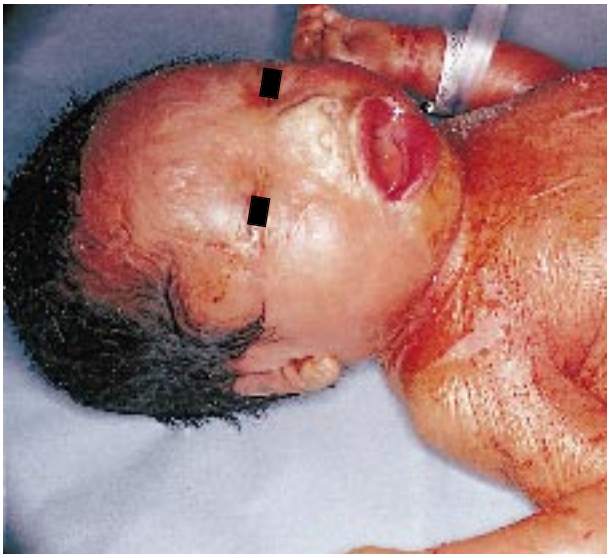

Figure 1.217. Another infant with a milder form of lamellar ichthyosis in which the parchment-like appearance of the skin is not as generalized. The skin develops widespread scaliness which may result in a generalized scaly erythroderma. If scaling and erythroderma are extensive, there may be excessive fluid loss resulting in hypernatremia, dehydration, and temperature instability. These infants are also more susceptible to infection.

1.218

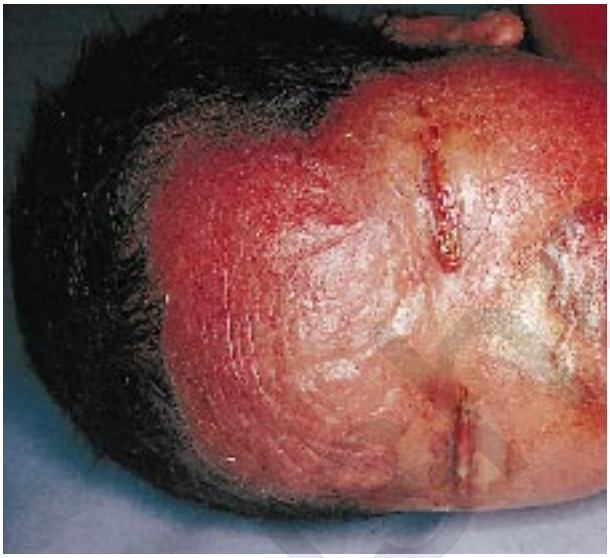

Figure 1.218. Close-up of the face of the same infant as in Figure 1.217, showing the parchment-like appearance of the skin and the mild ectropion.

1.219

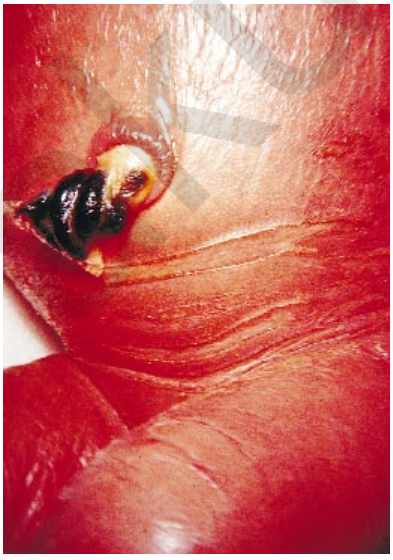

Figure 1.219. Close-up of the abdominal wall and thigh of the same infant as in Figures 1.217 and 1.218 with lamellar ichthyosis. Note the ichthyotic appearance of the skin, particularly in the upper abdomen, and the marked fissuring of the skin below as a result of spontaneous peeling. The underlying skin may be normal or may scale and form a new membrane. Lamellar scales are most prominent over the face, trunk, and extremities. Nail involvement is variable.

1.220

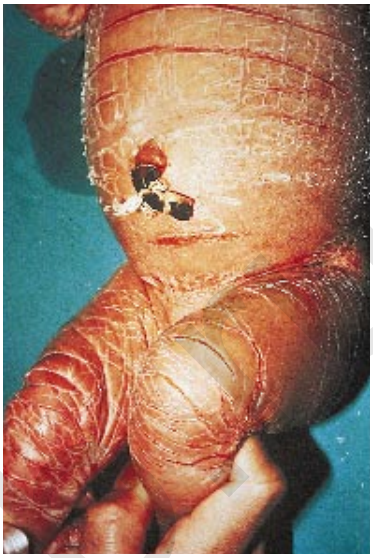

Figure 1.220. Congenital ichthyosis may present as a hyperkeratotic form in which widespread scaling occurs frequently with underlying erythroderma.

1.221

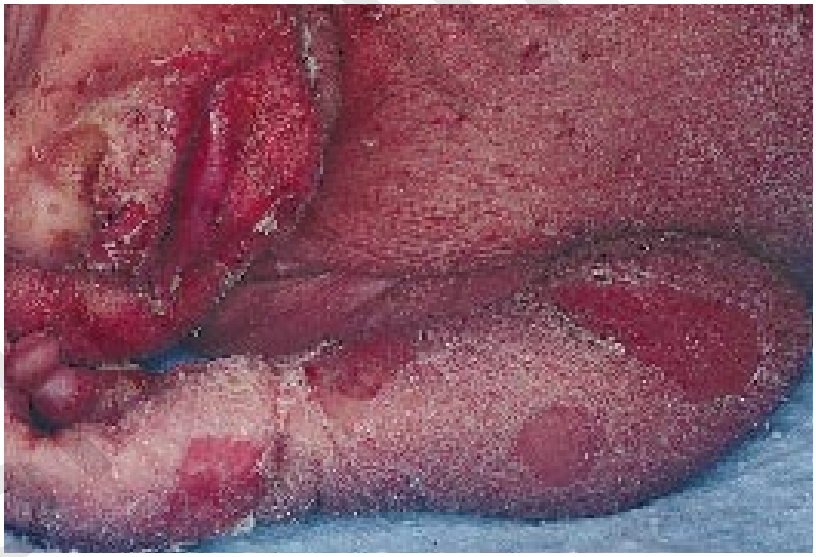

Figure 1.221. In bullous congenital ichthyosiform erythroderma (epidermolytic hyperkeratosis) there is a combination of bullous lesions, erythema, and desquamation. The presence of bullae is highly characteristic of this disorder. The blisters occur in crops and vary from 0.5 cm to several cm in diameter. They are superficial, tender, and when ruptured leave raw denuded areas. The bullous lesions present at birth and result in the erythema and scaling as noted here. The differential diagnosis includes epidermolysis bullosa, toxic epidermal necrolysis, and the different types of ichthyosis.

1.222

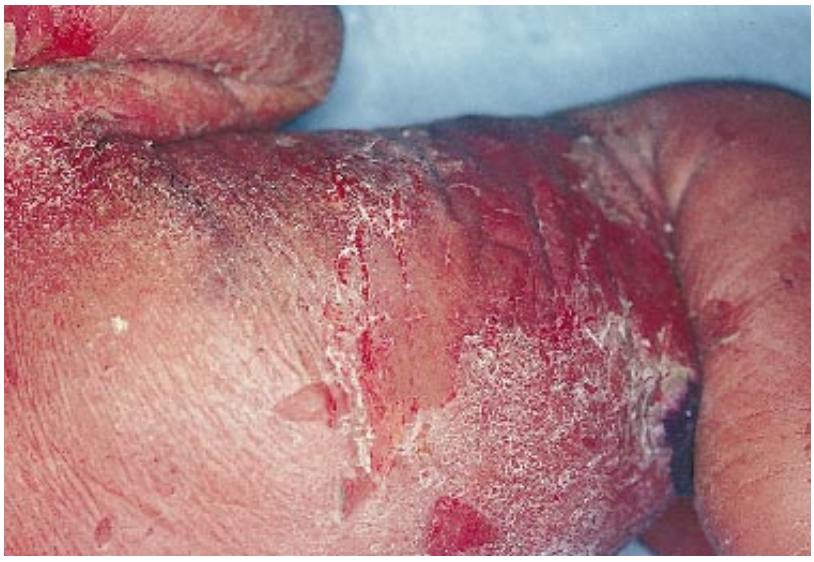

Figure 1.222. The torso of the same infant as in Figure 1.221 showing the typical erythema and desquamation following rupture of the bullous lesions. Improvement is rapid in these infants and with healing a generalized hyperkeratosis may remain. This consists of thick grayish-brown scales which cover most of the skin surface especially the flexural creases and intertriginous areas which may show marked involvement often with furrowed hyperkeratosis.

1.223

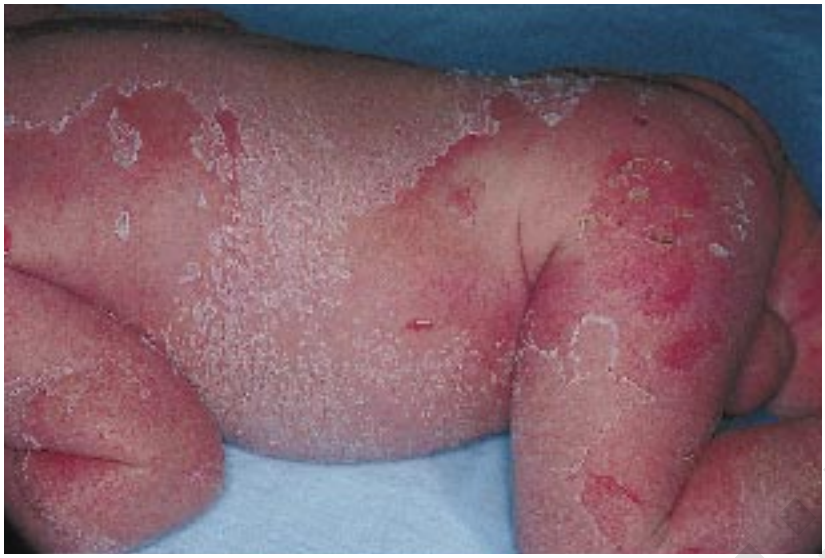

Figure 1.223. Another example of a milder form of the bullous congenital ichthyosiform erythroderma.

1.224

Figure 1.224. Harlequin fetus (congenital ichthyosis) is the most severe form of ichthyosis. It is an autosomal recessive condition which has generally been regarded as being incompatible with life. There is a tight constricting integument with a leather-like consistency. The skin, in addition to being thick and rigid, is cracked and hard with deep crevices. Survival is rare, with death occurring as a result of respiratory insufficiency due to thoracic rigidity, and infection. The harlequin fetus often has unexplained fever and failure to thrive.

1.225

Figure 1.225. Close-up of the head and upper trunk of the same infant as in Figure 1.224. Note the thick, dry, rigid, hardened, cracked skin with deep crevices. The division of the thickened grey- to yellow-colored skin into polygonal, triangular or diamond-shaped plaques by the deep reddish to purple fissures has been said to simulate the traditional costume of a harlequin. The skin has been likened to the bark of a tree, crocodile skin, or Moroccan leather.

1.226

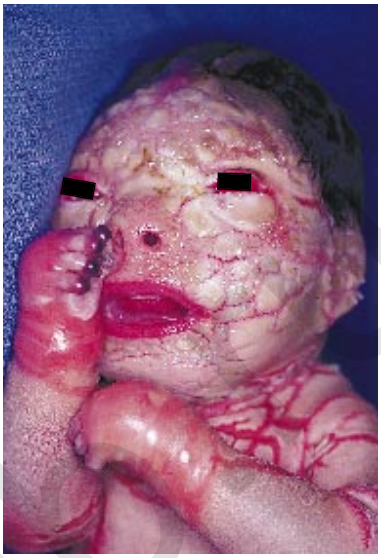

Figure 1.226. A close-up view of the face and left upper extremity of the same infant as in Figure 1.224 and 1.225. Note the marked ectropion resulting from rigidity of the skin about the eyes with conjunctival redness and edema. There is eclabium with some cracking and fissuring at the corners as a result of the unyielding skin. The right hand is severely affected and has resulted in gangrene of the fingers. The left hand has similar involvement.

1.227

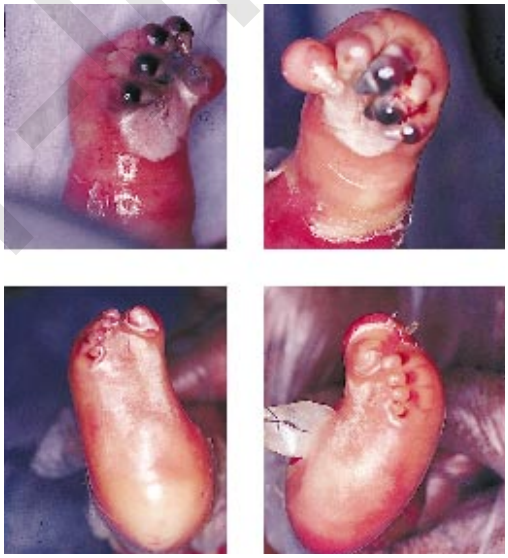

Figure 1.227. The hands and feet of the same harlequin fetus as in Figures 1.224, 1.225 and 1.226 show severe deformities which have occurred as a result of the tight constricting integument and compromise of the ectodermal structures, resulting in gangrene of the fingers and hypoplastic toes. The hands and feet are ischemic, hard, and waxy, often with poorly developed digits and an associated rigid and claw-like appearance of the limbs. The nails may be hypoplastic or absent.

1.228

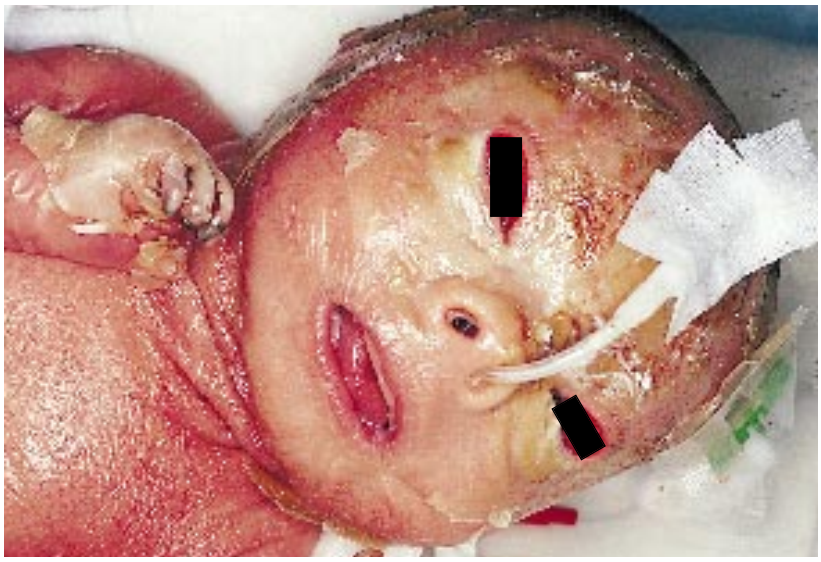

Figure 1.228. Another example of a harlequin fetus. Note the parchment-like skin, the ectropion, and eclabium. The mouth with the eclabium sometimes has a fish-like appearance. The unyielding skin has resulted in cracking and fissuring at the corners of the mouth and the left hand is severely affected. This infant was treated with the oral administration of etretinate and topical use of Eucerin™. Following use of this approach there has been prolonged survival in a few infants.

1.229

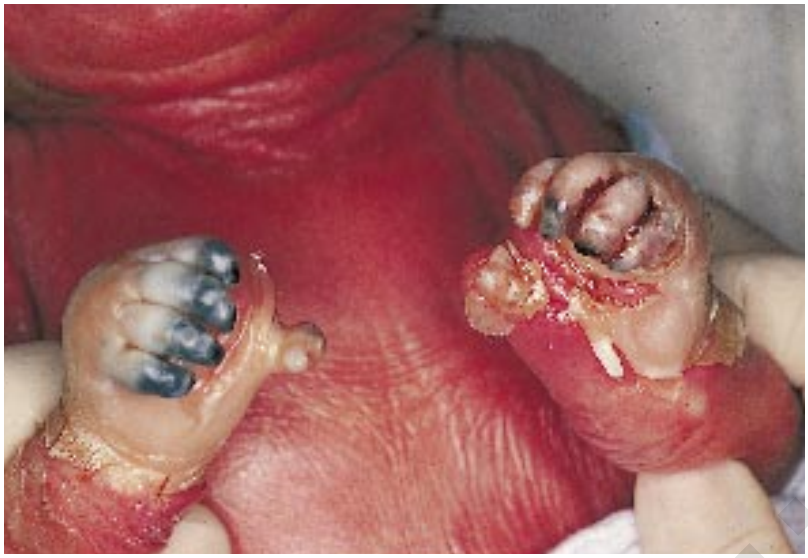

Figure 1.229. The hands of the same infant as in Figure 1.228. Note the pale, waxy, firm appearance and poorly developed digits which have become gangrenous. The nails may be hypoplastic or absent.

1.230

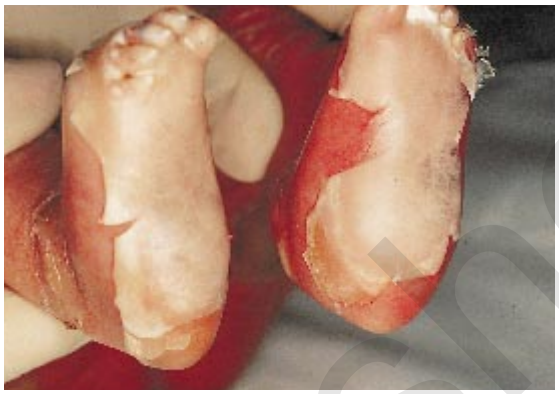

Figure 1.230. The feet of the same infant as in Figure 1.228 and 1.229 show the thick, rigid, hard, cracked skin and poorly developed toes with hypoplastic nails.

1.231

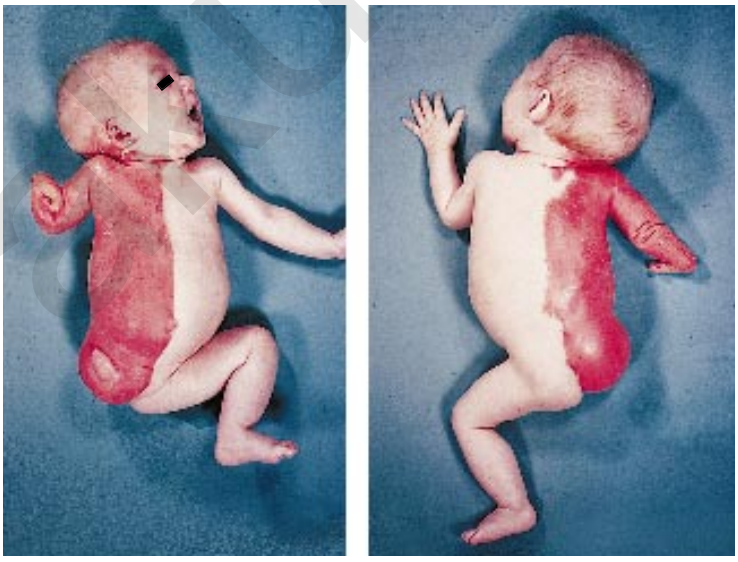

Figure 1.231. The CHILD syndrome is an X-linked dominant disorder (lethal to males) which is characterized by *c*ongenital *h*emidysplasia, with *i*chthyosiform erythroderma, and *l*imb *d*efects. The hallmark of the disorder is the sharp midline demarcation and the ipsilateral involvement of the skin and the extremities. The face is spared, and limb defects range in severity from hypoplasia of digits to complete agenesis of an extremity. In addition to the dermal and musculoskeletal involvement, other organs may be abnormal (viscera and occasionally the central nervous system).

1.232

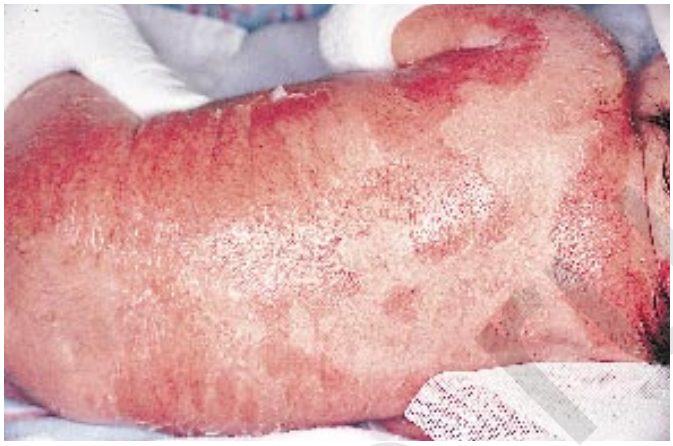

Figure 1.232. Following a spontaneous vaginal delivery in this term infant, desquamation of the skin was noted with the usual drying off in the delivery room. No bullae or blisters were noted. There was superficial desquamation over about 70% of the total body surface area. The Nikolsky's sign was positive. The diagnosis of "peeling skin syndrome" was confirmed by skin biopsy. This is an unusual congenital ichthyosis which is probably an autosomal recessive disease characterized by lifelong peeling of the epidermis with easy separation of the stratum corneum.

1.233

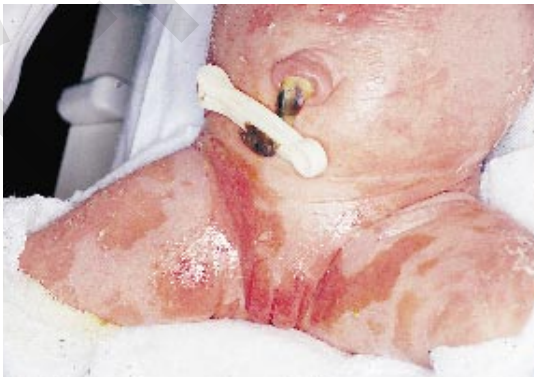

Figure 1.233. Another view of the same infant as in Figure 1.232 with the "peeling skin syndrome." This condition must be differentiated from non-bullous ichthyosiform erythroderma. Histopathologic features include intraepidermal separation between the stratum corneum and stratum granulosum. There may be a biochemical marker of moderate generalized aminoaciduria and low tryptophan levels.

OTHER DERMATOLOGIC PROBLEMS

1.234

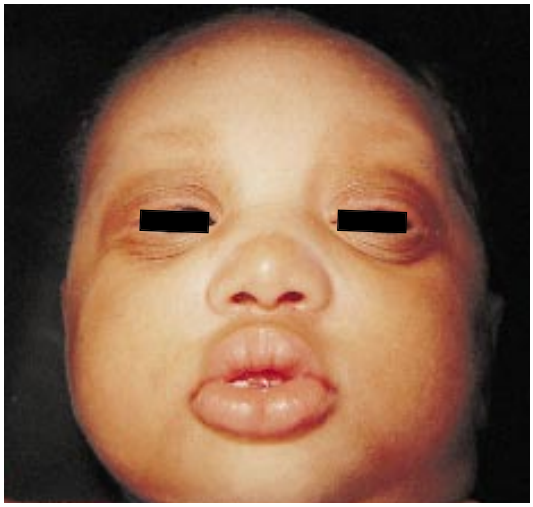

Figure 1.234. The typical facies of hypohidrotic (anhidrotic) ectodermal dysplasia is seen in this infant. Note the alopecia, absent eyebrows and eyelashes, square forehead with frontal bossing, hyperpigmented wrinkles around the eyes, flattened nasal bridge, and large conspicuous nostrils. There are wide cheek bones with depressed cheeks, thick everted lips, a prominent chin, and the ears may be small and pointed. These infants have a thin dry skin, decreased sweating, decreased tearing, and abnormal dentition. The nails are defective in a large percentage of these patients in that they may be thin, brittle, or ridged. If the absence of the sweat glands is generalized, they may have recurrent fever in high environmental temperatures.

1.235

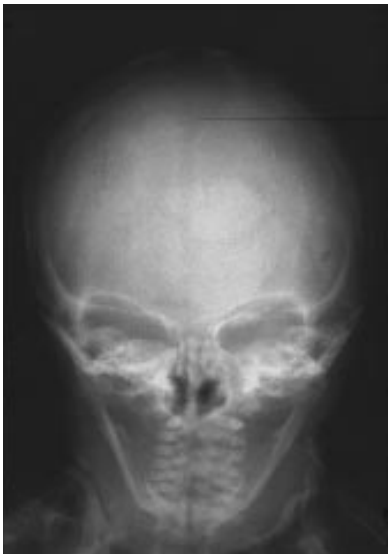

Figure 1.235. Radiograph of the face shows the typical hypoplasia of the maxillary alveolar processes and the lack of teeth (one of the hallmarks of hypohidrotic ectodermal dysplasia). Ectrodactyly-ectodermal dysplasia-clefting (EEC) syndrome should be considered in the differential diagnosis.

1.236

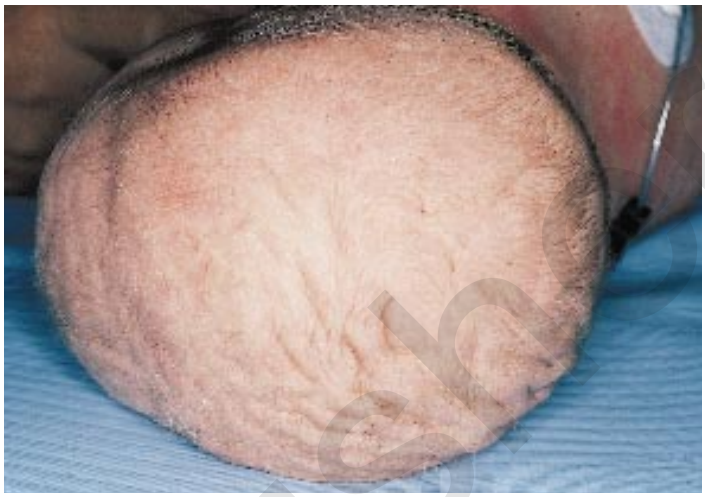

Figure 1.236. Cutis verticis gyrata is an unusual disorder characterized by coarse furrowing, most commonly of the vertex of the scalp and posterior aspect of the scalp and neck. The vertex usually has anteroposterior furrows whereas on the forehead and occiput they are transverse. The hair tends to be sparse on top of the folds and more profuse in the furrows. The entire scalp or only a small patch may have parallel folds of scalp skin furrowing with remarkable resemblance to the convolutions of the brain.

1.237

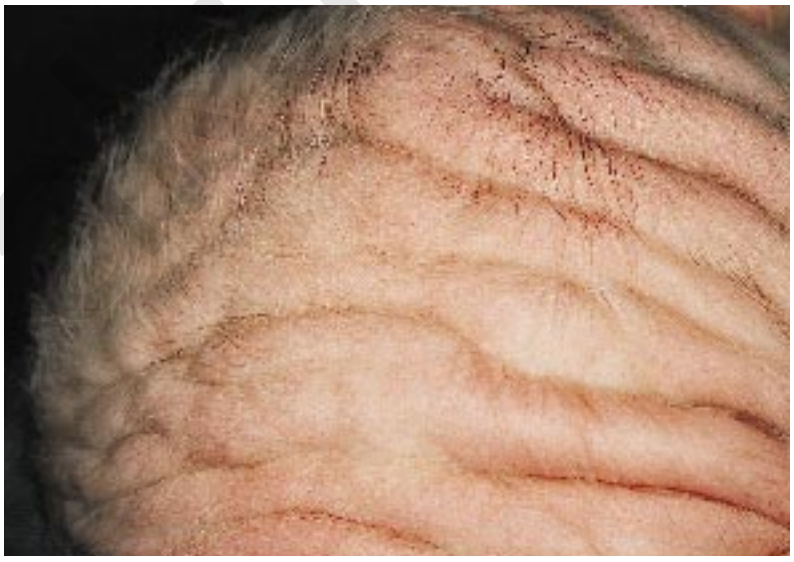

Figure 1.237. A close-up of cutis verticis gyrata in the same infant as in Figure 1.236. The condition is caused by an increase in dermal collagen and, as a result, excessive skin may buckle and form furrows and ridges that resemble gyri of the cerebral cortex. The condition may occur as a primary disorder without other associated abnormalities or it may be a manifestation of other pathology including Ehlers-Danlos syndrome, tuberous sclerosis, Apert's syndrome, hyperpituitarism, or pachydermomyositis.

1.238

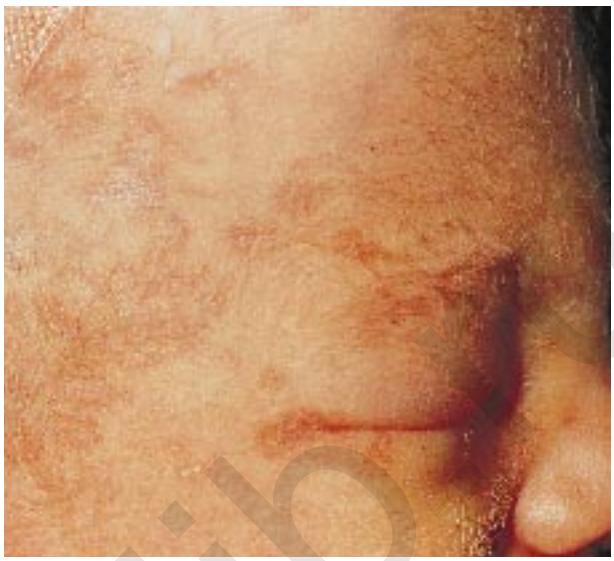

Figure 1.238. Neonatal lupus erythematosus is a unique variant of lupus erythematosus which occurs in infants born to mothers with or having a tendency for systemic lupus erythematosus, rheumatoid disease, etc. The majority of infants born to these mothers are usually normal, but they may have a lupus-like rash and lupus-associated hematologic and serologic abnormalities. The cutaneous lesions appear from birth (in two-thirds of cases) until about 12 weeks of age. The majority of infants have spontaneous resolution of the cutaneous lesions by about 6 to 12 months. In this infant note the diffuse erythema over the face and scalp, the scaly atrophic somewhat hypopigmented discoid lesions, and the alopecia which is a common finding in this disease. Cutaneous lesions of neonatal lupus erythematosus generally appear on the head and neck, extensor surfaces of the arms, and less frequently in other areas.

1.239

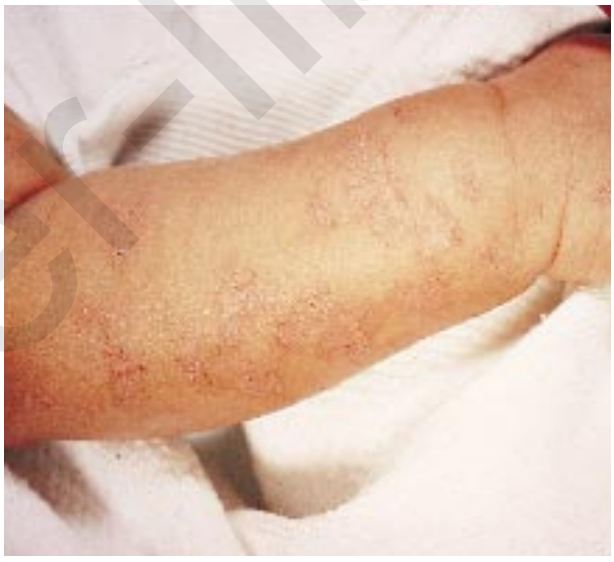

Figure 1.239. Sharply demarcated violaceous discoid lesions on the extensor surface of the forearm in another infant with neonatal lupus erythematosus. In neonatal lupus erythematosus about 15 to 30% of infants have congenital atrioventricular block, a complication which is usually irreversible with a high mortality rate (20 to 30% in the first few months of life.) During pregnancy the fetal ECG can be checked for heart block. Other systemic complications include cardiac malformations, hepatosplenomegaly, leukopenia, and thrombocytopenia. These infants have a positive Coombs' test and anti-Ro (SSA) antibodies are found in 95% of affected mother-infant pairs. Neonatal lupus was originally believed to be a transient disease but it is now apparent that continuing systemic involvement may occur.

1.240

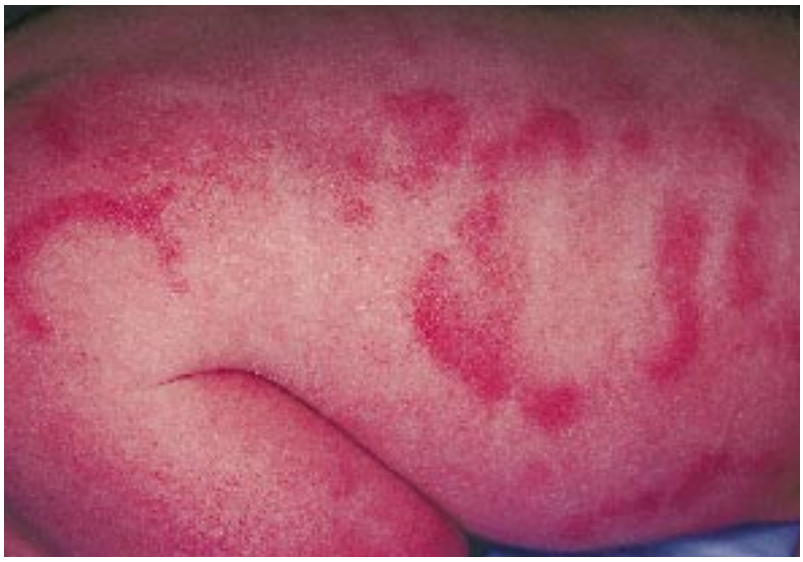

Figure 1.240. In erythema annulare centrifugum the lesions occur especially on the body, develop quickly, and can last for weeks. The lesions are erythematous and edematous, are of varying size and are partly ring-shaped in form. The centers of the lesions tend to fade and the lesions may spread out centrifugally and have a slightly scaly edge. The underlying etiology of this condition may be autoimmune disorders in the mother (such as lupus erythematosus), hypersensitivity to drugs, or fungal infection.

1.241

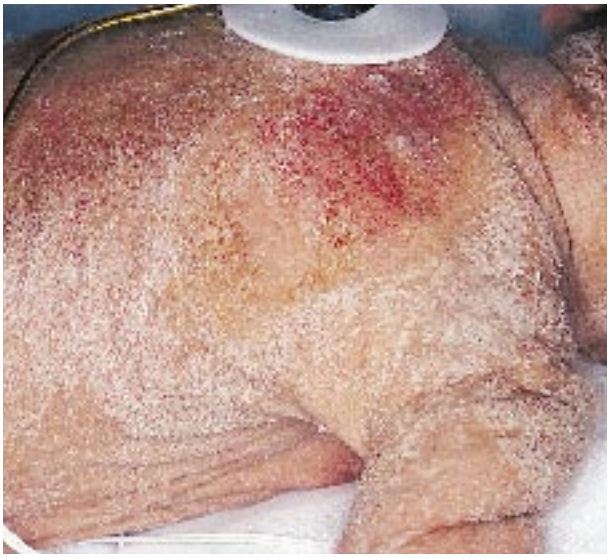

Figure 1.241. Exfoliative erythroderma occurred in this very small premature infant (birthweight 700 g) at 4 weeks of age following a blood transfusion for anemia at 3 weeks of age. He had a severe reaction and was critically ill for several days. There was marked blood eosinophilia and a diagnosis of graft-versus-host reaction was made. In acute graft-versus-host disease (GVHD) following transfusion, the findings include a generalized erythematous maculopapular exanthem with fine desquamation which later becomes a rough lamellar desquamation. There is no blister formation, and detachment of the nails may occur. Acute GVHD also affects the liver and may give abnormal liver function tests.

1.242

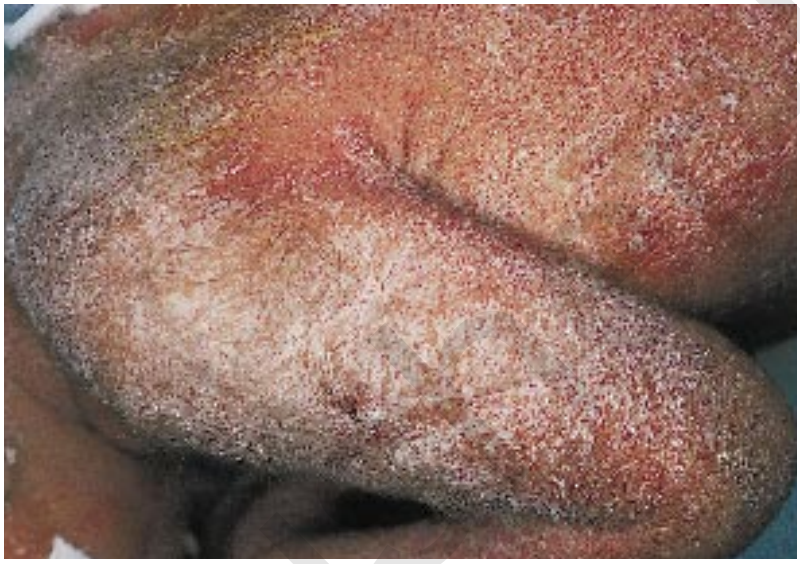

Figure 1.242. Close-up of the exfoliative erythroderma in the same infant as in Figure 1.241. This infant died at the age of 10 weeks, and at autopsy was found to have a primary immunodeficiency syndrome. Cutaneous manifestations of acute GVHD disease must be distinguished from drug eruptions or viral exanthems.

1.243

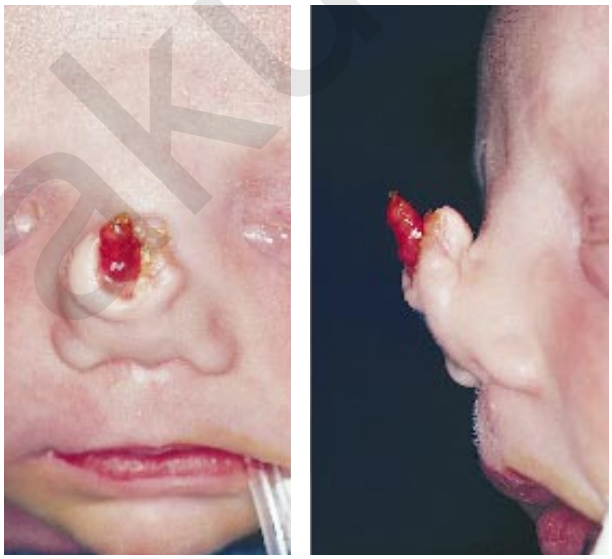

Figure 1.243. The diagnosis of a nasal dermoid in this infant was confirmed by biopsy. Dermoids are usually present at birth and occur particularly along the lines of embryonic fusion. They are most common on the head, especially around the eyes and the nose. Dermoid cysts may be attached to underlying structures. In any midline nasal mass, intracranial extension is common; thus, prior to removal of the mass, intracranial involvement should be excluded.

1.244

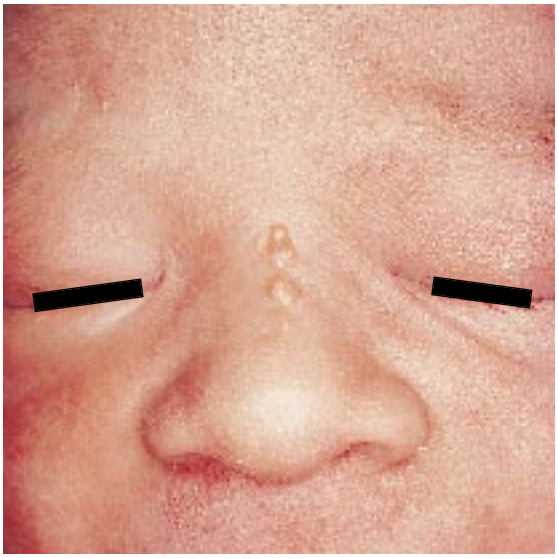

Figure 1.244. The diagnosis of a hamartoma of hair follicle origin was established by biopsy of the midline lesions of the nose in this infant.

1.245

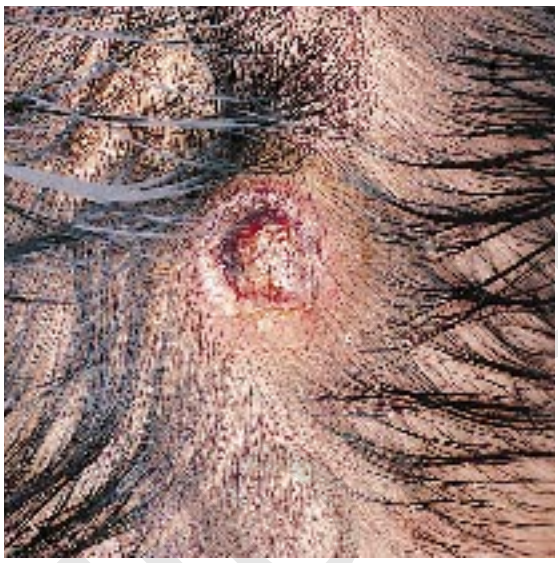

Figure 1.245. Congenital self-healing reticulohistiocytosis (Hashimoto-Pritzker disease) is a rare disease usually present at birth or within the first few days of life. It is characterized by solitary or multiple reddish-brown, pink, or purplish papulovesicular lesions mainly on the scalp, face, trunk, and extremities. They tend to break down in the center, form ulcerated craters, and involute spontaneously within 2 to 3 months leaving white atrophic scars. Although the course is benign and self-limiting, it is important to differentiate this condition from histiocytosis X and other histiocytic conditions. Diagnosis is confirmed by skin biopsy.

1.246

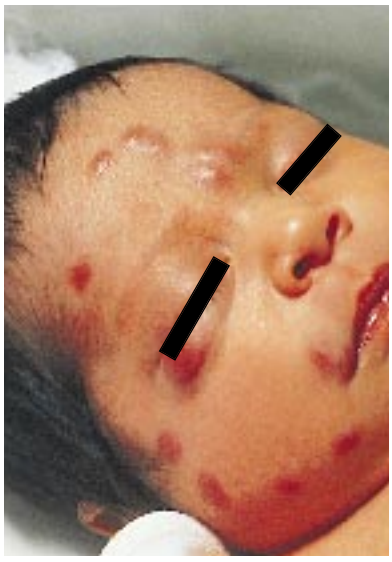

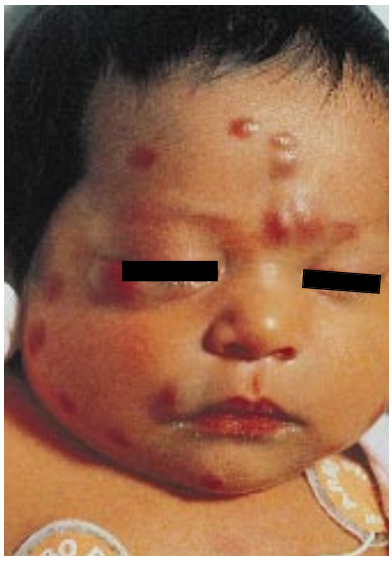

Figure 1.246. In juvenile xanthogranulomatosis the lesions are present at birth. They are characterized by solitary or multiple yellow to reddish-brown papules and nodules of the face, scalp, neck, and sometimes the sublingual areas and the proximal portions of the extremities or trunk. The lesions may enlarge and become bright yellow as they mature. Spontaneous regression usually occurs in the first year of life. Diagnosis is confirmed by biopsy which shows histiocytes of the non-Langerhans' cells and the presence of Touton giant cells. The lesions are harmless but should not be overlooked since there is an apparent association with neurofibromatosis. (Kenny, J.)

1.247

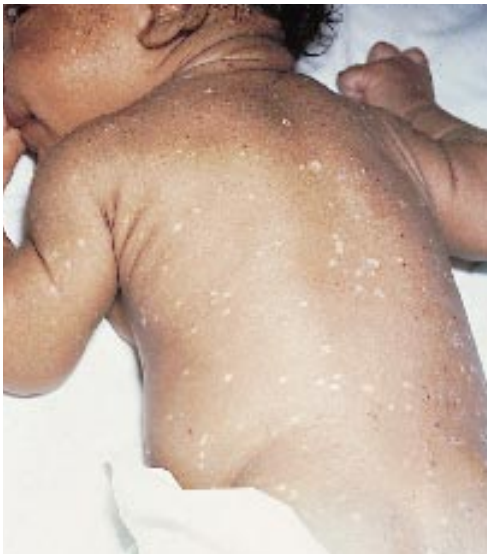

Figure 1.247. Skin lesions, present at birth in this infant with histiocytosis X, on biopsy showed the typical finding of the presence of histiocytes of the Langerhans' cell type and eosinophilia. The term "congenital histiocytosis" includes Letterer-Siwe disease, Hand-Schüller-Christian disease, and eosinophilic granuloma. These conditions are now grouped together as histiocytosis X.

1.248

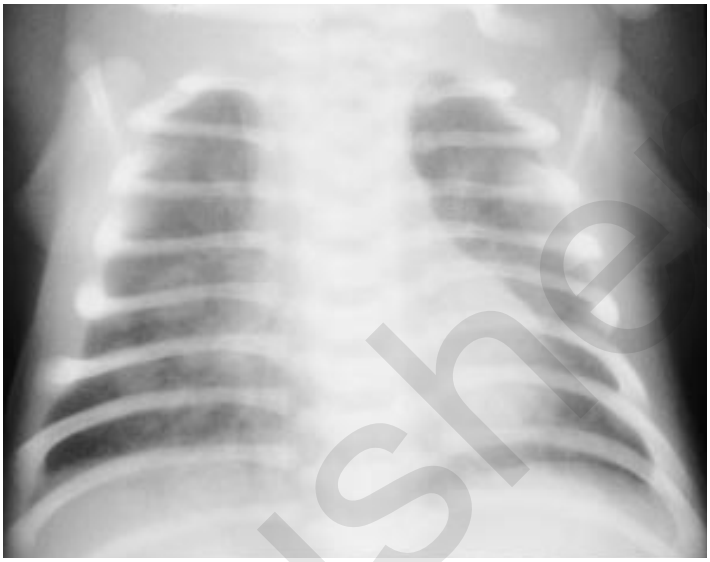

Figure 1.248. Chest radiograph in an infant at the age of 3 days with histiocytosis. Note the infiltrative coin-like lesions which are typical with pulmonary involvement in histiocytosis X. The presence of pulmonary and other systemic involvement worsens the prognosis.

1.249

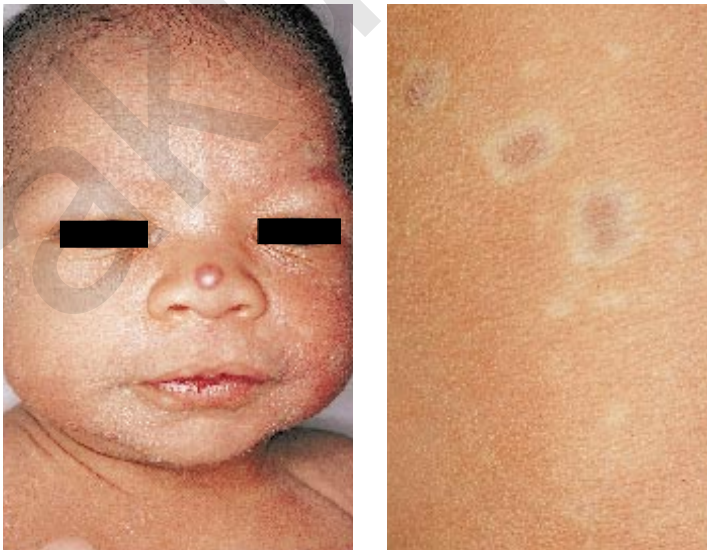

Figure 1.249. In this infant with congenital generalized fibromatosis, on the left note the lesion on the nose and the purplish area surrounded by a pale halo above the left eyebrow. On the right is a close-up of the lesions on the back of the same infant. The infants may also have firm hard nodules in the skin and subcutaneous tissue. In congenital generalized fibromatosis it is necessary to check the long bones and lungs for systemic involvement.

1.250

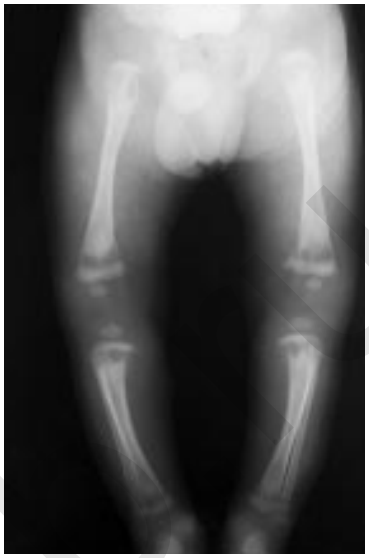

Figure 1.250. Radiograph of the long bones in another infant with congenital generalized fibromatosis showing the areas of erosion due to the presence of generalized fibromata.

1.251

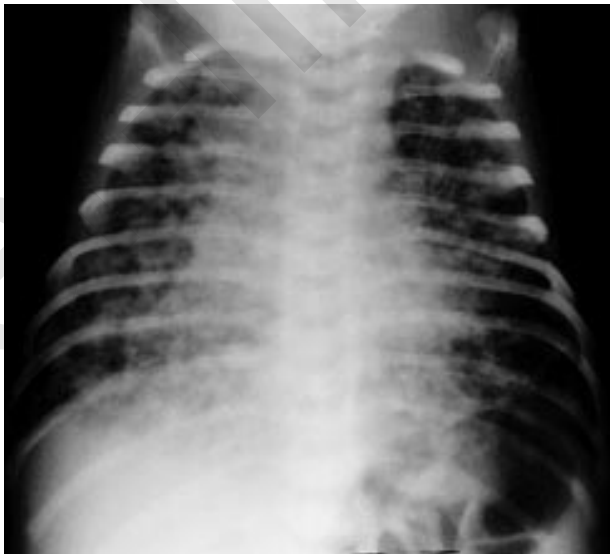

Figure 1.251. Chest radiograph showing extensive pulmonary involvement in an infant with congenital generalized fibromatosis. The presence of pulmonary involvement signifies a poor prognosis.

Chapter 2
Perinatal Infection

The immediate and long-term effects of perinatal infection are a major problem throughout the world. Perinatal infection is relatively common among the over 4 million births per year in the United States but the incidence is dependent upon the organism. One percent of newborn infants excrete cytomegalovirus. Fifteen percent are infected with *Chlamydia trachomatis*; one-third develop conjunctivitis and one-sixth, pneumonia. One to eight per 1,000 live births develop bacterial sepsis. In utero or perinatal infection with herpes simplex virus, *Toxoplasma gondii* and varicella-zoster virus occurs in about 1 per 1,000 live births and the sequelae may be severe. In-utero acquired infection may result in resorption of the embryo, abortion, stillbirth, malformation, intrauterine growth retardation, prematurity, and the numerous untoward sequelae associated with chronic infection. Infection acquired at or soon after birth may lead to death or persistent postnatal infection. Some infections may be inapparent at birth and present years later with signs (e.g., choreoretinitis of *T. gondii*, hearing loss of rubella virus, and immunologic defects of HIV). Early diagnosis and aggressive treatment of infection during pregnancy may lower the associated morbidity and mortality rates substantially.

2.1 BACTERIAL INFECTION

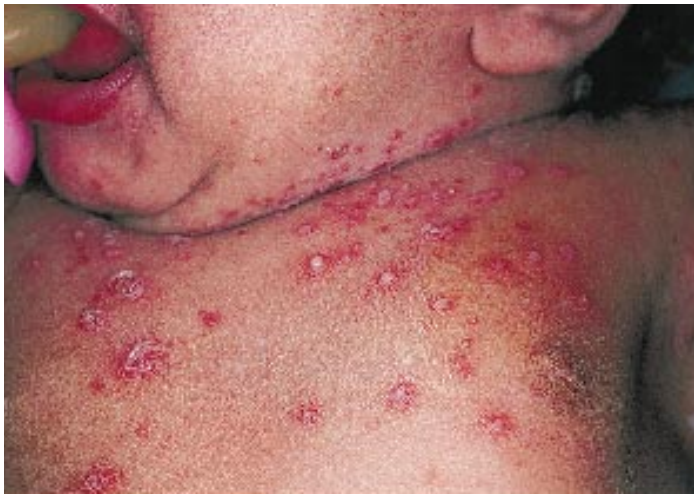

Figure 2.1. Staphylococcal furunculosis developed in this infant at the age of 6 days. A Gram stain of the material in the lesions showed numerous polymorphonuclear leukocytes and gram-positive cocci. The culture grew *Staphylococcus aureus*. Included in the differential diagnosis of these lesions are transient neonatal pustular melanosis and herpes.

2.2

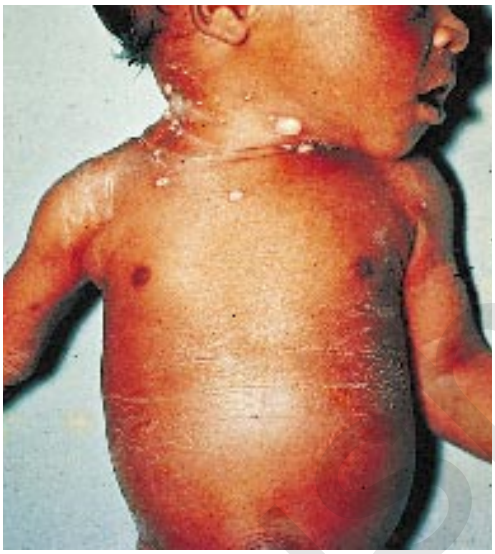

Figure 2.2. Staphylococcal pyoderma of the neck in an infant at the age of 8 days.

2.3

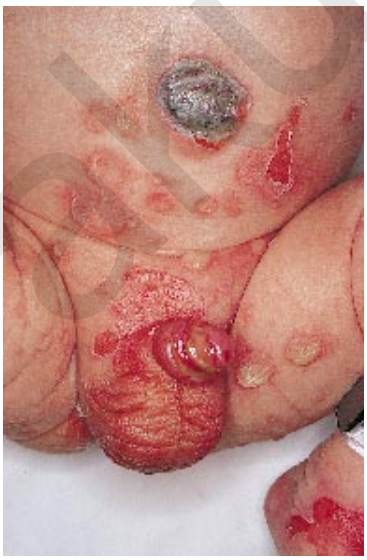

Figure 2.3. Bullous impetigo (pemphigus neonatorum) in a newborn infant at the age of 6 days. This infection may occur as early as the second day or as late as two weeks of life and may demonstrate both bullous and impetiginous lesions. It is most commonly due to a staphylococcal infection but, on occasion, is caused by *Streptococcus*. The lesions are more common in moist, warm areas such as the axillary folds of the neck or the groin and present as superficial bullae which are wrinkled, become flaccid, and rupture easily producing ulcers which become crusted. Note the impetigo of the umbilical area.

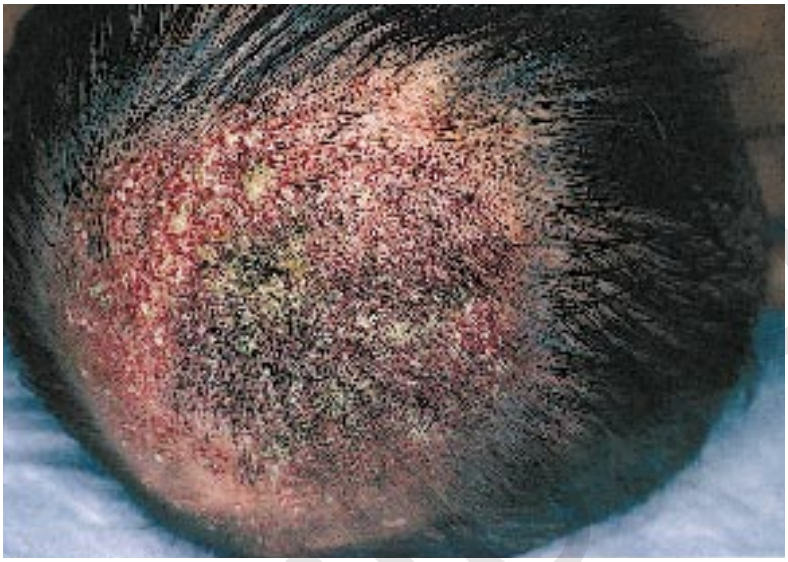

2.4

Figure 2.4. Scalp abscesses developed at 12 hours of age. Note the distribution over the area of the caput. In such an infant the diagnoses of herpes simplex and *Staphylococcus aureus* infection should be considered. Cultures from the lesions and the blood in this infant were positive for *Staphylococcus aureus*. The mother developed fever 24 hours postpartum, and *Staphylococcus aureus* was cultured from the episiotomy.

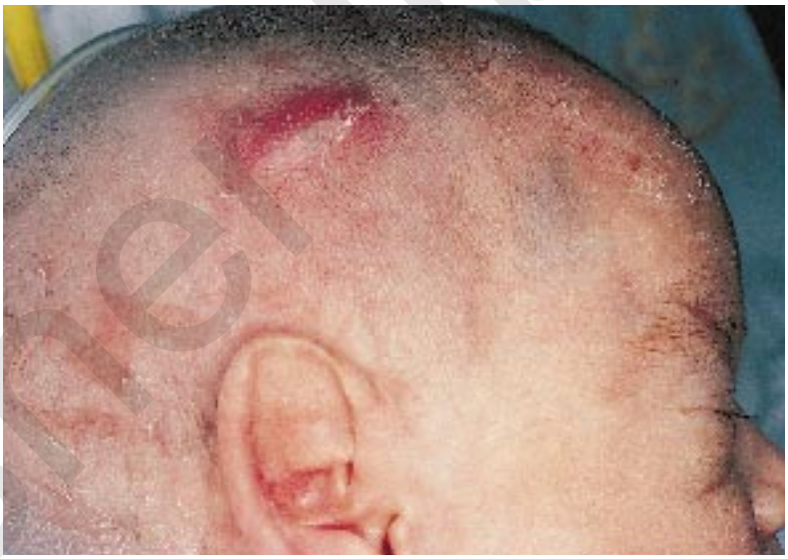

2.5

Figure 2.5. This nosocomial scalp abscess developed in a premature infant (birthweight 1000 g) at the age of 12 days. *Staphylococcus aureus* was cultured from both the abscess and the blood. The parietal area is the most frequent site for scalp abscess. Scalp abscesses frequently occur with the use of repeated scalp vein infusions.

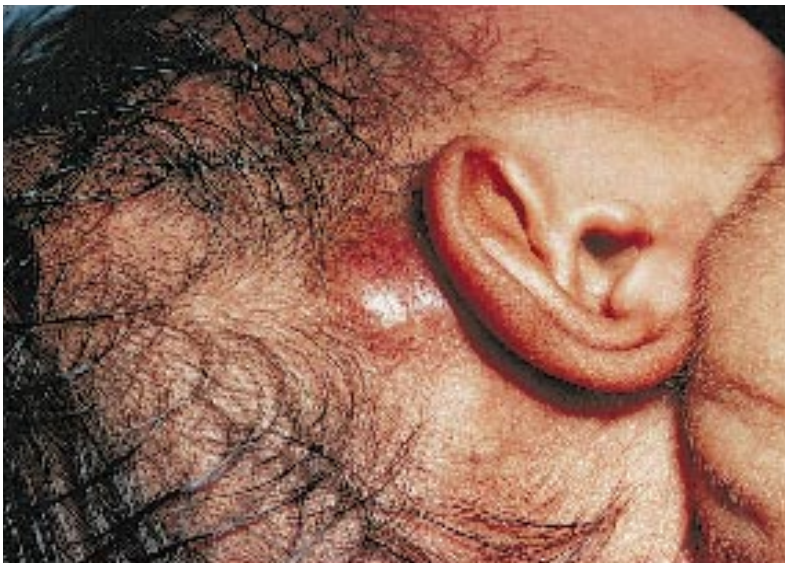

2.6

Figure 2.6. Postauricular scalp abscess in an infant due to *Staphylococcus aureus* infection as a result of forceps application.

2.7

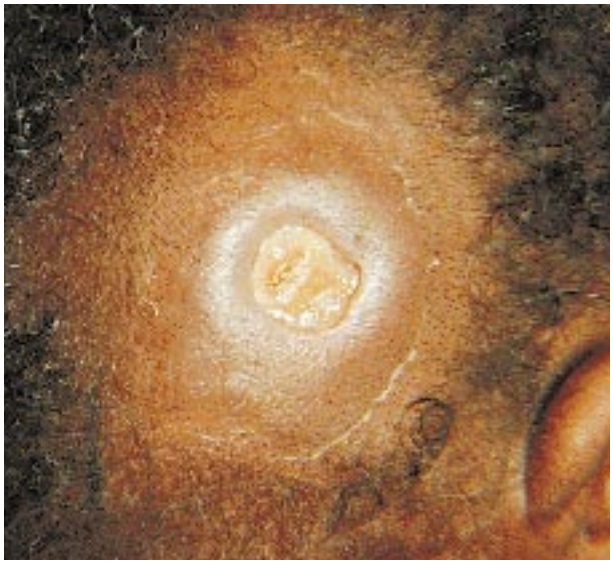

Figure 2.7. Healing staphylococcal abscess resulting from application of forceps during delivery. These usually are noted over the parietal area. Skin abrasions caused by application of forceps or scalp electrodes for fetal monitoring may become secondarily infected, resulting in the development of a scalp abscess.

2.8

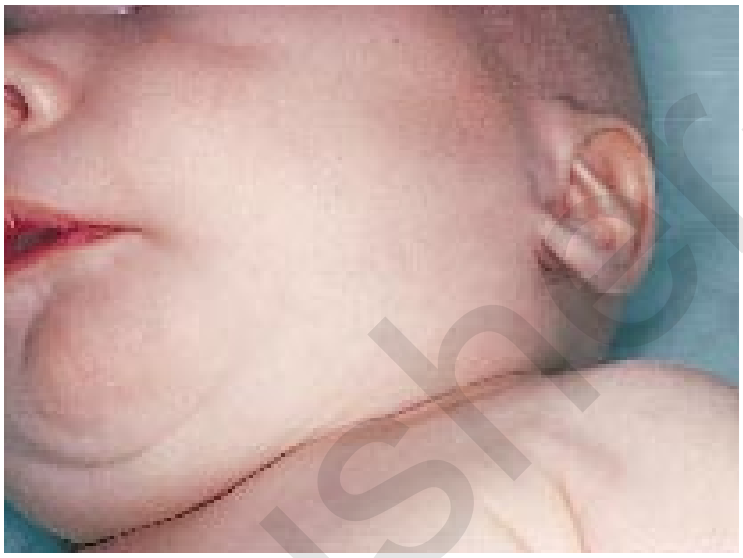

Figure 2.8. Staphylococcal parotitis in a two week old infant. Note the swelling over the parotid area.

2.9

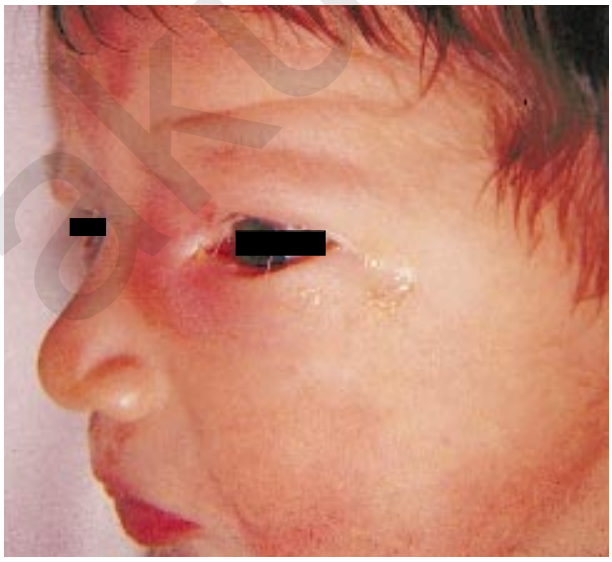

Figure 2.9. Acute staphylococcal dacryocystitis developed in this neonate at the age of 2 weeks. Note that in addition to the swelling over the lacrimal gland, there is conjunctival inflammatory change. Staphylococcal infection is the most common cause of this infection, but it may occur with infection by *Streptococcus* or *Neisseria*.

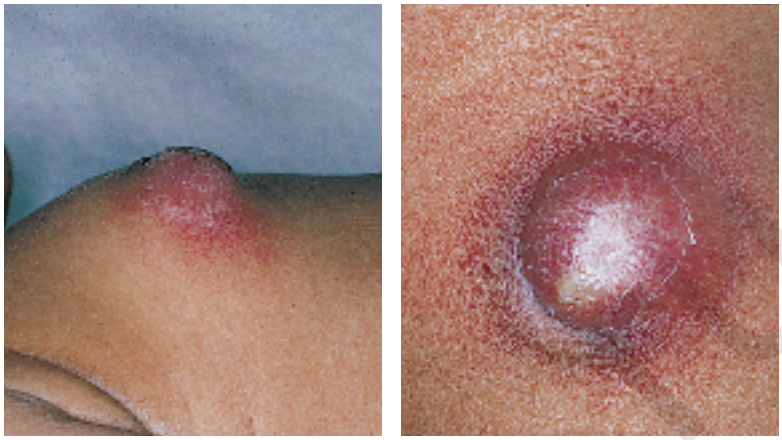

2.10

Figure 2.10. Breast abscess in a neonate due to *Staphylococcus aureus*. In the left figure note the infection as seen in the lateral view. A close-up of the abscess is shown in the right figure.

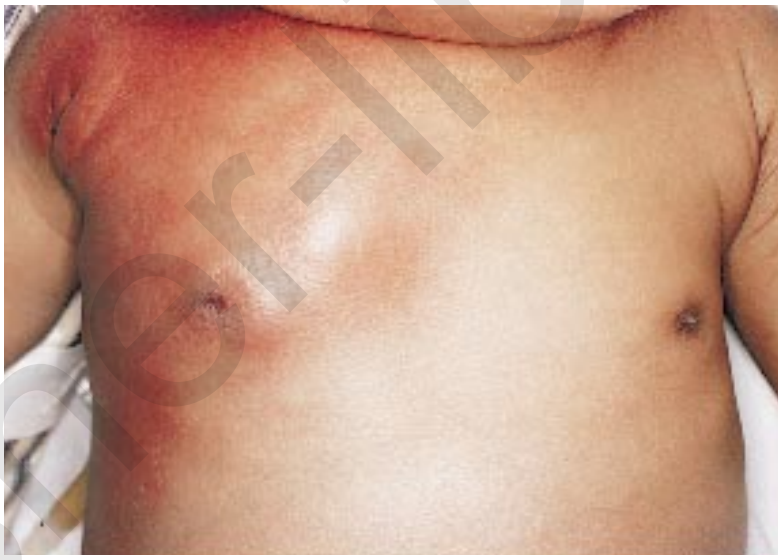

2.11

Figure 2.11. Mastitis of the right breast with abscess formation and cellulitis of the chest.

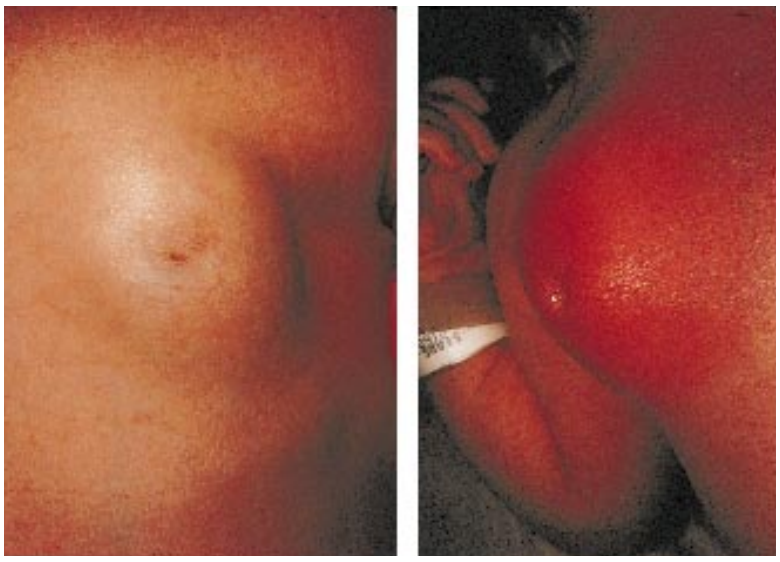

2.12

Figure 2.12. On the left note the normal physiologic engorgement of the breast. On the right there is a mastitis secondary to *Escherichia coli* infection. Although the most common cause of mastitis in the neonate is staphylococcal infection, other organisms may be responsible.

2.13

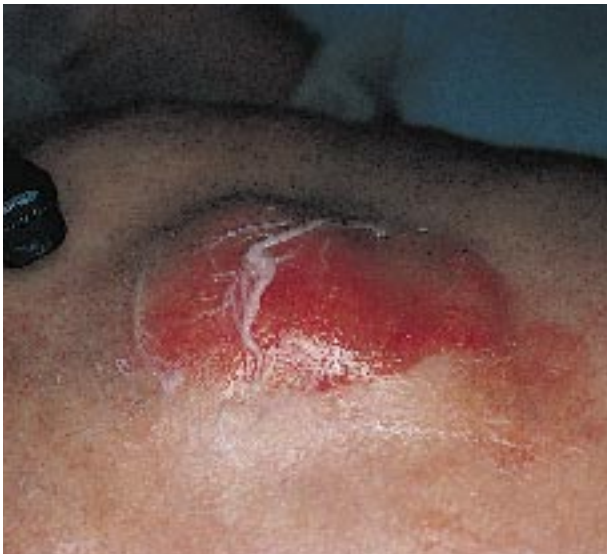

Figure 2.13. This large abscess over the xiphoid area developed at the age of 10 days in a neonate who had methicillin-sensitive *Staphylococcus aureus* sepsis.

2.14

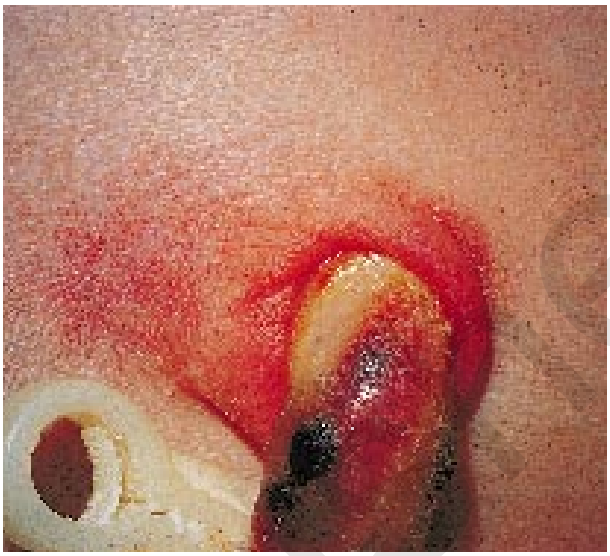

Figure 2.14. Staphylococcal omphalitis and funisitis in a neonate. The erythema of the skin surrounding the umbilical cord is due to omphalitis. Funisitis represents infection of the umbilical cord per se. Note the redness of the umbilical cord.

2.15

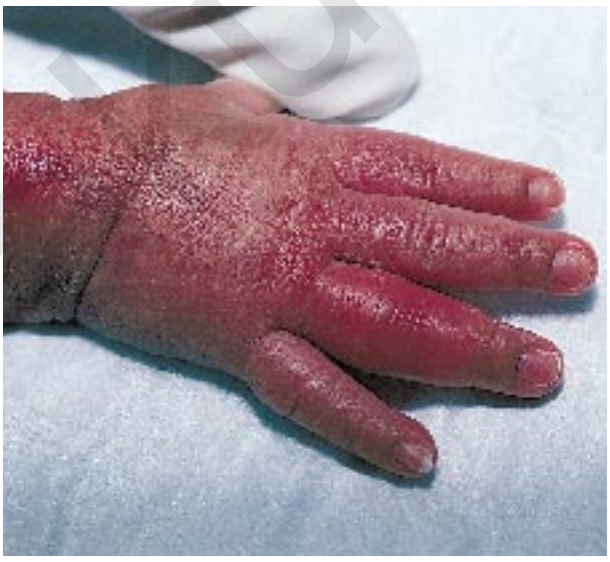

Figure 2.15. Nosocomial infection causing an abscess of the right wrist and cellulitis of the 4th finger in a premature infant (birth weight 1100 g) at the age of 35 days. This infant had methicillin-resistant *Staphylococcus aureus* bacteremia. There was no osseous involvement. The infant was successfully treated with vancomycin.

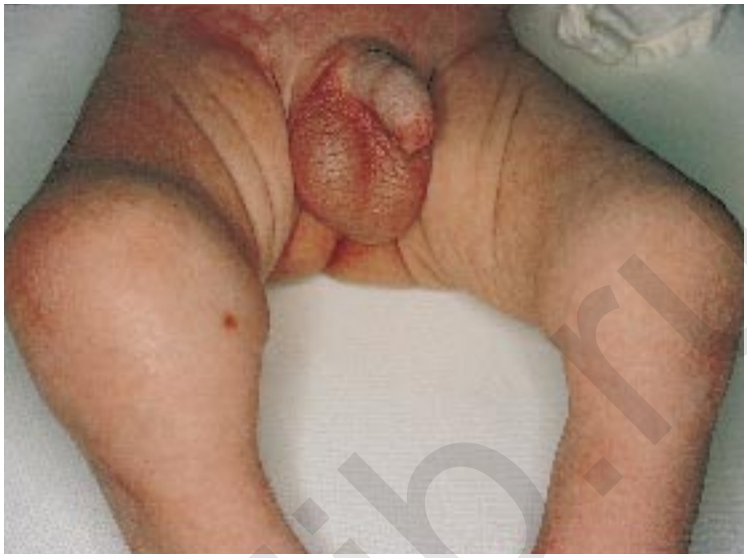

2.16

Figure 2.16. Acute osteomyelitis of the distal end of the right femur presenting with marked swelling of the right knee joint. Blood culture was positive for *Staphylococcus aureus*. The diagnosis of osteomyelitis must be excluded in any neonate with a swollen joint or who is reluctant to move a limb spontaneously. Neonatal osteomyelitis may occur 1) by direct inoculation, 2) by extension from infection in surrounding soft tissues (e.g., infected cephalhematoma), 3) by transplacental extension from maternal bacteremia (e.g., congenital syphilis), and 4) by blood-borne dissemination in neonatal septicemia (the major cause of neonatal osteomyelitis by metastatic seeding of the skeletal system through the nutrient arteries).

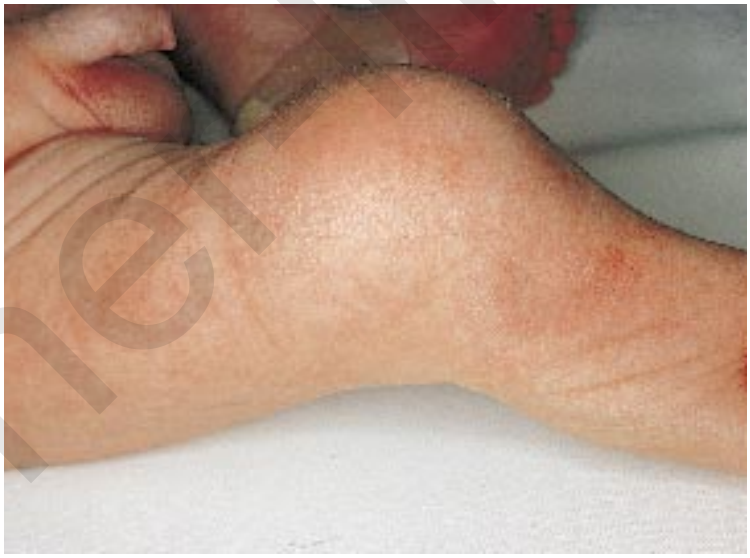

2.17

Figure 2.17. Lateral view of the right knee joint in the same infant demonstrates the marked joint swelling. The hips or knees or both are involved in 70% of cases of neonatal osteomyelitis. The higher incidence of sepsis in premature infants may contribute to the much higher incidence of osteomyelitis in premature infants.

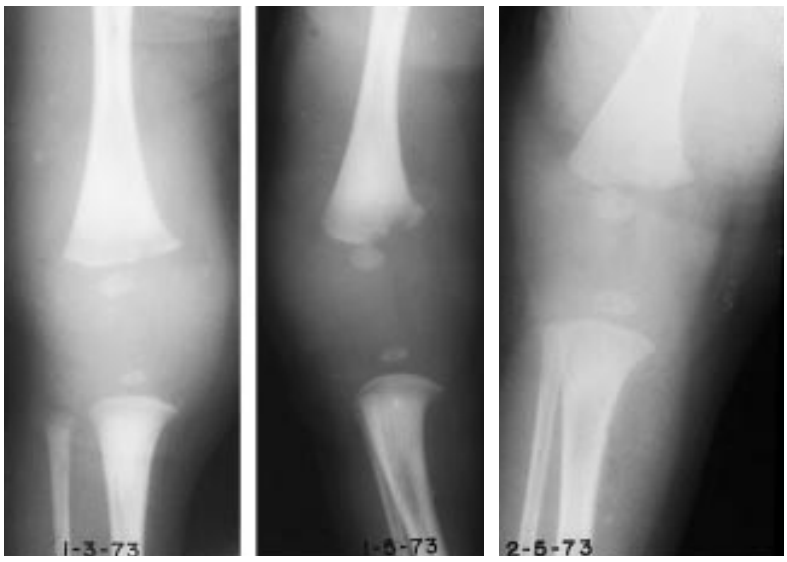

A B C

2.18

Figure 2.18. Radiographs of the same infant showing, left to right, *A)* marked swelling of the soft tissues and the joint with little evidence of bony change, *B)* two days later note early changes at the distal end of the femur, and *C)* marked improvement after 1 month of treatment. Unlike older children in which radiologic changes are delayed for several weeks, in the neonate changes of bone destruction are almost always present by the 7th to 10th day of illness. Capsular distention or widening of the joint is common. The reparative phase begins within 2 weeks after onset of infection, and the entire process from the first signs of rarefaction to restoration of the cortical structures may last no longer than 2 months.

2.19

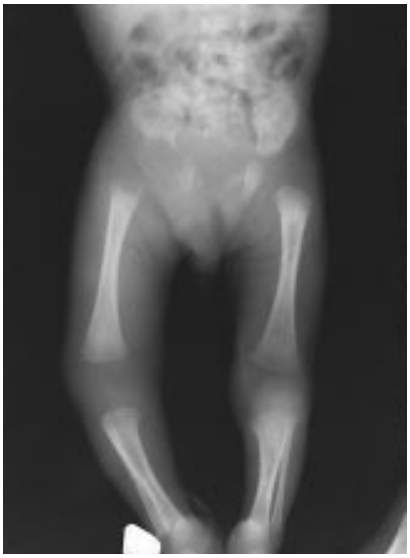

Figure 2.19. Osteomyelitis of the proximal end of the right femur with marked bony changes. Note the marked increase in the size of the hip joint. This again demonstrates that joint swelling may be the first indication of the development of osteomyelitis. The reason for the common involvement of joints in the neonatal period is that sinusoidal vessels, termed transphyseal vessels, connect the two separate circulatory systems seen in the bones of older children (the metaphyseal loops which derive from the diaphyseal nutrient artery and the epiphyseal vessels which course through the epiphyseal cartilage canals). With skeletal maturation the transphyseal vessels obliterate (8 to 18 months) and the epiphyseal and metaphyseal systems become totally separate.

2.20

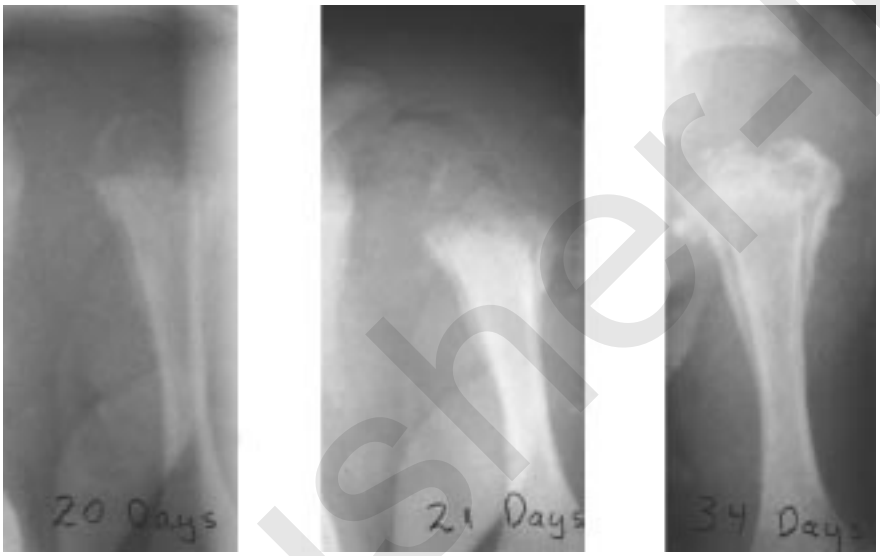

Figure 2.20. Neonatal osteomyelitis due to *Proteus mirabilis* infection. Although *Staphylococcus aureus* is the most common etiologic agent of osteomyelitis in the neonate, many other organisms such as group B *Streptococcus*, *E. coli*, *Klebsiella*, *Salmonella and Candida* have been implicated.

2.21

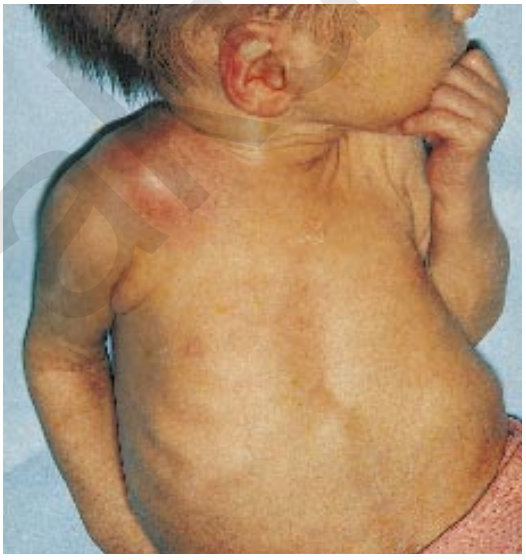

Figure 2.21. Osteomyelitis usually occurs in the long bones, but in the neonate frequently occurs in other bones such as the clavicle and ribs. This infant demonstrates inflammation and swelling over the right clavicle due to a staphylococcal osteomyelitis.

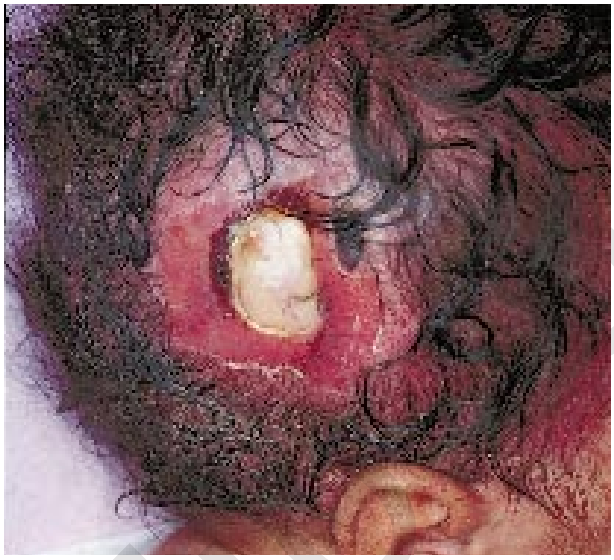

2.22

Figure 2.22. Severe scalp defect occurring as a result of an underlying staphylococcal osteomyelitis of the skull.

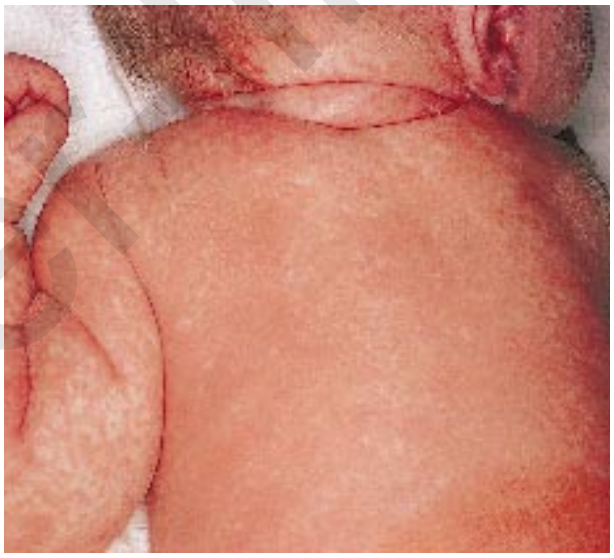

2.23

Figure 2.23. This infant presented with fever, lethargy and poor feeding at 4 days of age. He then developed a generalized rash which resembled scarlatina. Blood culture was positive for a *Staphylococcus aureus* phage type which produces an erythrogenic toxin, hence the appearance of the rash.

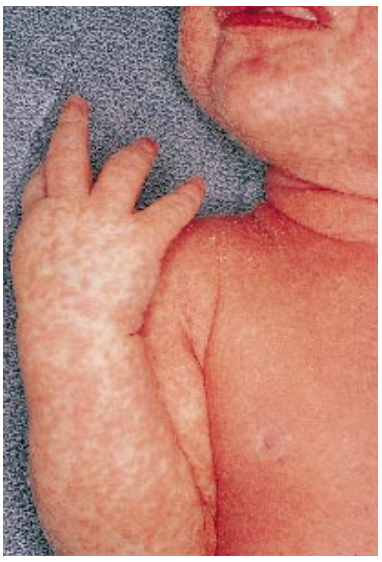

2.24

Figure 2.24. Close-up of the rash in the same infant.

2.25

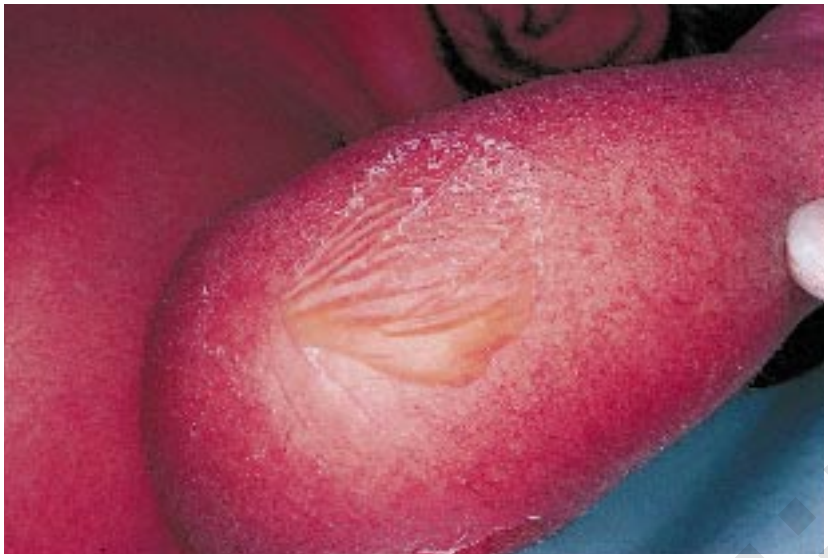

Figure 2.25. This infant who developed a mild scalded skin syndrome (toxic epidermal necrolysis; Ritter's disease) at the age of seven days had *Staphylococcus aureus* sepsis (methicillin-sensitive). Note the large bullae at this very early stage of the staphylococcal scalded skin syndrome. This is rapidly progressive. The skin is erythematous with vesicular and bullous formation, and there is widespread wrinkling and loosening of the epidermis, which results in the scalded skin appearance.

2.26

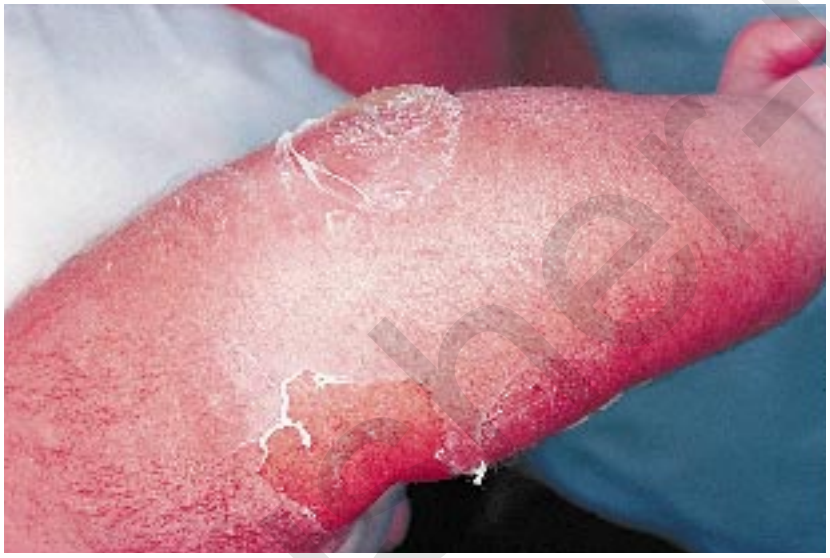

Figure 2.26. In the same infant there is rupture of the bullae. These infants present with the typical Nikolsky's sign in that there is skin exfoliation which peels on touch.

2.27

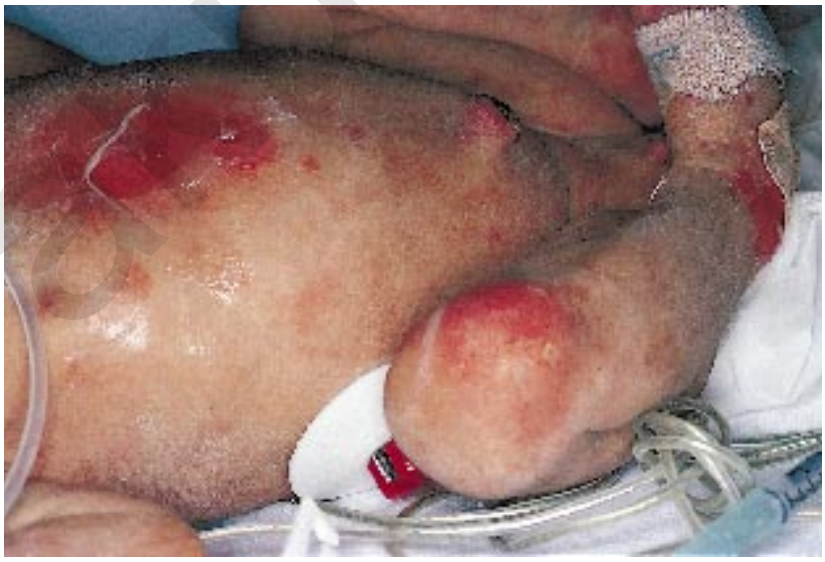

Figure 2.27. In this infant with the staphylococcal scalded skin syndrome, the bullous lesions have ruptured, resulting in the scalded skin appearance. Staphylococcal scalded skin syndrome is also known as Ritter's disease.

2.28

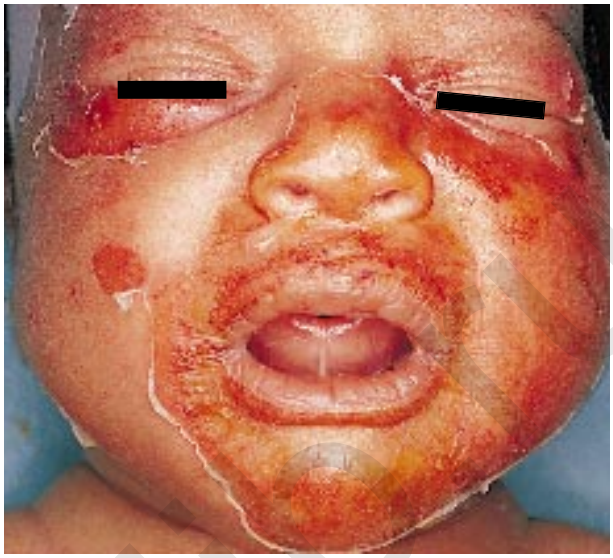

Figure 2.28. This infant had rapid progressive toxic epidermal necrolysis. The face is usually affected first and progression may rapidly become generalized. This condition is most commonly due to phage group type II staphylococci, and the toxin from the organism causes the severe exfoliative dermatitis which results in the systemic manifestations of fever, instability and water loss.

2.29

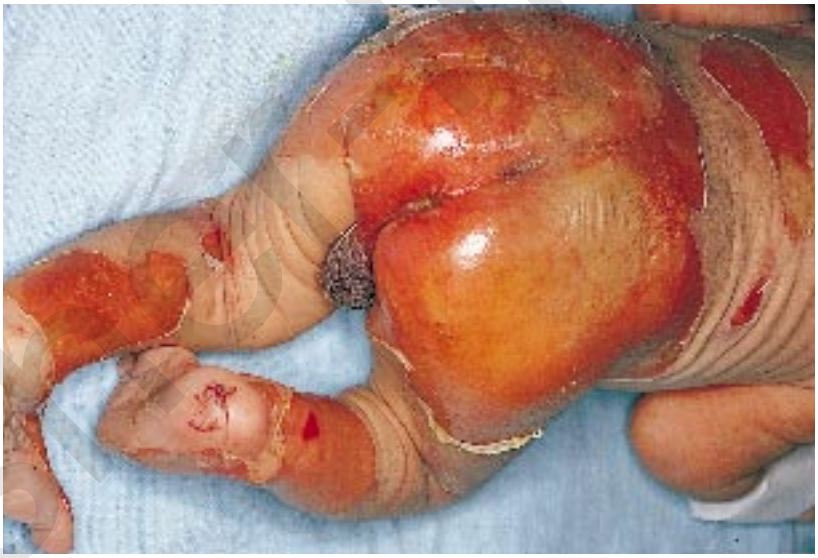

Figure 2.29. The body, buttocks and lower extremities of the same infant showing the very extensive "scalding" of the skin.

2.30

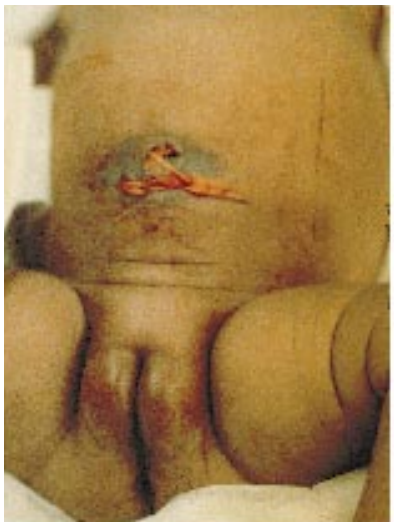

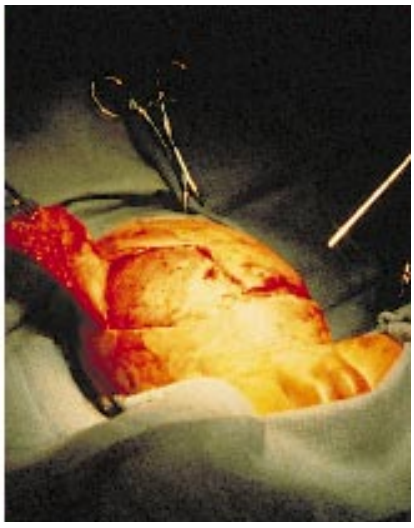

Figure 2.30. This infant has necrotizing fasciitis of the abdominal wall, which is a rapidly progressive acute necrotizing infection of the skin, subcutaneous tissue, muscle, and fascia. Necrotizing fasciitis usually presents as an area of cellulitis with fever, redness, and edema. It rapidly progresses to central patches of bluish discoloration followed by ulceration, gangrene, and toxicity. Necrotizing fasciitis is a surgical emergency as it is rapidly fatal if not treated aggressively by widespread incision and debridement. Infection in this condition has been associated with *Staphylococcus aureus*, anaerobic *Streptococcus*, *Bacteroides* and *Proteus*.

2.31

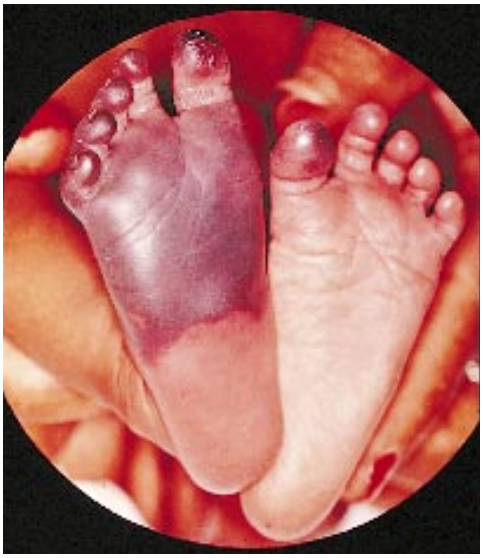

Figure 2.31. Staphylococcal sepsis resulting in gangrene of the right foot and left big toe. Umbilical catheters were not used in this infant.

2.32

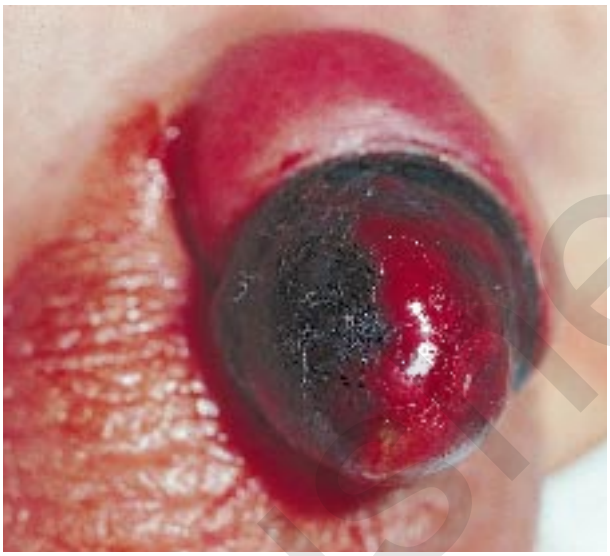

Figure 2.32. Forty-eight hours after circumcision at the age of 3 days, this infant developed cellulitis and inflammatory change of the glans and penis. There was thrombocytopenia and positive blood culture for *Staphylococcus aureus*.

2.33

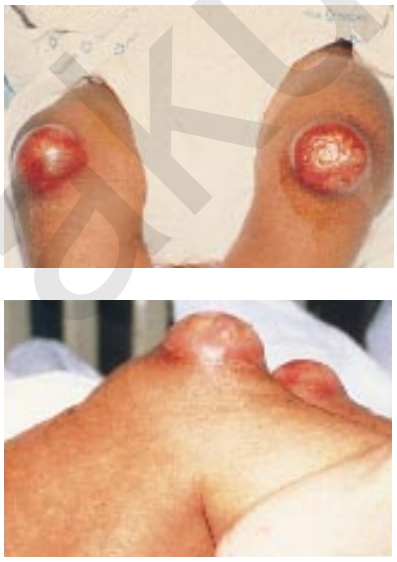

Figure 2.33. Bilateral prepatellar bursitis in a very active neonate who abraded her knees. Aspiration of the purulent material yielded group B *Streptococcus*. The knee joints, per se, were not affected. This complication is extremely rare. (Edwards, M.)

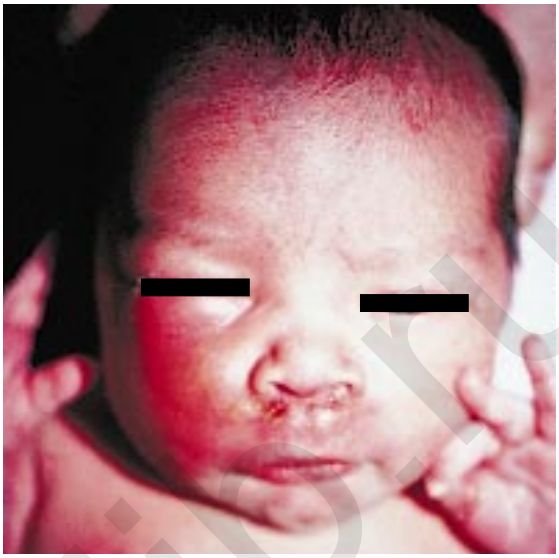

2.34

Figure 2.34. Marked cellulitis of the right side of the face in a neonate with group B streptococcal infection. There was a positive blood culture for group B *Streptococcus*.

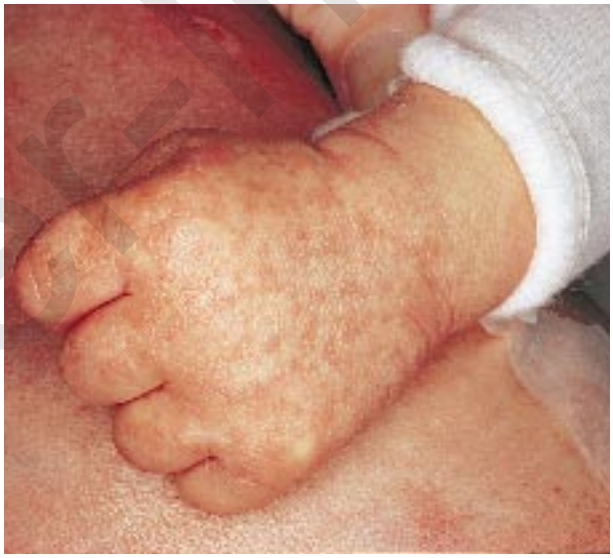

2.35

Figure 2.35. Beta hemolytic streptococcal sepsis is rare in neonates. This infant had a generalized scarlatiniform rash. Cultures were positive for group A *Streptococcus* (bacitracin-sensitive).

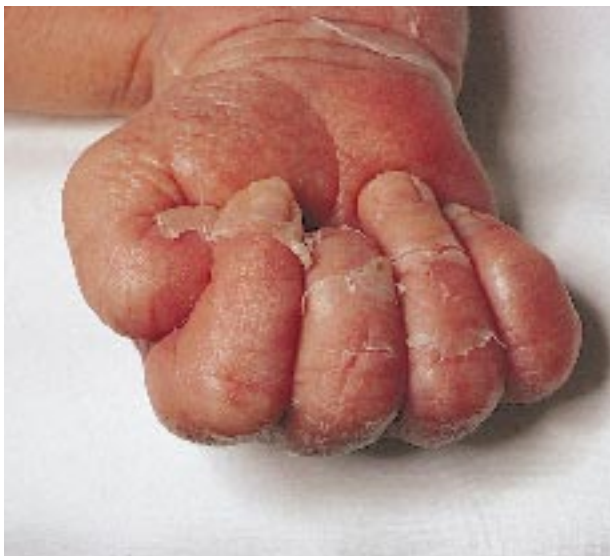

2.36

Figure 2.36. In the same infant as in Figure 2.35, note the marked desquamation of the skin 1 week later. This is similar to the typical desquamation in scarlatina in older children.

2.37

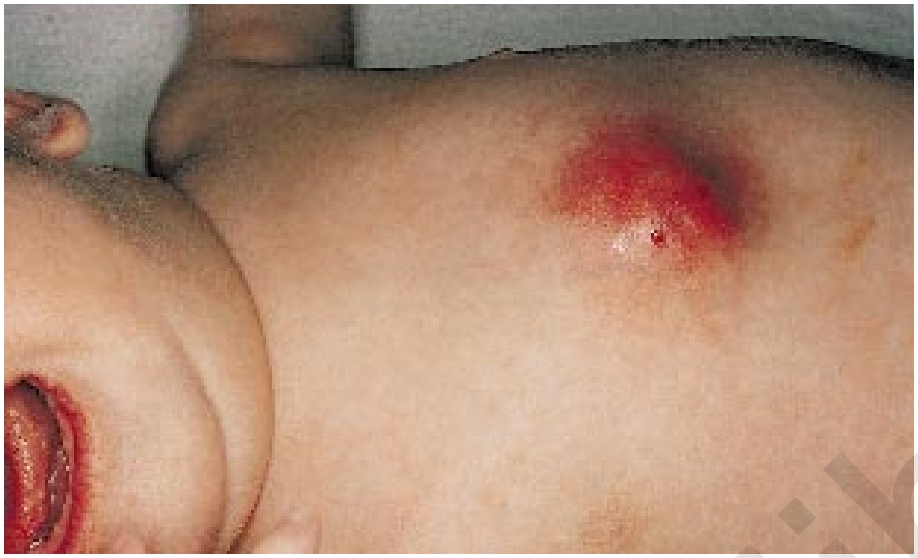

Figure 2.37. This infant with streptococcal sepsis developed cellulitis over a prominent xiphoid process.

2.38

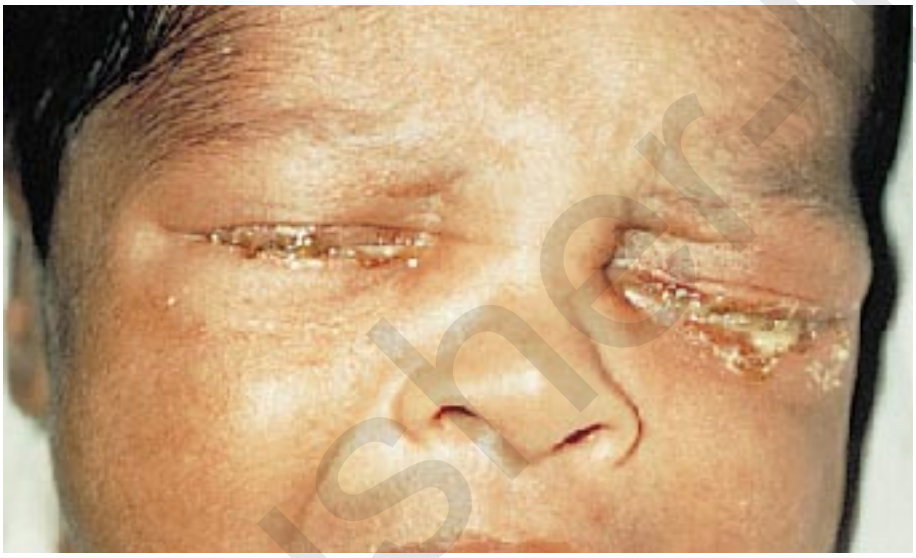

Figure 2.38. Gonococcal ophthalmia neonatorum in an infant at the age of 4 days. With prophylaxis this disease is rarely seen today. The most common cause of neonatal ophthalmia at the present time is staphylococcal infection.

2.39

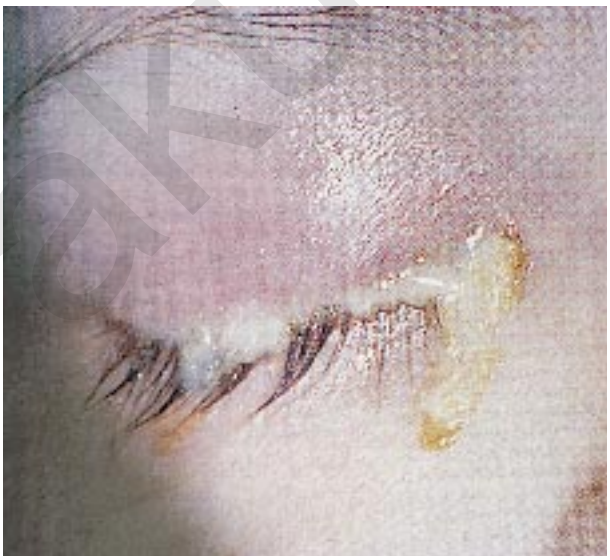

Figure 2.39. Close-up of an infant with marked purulent discharge caused by gonococcal ophthalmia neonatorum. Even with Credé's method, occasionally a breakthrough of gonococcal infection does occur in infants in that they may develop a mild conjunctivitis at the age of 7 to 14 days which is positive for *Neisseria*.

2.40

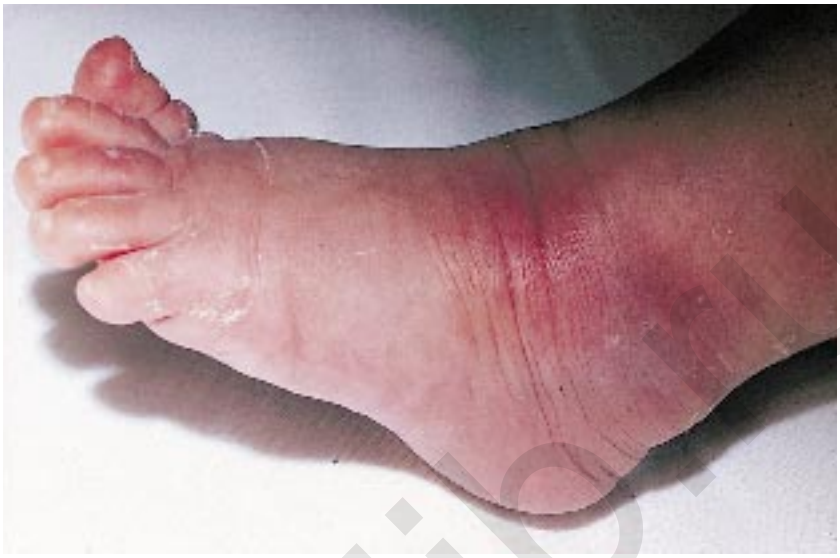

Figure 2.40. Gonococcal arthritis of the left ankle joint in an infant at the age of 2 weeks. As in the adult, neonatal gonococcal infection generally affects the large joints (knee, ankle, etc.).

2.41

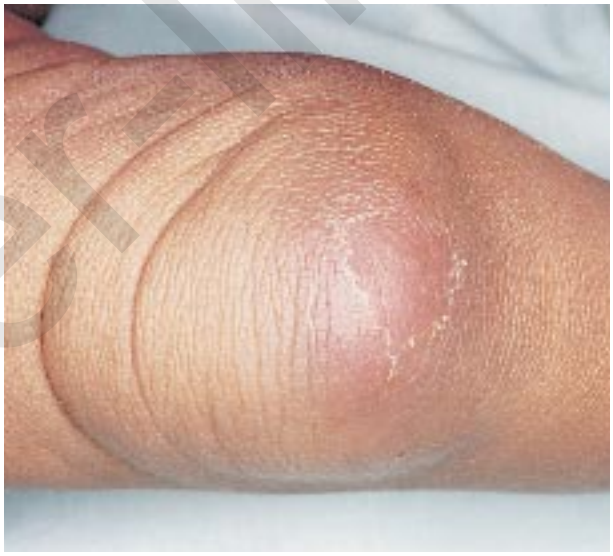

Figure 2.41. *Haemophilus influenzae* cellulitis of the prepatellar area in a neonate. Note the violaceous discoloration. This is very typical of *Haemophilus influenzae* cellulitis. The infant may be very ill with this type of infection. Cellulitis can occur as a result of infection with many other organisms.

2.42

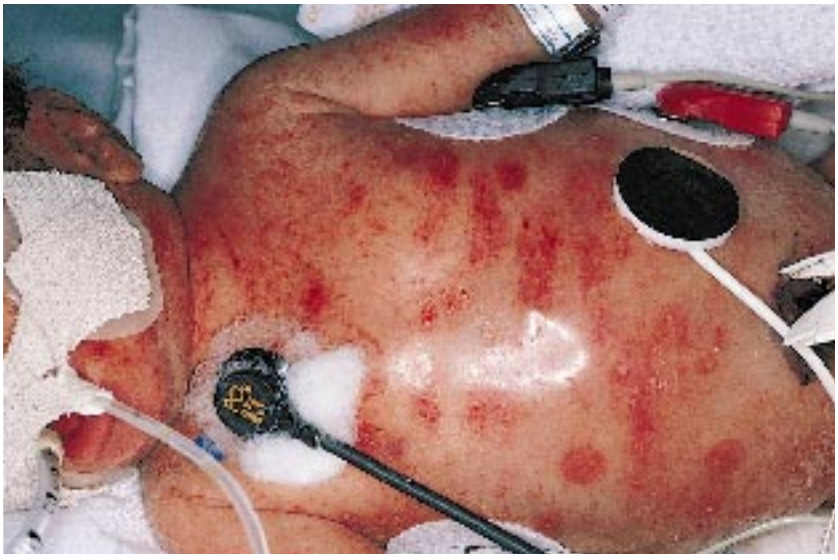

Figure 2.42. In this infant with congenital listeriosis, skin lesions were present over the entire body at birth. These increased in number. The infant had severe respiratory distress and had a congenital pneumonia due to listeriosis. The amniotic fluid was brown in color and *Listeria monocytogenes* was cultured from both skin lesions and the blood. Chocolate-brown amniotic fluid is typically seen in listeriosis. If meconium staining is reported in premature infants of less than 32 weeks gestation listerial infection may be the cause. A good site for culture of the organism is the meconium or stool.

2.43

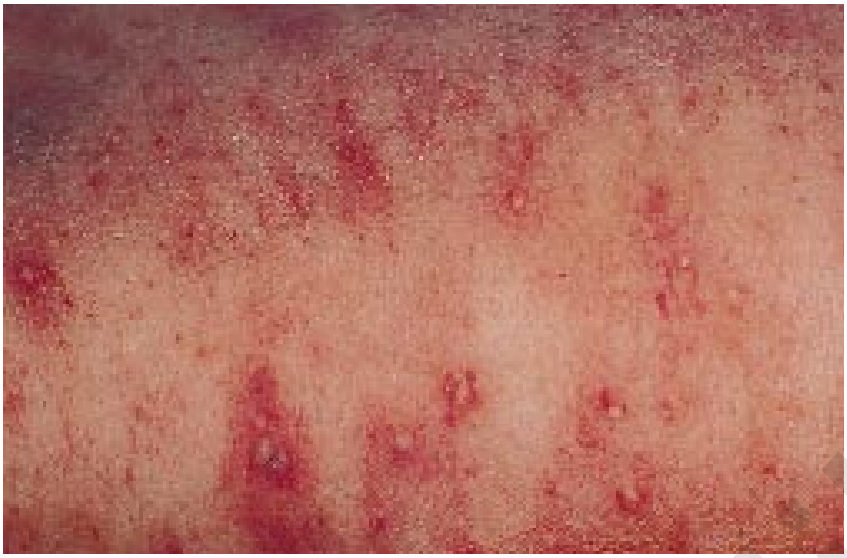

Figure 2.43. Close-up of the skin lesions of the same infant as in Figure 2.42. Note the macules, papules and vesicles. In the septicemic form of listeriosis, a cutaneous eruption of miliary abscesses resembling papules, pustules, or papulo-pustules may occur over the entire body with a predilection for the back. Culture of the lesions, the blood, or cerebrospinal fluid usually reveals *Listeria monocytogenes* as the offending agent.

2.44

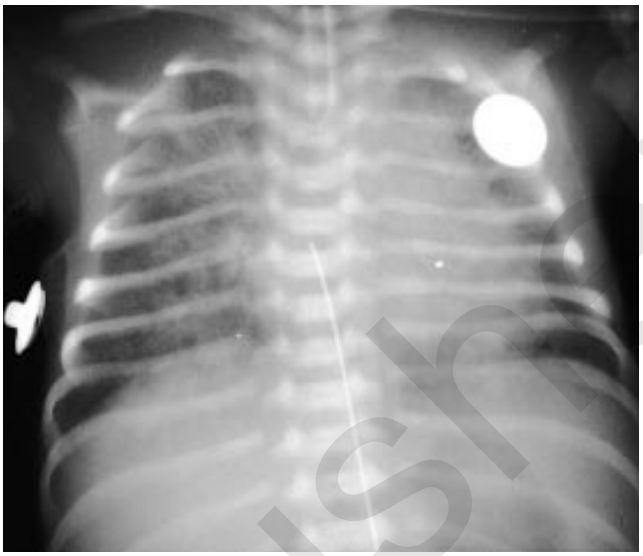

Figure 2.44. Chest radiograph in an infant who presented with severe respiratory distress from congenital pneumonia due to congenital listeriosis. The radiograph is not specific in that there may be peribronchial to wide-spread infiltration. In long-standing cases a coarse mottled or nodular pattern may be present.

2.45

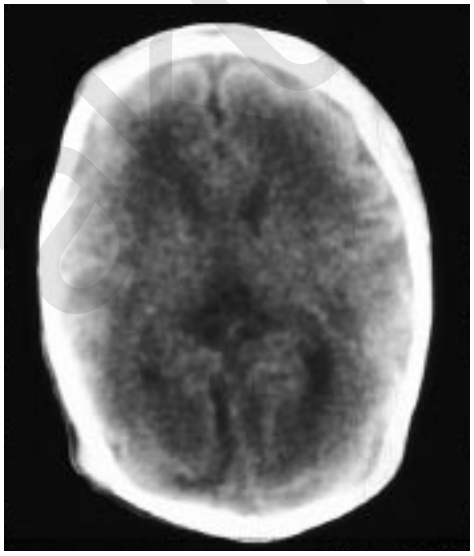

Figure 2.45. CT scan of a neonate who had listerial meningitis. Note the loss of morphology due to loss of white and gray matter differentiation. The villi are flattened out and there is evidence of some atrophy with fluid in the subarachnoid spaces. Listerial meningitis may present with early-onset disease (up to 7 days of age) usually associated with serotype I or late-onset disease (mean age 12 to 14 days) usually associated with serotype IV. Prognosis is poor in early-onset disease as seen in this infant. Note that late-onset listerial infection presents with fever in 90 to 95% of cases whereas hypothermia is much more common in other neonatal infections.

2.46

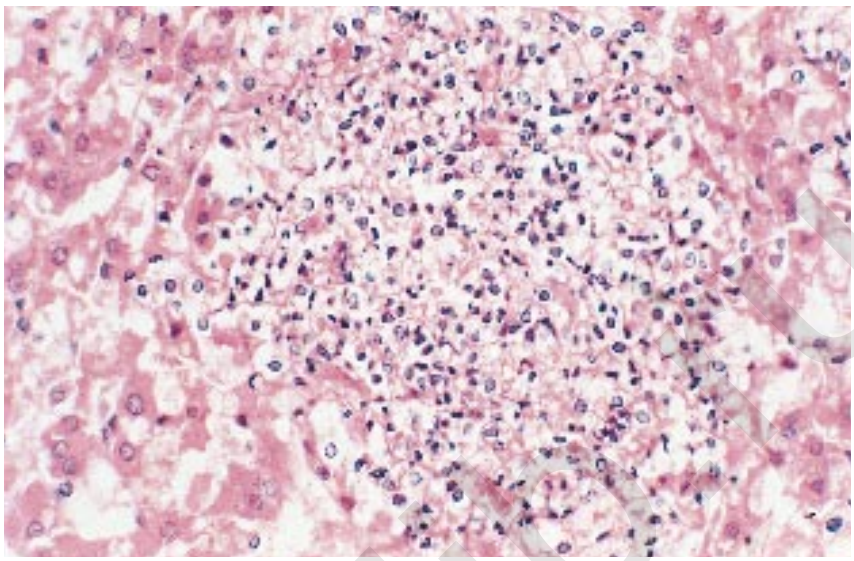

Figure 2.46. Histologic section of the liver shows the typical necrotic lesion of granuloma infantisepticum. Human listeriosis is characterized by the formation of miliary granulomas and focal necrosis or suppuration in the affected tissues. *Listeria* organisms are detectable in the necrotic foci. These lesions of granuloma infantisepticum are classically observed in generalized listeriosis. Massive involvement of the liver is predominant, but the lesions are also seen in the spleen, adrenal glands, lungs and throughout other tissues.

2.47

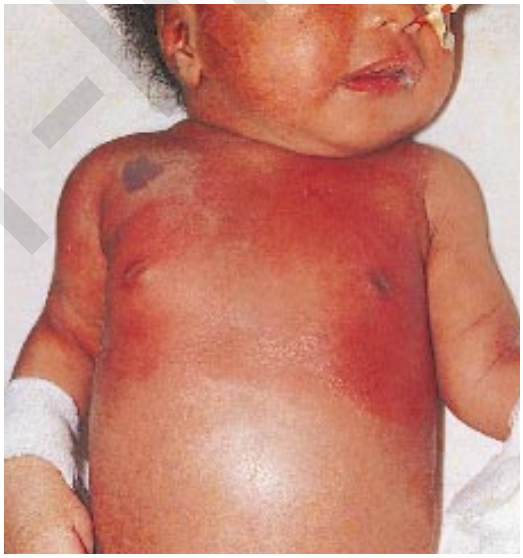

Figure 2.47. This term infant developed cellulitis of the upper chest and back at the age of 9 days. Note the very definite line of demarcation in the chest. At the same time the infant developed a purplish area over the infraclavicular and scapular areas. A sepsis evaluation was performed and cultures were positive for a gram-negative infection due to *Paracolobactrum*. (*Paracolobactrum* is in the same group as *Escherichia*, differing in that it has delayed fermentation of lactose. At the present time, it is included in the *Salmonella-Arizona* group of Enterobacteriaceae.) Prior to the report of the blood culture, differential diagnosis included erysipelas, as the line of demarcation was slightly raised, and gram-negative sepsis due to *Achromobacter*.

2.48

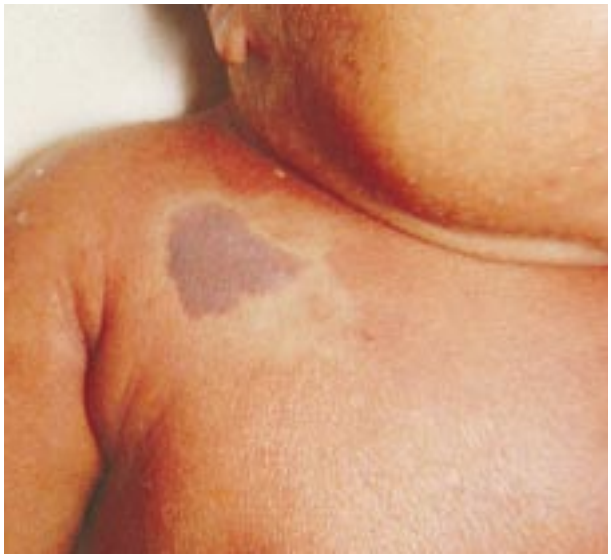

Figure 2.48. A close-up of the lesion 1 day later in the same infant as in Figure 2.47. The lesion is more violaceous in color and the diagnosis of fasciitis was made.

2.49

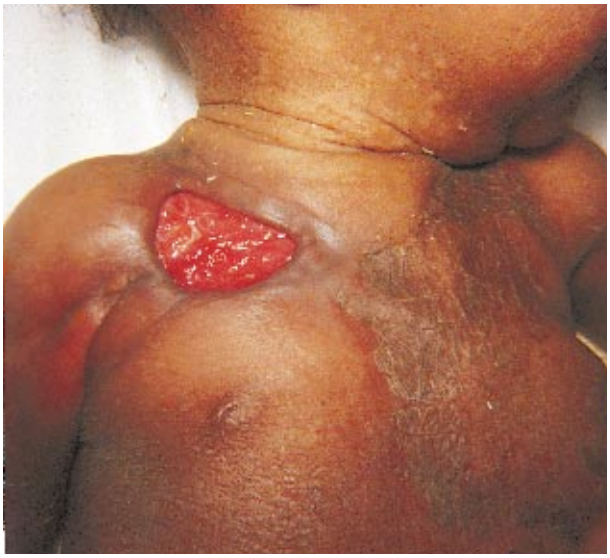

Figure 2.49. In the same infant as in Figure 2.47 and 2.48, the infraclavicular lesion broke down with severe damage to the underlying subcutaneous tissue and muscle ulceration developed; this healed with scarring over time. Note the lesion at the age of 37 days.

2.50

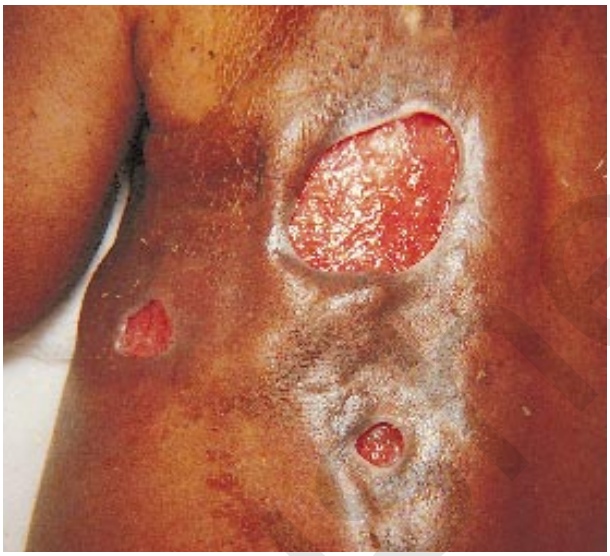

Figure 2.50. The same infant as in Figure 2.47 to 2.49 at the age of 57 days showing the lesions with breakdown and healing on the back.

2.51

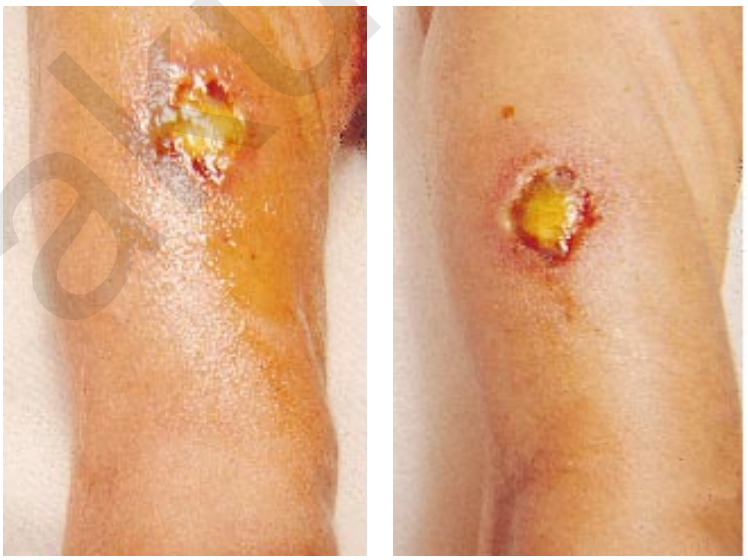

Figure 2.51. Typical "fried egg" appearance (necrotic center with surrounding inflammation) of skin lesions associated with *Pseudomonas* infection are seen in this 4-day-old neonate. This lesion developed at the site of a Vitamin K injection. *Pseudomonas aeruginosa* is usually a cause of late-onset disease in infants who are presumably infected via equipment, aqueous solutions or, on occasion, the hands of health care personnel.
The same infant with *Pseudomonas* infection shows healing at the age of nine days. Note the necrotic center. These lesions are indolent and slow healing.

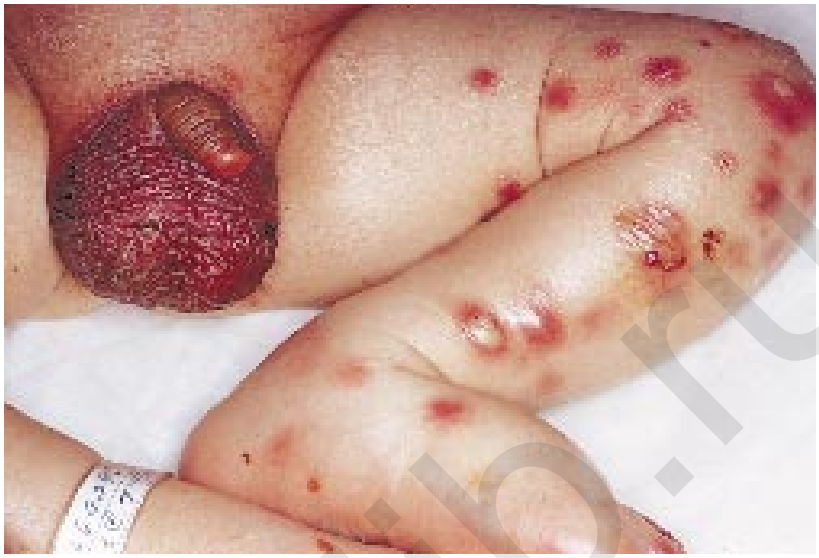

2.52

Figure 2.52. This infant with *Pseudomonas aeruginosa* sepsis and meningitis was acutely ill and had convulsions. He developed multiple skin lesions at the age of 12 days. Convulsions were controlled with difficulty and the infant died one week later. Although it is very uncommon, *Pseudomonas* conjunctivitis (a very purulent conjunctivitis) may be a devastating disease and if not promptly recognized and treated there may be rapid progression to septicemia, shock, and death. *Pseudomonas* sepsis may also cause purpura fulminans (thrombocytopenia, and clinical and laboratory signs of disseminated intravascular coagulopathy).

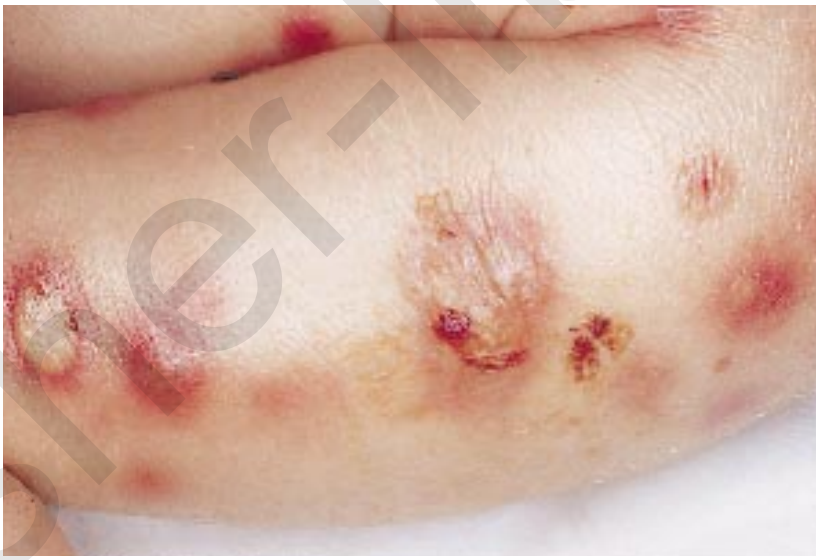

2.53

Figure 2.53. Close-up view of the typical lesions in the same infant. The cutaneous eruption in *Pseudomonas* infection consists of pearly vesicles on an erythematous background, which rapidly become purulent green or hemorrhagic. When the lesion ruptures, a circumscribed ulcer with a necrotic base appears and may persist surrounded by a purplish cellulitis.

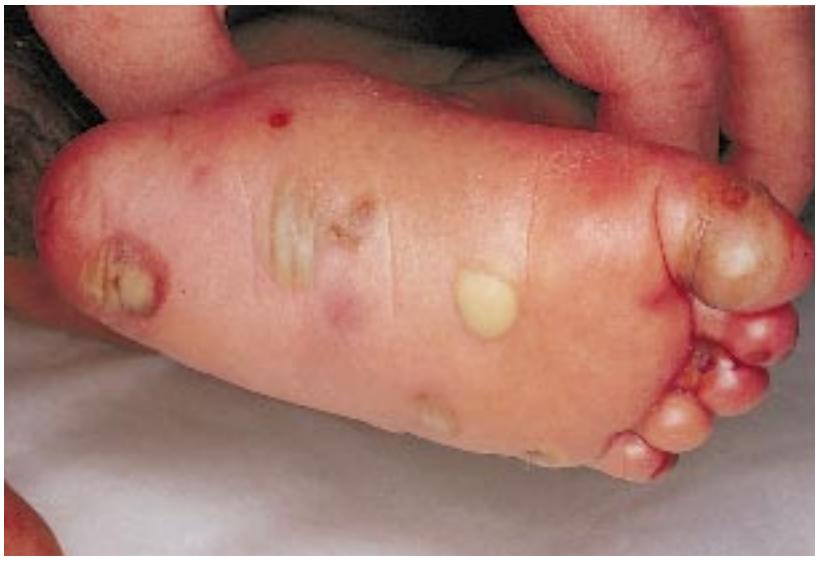

2.54

Figure 2.54. The typical lesions were also present on the soles of the feet. These lesions should not be confused with the lesions of syphilitic pemphigus.

2.55

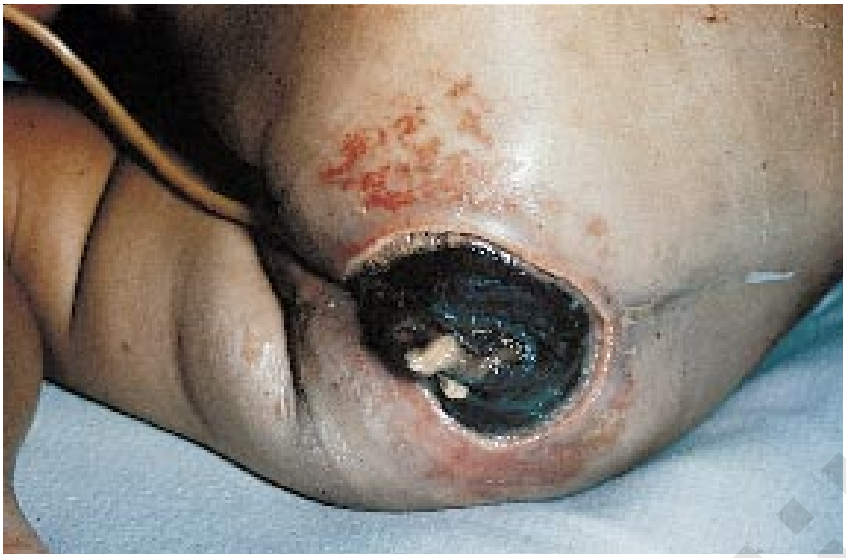

Figure 2.55. These gangrenous lesions associated with bacteremia caused by *Pseudomonas aeruginosa* demonstrate how devastating this infection can be.

2.56

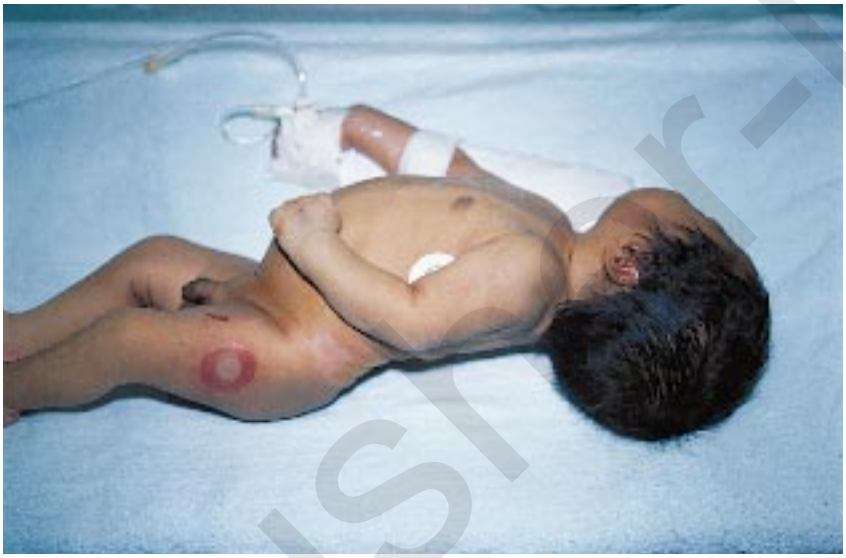

Figure 2.56. The typical opisthotonic appearance in an infant with neonatal tetanus. Note the head retraction, arching of the spine, and the hyperextension of the extremities resulting in a rigid posture. Neonatal tetanus is caused by gram-positive anaerobic spores of *Clostridium tetani*, present in the soil and in animal and human feces. Infection usually occurs after contamination of the umbilical stump that may result from unsanitary delivery or unclean handling of the cord. In developing countries the incidence of neonatal tetanus remains high.

2.57

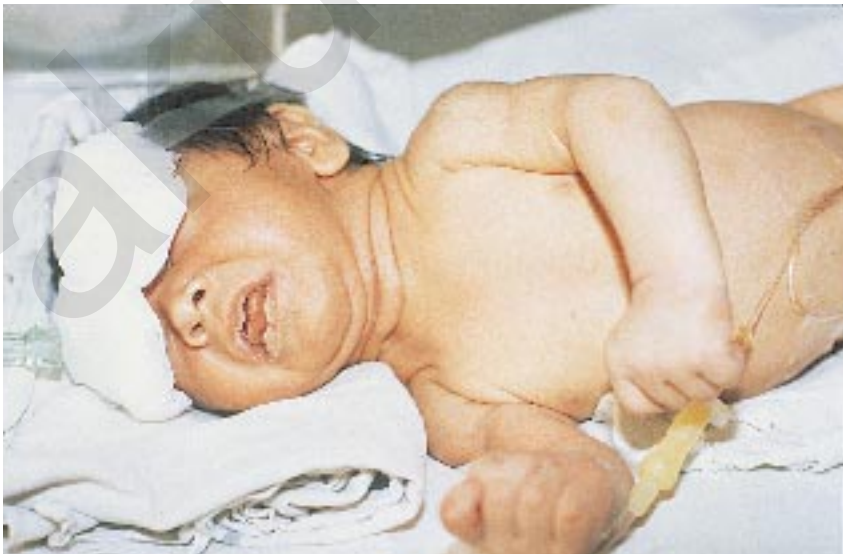

Figure 2.57. This infant with neonatal tetanus has the typical trismus giving rise to the risus sardonicus and tetanic spasm. Especially note the hands. Risus sardonicus is a grinning expression produced by spasm of the facial muscles.

2.58

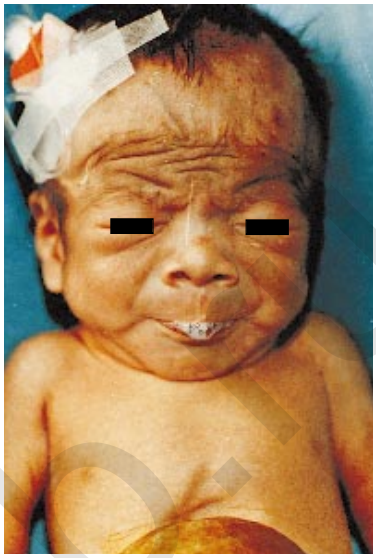

Figure 2.58. This infant with an omphalocele was delivered by a lay midwife under poor hygienic conditions. He developed tetanus at the age of 4 days and shows the typical risus sardonicus. (Cabrera-Meza, G.)

2.59

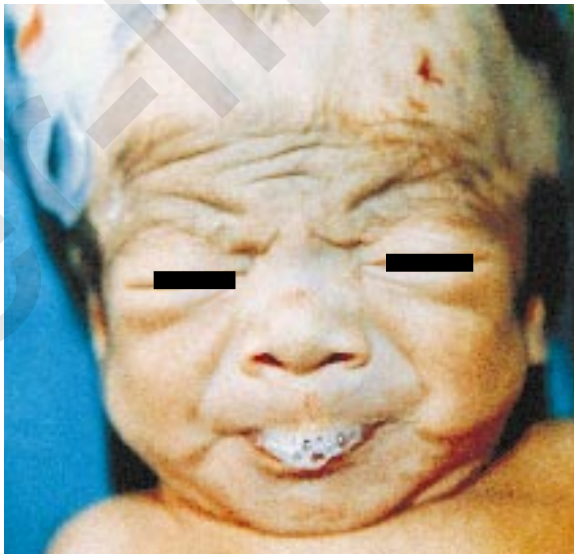

Figure 2.59. Close-up view of the face of the same infant as in Figure 2.58 showing the risus sardonicus. Note the excess secretions. (Cabrera-Meza, G.)

2.60

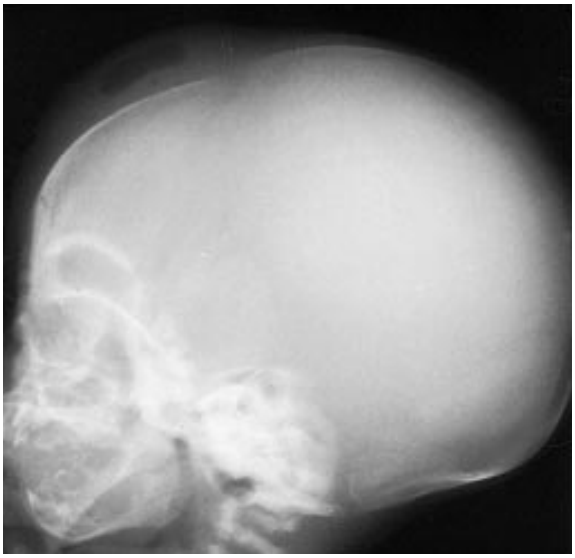

Figure 2.60. Lateral radiograph of a skull. Note the gas in a scalp abscess caused by a localized infection by a gas-forming organism.

2.61

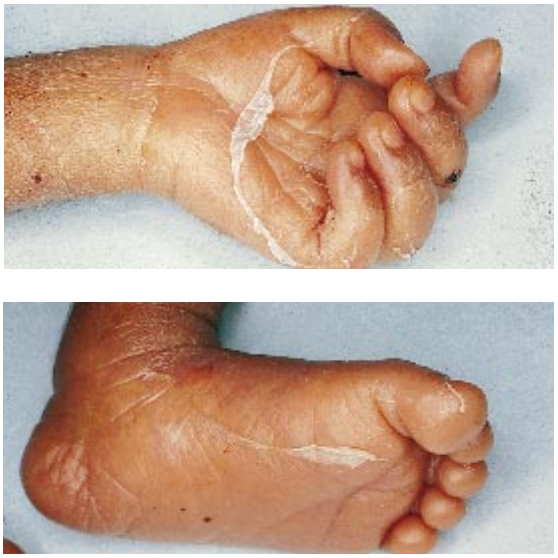

Figure 2.61. Note the desquamation of the palms and soles in a neonate. There were no other dermatologic lesions elsewhere. The VDRL (Venereal Disease Research Laboratory) test showed maternal blood to be reactive with a titer of 1:32 and the infant had a titer of 1:1024. Lesions on the palms and soles should be considered syphilitic until proven otherwise. The spectrum of cutaneous lesions which occur in 30 to 40% of infants with congenital syphilis can be extremely variable. There may be mild desquamation, annular or circinate lesions or vesiculobullous manifestations.

2.62

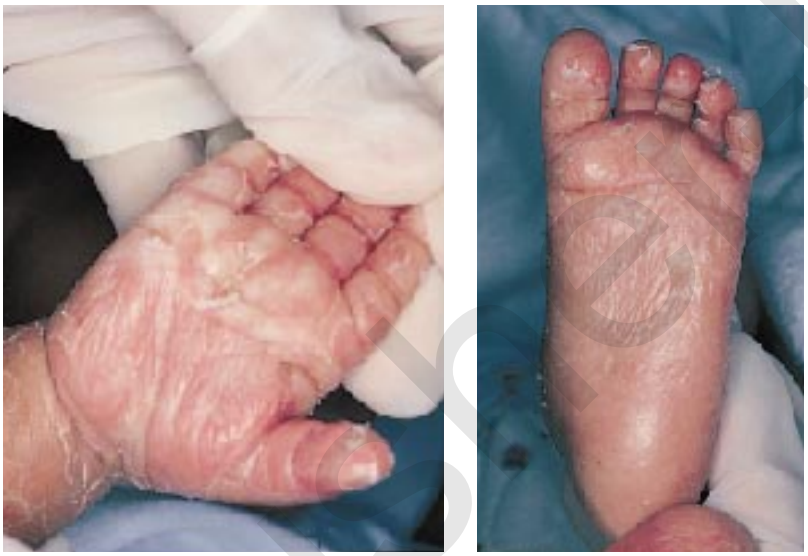

Figure 2.62. Desquamation on the palms and soles with no rash or desquamation elsewhere is very suggestive of congenital syphilis. The palms and soles may be fissured and erythematous and, as a result of subcutaneous edema, may have a shiny appearance.

2.63

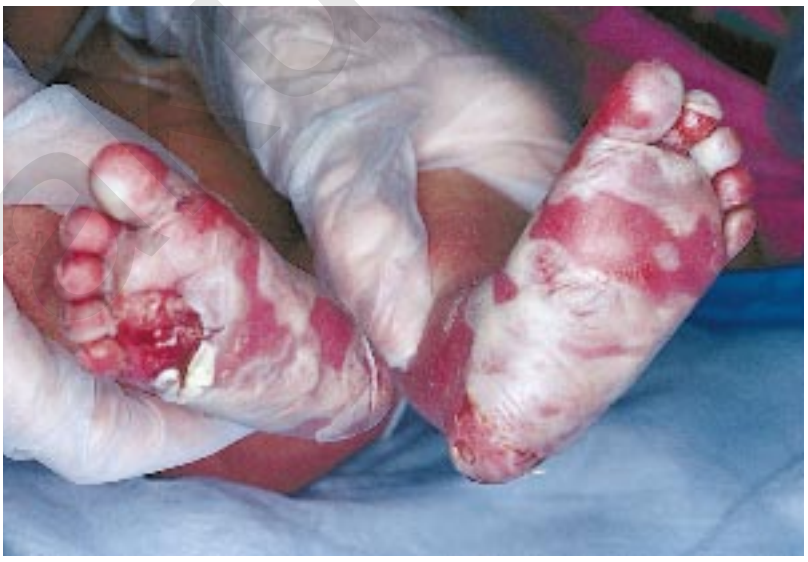

Figure 2.63. Syphilitic pemphigus showing the large vesiculobullous hemorrhagic lesions on the soles of both feet. These lesions are relatively rare but, especially when seen on the palms and soles, are highly diagnostic of this disease. The lesions may contain a cloudy hemorrhagic fluid that teems with organisms and is highly contagious. With bullous lesions such as these, other dermatologic diagnoses should be excluded (bullous impetigo, epidermolysis bullosa, congenital bullous ichthyosiform erythroderma, etc.).

2.64

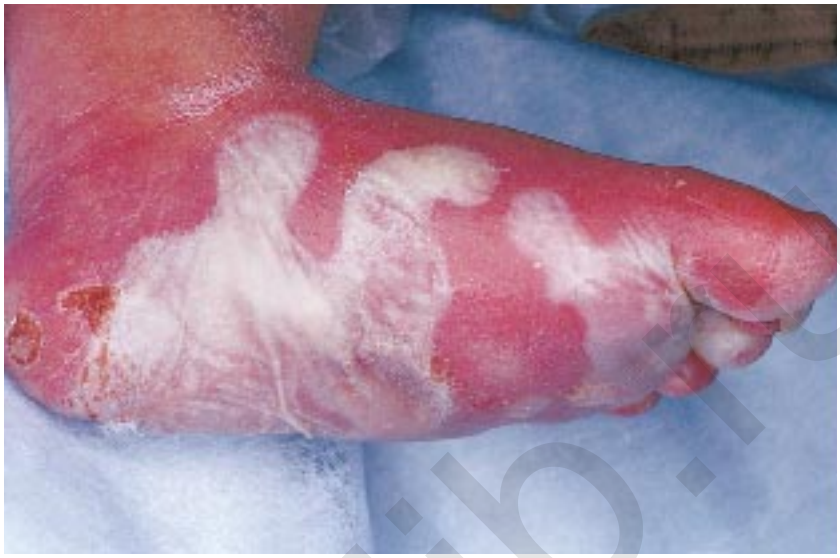

Figure 2.64. A close-up of the foot of the same infant as in Figure 2.63 shows both bullae and ulcerated areas on the sole.

2.65

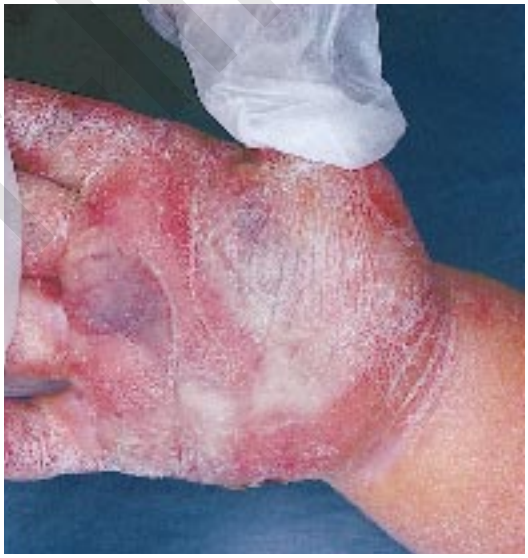

Figure 2.65. The same infant as in Figure 2.63 had bullae and ulcerations on the palms of both hands. When bullae rupture, they leave a denuded area that can undergo extensive maceration and crusting. It is unusual to see the bullae at birth as the majority have ruptured in utero.

2.66

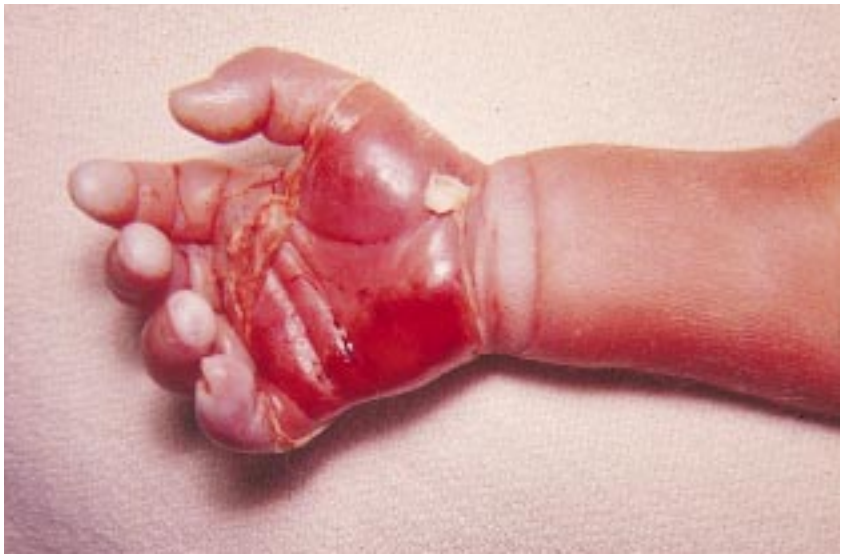

Figure 2.66. This infant with congenital syphilis had vesiculobullous hemorrhagic lesions which ruptured in utero and presented with the typical raw, hemorrhagic appearance of the palms and soles at birth. These lesions are highly infectious.

2.67

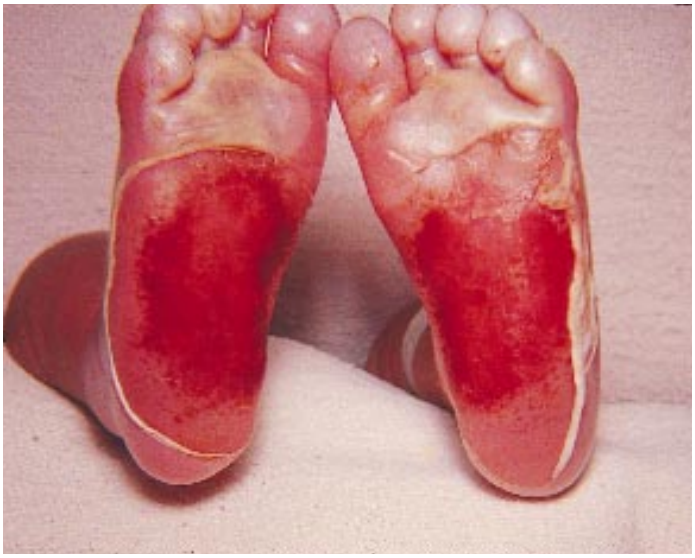

Figure 2.67. The raw hemorrhagic appearance of the lesions on the soles of the same infant as in Figure 2.66. In general, the more florid the manifestations of congenital syphilis at birth, the worse the prognosis.

2.68

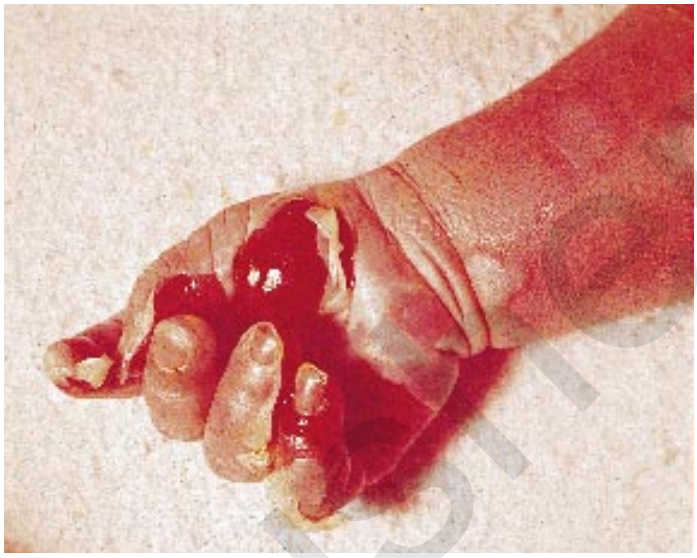

Figure 2.68. Characteristic circinate lesions involving the distal forearm in congenital syphilis. Syphilitic pemphigus of the palm is also present. The cutaneous manifestations may appear as large round or oval maculopapular (circinate) lesions. These are comparable to the lesions seen in secondary syphilis in the adult. It is unusual for them to be present at birth as they usually present between the age of 3 to 6 weeks in infants with congenital syphilis.

2.69

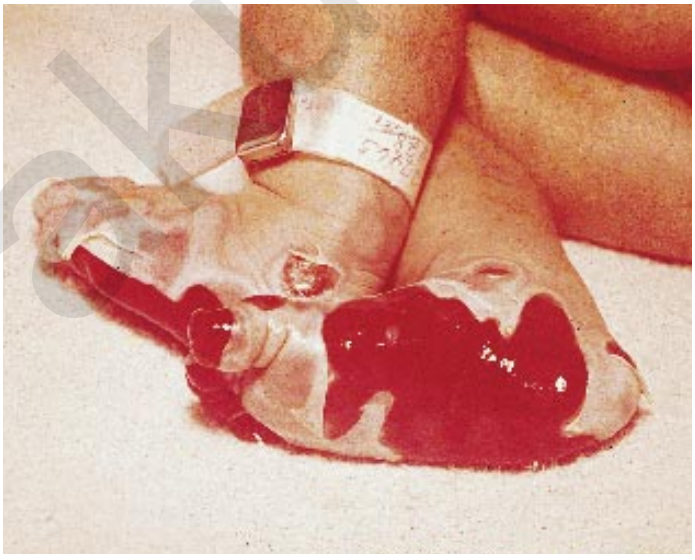

Figure 2.69. Circinate lesions and syphilitic pemphigus of the soles present at birth in the same infant as in Figure 2.68.

2.70

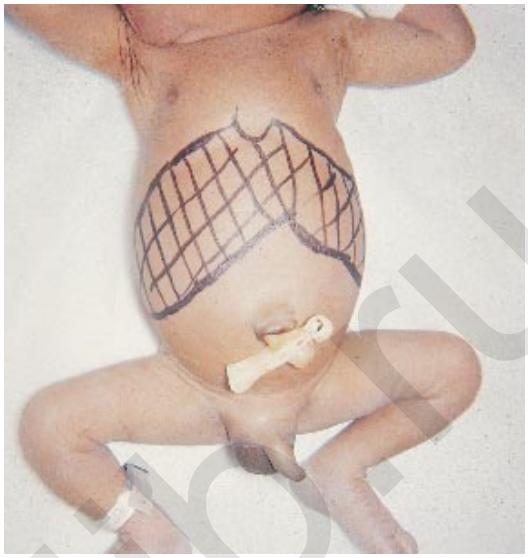

Figure 2.70. Marked hepatosplenomegaly in an infant with congenital syphilis. Hepatomegaly occurs in 50 to 60% of affected infants. It is frequently associated with jaundice, anemia, splenomegaly and ascites. In the spectrum of congenital syphilis there may be no clinical signs of disease at birth or there may be many clinical manifestations which include intrauterine growth retardation, skin manifestations, hepatosplenomegaly, jaundice, anemia, thrombocytopenia, and osseous changes.

2.71

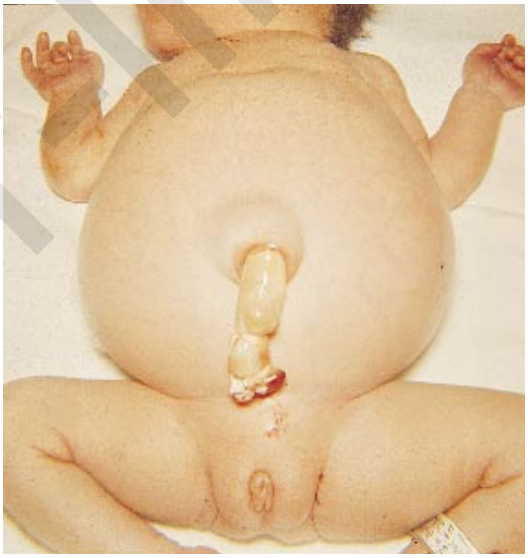

Figure 2.71. This infant with massive ascites secondary to congenital syphilis associated with respiratory distress, improved dramatically after abdominal paracentesis. This degree of ascites caused dystocia, necessitating a cesarean delivery.

2.72

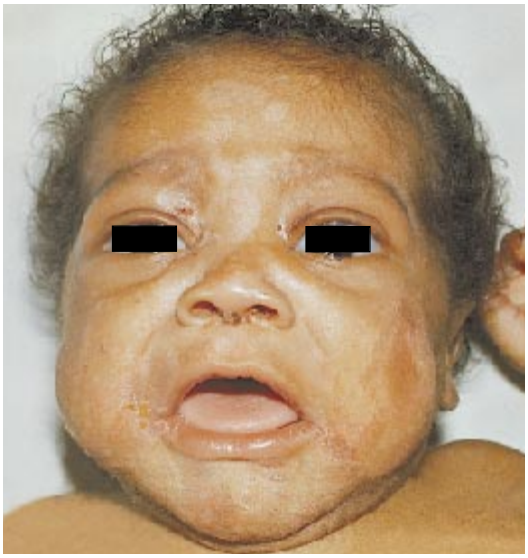

Figure 2.72. In an infant aged 6 weeks with the typical findings of congenital syphilis, note the circinate lesions over the forehead, the excoriation at the nose due to rhinitis, and the cheilitis at the corners of the mouth. Rhinitis ("snuffles") usually appears between the 2nd to 6th week of life and is the result of ulceration of the nasal mucosa. When the ulceration is deep enough to involve the cartilage of the nasal bone, the architecture is destroyed, thus giving rise to the classic saddle nose deformity. Mucous membrane patches are seen in approximately one-third of infants with congenital syphilis. At the mucocutaneous junctions these lesions tend to weep and may cause fissures (cheilitis) which often extend from the lips in a radiating fashion over the surrounding skin. When deep, these lesions may leave residual scars (rhagades).

2.73

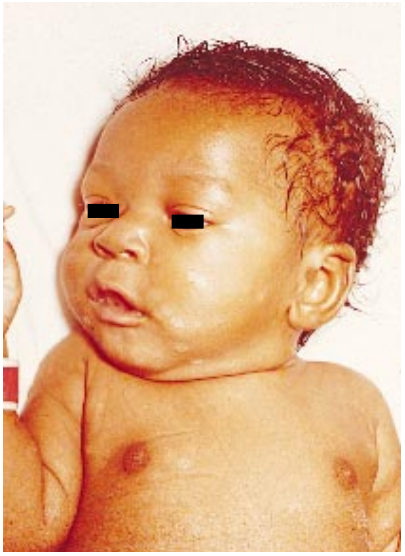

Figure 2.73. This infant developed a skin rash of congenital syphilis at the age of 7 weeks. These annular and circinate lesions healed but left areas of hypopigmentation. This type of cutaneous lesion, rarely present at birth, generally develops as a dark pink or red rash from the age of 3 to 6 weeks; it gradually fades to a coppery-brown lesion which disappears over a period of 1 to 2 months but often leaves an area of hyperpigmentation or hypopigmentation. The lesions may occur on any part of the body, but are usually most pronounced on the face and the dorsal surface of the trunk and legs.

2.74

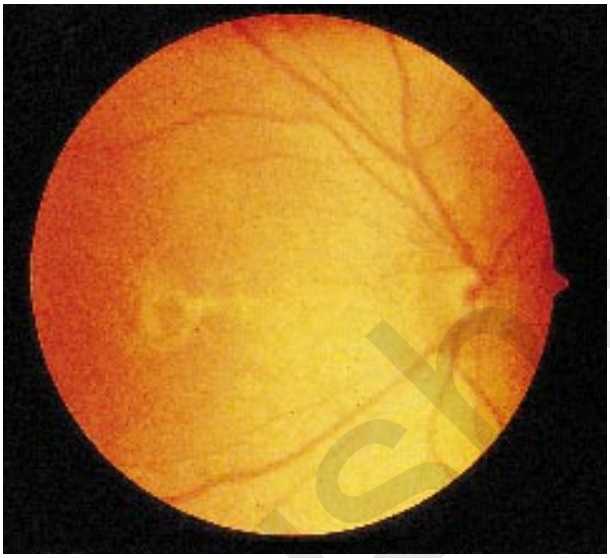

Figure 2.74. Congenital syphilitic chorioretinitis of the right eye. Note the abnormal scarring in the macular area. Optic atrophy, if present, is usually seen in conjunction with neurosyphilis. These findings are extremely rare in congenital syphilis. Other stigmata of congenital syphilis present much later. The deciduous teeth of children with early congenital syphilis are prone to caries but show no other abnormality. The stigmata of Hutchinson's triad (Hutchinson's incisors, interstitial keratitis, and eighth nerve deafness) occur later. Dental changes of Hutchinson's incisors and Moon's (mulberry) molars occur with secondary dentition.

2.75

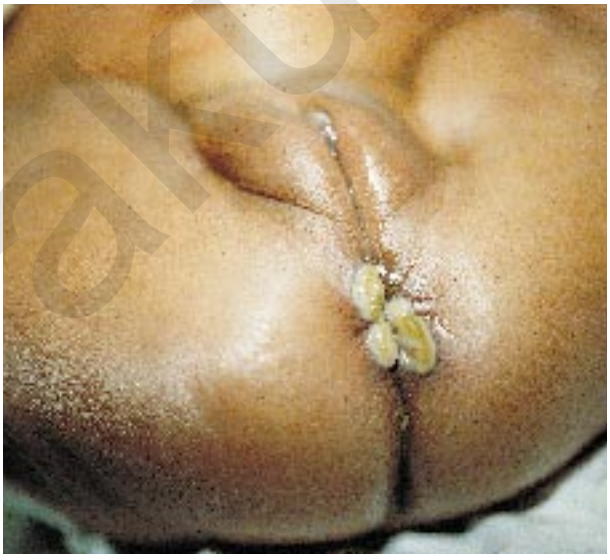

Figure 2.75. Condylomata lata presenting at the age of 6 weeks in an infant with congenital syphilis. The RPR (rapid plasma reagin) was negative at birth but at 6 weeks was reactive with a titer of 1:512. The infant was anemic with a hemoglobin of 4.8 mg/dL, three-plus hematuria, CSF (cerebrospinal fluid) pleocytosis, and a positive CSF VDRL. Lesions responded to penicillin 3 days after treatment was initiated. Condylomata lata appear as flat or raised, moist, wart-like cutaneous lesions, grayish-pink in color. They are smooth, round or oval, and wide-based, often mushroom-like, lesions which may be single or multiple. They occur in moist areas, especially the anogenital regions. They heal without scarring and are highly infectious and must be differentiated from condylomata accuminata which are covered by digitate vegetations.

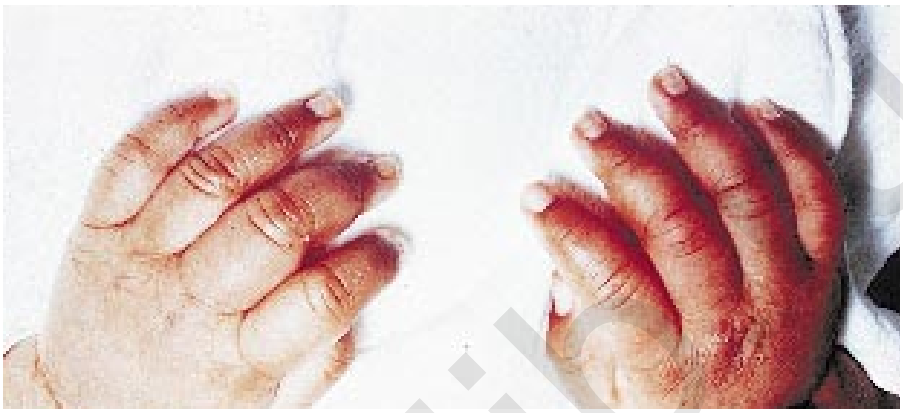

2.76

Figure 2.76. Dactylitis may be a rare finding in congenital syphilis. Note the spindle-shaped appearance of the fingers. This is a rare form of osteochondritis of the small bones of the hands and feet which usually appears between 6 months and 2 years of age. It is commonly found in the metacarpals, proximal phalanges of the hands, and the metatarsals. The swelling gives rise to little pain or discomfort.

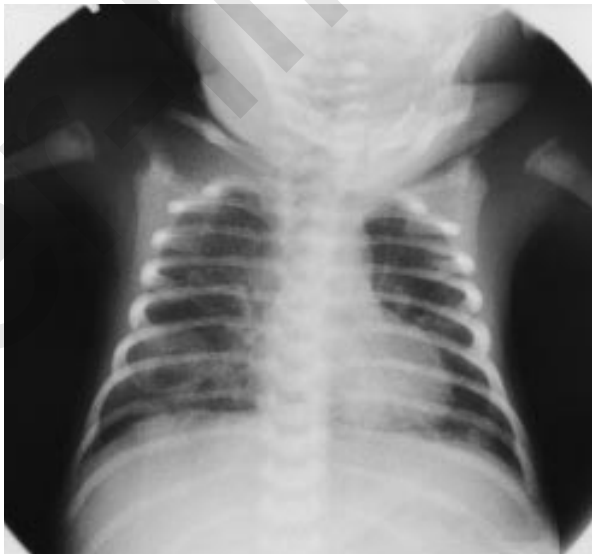

2.77

Figure 2.77. Radiograph of the chest in an infant at age 7 days. The interstitial pneumonia (pneumonia alba) of congenital syphilis is present. This is characterized pathologically by yellowish-white, heavy, firm and grossly enlarged lungs. Note the osseous changes of congenital syphilis at the proximal ends of the humeri.

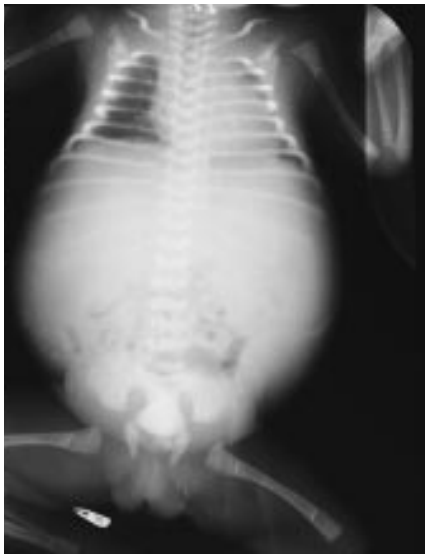

2.78

Figure 2.78. Radiograph of an infant with cogenital syphilis showing massive ascites and growth arrest lines at the ends of long bones.

2.79

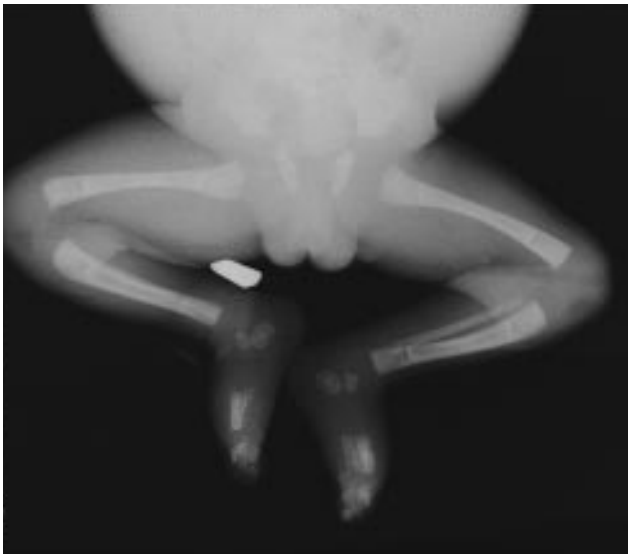

Figure 2.79. This radiograph in the same infant as in Figure 2.78 shows growth arrest lines in the lower extremity long bones. The growth arrest lines at the ends of the long bones are a nonspecific finding in that they signify interference with growth of the fetus in utero and, although commonly seen in congenital syphilis, may occur in many other conditions such as congenital viral infections and erythroblastosis fetalis.

2.80

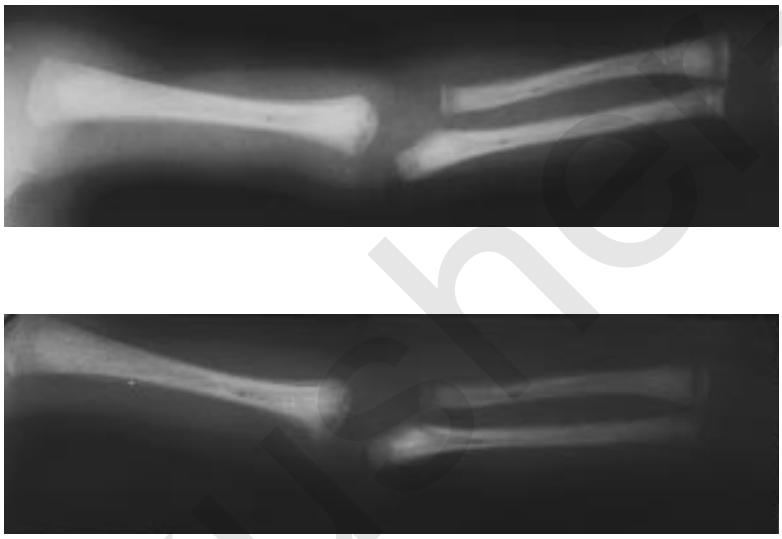

Figure 2.80. Growth arrest lines found in the upper extremities in an infant with congenital syphilis. Growth arrest lines show an enhanced zone of provisional calcification (radiopaque band) which is associated with osteoporosis immediately below the dense zone. The growth arrest line may be smooth or serrated. A serrated appearance is known as Wegner's sign.

2.81

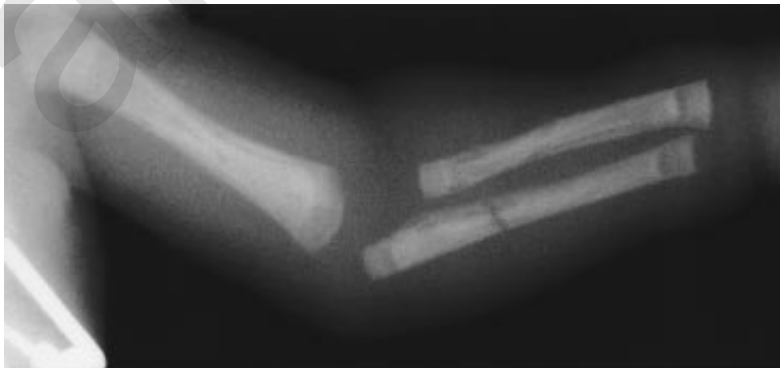

Figure 2.81. Radiograph of the upper extremity of an infant with congenital syphilis showing growth arrest lines, periostitis, and fracture of the ulna. Periostitis is seldom visualized at birth because of lack of sufficient calcification at that time to cast a shadow. It is more commonly seen at 4 to 6 weeks of age and, at that time, must be distinguished from that seen in healing rickets, child abuse, and infantile cortical hyperostosis. As the bone is more fragile with syphilitic infection, bone trauma is more common.

2.82

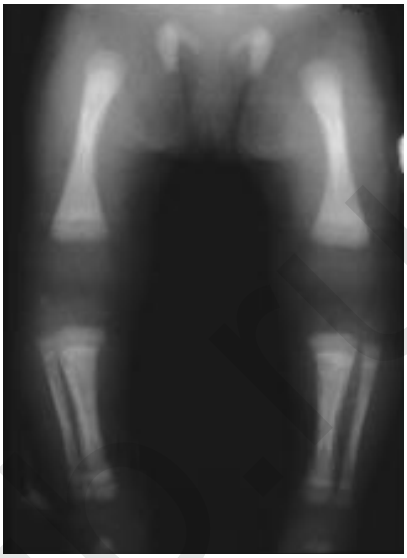

Figure 2.82. This radiograph demonstrates the lack of ossification centers and the presence of growth arrest lines in the lower extremities of a term infant with congenital syphilis. In congenital syphilis, some growth retardation may occur and it is not unusual to see a delay in appearance of the ossification centers. The bony involvement tends to be multiple and symmetrical. Characteristically bony involvement is widespread and includes the long bones, cranium and ribs. In most cases the osseous lesions are asymptomatic, but in some infants severe involvement may lead to subepiphyseal fractures with epiphyseal dislocation resulting in a painful pseudoparalysis (Parrot's atrophy of newborn). This may mimic Erb's palsy.

2.83

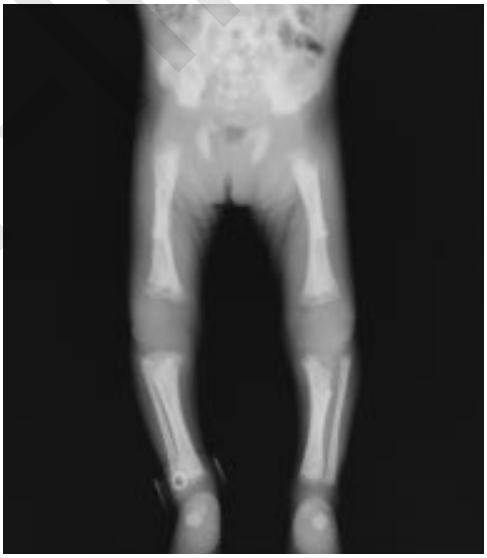

Figure 2.83. Lower extremity radiograph showing characteristic erosions of syphilitic osteochondritis at the metaphyses of the distal ends of the long bones. About 15% of infants with osteochondritis will show signs at birth. Ninety percent will show radiologic evidence of osteochondritis and periostitis after the first month of life. In osteochondritis, there is increased widening of the epiphyseal lines with increased density of the shafts, spotty areas of radiolucency, and a resultant moth-eaten appearance.

2.84

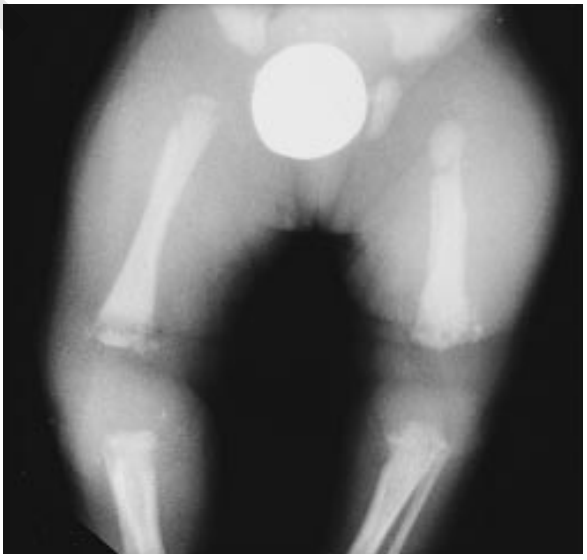

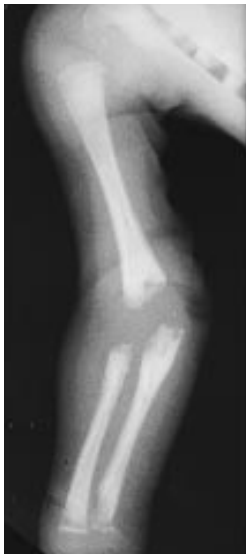

Figure 2.84. Radiograph of lower extremities and right upper extremity in this infant at the age of 7 days shows the typical syphilitic osteochondritis and some periosteal reaction, especially of the femora. The osteochondritis may be present at birth or may appear during the first month of life. It is most clearly seen in the long bones. The changes seen are fragmentation and apparent destruction with mottled areas of radiolucency.

2.85

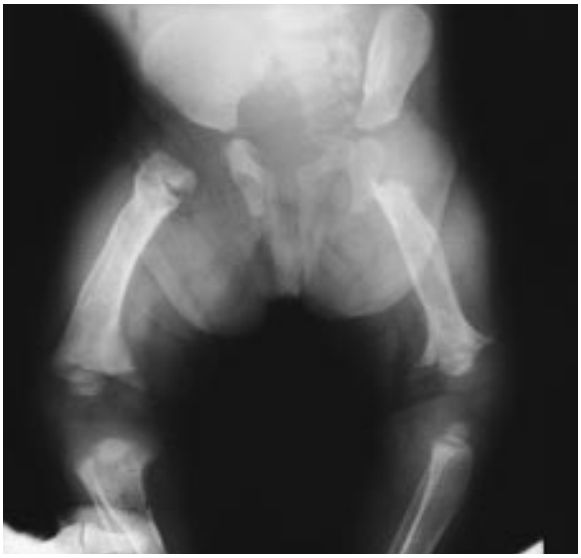

Figure 2.85. Radiograph of the lower extremities of the same infant as in Figure 2.84 at age 6 months. Note the marked alterations of the contour and thickness of the femora. The cortex is thin and the medullary cavity is expanded. The proximal end of the left femur is severely damaged due to syphilitic osteomyelitis. This may present as a syphilitic arthritis of the hip. In spite of these extensive changes, infantile luetic osteitis usually improves remarkably.

2.86

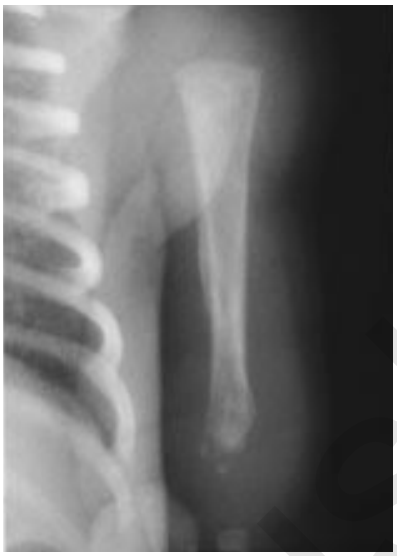

Figure 2.86. Radiograph of the left humerus in an infant with congenital syphilis showing periostitis which was present at birth. The lesions of periostitis are usually diffuse and frequently extend over the entire length of the involved bone. It is first seen as a thin even line of calcification outside the cortex of the involved bone; the lesions progress and eventually produce calcification and thickening of the cortex. When severe, this leads to a permanent deformity such as anterior bowing of the tibia (saber shins). Periostitis of the frontal bones of the skull, when severe, is responsible for the flat overhanging forehead that may persist as a stigma of congenital syphilis in infancy.

2.87

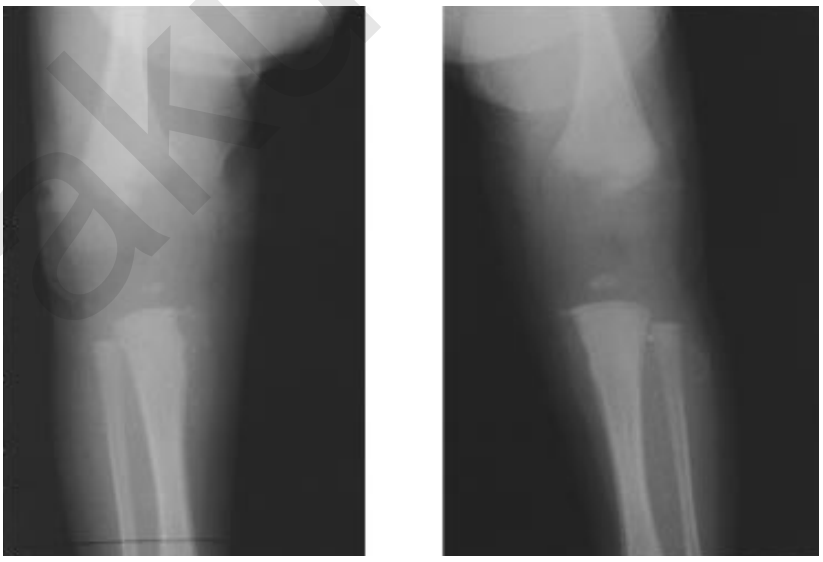

Figure 2.87. Wimberger's sign in an infant with congenital syphilis is recognized by radiolucency due to erosion of the medial aspect of the proximal tibial metaphysis. Painless effusion in one or both knees (Clutton's joints) generally becomes apparent between 8 to 15 years of age, involutes spontaneously and leaves no residual effects.

2.88

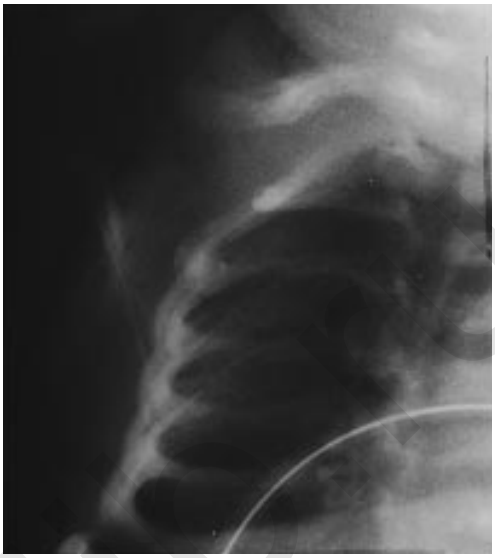

Figure 2.88. Higouménaki's sign refers to periostitis of the clavicle. This may be observed clinically or radiographically and is a diagnostic finding in congenital syphilis. Note also the periostitis of the ribs. Fracture of the clavicle with callus formation should be a consideration in the differential diagnosis.

VIRAL INFECTION

2.89

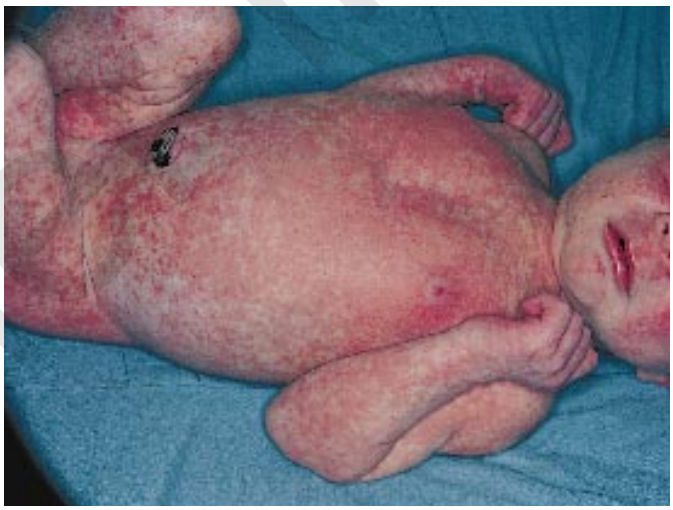

Figure 2.89. This infant at age 5 days developed fever, lethargy and poor feeding. On sepsis evaluation there was a pleocytosis of 120 WBCs in the cerebrospinal fluid indicative of meningoencephalitis. There was no evidence of cardiac involvement. The following day the infant developed a generalized maculopapular rash and loose stools. He recovered without treatment. Stool culture grew Coxsackie virus.

2.90

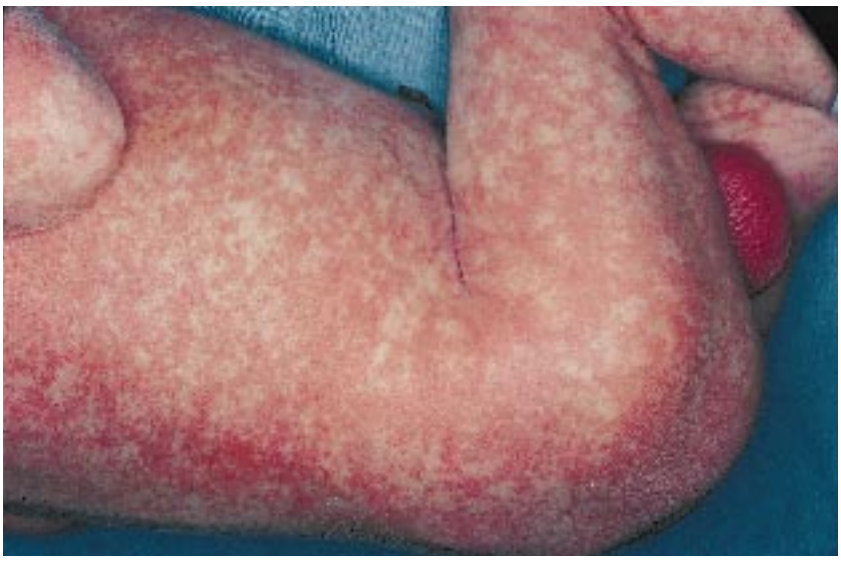

Figure 2.90. Close-up view of the rash from the same infant as in Figure 2.89 with Coxsackie virus infection.

2.91

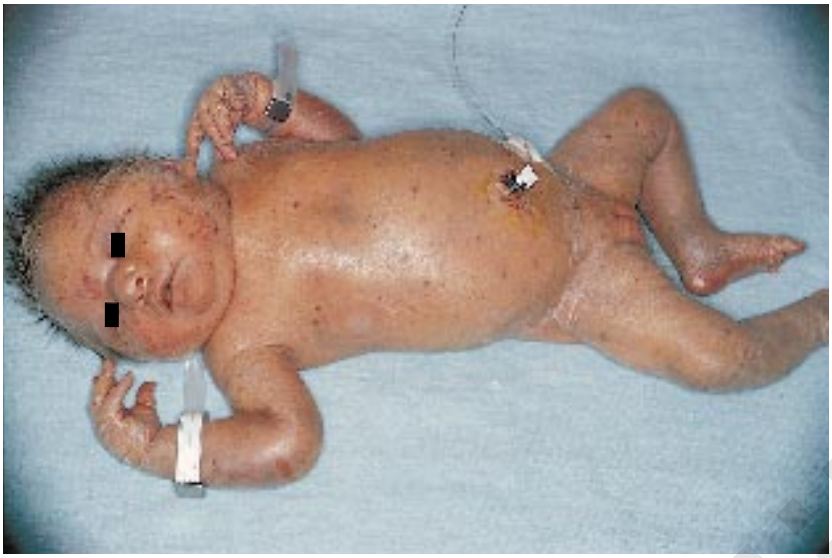

Figure 2.91. This infant with cytomegalovirus infection has a low birthweight due to intrauterine growth retardation and shows the "blueberry muffin" appearance, microcephaly, and abdominal distention due to marked hepatosplenomegaly. Cytomegalovirus infection is asymptomatic in approximately 90% of infected infants at birth. Of these, 5 to 10% develop late-onset sequelae such as hearing loss, chorioretinitis, mental retardation, and neurologic sequelae. The remaining 10% may have mild to severe and occasionally fatal disease.

2.92

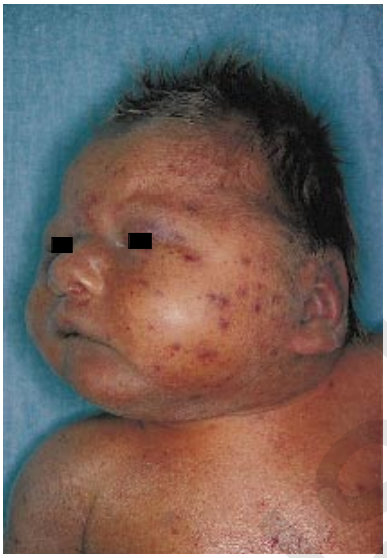

Figure 2.92. A close-up of the head and face of the same infant as in Figure 2.91 with microcephaly and the typical "blueberry muffin" lesions. These lesions represent areas of dermal erythropoiesis. Cutaneous manifestations include petechiae, purpura, "blueberry muffin" lesions (also seen in congenital rubella and other conditions), and vasculitis.

2.93

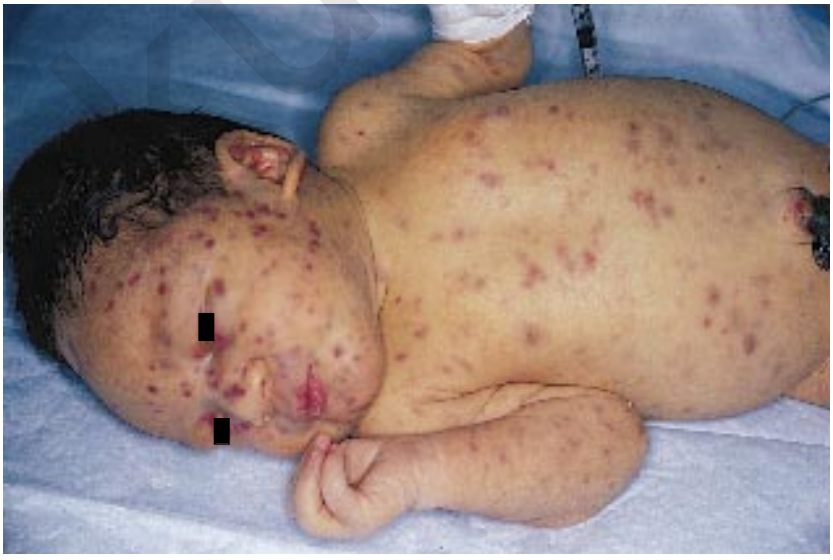

Figure 2.93. Another infant with cytomegalovirus infection showing the typical "blueberry muffin" appearance and jaundice soon after birth. Note that the head size is normal. Since most infections are asymptomatic, early diagnosis is only made in the full-blown syndrome manifested by the appearance of jaundice within the first 24 hours of life, hepatosplenomegaly, abdominal distention, anemia, thrombocytopenia, respiratory distress and neurologic changes.

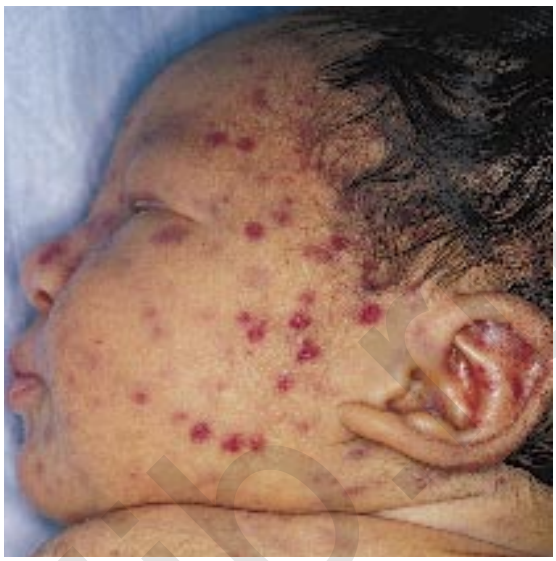

2.94

Figure 2.94. Close-up of the face of the same infant as in Figure 2.93 showing the typical "blueberry muffin" appearance.

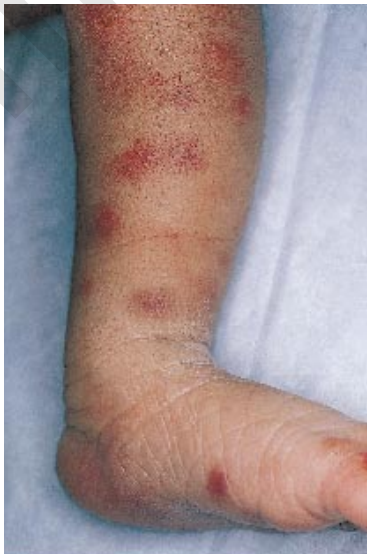

2.95

Figure 2.95. This infant presented with areas of skin involvement on the extremities only. The lesions were asymmetrical in that they were present on the right leg and left arm. Vasculitis, a less common manifestation of skin involvement by cytomegalovirus infection, was confirmed by skin biopsy.

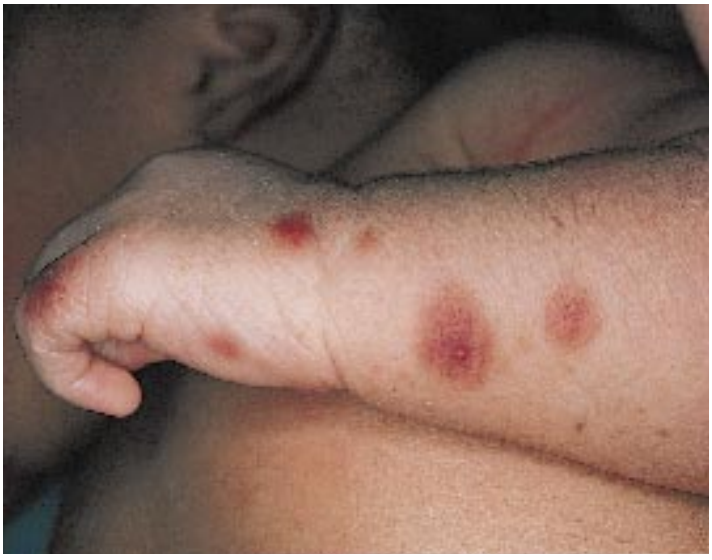

2.96

Figure 2.96. Lesions on the left arm of the same infant as in Figure 2.95 show the vasculitis.

2.97

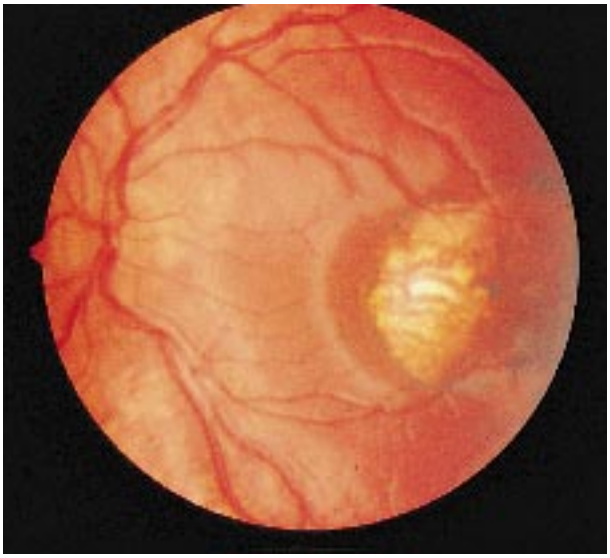

Figure 2.97. Macular chorioretinitis which is typical of cytomegalovirus infection.

2.98

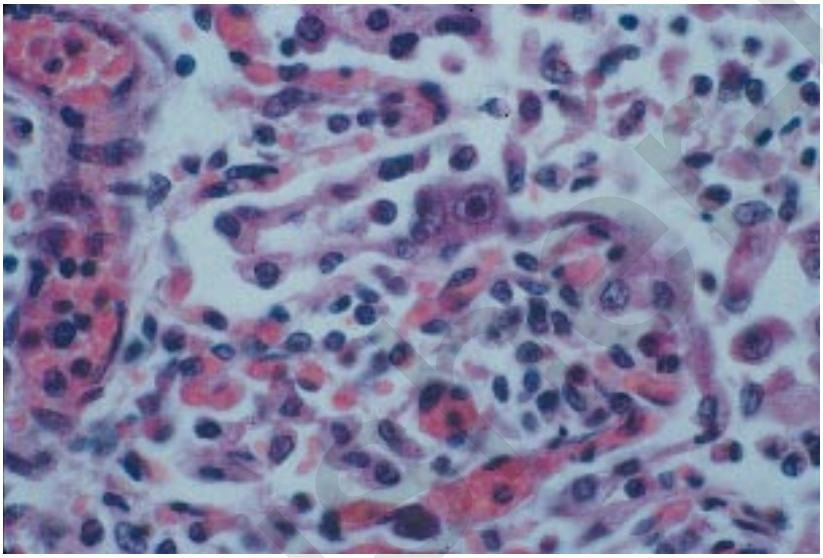

Figure 2.98. Histopathologic section of lung demonstrating the typical "owl's eye" appearance of cells infected with cytomegalovirus. Postnatally acquired cytomegalovirus infection can occur in infants with primary immunodeficiencies or following transfusion with cytomegalovirus-positive blood, etc. (Langston, C.)

2.99

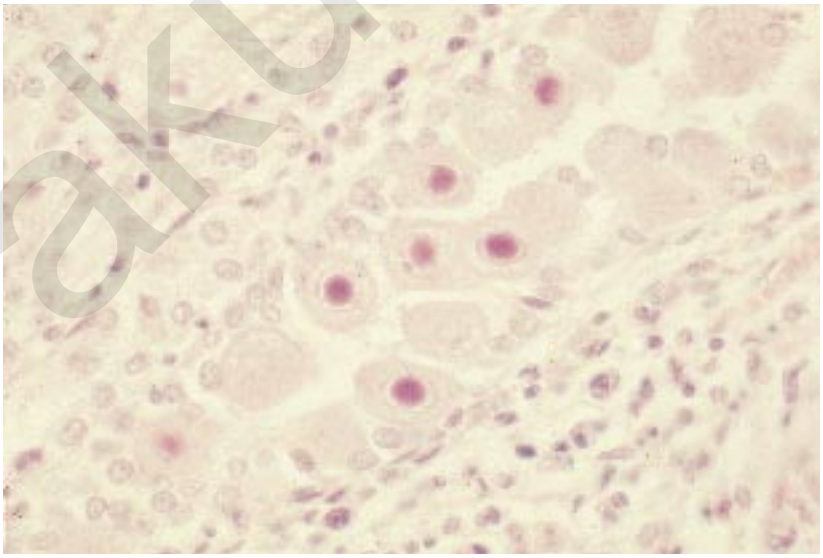

Figure 2.99. "Owl's eye" appearance in a histopathologic section of the kidney. Note the large cellular size which results from an increase in volume of both the nucleus and the cytoplasm. The nuclear inclusion is located centrally and corresponds to the shape of the cell. The nucleolus is usually displaced peripherally in infected cells. There is no necrosis of cells. (Langston, C.)

2.100

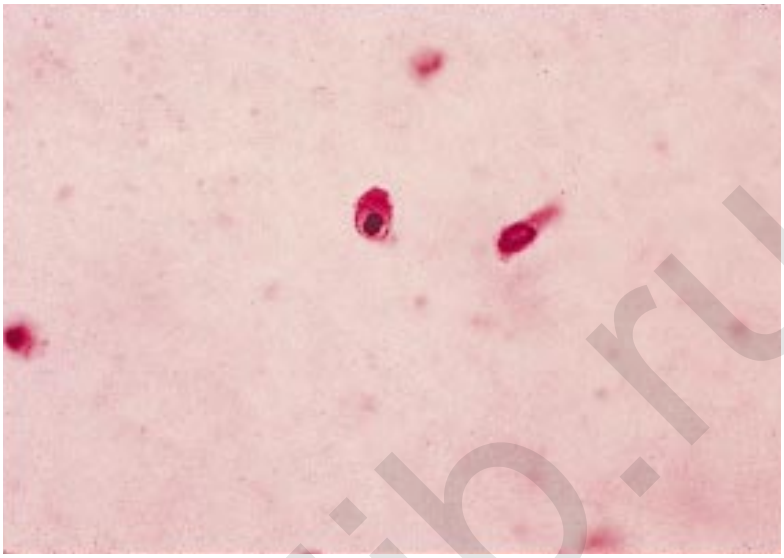

Figure 2.100. Typical "owl's eye" cells in the urine in an infant infected with cytomegalovirus. These cells are distinctive and large, containing intranuclear and cytoplasmic inclusions. (Langston, C.)

2.101

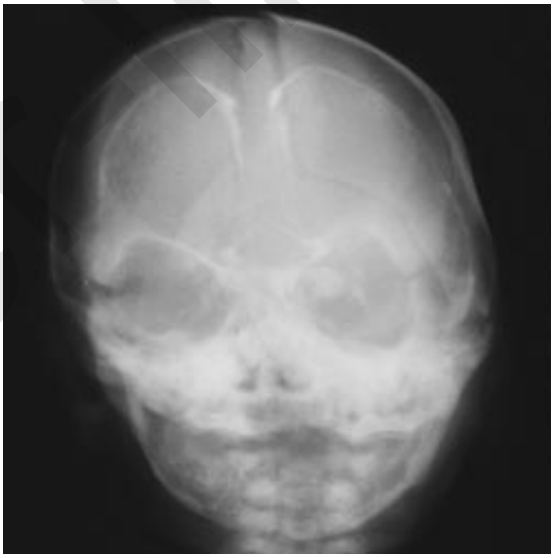

Figure 2.101. Radiograph showing the postero-anterior view of the skull of an infant infected with cytomegalovirus. Note the severe microcephaly and periventricular calcifications. These calcifications demonstrate the marked enlargement of both lateral ventricles. The changes were present at birth.

2.102

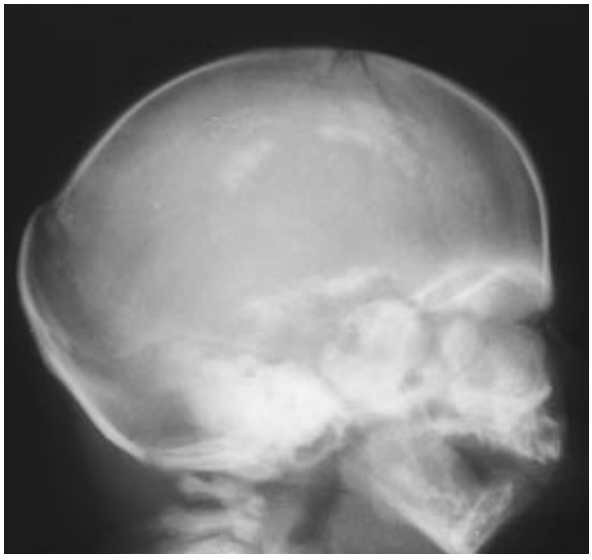

Figure 2.102. Lateral radiograph of the skull of the same infant as in Figure 2.101, again demonstrating microcephaly and periventricular calcifications. Periventricular calcification is seen most commonly in congenital cytomegalovirus infection whereas intracranial calcification in congenital toxoplasmosis is usually more generalized.

2.103

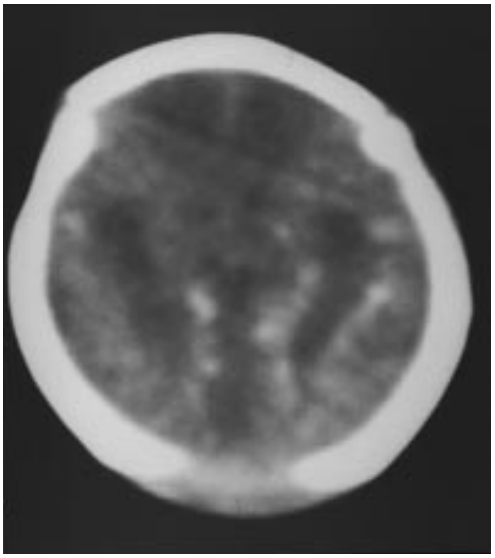

Figure 2.103. CT scan of the head shows periventricular calcifications and dilatation of the ventricles in an infant infected with cytomegalovirus. Intracranial calcification is present in about 20% of infected infants and may be noted much earlier on CT than on initial skull radiographs.

2.104

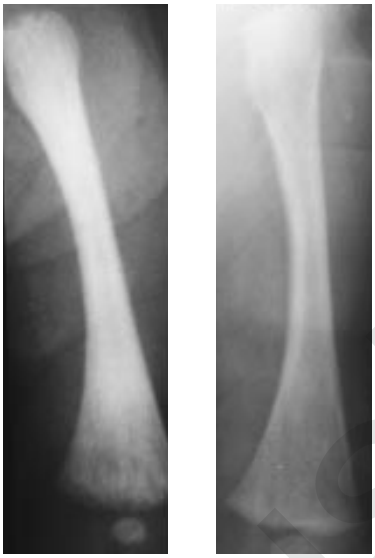

Figure 2.104. The radiograph on the left shows the typical "celery stalk" appearance at the distal end of the femur. This appearance is commonly found in infants with congenital rubella, but on rare occasions can be seen in infants infected with cytomegalovirus. The radiograph on the right shows resolution of the abnormal findings at 1 month of age.

2.105

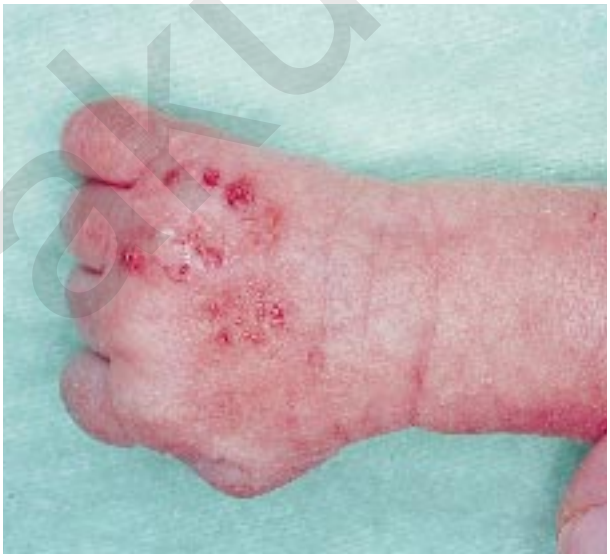

Figure 2.105. Herpetic lesions which appeared on the hand of an infant at the age of 5 days. The skin only was involved in this infant. There was rapid improvement on treatment with intravenous acyclovir. Infection may be acquired as the fetus passes through the birth canal. Thus, although skin lesions may be present at birth, the clinical picture of herpes in the newborn is frequently that of an apparently well infant who becomes symptomatic on the 4th to 8th day of life. The spectrum of illness in herpes simplex virus infection is broad ranging, from death or recovery with severe central nervous system or ocular damage to mild or asymptomatic infection with apparent complete recovery.

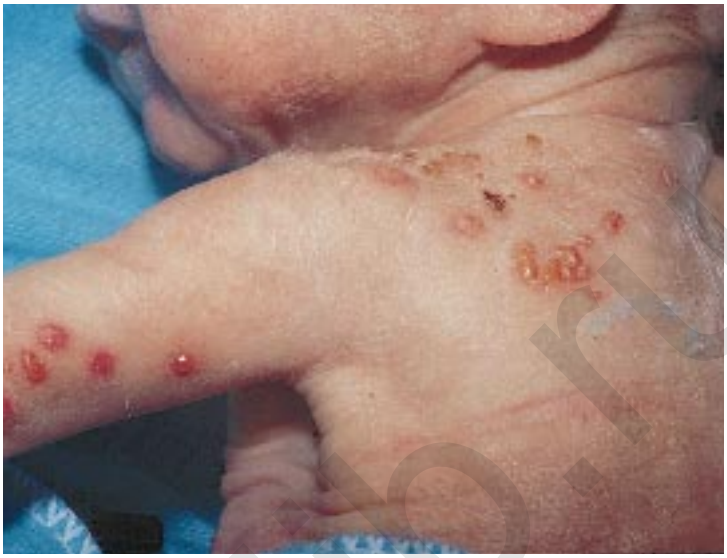

2.106

Figure 2.106. Herpetic lesions which appeared on the skin at 7 days of age in an infant who developed disseminated herpes simplex. Herpetic skin lesions are confluent, fluid-filled vesicles with an erythematous halo around the base. These vesicles become pustular after 24 to 48 hours and eventually become crusted or ulcerated. Most neonatal herpes simplex virus infections (80%) are caused by Type II (genital) herpes virus, acquired either by ascending infection from the mother's genital area to the fetus or by spread during delivery through the birth canal of the infected mother. Infection may be acquired by transplacental spread (about 5% of cases) or by postnatal contact with other infants or personnel with oral herpes simplex virus infections.

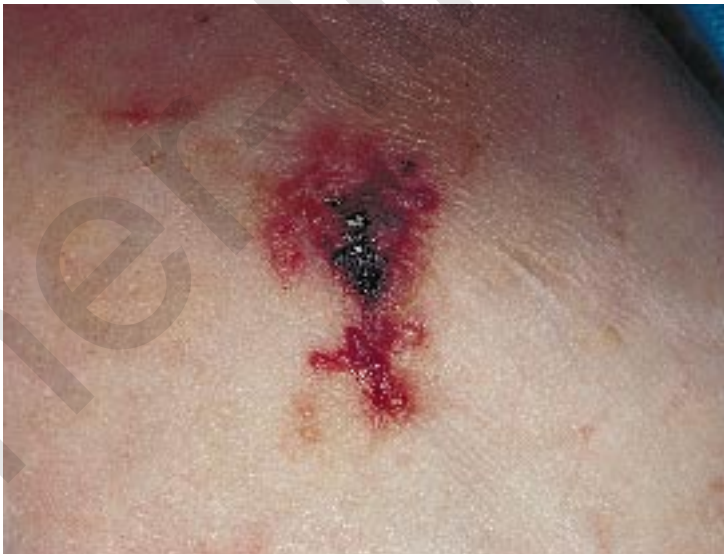

2.107

Figure 2.107. The same infant as in Figure 2.106 developed a fresh crop of skin lesions in the periumbilical area five days later while on systemic therapy. This is not uncommon as herpetic lesions often appear in crops. This infant also had herpes simplex encephalitis. Seventy percent of infants with neonatal herpes simplex virus infection have skin lesions, and 70% of these, if left untreated, will progress to systemic infection. Therefore, treat early.

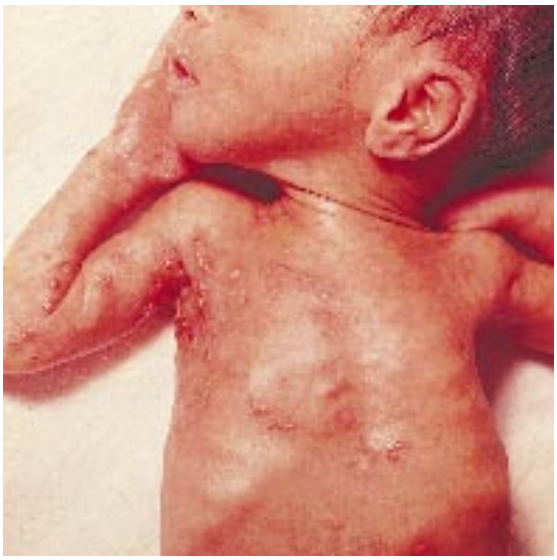

2.108

Figure 2.108. Disseminated neonatal herpes simplex infection in a premature infant who presented with skin involvement at age 6 days. The eruption is zosteriform and has been described in infants with herpes simplex virus infection. Skin lesions that may occur include petechiae, purpura, zosteriform lesions, erythematous macular lesions that eventually develop vesicles within the macules, pustular erosions, and large bullae. About 80% of infected babies develop skin lesions between 1 and 4 weeks of age.

2.109

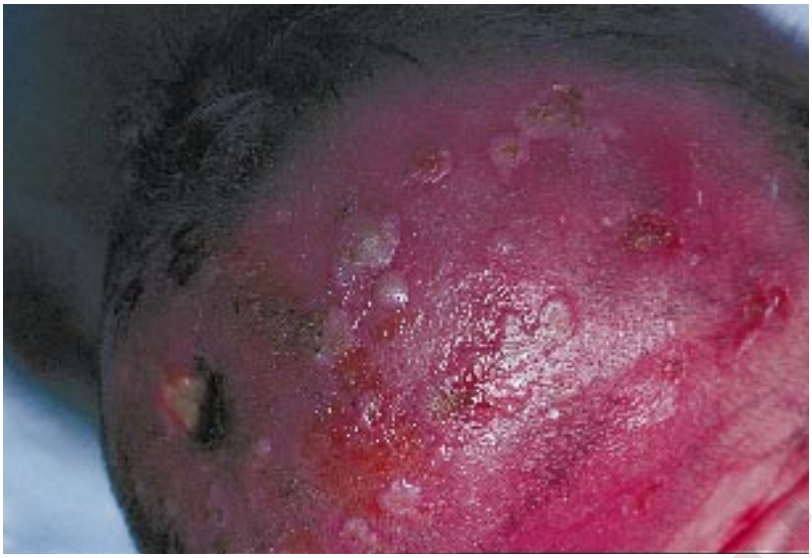

Figure 2.109. Herpetic skin lesions on the scalp in a premature infant (birthweight 1450 g). These lesions on the scalp appeared at the age of 4 days. Occasionally the presenting part of the infant at delivery may be covered by a diffuse edematous swelling resembling that seen in a caput succedaneum. Rather than resolving during the first week, this may become boggy and necrotic with a resultant draining sinus or eschar formation and tense irregular herpetic vesicles.

2.110

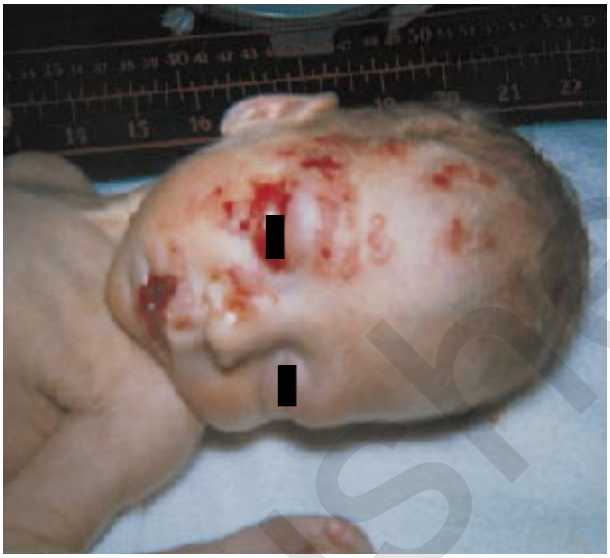

Figure 2.110. Disseminated neonatal herpes simplex infection with skin lesions on the face and eyelids. This infant had keratitis and encephalitis. At times conjunctivitis and keratoconjunctivitis may be seen as the first presenting signs of neonatal herpes infection. This is subsequently followed by lethargy, poor feeding, temperature instability, jaundice, hepatosplenomegaly, and widespread herpes simplex dissemination.

2.111

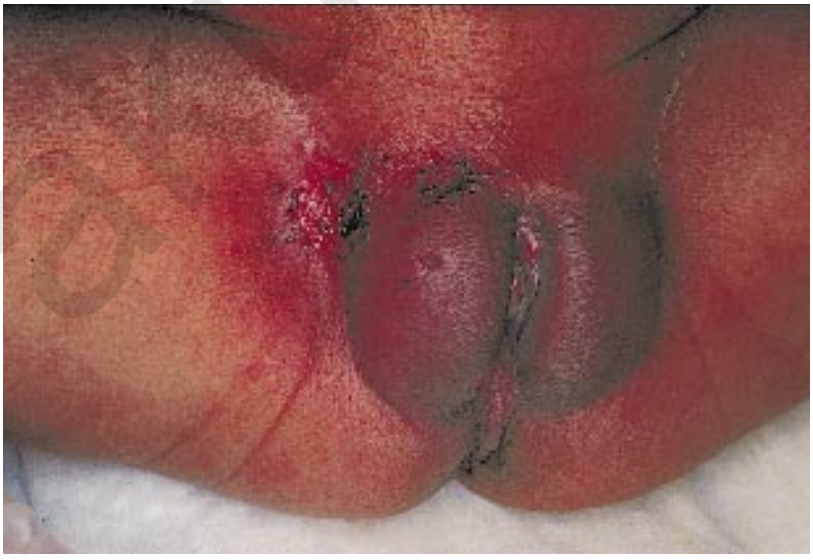

Figure 2.111. Herpetic lesions present on the vulva following a breech presentation. Note also the presence of ecchymoses. Skin lesions occur most often on the scalp and face, the areas which are closest to and in longest contact with the cervical area from which infection is transmitted. Involvement of the cornea in vertex presentations and the genitalia in breech presentations is thus common in herpetic infection.

2.112

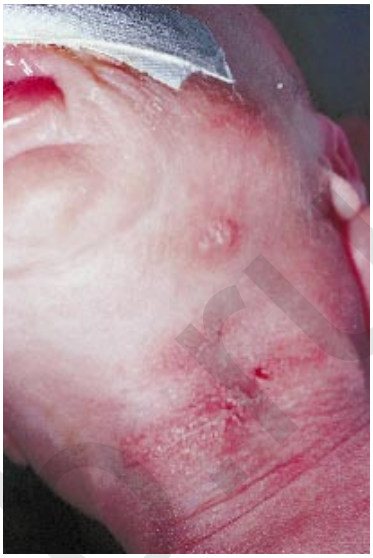

Figure 2.112. Herpetic skin lesions on the neck of a premature infant. A simple Gram stain or Tzanck test would differentiate this from staphylococcal infection. The presence of multinucleated giant cells containing intranuclear inclusions (balloon cells) are characteristic of viral infection.

2.113

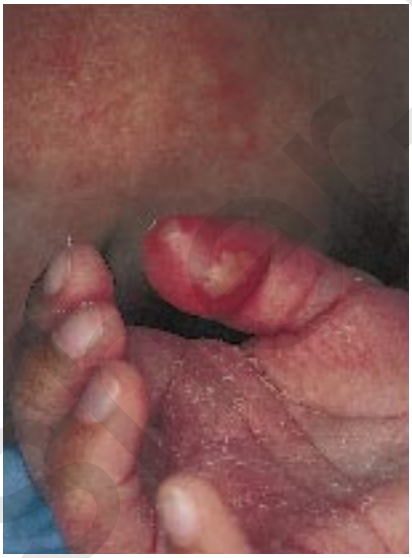

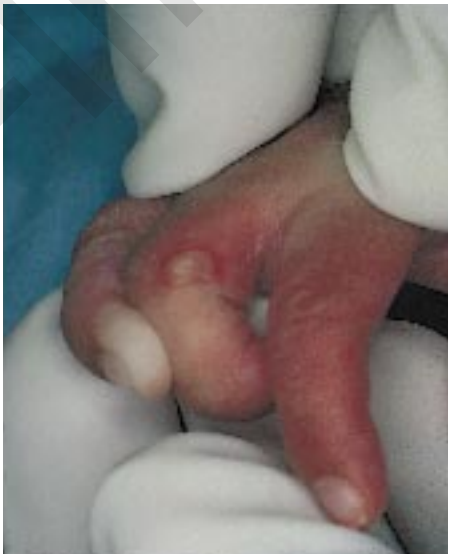

Figure 2.113. This infant with severe intrauterine growth retardation developed herpetic skin lesions and encephalitis. The infant was treated with acyclovir and improved, but the EEG and CT scan were grossly abnormal. One month following treatment he developed a fresh crop of lesions on the right hand (vesicles with paronychia) with resolution after a second course of acyclovir.

2.114

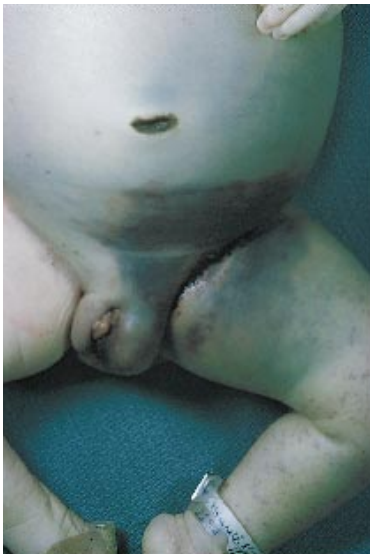

Figure 2.114. This infant presented with cardiovasular collapse and disseminated intravascular coagulopathy. She was well until age 12 days at which time she developed massive ecchymoses and petechiae with bleeding from the umbilical stump and rectum. There was rapid deterioration and death within 2 hours. Autopsy showed disseminated herpetic lesions. There may be hepatitis, pneumonia, coagulopathy with severe bleeding diathesis, and disease of the central nervous system (meningoencephalitis).

2.115

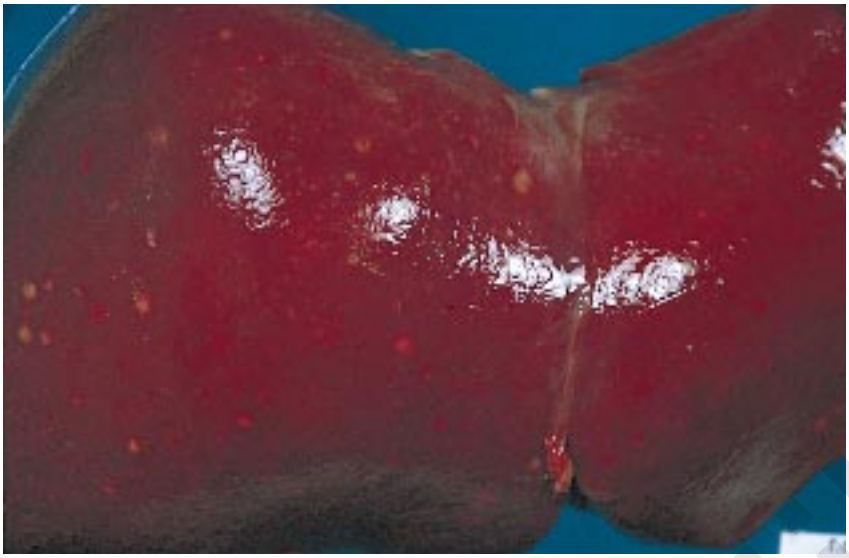

Figure 2.115. Gross pathologic specimen of the liver of the same infant as in Figure 2.114 showing herpetic lesions. The disseminated form of neonatal herpes simplex infection affects the visceral organs, chiefly the liver and adrenal glands. It may also involve the CNS and other organs, and results in a high mortality.

2.116

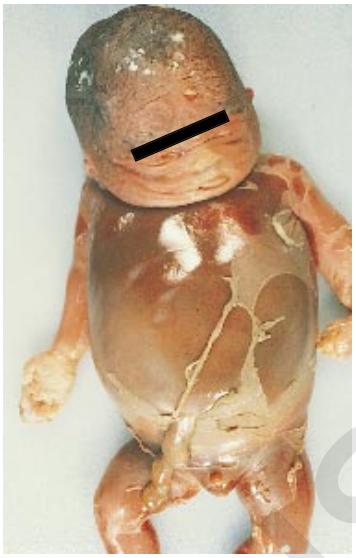

Figure 2.116. Parvovirus B19 infection resulting in intrauterine death in a hydropic stillbirth. Human parvovirus B19, the same virus that causes erythema infectiosum, has a special affinity for rapidly dividing cells, particularly erythroblasts; therefore, an infection may result in profound anemia, hydrops fetalis, and death in the fetus. (Singer, D.)

2.117

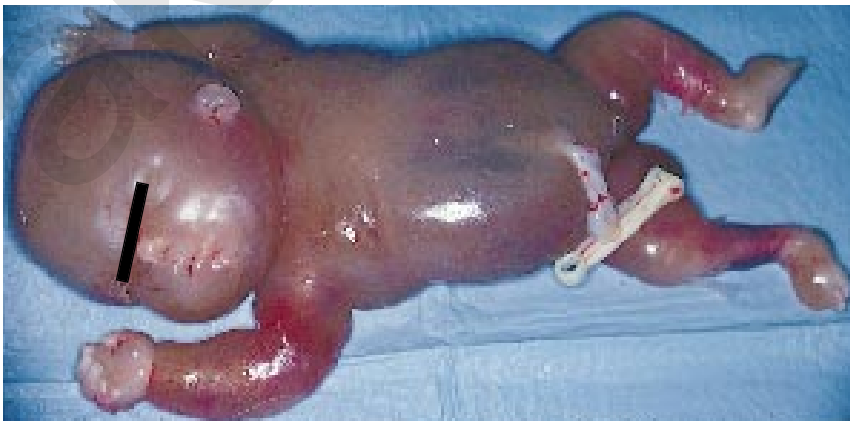

Figure 2.117. Nonimmune hydrops fetalis due to parvovirus B19 infection in a premature infant born at 24 weeks gestation. Note the gross hydrops fetalis. Laboratory analysis was remarkable for a hemoglobin level of 1.4 g/dL, hematocrit of 4%, platelet count of 10,000/mm^3, and WBC count of 6000/mm^3 (which, when corrected for nucleated red blood cells, showed a WBC count of 0).

2.118

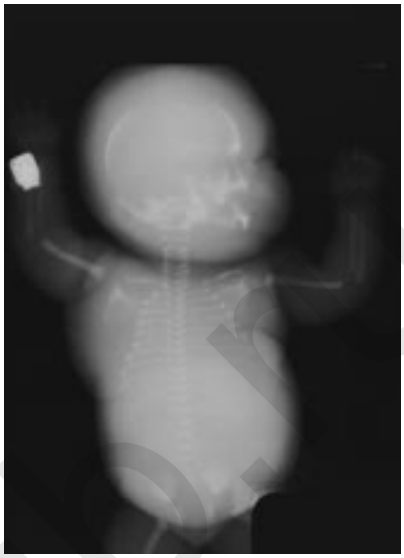

Figure 2.118. Radiograph of the same infant as in Figure 2.117 showing severe hydrops fetalis. Note the massive soft tissue edema. In pregnant women with evidence of infection, maternal serum alphafetoprotein concentration may provide a marker of fetal aplastic crisis. If the concentration is increased, serial ultrasonography may be used to check the possibility of fetal hydrops, and fetal sampling may indicate the severity of fetal anemia. Treatment is by in utero transfusion to the fetus.

2.119

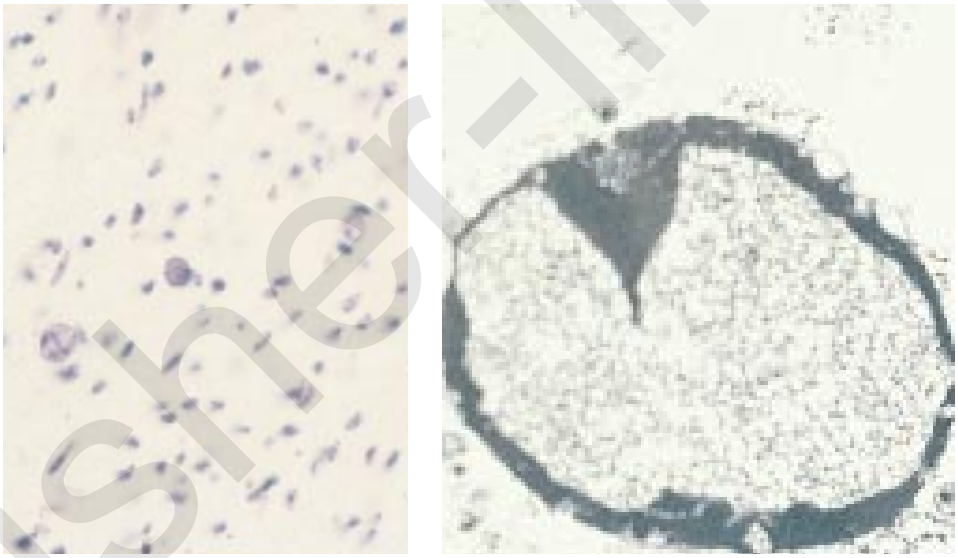

Figure 2.119. Pathologic slide of parvovirus B19 infection in erythroblasts. The virus can be clearly seen on the right in the electron micrograph of a nucleated red cell. (Singer, D.)

2.120

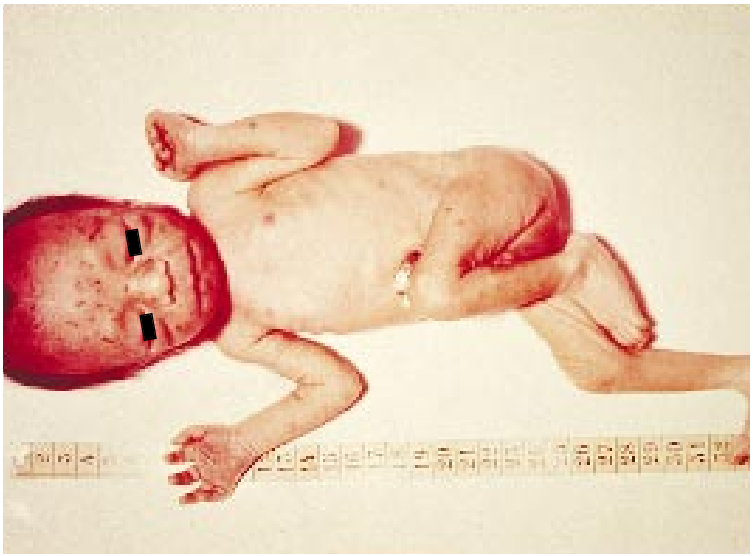

Figure 2.120. Congenital rubella in a term infant with severe intrauterine growth retardation (birthweight 1300 g). Note the "blueberry muffin" appearance. Infected infants are usually born at term, but with low birthweight. In addition to the "blueberry muffin" lesions there may be thrombocytopenic purpura, hyperbilirubinemia, hepatosplenomegaly, pneumonia, congenital cardiac defects (especially patent ductus arteriosus), eye disorders, deafness, and meningoencephalitis.

2.121

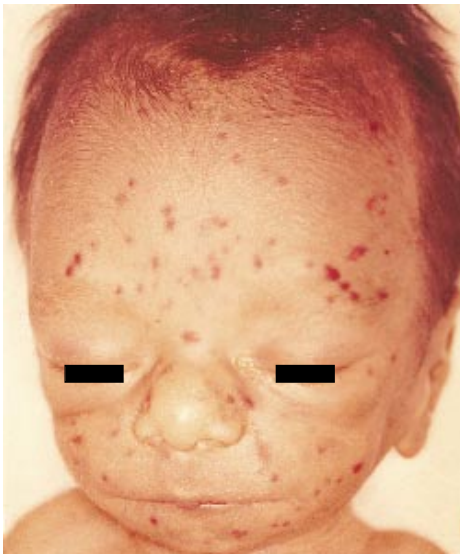

Figure 2.121. Close-up view of the face of the same infant as in Figure 2.120. Note that the "blueberry muffin" lesions in this infant were red rather than purple. In infants with fresh lesions the initial color is dark red but then changes to a bluish-red and dark blue color over the course of a few days. The lesions are infiltrated macules measuring 2 to 8 mm in diameter, are usually present at birth or within the first 24 hours, and new lesions are rare after 2 days.

2.122

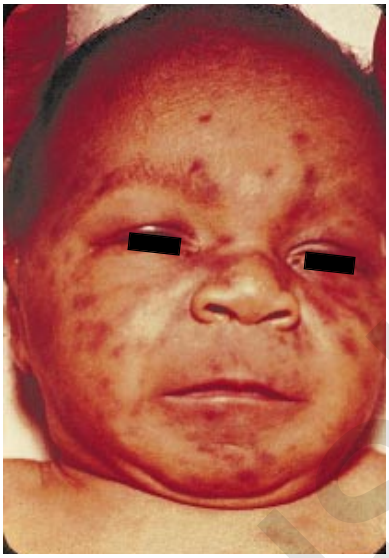

Figure 2.122. This infant shows the typical "blueberry muffin" skin lesions. Histologically, "blueberry muffin" lesions reveal discrete dermal aggregates of relatively large nucleated cells and non-nucleated erythrocytes. They are the result of dermal erythropoiesis (rather than true hemorrhage). These infiltrative lesions, characteristic of viral infections in the fetus, are not unique to infants with congenital rubella but may be seen in congenital cytomegalovirus infection and congenital toxoplasmosis. They also occur in erythroblastosis fetalis, congenital leukemia, etc.

2.123

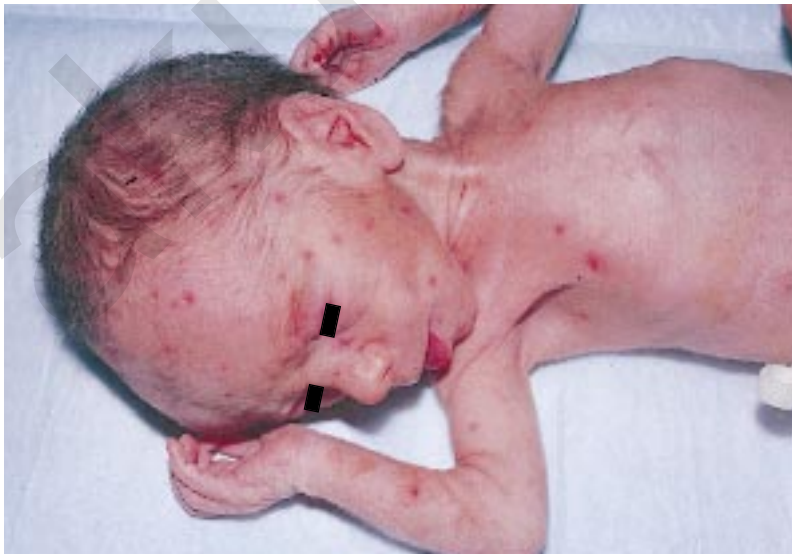

Figure 2.123. The intrauterine growth retardation in congenital rubella may be very striking as shown in this term infant with a birthweight of 860 g. The lesions of congenital rubella may be few or numerous and generally occur on the head, trunk, or extremities. Many of the larger lesions tend to be raised. They usually disappear within 3 to 4 weeks (the larger lesions more slowly than the small flat nodules).

2.124

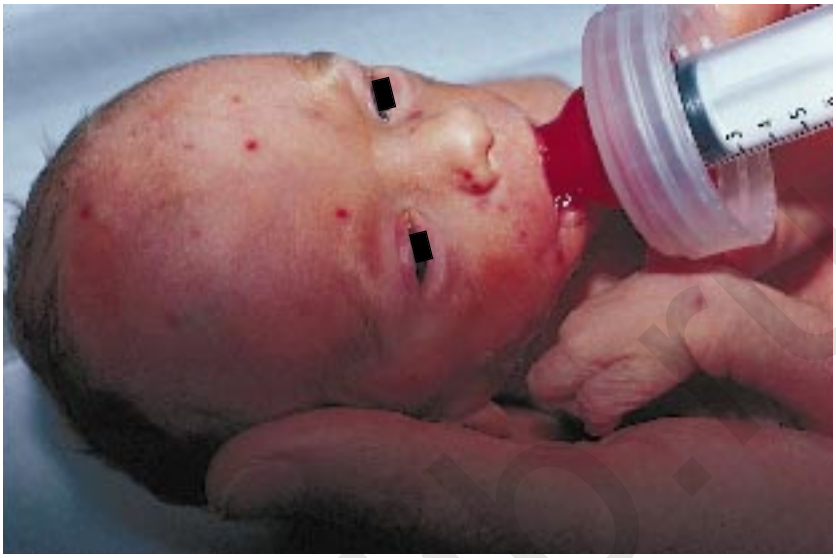

Figure 2.124. Although the infant with congenital rubella was of extremely low birthweight, he nippled all feeds well. Note the presence of a few "blueberry muffin" lesions.

2.125

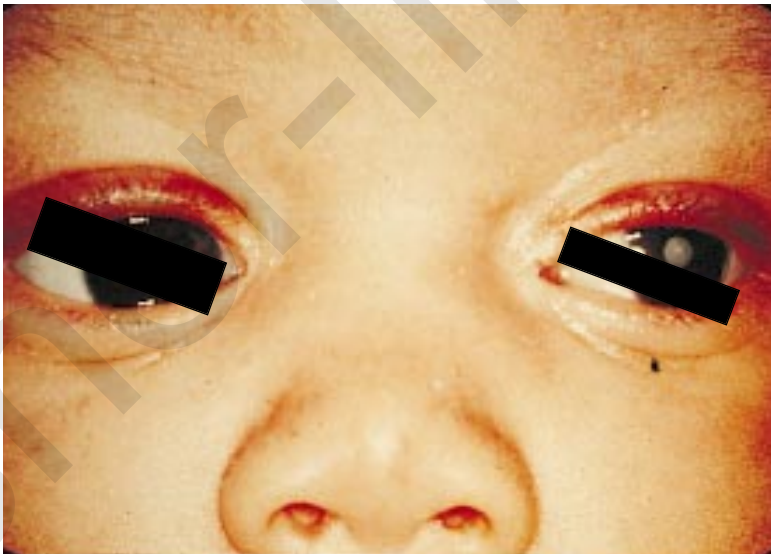

Figure 2.125. Microphthalmia and congenital cataract of the left eye in an infant with congenital rubella.

2.126

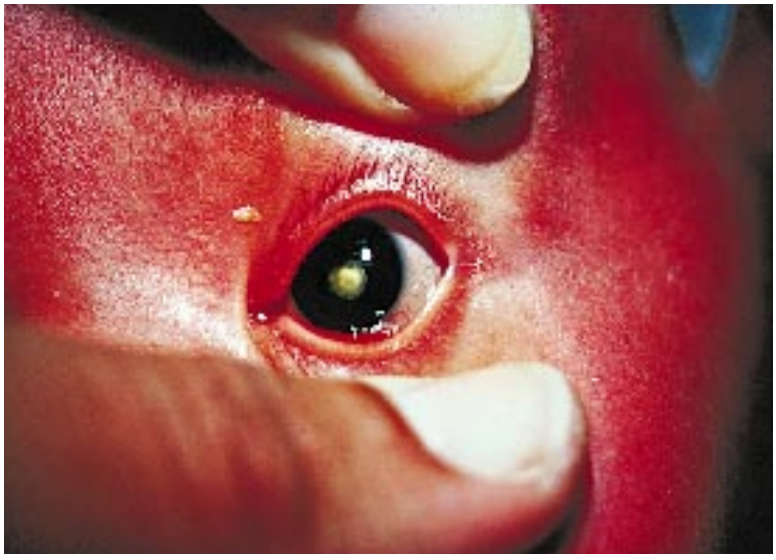

Figure 2.126. Congenital rubella cataract.

2.127

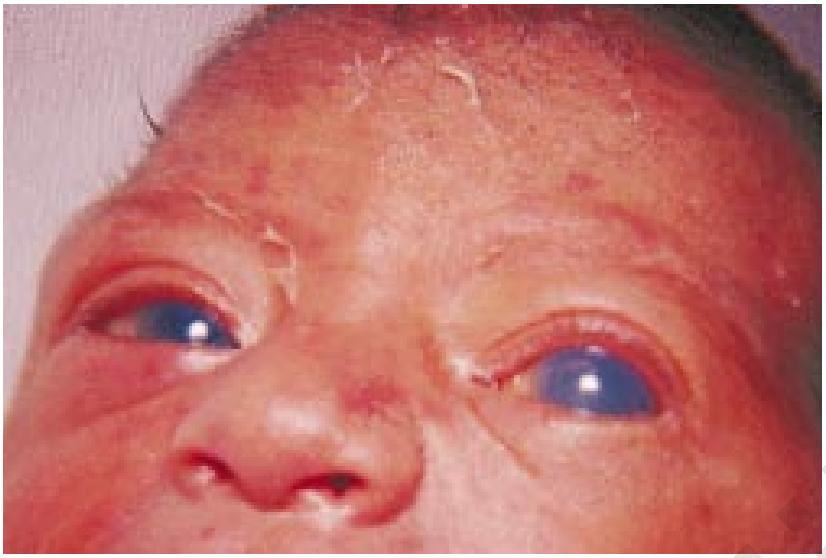

Figure 2.127. Corneal clouding and prominence of left eye due to glaucoma in an infant with congenital rubella. One should suspect glaucoma (buphthalmos) in any infant with a wide or cloudy cornea.

2.128

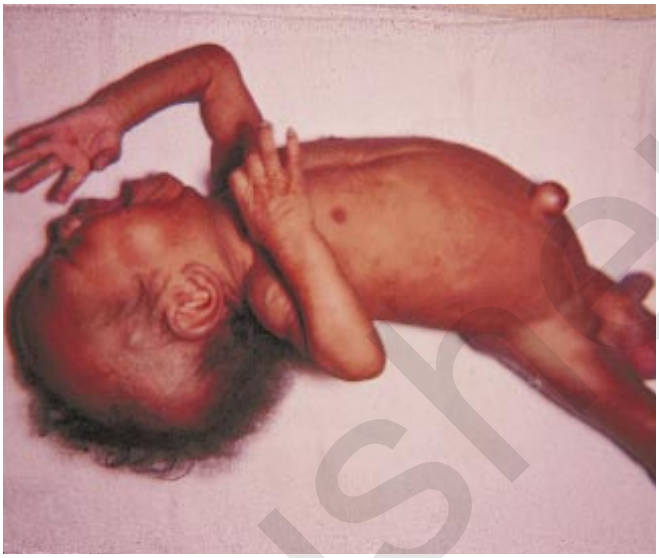

Figure 2.128. Opisthotonos in an infant with congenital rubella encephalitis. Viral culture from cerebrospinal fluid was positive.

2.129

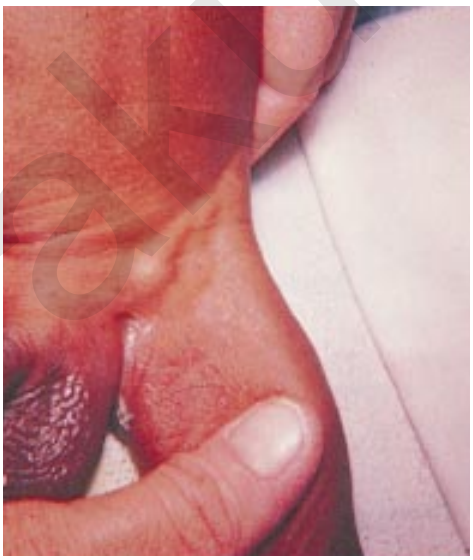

Figure 2.129. Adenopathy in an infant with congenital rubella. Enlargement of lymph nodes is uncommon in the neonate, but is described in infants with other viral syndromes and in congenital syphilis where the epitrochlear glands especially are enlarged.

2.130

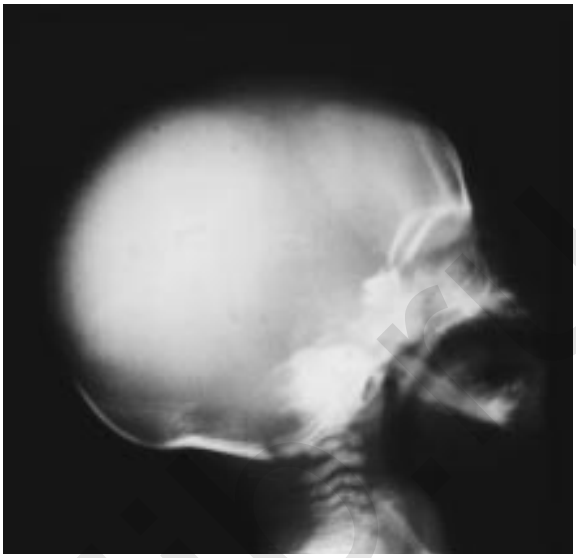

Figure 2.130. Lateral radiograph of the skull in an infant with congenital rubella. Note the very large anterior fontanelle, prominent sutures and poor mineralizaton of the calvaria. Bony abnormalities are seen at birth in up to 80% of infants with congenital rubella. These include the large anterior fontanelle and characteristic "celery stalk appearance." These bony abnormalities also resemble those of other fetal viral infections such as cytomegalovirus.

2.131

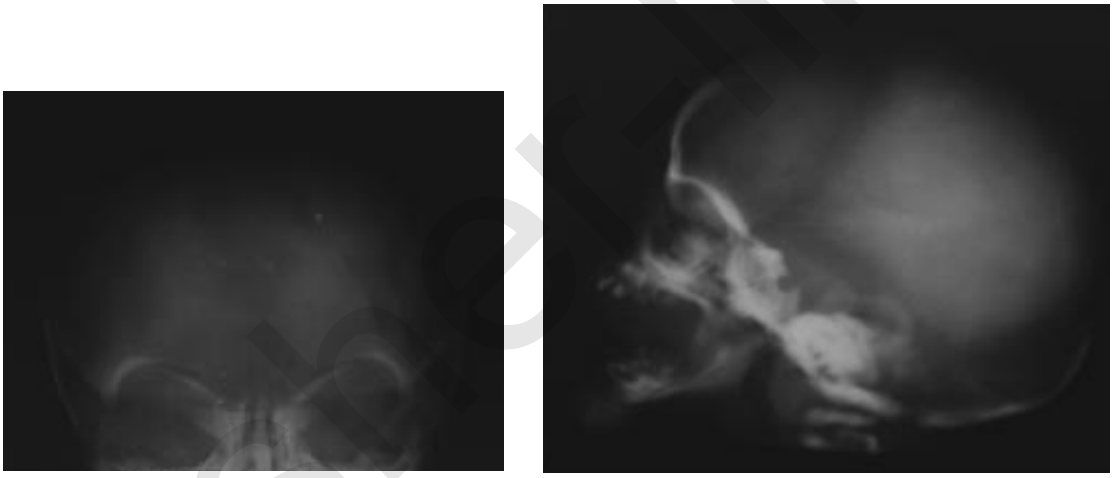

Figure 2.131. Anterior-posterior and lateral views of the skull in an infant with congenital rubella. Note the large anterior fontanelle which extends into the metopic suture with poor mineralization of the calvaria.

2.132

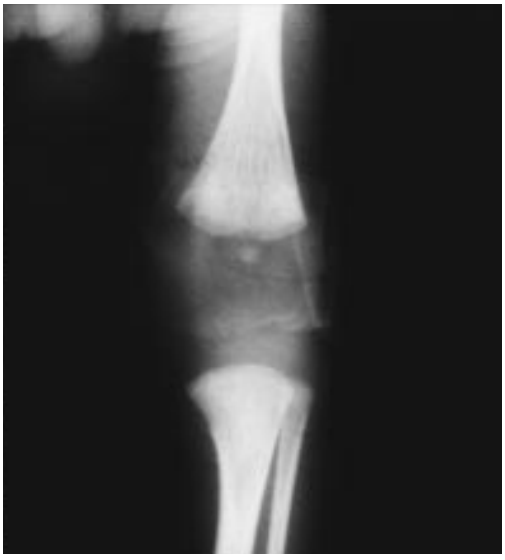

Figure 2.132. Lower extremity radiograph showing the typical "celery stalk" appearance particularly at the distal end of the femur. The longitudinal areas of radiolucency in the metaphyses of the long bones give rise to the radiographic appearance of "celery stalks." This appearance is especially noted at the distal ends of the femur or the proximal tibia.

2.133

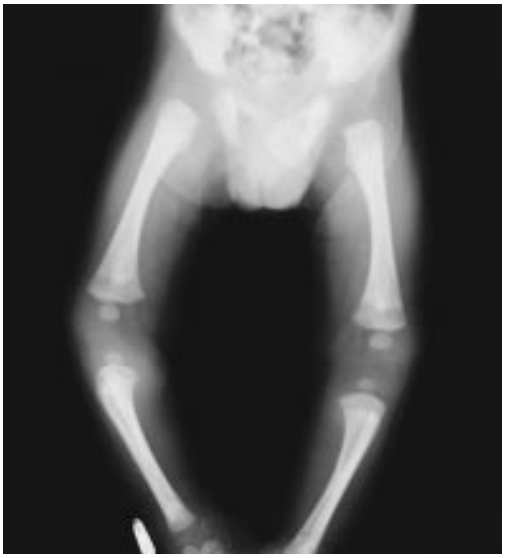

Figure 2.133. Lower extremity radiograph in an infant with congenital rubella at 3 weeks of age. Note the radiolucent zones paralleling the growth plates with residual irregular trabecular pattern. These are the nonspecific growth arrest lines which may be seen in any condition interfering with the growth of the fetus in utero.

2.134

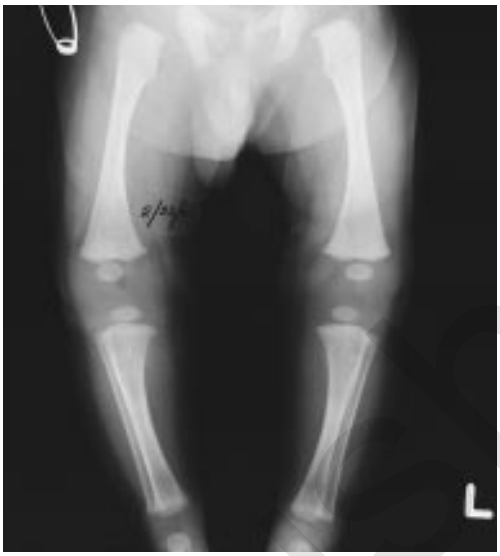

Figure 2.134. Repeat radiographs of the same infant as in Figure 2.133 at 2 months of age showing the regression of these changes.

2.135

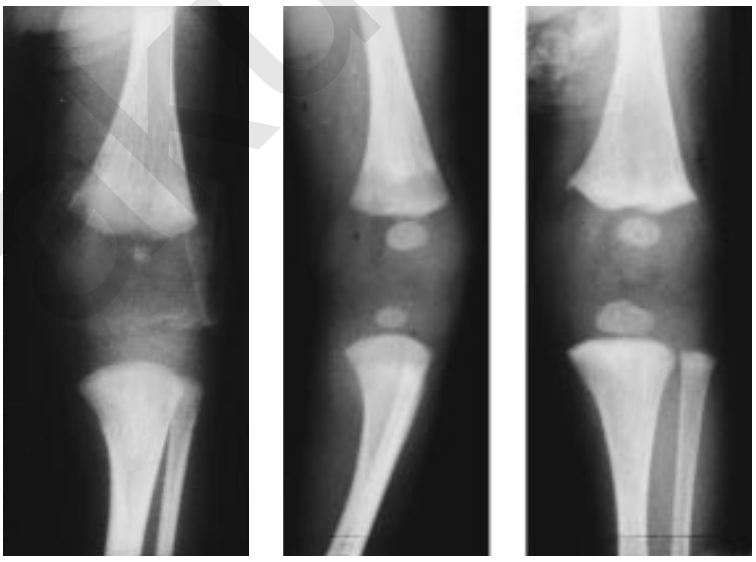

A) *B)* *C)*

Figure 2.135. Radiograph composite that demonstrates the types of bony changes found in congenital rubella syndrome: from left to right, *A)* "celery stalk" appearance; *B)* nonspecific growth arrest lines; *C)* a bony spicule at the medial condyle of the femur (an uncommon finding). All of these regress over the first few months postnatally.

2.136

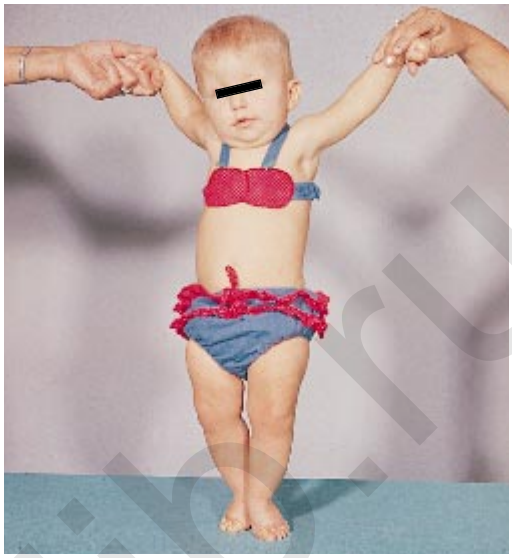

Figure 2.136. Children with congenital rubella may have a normal physical and neurodevelopmental outcome, although it is uncommon. Maternal rubella in the first 4 weeks of pregnancy carries a risk of congenital rubella of 50% (heart anomalies, eye defects, hearing problems, etc.); between the 12th and 16th weeks of pregnancy the risk decreases to 2 to 6%; and between the 18th to 20th weeks of pregnancy the risk is practically nil. Over 80% of babies with congenital rubella shed virus during the first month of life, and 5 to 10% (those severely affected), for one year.

2.137

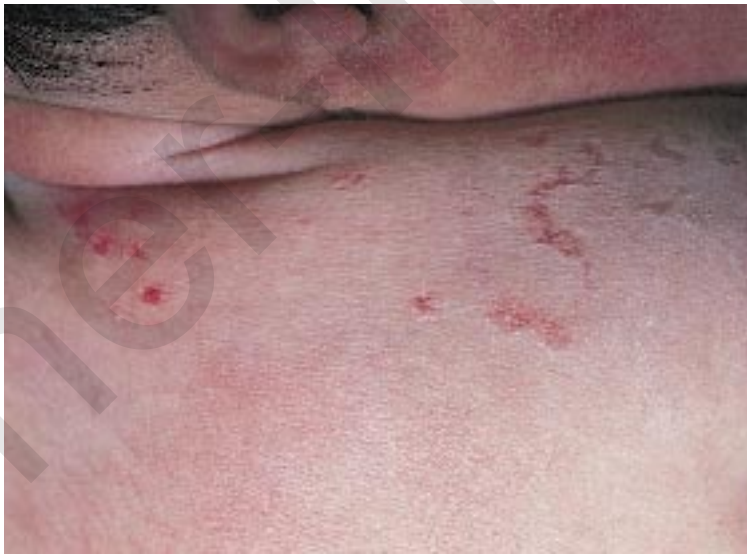

Figure 2.137. Cicatricial skin lesions of the neck and upper back in an otherwise normal infant following maternal varicella at 5 months gestation. These skin lesions are the most common finding after maternal varicella which presents in the 1st and early 2nd trimester. Maternal infection with varicella early in pregnancy is a cause of fetal malformations including reduction deformities of the limbs (hypoplastic limbs and/or contractures) and scars along the length of the affected limbs. The infant may be small for gestational age and demonstrate features of central nervous system involvement (encephalomyelitis) and eye defects (microphthalmia, cataracts, and chorioretinitis).

2.138

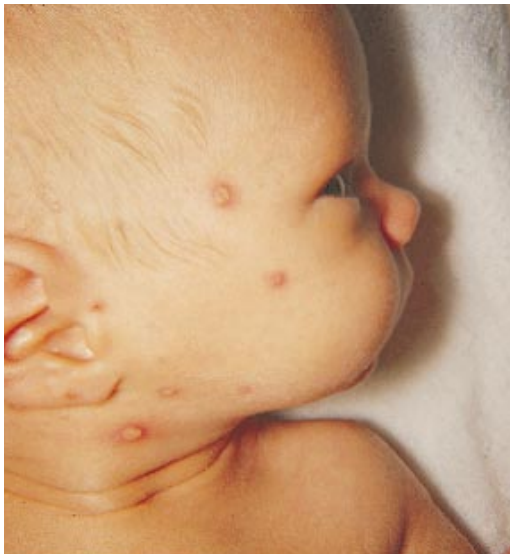

Figure 2.138. Congenital varicella in an infant which presented at the age of 7 days. Mother developed varicella 10 days prior to delivery. This infant had very few lesions and was not ill. If the onset in the mother is within 4 days prior to or within 48 hours after delivery, or if the onset in the newborn is between 5 to 10 days after birth, the infant's condition is usually more severe. In these cases, varicella-zoster immune globulin (VZIG) should be given as soon as possible after birth.

2.139

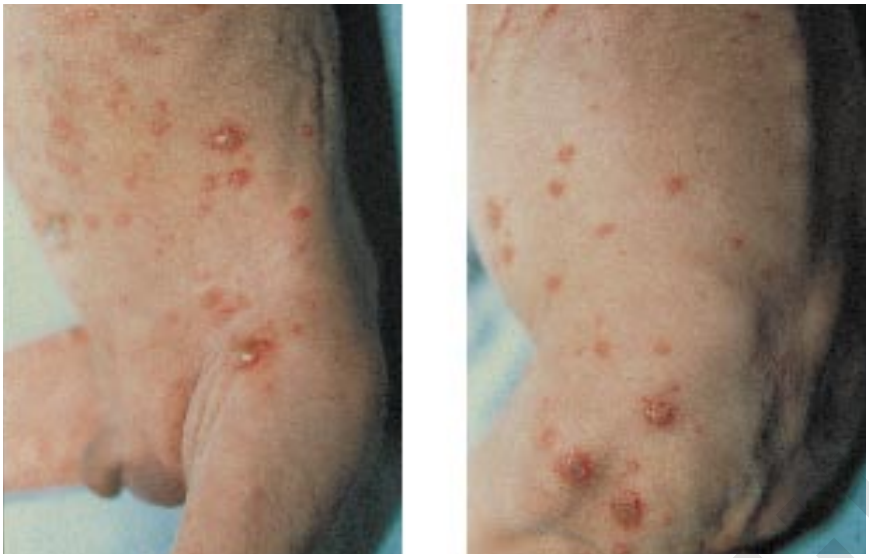

Figure 2.139. Another case of congenital varicella infection. Complications of congenital varicella may be disseminated and fulminant with pneumonia, hepatitis, or encephalomyelitis, and mortality is high. (Cabrera-Meza, G.)

2.140

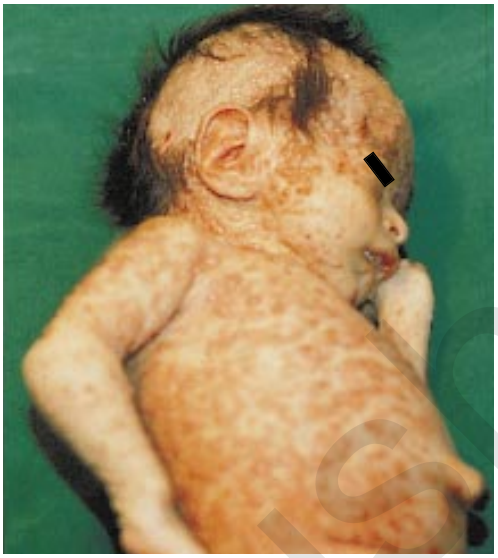

Figure 2.140. This neonate with congenital varicella has extensive skin involvement. (Cabrera-Meza, G.)

2.141

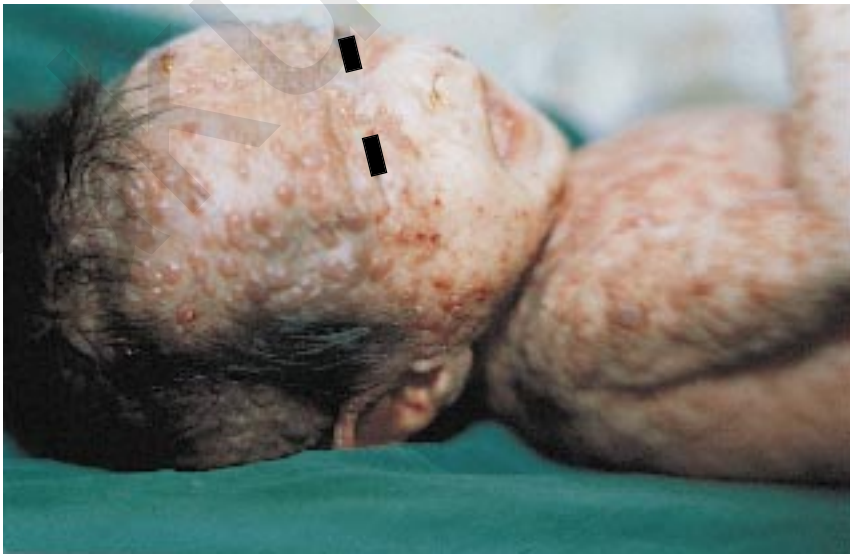

Figure 2.141. Close-up of the same infant as in Figure 2.140 with congenital varicella, showing extensive skin lesions at different stages. (Cabrera-Meza, G.)

PROTOZOAL AND PARASITIC INFECTIONS

2.142

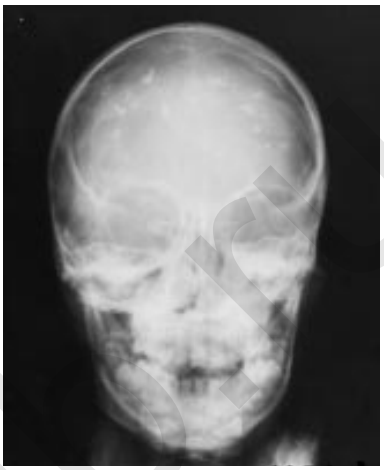

Figure 2.142. Anteroposterior (AP) skull radiograph in a child with congenital toxoplasmosis. Note the diffuse areas of intracranial calcification. This is characteristic of toxoplasmosis and may be associated subsequently with hydrocephalus or microcephaly. *Toxoplasma gondii* infection is transmitted to the fetus by invasion of the bloodstream during the stage of maternal parasitemia, and may result in a wide spectrum of clinical signs and symptoms. The fetus may be stillborn, born prematurely, or born at full term.

2.143

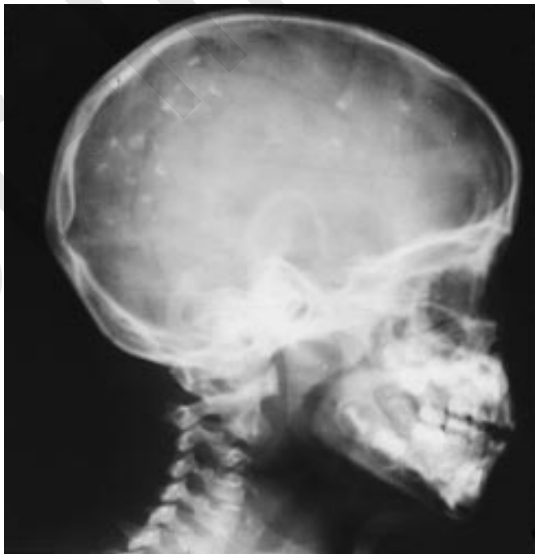

Figure 2.143. Lateral radiograph from the same child as in Figure 2.142, showing diffuse intracranial calcifications. Intracranial calcifications, in general, are diffuse and scattered in infants with congenital toxoplasmosis. Skull radiographs of infected infants frequently reveal this diffuse punctate intracranial calcification. The distribution of the calcification in infants with congenital cytomegalovirus infection is periventricular.

2.144

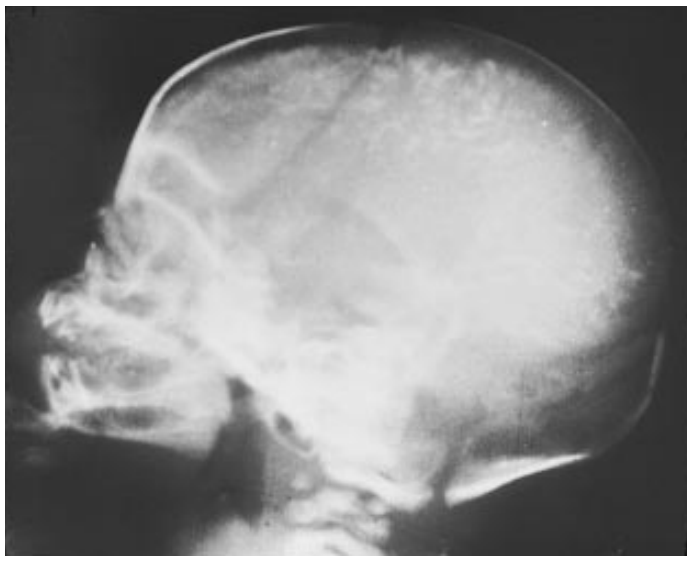

Figure 2.144. Lateral radiograph of the skull of a newborn infant infected with both toxoplasmosis and cytomegalovirus. Diffuse intracranial calcifications are present.

2.145

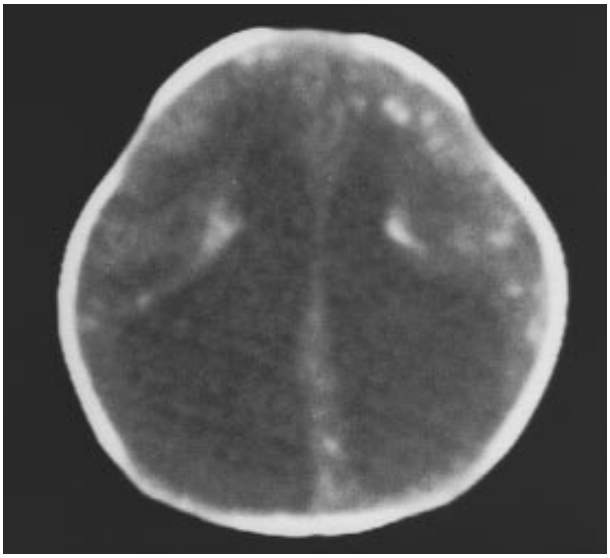

Figure 2.145. A CT scan in an infant with toxoplasmosis at the age of 22 days, showing the scattered intracranial calcification with some brain destruction.

2.146

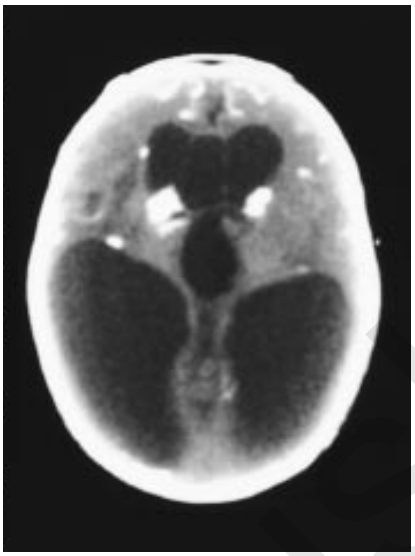

Figure 2.146. The CT scan of another infant at the age of 1 month showed marked brain destruction with scattered intracranial calcifications and hydrocephalus ex vacuo. The illness is usually apparent at birth in that the infant may have fever, poor feeding, vomiting and diarrhea, jaundice, and hepatosplenomegaly. There may be a maculopapular rash or "blueberry muffin" lesions as well as microphthalmia, cataracts, and chorioretinitis. The chorioretinitis is in the region of the macula and is seen in about 80% of infants with congenital toxoplasmosis.

2.147

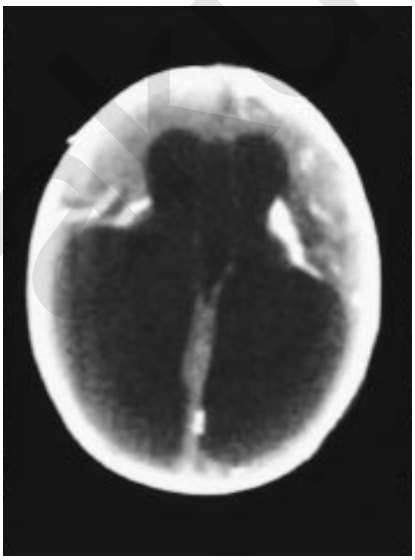

Figure 2.147. CT scan of the same infant several days later with congenital toxoplasmosis. Note the rapid progress with massive loss of brain parenchyma and multiple scattered areas of calcification. Peripheral white blood count was remarkable for 96% eosinophils. There were numerous eosinophils in the cerebrospinal fluid. In toxoplasmosis, anemia, thrombocytopenia, and at times severe leukopenia may be present. The cerebrospinal fluid is xanthochromic, has an elevated protein level, and may contain erythrocytes and leukocytes.

2.148

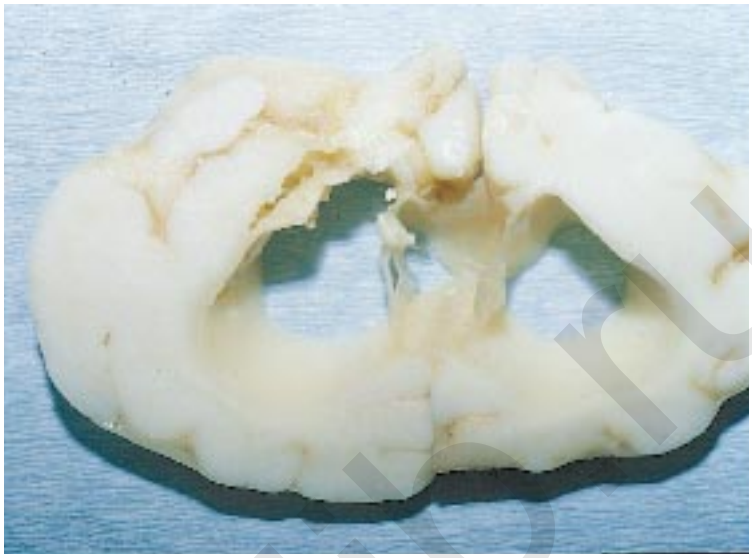

Figure 2.148. Pathologic specimen showing a section of the brain from the same infant as in Figure 2.147. Note the hydrocephalus and cortical necrosis present at autopsy.

2.149

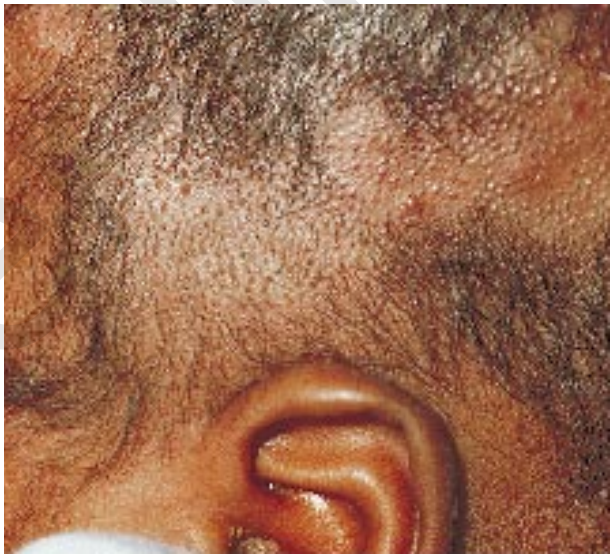

Figure 2.149. This infant has neonatal tinea capitis (ringworm), which was diagnosed at the age of 3 weeks. The condition is rarely seen in the neonate. Lesions are sharply outlined and ring- or disc-shaped, and there may be confluent areas of alopecia with areas of broken and brittle hair observed on an erythematous, scaling scalp (silvery scales). The diagnosis of ringworm of the scalp can frequently be made by the presence of fluorescence under a Wood's light (the affected scalp appears green due to fluorescence of the infected hairs) or by microscopic examination of infected hairs. In the neonate, the infection is usually produced by *Microsporon canis*, *M. audouinii*, or *Trichophyton tonsurans*. The hair does not fluoresce in a *Trychophyton tonsurans* infection. (Levy, M., Moise, K.)

2.150

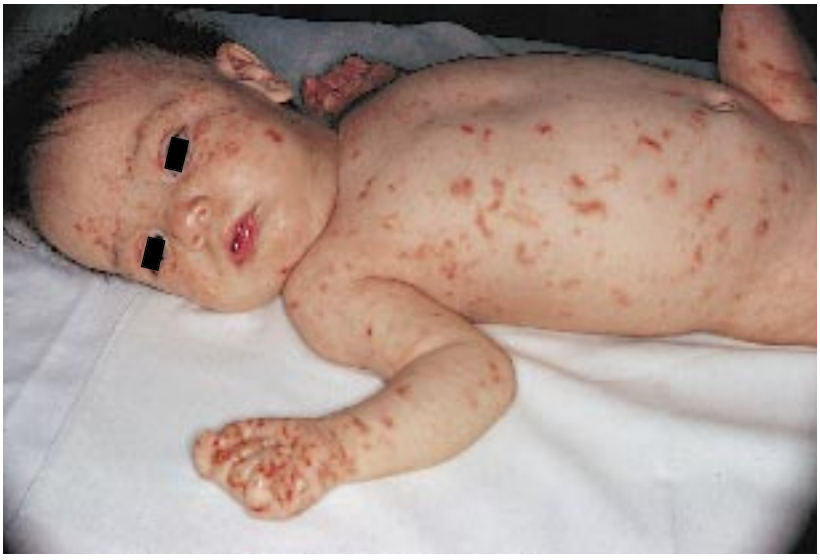

Figure 2.150. This infant presented with scabies at the age of 17 days. The mother had scabies. This parasitic infection is uncommon in the neonate. The distribution of the lesions is different from that of the older child in that the face, head, and neck may be involved, especially if the mother is breastfeeding. There may be scabetic burrows, papules, and vesicular lesions. In addition there is involvement of the usual areas such as the flexor surfaces of the extremities, the interdigital spaces, the groins and the axilla.

2.151

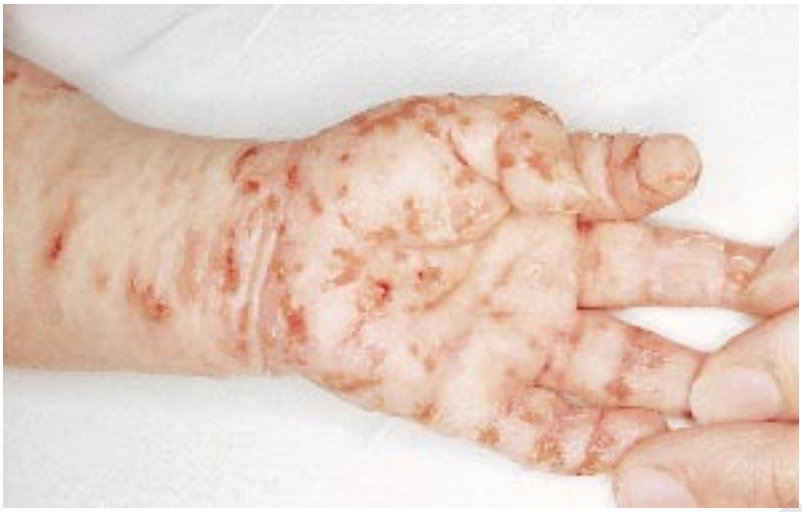

Figure 2.151. A close-up of the hand in the same infant as in Figure 2.150 showing the typical scabetic lesions. Primary lesions are burrows, papules, and vesicular lesions. Secondary bacterial infection causing pustules may occur.

2.152

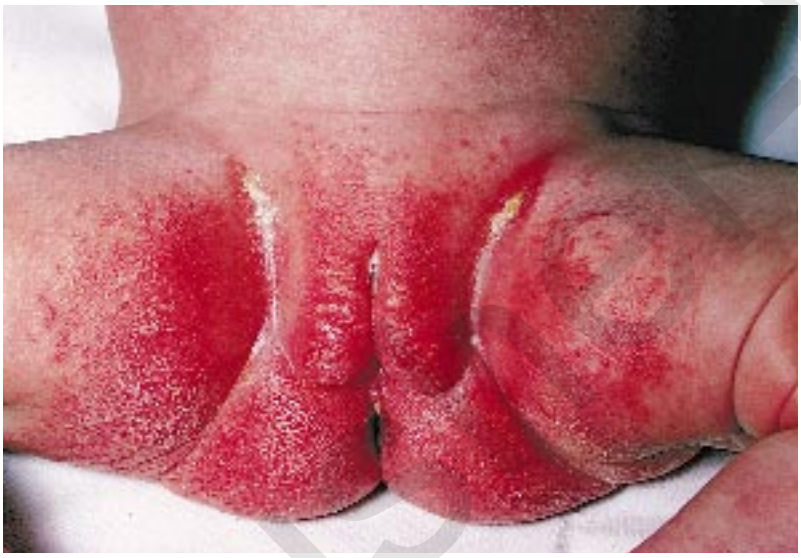

Figure 2.152. Typical candidal diaper dermatitis. Note the symmetric distribution of the rash with involvement of the intertriginous areas. Satellite lesions are often present. The skin is erythematous, swollen and slightly scaly. With healing, areas of depigmentation may occur. This should be differentiated from an ammoniacal diaper dermatitis where the rash is generally asymmetric, the intertriginous areas are spared, and satellite lesions are absent as it is a contact dermatitis.

2.153

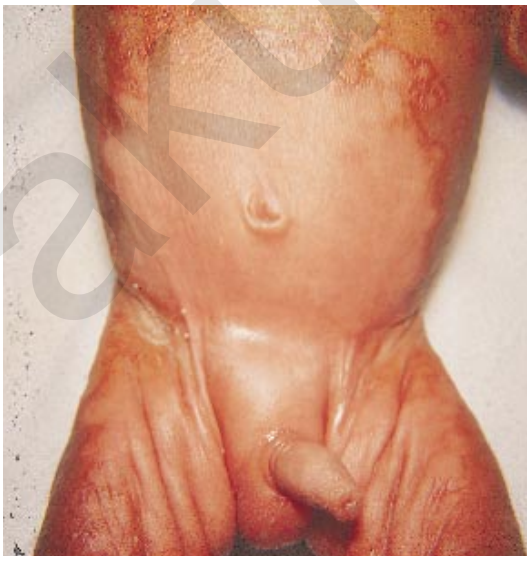

Figure 2.153. An infant with healed candidal dermatitis showing symmetrical depigmentation. Note the healed satellite areas. Candidal (monilial) dermatitis is a commonly overlooked disorder and should be suspected whenever a diaper rash fails to respond to usual measures.

2.154

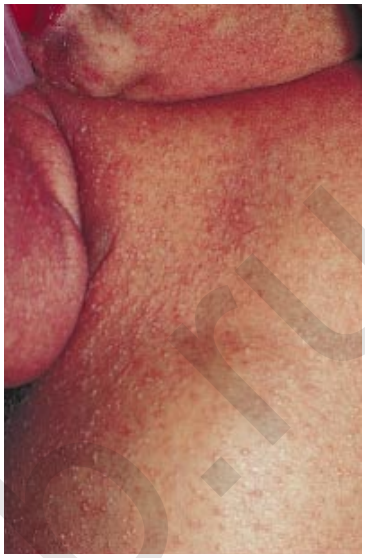

Figure 2.154. Congenital cutaneous candidiasis in an infant at age 3 days. Potassium hydroxide (KOH) scrapings of the skin were positive for hyphae. Mucocutaneous candidiasis may present as a vesicular dermatitis in the first week of life. The vesicular lesions become confluent and rupture, leaving a denuded area surrounded by satellite lesions or pustules. Congenital candidiasis may have only skin manifestations or there may be severe systemic involvement following the intrauterine infection.

2.155

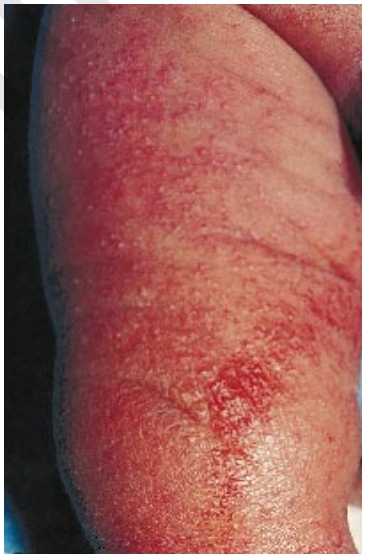

Figure 2.155. Close-up of the skin of the same infant as in Figure 2.154. Note the pinpoint pustulovesicular lesions. Diagnosis can be confirmed by culture on Sabouraud's or Nickerson's media.

2.156

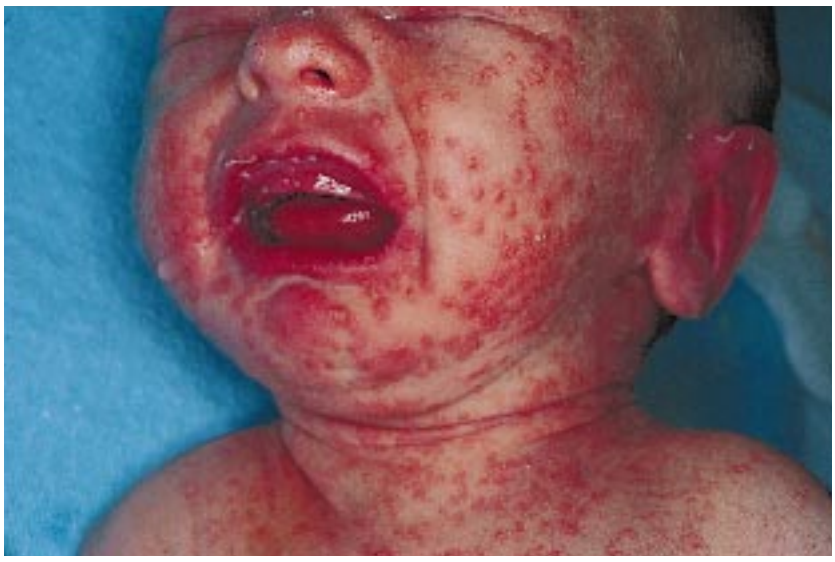

Figure 2.156. Congenital disseminated mucocutaneous candidiasis in an infant at age 5 days. Note the thrush with the generalized skin rash. These infants are generally well and have no systemic involvement. Although cutaneous candidiasis frequently occurs in association with oral thrush, commonly the mouth is bypassed and the infection is confined exclusively to the diaper area. Infants harbor *Candida albicans* in the lower intestine, and it is from this focus that infected feces present the primary source for candidal diaper rash.

2.157

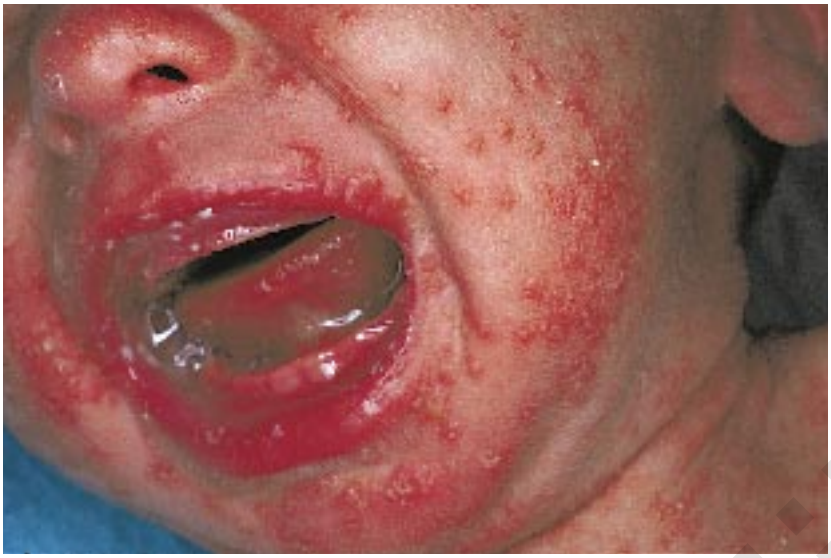

Figure 2.157. Close-up of the mouth and face in the same infant as in Figure 2.156. The white plaques on the tongue and buccal mucosa resemble milk curds; they are difficult to detach from the mucosa and leave a raw erythematous base.

2.158

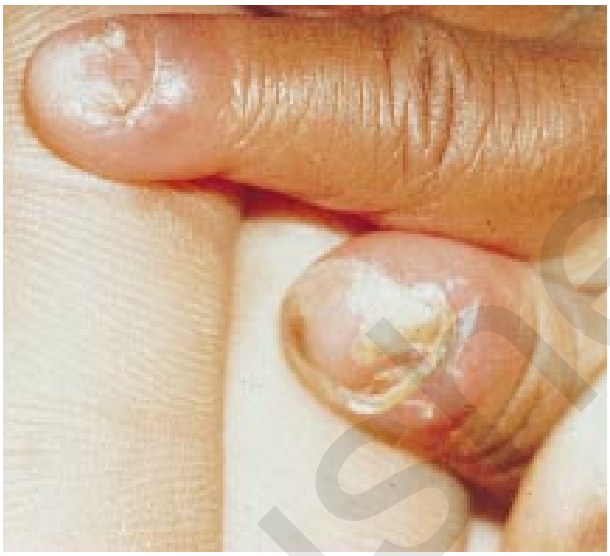

Figure 2.158. This premature infant developed candidal infection of the nails (onychomycosis) at the age of 3 weeks. Premature infants with thrush are more likely to develop infection of the nails from hand-mouth contact. Candidal infection almost exclusively affects the fingernails, whereas tineal infection more frequently affects toenails. In candidal infection the nail plate may be fragile and thick and may show grayish-white spots or brown discoloration of the nail edge. As there frequently is an associated paronychia in candidal infection, the adjacent cuticle is pink, swollen, and tender (caused by secondary staphyloccal infection). (Levy, M., Moise, K.)

2.159

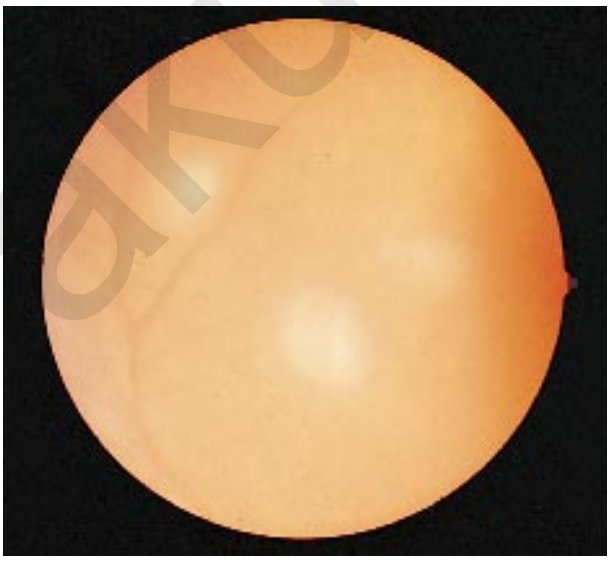

Figure 2.159. Candidal endophthalmitis as represented by the appearance of "cotton" patches is observed in an infant with systemic candidiasis. These lesions are diagnostic of a systemic candidal infection.

2.160

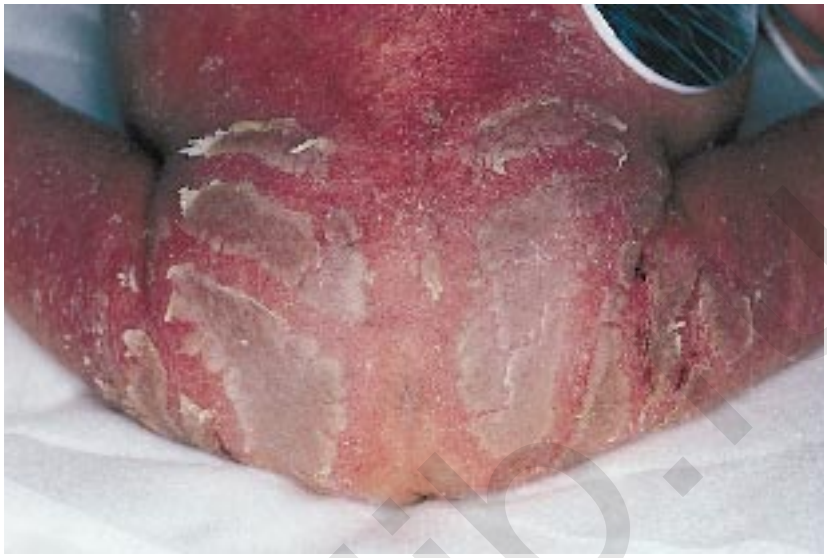

Figure 2.160. Candidal infection of the back and buttocks in a small premature infant (birthweight 775 g) at the age of 10 days. Hyphae were present both on the skin and in the urine.

2.161

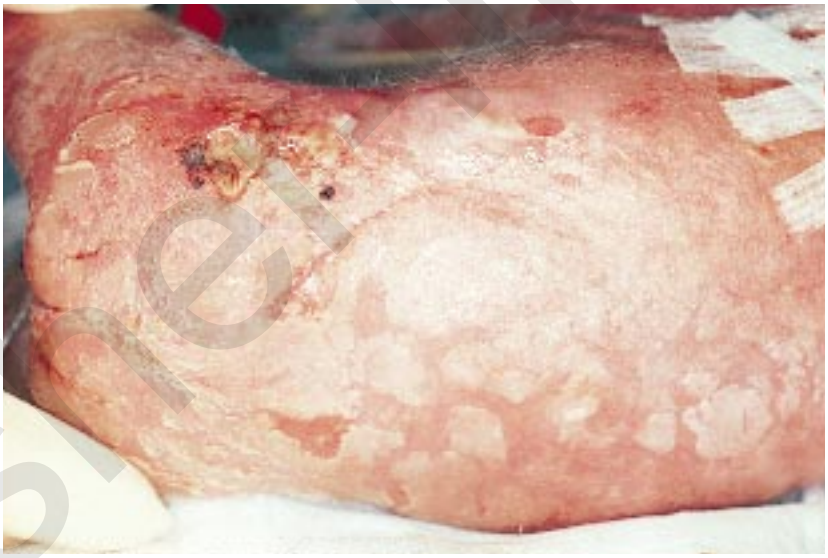

Figure 2.161. Candidal infection of the back in a premature infant of 24 weeks gestation (birthweight 680 g). The severe skin involvement was noted at 9 days of age when the condition of the infant was stable. There was minimal handling of the infant prior to this. This infant developed a patent ductus arteriosus which required ligation. Intravenous therapy with amphotericin was not successful.

2.162

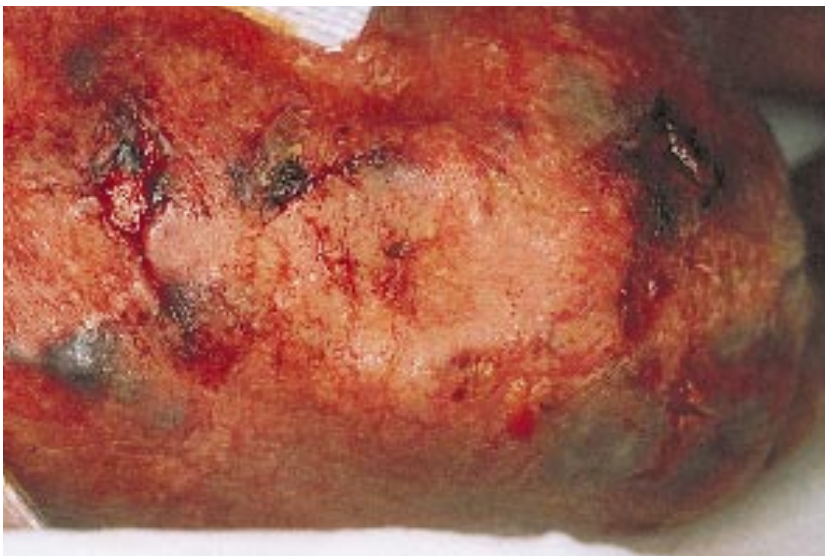

Figure 2.162. Severe disseminated candidiasis in a premature infant (birthweight 690 g). On the 13th day of life he developed the severe rash on his back. Hyphae were present in these lesions. The infant had resolution of fungemia and skin involvement with amphotericin therapy.

2.163

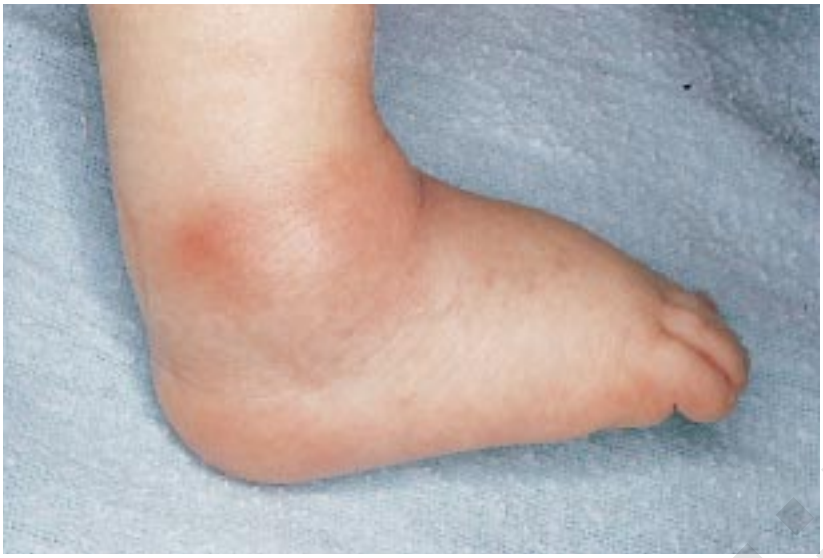

Figure 2.163. Candidal arthritis of the right ankle in an infant who developed candidal sepsis while on prolonged total parenteral nutrition for short bowel syndrome.

2.164

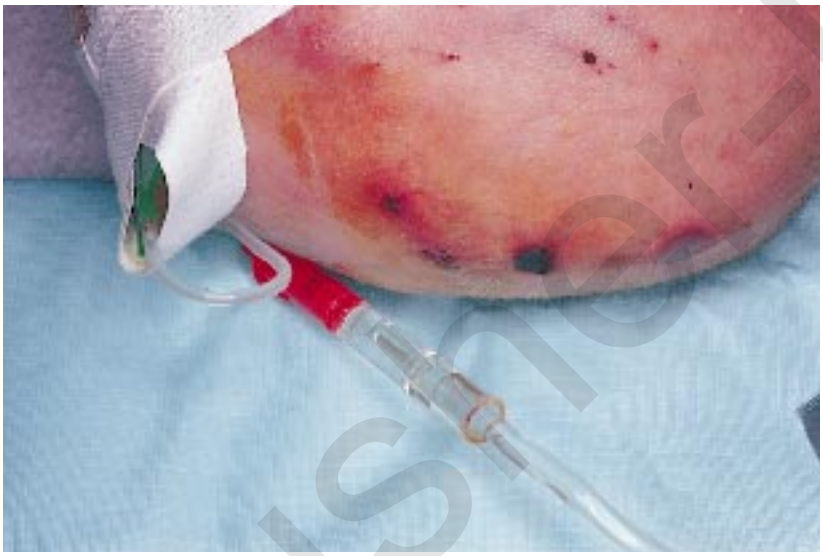

Figure 2.164. Candidal scalp infection in an infant on peripheral parenteral nutrition. The abscesses were recurrent until the cloudy appearance of the infusion solution was noted. Hyphae were seen on examinaton of this fluid. The abscesses resolved with discontinuation of the concentrated glucose solution.

2.165

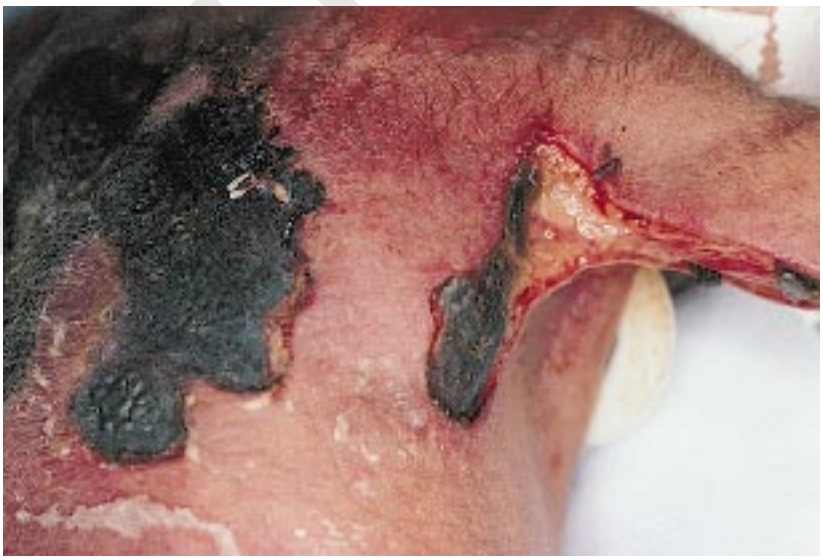

Figure 2.165. Invasive aspergillosis of the skin in a small premature infant (birthweight 785 g) at the age of 7 days. Note the involvement of the back and the right axilla. Infant was treated with amphotericin.

2.166

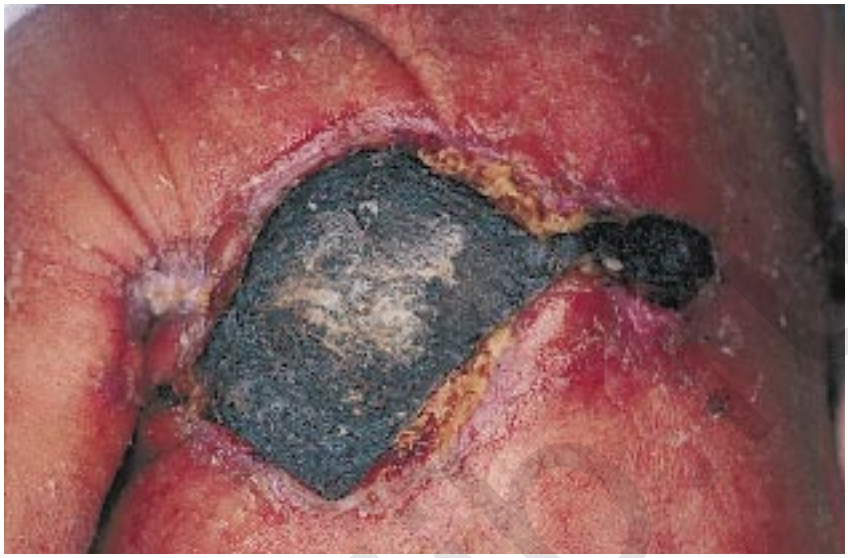

Figure 2.166. The same infant as in Figure 2.165 at the age of 5 weeks, showing healing of the lesions.

2.167

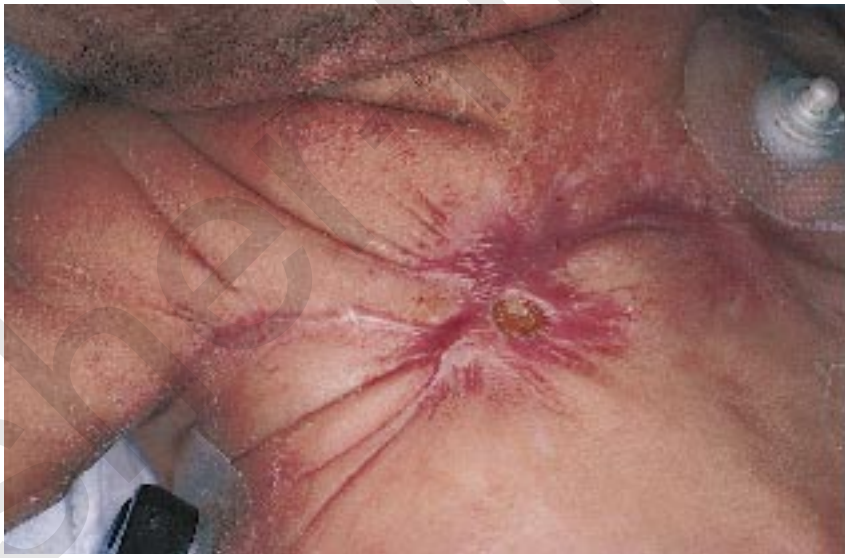

Figure 2.167. The same infant as in Figure 2.165 and 2.166 at the age of 10 weeks with good healing of the skin of the back and axilla. However, the contractures that were present necessitated plastic surgery at a later date.

2.168

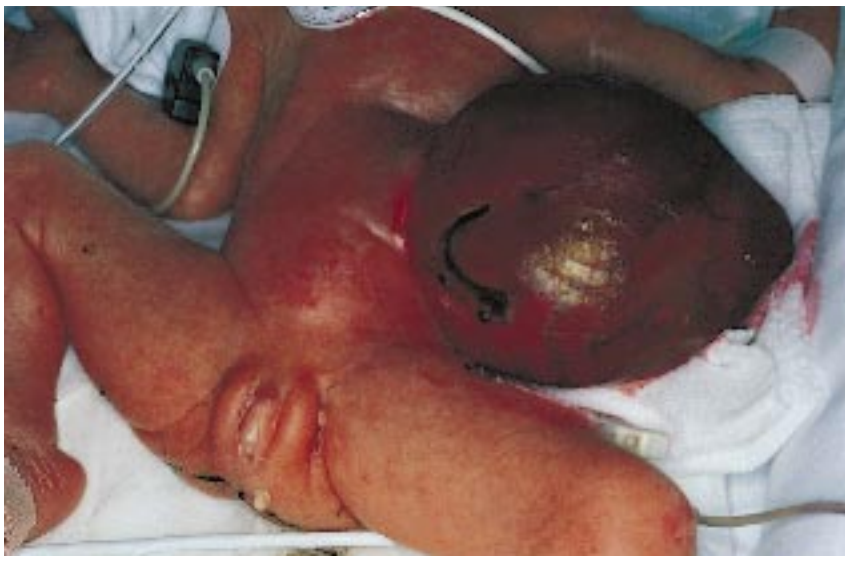

Figure 2.168. Premature infant (birthweight 1000 g) with severe hyaline membrane disease with giant omphalocele. Respiratory problems precluded surgical intervention. The omphalocele was managed medically with the application of mercurochrome. The infant developed mercury intoxication from excessive absorption of the mercurochrome.

2.169

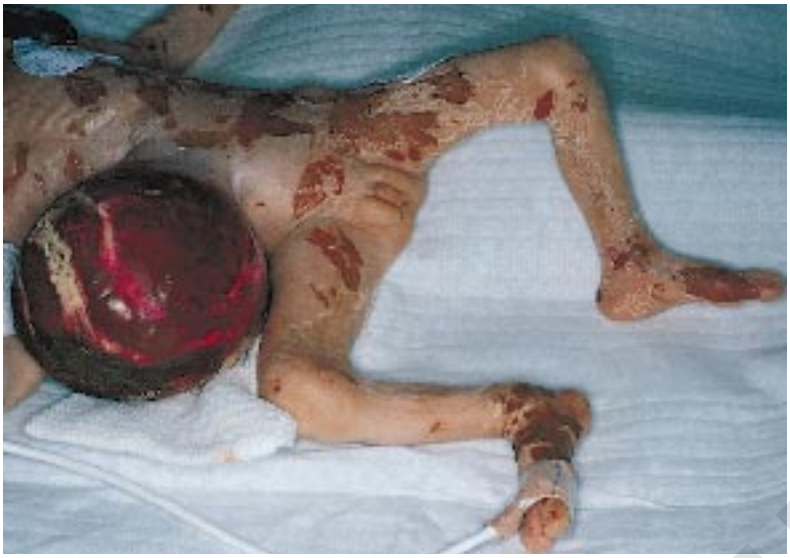

Figure 2.169. The same infant as in Figure 2.168 at the age of 11 days. Note the fungus on the omphalocele. KOH scrapings were positive for hyphae, and culture grew *Aspergillus fumigatus*. Aspergillosis is an uncommon opportunistic fungal disease. *Aspergillus fumigatus* is the most common, but the incidence of *Aspergillus niger* and other species is increasing. These fungi are ubiquitous and normally nonpathogenic. Primarily they affect debilitated individuals.

2.170

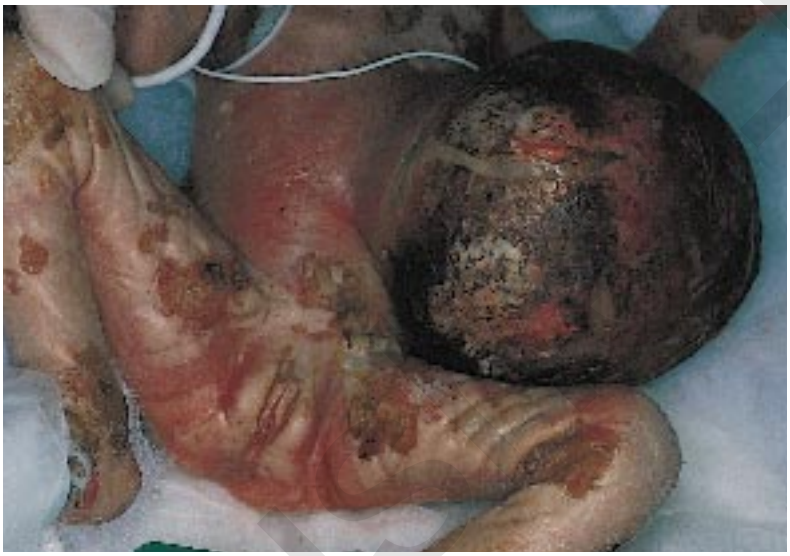

Figure 2.170. The same infant as in Figure 2.168 and 2.169 at the age of 18 days showing generalized involvement of the skin. The skin lesions are characterized by erythematous papules which develop into hemorrhagic bullae and then become violaceous plaques with central necrosis.

2.171

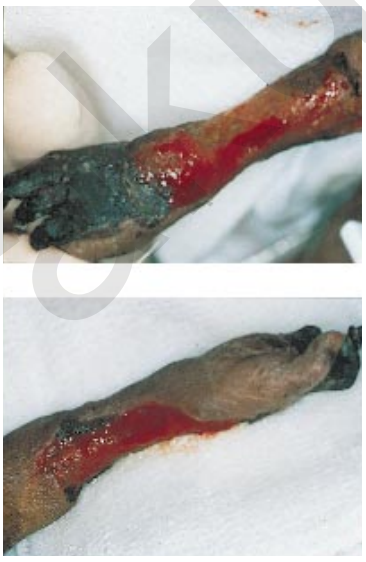

Figure 2.171. This small premature infant born at 23 weeks gestation (birthweight of 580 g) had severe hyaline membrane disease and a large ductus arteriosus. She was referred at the age of 33 days, having developed a *Staphylococcus epidermidis* bacteremia, bilateral grade III intraventricular hemorrhages, and bronchopulmonary dysplasia. Shortly after admission, infection of the right forearm and hand developed which was progressive, becoming gangrenous. *Rhizopus* infection was shown to be the etiology. She died at the age of 83 days.

2.172

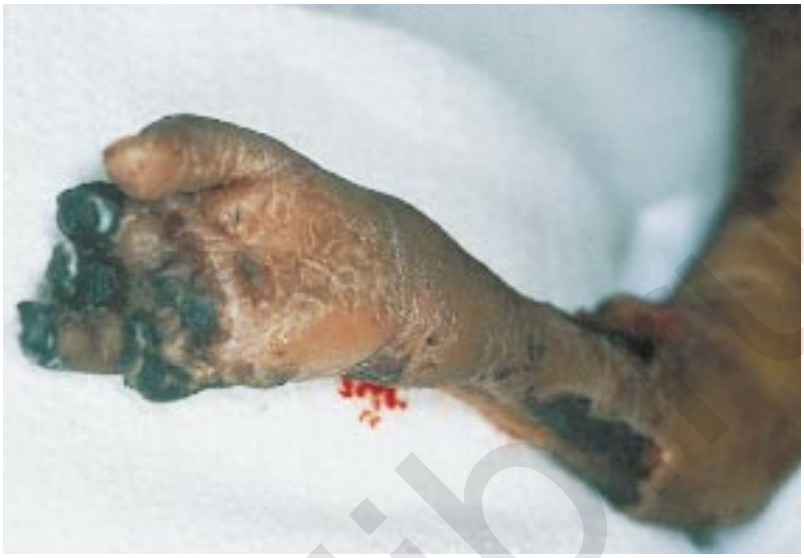

Figure 2.172. Another view of the arm and hand of the same infant as in Figure 2.171. Phycomycosis is very rare in neonates. The most common genera include *Mucor, Absidia,* and *Rhizopus*. Fungi of this class are frequently found in refrigerators and are commonly known as bread molds. Phycomycetes have the same affinity for vascular invasion, hemorrhage, necrosis, and suppuration as *Aspergillus*. There are few reports in the neonatal period, and the majority of these infants have died.

Index

VOLUME 5

Thorax, Abdomen, Blood, Endocrine, and Metabolic Disorders

Atlas of the Newborn

Rudolph

VOLUME 5

Thorax, Abdomen, Blood, Endocrine and Metabolic Disorders

Atlas of the Newborn

Arnold J. Rudolph, M.D.
(1918-1995)
Professor of Pediatrics and
Obstetrics and Gynecology
Baylor College of Medicine
Houston, Texas

VOLUME 5

Thorax, Abdomen, Blood, Endocrine and Metabolic Disorders

Atlas of the Newborn

Arnold J. Rudolph, M.D.
1918-1995

1997
B.C. Decker Inc.
Hamilton • London

B.C. Decker Inc.
4 Hughson Street South
P.O. Box 620, L.C.D. 1
Hamilton, Ontario L8N 3K7
Tel: 905 522-7017
Fax: 905 522-7839
e-mail: info@bcdecker.com

Printed in Canada

97 98 99 00/BP/9 8 7 6 5 4 3 2 1

ISBN 1-55009-035-6

Sales and distribution

United States
Blackwell Science Inc.
Commerce Place
350 Main Street
Malden, MA 02148
U.S.A.
Tel: 1-800-215-1000

Canada
Copp Clark Ltd.
200 Adelaide Street West
3rd Floor
Toronto, Ontario
Canada M5H 1W7
Tel: 1-800-815-9417

Japan
Igaku-Shoin Ltd.
Tokyo International P.O. Box 5063
1-28-36 Hongo, Bunkyo-ku
Tokyo 113, Japan
Tel: 3 3817 5680
Fax: 3 3815 7805

U.K., Europe, Scandinavia, Middle East
Blackwell Science Ltd.
c/o Marston Book Services Ltd.
P.O. Box 87
Oxford OX2 0DT
England
Tel: 44-1865-79115

Australia
Blackwell Science Pty, Ltd.
54 University Street
Carleton, Victoria 3053
Australia
Tel: 03 9347 0300
Fax: 03 9349 3016

India
Jaypee Bros. Medical Publishers (PUT) Ltd.
B-3 EMCA House, 23/23B Ansari Road
Daryaganj
P.B. 7193, New Delhi, -11002 India
Tel: 327 2143, 328 2021
Fax: 327 6490

Notice: the authors and publisher have made every effort to ensure that the patient care recommended herein, including choice of drugs and drug dosages, is in accord with the accepted standard and practice at the time of publication. However, since research and regulation constantly change clinical standards, the reader is urged to check the product information sheet included in the package of each drug, which includes recommended doses, warnings, and contraindications. This is particularly important with new or infrequently used drugs.

Foreword

Sir William Osler stated, "There is no more difficult task in medicine than the art of observation." The late Arnold Jack Rudolph was an internationally renowned neonatologist, a teacher's teacher, and, above all, one who constantly reminded us about how much could be learned by simply observing, in his case, the newborn infant.

This color atlas of neonatology represents a distillation of more than 50 years of observing normal and abnormal newborn infants. The *Atlas* begins with a section on the placenta, its membranes, and the umbilical cord. Jack Rudolph delighted in giving a lecture entitled "Don't Make Mirth of the Afterbirth," in which he captivated audiences by showing them how much you could learn about the newborn infant from simply observing the placenta, its membranes, and the umbilical cord.

In a few more than 60 photomicrographs, we learn to read the placenta and gain insight into such disorders as intrauterine growth retardation, omphalitis, cytomegalic inclusion disease, congenital syphilis, and congenital neuroblastoma. Congenital abnormalities of every organ system are depicted along with the appearance of newborn infants who have been subjected in utero to a variety of different drugs, toxins, or chemicals. We also learn to appreciate the manifestations of birth trauma and abnormalities caused by abnormal intrauterine positioning.

More than 250 photographs are used to illustrate the field of neonatal dermatology. The collection of photographs used in this section is superior to that which I have seen in any other textbook or atlas of neonatology or dermatology; this section alone makes this reference a required addition to the library of any clinician interested in the care of infants and children. Photographs of the Kasabach-Merritt syndrome (cavernous hemangioma with thrombocytopenia), Klippel-Trénaunay syndrome, Turner's syndrome, Waardenburg's syndrome, neurocutaneous melanosis, mastocytosis (urticaria pigmentosa), and incontinentia pigmenti (Bloch-Sulzberger syndrome) are among the best that I have seen.

Cutaneous manifestations are associated with many perinatal infections. The varied manifestations of staphylococcal infection of the newborn are depicted vividly in photomicrographs of furunculosis, pyoderma, bullous impetigo, abscesses, parotitis, dacryocystitis, inastitis, cellulitis, omphalitis, and funisitis. Streptococcal cellulitis, *Haemophilus influenzae* cellulitis, and cutaneous manifestations of listeriosis all are depicted. There are numerous photomicrographs of congenital syphilis, showing the typical peripheral desquamative rash on the palms and soles, as well as other potential skin manifestations of congenital syphilis which may produce either vesicular, bullous, or ulcerative lesions. The various radiologic manifestations of congenital syphilis, including pneumonia alba, ascites, growth arrest lines, Wegner's sign, periostitis, and syphilitic osteochondritis, are depicted. Periostitis of the clavicle (Higouménaki's sign) is shown in a photograph that also depicts periostitis of the ribs. A beautiful photomicrograph of Wimberger's sign also has been included; this sign, which may appear in an infant with congenital syphilis, reveals radiolucency due to erosion of the medial aspect of the proximal tibial metaphysis.

The *Atlas* also includes a beautiful set of photographs which delineate the ophthalmologic examination of the newborn. Lesions which may result from trauma, infection, or congenital abnormalities are included. There are numerous photographs of the ocular manifestations of a variety of systemic diseases, such as Tay-Sachs disease, tuberous sclerosis, tyrosinase deficiency, and many more.

Photographs of disturbances of each of the various organ systems, or disorders affecting such organ systems, also are included along with numerous photographs of different forms of dwarfism, nonchromosomal syndromes and associations, and chromosomal disorders. In short, this *Atlas* is the complete visual textbook of neonatology and will provide any physician, nurse, or student with a distillation of 50 years of neonatal experience as viewed through the eyes of a master clinician.

Arnold Jack Rudolph was born in 1918, grew up in South Africa, and graduated from the Witwatersrand Medical School in 1940. Following residency training in pediatrics at the Transvaal Memorial Hospital for Children, he entered private pediatric practice in Johannesburg, South Africa. After almost a decade, he left South Africa and moved to Boston, where he served as a Senior Assistant Resident in Medicine at the Children's Medical Center in Boston, Massachusetts, and subsequently pursued fellowship training in neonatology at the same institution and at the Boston Lying-In Hospital, Children's Medical Center and Harvard Medical School under Dr. Clement A. Smith.

In 1961, Dr. Rudolph came to Baylor College of Medicine in Houston, Texas, the school at which he spent the remainder of his career. He was a master teacher, who received the outstanding teacher award from pediatric medical students on so many occasions that he was elected to the Outstanding Faculty Hall of Fame in 1982. Dr. Rudolph also received numerous awards over the years from the pediatric house staffs for his superb teaching skills.

He was the Director of the Newborn Section in the Department of Pediatrics at Baylor College of Medicine for many years, until he voluntarily relinquished that position in 1986 for reasons related to his health. Nevertheless, Jack Rudolph continued to work extraordinarily long hours in the care of the newborn infant, and was at the bedside teaching both students and house staff, as well as his colleagues, on a daily basis until just a few months before his death in July 1995.

Although Dr. Rudolph was the author or co-author of more than 100 published papers that appeared in the peer-reviewed medical literature, his most lasting contribution to neonatology and to pediatrics is in the legacy of the numerous medical students, house staff, fellows, and other colleagues whom he taught incessantly about how much one could learn from simply observing the newborn infant. This *Atlas* is a tour de force; it is a spectacular teaching tool that has been developed, collated, and presented by one of the finest clinical neonatologists in the history of medicine. It is an intensely personal volume that, as Dr. Rudolph himself states, "is not intended to rival standard neonatology texts," but rather to supplement them. This statement reveals Dr. Rudolph's innate modesty, since with the exception of some discussion on pathogenesis and treatment, it surpasses most neonatology texts in the wealth of clinical information that one can derive from viewing and imbibing its contents. We owe Dr. Rudolph and those who aided him in this work a debt of gratitude for making available to the medical community an unparalleled visual reference on the normal and abnormal newborn infant.

Ralph D. Feigin, M.D.
June 13, 1996

Preface

I first became attracted to the idea of producing a color atlas of neonatology many years ago. However, the impetus to synthesize my experience and compile this current collection was inspired by the frequent requests from medical students, pediatric house staff, nurses and others to provide them with a color atlas of the clinical material provided in my "slide shows." For the past few decades I have used the medium of color slides and radiographs as a teaching tool. In these weekly "slide shows" the normal and abnormal, as words never can, are illustrated.

"I cannot define an elephant but I know one when I see one."[1]

The collection of material used has been added to constantly with the support of the pediatric house staff who inform me to "bring your camera" whenever they see an unusual clinical finding or syndrome in the nurseries.

A thorough routine neonatal examination is the inalienable right of every infant. Most newborn babies are healthy and only a relatively small number may require special care. It is important to have the ability to distinguish normal variations and minor findings from the subtle early signs of problems. The theme that recurs most often is that careful clinical assessment, in the traditional sense, is the prerequisite and the essential foundation for understanding the disorders of the newborn. It requires familiarity with the wide range of normal, as well as dermatologic, cardiac, pulmonary, gastrointestinal, genitourinary, neurologic, and musculoskeletal disorders, genetics and syndromes. A background in general pediatrics and a working knowledge of obstetrics are essential. The general layout of the atlas is based on the above. Diseases are assigned to each section on the basis of the most frequent and obvious presenting sign. It seems probable that the findings depicted will change significantly in the decades to come. In this way duplication has been kept to a minimum. Additional space has been devoted to those areas of neonatal pathology (e.g., examination of the placenta, multiple births and iatrogenesis) which pose particular problems or cause clinical concern.

Obviously, because of limitations of space, it is impossible to be comprehensive and include every rare disorder or syndrome. I have tried to select both typical findings and variations in normal infants and those found in uncommon conditions. Some relevant conditions where individual variations need to be demonstrated are shown in more than one case.

As the present volume is essentially one of my personal experience, it is not intended to rival standard neonatology texts, but is presented as a supplement to them. It seems logical that references should be to standard texts or reviews where discussion on pathogenesis, treatment, and references to original works may be found.

Helen Mintz Hittner, M.D., has been kind enough to contribute the outstanding section on neonatal ophthalmology.

I have done my best to make the necessary acknowledgements to the various sources for the clinical material. If I have inadvertently omitted any of those, I apologize. My most sincere appreciation and thanks to Donna Hamburg, M.D., Kru Ferry, M.D., Michael Gomez, M.D., Virginia Schneider, PA, and Jeff Murray, M.D., who have spent innumerable hours in organizing and culling the material from my large collection. We wish to thank Abraham M. Rudolph, M.D., for his assistance in reviewing the material.

We also wish to thank the following people for their photo contributions to this work: Cirilo Sotelo-Avila, Gerardo Cabrera-Meza, Ed Gonzalez, Vicky Gresik, Claire Langston, Edward Singleton, and Milton Wagner.

It is hoped that this atlas will provide neonatologists, pediatricians, family physicians, medical students and nurses with a basis for recognizing a broad spectrum of normal variations and clinical problems as well as provide them with an overall perspective of neonatology, a field in which there continues to be a rapid acceleration of knowledge and technology. One must bear in mind the caveat that pictures cannot supplant clinical experience in mastering the skill of visual recall.

1. Senile dementia of Alzheimer's type — normal aging or disease? (Editorial) *Lancet* 1989; i:476-477.

Arnold J. Rudolph, M.D.

CONTENTS

Volume 5
Thorax, Abdomen, Blood, Endocrine and Metabolic Disorders

Introduction

Although several texts provide extensive descriptions of the newborn infant, the senses of touch, hearing, and especially sight, create the most lasting impressions. Over a period of almost five decades, my brother Jack Rudolph diligently recorded, in pictorial form, his vast experiences in physical examination of the newborn infant. *Atlas of the Newborn* reflects his selection from the thousands of color slides in his collection. It truly represents the "art of medicine" as applied to neonatology. A number of unusual or rare conditions are included in this atlas. I consider this fully justified, because if one has not seen or heard of a condition, one will never be able to diagnose it.

This fifth volume of the five-volume series covers, in excellent detail, disorders of the cardiorespiratory, gastrointestinal and genitourinary systems, disorders of endocrinology and metabolism, and nutritional disorders. In addition, hematology, jaundice, and oncology are clearly depicted in this volume.

The first chapter of this volume concentrates on disorders of the heart and lungs. It depicts the various factors which cause cyanosis in the neonate, and presents a magnificent collection of radiographs demonstrating specific features of lung disorders peculiar to the newborn infant. Also shown are disturbances of muscle function and bony chest development that may interfere with respiratory function.

The chapters dedicated to the gastrointestinal and genitourinary tracts graphically present both the clinical aspects and the radiological features of numerous congenital anomalies which may occur in these systems. Also included in this chapter are outstanding presentations of the various abnormalities that can affect the male and female genitalia, and ambiguous genitalia.

Although many of the nutritional, hormonal, and metabolic disorders of the newborn are diagnosed by analysis of blood samples, several present with clinical features which are excellently documented in this volume.

Volume V of *Atlas of the Newborn* will be extremely valuable to neonatologists, obstetricians, and nurses involved in perinatal care, and also valuable to pediatric pulmonologists, cardiologists, gastroenterologists, nephrologists, geneticists and surgeons involved in the care of the newborn infant.

Abraham M. Rudolph, M.D.

Chapter 1
Cardiorespiratory System

Following birth, the function of gas exchange is transferred from the placenta to the lungs. Oxygen supply to the newborn infant depends upon the establishment of rhythmic breathing, expansion of the lungs with air, adequate pulmonary blood flow to pick up oxygen from the lungs, and systemic blood flow to transport oxygen to the tissues.

Normal respiration requires that the central and peripheral nervous systems involved in breathing are appropriately developed, that respiratory muscle function, especially of the diaphragm, is normal, and that the bony chest cage is normal both in size and stability. The airways are filled with fluid before birth, and this fluid must be effectively cleared to allow entry of air into the lungs. The presence of pulmonary surfactant is essential to reduce alveolar surface tension and facilitate lung expansion.

Oxygen is predominantly transported in the blood through its attachment to hemoglobin. Hemoglobin deficiency due to blood loss or hemolysis of red cells may thus reduce oxygen transport. Oxygen transport may also be reduced due to hemoglobin abnormalities, such as methemoglobinemia, which impair the oxygen-carrying capacity of the blood.

The proper circulatory pathways must also be established following birth in order to ensure adequate pulmonary blood flow. The normal increase in pulmonary blood flow after birth may be prevented by a failure of pulmonary vascular resistance to fall, as in persistent pulmonary hypertension of the newborn, or in congenital heart disease, where there is an obstruction of systemic venous blood flow into the lungs as occurs in pulmonary atresia. Furthermore, oxygen transport to the tissues may be inadequate because systemic arterial supply is reduced by myocardial failure, or by congenital heart lesions in which left ventricular output is impaired, as with severe aortic stenosis or aortic atresia.

Despite the complexity of these systems, the adaptations to birth usually occur uneventfully. The purpose of the resuscitation team is to prepare for those unusual occasions when the normal transition from intrauterine to extrauterine life does not proceed smoothly.

1.1

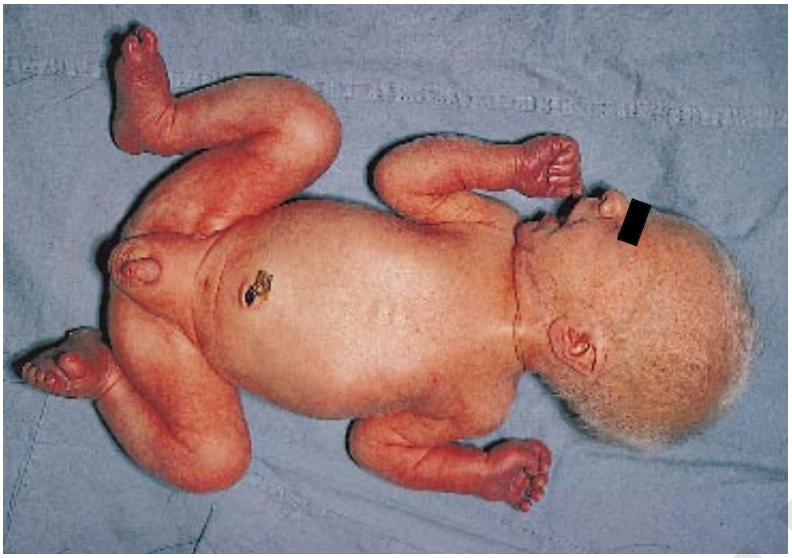

Figure 1.1. Acrocyanosis is the blue discoloration of the distal extremities noted in many normal infants, but it can be observed in older babies with cold stress, infection, or heart failure. Peripheral cyanosis of the hands and feet is a common clinical finding in normal infants in the first 24 hours of life, but may be a nonspecific sign of illness. This finding is the result of a combination of high fetal hemoglobin concentrations and relatively sluggish peripheral circulation from arteriolar vasoconstriction. Note that the infant's face, lips, and trunk appear pink. Spontaneous improvement always occurs. Gentle stroking induces a rapid vasomotor reaction resulting in the sudden dispersal of peripheral cyanosis.

1.2

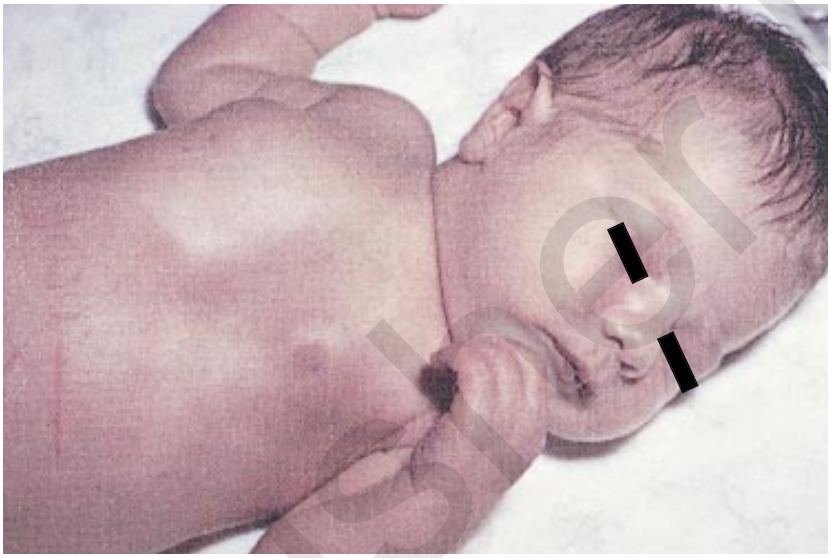

Figure 1.2. This infant's trunk, face and extremities are cyanotic, indicating a reduced hemoglobin oxygen content of at least 5 g/dL. Cyanosis is easier to detect in infants with polycythemia than in those with anemia, although oxygen saturation may be higher in the former and reduced in the latter.

1.3

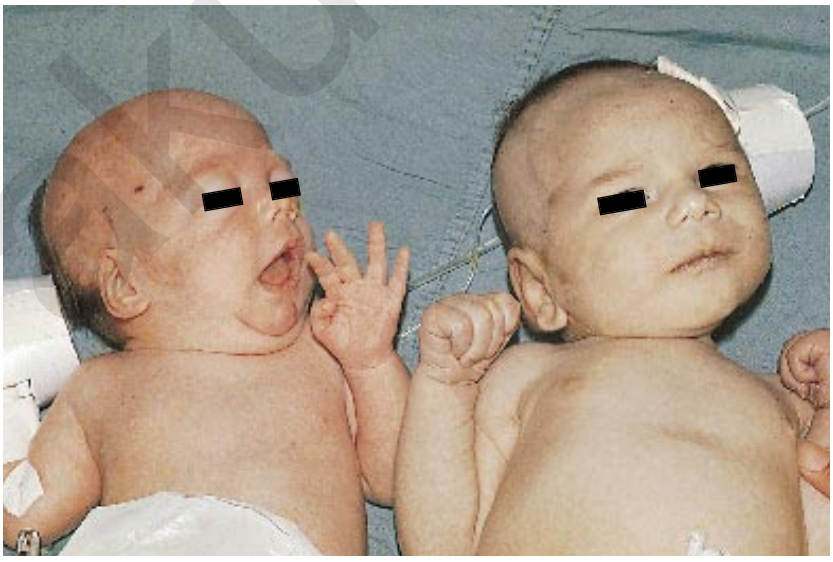

Figure 1.3. Methemoglobinemia is a condition which results in oxidized iron in hemoglobin being rendered unable to carry oxygen. Though the partial pressure of oxygen may be normal, oxygen content is low. Compare the color of the normal infant on the left with the typical slate grey color of the methemoglobinemic infant on the right. Distress may not be evident in infants until methemoglobin is 50% of the total hemoglobin. Methemoglobinemia is most commonly caused by postnatal exposure to toxins, such as nitrates or aniline dyes, but can also be congenital.

1.4

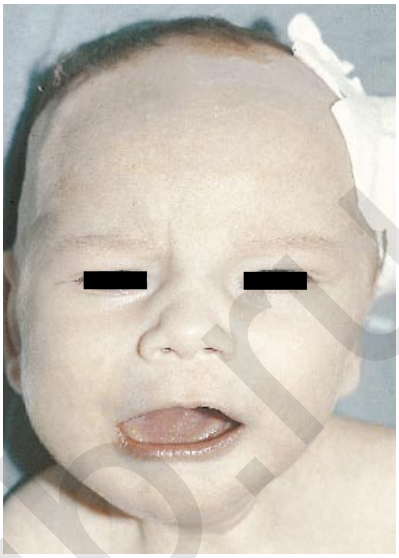

Figure 1.4. Methemoglobinemia occurred in this infant after the administration of intravenous nitrofurantoin. Methemoglobin was 45% of the total hemoglobin, resulting in the slate grey color. Poor oxygen delivery can lead to severe metabolic acidosis. Treatment is intravenous methylene blue or ascorbic acid.

1.5

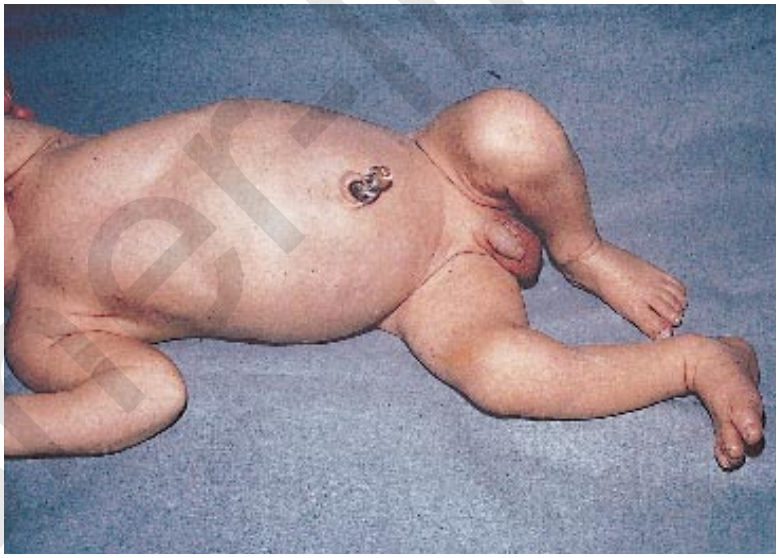

Figure 1.5. Differential cyanosis in an infant with congenital heart disease. Note the line of demarcation in the midabdomen showing the pink body proximally and the cyanosis distally (this infant had pink hands and blue feet). This occurs in infants with aortic obstruction (coarctation of the aorta, interrupted aorta) with a patent ductus arteriosus supplying the descending aorta.

1.6

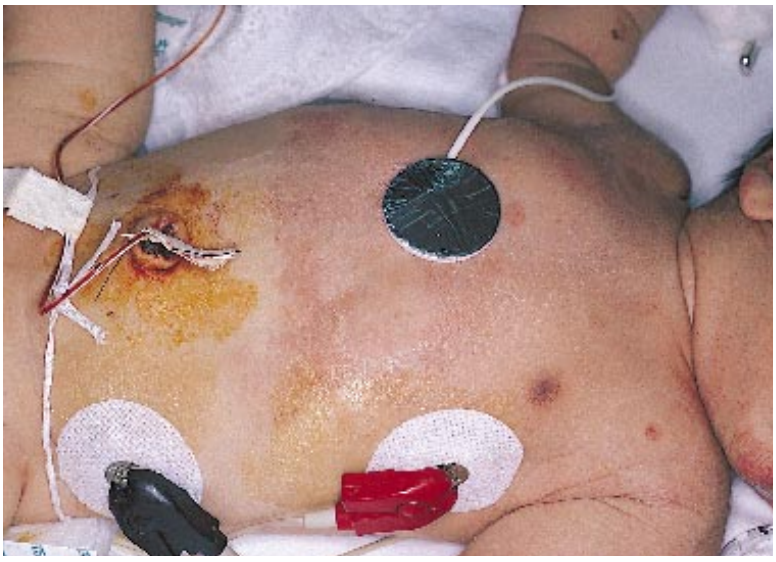

Figure 1.6. Differential cyanosis in an infant with congenital heart disease. Note the demarcation line in the midabdomen, and that the proximal part of the body is cyanotic, but the distal portion is pink (this infant had blue hands and pink feet). In this infant, this was due to aortopulmonary transposition, coarctation of the aorta, patent ductus arteriosus and pulmonary arterial hypertension. Well-oxygenated blood from the pulmonary artery passes through the ductus to the descending aorta, but the ascending aorta receives poorly-oxygenated blood from the right ventricle.

1.7

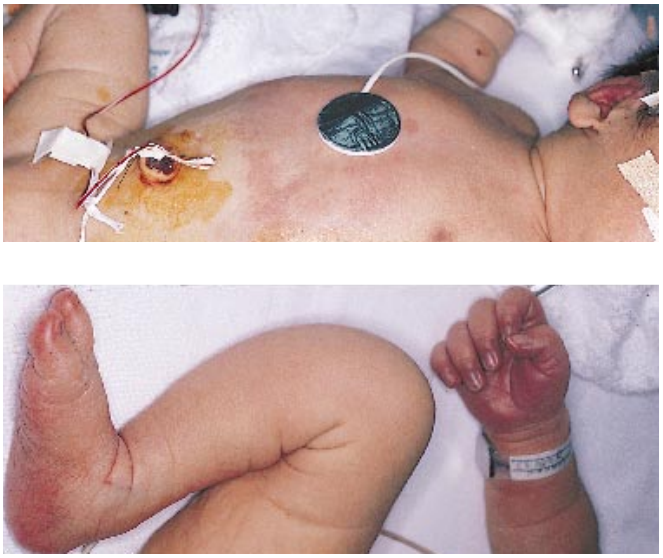

Figure 1.7. The same infant as in Figure 1.6 showing the differential cyanosis at the mid-abdomen as well as the blue hands and pink feet.

1.8

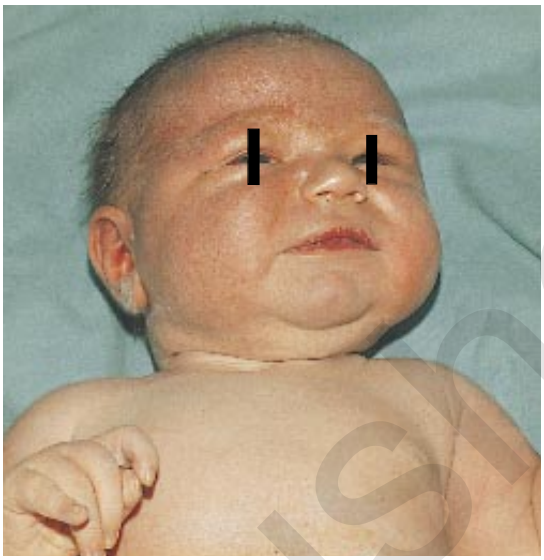

Figure 1.8. This infant developed venous congestion and numerous petechial hemorrhages as a result of a nuchal cord, which is the cause of the red or plethoric face and head. Subconjunctival hemorrhages are also present.

1.9

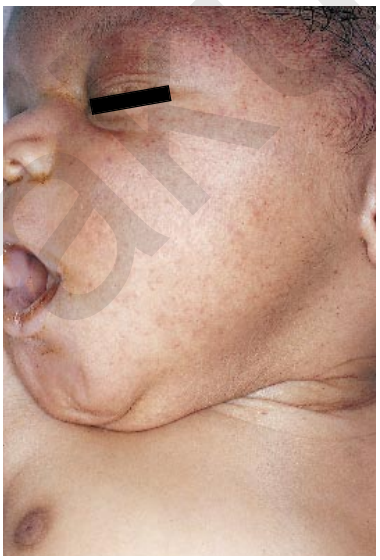

Figure 1.9. Tight nuchal cords can cause excess venous pressure in the head, and result in the rupture of small capillaries in the face causing petechiae and suffusion. These findings typically resolve spontaneously in a few days.

1.10

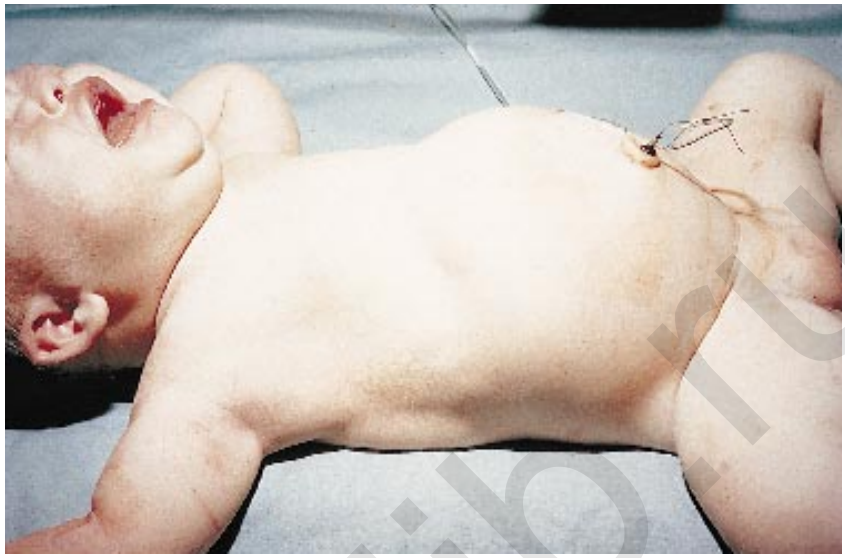

Figure 1.10. Following a difficult breech extraction, there was injury to the spinal cord at C7. This resulted in marked hypotonia (the infant is lying in the "pithed frog" position). Note that the infant is crying, and that a normal infant would usually flex extremities when disturbed. The abdominal distention is due to lack of abdominal muscle tone and an enlarged, paralyzed bladder.

1.11

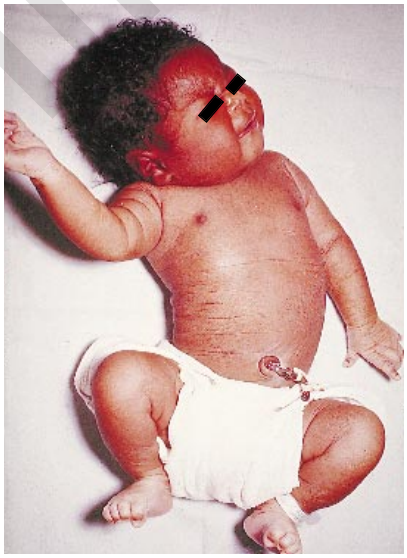

Figure 1.11. Erb's palsy is the result of trauma to the upper brachial plexus (nerve roots C4–7) at delivery. The infant's left arm is flaccid with the shoulder adducted and the arm internally rotated. The extended elbow follows down to a pronated forearm and flexed wrist. Spontaneous resolution is seen in 70 to 90% of cases within 30 days. Rarely is the injury permanent. Infants with Erb's palsy should have a chest radiograph taken to check for involvement of the ipsilateral diaphragm due to paralysis of the phrenic nerve (C3, 4 and 5).

1.12

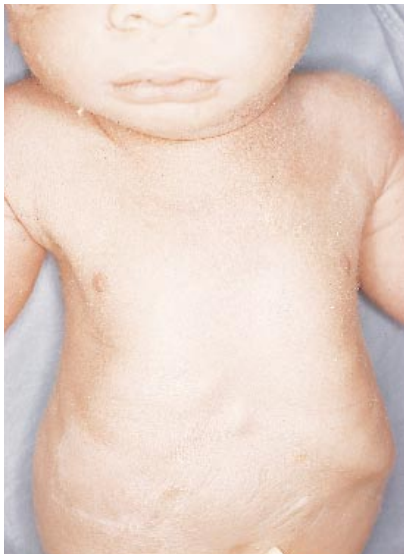

Figure 1.12. Lack of fetal movement in utero can result in positional deformities of the chest wall. Positional deformities, per se, do not cause respiratory distress, but if the changes are due to neuromuscular or osseous problems, respiratory distress may occur.

1.13

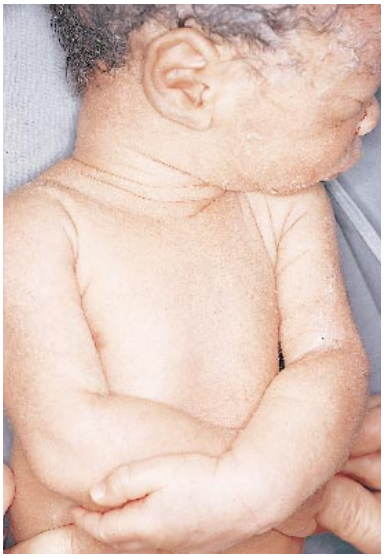

Figure 1.13. In the same infant as in Figure 1.12, note how the folded arm compressed the chest causing this change in the chest wall. Decreased fetal movement should alert one to neuromuscular conditions such as spinal muscular atrophy or myotonic dystrophy.

1.14

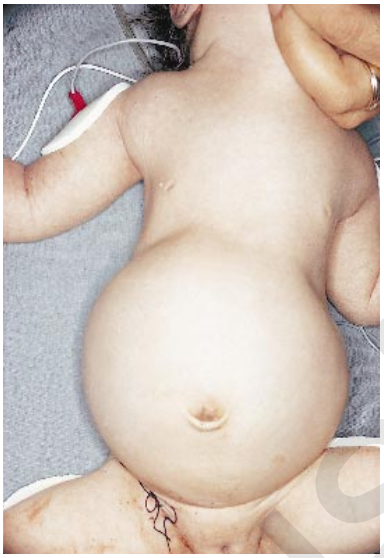

Figure 1.14. This is an infant with asphyxiating thoracic dystrophy, an autosomal recessive condition which severely restricts chest growth. The congenital deformity of the chest due to the short ribs results in a small chest which limits pulmonary expansion and severely restricts respiration. Because of the small thorax, the whole liver lies in the abdomen, producing the rounded and enlarged appearance seen in this infant.

1.15

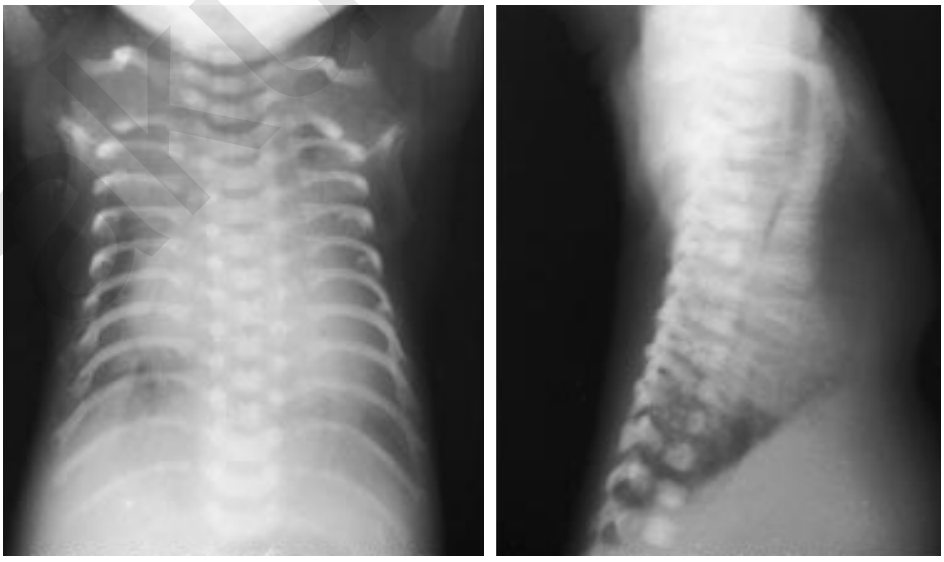

Figure 1.15. In the anteroposterior and lateral radiograph of an infant with asphyxiating thoracic dystrophy, note the thin, abnormally short, straight ribs and small chest wall with protuberant abdomen. This bell-shaped appearance occurs in a variety of conditions because of prenatal weakness of the muscles or a neurologic abnormality.

1.16

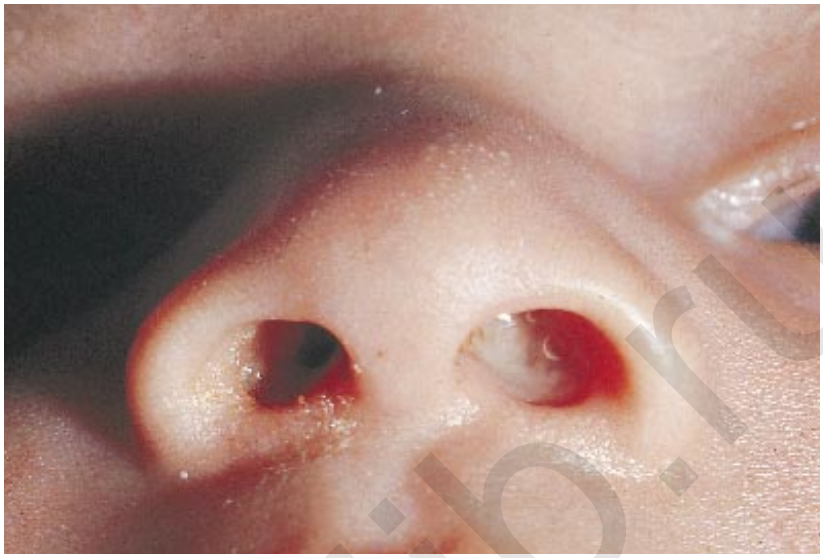

Figure 1.16. Nasal obstruction by a glioma in the left nostril caused respiratory distress in this infant. This neural tissue typically comes through the cribriform plate.

1.17

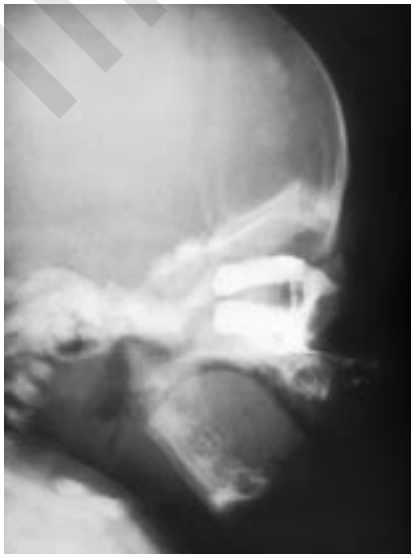

Figure 1.17. Choanal atresia results from blockage of one or both choanae and may present shortly after birth with cyanosis which is relieved when the infant cries. Unilateral choanal atresia may present later in life with the inability to breathe through one side of the nose. Narrowing occurs to some degree within the choanae of many infants. In this radiograph, contrast medium instilled into the nasal cavity did not reach the nasopharynx, indicating obstruction of the choana, most likely from atresia. Atresia is unilateral in 90% of cases (twice as frequent on the right side), and is more common in female infants. Associations occur with facial anomaly syndromes such as Apert's and Treacher-Collins, and with the CHARGE sequence (*c*oloboma, *h*eart disease, *a*tresia of the choanae, *r*etarded postnatal growth and development, *g*enitourinary anomalies, and *e*ar anomalies and deafness).

1.18

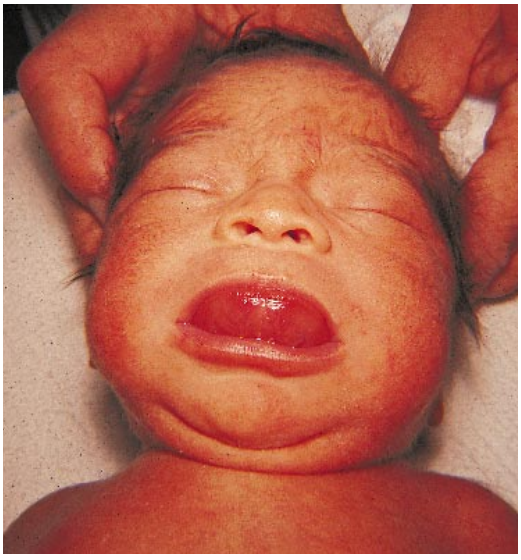

Figure 1.18. Macroglossia can result from trauma, hypothyroidism, storage diseases (such as Pompe's), Beckwith-Wiedemann syndrome, hemangiomas, and lymphangiomas, but occurs most often as an idiopathic finding. In the Pierre Robin sequence, the large tongue is exaggerated because of the mandibular hypoplasia.

1.19

Figure 1.19. A lateral radiograph of the head and neck in an infant with Beckwith-Wiedemann syndrome shows the macroglossia which encroaches on the oropharynx with resulting respiratory distress. (Singleton, E., Wagner, M.)

1.20

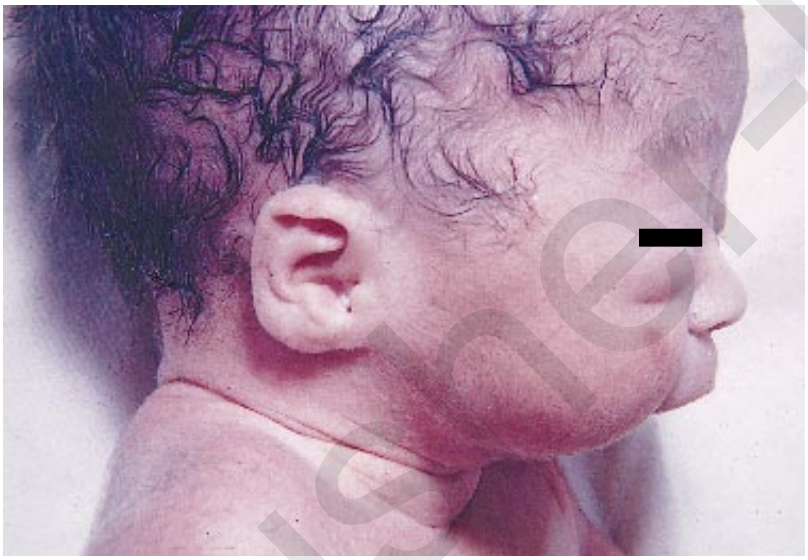

Figure 1.20. Mandibular hypoplasia, a small underdeveloped mandible, can be an isolated finding or part of a sequence such as Pierre Robin, Treacher-Collins, Hallermann Streiff, or trisomy 18. This may cause severe respiratory distress.

1.21

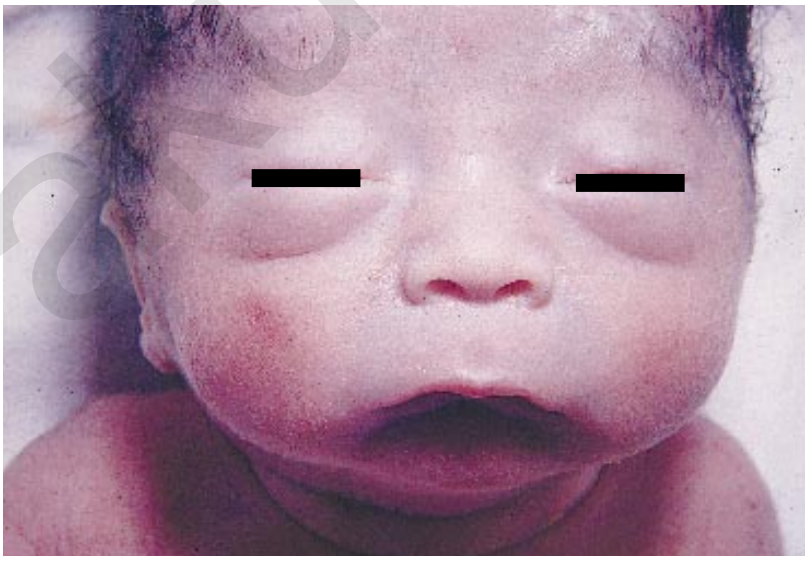

Figure 1.21. The same infant showing the Pierre Robin sequence: micrognathia, macroglossia, a protruding tongue, and a cleft palate which is often posterior. Cyanosis is often due to the tongue falling back and obstructing the posterior oropharynx. The infant should be managed in a prone position to avoid breathing problems. Micrognathia improves significantly over time.

1.22

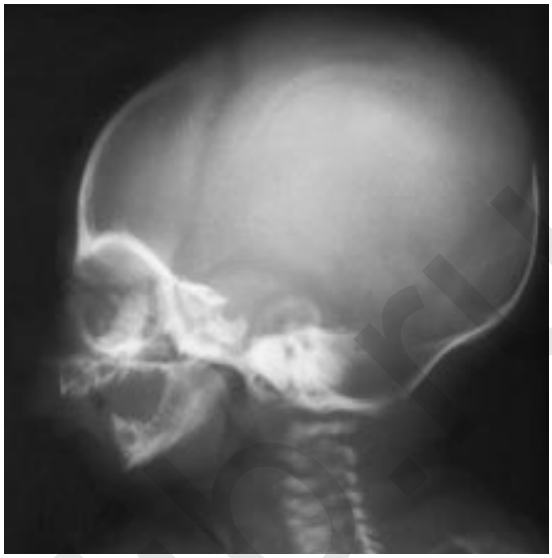

Figure 1.22. A lateral radiograph of the head and neck showing mandibular hypoplasia in an infant with trisomy 18. This caused severe respiratory distress because the hypoplastic mandible is associated with narrowing of the nasopharyngeal air passages. (Singleton, E., Wagner, M.)

1.23

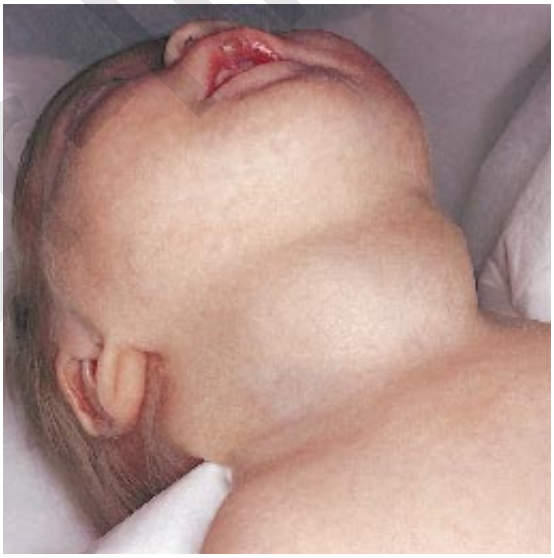

Figure 1.23. Congenital goiter is most commonly seen in an infant when there is a history of maternal ingestion of goitrogens such as antithyroid medications or iodides. Goiters can occur endemically in areas with insufficient maternal dietary iodine intake. This neck mass is symmetric about the midline of the neck.

1.24

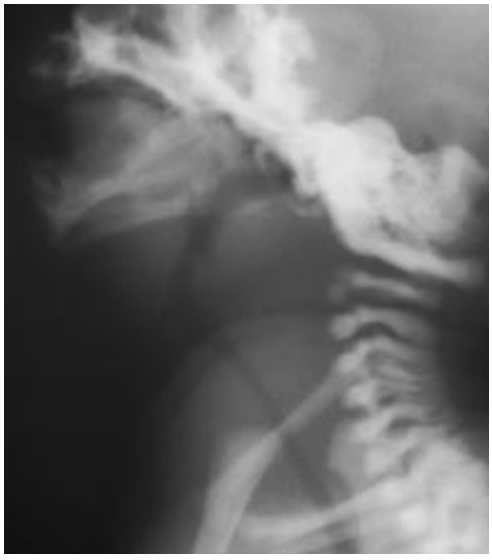

Figure 1.24. A radiograph of the neck in another infant who developed a very large congenital goiter as a result of maternal use of an iodide-containing medication. It compromised the airway, causing severe respiratory distress.

1.25

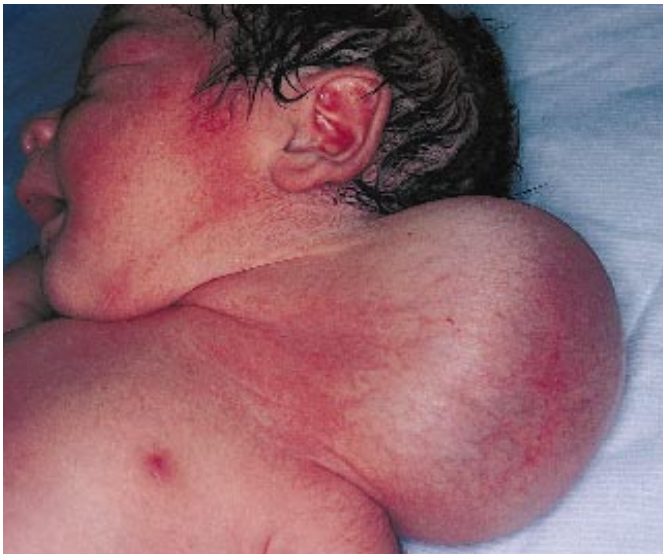

Figure 1.25. Cystic hygromas are typically benign unilateral masses in the lateral neck and are lymphatic in origin. They characteristically involve the face and upper trunk. They can occur as an isolated finding or may be associated with Turner's syndrome. The cervical variety can extend into the anterior and middle mediastinum, thus producing respiratory distress.

1.26

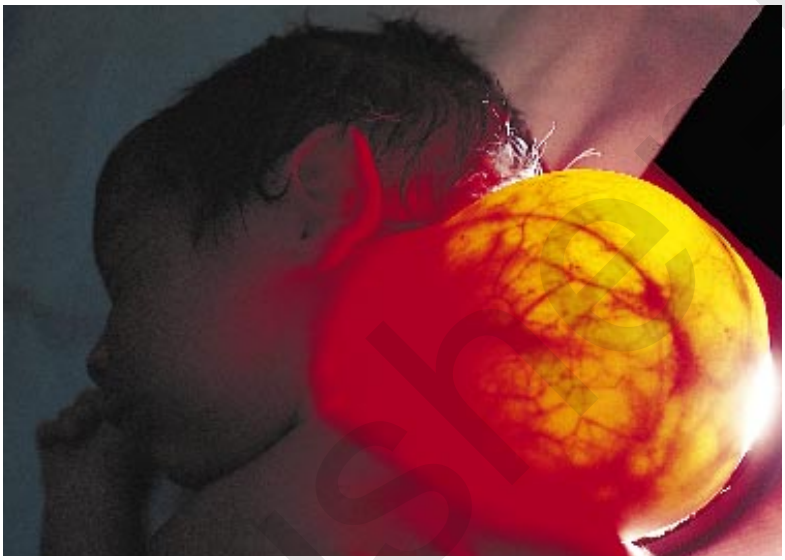

Figure 1.26. Transillumination of the cystic hygroma in the same infant as in Figure 1.25 reveals that the hygroma is filled with clear lymphatic fluid.

1.27

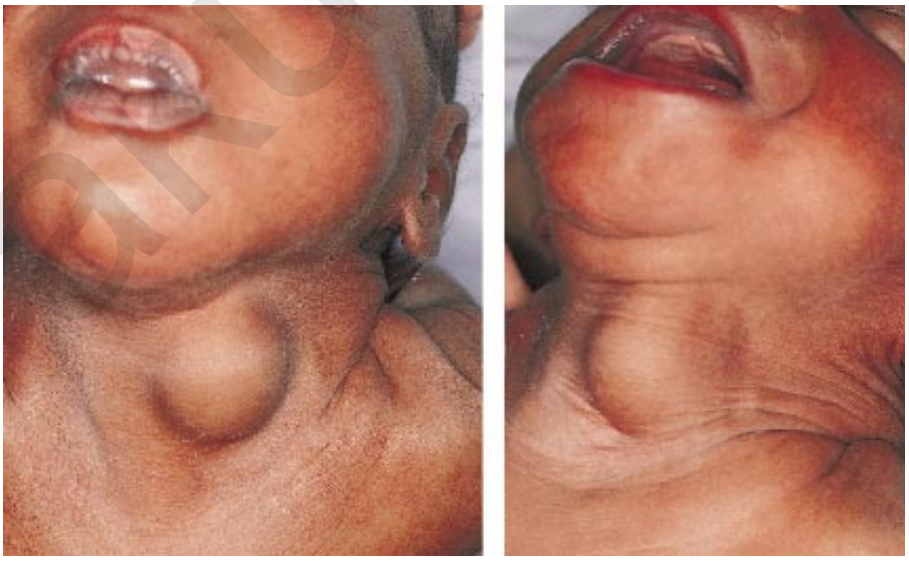

Figure 1.27. A branchial cleft cyst is a condition which arises from a persistent cervical sinus or second branchial groove. It is always located along the sternocleidomastoid muscle and is generally painless unless infected. If large, it can cause respiratory distress.

1.28

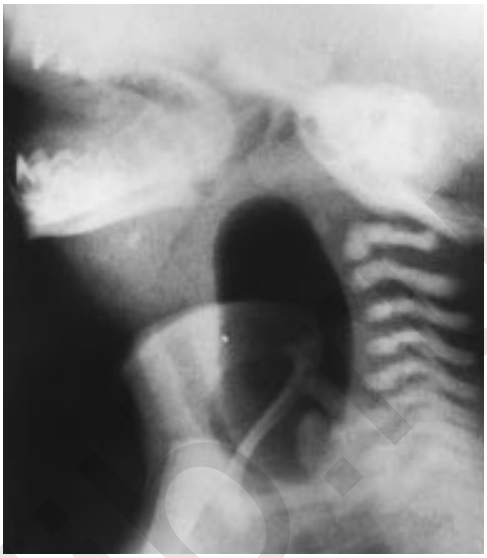

Figure 1.28. Radiograph of a branchiogenic cyst which is a product of ectopic branchial epithelium. It can be air- or fluid-filled. Enlarging cysts with mucinous secretions can lead to airway compromise. Bronchogenic cysts are most commonly located near the carina.

1.29

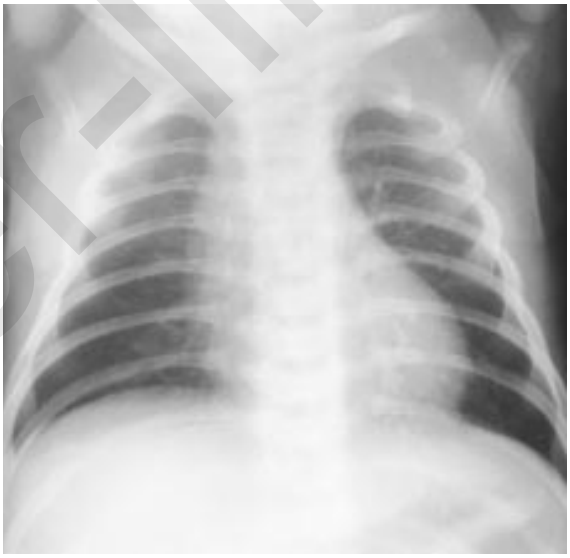

Figure 1.29. This anteroposterior radiograph of a normal chest shows the heart on the left, and complete aeration of the lungs with the diaphragm at the level of the 8th intercostal space. The diaphragm of the normal infant is usually rounded smoothly on both frontal and lateral radiographs, and the anterior costophrenic angle is usually quite shallow. The trachea is displaced slightly to the right of the midline by the left aortic arch.

1.30

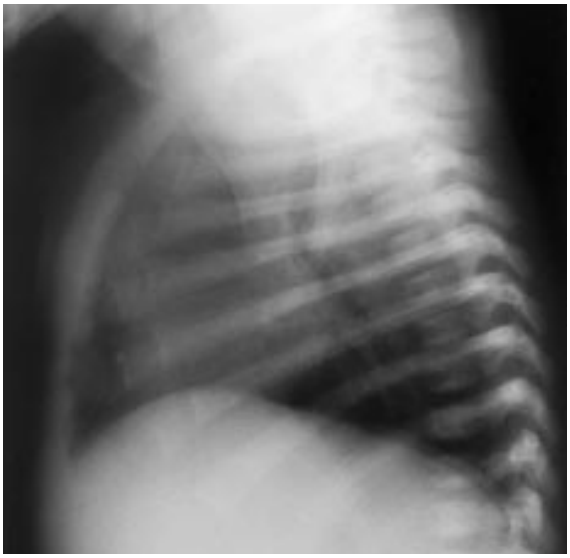

Figure 1.30. A lateral radiograph of a normal chest in an infant showing that the anteroposterior diameter is approximately the same as the thoracic diameter. Note the rounded diaphragm.

1.31

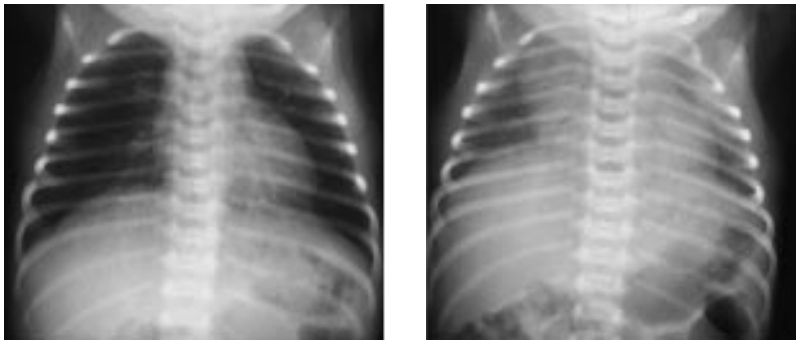

Figure 1.31. Normal chest radiographs of the same infant, showing an inspiratory view on the left and an expiratory view on the right. There can be dramatic differences in chest shape, cardiac and thymic shadow location, and degree of lung expansion, depending on the timing of the exposure. Incomplete aeration of the lungs may simulate pneumonia, and the thymus may appear large. The caliber of the trachea varies with respiration.

1.32

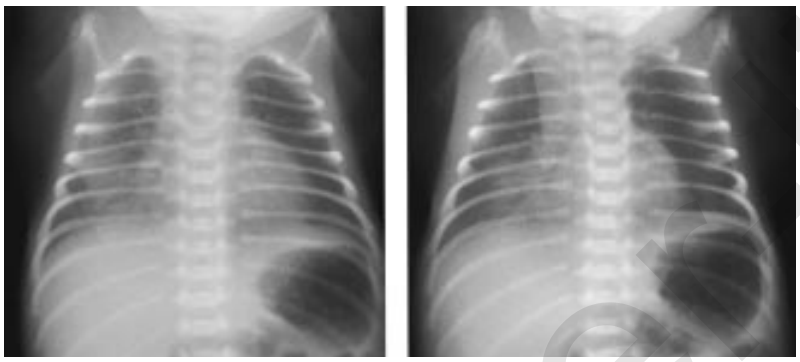

Figure 1.32. Chest radiographs of the same infant as in Figure 1.31 taken in sequence show a skin fold. Note the linear nature of this shadow across the right lung and diaphragm in the view on the left and the normal appearance of the chest in the view on the right. Skin folds should be recognized as normal artifacts and should not be mistaken for pathologic conditions.

1.33

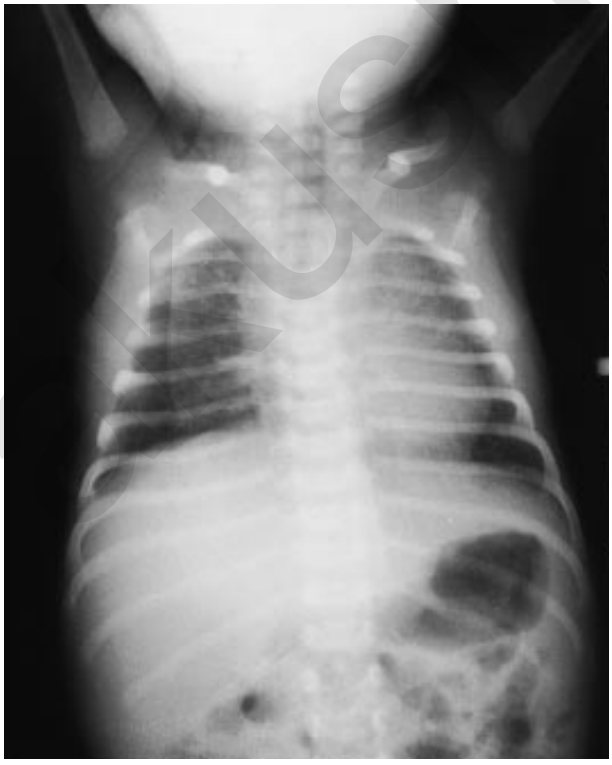

Figure 1.33. This is another example of a skin fold seen on a radiograph of the right chest. Despite the abnormal appearance of the radiograph, the infant was asymptomatic.

1.34

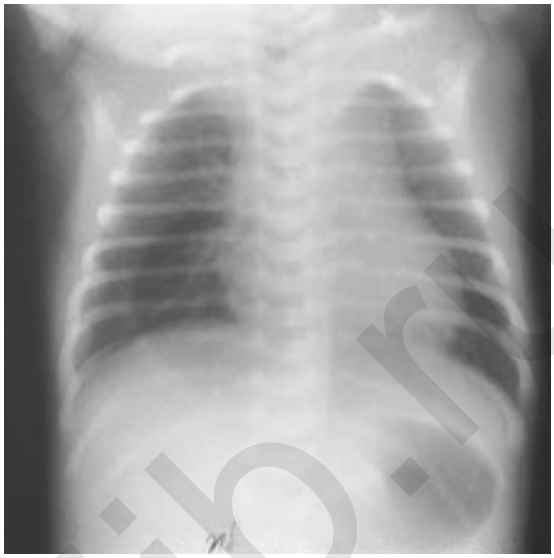

Figure 1.34. The perfect roundness and symmetry of the radiolucent defect in the right hemithorax and diaphragm in this radiograph suggest that this is an artifact created by a hole in the top of the incubator. This is not an uncommon finding when the radiograph is taken through the top of the incubator. (Singleton, E., Wagner, M.)

1.35

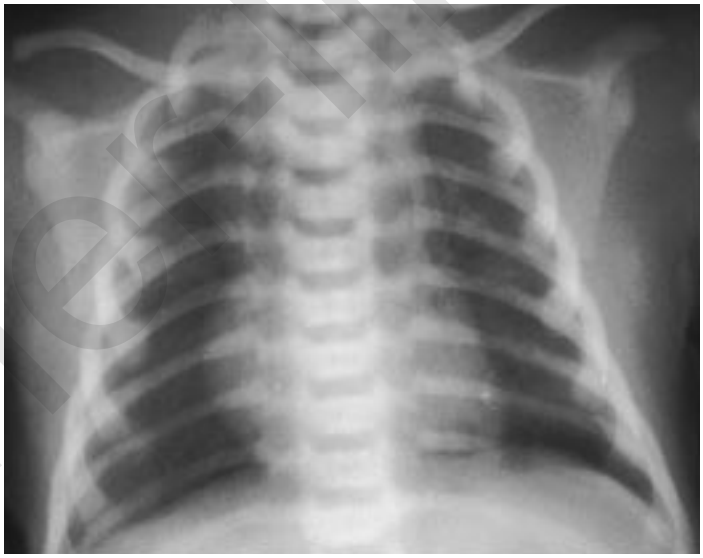

Figure 1.35. This is another example of a chest radiograph showing the "hole" in the incubator. This artifact lies directly over the mediastinum and should not be considered pathologic.

1.36

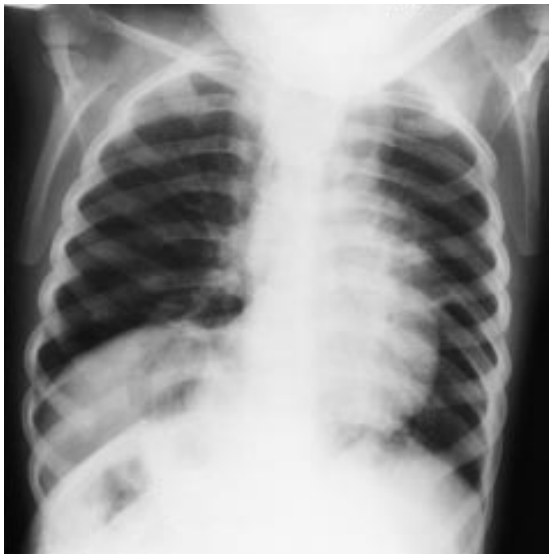

Figure 1.36. In this chest radiograph there is a symmetric round shadow overlying the mediastinum. This is an artifact caused by a pacifier lying directly on the infant's chest.

1.37

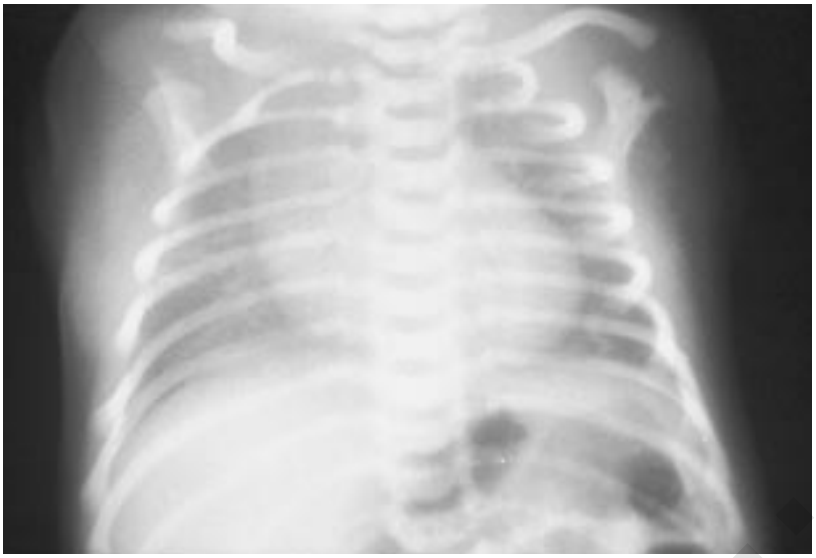

Figure 1.37. Chest radiograph of this infant shows a normal chest, but the scapulae are abnormal and there is amelia of the upper extremities bilaterally. This illustrates the importance of evaluating all osseous structures in any radiograph.

1.38

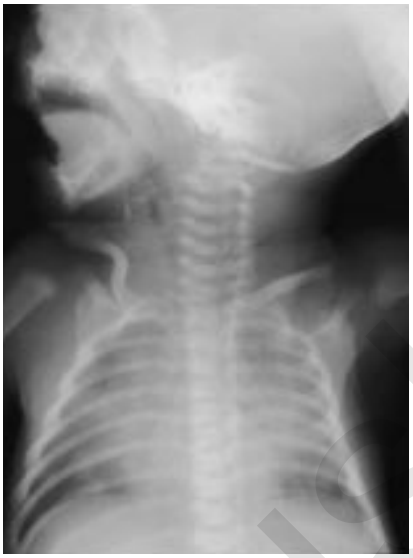

Figure 1.38. The lack of enamel and tooth buds is noted in this lateral radiograph. This infant had a chest radiograph taken for mild respiratory distress, and when the lack of tooth buds was noted, the diagnosis of ectodermal dysplasia was suspected and later confirmed.

1.39

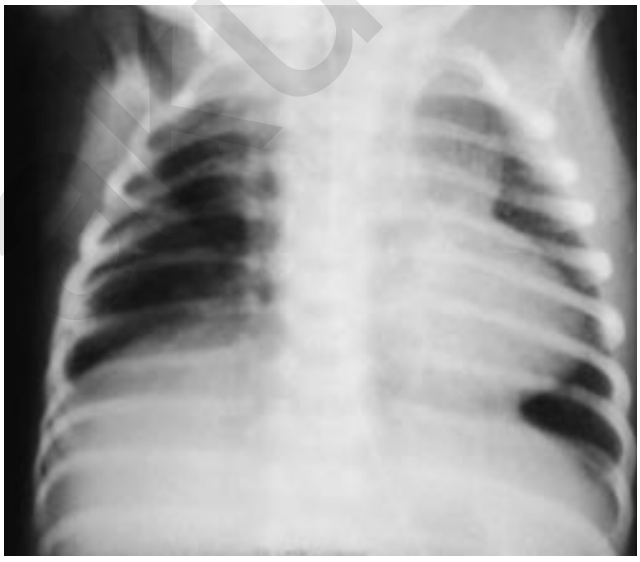

Figure 1.39. A chest radiograph was taken of this infant with Poland's anomaly to check for any abnormalities of the ribs. Note the increased lucency of the right upper part of the chest and loss of soft tissue shadow caused by the absence of the sternocostal head of the pectoralis muscle. Also note how clearly the scapula can be seen on the right side, also because of the absence of the pectoralis muscle.

1.40

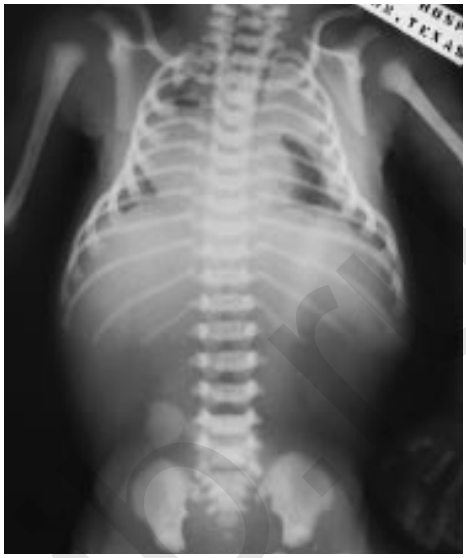

Figure 1.40. A small, bell-shaped thorax is seen in this infant with severe lung hypoplasia. After attempted resuscitation, air leaked into the thoracic and mediastinal spaces. Elevation of the lobes of the thymus created a "butterfly wing" appearance caused by mediastinal air. The abdomen is gasless and the opaque area to the right of the midline above the brim of the pelvis is the umbilical cord. The lung hypoplasia, confirmed at autopsy, occurred as a result of renal agenesis and oligohydramnios.
Difficulty in initiating respiration with minimal chest wall excursion, decreased lung expansion, decreased or absent air entry on auscultation, and persistent cyanosis should alert one to the possibility of lung hypoplasia.

1.41

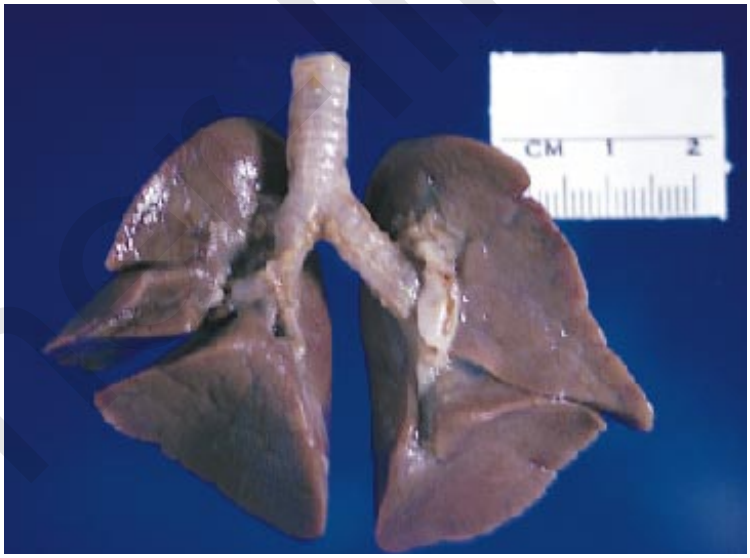

Figure 1.41. The lungs usually comprise 2% of total body weight in infants. This abdominal pregnancy resulted in severe oligohydramnios and severe hypoplasia of the lungs. The lungs weighed only 1% of total body weight in this infant.

1.42

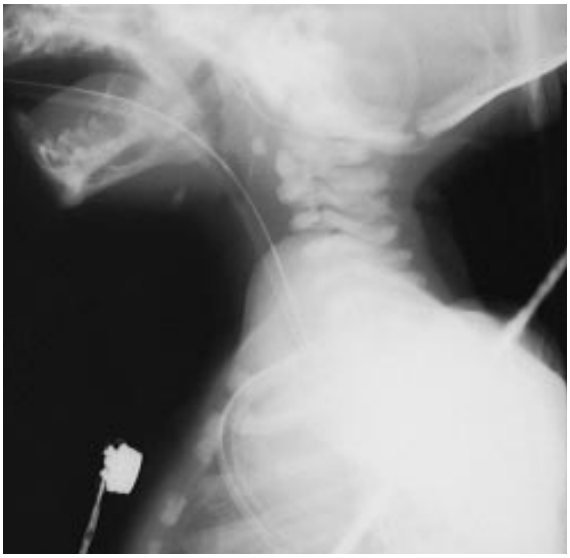

Figure 1.42. Radiograph of the head and neck in an infant with tracheal agenesis. An endotracheal tube could not be passed below the proximal tracheal obstruction. This lethal condition occurs when there is unequal division of the foregut between the esophagus and trachea. Affected infants are usually live-born; they may gasp but cannot introduce air into the lungs. Polyhydramnios is common. The lung architecture below the obstruction is suprisingly normal, and the lungs are typically larger than predicted for age. There may be an associated broncho- or tracheoesophageal fistula. If this is present, the infant may survive for a few hours by exchanging air through the fistula that communicates with the esophagus. Note the tube in the esophagus.

1.43

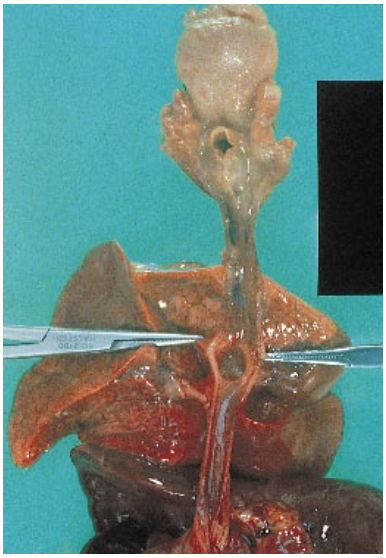

Figure 1.43. In the extremely rare condition of tracheal agenesis, the trachea and esophagus arise from the endoderm of the laryngotracheal tube. Note the communication that abnormally persists between these two structures.

1.44

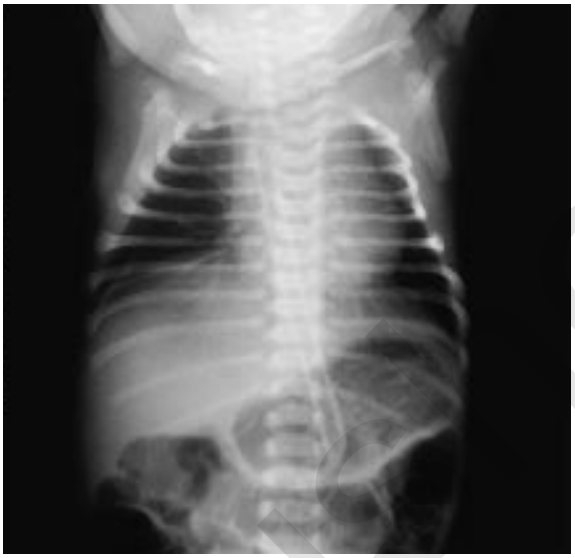

Figure 1.44. This radiograph depicts a swallowed cuffed endotracheal tube in the stomach. Attempts to resuscitate this infant by endotracheal intubation by the physician in attendance at delivery were unsuccessful. Leaving the tube in place, he called for assistance and the infant was intubated, responding immediately to positive pressure ventilation. In the nursery, attempts to feed the infant resulted in vomiting. This radiograph of the chest was taken and showed the endotracheal tube in the esophagus and stomach. Unbeknownst to the doctors, between attempts at resuscitation, the infant had swallowed the endotracheal tube that had been placed initially in his esophagus. The tube was successfully removed.

1.45

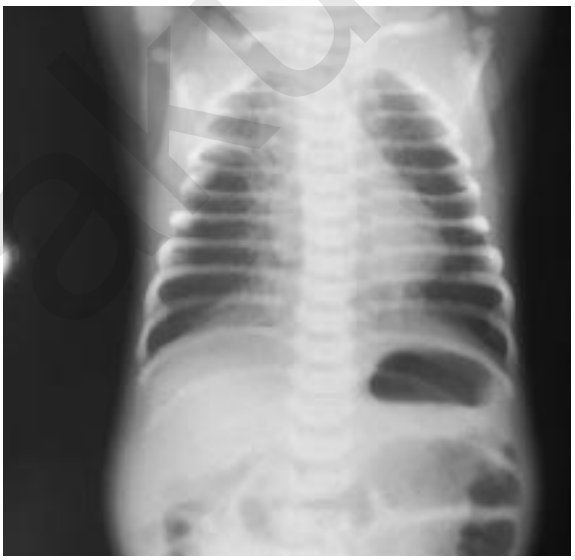

Figure 1.45. This infant presented with respiratory distress, respiratory stridor, and hyperextension of the neck. With these findings, consideration should be given to the diagnosis of vascular ring, which causes compression of the esophagus and trachea. It is most commonly due to a double aortic arch or right aortic arch with a left ductus arteriosus. Dysphagia is not a common presentation in infancy. Rather, it presents with stridor, respiratory distress, and sometimes recurrent pneumonia.

1.46

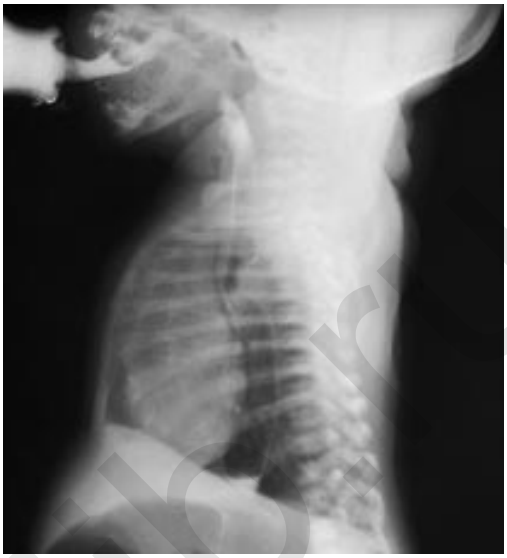

Figure 1.46. A lateral contrast radiograph of the chest in the same infant demonstrates the indentation of the esophagus by the obstructing vascular ring just below the thoracic inlet. A vascular ring is usually associated with a right-sided or double aortic arch. Usually a right aortic arch exists as an isolated anomaly but it may be associated with congenital heart disease. A double aortic arch which encircles the trachea and esophagus is the type of ring most likely to cause symptoms in early infancy.

1.47

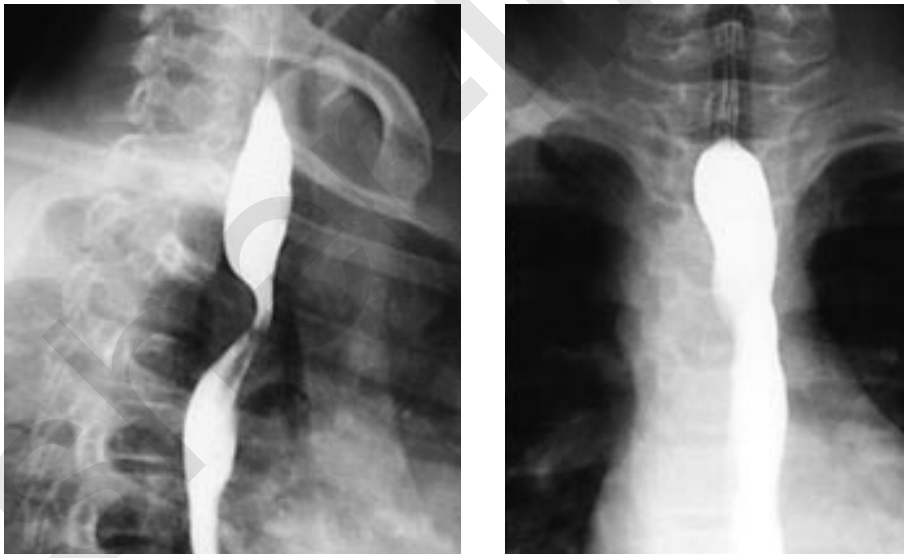

Figure 1.47. Lateral and anteroposterior views of a vascular ring demonstrate how it indents the upper esophagus. The lateral view offers the best opportunity to diagnose this condition. Symptomatic vascular rings should be resected.

1.48

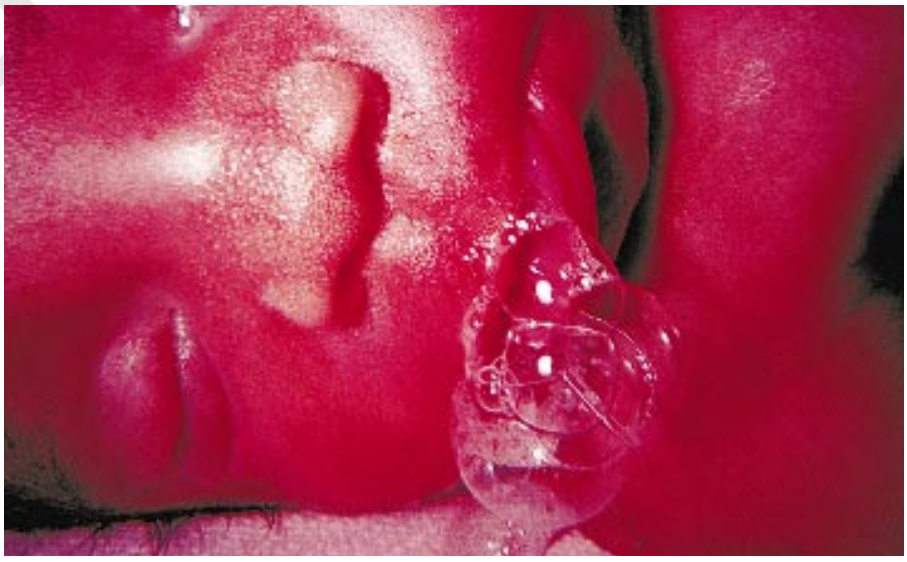

Figure 1.48. In any infant with excess secretions of mucus, the diagnosis of an esophageal atresia with a blind pouch or tracheoesophageal fistula should be considered. Infants may "spit-up" excessive amounts of mucus during normal transition. See this volume, Chapter 2, "Gastrointestinal System," for examples of tracheoesophageal fistulae.

1.49

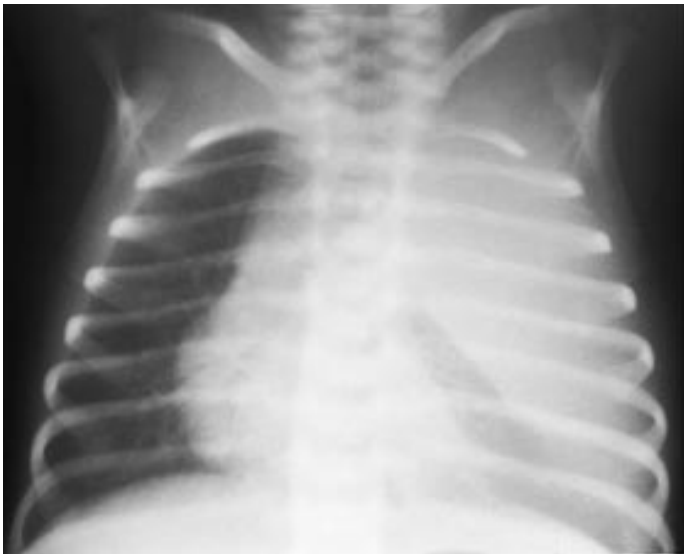

Figure 1.49. This chest radiograph demonstrates bronchial atresia. The atretic bronchus presents as a fluid-filled density of the area of the left upper lobe of the lung. The absent upper lung is replaced by pleural fluid. (Singleton, E., Wagner, M.)

1.50

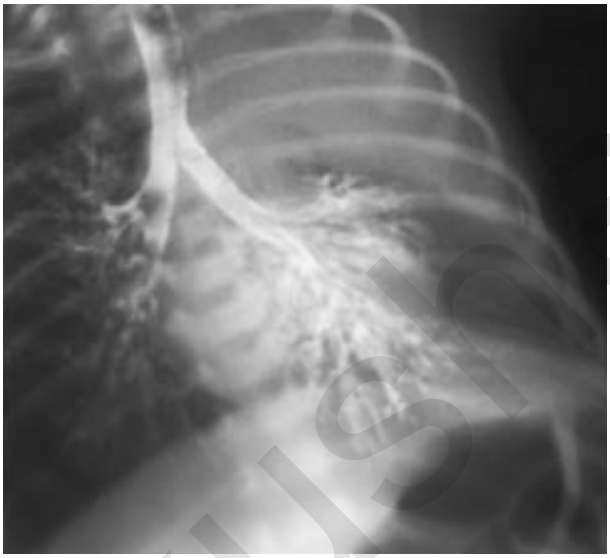

Figure 1.50. Bronchogram of the same infant as in Figure 1.49 demonstrates the normal bronchial segments. Note the normal right lung architecture with three lobes, but only the lower bronchus on the left side. There is an anomalous atretic bronchus with fluid in the lung distal to this. (Singleton, E., Wagner, M.)

1.51

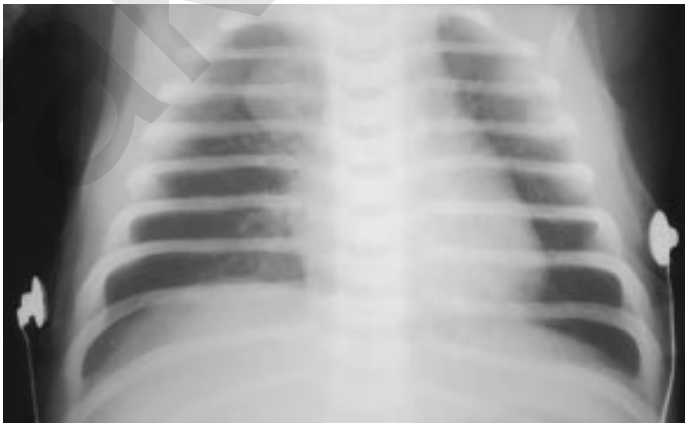

Figure 1.51. Radiograph of the chest shows a bronchogenic cyst on the right side. Such cysts are collections of bronchial epithelial tissue that assume a round, regular appearance. Communication with the large airways can result in spontaneous, intermittent drainage of purulent contents. Congenital bronchogenic cysts arise from abnormal budding of the primitive trachea or abnormal branching of the tracheobronchial tree. They are more common in an area contiguous to the mediastinum, especially in the subcarinal area. If the cyst is completely filled with fluid, it appears as a solid mass.

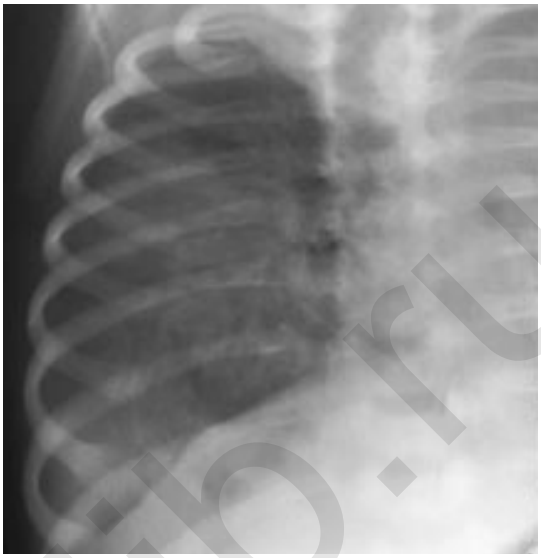

1.52

Figure 1.52. This chest radiograph demonstrates a lobar sequestration at the right lung base. The infant presented with respiratory distress which did not improve, and the density at the right base remained unchanged. Further work-up was undertaken. In many of these infants, clinical manifestations may not occur early. Pulmonary sequestration is a congenital malformation of the respiratory tract; the sequestered area does not communicate with the normal tracheobronchial tree and has a separate blood supply from systemic arteries. Resection of the sequestered lobe is necessary because it is prone to repeated infection.

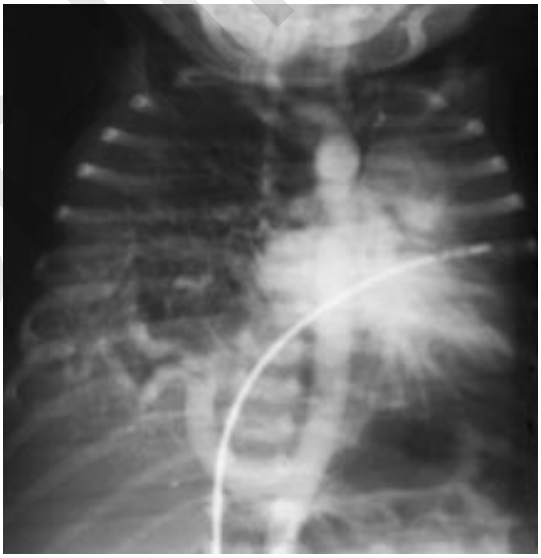

1.53

Figure 1.53. Angiography in the same infant as in Figure 1.52 demonstrates the anomalous vascular connection from the aorta to the sequestered lobe of the lung. This is an excellent example of an intralobar sequestration. The sequestered lung segment typically migrates to an improper position in either the chest or abdomen and has an abnormal systemic blood supply from the aorta. Sequestration, especially the more common intralobar type, occurs most often in the lower lobe areas within the normal visceral pleura. The less common extralobar type of lung sequestration, which is accessory lung tissue outside of the normal pleural boundaries, has been reported in nearly every portion of the thorax and even in the upper abdomen.

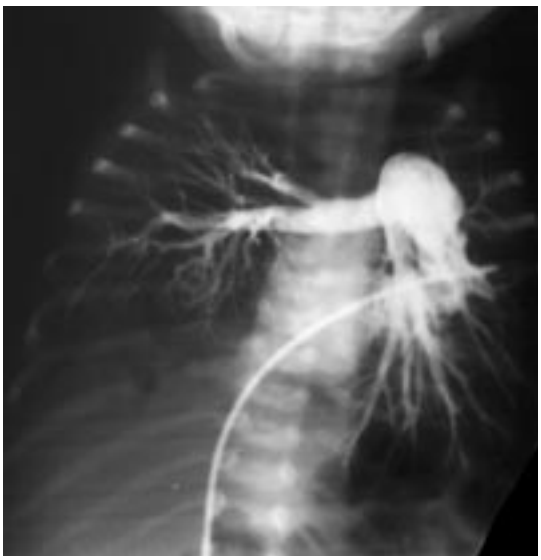

1.54

Figure 1.54. An angiogram of the same infant as in Figures 1.52 and 1.53 shows the heart on the left with crowding of the pulmonary vessels on the left and the lack of pulmonary vessels in the right lung base. This configuration results in the lack of pulmonary artery blood flow to the right lung base, confirming the diagnosis of sequestration.

1.55

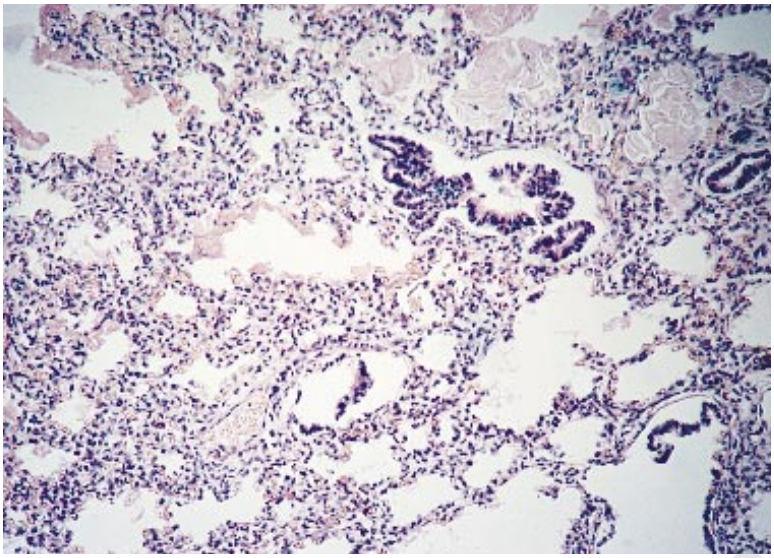

Figure 1.55. In an infant with intralobar sequestration who develops hyaline membrane disease, histologically there is hyaline membrane formation in the nonsequestered lung, but in the sequestered lobe there is no hyaline membrane formation because of its lack of communication with the airway. This photomicrograph shows the hyaline membrane formation in the normal lung, and at the lower right the lack of hyaline membrane in the sequestered lobe. It is possible for partial aeration to occur as a result of fistulous communications with normal lung tissue. This usually occurs following infection.

1.56

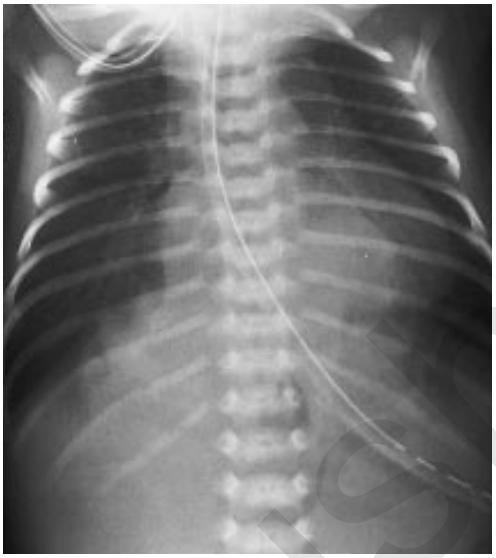

Figure 1.56. In this chest radiograph of an infant who presented with severe respiratory distress and congestive heart failure, note the bilateral posterior mediastinal masses and the hyperinflated lungs. These findings are consistent with large airway obstruction from extrapulmonary sequestration.

1.57

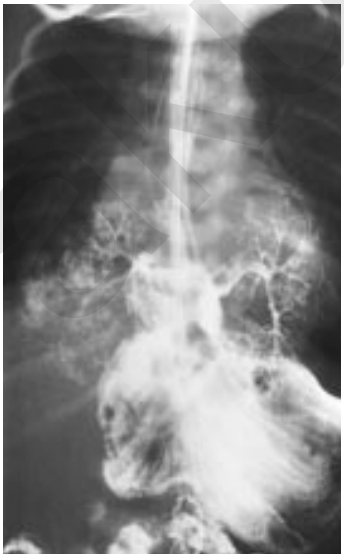

Figure 1.57. A contrast study of the chest and abdomen in the same infant as in Figure 1.56 shows that the extrapulmonary sequestration has bronchi originating bilaterally from the esophagus and esophageal bronchi. Both structures have their origin in the tracheoesophageal tube. This anomaly occurs as a result of a congenital foregut malformation.

1.58

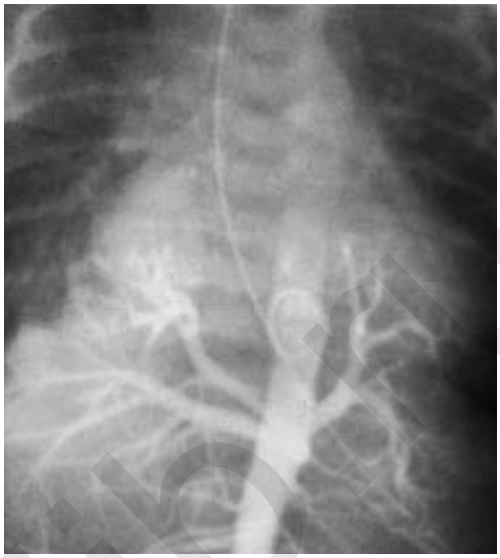

Figure 1.58. An aortogram in the same infant as in Figure 1.56 and 1.57 shows a single systemic artery to the left sequestered lobe and two arteries to the right sequestered lobe.

1.59

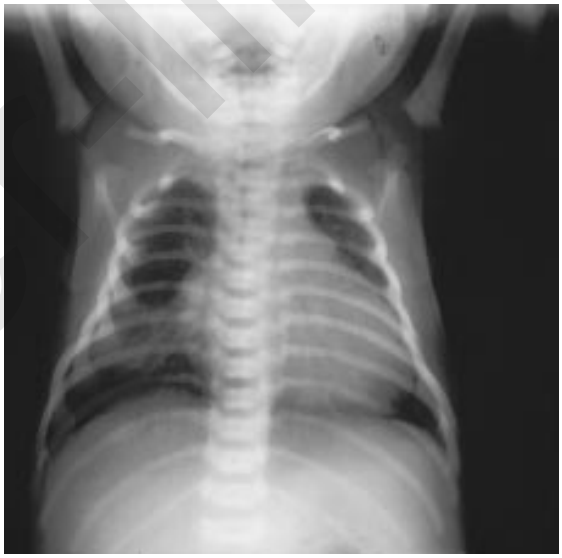

Figure 1.59. In this infant who presented with severe respiratory distress, a radiograph shows a right lower lobe infiltrate which is due to a pulmonary arteriovenous malformation. Congenital pulmonary arteriovenous fistulae may be single or multiple lesions. They present as homogenous densities of variable size and shape and are frequently in continuity with the hilar vascular shadows. They apparently result from persistence of fetal anastamotic capillaries. Frequently there may be associated hemangiomas in other parts of the body.

1.60

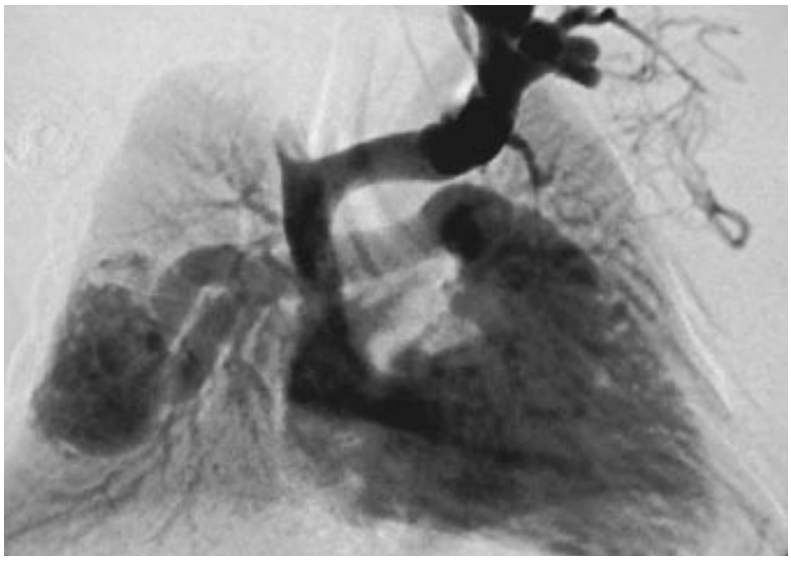

Figure 1.60. Angiography confirms the diagnosis of an arteriovenous malformation of the right lower lobe of the lung. Note the feeder artery from the right pulmonary artery and the direct venous connection going from the malformation into the left atrium. In some of these infants, a continuous bruit may be heard over the site of the arteriovenous malformation.

1.61

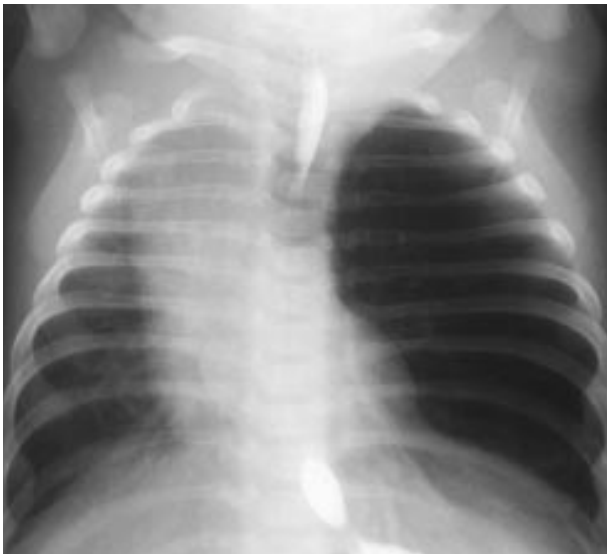

Figure 1.61. Congenital lobar emphysema most commonly involves the left upper lobe of the lung (47%). In general, the distribution is slightly greater in the right lung than in the left. The left upper lobe in this infant is hyperinflated and displaces the mediastinum to the right. The left hemithorax is larger than the right, but the absence of increased pulmonary vascular markings on the left and respiratory distress suggests the diagnosis of congenital lobar emphysema. (Singleton, E., Wagner, M.)

1.62

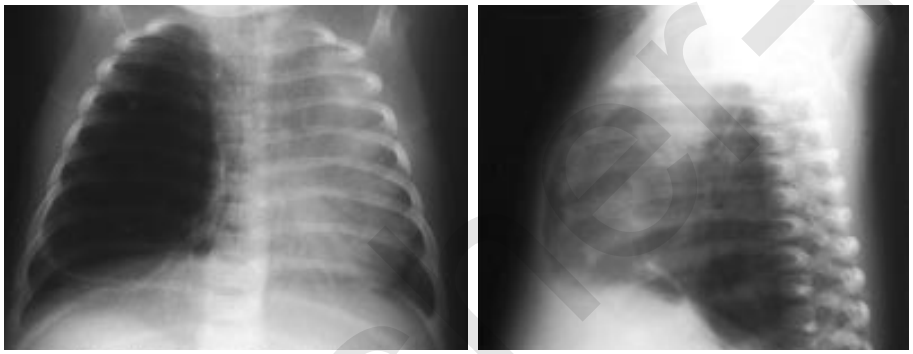

Figure 1.62. Anteroposterior and lateral chest radiographs in an infant with congenital lobar emphysema of the upper lobe of the right lung. Right upper lung lobe involvement occurs in 20% of the cases. Note the hyperinflated right hemithorax with the lack of vascular markings and the displacement of the mediastinum to the left.

1.63

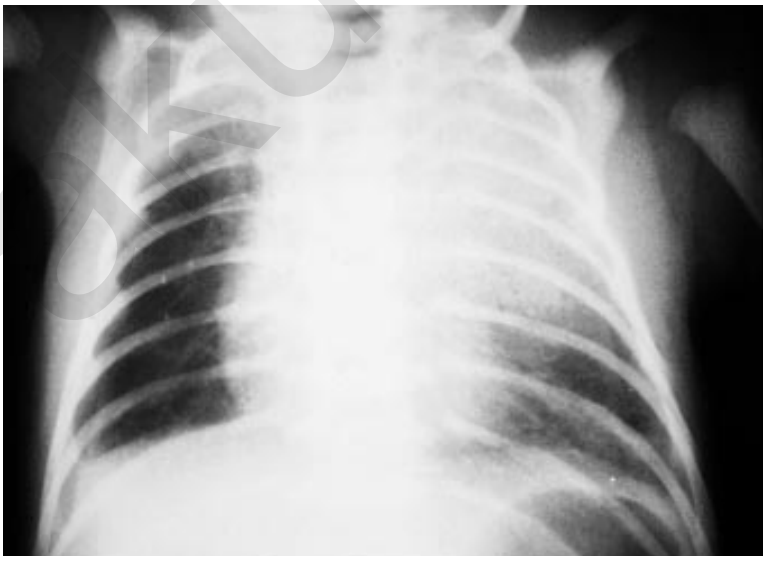

Figure 1.63. At birth, congenital lobar emphysema may present as an opacity due to the presence of retained fetal fluid as noted in this radiograph. When the fluid clears, the typical appearance of lobar emphysema becomes apparent. (Singleton, E., Wagner, M.)

1.64

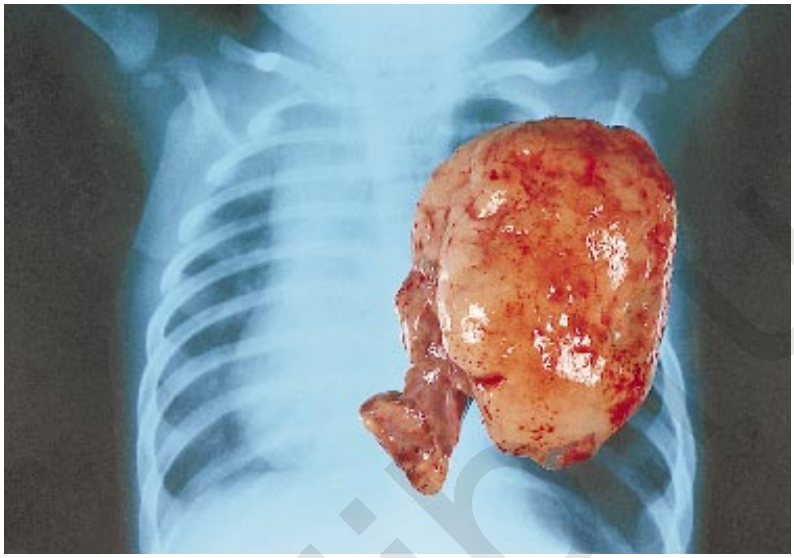

Figure 1.64. The surgical specimen of the emphysematous lobe shows its gross size in comparison to the chest radiograph.

1.65

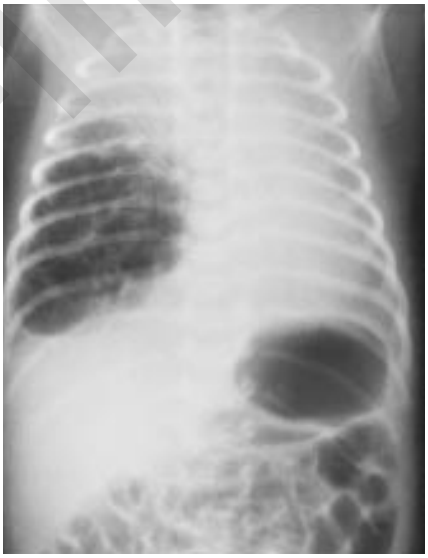

Figure 1.65. In this infant who presented with mild respiratory distress, note the congenital cyst of the right lung. The cyst has discrete septations, it does not fill the entire hemithorax, and does not appear under pressure as does the lung with lobar emphysema. Many of these infants may be asymptomatic.
Pulmonary cysts are large, thin-walled cysts. They are rare, are more commonly noted in the lung periphery, and probably represent a disorder of bronchial growth at a later stage in fetal life than do the more central bronchogenic cysts.

1.66

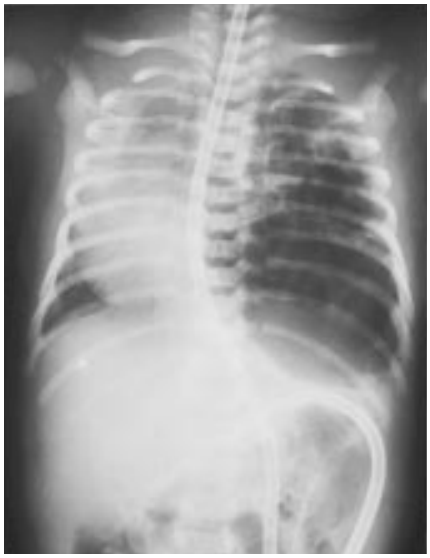

Figure 1.66. In infants with congenital cystic adenomatoid malformation of the lung, there may be no or minimal respiratory distress at birth. The respiratory distress becomes progressively worse with gaseous overdistention of the lung and mediastinal shift. In the radiograph of this infant, note the multiple loculi of areas of air in the left hemithorax with gaseous overdistention and the shift of the mediastinum to the right. The areas of loculated air may simulate a diaphragmatic hernia; however, the intestinal gas pattern is normal and the orogastric tube is clearly seen coiled in the stomach. (Singleton, E., Wagner, M.)

1.67

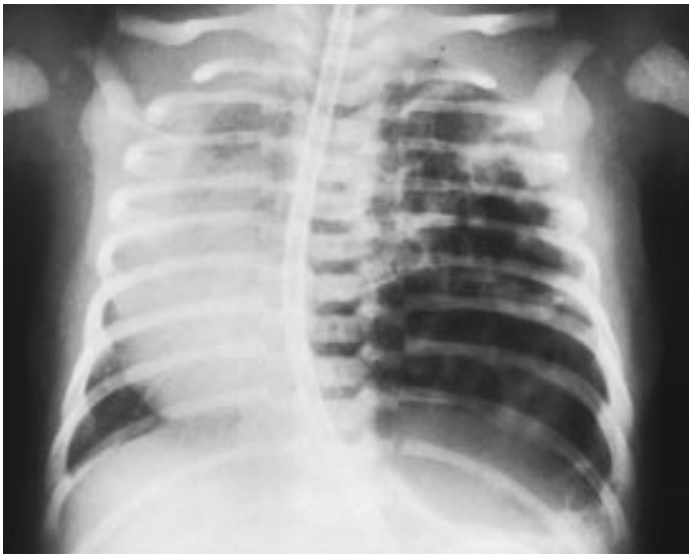

Figure 1.67. Radiograph of another infant with congenital cystic adenomatoid malformation of the lung on the left side. This infant developed increasingly severe respiratory distress within 18 hours of birth as a result of progressive air trapping and hyperinflation. In these infants, surgical removal of the malformation is essential.
Congenital cystic adenomatoid malformation may present initially as an intrapulmonary mass which appears solid or has a few scattered translucent areas, but this progresses to give the typical appearance of congenital cystic adenomatoid malformation.

1.68

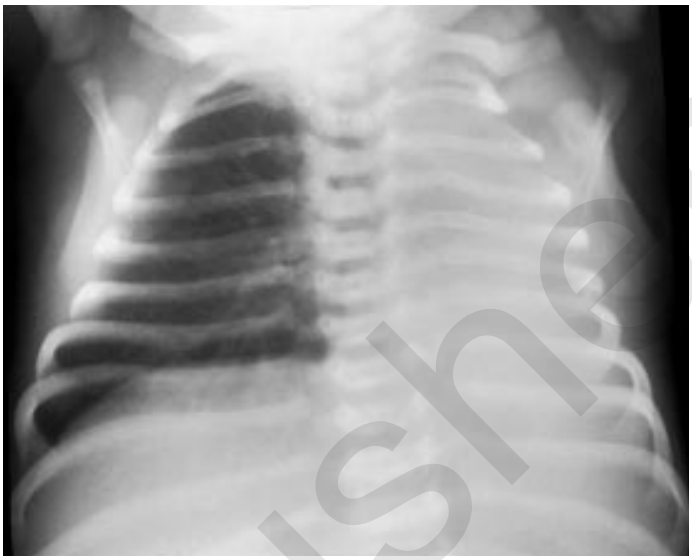

Figure 1.68. This chest radiograph shows pulmonary agenesis on the left side. Note the hyperinflated right lung with widening of the intercostal spaces and splaying of the ribs. The heart is displaced to the left side. In pulmonary agenesis the affected hemithorax is opaque, and the mediastinal structures occupy the airless space. Total agenesis of both lungs is very rare. Absence of the left lung is more frequent than of the right lung. The remaining lung is larger than normal and often herniates into the contralateral chest. Soon after a groove develops in the laryngotracheal tube, the tracheal portion bifurcates into the right and left lung bronchi. Failure to do so may result in agenesis. The presence of another anomaly, such as a vertebral defect, strongly supports the diagnosis of agenesis.

1.69

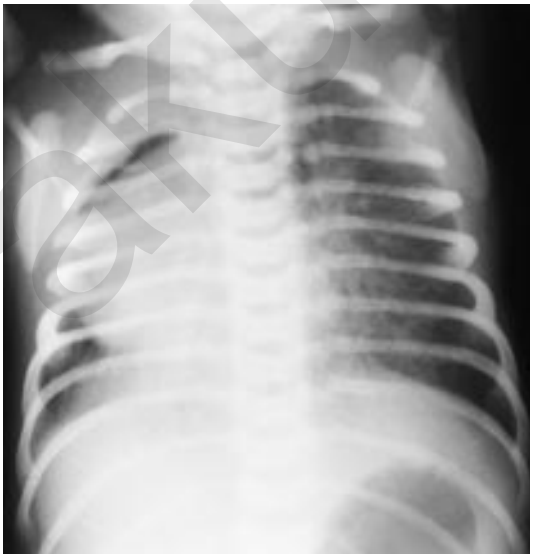

Figure 1.69. This infant had minimal respiratory distress, but on physical examination was noted to have asymmetry of the chest. A chest radiograph showed a marked difference in the width of the intercostal spaces between the left and right side of the chest. The right lung is opacified and the right hemithorax is small; the left lung is hyperexpanded. Hypogenetic lung syndrome (alveolar hypoplasia) is a variant of pulmonary agenesis. Congenital heart disease is apparently more common with right than with left lung hypogenesis. In this infant there was dextrocardia, pulmonary artery hypoplasia, and anomalous systemic arterial supply to the right lower lobe with anomalous venous drainage.

1.70

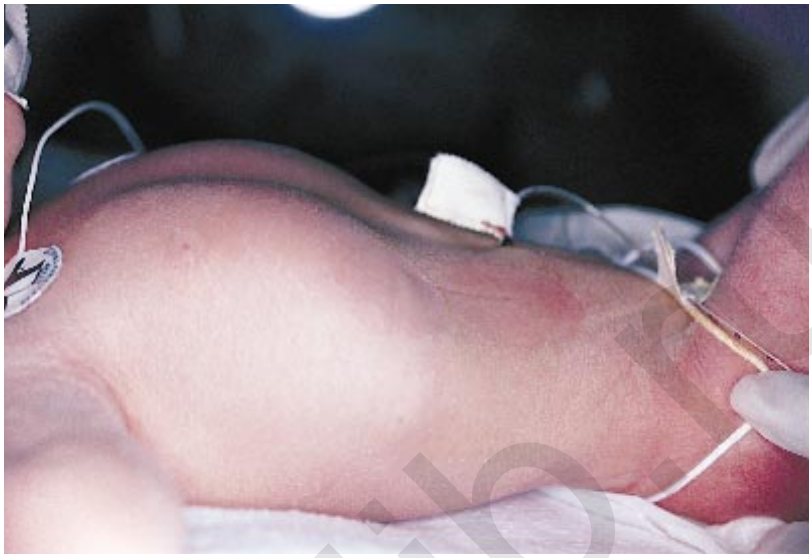

Figure 1.70. This infant with a scaphoid abdomen and barrelling of the chest had a diaphragmatic hernia. In any infant with a scaphoid abdomen, two surgical emergencies should be excluded – congenital diaphragmatic hernia, and esophageal atresia with a blind pouch and no communication with the gastrointestinal tract. Normally, the passage of air into the gastrointestinal tract after birth distends the scaphoid abdomen. In severe neuromuscular disease or central nervous system depression, air is not swallowed, hence the abdomen also remains scaphoid.

1.71

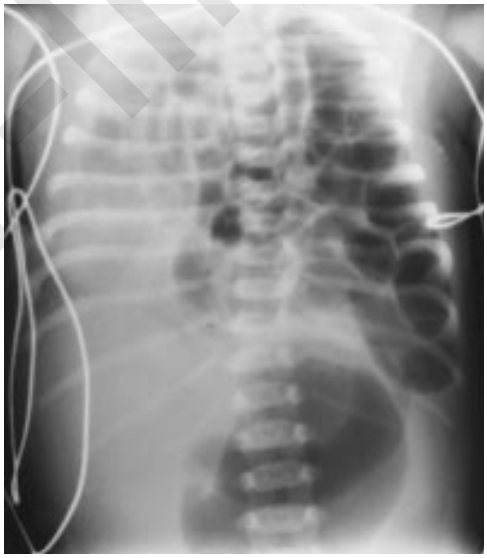

Figure 1.71. A radiograph of an infant with a Bochdalek-type congenital diaphragmatic hernia shows a midline abdominal stomach and multiple fluid and air-filled loops of bowel in the left hemithorax. Left-sided herniae occur five times more frequently than right-sided herniae. The incidence of this defect is 1:4000 live births and it constitutes a neonatal emergency if there is severe respiratory distress in the first hour of life. The infant swallows air which inflates the stomach and small bowel, causing collapse of the lung and displacement of the mediastinum. In severe cases, the stomach, small bowel, and left lobe of the liver may lie in the hemithorax during fetal life, resulting in hypoplasia of the lungs.

1.72

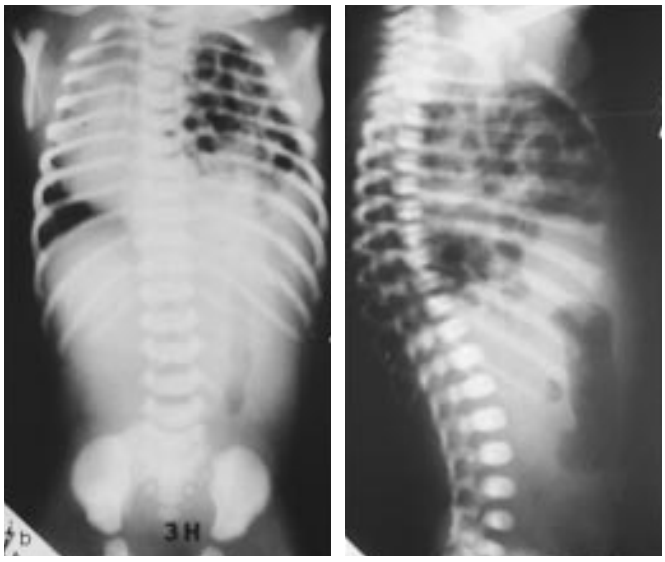

Figure 1.72. Anteroposterior and lateral radiographs of an infant with a diaphragmatic hernia who presented with severe respiratory distress at birth. Note the displacement of the heart to the right and the lack of gas in the gastrointestinal tract. In the lateral view, note the scaphoid appearance of the abdomen.

1.73

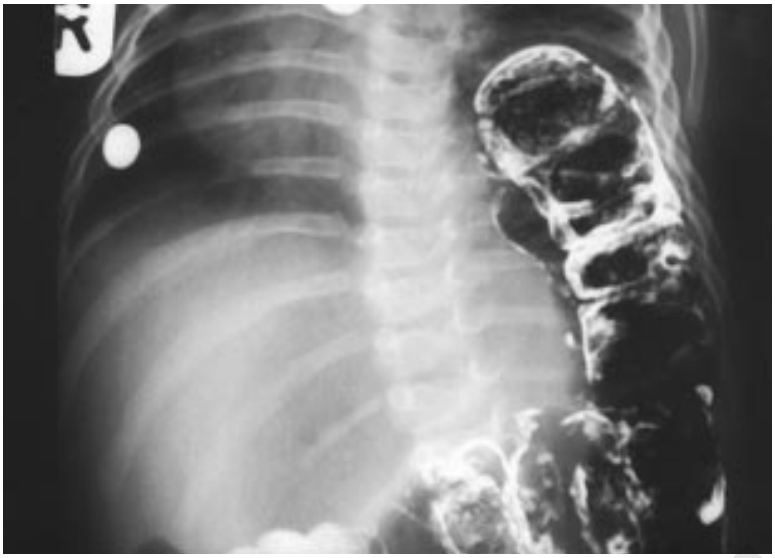

Figure 1.73. Infants with diaphragmatic herniae may present with a wide spectrum of symptoms. This infant had minimal respiratory distress, but some abdominal distention and vomiting. A contrast study of the colon demonstrates its location in the left hemithorax, confirming the diagnosis of a congenital diaphragmatic hernia.

1.74

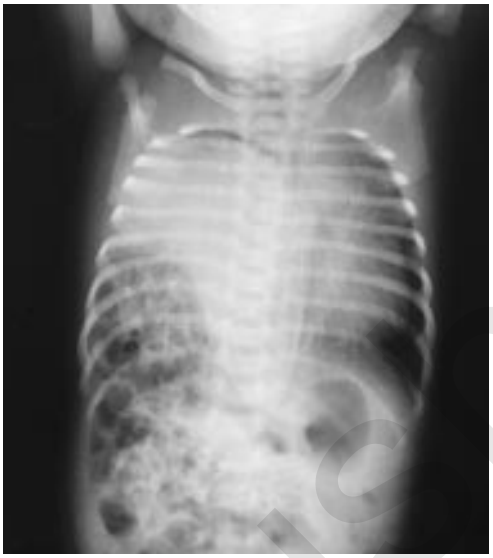

Figure 1.74. In this radiograph note a right-sided diaphragmatic hernia with the liver and bowel in the right side of the chest. Bochdalek-type herniae are typically large and involve a posterolateral defect in the foramen of Bochdalek. Morgagni herniae are retrosternal and involve the foramen of Morgagni. Ninety-eight percent of all defects are the Bochdalek type. Symptoms are generally less severe when the hernia is on the right side.

1.75

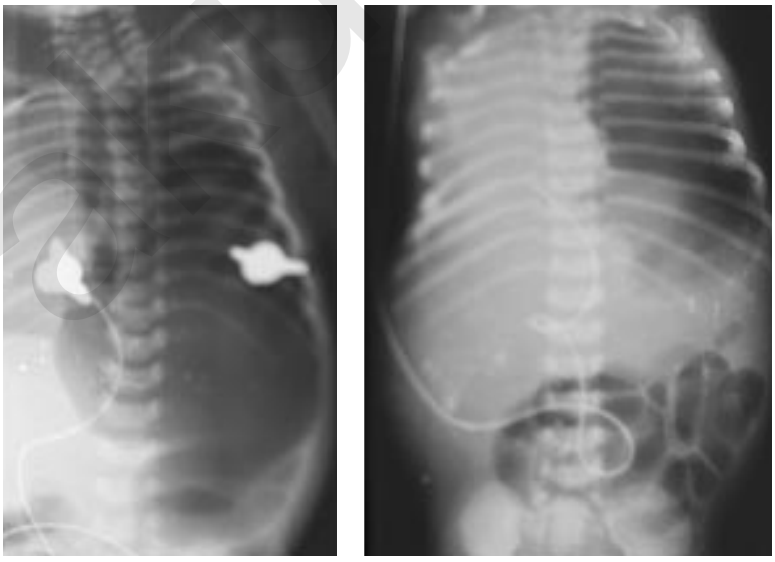

Figure 1.75. In this infant with a congenital diaphragmatic hernia, there was vigorous resuscitation at birth. Prolonged bag-mask ventilation can distend the stomach and intestine with air, thus increasing the respiratory distress. Note that the mediastinum and heart are shifted to the right even after decompression and that the markedly distended stomach is in the thoracic cavity. Gastric aspiration relieved the distention as noted in the radiograph on the right. Infants with congenital diaphragmatic hernia often require vigorous resuscitation; thus it is important to place an orogastric tube during resuscitation if diaphragmatic hernia is suspected.

1.76

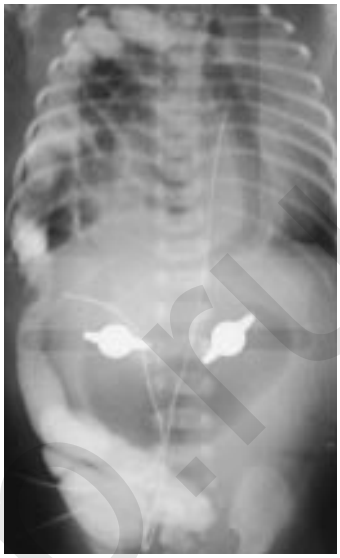

Figure 1.76. In this infant with Rh isoimmunization and a congenital diaphragmatic hernia, contrast was injected into the amniotic fluid of the fetus to permit swallowing of the contrast for confirmation of the position of the fetal bowel prior to intrauterine transfusion. At birth, the infant was noted to have respiratory distress, and a plain radiograph of the chest and abdomen showed the contrast-filled bowel lying in the chest, confirming the diagnosis of a diaphragmatic hernia. This is of historic interest only because this practice has been replaced by the use of ultrasound during the procedure of intrauterine transfusion.

1.77

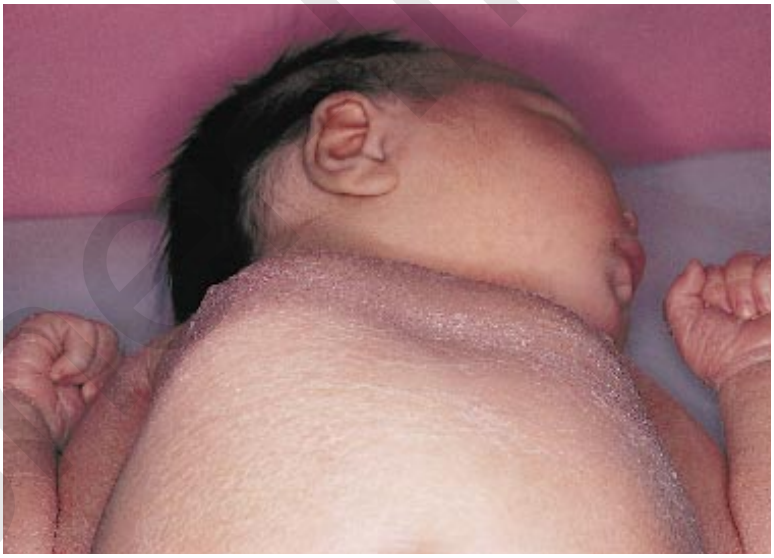

Figure 1.77. The asymmetry of the chest in this infant is a result of eventration of the diaphragm. Note the elevation with ballooning of the chest on the right side. Eventration is a congenital thinning of the muscle of the pleuroperitoneal membrane portion of the diaphragm. Thinning allows upward displacement of the liver, thereby elevating the ribs on the affected side. It is usually unilateral, rarely bilateral. If respiratory distress is not severe, these infants may be treated conservatively.

1.78

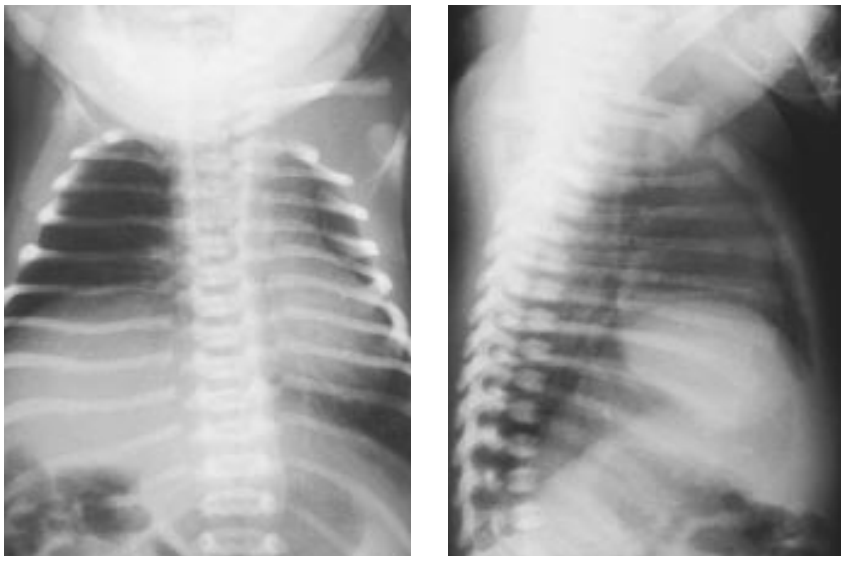

Figure 1.78. An anteroposterior and lateral radiograph of the chest of an infant with eventration of the diaphragm. Note the right diaphragm elevated well above the left with the increased density of the liver below it. Eventration of the diaphragm should be differentiated from paralysis of the diaphragm. On fluoroscopic examination, if the diagnosis is eventration of the diaphragm, there is movement of the diaphragm with respiration whereas, if the diagnosis is paralysis of the diaphragm, there is lack of movement. Currently, the diagnosis is made by ultrasonography.

1.79

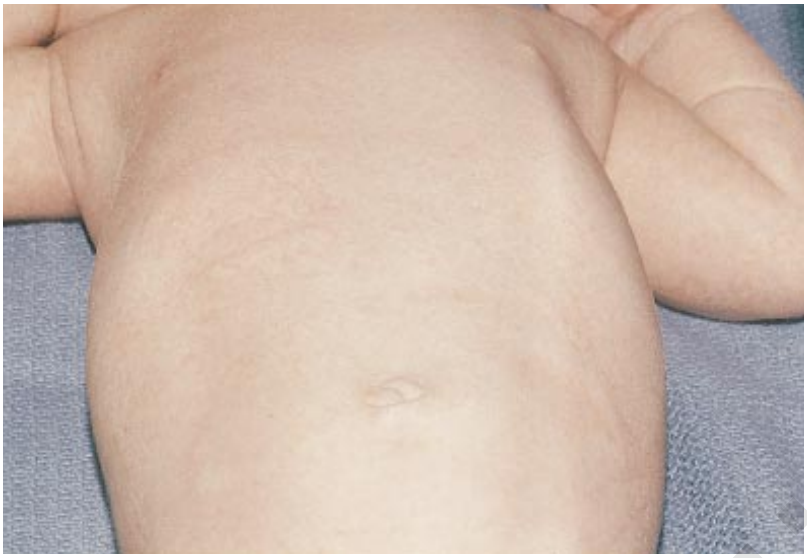

Figure 1.79. In this infant with a unilateral paralysis of the right diaphragm, note the elevation of the ribs on the affected side of the chest. The chest is asymmetrical and, with inspiration, chest expansion occurred only on the normal side. In general, this condition is functional and may resolve spontaneously.

1.80

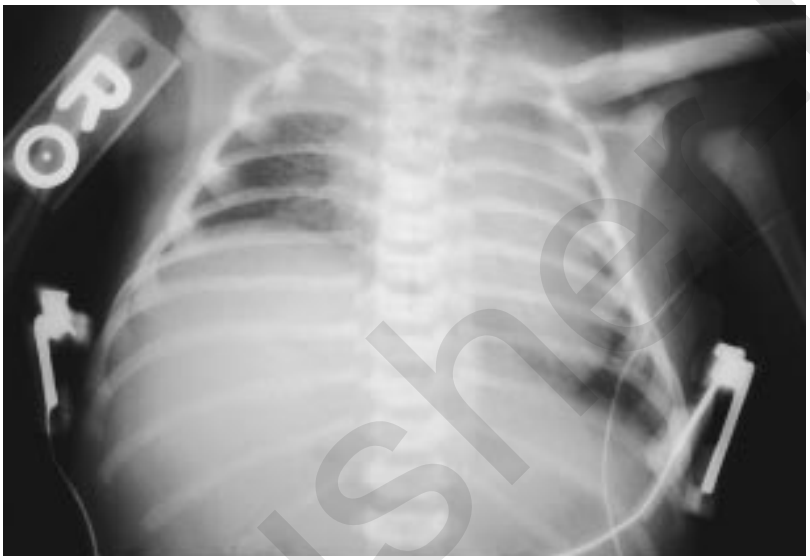

Figure 1.80. A radiograph of an infant with paralysis of the right diaphragm which occurred as a result of phrenic nerve palsy (C3, C4, C5) associated with a right Erb's palsy (C4, C5, C6). If this radiograph is compared with that of an eventration of the diaphragm, it is noted that it is important to do an ultrasonographic study. Paralysis of the diaphragm is more common in large infants and is clearly related to dystocia.

1.81

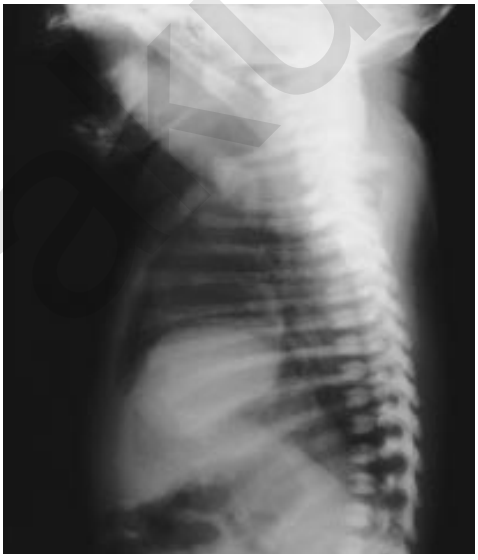

Figure 1.81. A lateral radiograph shows that the right diaphragm is elevated well above the left. Lack of movement can be appreciated under fluoroscopy or by ultrasonography. Paralysis of the diaphragm occurs on the right side versus the left side at a ratio of 4:1.

1.82

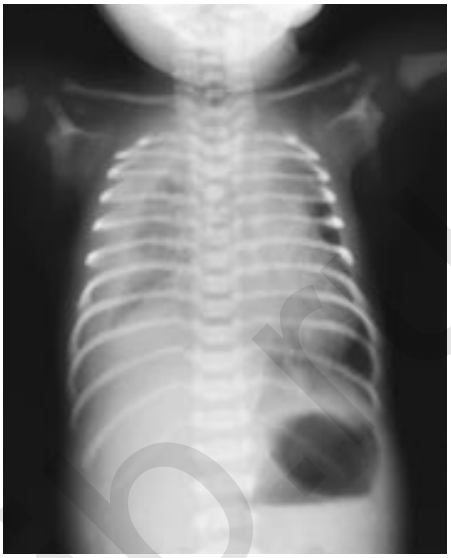

Figure 1.82. A large right pleural effusion obscures most lung markings. Air is appreciated centrally as the infant is supine and the entire hemithorax is not filled with fluid. Note that the cardiac shadow is displaced to the left. The etiology was unknown. Pleural effusions occur with chylothorax, hydrops fetalis, congestive heart failure, transient tachypnea of the newborn, complications of central total parenteral nutrition, and intrauterine viral infections.

1.83

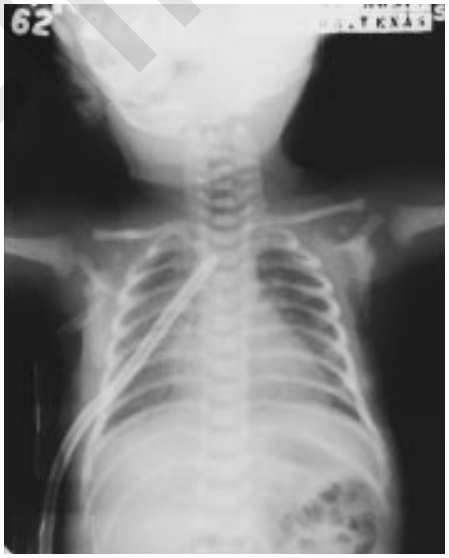

Figure 1.83. The same infant as seen in Figure 1.82 showed rapid improvement after a thoracostomy tube drainage was performed. The lung reinflated and the cardiac shadow returned to its normal position with relief of the respiratory distress.

1.84

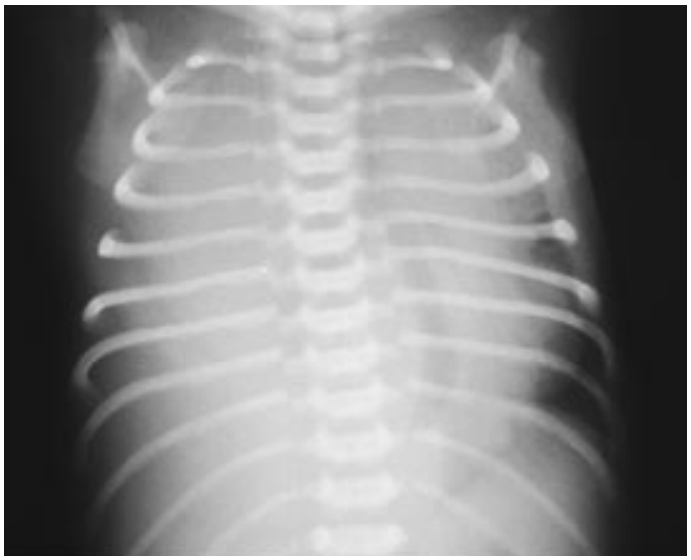

Figure 1.84. This infant presented with severe respiratory distress at birth. A chest radiograph showed marked opacification of the right hemithorax with displacement of the trachea and cardiac shadow to the left. All lung markings were obscured. The appearance was that of a massive pleural effusion, and the diagnosis of congenital chylothorax was made by thoracentesis performed on the right chest with removal of about 300 ml of straw-colored fluid. This resulted in rapid relief of the respiratory distress. Congenital chylothorax results from the leakage of chyle into the pleural space and is presumably caused by congenital defects in the thoracic duct or by trauma. The other lymphatic vessels are usually normal.

1.85

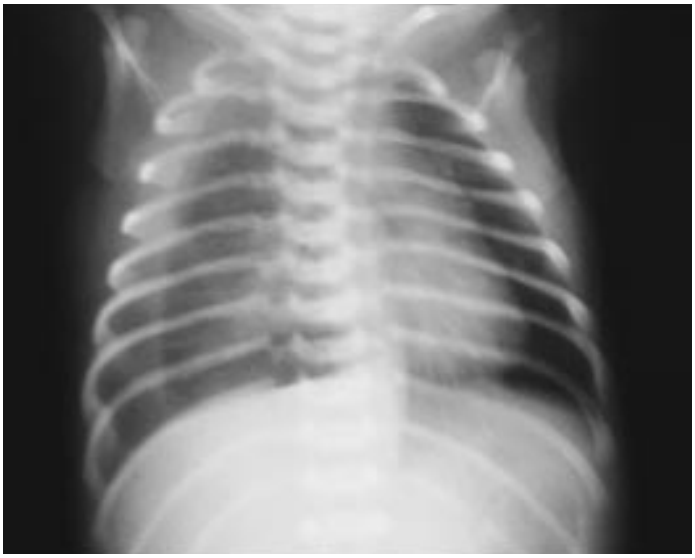

Figure 1.85. Radiograph of the same infant as in Figure 1.84 at the age of eight hours, following thoracentesis at the age of 4 hours. Note marked improvement, although some fluid is still present.

1.86

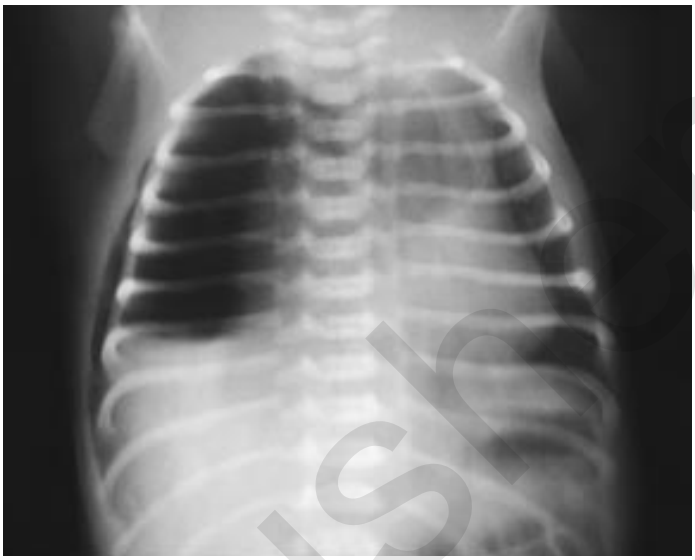

Figure 1.86. The same infant as in Figure 1.84 and 1.85 later required a second thoracentesis at the age of 48 hours. In this chest radiograph following aspiration of the chylothorax, a subcutaneous collection of air and a small residual pneumothorax persisted.

1.87

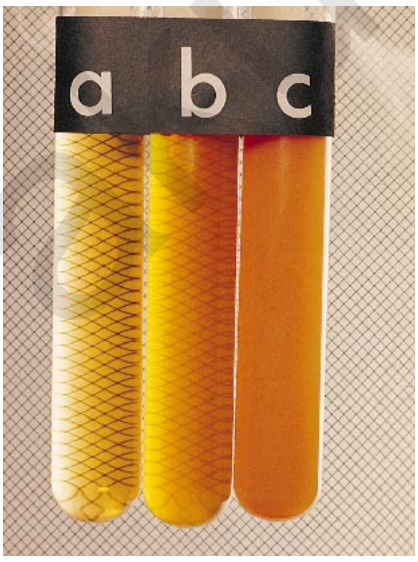

Figure 1.87. Comparisons of the clarity of chylous fluid at (a) the age of 4 hours, and prior to feeding, (b) 48 hours and after several milk feeds, and (c) after feeding has been well established. Note the progressive increase in turbidity associated with appearance of fat-laden chylomicrons after initiation of oral dietary fat intake. Chylous fluid is also high in protein and white blood cells. Management of this infant would include feeds with medium-chain triglycerides and total parenteral nutrition rather than the use of regular formula.

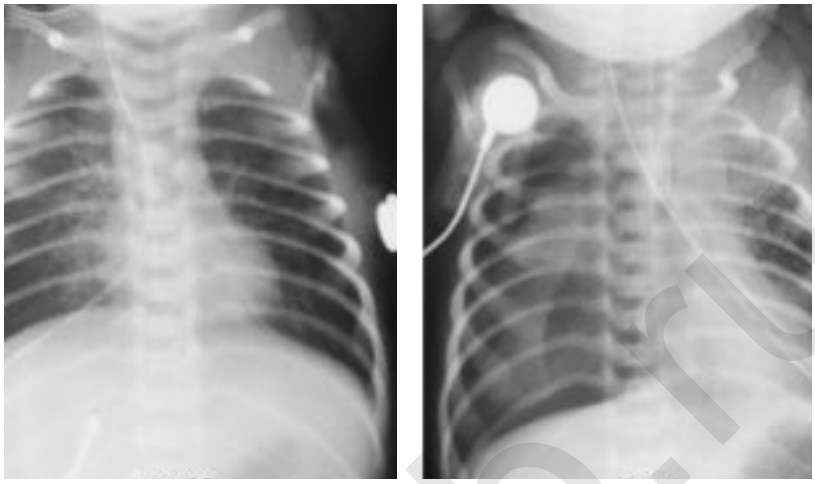

1.88

Figure 1.88. A tear in the hypopharynx of this infant occurred from erosion by a feeding tube. The tube went through a tear in the hypopharynx into the right pleural cavity (left radiograph). The tube was withdrawn and reinserted the following day, going through the tear into the left pleural cavity (right radiograph). Note the pneumothorax in the right chest in the radiograph on the right. A complication of gastric and endotracheal tube placement is a tear in the esophagus that allows the tube to be placed into the mediastinum, often resulting in a pneumothorax.

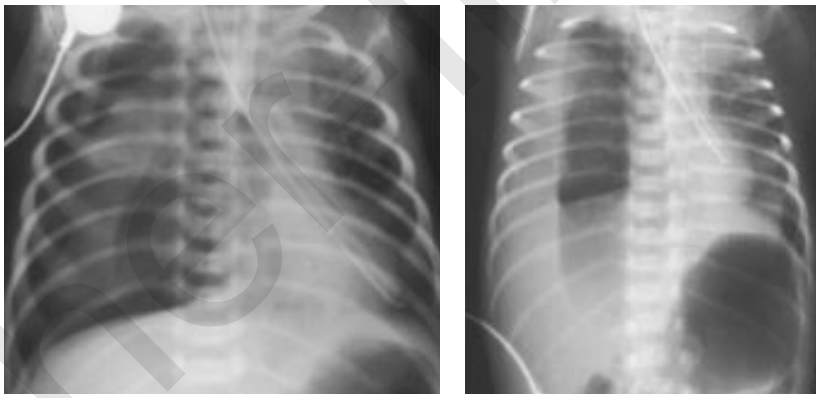

1.89

Figure 1.89. These anteroposterior and left lateral decubitus chest radiographs demonstrate a right hydropneumothorax caused by a malpositioned nasotracheal tube that tore through the hypopharynx.

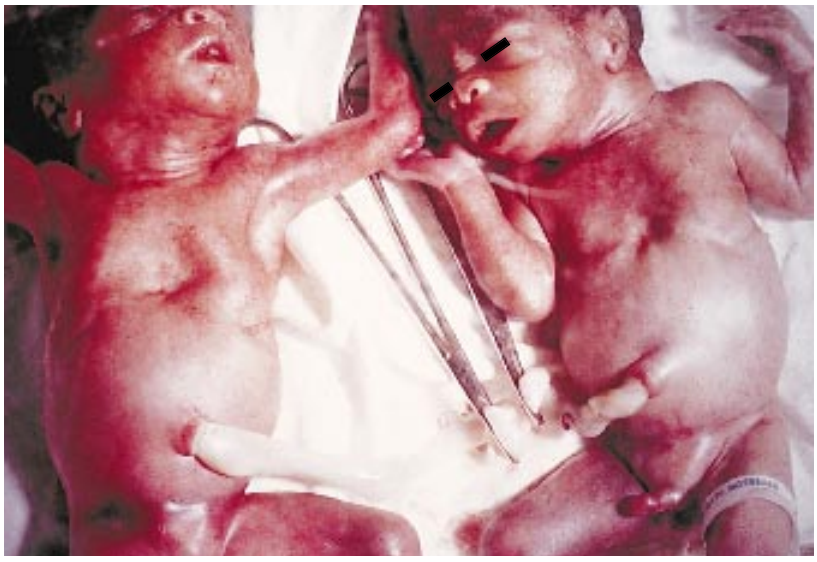

1.90

Figure 1.90. These twin premature infants with severe hyaline membrane disease developed respiratory distress soon after birth. Note the glistening, gelatinous appearance of the skin due to edema; severe nasal flaring; and intercostal, subcostal, and xyphoid retractions because of the pliability of the chest wall. This reflects the stiffness of the lungs and worsens over the first two to three days. Clinically, the infants have tachypnea with a "see-saw" pattern of breathing and an expiratory grunt.

1.91

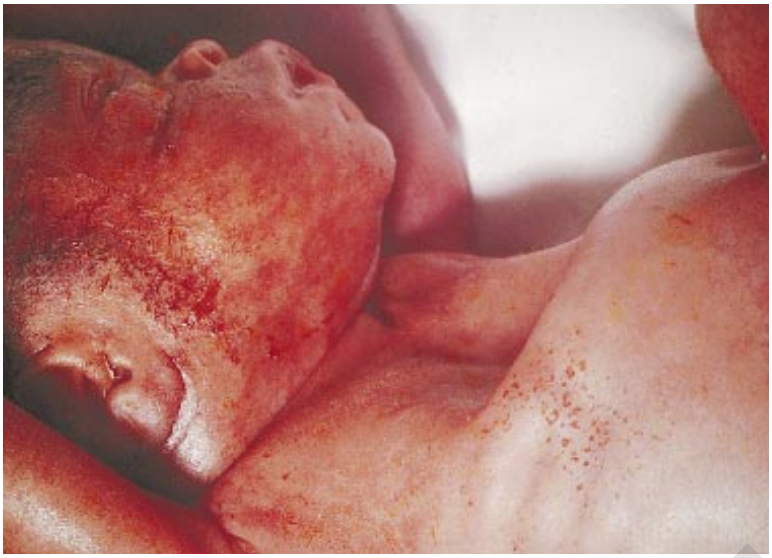

Figure 1.91. Severe xyphoid, subcostal, and intercostal retractions are shown in this infant with hyaline membrane disease. The stomach progressively dilates with swallowed air.

1.92

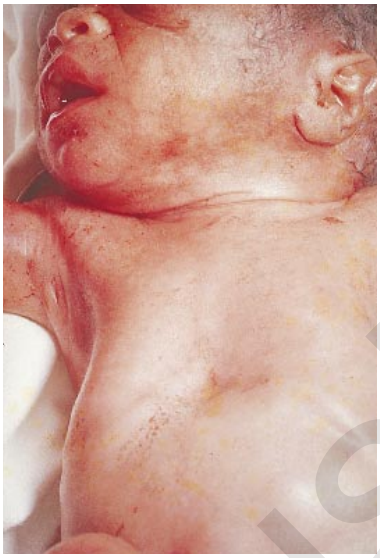

Figure 1.92. In this infant with hyaline membrane disease, the alae nasi are widely flared, the mouth is open, and there are severe retractions of the sternum and intercostal spaces. These reflect the severity of the respiratory distress. With severe distress, the alae nasi remain open and no flaring is noted. The mouth is open because of the infant's lack of tone and, with improvement in the infant's condition, flaring of the alae nasi is again noted.

1.93

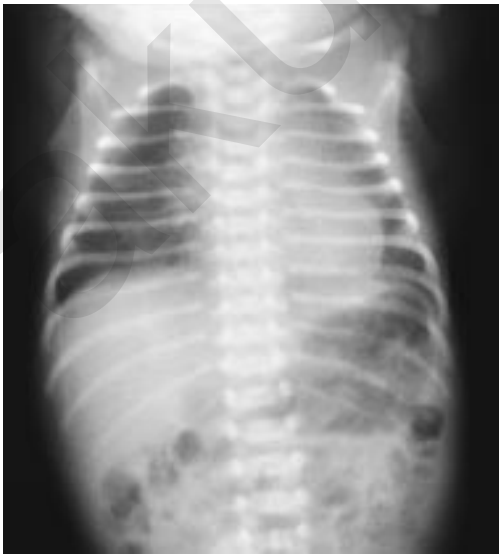

Figure 1.93. This radiograph taken at 20 minutes of age in an infant with mild hyaline membrane disease demonstrates that most of the lung fluid has been cleared. It does not yet reflect the volume loss and consolidation of the lung typical of surfactant deficiency and pulmonary edema.

1.94

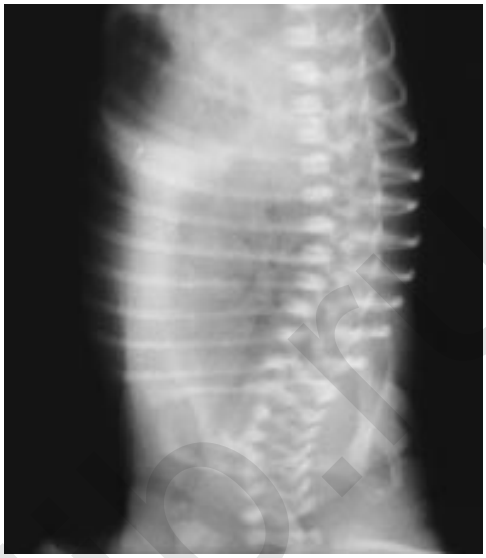

Figure 1.94. A lateral radiograph of the same infant as in Figure 1.93 shows the sternal retraction, and there is a mild air bronchogram.

1.95

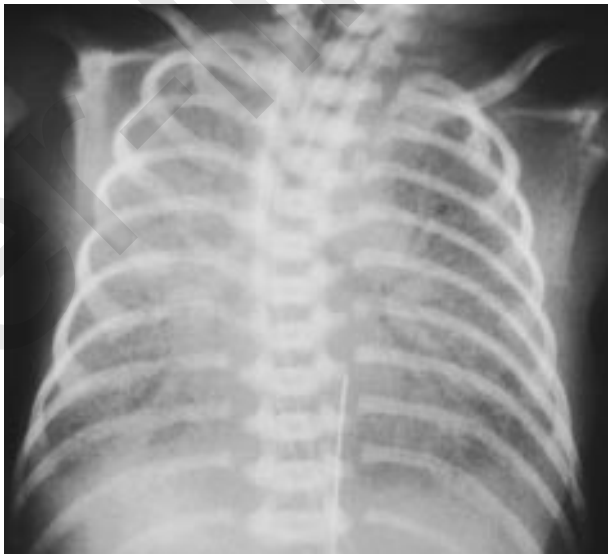

Figure 1.95. Over the ensuing several hours, surfactant deficiency results in severe lung injury with hyaline membrane formation, loss of lung volume, and air bronchograms on the chest radiograph along with the development of a reticulogranular pattern of the lung parenchyma. The reticulogranular pattern consists of diffuse, symmetrical areas of alveolar atelectasis interspersed with aerated bronchioles and alveolar ducts.

1.96

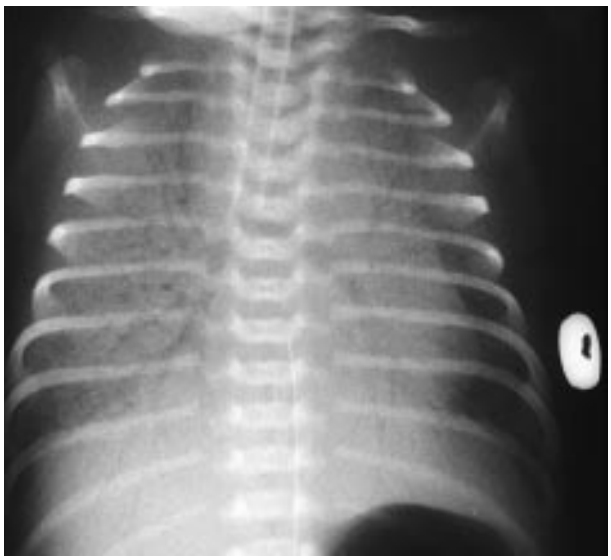

Figure 1.96. Hyaline membrane disease is a heterogeneous process involving only some alveoli while others are unaffected. In this instance, a radiograph demonstrates a more severely affected right lung. The typical radiologic appearance of hyaline membrane disease may vary from the typical reticulogranular ("ground glass") appearance of the lung fields with air bronchograms to complete opacification of the chest.

1.97

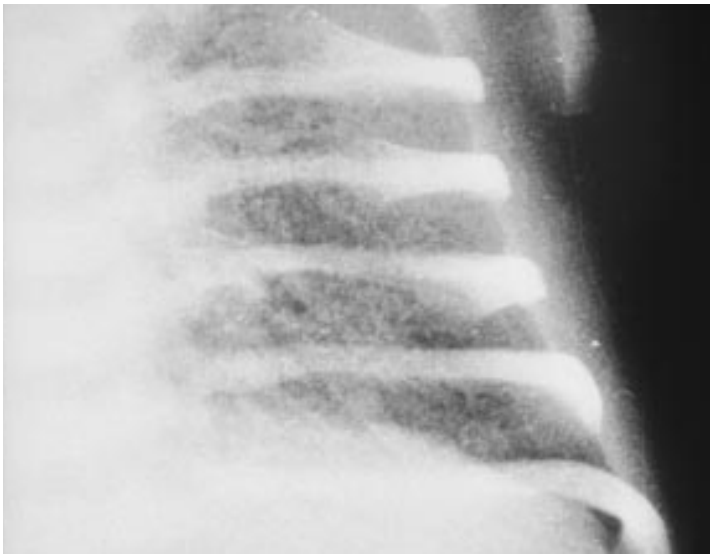

Figure 1.97. A detailed view of the left cardiophrenic angle in this radiograph demonstrates the reticulogranular pattern of the lung parenchyma in hyaline membrane disease. With progression of the disease, the reticulogranular pattern becomes more prominent, and coalescence of many of the small atelectatic areas occurs resulting in more opaque lung fields.

1.98

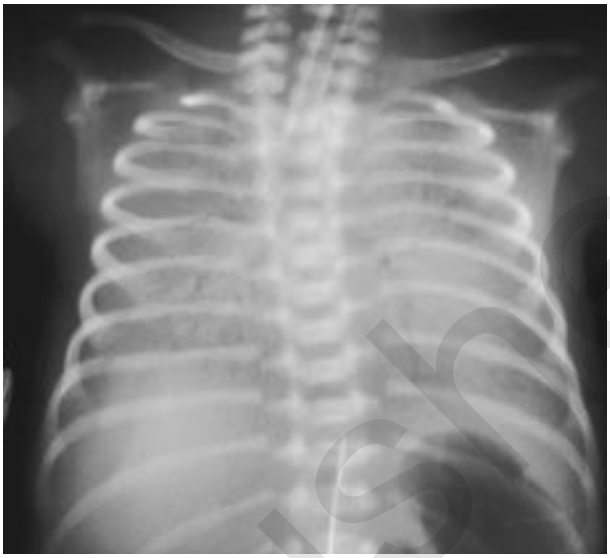

Figure 1.98. Lung volume in hyaline membrane disease is progressively lost, resulting in opacification as seen in this radiograph, and can be difficult to recruit again despite the use of vigorous positive pressure ventilation via an endotracheal tube.

1.99

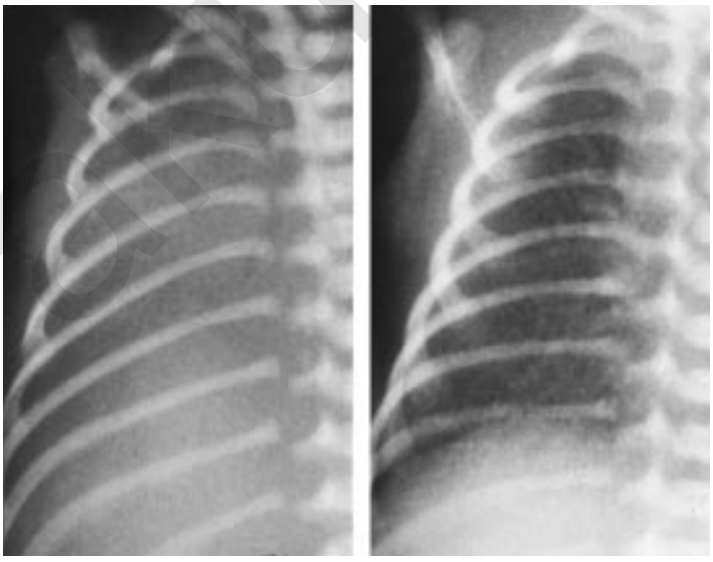

Figure 1.99. The appearance of hyaline membrane disease, seen in the radiograph on the left, can be altered dramatically with the application of positive pressure ventilation (radiograph on the right). The application of continuous positive airway pressure (CPAP) can result in a dramatic increase in lung volume and clearing of fluid from the lung fields. (Singleton, E., Wagner, M.)

1.100

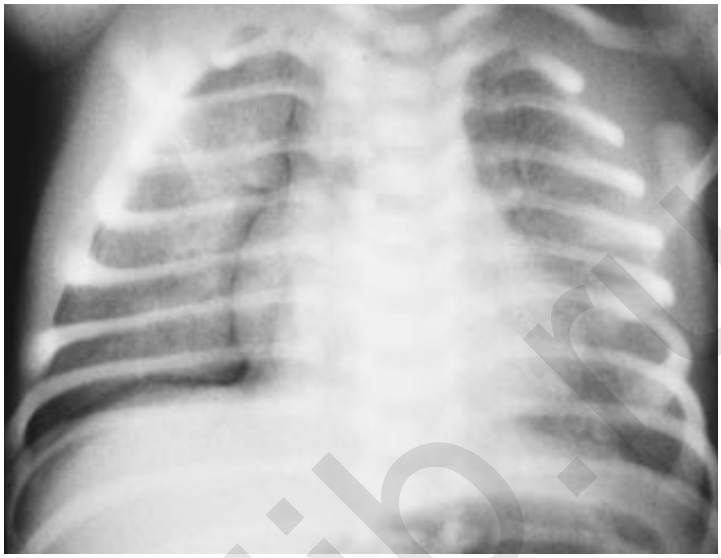

Figure 1.100. Pulmonary interstitial emphysema occurs as a complication in infants with hyaline membrane disease on ventilatory support. This may progress to other manifestations of the airblock syndrome (pneumothorax, pneumomediastinum, etc.). In this radiograph, note the pulmonary interstitial emphysema and pneumothorax on the right. Typically, the "solid lung" of infants with hyaline membrane disease does not collapse if they develop the airblock syndrome. The amount of free air in a pneumothorax may appear to be small because of the inability of the lungs to collapse.

1.101

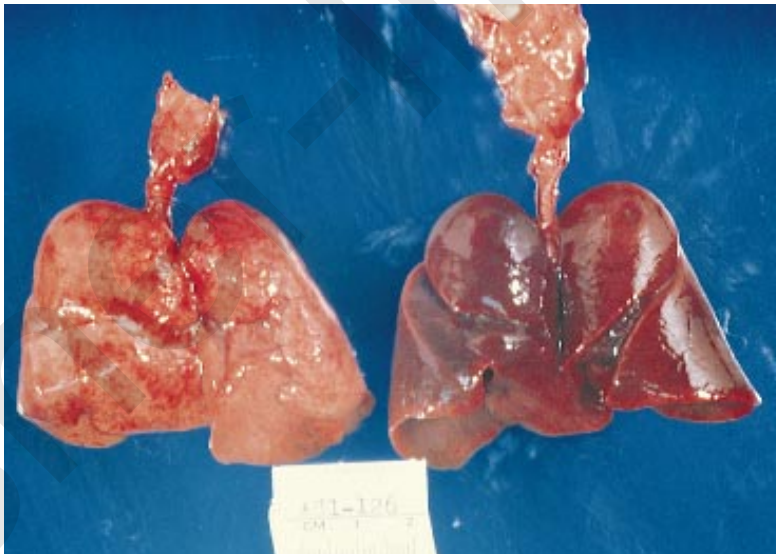

Figure 1.101. These pathologic specimens demonstrate the gross appearance of hyaline membrane disease. The lungs on the left are normal; those on the right are severely affected with hyaline membrane disease. They are cyanotic and engorged with edema fluid and are described as having the consistency and appearance of liver.

1.102

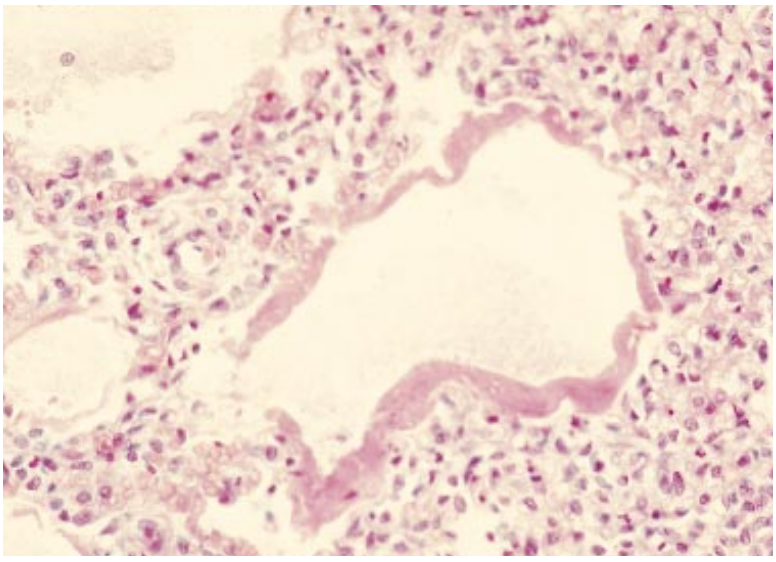

Figure 1.102. This photomicrograph shows hyaline membrane formation and edema fluid within the alveolus. The surrounding alveoli are thickened and atelectatic. Hyaline membranes are proteinaceous exudate from injured type I alveolar cells not lined with surfactant. The lack of surfactant represents immaturity of the type II alveolar cell.

1.103

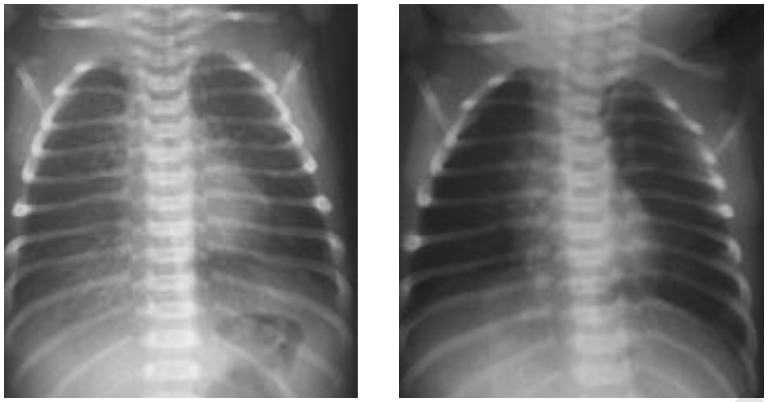

Figure 1.103. Transient tachypnea of the newborn ("wet lung" syndrome) may occur at all gestational ages (most common in term infants) and must be differentiated from hyaline membrane disease. The delayed clearance of excess fetal lung fluid, which normally is partly expelled by the trachea and partly absorbed by the pulmonary lymphatics, describes the physiologic basis for this condition which is most often associated with cesarean births. Prominent vascular markings radiating from the hilar area give rise to the typical "sunburst" appearance. The heart size is borderline or slightly enlarged. In several days (radiograph on the right) the prominence of the pulmonary vascular channels and the heart size decreases.

1.104

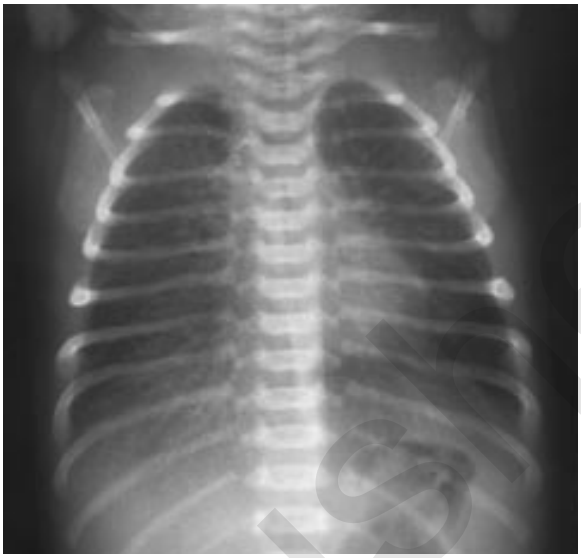

Figure 1.104. An anteroposterior radiograph of another infant with transient tachypnea of the newborn showing, in addition to the "sunburst" appearance, fluid in the transverse fissure and a right pleural effusion. Clearing of fetal lung fluid is probably mediated humorally and not by squeezing of the chest at expulsion during vaginal delivery. Other factors such as prematurity and depression of fetal breathing movements with anesthetics can contribute to this condition.

1.105

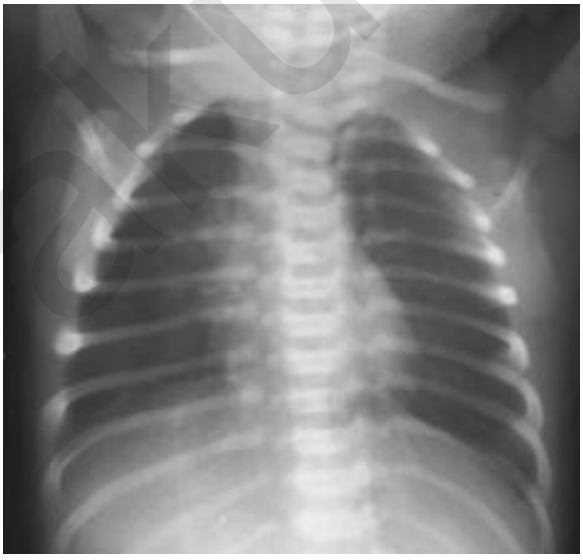

Figure 1.105. The same infant as in Figure 1.104, 24 hours later, showing the rapid improvement in the infant's condition. This was also apparent clinically.

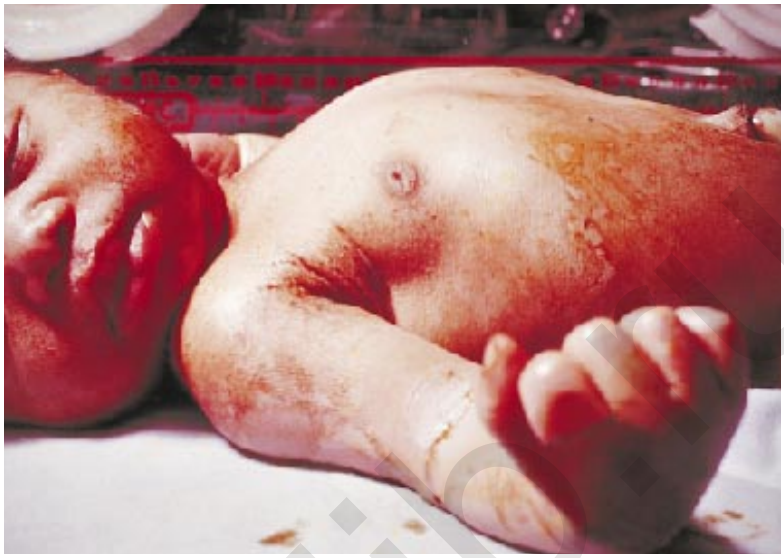

1.106

Figure 1.106. This infant, with meconium aspiration syndrome, has a barrelled chest with increased anteroposterior diameter and increased convexity of the anterior chest wall similar to that seen with other forms of obstructive emphysema. Note the meconium staining of the skin. Aspiration syndrome occurs when amniotic fluid which may or may not be meconium-stained extends into the respiratory tract. A certain amount of particulate matter in the form of squamous cells and lanugo may be aspirated, but these do not cause distress. If the aspiration is associated with meconium, there may be severe fetal distress. Meconium aspiration is more common in term and postmature infants and may cause a severe chemical pneumonitis.

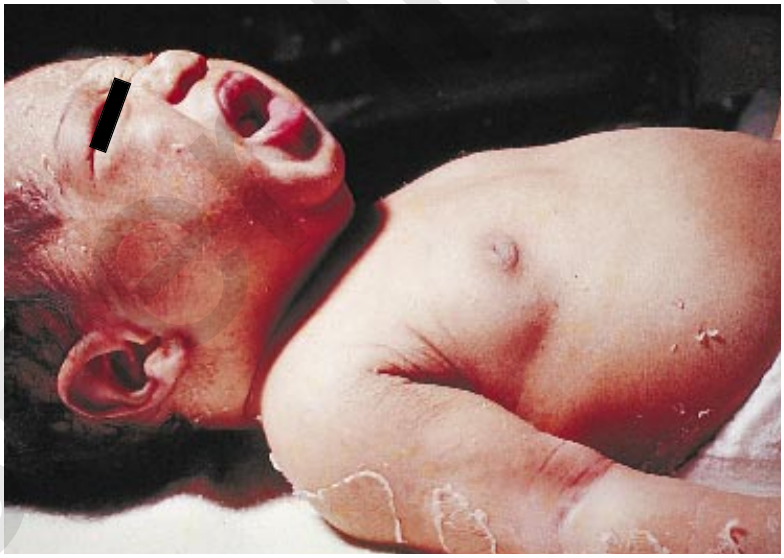

1.107

Figure 1.107. Once the meconium is cleared from the airways, there is generally less hyperinflation and some resolution of the respiratory distress symptoms. Note that the same infant as in Figure 1.106 has improved markedly within 48 hours. The barrelling of the chest and increased anteroposterior diameter are much improved.

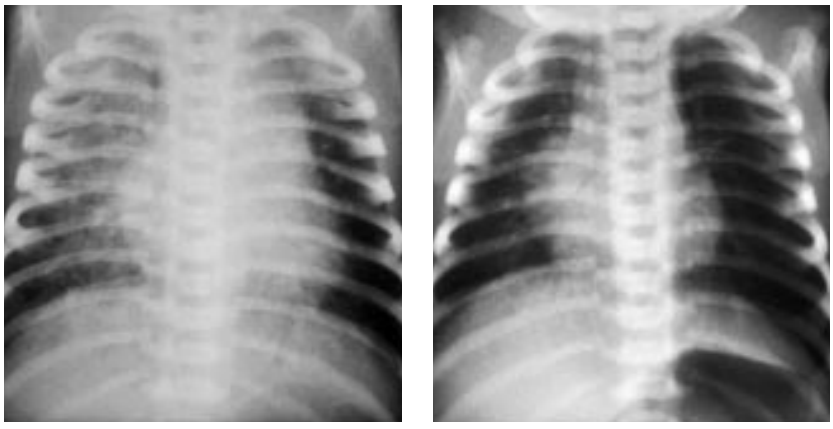

1.108

Figure 1.108. In the radiograph on the left, note the typical appearance of meconium aspiration pneumonia. The radiograph on the right, at 3 days later, shows a marked improvement. Regardless of contents aspirated (meconium, blood, amniotic fluid, or gastric contents), chest radiographs can demonstrate patchy diffuse infiltrates.

1.109

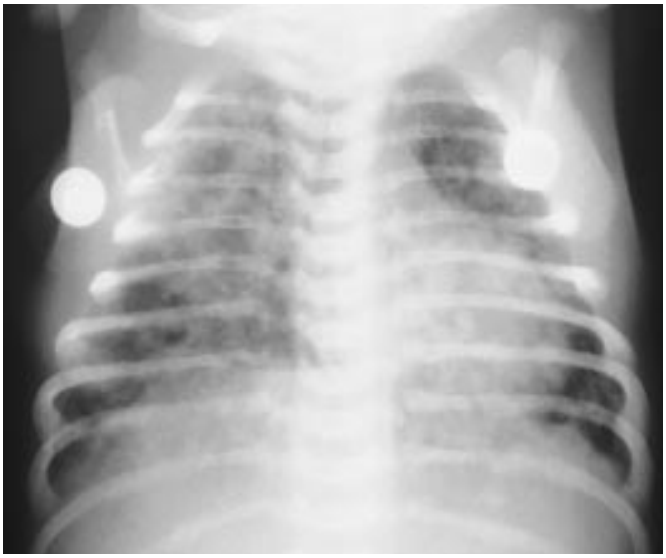

Figure 1.109. Meconium pneumonitis can occur when aspirated contents cause chemical inflammation of portions of the lung, resulting not only in hyperinflation from obstruction of airways but in patchy interstitial infiltrates extending out to the periphery. In meconium aspiration syndrome, the radiologic changes vary from lobar consolidation to widespread opacities involving both lung fields. There may be asymmetry of the patchy densities in both lung fields as seen in this radiograph. The radiologic findings in meconium aspiration syndrome may be identical to those seen in infectious pneumonia of the newborn. Aspiration pneumonitis may be secondary to esophageal atresia, pharyngeal incoordination, a vascular ring, and central nervous system abnormalities.

1.110

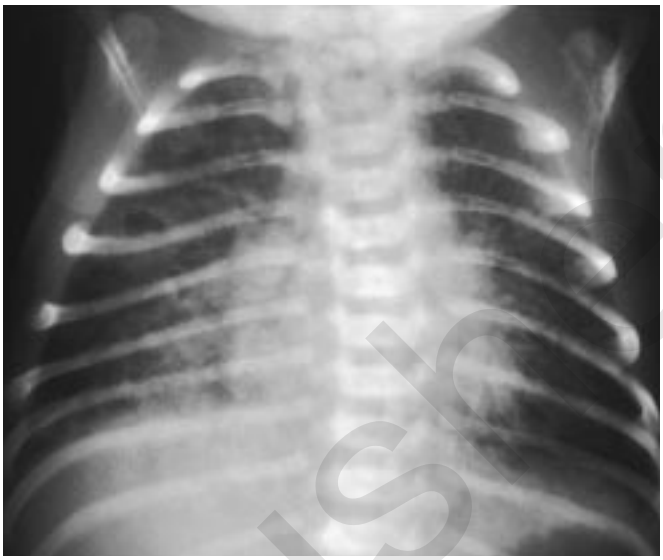

Figure 1.110. The sequelae of meconium aspiration syndrome are noted in this radiograph. There are areas of infiltrate and blebs seen in the right lung field. Pneumothorax and pneumomediastinum are common complications.

1.111

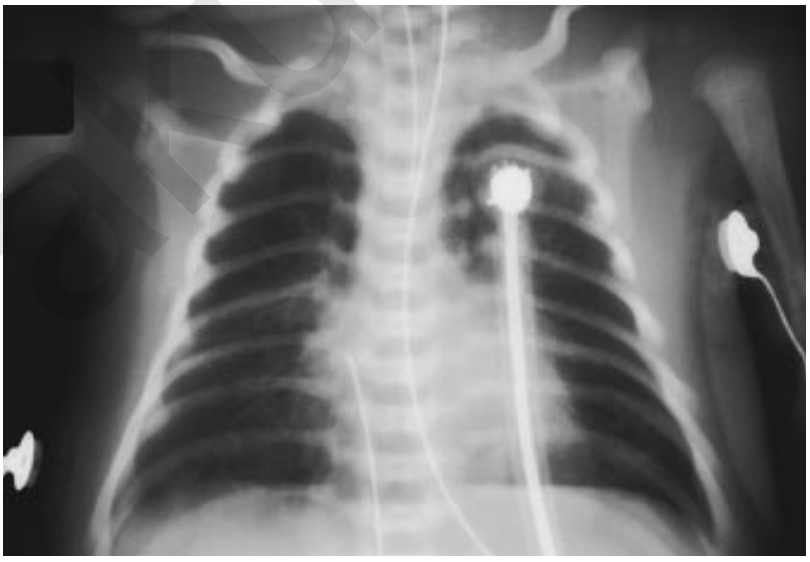

Figure 1.111. Persistent pulmonary hypertension of the newborn (persistent fetal circulation) is a condition in which there is persistence of the fetal high pulmonary vascular resistance. The condition can be primary, but is generally secondary to other causes such as meconium aspiration or diaphragmatic hernia. This chest radiograph shows no significant pulmonary pathology. There is decreased vascularity with mild cardiomegaly. There is severe respiratory distress and cyanosis, and the response to oxygen is initially poor.

1.112

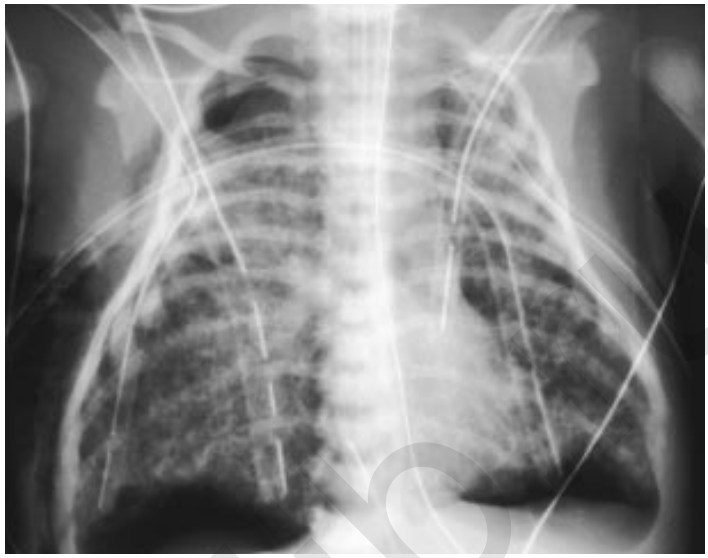

Figure 1.112. Medical therapy of persistent pulmonary hypertension of the newborn can cause severe complications as depicted in this radiograph. Vigorous positive pressure ventilation resulted in the development of interstitial emphysema and bilateral pneumothoraces. Persistent shunt pathways (shunting at the foramen ovale and ductus arteriosus) and high pulmonary vascular resistance make the condition poorly responsive to medical therapy with a mortality of 30 to 50%.

1.113

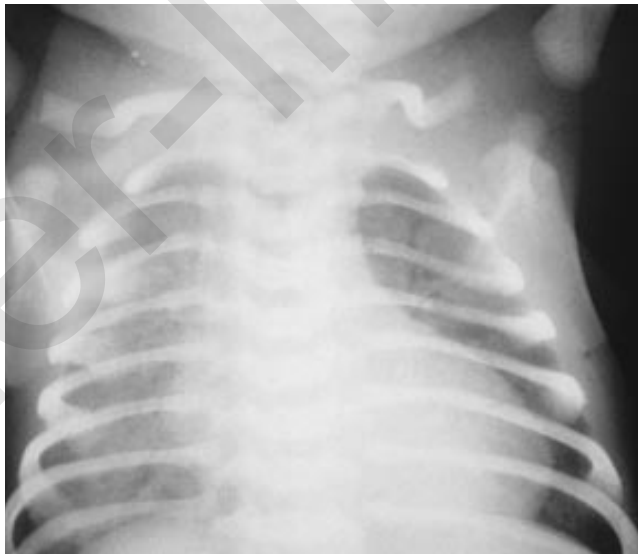

Figure 1.113. Pulmonary hemorrhage frequently develops in infants with hyaline membrane disease and is common in small-for-date infants. It also occurs with other conditions such as asphyxia, cold stress, or cerebral edema. The clinical picture is that of respiratory distress associated with the coughing or aspiration of frothy bloody mucus from the trachea. Chest radiographs demonstrate homogeneous bilateral hazy infiltrates which may affect one or more pulmonary segments and give the appearance of hyaline membrane disease or consolidation. The combination of hypoxia and increased lung capillary pressure is thought to contribute to the development of this condition.

1.114

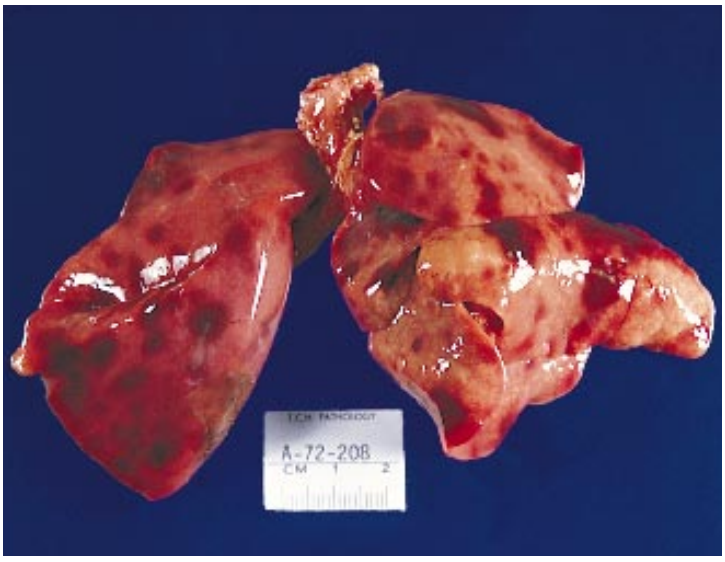

Figure 1.114. In this gross specimen is severe hemorrhage with an irregular distribution over the surface of the lung. It may be associated with a bleeding diathesis or can occur independently. In most cases, it reflects the massive accumulation of edema thereby explaining a generally lower hematocrit in the trachea's effluent than in venous blood (about 10% lower). True hemorrhage, however, can occur.

1.115

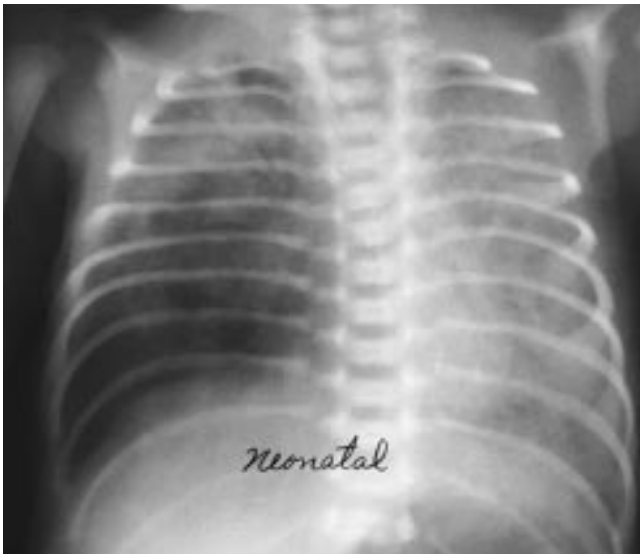

Figure 1.115. Neonatal pneumonia is most commonly caused by group B *Streptococcus*, but can be due to *Escherichia coli*, *Staphylococcus aureus*, or *Listeria monocytogenes*, etc. Ascending infection and aspiration of infected amniotic fluid is the postulated mechanism of infection. The radiographic appearance of intrauterine pneumonia is very similar to that of meconium aspiration syndrome. There are coarse linear areas of density, segmental areas of consolidation, atelectasis, and air trapping. The lungs are overinflated and, consequently, the diaphragm is at a low position. (Singleton, E., Wagner, M.)

1.116

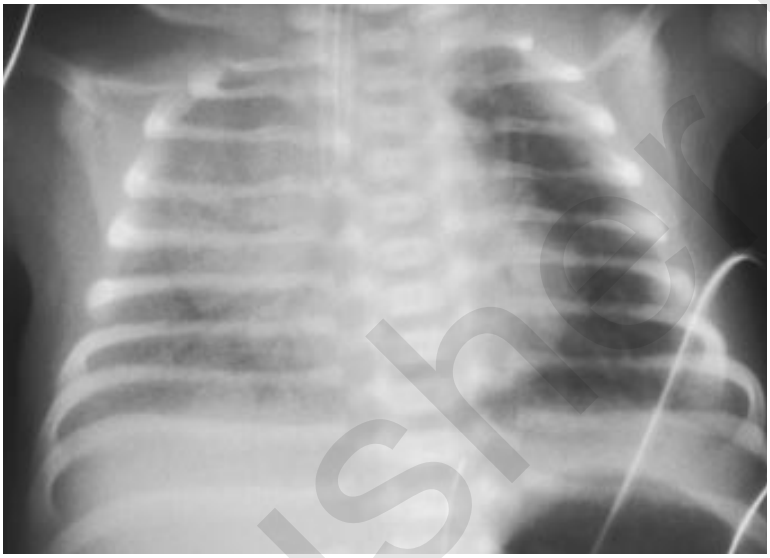

Figure 1.116. This radiograph is an example of group B streptococcal pneumonia. This chest radiograph demonstrates adequate lung expansion, but a diffuse, generalized reticulogranular pattern is noted over the lung fields making the condition difficult to distinguish from hyaline membrane disease.

1.117

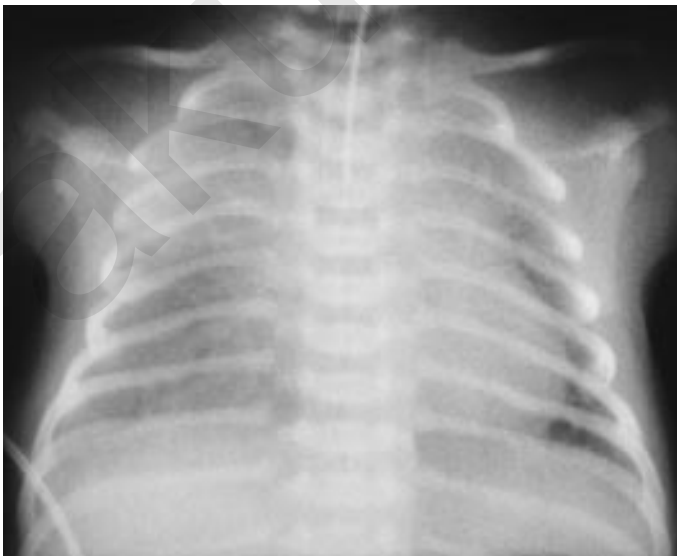

Figure 1.117. This radiograph is another example of group B streptococcal pneumonia indistinguishable from hyaline membrane disease. Only 50% of blood cultures are positive with congenital pneumonia. The diagnosis of group B streptococcal pneumonia was suggested by a positive tracheal aspirate and urine counterimmune electrophoresis (CIE).

1.118

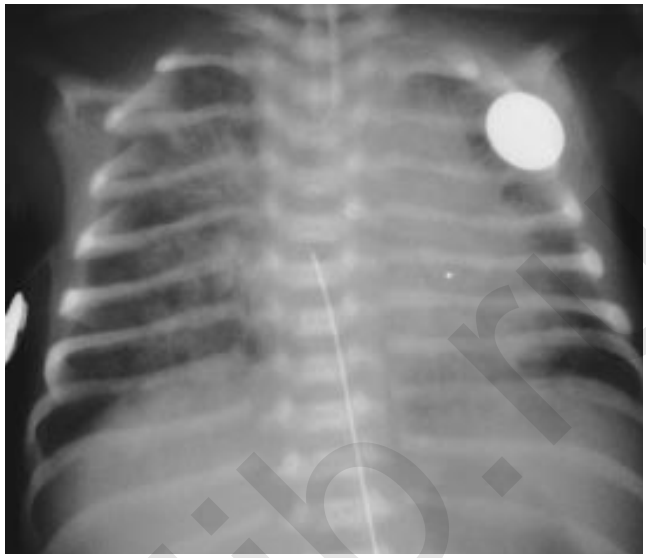

Figure 1.118. In this infant with congenital *Listeria monocytogenes* pneumonia the radiograph is indistinguishable from other types of pneumonia, but the infant had typical listerial skin lesions at birth and positive blood and spinal fluid cultures.

1.119

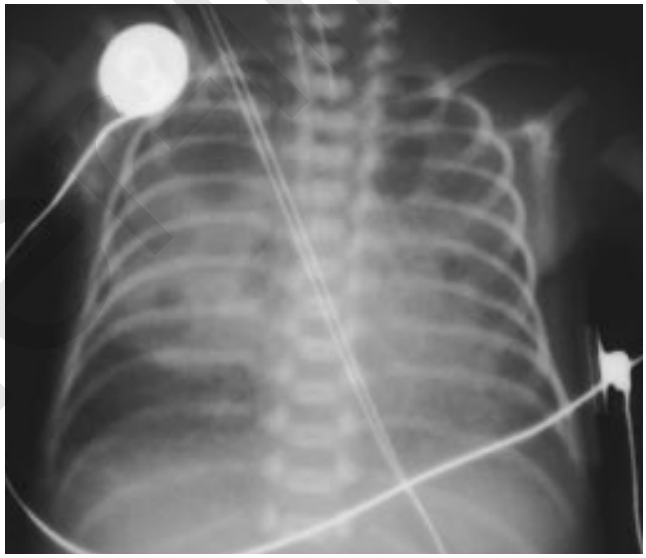

Figure 1.119. This infant with a birth weight of 700 g developed *Staphylococcus aureus* osteomyelitis and pneumonia. In this radiograph of the chest, note the consolidation and early pneumatocele formation. There was improvement with antibiotic treatment. At the present time, staphylococcal pneumonia in the neonate is not a major problem. Large outbreaks of staphylococcal infections in nurseries occurred several decades ago, often causing pneumonia and the development of pneumatoceles. Development of air-filled cystic pneumatoceles is quite characteristic of staphylococcal pneumonia. They generally are a sign of healing and require no specific therapy other than the appropriate antibiotics. Rarely they may rupture into the thorax producing a pneumothorax and the acute onset of distress. This complication suggests that therapy has been inadequate.

1.120

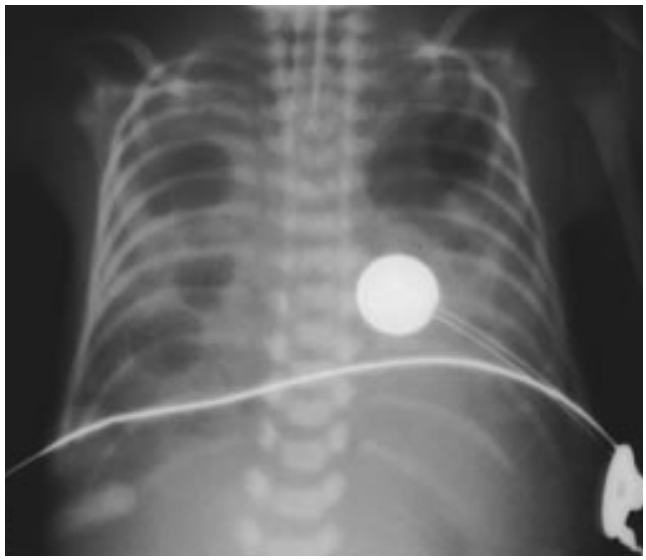

Figure 1.120. A chest radiograph of the same infant as in Figure 1.119 shows the pneumatoceles two days later when the infant generally was improving. Fluid levels may occasionally be seen in pneumatoceles. Residual fluid levels presumably represent persistent infection. Pneumatoceles must be differentiated from cystic emphysema which has developed as a sequel to interstitial emphysema or bronchopulmonary dysplasia. The cysts in these conditions are diffuse and bilateral. Serial films demonstrate evidence of prolonged respirator therapy with interstitial emphysema which then progresses to emphysematous bullae.

1.121

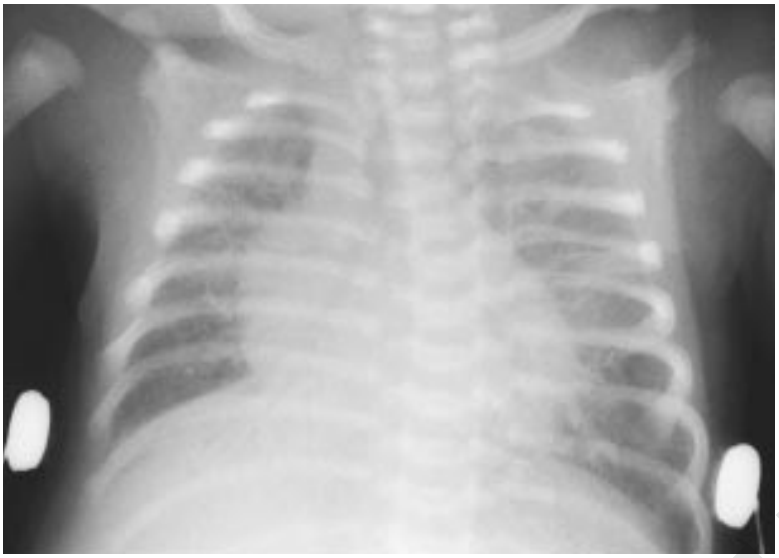

Figure 1.121. A radiograph of the chest of an infant with congenital syphilis demonstrates the typical interstitial pneumonia (pneumonia alba) and the osseous changes of growth arrest lines at the proximal ends of the humeri and periostitis of the clavicles (Higouménakis' sign).

1.122

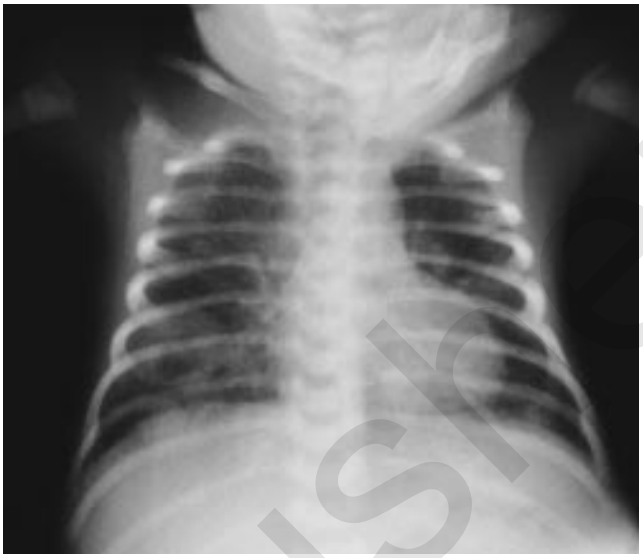

Figure 1.122. This infant who had severe congenital syphilis at birth with generalized osseous changes of all extremities shows pneumonia alba and bony changes in the proximal parts of the humerus in this chest radiograph. This stresses the importance of checking for any skeletal changes when reviewing a chest radiograph. (Singleton, E., Wagner, M.)

1.123

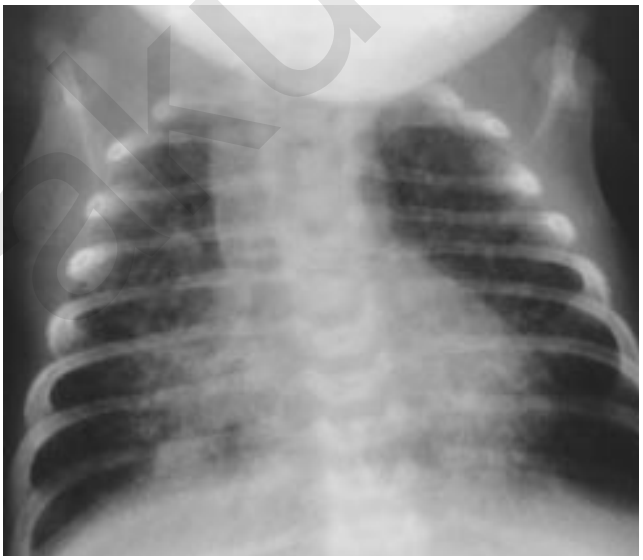

Figure 1.123. In this radiograph of an infant with chlamydia pneumonia note the bilateral interstitial infiltrates. He developed a stacatto cough, low grade fever, and purulent eye drainage at the age of 2 to 3 weeks and had positive cultures for *Chlamydia trachomatis* from the nasopharynx.

1.124

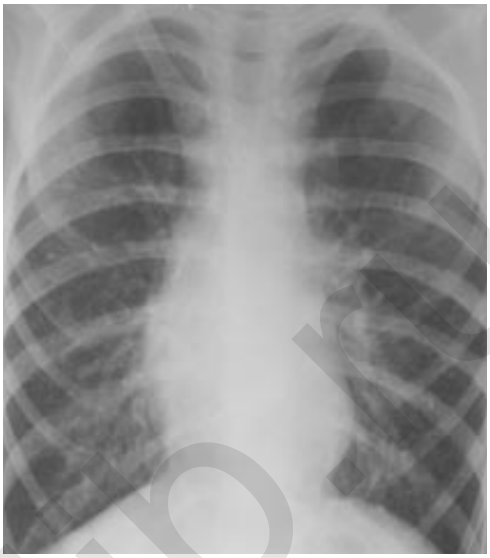

Figure 1.124. Pulmonary lymphangiectasia is a rare condition in which dysplastic, malformed lymphatics of the lungs result in poor lymph drainage with interstitial engorgement and hyperinflation. Lymphatic tissue proliferates in the lungs, thereby compromising the normal pulmonary ventilation. The condition is usually not recognized until later in childhood and, in its severe form, is incompatible with life. Bacterial pneumonias are a common complication. (Singleton, E., Wagner, M.)

1.125

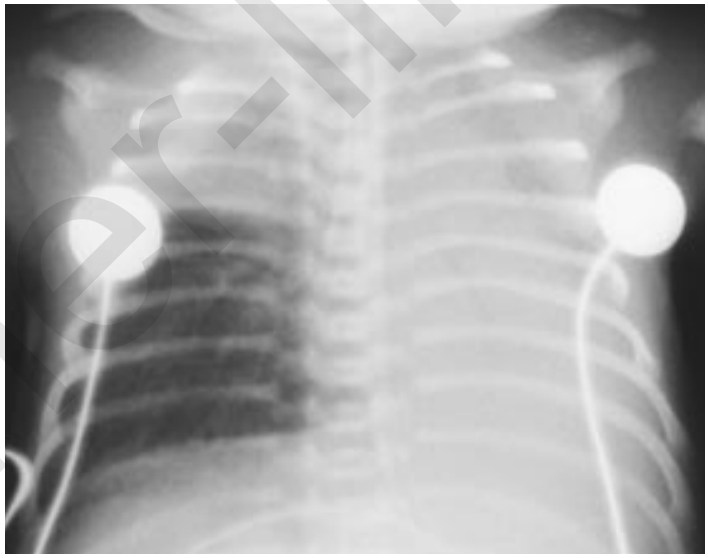

Figure 1.125. This infant had an endotracheal tube placed in his right mainstem bronchus as seen in this radiograph. Note the complete collapse of the left lung and collapse of the upper lobe of the right lung as a result of the obstructed airways.

1.126

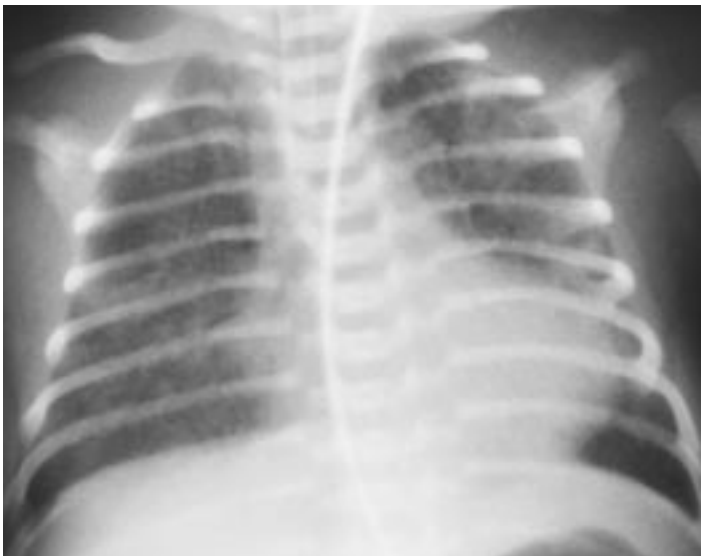

Figure 1.126. The same infant as in Figure 1.125 shows re-expansion 2 hours later of all of the collapsed areas after repositioning the endotracheal tube to the midtrachea.

1.127

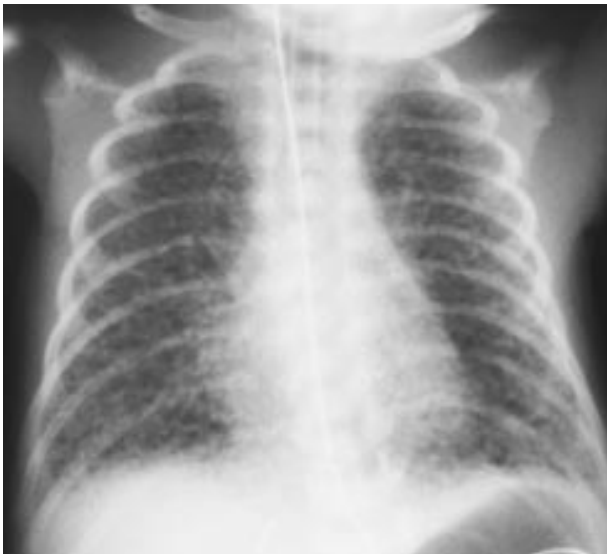

Figure 1.127. This infant with severe hyaline membrane disease developed severe diffuse bilateral pulmonary interstitial emphysema (PIE). Clinically, it behaves like other types of airblock-producing hypercarbia initially with hypoxemia and systemic hypotension when severe. The heart may be compressed by severe bilateral pulmonary interstitial emphysema. Systemic venous return and cardiac output may be severely compromised, resulting in a small heart shadow on chest radiograph. Loose connective tissue in the wide interstitial spaces of the preterm lung results in the accumulation of interstitial air. The onset may be gradual or sudden, resulting in decreased chest excursion with thoracic distention.

1.128

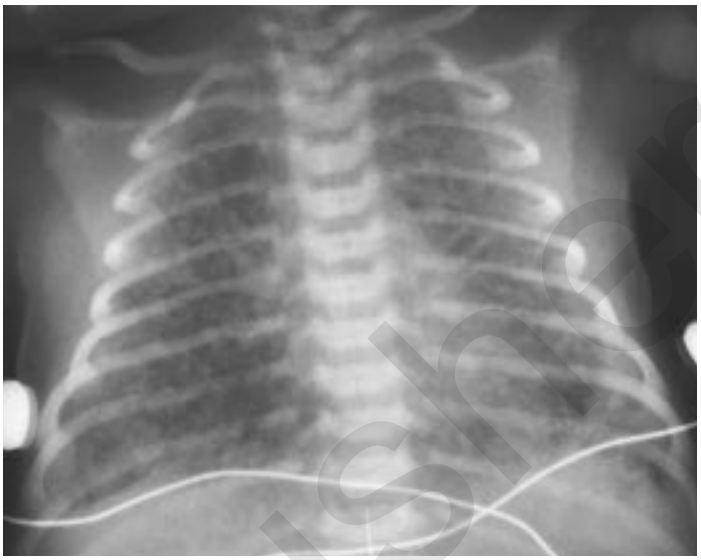

Figure 1.128. Bilateral pulmonary interstitial emphysema in another infant in which the radiograph shows the typical findings of hyperinflation and diffuse hyperlucencies within the lung parenchyma. This complication of hyaline membrane disease occurs most commonly as a complication of mechanically assisted ventilation and rarely occurs spontaneously. There is widespread rupture of alveoli resulting in accumulation of air in the interstitial lung tissue.

1.129

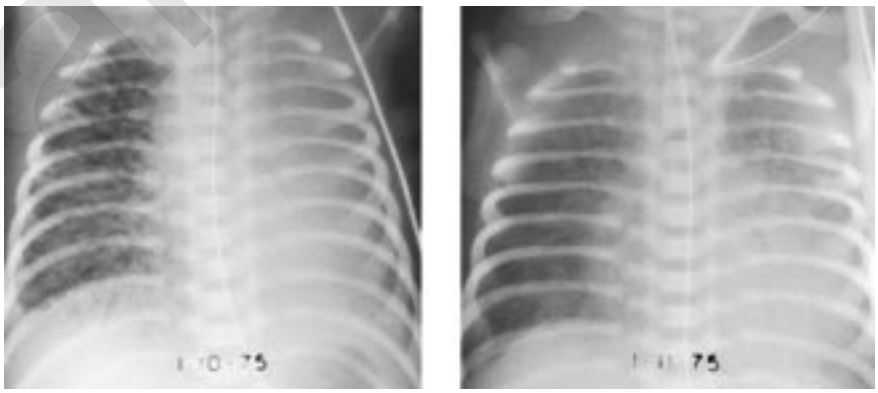

Figure 1.129. The radiograph on the left shows severe hyaline membrane disease in the left lung and pulmonary interstitial emphysema in the right lung. This is an example of unilateral PIE in an infant with hyaline membrane disease. Within 24 hours, the hyaline membrane disease is resolving, as is the PIE. On chest radiograph, the irregular linear streakiness of pulmonary interstitial emphysema is typical of air dissecting into the large interstitial spaces of the lung.

1.130

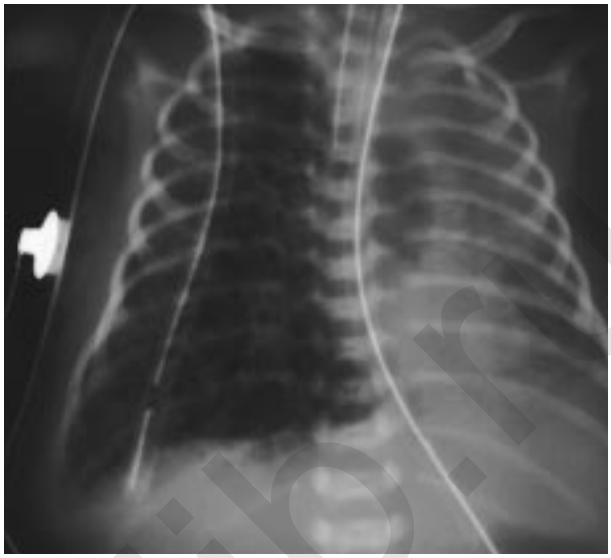

Figure 1.130. In more severe cases of pulmonary interstitial emphysema, air can accumulate in the interstitium to the extent that it causes herniation of an involved lung across the midline. The incidence of severe interstitial emphysema has significantly decreased with widespread use of exogenous surfactant replacement.

1.131

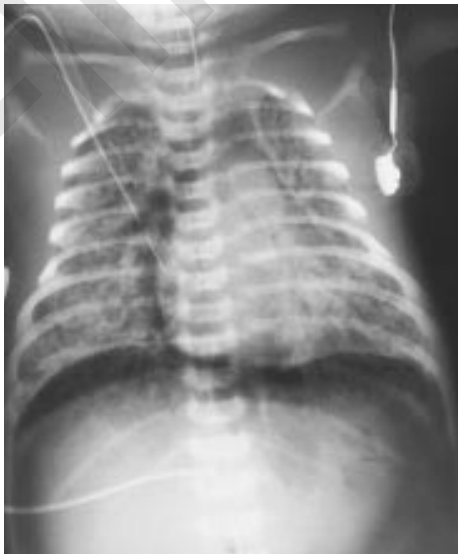

Figure 1.131. In pulmonary interstitial emphysema, the complications of pneumothorax and pneumomediastinum are not uncommon, with the result that air may extend into the pleural spaces, mediastinal space, pericardial space and even dissect down tissue planes into the abdominal cavity. Note the pulmonary interstitial emphysema, pneumomediastinum, and pneumoperitoneum.

1.132

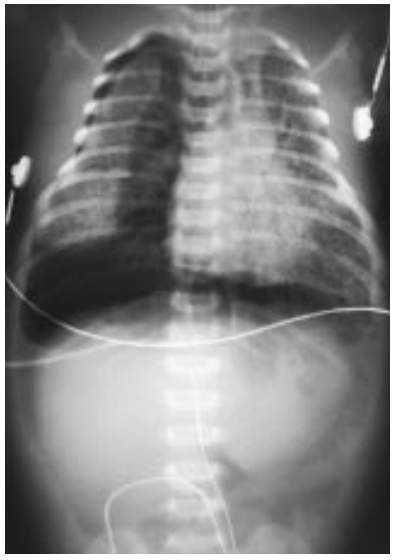

Figure 1.132. Radiograph of the same infant as in Figure 1.131 2 hours later showing the pulmonary interstitial emphysema on the left side and a large pneumothorax on the right side with collapse of the lung and the continued presence of the pneumomediastinum and pneumoperitoneum.

1.133

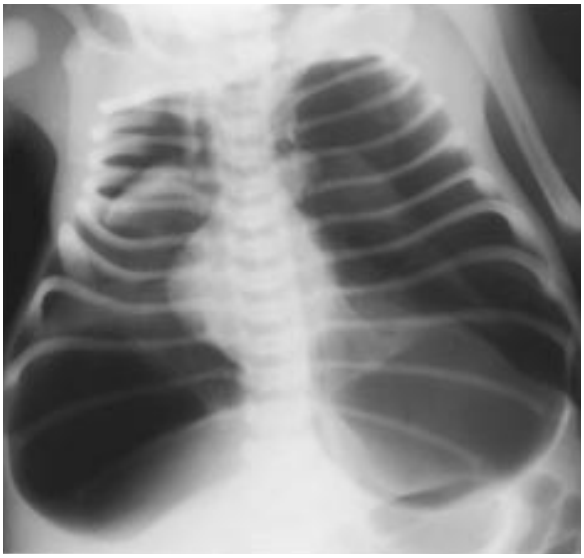

Figure 1.133. This radiograph of the chest shows massive bilateral pneumothoraces after resuscitative efforts. Note that these are both severe tension pneumothoraces in that both lungs have collapsed and both sides of the diaphragm are concave. In general, if the pneumothorax is not severe, there will be no concavity of the diaphragm. (Singleton, E., Wagner, M.)

1.134

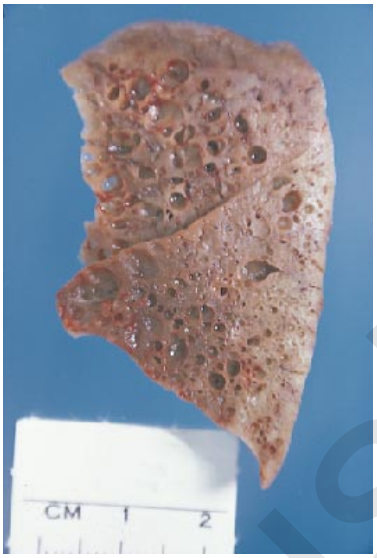

Figure 1.134. A gross specimen of the lung shows the severe extent of the pulmonary interstitial emphysema. Note that the upper lobe of the lung appears more affected.

1.135

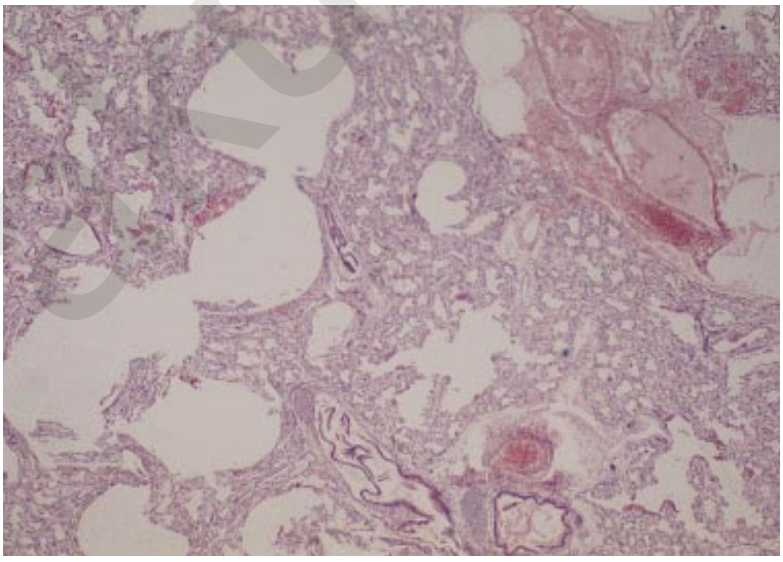

Figure 1.135. Histopathology of the lung shows the massively dilated, air-filled interstitial spaces and markedly thickened alveolar sacs in pulmonary interstitial emphysema.

1.136

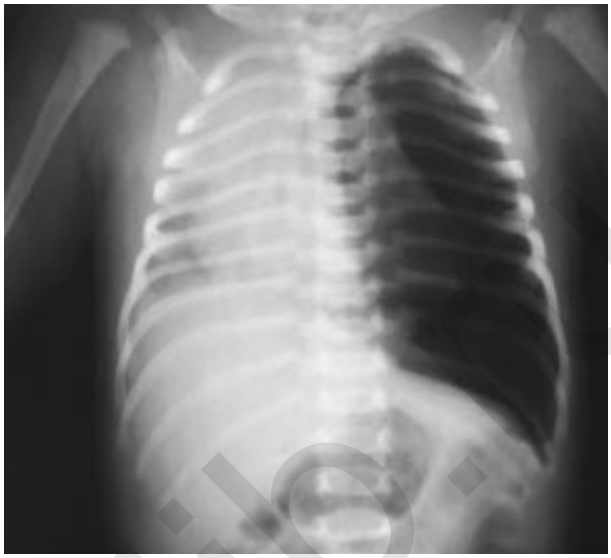

Figure 1.136. Clinical findings suggesting the diagnosis of pneumothorax include increasing respiratory distress, a unilateral chest bulge, diminished breath sounds on the affected side, and especially restlessness or irritability. If there is a large tension pneumothorax, there is decreased cardiac output and an elevated central venous pressure with profound circulatory collapse. In this radiograph there is a large left tension pneumothorax pushing the mediastinum and heart to the right. Note the marked depression of the diaphragm.

1.137

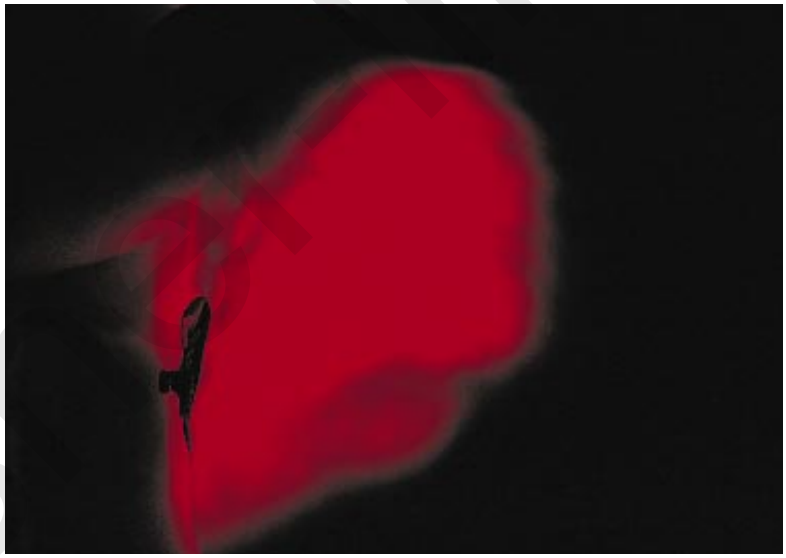

Figure 1.137. The diagnosis of pneumothorax can be rapidly established by the use of a bright light source for transillumination, especially in premature infants. This approach results in prompt recognition of the pneumothorax and can quickly direct appropriate therapy. In this figure, note the outline of the chest wall with the electrode attached and the total collapse of the right lung. Pneumothorax may occur spontaneously in infants who did not receive resuscitative measures or, more commonly, as a complication of assisted ventilation of preterm infants. A large tension pneumothorax should be promptly evacuated with a thoracostomy tube. A small pneumothorax, especially in the absence of symptoms, does not require treatment.

1.138

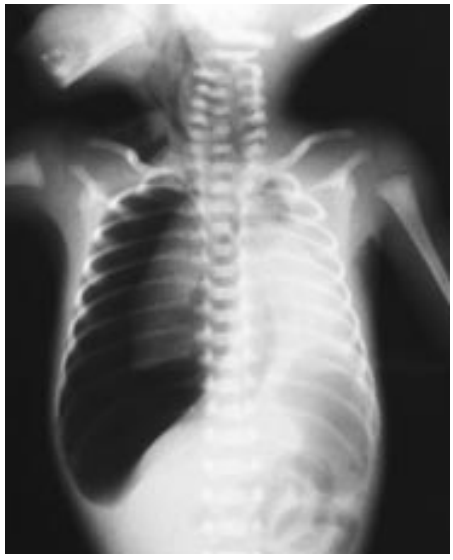

Figure 1.138. A radiograph of this infant with severe hyaline membrane disease shows the complications of positive pressure ventilation. There is a large right tension pneumothorax, pneumomediastinum, and subcutaneous air in the neck. Note that although there is collapse of lung with a severe pneumothorax, total collapse has not occurred because of the poor compliance of the lung. If the pneumothorax is associated with a positive pressure air leak, there is rapid clinical deterioration with mediastinal shift and collapse of the lungs. Placement of a thoracostomy tube results in rapid clinical improvement.

1.139

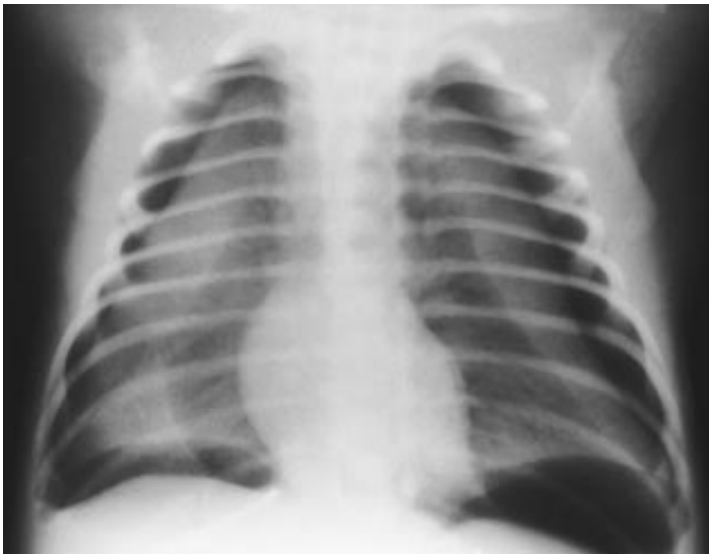

Figure 1.139. This radiograph shows bilateral pneumothoraces with accumulation of air on both the medial and lateral sides of the lung in an infant lying supine. Again, note that the lungs are not completely collapsed because of the severe degree of lung disease.

1.140

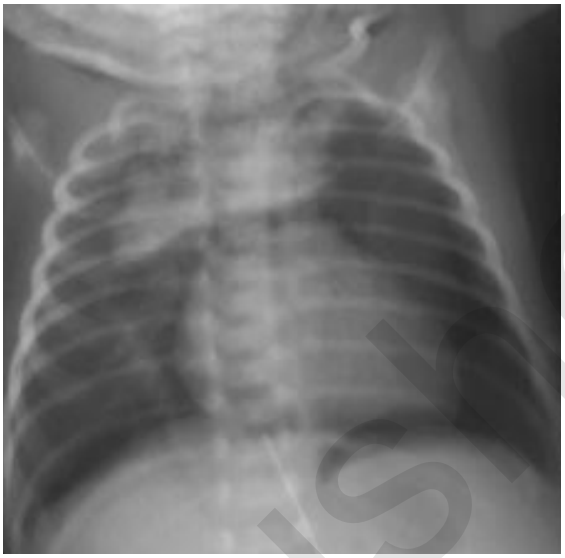

Figure 1.140. Air dissecting into the thorax and mediastinum may elevate the lobes of the thymus, resulting in the "butterfly wing" appearance of the lobes of the thymus gland. Clinically, pneumomediastinum is usually asymptomatic but findings may include a sternal bulge, restlessness or irritability, tachypnea, and distant heart sounds. Hamman's sign (a crunchy sound synchronous with the heart beat) is rarely present in the newborn period. Rupture of alveoli into the mediastinal space with accumulation of air around the heart does not usually require active management, except in extreme cases. (Singleton, E., Wagner, M.)

1.141

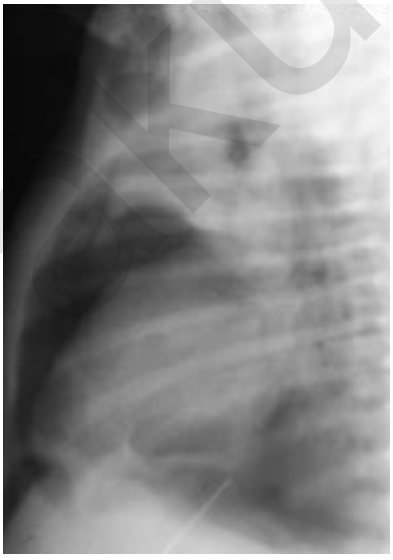

Figure 1.141. A lateral chest radiograph of the same infant as in Figure 1.140 shows air in the anterior mediastinum behind the sternum with elevation of the thymus. Note the well-outlined thymus gland and the subcutaneous air in the neck. (Singleton, E., Wagner, M.)

1.142

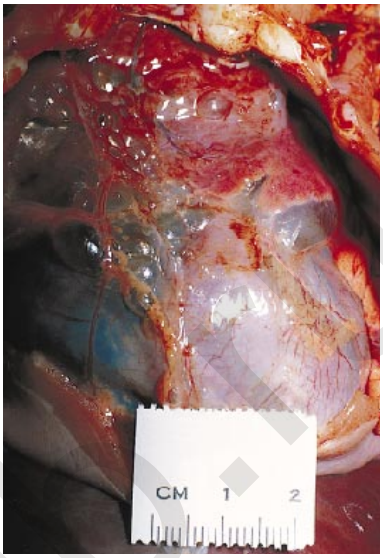

Figure 1.142. In this pathologic specimen note the multiple blebs dissecting through the soft tissue planes of the mediastinum as a result of a pneumomediastinum.

1.143

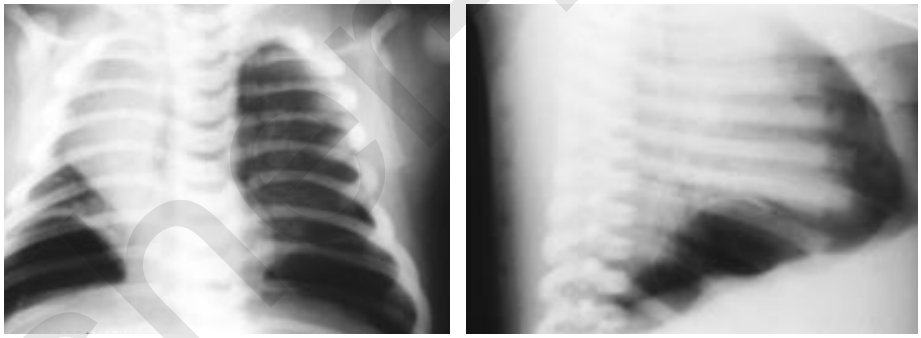

Figure 1.143. A rare complication associated with a pneumomediastinum is a subpleural collection of air. The air tracks between the parietal pleura and the diaphragm as seen in the anteroposterior and lateral radiographs of this infant.

1.144

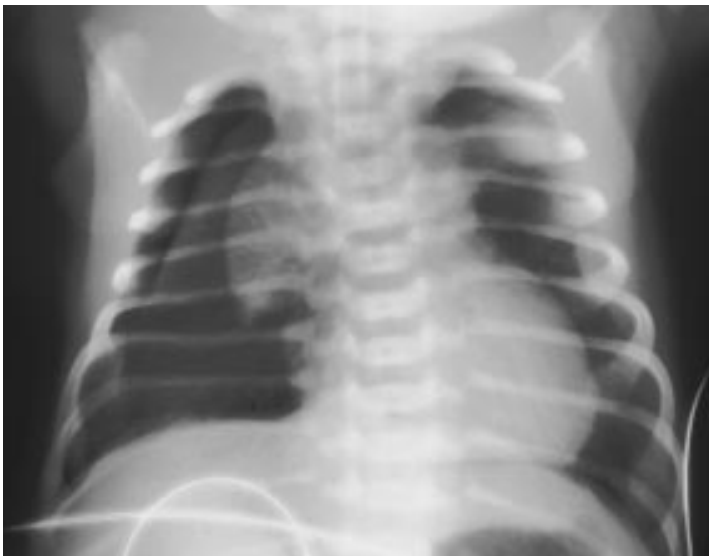

Figure 1.144. The chest radiograph of this infant shows a right pneumothorax and a pneumomediastinum. Note the lobes of the thymus gland displaced superiorly by the pneumomediastinum giving the "butterfly wing" appearance.

1.145

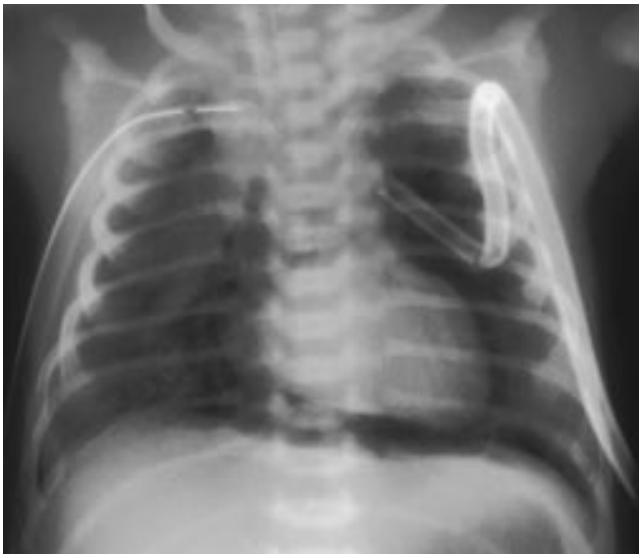

Figure 1.145. Three hours after the radiograph in Figure 1.144 was taken, the infant's condition had deteriorated and a repeat radiograph showed progression of the airblock with the development of a pneumopericardium. Clinically there is sudden deterioration with a marked decrease in peripheral circulation, marked decrease in blood and pulse pressure, and an elevated central venous pressure.

1.146

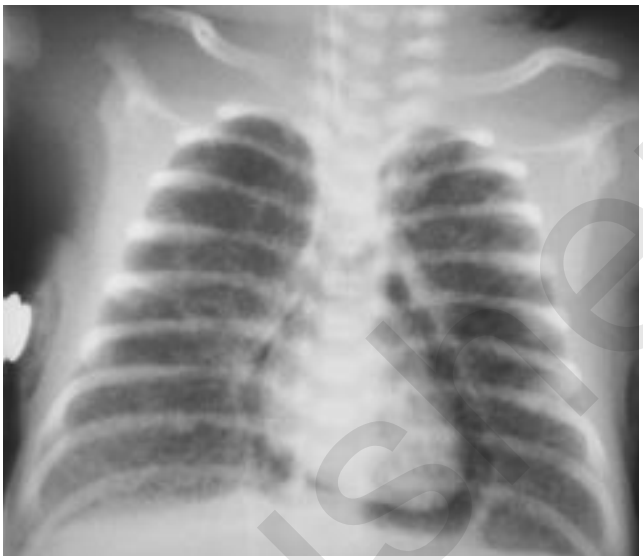

Figure 1.146. Pneumopericardium is a rare, but potentially fatal, form of airblock with accumulation of air around the heart. There are distant or absent heart sounds. Rupture of alveoli leads to interstitial emphysema and tracking of air along the pulmonary veins into the pericardial sac. This may resolve spontaneously or may result in cardiac tamponade with muffled heart sounds and poor cardiac output. The pericardium is readily seen as a line of increased density between the air surrounding the heart and the air infiltrating the lung.

1.147

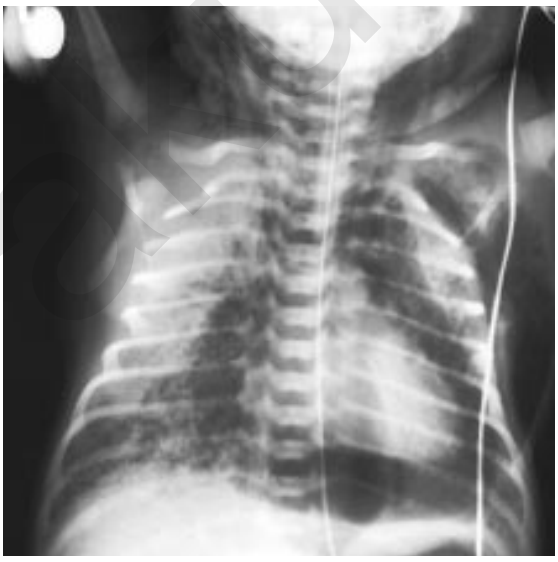

Figure 1.147. This infant on positive pressure ventilation developed a pneumothorax, pneumomediastinum, massive pneumopericardium, and subcutaneous emphysema in the neck, and especially on the left side of the chest. A massive pneumopericardium such as this always results in cardiac tamponade. Subcutaneous emphysema can be recognized clinically by crepitant bulging in the neck or over the chest, and results from the dissection of air from a pneumomediastinum. See Figure 7.71 in Volume I, Chapter 7.

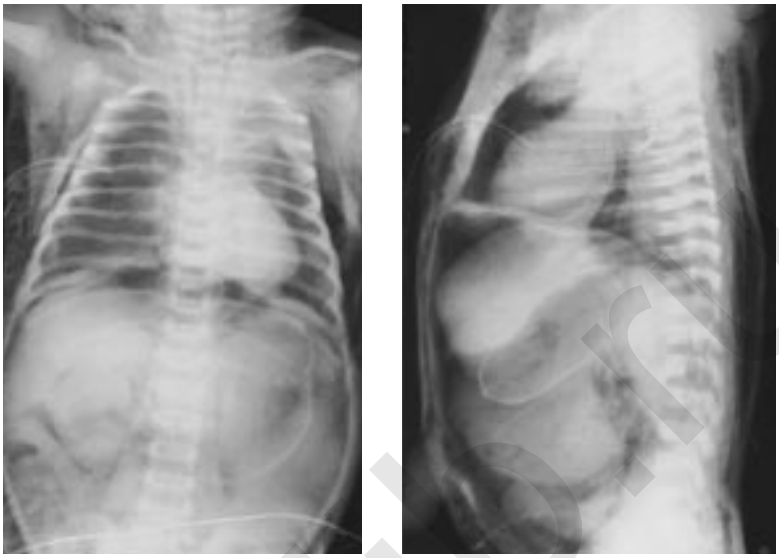

1.148

Figure 1.148. Poor lung compliance with hyaline membrane disease and positive pressure ventilation can lead to the development of severe air leaks. In this instance, air has dissected into the mediastinum, the abdominal cavity, and the subcutaneous tissue. In the lateral radiograph, the pneumomediastinum outlines the thymus gland. The air in the peritoneal cavity must be distinguished from that of a ruptured viscus. Thoracic air can dissect through any or all of the diaphragmatic apertures: the vena cava, aorta or esophagus. Especially on the lateral radiograph, note the large amount of subcutaneous air.

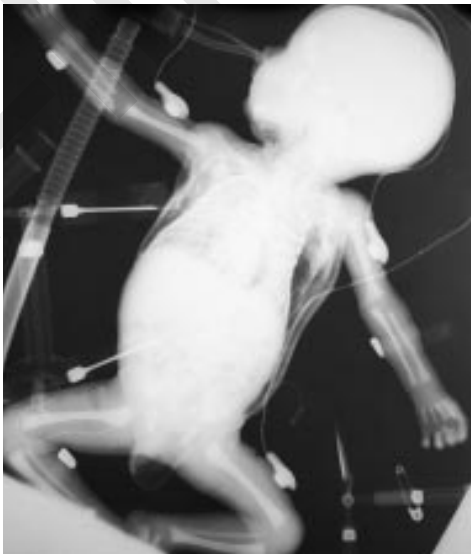

1.149

Figure 1.149. Extensive air leaks occurred in this male infant on positive pressure ventilation. Note the subcutaneous air over the scalp, chest and abdominal walls, and in the scrotum. In pneumoperitoneum associated with tracking down of air from a pneumomediastinum, no air/fluid levels are seen in the abdomen. With pneumoperitoneum associated with a perforation, air/fluid levels are present. In a pneumoperitoneum, air enters the scrotum via the patent processus vaginalis.

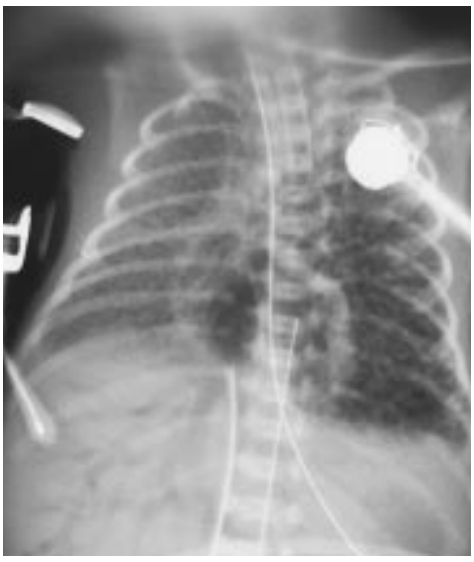

1.150

Figure 1.150. In the most severe cases, air can dissect into the intravascular spaces. In this radiograph, note that the air has dissected into the venous system causing massive air embolism to the heart. Note that the portal venous system is also filled with air.

1.151

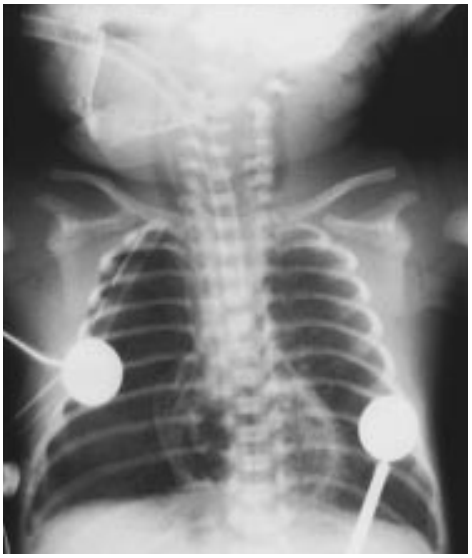

Figure 1.151. Massive air embolism occurs as a result of air dissecting into the vascular system and accumulating in the heart displacing blood. In this infant, note the air in the chambers of the heart and along the vessels in the neck and arms. Sudden fatal extravasation of gas into the circulatory system may occur apparently due to rupture of pulmonary veins in conjunction with high intra-alveolar pressures from positive pressure ventilation.

1.152

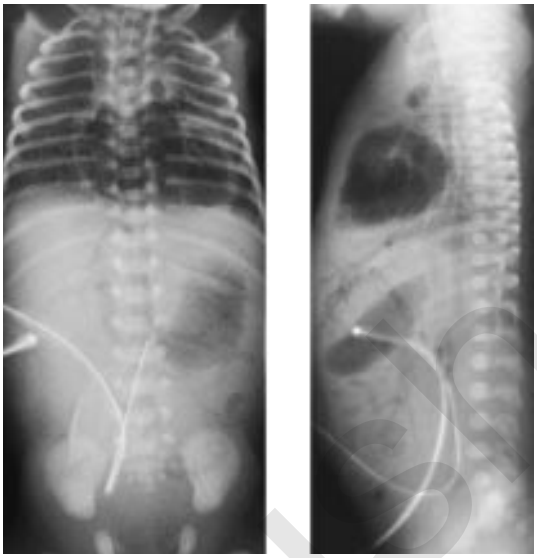

Figure 1.152. This is another example of a massive air embolism showing air dissecting into the vascular system. Note the air not only in the heart but also in the major vessels as clearly seen in the lateral radiograph.

1.153

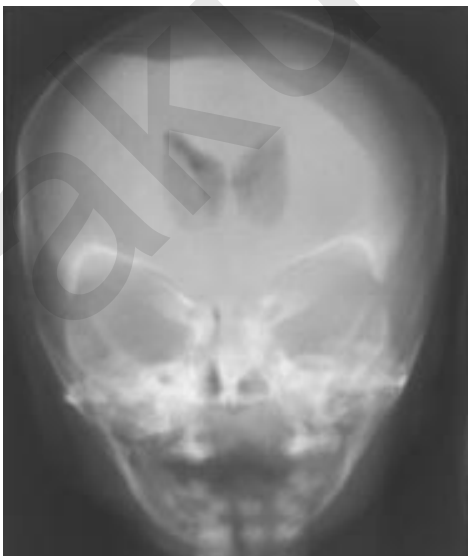

Figure 1.153. A skull radiograph of the same infant as in Figure 1.152 shows a pneumoencephalogram produced by the massive air embolism introducing air into the ventricular system. There was an associated intraventricular hemorrhage.

1.154

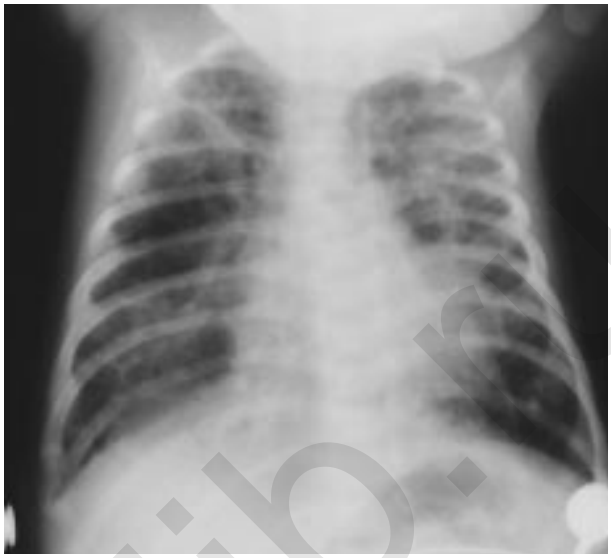

Figure 1.154. Bronchopulmonary dysplasia (BPD) is a form of chronic lung disease which occurs in infants who receive prolonged exposure to oxygen with positive pressure ventilation. There are four radiologic stages. Stage I occurs from 1 to 3 days of age and is indistinguishable from severe hyaline membrane disease. Stage II occurs between 4 to 10 days of age when the lungs become homogeneously opacified. Stage III occurs between 10 to 30 days of age when multiple small rounded areas of radiolucency appear as a result of focal alveolar emphysema somewhat similar to the "bubbly" appearance of the lung in Wilson-Mikity syndrome. Stage IV occurs after 30 days of age when the cystic areas of the lung coalesce into larger cysts particularly in the upper lobes, and streaky, linear areas of scarring appear.

1.155

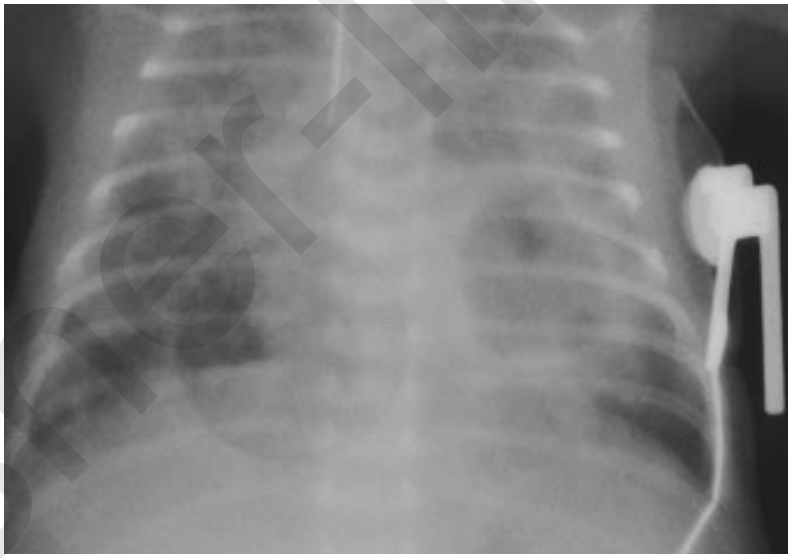

Figure 1.155. This chest radiograph of an infant with Stage IV BPD demonstrates pneumatocele formation in the left chest, prominent interstitial markings, and pulmonary edema. The circular hyperlucency seen over the mediastinum and right chest is an artifact caused by the hole in the incubator when the radiograph is taken from above.

1.156

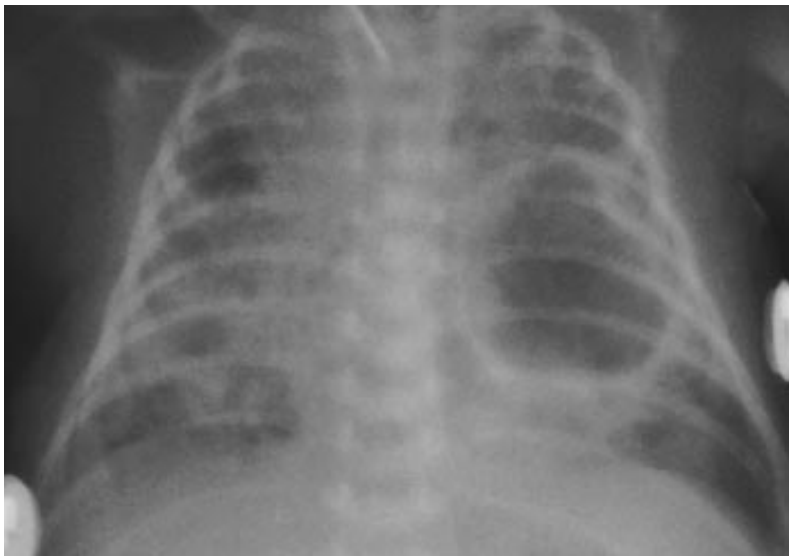

Figure 1.156. Twenty-four hours later, the same infant as in Figure 1.155 had an increase in the cystic areas and the pneumatocele on the left was larger.

1.157

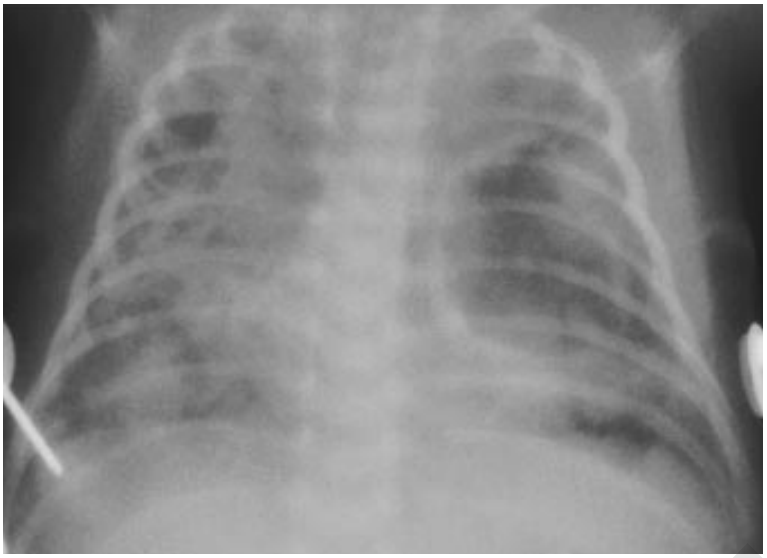

Figure 1.157. A radiograph of the chest of the same infant as in Figure 1.155 and 1.156 5 days later shows progression to the chronic changes of scarring and pulmonary edema. Lung injury this severe is often complicated by cor pulmonale. The overall prognosis for these infants is that approximately one-third recover, one-third develop chronic respiratory disease, and one-third die of respiratory failure.

1.158

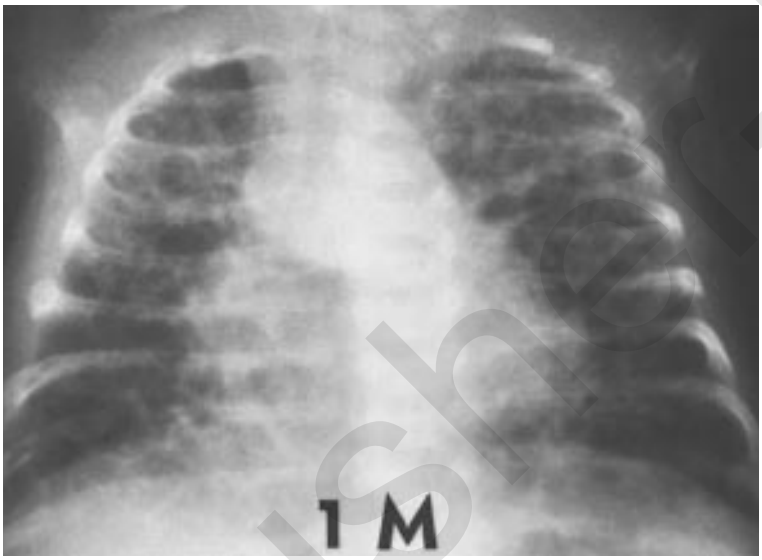

Figure 1.158. Wilson-Mikity syndrome (pulmonary dysmaturity, "bubbly" lung syndrome) shares many of the same radiologic features as Stage III BPD but there is no history of preceding hyaline membrane disease or of excessive oxygen therapy. The lungs are somewhat hyperinflated and there is a prominence of interstitial markings. Wilson-Mikity syndrome is not currently recognized as a disease entity.

1.159

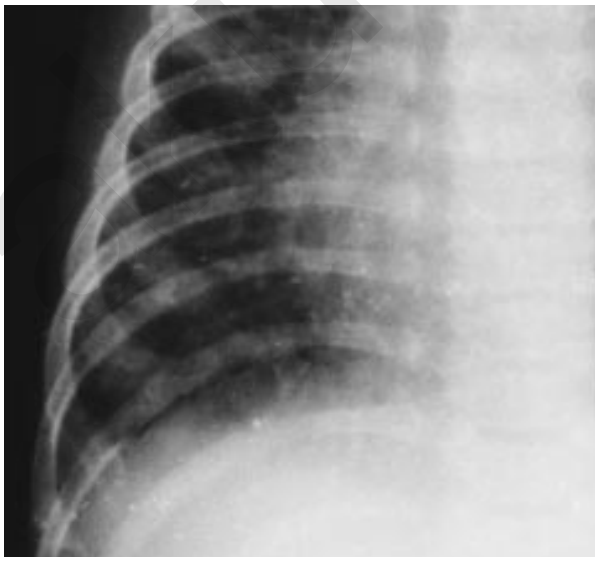

Figure 1.159. In an enlarged radiograph of lung markings at the costophrenic angle in the same infant as in Figure 1.158, the "bubbly" appearance of the lungs is noted. These radiographic features are usually pathognomonic in that they show diffuse linear and reticular areas of density within which are multiple cyst-like areas of hyperaeration.

1.160

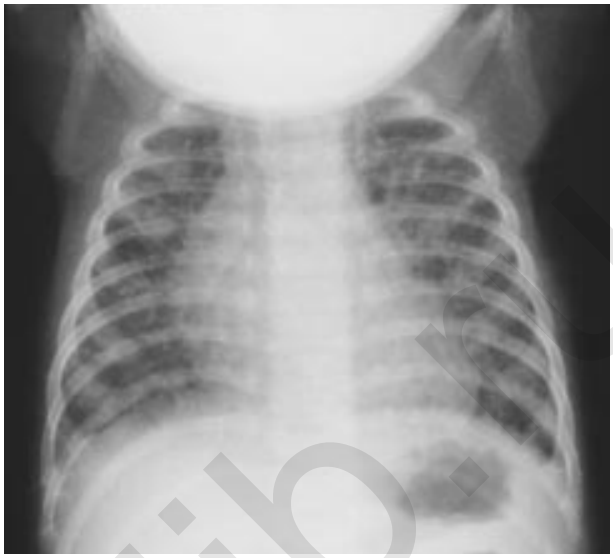

Figure 1.160. Wilson-Mikity syndrome is often confused with BPD because of the similar appearance on chest x-ray. This syndrome typically begins with no sign of respiratory distress. Clinical evidence of respiratory distress may occur in the first few days of life, especially in premature infants. However, the syndrome may not become evident until several weeks after birth, with the onset of respiratory distress which is usually not as severe as is seen in hyaline membrane disease. Oxygen requirements are usually not high.

1.161

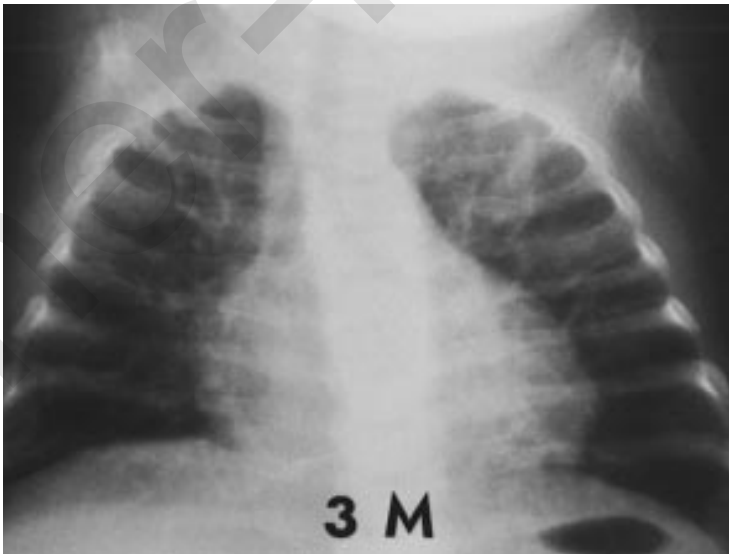

Figure 1.161. This chest radiograph in the same infant as in Figure 1.160 at the age of 3 months demonstrates persistent hyperinflation and prominent lung markings. The infant gradually improved over a period of 6 months and oxygen requirements were minimal.

1.162

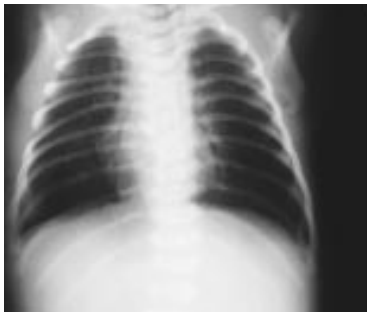

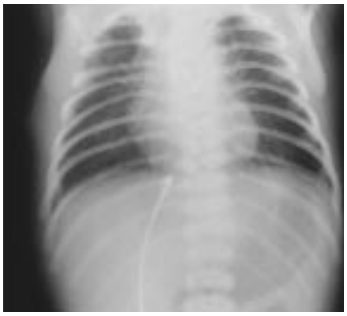

Figure 1.162. This infant was normal at birth, but at 1 week of age developed severe dehydration with cardiovascular symptoms and a severe metabolic acidosis. The chest radiograph on the left shows the markedly hyperinflated lungs with a small cardiac silhouette. The diagnosis of a salt-losing congenital adrenal hyperplasia was established. There was rapid improvement following rehydration and base administration, as noted in the chest radiograph on the right taken 2 hours later in which the lung fields and heart size appear normal. Severe dehydration associated with gastroenteritis can result in a similar problem.

1.163

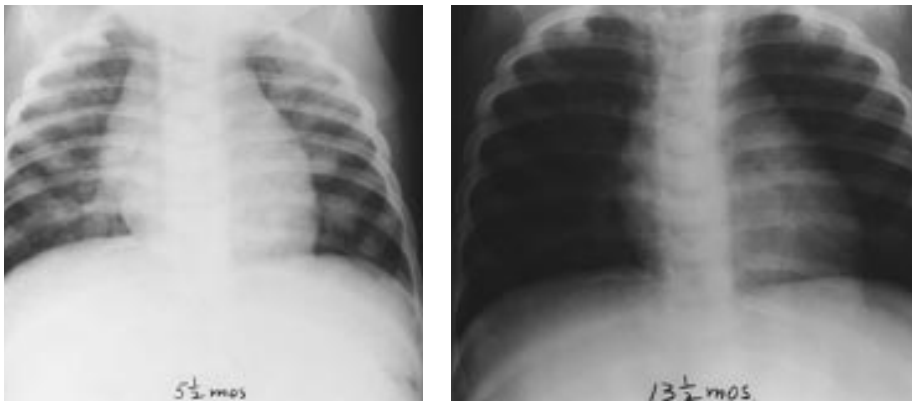

Figure 1.163. Congenital generalized fibromatosis can involve the skin, subcutaneous tissue, muscle, bone and visceral organs. The radiograph on the left demonstrates multiple fibromas in the chest of a 5 1/2-month-old child. There was complete resolution by 13 months of age, as seen in the radiograph on the right. Congenital generalized fibromatosi usually resolves spontaneously but is often fatal when visceral organs are involved, especially the lungs.

1.164

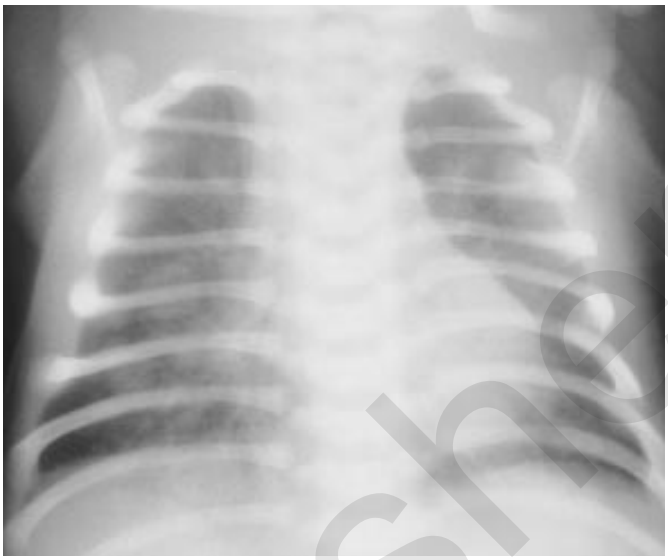

Figure 1.164. Reticuloendothelioses or histiocytosis X represents a variety of conditions which show clinical and pathologic overlap. There is a spectrum of widely disseminated monoblastic leukemia formerly called Letterer-Siwe disease. The lung is involved in only 2% of all cases. In this chest radiograph, note the bilateral lung nodules.

1.165

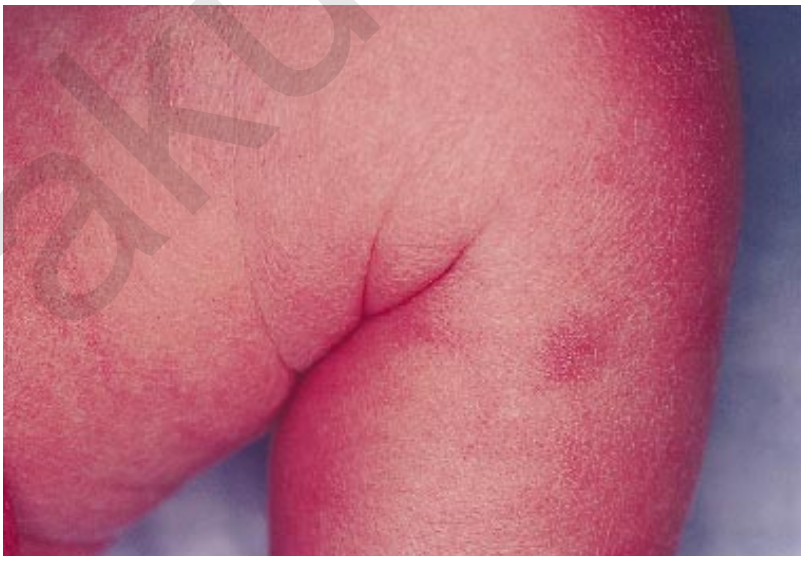

Figure 1.165. Histiocytosis X skin lesions are discrete, flat macules that occur when the cells invade the papillary dermis as seen in this same infant as in Figure 1.164. The infant did well on therapy.

1.166

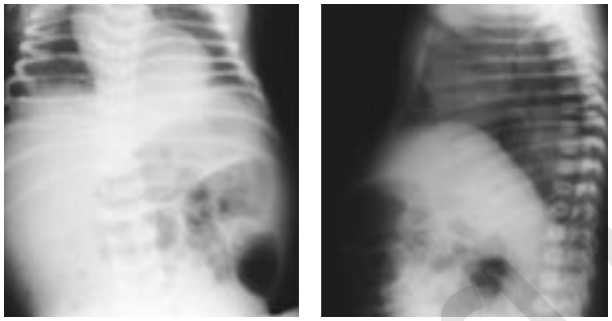

Figure 1.166. A left intrathoracic kidney is noted in this chest radiograph. The kidney arises embryologically from mesodermal tissue in the pelvis. It migrates caudally, passing along its blood supply to progressively higher levels of the aorta. Excessive migration can result in a thoracic location. Intrathoracic kidneys are generally asymptomatic. This infant had a chest radiograph performed at the age of 1 week because he had some abdominal distention.

1.167

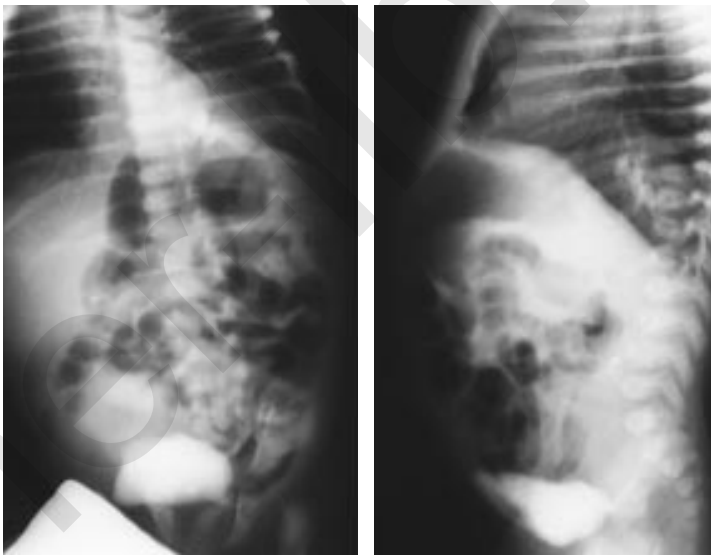

Figure 1.167. An intravenous pyelogram in the same infant as in Figure 1.166 demonstrates the location of the kidney in the thorax. Currently the diagnosis would be confirmed with the use of ultrasonography rather than a pyelogram.

1.168

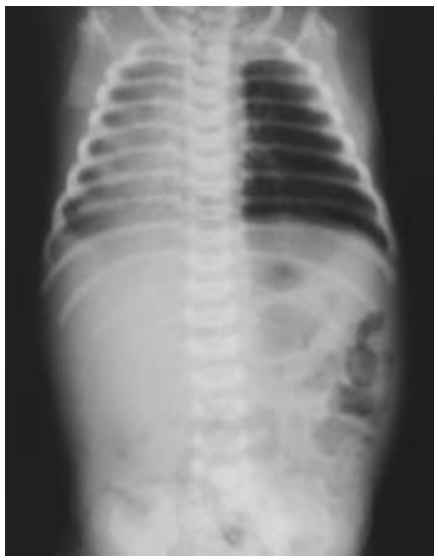

Figure 1.168. In isolated dextrocardia, the apex of the heart is in the right side of the chest. Situs solitus is the rotation of viscera embryologically so that the heart lies in the left hemithorax and the abdominal organs are in their proper relationships (stomach on the left side and liver on the right). Situs inversus results when the heart and stomach are on the right and the liver is on the left. Infants with isolated dextrocardia have an increased incidence of congenital heart disease.

1.169

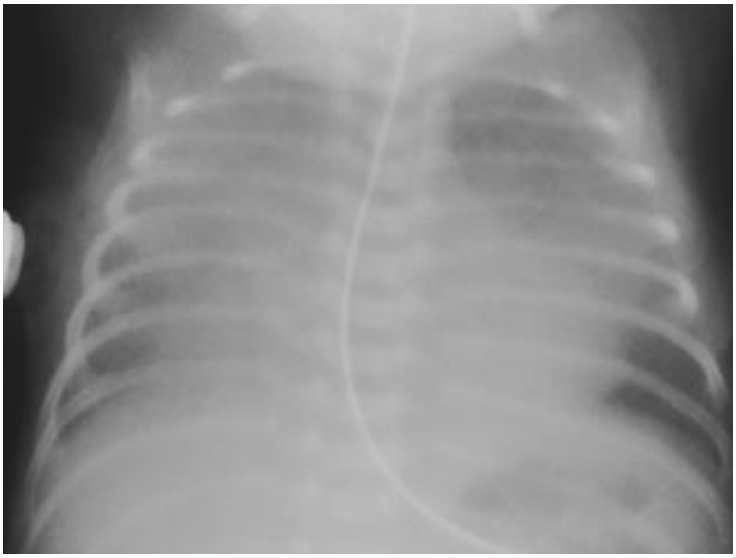

Figure 1.169. Patent ductus arteriosus (PDA) occurs commonly in preterm infants, but is rare in term infants. It can cause severe pulmonary overcirculation and systemic steal of blood flow resulting in shock, pulmonary edema and pulmonary hemorrhage. This radiograph shows an enlarged heart and hazy lung parenchyma because of a PDA and congestive heart failure.

1.170

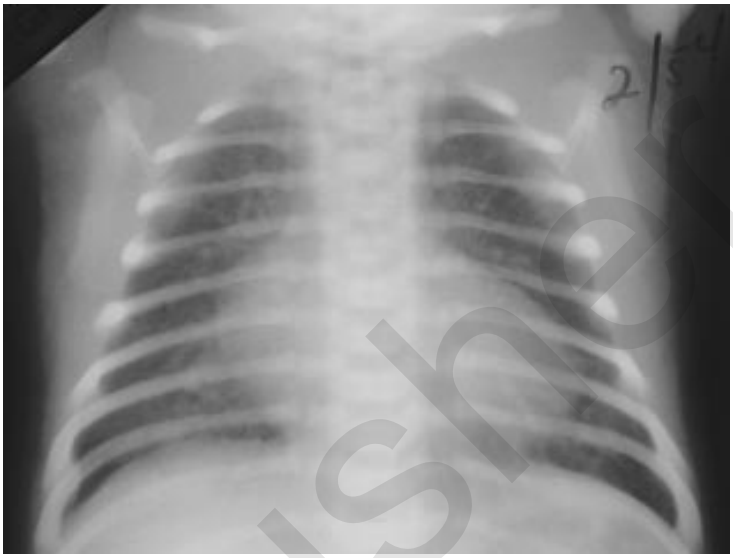

Figure 1.170. This is a chest radiograph of an infant with transposition of the great vessels. The heart is large and egg-shaped and the mediastinum is narrow on the anteroposterior view ("egg on a string"). The pulmonary artery segment is relatively flat and the pulmonary vascular markings are somewhat increased, compatible with the increased pulmonary blood flow in this condition.

1.171

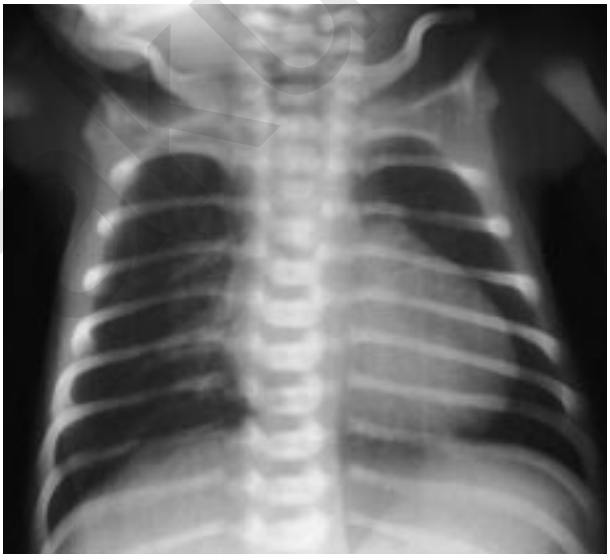

Figure 1.171. In tricuspid atresia, there is a marked decrease in pulmonary artery vascularity, hence the nearly absent lung markings in this chest radiograph. The right heart border is relatively straight, and the cardiac apex is blunt and rounded with a concave pulmonary artery segment.

1.172

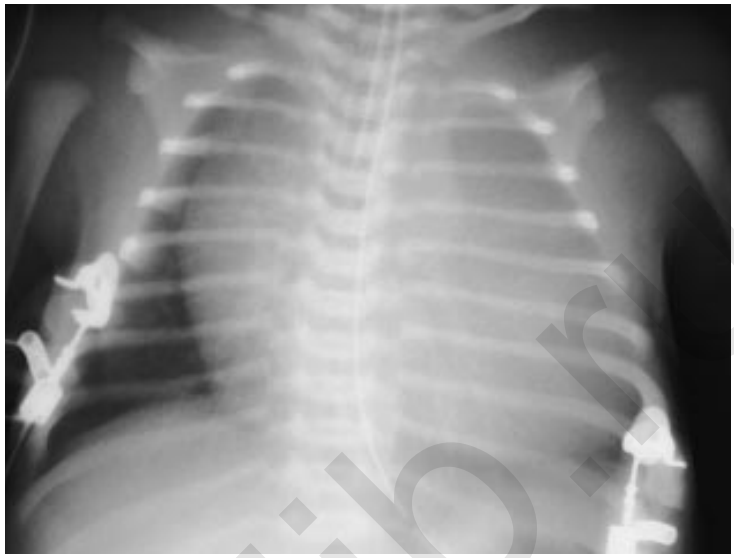

Figure 1.172. Ebstein's anomaly results in a massively dilated heart from tricuspid valve malformation, with tricuspid insufficiency, and sometimes right ventricular outflow tract obstruction. Clinically, the infants are profoundly cyanotic with severe respiratory distress. In Ebstein's anomaly the pulmonary vascularity is decreased and the right atrium is prominent.

1.173

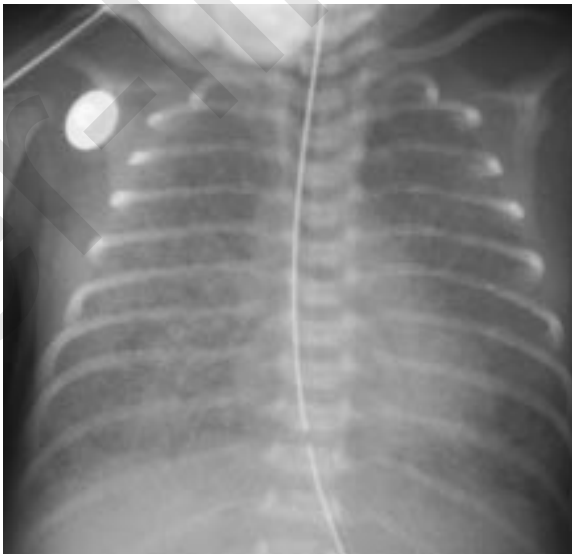

Figure 1.173. Anomalous pulmonary venous return below the diaphragm typically presents with respiratory distress. The infant presents with gross cyanosis, a normal cardiac outline, and plethoric lung fields (pulmonary edema) due to obstruction of the pulmonary venous drainage. The chest radiograph can mimic hyaline membrane disease or, rarely, meconium aspiration syndrome. Lack of improvement over the course of a few days should suggest the diagnosis. Mortality is high when the veins return to the inferior vena cava in a subdiaphragmatic position and are obstructed.

1.174

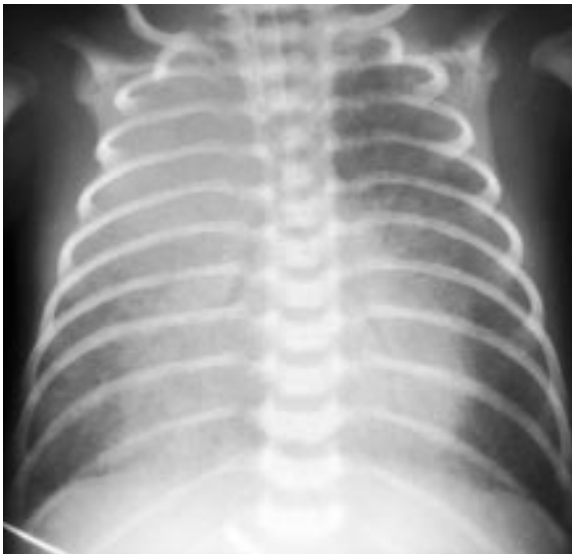

Figure 1.174. At 1 week of age, there was no clinical or radiographic improvement in the infant shown in Figure 1.173, suggesting the diagnosis of total anomalous pulmonary venous return below the diaphragm with obstruction. This was later confirmed by cardiac catheterization.

1.175

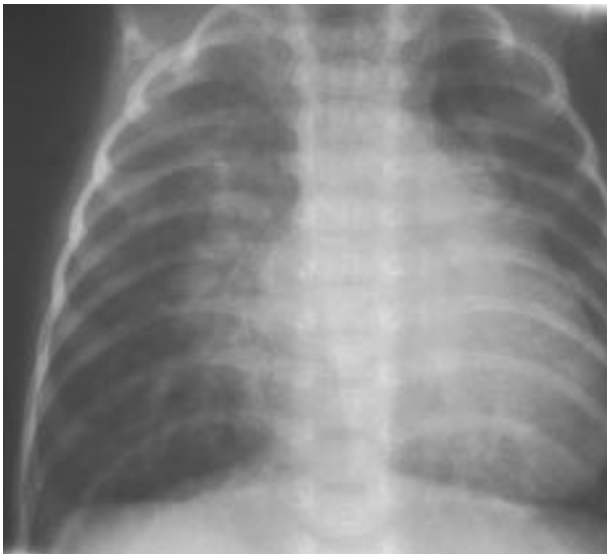

Figure 1.175. This infant with a large ventricular septal defect developed severe congestive heart failure. The cardiac silhouette is markedly enlarged and the lung fields are hazy from pulmonary edema.

1.176

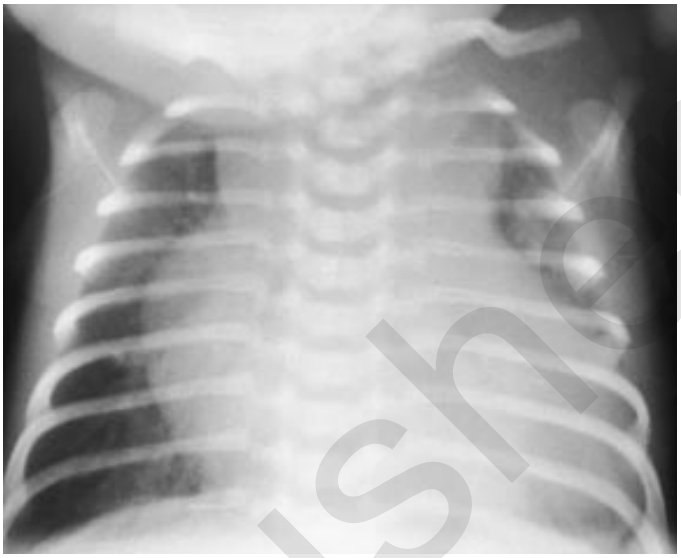

Figure 1.176. This infant presented with marked cardiomegaly and congestive heart failure from an arteriovenous malformation of the liver. In addition to congenital heart disease or myocarditis, the diagnosis of a large arteriovenous malformation should be included in the differential diagnosis of cardiomegaly. Clinical examination should include a careful auscultation for bruits over the skull, liver, and lungs and examination of the skin for shunts in large hemangiomas.

1.177

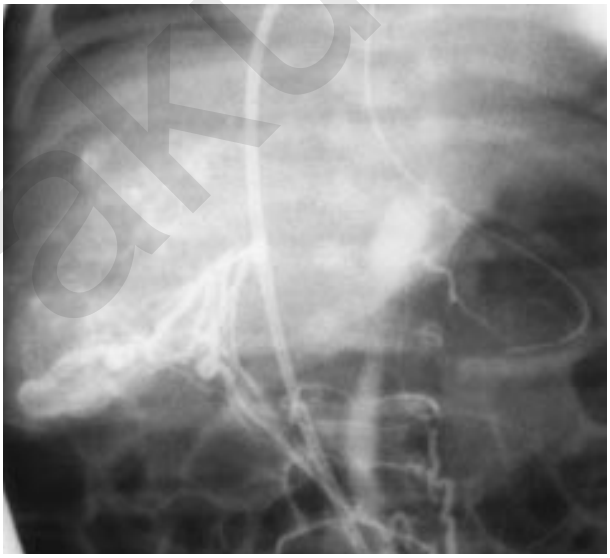

Figure 1.177. In the same infant as in Figure 1.176, angiography demonstrates venous filling of the arteriovenous malformation with rapid run-off of systemic arterial blood to the low resistance venous vessels. A bruit over the liver may not be heard on auscultation in every case.

1.178

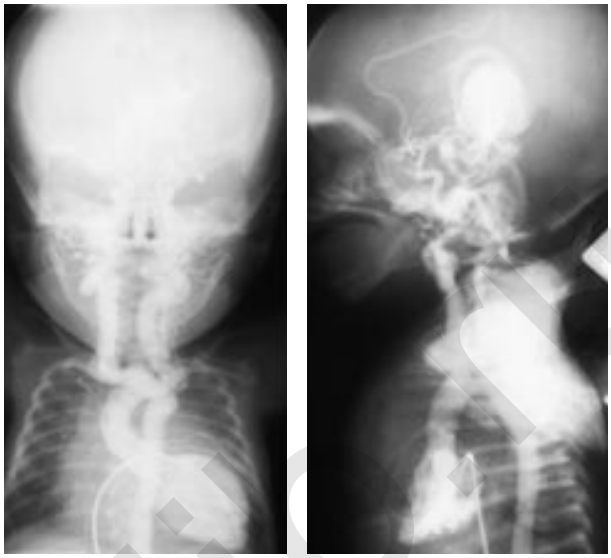

Figure 1.178. Congestive heart failure due to a large arteriovenous malformation of the vein of Galen resulted in massive cardiomegaly as noted in the angiograph on the left. The angiograph on the right demonstrates the massive aneurysmal dilatation 1.3 seconds after an arterial injection. Arteriovenous malformations are now recognized prenatally with the use of fetal ultrasonography, and the diagnosis can be made postnatally with ultrasonography and computed tomography.

1.179

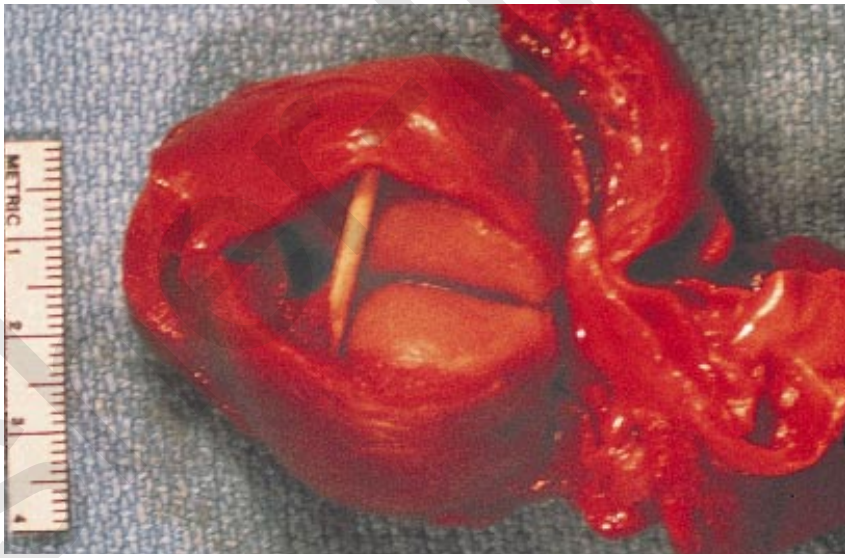

Figure 1.179. Tuberous sclerosis is a neurocutaneous syndrome in which there are skin lesions, as well as tumors of the brain, kidney, and the heart. This gross pathologic specimen shows a large rhabdomyoma lying within the atria. This syndrome may be recognized prenatally with the use of fetal ultrasonography.

1.180

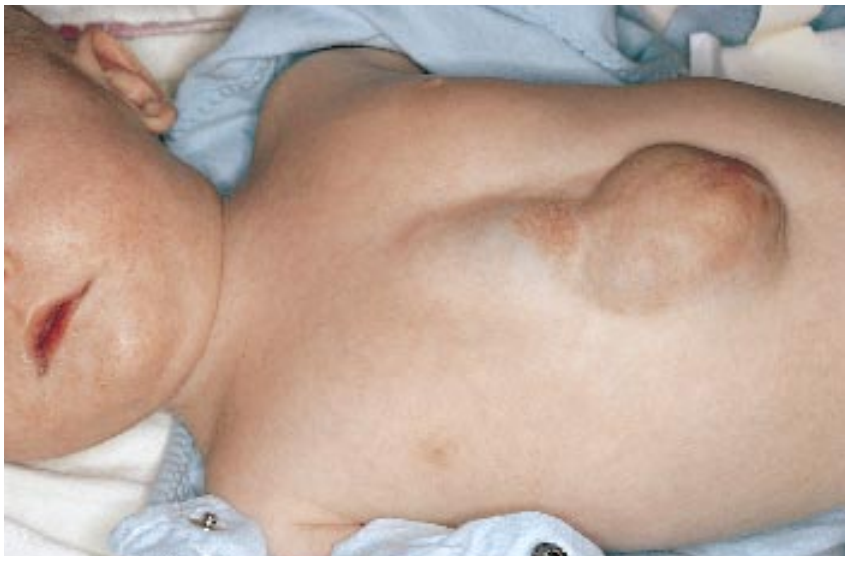

Figure 1.180. A diverticulum of the left ventricle presented as a thoracoabdominal swelling in this infant. Cardiac activity was visible through the skin.

1.181

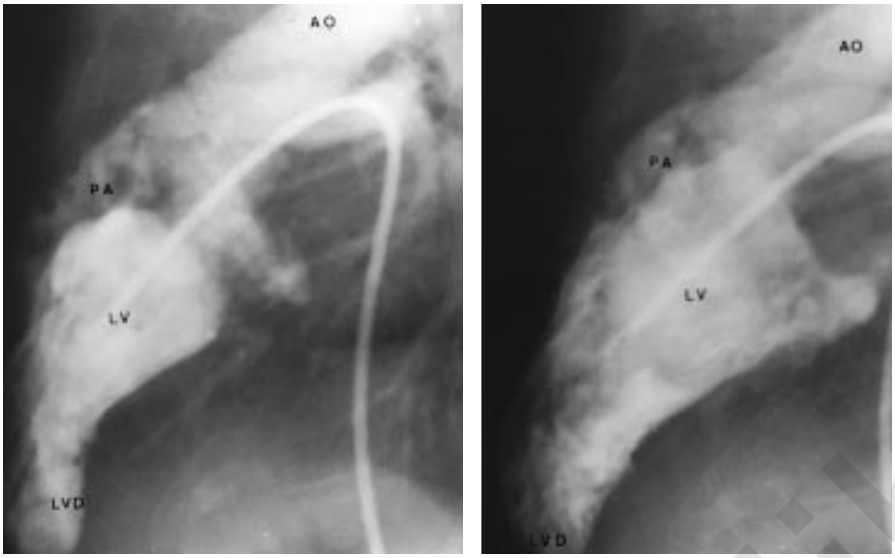

Figure 1.181. In the same infant as in Figure 1.180, the diagnosis of diverticulum of the left ventricle was confirmed by angiogram.

1.182

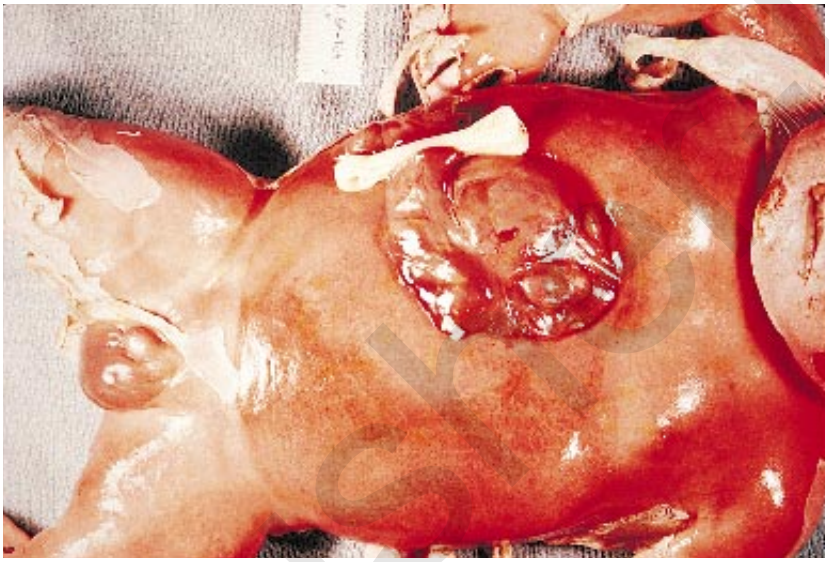

Figure 1.182. In this stillborn infant with ectopia cordis, the heart lies outside the thoracoabdominal wall. The heart typically has severe defects, such as in this case, with tetralogy of Fallot, secundum atrial septal defect, persistent left superior vena cava, and absent ductus arteriosus.

1.183

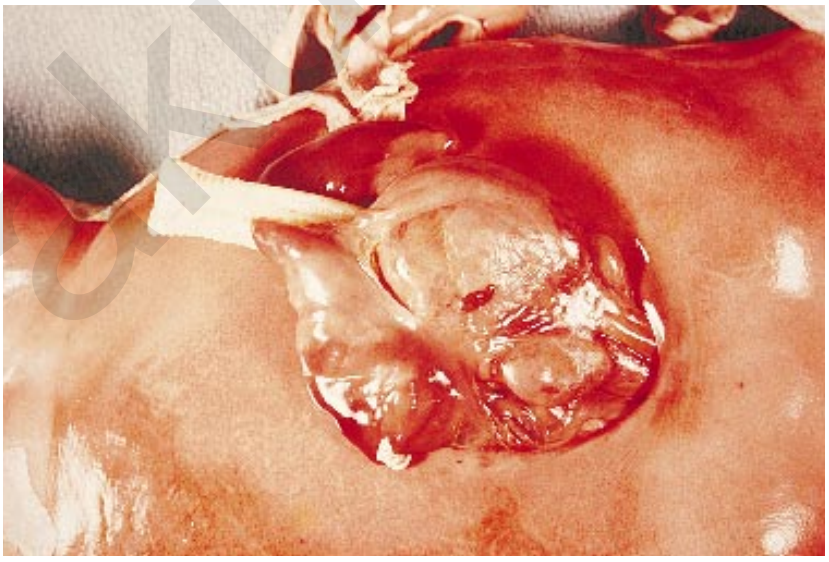

Figure 1.183. In another view of the same infant as in Figure 1.182, the heart is lying outside the skin over the chest and abdominal wall and is connected to the infant's circulation by a single small vessel. Attachment of the umbilical cord is also abnormal as there are severe circulatory anomalies. Surgical correction is not possible due to the small thoracic cavity and the possibility of compromising blood flow to the great vessels.

Chapter 2
Gastrointestinal System

The gastrointestinal tract absorbs and digests nutrients, maintains fluid and electrolyte balance, and protects the newborn from pathogens and toxins. Anatomic malformations of this system may be numerous and affect the pharynx, diaphragm, esophagus, stomach, small or large bowel, pancreas, liver, and spleen. The development of the gastrointestinal system is in close proximity and timing to the development of the respiratory and urogenital systems, and frequently malformations occurring in these systems are related. Normally the fetus is able to swallow and move amniotic fluid through the gastrointestinal tract at 12 weeks gestation, helping to regulate the amount of fluid in the amniotic sac. Maternal polyhydramnios may indicate that this regulation is not taking place and suggests a high intestinal obstruction in the fetus. Imaging studies, including radiographs, ultrasound, contrast, and magnetic resonance, may be necessary to define these disorders of the newborn gastrointestinal tract. During the second and third trimester, the fetal gut elongates and its glandular and functional development continues. Premature birth interrupts this development and poses special problems for the feeding, growth, and development of the infant.

2.1

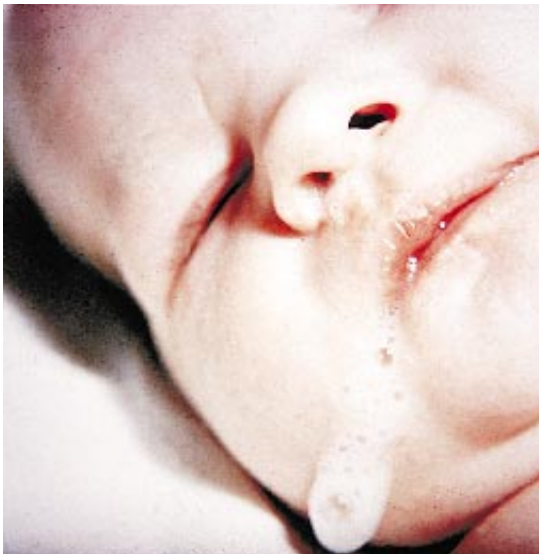

Figure 2.1. Excess mucus secretion in an infant with esophageal atresia. The diagnosis of esophageal atresia or tracheoesophageal fistula should be considered in any infant spitting up a lot of mucus. During transition, normal infants may spit up a lot of mucus.

2.2

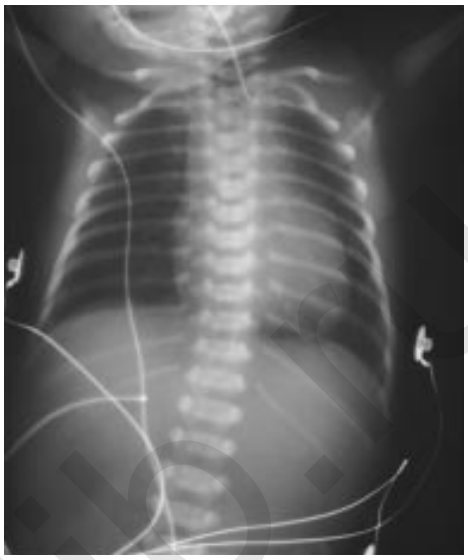

Figure 2.2. Radiograph of the chest of an infant showing esophageal atresia with a blind pouch. Note the tip of the catheter in the blind esophageal pouch. A gasless abdomen, which remains scaphoid, typically is seen in esophageal atresia because of the lack of communication between the respiratory and gastrointestinal tract.

2.3

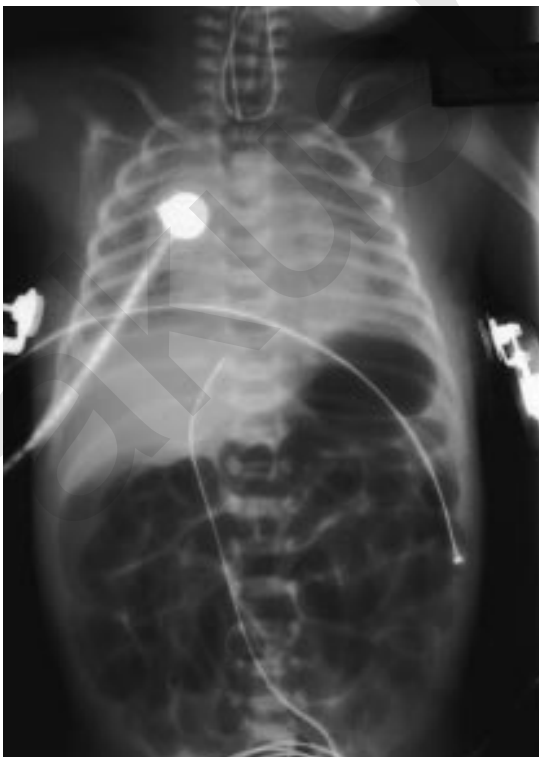

Figure 2.3. Radiograph of the chest and abdomen in an infant with esophageal atresia. Note the coiled catheter in the air-filled blind pouch in the upper mediastinum and the excessive amount of gas in the abdomen. Lack of abdominal gas would, therefore, suggest the diagnosis of an esophageal atresia with a blind pouch; whereas air in the stomach and abdomen indicates communication between the trachea and esophagus, suggesting the diagnosis of tracheoesophageal fistula.

2.4

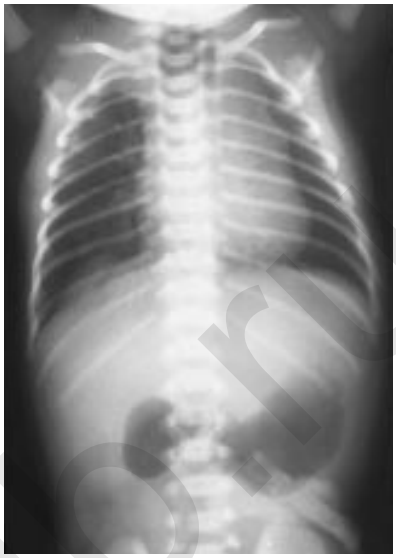

Figure 2.4. Radiograph of the chest and abdomen in an infant with a tracheoesophageal fistula and a double bubble of duodenal atresia. This combination of malformations is not uncommon in that both defects involve disorders of cannulation of the respective anlage. This infant had a type A tracheoesophageal fistula. These comprise 90% of tracheoesophageal fistulae.

2.5

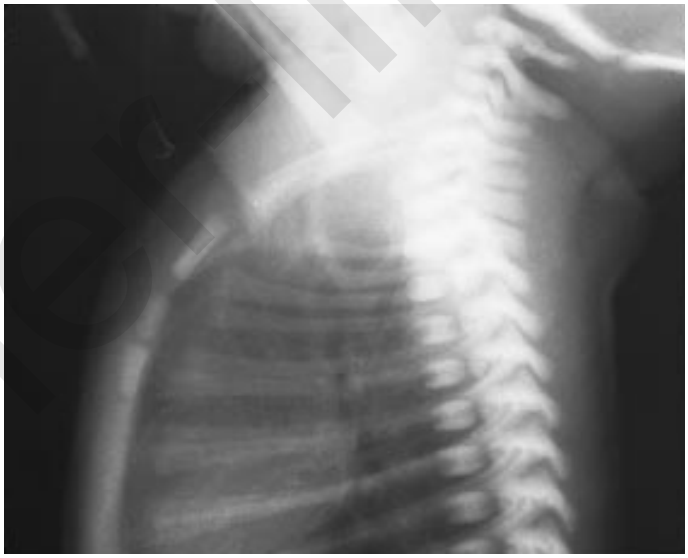

Figure 2.5. Lateral chest radiograph view of the same infant as in Figure 2.4 clearly demonstrates the blind pouch of the tracheoesophageal fistula. Note that the tracheal air column is present, but the esophageal air column is absent.

2.6

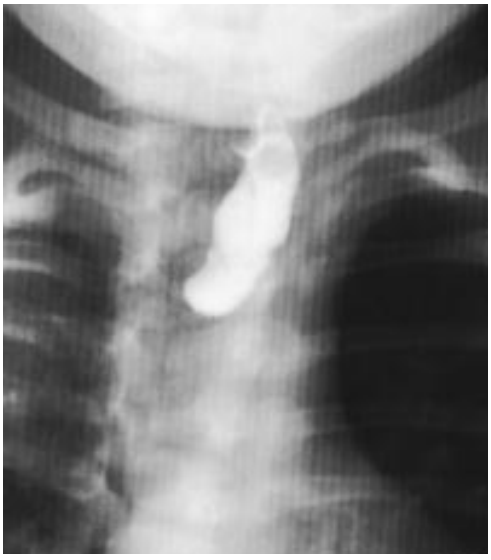

Figure 2.6. Contrast study of the blind pouch in an infant with a type A tracheoesophageal fistula.

2.7

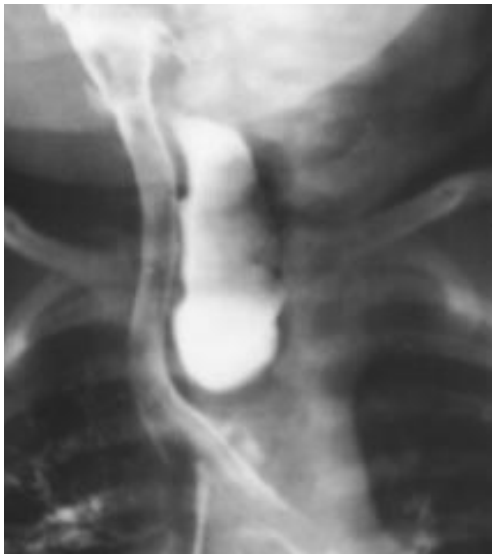

Figure 2.7. Contrast study more clearly delineates the abnormal pouch. This procedure is often not needed and carries increased risk. Note the communication with spillage of barium into the respiratory tract as an excessive amount of contrast was used. This aspiration of contrast into the lungs via the tracheoesophageal connection is typical of type C and D tracheoesophageal fistulae, but can occur with any type.

2.8

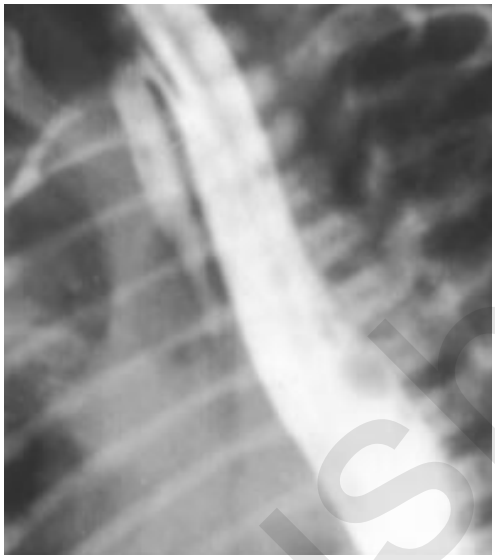

Figure 2.8. Contrast study showing the typical H-type fistula (type B tracheoesophageal fistula). Note that the "H" looks like a reversed "N." This occurs as a result of unequal growth of the trachea and esophagus. This type is rare and occurs in less than 5% of cases.

2.9

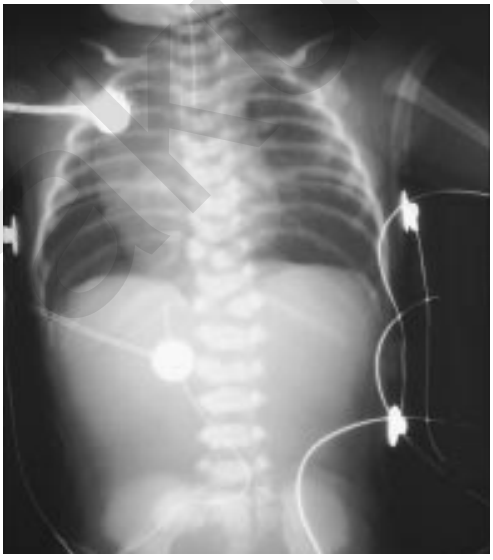

Figure 2.9. In infants with tracheoesophageal fistula, consideration should be given to whether this is a part of the VACTERL (*v*ertebral defects, imperforate *a*nus, *c*ardiac defects, *t*racheoesophageal fistula, *r*enal anomalies, and *l*imb defects) or VATER (*v*ertebral defects, imperforate *a*nus, *t*racheoesophageal fistula, and *r*adial and *r*enal dysplasia) syndrome. This chest radiograph shows an infant with the VACTERL syndrome. Note the vertebral and rib anomalies, the blind pouch and gasless abdomen associated with esophageal atresia, and the dextrocardia. The infant also had an imperforate anus.

2.10

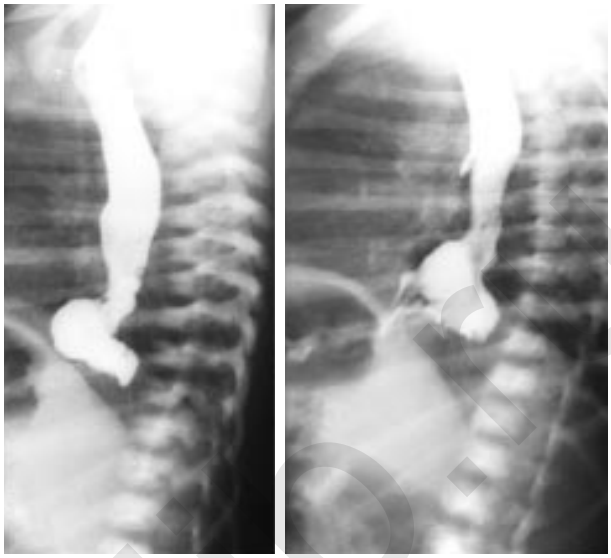

Figure 2.10. In a neonate who was vomiting at 4 days of age, the barium study demonstrates a hiatal hernia (congenital short esophagus).

2.11

Figure 2.11. Intestinal obstruction beyond the ampulla of Vater should be excluded in any neonate with bile-stained vomitus. Bile-stained vomitus can also occur in infants with sepsis or necrotizing enterocolitis.

2.12

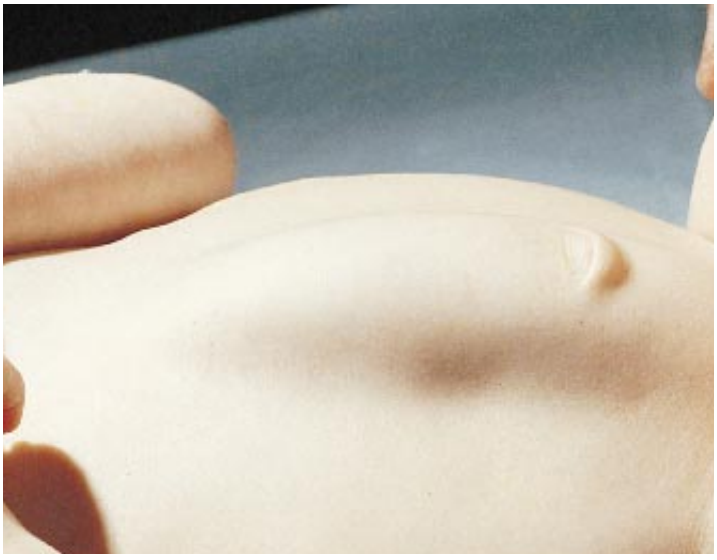

Figure 2.12. Diastasis recti (divarication of the recti muscles) in a term infant. This is a widened space between the rectus abdominis muscles. Lying between the umbilicus and the xiphoid process, it presents as a bulge especially with straining or crying. Varying degrees of separation may be found in nomal infants.

2.13

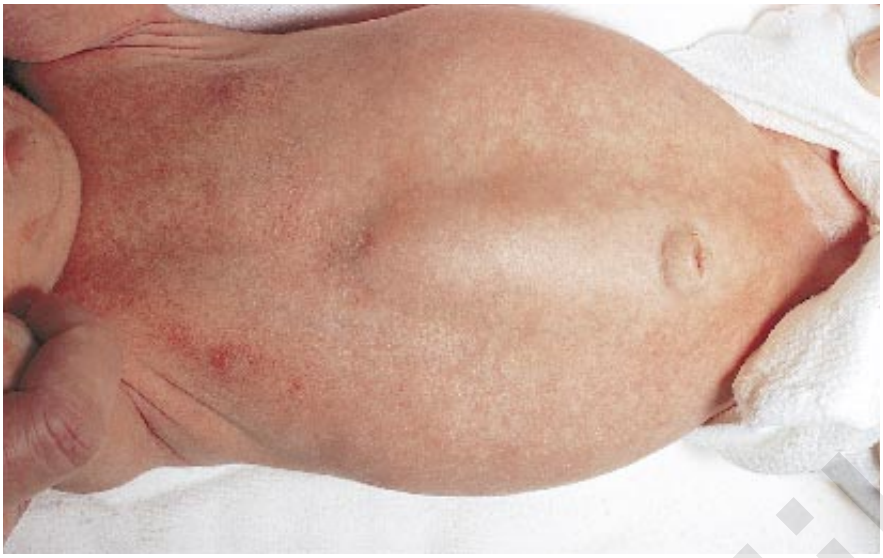

Figure 2.13. Diastasis recti in a premature infant. This condition is more frequently observed in low-birthweight infants and improves with maturation.

2.14

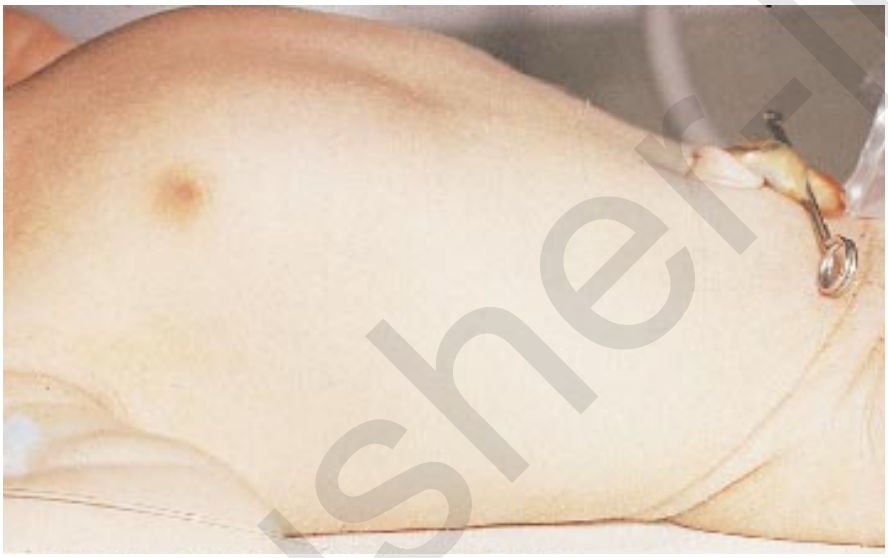

Figure 2.14. The abdomen is usually scaphoid at birth but as loops of bowel are filled with gas from swallowed air and the liver is displaced downward by postnatal expansion of the lungs, the abdomen soon becomes moderately protuberant. In this infant with a scaphoid abdomen, a diaphragmatic hernia was present. Differential diagnosis of a scaphoid abdomen includes severe CNS depression, congenital diaphragmatic hernia, and esophageal atresia with a blind pouch.

2.15

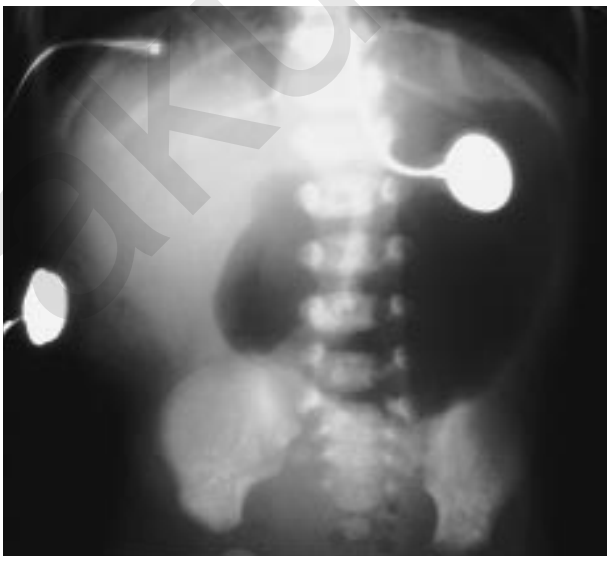

Figure 2.15. Radiograph of an infant with pyloric atresia. Note the large dilated stomach ("single bubble") with no gas distal to the obstruction. There is an association of pyloric atresia with epidermolysis bullosa.

2.16

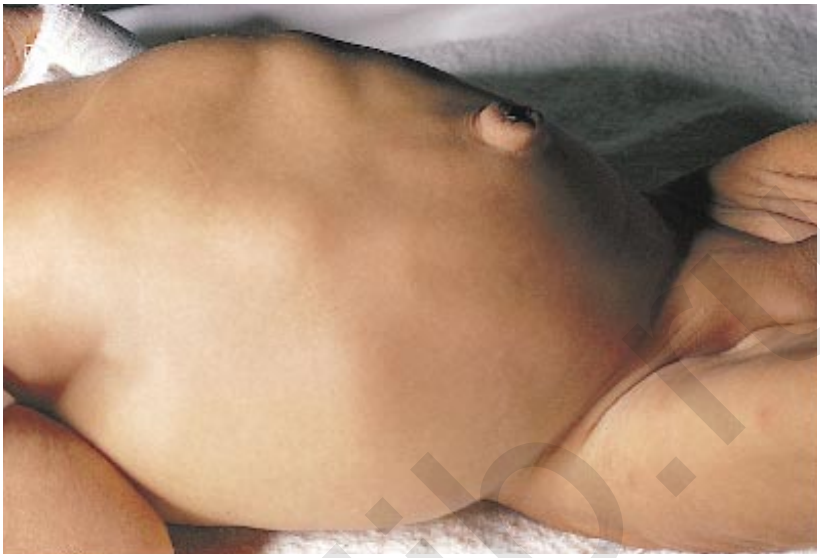

Figure 2.16. Note the typical gastric peristalsis in a 10-day-old infant with pyloric stenosis. There was a history of projectile vomiting, constipation, and an "olive" was palpable. It is unusual for pyloric stenosis to present at this early age.

2.17

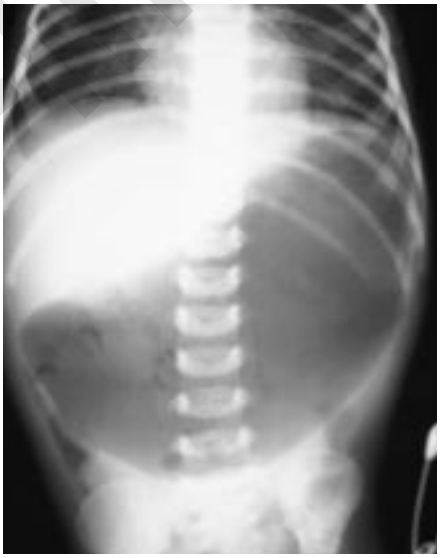

Figure 2.17. Radiograph of the same infant as in Figure 2.16 with pyloric stenosis. Note the large dilated stomach which is typical unless the infant has vomited recently. Note the gas in the gastrointestinal tract distal to the stomach as compared with the infant with pyloric atresia shown in Figure 2.15.

2.18

Figure 2.18. Contrast radiograph in a 3-day-old infant who presented with projectile vomiting. Pyloric stenosis generally does not present at this early age. At surgery a pyloric membrane was found. Note the "string" sign at the pylorus.

2.19

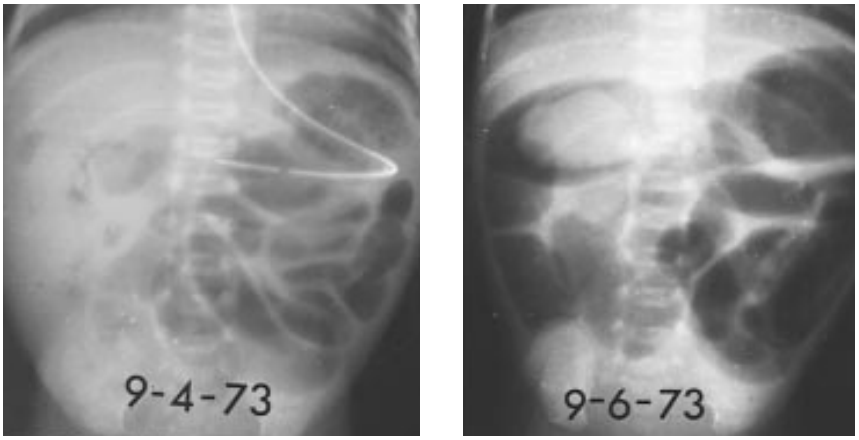

Figure 2.19. Radiograph of an infant with the inspissated milk syndrome. Note the multiple air fluid levels. This probably occurs with the use of formula containing excess long-chain fatty acids which form insoluble soaps resulting in indigestible milk curds. Note the lactobezoar with a marked increase in the size of the lactobezoar over the course of 2 to 3 days.

2.20

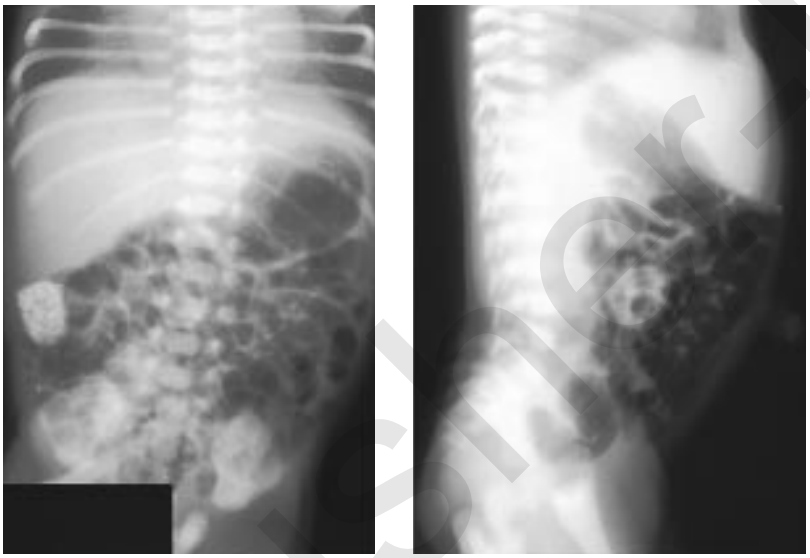

Figure 2.20. Anteroposterior and lateral radiograph showing a lactobezoar in an infant with the inspissated milk syndrome.

2.21

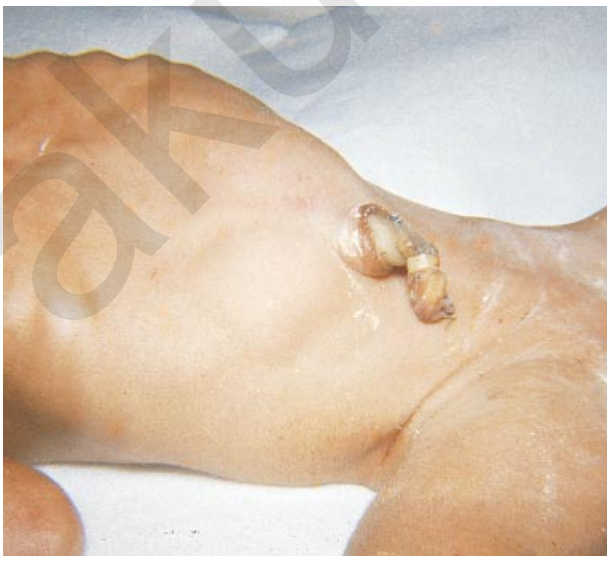

Figure 2.21. Duodenal atresia observed clinically in an infant at the age of 6 hours. Note the dilated stomach and dilated proximal duodenum giving rise to the "double bubble" appearance. At this early age, the infant also has a scaphoid lower abdomen. Thirty percent of infants with duodenal atresia will have other major anomalies, especially chromosomal abnormalities (e.g., Down syndrome).

2.22

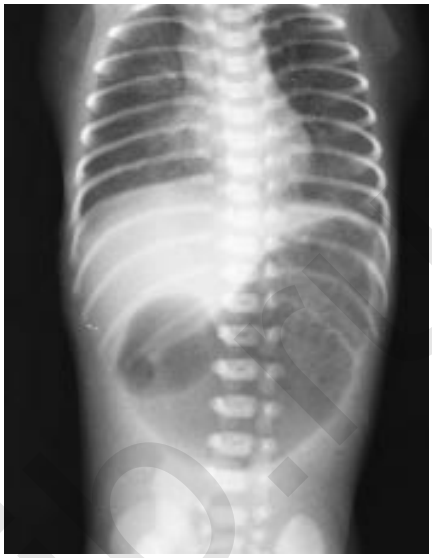

Figure 2.22. Radiograph of the same infant as in Figure 2.21 with duodenal atresia showing the classic "double bubble" appearance. Note that there is no gas distal to the obstruction at the duodenum. The opacity in the right lower quadrant represents the soft tissue shadow of the umbilical cord. This shadow is normally obscured in a gas-filled abdomen.

2.23

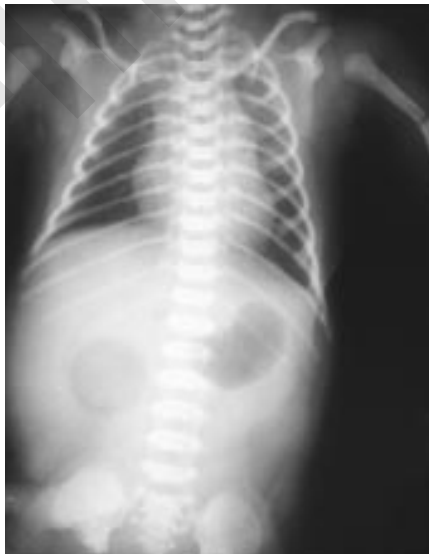

Figure 2.23. Radiograph of a normal infant at the age of 2 hours. The appearance suggests a "double bubble." This is an artifact as the radiograph was taken through the top of the incubator. The very circular lucency seen in the right abdomen represents the hole in the incubator.

2.24

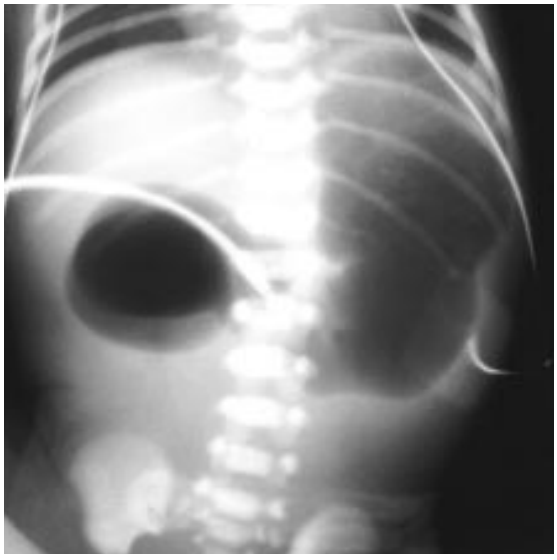

Figure 2.24. Radiograph of an infant with a duodenal web and windsock deformity resulting in the typical "double bubble" appearance. One can see a similar appearance in an annular pancreas causing complete obstruction.

2.25

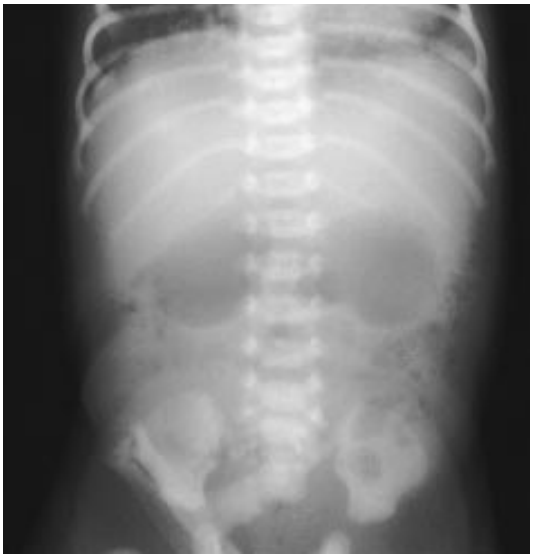

Figure 2.25. Radiograph of infant with duodenal stenosis. Note the presence of gas distal to the "double bubble." This appearance is also seen in infants with annular pancreas and malrotation with Ladd's bands.

2.26

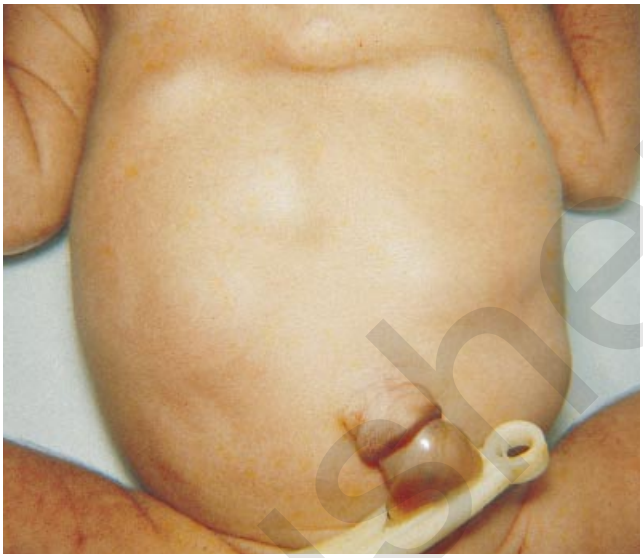

Figure 2.26. Clinical appearance of an infant at the age of 8 hours with jejunal atresia. Note the dilated stomach, dilated duodenum and dilated proximal jejunum giving the typical "triple bubble" appearance. Since jejunal and ileal atresias are due to vascular accidents, they are rarely associated with anomalies.

2.27

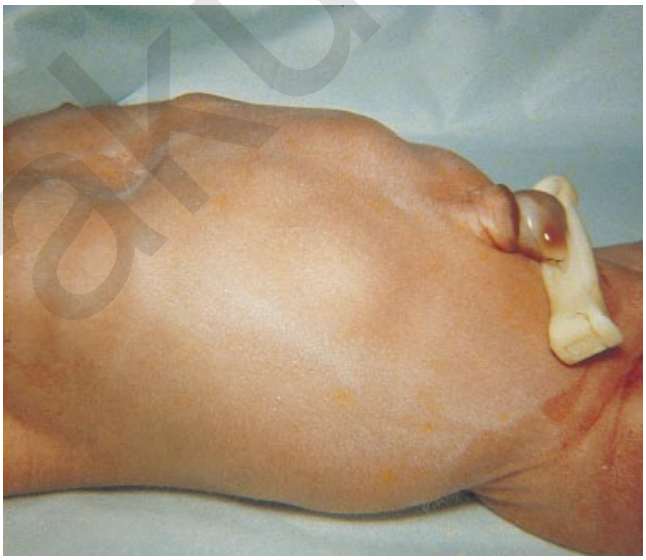

Figure 2.27. Lateral view of the same infant as in Figure 2.26 showing the typical "triple bubble" appearance. Note the scaphoid appearance of the lower abdomen in the infant at this early age.

2.28

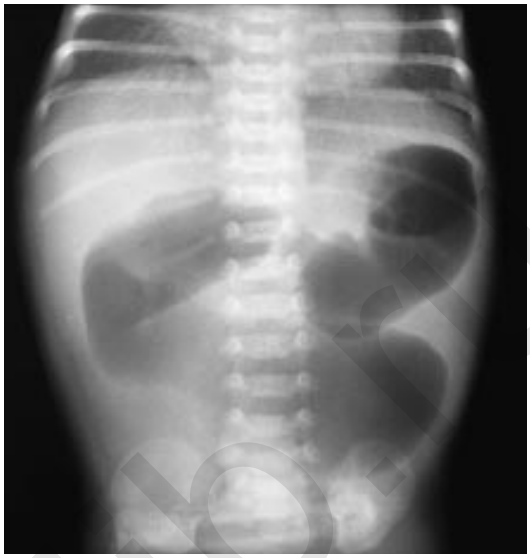

Figure 2.28. Radiographic appearance of jejunal atresia showing the typical "triple bubble." The dilated stomach, dilated duodenum and dilated proximal part of the jejunum are easily observed.

2.29

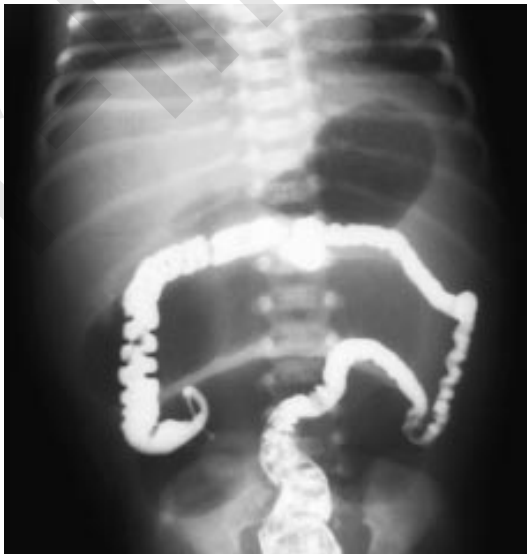

Figure 2.29. Barium contrast enema in the same infant with jejunal atresia as in Figure 2.28. Note the "triple bubble" in the background and the microcolon demonstrated by the contrast medium. The microcolon is due to the lack of passage of bowel contents distal to an intestinal obstruction. It may occur in distal jejunal atresia, ileal atresia, or atresia of the proximal colon. Following relief of the obstruction, the caliber and function of the colon are normal.

2.30

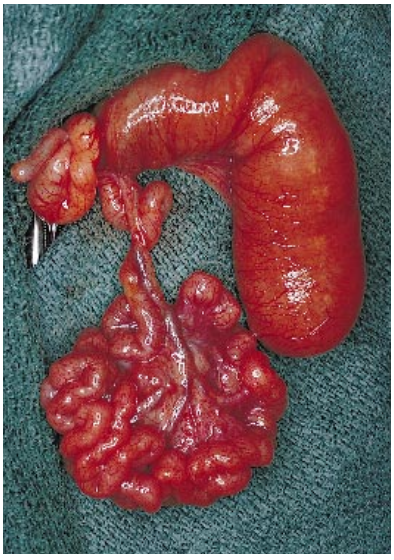

Figure 2.30. Surgical specimen in an infant with jejunal atresia showing the "Christmas tree" deformity (also called "apple peel" deformity). The loops of small bowel encircle a very short mesentery the way lights are draped on a Christmas tree. Note that there is no intestinal continuity and the proximal jejunum is approximately five times the size of the colon.

2.31

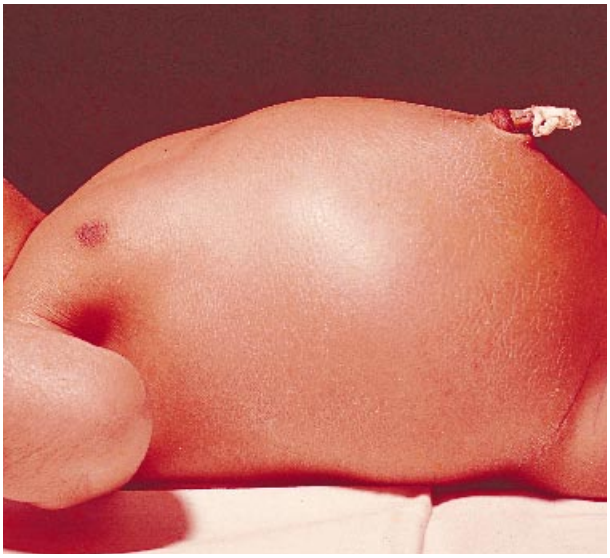

Figure 2.31. Marked abdominal distension in an infant with aganglionosis (Hirschsprung's disease) at the age of 4 days. Differential diagnosis includes intestinal obstruction, sepsis (ileus), ascites, and abdominal masses (hydronephrosis, ovarian tumors, etc.).

2.32

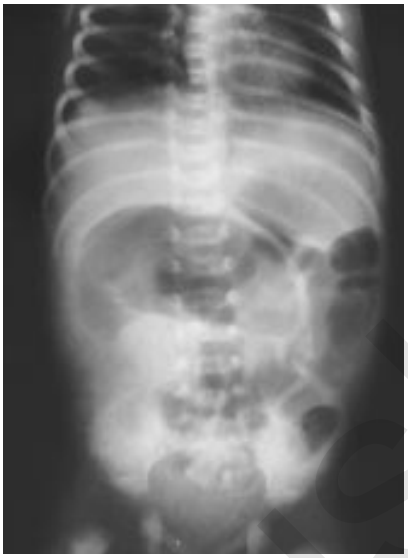

Figure 2.32. Abdominal radiograph of an infant who presented with marked distension and failure to pass stool due to ileal atresia. Note the large dilated loops of bowel. Differential diagnosis includes atresia of the colon and imperforate anus. It may be difficult to differentiate between loops of small and large bowel radiographically in a neonate since haustrations are not present at this early age.

2.33

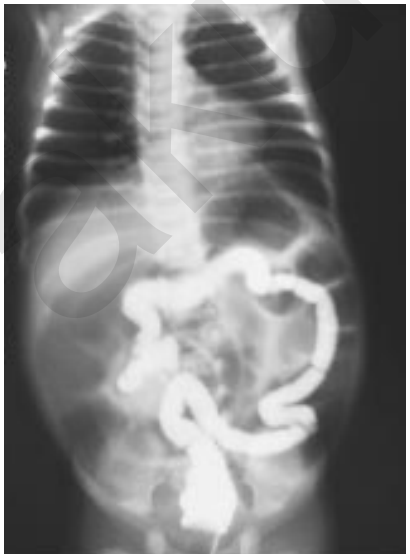

Figure 2.33. Barium enema in the same infant as in Figure 2.32, showing a typical microcolon. Microcolon occurs as a result of lack of passage of bowel contents distal to the obstruction.

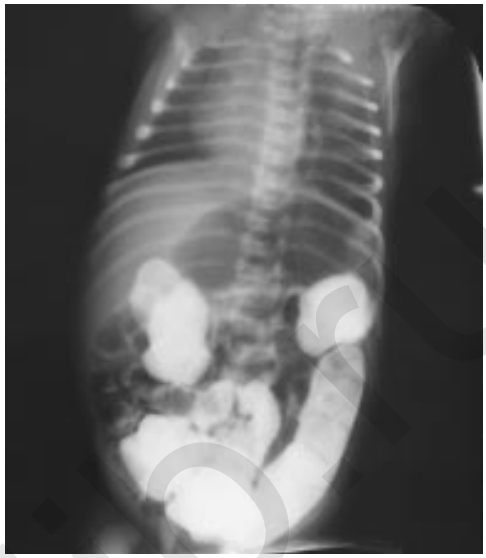

2.34

Figure 2.34. Barium enema in an infant with a normal colon. Note the difference in the caliber compared to that of a microcolon (Fig. 2.33). Note the isolated dextrocardia.

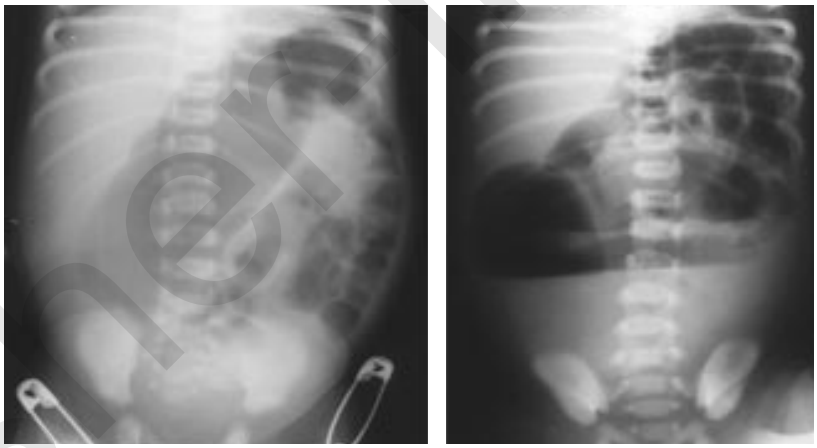

2.35

Figure 2.35. Abdominal radiograph in an infant who presented at the age of 3 days with massive abdominal distension, lack of stool, and vomiting. This infant has atresia of the colon. Note the large distended loop of bowel in the radiograph on the left. The upright radiograph on the right demonstrates air/fluid levels due to the obstruction. (Singleton, E., Wagner, M.)

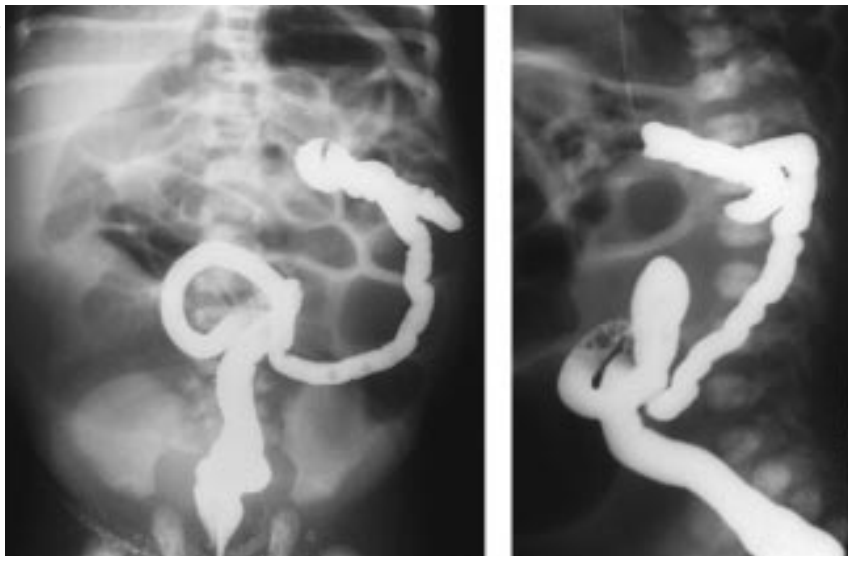

2.36

Figure 2.36. Barium enema in the same infant as in Figure 2.35 shows a microcolon with abrupt termination at the splenic flexure, confirming the diagnosis of atresia of the colon. (Singleton, E., Wagner, M.)

2.37

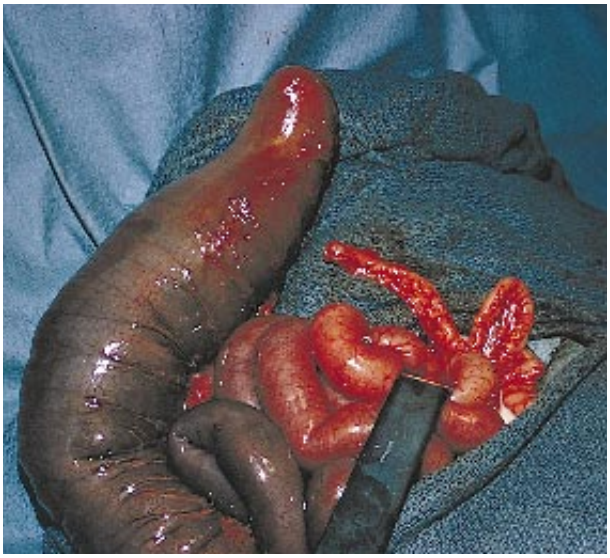

Figure 2.37. Appearance of atresia of the colon at surgery in the same infant as in Figures 2.35 and 2.36. Note the large dilated colon proximal to the atresia. Compare this with the preceding radiograph in Figure 2.29. Note the distal microcolon. The vascular insult in this infant resulted in complete separation of the proximal and distal segments of the colon. Decompression and colostomy permitted successful re-anastomosis one week postoperatively.

2.38

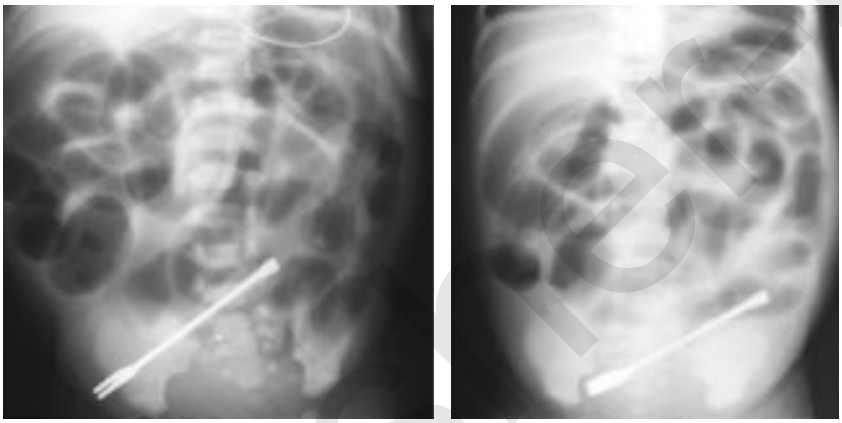

Figure 2.38. Radiograph of an infant with aganglionosis (Hirschsprung's disease). Massive dilated loops of bowel are seen on the flat plate film on the left and the upright film on the right. Upright films reveal no gas visible in the rectum.(Singleton, E., Wagner, M.)

2.39

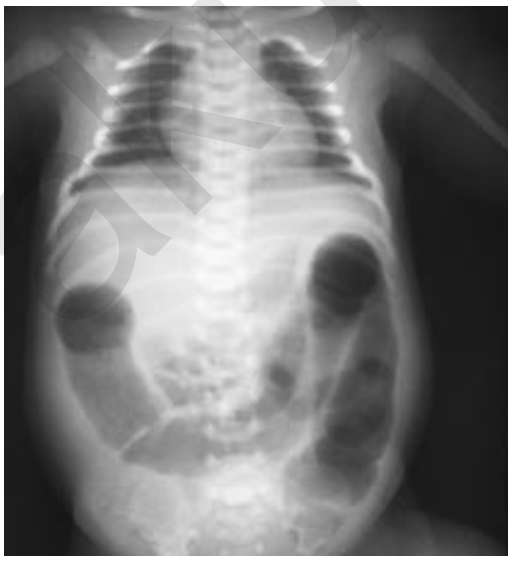

Figure 2.39. Radiograph of another infant with Hirschsprung's disease. Note the markedly dilated loops of bowel, particularly the transverse and descending colon. This infant presented with severe abdominal distension (see Figure 2.31) and delayed passage of meconium.

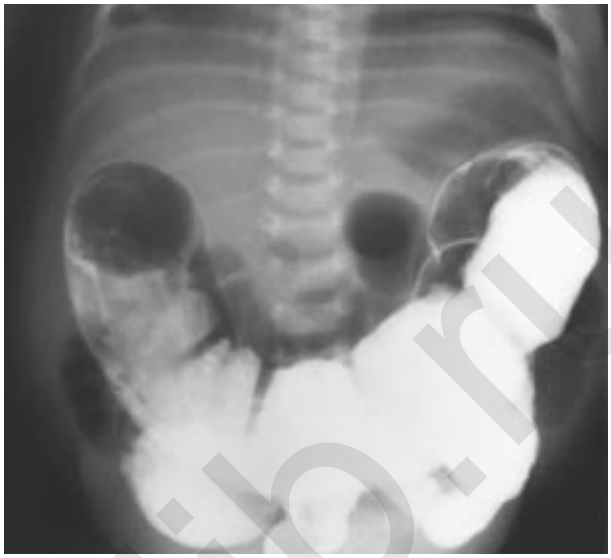

2.40

Figure 2.40. Barium enema of the same infant as in Figure 2.39 showing the gross dilatation of the large bowel proximal to the short aganglionic segment.

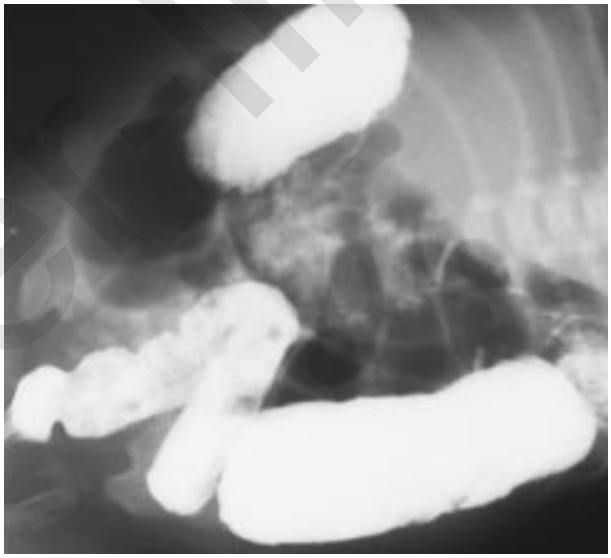

2.41

Figure 2.41. Oblique view of the barium study in the same infant as in Figures 2.39 and 2.40 better demonstrates the aganglionic segment.

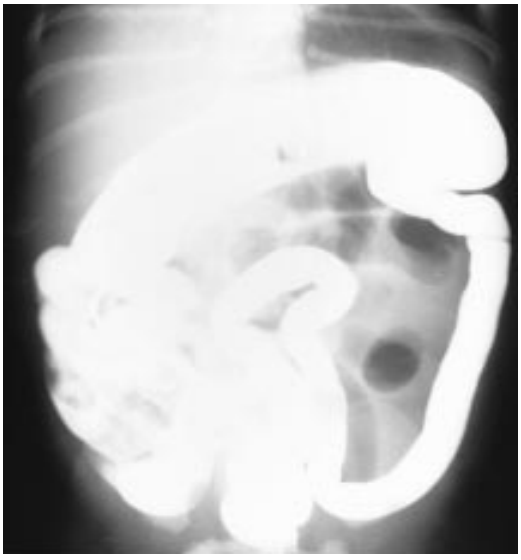

2.42

Figure 2.42. Barium enema in an infant of a diabetic mother with the small left colon syndrome. In the small left colon syndrome, there is a microcolon distal to the splenic flexure. Note the lack of haustrations which is normal for an infant. (Singleton, E., Wagner, M.)

2.43

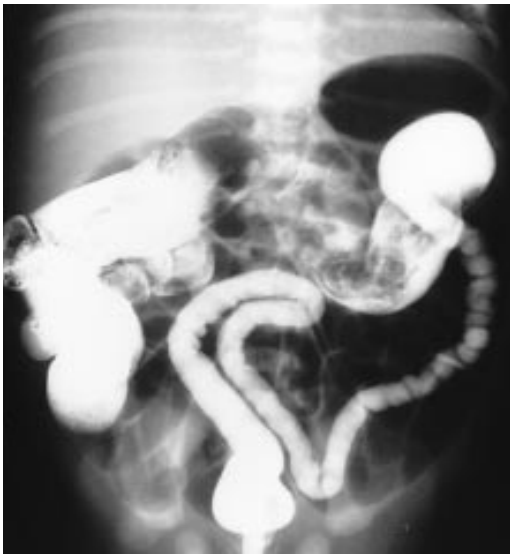

Figure 2.43. Another example of a barium enema in an infant with the small left colon syndrome. This condition is commonly seen in infants of diabetic mothers. Note the microcolon distal to the splenic flexure. Management of this condition is nonoperative, with slow enteral feedings and total parenteral nutrition support until the colon dilates to a more functional size.

2.44

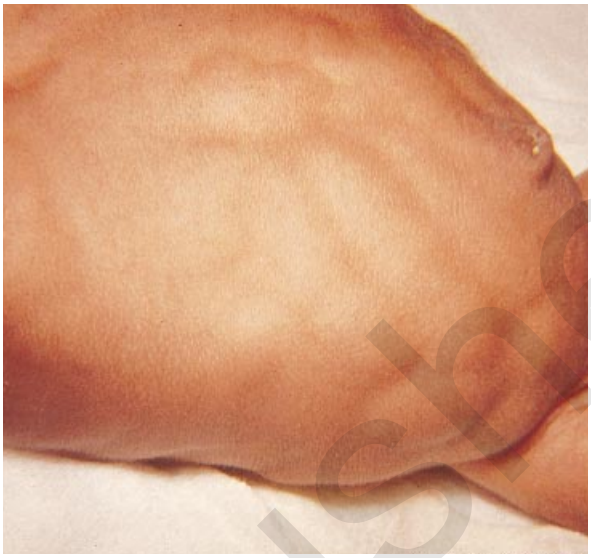

Figure 2.44. Abdominal distension with prominent loops of the bowel in a premature infant. This so-called "pseudoparalytic ileus" of prematurity occurs as a result of poor muscle development in both the abdominal wall and intestinal wall. The infants develop temporary distention with prominent loops of bowel, especially at feeding times. The condition improves with increasing maturity. Persistent distention in a premature infant could be associated with delay in passing meconium.

2.45

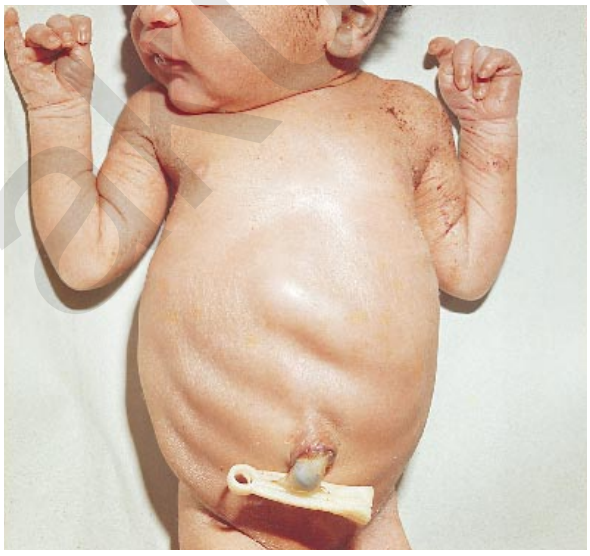

Figure 2.45. Intestinal obstruction in a term infant. Note the "ladder pattern" of the dilated loops of bowel. Distention and dilated loops of bowel can occur with any type of intestinal obstruction. In this instance they are secondary to a meconium plug. This appearance is pathologic as compared with the "pseudoparalytic ileus" of prematurity.

2.46

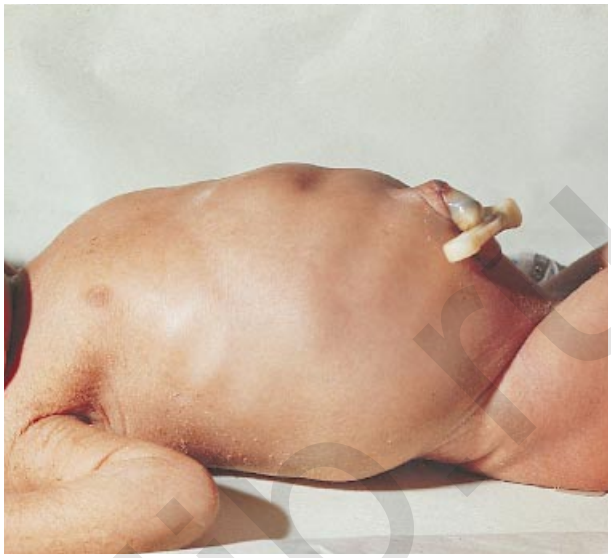

Figure 2.46. Lateral view of the same infant as in Figure 2.45. Note the abdominal distention and the "ladder pattern" of the dilated loops. Differential diagnosis includes other forms of intestinal atresia or obstruction.

2.47

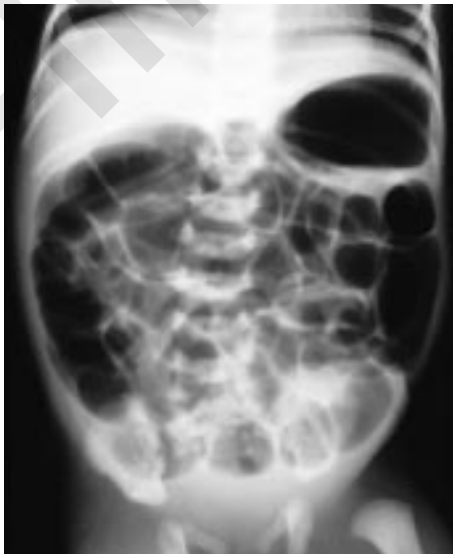

Figure 2.47. Abdominal radiograph of an infant with the meconium plug syndrome. Note the generalized distention due to the dilated loops of bowel and the lack of gas in the pelvis. This would suggest the presence of an obstruction in the distal part of the large bowel.

2.48

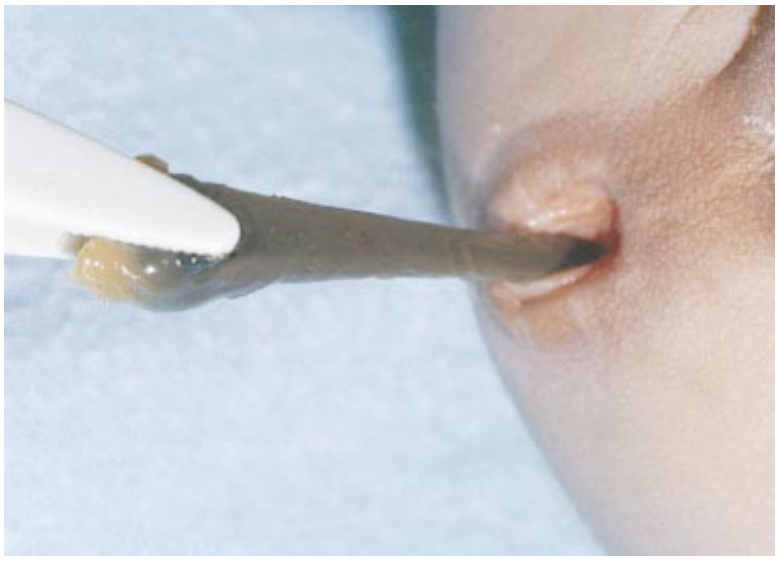

Figure 2.48. The same infant as in Figure 2.47, after a gentle saline enema, passed a large meconium plug. This meconium plug consists of inspissated meconium which obstructs the bowel lumen. In infants with meconium plug syndrome, the differential diagnosis includes meconium ileus (cystic fibrosis) and Hirschsprung's disease. Meconium plugs have also been reported in infants born to mothers treated with magnesium sulfate for toxemia of pregnancy.

2.49

Figure 2.49. Mucous and meconium plug in an infant. A mucous plug forms earlier in gestation and is gray to greenish in appearance. This occurs because of lack of bile formation early in gestation. The true meconium plug occurs later in gestation. This figure demonstrates a combination of a mucous and meconium plug. With passage of the plug, the mucous portion of the plug appears first because it develops earlier.

2.50

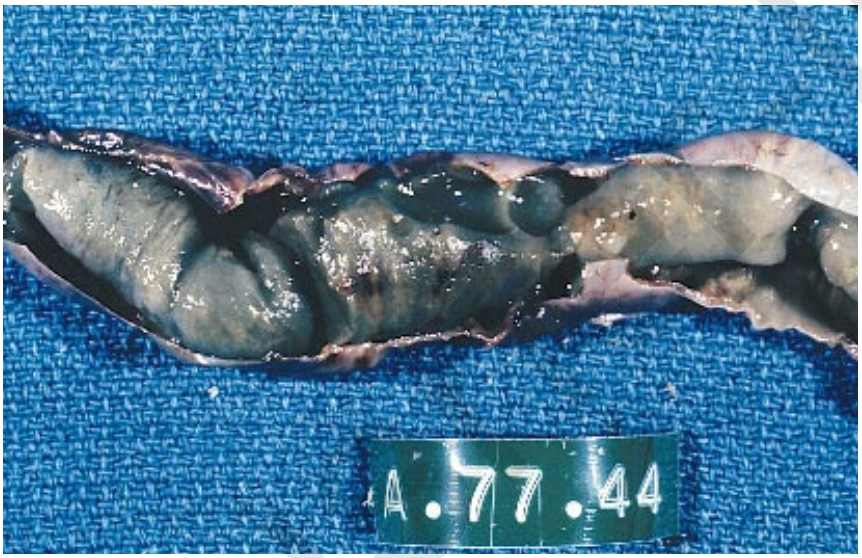

Figure 2.50. Pathologic appearance of a large meconium plug in the mid-jejunum. The plug was associated with intraluminal hemorrhage and colitis. This infant died of necrotizing enterocolitis.

2.51

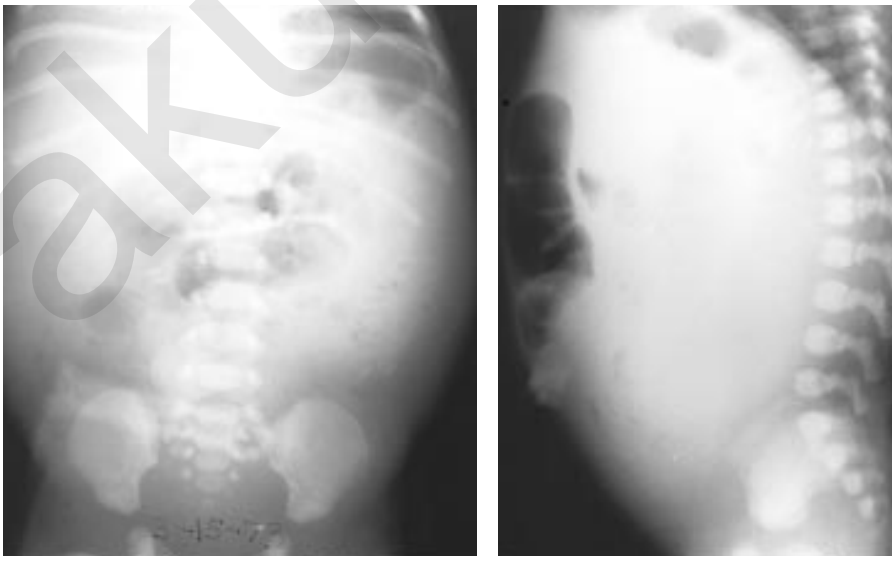

Figure 2.51. Radiographs of an infant with abdominal distention as a result of meconium ileus. Note the opacification of the bowel lumen with relative paucity of air because of the presence of a large amount of inspissated meconium. In infants with meconium ileus, the diagnosis of cystic fibrosis and Hirschsprung's disease should always be excluded. (Singleton, E., Wagner, M.)

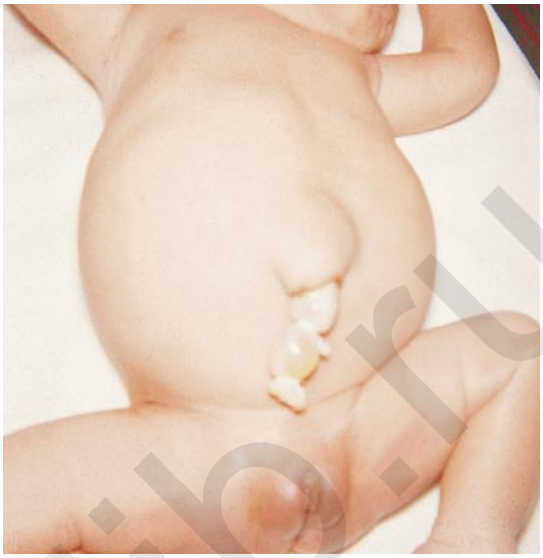

2.52

Figure 2.52. Differential diagnosis of abdominal distention at birth includes ascites due to multiple causes, meconium peritonitis, and abdominal masses. In this infant the abdominal distention was due to meconium peritonitis, which arises in utero when there is a perforation of the bowel wall with passage of meconium into the peritoneal cavity. The infant also had severe respiratory distress due to pressure on the diaphragm. The classic association is with either perforation and meconium ileus or perforation with bowel atresia. Often no cause is found.

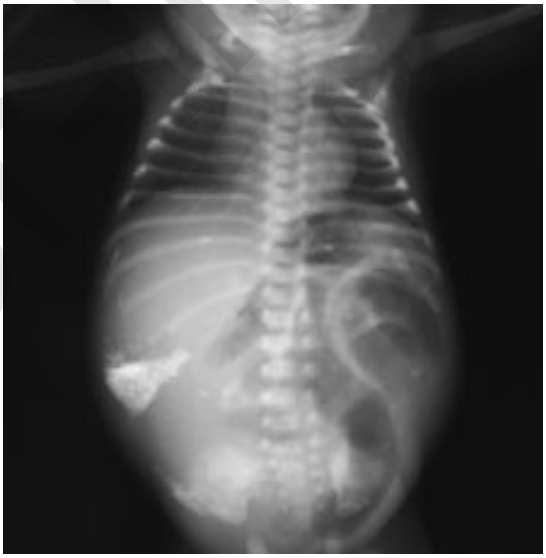

2.53

Figure 2.53. Radiograph of an infant with meconium peritonitis. Note the diffuse calcifications in the peritoneal cavity. This is a classic radiographic sign of this condition. As the bowel perforation occurs in utero, on rare occasions the meconium tracks down the inguinal canal into the scrotum and areas of calcification may be seen in the scrotum.

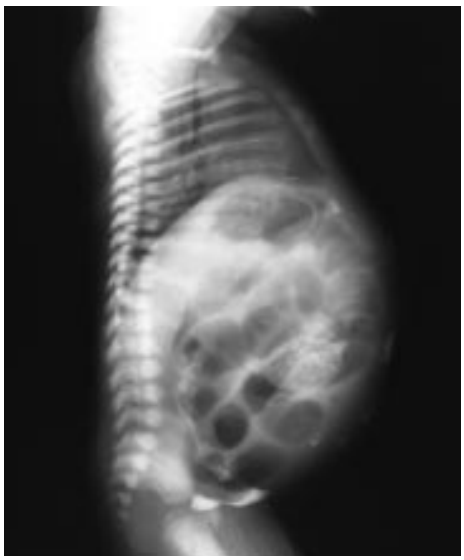

2.54

Figure 2.54. Lateral view of the same infant as in Figure 2.53 with meconium peritonitis. Note the abdominal distention with diffuse calcifications.

2.55

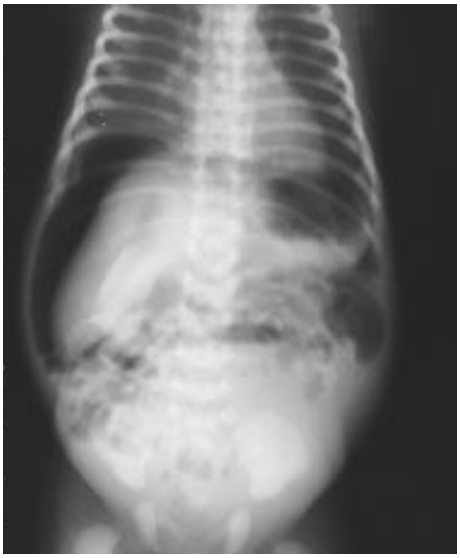

Figure 2.55. Upright radiograph of an infant with meconium peritonitis associated with perforation of the colon and pneumoperitoneum. Also note the diffuse calcification especially over the area of the liver.

2.56

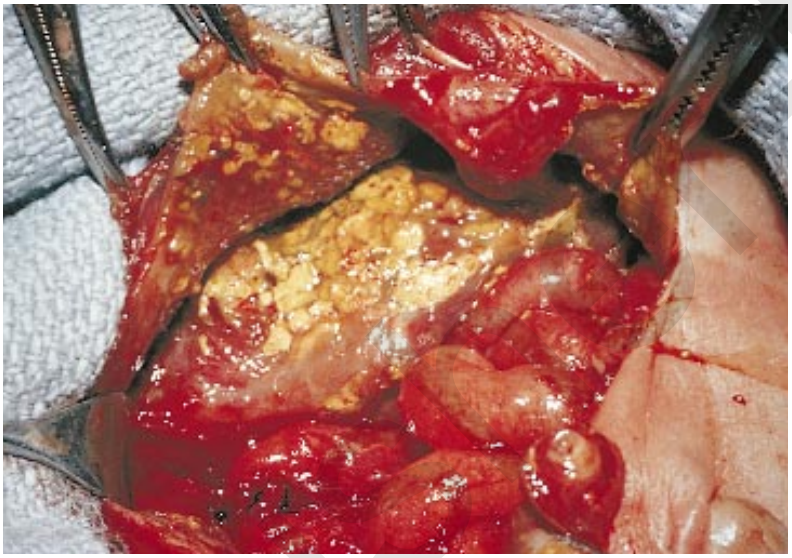

Figure 2.56. Surgical appearance of meconium peritonitis. Note the areas of calcification over the liver and in the peritoneal cavity.

2.57

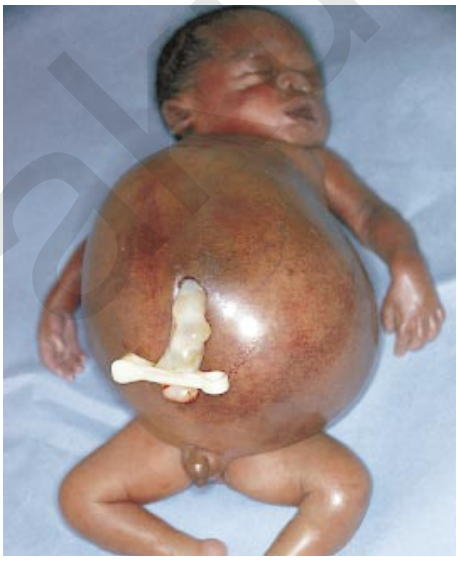

Figure 2.57. This infant presented with severe abdominal distention at birth. The diagnosis of a giant cystic meconium peritonitis was confirmed radiologically and at surgery. A meconium pseudocyst occurs as a result of a late intrauterine perforation with pouring of meconium into the peritoneal cavity.

2.58

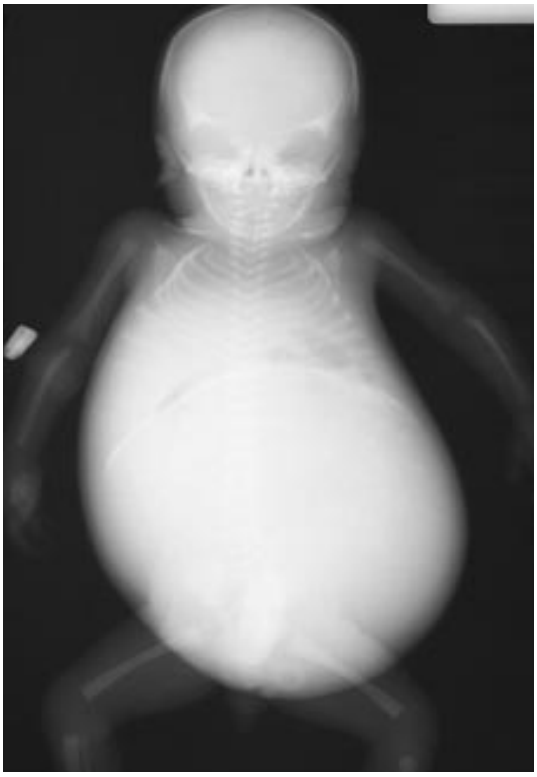

Figure 2.58. Radiograph of the same infant as in Figure 2.57 showing the rim of calcification outlining the giant meconium pseudocyst. There may be large air/fluid levels.

2.59

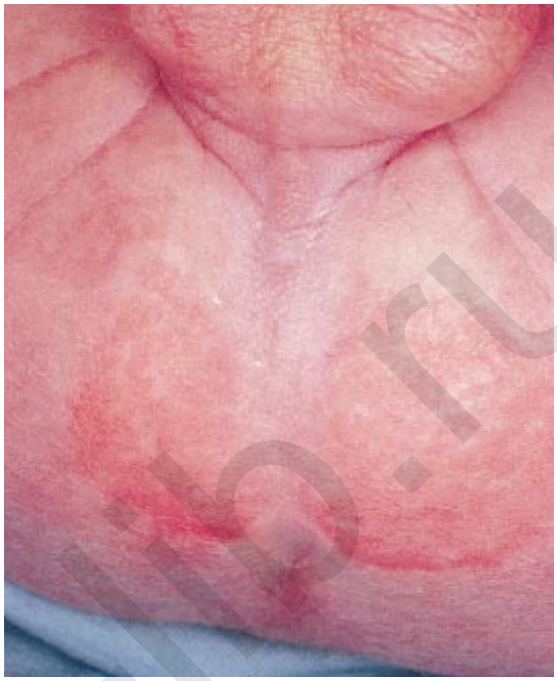

Figure 2.59. Imperforate anus (anal atresia) in an infant. Imperforate anus may appear in two forms: the rare membranous atresia, which probably results from failure of perforation of the anal membrane early in gestation; and the much more common anorectal atresia, in which the rectum ends blindly some distance above the perineum. In this type a fistula usually joins the blind pouch to the skin and the anal sphincter is usually intact and in its normal location. On the surface a remnant of the anal canal may be seen as a shallow dimple as in this infant.

2.60

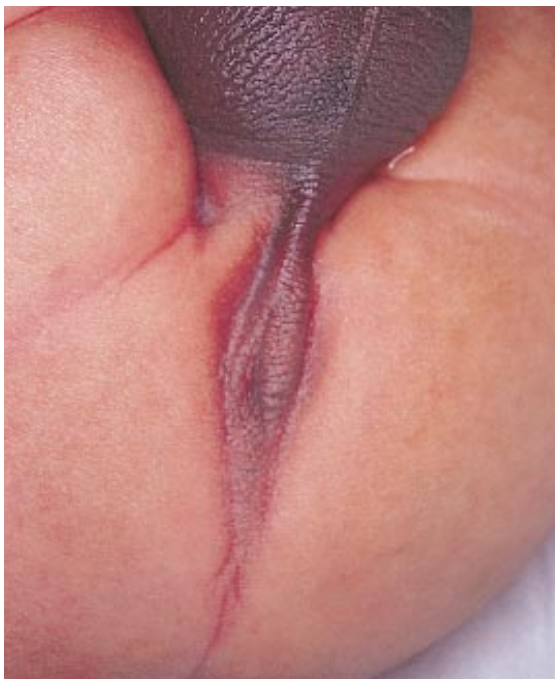

Figure 2.60. Extension of the median raphe in an infant with imperforate anus. In low anal atresias there may be a fistula to the anal cleft. Location may be "high" or "low" depending on whether the atresia is above ("high") or below ("low") the puborectalis muscle.

2.61

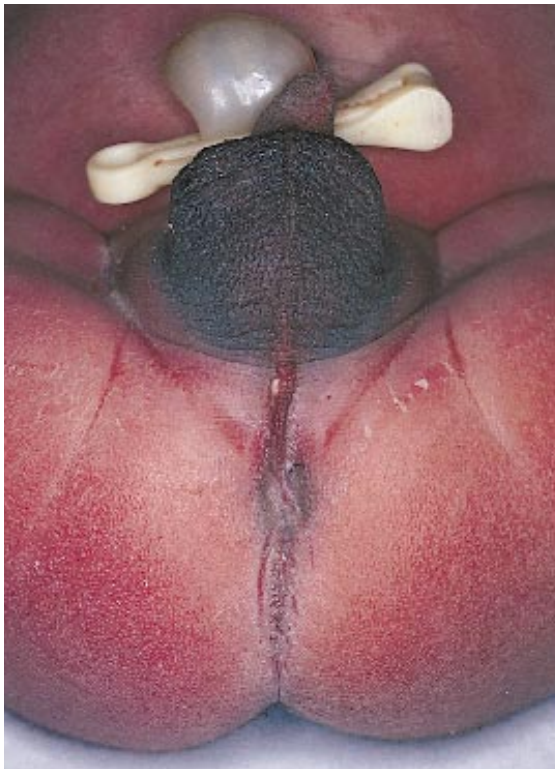

Figure 2.61. Median raphe with small inclusion cysts and an imperforate anus. Without careful examination, the diagnosis of imperforate anus may easily be missed.

2.62

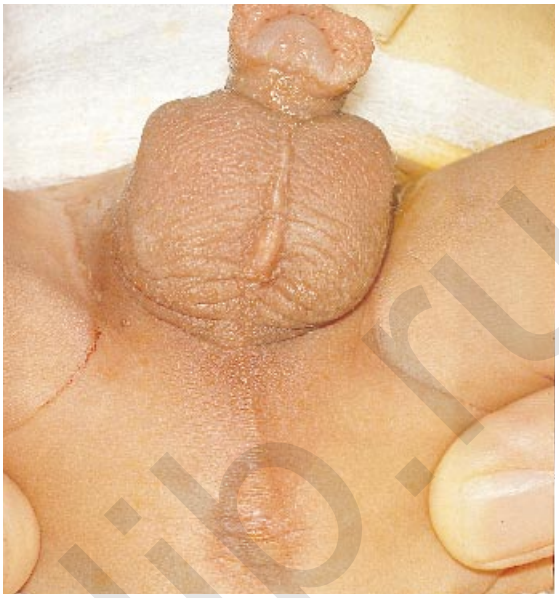

Figure 2.62. This is another example of an infant with imperforate anus. Note the anal dimple and in addition there is a hypospadias involving the glans. Anal atresia is often associated with other anomalies, primarily genitourinary tract or vertebral anomalies. It is also observed in the VACTERL syndrome.

2.63

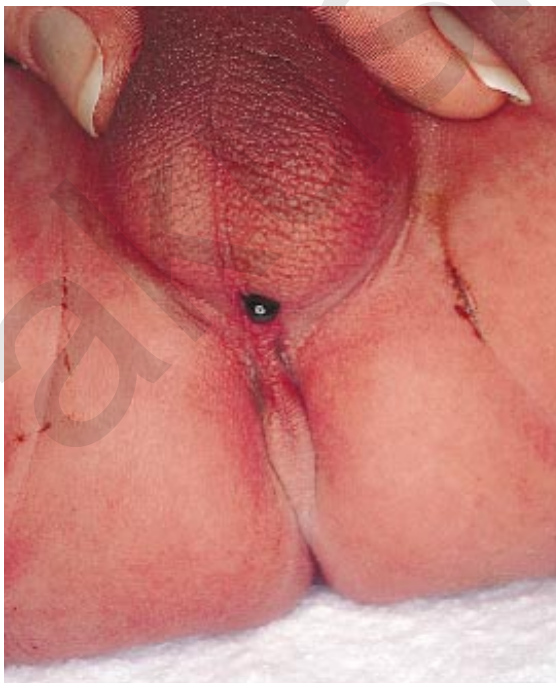

Figure 2.63. Imperforate anus with a superficial fistula running anteriorly from the anus along the midline of the perineum to the scrotum.

2.64

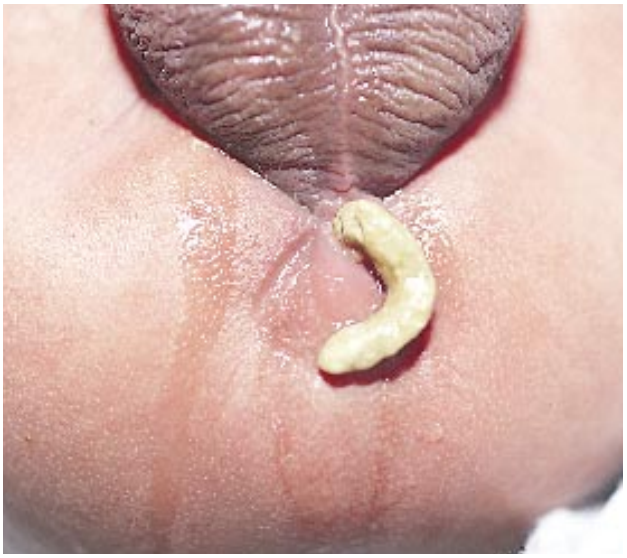

Figure 2.64. Imperforate anus with a rectoperineal fistula from which there was passage of meconium and later stool.

2.65

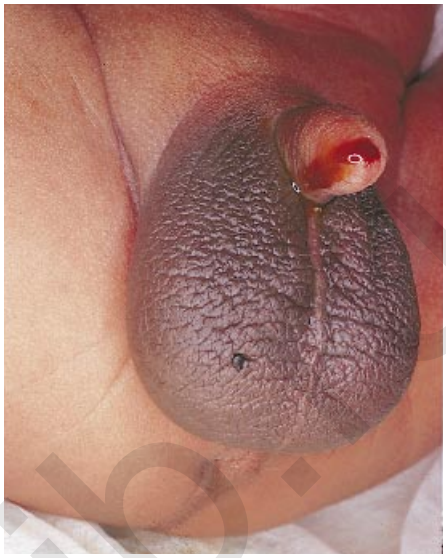

Figure 2.65. Imperforate anus with a rectourethral fistula. The majority of high anal atresias have a fistulous connection with the bladder or urethra in males or the vagina in females. This leads to passage of meconium from the urethra or from the vagina. If there is a fistulous connection to the bladder (rectovesical) the urine is mixed with meconium on voiding. If the fistulous connection is to the urethra (rectourethral), meconium trickles out of the urethra.

2.66

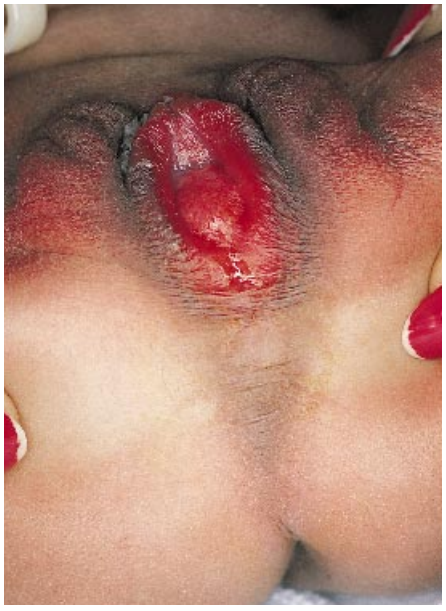

Figure 2.66. This infant with an imperforate anus has a rectovaginal fistula. In addition note the imperforate hymen. Because meconium may be passed through the fistula and out through the vagina, the diagnosis may be missed without careful inspection.

2.67

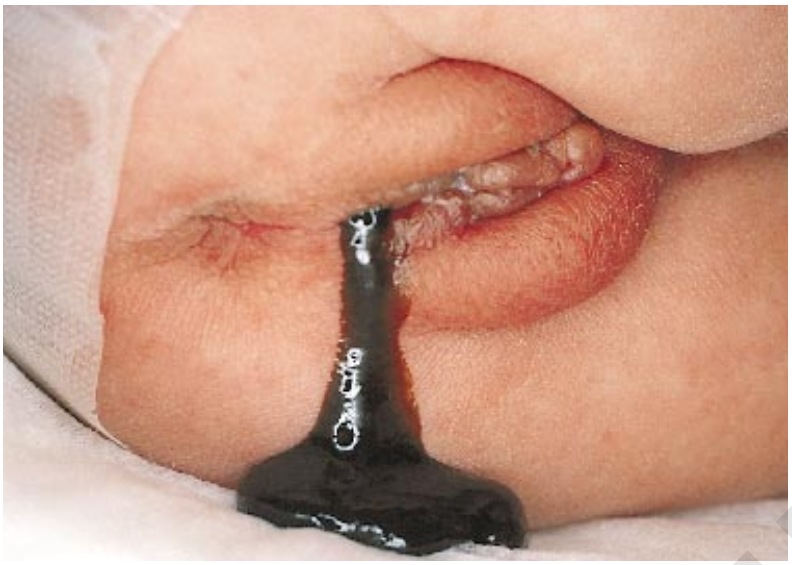

Figure 2.67. Imperforate anus with a rectovaginal fistula. The large fistulous tract allows for free passage of meconium hence this infant had no abdominal distention.

2.68

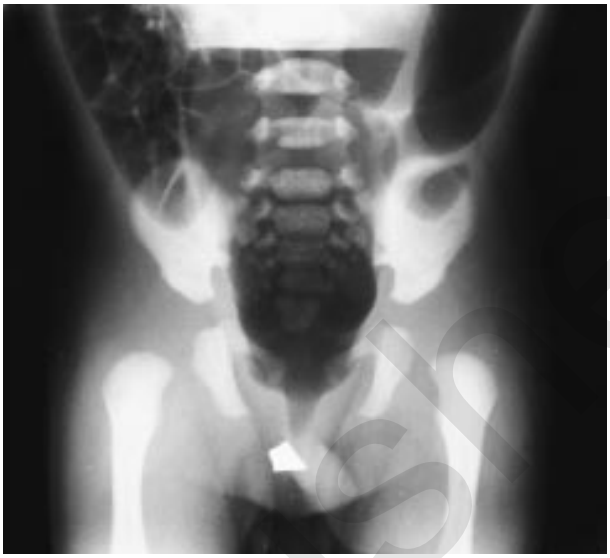

Figure 2.68. Radiograph of an infant with imperforate anus. The Wangensteen technique for diagnosis of high or low location of an imperforate anus places the infant in a head-down position using air as a contrast medium. A radio-opaque marker is placed over the external anal dimple. Presence of an air column, as this figure demonstrates, shows a "low" imperforate anus. Failure of gas to fill the rectum and anal canal demonstrates a "high" imperforate anus. (Singleton, E., Wagner, M.)

2.69

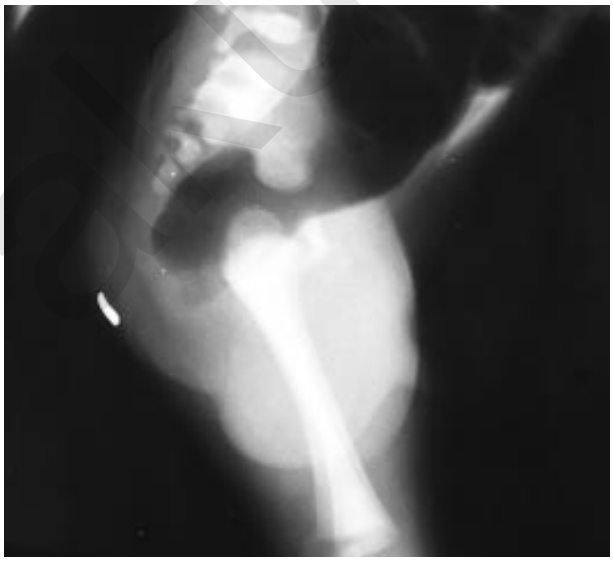

Figure 2.69. Lateral radiograph of the same infant as in Figure 2.68 shows the marker placed over the imperforate anus superficially with the air column demonstrating a "low" obstruction, as the air column is distal to the anatomic position of the puborectalis muscle. This technique may not demonstrate a fistulous tract. (Singleton, E., Wagner, M.)

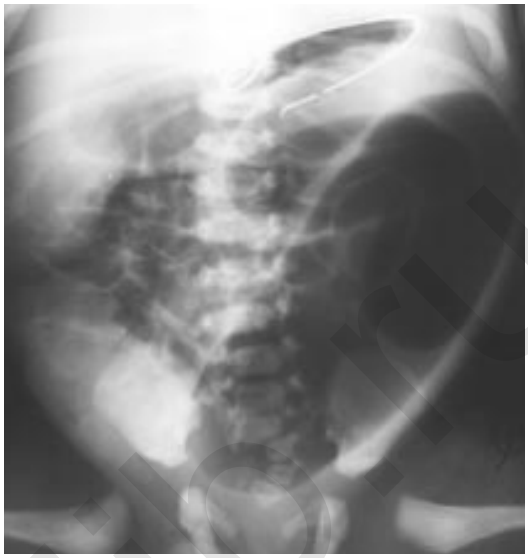

2.70

Figure 2.70. Imperforate anus with a large left obstructed colon. Note the anomalies of the lumbosacral spine. The spinal column should be checked in any infant with anal atresia.

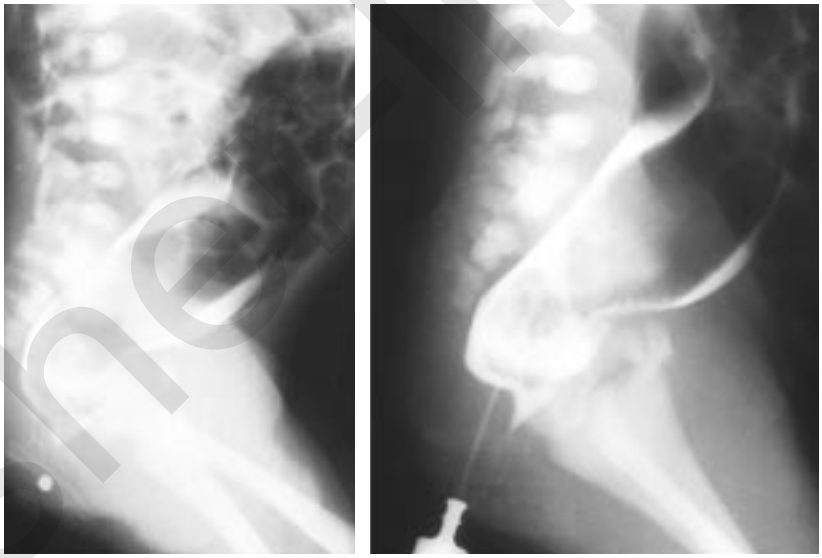

2.71

Figure 2.71. Contrast radiograph of an infant with an imperforate anus. The fistulous tract may be visualized under fluoroscopy. The technique is to inject a small amount of contrast medium (using the anal dimple as a marker) into the distal rectum from the skin. (Singleton, E., Wagner, M.)

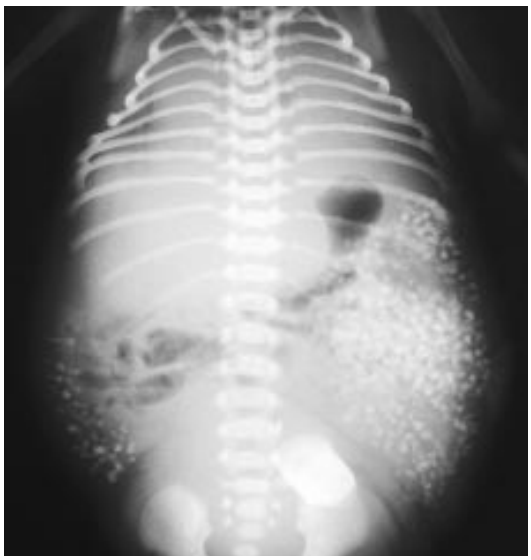

2.72

Figure 2.72. Radiograph of a male infant with an imperforate anus and a rectovesical fistula. Note the calcifications in the abdomen. Urine passage into the colon results in the typical "popcorn" calcifications which are contained in the colon. This differs from the extraluminal calcification seen in patients with meconium peritonitis. Also note the opacity in the left lower abdomen which is the umbilical cord being visualized on an opaque background.

2.73

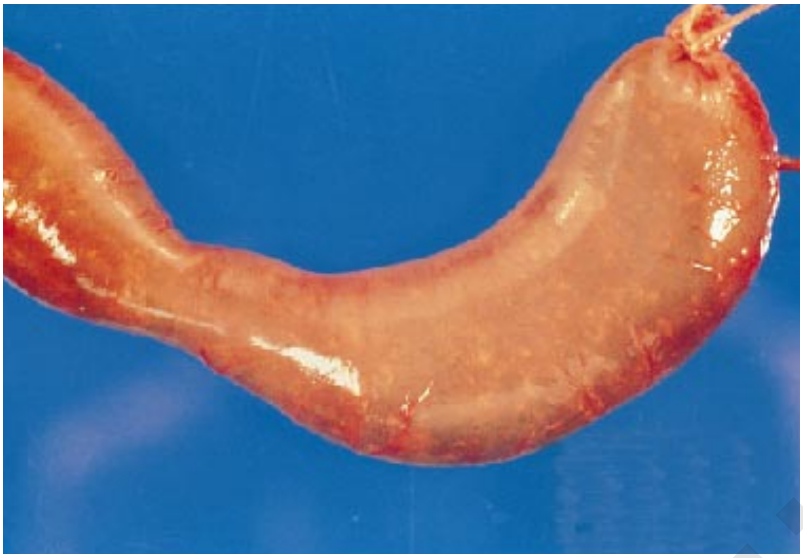

Figure 2.73. Autopsy specimen of the colon in an infant who had anal atresia with a rectovesical fistula. Note the colonic contents showing calcified meconium due to the anomalous communication between the bowel and genitourinary tract. This infant had caudal regression syndrome. (Langston, C.)

2.74

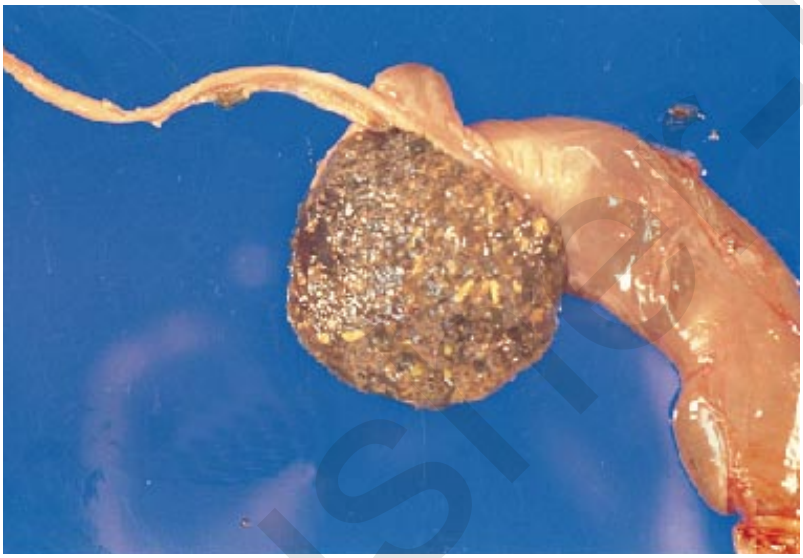

Figure 2.74. Appearance of calcified colonic contents after dissection of the bowel. (Langston, C.)

2.75

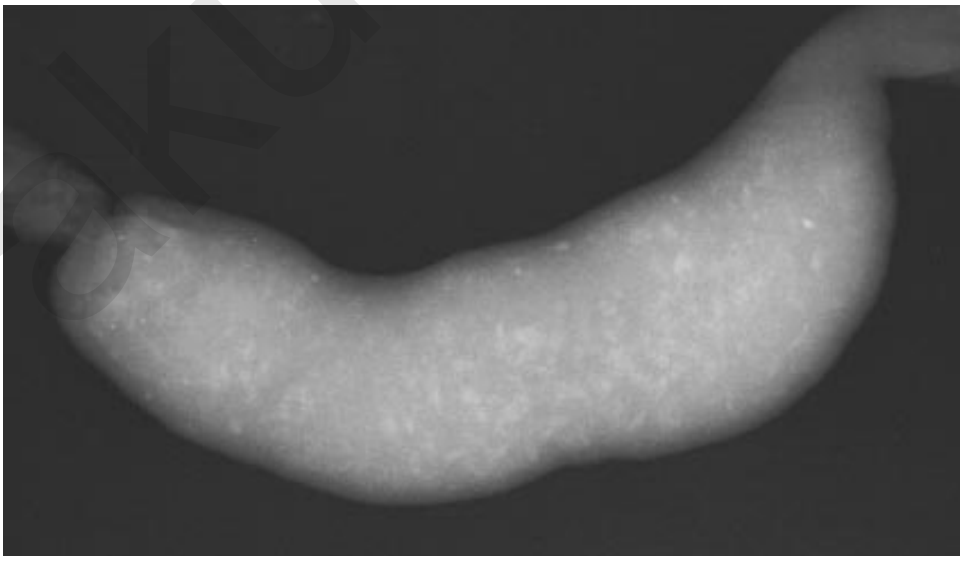

Figure 2.75. Radiograph of the autopsy specimen seen in Figure 2.73, showing the calcified colonic contents ("popcorn" appearance). (Langston, C.)

2.76

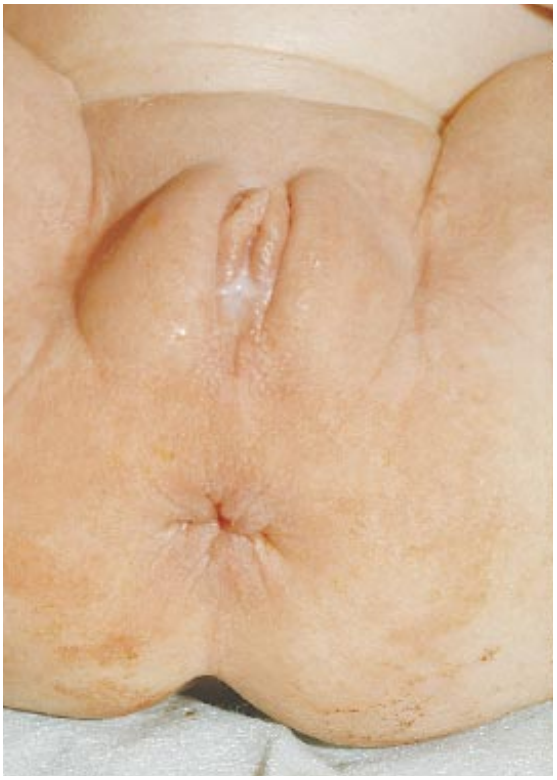

Figure 2.76. This infant presented with a patulous appearance of the anal sphincter. This may denote an abnormality of the innervation to the perineum. On rectal examination an obstruction was detected approximately 1 cm from the anal orifice as the result of an imperforate anal membrane.

2.77

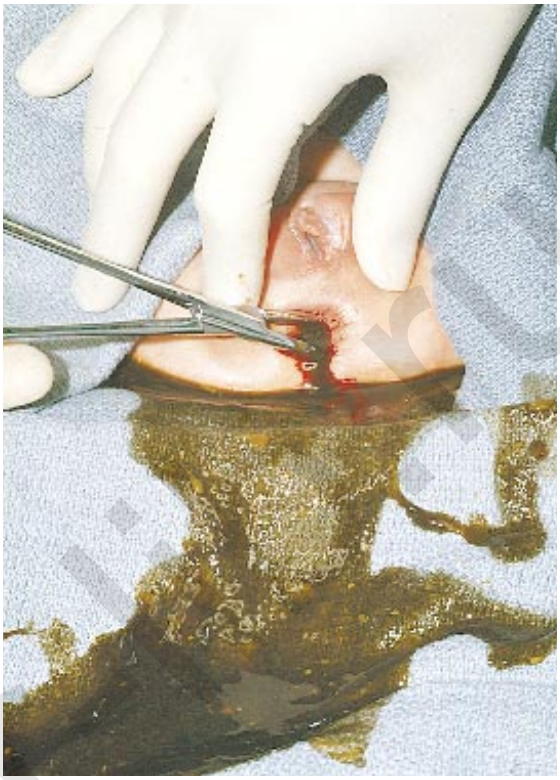

Figure 2.77. Following puncture of the membrane with a hemostat in the same infant as in Figure 2.76, there was rapid passage of meconium with no further problems.

2.78

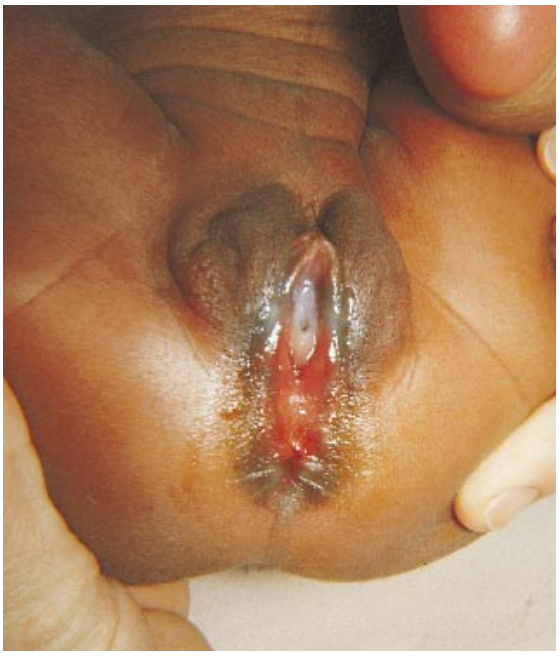

Figure 2.78. Failure of fusion of the perineal raphe involving the rectal sphincter.

2.79

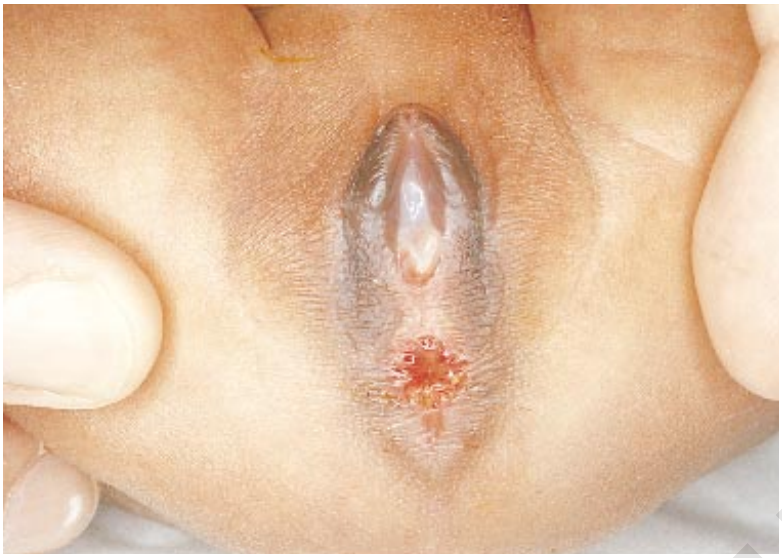

Figure 2.79. Anterior placement of the anus in an infant. This occurs when there is an abnormality of fusion between the urorectal septum and the cloacal membrane. If there is inadequate development of the urorectal septum and if its junction with the cloacal membrane is too far anteriorly, the anus is displaced forward and may open anywhere along the perineum. The anal opening is generally much smaller than normal.

2.80

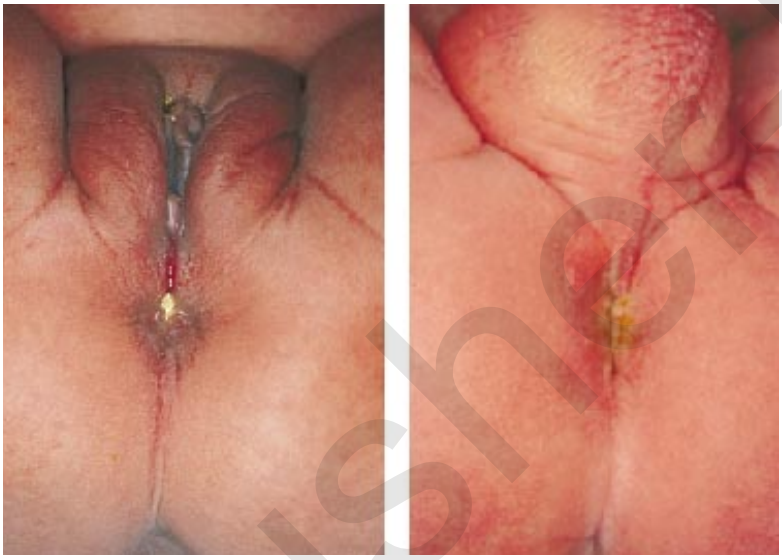

Figure 2.80. Anterior placement of the anus in a female infant on the left and in a male infant on the right. Ectopic anus may rarely be seen in the form of posterior displacement of the anus producing an abnormally long perineum.

2.81

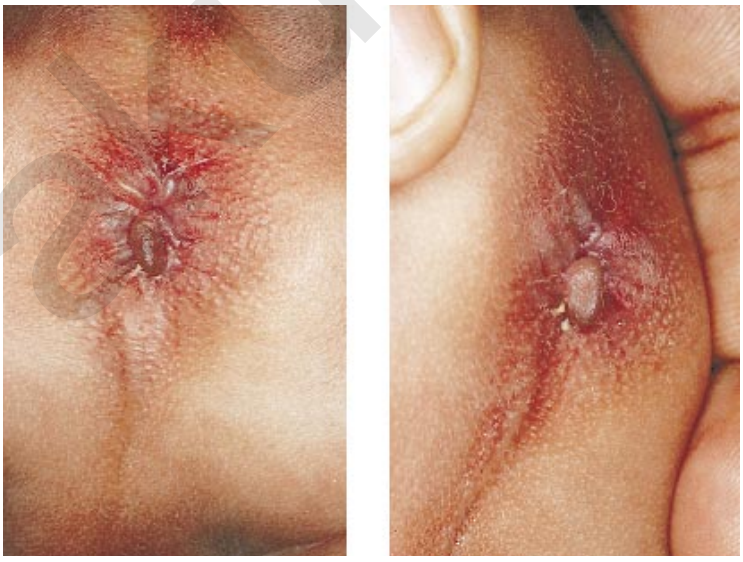

Figure 2.81. Anal skin tags are small outgrowths of the mucosa arising from the anal margin. They are relatively common and have no pathologic significance.

2.82

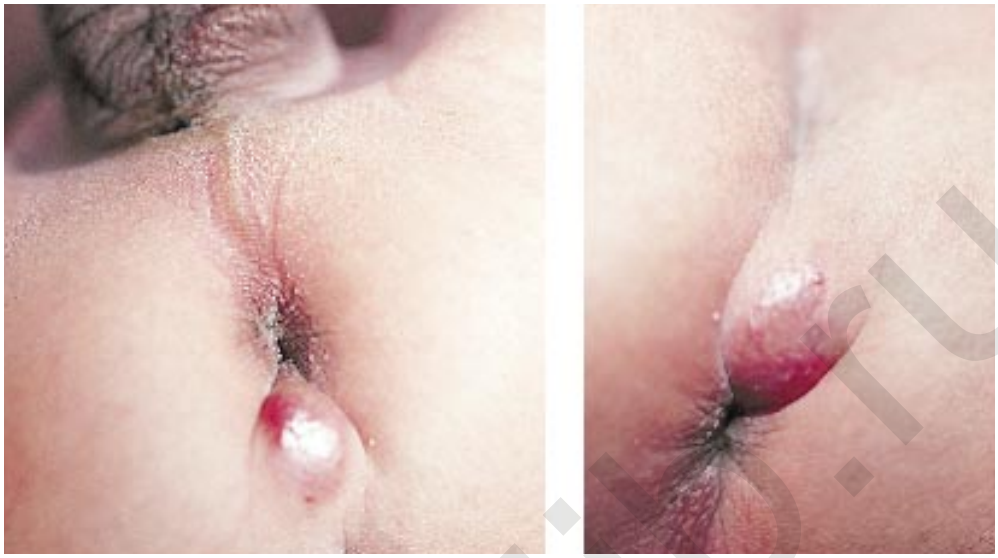

Figure 2.82. Perianal abscess in a neonate at 10 days of age. The etiology was undetermined but it healed rapidly following drainage.

2.83

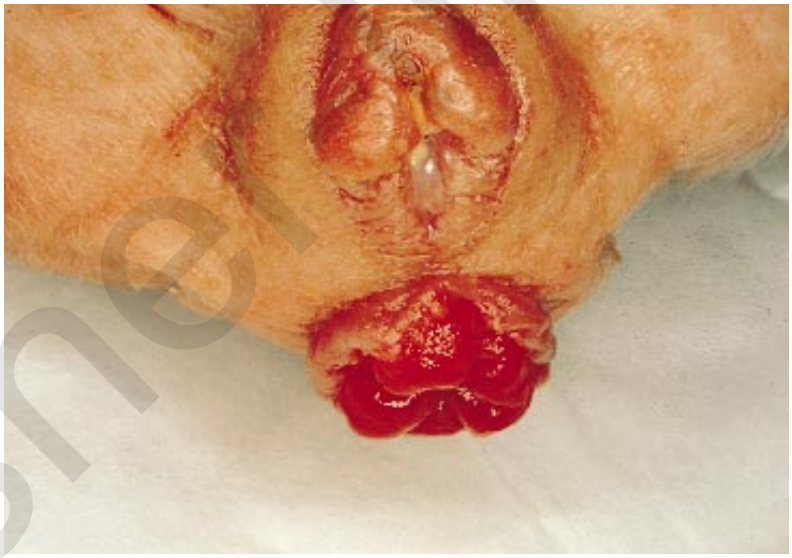

Figure 2.83. Coincidental rectal prolapse in a severely growth-retarded infant with leprechaunism. Rectal prolapse is very rare in a neonate, but if it occurs in the first few months of life a diagnosis of cystic fibrosis should be excluded. It may be seen in association with anomalies such as bladder exstrophy or any other condition causing raised intra-abdominal pressure and usually improves spontaneously.

2.84

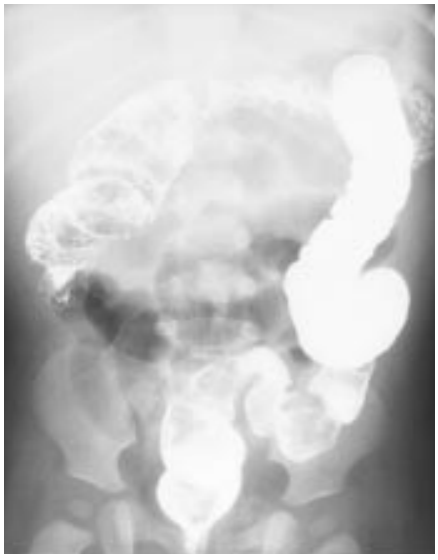

Figure 2.84. Barium enema in an infant with malrotation and volvulus. Note the anterior placement of the descending colon with failure to fill the ascending colon as a result of the volvulus.

2.85

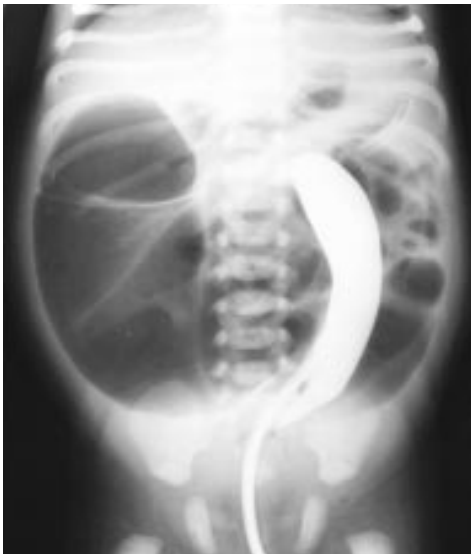

Figure 2.85. Contrast radiograph of an infant with a sigmoid volvulus. Note the failure of passage of barium into the descending and transverse colon with proximal dilated air-filled loops. It occurs as a result of a mesenteric abnormality in which the bowel is not attached to the posterior abdominal wall except at the duodenum and proximal colon. Consequently, the bowel may twist on itself resulting in obstruction and possible gangrene. (Singleton, E., Wagner, M.)

2.86

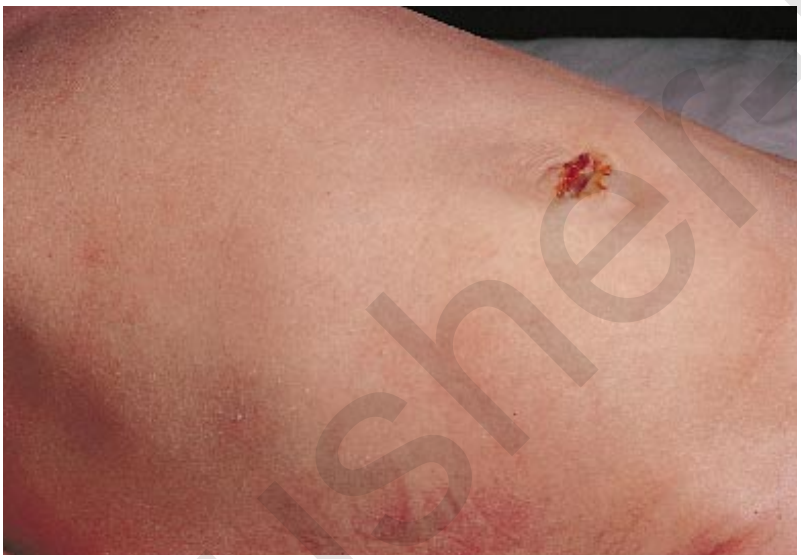

Figure 2.86. This infant presented at the age of 6 days with jaundice and vomiting. Clinically, note the mass in the right upper quadrant. At surgery a diagnosis of duodenal duplication was made.

2.87

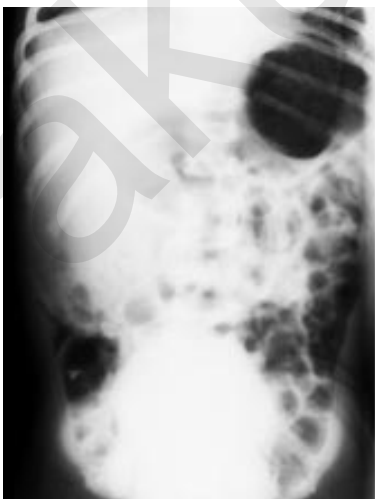

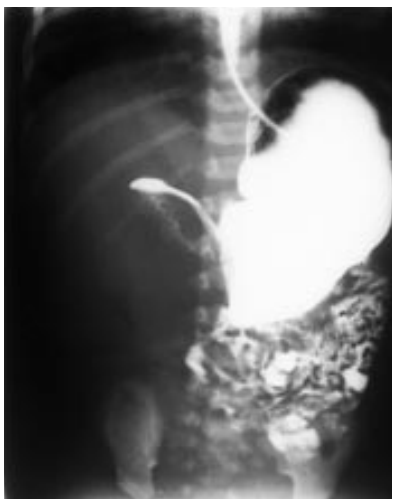

Figure 2.87. Radiographs from the same infant as in Figure 2.86. The flat film on the left shows displacement of the bowel gas to the left. The barium contrast study shows that there is upper displacement of the gastric antrum and duodenal bulb by a large mass. Differential diagnosis includes duodenal duplication and choledochal cyst which displaces the gastric antrum and duodenal bulb downward and medially. On plain radiographs, duplications within the abdomen often appear as soft tissue masses displacing the adjacent bowel. They are more commonly cystic rather than solid masses. (Singleton, E., Wagner, M.)

2.88

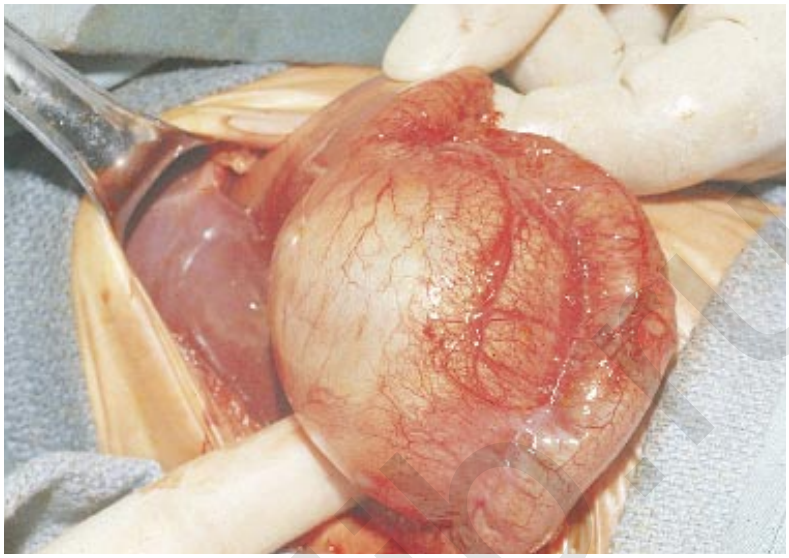

Figure 2.88. Duplication of the duodenum at surgery of the same infant as in Figure 2.87. The duodenum per se is not visible, and note the colon on the left. Duplications of foregut derivation may have associated skeletal malformations (thoracic and cervical vertebrae). With duplications of midgut and hindgut derivation, there are often associated anomalies of the gastrointestinal and genitourinary tracts but *no* skeletal abnormalities.

2.89

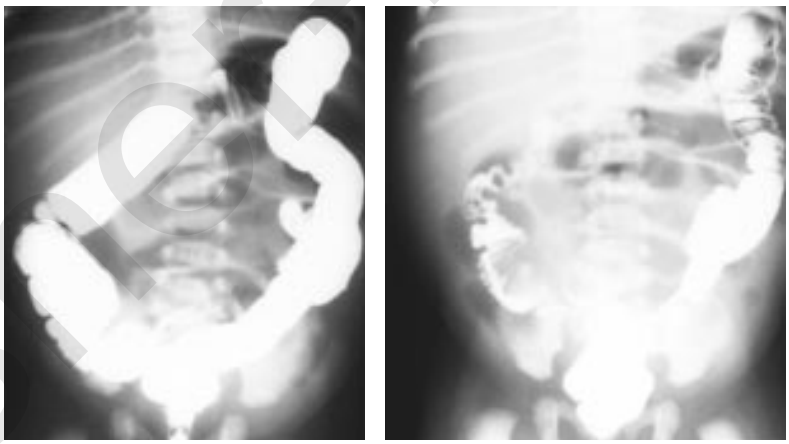

Figure 2.89. This infant presented with vomiting at the age of 5 days. Radiographs with contrast medium demonstrate the duplication of the ileum. Duplications may accumulate secretions in the closed lumen. This leads to distention and consequent obstruction of the normal neighboring bowel. Occasionally the torsion produced by the weight of the duplication leads to small bowel volvulus. (Singleton, E., Wagner, M.)

2.90

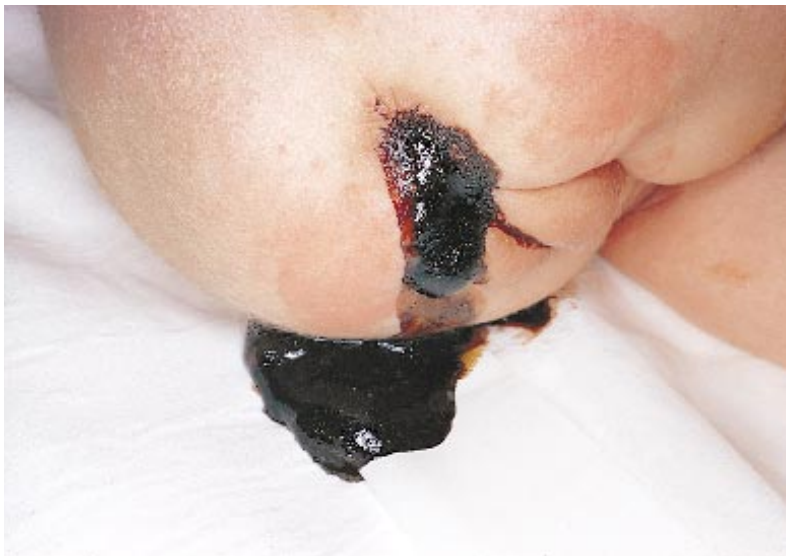

Figure 2.90. This infant presented with melena at the age of 3 days. Differential diagnosis includes ingested maternal blood, hemorrhagic disease of the newborn, infection with colitis (e.g., salmonella, shigella), necrotizing enterocolitis, and Meckel's diverticulum. Intussusception is very rare in the neonate.

2.91

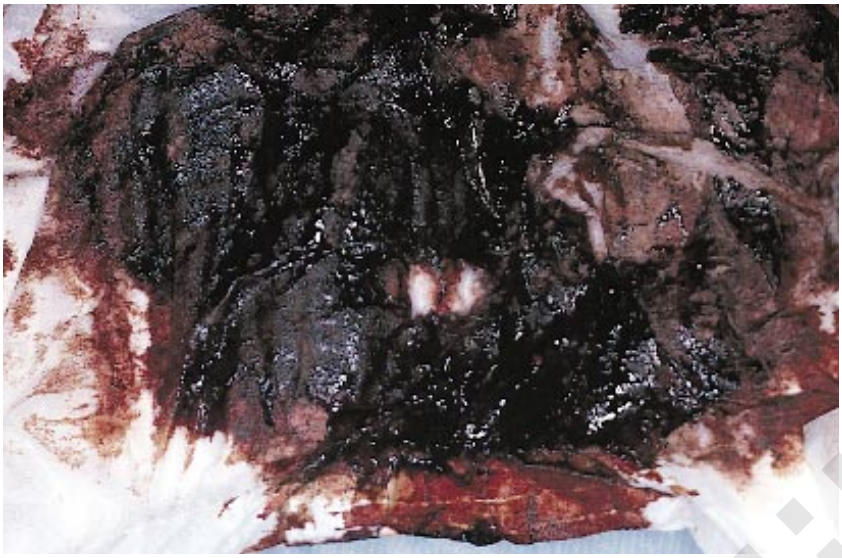

Figure 2.91. Melena neonatorum occurred in this infant at 24 hours of age. The most common cause of melena neonatorum is ingested maternal blood, and the diagnosis can be confirmed by the Apt test.

2.92

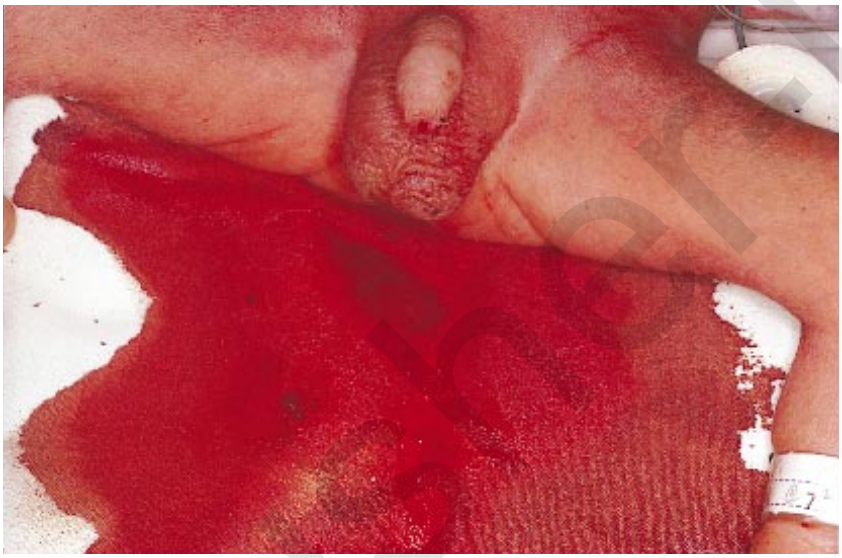

Figure 2.92. Bloody stools in an infant at the age of 3 days showing the gross bleeding from the rectum and the urethra. The etiology in this infant was hemorrhagic disease of the newborn. A vitamin K injection was not given at birth, and the infant developed hypoprothrombinemia.

2.93

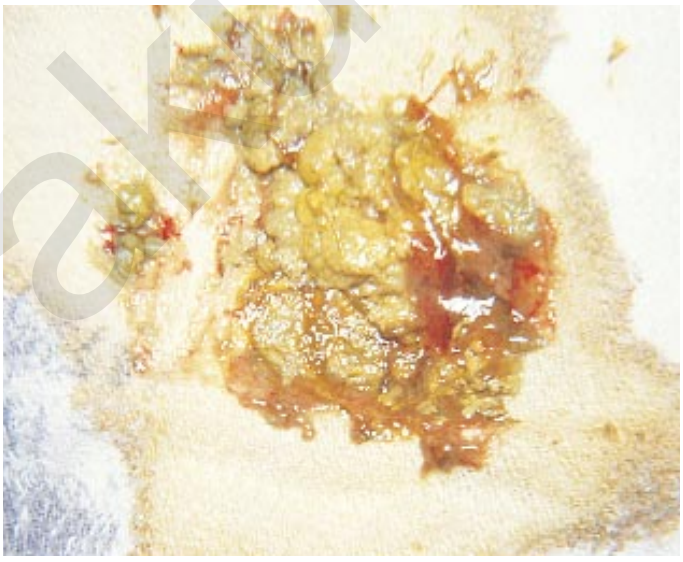

Figure 2.93. Bloody stools in this otherwise normal infant at the age of 48 hours were not caused by ingested maternal blood. Differential diagnosis includes infection, necrotizing enterocolitis, and anal fissure. Etiology was not determined and the infant did well.

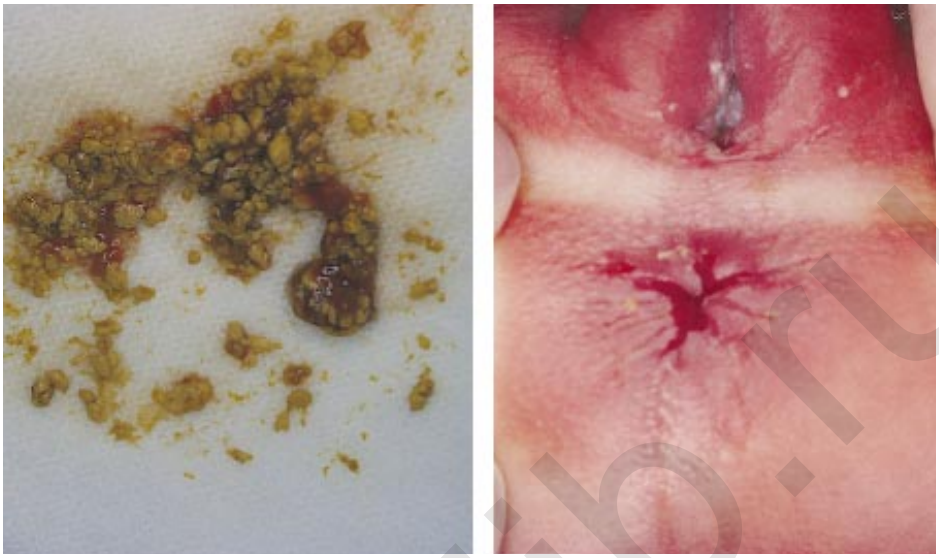

2.94

Figure 2.94. This premature infant with no symptoms at 3 weeks presented with blood in the stool. Note that the blood is not mixed in the stool. Inspection of the anal mucosa revealed fissures which caused the presence of blood in the stool. The most common cause of blood in the stool in the neonate is ingested maternal blood; the next most common cause is an anal fissure.

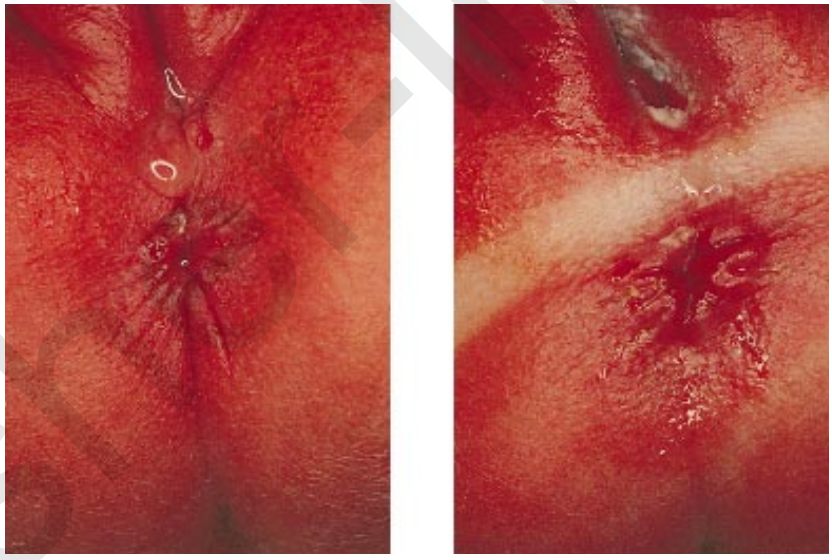

2.95

Figure 2.95. Normal appearance of the anus of a premature infant with bloody stools. As noted in the figure on the right, it is extremely important to spread the buttocks to permit careful inspection of the anus. Multiple fissures are noted in this same infant.

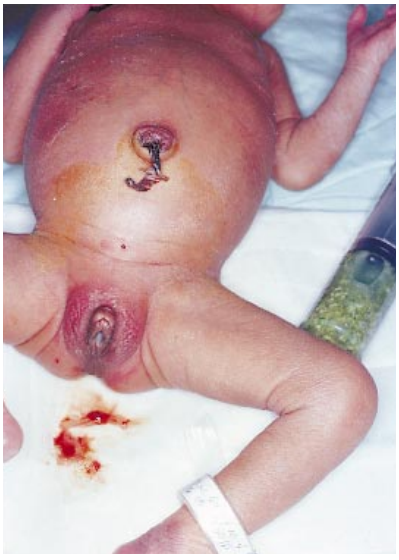

2.96

Figure 2.96. Bloody stools in an infant with necrotizing enterocolitis. Note the marked abdominal distention and the bile-stained gastric drainage.

2.97

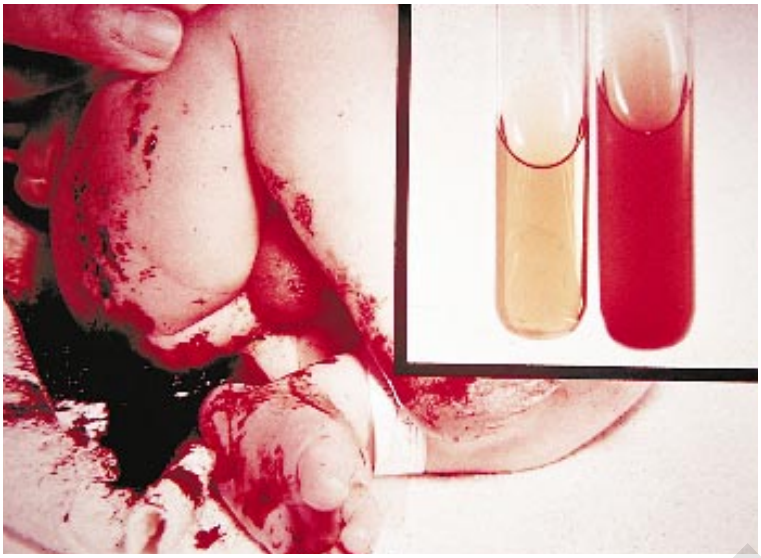

Figure 2.97. The Apt test diagnoses melena neonatorum caused by ingested maternal blood (see inset). Fetal hemoglobin in the presence of alkali remains pink and is not denatured. Adult hemoglobin in the presence of alkali denatures and changes to a yellow-brown color. Note the inset with adult hemoglobin on the left and fetal hemoglobin on the right.

2.98

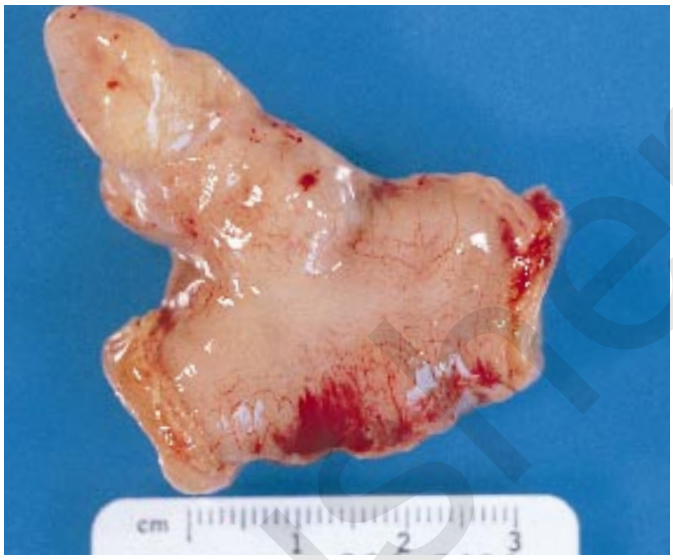

Figure 2.98. Surgical removal of a Meckel's diverticulum in an infant that presented with bloody stools. Meckel's diverticulum is rarely symptomatic in the neonate. It occurs when the proximal part of the mesenteric duct fails to obliterate. The diverticulum usually arises from the ileum and occurs in 1 to 2% of the population. Of these patients, 1 to 2% may be symptomatic in that there may be hemorrhage or perforation. Ectopic gastric mucosa is commonly present in the diverticulum and, hence, technetium studies may be used in making the diagnosis. (Langston, C.)

2.99

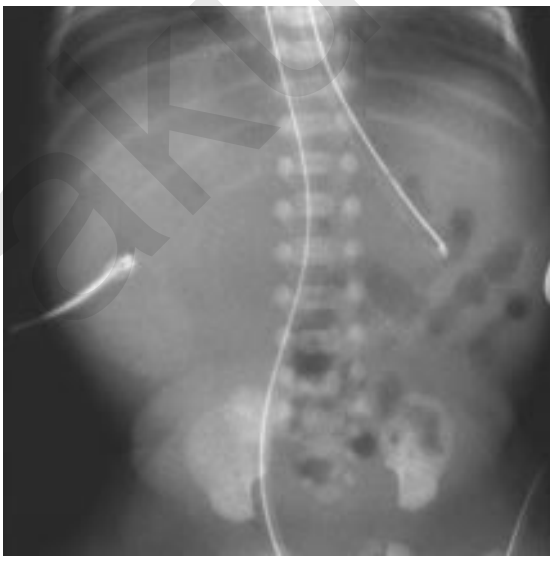

Figure 2.99. Radiograph of an infant with early signs of necrotizing enterocolitis. Clinically these include abdominal distention and blood in stool which may initially be microscopic. Radiographically there is paucity of bowel gas and separation of loops of bowel due to edema of the bowel wall. Late clinical signs include vomiting, ileus, and abdominal tenderness.

2.100

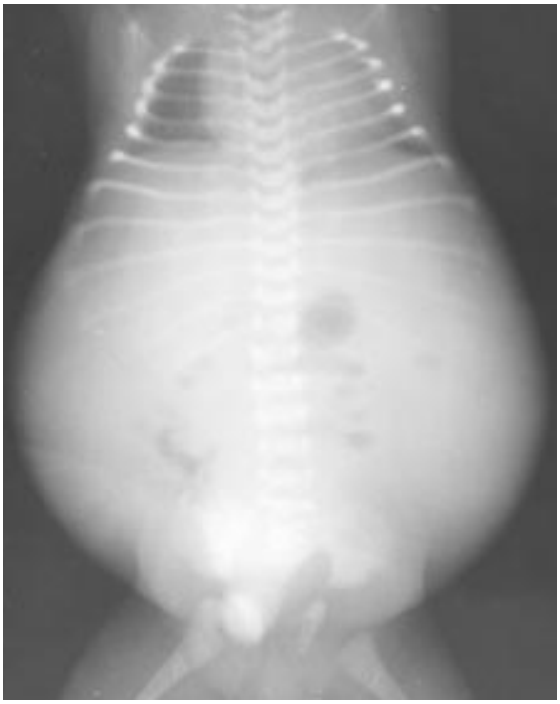

Figure 2.100. Radiograph of another infant with necrotizing enterocolitis. Note the subserosal and submucosal accumulation of gas (pneumatosis cystoides intestinalis) with associated portal gas. The gas in the wall of the intestine is mainly hydrogen and this most commonly reabsorbs without bowel perforation.

2.101

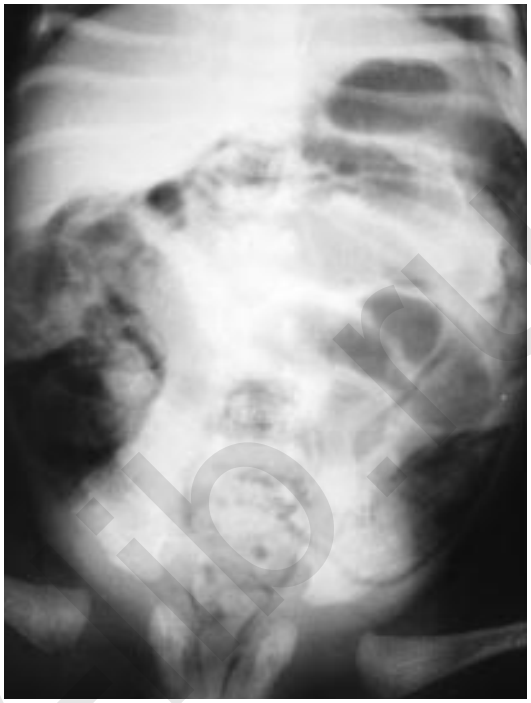

Figure 2.101. Severe pneumatosis cystoides intestinalis in an infant with necrotizing enterocolitis. Note that this clearly shows the subserosal air. (Singleton, E., Wagner, M.)

2.102

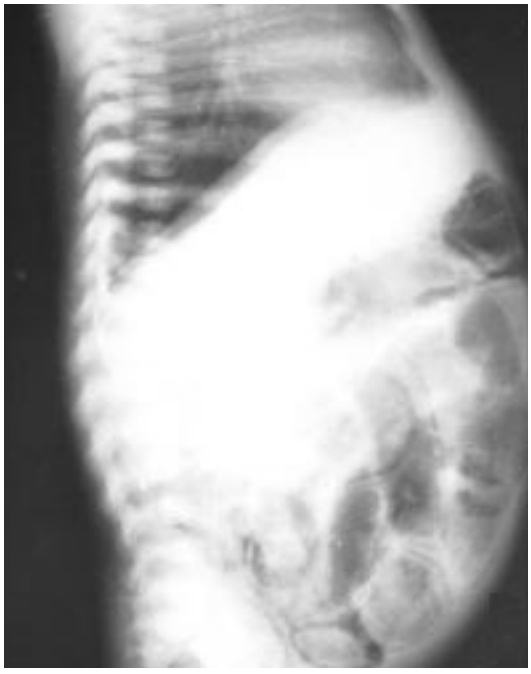

Figure 2.102. Lateral radiograph of the same infant as in Figure 2.101 with subserosal pneumatosis cystoides intestinalis in necrotizing enterocolitis. (Singleton, E., Wagner, M.)

2.103

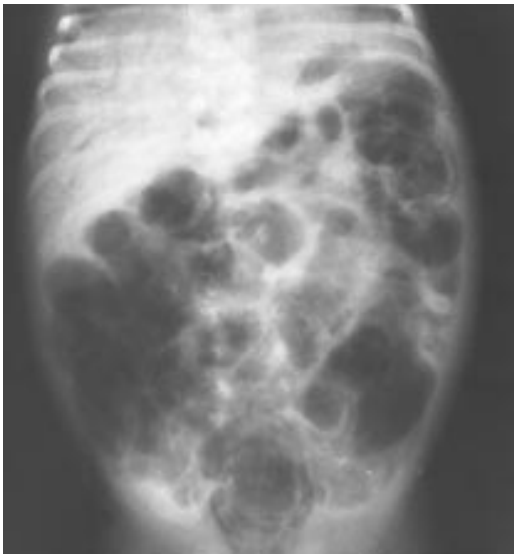

Figure 2.103. Radiograph of an infant with necrotizing enterocolitis. Gas is seen in the portal venous system. This occurs in more severe cases but often resolves spontaneously. In addition note the subserosal pneumatosis cystoides intestinalis.

2.104

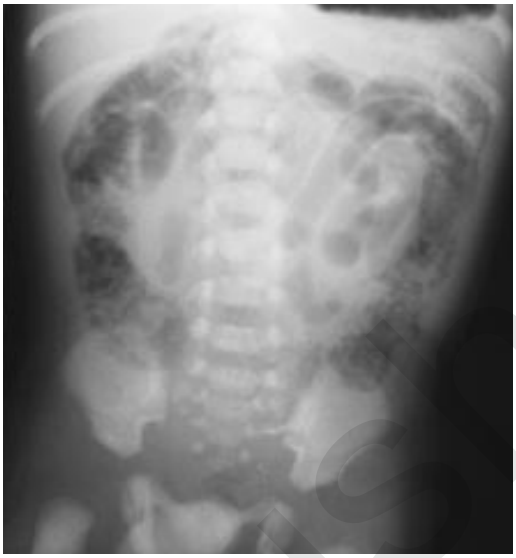

Figure 2.104. Upright abdominal radiograph of an infant with necrotizing enterocolitis. Note both the submucosal and subserosal pneumatosis cystoides intestinalis in the bowel. Submucosal pneumatosis characteristically gives the appearance of little bubbles as demonstrated in this figure, especially in both lower quadrants. Subserosal pneumatosis presents as linear areas in the wall of the bowel.

2.105

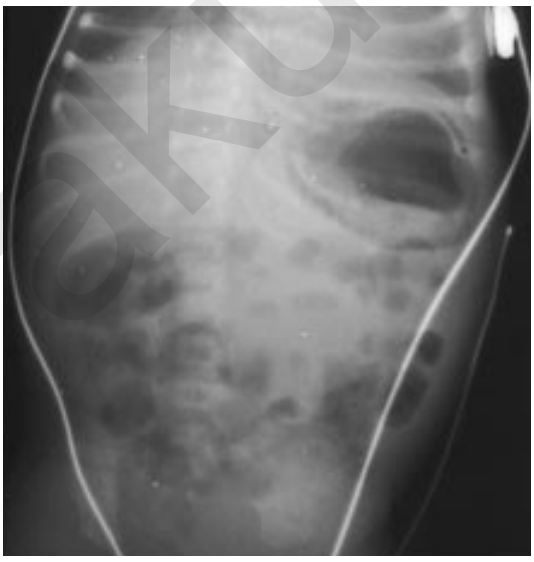

Figure 2.105. Abdominal radiograph of an infant with necrotizing enterocolitis showing gastric pneumatosis. This is not as common as pneumatosis cystoides intestinalis.

2.106

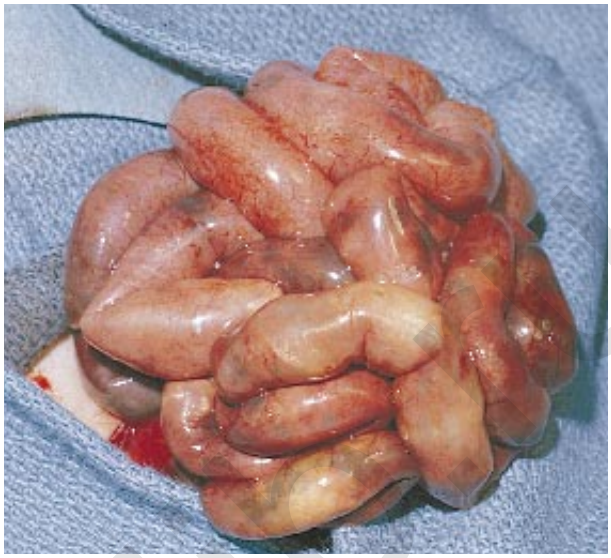

Figure 2.106. Surgical appearance of the bowel of an infant with necrotizing enterocolitis. There is discoloration of the bowel wall as a result of impairment of the vascular supply. Note the subserosal cysts which correlate with the pneumatosis cystoides intestinalis seen in radiographs.

2.107

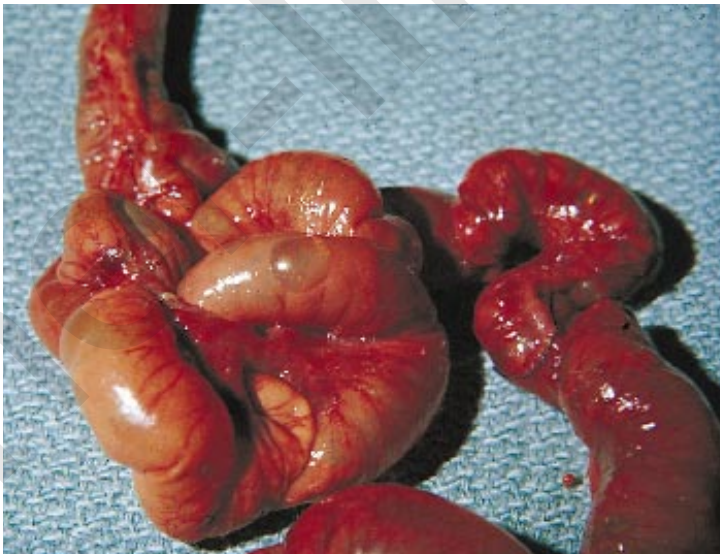

Figure 2.107. Another example of the surgical appearance of the bowel showing the subserosal cysts in an infant with necrotizing enterocolitis.

2.108

Figure 2.108. Pathologic specimen of the small bowel of an infant who had necrotizing enterocolitis. Note the submucosal blebs with a scattered distribution.

2.109

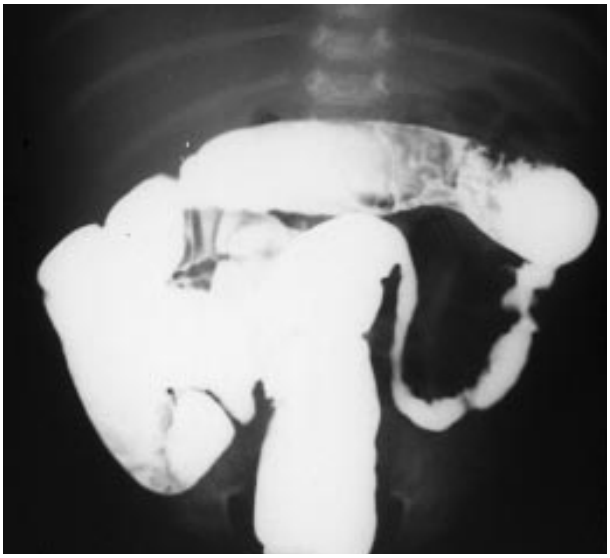

Figure 2.109. A contrast enema in an infant who had recovered from necrotizing enterocolitis. Note the stricture formation in the descending colon with proximal bowel dilatation. This has been reported to occur in about 20% of infants who recover from necrotizing enterocolitis, but the majority of these infants do not develop obstruction. The strictures may occur in the large or small bowel.

2.110

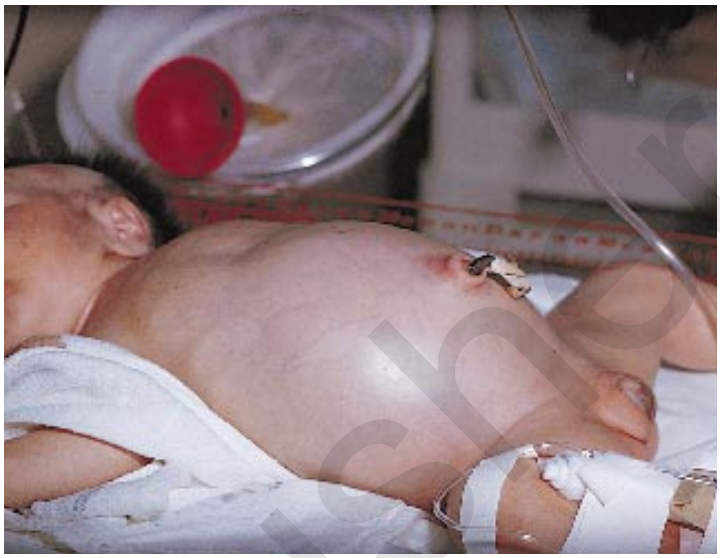

Figure 2.110. Following perforation of the bowel and resulting peritonitis, this infant developed marked abdominal distention and edema of the abdominal wall. This may occur in an infant with a perforated viscus or in low birthweight infants with necrotizing enterocolitis.

2.111

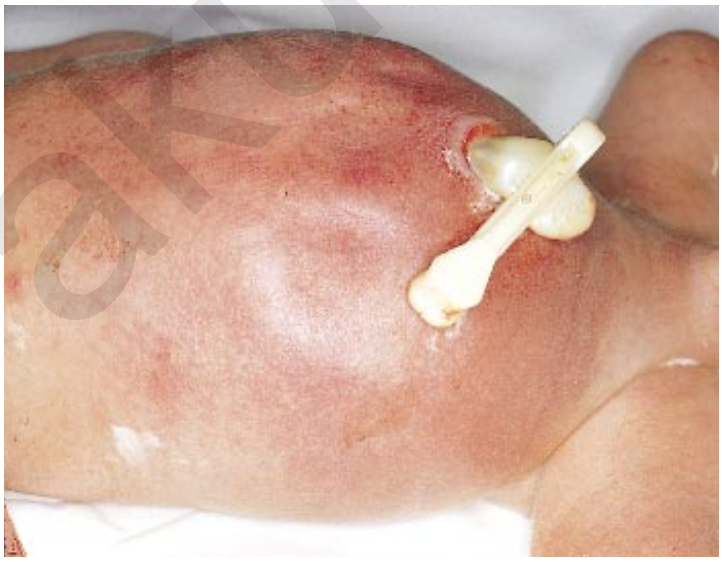

Figure 2.111. Cellulitis and edema of the abdominal wall in an infant with peritonitis which developed after perforation of the ileum.

2.112

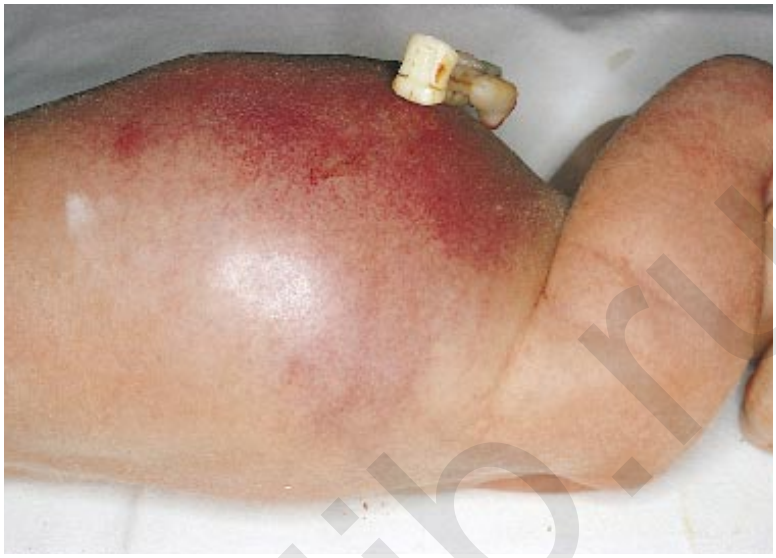

Figure 2.112. Lateral view of the abdomen in the same infant as in Figure 2.111, demonstrating the marked abdominal distention and cellulitis.

2.113

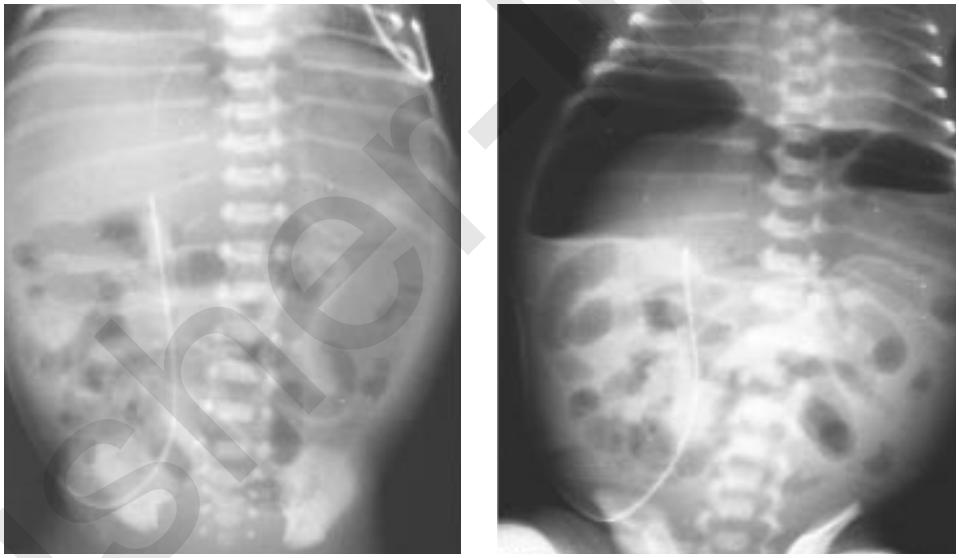

Figure 2.113. Abdominal radiographs of an infant with bowel perforation. In the flat plate film on the left, note the decreased density especially over the liver due to the presence of free air (free air floats to the top). The diagnosis may be easily missed on this film. In the upright plate on the right, the pneumoperitoneum, with subdiaphragmatic air and air/fluid level, is easily appreciated. (Singleton, E., Wagner, M.)

2.114

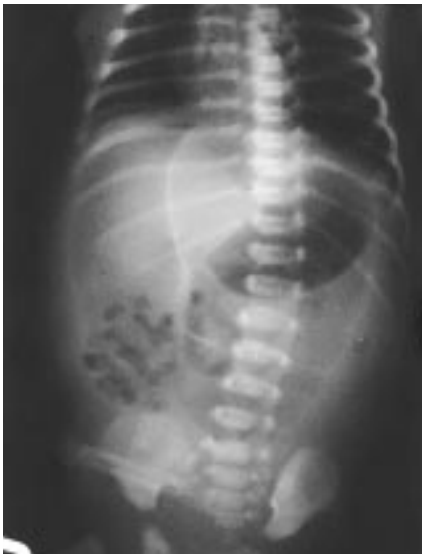

Figure 2.114. Pneumoperitoneum in an infant with perforation of the colon. Note the large central translucent collection of air referred to as the "football sign" with sharp demarcation of the falciform ligament.

2.115

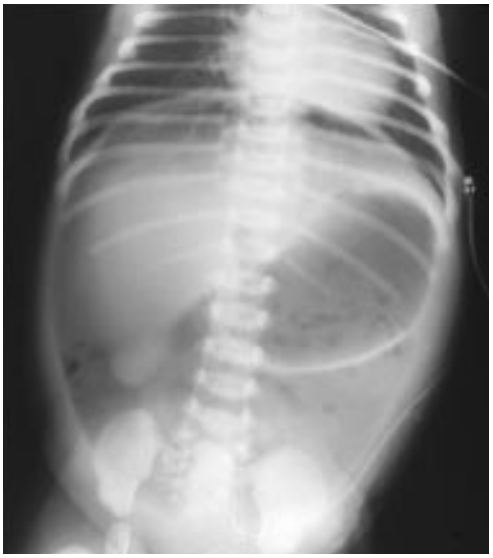

Figure 2.115. Flat abdominal radiograph in an infant with perforation of the colon, showing the marked pneumoperitoneum. The liver and gallbladder are well outlined in this film, and the subdiaphragmatic air is apparent. The diagnosis of free air is apparent on the flat plate film but is more dramatic in the upright film.

2.116

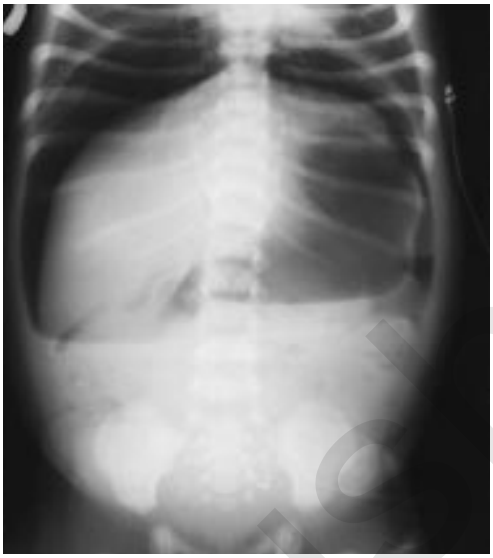

Figure 2.116. Upright abdominal radiograph of the same infant as in Figure 2.115. Note the subdiaphragmatic air and presence of air/fluid levels.

2.117

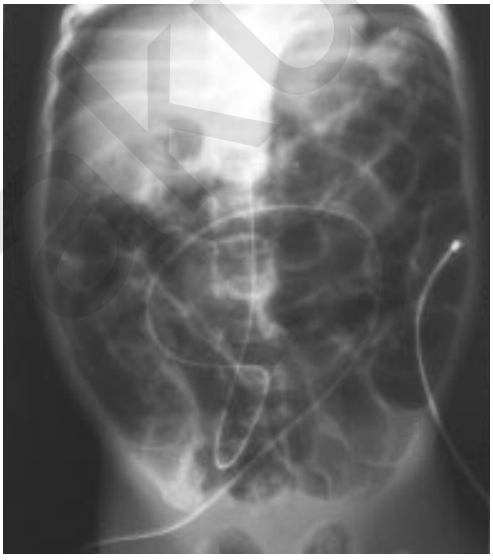

Figure 2.117. Abdominal radiograph of an infant with pneumoperitoneum due to perforation of the bowel. Note the subdiaphragmatic air, and in this infant the free air has also tracked down into the scrotum.

2.118

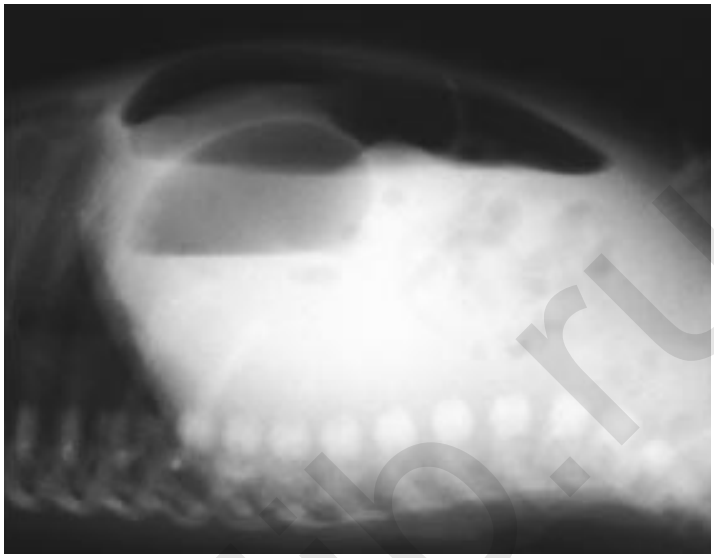

Figure 2.118. Cross-table lateral radiograph of an infant with pneumoperitoneum. This view may be of value in making the diagnosis when other radiographs are inconclusive. Note the lucent area below the abdominal wall superior to the gastric air bubble and bowel gas pattern.

2.119

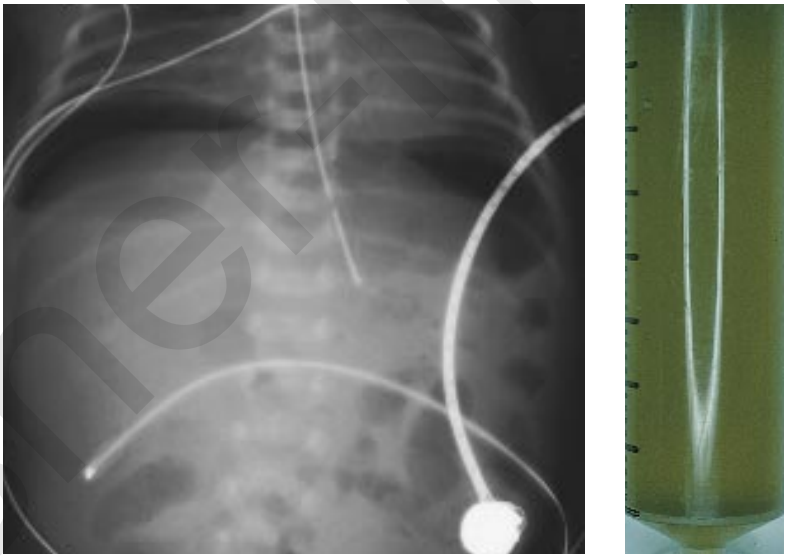

Figure 2.119. Abdominal radiograph of another infant with pneumoperitoneum. Note the subdiaphragmatic collection of free air. Photograph on the right shows the green urine voided by this infant. This association has been reported in cases of bowel perforation.

2.120

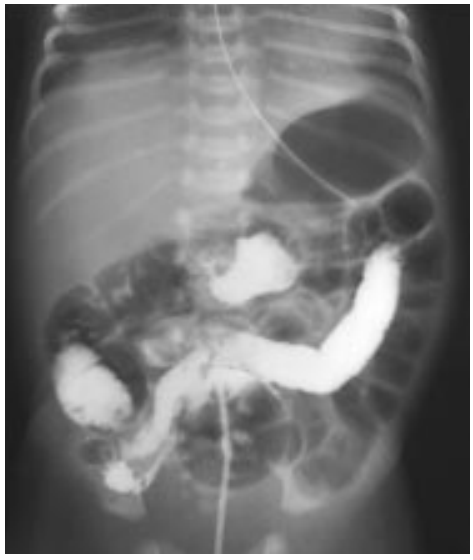

Figure 2.120. This infant presented with abdominal distention. A physician in a small community hospital performed a contrast enema which he accomplished by instilling barium into the rectum using a balloon catheter. This caused an iatrogenic perforation of the rectum with spillage of barium into the peritoneal cavity, resulting in barium peritonitis. Note the radiographic shadow of the catheter and balloon in the rectum.

2.121

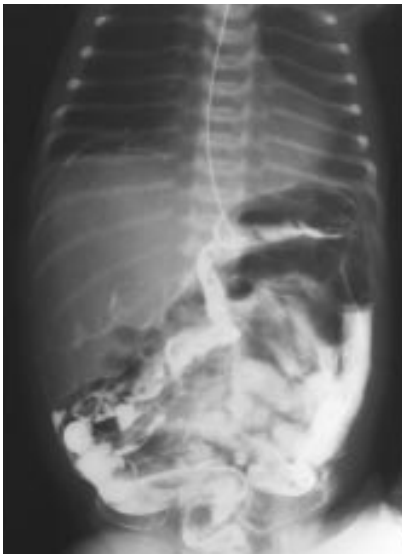

Figure 2.121. A follow-up contrast radiograph of the same infant as in Figure 2.120, demonstrating the extraluminal barium, particularly in the area of the liver and subdiaphragmatically. The technique of instilling barium with a ballon catheter is inappropriate; however, the infant did well following surgery.

2.122

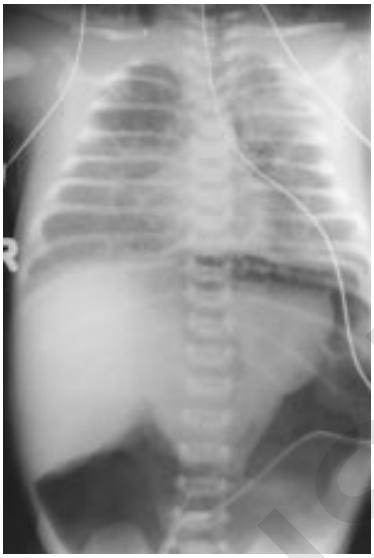

Figure 2.122. Radiograph of an infant with pulmonary interstitial emphysema, pneumomediastinum, and pneumoperitoneum. Air can track down from the respiratory system to the peritoneum without the perforation of an abdominal viscus. The pneumoperitoneum present in this infant is not the result of perforation. In pneumoperitoneum due to tracking down of air there are *no* air/fluid levels, whereas if it is associated with bowel perforation, air/fluid levels are present. If gas is present in the thorax with a pneumoperitoneum, surgery may not be indicated.

1.123

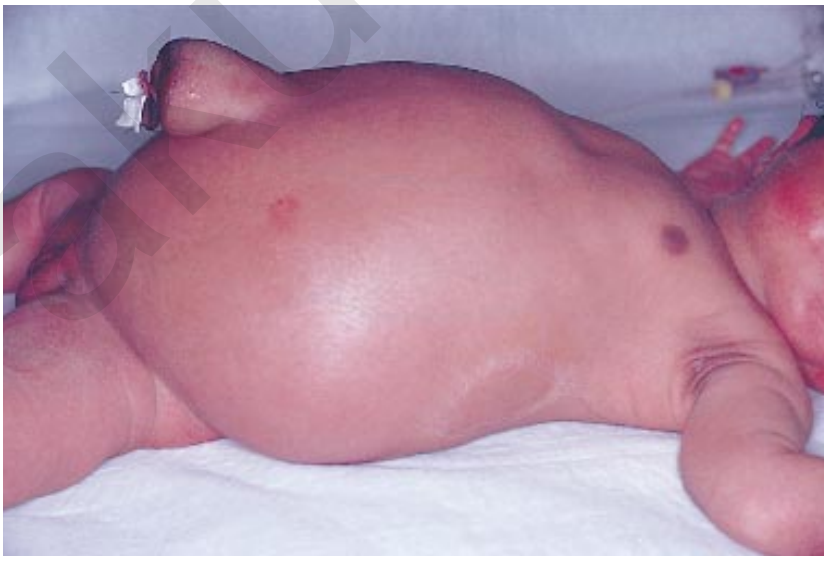

Figure 2.123. Marked abdominal distention present at birth in an infant with chylous ascites. Ascites may be caused by many conditions such as chylous ascites, urinary ascites, biliary ascites, hydrops fetalis, and infection.

2.124

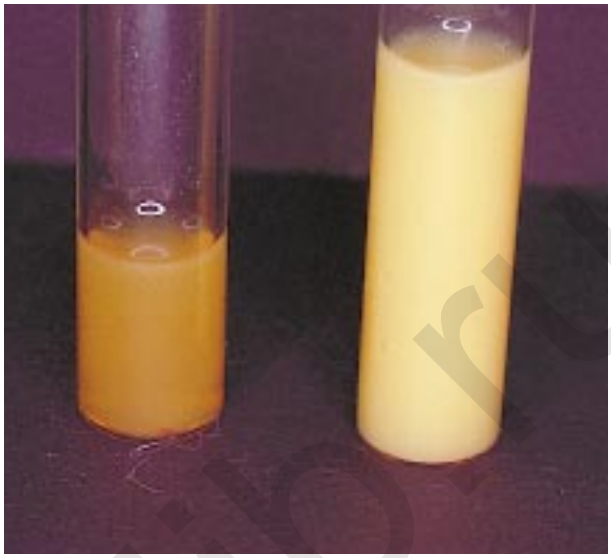

Figure 2.124. Ascitic fluid obtained before (left) and after (right) feedings. The change from a straw-colored fluid to a milky-white opaque fluid after feeds is consistent with a diagnosis of chylous ascites. Today, such an infant would not be placed on regular feedings but would be fed formula containing medium-chain triglycerides and these changes would not occur.

2.125

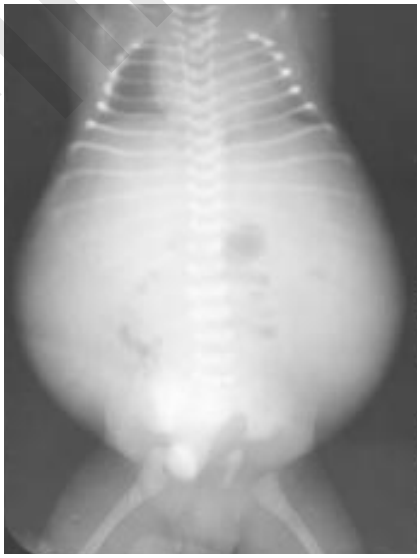

Figure 2.125. Radiograph of an infant with syphilitic ascites. Note the opacification of the abdomen with marked bulging of the flanks and central pooling of bowel gas. The loops of intestine "float" in the middle portion of the abdomen because of the large volume of ascitic fluid. Note the decrease in lung volume as a result of ascites.

2.126

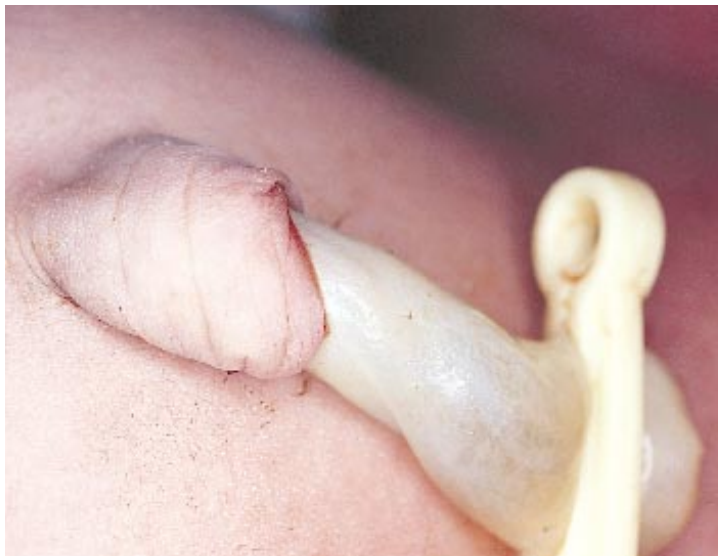

Figure 2.126. Umbilicus cutis or skin navel ("outie") in a normal neonate. Note the tubular projection of the skin up to about 2.5 cm in length. The hard stump is the remnant of the cord covered with skin. Normally the cord is a bluish-white color at birth, or sometimes faintly yellow, especially in postmature infants.

2.127

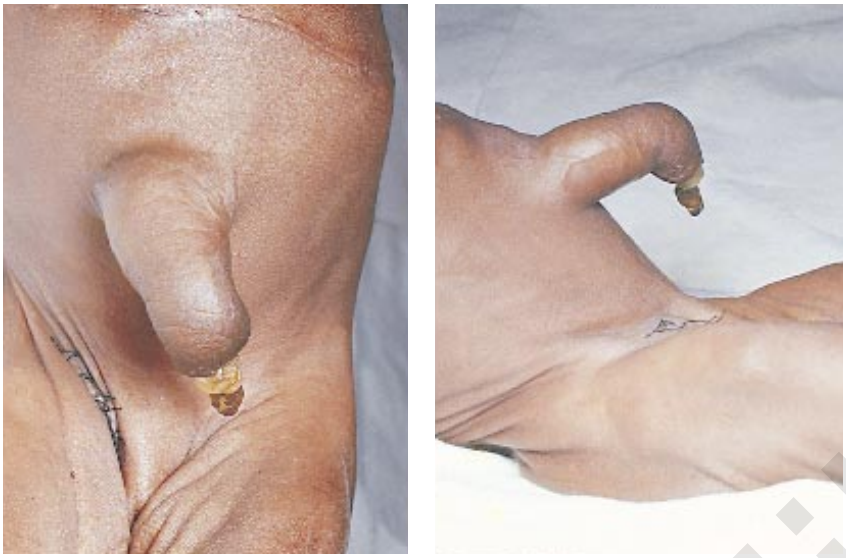

Figure 2.127. Superior and lateral view of umbilicus cutis in another infant. "Outies" or skin navels are more common in black infants. This protrusion is not reducible in contrast to infants with umbilical herniae. Umbilical herniae arise due to separation of the rectus muscles with herniation of the omentum and, on some occasions, bowel. Umbilical herniae resolve spontaneously as the rectus muscles become stronger, usually by the age of 18 months to 2 years.

2.128

Figure 2.128. Umbilicus amnioticus or amniotic navel ("innie") in an infant at the age of 5 days. This is less common. The amniotic portion of the umbilical cord extends to the abdominal wall and this results in a true belly button.

2.129

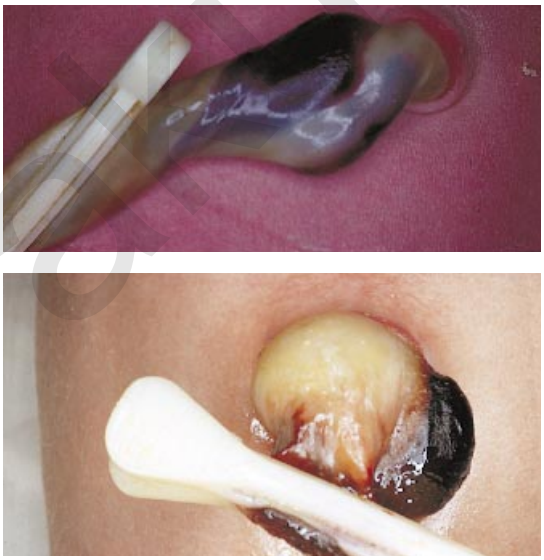

Figure 2.129. Examples of hematoma of the umbilical cord as a result of trauma. These can be a source of significant blood loss if rupture occurs early in the neonatal period.

2.130

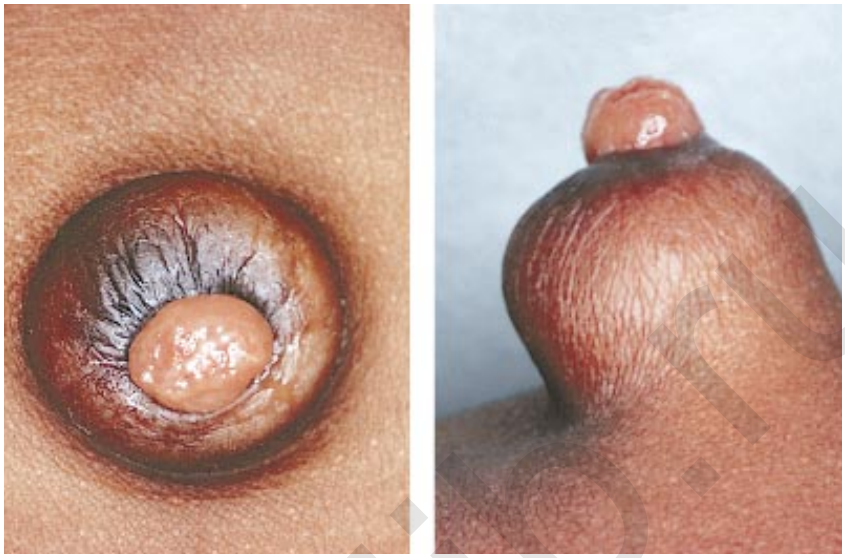

Figure 2.130. Umbilical granuloma in an infant with umbilicus cutis. This results from overgrowth of granulomatous tissue at the umbilicus when the cord separates. These occur more commonly in infants with large, thick umbilical cords. The tissue may be friable and bleeds easily. This can be treated with silver nitrate cauterization. Infants who have discharge or foul odor at the umbilicus may have umbilical granulomas or a patent omphalomesenteric duct (patent vitellointestinal duct).

2.131

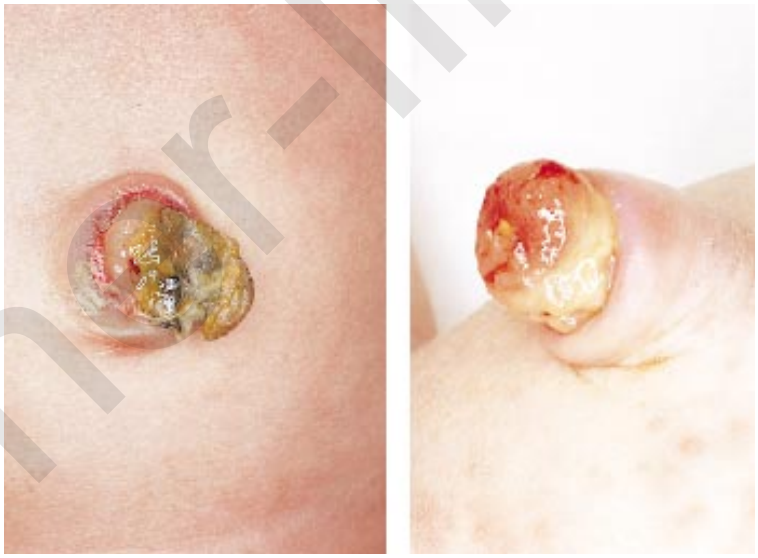

Figure 2.131. Patent omphalomesenteric duct in an infant with stool draining at the umbilicus. During early embryonic life the vitelline duct connects the yolk sac to the primitive bowel. It normally obliterates and atrophies in the course of fetal development. If it persists, it may present as a lumen through which intestinal contents pass from the umbilicus.

2.132

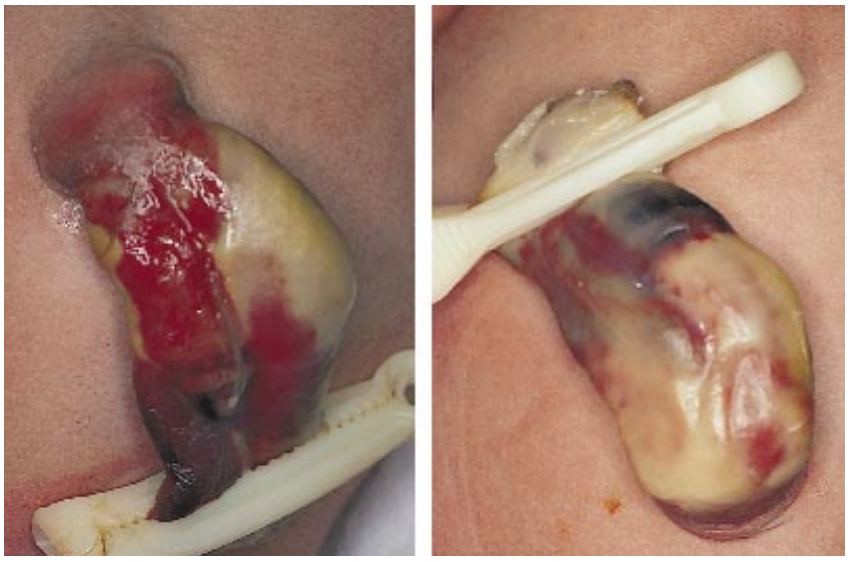

Figure 2.132. This abnormal appearance of an umbilical cord which showed a bright red surface was shown histologically to be a granulomatous omphalomesenteric duct remnant.

2.133

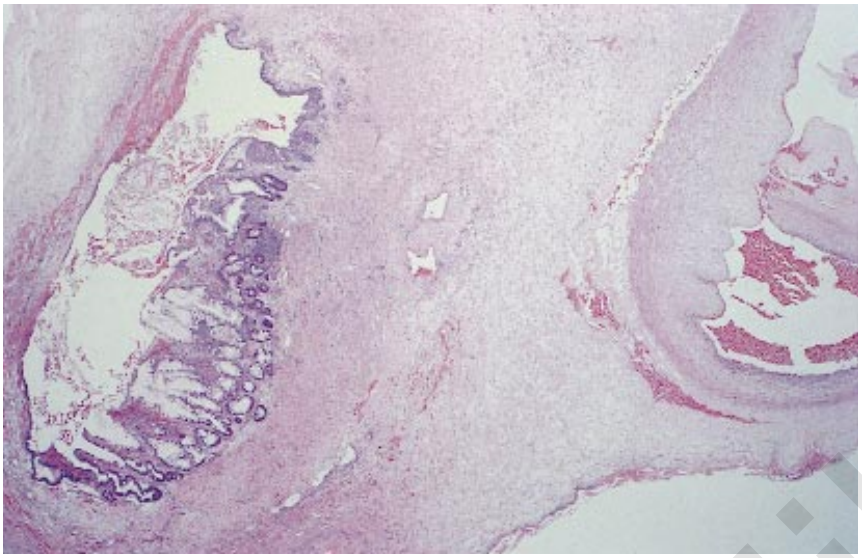

Figure 2.133. Histologic specimen of the same umbilical cord as in Figure 2.132 showing the omphalomesenteric duct remnant. Note the presence of columnar epithelium as seen elsewhere in the intestinal wall.

2.134

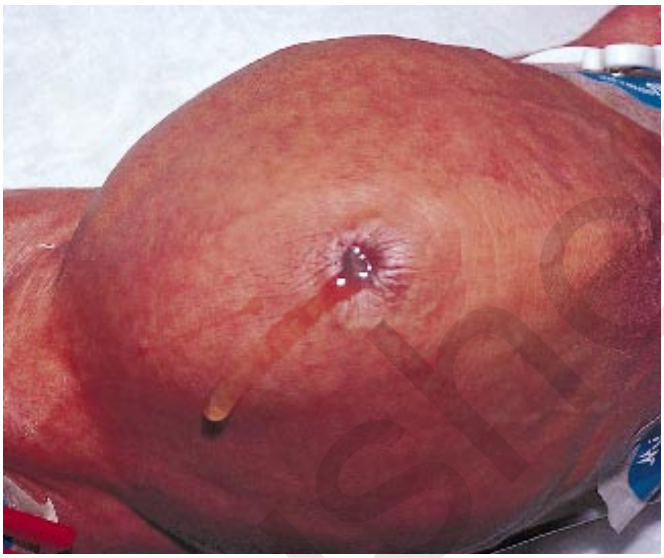

Figure 2.134. Note drainage of urine from the umbilicus due to a patent urachus. The marked abdominal distention in this infant was associated with absence of the abdominal musculature.

2.135

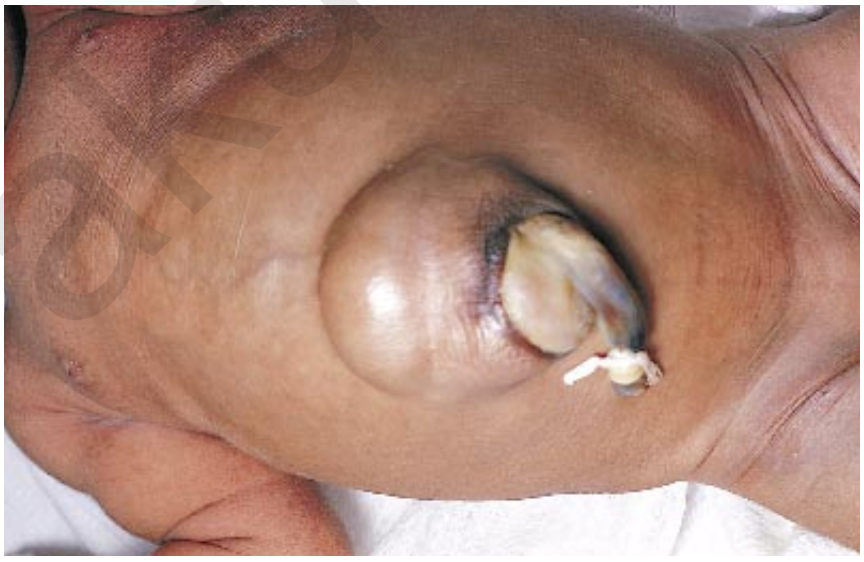

Figure 2.135. Umbilical hernia in a black infant at the age of 3 days. Umbilical herniae arise due to a separation of the rectus muscle with herniation of the omentum and, on some occasions, bowel.

2.136

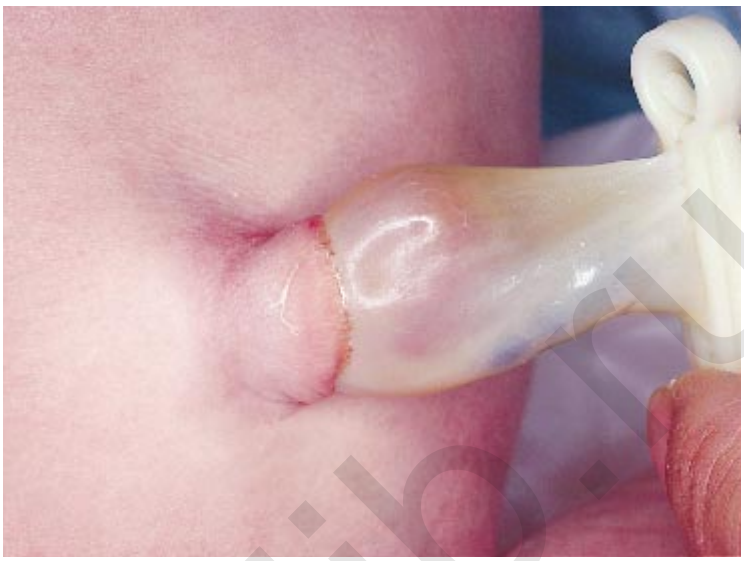

Figure 2.136. Omphaloceles can be quite small in infants and can resemble a Wharton's jelly cyst. The sac may contain a single loop of bowel as noted in this infant. Because of this risk of an omphalocele, the cord should not be cut or clamped close to its insertion.

2.137

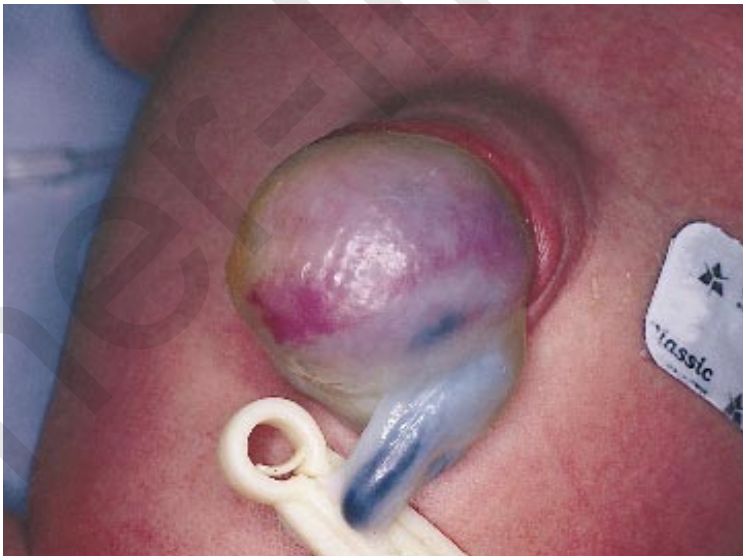

Figure 2.137. This infant has a moderate-sized omphalocele. The sac may contain a single loop of bowel or most of the intestine and liver. An omphalocele is caused by failure of the complete return of intestines to the abdominal cavity in early fetal life (10 weeks). Extra-abdominal contents are positioned midline. The umbilical cord is incorporated and a sac is present. Intestinal malrotation is a frequent associated finding. Omphaloceles may occur as isolated findings or can be associated with other congenital and chromosomal abnormalities. It is frequently seen in trisomy 13 and in Beckwith-Wiedemann syndrome.

2.138

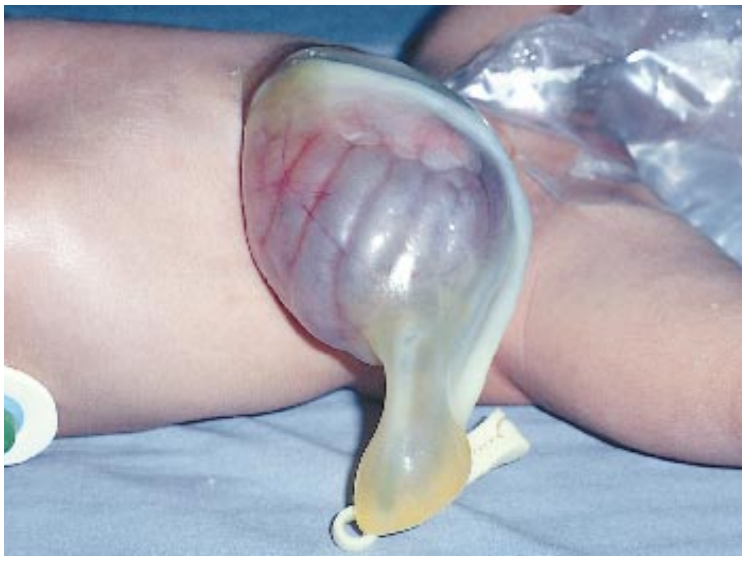

Figure 2.138. Infant with Beckwith-Wiedemann syndrome with an omphalocele. As noted in the preceding photographs of infants with omphaloceles, the defect is covered only by peritoneum without overlying skin. Note the many loops of bowel. This thin membranous sac may rupture.

2.139

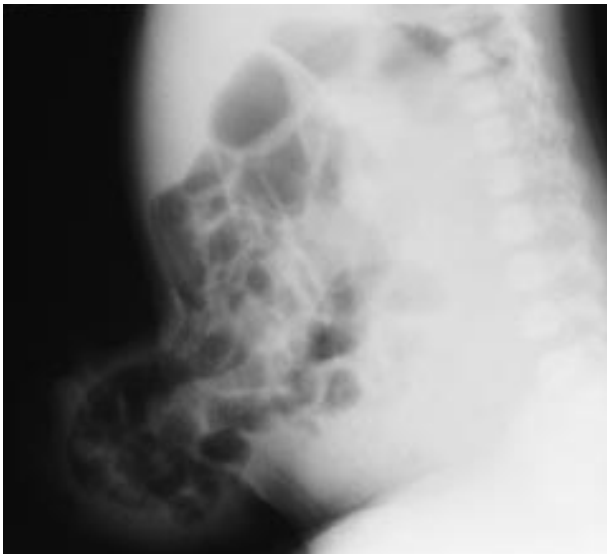

Figure 2.139. Lateral radiograph showing the omphalocele with bowel contents in an infant with Beckwith-Wiedemann syndrome.

2.140

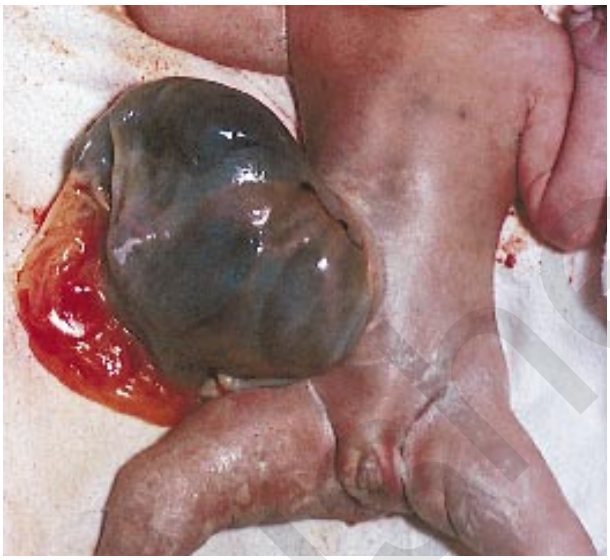

Figure 2.140. This infant has a giant omphalocele. Note that in addition to bowel the liver is present in the omphalocele and that the overlying membranous sac has ruptured. The incorporation of umbilical cord differentiates this from gastroschisis.

2.141

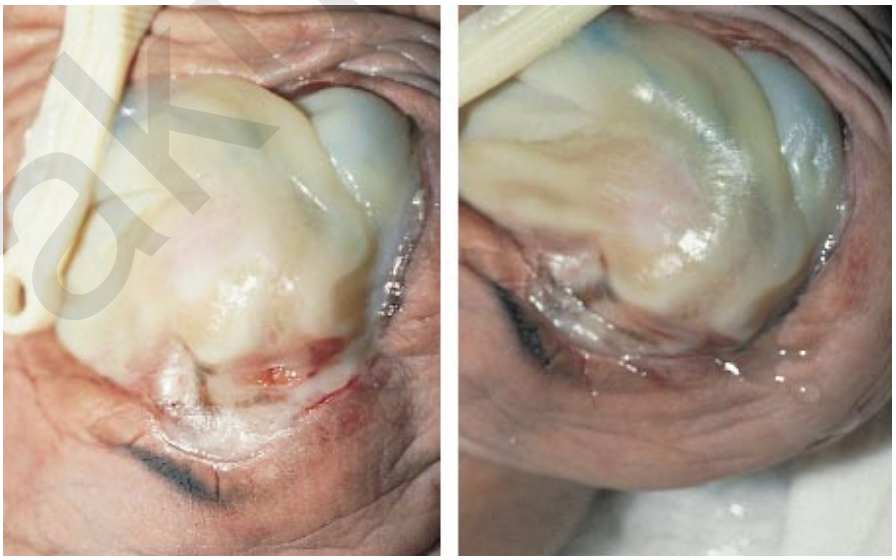

Figure 2.141. This infant with absence of the abdominal musculature (prune belly syndrome) had both an omphalocele and a patent urachus. On the left note the omphalocele with the opening of the urachus in the lower portion. On the right note the omphalocele and drainage of urine from the patent urachus.

2.142

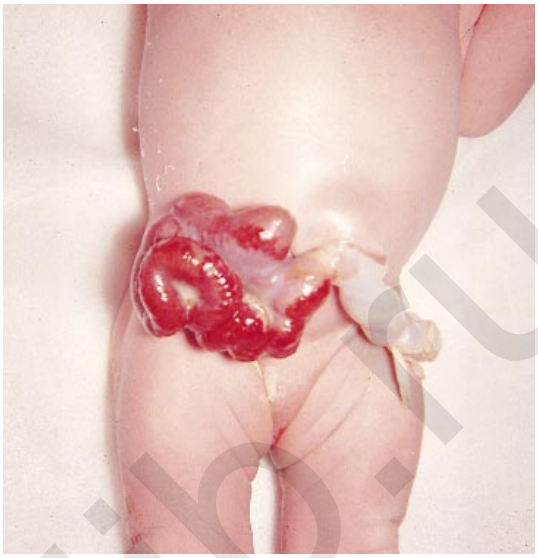

Figure 2.142. In gastroschisis there is no covering membrane. Gastroschisis is the result of an anterior abdominal wall defect which is usually paramedian to the right of the umbilical cord insertion. Gastroschisis is rarely associated with other congenital anomalies. There may be an associated intestinal malrotation and occasionally there are atretic portions of the extra-abdominal bowel. The stomach, bowel, and bladder may be outside the abdomen and completely uncovered. Note that the liver is *never* outside the abdominal cavity in an infant with gastroschisis.

2.143

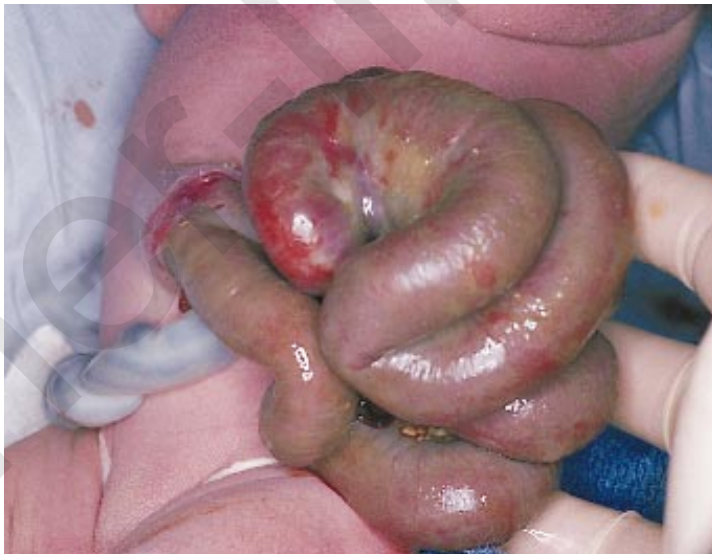

Figure 2.143. In this infant with gastroschisis note the dilated and thickened loops of bowel. This is common in infants with gastroschisis since the loops of bowel lie free in the amniotic fluid.

2.144

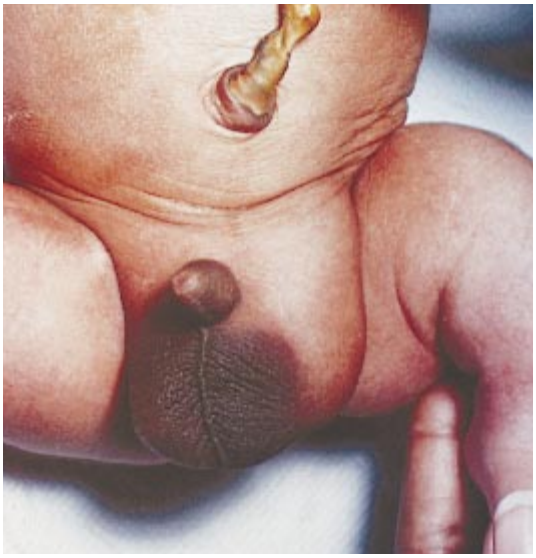

Figure 2.144. A left inguinal hernia which was present at birth in a male infant. Herniae are usually indirect, and are much more common in male and in premature infants. The risk of non–surgically-treated hernias include inability to reduce herniated bowel contents leading to potential strangulation and incarceration.

2.145

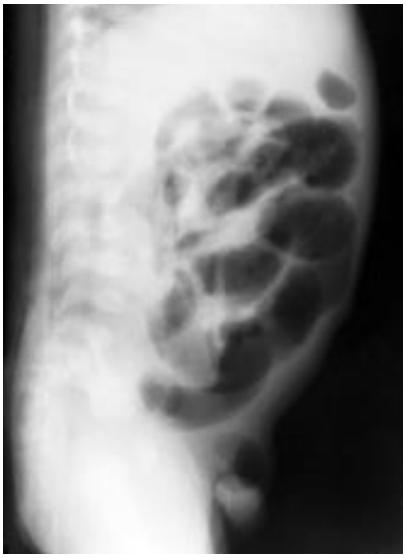

Figure 2.145. Abdominal radiograph of an infant with intestinal obstruction as the result of an incarcerated inguinal hernia. Note the bowel gas in the scrotum. It is important to examine the scrotum of male infants who present with abdominal distention due to intestinal obstruction.

2.146

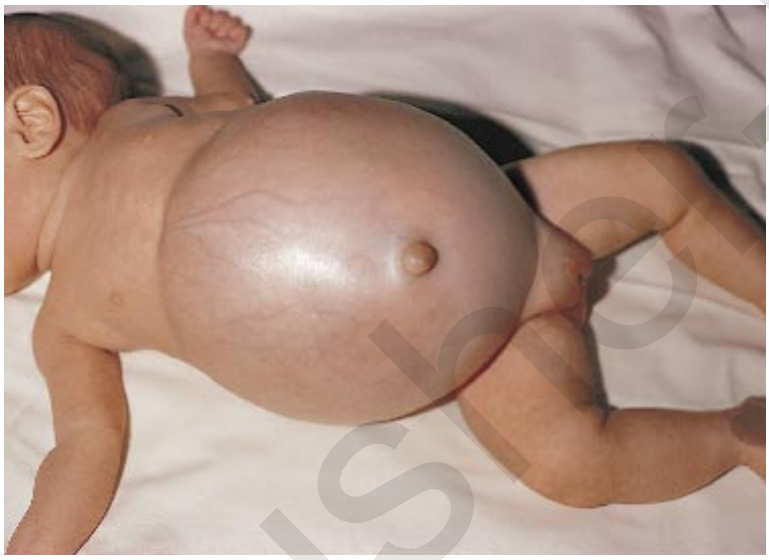

Figure 2.146. Marked abdominal distention in an infant with multiple hemangiomatosis. The abdominal distention was due to massive enlargement of the liver. This infant also had numerous hemangiomas of the skin.

2.147

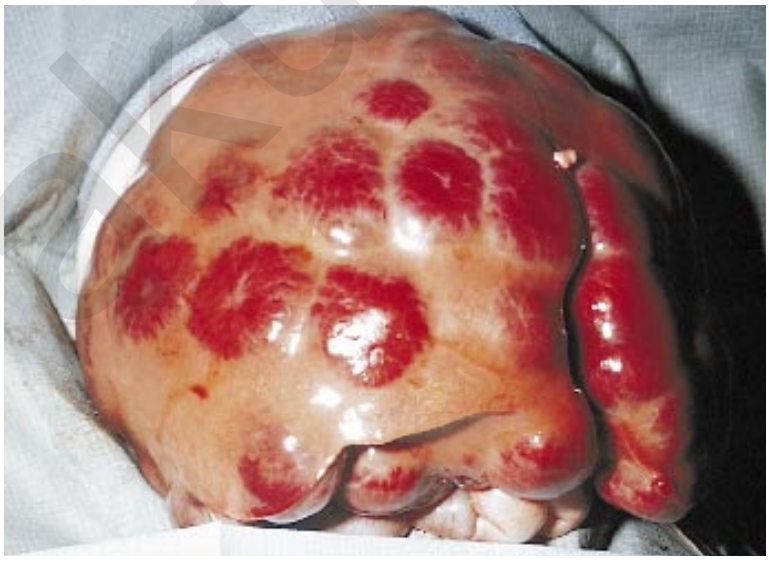

Figure 2.147. The multiple massive hemangiomas involving the liver are noted at surgery.

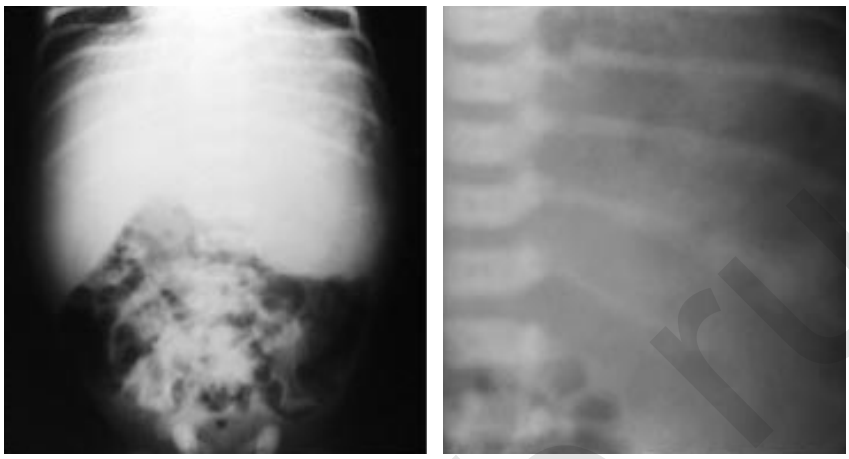

2.148

Figure 2.148. Radiograph of an infant who presented with abdominal distention. On the left note the marked enlargement of the liver and on the right note the calcifications in the right upper quadrant with inferior displacement of the normal bowel gas. This infant had a large hemangioma involving the left lobe of the liver.

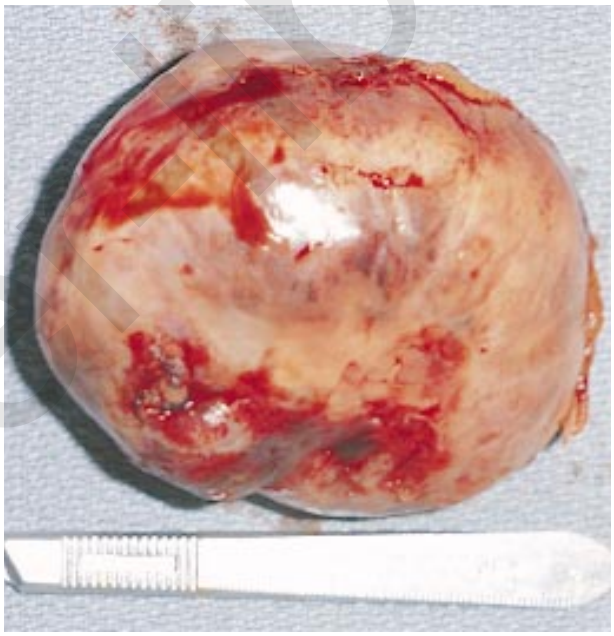

2.149

Figure 2.149. Pathologic specimen from the liver of the same infant as in Figure 2.148 showing the large hemangioma which was successfully removed.

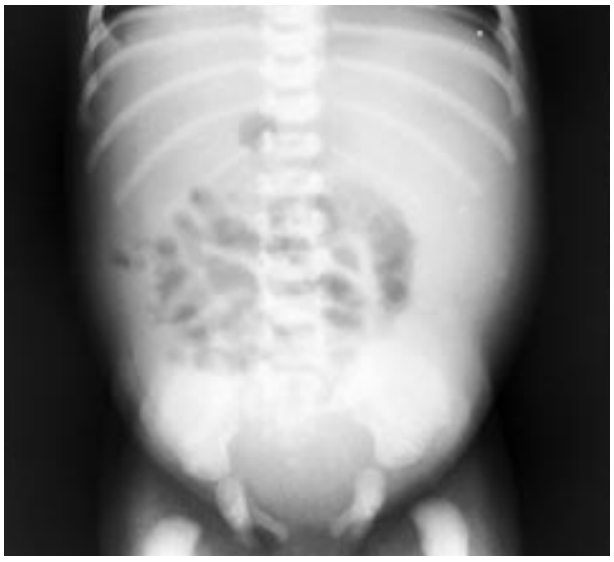

2.150

Figure 2.150. Radiograph of an infant who presented with marked abdominal distention and pallor at 3 days of age associated with a rupture of the spleen. The radiograph shows the marked diffuse opacification of the abdomen with central pooling of the bowel gas associated with a large hemoperitoneum. Pooling of gas is due to loops of bowel floating in the fluid in the peritoneal cavity and, thus, is seen most commonly with ascites.

2.151

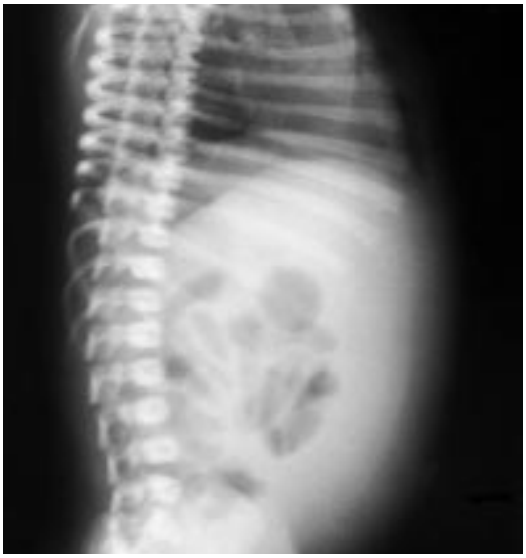

Figure 2.151. Lateral radiograph of the same infant as in Figure 2.150 demonstrating abdominal distention and pooling of bowel gas. The pooling of the gas in this infant was due to a hemoperitoneum rather than ascites.

2.152

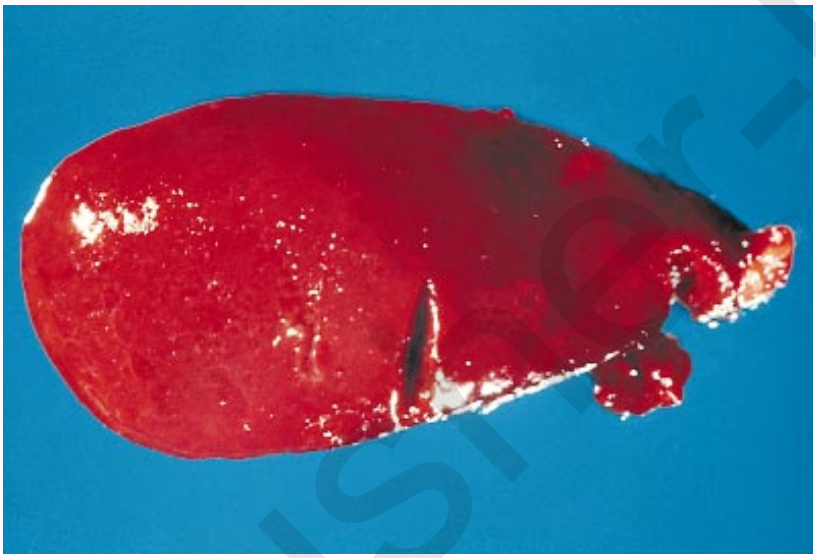

Figure 2.152. Surgical specimen of the spleen of the same infant as in Figure 2.150 and 2.151. Note that the rupture has occurred in the right inferior portion of the spleen. The midline defect is iatrogenic. Hemoperitoneum may occur as the result of rupture of a subcapsular hematoma of the liver and is more common in premature infants, especially with breech delivery. Rupture of the spleen in a normal term infant is rare.

Chapter 3
Nutritional Disorders

The gastrointestinal tract of the newborn must process a relatively large amount and variety of foods soon after birth. The average term infant takes about 540 cc (18 ounces) of food daily by two weeks of age. In adults, correcting for body surface area, this would equal approximately 10 liters of fluid per day. In proportion to its size, the premature infant processes an even greater load. The infant's diet must contain the appropriate quantity of protein, carbohydrates, fats, minerals, vitamins, trace elements and water. The complexity of this task is especially obvious in the premature infant where the child's nutritional reserves are limited and the margin for error is small. Advances in perinatal medicine have resulted in the increased survival of smaller and smaller infants. This poses several special considerations when designing a nutritional plan for these infants, including: the need for rapid growth, the immature functional development of the gut, and the presence of diseases that add additional stress or needs.

3.1

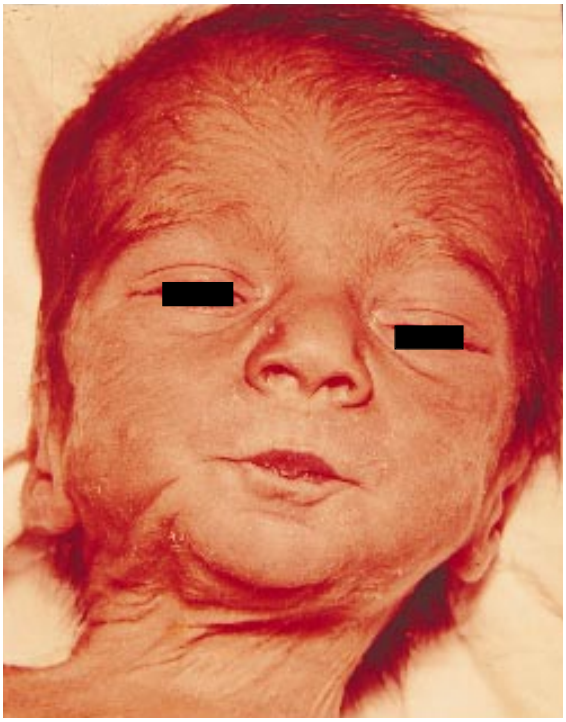

Figure 3.1. Severe intrauterine growth retardation (IUGR) in a post-term baby with a birth weight of 1800 g. Note the typical wizened appearance. The hyperalert expression is also common in postmaturity.

3.2

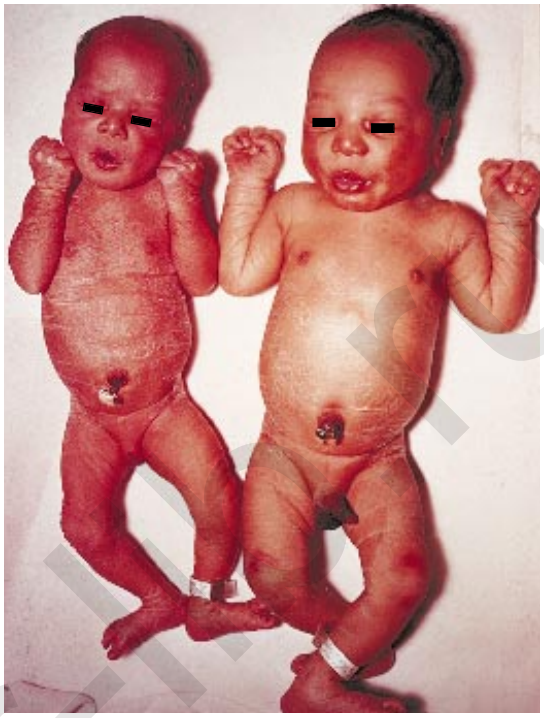

Figure 3.2. These discordant dizygotic twins demonstrate the condition of unequal size. One twin weighed 3200 g; the other twin weighed 2040 g.

3.3

Figure 3.3. Protein calorie malnutrition (kwashiorkor). This premature infant developed the typical appearance of kwashiorkor at the age of 3 months while in the nursery. She was treated in the pre-parenteral nutrition era.

3.4

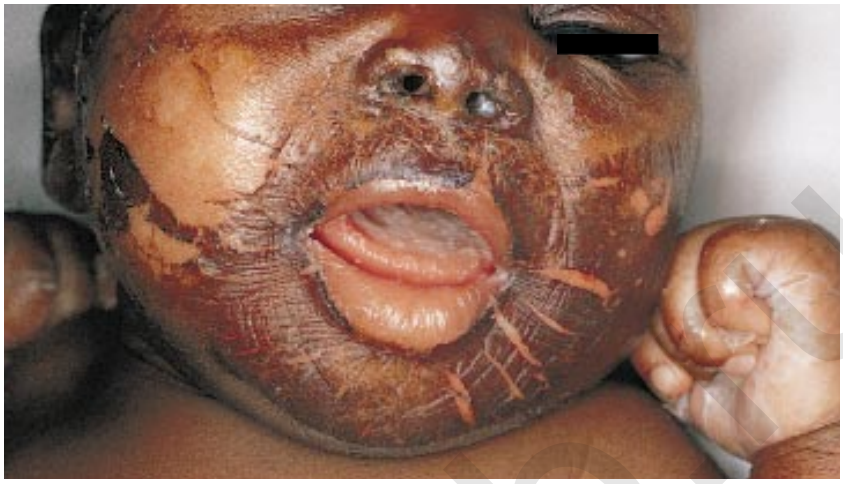

Figure 3.4. A close-up of the face of the same infant as in Figure 3.3 showing the earliest appearance of nutritional dermatitis with the copper color and blanching on pressure. Also note the edema, especially of the hand.

3.5

Figure 3.5. In the same infant as in Figure 3.3 and 3.4, note the frank desquamation with raw areas and edema.

3.6

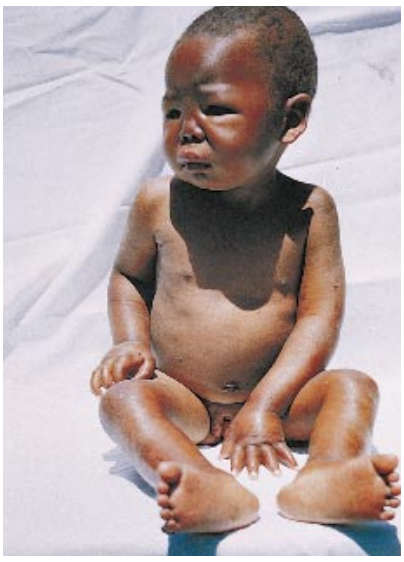

Figure 3.6. Protein calorie malnutrition in an infant. Note the marked edema, the picture of abject misery, and the "pot belly." No dermatitis is present.

3.7

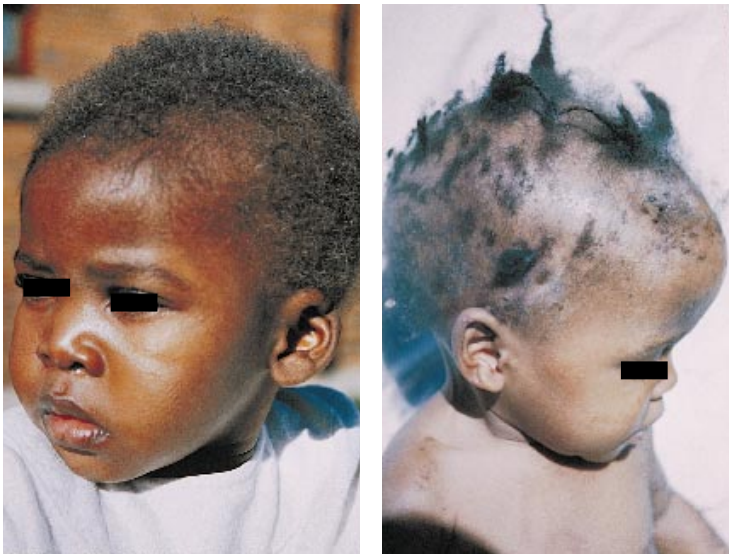

Figure 3.7. The infant on the left with protein calorie malnutrition shows the characteristic gray and atrophic hair. The infant on the right has lost most of his hair, but there are still patches of both atrophic and healthy hair attached to the skin by thin atrophic roots.

3.8

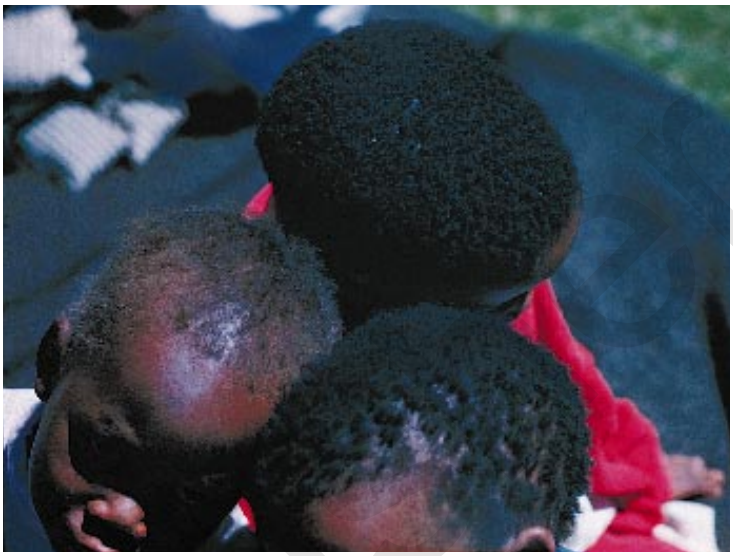

Figure 3.8. The characteristic hair changes are compared. Note the head of a normal infant, one with patchy alopecia, and one with gray and atrophic hair.

3.9

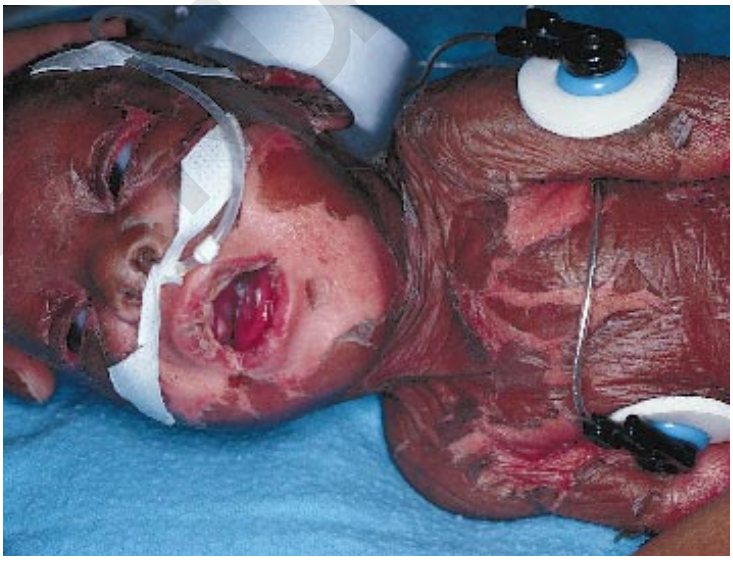

Figure 3.9. A 6-week-old premature infant (birth weight 1400 g) developed marked hyperpigmentation and desquamation of the skin while in the nursery. She was being treated for bronchopulmonary dysplasia with oxygen by cannula and receiving peripheral parenteral nutrition. Her condition improved when trace elements were added to her diet.

3.10

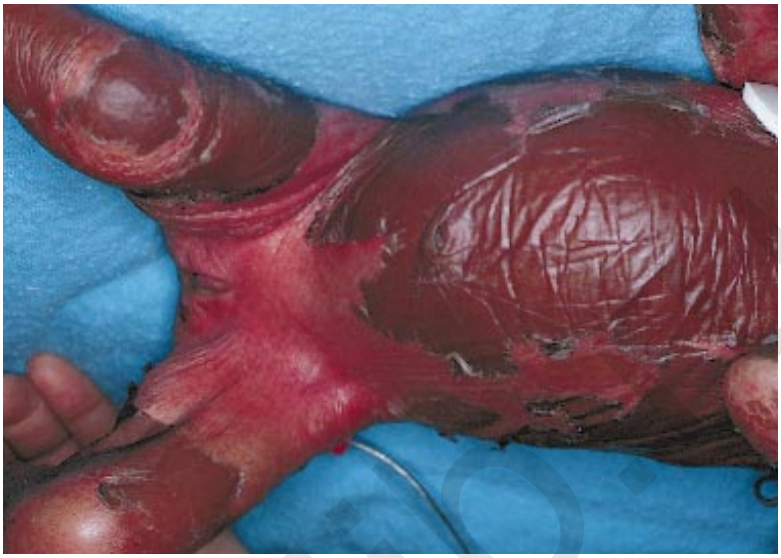

Figure 3.10. Another view of the same infant as in Figure 3.9 shows the marked hyperpigmentation and desquamation of the skin on the abdomen and lower extremities.

3.11

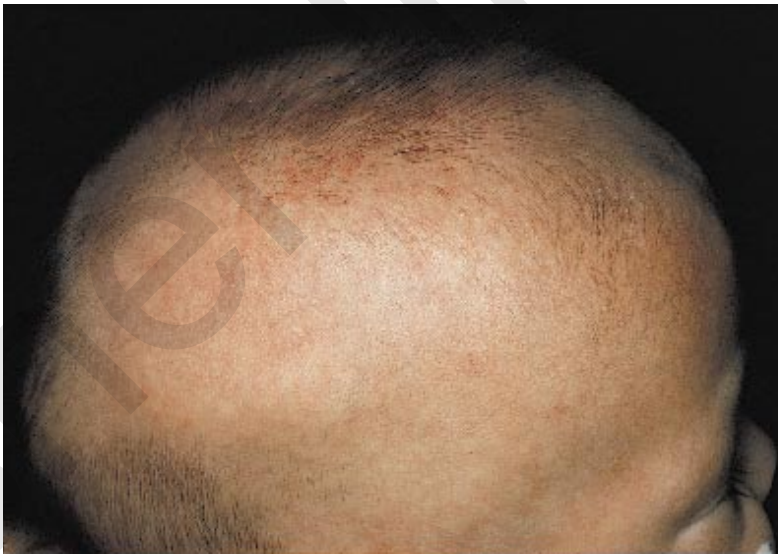

Figure 3.11. A low birthweight infant during the course of her treatment for bronchopulmonary dysplasia developed rickets at the age of 3 months. Note the typical "hot cross bun" head.

3.12

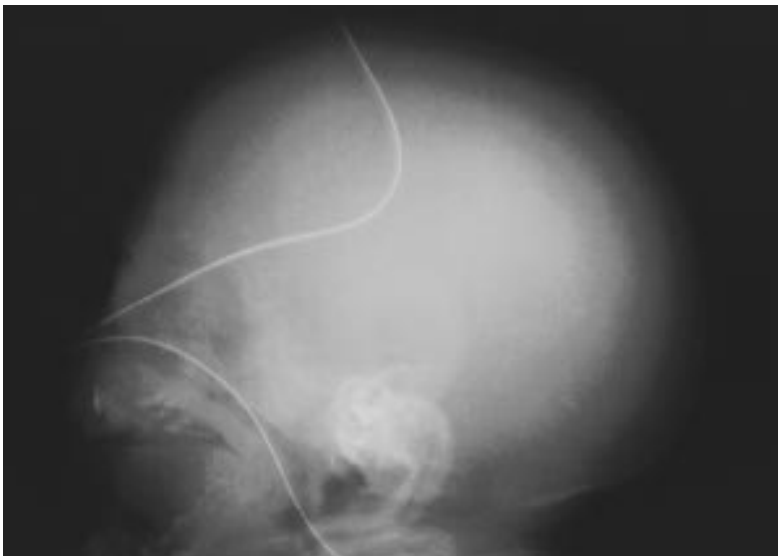

Figure 3.12. A radiograph of the skull of the same infant as in Figure 3.11 showing the marked lack of mineralization of the skull.

3.13

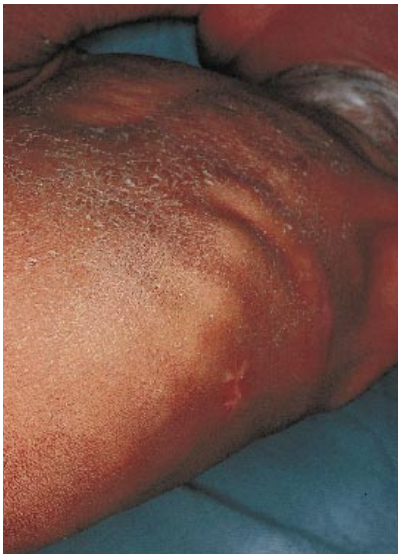

Figure 3.13. This infant with rickets shows the typical rachitic rosary (beading of the ribs at the costochondral junctions). This occurred as a result of prolonged furosemide use for bronchopulmonary dysplasia. Beaded ribs are also seen in hypophosphatasia and chondrodystrophia.

3.14

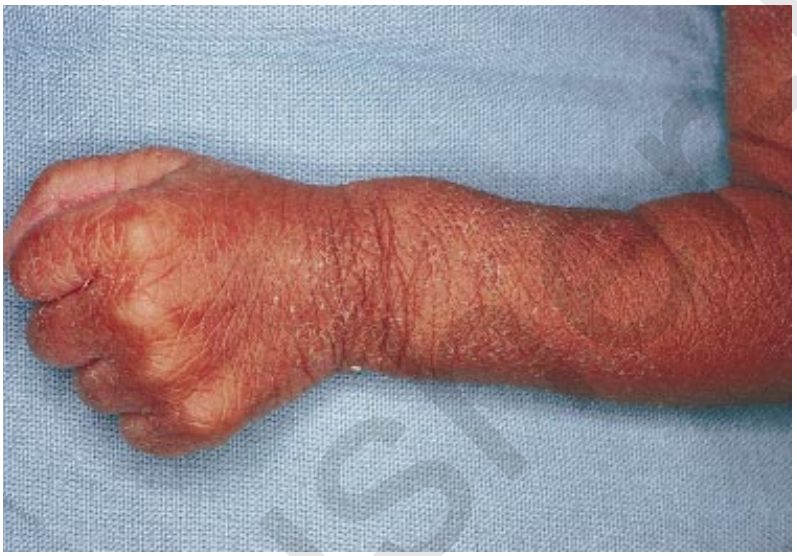

Figure 3.14. The wrist of the same infant as in Figure 3.13 demonstrates the very obvious broadening of the long bone epiphyses following the use of parenteral nutrition with insufficient vitamin D supplementation and the use of furosemide.

3.15

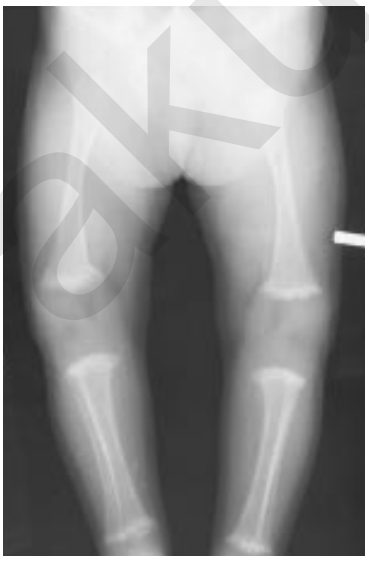

Figure 3.15. A radiograph of the lower extremities of a premature infant who developed rickets. Note the marked flaring and the ragged appearance of the epiphyses of the distal end of the long bones with widening of the joint space and demineralization.

3.16

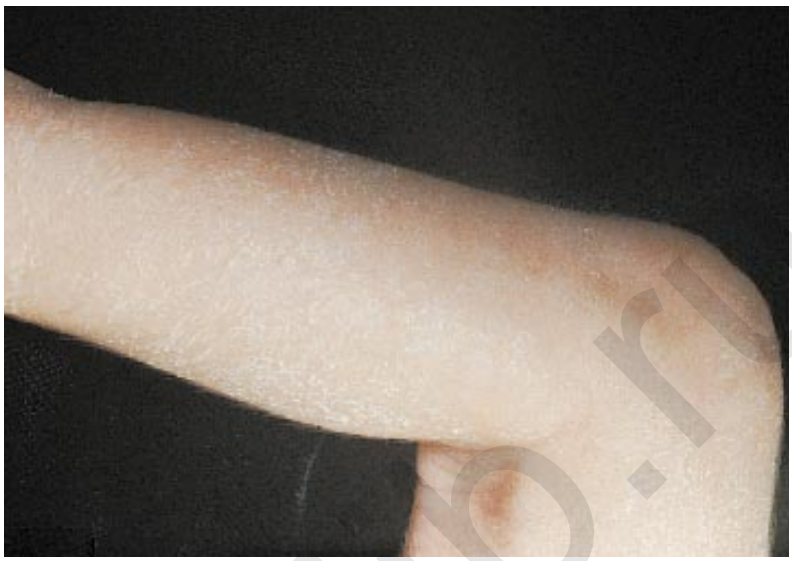

Figure 3.16. Linoleic acid deficiency. Note the fine branny desquamation in this infant with essential fatty acid deficiency.

3.17

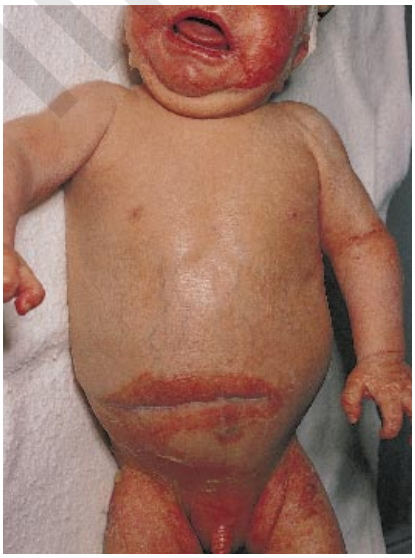

Figure 3.17. This infant with cystic fibrosis presented with perforation of the bowel and meconium peritonitis. He was treated for a prolonged period on parenteral nutrition. His abdominal wound healed poorly and he developed a perioral and perianal rash. He also had loose stools. The diagnosis of acrodermatitis enteropathica was confirmed by the addition of zinc to the parenteral nutrition, resulting in clinical improvement. At the time of this infant's hospitalization, trace minerals were not routinely added to parenteral nutrition.

3.18

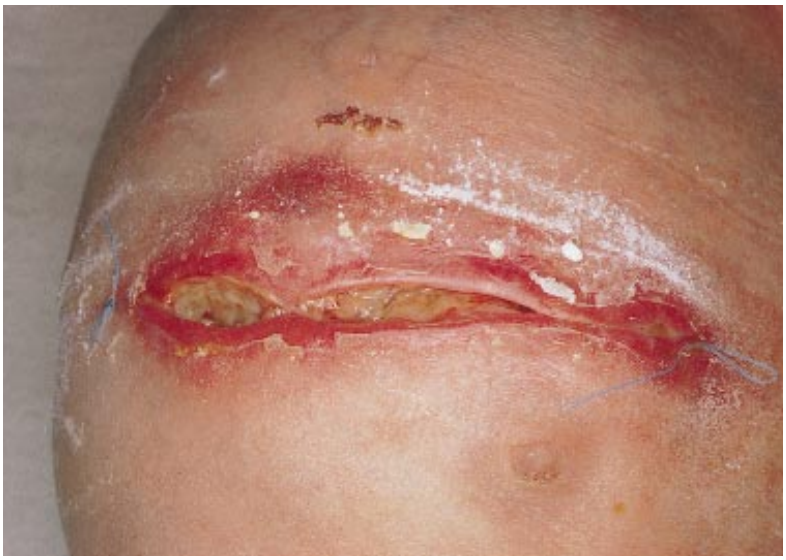

Figure 3.18. Note the poor healing of the surgical wound in the same infant as in Figure 3.17.

3.19

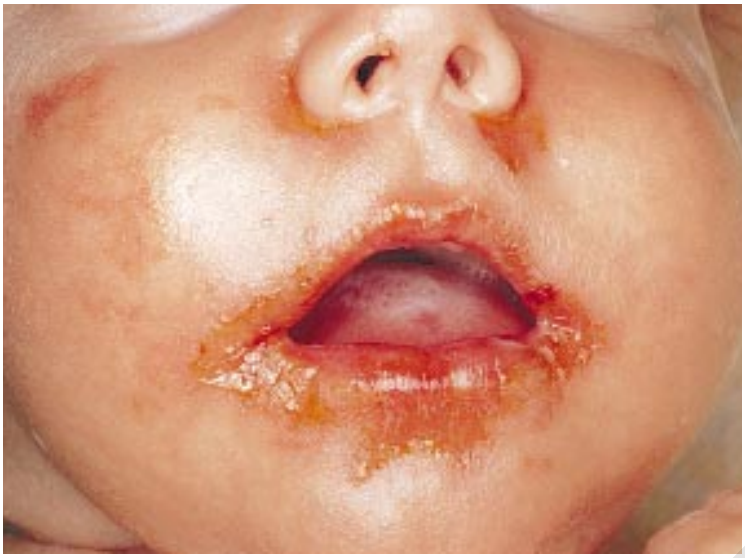

Figure 3.19. A close-up view of the same infant as in Figures 3.17 and 3.18 shows the perioral lesions in acrodermatitis enteropathica. There are extensive, sharply outlined, erythematous areas of skin partially covered with scales and crusts. Typically the lesions are located in the areas of the mouth, nose, and anogenital region. Initially the skin changes are vesicular or bullous. This condition must be distinguished from epidermolysis bullosa and impetigo.

3.20

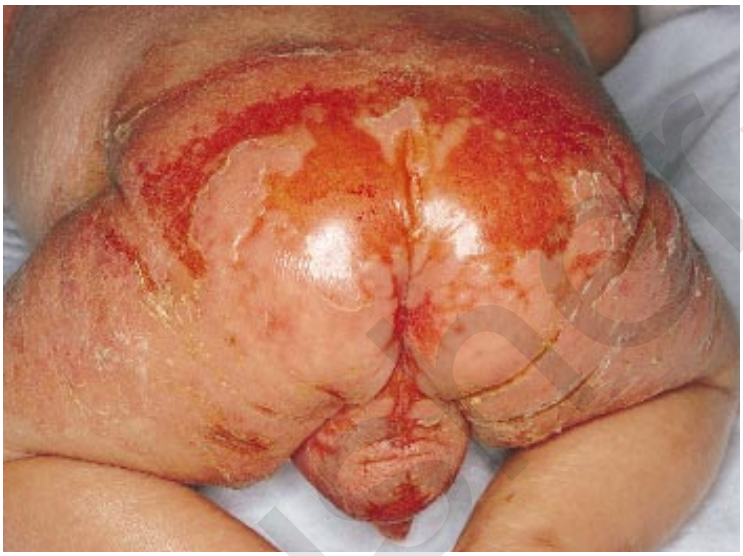

Figure 3.20. A close-up view shows the perianal lesions in the same infant as in Figures 3.17 to 3.19. Secondary infection with *Candida* is common in this condition.

Chapter 4
Genitourinary System

The genitourinary system excretes waste products, helps maintain fluid and electrolyte balance, and is the basis for later normal sexual development. Anatomic malformations of this system may be numerous and include the kidneys, ureters, bladder, urethra, or external and internal genitalia. Normally, the fetus is able to urinate into the amniotic sac by 10 weeks gestation. Maternal oligohydramnios may indicate that this is not occurring, and suggests an obstruction of the fetal genitourinary system. Failure to urinate by 24 hours of age may indicate an anatomic or functional disorder in the neonate. Acute and chronic renal dysfunction must also be considered in infants with excessive or decreased urinary excretion. Imaging studies, including radiographs, contrast studies (e.g., intravenous pyelogram, voiding cystourethrogram), ultrasonography, or radionucleotide scan may be necessary to define disorders of this system. Analysis of the urine, including microscopic, biochemical and culture, may also be necessary to delineate some of these disorders. Finally, evaluation of ambiguous genitalia may require complex endocrine evaluation as well as chromosomal analysis.

4.1

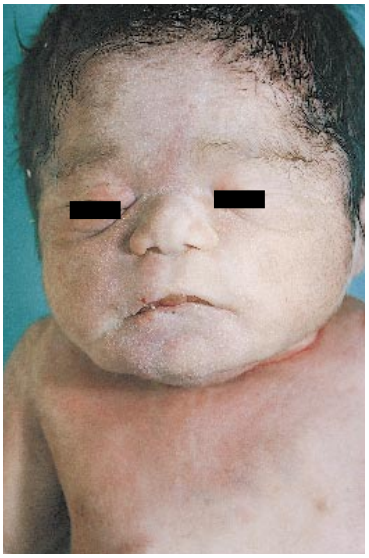

Figure 4.1. Frontal view of an infant with renal agenesis showing the typical Potter facies. The facies results from oligohydramnios causing prolonged intrauterine compression on the entire face. The nose is flattened, there are large vertical creases below the eyes, the ears are low set and dysplastic, and there is mild micrognathia.

4.2

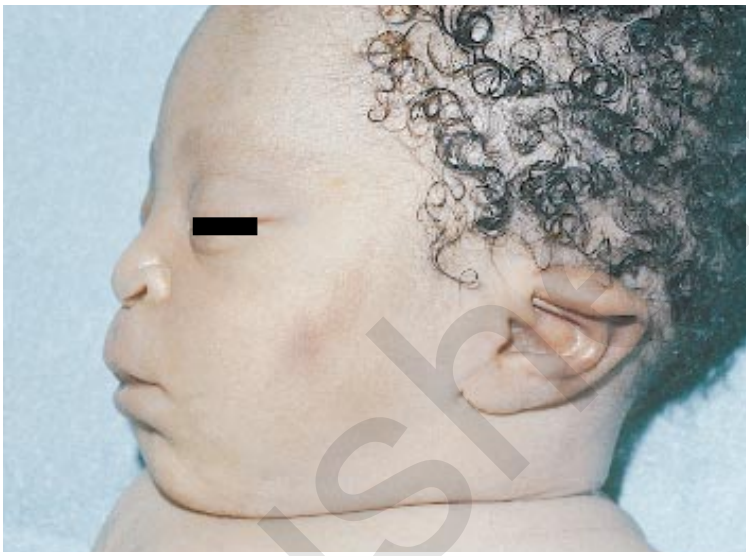

Figure 4.2. Lateral view of another infant with renal agenesis causing the Potter facies. Note the flattening of the nose and the low-set ears. Pressure deformity from the oligohydramnios in these infants may cause limb deformities (congenital dislocation of the hips, genu recurvatum, talipes equinovarus). The oligohydramnios may result in pulmonary hypoplasia, and amnion nodosum may be present on the fetal surface of the placenta.

4.3

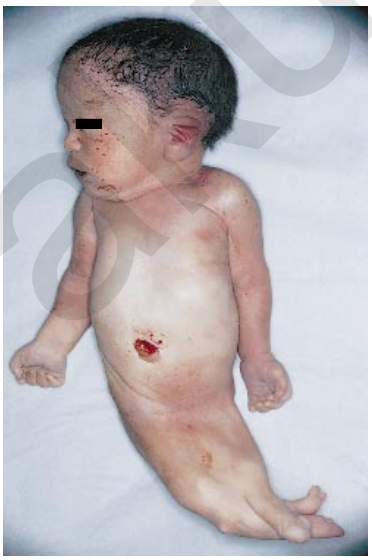

Figure 4.3. This infant with sirenomelia ("mermaid fetus") has the typical Potter facies, as renal agenesis with resulting oligohydramnios is always present. Sirenomelia is characterized by fusion of all or part of the lower limbs and is a condition incompatible with life.

4.4

Figure 4.4. Fetal surface of the placenta showing amnion nodosum. Note the small nodules which occur as a result of the oligohydramnios. The nodules consist of vernix caseosa, lanugo, and squamous epithelial cells from the fetal skin. (Sotelo-Avila, C)

4.5

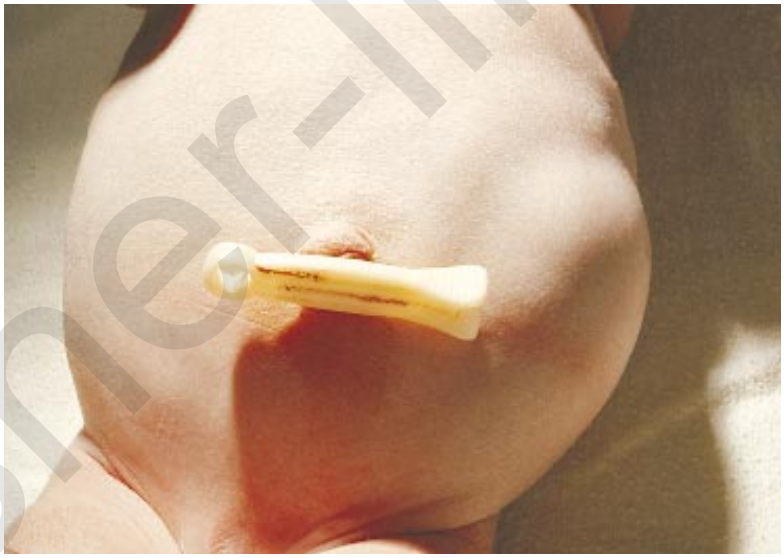

Figure 4.5. Abdominal distention with a large mass on the left side. This was a large multicystic kidney. Differential diagnosis of abdominal masses includes hydrometrocolpos, ovarian masses, sacrococcygeal teratoma, urinary tract abnormalities, and neuroblastoma.

4.6

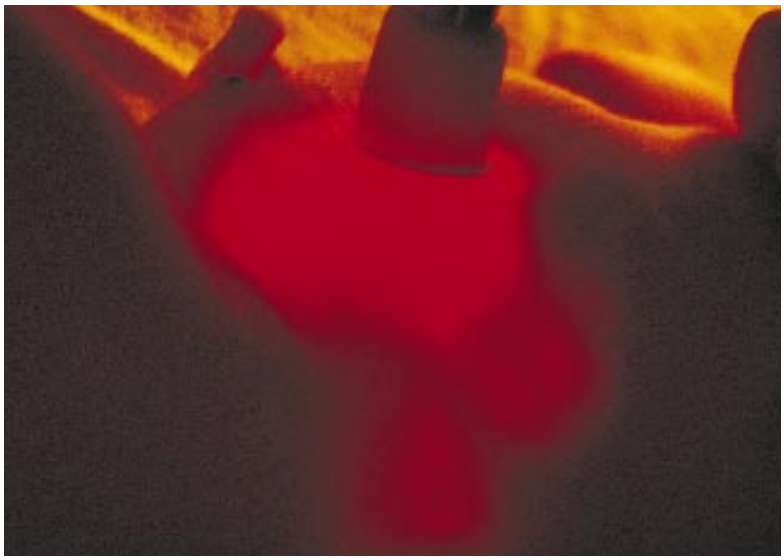

Figure 4.6. Transillumination of the abdomen in the same infant as in Figure 4.5 shows a large cystic mass on the left side. Abdominal masses in the newborn are most commonly cystic rather than solid.

4.7

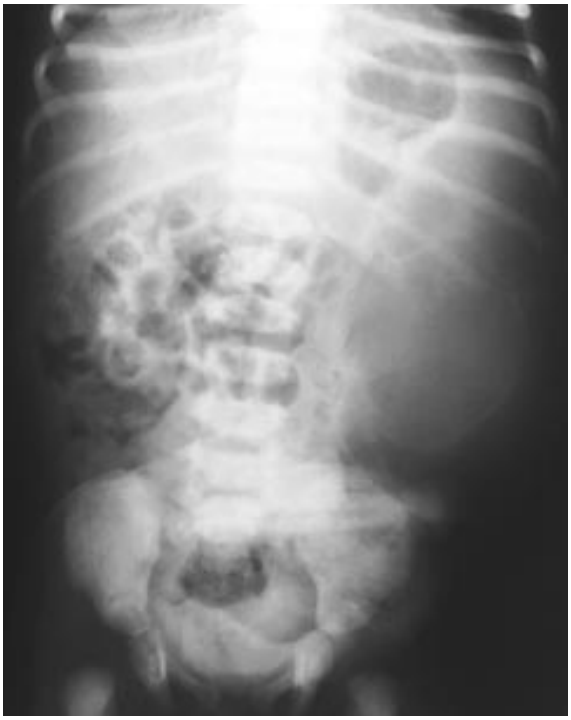

Figure 4.7. Abdominal radiograph of the same infant as in Figures 4.5 and 4.6 showing the opacity on the left caused by a multicystic kidney. Note the displacement of the normal bowel gas pattern to the right.

4.8

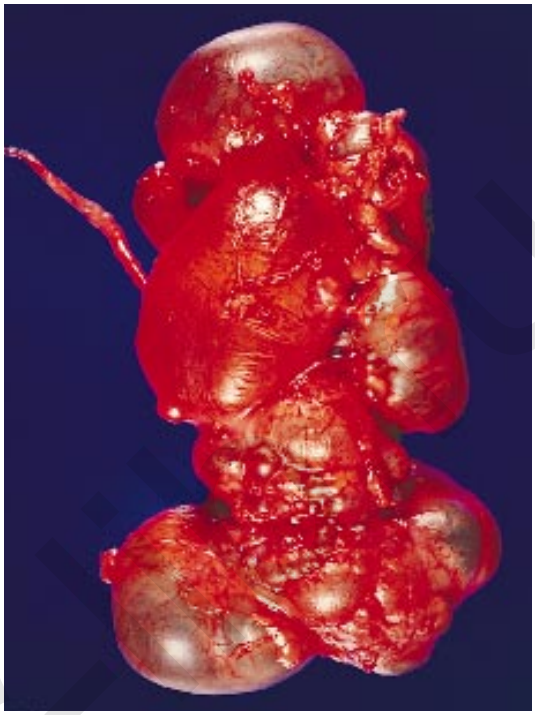

Figure 4.8. Surgical specimen of a large multicystic kidney. Note the numerous multiloculated cysts. Multicystic kidneys show no renal function and are generally unilateral but, on occasion, there may be bilateral involvement. Dysplastic kidneys may have delayed function.

4.9

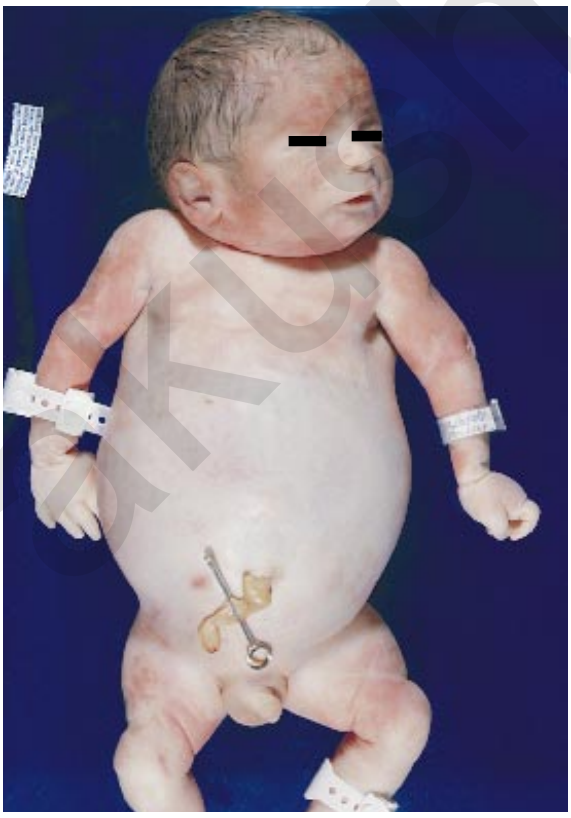

Figure 4.9. Marked abdominal distention in an infant with urinary ascites and bilateral multicystic kidneys.

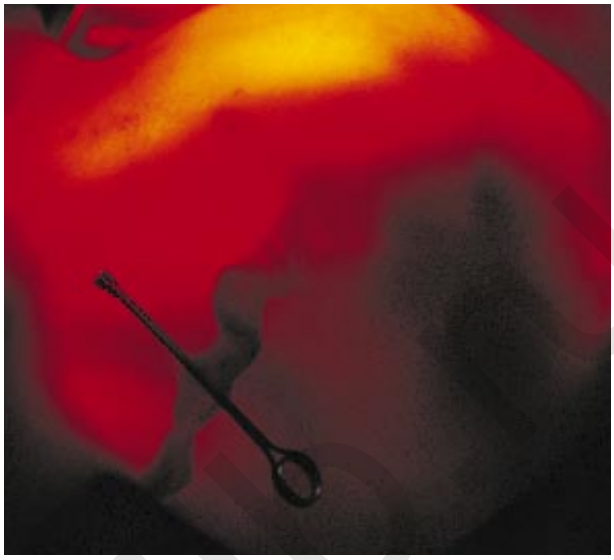

4.10

Figure 4.10. Transillumination of the abdomen in the same infant as in Figure 4.9 showing the large amount of ascitic fluid.

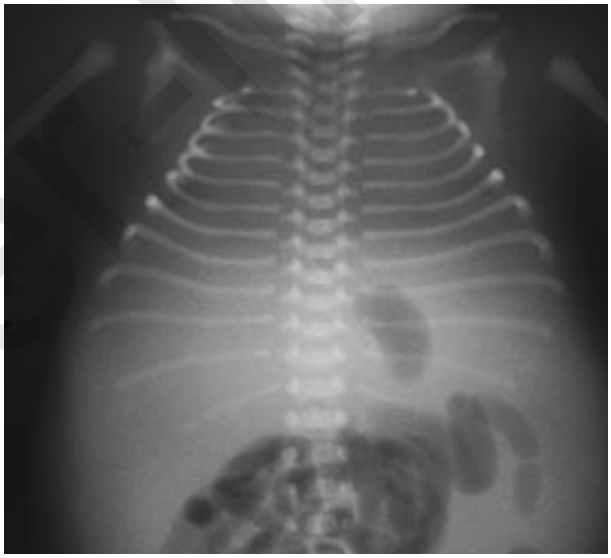

4.11

Figure 4.11. Radiograph showing the marked abdominal distention with bulging opacified flanks and central pooling of the loops of bowel. This radiograph is characteristic of any infant with ascites of any etiology.

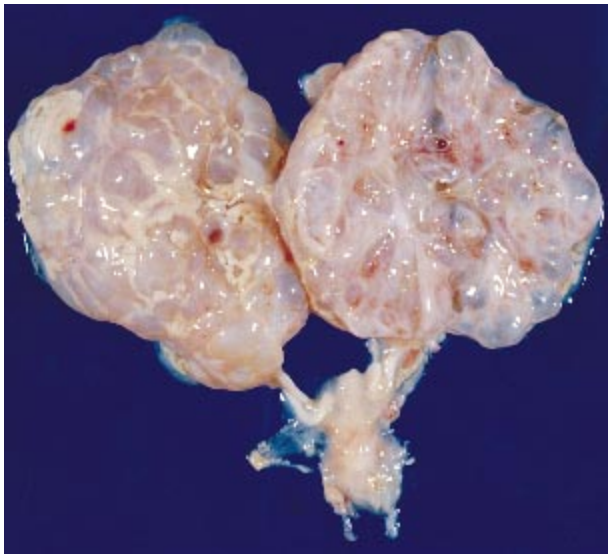

4.12

Figure 4.12. Pathologic specimen of the same infant as in Figure 4.11 with bilateral multicystic kidneys.

4.13

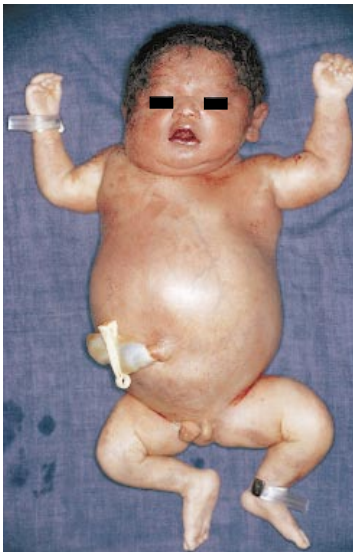

Figure 4.13. Marked abdominal distention in an infant with massive polycystic kidneys. This infant died soon after birth. Infants with polycystic kidneys typically have an autosomal dominant pattern of inheritance in contrast to the autosomal recessive pattern in adult polycystic kidney disease. If little urine is produced, the fetus may exhibit the Potter sequence with fetal compression and pulmonary hypoplasia.

4.14

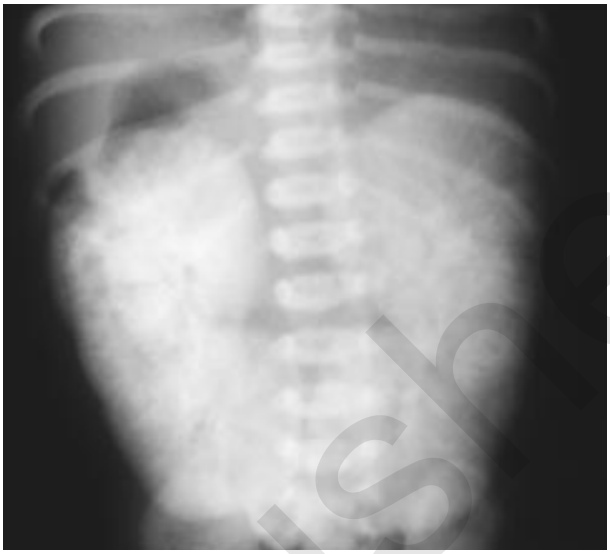

Figure 4.14. Radiograph taken 24 hours after contrast medium was given for an intravenous pyelogram. The contrast dye is contained in the hyperplastic dilated tubules without dye noted in the calyces or bladder. The dye was finally excreted several days later.

4.15

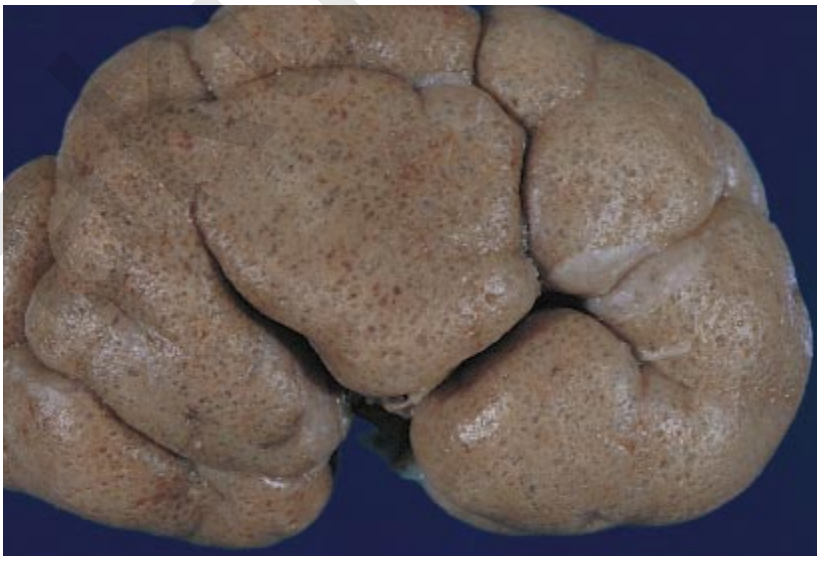

Figure 4.15. An autopsy specimen of a large infantile polycystic kidney. Note the fetal lobulation of the kidney with the visible cysts.

4.16

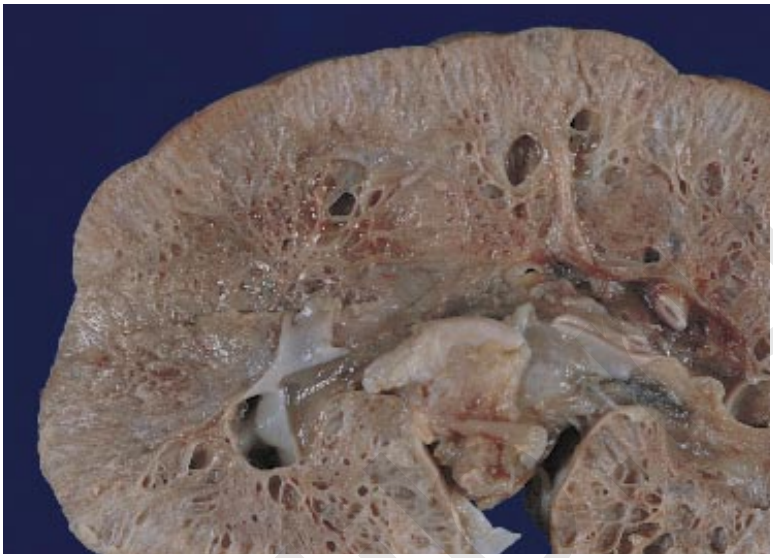

Figure 4.16. A sagittal section through the same specimen as in Figure 4.15. Cysts are noted throughout the whole kidney with the highest concentration in the medulla. This is the anatomic location of the hyperplastic tubules.

4.17

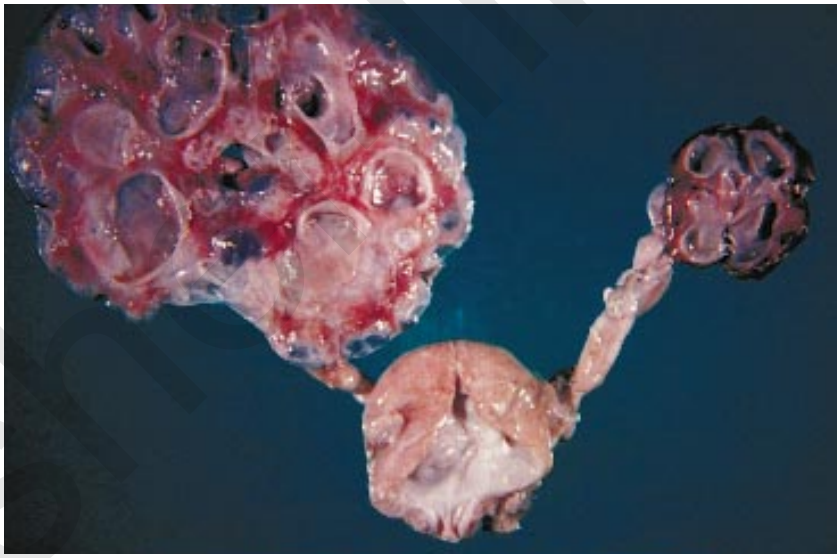

Figure 4.17. Autopsy specimen of an infant showing cystic dysplasia of the kidneys. As compared to multicystic kidneys where there is no renal function, dysplastic kidneys may show some delayed renal function.

4.18

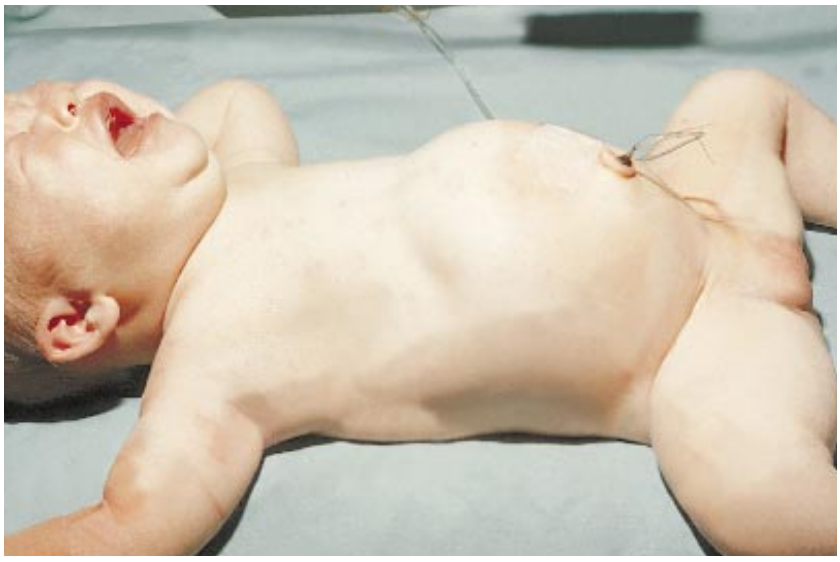

Figure 4.18. This term infant, the product of a breech extraction, presented with marked abdominal distention and respiratory distress. Note the marked hypotonia and "pithed-frog" appearance in a crying infant. Normally, a crying infant does not lie motionless. On examination of the abdomen, a markedly enlarged neurogenic bladder was palpable. This infant had a cervical cord injury at C7 to T1 with associated quadriplegia.

4.19

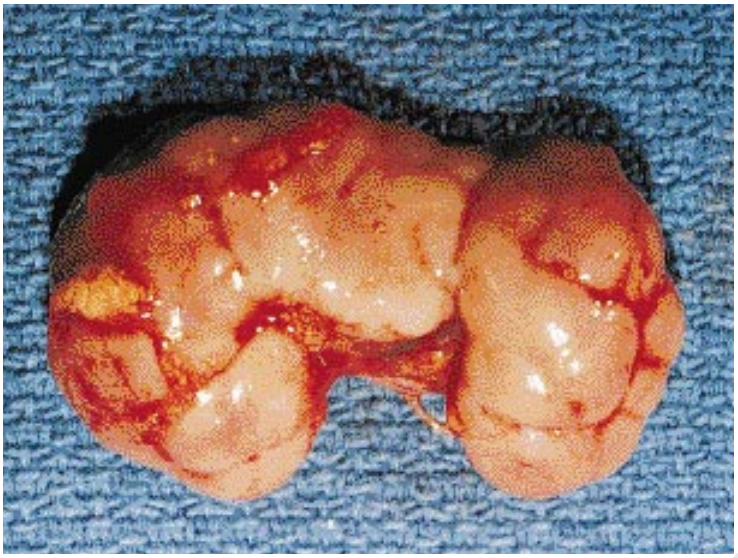

Figure 4.19. Pathologic specimen of a horseshoe kidney. This is not uncommon and is usually asymptomatic. Note the normal fetal lobulation.

4.20

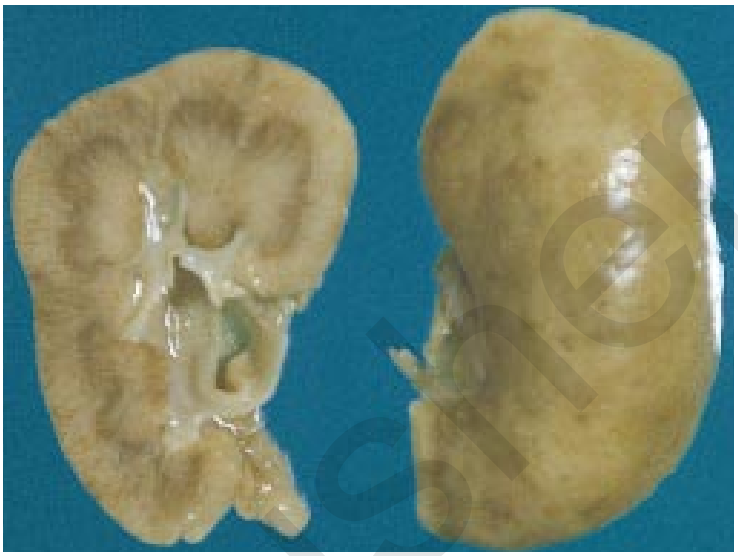

Figure 4.20. An autopsy specimen of "doll's" kidneys. Doll's kidneys refer to hypoplastic kidneys that function well. The cause of death in this infant was unrelated to renal function. This infant had intrauterine growth retardation, a birthweight of 1600 g, and a gestational age of 42 weeks.

4.21

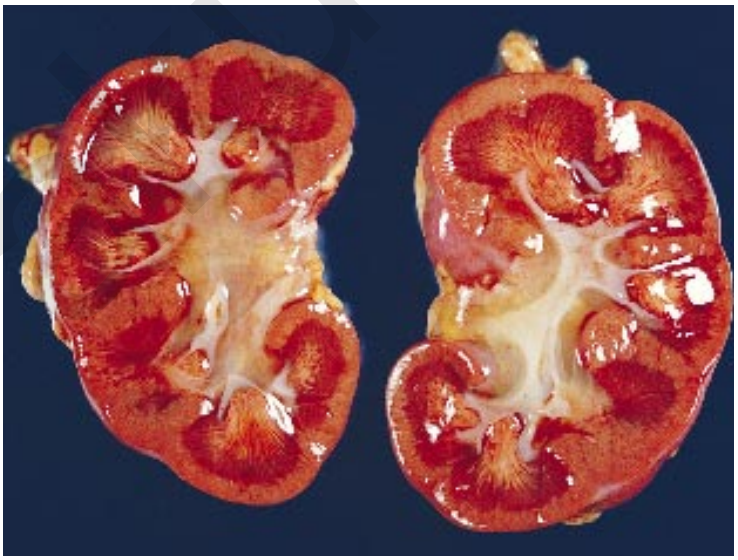

Figure 4.21. Sagittal section through an abnormal kidney. Note the urate deposits which are present as crystals in the collecting tubules and form golden brown aggregates described as "uric acid infarcts." They are obvious to the naked eye in about 15 to 20% of autopsies, but are washed out when the kidneys are fixed. Uric acid infarcts in neonatal kidneys are frequent in dehydration, sepsis, and erythroblastosis fetalis.

4.22

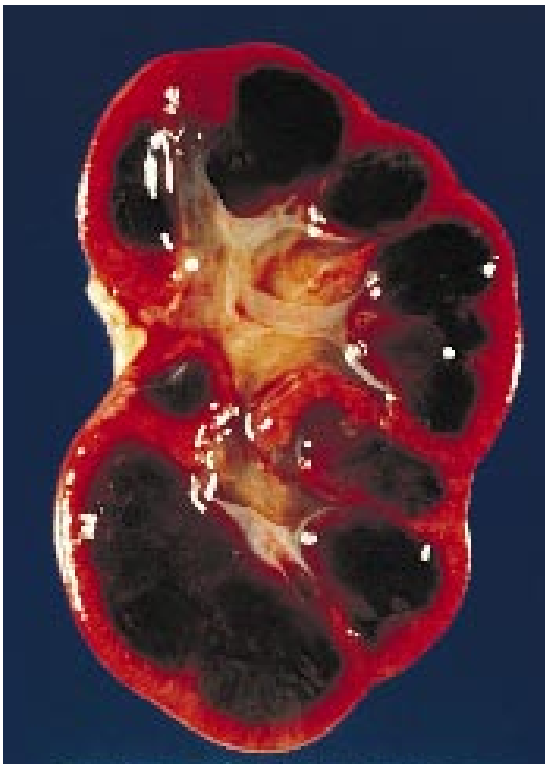

Figure 4.22. Sagittal section of an infant's kidney showing severe medullary hemorrhage secondary to hypoperfusion.

4.23

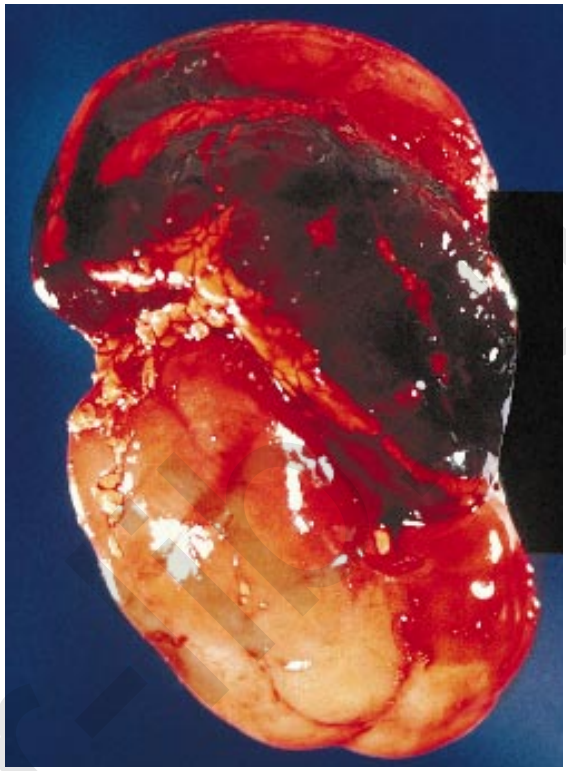

Figure 4.23. Autopsy specimen of the right kidney and adrenal gland in an infant who died from early onset group B streptococcal sepsis with disseminated intravascular coagulopathy. There is a massive adrenal hemorrhage which completely destroyed the adrenal gland by hemorrhagic necrosis. Note the normal kidney with fetal lobulation and the markedly enlarged adrenal gland.

4.24

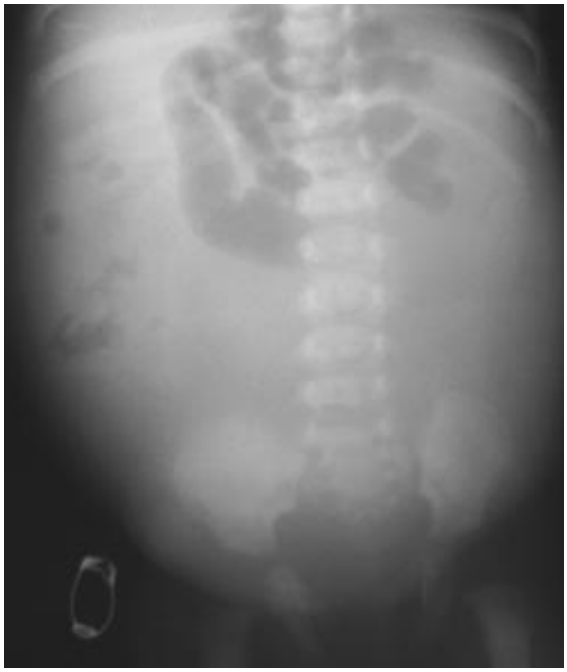

Figure 4.24. Radiograph showing a large distended abdomen secondary to urinary ascites. Note the bulging flanks with lack of definition of structures and the centralized pooling of bowel gas. Urinary ascites may be due to a traumatic tear in the calyx of the kidney or due to pyelolymphatic backflow. (Singleton, E.)

4.25

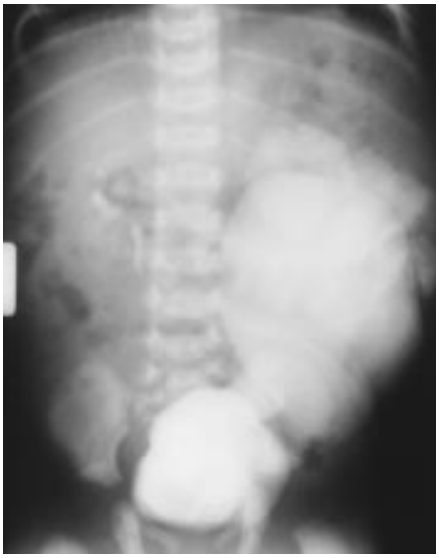

Figure 4.25. The intravenous pyelogram in this infant shows a left-sided ureterovesical obstruction resulting in a left hydroureter and severe left hydronephrosis. The radiograph was taken 3 hours after injection of the dye. Note that the calyceal pattern on the right side is normal and the bladder is not very enlarged. Hydronephrosis in the newborn is most commonly due to obstruction at the bladder neck or at the ureterovesical junction. With the advent of ultrasonography, intravenous pyelograms now are rarely performed. (Singleton, E.)

4.26

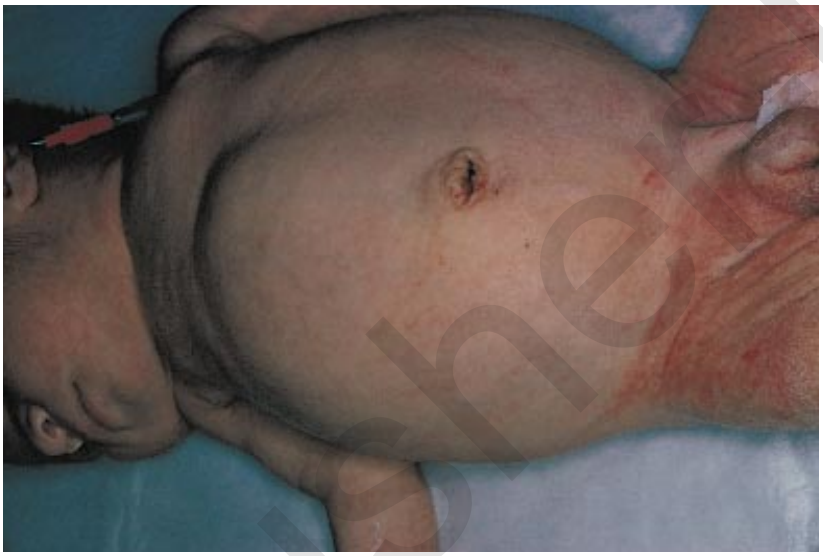

Figure 4.26. This infant with massive abdominal enlargement, especially on the right side, had congenital posterior urethral valves causing bilateral hydronephrosis and hydroureter, both more severe on the right side. Urethral atresia could give the same appearance of gross distention of the bladder, ureters, and kidneys.

4.27

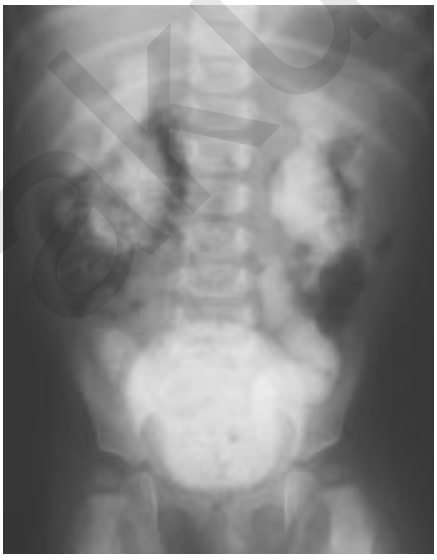

Figure 4.27. The intravenous pyelogram in this infant with congenital posterior urethral valves demonstrates bilateral hydronephrosis, bilateral hydroureters, and a large dilated bladder. Obstructions at the ureterovesical junction result in unilateral involvement of the ureter and kidney and a normal bladder, whereas obstruction in the urethra results in bilateral involvement of the ureters and kidneys and bladder enlargement. (Singleton, E.)

4.28

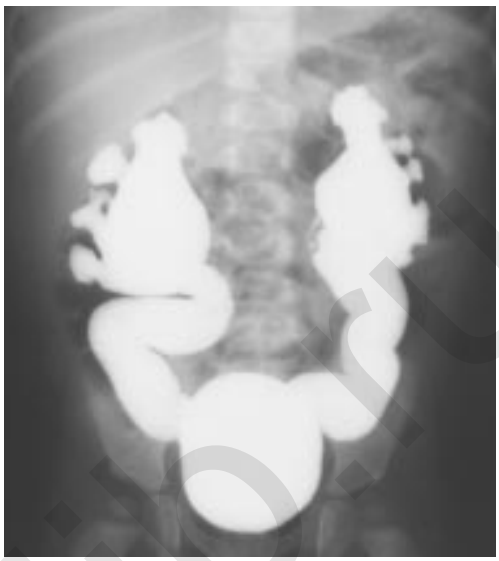

Figure 4.28. A cystogram in the same infant as in Figure 4.27 with posterior urethral valves shows extensive vesicoureteral reflux and bilateral hydroureter and hydronephrosis.

4.29

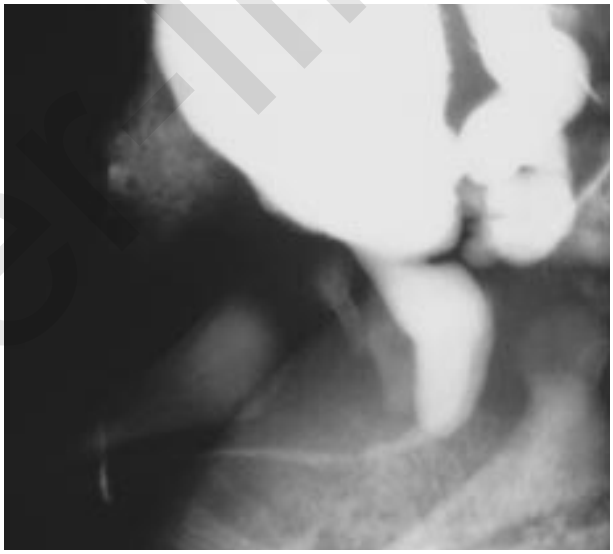

Figure 4.29. Lateral excretory contrast radiograph in an infant with posterior urethral valves. Note the markedly enlarged bladder and large dilated prostatic urethra proximal to the urethral valve. (Singleton, E.)

4.30

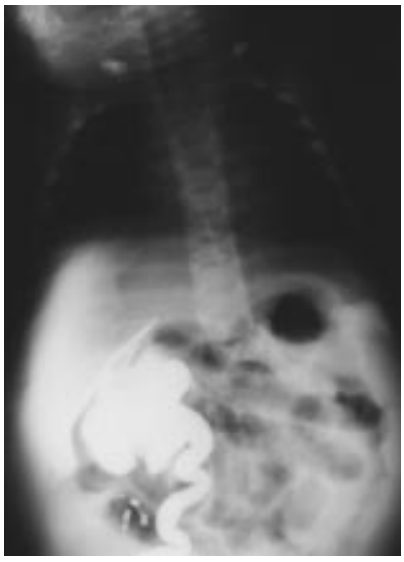

Figure 4.30. This infant with urinary ascites had congenital posterior urethral valves. In the cystogram study note the traumatic rupture of the calyx with extravasation of dye from the renal pelvis. (Singleton, E.)

4.31

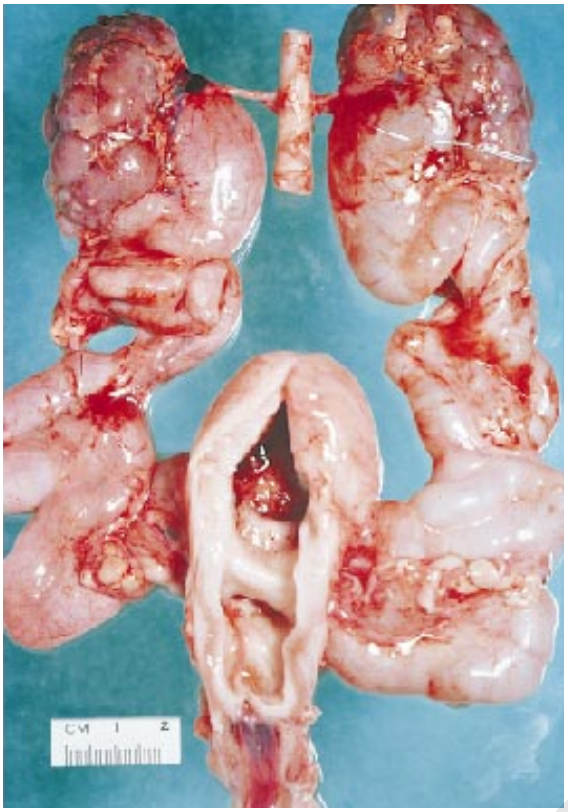

Figure 4.31. Autopsy specimen of the same infant as in Figure 4.30 with congenital posterior urethral valves. Note the urethral valves, enlarged bladder, bilateral hydroureter, and bilateral hydronephrosis.

4.32

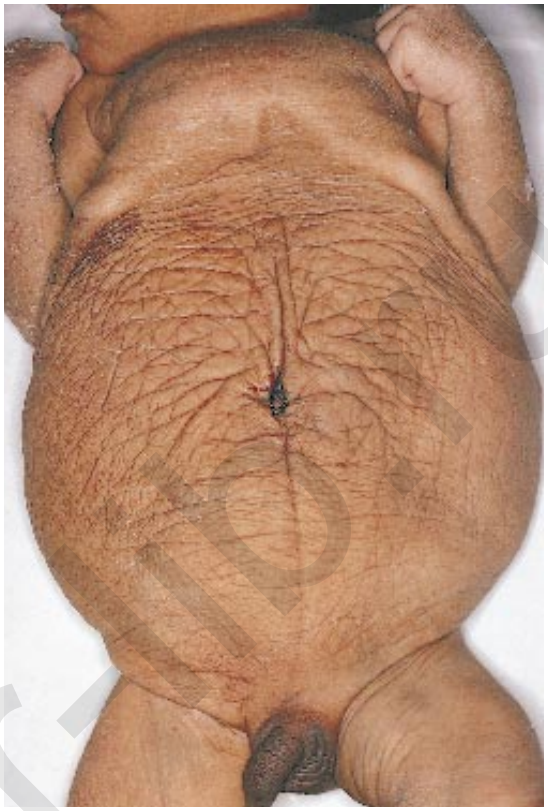

Figure 4.32. An infant with the prune belly syndrome (Eagle-Barrett syndrome; triad syndrome) shows the marked wrinkling of the skin and flaccid abdominal wall which bulges laterally as a result of lack of the underlying abdominal muscles. The triad of findings include absence of the abdominal muscles, urinary tract abnormalities, and cryptorchidism. The abdomen has a doughy consistency on palpation, and the abdominal viscera can be felt with unusual ease.

4.33

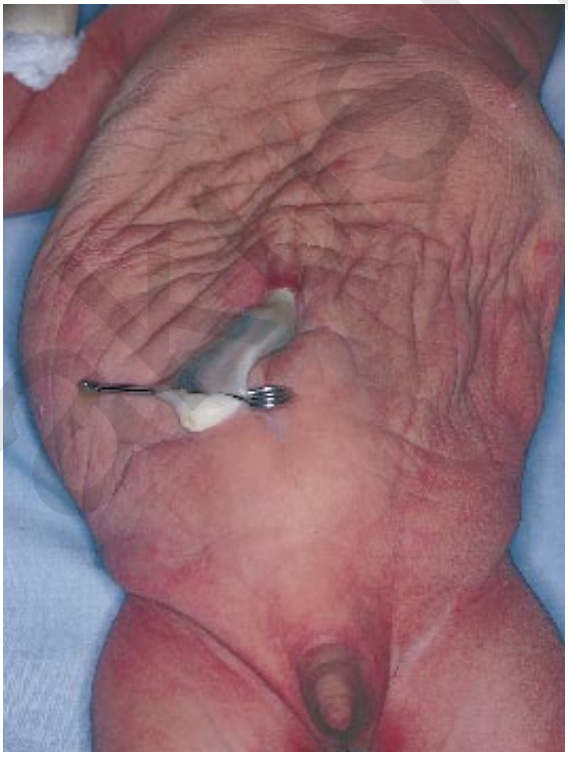

Figure 4.33. Another example of the prune belly syndrome showing the outlines of loops of bowel. The genitourinary tract findings are most frequently the result of obstruction of the distal urethra which causes marked distention of the bladder, and the ureters are dilated and tortuous. Currently it is thought that the marked distention of the bladder and ureters and renal involvement result in the ablation of the abdominal muscles, especially the recti. The kidneys may be hypoplastic or severely hydronephrotic as a result of the obstruction.

4.34

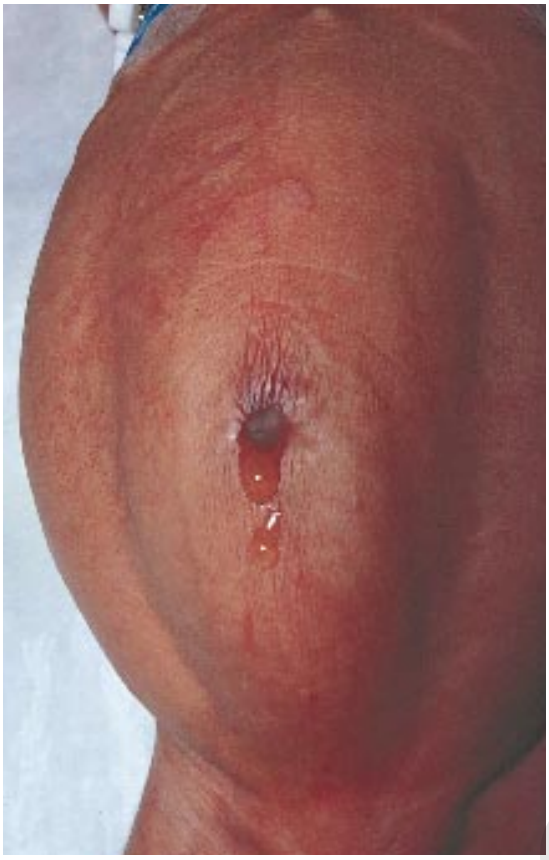

Figure 4.34. Patent urachus in an infant with absence of the abdominal musculature. The urachus is a persistence of the embryologic tract between the fundus of the bladder and the allantoic sac. A patent urachus results from failure of the tract to close and should be suspected when there is urinary drainage through the umbilicus. This finding is not uncommon in the prune belly syndrome.

4.35

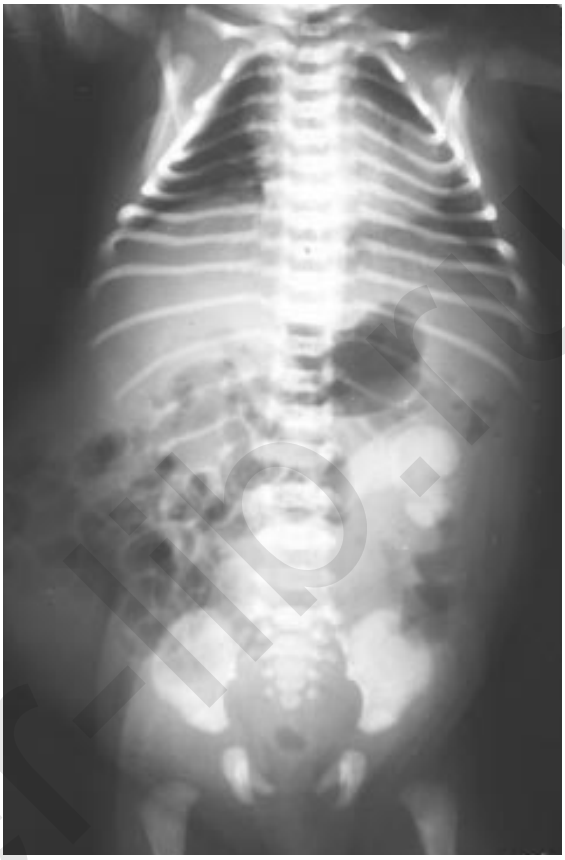

Figure 4.35. Abdominal radiograph in an infant with the prune belly syndrome. Note the marked asymmetrical bulging of the flanks.

4.36

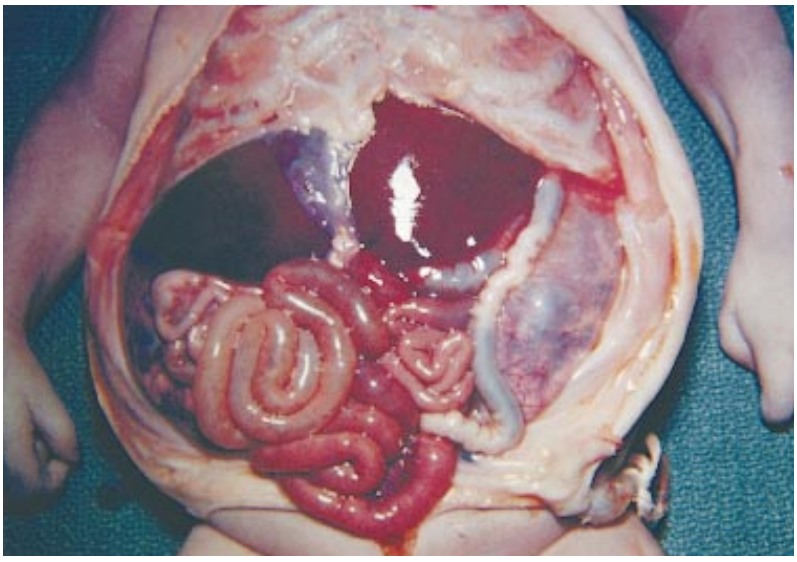

Figure 4.36. Autopsy specimen in an infant with the prune belly syndrome showing the marked bulging of the flanks, lack of abdominal muscles, and bilateral polycystic kidneys.

4.37

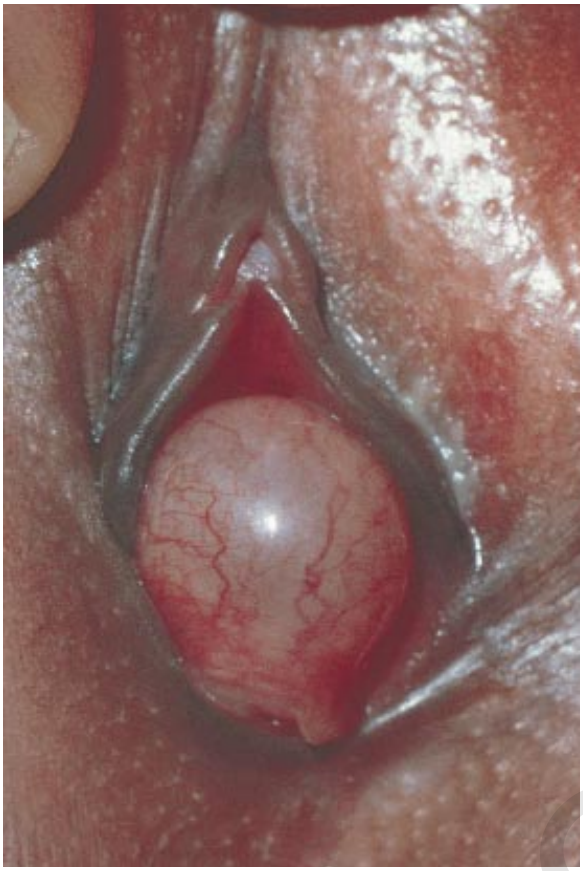

Figure 4.37. This female infant presented with a genital mass superior to the vaginal introitus. The mass is a large ureterocele coming out of the vagina. (Gonzalez, E.)

4.38

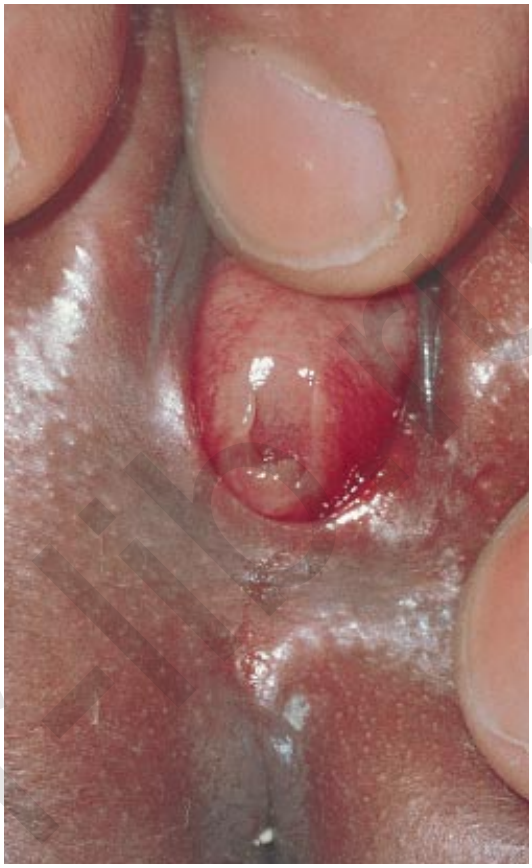

Figure 4.38. The mass is raised superiorly in the same infant as in Figure 4.37 to demonstrate a normal vaginal introitus. (Gonzalez, E.)

4.39

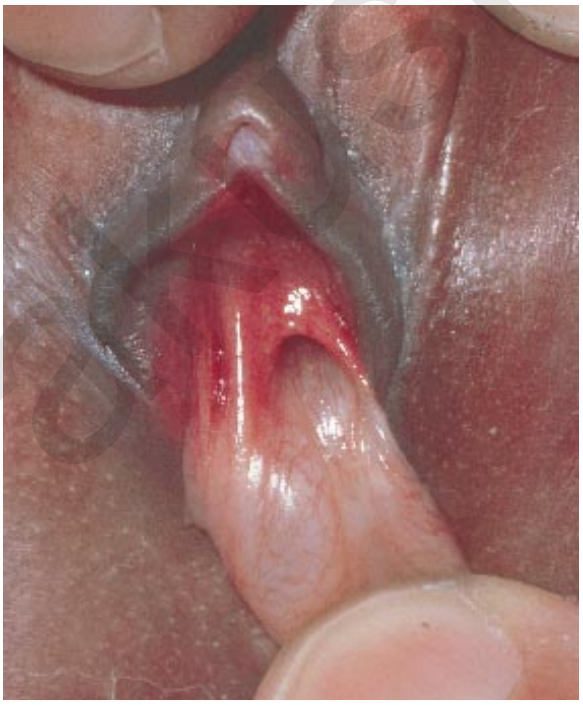

Figure 4.39. Gentle traction on the urethra of the same infant as in Figures 4.37 and 4.38 delineates the association of the cystic mass arising from the floor of the urethra. (Gonzalez, E.)

4.40

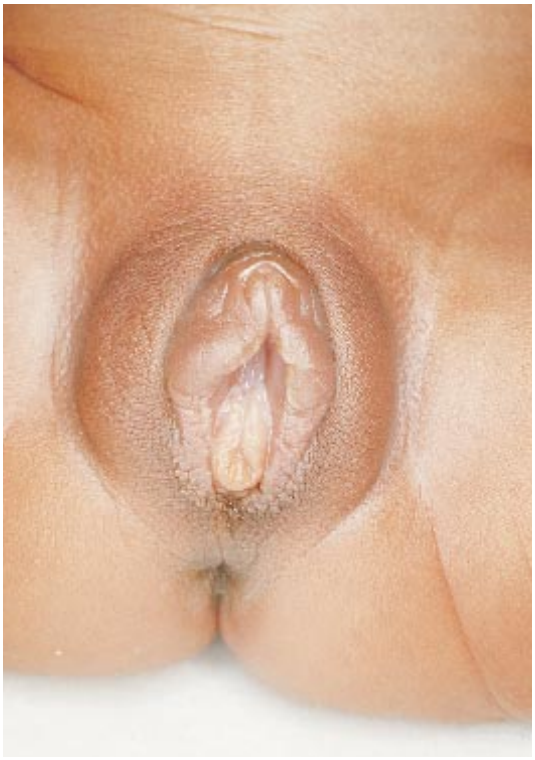

Figure 4.40. The genitalia of the normal female infant gape, partially revealing the labia minora and, perhaps, the clitoris. The labia majora are full, and the thickened labia minora protrude between them. The mucosa normally is pink and a mucoid vaginal secretion is common.

4.41

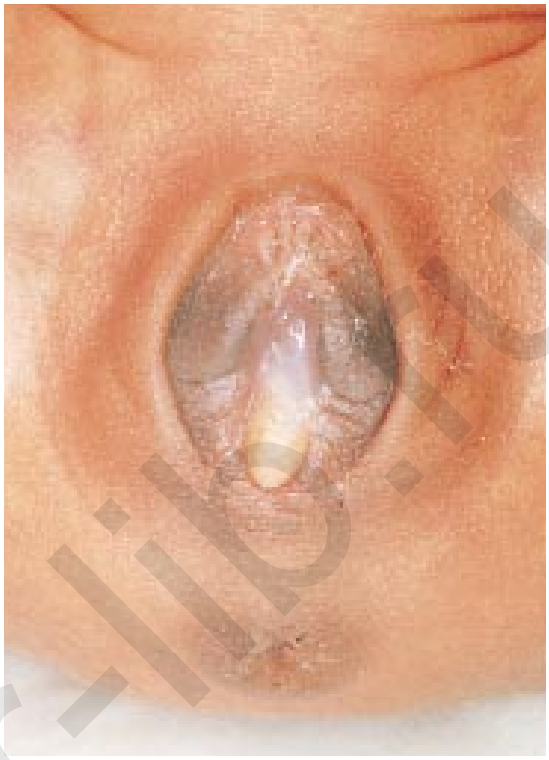

Figure 4.41. Normal external female genitalia in a premature infant. Note the prominence of the labia minora. The clitoris is large in preterm babies with the result that the inexperienced physician may suspect ambiguous genitalia.

4.42

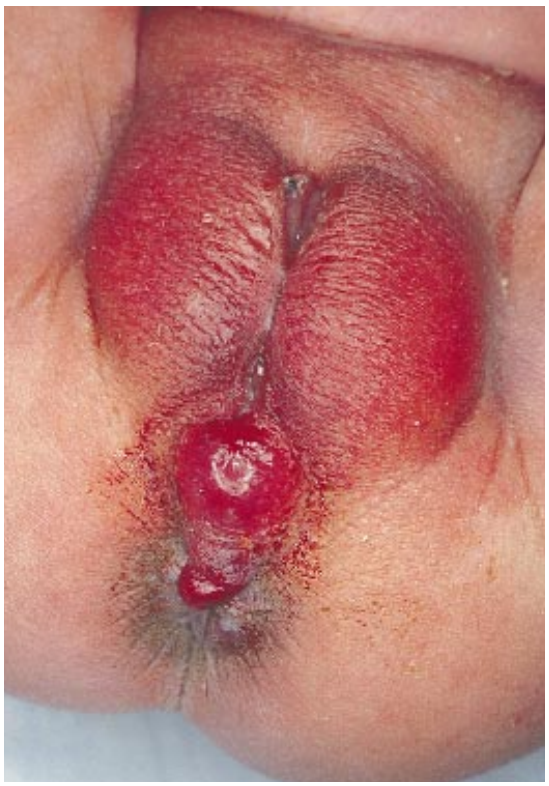

Figure 4.42. Marked swelling and bruising of the external genitalia in a normal female infant born via breech extraction. Some of the trauma may occur during vaginal exam of the mother during labor. This usually improves rapidly.

4.43

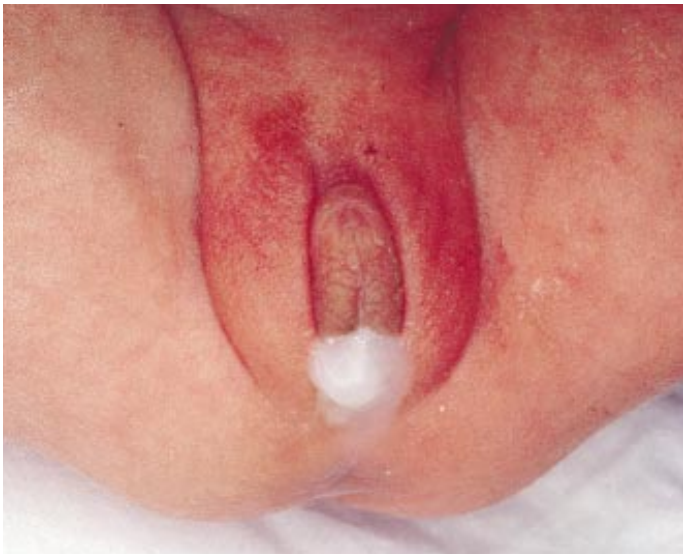

Figure 4.43. Normal mucoid vaginal discharge in a normal female infant. This results from the "withdrawal effect" from the in utero environment.

4.44

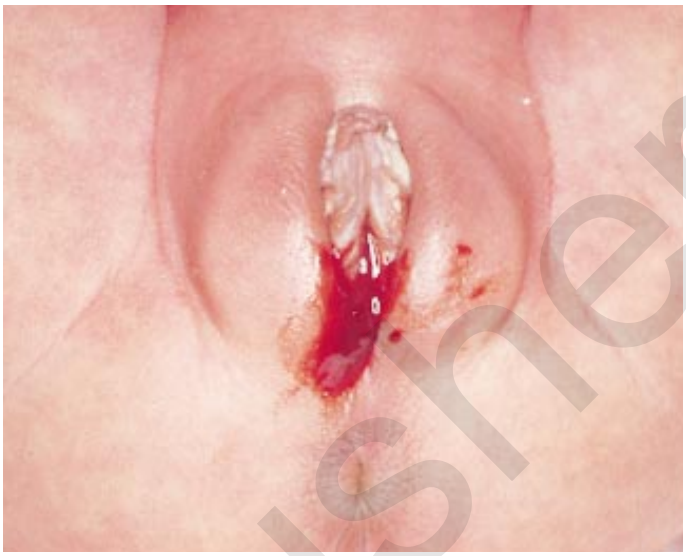

Figure 4.44. "Withdrawal" bleeding in a normal female neonate. Vaginal bleeding is not uncommon in the first week of life. It is caused by the withdrawal of the high maternal estrogen level to which the baby has been exposed in utero. Vaginal bleeding is self-limited in that transplacental hormone withdrawal effect starts on the third to fourth day of life and continues for 2 to 3 days.

4.45

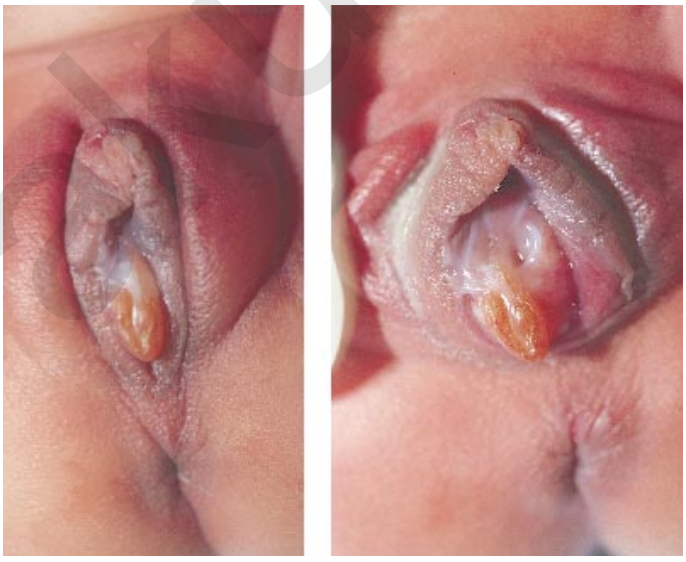

Figure 4.45. This normal female infant has a hymenal tag, which is a protrusion of redundant vaginal mucosa. Hymenal tags are a common finding and usually resolve spontaneously.

4.46

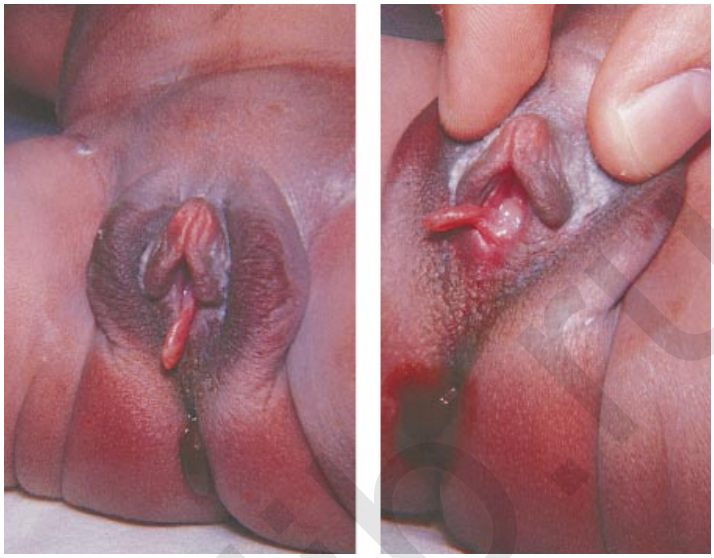

Figure 4.46. Another variant of a hymenal tag in a normal female infant. Hymenal remnants usually resolve spontaneously.

4.47

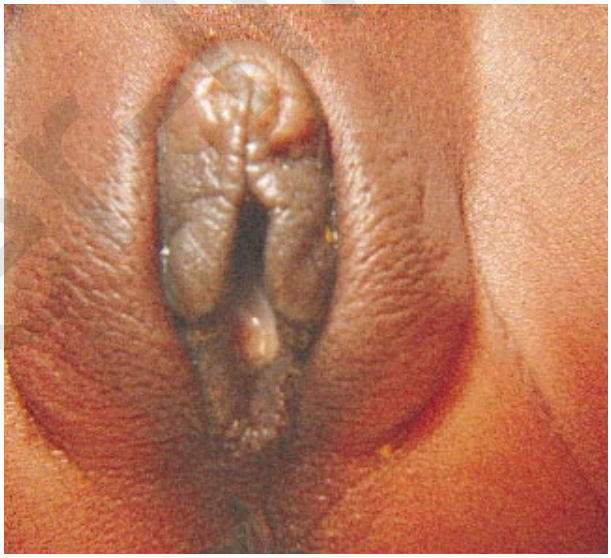

Figure 4.47. Clitoral hypertrophy giving the appearance of ambiguous genitalia. Potentially life-threatening adrenal abnormalities must be ruled out. Clitoral hypertrophy is the result of increased androgen stimulation as a result of a luteoma of pregnancy. This resolves after pregnancy. There was no adrenal anomaly in this infant.

4.48

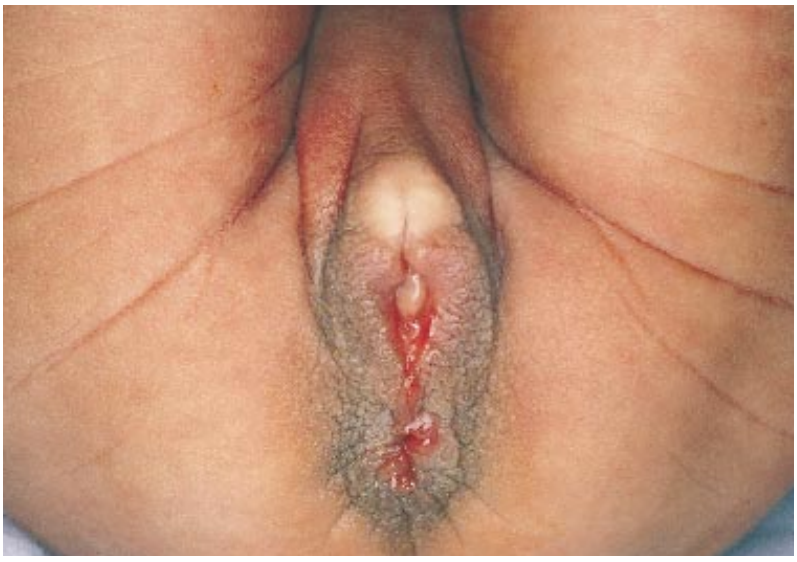

Figure 4.48. Abnormal female genitalia in this infant with prominent labia minora, clitoral enlargement, and anterior placement of the anus. Hypoplasia of the labia majora may give rise to the false impression of a large clitoris.

4.49

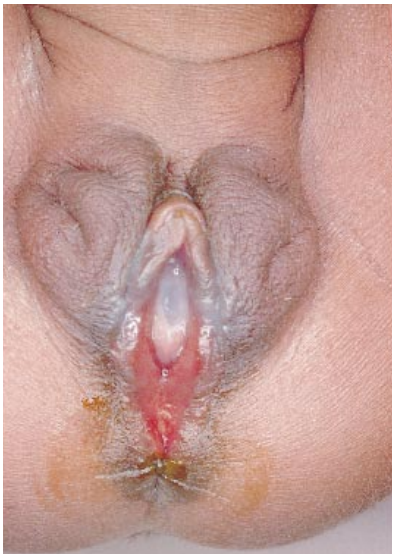

Figure 4.49. Abnormal anus as the result of failure of the fusion of the perineal raphe involving the external sphincter. The labia majora are very prominent and give the impression of scrotalization.

4.50

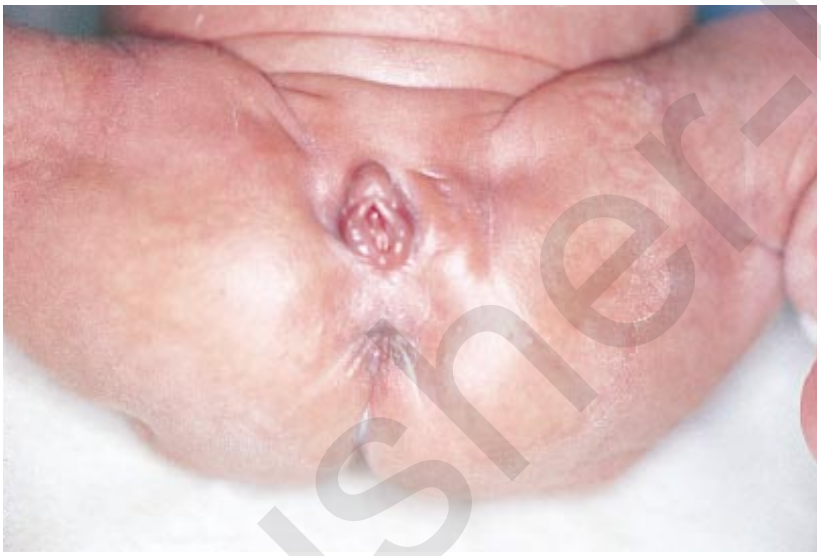

Figure 4.50. Absence of the labia majora in an infant with the popliteal pterygium syndrome.

4.51

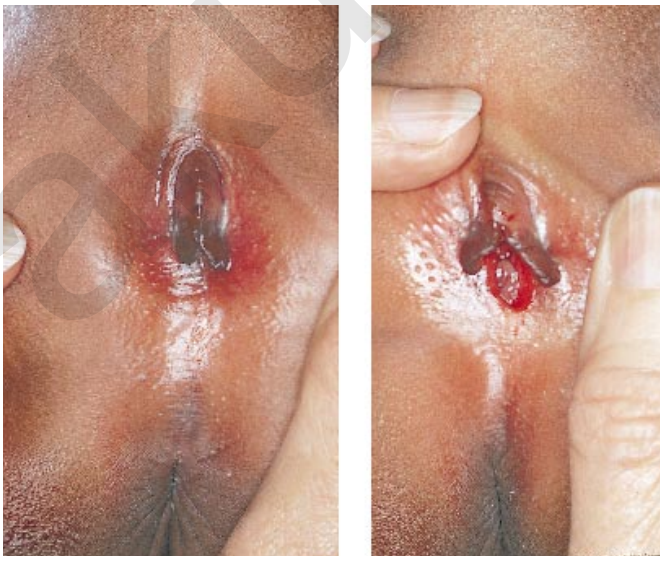

Figure 4.51. This female infant shows, on the left, adhesions of the labia minora (synechia of the labia). On the right the adhesions have been separated. These adhesions are sometimes present at birth and often can be separated, as in this infant, by gentle traction with the fingers. They are thought to occur as a result of maternal hormone effect.

4.52

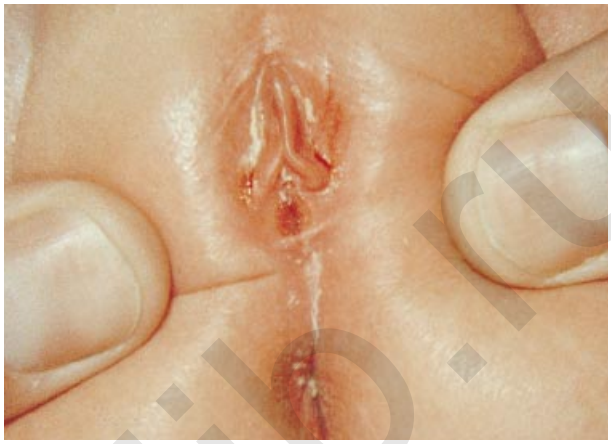

Figure 4.52. Adhesions of the labia minora (synechia of the labia) with some associated normal mucoid vaginal secretions. These adhesions could not be separated readily by the fingers. Separation was accomplished by inserting a probe behind the fusion and pulling forward.

4.53

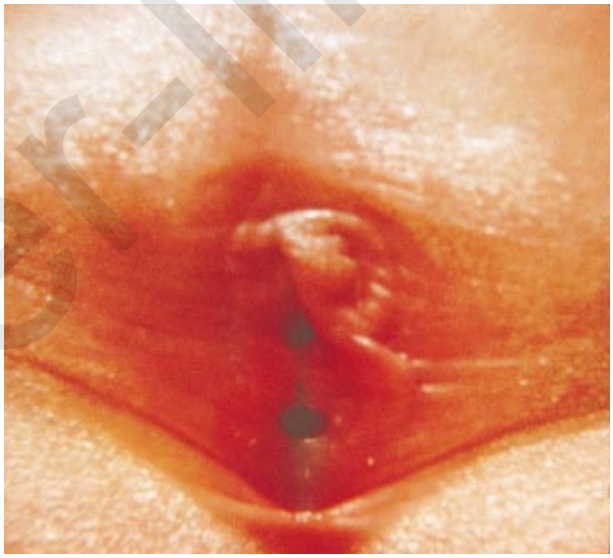

Figure 4.53. Close-up view of labial adhesions in another newborn infant. Rarely complete closure of the vaginal orifice can result in urinary retention.

4.54

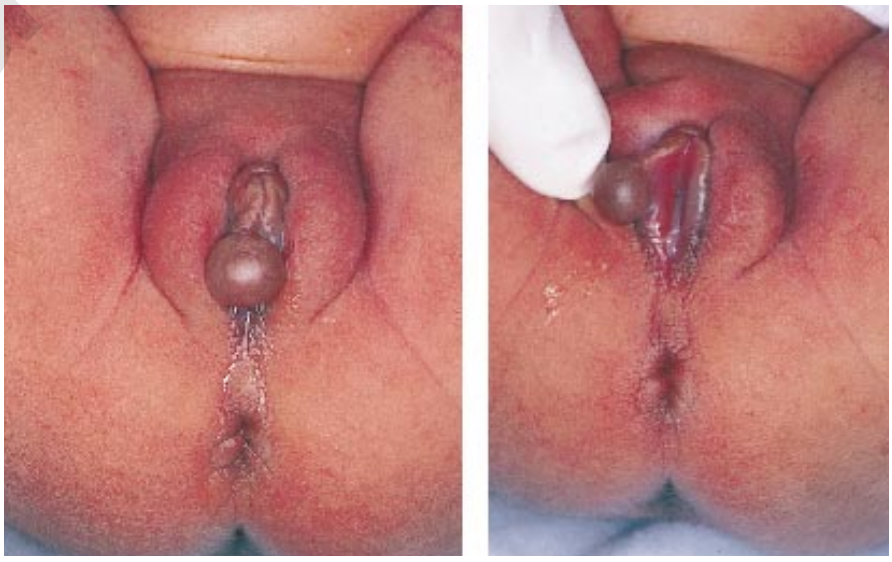

Figure 4.54. A cyst arising in the wall of the right labium minora. The cyst was removed and identified as a retention cyst.

4.55

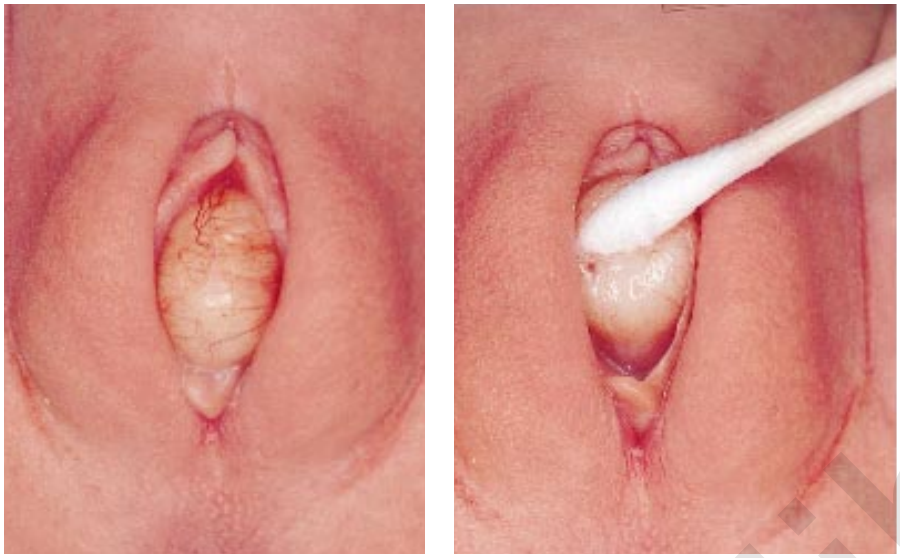

Figure 4.55. A left-sided Skene's gland cyst. In the figure on the left this appears to be midline and would raise concerns about the diagnosis of hydrocolpos. In the figure on the right, the diagnosis of a Skene's gland cyst on the left side is confirmed by the inability to pass a cotton-tip swab on the left side.

4.56

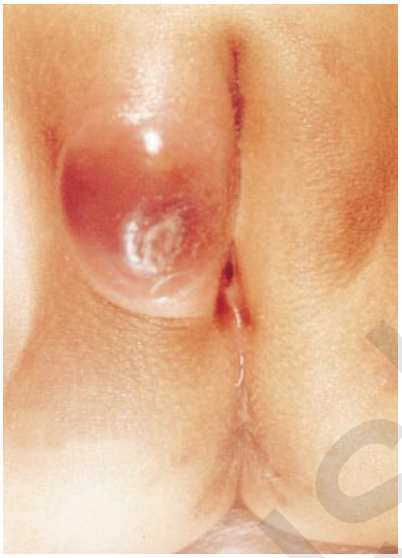

Figure 4.56. Involvement of Bartholin's gland is extremely rare in the neonate. This infant at the age of 2 weeks developed a Bartholin's cyst abscess.

4.57

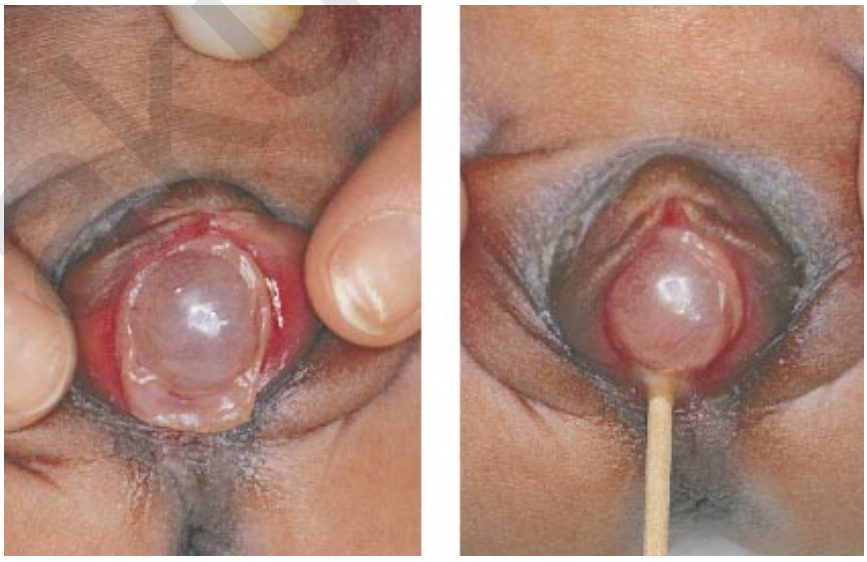

Figure 4.57. This infant presented with a swelling in the vagina. On the left note the typical appearance of a hydrocolpos. On the right, the use of the blunt end of a cotton tip swab demonstrates no obstruction on either side of the cystic swelling; therefore the cyst did not arise from the vaginal wall and the diagnosis is hydrocolpos.

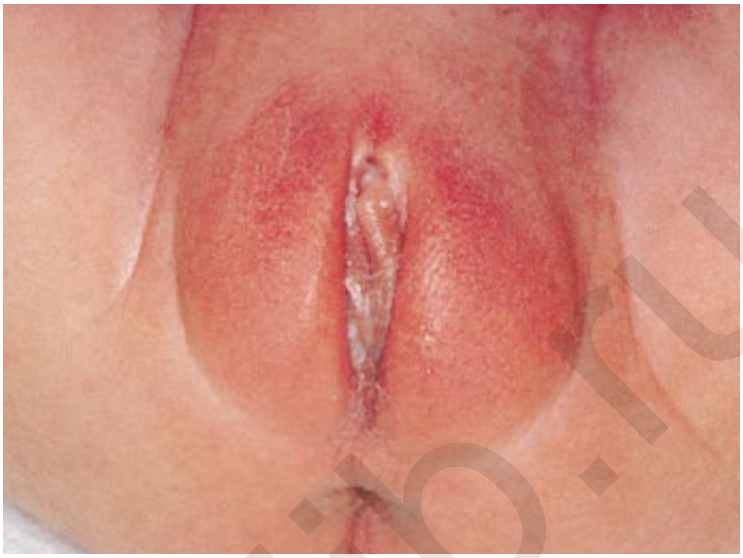

4.58

Figure 4.58. Normal appearance of the external female genitalia in an infant who presented with abdominal distention. The infant had hydrometrocolpos. The diagnosis can be missed if the external genitalia are not carefully examined. This stresses the importance of doing a careful examination on the external female genitalia.

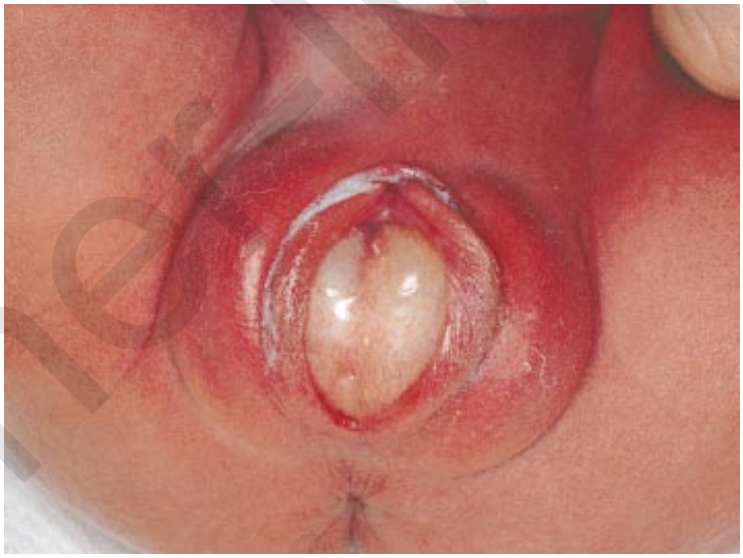

4.59

Figure 4.59. In the same infant as in Figure 4.58, with application of external abdominal pressure and spreading of the labia majora, a large cystic mass is revealed at the introitus. The abdominal distention is the result of hydrometrocolpos. Hydrocolpos is caused by a firm membrane (imperforate hymen) that covers the vaginal outlet, preventing drainage and thus resulting in accumulation of vaginal secretions in the vagina. If the secretions extend into the uterine cavity causing uterine enlargement, the diagnosis is hydrometrocolpos. Occasionally, maternal hormone secretion may cause pseudomenses, resulting in a reddish- or bluish-colored material behind the membrane (hematocolpos or hematometrocolpos).

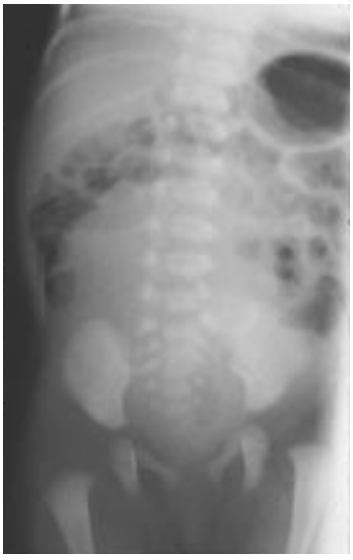

4.60

Figure 4.60. An abdominal radiograph of an infant with hydrometrocolpos. Note the superior and lateral displacement of the normal loops of bowel and the associated central opacification due to the enlarged uterus. Diagnosis is confirmed by examining the vagina.

4.61

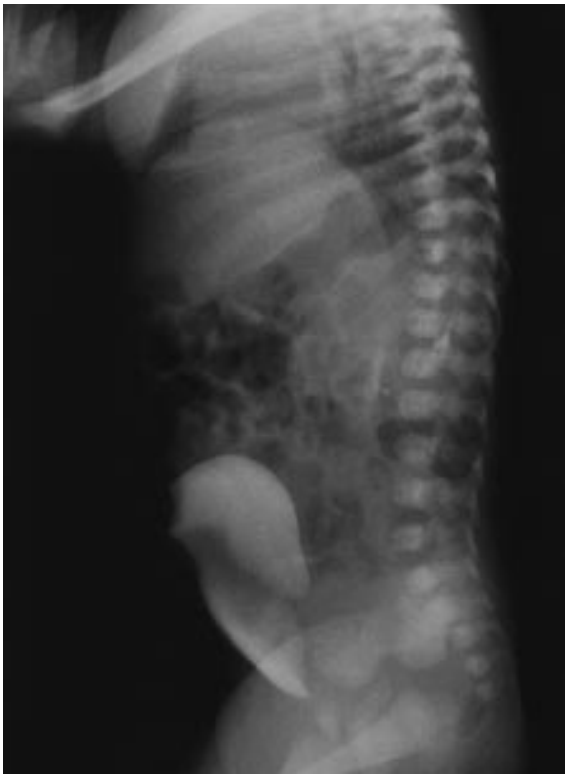

Figure 4.61. Contrast dye study in the same infant as in Figure 4.60 with hydrometrocolpos. Note the outline of the enlarged uterine cavity. This can cause pressure on the ureters, resulting in hydroureter and hydronephrosis.

4.62

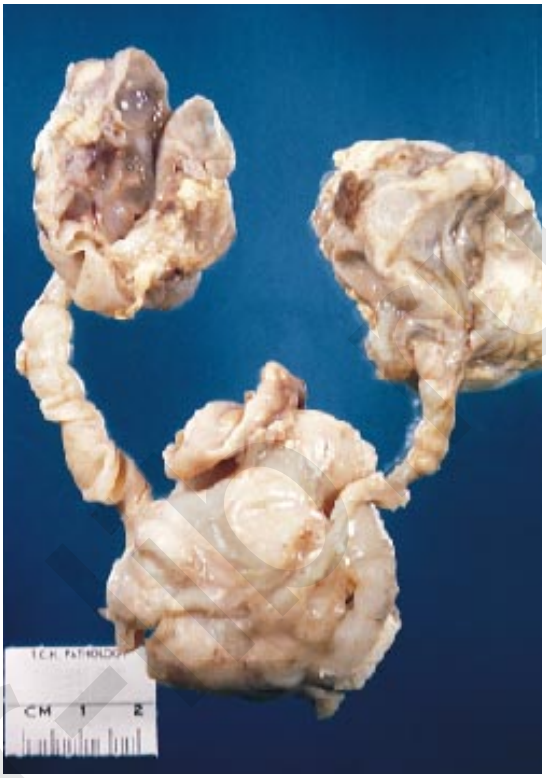

Figure 4.62. Autopsy specimen of an infant with bilateral hydronephrosis and hydroureter as a result of severe hydrometrocolpos causing pressure on both ureters. Note the markedly enlarged uterus.

4.63

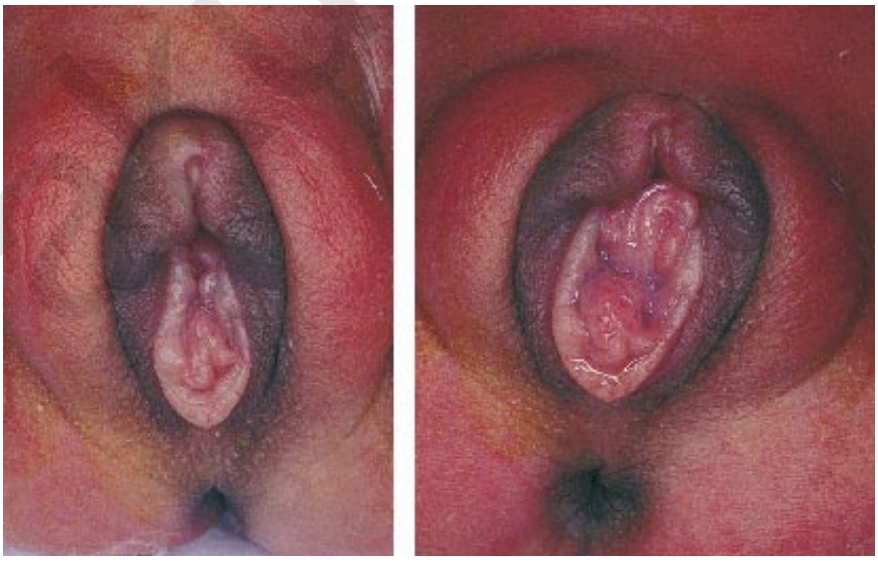

Figure 4.63. Mild procidentia (prolapse of the uterus) in an otherwise normal newborn.

4.64

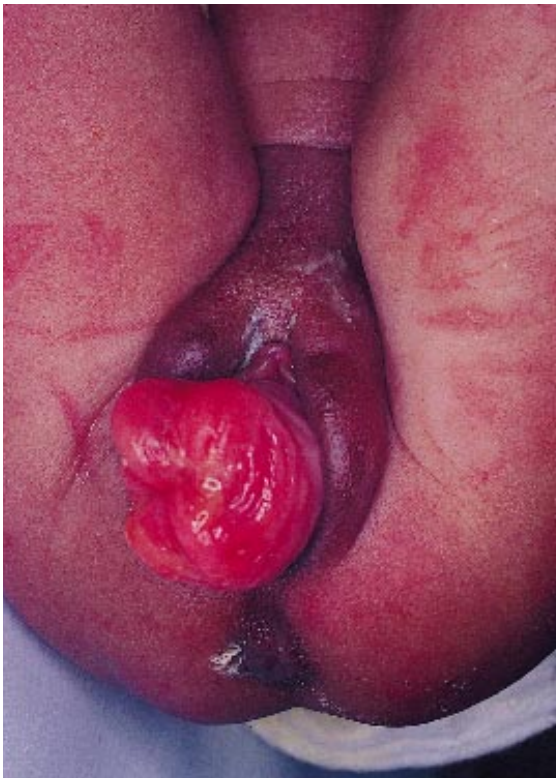

Figure 4.64. This neonate has a severe procidentia (prolapse of the uterus) to such a degree that the cervix protrudes from the vaginal outlet. The infant had an associated meningomyelocele. Procidentia in the newborn is almost invariably associated with neural tube defects.

4.65

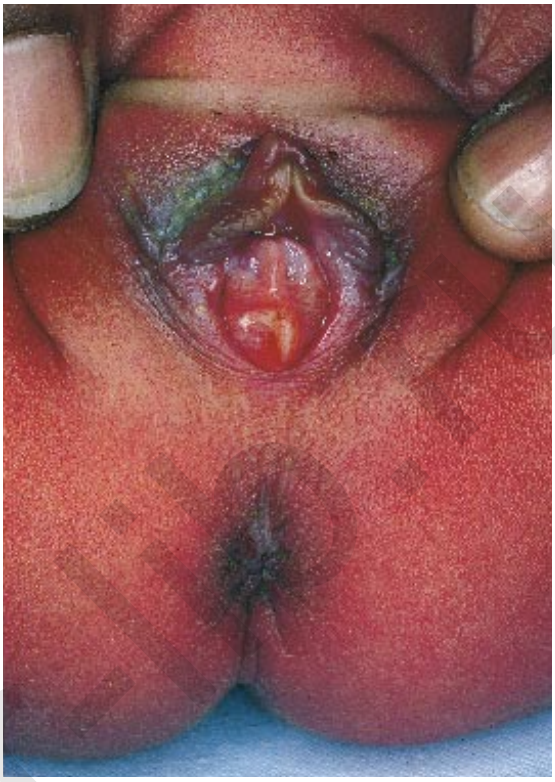

Figure 4.65. In this infant there is duplication of the external genitalia. Note the two vaginal orifices. Duplication of the external genitalia is extremely rare. It has been reported as part of an apparent sagittal mirror-image doubling of the posterior axis of the embryo. Partial or complete duplication of the vagina, labia, penis or scrotum may be caused by inadequate androgenic stimulation or end-organ unresponsiveness during late fetal life.

4.66

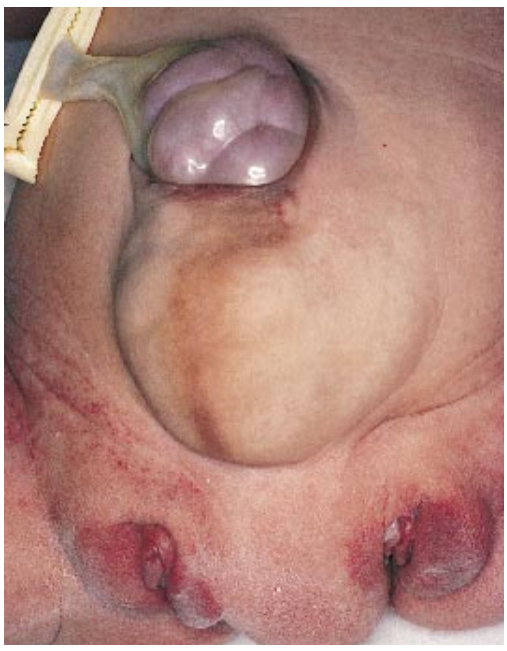

Figure 4.66. This infant has duplication of the external female genital tract with other associated anomalies which include omphalocele, absent rectus muscle, and congenital heart disease.

4.67

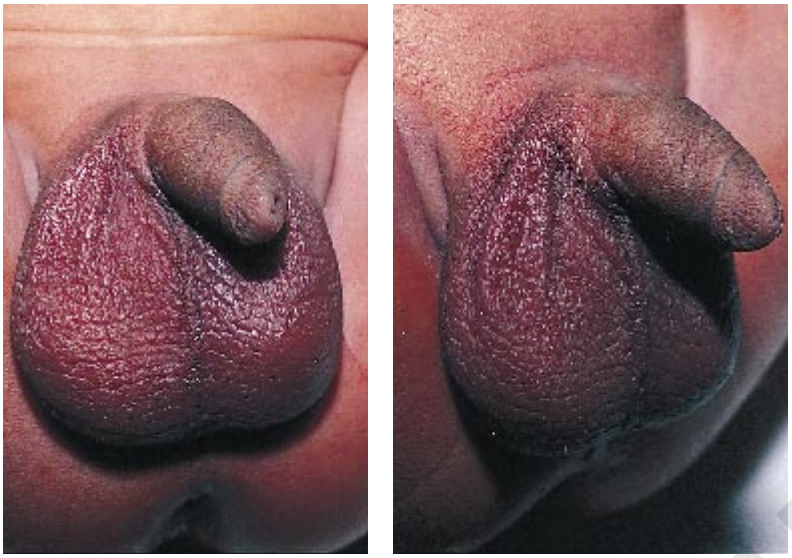

Figure 4.67. Normal external genitalia in a term male infant. In the newborn male, the relatively large size of the phallus gives the baby the appearance of being "well-endowed." On examination note the size of the phallus and the presence or absence of testes in the scrotum. An unusually large phallus for age usually indicates abnormal androgenic stimulation of testicular or adrenal origin. A true micropenis may represent either deficient hormonal stimulation during growth or a failure of early morphogenesis. Midline hypopigmentation may be noted on the gonads of dark-skinned newborn infants. They may have no other areas of hypopigmentation.

4.68

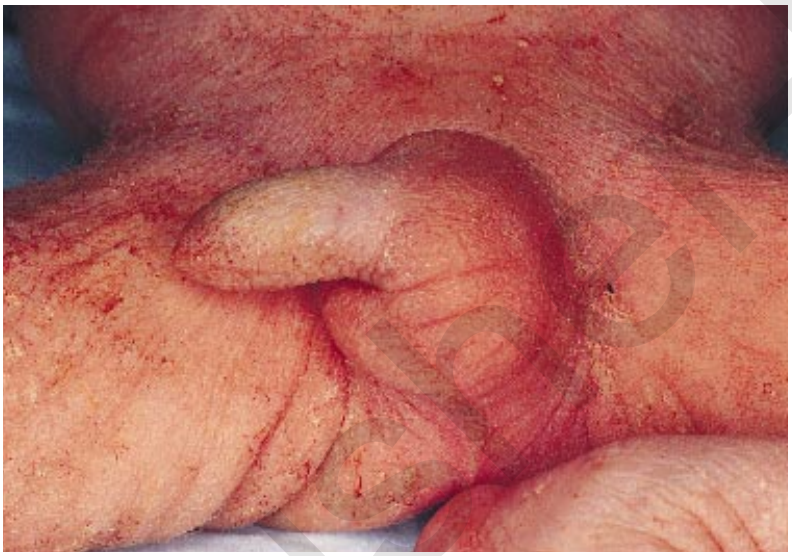

Figure 4.68. Normal male genitalia in a premature infant with a gestational age of 34 weeks. Note the lack of fullness of the scrotum due to the undescended testes. Note the presence of few rugae which are only on the undersurface of the scrotum. This appearance is consistent with the gestational age of 34 weeks.

4.69

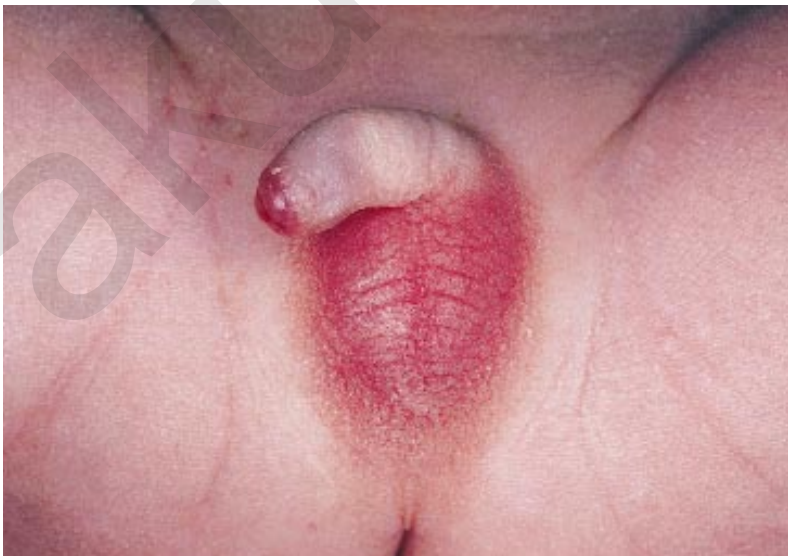

Figure 4.69. Bilateral undescended testes with an empty scrotum in a term male infant.

4.70

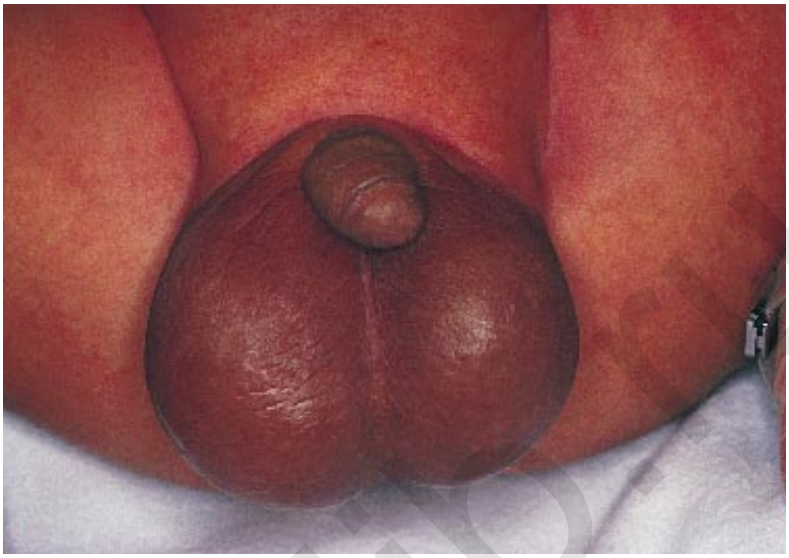

Figure 4.70. Bilateral hydroceles in a term male infant. Hydroceles arise from an abnormal collection of fluid in the tunica vaginalis which has failed to invaginate following descent of the testis. This is recognized clinically as a scrotal mass that transilluminates. At birth, up to 15 to 20% of male infants may have some degree of hydrocele. Complete spontaneous resolution is to be expected over a period of a few weeks to months.

4.71

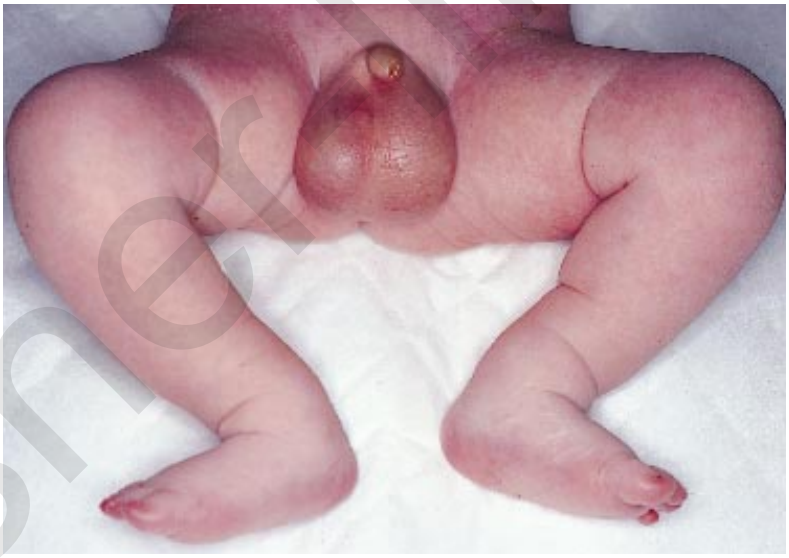

Figure 4.71. Bilateral hydroceles in a term infant with micropenis. The diagnosis of micropenis should be made after careful examination, as a normal penile shaft may be partially buried in the pubic fat pad in a neonate. Micropenis denotes a truly hypoplastic penile shaft.

4.72

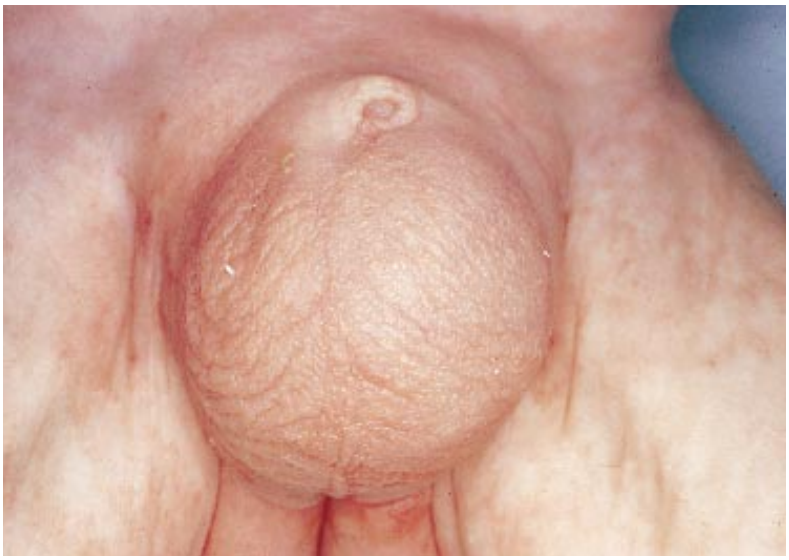

Figure 4.72. Large bilateral hydroceles in a premature infant with a normal-sized penis. In infants with hydrocele of the spermatic cord, the swelling is also noted in the groin and thus a hydrocele of the cord must be distinguished from an inguinal hernia.

4.73

Figure 4.73. Transillumination of bilateral hydroceles in a term infant. In the case of an indirect hernia, transillumination is negative.

4.74

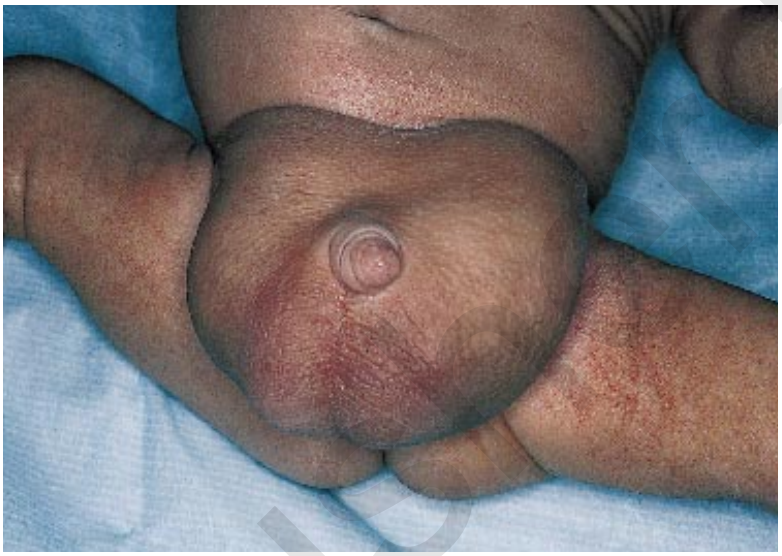

Figure 4.74. Massive bilateral inguinal herniae in a 10-week-old (weight 1900 g) premature infant with a birthweight of 700 g. Inguinal herniae occur commonly in neonates but rarely are present at birth. They are much more common in male infants and premature infants, and there is a risk of irreducibility and strangulation.

4.75

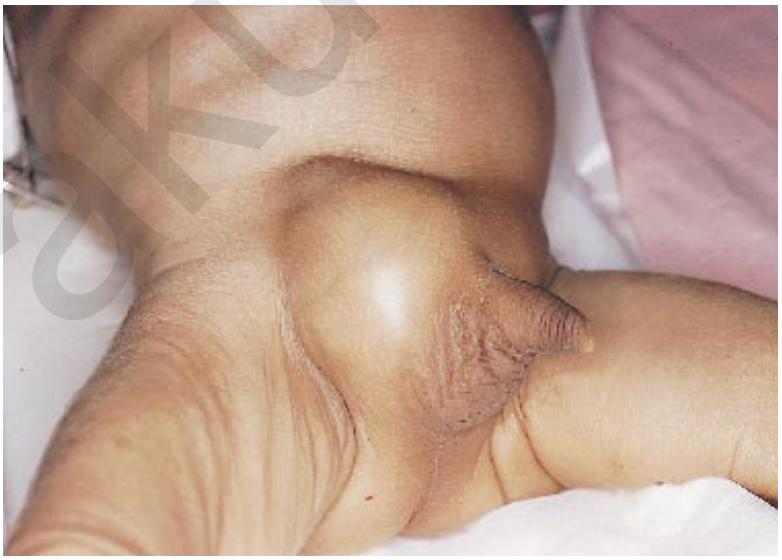

Figure 4.75. A unilateral right inguinal hernia in a male infant with trisomy 13.

4.76

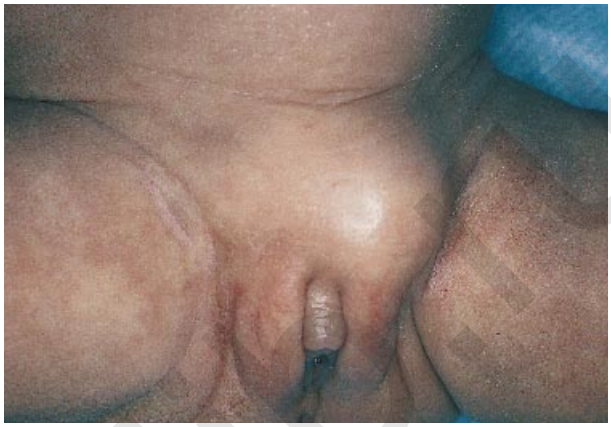

Figure 4.76. Large left-sided inguinal hernia in a 9-week-old (weight 1800 g) female premature infant with a birthweight of 750 g. Inguinal herniae are much less common in female infants. Prematurity and increased abdominal pressure increase the incidence. A mass, which is usually an ovary, may be present in the hernial sac.

4.77

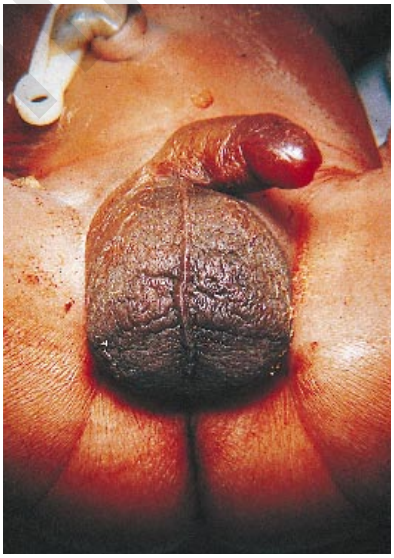

Figure 4.77. Marked edema and bruising of the external genitalia of a male infant delivered as a breech presentation. This infant had problems with voiding for the first 48 hours of life and required catheterization.

4.78

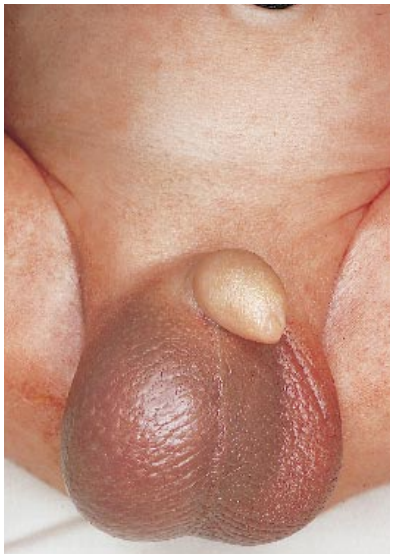

Figure 4.78. This infant, delivered as a breech presentation, developed marked swelling of the right side of the scrotum. There was a purplish-blue discoloration and a hard firm tender mass was palpated. The differential diagnosis included torsion of the testis and hematoma. Note that the swelling and discoloration extend beyond the midline to a portion of the left side of the scrotum. This would exclude the diagnosis of torsion of the testis and confirm a diagnosis of hematoma.

4.79

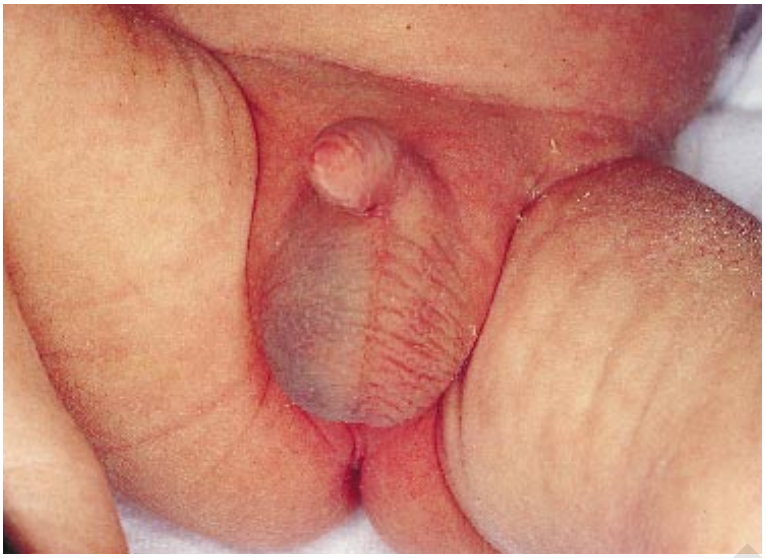

Figure 4.79. Another infant with a hematoma of the right side of the scrotum. In this case, note that the purplish-blue discoloration and swelling do not cross the midline. It would be more difficult to exclude a torsion of the testis in this case. The diagnosis of hematoma was confirmed at surgery.

4.80

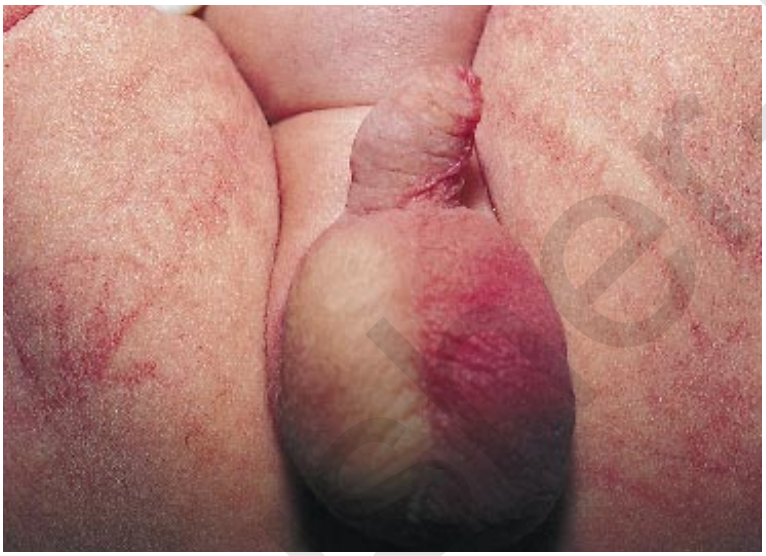

Figure 4.80. Torsion of the left testis which was present at birth. The left side felt firm and tender and there was purplish scrotal discoloration which did not cross the midline. The testicular scan may show the characteristic "bull's eye" sign of the vascular supply. With the advent of ultrasonography, the diagnosis is readily confirmed and a scan is not required. This represents a surgical emergency, but the testis usually sustains too much vascular compromise and cannot be salvaged.

4.81

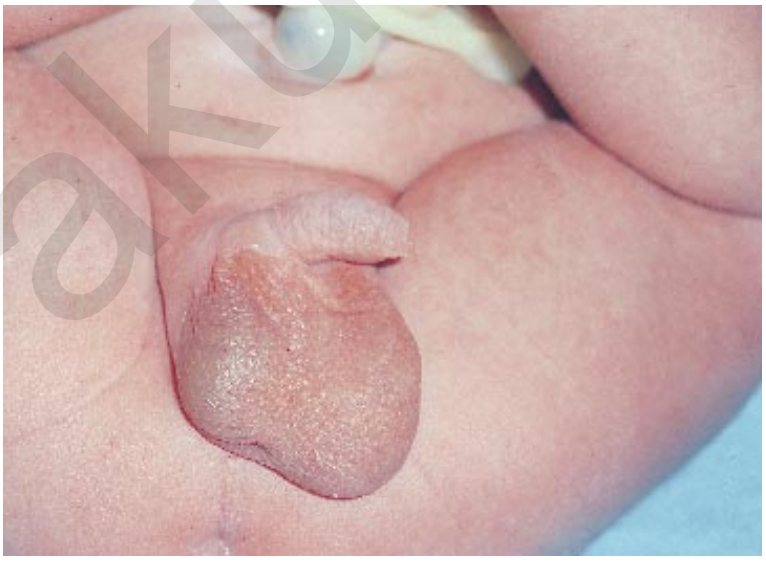

Figure 4.81. This infant has a torsion of the right testis. Note the purplish-blue appearance of the right testis which was firm and tender. The testis usually "rides high" with a torsion. The infant has a hydrocele on the left side. Torsion can lead to irreversible damage of the testis within 6 hours of the occurrence. Testicular salvage is almost unheard of because the torsion often occurs prenatally during the process of testicular decent.

4.82

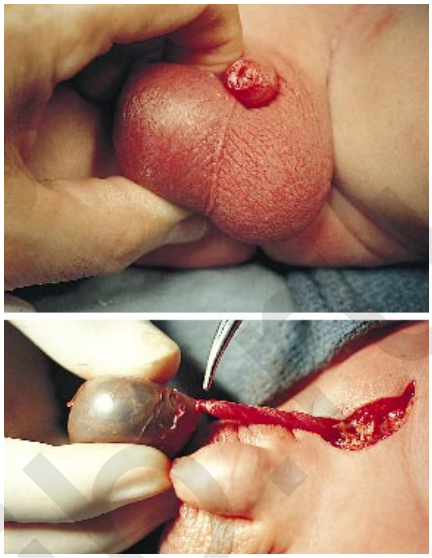

Figure 4.82. At surgery in this same infant as in Figure 4.81, note the gangrene of the right testis and its spermatic cord. It is impossible to salvage such a testis. (Gonzalez, E.)

4.83

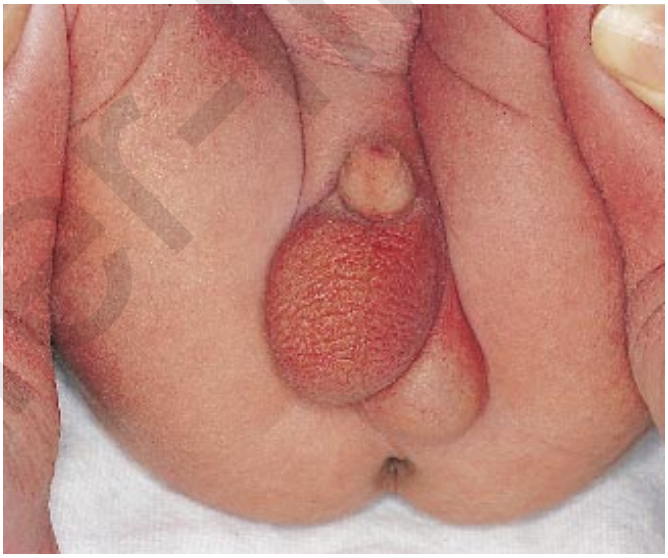

Figure 4.83. This infant has a left ectopic testis located in the perineum. The testes migrate from the abdominal cavity to the scrotum in the last trimester of pregnancy. Occasionally one testis fails to descend normally and migrates to an abnormal site. Note the emptiness of the left scrotal sac.

4.84

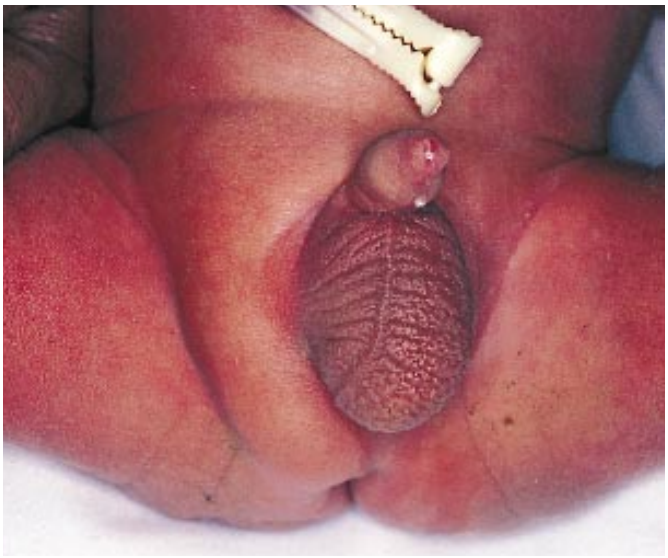

Figure 4.84. There is an ectopic testis on the right side in this infant. Note the normal scrotal sac on the left with a palpable testis. There was an empty scrotal sac on the right side and the testis was palpable in the perineum.

4.85

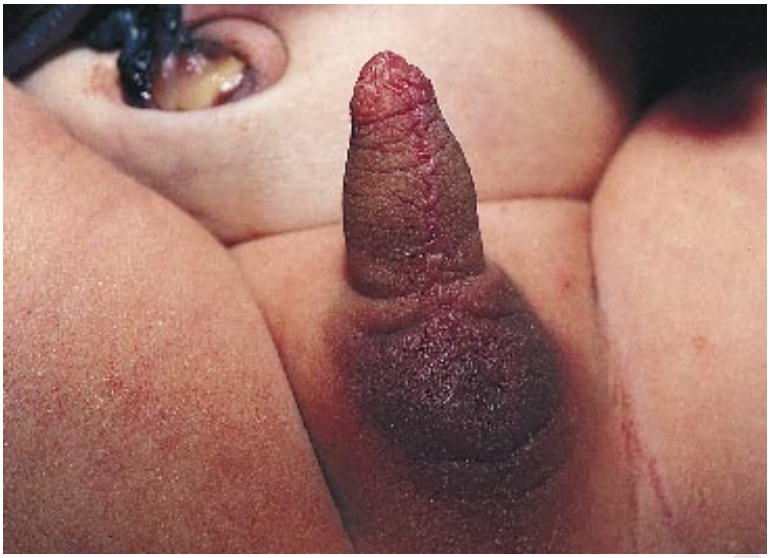

Figure 4.85. Bilateral cryptorchidism in a term infant with a normal penis. Note the empty scrotal sacs and the median raphe which traverses the underside of the penile shaft and scrotum. Babies of the youngest gestational ages have the highest rate of undescended testes or cryptorchidism. Even at term, about 3% of male infants have an incompletely descended testis on one side (nearly twice as often on the right as on the left). The majority descend within the first year.

4.86

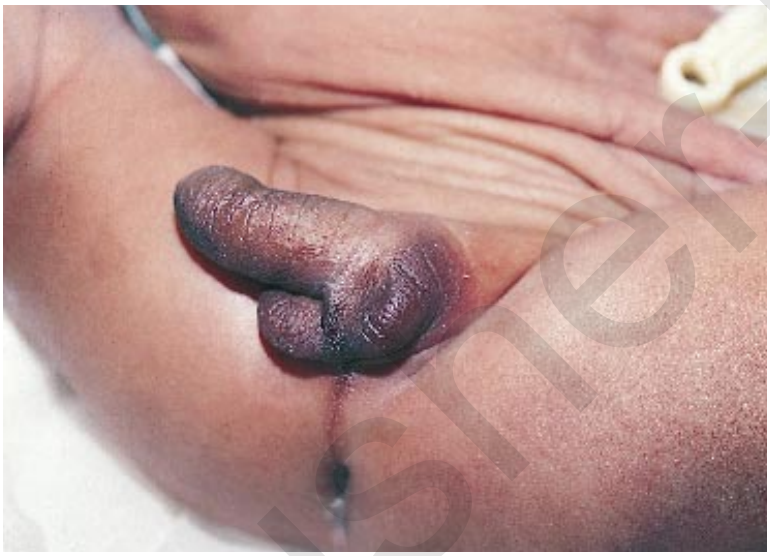

Figure 4.86. Cryptorchidism in an infant with prune belly syndrome. This is part of the triad of absence of abdominal musculature, genitourinary tract abnormalities, and cryptorchidism.

4.87

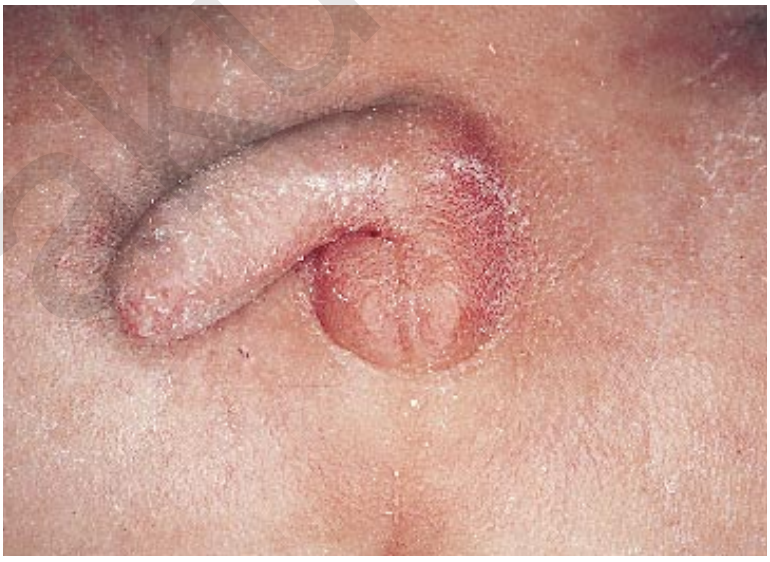

Figure 4.87. Cryptorchidism in an infant with Prader-Willi syndrome. This finding and hypotonia should alert one to consideration of the diagnosis of Prader-Willi syndrome in the neonatal period.

4.88

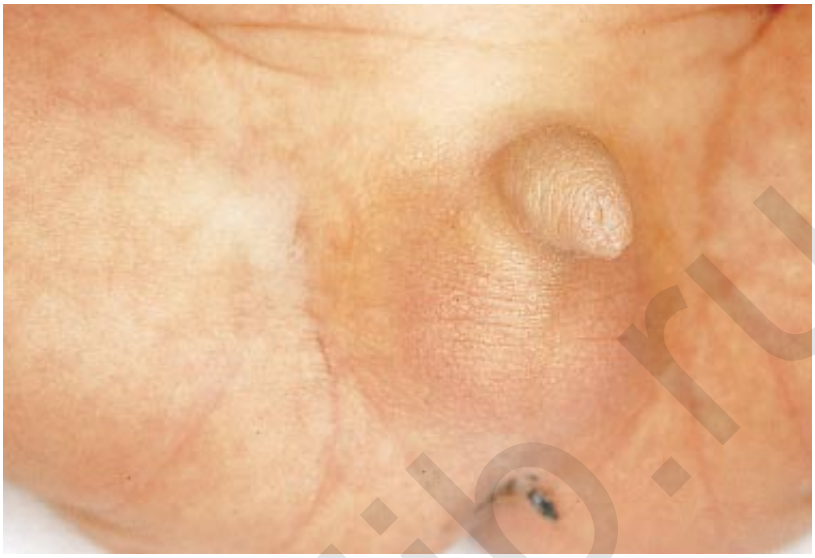

Figure 4.88. Hypogonadism in a term infant. Note the small penis and empty scrotal sacs.

4.89

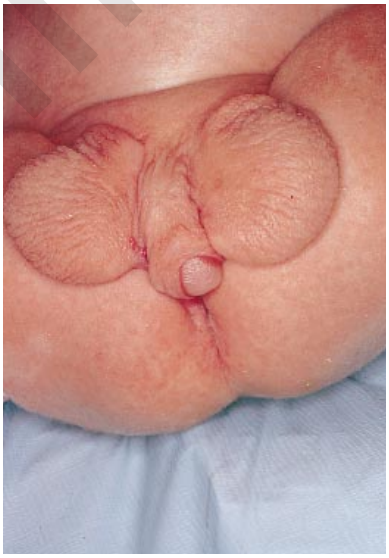

Figure 4.89. This infant has a bifid scrotum which indicates failure of the testosterone-induced fusion of the two labioscrotal folds at about 10 to 11 weeks of gestation with partial penoscrotal transposition. The scrotum is divided into two halves, each containing a testis; this condition may be associated with other perineal abnormalities such as hypospadias or imperforate anus.

4.90

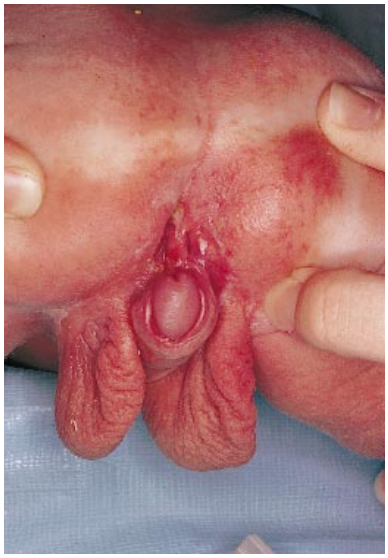

Figure 4.90. Another view of the same infant as in Figure 4.89 with the infant lying on his abdomen showing the bifid scrotum and penoscrotal transposition. Genitalia in which the urethral meatus opens between the two halves of a bifid scrotum (sacral hypospadias) constitute one form of ambiguous genitalia. This is especially worrisome if the testes cannot be palpated.

4.91

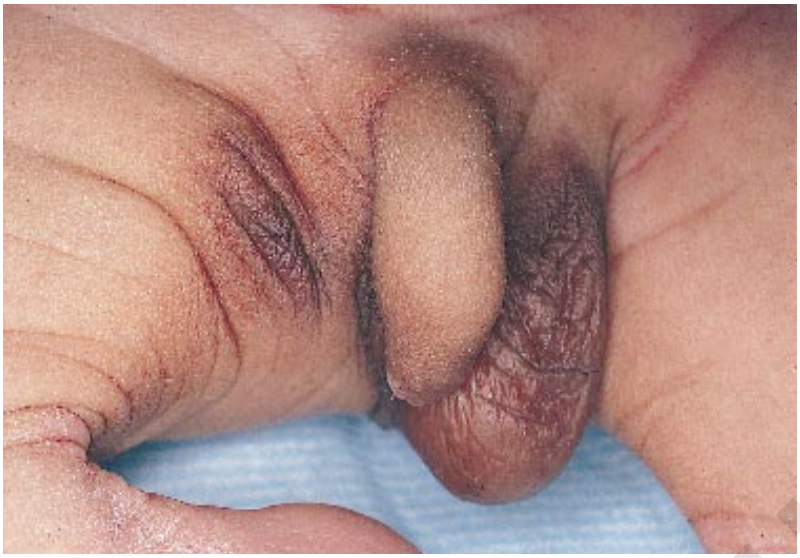

Figure 4.91. A right-sided ectopic scrotum with left hemiscrotum in an infant with the popliteal pterygium syndrome. The scrotum is thus divided and there is cryptorchidism on the right. The testis is palpable on the left side.

4.92

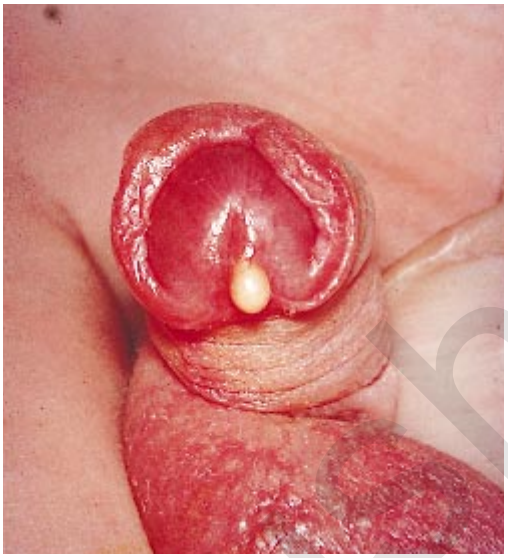

Figure 4.92. In this male infant there is a urethral retention cyst (Epstein's pearl) with a hooded foreskin. Epstein's pearls are small retention cysts most commonly found on the palate but also seen on the penis or scrotum or the nipples. The hooded foreskin should not be confused with a shawl scrotum.

4.93

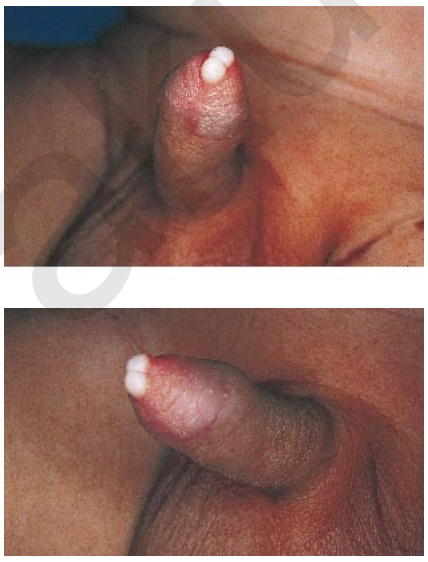

Figure 4.93. Another example of a male infant with urethral retention cysts. These do not interfere with micturition and resolve spontaneously.

4.94

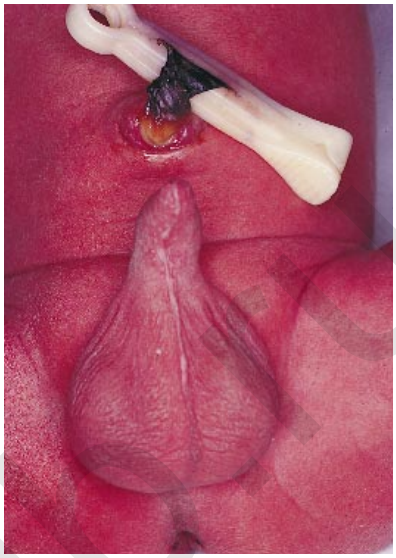

Figure 4.94. In this infant there is a white ridge on the scrotal raphe which probably represents retention cysts.

4.95

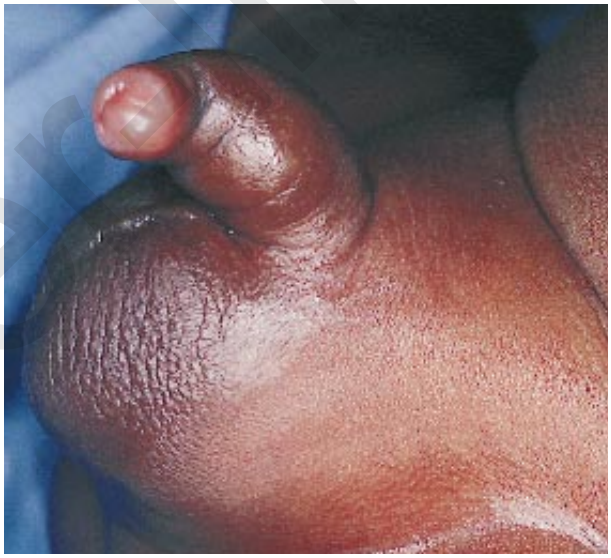

Figure 4.95. Redundant normal foreskin in a premature infant. The glans is normal and redundant foreskin is a frequent normal finding. Phimosis (narrowing of the opening of the foreskin preventing retraction) is physiologic in the normal neonate. Normal development releases the adhesions by the age of 2 to 3 years when the foreskin can be fully retracted. Parents should be told not to retract the foreskin in a normal newborn.

4.96

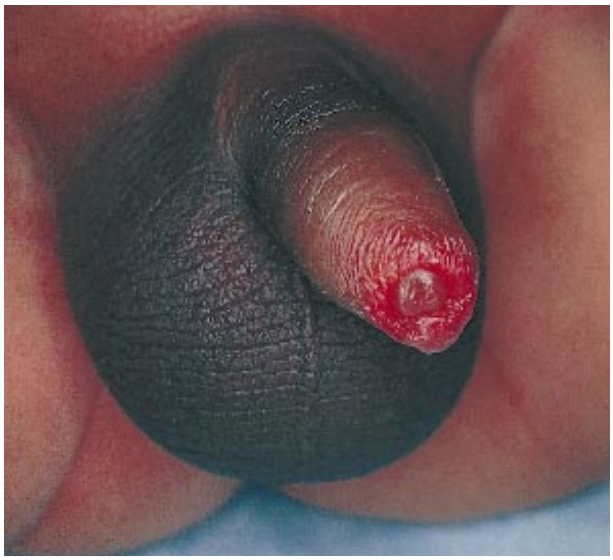

Figure 4.96. Balanoposthitis causing erythema and swelling of the prepuce and glans secondary to inflammation. Balanitis is inflammation of the glans and posthitis is inflammation of the foreskin. This change is frequently due to *Candida* infection but can occur with *Trichomonas* or herpes simplex virus infection. Balanitis should not be confused with a meatal ulceration, which is usually seen in circumcised male infants. In infants with meatal ulceration there is superficial ulceration often resulting from ammoniacal dermatitis. These usually heal spontaneously, but meatal stenosis may result.

4.97

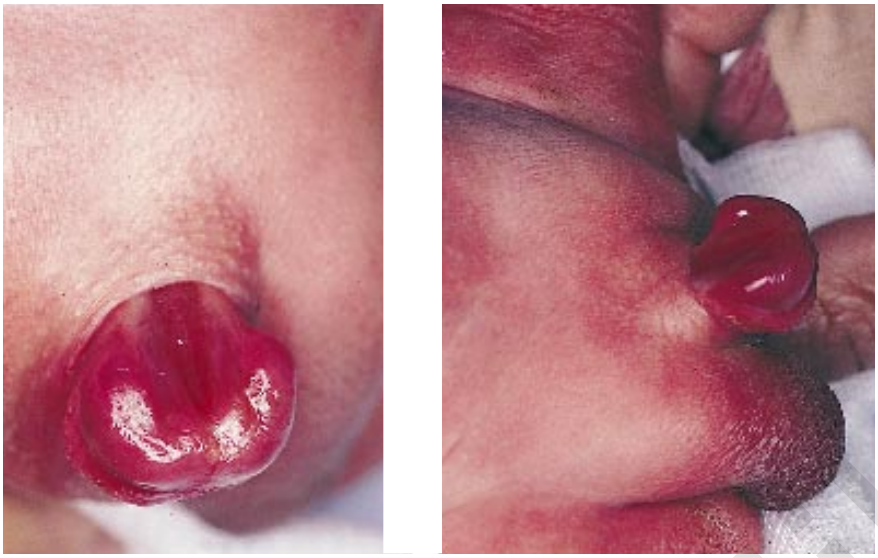

Figure 4.97. This infant has an isolated epispadias. Note that in epispadias the urethral opening is on the dorsal aspect of the phallus. The opening may be either small or large enough to form a furrow bisecting the glans and penis. This is rarely seen as an isolated anomaly, but is more frequently seen in association with extrophy of the bladder.

4.98

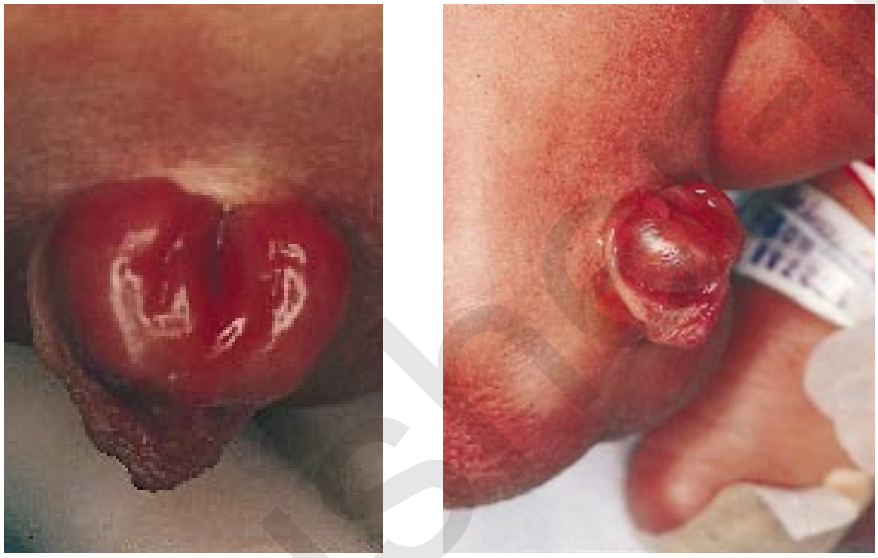

Figure 4.98. Epispadias in an infant with bilateral hydroceles.

4.99

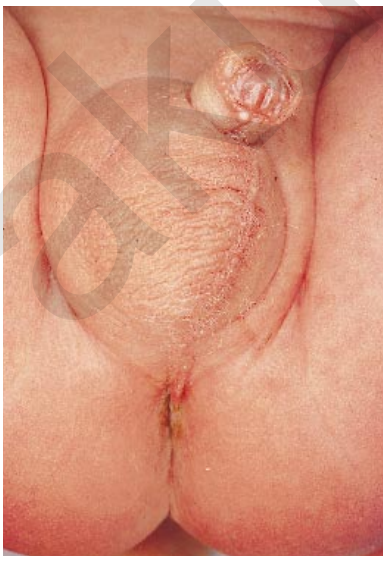

Figure 4.99. In this infant who has a mild glanular hypospadias, the prepuce has failed to fuse, resulting in a "hooded" penis. Hypospadias is the second most common genital abnormality (after cryptorchidism) in males. The incidence varies from 0.5 to 0.75% and it occurs much less frequently in black infants. The types of hypospadias are comprised of 87% glanular or coronal, 10% penile, and 3% penoscrotal and perineal.

4.100

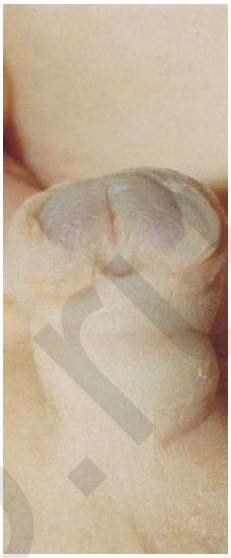

Figure 4.100. A glanular hypospadias in an infant with Russell-Silver dwarfism. This type of hypospadias is of minimal significance.

4.101

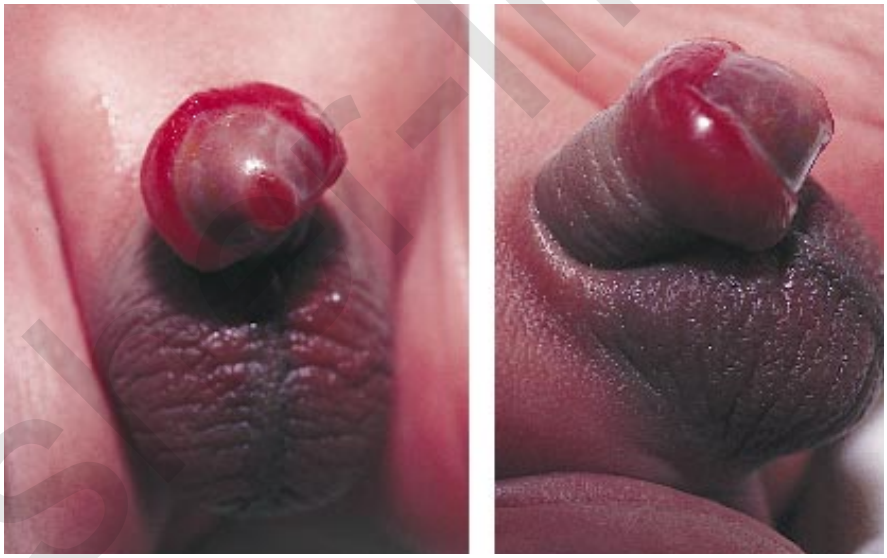

Figure 4.101. This 4-day-old term infant has a glanular hypospadias with an incomplete prepuce and has developed balanoposthitis (inflammation of the glans and prepuce).

4.102

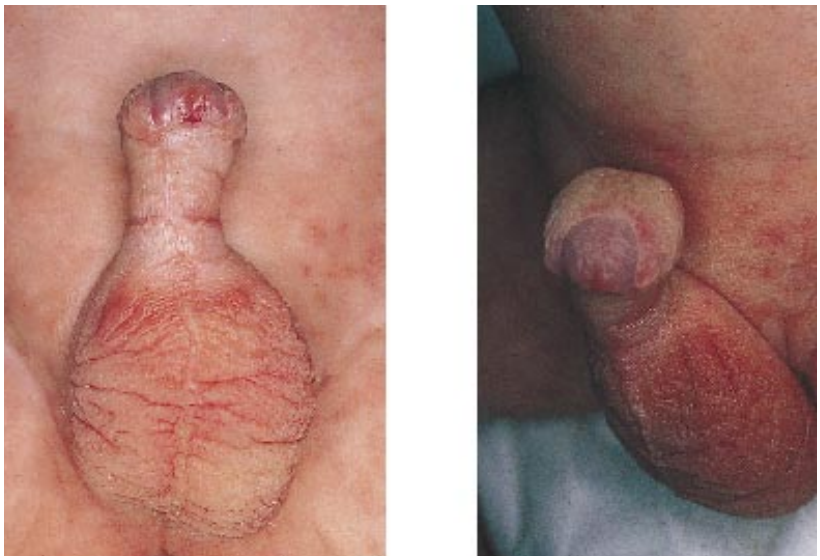

Figure 4.102. Glanular hypospadias with a hooded foreskin in a term infant. Circumcision is contraindicated in any infant with hypospadias as the foreskin may be required to repair the hypospadias.

4.103

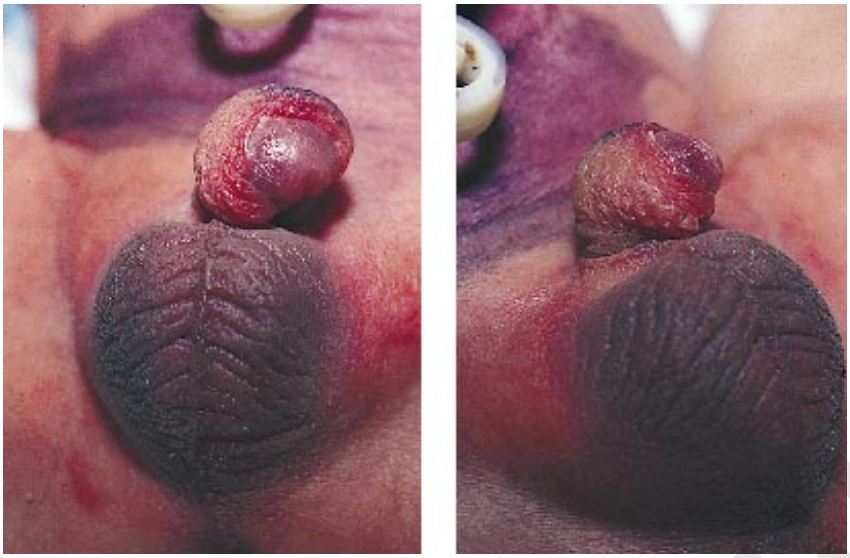

Figure 4.103. Glanular hypospadias with a hooded prepuce (incomplete foreskin) with chordee. Note that the whole ventral surface of the glans is uncovered, with prepuce covering only the dorsum of the glans like a hood. This defect invariably has an accompanying hypospadias. Chordee refers to the ventral curvature of the penile shaft. Severe hypospadias with chordee has more important implications both for its association with other malformations and for urologic repair. The pathogenesis of hypospadias is essentially the same for all degrees of severity in that there is a failure of complete fusion of the margins of the urogenital folds to form the penile urethra.

4.104

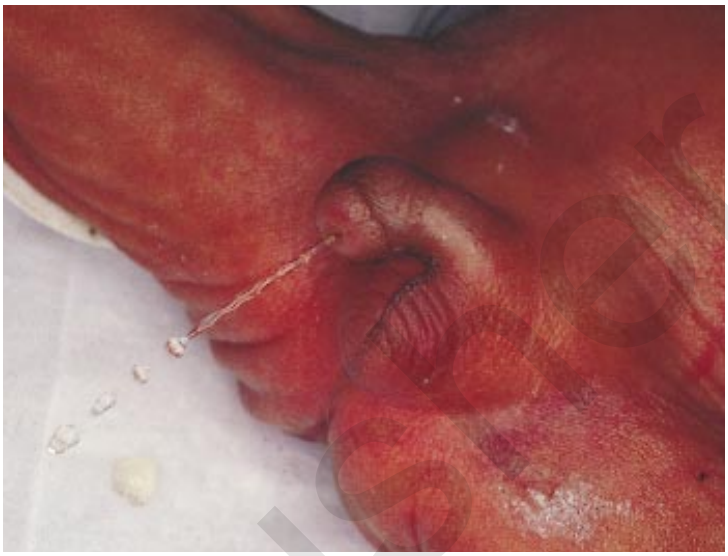

Figure 4.104. A premature infant with a glanular hypospadias and chordee in the act of voiding. Note that the chordee results in a stream of urine always pointing downward, hence the importance of correcting this defect. Note the normal appearance of the developing premature scrotum.

4.105

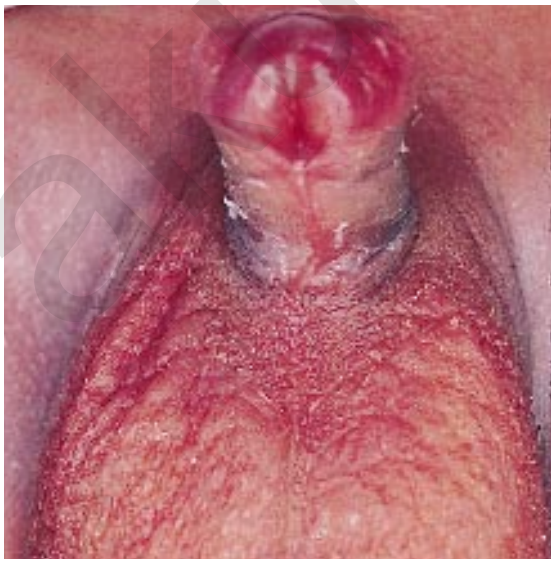

Figure 4.105. A coronal hypospadias. Note that the urethral sulcus is between the glans and the penile shaft.

4.106

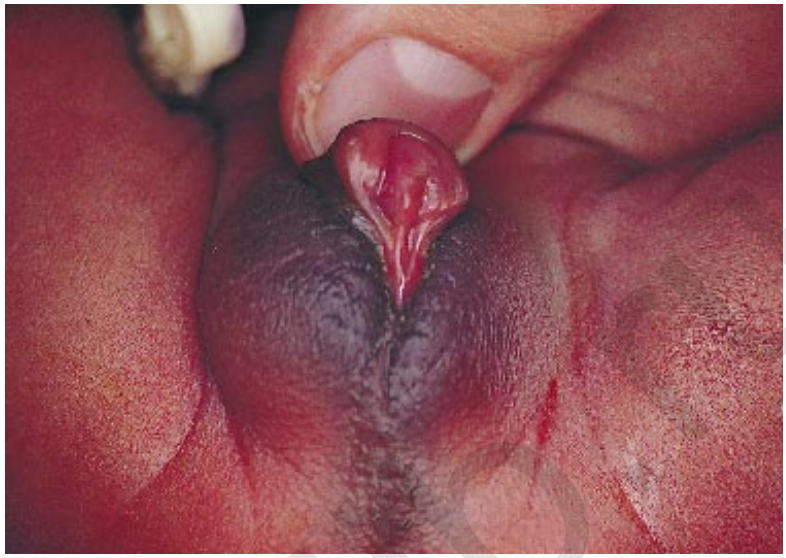

Figure 4.106. Penoscrotal hypospadias occurring in the mid or distal penile shaft in a male infant. Infants with penoscrotal or perineal hypospadias may present with the diagnosis of ambiguous genitalia. Both penoscrotal and perineal hypospadias have a strong association with other structural abnormalities of the genitourinary tract.

4.107

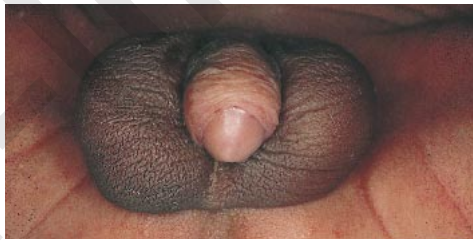

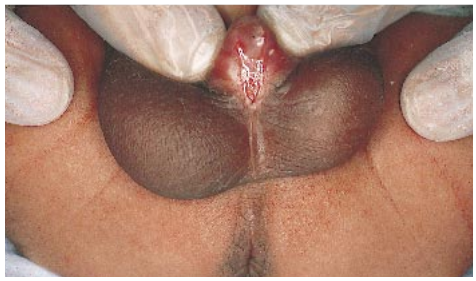

Figure 4.107. In this infant with a penoscrotal hypospadias with chordee and some bifurcation of the scrotum, the diagnosis of ambiguous genitalia needs to be considered. The upper portion of the figure shows the genitalia which appear to be fairly normal. In the lower figure, elevation of the penis and separation of the scrotal sacs show the penoscrotal hypospadias. Beware of assuming the gonads are testes in patients in whom the external genitalia are not totally normal. Karyotyping is essential. In this infant the karyotype was XY.

4.108

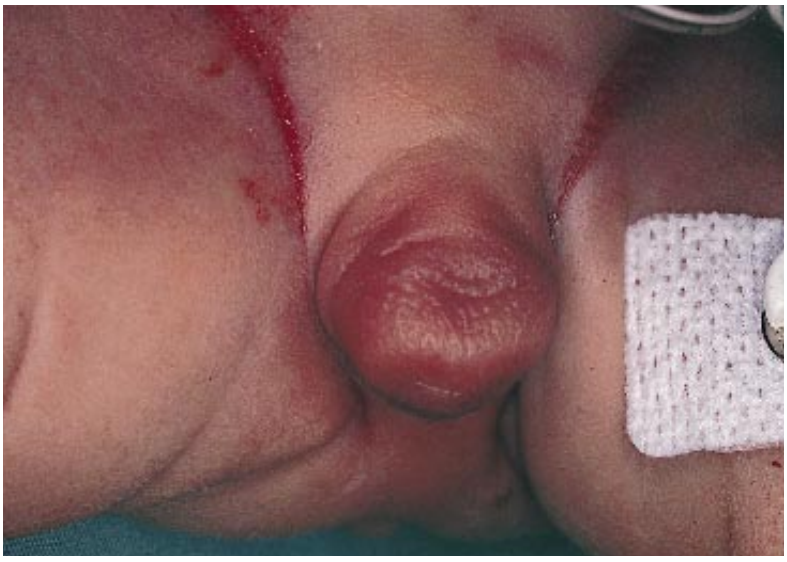

Figure 4.108. In agenesis of the phallus, there is no urethral meatus or anal opening. Note the single scrotal sac with rugal folds. Autopsy findings included renal agenesis, high anal atresia, small bladder, and no urethra.

4.109

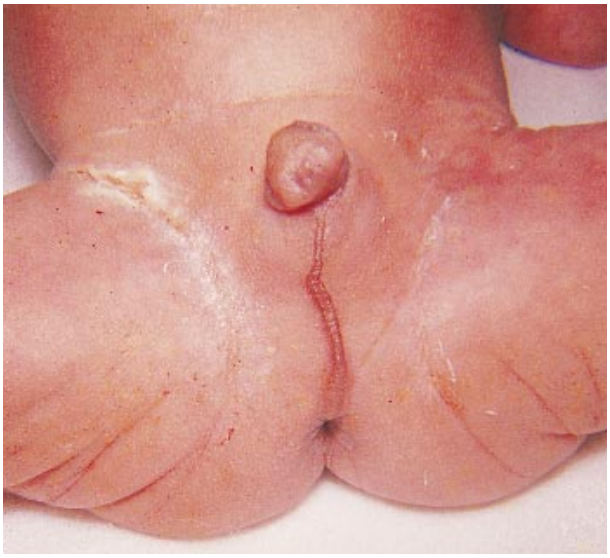

Figure 4.109. Penile agenesis with anterior displacement of an empty scrotum. The urethra appears at the top of the scrotal raphe. Agenesis of the phallus occurs as a result of failure of formation of the genital tubercle. The scrotum is usually present but may lack rugae, and descent of the testes is variable. This malformation has been reported most commonly in sirenomelia.

4.110

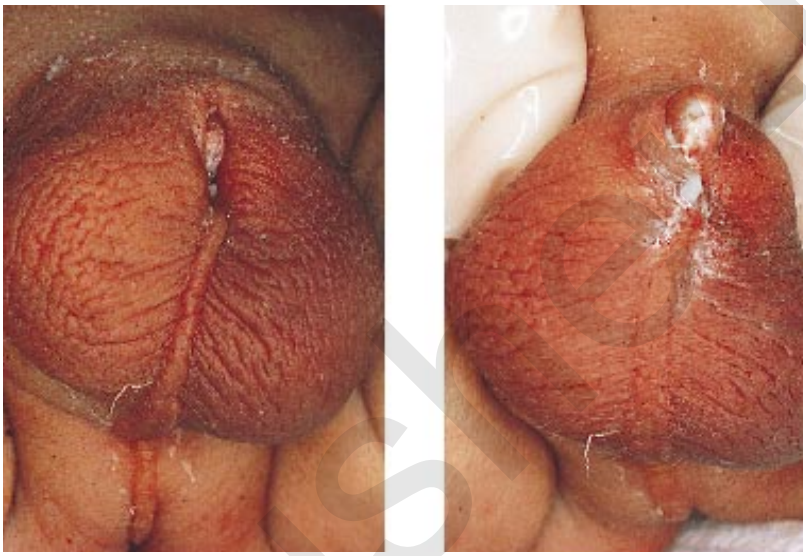

Figure 4.110. Ambiguous genitalia in a male infant with bilaterally descended testes and micropenis. The testosterone level was within normal limits for the newborn. Human chorionic growth hormone stimulation test (performed to see if the testes could respond to and produce testosterone) revealed inadequate testicular function. Exogenous administration of testosterone gave a good response with normal development of male genitalia.

4.111

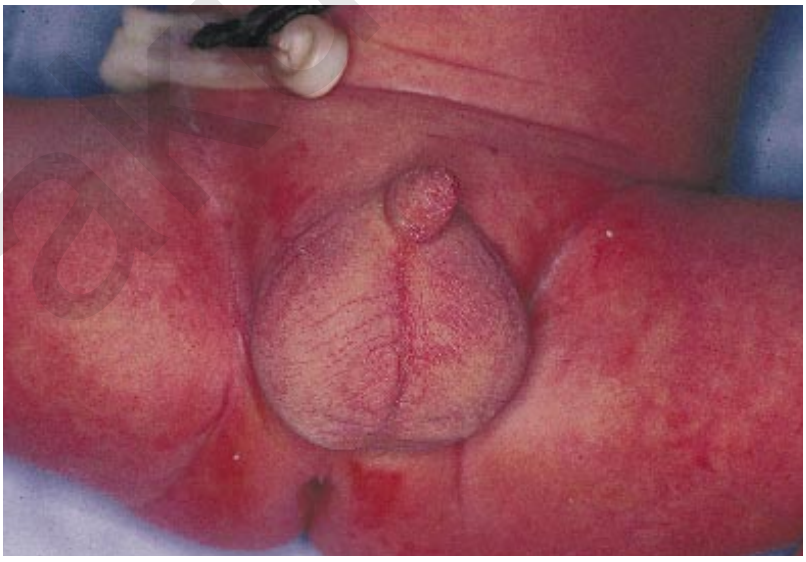

Figure 4.111. This infant presented with severe hypoglycemia and a micropenis with a normal scrotum. The diagnosis of hypopituitarism should always be considered in an infant with micropenis and hypoglycemia. Endocrine studies confirmed the diagnosis of hypopituitarism in this infant.

4.112

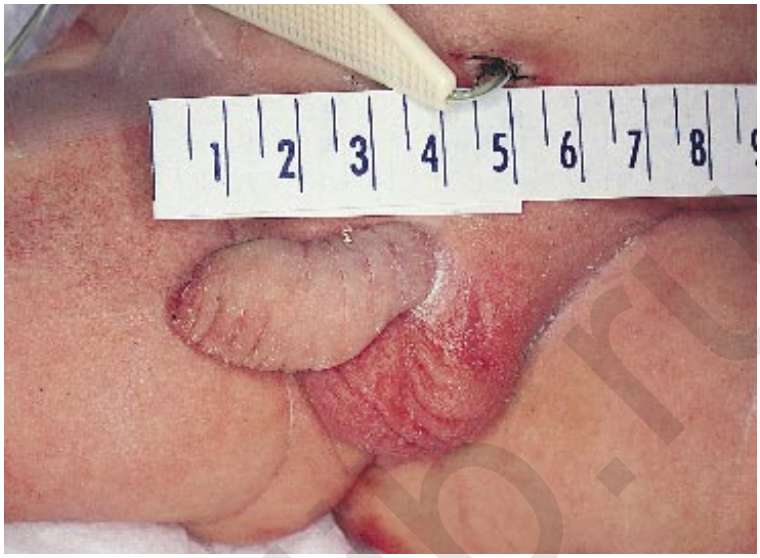

Figure 4.112. Enlargement of the penis. Minimal length of the normal stretched penis is 2.5 cm with a maximum length of 4.0 cm.

4.113

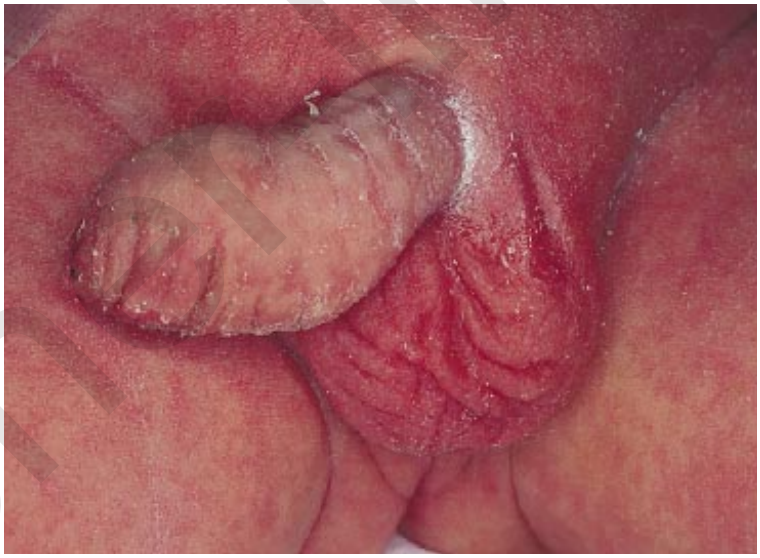

Figure 4.113. There is a markedly enlarged penis in this infant. In these infants the diagnosis of megalourethra should be considered.

4.114

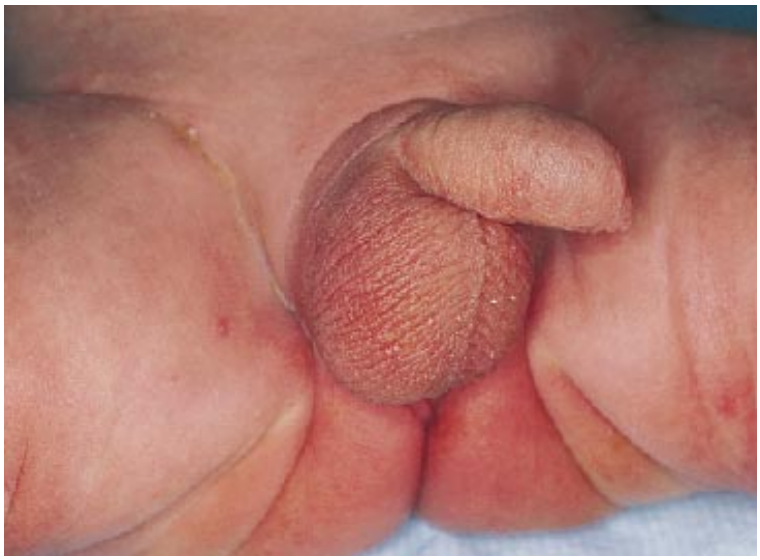

Figure 4.114. This infant has a large penis (8 cm) with left cryptorchidism. Note that the scrotal sac is full on the right and empty on the left.

4.115

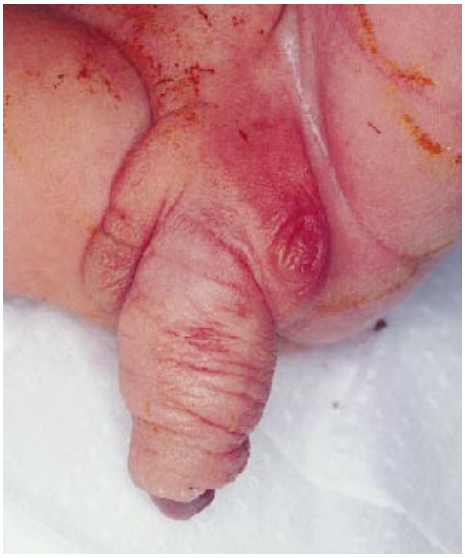

Figure 4.115. If there is a markedly enlarged penis and bifid scrotum, the diagnosis of megalopenis and megalourethra should be considered. In the more common variety of this unusual anomaly, the corpus spongiosum is absent and the abnormally large penis has a scaphoid shape. The upturned glans penis is normally formed and the urethral meatus is normal in site and in size, without demonstrable obstruction to voiding.

4.116

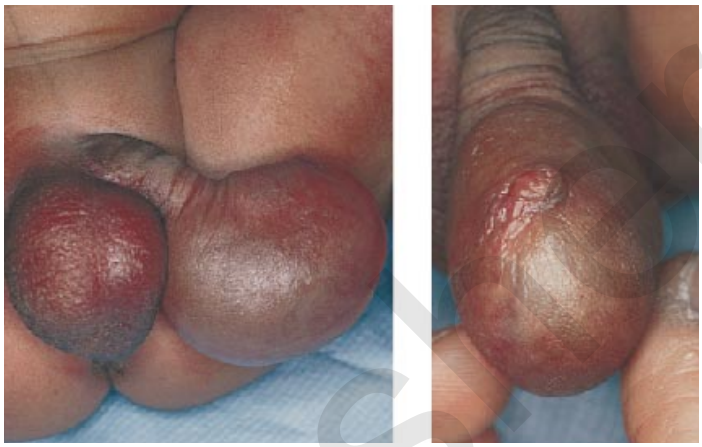

Figure 4.116. In this infant with a markedly enlarged penis and urethra (megalopenis and megalourethra), the penile urethra forms a large flabby sac on the ventrum of the penis which balloons in a striking fashion during micturition. This condition is non-obstructing and is present at birth as a swelling of variable size. The urine accumulated in about two hours, could be expressed easily, and then reaccumulated. Other abnormalities often coexist (e.g., bilateral refluxing mega-ureters, vesical diverticulum, and defective abdominal wall musculature). In this type of megalourethra, both the corpora cavernosa and corpus spongiosum are absent and the dilated penile urethra has a fusiform shape. There is a danger of infection of the stagnant urine in the dilated urethra.

4.117

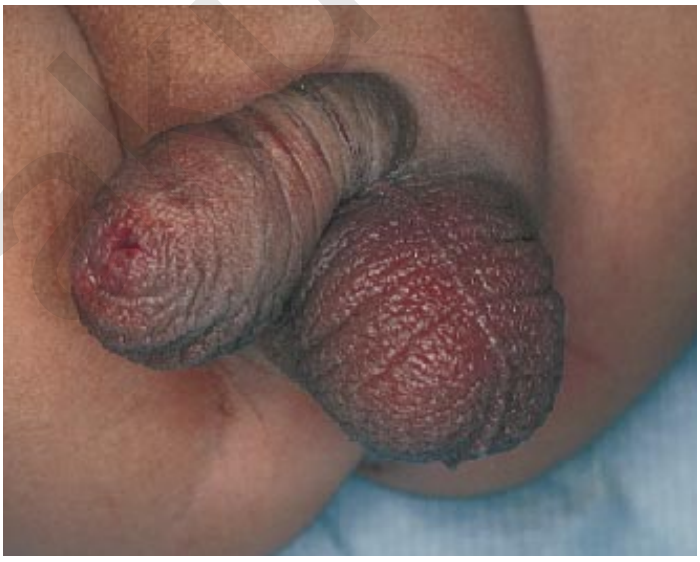

Figure 4.117. The same infant as in Figure 4.117 with megalopenis and megalourethra. After the infant voided, the penile size was more normal until the urine reaccumulated. As a rule, the enlarged penis does not grow proportionately with the child, and its proportions may appear relatively normal with time.

4.118

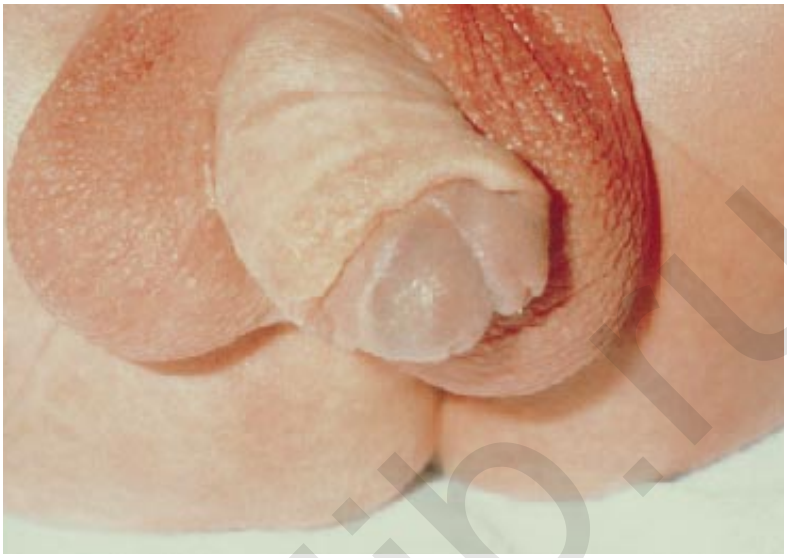

Figure 4.118. Duplication of the glans penis (diphallus) with a fused penile shaft in an infant. (Gonzalez, E.)

4.119

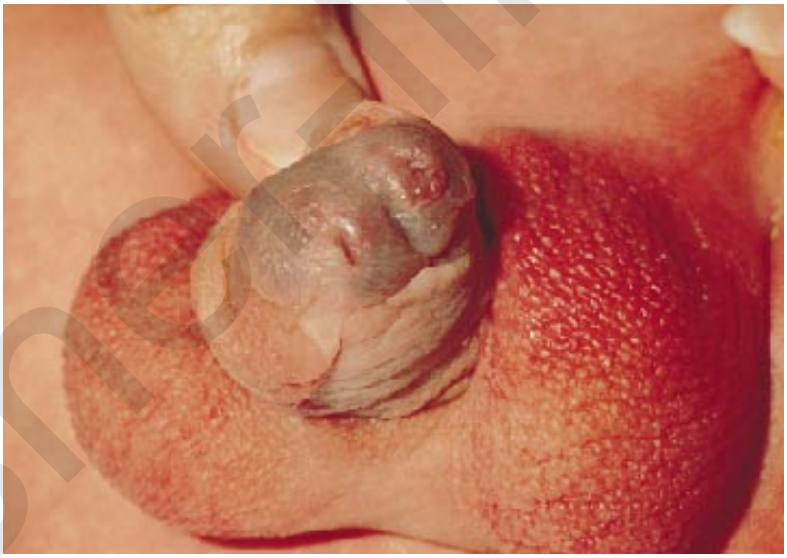

Figure 4.119. Duplication of the male genitalia. There were two bladders with one ureter going into each bladder from the two kidneys, and there was duplication of the urethras with three corpora spongiosum. (Gonzalez, E.)

4.120

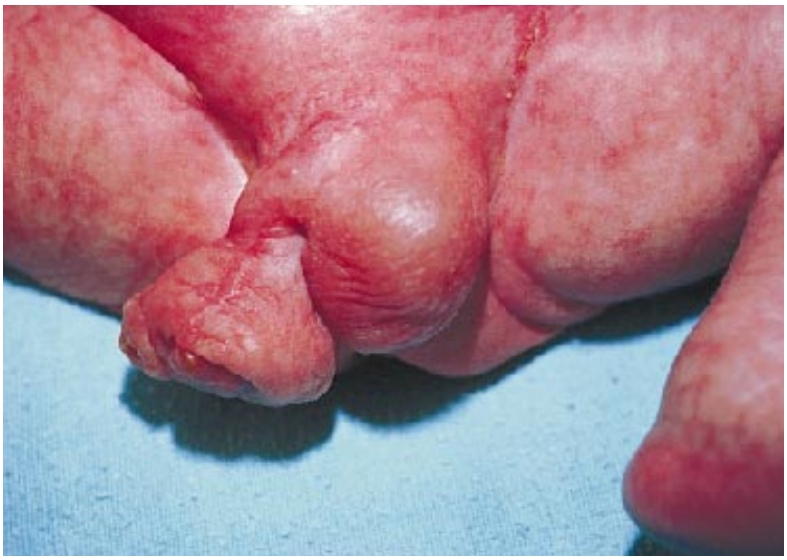

Figure 4.120. A term infant with abnormal penile foreskin and glans caused by a rhabdomyosarcoma involving the penile skin, rectal and bladder muscles, and mucous membranes.

4.121

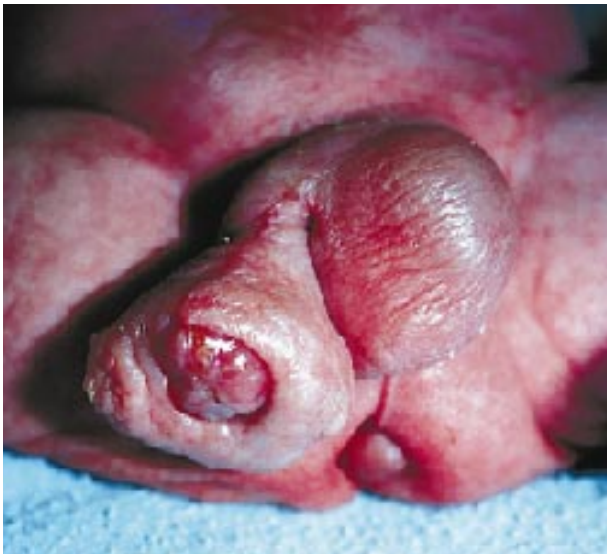

Figure 4.121. The same infant as in Figure 4.120 with rhabdomyosarcoma, showing the abnormal appearance of the glans and foreskin.

4.122

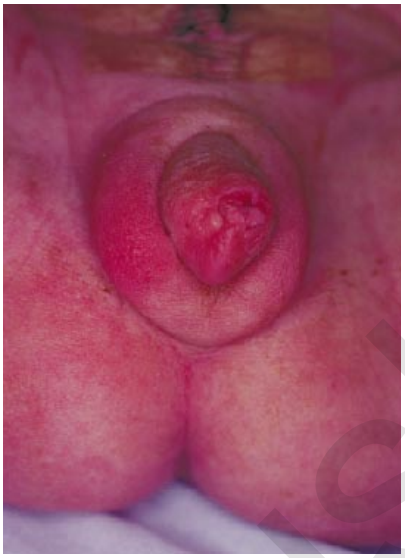

Figure 4.122. Ambiguous genitalia in a monozygotic female twin infant (the other twin was normal). There is imperforate anus and a blind vaginal pouch. This is an example of a "doughnut scrotum" which encircles the phallus. It is a form of penoscrotal transposition and is not of great consequence. This should be distinguished from a shawl scrotum which appears to represent a mild deficit in the full migration of the labioscrotal folds and may be accompanied by other signs of incomplete masculinization of the external genitalia. It is seen in Aarskog syndrome.

4.123

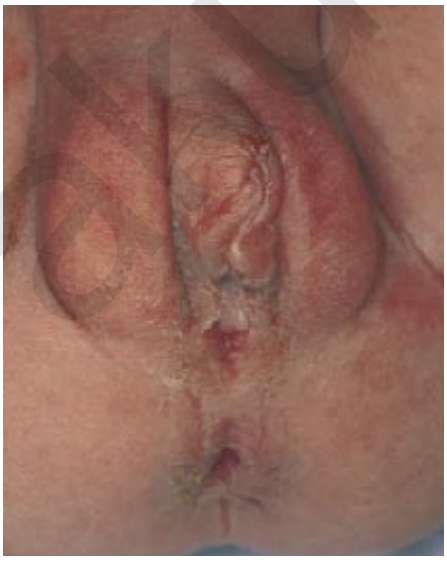

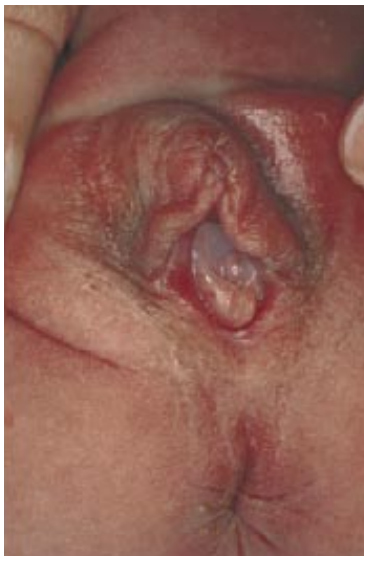

Figure 4.123. Congenital adrenal hyperplasia in a female infant with 21 hydroxylase deficiency. Examples of ambiguous genitalia are presented in Chapter 5.

4.124

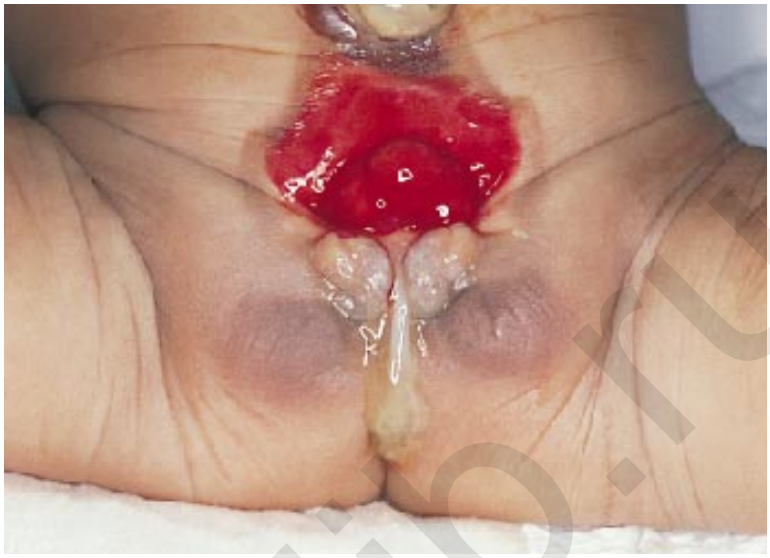

Figure 4.124. Bladder exstrophy (ectopia vesicae) in a female infant. This results from failure of midline fusion of the lower half of the abdominal wall, including the deep structures such as the symphysis pubis and anterior bladder wall. The trigone is exposed and inappropriate fusion may result in synechia vulva in the female infant or in associated epispadias in the male infant.

4.125

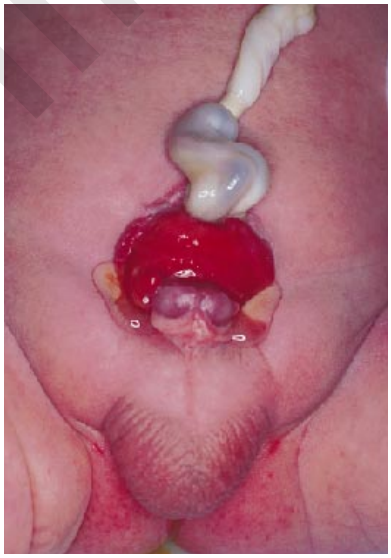

Figure 4.125. Ectopia vesicae (bladder exstrophy) in a male newborn infant. Note the exposed bladder and epispadias. Ectopia vesicae is most commonly seen in male infants. In the female it involves the bladder and vagina, and the labia are widely split.

4.126

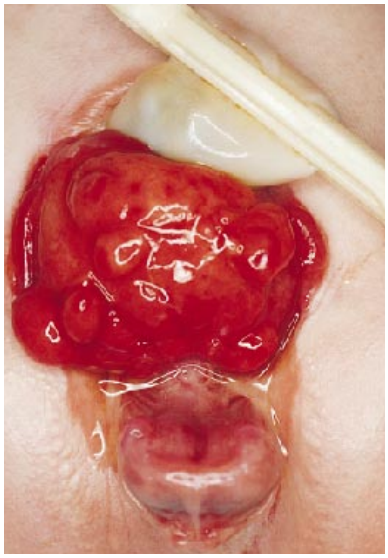

Figure 4.126. Close-up of exstrophy of the bladder in a male infant with a severe epispadias. The anterior wall of the bladder is absent and the posterior wall is exposed to the surface. The posterior wall is seen as a reddened granulomatous mass lying just above the pubic symphysis. The ureteral orifices can often be discerned laterally exuding urine onto the surface of the thickened and hypertrophic bladder mucosa. There is complete epispadias with the urethral opening on the dorsal side of an abnormally short penis.

4.127

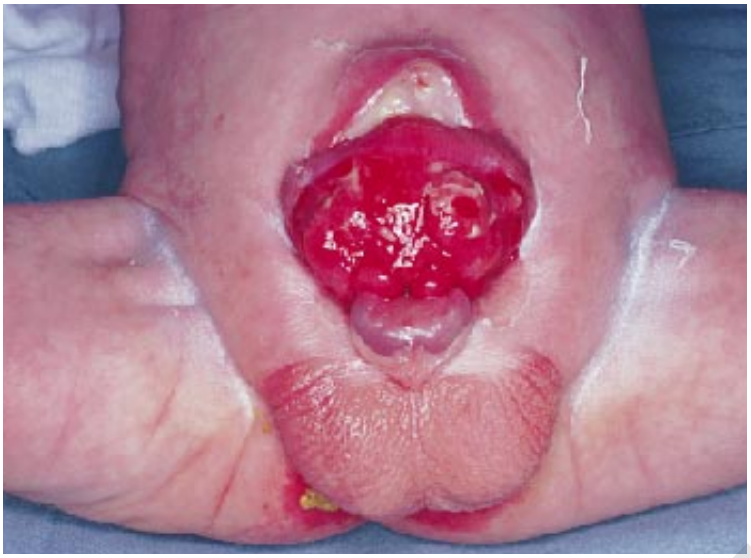

Figure 4.127. Another example of exstrophy of the bladder in a male infant who had meningomyelocele and developed an associated arthrogryposis.

4.128

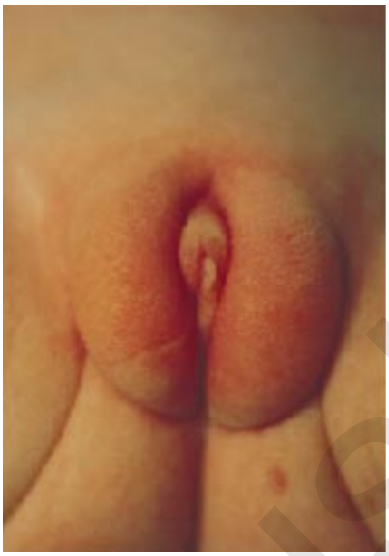

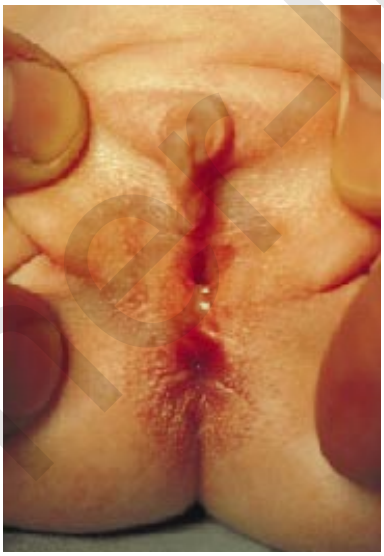

Figure 4.128. The cloacal dysgenesis sequence which represents a complete urogenital sac defect with a vesicointestinal fissure resulting from abnormal development of the lower half of the abdominal wall.

4.129

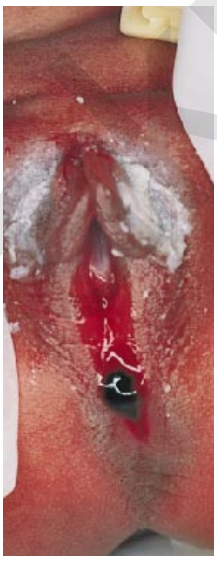

Figure 4.129. A urogenital sac defect which resulted in cloacal dysgenesis with anterior placement of the anus is present in this female infant. The features of cloacal dysgenesis include omphalocele, bladder exstrophy, and a blind colon which is associated with anorectal agenesis.

4.130

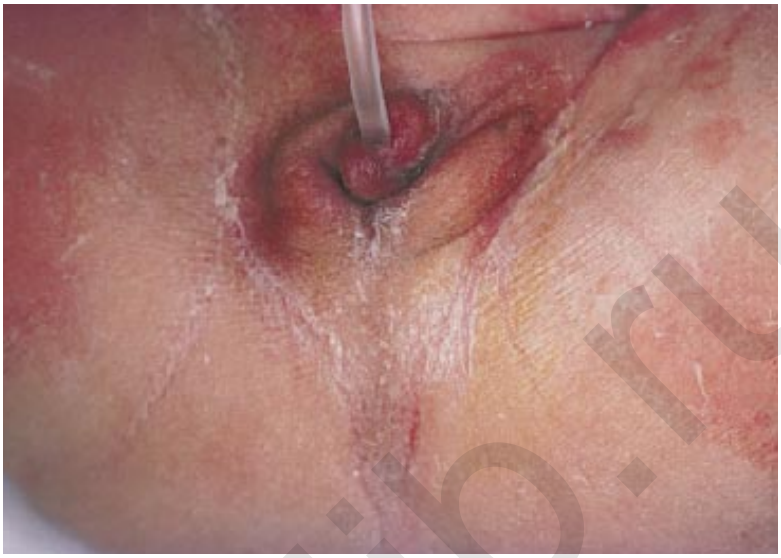

Figure 4.130. Ambiguous genitalia in a female infant with VACTERL syndrome. Note the cloacal sac with a single urogenital opening. The bladder is in free communication with the rectum. This infant also had congenital heart disease, a tracheoesophageal fistula, imperforate anus, and a right hydronephrosis. Karyotype was XX.

4.131

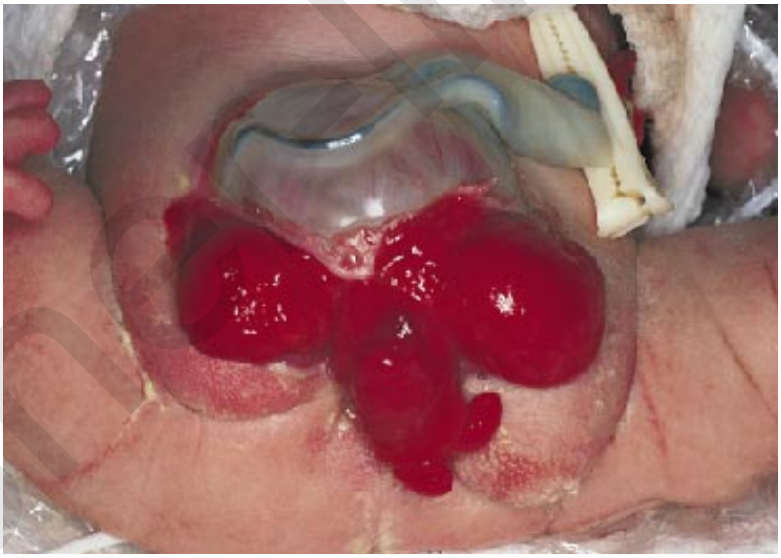

Figure 4.131. This infant has an omphalocele and exstrophy of the cloaca. The etiology for exstrophy of the cloaca (ectopia cloacae, vesicointestinal fissure) is similar to that of exstrophy of the bladder but the deficiency of mesenchymal migration is more severe and occurs before partitioning of the cloaca. Thus, the bladder is present only as lateral remnants which, along with the interior of the rectum, are exposed on the surface of the lower abdomen. The abdominal viscera, including the liver, may herniate through the intra-abdominal defect, and there is a wide gap between the pubic bones.

4.132

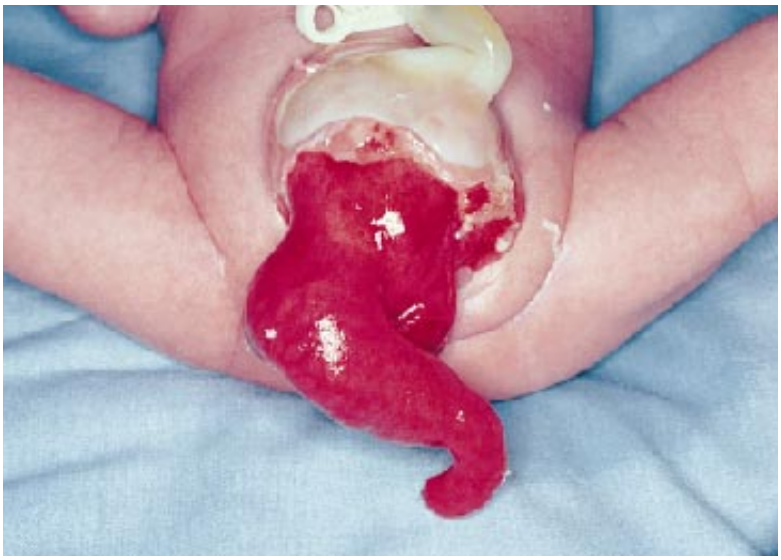

Figure 4.132. Exstrophy of the cloaca is a severe defect of the lower abdominal wall in which the exstrophic bladder is divided into a right and left half between which a field of intestinal mucosa is seen. The prolapsed ileum hangs like a trunk from the exposed field, the so-called "elephant trunk" deformity. In such cases the colon is short and ends blindly in an imperforate anus. This infant demonstrates an omphalocele, bladder exstrophy, a blind colon which is associated with anorectal agenesis, and the "elephant trunk" deformity.

4.133

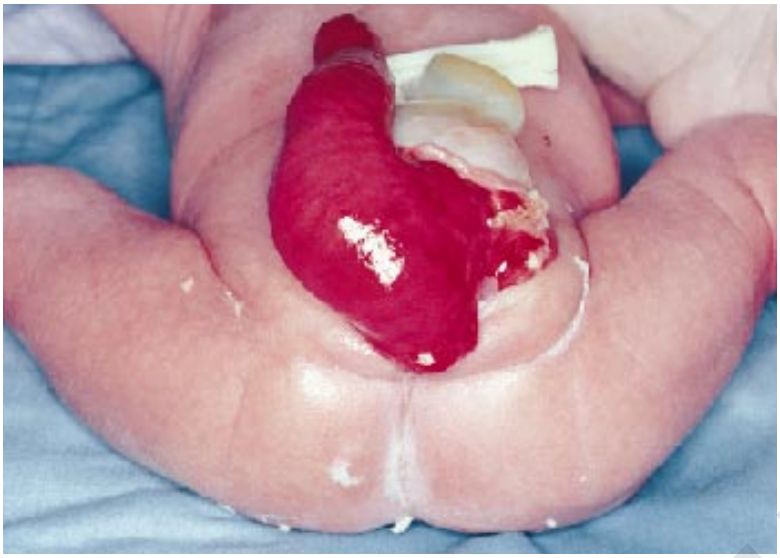

Figure 4.133. The same infant as in Figure 4.132 with exstrophy of the cloaca. Note the absence of an anal opening, the small omphalocele superiorly, and the "elephant trunk" deformity raised superiorly.

4.134

Figure 4.134. This female infant has exstrophy of the cloaca sequence which includes cloacal exstrophy with imperforate anus, ambiguous genitalia, and a lumbosacral myelocystocele (hydromelia). In addition to the exstrophy, the urinary tract may be involved by various anomalies such as hydronephrosis or cystic or absent kidney.

4.135

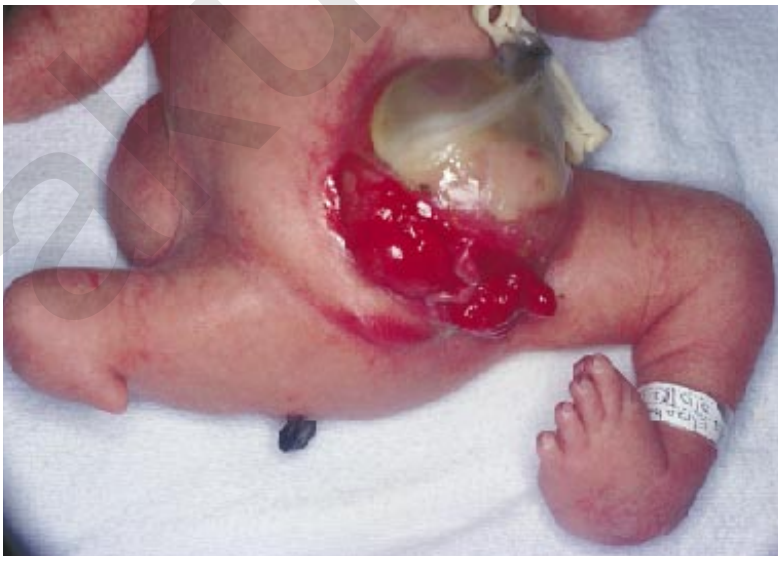

Figure 4.135. Another example of the exstrophy of the cloaca sequence. Note the exstrophy of the cloaca and hydromelia. This infant also developed an in utero amputation of the right lower extremity, probably from an amniotic band and had a gangrenous skin tag on the buttock. The left foot shows severe talipes equinovarus.

Chapter 5
Endocrine and Metabolic Disorders

Endocrine and metabolic processes are actively involved in the growth and development of the fetus from conception. Clinical disorders of endocrine and metabolic function in the neonate are most often based upon abnormal physiologic function in either the fetus or mother during gestation. The timing of these disturbances during gestation can result in varying clinical presentations. Endocrine system involvement may include the thyroid, pituitary, hypothalamus, parathyroid, testes, ovaries, and adrenal glands. Metabolic disorders may include carbohydrate, amino acid, fatty acid, calcium, phosphorus, and magnesium metabolism. Advances in the recognition, treatment and prevention of many endocrine and metabolic disorders make it imperative that the clinician be familiar with these disorders. Although screening programs exist for many of these disorders, many children remain undiagnosed. Clinicians must remain aware of these conditions so that infants may be diagnosed early and the condition treated, or genetic counseling can be provided to parents.

Endocrine Disorders

5.1

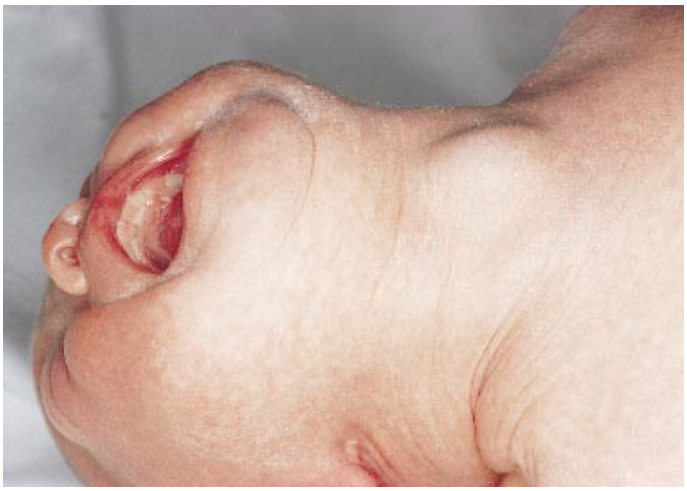

Figure 5.1. Midline neck mass in an infant with congenital goiter. Goiter may occur in the newborn period as a result of maternal iodine deficiency, drug ingestion (e.g., iodide during pregnancy for treatment of maternal asthma), maternal thyrotoxicosis, or inborn errors of thyroxine synthesis. The pressure effect of the enlarged thyroid on the trachea may result in respiratory distress. Medical treatment depends on whether the infant has hypothyroidism or hyperthyroidism.

5.2

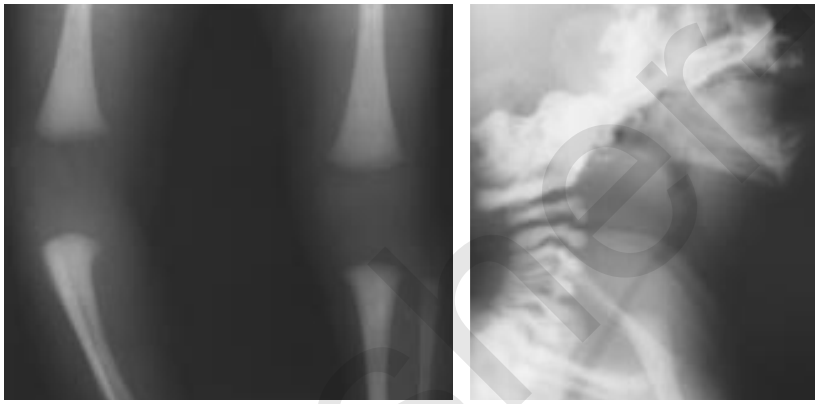

Figure 5.2. Left, radiograph of the long bones of the lower extremity in a term infant with congenital hypothyroidism. Note the lack of the ossification centers. The distal femoral ossification center usually appears at 36 weeks gestational age and the proximal tibial ossification center usually appears at 38 weeks gestational age. Right, lateral radiograph of the neck of the same infant showing the presence of a large congenital goiter which caused severe respiratory distress.

5.3

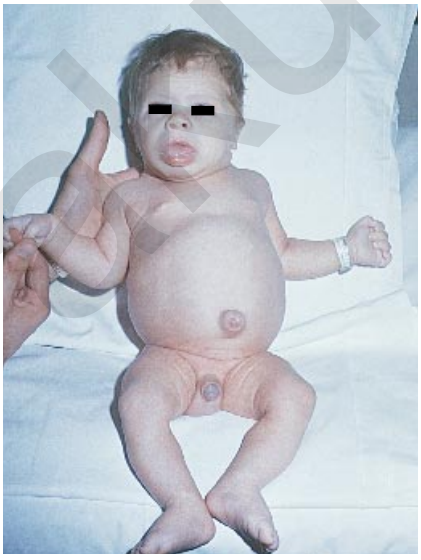

Figure 5.3. This 5-week-old infant with congenital hypothyroidism has generalized myxedema, dry skin, hoarse low-pitched cry, low body temperature, and constipation. Note the characteristic facies with enlarged tongue (macroglossia) and the protuberant abdomen ("pot belly") with umbilical hernia.

5.4

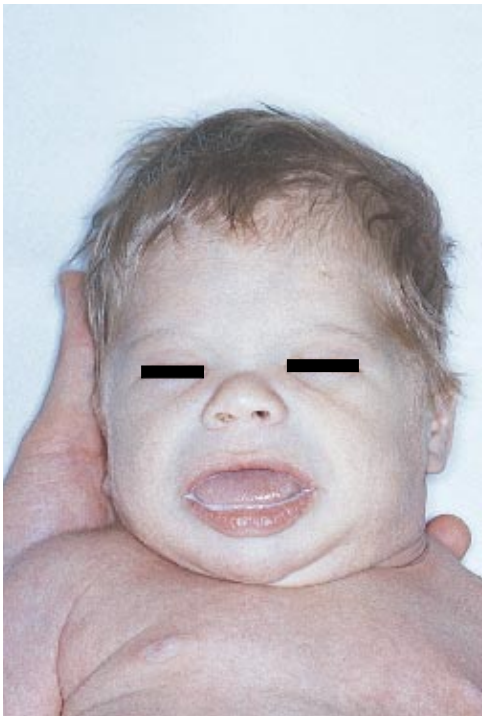

Figure 5.4. Typical facies of the same infant as in Figure 5.3 with congenital hypothyroidism. Note the coarse facial features with the macroglossia and the mottling of the skin (cutis marmorata). At birth there are usually no abnormal signs; the characteristic features of hypothyroidism develop at a few weeks to a few months of age. At the present time, neonatal screening has been invaluable in making an early diagnosis. The diagnosis must be considered in infants with persistent jaundice or constipation.

5.5

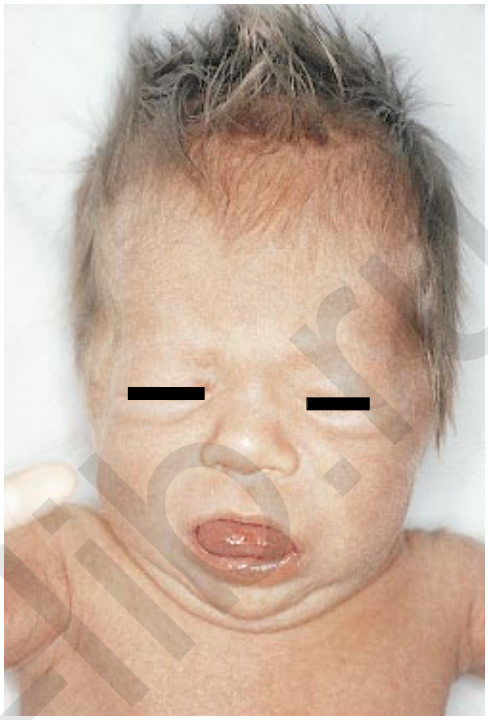

Figure 5.5. The face of another infant with congenital hypothyroidism. Note the coarse facies, coarse hair, puffiness of the eyes, and the macroglossia.

5.6

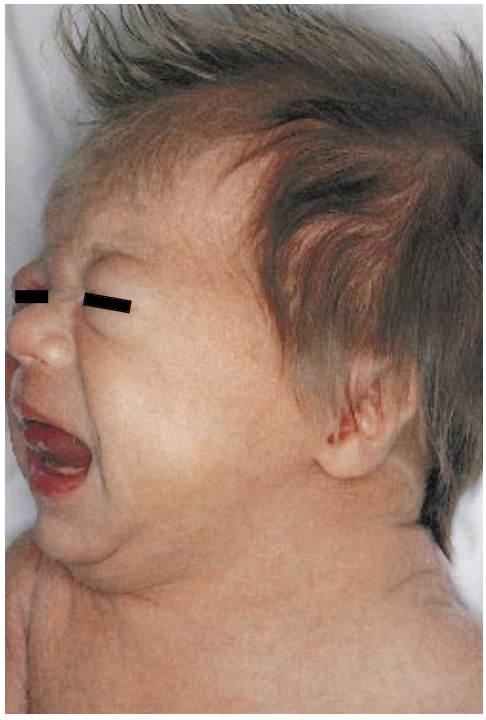

Figure 5.6. Lateral view of the head and face of the same infant as in Figure 5.5. Note the coarse facies, edema of the eyelids, and the macroglossia.

5.7

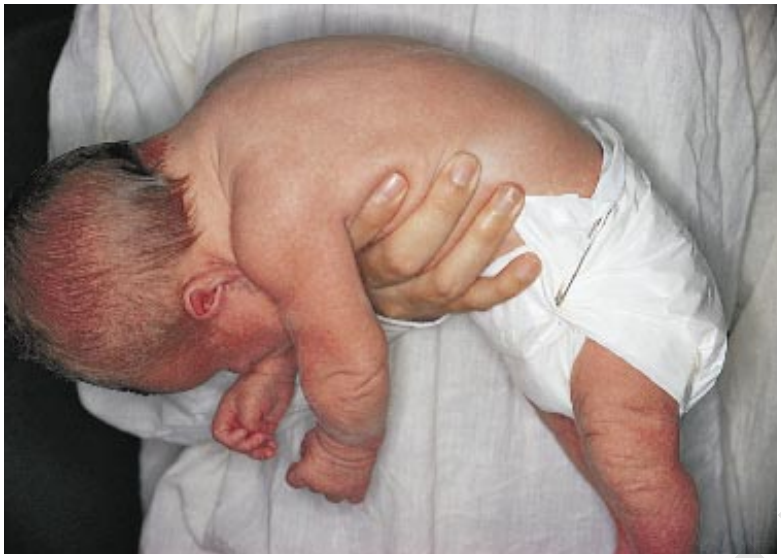

Figure 5.7. This infant with a goiter had decreased tone as the result of hypothyroidism.

5.8

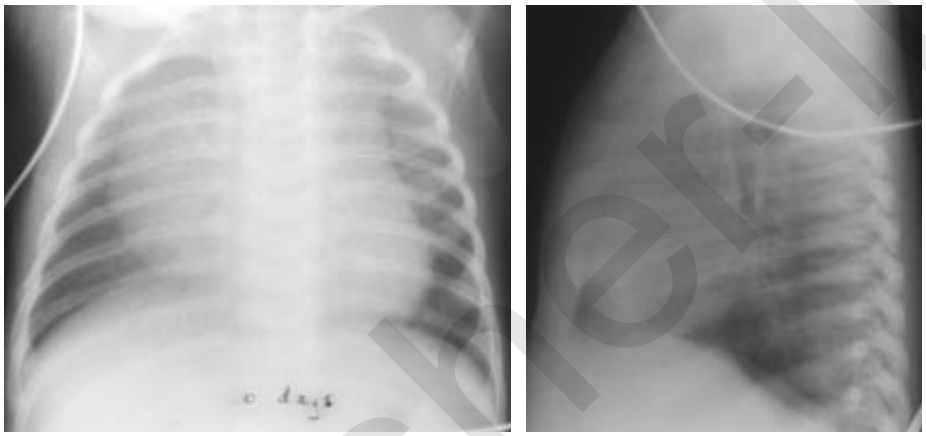

Figure 5.8. Antero-posterior and lateral radiographs of an infant with congenital hypothyroidism. Note the marked cardiomegaly as the result of congestive heart failure.

5.9

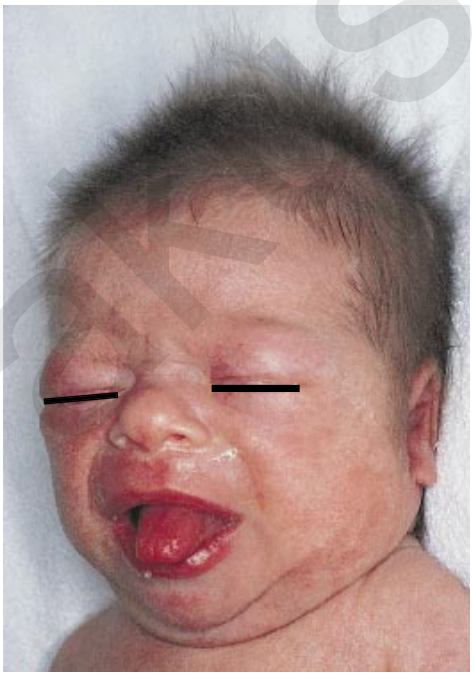

Figure 5.9. Typical appearance of infant at the age of 9 days with congenital hypothyroidism (coarse facial features, puffiness of the eyelids, macroglossia, and coarse hair). Infant presented at birth with cardiogenic shock. Hospital course was remarkable for seizures and death at age 12 days from a pulmonary hemorrhage. Infant had a low T4 (thyroxine) and increased TSH (thyroid-stimulating hormone). Autopsy findings revealed the presence of inflammation involving the heart, brain, liver, and kidneys. The thyroid gland was normal histologically. Adenovirus was detected with polymerase chain reaction (PCR) technology.

5.10

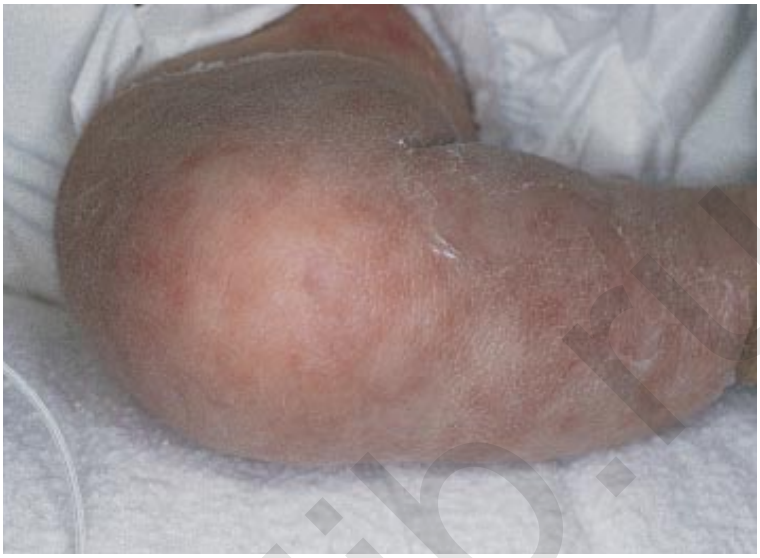

Figure 5.10. The same infant as in Figure 5.9 had marked cutis marmorata and non-pitting edema (myxedema) of the face, of the dorsum of the hand, and of the external genitalia.

5.11

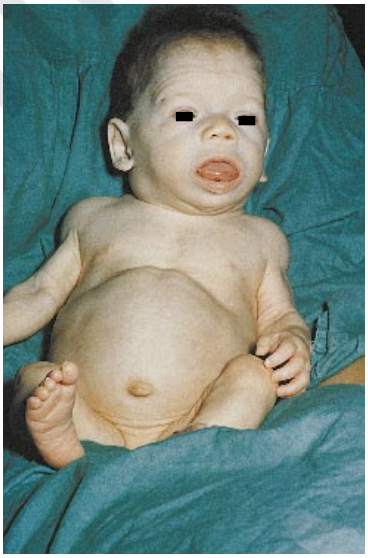

Figure 5.11. Congenital hypothyroidism. Note the classic facial features in association with generalized muscle hypertrophy. These are rare but classic findings in infants with the Kocher-Debré-Sémélaigne syndrome ("wrestler's" syndrome).

5.12

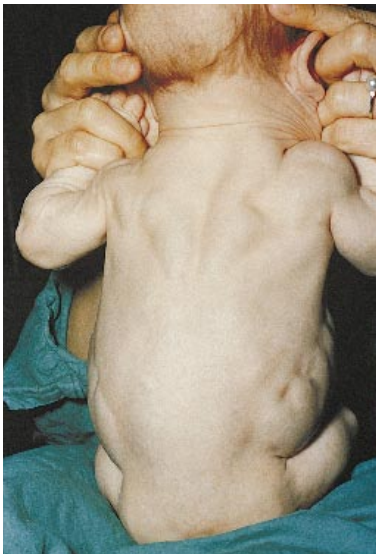

Figure 5.12. Posterior view of the same infant as in Figure 5.11 clearly demonstrating the generalized muscular hypertrophy.

5.13

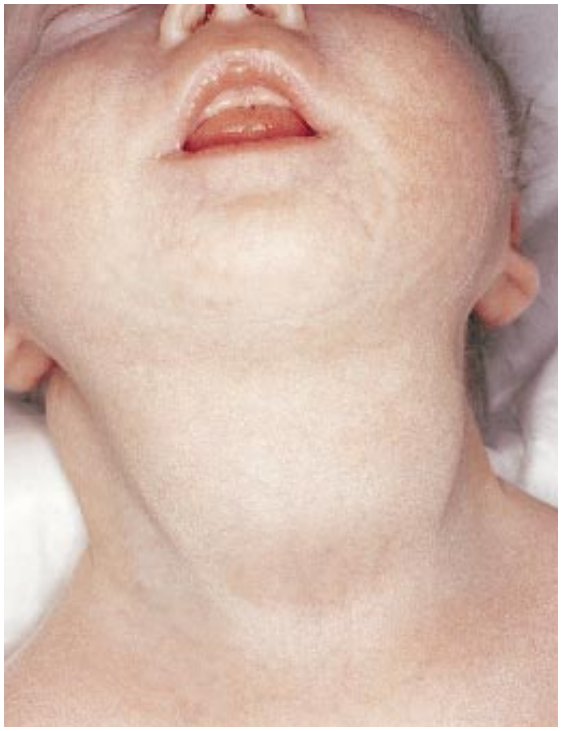

Figure 5.13. This infant with congenital hyperthyroidism had a large midline neck mass due to a congenital goiter. Congenital goiter can occur when there is a defect in the synthesis of thyroid hormone (due to fetal TSH stimulation causing intrauterine growth of the thyroid gland) or in cases of maternal hyperthyroidism (due to long-acting thyroid stimulator [LATS]) antibody crossing the placenta.

5.14

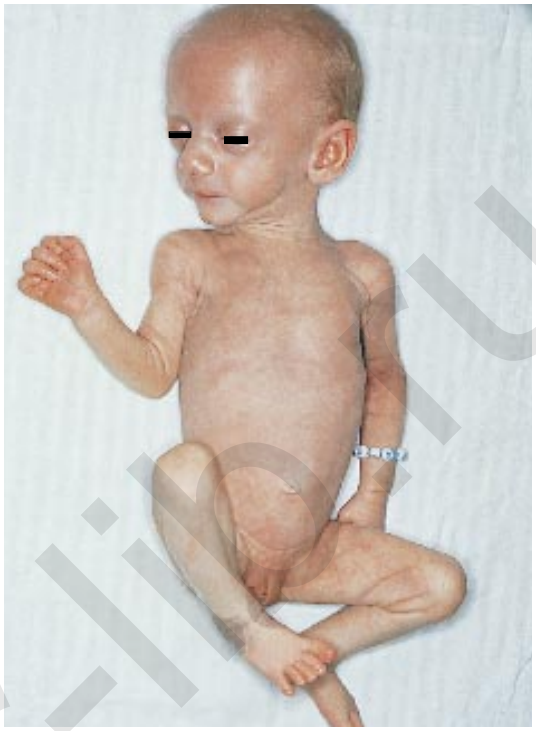

Figure 5.14. This hyperactive, term male infant with transient congenital hyperthyroidism had severe growth retardation. This infant's mother suffered from Graves' disease, and the maternal LATS antibodies were transmitted to the child. The symptoms include tachycardia, cardiac failure, abnormal eagerness for feedings, enlargement of the thyroid gland, and exophthalmos. Symptoms usually subside 4 to 6 weeks following birth concordant with the disappearance of maternal IgG antibodies. The onset of symptoms may be delayed for about a week as a result of prenatal therapy given to the mother.

5.15

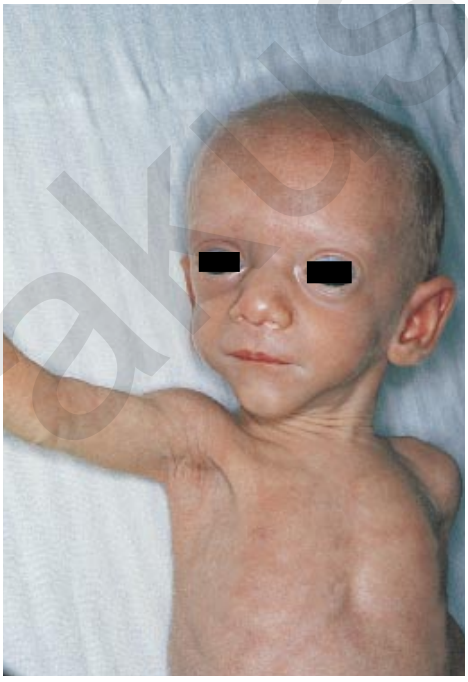

Figure 5.15. The same infant as in Figure 5.14 with congenital hyperthyroidism with exophthalmos and an alert expression failed to gain weight. Birth weight was 1560 g. At 5 weeks of age, this infant weighed 1655 g in spite of adequate caloric intake.

5.16

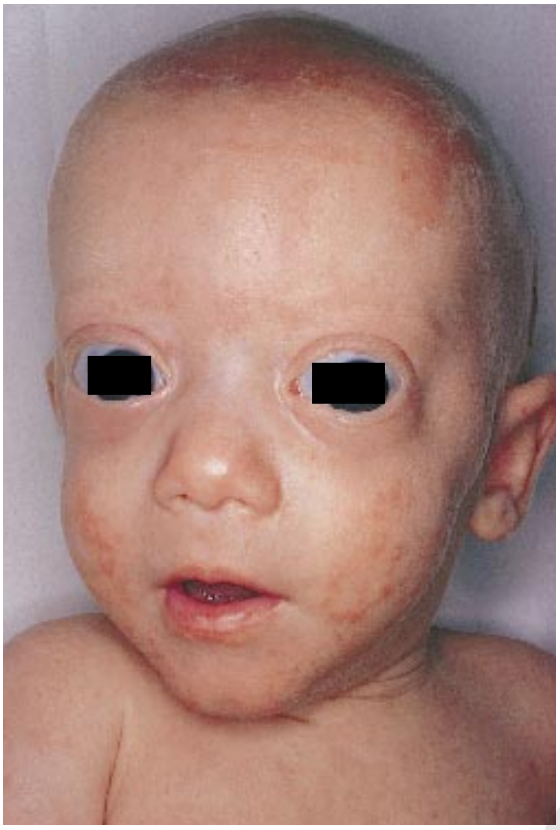

Figure 5.16. A close-up of the face of the same infant with congenital hyperthyroidism. Note the exophthalmos with retraction of the upper lids (Stellwag's sign).

5.17

Figure 5.17. Lateral view of the face of the same infant as in Figure 5.16 with exophthalmos. Stellwag's sign is demonstrated in this view.

5.18

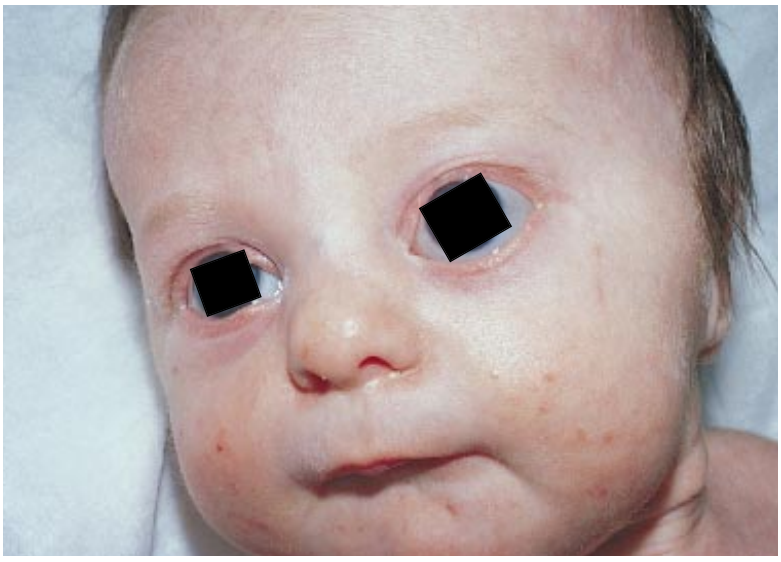

Figure 5.18. Unilateral exophthalmos can occur in infants with hypothyroidism. This infant had normal thyroid studies and an MRI of the orbit was normal. Differential diagnosis includes hemangioma, lymphangioma, anterior encephalocele, and intraorbital tumors (rhabdomyosarcoma, metastatic neuroblastoma, dermoid cysts).

5.19

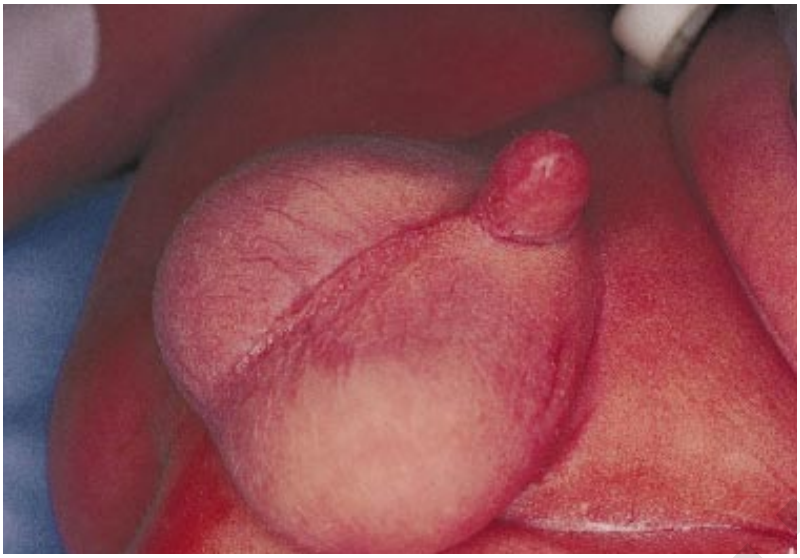

Figure 5.19. Micropenis with a normal scrotum in an infant who presented with severe hypoglycemia. This combination should alert one to the diagnosis of hypopituitarism. There is a higher incidence of hypopituitarism in patients with a variety of midline defects. Hypopituitarism was confirmed in this infant.

5.20

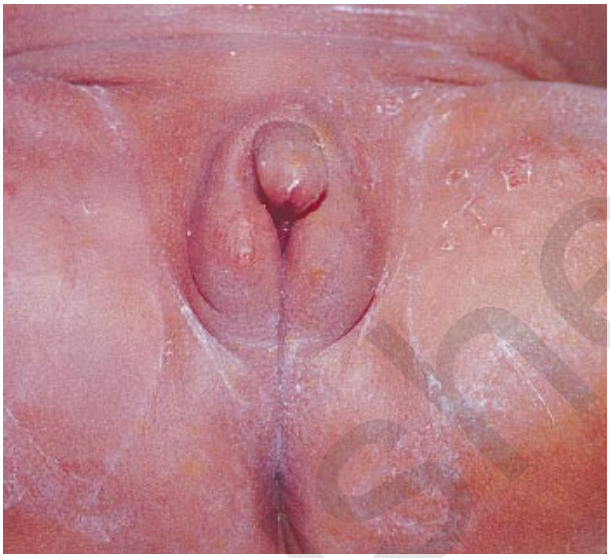

Figure 5.20. This female infant has ambiguous genitalia. The karyotype was XX. Difficulties in determining the sex of an infant may arise from abnormalities of the external genitalia. Ambiguous genitalia encompass a wide range of abnormalities having their origin before the 12th week of gestation. The phallus commonly shows hypospadias with chordee formation and appears large in proportion to the persisting labioscrotal folds which may or may not contain gonads (testis, ovotestis, or rarely a well-defined ovary). In females, the labia may be fused and the clitoris hypertrophied. This condition is known as pseudohermaphroditism.

5.21

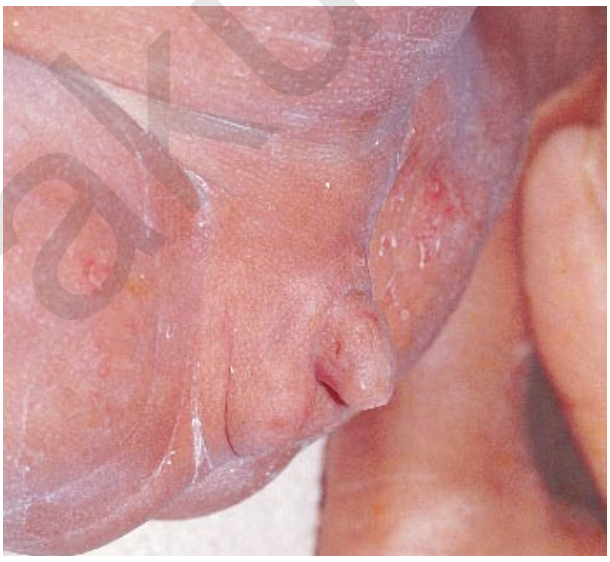

Figure 5.21. Lateral view of the same infant as in Figure 5.20 with ambiguous genitalia showing the marked clitoromegaly. Hermaphroditism (intersex) includes 1) true hermaphroditism, 2) female pseudohermaphroditism (virilizing adrenal hyperplasia), 3) male pseudohermaphroditism (the syndrome of incomplete testicular feminization; masculinization with 3-ß-hydroxysteroid dehydrogenase deficiency), 4) pseudohermaphroditism in syndromes (feminizing adrenal tumors).

5.22

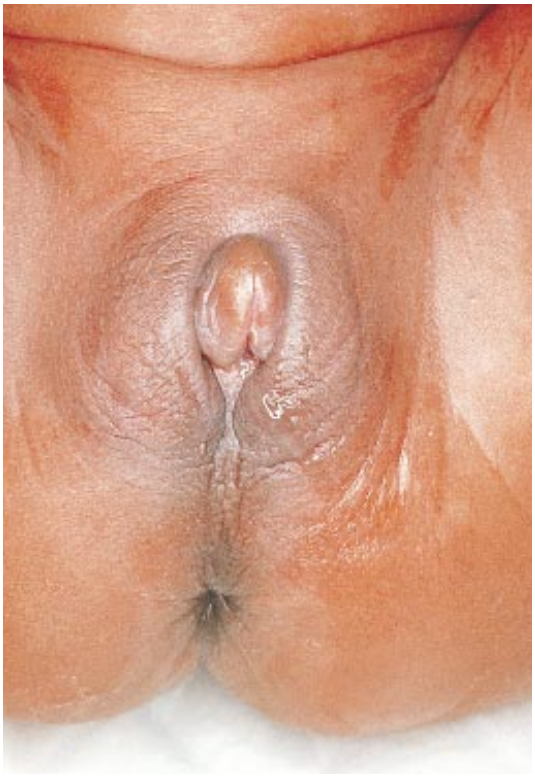

Figure 5.22. Ambiguous genitalia in a male pseudohermaphrodite with a karyotype of XY. Note the rugae in the labioscrotal folds. Gonads were not palpable.

5.23

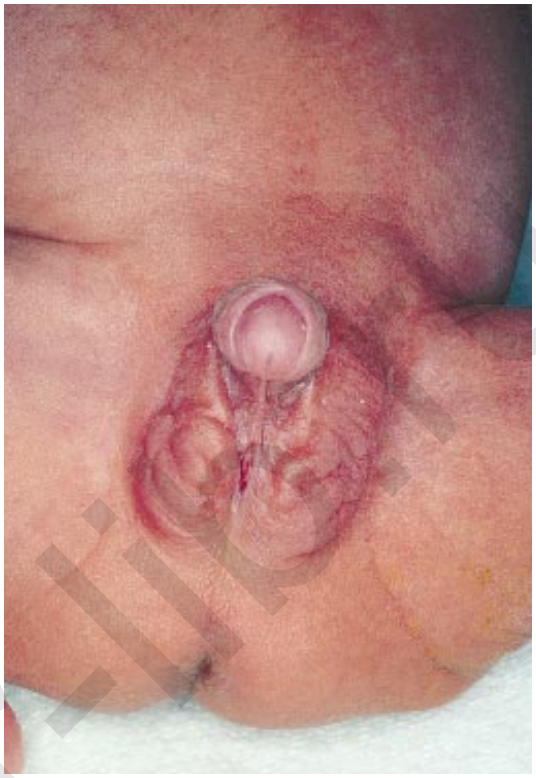

Figure 5.23. Another example of ambiguous genitalia in a male pseudohermaphrodite. Note the marked labioscrotal folds, absence of testes and presence of hypospadias.

5.24

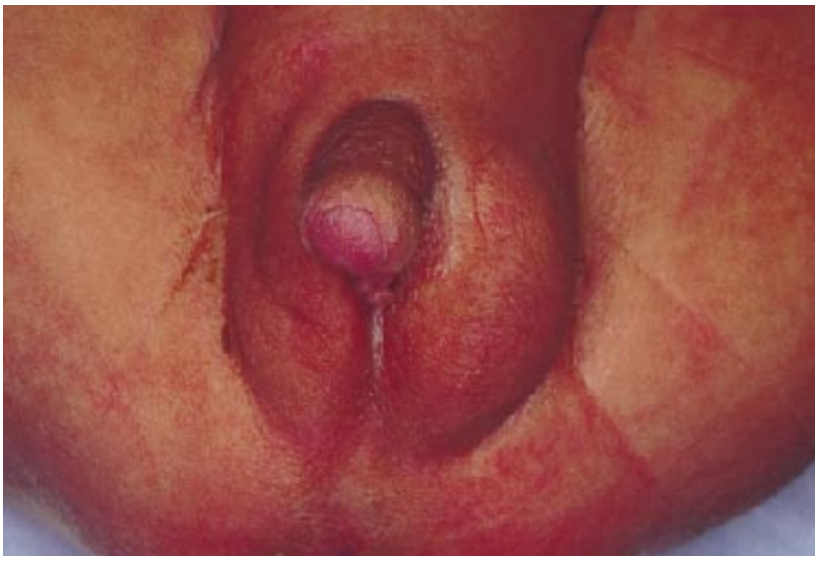

Figure 5.24. This infant with ambiguous genitalia is an example of incomplete testicular feminization in that there are normal-appearing female genitalia except for clitoral hypertrophy and a sinus urogenitalis. Because of the swelling of both labia majora an inguinal hernia may be suspected. At surgery the hernial sac was found to include both testes; no uterus was present. Karyotype was XY.

5.25

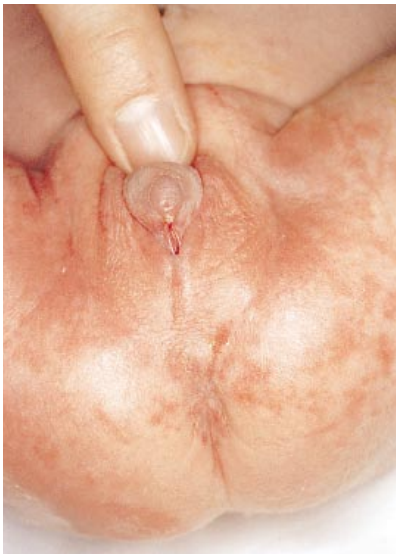

Figure 5.25. Another example of incomplete testicular feminization. Note the hypospadias. Karyotype was XY. In the syndrome of testicular feminization, the infants are genetic males: testes are located in the inguinal canal or in the labial folds. The external genitalia are female in configuration, and occasionally the clitoris is slightly enlarged; labioscrotal folds are partially fused and characteristically there is a blind vaginal pouch. The uterus may be rudimentary or absent. Incomplete variants of the syndrome do occur.

5.26

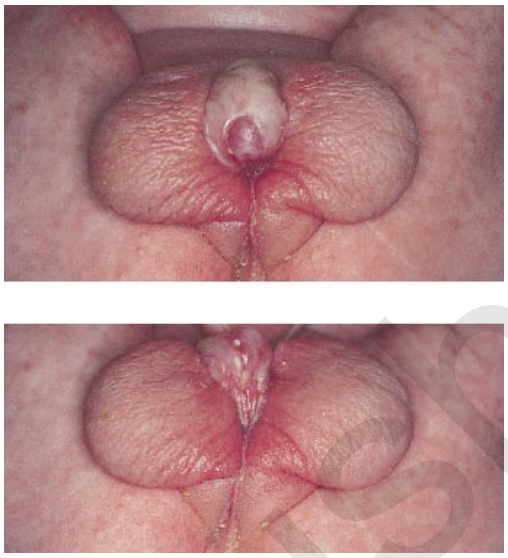

Figure 5.26. Ambiguous genitalia in an infant with a severe penoscrotal hypospadias. Karyotype was XY.

5.27

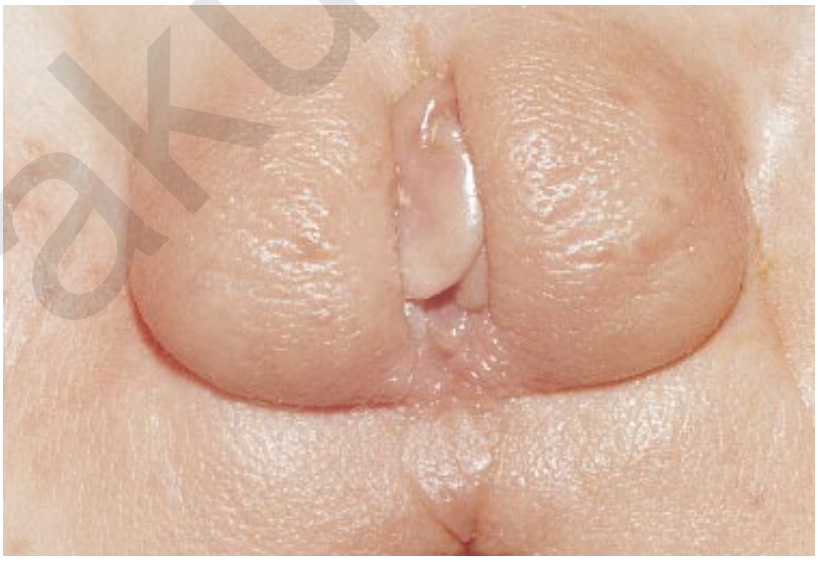

Figure 5.27. This infant with ambiguous genitalia had an XY karyotype and, thus, was a male pseudohermaphrodite. In male pseudohermaphroditism the appearance of the external genitalia varies from that of a normal female to that of a male with a penile urethra and either unilateral or bilateral cryptorchidism. Commonly there is perineal hypospadias, and the testes may be inside the abdomen, in the inguinal region, or in the labioscrotal folds.

5.28

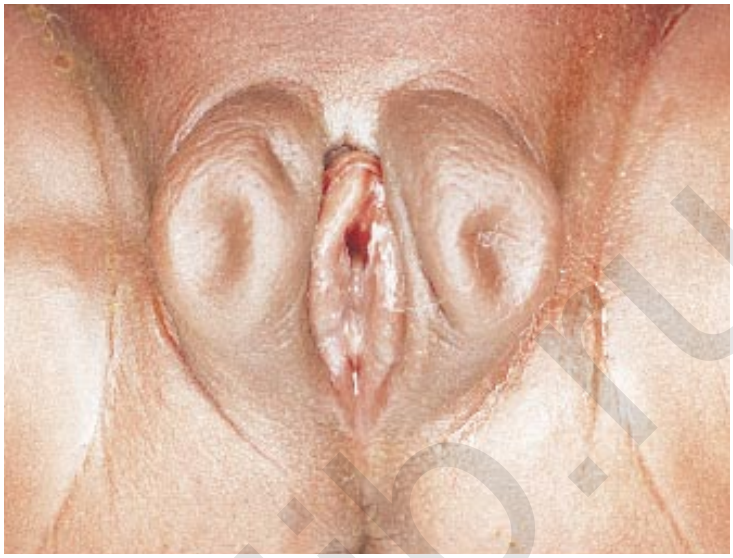

Figure 5.28. This infant with ambiguous genitalia had an XX karyotype. Gonads present in the labial folds (note the indentations) histologically were confirmed to be ovotestes.

5.29

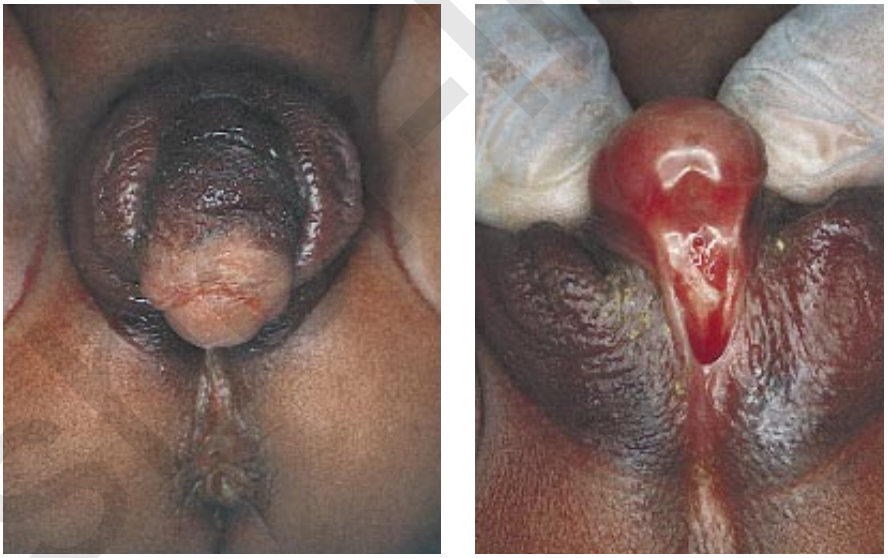

Figure 5.29. Ambiguous genitalia in this female pseudohermaphrodite was due to congenital virilizing adrenal hyperplasia. This female infant with 21-hydroxylase deficiency has clitoromegaly without fusion of the labial scrotal folds and separate vaginal and urethral openings. On the right the clitoris is raised to show the vaginal opening. The uterus was present on ultrasonography. Adrenogenital syndrome results from an enzymatic block of glucocorticoid biosynthesis resulting in excess secretion of androgens and masculinization of the female fetus.

5.30

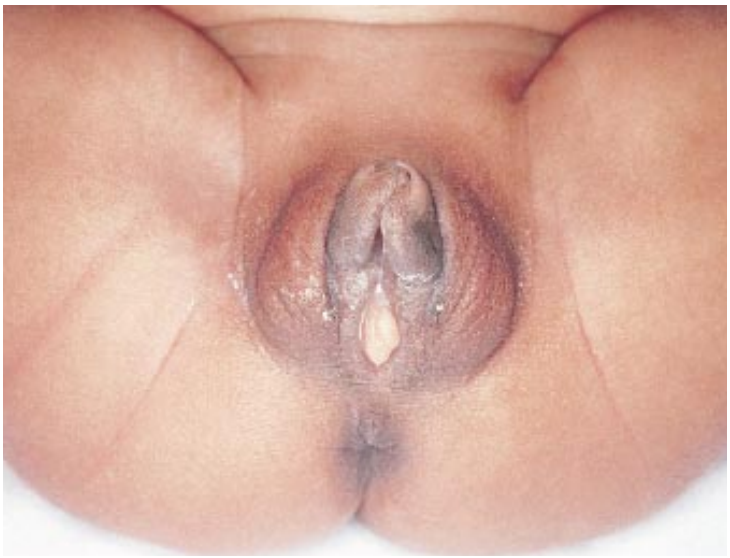

Figure 5.30. Another example of a female infant with ambiguous genitalia as the result of 21-hydroxylase deficiency. In female pseudohermaphroditism (masculinization of the external genitalia) findings include clitoral hypertrophy and fusion of the labia majora and a urogenital sinus (common opening of the urethra and vagina). In 21-hydroxylase deficiency there are elevated 17-hydroxyprogesterone levels with low urinary 17-hydroxysteroids. If there is also deficiency of mineralocorticoids, there may be abnormal urinary salt loss and hyponatremia. In 11-hydroxylase deficiency, clinical virilization of the female infant can also occur, but this is usually associated with hypertension resulting from an accumulation of deoxycorticosteroid which is a potent mineralocorticoid.

5.31

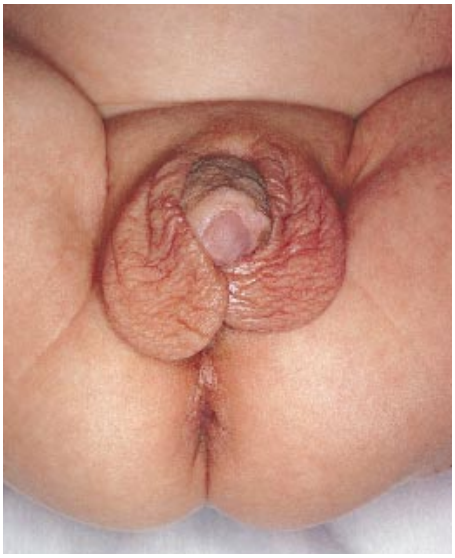

Figure 5.31. Another example of congenital adrenal hyperplasia in a female infant. Note the marked labioscrotal folds; testes were absent, and a hypospadias is present. In 21-hydroxylase deficiency, genitalia are conspicuously abnormal at birth. The degree of masculinization can be judged by the size of the clitoris and the degree of labioscrotal fusion, which determines the size of the urogenital sinus. The phallus is invariably enlarged, often approximating the size of a penis. It is generally bound with chordee, behind which a perineal hypospadias is situated. Commonly the labia majora have the appearance of a bifid scrotum. The orifices of the vagina and the urethra lie within the perineal opening of the urogenital sinus.

5.32

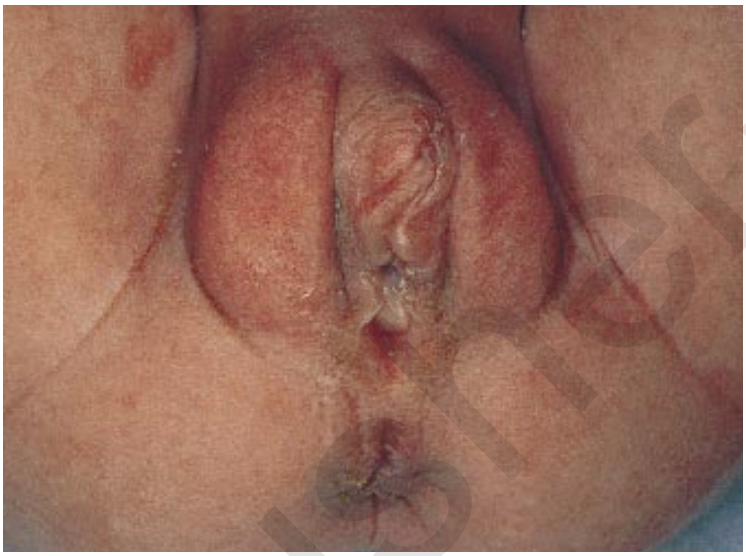

Figure 5.32. Another example of ambiguous genitalia in an infant with 21-hydroxylase deficiency. In female pseudohermaphroditism due to congenital adrenal hyperplasia, the following types of abnormalities may occur: Type I - only abnormality is an enlarged clitoris; Type II - there is partial labioscrotal fusion; Type III - a funnel-shaped urogenital sinus is present at the posterior end of a shallow vulva; Type IV - there is a very small urogenital sinus situated at the base of an enlarged phallus; Type V - a penile urethra is present.

5.33

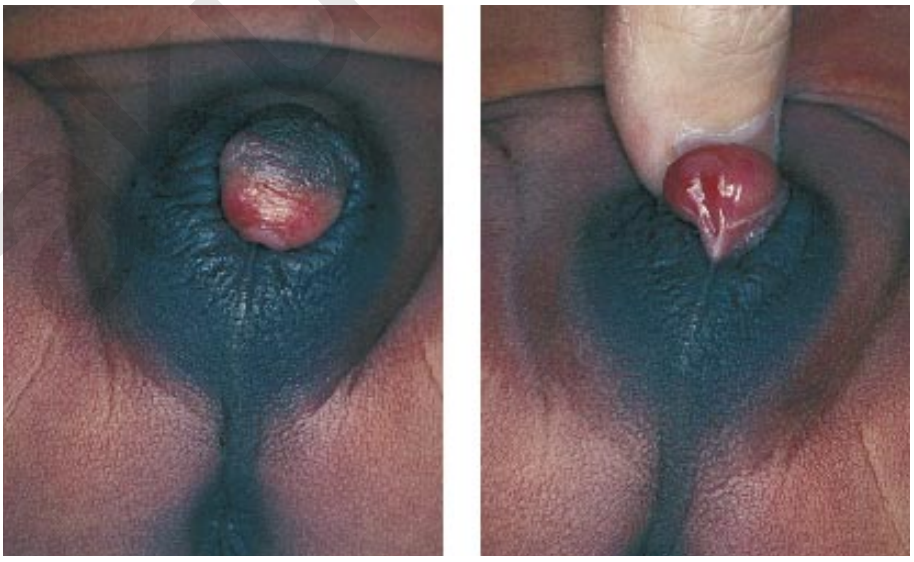

Figure 5.33. Hispanic female infant with ambiguous genitalia as a result of 21-hydroxylase deficiency. Infant presented on the 8th day of life with a serum potassium of 10 mEq/dL and a serum sodium of 108 mEq/dL due to congenital adrenal hyperplasia. Note the clitoromegaly and marked increase in pigmentation. Karyotype was 46 XX.

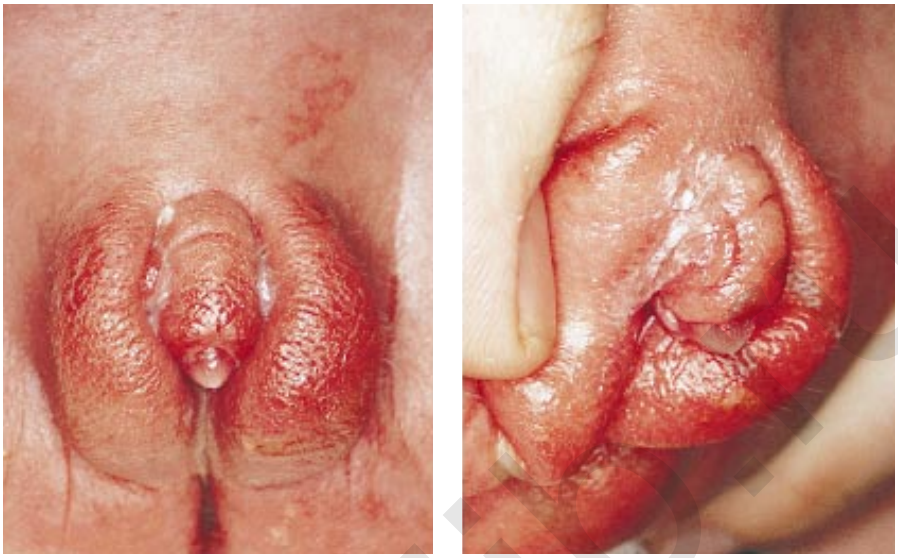

5.34

Figure 5.34. This female infant with ambiguous genitalia due to congenital adrenal hyperplasia presented in adrenal crisis at the age of 17 days with a serum potassium of 6.6 mEq/dL and a serum sodium of 117 mEq/dL. She responded rapidly to therapy.

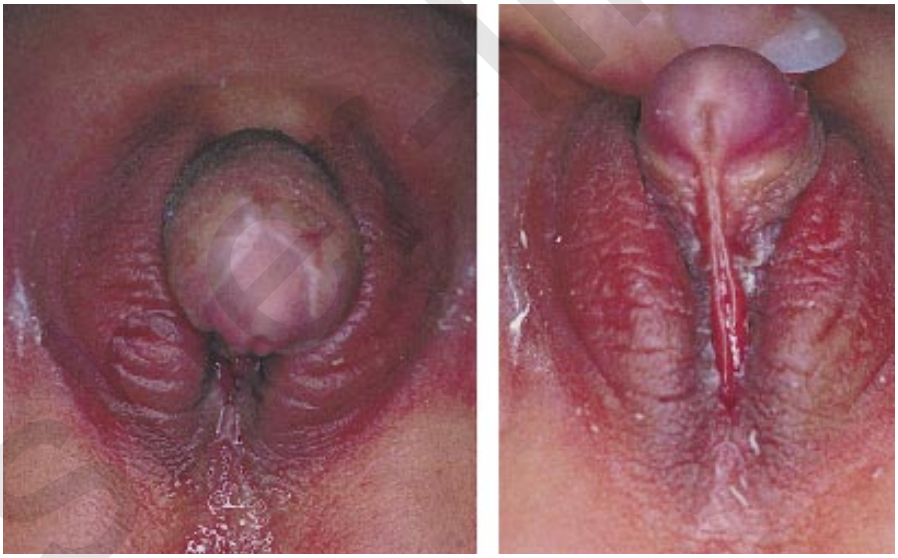

5.35

Figure 5.35. True hermaphroditism in an infant with an XX karyotype. Note the prominent phallus, lax labioscrotal folds, and urogenital sinus at the base of the phallus. Ovotestes were present in the abdomen. Most true hermaphrodites look more masculine than feminine. Cryptorchidism and inguinal herniae that contain a gonad or a vestigial uterus and fallopian tubes are present in about 50% of these infants.

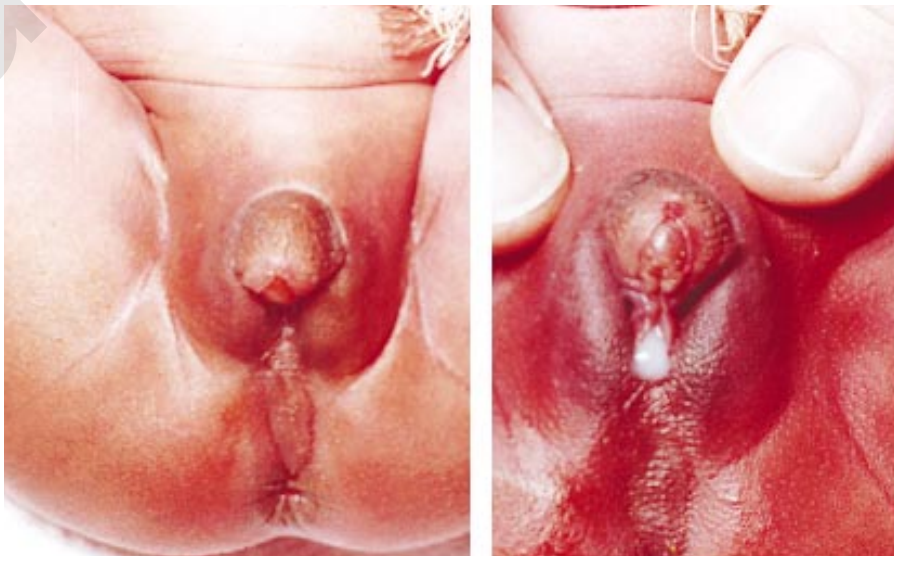

5.36

Figure 5.36. There was masculinization of this female infant following the use of diethylstilbestrol in the mother. Note the marked clitoromegaly. The presence of the vaginal secretion confirms the sex of this child. (See Volume I, Chapter 3, "Effects of Maternal Medication.")

5.37

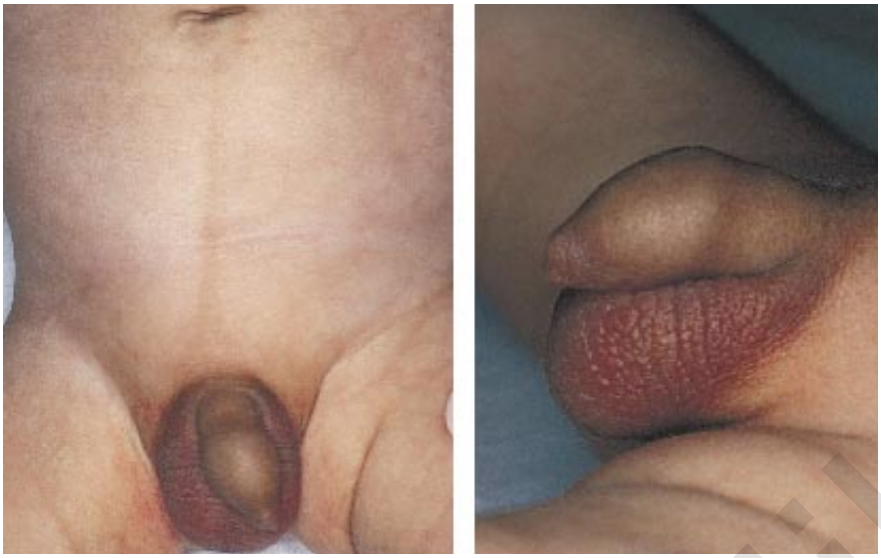

Figure 5.37. Enlarged penis and hyperpigmentation of this male infant with congenital adrenal hyperplasia. Note the prominent linea nigra.

5.38

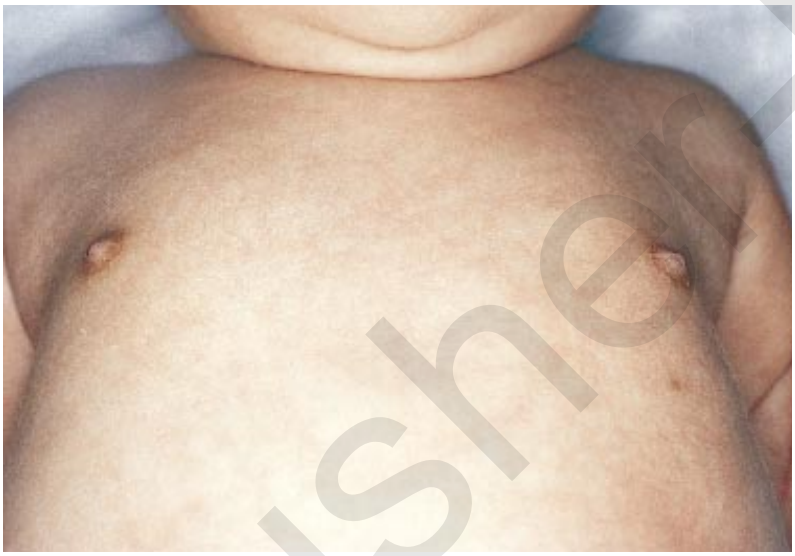

Figure 5.38. The same infant as in Figure 5.37 with hyperpigmentation of the nipples.

5.39

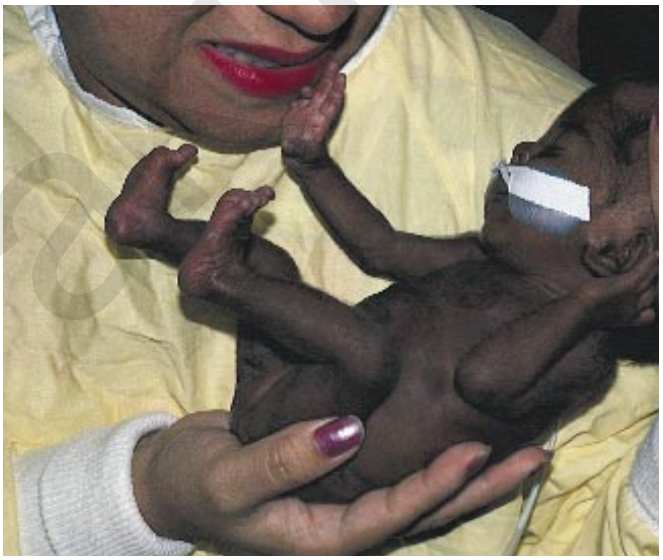

Figure 5.39. Thirty-three week gestational age infant with severe intrauterine growth retardation. This Hispanic infant was born at 33 weeks gestational age. There was oligohydramnios with severe intrauterine growth retardation (birth weight 1088 g). There was marked generalized hyperpigmentation of the skin (mother is holding infant) at age 4 weeks. This infant developed adrenal failure at 1 week of age, and the diagnosis of a primary adrenal hypoplasia was confirmed. The infant responded well to therapy, started to thrive, and the pigmentation was much decreased at 4 weeks of age and continued to improve.

Metabolic Disorders

5.40

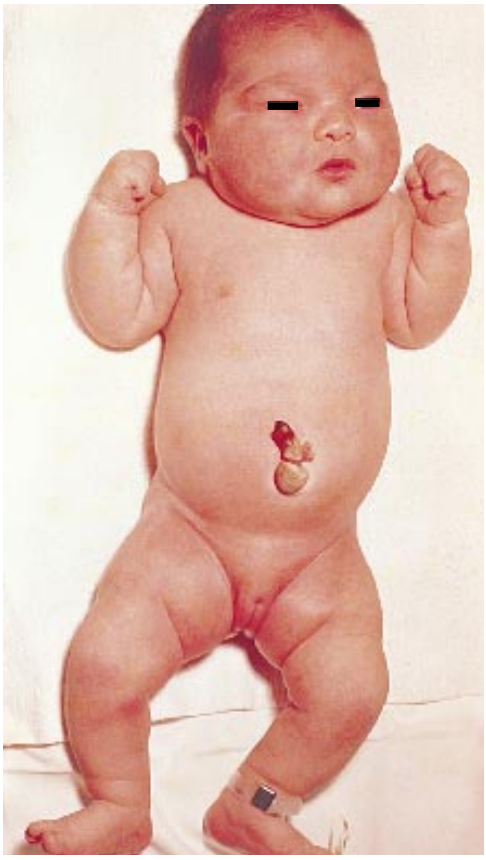

Figure 5.40. Infant of a diabetic mother. Infant is large for gestational age, has a cushingoid appearance, and is plethoric. Despite the deceptiveness of his size and appearance, the fact that the babies of diabetic mothers are often premature should not be disregarded.

5.41

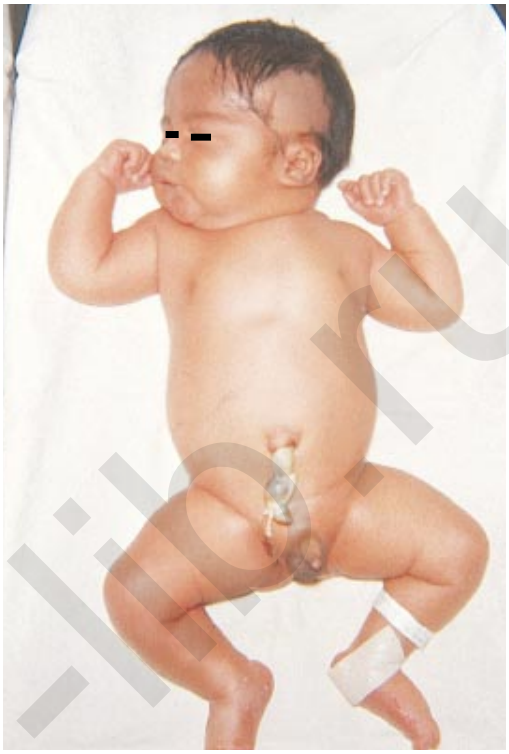

Figure 5.41. Infant of a diabetic mother showing macrosomia. The birthweight and body length are in excess of infants who are appropriate for gestational age. The macrosomic head of an infant of a diabetic mother may appear disporportionately small because brain size is not increased relative to gestational age. Macrosomia is also seen in Beckwith-Wiedemann syndrome, and Sotos' syndrome. Note the hypotonia which is common in these infants.

5.42

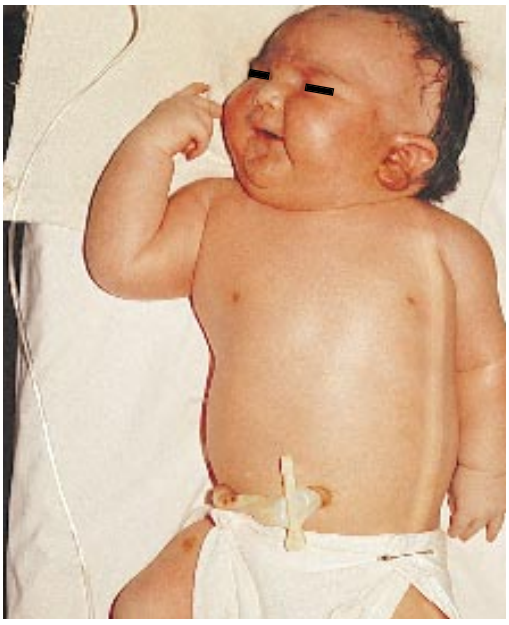

Figure 5.42. This infant of a diabetic mother has Erb's palsy of the left arm. Shoulder dystocia, which is common in these large-for-gestational-age infants, results in birth trauma such as fracture of the clavicle and brachial plexus injury. In general, there is an increased number of all congenital anomalies in infants of diabetic mothers. The caudal regression syndrome, sacral agenesis (see Volume II, Chapter 1, "Musculoskeletal Disorders"), and the small left colon syndrome (see this volume, Chapter 2) are malformations that occur almost exclusively in infants of diabetic mothers.

5.43

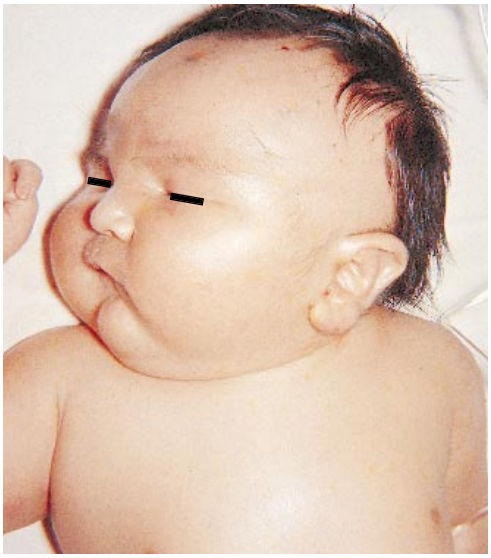

Figure 5.43. Classic facies of an infant of a diabetic mother. Note the shaved scalp with multiple venipuncture sites resulting from the need for intravenous glucose for hypoglycemia which occurs commonly in these infants. Therapy may also be required for hypocalcemia and hypomagnesemia.

5.44

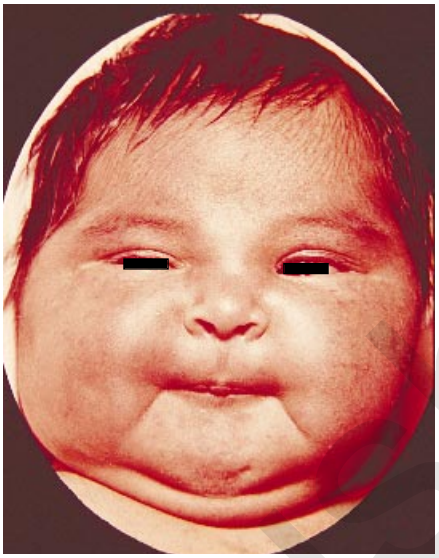

Figure 5.44. Classic cushingoid facies of an infant of a diabetic mother. Note the "balloon cheeks," dilated capillaries over the cheeks, and eyes that appear to be small. This infant also has a small subconjunctival hemorrhage of the left eye.

5.45

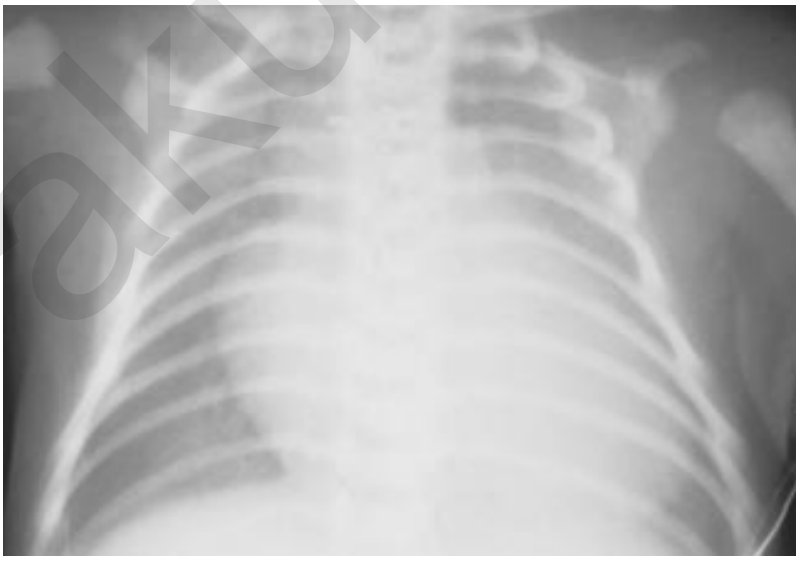

Figure 5.45. Chest radiograph of an infant of a diabetic mother presenting with tachypnea. Note the enlarged cardiac shadow. Infants of diabetic mothers may have cardiac enlargement due to a transient septal hypertrophy. The majority of these infants are asymptomatic, and the thickening is detected only by an electrocardiogram or echocardiography. With very marked septal thickening, left ventricular outflow obstruction may lead to left heart failure in the first few days after birth.

5.46

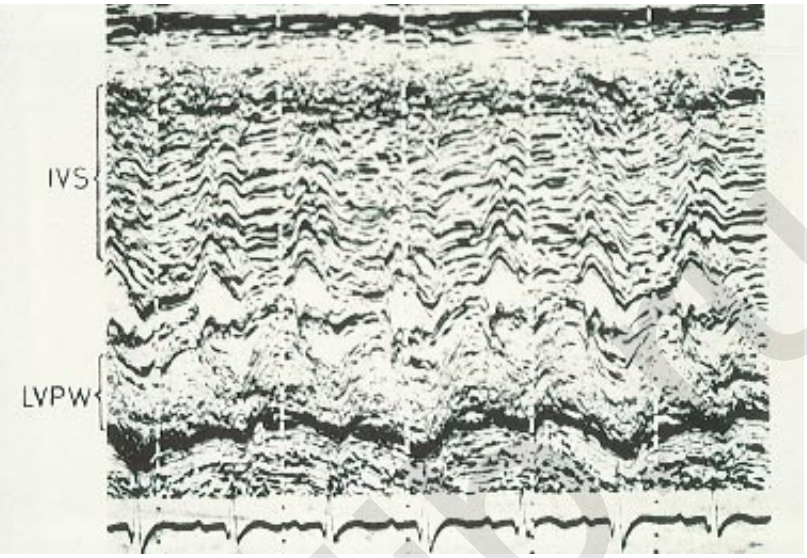

Figure 5.46. An echocardiogram of the same infant as in Figure 5.45 shows the marked thickening of the interventricular septum (interventricular septal hypertrophy). There may also be thickening of the left or right ventricular free wall. The changes generally regress after several months and the condition appears to leave no permanent effects on the myocardium. IVS interventricular septum LVPW left ventricular posterior wall.

5.47

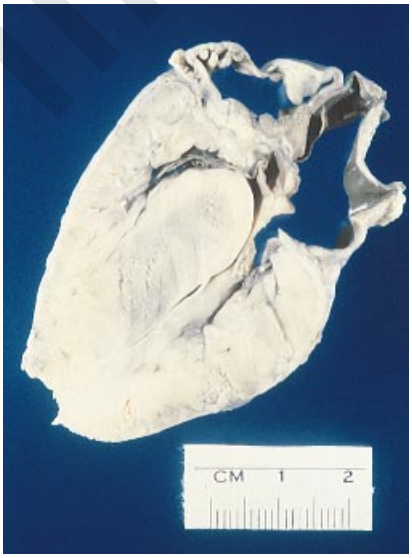

Figure 5.47. Autopsy specimen of a heart with marked interventricular septal hypertrophy in an infant of a diabetic mother.

5.48

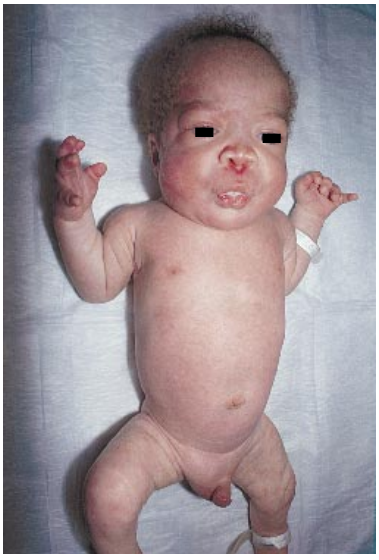

Figure 5.48. Infants with generalized gangliosidosis syndrome type I have a low birthweight and severe postnatal growth deficits. They have typical orofacial features and skeletal changes. The condition is autosomal recessive and has been shown to be due to a deficiency of ß-galactosidase. In this infant at the age of 16 days note the coarse features and growth deficiency.

5.49

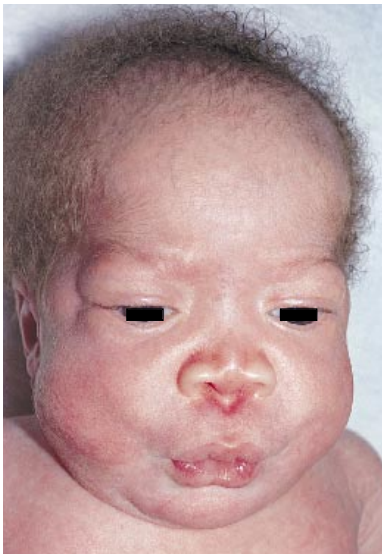

Figure 5.49. A close-up of the face of the same infant as in Figure 5.48 shows the coarse features with frontal bossing, puffiness of eyes, low nasal bridge, anteverted nostrils, and long philtrum.

5.50

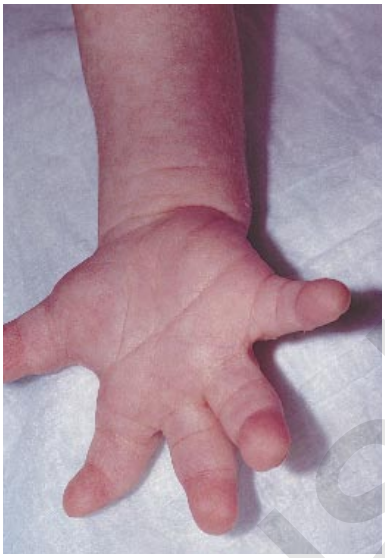

Figure 5.50. The right hand of the same infant as in Figures 5.48 and 5.49 shows the thickening of the wrists and a single palmar crease. Skeletal changes include moderate joint limitation with thick wrists, contractures at the elbows and knees, and development of a claw hand.

5.51

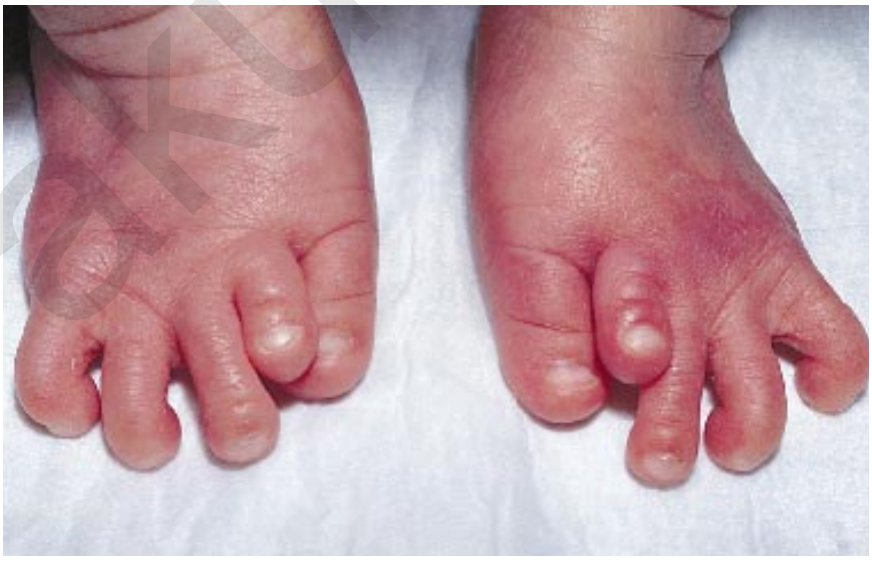

Figure 5.51. The feet of the same infant as in Figures 5.48–5.50 show the abnormalities of the toes. Radiologically the long bones are poorly mineralized and coarsely trabeculated, and some metaphyseal cupping and epiphyseal irregularity are usually present. The ribs are thick.

5.52

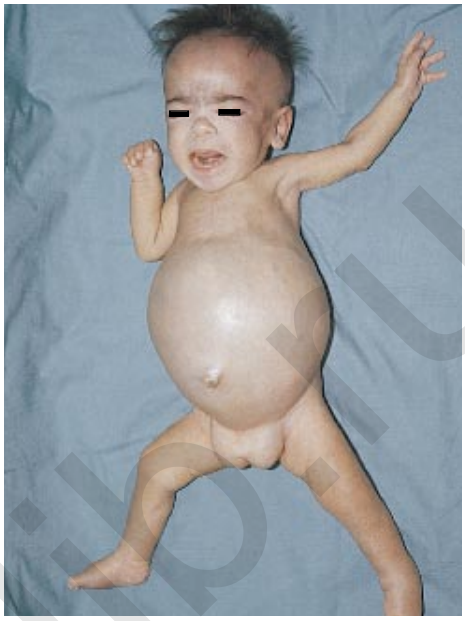

Figure 5.52. Infants with mucolipidosis type II (Leroy I-cell disease) have low birthweight and marked growth deficiency postnatally. Affected infants have the characteristic craniofacial features. There is moderate joint limitation in flexion of hips, kyphosis and broadening of the wrists and fingers. This infant at the age of 7 weeks shows the facial features and has marked ascites due to congestive cardiac failure. Death usually occurs from congestive cardiac failure.

5.53

Figure 5.53. In a lateral view of the same infant as in Figure 5.52 note the facial features, marked ascites, and labial edema.

5.54

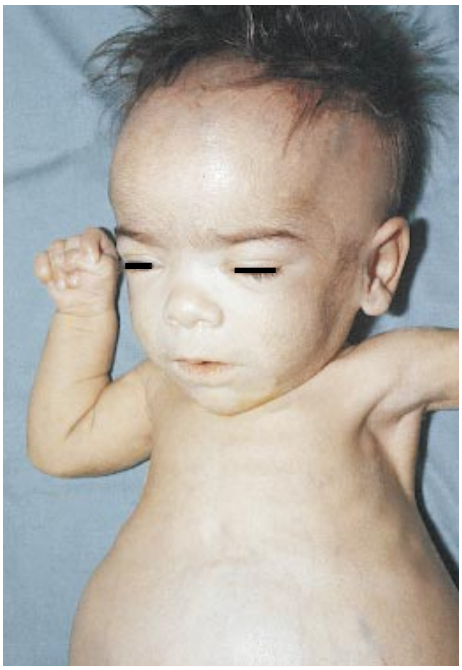

Figure 5.54. A close-up of the baby shows the typical facial features of high, narrow forehead, puffy eyelids, inner epicanthic folds, low nasal bridge, anteverted nostrils, a long philtrum, and progressive hypertrophy of the alveolar ridges.

5.55

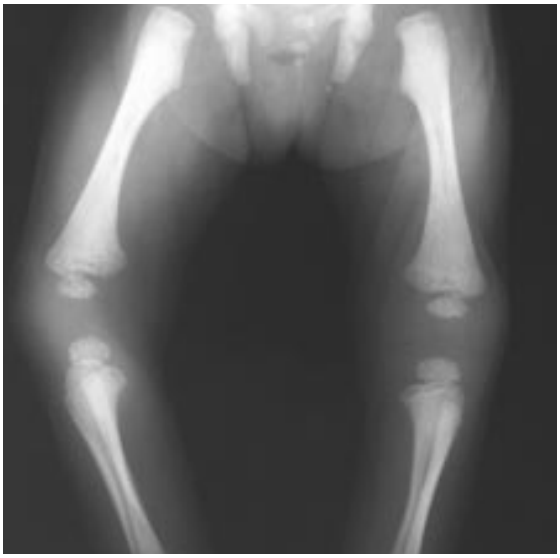

Figure 5.55. Radiograph of the lower extremities in Leroy I-cell disease shows discrete metaphyseal bands at the distal ends of the long bones.

5.56

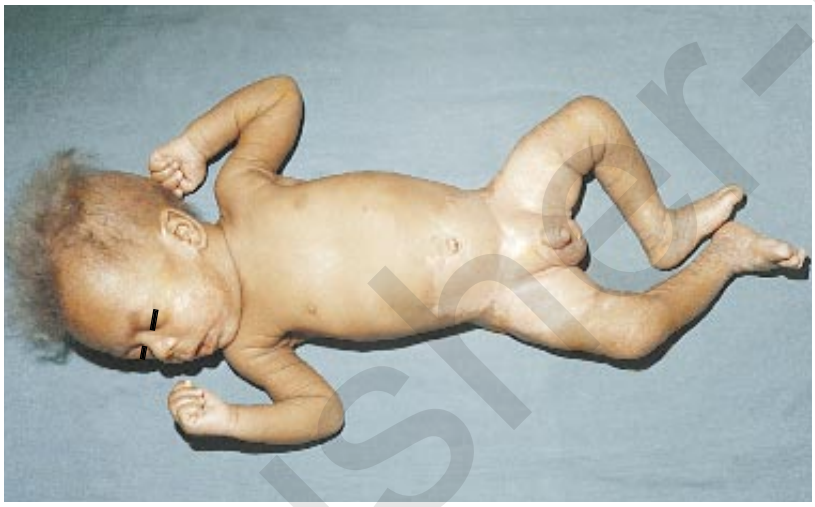

Figure 5.56. An infant with Menke's kinky-hair syndrome ("steely-hair" syndrome; trichopilodystrophy). Note the failure to thrive, and the abnormal hair pattern and skin lesions. These infants often present with seizures. It is a sex-linked recessive neurodegenerative disorder that affects male infants as a result of a copper deficiency and results in severe progressive neurologic deficit. There are low or absent copper and ceruloplasmin levels. Radiologically there may be widening of the metaphyses with spurring and frequent fractures, particularly of the ribs and femur. These may resemble the appearance of battered-child syndrome.

5.57

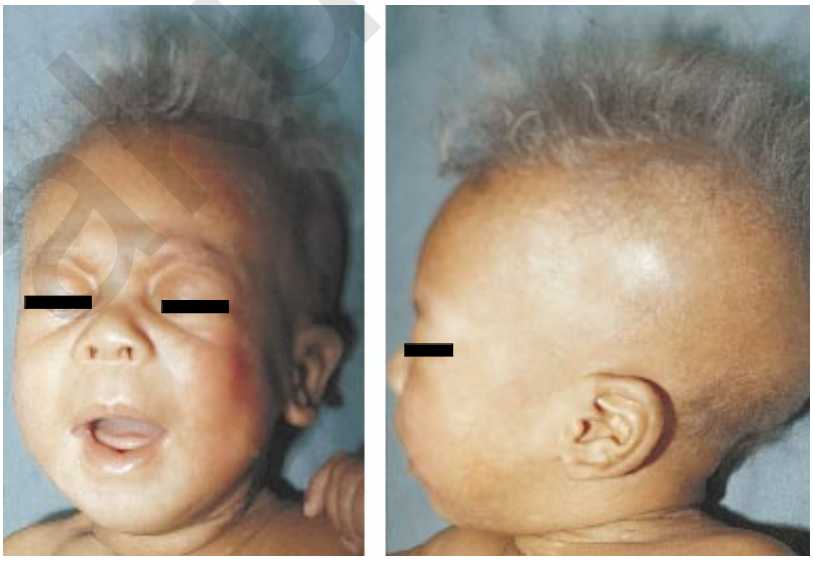

Figure 5.57. In this infant with Menke's syndrome note the pudgy cheeks, lack of expression and movement, marked areas of alopecia, and the short stubby hair which is lightly pigmented giving it a "steely" appearance.

5.58

Figure 5.58. A close-up of the hair in the same infant as in Figure 5.57 showing the "steely" appearance of the hair.

5.59

Figure 5.59. Another view of the scalp of the same infant as in Figures 5.57 and 5.58 showing hair which is fine, dull, sparse, and poorly pigmented. It stands on end and looks and feels like steel wool.

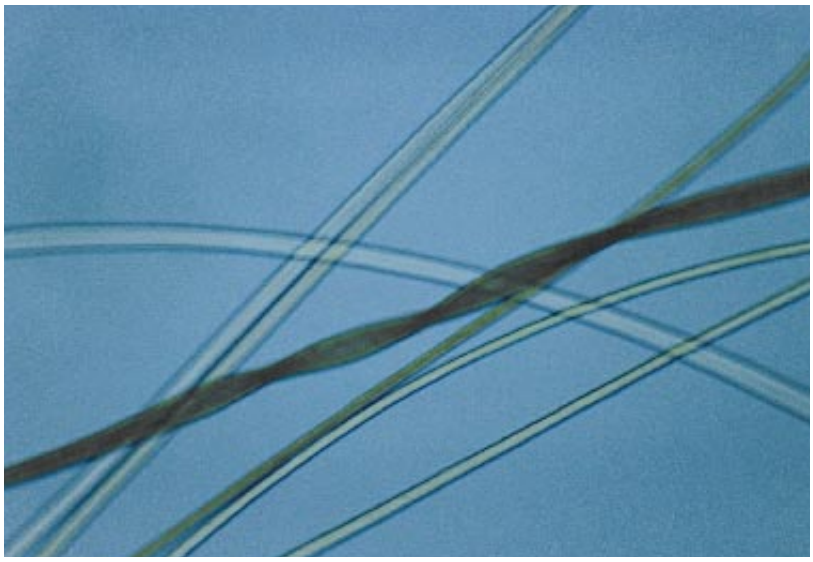

5.60

Figure 5.60. Microscopic examination of the hair shows the typical pilo torti. Note the dry fragile twisted hairs with partial breakage. This should not be confused with the apearance of the hair in argininosuccinicaciduria.

5.61

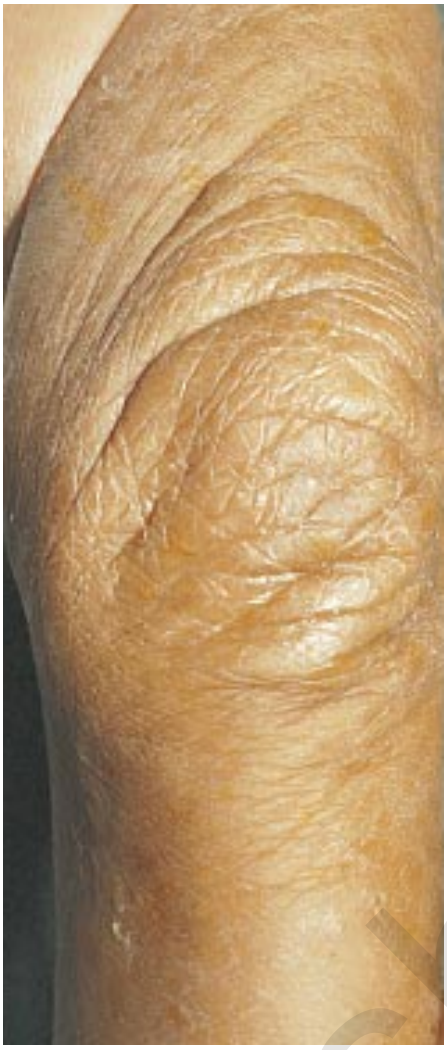

Figure 5.61. The same infant as in Figures 5.56 through 5.59 also had the typical eczema seen in infants with steely-hair syndrome. Pigmentation is often unequal and, additionally, there may be a seborrheic rash.

Chapter 6
Hematology, Jaundice, and Oncology

The neonate may suffer from hematologic conditions involving the erythrocyte, platelet, leukocyte, coagulation, and thrombosis. Many of these disturbances are life-threatening, some are primary, and some reflect other diseases. Jaundice is a common problem in the neonate, and it is rarely life-threatening or debilitating. It is of particular concern, because it frequently occurs in otherwise healthy infants, usually because the liver cannot clear sufficient bilirubin from the plasma. Neoplasias in the neonate are rare but frequently are unique in their diagnosis and treatment. They may be composed of persistent embryonal or fetal tissue, and may be associated with abnormalities of growth and congenital anomalies. The problems presented by these conditions relate to the difficulty in diagnosing a neoplasm from a poorly differentiated fetal tissue, and in the potential for long-term sequelae in the therapeutic interventions required.

6.1

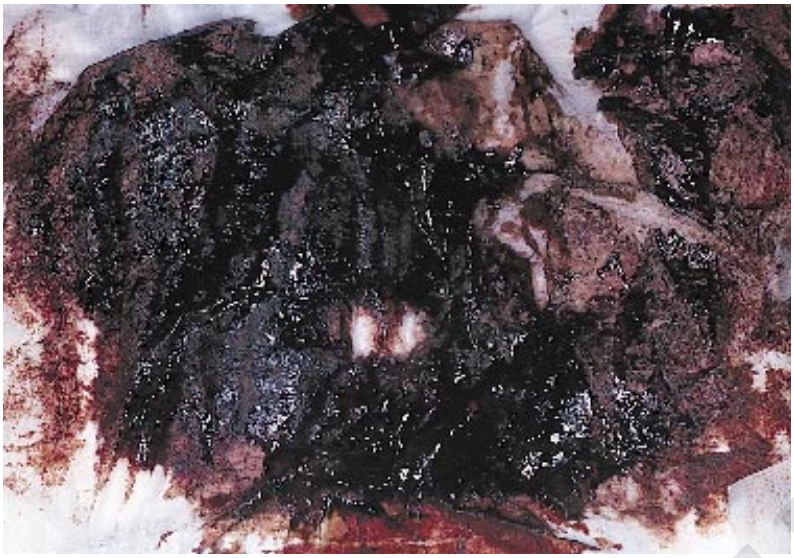

Figure 6.1. This infant had blood in the stools on the first day of life. The Apt test was positive, making the diagnosis one of ingested maternal blood.

6.2

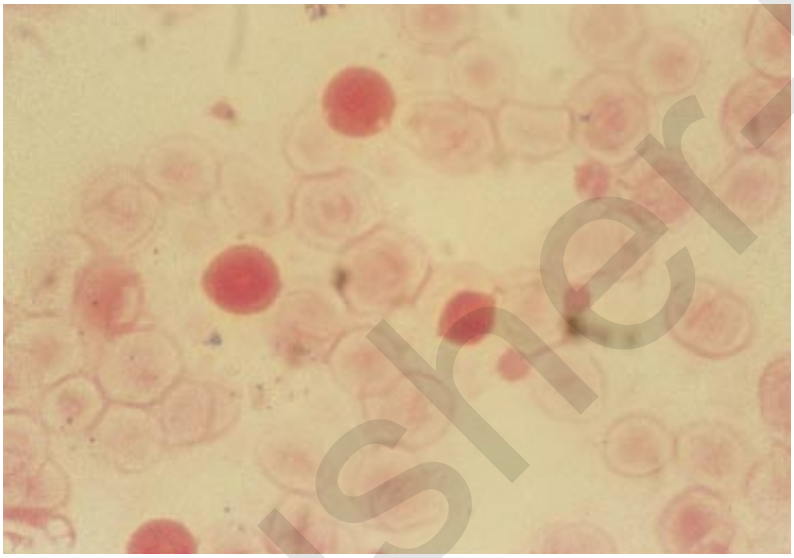

Figure 6.2. In infants with a feto-maternal hemorrhage, the Kleihauer-Betke test on maternal blood is positive as shown in this microscopic slide. Acid elution of maternal hemoglobin results in lysis of the red blood cells (creating "ghost" erythrocytes), while fetal red blood cells resist acid hydrolysis.

6.3

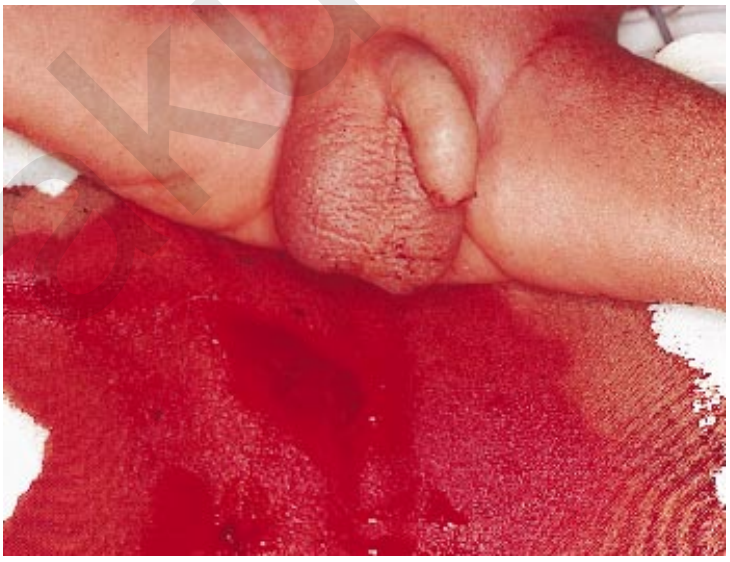

Figure 6.3. At the age of 3 days, this infant developed hematuria and bloody stools as a result of hemorrhagic disease of the newborn. This is due to a transitory prothrombin and vitamin K deficiency. The Apt test in such an infant would be negative for maternal blood. The condition is more common in black infants.

6.4

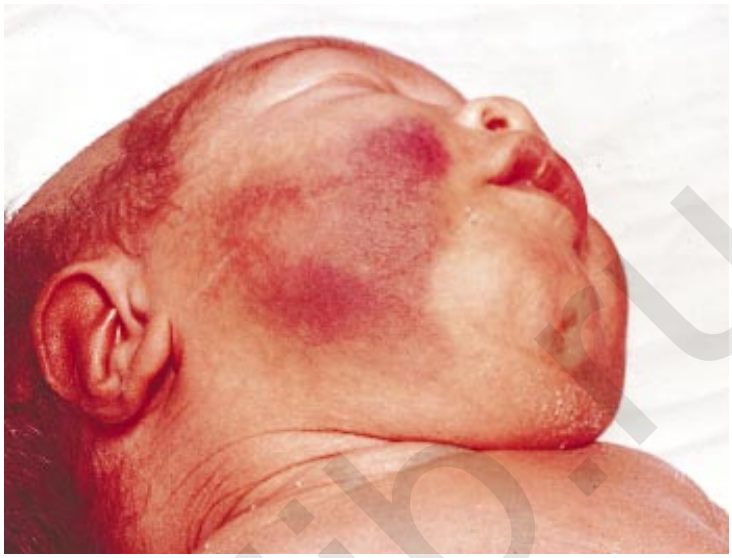

Figure 6.4. Hematoma of the right cheek following birth trauma. With a large hematoma there can be massive blood loss and trapping of platelets resulting in thrombocytopenia.

6.5

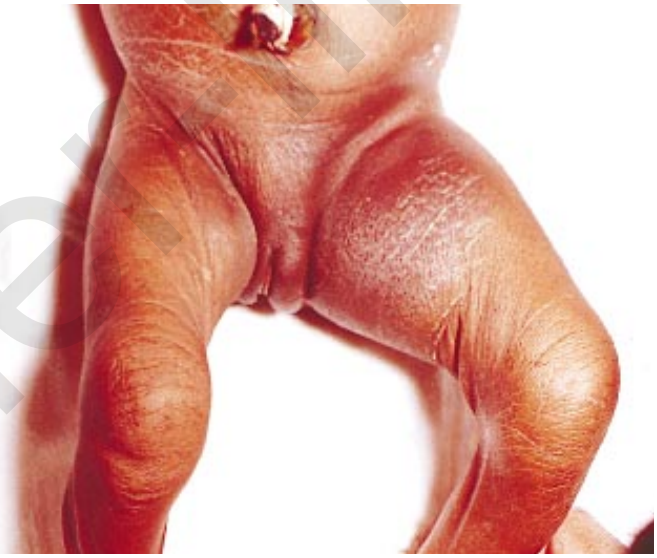

Figure 6.5. Large hematoma of the left thigh and groin.

6.6

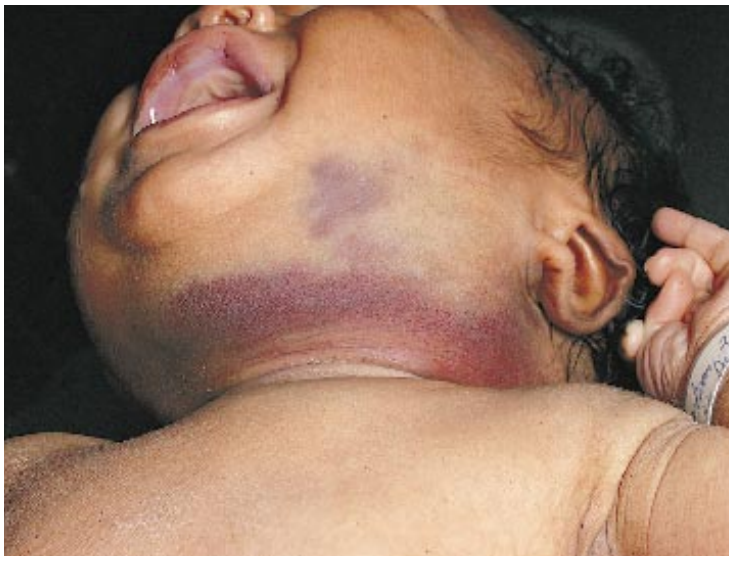

Figure 6.6. Hematoma with ecchymosis of the neck and face of an infant following birth trauma.

6.7

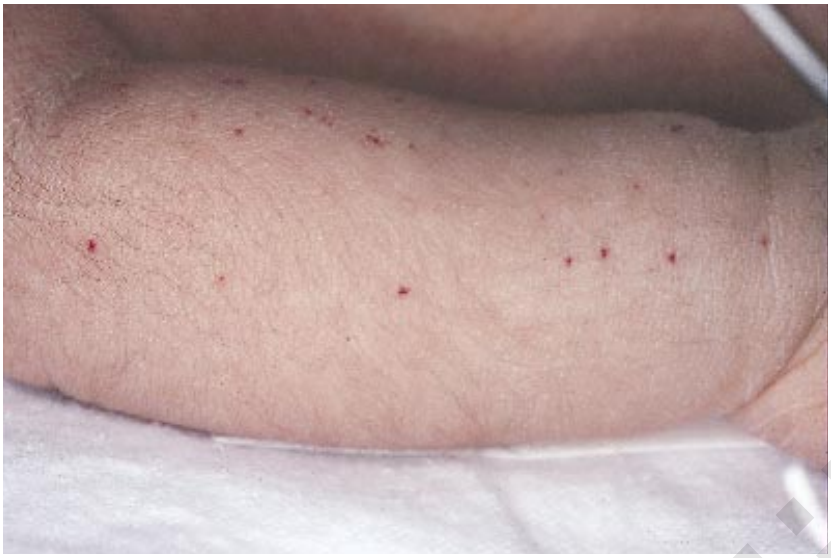

Figure 6.7. Petechiae on the forearm of an infant following severe birth asphyxia. The infant's platelet count was 90,000/mm^3 and returned to normal within a week.

6.8

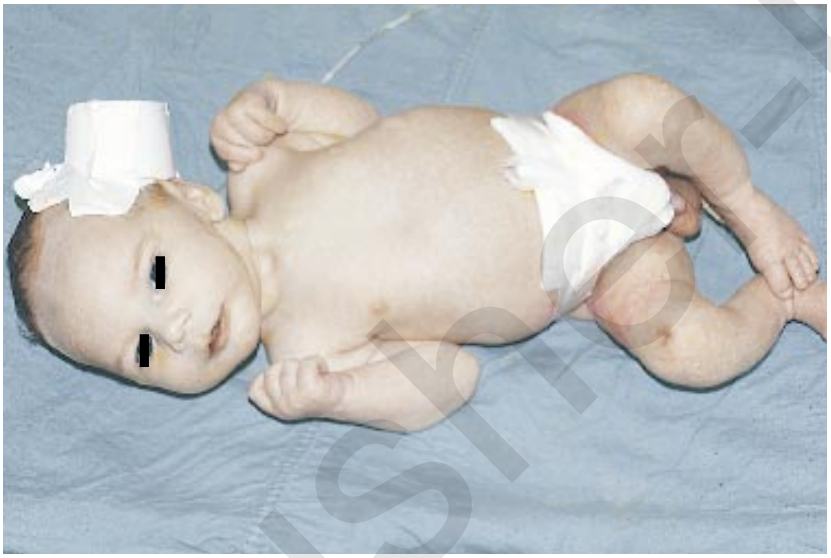

Figure 6.8. Note the slate gray discoloration of the skin in an infant with methemoglobinemia at the age of 9 days. Total hemoglobin was 10.4 gm/dL with 11% methemoglobin. The infant had been treated with intravenous nitrofurantoin for a urinary tract infection. There are many causes of methemoglobinemia in the neonate (see this volume, Chapter 1).

6.9

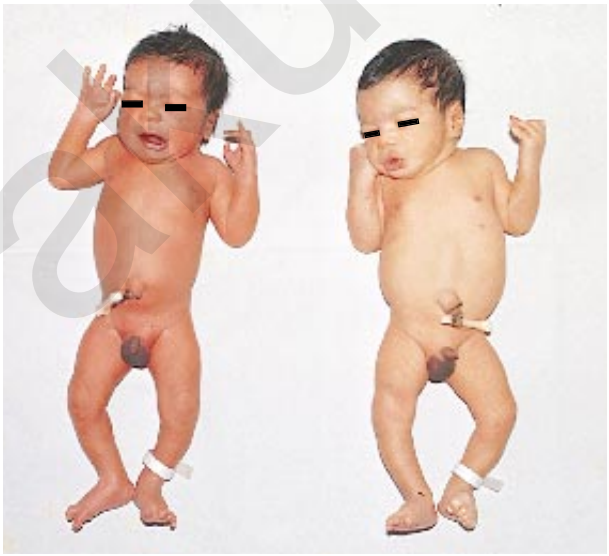

Figure 6.9. Feto-fetal (twin-twin) transfusion syndrome due to a vascular anastamosis in a monochorionic placenta. It results from abnormal placentation in identical twins in whom there is an arteriovenous anastamosis. As a result of the pressure differential, one twin becomes polycythemic and the other twin becomes anemic.

6.10

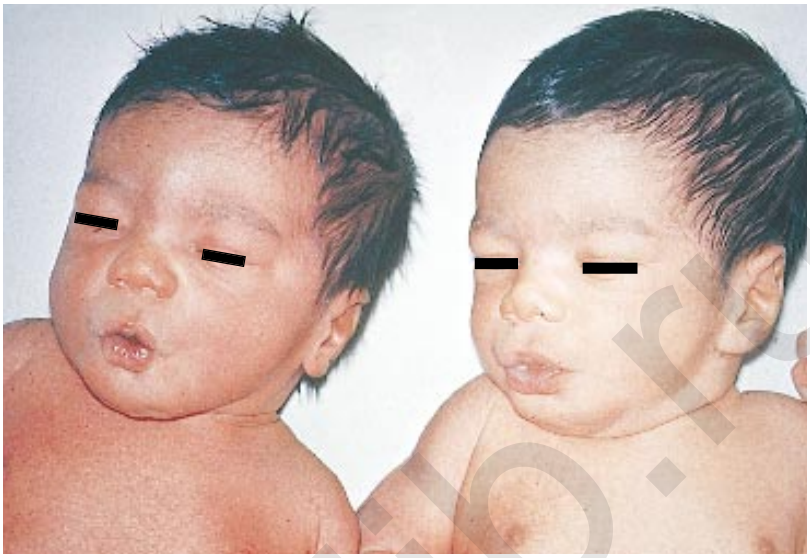

Figure 6.10. A close-up of the same infants as in Figure 6.9 shows the plethoric recipient twin on the left and pale donor twin on the right. Discordance is defined as a 20% difference in birthweight or a difference in hemoglobin of greater than 5 gm/dL. Morbidity is greater in the recipient twin. There may be intrauterine growth retardation in the donor twin due to a reduced blood supply.

6.11

Figure 6.11. Concordant female twin infants with a marked discrepancy in skin color due to a feto-fetal transfusion syndrome. The anemic twin on the right had a birthweight of 2530 g with a hemoglobin of 15.6 gm/dL and a hematocrit of 46%. The plethoric twin on the left had a birthweight of 2740 g with a hemoglobin of 27.4 gm/dL and a hematocrit of 84%.

6.12

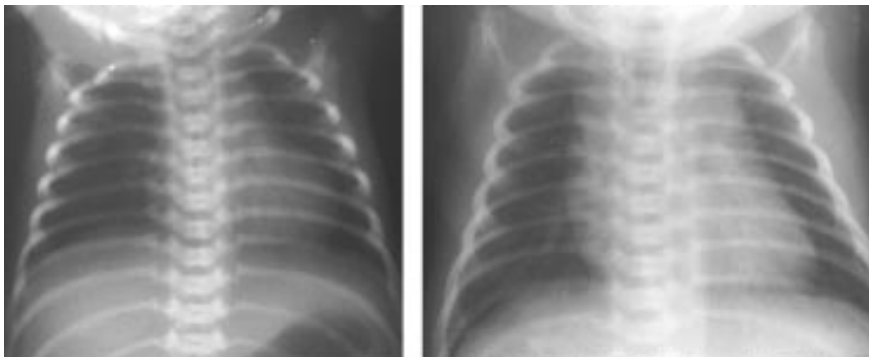

Figure 6.12. Chest radiographs of twin infants with feto-fetal transfusion syndrome. The radiograph on the left of the anemic twin is normal. The radiograph on the right of the polycythemic twin shows the increased pulmonary vascular markings with an enlarged cardiac shadow.

6.13

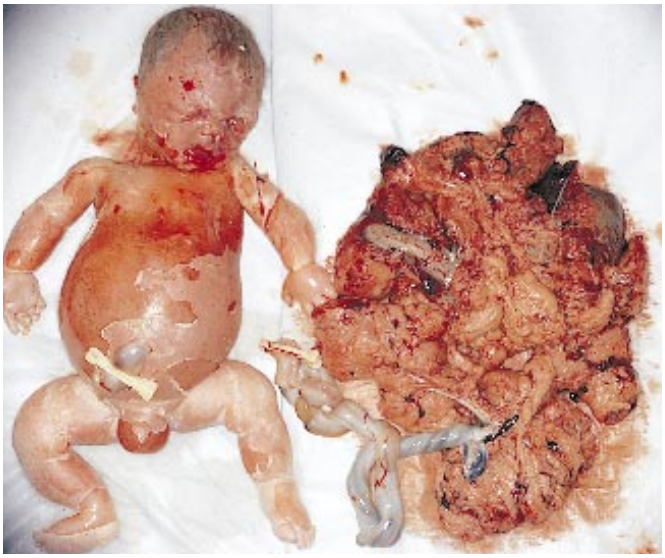

Figure 6.13. This is a macerated stillborn infant with its placenta markedly enlarged as a result of Rh isoimmunization. There is gross swelling and pallor of all parts of the body and hepatosplenomegaly. Whereas previously isoimmunization was the most common cause of hydrops fetalis, now with the use of Rhogam®, nonimmune causes of hydrops fetalis are much more common.

6.14

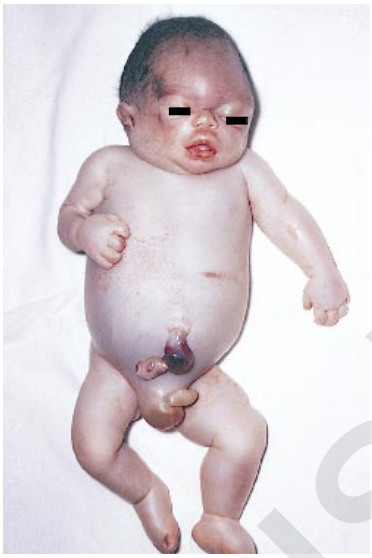

Figure 6.14. A pale hydropic newborn with Rh hemolytic disease of the newborn. Note the associated abdominal distension as a result of ascites and hepatosplenomegaly.

6.15

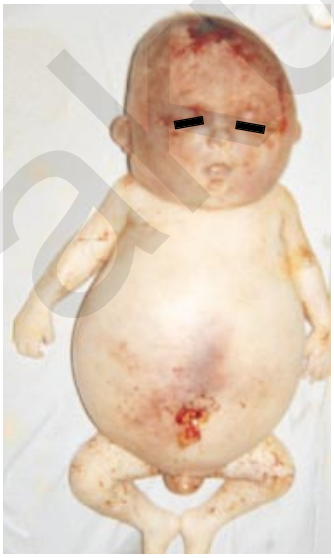

Figure 6.15. Nonimmune hydrops fetalis in an infant with congenital cytomegalovirus infection. Nonimmune hydrops fetalis has numerous causes including primary myocardial failure (cardiac malformation or arrhythmia), high output failure (anemia or arteriovenous malformation) and congenital infections.

6.16

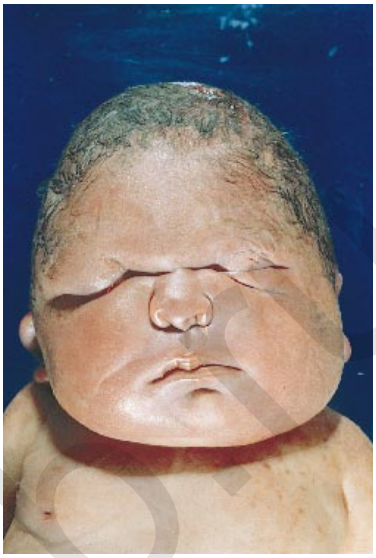

Figure 6.16. Hydrops fetalis in an infant with ß-glucuronidase deficiency.

6.17

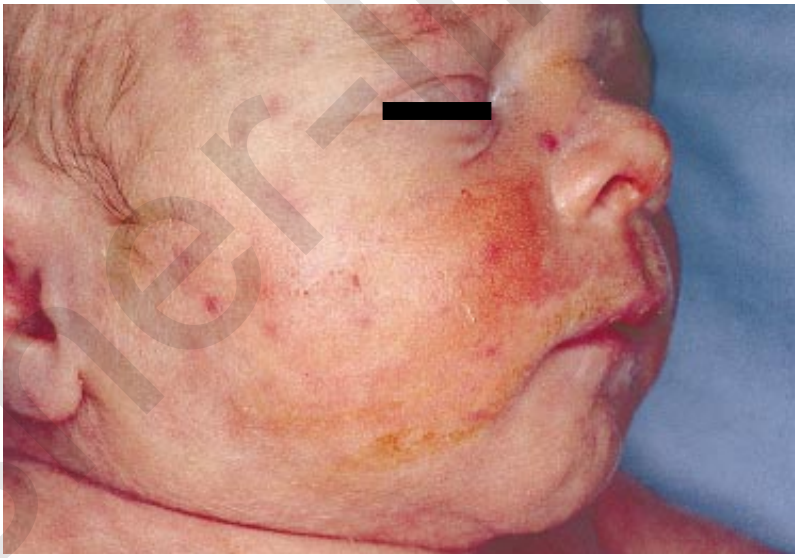

Figure 6.17. Purpuric lesions of the face and chin in an infant with Rh hemolytic disease of the newborn. Purpuric lesions represent extramedullary hematopoiesis and give rise to the "blueberry muffin" appearance. The blueberry muffin appearance may be seen in infants with other conditions. Differential diagnosis includes ABO incompatibility, TORCH infections, and isoimmune thrombocytopenia.

6.18

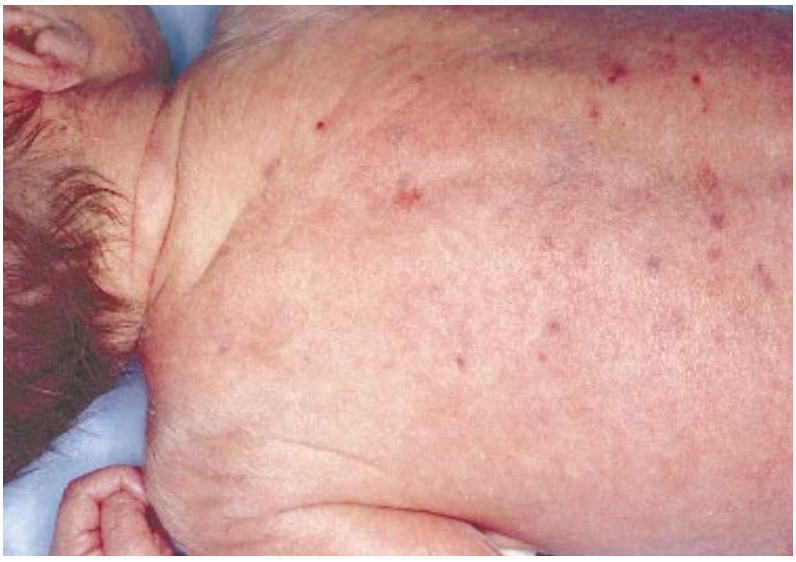

Figure 6.18. Purpuric lesions on the back of the same infant as in figure 6.17 with Rh hemolytic disease are the result of dermal erythropoiesis.

6.19

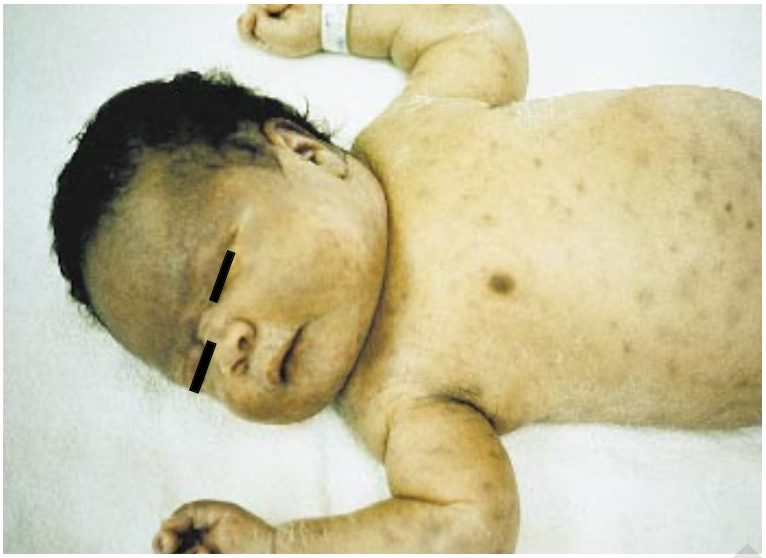

Figure 6.19. This infant with ABO incompatibility presented with the typical "blueberry muffin" appearance and hyperbilirubinemia. He had severe hemolysis with a bilirubin level of 18 mg/dL. The blueberry muffin appearance, due to extramedullary hematopoiesis, improved over the course of a few days.

6.20

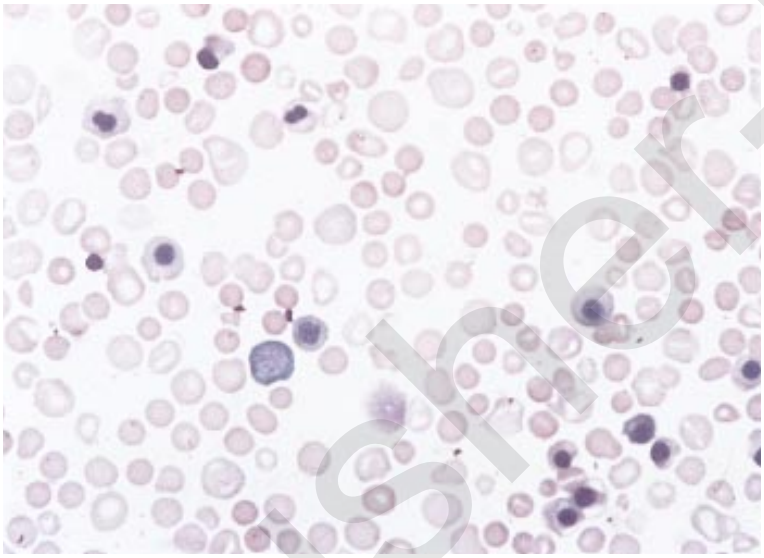

Figure 6.20. Photomicrograph of a peripheral blood smear in the same infant with a Coombs' positive ABO incompatibility. Note the microspherocytes, nucleated red blood cells, target cells, and polychromasia.

6.21

Figure 6.21. Skin coloration of infants in the first day of life who are not related. The infant on the left is jaundiced as a result of Rh hemolytic disease of the newborn. In comparison, note the normal pink skin of the infant with a large cephalhematoma on the right. The cephalhematoma can be a later cause of hyperbilirubinemia.

6.22

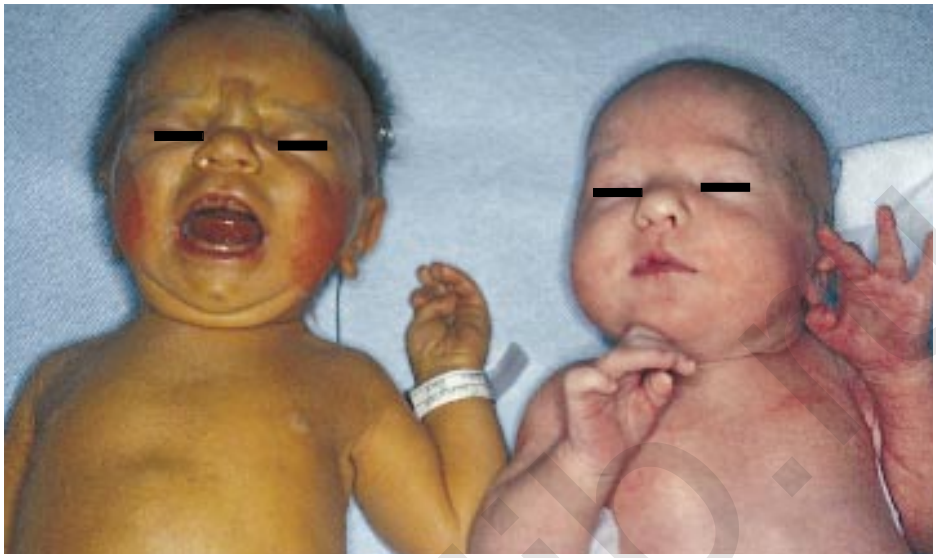

Figure 6.22. Markedly jaundiced appearance of the infant pictured on the left. This infant presented from home with a bilirubin of 50.6 mg/dL. Jaundice was the result of an anti-C alloimmunization. The infant on the right is normal.

6.23

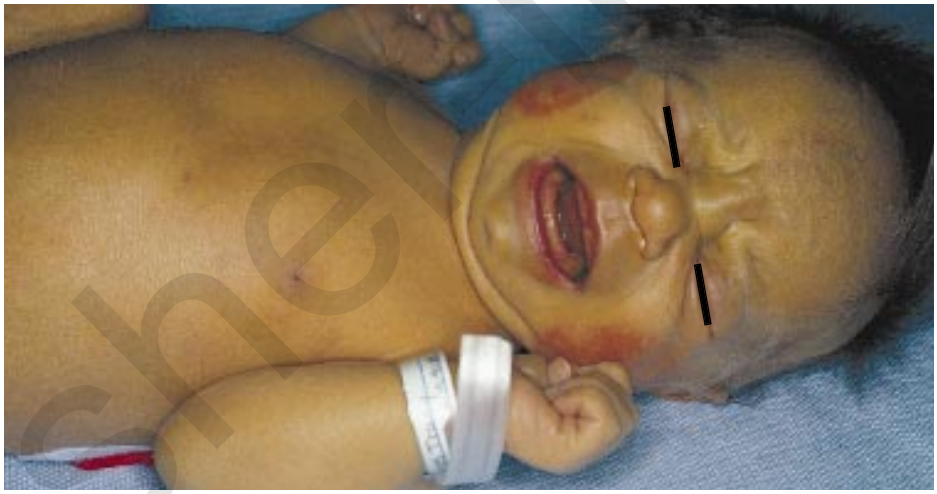

Figure 6.23. The same infant as in Figure 6.22 at age 3 days had a hematocrit of 23.7% with an unconjugated bilirubin of 8.4 mg/dL and a conjugated bilirubin of 4.8 mg/dL. At 4 days of age the infant's hematocrit had fallen to 18.5% and the conjugated bilirubin had increased to 50.6 mg/dL with an unconjugated level of 4.2 mg/dL.

6.24

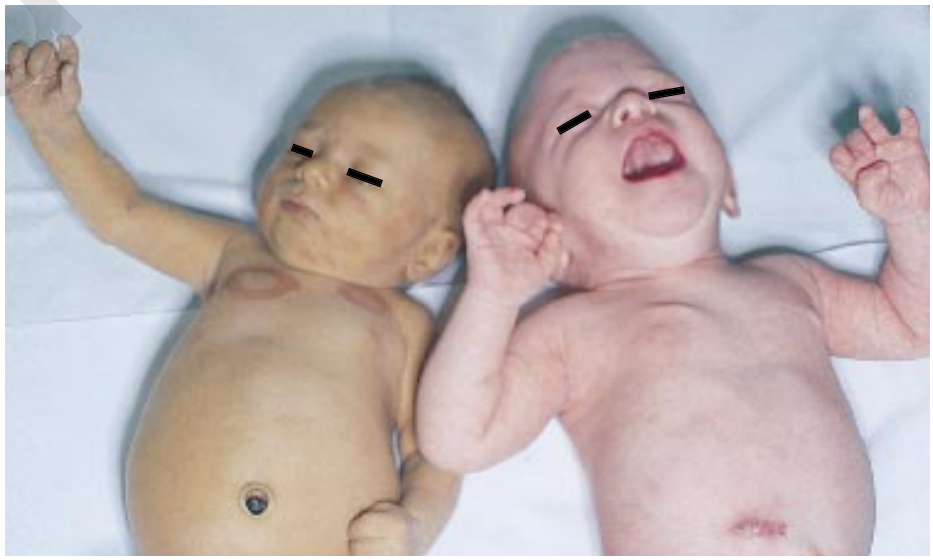

Figure 6.24. This infant with hemolytic disease of the newborn (left) developed persistent jaundice as a result of obstruction of bile channels (inspissated bile syndrome). Note the difference in coloration of the infant as compared to the normal infant on the right.

6.25

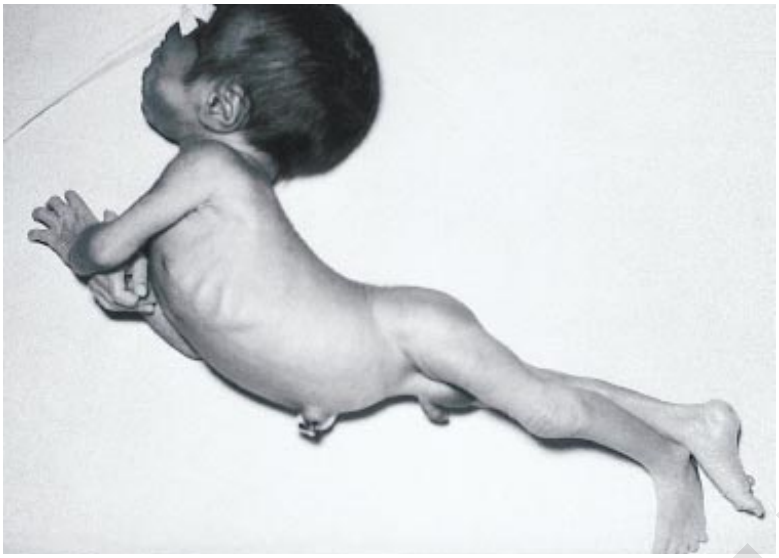

Figure 6.25. Opisthotonic posturing in an infant with erythroblastosis fetalis. Note the neck retraction and the hypertonic extensor spasm of the limbs with scissoring. This is the result of the development of kernicterus due to severe neonatal unconjugated hyperbilirubinemia.

6.26

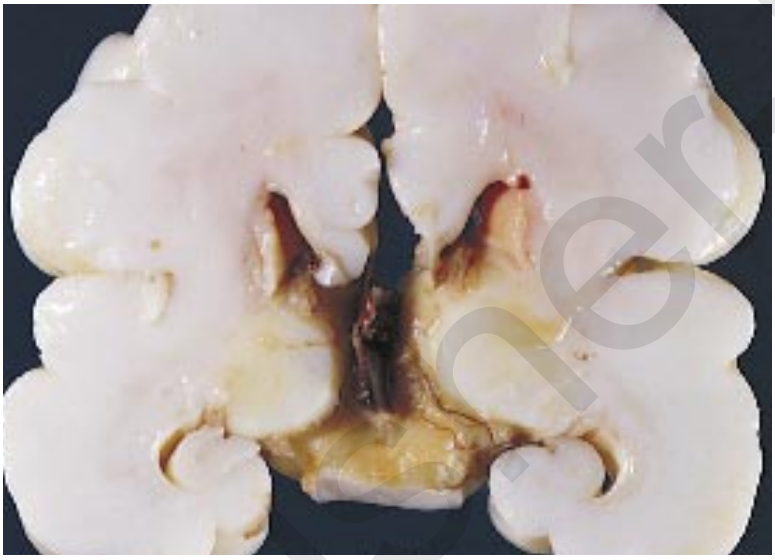

Figure 6.26. A section through the brain of a neonate who died from *Escherichia coli* sepsis shows yellow discoloration of the basal ganglia. This staining is referred to as kernicterus. Injury to the basal ganglia results in opisthotonos. Early manifestations of kernicterus are lethargy, hypotonia, poor feeding, fever, seizures, and possibly death. Late manifestations include spasticity, choreoathetosis, and deafness.

6.27

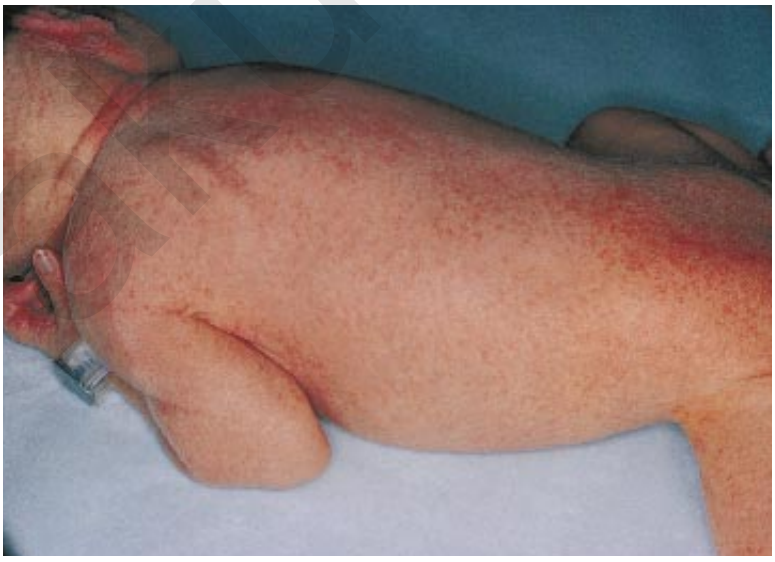

Figure 6.27. This infant with hyperbilirubinemia developed a fine erythematous maculopapular rash involving the trunk while being treated with phototherapy. This "bilirubin rash" improves rapidly. The bronze baby syndrome is a side effect of phototherapy when used in infants with an elevated direct reacting bilirubin. Natural skin color is restored after several months.

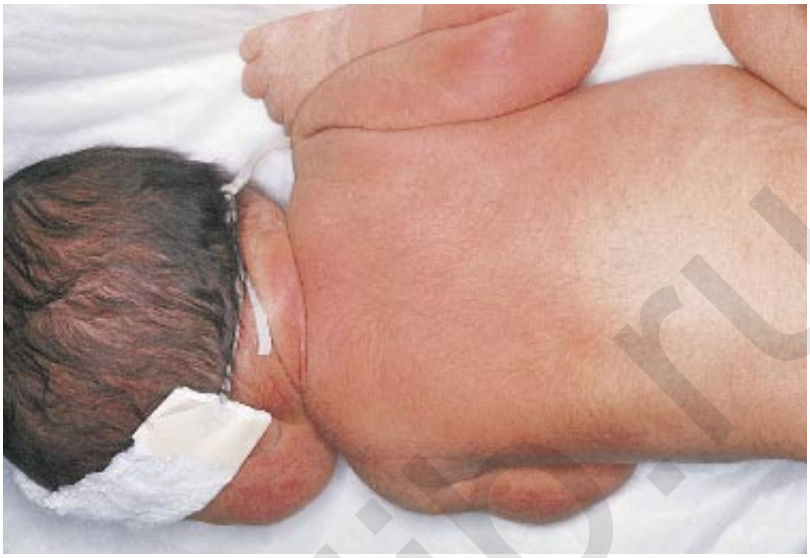

6.28

Figure 6.28. Erythema and edema of the trunk and neck of this infant with "phototherapy sunburn" as a result of placement under daylight fluorescent bulbs for hyperbilirubinemia. Phototherapy may cause hypopigmented spots in areas of the skin that are covered (for example, by electrode patches for monitoring).

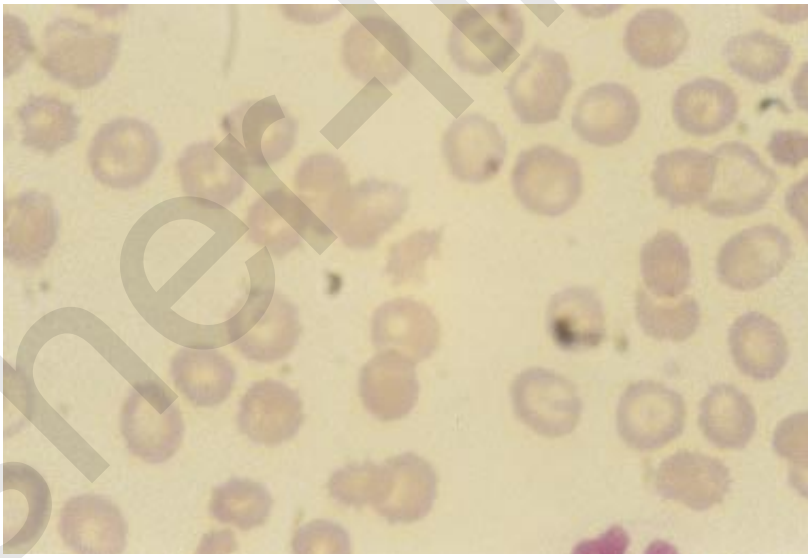

6.29

Figure 6.29. Peripheral blood smear from an infant with acanthocytosis due to vitamin E deficiency. Note the presence of target and burr cells. (Gresik, V.)

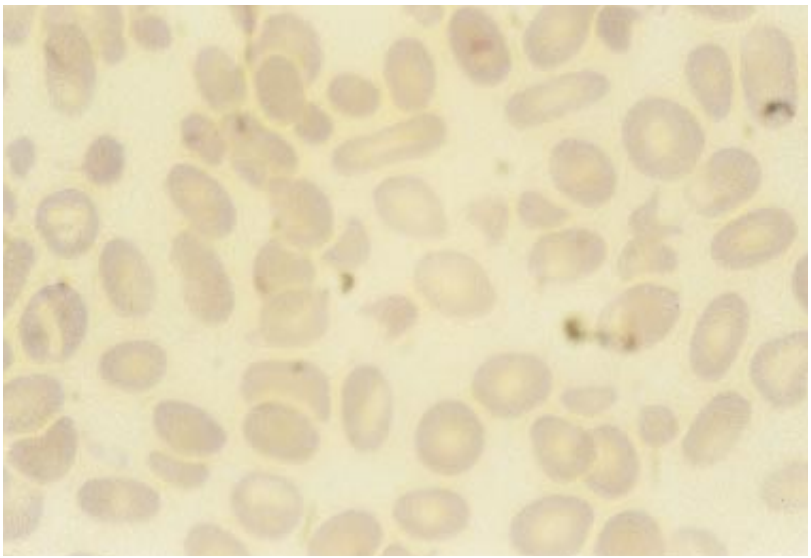

6.30

Figure 6.30. Peripheral blood smear from an infant with congenital elliptocytosis. This may be a cause of anemia or jaundice in the neonate. (Gresik, V.)

6.31

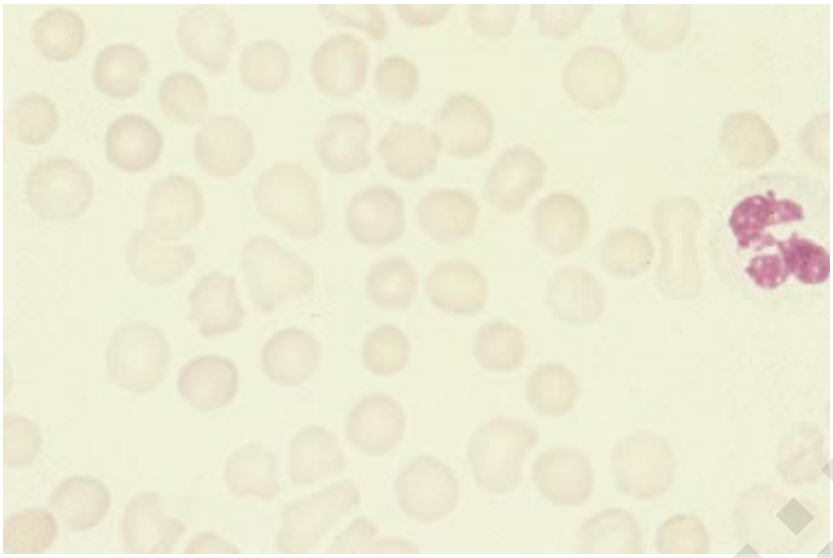

Figure 6.31. Peripheral blood smear from an infant with congenital hereditary spherocytosis. Note the microcytosis. (Gresik, V.)

6.32

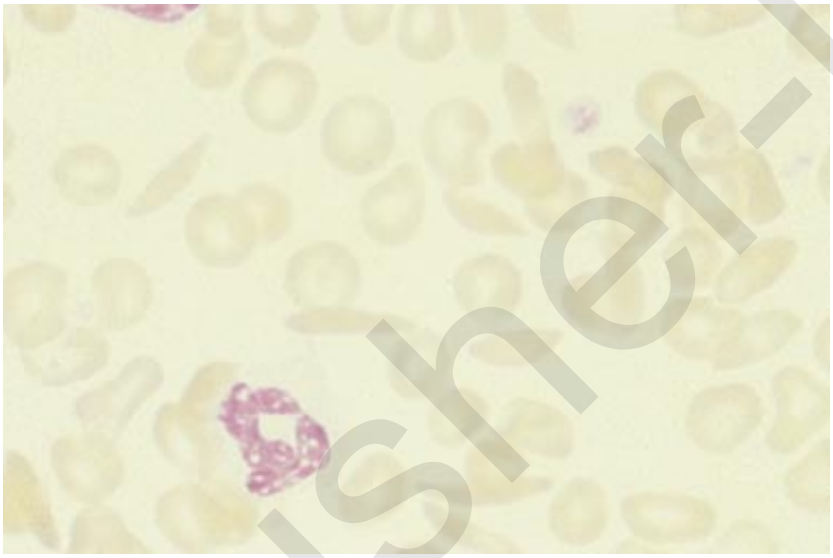

Figure 6.32. Peripheral blood smear from an older infant with sickle cell anemia. Neonates with sickle cell anemia do not have the typical sickling of cells due to the large percentage of fetal hemoglobin. (Gresik, V.)

6.33

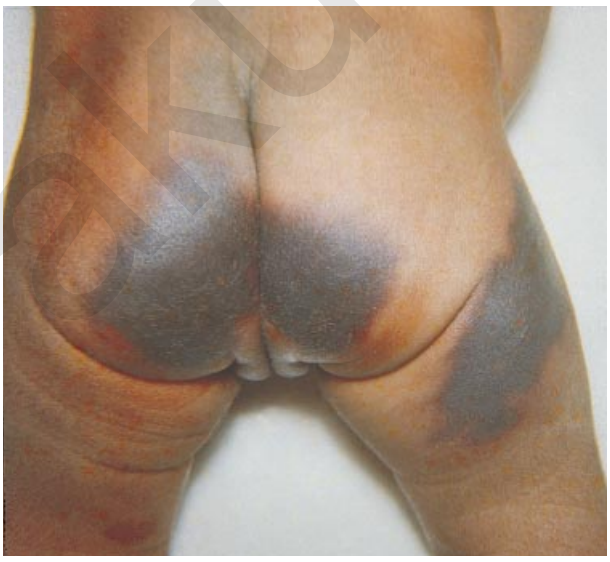

Figure 6.33. Discoloration of the buttocks and thighs in an infant at the age of 2 days with purpura fulminans as a result of sepsis. Purpura fulminans, a nonthrombocytopenic purpura, is characterized by acute, severe, often rapidly fatal, hemorrhagic infarction and necrosis of the skin. In the neonate, acquired or congenital protein C and protein S deficiency have been shown to cause purpura fulminans. It is usually triggered by a preceding infectious process in children.

6.34

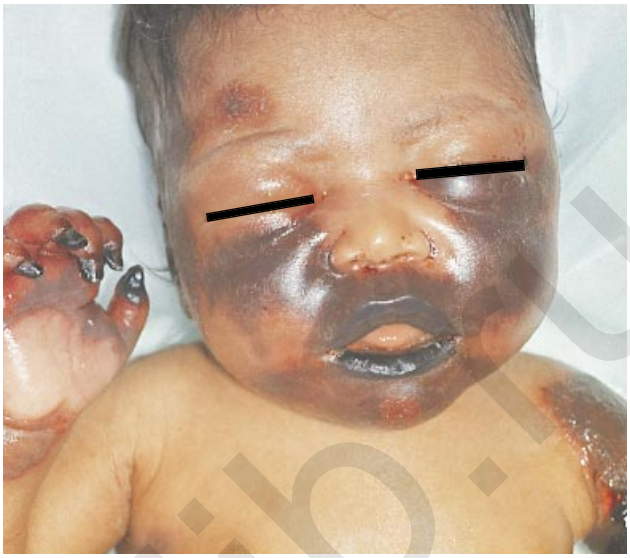

Figure 6.34. Discoloration of the face and necrosis of the fingertips in the same infant as in Figure 6.33 with purpura fulminans at the age of 10 days. Purpura fulminans is characterized by symmetrically distributed localized cutaneous ecchymoses, often with sharp irregular borders on the extremities. Lesions enlarge rapidly, coalesce, and develop central necrosis with hemorrhagic blebs and a raised edge with surrounding erythema. Visceral involvement with hematuria or gastrointestinal bleeding may occur.

6.35

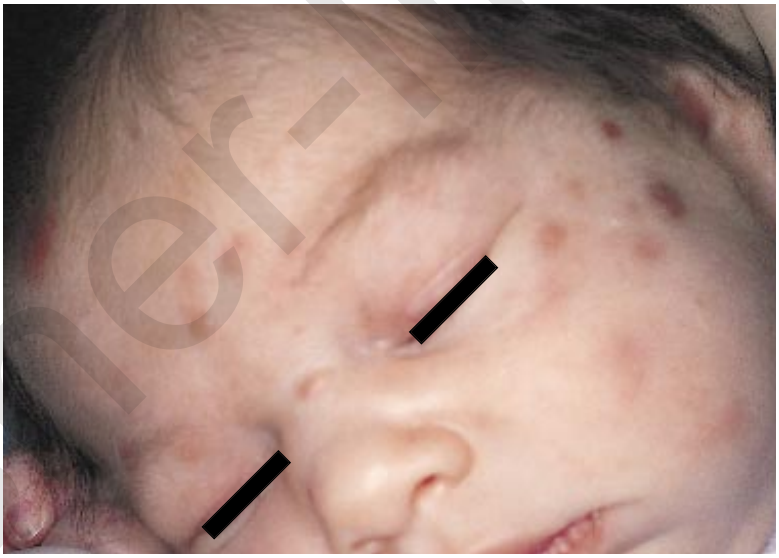

Figure 6.35. This infant with congenital monocytic leukemia was admitted to the hospital at age 20 days. Leukemic lesions are visible on the face of this infant and the peripheral blood smear demonstrated a marked leukocytosis and thrombocytopenia. The bone marrow confirmed the diagnosis of congenital monocytic leukemia.

6.36

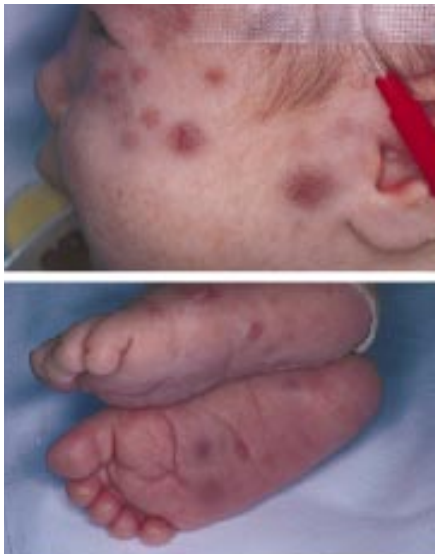

Figure 6.36. Skin lesions (leukemia cutis) on the feet and face of the same infant as in Figure 6.35 with congenital monocytic leukemia. The cutaneous lesions occur as discrete pink, red-brown, or purple macules, papules, or tumors. The tumors of monocytic leukemia tend to be large and purplish or "plum-colored," and are firm solid masses.

6.37

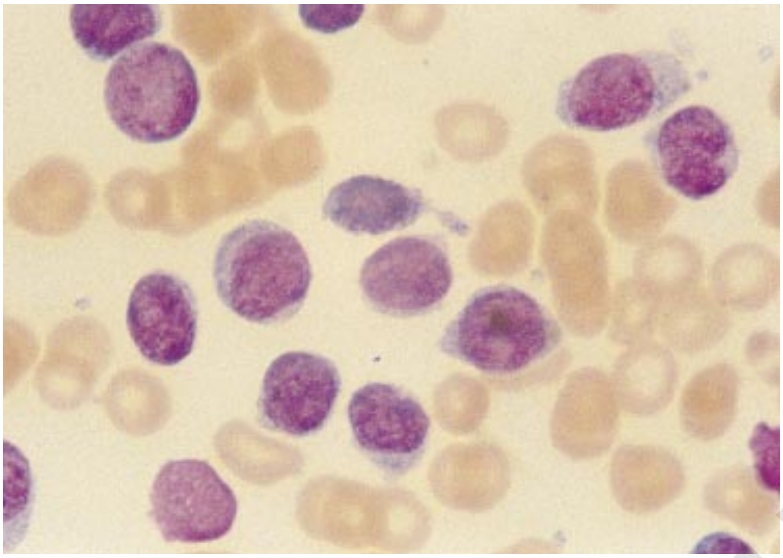

Figure 6.37. Bone marrow smear from the same infant as in Figures 6.35 and 6.36 showing numerous large immature monoblasts.

6.38

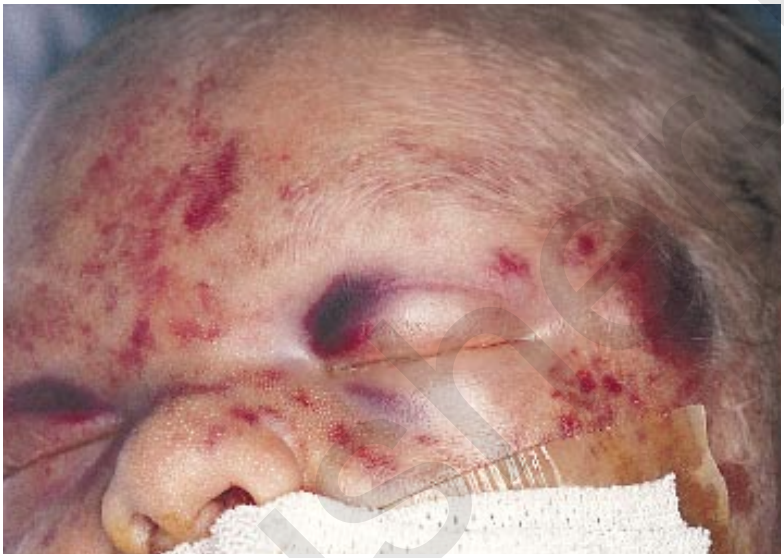

Figure 6.38. Petechiae, ecchymoses, leukemia cutis, and hepatosplenomegaly in an infant with lymphoblastic leukemia. The peripheral white blood cell count in this infant was 99,000/dL, of which 60% were blasts and the platelet count was 19,000/dL. The bone marrow confirmed the diagnosis of lymphoblastic leukemia.

6.39

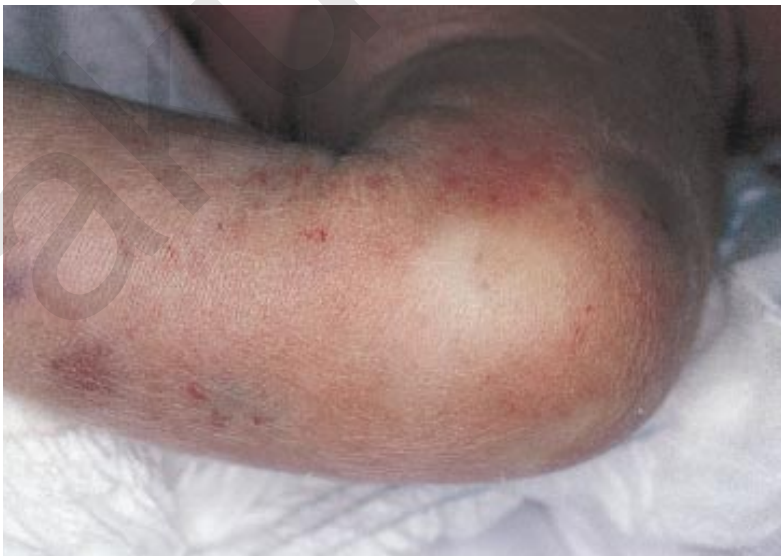

Figure 6.39. Skin nodules on the leg of the same infant as in Figure 6.38 with congenital lymphoblastic leukemia. Chromosome analysis of abnormal lymphoblasts showed a translocation between chromosomes 4 and 11.

6.40

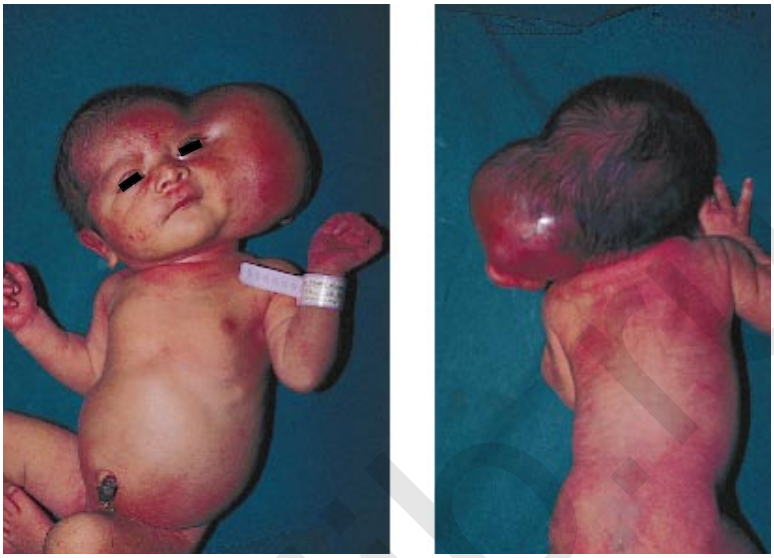

Figure 6.40. Supine and prone views of an infant with distortion of the left facial structures as the result of a large mass. Pathologic specimen confirmed the diagnosis of neuroblastoma which is the most common malignant tumor in infancy. The most common presentation is an abdominal mass. Cutaneous features are present in 50% of newborn infants with this disorder. (Cabrera-Meza, G.)

6.41

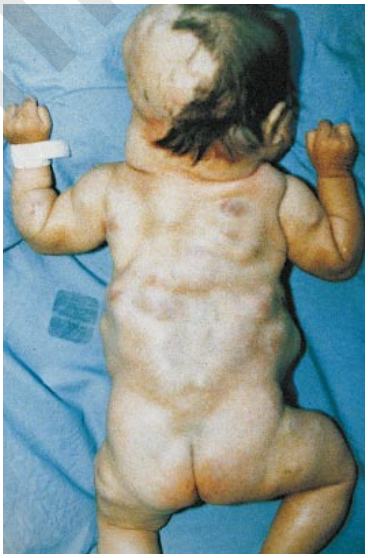

Figure 6.41. Skin metastases in the infant shown in figure 6.42 with congenital neuroblastoma at the age of six weeks. The nodules are characteristic in that they are firm, nontender, blue or grayish blue metastastic nodules that due to the release of catecholamines tend to blanch and develop a surrounding halo of erythema within 2 to 3 minutes after being palpated, stroked, or rubbed. (Cabrera-Meza, G.)

6.42

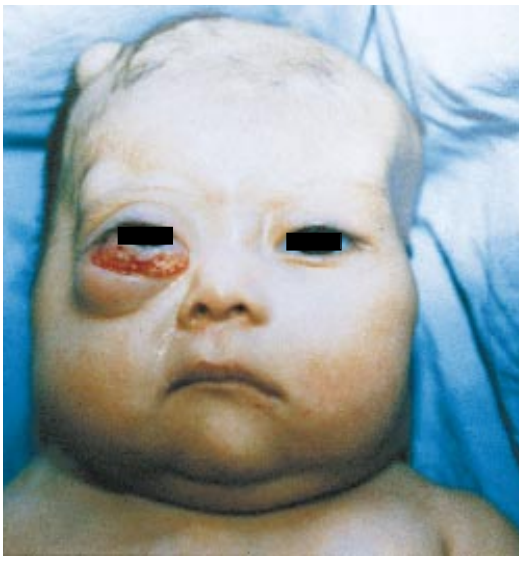

Figure 6.42. Metastases involving the orbit and scalp in the same infant as in Figure 6.41 with congenital neuroblastoma at the age of 6 weeks. The infant died at the age of 2 months. As a result of periorbital ecchymoses, which may occur from the orbital metastases, these infants may have the appearance of "raccoon eyes." (Cabrera-Meza, G.)

6.43

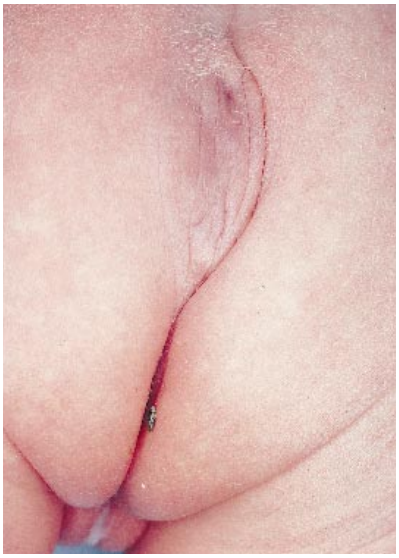

Figure 6.43. Midline cystic mass at the base of the spine. Surgical pathologic specimen confirmed the presence of a teratoma.

6.44

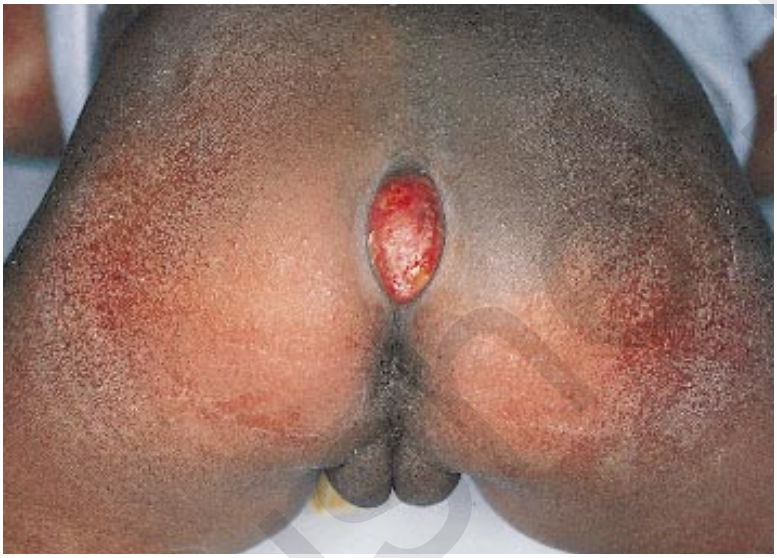

Figure 6.44. The most common solid tumor presenting in neonates at birth is a sacrococcygeal teratoma. Because the tumor arises from the coccyx, the spinal column and canal are spared. This infant has a very small midline spinal swelling. These may grow caudally, become very large, and displace the anus and genitalia. Pelvic extension may occur.

6.45

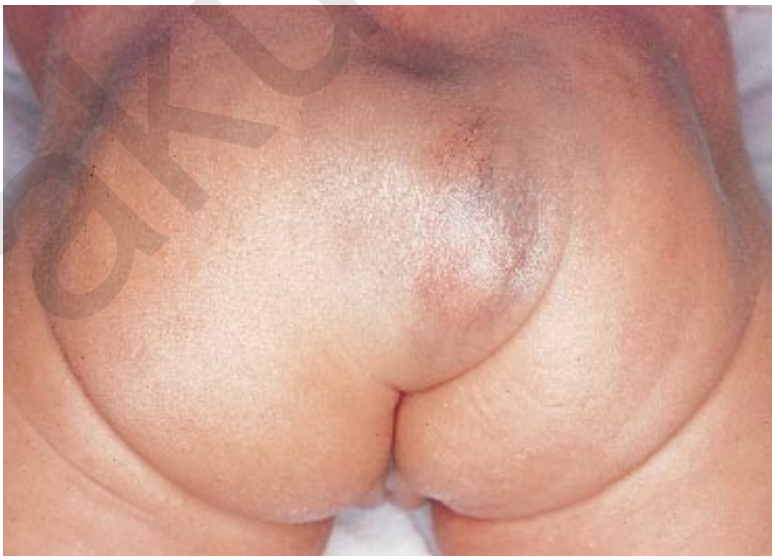

Figure 6.45. In this female infant there is a larger sacrococcygeal teratoma. These tumors are much more common in females. Differential diagnosis includes lipoma, neuroblastoma, cystic lymphangioma, and hemangioma.

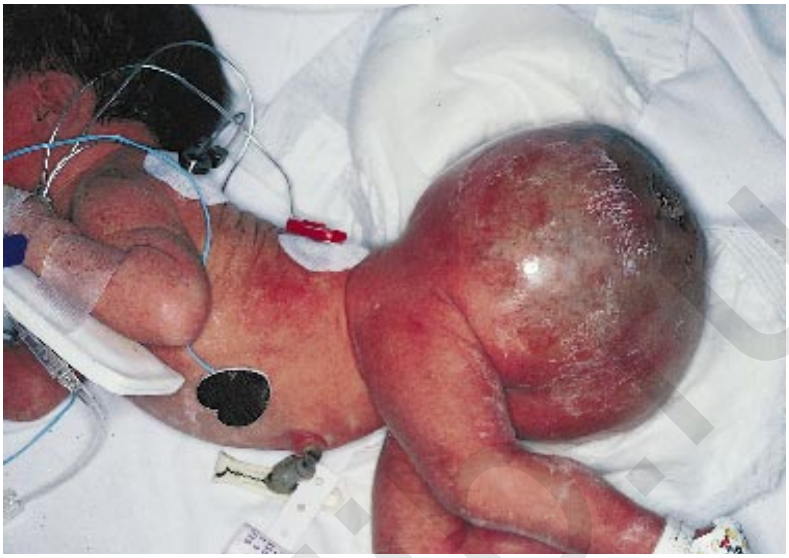

6.46

Figure 6.46. This 36-week-gestation premature infant with a large sacrococcygeal teratoma was delivered vaginally. Prompt surgical excision of the mass is advisable because of possible malignant transformation. Before the 4th month of life, the malignancy rate is 6%; between the 4th month and the 5th year of life, the malignancy rate increases to 50%.

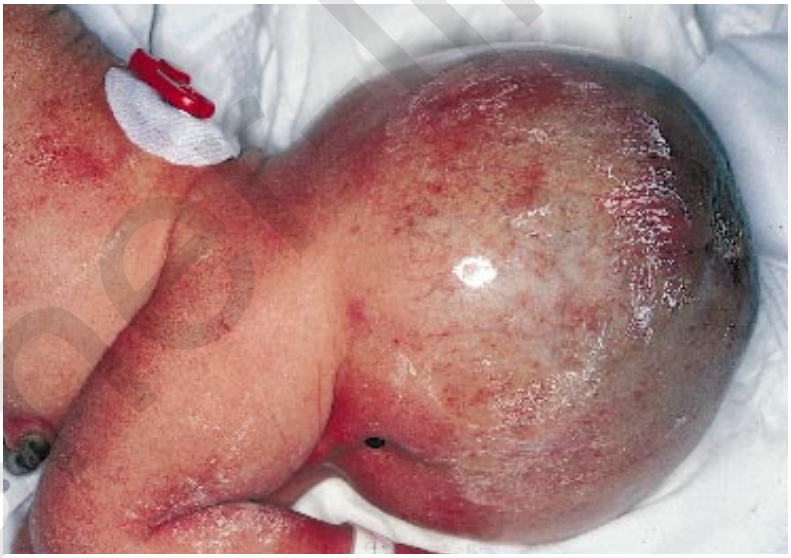

6.47

Figure 6.47. Close-up view of the same giant sacrococcygeal teratoma as in Figure 6.46 showing involvement of anus and genitalia. Pathologic specimen showed immature yolk sac elements with malignant changes.

6.48

Figure 6.48. Giant sacrococcygeal teratoma in a male infant.

6.49

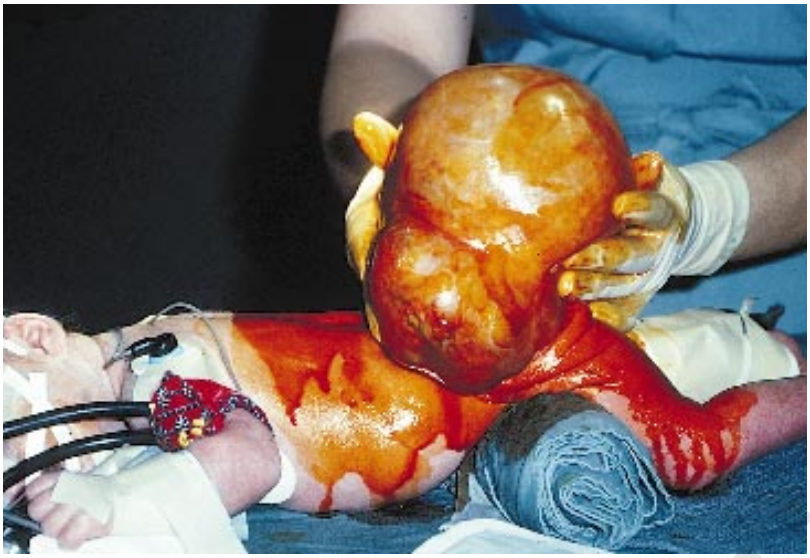

Figure 6.49. Complete surgical resection of the sacrococcygeal teratoma of the same infant as in Figure 6.48. Pathologic specimen was benign and the infant did well.

6.50

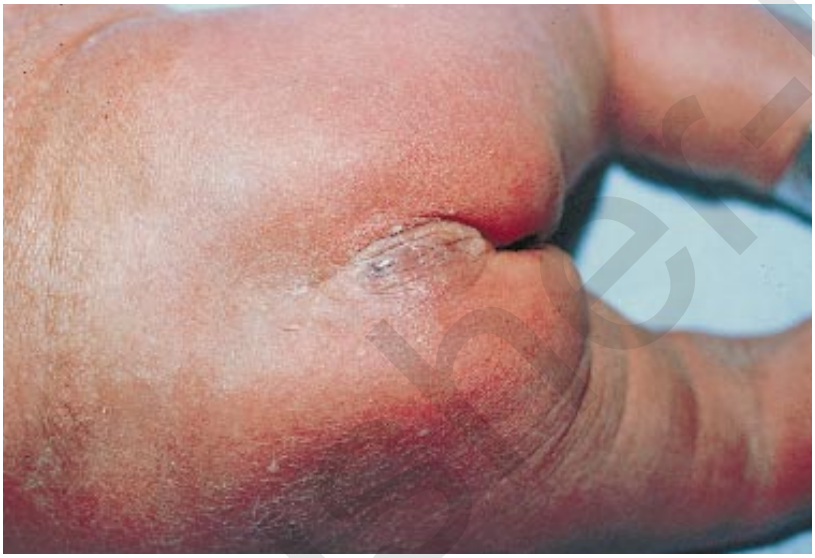

Figure 6.50. This female infant presented with a midline sacral mass which proved to be a chordoma. The infant also had a lymphangioma of the left upper extremity.

6.51

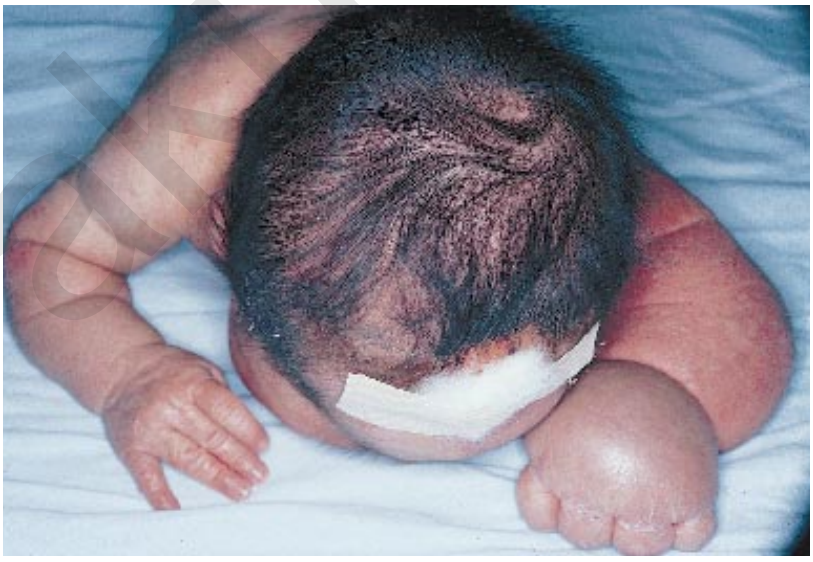

Figure 6.51. The same infant as in Figure 6.50 showing the edematous left upper extremity associated with the lymphangioma.

6.52

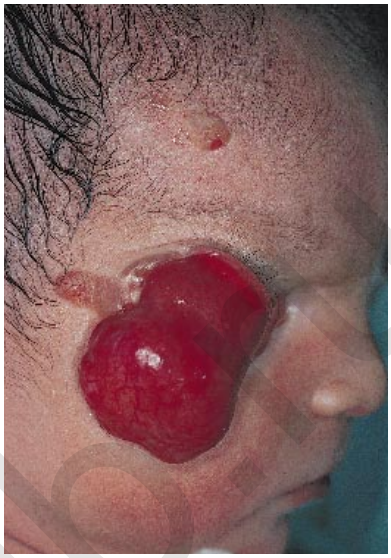

Figure 6.52. A term infant presented at birth with a large soft tissue mass (4 cm by 4 cm) protruding from the right orbit. An MRI showed a large irregular solid soft tissue mass which appeared to arise from or encompass and largely destroy the right globe. The retrobulbar fat was preserved, and the mass did not enter the intracranial space. On pathologic examination there was a malignant, primitive, embryonic tumor that had arisen in association with a congenital hamartomatous malformation of the globe.

6.53

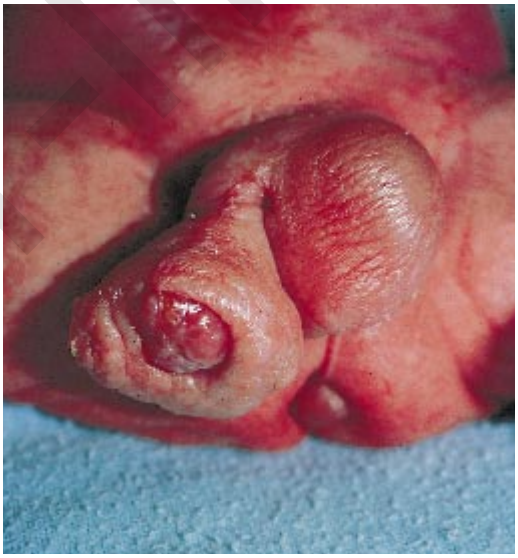

Figure 6.53. This neonate presented with a tumor involving the penile skin, the bladder, and the anal mucous membranes. Surgical removal showed this to be a rhabdomyosarcoma of the penis. The infant had a recurrence and died at the age of 3 years.

6.54

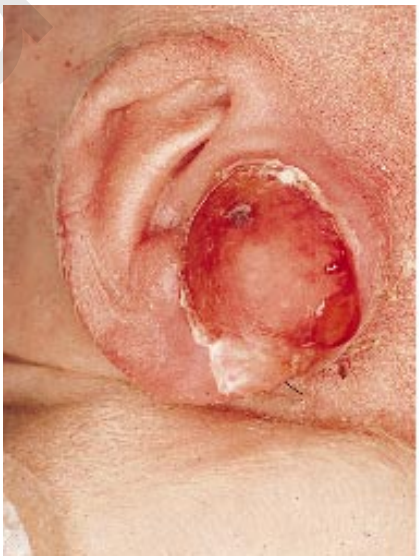

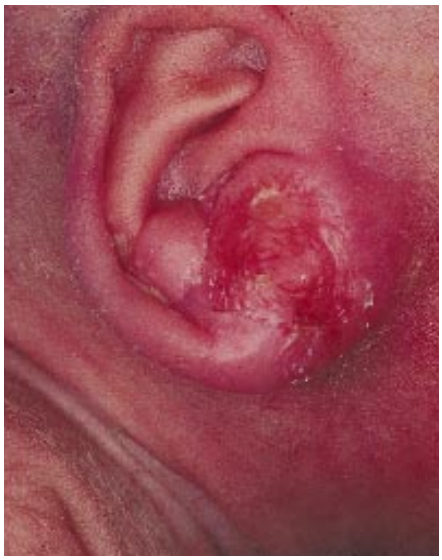

Figure 6.54. The left figure shows a mass involving the right ear of an infant. The biopsy diagnosis was myofibroma. The right figure is a view of the same ear 3 weeks later with regression without intervention. Congenital infantile myofibromatosis may present with multiple lesions that usually regress spontaneously or may present in a generalized form in which there is visceral involvement with a mortality of about 50%.

6.55

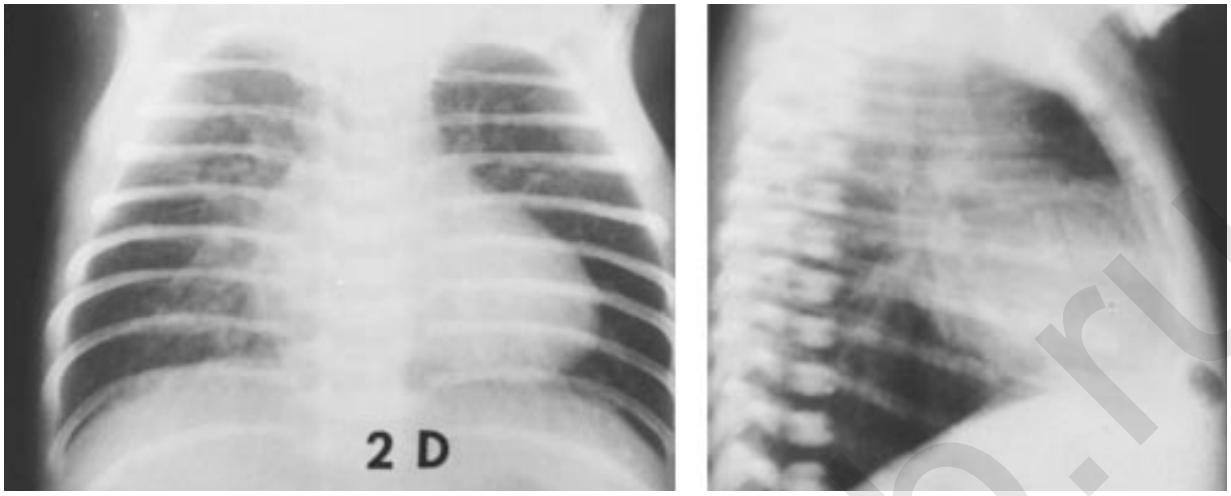

Figure 6.55. The anteroposterior and lateral chest radiographs in an infant with the DiGeorge syndrome. Note the absence of the thymic shadow on both projections. In the DiGeorge syndrome, an isolated T cell deficiency occurs as a result of a congenital malformation of the 3rd and 4th branchial arches. The acronym CATCH 22 syndrome lists the findings seen in DiGeorge syndrome: *c*ardiac defects, *a*bnormal facies, *t*hymic hypoplasia, *c*left palate, *h*ypocalcemia, and 22q11 deletion. The same chromosome abnormality—a deletion at chromosome 22q11 is manifested in velocardiofacial syndrome or Shprintzen's syndrome.

Index